VOLCANISM IN HAWAII

VOLUME 1

U. S. GEOLOGICAL SURVEY PROFESSIONAL PAPER 1350

DIAMOND JUBILEE (1912–1987)

HVO

HAWAIIAN VOLCANO OBSERVATORY

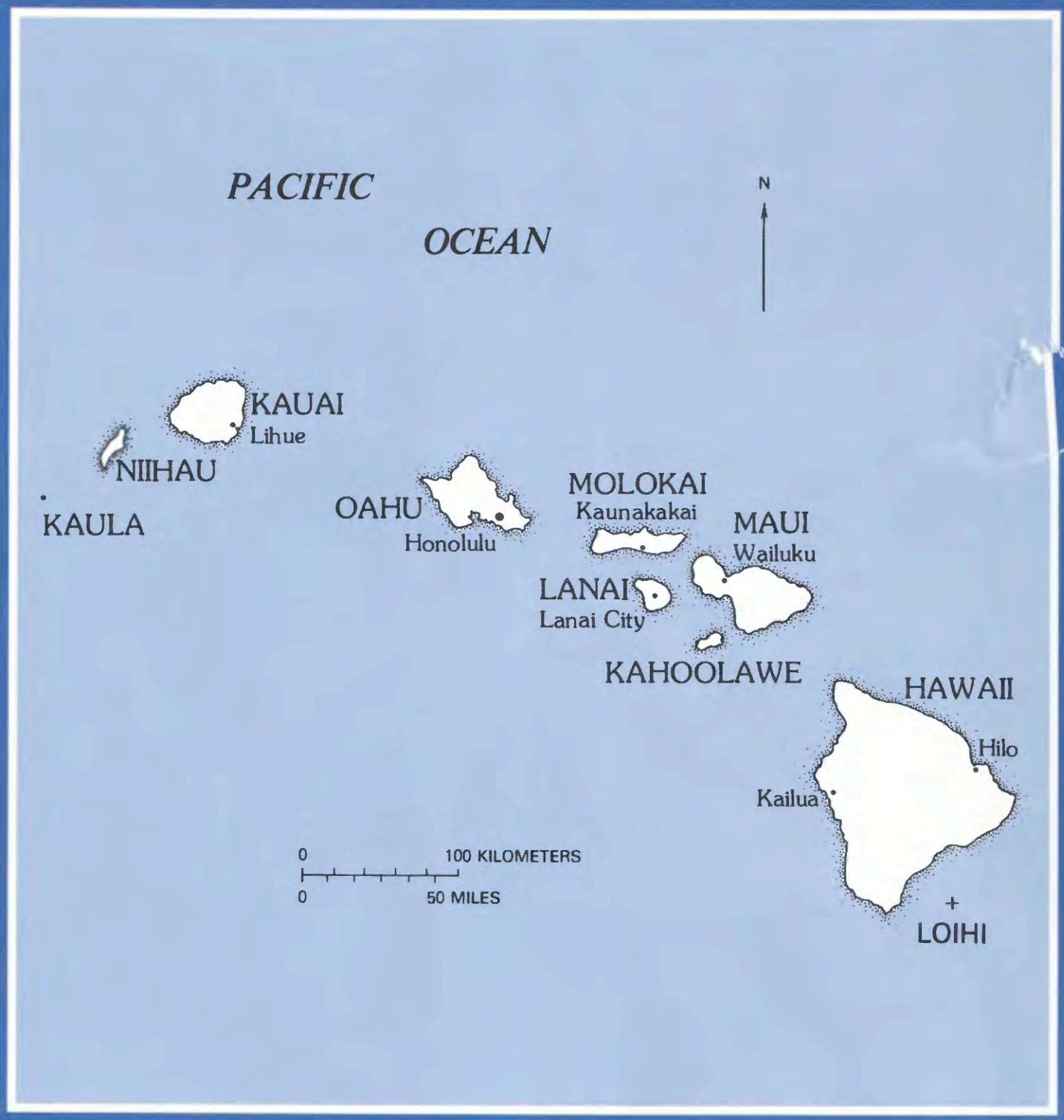

Hawaiian Islands

Cover: Low oblique aerial view of Puu Oo in eruption, east rift zone of Kilauea Volcano, January 31, 1984. View is toward southwest; flows are moving to the north and east. Fountain height is approximately 100 m above the vent. Photograph by J.D. Griggs.

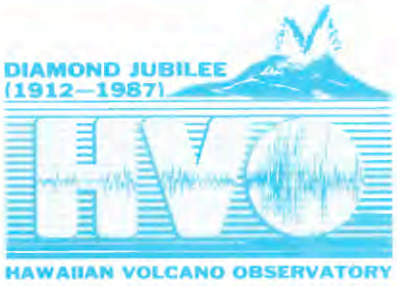

Volcanism in Hawaii

Papers to commemorate the 75th anniversary of the founding of the Hawaiian Volcano Observatory

Overleaf: Morphology of the sea floor in the northern Pacific Ocean, showing prominence and central position of Hawaiian-Emperor volcanic chain (compare with slope map in front of volume 2). From the map "World Ocean Floor" by Bruce C. Heezen and Marie Tharp, published 1977 by United States Navy (Office of Naval Research). Copyright 1977 by Marie Tharp, 1 Washington Avenue, South Nyack, NY 10960.

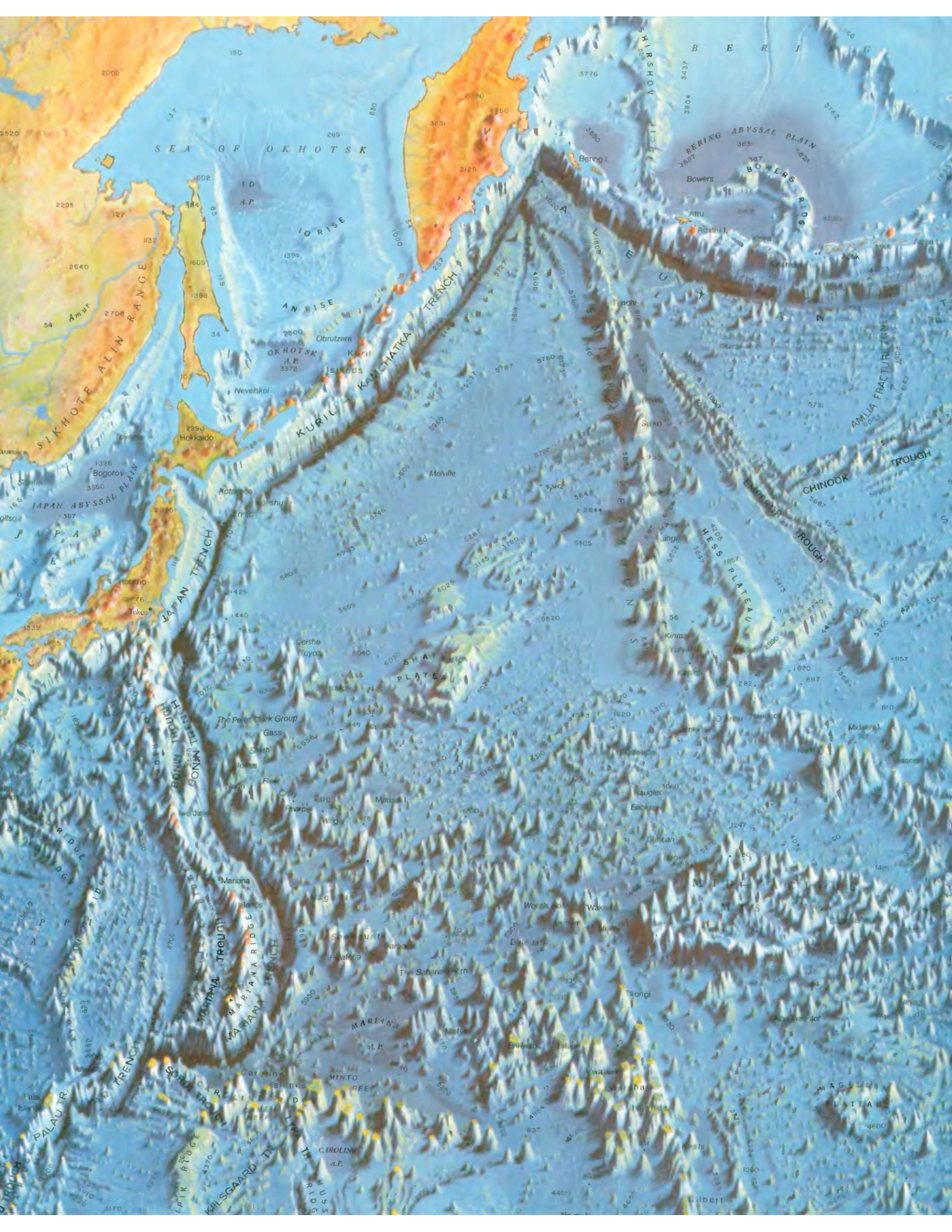
SEA OF OKHOTSK
BERING SEA
BERING ABYSSAL PLAIN
SHIRSHOV RIDGE
Bering I.
Bowers
BOWERS RIDGE
Attu
Attu I.
ALEUTIAN TRENCH
IORISE
ANISE
OKHOTSK A.P.
Obrutzeva
Kuril Islands
Nevelskoi
KURIL - KAMCHATKA TRENCH
SIKHOTE ALIN RANGE
Amur
Hokkaido
Bogorov
JAPAN ABYSSAL PLAIN
Aomori
Honshu
JAPAN TRENCH
Hakodate
Toky
Melville
Suiko
Kinmei
AMLIA FRACTURE ZONE
CHINOOK TROUGH
GIBBS FRACTURE ZONE
HESS PLATEAU
SHATSKY PLATEAU
Meiji
Daikan
Midway I.
The Peter Park Group
Gass
Smith
Francis
Maruyama I.
Baugler
Eastern
Duncan
Mariana
Islands
Wake I.
Wake
Darlac
The Scherm Islands
Tongi
Pilot
MARIANA TROUGH
MARIANA RIDGE
MARIANA TRENCH
SOUTH CHINA SEA BASIN
Caroline Islands
MINTO REEF
CAROLINE A.P.
PALAU TR.
KILSGAARD TR.
MUSSAU RIDGE
MAGELLAN PLATEAU
Gilbert

Nunivak I.
Kodiak
Paul I.
St. George I.
Unimak
Unalaska
Umnak
Surveyor Channel
Quinn
Pratt
Walker
Patton
Fans
Murray
Walls
Gilbert
Pathfinder
Scott
Dickins
Queen Charlotte Is.
Aleutian Abyssal Plain
Tufts Abyssal Plain
Horizon Channel
Mukluk Channel
Cascadia Channel
Juan de Fuca Ridge
Pioneer Fracture Zone
Murray Fracture Zone
Molokai Fracture Zone
Clarion Fracture Zone
Clipperton Fracture Zone
Rocky Mts.
Cascade Range
Sierra Nevada
Columbia
Colorado
San Francisco
Los Angeles
San Diego
Guide
Delgada Cone
California Borderland
Monterey Cone
Gulf of California
Aleutian Trench
Kauai
Oahu
Molokai
Maui
Hawaii
Nihoa
Gardner Pinnacles
French Frigate Shoals
Strauss
Bizet
Wagner
Seamount
Pensacola
Island

Volcanism in Hawaii

Edited by Robert W. Decker, Thomas L. Wright, *and* Peter H. Stauffer

Volume 1

- Physiography, Tectonics, and Submarine Geology
- Geology of the Island of Hawaii
- Petrogenesis and Volcanic Gases

U.S. GEOLOGICAL SURVEY PROFESSIONAL PAPER 1350

UNITED STATES GOVERNMENT PRINTING OFFICE, WASHINGTON : 1987

DEPARTMENT OF THE INTERIOR

DONALD PAUL HODEL, *Secretary*

U.S. GEOLOGICAL SURVEY

Dallas L. Peck, *Director*

Library of Congress Cataloging-in-Publication Data

Volcanism in Hawaii.

(U.S. Geological Survey Professional Paper 1350)
Contents: v.1. Physiography, tectonics, and submarine geology; Geology of the Island of Hawaii; Petrogenesis and volcanic gases. v.2. Structure; Dynamics; History of investigations of Hawaiian volcanism.
Supt. of Docs. no.: I 19.16:1350
1. Volcanism—Hawaii. 2. Volcanic ash, tuff, etc.—Hawaii. I. Decker, Robert Wayne, 1927–. II. Wright, Thomas Llewellyn, 1935–. III. Stauffer, Peter Herman, 1935–. IV. Series: United States. Geological Survey. Professional Paper 1350.
QE524.V65 1987 551.2'2'09969 86–600292

**For sale by the Books and Open-File Reports Section,
U.S. Geological Survey, Federal Center, Box 25425, Denver, CO 80225**

FOREWORD

When Thomas A. Jaggar established the Hawaiian Volcano Observatory (HVO) in 1912, he could not have imagined the extent to which his pioneering studies would expand in the next 75 years. He demonstrated great foresight in setting two major research goals for the observatory: (1) the conduct of systematic, scientific studies to understand more about volcanic processes, both during and between eruptions; and (2) the practical application of research results for mitigating hazards—the forecast of impending eruptions and paths of destructive lava flows and the evaluation of all other types of volcanic hazard. The results of studies by HVO staff and other scientists have been shared with the National Park Service since 1917, when Hawaii National Park was created by Congress, and I want to emphasize that the cooperation and support of the Park Service over the ensuing years have been exceptionally helpful for our scientific work and for the benefit of the public.

During these 75 years following the founding of HVO, scientists have pursued Jaggar's original goals with great success. In addition to developing volcano-monitoring techniques now used worldwide, the observatory also has served as a training center for volcanologists from many countries, as well as for the postgraduate training of a great number and variety of USGS scientists, myself included. The lessons learned at HVO became especially valuable when Mount St. Helens erupted catastrophically in 1980, and our cadre of HVO staffers past and present were able to provide monitoring and forecasting information for that volcano, resulting in the saving of many lives.

The papers in this volume reflect the greatly improved understanding of the behavior of Kilauea and Mauna Loa Volcanoes that has been developed since the early studies in Hawaii. The structure and tectonic setting of the volcanoes, the physical and chemical properties of the eruptive products, and the history of eruptive activity over the past several thousand years have all been investigated in great detail, and the results are summarized in this book. These volcanoes have served as unique natural laboratories for the study of volcanic phenomena and the development of new monitoring instruments, and the new methods and instruments in time became standards for monitoring in most other observatories around the world. The use of sophisticated instruments led to dramatic improvements in our ability to forecast the activity of Kilauea and Mauna Loa over the past 75 years. In particular, our ability to precisely monitor inflation-deflation cycles, the location of magma-generated microearthquakes, and volcanic tremor has moved from the subjective, intuitive stage to the level of being a science in itself. In recent decades, new technology for laser distance measuring, real-time analysis of telemetered seismic signals, and volcanic-gas analysis have greatly improved our forecasting capability. Currently we are pursuing new applications of computers to all the problems of volcano monitoring, including the generation of three-dimensional models of the volcanic "plumbing systems" for Kilauea and Mauna Loa.

All these exciting scientific accomplishments, though nourished by improved technology, have in fact been linked by a continuing thread of human ingenuity and dedication to science such as characterized the earliest work of Thomas Jaggar. His achievements and those of the people who succeeded him demonstrate the critical importance of individual imagination and creativity in earth-science research. I take great pride and personal pleasure in presenting these results of 75 years of research in Hawaiian volcanism to the scientific community and the public.

Dallas L. Peck
Director, U.S. Geological Survey

A Trip Around the Island
Hawaiian Petroglyph

PREFACE

"Stones rot; only the chants remain." This ancient Polynesian saying reflects the rapid changes that occur on volcanic islands. Young lava flows are soon covered by lush vegetation, and only the stories of their eruption, passed from generation to generation, survive. This collection of articles on Hawaiian volcanism commemorating the 75th anniversary of the Hawaiian Volcano Observatory is a chant to future generations. Much has been learned in these past 75 years, but much more is still to be discovered.

Scientific literature serves at least two purposes. From the standpoint of data it is, or should be, an archive of the truth. The data in these volumes are as close to the truth as is humanly possible. Interpretation of the data is another matter, and from this standpoint scientific literature should be a forum for debate. Readers of chapter 1, part I, and chapter 2 will discover that the authors reach different interpretations concerning the volume and propagation rates of Hawaiian volcanism during the past few million years. These authors base their respective conclusions largely on the same data. Eventually, additional data, strength of arguments, and the consideration and consensus of the readers may lead to acceptance of some interpretations and rejection of others. That is something for the scientific community, not the editors, to decide.

The staff and guest investigators at the Hawaiian Volcano Observatory over the past 75 years have represented many diverse scientific disciplines and backgrounds. There is great strength in this diversity. Working closely together on common problems, geologists, geochemists, geophysicists, biologists, oceanographers, meteorologists, and general scientific practitioners have learned a great deal about Hawaiian volcanoes as well as about the scientific methods of their colleagues. The whole has greatly exceeded the sum of the parts. Close cooperation among scientists with different backgrounds has led to conceptual models of volcanism that satisfy not only the geologic and geophysical field observations, but also the theoretical constraints of thermodynamics and rock mechanics.

The scope of articles in these volumes, and the many publications by guest investigators at the observatory during recent years, reflect the view that volcanoes can best be studied from a multidisciplinary approach. We hope that seismologists will read the chapters on Hawaiian petrology and volcanic gases and that, in turn, gas geochemists will read about the distribution and causes of earthquakes beneath the Island of Hawaii. The Hawaiian Volcano Observatory has made important gains in the cross-fertilization of science in the past, and as science becomes more and more specialized in the future, this role will become even more important.

Most place names in the Hawaiian Islands, and several geographical and descriptive terms used in volcanology, derive from the Hawaiian language. In the standard written form of that language, diacritical marks are used; these diacritical marks not only indicate the pronunciation, but in many cases are essential to distinguish between otherwise similar words of different meanings. However, the volcanological terms of Hawaiian origin (such as "aa" and "pahoehoe") are spelled in the English language without the diacritical marks, and the Board on Geographic Names in Washington, whose rulings the USGS follows, does not recognize such marks for Hawaiian place names. Hence no diacritical marks are used on Hawaiian words in the chapters of the present work. In order to acquaint those interested with the original Hawaiian spelling and pronunciation of these words, however, a pronunciation guide for Hawaiian words is included at the end of volume 2.

A work of the scale and complexity of the present one, compiled and produced with the aim of meeting short time deadlines, is clearly the product of many willing and skilled hands, from the authors to the printers. In the USGS Branch of Western Technical Reports, special contributions were made by Derrick Hirsch in editing, Jeff Troll in coordination and layout, Jim Pinkerton in overseeing the editing of figures, and Al Earnest and the entire drafting staff in preparing the hundreds of illustrations. The cooperation of the Branch of Eastern Technical Reports in helping prepare illustrations for certain chapters is also appreciated.

These volumes, readers, may be chants, but they are also intended to be steppingstones. The trail is yours.

Robert W. Decker, Thomas L. Wright, and Peter H. Stauffer
Editors

CONTENTS

VOLUME 1

PHYSIOGRAPHY, TECTONICS, AND SUBMARINE GEOLOGY

Chapter 1. The Hawaiian-Emperor volcanic chain

Part I. Geologic evolution *5*
David A. Clague and G. Brent Dalrymple

Part II. Stratigraphic framework of volcanic rocks of the Hawaiian Islands *55*
Virginia A.M. Langenheim and David A. Clague

2. Subsidence of the Hawaiian Ridge *85*
James G. Moore

3. Slopes of the Hawaiian Ridge *101*
Robert K. Mark and James G. Moore

4. Submarine topography around the Hawaiian Islands *109*
Daniel J. Fornari and J. Frisbee Campbell

5. The geomorphic and structural development of Hawaiian submarine rift zones *125*
Daniel J. Fornari

6. Geology of the summit of Loihi submarine volcano *133*
Alexander Malahoff

GEOLOGY OF THE ISLAND OF HAWAII

Chapter 7. Geologic history and evolution of geologic concepts, Island of Hawaii *149*
Donald W. Peterson and Richard B. Moore

8. Hawaii: The view from space *191*
George E. Ulrich, Peter J. Mouginis-Mark, and Jo-Ann Bowell

9. Effects of volcanic emanations on carbon-isotope content of modern plants near Kilauea Volcano *209*
Meyer Rubin, John P. Lockwood, and Irving Friedman

10. Hawaiian radiocarbon dates *213*
Meyer Rubin, Lea Kelley Gargulinski, and John P. McGeehin

11. Stratigraphy of Kilauea Volcano *243*
R. Michael Easton

12. Eruptive history and long-term behavior of Kilauea Volcano *261*
Robin T. Holcomb

Chapter 13. Stratigraphy and petrology of the Uwekahuna Bluff section, Kilauea caldera *351*
Thomas J. Casadevall and Daniel Dzurisin

14. Intrusive rocks of Kilauea caldera *377*
Thomas J. Casadevall and Daniel Dzurisin

15. An early 19th century reticulite pumice from Kilauea Volcano *395*
Robert P. Sharp, Daniel Dzurisin, and Michael C. Malin

16. The 1972–1974 Mauna Ulu eruption, Kilauea Volcano: An example of quasi-steady-state magma transfer *405*
Robert I. Tilling, Robert L. Christiansen, Wendell A. Duffield, Elliott T. Endo, Robin T. Holcomb, Robert Y. Koyanagi, Donald W. Peterson, and John D. Unger

17. The Puu Oo eruption of Kilauea Volcano, episodes 1–20, January 3, 1983, to June 8, 1984 *471*
Edward W. Wolfe, Michael O. Garcia, Dallas B. Jackson, Robert Y. Koyanagi, Christina A. Neal, and Arnold T. Okamura

18. Holocene eruptive history of Mauna Loa Volcano *509*
John P. Lockwood and Peter W. Lipman

19. Mauna Loa 1974–1984: A decade of intrusive and extrusive activity *537*
John P. Lockwood, John J. Dvorak, Thomas T. English, Robert Y. Koyanagi, Arnold T. Okamura, Marjorie L. Summers, and Wilfred R. Tanigawa

20. Hualalai Volcano: A preliminary summary of geologic, petrologic, and geophysical data *571*
Richard B. Moore, David A. Clague, Meyer Rubin, and Wendy A. Bohrson

21. Pleistocene subglacial eruptions on Mauna Kea *587*
Stephen C. Porter

22. Volcanic hazards in the Hawaiian Islands *599*
Donal R. Mullineaux, Donald W. Peterson, and Dwight R. Crandell

PETROGENESIS AND VOLCANIC GASES

Chapter 23. Recent advances in Hawaiian petrology and geochemistry *625*
Thomas L. Wright and Rosalind T. Helz

24. Trace-element chemistry of Kilauea and Mauna Loa lava in space and time: A reconnaissance *641*
Robert I. Tilling, Thomas L. Wright, and Hugh T. Millard, Jr.

25. Diverse olivine types in lava of the 1959 eruption of Kilauea Volcano and their bearing on eruption dynamics *691*
Rosalind Tuthill Helz

Chapter 26. Origin of the West Maui volcanic rocks inferred from Pb, Sr, and Nd isotopes and a multicomponent model for oceanic basalts *723*
Mitsunobu Tatsumoto, Ernst Hegner, and Daniel M. Unruh

27. Constraints on the characteristics of magma sources for Hawaiian volcanoes based on noble-gas systematics *745*
Ichiro Kaneoka

28. Hawaiian eruptive gases *759*
L. Paul Greenland

29. SO_2 and CO_2 emission rates at Kilauea Volcano, 1979–1984 *771*
Thomas J. Casadevall, J. Barry Stokes, L. Paul Greenland, Lawrence L. Malinconico, John R. Casadevall, and Bruce T. Furukawa

30. Composition of gases from the 1984 eruption of Mauna Loa Volcano *781*
L. Paul Greenland

31. Sulfur and carbon abundances in Hawaiian tholeiite lavas: 1972–1975 eruptions of Kilauea and 1975 eruption of Mauna Loa *791*
Karen J. Franczyk, Everett K. Gibson, Jr., and Robert I. Tilling

32. Variation of $\delta^{13}C$ in fumarolic gases from Kilauea Volcano *805*
Irving Friedman, Jim Gleason, and Trevor Jackson

33. Helium at Kilauea Volcano
Part I. Spatial and temporal variations at Sulphur Bank *809*
Irving Friedman and G. Michael Reimer
Part II. Distribution in the summit region *815*
G. Michael Reimer

34. Use of satellite telemetry for monitoring active volcanoes, with a case study of a gas-emission event at Kilauea Volcano, December 1982 *821*
Kenneth A. McGee, A. Jefferson Sutton, and Motoaki Sato

35. Hawaiian volcanoes and the biogeology of mercury *827*
Barbara Z. Siegel and Sanford M. Siegel

VOLUME 2

STRUCTURE

DYNAMICS

HISTORY OF INVESTIGATIONS OF HAWAIIAN VOLCANISM

Any use of trade names and trademarks in this publication is for descriptive purposes only and does not constitute endorsement by the U.S. Geological Survey.

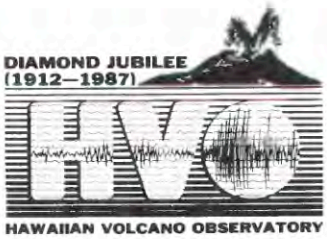
DIAMOND JUBILEE
(1912–1987)
HVO
HAWAIIAN VOLCANO OBSERVATORY

Volume 1

Aerial view of Laysan Island, the largest island in the northwestern (leeward) Hawaiian Chain. Photograph by George H. Balazs, National Marine Fisheries Service.

PHYSIOGRAPHY, TECTONICS, AND SUBMARINE GEOLOGY

The Hawaiian-Emperor volcanic chain is a dogleg ridge, largely submarine, that stretches nearly 6,000 km across the floor of the north Pacific Ocean. At the southeast end is the Island of Hawaii; from there it extends northwestward along the Hawaiian Ridge to a major bend beyond Kure Atoll. North of the bend the chain continues as the submarine ridge of the Emperor Seamounts. Volcanoes are active at the southeast end of the chain and become progressively older northwestward, reaching ages of 75–80 Ma at the north end of the Emperor Seamounts.

Nearly all of this volcanic chain, with an estimated total area of 1.2 million km^2, lies under water. Only the Hawaiian Islands and a few atolls of the Hawaiian Ridge, totaling some 16,878 km^2, rise above the ocean surface. Understandably, the chain has been explored largely by oceanographers. However, because many of the seamounts are similar to the island volcanoes of Hawaii, much has been learned by comparative studies.

The six chapters in this section deal with the origin and evolution of the Hawaiian-Emperor volcanic chain and the submarine geology of the Hawaiian Ridge. They begin with considering the entire chain and narrow down to the undersea summit of Loihi Volcano off the southeast coast of the Island of Hawaii.

Mother and Child
Hawaiian Petroglyph
Puako, Hawaii

THE HAWAIIAN-EMPEROR VOLCANIC CHAIN
Part I
Geologic Evolution

By David A. Clague *and* G. Brent Dalrymple

ABSTRACT

The Hawaiian-Emperor volcanic chain stretches nearly 6,000 km across the North Pacific Ocean and consists of at least 107 individual volcanoes with a total volume of about 1 million km³. The chain is age progressive with still-active volcanoes at the southeast end and 80–75-Ma volcanoes at the northwest end. The bend between the Hawaiian and Emperor Chains reflects a major change in Pacific plate motion at 43.1 ± 1.4 Ma and probably was caused by collision of the Indian subcontinent into Eurasia and the resulting reorganization of oceanic spreading centers and initiation of subduction zones in the western Pacific. The volcanoes of the chain were erupted onto the floor of the Pacific Ocean without regard for the age or preexisting structure of the ocean crust.

Hawaiian volcanoes erupt lava of distinct chemical compositions during four major stages in their evolution and growth. The earliest stage is a submarine alkalic preshield stage, which is followed by the tholeiitic shield stage. The shield stage probably accounts for >95 percent of the volume of each volcano. The shield stage is followed by an alkalic postshield stage during which a thin cap of alkalic basalt and associated differentiated lava covers the tholeiitic shield. After several million years of erosion, alkalic rejuvenated-stage lava erupts from isolated vents. An individual volcano may become extinct before the sequence is complete. The alkalic preshield stage is only known from recent study of Loihi Seamount. Lava from later eruptive stages has been identified from numerous submerged volcanoes located west of the principal Hawaiian Islands.

Volcanic propagation rates along the chain are 9.2 ± 0.3 cm/yr for the Hawaiian Chain and 7.2 ± 1.1 cm/yr for the Emperor Chain. A best fit through all the age data for both chains gives 8.6 ± 0.2 cm/yr. Alkalic rejuvenated-stage lava erupts on an older shield during the formation of a new large shield volcano 190 ± 30 km to the east. The duration of the quiescent period preceding eruption of rejuvenated-stage lava decreases systematically from 2.5 m.y. on Niihau to <0.4 m.y. at Haleakala, reflecting an increase in the rate of volcanic propagation during the last few million years. Rejuvenated-stage lava is generated during the rapid change from subsidence to uplift as the volcanoes override a flexural arch created by loading the new shield volcano on the ocean lithosphere.

Paleomagnetic data indicate that the Hawaiian hot spot has remained fixed during the last 40 m.y., but prior to that time the hot spot was apparently located at a more northerly latitude. The most reliable data suggest about 7° of southward movement of the hot spot between 65 and 40 Ma.

The numerous hypotheses to explain the mechanism of the hot spot fall into four types: propagating fracture hypotheses, thermal or chemical convection hypotheses, shear melting hypotheses, and heat injection hypotheses. A successful hypothesis must explain the propagation of volcanism along the chain, the near-fixity of the hot spot, the chemistry and timing of the eruptions from individual volcanoes, and the detailed geometry of volcanism. None of the geophysical hypotheses proposed to date are fully satisfactory. However, the existence of the Hawaiian swell suggests that hot spots are indeed hot. In addition, both geophysical and geochemical hypotheses suggest that primitive undegassed mantle material ascends beneath Hawaii. Petrologic models suggest that this primitive material reacts with the ocean lithosphere to produce the compositional range of Hawaiian lava.

INTRODUCTION

The Hawaiian Islands; the seamounts, banks, and islands of the Hawaiian Ridge; and the chain of Emperor Seamounts form an array of shield volcanoes that stretches nearly 6,000 km across the north Pacific Ocean (fig. 1.1). This unique geologic feature consists of more than 107 individual volcanoes with a combined volume slightly greater than 1 million km³ (Bargar and Jackson, 1974). The chain is age progressive with still-active volcanoes at the southeast end whereas those at the northwest end have ages of about 75–80 Ma. The volcanic ridge is surrounded by a symmetrical depression, the Hawaiian Deep, as much as 0.7 km deeper than the adjacent ocean floor (Hamilton, 1957). The Hawaiian Deep is in turn surrounded by the broad Hawaiian Arch.

At the southeast end of the chain lie the eight principal Hawaiian Islands. Place names for the islands and seamounts in the chain are shown in figure 1.1 (see also table 1.2). The Island of Hawaii includes the active volcanoes of Mauna Loa, which erupted in 1984, and Kilauea, which erupted in 1986. Loihi Seamount, located about 30 km off the southeast coast of Hawaii, is also active and considered to be an embryonic Hawaiian volcano (Malahoff, chapter 6; Moore and others, 1979, 1982). Hualalai Volcano on Hawaii and Haleakala Volcano on Maui have erupted in historical times. Between Niihau and Kure Island only a few of the volcanoes rise above the sea as small volcanic islets and coral atolls. Beyond Kure the volcanoes are entirely submerged beneath the sea. Approximately 3,450 km northwest of Kilauea, the Hawaiian Chain bends sharply to the north and becomes the Emperor Seamounts, which continue northward another 2,300 km.

It is now clear that this remarkable feature was formed during the past 70 m.y. or so as the Pacific lithospheric plate moved north and then west relative to a melting anomaly, called the Hawaiian hot spot, located in the asthenosphere. According to this hot-spot hypothesis, a trail of volcanoes was formed and left on the ocean

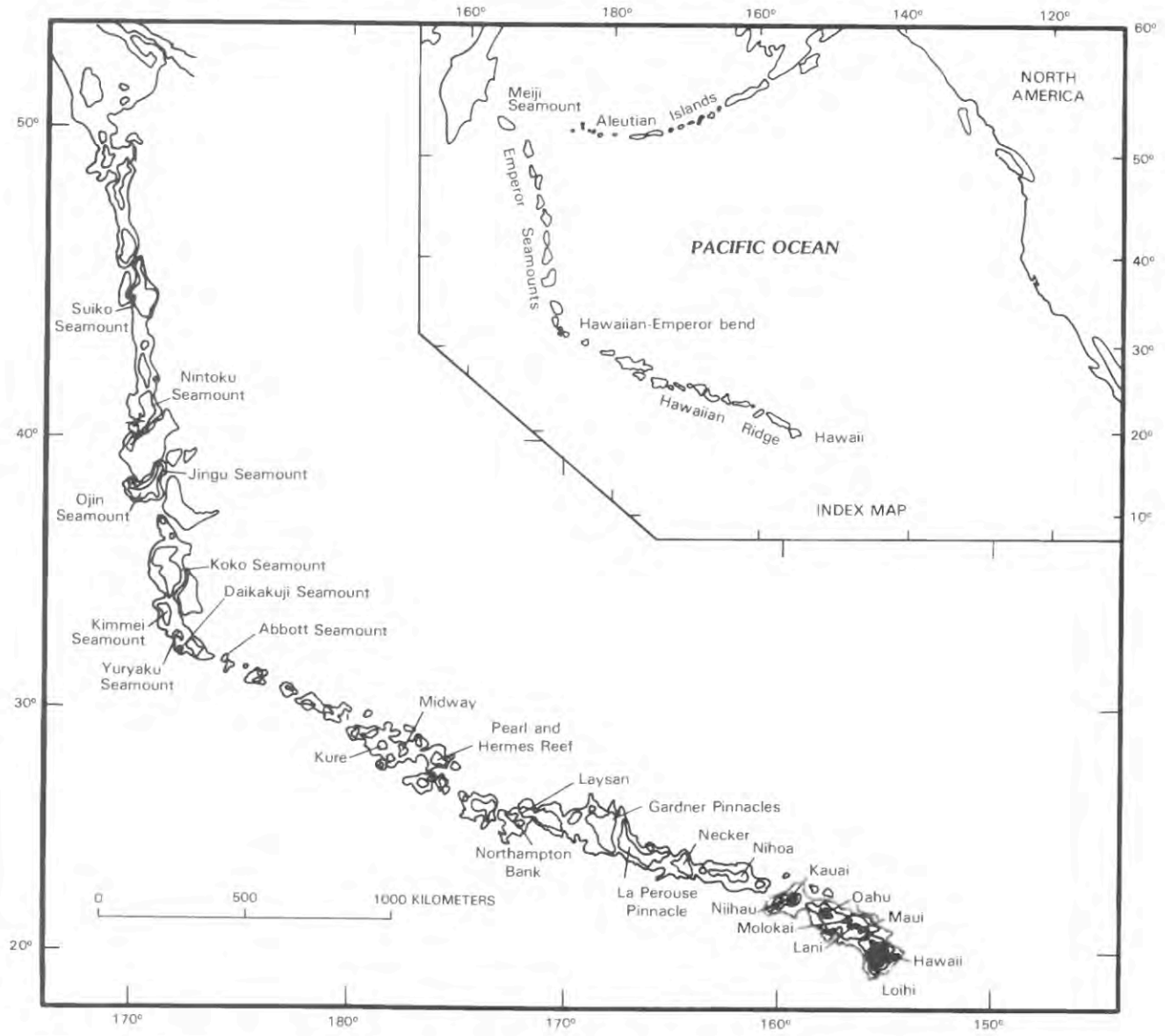

FIGURE 1.1.—Bathymetry of Hawaiian-Emperor volcanic chain modified from Chase and others (1970). Contours at 1-km and 2-km depths shown in area of the chain only. Inset shows location of chain (outlined by 2-km depth contour) in central North Pacific.

floor as each volcano was progressively cut off from its source of lava and a new volcano was born behind it.

Wilson (1963a, c) was the first to propose that the Hawaiian Islands and other parallel volcanic chains in the Pacific were formed by movement of the sea floor over sources of lava in the asthenosphere. Although the Emperor Chain was recognized as a northward continuation of the Hawaiian Chain by Bezrukov and Udintsev (1955) shortly after the Emperor Seamounts were first described by Tayama (1952) and Dietz (1954), Wilson confined his hypothesis to the volcanoes of the Hawaiian Islands and the Hawaiian Ridge. Christofferson (1968), who also coined the term "hot spot," extended Wilson's idea to include the Emperor Seamounts and suggested that the Hawaiian-Emperor bend represents a major change in the direction of sea-floor spreading from northward to westward. Morgan (1972a, b) proposed that the Hawaiian and other hot spots are thermal plumes of material rising from the deep mantle and that the worldwide system of hot spots constitutes a reference frame that is fixed relative to Earth's spin axis.

Although experimental testing of the various hypotheses proposed to explain hot spots has so far proven unproductive, the hot-

spot hypothesis has several important corollaries that can and have been tested to varying degrees. Foremost among these is that the volcanoes should become progressively older to the west and north as a function of distance from the hot spot. This progressive aging should be measurable with radiometric methods and also should be evident in the degree of erosion, subsidence, and geological evolution of the volcanoes along the chain. A second important corollary is that the latitude of formation of the volcanoes, as recorded in the magnetization of their lava flows, should reflect the present latitude of the hot spot rather than the present latitude of the volcanoes. Third, because the active mechanism is beneath the lithosphere, the Hawaiian-Emperor Chain should show no relation to the structure of the sea floor. Finally, the volcanic rocks of the volcanoes should be similar in both chemistry and sequence of eruption for each volcano along the chain, or should change in a systematic and coherent way.

In this paper we describe the Hawaiian-Emperor volcanic chain and those individual volcanoes that have been sampled and studied. We review the evidence that indicates that all of the corollaries mentioned above are true and, therefore, that the hot-spot hypothesis is a viable explanation of the origin of the chain. We will also describe the various hypotheses that have been proposed to explain the hot-spot mechanism and discuss their strengths and weaknesses.

ACKNOWLEDGMENTS

We thank Tom Wright and Jim Natland for their reviews, Kay McDaniel for her patience in typing it all, and Brigitta Fulop for drafting the figures.

STRUCTURE AND AGE OF THE UNDERLYING CRUST

The volcanoes of the Hawaiian-Emperor Chain were formed by eruption of lava onto the floor of the Pacific Ocean without regard for the age or preexisting structure of the ocean crust, or for the presence of preexisting volcanoes. The precise age of the ocean crust beneath much of the chain is poorly known because of the paucity of magnetic anomalies in the area (fig. 1.2). The Hawaiian Islands and Ridge east of about Midway Island lie on crust older than anomaly 34 but younger than anomaly M0. In a general way, both the Hawaiian seamounts and the underlying crust increase in age to the west so that the age of the crust beneath each volcano at the time it was built was between 80 and 90 m.y. (fig. 1.3). Volcanoes between Midway and the Hawaiian-Emperor bend and in the Emperor Seamounts south of Jingu Seamount are all built on crust whose age is between that of anomalies M0 and M3. Because the seamounts increase in age to the northwest but the underlying crust is roughly the same age, the age of the crust when the overlying volcano was built decreases systematically from about 80 m.y. at the bend to about 55 m.y. at Jingu Seamount. North of Jingu Seamount the age of the crust is not known, but plate reconstructions imply decreasing crustal ages to the north (Scientific Party DSDP 55, 1978; Byrne, 1979).

Northward from Jingu Seamount, we estimate that the crustal age at Suiko was roughly 40 m.y. and at the northernmost seamount, Meiji, was <20 m.y. when those volcanoes formed. If this extrapolation is extended beyond Meiji Seamount to hypothetical seamounts we presume existed once but which have been subducted or accreted in the Kuril Trench, we conclude that the Hawaiian hot spot was located, and perhaps originated, beneath the Kula-Pacific spreading axis at about 100–90 Ma.

Preexisting structures in and on the underlying crust appear to have had little or no influence on the formation of the Hawaiian-Emperor Chain (fig. 1.2). Several fracture zones, including the Mendocino, Murray, and Molokai, cross the chain, but none appears to have greatly affected the orientation of the chain, the rate of propagation of volcanism, or the volume of eruptive products. Likewise, the chain has overridden at least one Late Cretaceous seamount, again without obviously affecting the orientation, rate of propagation of volcanism, or the volumes of eruptive products (Clague and Dalrymple, 1975).

ERUPTIVE SEQUENCE

Hawaiian volcanoes erupt lava of distinct chemical compositions during four different stages in their evolution and growth (table 1.1). The three later stages are well studied and documented (Stearns, 1940a, b, c; Macdonald and Katsura, 1964; Macdonald, 1968), but the first (preshield) stage, which includes the early phase of the submarine history of the volcano, has only been examined recently (Moore and others, 1979, 1982).

The tholeiitic eruptive stage includes a long period of submarine eruption that forms a volcanic edifice with steep slopes and a subaerial eruptive phase that forms the shield-shaped volcano (Peterson and Moore, chapter 7). In this paper we refer to this entire stage of tholeiitic volcanism as the shield stage. In the shield stage, tholeiitic basalt flows construct the main volcanic edifice in the relatively short span of perhaps 1 m.y. or less (Jackson and others, 1972). Wright and others (1979) independently propose 200,000 yr as the duration of tholeiitic volcanism. Most of the mass of an individual volcano (95–98 percent) is formed from these voluminous eruptions. The shield stage usually includes caldera collapse and eruption of caldera-filling tholeiitic basalt. During the next stage, the alkalic postshield stage, alkalic basalt also may fill the caldera and form a thin cap of alkalic basalt and associated differentiated lava that covers the main shield. This alkalic lava accounts for less than 1 percent of the total volume of the volcano. After as much as a few million years of volcanic quiescence and erosion, very small amounts of SiO_2-poor lava may erupt from isolated vents; this stage is commonly called the posterosional stage; we refer to it here as the alkalic rejuvenated stage. An individual volcano may become extinct before this eruptive cycle is complete, but the general sequence is typical of the well-studied Hawaiian volcanoes (table 1.2). Some of these ideas are more than half a century old. Cross (1915) recognized that each of the Hawaiian volcanoes built a shield of lava, comparable to Kilauea flows, during a period of frequent voluminous eruptions. He also noted that this period was followed by a period of erosion and declining activity that produced cinder cones

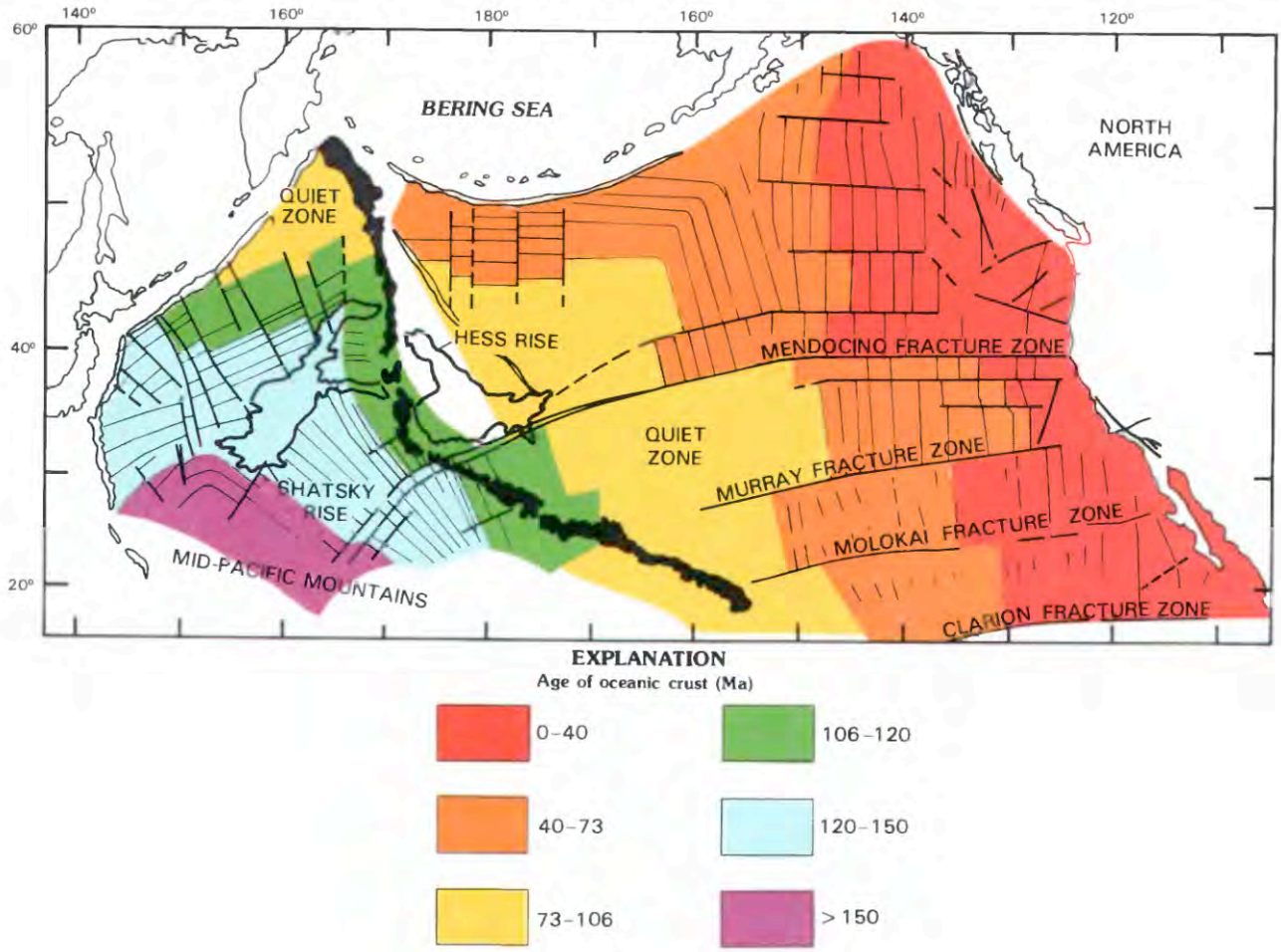

FIGURE 1.2.—Magnetic anomalies and structure of ocean floor crust in North Pacific modified from Hilde and others (1976). Hawaiian-Emperor Chain (black) crosscuts preexisting fracture zones and Mesozoic magnetic-anomaly sequence.

and small flows of lava richer in SiO_2 and FeO (these are the hawaiite and mugearite that characterize the alkalic postshield stage). S. Powers (1920) noted that eruptive centers of nepheline basalt on Kauai, Oahu, Molokai, and Maui were active long after the main volcano became quiet; he appears to have been the first to associate nepheline basalt with late-stage eruptions following an erosional hiatus.

New insight into the preshield stage has come from recent studies of Loihi Seamount, a small submarine volcano located about 30 km off the southeast coast of Hawaii. Its location, small size, seismic activity, and fresh, glassy lava all indicate that Loihi is an active volcano and the youngest in the Hawaiian-Emperor Chain. Some of the older lava samples recovered from Loihi Seamount are alkalic basalt and basanite, whereas the youngest lava samples recovered are tholeiitic and transitional basalt. This observation led Moore and others (1982) to conclude that Loihi Seamount, and perhaps all Hawaiian volcanoes, initially erupt alkalic basalt. Later, the bulk of the shield is built of tholeiitic basalt, but during declining activity the magma compositions revert to alkalic basalt. The alkalic preshield stage, like the alkalic postshield stage, produces only small volumes of lava, probably totaling less than a few percent of the volcano.

We have omitted the main caldera-collapse stage of Stearns (1966) from the eruption sequence because it can occur either during the shield stage or near the beginning of the alkalic postshield stage. The lava erupted may therefore be tholeiitic or alkalic basalt, or of both types.

GEOLOGY OF THE HAWAIIAN ISLANDS

Descriptions of volcanoes and their eruptions were made by nearly all the earliest visitors to the Hawaiian Islands. Descriptions of particular note are those of William Ellis (1823), George, Lord Byron (1826), Joseph Goodrich (1826, 1834), and Titus Coan

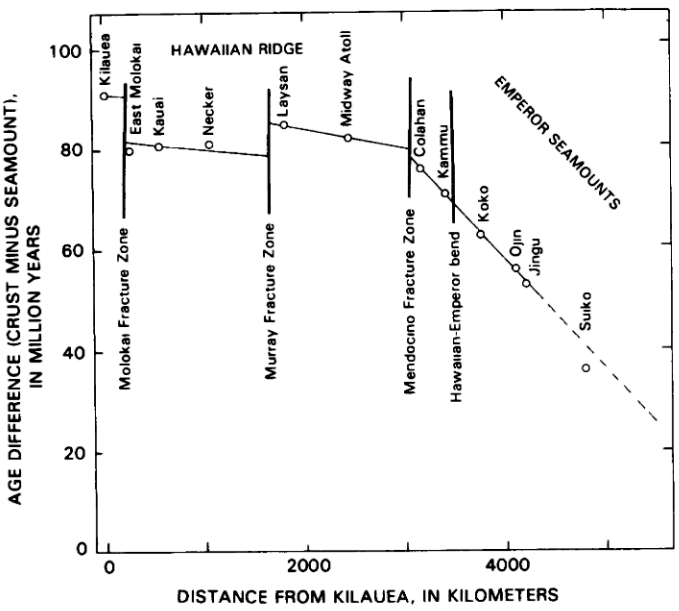

FIGURE 1.3.—Age of oceanic crust when overlying volcano formed, as a function of distance from Kilauea, for selected volcanoes in Hawaiian-Emperor Chain. Note offsets at fracture zones. Along Hawaiian Ridge both crust and volcanoes increase in age to west so crustal age when volcanoes formed is roughly constant. On the other hand, Emperor Seamounts increase in age to north but crust decreases in age; thus age of crust when seamounts formed decreases from roughly 75 Ma at the bend to less than 40 Ma at Suiko Seamount.

TABLE 1.1.—*Hawaiian eruptive products*

Eruptive stage	Rock types	Eruption rate	Volume (percent)
Rejuvenated --	alkalic basalt basanite nephelinite nepheline melilitite	Very low	<1
Postshield ---	alkalic basalt transitional basalt ankaramite hawaiite mugearite benmoreite trachyte phonolite	Low	~1
Shield -------	tholeiitic basalt olivine tholeiitic basalt picritic tholeiitic basalt icelandite (rare) rhyodacite (rare) [1]alkalic basalt (?)	High	95-98
Preshield ----	basanite alkalic basalt transitional basalt [1]tholeiitic basalt (?)	Low	~3

[1]Wright and Helz (chapter 23) suggest that the shield stage may include rare intercalated alkalic basalt and that the preshield stage includes tholeiitic basalt. We suspect that tholeiitic and alkalic basalt occur intercalated during the transitions from preshield to shield stage and from shield stage to postshield stage but that during the main shield stage only tholeiitic lava is erupted.

(1840 and other letters until 1882). Many of their letters describing the volcanoes were published in the American Journal of Science. Goodrich, in particular, provided detailed descriptions of the volcanoes on the Island of Hawaii. None of the earliest descriptions however, included information about the mineralogy or petrology of the lava.

The United States Exploring Expedition visited Hawaii in 1840–41. The commander of the expedition published a narrative (Wilkes, 1845) containing descriptions of caldera activity at Kilauea and new maps of both Kilauea and Mauna Loa calderas. James D. Dana, the geologist of the expedition, published a detailed report on the geology of the areas visited by the expedition (Dana, 1849). This report contains descriptions of lava flows including their mineralogy and flow morphology, in addition to numerous other observations on the active and inactive volcanoes that make up the islands. Later reports by Dutton (1884), J.D. Dana (1887, 1888, 1889), Green (1887), and Brigham (1909) added details on eruptions and expanded the geologic observations to other islands.

E.S. Dana (1877), Cross (1904), and Hitchcock (1911) presented detailed petrographic descriptions of lava from the islands. Daly (1911) and Cross (1915) described the mineralogy and petrology of Hawaiian lava flows at the time the Hawaiian Volcano Observatory was established, and Jagger (1917) described activity in Halemaumau lava lake. The paper by Cross (1915) is a milestone because it added detailed descriptions and chemical analyses of rocks from Hawaiian volcanoes other than Kilauea and Mauna Loa.

More detailed petrographic descriptions of lava from the islands were published by S. Powers (1920). Soon afterward, papers appeared by Washington (1923a, b, c) and Washington and Keyes (1926, 1928) with detailed accounts of the geology and petrology, new high-quality chemical analyses of lava from Hawaii and Maui, and a classification of Hawaiian volcanic rocks. Palmer (1927, 1936) added geologic descriptions and petrography of lava from Kaula and Lehua Islands, both of which are tuff cones of the alkalic rejuvenated stage. Lehua Island is just one of several rejuvenated-stage vents associated with Niihau, whereas Kaula Island sits atop a completely submerged shield.

These early, mainly descriptive and reconnaissance studies were superseded by detailed mapping of the islands beginning in the 1930's. H.T. Stearns and his coworkers, in a remarkable series of bulletins published by the Hawaii Division of Hydrography, published geologic maps and descriptions of Oahu (Stearns and Vaksvik, 1935; Stearns, 1939, 1940b), Lanai and Kahoolawe (Stearns, 1940c), Maui (Stearns and Macdonald, 1942), Hawaii (Stearns and Macdonald, 1946), Niihau (Stearns, 1947), and Molokai (Stearns and Macdonald, 1947). The bulletin on Kauai by Macdonald and others (1960) completed the monumental mapping job begun by Stearns; though Stearns did not coauthor the report, he did much of the mapping and is an author of the map. These maps and bulletins provide the geologic framework for all

TABLE 1.2.—*Eruptive stages represented on volcanoes of the Hawaiian-Emperor Chain*

[Volcano numbers from Bargar and Jackson (1974); numbers 0 and 65A added for consistency. Presence of stages: M, major unit; R, rare or of small volume; X, present but extent unknown; A, known to be absent; -, unknown. (T), transitional lava probably erupted during late shield stage or caldera-collapse phase of that stage. For volcanoes from Kilauea through Necker, data from detailed mapping and sampling; for remaining volcanoes, primarily from dredge and drill samples]

Volcano Number	Volcano Name	Eruptive Stages: Preshield (alkalic)	Shield (tholeiitic)	Postshield (alkalic)	Rejuvenated (alkalic)
	Hawaiian Islands				
0	Loihi	M	M	-	-
1	Kilauea	-	M	A	A
2	Mauna Loa	-	M	A	A
3	Mauna Kea	-	M	M	A
4	Hualalai	-	M	M	A
5	Kohala	-	M	M	A
6	East Maui	-	M	M	M
7	Kahoolawe	-	M	R	R
8	West Maui	-	M	R	R
9	Lanai	-	M	A	A
10	East Molokai	-	M	M	R
11	West Molokai	-	M	R	A
12	Koolau	-	M	A	M
13	Waianae	-	M	M	R
14	Kauai	-	M	R	M
15	Niihau	-	M	R	M
15A	Kaula	-	X	X	X
	Northwestern Hawaiian Islands and Hawaiian Ridge				
17	Nihoa	-	M	-	-
19	(Unnamed Seamount)	-	X(T)	-	-
20	(Unnamed Seamount)	-	X	-	X
21	(Unnamed Seamount)	-	X	-	-
23	Necker	-	M	X	X
26	La Perouse Pinnacles	-	X	-	-
28	Brooks Bank	-	X(T)	X	-
29	St. Rogatien Bank	-	-	X	-
30	Gardner Pinnacles	-	X	X	-
36	Laysan	-	-	X	-
37	Northampton Bank	-	X	-	-
39	Pioneer Bank	-	X	-	-
50	Pearl and Hermes Reef	-	-	X	-
51	Ladd Bank	-	-	-	X
52	Midway	-	M	X	-
53	Nero Bank	-	X	-	-
57	(Unnamed Seamount)	-	-	X	-
63	(Unnamed Seamount)	-	-	-	X
65	Colahan	-	X	-	X
65A	Abbott	-	X(T)	-	-
	Emperor Seamounts				
67	Daikakuji	-	X	-	-
69	Yuryaku	-	X	X	-
72	Kimmei	-	-	X	-
74	Koko (southern)	-	X	M	-
76	Koko (northwest)	-	X	-	-
81	Ojin	-	X	X	-
83	Jingu	-	-	X	-
86	Nintoku	-	-	X	-
90	Suiko (southern)	-	-	X	-
91	Suiko (central)	-	M	X	-
108	Meiji	-	M	-	-

subsequent studies of the islands and can also be used to put many of the earlier descriptions into a broader geological context. A number of derivative publications include summaries of the geology of the islands by Stearns (1946, 1966), an overview of the petrography of lava from the islands by Macdonald (1949), and a summary of the geology of the Hawaiian Islands by Macdonald and others (1983). The brief geologic summaries in appendix 1.1 have largely been extracted from the above publications. Additional unpublished observations by ourselves are included for Hualalai, East and West Molokai, Koolau, Kauai, and Niihau.

The maps of Stearns and coworkers separate rejuvenated-stage lava from earlier lava, but do not subdivide shield and postshield lava on the basis of chemical composition. The eruptive stages that are known to occur in each of the volcanoes of the Hawaiian Islands are summarized in table 1.2. Evidence for the alkalic preshield stage exists only at Loihi Seamount. If this stage is present in all Hawaiian volcanoes, it is completely buried by later, shield-stage tholeiitic lava. The tholeiitic shield stage is known to form the major portion of the subaerial and, we assume, the submarine part of each volcano. On the main islands, only Hualalai Volcano and Kaula Island do not have subaerial exposures of tholeiitic lava. Alkalic lava of the alkalic postshield stage occurs relatively late in the eruptive sequence and has not yet developed on Loihi Seamount or Kilauea and Mauna Loa Volcanoes. To the northwest of there it occurs on all volcanoes except Lanai and Koolau, although the volumes present on Kauai, Niihau, Kahoolawe, and West Molokai are small. Some volcanoes have predominantly mugearite, whereas others have predominantly hawaiite; these are called Kohala type and Haleakala type, respectively, by Macdonald and Katsura (1962). Wright and Clague (in press) propose two additional types: a Hualalai type with a bimodal trachyte-alkalic basalt lava distribution and a Koolau type with little or no alkalic postshield lava present.

Hawaiian volcanoes commonly have summit calderas and elongate curved rift zones from which much of the lava issues. Summit calderas exist on Loihi Seamount (Malahoff, chapter 6; Malahoff and others, 1982), Kilauea, and Mauna Loa. Each of these calderas is connected to two prominent rift zones. Not all Hawaiian volcanoes, however, had a summit caldera. West Molokai Volcano, in particular, shows no evidence of ever having had a caldera. Flat-lying lava ponded inside a caldera is not exposed on Hualalai, Mauna Kea, Kohala, or Niihau, but former calderas are inferred at those volcanoes from geophysical data (see Macdonald and others, 1983).

The formation and structure of the rift zones have been examined in an elegant paper by Fiske and Jackson (1972), who concluded that the orientation of the rift zones reflects local gravitational stresses within the volcanoes. Isolated shields such as Kauai and West Molokai had nearly symmetrical stress fields represented by generally radial dikes and thus have only poorly defined rift zones. The rift zones of these isolated volcanoes tend to align parallel to the orientation of the chain, suggesting the influence of a more regional stress field that also controls the orientation of the chain. In contrast, the rift zones of the other volcanoes tend to be aligned parallel to the flanks of the preexisting shields against which they abut.

GEOLOGY OF THE HAWAIIAN RIDGE

The Northwestern Hawaiian Islands were the focus of all geologic investigations along the Hawaiian Ridge west of Kauai until oceanographic techniques were applied to the area in the 1950's. Geological descriptions of the leeward islands include those of S. Powers (1920) for Nihoa and Necker Islands, and Washington and Keyes (1926) and Palmer (1927) for Nihoa, Necker, Gardner Pinnacles, and French Frigates Shoal (LaPerouse Pinnacles). These reports cite earlier sketchy descriptions. Macdonald (1949) reexamined Palmer's samples and added more detailed petrography. The petrology of the basaltic basement of Midway Atoll is described from two drill cores by Macdonald (1969) and Dalrymple and others (1974, 1977), whereas the geology of the site is detailed by Ladd and others (1967, 1969). Paleomagnetic data on flows and dikes from Nihoa and Necker Islands are given by Doell (1972), whereas similar data from the Midway drill core are given by Gromme and Vine (1972).

Marine geologic investigations of the Hawaiian Ridge began with Hamilton's pioneering work in 1957. Much subsequent work has focused on the structure of the oceanic crust in the vicinity of the chain, but few cruises have actually been conducted that dealt mainly with the geology of the Hawaiian Ridge. In the early 1970's, Scripps Institution of Oceanography and the Hawaii Institute of Geophysics conducted cruises to the Hawaiian Ridge. Samples collected by these cruises are described in Clague (1974a, 1974b) and Garcia, Grooms, and Naughton (in press). Subsequent cruises to the area by the Hawaii Institute of Geophysics and the U.S. Geological Survey are cited in appendix 1.1.

Lava samples recovered from the Hawaiian Ridge and Emperor Seamounts are more difficult to assign to volcanic stages because they are recovered by dredging and drilling or are collected from small islets and the field relations are usually unknown or only poorly known. Table 1.2 summarizes the available data from the Hawaiian Ridge. Based on the sequence and volumes of lava in the Hawaiian Islands, we have assumed that tholeiitic basalt always represents the shield stage and that strongly alkalic, SiO_2-poor lava represents the alkalic rejuvenated stage. Differentiated alkalic lava has been assigned to the alkalic postshield stage. Some alkalic basalt occurrences could be assigned to either the alkalic postshield or rejuvenated stages; they have been assigned on the basis of trace-element signatures and mineral chemistry using criteria outlined in a later section of this paper. No lava samples have been assigned to the alkalic preshield stage because we assume that the small volumes of such early lava have been buried by the later voluminous tholeiitic lava of the shield stage.

The samples recovered by dredging are probably not representative of the lava forming the bulk of the individual seamounts, but instead represent the youngest lava types erupted on the volcanoes. This natural sampling bias should result in an overrepresentation of alkalic lava from both the postshield and rejuvenated stages. In addition, selection of recovered samples for further study introduces another bias because the freshest samples are commonly alkalic lava, particularly hawaiite, mugearite, and trachyte. With these biases in mind, it is still possible to note general trends along the entire chain.

Tholeiitic basalt and picritic tholeiitic basalt, similar to those of the shield stage of subaerial Hawaiian volcanoes, have been recovered from 11 seamounts, banks, and islands in the Hawaiian Ridge west of Kauai and Niihau (table 1.2; appendix 1.1). The abundance of tholeiitic basalt from the Hawaiian Ridge implies that these volcanoes are genetically related to the Hawaiian Islands and that the general sequence of Hawaiian volcanism, in which tholeiitic basalt forms a major portion of each volcano, has occurred along the entire Hawaiian Chain.

GEOLOGY OF THE EMPEROR SEAMOUNTS

Little was known of the geology of the Emperor Seamounts until quite recently. The chain was recognized as the continuation of the Hawaiian Ridge by Bezrukov and Udintsev (1955), but not until 1968 were the first samples recovered from Suiko Seamount (Ozima and others, 1970). These samples are dominantly, if not completely, ice-rafted detritus. Subsequent studies included a cruise to the southern part of the chain by Scripps Institution of Oceanography in 1971 (ARIES Leg VII; Davies and others, 1971, 1972), Deep Sea Drilling Project (DSDP) Site 192 on Meiji Seamount (Creager and Scholl, 1973), DSDP Sites 308 and 309 on Koko Seamount (Larson and others, 1975), a cruise by the Hawaii Institute of Geophysics (Dalrymple and Garcia, 1980), a cruise by the U.S. Geological Survey in 1976 that surveyed the sites for Leg 55 of DSDP (Dalrymple and others, 1980a), and Leg 55 DSDP Sites 430, 431, 432, and 433 in the central part of the chain (Jackson and others, 1980). The Scripps Institution of Oceanography cruise ARIES VII in 1971 and the Leg 55 DSDP cruise in 1977 were particularly successful, and most of our knowledge of the Emperor Seamounts is derived from these two cruises.

The petrology of lava samples recovered by these two cruises is described in Clague (1974a) and Kirkpatrick and others (1980), respectively. A detailed seismic interpretation of the carbonate caps of many of the seamounts is given by Greene and others (1980), and overviews of the results of DSDP Leg 55 are given by Jackson and others (1980) and Clague (1981).

Table 1.2 summarizes the available data on eruptive stages represented by samples from the Emperor Seamounts, and details are given in appendix 1.1 for individual volcanoes. We have assumed that tholeiitic basalt represents the shield stage and that alkalic lava postdates the tholeiitic shield stage; only at Ojin and Suiko Seamounts does drilling show that the alkalic lava overlies the tholeiitic flows.

Tholeiitic basalt and picritic tholeiitic basalt similar to those of the shield stage of subaerial Hawaiian volcanoes have been recovered by drilling and dredging from six volcanic edifices in the Emperor Seamounts. The abundance of tholeiitic lava from the Emperor Seamounts is strong evidence that these volcanoes are genetically related to the Hawaiian Islands and Hawaiian Ridge. Likewise, the general eruptive model for the Hawaiian Islands is apparently applicable to the Emperor Seamounts.

Alkalic postshield-stage lava has been recovered by dredging and drilling from nine seamounts in the chain. In general these samples are alkalic basalt, hawaiite, mugearite, and trachyte similar to lava erupted in the Hawaiian Islands, but lava from Koko Seamount includes anorthoclase trachyte and phonolite that are interpreted to have erupted during the alkalic postshield stage (Clague, 1974a). Lava of the rejuvenated alkalic stage has not been identified from any of the Emperor Seamounts.

SUBSIDENCE OF THE VOLCANOES

Charles Darwin (1837, 1842) was the first to suggest that coral atolls might grow on subsiding platforms and that drowned atolls and certain deeply submerged banks with level tops could be explained by subsidence. Hess (1946) recognized that flat-topped submarine peaks, which he named guyots, were drowned islands. He thought that they were volcanic, bare of sediments and coral, and had been planed off by erosion at sea level. He attributed their depth to rising sea level caused by sediment deposition in the oceans. Menard and Dietz (1951) agreed with Hess that submergence was primarily due to a rise in sea level, but they thought that local subsidence might also play a role. Hamilton (1956), in his classic study of the Mid-Pacific Mountains, which included a program of dredging and coring, concluded that those (and other) guyots were formerly basaltic islands that had been wave and stream eroded and on which coral reefs subsequently grew. Their eventual submergence, he thought, was primarily caused by regional subsidence of the sea floor. It is now known that Darwin and Hamilton were basically correct about the steps leading to the formation of guyots, and about the predominant role of subsidence in the process.

The Hawaiian-Emperor volcanic chain is an excellent example of the gradual transformation of volcanic islands to guyots. From southeast to northwest there is a continuous progression from the active volcanoes such as Mauna Loa and Kilauea through the eroded remnants of Niihau, Nihoa, and Necker, through growing atolls like French Frigates Shoal and Midway Islands, to deeply submerged guyots like Ojin and Suiko. The progression can be observed not only along the chain but within the stratigraphy of individual seamounts. Drilling, dredging, and seismic observations have shown conclusively that the atolls and guyots of the chain are capped by carbonate deposits that overlie subaerial lava flows (see, for example, Ladd and others, 1967; Davies and others, 1971, 1972; Greene and others, 1980; Jackson and others, 1980).

The subsidence of Hawaiian volcanoes with time results from thermal aging of the lithosphere and isostatic response to local loading. The depth of the sea floor (and of volcanoes sitting upon it) increases away from spreading ridges because the lithosphere cools, thickens, and subsides as it moves away from the source of heat beneath the ridge (Parsons and Sclater, 1977; Schroeder, 1984). Detrick and Crough (1978) pointed out that the subsidence of many islands and seamounts, including those along the Hawaiian-Emperor Chain, was far in excess of that which could be accounted for by this normal lithospheric aging or by lithospheric loading. They proposed that the lithosphere is thermally reset locally as it passes over a hot spot and that the excess subsidence is largely a consequence of renewed lithospheric aging.

The Hawaiian-Emperor Chain rests on crust of Cretaceous age (circa 120–80 Ma) for which the depth should be about 5.5–5.9 km. The depth near Hawaii, however, is less than 4.5 km (fig. 1.4). The depth increases along the chain to about 5.3 km near the Hawaiian-Emperor bend in a manner consistent with the thermal resetting hypothesis. Thus, the subsidence of Hawaiian volcanoes as they move away from the hot spot is in part a function of their distance from the hot spot, that is, of the reset thermal age of the lithosphere beneath the chain. The volcanoes are passively riding away from the Hawaiian hot spot on cooling and thickening lithosphere that is subsiding at about 0.02 mm/yr.

Superimposed on the effect of crustal aging is subsidence caused by the immense and rapid loading of the lithosphere by the growing volcanoes (Moore, chapter 2). This effect is local, but while the volcano is active the rate of subsidence caused by loading may exceed that from lithospheric aging by more than two orders of magnitude. Moore (1970) found, from a study of tide-gage records in the Hawaiian Islands and on the west coast of North America, that Hilo on the Island of Hawaii has been subsiding at an absolute rate of 4.8 mm/yr since 1946. Recent data on drowned coral reefs near Kealakekua Bay indicate an absolute subsidence rate for the western side of Hawaii of 1.8 to 3+ mm/yr averaged over the past 300,000 yr and also indicate that the rate may have accelerated during that time (Moore and Fornari, 1984). Moore's (1970) tide-gage data also show that absolute subsidence decreases systematically away from the Island of Hawaii, with rates for Maui and Oahu of 1.7 mm/yr and 0 mm/yr, respectively. Some of this decrease in subsidence may be due to compensating uplift as the volcanoes are carried over the Hawaiian Arch, but an analysis of gravity data indicates that there is no appreciable viscous reaction to the seamount loads over time (Watts, 1978). Thus, it is probable that the volcanoes are isostatically compensated within a few million years of their birth, and that thermal aging of the lithosphere is the major cause of subsidence along the chain.

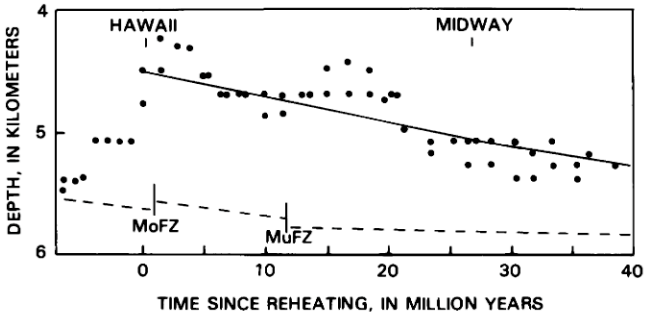

FIGURE 1.4.—Minimum depth to sea-floor swell as a function of time since reheating (or age of volcanoes along chain). Dashed line is predicted depth for normal aging of lithosphere away from spreading ridge. Solid line is predicted depth for thermally reset lithosphere 45 km thick. MoFZ and MuFZ, Molokai and Murray Fracture Zones, respectively. Modified from Detrick and Crough (1978) and Crough (1983).

GEOCHRONOLOGY AND PROPAGATION OF VOLCANISM

EARLY WORK: LEGENDS AND DEGREE OF EROSION

According to Hawaiian legend, the goddess Pele first inhabited Kauai, but then moved southeastward island by island to Kilauea Volcano, where she now resides (Bryan, 1915). The reasoning behind this legend is unknown, but it was probably based in large part on the relative appearance of age of the various volcanoes. Many centuries after this legend originated, J.D. Dana (1849) rendered the first scientific opinion confirming the general age progression implied by the legend.

Dana was not only the first geologist to conclude that the order of extinction of Hawaiian volcanoes was approximately from northwest to southeast, he also recognized that the Hawaiian Chain included the islets, atolls, and banks that stretch for some distance to the northwest of Kauai. Dana saw no reason to think that the volcanoes of the chain did not originate simultaneously: "No facts can be pointed to, which render it even probable that Hawaii is of more recent origin than Kauai" (Dana, 1849, p. 280). Their relative degree of erosion, however, provided ample evidence to indicate their order of extinction: "From Kauai to Mount Loa all may thus have simultaneously commenced their ejections, and have continued in operation during the same epoch till one after another became extinct. Now, the only burning summits out of the thirteen which were once in action from Niihau to Hawaii, are those of Loa and Hualalai: we might say farther that these are all out of a number unknown, which stretched along for fifteen hundred miles, the length of the whole range. This appears to be a correct view of the Hawaiian Islands" (Dana, 1849, p. 280). Subsequent workers agreed with Dana on the general order of extinction (for example, Brigham, 1868; Dutton, 1884; Hillebrand, 1888; Hitchcock, 1911; Cross, 1915; Martin and Pierce, 1915; Wentworth, 1927; Hinds, 1931; Stearns, 1946), although the sequences they proposed invariably differed in detail (table 1.3). Of these various workers only Stearns (1946), who studied the Hawaiian Islands in more detail than any of his predecessors, had the sequence exactly correct as judged by present data.

The idea that the volcanoes of the Hawaiian Chain originated simultaneously and only became extinct progressively seems to have persisted until a few decades ago. Stearns (1946), for example, mentions the lack of evidence to indicate when any of the Hawaiian volcanoes began but shows all of the main shields except Hualalai and Kilauea erupting simultaneously at the end of the Pliocene (Stearns, 1946, p. 97, fig. 25). Two exceptions were Cross (1904) and Wentworth (1927), who thought that the degree of erosion was probably a function of when the volcanoes emerged above the sea as well as of the elapsed time since they ceased to erupt. Cross (1904, p. 518) states: "It appears to me plausible to assume that the earliest eruptions occurred at or near the western limit of this zone (the more than 1000 mile expanse of the island chain), and that in a general way at least, the centers of activity have developed successively farther and farther to the east or southeast, until now the only active loci of eruption are those of Mauna Loa and Kilauea on the island of

TABLE 1.3.—*Early estimates of the order of extinction of the principal Hawaiian volcanoes*

[Criteria used are given beneath each source; volcanoes listed in proposed order of extinction, oldest at top]

Dana (1849) Erosion	Brigham (1868) Erosion	Dana (1888) Erosion	Hillebrand (1888) Floral diversity	Wentworth (1927) Erosion	Hinds (1931) Erosion	Stearns (1946) Erosion and stratigraphy
Kauai	West Kauai, Niihau	Kauai	West Oahu, Kauai	Koolau	Waianae	Kauai
Waianae	Waianae	Waianae	Molokai, East Oahu	Kauai	Koolau	Waianae
West Maui	East Kauai	West Maui	Kohala, West Maui	East Molokai	Niihau	Koolau
Koolau	West Molokai	Kohala	Mauna Kea	West Maui	Kauai	West Molokai
Mauna Kea	West Maui	Koolau	East Maui	Mauna Kea	West Molokai	East Molokai
East Maui	Kohala	East Maui	Hualalai	Waianae	East Molokai	West Maui, Lanai
Mauna Loa	Koolau	Mauna Kea	Mauna Loa, Kilauea	East Maui	Lanai	Kahoolawe
	East Molokai	Hualalai		Lanai	West Maui, Kohala	East Maui
	Mauna Kea	Mauna Loa, Kilauea		Niihau, West Molokai	Kahoolawe	Kohala
	Lanai, Kahoolawe			Kahoolawe	East Maui	Mauna Kea
	East Maui			Kohala	Mauna Kea	Haulalai, Mauna Loa, Kilauea
	Hualalai			Hualalai, Mauna Loa, Kilauea	Hualalai	
	Mauna Loa, Kilauea				Mauna Loa, Kilauea	

Hawaii." He specifically noted the difference between his hypothesis and that of Dana.

Estimates of the geologic ages of the Hawaiian volcanoes varied considerably among those early workers willing to hazard a guess on the basis of the meager data then available. Dana (1849) thought it likely that the eruptions commenced as early as early Carboniferous or Silurian time; this estimate was based on the concept that the Earth had cooled from a molten globe producing fissuring and volcanism, the apparent lack of post-Silurian volcanism in the interior of the North American continent, and the presumption that the oceans would cool after the continents. Cross (1904) speculated that the western part of the leeward islands formed in the early part of the Tertiary. Wentworth (1925, 1927) attempted to quantify erosion rates for several of the islands and estimated the extinction ages of some of the volcanoes as follows:

Lanai	0.15 Ma
Kohala	0.22 Ma
Koolau	1.00 Ma
Kauai	2.09 Ma

On the basis of physiographic evidence, Wentworth doubted that any part of the Hawaiian group emerged above sea level before late Tertiary time. Hinds (1931), like Cross (1904), recognized that the atolls and banks of the leeward islands were the remnants of once-larger volcanoes: "The landscapes of the leeward group—the volcanic stacks, the reef limestone and calcareous sand islands rising from submarine platforms, and submerged platforms from which no islands rise, represent the final stages in the destruction of a volcanic archipelago. Such a fate awaits the windward islands unless they be rejuvenated by volcanic or diastrophic forces" (Hinds, 1931, p. 196). He recognized that the amount of erosion and subsidence required to reduce a mammoth Hawaiian volcano to a coral atoll was probably considerable and concluded: "The complete or nearly complete destruction of the Leeward islands suggests that volcanism ceased there well back in the Tertiary, hence the mountains must have risen above the ocean long before, perhaps even in Mesozoic time" (Hinds, 1931, p. 205). On the basis of geomorphic considerations, Stearns (1946) thought that the volcanoes of the main Hawaiian Islands rose above sea level in the Tertiary.

RADIOMETRIC AND FOSSIL AGES

The first radiometric ages for Hawaiian volcanoes were determined by McDougall (1963), who measured ages of 2.8 to 3.6 Ma for his Middle and Upper Waianae Series on Oahu (all K-Ar ages have been converted to the new constants; Steiger and Jaeger, 1977). He also reported an age of 8.6 Ma for what he called the Mauna Kuwale Trachyte of the Lower Waianae Series(?), an age that later proved to be incorrect, probably because of excess argon in the biotite analyzed (Funkhouser and others, 1968). In subsequent studies McDougall and Tarling (1963) and (primarily) McDougall (1964) reported K-Ar ages of lava from 7 of the principal Hawaiian volcanoes and concluded that the ages of the shield stages were approximately:

Kauai	5.8–3.9 Ma
Waianae	3.5–2.8 Ma
Koolau	2.6–2.3 Ma
West Molokai	1.8 Ma
East Molokai	1.5–1.3 Ma
West Maui	1.3–1.15 Ma
East Maui	0.8 Ma
Hawaii (all 5 volcanoes)	<1 Ma

McDougall thus confirmed Stearns' extinction sequence and also suggested that the main shield stage of a Hawaiian volcano essentially was complete before the next volcano rose above the sea.

Since the pioneering work of McDougall, many additional radiometric ages have been determined for the volcanoes of the main islands, and the dating has been extended to the volcanoes of the

leeward islands, the western Hawaiian Ridge, and the Emperor Seamounts. In total, there are now reasonably precise radiometric age data for 35 of the volcanoes in the Hawaiian-Emperor Chain (see appendix 1.1). Radiometric ages of two volcanoes on the Hawaiian Ridge are not included in appendix 1.1 because it is probable that the samples are not from Hawaiian volcanoes (Clague and Dalrymple, 1975). These include a minimum age of 71 ± 5 Ma for altered basalt from Wentworth Seamount, 80 km northwest of Midway, and an age of 77.6 ± 1.7 Ma for a sample of rhyolite (probably an erratic, see appendix 1.1) dredged from the northern slope of Necker Island.

In addition to the radiometric age data, there are paleontologic ages for several of the Hawaiian-Emperor volcanoes based on material recovered by dredging and drilling programs. In general, these ages postdate volcanic activity and are consistent with the radiometric data. From southeast to northwest they include (1) an age of 28–31 Ma for late Oligocene nannofossils in volcanogenic sediments at DSDP Site 311 on the archipelagic sediment apron of an unnamed seamount (no. 58 of Bargar and Jackson, 1974) 240 km northwest of Midway (Bukry, 1975); (2) an age of 15–32 Ma (East Indies Tertiary stage Te) for larger foraminifers (Cole, 1969) and smaller foraminifers (Todd and Low, 1970) in reef limestone above basalt in a drill hole at Midway Atoll; (3) an age of 39–41 Ma for dredged late Eocene larger foraminifers from Kammu Seamount (Sachs, quoted in Clague and Jarrard, 1973); (4) an age of 50.5 ± 3.5 Ma for early Eocene coccoliths in volcanogenic sediments cored at DSDP Site 308 atop Koko Seamount (Bukry, 1975); (5) an age of 57–59 Ma for late Paleocene calcareous nannofossils (Takayama, 1980) and pelagic foraminifers (Hagn and others, 1980) in sediments above basalt at DSDP Site 430 on Ojin Seamount; (6) late Paleocene planktonic foraminifers and probable early Eocene benthic foraminifers in sediments above basalt at DSDP Site 432 on Nintoku Seamount (Butt, 1980); (7) an age of 59–61 Ma for middle Paleocene calcareous nannofossils in sediments above basalt at DSDP Site 433 on Suiko Seamount (Takayama, 1980); and (8) an age of 70–73 Ma for lower Maestrichtian nannofossils from sediments above basalt at DSDP Site 192 on Meiji Seamount at the northern end of the Emperor Seamounts (Worsley, 1973). None of these fossil ages is in conflict with the radiometric data.

On the other hand, Menard and others (1962) describe Miocene corals and pelagic foraminifers dredged from a submarine terrace 10 km southwest of Oahu. The authors note the difficulty in assigning an age to these samples and state that the "planktonic foraminifera *Globigerinoides quadralobates* [=*G. trilobus auct.*] *plexus* suggest a lower limit of early Miocene. The upper age limit is less definitive" (Menard and others, 1962, p. 896). Present nomenclature would identify these samples as *Globigerinoides triloba*, which ranges in age from early Miocene to Pleistocene (Kenneth and Srinivasan, 1983). Menard and others (1962) cite as additional evidence of the Miocene age of the sample the 60 percent of extinct coral species in the sample. We conclude that none of these criteria unequivocally supports a Miocene age and no conflict exists between the ages of the reef and that of the underlying volcanic basement of 1.8–2.7 Ma.

Two samples of Eocene terrigenous sediment recovered 250 km east of Hawaii and 100 km south of Kauai (Schreiber, 1969) are also anomalous. These samples were probably derived from volcanoes that predate the Hawaiian Chain, or they may have been reworked from sediment on the sea floor during formation of the Hawaiian volcanoes.

The available radiometric data are summarized in table 1.4 and plotted in figure 1.5 as a function of distance measured from Kilauea Volcano along the Hawaiian-Emperor trend. Because some of the volcanoes are unnamed and some seamounts and islands consist of more than one major volcanic edifice, each dated volcanic center is identified in the table with the number assigned to it by Bargar and Jackson (1974). The exceptions are Abbott Seamount, a small volcano between Colahan and Kammu Seamounts, and Kaula Island, which were not previously numbered and to which we have assigned numbers 65A and 15A, respectively.

As can be seen from figure 1.5, the age data confirm the general age progression along the chain as first suggested by Dana (1849) and required by the hot-spot hypothesis of Wilson (1963a), and they show that the progression is continuous from Kilauea at least to Suiko Seamount, more than half way up the Emperor Seamounts Chain and nearly 5,000 km from the active volcanoes of Mauna Loa and Kilauea. The data also substantiate the hypothesis that the Emperor Seamounts are a continuation of the Hawaiian Chain, as proposed by Christofferson (1968) and Morgan (1972a, b).

RATES OF VOLCANIC PROPAGATION

In order to determine accurately the rate of volcanic propagation along the Hawaiian-Emperor Chain, we would like to know the time that each tholeiitic shield volcano first erupted onto the sea floor, but such data clearly are not obtainable. What is available for the dated volcanoes is one or more radiometric age on lava flows erupted during one or more stage of volcanic activity (see appendix 1.1). In order to calculate propagation rates, therefore, it is necessary to adopt some consistent strategy for selecting the numerical age used to represent the age of each dated volcano. Different authors have approached this problem in different ways. McDougall (1971) used the youngest age of tholeiitic basalt as representing the time of cessation of volcanism for each dated volcano in the principal Hawaiian Islands. In contrast, Jackson and others (1972) and Dalrymple and others (1980b, 1981) used the oldest age for tholeiitic volcanism as the best available approximation of the age of the volcanoes. McDougall (1979) and McDougall and Duncan (1980) adopted yet another approach and used the average age of tholeiitic shield volcanism. For table 1.4, we have chosen the oldest reliable ages for tholeiitic volcanism available, but the choice of which ages to use is probably not critical when considering the data for the chain as a whole. The reason is that the existing data on the rate of formation of Hawaiian volcanoes indicate that the tholeiitic shields are probably built up from the sea floor in as little as 0.5–1.5 m.y. (see summary in Jackson and others, 1972). This amount of time is within the analytical uncertainty of the K-Ar ages at about 20 Ma, or less than one-third of the way along the dated

TABLE 1.4.—*Summary of K-Ar geochronology along the Hawaiian-Emperor volcanic chain*

[Volcano number and distance from Bargar and Jackson (1974) and K.E. Bargar (written commun., 1978). Best K-Ar age is oldest reliable age of tholeiitic basalt, where available; all data converted to new constants $\lambda\varepsilon + \lambda\varepsilon' = 0.581 \times 10^{-10}$/yr, $\lambda\beta = 4.962 \times 10^{-10}$/yr, $^{40}K/K = 1.167 \times 10^{-4}$ mol/mol]

Volcano Number	Volcano Name	Distance from Kilauea along trend of chain (km)	Best K-Ar age (Ma)	Data source	Remarks
1	Kilauea	0	0-0.4	--	Historical tholeiitic eruptions
3	Mauna Kea	54	0.375±0.05	1	Samples from tholeiitic shield (Hamakua Volcanics)
5	Kohala	100	0.43±0.02	2	Samples from tholeiitic shield (Pololu Basalt)
6	Haleakala	182	0.75±0.04	3	Samples from tholeiitic shield (Honomanu Basalt)
7	Kahoolawe	185	>1.03±0.18	3	Samples from alkalic postshield stage (upper part of Kanapou Volcanics)
8	West Maui	221	1.32±0.04	4	Samples from tholeiitic shield (Wailuku Basalt)
9	Lanai	226	1.28±0.04	5	Samples from tholeiitic shield (Lanai Basalt)
10	East Molokai	256	1.76±0.07	3	Samples from tholeiitic shield (lower member of East Molokai Volcanics)
11	West Molokai	280	1.90±0.06	3	Samples from tholeiitic shield (lower part of West Molokai Volcanics)
12	Koolau	339	2.6±0.1	4,6	Samples from tholeiitic shield (Koolau Basalt)
13	Waianae	374	3.7±0.1	6	Samples from tholeiitic shield (lower member of Waianae Volcanics)
14	Kauai	519	5.1±0.20	7	Sample from tholeiitic shield (Napali Member of Waimea Canyon Basalt)
15	Niihau	565	4.89±0.11	8	Samples from tholeiitic shield (Paniau Basalt)
15A	Kaula	600	4.0±0.2	21	Phonolite from postshield stage (?)
17	Nihoa	780	7.2±0.3	9	Samples from tholeiitic shield
20	Unnamed	913	9.2±0.8	20	Dredged samples of alkalic basalt
23	Necker	1,058	10.3±0.4	9	Samples from tholeiitic shield
26	La Perouse Pinnacles	1,209	12.0±0.4	9	Samples from tholeiitic shield
27	Brooks Bank	1,256	13.0±0.6	20	Dredged samples of hawaiite and alkalic basalt
30	Gardner Pinnacles	1,435	12.3±1.0	20	Dredged samples of alkalic and tholeiitic basalt
36	Laysan	1,818	19.9±0.3	10	Dredged samples of hawaiite and mugearite
37	Northampton Bank	1,841	26.6±2.7	10	Dredged samples of tholeiitic basalt
50	Pearl and Hermes Reef	2,281	20.6±0.5	11	Dredged samples of phonolite, hawaiite, and alkalic basalt
52	Midway	2,432	27.7±0.6	12	Samples of mugearite and hawaiite from conglomerate overlying tholeiitic basalt in drill hole
57	Unnamed	2,600	28.0±0.4	11	Dredged samples of alkalic basalt
63	Unnamed	2,825	27.4±0.5	11	Dredged samples of alkalic basalt
65	Colahan	3,128	38.6±0.3	13	Dredged samples of alkalic basalt
65A	Abbott	3,280	38.7±0.9	13	Dredged samples of tholeiitic (?) basalt
67	Daikakuji	3,493	42.4±2.3	14	Dredged samples of alkalic basalt
69	Yuryaku	3,520	43.4±1.6	11	Dredged samples of alkalic basalt
72	Kimmei	3,668	39.9±1.2	14	Dredged samples of alkalic basalt
74	Koko (southern)	3,758	48.1±0.8	14,15	Dredged samples of alkalic basalt, trachyte, and phonolite
81	Ojin	4,102	55.2±0.7	16	Samples of hawaiite and tholeiitic basalt from DSDP Site 430
83	Jingu	4,175	55.4±0.9	17	Dredged samples of hawaiite and mugearite
86	Nintoku	4,452	56.2±0.6	16	Samples of alkalic basalt from DSDP Site 432.
90	Suiko (southern)	4,794	59.6±0.6	18,19	Single dredged sample of mugearite
91	Suiko (central)	4,860	64.7±1.1	16	Samples of alkalic and tholeiitic basalt from DSDP Site 433

Data sources:

1. Porter and others (1977)
2. McDougall and Swanson (1972)
3. Naughton and others (1980)
4. McDougall (1964)
5. Bonhommet and others (1977)
6. Doell and Dalrymple (1973)
7. McDougall (1979)
8. G.B. Dalrymple (unpub. data, 1982)
9. Dalrymple and others (1974)
10. Dalrymple and others (1981)
11. Clague and others (1975)
12. Dalrymple and others (1977)
13. Duncan and Clague (1984)
14. Dalrymple and Clague (1976)
15. Clague and Dalrymple (1973)
16. Dalrymple and others (1980a)
17. Dalrymple and Garcia (1980)
18. Saito and Ozima (1975)
19. Saito and Ozima (1977)
20. Garcia and others (1986b)
21. Garcia and others (1986a)

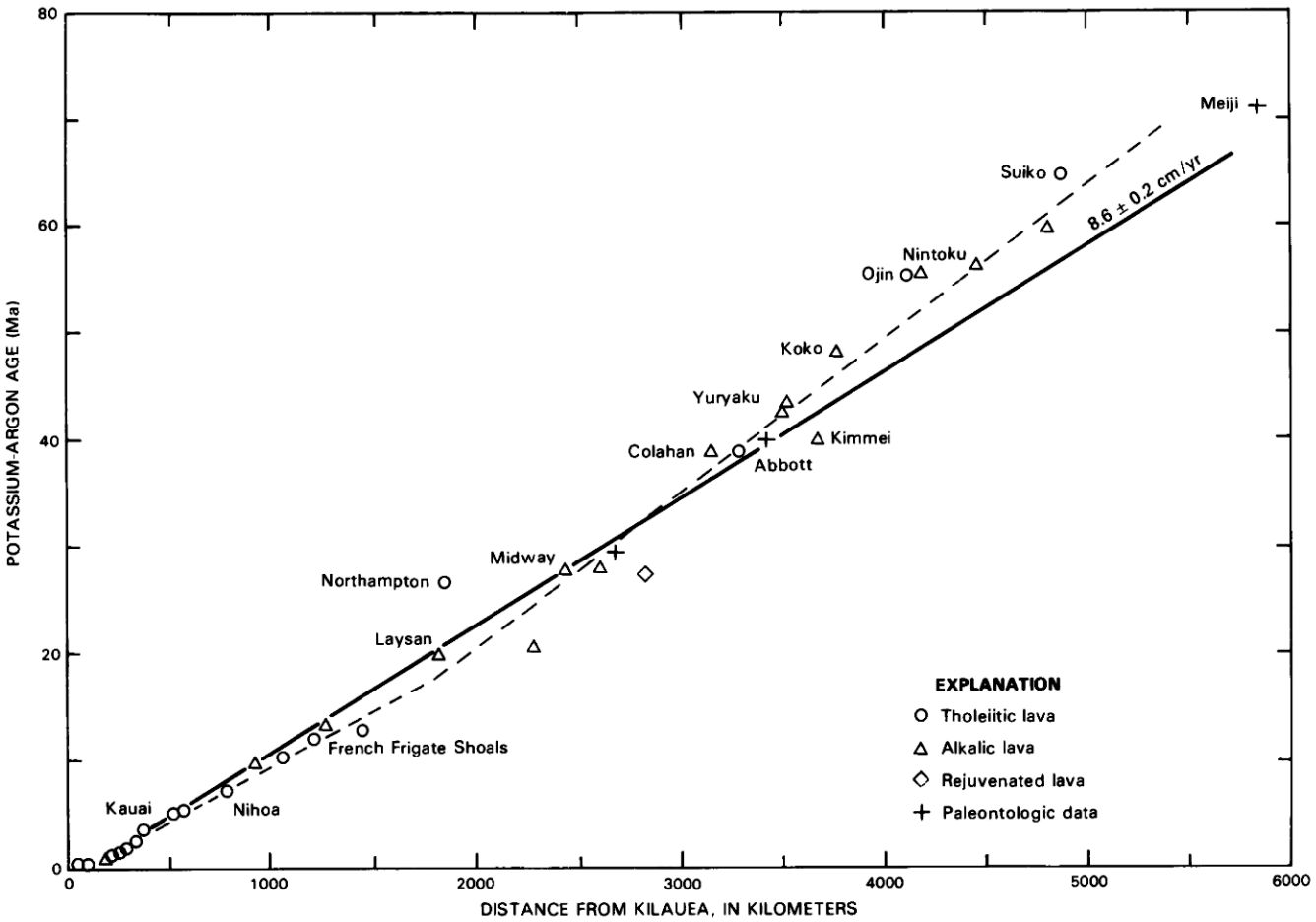

FIGURE 1.5.—Age of volcanoes in Hawaiian-Emperor Chain as a function of distance from Kilauea. Solid line is least-squares cubic fit (York 2) from table 1.5 and represents average rate of propagation of volcanism of 8.6 ± 0.2 cm/yr. Dashed line is two-segment fit using data from Kilauea to Gardner and Laysan to Suiko (table 1.5). Radiometric data from table 1.4, paleontologic data discussed in text.

part of the chain. The question of which ages to use is in any case moot for most of the volcanoes west of Kauai because so few suitable samples have been recovered that there is rarely a choice to make.

A majority of the age data from islands and seamounts west of French Frigates Shoal were obtained on alkalic rocks rather than on tholeiitic basalt. This is because the alkalic rocks, being younger than the tholeiitic basalt, are more likely to be recovered by dredging and drilling and are more resistant to submarine alteration than tholeiitic basalt. This bias toward ages of alkalic lava also probably makes very little difference because the difference between the ages of the postshield alkalic and youngest tholeiitic rocks is only a few hundred thousand years in the Hawaiian Islands (McDougall, 1964, 1969; Funkhouser and others, 1968; McDougall and Swanson, 1972; Doell and Dalrymple, 1973) and, presumably, in the other volcanoes of the Hawaiian-Emperor Chain. For one unnamed volcano on the western Hawaiian Ridge (63 in appendix 1.1 and table 1.4) the only data available are from lava erupted during the alkalic rejuvenated stage. In the principal Hawaiian Islands, lava erupted during the rejuvenated stage may postdate the tholeiitic shield and alkalic postshield stages by more than 4 m.y. (McDougall, 1964; G.B. Dalrymple, unpublished data, 1985), so the main shield of volcano 63 may be several million years older than indicated in table 1.4.

Previously, age-distance data along the Hawaiian-Emperor Chain have been regressed using a simple linear regression of age (dependent variable) on distance (independent variable), either unconstrained (for example, McDougall, 1971, 1979; Jackson and others, 1972; McDougall and Duncan, 1980) or forced through the origin (for example, Dalrymple and others, 1980b, 1981). The resulting volcanic propagation rates for the Hawaiian segment of the chain have ranged from as little as 6 cm/yr (Jackson and others, 1975) to as much as 15 cm/yr (McDougall, 1971; Jackson and others, 1972), although most recent estimates have been between 8 and 10 cm/yr (McDougall, 1979; McDougall and Duncan, 1980;

Dalrymple and others, 1981). Simple linear regression models have the disadvantages that they presume no error in distance and they do not take into account the experimental errors of individual determinations.

We have treated the data in table 1.4 using a two-error cubic fit (York 2), which allows for errors in both age and distance and weights the data accordingly (York, 1969). Errors for the age determinations are straightforward and are either provided in the original references or have been estimated by us from the array of data available on an individual volcano. Jackson and others (1975) estimated the cumulative errors in distance to be about 1.5 km at Kilauea to as much as 20 km near the western end of the Hawaiian Chain. We have interpolated and extrapolated these values to find errors for the distances in table 1.4. The results of both the York 2 regressions and the two simpler regression models for various segments of the Hawaiian-Emperor Chain are given in table 1.5. For the entire chain, the average rate of volcanic propagation is 8.6 ± 0.2 cm/yr with an intersection (that is, theoretical zero time) 89 km northwest of Kilauea using the York 2 regression. The simple regression models yield similar, though slightly lower, values of propagation rate.

Rates of propagation for the Hawaiian segment of the chain, that is, Kilauea through Abbott, have been calculated using both the maximum and minimum ages of tholeiitic volcanism. The results do not vary with model and range from 8.6 to 9.2 cm/yr. For comparison, we have included comparable calculations using the average ages of McDougall (1979). The resulting rates are somewhat higher than the rates calculated from either the maximum or

TABLE 1.5.—*Rates of propagation of volcanism along segments of the Hawaiian-Emperor Chain for several linear-regression models*

[Rates are in centimeters per year. Intercept, in kilometers, and correlation coefficient, r, given in parentheses where relevant. Simple regression is of age on distance, unweighted data; York 2 fit is two-error cubic, weighted data]

Chain segment	Data source	Simple regression		York 2 fit
		Unconstructed	Forced through origin	
Hawaiian-Emperor ---	table 1.4	7.8±0.2 (175, 0.992)	8.2±0.1	8.6±0.2 (89)
Hawaiian ----------	table 1.4 (maximum ages)	8.6±0.3 (102, 0.985)	9.1±0.2	9.2±0.3 (80)
	McDougall, 1979 (average ages)	9.4±0.3 (91, 0.994)	9.9±0.2	11.3±0.1 (3)
	appendix 1.1 (minimum ages)	8.6±0.3 (119, 0.986)	9.1±0.2	9.1±0.3 (97)
Emperor ----------	table 1.4	6.5±0.8	7.9±0.2	7.2±1.1
Kilauea to Gardner -	table 1.4	9.9±0.3 (57, 0.992)	10.6±0.3	9.6±0.4 (73)
Laysan to Suiko ----	table 1.4	6.9±0.4 (0.971)	8.1±0.2	6.8±0.3
Gardner to Waianae -	table 1.4	9.5±0.4 (54, 0.993)	10.1±0.2	10.1±0.8 (9)

minimum data, but the difference is largely a consequence of differences in the data sets, the ones in table 1.4 and appendix 1.1 being more current.

Rates calculated for the Emperor Chain, that is, Daikakuji through Suiko, are markedly lower than for the Hawaiian Chain, ranging from 6.5 to 7.2 cm/yr when not forced through the origin. Separate rates for these two major segments of the chain are only meaningful, however, if there was a rate change at the time of formation of the bend. This hypothesis can be tested by using the linear equations found from the York 2 regressions to predict the age of the bend, which we estimate to be 3,451 km from Kilauea at the position of volcano 68. The predicted ages for the bend are 36.7 Ma and and 43.0 Ma for the Hawaiian and Emperor segments, respectively. The Hawaiian prediction, which is similar to the value of 37.8 Ma found by McDougall (1979), differs significantly from the measured bend age of 43.1 ± 1.4 Ma as determined from the ages of Daikakuji and Yuryaku Seamounts. This suggests that if there was a significant change in volcanic propagation rate it did not occur at bend time, but some time after, a conclusion also reached by Epp (1978).

For some time, it has been apparent to us that a change in rate near or before the time of formation of Midway is consistent with the available data (Dalrymple and others, 1980b). For example, the fits of the data for the chain segments Kilauea-Gardner and Laysan-Suiko are slightly better than the fits for the Hawaiian and Emperor segments (table 1.5; fig. 1.5). The two former lines intersect near Gardner Pinnacles at an age of about 18 Ma. Epp (1978) concluded that a rate change occurred around 20–25 Ma. We have tried various ways to determine the most likely time for a change in the rate of volcanic propagation, including correlation with eruption volumes along the chain (see section below on eruption rates) and age-predictive models for the central parts of the chain, but we are not convinced that the results are meaningful. We can only conclude that the data imply, but do not require, a change of rate sometime after the formation of the Hawaiian-Emperor bend and before or near the time of formation of Laysan Volcano.

In addition to the possibility of a major change in the volcanic propagation rate, as discussed above, there are also indications of short-term departures from linearity. Short-term changes in the volcanic propagation rate were first proposed by Jackson and others (1972) to explain the apparent acceleration of propagation during the past 5 m.y. or so. They did not suggest that short-term variations in propagation rate reflected variations in relative motion of hot spot and plate. Shaw (1973) and Walcott (1976) proposed thermal feedback mechanisms to account for such variations without varying the relative rate of motion between the hot spot and the Pacific plate (see section below on models). Nonlinear models have been disputed by McDougall (1979) and McDougall and Duncan (1980), who argue that linear regressions fit the Hawaiian data so well that no other model needs to be considered.

It seems obvious to us from the geometry alone, however, that the volcanic propagation rates must be nonlinear in detail. If this were not so, then either the volcanism would have formed a ridge rather than individual volcanoes, or the volcanoes in the chain would be spaced in proportion to their ages along a single line. Neither is the case; the volcanoes are irregularly spaced within a band some 200–300 km wide, indicating clearly that volcanic propagation is irregular.

Although some of the irregularities in the age-distance data no doubt reflect dating errors and differences in the stage of volcanism sampled, some of the deviations appear to be larger than can reasonably be attributed to these causes. For example, the ages of Laysan and Northampton Bank should differ by only about 0.3 m.y. rather than the 6.7 m.y. indicated by their measured ages. A similar discrepancy occurs in the ages of volcanoes near the bend (table 1.4; fig. 1.5). There are also volcanoes in the chain that appear to have been active simultaneously even though they were separated by distances of hundreds of kilometers. Examples include Laysan, and Pearl and Hermes, as well as Midway and Northampton. Indeed, Mauna Loa, Kilauea, and Loihi are currently active, erupting tholeiitic basalt, and are separated by more than 80 km.

The primary reason that Jackson and others (1972) suggested short-term nonlinearities in propagation rates was the pronounced curvature in the age-distance data from the volcanoes of the principal Hawaiian Islands. When plotted as a function of distance from Kilauea, the ages for these volcanoes clearly indicate an acceleration of volcanic propagation over the past 5 m.y. (Jackson and others, 1972). This curvature is also one reason that virtually all regressions intersect the distance axis northwest of Kilauea (table 1.5) and predict a negative age for that volcano. McDougall (1979) has argued that the curvature is caused by a bias toward young ages for the less eroded volcanoes, but this cannot be so. Even though Kohala Mountain is relatively uneroded, it is deeply incised on the windward side by several canyons whose floors are near sea level, and it is unlikely that further erosion will expose lava significantly older than is now exposed. In addition, the rapid subsidence of Hawaii (Moore, 1970) may carry the oldest subaerial lava flows below sea level before they can be exposed by erosion. Similar arguments can be made for West Maui, Lanai, Kahoolawe, East Molokai, and Koolau Volcanoes, where lava deep within the subaerial part of the tholeiitic shield has been exposed by marine or stream erosion or by faulting.

We have plotted the known age range for tholeiitic shield, alkalic postshield, and alkalic rejuvenated-stage volcanism for the principal Hawaiian volcanoes in figure 1.6, from which the acceleration of volcanic propagation over the past 3–5 m.y. is evident. It is also clear from this figure that the curvature in the age-distance data is not a function of which eruption stage, tholeiitic shield or alkalic postshield, is chosen to represent the age of the volcanoes. Furthermore, a bias toward younger ages for the less eroded volcanoes, taken to include Kilauea through Haleakala, cannot produce the curvature because older ages for these volcanoes would exaggerate, not lessen, the apparent acceleration. Thus, the acceleration of volcanic propagation in the principal islands, as proposed by Jackson and others (1972), appears to us to be real.

While the overall rate of propagation of volcanism along the chain (or at least major segments of it) may be linear and reflect the relative motion between the Pacific plate and the Hawaiian hot spot, there also appears to be ample justification for retaining nonlinear

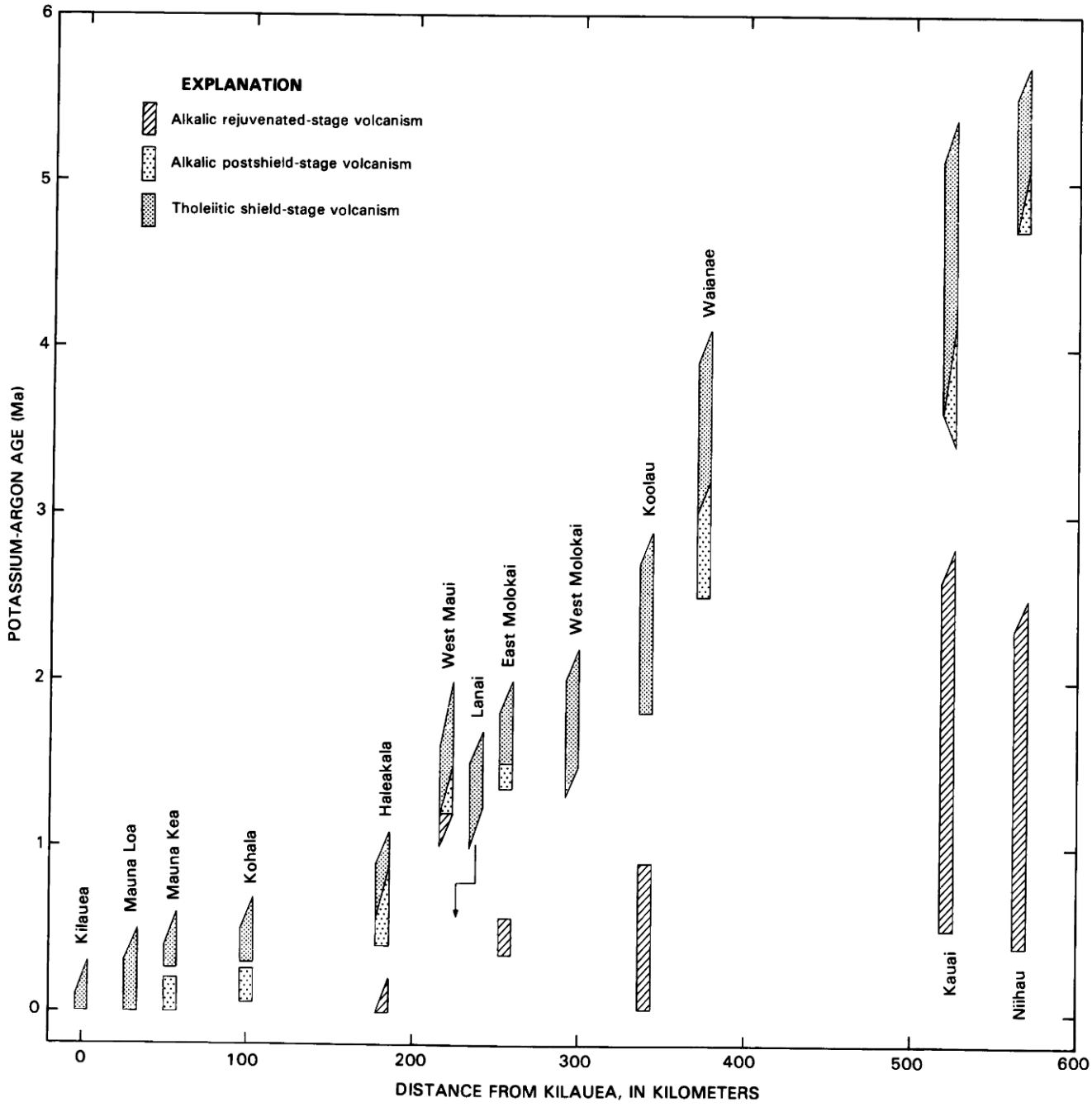

FIGURE 1.6.—Known durations of tholeiitic shield, alkalic postshield, and alkalic rejuvenated-stage volcanism for dated volcanoes of principal Hawaiian Islands. Angled lines indicate overlapping or uncertain ages or overlapping volcanism. Data from sources discussed in appendix 1.1. Data for Niihau and for Kauai (Koloa Volcanics) are from G.B. Dalrymple (unpublished data, 1985).

propagation on a small scale as a working hypothesis. It is unlikely that the cause of this nonlinear propagation, if real, will be known until more is learned about the hot-spot mechanism.

ERUPTION RATES ALONG THE CHAIN

The bathymetry of the chain as a whole is not well known, particularly for the western Hawaiian Ridge, and the 1970 charts for the North Pacific (Chase and others, 1970) and their 1973 derivative (Chase and others, 1973) are probably still the best published sources available. An updated bathymetric chart for the Emperor Seamounts (Clague and others, 1980) was based on the data used by Chase and others (1970) and additional geophysical profiles collected between 1970 and 1979; recently published bathymetry for much of the central part of the Emperor Seamounts (Smoot, 1982) is based on previously classified Navy multibeam

data. The gross structure of the Emperor Seamounts is little changed in the later charts, but the shapes and locations of some individual volcanoes changed dramatically (fig. 1.7).

Bargar and Jackson (1974) compiled volume data along the chain and identified individual volcanic centers and their rift systems using the bathymetry of Chase and others (1970). From the more accurate multibeam data it is clear that many of the volcanic centers and rift zones identified by Bargar and Jackson are incorrect in detail. Because the number and general sizes of the volcanoes change little on the later charts, we have used Bargar and Jackson's volume estimates rather than engage in the laborious process of calculating new ones from the newer data. We suspect that the volumes based on multibeam data would vary relatively little from those of Bargar and Jackson.

The cumulative volume of the volcanoes is plotted in figure 1.8 against distance from Kilauea beginning at Tenchi Seamount, 500 km north of Suiko. It is clear that the volume of eruptive products per unit distance along the chain has not been constant over the past 70 million years.

We have calculated dV/dx, where V is volume and x is distance, for segments of the chain, which are summarized in table 1.6. Also listed are dx/dt, where t is time, calculated from the age relations along the chain, and the derived quantity dV/dt for segments along the chain. These calculations clearly show that the volumes erupted per unit distance along the chain and per unit time increase from the Emperor Seamounts to the Hawaiian Ridge and to the Hawaiian Islands. The present-day eruption rate for Kilauea alone, when compared to eruption rates along the Hawaiian Ridge and Emperor Seamounts, demonstrates that the Hawaiian hot spot is presently producing large volumes of lava at the greatest eruption rates in its known history. The average eruption rate from Hualalai to Kilauea is 5 times that for the islands as a whole and nearly 22 times the rate for the entire chain. The only section of the chain where volumes do not increase toward the present is the westernmost section of the Hawaiian Ridge, which formed immediately following the change in plate motion recorded as the Hawaiian-Emperor bend. This change in plate motion was followed by a virtual cessation of volcanic activity that lasted for nearly 10 m.y.

PETROLOGY OF THE HAWAIIAN-EMPEROR VOLCANIC CHAIN

EARLY WORK: LAVA SERIES AND DIFFERENTIATES

Early observers of Hawaiian eruptions rather uniformly agreed that the lava originated "in the bowels of the earth." As time progressed this view was expanded upon, but it was not until the 1950's and 1960's that the lava source and the processes generating the various lava types were discussed in detail. S. Powers (1920) proposed that nepheline basalt and trachyte were formed by differentiation of basaltic magma because of their occurrence late in the eruptive sequence. He wrote (S. Powers, 1920, p. 280): "Each volcano has arisen at an intersection in a fracture system in the earth's crust, has been fed from the same primal source, and has finally lost connection with that source. When this takes place differentiation may proceed in the magma chambers of large volcanoes and the extreme products of Hawaiian volcanism, nepheline basalt and trachyte, may appear either at the close of the main volcanism or in a later phase after extensive erosion."

This viewpoint, that there was a single primary Hawaiian magma from which the varieties of lava evolved by means of differentiation, was popular well into the 1960's. H. Powers (1935) expressed a similar view, although he showed that fractional crystallization alone could not explain the differentiation of Hawaiian basalt. Macdonald (1949) proposed that the sole primary Hawaiian lava was olivine basalt, although his calculated average included both alkalic and tholeiitic olivine basalt analyses (which he did not distinguish at that time). He also proposed that andesine andesite (hawaiite), oligoclase andesite (mugearite), and trachyte were successive differentiates from an olivine basalt parental lava. This view is now known to be incorrect because Macdonald's calculated olivine basalt was basically a tholeiitic basalt in composition. He further inferred that picritic basalt of the oceanite type (here termed picritic tholeiitic basalt) formed by the accumulation of olivine and that ankaramite was not an oceanite that simply accumulated clinopyroxene. This last idea is correct, ankaramite being alkalic in composition whereas picritic basalt of the oceanite type is tholeiitic. In order to differentiate ankaramite and nepheline basalt from the parental olivine basalt, Macdonald (1949) proposed that limestone assimilation and selective remelting (wall-rock assimilation) were important processes. He correctly inferred that the dunite xenoliths so common in alkalic lava from the postshield and rejuvenated stages formed by accumulation of olivine followed by recrystallization.

Tilley (1950) recognized that the bulk of the primitive shields was made of tholeiitic basalt and that alkalic rocks erupted only during the declining stages of activity. He proposed that alkalic olivine basalt was derived from tholeiitic basalt by crystal fractionation. H. Powers (1935) had, however, earlier noted that primitive lava was silica saturated, whereas the late differentiated lava was silica undersaturated; he argued that these lavas could therefore not be simply related to one another by crystal fractionation.

New concepts important to understanding the origin of Hawaiian lava were introduced by H. Powers (1955). He clearly established that the abundant rocks termed olivine basalt in the shields are silica saturated and noted that they are compositionally distinct for individual volcanoes. He proposed the concept of magma batches to account for the subtle differences between the lava of different shields. He also reiterated that olivine basalt erupted during the declining stages of activity is silica undersaturated. His discussion of fractionation trends for tholeiitic and alkalic basalt is nearly identical to present-day views. He further recognized that earthquakes associated with volcanic activity gave a minimum depth of magma generation which he took to be 48–56 km (30–35 miles). His estimates of the source rocks that could be melted to produce basalt and of the causes of melting provided a framework for experimental research for many years. In particular, he noted that basalt could be generated at depth by wholesale melting of rocks of basaltic composition or by partial melting of peridotite. The models of melting he considered all assumed that it was caused by an increase in temperature. He dismissed exothermic nuclear processes

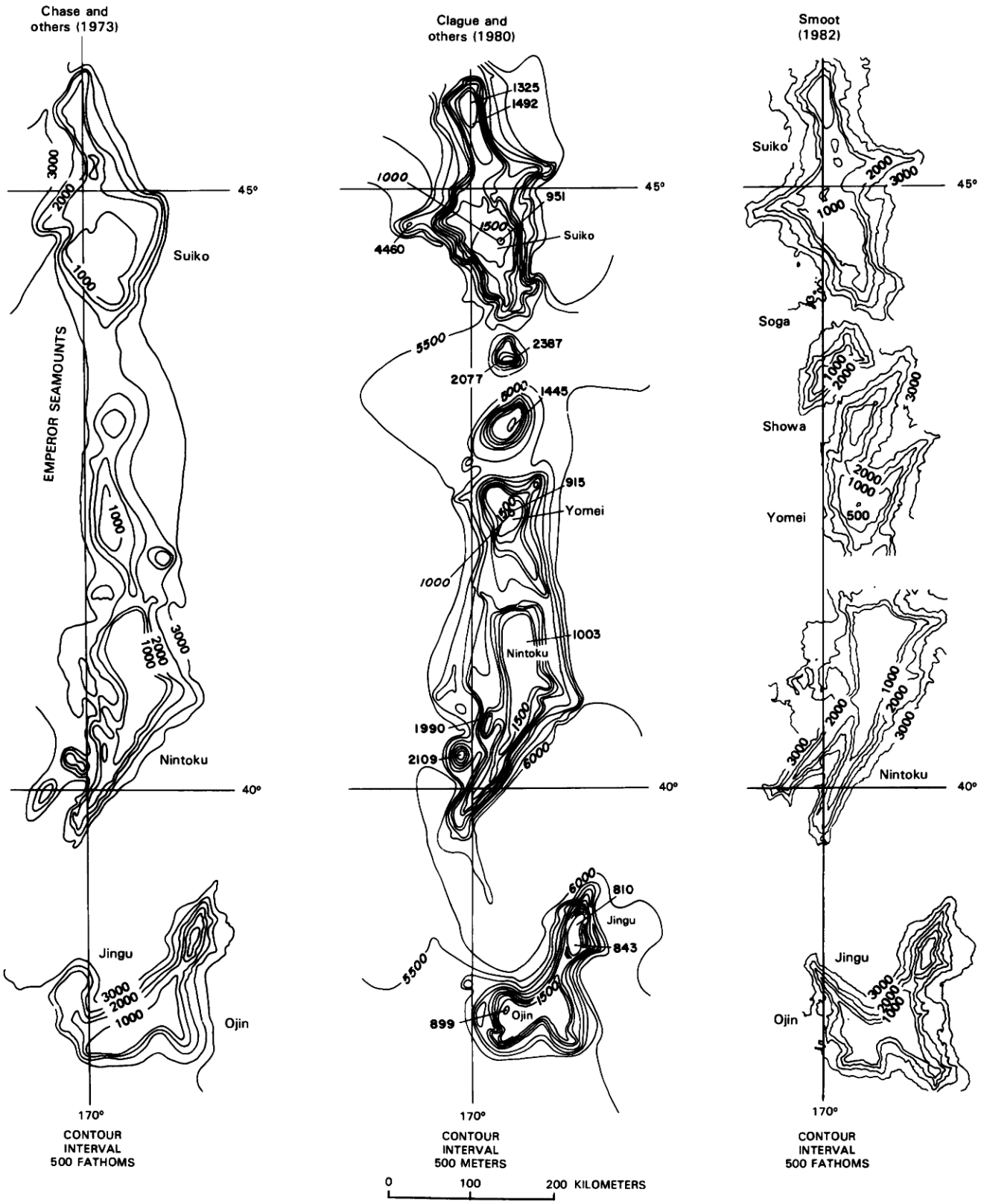

FIGURE 1.7.—Comparison of bathymetry of central Emperor Seamounts from Chase and others (1973; left), Clague and others (1980b; center) and Smoot (1982; right). General size and shape of seamounts were fairly well mapped by bathymetric sounding (left and center), but multibeam bathymetry (right) adds wealth of detail. Contour intervals are 500 fathoms for left and right figures and 500 m for center figure.

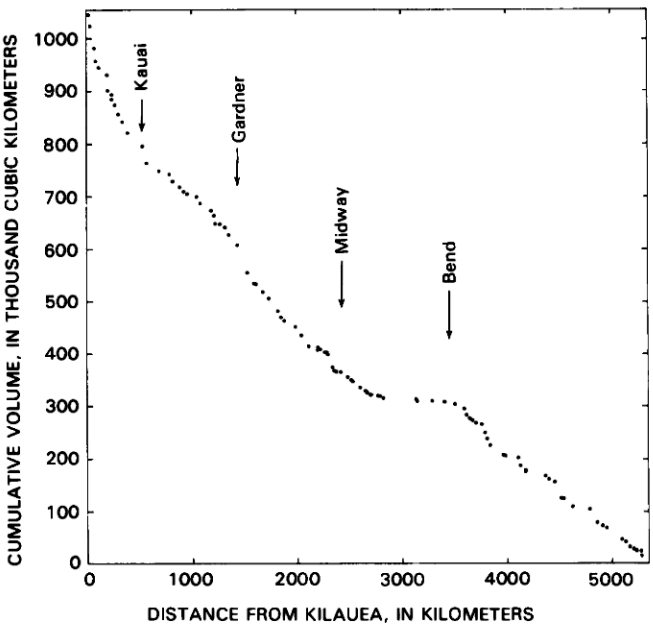

FIGURE 1.8.—Cumulative volcanic volume along Hawaiian-Emperor Chain plotted as a function of distance from Kilauea (along trend of chain). Average volume increment rate (dV/dx) for Emperor Chain is 0.16×10^3 km^3/km. Just east (left) of the bend there is a segment of very low volcanic productivity, in which only 0.02×10^3 km^3/km was erupted. Remainder of submarine portion of the Hawaiian Chain has an average dV/dx of 0.20×10^3 km^3/km. In Hawaiian Islands section from Kauai to Haleakala can be fit by 0.40×10^3 km^3/km and that from Haleakala to Kilauea by 1.1×10^3 km^3/km.

in the crust because Hawaiian lava is not enriched in U, Th, or K. He emphasized convection from hotter regions deep in the mantle and friction produced by dynamic processes (he proposed tides). His convection model is very similar to later plume models and his friction model to at least a part of later thermal-feedback models, both of which are discussed more thoroughly later in this paper.

Kuno and others (1957) clearly demonstrated that closed-system crystal fractionation of tholeiitic basalt led to generation of granophyre in the differentiation of thick lava bodies. They related picritic tholeiitic basalt, olivine tholeiitic basalt, tholeiitic basalt, and granophyre as one differentiation sequence and alkali olivine basalt, picrite basalt of ankaramite type (here called ankaramite), hawaiite, mugearite, and trachyte as another differentiation sequence. They presented trace-element data, which they used to evaluate the proposed fractionation trends. Most importantly, they dismissed any fractionation relation between tholeiitic and alkalic basalt and proposed that they originated independently "through melting of the earth's material under different sets of physical conditions" (Kuno and others, 1957, p. 214). They argued that both lava types were generated by partial melting of peridotite, but that alkalic basalt was derived at greater depth. Their discussion implies that the source rocks were homogeneous and that only the physical conditions of melting varied. In addition, the alkali-silica diagram, widely used to distinguish between tholeiitic and alkalic lava, was first presented in this paper.

Eaton and Murata (1960) published a detailed study locating earthquake epicenters as deep as 60 km beneath Kilauea using basically the same data cited by Powers (1955). These observations establish a minimum depth of magma generation for tholeiitic shield lava of greater than 60 km, although they still allow for selective melting (wall-rock reaction) at shallower depths (Macdonald, 1968).

Macdonald and Katsura (1962, 1964) established the tholeiitic character of the early lava on Kohala and West Maui, where the known late-stage lava is alkalic. They also demonstrated that the subtle variations in composition of the tholeiitic basalt from different volcanoes were unrelated to the type of alkalic cap that followed (Kohala or Haleakala type). In contrast to the interpretations of Tilley (1950), H. Powers (1955), and Kuno and others (1957), Macdonald and Katsura (1964) proposed that alkalic basalt formed by differentiation of tholeiitic basalt. They cited as evidence the interbedded sequence of tholeiitic and alkalic flows, including some of transitional composition, that occur in Haleakala-

TABLE 1.6.—*Eruptive rates along the Hawaiian-Emperor Chain*

[Volume/distance data from figure 1.8; propagation rate data from table 1.5, except for Kilauea to Hualalai; recent data for Kilauea from Dzurisin and others (1984), based on combined eruption-intrusion rate]

Segment	Volume/distance, dV/dx (10^3 km^3/km)	Propagation rate, dx/dt (km/m.y.)	Eruption rate dV/dt (10^3 km^3/m.y.)
Kilauea (1956-1983)	---	---	86
Kilauea to Hualalai	1,500	250	290
Hualalai to Waianae	400	101	40
Hawaiian Islands (0-5.5 Ma)	---	---	56
Waianae to Gardner Pinnacles	190	101	19
Gardner Pinnacles to volcano 57	200	68	14
Volcano 57 to Hawaiian-Emperor bend	20	68	1
Emperor Seamounts	160	72	12
Average for entire chain	---	---	13

type volcanoes between the tholeiitic shield lava and the later alkalic postshield-stage lava and proposed that volatile transfer might be an important differentiation process. They discussed thoroughly the fractionation sequences of both alkalic and tholeiitic lava and related the Mauna Kuwale rhyodacite to tholeiitic lava of the Waianae Range.

The years 1964–68 produced new insights from a variety of studies. The first isotopic data from Hawaiian lava (Lessing and Catanzaro, 1964; Hamilton, 1965; Powell and DeLong, 1966; Tatsumoto, 1966) clearly demonstrated that the source rocks for Hawaiian lava were heterogeneous. Experimental studies at high pressure and temperature (for example, O'Hara, 1965; Green and Ringwood, 1967) added new data bearing on the mineralogy of potential source rocks and the physical conditions of melting. At the same time, trace-element data began to be used to evaluate Hawaiian petrogenetic processes (Schilling and Winchester, 1966; Gast, 1968). Studies of Hawaiian xenoliths (White, 1966) added to the abundant new data being used to evaluate the petrogenesis of Hawaiian lava and the nature of the source rocks. This period marks a transition from relatively qualitative models of petrogenesis to modern quantitive modeling and testing of basalt petrogenesis. To a great degree present day petrogenic models are based on these same types of data and similar quantitative modeling techniques. However, because modern isotopic and trace-element data are more accurate and precise, the models proposed are more refined and complex.

Macdonald (1968) followed Green and Ringwood (1967) and proposed that the tholeiitic, alkalic, and nephelinitic lava types were derived from a single parent magma of olivine tholeiitic basalt composition. He proposed that the compositional variations reflect the depth at which fractional crystallization occurred with tholeiitic basalt fractionated at shallow depths, alkalic basalt at moderate depths, and nephelinitic lava at depths of several tens of kilometers. He further argued that the primary magma is olivine tholeiitic basalt rather than tholeiitic basalt because most lava has lost olivine, which accumulated within the magma chambers to form the high-density masses discovered by gravity surveys (summary and references in Jackson and others, 1972). Macdonald (1968) noted that the highest temperature lava from the Kilauea Iki eruption contained 27–30 percent olivine and proposed that this closely approximated primary magma. Wright (1973) calculated the bulk composition of the same eruption and proposed it as a representative parental (but not necessarily primary) composition for Kilauea tholeiitic basalt. Macdonald (1968) presented quantitative models showing that ankaramite is alkalic basalt plus olivine and clinopyroxene and that hawaiite is alkalic basalt minus olivine, clinopyroxene, plagioclase, and magnetite. This type of mass-balance approach was later refined by Wright (1971) and Wright and Fiske (1971) to demonstrate the roles of fractionation and hybridization in generating basalt at Kilauea and Mauna Loa. The debate about whether primary tholeiitic magma is olivine rich or olivine poor continues today (see Wright and Helz, chapter 23; Wright, 1984; Budahn and Schmitt, 1984). Extreme compositions are liquids with 20 percent MgO (Wright, 1984) and average tholeiitic basalt with 9 percent MgO (Powers, 1955).

Macdonald (1968) also calculated average compositions of Hawaiian lava from the different eruptive stages. His average compositions, recalculated on a dry-reduced normalized basis, are presented in table 1.7. These averages clearly show that lava of the tholeiitic shield stage is silica saturated and that of alkalic postshield and rejuvenated stages is silica undersaturated. The presence of normative hypersthene in the mugearite, benmoreite, and trachyte, which are derived from undersaturated alkalic basalt, reflects fractionation of Fe-Ti oxides, which enriches the residual melt in silica. Rejuvenated-stage alkalic basalt contains greater than 5 percent normative nepheline, and average nephelinite and nepheline melilitite contain normative leucite. Alkalic basalt of the preshield and rejuvenated stages are similar in composition. The preshield Loihi Seamount averages are calculated from Moore and others (1982), Frey and Clague (1983), and D.A. Clague (unpub. data, 1985).

XENOLITH DISTRIBUTIONS

In a detailed analysis of the xenolith populations in Hawaiian lava, Jackson (1968) subdivided the xenoliths into dikes and sills, cumulates, and metamorphic rocks. His breakdown of the relative abundances and types of xenoliths is given in table 1.8, modified to include xenoliths found in Loihi Seamount alkalic preshield lava. Jackson noted that only those xenoliths with metamorphic textures could represent either mantle source rocks or mantle residua left after partial melting. The dikes, sills, and some, but not all, of the cumulate rocks are cognate or from shallow depths. The cumulate xenoliths from Hualalai Volcano appear to come from a variety of sources, including cumulates formed as part of oceanic crustal layer 3, cumulates of tholeiitic Hawaiian shield lava, and cumulates of lava from the alkalic postshield stage (D.A. Clague, unpub. data, 1985). The single cumulate xenolith from Loihi Seamount presumably represents a cumulate of ocean crustal layer 3.

Jackson and Wright (1971) proposed that the abundant dunite xenoliths in the Honolulu Volcanics represent residue left after melting the mantle to form Koolau shield tholeiite, an interpretation with which we disagree. Jackson and Wright (1971) inferred that the garnet lherzolite and lherzolite found only in alkalic lava from the rejuvenated stage were potential mantle source rocks. The difference in xenolith populations for the three alkalic eruptive stages is striking since only the lava from the preshield stage and rejuvenated stage contain xenoliths that formed at depths greater than about 20 km. Although it would be useful if these xenolith populations reflected the mantle through which the lava ascends, it seems more likely that they reflect the development of shallow magma storage reservoirs, which act as hydraulic filters and remove xenoliths carried up from greater depths in much the same way as lakes remove sediment from rivers.

Lava stored in a shallow magma reservoir, either within a few kilometers of the surface or at the base of the oceanic crust, lose any xenoliths they may have acquired during ascent and from this point can only entrain xenoliths that occur at shallower levels in the volcanic system. However, lava of the preshield and rejuvenated stages erupts in small volumes at infrequent intervals and probably no shallow magma storage reservoirs exist. During the shield stage, tholeiitic lava erupts in large volumes at frequent intervals from a

TABLE 1.7.—*Average compositions and norms of major Hawaiian lava types*

[All figures in weight percent; -- not present. Normative components calculated with original FeO/Fe_2O_3 ratios. See Macdonald (1968) for remainder of norms for all but the alkalic preshield stage. Data for alkalic preshield stage from Frey and Clague (1983) and D.A. Clague (unpub. data, 1985)]

Stage	Alkalic preshield				Tholeiitic shield		Alkalic postshield						Alkalic rejuvenated			
Lava type	Tholeiite and olivine tholeiitic basalt	Transitional basalt	Alkalic basalt	Basanite	Picritic tholeiitic basalt	Tholeiitic and olivine tholeiitic basalt	Ankaramite	Alkalic basalt	Hawaiite	Mugearite	Benmoreite	Trachyte	Alkalic basalt	Basanite	Nephelinite	Melilitite
Chemical composition																
SiO_2 ------	48.4	48.3	45.6	43.5	46.7	50.0	44.6	45.9	48.6	52.1	58.3	62.8	45.2	44.6	40.6	37.8
Al_2O_3 -----	12.2	13.6	11.6	11.1	8.5	14.1	12.2	14.9	16.1	17.1	18.0	18.3	12.8	12.8	11.6	11.2
FeO* ------	12.0	12.3	12.4	13.6	12.1	11.3	12.6	13.0	12.2	10.0	7.5	4.5	12.4	12.5	13.3	14.6
MgO -------	11.2	7.5	13.5	12.2	20.9	8.5	13.1	7.9	4.9	3.3	1.6	.4	11.5	11.3	12.4	13.0
CaO -------	11.0	11.4	10.4	11.4	7.4	10.4	11.6	10.6	8.1	6.2	3.6	1.2	11.5	10.7	13.1	14.1
Na_2O ------	2.1	2.7	2.5	3.2	1.6	2.2	1.9	3.0	4.3	5.5	6.0	7.5	2.7	3.6	3.9	4.2
K_2O -------	.4	.7	.8	1.3	.3	.4	.7	1.0	1.5	2.1	2.9	4.3	.9	1.0	1.2	1.0
TiO_2 ------	2.3	3.1	2.7	3.1	2.0	2.5	2.7	3.0	3.4	2.4	1.2	.5	2.3	2.6	2.9	2.9
P_2O_5 ------	.2	.3	.3	.5	.2	.3	.3	.4	.7	1.1	.7	.2	.5	.5	.9	1.1
MnO -------	.2	.2	.2	.2	.2	.2	.2	.2	.2	0.2	.2	.2	.2	.2	.2	.1
Normative composition																
Q --------	--	--	--	--	--	2.2	--	--	--	--	--	--	--	--	--	--
Ne --------	--	--	2.7	11.8	--	--	2.6	2.6	0.3	--	--	--	6.0	10.5	17.3	18.7
Lc --------	--	--	--	--	--	--	--	--	--	--	--	--	--	--	5.7	4.8
Hy --------	14.3	6.3	--	--	15.9	21.5	--	--	--	2.7	4.0	.4	--	--	--	--
Ol --------	10.5	5.9	23.1	17.7	29.5	--	22.2	13.2	6.7	2.1	--	--	19.3	17.9	14.9	20.2

shallow magma storage reservoir and perhaps a deeper staging zone (see review by Decker, chapter 42). During the alkalic postshield stage, lava erupts in small volumes at infrequent intervals, though in larger volumes and at more frequent intervals than during the alkalic preshield or rejuvenated stages. During this stage, lava apparently resides in reservoirs below the base of the oceanic crust (Clague and others, 1981) for time periods sufficient for the dense peridotite xenoliths to settle out. Tholeiitic lava at Kilauea passes through two such filters, one an intermediate-depth (20–30 km) staging area, the second a well-defined and complex shallow reservoir system 3–7 km beneath the surface. After passing through these filters, the lava can only incorporate as xenoliths the wall rocks occurring at depths shallower than the shallowest reservoir (dikes, sills, and olivine cumulates). Alkalic lava of the postshield stage contains abundant xenoliths of dunite, which have CO_2 inclusions that were trapped at depths of at least 15 km, and cumulate xenoliths of rocks from oceanic crustal layer 3 (Roedder, 1965; D.A. Clague, unpub. data, 1985). These observations suggest that in the postshield stage any shallow magma chamber of the shield stage no longer exists but an intermediate staging area at 20–30 km, similar to that beneath Kilauea, acts as an effective filter that removes any lherzolite or garnet peridotite xenoliths. Lava may fractionate in this zone and, upon movement to the surface, entrain xenoliths of ocean crust rocks and cumulates formed in earlier volcanic stages at shallow depth. The presence of xenoliths that originate at great depth in alkalic lava of both the preshield and rejuvenated stages implies that neither shallow nor intermediate staging area acts as an effective filter in these stages. The near-primary character of the host lava also indicates that the lava was not stored at shallow depths but rather moved from its source region to the surface in short time periods (Clague and Frey, 1982).

This analysis leads us back to Jackson's (1968) conclusion that only the xenoliths with metamorphic textures could possibly be mantle source rocks or residua. We conclude that only the lherzolite and garnet peridotite xenoliths represent mantle rocks from below the magma storage zone that appears to have existed beneath Hawaiian shield volcanoes at depths of 20–30 km. The dunite and wehrlite xenoliths are either deformed cumulates formed during

TABLE 1.8.—*Distribution of Hawaiian xenolith types*

[Data from Jackson (1968) except the alkalic preshield stage which is from D.A. Clague (unpub. data, 1985)]

Eruptive stage	Lava type	Xenolith type (percent)		
		Dike rocks and vein fillings	Cumulates	Metamorphic rocks
Alkalic rejuvenated	alkalic basalt basanite nephelinite nepheline melilitite	(<1)	(1) olivine cumulates dominant	(99) dunite ≅ wehrlite ≅ lherzolite> harzburgite, garnet peridotite locally
Alkalic postshield	alkalic basalt	(3) veins dominant	(35) olivine cumulates> pyroxene cumulates	(62) dunite>> wehrlite
	ankaramite	(14) dikes and sills dominant	(53) pyroxene cumulates> olivine cumulates	(33) dunite>> wehrlite
	hawaiite mugeartie trachyte	(14) dikes and sills dominant	(57) pyroxene cumulates> olivine cumulates	(29) dunite>> wehrlite
Tholeiitic shield	tholeiitic basalt	(75) dikes and sills dominant	(25) olivine cumulates dominant	none
Alkalic preshield (Loihi)	alkalic basalt basanite	none	(1) olivine cumulates	(99) dunite>> lherzolite

earlier stages in the volcano's growth or cumulates formed during formation of oceanic crust (see Sen, 1983, 1985; Kurz and others, 1983; Sen and Presnall, 1985).

The remaining xenoliths of spinel lherzolite, rare harzburgite, and rare garnet peridotite that occur in alkalic lava of the rejuvenated stage and even more rarely in alkalic lava of the preshield stage therefore are the only xenoliths of deeper mantle material. Spinel lherzolite xenoliths have many characteristics that imply a close genetic relationship to midocean-ridge basalt; however, both the Sr-isotopic and rare-earth data indicate that these xenoliths have been enriched by mixing between residua left after formation of midocean-ridge basalt and an enriched magma or vapor (Frey 1980, 1984; Wright, 1984; Frey and Roden, in press). These xenoliths probably represent depleted oceanic lithosphere modified by processes related to Hawaiian magmatism.

The final group of xenoliths consists of pyroxenite, websterite, and garnet-bearing pyroxenite and websterite. These occur in only a few vents of the alkalic rejuvenated stage in the Honolulu Volcanics (Jackson and Wright, 1970) and on Kaula Island (Garcia, Frey, and Grooms, in press). These rocks occur both as separate xenoliths and as layers in xenoliths. Some of these xenoliths have been called garnet lherzolite (Jackson and Wright, 1970), but they are not merely a higher pressure assemblage of spinel lherzolite because their bulk compositions are distinct (Jackson and Wright, 1970; Sen, 1983). The iron-rich olivine in all the xenoliths of this group led Sen (1983) to argue that they represent neither source rocks nor residua related to Hawaiian lava. Frey (1980, 1984) has argued that they may represent crystal accumulates from alkaline Hawaiian magma. We conclude that none of the xenoliths found in Hawaiian lava represent mantle source rocks or residua related to Hawaiian volcanism. They do, however, provide insight into the conduit systems through which much of this lava passed.

Jackson and Wright (1970) demonstrated that xenoliths in the Honolulu Volcanics were compositionally zoned in a geographic sense with respect to the Koolau caldera; abundant dunite near the caldera grades into lherzolite and finally garnet-bearing websterite and pyroxenite away from the caldera. Jackson and Wright (1970) combined these observations with experimental petrologic and geophysical data to construct a cross section through the mantle and crust beneath Oahu (fig. 1.9). Their cross section emphasizes the mineralogic and compositional heterogeneity of the mantle beneath Hawaiian volcanoes. However, the origins of many of the rock types are now thought to be different from those proposed by Jackson and Wright (1970). A more recent model by Sen (1983) shows plagioclase lherzolite beneath the oceanic crust to a depth of about 30 km (defined by the limit of plagioclase stability), spinel lherzolite from 30 to nearly 50 km, and garnet lherzolite below about 50 km. The zone beneath the volcanoes includes cumulate dunite to depths

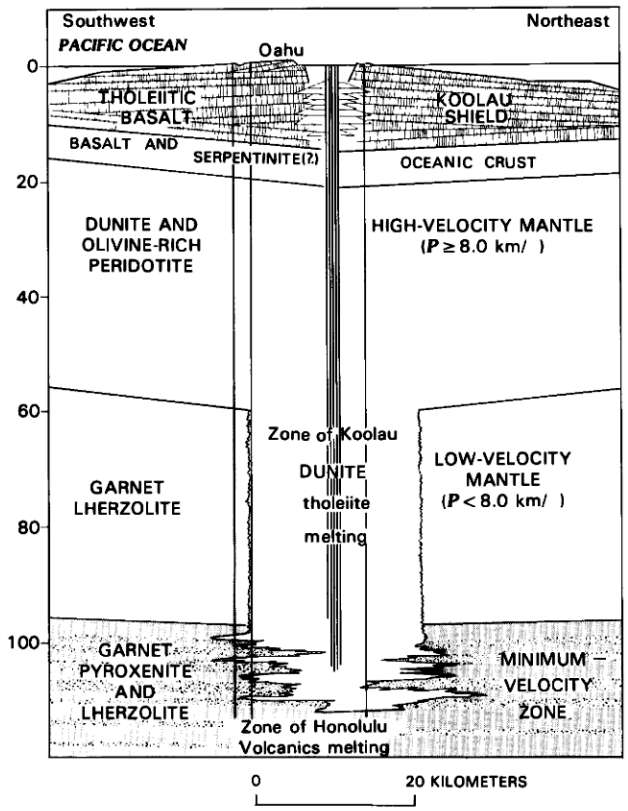

FIGURE 1.9.—Cross section beneath Oahu from Jackson and Wright (1970). Dunite zone inferred to be mantle residue left behind from partial melting that forms Koolau tholeiitic shield lava. Configuration of rock types and their mode of origin are far different from those shown in figure 1.10.

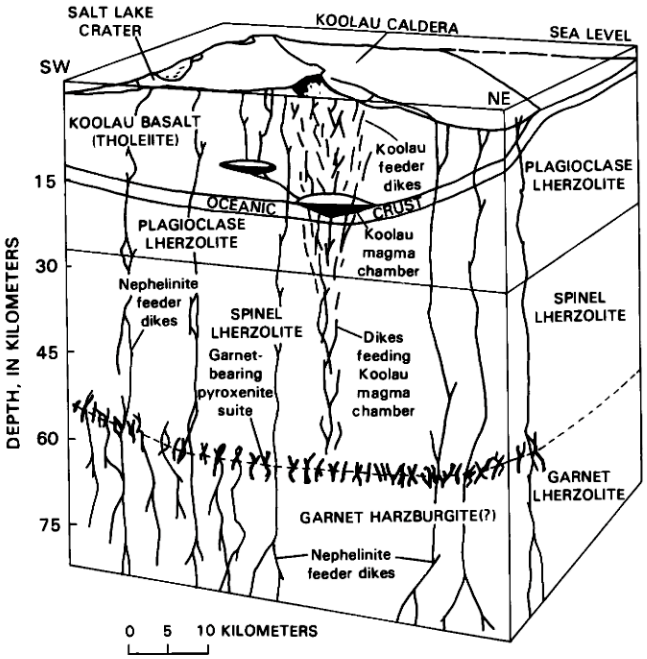

FIGURE 1.10.—Cross section beneath Oahu from Sen (1983) showing configuration of various mantle source and residual rocks brought to surface as xenoliths of abundant dunite, lherzolite, and garnet peridotite by rejuvenated-stage Honolulu Volcanics.

of about 15 km (fig. 1.10). The areal distribution of xenoliths observed by Jackson and Wright (1970) reflects passage of the Honolulu Volcanics lava through the zone of dunite cumulates.

PETROLOGY OF LAVAS ALONG THE VOLCANIC CHAIN

In the middle to late 1970's new studies added data to the already complex data array on Hawaiian volcanoes. Studies on lava recovered from the older submarine portions of the chain (Clague, 1974; Dalrymple and others, 1974, 1977, 1981; Clague and others, 1975; Dalrymple and Clague, 1976; Kirkpatrick and others, 1980; Clague and Frey, 1980; Lanphere and others, 1980; Dalrymple and Garcia, 1980; Garcia, Grooms, and Naughton, in press) clearly demonstrate that the volcanoes of the entire Hawaiian-Emperor volcanic chain erupted tholeiitic basalt and picritic tholeiitic basalt similar to those of the shield stage in the Hawaiian Islands. In addition, alkalic lava similar to that erupted during the postshield stage in the Hawaiian Islands, including hawaiite, mugearite and trachyte, is commonly recovered from the older volcanoes. In the drill holes on Ojin and Suiko, tholeiitic lava occurs below alkalic lava, as in the Hawaiian Islands. Some samples are chemically and mineralogically similar to alkalic rejuvenated-stage lava from the Hawaiian Islands (table 1.2). The identification of which dredged or drilled lava samples erupted during which eruptive stage relies on comparison of the major-element compositions to those of the various Hawaiian lava types (table 1.7) in conjunction with trace-element ratios (Clague and Beeson, 1980; Clague and others, 1980c; Frey and Clague, 1983) and mineral compositions (Keil and others, 1972; Fodor and others, 1975; Clague and others, 1980a). In particular, we have found that the composition of groundmass pyroxene and the K/Ba and P_2O_5/Zr ratios seem to separate alkalic basalt of the postshield and rejuvenated stages. Rejuvenated-stage alkalic basalt has lower K/Ba and higher P_2O_5/Zr ratios and pyroxene with more calcic compositions and higher concentrations of Na, Ti, and Al than postshield-stage alkalic basalt. Lava samples recovered from the volcanoes west of the principal Hawaiian Islands are discussed in appendix 1.1 and summarized in table 1.9.

Several conclusions may be drawn from these studies of samples from along the Hawaiian-Emperor Chain. The first conclusion is that the Hawaiian hot spot has produced very similar lava types in the same eruptive sequence for at least the last 65 m.y. (table 1.10). Samples from the same eruptive stage are similar to one another in both major- and trace-element compositions, including rare-earth elements (Clague and Frey, 1980; Frey and Roden, in press). Isotopic studies indicate, however, that small systematic changes occur over time (Lanphere and others, 1980; Unruh and

TABLE 1.9.—*Rock types and inferred volcanic stages represented along the Hawaiian-Emperor Chain*

[X, present; --, not present or not known; (T), transitional; volcano numbers from Bargar and Jackson (1974)]

Volcano Number	Volcano Name	Shield stage: Tholeiitic basalt	Shield stage: Picritic tholeiitic basalt	Shield stage: Rhyodacite	Alkalic postshield stage: Alkalic basalt	Alkalic postshield stage: Ankaramite	Alkalic postshield stage: Hawaiite	Alkalic postshield stage: Mugearite	Alkalic postshield stage: Trachyte	Alkalic postshield stage: Phonolite	Alkalic rejuvenated stage: Alkalic basalt	Alkalic rejuvenated stage: Basanite	Alkalic rejuvenated stage: Nephelinite	Alkalic rejuvenated stage: Melilitite	Alkalic rejuvenated stage: Tephrite
1	Kilauea	X	X	--	--	--	--	--	--	--	--	--	--	--	--
2	Mauna Loa	X	X	--	--	--	--	--	--	--	--	--	--	--	--
4	Hualalai	X	X	--	X	X	--	--	X	--	--	--	--	--	--
3	Mauna Kea	X	X	--	X	X	X	--	--	--	--	--	--	--	--
5	Kohala	X	--	--	--	--	--	X	X	--	--	--	--	--	--
6	Haleakala	X	--	--	X	X	X	X	--	--	X	X	--	--	--
7	Kahoolowe	X	X	--	--	X	--	--	--	--	X?	--	--	--	--
8	West Maui	X	X	--	X	X	--	X	X	--	--	X	--	--	--
10	East Molokai	X	X	--	X	X	X	X	X	--	X	X	--	--	--
9	Lanai	X	X	--	--	--	--	--	--	--	--	--	--	--	--
11	West Molokai	X	X	--	X	--	X	--	--	--	--	--	--	--	--
12	Koolau	X	X	--	--	--	--	--	--	--	X	X	X	X	--
13	Waianae	X	X	X	--	--	X	--	--	--	--	--	--	--	--
14	Kauai	X	X	--	--	--	X	--	--	--	X	X	X	X	--
15	Niihau	X	X	--	X	--	--	--	--	--	X	--	--	--	--
15A	Kaula	X	--	--	--	--	--	--	--	X	--	X	--	--	--
17	Nihoa	X	X	--	--	--	--	--	--	--	--	--	--	--	--
19	Unnamed Seamount	--	X	--	--	--	--	--	--	--	--	--	--	--	--
20	Unnamed Seamount	X	--	--	--	--	--	--	--	--	--	X	--	--	--
21	Unnamed Seamount	--	X	--	--	--	--	--	--	--	--	--	--	--	--
23	Necker	--	X	X?	--	--	X	--	--	--	--	--	--	--	X?
26	La Perouse Pinnacles	--	X	--	--	--	--	--	--	--	--	--	--	--	--
30	Gardner Pinnacles	--	X	--	X	--	--	--	--	--	--	--	--	--	--
38	Brooks Bank	X	--	--	--	--	X	--	--	--	--	--	--	--	--
29	St. Rogatein Bank	--	--	--	--	--	X	--	--	--	--	--	--	--	--
36	Laysan	--	--	--	--	--	X	X	--	--	--	--	--	--	--
37	Northampton Bank	X	X	--	--	--	--	--	--	--	--	--	--	--	--
39	Pioneer Bank	X	--	--	--	--	--	--	--	--	--	--	--	--	--
50	Pearl and Hermes Reef	--	--	--	X	--	X	--	--	X	--	--	--	--	--
51	Ladd Bank	--	--	--	--	--	--	--	--	--	--	--	X	--	--
52	Midway Island	X	--	--	--	--	X	X	--	--	--	--	--	--	--
53	Nero Bank	--	X	--	--	--	--	--	--	--	--	--	--	--	--
57	Unnamed Seamount	--	--	--	X	--	--	--	--	--	--	--	--	--	--
63	Unnamed Seamount	--	--	--	--	--	--	--	--	--	--	--	--	--	[1]X
65	Colahan Seamount	(T)	--	--	--	--	--	--	--	--	--	--	--	--	[1]X
65A	Abbott Seamount	(T)	--	--	--	--	--	--	--	--	--	--	--	--	--
67	Daikakiyi Seamount	X	--	--	X	--	--	--	--	--	--	--	--	--	--
69	Yuryaku Seamount	--	--	--	X	--	--	--	--	--	--	--	--	--	--
72	Kimmei Seamount	--	--	--	X	--	--	--	--	--	--	--	--	--	--
74	Koko Seamount (southeast)	X	--	--	X	--	X	X	X	X	--	--	--	--	--
76	Koko Seamount (northwest)	X	--	--	--	--	--	--	--	--	--	--	--	--	--
81	Ojin Seamount	X	--	--	--	--	X	--	--	--	--	--	--	--	--
89	Jingu Seamount	--	--	--	--	--	X	X	--	--	--	--	--	--	--
86	Nintoku Seamount	--	--	--	X	--	--	--	--	--	--	--	--	--	--
90	Suiko Seamount (southern)	--	--	--	--	--	--	X?	--	--	--	--	--	--	--
91	Suiko Seamount (central)	X	X	--	X	--	--	--	--	--	--	--	--	--	--
108	Meiji Seamount	X	--	--	--	--	--	--	--	--	--	--	--	--	--

[1]Dredges from unnamed seamount (63) and Colahan Seamount recovered ankaramite, tephrite, and amphibole-bearing hawaiite that are probably rejuvenated stage lava.

TABLE 1.10.—*Composition of tholeiitic basalt from volcanoes of the Hawaiian-Emperor Chain*

[All figures in weight percent, dry reduced normalized average analyses; olivine added or subtracted so that Mg/(Mg+0.85 Fe)=0.70; ..., not analyzed; P_2O_5 value in parentheses is high due to marine phosphatization]

Volcano	Kilauea	Mauna Loa	Mauna Kea	Hualalai	Kohala	East Maui	West Maui	Lanai	East Molokai	West Molokai	Koolau	Waianae (upper)	Waianae (lower)
SiO_2	48.9	50.5	46.4	49.4	48.2	49.7	47.3	49.0	46.4	49.2	51.5	46.9	47.9
Al_2O_3	12.1	12.2	12.8	11.8	13.5	13.3	12.6	12.8	12.9	11.8	13.2	13.4	14.1
FeO	11.4	11.0	12.3	11.9	11.8	10.9	12.2	11.0	12.4	11.9	10.4	11.9	11.2
MgO	12.7	12.3	13.6	13.4	13.1	12.1	13.7	12.3	13.8	13.2	11.7	13.2	12.5
CaO	9.7	9.2	9.9	9.2	9.4	9.6	9.8	8.8	9.7	8.9	8.3	9.1	9.6
Na_2O	1.99	1.98	1.82	1.84	1.62	1.76	1.66	2.13	1.89	2.42	2.47	2.07	1.86
K_2O	.44	.36	.28	.28	.10	.33	.23	.11	.20	.18	.27	.53	.26
TiO_2	2.34	1.85	2.40	1.75	1.93	2.01	2.14	1.66	2.22	2.08	1.68	2.46	2.20
P_2O_5	.22	.21	.23	.16	.20	.13	.20	.18	.25	--	.22	.35	.25
MnO	.17	.16	.17	.15	.18	.18	.17	.14	.18	.19	.15	.15	.17

Volcano	Kauai	Niihau	Nihoa	Unnamed (20)	Unnamed (21)	Necker Island	La Perouse Pinnacles	Gardner Pinnacles	Northampton Bank	Pioneer	Daikakiji	Suiko high TiO_2	Suiko low TiO_2
SiO_2	48.4	48.4	47.4	46.9	47.1	47.15	47.5	47.6	48.7	48.2	49.7	47.6	47.9
Al_2O_3	12.5	12.1	11.5	11.2	11.3	11.1	11.7	12.5	11.4	11.2	11.5	12.7	13.0
FeO	11.9	12.1	12.4	12.6	12.4	12.8	11.8	11.3	11.7	11.9	11.5	12.3	11.9
MgO	13.3	13.6	13.8	14.0	13.8	14.1	13.1	12.6	13.0	13.3	12.9	13.7	13.2
CaO	9.2	8.1	9.4	9.6	9.2	9.8	10.7	10.3	10.1	9.8	9.05	8.7	9.3
Na_2O	1.93	2.28	1.77	2.06	2.25	1.59	1.82	2.06	2.00	2.20	2.08	2.26	2.26
K_2O	.30	.49	.26	.24	.64	.38	.39	.16	.32	.67	.43	.28	.14
TiO_2	2.06	2.49	2.59	2.97	2.72	2.47	2.44	1.98	2.26	2.36	2.32	2.10	1.86
P_2O_5	.23	.31	(.70)	.28	.35	.36	.34	.26	.23	.17	.36	.22	.16
MnO	.17	.16	.15	.15	.15	.17	.20	.16	.16	.14	.16	.18	.18

others, 1983). The lower $^{87}Sr/^{86}Sr$ ratios and higher $^{143}Nd/^{144}Nd$ ratios of lava from the central Emperor Seamounts compared to those of lava from the Hawaiian Islands and Ridge imply that tholeiitic lava erupted 65 m.y. ago was derived from a more depleted source than that erupting today. Lanphere and others (1980) correlated this observation with the data shown in figure 1.3 to suggest that the chemistry of Hawaiian tholeiitic lava has varied as a function of the age and thickness of the oceanic lithosphere beneath each volcano when it was constructed. The correlation suggests that the oceanic lithosphere forms at least part of the source material for Hawaiian tholeiitic magma, or that the magma partially reequilibrates with the oceanic lithosphere. Wright (1984) proposes that Hawaiian magma originates from oceanic lithosphere converted to asthenosphere.

STRATIGRAPHIC STUDIES IN THE HAWAIIAN ISLANDS

Studies of stratigraphically controlled samples (Beeson, 1976; Clague and Beeson, 1980; Chen and Frey, 1983; Clague and others, 1983; Feigenson, 1984; Lanphere and Frey, 1985) have shown that major-element, trace-element, and isotopic ratios change systematically as a function of time at some Hawaiian volcanoes. These observations are not universal (Stille and others, 1983; Frey and others, 1984) in as much as Waianae and Mauna Kea erupted isotopically similar lava during the tholeiitic shield and alkalic postshield stages. Chen and Frey (1983) observed systematic stratigraphic trends in $^{87}Sr/^{86}Sr$, Rb/Sr, $^{143}Nd/^{144}Nd$, and Sm/Nd ratios in samples from East Maui Volcano. Their data indicate that the tholeiitic lava had higher $^{87}Sr/^{86}Sr$ and Sm/Nd ratios and lower $^{143}/Nd$ ^{144}Nd and Rb/Sr ratios than the later alkalic lava from the postshield and rejuvenated stages. They proposed a complex mixing model to explain the apparent paradox of having more radiogenic isotopic ratios combined with more depleted trace-element ratios in the same rocks. Their model proposes two sources, a primitive mantle-plume source and a depleted oceanic-lithosphere source, which can mix before melting or can produce partial melts which then mix. They argue that small amounts of small-percentage melts from the oceanic lithosphere (midocean-ridge source) are mixed with enriched mantle or with melts derived from enriched mantle. This model is similar to earlier selective-melting models qualitatively proposed by Green and Ringwood (1967) and Macdonald (1968). It would also be possible to mix small-percentage melts of enriched mantle with the oceanic-lithosphere source (basically an enrichment model) to create the source rocks for Hawaiian magma (Clague and others, 1983; Chen and Frey, 1985), although the measured and calculated compositions do not match as closely as in the model of Chen and Frey (1983). All these models predict a range of source compositions from which the lava is generated.

Other studies emphasize the bulk composition of the source rocks and the processes and physical conditions of the melting process. For example, Clague and Frey (1982), from a detailed trace-element analysis of the rejuvenated stage Honolulu Volcanics on Oahu, concluded that lava ranging from nepheline melilitite to alkalic basalt was generated by 2–11 percent partial melting of a homogeneous garnet (<10 percent) lherzolite source that was carbon bearing. The source had been recently enriched and had a chondrite-normalized La/Yb ratio of 4.4. During melting, phlo-

gopite, amphibole, and a Ti-rich phase (oxide?) remained in the residua, but apatite was completely melted. This model can be combined with the model of Chen and Frey (1983) to generate the source composition indicated for the Honolulu Volcanics (see Roden and others, 1984). The homogeneous composition of the mantle source for the Honolulu Volcanics implies that the recent enrichment event affects a large volume of depleted mantle from which the lava is then generated by partial melting. This is not the same process espoused in the model preferred by Chen and Frey (1983) in which enriched mantle or partial melts of enriched mantle mix with partial melts of depleted mantle. Note that all these models consider only two mixing end members, whereas the isotopic data clearly indicate that at least three distinct source compositions are required (Tatsumoto, 1978; Staudigel and others, 1984). Feigenson (1984) proposed three-end-member mixing models for Kauai lava but did not identify the trace-element signatures of the source components.

The generation of large volumes of tholeiitic lava has been the focus of recent studies by Wright (1984) and Budahn and Schmitt (1984), who used different approaches and reached dramatically different conclusions. Wright (1984) used mass-balance considerations to calculate the components and abundance of material that must be added to depleted lithosphere to generate Hawaiian tholeiitic basalt by large percentages of partial melting (35–42 percent melting). His models did not attempt to calculate the variations in source composition for tholeiitic basalt from the different volcanoes (Leeman and others, 1977, 1980; Basaltic Volcanism Study Project, 1981). Budahn and Schmitt (1984) used inverse procedures to estimate the variations in source composition required to generate the tholeiitic basalt from a number of Hawaiian volcanoes. Their estimated sources had 74–86 percent olivine plus orthopyroxene, 11–21 percent clinopyroxene, and 3–5 percent garnet. All the calculated sources had slightly enriched light-rare-earth-element contents, and low heavy-rare-earth abundances (0.9 to 1.6 times chondrites). They calculated the partial melting at 2–10 percent for these sources. Budahn and Schmitt (1984) did not address the processes that led to creation of these different source compositions, nor did they consider the volumes of mantle source regions required, or the constraints on the production of partial melts provided by Kilauea's magma supply and eruption processes. Wright's (1984) model follows from consideration of these additional constraints. The large difference between the models of Wright (1984) and Budahn and Schmitt (1984) emphasizes the uncertainties concerning the compositions and processes that create the source rocks and the lava of the Hawaiian Islands.

PETROLOGIC STUDIES OF LOIHI SEAMOUNT

Studies of Loihi Seamount have provided new insight in magma genesis in the Hawaiian Islands. Trace-element and isotopic studies demonstrate that the source rocks beneath a single volcano are heterogeneous and require at least three mantle components (Frey and Clague, 1983; Lanphere, 1983; Staudigel and others, 1984). Perhaps more important is the observation of very high $^3He/^4He$ ratios, which imply a primitive undegassed source of volatiles (Kaneoka, chapter 27; Kurz and others, 1983; Rison and Craig, 1983; Kaneoka and others, 1983). The ratio of $^3He/^4He$ is inversely related to the volume of the volcanoes on the Island of Hawaii (Kaneoka, chapter 27; Kurz and others, 1983), suggesting that at smaller volcanoes lava is generated from sources that are largely primitive and not degassed. Another observation is that Hawaiian volcanoes initially erupt alkalic lava generated from heterogeneous source compositions by rather small percentages of partial melting (Moore and others, 1982; Frey and Clague, 1983). The evolutionary sequence at a Hawaiian volcano is therefore from small-volume, infrequent eruptions of small-percentage melts to large-volume, frequent eruptions of large-percentage melts, and then back to small-volume, infrequent eruptions of small-percentage melts (Wise, 1982).

PETROLOGIC OVERVIEW

In summary, the petrology of lava from along the Hawaiian-Emperor Chain indicates that at least three source materials are involved in the generation of Hawaiian lava; one of these sources is apparently the depleted ocean lithosphere, whereas another is relatively primitive undegassed mantle. The third component is less well defined. Since multiple sources are required, mixing of these sources or of melts generated from these sources must occur. The compositions of lava along the chain apparently are related to the age (thickness) of the underlying oceanic lithosphere; the volcanoes formed on younger and thinner oceanic lithosphere were generated from a source with a larger component of the depleted ocean lithosphere. Detailed overviews of the petrology of Hawaiian tholeiitic lava and Hawaiian alkalic lava are presented in Wright and Helz (chapter 23) and Clague (in press), respectively.

Volcano volume reflects the degree of melting of the tholeiitic basalt and probably also the size and frequency of intrusion of magma batches. The inverse correlation of volcano volume with $^3He/^4He$ ratio in tholeiitic basalt indicates that smaller percentage melts are derived from sources with more of the primitive component and larger percentage melts are derived from sources with less of the primitive component. Volcano volumes and compositions of the shield tholeiitic basalt are also related, less-enriched tholeiitic basalt forms larger shields and more-enriched tholeiitic basalt forms smaller shields (Clague and Frey 1979), although this correlation is imperfect. Models developed in the future should address the problem of characterizing the isotopic and trace-element compositions of the three mantle components and address the timing and processes of mixing of these sources. The source volumes inferred from different melting models must be considered. Wright's (1984) model requires only modest source volumes, whereas the model of Budahn and Schmitt (1984) requires partial melting of a mantle zone 100 km thick and 100 km wide to generate the volcanoes of the principal Hawaiian Islands. Such enormous inferred volumes of mantle source rock pose numerous problems for models advocating small-percentage melting to generate the tholeiitic shields.

A separate problem is the cause of the alkalic rejuvenated stage. Jackson and Wright (1970) used tide-gage data from Moore (1970) to suggest that generation of the rejuvenated-stage Honolulu Volcanics might be caused by uplift as Oahu has passed over the

Hawaiian Arch. They argued that the Hawaiian Arch, an isostatic response to volcanic loading on the oceanic crust, follows the progression of active volcanic centers by several hundred kilometers and several million years. Clague and others (1982) showed that the duration of the quiescent period preceding eruption of the rejuvenated-stage lava has decreased systematically from nearly 2.5 m.y. on Niihau to <0.4 m.y. at Haleakala (see fig. 1.6). They suggested that a new mechanism should be sought to explain the age data. We have reexamined the data and conclude that they are consistent with the model proposed by Jackson and Wright (1970) because the rate of volcanic migration is increasing. The rejuvenated stage follows the formation of the shield not by a constant time but by a constant distance. The rejuvenated-stage Koloa Volcanics on Kauai and Kiekie Basalt on Niihau began erupting during formation of the Koolau shield located 180–225 km to the southeast. Likewise, the Honolulu Volcanics on the Koolau Range of Oahu began erupting during formation of the East Maui shield located 160 km to the southeast. The rejuvenated-stage Kalaupapa Volcanics on East Molokai erupted during formation of the Mauna Kea shield located 200 km to the southeast. Finally, the rejuvenated-stage Hana Volcanics on East Maui began erupting during formation of the Mauna Loa shield, located 160 km to the southeast. In each case, the lava of the rejuvenated stage began erupting during formation of a large shield 190 ± 30 km to the southeast. The Hawaiian Arch is about 250 km from the center of the volcanic ridge, but only 210 km to the east-southeast of Hawaii (Walcott, 1970). It is therefore likely that a factor in magma generation during the rejuvenated stage is the rapid change from subsidence to uplift as the volcanoes override the flexural arch created by formation of large shields. To the northwest of the Hawaiian Islands the rates of volcanic propagation were slower and more constant; we predict that lava of the rejuvenated stage will postdate the shield stage by 2–3 m.y. We also suggest that the apparent paucity of lava from the rejuvenated stage to the northwest of the Hawaiian Islands may reflect the absence of large volcanic edifices capable of flexing the lithosphere sufficiently. Likewise, the absence of any lava samples of the rejuvenated stage from the Emperor Seamounts may result from the rather wide spacing between volcanic edifices: by the time the next younger volcano formed, the previously constructed volcano was already beyond the arch. The fact that the Emperor volcanoes were constructed on young, thin lithosphere would amplify this effect because the distance from the load to the flexural arch decreases as the lithosphere becomes less rigid.

FIXITY OF THE HAWAIIAN HOT SPOT

Wilson's original hypothesis for the origin of the Hawaiian and other island chains by passage of the crust over a source of lava in the mantle (Wilson, 1963a, b, c) did not require that the hot spot be fixed, only that it have some motion relative to the crust above it. Morgan (1972a, b), on the other hand, specified that a worldwide system of thermal plumes (hot spots) was fixed in the mantle and that the relative movement between them was small or negligible. Several workers (for example, Minster and others, 1974; Gordon and Cape, 1981; Morgan, 1981) have shown from relative plate motions and paleomagnetic and other data that Morgan's hypothesis of relative hot-spot fixity is basically correct, but that the fixity of the hot-spot frame of reference with respect to the spin axis, particularly in early Cenozoic and Late Cretaceous times, is not established.

PALEOMAGNETIC TESTS OF HOT-SPOT FIXITY

Age data along the chain have shown that there has been more or less continuous relative motion between the Hawaiian hot spot and the Pacific plate, thereby proving the kinematic aspect of the hot-spot hypothesis, but these data have little or no bearing on the question of hot-spot fixity. The lava flows that form volcanoes of the Hawaiian-Emperor Chain, however, contain a nearly continuous magnetic record of the latitude of the Hawaiian hot spot for the entire Cenozoic and the latest Cretaceous. Although only a small fraction of this magnetic record has been read, there are now sufficient data to provide a partial test of the fixity hypothesis for the Hawaiian hot spot. Paleomagnetic data from volcanoes along the chain show that the Hawaiian hot spot (and thus presumably the worldwide hot-spot frame) has been, to a first approximation, fixed with respect to the spin axis since the time of formation of the Hawaiian-Emperor bend. The limited data indicate, however, that there was motion between the hot spot and the spin axis, that is, true polar wander, before that time.

The paleolatitudes of several Hawaiian-Emperor volcanoes, as determined from paleomagnetic studies on individual rock samples and from shipboard magnetic surveys, are given in table 1.11 and plotted in figure 1.11 as a function of volcano age. In general, the data indicate that the Hawaiian-Emperor volcanoes formed not at their present latitudes but at a latitude near the present latitude of Hawaii. Thus, the latitude of the Hawaiian hot spot has been approximately fixed throughout the Cenozoic. The data are not of uniform quality, however, and some care must be exercised in their interpretation.

The paleomagnetic data have been discussed and evaluated by Jackson and others (1980), Kono (1980), and Sager (1984), who point out that the paleomagnetic sampling of Meiji, Nintoku, Ojin, Midway, Nihoa, and the Island of Hawaii involved a small number of lava flows, making it doubtful that the secular variation is adequately averaged out. The errors for the Ojin and Nintoku sites reflect this uncertainty, but there is reason to suspect that the errors assigned to the paleolatitudes of Midway, Meiji, and Nihoa are too small. This is because of the unusually low dispersions and the likelihood of serial correlation of some of the flows, which further decreases the number of independent measurements from the sites.

The paleolatitude of 17.5° ± 5°, determined for Suiko by Kodama and others (1978) from magnetic survey data, is suspect for several reasons. First, the magnetic anomaly over Suiko is complex, resulting in a low statistical test of fit ($R = 1.1$) for the inversion. Second, it is likely that Suiko is constructed from several coalesced volcanoes (Bargar and Jackson, 1974), possibly of different ages, and the necessary assumption of uniform magnetization is probably invalid for this seamount. In addition, the paleolatitude is inconsistent with that obtained from the paleomagnetic study of

TABLE 1.11.—*Paleolatitudes determined for volcanoes of the Hawaiian-Emperor Chain*

[From paleomagnetic measurements on lava flows and from shipboard magnetic surveys (SM). Data from compilations by Kono (1980) and Sager (1984); the more reliable data (Sager, 1984) underlined; uncertainties are the values of α_{95}]

Volcano Number	Volcano Name	Number of flows determined	Present latitude (degrees north)	Paleolatitude (degrees north)
1,2,4,	Kilauea, Mauna Loa Hualalai (historical)	17	19.5	19.6±1.4
1,2,3	Kilauea, Mauna Loa Mauna Kea(^{14}C dated)	8	19.5	17.7±10.7
12	Koolau	33	21.4	16.8±3.6
13	Waianae	55	21.5	15.7±3.3
14	Kauai (Makaweli Member, Waimea Canyon Basalt)	25	22.0	15.6±3.1
14	Kauai (Napali Member, Waimea Canyon Basalt)	46	22.1	14.9±3.1
17	Nihoa	14	23.1	21.0±6.6
52	Midway	13	28.2	15.4±5.4
65A	Abbott	(SM)	31.8	17.5±2.4
81	Ojin	6	38.0	17.6±13.2
86	Nintoku	4	41.3	36.0±24.6
91	Suiko	(SM)	44.8	16.7±5
91	Suiko	65	44.8	27.1±3.5
108	Meiji	6	53.0	19.2±4.1

Suiko (Kono, 1980), which is the best study of its kind for any of the volcanoes in the chain.

Sager (1984) included in his compilation two additional determinations from the principal Hawaiian Islands that we have chosen to omit from table 1.11. These include a group of 129 flows from the Islands of Hawaii and Niihau, and a second group of 19 flows from Kauai. Both groups include flows from the rejuvenated stage that were erupted several million years after the hot spot had moved (relatively) southeastward to form new tholeiitic shields. Although both of these determinations were included by Sager in his list of more reliable paleolatitudes, they are so close to the present position of the hot spot that their elimination has no significant impact on the conclusions drawn from the data.

Taken at face value, the more reliable paleolatitude data (fig. 1.11) indicate that the Hawaiian hot spot may have been a few degrees south of its present position during the late Cenozoic, near its present position when Abbott Seamount formed at about 39 Ma, and 7° north of its present position at Suiko time, 65 Ma. Analyses of paleoequator (Sager, 1984) and worldwide paleomagnetic data (Livermore and others, 1983), however, show that there has been little or no motion of the spin axis relative to the worldwide hot-spot frame during the past 40 m.y. or so. From this comparison of independent data Sager (1984) concluded that the apparent southward displacement of the Hawaiian hot spot shown by the data from younger volcanoes in the chain (fig. 1.11) reflected changes in the magnetic field rather than relative movement between the hot spot and the spin axis.

The apparent displacement indicated by the Suiko data, however, is probably real. The Suiko paleolatitude is based on analysis of a large number of flows (table 1.11) recovered by coring over an interval of 550 m (Kono, 1980). Even when certain flows thought to represent a very short time interval are grouped, there are still a minimum of 40 independent data. There are also 12 places in the cores where the inclination changes by more than 15°, which indicates that at least 13 secular variation cycles have been sampled, making it likely that secular variation has been adequately averaged out. Other paleomagnetic stability indices indicate that 27.1°±3.5° is a highly reliable measure of the latitude of formation of Suiko Seamount (Kono, 1980).

BIOFACIES AND TEMPERATURE DATA FROM THE HAWAIIAN-EMPEROR CHAIN

Although northward displacement of the Hawaiian hot spot relative to the spin axis is only indicated by the single paleolatitude from Suiko, it is supported by a variety of additional data. Analysis of Pacific deep-sea sediment cores, for example, shows that the paleoequator was 10°–16° farther north than at present between about 75 Ma and 65 Ma (Sager, 1984).

Biofacies data from DSDP Leg 55 drilling in the Emperor Seamounts provide semiquantitative substantiation of the Suiko paleolatitude. The bioclastic sediment on Suiko, Nintoku, and Ojin Seamounts consists primarily of coralline algae and bryozoans with ostracodes, foraminifers, and assorted shell fragments typical of a shallow-water, high-energy environment (Jackson and others, 1980). Only a single coral was found in the Suiko material, and none was recovered from either Ojin or Nintoku, indicating that corals were not significant contributors to the carbonate buildups.

Schlanger and Konishi (1975) have pointed out that carbonate buildups in the Pacific can be divided into bryozoan-algal and coral-algal facies, the distribution of which depends largely on water temperature and solar insolation and thus is, to a large degree, a function of latitude. They observe that in the modern Pacific, the coral-algal facies dominates at latitudes less than about 20°, whereas the bryozoan-algal facies is predominant above about 30° latitude. They locate the boundary between these facies at about 25° latitude, but emphasize that the transition is gradual. In the central Pacific, the annual surface-water temperature at 25° latitude is about 22 °C (Muromtsev, 1958), which is usually considered the minimum for active coral-algal reef growth (Vaughn and Wells, 1943; Heckel, 1974). The optimum temperature for vigorous reef growth is 25–29 °C. Thus, the existence of carbonate buildups of the bryozoan-algal facies atop Ojin, Nintoku, and Suiko Seamounts indicates that the reefs atop the volcanoes formed in water temperatures less than about 22 °C.

Using the oxygen-isotope temperature data of Savin and others (1975) for the North Pacific, Greene and others (1978) reconstructed the approximate latitude variation through time for the 20 °C and 22 °C isotherms (fig. 1.12). They showed that if the Hawaiian hot spot were fixed, then Suiko Seamount would have formed in water warm enough to have developed active coral-algal reefs. Following the analysis of Greene and others (1978), Jackson and others (1980) showed that the Paleocene water temperature at the latitude determined by the paleomagnetic data from Suiko was appropriate for the bryozoan-algal carbonates that occur immediately above the basalt.

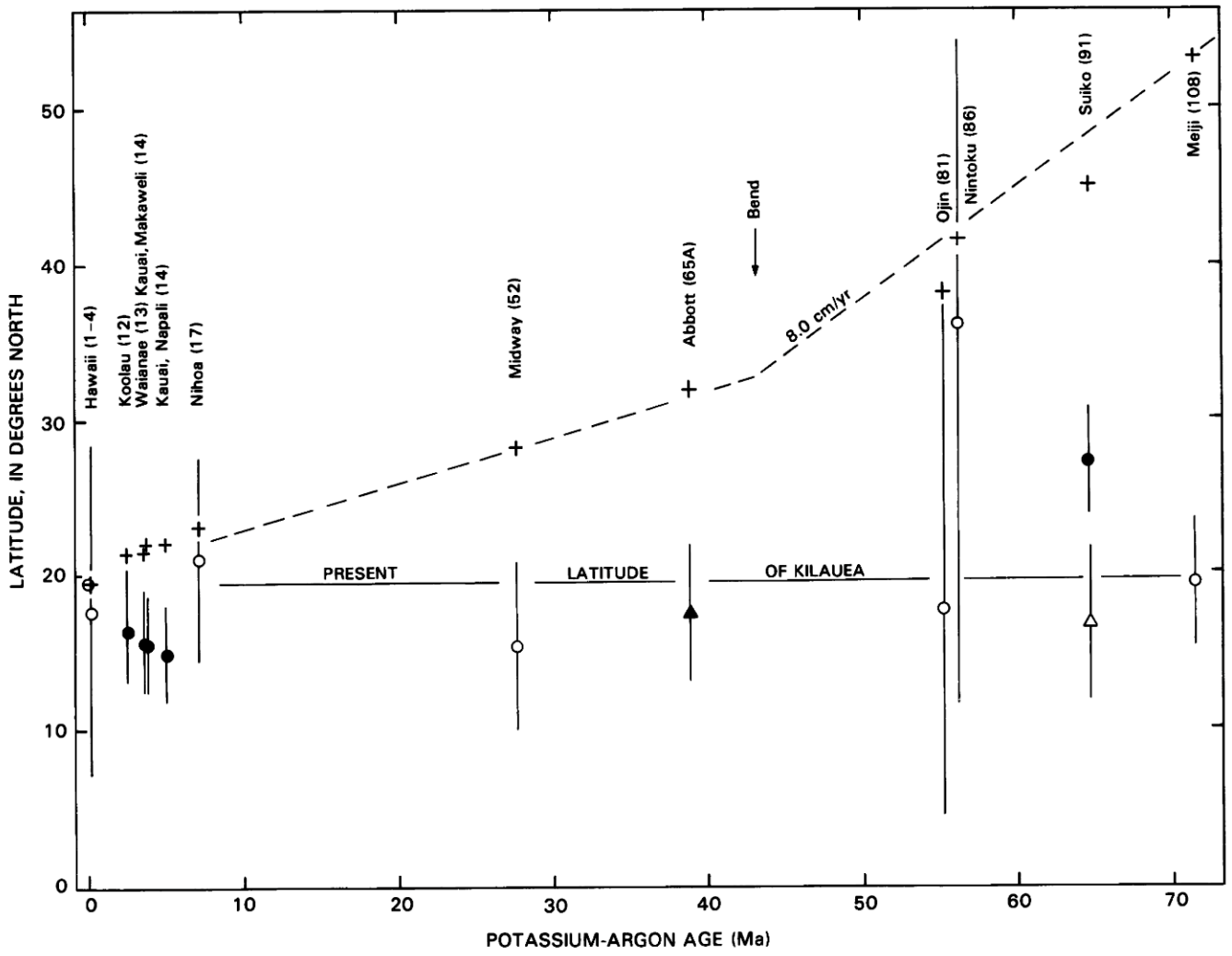

FIGURE 1.11.—Paleolatitude plotted against age for volcanoes along Hawaiian-Emperor Chain. Crosses, present latitude; dots and circles, paleolatitudes determined from paleomagnetic data; triangles, paleolatitudes determined from shipboard magnetic surveys. More reliable data indicated by solid symbols. Error bars show α_{95}. Dashed reference line is backtracked position of hot spot relative to Pacific plate assuming a constant velocity of 8 cm/yr. Paleomagnetic data from table 1.11, age data from table 1.4 and appendix 1.1.

The paucity of coral material on seamounts in the central Emperor Chain is in contrast to Koko and the seamounts on the bend, where corals are more common but still less abundant than in a region of vigorous coral reef growth (Davies and others, 1971, 1972; Matter and Gardner, 1975). Oxygen-isotope temperatures of carbonate diagenesis for Suiko, Nintoku, Ojin, and Kammu Seamounts (McKenzie and others, 1980) show a gradual warming from Suiko to Koko, at least in part caused by southward migration of the hot spot (Jackson and others, 1980). Thus, the biofacies and paleotemperature data from Leg 55 are consistent with the paleomagnetic data, indicating a latitude of 27° for the hot spot at Suiko time. The data are also consistent with Sager's (1984) suggestion that the hot spot had reached its approximate present latitude by the time Abbott Seamount formed just after formation of the Hawaiian-Emperor bend; the slightly cooler temperatures indicated by the carbonate facies and temperature data from the bend seamounts are probably related to the sudden drop in ocean temperature in the late Eocene rather than to a more northerly hot spot.

Thus, the paleomagnetic data from Suiko, the biofacies and temperature data from the central and southern Emperor Seamounts, and the Pacific paleoequator data all indicate southward migration of the Hawaiian hot spot in the early Tertiary and Late Cretaceous. This conclusion is consistent with previous findings, based on analysis of worldwide paleomagnetic data in the hot-spot frame of reference, of about 10° of southward movement of the hot-spot frame relative to the spin axis (that is, true polar wander)

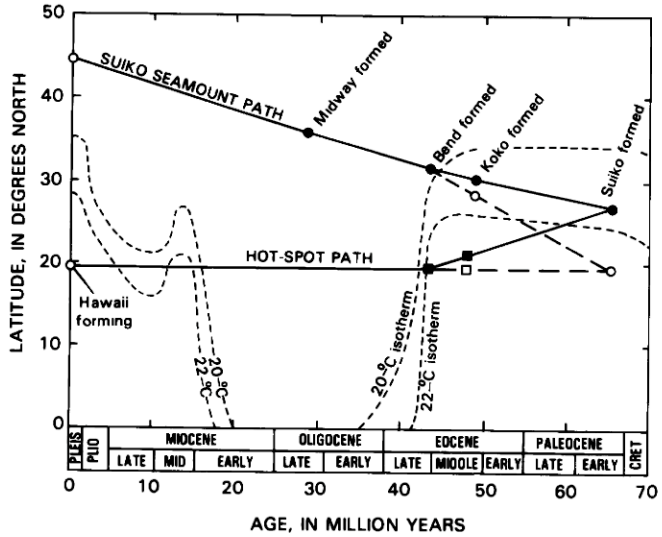

FIGURE 1.12.—Approximate position of 20 °C and 22 °C surface-water isotherms in north-central Pacific during Cenozoic, modified from Greene and others (1978), based on data of Savin and others (1975). Dots, paleolatitudes of Suiko Seamount assuming that Suiko formed at 27° N. and that hot spot has been fixed since time of bend formation. Circles, paleolatitudes for Suiko assuming a fixed hot spot for past 65 m.y. Squares, positions of formation of Koko Seamount and bend under same assumptions. Backtracking was about an Emperor pole at lat 17° N., long 107° W. and a Hawaiian pole at lat 69° N., long 68° W. (Clague and Jarrard, 1973). The 22 °C isotherm is approximate boundary between coral-algal (warmer) and bryozoan-algal (colder) facies of Schlanger and Konishi (1975).

during the latest Cretaceous and earliest Tertiary (for example, Gordon and Cape, 1981; Jurdy, 1981, 1983; Morgan, 1981; Gordon, 1982).

The paleolatitude of 17.5°±4.4° N. found for Abbott Seamount puts the Hawaiian hot spot at about its present latitude by 40 Ma, which is consistent with the conclusion of Livermore and others (1983) that true polar wander did not occur during the past 35 m.y. The paleoequator analysis of Sager (1984) suggests that there was no true polar wander after formation of the bend, that is, after 43 Ma. This requires approximately 7.6° of southward latitudinal motion of the hot spot between 65 Ma and 43 Ma and 5° of northward motion of the Pacific plate in order to satisfy the relative motion of about 0.65° latitude per million years indicated by the age-distance data.

COMPARISON TO OTHER PACIFIC LINEAR ISLAND CHAINS

Another way of evaluating the movement of hot spots is to compare the orientation and age progression quantitatively along volcanic chains formed during the same time period on the same plate. Several studies (Clague and Jarrard, 1973; Jackson, 1976; Jarrard and Clague, 1977; Epp, 1978; McDougall and Duncan, 1980; Turner and others, 1980; and Duncan and Clague, 1985) have attempted such evaluations for the Pacific plate since Morgan (1971) first proposed the technique. Most of the linear volcanic chains in the Pacific basin are oriented roughly west-northwest and apparently formed sequentially over nearly stationary hot spots during the last 43 m.y. as the Pacific plate rotated clockwise about a pole located near lat 69° N., long 68° W. (Clague and Jarrard, 1973). Another group of linear chains exhibit roughly north-trending orientations and apparently formed by the same mechanism between at least 80 Ma and 43 Ma as the Pacific plate rotated clockwise about a pole located near lat 17° N., long 107° W. (Clague and Jarrard, 1973).

The hot spots that formed the Hawaiian, Austral-Cook, Society, Marquesas, Caroline, Pitcairn-Gambier, Samoan, and Islas Revilla Gigedos island chains and the Pratt-Welker and Cobb-Eickelberg seamount chains moved very little with respect to one another (Duncan and Clague, 1985). The most convincing evidence that hot spots move with respect to one another comes from the orientation of the Marquesas Islands, which is discordant by about 25° with that predicted, implying motion of the Marquesas hot spot to the northeast with respect to the hot-spot reference frame at several centimeters per year (Jarrard and Clague, 1977) during the last 5 m.y. The rates of volcanic migration along the chains younger than 43 Ma fit a pole of rotation at lat 68° N., long 75° W. and an angular rotation rate of 0.95°±0.02°/m.y. (Duncan and Clague, 1985).

CAUSE OF THE HAWAIIAN-EMPEROR BEND

An especially knotty problem over the past decade has been the relationship between Pacific sea-floor spreading, worldwide plate motion, and the Hawaiian-Emperor bend. Since there is now firm evidence that the motion of the hot-spot frame was small during the early Cenozoic and has been negligible since then, the 120° angle in the Hawaiian-Emperor bend must represent a major (circa 60°) change in the absolute motion of the Pacific plate. Since the motions of individual plates are not independent, we would expect such a significant change to be part of a worldwide reorganization of both absolute and relative plate motions. Various authors have suggested that the bend might correlate with circum-Pacific tectonic events (Jackson and others, 1972; Clague and Jarrard, 1973; Moore, 1984), that it may be caused by the collision of India and Eurasia (Dalrymple and Clague, 1976), or that it may be the result of new subduction zones along the southwestern margin of the Pacific plate (Gordon and others, 1978). However, completely satisfactory correlations have not been achieved.

A major feature of the northeast Pacific magnetic-anomaly pattern is the major change in the trend of the magnetic anomalies, that is, the magnetic bight, between anomalies 24 and 21. Reconstruction of the Pacific plate shows that this change in the anomaly pattern is the result of a change in spreading about the Pacific-Kula-Farallon triple junction, in particular the cessation of spreading on the Kula Ridge (Scientific Party DSDP 55, 1978; Byrne, 1979). This occurred perhaps as early as anomaly 24 but no later than the time of anomaly 21, which is approximately the time of the major change in spreading direction between Greenland and Europe (Vogt

and Avery, 1974) and shortly before an apparent increase in the frequency of geomagnetic reversals (Jacobs, 1984). The change in anomaly orientation can also be correlated with numerous events associated with worldwide reorganization of plate motions (Rona and Richardson, 1978).

The early magnetic time scales of Heirtzler and others (1968) and LaBreque and others (1977) put anomaly 21 at about 54–53 Ma and 52–51 Ma (corrected for new K decay and abundance constants), respectively, which implies a lag of at least 10 m.y. between the reorganization of Pacific magnetic anomalies and the formation of the Hawaiian-Emperor bend at 43.1 ± 1.4 Ma (Dalrymple and Clague, 1976). More recent time scales, however, have narrowed this somewhat awkward gap. Ness and others (1980) put anomaly 21 at about 49–48 Ma, Lowrie and Alvarez (1981) at about 48.5–47.5 Ma, and Butler and Coney (1981) at about 47–46 Ma. As suggested by Butler and Coney, a lag of 3–4 m.y. is close enough to suggest a causal relationship between the relative motion change represented by the magnetic bight and the absolute change represented by the Hawaiian-Emperor bend.

Gordon and others (1978) suggested that the change in direction of the Pacific plate at ~43 Ma was caused by the development of new trenches along the southwestern boundary of the plate. These new trenches, which replaced an earlier set of ridges and transform faults, were the result of rifting of Australia from Antarctica and the accompanying convergence of the Australia-Indian and Pacific plates. Gordon and others (1978) suggest that some time would have elapsed before the subducting plate would have been long enough and dense enough to exert sufficient torque on the Pacific plate to change its direction of motion. This could explain the lag between the timing of reorientation of the magnetic anomalies, which record the change in relative plate motion, and the age of the Hawaiian-Emperor bend, which records the change in absolute plate motion. The duration of the lag time would depend on the rate of plate convergence. As noted by Gordon and others (1978) a lag time of perhaps as much as 10 m.y. might be explained if convergence were sufficiently slow. Their mechanism is more plausible, however, if the lag can be shortened to a few million years, as now seems likely.

HAWAIIAN HOT-SPOT MODELS

Although there is now little doubt that the Hawaiian-Emperor Chain owes its origin to a hot spot that has been approximately fixed with respect to the Earth's spin axis throughout the Cenozoic, there is scant information concerning the exact mechanism involved. Even the term "hot spot" may be misleading, for excess heat is not necessarily involved. Alternatively, it could be the result of pressure release in a mantle source area (Green, 1971; McDougall, 1971; Jackson and others, 1972).

A successful hypothesis for the Hawaiian hot-spot mechanism must explain the propagation of volcanism along the chain, the near-fixity of the hot spot, the chemistry and timing of the eruptions from individual volcanoes, and the detailed geometry of volcanism, including volcano spacing and departures from absolute linearity. Over the past decade or so several mechanisms have been advanced to explain how a linear chain of volcanoes might be progressively erupted onto the sea floor, but most are highly generalized and suffer from lack of detail. Few of the hypotheses address all of the kinematic and petrological issues, and none seems to be amenable to experimental test. Nonetheless, they are interesting speculations on solutions to an extremely difficult problem.

All of the proposed mechanisms can be grouped into four basic types:

1. Propagating fracture driven by lithospheric stresses.
2. Thermally or chemically driven convection.
3. Melting caused by shear between the lithosphere and the asthenosphere.
4. Mechanical injection of heat into the lithosphere.

PROPAGATING-FRACTURE HYPOTHESES

Dana (1849) was the first to associate the Hawaiian volcanic chain with crustal fracturing. He proposed that the Hawaiian and other volcanic chains in the Pacific were each emplaced along a series of short echelon fractures (or "rents") that were widest at the southeast end where volcanism was the most prolonged. He considered these fractures to be part of a worldwide system reflecting tension in the crust resulting from cooling of the Earth from an initially molten state. S. Powers (1917) agreed that the eruptions occurred through a superficial set of echelon fractures following the trend of the chain, but he attributed the trend to some deeper seated lines of weakness. Chubb (1934) thought that the Hawaiian swell represented the surface manifestation of a broad anticline trending in the direction of the chain and produced by compression oriented north-northeast and south-southwest. He proposed that the Hawaiian volcanoes erupted along strike faults and dip faults atop and aligned with the anticline.

Betz and Hess (1942) found no evidence of vertical displacement along fault scarps but thought that the chain might be the manifestation of a great transcurrent strike-slip fault resulting from crustal shortening within the Pacific basin caused by Tertiary volcanism along the margins of the basin. In view of the Earth's sphericity, the straightness of the chain indicated to them that the fault plane was essentially vertical. Considering the strength and thickness of the ocean crust, they thought that an anticline the dimensions of the Hawaiian swell was unlikely and proposed instead that the swell represented a thick lava pile related to the presumed fault zone. Dietz and Menard (1953) thought this idea improbable because of the enormous volume of lava that would be required to produce the swell.

Other early authors subscribed to the idea that the Hawaiian Chain developed atop a propagating fracture (for example, Stearns, 1946; Eaton and Murata, 1960; Jackson and Wright, 1970), but they were vague or noncommital as to the cause of the rupture.

Most recent authors who have advanced propagating-fracture hypotheses have attempted to relate the cause of the fracture to either local or regional stress fields within the Pacific plate. Green (1971) suggested that divergent flow vectors caused by the movement of the plate over an imperfect sphere, that is, an uneven upper mantle

surface, caused local tension and intermittent failure of the lithosphere. The fracturing would allow rapid upwelling and partial melting of material from the low-velocity zone. One problem with this hypothesis is the means by which the irregularities on the asthenosphere are maintained, but Menard (1973) suggested that such persistent asthenospheric "bumps" might be caused by a rising thermal plume in the mantle.

McDougall (1971), following the ideas of Green (1971), proposed that the physical feature that subjected the plate to local tension might be either a thermal high or an incipient upwelling caused by a local concentration of heat-producing radioisotopes. According to McDougall's model, fracturing results in the diapiric rise of peridotitic material from the asthenosphere into the lithosphere (fig. 1.13*A*, *B*), where partial melting then generates tholeiitic magma. Movement of the plate and counterflow of the asthenosphere eventually decapitate the diapir, but replacement of material from deeper levels of the asthenosphere perpetuates the high and a new diapir is created (fig. 1.13*C*, *D*). Noting that the rate of propagation of volcanism along the Hawaiian Chain is slightly more than twice the half-spreading rate of the East Pacific Rise, McDougall concluded that there must be counterflow of material in the asthenosphere in a zone of thickness comparable to that of the lithosphere. Jackson and others (1980) showed that it was not possible to reconcile equal-but-opposite hot-spot motion with the paleolatitude of Suiko Seamount if the counterflow had persisted throughout the history of the Hawaiian-Emperor Chain. Hot-spot countermovement until the time of the bend followed by latitudinal stability from then to the present is, however, kinematically permissible.

Another mechanism for producing a local stress field and lithospheric rupture was proposed by Walcott (1976), who related the stress to the volcanic load on the lithosphere. He suggested that large volcanoes will produce lithospheric stresses during growth that may be large enough to cause disruption of the plate. If the plate is under a normal state of horizontal compression, then the failure of the lithosphere will occur preferentially parallel to the direction of the compressive stress. The direction of rupture will remain linear as long as the ambient stress direction remains constant, and the rate of propagation will depend on the speed of formation of the load. Noting the rapidity with which Hawaiian volcanoes form, Walcott concluded that the propagation of volcanism along the Hawaiian chain must be limited by the availability of magma source material. Thus, the mechanism would be self-perpetuating and self-regulating. Although this mechanism will result in a line of volcanoes, it does not explain the observed age progression nor does it account for hot-spot fixity, but it might be locally important and explain the detailed distribution of volcanoes within the Hawaiian Chain (Walcott, 1976).

Expanding on the original idea of Dana (1849), Jackson and others (1972) observed that the individual volcanic centers of the Hawaiian-Emperor Chain appear to lie on short, sigmoidal, overlapping loci that are echelon in a clockwise sense in the Hawaiian Chain and in a counterclockwise sense in the Emperor Chain (fig. 1.14), although the latter was based on inadequate bathymetric data. They proposed that the pattern of loci may be caused by

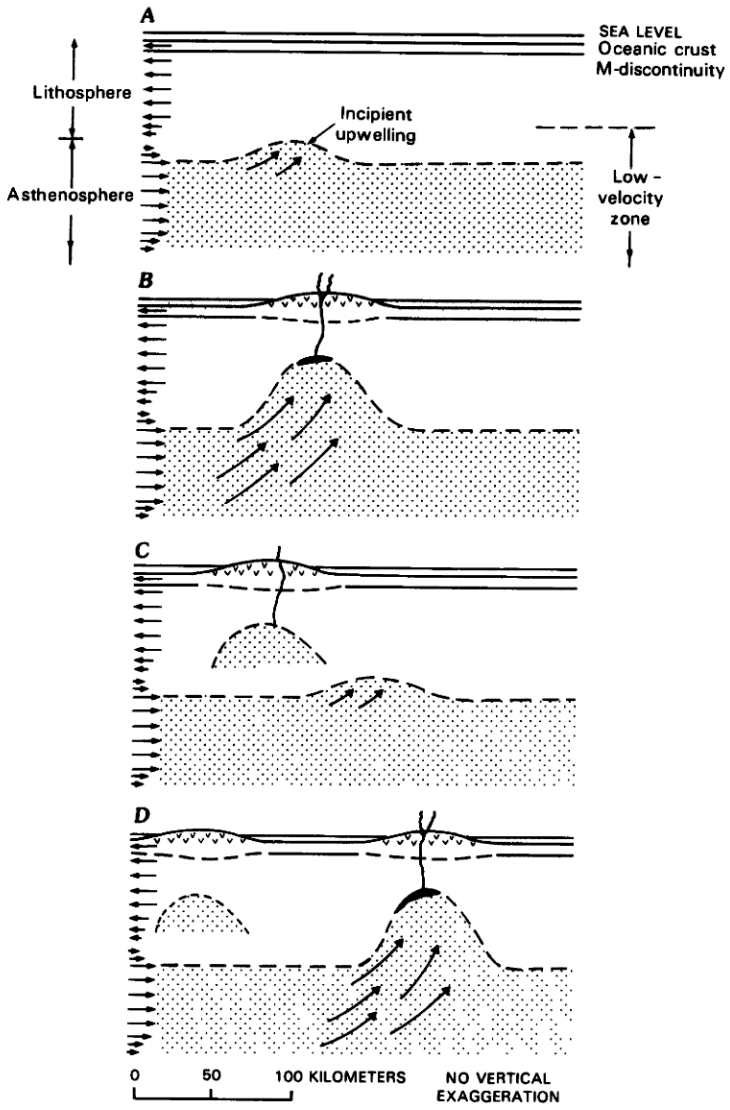

FIGURE 1.13.—Schematic diagram of McDougall's (1971) propagating-fracture hypothesis. Propagating tensional fracture allows diapiric upwelling from asthenosphere (***A***) and partial melting (***B***). Relative motion between lithosphere and asthenosphere (arrow along left margin) eventually decapitates diapir (***C***) and cycle begins at a new position (***D***). The shaded zone represents peridotitic material that is the source rock of the lava. From McDougall.

extensional strain resulting from tension within the Pacific plate, but they did not speculate on the ultimate cause of the stresses. Jackson and Shaw (1975) developed this idea more fully and extended it to other chains in the Pacific. They argued that linear hot-spot chains track and record the states of stress in the Pacific plate as a function of time, and that the stress was reflected in the detailed geometry of volcanoes within a chain, that is, in the orientation of the volcanic loci, which represent the injection of magma along lines perpendicular to least principal stress directions. On the basis of their analysis of the Hawaiian-Emperor, Pratt-Welker, Tuamotu, and

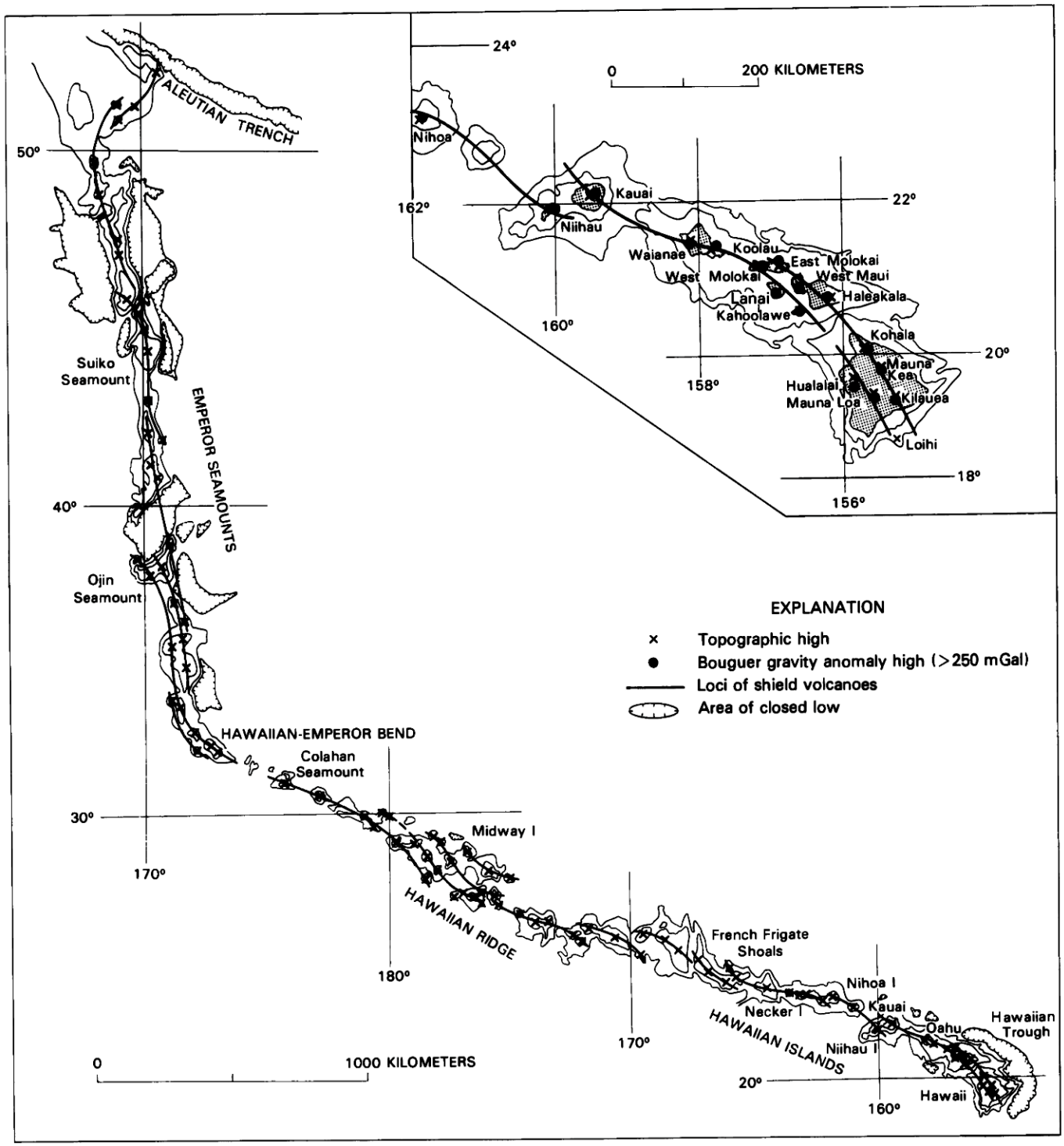

FIGURE 1.14.—Loci of shield volcanoes in Hawaiian-Emperor Chain according to Jackson and others (1972). Inset shows detailed relation between topographic highs, Bouguer gravity anomaly highs, and loci for principal Hawaiian Islands. Contour interval is 1 km; hachures indicate area of closed low.

Austral-Ellice-Gilbert-Marshall Chains, they concluded that the stress orientations since the time of formation of the Hawaiian-Emperor bend were caused by a right-lateral rotational couple acting within the plane of the Pacific plate. This couple resulted in the minimum principal stress oriented in a northeast-southwest direction. Before the time of the bend, the rotational couple was left-lateral and the minimum stress was oriented north-northwest and south-southeast. The curvature in the volcanic loci, they proposed, reflects episodic swings of the minimum-stress directions that averaged about 12 m.y. per episode and were perhaps a consequence of episodic changes in the force vectors at plate boundaries. Jackson and Shaw (1975) were uncertain about the exact causes of the stress field within the Pacific plate, but noted that possible contributors included convergence and divergence at plate boundaries, varying convection rates in the asthenosphere, and volume changes within the plate resulting from changing pressure and temperature.

On the basis of an analysis of volcano spacing and the relation of volcanic chains to preexisting plate structures, Vogt (1974) suggested that the factors that controlled the path of hot-spot chains are not clearly of one origin, but included simple shear, reactivated sea-floor-spreading structures, and local stresses. He concluded that the sigmoidal loci (fractures) postulated by Jackson and others (1972) for the Hawaiian Chain had no counterpart in other chains, although Jackson and Shaw (1975) claimed to have found a similar pattern on other chains in the Pacific.

Solomon and Sleep (1974) preferred the propagating-fracture hypothesis, in part because it avoided the necessity of an abnormal and unknown source of heat in the asthenosphere. They emphasized that the stresses in the Pacific plate can be explained entirely in terms of the forces acting on plate boundaries, and that such mechanisms have the attractive feature of being amenable to numerical treatment. They proposed that the continued motion of the plate with respect to the boundary force field and to secondary convection cells in the asthenosphere might cause a linear propagating fracture as new parts of the plate moved into zones of tension, and that such a tensional fracture would permit the passive upwelling of volcanic material from below. This model offers no explanation why Hawaii is located where it is. In addition, passive mantle upwelling seems inadequate to produce the enormous volume of lava that comprises the Hawaiian Islands.

Turcotte and Oxburgh (1973, 1976, 1978) also subscribed to propagating tensional fractures as a possible cause of linear midplate volcanism. They noted that although brittle failure may occur at the surface of a plate, plastic failure is more likely at depth where lithostatic pressure is large compared with the yield stress. Theoretically, plastic and brittle failure will occur at angles of 35° and 45°, respectively, to the direction of tension (fig. 1.15*A*). Possible causes of tension include thermal stresses in the cooling and thickening plate as it moves outward from the spreading ridge and membrane stresses caused by the movement of plates on the surface of the nonspherical Earth (fig. 1.15*B*, *C*). Turcotte and Oxburgh note that the angle between the Hawaiian Chain and the direction of sea-floor spreading, as deduced from magnetic anomalies and fracture zones, is 34°, in good agreement with the predicted value. They also note that the angle between the trend of the chain and the

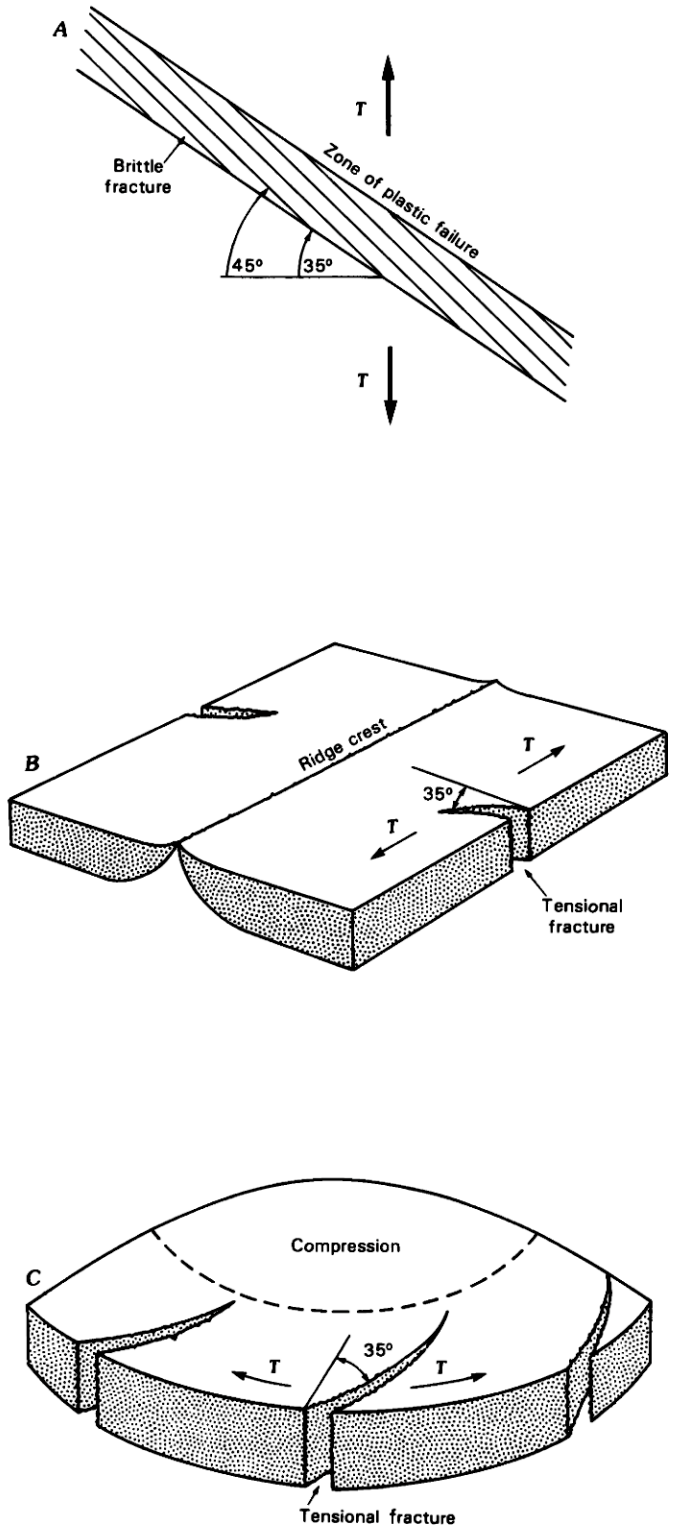

FIGURE 1.15.—Tensional stresses as a possible cause of propagating fractures in lithospheric plates. ***A***, Orientation of plastic and brittle failure in thin plate under tension (*T*) according to Turcotte and Oxburgh (1973, 1976, 1978). ***B***, Fracture in lithospheric plate from tensional stress caused by cooling and thickening of plate away from spreading ridge. ***C***, Fracture caused by membrane stresses in northward-moving plate on oblate Earth.

loci of Jackson and others (1972) is approximately correct for brittle fracture. The Cook-Austral, Tuamoto-Pitcairn, and Kodiak-Bowie Chains also lie at angles of between 31° and 42° to spreading directions, but the angle made by the Marquesas is 60°, which is much larger than that predicted by Turcotte and Oxburgh (1978).

Both plastic and brittle failure, as proposed by Turcotte and Oxburgh, provide a means of propagating a fracture as a function of plate motion and might account for some degree of hot-spot fixity. The thermal mechanism relies on cooling and thickening of the plate as a function of time and distance from the spreading ridge. Once started, the fracture will propagate from a point that remains at a fixed crustal age from the ridge. As these authors point out, fractures due to membrane stresses would be most likely in middle latitudes because the change in the radius of curvature of the Earth is a maximum at a latitude of about 45°. For a plate in the northern hemisphere moving northward, the fracture would propagate southward from a point that remains latitudinally fixed. This mechanism does not, however, account for the great variety of latitudes of active Pacific hot spots, the parallelism of Pacific volcanic chains, or the Hawaiian-Emperor bend (Solomon and Sleep, 1974).

Handschumacher (1973) advanced three fracture-related explanations for the Emperor Seamount Chain, but he did not extend them to include the Hawaiian Chain. Two of the mechanisms, extrusion along a strike-slip fault and interaction between a stable part of the Pacific plate on the west and a spreading ridge on the east, have since been disproved by the age progression (younger southward) of the Emperor volcanoes. The third mechanism, secondary activity along a zone of weakness between eastern and western parts of the plate, invokes preexisting structural control, but, like all propagating fracture hypotheses, does not provide any insight into the lava-producing mechanism.

THERMAL AND CHEMICAL CONVECTION HYPOTHESES

Numerous authors have associated the Hawaiian Chain with thermally driven convection in the asthenosphere. Among the earliest were Dietz and Menard (1953) and Menard (1955), who hypothesized that the Hawaiian Arch or swell occurred over the intersection of two upwelling and diverging convection cells. This would put the lithosphere under tension and produce fracturing as the volcanic load increased, providing a reasonable explanation for the geometry and form of the Hawaiian Arch, Ridge, and Deep. It does not, however, account for the constant rate of propagation of volcanism along the chain, although in 1955 this was poorly known. Although he did not discuss the Hawaiian Chain, Wilson (1962) showed it to be coincident with an early Tertiary ridge which he suggested formed by diverging convection cells.

Wilson (1963a, b, c, d) was the first to suggest a thermal convection mechanism that specifically addressed the age progression in the Hawaiian and eight other parallel chains in the Pacific. He speculated that the source of lava resided in the stagnant, or at least more slowly moving, region of a mantle convection cell (fig. 1.16). Spreading of the sea floor above this fixed source would result in an age-progressive chain of volcanoes. Wilson (1963a) tentatively put the source at a depth of about 200 km, below the low-velocity zone,

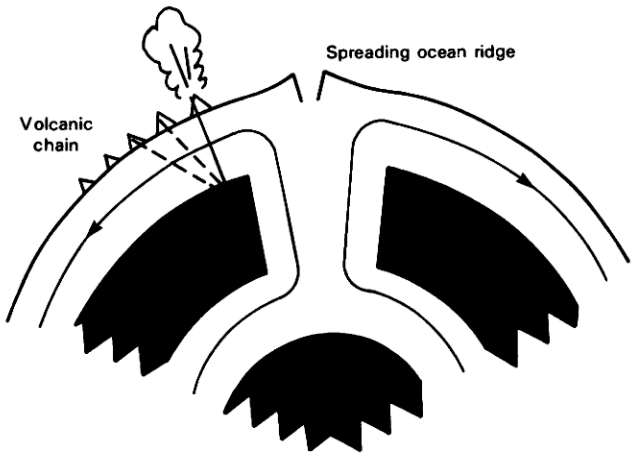

FIGURE 1.16.—Wilson's proposed possible origin of Hawaiian Chain. If lava is generated in stable core of mantle convection cell and surface is carried along by plate motion, then one source can give rise to a chain of successively extinct volcanoes. Modified from Wilson (1963), by permission of the National Research Council of Canada.

but did not speculate on the ultimate cause of the lava source.

The hypothesis that has undoubtedly received the most attention since Wilson's is that of Morgan (1971, 1972a, b) who proposed that the Hawaiian and other Pacific hot spots were narrow thermal zones of upwelling, which he termed "plumes," that originate deep within the Earth's mantle, possibly near the core. They arise because of thermal instabilities (excess heat), which cause upward convection of hot plumes of mantle rock in much the same way that thermal instabilities in the atmosphere cause thunderhead clouds. According to this hypothesis, the plumes are of relatively low viscosity, about 150 km in diameter, and convect upward at a rate of about 2 m/yr. In addition to providing lava for volcanic chains, plumes are considered by Morgan to be a driving force of plate tectonics, to be capable of rifting continents, and to occur on midocean ridges as well as in the middle of plates. Morgan identified about 20 hot spots, but subsequent authors have tended to be more generous (for example, Burke and Wilson, 1976; Crough, 1983).

One aspect of Morgan's hypothesis that has proven extremely important to the study of plate tectonics, whether or not hot spots are actually plumes, is the concept that hot spots are fixed relative to one another and to the Earth's spin axis. As we discussed earlier, hot-spot fixity appears to be generally true for long periods of geologic time, and thus hot spots provide a stable reference frame for studies of absolute plate motions.

Morgan (1972a, 1972b) observed that most hot spots were characterized by a positive gravity anomaly and a topographic high, both of which, he said, are symptomatic of rising thermal currents in the mantle. Morgan calculated that as few as 20 plumes could bring up from depth an estimated 500 km^3/yr of mantle material and half of the total heat flow from the Earth.

Wilson (1973) endorsed the plume hypothesis and likened plumes to other natural diapiric mechanisms such as salt domes, thunderheads, and volcanic pipes. Menard (1973) noted that the Hawaiian, Austral-Cook (Macdonald Seamount), and Gulf of Alaska hot spots all lie on the updrift side of asthenospheric bumps and concluded that equally persistent rising plumes were required to sustain the asthenospheric relief at sites not associated with hot spots. Strong (1974) noted that the compositions of Kilauea and Mauna Loa lava were not the same, concluded that the Hawaiian plume was probably not the direct source of lava, and questioned whether Morgan's plumes were necessarily zones of mass transport. Alternatively, he suggested they might be zones of high thermal conductivity or concentrated diffusion.

Morgan (1972b) proposed four tests of the plume hypothesis, including seismic detection, prediction of plate motions from plume dynamics, evaluation of the necessity of plumes for heat transport from the deep mantle, and correlation of changes in Cenozoic and Cretaceous spreading patterns with the disappearance or emergence of new hot spots. Of the four, only the seismic test had any real potential for yielding a conclusive answer. Davies and Sheppard (1972), Kanasewich and others (1972, 1973), and Kanasewich and Gutowski (1975) analyzed seismic rays passing beneath the Hawaiian Islands from earthquakes in the southwest Pacific. They concluded that there is a zone of abnormally high velocities near the core-mantle boundary beneath Hawaii and that the seismic data are generally consistent with Morgan's plume hypothesis, although there were no data indicating an extension of the velocity anomaly upward through the upper mantle. The interpretation of the seismic data was questioned by Wright (1975) and Green (1975), who concluded that the observed travel time anomalies were most likely the result of upper mantle inhomogeneities beneath the seismic detector arrays in western North America. From a study of teleseismic arrivals from 55 earthquakes recorded at 21 stations on Hawaii, however, Ellsworth and others (1975) found evidence of lower than average velocities at depths of 30–50 km beneath the island. Whether this anomaly extends into the asthenosphere is unknown. Thus, the seismic evidence for a thermal plume beneath Hawaii appears to be, at best, inconclusive.

One difficulty with the plume hypothesis is that narrowly confined convection is unstable in fluids with high Prandtl numbers (kinematic viscosity divided by thermal diffusivity) such as mantle material (Turcotte and Oxburgh, 1978). Narrow plumes might be sustained, however, if confined to the upper mantle and heated from below by a lower mantle source (Turcotte and Oxburgh, 1978). Another problem is that the amount of partial melting that would result from the adiabatic decompression of mantle material rising from the core-mantle boundary is much too high to result in Hawaiian basalt (Turcotte and Oxburgh, 1978). This objection might not apply if mantle plumes are a source of heat for melting of the lower lithosphere or the uppermost asthenosphere rather than a direct source of magma.

An alternative to thermal plumes, proposed by Anderson (1975), is that the plumes are relict compositional conduits. According to Anderson's hypothesis, the Earth accreted inhomogeneously and in the sequence in which compounds would condense from a cooling nebula. Thus, the primitive deep mantle was a material enriched in Ca, Al, Ti, and the refractory trace elements, including U and Th. This material, being less dense than the overlying layers, rose as chemical plumes through buoyancy early in Earth's history and partially melted to yield anorthosites. Present-day hot spots occur above the mantle residua of this partial melting. These plumes provide heat to the base of the lithosphere because they are enriched in heat-producing elements, principally U and Th, and so constitute what could be called radioactive hot spots. Chemical plumes might explain both asthenospheric bumps and also the episodic nature of volcanism. Anderson proposed that the rapid withdrawal of heat by magma could periodically outstrip heat production and therefore temporarily halt magma generation. However, one would think that the chemical inhomogeneities should be seismically detectable.

Richter (1973) and Richter and Parsons (1975) have suggested that the Hawaiian-Emperor Chain and other linear chains might be a consequence of the nonlinear interaction of two different scales of mantle convection, one involving sea-floor spreading and the return flow necessary to conserve mass, and the other a Rayleigh-Benard convection reaching to depths of about 650 km. This latter convection forms rolls whose axes initially are aligned perpendicular to the spreading direction. In time, however, the latitudinal rolls give way to longitudinal rolls with axes parallel to the direction of plate motion (fig. 1.17). The time for the transition to occur depends on the spreading velocity, but may be as short as about 20 m.y. for a fast (about 10 cm/yr) plate like the Pacific plate. Longitudinal rolls will generate alternating bands of tension and compression in the overlying plate. Linear volcanic chains might form along the zones of tension and, either because of modulation of convection amplitude along the roll or because of the fracture properties of the plate, could propagate opposite to the direction of spreading. A feature of this mechanism is that ages out of order can occur. In addition, an age gap of some tens of millions of years could occur near the bend in the Hawaiian-Emperor Chain because of the time required for a new set of longitudinal rolls to be established

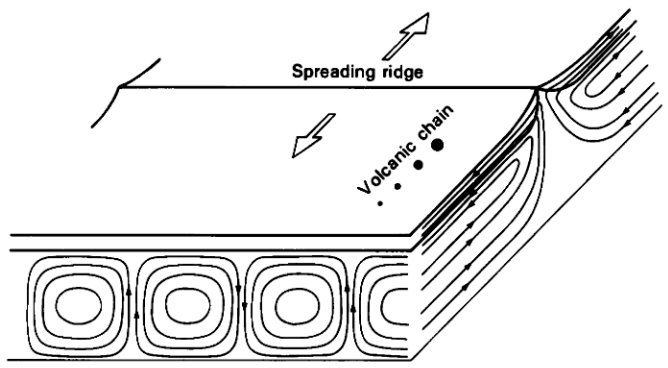

FIGURE 1.17.—Schematic diagram of large-scale asthenospheric flow related to sea-floor spreading and superimposed small-scale longitudinal rolls. Volcanic chain might occur in zone of tension between diverging rolls and would propagate opposite to direction of spreading. From Richter and Parsons (1975).

following a change in spreading direction. The age data for the Hawaiian-Emperor Chain (fig. 1.5), however, show that the propagation is continuous around the bend, although seamounts are sparse on the westernmost Hawaiian Ridge. Another feature of the longitudinal roll model is that parallel volcanic chains should be spaced at some multiple of twice the depth of the convecting layer, which is in accord with the geometry of the major Pacific chains for a convecting depth of about 600 km (Richter, 1973).

SHEAR-MELTING HYPOTHESES

Shear melting with thermal feedback to regulate the propagation rate was proposed by Shaw (1973) to explain the nonlinear time-distance-volume relations along the Hawaiian Chain noted by Jackson and others (1972) and Swanson (1972) (fig. 1.18). According to his hypothesis, the hot spot is the result of a delicately balanced thermomechanical process that derives energy from plate motion and is regulated by a feedback process inherent in the physical properties of the rocks involved. In principle, the idea is quite simple and is based on the observation that a viscous medium will rise in temperature when sheared. Shear occurs within a finite zone between the lower lithosphere and the upper asthenosphere because of their relative motion. As shear proceeds the temperature rises and the viscosity decreases within the shear zone. This allows an increase in the rate of shearing, which in turn produces a further increase in temperature. The increasing temperature eventually results in partial melting and the formation of magma, which rises to the surface to form the volcanoes. The magma carries off excess heat, the temperature decreases rapidly, viscosity increases, and melting stops temporarily as a new cycle is initiated. Each cycle lasts a few million years and is characterized by accelerating propagation of volcanism and eruption volume followed by a sudden halt.

A means of localizing shear melting and fixing the resulting hot spot relative to the mantle was advanced by Shaw and Jackson (1973). They proposed that once partial melting began the residua sinks, forming a type of gravitational anchor that reaches down into the mantle, perhaps to the core-mantle boundary (fig. 1.19). The downwelling anchor not only forms a geographic pinning point for the hot spot but also results in the inflow of fresh mantle material beneath the hot spot, which thus is not limited by supply. There is strong evidence, however, that the depleted residua from partial melting of the most likely parent rocks are less dense than the parent material and would not sink (see, for example, O'Hara, 1975; Boyd and McCallister, 1976; Jordan, 1979). Thus, unless the source of Hawaiian basalt is something quite unusual, the formation of a gravitational anchor seems unlikely, and the shear-melting hypothesis suffers from the lack of both a starting mechanism and a means of localization.

HEAT-INJECTION HYPOTHESIS

It has long been known that the Hawaiian hot spot, among others, is associated with a broad topographic anomaly on the ocean floor, the Hawaiian swell, which has been attributed to some sort of thermal anomaly for more than three decades (see, for example,

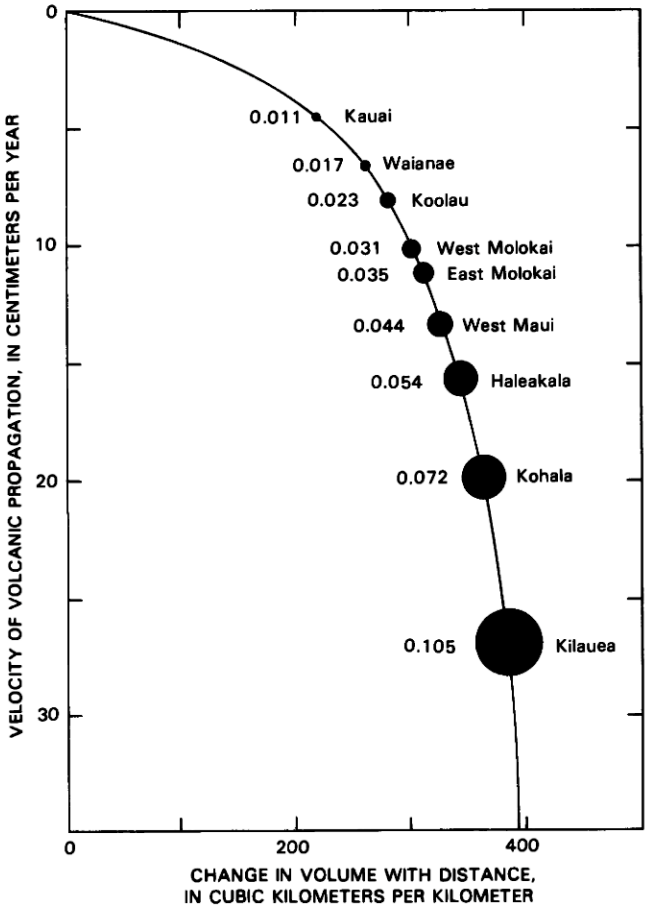

FIGURE 1.18.—Change in volume of lava with respect to unit distance versus change in distance with respect to time (velocity of volcanic propagation) for principal Hawaiian Islands. Diameter of circles approximately proportional to apparent eruption rates, which are also given (in cubic kilometers per year) next to circles. From Shaw (1973).

Dietz and Menard, 1953; Menard, 1955). Only recently, however, has it become clear that the swell may be the result of thermal resetting and thinning of the aging and thickening lithosphere. Detrick and Crough (1978) observed that long-term rates of subsidence of volcanoes in the Pacific are higher than can be accounted for by the subsidence that accompanies the cooling and thickening of the lithosphere as it moves away from the spreading ridge (Parsons and Sclater, 1977; Schroeder, 1984). They proposed that the excess subsidence is the result of thermal resetting of the lithosphere as the aging plate rides over the hot spot. The resetting is accompanied by lithospheric thinning and a rise in the elevation of the sea floor. The rapid subsequent subsidence then represents a gradual return of these shallow areas to normal depths, that is, depths commensurate with the age of the sea floor (see also Crough, 1979, 1983; Epp, 1984). The hypothesis of thermal resetting is supported by anomalously high heat flow along the

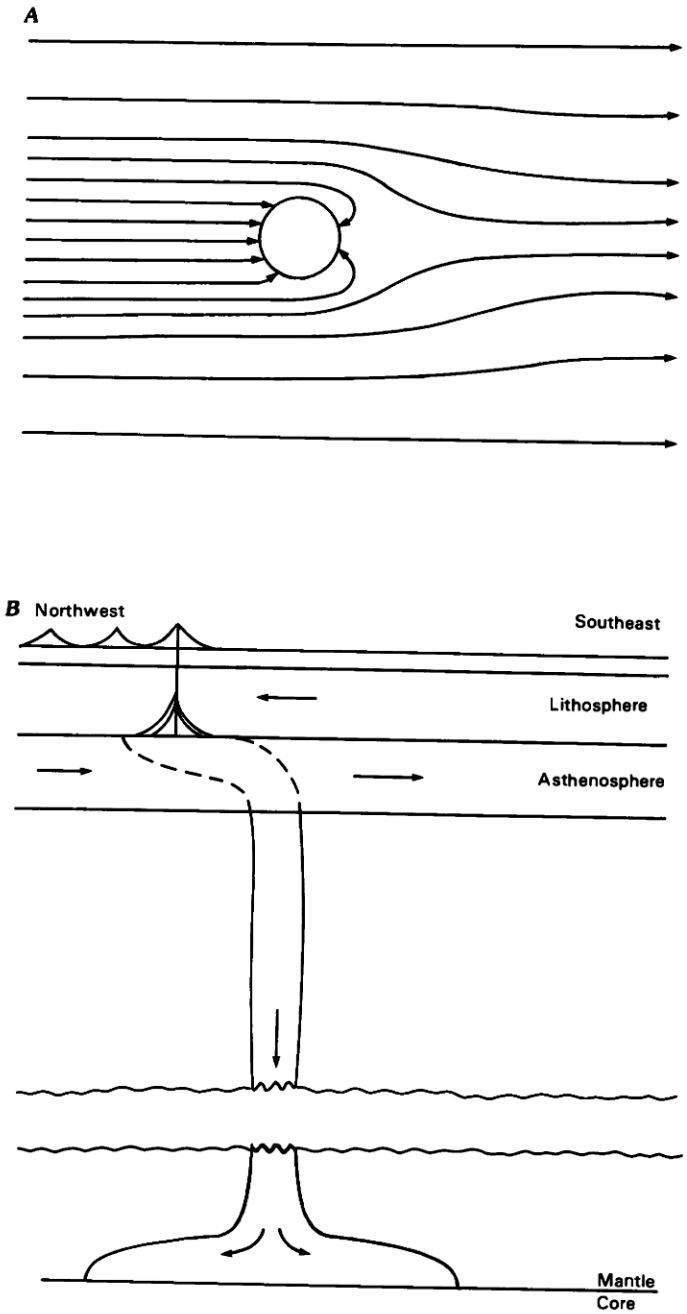

FIGURE 1.19.—Schematic views of possible downwelling of dense residua from tholeiitic melting. *A*, Plan view showing hypothetical flow lines in asthenosphere along horizontal plane taken at time near culmination of melting episode. *B*, Vertical section showing proposed gravitational anchor. From Shaw and Jackson (1973).

Hawaiian Ridge (Detrick and others, 1981). The concept of lithospheric thinning over hot spots is substantiated by the flexural data, which indicate that the lithosphere over hot spots is much thinner than that of comparable age flexed at subduction zones (McNutt, 1984).

Detrick and Crough (1978) recognized that the major problem with their thermal model for the Hawaiian swell is that it requires extremely rapid heating of the lithosphere; a heat flux more than 40 times normal is indicated, if the heating is entirely by conduction. This is because the kinematics of plate motion relative to the hot spot requires the swell to rise in only a few million years, whereas it would take about 100 m.y. at twice the normal heat flux to raise the swell. This problem, however, may not be as serious as it once seemed. More recent modeling by Nakiboglu and Lambeck (1985) demonstrates the sensitivity of these calculations to the lower boundary condition. They argue that most of the Hawaiian swell can be produced by thermal conduction, but a small dynamic component may also be required to support the swell. Another potential solution to this problem, proposed by McNutt (1984), is lithospheric delamination, a process invoked by Bird (1979) to explain volcanism in continental interiors. According to this hypothesis, a strip of the lower lithosphere separates from the upper lithosphere and descends into the asthenosphere. This produces the sudden rise in temperature at the base of the remaining lithosphere required to produce the swell without invoking an unreasonable heat flux. The lateral resistance of the descending strip might also provide the necessary stability of the hot spot with respect to the mantle. It is unclear how delamination might begin, but once started theory suggests that it can propagate at plate velocities (Bird and Baumgardner, 1981).

One problem with delamination is that it requires the sinking into the asthenosphere of the lower lithosphere, which is thought to be one component of the source of ocean-island basalt. For Hawaii the proposed depth of delamination, that is, the thickness of the lithosphere over the hot spot, is slightly less than 30 km (McNutt, 1984), a depth considered to be well above the source region of Hawaiian basalt. It is also clear from pressure-temperature relations that the descending slab would not melt (and if it did the residua would rise rather than sink). Therefore, Hawaiian basalt would have to be generated from the material of the upper asthenosphere, although at lower lithosphere depths, and the lithosphere-asthenosphere boundary would be a purely mechanical one (that is, with no compositional differences across the boundary).

In summary, geophysical models for the Hawaiian hot spot tend to be highly generalized and difficult if not impossible to test. None has yet been advanced that satisfactorily explains all of the geometric, kinematic, physical, and chemical observations from the Hawaiian-Emperor Chain. Although many intriguing and clever ideas have been advanced, the hot-spot mechanism is still somewhat mysterious. Detrick and Crough's (1978) idea that the Hawaiian swell is caused by thermal resetting of the aging ocean crust implies that hot spots are indeed hot. In addition, the possibility that the swell is dynamically supported (Detrick and Crough, 1978) implies that material wells up beneath the lithosphere. Petrologic studies indicate that Hawaiian lava is generated from mantle sources consisting of at least 3 geochemical components; one of these is a primitive undegassed component. The cause of the Hawaiian hot spot is still unknown, but present hypotheses are consistent with Morgan's plume hypothesis in which hot primitive mantle material ascends beneath the ocean lithosphere below Hawaii and reacts with

the lithosphere to produce the compositional range of Hawaiian lava.

REFERENCES

Anderson, D.L., 1975, Chemical plumes in the mantle: Geological Society of America Bulletin, v. 86, p. 1593-1600.

Bargar, K.E., and Jackson, E.D., 1974, Calculated volumes of individual shield volcanoes along the Hawaiian-Emperor Chain: U.S. Geological Survey Journal of Research, v. 2, p. 545-550.

Bargar, K.E., Marshall, M., and Trumbull, J.V.A., 1975, Bathymetry and ice-rafted pebbles from the northern end of the Emperor Seamount Chain: U.S. Geological Survey Open-File Report 75–609, 18 p.

Basaltic Volcanism Study Project, 1981, Basaltic Volcanism on the Terrestrial Planets: New York, Permagon Press, Inc., 1286 p.

Beeson, M.H., 1976, Petrology, mineralogy and geochemistry of the East Molokai Volcanic Series, Hawaii: U.S. Geological Survey Professional Paper 961, 53 p.

Betz, F., Jr., and Hess, H.H., 1942, The floor of the North Pacific Ocean: The Geographical Review, v. 32, p. 99-116.

Bezrukov, P.L., and Udintsev, G.B., 1955, The northern end of the Hawaiian suboceanic ridge: Doklady Akademiya Nauk, v. 103, no. 6, p. 1077-1080.

Bird, P., 1979, Continental delamination and the Colorado Plateau: Journal of Geophysical Research, v. 84, p. 7561-7571.

Bird, P., and Baumgardner, J., 1981, Steady propagation of delamination events: Journal of Geophysical Research, v. 86, p. 4891-4903.

Bonhommet, N., Beeson, M.H., and Dalrymple, G.B., 1977, A contribution to the geochronology and petrology of the Island of Lanai, Hawaii: Geological Society of America Bulletin, v. 88, p. 1282-1286.

Boyd, F.R., and McCallister, R.A., 1976, Densities of fertile and sterile garnet peridotite: Geophysical Research Letters, v. 3, p. 509-512.

Brigham, W.T., 1868, Notes on the Volcanic phenomena of the Hawaiian Islands: Boston, Society of Natural History, Memoir, 1, p. 341-472.

———1909, The volcanoes of Kilauea and Mauna Loa: Bernice Pauahi Bishop Museum, Memoir 2, no. 4, 222 p.

Bryan, W.A., 1915, Natural History of Hawaii: Honolulu, Hawaiian Gazette Co., 569 p.

Budahn, J.R., and Schmitt, R.A., 1984, Petrogenetic modelling of Hawaiian tholeiitic basalts: A geochemical approach: Geochimica et Cosmochimica Acta, v. 49, p. 67-87.

Bukry, D., 1975, Coccolith and silicoflagellate stratigraphy, northwestern Pacific Ocean, Deep Sea Drilling Project, Leg 32, *in* Larson, R.L., Moberly, R., and others, Initial Reports of the Deep Sea Drilling Project, v. 32: Washington, U.S. Government Printing Office, p. 677-701.

Burke, K.C., and Wilson, J.T., 1976, Hot spots on the Earth's surface: Scientific American, v. 235, no. 2, p. 46-57.

Butler, R. F., and Coney, P. J., 1981, A revised magnetic polarity time scale for the Paleocene and early Eocene and implications for Pacific plate motion: Geophysical Research Letters, v. 8, p. 301-304.

Butt, A., 1980, Biostratigraphic and paleoenvironment analyses of the sediments at the Emperor Seamounts, DSDP Leg 55, northwestern Pacific: Cenozoic foraminifers, *in* Jackson, E.D., Koizumi, I., and others, Initial Reports of the Deep Sea Drilling Project, v. 55: Washington, U.S. Government Printing Office, p. 289-325.

Byron, G., 1826, Voyage of the 'Blonde' to the Sandwich Islands: London, 260 p.

Byrne, T., 1979, Late Paleocene demise of the Kula-Pacific spreading center: Geology, v. 7, p. 341-344.

Campbell, F., DeCarlo, E., McMurtry, G., and Kroenke, L., 1984, Preliminary report on the assessment of the resource potential of selected seamounts in the Exclusive Economic Zone surrounding the Hawaiian Archipelago: Hawaii Institute of Geophysics Report, October 1984, 45 p.

Chase, T.E., Menard, H.W., and Mammerickx, J., 1970, Bathymetry of the North Pacific: La Jolla, Scripps Institution of Oceanography Charts 2, 7, 8.

———1973, Bathymetric atlas of the North Pacific Ocean, N.O. Pub. No. 1301-2-3.

Chen, C.-Y., and Frey, F.A, 1983, Origin of Hawaiian tholeiites and alkalic basalt: Nature, v. 302, p. 785-789.

———1985, Trace element and isotope geochemistry of lavas from Haleakala Volcano, East Maui: Implications for the origin of Hawaiian basalts: Journal Geophysical Research, v. 90, p. 8743-8768.

Christofferson, E., 1968, The relationship of sea-floor spreading in the Pacific to the origin of the Emperor Seamounts and the Hawaiian Island Chain [abs.]: American Geophysical Union Transactions, v. 49, p. 214.

Chubb, L.J., 1934, The structure of the Pacific basin: Geological Magazine, v. 71, p. 289-302.

Clague, D.A., 1974a, The Hawaiian-Emperor Seamount Chain: Its origin, petrology, and implications for plate tectonics: University of California, San Diego, Ph.D. thesis, 319 p.

———1974b, Nephelinic lavas dredged from the western Hawaiian Ridge: Geological Society of America Abstracts 6 (3), p. 156.

———1981, Linear island and seamount chains, aseismic ridges and intraplate volcanism: Results from DSDP: Society Economic Paleontologists and Mineralogists Special Publication No. 32, p. 7-22.

———1982, Petrology of tholeiitic basalt dredged from Hualalai Volcano, Hawaii: Eos, Transactions, American Geophysical Union, v. 63, p. 1138.

———in press, Hawaiian alkaline volcanism: Journal of the Geological Society of London.

Clague, D.A., and Beeson, M.H., 1980, Trace element geochemistry of the East Molokai Volcanic Series, Hawaii: American Journal of Science, v. 280-A, p. 820-844.

Clague, D.A., and Dalrymple, G.B., 1973, Age of Koko Seamount, Emperor Seamount Chain: Earth and Planetary Science Letters, v. 17, p. 411-415.

———1975, Cretaceous K-Ar ages of volcanic rocks from the Musicians Seamounts and the Hawaiian Ridge: Geophysical Research Letters, v. 2, p. 305-308.

Clague, D.A., Dalrymple, G.B., Greene, H.G., Wald, D., Kono, M., and Kroenke, L., 1980b, Bathymetry of the Emperor Seamounts, *in* Jackson, E.D., Koisumi, I., and others, Initial Reports of the Deep Sea Drilling Project, v. 55: Washington, U.S. Government Printing Office, p. 845-849.

Clague, D. A., Dalrymple, G. B., and Moberly, R., 1975, Petrography and K-Ar ages of dredged volcanic rocks from the western Hawaiian ridge and the southern Emperor Seamount Chain: Geological Society of America Bulletin, v. 86, p. 991-998.

Clague, D.A., Dao-Gong, C., Murnane, R., Beeson, M.H., Lanphere, M.A., Dalrymple, G.B., Friesen, W. and Holcomb, R.T., 1982, Age and petrology of the Kalaupapa Basalt, Molokai, Hawaii: Pacific Science, v. 36, p. 411-420.

Clague, D.A., Fisk, M.R., and Bence, A.E., 1980a, Mineral chemistry of basalts from Ojin, Nintoku, and Suiko Seamounts, Leg 55 DSDP, *in* Jackson, E.D., Koisumi, I., and others, Initial Reports of the Deep Sea Drilling Project, v. 55: Washington, U.S. Government Printing Office, p. 607-637.

Clague, D.A., and Frey, F.A., 1979, Petrology of the Hawaiian-Emperor volcanic chain: Hawaii Symposium on Intraplate volcanism and submarine volcanism, Abstracts Volume, p. 118.

———1980, Trace element geochemistry of tholeiitic basalts from site 433C, Suiko Seamount, *in* Jackson, E.D., Koisumi, I., and others, Initial Reports of the Deep Sea Drilling Project v. 55: Washington, U.S. Government Printing Office, p. 559-569

———1982, Petrology and trace element geochemistry of the Honolulu Volcanics, Oahu: Implications of the oceanic mantle beneath Hawaii: Journal of Petrology, v. 23, 447-504.

Clague, D.A., Frey, F.A., and Beeson, M.H., 1983, Rare-earth element and Sr isotopic evidence for the origin of the East Molokai volcanics, Hawaii: Eos, Transactions, American Geophysical Union, v. 64, p. 902.

Clague, D.A., Jackson, E.D., and Wright, T.L., 1980c, Petrology of Hualalai volcano, Hawaii: Implication for mantle composition: Bulletin Volcanologique, v. 43-4, p. 641-656.

Clague, D.A., and Jarrard, R.D., 1973, Tertiary Pacific plate motion deduced from the Hawaiian-Emperor Chain: Geological Society of America Bulletin, v. 84, p. 1135-1154.

Coan, T., 1840, Missionary Herald, xxxvii, p. 283.
Cole, W.S., 1969, Larger foraminifera from deep drill holes on Midway Atoll: U.S. Geological Survey Professional Paper 680-C, 15 p.
Creager, J.S., Scholl, D.W., 1973, Geological synthesis of Leg 19, Deep Sea Drilling Project, results: Far North Pacific, and Aleutian Ridge, and Bering Sea, *in* Creager, J.S., Scholl, D.W., and others, Initial Reports of the Deep Sea Drilling Project, v. 19: Washington, U.S. Government Printing Office, p. 897-913.
Cross, W., 1904, An occurrence of trachyte on the Island of Hawaii: Journal of Geology, v. 12, p. 510-523.
———1915, Lavas of Hawaii and their relations: U.S. Geological Survey Professional Paper 88, 97 p.
Crough, S.T., 1979, Hotspot epeirogeny: Tectonophysics, v. 61, p. 321-333.
———1983, Hotspot swells: Annual Reviews of Earth and Planetary Sciences, v. 11, p. 165-193.
Dalrymple, G.B., 1971, Potassium-argon ages from the Pololu Volcanic Series, Kohala Volcano, Hawaii: Geological Society of America Bulletin, v. 82, p. 1997-2000.
Dalrymple, G.B., and Clague, D.A., 1976, Age of the Hawaiian-Emperor bend: Earth and Planetary Science Letters, v. 31, p. 313-329.
Dalrymple, G.B., Clague, D.A., Garcia, M.O., and Bright, S.W., 1981, Petrology and K-Ar ages of dredged samples from Laysan Island and Northampton Bank volcanoes, Hawaiian Ridge, and evolution of the Hawaiian-Emperor Chain: Geological Society of America Bulletin Part II, v. 92, p. 884-933 (Summary in Part I, v. 92, p. 315-318).
Dalrymple, G.B., Clague, D.A., and Lanphere, M.A., 1977, Revised age for Midway volcano, Hawaiian volcanic chain: Earth and Planetary Science Letters, v. 37, p. 107-116.
Dalrymple, G.B., and Garcia, M.O., 1980, Age and chemistry of volcanic rocks dredged from Jingu Seamount, Emperor Seamount Chain, *in* Jackson, E.D., Koisumi, I., and others, Initial Reports of the Deep Sea Drilling Project, v. 55: Washington, U. S. Government Printing Office, p. 685-693.
Dalrymple, G.B., Greene, H.G., Ruppel, B.D., Bear, T.E., and Clague, D.A., 1980a, Pre-leg 55 site survey geophysical data from the Research Vessel S.P. *Lee* cruise LEE 8-76-NP, *in* Jackson, E.D., Koisumi, I., and others, Initial Reports of the Deep Sea Drilling Project, v. 55: Washington, U.S. Government Printing Office, p. 801-844.
Dalrymple, G.B., Lanphere, M.A., and Clague, D.A., 1980b, Conventional and $^{40}Ar/^{39}Ar$ K-Ar ages of volcanic rocks from Ojin (Site 430), Nintoku (Site 432), and Suiko (Site 433) Seamounts and the chronology of volcanic propagation along the Hawaiian-Emperor Chain, *in* Jackson, E.D., Koisumi, I., and others, Initial Reports of the Deep Sea Drilling Project, v. 55: Washington, U.S. Government Printing Office, p. 659-676.
Dalrymple, G.B., Lanphere, M.A., and Jackson, E.D., 1974, Contributions to the petrography and geochronology of volcanic rocks from the leeward Hawaiian Islands: Geological Society of America Bulletin, v. 85, p. 727-738.
Dalrymple, G.B., Lanphere, M.A., and Natland, J.H., 1980c, K-Ar minimum age for Meiji Guyot, Emperor Seamount Chain, *in* Jackson, E.D., Koisumi, I., and others, Initial Reports of the Deep Sea Drilling Project: v. 55: Washington, U.S. Government Printing Office, p. 677-683.
Dalrymple, G.B., Silver, E.A., and Jackson, E.D., 1973, Origin of the Hawaiian Islands: American Scientist, v. 61, p. 294-308.
Daly, R.A., 1911, The nature of volcanic action: American Academy of Arts and Sciences Proceedings, v. 47, no. 3, p. 45-122.
Dana, E.S., 1877, Contributions to the petrography of the Sandwich Islands: American Journal of Science, series 3, v. 37, p. 441-467.
Dana, J.D., 1849, United States Exploring Expedition During the Years 1838, 1839, 1840, 1841, 1842: New York, George P. Putnam, 756 p.
———1887, History of the changes in the Mt. Loa Craters, on Hawaii: American Journal of Sciences, series 3, v. 33, p. 433-451; v. 34, p. 81-97, p. 349-364.
———1888, History of the changes in the Mt. Loa Craters, on Hawaii: American Journal of Sciences, series 3, v. 35, p. 15-34, p. 213-228, p. 282-289; v. 36, p. 14-32, p. 81-112, p. 167-175.
———1889, Points on the geologic history of the islands Maui and Oahu: American Journal of Sciences, series 3, v. 37, p. 81-103.
Darwin, C. 1837, On certain areas of elevation and subsidence in the Pacific and Indian Oceans, as deduced from the study of coral formations: Proceedings of the Geological Society of London, v. 2, p. 552-554.
———1842, The Structure and Distribution of Coral Reefs: New York, Appleton.
Davies, D., and Sheppard, R.M., 1972, Lateral heterogeneity in the Earth's Mantle: Nature v. 239, p. 318-323.
Davies, T.A., Clague, D.A., and Wilde, P., 1971, Preliminary report on Leg VII of Aries expedition: Geological investigations in the western North Pacific: Scripps Institution of Oceanography Reference Series, No. 71-27.
Davies, T.A., Wilde, P., and Clague, D.A. 1972, Koko Seamount: A major guyot at the southern end of the Emperor Seamounts: Marine Geology, v. 13, p. 311-321.
Detrick, R.S., and Crough, S.T., 1978, Island subsidence, hot spots, and lithospheric thinning: Journal of Geophysical Research v. 83, p.1236-1244.
Detrick, R.S., von Herzen, R.P., Crough, S.T., Epp, D. and Felin, U., 1981, Heat flow on the Hawaiian swell and lithosphere reheating: Nature, v. 292, p. 142-143.
Dietz, R.S., 1954, Marine geology of northwestern Pacific: description of Japanese bathymetric chart 6901: Geological Society of America Bulletin, v. 65, p. 1199-1224.
Dietz, R.S., and Menard, H.W., 1953, Hawaiian swell, deep, and arch, and subsidence of the Hawaiian Islands: The Journal of Geology, v. 61, p. 99-113.
Doell, R.R., 1972, Paleomagnetism of volcanic rocks from Niihau, Nihoa, and Necker Islands, Hawaii: Journal of Geophysical Research, v. 77, p. 3725-3730.
Doell, R.R., and Dalrymple, G.B., 1973, Potassium-argon ages and paleomagnetism of the Waianae and Koolau Volcanic Series, Oahu, Hawaii: Geological Society of America Bulletin, v. 84, p. 1217-1242.
Duncan, R.A., and Clague, D.A., 1984, The earliest volcanism on the Hawaiian Ridge: Eos, Transactions, American Geophysical Union, v. 65, p. 1076.
———1985, Pacific plate motion recorded by linear volcanic chains, *in* Nairn, A.E.M., Stehli, F.G., and Uyeda, S., eds., The ocean basins and margins, v. 7A: New York, Plenum, p. 89-121.
Dutton, C.E., 1884, Hawaiian volcanoes: U.S. Geological Survey Annual Report, v. 4, p. 75-219.
Dzurisin, D., Koyanagi, R.Y., and English, T.T., 1984, Magma supply and storage at Kilauea Volcano, Hawaii, 1956-1983: Journal of Volcanology and Geothermal Research, v. 21, p. 177-206.
Eaton, J.P., and Murata, K.J., 1960, How volcanoes grow: Science, v. 132, p. 925-938.
Ellis, W., 1823, A narrative of tour through Hawaii: London, 367 p., reprinted Honolulu, 1917.
Ellsworth, W.L., Cipar, J.J., Ward, P.L., Aki, R., Koyanagi, R., and Unger, J., 1975, Crust and upper mantle structure of Kilauea Volcano, Hawaii: Grenoble, Abstracts of papers presented at the Interdisciplinary Symposia, International Union of Geodesy and Geophysics, XVI General Assembly, p. 109-110.
Epp, D., 1978, Age and tectonic relationships among volcanic chains on the Pacific plate: University of Hawaii, Ph.D. thesis, 199 p.
———1984, Implications of volcano and swell heights for thinning of the lithosphere by hotspots: Journal of Geophysical Research, v. 89, p. 9991-9996.
Evernden, J.F., Savage, D.E., Curtis, G.H., and James, G.T., 1964, Potassium-argon dates and the Cenozoic mammalian chronology of North America: American Journal of Science v. 262, p. 145-198.
Feigenson, M.D., 1984, Geochemistry of Kauai Volcanics and a mixing model for the origin of Hawaiian alkalic basalts: Contributions to Mineralogy and Petrology, v. 87, p. 109-119.
Feigenson, M.D., Hofmann, A.W. and Spera, F.J., 1983, Case studies on the origin of basalt II. The transition from tholeiitic to alkalic volcanism on Kohala Volcano, Hawaii: Contributions to Mineralogy and Petrology, v. 84, p. 390-405.
Fiske, R.S., and Jackson, E.D., 1972, Orientation and growth of Hawaiian volcanic rifts—the effect of regional structure and gravitational stresses: Royal Society of London, Proceedings, series A, v. 329, p. 299-326.

Fodor, R.V., Keil, K., and Bunch, T.E., 1975, Contributions to the mineral chemistry of Hawaiian rocks IV. Pyroxenes in rocks from Haleakala and West Maui Volcanoes, Maui, Hawaii: Contributions to Mineralogy and Petrology, v. 50, p. 173-195.

Frey, F.A., 1980, The origin of pyroxenites and garnet pyroxenites from Salt Lake Crater, Oahu, Hawaii: Trace element evidence: American Journal of Science, v. 280-A, 427-449.

———1984, Rare earth element abundances in upper mantle rocks, *in* Henderson, P., ed., Rare earth element geochemistry: Amsterdam, Elsevier, p. 153-203.

Frey, F.A., and Clague, D.A, 1983, Geochemistry of diverse basalt types from Loihi Seamount, Hawaii: Petrogenetic implications: Earth and Planetary Science Letters, v. 66, 337-355.

Frey, F.A., Kennedy, A., Garcia, M.O. West, H.B., Wise, W.S. and Kwon, S.-T., 1984, Mauna Kea Volcano, Hawaii: Lava compositions and their evolution: Eos, Transactions, American Geophysical Union, v. 65, p. 300.

Frey, F.A., and Roden, M.F., in press, The mantle source for the Hawaiian Islands: Constraints from the lavas and ultramafic inclusions, *in* Menzies, M., and Hawkesworth, C., eds., Mantle metasomatism.

Funkhouser, J.G., Barnes, I.L., and Naughton, J.J., 1968, The determination of a series of ages of Hawaiian volcanoes by the potassium-argon method: Pacific Science, v. 22, p. 369-372.

Garcia, M.O., Frey, F.A., and Grooms, D.G., in press, Petrology of volcanic rocks from Kaula Island, Hawaii: Implications for the origin of Hawaiian phonolites: Contributions to Mineralogy and Petrology.

Garcia, M.O., Grooms, D.G., and Naughton, J.J., in press, Petrology and geochronology of volcanic rocks from seamounts along and near the Hawaiian Ridge: Contributions to Mineralogy and Petrology.

Gast, P.W. 1968, Trace element fractionation and the origin of tholeiitic and alkaline magma types: Geochimica Cosmochimica Acta, v. 32, p. 1057-1086.

Goodrich, J., 1826, Notice of the volcanic character of the Island of Hawaii: American Journal of Science, v. 1, p. 1-36.

———1834, Letters of Rev. Joseph Goodrich: American Journal of Science, XXV, p. 199.

Gordon, R.G., 1982, The late Maastrichtian palaeomagnetic pole of the Pacific plate: Geophysical Journal of the Royal Astronomical Society, v. 70, p. 129-140.

Gordon, R.G., and Cape, C.D., 1981, Cenozoic latitudinal shift of the Hawaiian hotspot and its implications for true polar wander: Earth and Planetary Science Letters, v. 55, p. 37-47.

Gordon, R.G., Cox, A., and Harter, C.E., 1978, Absolute motion of an individual plate estimated from its ridge and trench boundaries: Nature, v. 274, p. 752-755.

Gramlich, J.W., Lewis, V.A., and Naughton, J.J., 1971, Potassium-argon dating of Holocene basalts of the Honolulu Volcanic Series: Geological Society of America Bulletin, v. 82, p. 1399-1404.

Green, A.G., 1975, On the postulated Hawaiian plume with emphasis on the limitations of seismic arrays for detecting deep mantle structure: Journal of Geophysical Research v. 80, p. 4028-4036.

Green, D.H., 1971, Composition of basaltic magmas as indicators of origin: Application to oceanic volcanism: Philosophical Transactions of the Royal Society of London, Series A, v. 268, p. 707-725.

Green, D.H., and Ringwood, A.E., 1967, The genesis of basaltic magmas: Contributions to Mineralogy and Petrology, v. 15, p. 103-190.

Green, W.L., 1887, Vestiges of the molten globe, pt. 2, The Earth's surface features and volcanic phenomena: Honolulu, 337 p.

Greene, H.G., Clague, D.A. and Dalrymple, G.B., 1980, Seismic stratigraphy and vertical tectonics of the Emperor Seamounts, DSDP Leg 55, *in* Jackson, E.D., Koisumi, I., and others, Initial Reports of the Deep Sea Drilling Project, v. 55: Washington, U.S. Government Printing Office, p. 759-788.

Greene, H.G., Dalrymple, G.B., and Clague, D.A., 1978, Evidence for northward movement of the Emperor Seamounts: Geology, v. 6, p. 70-74.

Gromme, S., and Vine, F.J., 1972, Paleomagnetism of Midway Atoll lavas and northward movement of the Pacific plate: Earth and Planetary Science Letters, v. 17, p. 159-168.

Hagn, H., Butt, A., and Malz, H., 1980, Paleocene shallow-water facies at Emperor Seamounts: DSDP Leg 55, Northwest Pacific, *in* Jackson, E.D., Koisumi, I., and others, Initial Reports of the Deep Sea Drilling Project, v. 55: Washington, U. S. Government Printing Office, p. 327-347.

Hamilton, E.I., 1965, Distribution of some trace elements and the isotopic composition of strontium in Hawaiian lavas: Nature, v. 206, no. 4981, p. 251-253.

Hamilton, E.L., 1956, Sunken Islands of the Mid-Pacific Mountains: Geological Society of America Memoir 64, 97 p.

———1957, Marine geology of the southern Hawaiian Ridge: Geological Society of America Bulletin, v. 68, p. 1011-1026.

Handschumacher, D., 1973, Formation of the Emperor Seamount Chain: Nature, v. 244, p. 150-152.

Heckel, P.H., 1974, Carbonate buildups in the geologic record: A review *in* Laporte, L.F., ed., Reefs in time and space: Society of Economic Paleontologists and Mineralogists, Special Publication no. 18, p. 90-154.

Heirtzler, J.R., Dickson, G.O., Herron, E.M., Pitman, W.C., III, and LePichon, X., 1968, Marine magnetic anomalies, geomagnetic reversals, and motions of the ocean floor and continents: Journal of Geophysical Research, v. 73, p. 2119-2136.

Hess, H.H., 1946, Drowned ancient islands of the Pacific basin: American Journal of Science, v. 244, p. 772-791.

Hilde, T.W.C., Isezaki, N. and Wageman, J.M., 1976, Mesozoic seafloor spreading in the North Pacific, *in* Sutton, G.H., Manghmani, M.H., and Moberly, R., American Geophysical Union, Geophysical Monogram, no. 19, p. 205-226.

Hillebrand, W., 1888, Flora of the Hawaiian Islands: London, Williams and Norgate, 673 p.

Hinds, N.E.A., 1931, The relative ages of the Hawaiian landscapes: University of California Publications in the Geological Sciences, v. 20, no. 6, p. 143-260.

Hitchcock, C.H., 1911, Hawaii and Its Volcanoes: Honolulu, The Hawaiian Gazette Co., 314 p.

Horibe, Y., Kim, K. and Craig, H., 1983, Off-ridge submarine hydrothermal vents: Back-arc spreading centers and hotspot seamounts: Eos, Transactions, American Geophysical Union, v. 64, p. 724.

Jackson, E.D., 1968, The character of the lower crust and upper mantle beneath the Hawaiian Islands: Prague, 23rd International Geological Conference, Proceeding 1, p. 135-150.

———1976, Linear volcanic chains on the Pacific plate, *in* Sutton, G.H., Manghnani, M.H., and Moberly, R., eds., The Geophysics of the Pacific Ocean Basin and its Margin: Washington, D.C., American Geophysical Union Monograph 19, p. 319-335.

Jackson, E.D., Koisumi, I., Dalrymple, G.B., Clague, D.A., Kirkpatrick, R.J., and Greene, H.G., 1980, Introduction and summary of results from DSDP Leg 55, the Hawaiian-Emperor Hot-Spot experiment, *in* Jackson, E.D., Koisumi, I., and others, Initial Reports of the Deep Sea Drilling Project, v. 55: Washington, U. S. Government Printing Office, p. 5-31.

Jackson, E.D., and Shaw, H.R., 1975, Stress fields in central portions of the Pacific plate: deliniated in time by linear volcanic chains: Journal of Geophysical Research, v. 80, p. 1861-1874.

Jackson, E.D., Shaw, H.R., and Bargar, K.E., 1975, Calculated geochronology and stress field orientations along the Hawaiian Chain: Earth and Planetary Science Letters, v. 26, p. 145-155.

Jackson, E.D., Silver, E.A., and Dalrymple, G.B., 1972, Hawaiian-Emperor Chain and its relation to Cenozoic circumpacific tectonics: Geological Society of America Bulletin, v. 83, p. 601-618.

Jackson, E.D., and Wright, T.L., 1970, Xenoliths in the Honolulu Volcanic Series, Hawaii: Journal of Petrology, v. 11, p. 405-430.

Jacobs, J.A., 1984, Reversals of the Earth's magnetic field: Bristol, Adam Hilger Ltd., 230 p.

Jaggar, T.A., 1917, Volcanological investigations at Kilauea: American Journal of Science, Series 4, v. 44, p. 161-220.

Jarrard, R.D., and Clague, D.A., 1977, Implications of Pacific Island and seamount ages for the origin of volcanic chains: Reviews of Geophysics and Space Physics, v. 15, p. 57-76.

Jordan, T.H., 1979, Mineralogies, densities, and seismic velocities of garnet

lherzolites and their geophysical applications, *in* Boyd, F.K., and Meyer, H.D.A., eds., The mantle sample: Inclusions in kimberlites and other volcanics: American Geophysical Union, Washington D.C., p. 1-14.

Jurdy, D.M., 1981, True polar wander: Tectonophysics, v. 74, p. 1-16.

———1983, Early Tertiary subduction zones and hot spots: Journal of Geophysical Research, v. 88, p. 6395-6402.

Kanasewich, E.R., Ellis, R.M., Chapman, C.H., and Gutowski, P.R., 1972, Teleseismic array evidence for inhomogeneities in the lower mantle and the origin of the Hawaiian Islands: Nature Physical Science, v. 239, p. 99-100.

———1973, Seismic array evidence of a core boundary source for the Hawaiian linear volcanic chain: Journal of Geophysical Research, v. 78, p. 1361-1371.

Kanasewich, E.R., and Gutowski, P.R., 1975, Detailed seismic analysis of a lateral mantle inhomogeneity: Earth and Planetary Science Letters v. 25, p. 379-384.

Kaneoka, I., Takaoka, N., and Clague, D.A. 1983, Nobel gas systematics for coexisting glass and olivine crystals in basalts and dunite xenoliths from Loihi Seamount: Earth and Planetary Science Letters, v. 66, p. 427-437.

Keil, K., Fodor, R.V., and Bunch T.E., 1972, Contribution to the mineral chemistry of Hawaiian rocks II. Feldspars and interstitial material in rocks from Haleakala and West Maui volcanoes, Maui, Hawaii: Contributions to Mineralogy and Petrology, v. 37, p. 253-276.

Kenneth, J.P. and Srinivasan, 1983, Neogene planktonic foraminifera: Strousber, Penn., Hutchinson Ross Publishing Co., p. 62-66.

Kim, K., and Craig, H., 1983, Methane: A "real-time" tracer for submarine hydrothermal systems: Eos, Transactions, American Geophysical Union, v. 64, p. 724.

Kirkpatrick, R.J., Clague, D.A., and Friesen, W., 1980, Petrology and geochemistry of volcanic rocks, DSDP Leg 55, Emperor Seamount Chain, *in* Jackson, E.D., Koisumi, I., and others, Initial Reports of the Deep Sea Drilling Project, v. 55: Washington, U.S. Government Printing Office, p. 509-557.

Klein, F.W., 1982, Earthquakes at Loihi Submarine volcano and the Hawaiian hot spot: Journal of Geophysical Research, v. 87, p. 7719-7726.

Klein, F.W., and Koyanagi, R.Y. 1979, Seismicity of Kilauea and Loihi Volcanoes, Hawaii: Hawaii Symposium on Intraplate Volcanism and Submarine Volcanism, Abstracts, p. 127.

Kodama, K., Uyeda, S., and Isezaki, N., 1978, Paleomagnetism of Suiko Seamount, Emperor Seamount Chain: Geophysical Research Letters, v. 5, p. 165-168.

Kono, M., 1980, Paleomagnetism of DSDP Leg 55 basalts and implications for the tectonics of the Pacific plate, *in* Jackson, E.D., Koisumi, I., and others, Initial Reports of the Deep Sea Drilling Project, v. 55: Washington, U.S. Government Printing Office, p. 737-758.

Kuno, H., Yamasaki, K., Iida, C., and Nagashima, K., 1957, Differentiation of Hawaiian magmas: Japanese Journal of Geology and Geography, v. 28, p. 179-218.

Kurz, M.D., Jenkins, W.J., Hart, S.R., and Clague, D., 1983, Helium isotopic variations in volcanic rocks from Loihi Seamount and the Island of Hawaii: Earth and Planetary Science Letters, v. 66, p. 388-406.

LaBrecque, J.L., Kent, D.V., and Cande, S.C., 1977, Revised magnetic polarity time scale for Late Cretaceous and Cenozoic time: Geology, v. 5, p. 330-335.

Ladd, H.S., Tracey, J.I., Jr., and Gross, M.G., 1967, Drilling on Midway Atoll, Hawaii: Science, v. 156, p. 1088-1094.

———1970, Deep drilling on Midway Atoll: U.S. Geological Survey Professional Paper 680–A, 22 p.

Lanphere, M.A., 1983, $^{87}Sr/^{86}Sr$ ratios for basalt from Loihi Seamount, Hawaii: Earth and Planetary Science Letters, v. 66, p. 380-387.

Lanphere, M.A., and Dalrymple, G.B., 1980, Age and strontium isotopic composition of the Honolulu Volcanic Series, Oahu, Hawaii: American Journal of Science, v. 280–A (Jackson Volume), p. 736-751.

Lanphere, M.A., Dalrymple, G.B., and Clague, D.A., 1980, Rb-Sr systematics of basalts from the Hawaiian-Emperor volcanic chain, *in* Jackson, E.D., Koisumi, I., and others, Initial Reports of the Deep Sea Drilling Project, v. 55: Washington, U.S. Government Printing Office, p. 695-706.

Lanphere, M.A., and Frey, F.A., in press, Geochemical Evolution of Kohala Volcano, Hawaii: Contributions to Mineralogy and Petrology.

Larson, R.L., Moberly, R., and others, 1975a, Initial Reports of the Deep Sea Drilling Project, v. 32: Washington, U.S. Government Printing Office.

———1975b, Site 311: Hawaiian magnetic lineations: Initial Reports of the Deep Sea Drilling Project, v. 32, Washington, U.S. Government Printing Office, p. 295-309.

Leeman, W.P., Budahn, J.R., Gerlach, D.C., Smith, D.R., and Powell, B.N., 1980, Origin of Hawaiian tholeiites: Trace element constraints: American Journal of Science, v. 280-A, p. 794-819.

Leeman, W.P., Murali, A.V., Ma, M.-S., and Schmitt, R.A., 1977, Mineral constitution of mantle source regions for Hawaiian basalts-rare earth element evidence for mantle heterogeneity, *in* Dick, H.J.B., ed., Magma genesis: Bulletin, Oregon Department of Geology and Mineral Industries, v. 96, p. 169-183.

Lessing, P., and Catanzaro, E.J., 1964, Sr^{87}/Sr^{86} ratios in Hawaiian lavas: Journal of Geophysical Research, v. 69, p. 1599-1601.

Livermore, R. A., Vine, F. J., and Smith, A. G., 1983, Plate motion and the geomagnetic field, I, Quaternary and late Tertiary: Geophysical Journal of the Royal Astronomical Society, v. 73, p. 151-171.

Lowrie, W., and Alvarez, W., 1981, One hundred million years of geomagnetic polarity history: Geology, v. 9, p. 392-397.

Macdonald, G.A., 1949, Hawaiian petrographic province: Geological Society of America Bulletin, v. 60, p. 1541-1596.

———1968, Composition and origin of Hawaiian lavas, *in* Coats, R.E., Hay, R.L., and Anderson, C.A., eds., Studies in volcanology: Geological Society of America Memoir, v. 116, p. 477-522.

———1969, Petrology of the basalt cores from Midway Atoll: U.S. Geological Survey Professional Paper 680–B, p. B1-B10.

Macdonald, G.A., Abbott, A.T., and Cox, D.C., 1983, Volcanoes in the Sea: Honolulu, University of Hawaii Press, 517 p.

Macdonald, G.A., Davis, D.A., and Cox, D.C., 1960, Geology and groundwater resources of the Island of Kauai, Hawaii (geologic map of Kauai enclosed): Hawaii Division of Hydrography, Bulletin 13, 207 p.

Macdonald, G.A., and Katsura, T., 1962, Relationship of petrographic suites in Hawaii: The crust of the Pacific Basin: American Geophysical Union, Geophysical Monograph 6, p. 187-195.

———1964, Chemical composition of Hawaiian lavas: Journal of Petrology, v. 5, p. 82-133.

Malahoff, A., McMurtry, G.M., Wiltshire, J.C., and Yeh, H.-W., 1982, Geology and geochemistry of hydrothermal deposits from active submarine volcano Loihi, Hawaii: Nature, v. 289, p. 234-239.

Martin, W.F., and Pierce, C.H., 1915, Water resources of Hawaii: U. S. Geological Survey Water Supply Paper 318.

Matter, A., and Gardner, J.V., 1975, Carbonate diagenesis at Site 308, Koko Guyot, *in* Larson, R.L., Moberly, R., and others, Initial Reports of the Deep Sea Drilling Project, v. 32: Washington, U. S. Government Printing Office, p. 521-535.

McDougall, I., 1963, Potassium-argon ages from western Oahu, Hawaii: Nature, v. 197, p. 344-345.

———1964, Potassium-argon ages from lavas of the Hawaiian Islands: Geological Society of America Bulletin, v. 75, p. 107-128.

———1969, Potassium-argon ages on lavas of Kohala Volcano, Hawaii: Geological Society of America Bulletin, v. 80, p. 2597-2600.

———1971, Volcanic island chains and sea floor spreading: Nature, v. 231, p. 141-144.

———1979, Age of shield-building volcanism of Kauai and linear migration of volcanism in the Hawaiian Island chain: Earth and Planetary Science Letters, v. 46, p. 31-42.

McDougall, I., and Duncan, R.A., 1980, Linear volcanic chains recording plate motions?: Tectonophysics, v. 63, p. 275-295.

McDougall, I., and Swanson, D.A., 1972, Potassium-argon ages of lavas from the Hawi and Pololu Volcanic Series, Kohala Volcano, Hawaii: Geological Society of America Bulletin, v. 83, p. 3731-3738.

McDougall, I., and Tarling, D.H., 1963, Dating of polarity zones in the Hawaiian Islands: Nature, v. 200, p. 54-56.

McDougall, I., and Ur-Rahman, A., 1972, Age of the Gauss-Matuyama boundary and the Kaena and Mammoth events: Earth and Planetary Science Letters, v. 14, p. 367-380.

McKenzie, J., Bernoulli, D., and Schlanger, S. O., 1980, Shallow-water carbonate sediments from the Emperor Seamounts: Their diagenesis and paleogeographic significance, *in* Jackson, E. D., Koisumi, I., and others, Initial Reports of the Deep Sea Drilling Project, v. 55: Washington, U.S. Government Printing Office, p. 415-455.

McNutt, M.K., 1984, Lithospheric flexure and thermal anomalies: Journal of Geophysical Research, v. 89, p. 11,180-11,194.

Menard, H.W., 1955, Deformation of the northeastern Pacific basin and the west coast of North America: Geological Society of America Bulletin, v. 66, p. 1149-1198.

———1973, Depth anomalies and the bobbing motion of drifting islands: Journal of Geophysical Research, v. 78, p. 5128-5137.

Menard, H.W., Allison, E.C., and Durham, J.W., 1962, A drowned Miocene terrace in the Hawaiian Islands: Science, v. 138, p. 896-897.

Menard, H.W., and Dietz, R.S., 1951, Submarine geology of the Gulf of Alaska: Geological Society of America Bulletin, v. 62, p. 1263-1286.

Minster, J.B., Jordan, T.H., Molnar, P., and Haines, E., 1974, Numerical modelling of instantaneous plate tectonics: Geophysical Journal of the Royal Astronomical Society, v. 36, p. 541-576.

Moore, G.W., 1984, Tertiary dismemberment of western North America: Proceedings of the Third Circum-Pacific Energy and Mineral Resources Conference, p. 607-612.

Moore, J.G., 1970, Relationship between subsidence and volcanic load, Hawaii: Bulletin Volcanologique, v. 34, p. 562-576.

Moore, J.G., Clague, D.A., and Normark, W.R., 1982, Diverse basalt types from Loihi Seamount, Hawaii: Geology, v. 10, p. 88-92.

Moore, J.G., and Fornari, D.J., 1984, Drowned reefs as indicators of the rate of subsidence of the Island of Hawaii: Journal of Geology, v. 92, p. 752-759.

Moore, J.G., Normark, W.R., and Lipman, P.W., 1979, Loihi Seamount—A young submarine Hawaiian volcano: Hawaii Symposium on Intraplate Volcanism and Submarine Volcanism, Abstracts, p. 127.

Morgan, W.J., 1971, Convection plumes in the lower mantle: Nature, v. 230, p. 42-43.

———1972a, Deep mantle convection plumes and plate motions: American Association of Petroleum Geologists Bulletin, v. 56, p. 203-213.

———1972b, Plate motions and deep mantle convection, *in* Shagam, R., and others, eds., Studies in Earth and Space Sciences: Geological Society of America Memoir 132 (Hess Volume), p. 7-22.

———1981, Hotspot tracks and the opening of the Atlantic and Indian Oceans, *in* Emiliani, C., ed., The Sea, v. 7, The Oceanic Lithosphere: New York, John Wiley and Sons, p. 443-487.

Muromtsev, A.M., 1958, The principal hydrologic features of the Pacific Ocean: Leningrad (Gidrometerologicheskoe Isdatel'stov)(from Russian, Jerusalem, 1963, Israel Prog. Sci. Trans.), 417 p.

Nakiboglu, S.M., and Lambeck, K., 1985, Thermal response of a moving lithosphere over a mantle heat source: Journal of Geophysical Research, v. 90, p. 2985-2994.

Naughton, J.J., Macdonald, G.A., and Greenberg, V.A., 1980, Some additional potassium-argon ages of Hawaiian rocks: the Maui volcanic complex of Molokai, Maui, Lanai, and Kahoolawe: Journal of Volcanology and Geothermal Research, v. 7, p. 339-355.

Ness, G., Levi, S., and Couch, R., 1980, Marine magnetic anomaly timescales for the Cenozoic and Late Cretaceous: A precise, critique and synthesis: Reviews of Geophysics and Space Physics, v. 19, p. 753-770.

O'Hara, M.J., 1965, Primary magmas and the origin of basalts: Scottish Journal of Geology, v. 1, p. 19-40.

———1975, Is there an Icelandic mantle plume?: Nature, v. 253, p. 708-710.

Oostdam, B.L., 1965, Age of lava flows on Haleakala, Maui, Hawaii: Geological Society of America Bulletin, v. 76, p. 393-394.

Ozima, M., Kaneoka, I., and Aramaki, S., 1970, K-Ar ages of submarine basalts dredged from seamounts in the western Pacific area and discussion of oceanic crust: Earth and Planetary Science Letters, v. 8, p. 237-249.

Palmer, H.S., 1927, Geology of Kaula, Nihoa, Necker, and Gardner Islands, and French Frigate Shoals: Bernice Pauhi Bishop Museum Bulletin 5 (Tanager Expedition Publication Number 4), 35 p.

———1936, Geology of Lehua and Kaula Islands: Bernice Pauhi Bishop Museum Occasional Papers, v. 12, no. 13, 36 p.

Parsons, B., and Sclater, J.G., 1977, An analysis of the variation of ocean floor bathymetry and heat flow with age: Journal of Geophysical Research v. 82, p. 803-827.

Porter, S.C., Stuvier, M., and Yang, I.C., 1977, Chronology of Hawaiian glaciations: Science, v. 195, p. 61-63.

Powell, J.L., and DeLong, S.E., 1966, Isotopic composition of strontium in volcanic rocks from Oahu: Science, v. 153, no. 3741, p. 1239-1242.

Powers, H.A., 1935, Differentiation of Hawaiian lavas: American Journal of Science 5th Series, v. 30, no. 175, p. 57-71.

———1955, Composition and origin of basaltic magma of the Hawaiian Islands: Geochimica et Cosmochimica Acta, v. 7. p. 77-107.

Powers, S., 1917, Tectonic lines in the Hawaiian Islands: Geological Society of America Bulletin, v. 28, p. 501-514.

———1920, Notes on Hawaiian petrology: American Journal of Science, 4th Series, v. 50, p. 256-280.

Richter, F.M., 1973, Convection and the large-scale circulation of the mantle: Journal of Geophysical Research, v. 78, p. 8735-8745.

Richter, F.M., and Parsons, B., 1975, On the interaction of two scales of convection in the mantle: Journal of Geophysical Research, v. 80, p. 2529-2541.

Rison, W., and Craig, H., 1983, Helium isotopes and mantle volatiles in Loihi Seamount and Hawaiian Island basalts and xenoliths: Earth and Planetary Science Letters, v. 66, p. 407-426.

Roden, M.F., Frey, F.A., and Clague, D.A., 1984, Geochemistry of tholeiitic and alkalic lavas from the Koolau Range, Oahu, Hawaii: Implications for Hawaiian Volcanism: Earth and Planetary Science Letters, v. 69, p. 141-158.

Roedder, E., 1965, Liquid CO_2 inclusions in olivine-bearing nodules and phenocrysts from basalts. American Mineralogist, v. 50, p. 1746-1782.

Rona, P.A., and Richardson, E. S., 1978, Early Cenozoic global plate reorganization: Earth and Planetary Science Letters, v. 40, p. 1-11.

Sager, W.W., 1984, Paleomagnetism of Abbott Seamount and implications for the latitudinal drift of the Hawaiian hot spot: Journal of Geophysical Research, v. 89, p. 6271-6284.

Saito, K., and Ozima, M., 1975, ^{40}Ar-^{39}Ar isochron age of a mugearite dredged from Suiko Seamount in the Emperor Chain: Rock Magnetism and Paleogeophysics, v. 3, p. 81-84.

———1977, ^{40}Ar-^{39}Ar geochronological studies on submarine rocks from the western Pacific area: Earth and Planetary Science Letters, v. 33, p. 353-369.

Savin, S.M., Douglas, R.G., and Stehli, F.G., 1975, Tertiary marine paleotemperatures: Geological Society of America Bulletin, v. 86, p. 1499-1510.

Schilling, J., and Winchester, J.W., 1966, Rare earths in Hawaiian basalts: Science, v. 153, p. 867-869.

Schlanger, S.O., and Konishi, K., 1975, The geographic boundary between the coral-algal and the bryozoan-algal limestone facies: A paleolatitude indicator: IX International Geological Congress of Sedimentology, Nice, Theme 1, Sedimentologic Indicators, p. 187-190.

Schreiber, B.C., 1969, New evidence concerning the age of the Hawaiian Ridge: Geological Society of America Bulletin, v. 80, p. 2601-2604.

Schroeder, W., 1984, The empirical age-depth relation and depth anomalies in the Pacific Ocean basin: Journal of Geophysical Research, v. 89, p. 9873-9883.

Scientific Party DSDP 55, 1978, Drilling confirms hot spot origins: Geotimes, v. 23, no. 2, p. 23-26.

Sen, G., 1983, A petrologic model for the constitution of the upper mantle and crust of the Koolau Shield, Oahu, Hawaii, and Hawaiian magmatism: Earth and Planetary Science Letters, v. 62, p. 215-228.

Sen, G., and Presnall, D.C., 1986, Petrogenesis of dunite xenoliths from Koolau Volcano, Oahu, Hawaii: Implications for Hawaiian Volcanism: Journal of Petrology, v. 27, p. 197-217.

Shaw, H.R., 1973, Mantle convection and volcanic peridocity in the Pacific;

evidence from Hawaii: Geological Society of America Bulletin, v. 84, p. 1505-1526.

Shaw, H.R., and Jackson, E.D., 1973, Linear island chains in the Pacific: Result of thermal plumes or gravitational anchors?: Journal of Geophysical Research, v. 78, p. 8634-8652.

Smoot, N.C., 1982, Guyots of the mid-Emperor Chain mapped with multibeam sonar: Marine Geology, v. 47, p. 153-163.

Solomon, S.C., and Sleep, N.H., 1974, Some simple physical models for absolute plate motions: Journal of Geophysical Research, v. 79, p. 2557-2567.

Staudigel, H., Zindler, A., Hart, S.R., Leslie, T., Chen, C.Y. and Clague, D., 1984, The isotope systematics of a juvenile intraplate volcano: Pb, Nd, and Sr isotope ratios of basalts from Loihi Seamount, Hawaii: Earth and Planetary Science Letters, v. 69, p. 13-29.

Stearns, H.T., 1939, Geologic map and guide of the Island of Oahu, Hawaii (geologic map of Oahu enclosed): Hawaiian Division of Hydrography, Bulletin 2, 75 p.

Stearns, H.T., 1940a, Four-phase volcanism in Hawaii [abs.]: Geological Society of America Bulletin, v. 51, p. 1947-1948.

———1940b, Supplement to the geology and ground-water resources of the Island of Oahu, Hawaii (includes chapters on geophysical investigations by J.H. Swartz, and petrography by G.A. Macdonald): Hawaii Division of Hydrography, Bulletin 5, 164 p.

———1940c, Geology and ground-water resources of the Islands of Lanai and Kahoolawe, Hawaii (includes chapters on geophysical investigations by J.H. Swartz, and petrography by G.A. Macdonald; geologic map of Lanai enclosed): Hawaii Division of Hydrography, Bulletin 6, 177 p.

———1946, Geology of the Hawaiian Islands: Hawaii Division of Hydrography Bulletin 8, 106 p.

———1947, Geology and ground-water resources of the Island of Niihau, Hawaii; also Macdonald, G.A. 1947. Petrography of Niihau (geologic map of Niihau enclosed): Hawaii Division of Hydrography, Bulletin 12, 51 p.

———1966, Geology of the State of Hawaii: Palo Alto, Pacific Books, 266 p.

Stearns, H.T., and Dalrymple, G.B., 1978, The K-Ar age of the Black Point dike on Oahu, Hawaii, and its relation to the Yarmouth Interglaciation: Occasional Papers of the Bernice Pauhi Bishop Museum, v. 24, p.307-313.

Stearns, H.T., and Macdonald, G.A., 1942, Geology and ground-water resources of the Island of Maui, Hawaii (geologic map of Maui enclosed): Hawaii Division of Hydrography, Bulletin 7, 344 p.

———1946, Geology and ground-water resources of the Island of Hawaii (geologic map of Hawaii enclosed): Hawaii Division of Hydrography, Bulletin, 9, 363 p.

———1947, Geology and ground-water resources of the Island of Molokai, Hawaii (geologic map of Molokai enclosed): Hawaii Division of Hydrography, Bulletin 11, 113 p.

Stearns, H.T., and Vaksvik, K.N., 1935, Geology and ground-water resources of the Island of Oahu, Hawaii: Hawaii Division of Hydrography, Bulletin 1, 479 p.

Steiger, R.H., and Jager, E., 1977, Subcommission on geochronology: Convention on the use of decay constants in geo and cosmochronlogy: Earth and Planetary Science Letters, v. 36, p. 359-362.

Stille, P., Unruh, D.M., and Tatsumoto, M., 1983, Pb, Sr, Nd, and Hf isotopic evidence of multiple sources for Oahu, Hawaii basalts: Nature, v. 304, p. 25-29.

Strong, D.F., 1974, Volcanic couples and deep mantle plumes: Nature, v. 247, p. 191-193.

Swanson, D.A., 1972, Magma supply note at Kilauea Volcano, 1952-1971: Science, v. 175, p. 169-170.

Takayama, T., 1980, Calcareous nannofossil biostratigraphy, Leg 55 of the Deep Sea Drilling Project, *in* Jackson, E. D., Koisumi, I., and others, Initial Reports of the Deep Sea Drilling Project, v. 55: Washington, U.S. Government Printing Office, p. 349-364.

Tatsumoto, M., 1966, Isotopic composition of lead in volcanic rocks from Hawaii, Iwo Jima, and Japan: Journal Geophysical Research, v. 71, p. 1721-1733.

———1978, Isotopic composition of lead in oceanic basalt and its implication to mantle evolution: Earth and Planetary Science Letters, v. 38, p. 63-87.

Tayama, R., 1952, On the near-Japan bathymetric chart (introduction to the submarine geography of the northwest Pacific): Hydrographic Magazine, no. 32, p. 160-167 and 201 (in Japanese).

Tilley, C.E., 1950, Some aspects of magmatic evolution: Geological Society of London Quarterly Journal, v. 106, p. 37-61.

Todd, R., and Low, D., 1970, Smaller foraminifera from Midway drill holes: U. S. Geological Survey Professional Paper 680–E, 46 p.

Turcotte, D.L., and Oxburgh, E.R., 1973, Mid-plate tectonics: Nature, v. 244, p. 337-339.

———1976, Stress accumulation in the lithosphere: Tectonophysics, v. 35, p. 183-199.

———1978, Intra-plate volcanism: Philosophical Transactions of the Royal Society of London, Series A, v. 288, p. 561-579.

Turner, D.L., Jarrard, R.D., and Forbes, R.S., 1980, Geochronology and origin of the Pratt-Welker Seamount Chain, Gulf of Alaska: a new pole of rotation for the Pacific Plate: Journal Geophysical Research, v. 85, p. 6547-6556.

Unruh, D.M., Stille, P., and Tatsumoto, M., 1983, Isotopic heterogeneity among Hawaiian-Emperor basalts: Eos, Transactions, American Geophysical Union, v. 64, 347-348.

Vaughan, T.W., and Wells, J.W., 1943, Revision of the suborders, families, and genera of the Scleractinia: Geological Society of America, Special Paper no. 44, 363 p.

Vogt, P.R., 1974, Volcano spacing, fracture, and thickness of the lithosphere: Earth and Planetary Science Letters, v. 21, p. 235-252.

Vogt, P. R., and Avery, O. E., 1974, Detailed magnetic surveys in the northeast Atlantic and Labrador Sea: Journal of Geophysical Research, v. 79, p. 363-389.

Walcott, R.I., 1970, Flexure of the lithosphere at Hawaii: Tectonophysics, v. 9, p. 435-446.

———1976, Lithospheric flexure, analysis of gravity anomalies, and the propagation of seamount chains, *in* Sutton, G.H., Manghnani, M.H., and Moberly, R., The Geophysics of the Pacific Ocean Basin and its margin: American Geophysical Union Monograph 19, p. 431-438.

Washington, H.S., 1923a, Petrology of the Hawaiian Islands; I. Kohala and Mauna Kea, Hawaii: American Journal of Science, Series 5, v. 5, p. 465-502.

———1923b, Petrology of the Hawaiian Islands; II Hualalai and Mauna Loa: American Journal of Science, Series 5, v. 6, p. 100-126.

———1923c, Petrology of the Hawaiian Islands; III, Kilauea and general petrology of Hawaii: American Journal of Science, Series 5, v. 6, p. 338-367.

Washington, H.S., and Keyes, M.G., 1926, Petrology of the Hawaiian Islands: V. The Leeward Islands: American Journal of Science, Series 5, v. 12, p. 336-352.

———1928, Petrology of the Hawaiian Islands: VI Maui: American Journal of Science, Series 5, v. 15, p. 199-220.

Watts, A.B., 1978, An analysis of isostacy in the world's oceans 1. Hawaiian-Emperor Seamount Chain: Journal of Geophysical Research, v. 83, p. 5989-6004.

Wentworth, C.K., 1925, The geology of Lanai: Bernice Pauhi Bishop Museum, Bulletin 24, 72 pp.

———1927, Estimates of marine and fluvial erosion in Hawaii: Journal of Geology v. 35, p. 117-133.

West, H.B., and Garcia, M.O., 1982, Composition and evolution of the alkalic cap stage lavas from Mauna Kea Volcano, Hawaii: Eos, Transactions, American Geophysical Union, v. 63, p. 1138.

White, R.W., 1966, Ultramafic inclusions in basaltic rocks from Hawaii: Mineralogie und Petrographie Mitt., v. 12, p. 245-314.

White, W.M., and Hofmann, A.W., 1982, Sr and Nd isotope geochemistry of oceanic basalts and mantle evolution: Nature, v. 296, p. 821-825.

Wilkes, C., 1845, Narrative of the United States Exploring Expedition, 1838-1842, *4*: Philadelphia, 539 p.

Wilson, J.T., 1962, Cabot Fault, an Appalachian equivalent of the San Andreas and Great Glen faults and some implications for continental displacement: Nature v. 195, p. 135-138.

———1963a, A possible origin of the Hawaiian Islands: Canadian Journal of Physics, v. 41, p. 863-870.

———1963b, Continental drift: Scientific American, v. 208, no. 4, p. 86-100.

———1963c, Evidence from islands on the spreading of ocean floors: Nature, v.

197, p. 536-538.
———1963d, Hypothesis of Earth's behavior: Nature, v. 198, p. 925-929.
———1973, Mantle plumes and plate motions: Tectonophysics, v. 19. p. 149-164.
Wise, W.S., 1982, A volume-time framework for the evolution of Mauna Kea Volcano, Hawaii: Eos, Transactions, American Geophysical Union, v. 63, p. 1137.
Worsley, J.R., 1973, Calcareous nannofossils: Leg 19 of the Deep Sea Drilling Project, *in* Creager, J.S., Scholl, D.W., and others, Initial Reports of the Deep Sea Drilling Project, v. 19: Washington, U.S. Government Printing Office, p. 741-750.
Wright, C., 1975, Comments on 'Seismic array evidence of a core boundary source for the Hawaiian linear volcanic chain' by E.R. Kanasewich and others: Journal of Geophysical Research v. 80, p. 1915-1919.
Wright, T.L., 1971, Chemistry of Kilauea and Mauna Loa lava in space and time: U.S. Geological Survey Professional Paper 735, 40 p.
———1973, Magma mixing as illustrated by the 1959 eruption, Kilauea Volcano, Hawaii: Geological Society of America Bulletin, v. 84, p. 849-858.
———1984, Origin of Hawaiian tholeiite: A metasomatic model: Journal of Geophysical Research, v. 89, p. 3233-3252.
Wright, T.L., and Clague, D.A., in press, Petrology of Hawaiian lava: Geologic Society of America, Decade of North American Geology, the Eastern Pacific Region.
Wright, T.L., and Fiske, R.S., 1971, Origin of the differentiated and hybrid lavas of Kilauea Volcano, Hawaii: Journal of Petrology, v. 12, p. 1-65.
Wright, T.L., Shaw, H.R., Tilling, R.I., and Fiske, R.S., 1979, Origin of Hawaiian tholeiitic basalt: a quantitative model: Hawaii Symposium on Intraplate Volcanism and Submarine Volcanism, Abstracts, p. 104.
York, D., 1969, Least squares fitting of a straight line with correlated errors: Earth and Planetrary Science Letters, v. 5, p. 320-324.

APPENDIX 1.1

NOTES ON THE GEOLOGY AND GEOCHRONOLOGY OF INDIVIDUAL VOLCANOES IN THE HAWAIIAN-EMPEROR CHAIN

Following are brief descriptions and comments on the geology and geochronology of all volcanoes in the Hawaiian-Emperor Chain that have been mapped or sampled. References to sources of data are included in the reference list of the main text of the paper. The radiometric ages are conventional K-Ar age determinations unless otherwise indicated; errors are the estimated standard deviations of precision. Volcanoes are discussed from southeast to northwest, that is, from youngest to oldest, using the numbering system (in parentheses) of Bargar and Jackson (1974). Stratigraphic nomenclature used here is from Langenheim and Clague (chapter 1, part II).

Loihi Seamount (no number).—Loihi Seamount is inferred to be the youngest Hawaiian volcano on the basis of its location and seismic activity, the presence of fresh glassy pillow lava, and the occurrence of hydrothermal discharge into the water column. Loihi is located on the southeast flank of Kilauea on the Island of Hawaii and is 30 km offshore and 60 km south-southeast from the summit of Mauna Loa. The seamount rises to 950 m below sea level and has a distinct north-south orientation, delineating two rift zones that extend from the roughly 2.8-km by 3.7-km summit caldera (Malahoff and others, 1982). The volcano is active seismically; persistent swarms of shallow earthquakes that are probably caused by volcanic intrusion or submarine eruptions (Klein, 1982) occur periodically near the summit (Klein and Koyanagi, 1979). Moore and others (1982) describe fresh glassy pillow lava recovered from Loihi Seamount that includes basanite, alkalic basalt, basalt transitional between alkalic and tholeiitic basalt, and tholeiitic basalt. They also demonstrated that the alkalic lava is generally older than the tholeiitic lava and suggested that Loihi Seamount, and presumably all Hawaiian volcanoes, have a stage of alkalic volcanism before the tholeiitic shield stage that is characterized by infrequent, small-volume eruptions of alkalic lava. Further evidence that Loihi Seamount is an active volcano is provided by the discovery of a plume of hydrothermal methane and helium in the water column above Loihi (Horibe and others, 1983; Kim and Craig, 1983) and the presence of water-temperature anomalies recorded by the ANGUS camera sled (Malahoff and others, 1982).

Kilauea Volcano (1).—The lava of Kilauea, currently active and historically the most active volcano in Hawaii, can be divided into the older Hilina Basalt and the younger Puna Basalt, which are separated by the Pahala Ash. The exposed lava consists of tholeiitic basalt and picritic tholeiitic basalt that issued from the 3-km by 5-km summit caldera and the two rift zones. The rift zones extend to the east and the southwest, with the east rift zone extending nearly 50 km from the summit caldera to Cape Kumikahi at the northeast corner of the island and for at least an additional 90 km beneath the sea.

Mauna Loa Volcano (2).—The lava of Mauna Loa is divided into the Ninole Basalt (oldest), the Kahuku Basalt, and the Kau Basalt (youngest). The Kahuku and Kau are separated by the Pahala Ash and are thought to be coeval with the Hilina Basalt and Puna Basalt, respectively, of Kilauea. The exposed lava is all tholeiitic basalt and picritic tholeiitic basalt that issued from the 2.5-km by 4-km summit caldera, named Mokuaweoweo, and two rift zones. The rift zones extend southwest and east-northeast. The southeastern and the southwestern slopes of Mauna Loa are steepened by downfaulting along the Kaoiki and Kealakakua fault systems. Mauna Loa last erupted in 1984. Possible remnants of two earlier shield volcanoes are exposed in the Ninole Hills (Ninole Basalt) and in the vicinity of Kulani. Neither of these earlier shield volcanoes is well delineated and both may be merely deeper parts of the Mauna Loa shield uplifted along normal faults in a manner analogous to that in the Hilina fault system near Puu Kapukapu. With the exception of numerous ^{14}C ages, the sole published age data for Mauna Loa were obtained by Evernden and others (1964) on two samples from the Ninole Basalt. One sample contained negligible radiogenic ^{40}Ar. The other sample had a radiogenic ^{40}Ar content of 2.5 percent and a calculated age of 0.54 Ma. No uncertainty was given for the age, but from the quality of the data we estimate a standard deviation of approximately 0.4 m.y. It seems unlikely that the Ninole Basalt is more than a few hundred thousand years old.

Mauna Kea Volcano (3).—Mauna Kea Volcano last erupted some 3,600 years ago (Porter and others, 1977). The volcano has a well exposed section of shield lava capped by postshield alkalic lava. The rocks are divided into the older Hamakua Volcanics and the younger Laupahoehoe Volcanics. The Hamakua Volcanics consists of shield-stage tholeiitic basalt, olivine tholeiitic basalt, and picritic tholeiitic basalt, and overlying postshield-stage alkalic basalt, ankaramite, and hawaiite. There is no clear boundary between the shield and postshield lavas; tholeiitic and alkalic lavas are intercalated near the boundary (Frey and others, 1984). Most of the surface of Mauna Kea is blanketed by the younger Laupahoehoe Volcanics which is mostly hawaiite, with much less ankaramite and alkalic basalt (West and Garcia, 1982). The Hamakua Volcanics is exposed only in deep erosional canyons.

The rift zones of Mauna Kea are not well defined, but cinder cones are roughly aligned in westerly and southerly directions from the summit. A nearly buried east rift zone is still clearly delineated by a submarine ridge extending nearly 40 km to sea. It is uncertain if a summit caldera existed, but the crude arcuate alignment of some cinder cones, coupled with a large gravity high just south of the summit, indicate that a former caldera may be buried beneath the Laupahoehoe Volcanics.

Porter and others (1977) obtained K-Ar ages on three samples from the Hamakua Volcanics. The two younger flows gave ages of 0.27 ± 0.04 Ma, whereas the older flow gave an age of 0.375 ± 0.050 Ma. K-Ar and ^{14}C ages for flows from the Laupahoehoe Volcanics range from about 0.19 Ma to 4.5 ka. Funkhouser and others (1968) reported a K-Ar age of 0.6 ± 0.3 Ma for a single sample of hawaiite from the Laupahoehoe Volcanics.

Hualalai Volcano (4).—Hualalai Volcano was last active in 1800-01 when two major and several smaller flows issued from a series of vents on the northwest rift zone. With the exception of a large trachyte cone and flow at Puu Waawaa (Waawaa Trachyte Member), the entire subaerial surface of the volcano consists of alkalic basalt flows of the alkalic postshield stage. All subaerial rocks of Hualalai are called the Hualalai Volcanics. A detailed study of the volcano (Moore and others, chapter 20) shows that nearly all the lava is alkalic basalt, with only a few flows that are

gradational to hawaiite. Some ^{14}C ages of charcoal from beneath many of these flows demonstrate the youth of the alkalic basalt surface. The structure of the volcano is poorly known, although the northwest and south rift zones are well defined. It is unknown if a summit caldera existed in the past. Recent studies on the submarine northwest rift zone recovered tholeiitic basalt and picritic tholeiitic basalt (Clague, 1982), indicating that Hualalai, like all other Hawaiian volcanoes, had a tholeiitic shield stage. The submarine portion of the rift is overlain by terrace deposits that are inferred to be as old as 120 ka (Moore and Fornari, 1984), which indicates that the tholeiitic shield stage had ended by this time.

Funkhouser and others (1968) reported an age of 0.4 ± 0.3 Ma for the Waawaa Trachyte Member of the Hualalai Volcanics; recent K-Ar results indicate the trachyte is about 105 ka (G.B. Dalrymple, unpub. data, 1985).

Kohala Volcano (5).—Kohala Volcano is composed of the older Pololu Basalt and the younger Hawi Volcanics. The Pololu Basalt is a succession of thin flows of tholeiitic basalt, olivine tholeiitic basalt, and picritic tholeiitic basalt except near the top of the section, where alkalic basalt occurs. Most of the Pololu Basalt represents the shield stage, whereas the uppermost, alkalic part represents the alkalic postshield stage. The younger Hawi Volcanics formed during the alkalic postshield stage and is separated from the Pololu Basalt by an erosional unconformity. Most of the Hawi lava is mugearite, but benmoreite and hawaiite are also present. Cinder cones of the Hawi Volcanics align along two rift zones trending northwest and southeast. Arcuate faults near the summit indicate that a caldera probably formed during eruption of Pololu lava, but Hawi lava has entirely buried it. A gravity high located southeast of the summit may correspond to the approximate location of this inferred caldera. Hawi lava is absent from an 11-km section on the northwest side of the volcano. Flows are deflected from this zone by a series of fault scarps in the summit region that bounds a northwest-trending graben 10 km long and 2–5 km wide. Lava erupted inside the graben, filled it, flowed to the northwest and southeast ends, and overflowed most of the southwest rim. Feigenson and others (1983) made a detailed petrologic study of stratigraphically controlled lava samples from the Pololu Volcanics, and Lanphere and Frey (1985) made a similar study of samples from the Pololu Basalt and Hawi Volcanics.

Evernden and others (1964) obtained an age of 0.43 Ma for one sample of tholeiitic basalt from the Pololu Basalt. Dalrymple (1971) obtained scattered age results that averaged 0.7 ± 0.15 Ma on five samples from the Pololu Basalt. The best data for lava of the Pololu is from McDougall and Swanson (1972), who dated nine flows ranging in age from 0.459 ± 0.028 to 0.304 ± 0.091 Ma. The average of the three oldest flows is 0.43 ± 0.02 Ma. Ages on 12 samples from the Hawi Volcanics (McDougall, 1969; McDougall and Swanson, 1972) range from 0.261 ± 0.005 to 0.061 ± 0.001 Ma.

East Maui Volcano (6).—East Maui Volcano is the youngest volcano in the Hawaiian Islands having rejuvenated-stage volcanics. The volcano was last active in about 1790 (Oostdam, 1965). The oldest unit is the Honomanu Basalt, a series of tholeiitic basalt, olivine tholeiitic basalt, and picritic tholeiitic basalt flows that represents the shield stage. Above sea level these flows are nearly completely buried by those of the overlying Kula Volcanics and Hana Volcanics. The Kula Volcanics is composed predominantly of hawaiite with some ankaramite and alkalic basalt and represents the alkalic postshield stage. There is little evidence of extensive erosion between the shield and postshield lavas. The Hana Volcanics is composed mostly of the same rock types as the Kula Volcanics, but it erupted after an erosional period; it represents an alkalic rejuvenated stage of volcanism. Three rift zones are delineated by the location of vents for the Kula and Hana Volcanics. The east and southwest rifts are characterized by vents of both these units, whereas the north rift has only Kula Volcanics vents. The Hana Volcanics is unique among Hawaiian rejuvenated stage volcanic rocks in that its vents are aligned along the preexisting rift zones, the duration of the erosional period is rather short (<0.4 m.y.), and ankaramite and hawaiite are present. Chen and Frey (1983, 1985) present a detailed geochemical study of lava from all three eruptive stages.

Naughton and others (1980) reported ages for 7 samples of the Honomanu Basalt from three localities. The individual sample ages range from 0.54 to 0.91 Ma. Probably the best age for the Honomanu Basalt is the mean of 0.75 ± 0.04 Ma of the four measurements on samples from the so-called crater of Haleakala. McDougall (1964) dated two samples of the Kula Volcanics at 0.46 and 0.86 Ma, whereas the mean of four samples from the Kula Volcanics dated by Naughton and others (1980) is 0.41 ± 0.09 Ma. No ages have been determined for the Hana Volcanics.

Kahoolawe (7).—The volcanic rocks of Kahoolawe have not been subdivided. The only formation, the Kanapou Volcanics, includes tholeiitic basalt and olivine tholeiitic basalt of the shield stage, tholeiitic and alkalic basalt of the caldera-filling phase, and alkalic basalt and hawaiite of the alkalic postshield stage. Five vents along the seacliff in Kanapou Bay erupted alkalic basalt following an extended period of volcanic quiescence; these vents presumably represent an alkalic rejuvenated stage. The volcano was built by eruptions along a prominent west-southwest rift zone and two less pronounced rifts trending east and north. Most of the vents have been removed by erosion, but remnants of about six vents remain. The caldera of 5 km diameter lies at the eastern end of the island and has been breached by the sea.

Naughton and others (1980) dated two samples collected by H.S. Palmer in 1925 from the upper (alkalic) part of the Kanapou Volcanics. The mean of the two measurements is 1.03 ± 0.18 Ma.

West Maui Volcano (8).—The volcanic rocks of West Maui are divided into the Wailuku Basalt, Honolua Volcanics, and Lahaina Volcanics. The Wailuku Basalt consists of tholeiitic basalt, olivine tholeiitic basalt, and picritic tholeiitic basalt of the shield stage and of alkalic basalt of a caldera-filling phase. The Honolua Volcanics, which represents an alkalic postshield stage, consists of a thin discontinuous cap of mugearite with some trachyte and hawaiite. The Lahaina Volcanics followed a long period of erosion and consists of the cones and flows of four small eruptions of basanite and olivine-rich basanite. The Lahaina Volcanics represents the alkalic rejuvenated stage. The volcano has ill-defined rift zones delineated by dike swarms trending northeast and south and by vents of the Honolua Volcanics trending north and south from the small central caldera. The caldera-filling lava is severely altered by late gases; erosion has preferentially removed these altered rocks in Iao Valley.

McDougall (1964) dated three samples of the Wailuku Basalt, and the ages all fall within the narrow range of 1.30–1.33 Ma with a mean of 1.32 ± 0.04 Ma. Naughton and others (1980) obtained ages of 1.58 and 1.97 Ma on two samples from the Wailuku, but the precision of the measurements is poor. The samples dated by Naughton and his colleagues may be from an older part of the shield than those dated by McDougall (Naughton and others, 1980). McDougall's results for four samples of the Honolua Volcanics range only from 1.18 to 1.20 Ma, whereas Naughton and others (1980) measured an age of 1.50 ± 0.13 Ma for a single sample of the Honolua Volcanics. Naughton and others (1980) dated one sample from the Lahaina Volcanics at 1.30 ± 0.10 Ma, an age which appears to be too old on stratigraphic grounds.

Lanai (9).—Only tholeiitic lava was erupted during the shield stage and caldera-collapse phase of Lanai Volcano; no later alkalic lava is known. The Lanai Basalt consists of tholeiitic basalt, olivine tholeiitic basalt, and picritic tholeiitic basalt that erupted from the northwest, southwest, and southeast rift zones and from the summit caldera underlying the present-day Palawai Basin. An extensive dike swarm marking the southwest rift crops out along the Kaholo Pali. Most of the dikes are nearly vertical and are about 30 cm thick.

Bonhommet and others (1977) measured ages for six samples of the Lanai Basalt that were collected on the southern part of the Lanai shield. The data fit a K-Ar isochron indicating an age for the Lanai Basalt of 1.28 ± 0.04 Ma. Naughton and others (1980) obtained ages of 0.71 ± 1.27 to 0.86 ± 0.55 Ma for three samples from the northeastern part of the island. They speculate that the northeastern part of the shield may be somewhat younger than the southern part, but the mean of their three ages (0.81 ± 0.66 Ma) is not significantly different from the more precise isochron age of Bonhommet and others (1977) at the 95-percent level of confidence.

East Molokai Volcano (10).—The lava of East Molokai is subdivided informally into an upper and a lower member of the East Molokai Volcanics. The lower member consists of tholeiitic basalt, olivine tholeiitic basalt, and picritic tholeiitic basalt characteristic of the shield stage, but alkalic basalt of the postshield stage occurs in the upper part of the lower member. Beeson (1976) and Clague and Beeson (1980) have shown that tholeiitic and alkalic basalt are intercalated in the upper part of the lower unit. The upper member consists predominantly of mugearite,

with smaller amounts of hawaiite and trachyte and represents the alkalic postshield stage. Following an extended erosional period, during which the 1,200-m cliffs on the north side of the island formed, alkalic basalt and basanite of the rejuvenated stage Kalaupapa Volcanics erupted to form the Kalaupapa Peninsula and Mokuhooniki Island, a tuff cone located offshore of the east end of the island. East Molokai Volcano was built by eruptions along eastward- and west-northwestward-extending rift zones and from a summit caldera about 2.5 km by 7 km in size. The caldera-filling lava flows are similar to those of the lower member except that they are horizontal, more massive, and more extensively altered.

McDougall (1964) dated two samples from the lower member of the East Molokai Volcanics. Both ages agree at 1.52 Ma. Naughton and others (1980) obtained an age of 1.76 ± 0.07 Ma based on several analyses of a single sample. McDougall also dated three samples of the upper member and obtained ages of 1.35 to 1.49 Ma. A basalt sample from the Kalaupapa Peninsula was dated at 1.24 ± 0.16 Ma by Naughton and others (1980), but this appears to be too old in view of the younger ages (0.35 ± 0.03 to 0.57 ± 0.02) obtained for three samples of the Kalaupapa Volcanics by Clague and others (1982).

West Molokai Volcano (11).—The volcanic rocks of West Molokai belong to the West Molokai Volcanics. Most of the exposed lava is tholeiitic basalt of the shield stage. This lava erupted from an east-northeast rift zone that crosses the summit area. A less pronounced rift trends toward the northwest. There is no evidence of a summit caldera. Alkalic lava of the postshield stage, predominately hawaiite with subordinate alkalic basalt, erupted from a series of cinder and spatter cones located mainly on the northwest rift zone. No rejuvenated-stage lava is known. A shoal area extends beneath the sea to the west-southwest nearly 65 km and includes Penguin Bank. This bank probably represents a separate volcanic center, but it has not been studied and little is known of its history.

McDougall (1964) dated one sample from the summit of the West Molokai shield at 1.89 Ma. From the sample locality, we conclude that it is from the tholeiitic shield (lower part of West Molokai Volcanics). Naughton and others (1980) dated six samples of the lower part of the West Molokai Volcanics from three localities. The three localities gave mean ages of 1.84 ± 0.07, 1.90 ± 0.06, and 1.52 ± 0.06 Ma.

Koolau Volcano (12).—Koolau Volcano on Oahu is composed of tholeiitic basalt, olivine tholeiitic basalt, and rather rare picritic tholeiitic basalt that erupted from a long rift system oriented northwest-southeast. These shield-building flows make up the Koolau Basalt. Lava that ponded in the 16-km by 13-km caldera is also tholeiitic and is called the Kailua Member of Koolau Basalt. The rift zones are identified by an extensive dike complex consisting of hundreds of nearly vertical dikes that average 60–90 cm thick. A few of the youngest flows of the Koolau Basalt appear to be transitional between tholeiitic and alkalic basalt. The rejuvenated-stage Honolulu Volcanics erupted from about 36 groups of vents following a long period of volcanic quiescence and erosion. The lava is strongly alkalic and ranges in composition from alkalic basalt, basanite, and nephelinite, to melilitite. The vents from which these rocks erupted show no relationship to the preexisting rift zones or caldera-bounding faults. Many of the vents formed by violent hydromagmatic eruptions that formed tuff cones commonly containing accidental blocks of Koolau Basalt and coral limestone. Clague and Frey (1982) presented a detailed trace-element geochemical study of the lava and summarized the geology of the Honolulu Volcanics.

K-Ar ages have been reported for a large number of samples from the Koolau Basalt by McDougall (1964), Funkhouser and others (1968), McDougall and Ur-Rahman (1972), and Doell and Dalrymple (1973), who also summarized and evaluated the ages. The best ages for the Koolau Basalt range from 1.8 to 2.7 Ma. Ages for lava of the rejuvenated-stage Honolulu Volcanics range from about 0.03 to 0.9 Ma (Funkhouser and others, 1968; Gramlich and others, 1971; Stearns and Dalrymple, 1978; Lanphere and Dalrymple, 1980).

Waianae Volcano (13).—Waianae Volcano is divided into the older Waianae Volcanics and the younger Kolekole Volcanics. The Waianae Volcanics is subdivided into the Lualualei, Kamaileunu, and Palehua Members. The Lualualei Member consists of tholeiitic basalt, olivine tholeiitic basalt, and picritic tholeiitic basalt of the shield stage. The Kamaileunu Member consists of rocks that accumulated inside the 14-km-wide caldera and is also composed mostly of tholeiitic lava, although alkalic rocks are present near the top. The Kamaileunu Member also includes the only occurrence of icelandite and rhyodacite (Mauna Kuwale-Rhyodacite Flow) in the Hawaiian Islands. The Palehua Member consists mainly of hawaiite with rather rare alkalic basalt flows; it represents the alkalic postshield stage. The Kolekole Volcanics represents the group of young cones near the southwest end of the island and a single flow of alkalic lava erupted in Kolekole Pass. The tholeiitic shield lava erupted from three rift zones trending northwest, south-southeast, and northeast. There is no unconformity between tholeiitic and alkalic lava within the caldera; the boundary is transitional and may be similar to the one on East Molokai. K-Ar ages have been determined for a large number of samples from the Waianae Volcanics by McDougall (1964), Funkhouser and others (1968), McDougall and Ur-Rahman (1972), and Doell and Dalrymple (1973), who also summarized and evaluated all of the data. Ages from the Lualualei and Kamaileunu Members range from about 3.0 to 3.9 Ma. Ages from the Palehua Member range from about 2.5 to 3.2 Ma.

Kauai (14).—The Island of Kauai consists of a single large shield volcano with a summit caldera 16–19 km across. The Waimea Canyon Basalt has been divided into four members, but all consist of tholeiitic basalt, olivine tholeiitic basalt, and abundant picritic tholeiitic basalt. The Napali Member represents the shield stage, whereas the Olokele and Makaweli Members represent the caldera-filling phase, having filled the summit caldera and a 6-km-wide graben on the south flank, respectively. Two other calderas formed on the flanks of the Kauai shield volcano: the Lihue depression, 11–16 km across, was apparently not filled by tholeiitic lava; the Haupu caldera, roughly 3 km across was filled with thick ponded flows called the Haupu Member of the Waimea Canyon Basalt. These are the only flank calderas known in the Hawaiian Islands. Near the top of the Olokele and Makaweli Members, a single flow of hawaiite rests on a soil 30–60 cm thick. This single flow apparently represents the alkalic postshield stage on Kauai. Unlike most Hawaiian volcanoes, Kauai has no well-defined rift zones; dikes radiate from the summit caldera in all directions, although they are more concentrated in the northeast and west-southwest directions.

Following a long period of volcanic quiescence and deep erosion, the alkalic rejuvenated stage Koloa Volcanics erupted from at least 40 vents concentrated on the south and east flanks of the shield. The lava ranges from alkalic basalt, basanite, and nephelinite, to melilitite. The abundant vents located along the southeast coast erupted almost entirely alkalic basalt.

McDougall (1964) reported ages for three samples from the Napali Member ranging from 3.63 to 5.77 Ma. Evernden and others (1964) obtained an age of 3.43 Ma for a single sample from the Napali. In a more recent study, McDougall (1979) reported K-Ar ages ranging from 3.81 ± 0.06 to 5.14 ± 0.20 Ma for 16 samples of the Napali collected from three localities. He concluded that some of the variation was probably due to differential Ar loss, that the Napali Member was erupted between about 5.1 and 4.3 Ma, and that the Napali lava in Waipio Valley was erupted over a short time interval at about 5.1 ± 0.2 Ma.

Ages of 4 samples from the Makaweli Member range from 3.60 to 4.15 Ma (McDougall, 1964). Only three samples from the Koloa Volcanics (rejuvenated stage) have been dated; two samples have ages of 0.62 and 1.21 Ma (Evernden and others, 1964) and another an age of 1.46 Ma (McDougall, 1964).

Niihau (15).—The Island of Niihau consists of a deeply eroded shield volcano mantled by lava of the alkalic rejuvenated stage on the north, west, and south sides. The Paniau Basalt consists of tholeiitic basalt and olivine tholeiitic basalt of the shield stage and the remnants of a single alkalic postshield stage vent at Kaeo. Several dikes exposed near the eastern coastline are also of alkalic basalt and presumably fed vents that have been completely removed by erosion. A magnificent dike swarm is exposed in the eastern seacliff (Dalrymple and others, 1973, fig. 5); these dikes trend southwest and represent a rift zone. The summit of the volcano was northeast of the present-day island, and the eastern side of the volcano has been removed by erosion or downfaulting. The period of volcanic quiescence and marine erosion that removed the eastern side of the shield was followed by eruption of the alkalic rejuvenated-stage lava of the Kiekie Basalt, which is entirely alkalic basalt. Lehua Island off the north shore is a breached tuff cone of the Kiekie Basalt.

Ages for Niihau have not been published, but data for 11 tholeiitic flows and dikes of the Paniau Basalt fit a K-Ar isochron with an age of 4.89 ± 0.11 Ma (G.B. Dalrymple, unpub. data, 1983).

Kaula Island (15A).—Kaula Island is a small tuff cone on a large submarine edifice. The edifice almost surely represents a separate shield volcano related to the Hawaiian Islands, but it has not been sampled. The tuff cone is probably a vent of the alkalic rejuvenated stage. Garcia, Frey and Grooms (in press) described accidental blocks of tholeiitic basalt, basanite, phonolite, and ultramafic xenoliths that occur in the tuff.

Garcia, Grooms, and Naughton (in press) obtained K-Ar ages for two phonolite blocks and a basanite from the tuff; they determined ages of 4.00 ± 0.09 and 4.22 ± 0.25 Ma for phonolite samples, 3.98 ± 0.70 Ma for a biotite separated from the phonolite, and 1.8 ± 0.2 Ma for the basanite.

On the basis of the composition and age of the phonolite, we propose that the phonolite is from the alkalic postshield stage, the basanite blocks are from rejuvenated-stage flows underlying the tuff cone (Garcia, Frey, and Grooms, in press), and tholeiitic basalt represents the shield stage.

Nihoa Island (17).—Nihoa Island is a remnant of a large tholeiitic shield with flows dipping 5°–10° to the southwest. All the flows exposed on Nihoa are of tholeiitic basalt, and they range from aphyric to porphyritic in texture (Dalrymple and others, 1974).

Funkhouser and others (1968) obtained an age of 7.5 ± 0.4 Ma for a single sample from Nihoa Island. Dalrymple and others (1974) reported a best weighted mean age of 7.2 ± 0.3 Ma for six samples of tholeiitic basalt from the island.

Unnamed Seamount (19).—A single sample dredged by the Hawaii Institute of Geophysics from this seamount has been analyzed (Garcia, Frey, and Naughton, in press). The samples in dredge 9-11 are moderately altered picritic tholeiitic to transitional basalt with about 30 percent olivine phenocrysts. These probably erupted during the late shield stage or the caldera-filling phase. The seamount is undated.

Unnamed Seamount (20).—On the second leg of the Hawaii Institute of Geophysics cruise 72-07-02, dredge 51 recovered tholeiitic basalt with 20 percent phenocrysts of augite, plagioclase, and olivine, and aphyric alkalic lava of basanite composition (Clague, 1974a; Garcia, Frey, and Naughton, in press). These rocks probably erupted during the shield and the alkalic rejuvenated stages, respectively. Garcia, Frey, and Naughton (in press) obtained a weighted mean age of 9.6 ± 0.8 Ma for four analyses of two of the dredged alkalic basalt samples.

Unnamed Seamount (21).—On the second leg of the Hawaii Institute of Geophysics cruise 72-07-02, dredge 49 recovered tholeiitic to transitional basalt containing 20 percent phenocrysts of olivine and augite (Clague, 1974a). This lava probably erupted during the shield stage. The volcano is undated.

Necker Island (23).—Samples have been collected from Necker Island (Dalrymple and others, 1974), and others have been dredged from the submarine flanks of the volcano during Hawaii Institute of Geophysics cruises 72-07-02 (second leg, dredge 48) and KK84-08-06-01 (Clague, 1974a; Campbell and others, 1984). The subaerial samples are mostly picritic tholeiitic basalt collected from flows dipping 5°–10° to the north-northwest. Palmer (1927) described two dikes that are alkalic lava. One is highly altered, but on the basis of chemical analysis appears to be a nephelinite; the other is described as a hawaiite. These two dikes probably fed vents during the alkalic rejuvenated stage and alkalic postshield stage, respectively. The single lava sample dredged in 1972 is a rhyolite porphyry (Clague and Dalrymple, 1975). This rock type is unknown from elsewhere in the Hawaiian-Emperor Chain, and we suspect that it is either an ice-rafted erratic or a piece of ship's ballast. The 1984 dredges have not yet been analyzed but contain calcareous sediment, volcaniclastic breccia, basalt, and hyaloclastite.

Funkhouser and others (1968) reported an age of 11.3 ± 0.6 Ma for a single sample of subaerial basalt. Dalrymple and others (1974) dated two samples of tholeiitic basalt from the island; they gave a mean age of 10.3 ± 0.4 Ma. The rhyolite porphyry has a Cretaceous age (Clague and Dalrymple, 1975).

La Perouse Pinnacle (French Frigates Shoal) (26).—La Perouse Pinnacle and an even smaller adjacent rock are the only subaerial exposures of volcanic rock within French Frigates Shoal, a coral atoll consisting of 15 or 16 small sand islets. La Perouse Pinnacle is a stack of lava flows that dip 1°–2° to the northwest. The subaerial flows are picritic tholeiitic basalt (Dalrymple and others, 1974) that probably erupted during the shield stage. Four dated samples have a mean age of 12.0 ± 0.4 Ma.

Brooks Bank (28).—Three samples have been analyzed from dredge 41 of the second leg of the Hawaii Institute of Geophysics cruise 72-07-02 (Clague, 1974a; Garcia, Frey, and Naughton, in press). Two of these samples are hawaiite, probably from the same flow, and the third sample is an olivine basalt transitional between tholeiitic and alkalic basalt. The hawaiite probably erupted during the alkalic postshield stage and the transitional basalt during either the late shield stage or the caldera-collapse phase. The hawaiite and alkalic basalt have a mean age of 13.0 ± 0.06 Ma.

St. Rogatien Bank (29).—A single sample has been analyzed from dredge 44 of the second leg of the Hawaii Institute of Geophysics cruise 72-07-02 (Clague, 1974a). The sample is an aphyric hawaiite that probably erupted during the alkalic postshield stage; it has not been dated.

Gardner Pinnacles (30).—The two rocks that constitute Gardner Pinnacles are the westernmost subaerial exposures of volcanic rock in the Hawaiian Chain. The alkalic basalt flows that make up the rocks dip 15° to the west and are cut by several east-trending dikes (Dalrymple and others, 1974). Dredged samples of geochemically similar, though less differentiated, alkalic basalt were recovered in dredge 37 from the second leg of the Hawaii Institute of Geophysics cruise 72-07-02 (Clague, 1974; Garcia, Frey, and Naughton, in press). A later dredge on the flank of Gardner Pinnacles (HIG dredge 6-7; see Garcia, Frey, and Naughton, in press) recovered largely unaltered picritic tholeiitic basalt. We infer that the picritic tholeiitic basalt erupted during the shield stage and the alkalic basalt flows during the postshield stage. Additional samples have recently been recovered during Hawaii Institute of Geophysics cruise KK84-04-28-05 from a number of dredge stations on Gardner Pinnacles, but these have yet to be analyzed (Campbell and others, 1984).

Samples from the island were too altered for dating (Dalrymple and others, 1974), but Garcia, Frey, and Naughton (in press) obtained a weighted mean age of 12.3 ± 1.0 Ma for two dredged samples of alkalic basalt and one of tholeiitic basalt.

Laysan Island (36).—A single dredge during U.S. Geological Survey cruise LEE8-76-NP recovered a variety of hawaiite and mugearite pebbles (Dalrymple and others, 1981) that probably erupted during the alkalic postshield stage. Conventional K-Ar and ^{40}Ar-^{39}Ar measurements on five of the samples fall within the range 18.8–21.4 Ma, and ^{40}Ar-^{39}Ar incremental heating experiments on three samples gave a mean age of 19.9 ± 0.3 Ma.

Northampton Bank (37).—A Hawaii Institute of Geophysics cruise sampled the south side of Northampton Bank and recovered coral-reef debris, picritic tholeiitic basalt, and olivine tholeiitic basalt that probably erupted during the shield stage. Dalrymple and others (1981) reported conventional K-Ar and ^{40}Ar-^{39}Ar age data for three dredged samples of tholeiitic basalt. Only one of the samples gave a ^{40}Ar-^{39}Ar age spectrum plateau. The inferred age for that sample is 26.6 ± 2.7 Ma.

Pioneer Bank (39).—On the second leg of the Hawaii Institute of Geophysics cruise 72-07-02, dredge 25 recovered pillow breccia of olivine tholeiitic basalt (Clague, 1974a) that probably erupted during the shield stage. The volcano is undated.

Pearl and Hermes Reef (50).—On the second leg of the Hawaii Institute of Geophysics cruise 72-07-02, dredge 24 recovered round clasts of alkalic basalt, hawaiite, and nepheline phonolite (Clague and others, 1975) that probably erupted during the alkalic postshield stage. It is possible that the phonolite sample erupted during an alkalic rejuvenated stage, although other phonolite samples from Koko Seamount in the Emperor Seamounts are all interpreted to have erupted during the alkalic postshield stage (Clague, 1974a). The weighted mean age of phonolite, hawaiite, and alkalic basalt is 20.6 ± 0.5 Ma.

Ladd Bank (51).—On the second leg of the Hawaii Institute of Geophysics cruise 72-07-02, dredge 23 recovered a single fresh clast of ankaramite vitrophyre that is compositionally similar to a basanite or nephelinite (Clague, 1974a). This sample probably erupted during an alkalic rejuvenated stage; it is undated.

Midway Island (52).—In 1965, two holes were drilled through the reef on Midway and into flows of tholeiitic basalt (Ladd and others, 1967). Analyses of the tholeiitic flows are presented in Dalrymple and others (1974) and of hawaiite and mugearite cobbles from a conglomerate overlying the flows in Dalrymple and others (1977). We infer that the tholeiitic flows erupted during the shield stage and the hawaiite and mugearite during an alkalic postshield stage.

Dalrymple and others (1974) reported ages for four samples of tholeiitic basalt from the reef drill hole at Midway. The ages ranged from 10.8 to 18.2 Ma. In the later study, Dalrymple and others (1977) reported an age for Midway of 27.7 ± 0.6 Ma based on conventional K-Ar and ^{40}Ar-^{39}Ar analyses of two unaltered samples of hawaiite and mugearite from the conglomerate. Incremental heating experiments showed that the conventional K-Ar ages obtained earlier for the tholeiitic basalt samples do not represent crystallization ages.

Nero Bank (53).—Scripps Institution of Oceanography cruise TASADAY III recovered a vitrophyre of picritic tholeiitic basalt that probably erupted during the shield stage (Clague, 1974a); it is undated.

Unnamed Seamount (57).—On the second leg of the Hawaii Institute of Geophysics cruise 72-07-02, dredge 20 recovered several samples of open-textured alkalic basalt that probably erupted during an alkalic postshield stage (Clague and others, 1975). Three samples of the basalt have concordant K-Ar ages with a mean of 28.0 ± 0.04 Ma.

Unnamed Seamount (58).—DSDP Site 311, located 240 km west of Midway Island, recovered volcanogenic deposits from the archipelagic apron of this volcano (Larson and others, 1975) that yielded a nannoplankton age of 31–28 Ma (Bukry, 1975).

Unnamed Seamount (63).—Scripps Institution of Oceanography cruise TASADAY III recovered a wide range of alkalic lava types including ankaramite, analcime tephrite, amphibole-bearing tephrite, and amphibole-bearing hawaiite (Clague, 1974a, 1974b; Clague and others, 1975). These strongly alkalic rocks probably originated by crystal fractionation from alkalic rejuvenated-stage basanitic parental magma. Clague and others (1975) obtained concordant K-Ar results from three samples of the alkalic lava; the mean age is 27.4 ± 0.05 Ma.

Hancock Seamount (64).—Hawaii Institute of Geophysics cruise KK84-04-28-05 recently recovered samples in a number of dredges from Hancock Seamount; these samples have not been analyzed or dated (Campbell and others, 1984).

Colahan Seamount (65).—On U.S. Geological Survey cruise L8-82-NP, dredge 4 recovered samples of transitional basalt, tephrite, and amphibole-bearing hawaiite (Duncan and Clague, 1984; D.A. Clague, unpub. data, 1983) that probably erupted during an alkalic rejuvenated stage. Analysis of these samples is still in progress; therefore the identification of eruptive stage is less certain than for the other seamounts. Duncan and Clague (1984) have reported ^{40}Ar-^{39}Ar total-fusion ages of 37.5 ± 0.3 and 39.8 ± 0.2 Ma for two alkalic basalt samples.

Abbott Seamount (65A).—On U.S. Geological Survey cruise L8-82-NP, dredges 2 and 3 recovered samples of transitional to alkalic basalt that probably erupted during the late shield stage or caldera-collapse phase (Duncan and Clague, 1984). Analysis of these samples is still in progress. Duncan and Clague (1984) reported ^{40}Ar-^{39}Ar total-fusion ages of 40.4 ± 0.5 and 36.3 ± 0.3 Ma for two of the samples.

Kammu Seamount (66).—On Scripps Institution of Oceanography cruise AIRES VII, dredge 54 recovered abundant carbonate reef debris but no volcanic rocks. N. Sachs (quoted in Clague and Jarrard, 1973) identified *Spiroclypeus variablis* Tan., a large foraminifer of late Eocene age.

Daikakuji Seamount (67).—On Scripps Institution of Oceanography cruise AIRES VII, dredge 55 recovered a range of lava samples including hypersthene-bearing tholeiitic basalt, basalt transitional between tholeiitic and alkalic basalt, and alkalic basalt (Clague, 1974a; Dalrymple and Clague, 1976). Microprobe analyses of glass rinds on some of these samples are in agreement with the published analyses on altered whole-rock samples. The tholeiitic basalt is interpreted to have erupted during the shield stage, the transitional basalt during the late shield stage or caldera-filling phase, and the alkalic basalt during the alkalic postshield stage.

Dalrymple and Clague (1976) made conventional K-Ar and ^{40}Ar-^{39}Ar age determinations on tholeiitic and alkalic basalt and on plagioclase separates. On the basis of ^{40}Ar-^{39}Ar incremental-heating results from the alkalic basalt and ^{40}Ar-^{39}Ar total-fusion analyses of the plagioclases samples, they concluded that the best age for the seamount was 42.4 ± 2.3 Ma.

Yuryaku Seamount (69).—On Scripps Institution of Oceanography cruise AIRES VII, dredge 53 recovered several fairly fresh pebbles of alkalic basalt (Clague, 1974a; Clague and others, 1975; Dalrymple and Clague, 1976). These samples probably erupted during the alkalic postshield stage.

Clague and others (1975) determined an age of 43.4 ± 1.6 Ma for Yuryaku on the basis of ^{40}Ar-^{39}Ar incremental-heating experiments on two dredged samples of alkalic basalt.

Kimmei Seamount (72).—On Scripps Institution of Oceanography cruise AIRES VII, dredges 51 and 52 recovered several samples of alkalic basalt that have been analyzed (Clague, 1974a; Dalrymple and Clague, 1976). Two of these samples are rather severely phosphatized, but all three probably erupted during the alkalic postshield stage.

Dalrymple and Clague concluded that the best age for Kimmei was 39.9 ± 1.2 Ma from ^{40}Ar-^{39}Ar incremental-heating experiments on three dredged samples of alkalic basalt.

Koko Seamount, southeast part (74).—On Scripps Institution of Oceanography cruise AIRES VII, dredge 43 recovered a large collection of rounded volcanic beach cobbles and abundant coral fragments. The volcanic cobbles include tholeiitic basalt, alkalic basalt, hawaiite, mugearite, trachyte, and phonolite (Clague, 1974a). The tholeiitic basalt probably erupted during the shield stage and the entire suite of related alkalic lava types probably erupted during the alkalic postshield stage. DSDP Leg 32 drilled two shallow holes on Koko Seamount, but neither reached volcanic basement (Larson and others, 1975). The structure and seismic stratigraphy of the seamount are described by Davies and others (1972) and Greene and others (1980).

Clague and Dalrymple (1973) obtained conventional K-Ar and ^{40}Ar-^{39}Ar total fusion data on seven dredged samples of sanidine trachyte, alkalic basalt, and phonolite. Krummenacher (cited in Clague and Jarrard, 1973) obtained K-Ar ages of sanidine from two trachyte samples. The data are concordant and have a mean of 48.1 ± 0.8 Ma (Dalrymple and Clague, 1976).

Koko Seamount, northwest flank (76).—On Scripps Institution of Oceanography cruise AIRES VII, dredge 44 recovered pillow fragments of differentiated tholeiitic basalt from the northwest flank of Koko Seamount (Clague and Dalrymple, 1972; Clague 1974a). This lava probably erupted from a rift zone during the shield stage.

Ojin Seamount (81).—DSDP Leg 55 drilled site 430 through a lagoonal sediment pond near the center of Ojin Seamount (Jackson and others, 1980). Five lava flows were penetrated, including four flows of aphyric to sparsely porphyritic hawaiite and an underlying flow of tholeiitic basalt (Kirkpatrick and others, 1980). The overlying sediment consists of shallow-water carbonate reef or bank deposits. The flows were clearly erupted subaerially: a red soil zone was recovered between two of them. The four hawaiite flows were apparently erupted rather rapidly, because their paleomagnetic inclinations are very similar (Kono, 1980). The lowermost tholeiitic flow probably erupted during the shield stage, whereas the hawaiite flows probably erupted during an alkalic postshield stage.

Dalrymple and others (1980) obtained an age of 55.2 ± 0.7 Ma for Ojin on the basis of ^{40}Ar-^{39}Ar incremental-heating results from two samples of hawaiite and one sample of tholeiitic basalt recovered during drilling of DSDP site 430.

Jingu Seamount (83).—A Hawaii Institute of Geophysics cruise in July 1977 recovered several fresh samples and abundant moderately altered samples of hawaiite and mugearite (Dalrymple and Garcia, 1980) that probably erupted during an

alkalic postshield stage.

Dalrymple and Garcia (1980) reported an age of 55.4±0.9 Ma for Jingu based on ^{40}Ar-^{39}Ar incremental-heating experiments on three of these dredged samples of hawaiite and mugearite.

Nintoku Seamount (86).—DSDP Leg 55 drilled site 432 into a lagoonal sediment pond on the top of Nintoku Seamount (Jackson and others, 1980). Samples of three lava flows were recovered from beneath sandstone, conglomerate, and a thin red clay horizon. The flows are all alkalic lava. The top two flows are identical feldspar-porphyritic alkalic basalt, and the bottom flow is transitional between alkalic basalt and hawaiite. All three flows probably erupted during the alkalic postshield stage. As on Ojin Seamount, these flows were clearly erupted subaerially.

Dalrymple and others (1980) obtained ^{40}Ar-^{39}Ar data from two samples recovered during drilling of DSDP site 432. Only one of the samples gave easily interpretable results, and that one indicated an age of 56.2±0.6 Ma.

Yomei Seamount (88).—DSDP Leg 55 drilled two holes at site 431 on a faulted terrace (Jackson and others, 1980). Neither hole reached volcanic basement. The upper 7.5 m consisted of fragments of manganese-oxide crust, authigenic silicates, phosphate, ice-rafted pebbles, and calcareous sand of Quaternary age. The lower 9.5 m consisted of authigenic silicates, manganese-oxide crust fragments, altered basalt clasts, and calcareous sand of middle Eocene age.

Suiko Seamount, southern part (90).—Saito and Ozima (1975, 1977) obtained a ^{40}Ar-^{39}Ar incremental-heating isochron age of 59.6±0.6 Ma for a single sample of mugearite dredged from the southern part of Suiko. The reliability of this age has been questioned, however, on the basis of (1) selection of the sample from a variety of ice-rafted material dredged from Suiko and (2) the unorthodox and potentially misleading treatment of the ^{40}Ar-^{39}Ar data (Dalrymple and others, 1980). Three conventional K-Ar determinations ranging from 22 Ma to 43 Ma on samples from the same dredged material (Ozima and others, 1970) are unreliable because of severe sample alteration. The sample of mugearite could represent lava of an alkalic postshield stage; however, the presence of abundant ice-rafted material (Ozima and others, 1970) creates obvious difficulties in identifying an indigenous sample from among the erratics.

Suiko Seamount, central part (91).—DSDP Leg 55 drilled a deep reentry hole (433C) in a lagoonal sediment pond (Jackson and others, 1980) on top of Suiko Seamount. The hole penetrated 550.5 m, the lower 387.5 m entirely in basalt. Samples of more than 100 flows or flow lobes were recovered, of which the upper three flow units are alkalic basalt and the remainder are tholeiitic basalt and picritic tholeiitic basalt. The three alkalic flows probably erupted during a postshield stage, whereas the thick sequence of tholeiitic lava represents the shield stage.

Dalrymple and others (1980) determined an age of 64.7±1.1 Ma for two samples of alkalic and tholeiitic basalt recovered during drilling of DSDP site 433C. The data were obtained by ^{40}Ar-^{39}Ar incremental heating.

Tenji Seamount (98).—A single dredge was obtained from Tenji Seamount by the U.S. Coast Guard Cutter *Glacier* in September 1971 (Bargar and others, 1975). The small group of rocks recovered included samples of basalt, crystal tuff, volcaniclastic sandstone, mudstone, graywacke, and a manganese nodule. Some of the lava samples could be derived from the seamount, but the rest are clearly glacial erratics. None of the samples was dated because of the uncertainty of their origin.

Meiji Seamount (108).—DSDP Leg 19 drilled site 192 on top of Meiji Seamount. A thickness of 13 m of pillow basalt with glassy margins was recovered; the rocks are highly altered, but interpretation of the immobile trace elements suggests that they are tholeiitic basalt erupted during the shield stage (Dalrymple and others, 1980b).

The only radiometric data available for Meiji is a minimum age of 61.9±5.0 Ma for highly altered basalt recovered during drilling of DSDP site 192 (Dalrymple and others, 1980b). This age is considerably less than the 70–68 Ma for overlying sediments based on nannoflora (Worsley, 1973).

THE HAWAIIAN-EMPEROR VOLCANIC CHAIN
Part II
Stratigraphic Framework of Volcanic Rocks of the Hawaiian Islands

By Virginia A.M. Langenheim *and* David A. Clague

ABSTRACT

Stratigraphy is an important tool for understanding the geologic history of the volcanoes of the Hawaiian Islands, providing a framework for much information from other geologic and related fields. Three major eruptive stages in a Hawaiian volcano's life—shield stage (tholeiitic), postshield stage (alkalic), and rejuvenated stage (alkalic)—have generally provided a basis for dividing the volcanic rocks into stratigraphic units. Such units are basic to stratigraphy, and suitable nomenclature for them helps promote unambiguous scientific communication regarding the spatial and temporal relations of rocks. The stratigraphic nomenclature of the Hawaiian Islands is herein reviewed and updated to reflect current scientific needs and to be consistent with the most recent (1983) North American Stratigraphic Code.

The major divisions of volcanic rocks on each island formerly called "Volcanic Series" are all considered to be of formational rank and renamed accordingly. Their names reflect either a predominant commonly accepted lithologic type (such as "Basalt") or the variety of volcanic lithologies in the unit (those units are called "Volcanics"). Only those subdivisions of the major units that are currently considered to be useful as formally named units of member or lesser rank are retained; others are considered to be informal. Principal and other reference localities are designated for those well-established units for which a type locality was not previously specified.

We give in tabular form a brief summary of each stratigraphic unit, including its lithology, occurrence, thickness, type and reference localities, stratigraphic relations, age, and any stratigraphic changes made herein.

INTRODUCTION

Stratigraphy is an important tool for understanding the geologic history of the Hawaiian Islands, providing a framework into which much of the scientific information contributed by other geologic and related fields can be fit in an organized manner.

The purpose of this paper is to present a brief summary of the volcanic stratigraphy of the islands, and, because the discrimination of stratigraphic units is basic to stratigraphy, to review the stratigraphic nomenclature for these rocks and update it as far as possible to reflect current scientific needs and to conform to the most recent North American Stratigraphic Code (North American Commission on Stratigraphic Nomenclature, 1983). In order to present a better view of the stratigraphy of the volcanic rocks of the islands, we begin with a short discussion of the geologic setting.

ACKNOWLEDGMENTS

We thank R.L. Christiansen and R.W. Decker for their constructive critical reviews. We also gratefully acknowledge the following persons for their helpful comments and suggestions: D.A. Brew, E.E. Brabb, T.J. Casadevall, G.B. Dalrymple, R.M. Easton, M.O. Garcia, R.T. Holcomb, P.W. Lipman, J.P. Lockwood, J.G. Moore, R.B. Moore, D.W. Peterson, S.C. Porter, J.M. Sinton, D.A. Swanson, G.P.L. Walker, and E.W. Wolfe.

We are deeply grateful to Cynthia Barclay and William Fedasko for their assistance in searching the literature and with the preparation of the typescript.

GEOLOGIC SETTING

The Hawaiian Islands consist of a chain of volcanoes that stretches about 2,700 km (1,700 mi) across the northern Pacific Ocean in a northwesterly direction from the Island of Hawaii to Kure Island (fig. 1.20). The principal (so-called Windward) Hawaiian Islands of Hawaii, Maui, Kahoolawe, Lanai, Molokai, Oahu, Kauai, Niihau, and Kaula lie at the southeastern end of the chain. All of these islands are formed by large volcanoes, though Kaula is only a small crescent-shaped erosional remnant of a tuff cone, presumably resting on a large submerged volcano. Some of the islands are formed by a single volcano, others by two or more coalesced volcanoes. The subaerial part of these volcanoes, which constitutes only a small fraction of the total mass of each volcano, is typically shield shaped. In older volcanoes, this shield shape is largely modified by erosion. The rocks of the southeastern islands are almost entirely of volcanic origin; only minor amounts of sedimentary rocks occur. Northwest of the Windward Islands lie the so-called Leeward Hawaiian Islands (fig. 1.20), which consist of small volcanic islets and atolls; only few of the volcanoes there rise above the sea.

The age of the volcanoes increases progressively from the southeast end, where the volcanoes are still active, to the northwest end, where the volcanoes are about 30 Ma. Most of the volcanoes have been extinct for millions of years. The only historical eruptions have been at East Maui (Haleakala) Volcano on the Island of Maui, and Hualalai, Mauna Loa, and Kilauea Volcanoes on the Island of Hawaii; Mauna Loa and Kilauea are frequently active.

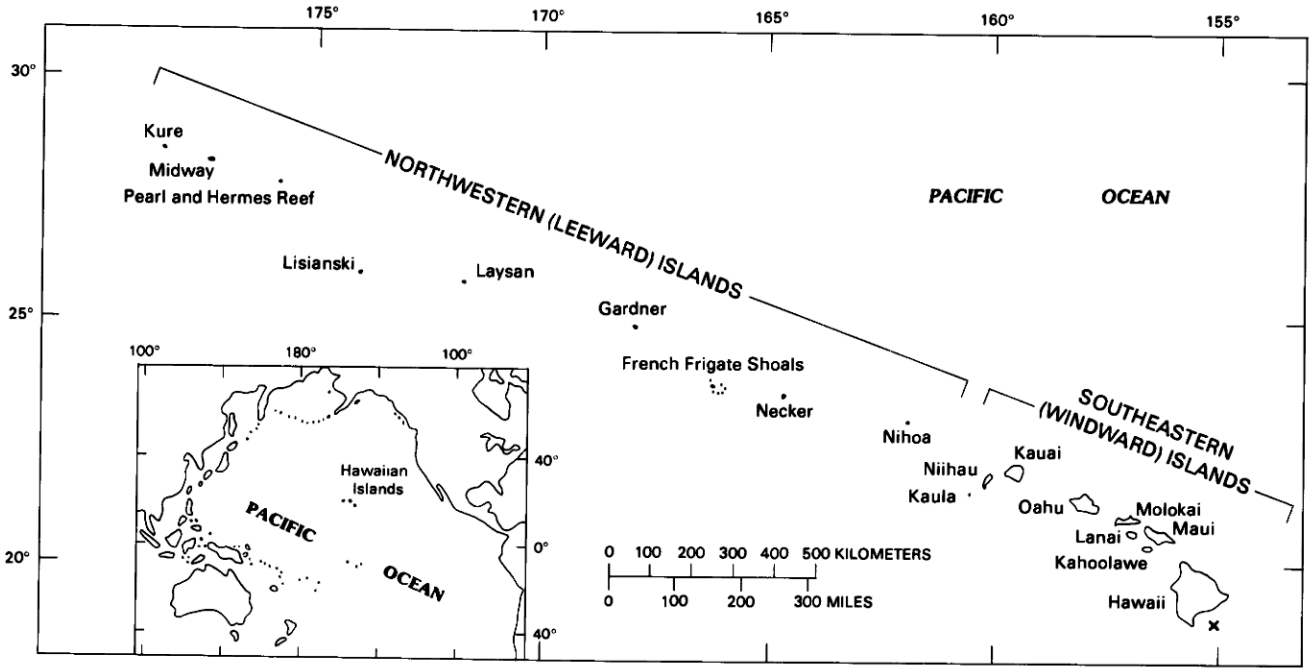

FIGURE 1.20.—Index map of Hawaiian Islands. x, Loihi Seamount.

Hawaiian volcanoes go through four major eruptive stages—preshield, shield, postshield, and rejuvenated stages—in their evolution and growth, and each stage is represented by rocks of distinct chemical and mineralogical composition. The stages used in this report are from Clague and Dalrymple (chapter 1, part I); see also Peterson and Moore (chapter 7) for discussion of alternative nomenclature. All but the preshield stage are well studied and documented (Stearns, 1940b; Macdonald and Katsura, 1964; Macdonald, 1968). Although an individual volcano may become extinct before all the stages are complete, the general sequence of stages is typical of well studied Hawaiian volcanoes.

Very little is known about the preshield stage, which includes the earliest phase of submarine activity and, in the one known example (Loihi Seamount, fig. 1.20), apparently consists of alkalic basalt and basanite (Moore and others, 1982). The main volcanic edifice (more than 95 percent of the total volume of the volcano) is constructed, in perhaps a million years or less, by voluminous eruptions of silica-rich tholeiitic basalt (and rare rhyodacite and icelandite) during the shield stage. The shield stage, as used here, includes the submarine eruption of tholeiitic basalt, which precedes the subaerial shield-forming eruptions. During the shield stage or at the beginning of the next stage, the postshield stage, a caldera may form and be filled with tholeiitic and (or) alkalic basalt. This process of caldera formation and filling was previously referred to as the caldera-filling or caldera-collapse stage, but is here considered to be a phase of the shield stage or postshield stage. During the postshield stage, a relatively thin cap of alkalic basalt and associated differentiated lava (ankaramite, hawaiite, mugearite, benmoreite, and trachyte) covers the main shield. This alkalic lava makes up less than 1 percent of the total volume of the volcano. Later, after a relatively long period of volcanic quiescence and erosion, a very small amount of silica-poor lava (alkalic basalt, basanite, nephelinite, and nepheline melilitite; rare ankaramite and hawaiite known on East Maui Volcano only) erupts from isolated vents; this stage is referred to here as the rejuvenated stage.

During the shield and postshield stages, eruptions are not confined to the summit area of a volcano, but also occur along extensive zones of fissures, called rift zones, that extend down the flanks of the volcano. These zones are usually marked at the surface by collapse craters, cinder and spatter cones, and grabens, and below the surface by large numbers of dikes. During the rejuvenated stage, however, eruptions occur at vents unassociated with the preexisting rift zones, with the exception of rejuvenated-stage lava on East Maui Volcano.

The shield stage is represented by lava that is dark colored and forms relatively long and thin flows. Most of these flows have sparse to abundant olivine phenocrysts, and some have abundant large phenocrysts of plagioclase. Pyroclastic deposits are minor components during the shield stage.

The postshield stage is represented by lava that is commonly lighter colored than shield-stage lava and contains pyroxene, olivine, and plagioclase phenocrysts. This lava forms shorter and thicker flows. Pyroclastic deposits are more abundant during the postshield stage. There is little evidence of erosion between the eruption of shield-stage lava and postshield-stage lava.

The lava that ponds in a caldera during the shield stage or at the beginning of the postshield stage is usually massive and may show columnar structure.

Rejuvenated-stage lava is also dark colored, but usually forms thick flows with few or no phenocrysts; pyroclastic deposits are

common during this stage.

The shield, postshield, and rejuvenated stages have generally formed the basis for the major stratigraphic divisions or subdivisions of the rocks of the Hawaiian volcanoes (fig. 1.21).

PREVIOUS STUDIES

The geology of the Hawaiian Islands has been studied for more than a hundred years (see Clague and Dalrymple, chapter 1, part I, and Peterson and Moore, chapter 7, for summaries of geologic investigations). Early geologic investigations concentrated on the main southeastern islands and were mainly reconnaissance and general descriptive studies. These early studies were superseded by detailed mapping of the eight major southeastern islands beginning in the 1930's and continuing for nearly 30 years. H.T. Stearns and his coworkers, in a series of bulletins published by the Hawaii Division of Hydrography, produced detailed geologic maps (at scale of 1:62,500, except Hawaii at 1:125,000) and descriptions of the Islands of Oahu (Stearns and Vaksvik, 1935; Stearns, 1939, 1940a), Lanai and Kahoolawe (Stearns, 1940b), Maui (Stearns and Macdonald, 1942), Hawaii (Stearns and Macdonald, 1946), Niihau (Stearns, 1947b), Molokai (Stearns and Macdonald, 1947), and Kauai (Macdonald and others, 1960; Stearns was not a coauthor of this report, but did much of the geologic mapping).

These bulletins have provided the basic stratigraphic framework for subsequent petrologic, mineralogic, geochemical, and geophysical investigations of the islands. Only a few stratigraphic studies have been done since publication of the bulletins, and those studies and detailed geologic mapping have been mainly on the Island of Hawaii.

STRATIGRAPHIC NOMENCLATURE

The classification and naming of stratigraphic units (used here as synonomous with lithostratigraphic units), although to some extent arbitrary and artificial, helps promote concise and unambiguous scientific communication as to the spatial and temporal relations of rocks. Stratigraphic units can be formally or informally named; both are useful in stratigraphic work. Formally named units, however, are named and defined in accordance with procedures outlined in the Code, and any major changes made to them, such as boundary or rank changes, need to be justified.

In the Hawaiian Islands, formal stratigraphic names have been applied only to rock units on the eight main southeastern Hawaiian Islands (Hawaii, Maui, Kahoolawe, Lanai, Molokai, Oahu, Kauai, and Niihau), and these names are almost entirely restricted to volcanic rocks and the sedimentary rocks closely associated with them. Other sedimentary units, such as beach and reef deposits, have been formally named, but they are not discussed here.

Stearns and his coworkers divided the rocks of each volcano into one or more major units that they formally named as "Volcanic Series" (see remarks column in table 1.12). These "Series" consisted of rocks resulting from a succession of extensive eruptions. Some of the "Series" consisted entirely of volcanic rocks, whereas others consisted of volcanic rocks, related intrusions, and their weathering products. Some of the "Series" were not subdivided, whereas others were subdivided either into formations or into members. Although the use of "Volcanic Series" as part of a formal name conformed to the "stratigraphic code" in use at the time the unit was named (Ashley and others, 1933), it does not conform to later codes, including the present (1983) code (American Commission on Stratigraphic Nomenclature, 1961, 1970; North American Commission on Stratigraphic Nomenclature, 1983), which restricts the use of the term "Series" to chronostratigraphic units.

The above inconsistencies, plus recent petrologic, mineralogical, and geochemical studies, have necessitated changes in the stratigraphic nomenclature for the volcanic rocks of the Hawaiian Islands[1] because (1) the lithic or descriptive terms of the names do not conform to the current stratigraphic code or do not reflect modern petrologic classification; (2) the ranks of the units are unclear or inappropriate; and (3) formalization of some names is not now considered to be necessary or useful.

The basic guidelines used in this report for updating the stratigraphic usage in the Hawaiian Islands are those recommended by the 1983 North American Stratigraphic Code (North American Commission of Stratigraphic Nomenclature, 1983). Any changes to the stratigraphic nomenclature made in this report, such as revision (change of rank or lower or upper boundary), redefinition (change of name), and abandonment of formally named stratigraphic units, have been approached as follows:

(1) Formal names are retained only for units that serve a useful purpose and require the stability of nomenclature that formalization affords. As stratigraphic units of any rank become established by repeated demonstration of their usefulness, those formal names that have not been used for a few decades or are currently not thought to serve a useful purpose are abandoned as formal names, but the geographic term of their name may be used informally to identify particular flows (and their associated cones) or beds.

(2) Major stratigraphic units on each volcano are all considered to be of formational rank, and are all formally named units. The ranks of stratigraphic units are important in that they give some concept of the scale of the units in relation to other units. Some of these units could have been considered to be units of group rank, but this does not seem necessary. The volcanic products of one volcano (except for some ash deposits) do not occur on other volcanoes, although they may overlap or interfinger at their boundaries where two or more volcanoes coalesce. Therefore, the units of a volcano can be considered to be essentially confined to one large "mountain," and group rank does not seem appropriate. This approach would also give some consistency to the stratigraphic nomenclature of all the islands.

(3) Formally named subdivisions of the major stratigraphic units are those units of member or lesser rank that are distinctive and (or) extensive. Many of the major units of the Hawaiian volcanoes are very often difficult to subdivide because of rapid lateral changes and lack of key beds.

[1]G.A. Macdonald had planned to revise the stratigraphic nomenclature of the Hawaiian Islands (written commun. to R.W. Kopf, 1976, 1977) before his untimely death in 1978.

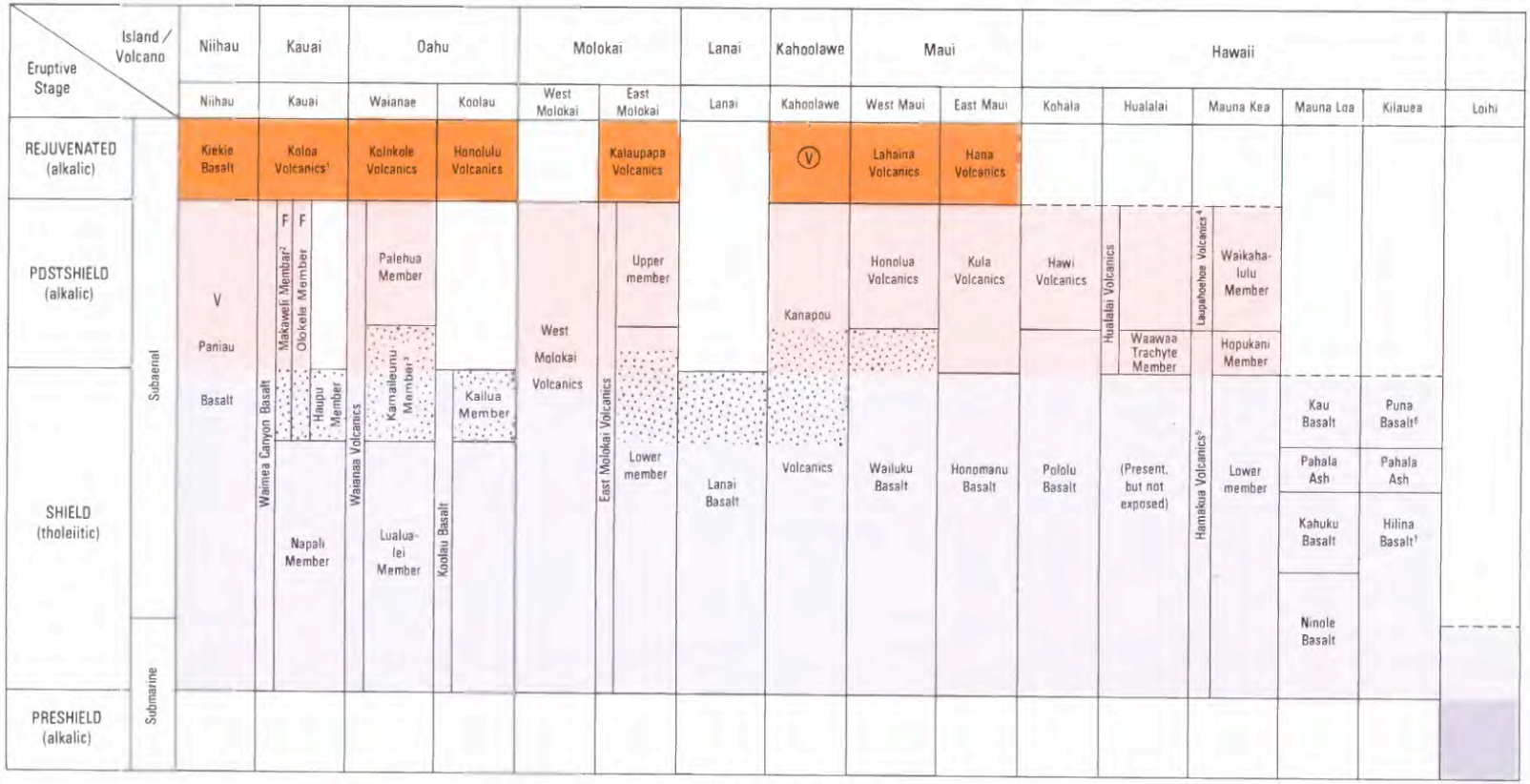

FIGURE 1.21.—Chart showing relations of eruptive stages to volcanoes and stratigraphic units, southeastern Hawaiian Islands, arranged approximately from northwest (left) to southeast (right) (see fig. 1.20 for location). No age correlation between units on different volcanoes implied. Dashed lines indicate end of stage not implied. Base of oldest unit on each volcano (except Loihi) assumed to be at the base of the shield stage.

(4) Formal names of the major stratigraphic units consist of a unique geographic term followed by a simple and generally accepted lithic term, such as "Basalt," or by the term "Volcanics." The initial letter of each term is capitalized. "Basalt" is used for units that consist entirely or almost entirely of basalt, whether tholeiitic or alkalic. An example is the Puna Basalt. The general term "Volcanics" (equivalent to the term "Formation") is used for units that do not have a predominant rock type or are composed of rock types such as hawaiite, mugearite, trachyte and basanite. Examples are the Lahaina Volcanics, Hamakua Volcanics, and Honolulu Volcanics (table 1.12).

The term "Formation" was not used because it does not convey that the unit is composed of volcanic rocks. The term "Volcanic Complex," which indicates a diverse assemblage of extrusive volcanic rocks, related intrusions, and their weathering products, could have been used for some units. However, we tentatively have opted for the term "Volcanics," because it is a shorter term, has precedence of use in the Hawaiian Islands, and does not introduce a new term until the need is confirmed by future investigations.

In general, the term "Basalt" is used for units that represent all or part of the shield stage, although a minor part of the postshield stage may also be represented. The term "Volcanics" is used for units that represent all or part of the postshield stage and for units that represent both shield stage and postshield stage. All units that represent the rejuvenated stage, with the exception of the Kiekie Basalt of Niihau Volcano, are termed "Volcanics."

(5) Formal names of subdivisions of the major units consist of a unique geographic term followed by the appropriate rank term—"Member," "Flow(s)," or "Bed(s)." An intervening lithic or descriptive term may be used in member names and is used in bed and flow names. The initial letter of each term is capitalized. Examples include the Napali Member, Kahele Ash Member, Makanaka Glacial Member, Mokuone Breccia Beds, and Mauna Kuwale Rhyodacite Flow.

Members, flows, and beds can also be informally named. Informal members are designated solely by their lithology or by their stratigraphic position, and none of the initial letters of their names is capitalized. Examples are ash member and lower member. The terms "historic member" and "prehistoric member" are not used in this report because age should play no part in differentiating lithostratigraphic units. Informal flows and beds are similarly designated, such as lower flow, upper flows, ash bed, and breccia beds, but may also combine a geographic term with the unit term or terms; only the initial letter of the geographic term is capitalized. Examples are the Kona ash beds, Kilea flow, and Makapipi flows. With one exception (see Waianae Volcano), all named flows in the Hawaiian Islands are considered to be informal in this report.

(6) A principal reference locality is herein designated for some well established units for which a type locality was never specified. For units that previously had more than one type locality specified, the one here considered to be the more accessible is retained as the type, and the other localities are redesignated as reference localities.

A designated stratotype (type section or type locality) is essential in the definition of a formal stratigraphic unit because it serves as the standard for the unit and constitutes the basis for its recognition. It should therefore be representative of the concept of the unit. Because of the nature of Hawaiian volcanic activity, the stratotype for many of the Hawaiian volcanic units is not truly representative of those units, and reference sections or localities become invaluable in illustrating the lithologic diversity within a unit or the stratigraphic relations with other units. We have not attempted to specify additional reference sections or localities in this report, but we hope this will be done in future stratigraphic studies.

STRATIGRAPHIC SUMMARY

The stratigraphy of the eight main Hawaiian Islands is briefly discussed below by island and volcano from southeast to northwest.

A summary of the formally named stratigraphic units used in this report is given in table 1.12, including a brief description of the lithology, occurrence, thickness, type and reference localities, stratigraphic relations, and age of each. The descriptions of the units were largely taken from the sources cited in the remarks column. Informal units are listed if they were previously formally named. Type localities are used throughout the table, even though some of the units have specified type sections.

Almost all of the isotopic ages shown in the table are K-Ar ages. Numerous radiocarbon ages have been determined for the youngest volcanoes but, with a few exceptions, are not shown. For a summary of radiocarbon ages for the Island of Hawaii, see Rubin and others (chapter 10). The relative ages assigned to the stratigraphic units are based on the Decade of North American Geology time scale (Palmer, 1983), which has the following epoch boundaries: Miocene-Pliocene, 5.3 Ma; Pliocene-Pleistocene, 1.6 Ma; and Pleistocene-Holocene, 10 ka. A correlation diagram of the major stratigraphic units is presented as figure 1.22.

Stratigraphic changes that are made in this report, using the guidelines of the Code and the approach discussed previously, are indicated in the remarks column and discussed below. Former names that have been applied to the units are also indicated in the remarks column. We have not used glottal stops in the geographic part of lithostratigraphic-unit names, although some authors have used them in other publications.

HAWAII

The Island of Hawaii, the largest of the Hawaiian Islands, consists of five coalesced volcanoes: Kilauea, Mauna Loa, Mauna Kea, Hualalai, and Kohala (fig. 1.23). Mauna Kea is the highest of these volcanoes; Mauna Loa is the largest by volume. Little erosion has occurred on these volcanoes except on the northeastern sides of Kohala and Mauna Kea.

KILAUEA VOLCANO

Kilauea, the youngest volcano of the island and still very active, consists entirely of shield-stage tholeiitic lava that issued from the summit caldera and the east and southwest rift zones. The rocks of the volcano are divided into the Hilina Basalt (older) and the

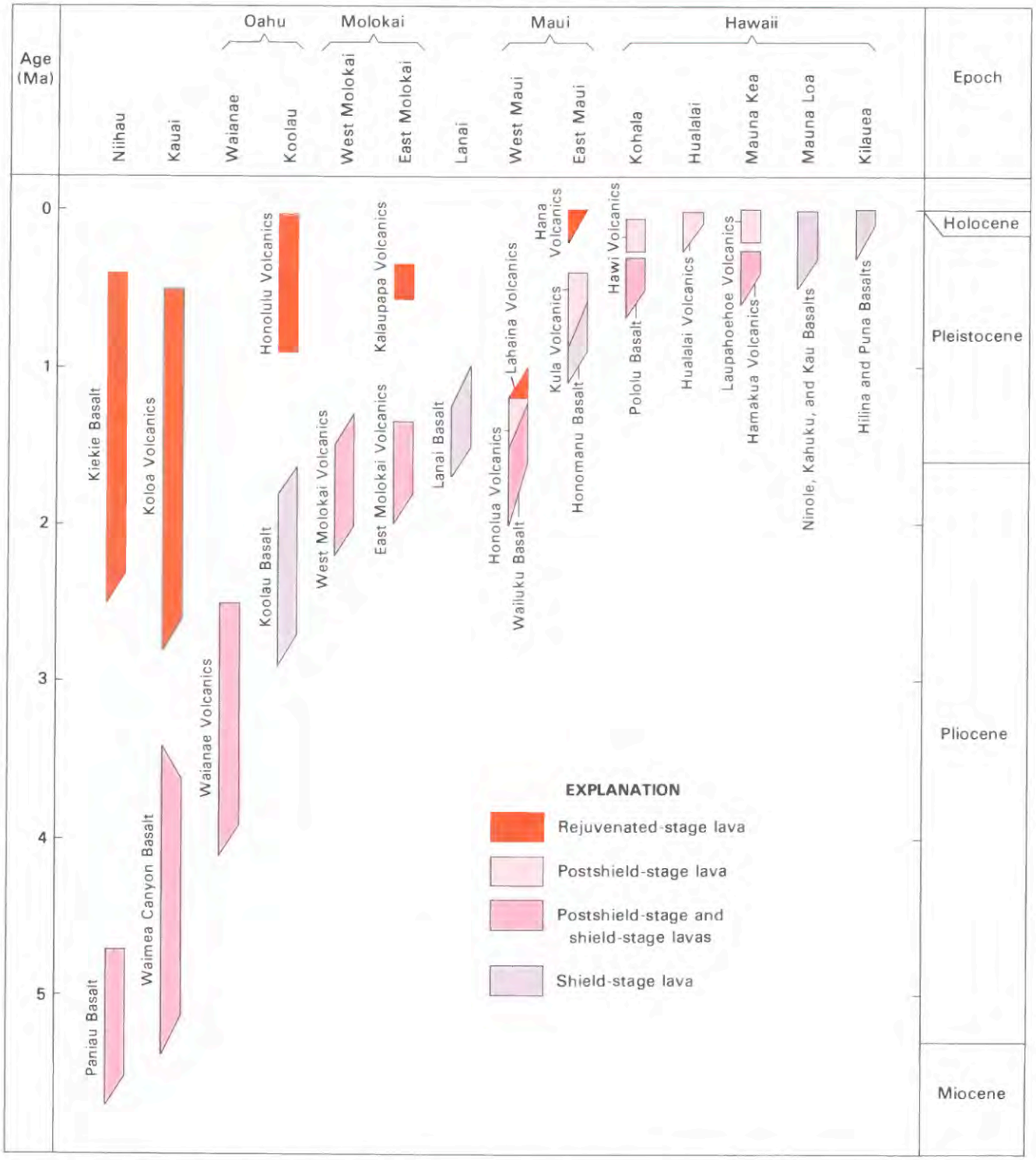

FIGURE 1.22.—Correlation diagram of isotopically dated major volcanic stratigraphic units of southeastern Hawaiian volcanoes. Modified from Clague and Dalrymple (chapter 1, part I, fig. 1.6). Diagonal lines indicate overlapping or uncertain ages. Epoch boundaries from Palmer (1983).

Puna Basalt (younger), generally separated from one another by the Pahala Ash (see subsection "Mauna Loa Volcano"; see also Easton, chapter 11). The Hilina Basalt is exposed only in fault scarps located along the south flank of the volcano. The Hilina Basalt includes the Halape (oldest), Kahele, Pohakaa, and Moo (youngest) Ash Members (Easton, chapter 11). The Puna Basalt covers almost the entire surface of Kilauea and essentially consists of all post-Pahala lava (see discussion below). The Puna includes the prehistoric Uwekahuna (older) and historical Keanakakoi (younger) Ash Members.

The ages of the Hilina and Puna Basalts are not well known. The Hilina Basalt is probably older than the approximately 31-ka

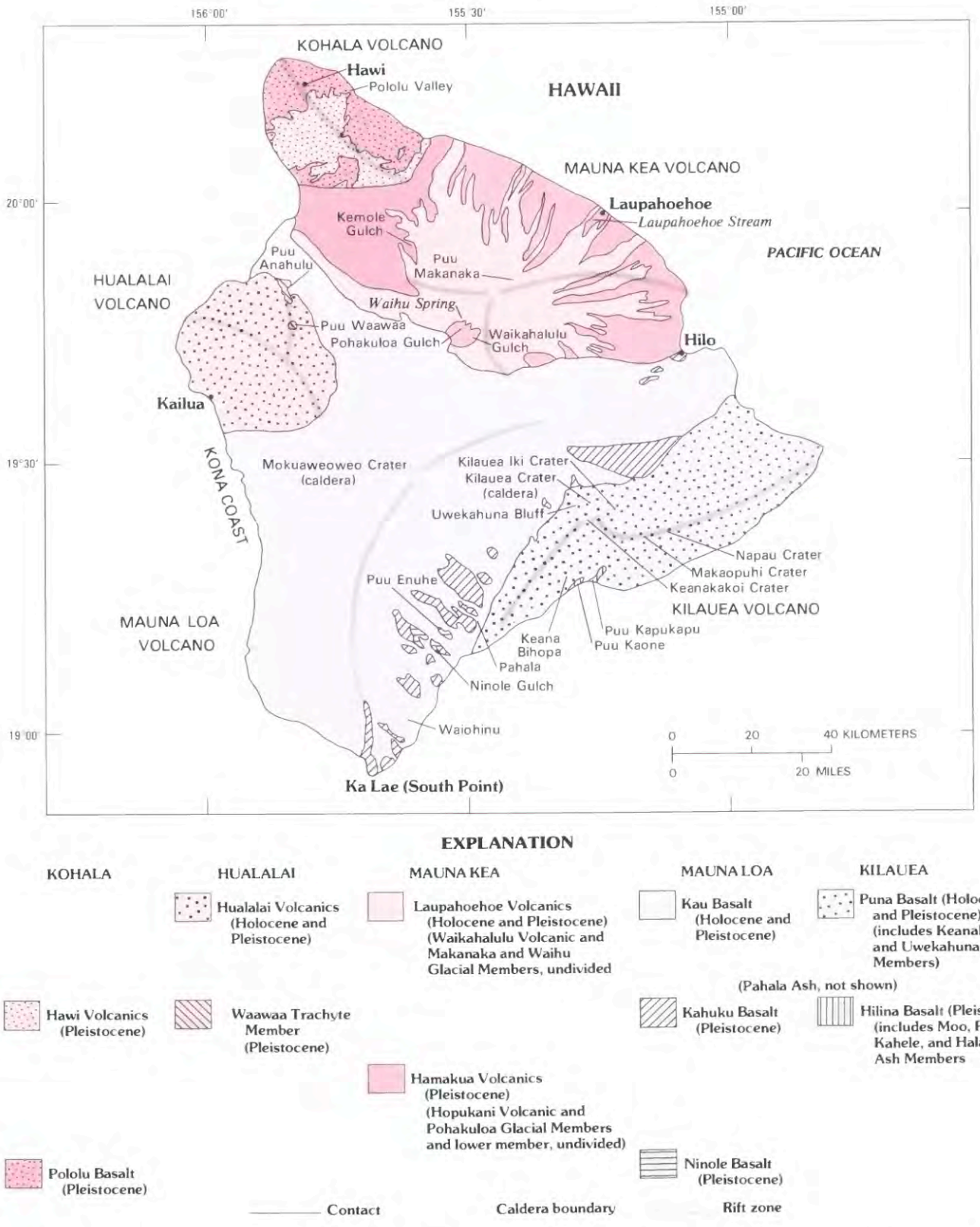

FIGURE 1.23.—Generalized geologic map of the Island of Hawaii, showing localities mentioned in text. Modified from Macdonald and others (1983), Easton (chapter 11), and Porter (1979a, 1979b). Rift zones from Fiske and Jackson (1972). Caldera boundary of Mauna Kea Volcano is inferred to be buried beneath younger lava (see Porter, 1972).

radiocarbon age obtained from the base of the Pahala Ash on Mauna Loa, and the oldest exposed Hilina flows are estimated to be about 100 ka (Easton, chapter 11). Most of the Puna Basalt was erupted during the last 10,000 years, but a Puna flow intercalated with the Pahala Ash at Puu Kaone was radiocarbon dated at about 22 ka (see Easton, chapter 11). The Uwekahuna Ash Member of the Puna Basalt has radiocarbon ages ranging from 2.17 ka to 1.04 ka; however, the age of the eruption or eruptions is uncertain. The ash could have been deposited about 2.1 ka (Casadevall and Dzurisin, chapter 13; Lockwood and Rubin, 1986) or about 1.5 ka (Holcomb, chapter 12).

MAUNA LOA VOLCANO

The lava of Mauna Loa, like that of Kilauea, is all shield-stage tholeiitic lava that has mostly issued from the summit caldera and southwest and northeast rift zones.

The oldest exposed rocks belong to the Ninole Basalt, which forms a series of steep-sided hills on the southeast flank of the volcano. The Ninole, which was originally named the Ninole Basalt by Stearns (1926), was later called the Ninole Volcanic Series by Stearns and Macdonald (1946). Recently, Lipman (1980) used the name Ninole Volcanics. As the Ninole is all tholeiitic basalt, the term used by Stearns (1926) is more informative and is used here. The Ninole was thought to represent remnants of an earlier shield volcano mostly buried by lavas from Mauna Loa (Stearns and Macdonald, 1946), but recent studies indicate that it may merely be deeper parts of the Mauna Loa shield, no more than a few hundred thousand years old, that have been uplifted along normal faults (Lipman, 1980).

Unconformably overlying the Ninole are the Kahuku Basalt (older) and Kau Basalt (younger) (table 1.12), which are separated by the Pahala Ash. Lipman (1980) recently used the terms Kahuku Volcanics and Kau Volcanics, but as these units are composed entirely of basalt, they are here renamed the Kahuku Basalt and Kau Basalt, respectively. The Kahuku Basalt crops out on the east and south sides of the volcano. The Kau Basalt covers most of the surface of Mauna Loa and consists of all post-Pahala lava.

The Pahala Ash is a distinctive yellowish vitric ash that has been largely altered by weathering to a reddish brown mixture of clay minerals and hydrated oxides. The thickness of the unit varies considerably, but it is locally more than 15 m thick (Easton, chapter 11).

These ash deposits were originally the uppermost part of what Noble and Clark (in Washington, 1923) called the Pahala Series, which also included the underlying flows. Stone (1926) used the term Pre-Kilauea Series for the uppermost ash and underlying flows, and restricted the name Pahala to the uppermost ash deposits, calling them the Pahala Ash. He applied the name Pahala Ash to ash deposits of Mauna Loa and Kilauea, but not to those of Mauna Kea. Stearns and Clark (1930) used the name Pahala Basalt for both the uppermost ash deposits and the underlying flows. The flows of their Pahala Basalt are herein called the Kahuku Basalt on Mauna Loa and the Hilina Basalt on Kilauea. Wentworth (1938) used the term Pahala Tuff in the same general sense as the Pahala Ash of Stone (1926), but also used the term Waiau Formation (recently abandoned by Porter, 1973) for equivalent ash on Mauna Kea and the term Glenwood Tuff for equivalent ash on parts of the east slope of Mauna Loa. Stearns and Macdonald (1946) and Davis and Macdonald (in Avias and others, 1956), however, considered the Pahala Ash to be a persistent ash formation that was derived from several sources. They believed the Pahala occurred on all the volcanoes, separating their major units on Kilauea (Hilina and Puna Volcanic Series), Mauna Loa (Kahuku and Kau Volcanic Series), and Mauna Kea (Hamakua and Laupahoehoe Volcanic Series) and capping the older unit (Pololu Volcanic Series) of Kohala and a member (Waawaa Volcanics) of the Hualalai Volcanic Series of Hualalai.

Current mapping on Mauna Kea, Hualalai, and Kohala indicates that the extensive surficial ash deposits on these volcanoes were locally derived and are genetically distinct from the Pahala Ash on Kilauea and Mauna Loa (E.W. Wolfe, oral commun., 1986). Therefore, we are geographically limiting the Pahala to the occurrences on Kilauea and Mauna Loa.

The age of the Ninole Basalt is considered to be no more than a few hundred thousand years. The single published K-Ar age of 0.54 Ma has an estimated uncertainty of 0.4 m.y. (see Clague and Dalrymple, chapter 1, part I). The Kahuku Basalt and the Kau Basalt are approximately coeval with the Hilina Basalt and Puna Basalt, respectively, of Kilauea. The Pahala Ash on Mauna Loa and Kilauea is considered by Easton (chapter 11) to be entirely of Pleistocene age (between about 30 ka and 10 ka).

MAUNA KEA VOLCANO

Mauna Kea last erupted about 3.6 ka (Porter, 1979a). The volcano passed through the shield stage into the postshield stage and produced a cap of differentiated lava that almost completely buried the original subaerial shield. It is uncertain if a summit caldera existed; however, a small caldera has been inferred to lie buried beneath the younger lava (Porter, 1972). Rift zones are less pronounced than on Kilauea and Mauna Loa, but westerly, southerly, and easterly rifts are suggested by alignments of cinder cones. The lower northeastern slope of the volcano has gulches cut into it, whereas the other slopes are generally little affected by erosion. The upper slopes of the volcano were glaciated during the Pleistocene.

The rocks of the volcano were divided into the Hamakua Volcanic Series and the overlying Laupahoehoe Volcanic Series by Stearns and Macdonald (1946). The Hamakua represents the shield stage and part of the postshield stage; the Laupahoehoe represents the rest of the postshield stage. These units, considered to be of formational rank by Stearns and Macdonald (1946), were subdivided by them into informal members.

Recently, Porter (1979a, 1979b; see also Porter, 1973, 1974; Porter and others, 1977) formally redefined the Hamakua and Laupahoehoe to include glacial deposits, raised them to group rank, and subdivided both units into formally named volcanic and glacial formations. They subdivided the upper part of the Hamakua Group into the Hopukani Formation (volcanic) and the Pohakuloa Formation (glacial), but Porter (1979a, 1979b) called the lower part of

the group the "lower member of Stearns and Macdonald (1946)." Porter and others (1977; see also Porter, 1973, 1974) originally subdivided their Laupahoehoe Group into three volcanic formations—Liloe (oldest), Hanaipoe, and Waikahalulu (youngest) Formations—and two interstratified glacial formations—Waihu and Makanaka Formations. The Makanaka included the Kemole Member, a volcanic unit. This usage was superseded by a threefold subdivision of the Laupahoehoe Group (Porter, 1979a, b), in which all of the volcanic rocks were assigned to the Waikahalulu Formation; the names Liloe, Hanaipoe, and Kemole were abandoned as formal names of lithostratigraphic units and were formally applied to chronostratigraphic units—the Liloean, Hanaipoean, and Kemolean Stages.

Because the use of the Hamakua and Laupahoehoe as units of group rank is not consistent with the approach used here for the rest of the volcanoes of the Hawaiian Islands, these units are here reduced to formation rank and renamed the Hamakua Volcanics and Laupahoehoe Volcanics. Their subdivisions are reduced to member rank and renamed to reflect the overall nature of their lithologies (see table 1.12).

The Hamakua is considered to be of Pleistocene age and the Laupahoehoe of Pleistocene and Holocene age on the basis of K-Ar and radiocarbon dating (Porter, 1979a) (table 1.12).

HUALALAI VOLCANO

Hualalai Volcano last erupted in 1800–1801, when several flows issued from the well-defined northwest rift zone. Less well defined rift zones trending north and southeast are marked by numerous cinder and spatter cones. It is not known whether the volcano had a summit caldera. Shield-stage tholeiitic lava is not exposed on Hualalai Volcano, but tholeiitic rocks are known to occur in the subsurface and in the submarine part of the volcano (Moore and others, chapter 20; Clague, 1982).

The entire subaerial surface of the volcano consists of postshield-stage alkalic basalt, with minor hawaiite and trachyte, named the Hualalai Volcanic Series by Stearns and Macdonald (1946). They included within the Hualalai a trachyte cone and flow, which they called the Waawaa Volcanics. Though they gave the Waawaa what is now considered to be a formational rank name, they clearly considered it to be a member of the Hualalai (Stearns and Macdonald, 1946, p. 143), and it is so considered here (table 1.12).

Stearns and Macdonald (1946) did not apply a name to the ash deposits that mantle the slopes of the volcano, although Wentworth (1938) had earlier called these deposits the Kona Tuff Formation. Later, Davis and Macdonald (in Avias and others, 1956) presumably included the Kona Tuff Formation within the Hualalai, effectively giving the Hualalai group status. R.B. Moore (oral commun., 1986) suggests that this unit should never have been formally named; it is here abandoned as a formal name and the unit is informally called the Kona ash beds. Thus, the Hualalai is here reduced to formational rank and renamed the Hualalai Volcanics.

The Hualalai Volcanics is largely of Holocene age, but the oldest flows are of Pleistocene age (Moore and others, chapter 20). The Waawaa Trachyte Member has a published K-Ar age of 0.4 ± 0.3 Ma (Funkhouser and others, 1968), but recent unpublished K-Ar determinations by G.B. Dalrymple (oral commun., 1986) indicate the trachyte is about 0.105 Ma.

KOHALA VOLCANO

Kohala Volcano is an oval volcano built up around northwest and southeast rift zones. It is deeply dissected on its northeast side. Arcuate faults near the summit of the volcano suggest that a caldera formed during the shield stage but was later buried by the younger lava in the postshield stage.

The volcanic rocks of Kohala Volcano were originally divided by Stearns and Macdonald (1946) into the Pololu Volcanic Series (older), composed of shield-stage tholeiitic basalt with caldera-filling postshield-stage alkalic basalt near the top, and the Hawi Volcanic Series (younger), consisting of differentiated alkalic lava of the postshield stage (table 1.12). Neither of these units has been subdivided, and they are here renamed the Pololu Basalt and Hawi Volcanics, respectively, to reflect their lithologies. The Pololu Basalt and Hawi Volcanics are of Pleistocene age on the basis of K-Ar determinations (McDougall, 1969; McDougall and Swanson, 1972) (table 1.12).

MAUI

The Island of Maui (fig. 1.24), the second largest of the Hawaiian Islands, consists of two large coalesced volcanoes, East Maui (or Haleakala) Volcano and West Maui Volcano, connected to one another by an isthmus formed when lava of East Maui banked against the already existing West Maui Volcano. The Maui volcanoes are more dissected than the volcanoes of the Island of Hawaii.

EAST MAUI (OR HALEAKALA) VOLCANO

East Maui Volcano last erupted about 200 years ago and has a large summit crater called Haleakala Crater, which is primarily of erosional origin (Macdonald and others, 1983). East Maui is the youngest Hawaiian volcano to have rejuvenated-stage lava.

The rocks of the volcano were originally divided by Stearns and Macdonald (1942) into the Honomanu Volcanic Series (oldest), Kula Volcanic Series, and Hana Volcanic Series (youngest), representing the shield, postshield, and rejuvenated stages, respectively (table 1.12). The Kula eruptions took place along southwest, east, and northwest rift zones. The Hana eruptions are unique among Hawaiian rejuvenated-stage eruptions because their vents are aligned along preexisting rift zones (southwest and northwest rift zones), the erosional period preceding these eruptions was rather short (<0.4 m.y.), and ankaramite and hawaiite are present.

The Honomanu Volcanic Series is almost completely buried by later lava and is only exposed in the seacliffs along part of the north coast. The Honomanu Volcanic Series was not subdivided by Stearns and Macdonald (1942), and it was more recently called the Honomanu Formation in the Haleakala Crater area by Macdonald

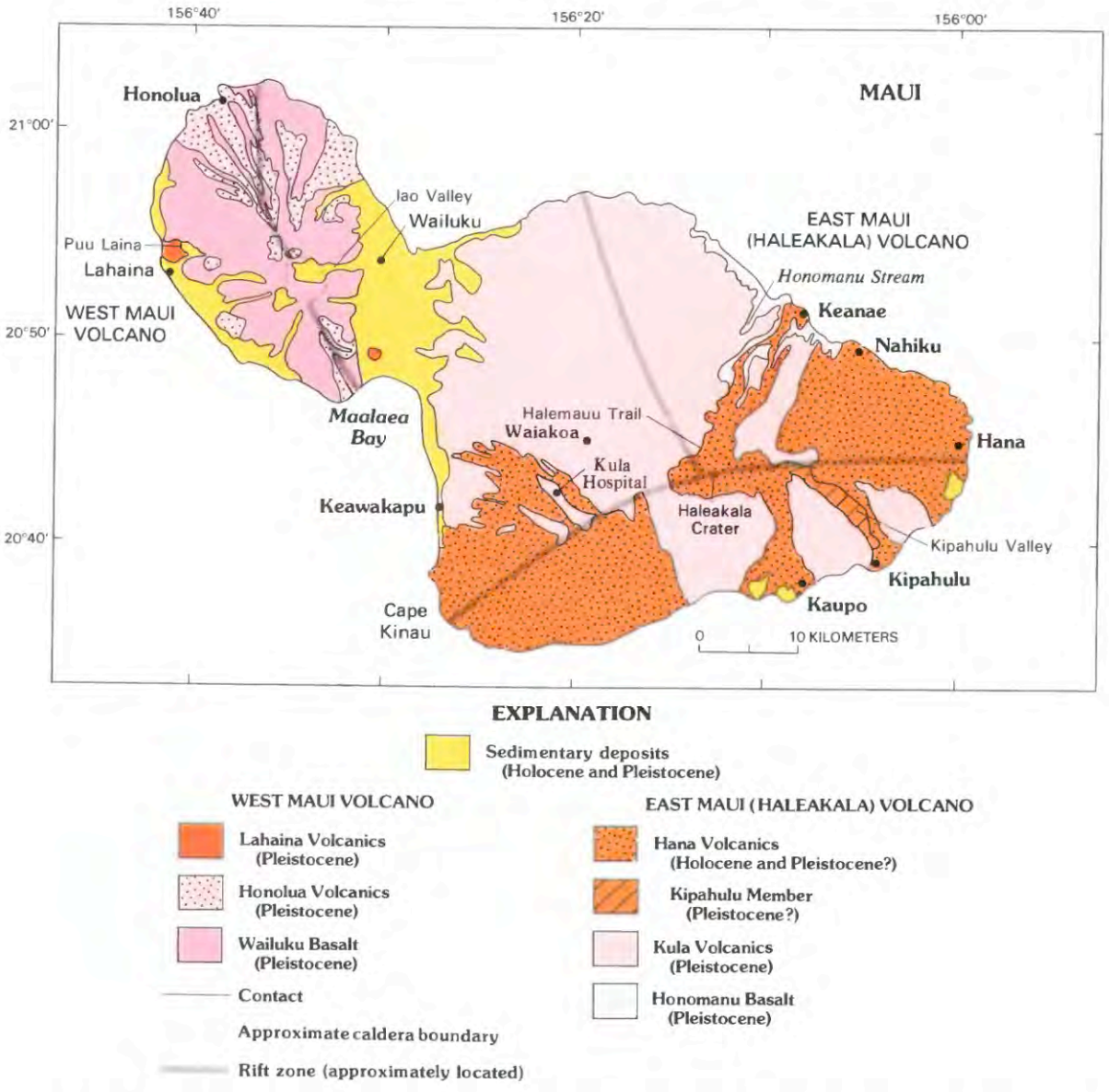

FIGURE 1.24.—Generalized geologic map of Maui, showing localities mentioned in text. Modified from Macdonald and others (1983). Rift zones from Fiske and Jackson (1972). West Maui Volcano caldera boundary from Macdonald and others (1983, fig. 20.4).

(1978). As it consists entirely of tholeiitic basalt, it is here renamed everywhere the Honomanu Basalt.

The Kula Volcanic Series of Stearns and Macdonald (1942), which was later called the Kula Formation by Macdonald (1978), is here renamed the Kula Volcanics to reflect its varied lithology. Rocks in the lower part of the south wall of Haleakala Crater that Stearns and Macdonald (1942) had originally assigned to the Honomanu were excluded from the Honomanu and named the Kumuiliahi Formation by Macdonald (1978). As these rocks appear more properly to belong to the Kula (Macdonald and others, 1983, p. 391), they are here tentatively included in the Kula, and the name Kumuiliahi Formation is not used.

The Kula was named by Stearns (1942) for the settlement of Kula (now called Waiakoa) along the roads leading to the Kula Sanatorium or Hospital on the west slope of the volcano, but he did not designate a type locality. Macdonald and Davis (in Avias and others, 1956), however, did specify the type locality as "Kula, a district on the west slope of East Maui Mountain." This "locality" is here considered to be along Highway 37 near Waiakoa (Kula Post Office), about 7 km northeast of Kula Hospital. Other accessible

sections of the Kula, according to Stearns, are along the Kaupo-Kipahulu road near Kipahulu and along Halemauu Trail in the Haleakala Crater area; these are here considered to be reference localities.

Stearns and Macdonald (1942) subdivided the Hana Volcanic Series into many local formally named units in the Keanae and Nahiku areas along the northeast coast. It was not clear whether they intended these units to be of member or formation rank (see Stearns and Macdonald, 1942, p. 94, 95), but they applied formational-rank names to these units. Macdonald and Davis (in Avias and others, 1956) considered them to be formations. In Kipahulu Valley in the southeastern part of the island, however, Stearns and Macdonald (1942) included only the Kipahulu Member within the Hana. The Kipahulu was later raised in rank by Macdonald and Davis (in Avias and others, 1956) to Kipahulu Formation, though in later publications by Macdonald and Abbott (1970), Macdonald and others (1983), and Stearns (1985) the term Kipahulu Member is used. Thus the Hana had previously been considered to be of group rank. Macdonald (1978) did reduce the rank of the Hana in the Haleakala Crater area, using the name Hana Formation, but he did not address the status of the formational rank units in the Keanae and Nahiku areas.

Therefore, the following changes are here made to the Hana: The Hana is reduced to formational rank everywhere and renamed the Hana Volcanics. Its subdivisions in the Keanae and Nahiku areas, being mainly single flows of very limited extent, are abandoned as formally named units and are used informally (table 1.12). The Kipahulu is retained as a member of the Hana because it is a fairly extensive unit and is separated from earlier Hana flows by an erosional unconformity. The historical lava flow of about 1790 in the Cape Kinau area (Oostdam, 1965) is considered to be part of the Hana, although it was not included in the Hana by Stearns and Macdonald (1942), and they gave "1750?" as the date of the flow. Finally, to correct an error in Keroher and others (1966, p. 1976), the Hana does not include the Kaupo Mudflow.

The Pleistocene age of the Honomanu Basalt and Kula Volcanics is well documented by K-Ar determinations (Naughton and others, 1980) (table 1.12). No isotopic ages have been determined for the Hana Volcanics, but it is here considered to be Pleistocene(?) and Holocene. The Kipahulu Member is probably Pleistocene, judging by its relations to older units.

WEST MAUI VOLCANO

West Maui Volcano is incised by deep valleys and is considered to be extinct. Lava was erupted from a small central caldera and from the north and southeast rift zones.

The rocks of West Maui Volcano were divided by Stearns and Macdonald (1942) into three major units—Wailuku Volcanic Series (oldest), Honolua Volcanic Series, and Lahaina Volcanic Series (youngest). These units represent the shield stage and postshield caldera-filling phase, the postshield stage, and the rejuvenated stage, respectively.

Stearns and Macdonald did not subdivide the Wailuku and Honolua, which are here renamed the Wailuku Basalt and Honolua Volcanics, respectively. They did, however, include two formational-rank units, the Kilea Volcanics and the Laina Volcanics, within their Lahaina Volcanic Series. The Lahaina was recently reduced to formational rank and renamed the Lahaina Volcanics by Clague and others (1982), but they did not address the status of the Kilea and Laina. The Kilea Volcanics and Laina Volcanics are two small flow units with associated cinder cones; because they are of such limited extent, they are here abandoned as formally named units and their names used informally (table 1.12). The name Lahaina Volcanics of Clague and others (1982) is retained here.

Isotopic age determinations of the Wailuku Basalt and Honolua Volcanics (McDougall, 1964; Naughton and others, 1980) (table 1.12) indicate a Pleistocene age for both units. The Lahaina Volcanics is less well dated, but it is also considered to be Pleistocene. The single K-Ar age of 1.30 ± 0.10 Ma (Naughton and others, 1980) is considered to be too old on stratigraphic grounds.

KAHOOLAWE AND LANAI

Each of these islands consists of a single shield volcano with a summit caldera, and each has been little dissected.

KAHOOLAWE VOLCANO

The lava of Kahoolawe Volcano was erupted along a prominent southwest rift zone (fig. 1.25). The caldera was almost completely buried beneath a cap of later lava.

The rocks that form essentially all of the Island of Kahoolawe, the smallest of the major islands, were called the Kanapou Volcanic Series by Stearns (1946). The Kanapou, which is not subdivided and is here renamed the Kanapou Volcanics, represents the shield stage, a caldera-filling phase of both the shield and postshield stages, and the postshield stage. The small rejuvenated-stage vents that occur in the sea cliffs on the west side of Kanapou Bay were not considered by Stearns (1946) to be part of the Kanapou, and they are not so considered here.

The alkalic part of the Kanapou Volcanics has been dated at about 1 Ma (Naughton and others, 1980); the tholeiitic part is undated, but is presumed here to be Pleistocene also. The rejuvenated-stage vents are not isotopically dated. They were considered to be of Holocene age by Macdonald and others (1983), but this age is probably too young.

LANAI VOLCANO

The Island of Lanai was built by eruptions from the summit and along northwest, southwest, and southeast rift zones (fig. 1.26). The caldera was mostly filled by lava flows, but its remnant is now covered by alluvium.

The volcanic rocks of Lanai represent the shield stage, including the caldera-filling phase, and they were called the Lanai Volcanic Series by Stearns (1946). Wentworth (1925) had originally applied the name Lanai Basalt to the lava flows of Lanai Volcano and the name Manele Basalt to the small crater remnant

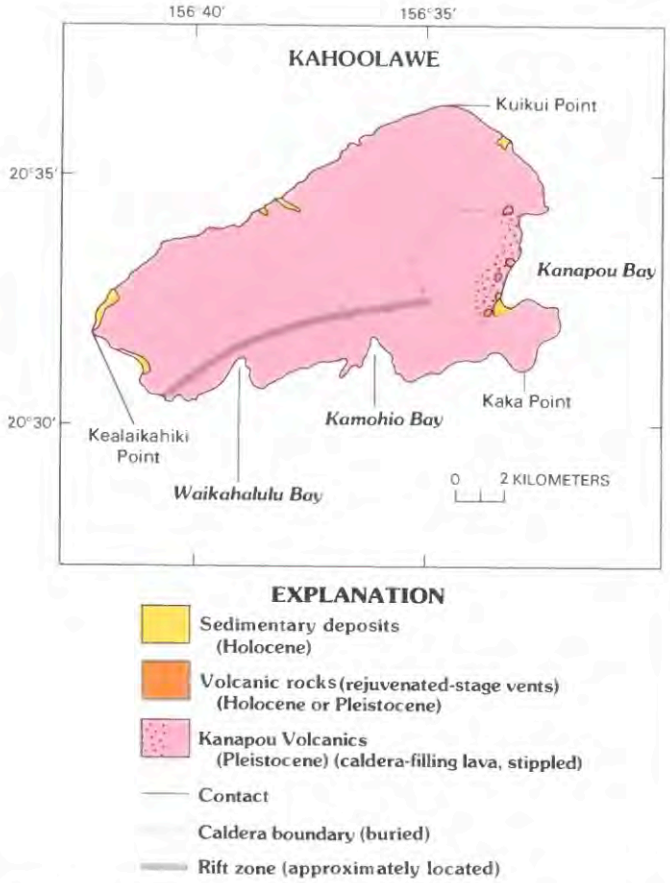

FIGURE 1.25.—Generalized geologic map of Kahoolawe, showing localities mentioned in text. Modified from Macdonald and others (1983). Rift zone from Fiske and Jackson (1972).

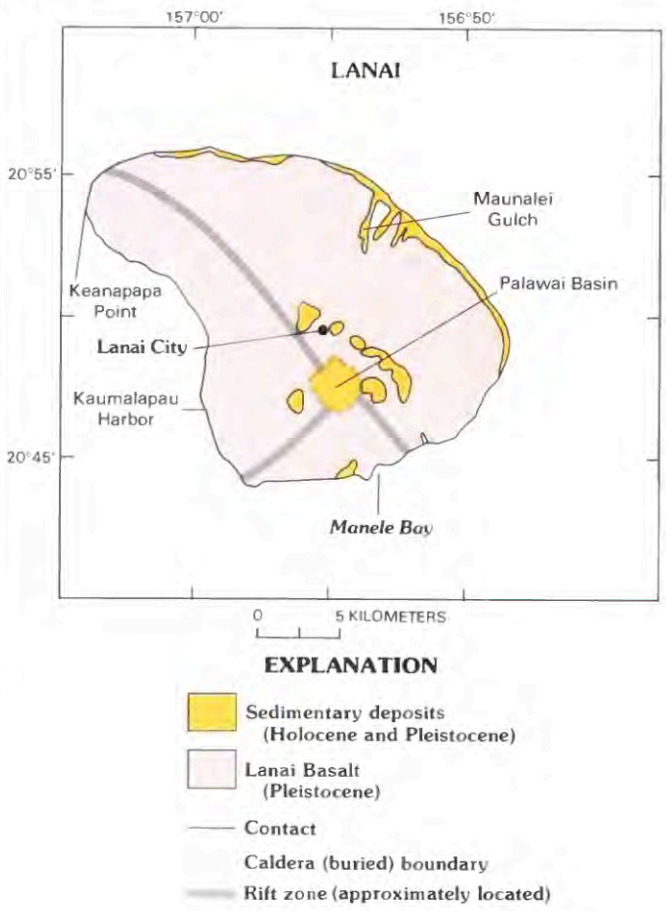

FIGURE 1.26.—Generalized geologic map of Lanai, showing localities mentioned in text. Modified from Macdonald and others (1983). Rift zones from Fiske and Jackson (1972). Caldera boundary inferred to be largely coincident with Palawai Basin.

that forms the headland southwest of Manele Bay. Stearns (1946) redefined the Lanai to include not only the lava flows but also other associated rocks (pyroclastic and intrusive rocks) in a unit he called the Lanai Volcanic Series; he did not include Wentworth's terms Lanai and Manele Basalts as part of the Lanai Volcanic Series. However, Macdonald and Davis (in Avias and others, 1956) included (improperly) the Lanai Basalt, which included Manele Basalt, in the Lanai Volcanic Series, seemingly giving group status to the later unit.

The Lanai Volcanic Series of Stearns (1946) is here reduced to formational rank and renamed the Lanai Basalt. Though there is a chance of confusion with the Lanai Basalt of Wentworth, which consisted only of the lava flows, it would be more misleading to call the unit "Lanai Volcanics" because it consists totally of shield-stage tholeiitic basalt.

The term Manele Basalt is here abandoned as a formal name because it has essentially the same lithology and same age as the Lanai Basalt, as used here, and is of extremely limited extent and the term has been applied to a former high stand of the sea.

The Lanai Basalt is of Pleistocene age based on a K-Ar isochron age of 1.28±0.4 Ma (Bonhommet and others, 1977) (table 1.12).

MOLOKAI

The Island of Molokai is another volcanic doublet, made up of two coalesced volcanoes—East Molokai and West Molokai Volcanoes (fig. 1.27). East Molokai Volcano had a summit caldera; there is no evidence that West Molokai Volcano had one. Both volcanoes are deeply dissected along their northern coasts.

EAST MOLOKAI VOLCANO

East Molokai Volcano was built principally by eruptions from the summit caldera and along east and northwest rift zones.

The volcanic rocks of East Molokai Volcano were divided by Stearns (1946, 1947a) into the East Molokai Volcanic Series (older) and the Kalaupapa Basalt (younger).

The East Molokai Volcanic Series, here renamed the East Molokai Volcanics, was subdivided by Stearns into two informal members—lower and upper members. The lower member represents the shield stage and part of the postshield stage; both stages include a caldera-filling phase. The upper member represents the rest of the postshield stage.

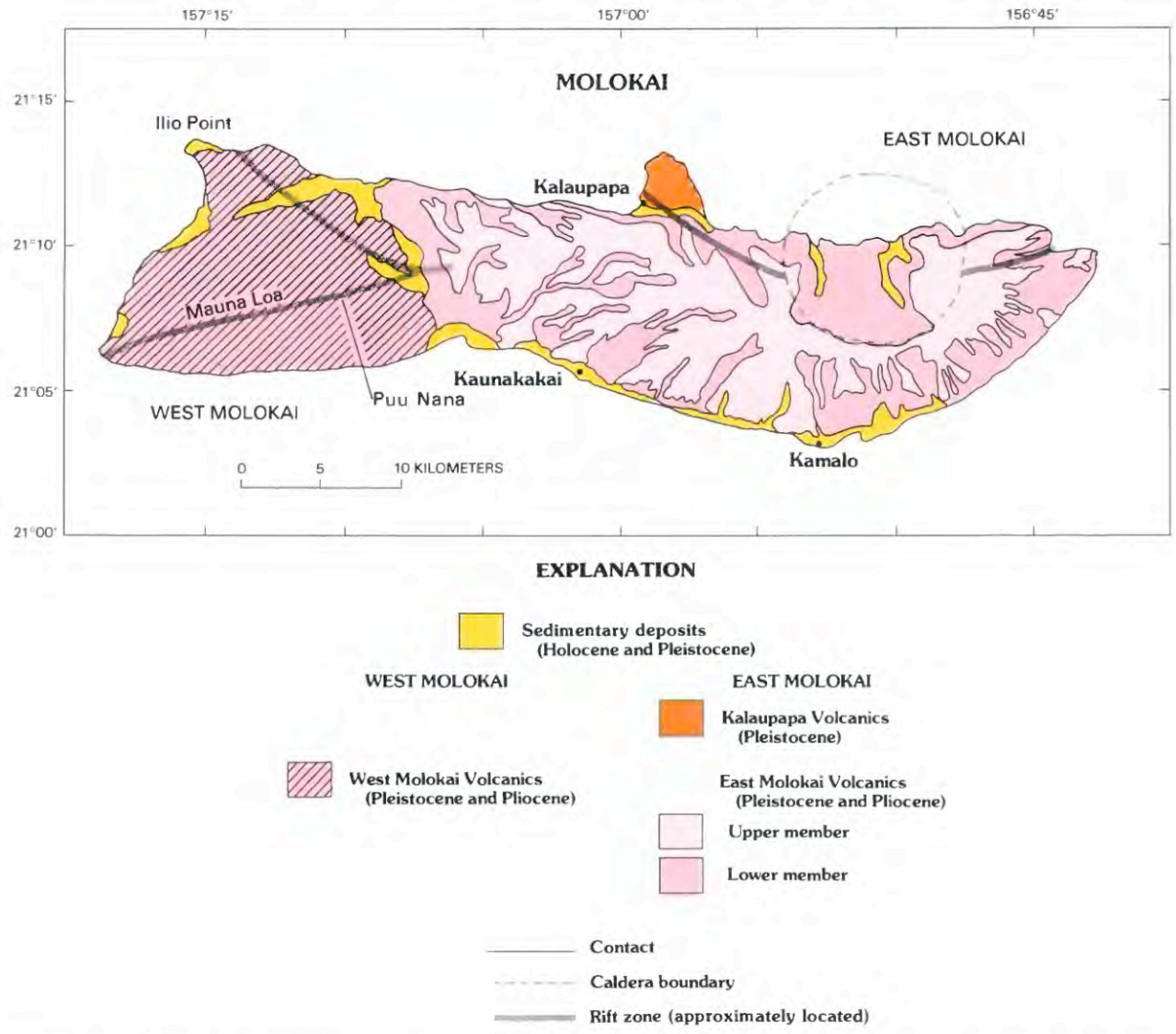

FIGURE 1.27.—Generalized geologic map of Molokai, showing localities mentioned in text. Modified from Macdonald and others (1983). Rift zones from Fiske and Jackson (1972). East Molokai Volcano caldera boundary from Holcomb (1985).

The Kalaupapa Basalt, which consists of alkalic basalt and basanite, is here renamed the Kalaupapa Volcanics to reflect the range of compositions present. The Kalaupapa has been proposed as a separate shield (see Macdonald and others, 1983; Holcomb, 1985), but it is here considered to represent a rejuvenated-stage vent associated with East Molokai Volcano on the basis of its age and chemistry (see Clague and others, 1982).

The East Molokai Volcanics is largely Pleistocene, but its lowermost flows are Pliocene on the basis of K-Ar age determinations on its lower and upper members (McDougall, 1964; Naughton and others, 1980) (table 1.12). The Kalaupapa Volcanics has a Pleistocene age based on K-Ar determinations of 0.57 ± 0.02 and 0.35 ± 0.03 Ma (Clague and others, 1982).

WEST MOLOKAI VOLCANO

West Molokai Volcano was built by eruptions principally along a northeast rift zone that crosses the summit area (Puu Nana) and along a northwest rift zone. There is no evidence of a summit caldera.

All of the volcanic rocks of West Molokai Volcano were called the West Molokai Volcanic Series by Stearns (1946, 1947a). The West Molokai Volcanic Series, which was not subdivided by Stearns, is here renamed the West Molokai Volcanics to reflect its varied rock types. The West Molokai Volcanics represents the shield and postshield eruptive stages.

The age of the West Molokai Volcanics is considered to be

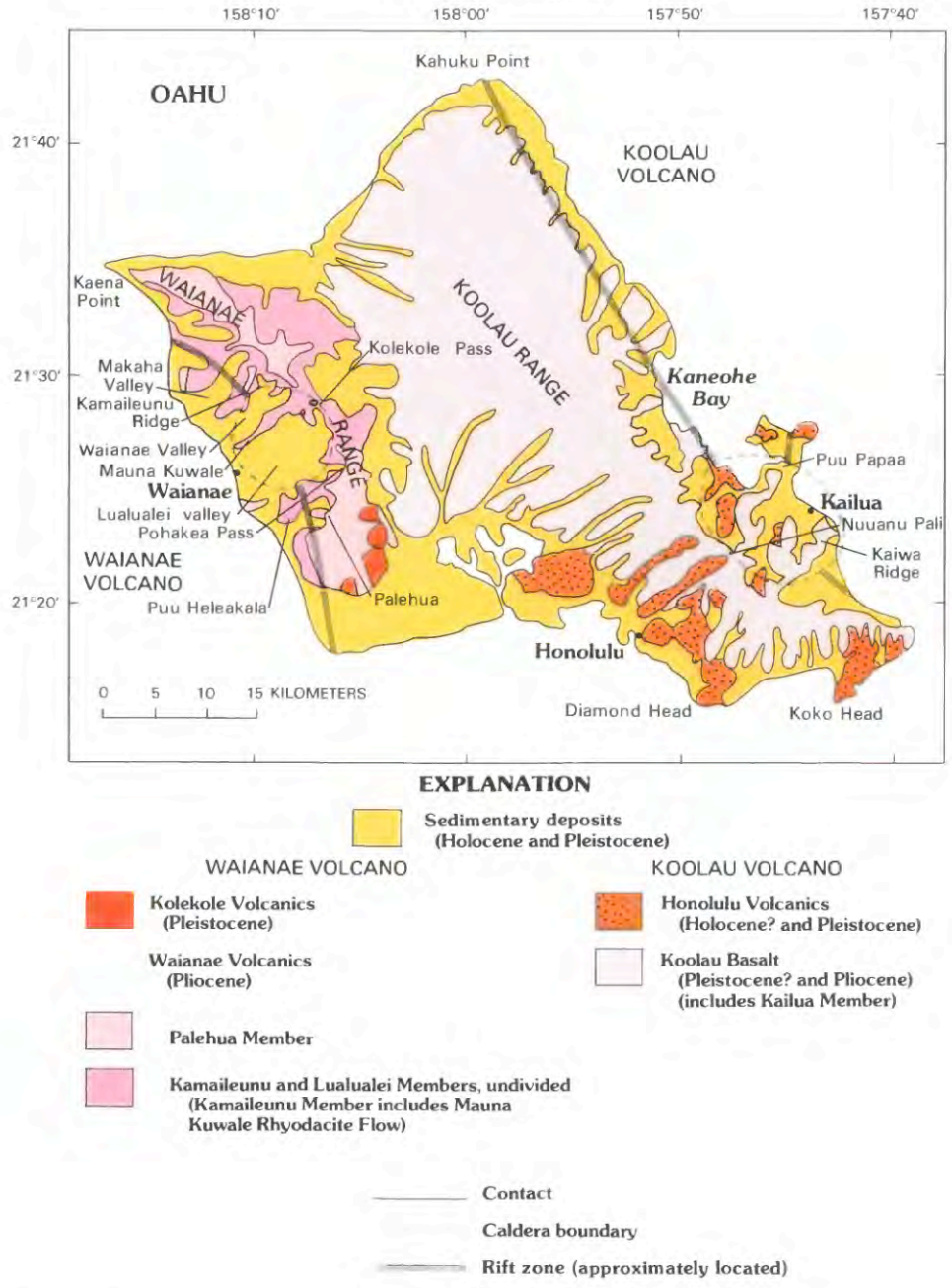

FIGURE 1.28.—Generalized geologic map of Oahu, showing localities mentioned in text. Modified from Macdonald and others (1983) and Sinton (in press). Rift zones from Fiske and Jackson (1972). Koolau Volcano caldera boundary from Clague and Frey (1982); Waianae Volcano caldera boundary from Sinton (in press).

Pliocene and Pleistocene on the basis of K-Ar determinations by Naughton and others (1980) (table 1.12).

OAHU

This island is made up of the highly dissected remnants of two shield volcanoes—Koolau Volcano (east) and Waianae Volcano (west) (fig. 1.28)—that have lost their original shield outline and are now two northwest-trending ridges shaped mainly by erosion. Both volcanoes had summit calderas.

KOOLAU VOLCANO

The lava of Koolau Volcano was principally erupted from the caldera and along the northwest and southeast rift zones. A major dike complex occurs in the rift zones (Walker, chapter 41). The vents

for the youngest lava (rejuvenated stage) show no relationship to the preexisting rift zones.

The rocks of this volcano were originally divided by Stearns (1935, 1939) into three major volcanic units—the Kailua Volcanic Series (oldest), the Koolau Volcanic Series, and the Honolulu Volcanic Series (youngest). The Koolau and the Honolulu represent the shield stage and rejuvenated stage, respectively. Stearns originally believed the Kailua Volcanic Series represented an older lava series that was under or close by the summit caldera of Koolau Volcano, but that it was not part of Koolau Volcano. He later (Stearns, 1940a) recognized that the Kailua was part of the Koolau Volcano, representing the caldera complex. Macdonald and Davis (in Avias and others, 1956) included (improperly) the Kailua Volcanic Series in the Koolau Volcanic Series. Although the ranks they intended for these units are not clear, it is here presumed that the Kailua Volcanic Series was of formational rank.

More recently the Koolau has been considered to be of formational rank. It was called the Koolau Formation by Wentworth (1951) and the Koolau Volcanics by Lanphere and Dalrymple (1979) (table 1.12). It is here renamed the Koolau Basalt because it consists entirely of shield-stage tholeiitic basalt. Although Wentworth (1926, fig. 15) also used the term "Koolau basalt" in the explanation of a page-size geologic map of a small area of Oahu, he did not describe the unit and there does not seem much chance of confusion with the Koolau Basalt as used here. The Kailua Volcanic Series is here reduced in rank and renamed the Kailua Member of the Koolau Basalt.

The Honolulu Volcanic Series was defined by Stearns (1935) to consist of rejuvenated-stage lava that erupted from more than 35 vents on the southern slopes of the volcano. These lavas are strongly alkalic and form a variety of cones (tuff, cinder, spatter), many with associated lava flows. The eruptions presumably did not come in rapid succession, but occurred over a long period of time. Their general sequence (Macdonald and others, 1983) (table 1.12) has been based largely on the relative degree of weathering and erosion and on relations to stands of the sea because few superpositional relations are known and isotopic ages are considered unreliable.

The Honolulu Volcanic Series was of group rank as defined by Stearns (1935, 1939) because it was made up of numerous formally named units of formational rank (table 1.12). Hay and Iijima (1968) and Clague and others (1982) also considered the Honolulu to be of group rank. Lanphere and Dalrymple (1979) and Clague and Frey (1982) used the formational-rank term Honolulu Volcanics, but did not address the status of its formally named subdivisions. The Honolulu is here considered to be of formational rank, and the term Honolulu Volcanics is retained to reflect its range of lithologic compositions.

The formally named eruptive units that make up the Honolulu could have been reduced in rank and retained as formally named members, but, because most are single flows of very limited extent, this seems unnecessary; they are here all considered to be informal units (table 1.12).

The age of the Koolau Basalt is Pliocene based on K-Ar ages ranging from 2.7 to 1.8 Ma (Doell and Dalrymple, 1973); however, a Pleistocene age cannot be ruled out for the youngest flows (table 1.12). The Kailua Member has not been isotopically dated, but is probably Pleistocene.

The K-Ar ages reported for the Honolulu Volcanics range from about 0.9 to about 0.03 Ma, but there are large differences (sometimes a factor of ten) in the ages reported by different investigators for the same eruptive units (see Clague and Dalrymple, chapter 1, part I; Macdonald and others, 1983). The Honolulu is certainly in part Pleistocene on the basis of published K-Ar ages, but because of the unreliability of some of the ages, a Holocene age cannot be ruled out for the youngest flows.

WAIANAE VOLCANO

Waianae Volcano was built by eruptions from the summit caldera and along the principal northwest and southeast rift zones.

The rocks of the volcano are divided into the Waianae Volcanics, representing the shield and postshield stages (both including a caldera- filling phase), and the Kolekole Volcanics, representing the rejuvenated stage (Sinton, in press). The Waianae was originally named the Waianae Volcanic Series and subdivided into three informal members (lower, middle, and upper) by Stearns (1935). He described these members but did not map them separately (Stearns, 1939). The Waianae has recently been subdivided by Sinton (in press) into three formally named members—the Lualualei (oldest), Kamaileunu, and Palehua (youngest) Members. These members are, for the most part, equivalent to Stearns' lower, middle, and upper members, respectively (table 1.12; see Sinton, in press). The Kamaileunu Member includes the Mauna Kuwale Rhyodacite Flow and several icelandite flows. These are the only known occurrences of rhyodacite and icelandite in the Hawaiian Islands. The rhyodacite flow was given formal status by Sinton (in press), and because it is of such distinctive lithology it is also considered to be formal here.

A Pliocene age for the Waianae Volcanics is inferred from K-Ar determinations ranging from 3.9 to 2.5 Ma (Doell and Dalrymple, 1973) (table 1.12). Funkhouser and others (1968) reported an average K-Ar age of about 2.4 Ma for the Mauna Kuwale Rhyodacite Flow, but this age is inconsistent with their reported ages for the overlying lava flow (4.3 Ma) and dikes (about 3 Ma) cutting the rhyodacite. According to Sinton (in press), the Mauna Kuwale probably has a minimum age of 3.2 Ma. The Kolekole Volcanics has not been isotopically dated but is tentatively considered by Sinton (in press) to be Pleistocene.

KAUAI

KAUAI VOLCANO

The Island of Kauai (fig. 1.29) consists of a single deeply eroded shield volcano with a summit caldera 15-20 km across, the largest in the Hawaiian Islands, and at least two flank calderas, the only ones known in the islands. Lava erupted not only in the calderas, but also from northwest and southeast rift zones. After a period of erosion, rejuvenated-stage lava erupted from about 40

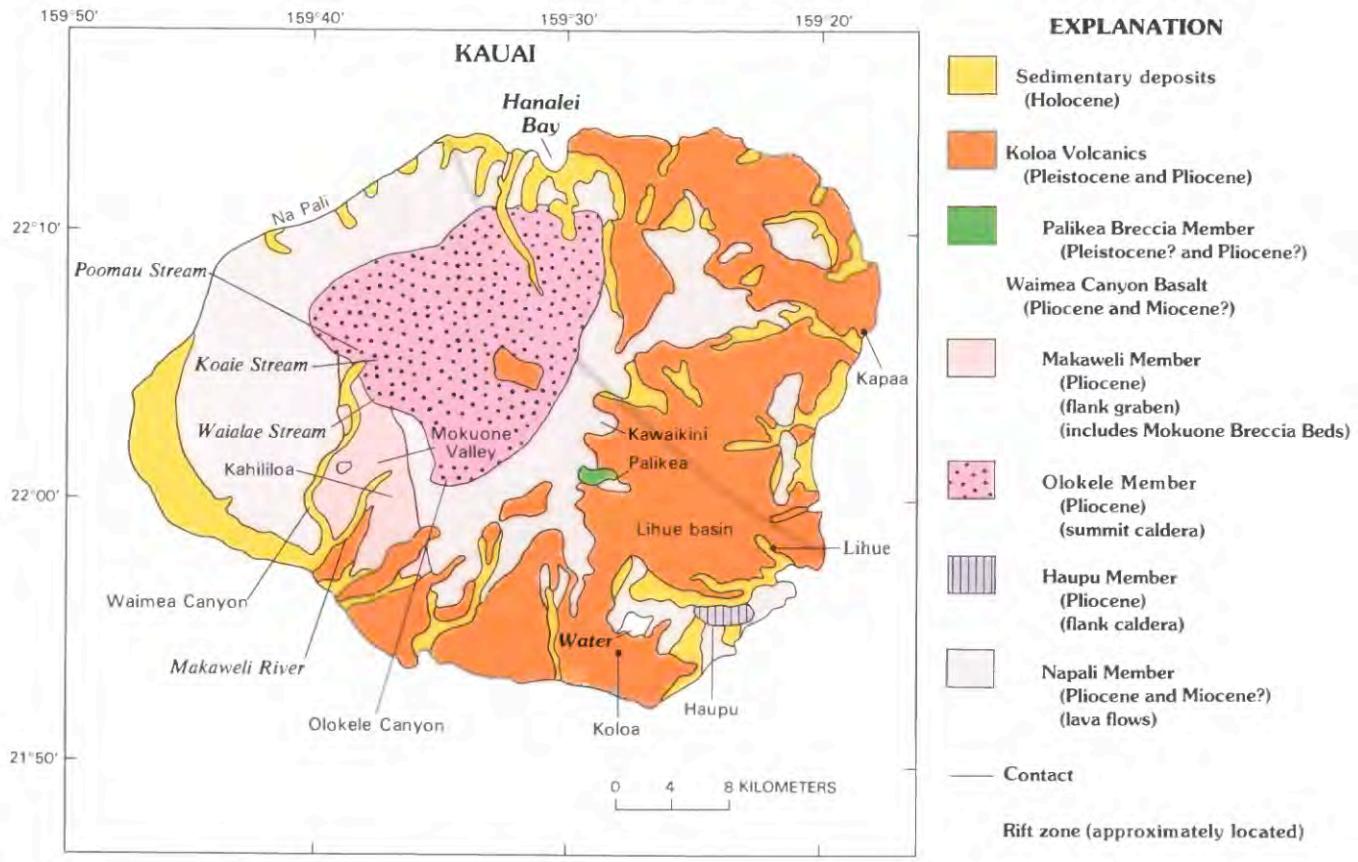

FIGURE 1.29.—Generalized geologic map of Kauai, showing localities mentioned in text. Modified from Macdonald and others (1983). Rift zones from Fiske and Jackson (1972). Summit caldera and southeast flank caldera are represented by Olokele Member and Haupu Member, respectively. Another flank caldera is represented by Lihue basin, a subcircular basin 10-15 km wide, which is almost bisected by southeast rift zone. There is no evidence that shield-stage or postshield-stage lava poured into this caldera, but it was later filled with rejuvenated-stage lava (Koloa Volcanics).

vents scattered over the eastern two-thirds of the island; these vents show no relation to the older rift zones.

The rocks of Kauai Volcano were originally divided by Stearns (1946) into the Waimea Volcanic Series (older), later renamed the Waimea Canyon Volcanic Series (Macdonald, 1949), and the Koloa Volcanic Series (younger). The Waimea Canyon represents the shield stage including the caldera-filling phase. Postshield-stage hawaiite is rare and occurs only at the top of the Waimea Canyon (fig. 1.21, table 1.12). The Koloa represents the rejuvenated stage.

The Waimea Canyon Volcanic Series was subdivided by Macdonald and others (1954, 1960) into four formally named formations—the Napali, Haupu, Olokele, and Makaweli Formations. The Makaweli Formation as defined by Macdonald and others (1960) included associated sedimentary deposits, which were called the Mokuone Member.

In order to have a nomenclature consistent with the other volcanoes of the Hawaiian Islands, the following changes are here made to the Waimea Canyon Volcanic Series: The Waimea Canyon is reduced to formational rank and renamed the Waimea Canyon Basalt to reflect its predominant lithology. Its subdivisions are reduced to member rank and called the Napali, Haupu, Olokele, and Makaweli Members. The sedimentary unit included within the Makaweli is reduced in rank and renamed the Mokuone Breccia Beds (table 1.12).

Although the Napali, Haupu, Olokele, and Makaweli Members consist of essentially the same rock types, they are distinguishable and extensive units. The Napali Member consists of thin-bedded flank flows, whereas the Olokele and Makaweli Members consist of massive or thick-bedded flows. The Olokele is separated from the Makaweli and from the Napali by faults. The Haupu, which presumably represents a small caldera on the southeast flank of the volcano, also consists of thick-bedded flows, but it is isolated from the Olokele and Makaweli Members and is surrounded by older thin-bedded flows of the Napali Member.

The Napali, Olokele, and Makaweli Members had more than one type locality specified by Davis and Macdonald (in Avias and others, 1956) and Macdonald and others (1960). One of the localities is here retained as the type locality for each unit, and the other localities are redesignated as reference localities (table 1.12.).

The Koloa Volcanic Series, as defined by Stearns (1946) and Macdonald and others (1960), included within it a sedimentary unit that they named the Palikea Formation. The Palikea Formation consists largely of breccia underlying and interbedded with Koloa lava flows. The breccia, which grades laterally in some places into stream-laid conglomerate, is primarily made up of fragments of the Waimea Canyon Basalt and represents the rapid shedding of debris from the steep slopes of the volcano before and during Koloa time. Clague and others (1982) reduced the Koloa Volcanic Series to formational rank and renamed it the Koloa Volcanics, but they did not discuss the status of the Palikea Formation. The Palikea is here reduced in rank and renamed the Palikea Breccia Member of the Koloa Volcanics.

The Waimea Canyon Basalt is largely of Pliocene age, but the oldest flows may be Miocene, as indicated by K-Ar ages ranging from about 5.1 to 3.6 Ma (McDougall, 1964; 1979). The age relations between the caldera-filling-phase members are not known, but the Olokele Member is considered to be older than the Makaweli Member, and the Haupu Member is thought to be coeval with the Olokele.

The Koloa Volcanics is largely Pleistocene, an age indicated by all the published K-Ar ages, but unpublished K-Ar ages of 2.59 and 2.01 Ma (G.B. Dalrymple, oral commun., 1986) suggest that the oldest flows are Pliocene. The age of the Palikea Breccia Member is not known, but it is probably Pliocene and Pleistocene on the basis of its stratigraphic relations to Koloa lava flows.

NIIHAU

NIIHAU VOLCANO

The Island of Niihau (fig. 1.30) is the deeply eroded remnant of a shield volcano. The central highland area, which consists of shield-stage tholeiitic lava, is fringed by a low coastal platform, which consists of rejuvenated-stage lava. The shield-stage lava was erupted from a southwest rift zone; the summit of the shield (and former caldera?) was presumably northeast of the present island.

The rocks of the volcano were divided by Stearns (1946, 1947b) into two major units—the Paniau Volcanic Series (older) and the Kiekie Volcanic Series (younger). The Paniau almost entirely represents the shield stage; a single postshield-stage vent that occurs at Kaeo and a couple postshield alkalic basalt dikes along the east coast of the island are also considered in this report to be part of the Paniau Basalt. These units are here renamed the Paniau Basalt and Kiekie Basalt, respectively. Although all of the rejuvenated-stage units on the other islands are called "Volcanics," the name Kiekie Volcanics is not used here because the Kiekie consists entirely of alkalic basalt.

No isotopic ages for the Island of Niihau have been published. However, unpublished K-Ar data for 11 flows of the Paniau indicate a Miocene and Pliocene age (G.B. Dalrymple, oral commun., 1986). The Kiekie Basalt was considered to be of Pleistocene age by Stearns (1947b) on the basis of its relations to Pleistocene shorelines, but unpublished K-Ar ages (G.B. Dalrymple, oral commun., 1986) indicate a Pliocene and Pleistocene age.

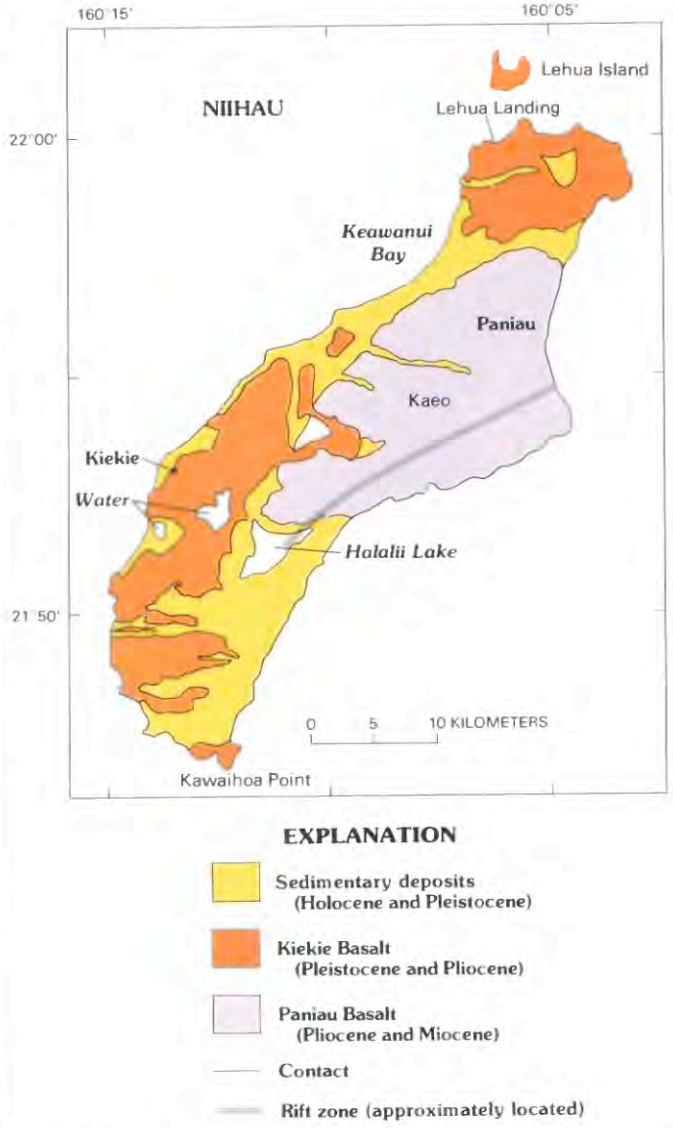

FIGURE 1.30.—Generalized geologic map of Niihau, showing localities mentioned in text. Modified from Macdonald and others (1983). Rift zone approximately follows dike swarm mapped by Stearns (1947b).

REFERENCES

American Commission on Stratigraphic Nomenclature, 1961, Code of Stratigraphic Nomenclature: American Association of Petroleum Geologists Bulletin, v. 45, no. 5, p. 645-665.

———1970, Code of Stratigraphic Nomenclature (revised): Tulsa, Oklahoma, American Association of Petroleum Geologists, 45 p.

Ashley, G.H., Cheney, M.G., Galloway, J.J., Gould, C.N., Hares, C.J., Howell, B.F., Levorsen, A.I., Miser, H.D., Moore, R.C., Reeside, J.B., Jr., Rubey, W.W., Stanton, T.W., Stose, G.W., and Twenhofel, W.H., 1933, Classification and nomenclature of rock units: Geological Society of America Bulletin, v. 44, p. 423-459.

Avias, J., Davis, D.A., Hanzawa, S., Ladd, H.S., Macdonald, G.A., and Obellianne, J.M., 1956, Oceanie proprement dite [Oceania properly speaking], pt. 2 of Oceanie, v. 6 of Lexique Stratigraphique International [International Stratigraphic Lexicon]: Paris, Centre National de la Recherche Scientifique, 286 p.

Bonhommet, N., Beeson, M.H., and Dalrymple, G.B., 1977, A contribution to the geochronology and petrology of the island of Lanai, Hawaii: Geological Society of America Bulletin, v. 88, p. 1282-1286.

Clague, D.A., 1982, Petrology of tholeiitic basalt dredged from Hualalai Volcano, Hawaii: Eos, Transactions American Geophysical Union, v. 63, p. 1138.

Clague, D.A., Dao-Gong, C., Murnane, R., Beeson, M.H., Lanphere, M.A., Dalrymple, G.B., Friesen, W., and Holcomb, R.T., 1982, Age and petrology of the Kalaupapa Basalt, Molokai, Hawaii: Pacific Science, v. 36, p. 411-420.

Clague, D.A., and Frey, F.A., 1982, Petrology and trace element geochemistry of the Honolulu Volcanics, Oahu: Implications for the oceanic mantle beneath Hawaii: Journal of Petrology, v. 23, p. 447-504.

Decker, R.W., and Christiansen, R.L., 1984, Explosive eruptions of Kilauea Volcano, Hawaii, *in* Explosive volcanism: Inception, evolution, and hazards (National Research Council Studies in Geophysics): Washington, National Academy Press, p. 122-132.

Doell, R.R., and Dalrymple, G.B., 1973, Potassium-argon ages and paleomagnetism of the Waianae and Koolau Volcanic Series, Oahu, Hawaii: Geological Society of America Bulletin, v. 84, p. 1217-1242.

Easton, R.M., and Garcia, M.O., 1980, Petrology of the Hilina Formation, Kilauea Volcano, Hawaii: Bulletin Volcanologique, v. 43-4, p. 657-673.

Fiske, R.S., and Jackson, E.D., 1972, Orientation and growth of Hawaiian volcanic rifts: The effect of regional structure and gravitational stresses: Proceedings of the Royal Society of London, ser. A. v. 329, p. 299-326.

Funkhouser, J.G., Barnes, I.L., and Naughton, J.J., 1968, The determination of a series of ages of Hawaiian volcanoes by the potassium-argon method: Pacific Science, v. 22, p. 369-372.

Hay, R.L., and Iijima, A., 1968, Nature and origin of palagonite tuffs of the Honolulu Group of Oahu, Hawaii, *in* Coats, R.R., Hay, R.L., and Anderson, C.A., eds., Studies in volcanology: Geological Society of America Memoir 116, p. 331-376.

Hinds, N.E.A., 1930, The geology of Kauai and Niihau: Bernice P.Bishop Museum Bulletin 71, 103 p.

Holcomb, R.T., 1985, The caldera of East Molokai Volcano, Hawaii: National Geographic Society Research Reports, v. 21, p. 81-87.

Keroher, G.C., and others, 1966, Lexicon of geologic names of the United States for 1936-1960: U.S. Geological Survey Bulletin 1200, p. 1449-2886.

Lanphere, M.A., and Dalrymple, G.B., 1979, Age and strontium isotopic composition of the Honolulu Volcanics, *in* Geological Survey Research 1979: U.S. Geological Survey Professional Paper 1150, p. 180.

Lipman, P.W., 1980, Rates of volcanic activity along the southwest rift zone of Mauna Loa Volcano, Hawaii: Bulletin Volcanologique, v. 43-4, p. 703-725.

Lockwood, J.P., and Rubin, Meyer, 1986, Distribution and age of the Uwekahuna Ash, Kilauea Volcano, Hawaii (abstract): International Volcanological Congress Feb. 1-9, 1986, New Zealand Abstracts, p. 112.

Macdonald, G.A., 1942, Geology and ground-water resources of the Nahiku area, East Maui: Hawaii Division of Hydrography Bulletin 7 (part 2), p. 223-274.

———1945, Ring structures at Mauna Kea, Hawaii: American Journal of Science, v. 243, no. 4, p. 210-217.

———1949, Hawaiian petrographic province: Geological Society of America Bulletin, v. 60, p. 1541-1595.

———1968, Composition and origin of Hawaiian lavas *in* Coats, R.E., Hay, R.L., and Anderson, C.A., eds., Studies in volcanology: Geological Society of America Memoir 116, p. 477-522.

———1978, Geologic map of the crater section of Haleakala National Park, Maui, Hawaii: U.S. Geological Survey Miscellaneous Investigations Series Map I-1088, scale 1:24,000.

Macdonald, G.A., and Abbott, A.T., 1970, Volcanoes in the sea: Honolulu, University of Hawaii Press, 441 p.

Macdonald, G.A., Abbott, A.T., and Peterson, F.L., 1983, Volcanoes in the sea: The geology of Hawaii (2nd ed.): Honolulu, University of Hawaii Press, 517 p.

Macdonald, G.A., Davis, D.A., and Cox, D.C., 1954, Kauai, an ancient Hawaiian volcano: The Volcano Letter, no. 526, p. 1-3.

———1960, Geology and ground-water resources of the Island of Kauai, Hawaii: Hawaii Division of Hydrography Bulletin 13, 212 p.

Macdonald, G.A., and Katsura, T., 1964, Chemical composition of Hawaiian lavas: Journal of Petrology, v. 5, pt. 1, p. 82-133.

Malin, M.C., Dzurisin, Daniel, and Sharp, R.P., 1983, Stripping of Keanakakoi tephra in Kilauea Volcano, Hawaii: Geological Society of America Bulletin, v. 94, p. 1148-1158.

McDougall, Ian, 1963, Potassium-argon ages from western Oahu, Hawaii: Nature, v. 197, p. 344-345.

———1964, Potassium-argon ages from lavas of the Hawaiian Islands: Geological Society of America Bulletin, v. 75, p. 107-128.

———1969, Potassium-argon ages on lavas of Kohala Volcano, Hawaii: Geological Society of America Bulletin, v. 80, p. 2597-2600.

———1979, Age of shield-building volcanism of Kauai and linear migration of volcanism in the Hawaiian Island chain: Earth and Planetary Science Letters, v. 46, p. 31-42.

McDougall, Ian, and Swanson, D.A., 1972, Potassium-argon ages of lavas from the Hawi and Pololu Volcanic Series, Kohala Volcano, Hawaii: Geological Society of America Bulletin, v. 83, p. 3731-3738.

Moore, J.G., Clague, D.A., and Normark, W.R., 1982, Diverse basalt types from Loihi seamount, Hawaii: Geology, v. 10, p. 88-92.

Naughton, J.J., Macdonald, G.A., and Greenberg, V.A., 1980, Some additional potassium-argon ages of Hawaiian rocks: the Maui volcanic complex of Molokai, Maui, Lanai, and Kahoolawe: Journal of Volcanology and Geothermal Research, v. 7, p. 339-355.

North American Commission on Stratigraphic Nomenclature, 1983, North American Stratigraphic Code: American Association of Petroleum Geologists Bulletin, v. 67, no. 5, p. 841-875.

Oostdam, B.L., 1965, Age of lava flows on Haleakala, Maui, Hawaii: Geological Society of America Bulletin, v. 76, p. 393-394.

Palmer, A.R., 1983, The Decade of North American Geology 1983 Time Scale: Geology, v. 11, p. 503-504.

Porter, S.C., 1971, Holocene eruptions of Mauna Kea Volcano: Science, v. 172, p. 375-377.

———1972, Buried caldera of Mauna Kea Volcano, Hawaii: Science, v. 175, p. 1458-1460.

———1973, Stratigraphy and chronology of late Quaternary tephra along the south rift zone of Mauna Kea Volcano, Hawaii: Geological Society of America Bulletin v. 84, p. 1923-1940.

———1974, Mauna Kea *in* Greely, R., ed., Guidebook to the Hawaiian Planetology Conference: Moffett Field, California, Ames Research Center (NASA), p. 239-246.

———1979a, Quaternary stratigraphy and chronology of Mauna Kea, Hawaii: A 380,000 year record of mid-Pacific volcanism and ice-cap glaciation: Geological Society of America Bulletin, v. 90, no. 7, pt. 1, p. 609-611; pt. 2, p. 980-1093.

———1979b, Geologic map of Mauna Kea Volcano, Hawaii: Geological Society of America Map and Chart Series, MC-30, scale 1:50,000.

Porter, S.C., Stuiver, Minze, and Yang, I.C., 1977, Chronology of Hawaiian glaciations: Science, v. 195, no. 1, p. 61-63.

Powers, H.A., 1948, A chronology of the explosive eruptions of Kilauea: Pacific Science, v. 2, no. 4, p. 278-292.

Sinton, J.M., in press, Revision of stratigraphic nomenclature of Waianae Volcano, Oahu, Hawaii: U.S. Geological Survey Bulletin 1775–A.

Stearns, H.T., 1926, Origin of the volcanoes of Mauna Loa and Kilauea (abstract): Geological Society of America Bulletin, v. 37, p. 150.

———1930, Geography and geology (part 1), *in* Stearns, H.T., and Clark, W.O., Geology and water resources of the Kau district: U.S. Geological Survey Water-Supply Paper 616, p. 29-165.

———1935, Geography and geology, *in* Stearns, H.T., and Vaksvik, K.N., Geology and ground-water resources of the Island of Oahu, Hawaii: Hawaii Division of Hydrography Bulletin 1, p.1-198.

———1939, Geologic map and guide of the Island of Oahu, Hawaii: Hawaii Division of Hydrography Bulletin 2, 75 p.

———1940a, Supplement to the geology and ground-water resources of the Island of Oahu, Hawaii: Hawaii Division of Hydrography Bulletin 5, 160 p.

———1940b, Geology and ground-water resources of the Islands of Lanai and Kahoolawe, Hawaii: Hawaii Division of Hydrography Bulletin 6, 177 p.

———1942, General geology and ground-water resources of Maui: Hawaii Division of Hydrography Bulletin 7 (part 1), p. 1-222.

———1945, Glaciation of Mauna Kea, Hawaii: Geological Society of America Bulletin, v. 56, p. 267-274.

———1946, Geology of the Hawaiian Islands (1st ed.): Hawaii Division of Hydrography Bulletin 8, 112 p.

———1947a, Geology (part 1) *in* Stearns, H.T., and Macdonald, G.A., Geology and ground-water resources of the Island of Molokai, Hawaii: Hawaii Division of Hydrography Bulletin, v. 11, p. 1-35.

———1947b, Geology and ground-water resources of the Island of Niihau, Hawaii: Hawaii Division of Hydrography Bulletin 12, p. 1-38.

———1967, Geology of the Hawaiian Islands (2nd ed.): Hawaii Division of Hydrography Bulletin 8, 112 p.

———1985, Geology of the State of Hawaii (2nd ed.): Palo Alto, Pacific Books, 335 p.

Stearns, H.T., and Clark, W.O., 1930, Geology and water resources of the Kau district, Hawaii: U.S. Geological Survey Water-Supply Paper 616, 194 p.

Stearns, H.T., and Macdonald, G.A., 1942, Geology and ground-water resources of the Island of Maui, Hawaii: Hawaii Division of Hydrography Bulletin 7, 344 p.

———1946, Geology and ground-water resources of the Island of Hawaii: Hawaii Division of Hydrography Bulletin 9, 363 p.

———1947, Geology and ground-water resources of the Island of Molokai, Hawaii: Hawaii Division of Hydrography Bulletin 11, 113 p.

Stearns, H.T., and Vaksvik, K.N., 1935, Geology and ground-water resources of the Island of Oahu, Hawaii: Hawaii Division of Hydrography Bulletin 1, 474 p.

Stone, J.B., 1926, The products and structure of Kilauea: Bernice P. Bishop Museum Bulletin 33, 60 p.

Washington, H.S., 1923, Petrology of the Hawaiian Islands: II, Hualalai and Mauna Loa: American Journal of Science, 5th series, v. 6, art. 10, p. 100-126.

Wentworth, C.K., 1925, The geology of Lanai: Bernice P. Bishop Museum Bulletin 24, 72 p.

———1926, Pyroclastic geology of Oahu: Bernice P. Bishop Museum Bulletin 30, 121 p.

———1938, Ash formations of the Island of Hawaii: Hawaiian Volcano Observatory, Special Report 3, 183 p.

———1951, Geology and ground-water resources of the Honolulu - Pearl Harbor area, Hawaii: Honolulu, Hawaii Board of Water Supply, 111 p.

Wentworth, C.K., and Jones, A.E., 1940, Intrusive rocks of the leeward slope of the Koolau Range, Oahu: Journal of Geology, v. 8, p. 975-1006.

Wentworth, C.K., and Powers, W.E., 1941, Multiple glaciations of Mauna Kea, Hawaii: Geological Society of America Bulletin, v. 52, p. 1193-1218.

Wentworth, C.K., and Winchell, Horace, 1947, Koolau Basalt Series, Oahu Hawaii: Geological Society of America Bulletin, v. 58, p. 49-78.

Winchell, Horace, 1947, Honolulu Series, Oahu, Hawaii: Geological Society of America Bulletin, v. 58, p. 1-48.

TABLE 1.12.—*Summary of stratigraphic units for main southeastern Hawaiian Islands*

[Volcanic rocks and closely associated intrusive rocks and sedimentary deposits only. Units on each volcano are listed from youngest to oldest; see text for further explanation. All isotopic ages (in parentheses) and K-Ar ages (in millions of years), recalculated from new decay constants, unless otherwise noted; see summary by Clague and Dalrymple (chapter 1, part I). The term "partly" (in parentheses) preceding a former name indicates that the unit as then defined is equivalent to only part of the unit as used here; the term "part" (in parentheses) following a former name indicates that the unit as used here is equivalent to only part of the unit as then defined]

Unit (this report)	Description	Age	Remarks
	HAWAII		
	Kilauea Volcano		
Puna Basalt	Shield-stage lava of tholeiitic basalt and picritic tholeiitic basalt. Historic and prehistoric lava flows and minor intercalated pyroclastic deposits. Exposed over most of surface of Kilauea. Maximum exposed thickness: > 100 m. Type locality: Uwekahuna Bluff at Kilauea Crater (caldera). Reference localities: at Napau, Makaopuhi, and Kilauea Iki Craters, and near Keana Bihopa (see Easton, chapter 11). Overlies and is locally intercalated with Pahala Ash; interfingers with Kau Basalt of Mauna Loa Volcano. Includes Keanakakoi Ash Member and Uwekahuna Ash Member:	Holocene and Pleistocene (^{14}C, 1.13-22.6 ka) (see text)	Puna Basalt (Easton, chapter 11). Formerly: Kamehame Basalt (part) (Stearns, 1926, 1930); Puna Volcanic Series (Stearns and Macdonald, 1946); Puna Formation (Easton and Garcia, 1980).
Keanakakoi Ash Member	Lithic and vitric ash. Pyroclastic surge and minor airfall deposits. Mainly represents explosive eruption of A.D. 1790, but has slightly older reticulite pumice at base and post-1790 but pre-1823 reticulite pumice at top. Occurs around Kilauea Crater (caldera). Maximum exposed thickness: ~11 m. Type locality: just southwest of Keanakakoi Crater. Is interbedded with historic Puna lava flows.	Holocene	Keanakakoi Ash Member (Easton, chapter 11). Formerly: Keanakakoi Formation (part) (Wentworth, 1938; Powers, 1948); "aa" [erroneously for ash?] member (part) of Puna Volcanic Series (Stearns and Macdonald 1946, p. 108); Keanakakoi Formation (part) of Puna Volcanic Series (Davis and Macdonald in Avias and others, 1956); Keanakakoi Member (part) of Puna Formation (Easton and Garcia, 1980); (partly) Keanakakoi Formation (Malin and others, 1983).
Uwekahuna Ash Member	Mostly ash. Mainly pyroclastic surge deposits Exposed near base of Kilauea Crater (caldera) and on southeast flank of Mauna Loa. Maximum exposed thickness: ~5 m. Type locality: Uwekahuna Bluff. Interbedded with prehistoric Puna lava flows.	Holocene (^{14}C, see text)	Uwekahuna Ash Member (Easton, chapter 11). Formerly: Uwekahuna Ash of Kilauea Series (Stone, 1926); Uwekahuna Formation (Wentworth, 1938; Powers, 1948); Uwekahuna Tuff of Puna Volcanic Series (Stearns and Macdonald, 1946, p. 194); Uwekahuna Ash of Puna Volcanic Series (Macdonald, 1949, p. 65, 67; Davis and Macdonald in Avias and others, 1956); Uwekahuna Member of Puna Formation (Easton and Garcia, 1980).
Pahala Ash	Vitric ash, largely palagonitized. Occurs on Mauna Loa and Kilauea Volcanoes (see text). Maximum exposed thickness: ~15 m. No type locality designated; named for exposures near town of Pahala on south slope of Mauna Loa. Principal reference locality: Moolelo, just southwest of Keana Bihopa; reference localities: Puu Kapukapu and Puu Kaone, all on Kilauea Volcano (see Easton, chapter 11). Overlies Hilina Basalt on Kilauea and Kahuku Basalt on Mauna Loa.	Pleistocene	Geographically restricted (see text). Pahala Ash (Easton, chapter 11). Formerly: Pahala Series (part) (Noble and Clark in Washington, 1923); Pahala Ash of Pre-Kilauea Series (Stone, 1926); Pahala Basalt or Formation (part) (Stearns, 1930); Pahala Tuff (Wentworth, 1938); Pahala Ash (part) (Stearns and Macdonald, 1946; Davis and Macdonald in Avias and others, 1956); Pahala Formation (Easton and Garcia, 1980).

TABLE 1.12.—*Summary of stratigraphic units for main southeastern Hawaiian Islands*—Continued

Unit (this report)	Description	Age	Remarks
	HAWAII--Continued		
	Kilauea Volcano--Continued		
Hilina Basalt	Shield-stage lava of tholeiitic basalt, olivine tholeiitic basalt, and picritic tholeiitic basalt. Predominantly flows with associated pyroclastic deposits. Exposed in Hilina fault system escarpments along south flank of volcano. Maximum exposed thickness: ~300 m. Type locality: just south of Keana Bihopa. Reference localities: Keana Bihopa and Puu Kapukapu. Base not exposed. Includes Moo, Pohakaa, Kahele, and Halepe Ash Members, all intercalated with Hilina lava flows.	Pleistocene (see text)	Hilina Basalt (Easton, chapter 11). Formerly: Pahala Basalt (part) (Stearns and Clark, 1930); Hilina Volcanic Series (Stearns and Macdonald, 1946); Hilina Formation (Easton and Garcia, 1980; Decker and Christiansen, 1984).
Moo Ash Member	Mostly yellow-brown ash and palagonite. Maximum exposed thickness: ~3 m. Type locality: Keana Bihopa. Reference locality: Puu Kapukapu.	Pleistocene	Moo Ash Member of Hilina Basalt (Easton, chapter 11). Formerly: Moo Member of Hilina Formation (Easton and Garcia, 1980).
Pohakaa Ash Member	Thickest of ash members. Yellow- to reddish-brown-weathering palagonite, vitric ash, and soil. Exposed thickness: 1-4 m. Type locality: Pohakaa Arroyo, about 3 km southwest of Keana Bihopa. Reference locality: Puu Kapukapu.	Pleistocene	Pohakaa Ash Member of Hilina Basalt (Easton, chapter 11). Formerly: Pohakaa Member of Hilina Formation (Easton and Garcia, 1980).
Kahele Ash Member	Crudely bedded red clay with palagonite. Exposed thickness: 10-125 cm. Type locality: Pohakaa Arroyo, about 3 km southwest of Keana Bihopa. Reference locality: Puu Kapukapu.	Pleistocene	Kahele Ash Member of Hilina Basalt (Easton, chapter 11). Formerly: Kahele Member of Hilina Formation (Easton and Garcia, 1980).
Halape Ash Member	Palagonite and poorly bedded clay. Exposed thickness: 10-50 cm. Type locality: Keana Bihopa. Reference locality: Puu Kapukapu.	Pleistocene	Halape Ash Member of Hilina Basalt (Easton, chapter 11). Formerly: Halape Member of Hilina Formation (Easton and Garcia, 1980).
	Mauna Loa Volcano		
Kau Basalt	Shield-stage lava of tholeiitic basalt, olivine tholeiitic basalt, and picritic tholeiitic basalt. Historic and prehistoric lava flows and minor intercalated pyroclastic deposits. Exposed over most of surface of Mauna Loa. Maximum exposed thickness: > 185 m. Type locality: west wall of Mokuaweoweo Crater (caldera). Overlies Pahala Ash and Kahuku Basalt; interfingers with Puna Basalt of Kilauea Volcano.	Holocene and Pleistocene	Renamed. Formerly: Kamehame Basalt (part) (Stearns, 1926, 1930); Kau Volcanic Series (Stearns and Macdonald, 1946); Kau Formation (Porter, 1971, 1974); Kau Volcanics (Lipman, 1980).
Pahala Ash	See description under Kilauea.	Pleistocene	See "Remarks" under Kilauea; see also text under Mauna Loa.
Kahuku Basalt	Shield-stage lava of tholeiitic basalt, olivine tholeiitic basalt, and picritic tholeiitic basalt. Lava flows and minor intercalated pyroclastic deposits. Exposed on east and south sides of Mauna Loa. Maximum exposed thickness: 180 m. Type locality: Kahuku Pali, a fault escarpment running north of Ka Lae. Overlies (fault or unconformity) Ninole Basalt.	Pleistocene	Renamed. Formerly: lower member of Pahala Basalt (part) (Stearns 1930); Kahuku Volcanic Series (Stearns and Macdonald, 1946); Kahuku Volcanics (Lipman, 1980).
Ninole Basalt	Shield-stage lava of tholeiitic basalt, olivine tholeiitic basalt, and picritic tholeiitic basalt. Lava flows with pyroclastic deposit near top. Exposed north of Waiohinu on southeast slope of Mauna Loa. Maximum exposed thickness: ~600 m. Type locality: walls of valley at Puu Enuhe, near Ninole Gulch. Base not exposed.	Pleistocene (0.54±0.4) (see text)	Ninole Basalt (Stearns, 1926, 1930) (see text). Formerly: (partly) Ninole Tuff (Wentworth, 1938); Ninole Volcanic Series (Stearns and Macdonald, 1946); Ninole Volcanics (Lipman, 1980).

TABLE 1.12.—*Summary of stratigraphic units for main southeastern Hawaiian Islands*—Continued

Unit (this report)	Description	Age	Remarks
	HAWAII--Continued		
	Mauna Kea Volcano		
Laupahoehoe Volcanics	Postshield-stage alkalic lava flows and associated volcanic and sedimentary deposits. Occurs on most of surface of Mauna Kea. Typical exposed thickness: 50-100 m. Type locality: near town of Laupahoehoe. Reference localities: in Waikahalulu and Pohakuloa Gulches. Conformably overlies Hamakua Volcanics. Divided into Waikahalulu Volcanic Member, and Makanaka and Waihu Glacial Members:	Holocene and Pleistocene	Reduced in rank and renamed (see text). Formerly: (partly) Laupahoehoe Volcanic Series (Macdonald, 1945; Stearns and Macdonald, 1946); Laupahoehoe Series (Porter, 1971); Laupahoehoe Group (Porter, 1973, 1974, 1979a, 1979b; Porter and others, 1977).
Waikahalulu Volcanic Member	Postshield-stage lava predominantly of hawaiite, but some alkalic basalt and ankaramite. Flows and associated pyroclastic deposits. Occurs on upper and lower slopes of volcano. Typical exposed thickness: 50-100 m. Type locality: in Waikahalulu Gulch. Reference locality: in Pohakuloa Gulch. Conformably, and locally unconformably, overlies Hamakua Volcanics. Interstratified with Makanaka and Waihu Glacial Members.	Holocene and Pleistocene (^{14}C and K-Ar, 0.0045-0.19)	Reduced in rank and renamed (see text). Formerly: (partly) Laupahoehoe Volcanic Series (Stearns and Macdonald, 1946); (partly) Waikahalulu Formation of Laupahoehoe Group (Porter, 1974, Porter and others, 1977); Waikahalulu Formation of Laupahoehoe Group (Porter, 1979a, 1979b).
Makanaka Glacial Member	Gravel and diamicton. Exposed on upper slopes of volcano. Exposed thickness: > 10 m. Type locality: Puu Makanaka. Reference localities: in Waikahalulu and Kemole Gulches. Intercalated with Waikahalulu lavas. Younger than Waihu Glacial Member.	Pleistocene	Reduced in rank and renamed (see text). Formerly: Makanaka Drift (Wentworth and Powers, 1941; see also Stearns, 1945); Makanaka Formation (part) of Laupahoehoe Group (Porter, 1974; Porter and others, 1977); Makanaka Formation of Laupahoehoe Group (Porter, 1979a, 1979b).
Waihu Glacial Member	Mainly conglomerate and diamictite. Exposed mainly on upper slopes below summit of Mauna Kea. Exposed thickness: generally < 30 m. Type locality: near Waihu Spring. Reference localities: in Pohakuloa Gulch and near Waihu Spring.	Pleistocene	Reduced in rank and renamed (see text). Formerly: Waihu Drift (Wentworth and Powers, 1941); Waihu Fanglomerate (Stearns, 1945); Waihu Formation of Laupahoehoe Group (Porter and others, 1977; Porter, 1974, 1979a, 1979b).
Hamakua Volcanics	Divided into three members: upper two formally-named members represent postshield-stage lava flows and pyroclastic cones and associated sedimentary (glacial) deposits; informal lower member represents shield-stage lava flows. Type locality: in south wall of Laupahoehoe Stream gulch. Reference locality: Pohakuloa Gulch.	Pleistocene	Reduced in rank and renamed (see text). Formerly: (partly) Hamakua Volcanic Series (Stearns and Macdonald, 1946); Hamakua Group (Porter, 1973, 1974, 1979a, 1979b; Porter and others, 1977) (see text).
Pohakuloa Glacial Member	Gravel and diamicton. Exposed mainly in Pohakuloa and Waikahalulu Gulches. Maximum exposed thickness: ~40 m. Type locality: west wall of upper Pohakuloa Gulch. Reference locality: in Waikahalulu Gulch. Locally overlies upper flows of Hopukani Volcanic Member.	Pleistocene	Reduced in rank and renamed (see text). Formerly: Pohakuloa Drift (Wentworth and Powers, 1941); Pohakuloa Formation of Hamakua Group (Porter, 1974, 1979a, 1979b; Porter and others, 1977)
Hopukani Volcanic Member	Postshield-stage lava of alkalic basalt, ankaramite, and hawaiite. Flows and cinder cones. Exposed mainly in gulches on lower windward slopes of Mauna Kea and in saddle between Mauna Kea and Kohala Volcanoes. Exposed thickness: ~25 m. Type locality: in south wall of Laupahoehoe Stream gulch. Reference localities: in Pohakuloa and Waikahalulu Gulches. Overlies lower member.	Pleistocene (0.27±0.04, 0.375±0.050)	Reduced in rank and renamed (see text). Formerly: upper member of Hamakua Volcanic Series (Stearns and Macdonald, 1946); Hopukani Formation of Hamakua Group (Porter, 1974, 1979a, 1979b; Porter and others, 1977).

TABLE 1.12.—*Summary of stratigraphic units for main southeastern Hawaiian Islands*—Continued

Unit (this report)	Description	Age	Remarks
	HAWAII--Continued		
	Mauna Kea Volcano--Continued		
lower member	Shield-stage lava of tholeiitic basalt, olivine tholeiitic basalt, and picritic tholeiitic basalt. Exposed in sea cliffs and gulches along northeast coast of Mauna Kea (so-called Hamakua coast) and near mouths of valleys between Hilo and Laupahoehoe. Exposed thickness: probably ~150 m. Base not exposed.	Pleistocene	Formerly: lower member of Hamakua Volcanic Series (Stearns and Macdonald, 1946, p. 154, fig. 31) (see text).
	Hualalai Volcano		
Hualalai Volcanics	Postshield-stage lava of alkalic basalt and rare hawaiite. Historic and prehistoric lava flows and associated pyroclastic deposits. Covers entire surface of Hualalai Volcano. Maximum exposed thickness: ~150 m. Type locality: around town of Kailua. Interfingers with Kau Basalt of Mauna Loa Volcano. Base not exposed. Includes Kona ash beds (informal) and Waawaa Trachyte Member (formal) (see text).	Holocene and Pleistocene	Reduced in rank and renamed (see text). Formerly: Hualalai Volcanic Series (Stearns and Macdonald, 1946).
	Kona ash beds		Abandoned as formally named unit (see text). Formerly: Kona Tuff Formation (Wentworth, 1938); unnamed unit of Hualalai Volcanic Series (Stearns and Macdonald, 1946); Kona Tuff Formation of Hualalai Volcanic Series (Davis and Macdonald *in* Avias and others, 1956).
Waawaa Trachyte Member	Trachyte cone and flow. Occurs in Puu Waawaa-Puu Anahulu area. Exposed thickness: ~275 m. Type locality: Puu Waawaa. Base not exposed.	Pleistocene (0.105, see text)	Renamed. Formerly Waawaa Volcanics [Member] of Hualalai Volcanic Series (Stearns and Macdonald, 1946, p. 143) (see text).
	Kohala Volcano		
Hawi Volcanics	Postshield-stage lava of mostly mugearite and hawaiite with some trachyte and benmoreite. Lava flows and associated pyroclastic deposits. Occurs in summit area and parts of slopes of Kohala Volcano. Exposed thickness of flows: ~30 m. Type locality: in Kumakua Gulch, about 1 km east of Hawi. Underlies Quaternary surficial deposits. Conformably, locally unconformably, overlies Pololu Basalt. Basalt.	Pleistocene (0.061±0.001, 0.261±0.005)	Renamed. Formerly: Hawi Volcanic Series (Stearns and Macdonald, 1946).
Pololu Basalt	Shield-stage lava of tholeiitic basalt, olivine tholeiitic basalt, and picritic tholeiitic basalt; postshield-stage caldera-filling alkalic basalt near top. Thin lava flows and associated pyroclastic deposits. Occurs on upper and lower slopes of Kohala. Maximum exposed thickness: ~900 m. Type locality: on northwest side of Pololu Valley. Base not exposed.	Pleistocene (0.304±0.091-0.459±0.028)	Renamed. Formerly: Pololu Volcanic Series (Stearns and Macdonald, 1946).

TABLE 1.12.—*Summary of stratigraphic units for main southeastern Hawaiian Islands*—Continued

Unit (this report)	Description	Age	Remarks
	MAUI		
	East Maui (Haleakala) Volcano		
Hana Volcanics	Rejuvenated-stage lava of alkalic basalt and basanite; rare ankaramite and hawaiite. Lava flows and associated intrusive rocks and pyroclastic and sedimentary deposits. Exposed in summit region and on eastern and southwestern slopes. Exposed thickness: > 300 m. Type locality: village of Hana. Unconformably overlies Kula Volcanics. Includes Kipahulu Member in Kipahulu Valley. Also includes historic flow of A.D. 1790 in Cape Kinau area and numerous informal flows in Nahiku and Keanae areas (see text) that are listed below in sequence (youngest to oldest) from Stearns and Macdonald (1942):	Holocene and Pleistocene(?)	Reduced in rank, revised to include historic (A.D. 1790) flow, and renamed (see text). Formerly: Hana Volcanic Series (Stearns, 1942); Hana Formation (Macdonald, 1978); Hana Group (Clague and others, 1982).
	Nahiku area: Hanawi flow Paakea flow Kuhiwa flow Mossman flow Kapaula flow Makaino flow Waiaaka flow Makapipi flows Big Falls flows		Abandoned as formally named units (see text). Formerly all in Hana Volcanic Series (see Macdonald, 1942; Macdonald and Davis in Avias and others, 1956): Hanawi Basaltic Andesite Paakea Basalt Kuhiwa Basaltic Andesite Mossman Picritic Basalt Kapaula Basaltic Andesite Makaino Basaltic Andesite Waiaaka Basaltic Andesite Makapipi Basalt(s) Big Falls Picritic Basalt(s)
	Keanae area: Keanae flow Waiokamilo flow Piinaau flow Ohia flow Wailuanui flow Pauwalu flow		Formerly all in Hana Volcanic Series (see Stearns, 1942): Keanae Basalt Waiokamilo Basalt Piinaau Basalt Ohia Basalt Wailuanui Basalt Pauwalu Basalt
Kipahulu Member	Late alkalic rejuvenated-stage lava of alkalic basalt and basanite; rare ankaramite and hawaiite. Lava flows. Exposed thickness: > 400 m. Type locality: Kipahulu Valley. Unconformably overlies Hana Volcanics (older flows), Kula Volcanics, and Honomanu Basalt.	Pleistocene(?)	See text. Formerly: Kipahulu Member of Hana Volcanic Series (Stearns, 1942); Kipahulu Formation of Hana Volcanic Series (Macdonald and Davis in Avias and others, 1956); Kipahulu Member of Hana Volcanic Series (Macdonald and Abbott, 1970; Macdonald and others, 1983; Stearns, 1985).
Kula Volcanics	Postshield-stage lava of hawaiite with some ankaramite and alkalic basalt. Lava flows with associated intrusive rocks and pyroclastic and sedimentary deposits. Exposed in summit region and on all slopes. Maximum exposed thickness: ~600 m. Type locality: near Waiakoa, on west slope of volcano; reference localities: near Kipahulu and along Halemauu Trail (see text). Overlies Honomanu Basalt.	Pleistocene (0.46-0.86, 0.41±0.09)	Renamed. Formerly: Kula Volcanic Series (Stearns, 1942); (partly) Kula Formation (Macdonald, 1978). Includes rocks formerly called Kumuiliahi Formation by Macdonald (1978) (see text).
Honomanu Basalt	Shield-stage lava of tholeiitic basalt, olivine tholeiitic basalt, and picritic tholeiitic basalt. Lava flows and associated intrusive rocks and rare pyroclastic deposits. Exposed in summit region and on north, northeast, and southwest slopes. Maximum exposed thickness: ~250 m. Type locality: in Honomanu Stream valley. Base not exposed.	Pleistocene (0.75±0.04)	Renamed. Formerly: Honomanu Volcanic Series (Stearns, 1942); (partly) Honomanu Formation (Macdonald, 1978).

TABLE 1.12.—*Summary of stratigraphic units for main southeastern Hawaiian Islands*—Continued

Unit (this report)	Description	Age	Remarks
	MAUI--Continued		
	West Maui Volcano		
Lahaina Volcanics	Rejuvenated-stage lava of basanite and picritic basanite. Lava flows and associated pyroclastic deposits. Exposed in small areas on west and southeast sides of West Maui. Exposed thickness of flows: 3-20 m; cones, ~45 m. No type locality designated. Principal reference locality[1]: Puu Laina. Unconformably overlies Honolua Volcanics. Locally includes two informal flows: Laina flows and cinder cone Kilea flow and cinder cone	Pleistocene (1.30±0.10, see text)	Lahaina Volcanics (Clague and others, 1982) (see text). Formerly: Lahaina Volcanic Series of Stearns (1942); Lahaina Group (Naughton and others, 1980). Abandoned as formally named units. Formerly of Lahaina Volcanic Series (Stearns, 1942): Laina Volcanics Kilea Volcanics
Honolua Volcanics	Postshield-stage lava of mugearite, trachyte, and hawaiite. Lava flows and associated domes dikes, and pyroclastic deposits. Caps ridges on all flanks of volcano. Maximum exposed thickness: ~300 m. Type locality: village of Honolua. Overlies Wailuku Volcanics.	Pleistocene (1.18-1.20, 1.50±0.13)	Renamed. Formerly: Honolua Volcanic Series (Stearns, 1942).
Wailuku Basalt	Shield-stage lava of tholeiitic basalt, olivine tholeiitic basalt, and picritic tholeiitic basalt, and postshield-stage caldera-filling lava of alkalic basalt. Lava flows with associated intrusive rocks and pyroclastic and sedimentary deposits. Widely exposed on West Maui Volcano. Maximum exposed thickness: > 1,500 m. Type locality: south wall of Iao Valley. Base not exposed.	Pleistocene (1.32±0.04, 1.58-1.97)	Renamed. Formerly: Waikulu Volcanic Series (Stearns, 1942).
	KAHOOLAWE		
	Kahoolawe Volcano		
Kanapou Volcanics	Postshield-stage lava of alkalic basalt and hawaiite; postshield-stage caldera-filling lava of alkalic basalt; shield-stage caldera-filling lava of tholeiitic basalt; shield-stage lava of tholeiitic basalt and olivine tholeiitic basalt. Lava flows and associated pyroclastic deposits and intrusive rocks. Forms essentially all of island. Maximum exposed thickness: ~450 m. Type locality: cliffs of Kanapou Bay. Base not exposed.	Pleistocene (upper alkalic part, 1.03±0.18)	Renamed. Formerly: Kanapou Volcanic Series (Stearns, 1946; Macdonald and Davis in Avias and others, 1956).
	LANAI		
	Lanai Volcano		
Lanai Basalt	Shield-stage (including caldera-filling phase) lava of tholeiitic basalt, olivine tholeiitic basalt, and picritic tholeiitic basalt. Lava flows and associated pyroclastic deposits and intrusive rocks. Forms almost all of island. Maximum exposed thickness: > 1,000 m. No type locality designated. Principal reference locality[1]: Maunalei Gulch on northeast side of island (J.G. Moore, oral commun., 1986). Base not exposed.	Pleistocene (1.28±0.4)	Reduced in rank and renamed (see text). Formerly: (partly) Lanai Basalt and Manele Basalt (Wentworth, 1925); Lanai Volcanic Series (Stearns, 1946); Lanai Volcanic Series (which [improperly] included Lanai Basalt, and Lanai Basalt [improperly] included Manele Basalt) Macdonald and Davis in Avias and others, 1956).

TABLE 1.12.—*Summary of stratigraphic units for main southeastern Hawaiian Islands*—Continued

Unit (this report)	Description	Age	Remarks
	LANAI--Continued		
	Lanai Volcano--Continued		
	(Manele crater remnant)		Abandoned as formally named unit (see text). Formerly: Manele Basalt (Wentworth, 1925); Manele Basalt of Lanai Basalt of Lanai Volcanic Series (Macdonald and Davis in Avias and others, 1956).
	MOLOKAI		
	East Molokai Volcano		
Kalaupapa Volcanics	Rejuvenated-stage lava of alkalic basalt and basanite. Lava flows and associated cone. Makes up Kalaupapa peninsula. Maximum exposed thickness: ~125 m. Type locality: Kalaupapa peninsula. Unconformably overlies East Molokai Volcanics.	Pleistocene (0.35±0.03, 0.57±0.02)	Renamed. Formerly: Kalaupapa Basalt (Stearns, 1946, 1947a; Clague and Frey, 1982).
East Molokai Volcanics	Divided into two informal members. Upper member: postshield-stage lava of mugearite, with lesser amounts of hawaiite and trachyte. Lava flows and associated pyroclastic deposits and intrusive rocks. Lower member: shield-stage (including caldera-filling phase) lava of tholeiitic basalt, olivine tholeiitic basalt, and picritic tholeiitic basalt, and postshield-stage (including caldera-filling phase) alkalic basalt. Lava flows and associated intrusive rocks and pyroclastic and sedimentary deposits. Makes up almost all of East Molokai. Maximum exposed thickness: > 1,500 m. Type locality: cliff south of Kalaupapa peninsula. Locally overlies West Molokai Volcanics of West Molokai Volcano. Base not exposed.	Pleistocene and Pliocene (1.35-1.49, upper member; 1.52 and 1.76±0.07, lower member)	Renamed. Formerly: East Molokai Volcanic Series (Stearns, 1946, 1947a).
	West Molokai Volcano		
West Molokai Volcanics	Postshield-stage lava of hawaiite and alkalic basalt; shield-stage lava of tholeiitic basalt. Lava flows and associated intrusive rocks and pyroclastic deposits. Forms most of West Molokai. Maximum exposed thickness: > 400 m. Type locality: West Molokai mountain (Mauna Loa). Locally overlapped by East Molokai Volcanics. Base not exposed.	Pleistocene and Pliocene 1.52±0.6, 1.89, 1.84±0.7, 1.90±0.06)	Renamed. Formerly: West Molokai Volcanic Series (Stearns, 1946; 1947a)
	OAHU		
	Koolau Volcano		
Honolulu Volcanics	Rejuvenated-stage lava, ranging from alkalic basalt, basanite, and nephelinite to melilitite. Exposed on southwest and northeast flanks of Koolau Range. No type locality designated; named for exposures in city and county of Honolulu. Honolulu Volcanics consists of an assemblage of local informally named lava flows, cinder, spatter, and tuff cones, and ash deposits (see text and below; sequence listed below from Macdonald and others, 1983). Unconformably overlies Koolau Basalt.	Holocene(?) and Pleistocene (0.03-0.9) (see text)	Honolulu Volcanics (Clague and Frey, 1982) [also Lanphere and Dalrymple, 1979]. Formerly: Honolulu Volcanic Series (Stearns, 1935, 1939); Honolulu Series (Winchell, 1947); Honolulu Group (Hay and Iijima, 1968; Clague and others, 1982).

TABLE 1.12.—*Summary of stratigraphic units for main southeastern Hawaiian Islands*—Continued

Unit (this report)	Description	Age	Remarks
	OAHU--Continued		
	Koolau Volcano--Continued		
			Abandoned as formally named units see text). Formerly all in Honolulu Volcanic Series (Stearns, 1935, 1939, 1940a; see also Avias and others, 1956, for other former names):
	Hawaiiloa flow (and associated cone)		Hawaiiloa Volcanics
	Pali Kilo flow (and associated cone?)		
	Pyramid Rock flow		Pyramid Rock Basalt
	Moku Manu tuff cone		Moku Manu Volcanics
	Ulupau tuff cone (and flow?)		Ulupau Tuff (also Ulupau Head Tuff); Mokapu Basalt (part)
	Mokolea flow		Mokolea [misspelled Mokulea by Stearns (1935)] Basalt; Mokapu Basalt (part)
	Kalihi flow (and associated cone)		Kalihi Volcanics
	Haiku flow (and associated cone)		Haiku Volcanics
	Rocky Hill flow (and associated cones)		Rocky Hill Volcanics (Basalt)
	Manoa cinder cone (and lava flow?)		
	Aliamanu flow (and associated cone)		Aliamanu Tuff (Basalt)
	Kaneohe flow (and associated cones)		Kaneohe Volcanics
	Luakaha flow (and associated cone)		Nuuanu Volcanics (Basalt) (part)
	Makuku flow (and associated cone)		Nuuanu Volcanics (Basalt) (part)
	Pali flow (and associated cone)		Pali Volcanics
	Makawao tuff and breccia deposits		Makawao Breccia
	Kaau flows (and associated tuff and mudflow deposits)		Kaau Volcanics (Basalt, Tuff)
	Mauumae flow (and associated cone)		Mauumae Volcanics
	Salt Lake tuff cone		Salt Lake Tuff
	Makalapa tuff cone		Makalapa Tuff
	Ainoni flow (and associated cone)		Ainoni Volcanics
	Castle flow (and associated cone)		Castle Volcanics
	Maunawili flow (and associated cone)		Maunawili Volcanics
	Training School flow (and associated cone)		Training School Volcanics
	Diamond Head tuff cone		Diamond Head Tuff [also Diamond Head Black Ash; Black Point Ash]
	Kaimuki flows		Kaimuki Volcanics (Basalt)
	Black Point flow		Black Point Basalt
	Kamanaiki flows		Kamanaiki Basalt
	Punchbowl flows (and associated cone)		Punchbowl Volcanics
	Manana tuff cone		Manana Tuff
	Koko Crater tuff cone		Koko Volcanics (part)
	Kahauloa flows (and associated cone)		
	Hanauma tuff cone		Koko Volcanics (part)
	Koko Head flow (and associated cone)		Koko Volcanics (part)
	Kalama flow (and associated cone)		Kalama Volcanics
	Kaohikaipu flow (and associated cone)		Kaohikaipu Volcanics
	Kaupo flow (and associated conelet)		Kaupo Basalt
	Round Top cinder and ash deposits		
	Sugarloaf flow (and associated cinder cone and ash deposits)		Sugar Loaf Basalt
	Tantalus flow (and associated cinder cone and ash deposits)		Tantalus Basalt
Koolau Basalt	Shield-stage lava of tholeiitic basalt, olivine tholeiitic basalt, and rare picritic tholeiitic basalt; near top, rocks transitional between tholeiitic and alkalic basalt. Lava flows (typically thin-bedded) with associated intrusive rocks (dikes) and minor pyroclastic and sedimentary deposits. Widely exposed in Koolau Range. Maximum exposed thickness of flows: probably > 1,000 m. No type locality designated. Principal reference locality[1]: Nuuanu Pali. Locally unconformably overlies Waianae Volcanics of Waianae Volcano. Base not exposed. Includes Kailua Member:	Pleistocene(?) and Pliocene (1.8-2.7)	Renamed (see text). Formerly: Koolau Basalt (Wentworth, 1926); Koolau Volcanic Series (Stearns, 1935); Koolau Series (Wentworth and Jones, 1940; Winchell, 1947); Koolau Basalt Series (Wentworth and Winchell, 1947); Koolau Formation (Wentworth, 1951); Koolau Volcanics (Lanphere and Dalrymple, 1979).

TABLE 1.12.—*Summary of stratigraphic units for main southeastern Hawaiian Islands*—Continued

Unit (this report)	Description	Age	Remarks
	OAHU--Continued		
	Koolau Volcano--Continued		
Kailua Member	Shield-stage caldera-filling tholeiitic basalt and olivine tholeiitic basalt. Thick-bedded lava flows and dikes cutting them. Exposed near town of Kailua. Exposed thickness: ~500 m. No type locality specified. Principal reference locality[1]: Kaiwa Ridge. Reference locality[1]: east side of Puu Papaa. In fault(?) contact with Koolau extracaldera flows. Base not exposed.	Pleistocene(?)	Reduced in rank (see text). Formerly: Kailua Volcanic Series (Stearns, 1935); Kailua Volcanic Series of Koolau Volcanic Series [improperly] (Macdonald and Davis in Avias and others, 1956).
	Waianae Volcano		
Kolekole Volcanics	Rejuvenated-stage alkalic lava. Flows and cones. Occurs near Kolekole Pass and at south end of Waianae Range. Thickness at type locality: ~2 m. Type locality: Kolekole Pass. Unconformably overlies flows of Waianae Volcanics and alluvium.	Pleistocene	Kolekole Volcanics (Sinton, in press). Formerly: (partly) Kolekole Volcanics (Stearns, 1946; Macdonald and Davis in Avias and others, 1956).
Waianae Volcanics	Postshield-stage lava of hawaiite with rare alkalic basalt and mugearite; postshield-stage caldera-filling lava of alkalic basalt; shield-stage caldera-filling lava of tholeiitic basalt; shield-stage lava of tholeiitic basalt, olivine tholeiitic basalt, and picritic tholeiitic basalt. Flows and associated intrusive, pyroclastic, and sedimentary rocks. Exposed over most of Waianae Range. Base not exposed. Divided into Palehua (youngest), Kamaileunu, and Lualualei (oldest) Members.	Pliocene	Waianae Volcanics (Sinton, in press) (see text). Formerly: Waianae Volcanic Series (part) (Stearns, 1935); Waianae Volcanic Series (Stearns, 1946).
Palehua Member	Postshield-stage lava of hawaiite with minor alkalic basalt and mugearite. Flows and associated pyroclastic deposits. Occurs at higher elevations throughout Waianae Range. Maximum exposed thickness: > 300 m. Type locality: near Palehua. Conformably, locally unconformably, overlies Kamaileunu Member.	Pliocene (2.5-3.2)	Palehua Member of Waianae Volcanics (Sinton, in press). Formerly: upper member (part) of Waianae Volcanic Series (Stearns, 1935); upper member of Waianae Volcanic Series (Stearns, 1946).
Kamaileunu Member	Postshield-stage caldera-filling lava of alkalic basalt, hawaiite, and rare ankaramite, grading down into shield-stage caldera-filling lava of tholeiitic basalt and rare icelandite. Thick flows and associated rocks. Well exposed in ridges bounding Waianae, Lualualei, and Makaha Valleys. Maximum exposed thickness: > 600 m. Type locality: Kamaileunu Ridge. Reference localities: near Puu Heleakala and Pohakea Pass. Conformably, locally unconformably, overlies Lualualei Member. Includes formally named Mauna Kuwale Rhyodacite Flow:	Pliocene (3.0-3.5)	Kamaileunu Member of Waianae Volcanics (Sinton, in press). Formerly: lower member (part) and middle member (part) of Waianae Volcanic Series (Stearns, 1935).
Mauna Kuwale Rhyodacite Flow	Rhyodacite. Exposed on Mauna Kuwale and Kauaopuu ridges. Exposed thickness: ~135 m. Type locality: Mauna Kuwale. Underlies hawaiite and overlies icelandite of Kamaileunu Member.	Pliocene (see text)	Mauna Kuwale Rhyodacite Flow of Kamaileunu Member (Sinton, in press). Formerly: part of lower member of Waianae Volcanic Series (Stearns, 1935); part of upper member of Waianae Volcanic Series (Stearns, 1940a); Mauna Kuwale Trachyte (McDougall, 1963, 1964); Mauna Kuwale Rhyodacite of upper Waianae Volcanic Series (Funkhouser and others, 1968).
Lualualei Member	Shield-stage lava of tholeiitic basalt, olivine tholeiitic basalt, and picritic tholeiitic basalt. Thin-bedded flows and associated rocks. Occurs mainly in Lualualei Valley. Exposed thickness: > 450 m. Type locality: Puu Heleakala. Base not exposed.	Pliocene (3.0-3.9)	Lualualei Member of Waianae Volcanics (Sinton, in press). Formerly: lower member (part) and middle member (part) of Waianae Volcanic Series (Stearns, 1935).

TABLE 1.12.—*Summary of stratigraphic units for main southeastern Hawaiian Islands*—Continued

Unit (this report)	Description	Age	Remarks
	KAUAI		
	Kauai Volcano		
Koloa Volcanics	Rejuvenated-stage lava of alkalic basalt, basanite, nephelinite, and melilitite. Lava flows and associated pyroclastic deposits. Widely exposed over eastern two-thirds of island. Maximum exposed thickness: ~650 m. Type locality: vicinity of town of Koloa. Unconformably overlies Waimea Canyon Basalt. Locally includes Palikea Breccia Member, which underlies and is intercalated with Koloa lava flows.	Pleistocene and Pliocene (0.62, 1.21, 1.46, 2.01, 2.59) (see text)	Koloa Volcanics (Clague and others, 1982) (see text). Formerly: Koloa Series (Hinds, 1930); Koloa Volcanic Series (Stearns, 1946; Macdonald, 1949; Macdonald and others, 1954, 1960; Macdonald and Davis in Avias and others, 1956).
Palikea Breccia Member	Breccia and lesser conglomerate. Exposed in narrow bands over eastern two-thirds of island. Maximum exposed thickness: ~215 m. Type locality: Palikea ridge, about 5 km southeast of Kawaikini peak.	Pleistocene(?) and Pliocene(?)	Reduced in rank and renamed (see text). Formerly: Palikea Formation of Koloa Volcanic Series Macdonald and others, 1954, 1960; Davis and Macdonald in Avias and others, 1956).
Waimea Canyon Basalt	Shield-stage lava of tholeiitic basalt, olivine tholeiitic basalt, and picritic tholeiitic basalt; rare postshield-stage hawaiite near top. Lava flows and minor pyroclastic deposits. Widely exposed. Total exposed thickness: ~800 m. Type locality: walls of Waimea Canyon. Divided into Makaweli, Olokele, Haupu, and Napali Members.	Pliocene and Miocene(?) (3.6-5.1)	Reduced in rank and renamed (see text). Formerly: Kauai Lavas (Hinds, 1930); Waimea Volcanic Series (Stearns, 1946); Waimea Canyon Volcanic Series (Macdonald, 1949; Macdonald and others, 1954, 1960; Davis and Macdonald in Avias and others, 1956; Stearns, 1967).
Makaweli Member	Shield-stage caldera-filling lava of tholeiitic basalt, olivine tholeiitic basalt, and picritic tholeiitic basalt; postshield-stage hawaiite flow near top of unit. Represents south flank graben. Predominantly thick-bedded flows. Exposed in southwestern part of island. Maximum exposed thickness: ~450 m. Type locality[1]: West wall of Makaweli River canyon. Reference locality[1]: east wall of lower Waimea Canyon. Includes Mokuone Breccia Beds at base of and intercalated with flows. In fault contact with Olokele and Napali Members.	Pliocene (3.60-4.15)	Reduced in rank (see text). Formerly: Makaweli Formation of Waimea Canyon Volcanic Series (Macdonald and others, 1954, 1960; Davis and Macdonald in Avias and others, 1956).
Mokuone Breccia Beds	Breccia with lesser conglomerate. Exposed in narrow bands in southwestern part of island. Maximum exposed thickness: ~300 m. Type locality: walls of Mokuone Valley, west of Kahililoa.	Pliocene	Reduced in rank and renamed (see text). Formerly: Mokuone Formation (Macdonald and others, 1954); Mokuone Member of Makaweli Formation (Davis and Macdonald in Avias and others, 1956; Macdonald and others, 1960).
Olokele Member	Shield-stage caldera-filling lava of tholeiitic basalt, olivine tholeiitic basalt, and picritic tholeiitic basalt; postshield-stage hawaiite flow near top. Represents large summit caldera. Thick-bedded flows and associated pyroclastic deposits. Exposed in central part of island. Maximum exposed thickness: ~800 m. Type locality[1]: walls of upper Olokele Canyon. Reference localities[1]: walls of Poomaa, Koaie, and Waialae Streams. In fault contact with Makaweli and Napali Members.	Pliocene	Reduced in rank (see text). Formerly: Olokele Formation of Waimea Canyon Volcanic Series (Macdonald and others, 1954, 1960; Davis and Macdonald in Avias and others, 1956).
Haupu Member	Shield-stage caldera-filling lava of tholeiitic basalt, olivine tholeiitic basalt, and picritic tholeiitic basalt. Represents southeast flank caldera. Thick-bedded flows exposed on Haupu ridge. Maximum exposed thickness: ~500 m. Type locality: south side of Haupu ridge. Separated from Napali Member by buried caldera faults(?).	Pliocene	Reduced in rank (see text) Formerly: Haupu Volcanic Series (part) (Stearns, 1946); Haupu Formation of Waimea Canyon Volcanic Series (Macdonald and others, 1954, 1960).

TABLE 1.12.—*Summary of stratigraphic units for main southeastern Hawaiian Islands*—Continued

Unit (this report)	Description	Age	Remarks
	KAUAI--Continued		
	Kauai Volcano--Continued		
Napali Member	Shield-stage lava of tholeiitic basalt, olivine tholeiitic basalt, and picritic tholeiitic basalt. Mostly thin-bedded flows and associated pyroclastic deposits. Widely exposed. Maximum exposed thickness: ~800 m. Type locality : west wall of Waimea Canyon. Reference locality : northwest coast of island (Napali coast). Base not exposed.	Pliocene and Miocene(?) (4.3-5.1)	Reduced in rank (see text). Formerly: Napali Formation of Waimea Canyon Volcanic Series (Macdonald and others, 1954, 1960).
	NIIHAU		
	Niihau Volcano		
Kiekie Basalt	Rejuvenated-stage lava of alkalic basalt. Lava flows and pyroclastic deposits. Forms low coastal plain. Maximum exposed thickness: ~90 m. Type locality: town of Kiekie. Unconformably overlies Paniau Basalt.	Pleistocene and Pliocene (see text)	Renamed. Formerly: Kiekie Volcanic Series (Stearns, 1946, 1947b); Kiekie Volcanics (Clague and others, 1982).
Paniau Basalt	Shield-stage lava of tholeiitic basalt, olivine tholeiitic basalt, and rare postshield-stage alkalic basalt. Lava flows and associated intrusive rocks, minor ash. Single post-caldera stage alkalic vent at Kaeo. Comprises central highlands of island. Maximum exposed thickness: ~350 m. Type locality: east side of Paniau hill. Base not exposed.	Pliocene and Miocene (see text)	Renamed. Formerly: Paniau Volcanic Series (Stearns, 1946, 1947b).

[1]Here designated.

Addendum

Some units on the Islands of Hawaii, Maui, and Oahu listed in table 1.12 and discussed in the text were also formerly called "Formations" as follows (listed in alphabetical order): Hana Formation (East Maui Volcano, Maui); Hawi Formation (Kohala Volcano, Hawaii); Honolua Formation (West Maui Volcano, Maui); Honolulu Formation (Koolau Volcano, Oahu); Honomanu Formation (East Maui Volcano, Maui); Hualalai Formation (Hualalai Volcano, Hawaii); Kahuku Formation (Mauna Loa Volcano, Hawaii); Kau Formation (Mauna Loa Volcano, Hawaii); Kolekole Formation (Waianae Volcano, Oahu); Koolau Formation (Koolau Volcano, Oahu); Kula Formation (East Maui Volcano, Maui); Lahaina Formation (West Maui Volcano, Maui); Ninole Formation (Mauna Loa Volcano, Hawaii); Pololu Formation (Kohala Volcano, Hawaii); Waawaa Formation (Hualalai Volcano, Hawaii); Waianae Formation (Waianae Volcano, Oahu); and Wailuku Formation (West Maui Volcano, Maui). See Easton, R.M., and Gaiswinkler-Easton, M., 1983, A guide to the geology of the Hawaiian Islands--Hawaii, Maui, and Oahu: Joint Annual Meeting of the Geological Association of Canada, Mineralogical Association of Canada, and Canadian Geophysical Union, Field Guidebook, v. 2, p. 1-91.

SUBSIDENCE OF THE HAWAIIAN RIDGE

By James G. Moore

ABSTRACT

The great load placed on the ocean floor by the Hawaiian volcanoes, combined with the removal of magma from depth to build the volcanoes, has caused the lithosphere to sag and the Hawaiian Ridge to subside. Constraints on the amount and age of subsidence have been derived from tide gauge measurements, geophysical measurements, and studies of submarine canyons, submerged carbonate reefs, drill holes, and dredge hauls. Most of the volcanoes have subsided 2–4 km since reaching the sea surface, and the bases of the volcanoes have subsided 5–8 km. The bulk of subsidence is complete about 1 m.y. after initiation of volcanism on the sea floor, and about one-half of the upbuilding of the volcanoes is reduced by subsidence. A substantial but unknown part of volcanic growth results from intrusion of dikes and sills into the volcanic edifice, and hence the subsidence of different parts of the volcanoes varies.

Major sea-level terraces form while the volcanoes are actively growing above sea level. As the site of volcanism and subsidence migrates toward the southeast, these terraces become tilted toward the point of active volcanic loading. This tilting makes it difficult to correlate terraces from volcano to volcano along the Hawaiian Ridge by use of depth alone.

The young volcanoes at the southeast end of the Hawaiian Ridge have not yet completed their growth and subsidence. Hence volcanic ages derived from them provide estimates of volcanic propagation rates that are too high. Likewise, volumes measured for the volcanoes only above the level of the ocean floor indicate eruption rates for the older, subsided volcanoes that are too low. These factors raise doubts about inferred increases in volcanic propagation rates and eruption rates during the last few million years.

Volcanic centers on the Hawaiian Ridge are commonly aligned along two or more curved loci roughly parallel to the ridge and approximately 40 km apart. These loci may mark the edges of downbending of the two sides of the lithospheric subsidence trough, where fracturing conducts magma to the surface. The curved map trends along the loci may be the result of interference in these subsidence-induced fractures by major pre-Hawaiian seamounts rafted into the area of active volcanism.

Some of the intense seismic activity concentrated at the southeastern end of the Hawaiian Ridge may result from bending and dislocation of the volcanic pile as its southeastern part subsides more rapidly than the part adjacent on the northwest.

INTRODUCTION

The Hawaiian Ridge is formed by the most vigorous volcanic center on Earth and consequently is one of the youngest, highest, and steepest topographic features on the planet. Northwestward movement of the Pacific plate relative to the mantle hot spot that produces the volcanic center carries the volcanic products away at a rate of about 10 cm/yr, thus forming the ridge. The combination of the weight of erupted material and the removal of material from depth to feed the volcanoes causes the lithosphere to flex downward and the volcanic islands to subside. Subsidence is also partly caused by cooling and contraction of the lithosphere as it moves away from the mantle hot spot.

The subsiding ridge has depressed the adjacent ocean floor more than one hundred kilometers away from the ridge axis. The volcanic products of the ridge fill the inner part of this depression, but the outer part remains a moat-like depression called the Hawaiian Deep. The axis of this deep parallels the ridge on each side and forms an arc around the southeast end of the ridge with a radius of about 140 km (fig. 2.1). The center of curvature falls on the island of Hawaii between the summits of Mauna Loa and Mauna Kea Volcanoes.

Outside of the Hawaiian Deep is a broad low upbowing of the ocean floor called the Hawaiian Arch. The arch probably formed mainly because mantle material squeezed out from beneath the sinking ridge and buoyed up the fairly rigid bend beyond the deep, but also perhaps partly through heating and uplift of mantle rocks as they encountered the Hawaiian hot spot.

The Hawaiian Ridge extends from its active southeast end at Kilauea, Mauna Loa, and Loihi Volcanoes nearly 3,500 km northwest across the central Pacific to the bend where the Emperor Seamounts begin. From this bend the seamount chain continues north for another 2,500 km to its end near the Aleutian Trench. The ages of volcanoes increase systematically from Kilauea toward the northwest; the age is about 43 Ma at the Hawaiian-Emperor bend and about 70 Ma at the north end of the Emperor Seamounts (Clague and Dalrymple, chapter 1). Across this same span of distance the volcano peaks become systematically lower in elevation (fig. 2.2): the highest at the young southeast end are more than 4 km above sea level; a large group located 1,000–3,000 km northwest are close to sea level; and the northern Emperor Seamounts are commonly about 3 km deep. Although the shape and height of the volcanoes have been modified by erosion and by growth of carbonate reefs, these elevation differences result mainly from subsidence.

ACKNOWLEDGMENTS

I thank Brent Dalrymple, David Clague, Donald Peterson, and Harold Stearns for helpful reviews. Thanks also to the many

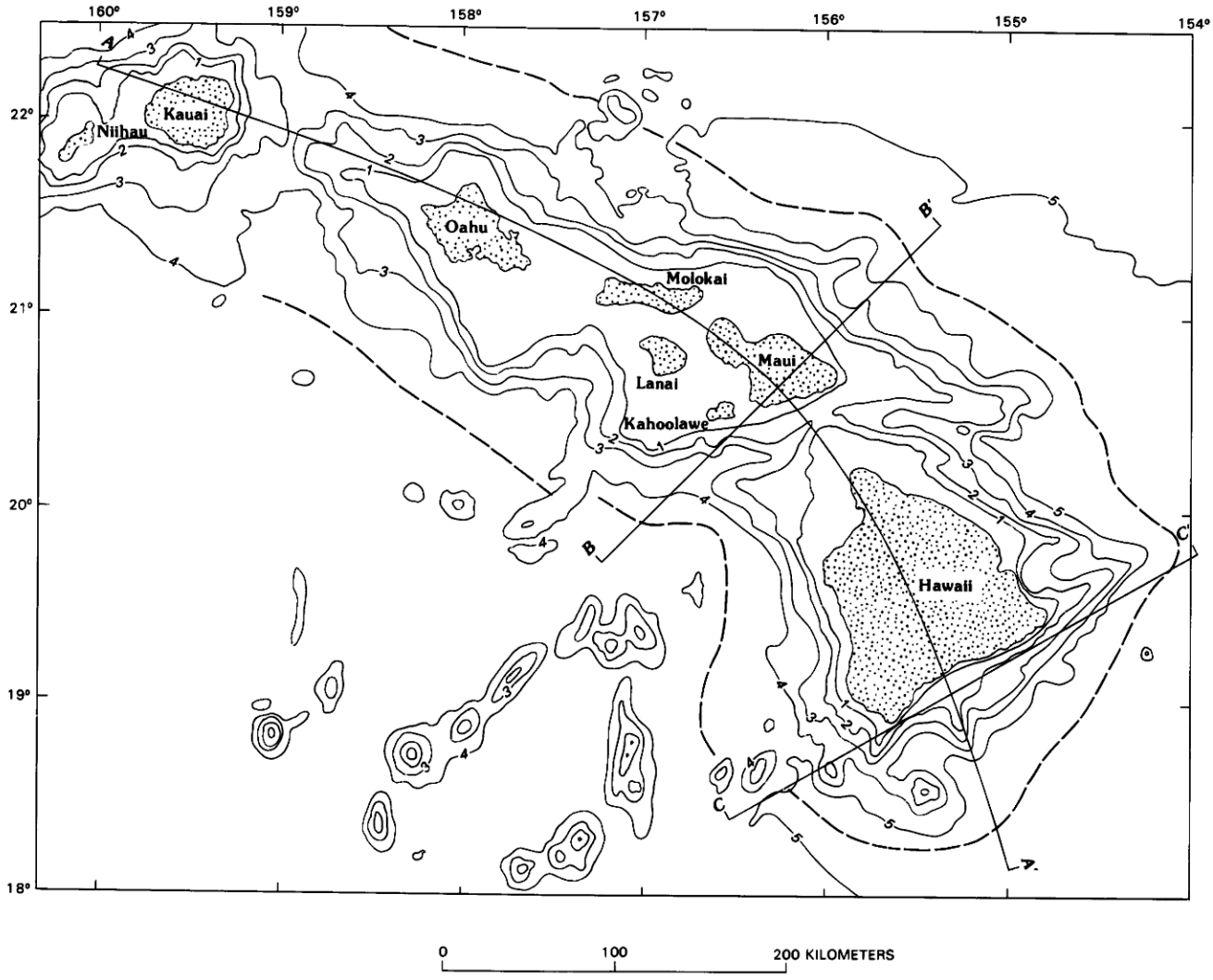

FIGURE 2.1.—Map of southeastern part of the Hawaiian Ridge showing axis of the Hawaiian Deep (dashed line) and section lines of figure 2.6. Depth contours in kilometers.

colleagues who have guided me through the intricacies and excitement of Hawaiian geology. The earliest and most effective of these were Donald Richter, Jerry Eaton, and Chester Wentworth.

TIDE GAUGE MEASUREMENTS

An analysis of tide-gauge data indicated that Honolulu on Oahu is approximately stable, because sea level at Honolulu is rising at a rate similar to that reported by many other stations that apparently reflect the worldwide eustatic rise (Moore, 1970). A reanalysis of Honolulu tidal data for the period 1935–83 indicates that sea level is rising there at a rate of 1.2 mm/yr. The close comparison of this rate with a recent estimate of global sea level increase of 1.5 mm/yr (Barnett, 1983) supports the notion that Honolulu is practically stable.

Some of the scatter inherent in tidal observations can be eliminated by comparing tide levels at other Hawaiian stations with those at the apparently stable Honolulu. Factors such as eustatic sea-level rise, barometric pressure, and sea temperature affect both Honolulu and other neighboring stations in the same way and hence are eliminated by using the differences in annual mean water levels for Honolulu and the neighboring stations. Such an analysis of measurements through 1967 indicated that sea level was rising at Hilo, Hawaii, at 4.1 mm/yr and at Kahului, Maui, at 1.7 mm/yr *relative to the assumed stable Honolulu* (Moore, 1970). Hence Hawaii and Maui were presumed to be undergoing absolute subsidence at those rates.

However, precise determination of sea level trends requires a long period of measurement. The 16 years of record for Kahului and the 21 years for Hilo utilized for the previous estimates were

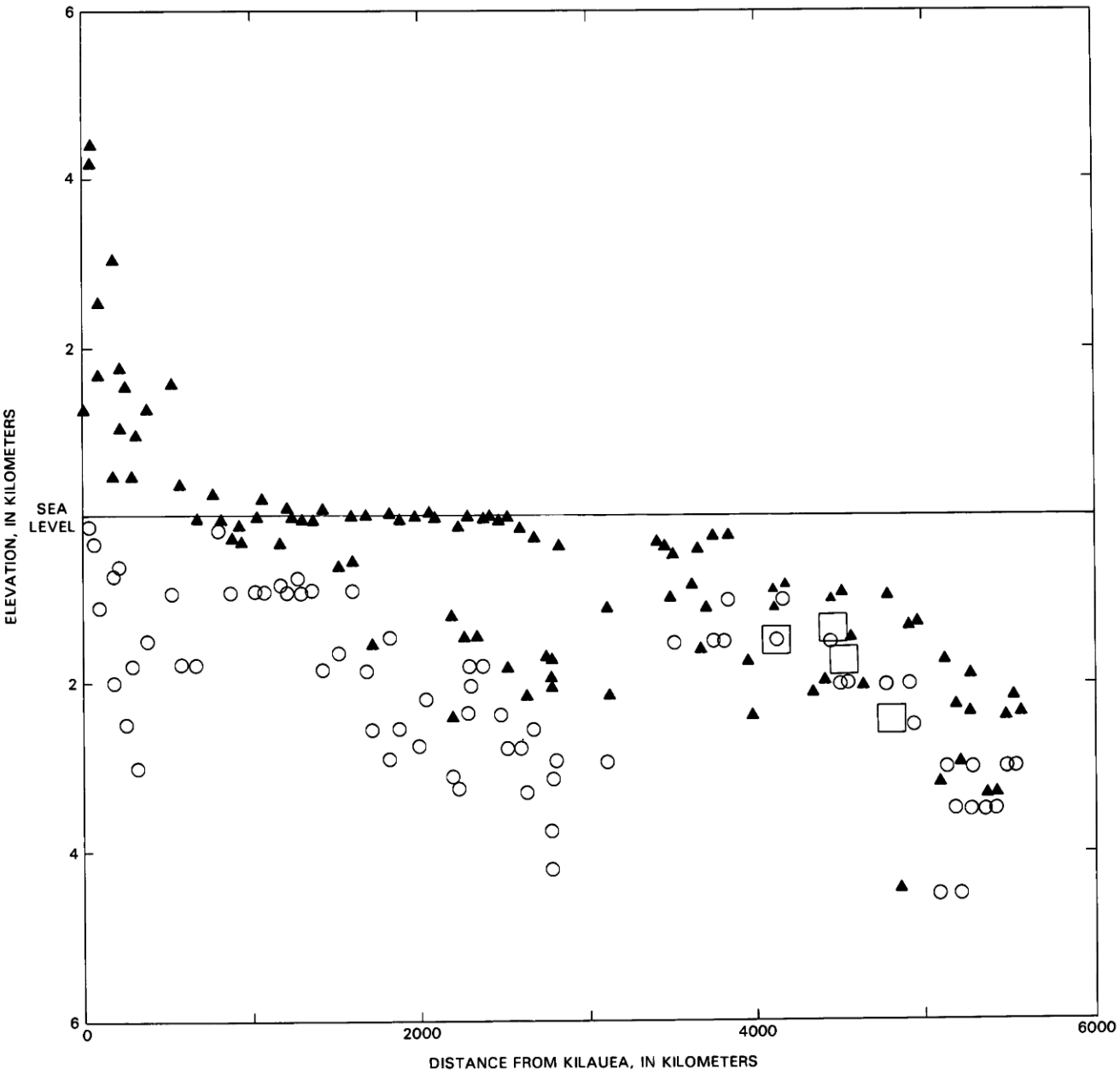

FIGURE 2.2.—Elevation and depth of volcanic features of the Hawaiian Ridge-Emperor Seamounts area. Triangles, tops of individual volcanoes; circles, depths of prominent terraces believed to have formed at sea level; squares, depth of penetration of drill holes on seamounts that encountered only subaerially erupted lava.

minimal. A reanalysis using the 17 additional years of measurements since 1967 provide a better data base for estimation of longer term trends in subsidence rates (fig. 2.3).

The primary measurement used is the annual mean of sea level at the various stations as reported by the U.S. National Ocean Survey. This annual mean is the stand of sea level relative to a fixed datum measured every hour and averaged for one year. The trends of differences of the annual mean of Hilo minus Honolulu and of Kahului minus Honolulu have been determined through 1983. Linear regression fits of this data indicate that Hilo is subsiding relative to Honolulu (assumed stable) at 2.4 mm/yr and Kahului at 0.3 mm/yr. The reason for the differences between the older estimates and these revised estimates is clear from the plot of annual means of sea level (fig. 2.3). The trend through 1967 was steeper than the longer trend through 1984. This change affects both the Kahului and Hilo stations, but is not a worldwide effect because the Honolulu means have been subtracted from the plotted data. The reason for this change in slope is unknown; it may reflect regional

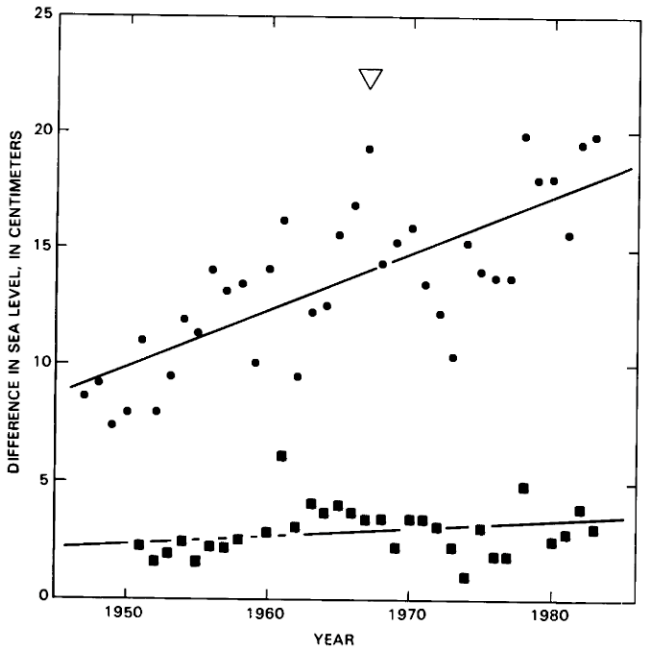

FIGURE 2.3.—Differences in annual means of sea level through 1983. Dots, means at Hilo, Hawaii, minus means at Honolulu, Oahu; squares, means at Kahului, Maui, minus means at Honolulu, Oahu. Open triangle, limit of data (1967) for analysis of Moore (1970).

variations in atmospheric or marine conditions on sea level or a real pulsation in subsidence rates.

In evaluating the subsidence of coastal stations such as Kahului and Hilo, the location of these stations relative to the deep subsiding trough underlying the Hawaiian Ridge must be considered (fig. 2.4). Subsidence varies between different locations on the island of Hawaii and probably reaches a maximum near the island center, where the base of the crust is depressed about three times as much as it is at Hilo on the coast. The surface subsidence at the island center may not actually be three times greater than it is at Hilo, however, because other processes taking place between the surface and the base of the crust, such as intrusion and variations in magma storage within shallow magma chambers, may affect surface subsidence.

DRILLING AND DREDGING

Many holes have been drilled on the Hawaiian Islands principally for the purpose of developing fresh water supplies. Most of these holes penetrate only a short distance below sea level, but a few deep research holes have been particularly valuable in providing information on the history of subsidence as well as on variations in sea level caused by other factors.

A hole drilled on the Ewa coastal plain, Oahu, reached a depth of 337 m and bottomed in red clinker and weathered vesicular subaerial basalt of the Koolau Volcano. The hole records a long period of subsidence and deposition of shallow marine and lagoonal muds, marsh deposits (lignite), and coral reefs, with intermittent periods of erosion and weathering (Stearns and Chamberlain, 1967).

Two holes were drilled on Midway Atoll in 1965. The deeper one penetrated limestone reef material until it encountered weathered basalt, overlain by basaltic conglomerate, at a depth of 384 m. The hole then went through a series of basaltic lava flows to the bottom at 504 m below sea level. The high vesicularity of these lavas (fig. 2.5) indicates that all were erupted subaerially.

A geothermal test well was drilled at an elevation of 182 m on the east rift zone of Kilauea Volcano in early 1976. This hole was 1,962 m deep and bottomed 1,780 m below sea level. The drill cuttings reveal the first appearance of pillow-like glass at 348 m below sea level, and the apparent transition zone between subaerially erupted and subaqueously erupted basalt is placed between 275 and 382 m below sea level (Stone, 1977). We will assume the change to be at 348 m. The age of the lavas encountered in the hole is not known, but it is evident that since the time the drill-hole region was at sea level, 182 + 348 = 530 m has been added to the upper surface of Kilauea Volcano. If the sea-level stand were the same then as now, the volcano has subsided 348 m. However, sea level may have been as much as 100 m below its present stand, in which case the volcano may have subsided only 248 m. One-half to two-thirds of the volcanic buildup of this part of the volcano has therefore been lost by subsidence. This ratio is similar to that for the southeastern Hawaiian Ridge as a whole. It now stands 5–6 km above the old ocean floor, which is depressed 5–8 km below the ridge axis (fig. 2.6). Hence about one-half of the buildup of the ridge has been lost by subsidence.

During Leg 55 of the Deep Sea Drilling Project (DSDP), holes were drilled on the tops of four seamounts of the Emperor chain (Jackson, Koisumi, and others, 1980). All of the core material recovered from these holes indicates that the lava flows were erupted subaerially and that the sediments are of shallow-water origin. Evidence for the subaerial nature of the lava flows is the presence of coarsely vesicular flow tops, red oxidized flow tops and bases, interbedded red tropical soils, and absence of pillow lavas; the sediments above the basalts contain shallow reef and littoral organisms and structures.

Because the water depth was great where these DSDP holes were started, they provide information on subsidence that is deeper than holes drilled on land (fig. 2.2). Hole 430 on Ojin Seamount (lat 37°59′ N.) reached 1,566 m below sea level and bottomed in material of subaerial origin. Hole 432 on Nintoku Seamount (lat 41°20′ N.) reached 1,327 m below sea level in lava flows with red oxidized tops interbedded with red tropical soil. Hole 433 on Suiko Seamount (lat 44°30′ N.) reached 2,422 m below sea level and penetrated a considerable thickness of reef limestone overlying subaerially erupted basalt. The Emperor DSDP holes document minimum subsidence of nearly 2.5 km after the volcanoes reached sea level and produced subaerially erupted lava.

Dredging of the submarine flanks of the Hawaiian volcanoes can also provide information on the amount of subsidence. Four dredge hauls from the submarine east rift zone of Mauna Kea Volcano recovered lavas that are much more vesicular than similar

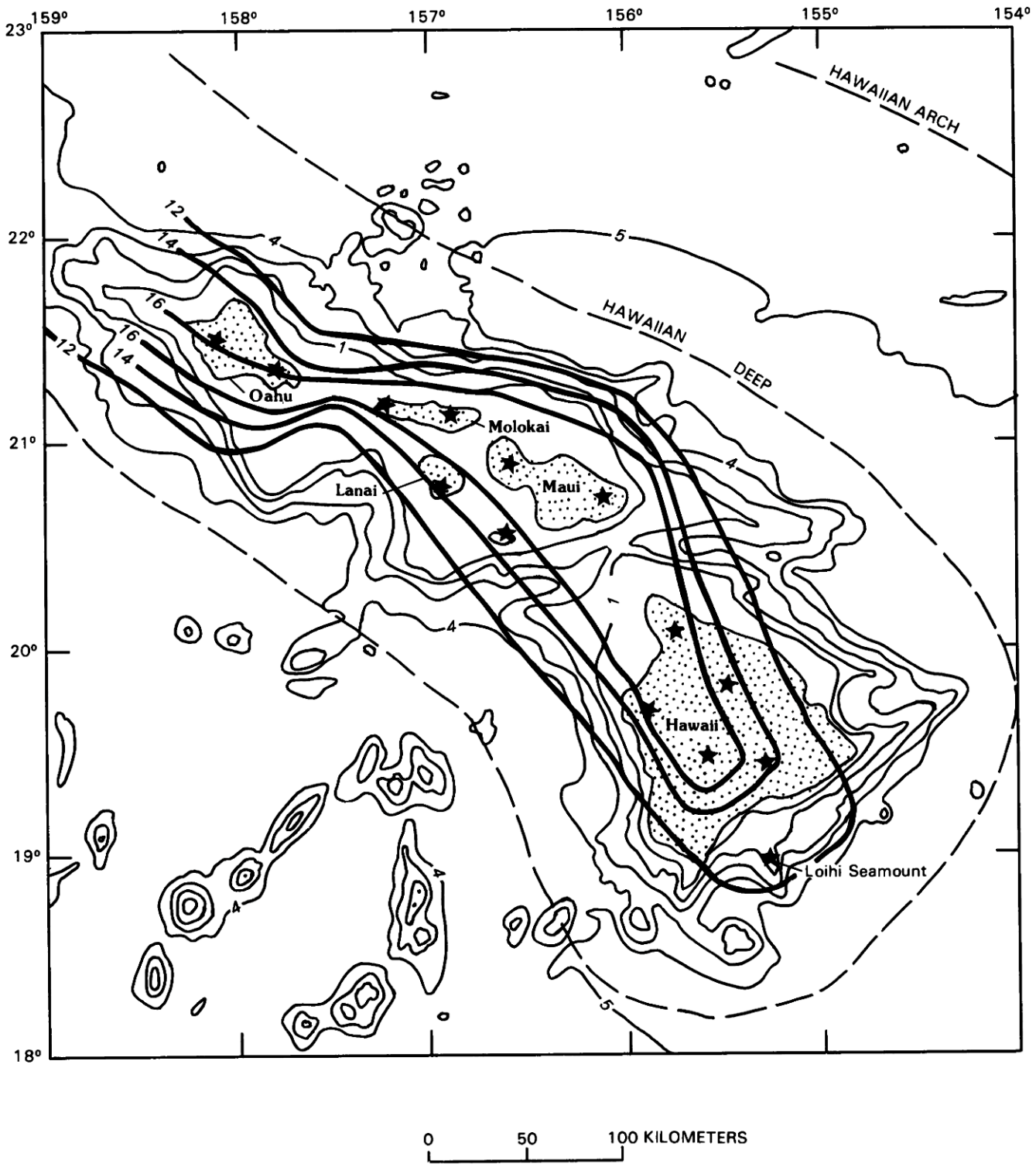

FIGURE 2.4.—Structure contours (heavy lines), in kilometers below sea level on the base of the crust, as determined by seismic refraction for the southeastern part of the Hawaiian Ridge. Data from Shor (1960), Furumoto and others (1973), and Zucca and others (1982). Depth contours in kilometers. Stars, volcanic centers.

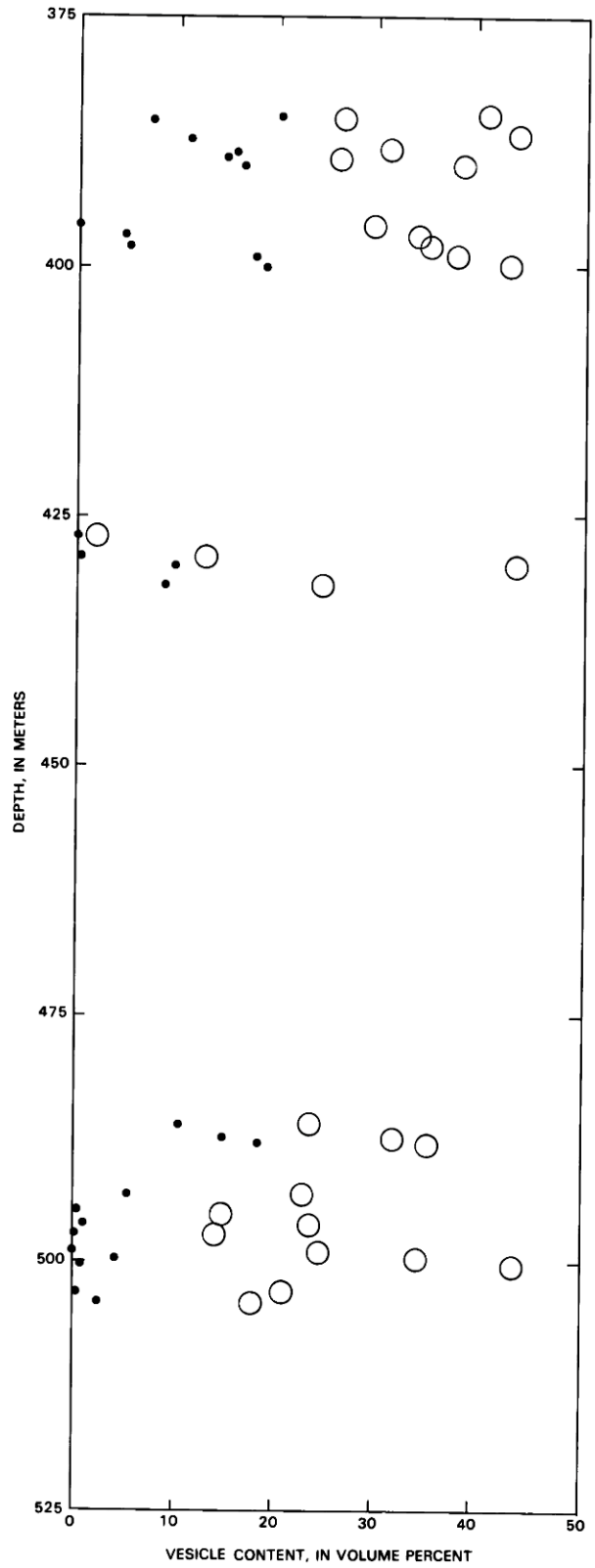

FIGURE 2.5.—Vesicularity of lava samples from 1965 drillhole on Midway Island. Open circles, volume percent of all vesicles; dots, volume percent of unfilled, open vesicles.

lavas collected from the same depth on the currently active rift zones of Kilauea and Mauna Loa Volcanoes. Comparison of vesicularity indicates that Mauna Kea has subsided about 1,000 m since extrusion of these lavas (Moore and Peck, 1965).

On the northwest rift of Hualalai Volcano, sulfur-poor degassed lavas have been dredged from depths down to 1,750 m. The low sulfur content of these lavas indicates that they were erupted under subaerial conditions and therefore that the volcano has subsided more than 1.7 km since their eruption (D.A. Clague, written commun., 1985).

ZONE OF ONGOING SUBSIDENCE

The southeast end of the Hawaiian Ridge, including the Island of Hawaii, is currently undergoing the most rapid subsidence. Tide gauge measurements indicate that Hilo has subsided at a rate of 2.4 mm/yr during the last 36 years. An analysis of the depth of reefs off the northwest coast in comparison with eustatic sea-level curves indicates that subsidence there has ranged from 1.8 to more than 3 mm/yr and has increased over the last 0.3 m.y. (Moore and Fornari, 1984). A study of submerged Hawaiian artifacts carved in lava flows indicates that Honaunau on the Kona coast of Hawaii is submerging at about 3 mm/yr (Apple and Macdonald, 1966). Photographs of the Kealakekua Bay region of west Hawaii taken in 1929 show a distinct sea-level algae line which is now 18.5 cm lower than the present-day line of the same character at the same place, indicating a submergence rate of 3.4 mm/yr (Moore and Fornari, 1984). Assuming that the current rise of sea level is 1.5 mm/yr, then these submergence rates translate to subsidence rates of 1.5 mm/yr for Honaunau and 1.9 mm/yr for Kealakekua Bay.

A growing body of data indicates that in addition to the general long-term subsidence, parts of the ridge are subject to landsliding and other forms of rapid subsidence. Such processes are an effective means of moving material to a lower elevation and of reducing the slope of the Hawaiian Ridge. During the November 1975 magnitude 7.2 earthquake, a 25-km-long zone along the southeast coast of Hawaii subsided as much as 3.5 m (Tilling and others, 1976). Such processes can be an efficient way of accommodating the rapid and dramatic subsidence that must be occurring on the southeast end of the ridge (fig. 2.6).

The Kalaupapa Peninsula on the north coast of Molokai is the exposed part of a small shield volcano that initially erupted below sea level, at the base of the giant northern sea cliff of the island. The vent in the center of the present peninsula erupted lava that covers a total area of about 20 km^2, half of which is now above sea level. Radiometric dating indicates that this activity occurred at 0.34–0.57 Ma (Clague and others, 1982). Available bathymetry (Mathewson, 1970) demonstrates that the submarine part of the shield has a markedly steeper slope below a depth of about 50 m (fig. 2.7). This slope break apparently marks the level of the sea at the time of volcanism (Mark and Moore, chapter 3). Therefore sea level is presently 50 m above its level during Kalaupapa volcanism. Sea level now stands relatively high compared to much of the Pleistocene when it probably averaged about 50 m below the present level. If we assume that sea level was at its present level

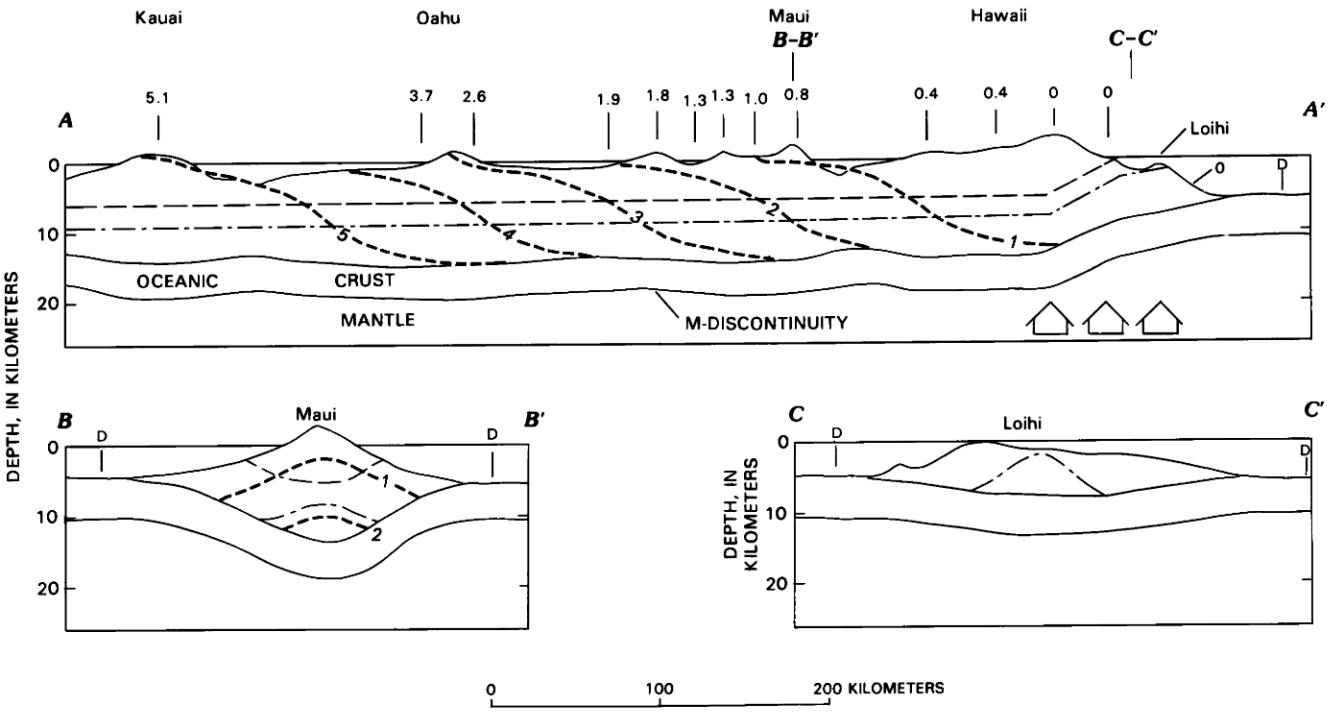

FIGURE 2.6.—Diagrammatic sections of the Hawaiian Ridge based primarily on seismic refraction and gravity measurements (Zucca and others, 1982). Location of sections shown in figure 2.1: *A–A'*, curved longitudinal crustal section along the length of the ridge; *B–B'*, transverse section through Haleakala Volcano on Maui; C–C', transverse section through Loihi Volcano south of Hawaii. Radiometric ages of volcanic rock series in Ma (Clague and Dalrymple, chapter 1) are shown above section *A–A'*. Heavy dashed lines, isochrons of volcanic products in Ma (note that the zero isochron is the present southeastern slope of the ridge); dashed line, boundary between subaerially and subaqueously erupted lava; dash-dot line, boundary between tholeiitic basalt above and early alkalic basalt below. D, axis of Hawaiian Deep. Vertical exaggeration, ×4. Magma chambers and volcanic conduits are omitted for clarity, but position of mantle hot-spot area shown by arrows in *A–A'*.

during growth of the Kalaupapa shield, then subsidence occurred at the low rate of about 0.1 mm/yr. If sea level was below its present level, as it was during much of the Pleistocene, then subsidence would be even less. The Kalaupapa evidence, therefore, indicates that subsidence of central Molokai has been 0.1 mm/yr or less during the last one-half million years.

The presence of coral reefs above sea level provides constraints on the timing and amount of subsidence of the Hawaiian Ridge, and this evidence consequently is critical to an understanding of the subsidence history. Recent studies have shown that coral deposits, previously believed to have been reefs uplifted hundreds of meters, were actually laid down by a giant wave that swept up on land more than 300 m high about 115,000 years ago (Moore and Moore, 1984; Moore and others, 1984). This evidence removes the need for the volcanoes to have risen tectonically hundreds of meters, as previously proposed (Stearns, 1978). Instead, rapid subsidence during volcano growth, and continuing perhaps 1 m.y. after growth, is consistent with most evidence.

Oahu is the southeasternmost island on which extensive coral reefs, clearly in growth position, occur above sea level. These reefs include the Waimanalo reef at 7.5 m above sea level dated at 125 ka, the Laie reef at 21.5 m, and the Kaena reef at 29–30 m dated at about 650 ka (Stearns, 1978). These reefs presumably grew and developed when sea level was higher than today owing to glacioeustatic causes, and they testify to the stability of Oahu and the lack of significant present-day subsidence. However, the presence of important terraces below sea level on Oahu, especially those below 150 m (fig. 2.8), which is commonly considered to be the lowest glacioeustatic stand of the sea, indicates that Oahu, like the other islands, subsided before the growth of reefs that now occur above sea level.

Available evidence therefore indicates that contemporary subsidence at rates of a few millimeters per year can be documented at several sites on the island of Hawaii, including Hilo and the west (Kona) coast. Subsidence on Maui, if occurring, is an order of magnitude less, and Molokai and Oahu have been virtually stable for a long period.

SUBMARINE TERRACES

A large number of submarine benches, terraces, and flat-topped ridges or seamounts appear on large- and small-scale bathymetric maps of parts of the Hawaiian Ridge. Many are rather subtle features, only visible on detailed bathymetric charts. Several

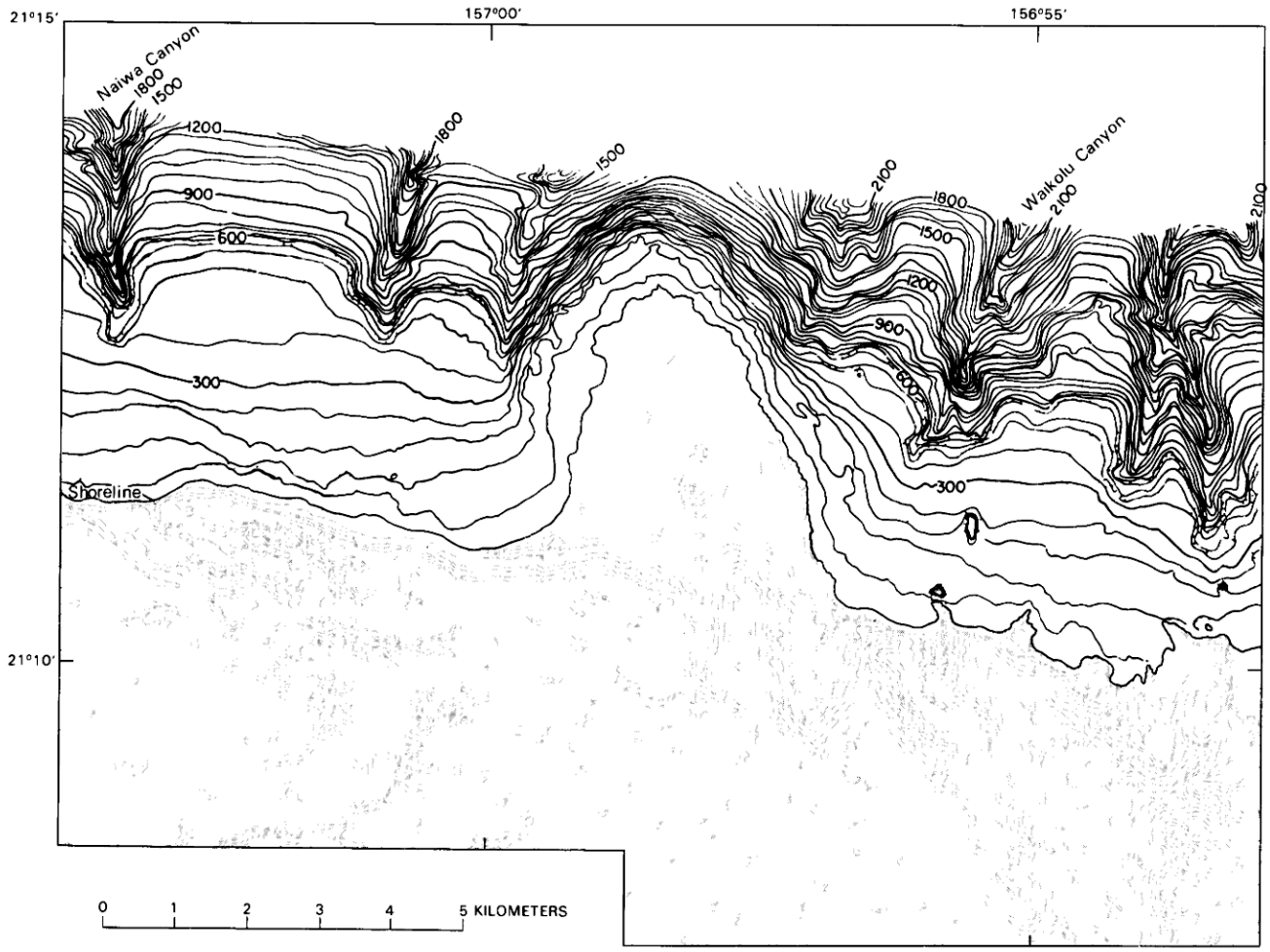

FIGURE 2.7.—Map of the Kalaupapa Peninsula on northern Molokai. Bathymetry after Mathewson (1970). Elevations and depths in feet; bathymetric contour interval, 60 ft.

of these that have been investigated by diving, dredging, and photography proved to be submerged coral reefs. A study of detailed nearshore bathymetric charts indicates that submarine terraces are common off several of the chief Hawaiian Islands at depths of 100–150 m. Curiously, deeper terraces in the depth range 200–500 m seem to be present only off the Island of Hawaii (fig. 2.8*A*). A prominent terrace at about 150-m depth occurs off west Hawaii on Kohala, Mauna Kea, and Hualalai Volcanoes, but younger lavas from Mauna Loa Volcano flood it south of lat 19°15′ N. Submersible dives reveal that it is a well-developed coral reef. Radiocarbon ages of the reef limestone show that the reef drowned 13,250 years ago (Moore and Fornari, 1984).

A second major reef terrace occurs at about 400-m depth off northwest Hawaii (Campbell, 1984) and is almost certainly correlative with the terrace at that depth off the northeast coast of Mauna Kea Volcano (figs. 2.1, 2.8). Submersible dives in 1985 off northwest Hawaii recovered reef limestone samples which yielded preliminary uranium-series ages of about 115 ka (B. Szabo, written commun., 1985).

These shallow reef terraces apparently deepen and become separated toward the southeast, forming an imbricate pattern tilted southeast (fig. 2.8). The terraces, which were presumably formed horizontally at sea level, have since been depressed more toward the southeast where subsequent subsidence has been greater. Toward the northwest, where Pleistocene subsidence occurred at only a very low rate, terraces of many different ages formed atop one another at the lower limit of the eustatically shifting sea, 100–150 m below present sea level.

Small-scale bathymetric charts of the Hawaiian Ridge show a series of large and prominent benches and terraces bounded below by a steep slope (fig. 2.9). The shapes of these abrupt slope changes indicate that they formed at the subaerial-subaqueous lava transition zone during island growth by grading of lava flows to sea level (Mark and Moore, chapter 3). A compilation of the depths of such

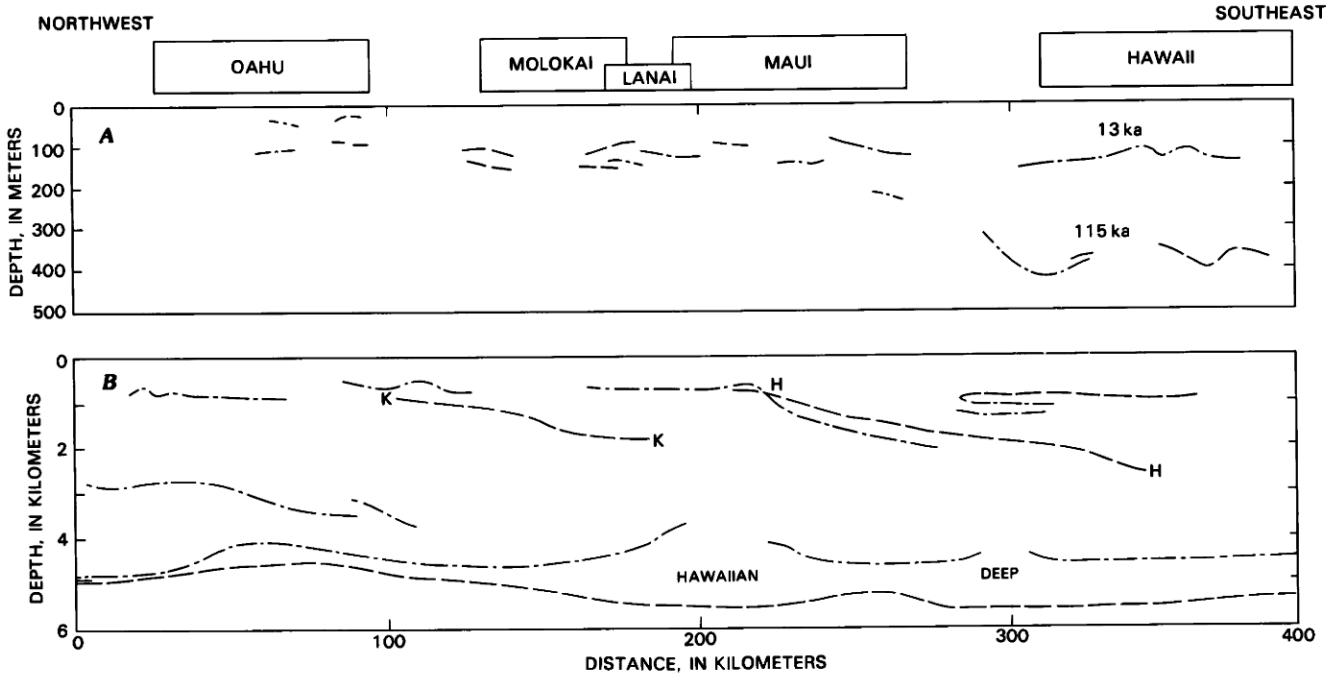

FIGURE 2.8.—Depths of terraces and axes of Hawaiian Deep projected onto a vertical plane striking N. 45° W. *A*, Terraces in upper 500 m, including two dated terraces off west Hawaii. *B*, All major terraces above Hawaiian Deep, including the tilted H and K terraces shown in figure 2.9. Dashed line, features on northeast side of ridge; dash-dot line, features on southwest side of ridge.

benches on the entire Hawaiian-Emperor chain indicates that they range from 1 to 4 km but are commonly 2–3 km (fig. 2.2). These depths, coupled with drill-hole evidence, suggest that the Hawaiian volcanoes have generally subsided 2–3 km after they had grown above sea level and could be marked by such sea-level features.

One of the more prominent benches surmounts the east Maui Ridge (called the Haleakala Ridge by Wilde and others, 1980). This terrace, here called the H terrace, is tilted down to the southeast and can be traced more than 150 km from north of west Maui at about 400-m depth to north of the Island of Hawaii at 2,000-m depth (figs. 2.8, 2.9). The terrace slopes about 1 km per 100 km, or about one-half degree, but it is believed to have been an original horizontal feature that has since tilted down toward the Hawaiian hot spot. A second such tilted terrace off north Molokai projects down beneath the H terrace and consequently is believed to be older (figs. 2.8, 2.9). This second feature, called the K terrace, can be traced nearly 100 km from about 900-m depth northwest of Molokai to 1,800-m depth northeast of Molokai. The K terrace is clearly younger than the proposed giant submarine landslide north of Molokai (Moore, 1964), but older than the Kalaupapa Volcano of north Molokai (0.34–0.57 Ma). The Molokai submarine canyons (see section "Submarine Canyons") could have been cut subaerially when the K terrace was about at sea level.

The ages of these tilted terraces are unknown, but they can be crudely approximated by comparing their depths with those of terraces of known ages in the same general area, assuming generally uniform rates of subsidence that are more rapid in the center than at the edge of the ridge. The H terrace, which was probably formed during the period when the present surface of Haleakala Volcano was developing, is about five times as deep as the 400-m terrace of Hawaii dated at 115 ka (fig. 2.8). Considering the lateral position of the H terrace, its age is probably 0.5–1.0 Ma. The K terrace, about twice as deep (and old) as the H terrace, probably formed when volcanism was active on Molokai at 1.8–1.9 Ma (Clague and Dalrymple, chapter 1). When the K terrace formed, the unsubsided Molokai volcanoes were more than 3 km above the sea, a height that may have led to gravitational instability and landsliding of the island's north flank.

SUBMARINE CANYONS

Submarine canyons have been identified off Kauai, Oahu, Molokai (Shepard and Dill, 1966), and Hawaii (this report), and doubtless many more will be found as improved bathymetric data become available. The Kauai submarine canyons head about 3.5 km offshore on the northwest coast and can be traced to depths of more than 2,200 m. The canyons are steep walled; Honopu Canyon has walls about 750 m high at an axial depth of 1,500 m.

Canyons off the northeast coast of Oahu head 3–4 km offshore and can be traced downward to depths exceeding 2,000 m. These canyons have been extensively filled by sediment in their upper parts, and they also passed sediment to fan deposits near the Hawaiian

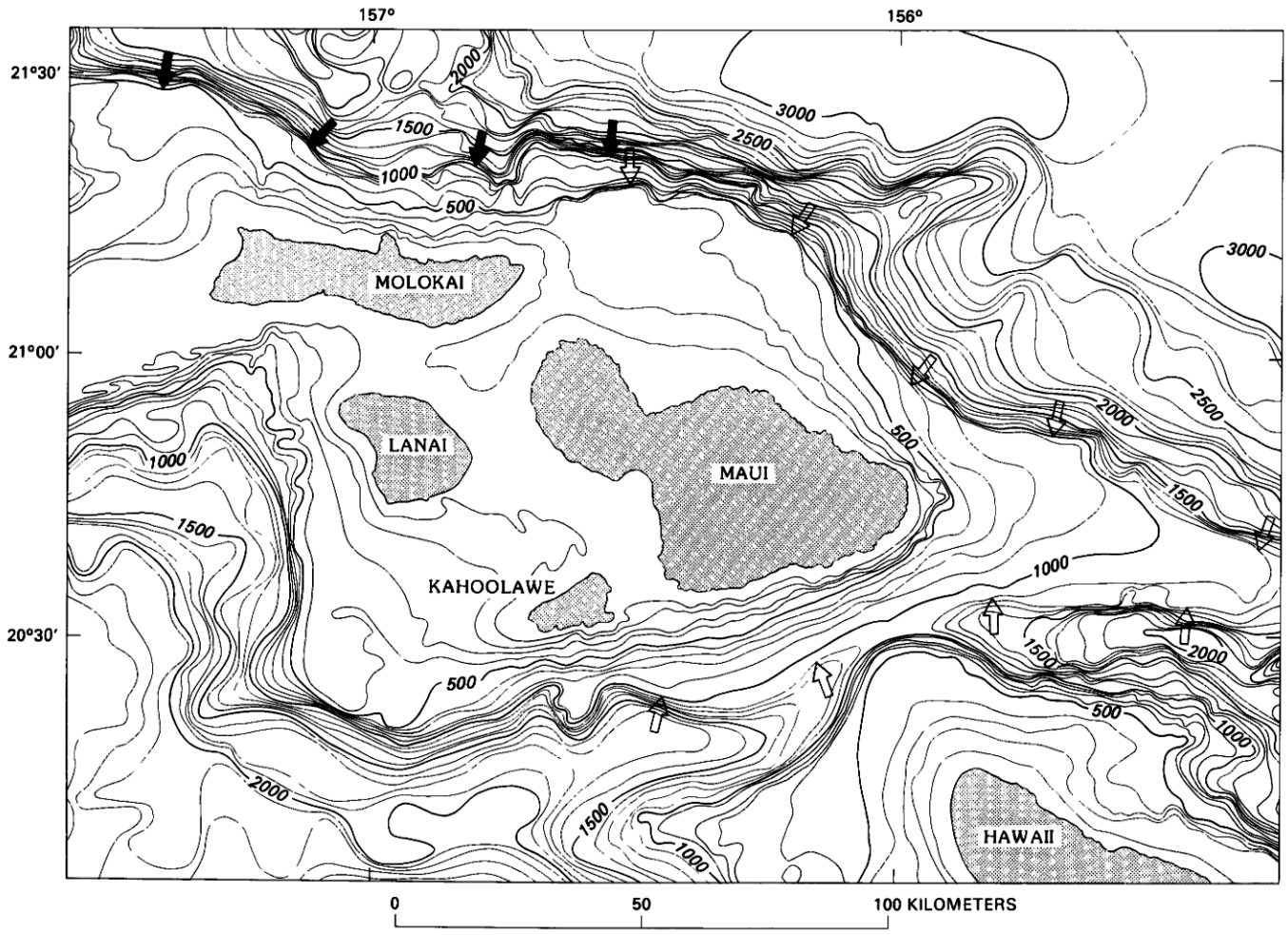

FIGURE 2.9.—Major tilted submarine terraces on southeastern Hawaiian Ridge. Open arrows, H terrace; solid arrows, K terrace. Contour interval, 100 fathoms (600 ft).

Deep (Andrews and Bainbridge, 1972). Ponds of such sediments occur between the blocky seamounts northeast of Oahu downslope from the canyons and indicate that these seamounts (variously interpreted as volcanoes or landslide blocks) predate canyon cutting.

The upper parts of 12 submarine canyons have been mapped in detail by Mathewson (1970) off the north coast of Molokai (fig. 2.7). Several of these canyons are directly offshore from major subaerial canyons and they head 1–2 km from shore. It is likely that the submarine canyons that flank the Kalaupapa Peninsula were cut before the peninsula was built at about 0.4 Ma (fig. 2.7).

A recent compilation of unpublished NOAA charts reveals three submarine canyons off windward Kohala Volcano (fig. 2.10). These canyons head less than 1 km from shore and can be traced downslope only to the limit of available bathymetry at a depth of 440 m. These submarine canyons are 40–80 m deep and hence are much less deeply incised than the 600-m-deep land canyons. This contrast can be attributed to the fact that the tops of the submarine canyons, as well as the upper part of the terrain between the canyons, has been planed off by erosional recession of the 400-m-high seacliff during subsidence. The canyons are offshore from major and minor subaerial canyons cut in Kohala Volcano. However, no submarine canyon lies offshore from Waipio Valley, the most southern Kohala canyon. This absence probably results from filling of the submarine continuation of Waipio Valley by lava from the younger, adjacent Mauna Kea Volcano (Stearns, 1966, p. 125).

Detailed bathymetric mapping off western Hawaii to locate anchor sites for an ocean thermal-energy conversion test platform has revealed a system of submarine canyons that generally head at depths greater than 1,000 m (Campbell and Erlandson, 1979). The western limit of this detailed mapping does not show the lower limit of these canyons, but several descend to depths greater than 1,600 m.

All who have investigated the Hawaiian submarine canyons note that they commonly align with present-day subaerial valleys but generally show little or no bathymetric expression across the near-

shore zone down to depths of about 100 m or more. Seismic-reflection profiling off windward Oahu (Coulbourn and others, 1974) shows that submarine troughs, filled and concealed by young sediments nearshore, connect the subaerial valleys with the visible submarine canyons. This fact provides support for a subaerial origin of at least some submarine canyons.

Hamilton (1957) and Macdonald and Abbott (1970) proposed erosion below sea level by submarine processes as the major cause of the Molokai submarine canyons, because the canyons extend deeper than any previously postulated estimate of submergence. On the other hand, other workers support subaerial erosion for the carving of all the canyons. Stearns (1966) believes submarine erosion simply could not cut such canyons in hard basalt; Mathewson (1970) points to the continuity of subaerial-submarine stream profiles to make the case for subaerial canyon cutting and later subsidence. Comparison of the depths of the lower ends of canyons with depths of major terraces believed to be sea-level features, as well as the evidence from drillholes (fig. 2.2). leaves little doubt that subsidence has been adequate to permit all of the canyons to have been cut by subaerial processes, although post-subsidence modification of the canyons by submarine processes is likely.

CRUSTAL STRUCTURE

Measurements of gravity and determinations of crustal structure by seismic refraction and reflection experiments have provided important constraints on the structure of the Hawaiian Ridge. This work shows that the depth to the base of the crust as marked by the M-discontinuity increases from about 10 km far from the ridge to as much as 20 km beneath the ridge. A 100-km-long seismic-refraction profile shot in 1978 offshore from the west coast of Hawaii indicates that the base of the crust has been depressed about 8 km beneath Mauna Loa Volcano (Zucca and others, 1982; Hill and Zucca, chapter 37). The base of the crust, normally 10–11 km below sea level away from the ridge, has been depressed to a depth of 13–14 km on both the west and south coasts of the island and down to 18.5 km beneath Mauna Loa (fig. 2.6). Seismic-refraction data farther northwest indicate that the M-discontinuity south of Oahu is about 20 km below sea level (Furumoto and Wollard, 1965; Watts and others, 1985).

The inferred lowering of the base of the crust beneath the ridge may be caused in part by injection of relatively low-density basaltic dikes and sills into the mantle beneath the original crustal layer. Such basaltic material would reduce the density and seismic velocity of the the upper mantle, convert it to a crustlike material, and cause a downward migration of the M-discontinuity. An interpretation based on seismic, gravity, and geoid data suggests that the lower 4 km of the depressed oceanic crust south of Oahu is composed of such a dense intrusive complex (Watts and others, 1985). This work also indicates that the old ocean floor on top of the oceanic crust has been warped down 5–7 km beneath the ridge to depths as great as 12 km below sea level.

Seismic refraction and gravity measurements have also shown that a significant mass fraction of the Mauna Loa and Kilauea volcanic edifices above the oceanic crust is composed of intrusive cores beneath the summit region and rift zones (Hill and Zucca, chapter 37). Intrusion of such material will add weight to the crust and cause subsidence of the volcano base, but will not cause the same degree of subsidence of the top of the volcanoes as it would if erupted subaerially as lava flows.

Depression of the top of the oceanic crust is 5–7 km near Oahu, and depression of the base of the oceanic crust is about 8 km beneath Mauna Loa, as revealed by seismic experiments. Despite the possibility that some of the apparent depression of the base of the crust is caused by intrusive activity, subsidence of the base of the volcanoes is probably 5–7 km and may be greater.

The major depression of the crust caused by the weight of the growing volcanoes atop the Hawaiian hot spot forms a giant trough or canoe-like crustal warp (fig. 2.4). This southeast-trending trough underlies the Hawaiian Ridge and terminates about 50 km southeast of the Island of Hawaii near the area where the Hawaiian Deep curves around the end of the ridge (fig. 2.1). The propagation of the Hawaiian Ridge and its underlying trough onto new virgin crust toward the southeast can be compared to the movement of a massive caterpillar tread over muddy ground (fig. 2.6). The sharp downflexing of the crust and lithosphere at the head of the caterpillar is probably the cause of some of the earthquakes concentrated around the volcanic front (fig. 2.11).

The edges of the deepest part of the downbowed crust are roughly coincident with the two or more loci, commonly about 40 km apart, that connect individual volcanic centers (fig. 2.4). Sharp bending of the crust and mantle on the two sides of the base of this trough may cause fractures that tap magmas from the hot spot and are related to the formation and progagation of these volcano loci. The changes in trend of these loci along the ridge (Shaw and others, 1980) are perhaps caused by the presence of major pre-Hawaiian volcanic seamounts that were rafted over the hot-spot area. Such seamounts and their underlying subsidence troughs could affect the downflexing of the lithosphere caused by the new volcanic load and perturb the positions of the fractures that conduct magma from the hot spot to the surface to feed the new volcanoes.

The prevolcanic sea floor underlying the Hawaiian Ridge is, like the underlying base of the crust, warped down into a trough. This trough, which is filled with material erupted from the volcanoes, extends beneath the level of the old ocean floor about as far down as the largest volcanoes presently rise above that level. The cross-sectional area of this trough beneath the level of the old ocean floor is about 750–1,000 km^2, equal to or somewhat greater than the cross-sectional area of the volcanic ridge above the old ocean floor. If the rate of plate motion is assumed to be 10 cm/yr, 0.075–0.1 km^3 of volcanic material subsides beneath the level of the old ocean floor per year. This volume is similar to or slightly less than the current measured output of Kilauea Volcano of 0.11 km^3/yr (Swanson, 1972). Hence the bulk of the material erupted from the Hawaiian hot spot is not only deeply buried, but has subsided below the general level of the surface on which it was originally deposited (the old ocean floor). Models considering the origin and structure of the ridge, and of the magmas that formed it, need take this fact into account.

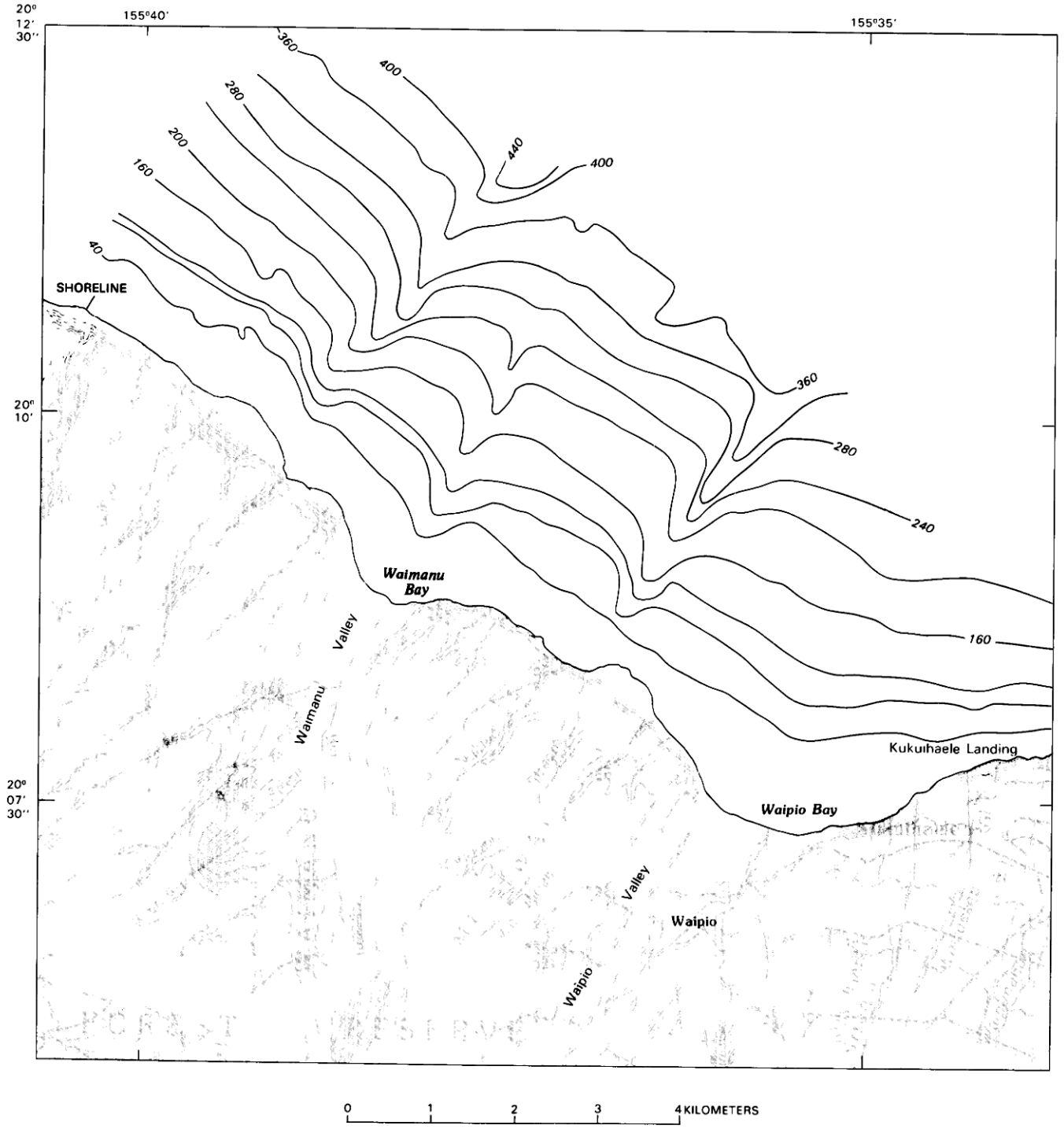

FIGURE 2.10.—Map of northeastern Kohala showing subaerial and submarine canyons. Bathymetric contour interval, 40 m.

The axis of the trough beneath the ridge has undergone most of its subsidence within a short distance (and hence time) from the unsubsided oceanic crust to the southeast. The base of the crust (and presumably also the old ocean floor) has subsided 7.5 km in the 100 km from the beginning of downwarping to the region beneath Mauna Loa (fig. 2.6). This is equivalent to a subsidence of 7.5 mm/yr if we assume that the volcanic system propagates laterally at a rate of 10 cm/yr relative to the crust.

The axis of the Hawaiian Deep becomes deeper northwest of the hot spot because of continued subsidence of the ridge and crust in

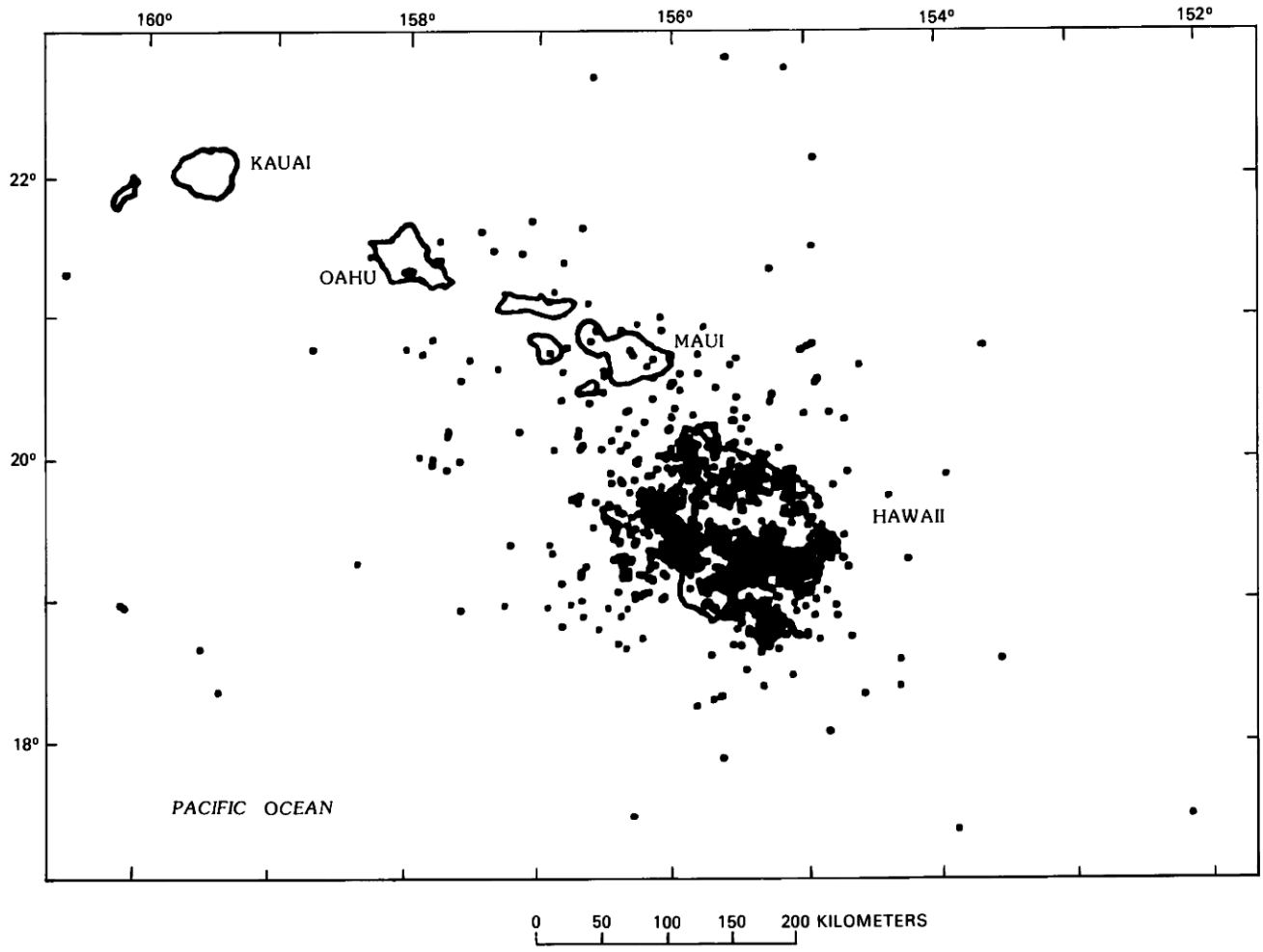

FIGURE 2.11.—Epicentral locations of earthquakes with magnitude 3 or larger in the Hawaiian region during 1968–83 (F.W. Klein, written commun., 1985).

response to the weight of erupted products. In addition, the lithosphere may have been reheated, and hence elevated adjacent to the hot spot to partly create the Hawaiian Arch (Von Herzen and others, 1982). Cooling and subsidence of the lithosphere northwest of the hot spot adds to the depression of the trough axis. Seismic refraction experiments indicating that the depth to the base of the crust south of Oahu is 20–23 km (Furumoto and Woollard, 1965) suggest the possibility of minor continued subsidence from Mauna Loa to Oahu.

CHARACTER OF SUBSIDENCE

The extent of the depression of the M-discontinuity from unaffected crust southeast of the ridge, through Kilauea, and northwestward to the older volcanoes provides information on the history and character of subsidence (fig. 2.6). Assuming a volcanic propagation rate of 10 cm/yr, each 100 km represents 1 m.y.

The bulk of subsidence occurred in about 1 m.y. The center of the base of the volcanic ridge subsides about 8 km, and the part of the volcano that first broke the sea surface subsides about 5 km. However, the sides of a volcano undergo considerably smaller amounts of subsidence than the center, producing a trough-like shape to the boundary between subaerially and submarine erupted basalt (fig. 2.6, section *B-B'*).

The southeast end of the ridge is downshearing against that part to the northwest because ongoing subsidence is greater to the southeast (fig. 2.6). This southeasterly dislocation probably occurs at all scales in southeast Hawaii and no doubt produces some of the seismic activity (fig. 2.11). Moreover, it must be an important process in shaping the geometry of volcanic conduits, magma chambers, and rift zones. Major fault systems such as the Kaoiki, which separates Mauna Loa from Kilauea, and the Hilina, on the south flank of Kilauea, are probably related to this process.

The general pattern of subsidence permits an estimate of the volume proportions of certain divisions of the volcanoes. A section

through the embryonic part of the ridge at Loihi Volcano (fig. 2.6) indicates a cross-sectional area of the ridge here of about 880 km^2 of basalt, all subaqueously erupted or intrusive. Petrologic studies (Moore and others, 1982) indicate that Loihi has recently undergone a transition from eruption of early alkalic lava to eruption of tholeiitic lava, and the section suggests that about 30 percent of the ridge here is composed of the early alkalic material. This estimate does not consider the possibility that much of the basal part of the volcano is composed of intrusive rock, possibly of a different composition. At this early stage already about 40 percent of the volume of the volcano has subsided beneath the level of the prevolcanic ocean floor.

In contrast, Haleakala Volcano on Maui has virtually completed its volcanic cycle, except for lingering small-scale eruption of late alkalic lavas. The cross-sectional area of the volcanic ridge here is about 1,450 km^2, of which about 16 percent is the early alkalic lava and only a few percent is late alkalic lava. Presently only 4 percent of the volcanic pile is above sea level, but 25 percent of the volume of the ridge here was erupted above sea level and built shield volcanoes largely of tholeiitic basalt. The other 75 percent of the volcanic ridge, although also composed principally of tholeiitic basalt, was erupted beneath the sea and is composed largely of pillowed lavas that predate the growth of the subaerial shield volcanoes and have steeper slopes (Moore and Fiske, 1969). About 53 percent of the volume of volcanic materials here has subsided beneath the level of the prevolcanic ocean floor.

The primary constraint on the measured rate of volcanic propagation along the Hawaiian Ridge is the body of radiometric ages of rocks collected from the volcanoes (Clague and Dalrymple, chapter 1). It is evident that virtually all of these samples are from near the top of the volcanoes. Wherever possible, tholeiitic lavas rather than the later alkalic lavas were collected and dated, so the ages more nearly define the age of the major shield-building stage of volcano growth.

Time-distance plots of the age data show an apparent acceleration of the volcanic propagation rate (as well as the volcanic eruption rate) in the last approximately one million years. Shaw and others (1980) find that the average rate of volcanic progression from the Hawaiian-Emperor bend to West Maui Volcano is 7.9 cm/yr, and the average rate from West Maui Volcano to Kilauea is 17.8 cm/yr. Clague and Dalrymple (chapter 1) support the notion of a relatively recent acceleration in the volcanic propagation rate and note that otherwise the curvature of the time-distance plot causes it to intersect the distance axis northwest of Kilauea and predict a negative age for that volcano.

However, the fact that the southeast end of the ridge has not undergone all of its subsidence is an important limitation to the use of unqualified time-distance plots to determine the propagation rate. The exposed and dated parts of the southeastern volcanoes will clearly submerge beneath the sea and be covered with younger lavas. When the first phase of rapid subsidence is complete for Kilauea, the present summit will be 1 km or more below sea level. Loihi Volcano (figs. 2.1 and 2.6). now 1 km below sea level, will have to grow more than 2 km up before it breaks the sea surface because more than one-half of its volcanic growth is offset by subsidence. In order for the ages of Kilauea and Mauna Loa to be comparable with those of the northwestern volcanoes, one must obtain samples of yet unerupted lavas that will mantle the presently exposed surface. Hence, if such unerupted future lava could be dated now it would have a negative age as suggested by Clague and Dalrymple. Until more is known about the volume and age of the submarine volcanic products, it seems premature to propose a dramatic increase in the rate of volcanic propagation in the last million years or so. Assuming that the rate has remained constant, then straight-line projection of age-distance data to Kilauea and on to Loihi suggests a negative (future) age for Loihi of 1–1.5 m.y. (Clague and Dalrymple, chapter 1). Since Loihi is already of finite age, the duration of the chief period of volcano growth is about 1.5–2 m.y. (fig. 2.6)

The proposed increase in the volume of volcanic products and hence eruption rates at the young end of the ridge (Clague and Dalrymple, chapter 1; Shaw and others, 1980) is also uncertain, because all of the previously measured volcanic volumes include only that part of the ridge above the level of the flat ocean floor surrounding the Hawaiian Ridge. The volume of volcanic material in the trough underlying the ridge has not been considered. Because the old ocean floor is fully depressed beneath the entire length of the ridge except at the extreme southeast end, it is not surprising that larger apparent volumes (and higher eruption rates) have been calculated for the unsubsided region.

The base of the volcanic material erupted between 1 Ma and the present is not depressed as much as that erupted between 2 and 1 or 3 and 2 Ma (fig. 2.6). The volume between the 1 Ma and zero isochrons is even further reduced if we consider the fact that the sides of the depressed zone loop around the end of the ridge (compare with fig. 2.4). This part of the ridge will subside many kilometers within the next one million years.

As the Hawaiian Ridge propagates southeasterly in the lithosphere by the northwesterly movement of the Pacific plate, the southeast end of the ridge and the surrounding ocean floor bend down toward the hot-spot area or toward the youngest volcano. Movement of the lithospheric plate away from the hot spot progressively removes a given island or volcano from the subsiding zone adjacent to the hot spot. At the present time Kahului, Maui, which is 180 km from Mauna Loa (near the hot-spot center), is not subsiding rapidly (fig. 2.3). and Molokai and Oahu appear to be stable. Hence the rapidly subsiding zone is largely in the vicinity of the Island of Hawaii, and it may be outlined by the concentration of recent earthquakes (fig. 2.11). Downwarping of the base of the crust begins about 100 km both southeast and southwest of Mauna Loa (Zucca and others, 1982). and available evidence suggests that the downwarping zone is roughly circular with a 100-km radius. The center of downwarping as defined by the curvature of the Hawaiian Deep (fig. 2.4) is about midway between the summits of Mauna Loa and Mauna Kea Volcanoes.

The manner of tilting of pre-existing terraces is clarified if we trace the history of a horizontal surface affected by this downwarping sag (fig. 2.12). Close to the center of the sag, assumed to be cone-like, the terrace will subside faster than on its edges where no subsidence occurs. As the terrace moves relatively northwest from the sag, progressively all subsidence will stop and the tilt will be

"frozen in" on the terrace. If we assume that the sag moves 10 cm/yr southeast relative to the crust, and that subsidence is 2.5 mm/yr at the cone center, then an original horizontal surface will finally end tilted toward the sag at about 1.5 km/100 km (fig. 2.12). This tilt is similar to that of the H terrace off east Maui (fig. 2.8).

The depression of the M-discontinuity beneath the Hawaiian Ridge is a measure of subsidence of the volcanoes. The high proportion of the volcanic pile that is below the level of the prevolcanic ocean floor even at the youngest, southeasternmost volcanoes indicates that subsidence is very rapid. Much of the subsidence occurs while the volcanoes are growing. A large part of the total subsidence has occurred by the time the volcanoes reach sea level; Loihi Volcano, still 1 km below sea level, has already subsided more than 1 km (fig. 2.6) and will presumably subside an additional 6 km if it grows to the size of Mauna Loa. However, subsidence is much more rapid after the volcanic products are deposited above sea level because the buoyancy of water does not affect this material and its effective weight is 1 g/cm^3 greater. This fact is demonstrated by the slope of the depressed M-discontinuity at the volcanic front. This slope becomes abruptly steeper beneath the southeast shoreline of Hawaii (fig. 2.6). These slopes (assuming a volcanic propagation rate of 10 cm/yr) indicate subsidence rates of 4 mm/yr for the submarine part of the volcano, and 12 mm/yr for the subaerial part of the volcano. Comparison of these slopes at the base of the crust with volcanic profiles at the top of the crust (fig. 2.6) indicates that downbowing of the crust is an almost immediate response to volcanic loading.

Through the life of the growing volcano, new material deposited on top undergoes progressively less subsidence than the older material below it. Hence when the volcano achieves enough mass above sea level to be marked by sea-level terraces, these features will undergo only a small part of the total subsidence experienced by the older, lower parts of the volcano.

CONCLUSIONS

Subsidence of the Hawaiian Ridge can be constrained by tide-gauge measurements, geophysical measurements of crustal structure, and information gained from submarine canyons, submerged carbonate reefs, deep drilling, and dredging. An analysis of these data indicates the following:

1. The Hawaiian Ridge has undergone rapid and dramatic subsidence. Most volcanoes have subsided 2–4 km since reaching the sea surface, and the bases of the volcanoes have subsided 5–8 km.

2. Between one-half and two-thirds of the upbuilding of the volcanoes is offset by subsidence.

3. Major sea-level terraces formed during the chief periods of volcanic growth above sea level tend to tilt toward the point of active volcanic loading, that is toward the southeast. Hence depth correlation of terraces along the island chain may be misleading.

4. Because the young volcanoes at the southeast end of the Hawaiian Ridge have not completed their subsidence and growth, volcanic ages derived from them provide estimates of volcanic propagation rates that are too high. Likewise, volumes measured for the volcanoes only above the level of the ocean floor indicate eruption rates for the older, subsided volcanoes that are too low. These factors raise doubts about both the proposed increase in volcanic propagation rate and eruption rate during the last few million years.

5. The alignment of volcanoes along two or more curving loci about 40 km apart and parallel to the Hawaiian Ridge may result from sharp bending of the crust and mantle on the two sides of the base of the subsided trough underlying the ridge. Such bending may

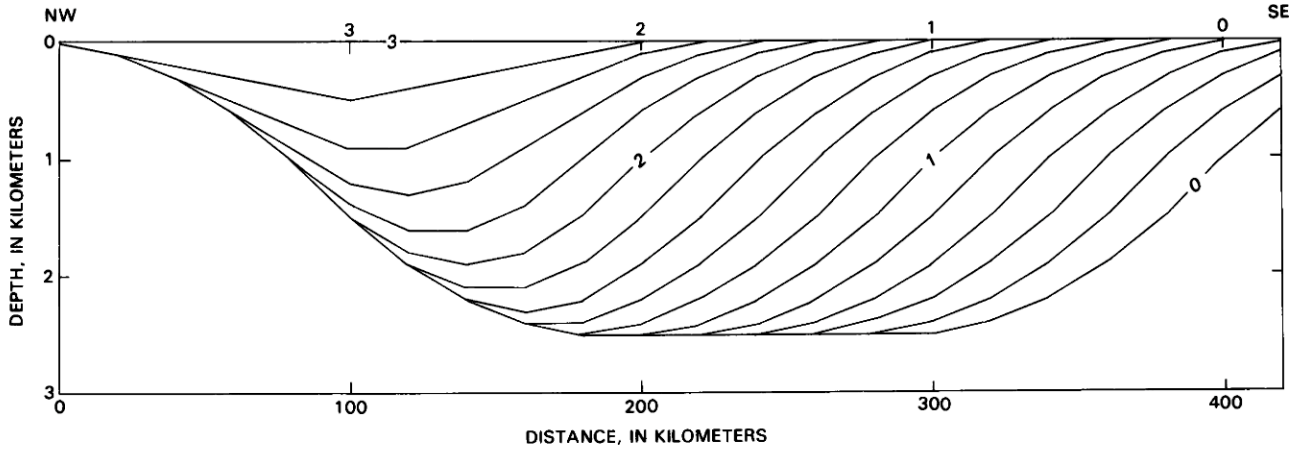

FIGURE 2.12.—Vertical section passing through center of migrating cone-like subsidence zone (100-km radius) that migrates southeast at 10 cm/yr; position of the center of the cone at specific times (Ma) is shown at top. The center of the cone subsides 2.5 mm/yr and subsidence and migration have occurred for 3 m.y. Profiles show successive shapes of a warped surface that was horizontal at 3 Ma; numbers give ages in Ma. Note the formation of a tilted terrace sloping about 1.5 km/100 km to the southeast that is left behind in the wake of the migrating subsidence zone. This model can apply to the deformation either of a sea-level terrace or of the ocean floor at the beginning of the propagation of the subsiding Hawaiian Ridge.

initiate fractures that tap magmas from the hot spot and feed the volcanoes. The changes in mapped trend of the loci may be caused by the rafting of pre-Hawaiian seamounts over the hot spot area, where they perturbed this downflexing of the lithosphere and the location of the conduit fractures.

6. An estimate of volumes based on patterns of subsidence indicate that as much as 16 percent of the volume of the ridge is early alkalic lava, about 25 percent was erupted subaerially, and about 53 percent has subsided beneath the level of the old ocean floor. These estimates may be reduced if a substantial volume of the volcanoes is composed of intrusive rather than extrusive rocks.

7. A part of the seismic activity that is centered at the southeastern end of the Ridge may result from bending and dislocation of the volcanic pile as the southeastern part subsides relative to that adjacent on the northwest.

REFERENCES CITED

Andrews, J.E., and Bainbridge, C., 1972, Submarine canyons off eastern Oahu: Pacific Science, v. 26, no. 1, p. 108–113.

Apple, R.A., and Macdonald, G.A., 1966, The rise of sea level in contemporary times at Honaunau, Kona, Hawaii: Pacific Science, v. 20, p. 125–136.

Barnett, T.P., 1983, Recent changes in sea level and their possible causes: Climate Change, v. 5, p. 15–38.

Campbell, J.F., 1984, Rapid subsidence of Kohala volcano and its effect on coral reef growth: Geo-Marine Letters, v. 4, p. 31–36.

Campbell, J.F., and Erlandson, D., 1979, OTEC-I anchor site survey: Hawaii Institute of Geophysics, v. HIG-79-6, 55 p.

Clague, D.A., Dalrymple, G.B., Green, H.G., Wald, D., Kono, M., and Kroenke, L.W., 1980, Bathymetry of the Emperor Seamounts, Leg 55 of the Deep Sea Drilling Project, *in* Jackson, E.D., Koisumi, I., and others, Initial reports of the Deep Sea Drilling Project, v. 55: Washington, U.S. Government Printing Office, p. 845–855.

Clague, D.A., Dao-gong, C., Murnane, R., Beeson, M.H., Lanphere, M.A., Dalrymple, G.B., Friesen, W., and Holcomb, R.T., 1982, Age and petrology of the Kalaupapa Basalt, Molokai, Hawaii: Pacific Science, v. 36, no. 4, p. 411–420.

Coulbourn, W.T., Campbell, J.F., and Moberly, R., 1974, Hawaiian submarine terraces, canyons, and Quaternary history evaluated by seismic-reflection profiling: Marine Geology, v. 17, p. 215–234.

Furumoto, A.S., Wiebenga, W.A., Webb, J.P., and Sutton, G.H., 1973, Crustal structure of the Hawaiian archipelago, northern Melanesia, and the central Pacific basin by seismic refraction methods: Tectonophysics, v. 20, p. 153–164.

Furumoto, A.S., and Woollard, G.P., 1965, Seismic refraction studies of the crustal structure of the Hawaiian archipelago: Pacific Science, v. 19, no. 3, p. 315–319.

Hamilton, E.L., 1957, Marine geology of the southern Hawaiian Ridge: Geological Society of America Bulletin, v. 68, p. 1011–1026.

Hill, D.P., 1969, Crustal structure of the island of Hawaii from seismic-refraction measurements: Bulletin of the Seismological Society of America, v. 59, no. 1, p. 101–130.

Jackson, E.D., and Koisumi, I., and others, 1980, Initial reports of the Deep Sea Drilling Project, v. 55: Washington, U.S. Government Printing Office.

Macdonald, G.A., and Abbott, A.T., 1970, Volcanoes in the sea: University of Hawaii Press, 441 p.

Mathewson, C.C., 1970, Submarine canyons and the shelf along the north coast of Molokai Island, Hawaiian ridge: Pacific Science, v. 24, p. 141–144.

Moore, J.G., 1964, Giant submarine landslides on the Hawaiian Ridge: U.S. Geological Survey Professional Paper 501-D, p. D95-D98.

———1970, Relationship between subsidence and volcanic load, Hawaii: Bulletin Volcanologique, v. 34, p. 562–576.

Moore, J.G., Clague, D.A., and Normark, W.R., 1982, Diverse basalt types from Loihi seamount, Hawaii: Geology, v. 10, p. 88–92.

Moore, J.G., and Fiske, R.S., 1969, Volcanic substructure inferred from dredge samples and ocean-bottom photographs, Hawaii: Geological Society of America Bulletin, v. 80, p. 1191–1202.

Moore J.G., and Fornari, D.J., 1984, Drowned reefs as indicators of the rate of subsidence of the Island of Hawaii: Journal of Geology, v. 92, p. 752–759.

Moore, J.G., and Moore, G.W., 1984, Deposit from a giant wave on the Island of Lanai, Hawaii: Science, v. 226, p. 1312–1315.

Moore, J.G., Moore, G.W., Szabo, B.J., 1984, Age of debris from a huge Pleistocene wave on Lanai, Hawaii [abs.]: EOS, v. 65, n. 45f, p. 1082.

Moore, J.G., and Peck, D.L., 1965, Submarine lavas from the east rift zone of Mauna Kea, Hawaii [abs.]: Geological Society of America Abstracts with Program, Cordilleran Section, Fresno, CA.

Shaw, H.R., Jackson, E.D., and Bargar, K.E., 1980, Volcanic periodicity along the Hawaiian-Emperor Chain: American Journal of Science, v. 280-A, p. 667–708.

Shepard, F.P., and Dill, R.F., 1966, Submarine canyons and other sea valleys: Chicago, Rand McNally and Company, 381 p.

Shor, G.G., 1960, Crustal structure of the Hawaiian ridge near Gardner Pinnacles: Bulletin of the Seismological Society of America, v. 50, no. 4, p. 563–573.

Stearns, H.T., 1966, Geology of the State of Hawaii: Palo Alto, California, Pacific Books, 266 p.

———1978, Quaternary shorelines in the Hawaiian Islands: Bernice P. Bishop Museum Bulletin 237, 57 p.

Stearns, H.T., and Chamberlain, T.K., 1967, Deep cores of Oahu, Hawaii and their bearing on the geologic history of the central Pacific basin: Pacific Science, v. 21, no. 2, p. 153–165.

Stone, C., 1977, Chemistry, petrography, and hydrothermal alteration of basalts from Hawaii geothermal project well-A, Kilauea, Hawaii: University of Hawaii Masters thesis, 84 p.

Stone, C., and Fan, P., 1978, Hydrothermal alteration of basalts from Hawaii geothermal project well-A, Hawaii: Geology, v. 6, p. 401–404.

Swanson, D.A., 1972, Magma supply rate at Kilauea Volcano, 1952-1971: Science, v. 175, p. 169–170.

Tilling, R.I., Koyanagi, R.Y., Lipman, P.W., Lockwood, J.P., Moore, J.G., and Swanson, D.A., 1976, Earthquakes and related catastrophic events, Island of Hawaii, November 29, 1975: A preliminary report: U.S. Geological Survey Circular 740, 33 p.

Von Herzen, R.P, Detrick, R.S., Crough, S.T., Epp, D., and Fehn, U., 1982, Thermal origin of the Hawaiian Swell: heat flow evidence and thermal models: Journal of Geophysical Research, v. 87, no. 8, p. 6711–6723.

Watts, A.B., Ten Brink, U.S., Buhl, P., and Brocher, T.M., 1985, A multichannel seismic study of lithospheric flexure across the Hawaiian-Emperor seamount chain: Nature v. 315, no. 6015, p. 105–111.

Wilde, P., Chase, T.E., Normark, W.R., Thomas, J.A., and Young, J.D., 1980, Oceanographic data off the southern Hawaiian Islands: Lawrence Berkeley Laboratory Publication 359, Lawrence Berkeley Laboratory, University of California, Berkeley.

Zucca, J.J., Hill, D.P., and Kovach, R.L., 1982, Crustal structure of Mauna Loa Volcano, Hawaii, from seismic refraction and gravity data: Bulletin of the Seismological Society of America, v. 72, no. 5, p. 1535–1550.

SLOPES OF THE HAWAIIAN RIDGE

By Robert K. Mark *and* James G. Moore

ABSTRACT

Slopes of the southeastern Hawaiian Ridge have been computed from elevation and bathymetric data digitized at 750-m spacing. Maps derived from these data show that most of the subaerial slopes of Mauna Loa shield volcano, built of tholeiitic basalt, are 3° to 6° and the steepest average slope is 8° at 3,300-m elevation. The lower slopes of much of Mauna Kea, capped by alkalic basalt, are also 3° to 6°, but they steepen to 6° to 9° on the east side, and the steepest average slope is 13° at 3,000-m elevation.

Submarine slopes are generally steeper than subaerial slopes on an active marine volcano, but both submarine and subaerial slopes become gentler downward. Consequently, submarine slopes are steepest slightly below sea level and merge upslope with the gentlest subaerial slopes. On Kilauea and Mauna Loa the average subaerial slope below 2,000-m elevation is 4°, but 500 m below sea level the slope increases to 13°. This sharp downward-slope increase at the subaerial-subaqueous transition results from several processes, but perhaps the most important depends on the buoyant effect of water on propagation of a lava flow. A flow cannot move downhill as readily underwater because gravity exerts less force on it, and so the flow will thicken, spread laterally, and build up the slope. Depression of this slope change in older volcanoes is a measure of subsidence of the volcano that has occurred since termination of the major period of shield growth.

Major submarine landslides commonly head in regions with regional slopes of 14° to 17°, but are flanked by slopes as great as 19°, the landslide having reduced the slope at its head. Arcs of anomalously steeper slopes at intermediate depths apparently mark gravitationally induced creep zones that bulge the volcano flank seaward.

INTRODUCTION

The present slope of landforms results from the equilibrium attained between the processes that built up the landform and those gravitationally induced processes that operate to reduce it to a flat plane. Volcanic activity, first on the sea floor and eventually on island peaks, is the chief process that built up the Hawaiian Ridge. Concurrently the ridge has undergone reduction by erosion, mass wasting, landsliding, and isostatic subsidence. An insight into all of these processes can be attained by analysis of slope.

Digitized topographic and bathymetric data (fig. 3.1) were employed to generate slope maps and plots of the southeast Hawaiian Ridge (figs. 3.2, 3.3). This proprietary data set, which includes over 42,000 scattered elevation values, was provided by Dynamic Graphics, Inc. Using the Surface Gridding Library (Dynamic Graphics, Inc., 1978), we computed a grid of 751 rows and 931 columns, with 750-m spacing, from the scattered data. Slopes were computed by fitting a quadratic surface to the three-by-three array around each grid point. Color separation negatives for publication were produced on the Scitex Response 280 System laser drum plotter.

The computer slope calculations determine the tangent of the angle of slope as measured from the horizontal. The color boundaries on the slope maps (figs. 3.2, 3.3) are in even increments of slope-angle tangent, which multiplied by 100 is equal to the percent grade. The equivalent angle in degrees is shown in table 3.1. Degrees are used in discussing slopes in the text because this is probably more meaningful to the average map user.

Rapid computer techniques were employed to determine the area-averaged slope for each 100-m interval of depth and elevation for the six segments of the age-progressive Hawaiian Ridge shown in figure 3.1. These average slopes were smoothed using RSMOOTH (Velleman and Hoagun, 1981) and plotted against depth (fig. 3.4). The slope-depth plots of the six segments, which are systematically older to the northwest, permit analysis of the changes in slope that occur through time.

ACKNOWLEDGMENTS

The digitized version of the topographic and bathymetric data used to generate the slope map and plots was provided by Dynamic Graphics, Inc. Careful reviews of the manuscript were made by D.A. Clague and M.A. Clynne. We are grateful for this help.

SUBAERIAL SLOPES

The unmodified subaerial slopes of Mauna Loa shield volcano are mostly very gentle (fig. 3.2). Substantial parts of the the lower slopes are between 3° and 6°, and slopes near the summit are rarely steeper than 11°. The steepest average slope is 8° and occurs at 3,300-m elevation (fig. 3.4). Flatter surfaces occur in saddles between Mauna Loa and the neighboring volcanoes Mauna Kea and Hualalai, where lavas are ponded. The smaller tholeiitic shield of Kilauea, which is built on the south side of Mauna Loa, shows gentle slopes generally less than 3°. In part this gentle slope is probably caused by ponding of both Mauna Loa and Kilauea lavas between the southeast flank of Mauna Loa and the summit and east rift zone of Kilauea. The flat area that covers much of the southeast part of the island (Puna) results from such lava flows ponded north of the east-rift-zone ridge of Kilauea. This area generally slopes less than 3° and is the largest such gently sloping area on the Hawaiian Islands.

The southern coastal part of Kilauea shows anomalously steep slopes exceeding 9° and locally exceeding 17°. These steep areas are clearly related to the Hilina fault system, in which steep fault scarps are common. A similar coastal region of steep terrain occurs on the west side of Mauna Loa and probably represents lava-mantled fault scarps (Normark and others, 1979).

In contrast to Mauna Loa and Kilauea, the central part of Mauna Kea Volcano is capped by alkalic lava that produces steeper slopes. Though much of the lower parts of this volcano has slopes between 3° and 6°, they steepen to 6° to 9° on the east side. The upper central part, however, commonly reaches a maximum slope of 14°. The steepest average slope is 13° and occurs at an elevation of 3,000 m (fig. 3.4).

This steeper central region of Mauna Kea is a result of several factors. Firstly, the alkalic lava flows, particularly hawaiite that erupted from vents on the upper slopes, are generally somewhat richer in SiO_2 and hence more viscous than the alkali basalt flows of the lower slopes or the tholeiitic basalt flows of Mauna Loa. Consequently the flows are thicker and pile up closer to the vent. Secondly, many of the alkalic flows are of smaller volume than tholeiitic flows and hence flow a shorter distance, thereby piling up near the summit. Thirdly, the younger lava flows of Mauna Kea were not erupted from long rift zones as on Mauna Loa, but from vents clustered near the summit. Finally, the alkalic lava of Mauna Kea is apparently rich in gas and has built dozens of rather large cinder cones on the upper parts of the volcano. These steep pyroclastic cones are concentrated on the upper part of the volcano and, with the lava flows that pond between them and cover them, tend to produce a steep cap to the volcano.

Haleakala Volcano on East Maui (fig. 3.3) is steep like Mauna Kea, also in part because of its cap of alkalic lava. The volcano is asymmetric, being steeper on the south side, both above and below sea level. This steep south side may result from faulting or landsliding. Slopes on the upper part of the volcano commonly exceed 17° and parts of the south slope exceed 19°. The steepest average slope is 14° and occurs at 1,700-m elevation (fig. 3.4).

Some of the localized areas of steep subaerial slope result from erosion of deep canyons. The young volcanoes of the Island of Hawaii are little eroded except for Kohala. Steep slopes on northeast Kohala result from several major stream-cut canyons. The canyons of north Kauai and east Molokai also generate moderate areas of steep slope (fig. 3.3).

SUBMARINE SLOPES

On average, submarine slopes on the Hawaiian volcanoes are steeper than subaerial slopes but, like their subaerial counterparts, generally flatten downward. Consequently the submarine slopes are steepest slightly below sea level on a young volcano, and near sea level this steep subaqueous slope meets the more gentle subaerial slope. The average subaerial slope from the shoreline of Kilauea and Mauna Loa up to about 2,000-m elevation is about 4°. Below sea level this slope steepens abruptly to an average of 13° at 500-m depth (fig. 3.4).

Not only does the slope angle increase when a lava flow passes from land to sea, but a similar phenomenon occurs where a rift zone crosses the shoreline. Even though individual lava flows issue at many points along the rift zone, both above and below sea level, the axial crest of the rift-zone ridge plunges more steeply below sea level. The crest of the east rift zone of Kilauea plunges an average of 1.5° for 50 km from the summit caldera to the east cape of the island. Below sea level the rift zone extends another 80 km to its end at 5,500 m depth, and over this distance the crest plunges at an average angle of about 4°.

This marked slope change at the subaerial-subaqueous transition zone is the result of several processes, primarily volcanic. Regional slopes are modified at sea level by erosion and by growth of coral reefs. However, development of the steepening just below sea level on the young, active volcanoes Mauna Loa and Kilauea, where erosion and reef growth are minimal, indicates that volcanic processes must be the dominant cause. One process is the chilling effect of water on flowing lava. This tends to increase the flow's effective viscosity and cause it to thicken or divide into pillowed flow lobes and hence flow a shorter distance, thus steepening the general slope angle. A second process is the disturbance of a lava flow crossing the shoreline by vigorous surf action, which disrupts flow channels and lava tubes and causes the flow to divide, spread, and flow a shorter distance over a broader front. Both of these processes can cause a flow to break up into solid fragmental material, producing a flow-foot breccia (Moore and Fiske, 1969). A third, and perhaps the most important, process depends on the buoyant effect of water on the propagation of a lava flow. When a flow crosses the shoreline and enters the sea, its effective density drops by 1 g/cm^3. The flow cannot move downhill on the same slope as readily, because gravity exerts less force on it, and so the flow will thicken and spread laterally.

The net effect of these processes that inhibit flow of lava under water is to cause the shoreline to be extended seaward with a gentle subaerial slope and to pile lava up below sea level at shallow depth, thus creating a steep slope below sea level. This marked slope change caused by the subaerial-subaqueous lava transition can be identified on older volcanoes, where it occurs at considerable depth (fig. 3.4). The depth of the slope change is a measure of the subsidence that the volcano has undergone since the slope change was created. One of the more striking feaures of the slope map of the Hawaiian Ridge is the presence of a zone of steep slope surrounding all of the islands. The steep slope surrounding the islands of Maui, Kahoolawe, Lanai, Molokai, and Oahu marks the former shoreline of a giant island more than twice the size of the present Island of Hawaii (fig. 3.3).

LANDSLIDES

Because of its youth, great height, and steep slopes, the Hawaiian Ridge is the site of numerous landslides that occur at widely different scales. Many landslides head in the exceptionally steep zone originally formed just below sea level. Because lava flows apparently do not propagate readily underwater, mass movement

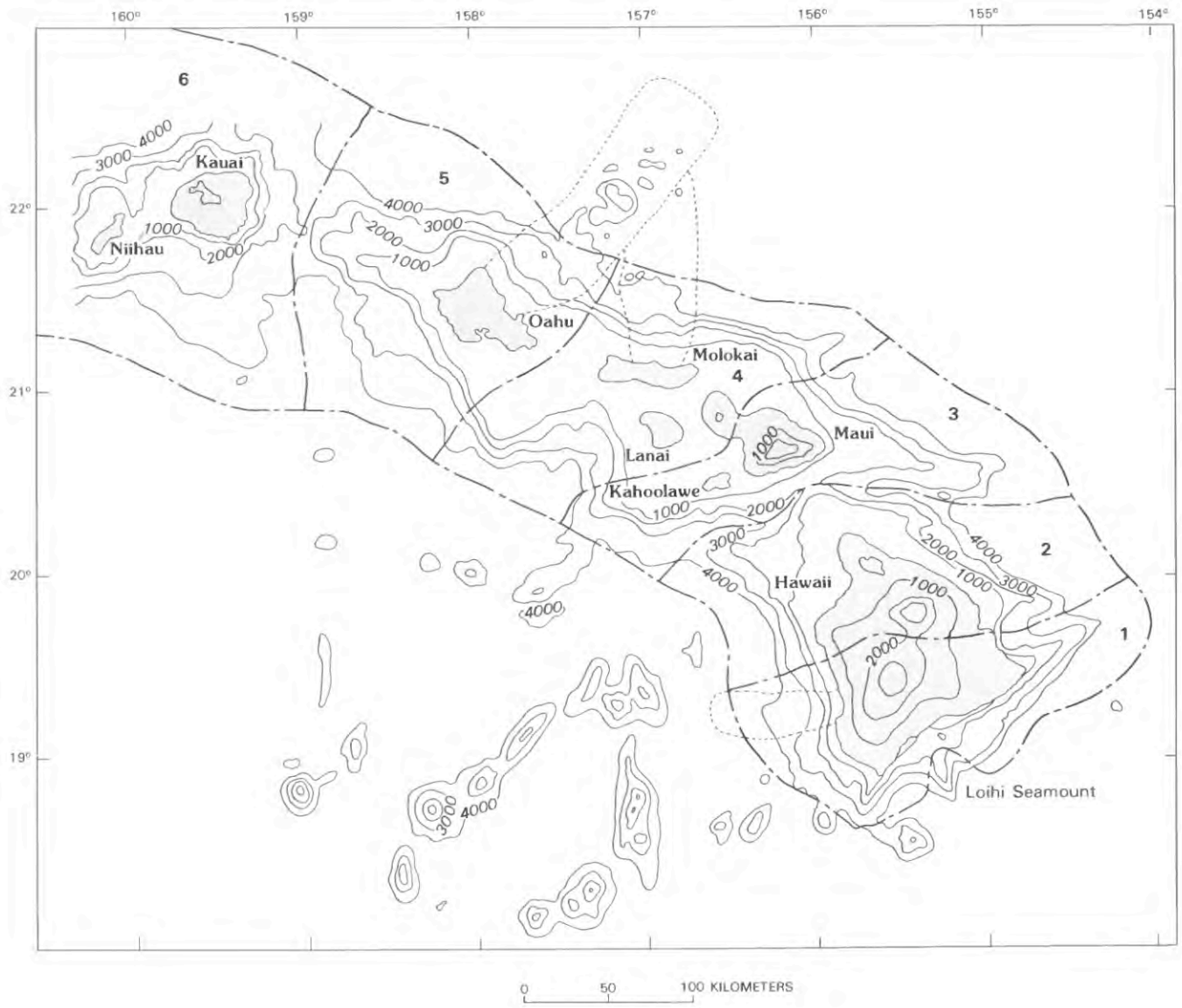

FIGURE 3.1.—Generalized topography and bathymetry of southeastern part of the Hawaiian Ridge. Contours in meters. Dotted lines bound major landslides; dash-dot lines bound age-progressive segments of ridge, numbered 1–6 (1 is youngest).

must be an important process in carrying volcanic material from near the shoreline to depth in order to maintain a slope in equilibrium.

Major landslides are suggested by two features of the slope map: They generally head on a particularly steep segment of the subaerial-subaqueous transition zone, but they are flanked by even steeper zones, the landslide having reduced the slope at its head. These relations are evident for the proposed landslides off the north coasts of Molokai and Oahu (fig. 3.1; Moore, 1964), and for the Alika landslide off the west coast of Hawaii. The landslide north of Molokai heads in a region where the maximum regional slope is about 17°, but it is flanked by steeper slopes exceeding 19°. The landslide northeast of Oahu likewise heads in a region with maximum slopes generally less than 14° but is flanked by slopes as steep as 19°. The Alika landslide off west Hawaii heads in a region with average slopes somewhat exceeding 14°, but it is flanked by slopes exceeding 19°. Additional steep offshore regions of Hawaii, prone to massive submarine landslides such as these three, are the east coast of Kilauea Volcano north of the the east cape of the island, and the south coast of Mauna Loa Volcano northeast of the south cape of the island (fig. 3.3).

Aside from these major landslides, other curious features of the slope map are probably related to downslope movement. These are arcs of steep slope at moderate depths that are separated from the main steep subaerial-subaqueous transition zone by a region of

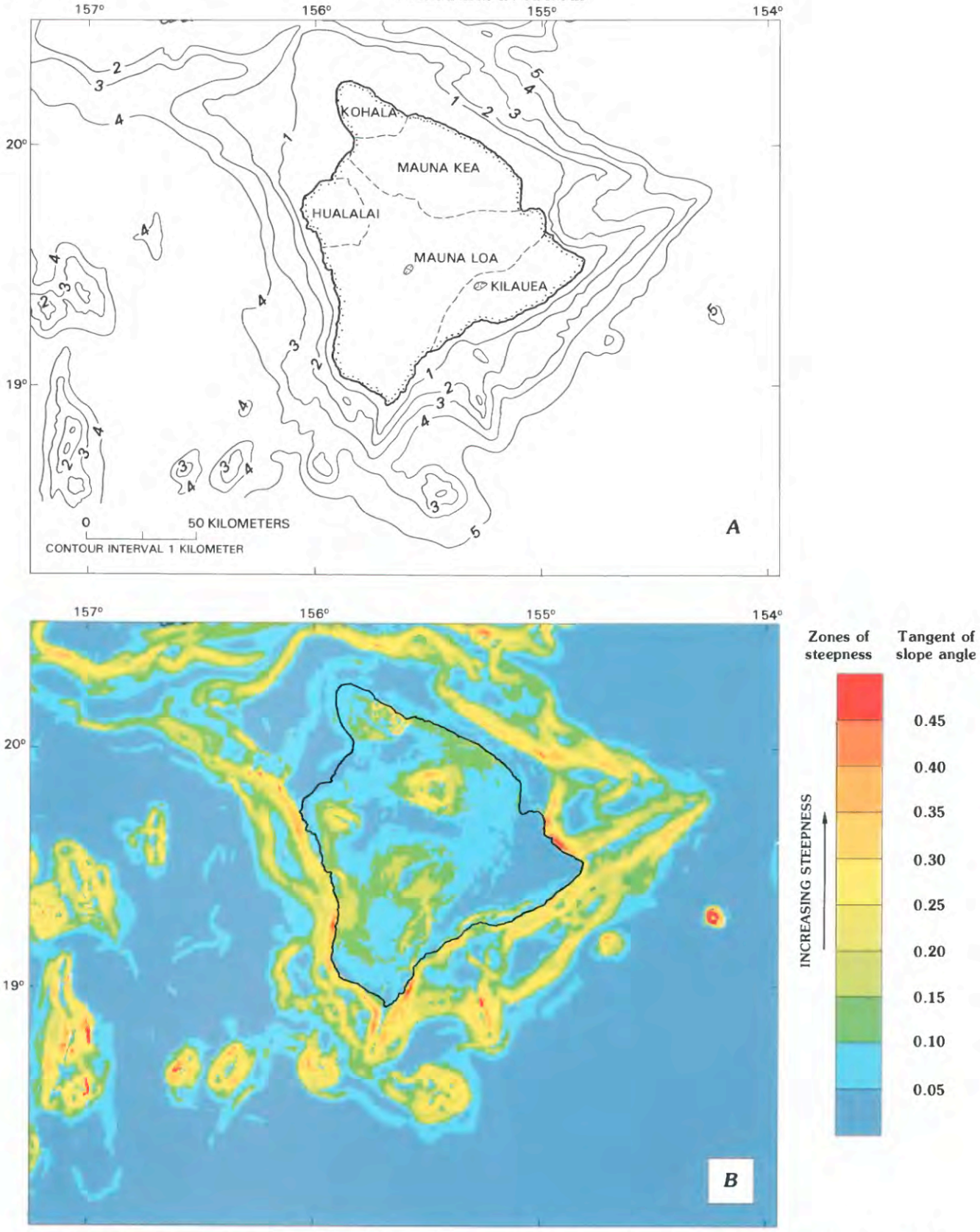

FIGURE 3.2.—Bathymetry and slopes around the Island of Hawaii. ***A***, Generalized bathymetric map. Dashed lines on the island are boundaries between the five volcanoes. ***B***, Computer-generated slope map of same region (including land areas). Slope steepness represented by color-coded intervals defined by tangents of slope angle measured from horizontal. Each color represents a slope-angle range of about 2.5° (see also table 3.1).

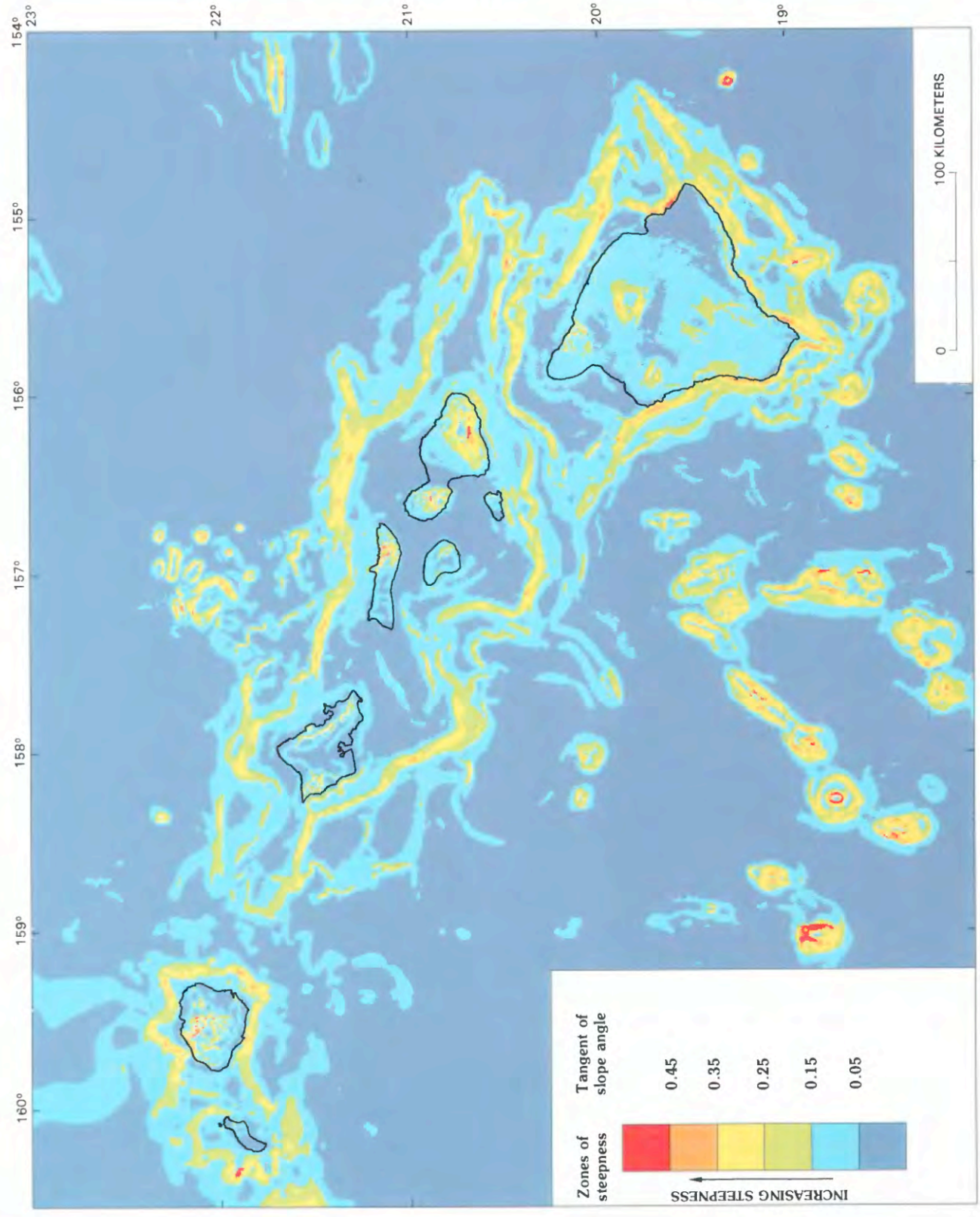

FIGURE 3.3.—Computer-generated slope map of southeastern part of the Hawaiian Ridge. Slope steepness represented by color-coded intervals defined by tangents of angle of slope. Each color represents a slope-angle range of about 5° (see also table 3.1).

TABLE 3.1.—*Angles of slope equivalent to values of tangent used as interval boundaries*

Tangent	Slope angle (degrees)
0.55	28.8
.50	26.6
.45	24.2
.40	21.8
.35	19.3
.30	16.7
.25	14.0
.20	11.3
.15	8.5
.10	5.7
.05	2.9

gentler slope. A prime example is the steep band at about 3,000-m depth that extends from Loihi Seamount off the south coast of the Island of Hawaii to near the east cape of the island (fig. 3.2). Others appear both north and south of the Alika landslide off west Hawaii. These arcs of anomalously steep terrane seem to mark gravitationally induced creep zones where the volcano flank is markedly bulged seaward. The probability of such bulges failing and producing major submarine landslides is not known.

SLOPE CHANGES WITH AGE

The bathymetric data have been compartmentalized into six segments (fig. 3.1) representing a volcanic age sequence becoming progressively older toward the northwest. The southeasternmost segment (number 1) includes Kilauea and Mauna Loa Volcanoes on the southern part of the Island of Hawaii. This segment is considered typical of youthful marine volcanoes because it includes the youngest, and currently most active, volcanic systems. The remaining segments with their included islands and general age of completion of major volcanic growth are, from southeast to northwest: (2) north Hawaii, 0.4 Ma; (3) east Maui and Kahoolawe, 0.8 Ma; (4) Molokai, Lanai, and west Maui, 1 Ma; (5) Oahu, 2.5 Ma and (6) Kauai and Niihau, 5 Ma. The slope-depth plot of each of these segments is compared to that of segment 1 so that departures from the assumed original volcanic condition can be evaluated (fig. 3.4). These departures apparently result from subsidence of the volcanoes and from erosional degradation.

The most extreme slope change of all the segments occurs in segment 1 near sea level and results from the subaerial-subaqueous lava transition. The average slope changes from about 4° at 200 m above sea level to 13° at 500 m below sea level. A similar abrupt change can be recognized in the other segments, although it is generally deeper and less distinct. The center of the slope change in segment 2 is 1.3 km below sea level; in 3, 2.1 km; in 4, 1.3 km; in 5, 1.3 km; and in 6, 1.0 km. These variations of the depth of the slope change from that in segment 1 are believed to be a measure of volcano subsidence since extension of the shoreline during a major period of volcano growth. Many of the areas of slope change are less distinct than that of segment 1. This results from the fact that the averaging technique includes different shorelines of different ages and

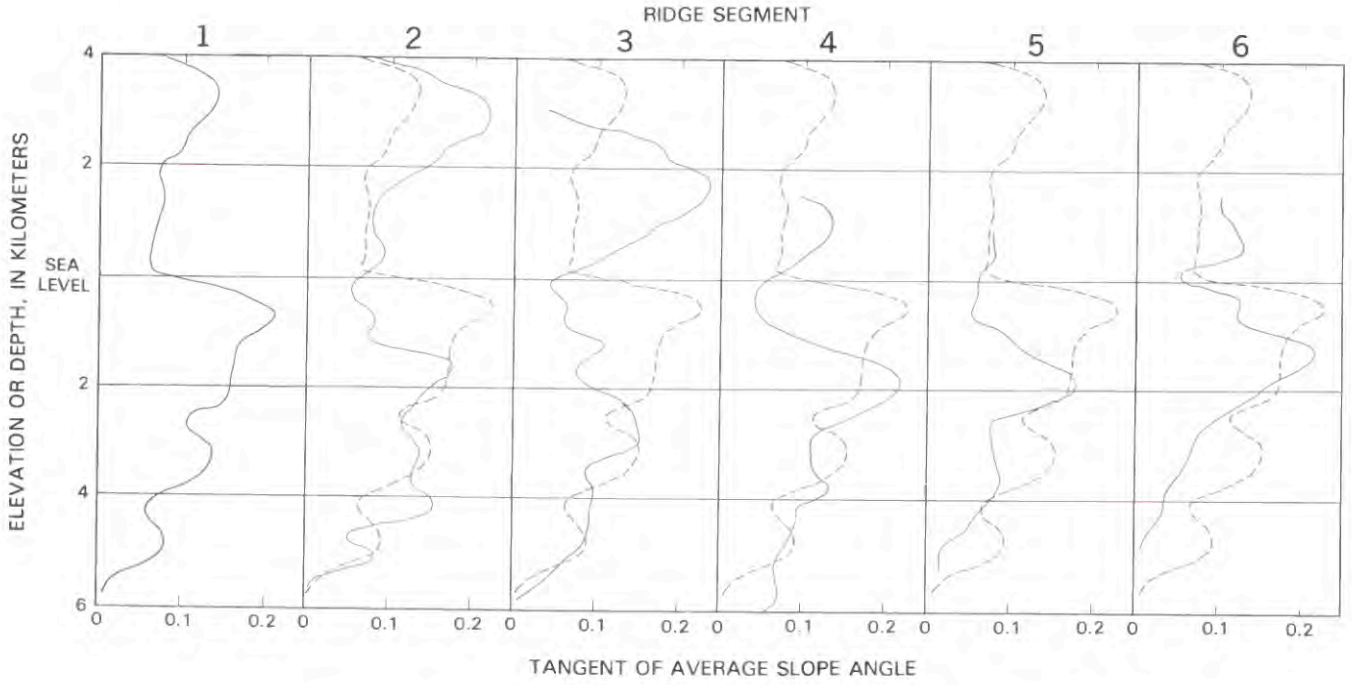

FIGURE 3.4.—Smoothed profiles of area-averaged slope against elevation for six segments of the Hawaiian Ridge (see figure 3.1). The trend of segment 1 (south Hawaii) is repeated as dashed line on the other five plots.

the same shoreline which has been warped and has subsided different amounts (Moore, chapter 2).

A marked smoothing of the lower submarine flanks of the volcanoes appears to proceed with age. On segment 1 the slope below the subaerial-subaqueous transition undergoes a general decrease with depth, which is interrupted twice by changes toward steeper slopes which are the bulges previously described. The first slope change increases the average slope 2.3° and the second about 1.7°. On segment 2 the slope decrease is interrupted 3 times by slope increases of 1.3°, 1.7°, and 2°. Segment 4 shows three zones of slope increase of 1.3°, 0.2°, and 0.4°. Segment 5 has only one, of 0.6°, and segment 6 has no zones of increase in slope below the transition zone.

Smoothing of the lower flanks is, moreover, accompanied by a general reduction of slope, so that all the zones of steep slope seem to have been removed (see segment 6 area on figures 3.3 and 3.4). The arcuate zones of steep slopes on the mid-depth submarine slopes of the younger volcanoes are missing on the older ones. Some form of mass wasting, requiring several million years to be effective, seems to smooth and flatten the lower slopes of these giant volcanoes.

REFERENCES CITED

Dynamic Graphics, Inc., 1978, User manual for the surface gridding library: 129 p.

Moore, J.G., 1964, Giant submarine landslides on the Hawaiian Ridge: U.S. Geological Survey Professional Paper 501–D, p. D95–D98.

Moore, J.G., and Fiske, R.S., 1969, Volcanic substructure inferred from dredge samples and ocean-bottom photographs, Hawaii: Geological Society of America Bulletin, v. 80, p. 1191–1202.

Normark, W.R., Lipman, P.W., and Moore, J.G., 1979, Regional slump structures on the west flank of Mauna Loa Volcano, Hawaii: [abs.]: Hawaii Symposium on Intraplate Volcanism and Submarine Volcanism, Hilo, Hawaii, July 16–22, 1979, Abstracts with Program, p. 72.

Velleman, P.G., and Hoagun, D.C., 1981, Applications, basics, and computing of exploratory data analysis: Boston, Mass., Duxbury Press, 354 p.

SUBMARINE TOPOGRAPHY AROUND THE HAWAIIAN ISLANDS

By Daniel J. Fornari[1] *and* J. Frisbee Campbell[2]

ABSTRACT

The submarine topography around the Hawaiian Islands reflects the time-integrated effects of volcanism, Pacific-plate tectonic fabric, island subsidence, sedimentation, gravitational collapse of unbuttressed volcano sides, and low-relief debris flows that transport shallow-water carbonate and volcanogenic sediment to greater depths on the submarine slope. First-order topographic relief around the islands is created by the submarine extensions of volcanic rift zones. The height above the surrounding abyssal sea floor and the topographic roughness of these rifts are inversely proportional to the age of the adjacent volcano. Second-order sea-floor relief around Hawaii is typified by Cretaceous seamounts that lie west of Hawaii and a few young volcanoes, including Loihi Seamount, direcly south of Hawaii. In addition to these obvious volcanic seamounts, a group of flat-topped mounts and small cones (Oahu Seamounts) extends to the northeast from the Island of Oahu. More subtle relief on the slumping of large sections of unbuttressed volcano flanks. These slumps form prominent steps on the otherwise regular, steep submarine slopes. Relief created by localized debris flows of surficial sediment and carbonate/volcanic rubble is usually less than 50 m; however, this process appears to be active on all Hawaiian submarine slopes investigated with Sea MARC II side-scan sonar and may be the principal agent for downslope sediment transport. Finally, reef development on the shallow parts of older, subsided volcanic foundations forms wide, low-gradient platforms that have karst-like microtopography.

INTRODUCTION

The strategic location of the Hawaiian Islands for oceanic exploration and the commerce that followed has resulted in the study of their natural history and geologic evolution since the 1700's. They have been a focus of marine research for the past 50 years, and much literature has been devoted to various aspects of Hawaiian marine geology and geophysics. The principal aim of this paper is to summarize the major topographic elements of the sea floor around Hawaii and to present new graphical and remote-sensing images of the sea floor around several of the islands. Only brief background information is offered, because much of the detailed information has already been discussed in the references we cite. In addition, other papers in this volume discuss specific topics that bear upon the development of the sea floor topography around the Hawaiian Islands. In particular, questions relating to island subsidence, carbonate-platform development, and submarine canyons are discussed in papers by Mark and Moore (chapter 3) and Moore (chapter 2). Data on Loihi Seamount is discussed by Malahoff (chapter 6), and the evolution of Hawaiian submarine rift zones is presented by Fornari (chapter 5).

ACKNOWLEDGMENTS

We thank the reviewers W. Dudley, R. Moberly, J.G. Moore, R. Pujalet, U. ten Brink, and A.B. Watts for their constructive comments. Paul White and Edwin Katibah of Dynamic Graphics Inc. were instrumental in providing the sea-floor graphics used to illustrate the paper. The management of Dynamic Graphics kindly provided all machine and personnel time needed to produce the images. M.A. Luckman expertly drafted and assisted in the preparation of all the figures. Support for Fornari was provided by the Office of Naval Research under contract number N00014-80-C-0098MM to the Lamont-Doherty Geological Observatory. Sea MARC II data in the Alenuihaha Channel were collected during the Hawaii Deep Water Cable Program, a project funded by the U.S. Department of Energy, grant number DE-AC01--82CE76214 to the Hawaiian Electric Company. Lamont-Doherty Geological Observatory Contribution No. 3841. Hawaii Institute of Geophysics Contribution No. 1592.

REGIONAL BATHYMETRY

The regional bathymetry around the Hawaiian Islands (fig. 4.1) has been mapped by numerous oceanographic institutions, the U.S. National Ocean Survey, and the U.S. Navy (see, for example, Chase and and others, 1971; Chase and others, 1980; Wilde and others, 1980, and references therein). The principal regional bathymetric features are the Hawaiian Deep and the Hawaiian Arch (fig. 4.2), which are topographic manifestations of lithospheric flexure, superimposed on the regional swell of the Hawaiian Ridge, that result from the load of the volcanic islands on the oceanic lithosphere (Betz and Hess, 1942; Dietz and Menard, 1953; Hamilton, 1957; Menard, 1964; Watts, 1976; Watts and others, 1985). The Molokai Fracture Zone (fig. 4.2) represents a diffuse zone of elongate troughs that reach depths below 5,000 m to

[1]Lamont-Doherty Geological Observatory of Columbia University, Palisades, New York 10964.
[2]Hawaii Institute of Geophysics, University of Hawaii, Honolulu, Hawaii 96822.

FIGURE 4.1.—Computer-drawn perspective model of the ocean floor around the Hawaiian Islands. Data base from Chase and others (1980) and Wilde and others (1980) and bathymetric charts of the U.S. National Ocean Survey (Nautical Chart Catalog No. 2, Panels, B, C, E). Bathymetric contour interval 1,000 m; grid spacings between nodal points (E.-W.) 1,667.18 m, and (N.-S.) 1,674.87 m. Subaerial contours from U.S. Geological Survey topographic map series. Black areas on land, historical lava flows (drawn from U.S. Geological Survey 1:100,000 series maps and Scientific Event Alert Network Bulletin, Smithsonian Institution, June 30, 1983). Red areas on land, 1983 lava flows from the east rift zone of Kilauea. Green areas, older slopes of inactive volcanoes. See figure 4.2 for geographic names. Vertical exaggeration ×5. Provided by Dynamic Graphics Inc., Berkeley, Calif.

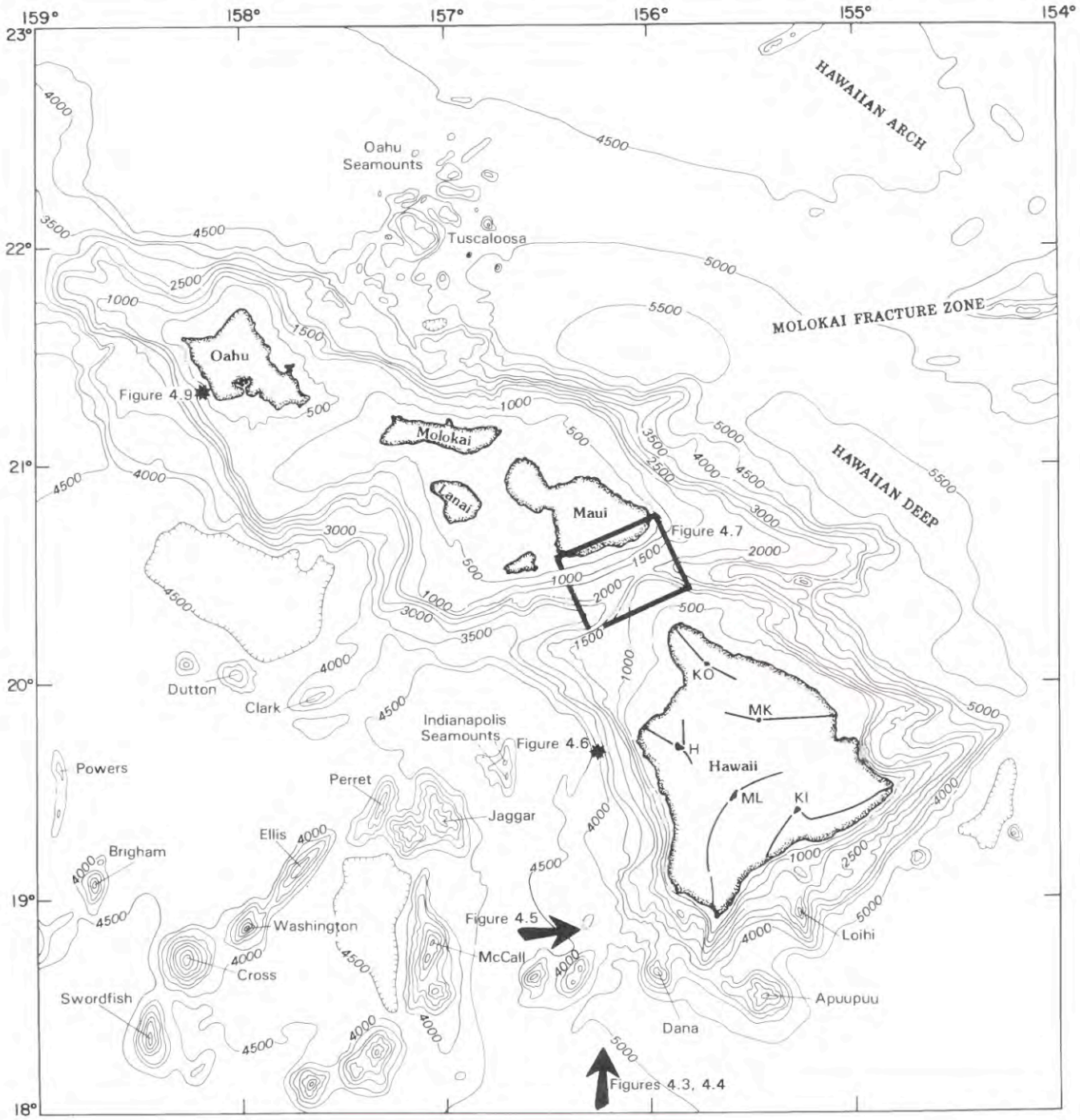

FIGURE 4.2.—Bathymetry around the principal Hawaiian Islands. Contour interval 500 m, simplified from Wilde and others (1980). Sites, viewing directions, and areas covered in some other figures are also indicated. Volcanoes on the Island of Hawaii: KO, Kohala; MK, Mauna Kea; H, Hualalai; ML, Mauna Loa; KI, Kilauea.

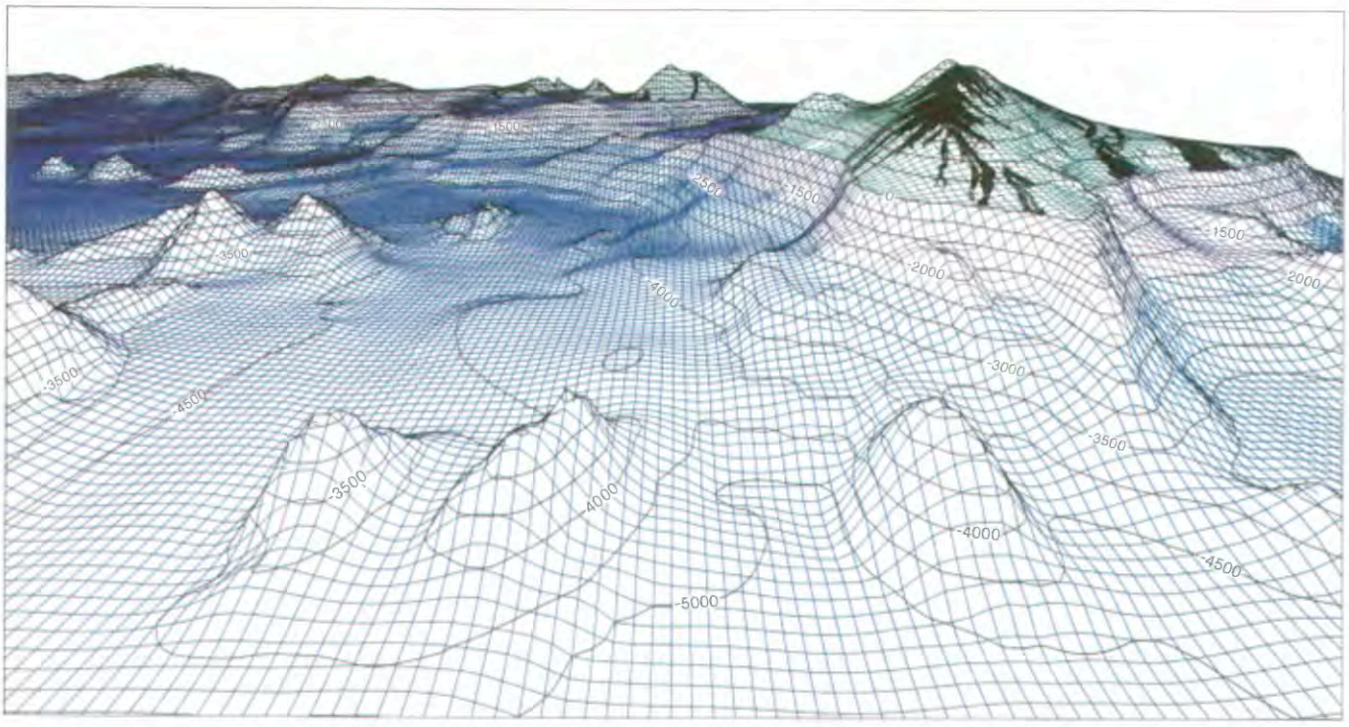

FIGURE 4.3.—Computer-drawn perspective model of the sea floor on western flank of Hawaiian Ridge from Hawaii to Oahu, looking approximately north. Contour interval 500 m. View point and direction marked on figure 4.2. Elevation of view point is 5,285 m above sea level. Data base is same as for figure 4.1. Vertical exaggeration ×5. Provided by Dynamic Graphics Inc., Berkeley, Calif.

the east of the Hawaiian Arch. The fracture zone topography narrows considerably within the arch and is likely to be responsible for the lineated contour pattern, trending west-northwest, found on the carbonate platform east of Molokai. Indeed, the principal trends of the subaerial and submarine rift zones of the East and West Molokai Volcanoes are subparallel to the fracture-zone trend and are likely to have been partly controlled by it (Furumoto and Woollard, 1965; Strange and others, 1965; Moberly and McCoy, 1966; Malahoff and Woollard, 1968).

DETAILED SEA-FLOOR TOPOGRAPHY, HAWAII TO OAHU

A computer-drawn perspective model of the sea floor around the southern Hawaiian Islands (produced by Dynamic Graphics Inc., of Berkeley, California) is shown in figure 4.1. The data base used to generate this figure is from Chase and others (1980), Wilde and others (1980), and bathymetric charts of the U.S. National Ocean Survey. The bathymetric data were gridded, digitized as a set of 43,000 x, y, and z coordinates, and then used to calculate a surface model of least tension in the form of a rectangular grid. The grid model contains 480,000 grid points (800 × 600) and was calculated by the Surface Gridding Library program of DGI. The bathymetric map in figure 4.2 shows the plan-view contours of most of the area of figure 4.1 and serves to locate the islands and seamounts, the starting points and azimuths of the perspective views shown in figures 4.3–4.5, and the location of other figure areas.

Three principal topographic elements are present on the sea floor shown in figure 4.1. They are (1) the submarine extensions of subaerial volcanic rift zones; (2) old and young seamounts; and (3) carbonate platforms. In addition to these major topographic features, there are several subtle steps in the western submarine slope of Hawaii (see figs. 4.3-4.5) that we interpret to be large-scale gravitational slumps of parts of Mauna Loa and Hualalai Volcanoes. One of these features is the already recognized Alika slide of Normark and others (1979).

SUBMARINE RIFT ZONES

Each principal island within the Hawaiian chain is composed of several volcanoes; consequently, the submarine flanks of each island are dominated by rift-zone ridges that may have as much as 3,000 m of relief above the surrounding abyssal sea floor. These submarine ridges are oriented in three principal directions: east to northeast, south-southwest, and northwest. A detailed discussion of the submarine topography and structure of the submarine rifts of Hawaii is presented in Fornari (chapter 5). In general, however, the total relief and topographic roughness of Hawaiian submarine rifts is

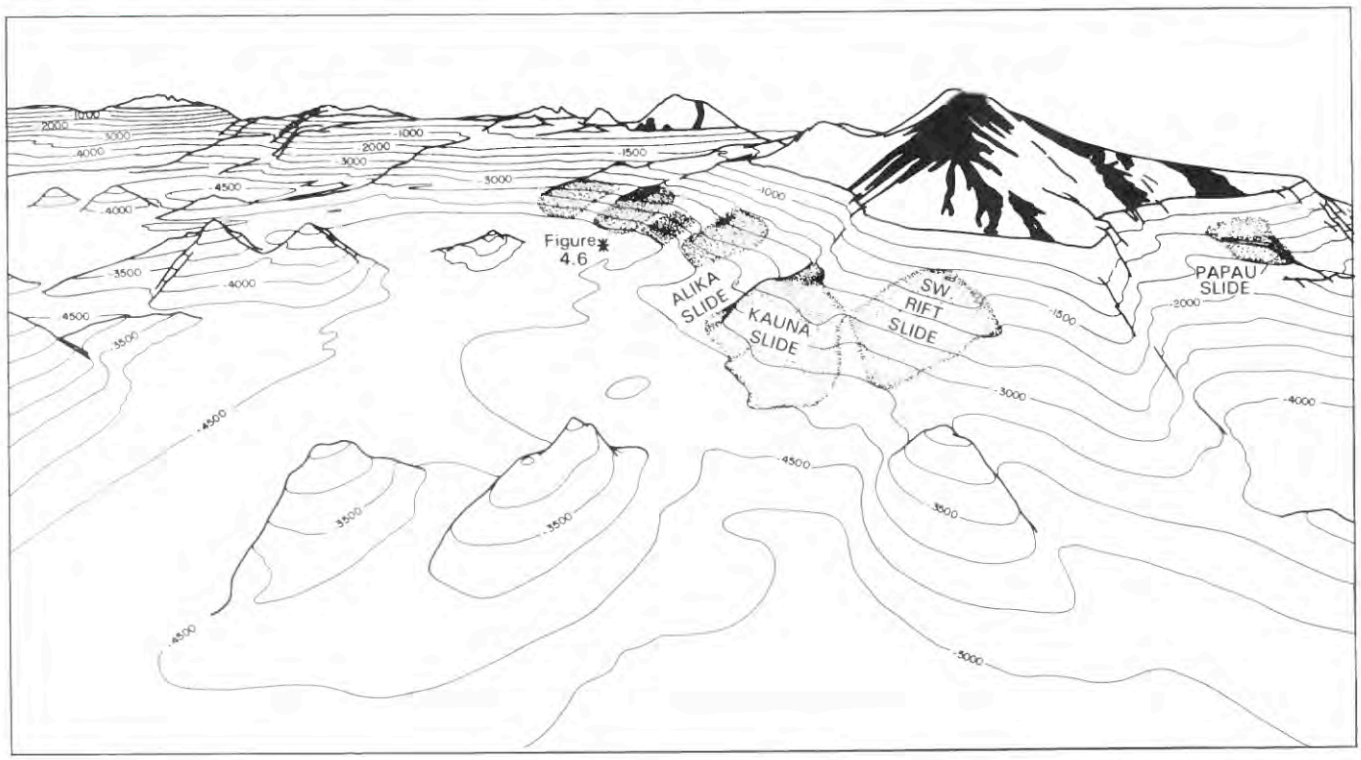

FIGURE 4.4.—Interpretative sketch of view seen in figure 4.3 showing positions of large gravitational slide blocks on the west flank of Island of Hawaii. Contour interval 500 m.

greatest next to the most active volcanic centers. The prominent asymmetry in the across-strike profiles of some of these submarine ridges can be directly attributed to the mobility of ridge flanks that are not buttressed by an adjacent volcano (Fornari, chapter 5; Stearns and Macdonald, 1946; Fiske and Kinoshita, 1969; Fiske and Jackson, 1972; Koyanagi and others, 1972; Swanson and others, 1976; Lockwood, 1979; Lipman, 1980).

The nearshore morphology of the submarine rifts changes as the islands subside (figs. 4.1, 4.2; Moore, chapter 2; Moore, 1970; Moore and Fornari, 1984). The shape and development of the carbonate platform that surrounds and lies between the Islands of Maui and Oahu have been largely controlled by the rift topography of East and West Molokai Volcanoes, as well as that of Waianae, Koolau and Penguin Banks(?) Volcanoes, parts of which now lie buried beneath a carbonate and sediment cover (Gregory and Kroenke, 1982). Off northwestern Hawaii, the northwest rift zone of Hualalai forms the southern boundary of the Kohala terrace, the wide platform that extends northwestward between Hualalai and Kohala Volcanoes. Flows ponded between Hualalai's rift and Kohala's northern rift zone created a broad, buttressed volcanic foundation that gradually subsided but was not subject to large-scale gravitational slumping; hence this was an ideal environment for reef buildup and platform development (Campbell and Erlandson, 1979, 1981; Campbell, 1984). For a further discussion of the subsidence history of the Hawaiian Islands and the development of carbonate platforms and reef terraces the reader is referred to Moore (chapter 2).

SEAMOUNTS

Important second-order topography around the Hawaiian Islands that is created by seamounts is also depicted in figures 4.1 and 4.2. Most of the seamounts that lie west of Hawaii are older features (see, for example, Moore, 1965; Francheteau and others, 1970), generally considered to be approximately Cretaceous in age, that were probably created at or near a ridge axis. The alignment of the main cluster of seamounts is generally northeast-southwest; however, two separate lineaments appear to meet at Perret and Jagger Seamounts to form a V shape pointing northeast. This V shape and the curious butterfly-like shape of Perret-Jagger Seamounts (fig. 4.2) imply a possible tectonic control on volcanism (the lineation is oblique to the trend of the Molokai Fracture Zone). These seamounts have not been studied in great detail, however, and their precise origin and volcanic history are unknown.

A few seamounts south of Hawaii (Dana and Apuupuu) may be genetically related to Hawaiian volcanism. Loihi Seamount, located 35 km south of Kilauea's south flank, is clearly a Hawaiian volcano and has been the subject of several deep-sea camera, dredging, and bathymetric surveys, and earthquake studies (Malahoff, chapter 6; Moore and others, 1979; Malahoff and others,

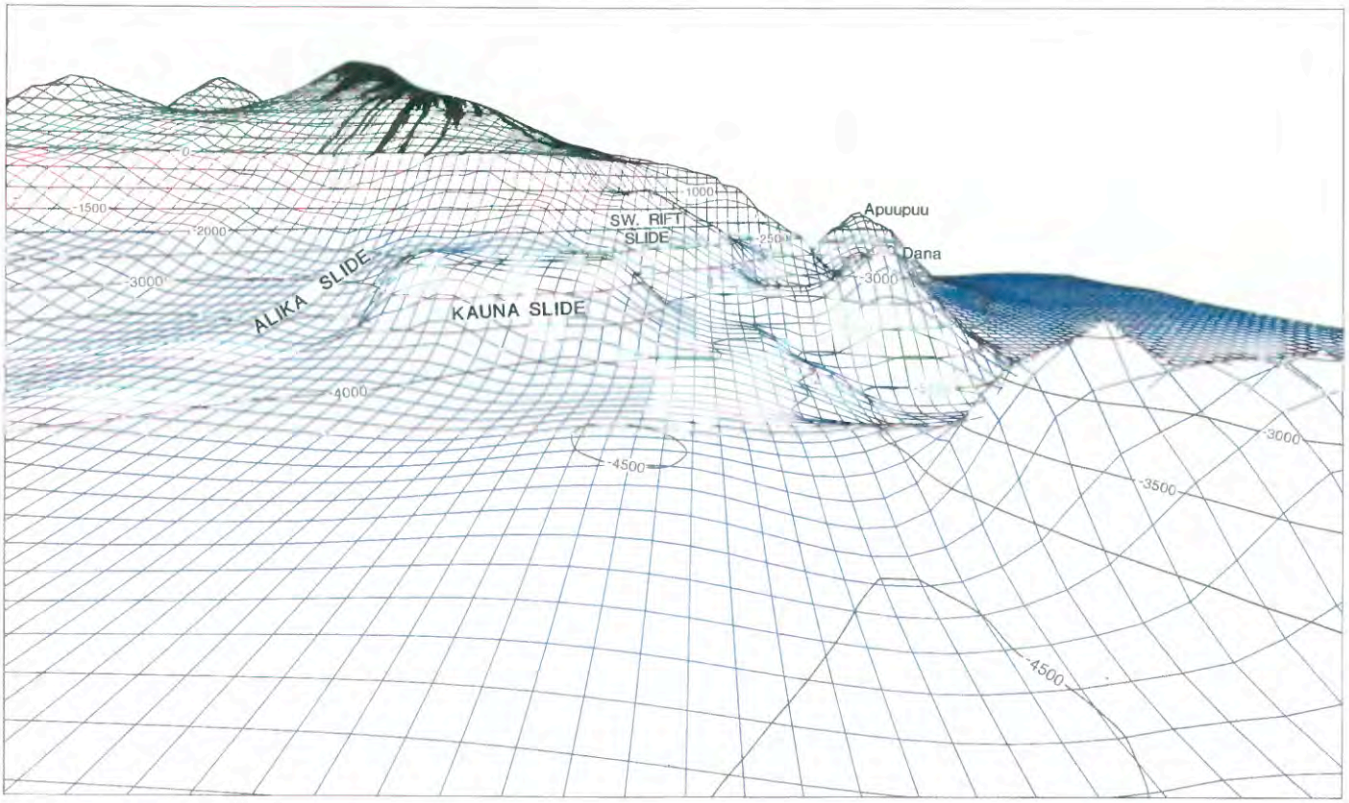

FIGURE 4.5.—Computer-drawn model of sea floor off southwestern part of Island of Hawaii, showing prominent step and bulge in the slope created by the Kauna slide. Alika slide of Normark and others (1979) is low, broad bulge to north of Kauna block. Contour interval 500 m. View point of perspective located 1,162 m below sea level; it and direction of view marked on figure 4.2. Apuupuu Seamount in background. Loihi Seamount hidden behind ridge created by submarine continuation of Mauna Loa's southwest rift zone. Vertical exaggeration × 5. Provided by Dynamic Graphics Inc., Berkeley, Calif.

1982; Moore and others, 1982; Klein, 1982). This submarine volcano rises 4,000 m above the surrounding abyssal floor and its topography is dominated by an elongate rift-zone ridge that extends to the south from summit pit craters. The diverse suite of alkalic to tholeiitic pillow basalts recovered from Loihi has led to new perspectives on the classical so-called thoeliitic shield-building stage of Hawaiian volcanism, and the chemistry of mafic inclusions recovered in the dredge hauls promises to further refine models of Hawaiian petrogenesis and volcanic history (Moore and others, 1982; Staudigel and others, 1984). Detailed U.S. Navy SASS multibeam bathymetry and ANGUS camera tows over Loihi (Malahoff, chapter 6; Malahoff and others, 1982) reveal that most constructional volcanism is restricted to the summit pit craters and shallower parts of the southern and northern rift zones, whereas most of the flanks are covered by clastic volcanic rocks and hemipelagic sediment. These data suggest that Hawaiian volcanoes develop submarine rift zones and shallow-level magma reservoirs early in their development. Additionally, the north-south elongation of Loihi appears to be partially controlled by the presence of Mauna Loa's southwest rift zone to the west. This physiography agrees with the predictions made by Fiske and Jackson (1972) regarding volcano shape and rift zone orientation and the genetic dependence of these two parameters on the locations of preexisting edifices.

A group of flat-topped seamounts of more problematic origin is located northeast of Oahu (Oahu seamounts, see figs. 4.1, 4.2). After analyzing bathymetric charts of this area, Moore (1964) suggested that these topographic highs are landslide blocks created by large slumps that affected the northeastern slope of Oahu and, to a lesser extent, the northern slope of Molokai. A close inspection of the sea-floor topography in figure 4.1 and the contours in figure 4.2 shows two prominent tongue-like features at the base of the northeast slopes of Oahu and Molokai. One feature extends northeast from Oahu at depths between 2,000 m and 4,000 m, and the other extends north from Molokai at depths between 3,000 m and 4,000 m. At the head of each tongue is an amphitheater-like reentrant in the regional slope contours (fig. 4.2). These bathymetric features could represent large gravitational slides that have affected the unbuttressed parts of volcanoes on each island. This area has been resurveyed using sparker and air-gun reflection profiling equipment (Andrews and Bainbridge, 1972) and more recently with multichannel seismic reflection methods (A.B. Watts, oral commun., 1985). Andrews and Bainbridge (1972) concluded that the lobate

structures at the base of Oahu's northeast slope resulted from transport of detrital sediment by turbidity currents that were channelled down submarine canyons and deposited their load over preexisting basement highs.

We agree with Moore (1964) that these basement highs could be large slump blocks. The prominent disruption of bathymetric contour trends along the northeast coast of Oahu and north coast of Molokai indicates that these island flanks have probably been subjected to gravitational mass-wasting processes and that surficial sediment has been transported downslope by rubble slides and turbidity currents (Mathewson, 1970; Andrews and Bainbridge, 1972).

The origin of the seamounts that extend seaward from the edges of these probable slump blocks is, however, quite different. Available bathymetric data indicate that several of the smaller topographic highs form well-developed closed-contour peaks similar to many small volcanic seamounts that dot the Pacific Basin. The larger features seem to have been formed by two volcanoes coalescing together to form a crude figure 8 or bow-tie shape. The prominent flat top of Tuscaloosa Seamount, the principal topographic high in the group, is rather large but not unusually so in the context of Pacific guyots (see, for example, Menard, 1984; Vogt and Smoot, 1984). In addition, Andrews and Bainbridge (1972) determined that the topographic highs in the Oahu Seamount group have controlled sediment deposition around the seamounts and that the sedimentary layers seen on seismic reflection records are not distorted or chaotic, as would be expected if they had been emplaced by slumping or sliding. Unpublished multichannel seismic records from north and east of Oahu (A.B. Watts, oral commun., 1985) do not show any evidence of lystric or other faults between the seamounts or of distortion of sedimentary layers. In addition, the large distance between Tuscaloosa Seamount and the Oahu shelf (approx. 85 km) decreases, in our opinion, the probability that such large volumes of material could be transported across the slope.

Whereas the topography at the southwest end of the Oahu seamounts is likely to have been created by large landslides, we suggest (along with Andrews and Bainbridge, 1972) that the isolated topographic highs in the central and northeastern part of the group are older (Cretaceous?), partially buried volcanic edifices and that some may be guyots. These seamounts are not aligned along any known rift zone that extends from Oahu. In fact, the trend of the group is perpendicular to the strike of the Koolau volcanic range. The Oahu seamounts have summit depths and shapes that are similar to those of seamounts in the Musicians Seamount group, located north of Oahu (Rea and Naugler, 1970).

GRAVITATIONAL SLUMP BLOCKS

A model produced by DGI of the west flank of the Hawaiian Ridge is shown in figure 4.3. The starting viewpoint and azimuth of the perspective shown in figure 4.3 are marked on figure 4.2. The most interesting features displayed by this bathymetric compilation are the pronounced steps in the morphology of the basal slope of the ridge. These prominent steps in the otherwise steep slopes of the Hawaiian Ridge are likely to reflect large-scale gravitational slumping of parts of the volcanoes that have not been buttressed during their growth and development. A line drawing of the model shown in figure 4.3 appears as figure 4.4 on which the most obvious slump blocks have been shaded. It is apparent from these graphical representations of bathymetry that the tops of most slide blocks lie at depths of 2,000–2,500 m. The exception is the southwest-rift slide (fig. 4.3), which is much shallower (1,000–1,500 m) and is probably the youngest feature of this kind on the western flank of Hawaii. The shallower depth of the southwest-rift slide is likely to result from its position near the submarine extension of Mauna Loa's southwest rift zone and the short time over which it could have subsided since its formation. The coincidence in top depths of most of the slide blocks shown in figure 4.4 may be a function of the integrated effects of volcano growth, island subsidence, and oversteepening of the flanks to a critical point after which they are gravitationally unstable.

The Alika slide (Normark and others, 1979) is the best studied slump in this area; it shows up on figures 4.3–4.5 as a broad, low bulge in the lower southwest flank of Hawaii. This feature covers a depth range between 2,000 m and the base of the island slope at 4,000 m. Normark and others (1979) have mapped the entire area of the slide using airgun, 3.5-kHz echo-sounder, and gravity measurements and found that it is approximately 200 m thick at the toe and covers an area 20–25 km wide and nearly 80 km long.

The Kauna slide is a more prominent bulge to the south of the Alika slide and has nearly 2,000 m of relief from the top of the step to the foot of the block (figs. 4.3–4.5). Emplacement of the Kauna block most likely predated the movement of the Alika slide, because it appears to have channelled the Alika flow along its northern margin.

A similar but much less prominent step is present on the central south flank of Hawaii, between 2,500-m and 3,000-m depth (figs. 4.1, 4.2; see also, Moore, chapter 2), southeast of the Papau slide (Fornari and others, 1979b). On the southwest side of Oahu (figs. 4.1, 4.2), a prominent break in the slope at 2,500-m depth is likely to represent the top of a major slump block or group of blocks that developed on the unbuttressed southwest flank of the Waianae Range. Alternatively this feature may be the top of an older volcano that is now partially buried by the Waianae Range.

The development of these large slump-block features on the flanks of Hawaiian volcanoes suggests that gravitational failure of the slopes is an important process that alters the original constructional slopes of volcanoes during the early and mature shield-building stages. This process restabilizes the edifice, widening its base, and creates prominent steps in the steep submarine slopes. It is not known if the gravitational failures take place principally subaqueously or subaerially, nor whether the relief created by these features represents the aggregate of many episodes of slumping and mass-wasting or only a few events of enormous proportions.

A possible answer to these questions may be found through the study of the Hilina fault system, a series of subparallel and echelon faults that trend northeast on the south flank of Kilauea Volcano. Swanson and others (1976) and Tilling and others (1976) have demonstrated that the Hilina faults result from gravitational slumping

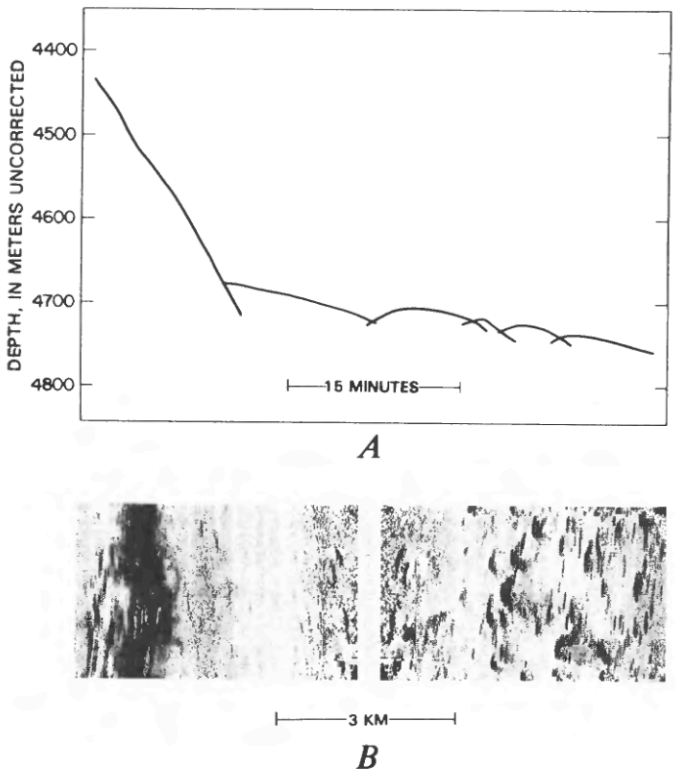

FIGURE 4.6.—Character of sea bottom off west coast of Island of Hawaii. ***A***, Tracing of 3.5-kHz echo-sounding profile (see figures 4.2 and 4.4 for location). Steep slope at left is base of Hualalai Volcano. Just seaward of slope is smooth sediment pond that appears to cover large blocks, represented by hyperbolic echos, that appear farther offshore. Horizontal scale is time; ship was moving at approximately 10 knots. ***B***, Sea MARC II side-scan sonar record of approximate area shown in *A*. Steep slope is represented by strong reflection at left of image, the large blocks as discrete reflections to right.

of the south flank of Kilauea. The slumping is induced by injection of magma into the east rift zone, thereby dilating the rift and forcing it to expand southward, in the direction it is not buttressed. These faults are a part of the initial stage of synconstructional edifice modification; they are known to continue out onto the submarine slope and have probably localized subsequent gravitational failures along their fault planes. The total relief created by the Hilina fault system is approximately 600 m, and the relief on a few individual scarps is as high as 300–450 m (Macdonald and others, 1983). The faults of the Hilina system may be viewed as modern-day analogs of faults (and fault systems) that now lie buried on the west flank of the Island of Hawaii whose cumulative activity and relief have created the large-scale gravitational slumps mapped on figures 4.3–4.5. Smaller scale features such as the Alika slide and Papau slide are likely to represent individual slide events in an area prone to gravitational collapse.

The development of prominent steps on the basal flanks of many of the Hawaiian Islands (and probably other volcanic oceanic islands) is controlled by the distribution of buttressing rift zones and gravitational mass-wasting of unbuttressed volcano sides. Clearly, large-scale gravitational mass-wasting of volcano flanks is responsible for the development of subtle but nonetheless important bathymetric features around Hawaii and probably around other oceanic volcanic islands as well (for example, Reunion Island, Duffield and others, 1982; Dallas Jackson, written commun., 1985).

LOW-RELIEF SUBMARINE RUBBLE AND DEBRIS FLOWS

The large-scale topographic features of the sea floor around Hawaii that are discussed above are easily resolved with standard bathymetric sonar tools. The investigation of smaller relief features and the microtopography of the sea floor has necessitated the development and use of sophisticated side-looking sonar systems that measure the acoustic reflectivity of the sea floor. The most successful system of this kind is the Sea MARC system, developed by International Submarine Technology of Redmond, Washington.

The Sea MARC II system, operated by the Hawaii Institute of Geophysics of the University of Hawaii, has been used in several surveys of the submarine flanks of Hawaiian volcanoes (Blackinton and others, 1983; Campbell, 1983; Campbell and Hussong, 1983; Fornari, 1984; Niedoroda and others, 1985). The technical details of the system have been described by Kosalos and others (1982) and Blackinton and others (1983). This system operates at 12 kHz, can insonify a swath of sea floor as large as 10 km wide, and can resolve linear sea floor topopgraphic features as small as 5–10 m high and several tens of meters long at survey speeds as great as 8 knots. Lateral changes in sea-floor reflectivity can be mapped and correlated to possible structural, morphologic, and sedimentologic facies.

An example of the use of the Sea MARC II system is presented in figure 4.6, which shows a 5-km-wide swath of sea floor in the Hawaiian Deep, west of Keahole Point on the Island of Hawaii. The Sea MARC II data show blocks as large as one kilometer in length and several tens of meters high that appear to be randomly scattered on the bottom. A dive made near this location by the Navy submersible *Trieste* found blocks reported to be the size of houses scattered on the bottom. These blocks are likely to be the deposits that were generated by one of the large gravitational slides located along this unbuttressed part of Hualalai Volcano.

Another principal result of the Sea MARC II surveys around the Hawaiian Islands has been the recognition of extensive rubble and debris flows and their deposits on the steep submarine flanks of the volcanoes. A mosaic of Sea MARC II side-scan sonar images (fig. 4.7) shows part of the Alenuihaha Channel and the deep channel that separates the Island of Maui from Hawaii, and an interpretative geologic sketch map of the principal features of this sonar mosaic is shown in figure 4.8.

Three major bathymetric features are present in the area shown in figure 4.8. These are the Kohala terrace, the northern slope of Kohala Volcano, and the southern slope of Haleakala Volcano on Maui. As can be seen on figure 4.7, nearly the entire submarine slope of Haleakala is covered by sinuous and branching patterns of high reflectivity, separated by linear acoustic shadows, which we have interpreted as being debris flow-lobes and channels. In several

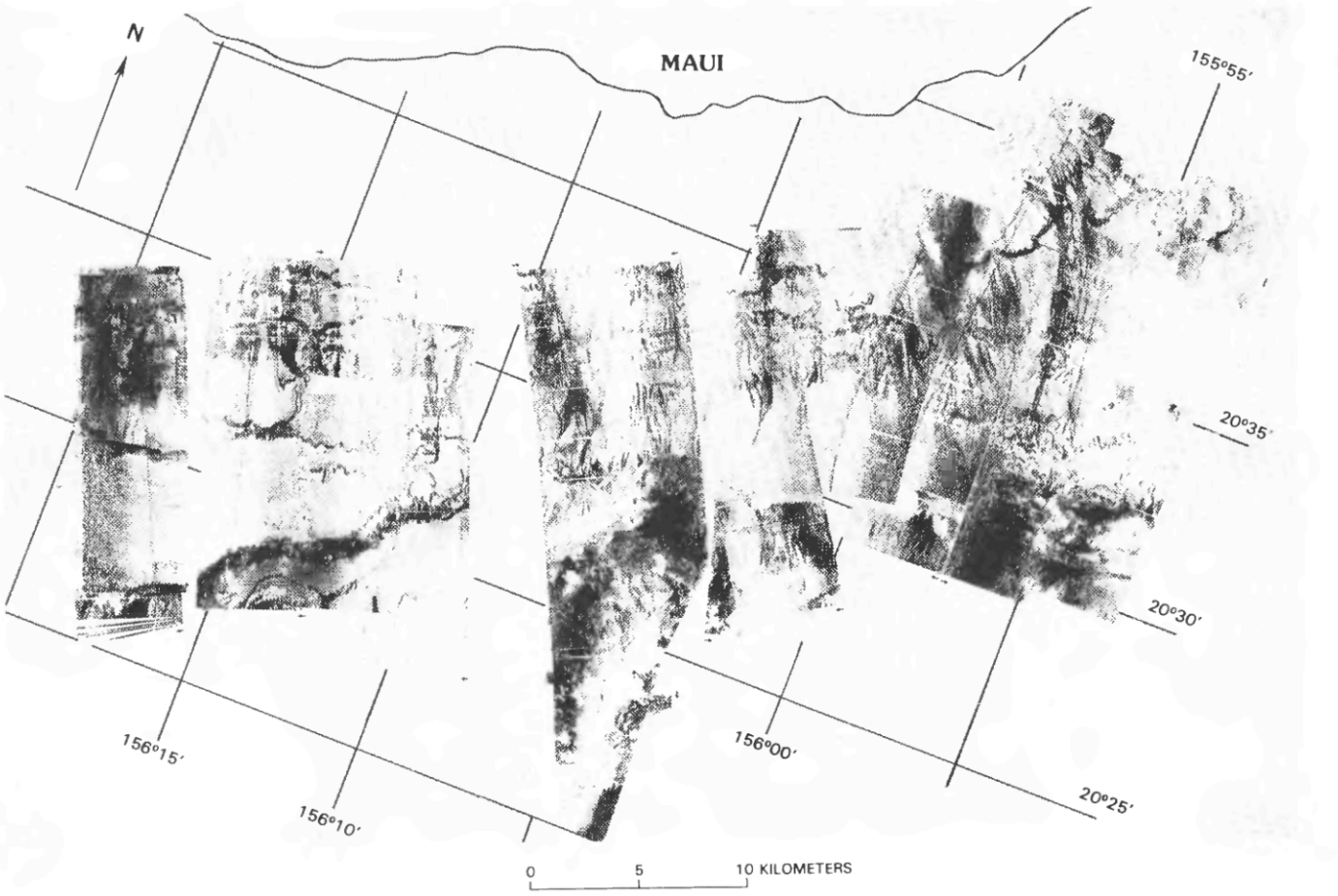

FIGURE 4.7.—Sea MARC II side-scan sonar image of the Alenuihaha Channel to south of Island of Maui. Dark areas on records are reflections from either hard, reverberant sea floor (such as volcanic rock or pavements with little sediment cover), or from linear relief that rises above surrounding sea floor. Light areas are acoustically less reflective and represent sediment-covered bottom or sea floor in complete or partial acoustic shadow (varied shades of gray). See figure 4.8 for interpretative map and Campbell (1983) for detailed description of this sea-floor area.

cases one can see that debris flows have been channelled by cuts and reentrants in flow fronts or scarps that trend across the slope. These flow fronts or scarps create strong reflections on the sonar images, implying that they have vertical or near-vertical faces. The total relief of these features may be as much as 100–200 m; the relief on individual flow fronts or scarps, however, is likely to be on the order of a few tens of meters, given the width of the returned signal and the difficulty in resolving these narrow features by conventional echo sounding. In comparison, the Sea MARC II image of the northern submarine flank of Kohala consists principally of strong returns suggestive of volcanic sea floor (Campbell, 1983), with very little dendritic fabric that could represent reflections from debris slides or channels. The northwestern edge of the Kohala terrace (Campbell and Erlandson, 1981; Campbell, 1984) has low reflectivity similar to the Alenuihaha Channel axis and other areas with gentle slopes that are covered with sediment. It is likely that the axis of the Alenuihaha Channel is largely filled with volcanic and coralline debris shed from Haleakala's southern slope. These sediments have been transported in fluvial erosional channels on land, in shallow submarine canyons on the upper slopes, and by debris flows and turbidity currents down the middle and lower submarine slopes (Campbell, 1983).

A Sea MARC II side-scan sonar mosaic of the sea floor off southwestern Oahu is shown in figure 4.9. There are several prominent morphological features in this area, including (1) the shelf-terrace area that lies between the shoreline and the top edge of the carbonate escarpment; (2) the continuous steep carbonate escarpment, which marks the western edge of a relict carbonate platform; (3) reflective ridge-and-gully terrain that lies seaward of the base of the escarpment; (4) highly reflective swaths of terrain that trend up and down the slope and are located seaward of the base of the escarpment; and (5) digitate lobes of alternating high- and low-reflectivity sea floor, located near the break in the slope between 1,500 m and 2,250 m at the downslope ends of the highly reflective

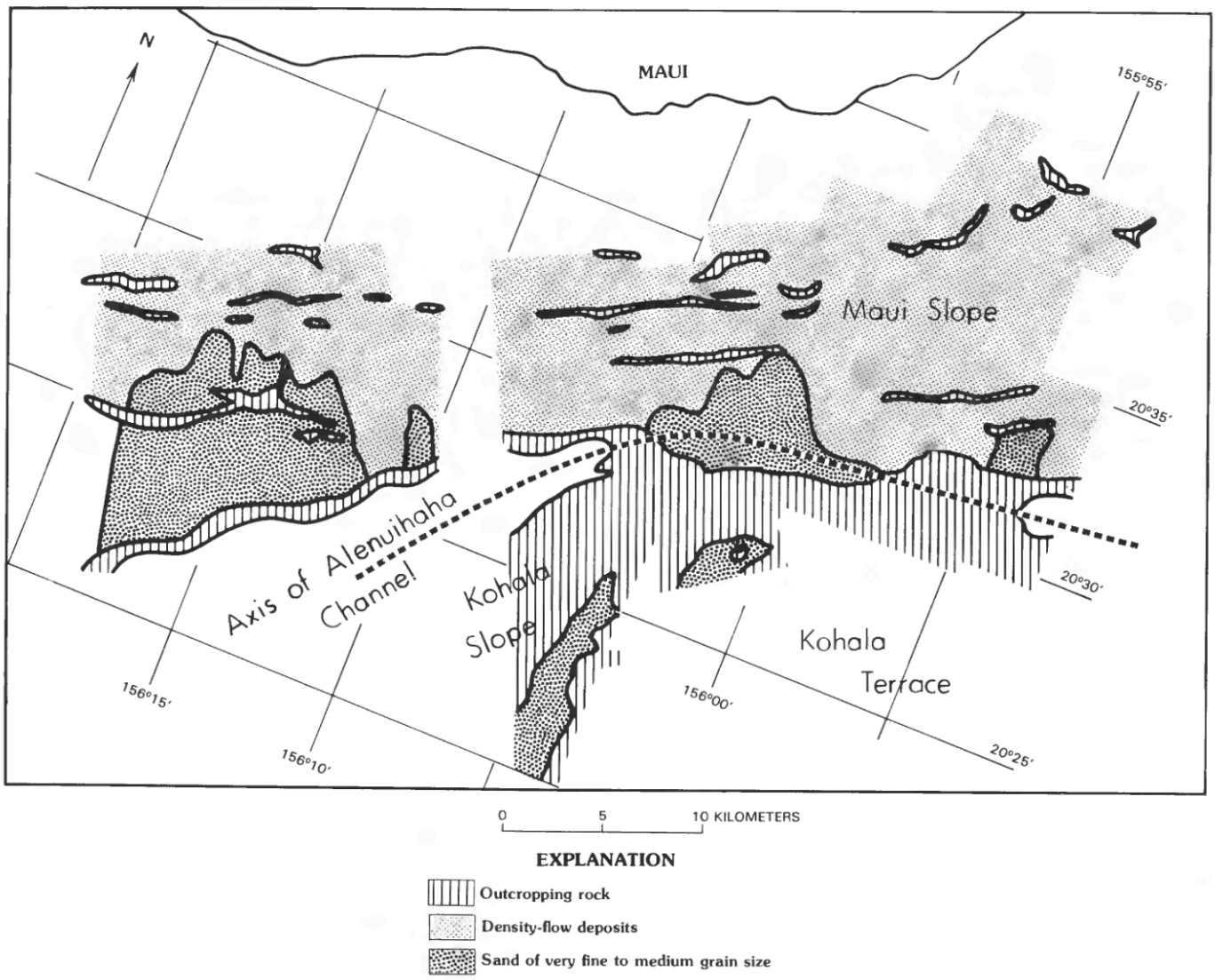

FIGURE 4.8.—Interpretative map of area of Sea MARC II images shown in figure 4.7. Note extensive linear, branching reflections and intervening acoustic shadows on south flank of Maui that we interpret as debris flows. Northern flank of Kohala Volcano forms a distinctly separate acoustic province. Samples, deep-sea photography, and Sea MARC II survey indicate that this submarine slope consists largely of outcropping volcanic flows and flow fronts with some volcanogenic and carbonate sediment on small terraces.

swaths, that are likely to represent localized landslide lobes (Fornari, 1983, 1984). The details of the sea-floor geology in this area have been studied with marine geophysical methods (Normark and others, 1982; Niedoroda and others, 1985) and with submersibles (Coles, 1982; Fornari, 1982, 1983, 1984).

The mosaic image in figure 4.9 and the interpretative maps in figures 4.10 and 4.11 provide an insight into the contemporary processes that act to shape the submarine shelf and slope areas on an older Hawaiian island such as Oahu. Also indicated on figure 4.10 are the telephone cable breaks that occurred during a hurricane on November 23, 1982. The reader is referred to Noda (1983), Fornari (1983), and Hollister (1984) for a detailed treatment of the cable-break data and the relation between cable breaks, sea-floor topography, and ocean-floor sediment dynamics.

Seaward of the base of the carbonate escarpment shown in figures 4.9 and 4.10 there are numerous zones of slightly higher reflectivity (fig. 4.10, unit C) that form crudely fan-shaped swaths of terrain interpreted to be more cobbly sea floor within the ridge-and-gully terrain identified on DSV *Turtle* dives (Fornari, 1982; 1983). These swaths of sea floor are characterized by linear patterns on the side-scan sonar records, and some swaths trend into the axes of the bathymetric reentrants typical along this southwestern coast of Oahu (Niedoroda and others, 1985). Seaward of these unit C acoustic reflectivity zones, swaths of terrain with much higher reflectivity (fig.

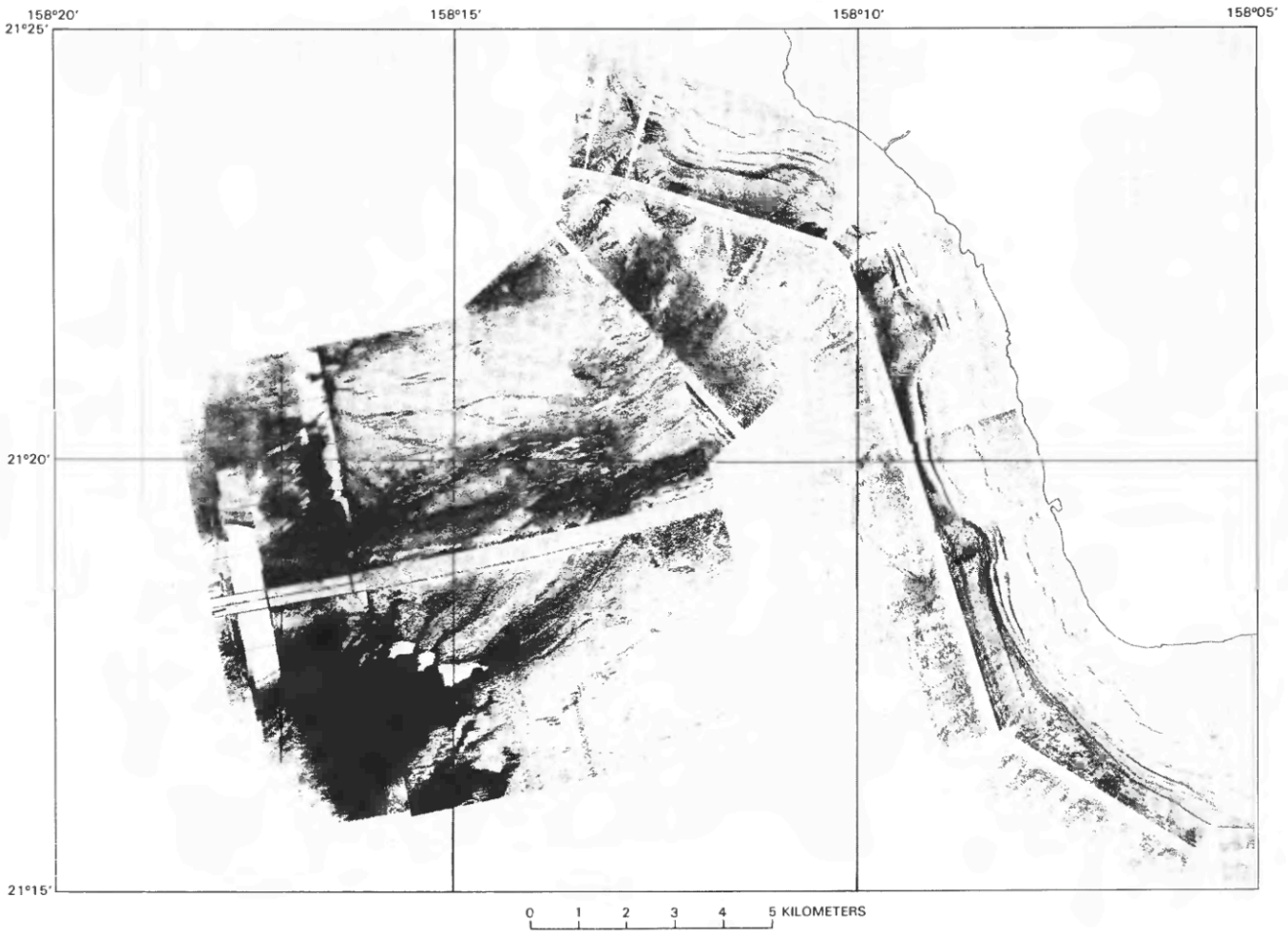

FIGURE 4.9.—Sea MARC II side-scan sonar image of the sea floor off Kahe Point, Oahu. See figure 4.10 for interpretation and Fornari (1984) for complete discussion of these data.

4.10, unit R) are likely to be areas of sea floor consisting of either gravelly or hard sediment (possibly indurated, cemented carbonate or manganese pavement). The acoustic contrast between the R and C zones is easily seen on figure 4.9, as is the higher reflectivity of these areas compared to the N zones (nonreflective). Near the southwestern edge of the sonar image in figure 4.9 there are several finger-like zones of sea floor characterized by narrow, alternating swaths of high and low reflectivity that create prominent acoustic shadows (figs. 4.9 and 4.10). These zones have been mapped by the symbol L on figure 4.10, and they appear to lie directly downslope from the R acoustic-facies zones.

A comparison between the Sea MARC II image in figure 4.7 and that in figure 4.9 points to the similarity in acoustic character of the sea-floor areas affected by low-relief rubble and debris flows. The importance of downslope transport of sediment by these processes on the flanks of Hawaiian volcanoes (Fornari and others, 1979b; Campbell, 1983; Campbell and Hussong, 1983) is suggested by the sinuous outline of the flow lobes and the delicate branching reflectors separated by intervening areas of low reflectivity that are likely to represent dendritic flow lobes and channels. Relief created by the debris flows is not great, usually on the order of a few tens of meters or less above the surrounding sea floor (Niedoroda and others, 1985). In most cases these features cannot be resolved with standard bathymetric echo sounding from the sea surface.

Thick wedges of clastic sediment, transported by debris flows and deposited on the submarine flanks of volcanoes, are important components of the gross stratigraphy of oceanic volcanoes and result from gravitational mass-wasting of large sections of unbuttressed volcano flanks and downslope movement of sediment in rubble and debris flows.

CARBONATE ESCARPMENTS

An interpretative sketch is shown in figure 4.12 of the stratigraphy viewed from the submersible *Makali'i* during several dives on

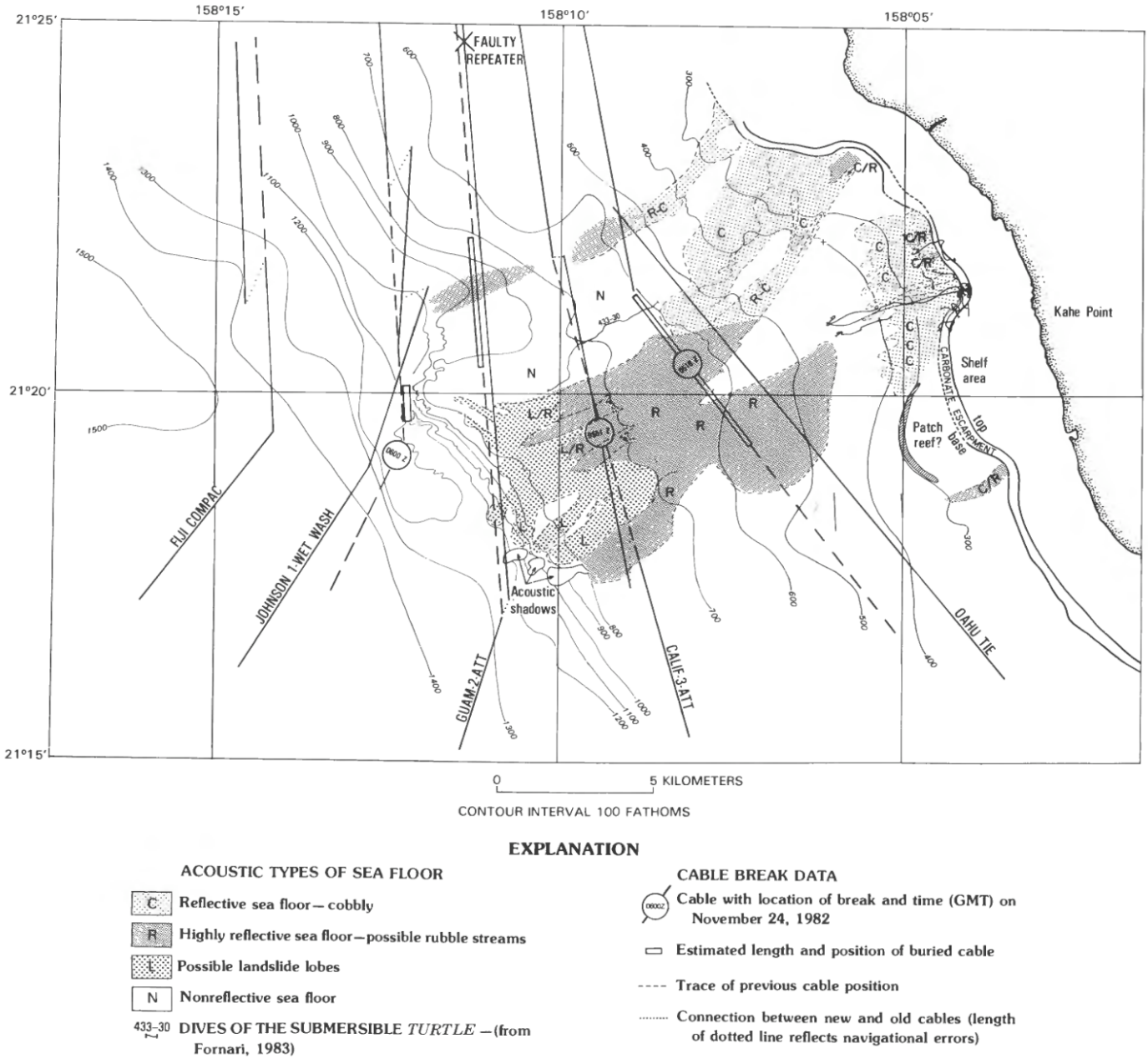

FIGURE 4.10.—Interpretative map of area of Sea MARC II image shown in figure 4.9. Major changes in acoustic reflectance relate to changes in surface sediment and depositional process. Prominent landslide lobes show analogous acoustic character to similar features on the south flank of Maui (see fig. 4.7). Reflective cobbly zones coincide with probable areas of active downslope transport of coarse volcanic and coralline rubble in traction carpets or rubble streams. See Fornari (1983, 1984) for further details and discussion of cable-break data.

the carbonate escarpment that is located just seaward of Kealakekua Bay, Hawaii (Moore and Fornari, 1984). During the traverse of *Makali'i* dive 164 (Moore and Fornari, 1984) a prominent cliff 3–10 m high was found in depths between 350 and 360 m. This cliff is continuous in a northwest direction along a contour-parallel trend, is subparallel to the escarpment, and exposes a volcanic conglomerate (fig. 4.12). The conglomerate consists of angular to subangular volcanic clasts that range in size from 0.5 cm to 0.5 m, with the median size being 0.5–2 cm, in a matrix of finer volcanic and biogenic carbonate silt and sand. Few bedding planes or graded beds were observed in the exposures; however, abundant fractures parallel to the original depositional surface indicate that crude bedding is probably present in the deposit and that it was laid down in successive episodes. Outcrops of the reef carbonate on the

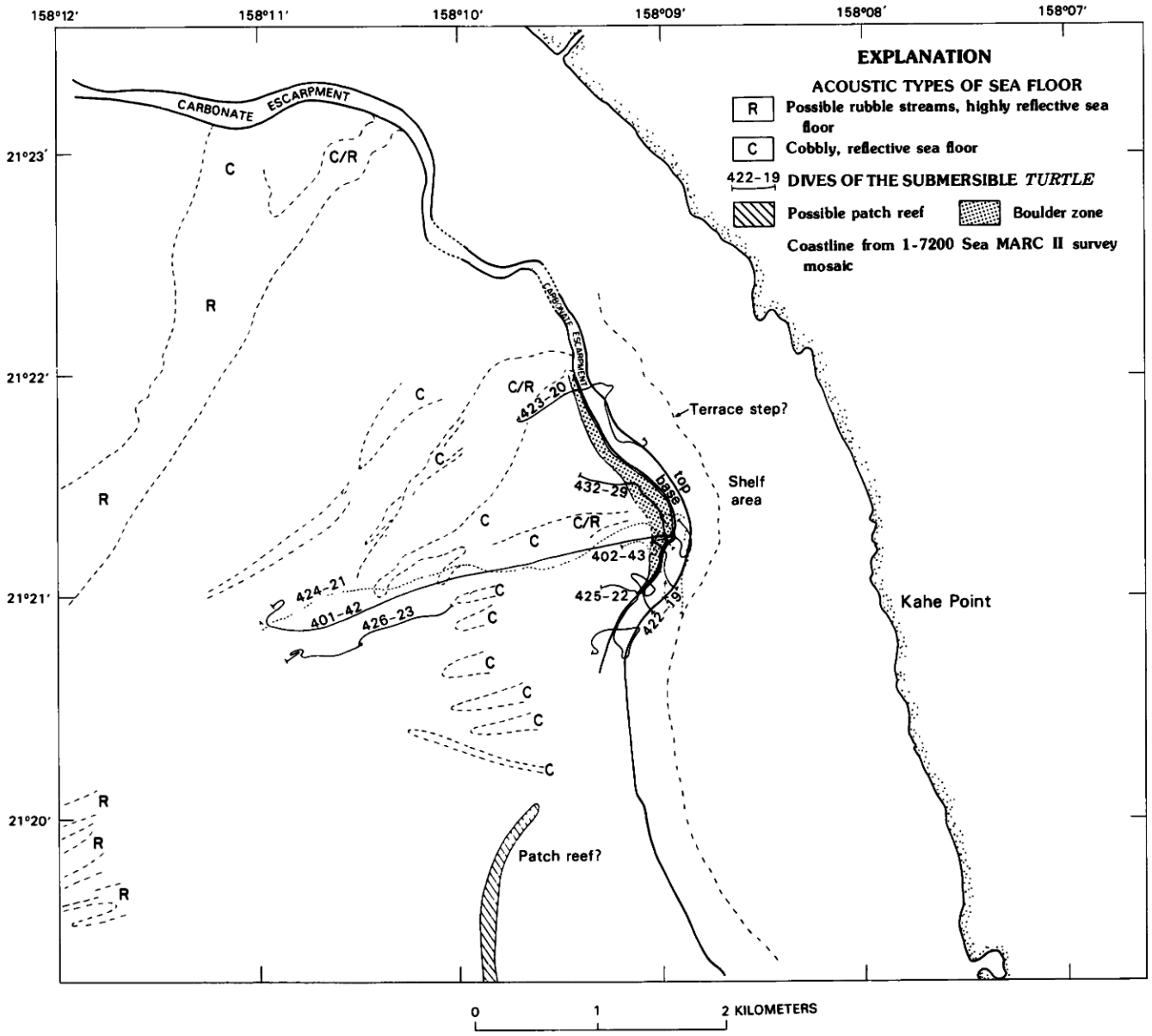

FIGURE 4.11.—Schematic map of nearshore part of area covered by Sea MARC II image off Kahe Point, Oahu, shown in figure 4.10. Submersible dive tracks and details of the sonar image have been mapped. See Fornari (1983, 1984) for further details.

escarpment above this cliff indicate that the conglomeratic deposit underlies and is the foundation for the massive limestone terrace (fig. 4.12). The instability of the volcaniclastic deposit in Kealakekua Bay is suggested by the common occurrence of large tabular blocks of the conglomerate on the sea floor immediately west of the cliff that were probably spalled off the vertical face. In some cases the base of the cliff was observed to have been undercut by as much as several meters, a process that certainly must accelerate the shedding of blocks from the escarpment.

This volcaniclastic deposit and exposures of other similar sedimentary sequences along the shallow submarine slope of Hawaii (Fornari and Perfit, unpub. data) indicate that erosion of the volcanic foundation takes place at a rapid rate. Deposition of clastic volcanogenic sediment by debris flows down the slopes leads to seaward-thinning wedges of mechanically weak clastic deposits that, when covered by successive sequences of lava, may provide an ideal surface on which seismically induced gravitational slumping can occur. This notion is supported by earthquake studies (Crosson and

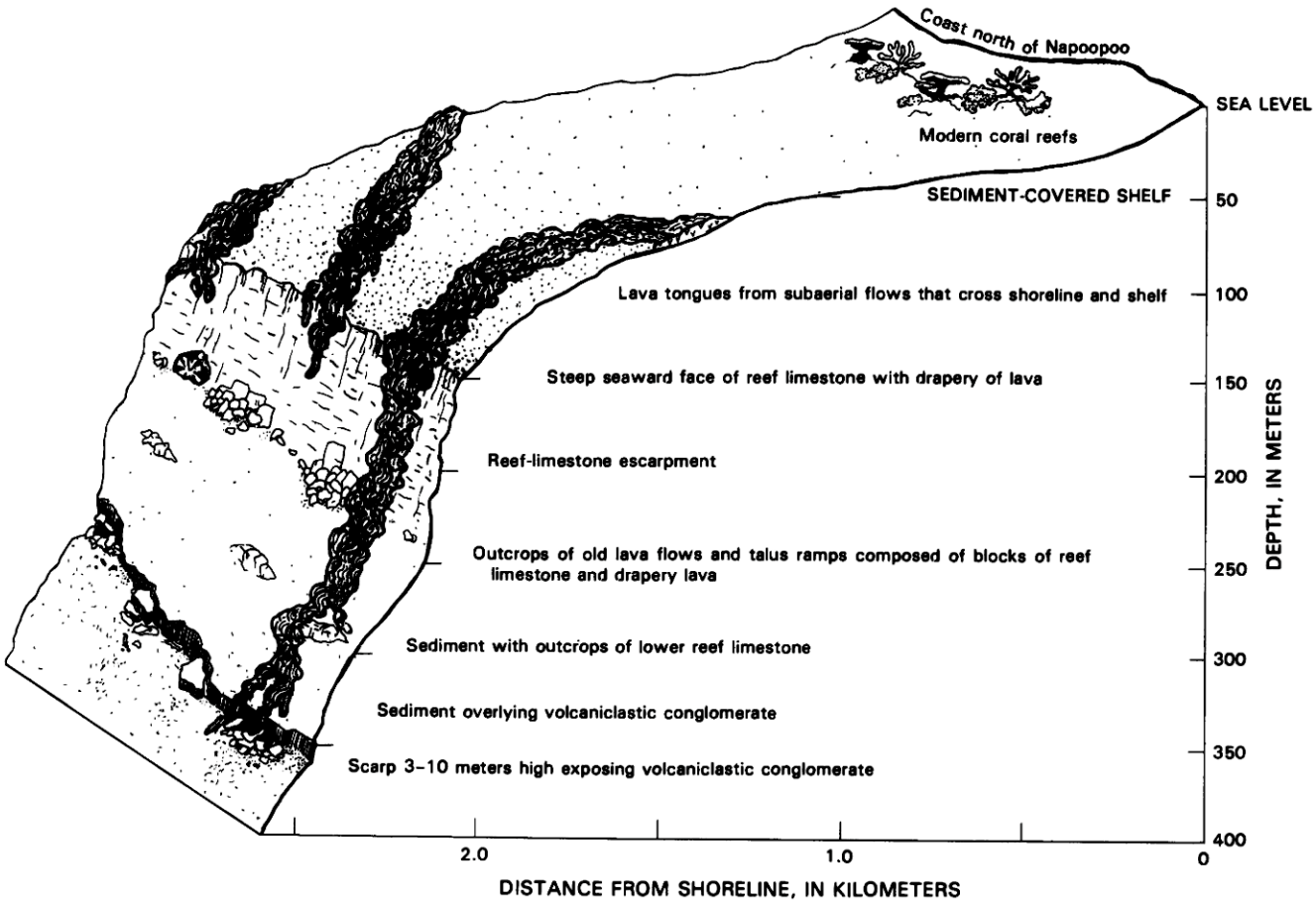

FIGURE 4.12.—Interpretative drawing of sea floor to 400-m depth off Kealakekua Bay, Hawaii, based on *Makali'i* dives (Moore and Fornari, 1984). Lava at base of carbonate escarpment is surrounded by reef limestone. This type of intercalation results from flows crossing an actively growing reef and being covered by later reef growth as subsidence occurs. Note volcaniclastic conglomerate bed 3–10 m thick that forms a continuous scarp along the base of the subsided reef terrace. This deposit was created by erosion of volcanic and carbonate outcrops on the slope and shore and deposited by rubble flows. Drawn by C.L. Fornari.

Endo, 1982) that indicate that focal mechanisms associated with nonvolcanic earthquakes on Kilauea's south flank occur within a slip plane that is coincident with a weak layer above old oceanic crust.

CONCLUSIONS

The sea floor around the Hawaiian Islands comprises several major classes of topography that are intimately related to (1) constructional volcanism that built the islands; (2) the preexisting fabric of the oceanic crust upon which the islands are built; (3) island subsidence; (4) gravitational collapse of unbuttressed volcano sides; and (5) low-relief debris flows that transport clastic sediment down the submarine slopes. The submarine continuations of subaerial rift zones create the most prominent relief around the islands. The topographic roughness and regional slope of each submarine rift is directly proportional to the age of the adjacent volcano. Seamounts around the Hawaiian Islands are largely older (Cretaceous) volcanoes that have been been partially buried by sediment. Some of these features may be drowned guyots. Several young seamounts that are genetically related to Hawaiian volcanism lie south of the Island of Hawaii. More subtle topographic features are present on the basal flanks of the Hawaiian Ridge and form steps and bulges in the lower slopes. These features were created by large-scale gravitational mass wasting of volcano flanks not buttressed by adjacent edifices. Low-relief debris flows appear to be the principal mechanism whereby clastic sediment is transported down the submarine flanks of oceanic volcanoes.

REFERENCES CITED

Andrews, J.E., and Bainbridge, C., 1972, Submarine canyons off eastern Oahu: Pacific Science, v. 26, p. 108–113.

Betz, F., and Hess, H.H., 1942, The floor of the north Pacific Ocean: Geographical Review, v. 32, p. 99–116.

Blackinton, J.G., Hussong, D.M., and Kosalos, J.G., 1983, First results from a combination side-scan sonar and seafloor mapping system (Sea MARC II):

Offshore Technology Conference, 15th, Houston, May 2-5, 1983, Appendix A, Proceedings, p. 309–314.

Campbell, J.F., 1983, Hawaii deep water cable program, phase II—at sea route surveys: Hawaii Institute of Geophysics Report, HIG–83-4, 50 p.

———1984, Rapid subsidence of Kohala Volcano and its effect on coral reef growth: Geo-Marine Letters, v. 4, p. 31–36.

Campbell, J.F., and Erlandson, D.L., 1979, Ocean Thermal Energy Conversion–1 (OTEC–1) Anchor site survey: Hawaii Institute of Geophysics Report, HIG–79-6, pp. 55.

———1981, Geology of Kohala submarine terrace, Hawaii: Marine Geology, v. 4, p. 63–72.

Campbell, J.F., and Hussong, D.M., 1983, Submarine geology of the Alenuihaha channel, the results of a Sea MARC II survey [abst.]: Eos, Transactions, American Geophysical Union, v. 64, p. 1032.

Chase, T.E., Menard, H.W., and Mammerickx, J., 1971, Bathymetric atlas of the north-central Pacific: Washington, H.O. Publication 1302, U.S. Naval Oceanographic Office.

———1980, Bathymetry of the North Pacific: La Jolla, Scripps Institution of Oceanography and Institute of Marine Resources, Chart No. 8.

Coles, S.L., 1982, A visual reconnaissance of the bottom between 20 and 365 m depth offshore of Kahe Point, Oahu for the purpose of OTEC pipeline/cable routing: unpublished report prepared for the Hawaiian Electric Co., Honolulu.

Crosson, R.S., and Endo, E.T., 1982, Focal mechanisms and locations of earthquakes in the vicinity of the 1975 Kalapana earthquake aftershock zone 1970–1979: implications for tectonics of the south flank of Kilauea Volcano, Island of Hawaii: Tectonics, v. 1, no. 6, p. 495–542.

Dietz, R.S., and Menard, H.W., 1953, Hawaiian swell, deep and arch, and subsidence of the Hawaiian Islands: Journal of Geology v. 61, p. 314–333.

Duffield, W.A., Stieltjes, L., and Varet, J., 1982, Huge landslide blocks in the growth of Piton de la Fournaise, La Reunion and Kilauea Volcano, Hawaii: Journal of Volcanology and Geothermal Research, v. 12, p. 147–160.

Fiske, R.S., and Jackson, E.D., 1972, Orientation and growth of Hawaiian rifts: the effects of regional structure and gravitational stresses: Royal Society of London, Proceedings, Series A., v. 329, p. 299–326.

Fiske, R.S., and Kinoshita, W.T., 1969, Rift dilation and seaward displacement of the south flank of Kilauea Volcano, Hawaii [abs.]: Symposium on volcanoes and their roots, Oxford, International Association of Volcanology and Chemistry of the Earth's Interior, p. 53–54.

Fornari, D.J., 1982, Deep-Submergence Vehicle *Turtle* dives off Keahole Pt., Hawaii, geological investigations of submarine slope micromorphology: baseline studies to assist in future OTEC cold-water pipe designs and deployments: Canoga Park, Ca; Rockwell International Energy Systems Group Technical Report.

———1983, Final Report, Deep-Submergence Vehicle *Turtle* dives off Kahe Point, Oahu, Hawaii: Chatham, N.Y., unpublished technical report, Offshore Investigations Limited, 60 p.

———1984, Preliminary Report, Sea MARC II side scan sonar image of the seafloor off Kahe Point, Oahu, Hawaii: Chatham, N.Y. unpublished technical report, Offshore Investigations Limited, 19 p.

Fornari, D.J., Malahoff, A., and Heezen, B.C., 1979a, Submarine slope micromorphology and volcanic substructure of the Island of Hawaii inferred from visual observations made from U.S. Navy Deep-Submergence Vehicle (DSV) *Sea Cliff*: Marine Geology v. 32, p. 1–20.

Fornari, D.J., Moore, J.G., and Calk, L., 1979b, A large submarine sand-rubble flow on Kilauea Volcano, Hawaii: Journal of Volcanology and Geothermal Research, v. 5, p. 239–256.

Francheteau, J., Harrison, C.G.H., Sclater, J.G., and Richards, M.L., 1970, Magnetizations of Pacific seamounts: A preliminary polar curve for the northeastern Pacific: Journal of Geophysical Research, v. 75, p. 2035–2061.

Furumoto, A., and Woollard, G.P., 1965, Seismic refraction studies of the crustal structure of the Hawaiian Archipelago: Pacific Science, v. 19, p. 315–319.

Gregory, A.E., and Kroenke, L.W., 1982, Reef development on a mid-oceanic island: Reflection profiling studies of the 500-meter shelf south of Oahu: American Association of Petroleum Geologists Bulletin, v. 66, p. 843–859.

Hamilton, E.L., 1957, Marine geology of the southern Hawaiian ridge: Geological Society of America Bulletin, v. 68, p. 1011–1026.

Hollister, C.D., 1984, Cable failures off Oahu caused by Hurricane Iwa: AT&T Communications, unpublished technical report.

Klein, F., 1982, Earthquakes at Loihi submarine volcano and the Hawaiian hot spot: Journal of Geophysical Research, v. 87, p. 7719–7726.

Kosalos, J.G., Blakinton, J.G., Hussong, D.M., and Fryer, P., 1982, The Sea MARC II seafloor reconnaissance system [abs.]: Eos, Transactions, American Geophysical Union, v. 63, p. 983.

Koyanagi, R.I., Swanson, D.A., and Endo, E.T., 1972, Distribution of earthquakes related to mobility of the south flank of Kilauea Volcano, Hawaii: U.S. Geological Survey Professional Paper 800–D, p. D89–D97.

Lipman, P., 1980, The southwest rift zone of Mauna Loa: implications for structural evolution of Hawaiian volcanoes: American Journal of Science, v. 280–A, p. 752–776.

Lockwood, J.P., 1979, Geologic asymmetry of the northeast rift zone of Mauna Loa Volcano, Hawaii—evidence for a mobile south flank [abs.]: Hilo, Hawaii Symposium on Intraplate Volcanism, p. 170.

Macdonald, G.A., Abbott, A.T., and Peterson, F.L., 1983, Volcanoes in the Sea, The Geology of Hawaii (2d ed.): Honolulu, University of Hawaii Press, pp. 517.

Malahoff, A., McMurtry, G., Wiltshire, J., and Yeh, H., 1982, Geology and chemistry of hydrothermal deposits from active submarine volcano Loihi, Hawaii: Nature, no. 298, p. 234–239.

Malahoff, A., and Woollard, G.P., 1968, Magnetic and tectonic trends over the Hawaiian Ridge, *in* Knopoff, L., Drake, C.L., and Hart, P.J., eds., The crust and upper mantle of the Pacific area: American Geophysical Union Monograph 12, p. 241–276.

Mathewson, C.C., 1970, Submarine canyons and the shelf along the north coast of Molokai Island, Hawaiian ridge: Pacific Science, v. 24, p. 235–244.

Menard, H.W., 1964, Marine Geology of the Pacific: New York, McGraw-Hill, 271 p.

———1984, Origin of guyots: the Beagle to Seabeam: Journal of Geophysical Research, v. 89, p. 11,117–11,123.

Moberly, R., and McCoy, F.W., 1966, The sea floor north of the eastern Hawaiian Islands, Marine Geology, v. 4, p. 21–48.

Moore, J.G., 1964, Giant submarine landslides on the Hawaiian ridge: U.S. Geological Survey Professional Paper 501–D, p. D95–D98.

———1965, Petrology of deep-sea basalt near Hawaii: American Journal of Science, v. 263, p. 40–52.

———1970, Relationship between subsidence and volcanic load, Hawaii: Bulletin Volcanologique, v. 34, p. 562–576.

Moore, J.G., Clague, D., and Normark, W.R., 1982, Diverse basalt types from Loihi Seamount, Hawaii: Geology, v. 10, p. 88–92.

Moore, J.G., and Fiske, R.S., 1969, Volcanic substructure inferred from dredge samples and ocean bottom photographs: Geological Society of America Bulletin, v. 80, p. 1191–1202.

Moore, J.G., and Fornari, D.J., 1984, Drowned reefs as indicators of the rate of subsidence of the Island of Hawaii: Journal of Geology, v. 92, p. 752–759.

Moore, J.G., Normark, W.R., and Lipman, P.W., 1979, Loihi Seamount—a young submarine Hawaiian volcano [abs.]: Hilo, Hawaii Symposium on Intraplate Volcanism, p. 127.

Niedoroda, A.W., Palmer, A.C., Pittman, J.R., Vandermeulen, J.P., and Campbell, J.F., in press, Oahu OTEC preliminary design: sea floor surveys: Proceedings of Offshore Site Investigations 1985.

Noda, E., 1983, Effects of Hurricane Iwa, November 23, 1982, offshore Kahe Point, Hawaii: (unpublished report submitted to RCUH, University of Hawaii).

Normark, W.R., Chase, T.E., Wilde, P., Hampton, C.E., Butmacher, B., Seekins, A., and Johnson, K.H., 1982, Geologic report for the O'OTEC site off Kahe Point, Oahu, Hawaii: U.S. Geological Survey Open-File Report 82–468A, 9 p.

Normark, W.R., Lipman, P., and Moore, J.G., 1979, Regional slump structures on the west flank of Mauna Loa Volcano, Hawaii [abs.]: Hawaii Symposium on Intraplate and Submarine Volcanism, Abstract volume, p. 172.

Rea, D.K., and Naugler, F.P., 1970, Musicians seamount province and related crustal structures north of the Hawaiian Ridge: Marine Geology, v. 10, p. 89–111.

Staudigel, H., Zindler, A., Hart, S.R., Leslie, T., Chen, C.-Y., and Clague, D.A., 1984, The isotope systematics of a juvenile intraplate volcano: Pb, Nd, and Sr isotope ratios of basalts from Loihi Seamount, Hawaii: Earth and Planetary Science Letters, v. 69, p. 13–29.

Stearns, H.T., and Macdonald, G.A., 1946, Geology and groundwater resources of the Island of Hawaii: Hawaii Division of Hydrography Bulletin, v. 9, 363p.

Strange, W.E., Woollard, G.P., and Rose, J.C., 1965, An analysis of the gravity field over the Hawaiian Islands in terms of crustal structure: Pacific Science, v. 19, p. 381–389.

Swanson, D.A., Duffield, W.A., and Fiske, R.S., 1976, Displacement of the south flank of Kilauea Volcano: the result of forceful intrusion of magma into the rift zones: U.S. Geological Survey Professional Paper 963, 39 p.

Tilling, R.I., Koyanagi, R.Y., Lipman, P.W., Lockwood, J.P., Moore, J.G., and Swanson, D.A., 1976, Earthquake and related catastrophic events, Island of Hawaii, November 29, 1975: a preliminary report: U.S. Geological Survey Circular 740, 33 p.

Vogt, P.R. and Smoot, N.C., 1984, The Geisha Guyots: multibeam bathymetry and morphometric interpretation: Journal of Geophysical Research, v. 89, p. 11,085–11,107.

Watts, A.B., 1976, Gravity and bathymetry in the central Pacific Ocean: Journal of Geophysical Research, v. 81, p. 1533–1553.

Watts, A.B., ten Brink, U.S., Buhl, P., and Brocher, T.M., 1985, A multichannel seismic study of lithospheric flexure across the Hawaiian-Emperor Seamount Chain: Nature, v. 315, p. 105–111.

Wilde, P., Chase, T.E., Normark, W.R., Thomas, J.A., and Young, J.D., 1980, Oceanographic data off the southern Hawaiian Islands: Berkeley, Lawrence Berkeley Laboratory, University of California, LBL Publication No. 359.

THE GEOMORPHIC AND STRUCTURAL DEVELOPMENT OF HAWAIIAN SUBMARINE RIFT ZONES

By Daniel J. Fornari[1]

ABSTRACT

The structure and morphology of Hawaiian submarine rift zones reflect the time-integrated effects of constructional volcanic processes, island subsidence, destructive gravitational slumping of unbuttressed volcano sides, and reef buildup and sedimentation. Structural modification of submarine rift flanks begins during initial stages of eruptive history and reaches a maximum during the shield-building stage. This process is exemplified by faults on the south submarine flank of Kilauea's east rift zone, debris slides like the Papau slide on the south flank of Hawaii, and large gravitational slump features, like the Kauna and Alika slides, on the southwest flank of Mauna Loa. The submarine northwest rift of Hualalai and Mauna Kea's submarine east rift have morphological characteristics indicating that their structural evolution is largely complete. Further changes to these evolved submarine rift zones and to older Hawaiian submarine slopes will be caused principally by subsidence, burial beneath carbonate platforms and sediments, and erosion and redeposition of hemipelagic and volcanogenic sediments by rubble flows and debris slides that transport sediments down steep submarine slopes.

INTRODUCTION

The submarine slopes of three shield volcanoes on the Island of Hawaii have been investigated since 1974 using the U.S. Navy submersibles DSV *Turtle* and DSV *Sea Cliff* (Fornari and others, 1979a). The resulting data have increased our understanding of volcanic and morphologic features on the submarine slopes of Kilauea, Mauna Loa, and Hualalai Volcanoes, and have led to the development of basic models of oceanic-island structure using submarine flank terrains as modern analogs of past volcanic episodes and processes (Fornari and others, 1979a).

The east rift of Kilauea (known offshore as the Puna Ridge) (Fornari and others, 1978) and the southwest rift of Mauna Loa (figs. 5.1, 5.2; Fornari and others, 1979b) were studied previously using U.S. Navy submersibles. With the analysis of data from seven dives on the south flank of the northwest rift of Hualalai Volcano (Schwartz and Fornari, 1982) and additional dredge and surface-ship (remote sensing) studies (Campbell and Erlandson, 1981; Clague, 1982), it has been possible to compare the morphological and structural evolution of these submarine features. That comparison forms the focus of this paper; it is especially interesting because of the age difference among the three Hawaiian submarine rifts, Hualalai's being the oldest and Kilauea's the youngest.

ACKNOWLEDGMENTS

E. Wolfe, R. Moore, J.G. Moore, D. Clague and G.P.L. Walker read various drafts of an earlier manucript and their constructive comments greatly improved this paper. I thank D. Christie, R. Decker, B. Decker and A. Malahoff for constructive comments on the final draft. D. Schwartz provided valuable assistance in reducing data from submersible dives on Hualalai. M.A. Luckman drafted the figures. Field and laboratory studies that were the basis for this synthesis have been supported by the U.S. Navy Office of Naval Research, Grant N00014-80-C-0098MM to the Lamont-Doherty Geological Observatory. Lamont-Doherty Geological Observatory Contribution No. 3840.

HAWAIIAN RIFT ZONES

SUBAERIAL PORTIONS

Hawaiian rift zones form swaths of tectonically disrupted terrain with rugged topography that consists of eruptive fissures, spatter ramparts and cones, and open cracks and collapse features (Stearns and Macdonald, 1946; Macdonald and Abbott, 1970; Lipman, 1980). The surficial expression of rift zone volcanism is usually a zone 3–4 km wide showing constructional and extensional features and normally coincident with a topographic ridge.

Geophysical anomalies (principally Bouguer gravity and magnetic anomalies) are useful in delineating the width of the intrusion zone, a steeply dipping plexus of dikes through which magma rises to the surface from shallow reservoirs located 2–6 km beneath the summit area (Swanson and others 1976; Ryan and others, 1981). Gravity and magnetic studies indicate that the intrusive dike complex beneath the narrow zone of surface rifting may be as wide as 12–17 km at depths of 3–4 km (Malahoff and Woollard, 1968; Broyles and others, 1979).

The positions of individual rift zones with respect to their volcanic centers and to neighboring volcanoes were investigated by Fiske and Jackson (1972) and in later field studies by Broyles and others (1979) and Lipman (1980a, b). Their conclusions are that

[1]Lamont-Doherty Geological Observatory of Columbia University, Palisades, New York 10964

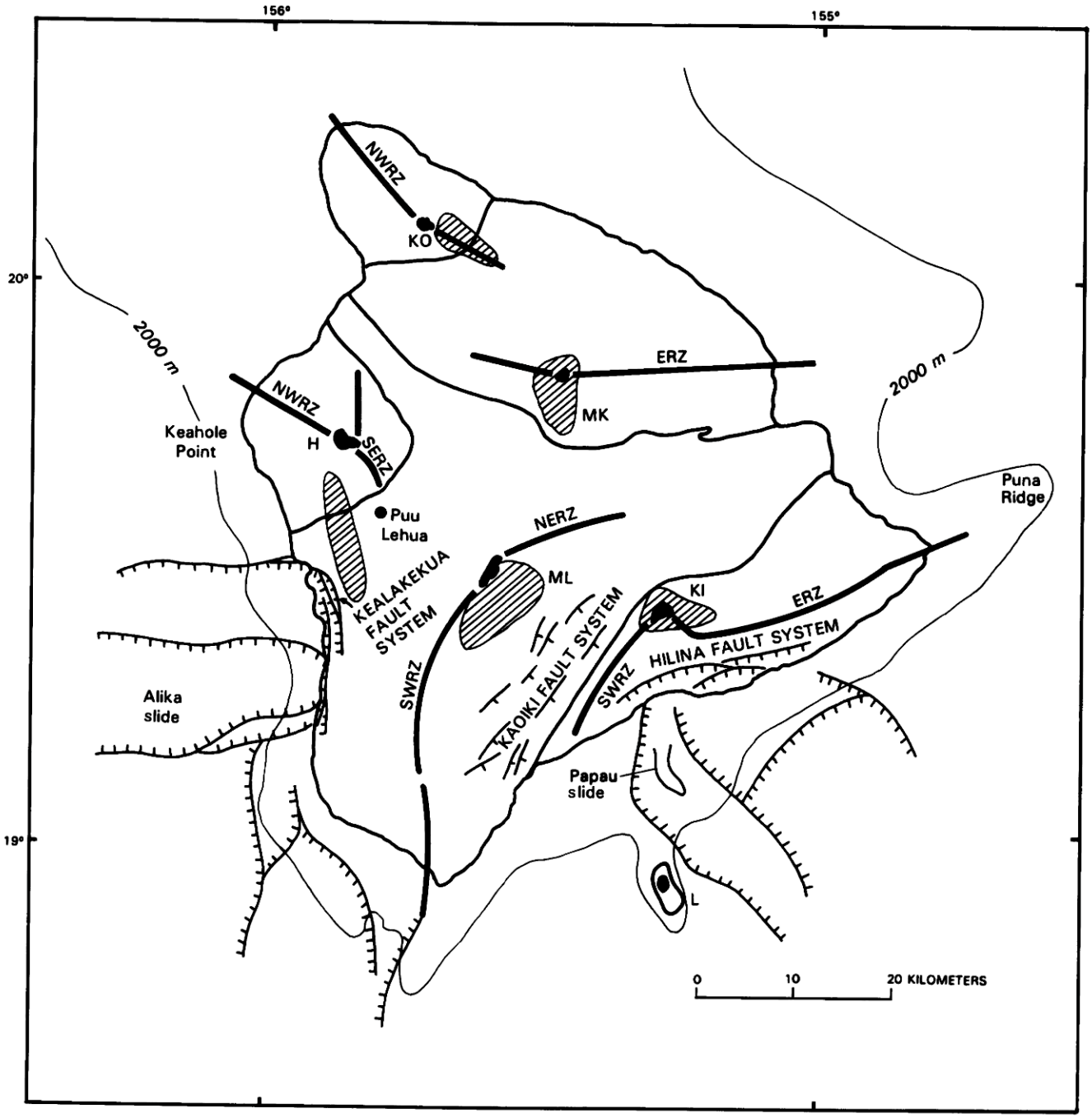

FIGURE 5.1.—Island of Hawaii showing boundaries between volcanoes, traces of rift zones, some fault systems, and areas of closed-contour Bouguer gravity highs (lined) from Kinoshita and others (1963). Volcanoes: KI, Kilauea; ML, Mauna Loa; H, Hualalai; MK, Mauna Kea; KO, Kohala; L, Loihi Seamount. Boundaries of submarine slump structures (ticks on downthrown side) are from Normark and others (1979). NWRZ, northwest rift zone; SWRZ, southwest rift zone; SERZ, southeast rift zone; ERZ, east rift zone; NERZ, northeast rift zone.

Hawaiian rift zones are shallow-level features whose locations are principally dictated by gravitational stresses within an edifice, but also indirectly by the shapes and positions of preexisting shields whose flanks have served as foundations for nascent volcanoes. As a result, the rifts vary in length; Kilauea's east rift zone and Mauna Loa's southwest rift zone are more than 100 km long including their submarine portions. Variation in rift-zone length may be attributed to the distribution of surrounding edifices that are large enough to inhibit or attenuate the development of a young rift zone. For example, Kilauea's southwest rift zone is sandwiched between Loihi

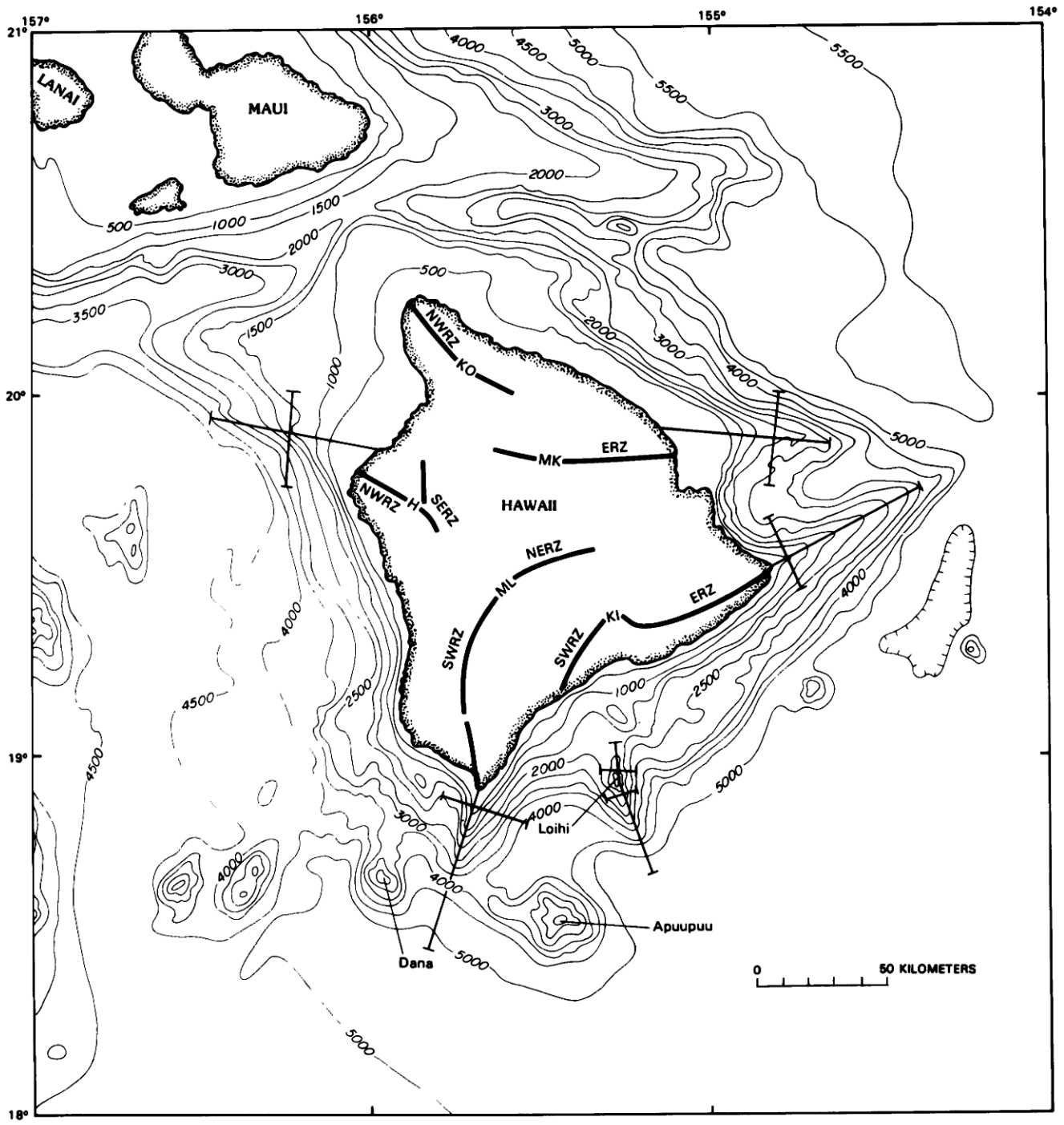

FIGURE 5.2.—Island of Hawaii showing 500-m submarine contours (from Wilde and others, 1980), traces of principal subaerial rift zones from each volcano, and locations of profiles shown in figures 5.3 and 5.4. Volcanoes: KI, Kilauea; ML, Mauna Loa; H, Hualalai; MK, Mauna Kea; KO, Kohala. NWRZ, northwest rift zone; SWRZ, southwest rift zone; SERZ, southeast rift zone; ERZ, east rift zone; NERZ, northeast rift zone.

Seamount to the south and Mauna Loa's southwest rift zone to the north and west, and its evolution and growth have thus been hindered. As a result, the southwest rift zone of Kilauea is rather short (~25 km, on land) and has no substantive morphologic expression on the sea floor south of Hawaii (see Fornari and Campbell, Chapter 4). Fiske and Jackson (1972) have pointed out that a basic understanding of the temporal and spatial growth of individual volcanoes within a composite shield can be achieved by

studying the lengths and relative positions of each volcano's rift zones.

SUBMARINE PORTIONS

PUNA RIDGE

Surface ship studies (Malahoff and McCoy, 1967; Moore and Fiske, 1969) and submersible investigations (Fornari and others, 1978) have shown that Puna Ridge (the submarine continuation of Kilauea's east rift zone; figures 5.1, 5.2) consists of purely constructional volcanic terrain on its crest and upper flanks. This terrain is characterized by steep flow-front escarpments separated by constructional benches on the upper flanks and narrow, linear volcanic ridges (pillow walls) and subparallel tensional and eruptive fissures on the ridge crest. All these features strike N. 45° E., parallel to the trend of the ridge (Fornari and others, 1978). The flank and ridge-crest terrains differ significantly. At the ridge crest there is an almost total absence of sediment and a dominance of constructional volcanic features. The flank areas, in contrast, have progressively more sediment with increasing depth, extrusive features that appear slightly more weathered and older (glassy crusts on extrusive forms that are starting to devitrify and spall off), and more common evidence of contemporary faulting and disruption of the volcanic sea floor. On the southern flank of Puna Ridge, at depths shallower than about 500 m, there are southeast-dipping normal faults that appear to be continuations of fault-line scarps of the Hilina fault system (fig. 5.1; Malahoff and McCoy, 1967). The subaerial Hilina scarps represent headwalls of major landslide blocks (Swanson and others, 1976), and the shallow submarine scarps probably also reflect lateral, slump-block readjustment of the unbuttressed flank of Kilauea caused by magma injection and dilation.

The slumping and mass-wasting that affects Hawaii's south flank leads to a fault-block-like submarine topography having alternating linear highs and lows that generally trend in a northeast direction. One major result of the tectonic and erosional processes is the redeposition of large quantities of sediment on the lower south flank of Puna Ridge and on the island's submarine south flank. This sediment is augmented by coarse basaltic debris derived through wave erosion of lava flows along the south coast and by the downslope transport of this material by tidal currents and debris flows and slides such as the Papau slide (Moore and Fiske, 1969; Fornari and others, 1979c).

MAUNA LOA'S SOUTHWEST RIFT ZONE

The southwest rift zone of Mauna Loa (figs. 5.1, 5.2) has also been investigated by submersibles and by remote-sensing from surface ships. Geophysical data show the gross structure of the rift as a series of scarps with steep west-facing walls that have vertical relief of 100 m to nearly 2,000 m (Fornari and others, 1979b). The principal linear scarp continues out to sea for about 50 km, and its asymmetric and faulted morphology has been interpreted to be a result of gravitational slumping of the unbuttressed west flank of Mauna Loa (Fornari and Campbell, chapter 4; Fornari and others, 1979b; Normark and others, 1979; Lipman, 1980a). The face of this scarp was acsended on three submersible dives and found to be composed of pillow-lava sequences, exposed in steeply (60°–70°) sloping outcrops and surrounded by volcaniclastic sediment. Less steep benches (10°–30° slopes) separate the outcrops. The tops of the outcrops are often capped by vertical walls, 1–3 m wide and 10–60 m high, formed by exposed dikes that have been stripped of their surrounding volcanic cover (Fornari and others, 1979b, fig. 6). Mass wasting of scarps must be very active because the steeply sloping outcrops and vertical dikes are highly unstable and prone to collapse. During the dives, extensive evidence of undercutting and erosion was seen in the form of toppled dike walls and faceted blocks of diabase dike rock strewn around the sea floor at the base of the walls and on the sediment (Fornari and others, 1979b).

Geophysical records of the sea floor to the west of the main scarp (Fornari and others, 1979b, fig. 4) suggest that thick deposits of clastic sediment lie in structural fault-bounded basins created by gravitational slump tectonics. Farther offshore, along the southern part of Hawaii's west coast, similar large slump-block features (for example, the Kauna and Alika slides) have been recognized on bathymetric compilations and geophysical records (Fornari and Campbell, chapter 4; Normark and others, 1979).

HUALALAI'S NORTHWEST RIFT ZONE

The submarine extension of Hualalai's northwest rift zone (figs. 5.1, 5.2) has been previously studied using conventional echo sounding (Campbell and Erlandson, 1981), dredging (Clague, 1982), and submersible diving (Schwartz and Fornari, 1982). These studies revealed the gross bathymetric character of the rift, the morphology and structure of parts of the submarine slope, and also determined that the exposed volcanic rocks are largely tholeiite and picritic, tholeiitic pillow basalt. The geochemistry of these rocks indicate that they have probably been derived from mantle sources separate from those feeding the other volcanoes on Hawaii (Clague, 1982).

The northern submarine flank of the rift zone has a regional slope of 3°–7° (the Puna Ridge has an average slope of 10°; Moore, 1971) and rugged topography created by constructional volcanism operating principally on the crest and north flank of the rift (Campbell and Erlandson, 1981). The data of Campbell and Erlandson (1981) clearly show that volcanic flows coming from the north flank are ponded against the preexisting terrace topography of the Kohala shelf.

The south flank of the rift zone, as seen in profile C of Campbell and Erlandson (1981, fig. 4) and in unpublished profiles recorded by the Hawaii Institute of Geophysics, differs from the north flank in having a steeper regional slope (16°–26°) and smoother acoustic reflectivity with fewer hyperbolae.

The southeastern part of the rift zone's south flank forms the submarine slope west of Keahole Point (figs. 5.1, 5.2) and has been observed during three previously reported DSV *Turtle* dives (Fornari, 1982). This area has microtopographic relief of 1–3 m; however, at shallower depths (less than 300 m) the outcrops have relief of as much as 7 m. Much of this relief is created by the downslope ends or edges of subaerially derived lava flows. Average slope

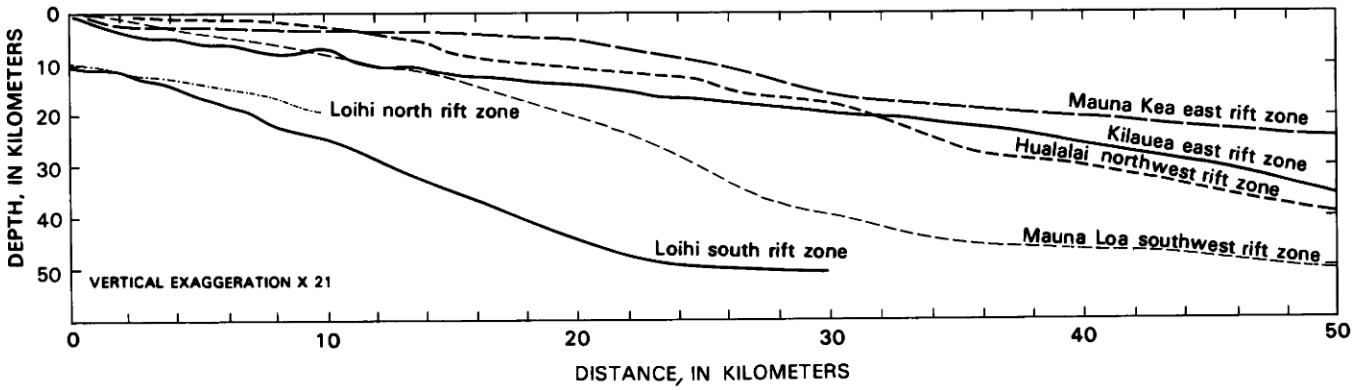

FIGURE 5.3.—Profiles of Hawaiian submarine rift zones taken along their strike. Drawn from published bathymetric maps (see references in text) and plotted following the axis of minimum depth of each rift. Data points were taken every 100 m of depth change. Horizontal distance is from the shoreline except for Loihi's rifts. Profile locations shown on figure 5.2.

angles for various segments of each dive traverse show that an abrupt increase in slope from approximately 15° to 27° occurs at about 750 m depth. This depth roughly conforms to the upslope onset of a ridge-and-gully terrain that is the principal sea-floor morphology in this area and apparently also occurs in similar depth ranges on other Hawaiian submarine slopes investigated with submersibles. The ridges and gullies are oriented parallel to the slope and usually have relief of 1–5 m (amplitude) and varied wavelengths. These features are likely to represent consequent topography developed over buried flow lobes (probably subaerial ones that have since subsided, although some may have originated from shallow submarine vents), which have subsequently served to channel tidal scouring in between the highs, thereby maintaining the troughs while sediment continued to accumulate on the low ridges.

This slope transition may be the result of basement faults, now largely buried, associated with earlier episodes of gravitational slumping of the west flank of Hualalai and its northwest rift zone. Only small fault scarps were observed during the submersible dives in this area, however, and those scarps are largely confined to depths below 1,000 m and have relief of 3–6 m. The scarp faces are smooth, in contrast to the rough, jagged flow fronts, and expose massive lava with occasional intercalations of carbonate, either as blocks or lenses several tens of centimeters thick (Fornari, 1982; Schwartz and Fornari, 1982). Alternatively, this slope change may reflect the general paleodepth to which subaerial flows were able to move. Historical subaerial flows (ranging in date from 1801 to 1950) that have flowed into the sea on the west flank of Hawaii have been mapped using a submersible, and they are known to have only reached depths of approximately 250 m (D.J. Fornari and M.R. Perfit, unpublished data).

Wide expanses of the sea floor in this area are covered by volcanic and carbonate clastic debris and sediment. These deposits bury most evidence of flow fronts and fault scarps; however, several southwest-facing ramps with 5–10 m of relief were traversed and are thought to have been formed by depositional draping over a preexisting basement structure. Much of the area examined during the dives between depths of 350 m and 1,000 m is covered by these clastic deposits. South of latitude 19° 48′ N. and below 1,500 m depth, the spacing between isobaths increases and the regional slope decreases to about 10° (fig. 5.2).

Extrapolation of dive observations, echo sounding, and bathymetric data indicate that the lower south flank of Hualalai's northwest rift zone is largely covered by volcanic and carbonate erosional debris and hemipelagic sediment. The net geomorphic effect has been to smooth and obscure nearly all of the constructional volcanic morphology through mass-wasting of flow fronts and scarp faces, resulting in deposition of talus and in downslope transport of erosional products. While indications of downslope movement of talus are present, no slump scars or discrete slump deposits were observed during the *Turtle* dives. The north flank of Hualalai's northwest rift zone, on the other hand, consists primarily of pillow lava and constructional volcanic topography that is variably covered by hemipelagic sediment.

DISCUSSION

Profiles drawn along the strike and across strike of several Hawaiian submarine rift zones are shown in figures 5.3 and 5.4, respectively. These profiles were constructed from 100-m bathymetric contour data (Chase and others, 1971; Moore, 1971; Wilde and others, 1980; Campbell and Erlandson, 1981; Malahoff and others, 1982; Moore and others, 1982). The differences between rift-zone profiles can largely be explained by age differences and differences in structural evolution. The profiles shown in figure 5.3 clearly show the differences in plunge angle as well as the localized effects of constructional volcanism along the crests of the youngest rifts (Puna Ridge and Loihi Seamount's north and south rifts).

The profile of Mauna Kea's east rift zone shows the effects of the carbonate reef buildup that has constructed a 20-km-wide shelf

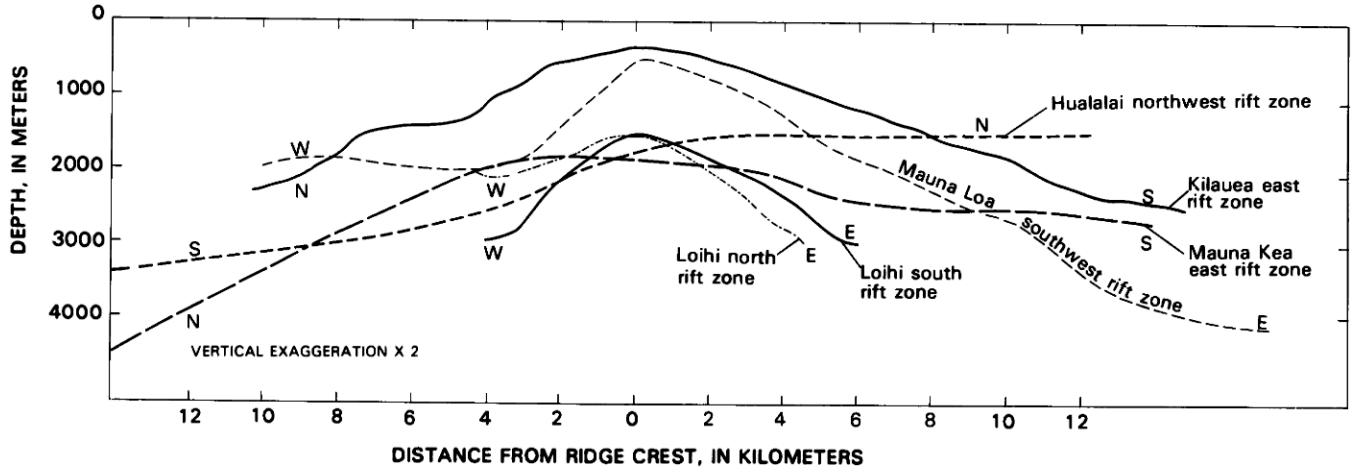

FIGURE 5.4.—Profiles of Hawaiian submarine rift zones taken across their strike. Drawn from same data set used in figure 5.3. Horizontal distance is centered on the topographic crest of each rift. Profile locations shown in figure 5.2. Approximate compass orientations of profiles indicated by labels on ends (N, north; E, east; S, south; W, west).

over the nearshore segment of this rift. Because volcanic activity has been absent along this rift for tens of thousands of years, the rough constructional topography of the rift has been buried by clastic and hemipelagic sediment and a coralline mantle. Mauna Kea's east rift zone shows two prominent slope transitions. The shallower one reflects the change from carbonate platform to a steeper slope that probably more closely reflects the original constructional rift slope. Farther seaward, the slope of the rift axis decreases abruptly about 30 km from the shoreline and then continues at this lower value past the end of the profile shown in figure 5.3. If the profile were extended (see fig. 5.2 for contours), one would see that Mauna Kea's profile consists of several steeper sections separated by wide, lower gradient benches that eventually merge onto the abyssal sea floor at approximately 5 km depth. This characteristic old-rift topography is similar to that of Hualalai's northwest rift zone, although the steeper ramp sections are smaller on Hualalai, possibly reflecting the smaller size of Hualalai Volcano compared to Mauna Kea.

Hualalai's northwest rift zone has a slightly steeper profile than Mauna Kea's east rift zone, but it also shows the effects of reef growth and carbonate terrace development. Along Hualalai's rift the terrace extends about 8 km from the shoreline; however, the Kohala terrace to the north is a much broader feature, whose morphology and development reflect the extended period of volcanic quiescence along the northwest coast of Hawaii and the older age of this portion of the island (Campbell and Erlandson, 1981). Hualalai's rift profile also appears rather smooth; but this is most likely a result of the use of wide-beam echo sounders to survey this area. A detailed inspection of echo-sounder records from the crest of Hualalai's northwest rift zone shows an abundance of overlapping hyperbolae suggestive of constructional volcanic sea floor (Campbell and Erlandson, 1981).

Mauna Loa's southwest rift zone also has a smooth profile, but its regional slope is greater than that of all other rifts except Loihi's (fig. 5.2). The smoothness of this profile does reflect a general absence of recent constructional volcanism on the rift-zone crest; however, young-looking volcanic flow fronts and outcrops are present on the west flank of the rift (Fornari and others, 1979b). The absence of a carbonate shelf on Mauna Loa's southwest rift zone indicates that this part of the island is still too young (volcanically active) and gravitationally unstable to allow carbonate reef terraces to grow and develop.

Kilauea's east rift zone (Puna Ridge) shows much more local irregularity than do the rifts of Mauna Kea, Hualalai, and Mauna Loa (fig. 5.3), undoubtedly because it is linked to the most active volcano and subaerial rift zone on Hawaii. Because of its young age, Puna Ridge does not possess a carbonate terrace (fig. 5.3). The rather constant gradient of this rift zone out to 50 km from shore and its greater elevation above the surrounding sea floor (for corresponding distances from shore) compared to Mauna Loa's southwest rift zone, probably result from the buoyant effects of magma intrusion and lack of subsidence, similar to the manner in which the crest of the East Pacific Rise is supported and elevated by accretionary magmatism (see Macdonald and others, 1984, and references therein).

Loihi Seamount's north and south rift zones are excellent examples of juvenile Hawaiian submarine rift zones. Both have steep plunge angles and local topographic roughness created by constructional volcanism on the rift crests. The north rift is not as steep as the south rift because of the constraining effects of Kilauea's south flank and southwest rift on its development. The crests of Loihi's rifts are known from deep-sea photography (Malahoff and others, 1982) to consist of pillow-lava flows, while the flanks of the rift zones and much of the volcano sides are covered with coarse pillow-lava talus.

Profiles across the strikes of these Hawaiian rifts are shown in figure 5.4. The most important feature of these profiles is the

consistently asymmetric character of the rifts. In all cases the rift flank that is not buttressed is steeper, indicating that gravitational slumping of rift flanks fundamentally alters the geometry of a rift zone. As exemplified by Loihi Seamount's rifts, this process is initiated at a very early stage in a rift zone's growth and continues through the volcano's early-mature stage of development.

Hence, Hawaiian rift zones initially develop and grow purely through constructional volcanism; however, early in the rift zone's active life the influence of adjacent volcanoes on its growth becomes important. The following model illustrates the importance of gravitational slumping and preexisting volcano location to the development of rift zones and volcano flank morphology and structure. In addition, this model offers an explanation for the absence of large-scale gravitational slumps on the west flank of Mauna Loa north of approximately latitude 19° 30′ N.

Fiske and Jackson (1972), who used the gravity data of Kinoshita and others (1963) to support their thesis, suggested that Hualalai's southeast rift zone has played a dominant role in the construction of the original Hualalai edifice, much of which is now buried beneath the flank of Mauna Loa (fig. 5.1, 5.2). The Bouguer gravity map of Hawaii (Kinoshita and others, 1963) shows an elongate north-south gravity high (265 mGal closed contour) that continues south of the surficial boundary between Hualalai and Mauna Loa and reaches latitude 19° 25′ N (fig. 5.1). South of the summit of Hualalai, the gravity high is west of the surface position of the rift zone, and the gravity maximum is the lowest of the five gravity highs on the island. This may be in part because the dense dike rocks are buried under 1–2 km of Mauna Loa lava and clastic deposits. The location of the gravity high, offset to the west with respect to the present surface rift, is still within the 12- to 17-km width of the dike complex proposed by Broyles and others (1979). However, the buttressing of Mauna Loa's west flank (see Lipman, 1980a, b) would lead one to expect the surface rift to lie west of the gravity high, in the direction that can most easily accommodate extensional tectonics because it is not buttressed.

I suggest that the dike complex under Hualalai's gravity high is a foundation that buttresses the northern part of the west flank of Mauna Loa. Deep-seated gravitational slumping on the west flank of Mauna Loa is, therefore, restricted to the area south of the end of the gravity high (approximate latitude 19° 25′ N. fig. 5.1). The extension of the Kealakekua fault north of latitude 19° 25′ N. may represent gravitational slump-block failure (Normark and others, 1979; Lipman, 1980a) of just the upper few kilometers of Mauna Loa's west flank that are unbuttressed by Hualalai's southern rift dike complex. In addition, the abrupt development of a carbonate terrace north of latitude 19° 30′ N. (fig. 5.2) probably results partially from the relative stability and low rate of volcanic activity along Hualalai's west flank as compared to Mauna Loa's gravitationally unstable west flank south of Kealakekua Bay.

CONCLUSION

There are several morphologic similarities between the youthful Puna Ridge and Hualalai's older northwest rift zone. Echo reflection characteristics and data from dives and dredges in the summit areas of both rifts reveal a predominance of fresh pillow lava and constructional morphology on the ridge crests. The unbuttressed south flanks of both rifts are mantled by volcaniclastic deposits resulting from mass wasting of constructional topography and from gravitational slumping. The latter process has disrupted the constructional slopes and widened the bases of the topographic ridges.

Because these two rifts are near opposite ends of the age spectrum for the Island of Hawaii, it is apparent that the processes of constructional volcanism (centered on a line source along the rift axis) and mass wasting of the unbuttressed rift flank are fundamental to the evolution of submarine rift-zone morphology and structure. The principal difference between Hualalai's northwest rift zone and Puna Ridge is the nearly complete burial of the headwalls of slump blocks on Hualalai's rift by subsequent volcaniclastic deposits that cover nearly all of the original constructional relief and fault scarps.

The morphology and structure of the submarine continuation of Mauna Loa's southwest rift zone are quite different from those of Puna Ridge and of Hualalai's northwest rift zone. The unbuttressed west flank of the southwest rift is very unstable at this stage in Mauna Loa's shield-building history, and gravitational slumping has created a prominent asymmetric scarp topography rather than a more symmetric constructional rift topography (fig. 5.4). The large vertical offsets and horizontal extent of the slumping indicate that this reconfiguration of the cross-sectional and plan-view structure and morphology of the rift zone is deep seated and extends well down into the volcanic pile. The abundance of these large-scale gravitational slump features (for example, Kauna and southwest rift slides) on the west flank of Mauna Loa attests to the predominance of this process during the mature phase of shield building (Fornari and Campbell, chapter 4). The size of gravitational slumps on volcano flanks is probably controlled by edifice size and by the constraining influence of adjacent volcanoes, which act to buttress parts of the volcanic pile.

The structure and morphology of Hawaiian submarine rift zones are primarily the result of a time-integrated sequence of volcanic constructional processes and gravitational tectonics. Initially constructional volcanism dominates, although parts of a rift may begin to be modified by gravitational slumping even during the juvenile stage. Early in a volcano's mature shield-building stage, however, the instability of the subaerial shield (whose foundation is the clastic volcanic sequences laid down during the volcano's emergence) results in the dominance of destructional gravitational slumping over constructional processes and the drastic reshaping of the submarine rift. At a still later date the combined effects of repeated slumping, minor renewed volcanism, the possible growth of a new volcano nearby, subsidence of the island, and development of a carbonate reef terrace result in a mature submarine rift like that of Mauna Kea's east rift zone or Hualalai's northwest rift zone.

REFERENCES CITED

Broyles, M.L., Suyenaga, W., and Furumoto, A.S., 1979, Structure of the lower east rift zone of Kilauea Volcano, Hawaii, from seismic and gravity data: Journal of Volcanology and Geothermal Research, v. 5, p. 317–336.

Campbell, J.F., and Erlandson, D.L., 1981, Geology of Kohala submarine terrace, Hawaii: Marine Geology, v. 4, p. 63–72.

Chase, T.E., Menard, H.W., and Mammerickx, J., 1971, Bathymetric atlas of the north-central Pacific: Washington, D.C., U.S. Naval Oceanographic Office, H.O. Publication 1302.

Clague, D.A., 1982, Petrology of tholeiitic basalt dredged from Hualalai Volcano, Hawaii [abs.]: Eos (Transactions of the American Geophysical Union),v. 63, no. 45, p. 1138.

Clague, D.A., Jackson, E.D. and Wright, T.W, 1980, Petrology of Hualalai Volcano, Hawaii: implication for mantle composition: Bulletin Volcanologique , v. 43-4, p. 641–656.

Fiske, R.S., and Jackson, E.D., 1972, Orientation and growth of Hawaiian rifts: the effects of regional structure and gravitational stresses: Proceedings of the Royal Society of London, Series A., v. 329, p. 299–326.

Fornari, D.J., Malahoff, A., and Heezen, B.C., 1978, Volcanic structure of the crest of the Puna Ridge, Hawaii: geophysical implications of submarine volcanic terrain: Geological Society of America Bulleltin, v. 89, p. 605–616.

———1979a, Submarine slope micromorphology and volcanic substructure of the Island of Hawaii inferred from visual observations made from U.S. Navy deep-submergence vehicle (DSV) *Sea Cliff*: Marine Geology, v. 32, p. 1–20.

———1979b, Submarine extension of the southwest rift zone of Mauna Loa Volcano, Hawaii: visual observations from U.S. Navy deep submergence vehicle DSV *Sea Cliff*: Geological Society of America Bulletin, v. 90, p. 435–443.

Fornari, D.J., Moore, J.G., and Calk, L., 1979c, A large submarine sand-rubble flow on Kilauea Volcano, Hawaii: Journal of Volcanology and Geothermal Research, v., 5, p. 239–256.

Fornari, D.J., 1982, DSV *Turtle* dives off Keahole Point, Hawaii, geological investigations of submarine slope micromorphology: baseline studies to assist in future OTEC cold-water pipe designs and deployments: Rockwell International Energy Systems Group Technical Report, Canoga Park, Ca.

Kinoshita, W.T., Krivoy, H.L., Mabey, D.R., and MacDonald, R.R., 1963, Gravity survey of the Island of Hawaii: U.S. Geological Survey Professional Paper 475–C, p. 114–116.

Lipman, P., 1980a, The southwest rift zone of Mauna Loa: implications for structural evolution of Hawaiian volcanoes: American Journal of Science, v. 280-A, p. 752–776.

———1980b, Rates of volcanic activity along the southwest rift zone of Mauna Loa Volcano, Hawaii: Bulletin Volcanologique, v. 43-4, p. 703–725.

Macdonald, G.A., and Abbott, A.T., 1970, Volcanoes in the Sea—the geology of Hawaii: Honolulu, University of Hawaii Press, 441 p.

Macdonald, K., Sempere, J-C., and Fox, P.J., 1984, East Pacific Rise from Siqueiros to Orozco fracture zones: Along-strike continuity of axial neovolcanic zone and structure and evolution of overlapping spreading centers: Journnal of Geophysical Research, v. 89, p. 6049–6069 and p. 6301–6305.

Malahoff, A., and McCoy, 1967, The geologic structure of the Puna submarine ridge: Journal of Geophysical Research, v. 72, p. 541–548.

Malahoff, A., McMurtry, G., Wiltshire, J., and Yeh, H., 1982, Geology and chemistry of hydrothermal deposits from active submarine volcano Loihi, Hawaii: Nature, no. 298, p. 234–239.

Malahoff, A., and Woollard, G.P., 1968, Magnetic and tectonic trends over the Hawaiian Ridge, *in* Knopoff, L., Drake, C.L., and Hart, P.J., eds., The crust and upper mantle of the Pacific area: American Geophysical Union Monograph no. 12, p. 241–276.

Moore, J.G., 1971, Bathymetry and geology—east cape of Hawaii: U.S. Geological Survey Miscellaneous Geological Investigations Map, I–677, scale 1:62,500.

Moore, J.G., Clague, D., and Normark, W. R., 1982, Diverse basalt types from Loihi Seamount, Hawaii: Geology, v. 10, p. 88–92.

Moore, J.G., and Fiske, R.S., 1969, Volcanic substructure inferred from dredge samples and ocean bottom photographs: Geological Society of America Bulletin, v, 88, p. 1191–1202.

Normark, W.R., Lipman, P., and Moore, J.G., 1979, Regional slump structures on the west flank of Mauna Loa Volcano, Hawaii [abs.]: Hawaii Symposium on Intraplate and Submarine Volcanoes, Abstract volume, p. 172.

Ryan, M.P., Koyanagi, R.Y., and Fiske, R.S., 1981, Modeling the three-dimensional structure of macroscopic magma transport systems: applications to Kilauea, Hawaii: Journal of Geophysical Research, v. 86, p. 7111–7129.

Schwartz, D., and Fornari, D.J., 1982, Submersible investigations of the northwest rift zone of Hualalai Volcano, Hawaii: Eos (Transactions of the American Geophysical Union), v. 63, p. 1138.

Stearns, H.T., and Macdonald, G.A., 1946, Geology and groundwater resources of the Island of Hawaii: Hawaii Division of Hydrography Bulletin, v. 9, 363 p.

Swanson, D.A., Duffield, W.A., and Fiske, R.S., 1976, Displacement of the south flank of Kilauea Volcano: the result of forceful intrusion of magma into the rift zones: U.S. Geological Survey Professional Paper 963, 39 p.

Wilde, P., Chase, T.E., Normark, W.R., Thomas, J.A., and Young, J.D., 1980, Oceanographic data off the southern Hawaiian Islands: Berkeley, University of California, Lawrence Berkeley Laboratory, LBL Publication 359.

GEOLOGY OF THE SUMMIT OF LOIHI SUBMARINE VOLCANO

By Alexander Malahoff[1]

ABSTRACT

Loihi submarine volcano is a seismically active seamount whose summit is at a water depth of 969 m (530 fathoms), 28 km (15 miles) southeast of the Island of Hawaii at 18°56′ N., 155°15.9′ E. Loihi is on the southernmost extension of the Kahoolawe-Hualalai-Mauna Loa volcanic line and probably marks the latest activity of the Hawaiian hot spot. The base of the volcanic edifice is 4,023 m (2,200 fathoms) below sea level. Loihi has formed through periodic volcanism along a northwest- to southeast-striking 31-km-long rift. High-resolution, shipboard hydrographic survey techniques supplemented by narrow, multibeam acoustic bottom surveys were followed by transponder-navigated bottom photography and ocean-floor dredge sampling. The combined data have produced a detailed picture of an emerging Pacific island. The summit of the volcano contains a calderalike depression 2.8 km wide and 3.7 km long with steep inner and outer walls. Within the depression, there are two pit craters; one is 0.6 km in diameter and 73 m deep, the other is 1.2 km in diameter and 146 m deep.

Shipboard and aeromagnetic studies show the presence of a 3,900-nT peak-to-peak normal bipole residual magnetic anomaly over its edifice. Superposed upon the normally polarized anomaly is a short wavelength, reversely polarized anomaly with peak-to-peak amplitude of 1,600 nT located directly over the summit of Loihi. Modeling of the reversely polarized anomaly suggests the source to be a nonmagnetic body, possibly a near-surface magma chamber below the summit of Loihi. Extensive bottom photography shows newly formed, glass-encrusted lava flows with pillow, sheet, lobate and aa forms erupted along the southeast slopes of the summit. The slopes of the volcano show evidence of recent, large-scale landslides that have scarred the volcano along its eastern and western slopes. Along the eastern edges of the summit depression, photographs show the presence of both hydrothermal activity and mineral precipitation with chimney forms similar to those mapped along the active rift systems of the East Pacific Rise and the Juan de Fuca Ridge. Orange to yellow iron-rich precipitates mark extensive hydrothermal vents around the central calderalike depression where water temperature anomalies in excess of several degrees Celsius have been detected. No exotic, hydrothermally associated, benthic animal communities have been detected in the present study. Photographic evidence suggests that forms of hydrothermal metallic precipitates found on Loihi may be similar to those found along the East Pacific Rise and that similar precipitates may be found at depths on other seamounts and volcanic islands.

INTRODUCTION

Loihi Seamount is a young (probably less than 0.5 Ma), active, submarine volcano on the southern extension of the Hawaiian hot spot (Jackson and others, 1972) along the Kahoolawe-Hualalai-Mauna Loa volcanic line; it is the youngest volcano in the Hawaiian Island chain and is the possible site for the next emerging island (fig. 6.1). The name Loihi, meaning long in Hawaiian, was first introduced by Emery (1955) to explain the elongate shape of the seamount. Loihi is seismically active, with shallow earthquake swarms that are distinct from the seismic activity of Kilauea (Klein, 1982), the nearest active volcano. A zone of deep earthquakes at a depth of 60 km between Kilauea, Loihi and Mauna Loa suggest a common deep source for the magma supply of the three volcanoes from the Hawaiian hot spot. Petrologic studies of basalt dredged from the volcanic edifice by Moore and others (1982) show these rocks to be glassy, tholeiitic pillow basalt, tholeiitic-alkalic transitional basalt, alkali basalt, and basanite. Most of the rocks sampled from the summit appear to be weakly vesicular, suggesting the possibility of mild explosive activity at the summit of Loihi (Moore and others, 1982). Extensive bottom photography and photointerpretation of surficial geology were performed by the author using the Woods Hole Oceanographic Institution's underwater camera system (ANGUS) deployed from the research vessel *Kana Keoki*. These data show the presence of fresh pillow lava, fresh sheet and lobate flows, and fresh aa and pahoehoe flows emerging from the summit of Loihi. Bottom transponder-controlled dredging (shipboard) of prospective hydrothermal deposit sites on the summit showed the presence of copper-enriched nontronite deposits (Malahoff and others, 1982). The nontronite was identified using bottom photography. The deposits were found to be associated with the freshest lava flows at several sites near the summit.

In order to map Loihi submarine volcano, detailed high-resolution bathymetric surveys were conducted over its summit by the National Oceanic and Atmospheric Administration (NOAA) vessels *Fairweather* and *Rainier*. The bathymetric surveys used shipboard traverses spaced 400 to 800 m apart. Navigation was by miniranger, with the network tied to the old Hawaiian datum. The details of the summit crater bathymetry were also mapped using the

[1]Department of Oceanography and Hawaii Institute of Geophysics, University of Hawaii, Honolulu, Hawaii 96822.

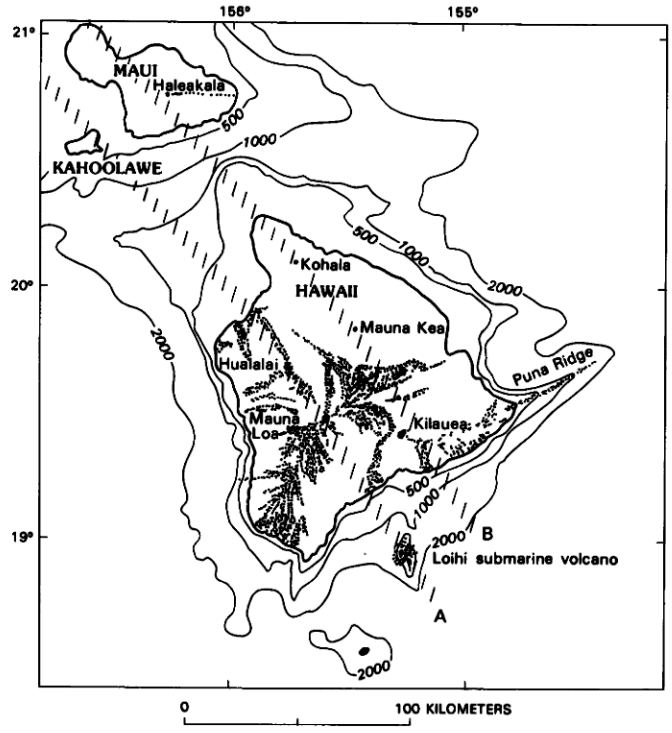

FIGURE 6.1.—Location of twin traces (hachures) of the Hawaiian hot spot showing Loihi submarine volcano at south end of Kahoolawe-Hualalai-Mauna Loa-Loihi trace (A), and the Haleakala-Kohala-Mauna Kea-Kilauea trace (B). Historical Hawaiian lava flows shown by dotted pattern. Bathymetric contours are in meters.

acoustic transponder and altimeter on the ANGUS photographic system. Bathymetric details of the whole volcanic edifice (see fig. 6.3) were determined through a U.S. Navy-conducted, high-resolution, narrow-beam, 64-beam Sonar Array Survey System (SASS) aboard the U.S. Navy (USN) ship *Hess*. All surveys were performed between 1978 and 1981. The depths for both the NOAA and the USN bathymetric surveys were plotted using fathoms as the depth unit. Airborne magnetic studies of Loihi were performed earlier by Malahoff and Woollard (1968, 1970) and were supplemented by shipboard magnetic traverses by vessels of the Hawaii Institute of Geophysics. This paper focuses on the surficial morphology and structure of Loihi as an example of the early stages of the structural development of a Hawaiian island as a submarine volcano.

ACKNOWLEDGMENTS

The research described in this paper was supported by funding from the National Ocean Survey (NOS) of the National Oceanic and Atmospheric Administration (NOAA). The United States Navy provided ship time aboard the USN ship *Hess* to conduct the multibeam, narrow-beam surveys over the flanks of Loihi. The bottom photographic surveys were performed by the ANGUS group of the Woods Hole Oceanographic Institution in October 1980 aboard the University of Hawaii's research vessel *Kana Keoki*. It was through the dedication and professionalism of the ANGUS team that such excellent photographic data were obtained during adverse weather conditions. I would like to thank Dr. Frisbee J. Campbell of the Hawaii Institute of Geophysics, University of Hawaii, and Captain William King of the research vessel *Kana Keoki* for their assistance in organizing the shipboard operations, and also the commanding officers of the NOAA ships *Rainier* and *Fairweather* for the excellent hydrographic coverage obtained over the summit of Loihi. I am grateful for the assistance and discussions offered during the cruise by Dr. Stephen Hammond and Dr. Robin Holcomb, for critical reviews of this paper by Dr. Gary McMurtry, and also for the help of Ms. Cheryl Komenaka in the preparation and compilation of the manuscript.

MORPHOLOGY OF THE VOLCANIC EDIFICE

Loihi is on the eastern flank of the southern extension of Mauna Loa volcano (fig. 6.1). Its northern base is 1,900 m below sea level, whereas the southern base is 4,755 m below sea level, showing that the edifice of Loihi was built on an original submarine slope of about 5°. The volcano apparently grows through continued volcanism, not only from a caldera or summit craters, but also from an elongate rift system consisting of a 17-km-long southern rift limb and a 7-km-long northern rift limb (fig. 6.2). The Loihi rift and crater system is not unlike those for the summits of the neighboring Mauna Loa and Kilauea Volcanoes.

The steepness of the southwestern and northeastern slopes of the volcano (35° to 40° between the water depths of 1,830 and 3,290 m) and the presence of armchairlike indentations into the edifice (at 155°14′ W., 18°47.5′ N., at 155°17.5′ W., 18°52.5′ N. and at 155°15′ W., 18°57.5′ N.) suggest that extensive erosion in the form of downslope mass wasting has occurred contemporaneously with the growth of the edifice by submarine volcanism. Bottom photographs of the upper flanks of Loihi show the development of talus slopes through the breakup of pillow basalt and sheet and lobate flows. The sheet and lobate flows frequently exhibit the photographic characteristics of pahoehoe and aa lava at the summit. The shaded areas in figure 6.2 indicate sites of talus slope and downslope mass wasting as interpreted from the study of bottom photography and bathymetry. Examination of the bathymetric data does not show the presence of any extensive flank cones on Loihi. This evidence, however, does not preclude the possible presence of flank fissures. The process of talus generation and downslope mass wasting appears to be steady and extensive. Therefore, the upward growth of the volcano is dependent upon a constant source of extrusive magma from the summit crater and the upper rift zones.

The detailed bathymetric map of the Loihi summit (fig. 6.3) was prepared from the total bathymetric data base, including the NOAA hydrographic survey, the Woods Hole Oceanographic Institution ANGUS camera data, and the USN SASS surveys. The combined bathymetric data suggest that the summit of Loihi has an oval configuration with the long axis parallel to the rift zone. A summit depression about 2,800 m wide and 3,700 m long appears

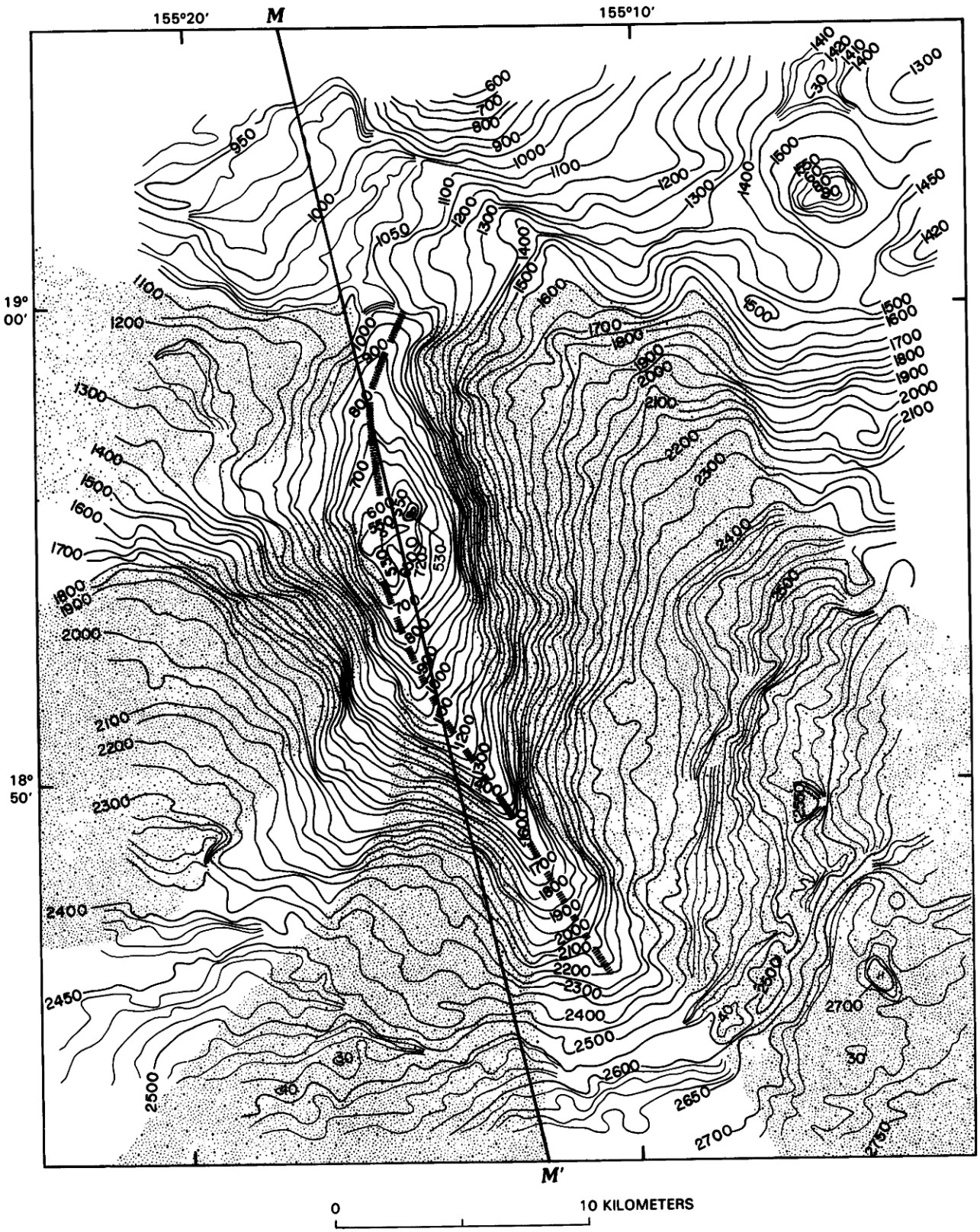

FIGURE 6.2.—Bathymetric map of Loihi, constructed from narrow-beam, multibeam surveys carried out aboard the U.S. Navy ship *Hess*. Water depth in fathoms (1 fathom = 1.83 m). Dotted pattern shows flanks of volcano that may have been subjected to mass wasting and talus formation. Heavy hachured line indicates the location of north and southeast rift zones of Loihi. Profile *M–M'* refers to figure 6.6.

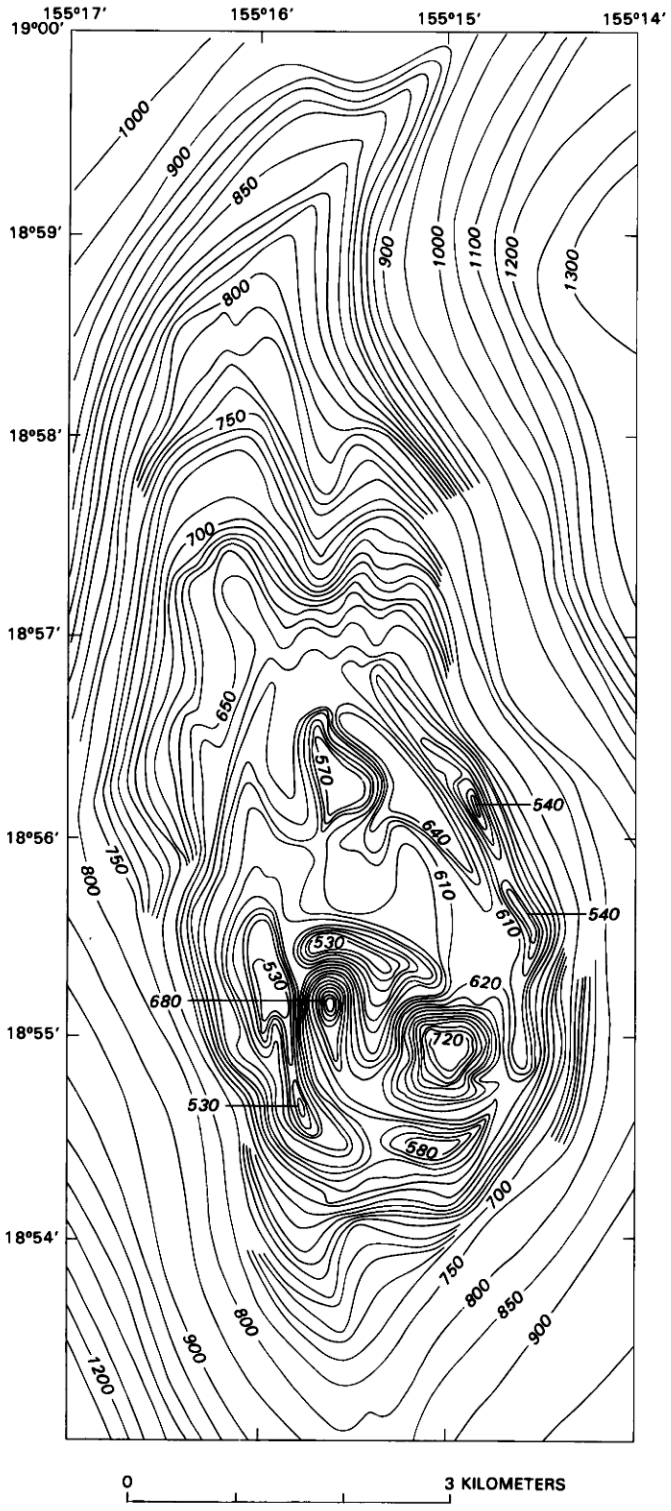

FIGURE 6.3.—Detailed bathymetric map in fathoms of summit area of Loihi, drawn from narrow-beam, multibeam surveys by the U.S. Navy ship *Hess* and narrow-beam surveys over summit area by the NOAA ships *Fairweather* and *Rainier*. Contour interval: 10 fathoms at summit and 50 fathoms on flanks.

to be structurally offset to the east of the north-south rift system. This depression, possibly a summit caldera, is approximately 128 m deep from rim to floor. The shallowest point along the rim is 969 m below sea level. Two pit craters within the caldera-like depression are 73 and 146 m deep. The Loihi summit depression may be a young caldera similar in its geologic structure to that of Kilauea caldera. Macdonald and Abbott (1970) suggest that the development of a caldera in a developing Hawaiian volcano, such as Kilauea, could begin early in the life of the volcanic edifice, which could be the case for young submarine volcanoes such as Loihi.

The geographic proximity of Kilauea and Loihi and the common deep magmatic source (Klein, 1982) suggest that both Kilauea and Loihi are in their early stages of edifice development. Indeed, the location and size of Loihi indicate that it may, in fact, be the youngest Hawaiian volcano. Therefore, the Loihi summit may be undergoing periods of swelling and shrinking as a result of shallow magmatic injection and removal through flank eruptions, similar to those that occur at Kilauea. Such magmatic processes could result in the formation of a subsidence caldera on Loihi. The summit depression of Loihi is surrounded by an oval ring of bathymetric highs (fig. 6.3) that could mark the outer rim of the caldera. Alternatively, the bathymetric highs could also mark a ring of individual volcanic cones or vents on the summit. A physiographic diagram of the summit of Loihi, based upon the high-resolution bathymetric data, was drawn by the author (fig. 6.4) to show the structural relation between the location of the summit depression and the flank rift zones (Malahoff and others, 1982). As in the case of Kilauea, the two pit craters appear to have been formed on the floor of the Loihi summit depression. The structural setting of the summit depression, based upon analyses of the bathymetric data, suggests an offset between the north flank and south flank rifts at the summit of Loihi.

STRUCTURE OF THE LOIHI EDIFICE

Studies of earthquake distribution beneath the summits of Mauna Loa, Kilauea and Loihi by Klein (1982) indicate that between the surface of the Island of Hawaii and a depth of about 40 km these volcanoes have separate volcanic conduits. Below that depth the earthquake hypocenters form a more common zone. The Hawaiian hot spot is interpreted by Klein (1982) to be at a depth of 60 km between and beneath the three volcanoes. Magmatic activity at the three volcanic sites can be explained by a dynamic model of an idealized Hawaiian volcano developed by Eaton and Murata (1960) and Eaton (1962), and by Klein (1982) from interpretation of seismic events associated with Kilauea and Loihi. This model shows the location of a magma reservoir to be 2 to 3 km beneath the summit caldera. This magma reservoir is refilled with magma from the 60-km-deep hot spot source. In this model, flank eruptions are followed by the partial emptying of the reservoir and, in the case of large flank eruptions, by the formation of pit craters at the summit. Growth of the volcanic edifice occurs as surface lava flows emanate from the summit and the flank rifts, and the intrusion of magma forms dike complexes within the rift zones. The source for these

magmatic events in the model appears to be a summit magma reservoir. It is assumed in this paper that the magmatic plumbing of Loihi is similar to that of the model.

Magnetic anomalies have been used in the past to study the size and shape of dike complexes within active and extinct volcanic centers of the Hawaiian Islands (Malahoff and Woollard 1968, 1970). Aeromagnetic studies of the active volcanoes along the Islands of Vanuatu (Malahoff 1970) showed the superposition of short-wavelength, reversed magnetic anomalies on the normally magnetized bipole anomalies located over the edifices of the volcanoes. Models based upon the wavelength of the observed magnetic anomaly, the magnetization of the volcanic edifice, and the contained dike complex were used by Malahoff and Woollard (1968, 1971) to construct calculated anomalies that were matched to those observed above the volcanic centers of Hawaii. Johnson and Malahoff (1971) conducted magnetic anomaly studies over Macdonald submarine volcano, at the southern end of the Austral Island chain. Macdonald Volcano marks the active volcanic center of the Austral Islands hot spot. A 500-nanotesla (nT), reversely polarized magnetic anomaly is superposed upon the normally polarized bipole of the volcano. In the aeromagnetic study of the Vanuatu volcanoes, Malahoff (1970) detected a similar reversely magnetized short-wavelength anomaly over the active Ambrym Volcano and interpreted that anomaly to reflect the presence of rocks having temperatures above the Curie point, approximately 578 °C for magnetite (Nagata, 1961), within the edifice of the volcano. Johnson and Malahoff (1971) interpreted the origin of the observed, reversely polarized, secondary magnetic anomaly above Macdonald Volcano to also be due to the presence of volcanic rocks heated above the Curie point within the edifice of the volcano, thus possibly marking the site of a magma reservoir.

The compilation of the residual magnetic anomaly data over the southern end of the Hawaiian Island chain is depicted in figure 6.5. All volcanoes on the Island of Hawaii show the presence of normally polarized, high-amplitude magnetic anomalies, such as 750 nT for Kohala Volcano, 1,250 nT for the east rift zone of Kilauea, 900 nT for Mauna Kea, 100 nT for Kilauea, 600 nT for Hualalai, 800 nT for Mauna Loa and 1,100 nT for Loihi. The high-amplitude anomalies are formed by the combined magnetic effects of the volcanic edifice and the intrusive dike systems within the edifice. The aeromagnetic profiles over Loihi were flown at an altitude of 2,800 m. A northwest- to southeast-oriented magnetic anomaly profile was also taken aboard the research vessel *Kana Keoki* across the summit of Loihi and approximately above the long axis of the edifice (profile *M–M'*, fig. 6.2). Figure 6.6 illustrates the wavelength and amplitude of the residual magnetic anomaly of this profile. At sea level, the total amplitude of the normally polarized, residual magnetic anomaly above Loihi is 3,900 nT (peak-to-peak). It is assumed that the normal polarity of the residual magnetic anomaly is due to the presence of flow and dike basalt younger than 0.7 Ma, the age of the present normal magnetic polarity epoch (LaBrecque and others, 1977).

It is interesting to note that superposed upon the normally polarized magnetic bipole anomaly is a reversely magnetized bipole anomaly with a peak-to-peak amplitude of 1,600 nT. As with

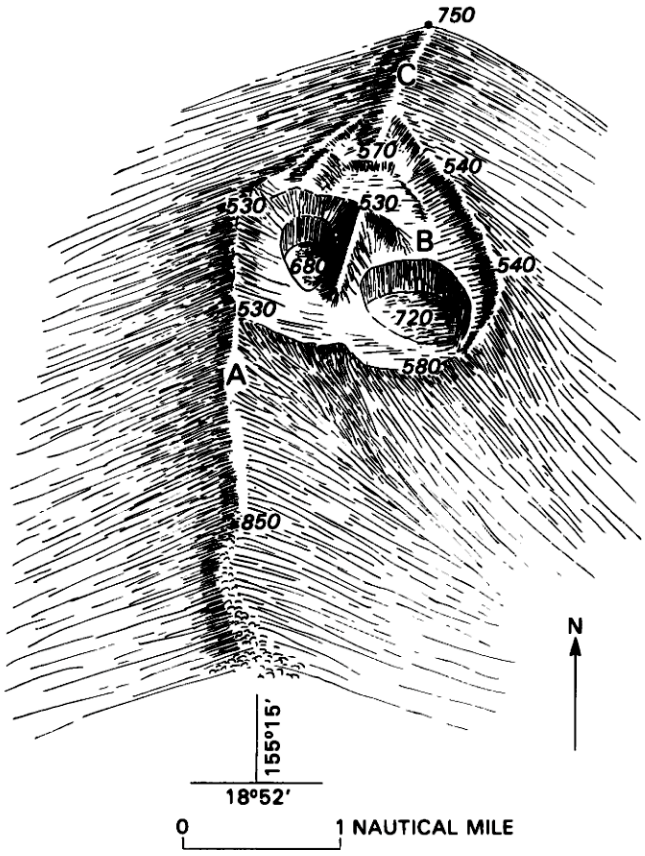

FIGURE 6.4.—Perspective physiographic drawing of summit of Loihi, constructed from bathymetric data base shown in figure 6.3. Spot depths in fathoms. Principal physiographic features: A, southeast flank rift; B, summit caldera with pit craters; C, north flank rift.

similar studies of secondary bipole residual magnetic anomalies observed over active volcanoes (Malahoff, 1970; Johnson and Malahoff, 1971), the interpretation of the observed magnetic anomaly is based upon several speculative source models. Using a two-dimensional model technique (Heirtzler and others, 1962) and the assumption of only a terrain effect for the normally magnetized bipole anomaly, a bulk rock magnetization of 75×10^{-3} emu was required to construct a calculated anomaly for the edifice of Loihi that would match the observed bipole anomaly. The assumed magnetization of 75×10^{-3} emu for the volcanic edifice of Loihi falls within the range of 20×10^{-3} emu to 150×10^{-3} emu measured by Johnson and Clague (1981) for the magnetization of samples recovered by rock dredging from Loihi. The observed anomaly can also be matched with a calculated anomaly based upon a terrain model with an associated dike complex having a magnetization contrast of 15×10^{-3} emu, extending to a depth of 40 km below the summit. In both of these terrain-effect calculations, however, the reversely magnetized, superposed bipole anomaly (fig. 6.6) is difficult to account for. As a speculation, the reversely polarized anomaly was modeled by using a nonmagnetic block (rocks heated

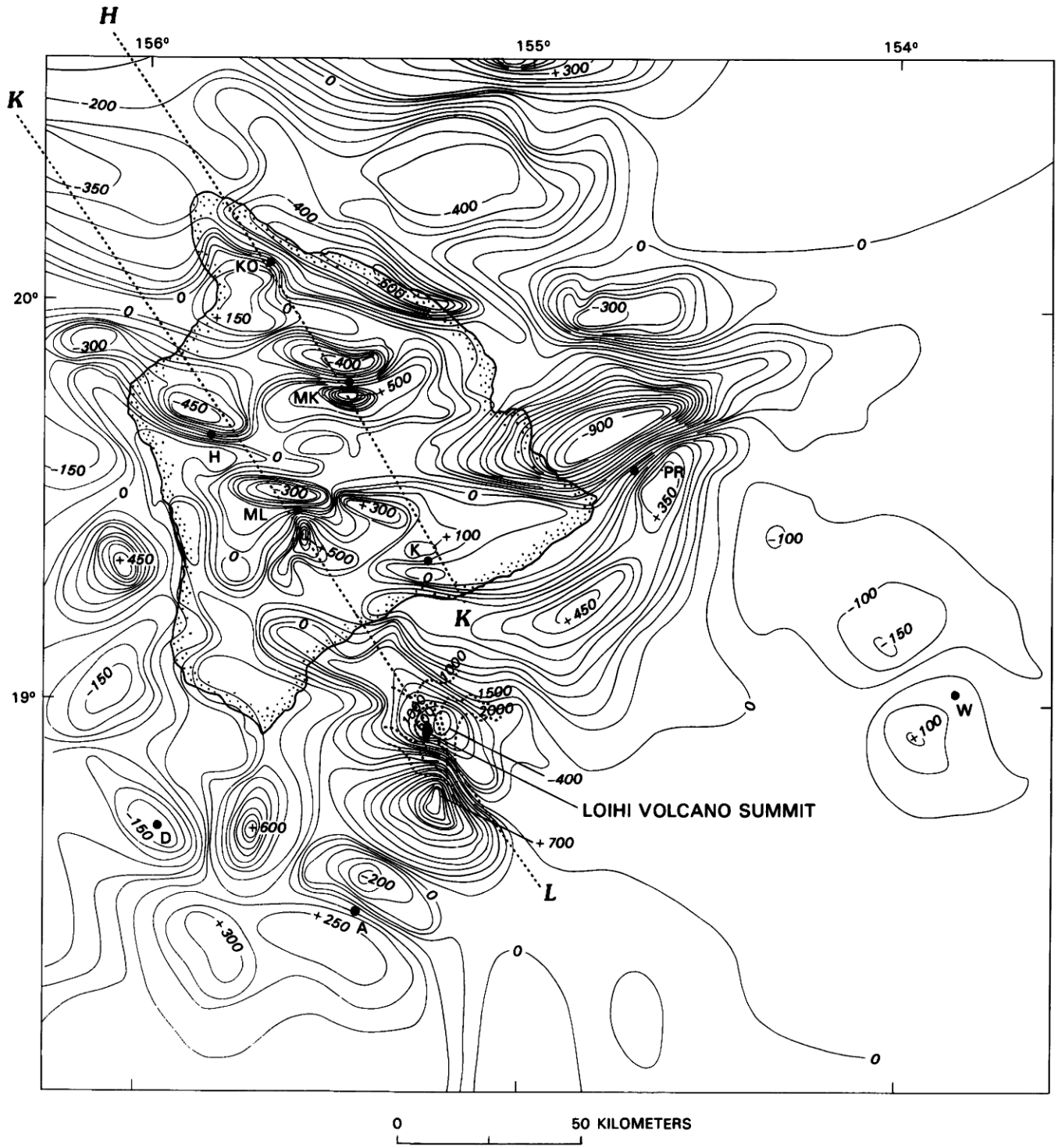

FIGURE 6.5.—Residual total-force magnetic anomaly map of Island of Hawaii and surrounding ocean areas; intensity in nanoteslas (nT). Data obtained from aeromagnetic flights, altitude 2,000 m above sea level over ocean and lower slopes of island. Flight altitude 3,000 m above Mauna Kea (MK) and Mauna Loa (ML). Other volcanic centers: KO, Kohala; H, Hualalai; K, Kilauea; PR, Puna Ridge; W, Wini Seamount; A, Apuupuu Seamount; D, Day Seamount. Dotted contour lines over Loihi summit show general bathymetry in fathoms. Haleakala-Mauna Kea-Kilauea trace of hot spot shown by line *H–K*; the Kahoolawe-Hualalai-Mauna Loa-Loihi trace shown by line *K–L*. Aeromagnetic data from Malahoff and Woollard (1970).

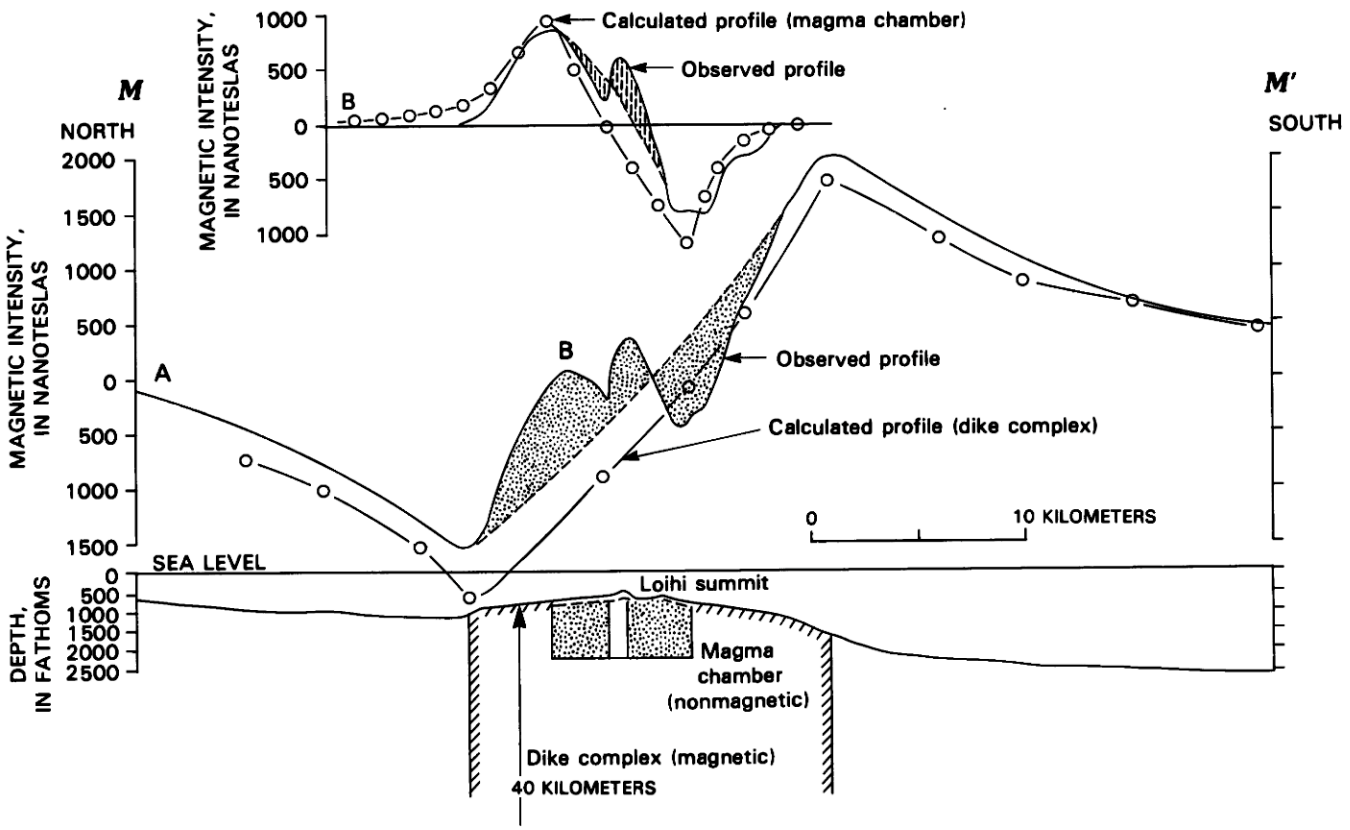

FIGURE 6.6.—Residual total-force magnetic-anomaly profile, M–M' (see location on fig. 6.2), observed at sea level above flank rifts and summit of Loihi. Magnetic intensity in nanoteslas (nT). Principal components of profile: profile A, normally polarized residual total-force magnetic anomaly; profile B, stippled area representing reversely magnetized section along profile A. Profile B also shown in upper diagram in form of residual anomaly subtracted from profile A. Calculated profile, lower diagram, based on model of surficial terrain effect and a magnetic dike complex, with assumed magnetization contrast of 15×10^{-3} emu extending to depth of 40 km. Calculated profile, upper diagram, is based on model of nonmagnetic magma chamber within Loihi edifice. Dashed area (upper diagram) represents normally polarized anomaly segment within profile B assumed to reflect small magnetic body within magma chamber.

above the Curie point) 7 km wide, possibly 3 km in vertical extent, located beneath the surface of the Loihi summit and divided in half by a vertical rock body less than 1 km wide having temperatures below the Curie point (normally polarized; fig. 6.6). This speculative interpretation of the observed residual magnetic anomaly profile over Loihi is based upon one of a number of models and suggests the presence of a heated rock body within the edifice of Loihi Volcano. This rock body could be a shallow summit magma reservoir that, as at Kilauea, may be structurally expressed at the summit by the presence of a caldera and pit craters.

NEOVOLCANIC ZONES OF THE LOIHI SUMMIT

The geologic interpretation of bottom photographic data (fig. 6.7) from the summit of Loihi shows a broad range of lava types and vents present on the summit. The photographic data were obtained using the Woods Hole Oceanographic Institution's ANGUS camera system, with a bottom-transponder navigation network and tow altitudes of 5 to 20 m above the ocean floor. The data were visually examined for the presence of geologic features such as fresh or broken pillow lava, lobate, sheet, aa and pahoehoe lava flows, talus, exposed dike systems, smooth or rippled sediment, visible structural features such as faults and fissures, and evidence of hydrothermal activity, such as yellow, orange or green precipitates (that is, nontronite; Malahoff and others, 1982), or the presence of hydrothermal chimneys. Photointerpretation techniques used in this study were similar to those used by Ballard and others (1979, 1982) and Crane and Ballard (1980) for ANGUS photographic data taken over the neovolcanic zone of the Galapagos Rift. Photographs were analyzed, frame by frame, and condensed into the interpretative geologic map shown in figure 6.7. The most interesting observation derived from the study of the photographic data over the Loihi summit is the relatively small area covered by fresh lava flows. The

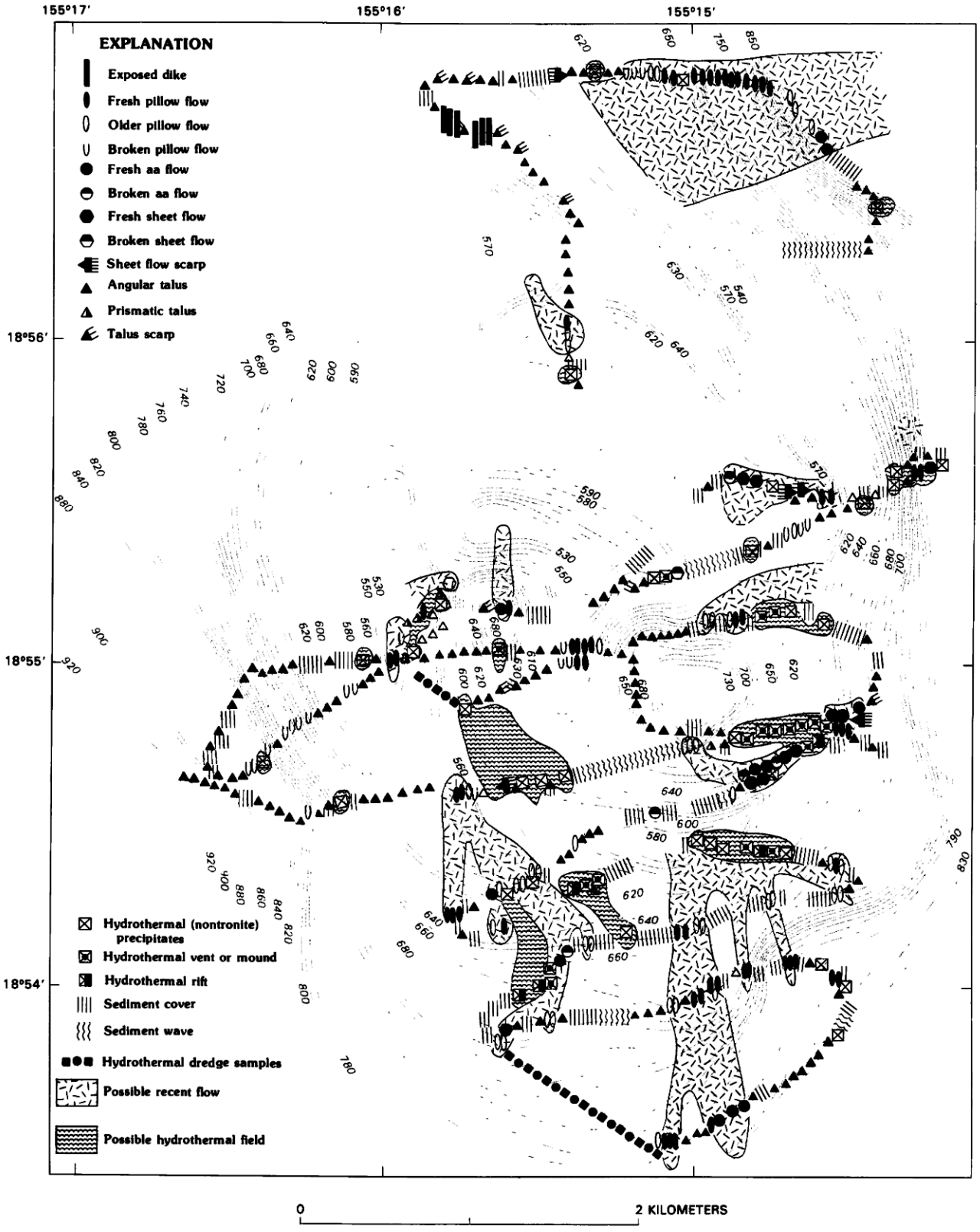

FIGURE 6.7.—Interpretive geologic map of Loihi summit area. Geologic symbols are drawn along tracklines of ANGUS camera system. Geologic data are superposed upon high-resolution bathymetric map (contour interval, 10 fathoms).

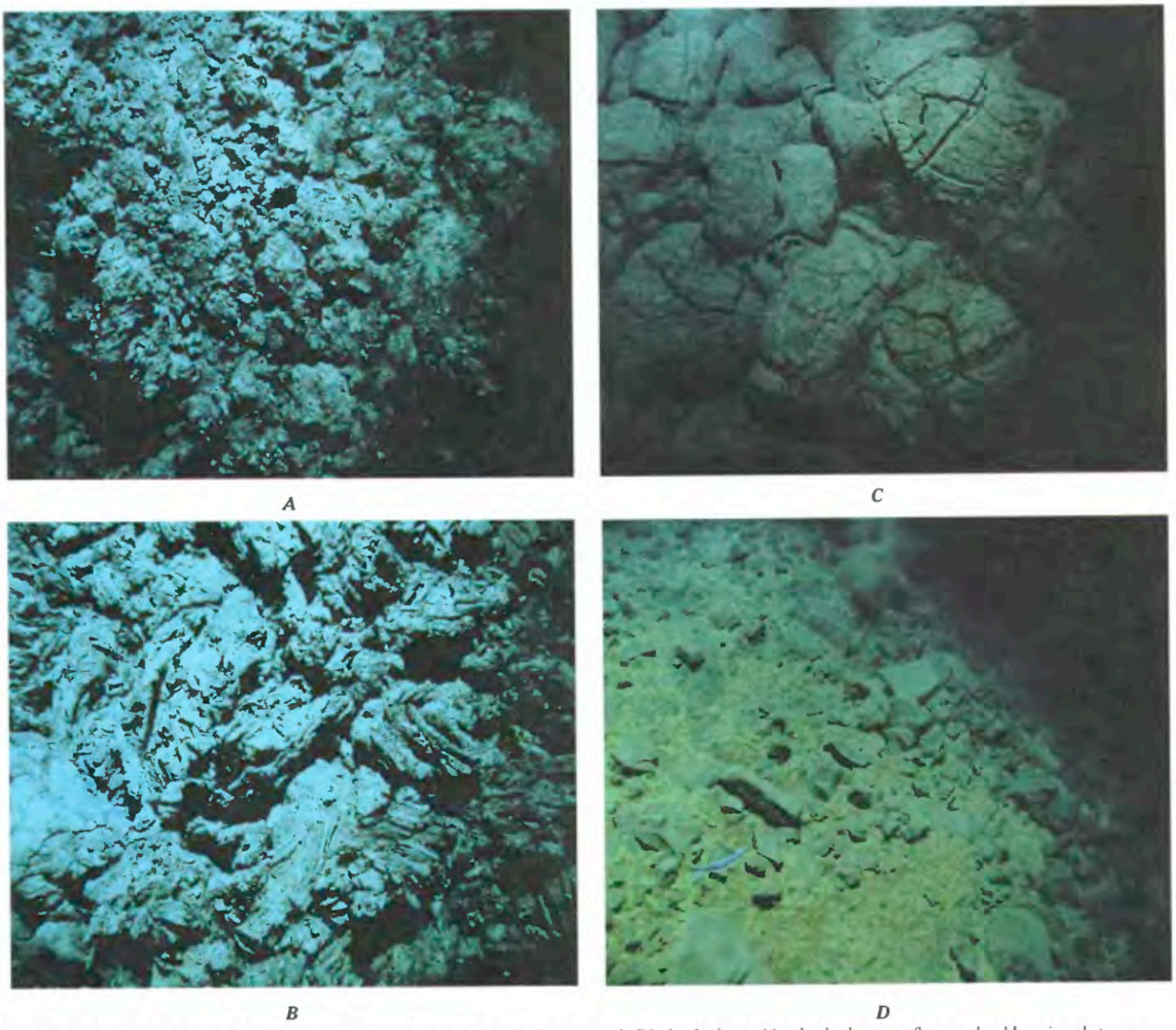

FIGURE 6.8.—Ocean-floor photographs of aa and pillow flows and talus, Loihi summit. ***A***, Blocky, fresh transitional pahoehoe to aa flow, south caldera rim; photocoverage 14 by 22 m, location at 155°14.9′ W., 18°53.7′ N. ***B***, Blocky, fresh transitional from pahoehoe to aa flow; photocoverage 7 by 11 m; location same as in 8*A*. ***C***, Fresh pillow basalt, northeast rim of Loihi caldera; photocoverage 10 by 14 m; location at 155°14.9′ W., 18°56.8′ N. ***D***, Talus along western inner margin of the summit depression; photocoverage 10 by 14 m. Yellow to orange hydrothermal nontronite covers much of central area of photograph; location at 155°15.95′ W., 18°55′ N.

freshest lava flows, those with high photoreflectivity and no visible sign of sediment coverage (fig. 6.8*A*, *B*), were found to originate from volcanic centers along the southern edge of the Loihi summit depression. The two longest lava flows appear to extend a maximum distance of 1,800 m from their sources, which are at water depths of 970 to 1,060 m. The photographic data suggest that these lava flows consist largely of pillow (fig. 6.8*C*) and lobate flows at the vent sites and transform into lava types similar to aa or broken sheet flows (fig. 6.8*A*, 6.9*B*) downslope from the vent site.

The steeper slopes of Loihi outside the summit depression are covered by talus, as are the steeper, inside slopes of the pit craters (fig. 6.9*B*). The floors of the two pit craters appear to be covered by sediment. Talus appears to be common in the photographic data. Sheet flows, similar in their photographic appearance to those observed by Ballard and others (1979, 1982) over the Galapagos Ridge, were photographed at several sites at the northeastern rim of the summit depression (fig. 6.9*A*). Sheet flows appear to form at the site of submarine volcanic eruptions where higher magmatic volumes and higher extrusion temperatures may have occurred. These flows occupy areas of the Loihi summit that are less than a few thousand square meters in area. They appear to undergo mechanical breakup soon after extrusion, with the downslope mass wasting resulting in the formation of talus (fig. 6.9*B*). Downslope mass-wasting talus development has apparently been extensive enough to expose the

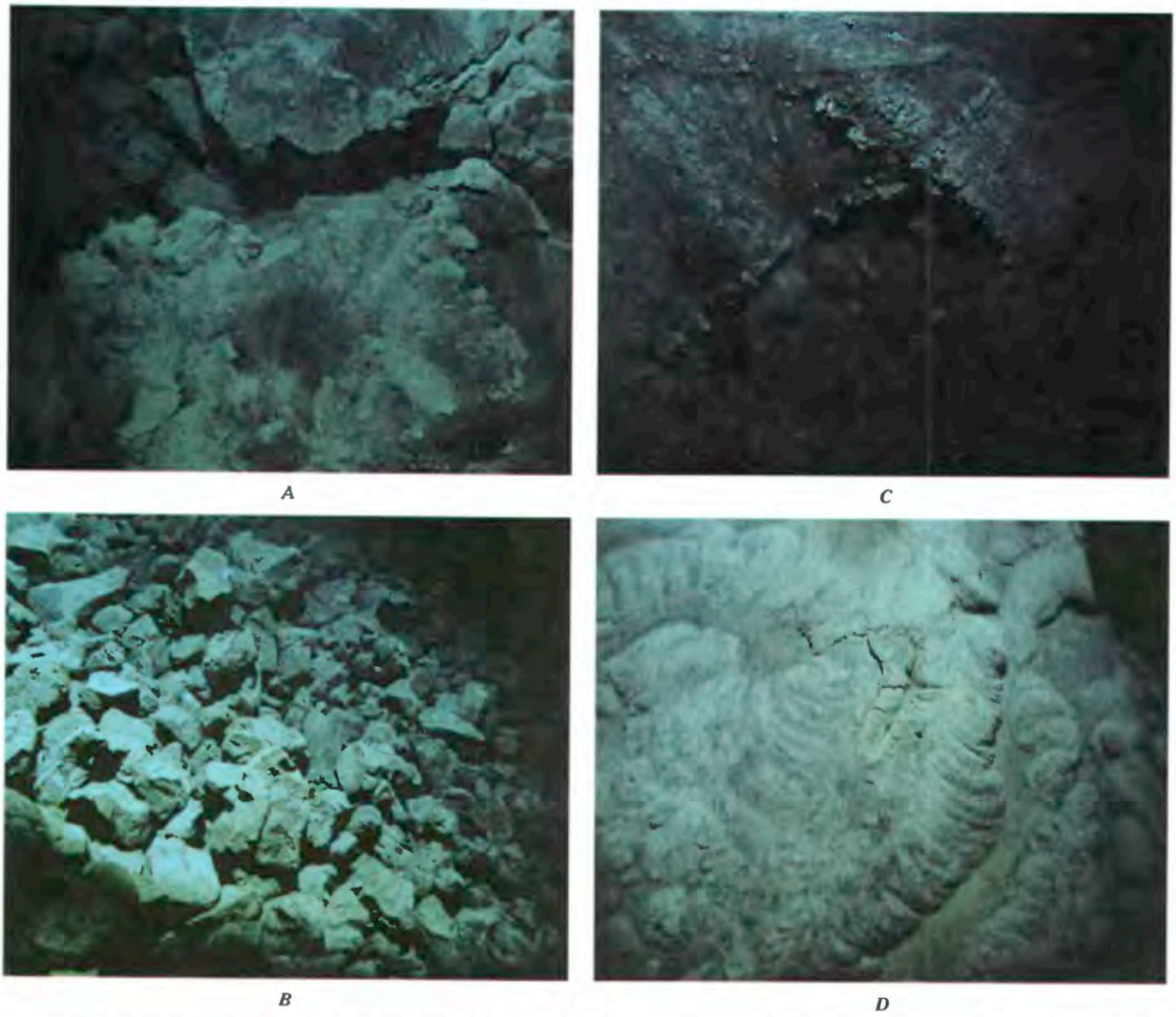

FIGURE 6.9.—Ocean-floor photographs of fresh sheet flows, broken sheet flows, exposed dikes, and lobate flows, Loihi summit. ***A***, Fresh sheet flow, showing initial stages of mechanical breakup; photocoverage 13 by 20 m; location at 155°14.8′ W., 18°54.65′ N. ***B***, Talus derived from broken sheet flow; photocoverage 10 by 14 m; location same as in 9*A*. ***C***, Exposed dike rocks, north rim Loihi caldera; photocoverage 24 by 36 m; location at 155°15.7′ W., 18°50.7′ N. ***D***, Ponded lobate and pillow flows; photocoverage 17 by 25 m, location at 155°15.4′ W., 18°56′ N.

underlying dike structure (fig. 6.9C) at the northern edge of the summit depression. Ponded lava is also observed (fig. 6.9*D*). Incipient lobate flows appear to have developed in association with the lateral lava drainage out of the lava ponds, that formed in flat-lying areas of the summit depression.

The slopes of the two pit craters within the summit depression appear to be covered by talus. Rippled sediment and talus cover large areas of the basaltic floor of the summit depression and the pit craters. Lava flows with the freshest appearance in the photographs are on the southern rim of the summit depression. The lava appears to have erupted from vents on the local highs that have the appearance of cones.

Extensive patches of hydrothermally precipitated yellow, red or green iron oxide and nontronite (Malahoff and others, 1982; DeCarlo and others, 1983) cover areas of the talus slopes (fig. 6.8*D*) and also form fields of individual chimneys 0.5 to 2.0 m high (fig. 6.10). Transponder-controlled shipboard dredging of two of the hydrothermal vent sites along the southern edge of the summit depression produced samples of yellow-brown goethite and nontronite, similar in composition to the iron-rich montmorillonite-nontronite recovered from the Red Sea Rift, the East Pacific Rise and the Galapagos hydrothermal mounds (Malahoff and others, 1982), as well as from the caldera of Axial Volcano on the Juan de Fuca Ridge (McMurtry and others, 1984). The shape and size of

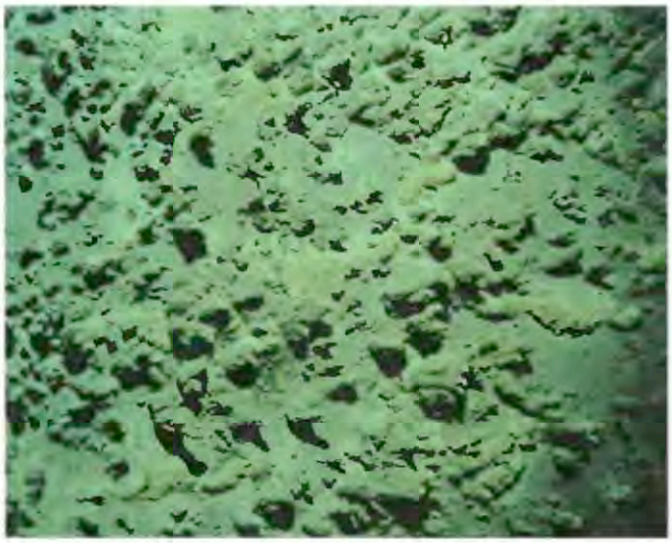

FIGURE 6.10.—Ocean-floor photograph of hydrothermal field, southeast edge, Loihi summit depression. Hydrothermal chimneys 0.5 to 2 m high. Dark areas to side of chimneys are shadows cast by camera strobe lights; photocoverage 14 by 22 m, location at 155°14.75′ W., 18°54.45′ N.

the low temperature hydrothermal chimneys of Axial caldera are similar to those photographed by the ANGUS system over Loihi. More than 100 chimneys can be counted in the photograph of figure 6.10, which covers an area of approximately 22 by 14 m.

The hydrothermal vent fields on the summit of Loihi are as long as 600 m. Malahoff and others (1982) measured water temperature anomalies of greater than 1 °C at a water depth of 10 m above the ocean floor where the nontronite-iron oxide deposits are situated, suggesting an extrapolated temperature of about 30 °C at the vent sites on the ocean floor. Most of the hydrothermal fields mapped in this study are characterized by the presence of reddish-yellow hydrothermal precipitates deposited on the surface of sediments (fig. 6.10), on talus (fig. 6.8*D*) or along cracks and fissures of sheet flows. All the hydrothermal vents with identifiable chimneys mapped in this study are adjacent to fresh lava flows (fig. 6.7). The association between fresh lava flows, visible hydrothermal vent fields and water temperature anomalies is common at midocean ridge-crest sites (Haymon and Kastner, 1980; Lonsdale and others, 1980; Ballard and others, 1981; Bäcker and others, 1985; Hekinian and Fouquet, 1985) and ridge-crest submarine volcanoes such as Axial (Malahoff and others, 1984; McMurtry and others, 1984) and along off-ridge seamounts such as the Red and Green Seamounts off the East Pacific Rise at 20°50′ N. (Lonsdale and others, 1982). At the active vent sites of Axial caldera, outer zones of disaggregated nontronite precipitates are found beyond the inner zone of sulfide precipitation and the middle zone of nontronite chimneys (McMurtry and others, 1984; Arquit and others, 1985). A similar outer zone, consisting of isolated patches of nontronite deposits, is found precipitated on the upper talus-covered slopes of Loihi, and thus probably marks the outer zones of Loihi hydrothermal fields.

The depth of the hydrothermal vent fields on Loihi mapped in this study ranges from a shallow point of 1,043 m below sea level at the southern rim of the summit depression to 1,500 m below sea level along the flanks of Loihi. Other hydrothermal vent sites may be present along the north flank and south flank rifts of Loihi.

To date, no high-temperature hydrothermal minerals, such as polymetallic sulfides, have been sampled during this or other shipboard rock-dredging expeditions on Loihi (Moore and others, 1982; DeCarlo and others, 1983), although it is possible that polymetallic sulfides may have been precipitated as chimneys (observed in the bottom photographs) or beneath the surface of Loihi (DeCarlo and others, 1983). High-temperature water anomalies were not detected over the summit of Loihi during the current studies, and no evidence for hydrothermal vent macro-organisms, such as worms or clams, has been observed in the current photographic data set taken over the summit of Loihi.

DISCUSSION

Loihi submarine volcano is a young Hawaiian volcano that is 969 m below sea level at the southern end of the Kahoolawe-Hualalai-Mauna Loa limb of the Hawaiian hot spot trace. The comprehensive bathymetric, photographic, geologic, and magnetic studies conducted over the Loihi summit show the volcano has structural similarities to the young subaerial volcanoes of Hawaii. The 2.8-km-wide summit depression, with a rim depth of 969 m below sea level and a floor depth of 1,134 m below sea level could represent the initial stages of submarine caldera development. Two pit craters within the summit depression are similar in their structural setting to craters on the summit of Kilauea Volcano. The summit depression of Loihi appears to be at the intersection of two flank rifts. Most of the volcanic extrusions that have built the edifice of Loihi probably erupted from the two flank rifts and from summit vents, thus giving Loihi its elongate shape. Although seismic studies show that the magma supply for Mauna Loa, Kilauea and Loihi originates from a common source (probably the Hawaiian hot spot) at a depth of 60 km or more beneath the surface, all three volcanoes apparently have individual conduits and seismic further showing that the magmatic cycles of the three volcanoes are largely independent of each other. A pronounced 3,900-nT peak-to-peak residual total-force magnetic anomaly is also observed over the edifice of Loihi. Within the configuration of this normally polarized, bipole anomaly, a shorter wavelength anomaly of amplitude 1,600 nT and having a reversed polarization is observed. The configuration of reversed polarization within a normally polarized magnetic anomaly profile has been observed over other active subaerial and submarine volcanoes. A speculative interpretation of the residual total-force magnetic anomaly observed over Loihi suggests the presence of a heated rock body or magma source, with temperatures above 578 °C, 7 km wide and 3 km thick located within the edifice.

Visual examination of the photographic data reveals the most common rock type to be volcanic talus. Ten fresh lava flows were mapped in this study with their vent sources traced to volcanic mounds located in and around the summit depression. The most extensively mapped lava flows with the freshest appearance are

about 2 km long and are along the southern rim of the depression; this lava appears to have erupted from 100- to 150-meter-high volcanic mounds. The lava mapped within these areas consists of sheet, lobate and pillow flows, with aa flows or broken sheet flows mapped along the steeper slopes of the summit. The freshest flows have been identified by Moore and others (1982) as tholeiitic in composition, as compared to older alkalic lava dredged from the Loihi edifice. The broken ends of fresh lava flows frequently observed directly above the talus piles on Loihi indicate that new lava is mechanically disintegrated into talus along the summit slopes shortly after formation, thereby building a submarine volcanic edifice that may be composed of alternating layers of talus and lava flows. Fields of hydrothermal precipitates consisting of blankets and chimneys are all found to be associated with fresh lava flows. No visible hydrothermal vent communities, such as the worm and clam communities observed at the East Pacific Rise or the Juan de Fuca hydrothermal vent sites, were observed in this study. Similarly, no high water temperatures were detected with the acoustic thermometer mounted on the camera sled. Bottom-transponder navigation-controlled dredging of the hydrothermal vent sites produced samples of nontronite; therefore, the hydrothermal blankets and chimneys observed in the photographs are probably constructed of nontronite, iron oxide, and other low-temperature hydrothermal precipitates. Higher temperature polymetallic sulfide deposition may have taken place within the edifice of Loihi during the upward migration of the hydrothermal fluids to the surface. The data described in these studies do not preclude the presence of unmapped high temperature smokers on Loihi. The tectonic, volcanic, and hydrothermal processes observed over the summit of Loihi probably represent submarine geologic processes that may be typical of those active along the summits of emerging hot spot volcanic islands and other major submarine basaltic volcanoes.

REFERENCES

Arquit, A., Malahoff, A., and McMurtry, G.M., 1985, Chemical and biological halos of a hydrothermal vent system, Axial caldera, Juan de Fuca Ridge: American Geophysical Union, Eos, v. 66, p. 401.

Bäcker, H., Lange, J., and Marchig, V., 1985, Hydrothermal activity and sulphide formation in axial valleys of the East Pacific Rise crest between 18 and 22° S.: Earth and Planetary Science Letters, v. 72, p. 9–22.

Ballard, R.D., Holcomb, R.T., and van Andel, T.H., 1979, The Galapagos Rift at 86° W.: 3. Sheet flows, collapse pits, and lava lakes of the rift valley: Journal of Geophysical Research, v. 84, p. 5407–5422.

Ballard, R.D., Francheteau, J., Juteau, T., Rangan, C., and Normark, W., 1981, East Pacific Rise at 21° N.: the volcanic, tectonic, and hydrothermal processes of the central axis: Earth and Planetary Science Letters, v. 55, p. 1–10.

Ballard, R.D., van Andel, T.H., and Holcomb, R.T., 1982, The Galapagos Rift at 86° W.: 5. Variations in volcanism, structure, and hydrothermal activity along a 30-kilometer segment of the rift valley: Journal of Geophysical Research, v. 87, p. 1149–1161.

Crane, K., and Ballard, R.D., 1980, The Galapagos Rift at 86° W.: 4. Structure and morphology of hydrothermal fields and their relationship to the volcanic and tectonic processes of the rift valley: Journal of Geophysical Research, v. 85, p. 1443–1454.

DeCarlo, E.H., McMurtry, G.M., and Yeh, H.-W., 1983, Geochemistry of hydrothermal deposits from Loihi submarine volcano, Hawaii: Earth and Planetary Science Letters, v. 66, p. 438–449.

Eaton, J.P., 1962, Crustal structure and volcanism in Hawaii, *in* The Crust of the Pacific Basin: American Geophysical Union Monograph 6, p. 13–29.

Eaton, J.P., and Murata, K.J., 1960, How volcanoes grow: Science, v. 132, p. 925.

Emery, K.O., 1955, Submarine topography south of Hawaii: Pacific Science, p. 286–291.

Haymon, R.M., and Kastner, M., 1980, Hot spring deposits on the East Pacific Rise at 21° N.: preliminary description of mineralogy and genesis: Earth and Planetary Science Letters, v. 53, p. 363–381.

Heirtzler, J.R., Peter, G., Talwani, M., and Zurflueh, E.G., 1962, Magnetic anomalies caused by two dimensional structure; their computation by digital computers and their interpretation: New York, Columbia University Technical Reports, v. 6, p. 6–62.

Hekinian, R., and Fouquet, Y., 1985, Volcanism and metallogenesis of axial and off-axial structures on the East Pacific Rise near 13° N.: Economic Geology, v. 80, p. 221–229.

Jackson, E.S., Silver, E.A., and Dalrymple, G.B., 1972, Hawaiian-Emperor chain and its relation to Cenozoic circum-Pacific tectonics: Geological Society of America Bulletin, v. 83, p. 601–617.

Johnson, H.P., and Clague, D.A., 1981, Magnetic properties of submarine basalt as a function of rock geochemistry: samples from Loihi Seamount, Hawaii: American Geophysical Union, Eos, v. 62, p. 1082.

Johnson, R., and Malahoff, A., 1971, Relation of Macdonald Volcano to migration of volcanism along the Austral Chain: Journal of Geophysical Research, v. 76, p. 3282–3290.

Klein, F.W., 1982, Earthquakes at Loihi submarine volcano and the Hawaiian hot spot: Journal of Geophysical Research, v. 87, p. 7719–7726.

LaBrecque, J.L., Kent, D.V., and Cande, S.C., 1977, Revised magnetic polarity time scale for the Late Cretaceous and Cenozoic time: Geology, v. 5, no. 6, p. 330–335.

Lonsdale, P.F., Batiza, R., and Simkin, T., 1982, Metallogenesis at seamounts on the East Pacific Rise: Marine Technology Society Journal, v. 16, p. 54–61.

Lonsdale, P.F., Bischoff, J.L., Burns, V.M., Kastner, M., and Sweeney, R.E., 1980, A high-temperature hydrothermal deposit on the seabed at a Gulf of California spreading center: Earth and Planetary Science Letters, v. 49, p. 8–20.

Macdonald, G.A., and Abbott, A.T., 1970, Volcanoes in the sea—the Geology of Hawaii: Honolulu, University of Hawaii Press, 441 p.

Malahoff, A., 1970, Gravity and magnetic studies of the New Hebrides Island Arc: New Hebrides, British Service, 67 p.

Malahoff, A., McMurtry, G.M., Hammond, S., and Embley, R.W., 1984, High temperature hydrothermal fields; Juan de Fuca Ridge axial volcano: American Geophysical Union, Eos, v. 65, p. 1112.

Malahoff, A., McMurtry, G.M., Wiltshire, J.C., and Yeh, H.-W., 1982, Geology and chemistry of hydrothermal deposits from active submarine volcano Loihi, Hawaii: Nature, v. 298, p. 234–239.

Malahoff, A., and Woollard, G.P., 1968, Magnetic and tectonic trends over the Hawaiian Ridge, *in* Knopoff, L., Drake, C.L., Hart, P.J., ed., The Crust and Upper Mantle of the Pacific Area: Washington, D.C., American Geophysical Union, Monograph 12, p. 241–276.

——— 1970, Geophysical studies of the Hawaiian Ridge and Murray Fracture Zone, *in* Maxwell, A.E., ed., The Sea-Ideas and observations on the progress in the study of the seas: New York, Interscience Publishers, p. 73–131.

McMurtry, G.M., Malahoff, A., Feely, R.A., and Massoth, G.J., 1984, Geology and chemistry of the hydrothermal nontronite deposits from the Juan de Fuca Ridge: American Geophysical Union, Eos, v. 65, p. 1112.

Moore, J.G., Clague, D.A., and Normark, W.R., 1982, Diverse basalt types from Loihi Seamount, Hawaii: Geology, v. 10, p. 88–92.

Nagata, T., 1961, Rock Magnetism: Tokyo, Maruzen Company, Ltd., 350 p.

Landsat image of the Island of Hawaii, taken February 11, 1973. This rendition, made at the USGS Flagstaff image-processing facility, is a simulation of the true color; the blue component, not measured by Landsat, was artificially derived by extrapolation from the red and green channels. Clearly visible in lower center are lava flows from the southwest and northeast rift zones of Mauna Loa Volcano, radiating from its summit caldera.

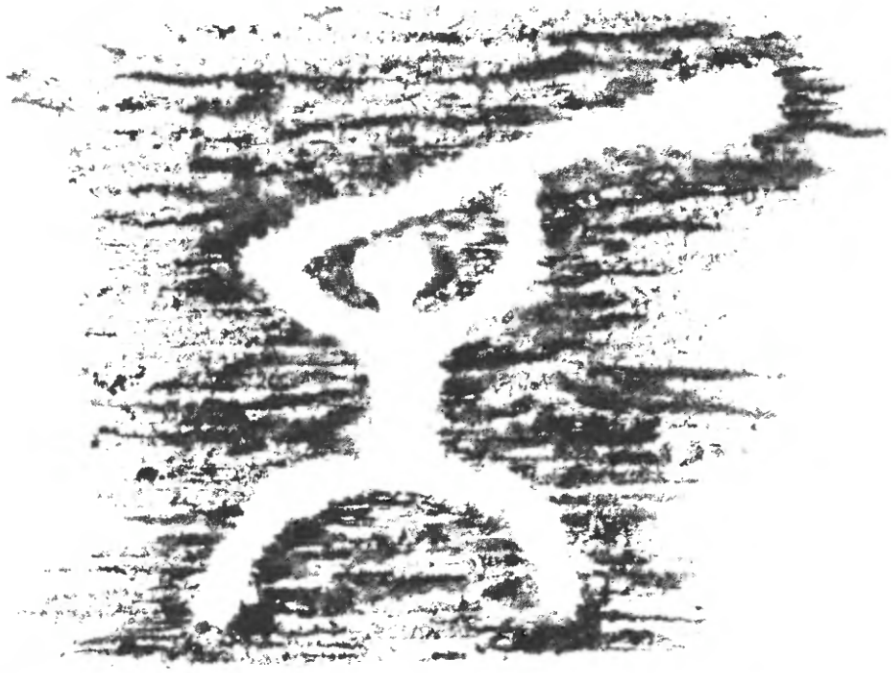

Man with Paddle
Hawaiian Petroglyph
Puna, Hawaii

GEOLOGY OF THE ISLAND OF HAWAII

The Island of Hawaii, aptly termed the "Big Island," is the setting for all current and most historical volcanic activity in the Hawaiian Chain, and the work of the Hawaiian Volcano Observatory has of necessity been concerned largely with the active volcanoes. Modern volcanism can only be understood, however, through study of past volcanic activity. Accordingly, many workers at HVO have participated in mapping projects that extend our knowledge of Hawaiian volcanic history at least back to the emergence of the volcanoes above sea level.

The latest geologic map of the Island of Hawaii was published by Harold Stearns and Gordon Macdonald in 1946 as part of a series of maps and descriptive bulletins for all the Hawaiian Islands. A revision of that map currently being prepared by a consortium of USGS and university geologists will incorporate information from a number of chapters in this section.

The section begins with a broad view of where we are now and where we have been in our understanding of the geology of Hawaii. With modern satellites we no longer have to confine ourselves to earthbound observation—chapter 8 gives us a view from space. Chapters 9 and 10 treat radiocarbon dating, a technique that has been essential in unraveling the prehistoric record of Hawaiian volcanism. Kilauea is the most active Hawaiian volcano in recent times, and chapters 11 through 17 discuss its activity from the most recent to the most ancient. Two following chapters on Mauna Loa provide comparable insight into both the historical and prehistoric behavior of that largest volcano in the Hawaiian Chain. The third volcano on the Big Island that can be considered active is Hualalai; chapter 20 provides the first modern assessment of its geologic history. Mauna Kea, dormant for about 4,000 years, underwent Pleistocene glaciation as well as volcanic activity—the relation between the two is discussed in chapter 21.

The section concludes with a revised assessment of volcanic hazards in the Hawaiian Islands; such hazards are mostly associated with the active volcanoes on the Island of Hawaii. Revised hazard-zone maps should be of value to all concerned with use of the precious and fragile land resources on the Big Island.

GEOLOGIC HISTORY AND EVOLUTION OF GEOLOGIC CONCEPTS, ISLAND OF HAWAII

By Donald W. Peterson *and* Richard B. Moore

ABSTRACT

The Island of Hawaii consists of five Quaternary shield volcanoes: Kohala, Mauna Kea, Hualalai, Mauna Loa, and Kilauea, in order of latest activity. Loihi Seamount, an active volcano 25–30 km south of the island, may eventually grow to merge with the Island of Hawaii.

Early Polynesian settlers on Hawaii kept no written records, and the visits of the earliest European explorers were too brief to contribute much information about the volcanoes. Systematic observations of Hawaiian volcanic activity began in the 1820's, and records by missionaries, explorers, botanists, and geologists described the general characteristics of Hawaiian eruptions and the morphology of the volcanoes. During the 19th century, the geologists J.D. Dana and C.E. Dutton developed basic concepts of Hawaiian volcanic processes that differed considerably from ideas then commonly held about volcanism. The Hawaiian Volcano Observatory, founded in 1912 under the direction of T.A. Jaggar, launched a program of continuous, systematic surveillance of Kilauea and Mauna Loa Volcanoes, which has continued until the present time.

During the first half of the 20th century, understanding of the geologic history of the island advanced by means of frequent observations of eruptions, recognition and study of contrasting rock types, and comprehensive reconnaissance mapping that charted the distribution of rock types and the structure of the volcanoes. More recently, additional understanding has been achieved through geophysical studies, offshore submarine investigations, numerical dating of rocks, advances in petrology and geochemistry, continuous surveillance and monitoring of eruptions, and more detailed geologic mapping.

These continuing advances have permitted earlier concepts on the evolution of Hawaiian volcanoes to be gradually modified, and the order of events, as currently understood, follows this sequence:

1. Initial stage. Basanite, alkalic basalt, and lava transitional to tholeiite build a moderately steep-sided edifice from the deep ocean floor.
2. Shield-building stage. Principal development of shield volcano; eruptions are frequent and voluminous from vents in summit area and along radial rift zones; repeated cycles of caldera formation and filling; weight of growing edifice causes regional subsidence. Three substages: (a) submarine—pillow lavas build moderately sloping submarine edifice; (b) sea-level—vigorous interaction between degassing molten lava and ocean waves, lava-steam explosions, hyaloclastite deposits; (c) subaerial—pahoehoe and aa lava flows build gently sloping shield volcano; processes of substages a and b may continue below and at sea level.
3. Capping stage. Alkalic basalt and related differentiated rocks build steeply sloping cap over tholeiitic shield; eruption frequency diminishes, explosive eruptions increase; final caldera buried.
4. Erosional stage. Frequency of eruptions declines to zero; stream and wave erosion cuts valleys and cliffs; coral reefs may form offshore.
5. Renewed volcanism stage. After long quiescence, highly differentiated lava and tephra erupt intermittently; erosion and reef building continue.
6. Atoll stage. Volcano is eroded to sea level abetted by regional subsidence; structure encircled and capped by coral reefs.
7. Late seamount stage. Regional subsidence eventually causes edifice to sink below sea level where it quietly remains as a seamount.

The volcanoes of the Island of Hawaii represent only the first four stages. Loihi is at stage 1 or 2a, Kilauea and Mauna Loa are at 2c, Hualalai and Mauna Kea at 3, and Kohala at 4.

The petrologic history of each Hawaiian volcano is summarized by silica- and magnesia-variation diagrams. These diagrams also illustrate chemical differences and similarities among the volcanoes, the differentiation trends of basaltic magmas, and the major role played by olivine in controlling basalt composition.

Though volcanic activity has dominated the development of the island, other geologic agents have also been at work. Subsidence caused by volcanic loading occurs at a rate of a few millimeters per year. Eustatic changes of sea level, chiefly during the Pleistocene, gave rise to marine terraces, most of which are below the modern strandline. High rainfall on the windward side has caused erosion of deep canyons having thick deposits of sediment in their lower reaches. Pleistocene glacial deposits cap Mauna Kea. Fault scarps are common on the active volcanoes Mauna Loa and Kilauea. Tsunamis generated by local and distant earthquakes have caused coastline erosion and redeposition every few decades through historical time and, by inference, throughout the entire life of the island.

INTRODUCTION

Hawaii, one of the world's largest volcanic islands, lies at the southeastern end of the Hawaiian Ridge, a linear chain of mostly submarine volcanic mountains that extends for 3,500 km through the central Pacific Ocean (fig. 7.1). The eight main Hawaiian islands span about 640 km from southeast to northwest; numerous small islands, atolls, reefs, and shoals lie farther northwest, extending the archipelago proper to about 2,600 km. The exclusively submarine portion of the Hawaiian Ridge continues northwestward for another

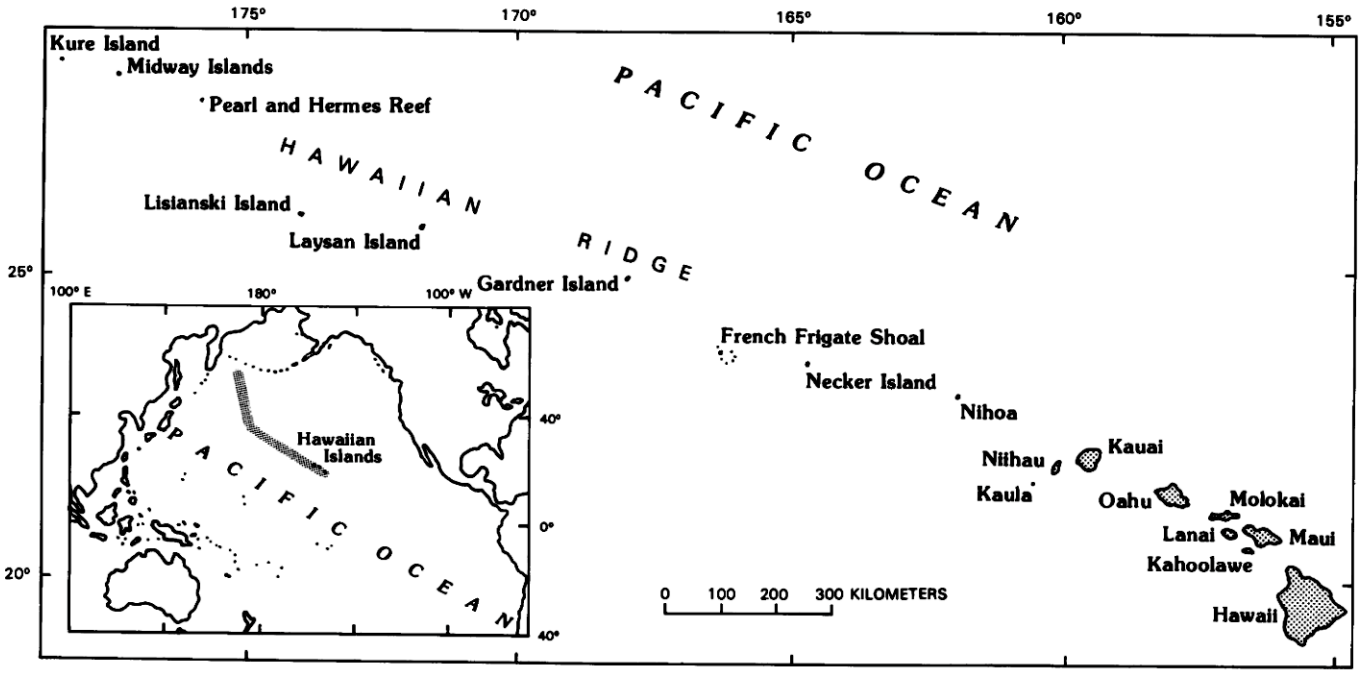

FIGURE 7.1.—Hawaiian archipelago showing location of eight main Hawaiian Islands at southeast end and small islands, atolls, and reefs that extend northwestward along Hawaiian Ridge. Pattern of inset shows location of Hawaiian-Emperor Chain.

900 km, then bends sharply northward to become the Emperor Seamounts, a similar linear chain that extends for another 2,500 km as far as the Aleutian Trench (fig. 7.1). The combined Hawaiian-Emperor volcanic chain is thought to record the persistent movement of the Pacific plate over a stationary melting spot beneath the crust (Dalrymple and others, 1973). The magma generated erupts to build volcanoes at the surface of the plate above the melting spot; as the plate moves on, these volcanoes cease growing but new ones begin. The Island of Hawaii is now thought to lie just north of the melting spot. The origin of the Hawaiian-Emperor Chain is reviewed by Clague and Dalrymple (chapter 1, part I).

Hawaii consists of five individual volcanoes: Kohala, Mauna Kea, Hualalai, Mauna Loa, and Kilauea (fig. 7.2; table 7.1). They rise from the sea floor, which lies here at a depth of about 5–6 km; the island is only their uppermost part, and by far the greatest part of their bulk lies beneath the ocean surface (table 7.2). The subaerial part of each volcano is typically shield shaped, though some have been modified by erosion.

Of the five volcanoes, Kohala, which forms the northernmost part of the island (fig. 7.2), has been inactive the longest. Stream erosion has deeply incised its northeastern flank, though the other flanks are less dissected. Cinder cones stud the upper part of the shield. Kohala last erupted at about 60 ka (McDougall and Swanson, 1972). Adjoining Kohala on the southeast is Mauna Kea, whose summit (4206 m) is the highest point on the island. Cinder cones are abundant on Mauna Kea; its most recent eruptions were at about 3.6 ka (Porter and others, 1979b). Several canyons incise the lower portions of its northeastern flank, whereas the remainder of the volcano has been little affected by erosion.

South of Mauna Kea is Mauna Loa, whose surface accounts for more than half the area of the island (table 7.1). A caldera occupies its summit, several pit craters indent the surface near the summit, and prominent rift zones, consisting of cinder and spatter cones, spatter ramparts, fissures, and small craters, extend northeast and southwest from the summit. Mauna Loa has erupted frequently in historical time, most recently in 1984 (Lockwood and others, chapter 19, 1985), and most of its surface is not eroded. Northwest of Mauna Loa is Hualalai, a relatively steep-sided shield with many cinder cones on its upper parts; it is essentially undissected by erosion. It has erupted once in historical time (1800–1801), from vents along its northwest rift zone. Abutting Mauna Loa's southeast flank is Kilauea, the most readily accessible and best studied of Hawaii's volcanoes. A caldera occupies its summit area, and several large pit craters indent the summit area and upper east rift zone. Rift zones extend from the caldera to beyond the shoreline both east and southwest from the summit. Kilauea, like Mauna Loa, has erupted frequently throughout historical time; the eruptions of these two volcanoes have provided much significant information about processes of basaltic volcanism.

Loihi is a seamount located 30 km south of the south coast of Hawaii (figs. 7.2, 7.8). Its highest point reaches to within about 950 m of the ocean surface. Ongoing studies have revealed evidence of its recent eruptive activity and demonstrate that it is a growing submarine volcano (Malahoff, chapter 6; Malahoff and others, 1982; Moore and others, 1982).

The geologic history of a basaltic volcanic island superficially may appear to be quite simple—a long sequence of repeated lava flows has constructed a broad, layered volcanic edifice. The wide

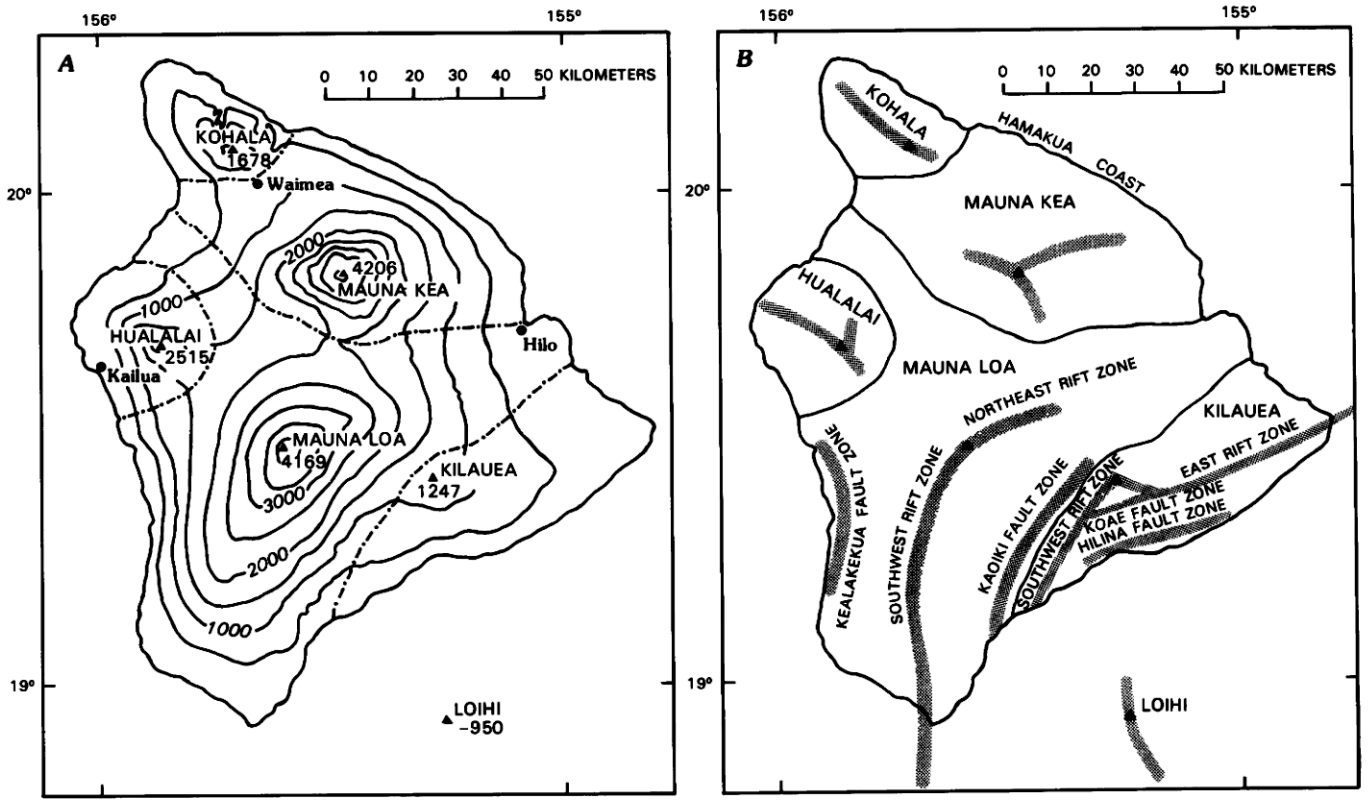

FIGURE 7.2.—Island of Hawaii and Loihi Seamount showing major geographic and geologic features. *A*, Generalized topography and boundaries of five volcanoes. Contours and summit elevations in meters. *B*, Major rift zones and fault zones; those on Kilauea and Mauna Loa are named.

TABLE 7.1.—*Physical dimensions of the subaerial portions of Hawaii's volcanoes*

[Adapted from Stearns and Macdonald, 1946, p. 24]

Volcano	Elevation of highest point (m)	Area (km^2)	Percent of area of island
Mauna Loa	4,169	5,271	50.5
Kilauea	1,247	1,430	13.7
Hualalai	2,521	751	7.2
Mauna Kea	4,206	2,380	22.8
Kohala	1,670	606	5.8
Entire island	4,206	10,438	100

TABLE 7.2.—*Volume and relative percentages of subaerial and submarine mass of each volcano and for entire Island of Hawaii*

[Volumetric data from Bargar and Jackson, 1974, table 1; sea floor assumed approximately level at depth of 5 km below sea level]

	Subaerial part		Submarine part		Total	
Volcano	Volume above sea level (10^3 km)	Fraction above sea level (percent)	Volume below sea level (10^3 km)	Fraction below sea level (percent)	Volume above plus below sea level (10^3 km)	Fraction of entire island mass (percent)
Mauna Loa	7.5	17.6	35.0	82.4	42.5	38
Kilauea	0.7	3.6	18.7	96.4	19.4	17
Hualalai	0.6	4.8	11.8	95.2	12.4	11
Mauna Kea	3.1	12.5	21.7	87.5	24.8	22
Kohala	0.4	2.9	13.6	97.1	14.0	12
Entire Island	12.3	10.9	100.8	89.1	113.1	100

variety of subjects covered by the succeeding papers in this section, however, demonstrates that such a view is oversimplified, and the geologic history actually includes a rich diversity of processes and events that were deciphered through the efforts of a long succession of geologists and other workers. Hence the geologic history of the Island of Hawaii will here be related from the point of view of how the concepts evolved during the last two centuries—in essence, a history of the development of the understanding of Hawaii's geologic history.

ACKNOWLEDGMENTS

Ideas summarized in this paper stem from the long progression of geologists who have worked on Hawaii, far too numerous to mention individually, but who merit sincere gratitude and are here collectively recognized. Special thanks are given to R.W. Decker, who stimulated the production of the paper, and to R.T. Holcomb, who served as a ready source of information, ideas, and constructive criticism. We also particularly thank R.I. Tilling and W. A. Duffield, who greatly improved the paper by their incisive and thorough reviews.

DEVELOPMENT OF CONCEPTS OF THE GEOLOGIC HISTORY OF HAWAII

PROGRESS FROM THE LATE 18TH CENTURY TO THE MID-20TH CENTURY

It is possible to summarize simplistically the geologic history of Hawaii in a single sentence: Hawaii has been built of adjacent and partly overlapping mounds of basaltic lava flows and small amounts of tephra, which originated on the ocean floor and successively grew above the sea to form the five distinct volcanoes that compose the still-evolving island. However, such a condensed history does not consider related processes and conditions that have shaped these volcanoes, such as changes in composition of the magma, shifts in vent location, causes and manifestations of stresses within the volcanoes, diversity of eruptive style and flow behavior, variations in duration of inactive intervals, and interactions between eruptive products and sea water. Underlying the development of the island, however, is the fundamental process of volcanism, for without countless and repeated volcanic eruptions, the Island of Hawaii would not exist.

Evidence of recent volcanism was noticed by even the earliest European visitors. The journals of Captain James Cook, who was the first European to visit Hawaii in 1778, emphasized navigation, geographic discovery, flora, fauna, and the nature of the endemic people, noted the volcanic characteristics of the island (Beaglehole, 1967, p. 486): "The coast of the Kau district presents a prospect of the most horrid and dreary kind: the whole country appearing to have undergone a dreadful convulsion. The ground is covered with cinders and intersected with black streaks which mark the course of lava that has flowed, not many ages back, from the mountain to the sea. The southern promontory looks like the dregs of a volcano." One of Cook's sailors, John Ledyard, led a field party to the interior of the island, where fresh lava flows and other signs of recent volcanic activity were encountered. Ledyard (1783) expressed the astute opinion that the entire island was of volcanic origin. However, members of the Cook expedition seemed unaware that the island included active volcanoes. Captain George Vancouver, on an expedition to Hawaii in 1793–94, was the first to record volcanic activity on the island (Vancouver, 1798, p. 8). Archibald Menzies, the botanist on the Vancouver expedition, explored part of the interior of the island and led ascents of Hualalai and Mauna Loa. Menzies' account of this first recorded ascent of Mauna Loa is a fascinating tale of hardship and persistence (see Hitchcock, 1909, p. 63–79). Menzies described the volcanic character of Mauna Loa, particularly the summit region, and he noted fume clouds and ash issuing from Kilauea.

The first detailed descriptions of Hawaiian volcanic activity were written by missionaries and were based in particular on a notable trip around the island trip in 1823. William Ellis (1827) described the characteristics of rocks and landforms and provided sketches and vivid impressions of the vigorous behavior of lava lakes and vents on the floor of Kilauea caldera. Joseph Goodrich (1826), an American missionary stationed at Hilo, wrote to Benjamin Silliman, editor of the American Journal of Science, with information about Kilauea; his earliest letter recounted the same journey described by Ellis. Based on the volcanic activity and the landforms they observed throughout the trip, these missionaries ascribed the origin of the entire island to volcanism. Ellis summarized this conclusion as follows (Ellis, 1827, p. 181): "The whole island of Hawaii, covering a space of four thousand square miles, from the summits of its lofty mountains * * * down to the beach, is, according to every observation we could make, one complete mass of lava, or other volcanic matter, in different stages of decomposition. Perforated with innumerable apertures in the shape of craters, the island forms a hollow cone over one vast furnace, situated in the heart of a stupendous submarine mountain, rising from the bottom of the sea * * *."

During the following years, sporadic visits to the volcanoes were reported by missionaries, sea captains, and a few other persons. The accounts of most of these visits are conveniently summarized by Dana (1890), Brigham (1909), and Hitchcock (1909). The accounts of several missionaries of this period, notably Goodrich and C.S. Stewart, were published in the American Journal of Science, the Missionary Herald, and a few other journals (see Macdonald, 1947). The botanist David Douglas described his visits to Kilauea and Mauna Loa in 1834 (Douglas, 1914; Harvey, 1947, p. 220-231). These accounts document the major changes in the morphology of Kilauea caldera and the persistent action of the lava lake and other vents on the caldera floor during the early and middle decades of the nineteenth century.

The first systematic exploration of the Hawaiian volcanoes was carried out by members of the Wilkes expedition during 1840–41. Wilkes' (1845) own narrative includes fascinating accounts of the exploration and of specific trips to the volcanoes, but J.D. Dana (1849) provided geological insight into the volcanoes and their role in the development of the island (Appleman, chapter 60). Dana noted the generally quiet behavior of Hawaiian volcanoes, their gently sloping flanks, and the scarcity of products from explosive eruptions. He correctly ascribed these features to the high fluidity of the Hawaiian lava in contrast to the more viscous lava of steeper sided volcanoes with more explosive habits. He also described the concentration of vents in the summit areas and along narrow linear zones radiating from the summits (the concept of the rift zone), and he correlated flank eruptions of Kilauea with concurrent subsidence of the lava lake and caldera floor—evidence of possible connection between flank and summit magma conduits. Even so, Dana regarded Kilauea as only a vent of Mauna Loa, rather than an independent volcano. For example, he described the island of Hawaii as being made up of three volcanoes, "Mount" Kea, "Mount" Loa, and Hualalai (Dana, 1849, p. 159), and he stated that volcanic activity was "confined to Loa and Hualalai" (p. 168). Furthermore, he included his general discussion of Kilauea (p. 171–206) in the section on Mauna Loa (p. 168–214). Nevertheless, he wondered about the lack of correlation in their activity and was puzzled that lava could be elevated to erupt at the summit of Mauna Loa while nearly 10,000 feet lower an open, constantly active conduit fed the lava lake at Kilauea. Although he proposed a separation of conduits (p. 218–221), he did not suggest that Kilauea might be an independent volcano. Finally, he described Kohala as a ridge separated from Mauna Kea by a scarp, but he

did not define it as a separate volcano or even as part of the three volcanoes making up the island.

The eruptive activity of Kilauea and Mauna Loa during the next four decades (1840–1880) was reasonably well documented, in spite of only irregular visits and the lack of an established system of surveillance. This documentation is chiefly owing to Titus Coan, a missionary stationed at Hilo and a perceptive and dedicated volcano observer. His missionary duties required frequent trips past Kilauea, and from 1840 to the early 1880's he recorded the volcano's activity. From the 1850's he summarized his observations in letters to his friend, J.D. Dana, who became the editor of the American Journal of Science, and Coan's graphic descriptions regularly found their way into the pages of that journal. He also observed the activity of Mauna Loa, although access there was much more difficult; he recorded the dates of eruption, and for most of the significant ones was able to visit the scene of the action. Several other missionaries, a few scientists, and an occasional tourist also made observations that were published. These reports were compiled by Dana (1890), Hitchcock (1909), Brigham (1909), and Macdonald (1947). Nearly all accounts from those of the Wilkes expedition to Dutton's study in 1882 were purely descriptive, but the record they chronicled provided evidence supporting the concept that the long-term growth of the island was the product of episodic lava flows from the active volcanoes.

C.E. Dutton carried out the most extensive geologic studies of Hawaii in the 19th century (Dutton, 1884). He described the surface morphology and structure of the five volcanoes. He recognized that Kilauea is a separate volcano, distinct from Mauna Loa (Dutton, 1884, p. 120–121) for the following reasons: (1) The distance between Kilauea and Mauna Loa is about the same as the distance between other pairs of adjacent volcanoes of the island; (2) according to hydrostatic principles, the difference in elevation between lava lakes at Kilauea and the summit of Mauna Loa is too great to permit liquid continuity; (3) Kilauea caldera "is situated on a totally distinct mountain pile," the top of which stands topographically above a saddle that separates the two volcanoes. Dutton observed that flows from the two volcanoes are intercalated and thus that the two volcanoes are intergrown. He concurred with Dana that Hawaiian volcanoes have gentler flanks than many other well-known volcanoes. Dutton emphasized the immense size of Mauna Loa, especially in view of its apparently huge submarine part, and he reasoned that Mauna Kea, which rises higher than Mauna Loa but has steeper sides and a smaller base, is considerably smaller in volume.

The distinction between the basaltic lava types of pahoehoe and aa commonly is credited to Dutton (1884 cited by Macdonald, 1972, p. 71; Peterson and Tilling, 1980, p. 272), although Dana (1849, p. 161–163) accurately described "pahoihoi" and "clinkers" several decades earlier. However, Dutton (1884, p. 95) apparently first introduced the Hawaiian term aa for the slaggy, rough, clinkery type. After Dutton's report, the terms aa and pahoehoe came into common use. Dutton (1884) suggested that the two lava types form because of contrasts in the dimensions of the lava flows and in the relations among lava movement, cooling, and solidification. He also (p. 105) proposed that the term caldera is more appropriate than the term crater to describe the large depressions at the summits of Kilauea and Mauna Loa.

During the 19th century, Kilauea's intracaldera lava lake, which was active for many decades, received the most attention. Dutton described his own observations and quoted extensively from the writings of others in summarizing activity that included vigorous fountaining and lava flows, quiet circulation within multiple lava lakes, updoming of portions of the caldera floor, and noisy and sometimes spattering "blowing cones," all of which were interspersed with major episodes of lava withdrawal and partial collapse of the solid floor of the caldera (Dutton, 1884, p. 106–119). Such behavior led him to speculate (p. 126) that the caldera formed as a consequence of repeated fluctuations in the height of the lava column. He reasoned that when the column was high, wall rocks were softened or melted by magmatic heat, and when the column lowered, such weakened rock spalled off and sank; thus repeated oscillations of the lava-column height caused the depression to enlarge. He seems to have visualized a magma column nearly as wide as the caldera. While not every facet of his explanation finds favor today, Dutton deserves credit for recognizing the process of collapse as essential to the development of the caldera. Like Dana, he recognized that linear zones of weakness (now called rift zones) radiate from the summit and noted that eruptions along these zones were accompanied by lowering of the lava column in the caldera.

Dutton (1884) visited the source of the 1880–81 eruption of lava from the northeast flank of Mauna Loa, and he accurately described the structure and character of the rift zone there. He was impressed by the large volume of lava produced during this 11-month-long eruption and by the small proportion that remained near the vents. He identified vent areas of earlier eruptions and thus gained considerable insight into the manner in which the volcano, and indeed the island, grew from rift eruptions. A brief excerpt is appropriate to summarize the concept he visualized (Dutton, 1884, p. 134–135):

> There is a strange fascination in wandering over this vast expanse of desolation. No doubt the dominant idea is the immensity of it. The best conception of the magnitude of Mauna Loa is to be obtained by attempting to traverse any limited district of it on foot. Mile after mile may be traversed but the landscape seems ever the same. All the great landmarks seem to stand just where they stood an hour before * * *. The only alternations are from aa to pahoehoe. Traces of recent eruptions are seen everywhere, but all the views are fragmentary. So extensive has each and every one of them been that the greater portions of them always reach far beyond the limits of vision, and mingling together are lost in the confusion of multitude. The imagination is discouraged at the thought that this colossal pile has been built up by thousands upon thousands of these eruptions.

Dutton himself saw no eruption in Mokuaweoweo, the summit caldera of Mauna Loa. However, from his review of the observations of others, he concluded that activity at the summit generally preceded flank eruptions and that summit activity declined and ended when lava broke out on the flanks, suggesting hydraulic connections among various vents of the volcano. As he had for the caldera of Kilauea, Dutton advocated for Mokuaweoweo an origin by collapse, citing a lack of evidence for explosive origin and the abundance of partly subsided blocks. He speculated that a caldera would tend to develop at the summit of a volcano when it grew large

enough for flank eruptions to occur and draw lava from a summit magma reservoir, thus reducing support beneath the central orifice. He therefore proposed that summit depressions could have existed at both Mauna Loa and Kilauea throughout much of their development (Dutton, 1884, p. 142–143).

Dutton concluded that Mauna Kea had long been inactive, because the rocks are deeply weathered, soil cover is common, and ravines and canyons disrupt the profile of the flanks, particularly on the northeastern, windward side (Dutton, 1884, p. 160, 168–170). He described the abundant cinder cones in the summit area of Mauna Kea and took note of the nearby flows of unusually hard and flinty lava that was used by Hawaiians for tools and weapons (p. 163–164). In recent years these distinctive rocks have been recognized as products of magmatic differentiation, but the idea of differentiation was spawned long after Dutton's time and he did not speculate on the cause of the somewhat unusual character of the quarried rock.

Dutton mentioned Kohala only briefly, recognizing it as the volcano longest inactive on the island, as demonstrated by its deeply incised canyons and its thick soil (Dutton, 1884, p. 171). He described Kohala lava as basalt with a tendency toward andesite, and he noted its many cinder cones. Similarly, his description of Hualalai is brief; he noted the abundant cinder cones in its summit region, the basaltic character of its lava, and the common occurrence of olivine (p. 173–174). He stated (p. 83) that Hualalai erupted three times in the early 19th century, later giving dates of 1801 (p. 181) and of 1805 and 1811 (p. 173), but he did not cite a source for these dates, which are in part at variance with the now commonly accepted time of eruption during 1800–1801 (Moore and others, chapter 20; Ellis, 1827, p. 38; Stearns and Macdonald, 1946, p. 146).

Stimulated by his participation in the Wilkes expedition, Professor James Dwight Dana of Yale University maintained a lively interest in Hawaii throughout his long and distinguished career. He kept himself informed about virtually every reliable observation of activity at Kilauea and Mauna Loa and published many accounts of it in the American Journal of Science. Dana made his second journey to the islands in 1887 at the age of 74 and later published a book (Dana, 1890) that served for years as the definitive work on Hawaiian volcanoes. Dana's general ideas on the geologic history of the volcanoes remained similar to those he developed on the Wilkes expedition, which were summarized above. However, he ultimately accepted the evidence offered by Dutton and others that Kilauea is a separate volcano and not part of Mauna Loa. This change in opinion was evidently not easy for him, as in the process of acquiescing he devoted several pages (Dana, 1890, p. 258–264) to recounting the virtues of his original views.

About two decades later, two major volumes were published about the volcanoes of Hawaii (Brigham, 1909; Hitchcock, 1909); each includes a chronological narrative of the activity of Kilauea and Mauna Loa, and each includes many photographs of volcanic features, as well as maps that illustrate the changes in caldera morphology through the years. Brigham's work also contains many of his own personal observations and experiences. Hitchcock's personal observations are fewer, but he was particularly diligent in documenting information, and the usefulness of his volume is enhanced because of extensive quotations from sources now hard to find. Although neither author developed new concepts on volcano development, their descriptive chronologies are very valuable. The timing of their publication was serendipitous, as these unique reference volumes appeared just before the establishment of the Hawaiian Volcano Observatory (HVO) in January 1912.

The founding of the HVO by T.A. Jaggar began the modern era of continuous surveillance and systematic documentation of the Hawaiian volcanoes (Apple, chapter 61). Jaggar and other HVO staff members made detailed daily observations of Halemaumau, and various scientific instruments were introduced to complement the regular program of observation. The easily accessible lava lake at Halemaumau offered abundant opportunities for observation and experimentation, and Jaggar collaborated with visiting scientists to build a new understanding of the behavior of Hawaiian volcanoes. Vast amounts of data were collected on the circulation and the rise and fall of the lava lake, composition of lava, character of seismicity, ground deformation, gas chemistry, and lava temperatures. In addition to the activities of the lava lake, all eruptions of Mauna Loa and Kilauea were thoroughly documented. Jaggar made several successful long-range forecasts of Mauna Loa activity.

Jaggar was a geologist and a geophysicist; he was a keen observer of eruptive phenomena, and he was much interested in experimentation and development of instruments. He and his collaborators led volcanology from a science of description to a science of quantitative measurement, experimentation, and interpretation. He wrote prolifically (see, for example, Jaggar, 1947); a convenient summary of his major writings appears in Macdonald (1947, p. 83–103).

Jaggar proposed that the magma column of Halemaumau consists of (1) hypomagma, a homogeneous, aphyric fluid from a source deep within the Earth, with gas contained in solution; (2) pyromagma, a vesiculating gas-rich foam, which constitutes the highly fluid portion of lava lakes and includes the lava of erupting fountains and; (3) epimagma, which he also called bench magma, a highly crystalline, pasty, largely degassed but still-incandescent lava forming the floor and lining of lava lakes; he visualized epimagma as forming the contact sheath of the magma conduit. Although Jaggar's terms are chiefly applicable to active lava lakes and have been but little used, they help to illustrate his key concept that the rate and amount of gas vesiculation determine the behavior of erupting lava.

Jaggar postulated a tidal influence on the behavior of Halemaumau lava lake, which led him to propose that activity peaked at solar equinoxes and solstices. Subsequent workers have found little evidence to substantiate the latter proposal, although investigations continue into the possibility that tidal maxima serve as a trigger for some eruptions (Shimozuru, chapter 49; Dzurisin, 1980). Jaggar sought diligently for evidence of cyclicity in eruptive behavior, and he was convinced that changes in behavior were governed by the 11.1-yr sunspot cycle, upon which was superimposed a 134-year cycle defined by the interval between the explosive eruptions of Kilauea in 1790 and 1924. Reexamination of his evidence and the timing of subsequent eruptions have failed to support his concepts regarding the sunspot cycle.

He was impressed by certain coincidences of eruptive events at Mauna Loa and Kilauea; although they rarely erupted simultaneously, Jaggar thought he recognized lowering of the Halemaumau lava lake during eruptions of Mauna Loa. Hence he advocated the view that Kilauea and Mauna Loa are closely interconnected (Jaggar, 1947, p. 90, 200), even though he clearly regarded them as independent systems. He interpreted the island to be arranged as a cross (Jaggar, 1920, p. 193–195; 1947, p. 90), in which the north-northeast-trending upright extends from Mauna Kea summit through the summit and along the southwest rift zone of Mauna Loa to South Point. The transverse arm of the cross extends between Hualalai and Kilauea summits, which are symmetrical about the upright, and the summit of Mauna Loa lies near the intersection of the two elements. Kohala is not part of this structure. (This cross pattern can be recognized by noting the geographical relations of the four volcanoes, see fig. 7.2). The supposed geographic symmetry of Hualalai and Kilauea, the record of occasional explosive eruptions of Kilauea, and Kilauea's lesser output of lava than Mauna Loa convinced Jaggar that Kilauea is older than Mauna Loa and that it is approaching the same state of "decadence" as Hualalai has achieved (Jaggar, 1920, p. 191–198).

Stearns and Macdonald (1946, p. 135) demonstrated that Kilauea and Hualalai behave quite independently of one another. Kilauea's many eruptions since the 1950's, as well as petrogenetic considerations developed after Jaggar's time and discussed later herein, refute any suggestion that the volcano is in late decline. Even though not all of Jaggar's hypotheses have withstood the test of time, his contributions remain monumental. His many observations and thorough documentation of the activity of Kilauea and Mauna Loa constitute a permanent record of the growth processes of Hawaiian volcanoes.

Other scientists made many contributions in studies of Hawaiian volcanism during the decades of the 1910's to 1940's. The petrologic studies of Daly (1911, 1914, 1933, 1944), Cross (1915), and Washington (1923a, b, c) demonstrated the near-constant composition of highly fluid lava throughout most of the subaerial growth of the volcanoes and the variable composition of the late differentiated lava. Through integrated field and laboratory studies, Sidney Powers (1916, 1920) helped document the relations between lava composition and eruptive behavior. Stone (1926) reviewed published reports of Kilauea and was perhaps the first to describe the geology and geologic history of the whole of Kilauea. H.A. Powers (1935) evaluated the differentiation processes and pointed out that crystal fractionation alone could not account for Hawaiian differentiated rocks. Wentworth (1938) examined geomorphic processes and the products of explosive eruptions. Harold T. Stearns and colleagues began systematic geologic mapping in the 1920's, which led to the first geologic map of a part of the island (Stearns and Clark, 1930) and eventually to a comprehensive geologic report about the entire island (Stearns and Macdonald, 1946). Their geologic map of the island (scale 1:125,000) established a consistent stratigraphic nomenclature and thus provided a basis for examining the stratigraphic relations among the five volcanoes (figs. 7.3 and 7.4). The mapping was complemented by petrologic and petrographic studies (Macdonald, 1949a, b). The combined results are the foundation upon which all further geologic investigations of Hawaii have been built.

From his studies throughout the islands, Stearns (1940) defined a progression of four stages of volcanism, which he later (1946, p. 17–20; 1966) expanded to a series of eight stages that describe the growth, erosion, submergence, reef development and posterosion volcanism of the Hawaiian and other islands of the central Pacific (fig. 7.5). The following summary reviews Stearns' ideas as expressed in 1946; their subsequent modifications are discussed later.

Stage 1 involves building the volcano from the ocean floor to sea level. The volcano produces mostly pillow lava, and Stearns believed then that the submarine deposits include extensive tuff from explosive interaction between molten lava and seawater. The first material to emerge above sea level is poorly consolidated ash that erodes rapidly. Eventually subaerial lava flows veneer this material, reducing the rate of wave erosion.

Stage 2 is the subaerial growth of the volcano. Countless thin sheets of highly fluid, compositionally uniform primitive olivine basalt erupt from rift zones and a central crater to build the volcano; Stearns (1946, p. 17) described the edifice as a shield-shaped dome. Eruptions are closely spaced in time; because of this and the high surface porosity that minimizes runoff, virtually no stream erosion occurs. Rare explosive eruptions may occur. All the volcanoes on Hawaii have already passed through this youthful stage.

Stage 3 of Stearns is characterized by collapse around the summit vent areas to form a caldera and subsidence along the rift zones to form craters and grabens. Eruptions continue to be frequent, and the lava continues to be of uniform composition. Explosive eruptions may occur slightly more frequently than during stage 2. Caldera walls prevent overflows of lava onto the flanks behind them, and so localized erosion and stream drainage may develop on sectors of the volcano not frequently covered by new lava. Kilauea and Mauna Loa are now in this stage.

Stage 4 is characterized by change in lava composition from primitive basalt to more alkalic types such as andesite and trachyte. These more viscous lavas fill any caldera, craters, and grabens and build a steeper sided cap. Explosive eruptions are common, ash is interbedded with lava, and cinder cones may be abundant. Intervals between eruptions are longer, and erosion increases; disconformities may separate successive flows and ash layers. Stearns (1946, p. 19) regarded Hualalai, Mauna Kea, and Kohala to be in this stage.

Stage 5 is dominated by stream and marine erosion. Local climate and exposure to prevailing winds and ocean currents determine the rate of erosion. The subsequent stages 6 (subsidence and reef building), 7 (emergence and renewed volcanism), and 8 (atoll and resubmergence) (fig. 7.5) have not yet been reached by the volcanoes of Hawaii; they are represented by volcanoes on other islands to the northwest.

This order of stages as proposed by Stearns (1946, 1966) culminated a century and a half of gradually improved understanding of the processes of growth and development of Hawaii and its sister islands. Subsequent studies have modified or redefined some of the stages, but much of the early foundation remains firm to the present day.

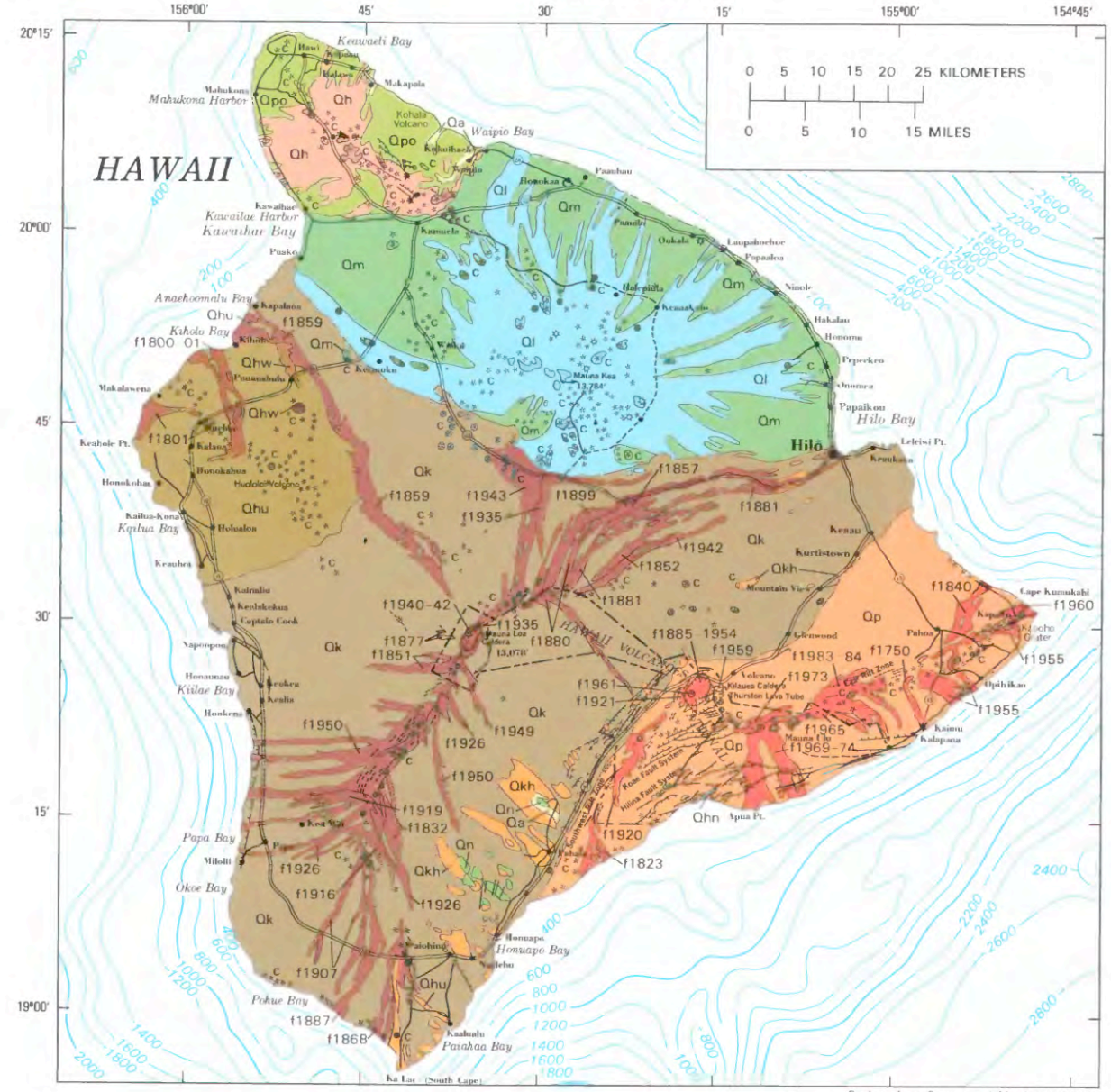

EXPLANATION

Kohala

Qa — Unconsolidated sediment

Qh — Hawi Volcanics c, cones and domes

Qpo — Pololu Basalt c, cones and domes

Mauna Kea

Ql — Laupahoehoe Volcanics c, cones and domes

Qm — Hamakua Volcanics c, cones

Hualalai

f / Qhu / Qhw — Hualalai Volcanics f, historical flows (year given) c, cones; Qhw, Waawaa Trachyte Member

Mauna Loa

f / Qk — Kau Basalt f, historical flows (year given); c, cones and pit craters

Qkh — Kahuku Basalt c, cones and pit craters

Qn — Ninole Basalt

Kilauea

f / Qp — Puna Basalt f, historical flows (year given); c, cones and pit craters

Qhn — Hilina Basalt

Cinder, spatter, or littoral cone — Pit crater or caldera — 100 Depth contours in fathoms — Fault lines and borders of calderas Hachures on downthrown side

FIGURE 7.3.—Geologic map of Island of Hawaii. Geology from Stearns and Macdonald (1946), with lava flows from 1946 to 1984 added. Taken from American Association of Petroleum Geologists Geological Highway Map: Alaska and Hawaii (Circum-Pacific Edition, 1974); modified with permission from the American Association of Petroleum Geologists. Stratigraphic nomenclature from Langenheim and Clague (chapter 1, part II). Figure 7.4 shows correlation of geologic units among several volcanoes.

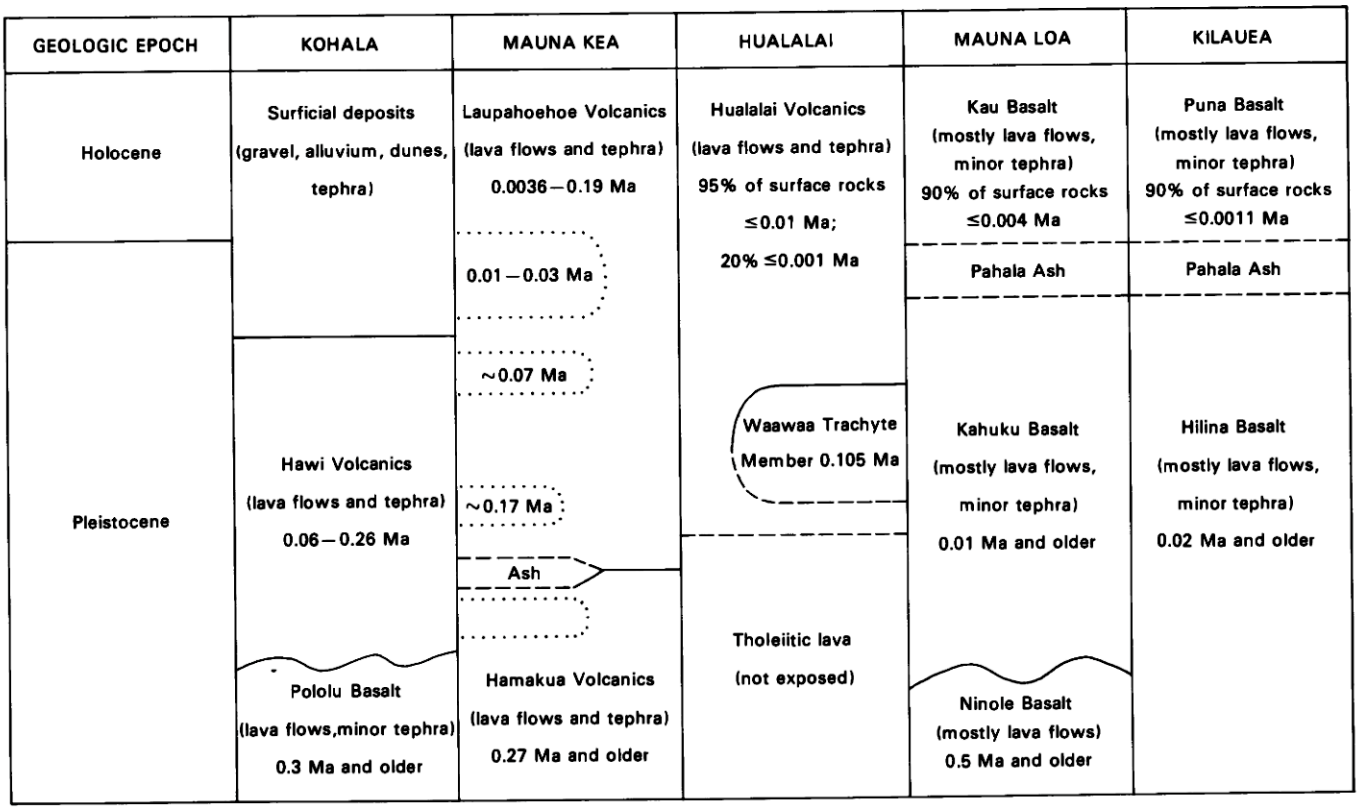

FIGURE 7.4.—Correlation chart showing major rock units on Island of Hawaii and their relative stratigraphic positions. Most names established initially by Stearns and Macdonald (1946), some units redefined by subsequent authors; relations shown here and nomenclature from Langenheim and Clague (chapter 1, part II). Numerical ages generalized from radiometric values given by various references cited in text. Dashed lines: indefinite, gradational, or controversial boundaries; dotted lines: glacial deposits (at Mauna Kea; from Porter, 1979a, 1979b); wavy lines: distinct hiatus.

DEVELOPMENTS SINCE THE MID-20TH CENTURY

The recognition and definition of the stages of island growth by Stearns (1946, 1966) were achieved in spite of severe limitations in the available evidence bearing on geologic history. The most significant limitations were these: (1) The submarine part of each volcano, which records the early geologic history, was inaccessible. (2) Present exposures reveal only the youngest rocks on most of the island's volcanoes. (3) Precise methods for dating basaltic lava had not been developed. We will consider the consequences of each of these limitations.

(1) Volcanoes are roughly conical in shape, so most of the volume of volcanic islands in the deep ocean lies below sea level. Bargar and Jackson (1974) used topography and bathymetry to measure the volumes of subaerial and submarine portions of the volcanoes of the Hawaiian-Emperor Chain; their results for the Island of Hawaii are shown in table 7.2. Only about 11 percent of the volume of the volcanoes of the island is above sea level, yet only the rocks and surface morphology of this part were available to Stearns and his associates for study. It is this small fraction that provided the evidence for Stearns' scheme of growth stages.

(2) Of this small subaerial fraction, erosion has penetrated the surface lavas only slightly or not at all on most volcanoes of the island. Even on Kohala and Mauna Kea, the most deeply eroded volcanoes, the exposed sections reveal but a small fraction of the geologic history. Hence the growth stages have been inferred chiefly from the most recent events as recorded by surface lavas and by analogy to the older, more deeply eroded volcanoes on the other islands. Even on older islands, however, erosion has only partly uncovered the subsurface rocks.

(3) Until the mid-20th century, fossils were the chief tool for determining rock ages, and few Hawaiian rocks contain fossils. Hence the only rocks that could be dated with much confidence were flows that had been emplaced during historical time. The dates of other geologic events were estimated by extrapolation of recurrence intervals of historical eruptions or inferred from rates of weathering, relative amounts of vegetation growing on old lava, degree and estimated rates of erosion, and stratigraphic relations among the exposed rocks. Even though such methods permitted conclusions to be reached, the lack of a way to measure numerical ages of basalt placed severe constraints on many geologic interpretations.

Since the time of the reports by Stearns (1946) and Stearns and Macdonald (1946), the gaps in knowledge have been narrowed through advances in a variety of disciplines, including geophysics, petrology, submarine geology, and radiometric and other dating techniques. Additional insights have been achieved through detailed

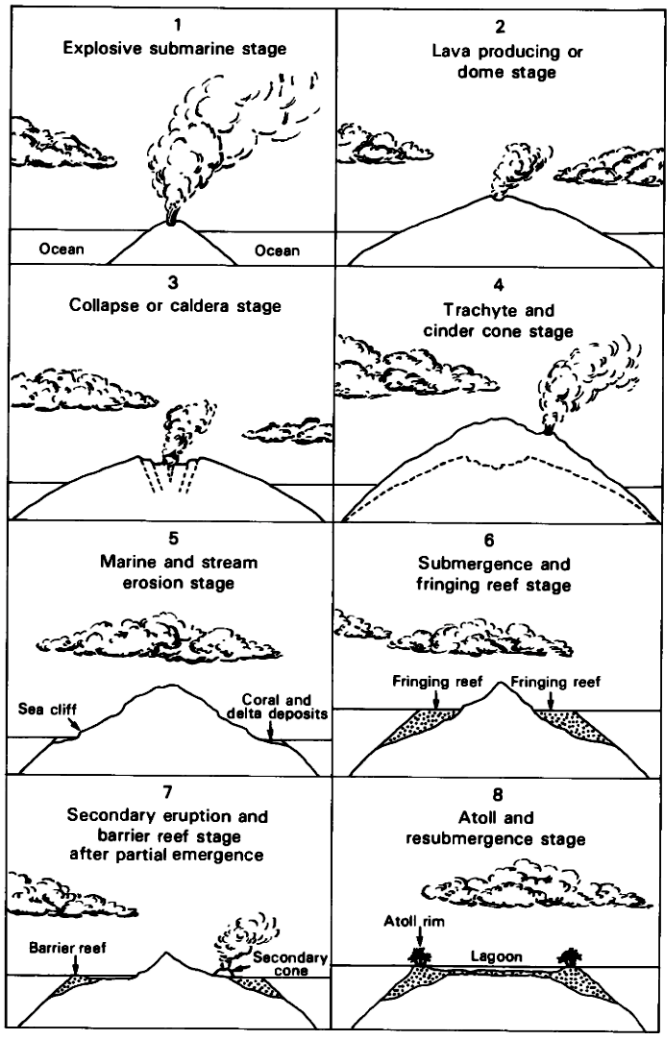

FIGURE 7.5.—Eight stages proposed by Stearns (1946) for geologic history of a volcanic island in the central Pacific.

geologic mapping of many areas, sophisticated applications of aerial photography, and sustained critical observations of a wide variety of eruptive activity. Findings at Loihi Seamount, 30 km offshore from the south coast of Hawaii, and its recognition as an active volcano have been of special value.

SUBMARINE INVESTIGATIONS

Investigations of submarine volcanism around Hawaii, including sea bottom photographs and studies of dredged samples, were begun in the 1960's. J.G. Moore and collaborators showed, for example, that at depths from 490 m to 5,190 m along the submarine extension of the east rift zone of Kilauea, virtually all the sea-floor material is fresh pillow lava, some of which is fragmental; nearby seamounts are composed of similar material, although most is less fresh and mantled with sediment (Moore and Reed, 1963; Moore, 1965). These studies found no indication of chemical exchange between erupting lava and sea water; rock composition, including water content, did not vary with depth. A progressive decrease in vesicle size, however, was observed to a depth of about 800 m, below which only microscopic vesicles were found. These findings confirmed the long-held inference that pillow lava is the dominant product of undersea basaltic eruptions of Hawaiian volcanoes. Pillow lava may also form when subaerially erupted lava enters the sea (Moore, 1975). The systematic relation between water depth and vesicle size apparently provided a tool by which the depth of eruption of submarine lava might be estimated. It was later found, however, that alkalic basalt dredged from Loihi at depths of 1–2 km has high vesicularity in comparison with tholeiitic samples collected at comparable depth (Moore and others, 1982, p. 91), demonstrating that vesicle size is a function of more than just depth of eruption.

The restricted development of vesicles in submarine tholeiites suggests that hydrostatic pressure of sea water inhibits vesiculation and explosive eruptions at depths below a few hundred meters (Moore, 1965). In contrast, explosive activity is common at the shoreline and in shallow depths, and it produces a zone of clastic debris intermixed with lava that extends from sea level to depths of several hundred meters (fig. 7.6). Explosive interactions occur between molten lava and sea water during shallow-water eruptions and also when subaerial lava flows enter the sea; the fragmented material may then be transported to cover deeper slopes. Fragmentation processes of explosion, implosion, thermal shock, and wave abrasion were observed at Kilauea from 1969 to 1973 during flows into the sea from Mauna Ulu (Moore and others, 1973; Peterson, 1976); the fragmented products are interleaved with coherent subaqueous lava flows, including pillow lava. Constructional submarine slopes are steep enough that slumping and landslides are common processes (Moore, chapter 2); near Oahu and Molokai, evidence has been found for truly huge submarine landslides (Moore, 1964). Slopes of the subaerial shields of the volcanoes are more gentle, in distinct contrast to steeper submarine slopes (Moore and Fiske, 1969). As the edifice grows through continuing eruptions, the clastic zone is covered by subaerially erupted lava, and it forms a layer between the submarine and subaerial lava that is a marker horizon extending through the volcano, preserving a record of the littoral and shallow-water processes and of subsidence of the island (fig. 7.6).

These and other investigations helped to characterize the submarine platform upon which the island rests and the behavior of lava in the presence of seawater. They are limited, however, to the exposed carapace and so do not give direct information about the internal core and the early history of the volcanoes. The recent recognition of Loihi Seamount as an active volcano, however, has furnished an opportunity to study an earlier stage in the growth of a Hawaiian shield volcano.

PETROLOGIC INVESTIGATIONS

Studies of Hawaiian lavas have made major contributions to igneous petrology during recent decades. The lavas are ideal for detailed investigations, because they reflect magma-generation and

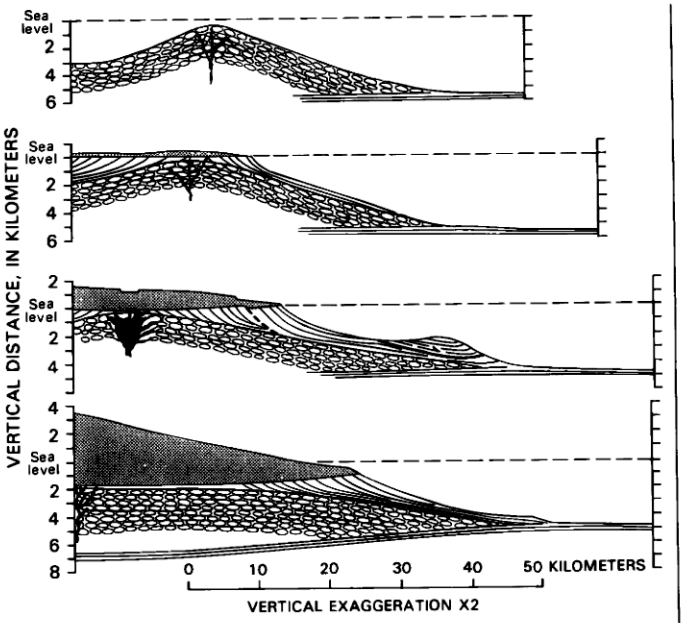

FIGURE 7.6.—Cross sections illustrating oceanic volcanic islands in submarine, sea-level, and subaerial stages of evolution (reproduced from Moore and Fiske, 1969, fig. 3, p. 1200). Patterns indicate rock types: ovals, pillow lavas with included pillow fragments and sediment; lined pattern, clastic rocks, including phreatic-explosion ash, littoral-cone ash, and flow-foot breccia and including some pillowed flows and pillow breccias; dark pattern, subaerial lava flows with minor ash; solid black, intrusive rock. Note contrast between submarine and subaerial slopes, continuation of clastic layer beneath subaerial shield, and downbowing of sea floor by subsidence caused by volcanic loading. Depth and elevation figures left side are in feet.

petrogenetic processes uncontaminated by assimilation of continental crustal rocks. Recent petrologic investigations of Hawaiian lavas are discussed in several papers elsewhere in this work (for example, Wright and Helz, chapter 23; Tilling and others, chapter 24), and the general petrologic development of the individual volcanoes of Hawaii is summarized later in this paper. Here we relate the growth stages established by Stearns (1946, 1966) to modern petrologic concepts and terminology.

The terminology applied to the lavas of Hawaii has shifted considerably during recent decades. In this paper we use the terms tholeiite and alkalic basalt and names for the other more differentiated lavas according to the usage adopted by Macdonald (1960) and Macdonald and Katsura (1961, 1962, 1964). They concurred with Powers (1935, 1955) that crystal fractionation alone cannot explain all of the chemical variation in rocks of the alkalic suite. Because no source materials for assimilation are available, Macdonald and Katsura (1961, 1962) suggested that volatile transfer and thermodiffusion might play a role in the differentiation processes. Another proposal was that wholly independent parent magmas produced the tholeiitic and alkalic suites (Kuno and others, 1957), but Macdonald and Katsura (1962) opposed this idea because of the small proportion of rocks representing alkalic magma. These and subsequent studies have retained the concept that voluminous and frequent eruptions of tholeiitic lava build a shield volcano (stage 2 of Stearns, 1946), with or without a summit caldera, and that this is followed by a transition to less frequent and less voluminous eruptions of more alkalic lava and tephra, which build a steeper sided carapace atop the shield (stage 4 of Stearns, 1946).

Petrologists have long sought to explain the origin of these two suites of lava. Samples of lava erupted at Kilauea Volcano from the 1950's to the present have helped relate eruptive behavior to the petrogenesis of tholeiitic magma (for example, Macdonald and Katsura, 1961; Murata and Richter, 1966; and Wright, 1973). Lava of the tholeiitic suite exhibits small but distinct chemical and mineralogical variations; most of these variations can be explained by the addition or subtraction of olivine, and hence such lava is referred to as olivine-controlled lava.

Powers (1955) first proposed the concept of distinct batches of magma derived from different parts of the mantle to explain variations other than those caused by olivine control. It was subsequently shown that olivine-controlled tholeiites of Mauna Loa appear to have been derived from a single batch of magma, whereas olivine-controlled tholeiites of Kilauea seem to have come from several separate batches (Wright, 1971; Wright and Fiske, 1971). Later work identified ten different chemical variants (magma batches) of Kilauea magma, which are mixed in varying proportions to produce the lavas erupted between 1968 and 1974 (Wright and others, 1975; Wright and Tilling, 1980). Trace-element contents of the tholeiites of Mauna Loa and Kilauea indicate derivation from more than one parent magma, confirming Powers' (1955) earlier deduction; the magma for each volcano was generated by distinctive partial-melting processes in different mantle source regions (Leeman and others, 1980). More recently, trace-element data suggest that olivine-controlled lavas of Mauna Loa, like those of Kilauea, also exhibit long-term compositional changes with time (Tilling and others, chapter 24; Budahn and Schmitt, 1985).

Wright (1984) proposed that Hawaiian tholeiite is the product of partial melting of mantle material that is residual from the material that earlier yielded midocean-ridge tholeiite and to which new components have been metasomatically added from a deeper melting source beneath Hawaii. This proposal is consistent with the distribution of trace elements and isotopes in the different tholeiites. These concepts provide a sound basis for the astute inferences by early workers that most of the volcano's volume, including much of the hidden portion of the shield, is constructed of tholeiite.

The subtle but significant compositional variations in Hawaiian tholeiites now provide problems and challenges that earlier workers, such as Cross (1915) and Washington (1923a, b, c) never anticipated, but the petrogenesis of the more alkalic lava poses a continuing challenge. Although much of the work on problems of alkalic magma has centered on other islands where more highly differentiated rocks are well represented, three of the volcanoes of the Island of Hawaii include alkalic rocks. Macdonald (1968) has provided a useful summary of the evidence that the alkalic and later suites of lava could be derived from the tholeiitic suite and that such derivation is compatible with the overall patterns of eruptive behavior. These and subsequently developed concepts on the origin of the alkalic suite are summarized by Clague (in press).

Samples dredged from Loihi provided some information with surprising implications for the composition of the deep interior of Hawaiian volcanoes. In addition to the anticipated tholeiite, the dredge hauls included transitional basalt, alkalic basalt, and basanite (Moore and others, 1982; Frey and Clague, 1983). Geochemical studies have led to the inference that the earliest erupted material was alkalic basalt; the initial melted material marking the onset of a new volcano may normally be of that composition (Frey and Clague, 1983). The wide compositional variety of dredge samples suggests that a transition from alkalic volcanism to the tholeiitic volcanism typical of the main growth stage of the shield may now be in progress. Palagonite coatings on the samples of alkalic basalt are thicker than coatings on tholeiite, suggesting that alkalic basalt is the older (Frey and Clague, 1983). Frequent seismic swarms (Klein and Koyanagi, 1979) suggest that Loihi is actively growing. Stratigraphic relations cannot be examined, and an alternate interpretation is that Loihi may now be at the end of the tholeiitic stage and only now is passing into the alkalic stage. The frequent seismicity however, as well as the relative thickness of palagonite, render this less likely. Still further implications of the geochemistry and petrogenesis of Loihi are discussed by Clague (in press). If Loihi is indeed passing from an initial alkalic stage to a tholeiitic stage, as proposed by Frey and Clague (1983), then alkalic volcanism is not solely confined to the waning stages of the life cycle of Hawaiian volcanoes. Even though it now serves as but a single example, findings at Loihi Seamount suggest that the hidden inner cores of Hawaiian volcanoes may record histories more complex than previously assumed.

AGE DETERMINATIONS

Until very recently, the lack of a method to date young basalts, the difficulty of correlating laterally discontinuous lava flows, and the scarcity of marker horizons placed severe limitations on stratigraphic studies in Hawaii. Even when radiometric dating techniques began to be developed and applied in the 1950's and 1960's, their usefulness on Hawaii appeared to be limited. The utility of the K-Ar method is constrained because Hawaiian rocks are very young and very low in potassium. As recently as the early 1970's, radiocarbon dating appeared to be applicable only to the few pyroclastic layers, because they contained the only obvious organic material intercalated among the lava flows. In spite of the difficulties, however, these and other radiometric techniques have subsequently been utilized to obtain numerical ages for many of the prehistoric lavas.

McDougall (1964) obtained K-Ar ages for rocks from several of the older Hawaiian Islands, but his initial effort to date samples from Hawaii (Kohala Volcano) was unsuccessful. However, refined sample preparation and improved techniques enabled a later study to succeed (McDougall and Swanson, 1972). The ages of Kohala rocks in the exposed part of the tholeiitic suite range from about 0.46 to 0.30 Ma, and ages of rocks in the alkalic suite range from about 0.26 to 0.06 Ma. These results established a position in the geologic time scale for the subaerial portion of Kohala Volcano, providing information on its growth rate, the interval between tholeiitic and alkalic volcanism, the duration of alkalic volcanism, and the date of last activity. Perhaps the only other exposed basaltic rocks on Hawaii old enough to be within the range of the K-Ar method are those of the Ninole Basalt on the south flank of Mauna Loa; these have yielded K-Ar ages from more than 0.5 to less than 0.1 Ma (Evernden and others, 1964, p. 156–158). A chronology for both volcanism and glaciation on Mauna Kea was established with the aid of K-Ar and radiocarbon techniques (fig. 7.4; Porter, chapter 21, 1979a, 1979b; Porter and others, 1977).

Initial attempts at radiocarbon dating of Hawaiian samples in the 1960's were confined to carbonized residues found in ash layers; results were not then published. During the early systematic geologic mapping of Mauna Loa in the mid-1970's, methods for finding carbonized organic remains beneath lava flows were improved, providing considerable material for radiocarbon dating (Lockwood and Lipman, 1980). This led to many successful radiocarbon age determinations for lava flows on the volcanoes of Hawaii (Rubin and others, chapter 10; Kelley, 1979; Kelley and others, 1979). However, application of the radiocarbon method is constrained both by its upper limit of 30–40 ka, depending on sample characteristics, and by the restricted distribution of datable carbon associated with lava flows. Woody residues are confined to zones near the margins of lava flows that have invaded vegetated areas, so the method cannot be used for flows above the tree line or in other barren areas nor for portions of lava flows that do not lie near a margin.

Many lavas of Hawaii are too old for radiocarbon dating and too young for K-Ar age determination. A technique that may provide ages within this gap is thermoluminescence (TL). This technique relies on an incompletely understood phenomenon in which light is emitted by certain minerals as they are heated toward the point of incandescence (Berry, 1973; May, 1979). Berry (1973) conducted experiments testing the feasibility of TL as a dating technique for Hawaiian rocks and concluded that the method holds promise. Subsequently more elaborate experiments yielded reasonably consistent results for feldspar from rocks of the alkalic suite for ages from about 250 to 2.5 ka (May, 1979, p. 40). Results for feldspar-poor tholeiitic rocks were not as consistent, but May (1979, p. 41) expressed the belief that a dating technique using TL could ultimately be developed for tholeiites through a range from about 100 to 10 ka.

Another method of dating uses the secular variation of the earth's magnetic field. As iron-titanium oxides in newly erupted lava cool through the Curie temperature, they assume and preserve the direction of magnetism of the earth's field at that time and place. Geomagnetic studies take advantage of this characteristic to construct a history of the changes in orientation of the magnetic field, using rocks that can be dated independently. By matching the magnetic direction of a rock of unknown age to the local geomagnetic history, the possible age(s) of the unknown rock can be determined. Working with lavas already dated by the radiocarbon method, Holcomb (1980) derived the history of the secular variation of the magnetic field in Hawaii for the past 2,500 yr and in turn has applied it to obtain ages for most of the surface flows of Kilauea Volcano. Although this method ultimately depends on radiocarbon

ages, samples for study are not restricted to the vegetated zones where datable carbon may occur. The dates obtained through this approach enabled Holcomb (chapter 12, 1980) to determine that 90 percent of the surface rocks of Kilauea are younger than 1.1 ka.

The increasing degree of weathering with increasing age has long been used to estimate visually the relative ages of lava flows. To see if weathering could be used to derive numerical ages, Halbig and others (1979) correlated the thickness of alteration rinds on basaltic glass with radiocarbon ages of the same lavas. They found that the rind thickens at an average rate of about 1.05 mm/100 yr during the first 1,000 years; thereafter rates become unreliable because of mechanical attrition and spalling. They recognized the potential effects of variations in climate and glass composition but did not study those effects. This technique, even with its probable limitations, has the advantages of being quicker, simpler, and less expensive than radiometric and paleomagnetic age determination, and it may prove useful for qualitative and semiquantitative estimates of age.

CALDERAS AS RELATED TO VOLCANO DEVELOPMENT

Dutton (1884, p. 142–143) suggested that caldera formation was a recurring process during the growth of Hawaiian volcanoes, but the proposal by Stearns (1940, 1946) that a single caldera forms at the end of shield growth was tacitly accepted by most workers until recently (Holcomb, chapter 12, 1976, 1980). Macdonald (1965) reviewed possible mechanisms for the formation of Hawaiian calderas and concluded that most commonly piecemeal collapse occurs above a shallow magma reservoir when magma is withdrawn by either voluminous eruption or intrusion along a rift zone. Macdonald further reasoned, in accord with the ideas of Stearns, that a volcano must achieve a state of maturity for a magma reservoir to have grown to a sufficiently large size for magma withdrawal to be able to trigger collapse. Calderas exposed by erosion at older volcanoes, such as Kohala on Hawaii as well as some on other islands, formed originally within tholeiitic lavas but were later filled by transitional or alkalic lavas. Although such evidence is permissive only, it supports the idea that calderas form at the conclusion of tholeiitic shield building (Stearns, 1940, 1946, 1966; Macdonald, 1965).

Macdonald (1965) considered many hypotheses before selecting a preferred mechanism for caldera formation, but he did not explicitly consider the possibility that such formation might occur more than once. Powers (1948) had suggested the existence of an earlier caldera at Kilauea on the basis of discrepant elevations of young ash beds and partially obscured surface structures. Using additional evidence, Holcomb (chapter 12, 1976, 1980, p. 194) concluded that the present caldera of Kilauea is nested within a prehistoric caldera that had been filled and nearly buried. He also noted evidence for an earlier caldera at the summit of Mauna Loa (Holcomb, 1976). If his conclusions are correct, the presence of a caldera is neither a sufficient nor necessary condition to infer a specific stage in the life cycle of a volcano, and the possibility exists, within any Hawaiian volcano, that a succession of calderas may lie buried.

This viewpoint is supported by results from Loihi, where a bathymetric survey revealed a summit depression approximately 70 m deep, and measuring about 2.8 km by 3.7 km, which includes two pit craters of about 0.8 and 1.2 km in diameter, each of which is more than 250 m deep (Malahoff, chapter 6; Malahoff and others, 1982; summarized by Macdonald and others, 1983, p. 117–118). If Loihi is accepted as a volcano in an early stage of its evolution (see section "Petrologic Investigations"), it provides an additional example of caldera formation at a stage other than near the end of the main growth of a Hawaiian volcano.

This change in thinking is reflected by Macdonald and others (1983, p. 146–149), who no longer specify the development of a caldera as an individual stage in the development of a volcano, but rather include it simply as an event that may happen during the shield-building stage. We concur with this usage and further advocate avoiding the characterization of the transition from tholeiitic to alkalic magmatism by the use of terms such as "caldera-filling" and "post-caldera." These shifts in viewpoints are incorporated in our proposed modifications to the scheme of growth stages for Hawaiian volcanoes, outlined in a subsequent section.

STRUCTURAL DEVELOPMENT OF HAWAIIAN VOLCANOES

The shield volcanoes of Hawaii have broad bases in relation to their height and subaerial slopes in the tholeiitic stage, unmodified by faulting or erosion, generally of 3°–10° and averaging about 6°. Volcanoes with a steeper sided alkalic cap have summit slopes that locally approach 20° and average about 12°. The subaerial part of each volcano is built of tens or hundreds of thousands of discrete, overlapping lava flows of pahoehoe and aa that radiate outward from a central summit vent area and from two or more linear rift zones. Beds of tephra may be interlayered sporadically with the tholeiitic lava, and the proportion of tephra to lava increases during the growth of the alkalic cap.

Some descriptions state that lava flows have the form of sheets (see Stearns, 1946, p. 17; Stearns and Macdonald, 1946, p. 24), an impression easy to derive because their thickness is small compared to their lateral dimensions. However, the geologic map (fig. 7.3; Stearns and Macdonald, 1946, plate 1) shows that for most flows the ratio of length to width is large, and it seems preferable to visualize flows as elongated tongues or lobes (Peterson, 1971, p. 163–164). This visualization helps emphasize the across-flow discontinuity of Hawaiian flows, which is one of the major problems in efforts to establish consistent stratigraphic correlations. Adjacent volcanoes generally grow contemporaneously, and their flows are commonly interdigitated.

Slopes on the submarine part of the volcano are steeper than on the subaerial part; they are commonly 10°–20° (fig. 7.6). Submarine flows are dominantly of pillow lava and are assumed also to be tongue-shaped, like subaerial flows. Superimposed upon and incorporated within this primary edifice of overlapping lava flows and sporadic tephra layers are a number of structures that develop throughout the growth of the shield, including rift zones, faults, landslides, calderas, craters, and tephra and spatter cones.

Rift zones have long been recognized as integral structural elements of Hawaiian volcanoes (Dana, 1849; Dutton, 1884). The summit areas and rift zones include almost all vents through which lava is erupted, and the surfaces of the rift zones of Kilauea and Mauna Loa are marked by spatter cones, spatter ramparts, pit craters, grabens, faults, cracks, and fissures, which constitute a record of repeated active volcanism and related ground dislocations. Where the subsurface portions of rift zones have been exposed by erosion on the older islands, they are marked by abundant closely spaced subparallel dikes, which demonstrate that rift zones tend to maintain consistent orientation and position throughout the growth of a shield.

Fiske and Jackson (1972) proposed that the orientations of rift zones on volcanoes that grew from the ocean floor, distant from other volcanoes, is determined by regional stress patterns; at volcanoes that grew on the flank of an already existing edifice, the orientation of the rift zones is determined by the gravitational stress field influenced by the buttressing effect of the older volcano. Their hypothesis is supported by results of experiments with gelatin models and is basically consistent with the progression of development of the volcanoes on all the islands from Kauai to Hawaii (see, for example, Moore, chapter 2, fig. 2.6). Their analysis yields the following sequence of origin for the volcanoes of Hawaii: Kohala, Hualalai, Mauna Kea, Mauna Loa, and Kilauea (fig. 7. 7). This sequence of origin is not necessarily the same as either the order of petrogenetic development or the time progression of known eruptions; for example, hawaiite on Mauna Kea is more differentiated than alkalic basalt on Hualalai, and historical activity has occurred at Hualalai but not at Mauna Kea. These relations suggest that Mauna Kea has passed through the petrogenetic development sequence more rapidly than Hualalai.

The model of Fiske and Jackson (1972) provides a generally consistent explanation for the orientations of rift zones and for many aspects of the behavior of the different volcanoes. As adjacent volcanoes commonly grow contemporaneously, however, fluctuations of eruption rates and shifts of vent sites from summit to rift zone in one volcano may cause changes in slope direction or in the influence of buttressing, thereby affecting the prevailing stress fields of an adjacent volcano and influencing the development of its rift zones. Stearns and Clark (1930) noted, for example, that the growth of Kilauea against the southeast flank of Mauna Loa caused a change in the pattern of behavior of the nearby fault systems of Mauna Loa. Lipman (1980) concluded that the growth of Kilauea has, in effect, squeezed the northeast rift zone of Mauna Loa and effectively sealed off its lower, easternmost extension and that it has caused the

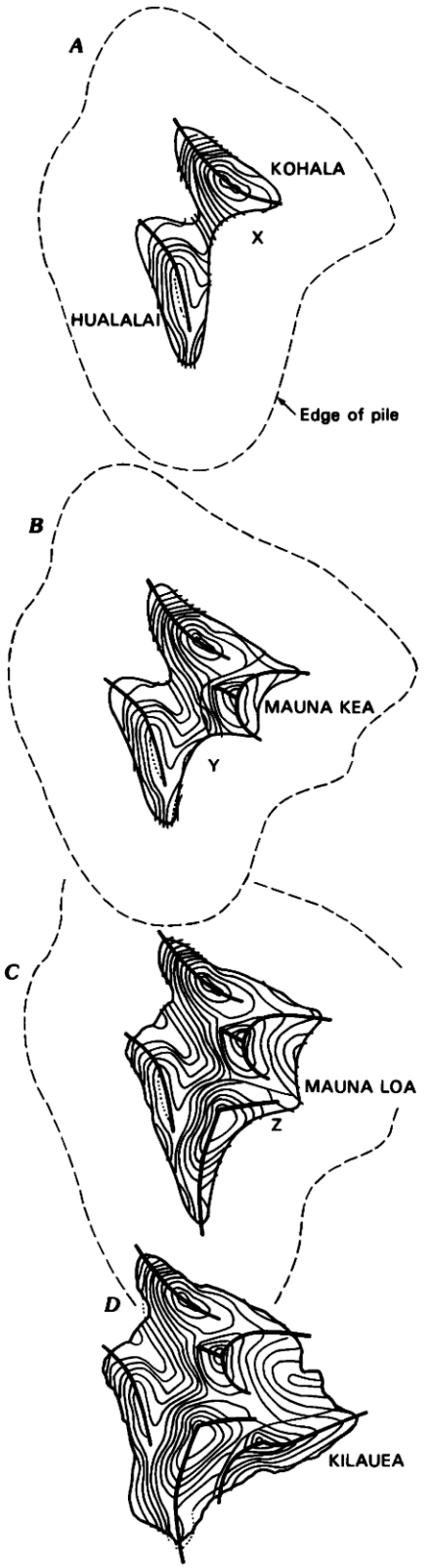

FIGURE 7.7.—Growth of Island of Hawaii as proposed by Fiske and Jackson (1972, fig. 11, p. 315). Reproduced by permission. ***A***, Early formed Kohala-Hualalai edifice; X marks site of future Mauna Kea. ***B***, Later stage; Y marks site of future Mauna Loa. ***C***, Still later stage; Z marks site of future Kilauea. ***D***, Present configuration. Each sketch shows orientations of rift zones, which developed in accord with prevailing regional or gravitational stress patterns.

southwest rift zone of Mauna Loa to migrate gradually westward. Such changes support the basic concept of Fiske and Jackson (1972) that rift zones develop in accord with the prevailing stress field, although they require modification of the idea that the rift zones remain fixed in position and orientation.

Pertinent to these issues is the orientation of the rift zones of Loihi Volcano. The bathymetric contours along the south flank of the island are oriented about N. 60° E. (fig. 7.8*A*); according to the concept of Fiske and Jackson (1972), the rift zones of Loihi should lie approximately parallel to this direction. Instead, the orientation of the elongate ridges inferred to mark the rift zones is mostly about N. 30° W., varying locally to due north and N. 10° E. (fig. 7.8*B*); it thus is chiefly almost at right angles to the expected orientation (Malahoff, chapter 6; Malahoff and others, 1982; Moore and others, 1982). Too little is known about the details of the structure and morphology of Loihi to fully evaluate this apparent discrepancy, but it may be noted that the rift zones of Loihi are approximately parallel to the line of the major loci of volcanoes to the northwest (fig. 7.8*A*; Malahoff, chapter 6). The central vent of Loihi lies approximately along the projection of the 4,000-m depth contour, approximately 1,000 m above the level of the regional ocean floor (fig. 7.8*A*). It may be that during the early growth of Loihi, the influence of the regional stress pattern predominated over that of the gravitational stress field on the flanks of the older volcanoes, or perhaps Loihi began before the submarine slopes of Kilauea and Mauna Loa had advanced to the Loihi site. As Loihi grows, it will offer a variety of tests for the Fiske-Jackson (1972) hypothesis and will be a fascinating subject for study by future generations of scientists.

The gravitational stress field on volcano flanks influences the structure in still another important way. Landslides have long been recognized as a hazard in Hawaii, occurring chiefly on steep slopes such as seacliffs and stream-cut valley walls; they are commonly induced by saturation of the ground by heavy rains, by shaking from earthquakes, or especially by the two in combination. In contrast to these relatively small, frequent landslides, Moore (1964) advocated large-scale landsliding as the origin for extensive areas of irregular submarine topography offshore from several islands, including Hawaii. Masses covering several thousand square kilometers north of Molokai and north of Oahu are inferred to be two immense landslides that moved more than 100 km along slide planes with an average slope of about 2°. As more detailed bathymetry has become available for offshore areas around Hawaii, it has been recognized that landslides are common on the submarine flanks of volcanoes. Some large-scale slumping events may be related to step-faulting on the subaerial seaward flanks of volcanoes, such as in the Hilina fault system on the south flank of Kilauea (Moore and Fiske, 1969, p. 1199–1200). Certain bathymetric details of Loihi are also inferred to be the result of submarine landslides (Malahoff, chapter 6).

Moore and Krivoy (1964) proposed that gravity-induced seaward movement of the south flank of Kilauea caused dilation of its east rift zone, leading to permissive emplacement of dikes by magma from the summit reservoir. This idea was tested when detailed analyses of the displacements of points on the east rift zone, the

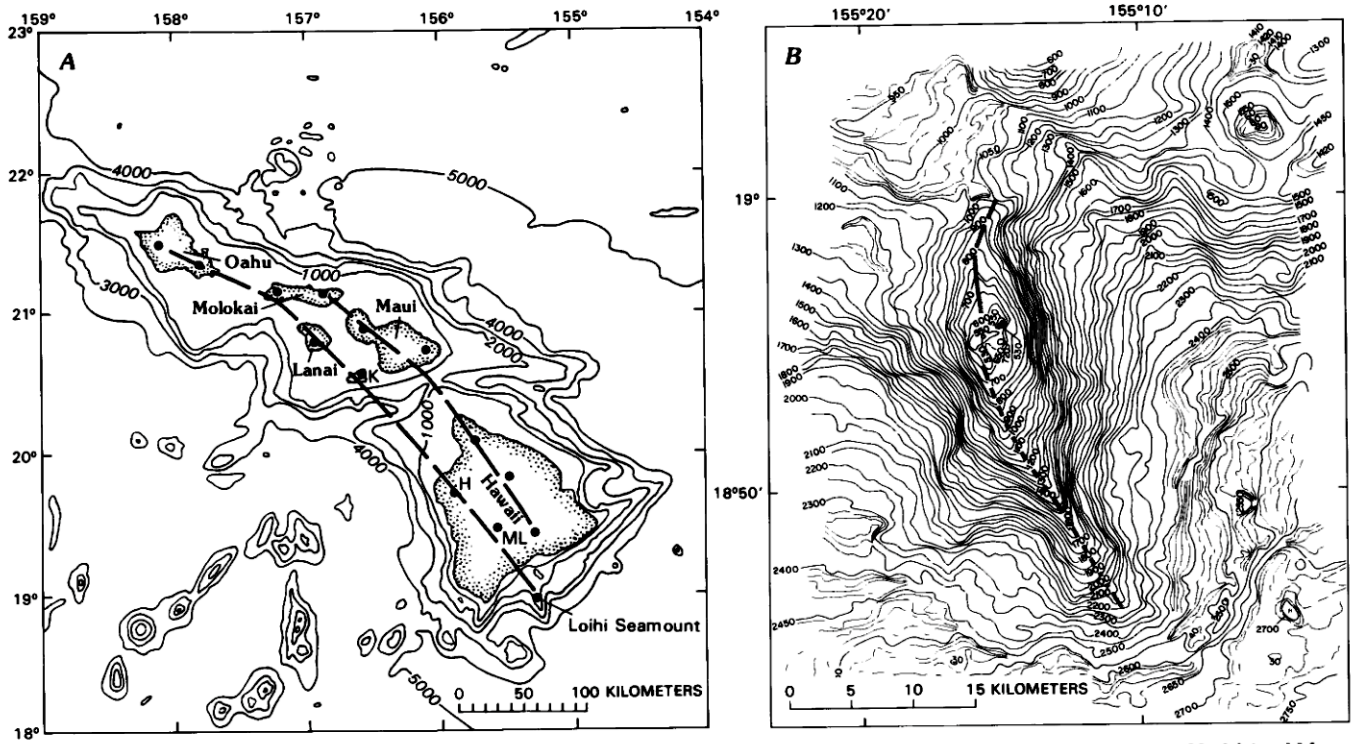

FIGURE 7.8.—Loihi Seamount. ***A***, Position along regional curved locus extending through western line of volcanoes from Oahu to Hawaii, including Hualalai and Mauna Loa Volcanoes (after Moore and others, 1982). Bathymetric contours in meters. ***B***, Bathymetric map (after Malahoff and others, 1982). Elongate ridges extending south-southeast and north from summit are major rift zones of volcano. They lie subparallel to volcano locus shown in *A* instead of parallel to submarine contours of island platform. Depth contours in fathoms (1 fathom = 1.83 m).

Koae and Hilina fault systems, and other parts of the south flank were made by Duffield (1975) and Swanson and others (1976a). They examined the amount, direction, and time of displacement as related to the time and place of eruptions and concluded that displacements on the rift zone and south flank were caused by forcible injection of magma into the rift zone, rather than the rift zone being dilated as a result of faulting and sliding of the south flank and permissively allowing magma to enter. Nevertheless, gravity plays an important role, because displacements are toward the sea in the unbuttressed direction. Hence these findings are compatible with those of Fiske and Jackson (1972) concerning the role of gravity in the development of the east rift zone.

The $M=7.2$ earthquake at Kilauea on November 29, 1975, was probably related to strains accumulated throughout the south flank from intrusion of dikes into the rift zone (Swanson and others, 1976a; Tilling and others, 1976). However, the earthquake itself has been determined to be the result of abrupt southward movement of the south flank edifice across the underlying oceanic crust (Ando, 1979; Furumoto and Kovach, 1979; Crosson and Endo, 1981, 1982). This movement induced extensive displacements throughout the Hilina and other fault systems (Tilling and others, 1976).

Marine terraces positioned both above and below sea level (Stearns and Macdonald, 1946) have long suggested that the level of the sea fluctuated over extended periods of time; they have been interpreted both as eustatic and as related to local crustal movements. Submergence of cultural artifacts of the early Hawaiian people indicates that Hawaii is currently subsiding (Apple and Macdonald, 1966). This inference was supported by a study of tide-gage records, which yielded a rate of subsidence at the Hilo tide gage of about 4.1 mm/yr, implying an annual volume rate of subsidence of the east end of the Hawaiian Ridge of about 0.27 km^3/yr (Moore, 1970). The rate of subsidence at Hilo has subsequently been redetermined to be 2.4 mm/yr, giving a recalculated volume rate of subsidence of 0.075–0.1 km^3/yr (Moore, chapter 2). The sinking of Hawaii is interpreted to be the result of crustal loading by the erupted products. The new volume rate of subsidence agrees closely with the figure of 0.11 km^3/yr, which recently has been the average annual volume of lava erupted by Kilauea (Swanson, 1972).

Marine deposits now above sea level are difficult to explain if progressive subsidence is the result of eruption and crustal loading. However, recent reinterpretation of such deposits as resulting from a giant ocean wave permits the interpretation that Hawaii, instead of alternately rising and sinking, has indeed been sinking persistently in response to long-sustained crustal loading (Moore and Moore, 1984).

Moore (chapter 2) demonstrates that the constructional volcanic edifices, instead of merely resting on the deep ocean floor at a depth of 5–6 km as previously believed, have bowed the crust downward during and after their growth, that most of their bases have subsided about 8–10 km, and that since reaching the sea surface the volcanoes have subsided 2–5 km. Hence a substantial part of their mass that is now below sea level was erupted subaerially.

HISTORICAL ACTIVITY

Among Hawaii's volcanoes, only Kilauea and Mauna Loa have erupted since the time of the missionaries, but they have in that interval been among the world's most active volcanoes. A summary of their activity is provided in tables 7.3 and 7.4.

When first known to the outside world, Kilauea became famous for its long-lasting lava lake in the crater and vent complex of Halemaumau inside the summit caldera. Lava in the lake circulated, fountained, and alternately rose and fell within Halemaumau Crater. The lake episodically overflowed onto the caldera floor and, during its 101-year life span, added about 2 km^3 of lava to the caldera, raising the floor several hundred meters. This lava constructed a gently sloping shield volcano inside the caldera, with the summit at Halemaumau. A few eruptions also occurred during this time along the east and southwest rift zones of Kilauea, but most activity was concentrated in the summit caldera. The lava-lake activity ended in 1924 with subsidence and explosive eruptions at Halemaumau, which left the pit crater more than 400 m deep.

During the next few years, brief episodic eruptions occurred at Halemaumau and partly filled the pit crater formed in 1924, but a period of repose followed from the mid-1930's to 1952. Since then, Kilauea has had more than two dozen eruptions within the caldera and nearby summit area as well as along both rift zones, extruded more than 1.3 km^3 of lava, and exhibited a very wide variety of behavior (see references in table 7.3). Most eruptions since the 1960's have occurred along the east rift zone. Individual eruptions have lasted from less than a day to more than two years. Episodic activity at Puu Oo, in the central east rift zone, began in January 1983 and continues as of early 1986 (Wolfe and others, chapter 17).

Mauna Loa erupted 35 times between 1832 and 1950 (table 7.4), an average of one eruption every 3.4 years. Eruptions showed a tendency to alternate between the summit area and either the northeast or southwest rift zone. Intervals between eruptions ranged from as brief as 4 months to as long as 11 years, and eruptions lasted from less than a day to 547 days. The native Hawaiians had no traditions or stories about Mauna Loa eruptions, so the length of the period of quiescence preceding 1832 is not known. Because the summit and upper rift zones are remote from Hawaiian villages, small eruptions may have gone unobserved; alternatively, a prolonged period of actual quiet may have prevailed. The latter seems much more likely, as eruptions of the type occurring in the nineteenth and twentieth centuries would have been obvious to the Hawaiians and would have influenced their activities. Following the eruption of 1950, the volcano did not erupt again until 1975, when a one-day-long eruption ended the longest period of quiet in historical time (Lockwood and others, chapter 19, 1976). The most recent activity occurred in 1984, when a 22-day-long eruption sent lava flows to within 18 km of the waterfront at Hilo and 6 km of the outskirts of the city (Lockwood and others, chapter 19, 1985)

The frequent activity of both these volcanoes suggests that similar patterns of behavior are likely to continue during the near future. Holcomb (chapter 12, 1980), however, has analyzed the long-range shifts in type and location of activity of Kilauea and has

developed a model indicating major shifts from summit growth and caldera filling to rift-zone growth and summit collapse. Equivalent patterns of shifting behavior at Mauna Loa are being reconstructed by Lockwood and Lipman (chapter 18).

REVISED SCHEME OF EVOLUTIONARY STAGES FOR HAWAIIAN VOLCANOES

The evolutionary stages defined by Stearns (1946) have served as a basic framework for Hawaiian geologic history for about four decades. Macdonald and Abbott (1970, p. 138) modified the stage boundaries to reflect improved knowledge of submarine processes and subdivided the first stage of Stearns into deep and shallow submarine stages. Later, Macdonald and others (1983, p. 147–149) recognized that calderas are not necessarily unique to a specific stage in the growth of the volcano, and their updated classification omitted the caldera stage.

Other investigators have emphasized four stages that are of significance in the petrologic evolution of Hawaiian volcanoes, roughly patterned after the initial definitions by Stearns (1940). Although the various workers have been consistent in designating four stages, they have selected different ways of defining their progression. Stearns (1940) initially defined them as (1) youthful, shield-building (chiefly olivine-bearing basalt); (2) mature, caldera formation (also olivine-bearing basalt); (3) old age, caldera filling (differentiated rocks); and (4) rejuvenated or post erosion (highly differentiated rocks); Stearns later (1946, 1966) added non-eruptive developmental stages. Tilley (1950) reiterated the same four stages of Hawaiian volcanism. Leeman and others (1980) redefined them as (1) shield-building stage (tholeiitic lava); (2) caldera-filling stage (tholeiitic, transitional, and mildly alkalic lava); (3) postcaldera stage (including alkali olivine basalt and related differentiates); and (4) posterosional stage (including basanitic and nephelinitic lavas). The chief difference in their scheme is that the formation of calderas has been included with shield building, and a caldera-filling stage has been substituted for the second stage and serves as the transition from tholeiitic to alkalic basalt. A different variant is offered by Clague and Dalrymple (chapter 1, part I, table 1.1). Their four stages are (1) preshield stage (including basanite, alkalic and transitional basalt); (2) shield stage (tholeiitic basalt and picritic tholeiitic basalt); (3) postshield alkalic stage (alkalic lavas of assorted composition); and (4) rejuvenated stage (alkalic lava and highly differentiated types such as basanite and nephelinite). Their stage (1) reflects the new findings at Loihi, and their stage (3) is equivalent to the latter part of stage (2) and all of stage (3) of Leeman and others (1980). The scheme of evolution to be offered here utilizes the four stages as defined by Clague and Dalrymple (chapter 1, part I), although the terms used for some of the stages are different, and additional stages are defined.

Earlier discussion (see section "Calderas as Related to Volcano Development") established our view that it is not appropriate to retain a separate stage of caldera formation. By the same arguments it is also inappropriate to designate another stage as postcaldera. For example, if either Kilauea or Loihi caldera is filled by new lava in the future, as seems quite likely, the subsequent activity in reality would be postcaldera, but the composition will most likely still be tholeiitic. This lava would certainly not meet the essential evolutionary criteria required of the so-called postcaldera stage, which some of the above authors have specified as reflecting the differentiation to alkalic magma. It is also possible for the magma of a volcano to undergo differentiation to the alkalic suite without the volcano having had a caldera (for example, no evidence has yet been found for a caldera at Hualalai, though it is possible that unknown filled calderas lie within the edifice). In view of these several considerations, we feel the name "postcaldera stage" is a misnomer and its use should be avoided.

Our intention is to propose a scheme of evolution with the same purpose as that by Stearns (1946) and subsequently modified by Macdonald and Abbott (1970) and Macdonald and others (1983)—to outline in simple form the major steps in development of a typical Hawaiian volcano. Such schemes are of necessity oversimplified because of the variations and exceptions followed by individual volcanoes, yet they are useful as a framework or standard of comparison, and most importantly they can serve as a spur in the search for improved understanding. The stages here include not only the growth of the volcano as reflected by petrogenetic developments reviewed just above, but they also include other significant geologic processes and environmental conditions. Some of the terms used by preceding authors have been retained, but others have been revised, either because of redefinition of a stage reflecting a modified current concept or simply because another term seemed more appropriate. The terms adopted avoid rock names because we find it difficult to apply a petrologic term without introducing some ambiguity. Furthermore, all reference to a caldera in the terms and in the definitions of stages has been removed because we hold the opinion that calderas may repeatedly form and be refilled at various times during the rapid growth of a shield; thus their development and filling is not sufficient to define a distinct stage. The terms here also avoid the prefixes pre- and post-, as associated with a process or a feature, because their use implies, sometimes erroneously, that this process or feature does not operate or exist at all during the designated stage. We wish to emphasize that the successive stages may overlap and intergrade, and the processes characteristic of two or more stages may be operating at different places on a volcano at the same time. Furthermore, volcanoes do not necessarily pass through every stage, nor do different volcanoes necessarily progress through stages at similar or consistent rates.

In spite of the advances since 1946, such as new geophysical and geochemical tools, improved investigative techniques, and extensive offshore submarine exploration, our concepts of volcano development are still based on facts derived from only a thin outer shell of the Hawaiian volcanoes. Petrological theories have made exciting and possibly valid inferences about the petrogenesis of magma and the growth of the volcanoes, but until these ideas can be tested by actually probing the deep interior and the base of several volcanoes, the concepts must remain speculative. So although the scheme proposed here represents an effort to reflect currently prevailing ideas as unabiguously as possible, it still suffers from some

TABLE 7.3.—*Historical eruptions of Kilauea through May 1985*

[Dashes (---), no data; query (?), questionable data]

Date eruption began Year	Month and day	Duration (days)	Location of major vent(s)	Approximate area (km^2)	Approximate volume ($m^3 \times 10^6$)	References
1750(?)	---	---	East rift	4.1	14.9	Holcomb, chapter 12, 1980.
1790(?)	---	---	-- do ----------	7.9	28.8	Holcomb, chapter 12, 1980.
1790	November (?)	---	Caldera (explosive)	(Blocks lapilli, ash)	---	Brigham, 1909, p. 36–39; Hitchcock, 1909, p. 165–167; Swanson and Christiansen, 1973; Decker and Christiansen, 1984.
1823	---	---	Southwest rift	10.0	11.5	Hitchcock, 1909, p. 163; Stearns, 1926.
1823	---	101 yr (intermittent)	Caldera, Halemaumau	8.2	2,000.0	Ellis, 1827, p. 163–176; Brigham, 1909, p. 40–222; Hitchcock, 1909, p. 179–182, 186–188, 191–194, 198–206, 210–260; Jaggar, 1947, p. 9–169, 216–314.
1832	January 14	---	East rim of caldera	---	---	Brigham, 1909, p. 46; Hitchcock, 1909, p. 182–185.
1840	May 30	26	East rift	17.1	215.0	Coan, 1841; Brigham, 1909, p. 50–55; Hitchcock, 1909, p. 188–190.
1868	April 2	---	Kilauea Iki	.2	---	Brigham, 1909, p. 106–110; Hitchcock, 1909, p. 207.
1868	April 2	---	Southwest rift	.1	.2	Brigham, 1909, p. 109–119; Hitchcock, 1909, p. 207–210; Coan, 1869.
1877	May 4	1	Caldera wall	---	---	Brigham, 1909, p. 131–132; Hitchcock, 1909, p. 217.
1877	May 21 (?)	---	Keanakakoi	.1	---	Brigham, 1909, p. 132; Hitchock, 1909, p. 217.
1884	January 22	1	East rift (submarine)	---	---	Stearns and Macdonald, 1946, p. 111; Macdonald and Abbott, 1970, p. 75.
1879	July 14	1 (?)	Distinct episodes of Halemaumau overflows and (or) caldera fissure outbreaks. These are part of the 1823 101-year-long summit eruption. Earlier lava buried; lava from those episodes locally exposed in caldera.	---	---	Brigham, 1909, p. 133, 140; Hitchcock, 1909, p. 219.
1882	September	3 yr		---	---	Brigham, 1909, p. 156–158; Hitchcock, 1909, p. 221–226.
1888	July	310		---	---	Dana, 1890, p. 123.
1892	April	730 (intermittent)		---	---	Brigham, 1909, p. 184–191.
1918	February 23	14		.1	.2	Jaggar, 1947, p. 112.
1919	February 7	294		4.1	26.0	Jaggar, 1947, p. 118–125.
1921	January	60 (approx)		2.0	6.7	Jaggar, 1947, p. 149–151.
1919	December 15	221	Southwest rift (Mauna Iki)	13.0	47.0	Jaggar, 1947, p. 137–146.
1922	May 28	2	East rift (Makaopuhi, Napau)	.1	---	Jaggar, 1947, p. 155–157.
1923	August 25	7	East rift	.5	.1	Jaggar, 1947, p. 161.
1924	May 10	17	Caldera (explosive)	(Blocks)	---	Jaggar and Finch, 1924; Jaggar, 1947, p. 162–168, 205–259; Decker and Christiansen, 1984.
1924	July 19	11	Halemaumau	.05	.24	Jaggar, 1947, p. 168–169.
1927	July 7	13	-- do ----------	.1	2.42	Jaggar, 1947, p. 175–176.
1929	February 20	2	-- do ----------	.15	1.47	Jaggar, 1947, p. 180–181.
1929	July 25	4	-- do ----------	.2	2.75	Jaggar, 1947, p. 181–182.
1930	November 19	19	-- do ----------	.23	6.48	Jaggar, 1947, p. 185–186.
1931	December 23	14	-- do ----------	.3	7.37	Jaggar, 1947, p. 186–189.
1934	September 6	33	-- do ----------	.4	7.26	Jaggar, 1947, p. 197.
1952	June 27	136	-- do ----------	.6	49.0	Macdonald, 1955, 1959.
1954	May 31	3	Halemaumau, caldera	1.1	6.5	Macdonald, 1959; Macdonald and Eaton, 1957.
1955	February 28	88	East rift	15.8	92.0	Macdonald, 1959; Macdonald and Eaton, 1964.
1959	November 14	36	Kilauea Iki	.6	51.0	Richter and Eaton, 1960; Macdonald, 1962; Richter and others, 1970.
1960	January 13	36	East rift	10.6	120.0	Do.
1961	February 24	1	Halemaumau	.05	.02	Richter and others, 1964.
1961	March 3	22	-- do ----------	.8	.27	Do.
1961	July 10	7	-- do ----------	1.0	13.2	Do.
1961	September 22	3	East rift	.8	2.3	Do.
1962	December 7	2	-- do ----------	.05	.33	Moore and Krivoy, 1964.
1963	August 21	2	East rift (Alae)	.2	.04	Peck and Kinoshita, 1976.
1963	October 5	1	East rift	3.4	6.9	Moore and Koyanagi, 1969.
1965	March 5	10	East rift (Makaopuhi, Napau)	7.8	18.0	Wright and others, 1968.
1965	December 24	1	East rift (Alae and vicinity)	.6	.9	Fiske and Koyanagi, 1968.
1967	November 5	251	Halemaumau	.65	84.1	Kinoshita and others, 1969.
1968	August 22	5	East rift	.03	.04	Jackson and others, 1975.
1968	October 7	15	-- do ----------	2.1	7.0	Do.
1969	February 22	6	-- do ----------	6.0	17.0	Swanson and others, 1976b.
1969	May 24	875	East rift (Mauna Ulu)	50.0	185.0	Swanson and others, 1971, 1979; Peterson and others, 1976, p. 647–648.
1971	August 14	1	Caldera	2.0	10.0	Peterson and others, 1976, p. 649–650; Duffield and others, 1982.
1971	September 24	5	Halemaumau, caldera, southwest rift	4.0	8.0	Peterson and others, 1976, p. 650; Duffield and others, 1982.
1972	February 3	455	East rift (Mauna Ulu)	35.0	125.0	Peterson and others, 1976, p. 651–652; Tilling and others, chapter 16.
1973	May 5	1	East rift (Pauahi, Hiiaka)	.14	1.0	Peterson and others, 1976, p. 651–652; Tilling and others, chapter 16.
1973	May 7	187	East rift (Mauna Ulu)	.5	2.5	Peterson and others, 1976, p. 652; Tilling and others, chapter 16.
1973	November 10	30	East rift (Pauahi and vicinity)	1.5	3.0	Peterson and others, 1976, p. 652–653; Tilling and others, chapter 16.

TABLE 7.3.—*Historical eruptions of Kilauea through May 1985*—Continued

Date eruption began Year	Month and day	Duration (days)	Location of major vent(s)	Approximate area (km^2)	Approximate volume ($m^3 \times 10^6$)	References
1973	December 12	222	East rift (Mauna Ulu)	8.0	30.0	Peterson and others, 1976, p. 653–654; Tilling and others, chapter 16.
1974	July 19	3	Caldera, Keanakakoi, and vicinity)	3.2	10.0	Peterson and others, 1976, p. 656; Lockwood and others, chapter 19.
1974	September 19	1	Halemaumau, caldera	1.1	11.0	Do.
1974	December 31	1	Southwest rift, Koae fault system	7.5	15.0	Do.
1975	November 29	1	Halemaumau, caldera	---	.25	Tilling and others, 1976, p. 15–17.
1977	September 12	20	East rift	8.0	35.0	Moore and others, 1980.
1979	November 16	1	East rift (Pauahi and vicinity)	.17	.7	Banks and others, 1981.
1980	March 11	1	East rift (near Mauna Ulu)	.0001	.000003	
1982	April 30	1	Halemaumau, caldera	.25	.5	Banks and others, 1983.
1982	September 23	1	South outer caldera	.75	4.0	Banks and others, 1983.
1983	January 3	continuing (August 1986)	East rift, Puu Oo	40 (approx)	350 (approx)	Wolfe and others, chapter 17.

of the same basic limitations as did that of Stearns (1946). New facts, as they become available, will inevitably modify current concepts, and we hope the progress will be at a rate such that this new scheme will require early revision.

We propose the following scheme of evolution for Hawaiian volcanoes (see fig. 7.9 and table 7.5)

1. Initial stage. Although little known, products apparently include a variety of differentiated, alkalic-type lavas. Calderas are possible.
2. Shield-building stage. Products are tholeiitic basalt and tholeiitic picrite, and major growth of the shield volcano occurs. Eruptions are frequent and voluminous. Three substages are recognized according to physical environment:
   a. Submarine substage; dominantly pillow lava and derivatives, relatively steep slopes.
   b. Sea-level substage; development of hyaloclastite rocks chiefly by explosive interaction between molten lava and seawater and by wave abrasion.
   c. Subaerial substage; pahoehoe and aa build gently sloping shield-shaped edifice; small percentage of tephra.

   Calderas and pit craters may form and be filled repeatedly during any of these substages.
3. Capping stage. Magma becomes differentiated to yield alkalic basalt and other alkalic rocks. Eruptions become less frequent, lava becomes more viscous and is interspersed with explosive products, and a steeper sided cap is built. Any existing caldera is filled. Eruptions decline and finally end.
4. Erosional stage. Erosion by streams and waves carves valleys, canyons, and seacliffs. Although erosion operates during stages (2) and (3), affecting any portion of the volcano not frequently covered by new eruptive products, it becomes the dominant process when eruptions end. Corals grow in the shallow water around the islands and may build large reefs when undisturbed by new lava.
5. Renewed volcanism stage. After long quiescence of hundreds of thousands to perhaps more than a million years, alkalic basalt and more highly differentiated lavas, such as basanite and nephelinite, may erupt intermittently, both as lava and tephra, through a span of perhaps thousands of years. Erosion and reef building continue in unaffected areas.
6. Atoll stage. After stream and wave erosion, coupled with subsidence induced by volcanic loading, have reduced the volcano to sea level, the former island typically is encircled by coral reefs. If subsidence continues, coral may build an edifice atop the eroded volcanic rock to thicknesses of hundreds of meters.
7. Late seamount stage. Rate of regional subsidence eventually exceeds rate of reef building; island sinks below sea level to become a seamount; pelagic sediments mantle edifice, which may survive quietly for millions of years.

Each Hawaiian volcano begins growing in a deep-ocean environment, but only a single example, Loihi, has provided clues to the composition and characteristics of the lava of the deep-sea stage. Loihi is as yet little explored, but it is already a large volcano, rising at least 3,000 m above its base. A wealth of petrologic information has been extracted from the dredged samples from Loihi, an innovative petrogenetic evolution has been suggested (Frey and Clague, 1983), and it is tempting to assume that all or most Hawaiian volcanoes have undergone this same petrogenesis. The assumption is reasonable, but the characteristics of later stages are all derived from the study of several or many volcanoes. Hence, until rocks similar to those of Loihi are found at other new seamounts or are encountered by deep drilling into the core of older volcanoes, the details and implications of stage (1) should be considered provisional.

Stage 1 begins with fissures or single vents erupting lava onto the ocean floor. Repeated flows build a submarine edifice (fig. 7.9), which consists mostly of pillow lava. If of alkalic composition, the edifice may have sides that are quite steep; the bathymetry of Loihi (Malahoff, chapter 6; Malahoff and others, 1982) shows some slopes approaching 45°. The first embryonic volcano in a region would grow independently of any influence by neighboring edifices. However, when one or more additional volcanoes develop nearby,

TABLE 7.4.—*Historical eruptions of Mauna Loa through 1985*

[Dashes (---), no data; query (?), questionable data]

Date eruption began Year	Month and day	Duration (days)	Location of major vent(s)	Approximate area (km^2)	Approximate volume ($m^3 \times 10^6$)	References
1832	June 20	21 (?)	Caldera	---	---	Stearns and Macdonald, 1946, p. 79.
1843	January 9	95	Northeast rift	53	191	Brigham, 1909, p. 63–65; Hitchcock, 1909, p. 84–85.
1849	May 15	15	Caldera	---	---	Coan, 1851; Brigham, 1909, p. 65; Hitchcock, 1909, p. 85
1851	August 8	21	-- do	18	69	Brigham, 1909, p. 65; Hitchcock, 1909, p. 85–86.
1852	February 17	21	Caldera, northeast rift	28	107	Coan, 1852; Brigham, 1909, p. 65–68; Hitchcock, 1909, p. 86–94.
1855	August 11	450	Northeast rift	31	115	Brigham, 1909, p. 68–71; Hitchcock, 1909, p. 94–100.
1859	January 23	300	North flank	85	459	Davis, 1859; Dana, 1859, 1860; Brigham, 1909, p. 75–80; Green, 1887; Hitchcock, 1909, p. 100–104.
1865	December 30	120	Caldera	---	---	Hitchcock, 1909, p. 104.
1868	March 27	16	Southwest rift	24	145	Coan, 1869; Brigham, 1909, p. 100–116; Hitchcock, 1909, p. 104–111; Moore and Ault, 1965, p. 5–7; Fisher, 1968.
1871	August 1	30	Caldera	---	---	Coan, 1871, p. 456.
1872	August 10	60	-- do	---	---	Brigham, 1909, p. 125; Hitchcock, 1909, p. 111–112.
1873	January 6	2 (?)	-- do	---	---	Brigham, 1909, p. 126; Hitchcock, 1909, p. 112–114.
1873	April 20	547	-- do	---	---	Brigham, 1909, p. 122–127; Hitchcock, 1909, p. 114–115.
1875	January 10	30	-- do	---	---	Brigham, 1909, p. 127; Hitchcock, 1909, p. 115; Coan, 1877.
1875	August 11	7	-- do	---	---	Do.
1876	February 13	1	-- do	---	---	Brigham, 1909, p. 127; Coan, 1877.
1877	February 14	11	Caldera, west flank (offshore)	---	---	Brigham, 1909, 127–128; Hitchcock, 1909, p. 115–116; Coan, 1877.
1880	May 1	6	Caldera	---	---	Brigham, 1909, p. 133, 145; Hitchcock, 1909, p. 116.
1880	November 1	280	Northeast rift	62	230	Brigham, 1909, p. 145–155; Hitchcock, 1909, p. 116–119.
1887	January 16	10	Southwest rift	29	230	Brigham, 1909, p. 165–168; Hitchcock, 1909, p. 123–127.
1892	November 30	3	Caldera	---	---	Brigham, 1909, p. 185.
1896	April 21	16	-- do	---	---	Brigham, 1909, p. 192–196; Hitchcock, 1909, p. 128–130.
1899	July 4	23	Caldera, northeast rift	42	153	Brigham, 1909, p. 196–199; Hitchcock, 1909, p. 132–138.
1903	October 6	60	Caldera	---	---	Brigham, 1909, p. 202–204; Hitchcock, 1909, p. 138–139.
1907	January 9	15	Caldera, southwest rift	21	76	Brigham, 1909, p. 206–209; Hitchcock, 1909, p. 142–146.
1914	November 25	48	Caldera	---	---	Jaggar, 1947, p. 99.
1916	May 19	14	Southwest rift	17	61	Jaggar, 1947, p. 104.
1919	September 26	42	Caldera, southwest rift	24	268	Jaggar, 1919, 1947, p. 125–133; Moore and Ault, 1965, p. 7.
1926	April 10	15	-- do	35	115	Jaggar, 1926, 1947, p. 171–173.
1933	December 2	17	Caldera	5	76	Jaggar, 1947, p. 195–196.
1935	November 21	42	Caldera, northeast rift	36	122	Jaggar, 1947, p. 197–200.
1940	April 7	133	Caldera	10	76	Macdonald, 1954; Macdonald and Abbott, 1970, p. 57–60.
1942	April 26	15	Caldera, northeast rift	28	76	Macdonald, 1954; Macdonald and Abbott, 1970, p. 60–65.
1949	January 6	145	Caldera	15	59	Macdonald and Orr, 1950; Finch and Macdonald, 1951; Macdonald and Abbott, 1970, p. 65–67.
1950	June 1	23	Southwest	91	460	Finch and Macdonald, 1953; Macdonald, 1954; Macdonald and Abbott, 1970, p. 9–11.
1975	July 5	1	Caldera, southwest and northeast rifts	14	30	Lockwood and others, chapter 19, 1976.
1984	March 25	22	Caldera, southwest rift, and, primarily, northeast rift	48	220	Lockwood and others, chapter 19, 1985.

the flows from two or more sources begin to interfinger, and the presence of each volcano would influence the path of flows from its neighbor. Linear rift zones develop, with their orientations determined by stress fields influenced both by regional tectonics and local gravitational forces (Fiske and Jackson, 1972).

The shield-building stage (2) includes the principal growth of the volcano; products consist almost exclusively of tholeiitic basalt and tholeiitic picrite (olivine-rich tholeiite). By far the greatest proportion of Hawaiian volcanoes consists of tholeiite erupted during the shield-building stage (fig. 7.9, table 7.5). Three substages have been designated submarine (2a), sea level (2b), and subaerial (2c); the behavior of the erupted products and their physical character is largely determined by which of these three environments they encounter.

The submarine substage (2a) involves the repeated voluminous extrusion of tholeiite, which assumes the form of pillow lava;

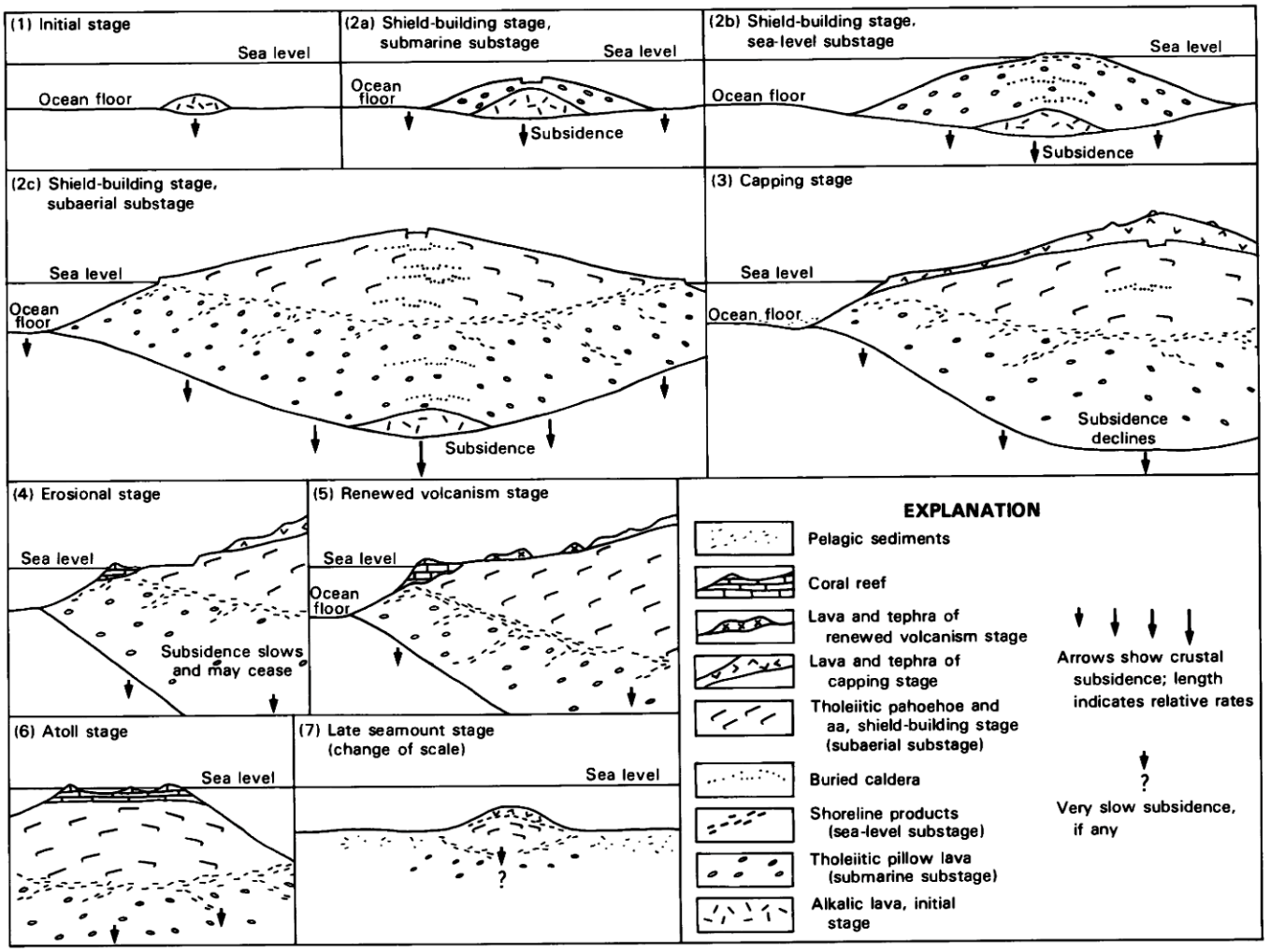

FIGURE 7.9.—Diagrams showing successive stages in evolution of a Hawaiian volcano as proposed in this paper. Changes between stages normally are transitional and gradational. For simplicity, feeder conduits and rift zones are omitted. Substantial crustal subsidence caused by volcanic loading occurs throughout growth stages (1) through (3); subsequent sea-level changes may be sporadic, but net subsidence continues into stage (7). Vertical exaggeration varies from approximately 2× to approximately 4×. Only stages (1) through (4) are represented on Hawaii. See text for additional details.

countless repeated flows build a submarine shield volcano. Lava issues from both summit vents and rift zones, and submarine eruptions probably exhibit as wide a variety of flow behavior as do subaerial eruptions, except that below a few hundred meters depth the pressure is sufficient to inhibit explosive activity, and any vesicles are only of microscopic size. Slopes of the edifice are generally 10° to 20°. The crust beneath the volcano subsides during rapid growth and volcanic loading; thus the length of time required for the summit to reach sea level is longer than previously thought, perhaps approaching a million years (Moore, chapter 2).

As the summit of the growing submarine shield approaches sea level, the sea-level substage (2b) begins. The hydrostatic head declines enough to allow the ocean water to boil when encountered by vesiculating molten lava. The abrupt production of steam disrupts the lava, sometimes explosively, and it is shattered to form tephra and hyaloclastite material (Moore and Fiske, 1969). As the process continues, a broad mound of mixed tephra and lava eventually emerges above sea level. Waves immediately begin to erode the tephra and fragment the lava, and initially the new island may be transitory. But if the supply of new material is steady and sufficiently large, the volcanic pile grows fast enough to keep ahead of wave erosion, and the new island enlarges. When the vent is sufficiently protected from sea water, explosions decline and coherent flows form a resistant veneer over the fragmental material, reducing the rate of wave erosion. The island of Surtsey, south of Iceland, is a well-observed example of the process by which a basaltic volcano initially emerges above the sea (Thorarinsson, 1967). Although the process has not been observed in Hawaii, basaltic volcanoes there would

TABLE 7.5.—*Revised evolutionary scheme for Hawaiian volcanoes*

Stage	Dominant composition of magma	Dominant geologic processes and characteristics[1]
(1) Initial	Alkalic basalt, basanite, transitional basalt	Initial activity of new volcano; rates and frequency of eruption and duration of stage not known; edifice may be steep sided (because only a single example is recognized, this stage is considered provisional).
(2) Shield-building	Tholeiitic basalt, tholeiitic picrite	Frequent voluminous eruptions from central vent and rift zones, historic examples suggest eruptive rates of 1–3 km^3/100 yr, frequency about 5–50 eruptions/100 yr; shield-shaped edifice built; caldera may form and be refilled repeatedly during any substage.
(2a) Submarine	-- do ----------	Products pillow lava and pillow fragments; moderately steeply sloping edifice.
(2b) Sea level	-- do ----------	Products hyaloclastites—the result of explosive interaction between sea water and molten lava, and wave abrasion.
(2c) Subaerial	-- do ----------	Products chiefly pahoehoe and aa lava flows, interspersed with sporadic tephra produced by occasional explosions; dominantly fluid lava builds gently sloping edifice; processes of 2a and 2b continue.
(3) Capping	Alkalic basalt, transitional basalt, other alkalic rocks[2]	Products initially pahoehoe and aa lava flows, increasing proportions of tephra-built cinder cones, gradual or abrupt change to smaller briefer eruptions; increasing lava viscosity (block flows); declining eruptive rates and frequency of eruptions, eventually at intervals exceeding 10^3 yr; capping structure steeper sided than stage 2c.
(4) Erosional	None	Lack of eruptions allows fluvial and marine erosion to carve valleys, canyons, cliffs, and so on; reefs may develop along some shorelines (erosion operates during all stages, but effects offset by repeated eruptions).
(5) Renewed volcanism	Alkalic basalt, basanite, nephelinite, nephiline melilitite	Sporadic eruptions, generally from vents not related to central conduit or rift zones, commonly explosive though some are effusive. Eruptions are of low volume and widely spaced in time. Erosion and reef building continue.
(6) Atoll	None	Abetted by regional subsidence, fluvial and marine erosion reduce volcano to sea level. Reef building continues, may form ring-shaped group of islands with interior lagoon.
(7) Late seamount	None	Rate of regional subsidence eventually exceeds rate of reef building and island sinks below sea level to become a seamount; gradually mantled by pelagic sediments; subdued edifice may survive for millions of years.

[1]In addition to processes listed, regional crustal subsidence caused by weight of growing volcanoes is nearly continuous, resulting in apparent rise in sea level. Episodes of glaciation cause a worldwide drop in sea level, temporarily offsetting steady regional subsidence.
[2]Other alkalic rocks may include hawaiite, mugearite, benmoreite, ankaramite, trachyte.

presumably emerge above the ocean in a like manner. The zone of tephra, fragmental lava, and hyaloclastite forms a distinctive horizon marking the transition from submarine to subaerial lava (Moore and Fiske, 1969). The behavior of lava at and below sea level was further reviewed above in the section "Submarine Investigations."

Once an island is established, the subaerial substage (2c) begins, which involves further growth of the shield by continued eruptions. The lava issues both from central vents and rift zones radial to the summit, and in composition the lava continues to be tholeiitic basalt. Slopes are generally from 3° to 10°, and they contrast distinctly with the steeper submarine slopes. Rate of growth is rapid, demonstrated by a general lack of both erosion and soils between successive flows. This substage is exemplified by frequent and well documented eruptions of Kilauea and Mauna Loa. As the subaerial shield grows, the processes of substages 2a and 2b continue below and at sea level as the volcano expands outward. Crustal subsidence continues (Moore, chapter 2), so that much of the subaerially erupted lava becomes part of the submarine edifice, and the hyaloclastite horizon assumes a broad, sagging profile (fig. 7.9). Calderas may form and be filled repeatedly throughout the tholeiitic lava stage.

The capping stage (3) begins as the magma eventually differentiates to yield alkalic basalt; at some volcanoes, lava transitional between tholeiitic and alkalic basalt is erupted (fig. 7.9, table 7.5). If a caldera is present, lava that fills it may be either tholeiite, transitional lava, or alkalic basalt. There is no theoretical reason why a caldera could not form during stage 3; calderas do occur in volcanoes of alkalic basaltic composition elsewhere in the world. However, they have not been observed to form during this stage in Hawaii, and in view of the declining volume rate of eruption characteristic of stage 3, caldera formation seems highly unlikely. With the change in composition, explosive eruptions become more common, and a steeper sided cap with slopes of as much as 20° is built over the shield. Differentiation may proceed further to yield one or more of the following: hawaiite, mugearite, benmoreite, trachyte, and ankaramite. Alkalic basalt, like tholeiite, forms pahoehoe and aa; the more differentiated lavas become increasingly viscous and may form block lava. Eruptions gradually become separated by progressively longer time intervals and finally end. Subsequent evolution of the volcanoes through the erosional stage (4), renewed volcanism stage (5), atoll stage (6), and late seamount stage (7) are briefly reviewed above, illustrated in figure 7.9, and outlined in table 7.5.

Of the volcanoes of Hawaii, Loihi seems to be at the end of stage 1, entering into stage 2a; Kilauea and Mauna Loa are in stage 2c; Hualalai is in stage 3; Mauna Kea is further along in stage 3, perhaps very late in the stage, and the processes of stage 4 are becoming dominant; and Kohala is in stage 4. None of these volcanoes has progressed beyond stage 4; the volcanoes of the other islands to the northwest are in various parts of stages 4 and 5, whereas stages 6 and 7 are represented by atolls, islets, and seamounts along the Hawaiian Ridge northwest of the main group of islands. Our stages 1, 2, 3, and 5 correspond to the four stages defined by Clague and Dalrymple (chapter 1, part I), although they are designated by different terms.

PETROLOGIC HISTORY OF INDIVIDUAL VOLCANOES

Though the volcanoes of Hawaii are broadly similar to one another in certain respects, each has achieved a specific position

within the hierarchy of growth stages by means of an individual course of petrologic development. Each volcano is basically a tholeiitic shield, but Kohala, Mauna Kea, and Hualalai Volcanoes have passed into or beyond the capping stage (3), whereas Mauna Loa and Kilauea are in the subaerial part of the shield-building stage (2c). Loihi cannot yet be termed a tholeiitic shield, though it appears to have completed the initial stage (1) and is entering the submarine part of the shield-building stage (2a). Among the volcanoes with alkalic caps, tholeiitic lavas of Kohala and Mauna Kea are exposed in a few canyons on the Hamakua coast, whereas Hualalai tholeiites are not exposed on the subaerial surface but have been found in a few water wells and along the submarine extension of the northwest rift zone (Clague, 1982).

The petrologic development is summarized here by showing (1) chemical variations and similarities among tholeiitic and alkalic basalts of the five island volcanoes plus Loihi; (2) differentiation processes by which basaltic magma produces rocks of other compositions; and (3) effects of olivine control on related lavas. To illustrate these processes we have selected five basic variation diagrams as follows: $Na_2O + K_2O$ vs. SiO_2 (fig. 7.10), CaO vs. SiO_2 (fig. 7.11), CaO vs. MgO (fig. 7.12), TiO_2 vs. MgO (fig. 7.13), and Na_2O vs. MgO (fig. 7.14). These diagrams are derived from 834 chemical analyses of rocks from Hawaii, distributed among the volcanoes as follows: Kohala, 36 analyses; Mauna Kea, 36; Hualalai, 293; Mauna Loa, 117; Kilauea, 340; Loihi, 12. Most analyses are from references listed in table 7.6; some are unpublished data of E.D. Jackson (Hualalai), T.L. Wright (Hualalai), and R.B. Moore (Hualalai and Kilauea).

In spite of documented long-term storage of Hawaiian tholeiitic magma in rift zone reservoirs, fractionation of such magma has rarely produced compositions more silicic than basalt (boundary at 52 percent SiO_2). The sole known exception is the Yellow Cone scoria (Kilauea southwest rift zone) with 55 percent SiO_2, which was produced by mixing of a differentiate with 60 percent SiO_2 and 2 percent MgO with a more olivine-rich magma (Wright and Fiske, 1971). Otherwise, andesitic or more silicic compositions of tholeiitic parentage are unknown on the Island of Hawaii, although rhyodacite occurs on Oahu (Macdonald and others, 1983).

Most of the subaerial part of Kohala and Mauna Kea and all of Hualalai are composed of alkali olivine basalt and its differentiates, and the average recurrence interval for eruptions on Hualalai in the Holocene has been about 50 yr, as evidenced by radiocarbon age data (Moore and others, chapter 20). These facts suggest that alkali olivine basalt has been generated frequently during late Pleistocene and Holocene time. Fractionation of alkali olivine basalt magma has been extensive; the most differentiated rocks at each volcano include trachyte on Hualalai, benmoreite and trachyte on Kohala, and a single reported occurrence of mugearite on Mauna Kea.

Macdonald and Katsura (1964) described separate compositional fields for alkalic and tholeiitic basalts for the whole Hawaiian island chain, and these fields for the Island of Hawaii are illustrated in the alkali-silica variation diagrams of figure 7.10. A few basalts from each volcano straddle the boundary between the fields. The alkali-silica diagrams further show that slightly andesitic melts are the most SiO_2-rich erupted from the tholeiitic suite on the island, and that trachyte is the most silicic rock produced by fractionation of the alkalic suite.

The lime-silica variation diagrams (fig. 7.11) show rather diverse trends among the different volcanoes. Kohala, Mauna Kea, Hualalai, and Loihi illustrate the general alkalic trend of decreasing CaO with increasing SiO_2, whereas the data for the tholeiitic Mauna Loa and Kilauea volcanoes produce bell-shaped curves that peak at about 50–51 percent SiO_2.

The lime-magnesia variation diagrams (fig. 7.12) document the major role played by olivine in the tholeiitic suite for MgO content above about 6.8 percent (Powers, 1955; Wright 1971; Wright and others, 1975; Wright and Tilling, 1980). The change in slope of the curves below this point indicates departure from olivine control and the coprecipitation of pyroxenes and plagioclase. Curves for the alkalic rocks of Kohala, Mauna Kea, and Hualalai change slope at about the same point as those of the tholeiitic suite, suggesting that olivine-controlled fractionation is also important among some basaltic rocks of the alkalic suite. Wide scatter in most of the plots at contents of MgO greater than 6.8 percent indicates that considerable mixing of different batches of olivine-controlled magma, or differentiation involving phases in addition to olivine, has occurred in both suites (except on Mauna Loa; see Rhodes, 1983).

The titania-magnesia variation diagrams (fig. 7.13) show considerable scatter, even at relatively high MgO values, reflecting the effects of possible mixing of magma in shallow storage chambers as well as temporal variations at given contents of MgO. The reason for the change in slope among the alkalic rocks at 5–6 percent MgO, instead of the more usual 6.8 percent in the tholeiitic suite (Wright and Fiske, 1971), is not clear, but this change may reflect the accumulation of titaniferous clinopyroxene in magmas that have fractionated olivine nearly to its possible limit. Olivine-controlled lavas of Mauna Kea and Kilauea generally are higher in TiO_2 than those of the other volcanoes; the differences do not seem to be related to differences between the alkalic and tholeiitic suites.

The soda-magnesia variation diagram for all volcanoes together (fig. 7.14) shows again the importance of olivine-controlled fractionation and of mixing in shallow magma chambers (the part of the plotted data showing the latter is dominated by analyses of Kilauea rocks). The diagram also demonstrates the generally higher soda values in alkalic rocks (dominated by analyses of Hualalai rocks).

Relatively recent reports on the petrology of individual Hawaiian volcanoes and on models for generation of tholeiitic and alkalic magmas are given in table 7.6. These studies are summarized by Wright and Helz (chapter 23) and will be treated only briefly here. Most workers, beginning with Stearns and Macdonald (1946), have suggested that alkalic rocks are related to tholeiitic basalts either by protracted fractional crystallization of tholeiitic magma or by varying degrees of partial melting of the mantle source. This conclusion was based partly on the small volume of alkalic rocks compared to tholeiites and on field relations, notably the occurrence of basalts of transitional composition stratigraphically between tholeiitic and alkalic basalts on Kohala and Mauna Kea and on other islands in the Hawaiian Chain. More recently,

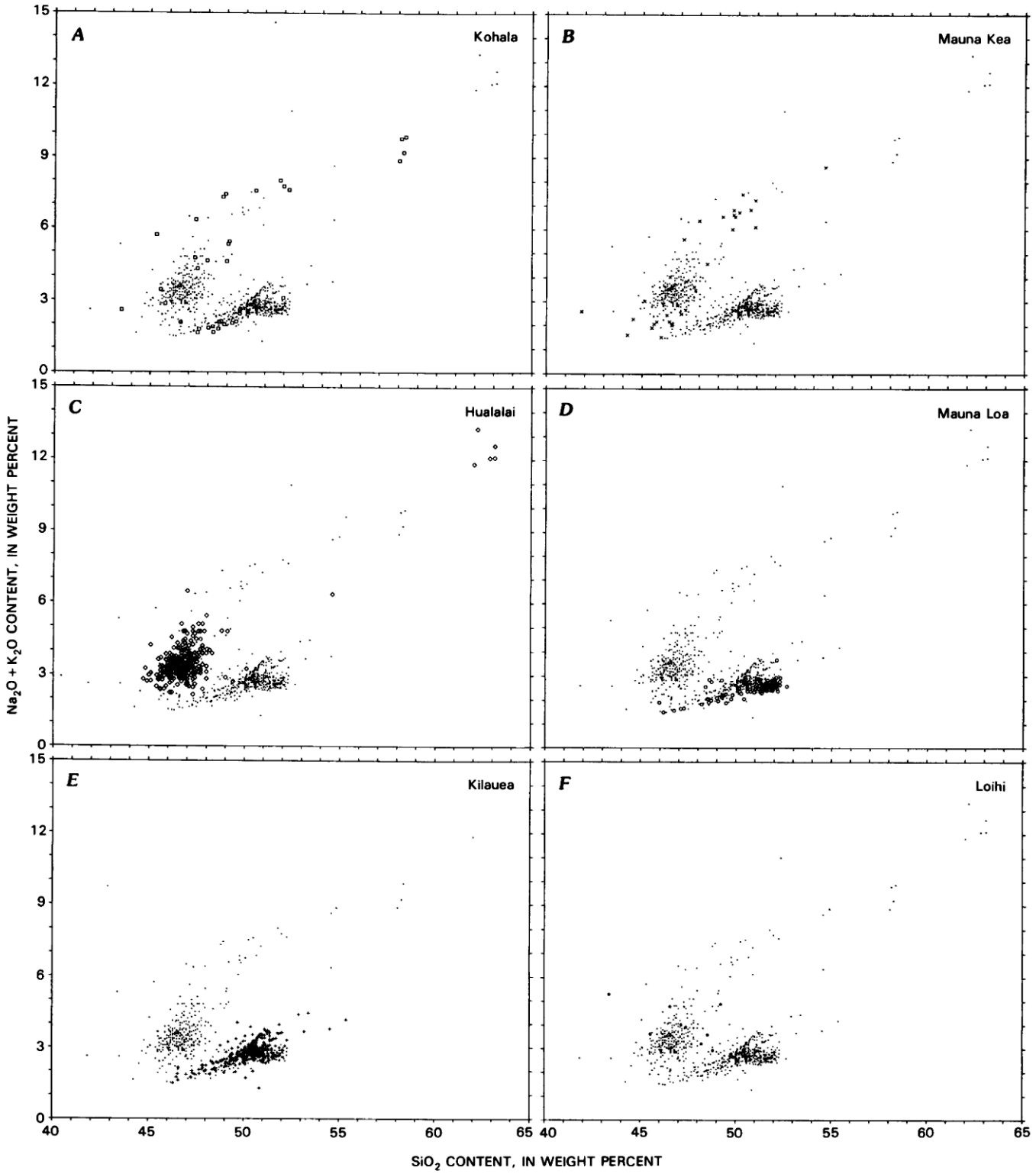

FIGURE 7.10.—Alkali-silica variation diagrams (Na_2O+K_2O vs. SiO_2) for volcanic rocks of Hawaii. ***A–F***, Plots for individual volcanoes as indicated. ***G***, Data for all six volcanoes combined. Individual diagrams show data for that volcano by heavy symbols and for comparison data for the other volcanoes by light dots. Analyses from published and unpublished sources.

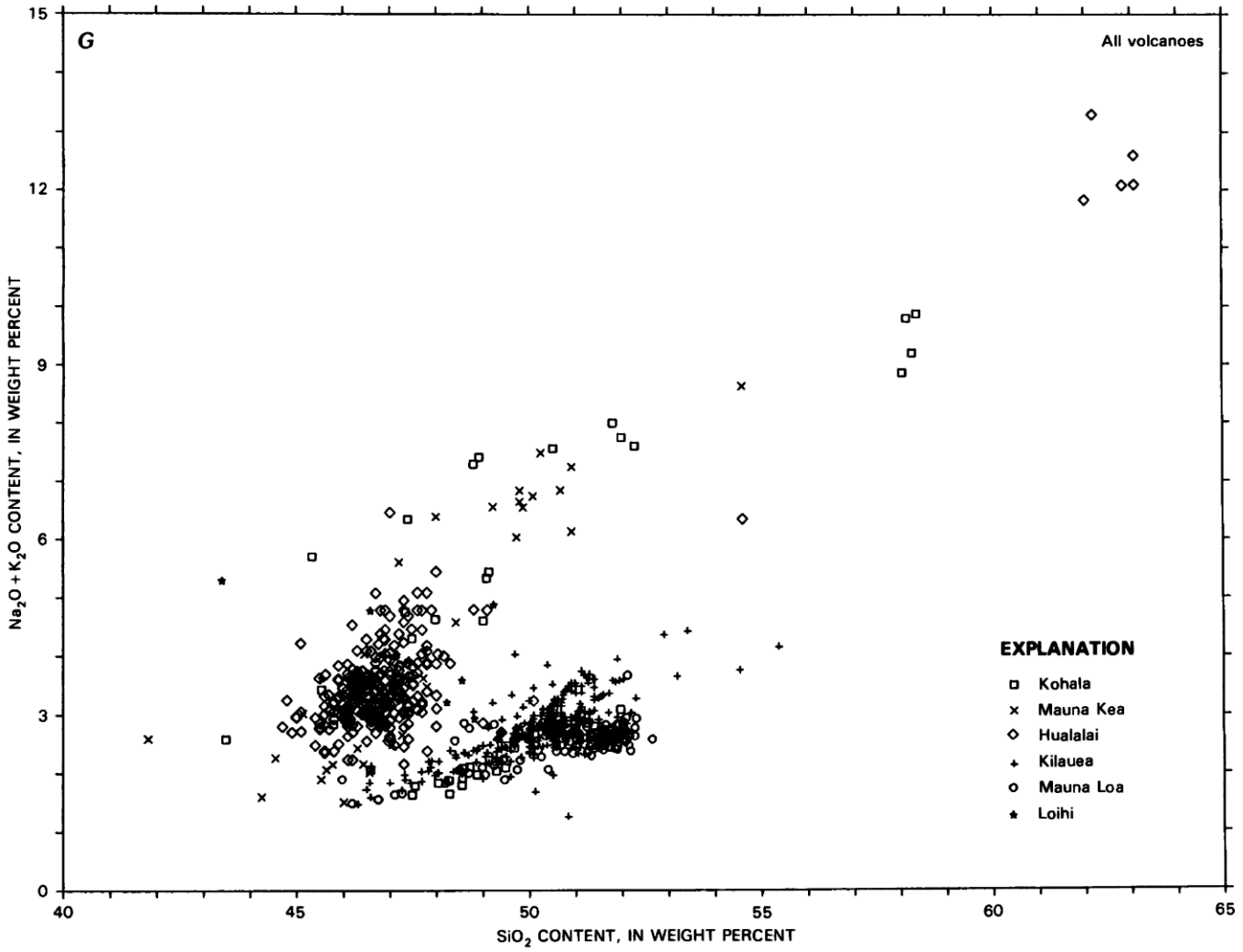

FIGURE 7.10.—Continued.

Lanphere and others (1980) concluded that alkalic and tholeiitic rocks are slightly different in terms of Rb and Sr abundances and isotopic compositions, suggesting intrinsic differences in mantle source regions. Lanphere (1983) has presented $^{87}Sr/^{86}Sr$ data for Loihi Seamount and concluded that the source materials for its divergent lavas are also isotopically distinct. Wright (1984) presented a metasomatic model for the origin of Hawaiian tholeiite that involves partial melting of a mantle source from which some mid-ocean-ridge basaltic liquid has been removed and to which has been added a nephelinitic fluid, amphibole, apatite, iron sulfide, and magnetite/ilmenite.

KOHALA

Kohala is the longest inactive and likely the oldest volcano on the Island of Hawaii, although, as noted by Lipman (1980), ages of basalts in the Ninole Hills in the south flank of Mauna Loa are similar to those of the oldest dated Kohala lavas (0.7–0.45 Ma; see Evernden and others, 1964; Dalrymple, 1971).

The geology of Kohala was mapped in reconnaissance by Stearns and Macdonald (1946); detailed mapping by M.O. Garcia and S.C. Porter is in progress. Stearns and Macdonald recognized two major groups of volcanic units; they termed the older of these the Pololu Volcanic Series, which they considered to be Pliocene to early Pleistocene in age, and the younger the Hawi Volcanic Series, which they considered middle Pleistocene. These units have been renamed the Pololu Basalt and the Hawi Volcanics by Langenheim and Clague (chapter 1, part II). Subsequent K-Ar dating (McDougall, 1964; Dalrymple, 1971; McDougall and Swanson, 1972) has established a Pleistocene age (0.7–0.06 Ma) for all of the subaerially exposed part of Kohala. McDougall and Swanson (1972) concluded that the Pololu shield-building stage ended at

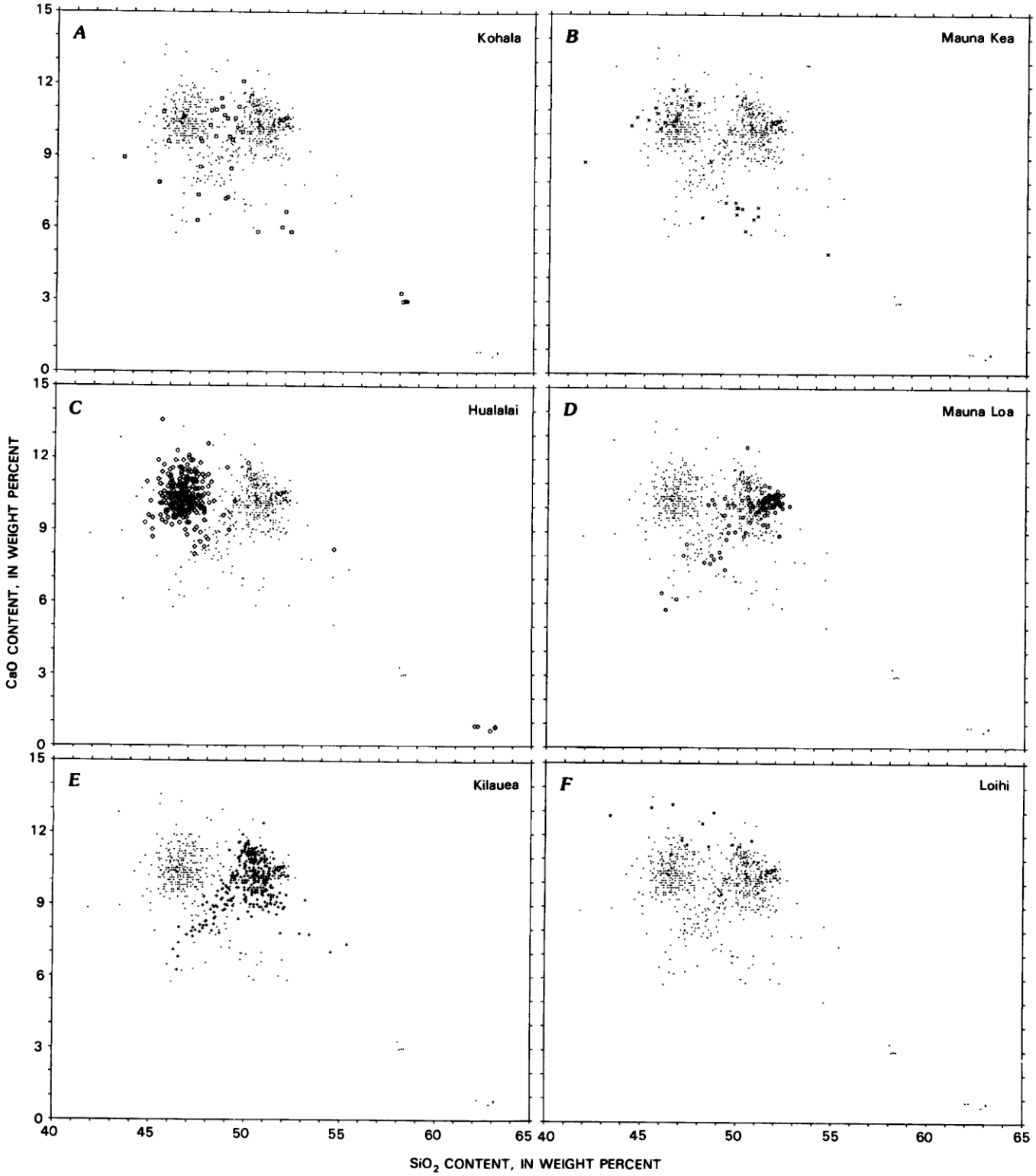

FIGURE 7.11.—Lime-silica variation diagrams (CaO vs. SiO_2) for volcanic rocks of Hawaii. ***A–F***, Plots for individual volcanoes, as indicated. ***G***, Data for all six volcanoes combined. Individual diagrams show data for that volcano by heavy symbols and for comparison data for other volcanoes by light dots. Analyses from published and unpublished sources.

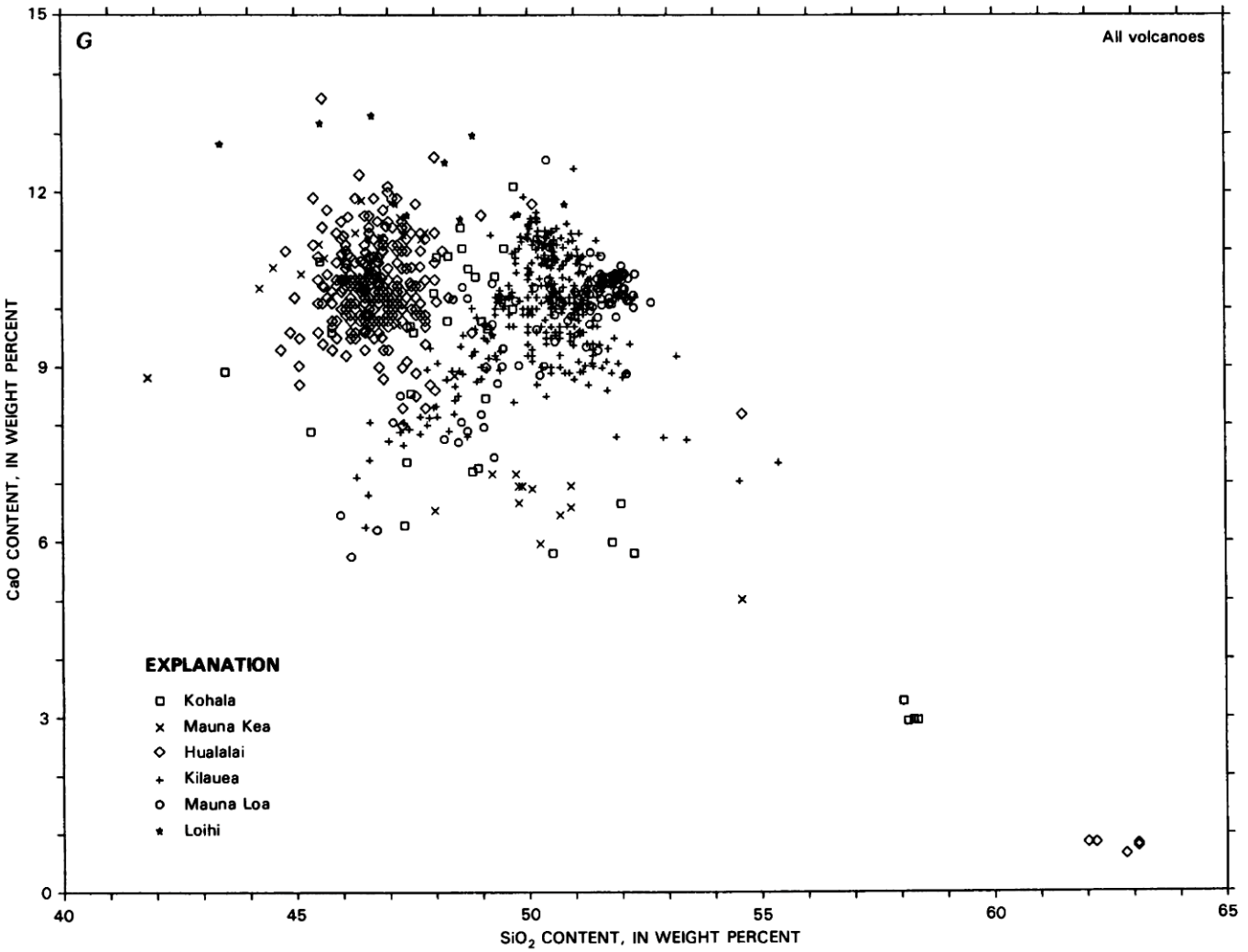

FIGURE 7.11.—Continued.

about 0.3 Ma and that the Hawi alkalic cap was formed by eruptions at 0.25–0.06 Ma (see fig. 7.4).

The lower part of the Pololu Basalt is tholeiitic (Macdonald and Katsura, 1964) and was extruded during the shield-building stage of the volcano; the younger volcanic materials are alkalic and characterized by larger proportions of intercalated cinders and ash. Variation diagrams (figures 7.10–7.14) suggest that some transitional basalts occur in the upper part of the Pololu Basalt.

The Hawi Volcanics is entirely alkalic and ranges in composition from alkali olivine basalt to benmoreite. Mugearites are particularly abundant, and more mafic rocks are rare. Feigenson and others (1983) report the occurrence of dunite xenoliths in some alkali basalt flows. Most of the Hawi vents are along Kohala's northwest-southeast-trending rift zone; the relation of this rift to the geometry of the tholeiitic shield is unknown, although probably the modern rift zone approximately coincides with the ancient one. A caldera that probably formed during Pololu time was buried by Hawi lavas (Stearns and Macdonald, 1946).

Variation diagrams (fig. 7.10–7.14) for Kohala rocks show that they generally are similar to rocks from Mauna Kea. Rocks of Kohala are somewhat more evolved, however; a single mugearite has been reported from Mauna Kea, whose subaerial lavas are dominated by hawaiite, ankaramite, and alkali olivine basalt.

The alkali-silica variation diagram for Kohala rocks (fig. 7.10*A*) shows the fields of tholeiitic and alkalic rocks and the differentiation products of alkali olivine basalt that include hawaiite, mugearite, and benmoreite. The lime-silica variation diagram for Kohala (fig. 7.11*A*) shows considerable scatter in the basalt range,

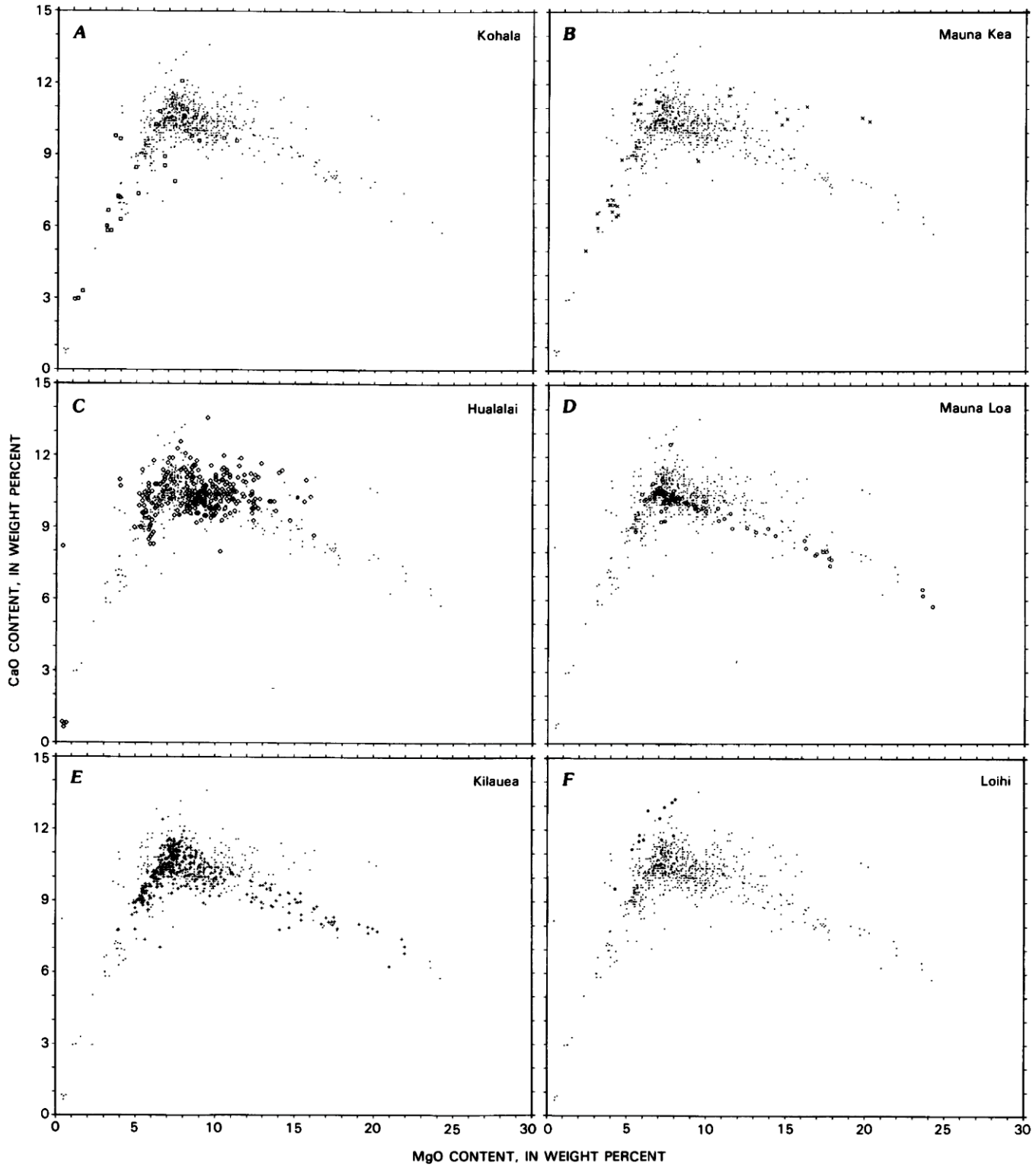

FIGURE 7.12.—Lime-magnesia variation diagrams (CaO vs. MgO) for volcanic rocks of Hawaii. ***A–F***, Plots for individual volcanoes, as indicated. ***G***, Data for all six volcanoes combined. Individual diagrams show data for that volcano by heavy symbols and for comparison data for other volcanoes by light dots. Analyses from published and unpublished sources.

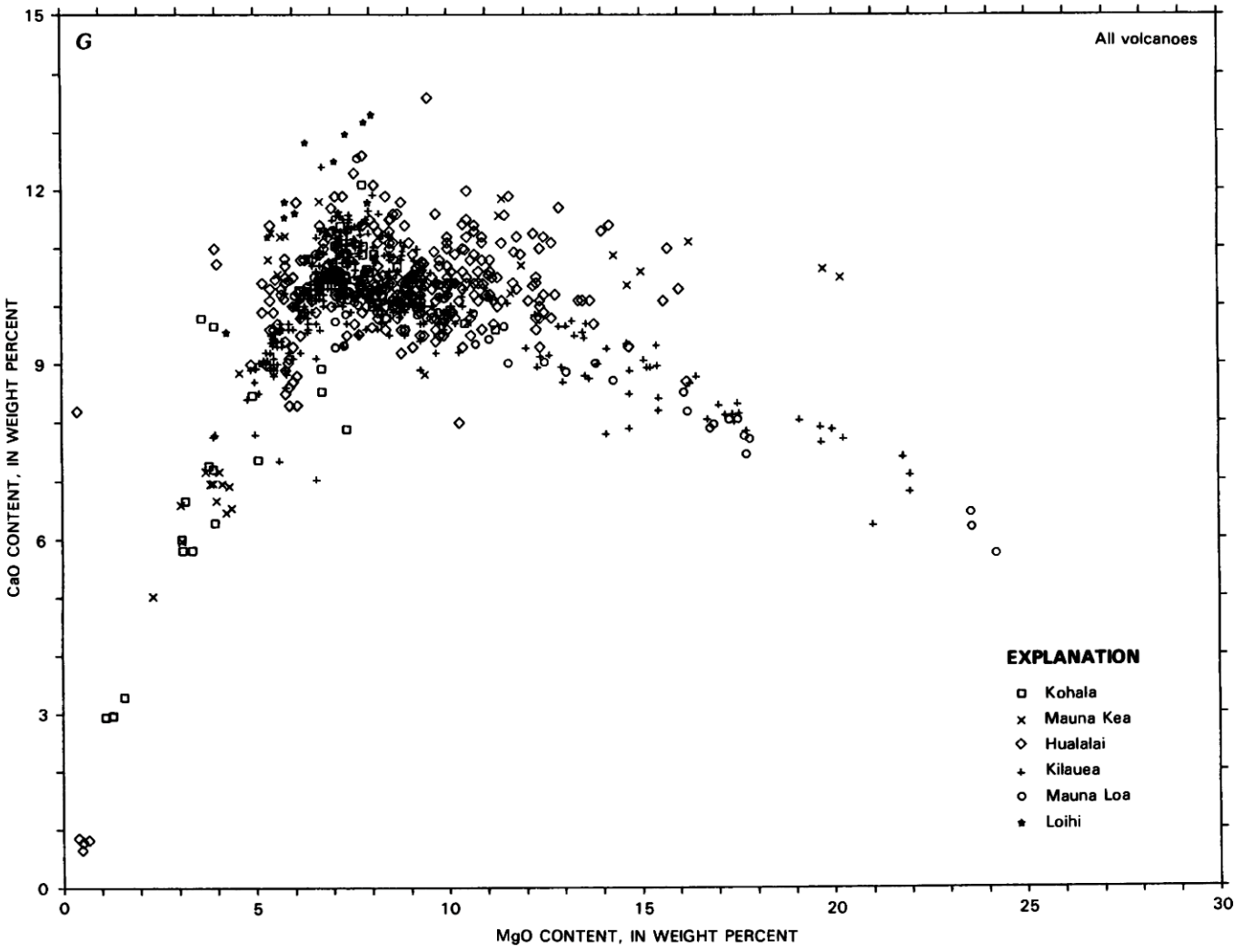

FIGURE 7.12.—Continued.

probably resulting from highly variable proportions of plagioclase and clinopyroxene phenocrysts. Mugearites and benmoreites of Kohala fall on a smooth trend. The lime-magnesia diagram (fig. 7.12 *A*) shows that Kohala tholeiites are similar to those from Hualalai, Mauna Loa, and Kilauea. The titania-magnesia diagram (fig. 7.13*A*) shows broad scatter among the Kohala rocks, suggesting that considerable mixing (Feigenson, 1984) and accumulation of Ti-rich phases (ilmenite, titanomagnetite, Ti-rich clinopyroxene) have occurred. Figure 7.14 (soda-magnesia diagram) further suggests that Kohala tholeiites are similar to those from Kilauea and Mauna Loa and that its alkalic rocks are generally similar to those from Hualalai and Mauna Kea.

MAUNA KEA

Mauna Kea has been inactive the second longest among volcanoes on the island of Hawaii. Some Mauna Kea lavas overlie rocks of Kohala on the east and south sides of Kohala; interlayering of lavas from the two sources likely occurs at depth. Stearns and Macdonald (1946) divided Mauna Kea lavas into the older Hamakua Volcanic Series (Pleistocene) and the younger Laupahoehoe Volcanic Series (Pleistocene and Holocene), now called the Hamakua Volcanics and Laupahoehoe Volcanics, respectively (fig. 7.4; Langenheim and Clague, chapter 1, part II). The two units locally are separated by as much as 5 m of weathered ash (originally called the Pahala Ash), most of which probably originated from proximal vents on Mauna Kea.

K-Ar ages reported by Porter and others (1977) range from 375±50 ka to 270±35 ka for the Hamakua Volcanics and 188±15 ka to 54.9±8.5 ka for the Laupahoehoe Volcanics. Radiocarbon ages by the same authors indicate that some Laupahoehoe lavas are as young as about 4.5 ka, and ash is as young as 3.6 ka (Porter, 1979b).

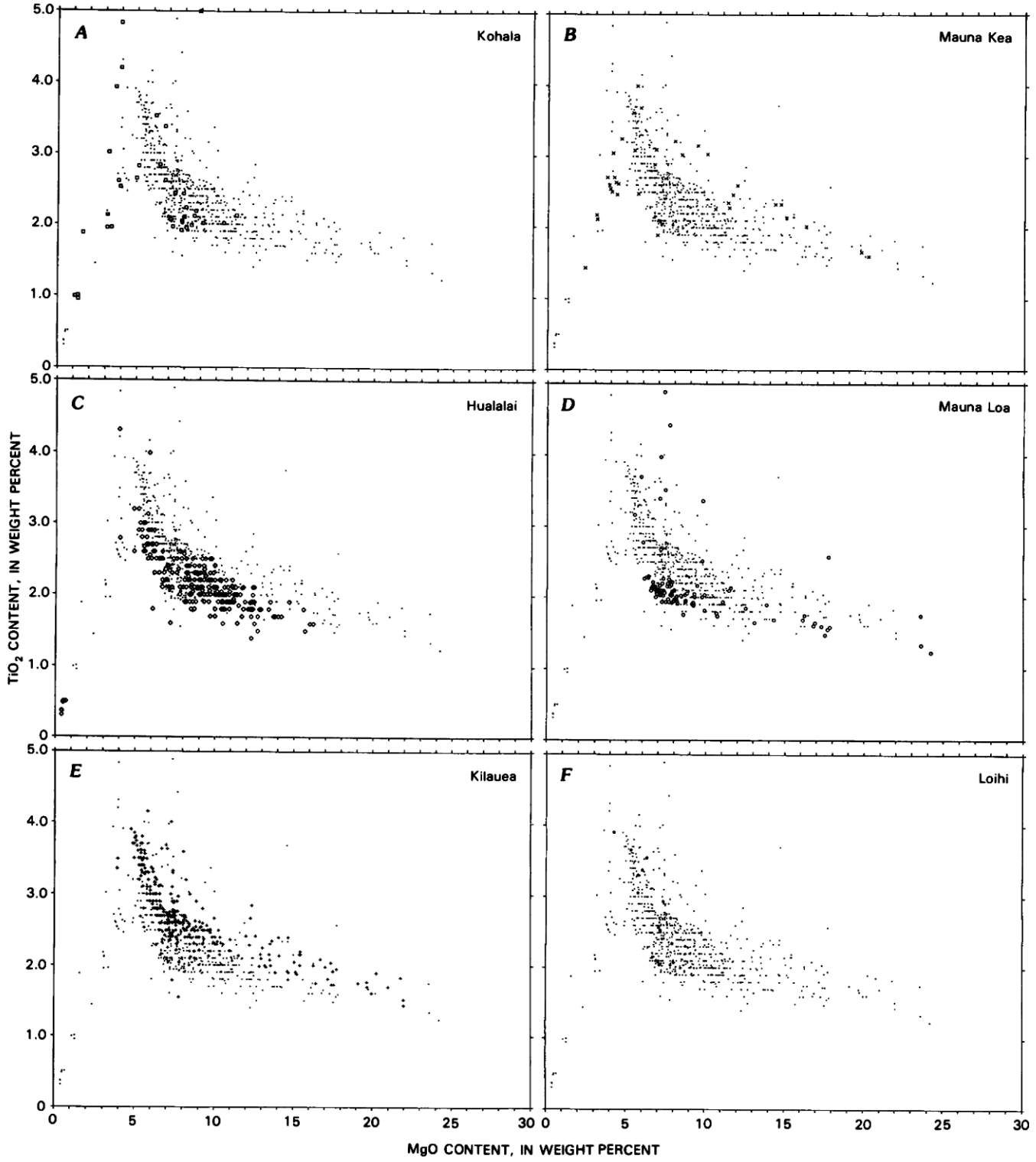

FIGURE 7.13.—Titania-magnesia variation diagrams (TiO_2 vs. MgO) for volcanic rocks of Hawaii. ***A–F***, Plots for individual volcanoes as indicated. ***G***, Data for all six volcanoes combined. Individual diagrams show data for that volcano by heavy symbols and for comparison data for volcanoes by light dots. Analyses from published and unpublished sources.

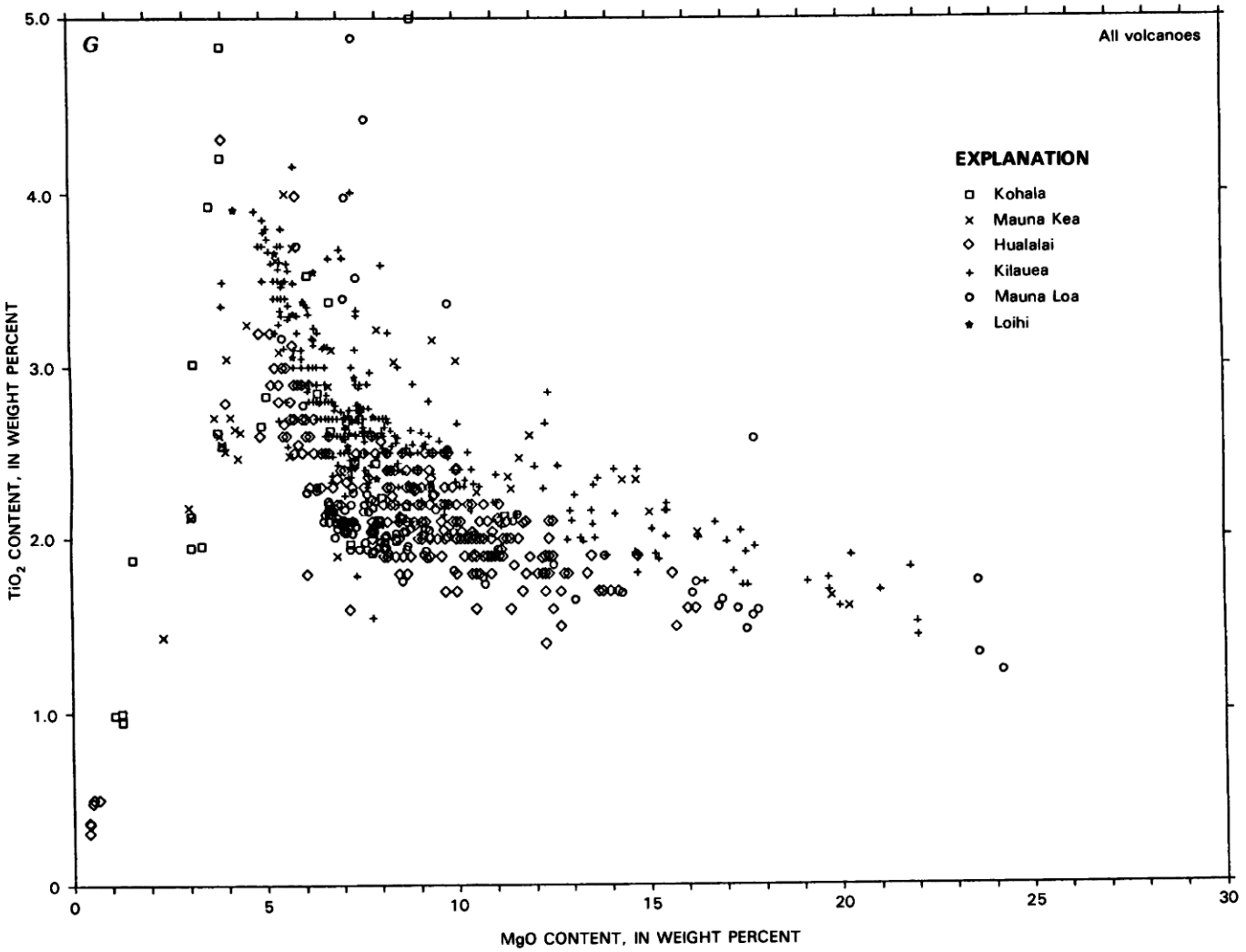

FIGURE 7.13.—Continued.

Tholeiitic basalts of the Hamakua Volcanics crop out only locally on the Hamakua (northeastern) coast of the island, where they commonly are interbedded with transitional and alkalic basalts (Macdonald and Katsura, 1964; Macdonald, 1968). The bulk of the subaerial part of the volcano, including all of the Laupahoehoe Volcanics, consists of transitional basalts, alkali olivine basalts, ankaramites, hawaiites, and a single known mugearite (Macdonald, 1968). Eruptions of alkali olivine basalt and derivative lavas produced cinder cones and lava flows (chiefly aa), widely distributed on the flanks and summit area of the volcano. Xenoliths of mafic and ultramafic rocks, commonly of cumulus origin, occur in several cones and flows (Jackson and others, 1982).

The early structural and eruptive history of Mauna Kea is conjectural, because alkalic lavas that constitute its cap have buried most structures. Porter (1972) recognized diffuse rift zones trending west, south-southeast, and east-northeast from an inferred buried caldera beneath the summit. It is not known whether these alignments of vents were inherited from the early tholeiitic, shield-building stage of the volcano.

As noted above, lavas of Mauna Kea are quite similar to, but generally less evolved than, those of Kohala (fig. 7.10–7.14). The alkali-silica variation diagram for Mauna Kea rocks (fig. 7.10*B*) indicates that virtually all analyzed lavas are alkalic. Fig. 7.11*B* shows that CaO decreases with increasing SiO_2, as with alkalic rocks from the other volcanoes. Wide scatter at the low-SiO_2 end suggests highly variable proportions of plagioclase and clinopyroxene phenocrysts. Figure 7.12*B* indicates that ankaramites from Mauna Kea with MgO greater than 11 percent are similar only to a few ankaramites from Hualalai. Fig. 7.13*B* shows that high-MgO Mauna Kea ankaramites and Kilauea tholeiites have similarly high

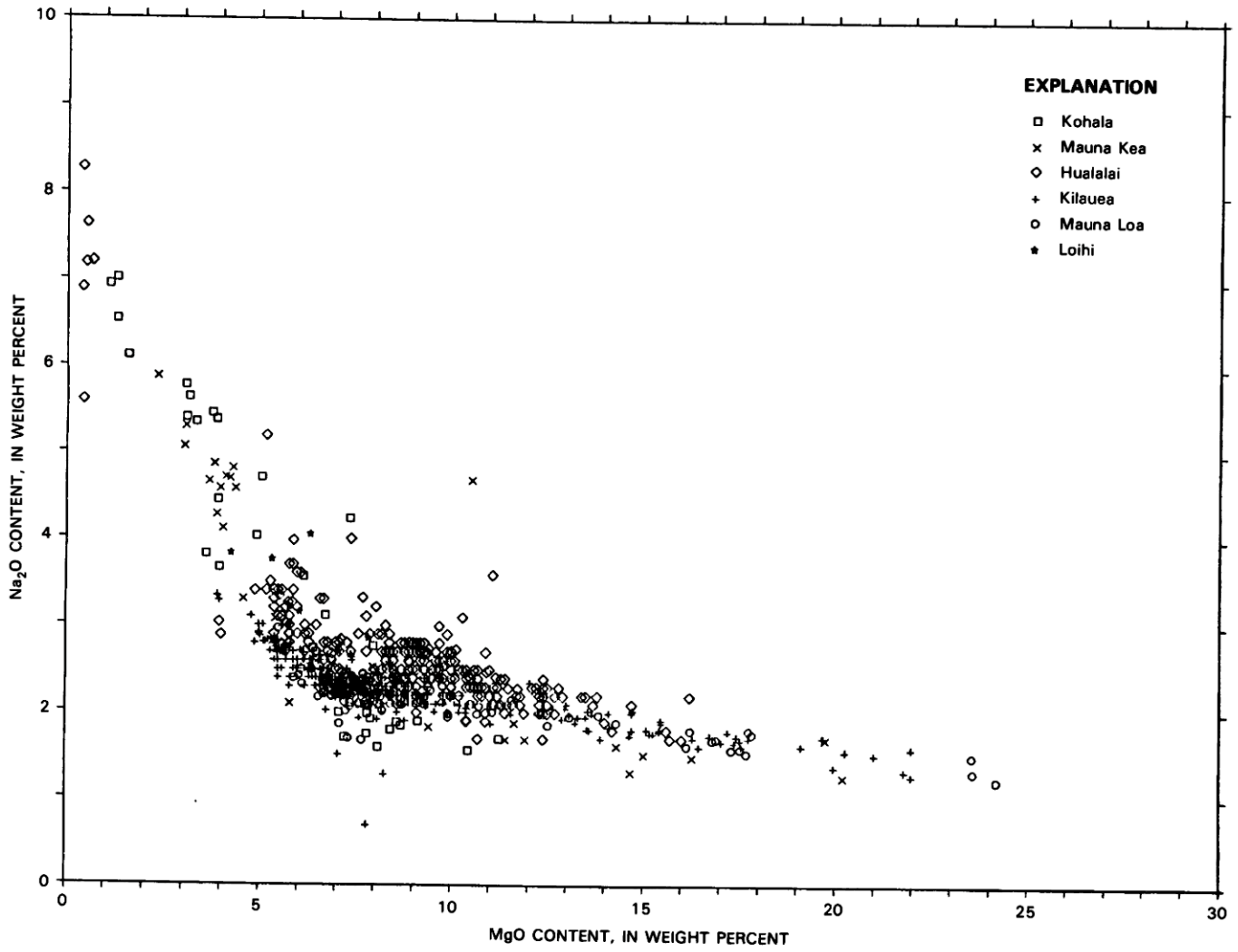

FIGURE 7.14.—Soda-magnesia variation diagram (Na_2O vs. MgO) for volcanic rocks of Hawaii. Analyses from published and unpublished sources.

TiO_2 contents; the two are distinct from the rocks of the other volcanoes. On figure 7.14 Mauna Kea rocks are seen to be similar to those of the other alkalic suites.

HUALALAI

Hualalai consists of a cap of alkalic lavas crowning an older tholeiitic shield (Moore and others, chapter 20). Exposed subaerial lavas are all alkalic; tholeiite has been recovered only from the submarine portion of the prominent northwest rift zone and (Clague, 1982) the bottoms of a few water wells. The geology of Hualalai was mapped in reconnaissance by Stearns and Macdonald (1946); detailed maps have been completed recently by D.A. Clague and by R.B. Moore.

About 5 km east of Hualalai's summit, a diffuse rift zone trends north from the principal northwest rift zone, which bends here and continues 13 km south-southeast. The subaerial portion of the northwest rift zone, 2–4 km wide, is 24 km long from the junction east of the summit to the ocean; bathymetry suggests that its submarine extension may be 70 km long. The north rift zone, about 10 km long and 5 km wide, contains less than 5 percent of the vents and has been inactive during the past 2,000 years. No ancient or modern caldera is evident, but there is, as on Mauna Kea, a concentration of vents in the summit area.

Trachyte, the most SiO_2-rich rock on the Island of Hawaii, crops out on the north rift zone of Hualalai at the Puu Waawaa cone and Puu Anahulu flow. Trachyte and microsyenite occur as xenoliths in basaltic deposits from four vents on the northwest and south-

TABLE 7.6.—*Selected references on the petrology and geochemistry of individual volcanoes of Hawaii*

Volcano	References
Kohala	Stearns and Macdonald (1946), Macdonald and Katsura (1964), Macdonald (1968), Feigenson and others (1983).
Mauna Kea	Stearns and Macdonald (1946), Macdonald and Katsura (1964), Macdonald (1968).
Hualalai	Moore and others (chapter 20), Stearns and Macdonald (1946), Macdonald (1968), Clague and others (1980).
Mauna Loa	Stearns and Macdonald (1946), Macdonald and Katsura (1964), Macdonald (1968), Wright (1971), Rhodes (1983).
Kilauea	Stearns and Macdonald (1946), Macdonald and Katsura (1964), Macdonald (1968), Wright (1971), Wright and Fiske (1971), Wright and others (1975), Wright and Tilling (1980), Wright 1984).
Loihi	Moore and others (1982), Frey and Clague (1983), Lanphere (1983).

southeast rift zones, and trachyte just above sea level was encountered in a drillhole on the northwest rift. A rather uncertain age for Puu Waawaa of 0.4 ± 0.3 Ma was obtained by Funkhouser and others (1968), but subsequently G.B. Dalrymple (written commun., 1985) determined an age of $0.106 \pm .006$ Ma. The steep topographic gradients in the area of the northwest rift zone suggest that other trachyte bodies may underlie a thin draping of more mafic lavas. Trachytes were produced during the Pleistocene, when magmatic activity was apparently much greater than it has been during the Holocene and much larger volumes of parental alkali olivine basalt were available for fractionation in shallow magma chambers.

Stearns and Macdonald (1946) mapped the alkalic rocks of Hualalai as the Hualalai Volcanic Series, which included the Waawaa Volcanics. These units are now called the Hualalai Volcanics and the Waawaa Trachyte Member, respectively (fig. 7.4; Langenheim and Clague, chapter 1, part II). Subsequent mapping and radiocarbon dating (Moore and others, chapter 20) have shown that about 95 percent of the surface is younger than 10 ka, and about 20 percent is younger than 1 ka. About 200 vents have erupted during Holocene time; the latest eruptions occurred in 1800–1801 (Stearns and Macdonald, 1946).

Hawaiite is the other differentiated lava that has been erupted by Hualalai; neither mugearite nor benmoreite, common on Kohala, has been found. The more silicic lavas are relatively old; during the last 5,000 years, most eruptions have produced olivine-controlled and differentiated alkali olivine basalt. Xenoliths include mafic and ultramafic rocks and are common in more than two dozen vents and associated flows. They are generally either rocks cognate to the volcano or fragments of oceanic crustal layer 3 (Jackson and others, 1981).

The alkali-silica variation diagram for Hualalai rocks (fig. 7.10C) shows that differentiation of alkalic magmas has produced the most silica-rich rocks on the island. It is possible that mugearites and benmoreites were formed during the period of trachyte volcanism, but they have never been found as flows, cones, or xenoliths.

Figure 7.11C shows the typical alkalic trend of decreasing CaO with increasing SiO_2, but it includes wide scatter at the basaltic end and a huge Daly gap (no lavas of intermediate silica content).

Figure 7.12C shows a wide scatter of CaO contents in the MgO range 5–15 percent, indicating that mixing of magmas has been an important process within Hualalai and reflecting the fact that phenocrysts of clinopyroxene and plagioclase locally are common. Figure 7.14 shows the higher soda content in alkalic rocks (analyses dominantly from Hualalai) vs. tholeiites.

MAUNA LOA

If the structurally high lavas in the Ninole Hills are considered to be part of Mauna Loa (Lipman, 1980), this volcano has been erupting above sea level for at least 400,000 years. Most of its surface, however, is Holocene, as mapped by Stearns and Macdonald (1946), Lipman and Swenson (1984), and Lockwood and others (1984, and unpublished data). Stearns and Macdonald (1946) divided Mauna Loa rocks into (1) the Pliocene Ninole Volcanic Series, shown by subsequent K-Ar dating (Evernden and others, 1964; Dalrymple, 1971) to be late Pleistocene; (2) the Pleistocene Kahuku Volcanic Series; and (3) the latest Pleistocene and Holocene Kau Volcanic Series. These units are now called the Ninole Basalt, the Kahuku Basalt, and the Kau Basalt (see fig. 7.4; Langenheim and Clague, chapter 1, part II). The Kahuku and Kau are separated by the Pahala Ash.

All known subaerial lavas of Mauna Loa are tholeiites, and most lavas are olivine controlled. Differentiated lavas are rare, in contrast to Kilauea (Wright, 1971). Figure 7.10*D* shows that a few of the more differentiated lavas plot close to the line separating alkalic from tholeiitic basalts (Macdonald and Katsura, 1964).

Figure 7.11*D* shows that CaO generally increases with increasing SiO_2 in Mauna Loa rocks, but begins to decrease as andesitic (52 percent SiO_2) compositions are approached. This trend reflects the removal of olivine (low in silica and lime) from tholeiitic melts. As andesitic compositions are approached, CaO begins to decrease, reflecting coprecipitation of pyroxene and (or) plagioclase, as in the alkalic trend.

Figure 7.12*D* (CaO vs. MgO) shows that most Mauna Loa tholeiites are olivine-controlled, as noted by Wright (1971) and Rhodes (1983). In a few cases, differentiated magmas (<6.8 percent MgO; Wright, 1971) have been mixed with olivine-controlled magmas to produce hybrid lavas whose compositions plot off the olivine-control line.

Figure 7.13*D* (TiO_2 vs. MgO) suggests that there are two trends among the Mauna Loa rocks. One has relatively low TiO_2 at specific MgO abundances and may reflect accumulation of ilmenite and (or) titanomagnetite.

KILAUEA

The oldest subaerial rocks of Kilauea were mapped as the Hilina Volcanic Series by Stearns and Macdonald (1946). The rocks in their lowermost exposures are thought to date from 100–70 ka (Easton and Garcia, 1980). Holcomb (1980) has determined

that 90 percent of the surface of Kilauea is younger than 1.1 ka, and 70 percent is younger than 0.5 ka. The youngest rocks of Kilauea were mapped as the Puna Volcanic Series by Stearns and Macdonald (1946). The Puna is of latest Pleistocene and Holocene age. These units have been renamed the Hilina Basalt and the Puna Basalt by Easton (chapter 11). The Hilina and the Puna are separated by the Pahala Ash (see fig. 7.4).

The known eruptive vents of Kilauea are confined to its summit caldera (3 km by 5 km in size) and two rift zones that extend east and southwest from the summit. The east rift zone, which initially trends southeast for 6 km from the summit and then turns east-northeastward and extends another 45 km, is the longer and historically more frequently active of the two (Duffield and others, 1982). It extends below sea level another 70 km beyond the eastern end of the island (Moore and Reed, 1963; Fornari and others, 1978). The subaerial part of the southwest rift zone is about 32 km long, and no extension has been identified offshore.

The south flank of Kilauea is unbuttressed, in contrast to its north side, and thus it is free to move southward in response to repeated injection of magma into storage chambers beneath the summit and rift zones (Swanson and others, 1976a). The large earthquakes of 1868 and 1975 were possibly related to accumulated stress caused by rift deformation. The normal fault scarps of the Hilina system record cumulative displacements of at least 300 m.

Eruptions of Kilauea and Mauna Loa are normally placid and nonexplosive, but Mauna Loa has had minor phreatic eruptions in Holocene time and Kilauea experienced violent explosive eruptions in 1790 and 1924 and doubtless many times previously (Swanson and Christiansen, 1973; Decker and Christiansen, 1984). The 1790 event was probably phreatomagmatic and may have been associated with a major collapse that formed the modern caldera (Holcomb, 1980). Lavas of that age cover much of the lower east rift zone (Moore, 1981, 1983); draining of the summit magma reservoir to feed the eruptions on the rift zone likely induced the collapse. The 1924 phreatic eruption was preceded by the injection of magma from the summit reservoir into the east rift zone, accompanied by ground subsidence at Kapoho, near the subaerial terminus of the rift; a submarine eruption may have occurred to the east-northeast. The event climaxed with a series of steam explosions at Halemaumau over the course of several days. The combination of lava withdrawal, explosions, and collapse of the walls greatly increased both the diameter and depth of Halemaumau Crater.

Other large explosive eruptions on Kilauea built the Kapoho cone, only 20 m above sea level, a few hundred years ago, and were associated with collapse of the three largest pit craters on the lower east rift zone in the time interval 1.3 to 0.2 ka (Moore, 1981, 1983).

Many historical eruptions of Kilauea have lasted only a few days to a few weeks, but three relatively long-lived eruptions have built satellitic shields and associated cones (Mauna Iki, Mauna Ulu, and Puu Oo) since 1919. Two late prehistoric satellitic shields (Kane Nui o Hamo and Heiheiahulu) lie along the east rift zone; similar shields probably formed throughout the growth of the volcano and now the older ones lie buried. Long-lived eruptions from central vents along rift zones apparently were less common during most of the last 1,500 years than they have been during historical (post-1820) time.

All known Kilauea lavas are only tholeiitic basalt; olivine-controlled, differentiated, and hybrid lavas have been erupted from its rift zones, while summit lavas are all olivine-controlled (Wright and Fiske, 1971). As with a few Mauna Loa lavas, a few Kilauea lavas fall in the transition zone between tholeiitic and alkalic Hawaiian rocks on the alkali-silica variation diagram (fig. 7.10*E*). It can also be seen from figure 7.10*E* that, despite its relative youth, Kilauea has erupted a few lavas that are somewhat more differentiated than any that have been found on Mauna Loa. It is not known why the rift zones of Kilauea are able to accommodate long-lived magma chambers whereas those of Mauna Loa do not, but the reason may be related to the different heights of the two volcanoes.

The variation diagram of CaO vs. SiO_2 shows that Kilauea tholeiites are similar to those from Mauna Loa. CaO increases with increasing SiO_2 until andesitic compositions are approached and then decreases with further increase of SiO_2. The lime content of Kilauea tholeiitic differentiates is markedly higher than that in alkalic differentiates of the other volcanoes.

Plots of the variation of CaO and TiO_2 with MgO (figs. 7.12*E*, 7.13*E*) show olivine-controlled differentiation down to MgO abundances of about 6.8 percent; departures from the straight trend reflect magma mixing in rift-zone storage chambers (Wright and Fiske, 1971). Melts erupted on the rift zones range as low as 4.1 percent MgO and include both differentiated and hybrid lavas (Wright and Fiske, 1971). TiO_2 is generally higher in MgO-rich Kilauea lavas than in those from Hualalai and Mauna Loa.

LOIHI

Because of its early stage of development, Loihi Seamount was expected to consist exclusively of tholeiitic rocks, but dredged samples included alkali olivine basalts and basanites, some with abundant ultramafic xenoliths, as well as tholeiites (Moore and others, 1982). From this it has been concluded that limited partial melting of mantle source material during the initial stages of formation of Hawaiian volcanoes may result in generation of alkalic basalts (Moore and others, 1982; Frey and Clague, 1983). With increased partial melting, tholeiitic melts would form, and Loihi appears to be in a transitional stage between the generation of these two types of basalt.

It is also possible, however, that the rocks of Loihi represent more than one mantle source. Lanphere (1983) reported $^{87}Sr/^{86}Sr$ ratios for the different groups of basalts recovered from Loihi and concluded that their mantle sources had different Sr-isotope compositions.

Analytical data reported by Moore and others (1982) are incorporated here in figures 7.10–7.14. The variation diagram of $Na_2O + K_2O$ vs. SiO_2 (fig. 7.10*F*) shows that Loihi alkalic and tholeiitic basalts are similar to those from other volcanoes on the Island of Hawaii, but no other basanites have been reported.

The field of high-CaO Loihi rocks is evident on figures 7.11*F* and 7.12*F*. Figures 7.13*F* and 7.14 further indicate that analyzed Loihi rocks are generally similar to those from other Hawaiian

volcanoes and that olivine-controlled differentiation and mixing of magmas have occurred.

NONERUPTIVE GEOLOGIC PROCESSES

Hawaii is the youngest island of the archipelago and the only one with appreciable historical volcanic activity, and any review of its geologic history necessarily deals chiefly with the growth and construction processes related to volcanism. However, geologic agents other than volcanism have also been at work, some constantly and others sporadically. During the active growth stages of a volcano their effects are commonly outstripped or covered by the effects of volcanism, but during the later evolutionary stages, when the frequency and volume rate of eruptions decline, the effects of these other geologic agents become more apparent.

EROSION AND SEDIMENTATION

Extensive discussions of the effects of erosion and sedimentation on the Island of Hawaii are given elsewhere, chiefly in Stearns and Macdonald (1946) and Macdonald and others (1983); we present only a brief summary here.

Annual rainfall on the windward side of Hawaii (east and northeast) is high, as much as 7,600 mm (300 inches). Erosion has been effective in cutting canyons on the windward slopes of the older volcanoes, Kohala and Mauna Kea, and to some extent in the old Ninole Hills on the south flank of Mauna Loa. In these areas of steep topography, soil creep and mudflows locally contribute to the process of erosion. The leeward (west and southwest) side of the island receives much less rainfall, locally as little as 250 mm (10 inches). As a consequence, the western flanks of Kohala and Mauna Kea are little dissected by streams. Hualalai, Kilauea, and most of Mauna Loa show little evidence of stream erosion, because the surface has been frequently renewed by Holocene volcanic activity. Another important factor inhibiting stream erosion is the porous nature of young volcanic rocks. Even heavy rain infiltrates young lava flows quickly, and surface runoff is minimal.

As noted by Stearns and Macdonald (1946), Macdonald and others (1983), and other workers, the locations of canyons on the northeastern side of Kohala are partly fault-controlled and partly consequent, initially cut near the edges of lava flows. Their local relief is as much as 500 m. Submergence of the island during latest Pleistocene and Holocene time has drowned the valley mouths, and the major canyons, including Waipio, Waimanu, Honokane Nui, and Pololu, contain thick sedimentary fill.

Canyons cut into the windward flank of Mauna Kea are not as deep (maximum 200 m) as those on Kohala, because the surface of Mauna Kea is younger. Radial drainage consequent upon the lava-flow topography dominates; slopes are thinly mantled by locally derived cinders, and the effect of structures, such as buried faults, appears to be minimal. The Wailuku River, which flows through part of Hilo, is primarily a consequent stream cut near the edges of Mauna Loa flows that lapped onto the flank of Mauna Kea.

The Ninole Hills, on the south flank of Mauna Loa, are either structurally high (Lipman, 1980) or erosional (Stearns and Macdonald, 1946) remnants of early Mauna Loa. Gulches that separate the hills are likely inherited from Pleistocene time; their positions can still be identified even though they have been buried by flows of the younger Kahuku and Kau Basalts.

Marine erosion has been vigorous, primarily on the windward sides of the island, and has formed sea cliffs as high as 400 m on Kohala and 100 m on Mauna Kea (Macdonald and others, 1983). Sea stacks and caves are common on the Hamakua coast. Wave action along the southeastern coast has formed sea cliffs several meters high on historic and prehistoric flows from vents on Kilauea's east rift zone. Erosion along this coast is so vigorous that a wave-cut face 1–3 m high was maintained even while lava from the east rift zone of Kilauea was still actively flowing into the sea (Peterson, 1976); within months of the cessation of activity, the newly created shoreline had been worn back appreciably. In contrast, marine erosion of flows from Kohala, Mauna Kea, Hualalai, and Mauna Loa on the western (leeward) side of the island has been slight, and sea cliffs higher than a few meters are rare, even on the older (Pleistocene) flows.

Eolian erosion and sedimentation have been of local importance on the island. Extensive areas on the west flank of Mauna Kea are covered by eolian silt, which originated chiefly as ash at vents and perhaps as glacial debris blown from the summit area. Dunes consisting of reworked Pahala ash are common in the South Point area on the southern flank of Mauna Loa. The Kau Desert, on the southwest flank of Kilauea, has many small active dunes that consist primarily of wind-blown pyroclastic debris originally ejected during the explosive eruptions of 1790 and 1924.

CHANGES OF SEA LEVEL

Many workers have studied changes of sea level in the Hawaiian Islands, especially H.T. Stearns and more recently J.G. Moore. The major controls on sea level have been (1) worldwide eustatic fluctuations caused by Quaternary climatic changes resulting in varying amounts of water stored in glaciers and (2) subsidence of the islands as a result of volcanic load (Moore, chapter 2, 1969).

Ancient shorelines have been identified throughout the Hawaiian Islands by wavecut terraces below and near sea level and by deposits above sea level inferred to represent marine terraces (Stearns, 1946, 1966, 1978; Macdonald and others, 1983). These widely separated stands of the sea suggested to Stearns that the crust has repeatedly oscillated up and down throughout Quaternary time. In view of the ongoing subsidence of the southeastern end of the island chain, readily shown to be caused by the persistent process of volcanic loading (Moore, chapter 2; Apple and Macdonald, 1966; Moore, 1970; Moore and Fornari, 1984), such large-amplitude fluctuations were puzzling. Moore and Moore (1984), however, have provided evidence showing that most or all of the supposed subaerial terrace deposits have instead resulted from a giant catastrophic wave, which avoids the need to explain high stands of sea level by crustal oscillation. Moore (chapter 2) discusses the subsidence processes in detail.

If, however, another major global glaciation occurs, sea level may drop faster than the ongoing subsidence. Canyon-cutting on the

Island of Hawaii would then become more vigorous, as streams become graded to the new lower sea level.

GLACIATION

Mauna Kea was glaciated during Pleistocene time, and the resulting deposits were studied by Wentworth and Powers (1941), Porter and others (1977), and Porter (1979a, b). These workers recognized the effects of four separate glaciations that occurred during the period 280–10 ka. Typical glacial features such as striated boulders, roches moutonnees, ground moraine, and lateral and terminal moraines are visible in the summit area of Mauna Kea. Porter (1979b) estimated that the maximum thickness of ice was 150–170 m.

Glaciers may have formed on Mauna Loa also, but any evidence of them has been buried by Holocene lavas (Macdonald and others, 1983).

EARTHQUAKES AND FLANK DISPLACEMENTS

Most earthquakes on and near the Island of Hawaii are the consequence of volcanic activity. Some are induced as magma moves into storage chambers beneath the summits of Mauna Loa and Kilauea, others as magma is intruded into the rift zones that radiate from the summit calderas. The intrusion of magma results in an accumulation of stress that must eventually be relieved. Some earthquakes occur when magma moves out of an area, resulting in local foundering of overlying rocks.

Large earthquakes (magnitude 6 or greater) in Hawaii have been concentrated in three principal areas: (1) the Kealakekua fault system on the west flank of Mauna Loa, (2) the Kaoiki fault system on the southeast flank of Mauna Loa, and (3) the Hilina fault system on the south flank of Kilauea. Each of these areas has experienced at least one earthquake of magnitude (M) greater than 6 since 1950. In addition, a deep (48-km) $M = 6.2$ earthquake struck the east flank of Mauna Kea in 1973 and apparently triggered sympathetic crustal aftershocks on the north flank of Mauna Kea, an area that has experienced occasional swarms for decades (Unger and Ward, 1979).

Earthquakes that occur on the Kealakekua and Hilina fault systems are, in large part, the result of gravitational sliding of parts of the volcanic edifices toward the sea. In these areas, there is no adjoining volcano to provide a buttress against such sliding; thus, when the volcano is overinflated (as Mauna Loa was in the aftermath of the great 1950 eruption and as the east rift zone of Kilauea was by the end of the 1969–1974 Mauna Ulu eruption), a condition of accumulated strain analogous to oversteepening results in failure of the volcano's flank (Swanson and others, 1976a).

Large earthquakes in the Kaoiki region probably are largely the result of inflation of the summit region and upper northeast rift zone of Mauna Loa. Here the strain release is accommodated by strike-slip faulting (Endo, 1985) rather than by normal faulting, because the presence of Kilauea provides a buttress resisting downward slippage of Mauna Loa's southeast flank.

Large fault scarps, as high as about 300 m, are the major surface expression of repeated faulting along the Hilina and Kealakekua systems. The Kaoiki system consists of upper and lower parts. The lower part is inactive seismically, and fault scarps there have been buried by lava flows as old as 9 ka (Lipman, 1980). The upper part, where modern seismicity is concentrated, is characterized by extensive ground cracking, but fault scarps of large displacement are absent (Endo, 1985).

TSUNAMIS

Tsunamis (seismic-induced sea waves) are the most dangerous and destructive natural hazards that affect Hawaii and its residents. Hawaiian tsunamis usually are caused by earthquakes of local or circum-Pacific origin that displace the ocean bottom; this displacement in turn generates a wave in the overlying water. These low-amplitude waves travel at speeds of several hundred kilometers per hour in deep ocean, but when they approach land masses they are slowed and build up to heights of many meters. The greatest recorded height of a wave striking the Island of Hawaii was 16.8 m at the mouth of Pololu Valley in 1946, although greater (but unmeasured) heights may have been reached in 1868 and at other times (Macdonald and others, 1983).

Tsunamis that have struck Hawaii since 1819 are listed in table 7.7. The average interval between tsunamis has been about five years, but the average interval separating the seven that have caused severe damage has been about 22 years. However, their recurrence interval has no regular pattern.

TABLE 7.7.—*Principal tsunamis observed in Hawaii during historical time*

[Adapted from Macdonald and others, 1947, 1983]

Date	Source	Damage in Hawaii
1819, April 12	Unknown	Unknown
1837, November 7	South America	SEVERE
1841, May 17	Kamchatka	Slight
1868, April 2	Hawaii	SEVERE
1868, August 13	South America	SEVERE
1869, July 25	South America (?)	Moderate
1872, August 23	Hawaii	Slight
1877, May 10	South America	SEVERE
1883, August 26	East Indies	Slight
1896, June 15	Japan	None
1901, August 9	Japan (?)	None
1906, January 31	Unknown	None
1906, August 16	South America	Slight
1918, September 7	Kamchatka	Slight
1919, April 30	Unknown	None
1922, November 11	South America	None
1923, February 3	Kamchatka	Moderate
1923, April 13	Kamchatka	None
1927, November 4	California	None
1927, December 28	Kamchatka	None
1928, June 16	Mexico	None
1929, March 6	Aleutian Islands	None
1931, October 3	Solomon Islands	None
1933, March 2	Japan	Slight
1938, November 10	Alaska	None
1944, December 7	Japan	None
1946, April 1	Aleutian Islands	SEVERE
1952, November 4	Kamchatka	Slight
1957, March 9	Aleutian Islands	Slight
1960, May 22	South America	SEVERE
1964, March 28	Alaska	None
1975, November 29	Hawaii	SEVERE

The effects of tsunamis are not likely to be preserved in the geologic record for very long. Vegetation generally grows rapidly in Hawaii and would mask debris. Boulders are thrown up on the tops of low sea cliffs also by severe storms, and these would be indistinguishable from those washed up by tsunamis. Deep narrow canyons (Pololu, Laupahoehoe) on the northeastern coast, which are most vulnerable to severe tsunami damage, are rapidly filled with new fluvial sediments. On the other hand, Moore and Moore (1984) interpreted a widespread gravel on Lanai, Maui, and northwest Hawaii as a deposit from a giant wave, possibly generated by a submarine landslide south of Lanai dating from about 100 ka. This event, however, was much larger and rarer than ordinary tsunamis.

FUTURE DEVELOPMENT

KOHALA

Kohala Volcano is generally considered extinct, because its last known eruption occurred at about 60 ka (McDougall and Swanson, 1972). However, renewed volcanism on other Hawaiian volcanoes has begun one million or more years after cessation of alkalic cap activity (Clague and Dalrymple, chapter 1, part I). Future eruptions of Kohala thus are possible; they might be alkalic basaltic, basanitic, or nephelinitic in composition.

Erosion is probably the major geologic process that will affect Kohala in the future. Unless parts are rebuilt by renewed volcanic activity, sustained fluvial and coastal erosion for millions of years will wear Kohala down to sea level. If regional subsidence continues in the future as it has in the past (Moore, chapter 2), subsidence will supplement the erosion process. Kohala will become a separate island long before it is leveled by erosion, if subsidence causes the saddle between it and Mauna Kea to be submerged.

MAUNA KEA

Mauna Kea may well erupt again, since it has been only about 4,500 years since it last erupted (Porter and others, 1977). The next eruptions may be similar in composition to the most recent (hawaiite), although it is possible that mugearite, benmoreite, or trachyte will appear in the future. Mauna Kea is still considered to be in the capping stage (3) although unless additional eruptions of alkalic rocks occur, it will have quietly completed the transition to the erosional stage (4).

As on Kohala, erosion will be the major geologic process occurring on Mauna Kea. Over the next few millions of years, erosion and subsidence probably will reduce the volcano to sea level.

HUALALAI

The average recurrence interval for eruptions of Hualalai in the Holocene has been about 50 yr (200 events in 10,000 yr), but clusters of eruptions separated by gaps of hundreds of years have apparently occurred. A few satellitic shields that probably took several years to form are present. Most of the recent eruptions have been of high volume (>0.25 km^3). Phreatic explosions have occurred at two vents within the past 700 years; the products of one covered an area of at least 10 km^2. Eruptions since at least 100 ka have been exclusively of alkali olivine basalt and its differentiates; no major change in chemical composition is expected for tens of thousands of years. Perhaps in hundreds of thousands of years Hualalai will erupt basanite and (or) nephelinite. An intense swarm of earthquakes beneath Hualalai in 1929 is believed to have been associated with underground movement of magma (Macdonald and Abbott, 1970, p. 53–54), and the volcano may have been close to having an eruption (Moore and others, chapter 20). Since 1929, however, neither ground deformation nor swarms of earthquakes have been detected on Hualalai, so it cannot be estimated when the next magmatic activity will occur.

Hualalai is virtually undissected, although a few intermittent streams are subject to flash flooding. Heavy rain in 1980 and 1981 resulted in deposition of several hundred cubic meters of debris in alluvial fans near the summit and downcutting of gullies by as much as 5 m. On the southwest flank of the volcano, gullying locally occurs on flows that are relatively old (13–5 ka). The surface renewal rate (18 km^2 per 100 yr for the last 3,000 yr) suggests that erosion will not have a pronounced effect on Hualalai's morphology for a long time, possibly tens of thousands of years.

MAUNA LOA

Mauna Loa has been active about 6 percent of the time since 1835, and a similar rate of activity likely will continue in the foreseeable future. Mauna Loa has erupted an average of 2.9 km^3 of lava per century during historical time, and most of its surface is younger than 4 ka (Lockwood and Lipman, chapter 18). Historical Mauna Loa eruptions have ranged in duration from a few hours to 450 days, and future eruptions from the summit, rift zones, and north and west flanks probably will be similar. Mauna Loa does not seem to build satellitic shields, in contrast to Kilauea. In view of the prevailing rate of crustal subsidence (Moore, chapter 2), it seems unlikely that the height of Mauna Loa above sea level will increase much more than a few tens or hundreds of meters; however, repeated filling and collapse of Mokuaweoweo Crater seems likely to occur.

If Mauna Loa follows the pattern of most other Hawaiian volcanoes, thousands to hundreds of thousands of years in the future, it will erupt alkalic basalts and their differentiates. As noted earlier, a few basalts of Mauna Loa already appear to be transitional in their chemical composition.

Mauna Loa is nearly undissected; until the output of the volcano decreases markedly, erosion will have negligible effect on its constructional landforms.

KILAUEA

Kilauea has been active about 60 percent of historical time and has extruded more than 1.2 km^3 of tholeiitic basalt since 1952. Three satellitic shields have formed during this century, and two others during the past few hundred years. In contrast to Mauna Loa, Kilauea has sustained long-term eruptions (at least 5 years). Magma will continue to be stored in its rift zones, where it will differentiate; perhaps more differentiates as extreme as the Yellow

Cone scoria will form and be erupted. Eventually, basalts more transitional in composition will be erupted, although Kilauea seems unlikely to erupt alkalic rocks until its present rate of magma production declines. That may be hundreds of thousands of years in the future.

Kilauea also is little eroded, although a few intermittent streams flood during heavy rains. Kilauea's historical output of about 2.2 km^3/100 yr seems likely to ensure that its surface will be frequently renewed; at present, 90 percent of its surface is younger than 1.1 ka (Holcomb, chapter 12).

LOIHI

If Loihi erupts in the future at a rate comparable to those of Kilauea and Mauna Loa, its summit will reach the ocean's surface in a few tens of thousands of years. Moore and others (1982) suggested that Loihi has been or may soon begin erupting tholeiitic basalt exclusively as the amount of partial melting of the mantle source increases. If it reaches sea level, it will initially form a separate island, but if eruptions continue, it could ultimately be joined with Hawaii. Loihi likely will follow the same eruptive pattern as other volcanoes along the island chain.

REFERENCES CITED

Ando, M., 1979, The Hawaii earthquake of November 29, 1975: low dip angle faulting due to forceful injection of magma: Journal of Geophysical Research, v. 84, no. B 13, p. 7616–7626.

Apple, R.A., and Macdonald, G.A., 1966, The rise of sea level in contemporary times at Honaunau, Kona, Hawaii: Pacific Science, v. 20, p. 125–136.

Banks, N.G., Klein, F.W., Moore, R.B., Jackson, D.B., and Okamura, A.T., 1981, Kilauea Volcano November 1979 eruption [abs]: Eos (American Geophysical Union Transactions), v. 62, no. 45, p. 1072.

Banks, N.G., Wolfe, E.W., Duggan, T.A., Okamura, A.T., Koyanagi, R.Y., Greenland, L.P., and Jackson, D.B., 1983, Magmatic events at Kilauea Volcano, Hawaii, 1982 [abs.]: Eos (American Geophysical Union Transactions), v. 64, no. 45, p. 901–902.

Bargar, K.E., and Jackson, E.D., 1974, Calculated volumes of individual shield volcanoes along the Hawaiian-Emperor Chain: U.S. Geological Survey Journal of Research, v. 2, p. 545–550.

Beaglehole, J.C., 1967, The journals of Captain Cook on his voyages of discovery; Volume III: The voyage of the Resolution and Discovery, 1776–1780: Cambridge University Press, 1647 p.

Berry, A.L., 1973, Thermoluminescence of Hawaiian basalts: Journal of Geophysical Research, v. 78, p. 6863–6867.

Brigham, W.T., 1909, The volcanoes of Kilauea and Mauna Loa: B.P. Bishop Museum Memoir, v. 2, no. 4, 222 p.

Budahn, J.R., and Schmitt, R.A., 1985, Petrogenetic modeling of Hawaiian tholeiitic basalts: a geochemical approach: Geochimica et Cosmochimica Acta, v. 49, p. 67–87.

Clague, D.A., 1982, Petrology of tholeiitic basalt dredged from Hualalai Volcano, Hawaii: Eos (American Geophysical Union Transactions), v. 63, p. 1138.

———in press, Hawaiian alkaline volcanism: Quarterly Journal, Geological Society of London.

Clague, D.A., Jackson, E.D., and Wright, T.L., 1980, Petrology of Hualalai Volcano, Hawaii: implication for mantle composition: Bulletin Volcanologique, v. 43, no. 4, p. 641–656.

Coan, T., 1841, Great eruption of the volcano of Kilauea: Missionary Herald, v. 37, p. 283–285.

———1851, Mauna Loa eruption of 1849: American Journal of Science, 2d ser., v. 12, p. 82.

———1852, On the eruption of Mauna Loa, Hawaii, February 1852: American Journal of Science, 2nd ser., v. 14, p. 106–107, 219–224.

———1869, Notes on the recent volcanic disturbances of Hawaii: American Journal of Science, 2nd ser., v. 47, p. 89–98.

———1871, On Kilauea and Mauna Loa: American Journal of Science, 3d ser., v. 2, p. 454–456.

———1877, Volcanic eruptions on Hawaii: American Journal of Science, 3d ser., v. 14, p. 68–69.

Cross, Whitman, 1915, Lavas of Hawaii and their relations: U.S. Geological Survey Professional Paper 88, 97 p.

Crosson, R.S., and Endo, E.T., 1981, Focal mechanisms of earthquakes related to the 29 November 1975 Kalapana, Hawaii, earthquake: the effect of structure models: Bulletin of the Seismological Society of America, v. 71, no. 3, p. 713–729.

———1982, Focal mechansims and locations of earthquakes in the vicinity of the 1975 Kalapana earthquake aftershock zone 1970–1979: implications for tectonics of the south flank of Kilauea Volcano, Island of Hawaii: Tectonics, v. 1, p. 495–542.

Dalrymple, G.B., 1971, Potassium-argon ages from the Pololu Volcanic Series, Kohala Volcano, Hawaii: Geological Society of America Bulletin, v. 82, p. 1997–1999.

Dalrymple, G.B., Silver, E.A., and Jackson, E.D., 1973, Origin of the Hawaiian Islands: American Scientist, v. 61, p. 294–308.

Daly, R.A., 1911, The nature of volcanic action: American Academy of Arts and Sciences, Proceedings, v. 47, p. 47–122.

———1914, Igneous rocks and their origin: New York, McGraw-Hill Book Co., 563 p.

———1933, Igneous rocks and the depths of the earth: New York, McGraw-Hill Book Co., Inc., 598 p.

———1944, Volcanism and petrogenesis as illustrated in the Hawaiian Islands: Geological Society of America Bulletin, v. 55, p. 1363–1400.

Dana, J.D., 1849, Geology: U.S. Exploring Expedition, under the command of Charles Wilkes, U.S.N., 1838–1842: v. 10, p. 156–226.

———1859, Eruption of Mauna Loa, Hawaii: American Journal of Science, 2d ser., v. 27, p. 410–415.

———1860, Eruption of Mauna Loa, Sandwich Islands: American Journal of Science, 2d ser., v. 29, p. 301–302.

———1890, Characteristics of Volcanoes: New York, Dodd, Mead Co., 399 p.

Davis, J.B., 1859, Great eruption of the volcano Mauna Loa, in the Island of Hawaii: Edinburgh New Philosophical Journal, new ser., v. 10, p. 94–97.

Decker, R.W., and Christiansen, R.L., 1984, Explosive eruptions of Kilauea Volcano, Hawaii: *in* Explosive volcanism: inception, evolution, and hazards: Washington, D.C., National Academy Press, p. 122–132.

Douglas, D., 1914, Journal kept by David Douglas during his travels in North America, 1833–1837, London, p. 298–317.

Duffield, W.A., 1975, Structure and origin of the Koae fault system, Kilauea Volcano, Hawaii: U.S. Geological Survey Professional Paper 856, 12 p.

Duffield, W.A., Christiansen, R.L., Koyanagi, R.Y., and Peterson, D.W., 1982, Storage, migration, and eruption of magma at Kilauea Volcano, Hawaii, 1971–1972: Journal of Volcanology and Geothermal Research, v. 13, p. 273–307.

Dutton, C.E., 1884, Hawaiian volcanoes: U.S. Geological Survey, 4th Annual Report, p. 75–219.

Dzurisin, Daniel, 1980, Influence of fortnightly earth tides at Kilauea Volcano, Hawaii: Geophysical Research Letters, v. 7, p. 925–928.

Easton, R.M., and Garcia, M.O., 1980, Petrology of the Hilina Formation, Kilauea Volcano, Hawaii: Bulletin Volcanologique, v. 43, p. 657–673.

Ellis, William, 1827, Journal of William Ellis, Narrative of a tour of Hawaii, with remarks on the history, traditions, manners, customs, and language of the inhabitants of the Sandwich Islands: Honolulu (1963), Advertiser Publishing Co., Ltd., reprint of the London 1827 edition, 342 p.

Endo, E.T., 1985, Seismotectonic framework for the southeast flank of Mauna Loa Volcano, Hawaii: Seattle, University of Washington, Ph.D. dissertation, 327 p.

Evernden, J.F., Savage, D.E., Curtis, G.H., and James, G.T., 1964, Potassium-argon dates and the Cenozoic mammalian chronology of North America:

American Journal of Science, v. 262, p. 145–198.
Feigenson, M.D., Hofmann, A.W., and Spera, F.J., 1983, Case studies on the origin of basalt, II. The transition from tholeiitic to alkalic volcanism on Kohala Volcano, Hawaii: Contributions to Mineralogy and Petrology, v. 84, p. 390–405.
Finch, R.H., and Macdonald, G.A., 1951, Report of the Hawaiian Volcano Observatory for 1948 and 1949: U.S. Geological Survey Bulletin 974–D, p. 103–133.
———1953, Hawaiian volcanoes during 1950: U.S. Geological Survey Bulletin 996–B, p. 27–89.
Fisher, R.V., 1968, Puu Hou littoral cones, Hawaii: Geologisches Rundschau, v. 57, p. 837–864.
Fiske, R.S., and Jackson, E.D., 1972, Orientation and growth of Hawaiian volcanic rifts: the effect of regional structure and gravitational stresses: Proceedings of the Royal Society of London, v. 329, p. 299–326.
Fiske, R.S., and Koyanagi, R.Y., 1968, The December 1965 eruption of Kilauea Volcano, Hawaii: U.S. Geological Survey Professional Paper 607, 21 p.
Fornari, D.J., Malahoff, A., and Heezen, B.C., 1978, Volcanic structure of the crest of the Puna Ridge, Hawaii: geophysical implications of submarine volcanic terrain: Geological Society of America Bulletin, v. 89, p. 605–616.
Frey, F.A., and Clague, D.A., 1983, Geochemistry of diverse basalt types from Loihi Seamount, Hawaii: petrogenetic implications: Earth and Planetary Science Letters, v. 66, p. 337–355.
Funkhouser, J.G., Barnes, I.L., and Naughton, J.J., 1968, The determination of a series of ages of Hawaiian volcanoes by the potassium-argon method: Pacific Science, v. 22, p. 369–372.
Furumoto, A.S., and Kovach, R.L., 1979, The Kalapana earthquake of November 29, 1975: an intra-plate earthquake and its relations to geothermal processes: Physics of the Earth and Planetary Interiors, v. 29, p. 355–364.
Goodrich, Joseph, 1826, Notice of the volcanic character of the Island of Hawaii: American Journal of Science, lst series, v. 11, p. 2–7.
Green, W.L., 1887, Vestiges of the molten globe, Pt. 2 of the Earth's surface features and volcanic phenomena: Honolulu, 377 p.
Halbig, J.B., Orr, J.B., and Lockwood, J.P., 1979, Use of alteration rind thickness to date prehistoric Hawaiian lavas: Hawaii Symposium on Intraplate Volcanism and Submarine Volcanism, Hilo, Hawaii, Abstract Volume, p. 163.
Harvey, A.G., 1947, Douglas of the fir, A biography of David Douglas, Botanist: Cambridge, Mass., Harvard University Press, 290 p.
Hitchcock, C.H., 1909, Hawaii and its volcanoes: Honolulu, The Hawaiian Gazette Co., Ltd., 314 p. (2nd edition with supplement, 1911).
Holcomb, R.T., 1976, Complexity and hazards of Hawaiian shield volcanoes [abs]: Geological Society of America, Abstracts with Program, v. 8, no. 6, p. 920–921.
———1980, Kilauea Volcano, Hawaii: chronology and morphology of the surficial lava flows: Stanford University, Ph.D. dissertation, 321 p., also U.S. Geological Survey Open-File Report 81–354, 1981.
Jackson, D.B., Swanson, D.A., Koyanagi, R.Y., and Wright, T.L., 1975, The August and October 1968 east rift eruptions of Kilauea Volcano, Hawaii: U.S. Geological Survey Professional Paper 890, 33 p.
Jackson, E.D., Beeson, M.H., and Clague, D.A., 1982, Xenoliths in volcanic rocks from Mauna Kea Volcano, Hawaii: U.S. Geological Survey Open-File Report 82–201, 19 p.
Jackson, E.D., Clague, D.A., Engleman, E., Friesen, W.B., and Norton, D., 1981, Xenoliths in the alkalic basalt flows from Hualalai Volcano, Hawaii: U.S. Geological Survey Open-File Report 81–1031, 32 p.
Jaggar, T.A., 1919, Activity of Mauna Loa: Hawaiian Volcano Observatory Bulletin, v. 7, no. 10, p. 128–158.
———1920, Seismometric investigation of the Hawaiian lava column: Seismological Society of America Bulletin, v. 10, p. 155–275.
———1926, Journal of Mauna Loa eruption: Hawaiian Volcano Observatory Bulletin, v. 14, p. 31–47, 54–57.
———1947, Origin and development of craters: Geological Society of America Memoir 21, 508 p.
Jaggar, T.A., and Finch, R.H., 1924, The explosive eruption of Kilauea in Hawaii, 1924: American Journal of Science, ser. 5, v. 8, p. 353–374.
Kelley, M.L., 1979, Radiocarbon dates from the Hawaiian Islands—a compilation: U.S. Geological Survey Open File Report 79–1700, 37 p.
Kelley, M.L., Spiker, E.C., Lipman, P.W., Lockwood, J.P., Holcomb, R.T., and Rubin, M., 1979, U.S. Geological Survey, Reston, Virginia, Radiocarbon dates XV: Mauna Loa and Kilauea Volcanoes, Hawaii: Radiocarbon, v. 21, p. 306–320.
Kinoshita, W.T., Koyanagi, R.Y., Wright, T.L., and Fiske, R.S., 1969, Kilauea Volcano; the 1967–1968 summit eruption: Science, v. 166, p. 459–468.
Klein, F.W., and Koyanagi, R.Y., 1979, Seismicity of Kilauea and Loihi Volcanoes, Hawaii: Hawaii Symposium on Intraplate Volcanism and Submarine Volcanism, Hilo, Hawaii, Abstract Volume, p. 124.
Kuno, H., Yamasake, K., Iida, C., and Nagashima, K., 1957, Differentiation of Hawaiian magmas: Japan Journal of Geology and Geography, v. 28, p. 179–218.
Lanphere, M.A., 1983, $^{87}Sr/^{86}Sr$ ratios for basalt from Loihi Seamount, Hawaii: Earth and Planetary Science Letters, v. 66, p. 380–387.
Lanphere, M.A., Dalrymple, G.B., and Clague, D.A., 1980, Rb-Sr systematics of basalts from the Hawaiian-Emporer volcanic chain: Initial Reports of the Deep Sea Drilling Project, 55, p. 695–706.
Ledyard, John, 1783, A journal of Captain Cook's last voyage to the Pacific Ocean and in quest of a northwest passage between Asia and America: Hartford, Conn., Nathaniel Patkon.
Leeman, W.P., Budahn, J.R., Gerlach, D.C., Smith, D.R., and Powell, B.N., 1980, Origin of Hawaiian tholeiites: Trace element constraints: American Journal of Science, v. 280-A, p. 794–819.
Lipman, P.W., 1980, The southwest rift zone of Mauna Loa: implications for structural evolution of Hawaiian volcanoes: American Journal of Science, v. 280-A, p. 752–776.
Lipman, P.W., and Swenson, Alan, 1984, Generalized geologic map of the southwest rift zone of Mauna Loa Volcano, Hawaii: U.S. Geological Survey Miscellaneous Investigations Series Map I– 1323, scale 1:100,000.
Lockwood, J.P., Banks, N.G., English, T.T., Greenland, L.P., Jackson, D.B., Johnson, D.J., Koyanagi, R.Y., McGee, K.A., Okamura, A.T., and Rhodes, J.M., 1985, The 1984 eruption of Mauna Loa Volcano, Hawaii: Eos, Transactions, American Geophysical Union, v. 66, no. 16, p. 169–171.
Lockwood, J.P., Koyanagi, R.Y., Tilling, R.I., Holcomb, R.T., and Peterson, D.W., 1976, Mauna Loa threatening: Geotimes, v. 21, no. 6, p. 12–15.
Lockwood, J.P., and Lipman, P.W., 1980, Recovery of datable charcoal beneath young lavas: lessons from Hawaii: Bulletin Volcanologique, v. 43, no. 3, p. 609–615.
Macdonald, G.A., 1947, Bibliography of the geology and water resources of the Island of Hawaii: Hawaii Division of Hydrography, Bulletin 10, 191 p.
———1949a, Petrography of the Island of Hawaii: U.S. Geological Survey Professional Paper 214–D, p. 51–95.
———1949b, Hawaiian Petrographic Province: Geological Society of America Bulletin, v. 60, p. 1541–1596.
———1954, Activity of Hawaiian volcanoes during the years 1940–1950: Bulletin Volcanologique, ser. 2, v. 15, p. 120–179.
———1955, Hawaiian Islands: Catalog of the active volcanoes of the world including solfatara fields, Part III, International Volcanological Association, Naples, Italy, 37 p.
———1959, The activity of Hawaiian volcanoes during the years 1951–1956: Bulletin Volcanologique, ser. 2, v. 22, p. 3–70.
———1960, Dissimilarity of continental and oceanic rock types: Journal of Petrology, v. 1, p. 172–177.
———1962, The 1959 and 1960 eruptions of Kilauea Volcano, Hawaii, and the construction of walls to restrict the spread of the lava flows: Bulletin Volcanologique, v. 24, p. 249–294.
———1965, Hawaiian calderas: Pacific Science, v. 19, p. 320–334.
———1968, Composition and origin of Hawaiian lavas: Geological Society of America Memoir 116, p. 477–522.
———1972, Volcanoes: Englewood Cliffs, N.J., Prentice-Hall, Inc., 510 p.
Macdonald, G.A., and Abbott, A.T., 1970, Volcanoes in the sea: Honolulu, University of Hawaii Press, 441 p.
Macdonald, G.A., Abbott, A.T., and Peterson, F.L., 1983, Volcanoes in the sea, second edition: Honolulu, University of Hawaii Press, 517 p.

Macdonald, G.A., and Eaton, J.P., 1957, Hawaiian volcanoes during 1954: U.S. Geological Survey Bulletin 1061–B, 17–72.

———1964, Hawaiian volcanoes during 1955: U.S. Geological Survey Bulletin 1171, 170 p.

Macdonald, G.A., and Katsura, T., 1961, Variations in the lava of the 1959 eruption in Kilauea Iki: Pacific Science, v. 15, p. 358–369.

———1962, Relationship of petrographic suites in Hawaii: Crust of the Pacific Basin, Geophysical Monograph no. 6, p. 187–195.

———1964, Chemical composition of Hawaiian lavas: Journal of Petrology, v. 5, p. 82–133.

Macdonald, G.A., and Orr, J.B., 1950, The 1949 summit eruption of Mauna Loa, Hawaii: U.S. Geological Survey Bulletin 974–A, p. 1–31.

Malahoff, A., McMurtry, G.M., Wiltshire, J.C., and Yeh, H.W., 1982, Geology and chemistry of hydrothermal deposits from active submarine volcano Loihi, Hawaii: Nature, v. 298, p. 234–239.

May, R.J., 1979, Thermoluminescence dating of Hawaiian basalt: U.S. Geological Survey Professional Paper 1095, 47 p.

McDougall, Ian, 1964, Potassium-argon ages from lavas of the Hawaiian Islands: Geological Society of America Bulletin, v. 75, p. 107–128.

McDougall, Ian, and Swanson, D.A., 1972, Potassium-argon ages of lavas from the Hawi and Pololu Volcanic Series, Kohala Volcano, Hawaii: Geological Society of America Bulletin, v. 83, p. 3731–3738.

Moore, J.G., 1964, Giant submarine landslides on the Hawaiian Ridge: U.S. Geological Survey Professional Paper 501–D, p. D95–D98.

———1965, Petrology of deep-sea basalt near Hawaii: American Journal of Science, v. 263, p. 40–52.

———1970, Relationship between subsidence and volcanic load, Hawaii: Bulletin Volcanologique, v. 34, p. 562–576.

———1975, Mechanism of formation of pillow lava: American Scientist, v. 63, p. 269–277.

Moore, J.G., and Ault, W.U., 1965, Historic littoral cones in Hawaii: Pacific Science, v. 19, p. 3–11.

Moore, J.G., Clague, D.A., and Normark, W.R., 1982, Diverse basalt types from Loihi Seamount, Hawaii: Geology, v. 10, p. 88–92.

Moore, J.G., and Fiske, R.S., 1969, Volcanic substructure inferred from dredge samples and ocean-bottom photographs, Hawaii: Geological Society of America Bulletin, v. 80, p. 1191–1202.

Moore, J.G., and Fornari, D.J., 1984, Drowned reefs as indicators of the rate of subsidence of the island of Hawaii: Journal of Geology, v. 92, p. 752–759.

Moore, J.G., and Koyanagi, R.Y., 1969, The October 1963 eruption of Kilauea Volcano, Hawaii: U.S. Geological Survey Professional Paper 614-C, 13 p.

Moore, J.G., and Krivoy, H.L., 1964, The 1962 flank eruption of Kilauea Volcano and structure of the east rift zone: Journal of Geophysical Research, v. 69, p. 2033–2045.

Moore, J.G., and Moore, G.W., 1984, Deposit from a giant wave on the Island of Lanai, Hawaii: Science, v. 226, p. 1312–1315.

Moore, J.G., Phillips, R.L., Grigg, R.W., Peterson, D.W., and Swanson, D. A., 1973, Flow of lava into the sea, 1969–1971, Kilauea Volcano, Hawaii: Geological Society of America Bulletin, v. 84, p. 537–546.

Moore, J.G., and Reed, R.K., 1963, Pillow structures of submarine basalts east of Hawaii: U.S. Geological Survey Professional Paper 475–B, p. B153–B157.

Moore, R.B., 1981, Preliminary geologic map of the Kapoho quadrangle, Hawaii: U.S. Geological Survey Open-File Report 81–947, scale 1:24,000.

———1983, Distribution of differentiated tholeiitic basalt on the lower east rift zone of Kilauea Volcano, Hawaii: a possible guide to geothermal exploration: Geology, v. 11, p. 136–140.

Moore, R.B., Helz, R.T., Dzurisin, D., Eaton, G.P., Koyanagi, R.Y., Lipman, P.W., Lockwood, J.P., and Puniwai, G.S., 1980, The 1977 eruption of Kilauea Volcano, Hawaii: Journal of Volcanology and Geothermal Research, v. 7, p. 189–210.

Murata, K.J., and Richter, D.H., 1966, Chemistry of the lavas of the 1959–60 eruption of Kilauea Volcano, Hawaii: U.S. Geological Survey Professional Paper 537–A, 26 p.

Peck, D.L., and Kinoshita, W.T., 1976, The eruption of August 1963 and the formation of Alae lava lake, Hawaii: U.S. Geological Survey Professional Paper 935–A, 33 p.

Peterson, D.W., 1971, Petroleum potential of Hawaii, *in* Cram, I. H., ed., Future Petroleum Provinces of the United States: American Association of Petroleum Geologists Memoir 15, p. 161–169.

———1976, Processes of volcanic island growth, Kilauea Volcano, Hawaii: International Association of Volcanology and Chemistry of the Earth's Interior, Proceedings of the Symposium on Andean and Antarctic Volcanology Problems, Special Series, p. 172–189.

Peterson, D.W., Christiansen, R.L., Duffield, W.A., Holcomb, R.T., and Tilling, R.I., 1976, Recent activity of Kilauea Volcano, Hawaii, *in* Gonzales-Ferran, O., ed., International Association Volcanology and Chemistry of the Earth's Interior, Symposium on Andean and Antarctic Volcanology Problems, 1974, Santiago, Chile, Proceedings: p. 646–656.

Peterson, D.W., and Tilling, R.I., 1980, Transition of basaltic lava from pahoehoe to aa, Kilauea Volcano, Hawaii: field observations and key factors: Journal of Volcanology and Geothermal Research, v. 7, p. 271–293.

Porter, S.C., 1972, Buried caldera of Mauna Kea Volcano, Hawaii: Science, v. 175, p. 1458–1460.

———1979a, Hawaiian glacial ages: Quaternary Research, v. 12, p. 161–187.

———1979b, Quaternary stratigraphy and chronology of Mauna Kea, Hawaii: a 380,000-yr record of mid-Pacific volcanism and ice-cap glaciation: Geological Society of America Bulletin, Part II, v. 90, p. 980–1093.

Porter, S.C., Stuiver, M., and Yang, I.C., 1977, Chronology of Hawaiian glaciations: Science, v. 195, p. 61–63.

Powers, H.A., 1935, Differentiation of Hawaiian lavas: American Journal of Science, 5th series, v. 30, p. 57–71.

———1948, A chronology of the explosive eruptions of Kilauea: Pacific Science, v. 2, p. 278–292.

———1955, Composition and origin of basaltic magma of the Hawaiian islands: Geochimica et Cosmochimica Acta, v. 7, p. 77–107.

Powers, Sidney, 1916, Explosive ejectamenta of Kilauea: American Journal of Science, 4th series, v. 41, p. 227–244.

———1920, Notes on Hawaiian petrology: American Journal of Science, 4th series, v.50, p. 256–280.

Rhodes, J.M., 1983, Homogeneity of lava flows: chemical data for historic Mauna Loan eruptions: Journal of Geophysical Research, v. 88, suppl. (2), p. A869–A879.

Richter, D.H., Ault, W.U., Eaton, J.P., and Moore, J.G., 1964, The 1961 eruption of Kilauea Volcano, Hawaii: U.S. Geological Survey Professional Paper 474–D, 34 p.

Richter, D.H., and Eaton, J.P., 1960, The 1959–60 eruption of Kilauea Volcano: New Scientist, v. 7, p. 994–997.

Richter, D.H., Eaton, J.P., Murata, K.J., Ault, W.U., and, Krivoy, H.L., 1970, Chronological narrative of the 1959–60 eruption of Kilauea Volcano, Hawaii: U.S. Geological Survey Professional Paper 539–E, 73 p.

Stearns, H.T., 1926, the Keaiwa or 1823 lava flow from Kilauea Volcano, Hawaii: Journal of Geology, v. 34, p. 336–351.

———1940, Four-phase volcanism in Hawaii [abs]: Geological Society of America Bulletin, v.51, p. 1947–1948.

———1946, Geology of the Hawaiian Islands: Hawaii Division of Hydrography, Bulletin 8, 105 p. (2nd printing, 1967, with supplement, 112 p.).

———1966, Geology of the State of Hawaii: Palo Alto, Ca., Pacific Books, 266 p.

———1978, Quaternary shorelines in the Hawaiian Islands: Bernice P. Bishop Museum Bulletin 237, 57 p.

Stearns, H.T., and Clark, W.O., 1930, Geology and water resources of the Kau District, Hawaii: U.S. Geological Survey Water-Supply Paper 616, 194 p.

Stearns, H.T., and Macdonald, G.A., 1946, Geology and ground-water resources of the Island of Hawaii: Hawaii Division of Hydrography, Bulletin 9, 363 p.

Stone, J.B., 1926, The products and structure of Kilauea: B.P. Bishop Museum, Bulletin 33, 59 p.

Swanson, D.A., 1972, Magma supply rate at Kilauea Volcano, 1952–1971: Science v. 175, p. 169–170.

Swanson, D.A., and Christiansen, R.L., 1973, Tragic base surge in 1790 at

Kilauea Volcano: Geology, v. 1, p. 83–86.

Swanson, D.A., Duffield, W.A., and Fiske, R. S., 1976a, Displacement of the south flank of Kilauea Volcano: the result of forceful intrusion of magma into the rift zones: U.S. Geological Survey Professional Paper 963, 39 p.

Swanson, D.A., Duffield, W.A., Jackson, D.B., and Peterson, D.W., 1979, Chronological narrative of the 1969–71 Mauna Ulu eruption of Kilauea Volcano, Hawaii: U.S. Geological Survey Professional Paper 1056, 55 p.

Swanson, D.A., Jackson, D.B., Duffield, W.A., and Peterson, D.W., 1971, Mauna Ulu eruption, Kilauea Volcano: Geotimes, v. 16, no. 5, p. 12–16.

Swanson, D.A., Jackson, D.B., Koyanagi, R.Y., and Wright, T.L., 1976b, The February 1969 east rift eruption of Kilauea Volcano, Hawaii: U.S. Geological Survey Professional Paper 891, 30 p.

Tilley, C.E., 1950, Some aspects of magmatic evolution: Quarterly Journal of the Geological Society of London, v. 106, p. 37–61.

Tilling, R.I., Koyanagi, R.Y., Lipman, P.W., Lockwood, J.P., Moore, J.G., and Swanson, D.A., 1976, Earthquake and related catastrophic events, Island of Hawaii, November 29, 1975: A preliminary report: U.S. Geological Survey Circular 740, 33 p.

Thorarinsson, S., 1967, Surtsey: New York, Viking Press, 47 p.

Unger, J.D., and Ward, P.L., 1979, A large, deep Hawaiian earthquake—the Honomu, Hawaii event of April 26, 1973: Seismological Society of America Bulletin, v. 69, p. 1771–1781.

Vancouver, G., 1798, A voyage of discovery to the north Pacific Ocean: New York, Da Capo Press (reprinted 1967), v. 3.

Washington, H.S., 1923a, Petrology of the Hawaiian Islands: I. Kohala and Mauna Kea, Hawaii: American Journal of Science, 5th series, v. 5, p. 465–502.

———1923b, Petrology of the Hawaiian Islands: II. Hualalai and Mauna Loa: American Journal of Science, 5th series, v. 6, p. 100–126.

———1923c, Petrology of the Hawaiian Islands: III. Kilauea and general petrology of Hawaii: American Journal of Science, 5th series, v. 6, p. 338–367.

Wentworth, C.K., 1938, Ash formations of the island Hawaii: Hawaiian Volcano Observatory, 3rd Special Report, 173 p.

Wentworth, C.K., and Powers, W.E., 1941, Multiple glaciation of Mauna Kea, Hawaii: Geological Society of America Bulletin, v. 52, p. 1193–1218.

Wilkes, C., 1845, Narrative of the U.S. Exploring Expedition, 1838–1842, Philadelphia, Lea and Blanchard, v. 4, p. 87–231.

Wright, T.L., 1971, Chemistry of Kilauea and Mauna Loa lava in space and time: U.S. Geological Survey Professional Paper 735, 39 p.

———1973, Magma mixing as illustrated by the 1959 eruption, Kilauea Volcano, Hawaii: Geological Society of America Bulletin, v. 84, p. 849–858.

———1984, Origin of Hawaiian tholeiite: a metasomatic model: Journal of Geophysical Research, v. 89, p. 3233–3252.

Wright, T.L., and Fiske, R.S., 1971, Origin of the differentiated and hybrid lavas of Kilauea Volcano, Hawaii: Journal of Petrology, v. 12, p. 1–65.

Wright, T.L., Kinoshita, W.T., and Peck, D.L., 1968, March 1965 eruption of Kilauea Volcano and the formation of Makaopuhi lava lake: Journal of Geophysical Research, v. 73, p. 3181–3205.

Wright, T.L., Swanson, D.A., and Duffield, W.A., 1975, Chemical compositions of Kilauea east-rift lava, 1968–1971: Journal of Petrology, v. 16, p. 110–133.

Wright, T.L., and Tilling, R.I., 1980, Chemical variations in Kilauea eruptions 1971–1974: American Journal of Science, v. 280-A, p. 777–793.

HAWAII: THE VIEW FROM SPACE

By George E. Ulrich, Peter J. Mouginis-Mark,[1] *and* Jo-Ann Bowell

ABSTRACT

Aerial portrayal of Hawaii has advanced dramatically in the 20th century through the use of aircraft, mapping cameras, and photogrammetric instruments. In the past two decades, Earth-orbiting spacecraft have added new dimensions to the study of Hawaii's volcanoes, including synoptic views of all or most of the Island of Hawaii from hundreds of kilometers above the surface and repetitive coverage from automated satellites that record changes on the Earth's surface with time.

Astronaut crews in Apollo, Skylab, and Shuttle spacecraft have taken valuable photographs of short-lived events such as the 1983–84 eruptions on Kilauea and Mauna Loa. Landsat satellites have provided several digital images of high quality, and improved sensors now in use on Landsat for many parts of the world may be transmitting pictures of Hawaii in the near future. Multispectral scanners and a synthetic aperture radar system have been used on recent Shuttle missions and have provided digital images showing subtle volcanic features and even textural differences between lava flows from orbital altitudes of 230 to 290 km. Radar is particularly attractive for Hawaiian volcanoes because it is independent of surface illumination and weather and thus is useful day or night and in cloud-covered areas. Experimentation during the next several years on the Space Shuttle flights will improve present coverage even more as new improved methods continue to be developed.

INTRODUCTION

Since man first arrived in the Hawaiian Islands, his understanding of them has progressed, along with his technology, to new and improved perspectives. Early Polynesian canoes from the Markesa Islands carried the first humans to within sight of the broad volcanic shields and eroded seacliffs. Their view from the sea—a profile on the horizon commonly shrouded in clouds and mist—was a local view, constantly changing with location and lighting. Songs and chants were the basis for description of the islands; early cartographic definition was very unlike the accurate maps and charts of today.

For several centuries after their discovery, the islands were charted by ships' navigators with only the stars and Earth's magnetic field as control. Early maps depended on the artistic talents of the mapmakers while onboard ship or, as likely as not, back in their home ports of Europe and America. More precise definition of the land was achieved when surveyors marked points at the shorelines, on the mountain tops, and along the valleys and ridges between. Before the advent of modern transportation, these surveys were accomplished only with tremendous physical effort and endurance, and they required years of labor to complete.

In the 20th century, the use of aircraft and aerial photography has revolutionized the cartographic profession. The birdseye view of the Hawaiian Islands could be recorded on film at selected scales and over large areas in several days of flying. These photographs were then systematically converted by photogrammetric methods to accurate topographic maps, as a basis for displaying present and future use of the land, and, on the Island of Hawaii for frequent revision, showing new volcanic deposits as they occurred.

In the last two decades, the mapping of Hawaii has been both a stimulus to and a beneficiary of space exploration. The volcanic history and landforms of Hawaii have served as analogs for the study of similar features on other planets. For example, a comparison with analogous features on Mars was the basis for presenting the many excellent examples of oblique and vertical photographic views of the volcanic shields of Hawaii by Greeley (1974) and Carr and Greeley (1980). These photographs were taken between 1942 and 1975 from various altitudes, none of which approached orbital heights.

In spite of the tremendous advances in mapping accuracy made possible by aerial photography, drawbacks remain. Many standard aerial photographs are required to cover the island. The distortion introduced by terrain relief and the inability of aircraft to remain perfectly horizontal preclude the use of these photographs as accurate planimetric maps. Stereoscopic models of overlapping photographs permit precise three-dimensional contour mapping, but the numerous models required are expensive and consume many months of labor.

The view from space adds a totally new perspective to the utility of aerial photography. If there is a single most important aspect of images taken from Earth orbit, it is probably the synoptic view it offers, namely the broad view of a large part of the Earth's surface at one moment in time. Though standard aerial photographs provide high-resolution coverage, they are necessarily limited in the size of the area shown; the view from space is valuable in its instantaneous portrayal of a much larger area albeit in less detail. A second important aspect of space images, the possibility of repeated coverage on subsequent orbits, has many useful applications. A sequence of photographs or digital pictures of phenomena that change with time intervals of days, months, or years can be produced at relatively low cost, once the spacecraft is available. Obvious examples are volcanic eruptions, weather systems, forest

[1]Planetary Geosciences Division, Hawaii Institute of Geophysics, University of Hawaii 96822.

fires, and agricultural conditions. Furthermore, special spectrometers can also view large areas in both the visible and infrared wavelengths to scan for zones of surface alteration, permitting concentrations of economically important minerals or potential geothermal resources to be identified.

The purpose of this paper is threefold: (1) to demonstrate some applications of space images for the improvement of existing maps; (2) to illustrate some aspects of the geology and structure of the Island of Hawaii, using a few examples of available photographs, satellite images, and radar data; and (3) to provide a selective listing of the better images available for the Hawaiian Island chain. Tables 8.1 and 8.2 list those images considered most useful based on minimum cloud coverage, geologic interest, and availabilty from the Earth Resources Observation Systems (EROS) Data Center as of this writing.

ACKNOWLEDGMENTS

Appreciation goes to Charles A. Wood for reviewing and recommending additions to the photographs listed in table 8.1. The authors are indebted to William R. Muehlberger for advice and information on the Skylab and Shuttle photographs, to Ellen M. Sanchez and Kathleen Edwards for direction in the processing of the Landsat images, and to Mary Ann Hager for copies of several important photographs. James D. Griggs provided valuable and always dependable advice and assistance on numerous photographic matters. Christina A. Neal and Ray M. Batson provided very helpful critical reviews of the manuscript, improving it significantly. P.J. Mouginis-Mark received support from NASA's Non-Renewable Resources Branch under NASA/JPL Grant No. 956925.

APOLLO, SKYLAB, AND SHUTTLE PHOTOGRAPHY

Early photographs of Hawaii from space, taken on the Apollo 9 mission in March 1969, formed a panoramic series of four oblique views showing mostly clouds and were published as a mosaic in Dalrymple and others (1973). One of the better photographs of the island was taken from the Skylab spacecraft at an altitude of 435 km (270 mi; see figure 8.1). This vertical view provided an excellent cartographic delineation of the island's shoreline. More recent photographs, from the Space Shuttle missions since 1983, have normally been taken from lower altitudes (230–300 km; 143–186 mi), although Shuttle mission 41–C in April 1984 returned photographs from orbits as high as 500 km (310 mi).

All photographs cited were taken with hand-held NASA-modified cameras, primarily the Hasselblad 500 EL/M, using 70-mm (2.75-in) Kodak Ektachrome film. Advantages in the use of hand-held cameras to view the Earth include the ability to point the lens at targets of opportunity and the flexibility to interchange lenses of different focal lengths. A majority of the hand-held photographs of Hawaii taken from space to date have been taken through a telephoto lens (see table 8.1). The nominal ground resolution from a typical Space Shuttle altitude (284 km; 177 mi) using a 250-mm focal-length lens is about 25 m; the resolution using a 100-mm lens is about 60 m (Mohler, 1983). An example of a telephoto view of Mauna Loa Volcano's summit caldera and most of its two rift zones is shown in figure 8.2 for comparison with the wider angle view of figure 8.3.

The documentation of volcanic activity during and following an eruption is an obvious application of remote-sensing techniques on Hawaii. The beginning of the March–April 1984 eruption of Mauna Loa was precisely marked by a thermal sensor on a military satellite. On the shorter, manned Space Shuttle missions, special events can be targeted for photographic coverage, but the combined requirements of timing and good visibility are largely a matter of luck and perseverance on the part of the flight crews. One such opportunity permitted the plumes from the Mauna Loa eruption of 1984 to be photographed on four different days (table 8.1; fig. 8.3). Less prominent but quite visible was the plume from an eruption on Kilauea Volcano in late 1983 (fig. 8.4).

Perhaps the most photogenic of the five shield volcanoes on the Island of Hawaii is Mauna Kea, the most cited example of a tholeiitic shield capped by alkalic cones and flows in its later stages of development. The distribution of cinder cones on the summit and flanks of this symmetrical shield are shown in figure 8.5. The diversion of younger lava flows from Mauna Loa to the east and west around the base of Mauna Kea is also illustrated.

TABLE 8.1.—*Selected photographs of the Hawaiian Island chain taken by Gemini, Apollo, Skylab, and Space Shuttle missions*

[Data for Shuttle missions are taken mainly from NASA documents (Nowakowski, 1984a, b; Palmer, 1984; and Nowakowski and Palmer, 1984) but are modified where more information was available]

Mo	Da	Yr	Space-craft	Mission	Scene identification	Orbit	Feature	Quality	Percent clouds	Center of scene Lat.	Long.
02	11	73	Landsat	1	8120320180500	67-46	North Hawaii	8888	30	20.22	155.43
02	11	73	Landsat	1	8120320182500	67-47	South Hawaii	8888	20	18.78	155.16
03	01	73	Landsat	1	8122120181500	67-46	North Hawaii	8888	20	20.28	155.50
03	01	73	Landsat	1	8122120183500	67-47	South Hawaii	8882	20	18.84	155.85
10	09	77	Landsat	2	8299119392500	67-47	South Hawaii	8888	30	18.83	155.72
01	07	78	Landsat	2	82108119354X0	67-46	North Hawaii	8888	20	20.18	155.39
01	07	78	Landsat	2	82108119360X0	67-47	South Hawaii	8888	30	18.74	155.74
09	07	78	Landsat	3	83018620064X0	67-46	North Hawaii	8888	30	20.18	155.37

1 Image quality is scaled from 1 (poorest) to 8 (best). Columns under Quality represent, in order, Multispectral Scanner bands 4 (wavelength 0.5 to 0.6 microns), 5 (0.6-0.7), 6 (0.7-0.8), and 7 (0.8-1.1).

Cloud patterns and ocean roughness are remarkably well portrayed in the synoptic view from space. The typical cloud pile-up on the windward side of Hawaii in contrast with the open sky and smoother ocean surface on the leeward or Kona side (fig. 8.6) produces the illusion of an island sailing northeastward across the Pacific. The disturbance of windflow (orographic effect) across and around the five volcanic shields provides a fruitful area of research for atmospheric scientists.

LANDSAT AND OTHER MULTISPECTRAL SATELLITE IMAGES

Digital images transmitted from Landsat, originally called Earth Resources Technology Satellite (or ERTS), provide repetitive coverage of the Earth from polar orbit using a scanner system that includes spectral bands from near infrared through the visible wavelengths. Landsats 1, 2, and 3 recorded scenes of Hawaii on four bands over the wavelength range of 0.5 to 1.1 microns. A typical image is approximately 185 km (115 mi) on each side and has a nominal resolution per picture element (pixel) of 80 m (Short and others, 1976). The amount of area included within Landsat images compared with photographs taken on Skylab and Shuttle missions is shown in figure 8.7.

In comparison with photographs taken from aircraft and manned spacecraft, the shortcomings of digital images from satellites are mainly their lower spatial resolution, their rigid format and direction of view, and the acquisition of data at only one lighting geometry (due to the sun-synchronous nature of the Landsat orbits; Short and others, 1976). The advantages of digital images recorded by satellites are: (1) they cover larger areas, (2) they have uniform resolution across the entire image, and (3) they include various spectral bands that can be filtered or enhanced after the image is recorded to delete atmospheric haze or to emphasize the surface distribution of different natural materials. In contrast, improvements to aerial photographs are normally made as the pictures are taken, requiring extensive experience and know-how. Corrections for haze, color, and lighting are difficult to apply in the photographic laboratory, but are generally possible for digital images via computer processing.

Image processing and enhancement of digital scenes such as from Landsat can be helpful in geologic interpretation and illustration of regional features on Earth as well as other planets. The Landsat scene shown in figure 8.8 was recorded in 1978. Other scenes (until late 1978; table 8.2) can be purchased from EROS in several formats. Repetitive overflights could eventually make it possible to acquire near-perfect images of the entire island chain, although the current spacecraft configuration prohibits the transmission of new images from Landsats 4 and 5.

Cartographic applications of Landsat data require that scenes be fitted to standard map projections and existing map products. Figure 8.8 has been geometrically adjusted to the universal transverse mercator projection, and the red and green color bands have been combined with an artificially generated blue band to create a simulated true-color rendition of Hawaii as described by Eliason and others (1974). Landsat scenes can be modified by computer to increase their interpretability. One example is the superposition of the scene on a digital elevation model (obtained from the U.S. Defense Mapping Agency) derived from the 1:250,000-scale map series. The registration procedure, whereby every pixel of the image is assigned a corresponding elevation value, is the most labor-intensive part of this technique.

The composite data set thus produced can be digitally rotated to an oblique aerial view. The vertical exaggeration, the vertical angle of the perspective view, and the look-azimuth desired can all be adjusted by an analyst for maximum interpretability. We chose the northwestward view shown in figure 8.9 to look across the rift structures of Mauna Loa and Kilauea Volcanoes. If one wanted to look for subtle structures (for example, parallel to a rift zone), the down-structure view could be generated just as easily. A three-times vertical exaggeration appears to best illustrate the relief of the volcanoes in this case. An additional processing technique, not developed in time for this report, is the removal of cloud cover from the image while retaining the terrain information from the elevation model. This effect can be created by digitally stenciling out the white pixels in the scene and replacing them with a digital shading of the elevation model.

A further enhancement of the oblique aerial view could include a second oblique view—slightly offset in azimuth but with other variables held constant—to provide a stereo pair. An example of this technique for another volcanic area is illustrated elsewhere (Anonymous, 1984a, 1984b). Subtle structures such as shallow craters and small cones and shields can be more easily recognized and interpreted in the stereoscopic view.

Unfortunately the number of geologically useful Landsat images of Hawaii is small due to the frequent canopy of clouds that cover much of the island. The Thematic Mappers on Landsats 4 and 5 have better spectral and spatial resolution than any previous Landsat. These spacecraft do not carry tape recorders, however, and the only areas on the Earth's surface that can be acquired are those in direct line of sight with a receiving station. As of this writing (1985) and because of the inability to record, there are no images of Hawaii yet available from these spacecraft (Landsats 4 or 5). This problem may be resolved when a tracking and data-relay satellite (TDRS-west) is launched in the near future. (Note: The TDRS satellite was lost in the shuttle *Challenger* accident in 1986, and its replacement and launching will be significantly delayed. Until that time, new Landsat images for the Hawaiian Islands will not be available.)

While Landsat is an established standard for orbital-digital images of the Earth, other sensors are under development, many of them using the Space Shuttle as a platform. One such experiment, the German MOMS–1 (Modular Optoelectronic Multispectral Scanner), was flown on the Shuttle in February 1984 and recorded the image of Hawaii reproduced in figure 8.10. The image has a spatial resolution of approximately 20 m in two spectral channels (0.60 and 0.90 microns), sufficient to identify features such as the new lava flows of the 1983–85 east-rift eruptions on Kilauea. Obvious applications for these images lie in their potential for mapping recent eruption areas, portraying patterns of flow distribu-

TABLE 8.2.—*Selected Landsat scenes of the Island of Hawaii*

[Images and photographs listed can be purchased from EROS Data Center, Sioux Falls, SD 57198]

Mo	Da	Yr	Space-craft	Mission identificat.	Scene identification 1	Orbit	Feature	Focal length	Percent clouds 2	Perspective 3	Direction	Stereo 4	Center of scene Lat 5	Long
08	24	65	Gemini	V	S-65-45616	51	Hawaii to Kauai	80	80	Oblique	SW	No	20.0	154.0
10	15	68	Apollo	7	AS7-7-1740	51	Niihau	80	--	---do---	NE	No	23.0	160.5
10	15	68	Apollo	7	AS7-7-1741	51	Oahu	80	--	---do---	NE	Yes	23.0	158.5
10	15	68	Apollo	7	AS7-7-1742	51	Oahu, Maui	80	--	---do---	NE	Yes	23.0	157.0
10	15	68	Apollo	7	AS7-7-1743	51	--do----------	80	--	---do---	NE	Yes	22.0	157.0
10	15	68	Apollo	7	AS7-7-1744	51	Maui, Hawaii	60	--	---do---	NE	Yes	22.0	156.5
10	15	68	Apollo	7	AS7-7-1745	51	Maui,Kahoolawe,Haw	80	--	---do---	NE	Yes	21.5	156.0
10	15	68	Apollo	7	AS7-7-1746	51	--do----------	80	--	---do---	NE	Yes	20.0	155.5
10	15	68	Apollo	7	AS7-7-1747	51	Hawaii	80	--	---do---	NE	Yes	21.5	155.0
02	03	69	Apollo	9	AS9-3505 to-8	--	Hawaii to Niihau	100(?)	50	---do---	SW	Yes	20.0	154.0
12	07	73	Skylab	4	SL4-139-3997	--	Hawaii	100	10	Vertical	--	No	19.6	155.5
04	05	83	Shuttle	STS-6, S-06	40-745	22	Mauna Loa	250	85	---do---	--	Yes	19.5	155.5
06	18	83	--do---	STS-7, S-07	20-1029	5	Oahu,Molakai,Lanai	100	30	Oblique	N	Yes	22.5	158.0
06	18	83	--do---	----do-----	20-1030	5	Molokai,Maui,Lanai	100	30	---do---	N	Yes	23.0	157.0
06	18	83	--do---	----do-----	22-1134	6	Niihau	250	30	---do---	NE	No	22.0	160.0
06	18	83	--do---	----do-----	22-1135	6	Kauai	250	20	---do---	E	No	22.0	159.5
06	18	83	--do---	----do-----	22-1136	6	Oahu	250	20	---do---	E	No	21.5	158.0
06	18	83	--do---	----do-----	22-1137	6	Molak,Lanai,Kahool	250	15	---do---	E	Yes	21.0	157.0
06	18	83	--do---	----do-----	22-1138	6	--do----------	250	25	---do---	E	Yes	21.0	157.0
06	18	83	--do---	----do-----	22-1139	6	Maui, Lanai	250	30	---do---	E	Yes	21.0	156.5
06	18	83	--do---	----do-----	22-1141	6	Hawaii	250	30	---do---	SE	Yes	20.0	155.5
06	18	83	--do---	----do-----	22-1142	6	--do----------	250	30	---do---	SE	Yes	19.5	155.5
06	18	83	--do---	----do-----	22-1144	6	Hawaii, Maui	250	506	---do---	NE	Yes	19.5	156.0
06	19	83	--do---	----do-----	03-0084	22	Niihau	250	10	Vertical	--	No	22.0	160.0
06	19	83	--do---	----do------	03-0085	22	Kauai	250	20	---do---	--	No	22.0	160.0
06	19	83	--do---	----do------	03-0886	22	Pearl Harbor	250	25	---do---	--	No	21.5	158.0
06	19	83	--do---	----do------	03-0087	22	Molokai, Lanai	250	15	---do---	--	Yes	21.0	157.0
06	19	83	--do---	----do------	03-0088	22	Maui, Kahoolawe	250	15	---do---	--	Yes	21.0	157.0
06	19	83	--do---	----do------	03-0089	22	--do----------	250	15	---do---	--	Yes	21.0	156.5
06	19	83	--do---	----do------	03-0090	22	Mauna Loa Volcano	250	15	---do---	--	Yes	19.5	155.5
06	19	83	--do---	----do------	03-0091	22	--do----------	250	15	---do---	--	Yes	19.5	155.5
06	19	83	--do---	----do------	03-0092	22	--do----------	250	15	---do---	--	Yes	19.5	155.5
06	19	83	--do---	----do------	03-0093	22	--do----------	250	15	---do--	--	Yes	19.5	155.5
06	19	83	--do---	----do------	03-0094	22	--do----------	250	15	---do---	--	Yes	19.5	155.5
06	19	83	--do---	----do------	19-0874	22	Kauai	100	10	---do---	--	No	22.0	160.0
06	19	83	--do---	----do------	19-0875	22	Molokai & adjacent	100	10	Oblique	N	No	21.0	157.5
06	19	83	--do---	----do------	19-0876	22	Maui & adjacent	100	15	Vertical	--	Yes	20.5	156.5
06	19	83	--do---	----do------	19-0877	22	--do----------	100	15	---do---	--	Yes	20.5	156.0
06	19	83	--do---	----do------	19-0878	22	Hawaii	100	15	---do---	--	Yes	20.0	155.5
06	19	83	--do---	----do------	19-0879	22	--do----------	100	15	---do---	--	Yes	19.5	155.5
06	19	83	--do---	----do------	19-0880	22	--do----------	100	15	---do---	--	Yes	19.5	155.5
06	20	83	--do---	----do------	03-0114	37	Mauna Kea Volcano	250	30	Oblique	SW	No	19.5	155.5
06	20	83	--do---	----do------	03-0115	37	--do----------	250	30	---do---	SW	No	19.5	155.5
11	28	83	--do---	STS-9, 41-A	31-1015	4	Mauna Loa Volcano	250	05	Vertical	--	No	19.5	155.5
11	28	83	--do---	----do-----	31-1016	4	--do----------	250	10	---do---	--	Yes	19.0	155.5
11	28	83	--do---	----do-----	31-1017	4	--do----------	250	20	---do---	--	Yes	19.5	155.5
11	28	83	--do---	----do-----	31-1018	4	M. Kea, Hilo Bay	250	20	Oblique	S	Yes	20.0	155.5
11	28	83	--do---	----do-----	31-1019	4	Hawaii coast	250	10	Vertical	--	Yes	20.0	155.5
11	28	83	--do---	----do-----	31-1020	4	Mauna Loa Volcano	250	10	Oblique	SW	Yes	19.5	155.5
11	28	83	--do---	----do-----	31-1021	4	--do----------	250	10	---do---	SW	Yes	19.5	155.5
11	28	83	--do---	----do-----	31-1022	4	Hawaii	250	10	---do---	SW	Yes	19.5	155.5
11	28	83	--do---	----do-----	31-1023	4	--do----------	250	10	---do---	SW	No	20.0	155.5
11	28	83	--do---	----do-----	31-1024	4	--do----------	250	10	---do---	SW	No	20.0	155.5
11	28	83	--do---	----do-----	32-1118	4	--do----------	100	20	---do---	SW	No	19.5	155.5
11	28	83	--do---	----do-----	32-1119	4	--do----------	100	20	---do---	SW	No	19.5	155.5
11	28	83	--do---	----do-----	32-1120	4	--do----------	100	20	---do---	SW	No	19.5	155.5
11	29	83	--do---	----do-----	35-1596	20	Hawaii, Maui	100	15	---do---	SE	Yes	20.0	156.0
11	29	83	Shuttle	STS-9, 41-A	35-1597	20	Haw,Maui,Molok,Lan	100	20	Oblique	E	Yes	21.0	156.5
11	29	83	--do---	----do-----	35-1598	20	Lanai,Molok,Maui	100	20	---do---	E	Yes	21.0	157.0
11	29	83	--do---	----do-----	35-1599	20	Molok,Oahu,Kahool	100	20	---do---	W	Yes	21.5	158.0
11	29	83	--do---	----do-----	35-1600	20	Kauai, Niihau	100	20	---do---	W	No	22.0	159.5
11	29	83	--do---	----do-----	46-1836	20	Haw,Maui,Lan,Molok	250	30	---do---	NE	No	21.0	156.5
11	29	83	--do---	----do-----	46-1837	20	Hawaii	250	20	---do---	NE	No	19.5	156.0
11	29	83	--do--	----do-----	46-1838	20	Molokai,Lanai,Maui	250	40	---do---	NE	No	21.0	157.0
11	29	83	--do---	----do-----	46-1840	20	SE Haw, Kil. plume	250	20	---do---	NE	Right	19.0	155.5
11	29	83	--do---	----do-----	46-1841	20	Hawaii, Kil. plume	250	20	---do---	NE	Ctr	19.5	155.5
11	29	83	--do---	----do-----	46-1842	20	NW Haw, Kohala	250	20	---do---	NE	Left	20.0	155.5
11	29	83	--do---	----do-----	46-1843	20	Maui, Kahoolawe	250	30	---do---	NE	No	20.5	156.5
11	29	83	--do---	----do-----	46-1844	20	Maui, Lanai	250	30	---do---	NE	No	21.0	156.5
11	29	83	--do---	----do-----	46-1845	20	Lanai, Maui, Molok	250	30	Vertical	--	No	21.0	156.5
11	29	83	--do---	----do-----	46-1846	20	Molokai, Lanai	250	30	---do---	--	No	21.0	157.0
11	29	83	--do---	----do-----	46-1848	20	Kauai	250	40	---do---	--	No	22.0	159.5
02	04	84	--do---	STS-11, 41-B	41-2351	22	Honolulu, Oahu	250	10	Oblique	--	Yes	21.5	158.0
02	04	84	--do---	----do------	41-2352	22	--do----------	250	10	---do---	--	Yes	21.5	158.0
02	04	84	--do---	----do------	41-2353	22	Molokai,Lanai,Maui	250	0	---do---	--	Yes	21.0	157.0
02	04	84	--do---	----do------	41-2354	22	Mol,Lan,Kahoo,Maui	250	10	---do---	--	Yes	21.0	157.0
02	04	84	--do---	----do------	41-2355	22	Maui, Kahoolawe	250	10	---do---	--	Yes	21.0	156.5

TABLE 8.2.— *Selected Landsat scenes of the Island of Hawaii*— Continued

Mo	Da	Yr	Space-craft	Mission identificat.	Scene identification [1]	Orbit	Feature	Focal length	Percent clouds [2]	Perspective [3]	Direction	Stereo [4]	Center of scene Lat [5]	Long
02	04	84	--do---	----do------	41-2356	22	Hawaii	250	30	---do---	--	Yes	19.5	155.5
02	06	84	--do---	----do------	33-1458	53	Kauai	100	30	Vertical	--	No	22.0	156.5
02	06	84	--do---	----do------	33-1459	53	Maui,Kahool,Lanai	100	30	---do---	--	No	21.0	156.5
02	06	84	--do---	----do------	33-1460	53	Hawaii	100	30	---do---	--	Yes	19.5	155.5
02	06	84	--do---	----do------	33-1461	53	--do----------	100	30	---do---	--	Yes	20.0	155.5
02	06	84	--do---	----do------	34-1554	53	Niihau	250	30	---do---	--	Yes	22.0	160.0
02	06	84	--do---	----do------	34-1555	53	Kauai	250	30	---do---	--	Yes	22.0	159.5
02	06	84	--do---	----do------	34-1556	53	Oahu	250	30	---do---	--	Yes	21.5	158.0
02	06	84	--do---	----do------	34-1557	53	--do----------	250	20	---do---	--	Yes	21.5	158.0
02	06	84	--do---	----do------	34-1558	53	--do----------	250	20	---do---	--	Yes	21.5	158.0
02	06	84	--do---	----do------	34-1561	53	Maui	250	30	---do---	--	Yes	21.0	156.5
02	06	84	--do---	----do------	34-1562	53	--do----------	250	20	---do---	--	Yes	21.0	156.5
02	06	84	--do---	----do------	34-1563	53	Hawaii	250	5	---do---	--	Yes	19.5	155.5
02	06	84	--do---	----do------	34-1564	53	--do----------	250	30	---do---	--	Yes	20.0	155.5
02	06	84	--do---	----do------	34-1565	53	--do----------	250	30	---do---	--	Yes	20.0	155.5
02	06	84	--do---	----do------	34-1566	53	--do----------	250	1	---do---	--	Yes	19.5	155.5
02	06	64	--do---	----do------	34-1567	53	--do----------	250	5	---do---	--	Yes	19.0	155.5
02	06	84	--do---	----do------	34-1568	53	--do----------	250	5	---do---	--	Yes	19.5	155.5
02	06	84	--do---	----do------	34-1569	53	--do----------	250	15	---do---	--	Yes	19.5	155.5
02	08	84	--do---	----do------	43-2625	84	Kauai	250	30	Oblique	--	No	22.0	159.5
02	08	84	--do---	----do------	43-2626	84	Oahu	250	20	---do---	--	No	21.5	158.5
02	08	84	--do---	----do------	43-2627	84	Molokai, Lanai	250	30	---do---	--	No	21.0	157.0
02	08	84	--do---	----do------	43-2629	84	Hawaii	250	30	---do---	--	Yes	19.5	155.5
02	08	84	--do---	----do------	43-2630	84	--do----------	250	30	---do---	--	Yes	19.5	155.5
02	09	84	--do---	----do------	45-2794	100	Hawaii Isl. chain	100	30	---do---	NW	No	19.5	155.5
02	09	84	--do---	----do------	45-2795	100	Hawaii	100	30	---do---	--	No	19.5	155.5
02	09	84	--do---	----do------	45-2796	100	--do----------	100	30	---do---	--	No	19.5	155.5
02	09	84	--do---	----do------	46-2923	100	--do----------	250	60	---do---	N	Yes	19.5	155.5
02	09	84	--do---	----do------	46-2924	100	--do----------	250	60	---do---	N	Yes	19.5	155.5
02	09	84	--do---	----do------	46-2925	100	--do----------	250	60	---do---	N	Yes	19.5	155.5
04	06	84	--do---	STS-13, 41-C	31-0968	6	Niihau	250	25	Vertical	--	No	22.0	160.0
04	06	84	--do---	----do------	31-0969	6	Kauai	250	25	---do---	--	No	22.0	159.5
04	06	84	--do---	----do------	31-0974	6	Mauna Loa plumes	250	80	Oblique	SW	Yes	19.5	155.5
04	06	84	--do---	----do------	31-0975	6	--do----------	250	80	---do---	SW	Yes	19.5	155.5
04	06	84	--do---	----do------	32-1087	6	--do----------	50	40	Vertical	--	No	22.0	160.0
04	06	84	--do---	----do------	51-2264	6	Kauai, Niihau	250	30	---do---	--	No	22.0	160.0
04	06	84	--do---	----do------	51-2265	6	Oahu	250	25	---do---	--	No	22.0	158.0
04	07	84	Shuttle	STS-13, 41-C	35-1538	21	Mauna Loa plumes	250	25	Oblique	SE	Yes	19.5	155.5
04	07	84	--do---	----do------	35-1539	21	--do----------	250	25	---do---	SE	Yes	19.5	155.5
04	07	84	--do---	----do------	35-1540	21	Mauna Loa plumes	250	25	Oblique	S?	Yes	19.5	155.5
04	07	84	--do---	----do------	36-1633	21	M. Loa plume, Maui	50	40	Vertical	--	No	22.0	160.0
04	07	84	--do---	----do------	36-1686	37	Mauna Loa plumes	50	60	Oblique	SW	No	21.0	155.0
04	08	84	--do---	----do------	34-1411	37	--do----------	250	30	---do---	NE	Yes	19.5	155.5
04	09	84	--do---	----do------	52-2537	51	--do----------	250	50	---do---	SE	No	20.5	157.0
04	09	84	--do---	----do------	52-2538	51	--do----------	250	50	---do---	SE	No	20.0	156.5
04	12	84	--do---	----do------	37-1807	96	--do----------	250	40	---do---	E	No	19.5	155.5
04	12	84	--do---	----do------	37-1808	96	--do----------	250	40	--do----	S	No	19.9	155.5
04	12	84	--do---	----do------	37-1809	96	Oahu	250	25	---do---	SW	No	21.5	158.0
04	12	84	--do---	----do------	37-1810	96	Hawaii	250	35	---do---	SW	No	19.5	155.5
04	12	84	--do---	----do------	52-2726	97	Mauna Loa plumes	250	40	---do---	NE	No	20.0	155.0
04	12	84	--do---	----do------	52-2727	97	--do----------	250	40	---do---	NE	No	19.5	155.0
04	12	84	--do---	----do------	52-2728	97	--do----------	250	40	---do---	NE	No	20.0	155.0
09	02	84	--do---	S84-14, 41-D	34-0075	53	--do----------	250	30	---do---	--	No	20.0	155.5
09	02	84	--do---	----do------	34-0076	53	--do----------	250	30	---do---	--	No	19.5	155.5
09	02	84	--do---	----do------	44-0093	84	Mauna Kea	250	10	Vertical	--	No	20.0	155.5
11	10	84	--do---	51-A	35-0013	38	Mauna Loa	250	15	Oblique	NE	Yes	19.5	155.5
11	10	84	--do---	----do------	35-0014	38	--do----------	250	15	---do---	NE	Yes	19.5	155.5
11	10	84	--do---	----do------	35-0015	38	--do----------	250	20	---do---	NE	Yes	19.5	155.5
11	10	84	--do---	----do------	35-0016	38	Hawaii	250	20	---do---	NW	Yes	19.5	155.5
11	10	84	--do---	----do------	35-0017	38	--do----------	250	20	---do---	NW	Yes	19.0	155.5
11	10	84	--do---	----do------	36-0016	38	Mauna Loa, M. Kea	100	15	---do---	NE	Yes	19.5	156.0
11	10	84	--do---	----do------	36-0017	38	--do----------	100	15	---do---	NE	Yes	19.0	155.5
04	14	85	--do---	51D	S85-23-40-62	35	Kauai, Niihau	250	40	---do---	SE	No	26.0	160.0
04	14	85	--do---	51D	S85-23-40-82	36	Hawaii, west side	250	40	Vertical	--	Yes	17.0	156.0
04	14	85	--do---	51D	S85-23-40-83	36	--do----------	250	40	---do---	--	Yes	17.0	156.0
04	16	85	--do---	51D	S85-23-42-98	66	Niihau, west Kauai	250	20	---do---	--	No		59.0
04	16	85	--do---	51D	S85-23-42-100	66	Hawaii, M. Loa	250	40	---do---	--	No	22.0	155.5
04	18	85	--do---	51D	S85-23-46-43	97	Hawaii to Oahu	250	50	---do---	--	No	16.0	152.0
06	21	85	--do---	51G	51G-47-13	100	Hawaii to Niihau	100	50	Oblique	E	Yes	-----	-----
06	21	85	--do---	51G	51G-48-15	100	--do----------	100	50	--do----	E	Yes	-----	-----

1 Numbers to left of hyphen indicate magazines; numbers to right of hyphen indicate frames.

2 Photos with ›30 percent cloud cover are not included except where known to have useful information. Percent areas covered by clouds are mainly from NASA documents and generally cover a higher percentage of the land area within a scene. Some estimates have been revised slightly.

3 Some photographs designated as vertical are slightly inclined from true vertical.

4 Stereo "yes" indicates some overlap with adjacent photograph on left or right.

5 Longitude values are west of the Greenwich Meridian. Latitudes are north.

tion, and measuring areas covered by new lava flows (compare figs. 8.10*B* and 8.10*C*).

RADAR IMAGES

Additional studies of part of Kilauea Volcano from space have been conducted using an imaging radar system (SIR-B) that was flown on board the Shuttle in October 1984. Data were acquired across the southeastern part of the Island of Hawaii, extending from South Point, across Kilauea caldera to Hilo Bay (fig. 8.11).

The SIR-B radar operated at a wavelength of 23 cm, complementing information gained at visible and near infrared wavelengths by Landsat and MOMS–1. It was similar to the synthetic aperture radars flown on the Seasat satellite in 1978 described by Elachi (1980), and the Shuttle Imaging Radar (SIR-A) experiment flown on the Space Shuttle in 1981 (Elachi and others, 1982).

However, unlike these earlier orbital radar systems, SIR-B had the capability to vary the angle at which the radar beam encountered the surface, and obtained images of Hawaii at incidence angles of 28 and 48 degrees. Because orbital radars provide their own illuminating energy and are capable of penetrating clouds, they can provide useful images at all times (day or night) as well as in areas of frequently poor weather, such as Kilauea's east rift zone. Because of the choice of spacecraft orbits and the short duration (8 days) of the mission, only two SIR-B radar images (swathwidths of approximately 20 and 30 km on the ground) were obtained during the Shuttle flight. More complete coverage is anticipated on the reflight of the SIR-B experiment (SIR-B′) scheduled for early 1987.

Radar images display, in part, variations in surface roughness at a scale of a few centimeters to a few decimeters with a pixel size of about 15–20 meters, and many of the individual pit craters and lava flows can be recognized within the national park (fig. 8.12). In particular, variations in the surface texture of lava flows is clearly seen in the SIR-B images. Two examples are identified in figure 8.12; the December 1974 lava flow and the multiple flows within Kilauea caldera show diverse radar backscatter properties. The December 1974 flow erupted as pahoehoe close to Kilauea caldera, but at a distance of approximately 5 km from the vent the flow passed through the transition to aa. This transition (at point A in fig. 8.12) is indicated by an increase in radar brightness associated with the greater backscatter from the rough aa surface. In comparison, the near-vent pahoehoe surface produces a dark radar signal because of its smooth, specular surface.

Kilauea caldera provides further insights into the capability of the SIR-B radar system to distinguish between different surface materials. The caldera rim and the edge of Kilauea Iki pit crater are distinctive (B in fig. 8.12) due to the contrast between the crater floor (low radar return) and the surrounding rain forest (high radar return). Less obvious are the September 1982 pahoehoe flow (C) and other pahoehoe flows within the caldera, due to the uniformly low radar returns from those features as viewed at an incidence angle of 48 degrees.

Such a variation in the radar signature of the different flows is attributed to the decimeter-scale roughness of the lava flow surfaces. Similarly, brightness variations around Halemaumau pit crater (D in fig. 8.12) are attributed to variations in the number and size of boulders (decimeters to meters in diameter) scattered across the caldera floor during the 1924 phreatic eruption.

SUMMARY

Images from space of active or young volcanic areas like Hawaii provide graphic information having several advantages over typical aerial and surface photographs. Considering the larger areas covered and the greater applicability of image-enhancement techniques, views from Earth-orbital altitudes have proved to be a relatively economical form of cartographic data having significant value for the earth sciences. Furthermore, the choice of spaceborne sensor (photography, digital multispectral images, or synthetic aperture radar) permits different physical and compositional attributes of the Earth's surface to be studied. Thus with future Space Shuttle flights and the orbiting of new and currently planned automated satellites (having names like TOPEX, ERS–1, SPOT–1, and Radarsat), the volcanoes of Hawaii will come under more detailed scrutiny from space in the next few years.

REFERENCES CITED

Anonymous, 1984a, Landsat vertical image yields a stereo oblique: Geotimes, v. 29, no. 4, p. 10–11.

———1984b, Image yields stereo oblique: Earth science, v. 37, no. 4, p.18–19.

Carr, M.H., and Greeley, Ronald, 1980, Volcanic features of Hawaii—a basis for comparison with Mars: National Aeronautics and Space Administration Special Paper, NASA SP–403, 211 p.

Dalrymple, G.B., Silver, E.A., and Jackson, E.D., 1973, Origin of the Hawaiian Islands: American Scientist, v. 61, p. 294–308.

Elachi, Charles, 1980, Spaceborne imaging radar: geologic and oceanographic applications: Science, v. 209, no. 4461, p. 1073–1082.

Elachi, Charles, Brown, W.E., Cimino, J.B., Dixon, T., Evans, D.L., Ford, J.P., Saunders, R.S., Breed, C., Masursky, H., McCauley, J.F., Schaber, G., Delwig, L., England, A., MacDonald, H., Martin-Kaye, P., and Sabins, F., 1982, Shuttle imaging radar experiment: Science, v. 218, p. 996–1003.

Eliason, E.M., Chavez, P.S., and Soderblom, L.A., 1974, Simulated "true color" images from ERTS data: Geology, v.2, no. 5, p. 231–234.

Greeley, Ronald, 1974, Aerial reconnaissance of the geology over the Island of Hawaii, *in* Greeley, Ronald, ed., Geologic Guide to the Island of Hawaii: National Aeronautics and Space Administration CR15 2416, p. 113–183.

Mohler, R.R.J., 1983, Catalog of Space Shuttle Earth observation hand-held photography: Space Transportation System 6 Mission: National Technical Information Service Report JSC–18897, 28 p.

Nowakowski, B.S., 1984a, Catalog of Space Shuttle Earth observation hand-held photography: Space Transportation System 7 Mission: National Technical Information Service Report JSC–18913, 31 p.

———1984b, Catalog of Space Shuttle Earth observations hand-held photography: Space Transportation System 9 Mission: National Technical Information Service Report JSC–20175, 51 p.

Nowakowski, B.S., and Palmer, W.F., 1984, Catalog of Space Shuttle Earth observations hand-held photography: Space Transportation System 41–C Mission: National Technical Information Service Report JSC–20056, 46 p.

Palmer, W.F., 1984, Catalog of Space Shuttle Earth observations hand-held photography: Space Transportation System 41–B Mission: National Technical Information Service Report JSC–20690, 44 p.

Short, N.M., Lowman, P.D., Freden, S.C., and Finch, W.A., 1976, Mission to Earth: Landsat views the world: National Aeronautics and Space Administration Special Publication SP–360, 459 p.

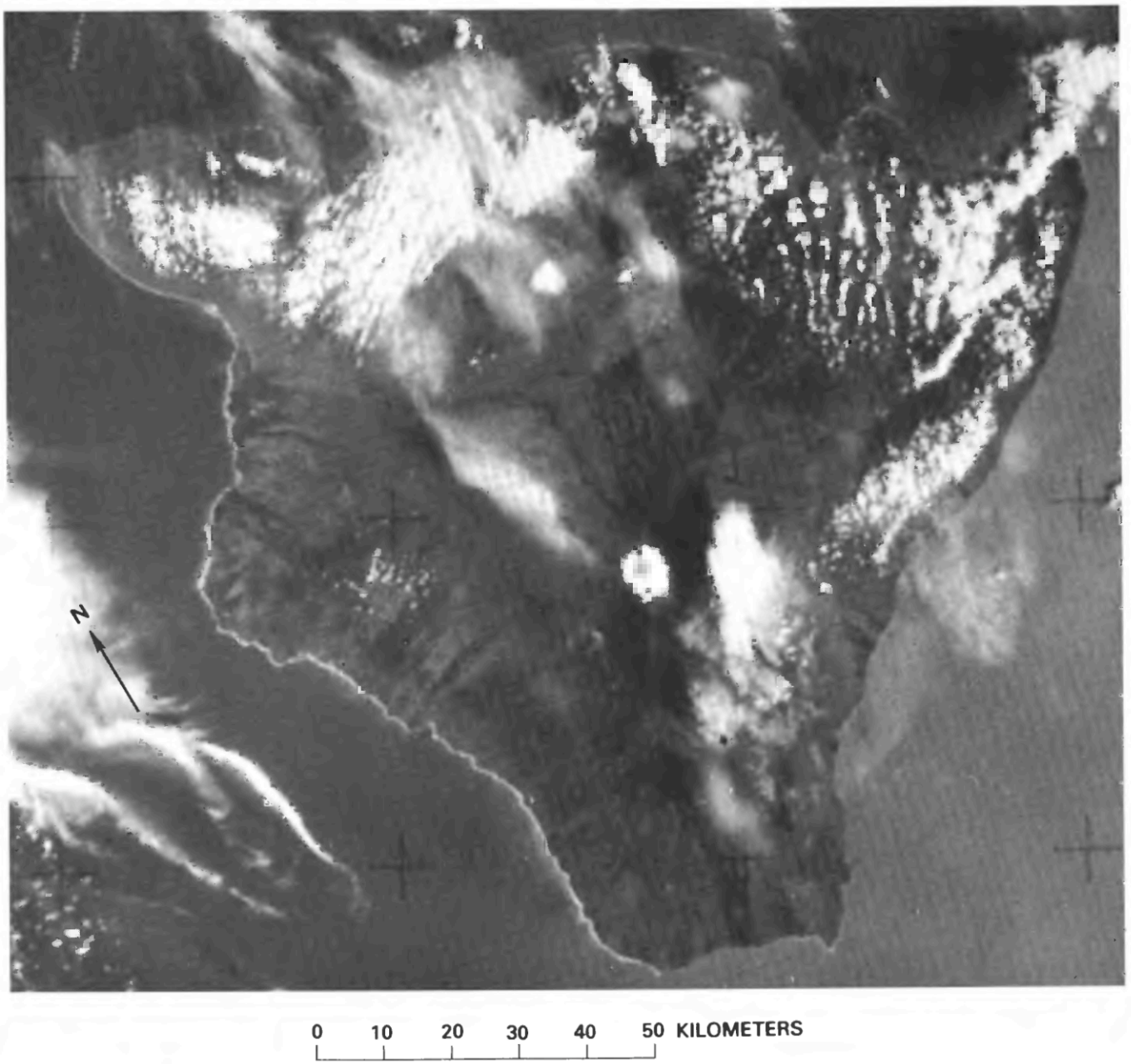

FIGURE 8.1.—View of Island of Hawaii taken on December 7, 1973, during Skylab 4 mission from altitude of about 435 km (270 mi). Snow-capped summits of Mauna Loa (4,170 m; 13,677 ft; center) and Mauna Kea (4,205 m; 13,796 ft; northeast) are 40 km (25 mi) apart. Reseau crosses provide calibration for photogrammetric applications. (NASA photograph SL4–139-3997; lens focal length, 100 mm).

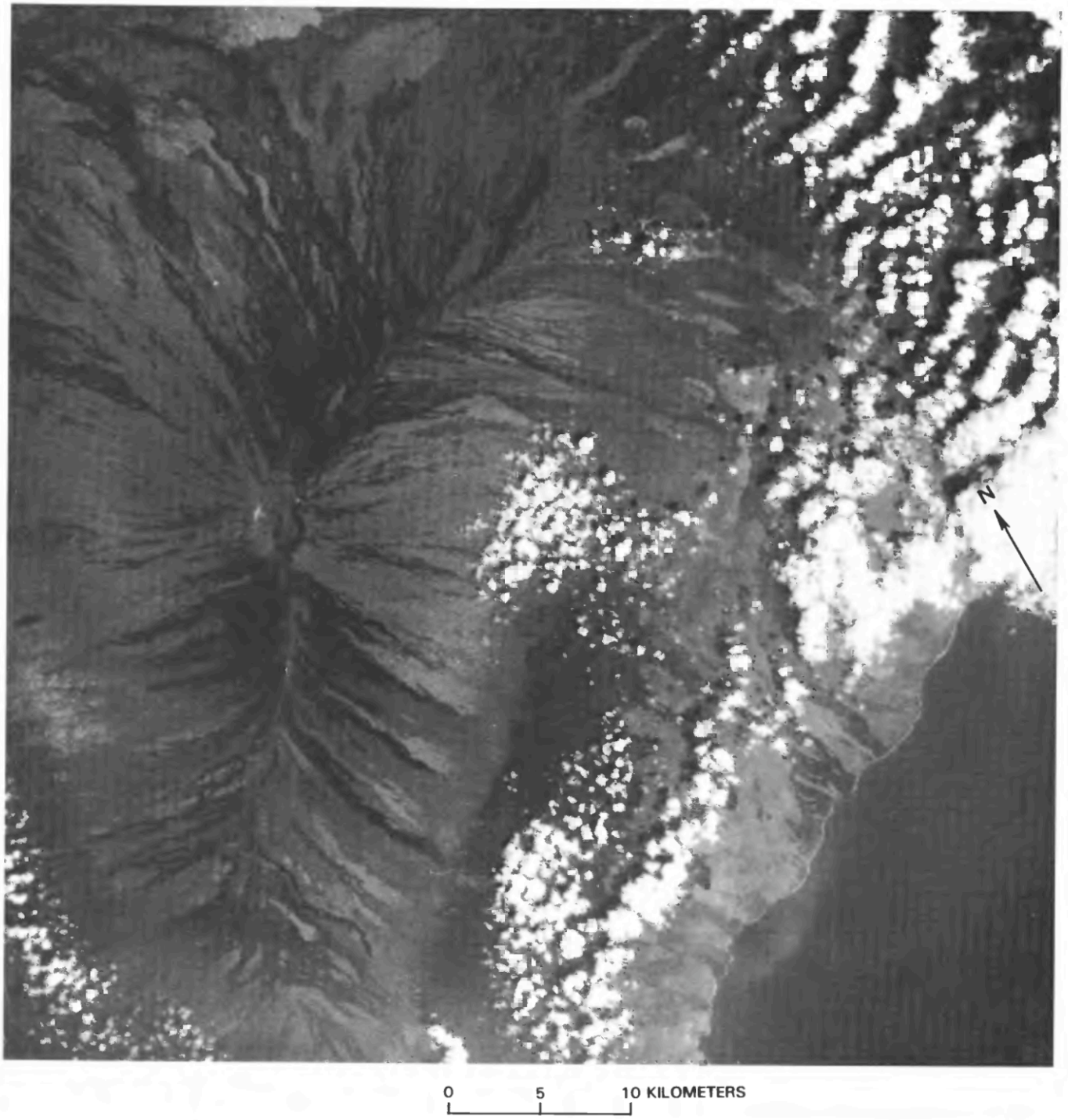

FIGURE 8.2.—Near-vertical view from Space Shuttle of Mauna Loa Volcano showing Mokuaweoweo caldera and young lava flows from northeast and southwest rift zones. (NASA photograph 41A–31-1017; lens focal length, 250 mm; November 1983).

FIGURE 8.3.—Oblique view from Space Shuttle of Island of Hawaii showing eruption plumes from Mauna Loa on April 7, 1984, twelve days after start of eruption. Higher plume (on right) is from degassing vent. Lower plume is from lava-producing vent (J.P. Lockwood, oral commun., 1985). Upper parts of new lava flows are visible as they move toward Hilo Bay (large reentrant on lower left). Active flow front is below clouds, lower on northeast rift. Often-present cloud bank obscures northeast rift zone of Mauna Loa and most of Kilauea Volcano to left. Mauna Kea Volcano is in central near-field. View southwest. (NASA photograph 41C–43-1539).

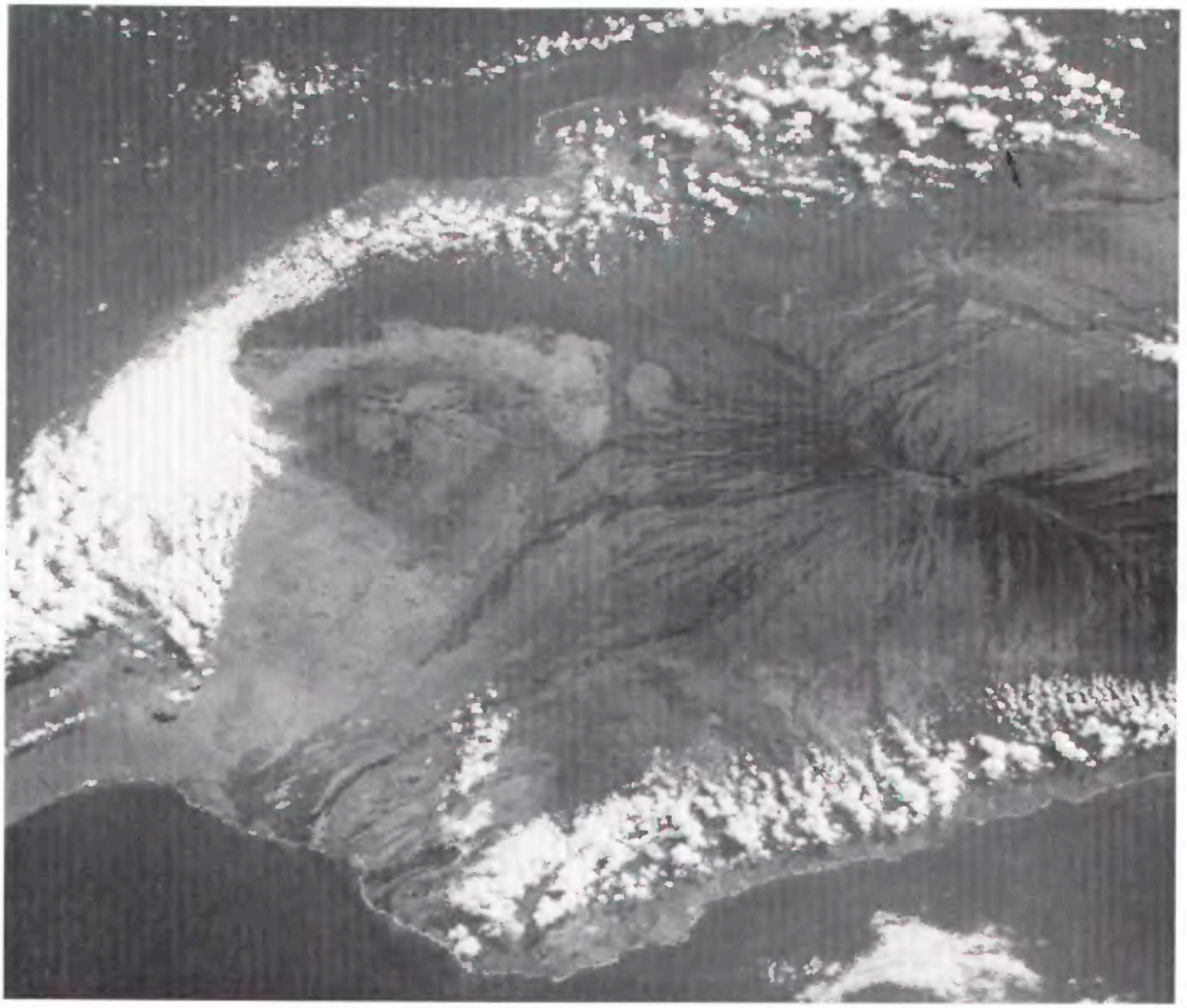

FIGURE 8.4.—Oblique view from Space Shuttle of Island of Hawaii, including Mauna Loa Volcano (right center), Kilauea Volcano and plume from phase 12 eruption of Puu Oo on the east rift zone (top right, arrow), Mauna Kea Volcano (left of center) with numerous cinder cones, Kohala Volcano (left edge), and Hualalai Volcano (bottom center, partly obscured by clouds), also with cinder cones. Note many young (dark) lava flows from Mauna Loa and Hualalai that have reached North Kona and South Kohala coasts. View east. (NASA photograph 41A–46-1841, November 30, 1983).

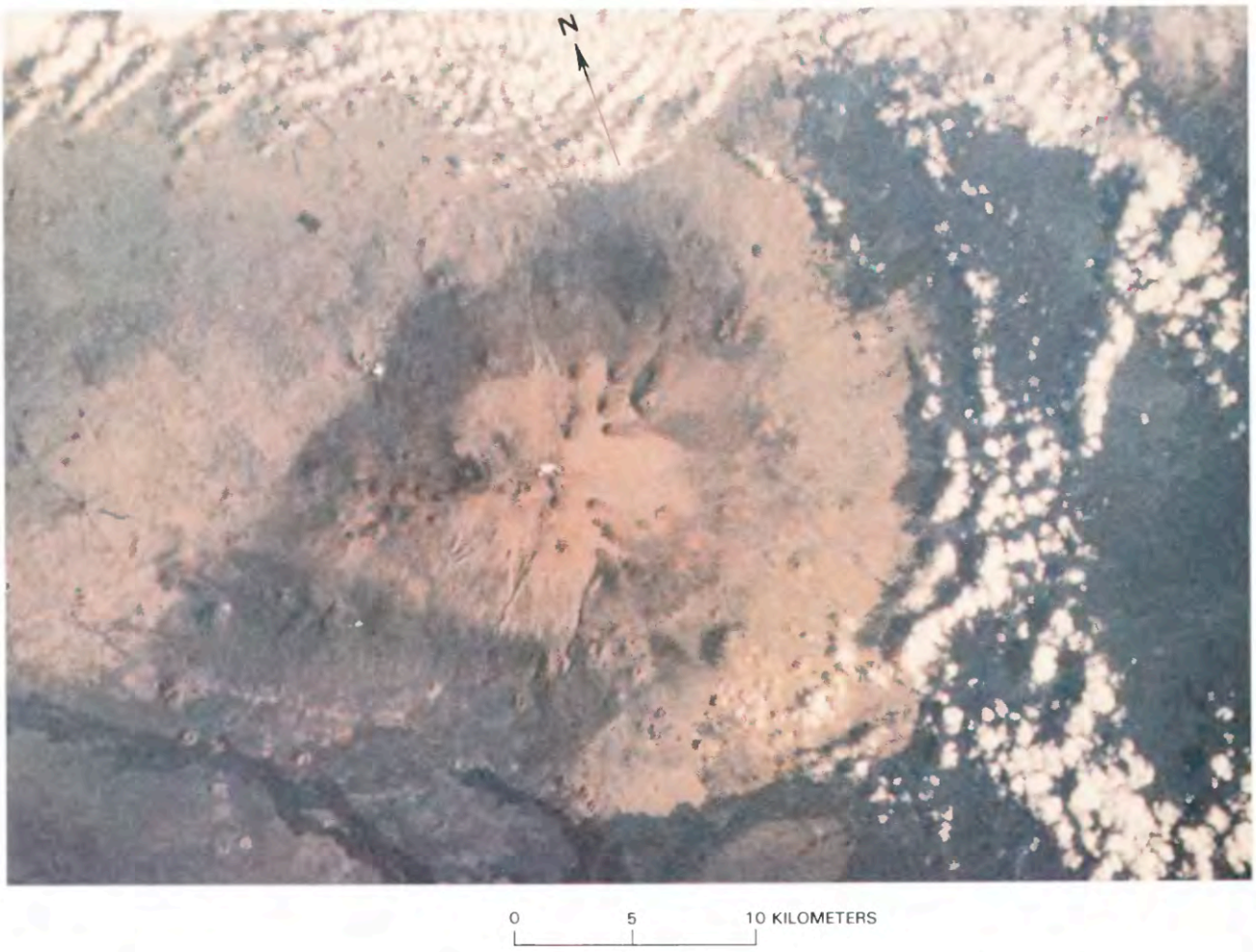

FIGURE 8.5.—View from Space Shuttle of Mauna Kea, showing distribution of alkalic cinder cones capping older tholeiitic shield. Young (dark) lava flows at bottom of photograph are from Mauna Loa. (NASA photograph 41B–34-1565, February 1984).

FIGURE 8.6.—Oblique view of Hawaii taken from Space Shuttle on December 3, 1983, at altitude of 240 km (150 mi). Cloud concentration is caused by northeasterly tradewinds against shield volcanoes, in contrast to clear sky and calm seas on leeward (Kona) side of island. Difference in ocean-surface texture is enhanced by sun illumination with respect to spacecraft. View southeast. (NASA photograph 41A–35-1596).

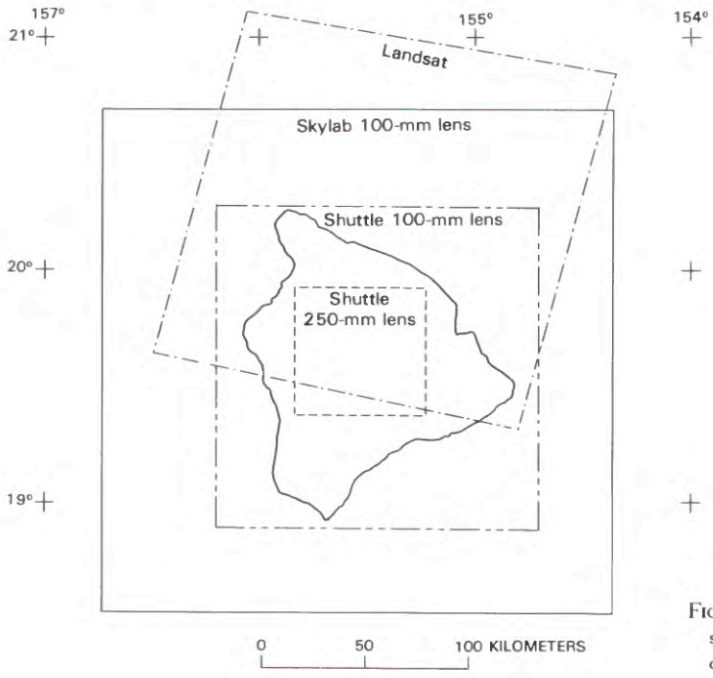

FIGURE 8.7.—Areas covered by typical Landsat, Skylab, and Space Shuttle scenes. The Skylab and Shuttle footprints are for a Hasselblad camera at altitudes of 435 km (270 mi) and 300 km (185 mi) respectively.

FIGURE 8.8.—Composite Landsat image of Island of Hawaii recorded on January 7, 1978, at altitude of about 915 km (570 mi). Image was geometrically corrected and processed to simulate true color by U.S. Geological Survey's Image Processing Facility at Flagstaff, Ariz. (Scene identification numbers 821081193-54X0 and -60X0).

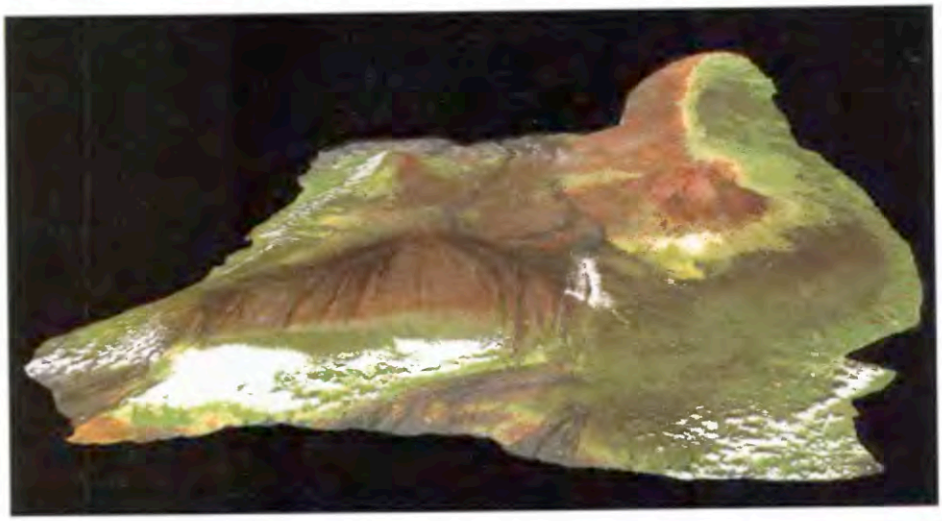

FIGURE 8.9.—Landsat image (same as fig. 8.8) digitally converted to oblique view looking northwest to illustrate Mauna Loa and Kilauea basaltic shields. Prepared by U.S. Geological Survey Image Processing Facility at Flagstaff, Ariz.

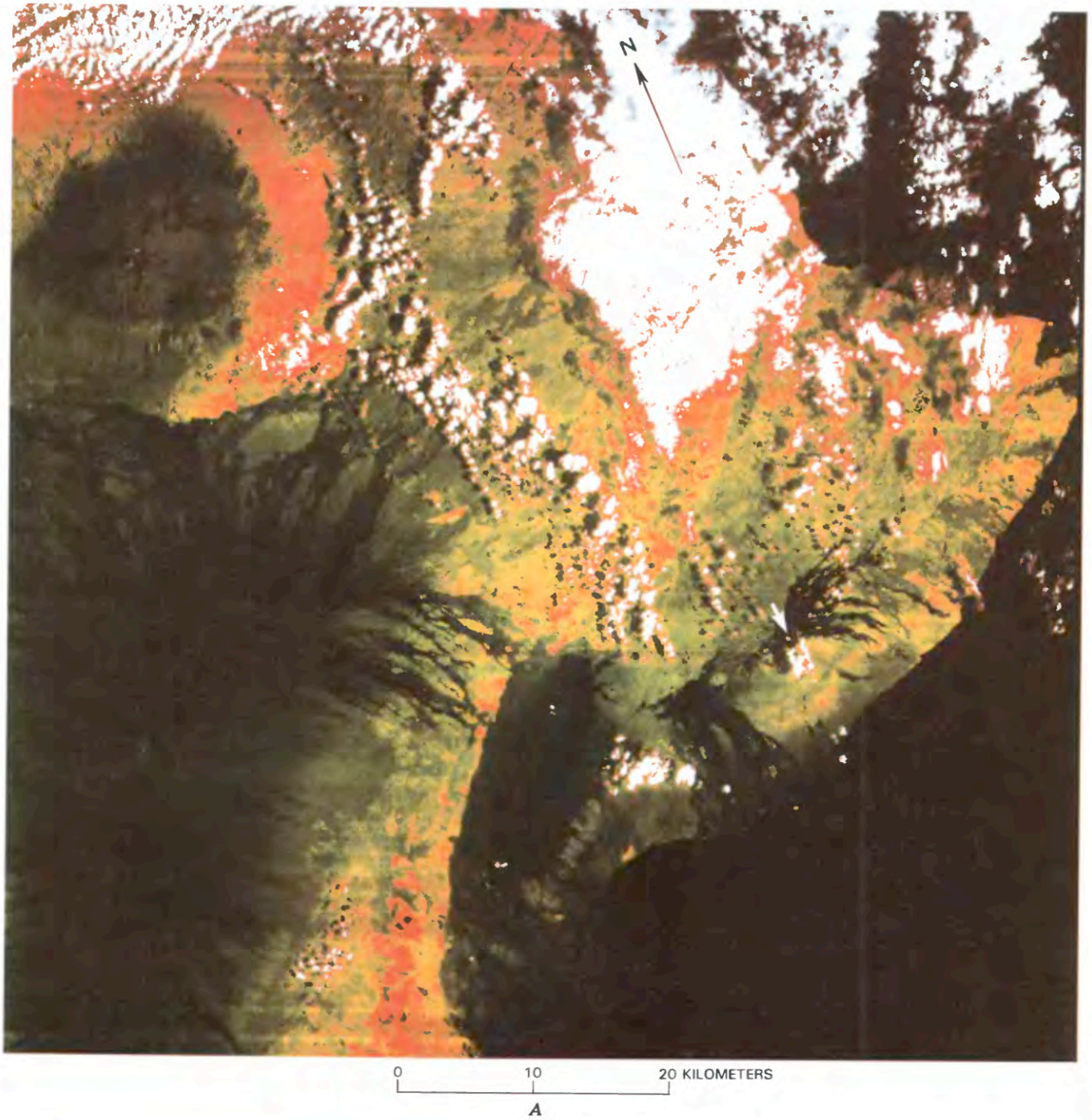

FIGURE 8.10.—Scene of eastern Hawaii from German MOMS–1 experiment on February 6, 1984, at 0930 H.s.t. from Space Shuttle. Lava flows are from Puu Oo vent (arrow in *A*). Color representation for two channels of MOMS–1 instrument is based on image-enhancement technique using HSI display mode (hue, saturation, and intensity shown in blue, green, and red channels of display system). Ratio between two channels (at 0.60 and 0.90 microns), combined with the HSI display mode, enhances weak variations in image contrast. White features are clouds. ***A***, Northeast quarter of original scene. ***B***, Enlarged subscene (750 by 750 pixels) of Puu Oo eruption area. ***C***, Eruption area (E.W. Wolfe, written commun.) showing new flows through episode 14 in January 1984, that can be directly compared with *B*.

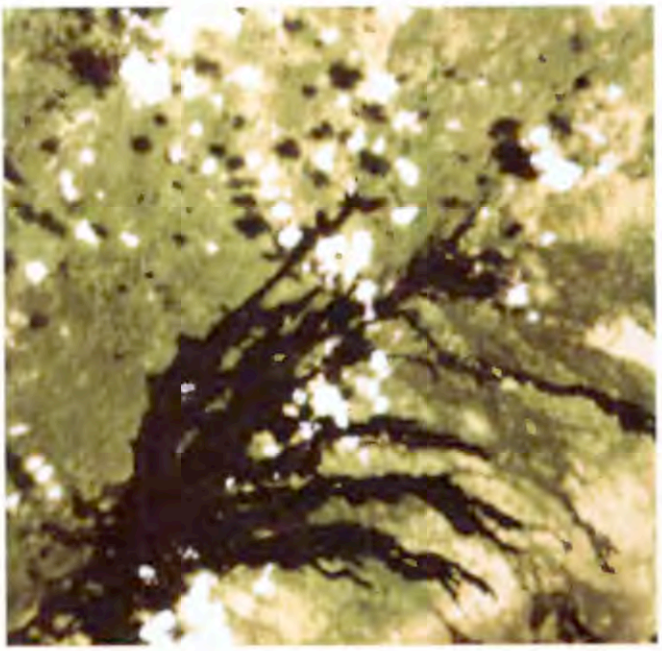

B

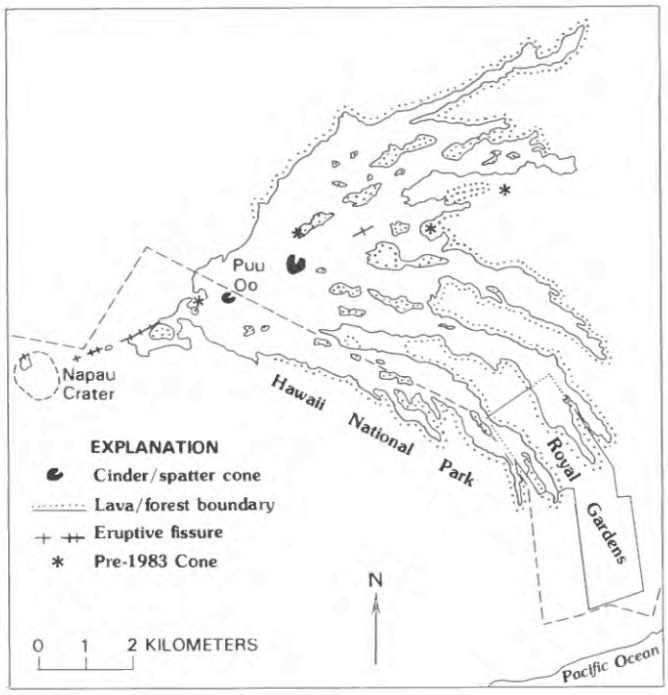

C

FIGURE 8.10.—Continued.

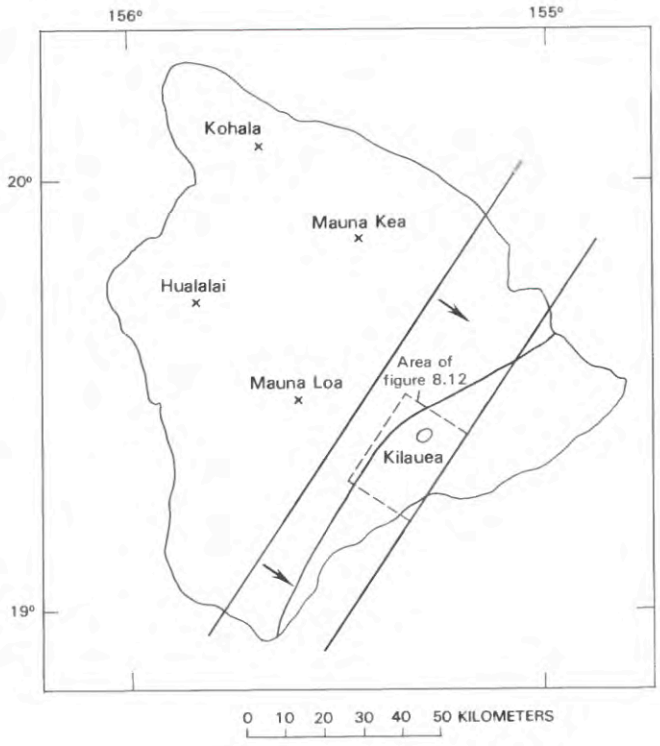

FIGURE 8.11.—Location of SIR-B radar images (area between parallel lines) that were acquired over southeast Hawaii in October 1984. Radar look-direction (arrowed) was toward southeast, and Shuttle flew from southwest to northeast on both data takes.

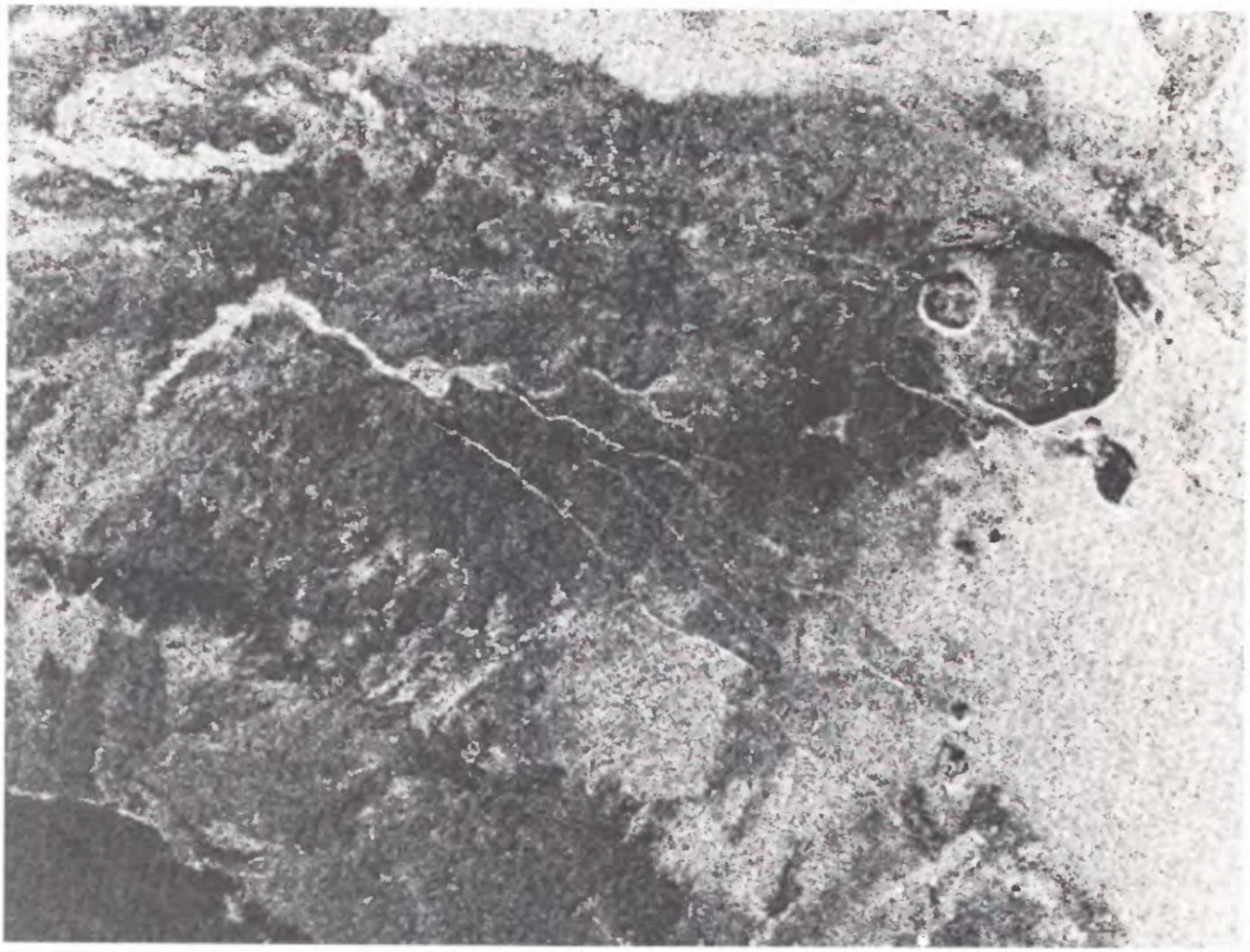

A

FIGURE 8.12.—Radar image and map of Kilauea summit area (see fig. 8.11 for location. ***A***, Subscene of SIR-B Data Take number 115.2, acquired at incidence angle of 48 degrees. Nominal image resolution is approximately 20 meters per pixel. ***B***, Same area indicating location of prominent lava flows, craters, and pali. A, transition from aa to pahoehoe on December 1974 lava flow; B, Kilauea Iki pit crater; C, September 1982 pahoehoe flows where low radar returns are evident; D, variations in radar brightness around Halemaumau pit crater (dotted line) are attributed to spatial variations in size and number of boulders ejected onto surrounding terrain by 1924 phreatic eruption of Halemaumau.

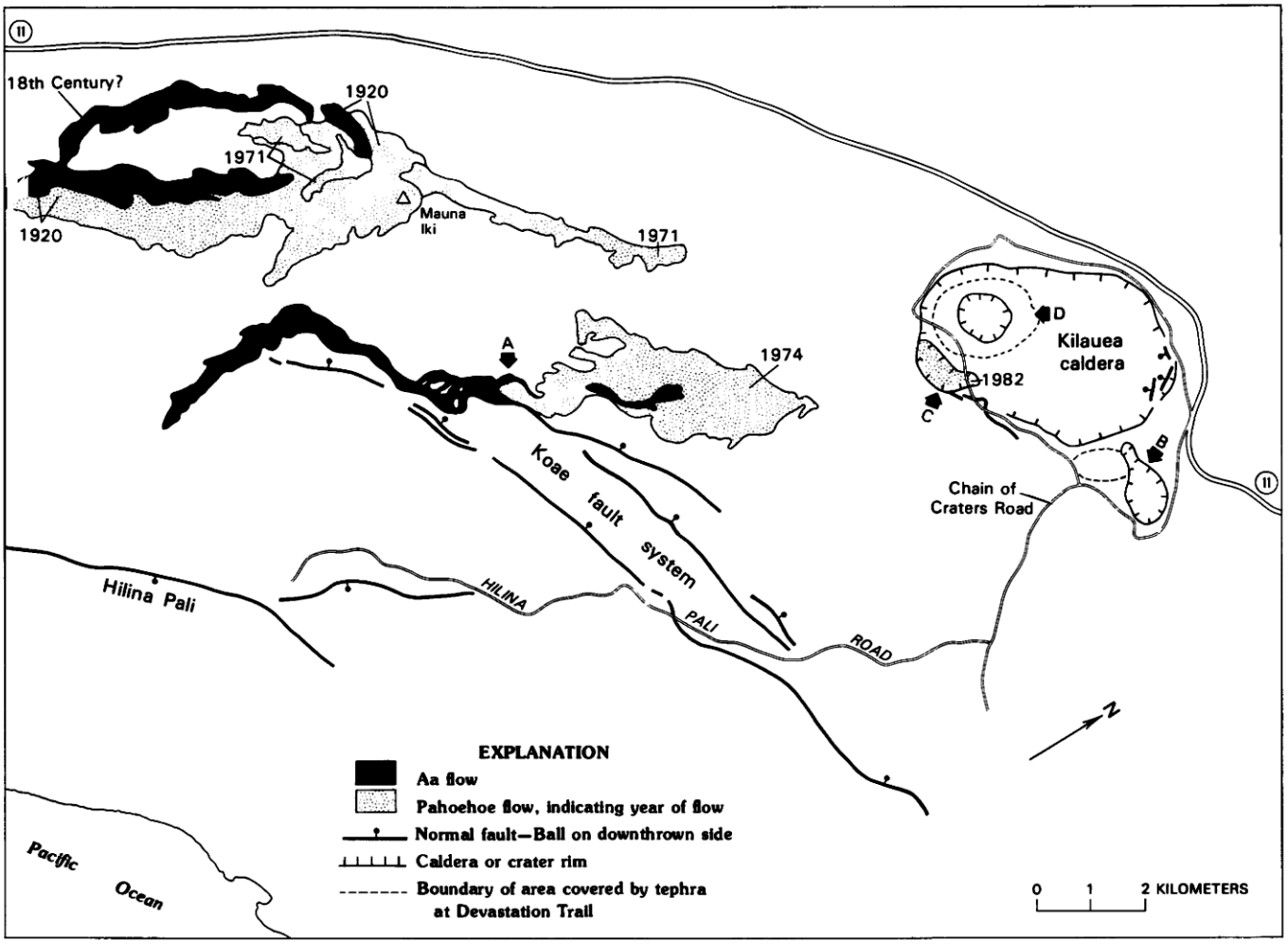

B

FIGURE 8.12.—Continued.

EFFECTS OF VOLCANIC EMANATIONS ON CARBON-ISOTOPE CONTENT OF MODERN PLANTS NEAR KILAUEA VOLCANO

By Meyer Rubin, John P. Lockwood, *and* Irving Friedman

ABSTRACT

Measurement of stable and unstable carbon isotopes were made on growing plants at various distances from fumarolic volcanic vents on the Island of Hawaii. Samples of CO_2 from volcanic gas vents were also measured, as well as control samples of unaffected atmosphere and plants. Results indicate that the proximity of the sample to the source of volcanic emanation does affect the ^{14}C concentration as anticipated, but for a variety of reasons the $^{13}C/^{12}C$ ratio, although significantly altered, does not relate directly to ^{14}C activity. Depending on how close a plant grows to fumaroles, the radiocarbon age can appear to be 1,400 years too old, with extremes of 4,000 years not unlikely.

INTRODUCTION

During investigations of the age of a pyroclastic ash on Kilauea (the mostly A.D. 1790 Keanakakoi Ash Member of the Puna Basalt) using buried charcoal, a negative correlation was observed between the radiocarbon age and the collection distance from the caldera (fig. 9.1). In order to test whether a $^{13}C/^{12}C$ ratio on the charcoal could give an indication of how much, or if any, non-radiogenic, juvenile carbon from volcanic vents was incorporated in the plants during growth, a series of samples was collected from living plants at various distances from active vents as well as control samples that could not have incorporated volcanic CO_2. From previous work

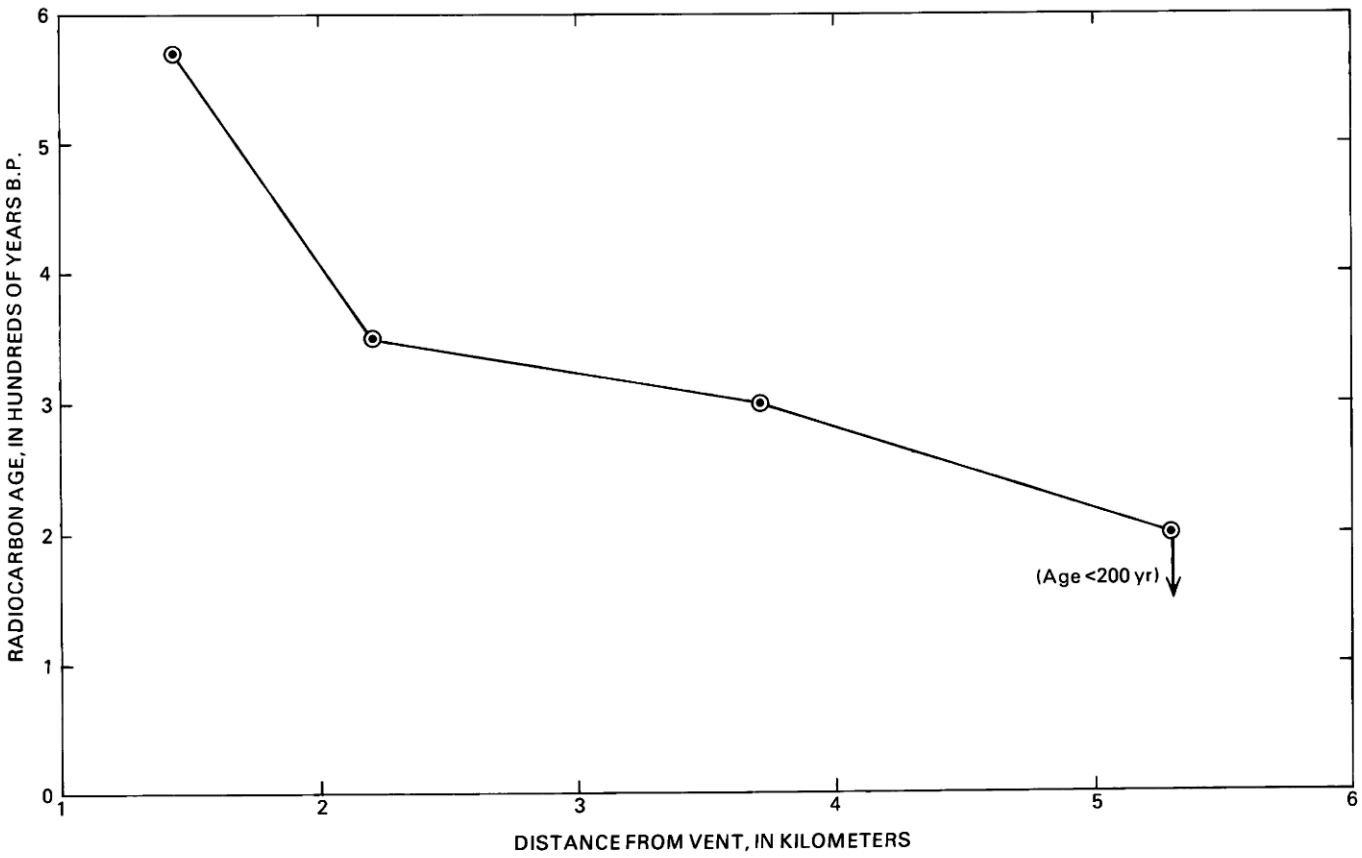

FIGURE 9.1.—Carbon-14 ages on charcoal from the mostly A.D. 1790 Keanakakoi Ash Member of the Puna Basalt as a function of collection distance from steam vents.

TABLE 9.1.—*Isotopic composition of Hawaiian plants*

Lab number	Description	$\delta^{13}C$ PDB (in permil)[1]	^{14}C (percent of modern)[2]	Apparent age (in ka)[3]
W-5476	Ohia[4] leaves from living trees overhanging the ocean on the windward Hamakua coast, Kukui Point.	-28.9	124	0
W-5477	Ohia leaves from anomalous kipuka south of Bird Park.	-24.5	124	0
W-5474	Ohia leaves from Puhimau Thermal Area.	-25.8	108	1.4
W-5482	Root of living Ohia tree at edge of fumarole at margin of Puhimau Thermal Area.	-26.3	108	1.4
W-5480	Fern[5] growing directly in hot steam at margin of fumarole at Puhimau Thermal Area.	-26.8	82	4.3
3464-6	Gas sample, Puhimau vent.	-3.0	--	--
3464-7	Gas sample, Halemaumau.	-3.5	--	--
W-1957	Gas sample, Sulfur Bank no. 2, Kilauea 1966.	-3.6	.1	>45
W-1958	Gas sample, Sulfur Bank no. 1.	--	.0	>45
W-3983	Gas sample, Sulfur Bank, 1971.	--	.2	>40
W-3989	Gas sample, 1971 fissure, Kilauea.	--	.5	>40

[1] CO_2 from samples of air collected weekly for 4 yr on Mauna Loa at 3,048 m elevation range from -7.1 to -8.4 permil.

$$\delta^{13}C_{PDB} = \left(\frac{R\ sample}{R\ standard}\right) - 1 \quad 1{,}000, \text{ where } R = \text{the ratio } {}^{13}C/{}^{12}C.$$

[2] Measured in comparison to the National Bureau of Standards 1960 oxalic acid standard. Modern equals 95 percent of the activity of this standard.

[3] Using present-day wood activity as 124 percent of modern.

[4] *Metrosideros polymorpha.*

[5] *Nephrolepsis exaltata.*

(Chatters and others, 1969; Sulerhitzky, 1970; Libby and Libby, 1972; Panichi and Tongiorgi, 1975; Michael, 1978; Weinstein and Betancourt, 1978; Puchelt and Hubberten, 1979; Bruns and others, 1980; Saupe and others, 1980), juvenile CO_2 from volcanic vents was found to be "dead" (contains no ^{14}C), and plants growing immediately adjacent to the vents could give anomalous ages as much as several thousand years too old. What was not known, however, was whether the ^{13}C measurements could help in determining possible old carbon contamination in the hundreds of previously dated samples from Hawaii.

METHODS

Grab samples were collected of living, native vegetation growing under different conditions of exposure to volcanic gases, from the worst case of ferns growing directly in the hot steam of a fumarole to leaves of trees overhanging the Hamakua coast bathed in the uncontaminated northeast trade winds (table 9.1). Samples were taken of first-year leafy growth to verify that the biologically fixed carbon was obtained from the atmosphere in the year of sampling (1983). The $^{13}C/^{12}C$ measurements were made in Denver, Colorado, on an aliquot of the same samples that were dated by ^{14}C measurements in Reston, Virginia. The dried plant material was oxidized at 900 °C and the purified CO_2 was analyzed on a 12-inch triple-collector magnetic-sector mass spectrometer. The analytical precision is ±0.1 percent (2 sigma). All $^{13}C/^{12}C$ ratios are reported in permil relative to the Peedee belemnite (PDB) standard. A value of −28.1 permil was obtained for NBS–21 graphite. The Sulfur Bank gas samples were collected in 1966 by Bruce

Hanshaw and Meyer Rubin and measured by the same methods. The 1971 gas samples were collected by Meyer Rubin and Elliott Spiker. The gas for ^{14}C determinations was collected by absorption in NaOH. The leaves, collected from several growing plants in a localized area, were only given a hot water wash as a pretreatment, then counted in gas proportional counters as acetylene.

DISCUSSION

As anticipated, the ^{14}C data show the dilution effect of the "dead" CO_2 of juvenile volcanic origin. The Sulfur Bank gas has a ^{14}C activity of juvenile gas. Within our background error of ± 1 percent, there is no measurable ^{14}C. The gas samples from Puhimau vent and Halemaumau crater as well as from Sulfur Bank and the 1971 fissure have $\delta^{13}C$ values ranging from -3.0 to -3.6 permil. Pure air has a $\delta^{13}C$ of approximately -8 ± 0.3 permil. This 5 permil difference between the pure air and the volcanic gas should show up in the $\delta^{13}C$ of the leaves if the plants incorporated the isotopically heavier volcanic gas. The Kilauea samples are about 2 permil heavier than those from a tree growing on the seacliff remote from volcanic CO_2. If 40 percent of the CO_2 assimilated by the plants was of volcanic origin, we would expect the $\delta^{13}C$ of the plant material to be heavier by about 2 permil. Inasmuch as Puhimau gas contains 1 to 5 percent CO_2 (L.P. Greenland, oral commun., 1985) only 1 percent of this gas mixed with 99 percent air (0.035 percent CO_2) could account for this change in $\delta^{13}C$. However, the $\delta^{13}C$ values of the leaves and roots are probably affected by factors such as moisture availability and temperature as well as the $\delta^{13}C$ of the ingested CO_2, and the $\delta^{13}C$ values of the samples collected on Kilauea do not relate directly to the ^{14}C activity, as can be seen in table 9.1.

The ^{14}C results (table 9.1) may appear slightly confusing because they are compared to 0.95 times the activity of an oxalic acid standard, which gives the modern or present-day atmospheric activity if there had been no bomb testing. The ^{14}C produced by the nuclear weapons tests since 1953 first elevated the activity to 200 percent of the 95 percent oxalic acid standard; absorption by the oceans and other buffering mechanisms has subsequently lowered it to approximately 124 percent (as of 1985).

If the present-day activity is represented by the two samples at 124 percent ^{14}C activity, then the samples growing in a thermal area are depressed by 16 percent, giving the plants an initial age of approximately 1.4 ka. The fern leaves growing at the very edge of a fumarole, a worst case situation, were depressed approximately 42 percent, differing from normal living plants by 4,300 years.

Thus, the charcoal from plants buried by an ash or lava flow could have an initial built-in age of as much as 4.3 ka, but more likely not more than 1.4 ka, depending on how close to a volcanic fumarole the plants grew at the time of burial. This dilution is also possible near central volcanic areas, particularly downwind, decreasing in effect rapidly away from the source of the dead CO_2 (fig 9.1). Nonmeteoric CO_2 is higher in abundance at Kilauea summit fumaroles, but decreases in abundance away from the caldera, along both the east and southwest rift zones (L.P. Greenland, written commun., 1985).

CONCLUSIONS

Carbonaceous samples dating volcanic activity are probably usually correct to within twice the stated one-sigma counting error. However, because one cannot always reconstruct the locations of volcanic fumaroles or determine the original juvenile CO_2 gas activity, radiocarbon samples from volcanic areas may appear too old by about 1,400 years. In rare situations samples may date 4,300 years too old.

Most contaminants of charcoal collected for radiocarbon chronology studies result in geologically young ages (modern rootlets, humic acids, and so on). Our studies show that samples collected from the immediate vicinity of CO_2-emitting volcanic fumaroles can also incorporate contaminants that result in radiocarbon ages that are too old. Considerable caution should be used in the evaluation of ages from central volcanic areas. Given the present sparse data one cannot use $\delta^{13}C$ to predict possible old carbon contamination.

REFERENCES CITED

Bruns, Michael, Levin, Ingeborg, Munnich, K.O., Hubberten, H.W., Fillipakis, S., 1980, Regional sources of volcanic carbon dioxide and their influence on ^{14}C content of present-day plant material: Radiocarbon, v. 22, no. 2, p. 532–536.

Chatters, R.M., Crosby, J.W., and Engstrand, L.G., 1969, Fumarole gaseous emanations their influence on carbon-14 dates: Washington State University College of Engineering Circular 32, 9 p.

Libby, L.M., and Libby, W.F., 1972, Volcanism and radiocarbon dates, *in* Rafter, T.A., and Grant-Taylor, T. eds., International Radiocarbon Conference, 8th, Proceedings: Wellington, Royal Society of New Zealand, v. 1, p. A72–A75.

Michael, H.N., 1978, Radiocarbon dates from Akrotiri, Thera, 1967–1977, *in* Doumas, D., ed., Thera and the Aegean World, I: International Science Conference, London, 2nd, Papers, p. 791–795.

Panichi, Costanzo, and Tongiorgi, Ezio, 1975, Carbon isotopic composition of CO_2 from springs, fumaroles, mofettes, and travertines of central and southern Italy: a preliminary prospection method of geothermal area: United Nations Symposium on Development and Use of Geothermal Resources, 2nd, Proceedings, San Francisco, Lawrence Berkeley Laboratory, University of California.

Puchelt, H., and Hubberten, H.W., 1979, Vulkanogenes Kohlendioxid: Aussagen und Herkunft aufgrund von Isotopenuntersuchungen, *in* Arbeitstagung, Isotope in der Natur., Leipzig, 1979, 2nd, Proceedings.

Saupe, Francis, Strappa, Osvaldo, Coppens. Rene, Guillet, Bernard, and Jaegy, Robert, 1980, A possible source of error in ^{14}C dates: volcanic emanations (examples from the Monte Amiata district, Provinces of Grosseto and Sienna, Italy): Radiocarbon, v. 22, no. 2, p. 525–531.

Sulerzhitzky, C.D., 1970, Radiocarbon dating of volcanoes: Bulletin Volcanologique, v. 35, p. 85–94.

Weinstein, G.A., and Betancourt, P.P., 1978, Problems of interpretation of the Akrotiri radiocarbon dates, *in* Doumas, C., ed., Thera and the Aegean World, I: International Science Congress, 2nd, London, Papers, p. 805–814.

HAWAIIAN RADIOCARBON DATES

By Meyer Rubin, Lea Kelley Gargulinski, *and* John P. McGeehin

ABSTRACT

Radiocarbon dates have been obtained from 306 geologic samples collected from the Island of Hawaii and analyzed by the U.S. Geological Survey laboratory at Reston, Virginia. The dates range from modern (present-day carbon) to greater than 38 ka. For convenience, the tabulated dates are grouped by volcano: 185 from Mauna Loa, 90 from Kilauea, 30 from Hualalai, and 1 from Mauna Kea. Maps show sample locations, and a selected bibliography of articles covers aspects of Hawaiian radiocarbon dates.

INTRODUCTION

Understanding the history of volcanism in Hawaii requires an understanding of the timing of the volcanic events. This article lists the radiocarbon dates from the Island of Hawaii, giving their sample locations, ages, significance, and stratigraphic relations in tabular form. Dates from each volcano on Hawaii are grouped in a separate table. These tables and the accompanying bibliography provide a comprehensive source of information on Hawaiian radiocarbon dates.

HISTORY OF ^{14}C DATING IN THE HAWAIIAN ISLANDS

Although radiocarbon dating methods have been available since the late 1940's, only a handful of dates were determined on material from Hawaiian lava flows before 1976. This was not because of lack of interest but because samples of datable organic material were not available. With improved understanding of the conditions of charcoal formation and preservation beneath basaltic lavas, opportunities for discovery increased. Lockwood and Lipman (1979) pioneered the recovery of such material, allowing the dating of many new samples. Dates from Hawaii before 1979 are listed in Kelley (1979) and Kelley and others (1979). In the present paper, we list all dates from Hawaii analyzed for volcano-stratigraphic purposes at the U.S. Geological Survey radiocarbon laboratory at Reston, Va. Many dates obtained for other purposes, such as archaeologic dates, geochemical dates related to volcanic gases and volcanic emanations affecting the biosphere, and dates on ground water are not listed here, as they are beyond the scope of this article.

A curve depicting the number of radiocarbon dates by year since 1950 would be a steeply rising one. The development of the new technique of tandem-accelerator mass spectrometry, with its attendant thousandfold decrease in the required sample size, will undoubtedly cause this curve to rise even more steeply. Many sites yield charcoal in insufficient quantity for a conventional radiocarbon age without large-scale quarrying operations, but the new method can provide a reliable date from a few milligrams of carbon. The experience of volcanologists indicates that many additional flows can be dated, now that the sample requirements have been reduced significantly.

Radiocarbon dates from Hawaii have revolutionized our understanding of the island's volcanic history. Previous workers had to be satisfied with relative ages, rather than numerical dates. In addition to directly dating the geologic deposit, ^{14}C dating has helped to calibrate other forms of dating, which then could be used as a substitute dating technique where carbon is not available. These alternate methods include paleomagnetic-age curves of various types and individual weathering indices developed by several workers. All of these are calibrated on ^{14}C-dated flows.

CARBON SOURCES

The ideal sample for radiocarbon dating of a flow would be a sample from a short-lived plant converted to vitreous charcoal by the heat of the advancing lava (Lockwood and Lipman, 1979). The plant should have been growing away from the influence of volcanic-source CO_2, which lacks the ^{14}C present in atmospheric CO_2, should be buried too deeply for surface rootlet penetration, and should not be soaked in ground water rich in organic components. Poor samples would be those from buried soils, poor in organic matter, having modern rootlets, or lying under the water table. Various enrichment and purification techniques for removing contaminants have been developed to analyze such poor-quality samples, but the results are not always reliable. Charcoal from post-flow fires commonly trickles down through the flow (most easily with aa) and can give the appearance of having been formed during the flow's advance, but such material will not date the actual flow.

VALIDITY OF THE DATES

The uncertainty given for the dates in the tables (the figure after the $\pm$) is the standard deviation (one sigma) based only on the counting statistics and not on analysis of replicate samples from the field. This counting error does not include variable factors, such as contamination, isotopic fractionation, and other laboratory uncertainties. Experience has shown that these factors raise the uncertainty to more than twice the quoted error.

Another type of error encountered in some samples taken from volcanic areas is that caused by dilution of the normal ^{14}C content in atmospheric CO_2 by volcanic emanations that contain no ^{14}C.

Plants take up this ^{14}C-poor CO_2 in their metabolism and therefore have an initial apparent age because of such deficient initial activity. This error in extreme cases can produce an apparent age of 3 ka in living plants (Rubin and others, chapter 9). However, common practice suggests that unless a plant is known to be growing immediately adjacent to a vent, it can be assumed to give a reasonably correct age.

HOW ^{14}C DATING HAS AFFECTED THE THINKING OF HAWAIIAN GEOLOGISTS

What surprises have been produced by the numerous ^{14}C dates obtained in recent years? In general, geologists did not have to revise greatly their age estimates for flows younger than 1 ka. By extrapolation of historical weathering rates, they had been able to estimate fairly accurately the ages of the younger flows. Flows having a very weathered appearance, however, had been estimated to be much older than the dates ultimately derived by ^{14}C measurements.

SUMMARY OF HAWAIIAN RADIOCARBON DATES AND THEIR SIGNIFICANCE

Sample locations, laboratory numbers, and ages of Hawaiian radiocarbon dates have been plotted (figs. 10.2–10.5; see also fig. 10.1) and are also listed by volcano (tables 10.1–10.4). The tables list samples in order of increasing age and also give additional information on location, geologic section, altitude and flow name. Only those samples that were processed at the U.S. Geological Survey radiocarbon laboratory at Reston, Va., and that have geologic significance are included in this compilation.

Much further information for each sample, including the complete geologic section and significance, the date of collection, and the collector's judgment as to whether the sample age appears to be a valid age for the overlying flow or ash is available from the U.S. Geological Survey laboratory at Reston or from the collector. All collectors are or were members of the U.S. Geological Survey. Other chapters in the present work make use of the dates collected here in their studies of separate volcanic areas, and they constitute prime sources of information on Hawaiian chronology.

MAUNA LOA

The numerous samples dating the flows of Mauna Loa (table 10.1; figs. 10.2–10.4) serve only to establish a foundation for further work. Of the hundreds of individual flows that have been mapped, many have been dated, but there are still many more flows to be dated. Where carbon is not available, or the age is beyond the range of ^{14}C dating, observational methods of relative dating will be used, with the radiocarbon dates as a calibration where possible.

Some tentative statements as to the activities of the various volcanoes can be made. Mauna Loa appears to have been more active during the brief period of its recorded history than during the several centuries immediately preceding 1840. Activity was also higher around 0.8–1.0 ka (800–1,000 years before present). Surface flows on Mauna Loa appear to be older than those of Kilauea. Areal percentages covered by various ages of flows are discussed by Lockwood and Lipman (chapter 18). Flows several thousand years old are common on Mauna Loa, but flows more than a few hundred years old are rare on Kilauea. About 30 percent of the surface of the southwest side of Mauna Loa has been covered by lava in the past 1,000 years, but about 90 percent of Kilauea's surface is younger than 1 ka.

Ages of Mauna Loa flows range from very recent to greater than 38 ka, the very oldest flows being exposed along deeply incised river channels and fault scarps.

KILAUEA

As is evident from the dates (table 10.2; fig. 10.5), Kilauea is a young, active volcano. Kilauea's surface is only about one-tenth as old as was thought previously. The northeast rift zone appears to be the same age as the southwest rift zone but has more bulk, erupting more often and with greater volume. The older rocks are, in general, found farther away from the rift zone. About 90 percent of the surface flows are younger than 1.1 ka (Holcomb, chapter 12). Kilauea is the youngest volcano on the Island of Hawaii, with dated eruptions from the present time back to about 23 ka.

HUALALAI

Although the flows of Hualalai (table 10.3; fig. 10.2) have not been as frequent as Kilauea in historical time, the flows in the past 1,500 years have been very large and cover 10–20 percent of the area. All of the approximately 200 cones on Hualalai are of Holocene age (less than 10 ka) and 95 percent of the surface flows are also Holocene in age. As much as 50 percent of the area is covered by flows younger than 5 ka. Hualalai is still an active volcano, with an average of one eruption every 50 years during Holocene time, and the last known eruption occurred in 1801. Ages range from less than 200 years to 13 ka.

MAUNA KEA

Mauna Kea is, next to Kohala Volcano, the oldest and least active of the Hawaiian volcanoes. The date from Mauna Kea (table 10.4; fig. 10.3) is Holocene in age, but this does not reflect the age of the majority of deposits (see Porter, chapter 21).

SELECTED BIBLIOGRAPHY

DATE LISTS

Buckley, J.D., 1973, Isotopes' radiocarbon measurements X: Radiocarbon, v. 15, p. 280–298.

Buckley, J.D., and Willis, E.H., 1969, Isotopes' radiocarbon measurements VII: Radiocarbon, v. 11, p. 53–105.

———1972, Isotopes' radiocarbon measurements IX: Radiocarbon, v. 14, p. 114–139.

Buddemeier, R.W., and Hufen, T.H., 1978, Hawaii Institute of Geophysics radiocarbon dates: Radiocarbon, v. 15, p. 68–74.

Crane, H.R., 1956, University of Michigan radiocarbon dates I: Science, v. 124, p. 664–672.
Crane, H.R., and Griffin, J.B., 1958, University of Michigan radiocarbon dates II: Science, v. 127, p. 1098–1105.
———1959, University of Michigan radiocarbon dates IV: Radiocarbon, v. 1, p. 173–198.
———1960, University of Michigan radiocarbon dates V: Radiocarbon, v. 2, p. 31–48.
———1962, University of Michigan radiocarbon dates VII: Radiocarbon, v. 4, p. 183–203.
———1963, University of Michigan radiocarbon dates VIII: Radiocarbon, v. 5, p. 228–253.
Fairhall, A.W., Young, A.W., and Erickson, J.L., 1976, University of Washington dates IV: Radiocarbon, v. 18, p. 221–239.
Hubbs, C.L., Bien, G.S., and Suess, H.E., 1962, La Jolla natural radiocarbon measurements II: Radiocarbon, v. 4, p. 204–238.
———1965, La Jolla natural radiocarbon measurements IV: Radiocarbon, v. 7, p. 66–117.
Ives, P.C., Levin, Betsy, Oman, C.L., and Rubin, Meyer, 1967, U.S. Geological Survey radiocarbon dates IX: Radiocarbon, v. 9, p. 505–529.
Ives, P.C., Levin, Betsy, Robinson, R.D., and Rubin, Meyer, 1964, U.S. Geological Survey radiocarbon dates VII: Radiocarbon, v. 6, p. 37–76.
Kelley, M.L., 1979, Radiocarbon dates from the Hawaiian Islands: A compilation: U.S. Geological Survey Open-File Report 79-1700, 39 p.
Kelley, M.L., Spiker, E.C., Lipman, P.W., Lockwood, J.P., Holcomb, R.T., and Rubin, Meyer, 1979, U.S. Geological Survey, Reston, Virginia, radiocarbon dates XV: Mauna Loa and Kilauea Volcanoes, Hawaii: Radiocarbon, v. 21, p. 306–320.
Kigoshi, Kunihiko, Tomikura, Yoshio, and Endo, Kunihiko, 1962, Gakushuin natural radiocarbon measurements I: Radiocarbon, v. 4, p. 84–94.
Krueger, H.W., and Weeks, C.E., 1966, Geochron Laboratories, Inc. radiocarbon measurements II: Radiocarbon, v. 8, p. 142–160.
Levin, Betsy, Ives, P.C., Oman, C.L., and Rubin, Meyer, 1965, U.S. Geological Survey radiocarbon dates VIII: Radiocarbon, v. 7, p. 372–398.
Libby, W.F., 1951, Radiocarbon dates III: Science, v. 114, p. 291–296.
———1954, Chicago radiocarbon dates V: Science, v. 120, p. 733–742.
Marsters, Beverly, Spiker, Elliott, and Rubin, Meyer, 1969, U.S. Geological Survey radiocarbon dates X: Radiocarbon, v. 11, p. 210–227.
Rubin, Meyer, and Alexander, Corrinne, 1958, U.S. Geological Survey radiocarbon dates IV: Science, v. 127, p. 1476–1487.
———1960, U.S. Geological Survey radiocarbon dates V: Radiocarbon, v. 2, p. 129–185.
Rubin, Meyer, and Berthold, S.M., 1961, U.S. Geological Survey radiocarbon dates VI: Radiocarbon, v. 3, p. 86–98.
Rubin, Meyer, and Suess, H.E., 1956, U.S. Geological Survey radiocarbon dates III: Science, v. 123, p. 442–448.
Stuckenrath, Jr., Robert, 1967, University of Pennsylvania radiocarbon dates X: Radiocarbon, v. 9, p. 333–345.
Sullivan, B.M., Spiker, Elliott, and Rubin, Meyer, 1970, U.S. Geological Survey radiocarbon dates XI: Radiocarbon, v. 12, p. 319–334.
Vogel, J.C., and Waterbolk, H.T., 1964, Groningen radiocarbon dates V: Radiocarbon, v. 6, p. 349–369.

SPECIFIC USES

Berry, A.L., 1973, Thermoluminescence of Hawaiian basalts: Journal of Geophysical Research, v. 78, p. 6863–6867.
Coe, R.S., Groome, Sherman, and Mankinen, E.A., 1978, Geomagnetic paleointensities from radiocarbon-dated lava flows on Hawaii and the question of the Pacific nondipole low: Journal of Geophysical Research, v. 83, no. B4, p. 1740–1756.
Doell, R.R., and Cox, Allan, 1965, Paleomagnetism of Hawaiian lava flows: Journal of Geophysical Research, v. 70, no. 14, p. 3377–3405.
May, R.J., 1975, Thermoluminescence dating of Hawaiian basalts: Palo Alto, Stanford University, Ph.D. dissertation, 156 p.
———1977, Thermoluminescence dating of Hawaiian alkalic basalts: Journal of Geophysical Research, v. 82, p. 3023–3029.
———1979, Thermoluminescence dating of Hawaiian basalt: U.S. Geological Survey Professional Paper 1095, 47 p.
McWilliams, M.O., Holcomb, R.T., and Champion, D.E., 1979, Holocene geomagnetic secular variation for Hawaii: Eos (American Geophysical Union, Trans.), v. 60, no. 18, 244 p.
———1982, Geomagnetic secular variation from ^{14}C-dated lava flows on Hawaii and the question of the Pacific non-dipole low, *in* Runcorn, S.K., Creer, K.M., and Jacobs, J.H., eds., The Earth's core: Its structure, evolution, and magnetic fields: Royal Society of London Series A, v. 306, p. 211–222.
Morgenstein, M., Riley, T.J., 1975, Hydration-rind dating of basaltic glass: A new method for archaeological chronologies: Hawaii University, Institute of Geophysics, Contributions, p. 1–18.

GENERAL TOPICS

Easton, R.M., 1978, The stratigraphy and petrology of the Hilina Formation: The oldest exposed lavas of Kilauea Volcano, Hawaii: Honolulu, University of Hawaii, m.s. thesis.
Holcomb, R.T., 1981, Kilauea Volcano, Hawaii: Chronology and morphology of the surficial lava flows: U.S. Geological Survey Open-File Report 81-0354, 383 p.
Inman, D.L., and Veeh, H.H., 1966, Dating the 10-fathom terrace off Hawaii [abs.]: American Geophysical Union Transactions: v. 47, p. 125.
Lockwood, J.P., and Lipman, P.W., 1979, Recovery of charcoal for ^{14}C dating from beneath lava—lessons from Hawaii: Journal of Volcanology and Geothermal Research, v. 4.
Macdonald, G.A., and Abbott, A.T., 1970, Volcanoes in the Sea: Honolulu, University of Hawaii Press, 441 p.
Macdonald, G.A., and Eaton, J.P., 1964, Hawaiian volcanoes during 1955: U.S. Geological Survey Bulletin 1171, p. 156–157.
Peterson, D.W., 1967, Geologic map of Kilauea Crater Quadrangle: U.S. Geological Survey GQ Map 667, scale 1:24,000.
Porter, S.C., 1971, Holocene eruptions of Mauna Kea Volcano, Hawaii: Science, v. 172, p. 375–377.
———1972, Buried caldera of Mauna Kea Volcano, Hawaii: Science, v. 175, p. 1458–1460.
———1973, Stratigraphy and chronology of late Quaternary tephra along the south rift zone of Mauna Kea Volcano, Hawaii: Geological Society of America Bulletin, v. 84, p. 1923–1940.
———1975, Late Quaternary glaciation and tephrochronology of Mauna Kea, Hawaii: Royal Society of New Zealand Bulletin 13, p. 247–251.
———1979, Quaternary stratigraphy and chronology of Mauna Kea, Hawaii: A 380,000-yr record of mid-Pacific volcanism and ice-cap glaciation: Summary: Geological Society of America Bulletin, v. 90, p. 609–611.
———1979, Hawaiian glacial ages: Quaternary Research, v. 12, p. 161–187.
Porter, S.C., Stuiver, Minze, and Yang, I.C., 1977, Chronology of Hawaiian glaciations: Science, v. 195, p. 61–63.
Woodcock, A.H., Rubin, Meyer, and Duce, R.A., 1966, Deep layer of sediments in alpine lake in the tropical mid-Pacific: Science, v. 154, p. 647–648

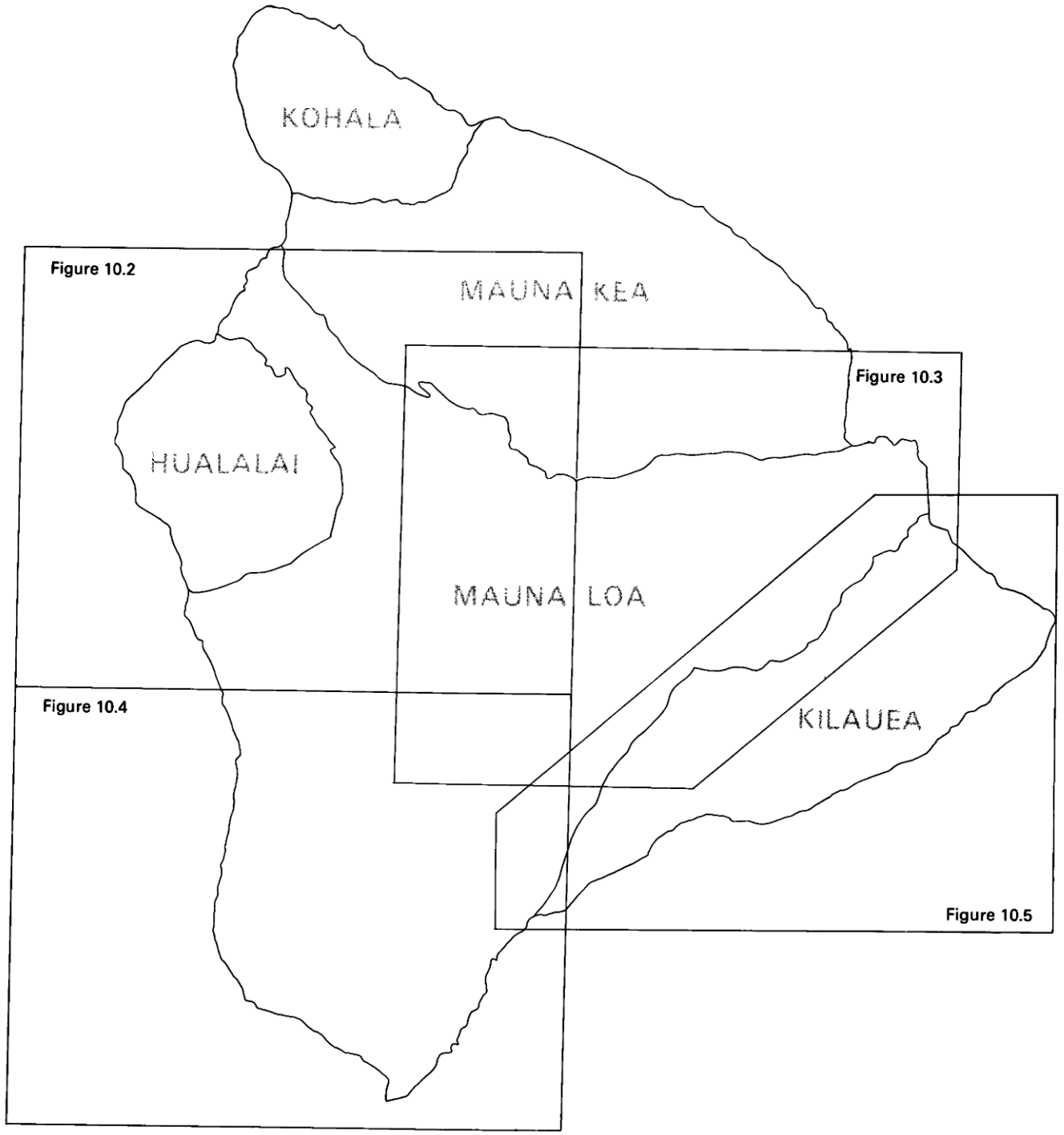

FIGURE 10.1.—Index map of Island of Hawaii showing areas covered by locality maps, figures 10.2.–10.5.

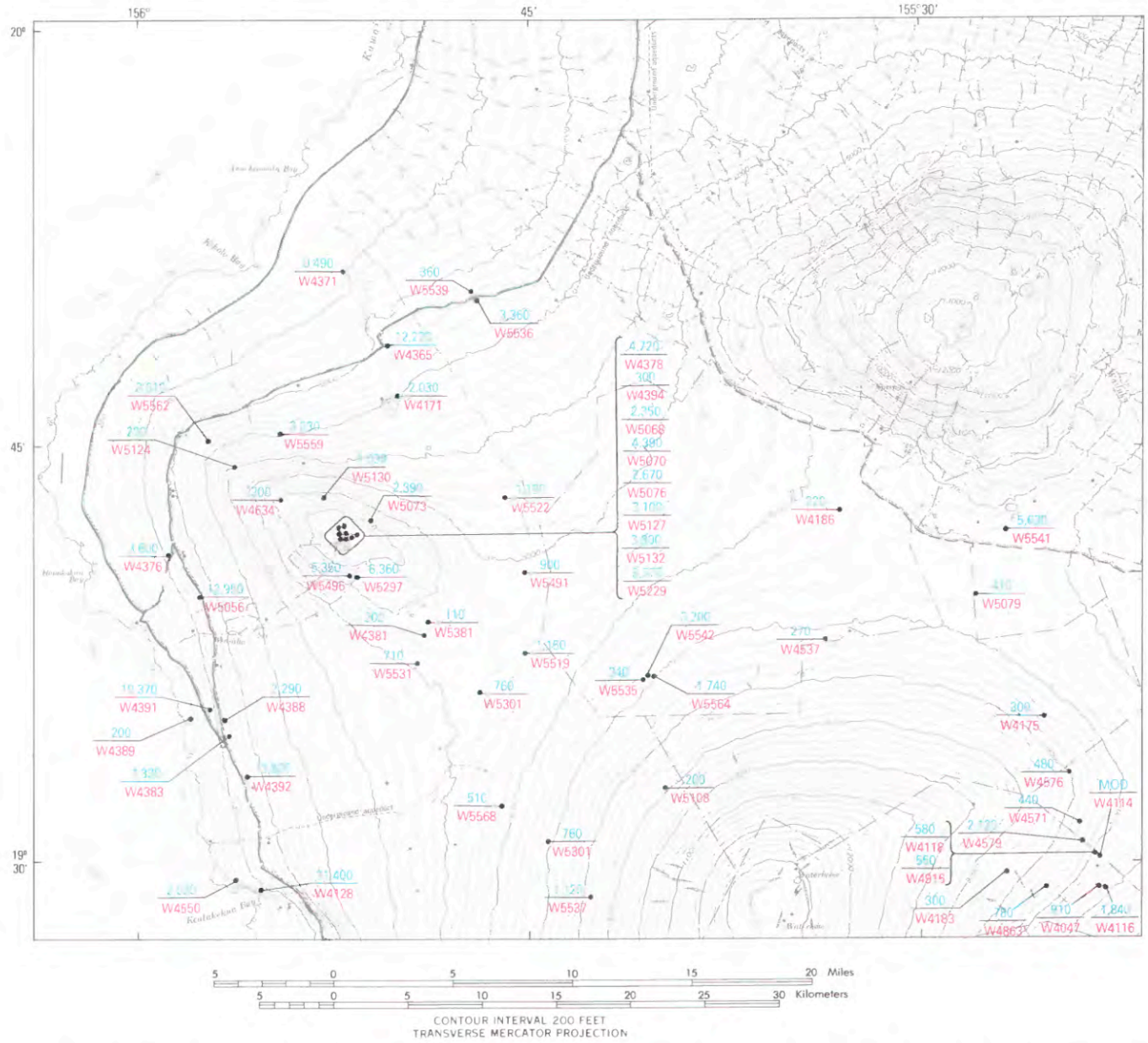

FIGURE 10.2.—Localities and ages of ^{14}C-dated samples on Hualalai Volcano and the northwestern part of Mauna Loa Volcano. Dots, sample localities; for each locality the ^{14}C age in years B.P. (blue) and the sample number (red) are given. For details of samples, see tables 10.1 and 10.3. MOD, modern.

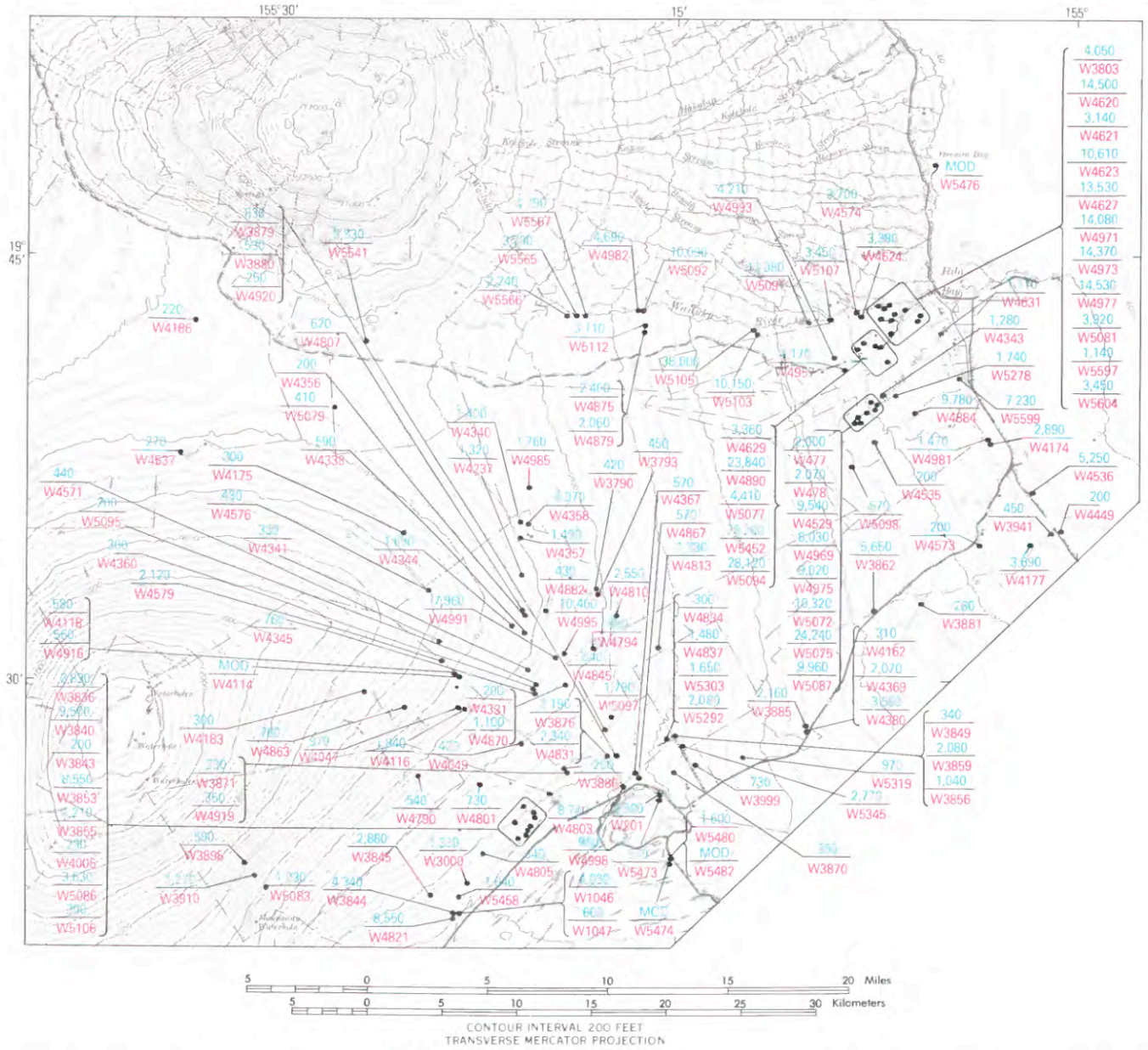

FIGURE 10.3.—Localities and ages of ^{14}C-dated samples on Mauna Kea Volcano, eastern part of Mauna Loa Volcano, and northwestern part of Kilauea Volcano. Dots, sample localities; for each locality the ^{14}C age in years B.P. (blue) and the sample number (red) are given. For details of samples, see tables 10.1, 10.2, and 10.4.

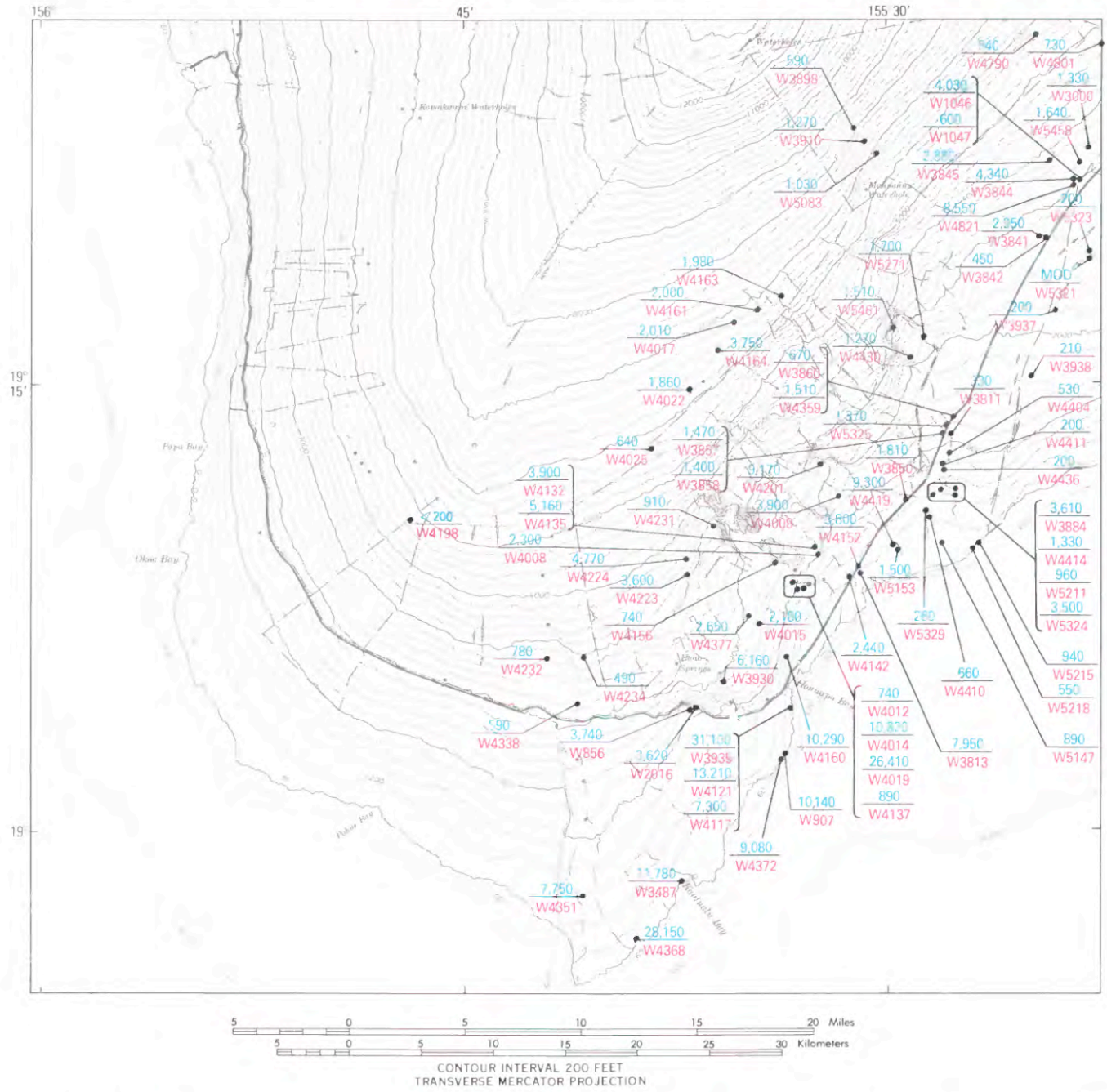
156°
45'
155°30'
19°15'
19°
Papa Bay
Okoe Bay
Pohue Bay
Kaaluhe Bay
Keamukuapaa Waterhole
Mauna Loa Weather Station
Hilo
Hawaiian Volcano Observatory
Kilauea Iki
Halemaumau
Crater
Kilauea Caldera
Chain of Craters Road
Hilina Pali Road
Kilauea Military Camp
Volcano
Kilauea Crater
Kilauea Iki Crater
Kilauea Iki Trail
Crater Rim Trail
Crater Rim Drive
Byron Ledge
Uwekahuna Bluff
Uwekahuna
Keanakakoi Crater
Keanakakoi Trail
Keanakakoi Ridge
Kilauea Overlook
Kilauea Visitor Center
Volcano House
Volcano Golf Course
Volcano Art Center
Volcano Village
Volcano Post Office
Volcano Elementary School
Volcano Community Hall
Volcano Community Church
Volcano Chapel
Volcano Cemetery
Volcano Airport
Volcano Airport Road
Volcano Road
Mauna Loa Road
Mauna Loa Trail
Mauna Loa Observatory
Mauna Loa Weather Observatory
Mauna Loa Trail
Mauna Loa Trail
Mauna Loa Trail

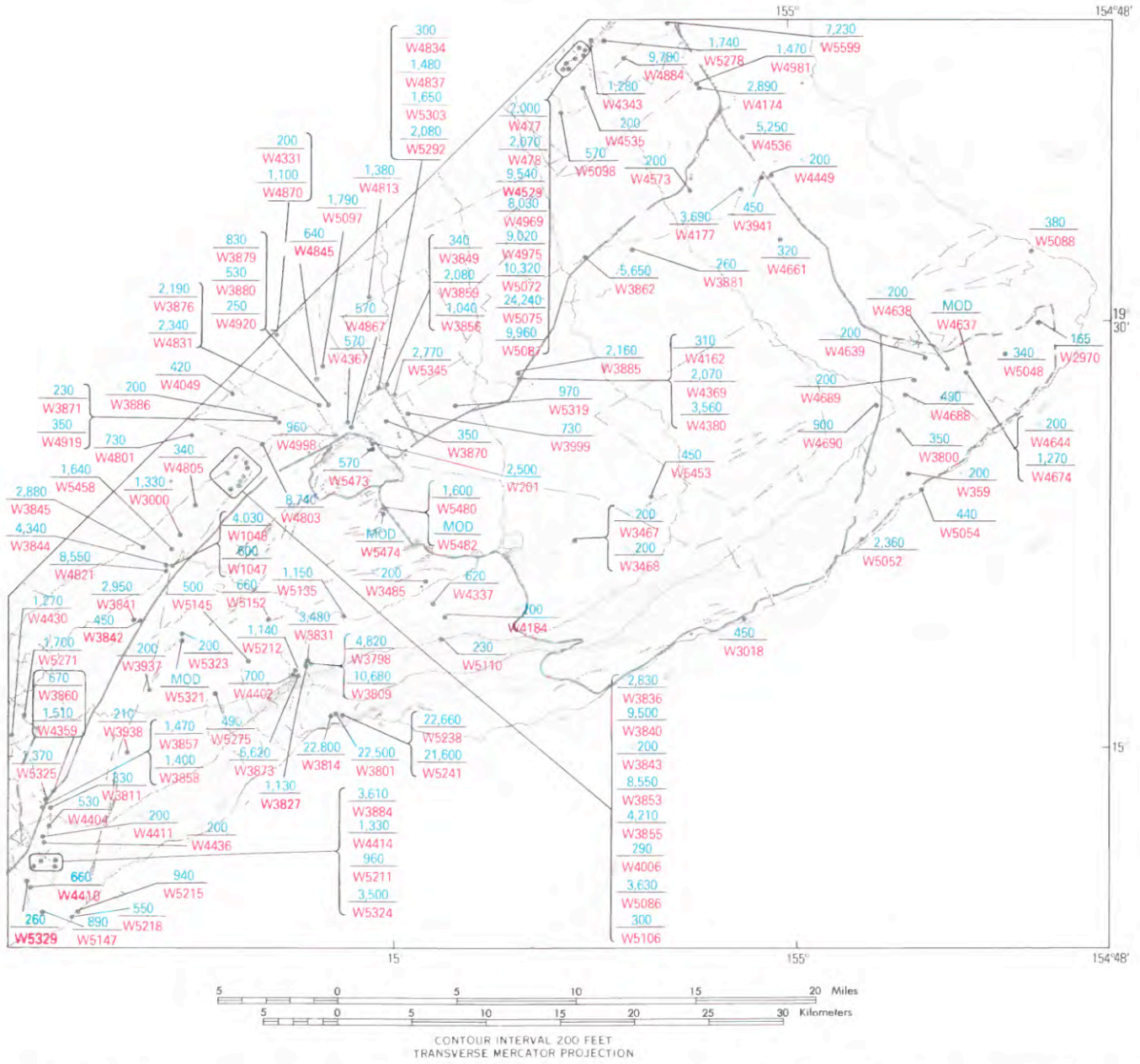

FIGURE 10.5.—Localities and ages of ^{14}C-dated samples on Kilauea Volcano and southeastern part of Mauna Loa Volcano. Dots, sample localities; for each locality the ^{14}C age in years B.P. (blue) and the sample number (red) are given. For details of samples, see tables 10.1 and 10.2.

TABLE 10.1—*Radiocarbon dates from Mauna Loa Volcano, Island of Hawaii*

[Samples listed in order of increasing age; uncertainty is one standard deviation, ± 1σ; modern age means sample is younger than AD 1950; ML = Mauna Loa; MK = Mauna Kea; mauka = toward the mountain, makai = toward the sea; see figs. 10.2–10.4 for localities. Stratigraphic nomenclature from Langenheim and Clague (chapter 1, part II)]

Sample	Radiocarbon age (years before present)	Location (latitude, longitude, quadrangle)	Elevation (m)	Sample and site description	Collector
W4114	Modern	19°30'09" 155°23'10" Puu Ulaula	2,070	Root fragments under margin of aa, Keamoku flow, 800 m N. of end of Strip Rd., 300 m E. of Puu Ulaula Trail.	J. P. Lockwood
W-3843	<200	19°24'32" 155°20'37" Kilauea Crater	1,050	Charcoal root fragments from Pahala Ash below flow of Kipuka Maunaiu, at head of gully, along contact with Keamoku flow, Chaikea Rd.	P. W. Lipman
W4198	<200	19°10'28" 155°46'37" Papa	1,481	Charcoal fragments along basal aa, at edge of Manuka flow, resting on pumice blanket from Hapaimanu, N. end of prominent kipuka, NW. of Pohakuloa.	P. W. Lipman
W4331	<200	19°29'52" 155°19'07" Kilauea Crater	1,542	Charcoal rootlets, in soil at base of pahoehoe, E. Keamoku flow, overlain by grey tube-fed pahoehoe, Puu Oo Trail, Keauhou Ranch Rd. pit, 4 km SE. of Keawewai Camp.	J. P. Lockwood
W4356	<200	19°32'20" 155°20'44" Kulani	1,913	Charcoal, at base of large tree mold, Solomon's Water Hole flow, overlain by aphanitic tube-fed pahoehoe, Powerline Rd., between pole 103 and 104.	J. P. Lockwood
W4411	<200	19°12'22" 155°28'02" Pahala	238	Charcoal roots under aa clinkers at edge of flow, SE. of Highway 11, NE. of Paauau Gulch.	N. G. Banks
W-4535	<200	19°38'31" 155°07'35" Piihonua	337	Charcoal roots, in red-orange sub-laterite soil, young Ainaola pahoehoe flow, overlain by very fine crystalline, near aphanitic dark grey pahoehoe, drainage ditch 10 m S. of Ainaola Dr.	J. P. Lockwood
W-5095	<200	19°29'46" 155°20'39" Kilauea Crater	1,684	Charcoal rootlets from edge of Keamoku flow, NW. of Kipuka Kekake, Powerline Rd., pole 140.	J. P. Lockwood
W5108	<200	19°30'42" 155°44'24" Puu O Uo	2,082	Charcoal twigs from Puu O Uo flow, along S. margin of the flow near uppermost ohia forest, 5 km WNW. from summit of Puu O Uo.	J. P. Lockwood
W-4186	220±60	19°42'41" 155°33'09" Puu Koli	1,914	Charcoal, beneath thin pahoehoe toes at contact with old MK aa around small kipuka, Red Leg Trail, 5 km SSE. of Pohakuloa cabins.	J. P. Lockwood
W3871	230±60	19°26'44" 155°19'07" Kilauea Crater	1,281	Charcoal roots in ash below Keamoku aa flow, from roadcuts in Kipuka Ki.	J. P. Lockwood
W4920	250±70	19°27'48" 155°17'04" Kilauea Crater	1,250	Charcoal (rerun of W-3879, age 830±60).	J. P. Lockwood
W5329	260±200	19°10'52" 155°28'41" Pahala	85	Charcoal, from soil beneath pahoehoe overlying Pahala Ash, top of Pahala section, at base of cliff below Puu Kalea.	N. G. Banks
W4537	270±60	19°37'49" 155°33'43" Puu Koli	2,243	Charcoal roots beneath aa margin of Keamuku flow, 3 km NNE. of Puu Kokoolau.	J. P. Lockwood

TABLE 10.1.—*Radiocarbon dates from Mauna Loa Volcano, Island of Hawaii*—Continued

Sample	Radiocarbon age (years before present)	Location (latitude, longitude, quadrangle)	Elevation (m)	Sample and site description	Collector
W4006	290±70	19°24'44" 155°20'33" Kilauea Crater	1,095	Charcoal roots in Pahala Ash, underlying Kipuka Maunaiu flow, Ohaikea Rd.	P. W. Lipman
W4183	300±60	19°29'44" 155°26'40" Kipuka Pakekake	2,550	Charcoal, SW. margin of prominent red pahoehoe kipuka on W. margin of Kau 1880 flow.	J. P. Lockwood
W4360	300±60	19°39'37" 155°20'41" Kilauea Crater	1,676	Charcoal underlying marginal blocks of aa, Keamoku flow, Powerline Rd., pole 142.	J. P. Lockwood
W4175	300±50	19°35'12" 155°25'17" Puu Ulaula	2,292	Charcoal underlying dark grey aa, Puu Kupanaha flow, overlain by 1880 lavas, Kulani-Mauna Loa Observatory Rd.	J. P. Lockwood
W5106	300±80	19°24'58" 155°20'59" Kilauea Crater	1,166	Coarse charcoal roots, beneath tree mold in base of flow, Lacey Cesspool picrite-rich flow overlain by basalt of Kipuka Maunaiu, Peter Lee Rd.	J. P. Lockwood
W4238	300±70	19°04'17" 155°40'57" Kahuku Ranch	688	Charcoal root fragments in olivine-rich pahoehoe, Puu Lokuana.	P. W. Lipman
W4341	330±60	19°30'29" 155°20'36" Kulani	1,766	Charcoal rootlets under aa at margin of pahoehoe flow, Puu Kulua flow, lowest unit in Keamoku suite, Powerline Rd., 1.6 km S. of Keawewai Camp.	J. P. Lockwood
W4805	340±60	19°23'50" 155°22'16" Kilauea Crater	1,155	Charcoal rootlets beneath thin edge of fresh pahoehoe flow, Ke A Poomoku Ohaikea, 3 m mauka of Powerline Rd.	J. P. Lockwood
W5535	340±150	19°36'14" 155°40'36" Puu O Uo	2,137	Charcoal roots at margin of loose shelly pahoehoe, under radial vent surrounded by 1859 lava.	J. P. Lockwood
W4919	350±70	19°26'44" 155°19'07" Kilauea Crater	1,281	Charcoal (rerun of W-3871, age 230±60).	P. W. Lipman
W5539	360±150	19°50'23" 155°47'23" Puu Anahulu	710	Bush fragments at basal contact of 1859 aa flow, Mamalahoa Highway, 37 km NE. of Kailua.	J. P. Lockwood
W5079	410±60	19°32'37" 155°27'56" Puu Oo	2,059	Charcoal roots in pocket of ash beneath thin pahoehoe toe above picrite, Humuulu flow, overlain by 1855 flow, 1 km E. of Mauna Loa Observatory Rd.	J. P. Lockwood
W4049	420±70	19°27'47" 155°20'48" Kilauea Crater	1,498	Vitreous charcoal from Keamoku flow, upper unit, underlying thin outlier of aa.	J. P. Lockwood
W3790	420±70	19°33'15" 155°18'04" Kulani	1,574	Charcoal from thin soil, developed on old spatter, underlying Kulani picrite, on high-standing dry hillock.	J. P. Lockwood
W4882	430±70	19°32'28" 155°19'54" Kulani	1,795	Coarse charcoal fragments in a horizontal tree mold at margin of tube-fed pahoehoe Kulaloa flow, Kilauea Forest Reserve lobe, overlain by Kulani picrite, 200 m SW. of Kilauea Forest Reserve Boundary Rd.	J. P. Lockwood

TABLE 10.1.—*Radiocarbon dates from Mauna Loa Volcano, Island of Hawaii*—Continued

Sample	Radiocarbon age (years before present)	Location (latitude, longitude, quadrangle)	Elevation (m)	Sample and site description	Collector
W4571	440±70	19°31'08" 155°23'42" Puu Ulaula	2,268	Charcoal rootlets beneath margin of aa breccia, W. Keamoku flow, 1.3 km NE. of Puu Ulaula Trail.	J. P. Lockwood
W3793	450±60	19°33'15" 155°18'07" Kulani	1,574	Charcoal from water-saturated spatter underlying 2 m of Kulani picrite.	J. P. Lockwood
W4576	480±60	19°33'19" 155°24'15" Puu Ulaula	2,414	Charcoal roots beneath Mauna Loa Boys' School flow, at crescent-shaped spatter cone, 1 km ENE. of Puu Kulua.	J. P. Lockwood
W4243	490±80	19°05'49" 155°40'43" Kahuku Ranch	829	Charcoal fragments in dirt and ash adjacent to flow margin, underlying aa containing small phenocrysts of plagioclase and olivine, Akihi.	J. P. Lockwood
W5568	510±150	19°31'52" 155°46'08" Puu Lehua	1,762	Vitreous twigs and fine rootlets, under slabby pahoehoe fragments at outer margin of thin pahoehoe squeeze-out, N. margin of Puu O Uo flow, 250 m NW. of prominent kipuka.	J. P. Lockwood
W3880	530±60	19°27'48" 155°17'04" Kilauea Crater	1,250	Organic debris and sooty soil directly underlying ropy pahoehoe.	J. P. Lockwood
W4790	540±70	19°26'25" 155°24'07" Kipuka Pakekake	1,609	Charcoal rootlets, Ke A Poomoku pahoehoe flow, W. edge of fresh flow, 1.3 km S. of National Park boundary, 700 m SE. of prominent rockwall.	J. P. Lockwood
W4916	560±70	19°30'11" 155°23'10" Puu Ulaula	2,079	Charcoal (rerun of W-4118, age 580±80).	J. P. Lockwood
W5098	570±60	19°37'37" 155°08'28" Piihonua	463	Charcoal twigs and roots, in muddy ash layer between Kulaloa and Panaewa pahoehoe flows, off Kulaloa Rd., Waiakea Homesteads.	J. P. Lockwood
W4367	570±70	19°26'33" 155°16'29" Kilauea Crater	1,238	Charcoal under basalt flow on Volcano Golf Course, Keamoku flow, 50 m W. of third green on golf course.	R. B. Moore
W4118	580±80	19°30'11" 155°23'10" Puu Ulaula	2,079	Charcoal from younger phase of Keamoku flow.	J. P. Lockwood
W4338	590±50	19°31'43" 155°20'48" Kulani	1,887	Coarse charcoal fragments from tree mold at margin of aa flow, Keawewai Camp flow, Powerline Rd., pole 112.	J. P. Lockwood
W3898	590±70	19°23'25" 155°30'53" Mauna Loa	2,428	Charcoal from pocket of baked ash, very young precaldera aa flow, Ainapo Trail.	J. P. Lockwood
W1047	600±250	19°21'54" 155°23'06" Wood Valley	910	Charcoal fragments in sandy ash, top of Pahala Ash, just below black sandy ash, Kaoiki Pali.	G. A. Macdonald
W4807	620±70	19°32'22" 155°20'44" Kulani	1,917	Charcoal roots in ash pockets of picrite-rich aa, at contact with aphanitic pahoehoe, Solomon's Water-hole flow, Powerline Rd., between pole 103 and 104, Puu Oo Trail.	J. P. Lockwood
W4025	640±45	19°13'09" 155°37'54" Puu Keokeo	1,774	Charcoal fragments at base of Pohina flow, where it rests on Pahala Ash at edge of Na Manua Haalou Swamp.	J. P. Lockwood

TABLE 10.1.—*Radiocarbon dates from Mauna Loa Volcano, Island of Hawaii*—Continued

Sample	Radiocarbon age (years before present)	Location (latitude, longitude, quadrangle)	Elevation (m)	Sample and site description	Collector
W4845	640±70	19°28'17" 155°17'44" Kilauea Crater	1,349	Charcoal rootlets in soot, beneath thick pahoehoe toe, Keamoku flow, Keauhou Ranch, Golf Course lobe.	J. P. Lockwood
W4410	660±70	19°10'37" 155°28'37" Pahala	53	Charcoal roots in Pahala Ash just below lava basalt flow, stream bed, Kanenelu flat, Hionamoa Gulch.	N. G. Banks
W4801	730±70	19°26'20" 155°22'21" Kilauea Crater	1,442	Charcoal fragments and soot, from small bush molds, upper part of deep ash below pahoehoe toe, picrite-rich Kipuka Maunaiu pahoehoe, overlying Ke A Poomoku flow, 1.5 km mauka of Powerline Rd.	J. P. Lockwood
W4156	740±60	19°09'02" 155°33'56" Punaluu	473	Charcoal roots from ash at base of Kipuka Nene flow, exposed in pothole along Hilea Gulch.	P. W. Lipman
W4012	740±60	19°08'17" 155°33'08" Punaluu	305	Charcoal roots from ash underlying thin variable-olivine pahoehoe flow at Kipuka Nene, Hilea Gulch.	P. W. Lipman
W5301	760±100	19°35'46" 155°47'11" Puu Lehua	1,561	Charcoal in soil on Hualalai cinder cone, overrun by picritic ML flow, 1 km NE. of Kanahaha.	R. B. Moore
W4345	760±70	19°29'34" 155°20'37" Kilauea Crater	1,661	Charcoal rootlets beneath thin pahoehoe lobe, Powerline Rd., pole 142.	J. P. Lockwood
W4232	780±70	19°05'41" 155°42'09" Kahuku Ranch	780	Small sparse hard charcoal, in thin marginal aa near its base, where lapping onto pumice from Kahuku picrite cone.	P. W. Lipman
W4863	780±70	19°29'12" 155°25'08" Kipuka Pakekake	2,254	Charcoal roots in discontinuous soil above picrite-rich aa where overlain by thin aphanitic tube-fed pahoehoe and vesicular aa, overlain by 1880 and Ke A Poomoku flows, E. margin of small kipuka 400 m ESE. of 1880 lobe distal end.	J. P. Lockwood
W3879	830±60	19°27'48" 155°17'04" Kilauea Crater	1,250	Charcoal from flaky roots in Pahala Ash, 15 cm beneath ropy pahoehoe.	J. P. Lockwood
W4794	880±60	19°31'11" 155°18'06" Kulani	1,533	Tiny vitreous fragments of ohia leaves and twigs in soot, from overlying tree canopy knocked off by falling spatter, Olaa Uka flow, dense rain forest in gully on S. edge of Kulani Cone.	J. P. Lockwood
W4137	890±60	19°08'30" 155°33'17" Punaluu	381	Charcoal roots from lens of Pahala-like ash, below thin olivine-rich pahoehoe, Kipuka Nene flow, Hilea Gulch.	P. W. Lipman
W4047	910±70	19°29'15" 155°23'11" Kipuka Pakekake	1,934	Charcoal under olivine-rich aa flow.	J. P. Lockwood
W4231	910±60	19°10'17" 155°36'05" Punaluu	878	Charcoal roots in Pahala Ash, underlying olivine-rich pahoehoe, and overlying phenocryst-poor aa, stream bed, Hilea Gulch gauging station.	P. W. Lipman

TABLE 10.1.—*Radiocarbon dates from Mauna Loa Volcano, Island of Hawaii*—Continued

Sample	Radiocarbon age (years before present)	Location (latitude, longitude, quadrangle)	Elevation (m)	Sample and site description	Collector
W5083	1,030±60	19°22'50" 155°30'17" Mauna Loa	2,091	Elongate charcoal fragments, beneath thin Keamoku pahoehoe toes, overlying discontinuous ash, Lower Ainapo Trail.	J. P. Lockwood
W4870	1,100±70	19°29'52" 155°19'07" Kilauea Crater	1,542	Coarse charcoal root fragments underlying thick pahoehoe, overlain by Keamoku flow, Puu Oo Trail, Keauhou Ranch Rd.	J. P. Lockwood
W4631	1,110±60	19°42'23" 155°05'10" Hilo	41	Charcoal roots underlying pahoehoe with round vesicles, at top of stream deposit, overlying thin Kulaloa pahoehoe flow, Waiakea Stream, S. of Kumakoa St. bridge.	J. M. Buchanan-Banks
W5537	1,120±200	19°28'44" 155°42'38" Sulphur Cone	2,499	Charcoal rootlets in small ash pocket below narrow young aphanitic pahoehoe toes, 2.8 km SW. of Puu O Uo.	J. P. Lockwood
W5597	1,140±300	19°42'50" 155°05'56" Hilo	67	Scattered charcoal fragments in ash deposit, overlain by Kinoole aa, Alenaio Stream at tributary E. of Komohana Street.	J. M. Buchanan-Banks
W5519	1,150±200	19°37'28" 155°45'22" Puu Lehua	1,649	Charcoal in soil on picritic pahoehoe, under young pahoehoe, SE. of Ahu a Umi Heiau.	R. B. Moore
W3910	1,270±60	19°23'22" 155°33'45" Mauna Loa	2,318	Charcoal in ash pocket underlying tree mold in tube-fed late prehistoric pahoehoe flow, Ainapo Trail, ML S. flank.	J. P. Lockwood
W4430	1,270±70	19°16'03" 155°29'06" Wood Valley	689	Charcoal roots in soil and ash below lava flow, overlain by crystal-poor pahoehoe, Pelelilii Gulch.	N. G. Banks
W4343	1,280±70	19°40'11" 155°07'20" Hilo	232	Charcoal roots beneath thin pahoehoe flow, young Waiakea-Uka pahoehoe, Waiakea-Uka School.	J. P. Lockwood
W4237	1,320±50	19°33'47" 155°20'42" Kulani	1,884	Vitreous narrow rootlets under pahoehoe toes, overlying weathered phenocryst-rich aa kipuka, and overlain by Kulani picrite.	J. P. Lockwood
W3000	1,330±70	19°22'29" 155°22'33" Wood Valley	915	Organic debris and charcoal, at uppermost part of yellow ash section, overridden by ML pahoehoe, Kaoiki Pali.	R. I. Tilling
W5325	1,370±200	19°13'55" 155°27'59" Pahala	389	Charcoal roots in soil and in ash and pahoehoe, Highway 11, Piukea Gulch.	N. G. Banks
W4813	1,380±60	19°31'08" 155°15'53" Kulani	1,297	Soot with scattered fragments of fern leaves, in deep ash above old spatter, under fresh spatter covered by fountain-fed pahoehoe, Olaa Uka flow, one day's hike S. of Stainback Highway.	J. P. Lockwood
W3858	1,400±60	19°13'26" 155°27'56" Pahala	457	Carbonized wood fragments (ohia lehu) in Pahala Ash, beneath young prehistoric ML pahoehoe flow, Kaalaala Gulch.	P. W. Lipman

TABLE 10.1.—*Radiocarbon dates from Mauna Loa Volcano, Island of Hawaii*—Continued

Sample	Radiocarbon age (years before present)	Location (latitude, longitude, quadrangle)	Elevation (m)	Sample and site description	Collector
W4340	1,400±70	19°35'43" 155°20'52" Kulani	1,779	Charcoal rootlets imbedded in soot at base of pahoehoe, overlain by nearly aphanitic tube-fed pahoehoe, overlain by 1942 aa, 1 km NW. of Mauna Loa Boys' School.	J. P. Lockwood
W4981	1,470±50	19°38'34" 155°03'23" Hilo	110	Charcoal rootlets in unoxidized pocket of older, coarse grey-black aa at base of Panaewa picrite flow, Allied Aggregates Quarry.	J. P. Lockwood
W3857	1,470±60	19°13'26" 155°27'56" Pahala	457	Charcoal fragments beneath young prehistoric ML pahoehoe flow, Kaalaala Gulch.	P. W. Lipman
W4357	1,490±50	19°35'03" 155°20'52" Kulani	1,812	Charcoal roots in soil beneath aphanitic pahoehoe, with uniform-size, spherical vesicles, 1 km E. of Mauna Loa Boys' School.	J. P. Lockwood
W5153	1,500±70	19°09'48" 155°27'46" Pahala	53	Charcoal roots in soil and ash under pahoehoe, Punaluu Gulch.	N. G. Banks
W5461	1,510±110	19°17'02" 155°29'50" Wood Valley	963	Charcoal roots in sooty zone at top of Pahala Ash, young Upper Wood Valley pahoehoe, overlies section exposed on Wood Valley headwall, Kapapala Ranch Water Tunnel Trail.	J. P. Lockwood
W5458	1,640±150	19°22'16" 155°22'49" Wood Valley	920	Charcoal roots in black sooty ash at top of Pahala Ash, Halfway House olivine-rich pahoehoe, Peter Lee Rd. and Highway 11 junction, 2 m above base of Kaoiki Pali, in fresh slump.	J. P. Lockwood
W4344	1,690±70	19°31'57" 155°21'13" Kulani	1,963	Large charcoal roots underlying marginal blocks of aa above old spatter on this mostly buried spatter cone, Powerline Rd., 5.5 km SW. of Kulani Prison Headquarters.	J. P. Lockwood
W5271	1,700±80	19°27'58" 155°48'14" Wood Valley	?	Charcoal rootlets in ash under pahoehoe, upper crossover of water-course along E. edge of Wood Valley.	N. G. Banks
W5278	1,740±100	19°40'12" 155°36'52" Hilo	201	Charcoal twigs and roots in pockets at top of ash deposit overlying aa, overlain by young pahoehoe flow, Kukuau flow, Waiakea Stream, N. of Hoaka Rd.	J. M. Buchanan-Banks
W5564	1,740±250	19°36'36" 155°40'17" Puu O Uo	2,140	Charcoal roots beneath thin pahoehoe sheets, W. of eastern 1859 lobe, 500 m SE. of P.T.A. Bobcat Trail.	J. P. Lockwood
W4985	1,760±60	19°36'49" 155°20'26" Kulani	1,666	Charcoal fragments beneath pahoehoe toes in ash pockets of aa, overlain by Punahoa flow, N. of 1942 flow, Powerline Rd.	J. P. Lockwood
W3850	1,810±80	19°11'14" 155°29'09" Pahala	137	Charcoal in Pahala Ash, overlain by phenocryst-poor ML pahoehoe from SW. rift zone, Moaula Gulch.	P. W. Lipman
W4116	1,840±60	19°29'10" 155°23'08" Kipuka Pakekake	1,940	Charcoal from thin soil at contact of pahoehoe and aa.	J. P. Lockwood

TABLE 10.1.—*Radiocarbon dates from Mauna Loa Volcano, Island of Hawaii*—Continued

Sample	Radiocarbon age (years before present)	Location (latitude, longitude, quadrangle)	Elevation (m)	Sample and site description	Collector
W4022	1,860±70	19°14'56" 155°36'50" Punaluu	1,891	Charcoal fragments at base of plagioclase porphyritic aa flow, Punaluu Kahawai.	P. W. Lipman
W4163	1,980±80	19°18'01" 155°33'43" Keaiwa Reservoir	2,036	Charcoal roots in Pahala Ash, at base of flow, underlying phenocryst-poor aa flow, collected where aa cascaded through small lava tube, Kauhuhuula Gulch.	P. W. Lipman
W4161	2,000±70	19°17'47" 155°34'12" Keaiwa Reservoir	2,060	Charcoal fragments from basal Hionamoa flow, a large phenocryst-poor unit, head of Makaka Ravine.	P. W. Lipman
W477	2,000±250	19°39'45" 155°08'06" Hilo	244	Charcoal of ohia buried in cinders of prehistoric vent of the last group of lavas of ML, Kau volcanic series, Waiakea Homesteads.	G. A. Macdonald
W4017	2,010±70	19°17'10" 155°35'24" Keaiwa Reservoir	2,074	Charcoal fragments from Pahala-like ash, underlying weathered phenocryst-poor pahoehoe, Hionamoa Gulch.	P. W. Lipman
W4550	2,030±60	19°29'13" 155°56'17" Honaunau	61	Carbonaceous soil underlying glassy pahoehoe flow and overlying the entire Kealakekua Pali sequence, Captain Cook Monument, Kaawaloa, Kealakekua Bay.	J. P. Lockwood
W478	2,070±250	19°39'45" 155°08'06" Hilo	244	Charcoal of tree fern, Kau Basalt, Waiakea Homesteads.	G. A. Macdonald
W4579	2,120±70	19°30'32" 155°23'45" Puu Ulaula	2,213	Charcoal roots beneath pahoehoe toes, overlain by all Keamoku flow units, Upper Strip Rd. pahoehoe, 250 m NE. of Puu Ulaula.	J. P. Lockwood
W4015	2,180±60	19°07'04" 155°34'28" Naalehu	534	Charred log, base of young aa flow containing large olivine phenocrysts.	P. W. Lipman
W3876	2,190±70	19°27'50" 155°17'36" Kilauea Crater	1,256	Charcoal from root underlying ML NE. rift aa flow, covering Pahala Ash on E. extension of Kaoiki fault, Puu Oo Trail.	J. P. Lockwood
W5566	2,240±150	19°42'07" 155°23'25" Puu Oo	1,742	Charcoal root fragments overlain by Puu Kahiliku picrite-rich flow, deep gully in ash along cow path, 50 m E. of Puu Oo Ranch access road.	J. P. Lockwood
W4008	2,300±60	19°09'23" 155°32'26" Punaluu	316	Carbonized wood fragments in ash at base of the plagioclase-porphyritic aa flow in the Ninole Gulch area, one of the last flows from this sector of ML to flow into ocean.	P. W. Lipman
W4831	2,340±70	19°27'50" 155°17'36" Kilauea Crater	1,256	Charcoal root in sooty ash, under Keauhou Ranch aa flow, overlain by all Keamoku flows, junction of Puu Oo Rd. and Kaoiki Pali.	J. P. Lockwood
W4142	2,440±60	19°08'36" 155°31'19" Punaluu	53	Charcoal fragments in Pahala-like ash, base of Ninole aa flow, Ninole Gulch.	P. W. Lipman

TABLE 10.1.—*Radiocarbon dates from Mauna Loa Volcano, Island of Hawaii*—Continued

Sample	Radiocarbon age (years before present)	Location (latitude, longitude, quadrangle)	Elevation (m)	Sample and site description	Collector
W4810	2,550±80	19°32'06" 155°17'20" Kulani	1,448	Charcoal and rootlets in organic mat at base of pahoehoe toes, overlain by dense tube-fed pahoehoe, N. of Kulani Cone, 2.5 km S. of Stainback Highway, Kulani Prison boundary road, S. of prominent picrite exposures.	J. P. Lockwood
W4377	2,650±50	19°07'04" 155°34'28" Naalehu	533	Carbonized wood fragment at base of olivine-rich aa flow, Kaalaiki quarry.	P. W. Lipman
W3836	2,830±60	19°26'28" 155°20'38" Kilauea Crater	1,064	Carbonaceous soil below aa of the Keamoku flow.	P. W. Lipman
W3845	2,880±70	19°22'20" 155°23'56" Wood Valley	1,083	Charcoal root fragments, top of Pahala Ash below olivine-rich ML pahoehoe flow, where draped over Kaoiki fault scarp, Kaoiki Pali.	P. W. Lipman
W4174	2,890±70	19°38'34" 155°02'53" Hilo	111	Amorphous sooty material underlying Panaewa flow, Hilo side of Allied Aggregates quarry.	J. P. Lockwood
W3841	2,950±80	19°20'02" 155°24'29" Wood Valley	793	Charcoal root fragments from Pahala Ash, overlain by olivine-rich pahoehoe, Puu Kuanene area.	P. W. Lipman
W5112	3,110±60	19°42'34" 155°16'22" Upper Piihonua	1,105	Charcoal rootlets in ash mixed with aa clasts at base of pahoehoe, overlain by upper Piihonua Punahoa flow, Wailuku River.	J. P. Lockwood
W4621	3,140±70	19°42'17" 155°07'01" Hilo	169	Charcoal root at contact between lava flow and ash deposit, overlain by pahoehoe with spherical vesicles, 698 Kaumana Dr.	J. M. Buchanan-Banks
W5542	3,200±200	19°36'25" 155°40'21" Puu O Uo	2,131	Charcoal roots beneath thick pahoehoe toes, overlain by Kaniku flow, Naiomamani Kipuka.	J. P. Lockwood
W4629	3,360±80	19°41'52" 155°07'29" Hilo	216	Charcoal roots beneath thin pahoehoe flow at contact with thick ash deposit, underlies 1880 flow and overlies ash, Waipahoehoe Stream, Ponahawai Homesteads, N. of Kaumana Dr.	J. M. Buchanan-Banks
W5536	3,360±200	19°50'47" 155°47'12" Puu Anahulu	756	Charcoal roots in basal aa breccia, under Mamalahoa Highway, Kaniku euhedral olivine laths with aa, Highway 190, E. of 1859 contact.	J. P. Lockwood
W4624	3,380±80	19°43'00" 155°08'08" Piihonua	256	Charcoal tree trunk in sealed tree mold, overlain by KPUA pahoehoe, Wailuku-Alenaio diversion canal, N. of Waianuenue Ave.	J. M. Buchanan-Banks
W5107	3,450±60	19°42'56" 155°09'11" Piihonua	299	Charcoal root at base of tree mold, Lauiole Falls pahoehoe, overlain by Waianuenue pahoehoe, Wailuku River, 20 m E. of Hilo County Water Department gauging ladder.	J. P. Lockwood
W5604	3,450±200	19°42'50" 155°05'56" Hilo	67	Charcoal (rerun of W-5081, age 3920±80).	J. M. Buchanan-Banks

TABLE 10.1.—*Radiocarbon dates from Mauna Loa Volcano, Island of Hawaii*—Continued

Sample	Radiocarbon age (years before present)	Location (latitude, longitude, quadrangle)	Elevation (m)	Sample and site description	Collector
W4223	3,600±70	19°08'41" 155°36'58" Punaluu	983	Charcoal roots in Pahala Ash, overlain by transitional aa-pahoehoe containing sparse large olivine and plagioclase phenocrysts, roadcut, Mountain House tunnel road.	P. W. Lipman
W2016	3,620±250	19°04'15" 155°36'52" Naalehu	326	Charcoal, depth 417 cm, underlying surface pahoehoe lava flow, Bishop Museum cesspool excavation, Waiohinu.	R. R. Doell
W5086	3,630±80	19°25'25" 155°20'50" Kilauea Crater	1,244	Charcoal roots in patches in unconsolidated oxidized ash, overlain by Upper Strip Rd. phenocryst-picrite pahoehoe, 1.9 km N. of Kapapala Ranch corral.	J. P. Lockwood
W4574	3,700±70	19°43'05" 155°08'18" Piihonua	263	Charcoal roots beneath young tube-fed pahoehoe, overlying massive olivine-rich aa, KPUA flow, Wailuku River, across from KPUA.	J. P. Lockwood
W856	3,740±250	19°04'00" 155°37'00" Naalehu	326	Charcoal, under pahoehoe flow in churchyard, Waiohinu.	K. J. Murata
W4164	3,750±70	19°16'02" 155°36'38" Keaiwa Reservoir	1,996	Charcoal fragments, base of aa flow which contains abundant small plagioclase phenocrysts, Puu Kinikini.	P. W. Lipman
W5565	3,790±200	19°42'56" 155°18'53" Upper Piihonua	1,314	Charcoal root fragments, at base of Wailuku River olivine-pahoehoe flow, S. bank of river, 500 m upstream from Water Gauging Station Trail.	J. P. Lockwood
W4152	3,800±90	19°08'53" 155°30'58" Punaluu	84	Charcoal fragments from thin lens of Pahala-like ash below transitional hummocky pahoehoe-aa flow, Highway 11 roadcut.	P. W. Lipman
W4009	3,900±80	19°11'22" 155°31'42" Punaluu	488	Carbonized wood, base of Punaluu aa flow, Punaluu Gulch.	P. W. Lipman
W4132	3,900±90	19°09'39" 155°32'33" Punaluu	372	Charcoal roots from thin lens of Pahala-like ash, below pahoehoe flow, Ninole Gulch.	P. W. Lipman
W5081	3,920±80	19°42'50" 155°05'56" Hilo	67	Charcoal from stream deposit between two pahoehoe flows, overlain by Kulaloa flow, Alenaio Stream at Komohana St.	J. M. Buchanan-Banks
W1046	4,030±350	19°21'54" 155°23'06" Wood Valley	911	Charcoal in sandy silty ash, top of Pahala Ash, Mamalahoa Highway, Kaoiki Pali.	G. A. Macdonald
W3803	4,050±50	19°42'48" 155°07'05" Hilo	152	Soil, rich in organic matter and containing bits of charcoal, from cesspool excavation, Kaumana area of Hilo.	J. P. Lockwood
W4358	4,070±70	19°35'41" 155°20'41" Kulani	1,762	Fine charcoal rootlets in sooty organic layer at base of Kulani pahoehoe, underlying thick lobe of pahoehoe, 1.2 km NW. of Mauna Loa Boys' School.	J. P. Lockwood
W4957	4,170±90	19°41'06" 155°08'46" Piihonua	354	Charcoal atop orange ash, Wilder Rd. pahoehoe, under Kulaloa flow, 400 m S. of Humuulu Saddle Rd.	J. P. Lockwood

TABLE 10.1.—*Radiocarbon dates from Mauna Loa Volcano, Island of Hawaii*—Continued

Sample	Radiocarbon age (years before present)	Location (latitude, longitude, quadrangle)	Elevation (m)	Sample and site description	Collector
W4993	4,210±80	19°41'29" 155°09'08" Piihonua	372	Charcoal exposed at base of pahoehoe by slumping of underlying ash along streambed, under Piihonua pahoehoe, W. of Akolea Rd., Kaliuiki Stream.	J. P. Lockwood
W3855	4,210±90	19°25'25" 155°20'22" Kilauea Crater	?	Charcoal from Pahala Ash, below phenocryst-poor aa flow draped on Kaoiki fault scarp.	P. W. Lipman
W3844	4,340±80	19°21'52" 155°23'16" Wood Valley	920	Charcoal fragments from soil zone below aa flow, draped over Kaoiki fault scarp.	P. W. Lipman
W5077	4,410±120	19°41'24" 155°07'12" Hilo	183	Vegetative mat beneath surficial pahoehoe at contact with underlying ash, overlain by Wilder Rd. pahoehoe, Brilhante property, Edita Rd.	J. M. Buchanan-Banks
W4982	4,690±60	19°43'07" 155°16'30" Piihonua	1,160	Charcoal from yellow-brown ash overlain by aa of MK hawaiite, N. bank of Wailuku River.	J. P. Lockwood
W4224	4,770±90	19°09'14" 155°36'59" Punaluu	1,044	Charcoal roots in Pahala Ash, overlain by phenocryst-poor pahoehoe flow, roadcut on Mountain House tunnel road.	P. W. Lipman
W5567	4,790±250	19°42'56" 155°18'30" Upper Piihonua	1,292	Charcoal root fragments in scattered pockets of soft MK ash at base of dense aphanitic aa of Upper Wailuku River, S. bank of river.	J. P. Lockwood
W4135	5,160±100	19°09'38" 155°32'33" Punaluu	369	Charcoal roots from thin layer of Pahala-like ash, overlain by phenocryst-poor pahoehoe flow, Ninole Gulch.	P. W. Lipman
W4536	5,250±100	19°36'40" 155°01'55" Mountain View	98	Large charcoal root, Puna Sugar Picrite aa, overlying yellow-red ash, 700 m SW. of plantation house, Keaau-Pahoa Rd.	J. P. Lockwood
W3862	5,650±90	19°32'34" 155°07'28" Mountain View	528	Charcoal fragments, top of Pahala-type ash overlain by young ML aa flow, SW. of Mountain View.	P. W. Lipman
W3930	6,160±110	19°25'05" 155°35'42" Naalehu	567	Charcoal root fragments in ash, overlain by transitional pahoehoe-aa ML flow, Alapai Gulch.	P. W. Lipman
W5599	7,230±230	19°40'48" 155°04'31" Hilo	76	Carbonaceous roots at top of ash layer, overlain by Malaai aa, Hilo Golf Course, drainage ditch N. of Haihai St.	J. M. Buchanan-Banks
W4117	7,300±100	19°04'19" 155°33'26" Naalehu	21	Carbonaceous soil from ash at base of top ML flow, bay S. of Kahukupoko Point.	P. W. Lipman
W4351	7,750±70	18°56'37" 155°40'48" Ka Lae	98	Charcoal and soil from top of Pahala Ash, along contact with flow in Kahawai Kolano gully, 0.6 km ENE. of Pacific Missile Range Facility.	J. P. Lockwood

TABLE 10.1.—*Radiocarbon dates from Mauna Loa Volcano, Island of Hawaii*—Continued

Sample	Radiocarbon age (years before present)	Location (latitude, longitude, quadrangle)	Elevation (m)	Sample and site description	Collector
W3813	7,950±110	19°08'45" 155°30'58" Punaluu	76	Black carbonaceous soil at top of Pahala Ash, Puehu quarry.	J. P. Lockwood
W4991	7,960±110	19°30'44" 155°19'36" Kulani	1,658	Charcoal rootlets at contact between Keauhou Ranch picrite and nearly buried spatter cone, middle of logging road, 900 m W. of Puu Lalaau.	J. P. Lockwood
W4969	8,030±70	19°39'16" 155°08'21" Piihonua	372	Organic matter in zones around aa clasts at base of D. Smith flow, Waiakea Stream, 1.9 km above Hoaka Rd. Bridge.	J. P. Lockwood
W4821	8,550±90	19°21'49" 155°23'18" Wood Valley	930	Rootlets and carbonaceous sooty ash, top of Pahala Ash, Halfway House picrite-rich pahoehoe that mantles Kaoiki Pali here, halfway up prominent gully at Old Halfway House.	J. P. Lockwood
W3853	8,550±100	19°25'11" 155°20'20" Kilauea Crater	1,122	Charcoal root fragments from soil zone, overlain by ML pahoehoe flow, interbedded with Pahala Ash, or reworked ash, Kaoiki Pali.	P. W. Lipman
W4803	8,740±100	19°26'08" 155°19'45" Kilauea Crater	1,219	Soft charcoal rootlets in soot below thick Strip Rd. pahoehoe, in prominent deep gully near National Park SW. boundary fence, 1.5 km SW. of Strip Rd. in Kipuku Ki.	J. P. Lockwood
W4975	9,020±130	19°39'38" 155°07'40" Piihonua	274	Charcoal rootlets in thin ash at base of flow, overlain by Puu Hoakalei picrite flow, Waiakea Stream, 500 m upstream from Hoaka Rd. bridge.	J. P. Lockwood
W4372	9,080±80	19°02'45" 155°33'32" Naalehu	37	Sooty soil at top of ash zone, Maniania Pali, overlain by olivine -rich pahoehoe, top of seacliff, 100 m NE. of contact with plagioclase -phyric flow.	P. W. Lipman
W4201	9,170±100	19°12'26" 155°32'17" Punaluu	652	Charcoal roots in Pahala Ash, overlain by phenocryst-poor pahoehoe flow, part of flow sequence from ML that laps out against eroded Ninole Hills, Upper Moaula Gulch.	P. W. Lipman
W4419	9,300±130	19°09'46" 155°29'51" Pahala	64	Charcoal roots in soil and ash below lava flow, under crystal-poor ML flow, in kipuka, Punaluu Gulch.	N. G. Banks
W3840	9,500±140	19°25'05" 155°24'29" Kilauea Crater	1,144	Charcoal rootlets and carbonaceous soil from Pahala Ash between two ML aa flows, draped over Kaoiki fault scarp, Kaoiki Pali.	P. W. Lipman
W4529	9,540±110	19°39'14" 155°08'22" Piihonua	379	Charcoal roots and wood fragments beneath capped tree mold, Old Waiakea Uka aphanitic pahoehoe, Waiakea Stream, between Hoaka and Ainaole Rds.	J. P. Lockwood
W4884	9,780±140	19°39'32" 155°06'03" Hilo	201	Charcoal tree root in thin ash deposit under plagioclase phyric pahoehoe, Waiakea Homesteads, streambed, Alaloa Rd.	J. M. Buchanan-Banks

TABLE 10.1.—*Radiocarbon dates from Mauna Loa Volcano, Island of Hawaii*—Continued

Sample	Radiocarbon age (years before present)	Location (latitude, longitude, quadrangle)	Elevation (m)	Sample and site description	Collector
W5087	9,960±70	19°39'19" 155°08'17" Piihonua	360	Charcoal in brown layer of thick yellow ash at base of pahoehoe, under very old pahoehoe of Waiakea Stream, 1.7 km upstream from Hoaka Rd. bridge.	J. P. Lockwood
W5092	10,090±120	19°43'06" 155°16'23" Upper Piihonua	1,097	Charcoal roots at base of Wailuku River pahoehoe, in ash deposit which overlies MK rocks, S. bank of Wailuku River.	J. P. Lockwood
W907	10,140±300	19°03'00" 155°35'00" Naalehu	61	Carbonaceous ash exposed in sea cliff, S. of Honuapu, top of Pahala Ash, which is underlain and overlain by basalt, Maniani Pali.	G. D. Fraser
W5103	10,150±80	19°42'23" 155°12'02" Piihonua	663	Coarse charcoal at base of tree mold, Upper Wailuku River young pahoehoe, under Punahoa flow, Wailuku River, 70 m above waterfall.	J. P. Lockwood
W4160	10,290±150	19°06'01" 155°33'34" Naalehu	186	Charcoal roots in Pahala Ash, overlain by phenocryst-poor pahoehoe flow, Honuapu.	P. W. Lipman
W5072	10,320±70	19°39'32" 155°07'51" Piihonua	305	Charcoal root beneath pahoehoe at contact with underlying ash deposit, overlain by D. Smith and University of Hawaii flows, Waiakea Stream in Waiakea-Uka, Kalana Place.	J. M. Buchanan-Banks
W4995	10,400±150	19°30'53" 155°19'11" Kulani	1,635	Root fragments under pahoehoe flow that overlies Puu Lalaau olivine-rich spatter, N. bank of water hole, 50 m NW. of Puu Lalaau.	J. P. Lockwood
W4623	10,610±150	19°43'24" 155°06'59" Hilo	140	Charcoal root at contact between lava rubble and ash, under Wailuku River channel aa, W. of Rainbow Falls.	J. M. Buchanan-Banks
W4014	10,820±90	19°08'18" 155°32'56" Punaluu	229	Charcoal roots in uppermost main Pahala Ash, near tree molds in overlying pahoehoe flow sequence, Hilea Gulch.	P. W. Lipman
W3487	11,780±100	18°58'18" 155°37'18" Ka Lae	5	Charcoal fragments in Pahala Ash overlain by an intercalated basalt flow, W. side of Kaaluala Bay, 9.2 km NE. of South Point.	J. P. Lockwood
W4121	13,210±190	19°04'20" 155°33'25" Naalehu	15	Carbonaceous soil from ash at base of middle flow sequence, bay S. of Kahukupoko Point.	P. W. Lipman
W4627	13,530±180	19°43'12" 155°06'32" Hilo	99	Crumbly rootlets at top of ash deposit at contact with overlying pahoehoe, Rainbow Falls intersection, Waianuenue Ave. and Kaumana Dr.	J. M. Buchanan-Banks
W4392	13,800±300	19°32'51" 155°55'57" Kealakekua	439	Charcoal from shrub in soil, on picritic basalt flow, under basalt flow from Hualalai in Honalo, E. side of Mamalahoa Highway.	R. B. Moore
W4971	14,080±150	19°43'14" 155°07'13" Hilo	162	Tree charcoal at contact between pahoehoe flow and basal ash, underlying picrite-porphyritic pahoehoe, parking lot of First Protestant Church, Waianuenue Ave.	J. M. Buchanan-Banks

TABLE 10.1.—*Radiocarbon dates from Mauna Loa Volcano, Island of Hawaii*—Continued

Sample	Radiocarbon age (years before present)	Location (latitude, longitude, quadrangle)	Elevation (m)	Sample and site description	Collector
W5091	14,080±160	19°42'41" 155°10'05" Piihonua	451	Charcoal roots at base of pahoehoe in kipuka of yellow ash, underlying Punahoa flow, Kahoama Stream, upstream from Wailuku River.	J. P. Lockwood
W4973	14,370±190	19°42'58" 155°07'25" Hilo	186	Charcoal tree root beneath pahoehoe flow at contact with underlying ash, overlain by porphyritic pahoehoe, Ainaloa Subdivision, Kaeokulani St.	J. M. Buchanan-Banks
W4620	14,500±200	19°45'20" 155°07'27" Hilo	163	Charcoal root at contact between ash unit and pahoehoe flows sequence, which underlies thick ash, saprolite, and lava from MK, Wailuku River.	J. M. Buchanan-Banks
W4977	14,530±120	19°43'05" 155°07'01" Hilo	146	Charcoal roots at contact between pahoehoe flow and underlying ash, overlain by picrite-porphyritic pahoehoe, Kaumana Springs, Waianuenue Ave.	J. M. Buchanan-Banks
W4894	21,900±270	19°39'32" 155°07'51" Piihonua	305	Charcoal root beneath pahoehoe in ash deposit, underlying picrite-rich and olivine-poor pahoehoe, Waiakea Stream in Waiakea-Uka, Kalana Place.	J. M. Buchanan-Banks
W4890	23,840±600	19°41'50" 155°07'25" Hilo	207	Charcoal root in ash deposit, between pahoehoe flows, Waipahoehoe Stream, Chong's Bridge.	J. M. Buchanan-Banks
W5075	24,240±500	19°39'40" 155°07'38" Piihonua	268	Charcoal roots beneath pahoehoe at contact with underlying ash deposit, underlies University of Hawaii and D. Smith aa flows, Waiakea Stream in Waiakea-Uka, Hoaka Rd.	J. M. Buchanan-Banks
W4019	26,410±390	19°08'19" 155°32'53" Punaluu	183	Thin carbonaceous mat, scraped from base of pahoehoe flow of the Ninole volcanic rocks, Hilea Gulch.	P. W. Lipman
W5094	28,120±400	19°41'53" 155°08'06" Piihonua	256	Charcoal rootlets at top of yellow ash, overlain by Punahoa flow, overlies old picrite-rich flow, Lower Kaluiiki Stream, 600 m W. of Chong's Bridge.	J. P. Lockwood
W4368	28,150±800	18°56'20" 155°38'50" Ka Lae	9	Carbonaceous soil under pahoehoe flow interlayered with main unit of Pahala Ash, sea cliff exposure, 75 m SW. of margin of Puu O Mahaua Cone.	P. W. Lipman
W5452	28,200±600	19°41'50" 155°08'14" Piihonua	287	Charcoal roots under aphanitic pahoehoe flow, Kaluiiki Stream.	J. P. Lockwood
W3935	31,100±900	19°04'16" 155°33'24" Naalehu	1.5	Charcoal roots in Pahala-like ash, at base of tree mold in overlying ML aa flow, base of sea cliff in bay S. of Kahukupoko Point.	P. W. Lipman
W4128	31,400±1,600	19°29'07" 155°55'53" Honaunau	5	Charcoal fragments in ash, overlain by small pahoehoe lobe of mainly aa flow, along prominent main ash bed exposed along Pali Kapu Keoua, Kealakekua scarp.	P. W. Lipman
W5105	>38,000	19°42'25" 155°12'06" Piihonua	664	Charcoal fragments at top of thick ash, overlain by Homelani ash, in turn overlain by Punahoa aphanitic pahoehoe, Upper Wailuku River.	J. P. Lockwood

TABLE 10.2—*Radiocarbon dates from Kilauea Volcano, Island of Hawaii*

[Samples listed in order of increasing age; uncertainty is one standard deviation, ± 1σ; modern age means sample is younger than AD 1950; ML = Mauna Loa; MK = Mauna Kea; mauka = toward the mountain, makai = toward the sea; see figs. 10.2–10.4 for localities. Stratigraphic nomenclature from Langenheim and Clague (chapter 1, part II)]

Sample	Radiocarbon age (years before present)	Location (latitude, longitude, quadrangle)	Elevation (m)	Sample and site description	Collector
W2999	Modern	19°24'18" 155°14'53" Volcano	1,166	Humus layer in yellow ash, overlying pahoehoe flow of prehistoric age, Thurston Lava Tube.	R. I. Tilling
W3481	Modern	19°24'00" 155°20'00" Kilauea Crater	1,076	Wood (ohia) from fallen tree in ohia-koa forest, in aa and ash.	J. P. Lockwood
W3486	Modern	19°22'00" 155°18'00" Kilauea Crater	1,257	Wood (ohia) from fallen tree in kipuka, overlying pahoehoe.	J. P. Lockwood
W4122	Modern	19°26'37" 155°15'05" Kilauea Crater	1,196	Charcoal, 60–80 cm above base in lithic ash of upper Keanakoi, makai side of Iiwi Road across from Lockwood house.	J. P. Lockwood
W4637	Modern	19°28'36" 154°53'25" Pahoa South	177	Charcoal rootlets, underlying thin Puu Pilau flow, W. side of quarry.	R. B. Moore
W5321	Modern	19°19'21" 155°22'46" Wood Valley	786	Wood and charcoal roots below tree mold underlying historical but undescribed shield, N. of 1920 lava flow.	N. G. Banks
W2970	<200	19°30'06" 154°51'48" Kapoho	61	Wood from Kapoho Cone, E. rift zone.	R. I. Tilling
W3467	<200	19°22'27" 155°08'10" Makaopuhi Crater	765	Charcoal underlying fountain-fed pahoehoe flow, SE. side of small crater SE. of Napau, E. rift zone.	R. T. Holcomb
W3468	<200	19°22'27" 155°08'10" Makaopuhi Crater	765	Charcoal in root mold where lava flowed into crack, underlying fountain-fed pahoehoe, E. rift zone.	R. T. Holcomb
W3480	<200	19°24'00" 155°20'00" Kilauea Crater	1,079	Wood (ohia) from kipuka of older aa lava surrounded by finer, fresher aa of the Keamoku flow.	J. P. Lockwood
W3483	<200	19°24'00" 155°20'00" Kilauea Crater	1,076	Wood (ohia) from standing tree in ohia-koa forest.	J. P. Lockwood
W3485	<200	19°21'00" 155°14'00" Makaopuhi Crater	920	Wood (ohia) from standing tall tree, in Ainahou Ranch pahoehoe.	J. P. Lockwood
W3886	<200	19°26'48" 155°19'09" Kilauea Crater	1,283	Charcoal fragments in Keanakakoi ash, from pit, Kipuka Ki.	P. W. Lipman
W359	<200	19°24'55" 154°55'50" Pahoa South	69	Charcoal in tree mold in prehistoric pahoehoe, E. rift zone, Puna.	G. A. Macdonald
W3937	<200	19°17'37" 155°24'24" Wood Valley	?	Charcoal from tree mold where lava ponded rapidly against the base of a fault scarp.	R. T. Holcomb
W4184	<200	19°19'48" 155°12'59" Makaopuhi Crater	765	Charcoal underlying tube-fed pahoehoe in large kipuka, E. rift zone, Ainahou Range.	J. P. Lockwood
W4436	<200	19°12'13" 155°27'58" Pahala	218	Charcoal roots in soil layer underlying young pahoehoe, 671 m E. of benchmark 803 on Highway 11 just N. of Pahala turnoff.	N. G. Banks

TABLE 10.2.—*Radiocarbon dates from Kilauea Volcano, Island of Hawaii*—Continued

Sample	Radiocarbon age (years before present)	Location (latitude, longitude, quadrangle)	Elevation (m)	Sample and site description	Collector
W4449	<200	19°35'16" 155°01'01" Mountain View	96	Charcoal roots in baked ash beneath surficial lava flow at Waipahoehoe Gulch, E. rift zone, S. bank of gulch along S. margin of Puna Sugar Co. field 20.	R. T. Holcomb
W4452	<200	19°15'35" 155°24'37" Wood Valley	530	Charred wood from within the hollow interior of sealed lava tree protruding from surface of Red Cone flow, along gaping eruptive fissures about 1 km uprift from Red Cones, along the SW. rift zone.	R. T. Holcomb
W4573	<200	19°34'53" 155°03'43" Mountain View	244	Charcoal roots in ash beneath thin tube-fed pahoehoe of the Kurtistown Kilauea flow, 400 m SW. of Kurtistown Assembly of God Church.	J. P. Lockwood
W4638	<200	19°28'28" 154°54'01" Pahoa South	204	Charcoal rootlets in young flow overlying Kiapu Cone in Leilani Estates.	R. B. Moore
W4639	<200	19°28'55" 154°55'00" Pahoa South	229	Charcoal under tree mold beneath pre-1790 flow in Leilani Estates, roadcut on Kahukai St., N. side of intersection with Kupono St.	R. B. Moore
W4644	<200	19°28'19" 154°53'31" Pahoa South	171	Charcoal roots in soil under surface lava flow, in roadcut W. side of Malama Homesteads road, 80 m S. of old Pohoiki Rd.	R. B. Moore
W4689	<200	19°28'03" 154°55'24" Pahoa South	242	Charcoal roots in thin soil underlying pre-1790 flow, roadcut, S. Pomaikai St., Leilani Estates.	R. B. Moore
W5323	<200	19°19'43" 155°22'49" Wood Valley	792	Wood and charcoal at edge of tree mold and in underlying roots, beneath 1920 lava flow, 700 m N. of 81-6 geodimeter station.	N. G. Banks
W3938	210±60	19°15'35" 155°24'37" Wood Valley	?	Charcoal in tree mold, 3 m from eruptive fissure.	R. T. Holcomb
W5110	230±60	19°19'01" 155°13'07" Makaopuhi Crater	512	Charcoal roots along vertical contact between Kamapuaa flow and pahoehoe at W. flow contact, at base of Poliokeawe Pali, below cascade drapery 125 m NE. of easternmost switchback in Ainahou Ranch.	J. P. Lockwood
W3881	260±70	19°32'47" 155°05'53" Mountain View	415	Charcoal root fragments in ash below phenocryst-poor Kilauea pahoehoe, in Fern Acres.	P. W. Lipman
W4834	300±70	19°27'55" 155°15'25" Kilauea Crater	1,187	Charcoal in thick organic mat underlying Keanakakoi Ash Member of Puna Basalt on east-west section of Wright Road.	J. P. Lockwood
W4162	310±70	19°28'17" 155°10'10" Volcano	784	Charcoal roots from ash at base of Kilauea pahoehoe flow, SE. side of Wung Ranch quarry.	P. W. Lipman
W4470	310±70	19°13'02" 155°27'42" Pahala	341	Charcoal root in ash underlying young pahoehoe lava flow exposed in gully, NE. edge of macadamia orchard.	R. T. Holcomb

TABLE 10.2.—*Radiocarbon dates from Kilauea Volcano, Island of Hawaii*—Continued

Sample	Radiocarbon age (years before present)	Location (latitude, longitude, quadrangle)	Elevation (m)	Sample and site description	Collector
W4661	320±70	19°33'09" 155°01'23" Mountain View	151	Charcoal in tree mold, enclosed in pahoehoe flow in Iki-Thurston lava tube area, located near private home 100 m W. of Melia St. in Orchid Land Estates.	R. B. Moore
W3811	330±60	19°13'02" 155°27'42" Pahala	341	Charcoal fragments from Kilauea pahoehoe flow, beneath young prehistoric ML pahoehoe flow exposed in gully.	J. P. Lockwood
W3849	340±60	19°28'02" 155°15'05" Kilauea Crater	1,177	Carbonaceous soil and charcoal, base of pyroclastic sequence, underlying basal reticulite of Keanakakoi Ash, Member of Puna Basalt in pit in Olaa Forest Reserve, depth 50 cm, Wright Rd.	P. W. Lipman
W5048	340±60	19°29'00" 154°52'05" Kapoho	110	Charcoal in tree mold underlying Honuaula flow, in new papaya field 100 m mauka of road connecting Pohoiki and Kapoho Rds.	R. B. Moore
W3800	350±150	19°26'14" 154°56'07" Pahoa South	174	Carbonaceous debris under prehistoric aa flow, depth 2 m, in cesspool excavation, Puna.	J. P. Lockwood
W3870	350±60	19°26'38" 155°15'07" Kilauea Crater	?	Clay, rich in organic matter and containing charcoal fragments near base of Keanakakoi Ash.	J. P. Lockwood
W5054	440±60	19°24'05" 154°55'15" Pahoa South	15	Charcoal fragments in soil underlying Kehena Beach Section, 50 m N. of small old quarry on makai side of Highway 137.	R. B. Moore
W3842	450±60	19°19'59" 155°24'20" Wood Valley	792	Charcoal fragments from soil below phenocryst-poor pahoehoe flow from Kilauea along base of Kaoiki Pali, old quarry, SW. rift zone.	P. W. Lipman
W3941	450±60	19°35'16" 155°01'06" Mountain View	518	Charcoal from top of ash layer beneath tube-fed pahoehoe flow partly filling old stream channel between two kipukas of ash-covered aa apparently derived from Mauna Loa.	R. T. Holcomb
W5453	450±110	19°24'00" 155°05'23" Kalalua	677	Charcoal roots overlain by prehistoric flow SE. of Puu Kahaualea, 250 m E. of crack that consumed January 1983 eruption.	J. P. Lockwood
W4688	490±60	19°27'26" 154°55'43" Pahoa South	274	Charcoal underlying young flow W. of Kaliu, Leilani Estates, South Kumakahi St., 40 m S. of intersection with Malama St.	R. B. Moore
W5275	490±150	19°17'17" 155°21'11" Kau Desert	640	Charcoal in soil layer recording old fire, buried by Keanakakoi Ash, Member of Puna Basalt, 15 km SW. of crater.	N. G. Banks
W5145	500±100	19°18'09" 155°20'29" Kau Desert	724	Charcoal roots in soil-ash pockets underlying Puu Koae aa.	N. G. Banks
W4404	530±70	19°12'48" 155°27'44" Pahala	271	Charcoal roots in soil beneath pahoehoe flow, 0.7 km SE. of Highway 11 in gulch that parallels the highway.	N. G. Banks

TABLE 10.2.—*Radiocarbon dates from Kilauea Volcano, Island of Hawaii*—Continued

Sample	Radiocarbon age (years before present)	Location (latitude, longitude, quadrangle)	Elevation (m)	Sample and site description	Collector
W5218	550±70	19°09'36" 155°26'50" Pahala	15	Charcoal in soil pockets underlying Ulekuwale Pueo.	N. G. Banks
W4867	570±70	19°26'35" 155°16'24" Kilauea Crater	1,238	Vitreous fern and ohia leaves in organic black soot lens, underlying Keanakakoi Ash, Member of Puna Basalt near cesspool excavation at SE. end of Dahlberg residence, 150 m NW. of golf course number 3 green.	J. P. Lockwood
W5423	570±100	19°25'58" 155°15'52 Kilauea Crater	1,201	Charcoal rootlets in soil developed within Keanakakoi surge deposit, on Sandalwood Trail between steaming bluff and Volcano House.	J. M. Buchanan-Banks
W4337	620±70	19°20'11" 155°13'25" Makaopuhi Crater	815	Charcoal rootlets at base of tube-fed Ainahou flow located 1.5 km SSE. of Ainahou Ranch House, Kamapuaa flow, 20 m E. of Poliokuwe Pali Rd.	J. P. Lockwood
W5152	660±70	19°19'41" 155°19'47" Kau Desert	853	Charcoal roots in mixed ash and eolian sand under pahoehoe.	N. G. Banks
W3860	670±60	19°13'02" 155°27'35" Pahala	399	Charcoal in Pahala Ash, below thin pahoehoe (one of the last major prehistoric flows on Kilauea SW. rift zone), along small gully, tributary to Kaalaala Gulch.	P. W. Lipman
W4402	700±70	19°17'44" 155°08'41" Kau Desert	658	Charcoal roots in soil and ash underlying pahoehoe flow, 325 m SW. of Hilina Pali Rd. end.	N. G. Banks
W3999	730±80	19°27'04" 155°14'19" Volcano	1,134	Carbonaceous soil containing small charcoal fragments from beneath toe of pahoehoe flow.	P. W. Lipman
W5147	890±70	19°09'52" 155°28'04" Pahala	45	Charcoal roots in ash pockets underlying pahoehoe, E. side of Puu Pili Rd., NW. of Puu Pili.	N. G. Banks
W4690	900±70	19°27'07" 154°56'55" Pahoa South	348	Charcoal underlying rootless lava flow located in cinder pit 500 m W. of Highway 13 in Kamaili Homesteads, SE. part of Norona Quarry.	R. B. Moore
W5215	940±70	19°09'79" 155°26'44" Pahala	46	Charcoal roots in discontinuous soil-ash layer under pahoehoe, E. of Ulekuwale Pueo.	N. G. Banks
W4998	960±60	19°26'11" 155°16'59" Kilauea Crater	1,225	Carbonized leaves in vitric ash rich in organic material, within Uwekahuna Ash Member of Puna Basalt 50 m E. of easternmost point of Tree Molds visitor area road.	J. P. Lockwood
W5211	960±70	19°11'34" 155°27'26" Pahala	145	Charcoal roots in soil and ash under pahoehoe, E. side of flood control ditch makai of aa gravel borrow pits.	N. G. Banks
W5319	970±120	19°27'20" 155°12'25" Volcano	968	Charcoal twigs and rootlets in black sooty soil at base of pahoehoe flow underlying Keanakakoi Ash Member of Puna Basalt located at Volcano Dump off Highway 11.	J. P. Lockwood
W3856	1,040±70	19°28'02" 155°15'05" Kilauea Crater	1,177	Carbonaceous clay and ash at base of pyroclastic base-surge sequence, Uwekahuna Ash Member of Puna Basalt just N. of Kilauea summit, in pit of Olaa Forest Reserve, depth 80 cm, Wright Rd.	P. W. Lipman

TABLE 10.2.—*Radiocarbon dates from Kilauea Volcano, Island of Hawaii*—Continued

Sample	Radiocarbon age (years before present)	Location (latitude, longitude, quadrangle)	Elevation (m)	Sample and site description	Collector
W3827	1,130±60	19°18'06" 155°18'23" Kau Desert	704	Charcoal beneath Kilauea basalt flow, overlying Hilina Series rocks exposed in Poliokeawe Pali.	J. P. Lockwood
W5212	1,140±70	19°17'53" 155°18'38" Kau Desert	693	Charcoal roots in soil, makai edge of trail W. of Hilina Pali parking lot in the first gully.	N. G. Banks
W5135	1,150±70	19°19'46" 155°16'51" Kau Desert	892	Charcoal roots in soil under pahoehoe, Kipuka Nene flow, surface flow in parking lot.	N. G. Banks
W4674	1,270±70	19°28'19" 154°53'31" Pahoa South	169	Charcoal rootlets in soil underlying lava flow in roadcut, W. side of Malama Homesteads Rd., 80 m S. of old Pohoiki Rd.	R. B. Moore
W4414	1,330±60	19°11'27" 155°27'29" Pahala	146	Charcoal of one tap root below a tree mold, Cinder Hills.	N. G. Banks
W4837	1,480±60	19°27'55" 155°15'25" Kilauea Crater	1,187	Organic soot within the Uwekahuna Ash Member of Puna Basalt on the east-west section of Wright Rd.	J. P. Lockwood
W4359	1,510±60	19°13'56" 155°27'35" Pahala	399	Carbonaceous soil under thin pahoehoe of Kilauea SE. rift zone, small gully, tributary to Kaalaala Gulch, 25 km mauka of Highway 11.	P. W. Lipman
W5303	1,650±150	19°27'55" 155°15'25" Kilauea Crater	1,187	Dark sooty ash with charcoal flakes (with small modern rootlets present) underlying the Wright Road Uwekahuna Ash Member of Puna Basalt on the east -west section of Wright Rd.	J. P. Lockwood
W5097	1,790±70	19°28'40" 155°17'23" Kilauea Crater	1,347	Black sooty soil from organic layer at base of weathered ash unit, overlain by Uwekahuna Ash, Member of Puna Basalt, Keauhou Ranch, 1.4 km E. of Puu Oo Trail, 2.2 km WSW. of end of Wright Rd.	J. P. Lockwood
W4119	1,800±80	19°14'48" 155°21'09" Maliikakani Point	50	Carbonaceous baked ash containing charred root fragments beneath aa flow mantling Pahala Ash on rim of Kukalauula Pali.	R. T. Holcomb
W4369	2,070±80	19°28'17" 155°10'10" Volcano	786	Charcoal near base of tree mold under pahoehoe flow exposed in quarry on Wung Rd., NW. of Highway 11.	P. W. Lipman
W3859	2,080±70	19°28'02" 155°15'05" Kilauea Crater	1,177	Carbonaceous clay and ash, underlying base-surge sequence, Uwekahuna Ash, Member of Puna Basalt just N. of Kilauea summit, from pit in Olaa Forest Reserve, depth 130 cm.	P. W. Lipman
W5292	2,080±150	19°27'55" 155°15'25" Kilauea Crater	1,187	Dark sooty ash with charcoal flakes (cleaned of modern rootlets) underlying the Uwekahuna Ash Member of Puna Basalt on Wright Road at the same location as W-5303 (age 1,650 ± 150).	J. P. Lockwood
W3885	2,160±70	19°28'17" 155°10'10" Volcano	786	Charcoal around base of tree mold in crystal-poor Kilauea pahoehoe, Wung Ranch quarry.	P. W. Lipman
W5052	2,360±90	19°22'55" 154°57'29" Kalapana	9	Charcoal in soil underlying early Heiheiahulu pahoehoe flow with tree molds exposed at Kalapana dump on mauka side of road.	R. B. Moore

TABLE 10.2.—*Radiocarbon dates from Kilauea Volcano, Island of Hawaii*—Continued

Sample	Radiocarbon age (years before present)	Location (latitude, longitude, quadrangle)	Elevation (m)	Sample and site description	Collector
W201	2,500±250	19°25'00" 155°20'00" Kilauea Crater	1,209	Fern mold underlying basaltic pumice, excavation for N. wing of Volcano House, Keanakakoi Ash Members of Puna Basalt.	H. A. Powers
W5345	2,770±150	19°27'37" 155°14'52" Volcano	1,160	Charcoal rootlets at base of pahoehoe flow buried by Uwekahuna Ash and Keanakakoi Ash Members of Puna Basalt, located 15 m E. of Wright Rd. and 3.5 km N. of Old Volcano Highway.	J. P. Lockwood
W3831	3,480±80	19°18'06" 155°18'22" Kau Desert	703	Charcoal beneath Kilauea basalt flow overlying rocks of the Hilina Basalt, exposed in Poliokeawe Pali.	J. P. Lockwood
W5324	3,500±200	19°11'23" 155°28'20" Pahala	137	Charcoal roots in soil under pahoehoe flow at right angle bend of Old Pahala Dump Rd., W. side of road, makai of bagasse flume.	N. G. Banks
W4380	3,560±60	19°28'17" 155°10'10" Volcano	782	Carbonaceous soil and charcoal fragments within Wung Quarry ash sequence on Wung Ranch, Uwekahuna Ash, Member of Puna Basalt, of Highway 11.	P. W. Lipman
W3884	3,610±60	19°12'44" 155°28'10" Pahala	177	Charcoal in ash below olivine-rich pahoehoe flow, Pahala vent.	P. W. Lipman
W4177	3,690±70	19°34'56" 155°01'49" Mountain View	142	Charcoal beneath pahoehoe exposed in trench, Puna Sugar Field 20, SE. from Keauu.	J. P. Lockwood
W3798	4,820±90	19°28'10" 155°18'20" Kau Desert	698	Carbonized charcoal tree fern (hapuu) from ash directly above lava dated by W-3809 (age 10,680 ± 130), from new scar formed during 1975 earthquake Hilina Pali.	J. P. Lockwood
W3873	6,620±150	19°17'11" 155°18'15" Kau Desert	?	Ash rich in organic material and containing charcoal fragments from uppermost level of thick Pahala Ash sequence, W. side Keana Bihopa Arroyo, Hilina Pali.	J. P. Lockwood
W3809	10,680±130	19°18'10" 155°18'20" Kau Desert	696	Charcoal beneath basalt and ash in upper Hilina Pali section, from new scar formed during 1975 earthquake.	J. P. Lockwood
W905	17,360±650	19°20'00" 155°20'00" Kau Desert	189	Carbonaceous ash from contact of lower Pahala Ash with overlying basalt, SE. end of seaward-facing Keone fault scarp, Keone Pali.	G. D. Fraser
W5241	21,600±600	19°16'39" 155°15'30" Kau Desert	107	Charcoal roots in black ash located at the top of the second ash layer above the base of Kapukapu cliff.	N. G. Banks
W3801	22,500±300	19°16'16" 155°17'10" Kau Desert	171	Charcoal from top of Pahala Ash section on Puu Keone.	J. P. Lockwood
W5238	22,660±600	19°16'38" 155°15'30" Kau Desert	91	Charcoal roots in black soil located above lowest ash layer in Kapukapu cliff.	N. G. Banks
W3814	22,800±340	19°16'14" 155°17'20" Kau Desert	183	Charcoal exposed in fresh outcrop created by massive slumping during 1975 earthquake, Puu Keone.	J. P. Lockwood

TABLE 10.3.—*Radiocarbon dates from Hualalai Volcano, Island of Hawaii*

[Samples listed in order of increasing age; uncertainty is one standard deviation, ± 1σ; modern age means sample is younger than AD 1950; ML = Mauna Loa; MK = Mauna Kea; mauka = toward the mountain, makai = toward the sea; see figs. 10.2–10.4 for localities. Stratigraphic nomenclature from Langenheim and Clague (chapter 1, part II)]

Sample	Radiocarbon age (years before present)	Location (latitude, longitude, quadrangle)	Elevation (m)	Sample and site description	Collector
W4634	<200	19°42'55" 155°54'35" Kailua	1,841	Charcoal rootlets from high-water mark of olivine basalt flow from Kaupulahu Crater along main road up NW. flank and rift zone of Hualalai.	R. B. Moore
W4381	<200	19°37'55" 155°48'50" Hualalai	1,667	Charcoal rootlets in soil developed on Puu Ikaaka cinders, overlain by pahoehoe flow, 700 m E. of Hualalai summit road along Judd Trail, 200 m S. of trail at N. base of Puu Ikaaka.	R. B. Moore
W4389	<200	19°35'00" 155°58'33" Kealakekua	3	Charcoal in soil separating two flows at Kahaluu Beach Park, on E. side of Alii Drive, below T.K. Cook's house.	R. B. Moore
W5124	<200	19°44'08" 155°56'25" Kailua	1,250	Charcoal in soil developed on old cone, overlain by young flow on Hualalai Ranch, N. of Moanuiahea near flower nursery.	R. B. Moore
W5381	110±60	19°38'46" 155°49'00" Hualalai	1,768	Charcoal in soil under Moore Crater flow, SE. side of airstrip.	R. B. Moore
W4394	300±60	19°41'50" 155°52'44" Kailua	2,316	Charcoal from under edge of Malekule flow at end of road on N. side of cinder cones, edge of flow against cinder cone.	R. B. Moore
W5531	710±150	19°37'00" 155°49'26" Puu Lehua	1,509	Charcoal in soil under toe of Waha Pale flow at E. edge of flow, 800 m S. of Bishop experimental plot.	R. B. Moore
W5491	900±110	19°40'27" 155°45'53" Hualalai	1,545	Charcoal in cinders under toe of Moore Crater flow, one of the largest on the Big Island.	R. B. Moore
W5130	1,030±60	19°43'03" 155°52'48" Kailua	1,987	Charcoal under North Jackson Crater flow between two old cones.	R. B. Moore
W5522	1,180±200	19°43'09" 155°46'11" Hualalai	1,378	Charcoal in soil on ML flow under pahoehoe overflow from channel of Trusdell Crater flow.	R. B. Moore
W4383	1,330±50	19°34'23" 155°55'00" Kealakekua	366	Charcoal from under highest basalt flow in Tanaka's quarry, E. side of quarry.	R. B. Moore
W4171	2,030±80	19°46'52" 155°50'00" Puu Anahulu	866	Charcoal in soil zone on top of trachyte cinders under olivine-bearing basalt flow, N. flank of Puu Waawaa.	R. B. Moore
W4388	2,290±70	19°34'58" 155°56'46" Kealakekua	354	Charcoal in soil on top of aa flow under basalt flow on E. side of Mamalahoa Highway, N. of Tanaka quarry.	R. B. Moore
W5068	2,350±80	19°41'47" 155°52'31" Hualalai	2,353	Charcoal under edge of older Luamakami pahoehoe flow overlying cinders in ditch in road 300 m W. of highest saddle N. of Hualalai summit.	R. B. Moore

TABLE 10.3.—*Radiocarbon dates from Hualalai Volcano, Island of Hawaii*—Continued

Sample	Radiocarbon age (years before present)	Location (latitude, longitude, quadrangle)	Elevation (m)	Sample and site description	Collector
W5073	2,390±60	19°42'18" 155°50'44" Hualalai	2,000	Charcoal under spatter bombs at edge of deposit from NE. Mawahine Cone along road between Bishop Estate and Puu Waawaa Ranch.	R. B. Moore
W5076	2,670±80	19°41'14" 155°51'55" Hualalai	2,377	Charcoal under 0.5 m bombs from the 8001-ft. cone on S. side of lower saddle on N. side of Hualalai summit.	R. B. Moore
W5559	3,030±200	19°45'07" 155°54'47" Kiholo	1,030	Charcoal in soil under Puu Waawaa Ranch flow at ranch road.	R. B. Moore
W5127	3,100±80	19°44'15" 155°52'40" Hualalai	2,292	Charcoal in soil developed on old cone, covered by flow, transected by pit crater, on E. side of pit crater 700 m NE. of Malekule.	R. B. Moore
W4376	3,600±70	19°40'55" 155°58'44" Kailua	341	Charcoal in soil on aa flow under basalt flow near Palani Junction, in roadcut on side of Highway 19, 0.8 km S. of Palani Junction.	R. B. Moore
W5562	3,610±200	19°45'05" 155°57'29" Kiholo	817	Charcoal in soil beneath old Hualalai Ranch flow along road W. of ranch office.	R. B. Moore
W5132	3,990±70	19°41'50" 155°52'17" Hualalai	2,390	Charcoal in soil developed on older spatter, covered by younger spatter on S. side of main Hualalai summit road, 100 m W. of highest saddle.	R. B. Moore
W5070	4,390±70	19°41'44" 155°52'59" Hualalai	2,256	Charcoal in cinders under edge of slabby pahoehoe flow SW. of Malekule in gully 200 m above main road down Kaupuleku side of Hualalai.	R. B. Moore
W4378	4,720±80	19°41'50" 155°52'47" Kailua	2,292	Charcoal in soil developed on cinders underlying edge of second flow down from West Malekule on E. wall of West Malekule pit crater.	R. B. Moore
W5496	5,350±180	19°40'16" 155°51'55" Hualalai	1,905	Charcoal in cinders from extensive cinder unit S. of Hualalai summit along road near W. boundary of quad.	R. B. Moore
W5297	6,360±100	19°40'13" 155°51'41" Hualalai	1,902	Charcoal under Puu Neneakolu flow along Waiaha Stream between road and Puu Hale.	R. B. Moore
W5299	8,770±200	19°41'45" 155°52'01" Hualalai	2,390	Charcoal in red soil under cinders in canyon above recent alluvial fan at Hualalai summit.	R. B. Moore
W4371	9,490±100	19°51'21" 155°52'15" Puu Anahulu	195	Charcoal under olivine-rich basalt 4 m thick at NW. end of Puu Anahulu Cone, 200 m W. of end of trail leading N. from Mamalahoa Highway.	R. B. Moore
W4391	10,370±150	19°35'25" 155°57'26" Kealakekua	199	Carbonaceous material in yellow to red cinders overlain by basalt flow at intersection of Kuakini Highway and Kam III Rd.	R. B. Moore
W4365	12,230±150	19°48'39" 155°50'30" Puu Anahulu	677	Charcoal roots in soil zone on top of trachyte lava flow, under olivine-rich basalt flow on W. side of Puu Anahulu, roadcut, 200 m E. of Mamalahoa Highway.	R. B. Moore
W5056	12,950±150	19°39'28" 155°57'37" Kailua	439	Charcoal in soil under Keopu flow 100 m W. of Mamalahoa Highway next to Keopu subdivision road.	R. B. Moore

TABLE 10.4—*Radiocarbon date from Mauna Kea Volcano, Island of Hawaii*

[Samples listed in order of increasing age; uncertainty is one standard deviation, ± 1σ; modern age means sample is younger than AD 1950; ML = Mauna Loa; MK = Mauna Kea; mauka = toward the mountain, makai = toward the sea; see figs. 10.2–10.4 for localities. Stratigraphic nomenclature from Langenheim and Clague (chapter 1, part II)]

Sample	Radiocarbon age (years before present)	Location (latitude, longitude, quadrangle)	Elevation (m)	Sample and site description	Collector
W5541	5,630±200	19°41'53" 155°26'41" Puu Oo	1,986	Charcoal root fragments at top of deep ash overlain by Puu Kalaieha flow on Parker Ranch land off Saddle Rd.	J. P. Lockwood

STRATIGRAPHY OF KILAUEA VOLCANO

By R. Michael Easton[1]

ABSTRACT

This paper reviews and revises the lithostratigraphic nomenclature of Kilauea Volcano. The major stratigraphic units of the volcano are redefined as the Hilina Basalt (oldest), Pahala Ash, and Puna Basalt (youngest) in accordance with the stratigraphic code. Four pyroclastic units within the Hilina Basalt can be used as stratigraphic markers; these are formally proposed and described here and given member rank. These new stratigraphic units are, from oldest to youngest, the Halape, Kahele, Pohakaa and Moo Ash Members. The Pohakaa has a similar distribution and lithology to the Pahala Ash and represents a major period of ash deposition on Kilauea at about 40–50 ka. Two pyroclastic units intercalated within the Puna Basalt are the circa 1.5-ka Uwekahuna Ash Member and the mostly A.D. 1790 Keanakakoi Ash Member. The origin and source of these pyroclastic units, particularly the Pahala Ash and the Pohakaa Ash Member, is briefly discussed, in light of new rare-earth-element and petrographic data from these units.

INTRODUCTION

A stratigraphic unit, whether it be a group, formation, member, or flow, becomes established through the repeated demonstration of its utility. Since the Hawaiian Volcano Observatory was established 75 years ago, a number of stratigraphic terms have been introduced to help geologists unravel the stratigraphy of Kilauea Volcano. Some of these terms have become well established through use; others, although widely used, do not meet all of the criteria required of formal stratigraphic units as outlined in Article 3 of the North American stratigraphic code (North American Commission on Stratigraphic Nomenclature, 1983).

The purpose of this paper is to review the stratigraphic nomenclature of Kilauea Volcano and to revise it so as to be consistent with the stratigraphic code and with current needs. Some new stratigraphic terms are herein formally proposed so that they will be available to the geologic community and their utility can be tested. Stratigraphy is an important tool in aiding our understanding of Kilauea Volcano, and I hope that this revision of stratigraphic nomenclature will make this tool even more effective.

ACKNOWLEDGMENTS

R.T. Holcomb was in large part responsible for this paper through his encouragement, and this paper has benefited from discussion over the years with M.O. Garcia, R.T. Holcomb, J.P. Lockwood, and G.A. Macdonald. As a historical note, it was G.A. Macdonald's intention to revise the stratigraphy of the Island of Hawaii and Kilauea Volcano in order to make the nomenclature consistent with the recommendations of the stratigraphic code, but this work was cut short by his untimely death. This paper was reviewed by R.L. Christiansen and R.T. Holcomb, and I thank them for their careful reading and helpful comments and suggestions.

PREVIOUS WORK

The various lithostratigraphic schemes that have been applied to Kilauea Volcano and correlations between them are summarized in figure 11.1. An essential element of all these schemes is the use of the Pahala Ash as a marker horizon to divide the lava of Kilauea Volcano into pre-Pahala and post-Pahala units. This usage arose because the Pahala Ash was considered to be the only stratigraphic unit found on several (four of the five) volcanoes on the Island of Hawaii (see Stearns and Macdonald, 1946). It has therefore been used as an important stratigraphic marker. As discussed in detail later, the Pahala Ash does not always meet the criteria required of a marker horizon, and this can present local correlation problems.

Stone (1926) divided Kilauea rocks into the pre-Kilauea Series, comprising all rocks below and including the unit he called the Pahala Ash, and the Kilauea Series, comprising prehistoric and historical lavas younger than the Pahala. L.F. Noble and W.O. Clark (unpub. data, 1920, in Washington, 1923) made a similar division, but used the terms Pahala Series and post-Pahala Series; this division was later revised in Stearns and Clark (1930). In both these works, the lavas of Kilauea and Mauna Loa were not differentiated stratigraphically. Stearns and Clark (1930) included lava and tuff of both volcanoes in the Pahala Basalt (which included the upper ash member now called the Pahala Ash) and the overlying Kamehame Basalt. The Kamehame Basalt was divided into a lower prehistoric part, which included all ash units above the Pahala Basalt, and an upper part composed essentially of historic flows (fig. 11.1).

Wentworth (1938), in his examination of Kilauea pyroclastic rocks, introduced the term Pahala Tuff for what has generally been called the Pahala Ash by workers both before and since. He also introduced the terms Uwekahuna Formation and Keanakakoi Formation for ash units of Kilauea stratigraphically above his Pahala Tuff.

[1]Ontario Geological Survey, Toronto, Ontario, Canada M53 1B3.

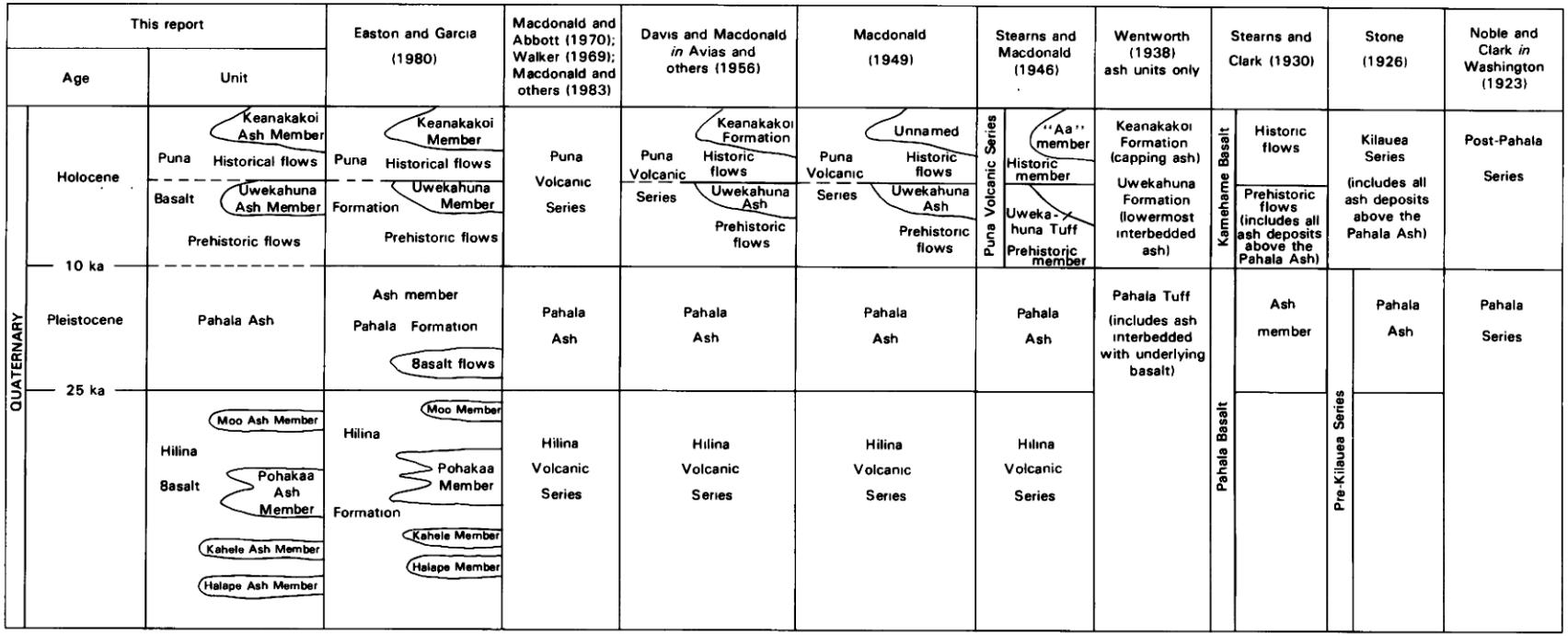

FIGURE 11.1.—Evolution of lithostratigraphic nomenclature for Kilauea Volcano. Stearns and Macdonald's (1946) "aa" member is probably erroneous for ash member. Dashed line between Puna Basalt and Pahala Ash of this report indicates that locally lowermost Puna flows are intercalated with Pahala Ash and are of Pleistocene age (see text).

Modern usage began when Stearns and Macdonald (1946) divided the rocks below the ash member of the Pahala Basalt (Stearns and Clark, 1930) into the Kahuku Volcanic Series for lava of Mauna Loa and the Hilina Volcanic Series for lava of Kilauea (fig. 11.1). In addition, they divided the rocks called the Kamehame Basalt by Stearns and Clark (1930), which overlie the Pahala on Mauna Loa and Kilauea and include the historical lava of the two volcanoes, into the Kau Volcanic Series on Mauna Loa and the Puna Volcanic Series on Kilauea (fig. 11.1), thus abandoning the term Kamehume Basalt. They included the Uwekahuna in the Puna and called it Uwekahuna Tuff, but treated rocks called the Keanakakoi Formation by Wentworth (1938) as an informal member. The Pahala Ash was used to separate these stratigraphic units. Macdonald (1949, p. 65, 67) also included the Uwekahuna in the Puna Volcanic Series but called it the Uwekahuna Ash. Davis and Macdonald (in Avias and others, 1956) included Wentworth's Keanakakoi Formation in the Puna. Walker (1969), Macdonald and Abbott (1970), and Macdonald and others (1983) essentially retained the nomenclature of Stearns and Macdonald (1946; fig. 11.1).

Easton and Garcia (1980) renamed the Hilina Volcanic Series and the Pahala Ash as the Hilina and Pahala Formations, respectively, and effectively reduced the rank of the Puna Volcanic Series (and its subdivisions) and renamed it the Puna Formation. Easton and Garcia (1980) also introduced new stratigraphic terms for several ash units within the Hilina Formation (fig. 11.1), but these terms were not formally proposed in the sense of Article 3 of the stratigraphic code.

STRATIGRAPHY OF KILAUEA VOLCANO

The revised stratigraphic nomenclature for Kilauea Volcano proposed in this paper is shown in figures 11.1 and 11.2. As the use of the term "Formation" does not indicate the predominant lithology or volcanic origin of each lithostratigraphic unit, the names Hilina Basalt, Pahala Ash, and Puna Basalt replace the names Hilina Formation, Pahala Formation, and Puna Formation of Easton and Garcia (1980), respectively. The name Pahala Ash is used in this report, although the ash is indurated and more properly could be called a tuff. However, the term ash is commonly applied to its indurated counterpart, and the name Pahala Ash is widely used.

Reference sections for each of the units are given in table 11.1; they are those of Stearns and Macdonald (1946) unless otherwise indicated. Short descriptions of the three major stratigraphic units are also given below.

In addition to the name changes of two main lithostratigraphic units of Kilauea Volcano, a number of subdivisions of these formations can be made (figs. 11.1, 11.2). These subdivisions are herein formally proposed as members and described in detail under the appropriate higher rank stratigraphic unit. Locations of reference sections for some of these units are given in table 11.1.

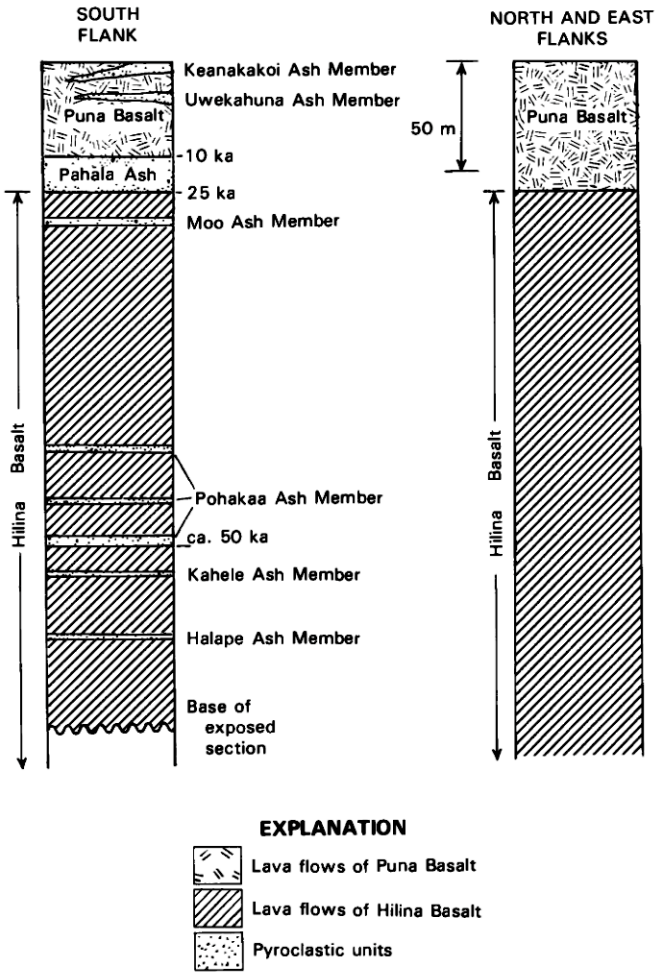

FIGURE 11.2.—Generalized stratigraphic column for south flank of Kilauea Volcano (left) based on sections measured along Hilina fault system (see fig. 11.4). Inferred stratigraphic column for north and east flanks of Kilauea Volcano shown on right. Absence of ash horizons on north flank indicated here reflects trade-wind patterns in Hawaiian region. Although Keanakakoi Ash Member of the Puna Basalt is present in Glenwood region on north flank of Kilauea, its distribution on east flank is unknown.

HILINA BASALT

The Hilina Basalt is exposed only in valleys along the Hilina fault system on the south flank of Kilauea Volcano (fig. 11.3). Exposures are limited to Puu Kapukapu, Puu Kaone, Puueo Pali, Hilina Pali, and a fault scarp north of Kalaeapuki (fig. 11.3). The Hilina Basalt consists predominantly (95 percent) of lava flows, but several major ash horizons are present.

Stone (1926) and Stearns and Clark (1930) examined the formation but gave only general descriptions. Macdonald described a section of the formation 1.6 km southwest of the end of Hilina Road (Stearns and Macdonald, 1946, appendix) and also gave brief petrographic descriptions of the lava (Macdonald, 1949).

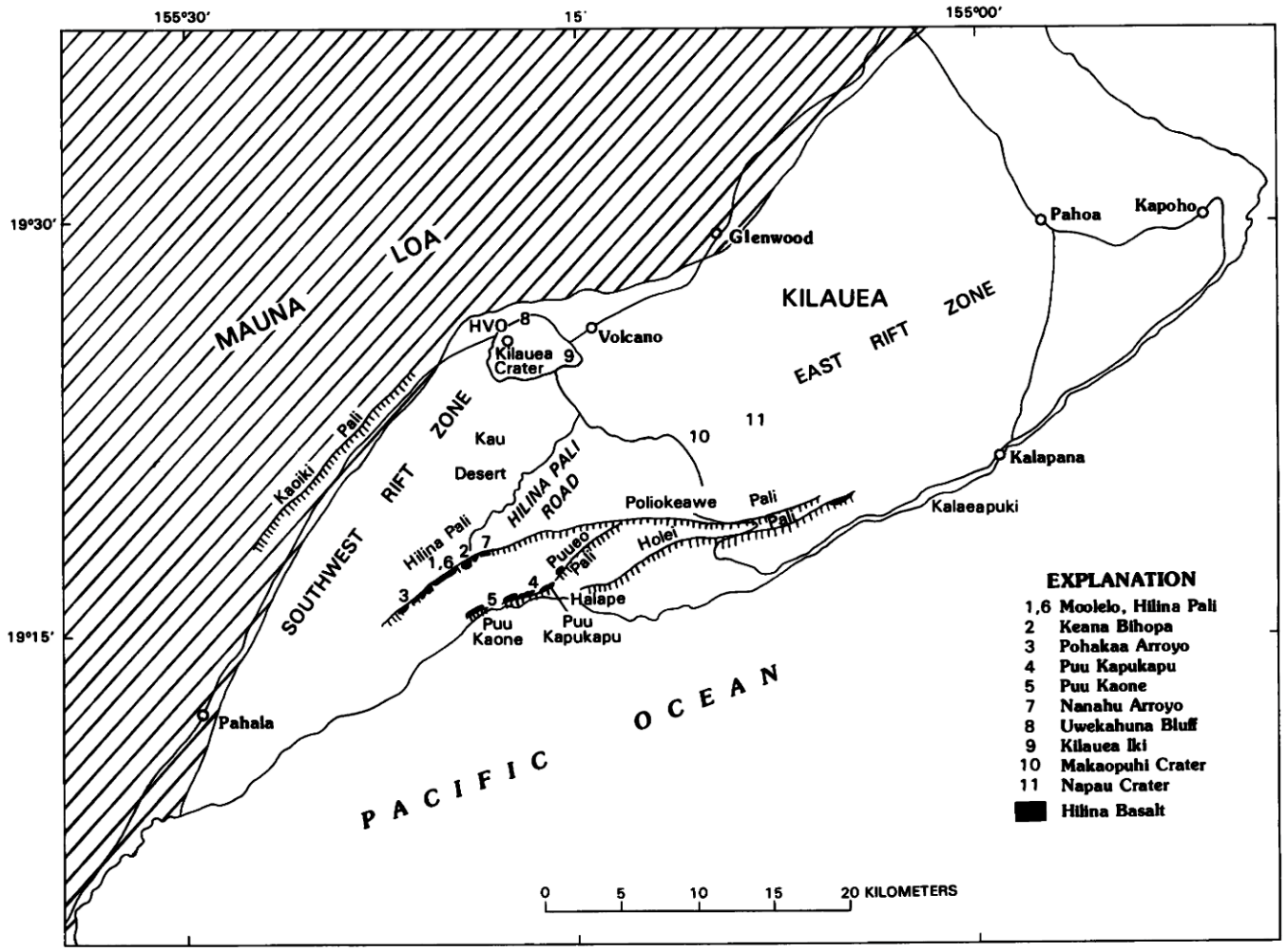

FIGURE 11.3.—Location of type and reference sections for stratigraphic units of Kilauea Volcano (see table 11.1).

PYROCLASTIC AND SEDIMENTARY DEPOSITS

The Hilina Basalt contains several altered and reworked ash horizons (fig. 11.4). The number of ash horizons varies between sections, reflecting intercalation of lava flows with the ash beds. More distal sections such as Puu Kapukapu contain fewer ash horizons because in these areas ash from occasional explosive eruptions could accumulate for longer periods without flow activity occurring. The overall thickness of the ash horizons is relatively constant in any area, but it decreases with distance from Kilauea's summit. The above features make bed-to-bed correlation difficult. Nevertheless, it is still possible to define at least three major ash events and one minor one, widely separated in space and time within the Hilina Basalt which can be correlated between sections over distances of tens of kilometers (figs. 11.2, 11.4).

HALAPE ASH MEMBER (NEW TERM)

This member is found at Puu Kapukapu and at Keana Bihopa near the base of the exposed Hilina section (figs. 11.3, 11.4). The name is derived from the Halape area at the base of Puu Kapukapu (Pukui and others, 1974). The type section is at Keana Bihopa (tables 11.1, 11.3). The unit is found at roughly the same stratigraphic level in both localities, but at each locality it varies laterally in thickness from 10 cm to 50 cm. At Puu Kapukapu, the unit grades downward into a deeply weathered aa clinker zone; at both localities it is overlain by aa flows.

The member is composed of red-weathering, poorly bedded, clayey soil and palagonite. Soil predominates at Puu Kapukapu, but at Keana Bihopa, brown beds of palagonite 0.5–1 cm thick are present. A section from Keana Bihopa is described in table 11.3.

TABLE 11.1.—*Type localities and reference localities of lithostratigraphic units, Kilauea Volcano*

[See figure 11.3 for localities]

Locality	Description
1	Type section of the Hilina Basalt (Stearns and Macdonald, 1946). 1.6 km southwest of end of Hilina Pali Road (approx. lat 19°17′00″ N., long 155°18′45″ W., Kau Desert 7.5-min quadrangle).
2a	Reference section of Hilina Basalt, Keana Bihopa, from base of pali (370 m elev) to top (640 m elev) (19°17′19″ N., 155°18′25″ W., Kau Desert 7.5-min quadrangle). 250 m south-southwest of end of Hilina Pali Road.
2b	Type section of Halape Ash Member, Hilina Basalt, Keana Bihopa, (395 m elev) (19°17′19″ N., 155°18′25″ W., Kau Desert 7.5-min quadrangle).
2c	Type section of Moo Ash Member, Hilina Basalt, Keana Bihopa (570 m elev) (19°17′19″ N., 155°18′25″ W., Kau Desert 7.5-min quadrangle).
2d	Reference section of Puna Basalt, Keana Bihopa (600–640 m elev) (19°17′19″ N., 155°18′25″ W., Kau Desert 7.5-min quadrangle).
3a	Type section of Kahele Ash member, Hilina Basalt, Pohakaa Arroyo (approx. 470 m elev) (19°16′40″ N., 155°20′00″ W., Kau Desert 7.5-min quadrangle).
3b	Type section of Pohakaa Ash Member, Hilina Basalt, Pohakaa Arroyo (approx. 425–450 m elev) (19°16′40″ N., 155°20′00″ W., Kau Desert 7.5-min quadrangle).
4a	Reference section of Hilina Basalt and Halape, Kahele, Pohakaa and Moo Ash Members, Puu Kapukapu, from base of pali (100 m elev) to top (300 m elev) (19°16′45″ N., 155°15′35″ W., Kau Desert 7.5-min quadrangle).
4b	Reference section of Pahala Ash, Puu Kapukapu (19°16′15″ N., 155°17′15″ W., Kau Desert 7.5-min quadrangle).
5	Reference section of Pahala Ash, Puu Kaone (19°16′15″ N., 155°17′15″ W., Kau Desert 7.5-min quadrangle).
6	Principal reference section of Pahala Ash, Moolelo, Hilina Pali (19°17′00″ N., 155°19′00″ W., Kau Desert 7.5-min quadrangle).
7	Reference section of Puna Basalt and Uwekahuna Ash Member, Nanahu Arroyo, Hilina Pali, 0.5 km northeast of end of Hilina Pali Road (19°18′15″ N., 155°18′34″ W., Kau Desert 7.5-min quadrangle).
8	Type sections of Puna Basalt and of Uwekahuna Ash Member, Uwekahuna Bluff, Kilauea caldera (Kilauea Crater 7.5-min quadrangle).
9	Reference section of Puna Basalt, Kilauea Iki Crater, summit lava (Volcano 7.5-min quadrangle).
10	Reference section of Puna Basalt, east-rift-zone lava, Makaopuhi Crater (Makaopuhi Crater 7.5-min quadrangle).
11	Reference section of Puna Basalt, east-rift-zone lava, Napau Crater (Volcano 7.5-min quadrangle).

Walker (1969) examined the Hilina while mapping the Kau Desert quadrangle. Easton and Garcia (1980) described the petrography and geochemistry of the Hilina lava in detail. Easton (1978) examined the Hilina in detail and measured sections through the formation at most exposures (Easton, 1978, fig. 3, appendix). The two most extensive and best exposed sections are at Keana Bihopa (Hilina Pali) and Puu Kapukapu (figs. 11.3, 11.4).

LAVA FLOWS

The exposed Hilina Basalt consists of a sequence of aa and pahoehoe flows. Individual pahoehoe flows are 0.5–3 m thick, averaging 2 m. Upper surfaces are commonly ropy and reddish to purplish, and surface crusts are rarely preserved, indicating minor erosion (1–10 cm of material removed) between flows. Pahoehoe sequences of mineralogically similar rocks 8–16 m thick are common, and it is difficult to distinguish individual flows in these sequences. These flow sequences, more abundant in the upper part of the Hilina Basalt, could represent different phases of the same eruption (much like the 1969–74 flows erupted from Mauna Ulu).

The aa flows are 1–6 m thick, averaging 4 m including the clinker zones; the core zone accounts for 20–80 percent of the flow thickness. The clinker zones are partially to totally weathered to reddish-brown clay and commonly contain soil or yellow palagonite horizons in their upper parts. The palagonite layers are probably remnants of ash pockets or lenses. Otherwise, all flow rocks are fresh, mainly because of the low rainfall in the area.

The relative amounts of aa and pahoehoe in the measured sections vary (fig. 11.4, table 11.2). In general, pahoehoe flows predominate in sections farthest away from the caldera (for example, Puueo Pali), supporting the suggestion of Swanson (1973) that only large volume, tube-fed pahoehoe eruptions are able to reach and flood large areas of Kilauea's south flank.

The relative abundances of rock types in the Hilina Basalt are also shown in table 11.2. Olivine basalt contains more than 5 percent olivine phenocrysts (Macdonald, 1949). Picrite basalt contains less than 35 percent modal plagioclase and more than 15 percent modal olivine (Macdonald, 1949; Wright, 1971). Olivine basalt is more abundant than other kinds of basalt in the sections examined (table 11.2). Hypersthene was only rarely observed in lava of the Hilina Basalt, and then only in small amounts. Picrite basalt and plagioclase porphyritic basalt are present only at Puueo Pali and Puu Kapukapu and may be derived from the nearby east rift zone (Macdonald, 1944). Further details on the petrography of Hilina Basalt lava are found in Easton and Garcia (1980).

The Hilina Basalt flows are chemically distinct from the overlying Puna Basalt flows, the former having higher FeO^t content for the same MgO content and lower K_2O/P_2O_5 ratio than the latter (Easton and Garcia, 1980). This distinction may aid in mapping the Hilina and Puna Basalts in areas where the intervening Pahala Ash is thin or absent. Easton (1978) and Easton and Garcia (1980) concluded on the basis of mapping and geochemistry that the Hilina Basalt exposed on the south flank of Kilauea was an intricately stacked sequence of flows derived from the summit caldera and from the east and southwest rift zones of Kilauea. Further details on the chemistry of Hilina Basalt lava are given in Easton and Garcia (1980).

The lower contact of the Hilina Basalt is not exposed, but at least 300 m of lava is exposed along the Hilina Pali. The upper contact of the Hilina Basalt has been defined as the base of the Pahala Ash (Stearns and Macdonald, 1946). The age of the Hilina Basalt is not well defined, but it is older than the radiocarbon age of 31 ± 0.9 ka obtained from the base of the Pahala Ash on Mauna Loa (Kelley and others, 1979). The base of the exposed Hilina Basalt lava at Puu Kapukapu may be estimated to be on the order of 100 ka from average eruption rates determined at Nanahu Arroyo[2] along the Hilina Pali (Easton, 1978).

[2]Name does not appear on current topographic map, but has recently been approved by the U.S. Board on Geographic Names (Donald J. Orth, written commun., 1986).

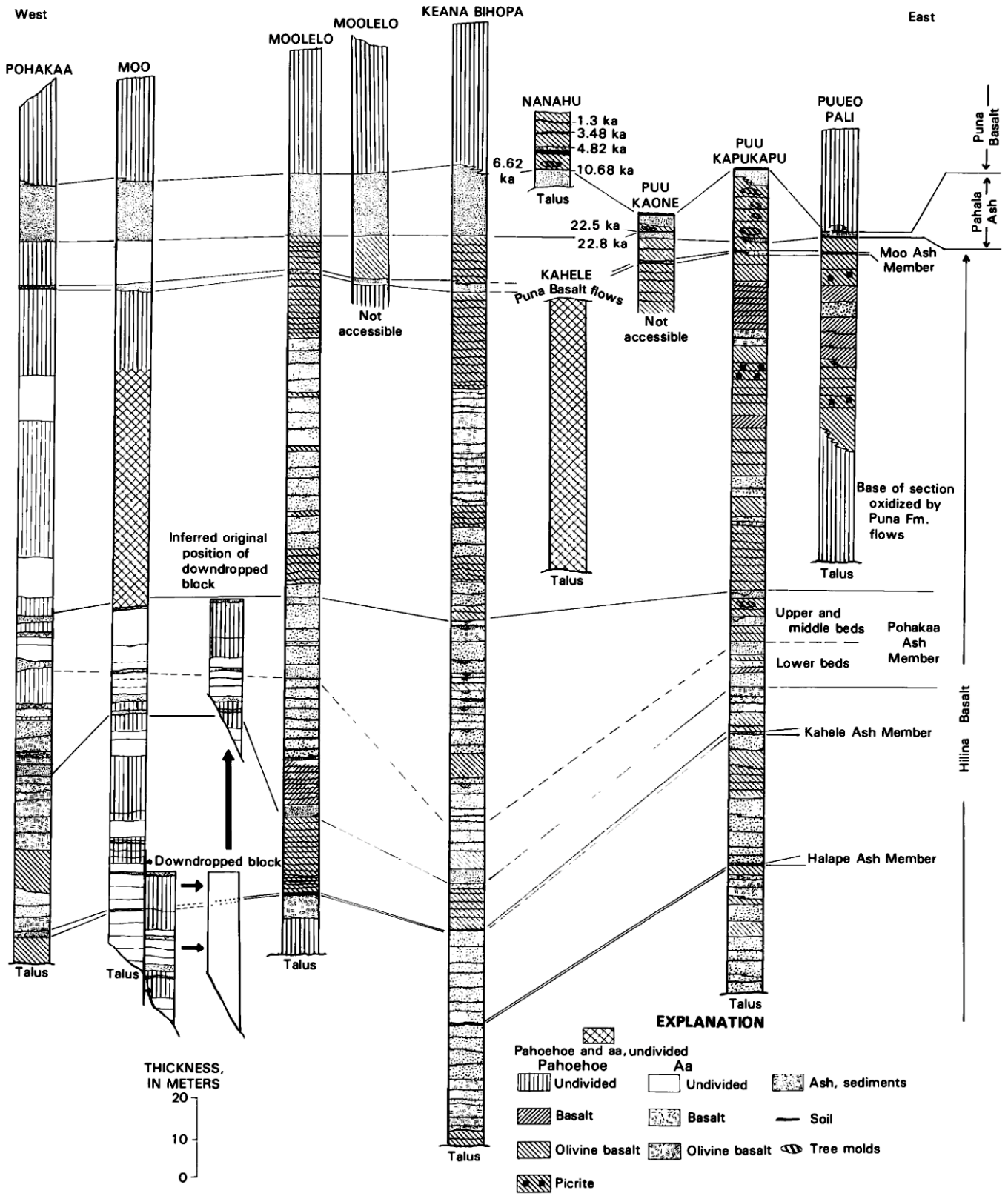

FIGURE 11.4.—Measured stratigraphic sections of Hilina Basalt along Hilina fault system, south flank of Kilauea Volcano. Data adapted from Easton (1978). Base of Hilina Basalt is nowhere exposed. Intercalated lava flows shown in sections of Pahala Ash and Pohakaa Ash Member are Puna Basalt flows and Hilina Basalt flows, respectively (see text).

TABLE 11.2.—*Abundance of rock and flow types exposed on Kilauea Volcano, in part modified from Easton and Garcia (1980)*

[All figures in percent; n.d., not determined]

Area or subdivision	Relative abundance of rock type exposed				Relative abundance of flow types exposed		Relative abundance of flow type in each rock type			
	Olivine basalt	Picrite basalt	Basalt	Hypersthene-bearing basalt	Aa	Pahoehoe	Basalt		Olivine basalt	
							Aa	Pahoehoe	Aa	Pahoehoe
Puna Basalt										
Historical flows	78	7	13	2	n.d.	[1]100	n.d.	n.d.	n.d.	n.d.
Prehistoric flows	71	5	22	2	n.d.	[1]100	n.d.	n.d.	n.d.	n.d.
Moolelo[2]	67	3	30	0	50	50	n.d.	n.d.	n.d.	n.d.
Hilina Basalt										
Keana Bihopa[3]	56	0	44	0	60	40	90	10	38	62
Pohakaa[4]	68	n.d.	32	n.d.	57	43	n.d.	n.d.	n.d.	n.d.
Kapukapu[5]	62	4	34	0	36	64	60	40	24	76
Puueo Pali[6]	67	8	25	n.d.	5	95	5	95	0	100

[1]Cliff sections, Hilina Pali and Kapukapu only.
[2]Difficult to estimate number of flows; pahoehoe, aa figures approximate. From Macdonald (1946).
[3]50 flows of olivine basalt: 20 aa, 30 pahoehoe; 40 flows of basalt: 35 aa, 5 pahoehoe.
[4]Lower half of section, top of Pohakaa Ash Member to base of section.
[5]50 flows of olivine basalt and picrite basalt: 12 aa, 30 pahoehoe, transition pahoehoe; 25 flows of basalt: 15 aa, 10 pahoehoe.
[6]Upper section, above top of the Pohakaa Ash Member: 16 flows of olivine basalt, 2 flows of picrite basalt, all pahoehoe; 6 flows of basalt, 5 pahoehoe, 1 aa.

The Halape Ash Member is lithologically similar to the better exposed Kahele Ash Member. Although the unit is thin, it can be correlated between palis (fig. 11.2). The age of the member is not known, but it is probably between 100 ka and 30 ka on the basis of the estimated age of the base of the Hilina Basalt (Easton, 1978).

KAHELE ASH MEMBER (NEW TERM)

This pyroclastic unit crops out all along the Hilina Pali and at Puu Kapukapu (fig. 11.4). The name is derived from Kahele Arroyo[2], a valley at approximately 19°18′00″ N. latitude and 155°17′10″ W. longitude located 1 km east-southeast of the Hilina Shelter. The type section is at Pohakaa Arroyo[2] (table 11.3). Thickness is variable, being only 10-50 cm at Keana Bihopa and Puu Kapukapu, but increasing along the Hilina Pali to 125 cm at Pohakaa Arroyo. Except at Pohakaa Arroyo, the unit is crudely bedded; bedding is better developed than in the Halape Ash Member. The Kahele Ash Member contains some brown and red-brown palagonite but consists mostly of a red clay; 10 to 25 percent more ash material is present than in the Halape Ash Member. At Pohakaa Arroyo the unit also includes a bed, 10–15 cm thick, of gray, coarse, crossbedded sand composed of rounded olivine and lava fragments (table 11.3; fig. 11.5). In addition, a bed of glassy, vesicular scoria and glass fragments only 2–5 cm thick is present; these materials are interpreted to be cinder-cone eruptive debris derived from the southwest rift zone of Kilauea. Eastward thinning of the Kahele Ash Member indicates a possible source in the southwest rift zone for much of this unit. A representative section of this unit is described in table 11.3. The age of this member is not known, but it is presumed to be between 100 ka and 30 ka. Both the Halape and Kahele Ash Members differ from ash units higher in the section in being more deeply weathered (possibly a result of greater age) and in consisting of red clay rather than yellow-brown palagonite. It is possible that the Halape and Kahele Ash Members may represent a period of soil development as well as ash deposition.

POHAKAA ASH MEMBER (NEW TERM)

The Pohakaa Ash Member represents a major period of ash production comparable in scale to that of the Pahala Ash. The name is derived from Pohakaa Arroyo[2] on the Hilina Pali. Pohakaa was a Hawaiian god who lived in precipitous places and who rolled down stones, frightening and injuring passersby (Kalakaua, 1888). The name is appropriate both to the exposure and to the lithology of the unit.

The Pohakaa Ash Member contains intercalated flows, but it is underlain and overlain by about 100 m of lava containing no ash units. The intercalated flows have no distinctive features and are not considered to be part of the Pohakaa Ash Member. At Pohakaa Arroyo, the member consists of six individual ash layers, each 1–4 m thick (total thickness 10–12 m), at Moolelo of five horizons (total 6.5 m), at Keana Bihopa three to five layers (total 7 m), and at Puu Kapukapu four layers (total 10 m). The Pohakaa Member is not exposed at Puueo Pali, probably because the section there is incomplete. The type section of the Pohakaa Member is at Pohakaa Arroyo (tables 11.1, 11.3), where it shows the greatest number, thickness, and lithologic variation of the ash layers; however, the member is more accessible at Keana Bihopa and Puu Kapukapu.

Although the Pohakaa Ash Member has an areal distribution on Kilauea and is lithologically similar to the Pahala Ash, it has been given member instead of formation rank for the following reasons: (1) The Pohakaa Ash Member is limited in present-day exposure and, unlike the Pahala Ash, has only been found on Kilauea Volcano; thus the unit is not as widespread as the Pahala Ash. (2) If the Pohakaa Ash Member were upgraded to formation rank, then the Hilina Basalt would need to be raised to group rank or split into an upper and lower formation separated by the Pohakaa ash layers. Such a division would cause confusion and would be unsuitable for areas where the Pohakaa Ash Member is thin or absent. As there is no compelling need to give the Pohakaa formational rank, the designation of the rank of member seems most adequate at present.

The Pohakaa Ash Member can be subdivided into lower, middle, and upper beds; however, it is not always possible locally to separate the middle and upper beds. These smaller units are not sufficiently characteristic to warrant formal designation as beds or members.

The total thickness of the member is 6–10 m at Puu Kapukapu, 7–15 m at Keana Bihopa, and 8–15 m at Pohakaa; it thus shows an eastward and southward thinning. This thinning is best defined when only the thickness of primary ash beds is included. It has been possible to distinguish reworked beds from primary ash beds within the Pohakaa Ash Member, the Pahala Ash, and younger ash horizons on Kilauea by means of the following criteria:

(1) Primary beds are regularly layered beds of palagonite, 1–30 cm thick, containing remnant small glass shards, distinct grains of pumice or accretionary lapilli, usually yellow-brown in color, and few olivine crystals or rock fragments.

TABLE 11.3.—*Descriptions of Hilina Basalt ash units, Kilauea Volcano*

[Descriptions from type sections; listed in order from oldest to youngest. Location of sections shown in figure 11.3.]

Thickness (cm)	Description
	Halape Ash Member—Keana Bihopa section
	Overlying aa flow
10–20	Red palagonite, grades downward into red-weathered clinker of underlying aa flow.
	Underlying aa flow.
	Kahele Ash Member—Pohakaa Arroyo
	Overlying lava flow.
20	Coarse, red-brown to black, glassy scoria, clinker and pumice, refractive index of glass 1.602±0.002, fragments as large as 20 mm.
40	Red-brown indurated palagonite, rare plagioclase grains, subhedral olivine phenocrysts, some glass shards with refractive index of 1.604.
5–10	Rippled, coarse-bedded, pink to white-gray pebble gravel; 40–50 percent olivine sand, rounded grains; also vesicular lava sand and gravel-size grains.
30	Yellow-red palagonite.
	Underlying lava flow.
	Pohakaa Ash Member—Keana Bihopa
	Overlying lava flow.
	Upper beds (may include parts of middle beds) (45–50 percent ash material; 1.25–1.5 m total thickness).
20	Brown palagonite, fining upward; minor clinker and pumice, mostly altered glass, refractive index of palagonite 1.548±0.002.
5–8	Gray, friable, sand-size lava fragments.
5–8	Pale red palagonite with black glassy cinders 0.5–1 mm large.
30	Gray, laminated, friable beds of fragments 2–4 mm large of rounded, red, gray, and black lava, minor rounded olivine.
35	Pale brown to yellow palagonite, cinders as large as 1 mm, some glass with refractive index 1.606±0.002.
50–100	Weathered aa clinker and red soil.
	Interstratified lava: 16 m of aa and transition pahoehoe olivine basalt and basalt flows (6 flows).
	Middle beds (30 percent ash material; 1.75 m total thickness). Unit cut by stream channels with many local unconformities.
10–20	Red-brown palagonite, with or without soil.
5	Gray, rounded, red and black lava fragments, beds of friable sand.
10	Yellow-brown palagonite.
30	Brown indurated palagonite in beds 1–2 cm thick, locally eroded and unconformably in contact with overlying flow.
8	Finely laminated, gray, friable sand-size rounded lava and olivine fragments, mantles underlying unit.
10 (locally 30–50)	Finely bedded and crossbedded; gray, rounded lava grains; fills channels cut in underlying beds.
10	Brown to red-brown palagonite, vitric cinders 1–2 mm large.
5	Coarse rounded sand-size lava fragments.
20	Brown to red-brown clay, palagonite, or soil.
20	Brown soil containing aa blocks and clinker.
	Interstratified lava: 18 m of aa and pahoehoe basalt and olivine basalt flows (6 flows).
	Lower beds (50 percent ash material; 2.75–3 m total thickness).
30	Brown to red-brown soil and palagonite.
10	Yellow-gray palagonite with black cinders as large as 3 mm.
25	Brown to red-brown palagonite with local beds of glassy cinders.
60	Beds 1–10 cm thick of gray, rounded olivine and lava fragments 2–3 mm large, locally beds 1–2 cm thick of yellow-brown palagonite.
25	Yellow-brown palagonite in beds 1–3 cm thick, brown beds contain glassy cinders 1–2 mm large.
10	Rounded lava and rock fragments, as large as 5 cm.
5	Gray to yellow-brown palagonite.
1–3	Red, black, and gray rounded lava fragments as large as 3 cm.
7	Gray-brown palagonite, bedding on 5-mm scale, vitric cinders as large as 1 mm.
12	Yellow-brown palagonite.
15	Red, black, and gray, vesicular, rounded basalt fragments.
3–7	Brown palagonite, vitric cinders 0.5–1 mm large.
20–50	Gray, finely laminated beds of olivine and lava sand and gravel.
20	Yellow-brown palagonite with rounded red and black lava fragments as large as 1 cm, weakly bedded.
5	Brown palagonite with vitric, angular cinders as large as 4 mm.
25	Brown palagonite.
30	Reddish to purplish-gray aa clinker, brown to pale yellow-brown ash and soil matrix.
	Underlying aa and pahoehoe flows.
	Moo Ash Member—Keana Bihopa (50 percent ash material, 2.5 m total thickness)
	Overlying pahoehoe flows.
10–15	Fine black sand, soil, brown palagonite.
6	Pale brown, accretionary lapilli 1–2 mm in diameter.
1	Purple-brown palagonite, vitric cinders 1–2 mm large.
5	Pink-brown palagonite, vitric cinders 1 mm large.
5	Purple-brown to brown palagonite, with red and black cinders 1 mm large, local carbonized roots.
2–3	Red-brown palagonite, pumice fragments 5–7 mm large.
5–7	Gray, rounded lava and olivine sand.
2	Purple-brown palagonite, vitric cinders 1 mm large.
2	Gray lava sand.
10	Accretionary lapilli 2–3 mm in diameter, local charcoal at base.
1–2	Reddish clay or soil.
5	Finely laminated beds (1–2 mm thick) of gray lava and olivine sand.
5	Brown accretionary lapilli.
1	Reddish soil.
25–30	Brown to purple-gray, red, and black altered flow fragments 10–25 mm large.
1–2	Reddish clay (soil?).
5	Brown, coarse, rounded lava fragments.
5	Brown, glassy, angular pahoehoe crusts 2–3 mm across.
10	Finely laminated gray lava and olivine sand.
5	Vitric black cinders 2–3 mm large.
5	Red-brown clay (soil?).
40–50	Gray, finely laminated beds of rounded flow and clinker material.
10–40	Yellow to red-brown palagonite, soil near base.
	Underlying aa flows.

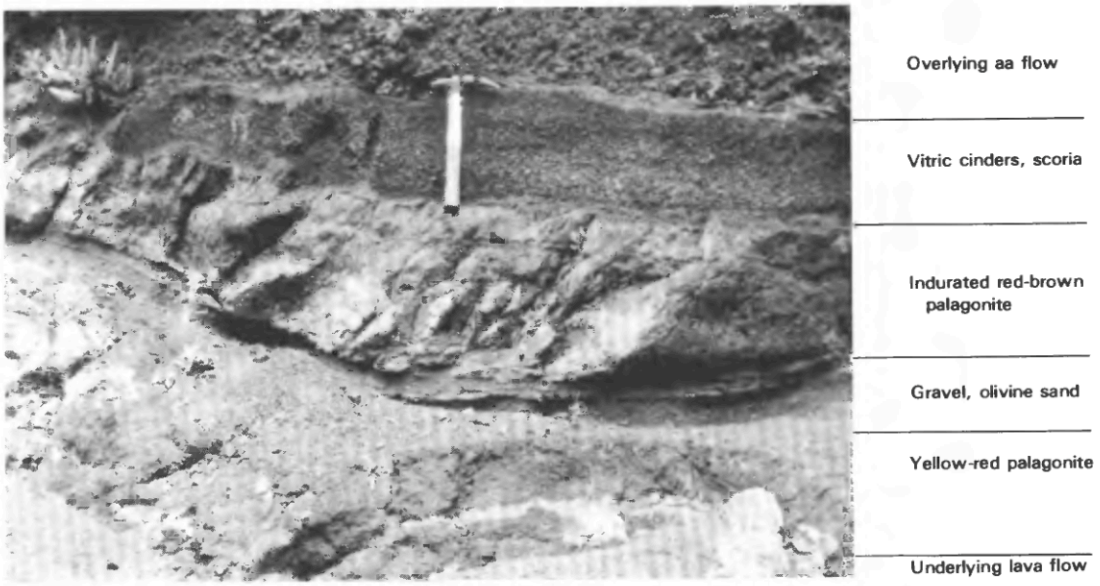

FIGURE 11.5.—Kahele Ash Member of Hilina Basalt at Pohakaa Arroyo, Hilina Pali. Entire thickness of member is shown.

(2) Reworked beds contain sedimentary and pyroclastic material, including: distinct rounded to angular fragments of flow rocks; broken pahoehoe crusts, scoria, and clinker; abundant subrounded olivine fragments (10 percent or more), commonly attached to rock; and minor plagioclase crystal fragments. The bedding layers are thin (1 mm to 5 cm), and crossbedding, undulatory bedding, truncated bedding, and local soil horizons are often present in local channels cut into palagonite. These reworked units are commonly found as friable, gray-weathering, fine-sand to granule-gravel beds.

(3) Surge deposits, which are present mainly in some of the younger ash units contain both primary and reworked layers. The characteristics of these deposits have been described by Swanson and Christiansen (1973) and Decker and Christiansen (1984). Primary and reworked material are intercalated on a fine scale, and it must be realized that most ash layers on Kilauea are a mixture of both types. Sedimentary material similar to that present in the older ash units is found on the surface throughout the Kau Desert region of Kilauea.

The lower beds of the Pohakaa Ash Member form the thickest part of the member (3–4 m) and constitute the first two ash horizons at Pohakaa, Moo, Moolelo, and Puu Kapukapu. At Keana Bihopa, these lower beds are thicker than at other localities. The lower beds consist of alternating beds (5–30 cm) of primary ash (table 11.3; fig. 11.6) and local interbeds of reworked ash and sediment. The lower beds of the Pohakaa Ash Member mark the first appearance of thick palagonitized ash horizons in the exposed Hilina Basalt; they are characterized by a greater proportion of yellow-brown palagonite than the middle and upper beds, by a greater proportion of primary ash beds (50 percent and more along the Hilina Pali, 25 percent and more at Puu Kapukapu), and by the absence of local unconformities, crossbedding, truncated beds, and large- and small-scale channels.

The middle beds of the Pohakaa Ash Member are characterized by a greater abundance of reworked ash beds and sediment (75 percent along the Hilina Pali, 90–95 percent at Puu Kapukapu), a greater abundance of brown and red-brown palagonite, more soil horizons, extensive development of small stream channels 5–50 cm deep, and the presence of crossbedding, truncated beds, channel filling by later ash beds, and filling of channels by lava flows and later primary ash beds (fig. 11.7). Local unconformities are also common in the middle beds.

The upper beds of the Pohakaa Ash Member are present only locally and are restricted almost entirely to large-scale stream channels as much as 10 m deep. These channels grade laterally into a yellow-brown palagonite matrix found in aa clinker layers (usually a red-brown soil matrix is present), indicating that eruption of ash and lava occurred concurrently, in contrast to the situation during formation of the Pahala Ash and the lower parts of the Pohakaa Ash Member. There is also more primary ash material in the upper beds than in the middle beds. Yellow-brown palagonite is more abundant in the upper beds, and small-scale channeling (less than 2 m across), crossbedding, and other sedimentary structures common to the middle beds are less pronounced in the upper beds. A section through the Pohakaa Ash Member at Pohakaa Arroyo is described in table 11.3.

The thickness of the middle and upper beds is difficult to establish. At Keana Bihopa and Pohakaa Arroyo, the middle and upper beds are thickest where located in the deepest parts of the valley chutes, central to the incised valleys. Aa flows are present locally in these channels, but they do not fill them. Along Moolelo and at Puu Kapukapu, the beds of the Pohakaa Ash Member are much more uniform in thickness, and they can be traced laterally with little variation in thickness. These latter two areas lack present-day stream channels. The presence of the thickest, best developed

FIGURE 11.6.—Closeup view of lower beds of Pohakaa Ash Member, Keana Bihopa, showing typical bedding and lithology. Pahala Ash beds are similar to those shown here.

FIGURE 11.7.—Middle beds of Pohakaa Ash Member of Hilina Basalt, Keana Bihopa. Stream channel and minor crossbeds to left of hammer (30 cm long) are mantled by later ash and stream deposits. Overlying aa flow (upper right) fills later channel developed within upper beds in photograph.

sections in current valley cuts and the absence of channels elsewhere along the palis indicate that the drainage system on the south flank of Kilauea has changed very little for several thousand years.

At Pohakaa Arroyo, in the middle beds of the Pohakaa Ash Member, a crossbedded, rippled, pale-gray unit of finely laminated beds containing lithic and crystal fragments forms a horizon 10–15 cm thick that is interbedded with the typical red and yellow-brown palagonite beds (fig. 11.8). This unit closely resembles an outcrop at the Lanai Lookout on Oahu described by Fisher (1977) and attributed to base-surge deposition. Unfortunately, there are no diagnostic textures present at the Pohakaa exposure that would confirm a base-surge origin for the deposit. The proximity of this outcrop to the southwest rift zone does indicate that a base-surge deposit could be present. No similar unit was found in any of the other Hilina sections.

Abundant soils, red-brown palagonite, and extensive stream development imply a more humid climate during the deposition of the Pohakaa Ash Member than at present. This is supported by the presence of *Metrosiderus* sp. (Ohia lehua) tree molds in flows overlying the middle beds of the Pohakaa Ash Member at Puu Kapukapu and at Pohakaa Arroyo. These are the only tree molds found in the Hilina section, other than those present in flows within and overlying the Pahala Ash.

The age of the Pohakaa Ash Member is not known. The member is older than 30 ka because it underlies the Pahala Ash (Kelley and others, 1979), and it may be on the order of 40–50 ka. This age is based on lava and ash accumulation rates obtained from Nanahu Arroyo[2] by Easton (1978): 1 cm/yr for 100 m lava; 1 cm/yr for 10 m of ash and soil. No chemical data are available on ash from the Pohakaa Ash Member. Refractive-index measurements of basaltic glass from the member are similar to those of other Kilauea glass samples (fig. 11.9). A Kilauea source is thus very likely for the primary ash units in the Pohakaa Ash Member, and

FIGURE 11.8.—Middle beds of Pohakaa Ash Member of Hilina Basalt, Pohakaa Arroyo. Undulating beds near hammer may be base-surge deposit. See text for additional details.

the distribution of ash material in the member is consistent with such a source. As discussed in further detail below in the section "Pahala Ash," a Mauna Loa source for both the Pahala and the Pohakaa cannot be ruled out.

MOO ASH MEMBER (NEW TERM)

The Moo Ash Member is well exposed along the Hilina Pali and is also present at Puu Kapukapu and Puueo Pali. The name is derived from Moo Arroyo[2], where the unit is exposed; Moo is the Hawaiian word for dragon. The type section is at Keana Bihopa and is described in tables 11.1 and 11.3.

At Keana Bihopa, the Moo Ash Member underlies a sequence of olivine basalt pahoehoe flows 10–12 m thick, which are capped by Pahala Ash. At this locality, the Moo Ash Member ranges in thickness from 2.5 m on the inward (north) side of the arroyo to 1.5 m near the face of the pali. The overlying flows thicken where the ash thins. It appears that the ash has been eroded away from the lip of the pali and later covered by flows that draped the pali. The Moo Ash Member is lithologically similar to the Pohakaa Ash Member and the Pahala Ash, being composed of a mixture of palagonite and vitric ash (primary ash beds) and reworked ash and sediment.

Criteria for distinguishing the Moo Ash Member from the Pahala Ash include the following: (1) The Pahala Ash is overlain by and intercalated with flows bearing tree molds of *Cibotium* sp. (tree ferns). No tree molds are found below the base of the Pahala Ash down to the middle beds of the Pohakaa Ash Member. (2) The Moo Ash Member is a tuff and sediment horizon 1–2 m thick located 10–15 m below the Pahala and separated from it by a series of mineralogically uniform basalt flows. (3) The Moo Ash Member contains several beds of accretionary lapilli, which are absent from the Pahala Ash on Kilauea.

The Moo Ash Member may be present at Puu Kapukapu and Puueo Pali (fig. 11.4) as a bed of yellow-brown palagonite and

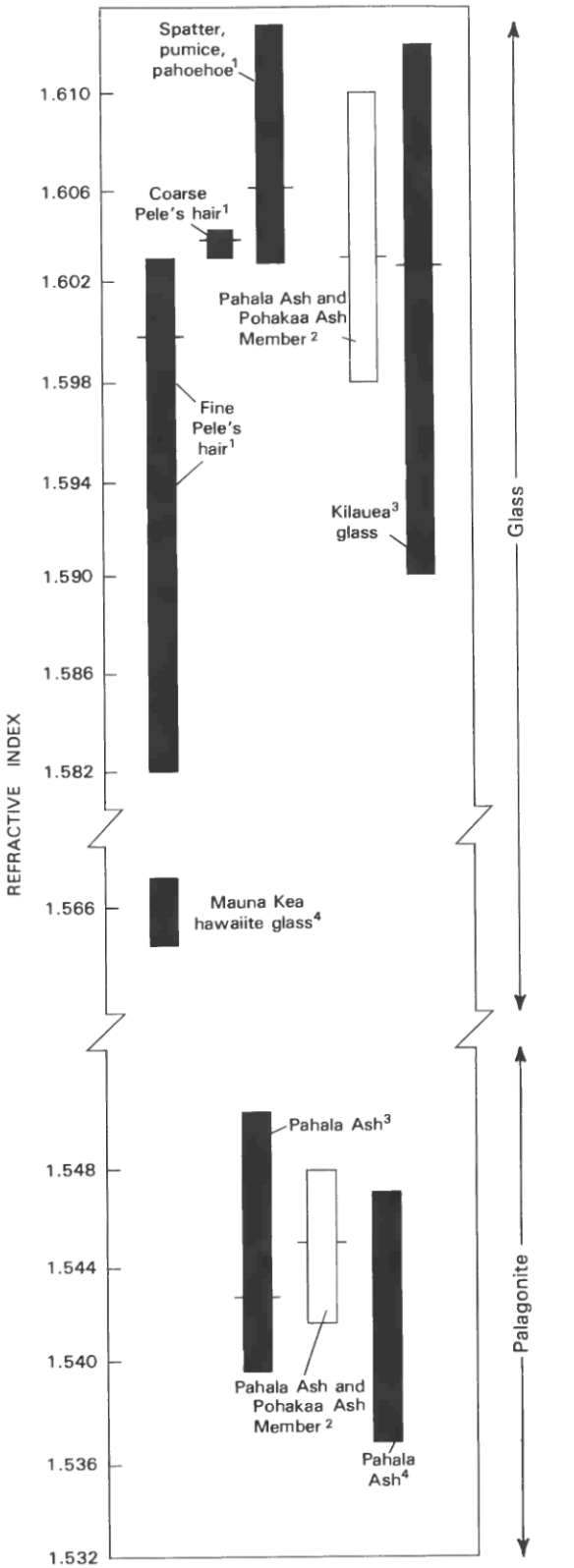

FIGURE 11.9.—Refractive-index measurements of Kilauea glass and palagonite and Mauna Kea glass showing basaltic nature of preserved glass in Pahala Ash and Pohakaa Ash Member. Sources identified by number: 1, Duffield and others (1977); 2, Easton (1978); 3, Wentworth (1938); 4, Macdonald (1949).

sediment 50–100 cm thick and located 3 m below the base of the Pahala Ash. At both these localities, and at Puu Kaone, this ash layer lacks accretionary lapilli, and its assignment to the Moo Ash Member is tentative.

In some areas the Moo Ash Member may be conformable with the lower part of the Pahala Ash, and in such instances it would be difficult to distinguish the two units without radiocarbon ages. At present, the Moo Ash Member is considered part of the Hilina Basalt, because the overlying lavas are similar chemically to those of the Hilina Basalt and distinct from Puna Basalt flows, and wherever the Moo Ash Member is exposed, it is separate from the Pahala Ash.

The age of the Moo Ash Member is not precisely known. It is older than the 24 ka age for the base of the Pahala Ash at Puu Kaone and the 30 ka age for the base of the Pahala Ash on Mauna Loa (Kelley and others, 1979). A reasonable estimate for the age of the Moo Ash Member is between 30–35 ka. Charcoal is present in the Moo Ash Member, but sufficient quantities have not yet been recovered for dating purposes. The Moo Ash Member is lithologically similar to the Pohakaa Ash Member and the Pahala Ash and probably had a similar origin and source.

PAHALA ASH

The Pahala Ash on Kilauea Volcano is only exposed atop fault scarps at Hilina Pali, Puueo Pali, Holei Pali, Puu Kapukapu, and Puu Kaone, and in the Glenwood District (figs. 11.3, 11.10). The distribution of the Pahala Ash on the Island of Hawaii is shown in figure 11.10. The Pahala Ash on Kilauea has been described by Stone (1926), Stearns and Clark (1930), Wentworth (1938), Stearns and Macdonald (1946), Fraser (1960), Walker (1969), and Easton (1978). Stearns and Macdonald (1946) review the older literature on the Pahala Ash on the Island of Hawaii, much of which is concerned with the origin and source of the ash. Wentworth (1938), Hay and Iijima (1968), and Hay and Jones (1972) present chemical analyses of the Pahala from Kilauea, although many of these samples were highly altered. Hay and Iijima (1968), Hay and Jones (1972), and Easton and Easton (1983) have examined the alteration of the Pahala Ash.

The formation was named for the town of Pahala on Mauna Loa Volcano, where the ash is exposed on the surface, but not in section (Wentworth, 1938). Stearns and Macdonald (1946) do not specify a type or reference locality but do present a section through the Pahala Ash at the base of Kaoiki Pali, 5 km southwest of Kilauea caldera. Wentworth (1938) describes a number of sections through the Pahala Ash. The Pahala Ash at Puu Kapukapu and Puu Kaone on Kilauea (fig. 11.3) is well exposed, and it is proposed that sections at these two localities be designated as reference sections for the Pahala Ash on Kilauea. A section through the Pahala Ash at Moolelo (fig. 11.11) is typical of the character of the formation on the south flank of Kilauea and is here designated as the principal reference section. It consists of a mixture of yellow-brown palagonite derived from weathered ash, and beds of reworked ash and sediment. The section at Puu Kaone (fig. 11.12) shows the presence of intercalated flows, which are present locally throughout the Pahala Ash.

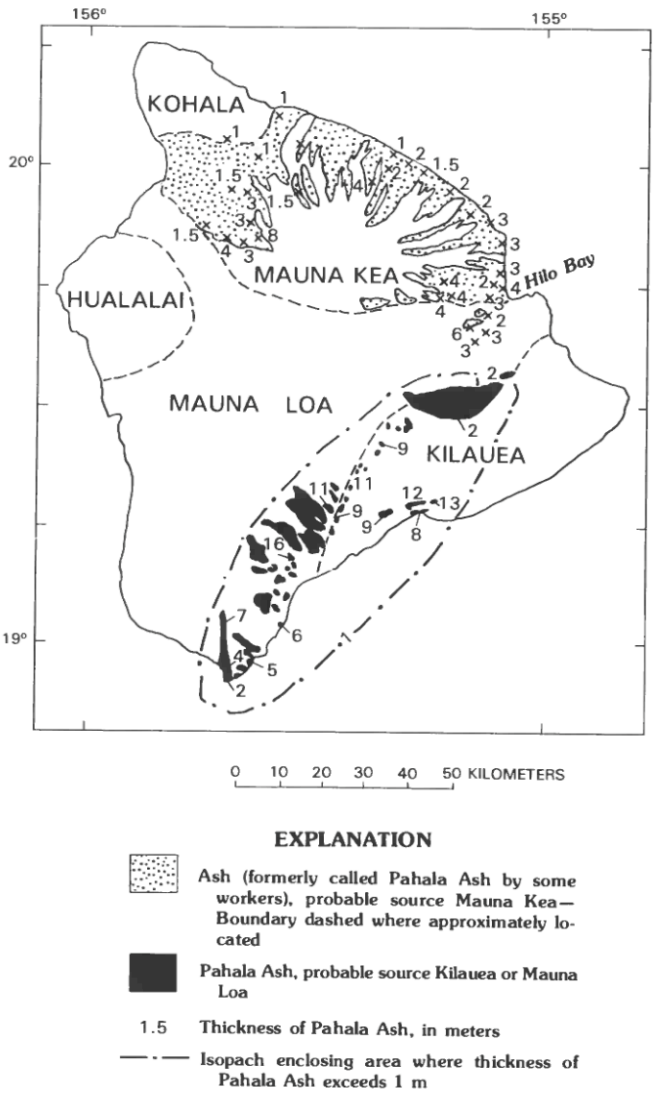

FIGURE 11.10.—Distribution of Pahala Ash on Island of Hawaii. Data from Stearns and Macdonald (1946) and Fraser (1960). The main period of Pahala Ash deposition on Kilauea and Mauna Loa was between 24 ka and 10 ka (Kelley and others, 1979). Distribution of Pahala Ash is also consistent with a Mauna Loa source instead of Kilauea source indicated here.

Flows are interbedded with or overlie the Pahala Ash at Puu Kaone, Puu Kapukapu, and in places along the Hilina Pali. Flows within the Pahala Ash are more abundant south and east of the summit area and are characterized by the presence of *Cibotium* sp. (tree fern) tree molds 15–25 cm in diameter. In addition, some flows contain hypersthene, a mineral rarely observed in the Hilina Basalt. Chemically, these lava flows are similar to Puna Basalt lava flows, and they are here considered to be part of the Puna Basalt. They are also mineralogically similar to the Puna Basalt flows, and they

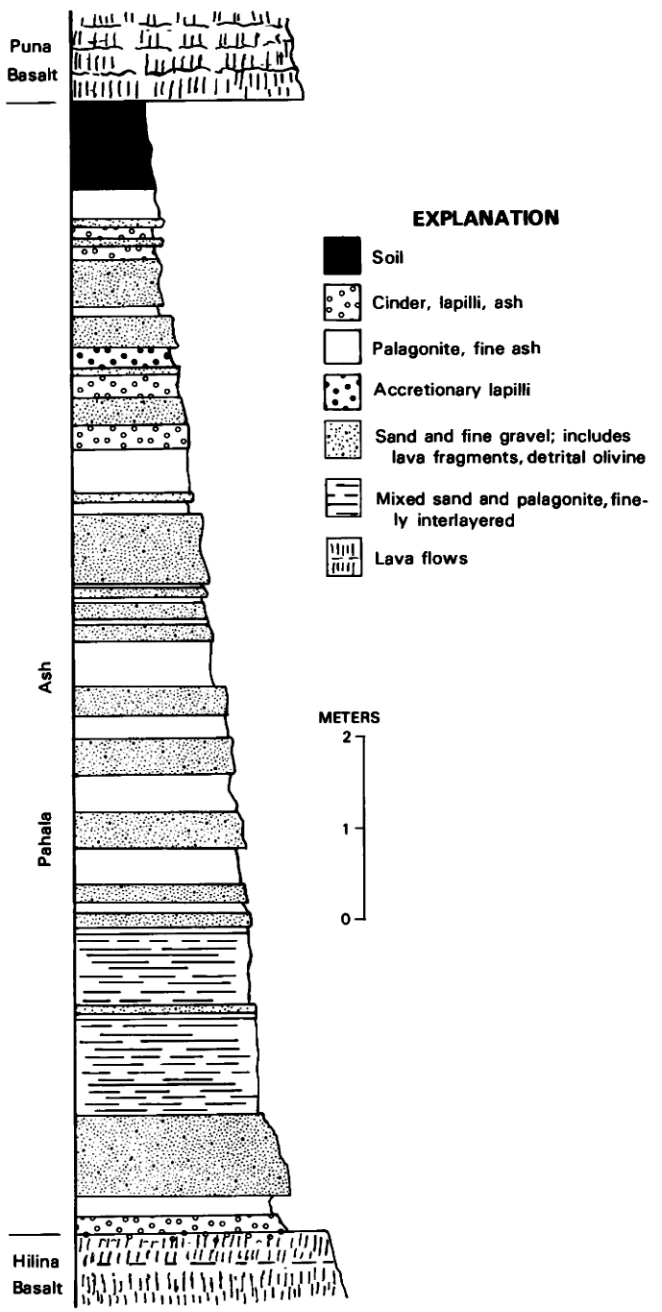

FIGURE 11.11.—Measured section of Pahala Ash exposure 14.25 m thick at Moolelo, Hilina Pali, 20 km south of Kilauea caldera (lat 19°17′ N., long 155°19′ W.), showing proportion of ash and reworked material (sand and gravel) in typical section.

differ only in the presence of tree molds. In areas where the Pahala Ash is absent, it is unlikely that these flows could be distinguished from other Puna Basalt flows. This supports the historical designation of the Pahala Ash as essentially a pyroclastic unit.

Pahala Ash beds at Puu Kapukapu are 1–2 m thick and are underlain by 6–8 m of basalt flows with *Cibotium* sp. tree molds. Farther east, the beds are 0–2 m thick and are overlain by 10–12 m of olivine basalt flows and capped by an additional 2–4 m of ash. The section at Puu Kaone (fig. 11.12) is similar in that it also contains interbedded Puna flows. At Puueo Pali, farther to the east, three 1-m-thick ash beds are interstratified with lava flows 30 m below the top of the pali. These beds contain coarser vitric fragments than are common to the west, and they may be related to fire-fountaining along the east rift zone. If this is the case, these ash beds may not be correlative with the Pahala Ash.

Widely varying thicknesses for the Pahala Ash at Puu Kaone (10–14 m) and Puu Kapukapu (6–12 m) have been reported in the literature (Stone, 1926; Stearns and Clark, 1930; Wentworth, 1938; Stearns and Macdonald, 1946), but these figures include the lava flows. Ground slumping in the area has moved blocks of ash downslope, burying underlying flows and coating flows with a thin veneer of ash. Both effects make the Pahala Ash appear thicker than it truly is.

The Pahala Ash exposed along the Hilina Pali averages 15 m in thickness. In addition, the amount of primary ash versus reworked ash and sediment is greater along the Hilina Pali (50 percent primary) than at Kapukapu (25–40 percent primary). Both effects are consistent with a source for the Pahala on Kilauea or Mauna Loa (see later discussion).

On Mauna Loa, the Pahala Ash contains fewer reworked or sedimentary beds than on Kilauea, and lapilli-size material is more common (Stearns and Macdonald, 1946). The thickness of the Pahala Ash on Mauna Loa varies (fig. 11.10), but locally it is as thick as on Kilauea. On parts of Mauna Loa, the ash resembles loess and may have been transported by wind either during or after deposition.

A charcoal sample collected by G. Fraser from the lower part of the Pahala Ash at Puu Kaone was dated at 17.36±0.65 ka (Rubin and Berthold, 1961). Resampling near this site in 1977 at the base of an olivine basalt flow (Puna Basalt) interbedded with the ash (fig. 11.12) yielded charcoal that was dated at 22.5±0.5 ka and 22.8±0.5 ka (Kelley and others, 1979). These ages are preferred over the previous age of 17.36 ka because three counters were used instead of one, and the earlier sample was diluted because of insufficient carbon (M. Rubin, written commun., 1978). The data indicate that the base of the Pahala Ash on Kilauea has an age of about 23–25 ka. An age of 31.1±0.9 ka has been reported from the base of Pahala Ash on Mauna Loa (Kelley and others, 1979). This is older than the age at Puu Kaone, and it is possible that these lowermost dated ash beds on Mauna Loa may be correlative with the Moo Ash Member of the Hilina Basalt on Kilauea.

The upper part of the Pahala Ash has been dated at several localities on Mauna Loa and Kilauea (see Kelley and others, 1979). The ages range from about 12 ka to 0.2 ka; such a range would be expected because these ages date the time the formation was first buried by lava. The oldest of these overlying flows have ages of 10–12 ka, indicating that the bulk of the ash was deposited between 24 ka and 10 ka on the two volcanoes. Little flow activity occurred on the south flank of Kilauea during this interval. The upper part of

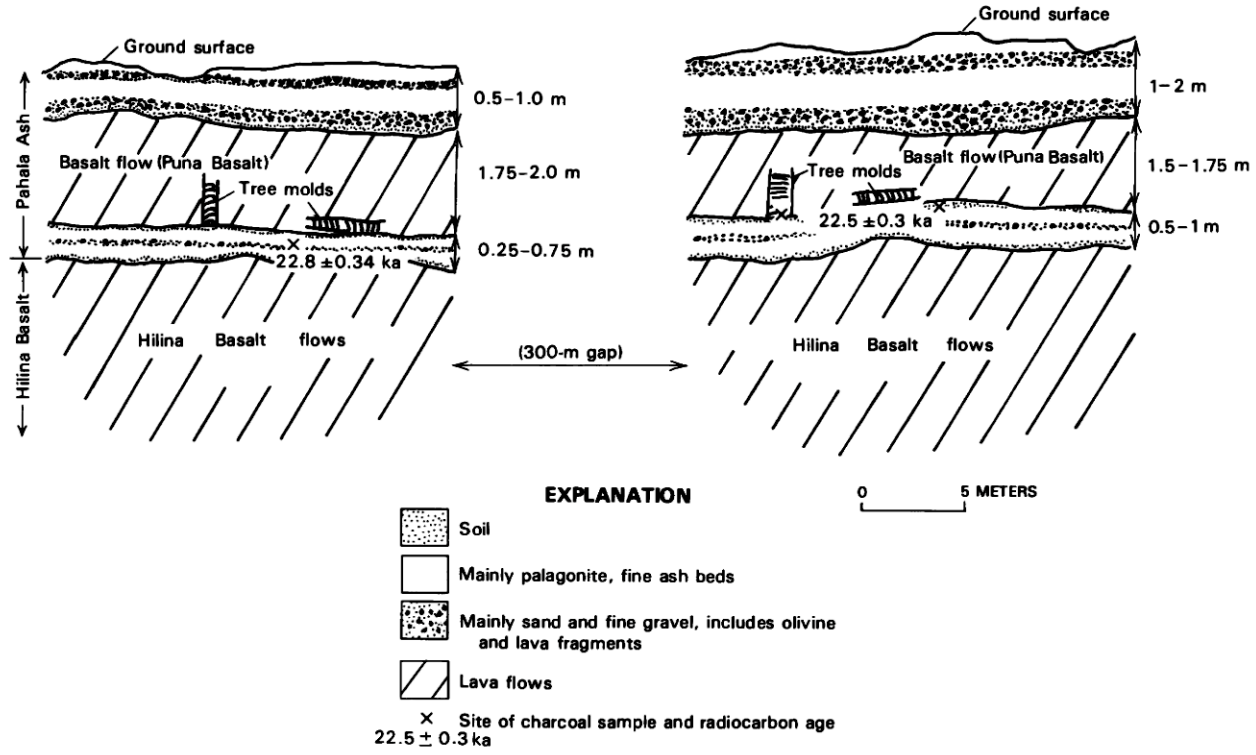

FIGURE 11.12.—Stratigraphic sections of Pahala Ash at Puu Kaone, Kilauea Volcano. Radiocarbon ages from Kelley and others (1979).

the Pahala Ash is obviously not useful as a time-stratigraphic horizon because of the long interval between deposition and burial of the ash. The base of the ash may mark a time-stratigraphic horizon, but additional ages are needed to confirm this. The origin of the ash is discussed later in the paper.

PUNA BASALT

The Puna Basalt covers most of Kilauea and was mostly erupted within the last 10,000 years following Pahala Ash deposition. Historical lava flows are included within the formation. The name is derived from the Puna District of Kilauea, where these flows are abundant (Stearns and Macdonald, 1946). Although Stearns and Macdonald defined the Puna as overlying the Pahala Ash, lava flows here considered to be part of the Puna are locally intercalated with the Pahala Ash (see section "Pahala Ash"). Thus, the base of the Puna Basalt generally overlies the Pahala, but locally may be present within the Pahala and may be as old as about 23 ka. No good sections of the prehistoric lava flows are present in the type locality designated by Stearns and Macdonald (1946, p. 193–194), in the walls of Kilauea caldera, although many surface exposures of flows are present.

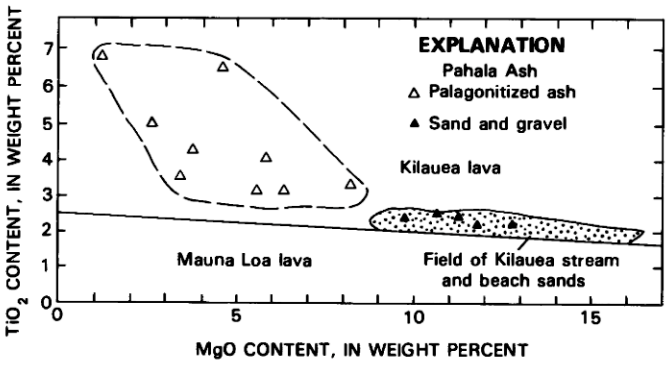

FIGURE 11.13.—TiO_2 content plotted against MgO content for two main lithologies in Pahala Ash. Palagonite beds show a wide range, in part because of in-place alteration (Hay and Jones, 1972; Easton and Easton, 1983). Detrital beds in Pahala Ash fall in field of recent Kilauea stream and beach sands and show less evidence of alteration (Easton and Easton, 1983). Straight line separates field of Kilauea and Mauna Loa lava flows (Wright, 1971; Easton and Garcia, 1980).

LAVA FLOWS

There are some slight chemical and mineralogical differences between Hilina Basalt and Puna Basalt lavas (see section above on Hilina Basalt; Easton and Garcia, 1980). Descriptions of Puna Basalt lava, particularly the historical flows, can be found in Stearns and Clark (1930), Stearns and Macdonald (1946), Easton and Garcia (1980), and Holcomb (1981). Chemical analyses of prehistoric flows of the Puna Basalt are given in Wright (1971). Sections through the prehistoric flows of the formation are present in the walls of Kilauea caldera, notably at Uwekahuna Bluff. Other sections through prehistoric flows are in pit craters along the east rift zone, including Kilauea Iki, Makaopuhi Crater, and Napau Crater; and along the Hilina Pali at the same locations as the Hilina Basalt exposures; these sections can be regarded as reference sections (table 11.1) for the Puna Basalt because they typify groups of flows originating from the summit, the east rift zone, or both areas of Kilauea.

PYROCLASTIC AND SEDIMENTARY DEPOSITS

Several prehistoric ash units are interbedded with lava flows of the Puna Basalt. Only two of these units have been given formal status as members of the Puna Basalt—the Keanakakoi Ash Member and the Uwekahuna Ash Member (renamed to indicate their dominant lithology; formerly the Keanakakoi and Uwekahuna Members of Easton and Garcia, 1980). These members are generally restricted to the summit region of Kilauea. Apart from these and several unnamed older ash layers, the products of the 1924 phreatic eruption in Kilauea crater are also present overlying the Keanakakoi Ash Member on the southwest flank of Kilauea (Decker and Christiansen, 1984). These very young deposits are considered to be part of the Puna Basalt.

OLDER ASH UNITS

At Nanahu Arroyo along the Hilina fault system (figs. 11.3, 11.14) several flow and ash units overlie the Pahala Ash. The uppermost of these units has a radiocarbon age of 1.13 ± 0.25 ka (Kelley and others, 1979) and may be correlative with the Uwekahuna Ash Member. The next lowest soil layer was overlain by lava at about 3.48 ± 0.25 ka (Kelley and others, 1979). A third unit consists of 65 cm of ash that overlies a 69-cm-thick soil horizon developed on a lava flow overlying the Pahala Ash. This ash unit was covered by lava at 4.82 ± 0.2 ka (Kelley and others, 1979).

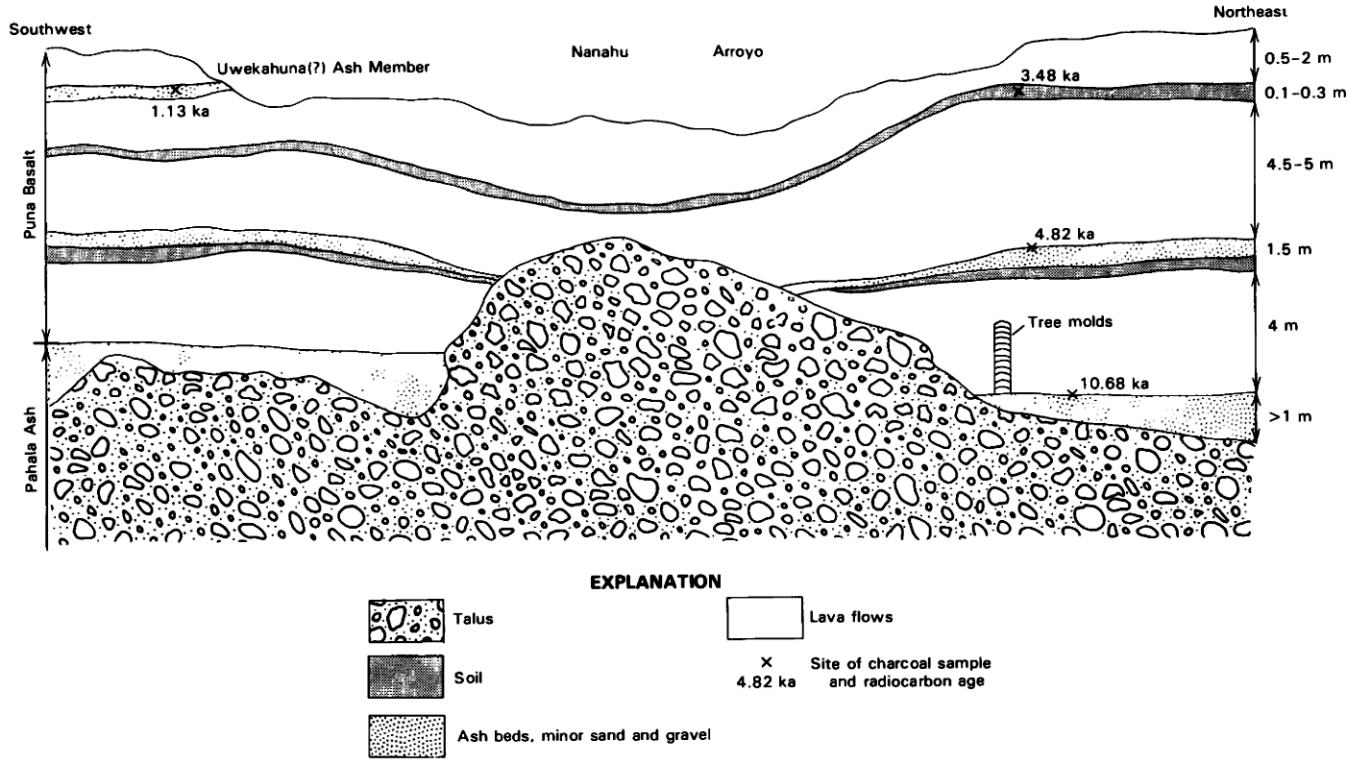

FIGURE 11.14.—Stratigraphic section through Puna Basalt at Nanahu Arroyo. Location of dated charcoal samples (Kelley and others, 1979) and Puna Basalt soil and ash units are shown. Only part of exposed Pahala Ash at this locality is shown.

Given the thick accumulation of soil beneath the ash and the minimal evidence of soil formation in the ash itself, this age may be close to the time of ash deposition. None of these older ash units is widespread enough to be given formal stratigraphic status at present, but they do indicate older explosive activity of Kilauea Volcano between the times the Pahala Ash and Uwekahuna Ash Member were deposited.

Uwekahuna Ash Member

The Uwekahuna Ash Member is a hydromagmatic deposit exposed near the base of the present caldera cliffs at Kilauea and on or near the surface of some areas on the southeast flank of Mauna Loa. The unit was named by Stone (1926) for Uwekahuna Bluff, where about 5 m was previously well exposed (see Powers, 1916). It was subsequently covered by lava and has been partly exposed (about 2 m) more recently (Casadevall and Dzurisin, chapter 13). The member has a distribution similar to that of the Keanakakoi Ash Member, and it probably had a similar origin (Decker and Christiansen, 1984). Radiocarbon ages on charcoal from overlying and underlying flows indicate an approximate age of 1.1–1.5 ka for this unit (Kelley and others, 1979). Descriptions of the unit are found in Casadevall and Dzurisin (chapter 13), and also in Powers (1916), Wentworth (1938), Stearns and Macdonald (1946), and Decker and Christiansen (1984). A reference section is here designated as shown in table 11.1.

Keanakakoi Ash Member

This unit was originally called the Keanakakoi Formation by Wentworth (1938), who considered it to comprise the whole series of ash layers southwest of Kilauea caldera, including ash of the 1790 and 1924 eruptions. The name is derived from Keanakakoi Crater near Kilauea caldera, and the unit is well exposed at its type locality along scarps southwest of Keanakakoi Crater. Powers (1948) also considered the unit to include all fragmental eruptive deposits southwest of Kilauea caldera, and he recognized that these deposits included a number of unconformities. Only the uppermost layer of the member was considered by Powers (1948) to be related to the 1790 eruption. Recent work by Swanson and Christiansen (1973), Christiansen (1979), and Decker and Christiansen (1984) indicate that the member consists of fallout, pyroclastic-surge, and reworked deposits, and were mostly deposited during the 1790 eruption. Recent radiocarbon dating has confirmed this interpretation (Kelley and others, 1979). Decker and Christiansen (1984) showed an idealized section of the member, Malin and others (1983) briefly described the member, and Stearns and Clark (1930) produced a map of its distribution.

Decker and Christiansen (1984) noted the following six major units within the Keanakakoi Ash Member, each unit separated from its neighbors by truncated surfaces: (1) Basal wind-redeposited Pele's hair and reticulite pumice. (2) Predominantly well sorted vitric ash with planar mantle bedding. (3) Less well sorted lithic-vitric ash, commonly with wavy and lenticular bedding, cross-stratification, and bedding sags beneath lithic blocks. (4) A local lava flow. (5) Lithic ash and blocks, with abundant accretionary lapilli and cross-stratification. (6) An uppermost deposit of fallout and wind-resorted pumice and Pele's hair. Units 1 and 2 correspond roughly to the "lower mixed unit" of Malin and others (1982); unit 3 is their "intermediate vitric unit"; and unit 5 is their "upper lithic unit." Malin and others (1982) suggested that the upper layer of fallout and wind-resorted pumice and Pele's hair was deposited between 1790 and 1823, but do not include it in their Keanakakoi.

The definition of the Keanakakoi in this report is that of Decker and Christiansen (1984), including both the lower and upper pumices. The Keanakakoi was mainly deposited during the 1790 eruption, but the basal pumice is slightly older (R.L. Christiansen, oral commun., 1986), and the overlying fallout and the unconformably overlying fallout and resorted pumice layer—the "golden pumice" of Sharp and others (chapter 15)— is circa A.D. 1820.

PALEOCLIMATE AND PALEOGEOGRAPHY

During the 10,000 to 15,000 years of Pahala Ash deposition on Kilauea, very few lava flows reached its south flank. This in part accounts for the thickness of the formation and is probably a result of diversion of lava away from the south flank by an incipient Kaoe fault zone, by entrapment of lava within a deep caldera, or by a prolonged period of mainly ash production at Kilauea caldera. This long period of deposition also allowed reworking of the ash and development of sheetwash plains consisting of reworked ash and broken flow material, much as is occurring today southwest of Kilauea caldera. Similar conditions probably also existed during deposition of the Pohakaa Ash Member of the Hilina Basalt.

In addition, lava flows intercalated with and immediately overlying the Pahala Ash and Pohakaa Ash Member contain abundant tree molds. The presence of *Cibotium* sp. (tree fern) molds as much as 25 cm in diameter within Pahala flows at Puu Kaone and Puu Kapukapu indicate that sufficient time elapsed between deposition of the ashes and the flows to produce forest growth (about 400 years; see Atkinson, 1971). Annual rainfall of about 200 cm is needed for the development of fern forests. The area of these molds now receives less than 50 cm of rain annually; hence a wetter climate probably existed during these periods of ash deposition. Tree molds are absent elsewhere in the Hilina Basalt. This paleoclimatic regime may also have been important in establishing conditions favorable for ash production (for example, by producing a higher ground-water table).

DISCUSSION

In the following discussion on the origin and source of the Pohakaa, Moo, and Pahala pyroclastic deposits, emphasis is placed on the better studied Pahala Ash. However, all of these units are similar in lithology and distribution, and the comments with regard to the Pahala Ash are probably applicable to the Pohakaa and Moo ashes as well.

The source of the Pahala Ash is controversial. Stearns and Clark (1930) and Wentworth (1938) attributed the ash to explosive eruptions of vents on Mauna Loa Volcano and elsewhere outside Kilauea. Stone (1926), Stearns and Macdonald (1946), Fraser

(1960), and Easton (1978) regarded the Pahala deposits southwest of Kilauea caldera as originating from Kilauea (fig. 11.10). Refractive-index measurements of Pahala Ash glass (fig. 11.9) and chemical analyses of the glass (Fraser, 1960; Hay and Iijima, 1968; Hay and Jones, 1972; Easton and Easton, 1983) confirm that the bulk of the ash is basaltic in composition; hence it is probably not derived from Mauna Kea, which would likely have glass erupted of hawaiite composition at that time (Porter, 1979). Isopach patterns of the Pahala Ash (fig. 11.10; Fraser, 1960) are also consistent with a Kilauea source, as is the greater proportion of ash versus detrital material closer to the summit of Kilauea caldera. However, the isopach data is also consistent with a Mauna Loa source for the Pahala Ash (R.T. Holcomb, written commun., 1983, 1984). Rare-earth-element data on the Pahala Ash (fig. 11.15; Easton and Easton, 1983) are inconclusive regarding the origin of the primary ash material. It is definitely basaltic in composition, but alteration makes it difficult to distinguish between a Kilauea and a Mauna Loa source (fig. 11.15). The detrital component of the Pahala Ash on Kilauea (fig. 11.13) is derived from the weathering of Kilauea lavas and is not as altered as the ash component of the formation (fig. 11.13; Easton and Easton, 1983).

Since the original nature of the Pahala Ash is difficult to decipher because of alteration, the origin of the ash has also remained controversial. Two suggested origins are as follows: (1) The ash may consist of magmatic fire-fountain debris (Stearns and Clark, 1930; Wentworth, 1938; Stearns and Macdonald, 1946); Stearns and Macdonald (1946) considered that most of the Pahala Ash was of fire-fountain origin, but allowed for the possibility of a phreatic or phreatomagmatic origin. (2) The ash may be the product of phreatic or phreatomagmatic eruptions of Kilauea that were similar to but of larger scale and duration than the 1790 and May 1924 eruptions of Kilauea's summit (Stone, 1926; Fraser, 1960).

Physical evidence for a phreatic or phreatomagmatic origin include the presence of accretionary lapilli and lithic and crystal fragments in the Pahala, Pohakaa, and Moo ashes in addition to the predominant vitric ash. Judging from the 1790 and 1924 eruptions, hydromagmatic activity at Kilauea's summit is an effective means of producing large quantities of ash; this process of origin is also consistent with a wetter climate during these periods of ash deposition. If the ash is from eruptions at Mauna Loa, then snow and ice in the summit area could also have been a significant factor in ash production (R.T Holcomb, written commun., 1983, 1984). Alternatively, G.A. Macdonald (written commun., 1978) reported that the fire-fountain debris for the 1959 Kilauea Iki eruption could be found as far south as Ka Lae (the southernmost point on the Island of Hawaii) on Mauna Loa, hence the extensive distribution of the Pahala Ash on Kilauea and Mauna Loa does not preclude a magmatic origin. However, this fire-fountain debris consists only of pumiceous shards and Pele's hair and does not include blocky shard fragments such as are common in the Pahala Ash. Possibly both origins are correct: the ash may be predominantly hydromagmatic in origin, but magmatic deposits may also be present locally within the formation.

Decker and Christiansen (1984) have discussed the significance of the number of pyroclastic deposits within the exposed Kilauea section with respect to future volcanic hazards. Holcomb (chapter 12) discusses how some of these ash deposits may be related to caldera collapse at Kilauea. The ash horizons are therefore important markers of Kilauea volcanic activity.

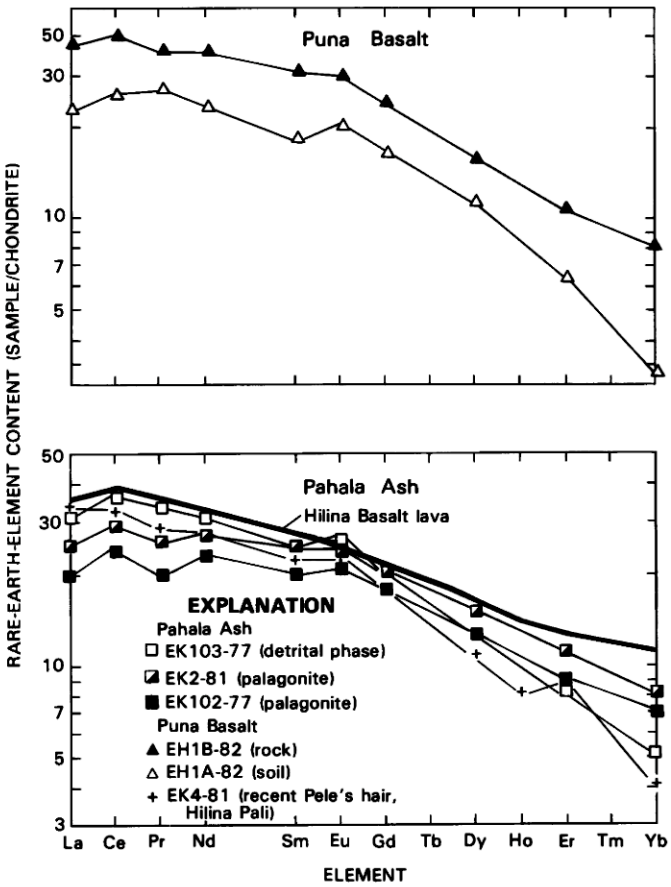

FIGURE 11.15.—Chondrite-normalized rare-earth-element (REE) data for Pahala Ash samples. Sample EK103-77 is a gray-weathering sand bed from Pahala Ash at Keana Bihopa, Hilina Pali. Its REE pattern is similar to typical Kilauea lava (for instance, Hilina Basalt lava shown) and modern Kilauea stream and sheetwash sands (not shown; Easton and Easton, 1983); low content of heavy REE in sample may be a result of presence of detrital olivine in the sample. Sample EK102-77 is palgonitized ash from Pahala Ash overlying EK103-77. Although the REE pattern is similar to that for Hilina Basalt lava, REE abundances are about 20–25 percent lower than in lava. The same is true of sample EK2-81, a Pahala Ash sample from Mauna Loa near town of Waiohinu. The REE loss in Pahala Ash palagonite is similar to that observed for soils developed over Puna Basalt lava flows from east rift zone of Kilauea (EH1A-82, EH1B-82) and is probably related to weathering and alteration. The REE data indicate a basaltic composition for Pahala Ash, but alteration, particularly with respect to light REE, prevents discrimination between Mauna Loa and Kilauea sources.

REFERENCES CITED

Atkinson, I.A.E., 1971, Successional trends in the coastal and lowland forests of Mauna Loa and Kilauea Volcano, Hawaii: Pacific Science, v. 23, p. 387–400.

Avias, J., Davis, D.A., Hanzawa, S., Ladd, H.S., Macdonald, G.A., and Obelliane, J.M., 1956, Oceanie proprement dite [Oceania properly speaking],

in Oceanie, Lexique Stratigraphique International [International Stratigraphic Lexicon], v. 6, pt. 2: Paris, Centre National de la Recherche Scientifique, 286 p.

Christiansen, R.L., 1979, Explosive eruption of Kilauea Volcano in 1790 [abs.], *in* Hawaii Symposium on Intraplate Volcanism and Submarine Volcanism, Hilo, Hawaii, July 16–22, 1979: p. 158.

Decker, R.W., and Christiansen, R.L., 1984, Explosive eruptions of Kilauea Volcano, Hawaii, *in* Explosive volcanism: Inception, evolution and hazards: Washington, National Research Council, National Academy Press, p. 122–132.

Duffield, W.A., Gibson, E.K., Jr., and Heiken, G.H., 1977, Some characteristics of Pele's hair: U.S. Geological Survey Journal of Research, v. 5, p. 93–101.

Easton, M.G., and Easton, R.M., 1983, Effects of weathering on trace and rare-earth element contents of volcanic sediments, Island of Hawaii, USA [abs.]: Geological Association of Canada Program with Abstracts, v. 8, p. A-19.

Easton, R.M., 1978, The stratigraphy and petrology of the Hilina Formation: The oldest exposed lavas of Kilauea Volcano, Hawaii: University of Hawaii, University of Hawaii, Honolulu, M.S. thesis, 274 p.

Easton, R.M., and Garcia, M.O., 1980, Petrology of the Hilina Formation, Kilauea Volcano, Hawaii: Bulletin Volcanologique, v. 43, p. 657–673.

Fisher, R.V., 1977, Erosion by volcanic base surge density currents: U-shaped channels: Geological Society of America Bulletin, v. 88, p. 1287–1297.

Fraser, G.D., 1960, Pahala Ash—an unusual deposit from Kilauea Volcano, Hawaii [art.] 163 *of* Short papers in the geological sciences: U.S. Geological Survey Professional Paper 400–B, p. B354–B355.

Hay, R.L., and Iijima, A., 1968, Nature and origin of palagonite tuffs of the Honolulu Group of Oahu, Hawaii, *in* Coats, R.R., Hay, R.L., and Anderson, C.A., eds., Studies in Volcanology: Geological Society of America Memoir 116, p. 331–376.

Hay, R.L., and Jones, B.F., 1972, Weathering of basaltic tephra on the Island of Hawaii: Geological Society of America Bulletin, v. 83, p. 317–332.

Holcomb, R.T., 1980, Preliminary geologic map of Kilauea Volcano, Hawaii: U.S. Geological Survey Open-File Report 80–796, 2 maps, 1:50,000 scale.

———1981, Kilauea Volcano, Hawaii: chronology and morphology of the surficial lava flows: U.S. Geological Survey Open-File Report 81–354, 321 p.

Kalakaua, K. D., 1888, The legends and myths of Hawaii: New York, Charles L. Webster and Co., 530 p. [reprinted 1972, Tokyo, Charles E. Tuttle Co.].

Kelley, M.L., Spiker, E.C., Lipman, P.W., Lockwood, J.P., Holcomb, R.T., and Rubin, M., 1979, U.S. Geological Survey Reston, Virginia, radiocarbon dates XV: Mauna Loa and Kilauea Volcanoes, Hawaii: Radiocarbon, v. 21, p. 306–320.

Macdonald, G.A., 1944, The 1840 eruption and crystal differentiation in the Kilauean magma column: American Journal of Science, v. 242, p. 177–189.

———1949, Petrography of the Island of Hawaii: U.S. Geological Survey Professional Paper 214–D, p. D51–D96.

Macdonald, G.A., and Abbott, A.T., 1970, Volcanoes in the Sea: Honolulu, University of Hawaii Press, 441 p.

Macdonald, G.A., Abbott, A.T., and Peterson, F.L., 1983, Volcanoes in the Sea, 2nd edition: Honolulu, University of Hawaii Press, 517 p.

Malin, M.C., Dzurisin, D., and Sharp, R.P., 1983, Stripping of Keanakakoi tephra on Kilauea Volcano, Hawaii: Geological Society of America Bulletin, v. 94, p. 1148–1158.

North American Commission on Stratigraphic Nomenclature, 1983, North American Stratigraphic Code, 1983 edition: American Association of Petroleum Geologists Bulletin, v. 67, p. 841–875.

Porter, S.C., 1979, Quaternary stratigraphy and chronology of Mauna Kea, Hawaii: A 380,000-yr record of mid-Pacific volcanism and ice-cap glaciation: Geological Society of America Bulletin, v. 90, pt. 2, p. 909–1093.

Powers, H.A., 1948, A chronology of explosive eruptions of Kilauea: Pacific Science, v. 2, p. 278–292.

Powers, S., 1916, Explosive ejectamenta of Kilauea: American Journal of Science, Series 4, v. 41, p. 227–244.

Pukui, M.K., Elbert, S.H., and Mookini, E.T., 1974, Place Names of Hawaii, 2nd edition: Honolulu, University of Hawaii Press, 289 p.

Rubin, M., and Berthold, S., 1961, U.S. Geological Survey radiocarbon dates, VI: Radiocarbon, v. 3, p. 93–94.

Stearns, H.T., and Clark, W.O., 1930, Geology and groundwater resources of the Kau District, Hawaii: U.S. Geological Survey Water Supply Paper 616, 183 p.

Stearns, H.T., and Macdonald, G.A., 1946, Geology and ground-water resources of the Island of Hawaii: Hawaii Division of Hydrography Bulletin 9, 363 p.

Stone, J.B., 1926, The products and structure of Kilauea: Honolulu, Bernice Pauhi Bishop Museum Bulletin 33, 60 p.

Swanson, D.A., 1973, Pahoehoe flows from the 1969–1971 Mauna Ulu eruption of Kilauea Volcano, Hawaii: Geological Society of America Bulletin, v. 84, p. 615–626.

Swanson, D.A., and Christiansen, R.L., 1973, Tragic base surge in 1790 at Kilauea Volcano: Geology, v. 1, p. 83–86.

Walker, G.W., 1969, Geological map of the Kau Desert quadrangle, Hawaii: U.S. Geological Survey Geologic Map GQ–827, scale 1:24,000.

Washington, H.S., 1923, Petrology of the Hawaiian Islands: II, Hualalai and Mauna Loa: American Journal of Science, 5th Series, v. 6, art. 10, p. 100–126.

Wentworth, C.K., 1938, Ash formations on the Island of Hawaii: Honolulu, 3rd Special Report of the Hawaiian Volcano Observatory, Hawaii Volcano Research Association, 183 p.

Wright, T.L., 1971, Chemistry of Kilauea and Mauna Loa in space and time: U.S. Geological Survey Professional Paper 735, 40 p.

ERUPTIVE HISTORY AND LONG-TERM BEHAVIOR OF KILAUEA VOLCANO

By Robin T. Holcomb

ABSTRACT

Long-term variations in Kilauea's eruptive behavior are revealed by mapping, paleomagnetic dating, and morphologic analysis of the surficial lava flows.

About 70 percent of Kilauea's surface is younger than 500 years, about 90 percent younger than 1,100 years. Much of its present caldera dates from the 18th century. An earlier caldera collapse about 1,500 years ago was followed by an eruptive hiatus outside the caldera until summit overflows began about 1,100 years ago.

Kilauea's surface is dominated by the products of sustained eruptions; it consists of 67 percent tube-fed pahoehoe, 14 percent surface-fed pahoehoe, and 16 percent aa. Eruptions are sustained longer at the summit and are briefer along the rift zones away from the magma reservoir beneath the summit. More than 50 percent of Kilauea is still covered by lava flows from long-sustained eruptions at the summit, despite an absence of such overflows in the last 250 years. Local variations in eruptive behavior along different rift structures probably reflect different connections to the principal reservoir.

Changes in eruptive behavior have occurred over intervals of decades and centuries. Some changes have been repeated, and some appear to have been evolutionary. Two caldera collapses and accompanying large explosive eruptions have been followed by intervals of little activity along the subaerial rift zones. Rift activity waxed as summit activity waned, and one waxing sequence resembles an evolutionary progression: rift eruptions, at first brief and widely separated in time and space, gradually became frequent along restricted segments of the rift zone and culminated in sustained activity at localities progressively farther from the summit. The current rift-zone activity resembles that which occurred in the 18th century preceding the explosive eruption of 1790.

The causes of long-term eruptive variation remain undetermined, though shifts in the sites of principal magma storage are probably involved. Slow development of integrated plumbing along the rift zones is probably interrupted by sudden subsidences of the summit and the unbuttressed south flank. Possible behavioral models are classified as evolutionary, cyclical, and stochastic; they differ greatly in their implications on long-range forecasting.

INTRODUCTION

By the early 1970's it was clear that an eruption history of Kilauea Volcano was needed for the period preceding the 19th century. The Polynesian oral history had been lost early in that century, and only a few scattered traditions had survived. During the following one hundred years Kilauea's eruptive behavior had shown little change, being nearly continuous and almost completely restricted to the caldera (fig. 12.1*A*). As a result, rift eruptions were thought rare and volcanic hazards small, and the Puna District was extensively developed (fig. 12.1*B*). However, summit activity had become episodic after collapse of Halemaumau and explosions in 1924, and a flurry of rift eruptions began in 1955. Continued rift activity through the 1960's raised the possibility of a higher long-term eruption frequency outside the caldera and of consequent greater hazard (fig. 12.1*C*). When I joined the staff of the Hawaiian Volcano Observatory in 1971 I began to reexamine the risk and the usefulness of the historical record for assessing it.

One impediment to study of long-term eruption histories had been a feeling that they could tell little about future behavior. According to the idealized life history of Hawaiian volcanoes (fig. 12.2), a shield undergoes distinct developmental stages, including a youthful growth stage and a mature caldera stage. The caldera develops when magma supply can no longer overcome a tendency for the summit to founder (Macdonald, 1965). Though eruptions may continue vigorously for some time afterward, caldera formation marks the end of shield growth. According to this view, Kilauea had recently entered its mature stage; behavior preceding caldera formation differed from that occurring now, so little could be learned about present hazards through study of precaldera events.

Powers (1948), however, had inferred that an ancient caldera was filled and buried before the present one formed. If there had been one earlier caldera there could have been many; perhaps the volcano had no distinct shield-building and caldera stages but underwent repeated caldera collapse and filling as it grew (Holcomb, 1976b). If so, Kilauea might continue to grow long into the future, and events that occurred before caldera formation might be repeated. In particular, collapses might interrupt dikes transporting magma into rift zones (Fiske and Jackson, 1972) and thereby cause changes in long-term eruption patterns. If repeated patterns occurred, they might tell much about the operation of the volcano and lead to better forecasts of its behavior. The work reported here was focused on those possibilities.

ACKNOWLEDGMENTS

Many friends and colleagues have provided assistance. R.L. Christiansen and D.W. Peterson have contributed frequent discussions since 1971. D.E. Champion and M.O. McWilliams collaborated in much of the paleomagnetic work. N.G. Banks, T.C. Casadevall, R.R. Doell, D. Dzurisin, R.M. Easton, P.W. Lipman, J.P. Lockwood, R.B. Moore, and M. Rubin provided unpublished ^{14}C ages, paleomagnetic data, and other information. Contributions were made also by many others, especially the staff of

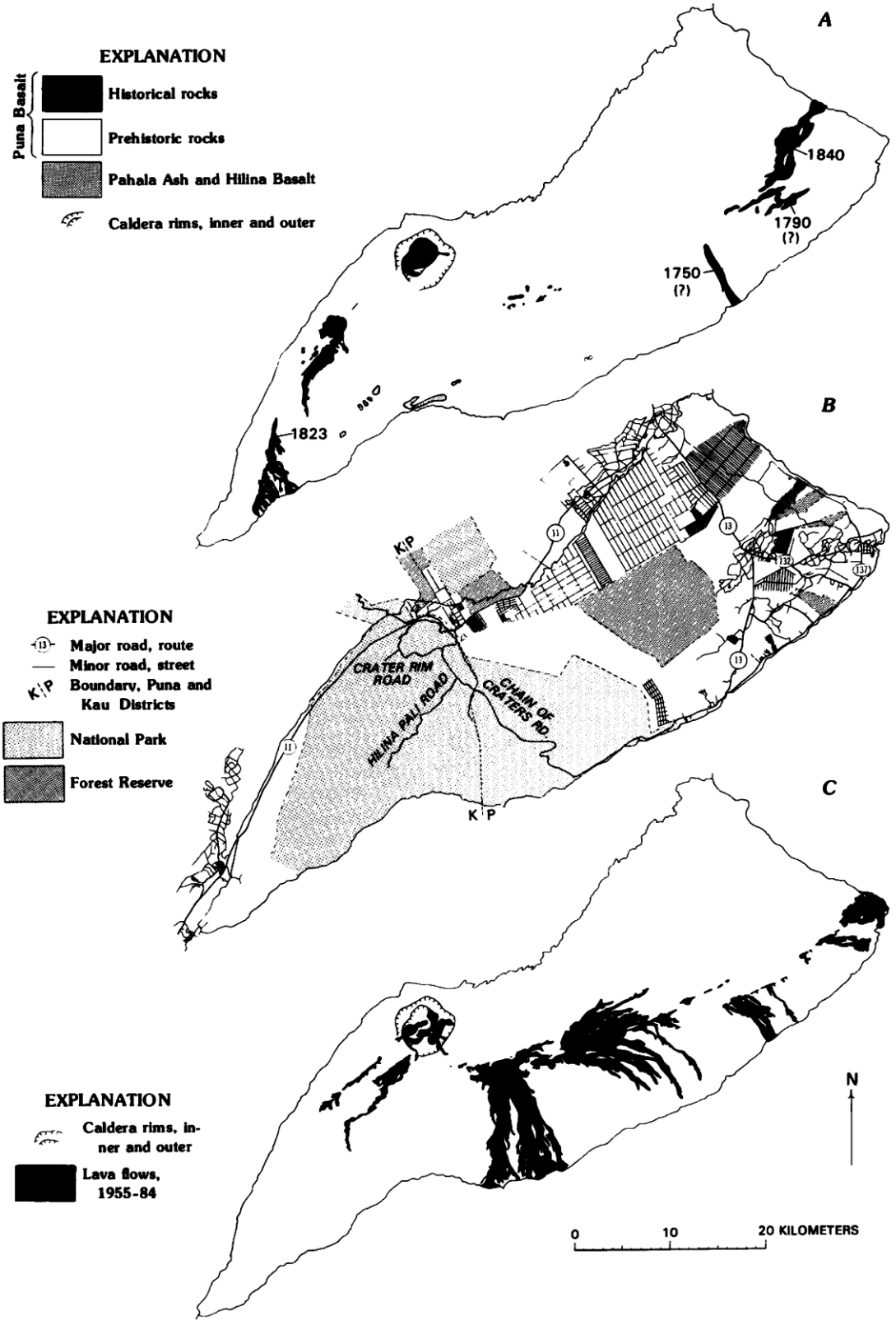

FIGURE 12.1.—Historical eruptions and property development on Kilauea Volcano. ***A***, Stratigraphy of Kilauea, showing historical lava flows erupted before 1954, with dates given for some flows, from Stearns and Macdonald (1946). ***B***, Property subdivisions, developed mostly after 1950. ***C***, Lava flows erupted during 1955–84.

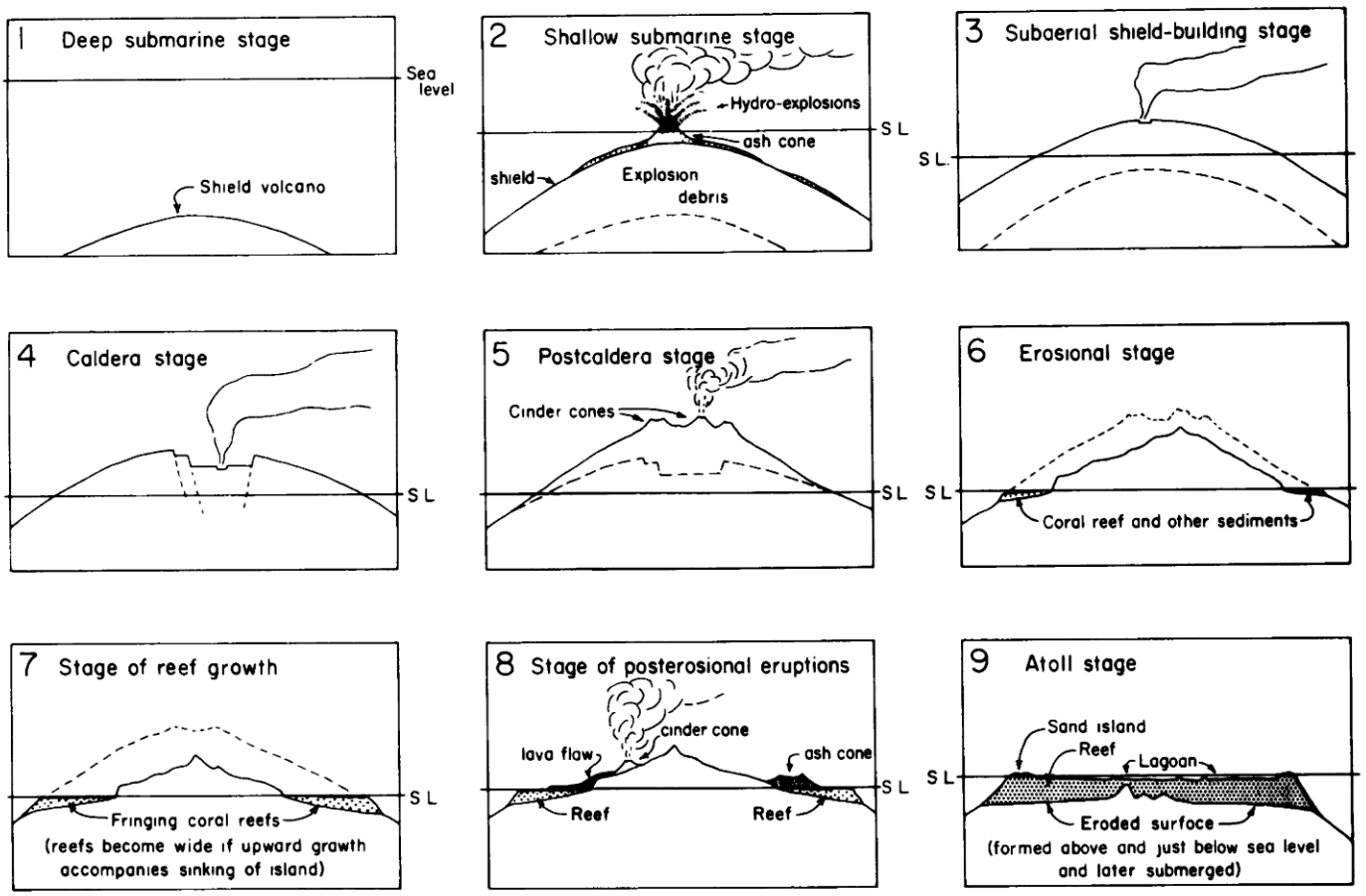

FIGURE 12.2.—Life cycle of a Hawaiian volcano, from Macdonald and Abbott (1970).

the Hawaiian Volcano Observatory, residents of Kilauea, and the faculty and students of Stanford University. Some of the work was supported by a grant from the Piton Foundation of Denver, Colorado. This report has benefited greatly from encouragement by R.W. Decker and reviews by D.E. Champion, R.L. Christiansen, D. Dzurisin, R.B. Moore, and D.W. Peterson. The maps were colored by B.M. Myers, G.R. Stoopes, and D.E. Wieprecht.

PURPOSE AND PROCEDURE

Kilauea's recent history has been surveyed to evaluate long-term eruptive changes. The work has focused on the interval recorded by the surficial lava flows; a tentative history for this interval has been derived from geologic mapping, age determinations, and morphologic analysis of eruption products (Holcomb, 1980b).

GEOLOGIC MAPPING

In order to establish stratigraphic sequences and gather other information, a reconnaissance geologic map of Kilauea's subaerial edifice was made at a scale of 1:50,000 (Holcomb, 1980a; many subsequent illustrations herein are adapted from that map, as indicated in fig. 12.3). Four years of general familiarization (1971–75) were followed by several months of systematic photograph interpretation (1975–76) and three months of ground checking (1977). Emphasis was placed on lava-flow morphology. Standard procedures were adapted to suit the particular goals of the work, time available, and characteristics of the mapped area.

The subaerial part of Kilauea is about 80 km long, averages about 20 km wide, and includes about 1,500 km^2. It is a long, domelike ridge rising to a summit elevation of about 1,240 m (fig. 12.4*A*). The orographic rainfall pattern renders it climatically and

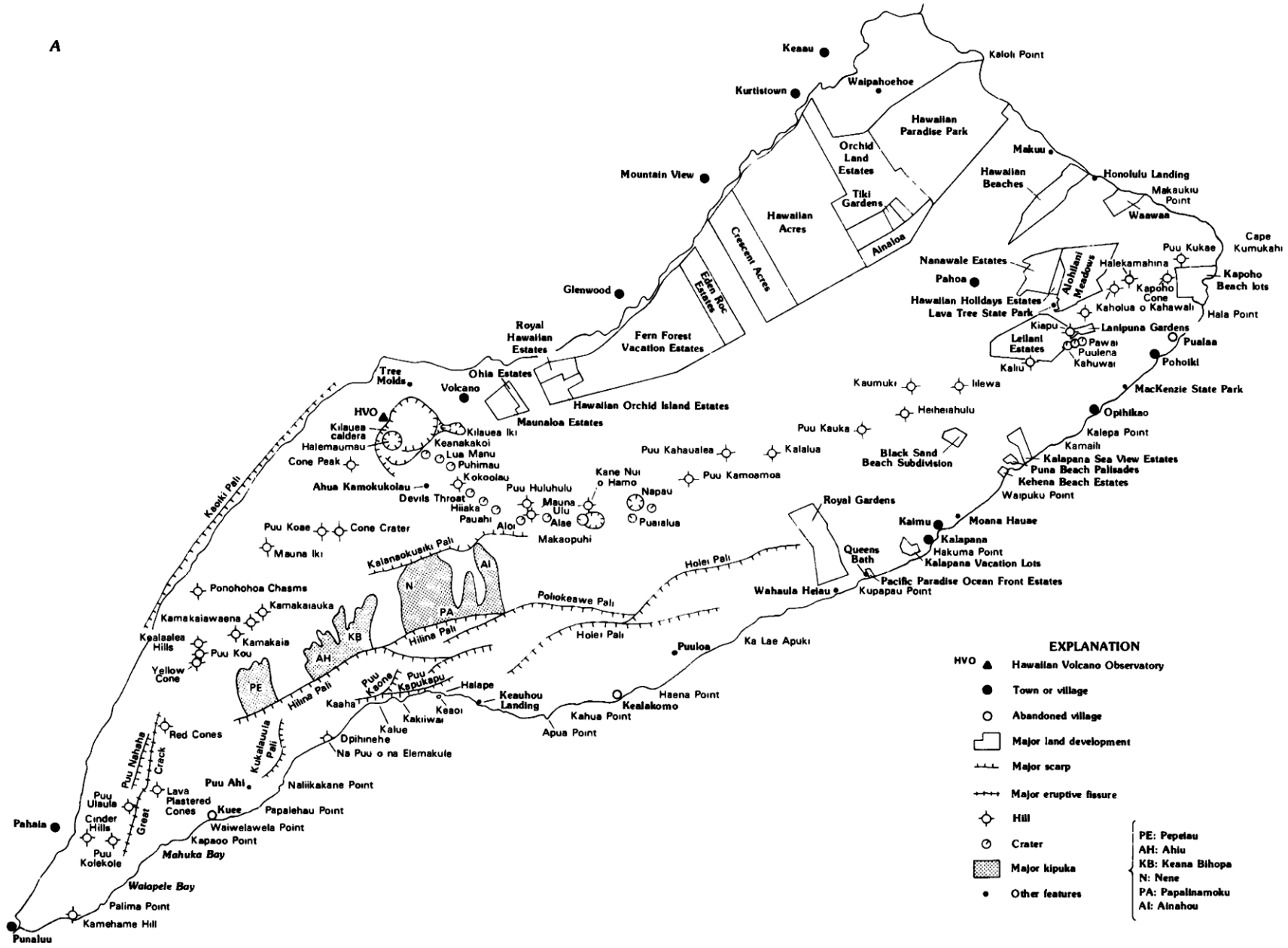

FIGURE 12.3.—Index maps for Kilauea Volcano. ***A***, Some named localities; others are shown on figure 12.5. ***B***, Coverage of map and aerial-photograph illustrations in this report; numbers refer to figure numbers.

FIGURE 12.3—Continued.

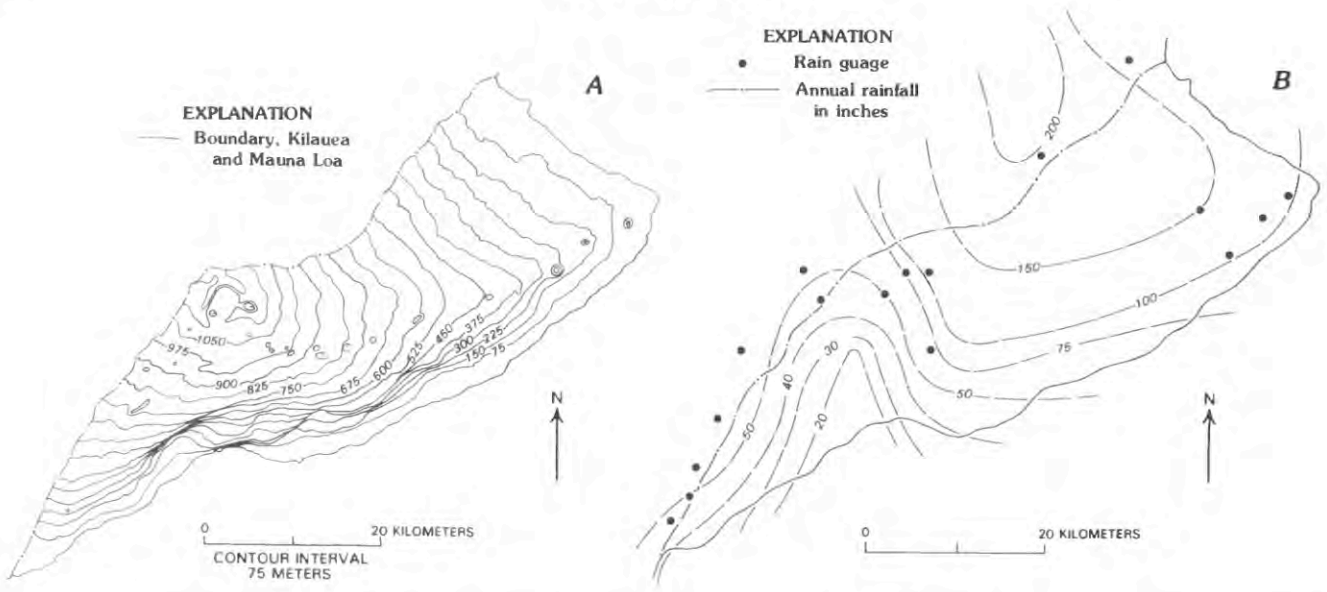

FIGURE 12.4.—Variation of geographic and mapping conditions on Kilauea Volcano. ***A***, Topography. ***B***, Annual rainfall, from Taliaferro (1959). ***C***, Vegetation, from Ripperton and Hosaka (1942). ***D***, Mapping confidence.

botanically diverse, and large parts range from tropical rain forest to barren desert (fig 12.4*B*,*C*). These variations made the mapping procedure very different from one flank to another, and as a result mapping confidence varies widely (fig. 12.4*D*).

A simplified version of the geologic map is presented here as figure 12.5. Though the original is more detailed than maps of most other shield volcanoes, it still represents merely a reconnaissance for the goal of a detailed eruption history.

CLASSIFICATION OF LAVA FLOWS AND ERUPTIONS

In order to examine more than simple eruption frequencies, the eruptions were classified according to their behavior. This was done through morphologic classification of eruption products (fig. 12.6) using interpretive principles developed during the Mauna Ulu eruptions of 1969–74. The morphology of a lava flow is influenced by the behavior of the eruption that produces it, with sustained effusion leading to a high degree of channelization and formation of lava tubes (fig. 12.7; Peterson and Swanson, 1974). Different kinds of eruptions produce different kinds of vent edifices and flow assemblages (Swanson, 1973; Holcomb, 1976a). Brief eruptions produce small edifices and simple assemblages of surface-fed pahoehoe and aa, while long-sustained eruptions produce large lava shields and assemblages dominated by tube-fed pahoehoe (table 12.1). Eruptions of intermediate duration, several weeks to a few years, typically produce small shields and complex assemblages of all three flow types. The flow assemblages and vent types were used to classify Kilauea's eruptions (fig. 12.8).

DATING

Most of the ages obtained in this work used a paleomagnetic method based on the secular variation of the Earth's magnetic field (Holcomb and others, 1986). Oriented rock samples were collected during four 2-week to 3-week trips in 1978, 1979, 1981, and 1983. Directions of remanent magnetization were measured first at 67 sites on lava flows dated previously by ^{14}C. Most of these sites were on the southeast flank of Mauna Loa (fig. 12.9), where many flows have spread over weathered ash well suited for charcoal preservation (Lockwood and Lipman, 1980). Results from these sites were used to define a history of Hawaiian secular variation during the last few thousand years (fig. 12.10). Kilauea flows of unknown age were then dated by comparing their magnetization with this history of secular variation.

Flows could not be dated precisely using this method, because of dispersion in the results between paleomagnetic sites on lava flows of similar ^{14}C age. Instead, it was necessary to infer approximate ages using a semi-quantitative classification procedure. When directions of dated flows younger than 2.5 ka were plotted on an equal-area projection, they defined fields mutually exclusive in age (fig. 12.11*A*). Undated flows were then assigned ages corresponding to fields in which they fell (fig. 12.11*B*–*F*). The chronology offered here is tentative; refinements in the history of magnetic secular variation will no doubt lead to revisions in the eruption history.

In this report the chronology of Holcomb and others (1986) has been revised using results from paleomagnetic sites not yet published. In paleomagnetic citations that follow, sites prefixed by

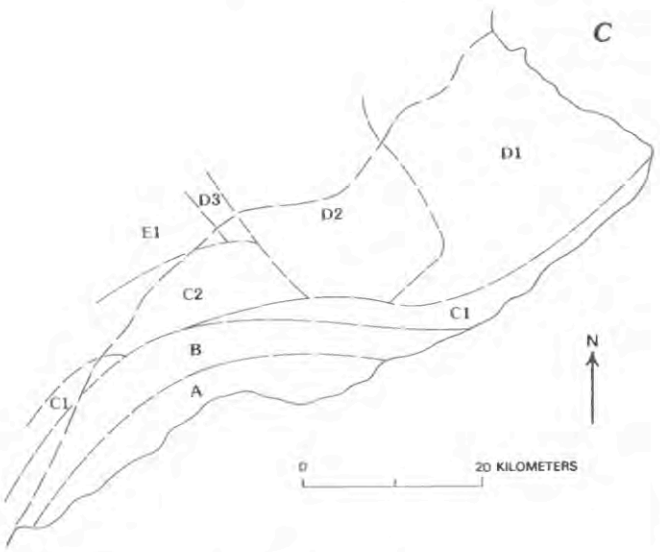

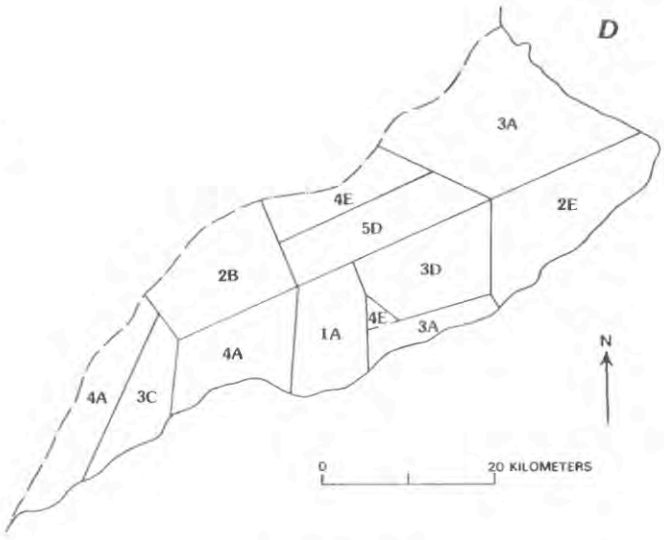

EXPLANATION

Vegetation zone	Approximate yearly rainfall (inches)	Approximate altitude limit (feet)	Characteristics of the vegetation: Natural cover	Typical plants
A	20	1,000	Xerophytic shrub with a coastal fringe of trees	Algaroba, koahaole, swollen fingergrass, feather fingergrass, piligrass, bristly foxtail
B	20-40	3,000	Xerophytic shrub with some trees in the upper part	Lantana, koahaole, klu, cactus, uhaloa, ilima, falsemallow, Natal redtop, piligrass, native panicums, kakonakona
C Low phase (C1)	40-60	2,500	Mixed open forest and shrubs	Koahaole, guava, lantana, Spanish clover, Bermudagrass, kukaipuaa, pilipiilula
High phase (C2)		2,500-4,000	Mixed open forest	Bermudagrass, Spanish clover, wild geranium, bristly-fruited mallow, plantain, rattail
D Low phase (D1)		1,500	Shrub and closed forest	Guava, sensitive plant, Boston fern, Hilograss, ricegrass, basketgrass, honohono, staghorn fern
Middle phase (D2)	60	Variable	Closed forest	Ohia lehua, tree fern, staghorn fern
High phase (D3)		4,000-7,000	Open forest	Koa, pukamole, sheepgrass, mountain pili, rattail, alapaio fern, tree fern
E Low phase (E1)	50	4,000-7,000	Open forest and shrub	Koa, mamani, heu pueo, mountain pili, large Hawaiian lovegrass, kalamaloa, sweet vernalgrass, bracken fern, alapaio fern, Kentucky bluegrass

EXPLANATION

GENERAL DEGREE OF CONFIDENCE	MAIN FACTOR LIMITING CONFIDENCE
1 Very good	A Adjacent pahoehoe flows have inherently obscure contacts
2 Good	B Tephra obscures relations between underlying units
3 Average	C Vegetal sparsity on nonadjacent flows obscures chronology based on plant succession
4 Poor	D Rain forest obscures geology
5 Very Poor	E Human forest modification obscures plant succession

FIGURE 12.4.—Continued.

8B and 9B were collected in 1978–79 and published by Holcomb and others (1986). Unpublished sites prefixed by 1B were collected by Holcomb and D.E. Champion in 1981; those prefixed by 3R were collected by Holcomb and J.D. Ward in 1983; one prefixed by 4A was collected by J.P. Lockwood in 1984.

Also used are ^{14}C ages by the U.S. Geological Survey radiocarbon laboratory in Reston, Virginia, directed by M. Rubin. Such ages are cited by their laboratory identification numbers prefixed by W. All of the cited ages are included in compilations by Kelley (1979), Kelley and others (1979), or Rubin and others (chapter 10). Though published originally with laboratory precision to the nearest 10 yr, most of the ages are expressed here only to about the nearest 100 yr. Replicate ages and comparisons with paleomagnetic data suggest that dating precision is about 200 yr

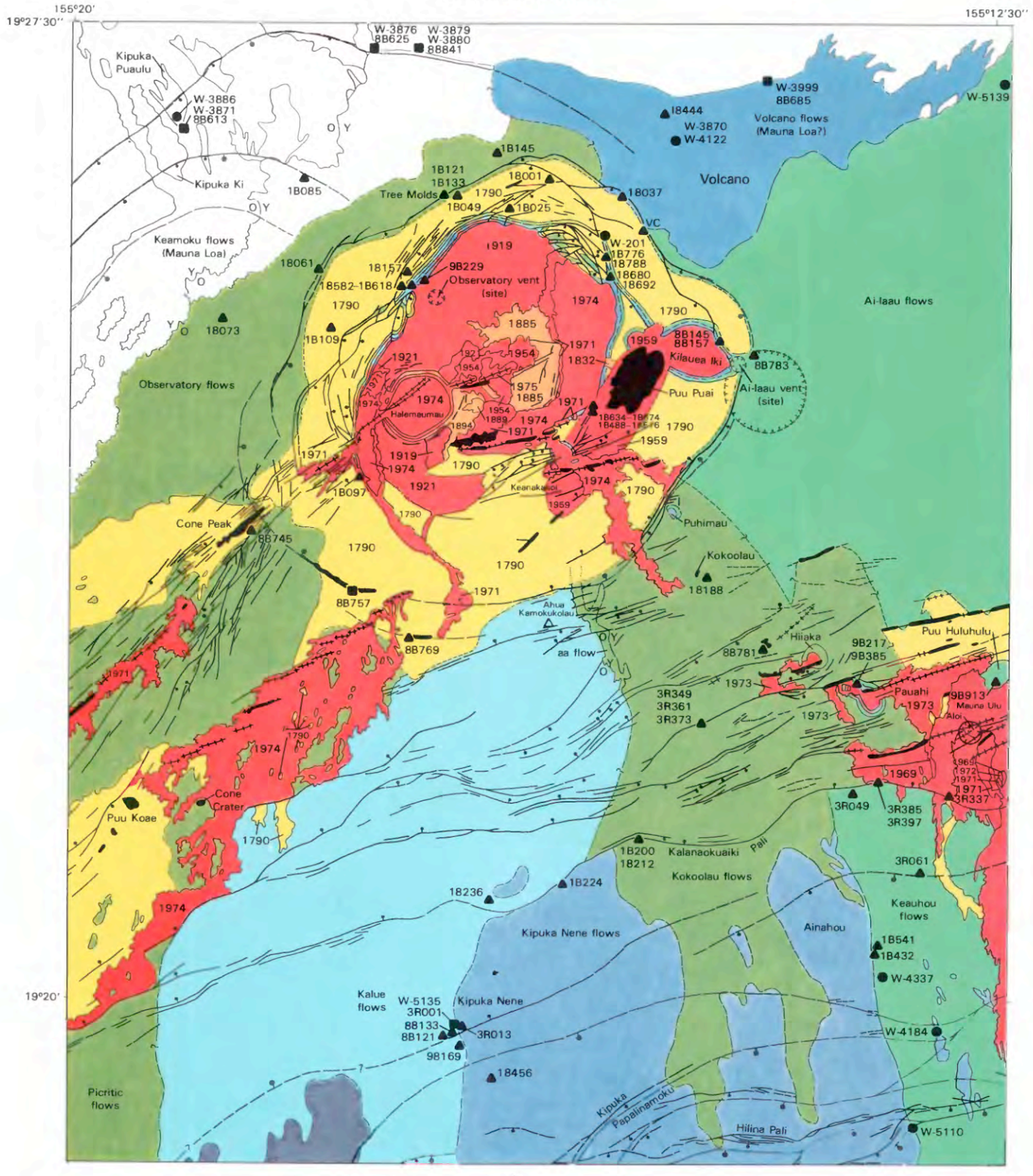

A

FIGURE 12.5.—Reconnaissance geologic map of Kilauea Volcano showing lavas erupted through 1977, revised and simplified from Holcomb (1980a), which also shows topography and cultural features. In this version, lava flows are classified only by age; in original map they were classified also by flow morphology and eruption type. Age uncertainties are discussed in text. Year of eruption is indicated for historical flows. ***A***, Summit region and Koae fault system. Volcano flows may have been fed by eruptions of Mauna Loa. VC, visitor center sampling site of Coe and others (1978). ***B***, Upper southwest rift zone. Some Observatory flows(?) may have been erupted

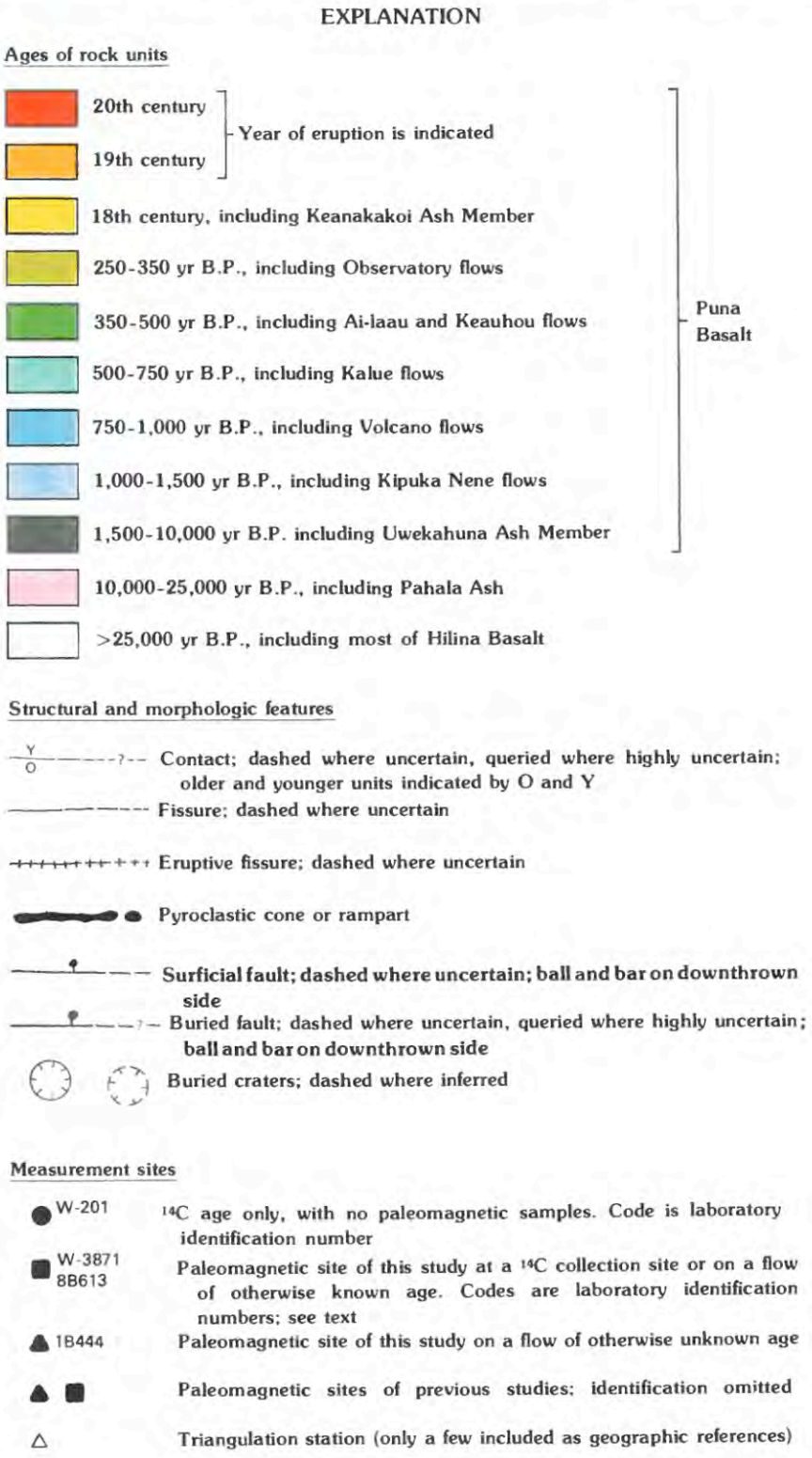

from Mauna Loa, as mapped by Stearns and Macdonald (1946). ***C***, Lower southwest rift zone. Flows west of Great Crack may belong to more age groups than indicated here. ***D***, Flank south of summit region. Area encompasses much of Hilina and Koae fault systems, and the Papau submarine landslide (Moore and Peck, 1965; Fornari and others, 1979) occurs offshore. ***E***, Upper east rift zone and south flank. Much of this area shown also in figure 12.35, in which lava flows are classified by morphology. ***F***, Part of middle east rift zone and south flank. South flank here covered largely by lava flows from Kane Nui o Hamo. ***G***, South flank and east rift zone from Heiheiahulu to Malama. Especially prominent in this area are 18th-century lava flows of Heiheiahulu, which in figure 12.40 are classified by morphology. ***H***, East rift zone from Kaliu to Cape Kumukahi. Flows of 17th and 18th centuries not distinguished confidently in this area. Transform fault as inferred by Zablocki (1977). ***I***, Part of flank north of middle east rift zone. This heavily forested area includes poorest known part of Kilauea. ***J***, North flank southeast of Keaau. All flows older than Ai-laau shield in northern part of this area may have been erupted on Mauna Loa.

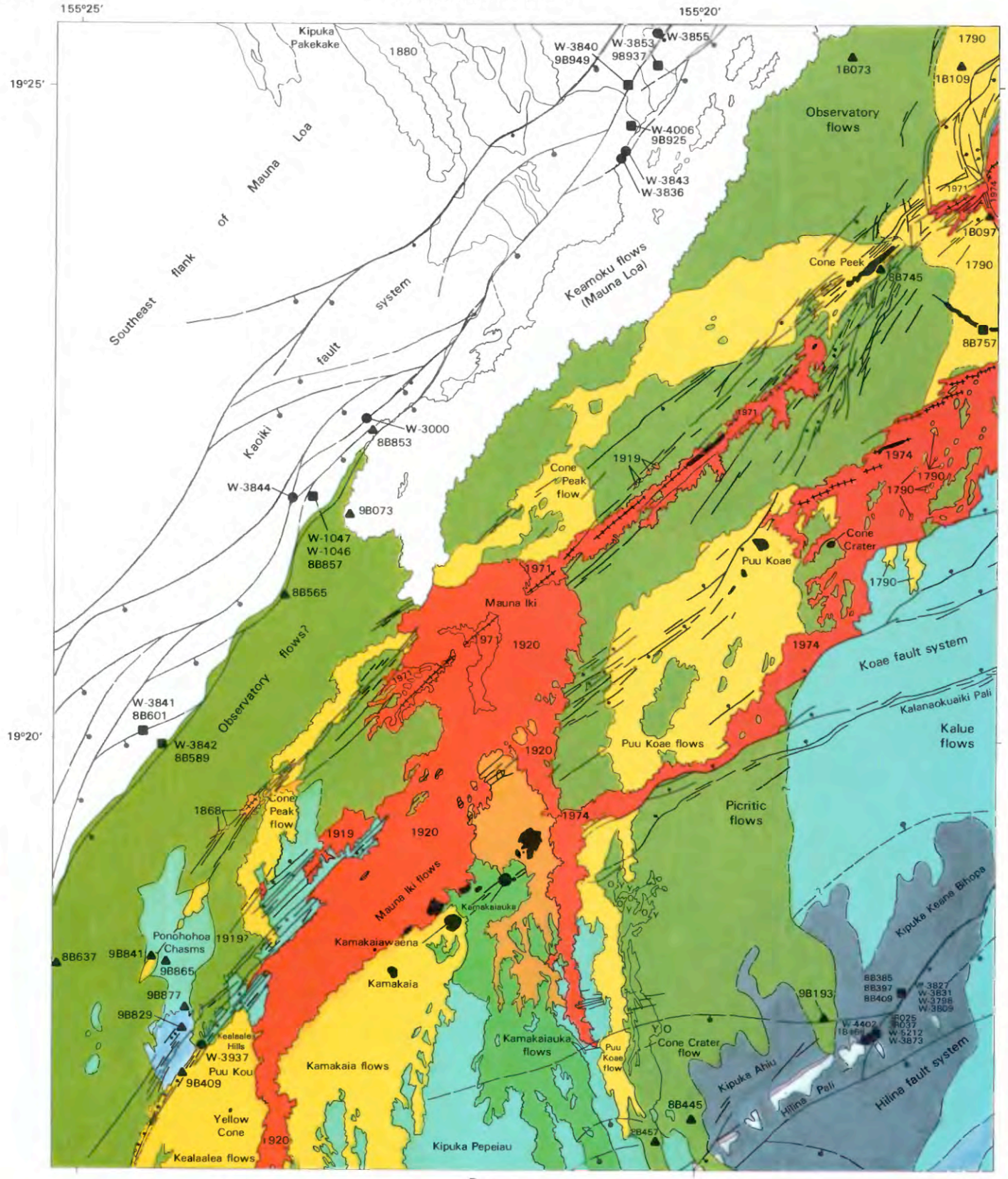

B

FIGURE 12.5.—Continued.

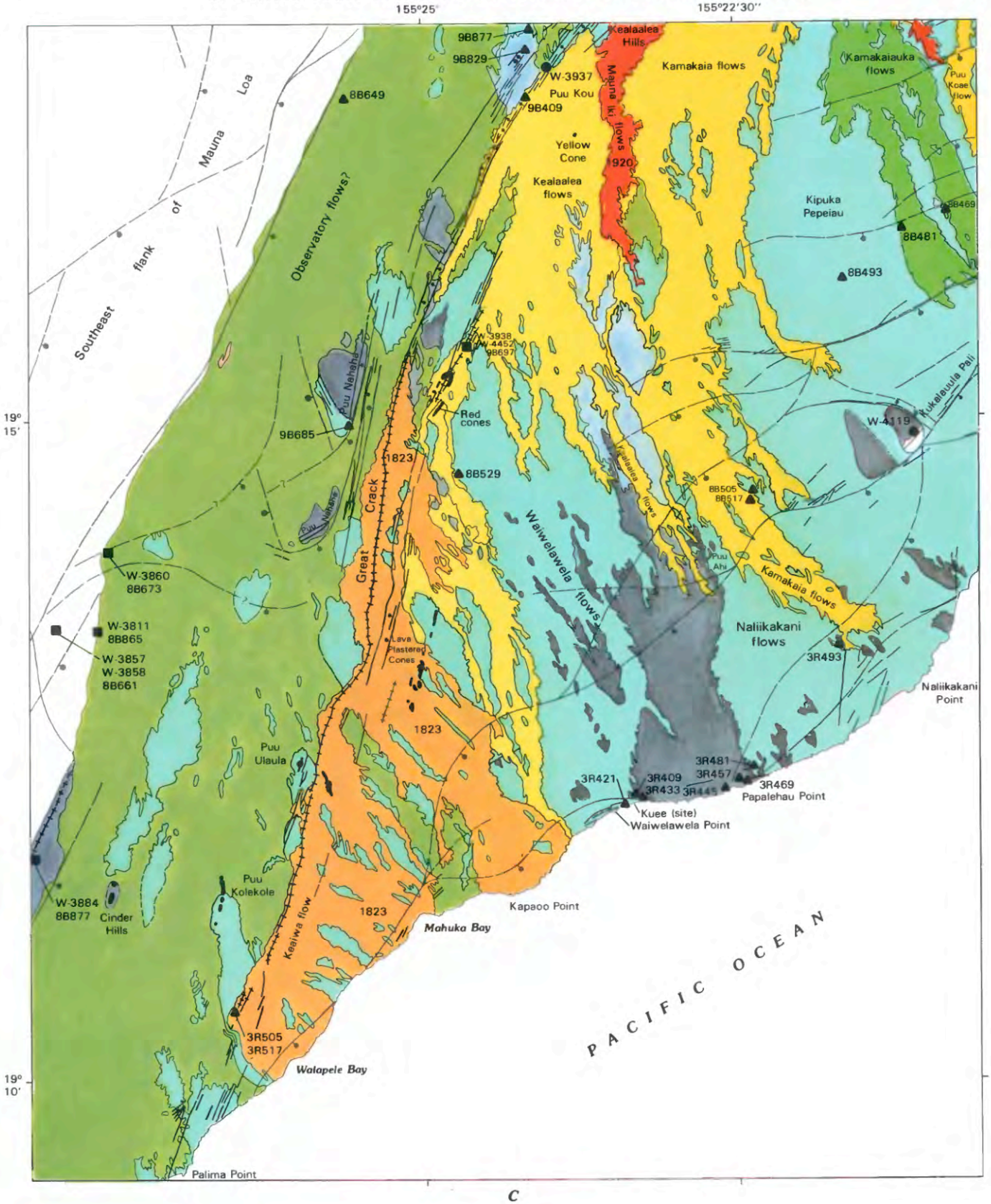

C

FIGURE 12.5.—Continued.

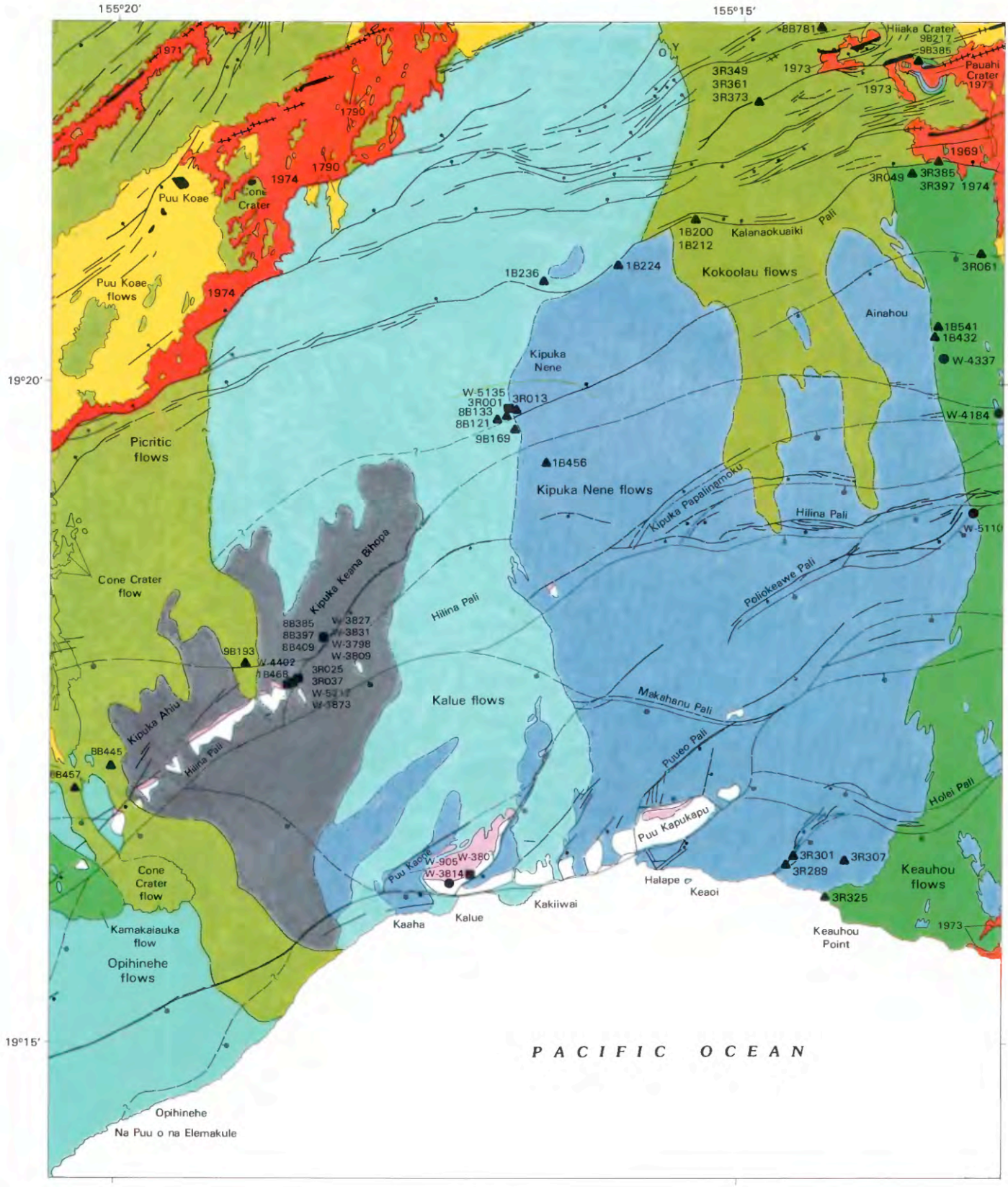

D

FIGURE 12.5.—Continued.

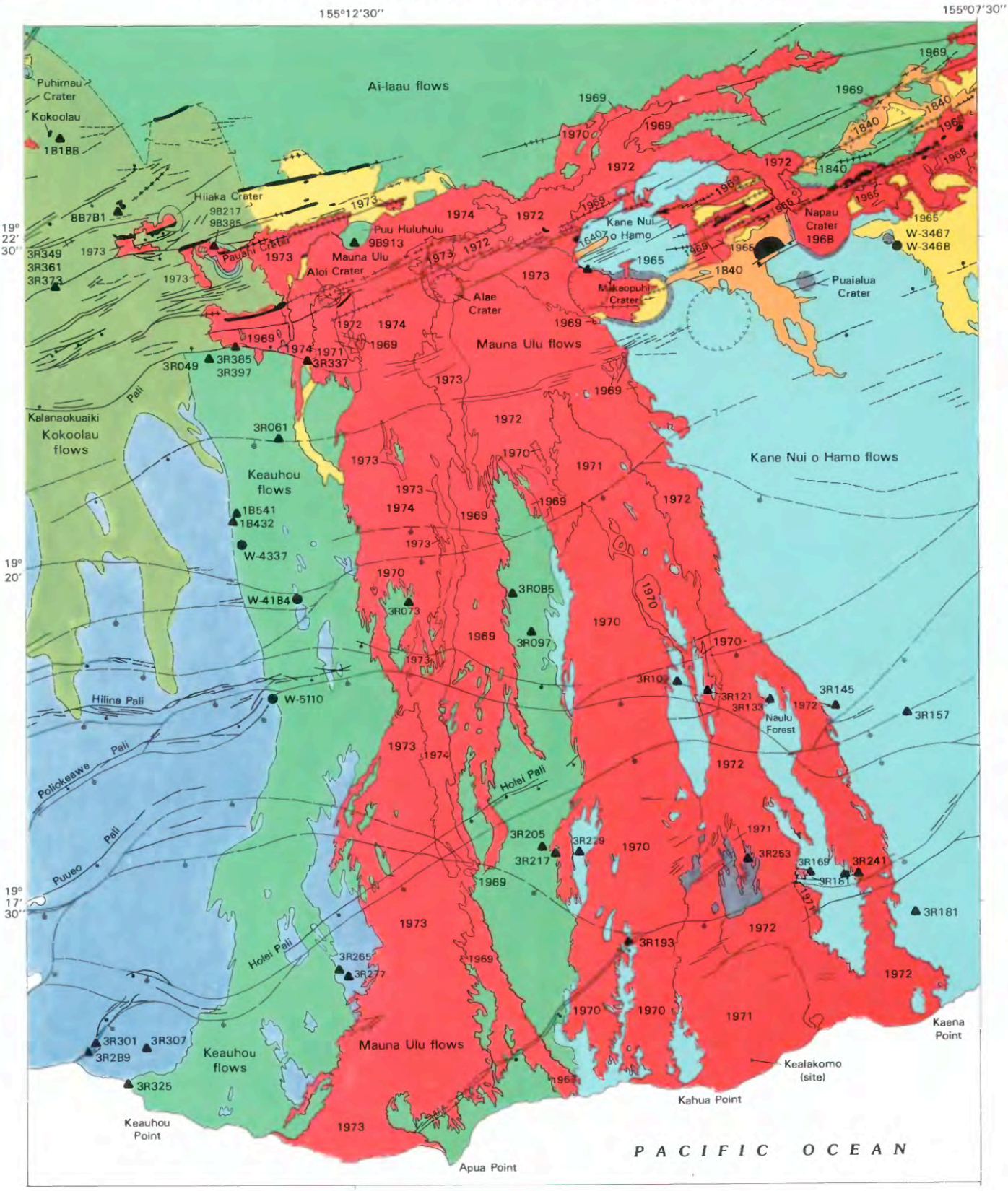

E

FIGURE 12.5.—Continued.

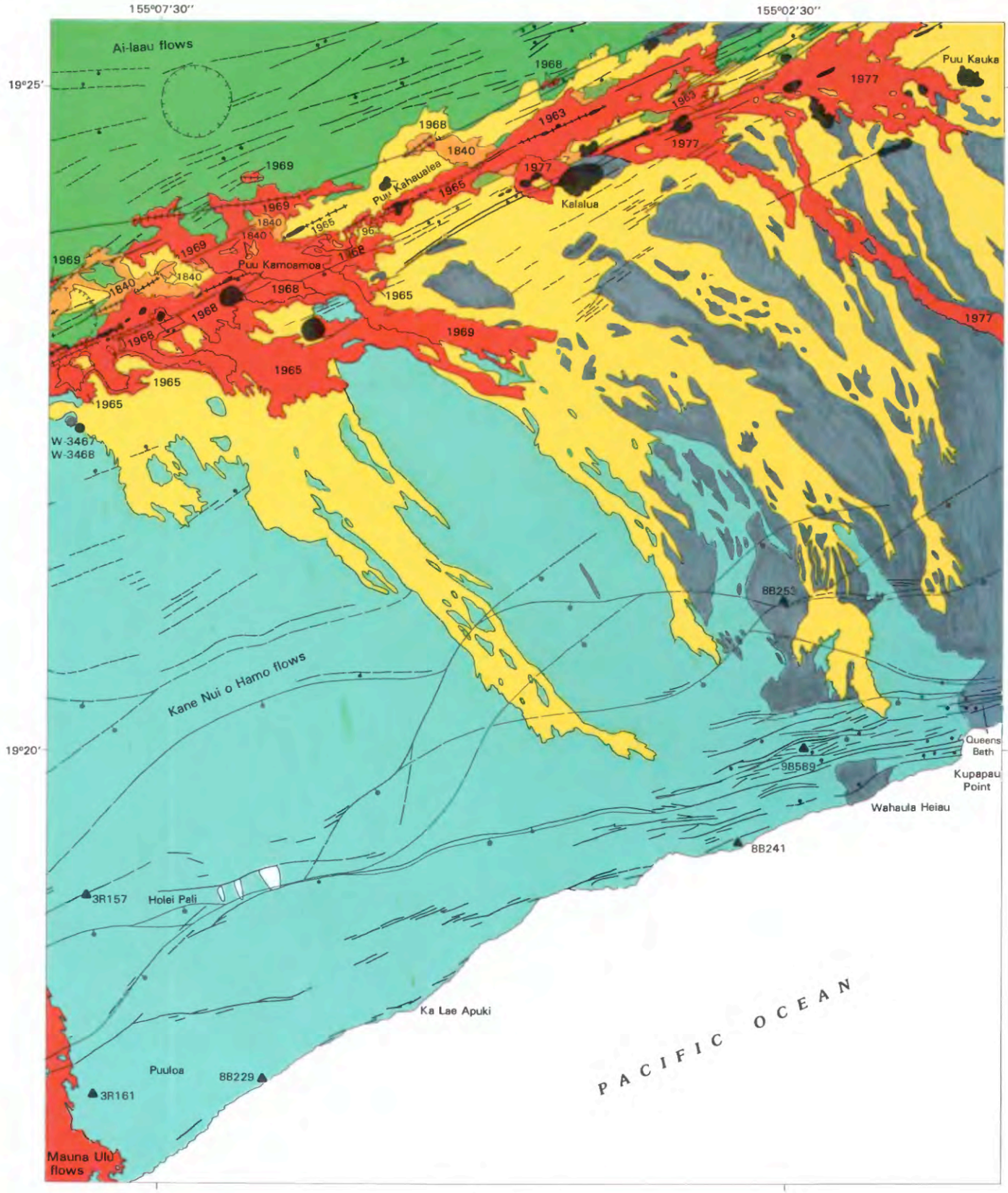

F

FIGURE 12.5—Continued.

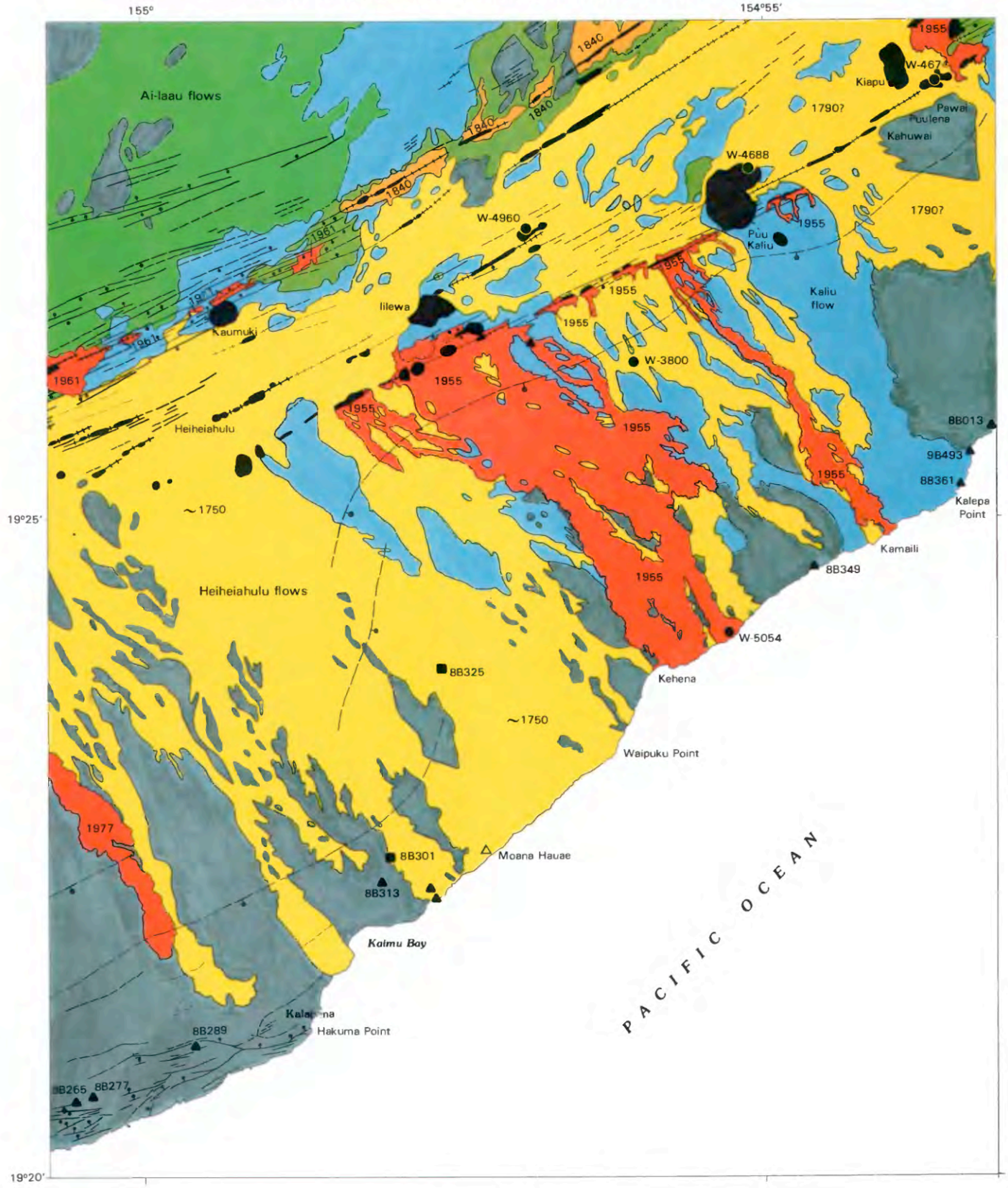

G

FIGURE 12.5—Continued.

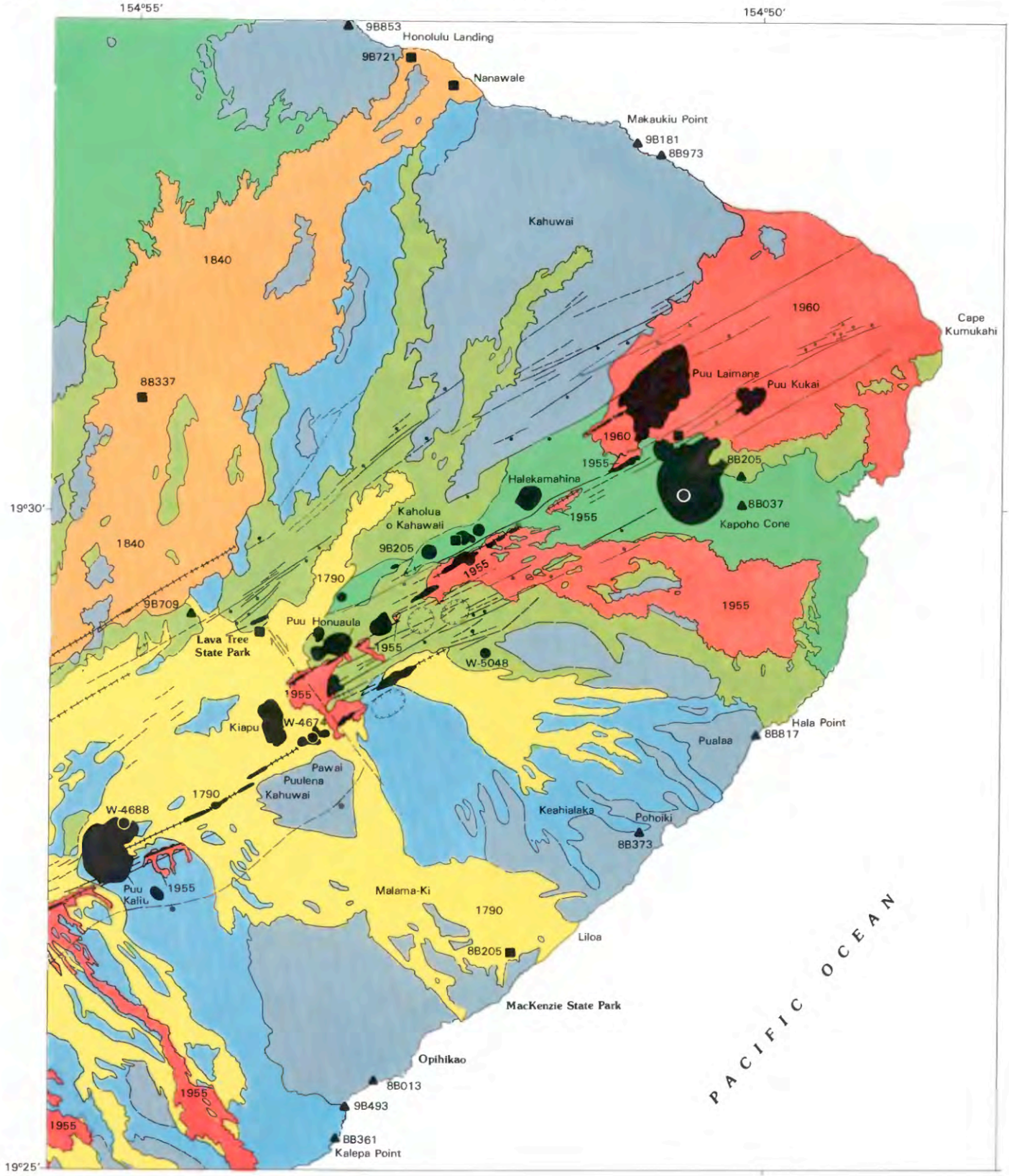

H

FIGURE 12.5—Continued.

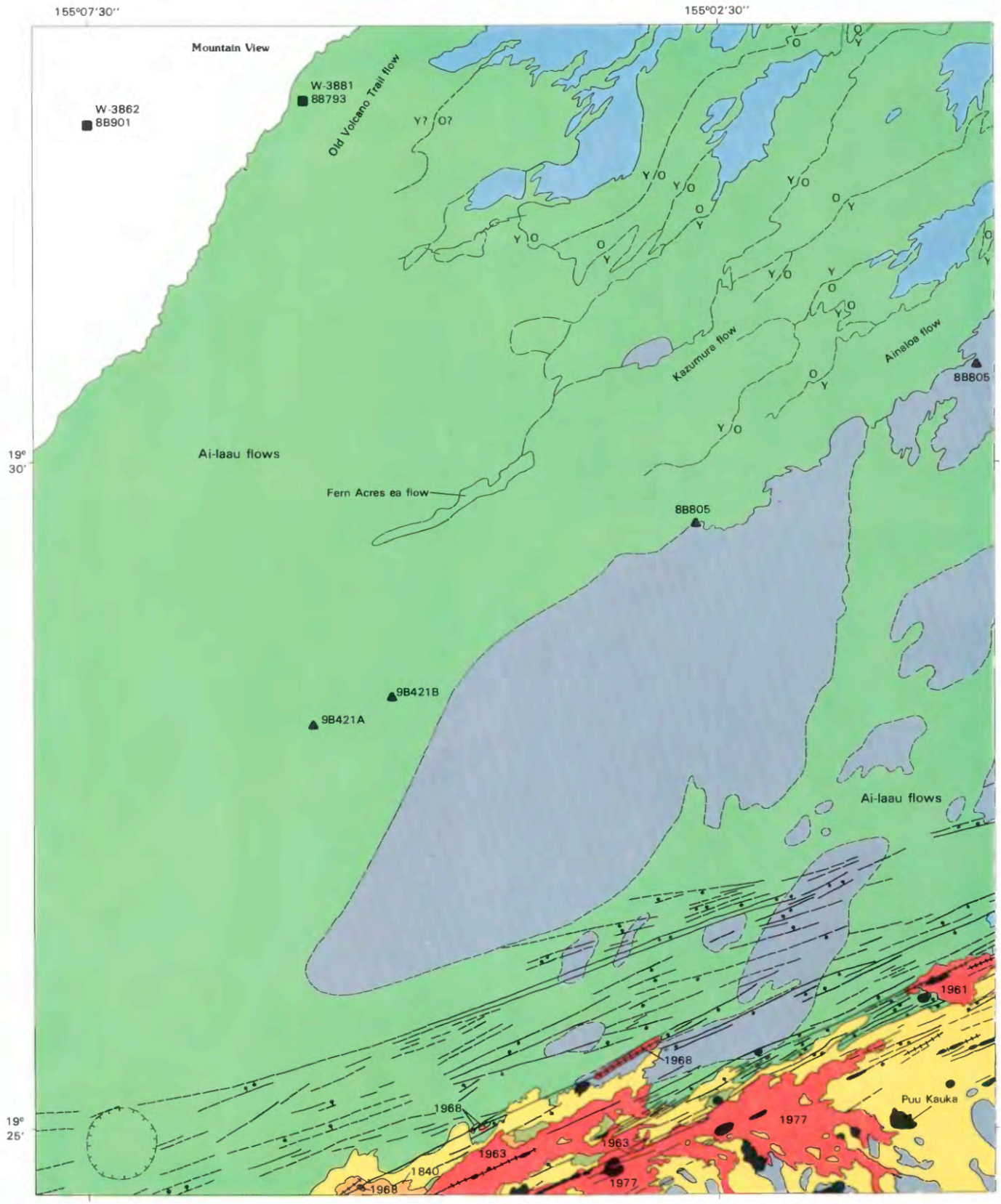

I

FIGURE 12.5—Continued.

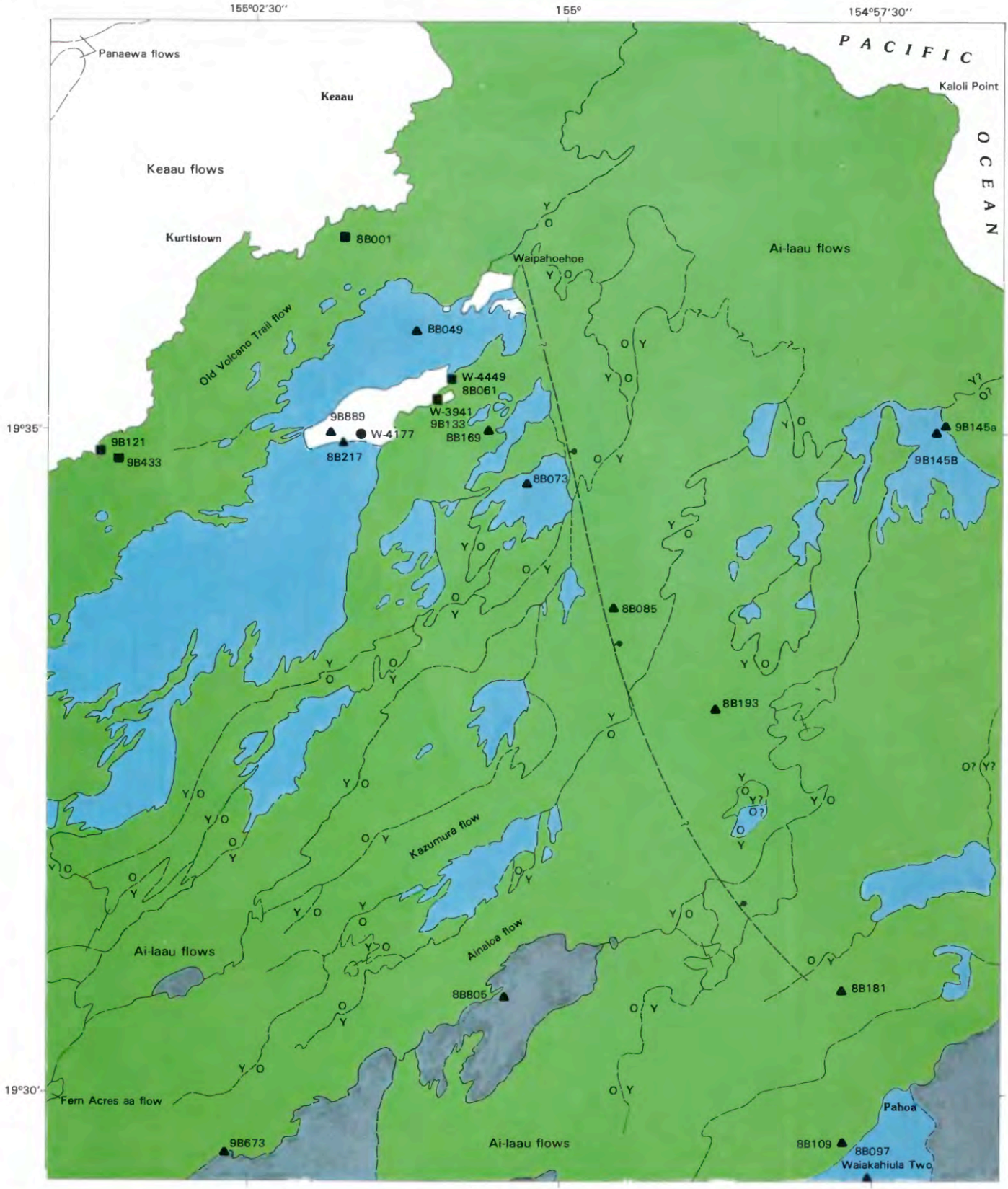

J

FIGURE 12.5—Continued.

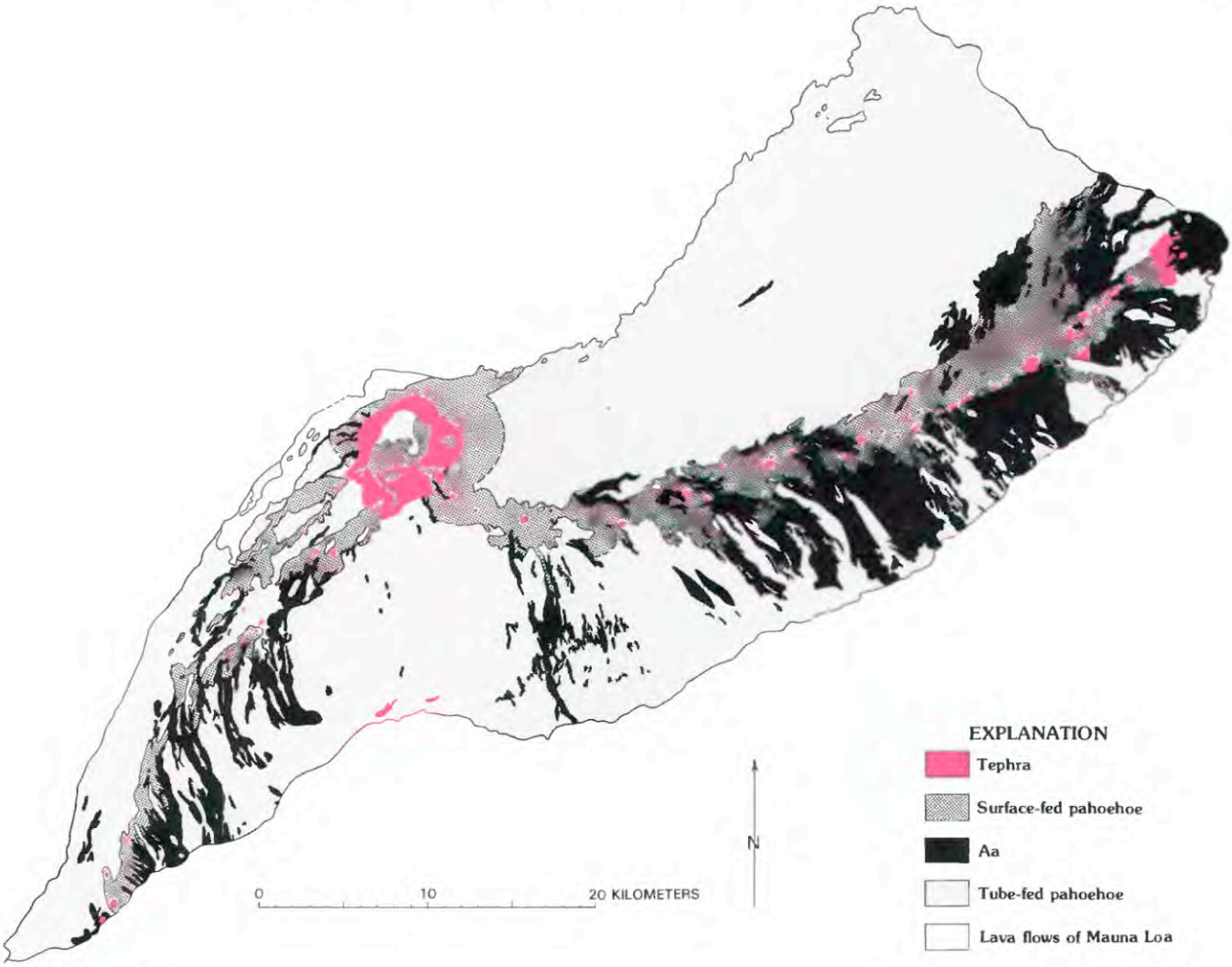

FIGURE 12.6.—Kilauea lava flows, classified by morphology; extensive tephra units are shown separately in red. Dashed lines, gradational or uncertain contacts.

(Holcomb and others, 1986). Large errors may arise from contamination by modern organisms in subtropical rainforest and by old fumarolic carbon elsewhere (Rubin and others, chapter 9).

AGE OF KILAUEA'S SURFACE

Most surficial flows have magnetization corresponding to ages of 250–1,100 yr (green hues on fig. 12.12). About 70 percent of the surface is younger than 500 yr, 90 percent younger than 1,100 yr (fig. 12.13; table 12.2). This is about ten times younger than was commonly believed as recently as a decade ago. When the mapping was begun, it was thought that a large part of Kilauea's surface was 5,000–10,000 yr old, largely because of a 2.57-ka ^{14}C age (now known to be erroneous) on the Keanakakoi Ash Member of the Puna Basalt near the rim of Kilauea'a present caldera (Rubin and Suess, 1956). The caldera is older than the ash because the ash is draped unbroken across caldera faults. Lava flows truncated by the caldera are older still; because vegetation patterns reveal clear age differences among these flows, many were thought to be much older than 2.5 ka. It was therefore puzzling when ^{14}C dating in the late 1970's found few ages older than 1 ka (Kelley and others, 1979). This dating suggested that Kilauea's surface was younger than expected, and when paleomagnetic work was planned in 1978 it was thought that a majority of surface flows were as young as 2–4 ka. The paleomagnetic results actually show that they are even younger.

This youthfulness is not inconsistent with other information about Kilauea's rate of magma supply. Assuming a supply rate of 9×10^6 m^3/mo (Swanson, 1972) and mean flow thickness of 2 m, an estimate for Kilauea's rate of surface coverage is 54,000 km^2/1,000 yr, 36 times the rate needed to cover the volcano's 1,450-km^2 subaerial surface during such an interval. This coverage rate is a

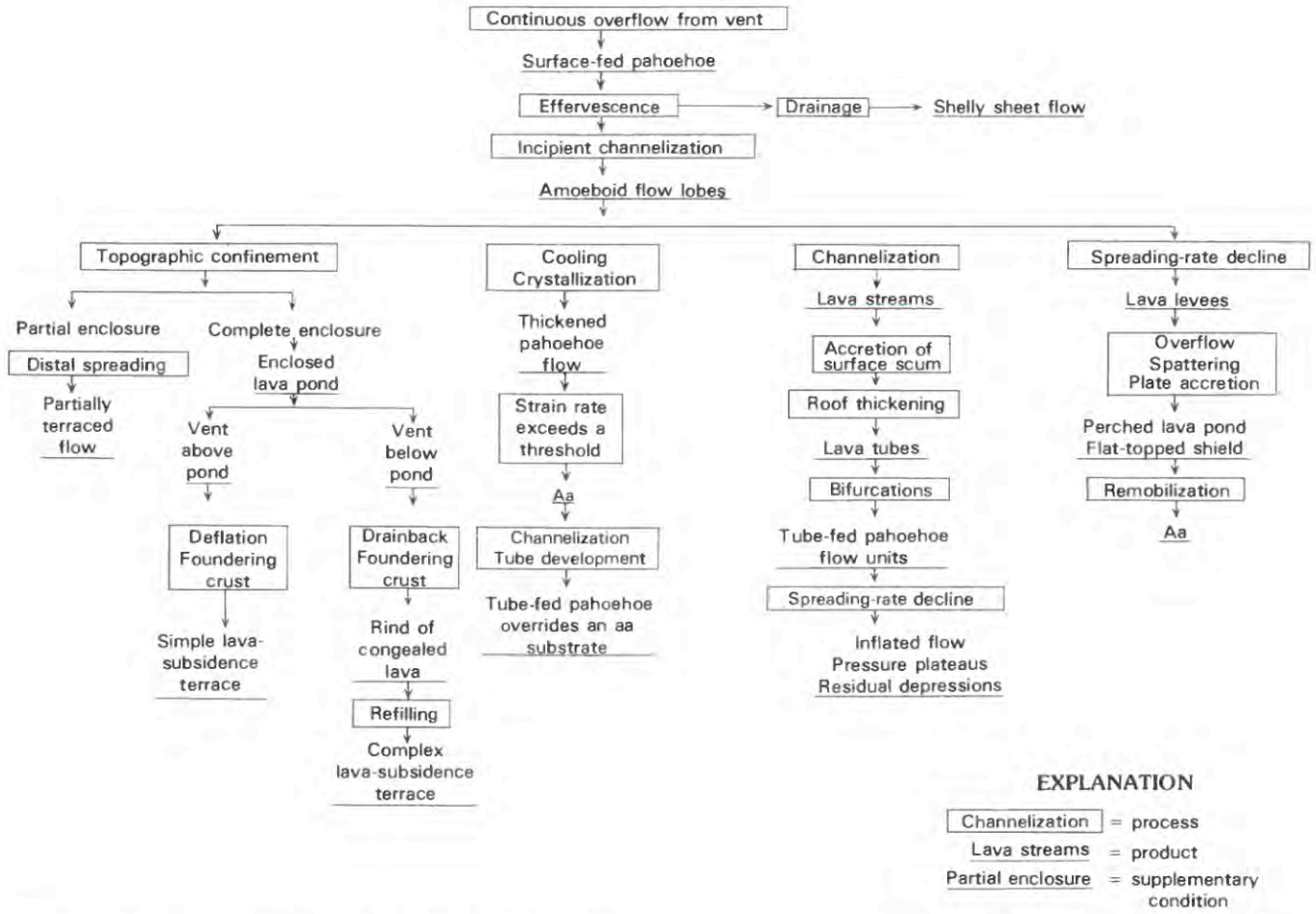

FIGURE 12.7.—Patterns of possible evolution of a lava flow. Summarized here are some processes and environmental factors affecting morphology of basaltic lava flows. In order to infer eruptive behavior it is necessary to distinguish between landforms resulting mainly from topographic influences and those resulting mainly from character of an eruption. Not all branches shown in this flow chart have been useful for interpreting eruptive behavior.

maximum value because it is not corrected for overlapping of flows or, extension of flows onto submarine flanks. Despite those omissions, however, the supply rate seems adequate to explain the rate of surface renewal graphed on figure 12.13.

STRUCTURAL SUBDIVISIONS

Different parts of Kilauea differ in eruptive behavior, so that temporal variations must be extracted from an overprint of spatial variation. Magma rises into Kilauea beneath its summit and then moves laterally for great distances along its rift zones (Fiske and Jackson, 1972). Different behaviors characterize different parts of the system, which is commonly divided into six structural subdivisions (fig. 12.14). A review of these subdivisions will provide a background for the historical account.

SUMMIT

The summit is dominated by collapse features (fig. 12.5*A*). Caldera faults form an annulus of arcuate blocks stepped downward toward an inner sink. All major displacements on caldera faults occurred before eruption of most of the Keanakakoi Ash Member in 1790 (Christiansen, 1979). Other collapse features include Kilauea Iki, Keanakakoi, and smaller prehistoric craters and the Halemaumau pit formed in 1924. Though most eruptive fissures trend east-northeast across caldera structures, other trends occur; some late prehistoric lava erupted from fissures concentric to the caldera.

Eruptions of all types occur in the summit area, but those of long duration are characteristic. Nearly continuous activity at Halemaumau for more than a century built a lava shield that filled the inner sink to overflowing by 1921. Similar eruptions buried an

earlier caldera; still preserved are parts of two lava shields, one surrounding a vent at the east end of Kilauea Iki (the Ai-laau shield), and the other centered in the northwest caldera (the Observatory shield). Tube-fed flows from these vents cover much of Kilauea. Explosive eruptions occur also at long intervals; a small one occurred in 1924, and several much larger ones occurred earlier (Decker and Christiansen, 1984).

EAST RIFT ZONE

The east rift zone forms a ridge extending more than 60 km beyond Cape Kumukahi, the easternmost point on the Island of Hawaii (fig. 12.15; Moore, 1971). Its subaerial part is 4–6 km wide and is loosely divided into an upper segment extending from the caldera to Napau Crater, a middle segment from Napau to Heiheiahulu lava shield, and a lower segment from Heiheiahulu to Cape Kumukahi. The upper segment is dominated by pit craters, and the other segments are marked by closely spaced fissures, faults, and grabens having net seaward subsidence.

The rift zone is straighter and wider than commonly portrayed. Kinks inferred in the lower segment (Skokan, 1974; Furumoto, 1976) are merely offsets in recent eruptive fissures, not in the rift zone as a whole (fig. 12.5*G*,*H*). Seaward migration of the middle segment (as suggested by Swanson and others, 1976a) has not occurred recently; historical eruptions have followed its axis, 18th-century lava having obscured the structures of its southern half (fig. 12.16). All recent flows from the middle segment have spread seaward because the rift zone has subsided below its northern margin, but some older flows of the north flank were erupted from it. The upper segment was almost entirely buried by lava from the Ai-laau vent about 400 years ago; it is probably wider and straighter than the curved chain of young pit craters, which may reflect recent localization to its southwest edge (fig. 12.5*E*). Magma intruding west along Koae faults (Unger and Koyanagi, 1979) may have produced westward widening of the rift zone.

Eruptions are briefer along the rift zone than at the summit. Flows from eruptions of moderate duration are prominent along the upper and middle rift segments, and less so along the lower segment. Brief eruptions are especially numerous along the middle and lower segments, and pyroclastic vents are more common there.

SOUTHWEST RIFT ZONE

The southwest rift zone does not form a distinct ridge like the east rift zone, its seaward subsidence is more obvious, and it does not extend far beyond the shoreline (Moore and Fiske, 1969). It parallels the Kaoiki fault system of Mauna Loa; its structures may follow buried Kaoiki faults. It consists of an inactive zone inland and an active zone seaward. The active zone contains strands of closely spaced fractures separated by unbroken blocks. The rift zone can be divided into segments where it bends near Yellow Cone; the upper segment trends about S. 50° W. and the lower segment trends about S. 15° W.

In the lower segment a seaward zone of recent rifting about 1 km wide is dominated by the Great Crack (fig. 12.5*C*). Other strands in the active zone extend through Puu Ulaula and Puu Kolekole (inland) and Red Cones and Lava Plastered Cones (seaward). Most faults are down to the southeast, toward the sea. More than 20 m of displacement has occurred on faults along the northwest side of the active zone; some landward blocks like Puu Nahaha stand high enough to escape draping by young flows from the rift, though they are draped by young flows from the summit. A seaward migration of eruptions may have occurred; all vents seaward of the faults appear young, while all inland vents are older than 1,000 years. But the most recently active Great Crack is inland from some other vents of the active zone.

The upper segment appears to be a broad graben or sag. It has no large pit craters, though a few small pits do occur. The seaward zone of active rifting flares from a width of 1 km in the southwest to more than 3 km in the northeast (fig. 12.5*B*). It is currently split into three strands converging downrift; each strand consists of closely spaced fractures breaking the sheet of late prehistoric summit flows.

The middle strand extends from the main center of summit tumescence (south of the caldera) through Cone Crater and Puu Koae to the lower segment of the rift zone. Eruptions from this strand have been vigorous and brief, producing spatter cones and aa flows but little tube-fed pahoehoe. The flows have olivine-controlled compositions similar to lavas erupted at the summit (Wright, 1971). This strand probably connects directly to a deeper magma reservoir and taps magma that is changed little by differentiation or loss of volatiles but cannot sustain eruption after the gas-rich fraction has escaped.

The northern strand passes from Halemaumau through Cone Peak and Mauna Iki. Its fissures end 5 km southwest of Mauna Iki without reaching the lower segment. Its historical eruptions have followed shortly after summit activity and have produced little tephra. Lava feeding the Mauna Iki eruption (1919–20) drained from Halemaumau along shallow fissures (Jaggar, 1947). This strand probably is connected to the deeper plumbing by way of Halemaumau so that its magma loses gas through summit eruptions and fumaroles. Eruptions can be sustained for months or years by drainage of degassed lava when Halemaumau acts as a shallow holding tank. (For supporting chemical and deformation data, see Duffield and others, 1982.)

The southern strand passes from the Koae faults through Kamakaia and Yellow Cone; it may intersect the middle strand where the latter bends into the lower rift segment. Its eruptions have been brief to moderately long, but they are unique on Kilauea because they produce cinder cones and viscous lava flows (fig. 12.17) of (for Kilauea) highly differentiated compositions (Wright and Fiske, 1971). This strand may have only a tenuous connection to the main plumbing, its magma residing at shallow depths for long intervals after backing up along Koae structures.

KOAE FAULT SYSTEM

The Koae fault system extends east-northeastward between the rift zones (fig. 12.5*A*,*D*). Its faults have their downthrown side mainly toward the caldera and have had recurrent movement (Duffield, 1975). Some scarps were large enough by the 18th

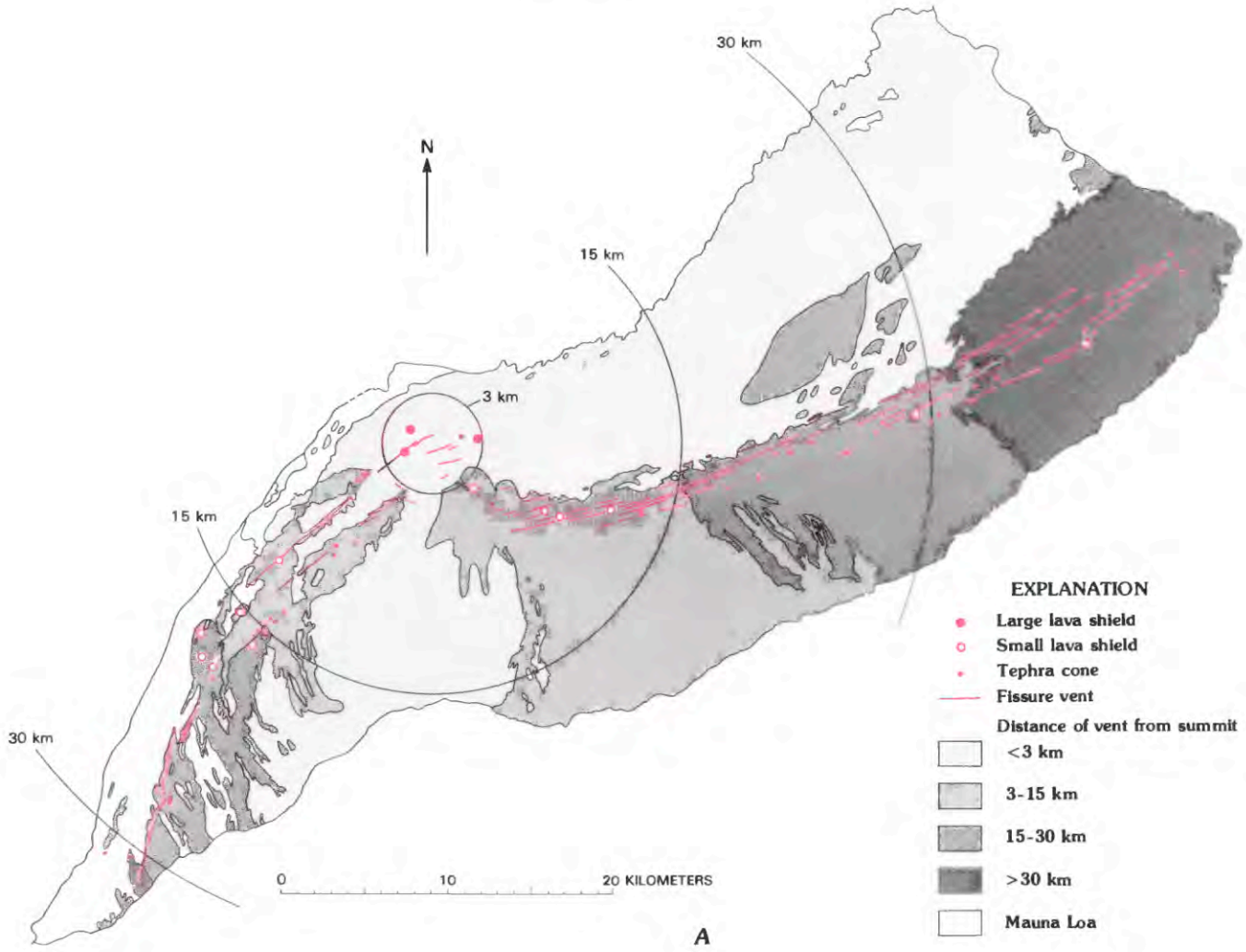

FIGURE 12.8.—Kilauea lava flows classified by location and by type of eruption. ***A***, Flows classified by location of eruption. Lava flows from summit cover large areas of north flank and southwest rift zone as well as flank south of summit. ***B***, Flows classified by eruption type. Eruptions tend to be briefer at greater distances from summit. Because it is difficult to group older flows into eruption assemblages, some older aa flows alone are inferred to represent brief eruptions and older tube-fed flows alone are inferred to represent sustained eruptions; these inferences may not always be correct.

century to deflect lava flows from Cone Crater and Puu Koae. Most present scarps postdate the Kalue flows thought to be 500–750 years old, but some scarps are older. A segment of Kalanaokuaiki Pali extending 2 km east of the Hilina Pali Road crossing is rimmed by Kipuka Nene flows thought to be about 1,100 years old (fig. 12.18); the younger Kalue flows failed to overtop the scarp, and lava tongues oozed down into the open fracture at its base. The southernmost Koae fault extending eastward from Kipuka Nene campground is overlapped by Kalue flows and has had little displacement during the subsequent 500 years.

Few eruptions are known from the Koae fault system, and most of them have been from near its intersection with the southwest rift zone. Some lava was erupted from eastern Koae structures in 1973 (Tilling and others, chapter 16). Spatter found beneath Kokoolau lava along Kalanaokuaiki Pali may be clots ejected by heated air or steam after surface flows invaded the fracture. It remains possible that true eruptions from the central Koae system have occurred and then been obscured by the younger flows from the summit.

The Koae fault system may be an ancient feature of Kilauea, or it may have been produced recently by contraction or migration of the rift zones and caldera. An anomalous area of caldera-concentric structures along the central Koae (Duffield, 1975) may reflect the buried rim of an earlier caldera, and the fault segments extending to the east and west may follow former eruptive-rift structures radial to

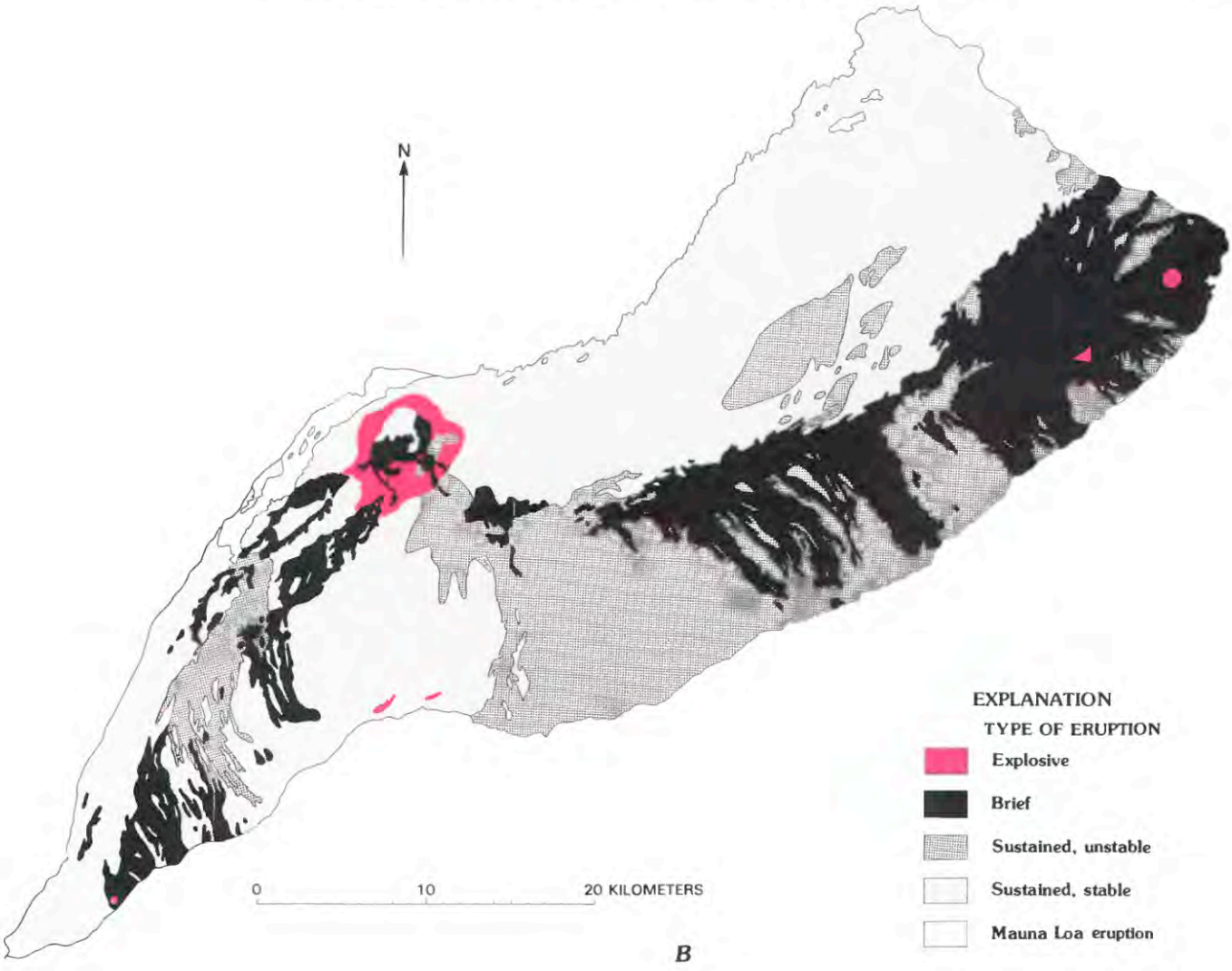

FIGURE 12.8.—Continued.

that caldera. If so, the bend in the east rift zone could have arisen from northward migration of summit collapse instead of southward migration of the rift zone.

SOUTH FLANK

The south flank is the area seaward of the rift zones and the Koae fault system. Faults of the south flank (Hilina fault system) mainly show displacement down to the south (fig. 12.5*C–F*). The most prominent faults, such as those of Hilina, Poliokeawe, and Holei Palis and of Puu Kapukapu, occur in the seaward part of the south flank; this has led to a distinction between faulted and unfaulted parts of the flank (Swanson and others, 1976a). Buried Hilina faults, however, inferred from steepened slopes, occur inland close to the Koae system and probably extend into each of the rift zones (Holcomb, 1980b). The Hilina fault system probably is not isolated from other Kilauea structures but grades into them; its apparent isolation arises from the restricted extent of its recent displacements.

The age of the Hilina system is not known. Stearns and Clark (1930) considered the faults to postdate the base of the Pahala Ash, about 23 ka (Easton, 1978), because the ash caps some blocks (Puu Kapukapu and Puu Kaone) truncated by the faults. Puu Kapukapu is about 300 m high. If the block seaward of Puu Kapukapu subsided to sea level in 3-m increments similar to the displacement of November 29, 1975 (Tilling and others, 1976), it would have required 100 such episodes recurring at intervals of about 230 years. The highest part of Hilina Pali undraped by younger lava also is about 300 m high, and the youngest Pahala Ash truncated by this fault could be as young as about 11 ka (Easton, 1978). That displacement could have been accomplished by 3-m subsidence episodes repeated every 110 years. These frequencies are reason-

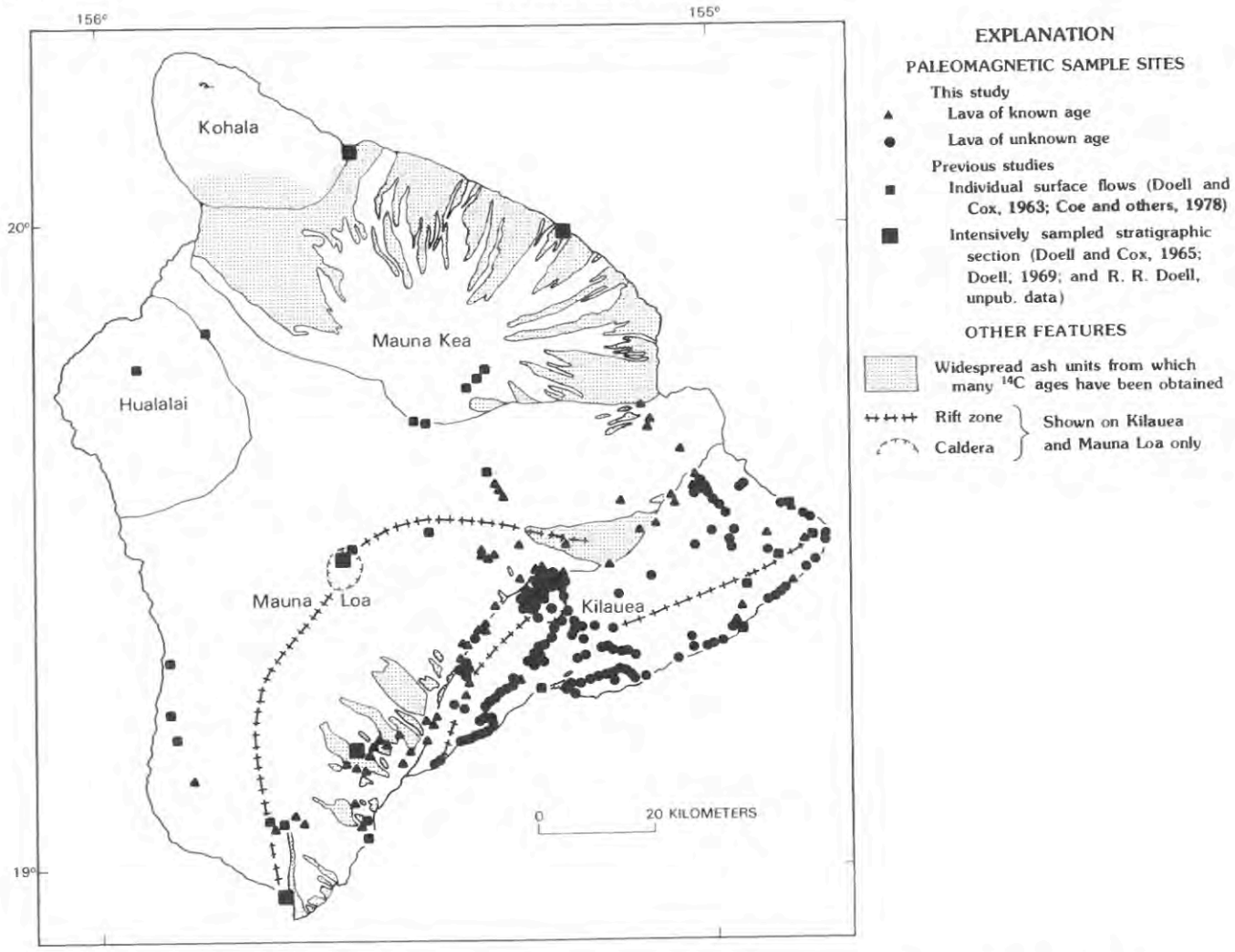

FIGURE 12.9.—Paleomagnetic sampling locations on five volcanoes that make up Hawaii. Map modified from Stearns and Macdonald (1946).

able, and the interpretation by Stearns and Clark may be correct. However, the faults could be younger and could have had large, catastrophic displacements earlier in their development, or they could be older and draped by Pahala Ash that is now buried or subsided beneath the sea. The Hilina fault system could be older than Kilauea and could have developed from seaward migration of the Kaoiki fault system as older inland faults were stabilized by the growing edifice.

No eruptions are known from the south flank; sparse dikes along Hilina Pali were fed by lava flows spreading down into open fissures (Walker, 1967; Easton and Lockwood, 1983). Nonetheless, episodes of Hilina displacement may affect Kilauea's eruptive behavior by dilating the rift zones and disrupting the magma plumbing system.

NORTH FLANK

The north flank does not show surficial structures, though inactive structures may be buried. Only one possible buried fault is inferred, with great uncertainty, subparallel to the coast at an elevation of about 60 m, 5 km inland from Kaloli Point (figs. 12.5*J*, 12.19). Several kipukas (inliers) in the youngest flows are truncated along this line, and no kipukas of older Mauna Loa lava occur seaward of it. The surface slope decreases across it from 1.6° inland to 1.0° seaward, and the seaward lava has assumed a thickened elephant-hide appearance (Stearns and Macdonald, 1946) below the break in slope. The discontinuity may be a normal fault, its downdropped eastern block buried by younger lava, or it may parallel a buried seacliff several dekameters high. Alternatively, it

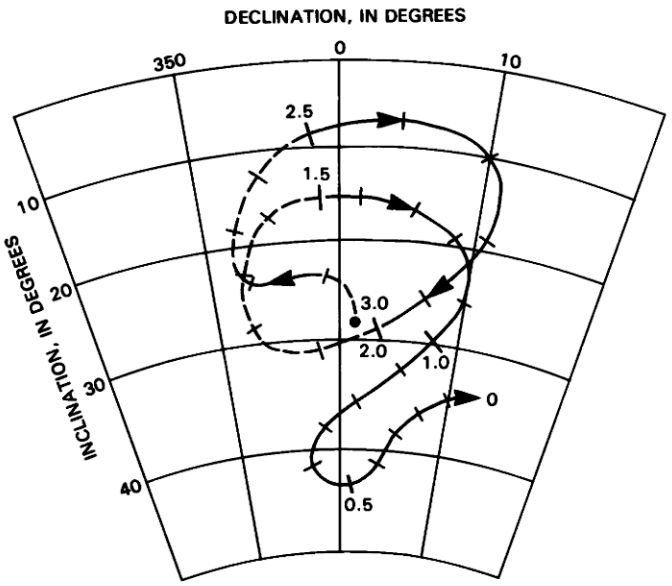

FIGURE 12.10.—Generalized history of Hawaiian geomagnetic secular variation during the last 3,000 years. Track dashed where confidence is less. Ticks are shown at approximate 100-yr intervals, and numbers indicate thousands of years before present. Unpublished data have been used to modify earlier version by Holcomb and others (1986).

could be the edge of a very broad, flat cone of lava banked against an older, steeper slope. Such a cone could develop from several causes; for example, a rise in relative sea level could have raised the baselevel to which the slope was formerly adjusted.

No eruptions are known from this flank; for at least the last few millenia it has passively accumulated lava, mostly as tube-fed flows from the summit.

EARLIER PREHISTORIC ACTIVITY

Because of incomplete exposures and dating uncertainties, a full eruption history of Kilauea is not yet possible, even for the last few thousand years. Available information does, however, permit a general history, having increased detail with younger age. The history is reviewed in the following sections, in which many dating uncertainties are discussed. Readers not interested in these details may want to skip ahead to the section entitled "Summary of Eruptive History."

PLEISTOCENE SHIELD GROWTH

Kilauea's early history was studied by Easton (chapter 11, 1978), who estimated that the volcano began to grow around 200–300 ka. Only the later subaerial part of shield growth has been available for study; it is recorded by the Hilina Basalt, Pahala Ash, and lower part of the Puna Basalt exposed in the Hilina fault scarps of the central south flank (fig. 12.20). The lowermost Hilina flows now exposed are estimated to have ages of 100 ka, and the Pahala Ash was deposited between 25 ka and 10 ka (Easton, chapter 11). Rocks below the Pahala Ash are mostly tube-fed pahoehoe flows, probably from sustained summit eruptions. Interspersed among the flows are ash layers, probably erupted at the summit in large explosions associated with successive caldera collapses. Little is known about rift-zone activity during this interval.

OLDER HOLOCENE FLOWS

About 10 percent of Kilauea's surface consists of rock older than about 1,100 years. Some of the older lava flows are veneered by ash deposits. Among these are kipukas of picritic aa of about 5.2 ka (W–4536) on the north flank southeast of Keaau (fig. 12.21), probably erupted from the northeast rift zone of Mauna Loa (Lockwood and Lipman, chapter 18). Pahoehoe above ash in one kipuka has been dated at about 3.7 ka (W–4177, fig. 12.5*J*). The source of this lava is unknown; it could have come from the summit of Kilauea or from the northeast rift zone of Mauna Loa. As discussed later, it may be coeval with flows previously thought to have been erupted 750–1,000 years ago. Buried flows resting on Pahala Ash below the rim of Hilina Pali have been dated at about 6.6 ka and 4.8 ka (W–3873 and W–3798, fig. 12.5*D*). Younger flows, separated from the older ones by thin ash and forming much of the surface in Kipuka Ahiu and Kipuka Keana Bihopa (fig. 12.22), have been dated at about 3.5 ka (W–3831, fig 12.5*D*). These flows are veneered by ash and eolian sand thick enough to support a carpet of high range grass and scattered ohia trees (*Metrosideros polymorpha*). The ash on and between these older Puna flows suggests that explosive eruptions occurred more than once between 6.6 and 1.5 ka, but the number of eruptions is not known. The flows have various directions of magnetization, but not enough ^{14}C ages are available to derive a continuous magnetic history.

Several vents still exposed in kipukas along the east rift zone may be older than 2,000 years; among them are Kapoho Crater, Kiapu, Iilewa, and Kalalua (fig. 12.5*F–H*). Some vents along the lower southwest rift zone may also be older. The Cinder Hills 2 km southeast of Pahala are overlapped by a lava flow dated by ^{14}C at about 3.5 ka (W–5324, fig. 12.5C). A thin lava flow issuing from a prominent fissure along the Kilauea-Mauna Loa boundary 1 km southeast of Pahala has been dated at about 3.6 ka (W–3884, fig. 12.5C); though Lipman and Swenson (1984) mapped this fissure as an eruptive vent, a lava flow erupted elsewhere could have flowed into it farther upslope and then overflowed its rim.

FLOWS BENEATH UWEKAHUNA ASH MEMBER OF PUNA BASALT

Much of Kilauea may have been covered by lava in a short interval preceding deposition of the Uwekahuna Ash Member. In stratigraphic sections of the summit and upper east rift zone, flows below the Uwekahuna Ash Member have remanent magnetizations (crosses, fig. 12.11C) distinct from those of flows of the last millenium. Examples occur in Uwekahuna Bluff (9B229A; sites 133 of Doell and Cox, 1965; 137D,E of Doell, unpublished work), Tree Molds (1B121), Kilauea Iki (8B145), and Pauahi (9B385). Surficial flows inland from Papalehau Point (3R457, fig. 12.5C) may have been erupted at the summit also.

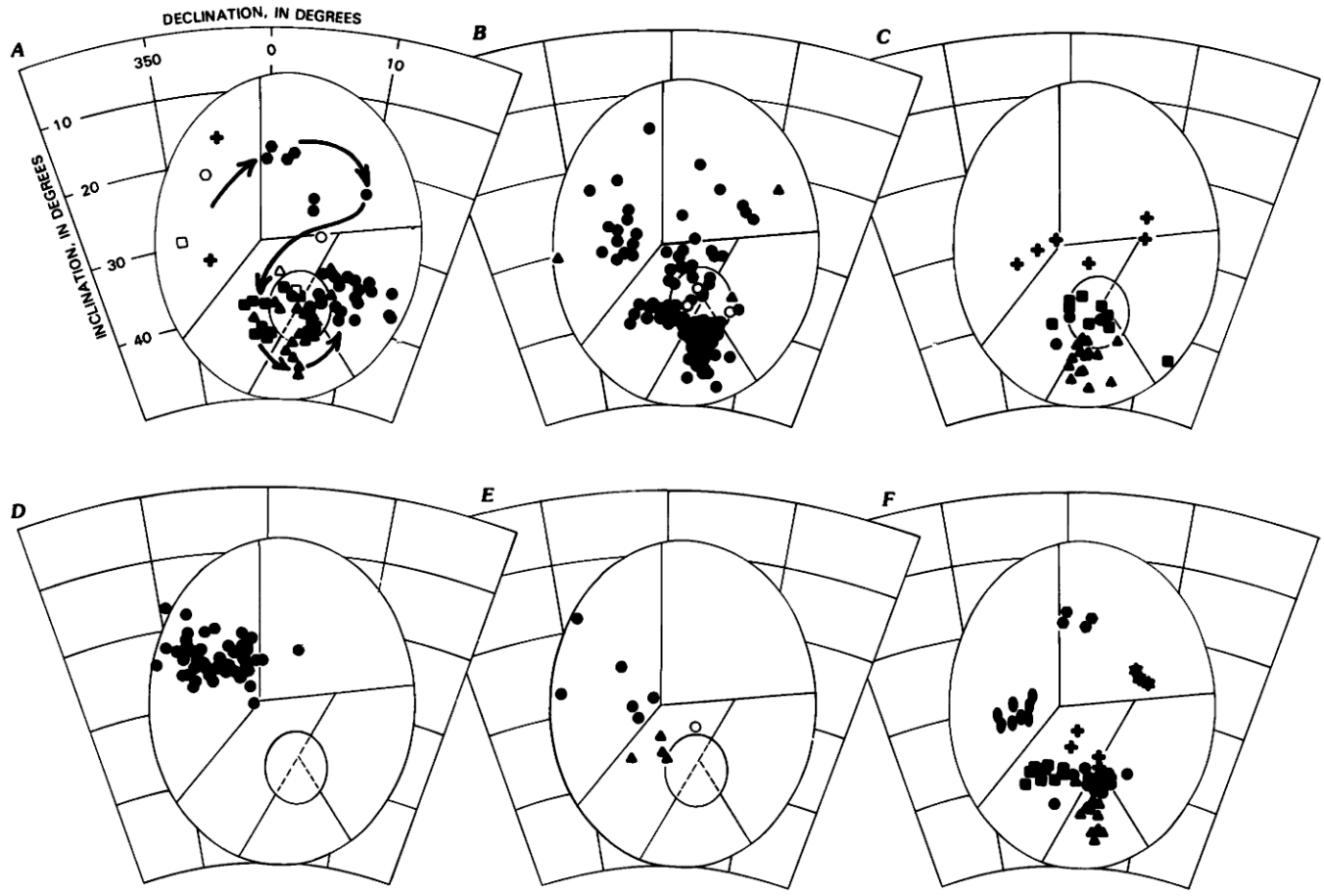

FIGURE 12.11.—Semiquantitative method used to infer ages of lava flows. Unpublished data have been used to modify version by Holcomb and others (1986). Large ellipse divided into fields containing sites of similar age; smaller ellipse is area of confusion having diverse ages clustered together. ***A***, Age classification from dated flows; symbols represent different ages: dots, younger than 250 years B.P.; triangles, 250–500 years B.P.; squares, 500–1,000 years B.P.; hexagons, 1,000–1,500 years B.P.; crosses, 1,500–2,000 years B.P. Open symbols are doubted results. Arrows approximate secular variation. ***B***, Site mean directions for undated surface flows of Kilauea. Dots, pahoehoe; triangles, aa. Open symbols indicate doubted results. ***C***, Stratigraphic section in Uwekahuna Bluff (Doell and Cox, 1965; R.R. Doell, unpublished work). Symbols denote different parts of section: crosses, below Uwekahuna Ash of Puna Basalt (nos. 131–133, 137C–137E); squares, lower section above Uwekahuna Ash Member (nos. 134–137B, 137F–137H); triangles, middle part of section; dots, upper part of section. ***D***, Stratigraphic section in west wall of Mokuaweoweo caldera, Mauna Loa Volcano (Doell, 1969). ***E***, Buried flows of Kilauea, exposed in walls of caldera and pit craters. Symbols indicate stratigraphic position: dots, below hiatus; triangles, above hiatus. Circle indicates anomalous magnetization below hiatus in Makaopuhi Crater. ***F***, Groups of surface flows thought from independent evidence to be closely similar in age: dots, Observatory; triangles, Ai-laau; squares, Kalue; crosses, Volcano; stars, Kipuka Nene; hexagons, Kukuau (Mauna Loa); ellipses, older flows of Kalapana.

Flows with similar magnetization crop out along both rift zones. Among them are a red tephra cone and lava flows (paleomagnetic site 9B345) exposed beneath a yellow tephra layer in the west wall of Pauahi Crater (fig. 12.23). Mixed flow assemblages (8B253, 8B349, 8B313, 8B289, 8B277) between Kaimu and Kupapau (fig. 12.5*F,G*; older Kalapana flows of fig. 12.11) indicate sustained eruption from the middle east rift zone near Kalalua, and other mixed flows around Kapoho (9B181, 8B973, 8B817) may represent sustained eruption from the lower east rift zone near Puu Honuaula (fig. 12.5*H*). Tube-fed flows with similar magnetization on the north flank in Hawaiian Beaches (9B853) and Ainaloa (8B805) subdivisions (fig. 12.5*H*) may have been erupted from the summit or from the middle east rift zone. This old north-flank lava supports a monotonous forest in which separate flows cannot be distinguished (figs. 12.24, 12.25); forest patchiness probably is caused by ohia dieback (Jacobi, 1983) rather than flow boundaries.

Their similar magnetizations suggest that these flows were erupted within a few centuries preceding the Uwekahuna Ash Member, but ages are not yet well constrained. Because a Mauna Loa flow (8B697) dated by ^{14}C at about 1.8 ka (W–3850) is magnetically similar, these Kilauea flows were assigned ages of 2.0–1.5 ka by Holcomb and others (1986). But Lockwood and Rubin (1986) now judge the Uwekahuna Ash Member above them

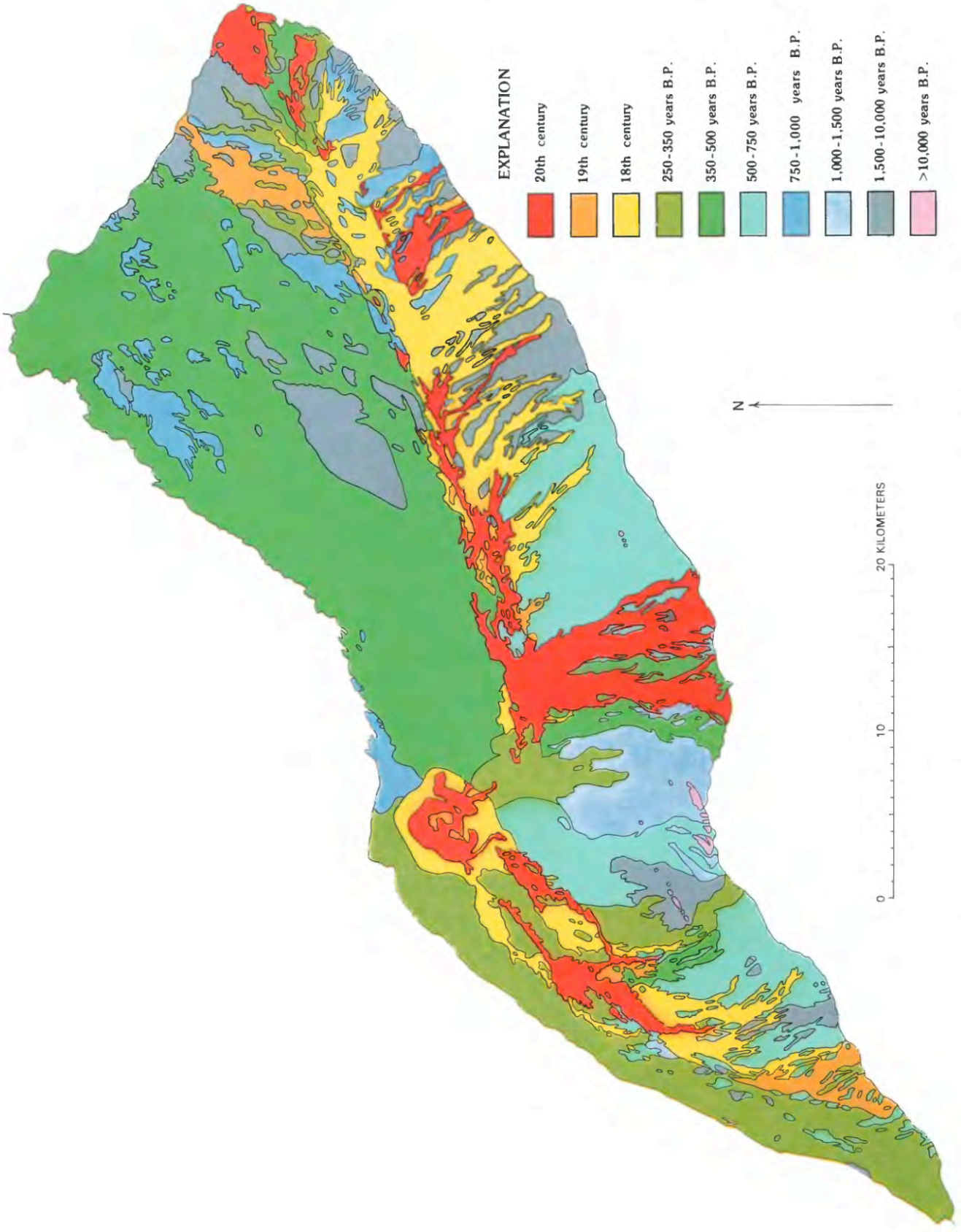

FIGURE 12.12.—Stratigraphic map of Kilauea, showing approximate ages of surficial lava flows. Modified from Holcomb (1980b).

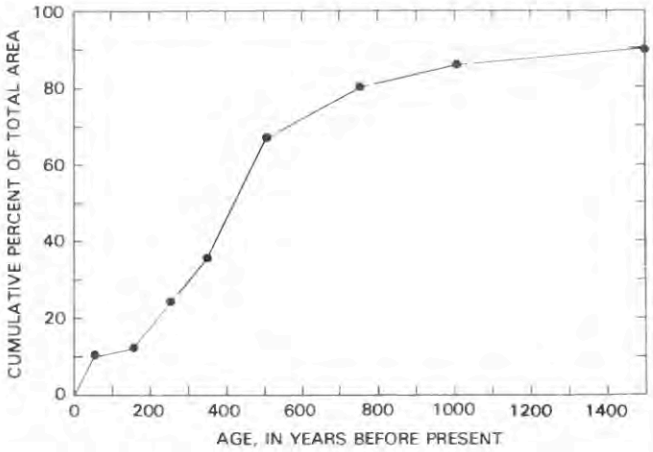

FIGURE 12.13.—Age of Kilauea's surface, a graphical presentation of data in table 12.2. Large variation is shown in rate of flooding, intervals 0–100 and 400–600 yr B.P. having high rates and intervals 100–200 and 1,000–1,500 yr B.P. having low rates. Lower apparent rates of earlier intervals arise partly from later coverage of older flows by younger lava.

to have an age of 2.1 ka, and stratigraphic relations permit most of the flows to be older. Lava east of Kaimu, possibly correlative with 8B313, has been dated at about 2.4 ka by ^{14}C (W–5052, fig. 12.5*G*). Ages of about 2.1 ka and 2.2 ka have been obtained for pahoehoe in a quarry at 786-m elevation along the northeast margin of Kilauea (W–4369 and W–3885). Ash-veneered aa on the rim of Kukalauula Pali is dated at about 1.8 ka (W–4119, fig. 12.5*C*), but its magnetization is not known. Though their ages remain uncertain, lava flows from the summit and east rift zone probably covered much of Kilauea within the few hundred years before the development of the Powers caldera.

POWERS CALDERA

That an ancient caldera was buried before the present one developed was inferred by Powers (1948) because the Uwekahuna Ash Member occurs in the base of Uwekahuna Bluff at an elevation of about 1,100 m, while at Tree Molds it occurs at about 1,220 m (Doerr, 1933). The exposure in Uwekahuna Bluff must cap an old caldera block that subsided about 120 m. This inference is confirmed by paleomagnetic data; flows above the Uwekahuna Ash Member are magnetically similar to Kilauea's surface flows (fig. 12.11*C*) and indicate rapid accumulation in the last millenium. If this thick section is coeval with the thin carapace elsewhere but is younger than higher flows beneath the Uwekahuna Ash Member at Tree Molds, it must fill a caldera.

The configuration of the Powers caldera is poorly known. A buried outer rim is inferred to coincide with the outermost structures of the modern caldera because the outer fault west of Uwekahuna predates the most recent collapse (fig. 12.5*A*). This outer rim did not bound a deep sink because it is little more than 100 m higher than older rock exposed beneath the Uwekahuna Ash Member in Uwekahuna Bluff; a shallow subsided annulus at least 1 km wide, similar to the present one, must have existed. Faulting within that annulus is suggested by draping of the Uwekahuna Ash Member over a step 30 m high formerly exposed in the face of Uwekahuna Bluff (Powers, 1948).

The age of the Powers caldera also is not yet well constrained. It is probably older than 1,300 years because its oldest overflows are thought to be about 1,100 years old, and at least a few hundred years of filling should have preceded overflow. The caldera and Uwekahuna Ash Member should be close in age if caldera collapse caused the explosive eruption. Holcomb and others (1986) inferred an age of about 1.5 ka for both caldera and ash, but they may be older. Eight ^{14}C ages currently available for the Uwekahuna Ash Member range from about 1.0 ka to about 2.2 ka. Lockwood and Rubin (1986) now believe that the younger ages reflect sample contamination and judge the age of the ash to be about 2.1 ka. An age of 1.5 ka is retained in this report; several generalizations herein may need revision if further work confirms the older age. Casadevall and Dzurisin (chapter 13) adopt the older age and discuss some of its possible consequences.

SUMMIT HIATUS

Collapse of the Powers caldera was followed by a caldera-filling interval in which no lava spread from the summit onto the flank. Dzurisin and Casadevall (1986) believe that this interval was very short (only a few years) because the uppermost pumice of the Uwekahuna Ash Member in Uwekahuna Bluff was not eroded before it was covered by lava. But the uneroded pumice could be much younger than the rest of the ash, and paleomagnetic data suggest a long interval between flows below and above the ash. Lava beneath the ash has magnetization consistent with an age greater than 1.5 ka (9B229A; sites 133, of Doell and Cox, 1965, and 137D,E of R.R. Doell, unpublished work), while lava above the ash has magnetization consistent with an age of about 0.75 ka (1B618; sites 137F,G,H of R.R. Doell, unpublished work).

A surface marking a hiatus is exposed also in three pit craters. In Kilauea Iki Crater (fig. 12.26) it lies between flows separated by a red cinder layer. In Pauahi Crater (fig. 12.27) and Makaopuhi Crater (fig. 12.28) it lies above weathered ash and debris on which a forest grew, so that tree molds were produced when the area was flooded by lava. Paleomagnetic samples have been collected from lava flows just above and just below the hiatus in each crater (Kilauea Iki, 8B145 below, 8B157 above; Pauahi, 9B385 below, 9B217 above; Makaopuhi, 9B157 below, 9B241 above). The flows above are all younger than 1.0 ka (fig. 12.11*E*). Flows below have directions indicating pre-Powers caldera ages older than 1.5 ka, except for one. The lower flow in Makaopuhi has a direction corresponding to less than 1.0 ka; if the direction is correct, it suggests only a brief hiatus and rapid forest growth there. But because no stratigraphic evidence bounds its age, the flow could be much older; alternatively, it may have been remagnetized during rapid accumulation and slow cooling of the Kane Nui o Hamo lava shield above it. With this possible exception, the hiatus is correlative

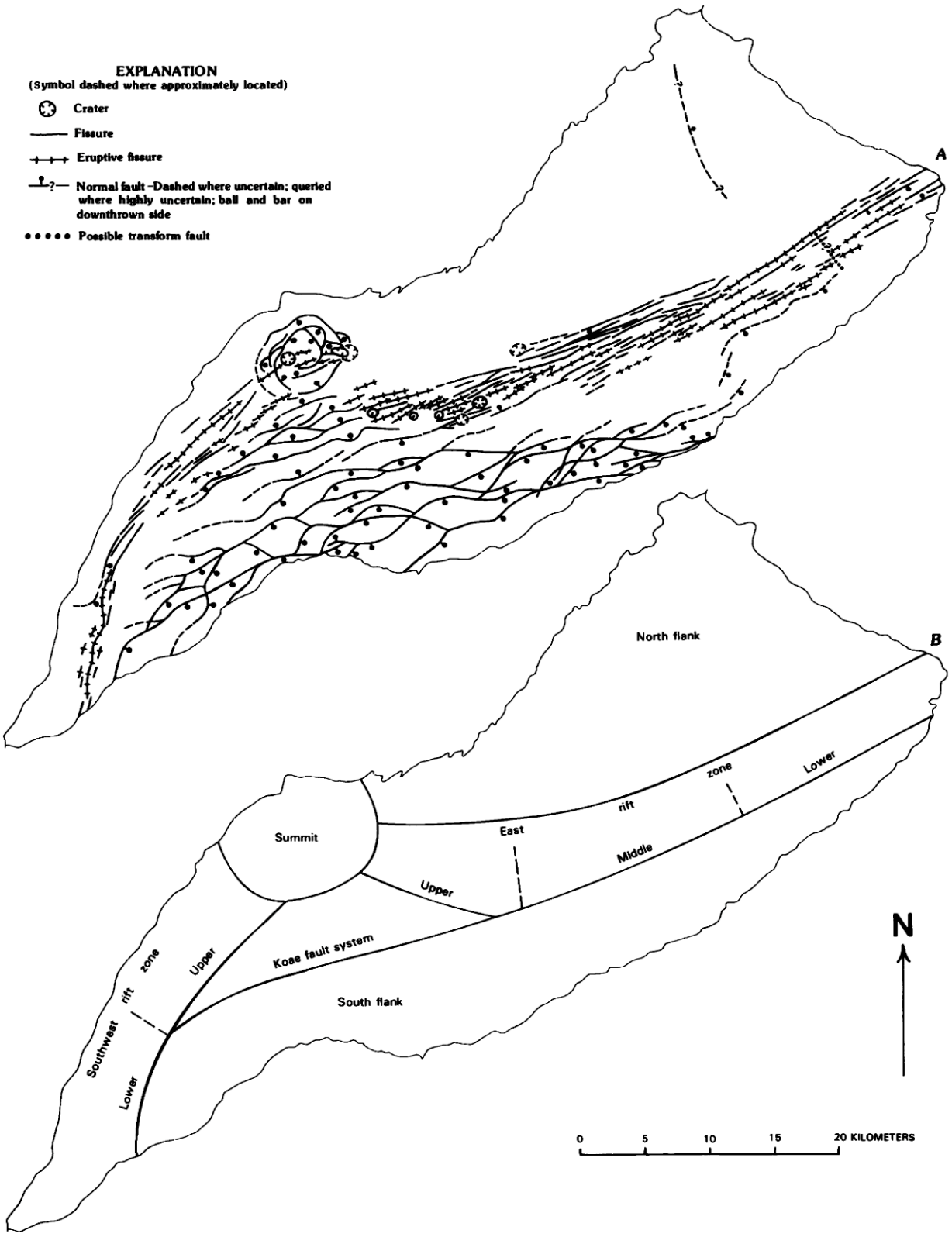

FIGURE 12.14.—Structure of Kilauea. *A*, Mapped structures, simplified from Holcomb (1980b). *B*, Structural subdivisions, modified from Swanson and others (1976a).

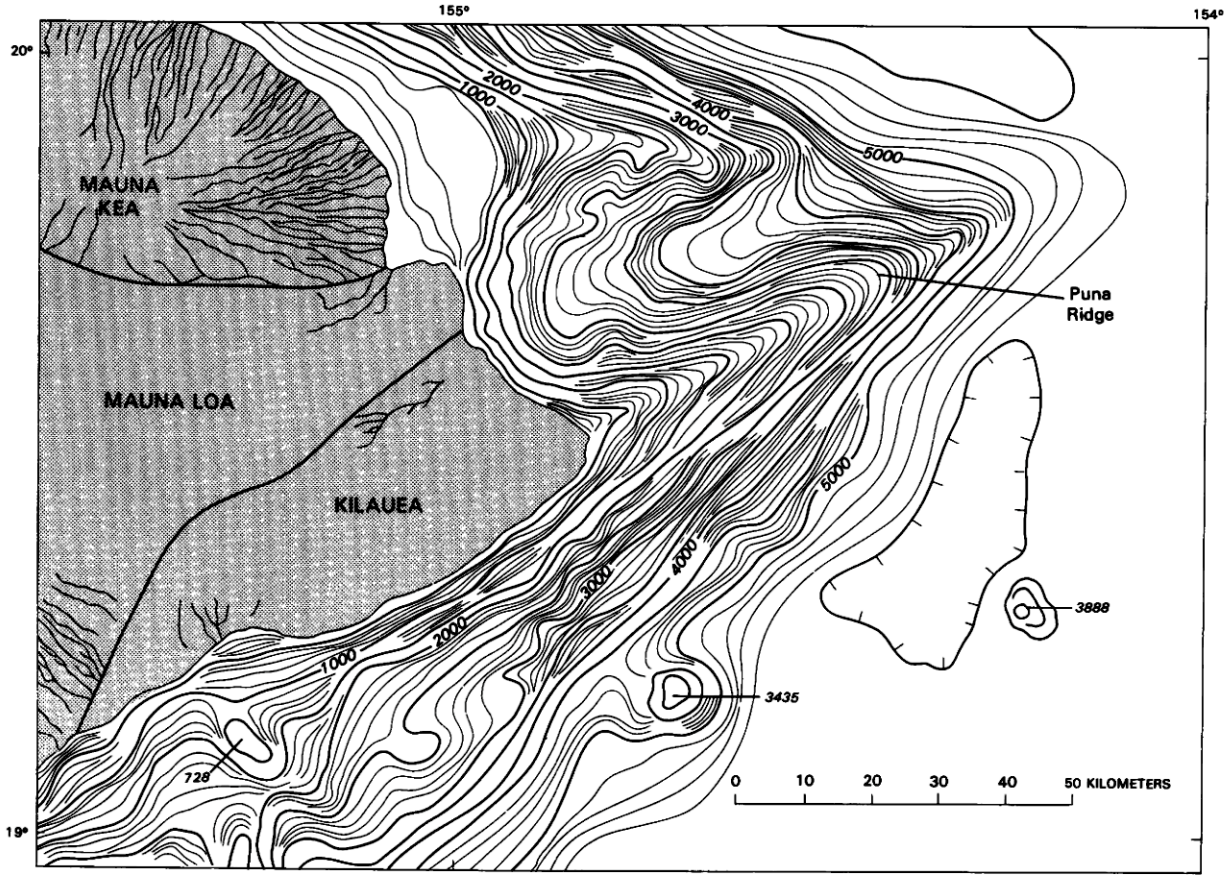

FIGURE 12.15.—Bathymetry around eastern part of Hawaii, showing Puna Ridge. From Wilde and others (1980); depths in meters; contour interval 100 m. Hachures indicate area of closed low depression.

at all sites and spans more than 500 years from more than 1.5 ka to less than 1.0 ka.

Coincident with this hiatus is a paucity of eruptions along subaerial parts of the rift zones. A small pyroclastic cone of the lower east rift zone east of Kiapu has been dated at about 1.3 ka by ^{14}C (W–4674, fig. 12.5*H*), and paleomagnetic data have suggested one group of flows (9B829, fig. 12.5*B*; 3R409, fig. 12.5*C*) in this interval along the southwest rift zone. No others are known, however; most eruptions in this interval were probably confined to a deep inner sink or submarine segments of the rift zones.

KIPUKA NENE FLOWS

The earliest overflows from the Powers caldera may be the tube-fed flows of Kipuka Nene and Kipuka Papalinamoku, which form much of the coast between Keauhou and Kaaha (fig. 12.5*D*). The flows have a distinctive magnetization (1B224, 1B456, 3R013; table 12.5) similar to Mauna Loa flows (4A276) dated at about 1.1 ka by ^{14}C (W–3910, 1,270 years B.P.; W–5083, 1,030 years B.P.). If the Kipuka Nene flows do postdate the Powers caldera, they are probably about 1.1 ka. Available stratigraphic evidence, however, does not require them to postdate the caldera. Additional uncertainty is caused by other nearby flows having different magnetizations but ^{14}C ages also of about 1.1 ka, as noted later in discussion of the Kalue flows.

Initial errors in dating the Kipuka Nene flows illustrate well the difficulties encountered in work of this kind. Though the Kipuka Nene flows are clearly veneered by surficial deposits and vegetation that are absent on overlying Kalue flows (fig. 12.29), it was difficult to find the exact boundary between them. Initially inferring the boundary to parallel the west side of a prominent band of trees, I collected paleomagnetic samples in 1978 from sites 8B121 and 8B133 on each side of this boundary (fig. 12.30*A*). The results revealed the same magnetization at both sites (table 12.5; fig. 12.30*B*). Wanting to make sure that I had really sampled the older flows, in 1979 I collected from site 9B169 south of a fault that extended through Kipuka Nene. This fault seemed to be overlapped to the west by the younger Kalue flows, and I reasoned that lava on the southern rim of the fault scarp must belong to the older flows. The results again gave virtually the identical magnetization, so I

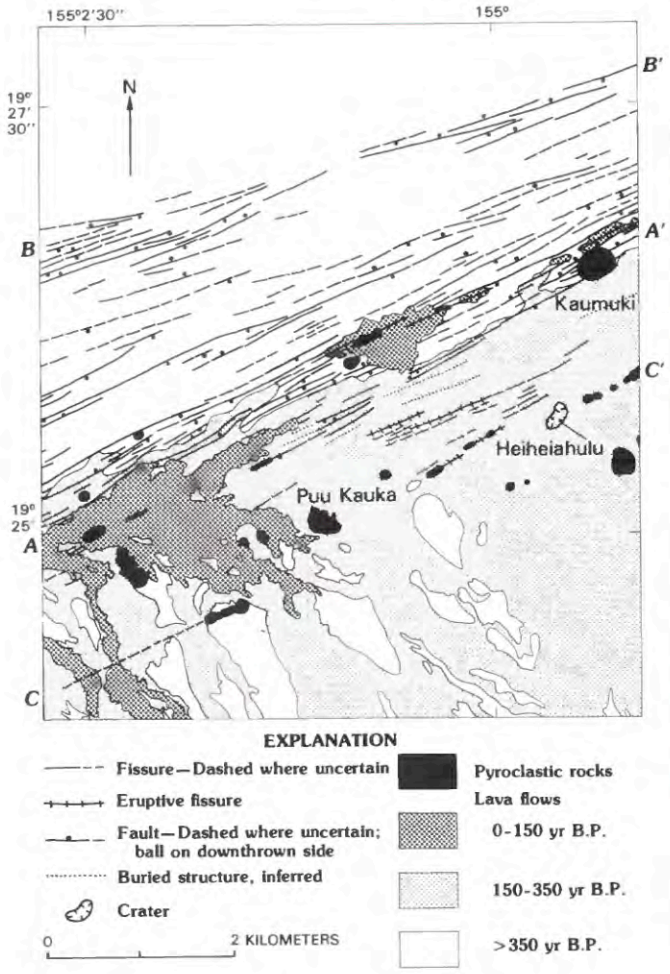

FIGURE 12.16.—Eastern part of middle east rift zone, with contrasting surficial structure north and south of active zone A–A'. North edge of rift zone is along B–B'; south edge along C–C'. Lava flows 350–500 years old north of A–A' broken by many fissures but no eruptive vents; flows 150–250 years old south of A–A' have many vents but few younger fissures. Flooding south of A–A' probably followed large dilation of rift zone a few hundred years ago.

A

B

FIGURE 12.17.—Unusual eruption products of Kamakaia Hills. Photographs by R.T. Holcomb, 1977. ***A***, Kamakaiwaena, one of several cinder cones found only in this area of Kilauea, and peculiar near-vent lava flow in foreground. View northeast (see figure 12.48 for location). ***B***, Closer view, looking west, of same flow, which consists of thick, cylindrical, toothpastelike extrusions that twisted back on themselves and then broke as they cooled. These protrusions are morphologically distinct from all other flow forms seen on Kilauea and resemble some elongate pillows of submarine lava flows. Scale indicated by aerial-photograph case (about 25 cm wide) perched on day pack.

assigned the Kipuka Nene flows a young age similar to that of the Kalue flows and tried to explain the difference in surficial cover by inferring that a tephra-producing eruption at Kane Nui o Hamo (which shares the same magnetization) had occurred during a short interval between the two sets of lava flows. However, still not being satisfied, in 1981 I collected from two more sites, 1B236 on the rim of Kalanaokuaiki Pali and 1B456 deep within Kipuka Nene. This time I found a distinctly different magnetization (fig. 12.30*B*). Then N.G. Banks found beside the Kipuka Nene picnic shelter a contact between two lava flows, with a thin deposit of ash between them. In 1983 I collected 3R001 and 3R013 on each side of this contact and found two different magnetizations corresponding to the two measured previously: the boundary had finally been discovered. Though I have not traced it away from the picnic shelter, it must extend roughly as shown in fig. 12.30*A*, about 100 m east of the contact inferred initially.

The distinctive Kipuka Nene magnetization is also shared by the flows of Opihikao (8B013; fig. 12.5*H*); they may have been erupted from Puulena or Kahuwai, which are notable for their phreatomagmatic ash blanket (Moore, 1983). Other eruptions of this age are not yet known from elsewhere along the rift zones.

VOLCANO FLOWS

Volcano village is built on flows forested differently from younger Ai-laau flows (fig. 12.31). One of these older flows is dated

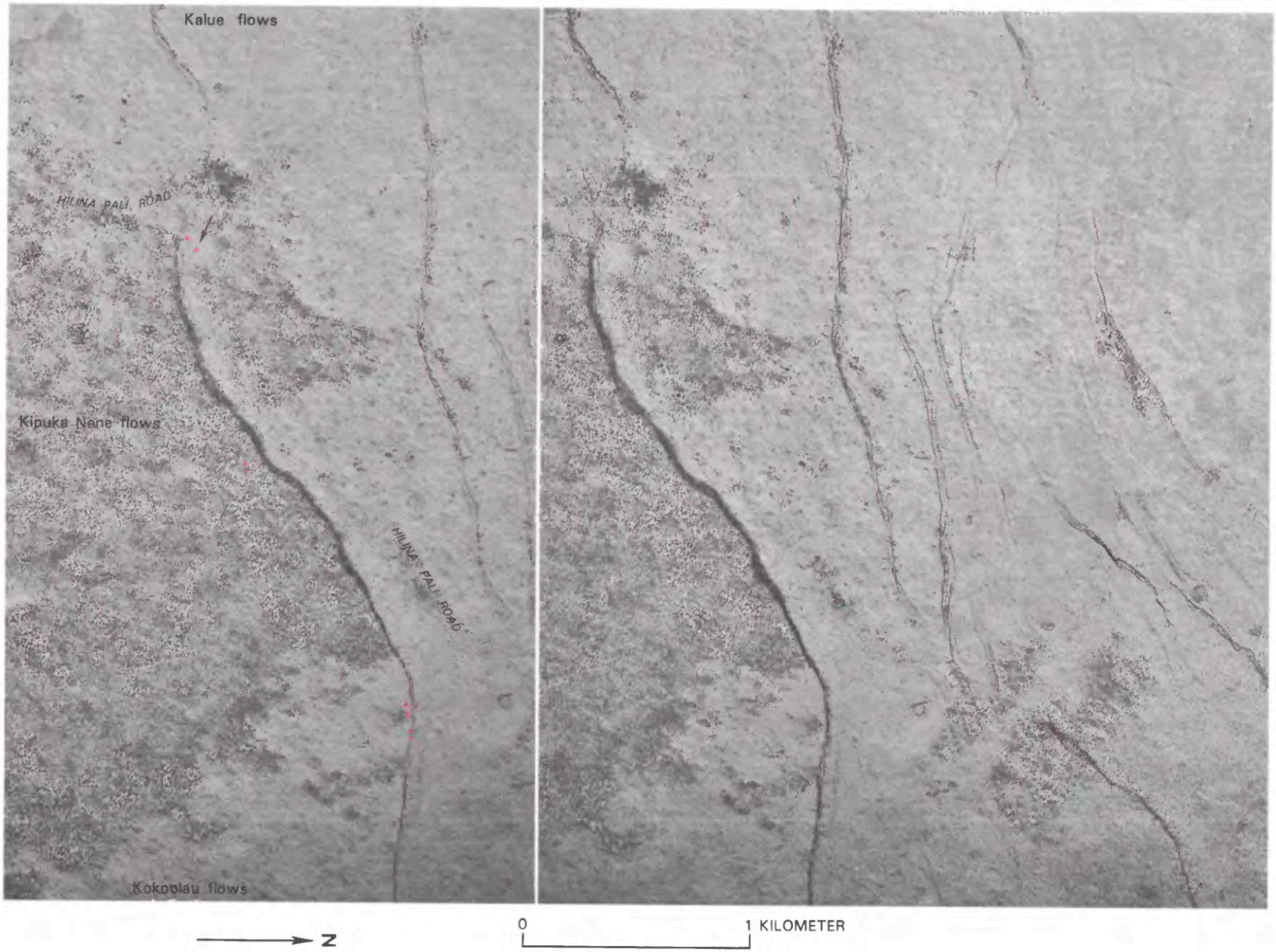

FIGURE 12.18.—Contrasting vegetation patterns along Kalanaokuaiki Pali. Barren Kalue and Kokoolau flows interpreted to postdate much of fault displacement, while tree-covered Kipuka Nene flows are thought to predate it. Pattern of polygonal plates (arrow) at base of cliff is characteristic of ponded lava. Duffield (1975, p. 10) argued against ponding because similar smooth surface is found on south side of fault, but smooth surface is not extensive there, lacks polygonal pattern, and could have formed from spreading of pond as it rose above scarp that initially held it back. Pairs of small red dots, paleomagnetic sample sites. Stereo pair prepared from frames 74, 75 of roll 14CC, USDA series EKL, 1965.

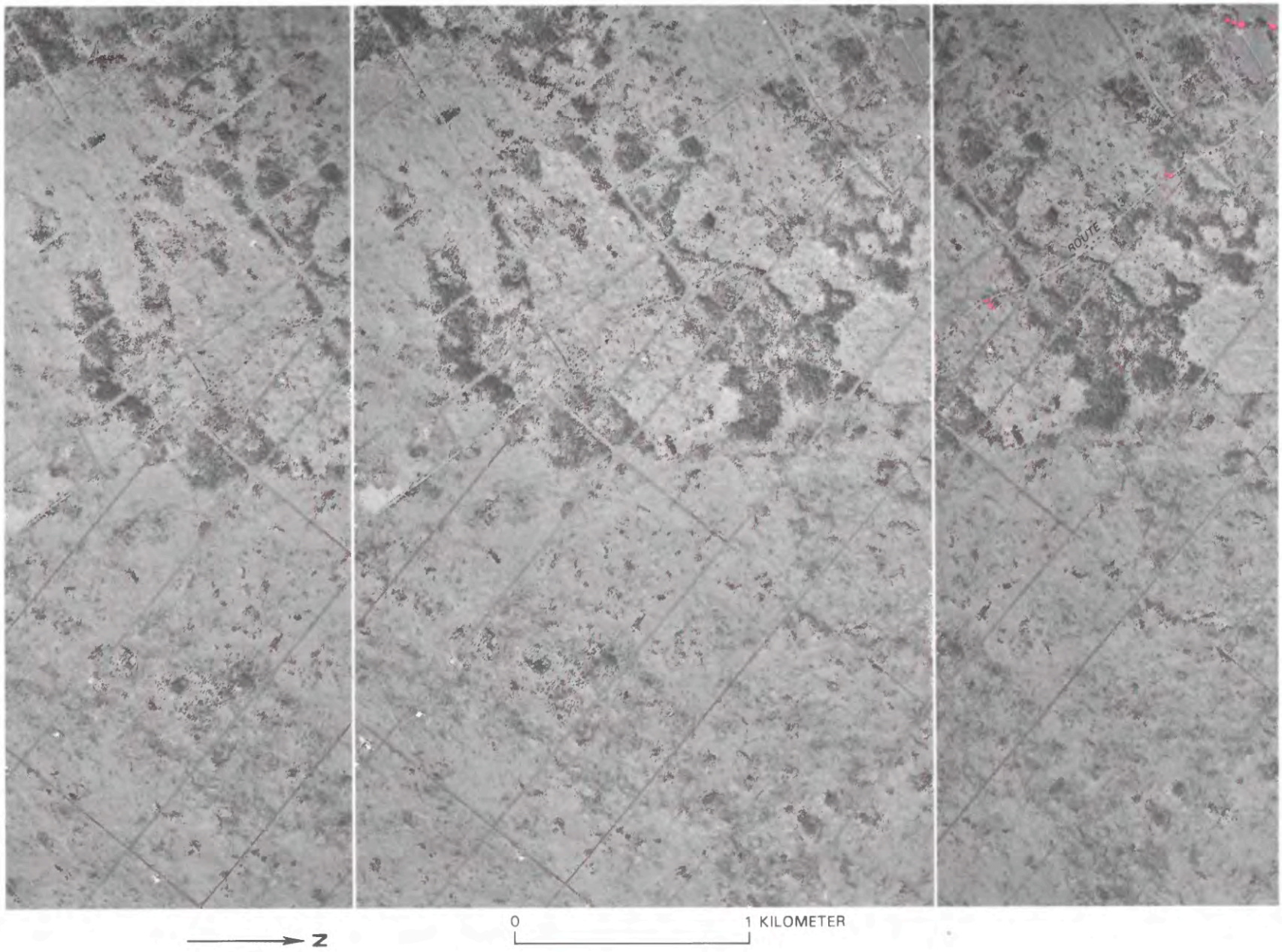

FIGURE 12.19.—Topographic and geologic discontinuity southeast of Keaau (see fig. 12.3). Sharp vegetation change extending north-south corresponds to flow boundary; young Ai-laau flows to east are highly inflated on a wide coastal plain, while older flows to west form kipukas elongate northeast-southwest between less inflated lobes of young lava extending down steeper slope to coastal plain. Pairs of small red dots, paleomagnetic sample sites; larger red dots, ^{14}C sample sites. Stereo triplet prepared from frames 64–66, roll 12CC, USDA series EKL, 1965.

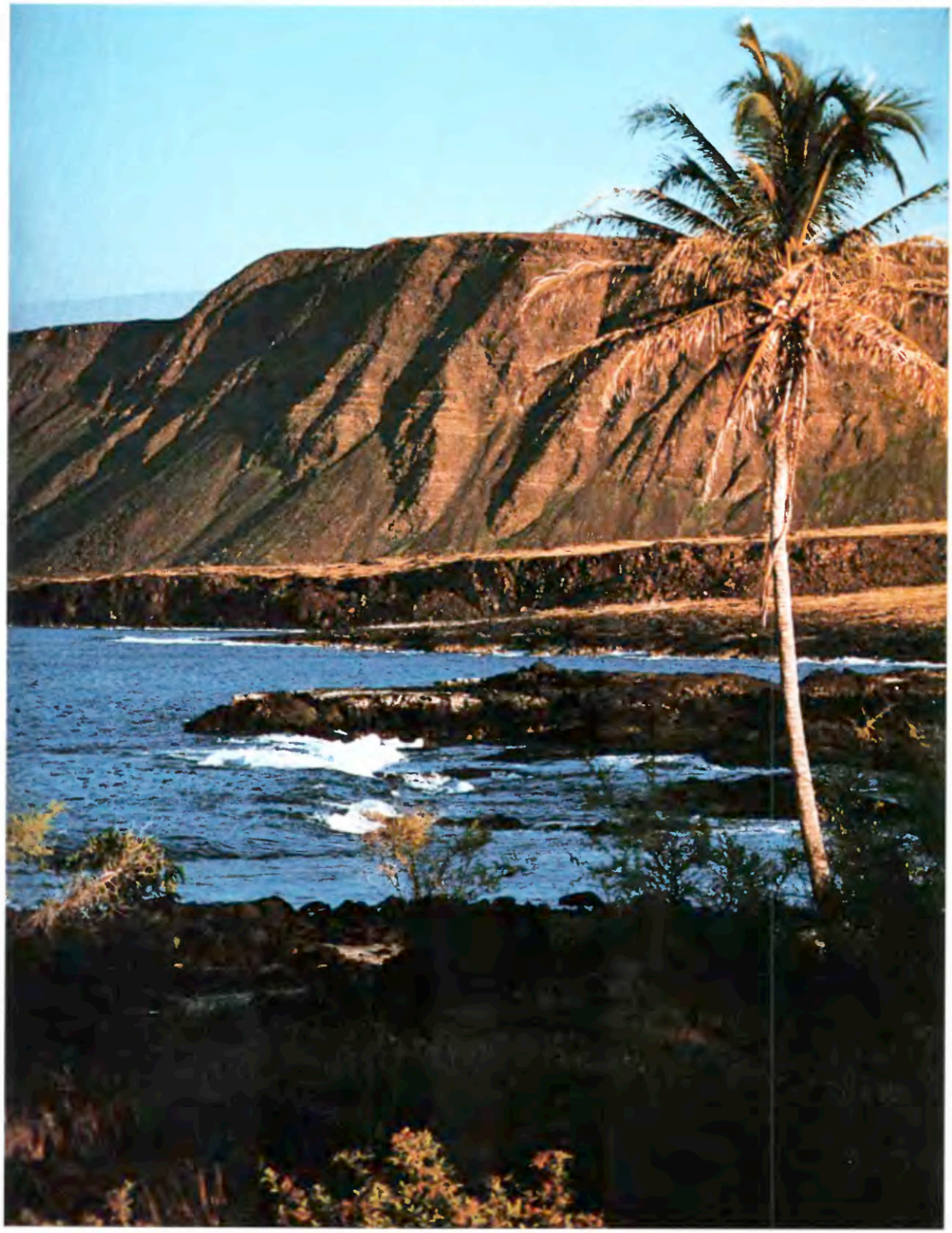

A

FIGURE 12.20.—Oldest rocks exposed on Kilauea. ***A***, Puu Kapukapu, viewed from Keauhou Landing. Most of visible stratigraphic section, about 300 m thick, is included in Hilina Basalt, with cap of Pahala Ash 10–20 m thick. Lower fault scarp in front of Puu Kapukapu displaces lava flows of Kipuka Papalinamoku thought to be about 1,100 yr old. Foreground, composed of lava 350–500 yr old, subsided beneath sea level during earthquake of November 29, 1975. Profile of Mauna Loa visible beyond Puu Kapukapu, to left. Photograph by R.T. Holcomb, April 1974. ***B***, Closer aerial view of Puu Kapukapu, showing lava flows and prominent ash layers in Hilina Basalt. Rim of Hilina Pali visible beyond Puu Kapukapu, to left. Photograph by D.A. Swanson, June 1971.

B

FIGURE 12.20—Continued.

at 730 ± 80 years B.P. by ^{14}C (W–3999), and its magnetization (8B685) is consistent with age of 750–1,000 years B.P. A flow resting above the Uwekahuna Ash Member in the Volcano rubbish dump has been dated at about 1,000 years B.P. by ^{14}C (W–5319). A source has not been established for these flows; Holcomb (1980a, b) interpreted them as caldera overflows, and this is consistent with their magnetic similarity to flows in the eastern caldera wall below Waldron Ledge (1B776, 1B788) and to the flow above the hiatus in Kilauea Iki (8B157). They could have come from the northeast rift zone of Mauna Loa, however; nearby Mauna Loa flows draped over a Kaoiki fault scarp 2 km north of Tree Molds (fig. 12.5*A*) have similar magnetization (8B841) and ^{14}C age (830 ± 60 and 530 ± 60 years B.P., W–3879 and W–3880, respectively). It is conceivable too that flows exposed in Kilauea Iki (8B157) and the eastern caldera (1B680, 1B692, 1B776, 1B788) also were erupted from Mauna Loa and flowed into the Powers caldera.

The Volcano flows may extend far down the flank of Kilauea. Much of the north flank is surfaced by younger Ai-laau flows, but older flows above the Pahala Ash are exposed in kipukas south of Keaau (fig. 12.5*J*). Aerial photographs reveal rudimentary fluvial drainage on the kipukas but not the younger flows (fig. 12.21). The

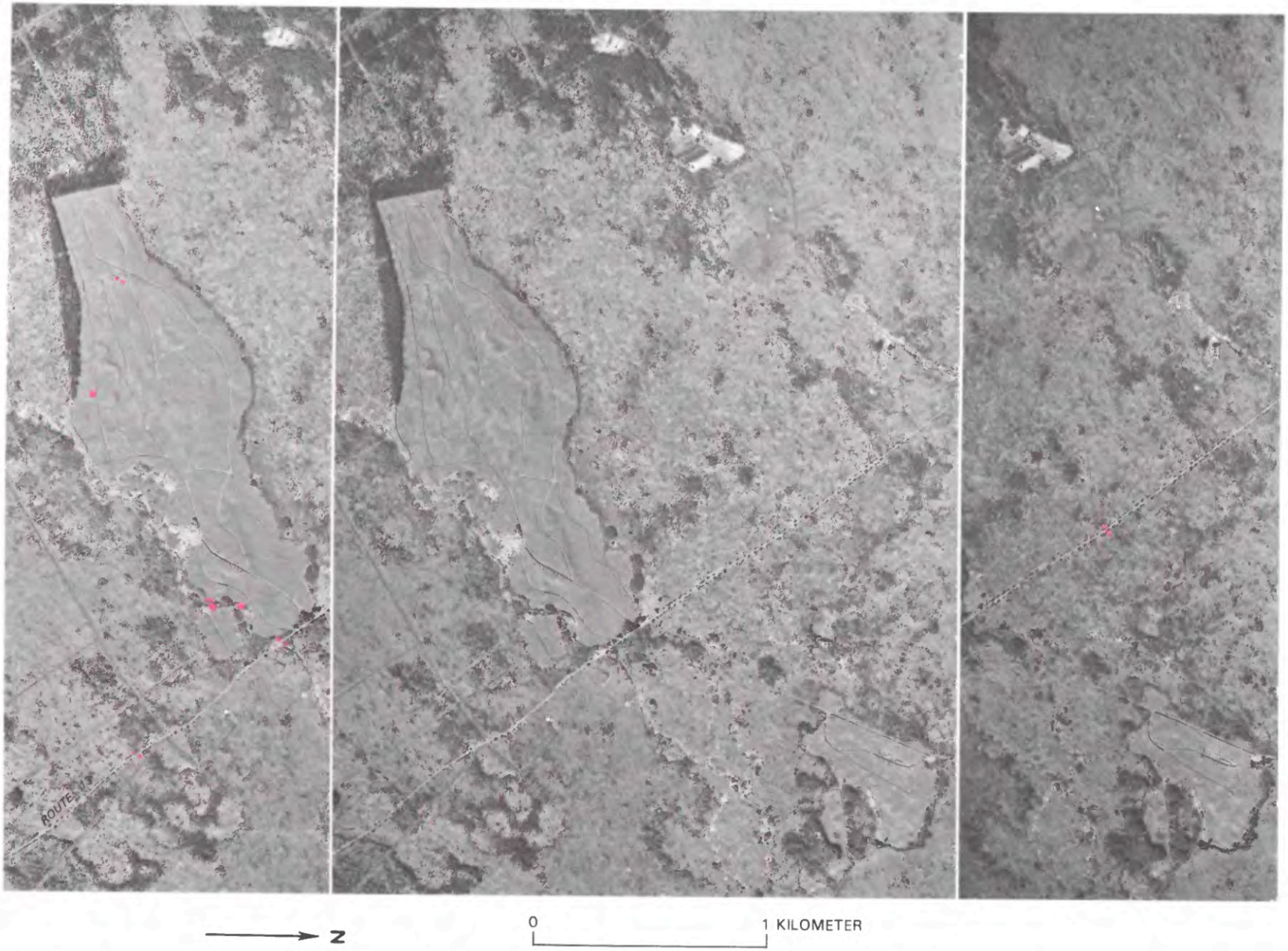

FIGURE 12.21.—Lava flows of three ages southeast of Keaau. Old ash-covered Mauna Loa flows are occupied by truck farms and fields of sugar cane, while Kilauea flows are uncultivated. Two groups of Kilauea flows differ in age and appearance: Older flows have blotchier vegetation pattern and incipient drainage channels absent on younger flows; ohia trees cluster atop younger flows near their margins. Flow groups differ in their directions of remanent magnetization. Large red dots, ^{14}C sample sites; pairs of small red dots, paleomagnetic sites. Some small clumps of ohia along axes of younger flows are known to occur above lava tubes. Thick stand of trees bordering southern and western sides of largest cane field is an artificial planting of Norfolk pines and other trees. Stereo triplet prepared from photographs 81–83, roll 12CC, USDA series EKL, 1965.

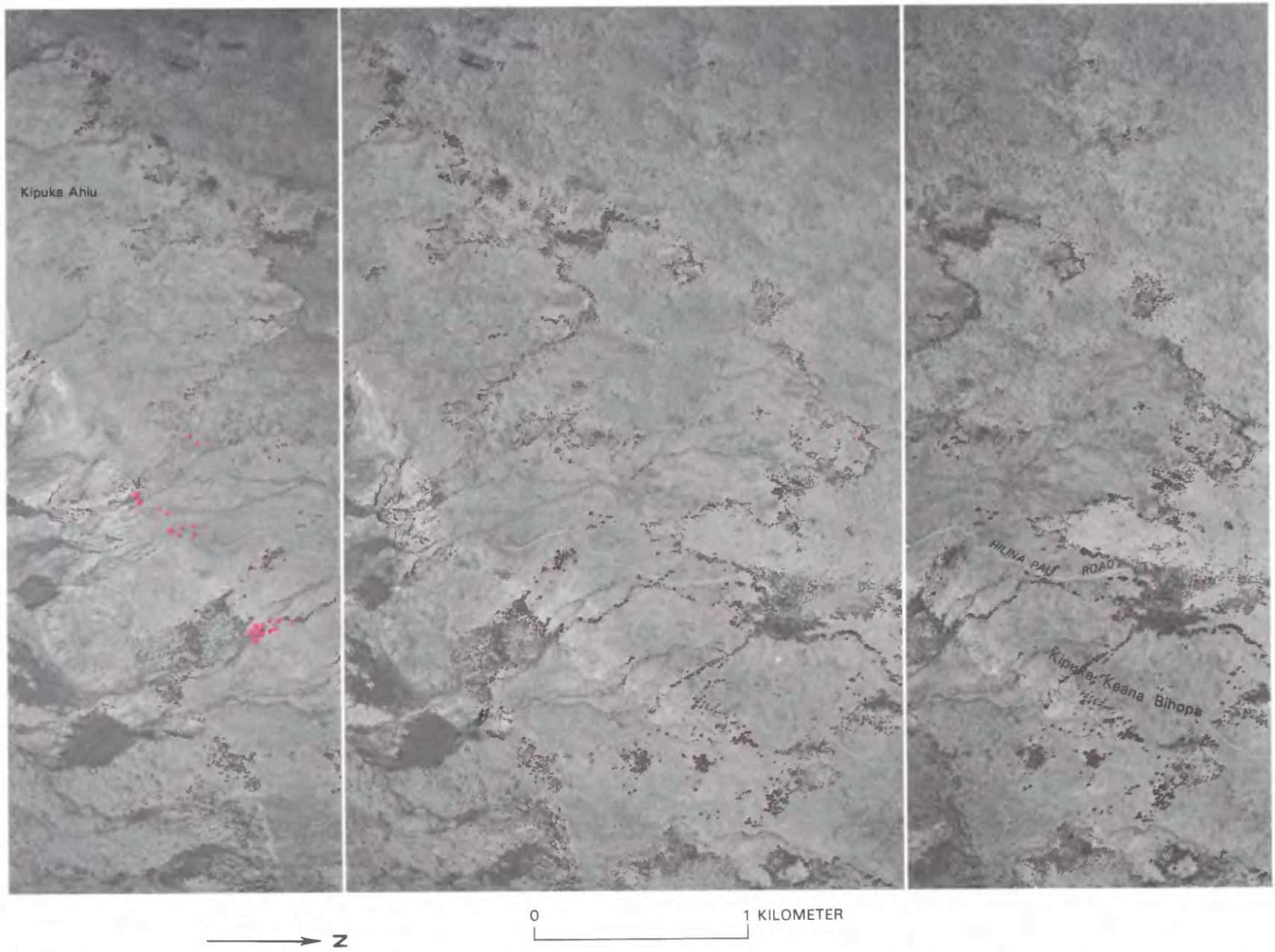

FIGURE 12.22.—Vegetation contrasts near end of Hilina Pali Road. Kipukas are carpeted by range grass on veneer of ash and sand, while barren areas to north are dotted only by low trees and shrubs. Walker (1967) thought contrasts arose from partial stripping of an ash deposit, but Holcomb (1980b) believed them to reflect lava flows of different ages. Some bare patches within kipukas may arise from stripping or nondeposition; others may be tongues of younger lava flows. N.G. Banks (unpublished work) has found lava younger than 1,000 yr at some places within kipukas. Large red dots, ^{14}C sample sites; pairs of small red dots, paleomagnetic sites. Stereo triplet prepared from frames 4–6, roll 5CC, USDA series EKL, 1965.

FIGURE 12.23.—Red tephra cone left of center exposed in west wall of Pauahi Crater. Crater of cone was choked with coarse debris and then filled by ponded lava, which cooled to produce massive block with radial jointing. Exquisitely detailed molds of tree ferns are found in lower part of pond. Yellow tephra layer of figure 12.27 occurs higher in wall on both sides of cone and dips down toward crater. Hiatus above yellow tephra is apparently correlative with hiatus beneath lava pond, and yellow tephra may be coeval with coarse debris within buried crater. People at upper left stand on overlook along Chain of Craters Road; overlook was later moved about 100 m to right. On crater floor at lower right is perched lava pond (Holcomb and others, 1974) active on this day. Workers on crater floor are measuring deformation of floor, which is crust of fresh lava lake being domed by continued injection of lava. Foreground, septum between west pit and larger central pit of Pauahi; septum is veneered by thin crustal plates of lava lake that subsided within central pit a few weeks earlier (Tilling and others, chapter 16). Lava has since broken through crust of west pit and dribbled across septum into central pit. Photograph by R.T. Holcomb, December 4, 1973.

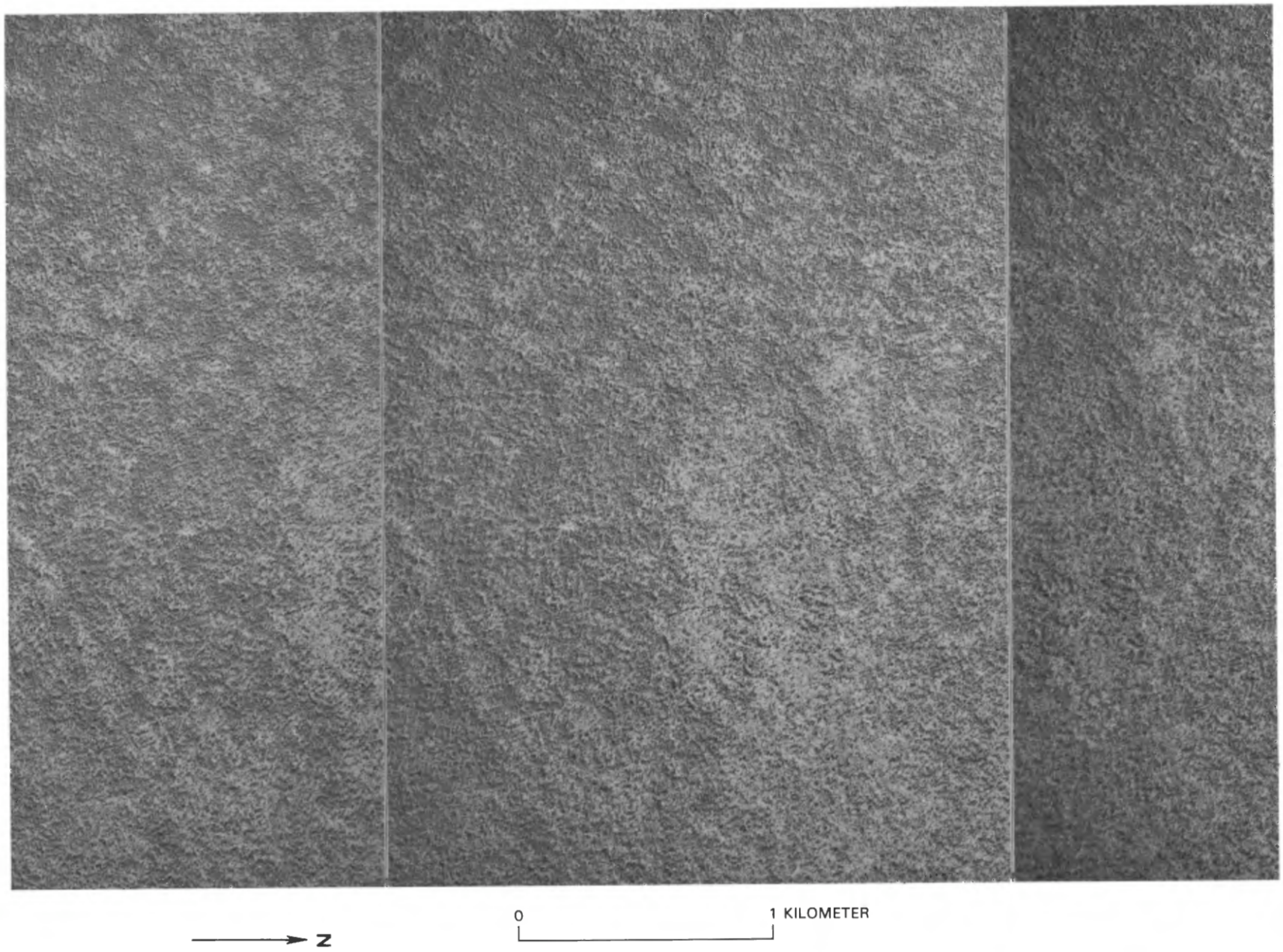

FIGURE 12.24.—Monotonous forest along north side of middle east rift zone, developed on lava flows older than 1,500 years. Aerial photographs could not be used to identify lava-flow boundaries here, but ground traverse showed that major boundaries must exist (fig. 12.25). Prominent rift structures are visible in southeast corner, and broad low swell, elongate east-northeast to west-southwest near center of this view, may be an ancient feature of rift zone. Stereo triplet prepared from frames 125–127, roll 12CC, USDA series EKL, 1965.

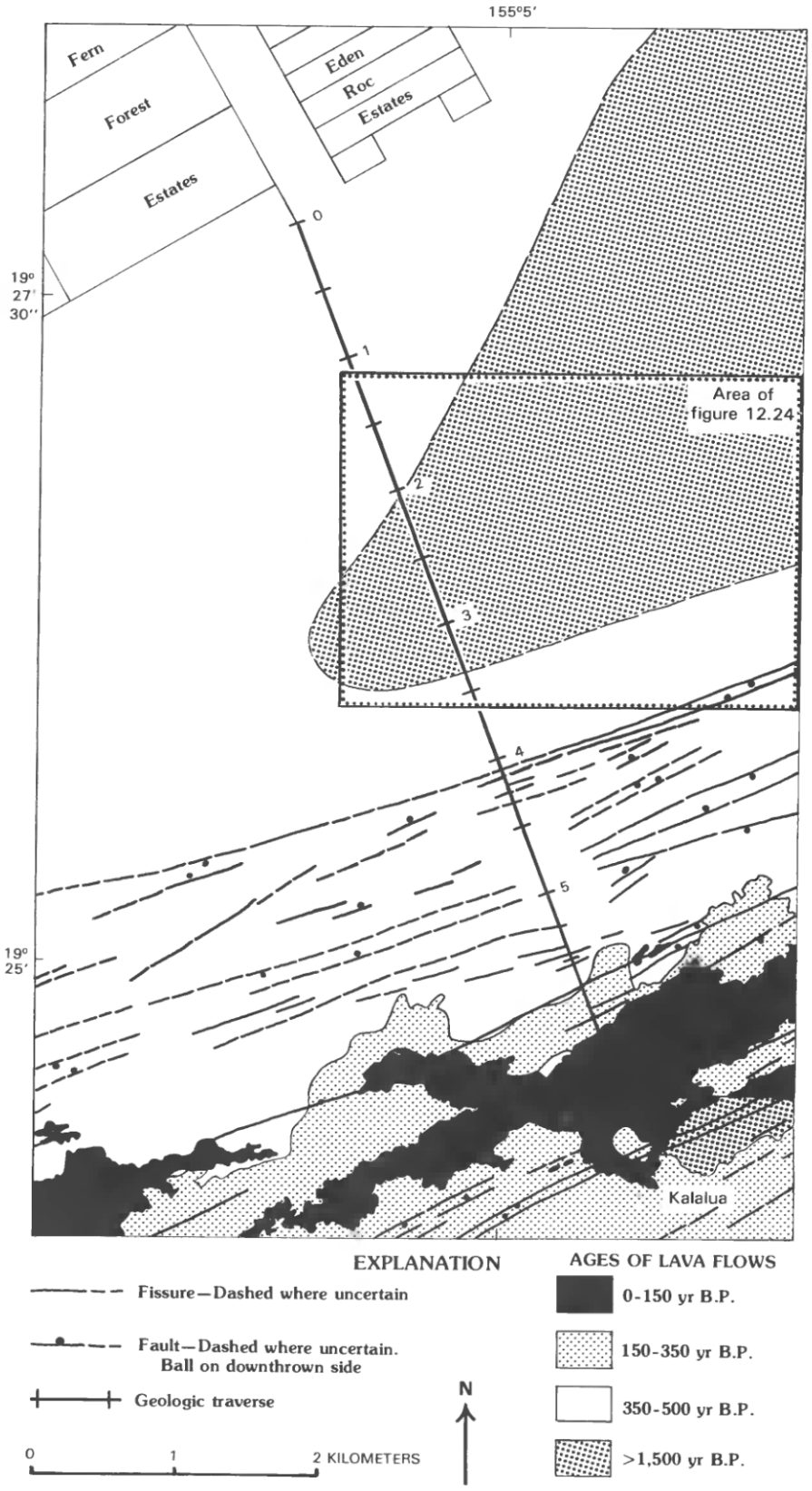

FIGURE 12.25.—Geologic map of Kilauea north flank adjacent to middle east rift zone. Contacts within area of figure 12.24 inferred from changes in rock type found along one tape-and-compass traverse through forest, indicated by heavy line marked at 0.5-km intervals.

older flows are more weathered and have a different vegetation pattern. Tree molds in the younger flows show that trees were growing on the older flows when they were flooded by the younger lava. The older flows have magnetization (8B049, 8B073, 8B217; fig. 12.11*F*, crosses) similar to those at Volcano, but they are similar also to 9B889 (fig. 12.5*J*), which is tentatively correlated with lava dated at about 3.7 ka (W–4177). They are also magnetically similar to a Mauna Loa flow (8B901) upslope from Mountain View dated at about 5.6 ka (W–3862). This magnetic direction is near that for a geocentric axial dipole; it is frequently repeated and is therefore not very diagnostic of age.

A few flows along Kilauea's rift zones are also magnetically similar. Among them is the flow above the hiatus in Pauahi Crater (9B217), which could represent an overflow from the summit. Another is the Kaliu flow (8B361 and 9B493, fig. 12.5*G*,*H*), which overlies the flows of Opihikao, but its measured magnetic dispersion is high and its age is therefore uncertain. Ash-covered pahoehoe of Waiakahiula Two (8B097, fig. 12.5*J*) above Pahoa also has this direction, as do flows of Keahialaka and Pohoiki (8B373, fig. 12.5*H*; Moore, 1981), but they could be older. A site (9B865, fig. 12.5*B*) on the lava shield of Ponohohoa Chasms also is similar, but here again the age is not constrained stratigraphically. An unnamed pyroclastic cone of the lower east rift zone, 2 km northeast of Iilewa Crater (fig. 12.5*G*), has been dated at about 900 years B.P. by ^{14}C (W–4690), but its magnetization is not known.

Tube-fed pahoehoe flows on the inland side of the lower southwest rift zone (fig. 12.5C) have yielded ^{14}C ages of about 900–1,000 years (W–5147, W–5211, W–5215). The source of these flows is uncertain; they could have spread down the west flank of Kilauea from a source on Mauna Loa, or they could have come from the summit of Kilauea. They may be coeval with the flows from the Observatory vent if that vent is older than the Ai-laau vent, as discussed in a later section, despite distinctly younger ^{14}C ages for the Observatory flows.

In summary, though several flows are tentatively assigned to Kilauea eruptions 750–1,000 years ago, most are equivocal. Stratigraphic uncertainty permits many to be older, and of those dated by ^{14}C, all except one could have been erupted from Mauna Loa.

KALUE FLOWS

Much of the Koae fault zone north and west of Kipuka Nene (figs. 12.18, 12.29) is surfaced by barren lava thought to have overflowed the southern caldera rim. These flows are not easily differentiated from other so-called regional pahoehoe (Walker, 1967) barren of vegetation above Hilina Pali, but they are magnetically distinct (fig. 12.11*F*, squares). Below the pali they are easily distinguished from older flows, being darker (fig. 12.32) and less green because of less weathering and less surficial cover. Between Hilina Pali and Puu Kaone they are split into four main lobes; two cascaded over the coastal cliffs to form the Kakiiwai and Kalue lava deltas, and a third forms the shoreline at Kaaha.

The magnetization of these flows is shared by others to the west (fig. 12.5C), including the pahoehoe of Kipuka Pepeiau (8B493), the Naliikakani flows (3R481), and the Waiwelawela flows (8B529; but site 3R421 on the Waiwelawela flows has yielded a different result). The Opihinehe flows (fig. 12.5*D*) are probably coeval. Because no lava shield of this age is known along the southwest rift zone, these extensive flows are inferred to come from the same summit source as the Kalue flows.

Similar magnetization is also shared by extensive pahoehoe seaward of the east rift zone (fig. 12.5*E*,*F*) from Kupapau to Kaena Point (8B229, 8B241, 3R157, 3R181) and beneath the eastern flows of Mauna Ulu (3R097, 3R109, 3R121, 3R133, 3R169, 3R193, 3R229). The eruption of Kane Nui o Hamo fed these flows. The size of the lava shield and large extent of its tube-fed flows suggest that this was the longest and most stable eruption of any known along either rift zone, but no other rift eruptions of similar age have been found.

The age of this group is uncertain, and because it illustrates the contradictions still existing among stratigraphic, paleomagnetic, and ^{14}C data, some details will now be given. The magnetization of this group is consistent with an age of 750–500 years, according to the preliminary chronology of Holcomb and others (1986), and the magnetically distinct Kipuka Nene flows beneath are judged from other evidence to have an age of 1.1 ka, as noted earlier. Yet charcoal from beneath one of the upper flows (3R001; fig. 12.30) in Kipuka Nene indicates an age of 1.15 ka (W–5135) for Kalue lava. The problem is compounded by two other flows in Kipuka Keana Bihopa (fig. 12.5*D*) with still different magnetizations but ^{14}C ages of 1.14 ka (W–5212) and 1.13 ka (W–3827). Though the magnetic inclinations of both latter flows (8B397, 3R025) differ from those of Kalue, their declinations are similar; they could be coeval with Kalue flows but have inclinations affected by a topographic magnetic anomaly along Hilina Pali. If so, the three ^{14}C dates would agree well in assigning an age of 1.14 ka to the Kalue flows instead of the 500–750 years adopted here. If this were true, then the magnetically distinct older flows of Kipuka Nene would have to be older than its assigned age, and possibly predate the Powers caldera.

AI-LAAU FLOWS

Much of Kilauea's north flank is covered by tube-fed flows extending northeast from the summit to the coast between Haena and Honolulu Landing. The Ainaloa, Kazumura, Old Volcano Trail, and other flows of this group are well-known for their large lava tubes. Despite high rainfall in this area, the flows are little weathered and support a juvenile forest (figs. 12.5*J*, 12.21) implying that they are young. Their vegetation was even lighter in the 19th century, eliciting comments from visitors. For example, Wilkes (1845, p. 119) observed in 1840 that "After leaving Olaa, we had no distinct path to follow; for the whole surface became a mass of lava, which retained all its metallic lustre, and appeared as if it had but just run over the ground—so small was the action of decomposition. There were only a few stunted bushes on our track." Even a critique accusing Wilkes of exaggeration (by "A.V." in the February 1, 1847, issue of a missionary journal, *The Friend*) described vegetation different from today, saying "the road from Olaa to the

A

FIGURE 12.26.—Hiatus exposed in Kilauea Iki Crater. Photographs by J.D. Griggs, December 1985. ***A***, Northeast wall of crater below Byron Ledge overlook, showing color change on face of cliff. Tree-covered recess at right is older Ai-laau part of crater. ***B***, Closer view of color change, which coincides with layer of red cinders. Debris from this layer mantles slopes below, reddening surface and supporting more plant growth than slopes above. Cinder unit is truncated at right by densely vegetated thin lava plaster on wall of Ai-laau crater; plaster may be dregs of subsided lava lake.

volcano is generally very distinct. Ohelo bushes grow much of the way, as other bushes, grass and small trees, on both sides of the road."

Of seven ^{14}C ages obtained from these lava flows (table 12.6), three that duplicate others are anomalous and are disregarded. Others range from 260 to 450 years and average 335 years B.P. They are distinctively magnetized (fig. 12.11*F*, triangles; sites 8B001, 8B061, 8B085, 8B169, 8B193, 8B421, 8B733, 8B793, 9B121, 9B133, 9B421, 9B433, 9B397, 9B673).

Ohia trees clustered along flow margins can be used to delineate individual tube-fed flows (figs. 12.5*J*, 12.21) up to elevations of about 500 m. Separate flows cannot be mapped above this; they disappear upslope into a monotonous young ohia-hapuu forest that extends to the summit region. Thurston Lava Tube and other tubes fanning eastward from the summit fed the multiple lobes distinguished at lower elevations.

The source of the flows is the eastern part of Kilauea Iki (figs. 12.5*A*, 12.33), which is an eruptive crater choked with talus. It is older than the other parts of Kilauea Iki and supports a more mature forest. It is also less deep and has lava plastered against its walls in some places. The rest of Kilauea Iki is deeper, steeper, and lacks wall plaster; it is a chain of later collapse pits. A sagged platform east of this Ai-laau vent resembles those developed above Alae and Aloi Craters after burial (Swanson and others, 1972; Holcomb and others, 1974); a buried pit crater is inferred beneath it. The presence of such a crater, filled with still-cooling lava, could explain a self-potential anomaly mapped by Zablocki (1976) in this area.

Also inferred to come from the Ai-laau vent are magnetically similar (8B109, 8B181, 9B145A) tube-fed flows extending northeast from the middle east rift zone near Kalalua to the coast around Makuu (fig. 12.5*G–J*). Initially these flows were assumed to have come from the rift zone, but no vent could be found; vents inferred by Moore and Koyanagi (1969) are younger fissures crossing the flows, while Kalalua and other pyroclastic cones are older and Puu Kahaualea is younger. Because their vegetation and magnetization are similar to those of the other flows from the Ai-laau vent, they are inferred to be of the same age and come from that same vent. If so, they must have spread east past the northeast side of Kane Nui o Hamo and along the northern part of the rift zone for several kilometers before moving northeast onto the north flank. Fissures, faults, and grabens may have prevented them from crossing the rift zone and spreading farther south. The many structures crossing them must be younger or had recurrent displacement after burial 350–500 years ago.

B

FIGURE 12.26—Continued.

The lightly vegetated Keauhou flows seaward of the upper east rift zone west of Kane Nui o Hamo (figs. 12.5*E*, 12.34, 12.35) have similar magnetization (8B541, 1B432, 3R049, 3R073, 3R085, 3R205, 3R217, 3R265, 3R325, 3R397) and ^{14}C ages (table 12.6). These flows could come from the Ai-laau vent, but they are smaller and include a more complex assemblage of flow types. They probably represent sustained, unstable eruption (table 12.1) from an upper-east-rift vent, most likely Puu Huluhulu. The spatter cone between Hiiaka and Devils Throat also has similar magnetization; this brief eruption may have preceded the sustained one (like the brief eruptions of 1968–69 that preceded the Mauna Ulu eruption of 1969–74) but a stratigraphic relationship has not been established. Some pit craters of the upper east rift zone must postdate these eruptions.

Other flank vents and flows are thought to have similar ages. Two assemblages have similar magnetization. One is the group of Kamakaiauka along the southern strand of the southwest rift zone (fig. 12.5*B*); its age assignment is tentative because only one paleomagnetic site (8B481) has been sampled from an aa flow. Another group along the lower east rift zone (fig. 12.5*H*) includes Kaholua o Kahawali (9B205) and its associated lava flows. A flow younger than Puu Kaliu but older than A.D. 1790 lava has been dated at about 500 years B.P. (W–4688), while a flow at Kehena has been dated by ^{14}C at about 450 years B.P. (W–5054). Puu Honuaula and a flow 2 km southwest of Puu Kaliu are dated at about 350 years B.P. (W–5048, W–3800).

Macdonald (1941) and Holcomb (1980a) included several other vents with Kaholua o Kahawali because the legend of Pele and Kahawali suggests that a long chain of vents erupted at the same time. But mapping by R.B. Moore (1981) has not confirmed this. Moore believes that Kaholua o Kahawali and an adjacent cone are significantly younger than Halekamahina and other nearby vents. Moore has also mapped as much older a flow having similar magnetization (8B037) east of Kapoho Crater.

One other Puna flow should be mentioned, the prominent aa flow of Makaukiu Point between Nanawale and Cape Kumukahi (fig. 12.5*H*). A ^{14}C age of 350 years B.P. (W–5088) has been obtained from charcoal beneath this flow, and chemical weathering data suggest an age of 300–350 years (Atkinson and Swindale, 1974). Moore (1981) has mapped it as one of the youngest prehistoric units in the Kapoho area because it still projects beyond the adjacent shoreline to form Makaukiu Point. However, this flow is clothed by a mature *Pandanus* forest that implies it is much older (Atkinson, 1970), and paleomagnetic data (8B973, 9B181) indicate that it and the flows beneath are older than 1.5 ka.

Dating is not yet precise enough to determine relative ages of eruptions within this interval, and it is not clear whether the rift eruptions are younger or older than the Ai-laau vent. Some Hawaiian traditions suggest a sequence: Kaholua o Kahawali and the flows seaward of Puu Huluhulu are associated with the current volcano goddess Pele (Ellis, 1827; Macdonald, 1941), while activity at Kilauea Iki is associated with Pele's predecessor, Ai-laau

A *B*

FIGURE 12.27.—Hiatus exposed in north wall of Pauahi Crater. Photographs by J.D. Griggs, October 1985. ***A***, Northwest wall of Pauahi, viewed from overlook shown in figure 12.23. Hiatus occurs atop yellow tephra layer. ***B***, Closeup view of yellow tephra, which is mixture of blocks and ash. This tephra may consist in part of Uwekahuna Ash Member, but because it grades laterally into coarse debris in crater of buried tephra cone nearby (fig. 12.23), at least some of it may have been ejected from local source. Organic ash is abundant atop tephra, and overlying lava flow contains many tree molds.

(Westervelt, 1916). If that chronology is correct, the rift eruptions followed the summit eruption.

OBSERVATORY FLOWS

Lightly vegetated prehistoric tube-fed flows in a band 4 km wide extend down the inland side of the southwest rift zone (fig. 12.5*B*,*C*). They are buried by Keamoku, Mauna Iki, and Cone Peak flows at elevations of 800–900 m but reappear higher up; flows with similar magnetization (1B001, 1B013, 1B025, 1B037, 1B049, 1B061, 1B073, 1B109, 1B133) form the northwest rim of the present caldera (fig. 12.5*A*) and the upper section of Uwekahuna Bluff (5 flows of 1B157; sites 145–148, Doell and Cox, 1965).

Though detailed mapping may show some of these flows to have been erupted on Mauna Loa (possibly more of the lava north of Tree Molds dated by W–3879 and W–3880), the source of at least some was a long-sustained vent located in what is now the northwest caldera near Uwekahuna Bluff. A large lava shield grew around this vent; it is well expressed west and northwest of the caldera rim by ground slopes, mappable aa lobes, and flow lineations radiating from a point about 1 km east of the Hawaiian Volcano Observatory (fig. 12.36). The crater of the Observatory vent may have extended close to Uwekahuna Bluff. Though the large shield and extensive tube-fed pahoehoe indicate that activity was long-sustained at the Observatory vent, the radiating aa lobes indicate some instability toward the end of its activity, like that observed at Mauna Ulu (Tilling and others, chapter 16; Holcomb, 1976a).

Flows of apparently similar age cover the south flank north and west of Kipuka Ahiu and extend over Hilina Pali to the coast west of Kaaha (fig. 12.5*B*,*D*). They consist of multiple units, aa flows from the southwest rift zone being interbedded with pahoehoe flows from the summit. Aa mapped by Walker (1967) as one unit from Puu Koae actually consists of two flows separated by pahoehoe from the summit (fig. 12.37). The western aa flow, traceable directly to Puu Koae, was erupted in the 18th century and lies atop the pahoehoe, while the eastern aa lobe, inferred to come from Cone Crater, lies below the pahoehoe. Another pahoehoe sheet occurs beneath the Cone Crater aa flow. The pahoehoe unit between the aa flows is distinctively picritic. Though Walker (1967) did not map the contact between the picritic unit and older pahoehoe, he did show extensive distribution of picritic basalt with separate symbols,

A

FIGURE 12.28.—Hiatus exposed in Makaopuhi Crater. ***A***, Northwest wall of crater, viewed from west rim, showing lower layer of yellow tephra separated by thin lava flows from upper layer of reddish tephra. Massive lava flows above red tephra occur in flank of Kane Nui o Hamo lava shield. Photograph by R.T. Holcomb, February 6, 1973. ***B***, Closeup view of upper tephra layer, which consists of red and green cinder beds. This layer appears to have been barren of vegetation when it was covered by lava. Photograph by R.T. Holcomb, March 24, 1974. ***C***, Closeup view of lower yellow tephra layer, which consists of blocks and ash. Large size of some blocks indicates they were ejected from local source, such as nearby pit crater ancestral to Makaopuhi. Upper part of this layer is rich in organic ash, and lava flow above it contains many molds of trees and ferns, indicating hiatus in accumulation of lava flows. Photograph by R.T. Holcomb, March 24, 1974. ***D***, Southwest wall of crater, viewed from mezzanine, showing two tephra layers and small tephra cone lower in section. Photograph by R.T. Holcomb, June 30, 1972, when lava from Mauna Ulu was cascading over crater rim to build talus-and-lava cones (Holcomb and others, 1974) against crater wall.

B

C

FIGURE 12.28.—Continued.

D

FIGURE 12.28.—Continued.

and picritic lava has been traced to the southwest rim of Kilauea caldera (T.L. Wright, oral commun., 1976), where it is the top unit beneath the Keanakakoi Ash Member. The Cone Crater aa (8B457) and the picritic unit (1B097) are magnetically similar to the Observatory flows; the older pahoehoe (8B445) is magnetically more similar to the flows of Volcano.

The Observatory flows are of uncertain age. They predate Cone Peak and other 18th-century flows of the southwest rift zone, but their age relative to Ai-laau flows is not yet certain. Vegetation is sparser on Observatory flows, but this probably arises from a rainfall contrast instead of a difference in age: annual rainfall on the north flank is 380 cm (150 in.) versus 75 cm (30 in.) on the southwest flank. Observatory flows have deeper weathering (J. Lockwood, oral commun., 1985), but because they are downwind from summit vents their weathering may have been accelerated by fumarolic acids.

Four ^{14}C ages have been obtained from Observatory flows (table 12.6), but one is anomalous. Sample W–4998 was collected within the caldera near Tree Molds (fig. 12.5*A*) and is the sample most likely contaminated by fumarolic carbon (Rubin and others, chapter 9; Chatters and others, 1969). The other three ages are similar to those for Ai-laau flows. Because the Observatory flows

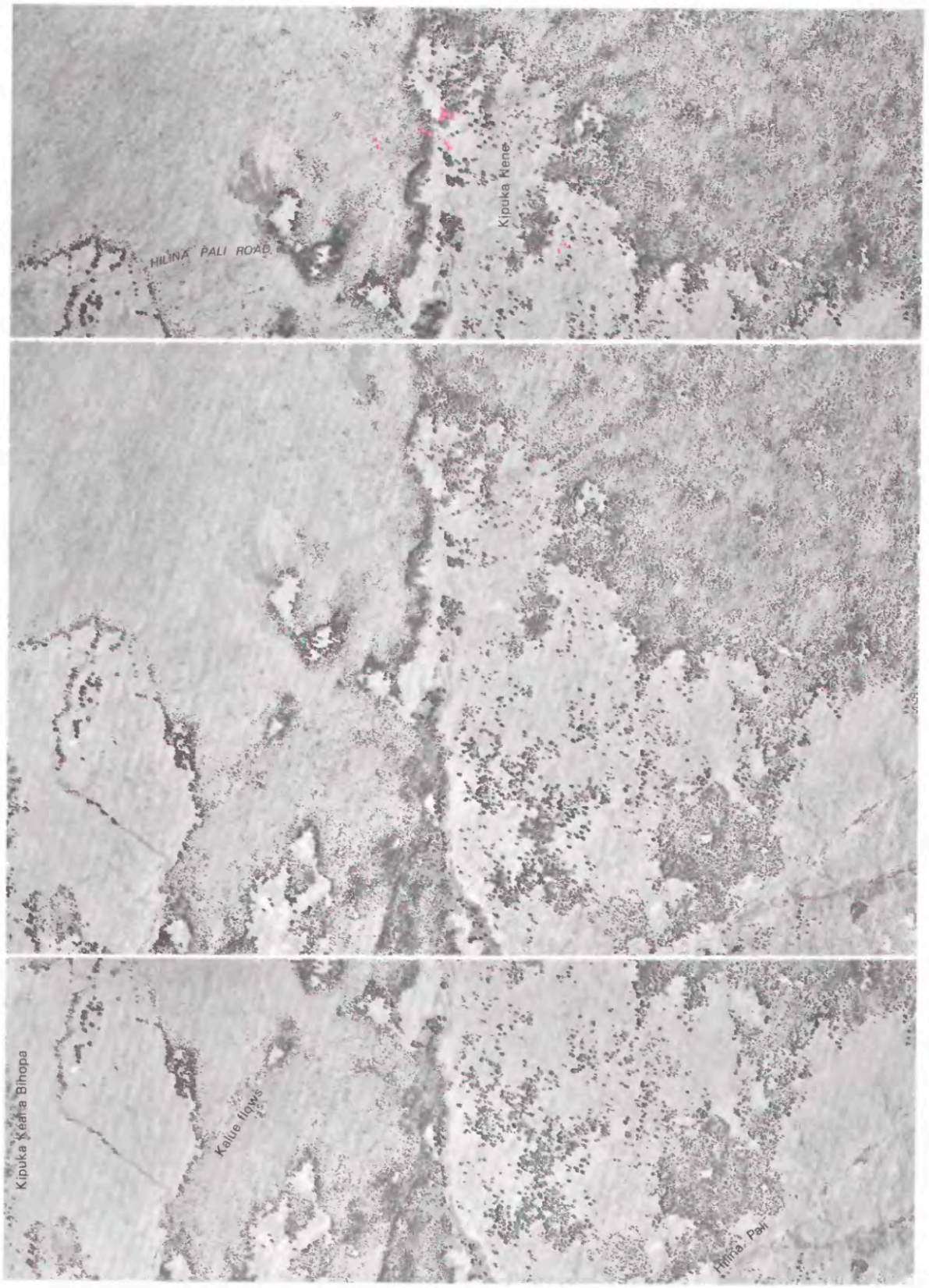

FIGURE 12.29.—Vegetation contrasts in Kipuka Nene area. Kipuka Nene and Kalue flows believed about 1,100 and 500–750 years old, respectively. Though vegetation contrasts generally seem to reflect different ages of lava flows, vegetation boundaries do not follow flow boundaries exactly, as shown in figure 12.30. Large red dot, ^{14}C sampling site; pairs of small red dots, paleomagnetic sampling sites. Stereo triplet prepared from frames 75–77, roll 14CC, USDA series EKL, 1965.

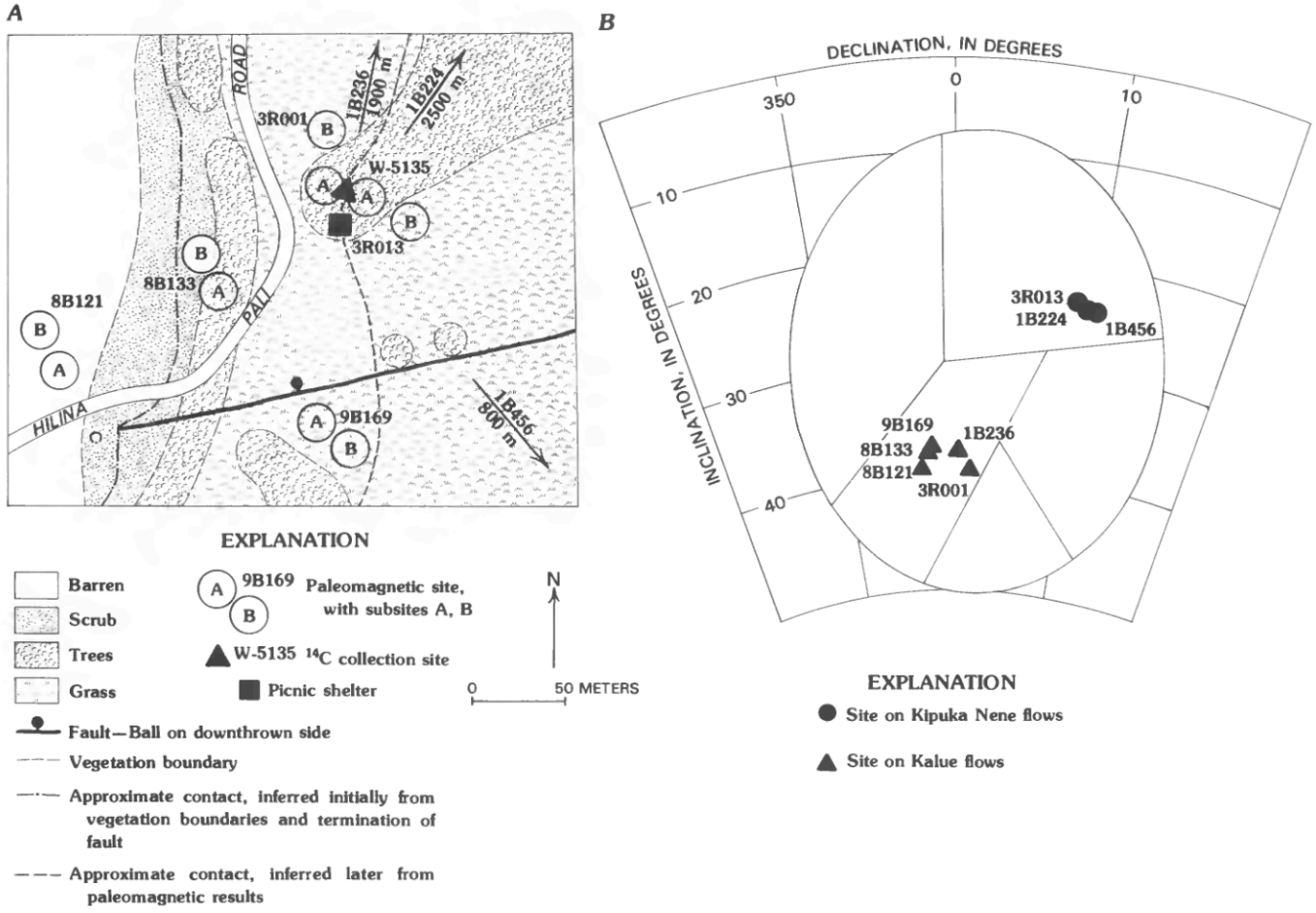

FIGURE 12.30.—Location of Kalue flow margin adjacent to Kipuka Nene. ***A***, Sketch map of Kipuka Nene picnic area, showing flow margin inferred initially and that inferred currently. Margin, traced with certainty only near picnic shelter, does not coincide exactly with vegetation boundary, causing earlier confusion about ages of Kipuka Nene and Kalue lava flows. Boundary between trees and barren lava may follow edge of thicker, inflated part of Kalue flows not easily penetrated by tree roots. Thinner marginal lobes may be penetrated easily by roots of trees but not roots of grass, and sand and soil beneath may provide water and nutrients enhancing tree growth. ***B***, Paleomagnetic results from Kipuka Nene area; Kipuka Nene and Kalue flows are magnetically distinct. Ellipse divided into fields containing sites of similar age, as defined in figure 12.11.

were sampled downwind from summit vents, their ^{14}C ages could be affected by fumarolic carbon, while samples beneath Ai-laau flows from the rainy windward flank could be contaminated by modern organisms. This suggests that the Observatory flows may be younger; but three older ages from the southwest rift zone could also represent Observatory flows (table 12.6), and they would raise the Observatory mean to more than 500 years.

The two flow groups differ magnetically (fig. 12.11*F*), the Observatory direction being intermediate between the Ai-laau and 18th century directions. However, the Observatory magnetization is not far from the axial dipole direction and alone is not diagnostic of age. Holcomb and others (1986) argued that the Observatory flows are younger than Ai-laau flows because lava in Uwekahuna Bluff beneath the Observatory flows seemed to have Ai-laau magnetization, according to the data of Doell and Cox (1965, flows 138–144) and R.R. Doell (unpublished work, flows 137I, 138A, 138B, 139A, 140A, 141A, 141B, 142A). But later sampling (1B582, 1B594, 1B606) has not confirmed the Ai-laau direction in Uwekahuna Bluff; it appears that the inferred Ai-laau samples of Doell and Cox were taken from a rotated fault block. Because the Observatory flows are magnetically not very different from the Volcano flows, they could be similar in age to the Volcano flows and thus 500 years older than judged by Holcomb and others (1986). Detailed mapping and chemical analyses should help sort out ages and sources of these various interfingered flows from Kilauea and Mauna Loa.

LATEST PREHISTORIC ERUPTIONS

Prominent widespread flows along both rift zones span a narrow range of ages. Most of them probably date from the 18th century, though some may be slightly older. This interval of frequent rift eruptions ended with a caldera collapse and explosive eruption at the summit.

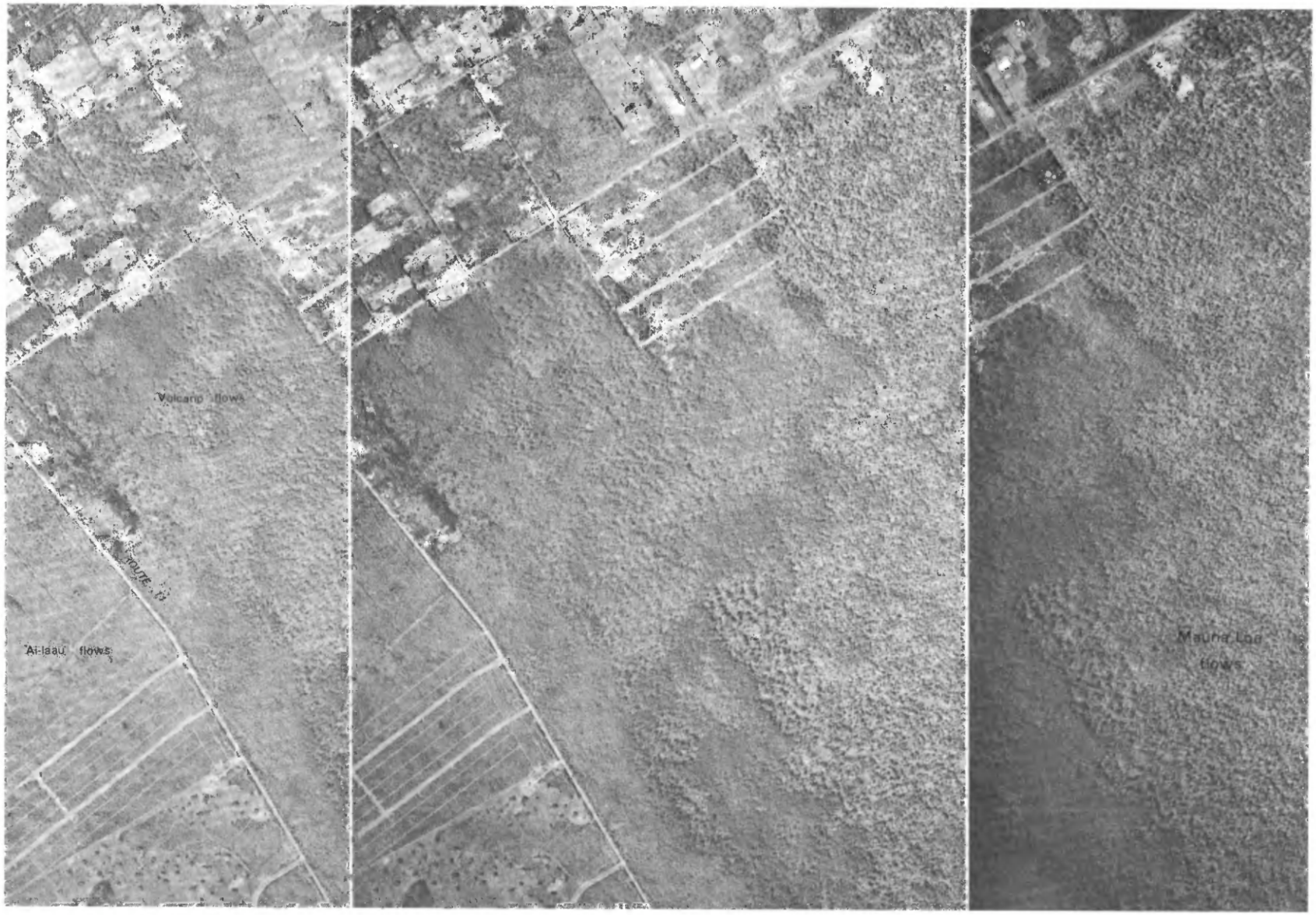

FIGURE 12.31.—Vegetation contrasts between flows of Volcano, older flows of Mauna Loa, and younger flows of Ai-laau vent. Large red dot, ^{14}C sample site; pair of smaller red dots, paleomagnetic sample site. Stereo triplet prepared from frames 183–185, roll 12CC, USDA series EKL, 1965.

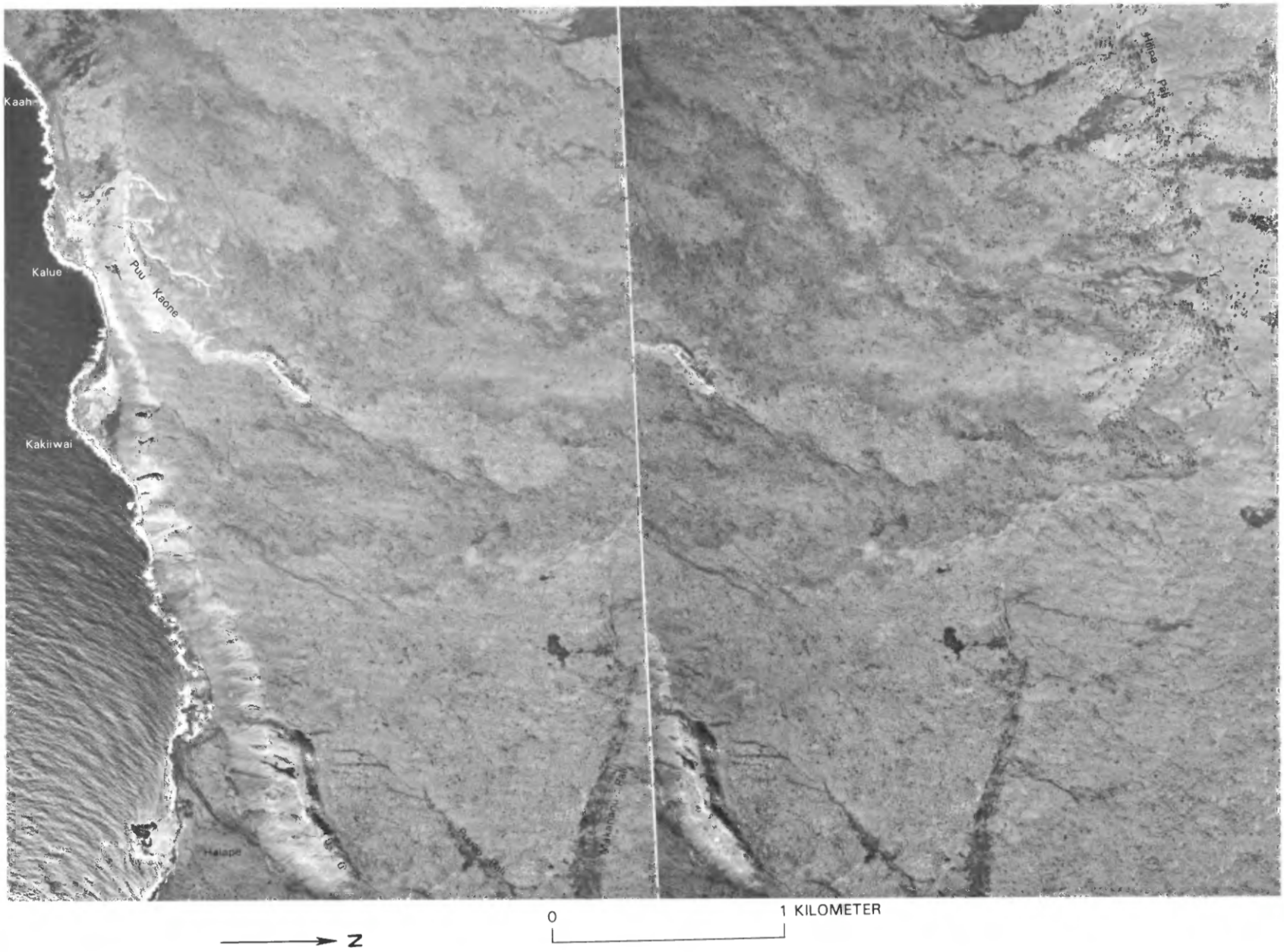

FIGURE 12.32.—Contrasting flow units in area between Hilina Pali and Puu Kaone. Two series of widespread surficial flows differ in photographic tone and surficial cover. Stereo pair prepared from frames 77, 78, roll 14CC, USDA series EKL, 1965.

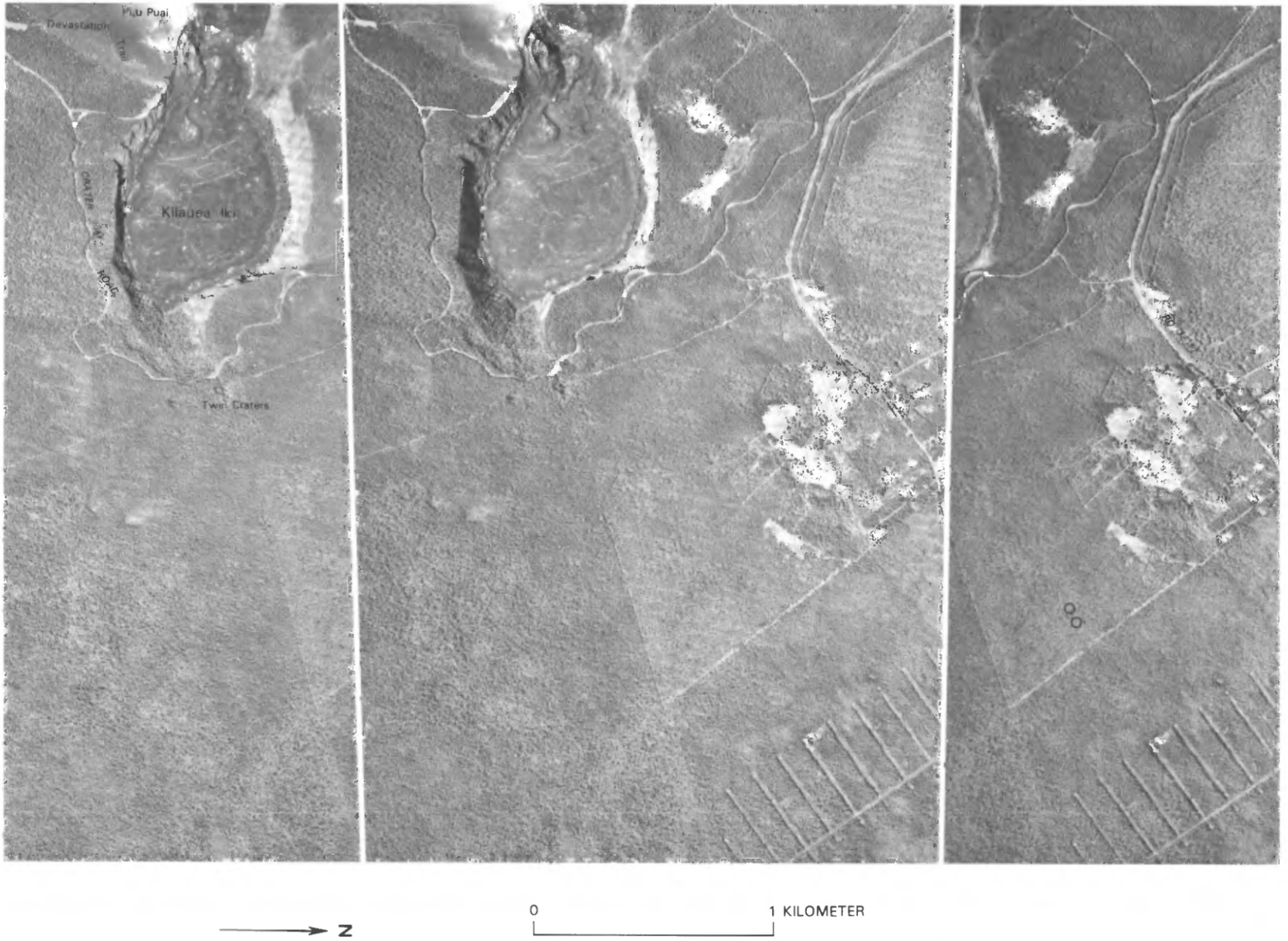

FIGURE 12.33.—Ai-laau vent and lava shield. Kilauea Iki is chain of three or four collapse structures extending eastward from inner sink of present caldera; it contains lava lake erupted in 1959. Ai-laau vent area includes east end of Kilauea Iki and small Twin Craters. Broad, shallow sag southeast of vent area is thought to overlie buried pit crater. Broad ridge with small axial pits (circled) extending northeast from vent area may represent path of major lava tube; similar ridges radiate south and southeast from broad sag, beyond this view. Paired red dots, paleomagnetic sample sites. Stereo triplet prepared from frames 185–187, roll 12CC, USDA series EKL, 1965.

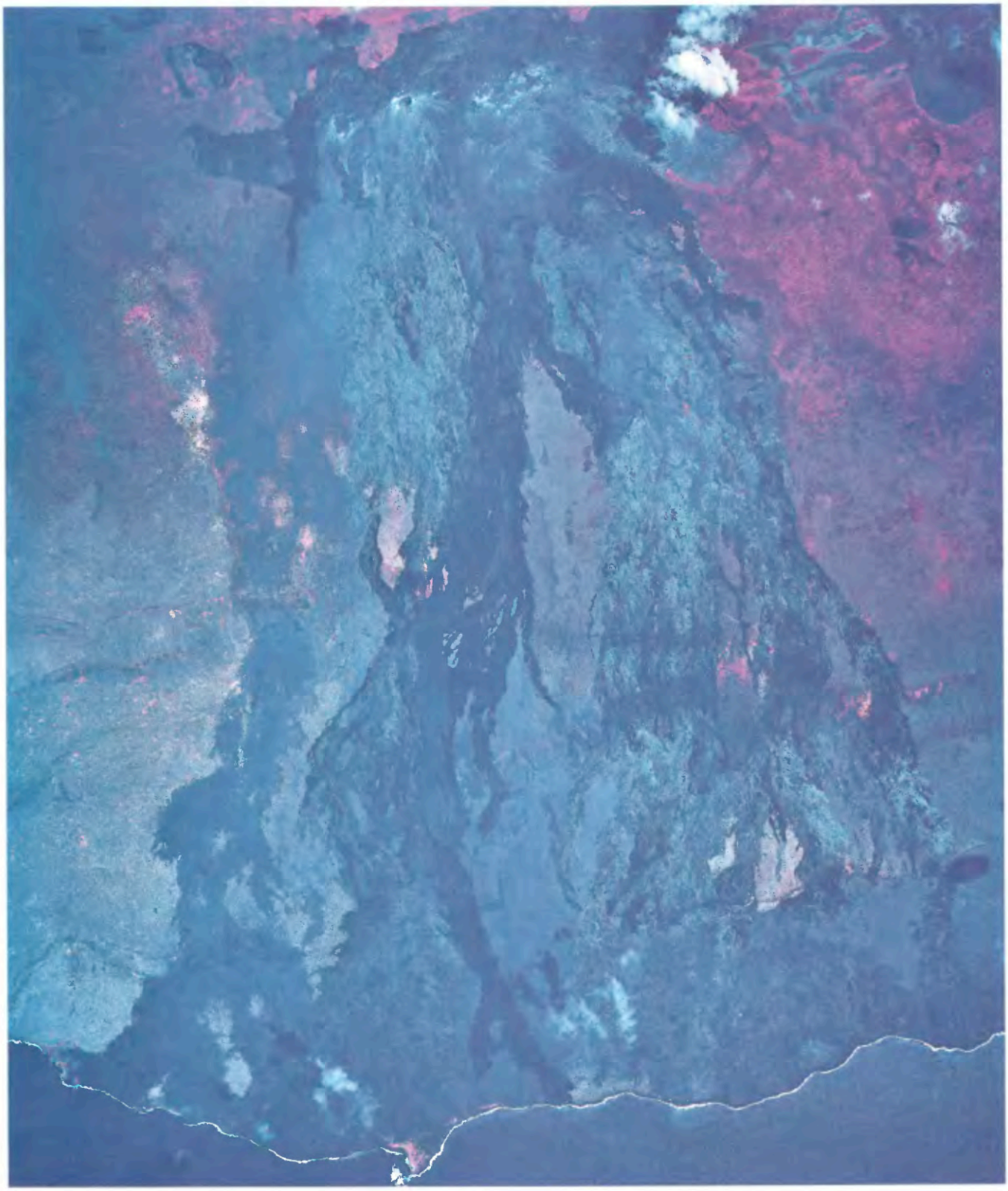

FIGURE 12.34.—Mauna Ulu region of upper east rift zone and south flank. High-altitude false-color infrared photograph showing bands of Mauna Ulu lava in center, flanked to left by Keauhou and Kipuka Nene flows, and to right by flows of Kane Nui o Hamo. Rain forest along rift zone is red; oldest grass-covered flows have very light tones. Barren lava flows are bluish gray and black. Darkest flows are aa; rest are pahoehoe. U2 photograph by NASA Ames Research Center, 1974.

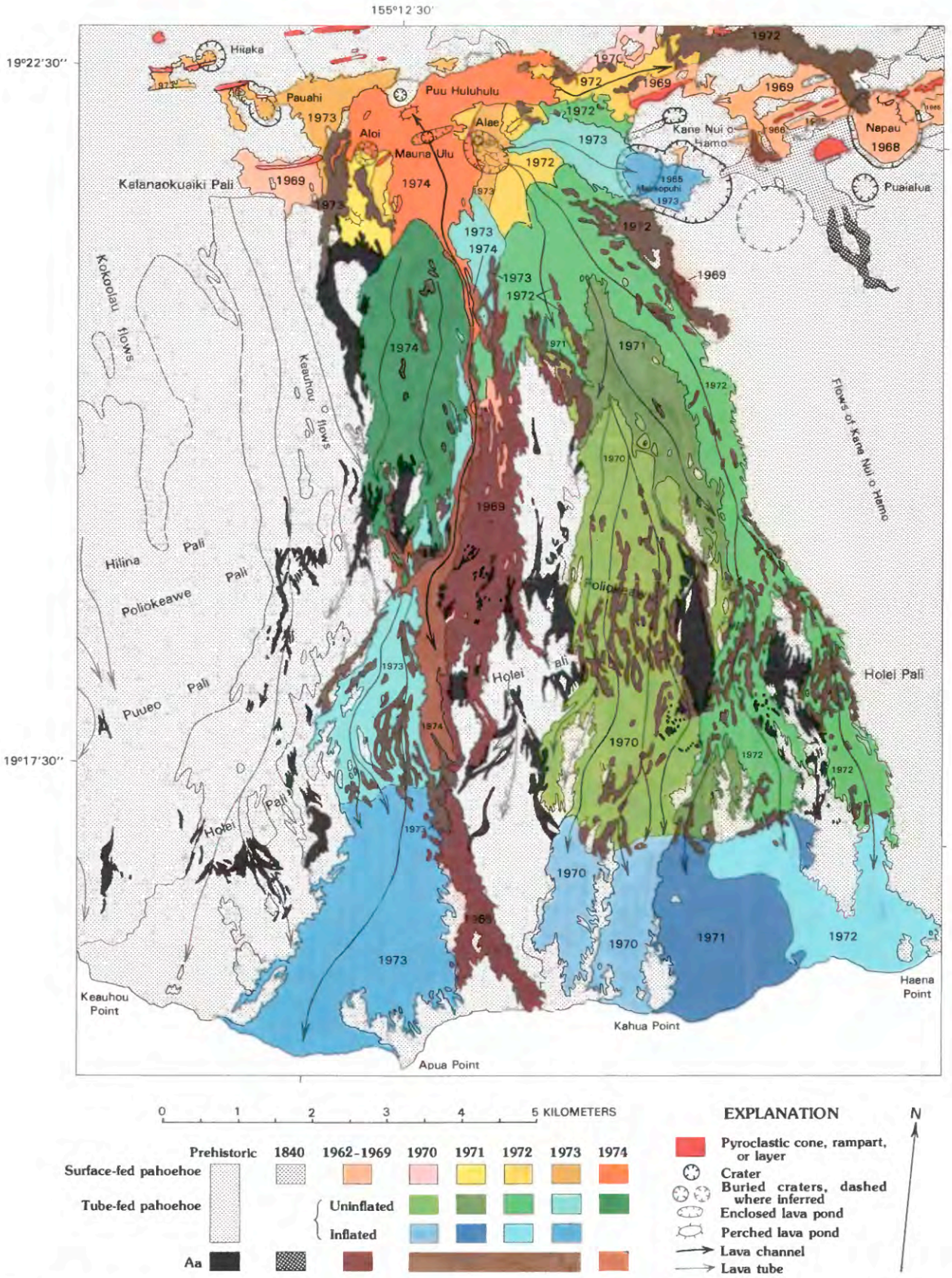

FIGURE 12.35.—Mauna Ulu region, with lava flows classified by their morphology. Shown also are boundaries between pahoehoe units of different age, as indicated on figure 12.5*E*, and eruption years of historical flows. Simplified from Holcomb (1976a, 1980a).

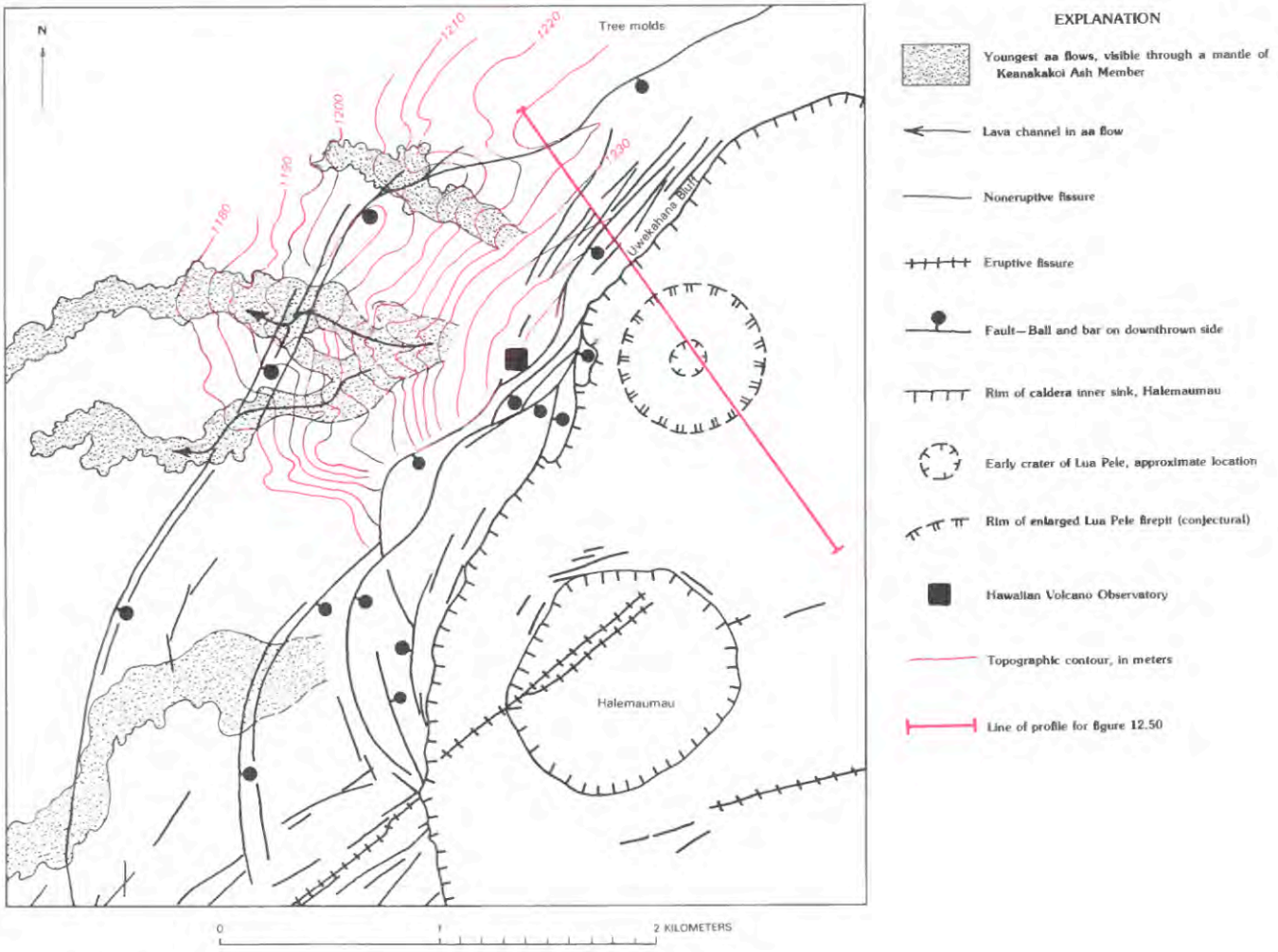

FIGURE 12.36.—Northwest sector of Kilauea caldera. Location of Observatory vent is inferred from radiating ground slopes and lava flows. Enlarged Observatory firepit is conjectural, its former existence suggested by remnants of concentric dikes on present caldera wall (fig. 12.49). Youngest aa flows and their channels (visible beneath mantle of Keanakakoi Ash Member) appear to have been deflected along fault scarp now cutting across them, indicating that displacement began before flows were erupted. This early deformation could have arisen from thermal contraction of lava filling older Powers caldera, as shown in figure 12.50.

KOKOOLAU ERUPTION

Superposition relations between Kokoolau (fig. 12.38) and surrounding lava flows are not yet clear. Holcomb (1980a) interpreted Kokoolau as a kipuka surrounded by flows from the Ai-laau vent, but paleomagnetic sites on Kokoolau (1B188, fig. 12.5*A*) and seaward flows (1B212, 3R349) extending into Kipuka Papalinamoku have shown that they are probably younger, dating from the late 17th century or early 18th century. An aa flow east of the Ahua Kamokukolau triangulation station (fig. 12.5*A*), atop Kalue lava and probably fed by a caldera-concentric vent mantled by A.D. 1790 ash south of Keanakakoi, is overlapped by pahoehoe on its east side (Peterson, 1967, and written commun., 1966). The younger pahoehoe is thought to come from Kokoolau; if so, Kokoolau is not only younger than the Kalue lava but also younger than at least one of the concentric vents. Kokoolau probably belongs to an extensive assemblage from the 17th and 18th centuries that extends the length of the east rift zone.

VEGETATION PATTERNS OF THE MIDDLE EAST RIFT ZONE

One reason for the age uncertainty of Kokoolau is a coincidental vegetation boundary caused by orographic rainfall variation. The rest of the east rift zone extends through an area of high rainfall and rapid forest growth, making it possible to differentiate lava flows using vegetation patterns (Atkinson, 1970). The latest prehistoric flows downrift from Kokoolau can be recognized from their distinctive vegetation. Although in rainy areas they are densely overgrown, their vegetal structure and floristic composition indicate that they are considerably younger than neighboring flows, including those from the Ai-laau vent (fig. 12.39).

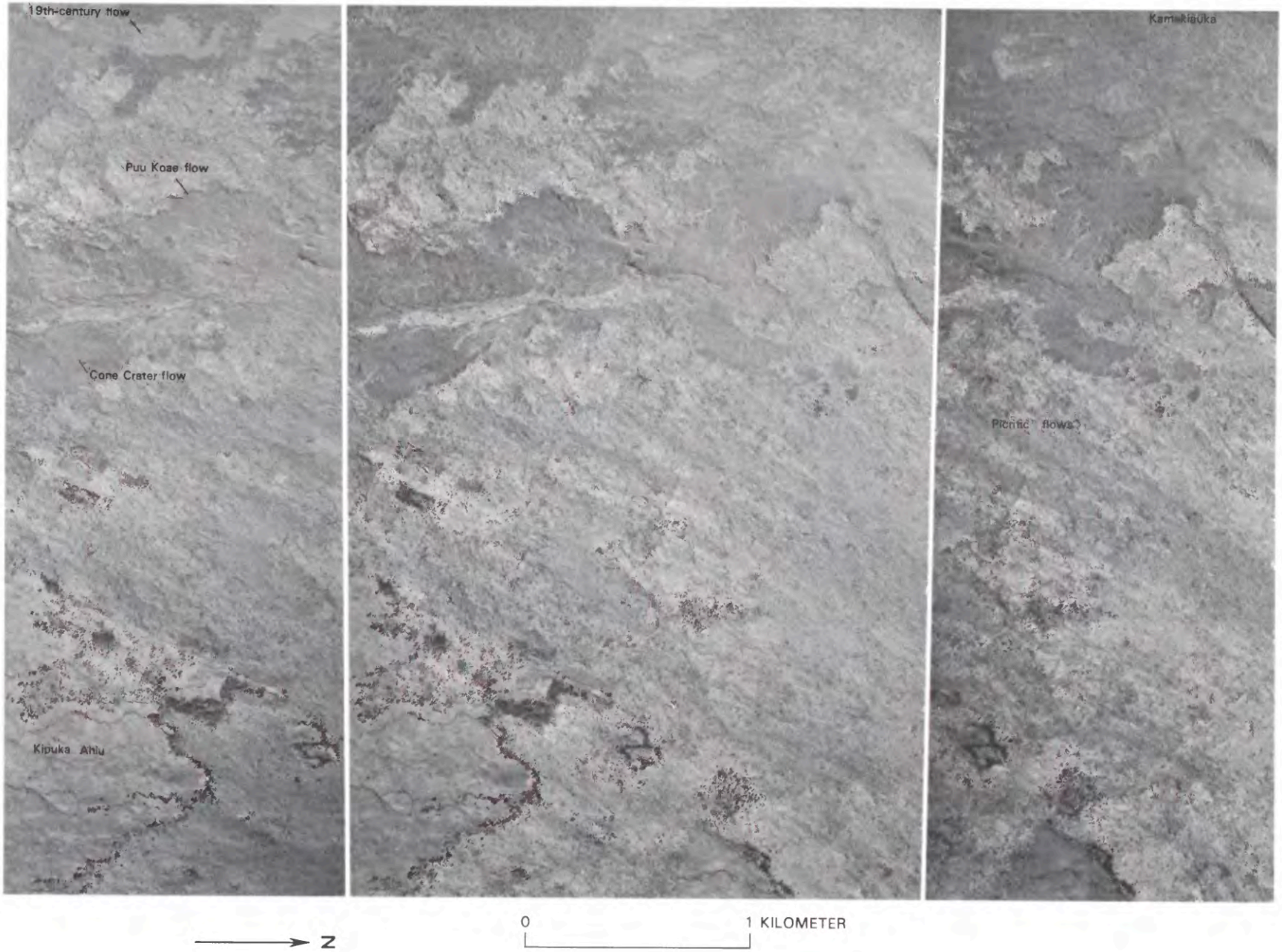

FIGURE 12.37.—Overlapping flows between Kamakaia and Kipuka Ahiu. Aa flows of two ages are present, with sheets of tube-fed pahoehoe between and beneath them. Both pahoehoe units inferred to originate from summit, upper aa from Puu Koae, lower aa from Cone Crater and chain of spatter ramparts to northeast (now covered by lava of 1974). Tonal stripes trending north-northeast to south-southwest at right represent variations in sand cover; dark bands contain more sand. Stereo triplet prepared from frames 201–203, roll 12CC, USDA series EKL, 1965.

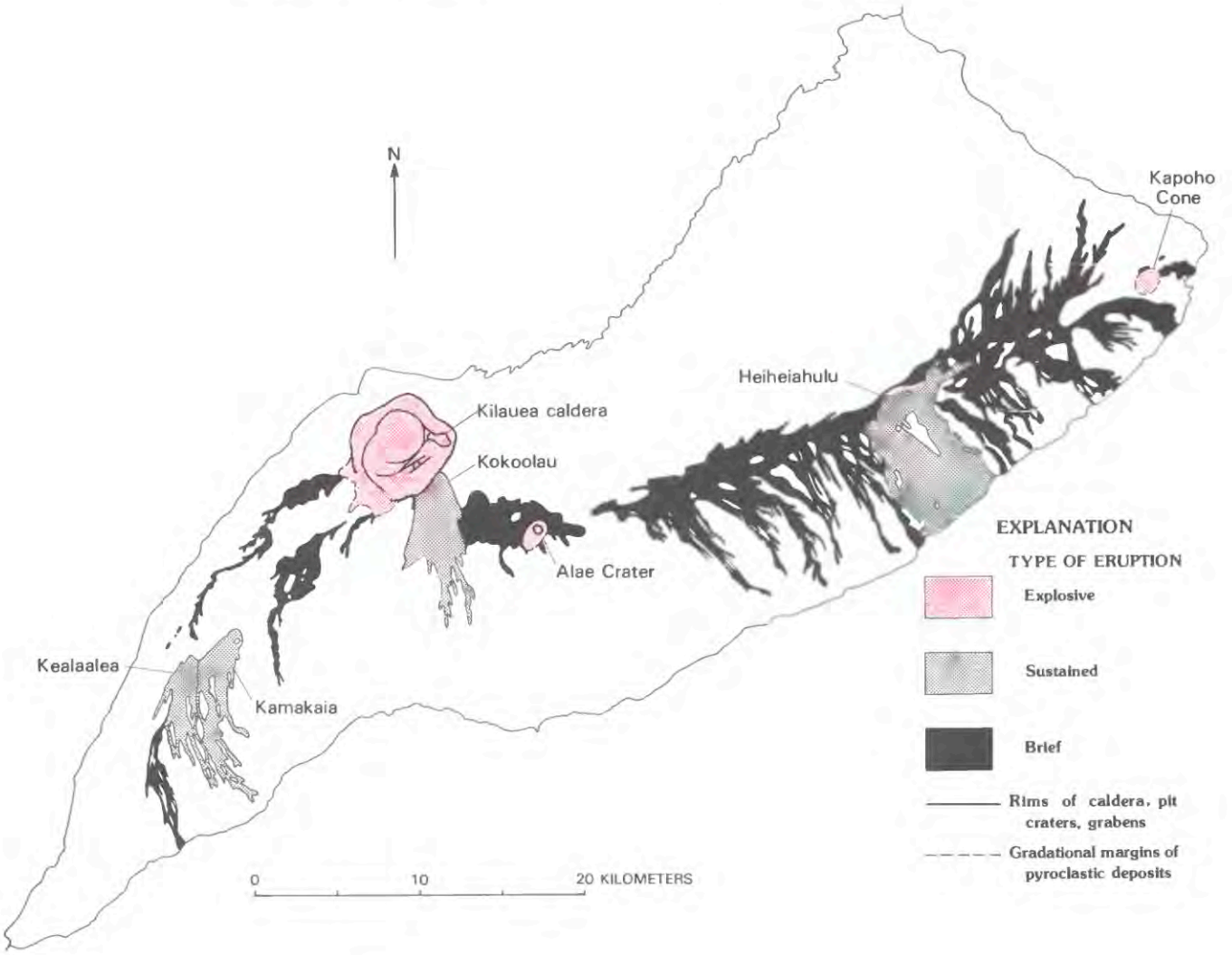

FIGURE 12.38.—Kokoolau and eruption products of 18th century.

Older flows display on aerial photographs a relatively coarse forest grain owing to greater spacing and crown heights of trees. Vegetation patterns have hectometer-scale patchiness, unrelated to flow morphology. When viewed on the ground, large ohia lehua trees (*Metrosideros polymorpha*) of older forests commonly are seen to be epiphytically rooted, indicating that they are not the first generation of trees on the flows. Older flows have more floral diversity; kukui trees (candlenut: *Aleurites moluccana*) are especially common in older forests at lower elevations and are easily detectable because of their high albedo. The younger flows possess a finer vegetation grain arising from close spacing of young trees, and the patchiness of the forest on them is closely related to flow margins and other features of the flow morphology.

Most of the younger flows date from the 18th century, though some could be slightly older. They are distinctly older than flows of 1840, which are also densely vegetated but with plants that are shorter and more closely spaced (fig. 12.39). Though they must be prehistoric, their ^{14}C ages are consistently less than 200 years B.P. (W–359, W–2970, W–3467, W–3468, W–4638, W–4639, W–4644, W–4689).

An 18th century age is indicated also by 19th-century accounts showing that the flows were then much less overgrown than now. Members of the United States Exploring Expedition in 1840–41 were able to walk the length of the middle east rift zone from Napau to Pahoa in a single day, traversing "old lava plains * * * covered with stunted shrubs" (Wilkes, 1845; see especially p. 181–183, 216). A similar trip in 1975 required two days of arduous travel through heavy forest, despite some barren areas of 20th-century lava. When Wilkes passed by the north side of Heiheiahulu lava shield (which he called "Kalalua") he could see that it was a volcanic cone surfaced by streams of pahoehoe even though he had no time to examine it at close range. Today the shield is so densely carpeted with small trees and uluhe (*Dicranopteris linearis*, a species of false staghorn fern) that its nature cannot be determined without climbing

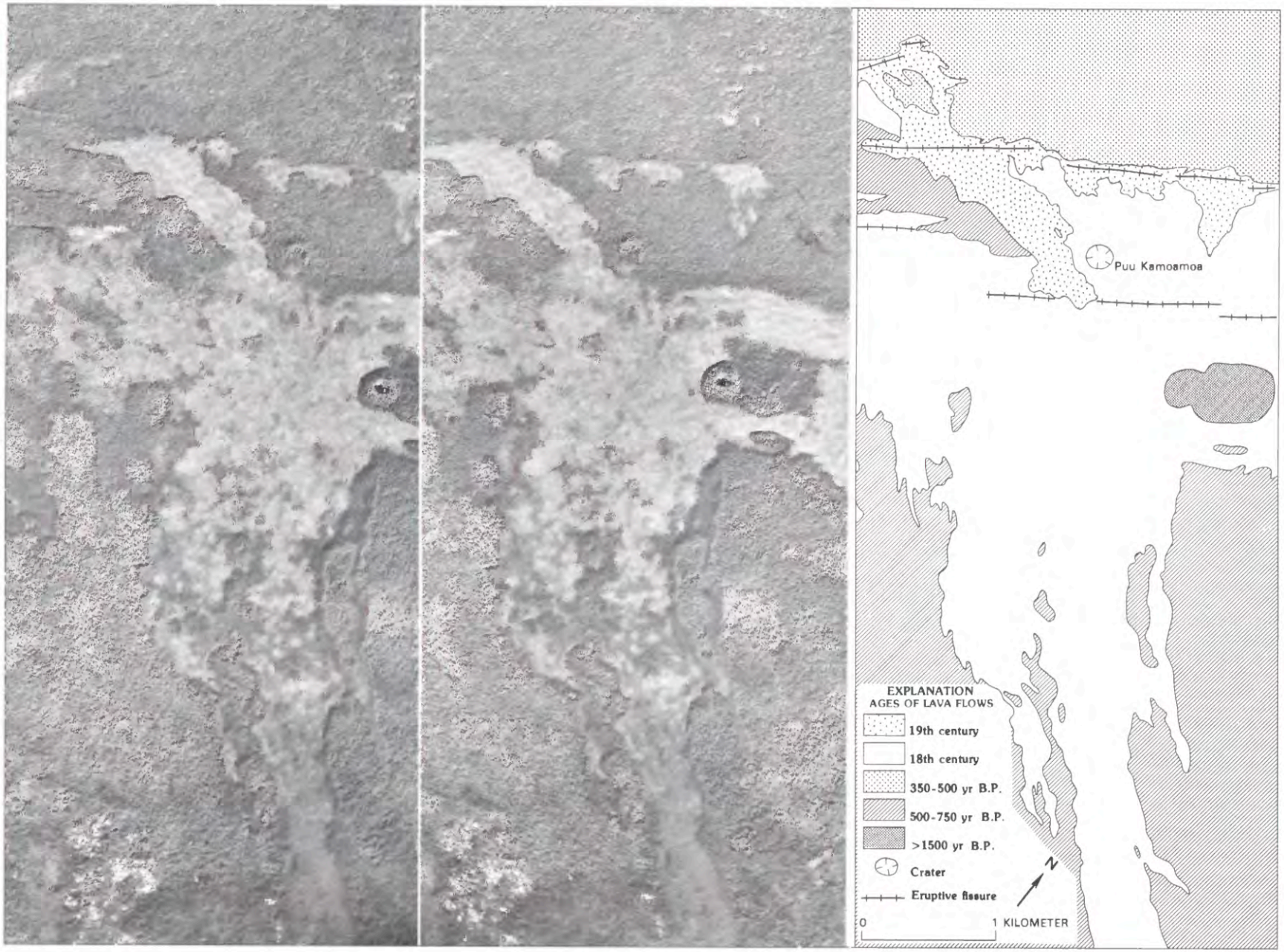

FIGURE 12.39.—Vegetation contrasts near Puu Kamoamoa before extensive flooding by 20th-century lava. All flows visible here are densely vegetated, and their forest patterns vary with age and surface morphology. Most trees are ohia, but light-toned ones in lower left are kukui on flow-mantled fault scarp. Where trees are small on young flows, unshaded understory is composed largely of uluhe; where trees are large, understory is generally dominated by hapuu. Stereo pair prepared from photographs 019, 020, roll 14, U.S. Navy series HAI, 1954.

its flank; in fact, the vegetation is so dense that Heiheiahulu and some smaller cones mentioned by Wilkes cannot even be seen from most places along the rift zone. Because of their vegetal sparsity then and dense vegetation now, most flows along the middle east rift zone must have been quite young when traversed in 1840.

In an earlier interpretation of these vegetation patterns, Moore and Koyanagi (1969) differentiated "late prehistoric" flows (older than about 300 years) from "very late prehistoric" flows older than 1840. However, the vegetation contrasts they used to differentiate the two groups arise from differences in flow morphology instead of age. This is demonstrated by vegetation patterns seaward of Heiheialulu lava shield, inland from Kaimu (fig. 12.40). Here oral history establishes the age, and ranges of climate and flow morphology reveal various rates of forest development for different conditions of rainfall and substrate.

HEIHEIAHULU ERUPTION, CIRCA A.D. 1750

In 1823 Ellis (1827) was told in Kaimu that "the district * * * was overflowed [by lava] in the days of Arapai." Because the reign of Alapai ["Arapai"] was less than a century earlier (approximately 1730–54, according to Hitchcock, 1911) this report should be reliable. Macdonald (1941) supposed the eruption of circa 1750 to be represented by a barren aa flow along the coast about 1 km east of Kaimu (fig. 12.41). Macdonald could not trace this flow directly to its source because it disappears into thick forest, but extrapolation upslope showed that its probable source was Heiheiahulu (Stearns and Macdonald, 1946).

Stratigraphic relations at the shoreline demonstrate that this flow is not the youngest one. Its eastern margin is overlain by pahoehoe of a lava delta (Moore and others, 1973) covering 3 km of shoreline eastward past the Moana Hauae triangulation station and Waipuku Point (figs. 12.41, 12.42). This delta was fed by a lava tube traceable to the upper flank of Heiheiahulu (fig. 12.43). Other tubes and channels radiate from Heiheiahulu; the shield and its flows comprise a diverse assemblage similar to that of Mauna Ulu. The Kaimu district was overflowed not by a single flow but by many, and by analogy with Mauna Ulu this 18th-century eruption was sustained for several months or a few years.

Though all of the Heiheiahulu flows are closely similar in age, their vegetation is highly diverse, varying with flow morphology and climate. The dominant trees on all flows are young ohia (*Metrosideros polymorpha*), but the flows vary widely in the size and spacing of their trees and the character of their understories. In a narrow relatively warm and dry band along the coast, the vegetation is light on all flows but is more dense on tube-fed pahoehoe than on aa. Aa is colonized only by scattered ohia and lichen, while adjacent pahoehoe has thickets of shrubs and grasses as well as more numerous ohia. The contrast is probably caused by differences in water retention; pahoehoe is less permeable and rainwater remains on it longer than on aa. Though vegetation is much more dense in wetter and cooler areas at higher elevations inland, vegetal contrast remains high between flow types. Ohia trees are taller and more closely spaced on aa flows than on pahoehoe. The broader spaces between trees on pahoehoe are generally overgrown by thick tangles of uluhe. Aa probably provides better substrate for trees where rainfall is abundant. Transitions in the vegetal cover on a single flow correspond to morphologic transitions, so that although Heiheiahulu lavas are densely forested, it is still possible to map morphologic transitions from vegetation patterns visible on aerial photographs. Trees grow faster along margins of flows than in their centers, probably because thinner margins are more easily penetrated by roots. Where flows are thick they commonly possess massive interiors that may prevent roots from reaching nutrients and moisture beneath the lava.

These vegetation patterns can be used to identify 18th-century flows along most of the east rift zone. Similar relations of vegetation to flow morphology and climate have been found on the 1868 flow of Mauna Loa (Juvik, 1976).

OTHER ERUPTIONS FROM THE EAST RIFT ZONE

A few flows have been included with the 18th-century group despite evidence that they may be somewhat older. On some flows the vegetation is slightly different, the ohia trees being taller and more widely spaced and giving the forest a coarser grain when viewed on aerial photographs. Some of these flows may be contemporaneous with the Observatory flows, but this is not yet certain; some of the flows differ for reasons other than age. An example just southeast of Napau (fig. 12.44) has a vegetation pattern coarser than most 18th-century flows, but ^{14}C samples W–3468 and W–3469 suggest an age younger than 200 years. This flow consists of surface-fed pahoehoe generally less than 1 m thick, penetrated by tree molds from which many of the present trees grow. These conditions may have permitted more diversity and rapid growth; if so, they prevent fine age distinctions based on vegetation differences.

Some age uncertainties arise from early historical descriptions. For example, the pahoehoe of Malama-Ki Forest Reserve, comprising the coastline between Lililoa and Mackenzie State Park (fig. 12.45), is included in the 18th-century group even though Ellis' (1827, p. 201, 205) account seems to preclude such an age. Ellis was told on passing through Malama that the area inland was inundated by an eruption in about A.D. 1790, but he observed that the coastal tract where he traveled "was covered with soil, and smiling with verdure." He was told later at the village of Pualaa that an eruption near the time of Cook's visit inundated much country along the lower east rift zone but was arrested by the contiguous hills of Kaliu, Malama (Kahuwai-Puulena), and Honuaula. Macdonald (1941) inferred from these accounts that the flows of circa 1790 were confined to the region north of Puu Kaliu and Malama, but aerial photographs show that Macdonald's fissure vent extending from Kaliu to Malama fed flows to the south as well as to the north. The two reports given to Ellis could have referred to two different eruptions in the late 18th century, so that the one confined north of the Kaliu-Malama complex differs from the one sending flows into the lower Malama district, resolving the apparent contradiction. But Ellis' implication that coastal Malama was not flooded is clearly inconsistent with the flow distribution shown on figure 12.45. More faith is placed here in the vegetation and flow morphology than in Ellis' inference. An 18th-century age for the Malama flow is also consistent with its direction of remanent magnetization (site 8B025). Ellis' verdant coastline may front another part of Malama, or

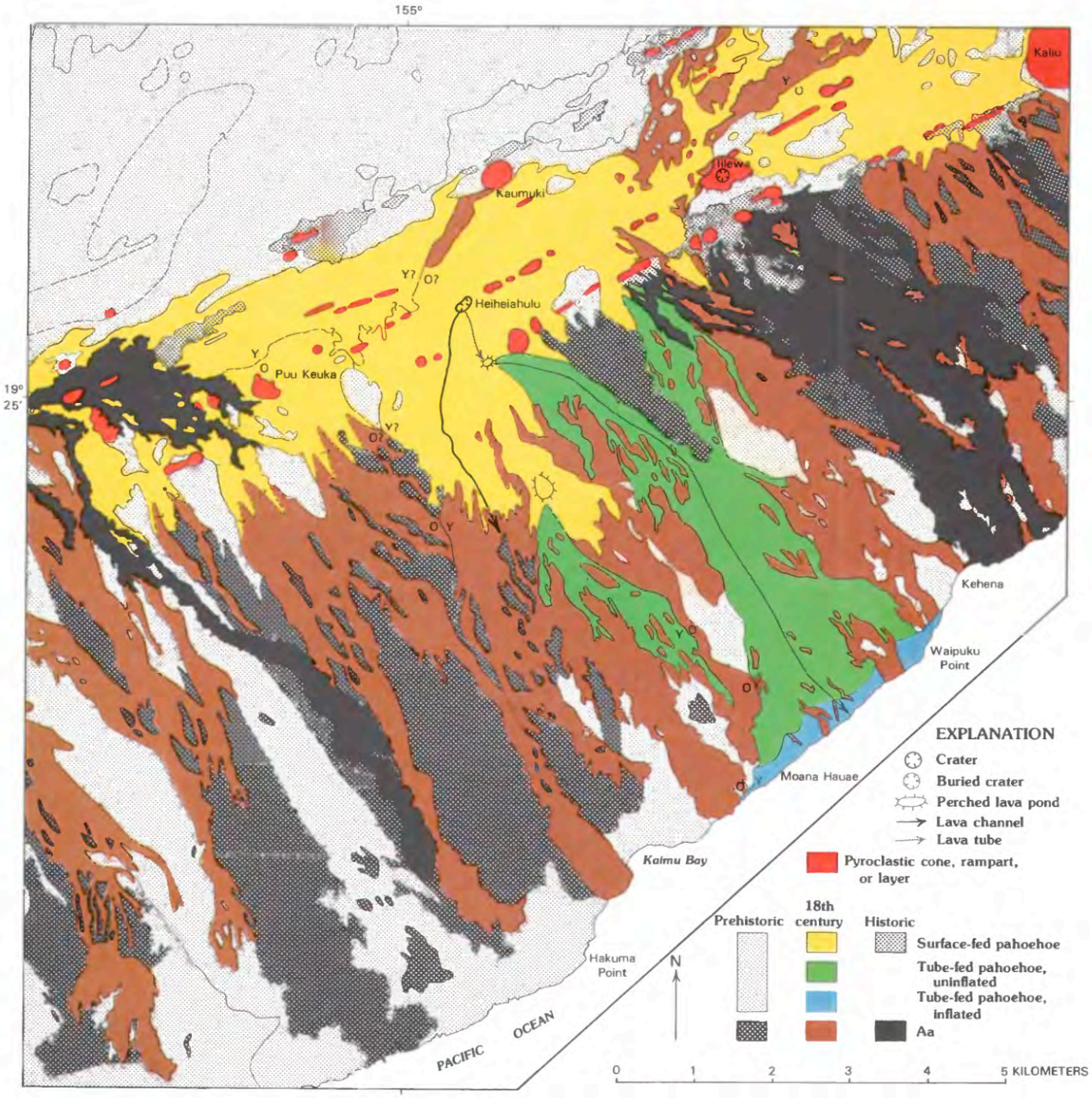

FIGURE 12.40.—Lava flows of circa 1750 eruption of Heiheiahulu, classified by their morphology. Relative ages indicated at some contacts: Y, younger; O, older; queried where uncertain.

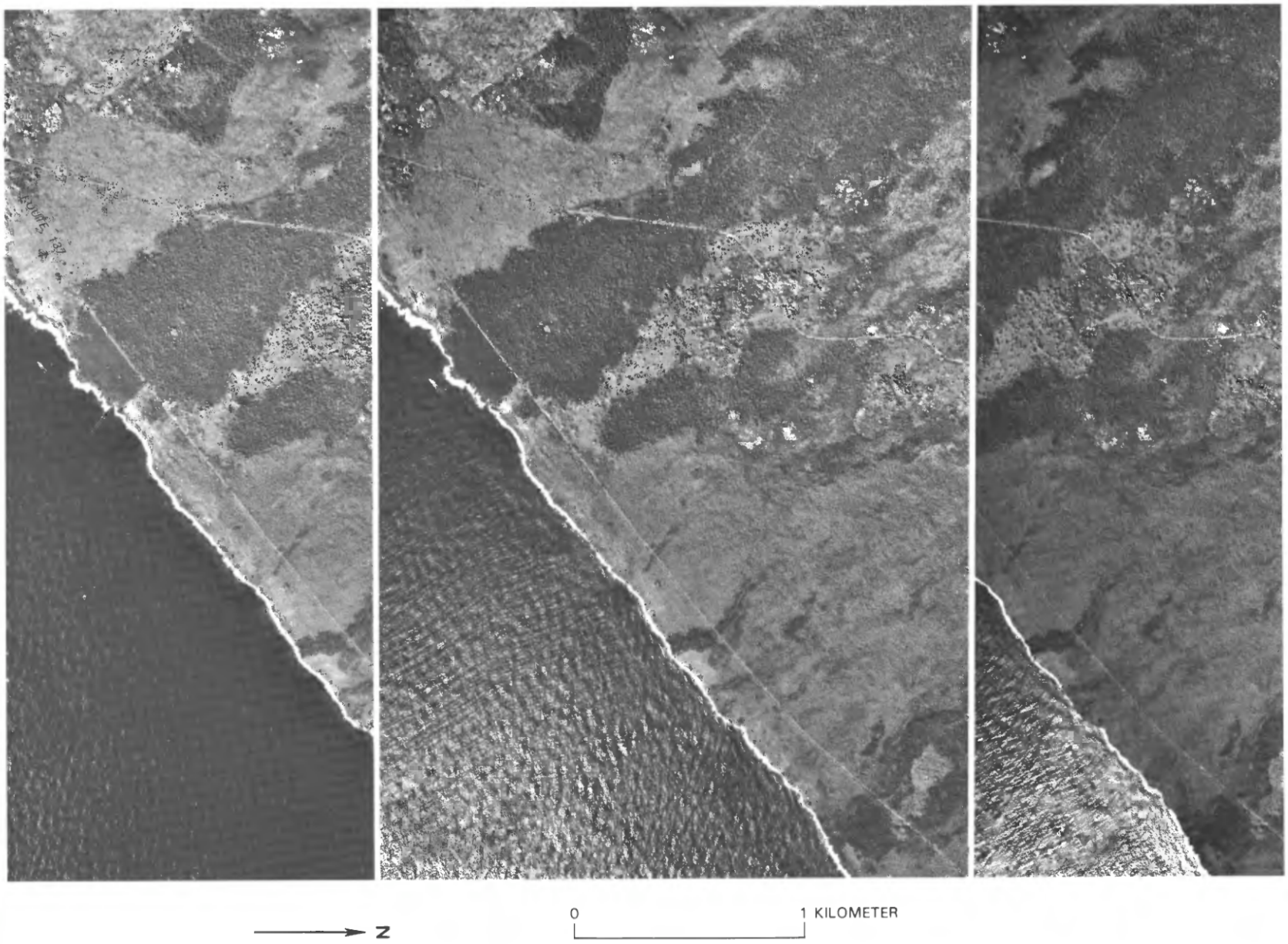

FIGURE 12.41.—Coastal flows between Kaimu and Waipuku Point. Prominent dark flow was only one designated as circa 1750 by Macdonald (1941), but flow morphology and superposition relations indicate that many other flows are of similar age and also erupted at Heiheiahulu. Spacing of ohia on 18th-century aa decreases with increasing elevation inland. Dark-gray, fine-textured tube-fed flows of 18th century are sparsely overgrown with shrubs and grasses between small ohia. Light-toned older flows are densely vegetated, with scattered large trees being prominent. Distinctive globular trees are mango; very light trees are kukui. Arrow indicates small cove whose northeast edge is shown in figure 12.42B. Pairs of red dots are paleomagnetic sample sites, each dot representing a subsite. Stereo triplet prepared from photographs 47–49, roll 12CC, USDA series EKL, 1965.

A

B

FIGURE 12.42.—Stratigraphic relation of circa 1750 flows at shoreline. ***A***, Oblique aerial view showing circa 1750 flow of Macdonald (1941) on left and tube-fed flow of Moana Hauae/Waipuku Point lava delta on right. Narrow, light-toned horn of pahoehoe extends along shoreline from delta to front of aa flow. Horns typically form when surf retards spreading of delta front but permits lava to spread along shore. Photograph by J.P. Lockwood, June 1974. ***B***, Seaward view from atop aa flow in contact with pahoehoe delta. Marine erosion has removed clinkery top of aa flow, producing small cove indicated on figure 12.41, which extends to right of this view. Rock hammer at left (circled) is on contact between flows. Pahoehoe is molded around underlying clinkers. Photograph by J.P. Lockwood, June 1976.

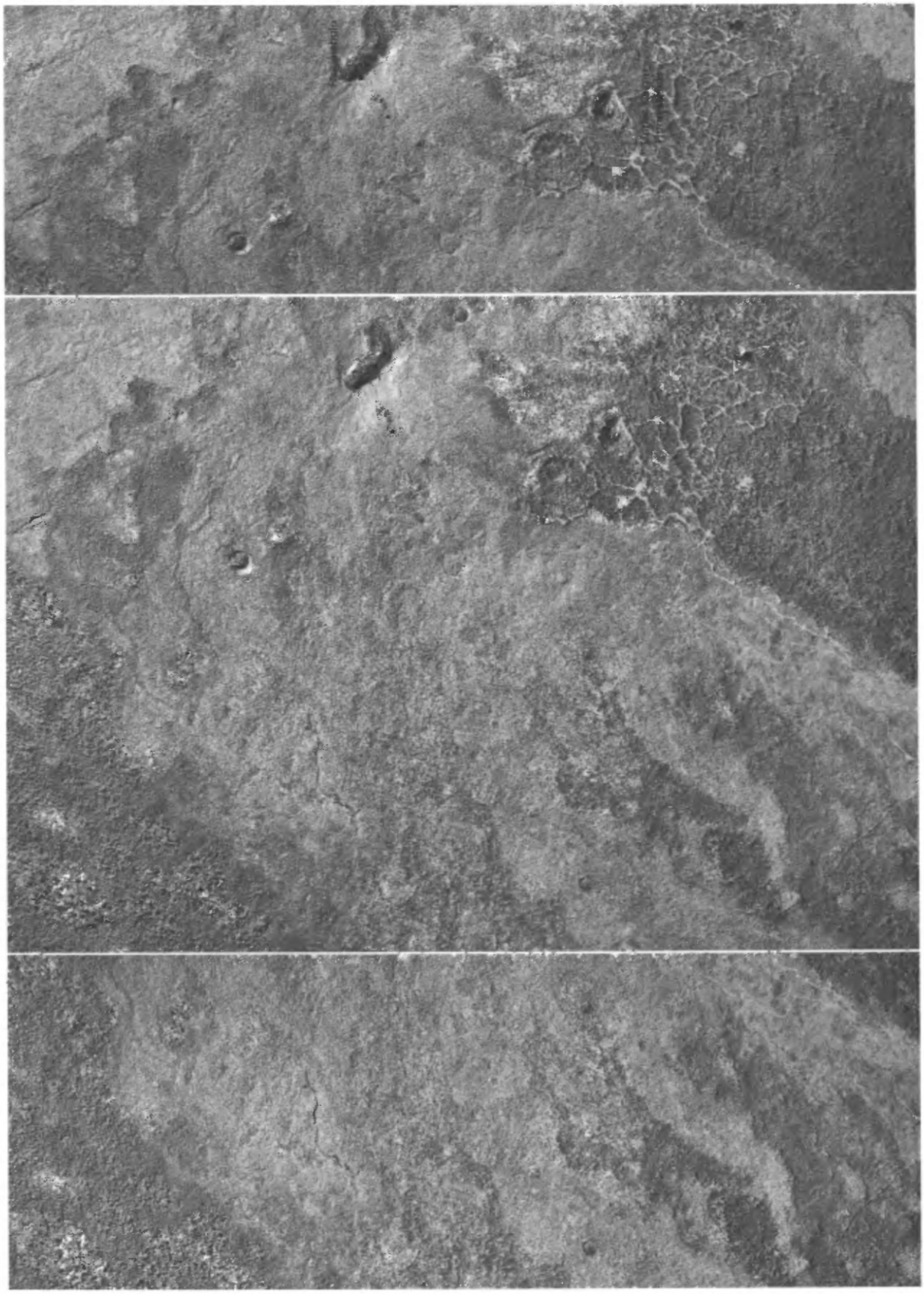

FIGURE 12.43.—Seaward flank of Heiheiahulu. Dark-toned aa supports dense ohia forest, while pahoehoe is covered by uluhe thickets and more widely spaced ohia. Stereo triplet prepared from photographs 55–57, roll 12CC, USDA series EKL, 1965.

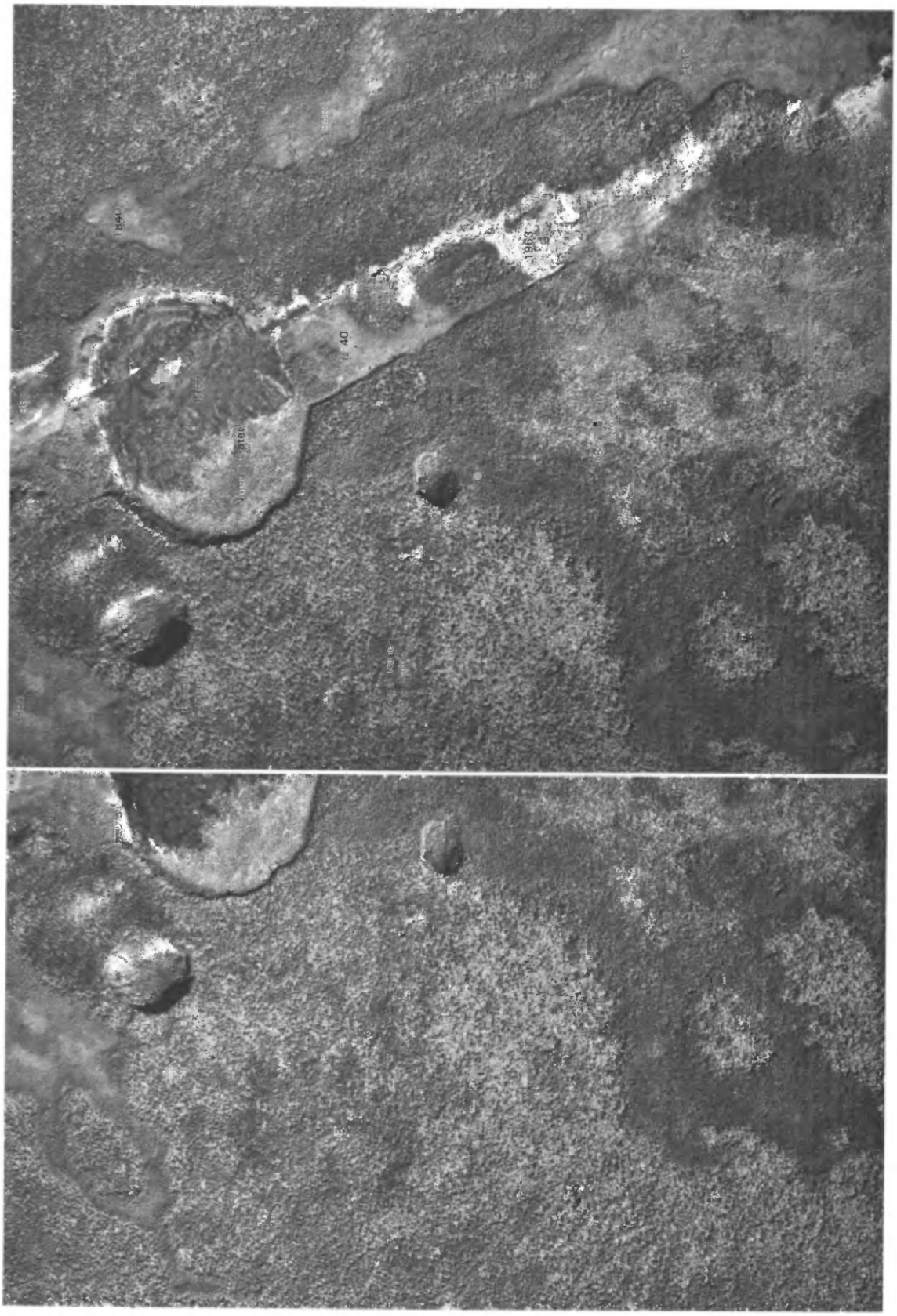
1984
1983
1840
1840
1840

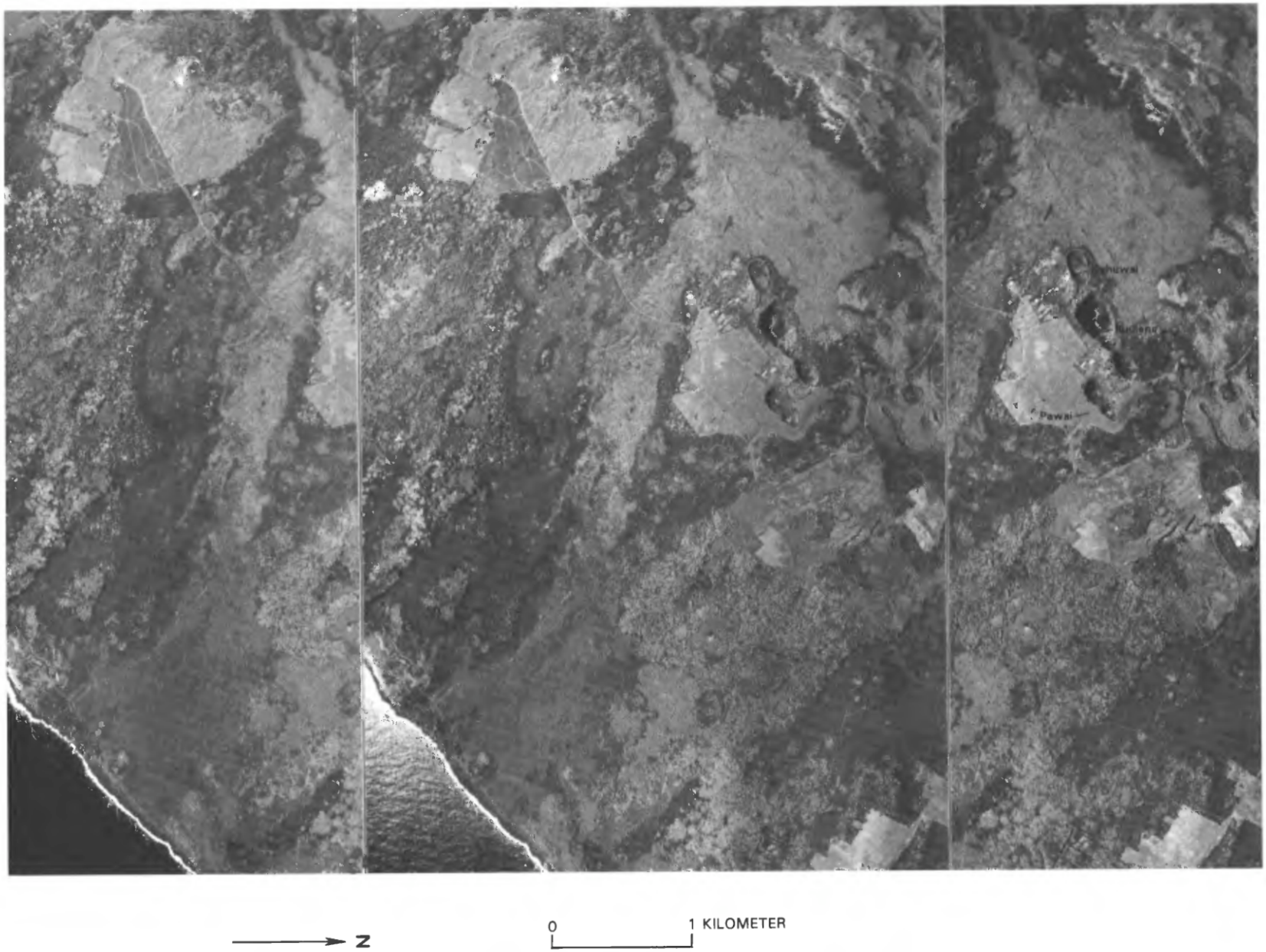

FIGURE 12.45.—Late prehistoric Malama flows, erupted from fissure extending east-northeast from Kaliu past Kahuwai and Puulena. Macdonald (1941) attributed flows inland of fissure to eruption of circa 1790, but their vegetation and morphology show that seaward flows are coeval. Open fissures and spatter ramparts occur together with a tube system; evidently criteria of table 12.1 can be contradictory in some cases. Holcomb (1980b) used vegetation differences to assign 17th-century age to flow east of Pawai Crater, but R.B. Moore (1985) has shown it to be from same eruption of circa 1790. Large red dot, ^{14}C sample site; pair of small red dots, paleomagnetic sample site. Stereo triplet prepared from photographs 128–130, roll 23, U.S. Navy series HAI, 1954.

vegetation may have been reestablished quickly along the coast. Kaliu, Malama, and Honuaula could have dammed a flood of lava and yet permitted some tongues to flow through the gaps between them.

The most recent activity in Kapoho Crater (fig. 12.46) is of uncertain age but probably occurred in the early 18th century or 17th century. An age significantly earlier than A.D. 1800 seems required by the account of Ellis (1827), who in 1823 recognized the volcanic nature of the tuff cone and questioned local residents about its last eruption. Though tradition described it as a seat of volcanism, the people living there could give no specific information about the last eruption, which suggests that it had occurred long before. There had certainly been enough time for thick vegetation to grow, because Ellis described the tuff cone as "overhung with trees, and clothed with herbage" (Ellis, 1827, p. 205–206). On the other hand, the aa flow extending east from the cone (fig. 12.47) is magnetized (8B205) in a direction similar to the Observatory flows, and a ^{14}C age of less than 200 years B.P. (W–2970) has been obtained from charcoal beneath a thick pyroclastic layer within the cone. Given the uncertainty in the ^{14}C and paleomagnetic ages, a single eruption could have produced both the flow and pyroclastics a century or so before Ellis' visit.

The morphologies of flows and vents indicate that all of these latest prehistoric eruptions, except for those of Kokoolau and Heiheiahulu, and perhaps the one of circa 1790, had high discharges and short durations. Though the flows typically extend several kilometers from their fissure vents and terminate as aa lobes, they are remarkably free of mappable lava channels.

ERUPTIONS FROM THE SOUTHWEST RIFT ZONE

The 18th century saw frequent and sustained eruptions from the southwest rift zone as well as the east rift zone, with eruptions occurring from all of its active parts.

Brief eruptions were widespread (fig. 12.5*B*). A vigorous one from the northern strand produced the Cone Peak ramparts (8B745) and flows that extended nearly to Kamakaia. Subdued eruptions near the end of the same strand built small shields and lava pads (9B841), similar to those of 1868, inland from Kamakaia; some of the pads overlap the Cone Peak aa flow. Vigorous eruption from the central strand produced Puu Koae and other spatter cones and aa flows extending to about 1 km from Hilina Pali.

Another brief eruption occurred from the lower segment about 1.3 km east of Puu Nahaha and 600 m east of the upper end of the Keaiwa flow of 1823 (fig. 12.5C). Lava flows from this eruption reached the sea between Kapaoo Point and Waiwelawela Point. They are more weathered than the overlying Keaiwa flow and have been dated by ^{14}C at about 200 years B.P. (W–3938, W–4452). The Red Cones and their aa flows, which also overlie these flows, are undated, but they too are overlapped by the Keaiwa flow. Both the Red Cones and the earlier unnamed flows probably date from the 18th century. Their eruptive fissures appear to have extended through Yellow Cone from the southern strand of the upper segment, but they cannot be traced far uprift because they are buried by other 18th-century lava flows of sustained eruptions.

The late prehistoric lava commonly termed the Kamooalii flow (see Stearns, 1926) consists of two assemblages of similar age from different strands of the rift zone. A sustained eruption from the central strand built a lava shield at Puu Kou and Kealaalea Hills (fig. 12.5*B*), and a complex flow assemblage extending seaward across the Kau Trail and past the west side of Puu Ahi (fig. 12.5C). The eastern part of the Kamooalii flow is another complex assemblage fed by vents of the southern strand, including Kamakaia and Kamakaiawaena (fig. 12.48). Kamakaia flows overlap those of Kealaalea. Magnetization of Kealaalea (9B409) and Kamakaia (8B517) flows is consistent with an 18th-century age, and the Kealaalea flows have been dated by ^{14}C as younger than 200 years B.P. (W–3937). Both flow assemblages probably represent sustained, unstable eruptions during the 18th century.

Yellow Cone is a small kipuka of pyroclastic material protruding through the flank of the Kealaalea shield (fig. 12.5*B*). It may predate the 18th century; no young flows have been found seaward of it beneath the flows of Kealaalea. While the lavas of Yellow Cone, Red Cones, Kamakaia, Kamakaiawaena, and Kamakaiauka along the southern strand of the southwest rift zone all have differentiated compositions, the analyzed flows from the Great Crack and central strand of the upper southwest rift do not (Wright and Fiske, 1971).

FIGURE 12.46.—Kapoho Crater, looking northeast from distance of about 1 km. Photograph by R.T. Holcomb, 1977.

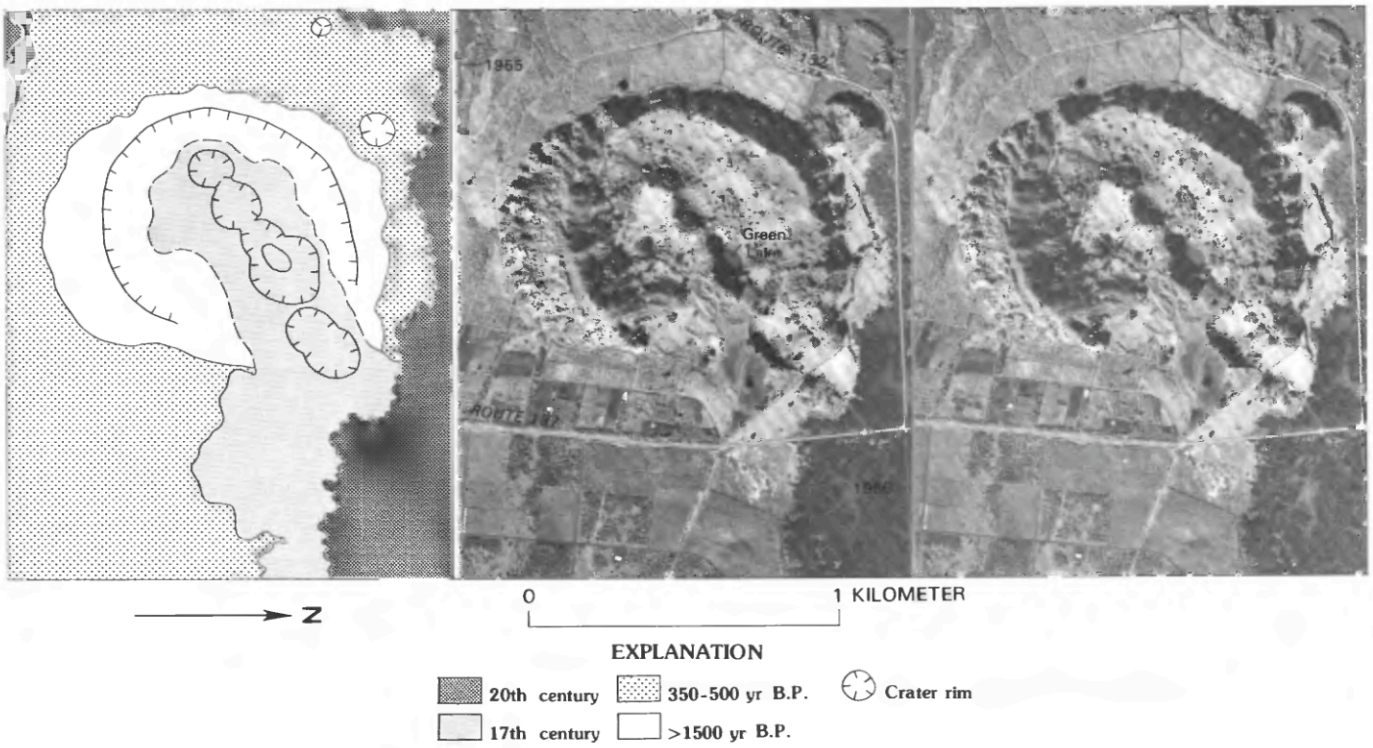

FIGURE 12.47.—Vertical view of Kapoho Crater. Tuff cone is incomplete, possessing gap on its eastern side through which thick prehistoric aa flow extends east about 1.5 km to present shoreline. This aa flow probably was erupted during 17th century and sits atop pahoehoe flows that have direction of magnetization consistent with age of 350–500 yr B.P. (pairs of small red dots, paleomagnetic sample sites). Both flows veneered by ash distributed around tuff cone, suggesting that pyroclastics postdate flows, but aa flow must be younger than cone if it has extended through gap in cone, and sharp break in slope around outer base of cone suggests that cone protrudes through pahoehoe flows and predates them as well. A ^{14}C age of less than 200 yr B.P. was obtained from charred log beneath ash on interior slope of tuff cone (large red dot). Both aa flow and its ash veneer may have been erupted during 17th century from chain of craters within cone, while bulk of cone is older than pahoehoe flows. Crater containing Green Lake is thickly rimmed by ash. Ellis (1827, p. 206) described within Kapoho Crater "a smaller circle of hills, equally verdant, and ornamented with trees" that may have comprised an inner tuff ring (not now definable as morphologic feature, possibly destroyed by quarrying). Aa flow and young ash deposits around chain of craters may be products of single eruption.

The compositions of the 18th-century flows beneath Red Cones, and of flows from other seaward vents such as the Lava Plastered Cones, are not known.

In summary, the latest prehistoric interval saw from the northern strand of the upper southwest rift zone a brief but vigorous eruption at Cone Peak followed by brief, less vigorous eruptions farther downrift. The central strand saw brief, vigorous eruption at Puu Koae and sustained, unstable eruption at Kealaalea, with their sequence not yet known. The southern strand saw a vigorous brief eruption east of Puu Nahaha followed by a smaller eruption of Red Cones and sustained eruption at Kamakaia farther uprift.

THE MODERN CALDERA

The age of the modern caldera and the timing of collapse with respect to the explosive eruption of A.D. 1790 are not yet known. There still remains much room for alternative sequences and mechanisms.

Much—maybe all—of the collapse preceded the explosive eruption, because all of the 1790 ash now exposed is draped unbroken across the modern caldera faults surrounding the inner sink (Christiansen, 1979). Within the sink, the so-called sand spit between Keanakakoi and Halemaumau and the deeply subsided blocks adjacent to Uwekahuna Bluff and Waldron Ledge also are draped by the ash. However, higher caldera walls in several places lack ashy plaster and may have seen local collapse following ash deposition. It remains possible that most of the collapse occurred only a short time (hours or days) before the onset of explosive eruption. It also remains possible that much collapse occurred within the inner sink during, or even following, the explosive eruption without continued displacement along the outer caldera structures.

Alternatively, the inner sink could have reached essentially its present diameter sometime earlier than 1790. Incipient smaller scale collapse probably did begin earlier, with alternating rise and fall of the magma column. Many dikes and other intrusive bodies are exposed along the north wall of the modern caldera (Powers, 1916); those rising high through the stratigraphic section must postdate the Observatory vent (Casadevall and Dzurisin, chapter 14). Some dikes appear to follow structures bounding the inner sink of the modern caldera: Some occurrences thought by Powers to be intru-

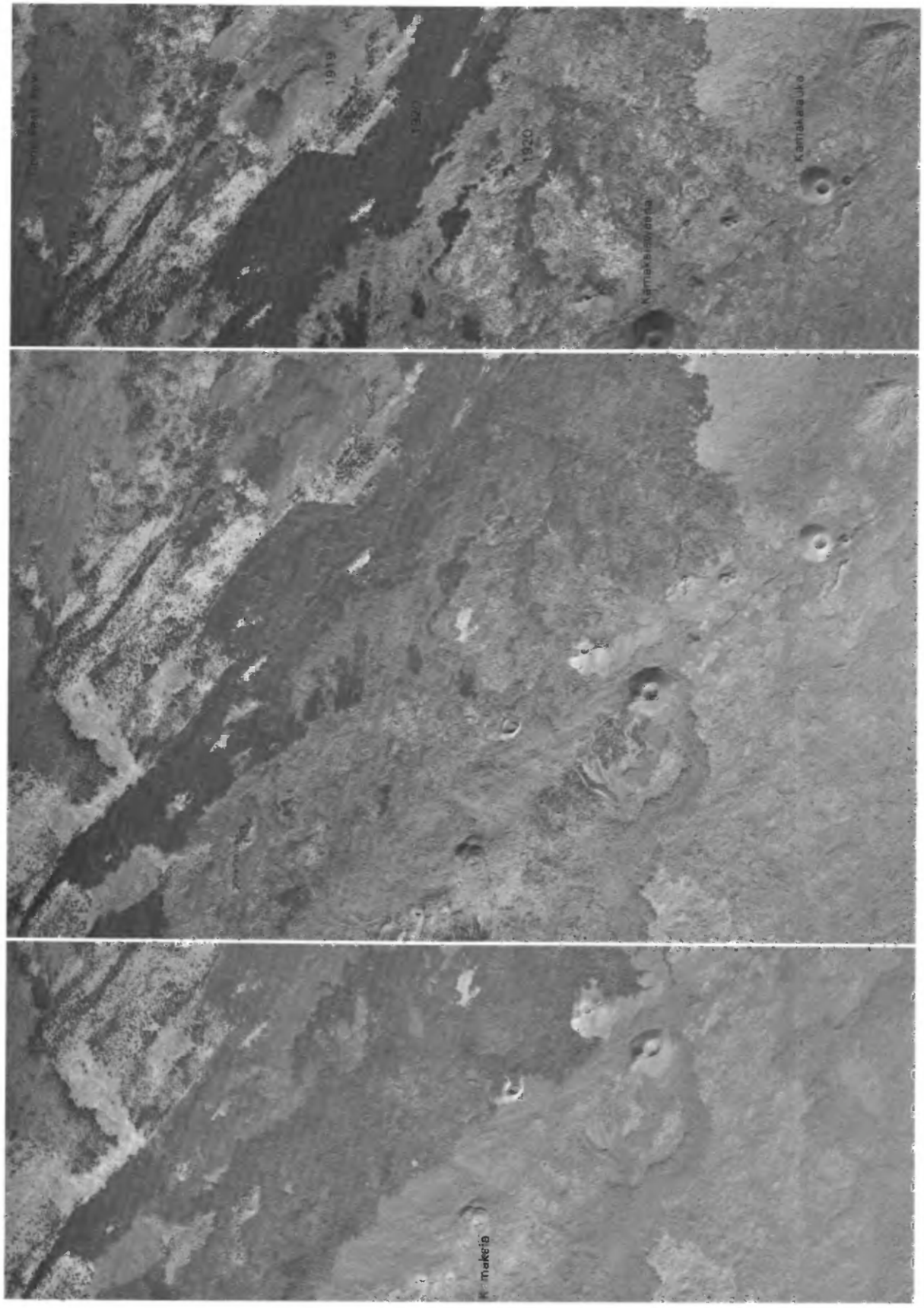

FIGURE 12.48.—Kamakaia Hills. Red dot indicates approximate viewpoint for figure 12.17. Stereo triplet prepared from frames 41–43, roll 5CC, USDA series EKL, 1965.

sions within the truncated stratigraphic section are actually veneer a few meters thick adhering to the caldera wall (fig. 12.49). These probably are remnants of dikes intruded along older fissures concentric to the Observatory vent. Some thinner dikes seem to extend irregularly into the wall away from these thicker concentric dikes instead of rising vertically through fissures radial to the caldera. The concentric fissures may have formed when the magma column subsided to produce an enlarged Observatory pit like Halemaumau, and dikes may have been intruded along these fissures later when the magma column rose again. The column could have oscillated several times, and successive collapses could have enlarged the sink to nearly its present size long before the climactic explosive eruption in 1790. (It was suggested by de St. Ours, 1979, that multiple collapses occurred at different centers; see also, de St. Ours, 1982.) An active lava lake may have been present much of the time in this sink; reticulite at the base of the Keanakakoi Ash Member shows that high lava fountains occurred near the summit sometime before the 1790 explosions (Decker and Christiansen, 1984). A hypothetical sequence showing the enlargement of an Observatory firepit followed by a larger scale collapse to form the present inner caldera sink is sketched in figure 12.50. This sequence was drawn assuming a 17th-century age for the Observatory flows, but other ages and other sequences are possible.

FIGURE 12.49.—Part of north caldera wall of Kilauea, showing light-toned rectangular rock body that Powers (1916) interpreted as sill-like intrusion projecting into cliff face. Close inspection has shown instead that it adheres like plaster on cliff face. Cliff and trees on its rim are 120 m and 10 m high, respectively. Steam in foreground rises through lava flows of 1919. Photograph by J.D. Griggs, May 1979.

Stratigraphic constraints on the age of the northwest part of the inner caldera sink turn largely on the age of the Observatory lava shield. Much of the caldera here must have developed after the Observatory shield ceased to grow, because much of the shield was engulfed by the collapse of the inner sink. If the Observatory flows do date from the 17th century, they constrain caldera development to the late 17th century and 18th century. But if the Observatory flows are older than 700 years, the caldera could have begun to grow long before the 18th century.

Neither is the age of caldera formation well constrained to the south. A few eruptions from fissures concentric to the caldera probably occurred after extensive collapse in the summit region. One flow from a concentric fissure southwest of the caldera and having 18th-century magnetization (8B757) occurs between layers of the Keanakakoi Ash Member and must date from 1790. Others predate the ash by unknown amounts; magnetization of one (8B769) south-southwest of the caldera implies that it could date from the 17th century, but its large within-site dispersion (4.7°) permits it to be a century younger. An aa flow east of the Ahua Kamokukolau triangulation station was probably fed by a concentric vent south of Keanakakoi; as discussed earlier, the east side of this flow is overlapped by pahoehoe probably from Kokoolau. Two of these flows from caldera-concentric vents were deflected by preexisting Koae fault scarps and then broken by recurrent displacements on those scarps.

PIT CRATERS OF THE UPPER EAST RIFT ZONE

Subsidence and dilation of both rift zones also occurred during the past few centuries, but the timing of these events with respect to summit collapse is not yet known. Especially prominent are several pit craters of the upper east rift zone. Some craters probably collapsed in the 18th century, though a few show signs of complex development that began earlier. Makaopuhi and Alae illustrate the complexity especially well.

The coarse ejecta exposed in the wall of Makaopuhi (fig. 12.28C) indicate that an earlier pit existed at or near the site of the present one. The present crater consists of two parts indenting the flank of Kane Nui o Hamo (figs. 12.51, 12.52; see Aramaki and Moore, 1969, fig. 7). The eastern pit may be older than 500 years; it was partly filled by a thick lava lake followed by four thinner flows (Stone, 1925). The lowermost of these flows sent dikes down into columnar joints of the lake far enough to suggest that the lake cooled for at least a few decades before it was covered (Moore and Evans, 1967). The uppermost flow may have been erupted from the southwest crater wall; its surface slopes slightly (0.3°) away from

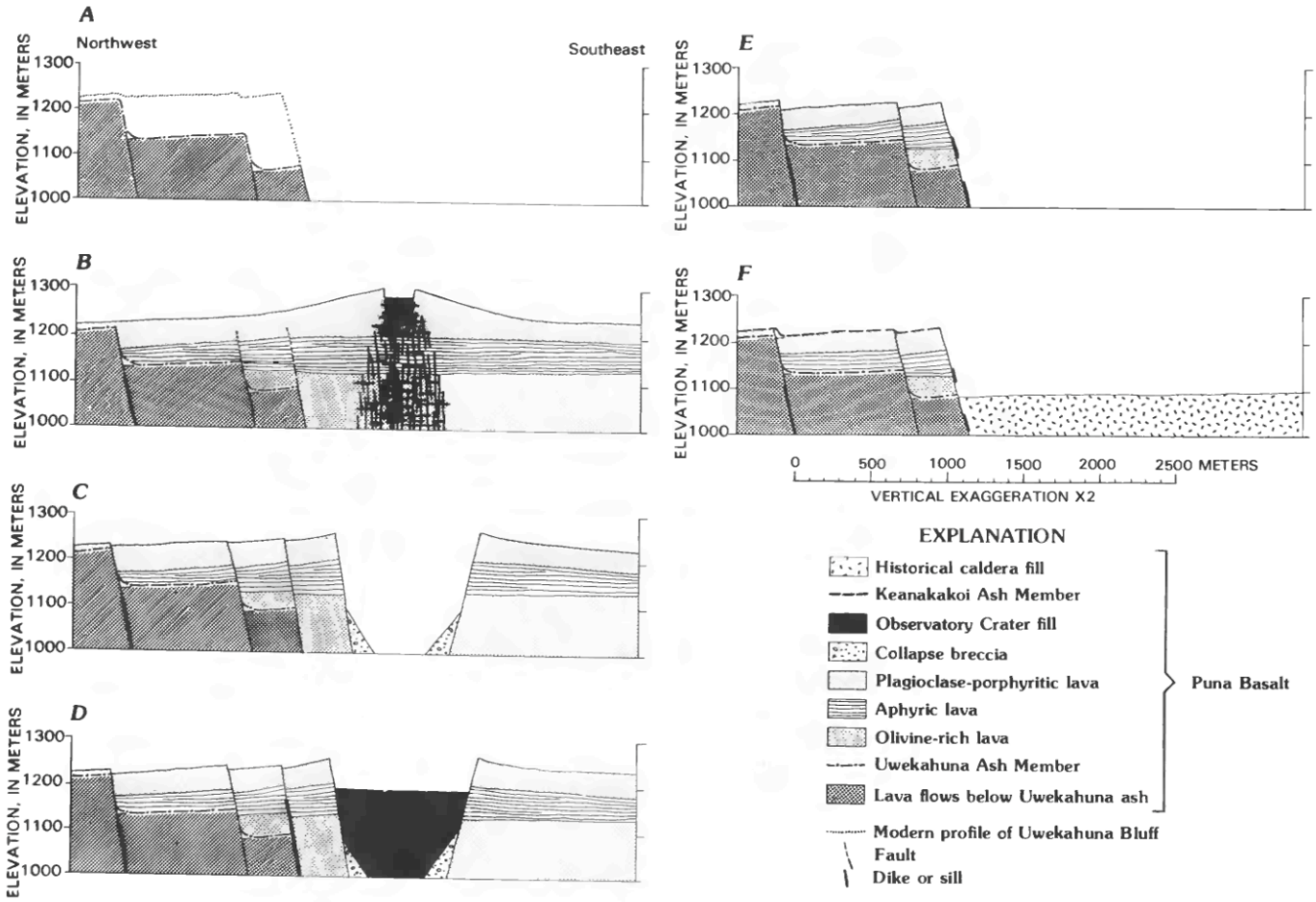

FIGURE 12.50.—Cross sections showing possible developmental sequence for Uwekahuna Bluff, assuming that Observatory shield ceased to grow during 17th century. Line of profile shown on figure 12.36. ***A***, About 1,500 years ago. Powers caldera mantled by Uwekahuna Ash Member. Profile of modern caldera shown for comparison. ***B***, About 300 years ago. Powers caldera filled by flows of three successive groups (Casadevall and Dzurisin, chapter 13). Lower fill broken by differential thermal contraction above buried fault scarps. Dikes and sills surround magma column beneath Observatory lava shield, and dikes intrude along some peripheral caldera faults. ***C***, About 275 years ago. Drainage of magma has produced enlarged firepit. Continued contraction of caldera fill has broken surficial lava flows, forming low scarps above buried faults. ***D***, About 250 years ago. Magma has risen again into firepit and has fed dikes along fractures around pit. ***E***, About 200 years ago. Inner sink rejuvenated by caldera collapse, and dike remnants adhere to its wall. ***F***, Present time. Modern caldera mantled by Keanakakoi Ash Member and partially filled by historical lava flows.

lava drapery and spatter along a fissure in the wall. Lava also issued from a fissure on the crater floor to form small pads atop the upper flow. Another collapse then produced a western pit with the older crater fill forming a mezzanine on its eastern side. The age of the western pit is not known; though it is prehistoric, it must be fairly young. Vegetation on the earlier mezzanine is similar to that developed elsewhere on lava flows of the 18th century.

Alae also was a compound crater (figs. 12.53, 12.54). It appears on aerial photographs that the older pit postdates Puu Huluhulu and the flows of Keauhou; it may therefore be younger than 350 years. The crater was partly filled by a lava lake capped by thinner flows, and then a new collapse formed an inner pit bordered by a western mezzanine. Phreatic explosions from the inner pit deposited a layer of lapilli 15 cm thick on the crater rim and ejected blocks up to 1 m in diameter, some of them to nearly 1 km west of the crater (Stearns and Clark, 1930, p. 143). The debris was partly covered by lava that extruded from a fissure on the northwest rim and flowed into the crater. This lava was overlaid by additional ejecta, possibly from the caldera eruption of 1790, which in turn was overlapped by more lava in 1840 that flowed across the mezzanine into the inner pit. On aerial photographs, the vegetation on a part of Alae mezzanine appears similar to that of 18th-century flows elsewhere, but this cannot be confirmed; the inner pit was floored by a new lava lake in 1963 (Peck and others, 1966), and the entire crater was buried in 1969–71 (Swanson and others, 1972).

Pauahi and Hiiaka are compound craters too (figs. 12.55, 12.56). Before it was buried in 1973, a small lava lake in the central pit of Pauahi supported vegetation typical of 18th-century age, while the lightly vegetated walls of the west pit appeared fresher. The outer compartment of Hiiaka is a sag instead of a sharp-rimmed

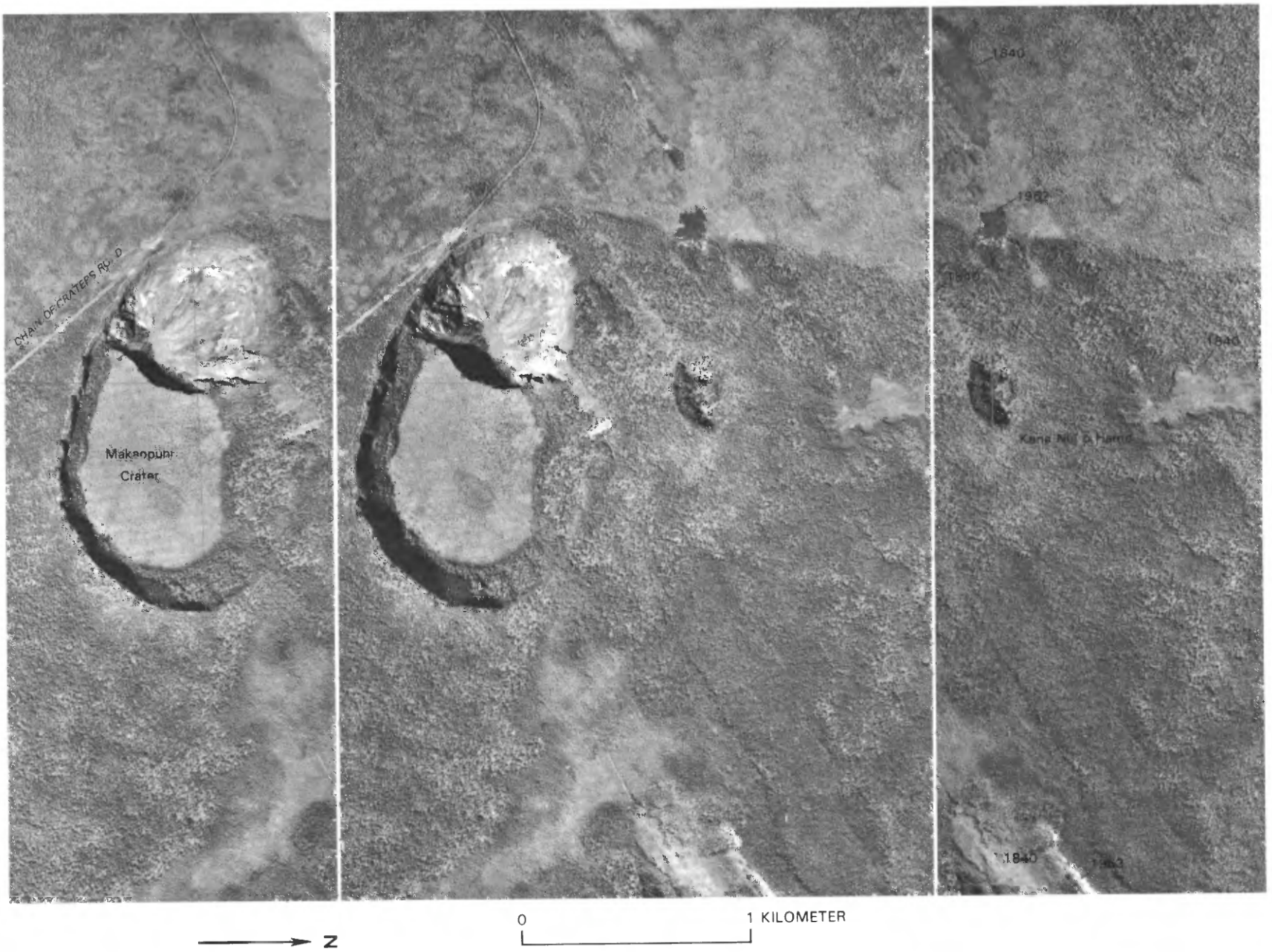

FIGURE 12.51.—Makaopuhi Crater area before much of it was covered by 20th-century lava flows. West pit of Makaopuhi in this view contains very small flat floor of ponded lava erupted in 1922; west pit was later filled and western part of mezzanine covered during eruptions from 1965 to 1974. Red dots, paleomagnetic sample sites above and below yellow tephra layer. Also shown in red are lines of profile for figure 12.52. Ovate, slightly darker area on eastern mezzanine is prehistoric lava pad extruded from fissure extending northeast across mezzanine. Northeast-trending lineament west of this pad is another fissure from which another pad was extruded in August 1972 (fig. 12.52). Stereo triplet prepared from frames 159–161, roll 12CC, USDA series EKL, 1965.

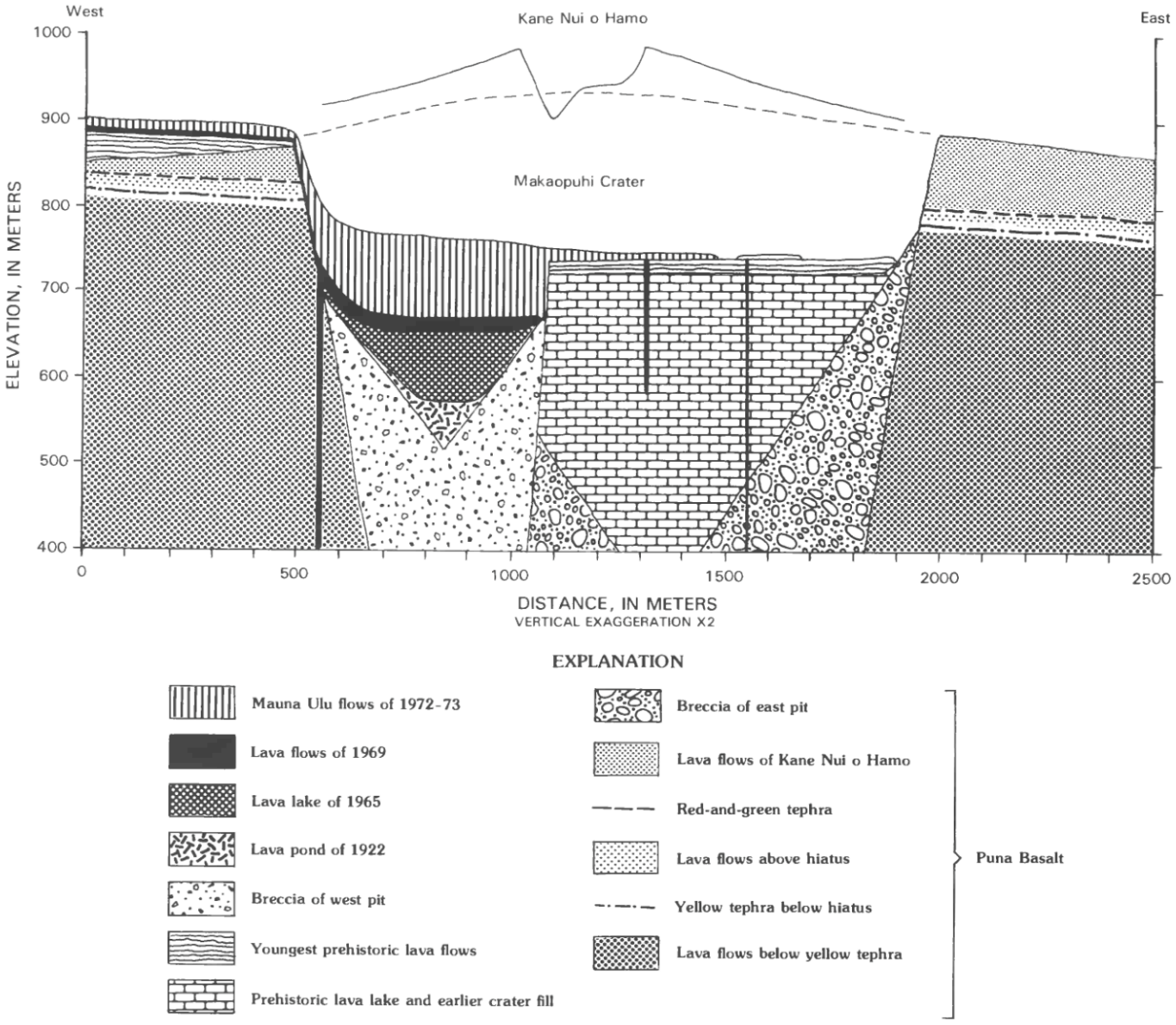

FIGURE 12.52.—Cross section of Makaopuhi Crater, along longer red line of figure 12.51. Also shown are inferred precollapse profile (dashed line) along this section, and present profile (solid line) across crater of Kane Nui o Hamo lava shield 800 m to the north (shorter red line of figure 12.51). Thick vertical lines are dikes that fed prehistoric lava pad on mezzanine (east; see fig. 12.51), eruptions of 1922 and 1965 (west), and eruption on mezzanine in August 1972 (center). Dike of 1972 is shown as rootless because it was probably fed laterally by Mauna Ulu lava ponded in west pit (Tilling and others, chapter 16).

crater (figs. 12.55, 12.56). Stearns and Clark (1930, p. 128) attributed the sagging to subsidence of an intact block preceding collapse of the inner pit, but other interpretations are possible. In the alternative shown in figure 12.56, the sag developed by thermal contraction of lava filling a buried crater, similar to the sag now developed at Alae. A buried crater of this sort could be a source of tephra now exposed in the wall of Pauahi (fig. 12.27).

The complex histories of several pit craters, and the coarse ejecta exposed in the walls of some, indicate that they have long been sites of repeated collapse and phreatic explosion. Nodes in the plumbing system may occur at these places, developed where Koae faults intersect the rift zone. Such nodes could form reservoirs for producing differentiated and hybrid magmas along the rift zone (Wright and Fiske, 1971; Swanson and others, 1976b, p. 28).

Though they are prehistoric, several of the simple craters and younger pits of the compound craters must be very young. They could have formed at the same time as a caldera collapse in or before 1790, all of them resulting from one drainage event lower along the

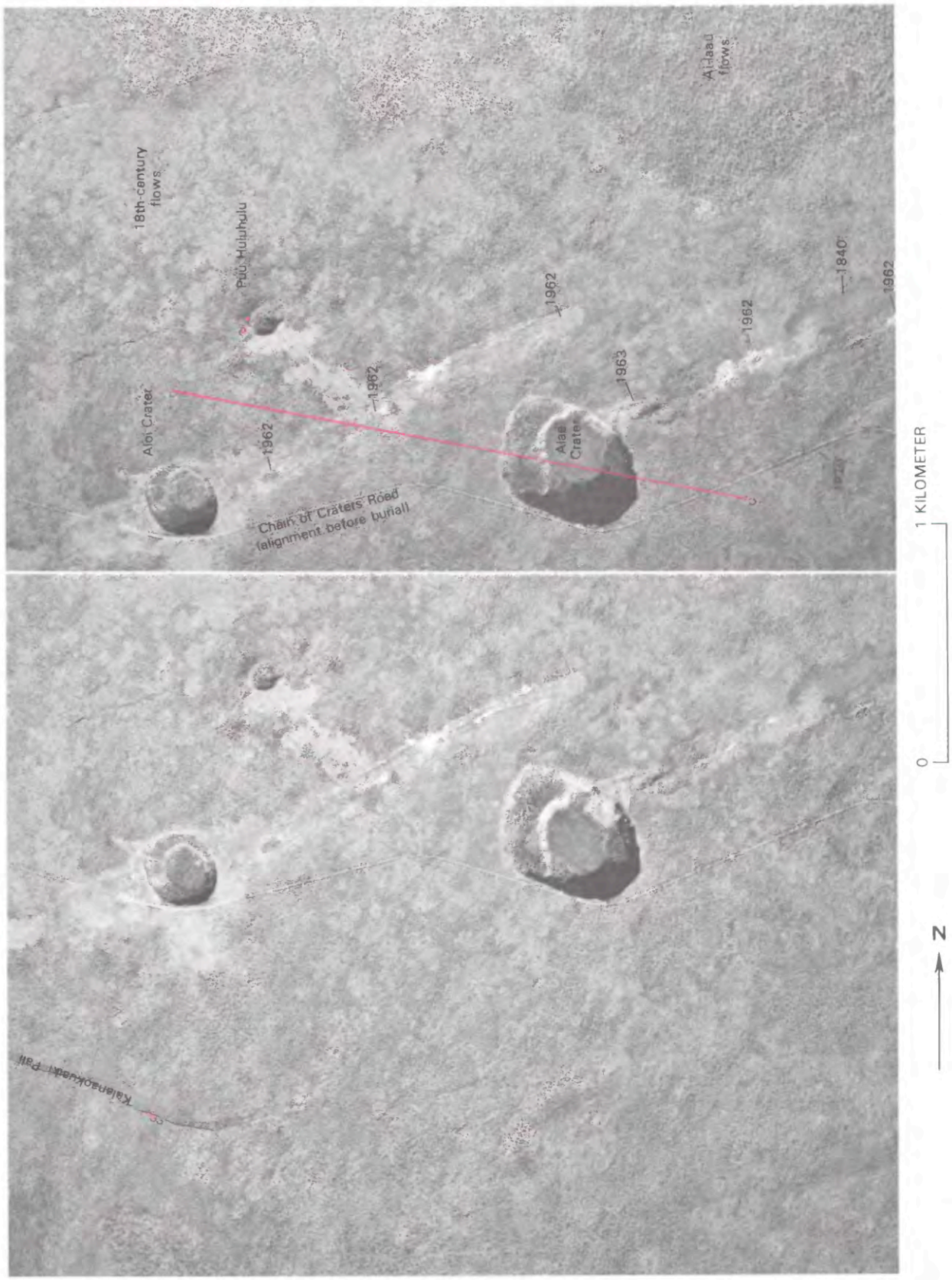

FIGURE 12.53.—Alae Crater, Aloi Crater, and Puu Huluhulu before craters were buried by growth of Mauna Ulu. Red dots, paleomagnetic sampling sites. Also shown in red is line of profile for figure 12.54. Stereo pair prepared from frames 174 and 175, roll 12CC, USDA series EKL, 1965.

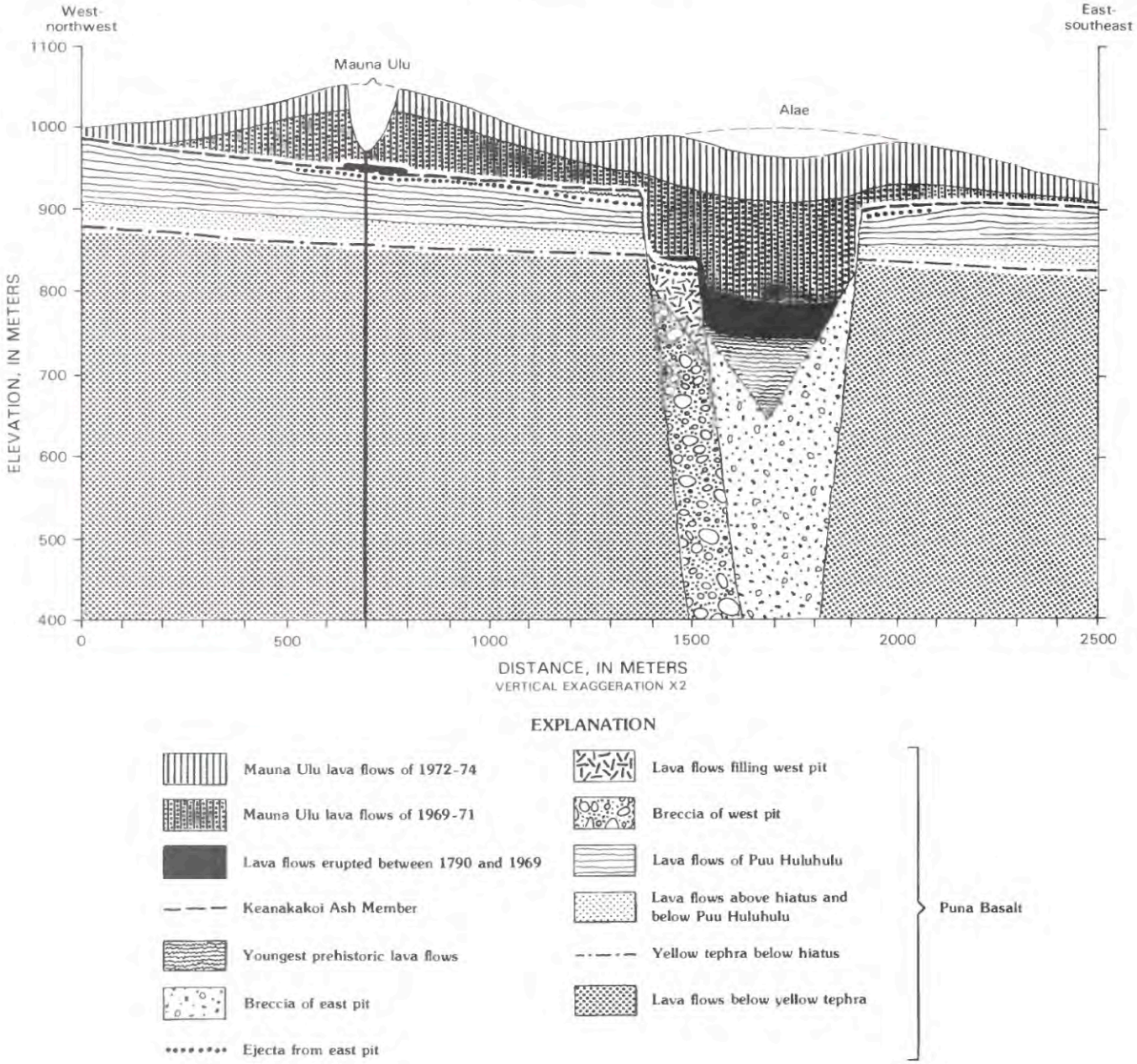

FIGURE 12.54.—Cross section of Mauna Ulu and buried Alae Crater, along line shown on figure 12.53. Dashed lines show profiles before crater formation on Mauna Ulu and sagging of lava shield above Alae Crater. Thick vertical line represents dike that fed Mauna Ulu. Hiatus and yellow tephra layer correlative with Uwekahuna Ash Member are inferred from their known occurrence in Makaopuhi Crater to east and Pauahi Crater to west. Thin layers of prehistoric ejecta and lava on rim of Alae are inferred from description by Stearns and Clark (1930); their thickness is exaggerated in this illustration.

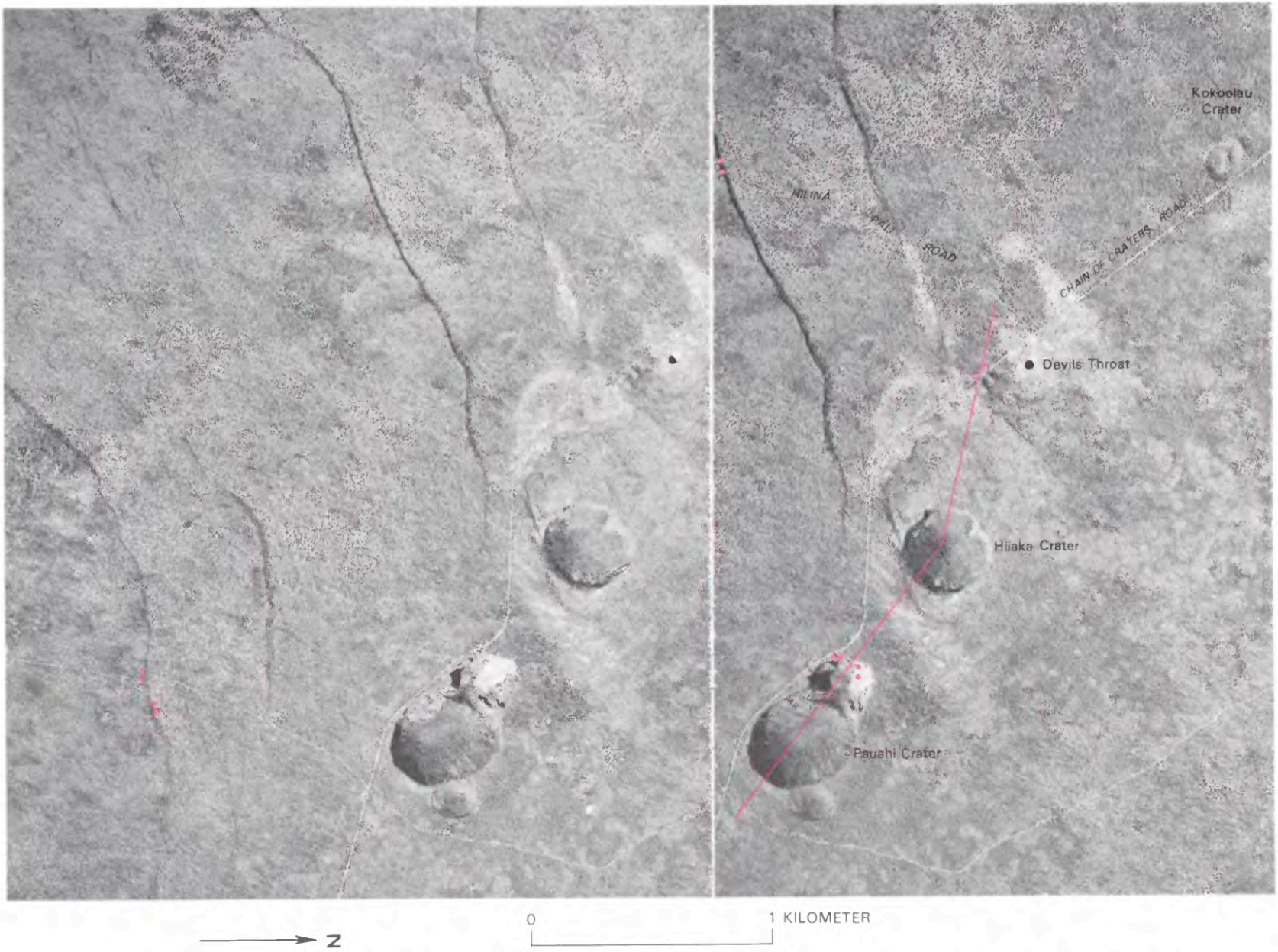

FIGURE 12.55.—Pauahi and Hiiaka before these craters were partly filled by lava during 1968–79. Larger central pit of Pauahi was floored by prehistoric lava lake. Pairs of red dots, paleomagnetic sample sites. Also shown in red is line of profile for figure 12.56. Stereo pair prepared from frames 188 and 189, roll 12CC, USDA series EKL, 1965.

east rift zone, but this has not been proved. Similar pits may form in the future, especially near sites of sustained eruption such as Mauna Ulu and Puu Oo.

SUMMIT ERUPTION OF A.D. 1790

Except for thin deposits of older and younger basaltic pumice at its base and top, the Keanakakoi Ash Member was produced by a series of explosions in 1790 (Decker and Christiansen, 1984). This eruption was still remembered well when Europeans first visited Kilauea in 1823, and it was notable for wiping out a detachment of Keoua's Puna army (Swanson and Christiansen, 1973). Deposited in quick succession were well-sorted vitric ash, less well sorted lithic-vitric ash, a local lava flow from a circumferential fissure, and poorly sorted lithic ash and blocks. Hawaiian accounts suggest that the main explosive phase continued for two or three days. The explosions were probably caused by rapid lowering of the summit magma column and entrance of subsurface water into the emptying magma conduits. Lowering of the magma column may have been associated with the voluminous eruptions of circa 1790 low on the subaerial east rift zone, but the relative timing of the summit and rift events has not been established.

It appears that the two most recent episodes of large caldera collapse and ash eruption were separated in time by about 1,500 years. Several smaller collapses and explosive eruptions could have occurred between them but have not yet been recognized.

AFTERMATH OF THE 1790 ERUPTION

More than 30 years passed between the eruption of 1790 and Ellis' visit in 1823. Little is known about this interval, but at some point eruptive activity had resumed at the summit, within the inner sink of the modern caldera. During this interval, lava fountains probably produced the golden pumice at the top of the Keanakakoi Ash Member (Sharp and others, chapter 15). By the time of Ellis' visit, the inner sink had filled with lava to within 160 m of the

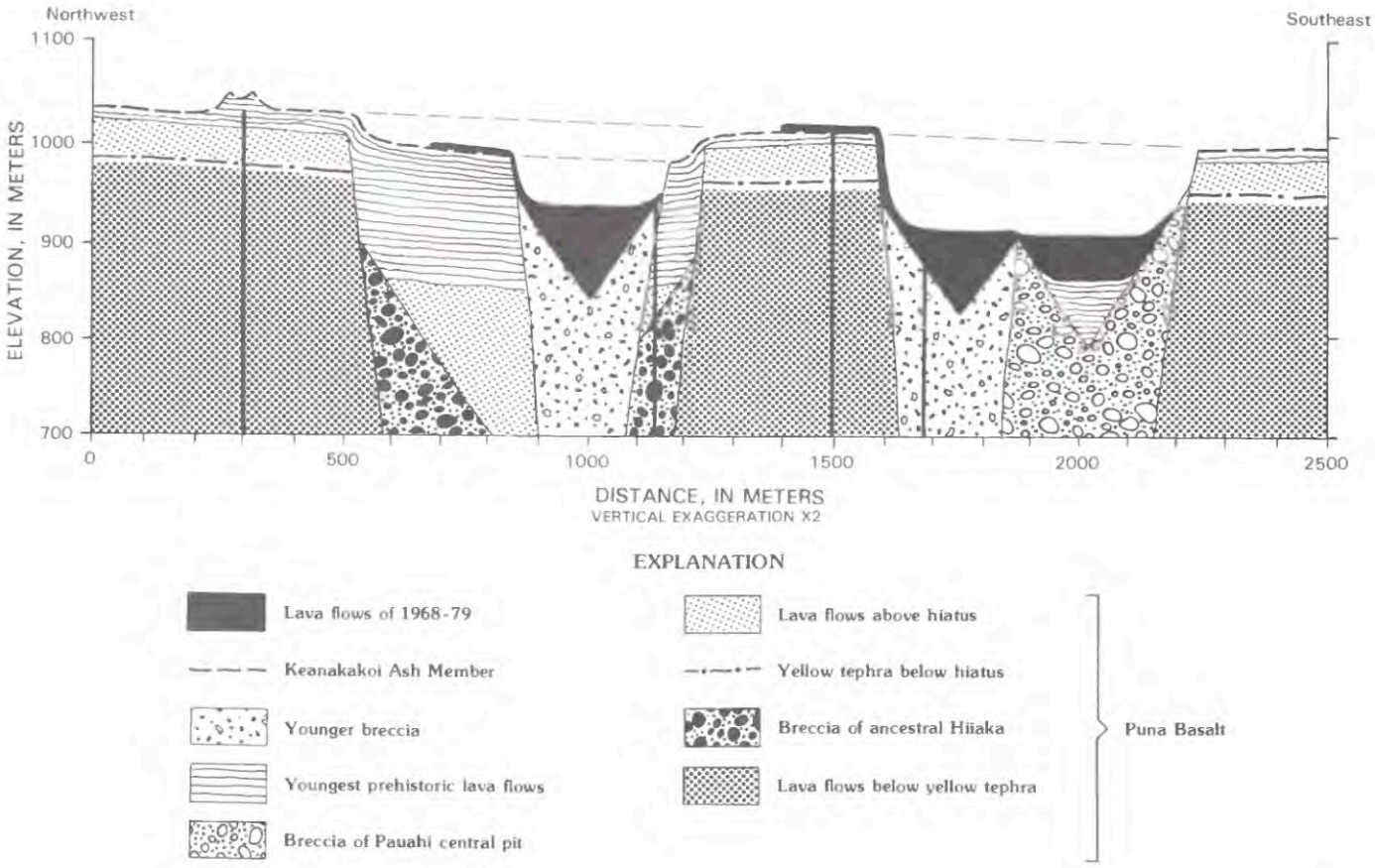

FIGURE 12.56.—Cross section through Pauahi, Hiiaka, and unnamed spatter cone near Devils Throat, along red line shown in figure 12.55. Ash and hiatus exposed in west wall of Pauahi have not been found in Hiiaka, where they are inferred to be hidden behind crater fill. Hiiaka is interpreted here as complex crater formed by two collapses, with earlier crater rim buried by prehistoric lava flows that sagged from thermal contraction. This has not been proved, however; other interpretations are possible. Ash and debris exposed in west wall of Pauahi may consist partly of Uwekahuna Ash Member ejected from Powers caldera, and partly of material ejected from local source such as older crater of Hiiaka. Dashed lines show profiles before sagging and collapse. Thick vertical lines represent dikes that fed younger lava flows.

northern rim, and then subsided again to leave a congealed terrace called the Black Ledge. This subsidence probably occurred during the southwest rift eruption of 1823, shortly before Ellis' visit. No other flank eruptions have been definitely tied to this interval, though some of the 18th-century flows may have been erupted then. Ellis' Hawaiian guides told him that several places had been overflowed by lava since the explosions of 1790. Other activity had occurred too, including a memorable earthquake and ground cracking at Kaimu.

HAWAIIAN TRADITIONS

Much of the Polynesian oral history has been lost, and many surviving fragments are contradictory, ambiguous, or unspecific. Some accounts still preserved, however, provide provocative comparisons with geologic information.

ELLIS' GENERAL ACCOUNT

The most authoritative summary was recorded in 1823 by Ellis (1827, p. 171–172) on the caldera rim. This history was given by Ellis' Hawaiian guides, according to whom Kilauea

> had been burning from time immemorial, or, to use their own words, 'mai ka po mai,' from chaos till now, * * * and had overflowed some part of the country during the reign of every king that had governed Hawaii: that in earlier ages it used to boil up, overflow its banks, and inundate the adjacent country—but that, for many kings' reigns past, it had kept below the level of the surrounding plain, continually extending its surface and increasing its depth, and occasionally throwing up, with violent explosion, huge rocks or red-hot stones. These eruptions, they said, were always accompanied by dreadful earthquakes, loud claps of thunder, with vivid and quick-succeeding lightning. No great explosion, they added, had taken place since the days of Keoua [1790]; but many places near the sea had since been overflowed, on which occasions they supposed Pele went by a road underground from her house in the crater to the shore.

Confirmation of the story was provided to Ellis (1827, p. 194) a few days later at Kaimu, along the southern coast of Puna, where

> the evenings we spent with the people of the place in conversation on various subjects, but principally respecting the volcano which we had recently visited. They corroborated the accounts we had before heard, by telling us it had been burning from time immemorial, and added, that eruptions from it had taken place during every king's reign, whose name was preserved in tradition, or song, from Akea, first king of the island, down to the present monarch.

This account is especially valuable because it is the earliest one known and was taken from local informants at Kilauea. As a result, it is the one least likely to have been distorted by distance, time, or Western preconceptions. But much uncertainty remains in its interpretation. It is difficult to say how much of it is a simple summary of witnessed events and how much is interpretation by Ellis of what was said to him or by Hawaiians of phenomena observed by them.

Especially troublesome is the possibility of Hawaiian interpretation, because evidence indicates that other traditions do include geologic inferences from the natural record. The Hawaiian account of Pele's successive homes agrees well with the progression of island volcanism, even though the sequence could not have been witnessed directly. Unless the agreement between fact and legend is coincidental, the legend must rest on inferences from nature by Hawaiians. If traditions could include inferences about the history of the archipelago they could also include inferences about the history of Kilauea.

Despite this uncertainty, however, Ellis' acount merits serious consideration. Hawaiians were probably living on Kilauea throughout the millenium in which most surficial lava flows were erupted, and they should have seen the eruptions. Widespread consistency in genealogies suggest that oral traditions can be very precise. It is worthwhile to compare Ellis' account with modern information.

Agreement between tradition and geologic information appears generally to be good. Tradition agrees well with the other evidence in stating that Kilauea had been active for a long time, had had frequent eruptions, had undergone a change in behavior from frequent overflows to summit confinement, and had had explosive eruptions.

Ellis' account is more specific than the other evidence in at least four ways. First, Ellis states that eruptions were so frequent as to occur during every king's reign, while the geologic record could permit dormant intervals of several decades or more. Second, Ellis says that the caldera developed gradually over some extended interval, while the geologic record permits sudden caldera development shortly before the explosive eruption of 1790. Third, Ellis says that explosive eruptions had occurred more than once and at intervals, while the geologic information requires no explosive eruptions between those of the Uwekahuna Ash Member (probably pre-Polynesian) and the Keanakakoi Ash Member in A.D. 1790 (Christiansen, 1979). Fourth, Ellis' account states that many coastal areas (on more than one occasion?) had been overflowed by lava since 1790, while the geologic evidence requires no such eruptions between 1790 and 1823. (Several flows in Puna and a few along the southwest rift zone could date from this interval, but the evidence available also permits them to be older.)

There are no definite contradictions between Ellis' account and currently available geologic evidence, but potential conflicts exist, especially in regard to the timing of the last summit overflows. While the tradition states explicitly that the summit had not overflowed "for many kings' reigns past," the paleomagnetic evidence indicates that such overflows had occurred as recently as the 17th century or even the early 18th century, within 100–150 years of Ellis' visit. This seems a rather short interval to include the reigns of many kings, and in fact Kalakaua's (1888, p. 31) history lists the reigns of only five kings of Hawaii between A.D. 1685 and 1824. Despite this potential disagreement and the uncertain derivation of Ellis' account, however, there are few concrete reasons to doubt the veracity of the tradition, and it appears to have potential value in supplying information not yet available from other kinds of evidence.

WESTERVELT'S EMBELLISHMENTS

Other traditions seem less reliable. Some cited by Westervelt (1916) give many details not included in Ellis' account. For example, Westervelt describes specific changes in the focus of summit eruptions, and particular explosive eruptions, not mentioned by Ellis. According to Westervelt (1916, p. 1–3):

> When Pele came to the island Hawaii, seeking a permanent home, she found another god of fire already in possession of the territory. Ai-laau was known and feared by all the people. *Ai* means 'the one who eats or devours.' *Laau* means 'tree' or a 'forest.'

Ai-laau was, therefore, the fire-god devouring forests. Time and again he laid the districts of south Hawaii desolate by the lava he poured out from his fire-pits.

* * * * *

He lived, the legends say, for a long time in a very ancient part of Kilauea, on the large island of Hawaii, now separated by a narrow ledge from the great crater and called Kilauea-iki (Little Kilauea). This seems to be the first and greatest of a number of craters extending in a line from the great lake of fire in Kilauea to the seacoast many miles away * * *.

After a time, Ai-laau left these pit craters and went into the great crater and was said to be living there when Pele came to the seashore far below.

In one of the Pele stories is the following literal translation of the account of her taking Kilauea:

'When Pele came to the island Hawaii, she first stopped at a place called Ke-ahi-a-laka in the district of Puna. From this place she began her inland journey toward the mountains. As she passed on her way there grew within her an intense desire to go at once and see Ai-laau, the god to whom Kilauea belonged, and find a resting place with him as the end of her journey. She came up, but Ai-laau was not in his home. Of a truth he had made himself thoroughly lost. He had vanished because he knew that this one coming toward him was Pele. He had seen her toiling down by the sea at Ke-ahi-a-laka. Trembling dread and heavy fear overpowered him. He ran away and was entirely lost. When Pele came to that pit she laid out the plan for her abiding home, beginning at once to dig up the foundations. She dug day and night and found that this place fulfilled all her desires. Therefore, she fastened herself tight to Hawaii for all time'

Elsewhere in this book, after quoting Ellis' account presented above, Westervelt (1916, p. 191–192) states that

When the crater was 'boiling up, overflowing its banks, and inundating the adjacent territory,' as the natives said, it poured out lava which became solid rock. As it went westward, the character of its overflow changed, becoming explosive, hurling out cinders and ashes instead of boiling lava, so that all the land, especially toward the south and west, is covered with volcanic ash.

Westervelt's account can be interpreted in many ways, one of which is the following: Long ago much of Kilauea was forested (because of a hiatus in summit overflows?), but then frequent overflows from the summit destroyed more and more of the forest. For a long time the eruptions were focused in the vicinity of Kilauea Iki, but eventually the site of eruption shifted to the west, somewhere within the perimeter of the present caldera. Eventually a series of eruptions occurred along the east rift zone, the site of eruption progressing uprift from the coast. As these eruptions occurred, the summit was shaken by tremors and a summit pool of lava drained away, leaving behind an empty, growing crater. Following a series of explosive eruptions, lava returned to the enlarged crater, which became a new site of long-sustained activity.

This account is highly provocative, and it is tempting to relate particular events of the tradition to events inferred from geologic evidence. However, this would be dangerous because the reliability of Westervelt's account is highly uncertain, for several reasons.

First, Westervelt cites no sources, though comments elsewhere in his book suggest that he had consulted Hawaiian-language newpapers of the late 19th century in Honolulu. With the sources unknown, there is no way to judge their reliability.

It appears that some material is Westervelt's own synthesis of several different accounts, and there is a strong possibility that his own preconceptions were incorporated. For example, the westward shift in the focus of summit volcanism may not have come from tradition but from his own understanding of summit events. A few decades earlier Dutton (1884, p. 121) had used geologic evidence to infer such a shift of the eruptive focus.

Westervelt's accounts could have been earlier degraded by Hawaiian storytellers, especially if his sources were newspaper accounts from the late 19th century in Honolulu, a time and locale far removed from the Kilauea of pre-Western influence. During the disintegration of Polynesian society following Captain Cook's arrival, an apparently well-preserved oral history was adulterated and partly lost. It is possible, for example, that the westward shift in eruptive activity really was mentioned by Westervelt's sources, but that these sources themselves were influenced by Dutton's interpretation.

Finally, Westervelt's account is inconsistent with traditions given elsewhere. Other sources, for example, describe Pele's arrival in very different ways and make no mention at all of Ai-laau. Until the ancestry of Westervelt's account can be established and evaluated, it can be given little credence. This is also true of many other provocative traditions.

SOME OTHER TRADITIONS

Though specific details of most traditions cannot be taken as literal truth, some traditions probably allude to real eruptions, especially those traditions Ellis recorded as associated with specific lava flows. Examples are the late prehistoric Keauhou flows west of Kealakomo (associated with a legendary conflict between Pele and Kamapua'a; Ellis, 1827, p. 183), the vent and flows of Kaholua o Kahawali (tied to the legend of Kahawali; Ellis, 1827, p. 207–210), and a flow formerly forming Cape Kumukahi (associated with Pele's rejection by the Puna Chief Kumu-kahi; Westervelt, 1916, p. 27–28). Some traditions state a time in history for a particular lava flow, for example, that Pele's action occurred during the reign of a particular king whose dates have been inferred from well-kept genealogies. Such statements could provide especially valuable checks on the geologic evidence, but even here confusion can arise.

An example of possible contradition in the most authentic traditions concerns the age of Puu Huluhulu (fig. 12.57), which paleomagnetic evidence suggests is 350 to 500 years (9B913). Seaward of Puu Huluhulu and of similar age are the Keauhou lava flows. Ellis (1827, p. 183) notes this flood of lava as dating from Pele's struggle with Kamapua'a, which Kalakaua (1888, p. 140) attributes approximately to the year A.D. 1200 in the reign of Kamaiole. But Ellis' comments elsewhere (p. 182) suggest a different age for Puu Huluhulu:

Within a few miles of Kirauea, we passed three or four high and extinct craters. One of them, Keanakakoi, the natives told us, sent forth, in the days of Riroa, king of Hawaii about fourteen generations back, most of the lava over which we were travelling. The sides of these craters were generally covered with verdure, while the brown irregular-shaped rocks on their indented summits frowned like the battlements of an ancient castle in ruins.

The crater of Liloa's reign cannot be the pit now known as Keanakakoi because Ellis (1827, p. 179) had earlier clearly stated that the only deep crater he saw besides the caldera was Kilauea Iki; he saw no others, though his guides said there were many in the

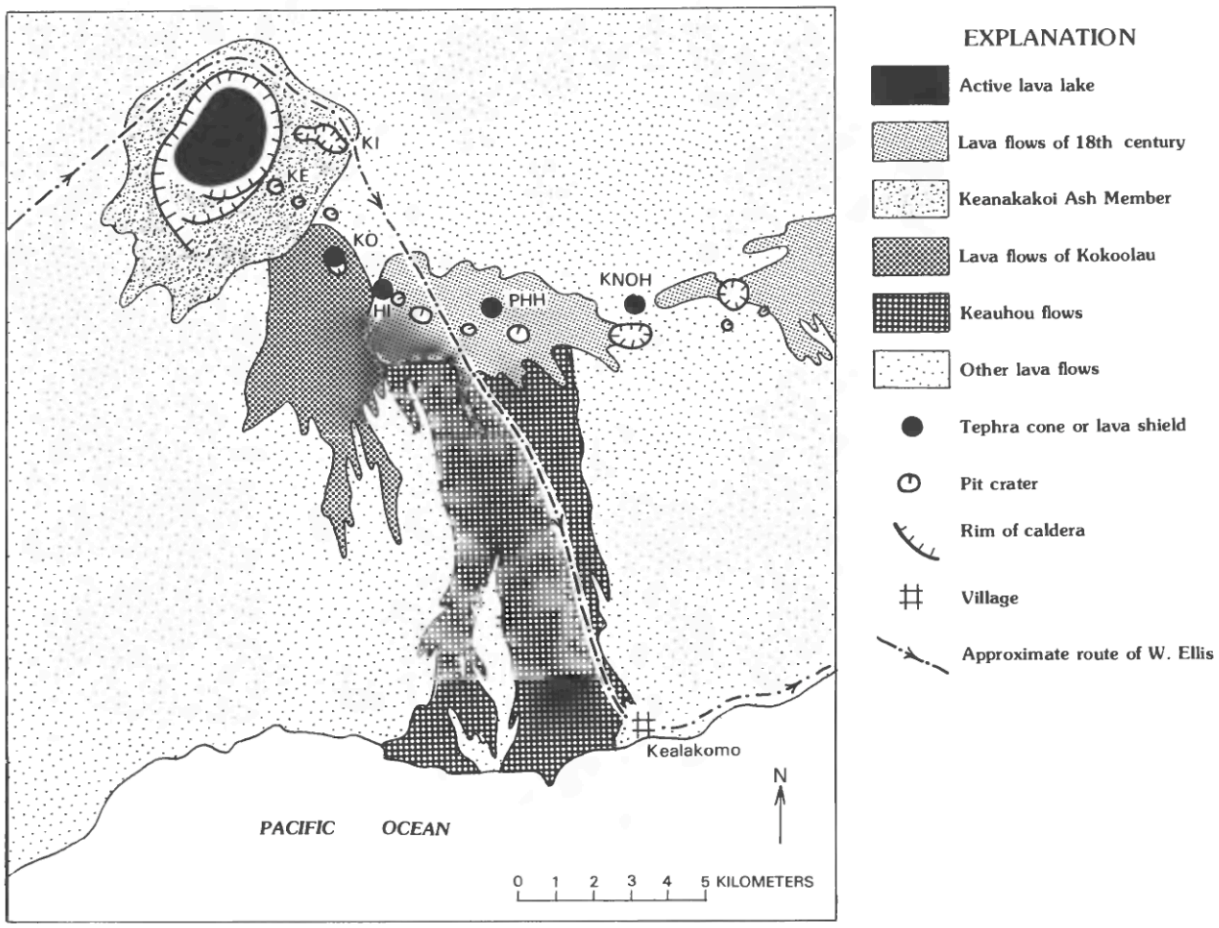

FIGURE 12.57.—Approximate route and features probably observed by William Ellis on his trek from Kilauea caldera to Kealakomo in 1823. He saw "three or four high and extinct craters" but no "deep" craters besides Kilauea Iki, though he was told that others were nearby (Ellis, 1827, p. 179, 182). Geographic features: KI, Kilauea Iki; KE, Keanakakoi; KO, Kokoolau; HI, Hiiaka; PHH, Puu Huluhulu; KNOH, Kane Nui o Hamo.

neighborhood. Moreover, Ellis described this and some other craters as high-standing edifices. Along the route that Ellis travelled from the caldera to the coast are three such features: Kokoolau, Puu Huluhulu, and the spatter cone near Devils Throat. Ellis would also have seen Kane Nui o Hamo in the distance.

If Puu Huluhulu was the crater at issue it would contradict Ellis' other comments because Liloa's reign occurred long after the inferred time of conflict between Pele and Kamapua'a. According to Kalakaua's (1888) chronology Liloa preceded Liholiho (reigning during Ellis' visit of 1823) by 14 reigns, while Kamaiole preceded Liloa by another eight reigns. Kalakaua believed Kamaiole to have reigned around A.D. 1200 and Liloa around A.D. 1475. While Liloa's reign falls into the range indicated by the paleomagnetic data (350–500 years B.P.), Kamaiole's reign does not. If Puu Huluhulu is the source of flows tied to Kamapua'a, the two traditions are in conflict. Moreover, Kane Nui o Hamo should not be the active vent of Liloa's reign because it is clearly older than Puu Huluhulu.

Other interpretatiouns are possible. The Pele-Kamapua'a tradition could refer to Kane Nui o Hamo, whose lava flows have a paleomagnetic direction consistent with the dates assigned to Kamaiole's reign. Ellis clearly stated, however, that the Pele-Kamapua'a conflict was associated with the young, dark lava flows west of Kealakomo (the Keauhou flows), and these flows could not have come from Kane Nui o Hamo; the flows from Kane Nui o Hamo are the older ones upon which Kealakomo sat.

Another alternative would have Kokoolau as the vent of Liloa's reign and Puu Huluhulu the older source of the Kamapua'a flows. This would preserve the chronology implied by the traditions; but then both Kokoolau and Puu Huluhulu would be older than expected from their paleomagnetic data, unless the reigns were briefer than believed by Kalakaua.

From the discussion above it should be clear that caution must be used in extracting eruption history from the traditions. In fact, the most useful comparisons between traditions and geologic information may proceed in the opposite direction, the geologic data providing a firmer base for reconstructing the social history.

HISTORICAL ERUPTIONS

The historical activity of Kilauea has been reviewed in detail several times previously (Dana, 1890; Brigham, 1909; Hitchcock, 1909; Stearns and Clark, 1930; Stearns and Macdonald, 1946; Macdonald and Abbott, 1970). Only a brief summary is given here.

LONG-SUSTAINED SUMMIT ERUPTIONS, 1823–1924

Though brief references to Hawaiian volcanism were recorded in the late 18th century (Ledyard, 1783; Beaglehole, 1967; Vancouver, 1798; A. Menzies, in Hitchcock, 1909), the historical record really began with Ellis' (1827) description of Kilauea in 1823. At that time a sustained eruption was in progress, and most of the inner sink was occupied by an active lava lake standing about 270 m below the north rim. About 90 m above the lake surface was the Black Ledge a terrace of freshly congealed lava thought to represent the level reached by caldera filling a short time before. The caldera floor probably had subsided in the spring of 1823, when a brief but voluminous eruption from the Great Crack flooded the western south flank with lava (the Keaiwa flow, which reached the sea from Kapaoo Point to Waiapele Bay). The subsidence of the caldera floor apparently did not generate large explosions at the summit, though small phreatic explosions deposited tephra at two places along the Great Crack (Stearns, 1926).

Continued activity after 1823 refilled the caldera to a level about 15 m above the Black Ledge by 1832, when a small eruption occurred on Byron Ledge and the caldera floor subsided again, this time about 300 m (Goodrich, 1833). Filling then recommenced, and in 1834 the caldera was much the way it had been in 1823, with an inner pit 113 m deep surrounded by a black ledge (Douglas, 1905). Continued activity filled the pit and apparently overflowed the black ledge so that it was no longer visible late in 1838 (Strzelecki, 1845). At this time the activity had become confined to 5 lava lakes, the largest of them called Hau-mau-mau in the southwestern part of the caldera on the site of the pit crater now called Halemaumau.

Vigorous summit activity in the spring of 1840 was followed by another subsidence of the caldera floor and a rapid series of brief eruptions along the east rift zone. The last eruption from the lower east rift zone was especially voluminous and sent surface-fed lava flows northeastward from the vicinity of Pahoa to the coast at Nanawale (Coan, 1841). Shortly afterward Kilauea was visited and described by members of the United States Exploring Expedition (Wilkes, 1845; Dana, 1849). The subsided inner sink at this time was about 100 m deep and was surrounded by a new black ledge about 480 m wide rising to about 180 m below the western caldera rim. By 1846 the inner basin had filled again (Dana, 1850), and by 1848 a lava shield at the site of Halemaumau had grown nearly as high as the lowest part of the caldera rim (Coan, 1851).

The next subsidence of the caldera floor occurred in 1868, when large earthquakes shook the southern part of Hawaii and simultaneous eruptions occurred from Mauna Loa and Kilauea (Coan, 1868). One Kilauea outbreak produced a chain of small lava pads near the distal end of the northern strand of the upper southwest rift zone. Another small eruption from Byron Ledge fed a lava flow that ponded on the floor of Kilauea Iki. An area about 1,900 m wide on the central caldera floor sagged about 100 m, and a deeper conical pit about 900 m wide and about 200 m deep developed at its southwest end at Halemaumau (Hitchcock, 1909). The pit again filled, and by 1874 a lava shield at Halemaumau had once again grown to about the elevation of the southern caldera rim (Coan, 1874). Minor subsidences in and around Halemaumau occurred again in 1879, 1886, 1891, and 1894 (Hitchcock, 1909). None of those episodes was associated with known eruptions from the rift zones, though some undated post-1790 flows south of Mauna Iki (fig. 12.5*B*; Holcomb, 1980b) could have been erupted at one of those times.

The subsidence of 1894 was followed by 13 years of dormancy and very subdued, episodic activity within the pit of Halemaumau (Hitchcock, 1909). In 1908 the activity once again became more vigorous, and it was nearly continuous until 1924, with minor subsidences of the lava column occurring in 1916, 1919, 1922, and 1923 (Jaggar, 1947). The 1919 subsidence was followed by the 1919–20 eruption of Mauna Iki along the southwest rift, the first sustained eruption along either rift zone during the historical interval and probably the first since the Heiheiahulu eruption of circa 1750. The 1922 subsidence was associated with small eruptions from Makaopuhi to Napau, and the 1923 event was followed by another small eruption between Makaopuhi and Alae. The summit activity once again built a broad lava shield that occupied the entire inner sink of the modern caldera, with Halemaumau at its summit.

INTERMITTENT SUMMIT AND FLANK ERUPTIONS, 1924–1968

The century-long interval of nearly continuous activity in the caldera ended in 1924 (Jaggar and Finch, 1924; Stearns, 1925). In the spring of that year an 80-m drop of the magma column was followed by a swarm of earthquakes that migrated from the summit along the east rift zone past Kapoho. Though much ground deformation developed near Kapoho, a subaerial eruption did not occur; a submarine eruption may have occurred somewhere beyond Cape Kumukahi. Renewed subsidence of the magma column at Halemaumau was then followed by 17 days of repeated phreatic explosions and collapse of the caldera floor around Halemaumau.

Lava returned to Halemaumau shortly after the 1924 explosions ceased, but instead of being sustained the activity was now episodic. A series of seven brief eruptions in the next 10 years (Jaggar, 1947) reduced the depth of Halemaumau from 390 to 150 m, and then no eruptions occurred for 18 years, from 1934 to 1952. Sustained eruption from June to November of 1952 filled Halemaumau with another 120 m of lava. A brief eruption in May–June 1954 added 6 m of lava in Halemaumau and a thin lava flow on the caldera floor to the east (Macdonald, 1955).

Then, after at least 150 years of infrequent eruption and 33 years of no eruption, the subaerial part of Kilauea's east rift zone resumed frequent activity in February–May 1955 with a series of eruptions along its lower segment (fig. 12.58*A*; Macdonald and Eaton, 1964). These were followed by a sustained eruption in Kilauea Iki in 1959 and then by eruptions from the middle and lower segments of the east rift zone in January–February 1960 (fig. 12.58*B*; Richter and others, 1970). Brief eruptions at Halemaumau in February–March 1961 were followed by a series of outbreaks at 13 places along the middle and lower east rift zone in September 1961 (Richter and others, 1964), and further eruptions from the upper and middle east rift zone occurred in December 1962, August 1963, and March and December 1965 (fig. 12.58*C*; Moore and Krivoy, 1964; Peck and others, 1966; Fiske and Koyanagi, 1968; Wright and others, 1968). A sustained eruption then occurred in Halemaumau from November 1967 to

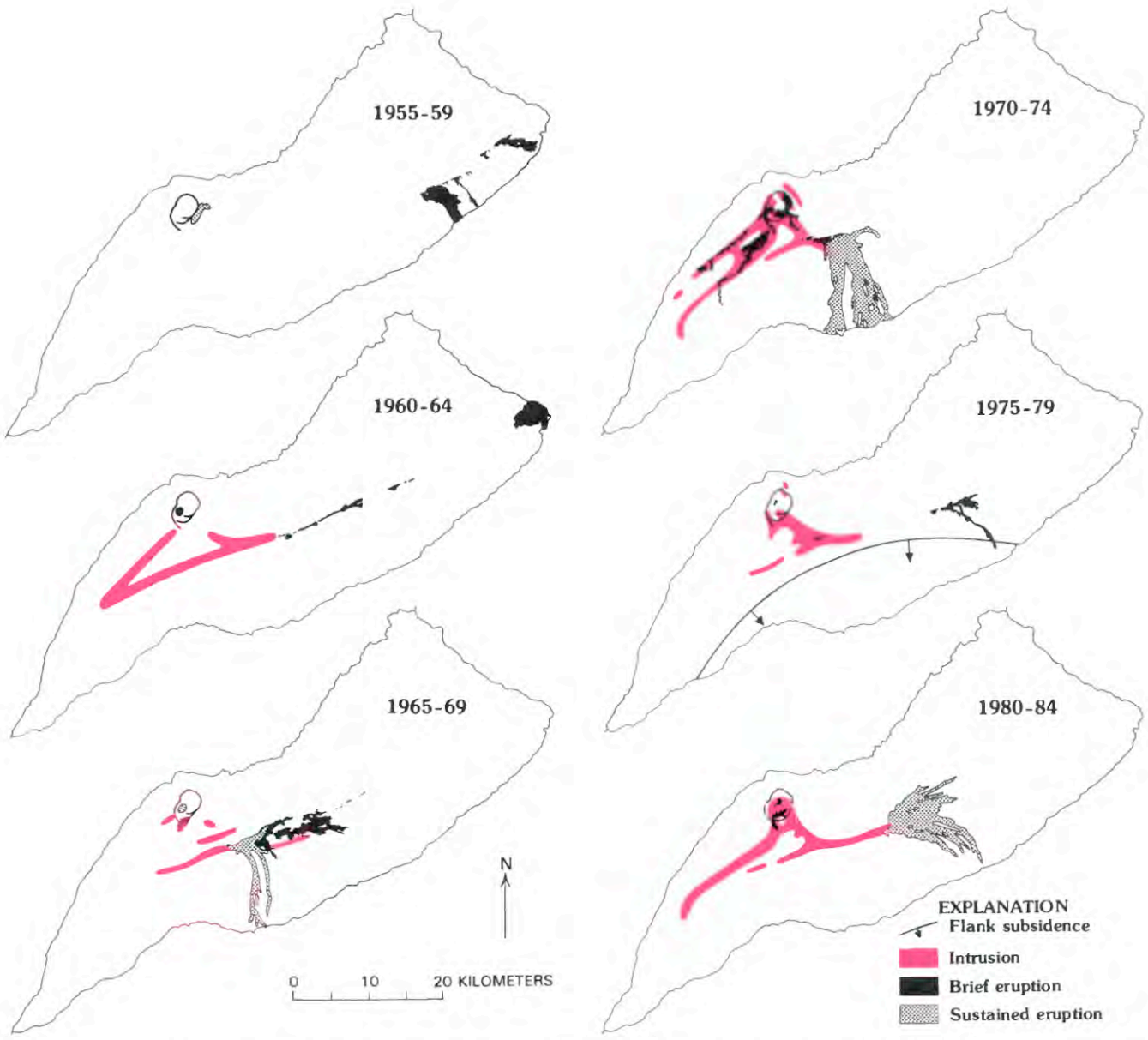

FIGURE 12.58.—Lava flows and intrusions during the interval 1955–1984 at Kilauea. Intrusions since 1962 are inferred from locations of shallow earthquake swarms compiled by Klein and others (chapter 43).

July 1968 (Kinoshita and others, 1969). This was the last sustained eruption in the summit region; sustained activity since then has occurred only along the east rift zone.

FREQUENT AND SUSTAINED FLANK ERUPTIONS, 1968–1985

The 1967–68 summit eruption was followed by a succession of brief eruptions from the upper and middle east rift zone in August and October 1968, and February 1969 (Moore and Koyanagi, 1969; Jackson and others, 1975; Swanson and others, 1976b). While the flank eruptions of 1955–1963 were widely distributed along the east rift zone and interspersed with sustained eruptions at the summit, the 1968–69 eruptions were concentrated along a short segment of the rift zone between Hiiaka and Napau pit craters. As the locus of eruptions contracted, the intervals between eruption decreased to a few months. The sequence culminated in a sustained eruption that began in May 1969 and continued, with brief interruptions, until June 1974, building the lava shield of Mauna Ulu (figs. 12.34, 12.35, 12.58*D*; Swanson and others, 1979; Tilling and others, chapter 16). An interruption in the second half of 1971 saw two brief eruptions from the summit and northern strand of the upper southwest rift zone (Duffield and others, 1982). Other interruptions saw brief eruptions higher up the east rift zone in May and November 1973 (Tilling and others, chapter 16). The final cessation of activity at Mauna Ulu in June 1974 was followed by brief eruptions from the summit and middle strand of the upper southwest rift zone in July, September, and December 1974.

A magnitude 7.2 earthquake and subsidence along the south coast on November 29, 1975 (fig. 12.58*E*; Tilling and others, 1976) was followed by episodes of summit deflation and rift intrusion in June, July, and August 1976 and February 1977 (Dzurisin and others, 1980) and then a brief eruption from the middle east rift zone in September 1977 (Moore and others, 1980). An intrusion of magma into the upper east rift zone in May 1979 was followed by a brief eruption at Pauahi and vicinity in November 1979, and five more intrusive episodes along the upper east rift zone in March (two episodes), August, October, and November 1980 (Dzurisin and others, 1984; Banks and others, 1981). Activity then shifted to the southwest rift zone, with intrusive episodes occurring there in January and August 1981 and June 1982. Brief eruptions occurred at the summit in April and September 1982 (Banks and others, 1983).

Following the 1982 summit eruptions, activity shifted once again to the east rift zone. An intrusion into the upper east rift zone in December 1982 was followed in January 1983 by an eruption near Puu Kahaualea on the middle east rift zone. That eruption was sustained, building a vent edifice called Puu Oo (Wolfe and others, chapter 17); it still continues at this writing in March 1986.

SUMMARY OF ERUPTIVE HISTORY

Kilauea saw subaerial shield growth punctuated by large explosions 100,000–10,000 years ago (Hilina Basalt and Pahala Ash); long-sustained summit eruptions and briefer rift eruptions 10,000–2,000 years ago (scattered kipukas); sustained eruptions from the summit and rift zones 2,000–1,500 years ago; caldera collapse and filling 1,500–1,100 years ago (Uwekahuna Ash Member of the Puna Basalt and hiatus); extensive caldera overflows and numerous rift eruptions, with no patterns of summit-flank interrelation yet discerned, 1,000–350 years ago (Volcano, Kalue, Ai-laau flows); sustained summit activity followed by extensive rift eruptions accompanying caldera collapse, followed by summit explosion, 350–200 years ago (Observatory flows, Keanakakoi Ash Member of Puna Basalt); and long-sustained summit eruption followed by frequent rift eruptions during the last 200 years (historical records).

The recent eruption history is summarized in figure 12.59. About 1,500 years ago the Powers caldera developed, truncating lava flows assigned paleomagnetically to the interval 2,000–1,500 years B.P. The Uwekahuna Ash Member was draped onto the rim and step faults of the caldera. Little is known about Kilauea's eruptions of about 1,500–1,100 years B.P.; only a few flows along the rift zones are known from this interval, and the summit region was remarkably devoid of eruptions outside the Powers caldera. Unless the magma supply was cut off during this interval, most of the eruptive activity must have been confined to the caldera and to submarine parts of the volcano. The Powers caldera began to overflow about 1,200–1,100 years ago and continued to do so intermittently until the 18th century. These overflows covered much of Kilauea's surface. The overflows on different flanks have different ages, indicating that activity was concentrated on one side of the summit for a few decades or centuries and then shifted to another side to cover a different sector. Progressive time relations between summit activity and rift activity are not yet resolved during this interval.

Such progressions do appear beginning about 500–350 years ago. Although paleomagnetic dating does not yet resolve a summit-rift progression at that time, traditions cited by Westervelt (1916) suggest that long-lived activity at the Ai-laau vent was followed by rift eruptions and summit collapse, which were in turn followed by sustained activity at the Observatory vent.

The Observatory activity was followed by many brief eruptions and a few sustained eruptions along both rift zones, especially the east rift zone. This flurry of flank eruptions must have been accompanied by growth of the modern caldera, much of which postdates the Observatory shield. Caldera collapse climaxed with phreatomagmatic eruption of the Keanakakoi Ash Member in A.D. 1790.

Following the 1790 eruption, Kilauea's behavior changed again, and for more than a century almost all subaerial activity was confined to the caldera. During this interval, only two large flank eruptions are known, in 1823 and 1840, wheras activity within the caldera was sustained almost continuously.

Kilauea's famous 19th-century pattern of continuous summit activity ceased in 1924, possibly following a submarine eruption from the east rift zone that coincided with summit collapse. Since then summit eruptions have been infrequent and relatively brief, while eruptions from the rift zones have become more frequent and more sustained.

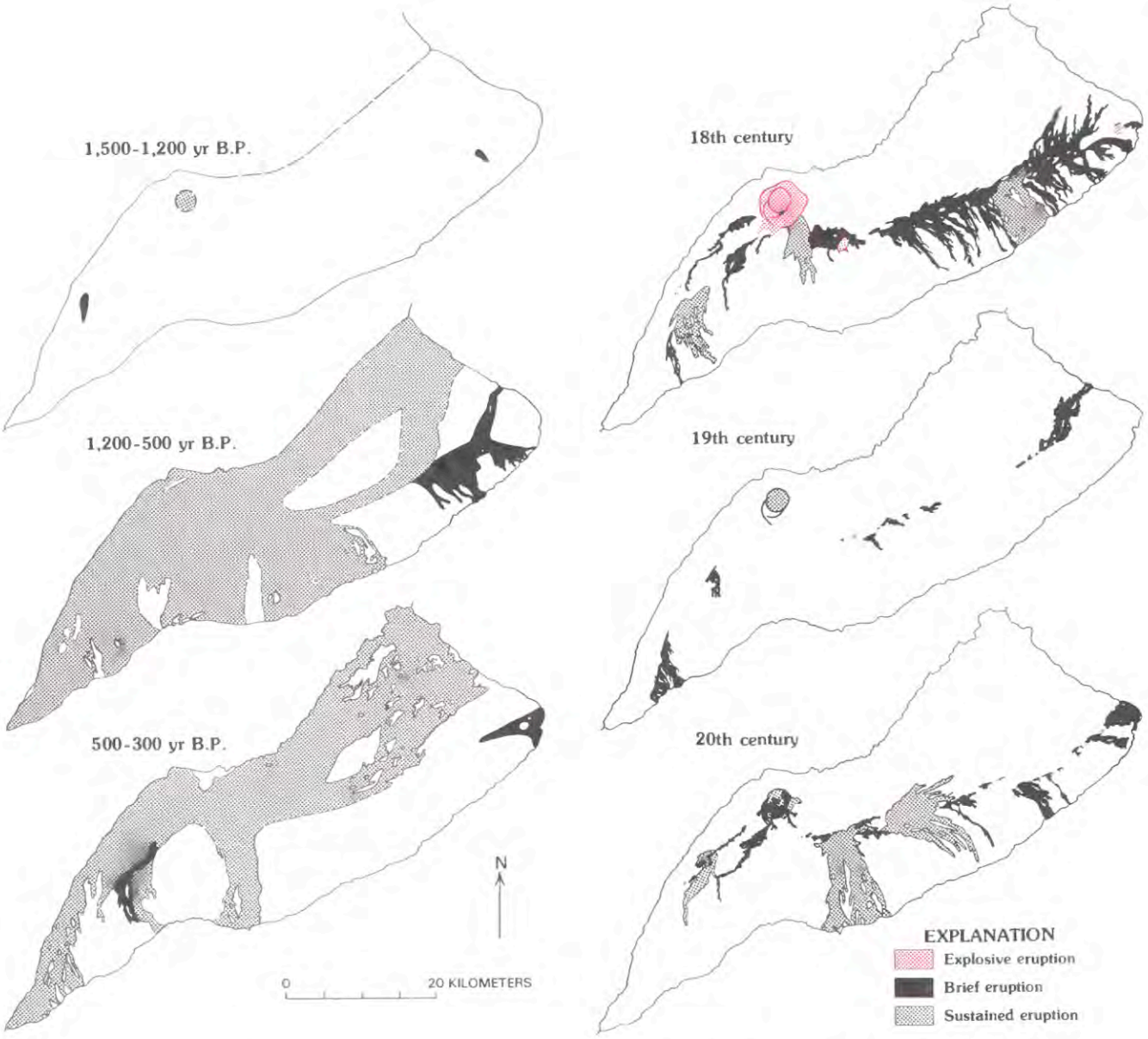

FIGURE 12.59.—Series of maps summarizing Kilauea's eruption history during the last 1,500 years, generalized from information in figures 12.5, 12.6, and 12.8.

MODELS FOR LONG-TERM BEHAVIOR

It may be useful here to speculate a little about the causes of temporal variation in eruptive behavior. Those causes will be a topic of future research because they may lead to better eruption forecasts.

Many models can be visualized, and they can be classified in various ways. For example, we can distinguish evolutionary, cyclical, and steady-state models differing in their forecasting utility.

A cyclical model is shown in figure 12.60. This caldera-dominated model features shifts in magma storage as successive calderas form and fill. In this model caldera collapse arises from changes in magma plumbing, and collapse in turn causes changes in the plumbing, acting as a feedback mechanism of an oscillatory system. Kilauea's history between about 1,500 and 200 years B.P. could represent one long cycle, and its history since 200 years B.P. could represent another shorter one, with the volcano's current state corresponding to stage 2 or stage 3 of the model (fig. 12.60).

Another cyclical model is shown in figure 12.61. This slumping-dominated model focuses on Kilauea's unbuttressed south flank, which the caldera model ignores. Eruptive behavior in this model responds to changes in magma storage arising from flank deformation. It was suggested more than 20 years ago that magma storage in the rift zones is controlled by recurrent slumping of the south flank (Moore and Krivoy, 1964). Later it was concluded from the timing

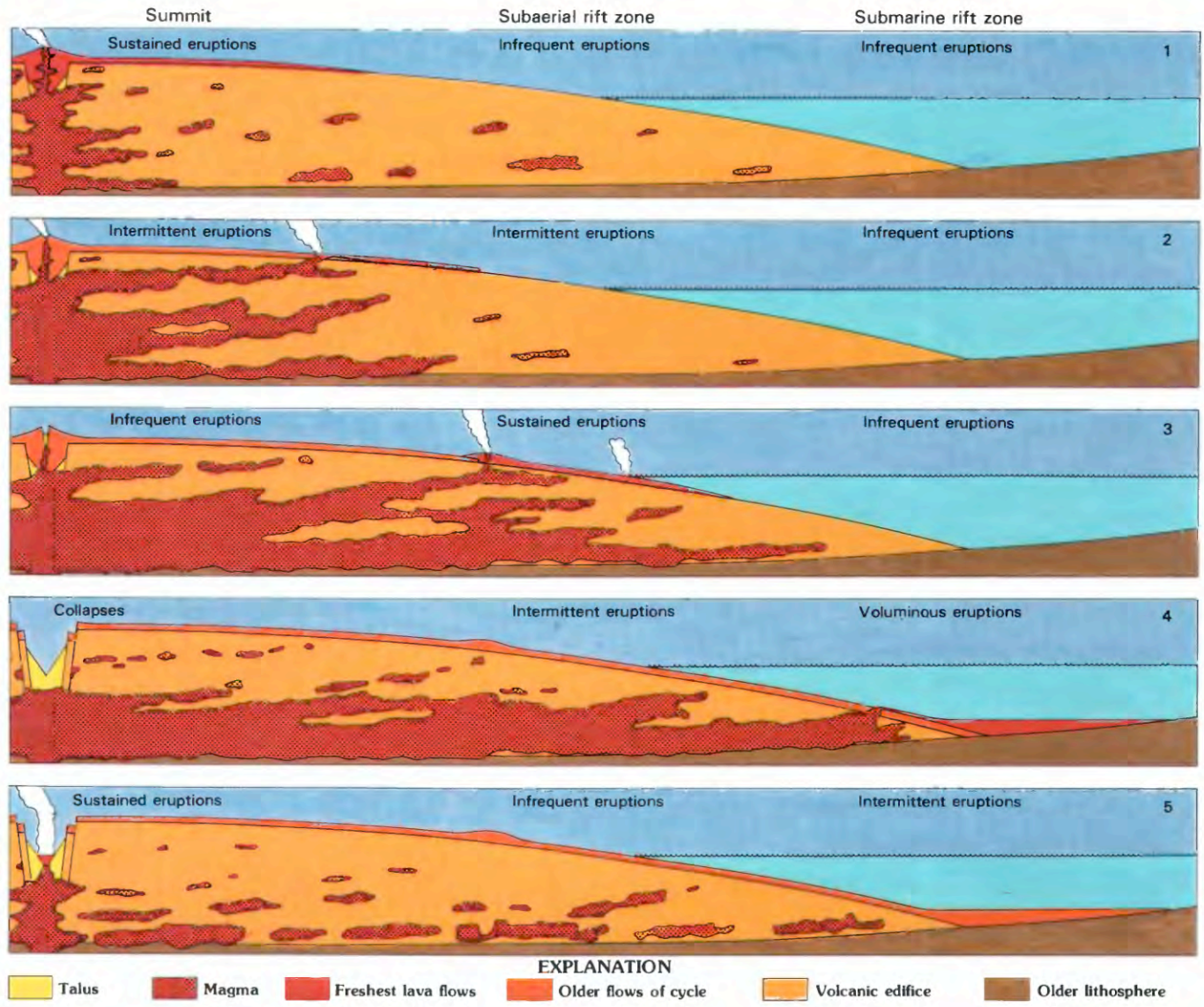

FIGURE 12.60.—Cyclical model for long-term behavior of Kilauea, based on repeated episodes of caldera collapse and filling. Schematic longitudinal profiles of rift zone show five stages in cycle, which could represent dynamic equilibrium between hydrostatic, thermal, and frictional factors. **Stage 1.** Eruptions are long-sustained and restricted to caldera, filling it so that most magma is stored beneath summit. As magma column rises, however, dikes are injected laterally under increasing head and penetrate into rift zones. **Stage 2.** Summit eruptions are less sustained and rift eruptions more frequent as more magma is diverted into rift zones. **Stage 3.** As better continuity is developed in plumbing of rift zone, longer eruptions occur farther from summit. As lava is erupted at lower elevations, magma column subsides beneath summit, and caldera-filling lava slowly cools. **Stage 4.** Voluminous eruptions from rift zones drain magma from upper parts of edifice, and collapse ensues. Collapse at summit rejuvenates caldera, and collapse along rift zones reduces continuity of their plumbing systems. **Stage 5.** Magma rising from deep beneath summit now finds its easiest escape into newly deepened caldera; activity is once again sustained within caldera, and continuity is further reduced in rift plumbing system as dikes solidify.

of flank deformation that slumping is a passive response to forceful intrusion of magma into the rift zones (Swanson and others, 1976a). But that conclusion was based on observations of just the past century; long-term changes in flank behavior might accompany long-term changes in eruptive behavior. Some intervals might be dominated by forceful intrusion and passive deformation and other intervals by active slumping and permissive intrusion. The true state of the edifice might be a quasi-equilibrium perturbable in either direction, with feedback mechanisms forcing an oscillation.

Still other models could be fundamentally cyclical but made complex from the interplay of various mechanisms. For example, slumping cycles and caldera cycles could both operate, independently or in rhythm. If episodes of slumping occurred more often than episodes of caldera collapse, with each perturbation disrupting the

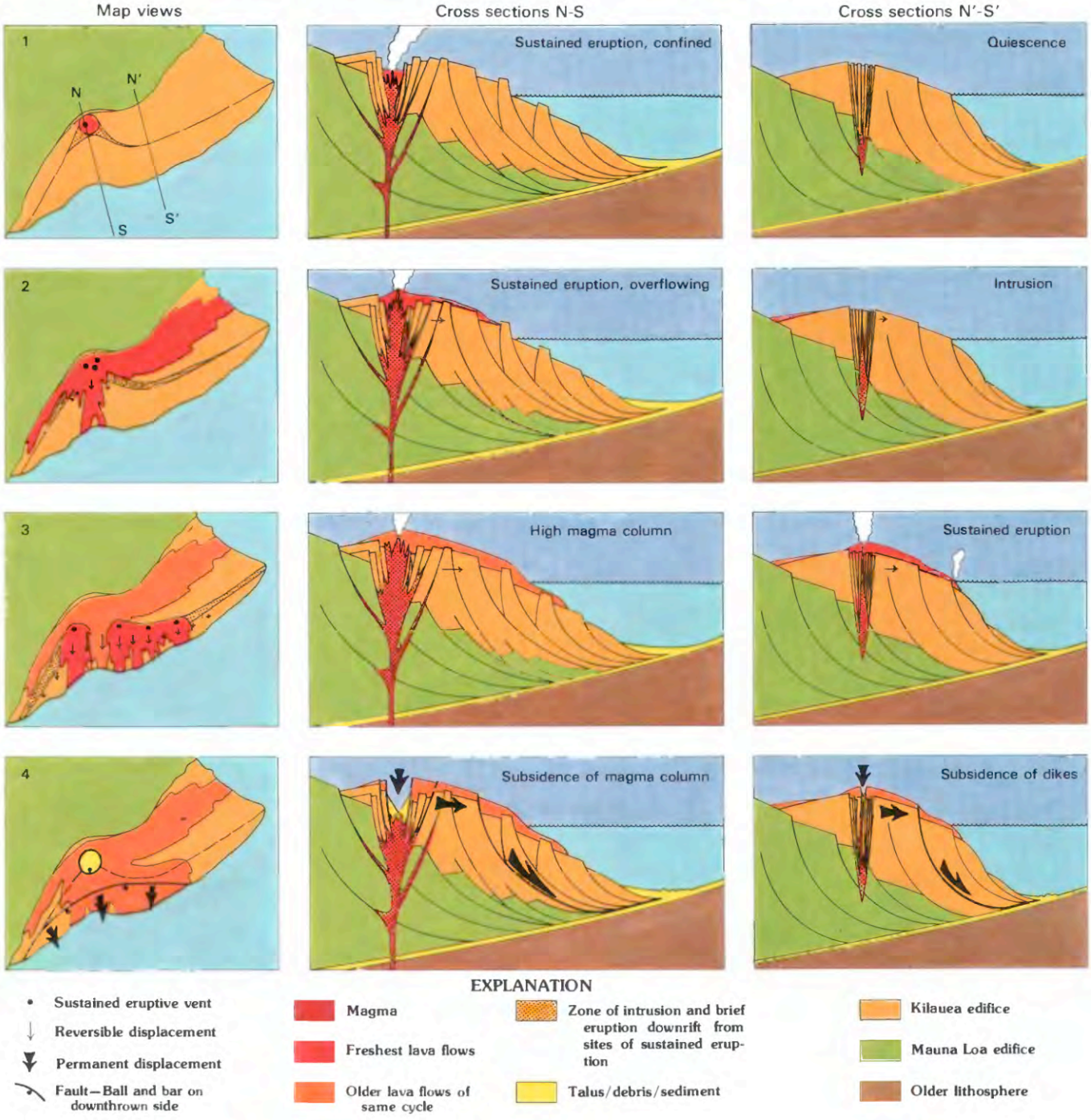

FIGURE 12.61.—Cyclical model based on seaward displacement of south flank. Schematic maps and transverse cross sections show four stages in cycle. Slumping cycles of this sort could occur over intervals as short as a few years, and they might be superimposed on long-term caldera cycles. Slumping episodes might sometimes induce caldera subsidence. Slippage might be concentrated within a layer of oceanic sediment several hundred meters thick beneath the volcano, as suggested by Nakamura (1982). **Stage 1.** Volcanic edifice is in repose as magma column rises passively to fill summit reservoir. **Stage 2.** Summit magma column rises high and overflows. Magma is forcefully intruded under rising head into rift zones, and south flank is displaced. Much of this flank deformation can be reversed if magma withdraws. **Stage 3.** Continued intrusion initiates sustained eruptions along rift zones and displaces south flank further. Flank is made increasingly unstable by steepening its slope and loading its surface, but permanent displacement does not occur until frictional threshold is overcome. **Stage 4.** Oversteepening and loading of flank by extrusion and forceful intrusion overcome sliding resistance, and permanent slumping displacement occurs along flank faults. Lateral expansion of magma reservoir causes summit magma column to subside, and head loss causes magma also to subside far out along rift zones. Magma pressure drops rapidly and stops driving permanent displacement, but slumping continues until frictional resistance overcomes inertia of sliding block. Magma resumes passive filling of space made available by slumping episode.

plumbing system and followed by evolutionary reintegration of the plumbing system, very complicated but possibly predictable harmonic patterns of eruption might ensue.

Cyclical models imply the possibility of long-range forecasts, but steady-state or stochastic models do not. By itself, stage 3 of figure 12.60 could represent such a model, with much magma always stored throughout a plumbing system that is never seriously disrupted. Eruptions of any type could occur from any part of the system at any time. In this model there would be no systematic evolution of the plumbing system over decades or centuries; instead, the variations in eruptive behavior would arise merely from chance developments such as the times when individual dikes happened to intersect the surface. If a model like this best described the volcano's behavior, it might not be possible to predict long-term changes using the previous history.

Alternative noncyclical models could blend evolutionary processes with random events. Random behavior might be superimposed upon, or reset, evolutionary progressions, and evolutionary behavior might characterize some intervals but not others. For example, the magma plumbing system might respond in a predictable, evolutionary way to a major submarine eruption or flank subsidence not caused by feedback mechanisms within the system. Although major perturbations would remain unpredictable, evolutionary trends following them might permit forecasts of long-term behavior between them. That is, we might be able to forecast long intervals of dominantly summit activity versus long intervals of dominantly rift activity. Predictive success would be achieved much of the time even though major perturbations remained unpredictable.

CONCLUSIONS

Kilauea's surface is about 10 times younger than was thought previously (table 12.2); 70 percent is younger than 500 years, 90 percent younger than 1,100 years. A major hiatus in summit overflows occurred between about 1,500 and 1,100 years ago. Much of the present caldera dates from the 18th century, but it was preceded by at least one earlier caldera that developed about 1,500 years B.P. and was later filled.

The various subdivisions of Kilauea are covered by lava flows of different types (table 12.3) produced by eruptions of different kinds from different parts of the magma plumbing system (table 12.4). Kilauea's surface is dominated by tube-fed pahoehoe (67 percent), while surface-fed pahoehoe (14 percent) is mainly limited to near vents along the rift zones, and aa (16 percent) occurs mainly on the south flank seaward of the rift zones. Surface coverage has been dominated by tube-fed lava flows from long-sustained eruptions at the summit; 51 percent of the volcano's surface still consists of such lava even though summit overflows have not occurred for the last 200 years. About 30 percent of Kilauea was covered by lava from just one long eruption at the Ai-laau vent a few hundred years ago. Surface coverage by brief eruptions is minor (22 percent), despite the high frequency of such eruptions in recent decades.

Different parts of Kilauea have differed in eruptive behavior. The most notable difference is between the summit and rift zones, with most long-sustained eruptions occurring at summit vents. Sustained unstable eruptions are more numerous along the upper parts of the rift zones than along their lower parts. Pyroclastic central vents are more common along the lower parts of the rift zones, especially below elevations of 500 m. The briefest fissure eruptions have occurred all along the rift zones and at the summit, displaying on average no obvious affinity for any part of the volcano. During particular decades or centuries, however, they have been concentrated in restricted regions. Other spatial variations appear to have been characteristic of particular localities, such as the southern strand of the southwest rift zone.

Different intervals of Kilauea's history have been dominated by different eruptive behaviors. Behavioral changes have occurred over intervals of decades and centuries. The changes include variations in both frequency and type of eruption. Some changes have been repeated at long intervals, and some may have occurred in evolutionary sequences. Two explosive eruptions large enough to produce extensive pyroclastic sheets seem to have been followed by intervals longer than a century in which most eruptive activity was confined to a summit caldera. While the caldera slowly filled, vegetation became well established on the volcano's flanks. Rift activity waxed as summit activity waned, and in the recent historical example the waxing sequence resembles an evolutionary progression: rift eruptions were at first brief and widely separated in space and time, but gradually they became frequent along a restricted segment of the rift zone and culminated in sustained activity at one locality.

During the past 500 years, when the eruptive pattern can best be defined, there has been a repeated pattern of sympathetic behavior between the summit and rift zones. Little flank activity has occurred when summit activity was sustained, and sustained summit activity has ceased when there was much activity on the rift zones. Rift activity has been accompanied by subsidence at the summit, and large summit collapses have been followed by phreatomagmatic eruption. Events following explosive eruptions, however, have displayed no consistent pattern. The large explosive eruption of 1790 was preceded by much rift activity and followed by much summit activity, but the smaller eruption of 1924 was preceded by much summit activity and followed by little such activity. The current rift activity resembles that which occurred in the 18th century before the explosive eruption of 1790.

TABLE 12.1.—*Classification of Kilauea eruptions*

[Types of lava flow: PS, surface-fed pahoehoe; PT, tube-fed pahoehoe; A, aa]

Type	Duration	Character of effusion	Vents	Lava flows
Brief, fissure	Hours to days	Simple waxing, waning; small fountains.	Open fissures, ramparts.	Few; PS and A.
Brief, localized	Days to weeks	Simple waxing, waning or pulses; large fountains.	Pyroclastic cones, mounds.	Several; PS and A.
Sustained, unstable	Months to years	Complex sequence; waxing, pulses, waning.	Small shields.	Many; PS, PT, and A.
Sustained, stable	Decades to centuries	Mainly slow, steady; some interruptions.	Large shield.	Many; mainly PT.
Explosive	Days to weeks	Successive explosions.	Crater.	Few or none.

TABLE 12.2.—*Age distribution of Kilauea's surface*

[Areas measured by digitizer on a generalized map at scale of 1:50,000]

Age (yr B.P.)	Area		Cumulative area	
	(km²)	(percent)	(km²)	(percent)
0–50	146.5	10.1	146.5	10.1
50–150	38.2	2.6	184.7	12.7
150–250	168.2	11.6	352.9	24.3
250–350	167.6	11.5	520.5	35.8
350–500	454.5	31.3	975.0	67.1
500–750	190.6	13.1	1,165.6	80.2
750–1,000	89.6	6.2	1,255.3	86.4
1,000–1,500	50.4	3.5	1,395.6	89.9
>1,500	146.0	10.1	[1]1,451.6	100.0

[1]A separate measurement of total area on the same map gave 1,451.0 km².

TABLE 12.3.—*Distribution of lava types on Kilauea's subaerial surface*

[Areas measured by digitizer on a generalized map at scale of 1:50,000. Types of lava: PS, surface-fed pahoehoe; PT, tube-fed pahoehoe; A, aa: T, pyroclastics; ML, all types erupted from Mauna Loa]

Structural subdivision	Area		Lava type	Area	
	(km²)	Percent of Kilauea		(km²)	Percent of subdivision
Summit	51.6	3.6	PS	19.4	37.5
			PT	5.0	9.6
			A	1.5	3.0
			T	18.3	35.6
			ML	7.4	14.3
Koae fault system	65.7	4.5	PS	7.8	11.9
			PT	51.1	77.7
			A	6.3	9.6
			T	.5	.8
Upper southwest rift zone	88.4	6.1	PS	21.3	24.1
			PT	46.6	52.7
			A	7.5	8.5
			T	1.1	1.2
			ML	11.9	13.5
Lower southwest rift zone	91.5	6.3	PS	13.8	15.1
			PT	64.0	69.9
			A	13.7	15.0
Upper east rift zone	55.1	3.8	PS	20.9	38.0
			PT	31.2	56.6
			A	2.8	5.0
			T	.2	.4
Middle east rift zone	91.5	6.3	PS	36.7	40.1
			PT	42.8	46.8
			A	10.7	11.7
			T	1.2	1.4
Lower east rift zone	81.8	5.7	PS	43.0	52.5
			PT	8.1	9.9
			A	25.9	31.7
			T	4.9	5.9
North flank	445.7	30.8	PS	19.1	4.3
			PT	403.4	90.5
			A	21.4	4.8
			ML	1.8	.4
South flank	475.9	32.9	PS	17.4	3.7
			PT	316.9	66.6
			A	141.1	29.6
			T	.6	.1
Total subaerial Kilauea	[1]1,447.3	100.0	PS	199.4	13.8
			PT	969.1	67.0
			A	230.9	16.0
			T	26.8	1.9
			ML	21.1	1.5

[1]A separate measurement of total area on the same map gave 1,447.9 km².

TABLE 12.4.—*Distribution of lava on Kilauea's surface from different types of eruption*

[Areas measured by digitizer on a generalized map at scale of 1:50,000]

Location of vents	Area covered by eruption type									
	Brief		Sustained, stable		Sustained, unstable		Explosive		Total	
	(km²)	(percent)	(km²)	(percent)	(km²)	(percent)	(km²)	(percent)	(km²)	(percent)
Summit	10.2	0.7	732.9	50.6	0	0	18.5	1.3	761.6	52.6
Upper southwest rift zone	35.8	2.5	0	0	34.0	2.3	0	0	69.8	4.8
Lower southwest rift zone	28.0	1.9	0	0	0	0	.0	.0	28.0	1.9
Upper east rift zone	7.5	.5	0	0	183.3	12.6	0	0	190.8	13.1
Middle east rift zone	93.9	6.5	0	0	100.2	6.9	0	0	194.1	13.4
Lower east rift zone	154.5	10.7	0	0	25.0	1.7	.0	.0	179.5	12.4
Mauna Loa	-----	----	-----	----	-----	----	----	---	21.3	1.5
Undetermined	-----	----	-----	----	-----	----	----	---	2.6	.2
Total	329.9	22.8	732.9	50.6	342.5	23.5	18.5	1.3	[1]1,449.4	99.9

[1]A separate measurement of total area on the same map gave 1,450.4 km².

TABLE 12.5.—*Paleomagnetic results from lava flows in the Kipuka Nene area of Kilauea*

[D and I are respectively, mean declination and inclination, in degrees, of remanent magnetization in 12 specimens from each site. α_{95} is circle of 95-percent confidence around the mean direction]

Site	D	I	α_{95}
Kalue flows			
1B224	9.5	24.6	1.7
1B456	10.2	24.6	1.8
3R013	8.7	24.1	2.6
Kipuka Nene flows			
8B121	357.0	39.2	1.6
8B133	357.5	37.9	1.2
9B169	357.9	37.4	1.6
3R001	1.9	39.2	2.1

TABLE 12.6.—*^{14}C ages of material related to the Ai-laau and Observatory vents*

Source of flow	Sample	Age (yr B.P.)
Ai-laau vent	[1]W–4449	<200
	[2]W–4573	<200
	W–3881	260 ± 70
	W–4162	310 ± 70
	W–4661	320 ± 70
	W–3941	450 ± 60
	[2]W–3885	2,160 ± 70
Probably Puu Huluhulu	W–4184	<200
	W–5110	230 ± 60
	W–4337	620 ± 70
Observatory vent	W–4470	310 ± 70
	W–3811	330 ± 60
	W–3852	450 ± 60
	[3]W–4998	960 ± 60
Possibly Observatory vent	W–4404	530 ± 70
	W–5218	550 ± 70
	W–3860	670 ± 60

[1]Same prehistoric flow as W–3941; disregarded.
[2]Same prehistoric flow as W–4162; disregarded.
[3]Anomalous, possibly contaminated by fumaroles.

REFERENCES CITED

Aramaki, S., and Moore, J.G., 1969, Chemical composition of prehistoric lavas at Makaopuhi Crater, Kilauea Volcano, and periodic change in alkalai content of Hawaiian tholeiitic lavas: Tokyo, Bulletin of the Earthquake Research Institute, v. 47, p. 257–270.

Atkinson, I.A.E., 1970, Successional trends in the coastal and lowland forest of Mauna Loa and Kilauea Volcanoes, Hawaii: Pacific Science, v. 24, p. 387–400.

Atkinson, I.A.E., and Swindale, L.D., 1974, Age determinations of some prehistoric lava flows in Hawaii: Hawaii Agricultural Experiment Station Technical Bulletin 90, 43 p.

Banks, N.G., Klein, F.W., Moore, R.B., Jackson, D.B., and Okamura, A.T., 1981, Kilauea Volcano's November 1979 eruption [abs.]: Eos, American Geophysical Union Transactions, v. 62, p. 1072.

Banks, N.G., Wolfe, E.W., Duggan, T.A., Okamura, A.T., Koyanagi, R.Y., Greenland, L.P., and Jackson, D.B., 1983, Magmatic events at Kilauea Volcano, Hawaii [abs.]: Eos, American Geophysical Union Transactions, v. 64, p. 901–902.

Beaglehole, J.C., 1967, The journals of Captain James Cook on his voyages of Discovery, 1776–1780, v. 3, The voyage of the Resolution and Discovery, 1776–1780: New York, Cambridge University Press, 1,647 p.

Brigham, W.T., 1909, The volcanoes of Kilauea and Mauna Loa: Honolulu, Bernice P. Bishop Museum Memoirs, v. 2, no. 4, 222 p.

Chatters, R.M., Crosby, J.W., III, and Engstrand, L.G., 1969, Fumarole gaseous emanations: Their influence on carbon-14 dates: Washington State University, College of Engineering, Circular 93.

Christiansen, R.L., 1979, Explosive eruption of Kilauea volcano in 1790 [abs.]: Hawaii Symposium on Intraplate Volcanism and Submarine Volcanism, Hilo, Hawaii, July 16–22, 1979, Abstract volume, p. 158.

Coan, T., 1841, Great eruption of the volcano of Kilauea, Missionary Herald, v. 37, p. 283–285.

———1851, [On Kilauea]: American Journal of Science, 2nd series, v. 12, p. 80–82.

———1868, [On the earthquakes and eruption of 1868]: American Journal of Science, 2nd series, v. 46, p. 106–109.

———1874, Note on the Hawaiian volcanoes: American Journal of Science, 3rd series, v. 8, p. 467.

Coe, R.S., Grommé, C.S., and Mankinen, E.A., 1978, Geomagnetic paleointensities from radiocarbon-dated lava flows on Hawaii and the question of the Pacific nondipole low: Journal of Geophysical Research, v. 83, p. 1740–1756.

Dana, J.D., 1849, Geology, United States Exploring Expedition, during the years 1838, 1839, 1840, 1841, 1842, under the command of Charles Wilkes, U.S.N.: Philadelphia, v. 10, 756 p.

———1850, Historical account of the eruptions on Hawaii: American Journal of Science, ser. 2, v. 9, p. 347–364.

———1890, Characteristics of volcanoes: New York, Dodd, Mead, 399 p.

Decker, R.W., and Christiansen, R.L., 1984, Explosive eruptions of Kilauea Volcano, Hawaii, *in* Explosive volcanism: Inception, evolution, and hazards: Washington, D.C., National Academy Press, p. 122–132.

Doell, R.R., 1969, Paleomagnetism of the Kau volcanic series, Hawaii: Journal of Geophysical Research, v. 74, p. 4857–4868.

Doell, R.R., and Cox, A.V., 1963, The accuracy of the paleomagnetic method as evaluated from historic Hawaiian lava flows: Journal of Geophysical Research, v. 68, p. 1997–2009.

———1965, Paleomagnetism of Hawaiian lava flows: Journal of Geophysical Research, v. 70, p. 3377–3405.

Doerr, J.E., Jr., 1933, Tree molds in the Volcano golf course: Hawaii National Park Notes, v. 3, p. 3–7.

Douglas, D., 1905, Sketch of a second journey to the northwestern parts of the continent of North America and to the Sandwich Islands during the years 1829–'30–'31–'32–'33–'34, Part VI: Oregon Historical Quarterly, v. 6, p. 417–449.

Duffield, W.A., 1975, Structure and origin of the Koae fault system, Kilauea Volcano, Hawaii: U.S. Geological Survey Professional Paper 856, 12 p.

Duffield, W.A., Christiansen, R.L., Koyanagi, R.Y., and Peterson, D.W., 1982, Storage, migration, and eruption of magma at Kilauea Volcano, Hawaii, 1971–1972: Journal of Volcanology and Geothermal Research, v. 13, p. 273–307.

Dutton, C.E., 1884, Hawaiian volcanoes: U.S. Geological Survey 4th Annual Report, p. 75–219.

Dzurisin, D., Anderson, L.A., Eaton, G.P., Koyanagi, R.Y., Lipman, P.W., Lockwood, J.P., Okamura, R.T., Puniwai, G.S., Sako, M.K., and Yamashita, K.M., 1980, Geophysical observations of Kilauea Volcano, Hawaii, 2. Constraints on the magma supply during November 1975–September 1977: Journal of Volcanology and Geothermal Research, v. 7, p. 241–269.

Dzurisin, D., and Casadevall, T.C., 1986, Stratigraphy and chemistry of the Uwekahuna Ash: Product of prehistoric phreatomagmatic eruptions at Kilauea Volcano, Hawaii [abs.]: International Association of Volcanology and Chemistry of the Earth's Interior, Aukland-Hamilton-Rotorua, New Zealand, February 1–9, 1986, Abstracts, p. 100.

Dzurisin, D., Koyanagi, R.Y., and English, T.T., 1984, Magma supply and storage at Kilauea Volcano, Hawaii, 1956–1983: Journal of Volcanology and Geothermal Research, v. 21, p. 177–206.

Easton, R.M., 1978, The stratigraphy and petrology of the Hilina Formation: the oldest exposed lavas of Kilauea Volcano, Hawaii: Honolulu, University of Hawaii, M.S. thesis, 274 p.

Easton, R.M., and Lockwood, J.P., 1983, "Surface-fed dikes"—the origin of some unusual dikes along the Hilina fault zone, Kilauea Volcano, Hawaii: Bulletin Volcanologique, v. 46, p. 45–53.

Ellis, W., 1827, Journal of William Ellis, narrative of a tour of Hawaii, or Owhyhee; with remarks on the history, traditions, manners, customs and language of the inhabitants of the Sandwich Islands: Honolulu Advertiser, 342 p., reprinted 1963.

Fiske, R.S., and Jackson, E.D., 1972, Orientation and growth of Hawaiian volcanic rifts: The effect of regional structure and gravitational stresses: Royal Society of London Proceedings, v. A329, p. 299–326.

Fiske, R.S., and Koyanagi, R.Y., 1968, The December 1965 eruption of Kilauea Volcano, Hawaii: U.S. Geological Survey Professional Paper 607, 21 p.

Fornari, D.J., Moore, J.G., and Calk, L., 1979, A large submarine sand-rubble flow on Kilauea Volcano, Hawaii: Journal of Volcanology and Geothermal Research, v. 5, p. 239–256.

Furumoto, A.S., 1976, A coordinated exploration program for geothermal sources on the Island of Hawaii, *in* United Nations Symposium on the Development and Use of Geothermal Resources, 2nd, San Francisco, California, May 1975: Proceedings, v. 2, p. 993–1001.

Goodrich, J., 1833, Volcanoes and volcanic phenomena of Hawaii: American Journal of Science, v. 25, p. 199–203.

Hitchcock, C.H., 1909, Hawaii and its volcanoes: Honolulu, Hawaiian Gazette, 2nd edition 1911, 314 p.

Holcomb, R.T., 1976a, Preliminary map showing products of eruptions, 1962–1974, from the upper east rift zone of Kilauea Volcano, Hawaii: U.S. Geological Survey Miscellaneous Field Studies Map MF–811, scale 1:24,000.

———1976b, Complexity and hazards of Hawaiian shield volcanoes [abs.]: Geological Society of America, Abstracts with Programs, v. 8, no. 6, p. 920–921.

———1980a Preliminary geologic map of Kilauea Volcano, Hawaii: U.S. Geological Survey Open-File Report 80-796, 2 sheets, scale 1:50,000.

———1980b, Kilauea Volcano, Hawaii: Chronology and morphology of the surficial lava flows: Palo Alto, Stanford University, Ph.D. thesis, 321 p. Also released as U.S. Geological Survey Open-File Report 81–354.

Holcomb, R.T., Champion, D.E., and McWilliams, M.O., 1986, Dating recent Hawaiian lava flows using paleomagnetic secular variation: Geological Society of America Bulletin, v. 97, p. 829–839.

Holcomb, R.T., Peterson, D.W., and Tilling, R.I., 1974, Recent landforms at Kilauea Volcano, a selected photographic compilation, *in* Guidebook to the Hawaiian Planetology Conference: Hilo, Hawaii, October 1974, p. 49–86.

Jackson, D.B., Swanson, D.A., Koyanagi, R.Y., and Wright, T.L., 1975, The August and October, 1968, east rift eruptions of Kilauea Volcano, Hawaii: U.S. Geological Survey Professional Paper 890, 33 p.

Jacobi, J.D., 1983, *Metrosideros* dieback in Hawaii: A comparison of adjacent dieback and non-dieback rain forest stands: New Zealand Journal of Ecology, v. 6, p. 79–97.

Jaggar, T.A., 1947, Origin and development of craters: Geological Society of America Memoir 21, 508 p.

Jaggar, T.A., and Finch, R.H., 1924, The explosive eruption of Kilauea in Hawaii, 1924: American Journal of Science, ser. 5, v. 8, p. 353–374.

Juvik, J.O., 1976, A substrate control model for vegetation succession on recent volcanic deposits in the Hawaiian and Mascarene Islands: Yearbook of the Association of Pacific Coast Geographers, v. 38, p. 125.

Kalakaua, D., 1888, The legends and myths of Hawaii: New York, Charles L. Webster (reprinted 1972, Tokyo, Charles E. Tuttle), 530 p.

Kelley, M.L., 1979, Radiocarbon dates from the Hawaiian Islands—a compilation: U.S. Geological Survey Open-File Report 79–1700, 37 p.

Kelley, M.L., Spiker, E.C., Lipman, P.W., Lockwood, J.P., Holcomb, R.T., and Rubin, M., 1979, U.S. Geological Survey radiocarbon dates XV: Mauna Loa and Kilauea Volcanoes, Hawaii: Radiocarbon, v. 21, p. 306–320.

Kinoshita, W.T., Koyanagi, R.Y., Wright, T.L., and Fiske, R.S., 1969, Kilauea Volcano: the 1967–68 summit eruption: Science, v. 166, p. 459–468.

Ledyard, J., 1783, A journal of Captain Cook's last voyage to the Pacific Ocean and in quest of a northwest passage between Asia and America: Hartford, Conn., Nathaniel Patkon.

Lipman, P.W., and Swenson, A., 1984, Generalized geologic map of the southwest rift zone of Mauna Loa Volcano, Hawaii: U.S. Geological Survey Miscellaneous Investigations Map I–1323, scale 1:100,000.

Lockwood, J.P., and Lipman, P.W., 1980, Recovery of charcoal for ^{14}C dating from beneath lava—lessons from Hawaii: Bulletin Volcanologique, v. 43, p. 609–615.

Lockwood, J.P., and Rubin, M., 1986, Distribution and age of the Uwekahuna Ash, Kilauea Volcano, Hawaii [abs.]: International Association of Volcanology and Chemistry of the Earth's Interior, Aukland-Hamilton-Rotorua, New Zealand, February 1–9, 1986, Abstracts, p. 112.

Macdonald, G.A., 1941, Lava flows in eastern Puna: Volcano Letter, no. 474, p. 1–3.

———1955, Hawaiian volcanoes during 1952: U.S. Geological Survey Bulletin 1021–B, p. 15–108.

———1965, Hawaiian calderas: Pacific Science, v. 19, p. 320–331.

Macdonald, G.A., and Abbott, A.T., 1970, Volcanoes in the sea—the geology of Hawaii: Honolulu, University of Hawaii Press, 441 p.

Macdonald, G.A., and Eaton, J.P., 1964, Hawaiian volcanoes during 1955: U.S. Geological Survey Bulletin 1171, 170 p.

Moore, J.G., 1971, Bathymetry and geology—East Cape of the Island of Hawaii: U.S. Geological Survey Map I–677, scale 1:62,500.

Moore, J.G., and Evans, B.W., 1967, The role of olivine in the crystallization of the prehistoric Makaopuhi tholeiitic lava lake, Hawaii: Contributions to Mineralogy and Petrology, v. 15, p. 202–223.

Moore, J.G., and Fiske, R.S., 1969, Volcanic structure inferred from dredge samples and ocean-bottom photographs, Hawaii: Geological Society of America Bulletin, v. 80, p. 1191–1202.

Moore, J.G., and Koyanagi, R.Y., 1969, The October 1963 eruption of Kilauea Volcano, Hawaii: U.S. Geological Survey Professional Paper 614–C, 13 p.

Moore, J.G., and Krivoy, H.L., 1964, The 1962 flank eruption of Kilauea and structure of the east rift zone: Journal of Geophysical Research, v. 69, p. 2033–2045.

Moore, J.G., and Peck, D.L., 1965, Bathymetric, topographic, and structural map of the south-central flank of Kilauea Volcano, Hawaii: U.S. Geological Survey Miscellaneous Investigations Map I–456, scale 1:62,500.

Moore, J.G., Phillips, R.L., Grigg, R.W., Peterson, D.W., and Swanson, D.A., 1973, Flow of lava into the sea, 1969–1971, Kilauea Volcano, Hawaii: Geological Society of America Bulletin, v. 84, p. 537–546.

Moore, R.B., 1981, Preliminary geologic map of the Kapoho quadrangle, Hawaii: U.S. Geological Survey Open-File Report 81–947, 1 sheet, scale 1:24,000.

———1983, Distribution of differentiated tholeiitic basalts on the lower east rift zone of Kilauea Volcano, Hawaii: A possible guide to geothermal exploration: Geology, v. 11, p. 136–140.

———1985, Preliminary geologic map of the Pahoa South quadrangle, Hawaii: U.S. Geological Survey Open-File Report 85–715, 1 sheet, scale 1:24,000.

Moore, R.B., Helz, R.T., Dzurisin, D., Eaton, G.P., Koyanagi, R.Y., Lipman, P.W., Lockwood, J.P., and Puniwai, G.S., 1980, The 1977 eruption of Kilauea Volcano, Hawaii: Journal of Volcanology and Geothermal Research, v. 7, p. 189–210.

Nakamura, K., 1982, Why do long rift zones develop better in Hawaiian volcanoes—a possible role of thick sediments, *in* Proceedings, International Association of Volcanology and Chemistry of the Earth's Interior 1980 Symposium on the Activity of Ocean Volcanoes, Ponta Delgada, Azores, Universidade dos Acores, p. 59–73.

Peck, D.L., Wright, T.L., and Moore J.G., 1966, Crystallization of tholeiitic basalt in Alae lava lake, Hawaii, *in* International Symposium on Volcanology, New Zealand, 1965: Bulletin Volcanologique, v. 29, p. 629–656.

Peterson, D.W., 1967, Geologic map of the Kilauea Crater quadrangle, Hawaii: U.S. Geological Survey Geologic Quadrangle Map GQ–667, scale

1:24,000.

Peterson, D.W., and Swanson, D.A., 1974, Observed formation of lava tubes during 1970–1971 at Kilauea Volcano, Hawaii: Studies in Speleology, v. 2, p. 209–222.

Powers, H.A., 1948, A chronology of explosive eruptions of Kilauea: Pacific Science, v. 2, p. 278–292.

Powers, S., 1916, Intrusive bodies at Kilauea: Zeitschrift fur Vulkanologie, v. 3, p. 28–33.

Richter, D.H., Ault, W.U., Eaton, J.P., and Moore, J.G., 1964, The 1961 eruption of Kilauea Volcano, Hawaii: U.S. Geological Survey Professional Paper 474–D, 34 p.

Richter, D.H., Eaton, J.P., Murata, K.J., Ault, W.U., and Krivoy, H. L., 1970, Chronological narrative of the 1959–60 eruption of Kilauea Volcano, Hawaii: U.S. Geological Survey Professional Paper 537–E, 73 p.

Ripperton, J.C., and Hosaka, E.Y., 1942, Vegetation zones of Hawaii: Hawaii Agricultural Experiment Station Bulletin 89, p. 1–60.

Rubin, M., and Suess, H.E., 1956, U.S. Geological Survey radiocarbon dates, 3: Science, v. 123, p. 442–448.

de Saint Ours, P.J., 1979, Analyse morpho-structurale et surveillance tectonique d'un volcan actif: Exemple du Kilauea, Hawaii: Orsay, France, l'Universite de Paris-Sud, Centre d'Orsay, Docteur 3eme cycle [thesis], 250 p.

———1982, Map of tectonic features of Kilauea Volcano summit region, Hawaii: U.S. Geological Survey Miscellaneous Field Studies Map MF–1368.

Skokan, C.K., 1974, A time domain electromagnetic survey of the east rift zone, Kilauea Volcano, Hawaii: Golden, Colorado School of Mines, Ph.D. dissertation no. T–1700, 152 p.

Stearns, H.T., 1925, The explosive phase of Kilauea Volcano, Hawaii, in 1924: Bulletin Volcanologique, v. 2, p. 193–209.

———1926, The Keaiwa or 1823 lava flow from Kilauea volcano, Hawaii: Journal of Geology, v. 134, p. 336–351.

Stearns, H.T., and Clark, W.O., 1930, Geology and water resources of the Kau district, Hawaii: U.S. Geological Survey Water-Supply Paper 616, 194 p.

Stearns, H.T., and Macdonald, G.A., 1946, Geology and ground-water resources of the Island of Hawaii: Hawaii Division of Hydrography Bulletin 9, 363 p.

Stone, J.B., 1925, Interior of Makaopuhi Crater: The Volcano Letter, no. 47.

Strzelecki, Count, 1845, New South Wales and Van Diemen's Land: London, p. 106.

Swanson, D.A., 1972, Magma supply rate at Kilauea Volcano, 1952–1971: Science, v. 175, p. 163–170.

———1973, Pahoehoe flows from the 1969–1971 Mauna Ulu eruption, Kilauea Volcano, Hawaii: Geological Society of America Bulletin, v. 84, p. 615–626.

Swanson, D.A., and Christiansen, R.L., 1973, Tragic base surge in 1790 at Kilauea Volcano: Geology, v. 1, p. 83–86.

Swanson, D.A., Duffield, W.A., and Fiske, R.S., 1976a, Displacement of the south flank of Kilauea Volcano, Hawaii: the result of forceful intrusion of magma into rift zones: U.S. Geological Survey Professional Paper 963, 39 p.

Swanson, D.A., Duffield, W.A., Jackson, D.B., and Peterson, D.W., 1972, The complex filling of Alae Crater, Kilauea Volcano, Hawaii: Bulletin Volcanologique, v. 36, p. 105–126.

———1979, Chronological narrative of the 1969–1971 Mauna Ulu eruption of Kilauea Volcano, Hawaii: U.S. Geological Survey Professional Paper 1056, 55 p.

Swanson, D.A., Jackson, D.B., Koyanagi, R.Y., and Wright, T.L., 1976b, The February 1969 east rift eruption of Kilauea Volcano, Hawaii: U.S. Geological Survey Professional Paper 891, 30 p.

Taliaferro, W.J., 1959, Rainfall of the Hawaiian Islands: Honolulu, Hawaii Water Authority.

Tilling, R.I., Koyanagi, R.Y., Lipman, P.W., Lockwood, J.P., Moore, J.G., and Swanson, D.A., 1976, Earthquake and related catastrophic events, Island of Hawaii, November 29, 1975: A preliminary report: U.S. Geological Survey Circular 740, 33 p.

Unger, J.D., and Koyanagi, R.Y., 1979, Evidence of the effects of shallow magma intrusion in Kilauea Volcano: Hawaii Symposium on Intraplate Volcanism and Submarine Volcanism, Hilo, Hawaii, July 16–22, 1979, Abstract Volume, p. 176.

Vancouver, G., 1798, A voyage of discovery to the north Pacific Ocean: New York, Da Capo Press, reprinted 1967.

Walker, G.W., 1967, Geologic map of the Kau Desert quadrangle, Hawaii: U.S. Geological Survey Geologic Quadrangle Map GQ–827, scale 1:24,000.

Westervelt, W.D., 1916, Hawaiian legends of volcanoes: Honolulu, Charles E. Tuttle, 205 p., reprinted 1963 (Tokyo).

Wilde, P., Chase, T.E., Normark, W.R., Thomas, J.A., and Young, J.D., 1980, Oceanographic data off southern Hawaiian Islands: Lawrence Berkeley Laboratory Publication 359.

Wilkes, C., 1845, Narrative of the United States Exploring Expedition during the years 1838, 1839, 1840, 1841, 1842, v. IV: Philadelphia, Lea and Blanchard.

Wright, T.L., 1971, Chemistry of Kilauea and Mauna Loa lava in space and time: U.S. Geological Survey Professional Paper 735, 40 p.

Wright, T.L., and Fiske, R.S., 1971, Origin of the differentiated and hybrid lavas of Kilauea Volcano, Hawaii: Journal of Petrology, v. 12, p. 1–65.

Wright, T.L., Kinoshita, W.T., and Peck, D.L., 1968, March 1965 eruption of Kilauea Volcano and the formation of Makaopuhi lava lake: Journal of Geophysical Research, v. 73, p. 3181–3205.

Zablocki, C.J., 1976, Mapping thermal anomalies on an active volcano by the self-potential method, Kilauea, Hawaii, *in* United Nations Symposium on the Development and Use of Geothermal Resources, 2nd, San Francisco, California, May 20–29, 1975, Proceedings, v. 2, p. 1299–1309.

———1977, Self-potential studies in east Puna, Hawaii, *in* Keller, G.V., Skokan, C.K., Skokan, J.J., Daniels, J., Kauahikaua, J.P., Klein, D.P., and Zablocki, C.J., Geoelectric studies on the east rift, Kilauea Volcano, Hawaii Island: Honolulu, Hawaii Institute of Geophysics, Geothermal Resources Exploration in Hawaii, Report Number 3, p. 175–195.

STRATIGRAPHY AND PETROLOGY OF THE UWEKAHUNA BLUFF SECTION, KILAUEA CALDERA

By Thomas J. Casadevall *and* Daniel Dzurisin

ABSTRACT

Samples from 63 lava flows in a 135-m vertical section at Uwekahuna Bluff within Kilauea caldera were analyzed for major oxides, trace elements, and rare-earth elements. Four stratigraphically defined suites of subaerial lava flows are present: (A) units 1–14 (youngest suite), plagioclase-porphyritic flows (6.4–7.3 weight percent MgO); (B) units 15–30, aphyric flows (6.5–8.0 weight percent MgO); (C) units 31–51, olivine-rich flows (9.0–19.7 weight percent MgO) with the Uwekahuna Ash Member of the Puna Basalt at base; (D) units 44A–52A (oldest suite), nonvesicular, aphyric flows (7.1–7.8 weight percent MgO).

Suite D flows were erupted at about 2.8 ka, probably in an ancient caldera. At about 2.1 ka, catastrophic eruption of the Uwekahuna Ash Member may have unloaded Kilauea's deep magma-transport system and triggered extrusion of olivine-porphyritic lavas of suite C. Suites A and B may be genetically related, possibly from the top of a single reservoir; the plagioclase-porphyritic flows of suite A may represent the later eruptive product of a shallow reservoir that earlier was the source for the aphyric lavas of suite B. We interpret this sequence of aphyric lavas followed by plagioclase-porphyritic lavas as indicating a two-stage drawdown of a post-Uwekahuna Ash Member magma reservoir.

Comparison of published major- and trace-element data from Kilauea and Mauna Loa with data for the Uwekahuna Bluff flows indicates the latter are all from a Kilauea source; apparently no Mauna Loa flows occur in the west wall of Kilauea caldera, although surface flows from Mauna Loa have been mapped within 1 km of the caldera rim.

INTRODUCTION

Kilauea Volcano, on the southeast flank of much larger Mauna Loa Volcano (fig. 13.1), has a broad, gently sloping summit region 1,260 m above sea level and two rift zones that extend outward from a 3 × 5-km summit caldera. The western wall of Kilauea caldera is easily accessible and contains the largest cross-sectional exposure of the summit area (fig. 13.1). This exposure comprises numerous lava flows, at least 18 dikes (Casadevall and Dzurisin, chapter 14), the Uwekahuna laccolith (Murata and Richter, 1961), and three pyroclastic units—the A.D. 1924 lithic ash and the mostly A.D. 1790 Keanakakoi and 2.1-ka Uwekahuna Ash Members of the Puna Basalt (Powers, 1948; Dzurisin and Casadevall, 1986; Lockwood and Rubin, 1986). The wall extends from the area known as the Outlet roughly 6 km northward to the Steaming Bluff area and includes the 135-m-high Uwekahuna Bluff (fig. 13.2). From Uwekahuna Bluff north to Steaming Bluff, the western wall is an unbroken and near-vertical slice through the summit area of Kilauea shield (fig. 13.1). South of Uwekahuna Bluff, however, the wall has a stepped profile attributed to normal faulting (Dutton, 1884; Peterson, 1967; Holcomb, 1981; de Saint Ours, 1982).

We report here the results of field and laboratory studies of rocks in the Uwekahuna Bluff area of Kilauea's summit caldera. Using chemistry, field occurrence, and petrography, we distinguish flows and attempt to identify systematic chemical variations in the composition of summit lava flows. We have examined the data to see whether they allow extension of the secular chemical variation recognized for historical flows (Wright, 1971) further back in time and to see whether they support the hypothesis that more than one long-lived eruptive center was active in the Kiluaea summit area during the past several thousand years (Holcomb, 1981).

Considering the proximity of Mauna Loa surface lavas to the present western rim of Kilauea caldera (Peterson, 1967; J.P. Lockwood, written commun., 1980), we have also scrutinized the data to determine if any flow at Uwekahuna Bluff might have come from Mauna Loa. Previous work has suggested that historical lavas from Kilauea and Mauna Loa can be distinguished by major-element chemistry (Powers, 1955; Wright, 1971; Basaltic Volcanism Study Project, 1981) and rare-earth-element chemistry (Leeman and others, 1977, 1980; Basaltic Volcanism Study Project, 1981).

This study is a companion to two others conducted concurrently. One focuses on the age, distribution, and eruptive mechanism of the Uwekahuna Ash Member of the Puna Basalt, a product of large phreatomagmatic eruptions in the Kilauea summit area (Dzurisin and Casadevall, 1986; Lockwood and Rubin, 1986). The other describes the distribution and petrology of intrusive bodies in Kilauea caldera and assesses the importance of intrusions to the growth of the summit region of Kilauea (Casadevall and Dzurisin, chapter 14).

PREVIOUS STUDIES

Although geologic mapping of Kilauea's summit area has focused on young surface flows (Peterson, 1967; Walker, 1969;

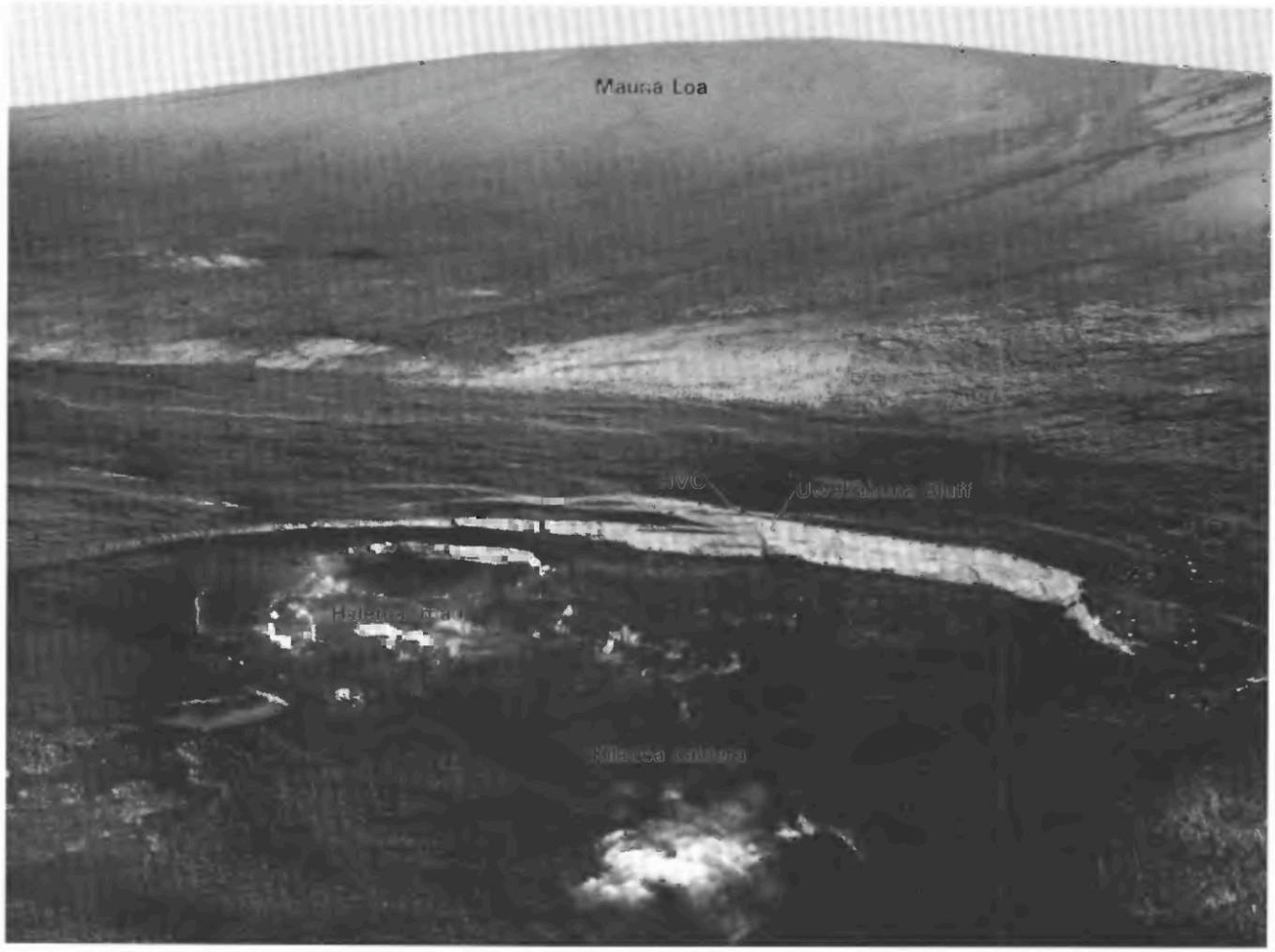

FIGURE 13.1.—Aerial view looking southwest over Kilauea caldera toward the east flank of Mauna Loa, showing location of Uwekahuna Bluff section and Hawaiian Volcano Observatory (HVO). Photograph by J.P. Lockwood, U.S. Geological Survey.

Holcomb, 1981) and on the structural setting of the summit region (de Saint Ours, 1982), some studies have concerned the walls of the caldera and nearby pit craters. Macdonald described the sequence of flows exposed at Uwekahuna Bluff (Stearns and Macdonald, 1946; Macdonald, 1949), Doell sampled the Uwekahuna section for paleomagnetic studies (Doell and Cox, 1965, 1972), and Wright (1971) reported on the chemistry of several of Doell's samples.

Stearns and Macdonald (1946, p. 99–111) placed the three widespread tephra deposits at Kilauea into a stratigraphic framework for the volcano. The Uwekahuna Ash Member of the Puna Basalt is the oldest at 2.1 ka (Lockwood and Rubin, 1986). At Uwekahuna Bluff the ash is overlain by 105–135 m of lava flows, capped by the mostly A.D. 1790 Keanakakoi Ash Member and by traces of A.D. 1924 lithic ash.

ACKNOWLEDGMENTS

We greatly appreciate the interest and advice received from many colleagues, in particular T.L. Wright, which have been helpful in clarifying our ideas. We also wish to thank J. Arth, D.E. Champion, D.A. Clague, R.T. Holcomb, J.P. Lockwood, D.W. Peterson, D.A. Swanson, and R.I. Tilling. Initial thin section descriptions and point counts for figure 13.4 were made by J.E. Ewert. Major-element chemistry was determined by J. Reid and D. Kay; instrumental neutron activation analyses were performed by L.J. Schwarz; and atomic absorption analyses were performed by D.W. Golightly and P. Aruscavage; we greatly appreciate their considerable analytical effort. M. Mangan and D. Johnson helped with computer plots of the data. Reviews of this paper by D.A. Swanson and T.L. Wright have substantially improved the presentation of our results.

METHODS OF STUDY

We sampled and described the succession of flows in the Uwekahuna Bluff section (fig. 13.3) in sequence, starting immediately below the Uwekahuna triangulation station on the caldera rim. Each flow unit was marked with a small aluminum tag bearing the appropriate unit number so that our sampling sites could be precisely revisited. We followed an existing trail near the top of the section down to about unit 12, below which we diverted to the north margin of a prominent talus cone (fig. 13.3) for the remainder of the

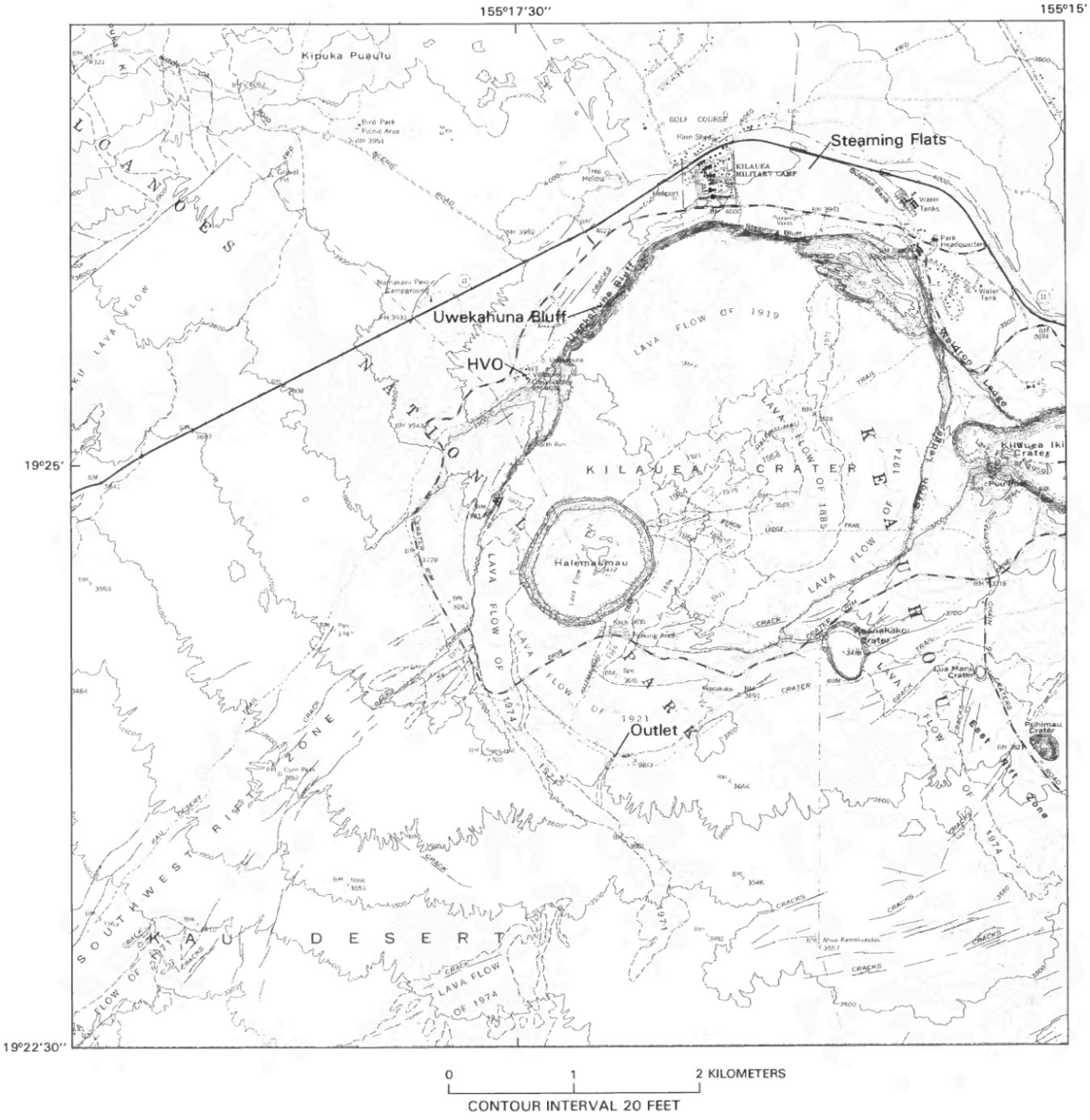

FIGURE 13.2.—Summit area of Kilauea, showing the location of segments of caldera wall examined in this study. Modified from U.S. Geological Survey Kilauea Crater 7.5-minute topographic map, 1981.

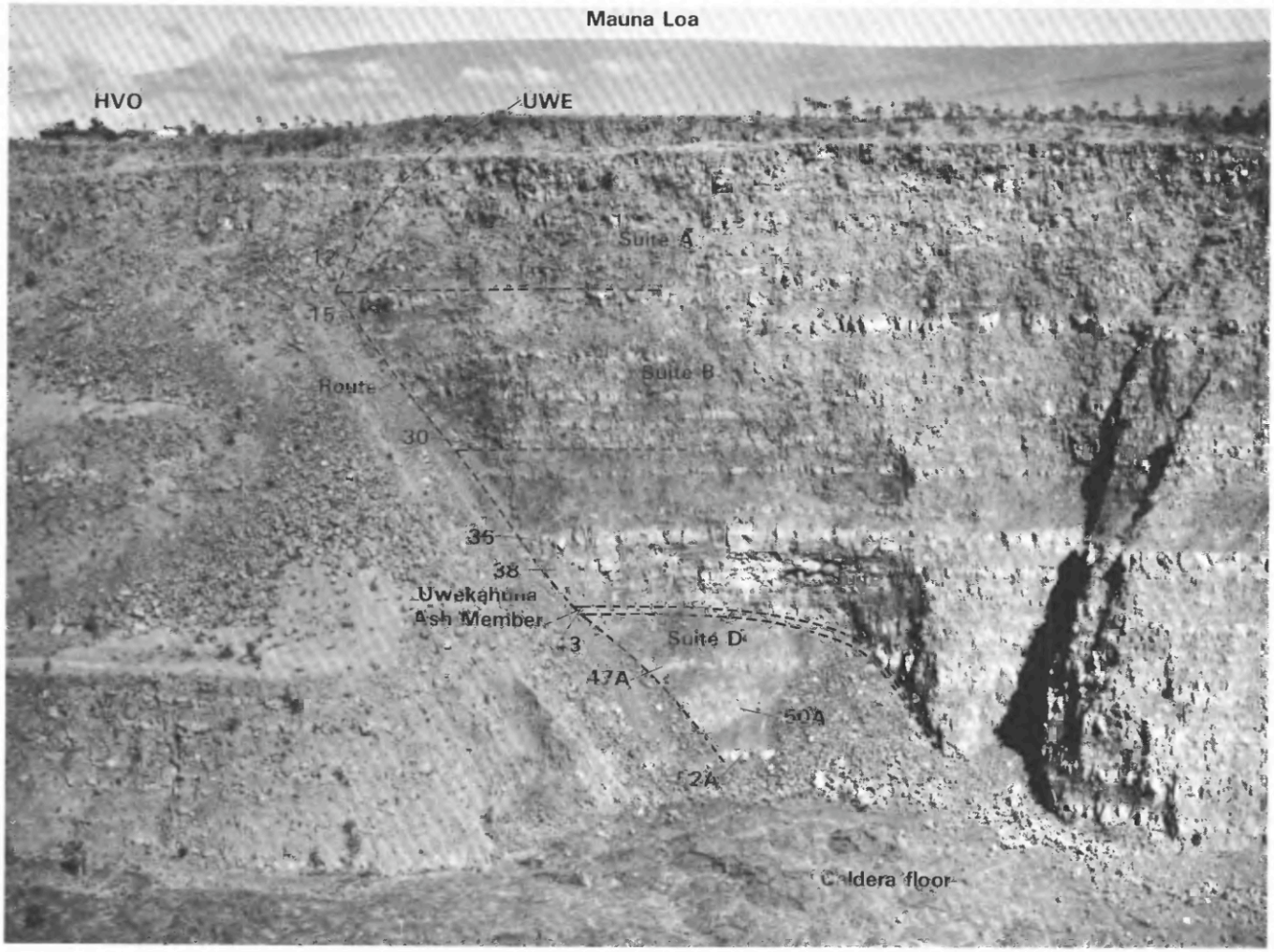

FIGURE 13.3.—Stratigraphic section exposed at Uwekahuna Bluff, with summit of Mauna Loa in distant background. Boundaries of lava suites A–D and position of the Uwekahuna Ash Member of the Puna Basalt are indicated. Selected units are labeled by number. Sampling route is shown by diagonal dashed line descending from Uwekahuna triangulation tower (UWE). HVO, Hawaiian Volcano Observatory. Height of cliff, from unit 52A up to rim, is 135 m.

section. After our sampling of the section in 1980, an earthquake in 1983 triggered rockfalls that buried the lower 50 m of the section, including all units below unit 38 (fig. 13.3).

Field criteria used to delineate lava flows and to distinguish between flows and sills include contact relations, particularly evidence for crosscutting and deformation of host rocks, and the textures of the top and bottom surfaces of a unit. Other features such as color, texture, mineralogy, and vesicle abundance and distribution, were occasionally helpful in tracing a flow unit. When viewed from a distance, the section appeared to have light-colored sills similar to the Uwekahuna laccolith. However, close examination of these suspected sills invariably revealed contact relationships that indicated an extrusive origin. We attempted to subdivide the Uwekahuna Bluff section as thoroughly as possible on the basis of field observations, while recognizing that petrologic considerations might eventually lead us to combine similar flow units into more generalized groups of flows.

The Uwekahuna Bluff section measured by Macdonald (Stearns and Macdonald, 1946, p. 193–194) differs from ours in detail, perhaps owing to different criteria used to distinguish flow units or to a different path selected for descent to the caldera floor.

FIELD OBSERVATIONS

Major features of the lava flows in the Uwekahuna Bluff section are summarized in table 13.1. The stratigraphic section at Uwekahuna Bluff consists of at least 63 flow units and 2 thick tephra deposits. The section is capped by the mostly A.D. 1790 Keanakakoi Ash Member, interpreted as the product of a large phreatomagmatic eruption possibly accompanied by partial caldera collapse (Swanson and Christiansen, 1973; Christiansen, 1979). The basal part of the Uwekahuna Ash Member exposed near the bottom of the bluff section has been assigned an age of 2.1 ka on the basis of radiocarbon dating of material from an inferred correlative

TABLE 13.1.—*Description of rock units from Uwekahuna Bluff section, Kilauea caldera, Hawaii*

[n.d., not determined]

Unit	Thickness (meters)	MgO content (wt percent)	Field description
			Keanakakoi Ash Member
0	0.3–1.0	n.d.	Ash from eruption circa A.D. 1790.
			Suite A flows
1	0.6	6.6	Flow varying in thickness from 0.3 to 1.3 m; vesicular pahoehoe with sparse olivine phenocrysts; reddish, oxidized ropy surface.
2	.9	6.6	Vesicular pahoehoe flow with sparse olivine phenocrysts.
3	4.9	6.6	Massive blocky flow with vesicular top, dense interior, and olivine phenocrysts.
4	2.75	6.8	Vesicular, ropy lava flow with red, ropy top and bottom; well-layered vesicularity; lower 0.6 m of unit is massive, dense; top and bottom flow surfaces dip toward caldera.
5	1.2	6.4	Vesicular, ropy lava flow; no layering of vesicles; similar to unit 4; flow contacts dip toward caldera.
6	4.25	6.7	Vesicular lava flow; top of flow is undulating and shows zones of vesicularity about 0.6 m wide; most of flow interior is dense.
7	.9	6.9	Vesicular flow that pinches out laterally; notably lenticular.
8	.6	6.8	Similar to flow 7.
9	1.5	7.0	Similar to flow 7.
10	3.35	6.7	Dense vesicular flow with rare zones 0.6–0.9 m thick, of dense nonvesicular material; lower 1.3 m is made of 1–3 reddish, oxidized, vesicular layers; base of unit is glassy.
11	4.1	7.3	Dense flow with rubbly, blocky aspect near top; in small gully, flow dips steeply toward crater, and measurement of true thickness is difficult.
12	5.0	6.3	Flow that dips toward caldera 27°–33°; rubble and talus cover in gully; large blocks and boulders cover this interval.
13	.3	6.6	Thin flow with glassy top and bottom.
14	.6	6.4	Thin flow with glassy top and bottom overlying reddish, highly oxidized zone.
			Suite B flows
15	1.7–10.5	7.0	Prominent red, oxidized layer with sharp upper contact; does not extend to south; may be faulted out or covered by rubble; may include several flows; oxidation occurs on fracture surfaces and in vesicles; flows dip toward caldera (maximum dip, 40°, average dip, 25°); reddish layers have a total thickness of 10.5 m; abundant loose blocks make it difficult to distinguish true bedrock.
16	.8	7.3	Distinct, thin flow unit with glassy top and bottom.
17	2.3	7.5	Light-gray rock with tiny olivine phenocrysts and irregular-shaped vesicles.
18	3.3	7.4	Massive flow with glassy top and bottom and dense zones or bands of nonvesicular material.
19	1.45	7.1	Flow with prominent irregular vesicles as large as 3 cm near top; rests on red, oxidized flow top that extends into cliff face to north.
20	.65	7.2	Thin flow, brownish gray and vesicular, that arches over an eye-shaped massive lens (tumulus?) and is overlain by prominent red, oxidized flow top.
21	2.5	7.4	Massive lens; thins rapidly to north.
22	.8	6.7	Unit composed of four thin, glassy vesicular flows with glassy tops.
23	.9–1.5	6.9	Unit of varying thickness, perhaps multiple flow units; highly vesicular with glassy flow tops and bottoms; thickens to north.
24	1.4	7.7	Vesicular flow with glassy top and red, oxidized glassy bottom; surface dips toward caldera.
25	2.1	8.0	Lens-like massive flow that thickens toward gully to south; may be an inflated pahoehoe flow.
26	4.4	7.8	Massive lens(?) of lava between two red, oxidized, vesicular flow contacts; open vugs as large as 1 cm; pipe vesicles in lower 2 m of flow.
27	4.3	7.0	Several thin (less than 1 m) red flows; highly vesicular; flow contacts dip 37°–39° and strike N. 35° E; this unit may be a tumulus.
28	2.4	7.5	Brown flow with irregular vesicles as large as 2 cm near top and dense interior with well-developed pipe vesicles; no coarse-grained zones; vesicles throughout; from a distance this unit may appear to be intrusive; to south this unit dips into gully; to north unit appears to thicken but is in cliff face and not accessible for measurement.
29	2.1	7.3	Similar in appearance to unit 28; massive, vesicular, brown, with glassy vesicular top; note 5 paleomagnetic drill holes 8X080 to 8X084; unit has prominent red, oxidized top and bottom surfaces that dip 21°–24° towards caldera and strike N. 38° E; this unit may be a tumulus.
30	1.9	7.4	Massive flow that thickens to 3.1 m in a 5-m lateral distance; vesicular throughout and highly fractured; brown-red color; a single flow with nearly horizontal top; to north along the cliff face unit appears more dense.
			Suite C flows
31	2.3	17.6	Package of thin, collapsed, shelly pahoehoe flows with excellent continuity to the north; highly vesicular with some ropy surfaces; individual flows from 4–10 cm in thickness; portions of unit contain abundant olivine phenocrysts (20 percent) as large as 5 mm.
32	1.5	18.1	Dense lava flow with obvious northward continuity and abundant olivine; paleomagnetic drill holes 8X075–8X079.
33	6.9	17.2	Prominent unit of numerous thin flows, probably collapsed shelly pahoehoe; flows highly vesicular, reddish, oxidized material, very friable; abundant olivine; flows dip about 5° away from caldera.
34	1.5	14.5	Prominent thin, dense, olivine-bearing lava flow, moderately vesicular; paleomagnetic drill holes 8X070–8X074; unit extends to north along cliff face.
35	2.5	13.7	Thin flows of collapsed shelly pahoehoe with prominent olivine phenocrysts (5–10 percent); unit dips 22° toward caldera.
36	3.3	13.2	Massive gray flow unit with lateral continuity to north; vesicular with prominent curving fractures; paleomagnetic drill holes 8X065–8X069; contains less olivine (up to 5 percent phenocrysts as large as 3 mm) than overlying units.
37	3.0	17.3	Gray-brown massive flow unit with large vesicles near top and dense interior; dips 10° toward caldera; poor lateral continuity, may be a lens; paleomagnetic drill holes 8X060–8X064.
38	2.4	9.0	Flow that interfingers with unit 37 to north, where units become difficult to distinguish; both have red, oxidized tops.
39	2.3	14.5	Unit composed of several thin horizontal layers 0.2–0.3 m thick; abundant (10 percent) olvine phenocrysts as large as 4 mm; paleomagnetic drill holes 1D070–1D075.
40	3.0	10.1	Massive, vesicular unit that becomes indistinct to north; contains abundant olivine (5 percent) as large as 2 mm but mostly less than 1 mm.
41	3.1	14.0	Vesicular unit that looks like aa flow, jumble of thin flows, and rubble; lower contact is red surface; contact with overlying flow is indistinct; contains abundant (5–10 percent) olivine as large as 3 mm.
42	1.3	19.7	Dense, vesicular flow above Uwekahuna Ash Member; paleomagnetic drill holes 1D076–1D083; abundant (10–15 percent) olivine phenocrysts with some lenses and pods containing as much as 50 percent olivine.

TABLE 13.1.—*Description of rock units from Uwekahuna Bluff section, Kilauea caldera, Hawaii*—Continued

Unit	Thickness (meters)	MgO content (wt percent)	Field description
			Beneath unit 42
43	1.5–2.2	6.5–9.7	Uwekahuna Ash Member.
			Flows of suite C ponded against Uwekahuna Ash Member
44	3.6	9.2	Upper 0.9 m, red rubble and vesicular flow with pipe vesicles; middle 1.2 m, massive flow with large, irregular vesicles; lower 1.5 m, dense, massive flow unit with finger-shaped gas vesicles.
45	7.1	13.0	Thick, massive unit overlain by 0.2–0.6 m, of reddish rubble; unit contains trains of vesicles in middle 1.5–2 m; olivine phenocrysts as large as 5 mm locally make up 10–15 percent of rock; obvious lateral continuity to north; flow has shattered or fractured appearance; bottom of unit rests on red, rubbly oxidized flow top.
46	1.8	13.3	Red, vesicular, blocky flows; several lobes of one or more flows, each with a well-preserved black glassy surface; fractured, with abundant olivine.
47	1.3	13.0	Gray-green massive flow with large irregular vesicles; olivine phenocrysts as large as 7 mm make up about 15 percent of rock; lower contact is glassy top of underlying flow unit 48.
48	3.2	9.8	Gray-green vesicular massive flow with abundant olivine as large as 3 mm.
49	.6	10.4	Olivine-rich (phenocrysts as large as 2 mm) pahoehoe flow overlying an aa flow.
50	2.7	10.1	Aa flow; top 1.5 m is rubble overlying dense interior; white sublimates on surface of blocks in rubble.
51	2.0	7.5	Dense flow overlying ash; contains portions of what may be foundered crust.
			Uwekahuna Ash Member beneath unit 51
---	4.8	---	Uwekahuna Ash Member here is 1.4 m thick; base of ash covered by 3.4 m of talus extending down to 1919 flows on caldera floor.
			Suite D flows
44A	0.6	n.d.	Scoriaceous rubble; possibly an aa flow top or scoria from nearby vent.
45A	2.4	n.d.	Massive, non-porphyritic, vesicular lava flow; lower 1.5 m forms prominent bench.
46A	1.6	n.d.	Mantled rubble, possibly infiltrated by tephra from unit 43; lower contact indistinct and highly oxidized, with some smooth, glassy (pahoehoe?) surfaces.
47A	2.4	7.1	Prominent massive flow clearly visible in fig. 13.3; fine-grained and vesicular, with weathered surface that is light colored; two paleomagnetic drill holes 1.2 m from lower contact, others may be covered by talus from the November 1975 earthquake; sample from dense lower portion of flow near paleomagnetic holes.
48A	4.2	n.d.	Rubble-covered flow; massive and vesicular; interior mostly covered by talus and ash from above, but appears to be dense and blocky; two paleomagnetic drill holes in lower portion of unit may be in an erratic boulder.
49A	1.8	n.d.	Massive, vesicular lava flow with buff weathered surface; flinty or glassy surface at top; unit contains eight paleomagnetic drill holes about 20 cm from lower contact.
50A	2.5	7.4	Massive flow unit with both vesicular and dense portions; dark gray in fresh outcop, but buff on weathered surface; sampled near base of flow.
51A	4.2	n.d.	Flow 1.5 m below base of unit 50A; surface dips 32° toward caldera; most of interval is covered by rubble and talus overlying massive, buff unit 52A.
52A	2.2	7.8	Massive, dense unit at base of section; contains unusual texture, similar to that of foundered crust from Kilauea Iki drill holes—dense non-vesicular lenses interlayed with vesicular material; samples from middle of unit.
53A	4.1	n.d.	Talus-covered slope to caldera floor, which here consists of 1919 flow.

unit outside of the caldera (Lockwood and Rubin, 1986). Based on the wider dispersal of the Uwekahuna Ash Member, its eruptions were probably more violent than eruption of the Keanakakoi (Dzurisin and Casadevall, 1986).

Flows in the Uwekahuna Bluff section can be grouped into four suites differing in hand-specimen mineralogy and field occurrence (fig. 13.3). Suite A (units 1–14), at the top of the section, includes numerous thin lenticular pahoehoe flows containing small (less than 5 mm) plagioclase laths and rare olivine phenocrysts. A few thicker and more massive flows occur in this suite, but these usually lack the lateral persistence of similar massive flows lower in the section.

Suite B (units 15–30) consists of flows that contain rare phenocrysts of olivine and plagioclase. The glassy upper surface of flow 15, the youngest in suite B, is strongly weathered and pale yellow to red-brown. The texture of this surface is preserved, and no soil was found on it. This weathered surface is the only physical evidence we discovered for a significant time break within the Uwekahuna Bluff section; it correlates with the change from the mostly aphyric flows of suite B to the porphyritic flows of suite A.

Suite C (units 31–42 and 44–51; unit 43 is the Uwekahuna Ash Member) contains flows having abundant olivine phenocrysts and little or no plagioclase visible in hand specimen. The olivine content in individual flows varies greatly and probably reflects crystal settling during flow (Fuller, 1939). We generally selected only one sample from each flow, and this is insufficient to characterize the olivine content of the entire flow. Several units consist of packages of thin (a few centimeters thick) highly vesicular layers interpreted as near-vent shelly pahoehoe flows that collapsed because of degassing and the weight of overlying flows (Swanson, 1973). A few units (for example, unit 36) are more massive and have dense interiors. These usually have appreciable lateral continuity and can be traced northward in the wall for as much as 2 km.

The Uwekahuna Ash Member (unit 43) underlies suite C. Along the south side of Uwekahuna Bluff, the ash directly underlies unit 42, about 35 m above the caldera floor (fig. 13.3). Farther north, the ash mantles an old northeast-facing slope and drops to within a few meters of the caldera floor (fig. 13.3). Ponded against this slope and overlying the ash are olivine-rich aa and pahoehoe lava flows (units 44–51), which petrographically and chemically resemble units 31–42.

Suite D (units 44A–52A) contains fairly massive and sparsely vesicular aphyric flows beneath the Uwekahuna Ash Member. Most are poorly exposed because of mantling by talus and ash from above. The near absence of olivine phenocrysts makes these flows petrographically distinct from those of suite C. Flows of suite D are

exposed in a 30-m-thick section that is cut off by a northeast-facing slope mantled by the Uwekahuna Ash Member and buried by the flows of suite C (fig. 13.3). North of Uwekahuna Bluff, the ash is essentially horizontal and extends for more than 1.5 km at a constant level above the caldera floor (Powers, 1948), which level corresponds to the lower elevation of the ash in the bluff section. The horizontal ash layer probably covered a broad, relatively flat surface, similar to that of the present caldera floor.

PETROGRAPHY

We examined 57 thin sections of rocks from Uwekahuna Bluff. Nearly all samples contain olivine phenocrysts in a holohyaline to holocrystalline groundmass. Most groundmass textures are intersertal, with brown glass between microlites. Intergranular texture is most common in the dense flow interiors, particularly in those from picritic units 44–51. Crystallinity ranges from about 25 to 85 percent. In the more crystalline samples, the groundmass consists of clinopyroxene and plagioclase in overlapping or felted microlites too small for individual crystals to be recognized. Most samples contain dark brown glass and scattered small anhedral opaque grains. Olivine is present as euhedral to subhedral phenocrysts that range in shape from stout and prismatic to elongate and lathlike. In most flows, a few olivine crystals occur in the microcrystalline groundmass. The olivine microlites and phenocrysts are in general partly resorbed and corroded. Clinopyroxene and plagioclase occur as coarse granular aggregates of subhedal crystals in which pyroxene subophitically or ophitically encloses plagioclase, as rosettes or sprays of clinopyroxene and plagioclase, and less commonly as individual phenocrysts and microlites.

Modal abundances for thin sections from 21 flows were determined by standard point-count methods (fig. 13.4). Microlites (0.05–1 mm) of plagioclase, clinopyroxene, and olivine; phenocrysts (greater than 1 mm) of plagioclase, clinopyroxene, and olivine; groundmass (microlites less than 0.05 mm); and vesicles were counted. Hypersthene was looked for but not found. Flows of suite C form a distinct cluster because of their high olivine content. Flows of suites B and D contain only sparse olivine and plagioclase, and flows of suite A are similar to the aphyric lavas except in their greater abundance of plagioclase.

CHEMISTRY

The basalt lavas of Uwekahuna Bluff are olivine tholeiite similar to other Kilauea summit flows (Macdonald, 1949; Wright, 1971; Wright and Tilling, 1980). Units 1–51 and 47A, 50A, and 52A were analyzed for major-element composition by rapid rock-analytical methods (Shapiro, 1975) and for trace-element and rare-earth-element compositions by instrumental neutron-activation (Baedecker, 1979) and atomic-absorption techniques (table 13.2). Precisions for major-element oxides (variation in percent of reported weight percent value) in rocks of basaltic composition are as follows: SiO_2 (0.3), Al_2O_3 (0.2), CaO (0.2), MgO (0.1), Na_2O (0.1), K_2O (0.1), Fe total (0.1), TiO_2 (0.05), P_2O_5 (0.04), MnO (0.04). Error limits (variation in percent of reported ppm value) for trace-element analyses for one standard deviation (one sigma) are as follows: Ba (10–20), Co (1), Cr (1), Hf (2), Rb (25–30), Ta (3), Th (6–12), Zn (2), Zr (10), Sc (1), La (1–2), Ce (2), Nd (7–17), Sm (1), Eu (1), Gd (8–25), Tb (2–3), Tm (5–15), Yb (3), Lu (3). For Cu, Co, and Ni values determined by atomic absorption methods, uncertainties are ± 2 percent of reported ppm value. To facilitate comparison of chemical data, we have recalculated all analyses from table 13.2 on a dry-weight basis after converting iron to FeO_t ($FeO_t = FeO + 0.9Fe_2O_3$). The recalculated analyses are plotted on MgO variation diagrams (fig. 13.5), following Powers (1955) and Wright (1971, 1974).

MAJOR-ELEMENT CHEMISTRY

The major-element compositions of units 1–30 (suites A and B) and 47A, 50A, and 52A (suite D) are broadly similar (fig. 13.5A) and vary only slightly with stratigraphic position (fig. 13.6A). The MgO contents in all these units lie between 6.4 and 8.0 weight percent (table 13.2). Flow units 31 through 51 (suite C), however, contain various amounts of olivine, and their MgO contents range from 7.5 to 19.7 weight percent. The chemistries of units 31–51 show considerable variation with stratigraphic position (fig. 13.6A) because of differing olivine contents within each picritic flow. This wide range in olivine content for the picritic flows of suite C facilitates precise calculation of olivine-control lines by linear least-squares regression. This procedure yields equations of the form $y = ax + b$, where y is the major oxide or element, x is the MgO content, a is the slope, and b is the y intercept value at MgO = 0 weight percent (table 13.3). Most oxides correlate negatively with MgO (fig. 13.5A), indicating the diluting effect of increasing olivine content on elements that do not enter the olivine crystal structure.

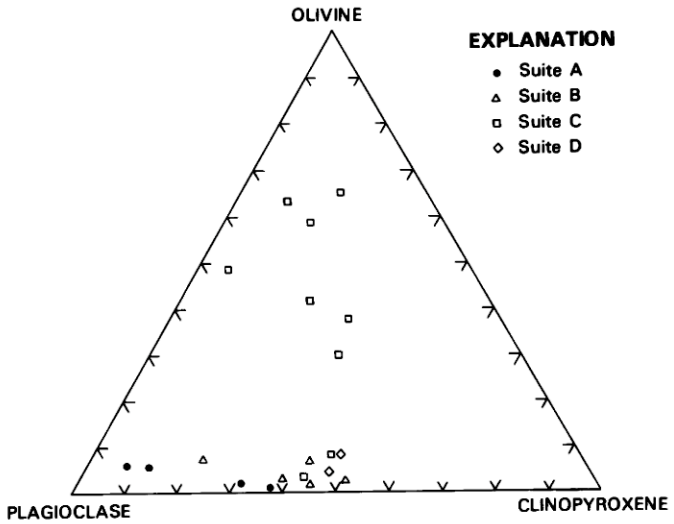

FIGURE 13.4.—Ternary diagram (clinopyroxene-olivine-plagioclase) derived from volumetric modal analyses (1,000 points per thin section) of 21 flows from Uwekahuna Bluff section.

TABLE 13.2.—*Chemical analyses of Uwekahuna Bluff samples*

[Values for oxides in weight percent; values for trace elements in parts per million. Symbols P, X, O, A, and U used to distinguish lava suites A–D and Uwekahuna Ash Member, respectively, in figs. 13.4–13.6 and 13.10. INAA, neutron-activation analysis; AA, atomic-absorption analysis; n.d., not determined; <, less than]

Sample symbol	UWE-1 P	UWE-2 P	UWE-3 P	UWE-4 P	UWE-5 P	UWE-6 P	UWE-7 P	UWE-8 P	UWE-9 P	UWE-10 P	UWE-11 P	UWE-12 P
SiO_2	50.8	51.1	51.0	50.4	51.6	51.1	51.2	51.2	51.3	50.8	50.4	51.3
Al_2O_3	14.0	14.0	13.8	13.9	13.8	13.8	13.7	13.6	13.9	13.8	13.6	13.8
Fe_2O_3	2.5	5.7	2.9	6.7	5.3	5.2	6.6	4.3	4.1	4.5	3.2	6.7
FeO	8.9	5.9	9.1	5.8	7.4	7.2	5.6	7.5	7.7	8.0	8.4	5.7
MgO	6.6	6.6	6.6	6.8	6.4	6.7	6.9	6.8	7.0	6.7	7.3	6.3
CaO	10.5	10.7	10.6	10.5	10.6	10.7	10.7	10.7	10.5	10.7	11.2	10.7
Na_2O	2.5	2.3	2.4	2.4	2.5	2.4	2.4	2.4	2.4	2.5	2.3	2.5
K_2O	.47	.44	.47	.46	.46	.47	.44	.44	.44	.45	.42	.42
H_2O	.16	.21	.16	.18	.03	.30	.15	.10	.11	.17	.12	.29
TiO_2	2.6	2.5	2.6	2.5	2.6	2.6	2.4	2.6	2.4	2.5	2.3	2.6
P_2O_5	.31	.32	.32	.31	.32	.30	.29	.31	.30	.31	.29	.32
MnO	.22	.16	.18	.20	.18	.17	.17	.17	.18	.17	.16	.18
Ba	152	104	135	144	106	139	132	111	104	116	105	124
Co (INAA)	43	43	43	42	43	42	44	44	43	43	44	43
Co (AA)	44	44	44	46	42	44	43	46	44	42	42	44
Cr	353	336	309	338	313	327	366	331	351	313	354	235
Ni	96	100	93	91	80	91	110	98	100	87	93	82
Cu	130	120	99	130	130	95	120	130	130	120	92	140
Hf	4.06	3.93	4.05	3.85	4.13	4.00	3.85	4.02	3.92	4.00	3.57	4.05
Rb	<8	<20	16	10	9	12	15	13	13	14	<20	8
Ta	.94	.96	.95	.86	.97	.92	.88	.86	.81	.91	.83	.85
Th	.98	.84	.94	.88	.90	.83	.92	.78	.90	.89	.82	.83
U	<0.3	<0.3	<0.3	<0.3	.5	<0.3	<0.3	<0.3	<0.3	<0.3	<0.3	<0.4
Zn	112	108	111	105	118	111	108	113	110	110	109	116
Zr	152	164	181	158	152	159	138	159	151	182	145	117
Sc	31.0	31.0	30.7	30.8	32.1	30.7	30.6	31.6	31.0	31.7	33.4	33.0
La	12.7	12.7	12.9	11.9	12.8	11.8	11.7	11.8	11.6	11.8	10.8	10.9
Ce	31.6	29.9	30.3	28.5	31.3	29.5	29.5	28.9	28.2	29.7	26.5	27.8
Nd	19	21	20	12	22	20	20	21	22	24	20	18
Sm	5.83	5.76	5.89	5.66	6.09	5.66	5.68	5.81	5.57	5.80	5.28	5.80
Eu	1.93	1.89	1.91	1.83	2.04	1.88	1.90	1.92	1.89	1.92	1.78	1.93
Gd	5.8	6.6	5.8	6.1	7.4	6.4	5.8	6.4	7.1	6.9	5.9	6.0
Tb	1.02	.96	.98	.96	1.02	.95	.92	.96	.88	1.00	.88	1.01
Tm	.33	.17	.29	.29	.31	.35	.34	.39	.34	.39	.34	.41
Yb	2.22	2.25	2.18	2.26	2.48	2.17	2.25	2.31	2.09	2.18	2.08	2.48
Lu	.311	.299	.308	.301	.307	.290	.294	.309	.287	.319	.296	.340

Sample symbol	UWE-13 P	UWE-14 P	UWE-15-1 X	UWE-15-2 X	UWE-16 X	UWE-17 X	UWE-18 X	UWE-19 X	UWE-20 X	UWE-21 X	UWE-22 X	UWE-23 X
SiO_2	51.4	50.8	51.6	51.2	50.3	51.1	51.7	50.8	50.4	51.3	50.4	50.7
Al_2O_3	13.7	14.0	13.5	13.7	13.7	13.7	13.6	13.6	13.8	13.4	13.6	13.3
Fe_2O_3	7.7	4.9	4.4	3.3	4.1	3.4	2.6	5.1	4.8	3.0	4.0	3.0
FeO	5.2	7.4	8.1	8.6	8.1	8.7	9.1	6.5	7.3	9.4	8.1	9.4
MgO	6.6	6.4	7.0	6.5	7.3	7.5	7.4	7.1	7.2	7.4	6.7	6.9
CaO	10.7	10.6	10.5	10.6	10.6	10.7	10.6	10.6	10.8	10.9	10.8	10.8
Na_2O	2.5	2.4	2.4	2.3	2.3	2.3	2.3	2.3	2.3	2.3	2.4	2.3
K_2O	.44	.43	.40	.40	.38	.38	.39	.38	.42	.42	.46	.47
H_2O	.06	.10	.05	.09	.14	.11	.07	.52	.29	.14	.25	.03
TiO_2	2.6	2.5	2.6	2.5	2.4	2.4	2.4	2.4	2.4	2.5	2.7	2.7
P_2O_5	.32	.30	.31	.28	.30	.30	.29	.28	.30	.30	.31	.30
MnO	.18	.18	.17	.17	.17	.16	.17	.17	.17	.17	.18	.17
Ba	90	97	<200	81	108	83	89	105	115	118	137	129
Co (INAA)	42	41	45	44	46	45	46	45	44	46	45	45
Co (AA)	42	42	44	44	46	48	46	48	44	46	44	48
Cr	266	235	415	287	354	386	354	351	344	316	252	265
Ni	91	84	100	96	100	110	110	100	110	110	80	87
Cu	140	140	120	110	120	100	110	120	120	98	140	120
Hf	3.74	3.76	3.68	3.81	3.67	3.48	3.66	3.67	3.59	4.00	4.05	4.06
Rb	12	9	<20	<20	<20	11	<20	<20	<20	12	11	<20
Ta	.80	.76	.74	.77	.74	.75	.77	.75	.79	.86	1.05	.99
Th	.73	.83	.66	.74	.74	.70	.77	.71	.69	.74	.91	.91
U	<0.3	0.30	<0.4	<0.4	<0.4	<0.3	<0.4	<0.4	<0.4	<0.4	0.30	<0.4
Zn	110	110	113	109	107	109	108	113	104	110	113	113
Zr	130	161	148	120	142	152	132	129	135	121	149	140
Sc	32.0	31.4	32.4	33.1	33.0	32.1	32.4	32.0	31.8	33.5	32.8	32.3
La	10.7	10.8	10.1	10.4	9.9	10.2	10.5	10.4	10.5	13.0	12.1	12.8
Ce	26.5	26.8	25.6	26.5	25.8	25.6	26.6	26.0	26.8	27.9	31.1	30.4
Nd	16	21	18	19	16	19	19	19	19	23	20	23
Sm	5.61	5.70	5.50	5.44	5.26	5.26	5.40	5.40	5.40	5.80	5.90	5.90
Eu	1.83	1.85	1.82	1.82	1.76	1.75	1.79	1.76	1.77	1.87	1.94	1.95
Gd	7.1	7.1	5.5	5.4	6.2	6.7	6.1	6.1	5.8	4.3	7.9	7.5
Tb	.93	.94	.97	.96	1.01	.91	.95	.93	.94	.98	.99	.95
Tm	.35	.39	.38	.35	.33	.32	.31	.26	.33	.30	.43	.29
Yb	2.25	2.34	2.35	2.12	2.19	2.17	2.27	2.10	2.03	2.42	2.37	2.20
Lu	.340	.319	.312	.299	.303	.301	.306	.301	.301	.300	.301	.322

Sample symbol	UWE-24 X	UWE-25-1 X	UWE-25-2 X	UWE-26 X	UWE-27 X	UWE-28 X	UWE-29 X	UWE-30-1 X	UWE-30-2 X	UWE-31 O	UWE-32 O	UWE-33 O
SiO_2	50.0	50.7	50.6	50.9	50.6	50.5	50.8	50.5	50.8	47.6	47.7	47.7
Al_2O_3	13.4	13.5	13.3	13.3	13.7	13.5	13.2	13.3	14.0	9.9	10.2	10.1
Fe_2O_3	4.4	2.6	3.3	4.0	6.9	4.7	5.3	5.0	3.3	3.4	3.2	6.0
FeO	8.1	9.4	9.2	8.7	6.0	8.0	7.6	7.1	8.5	8.5	8.7	6.9
MgO	7.7	8.0	7.8	7.8	7.0	7.5	7.3	7.4	6.5	17.6	18.1	17.2
CaO	11.1	11.4	11.1	10.9	11.0	10.9	11.0	10.9	10.6	7.9	9.0	9.0
Na_2O	2.0	2.3	2.3	2.2	2.4	2.5	2.5	2.2	2.5	1.5	1.6	1.6

TABLE 13.2.—*Chemical analyses of Uwekahuna Bluff samples*—Continued

Sample symbol	UWE-1 P	UWE-2 P	UWE-3 P	UWE-4 P	UWE-5 P	UWE-6 P	UWE-7 P	UWE-8 P	UWE-9 P	UWE-10 P	UWE-11 P	UWE-12 P
K_2O	.45	.43	.43	.42	.44	.50	.47	.43	.45	.30	.29	.30
H_2O	.14	.08	.50	.07	.23	.24	.09	.22	.12	.41	.19	.28
TiO_2	2.1	2.4	2.4	2.4	2.6	2.5	2.6	2.5	2.5	1.8	1.8	1.9
P_2O_5	.29	.26	.28	.28	.29	.29	.31	.29	.31	.18	.21	.23
MnO	.20	.18	.17	.16	.18	.17	.18	.18	.17	.16	.15	.17
Ba	106	114	108	131	142	132	155	151	95	n.d.	140	96
Co (INAA)	46	48	47	48	44	45	46	45	43	n.d.	76	72
Co (AA)	49	49	48	49	46	46	44	44	44	n.d.	74	74
Cr	403	440	456	461	321	332	346	372	309	n.d.	1100	1040
Ni	110	120	120	130	89	96	100	110	89	n.d.	760	740
Cu	120	95	91	110	120	130	120	130	110	n.d.	90	96
Hf	3.83	3.57	3.61	3.69	3.90	3.97	3.86	3.74	4.01	n.d.	2.98	2.95
Rb	15	<20	<20	13	13	12	<20	<20	<10	n.d.	<20	14
Ta	.92	.82	.84	.94	1.01	.98	1.01	1.02	.85	n.d.	.72	.75
Th	.85	.88	.64	.88	.99	.84	.86	.85	.81	n.d.	.52	.60
U	<0.4	<0.4	<0.4	.16	<0.5	.27	.21	.24	.30	n.d.	<0.5	.27
Zn	111	110	109	107	111	109	114	109	108	n.d.	105	102
Zr	144	146	168	135	167	162	127	166	147	n.d.	131	103
Sc	31.5	32.8	32.7	32.7	32.0	31.6	32.5	33.0	31.4	n.d.	26.0	25.3
La	12.2	10.6	11.0	11.4	12.7	12.4	13.3	12.6	12.2	n.d.	8.9	9.29
Ce	28.0	26.1	26.6	27.4	30.7	30.5	30.6	30.5	29.7	n.d.	22.7	22.9
Nd	22	18	16	23	23	22	21	21	26	n.d.	18	15.8
Sm	5.84	5.30	5.40	5.50	6.10	5.80	6.00	5.85	6.00	n.d.	4.42	4.23
Eu	1.81	1.70	1.73	1.79	1.85	1.86	1.84	1.80	1.92	n.d.	1.38	1.37
Gd	6.7	5.6	6.4	5.2	5.2	6.6	5.7	5.9	7.2	n.d.	3.4	3.6
Tb	.99	.87	.87	.88	.94	.92	.97	.91	1.00	n.d.	.79	.65
Tm	.35	.35	.39	.32	.33	.31	.32	.33	.37	n.d.	.31	.213
Yb	2.03	2.02	2.11	2.09	2.19	2.05	2.07	2.00	2.47	n.d.	1.73	1.65
Lu	.299	.270	.280	.310	.313	.309	.34	.27	.317	n.d.	.26	.238

Sample symbol	UWE-34 O	UWE-35 O	UWE-36 O	UWE-37 O	UWE-38 O	UWE-39 O	UWE-40 O	UWE-41 O	UWE-42 O	UWE-43 U	UWE-44 O	UWE-45 O
SiO_2	48.6	48.6	48.8	48.0	50.5	49.0	49.4	48.9	47.2	50.8	50.8	49.2
Al_2O_3	11.2	11.4	11.6	10.0	13.2	10.8	12.4	11.6	9.4	13.2	13.0	10.7
Fe_2O_3	5.4	8.1	4.8	3.0	4.8	4.0	4.0	5.8	3.3	3.1	4.0	3.3
FeO	6.8	4.6	7.4	9.3	6.5	8.8	7.9	6.4	9.6	8.0	7.6	9.7
MgO	14.5	13.7	13.2	17.3	9.0	14.5	10.1	14.0	19.7	9.5	9.2	13.0
CaO	9.6	9.5	10.0	8.4	10.5	8.9	10.5	9.5	8.3	10.2	10.9	8.8
Na_2O	1.7	1.8	1.9	1.7	2.2	1.8	2.0	2.0	1.5	1.9	2.2	2.0
K_2O	.30	.35	.39	.34	.41	.39	.43	.37	.26	.42	.42	.46
H_2O	.11	.19	.64	.18	.30	.27	.40	.15	.27	.27	.20	.24
TiO_2	2.1	2.2	2.2	1.8	2.5	2.2	2.4	2.2	1.5	2.4	2.5	2.8
P_2O_5	.23	.25	.26	.22	.29	.25	.31	.27	.17	.29	.29	.36
MnO	.19	.15	.18	.17	.17	.16	.16	.14	.18	.16	.16	.16
Ba	99	96	<100	<200	<200	<200	86	90	<200	107	81	120
Co (INAA)	65	62	63	76	48	71	53	62	85	50	45	64
Co (AA)	66	63	66	79	50	72	58	68	85	53	50	68
Cr	961	869	887	1090	602	987	687	861	1260	535	626	790
Ni	580	490	490	790	230	600	320	490	870	230	220	500
Cu	100	95	89	78	120	100	110	110	53	110	120	120
Hf	3.06	3.26	3.43	2.72	3.8	3.30	3.61	3.32	2.33	3.30	3.7	4.15
Rb	11	10	<30	13	18	<30	11	<30	<30	8	<30	13
Ta	.79	.81	.87	.64	.91	.87	.91	.86	.56	.85	.95	1.09
Th	.67	.70	.65	.51	.75	.65	.67	.60	.52	.82	.73	.70
U	<0.5	.35	<0.4	<0.5	.23	<0.3	<0.5	.33	<0.4	.40	.44	.31
Zn	104	106	112	108	119	107	109	109	108	103	100	122
Zr	104	103	140	<100	131	<200	148	178	120	154	136	152
Sc	27.1	27.2	27.7	24.6	31.2	27.3	29.6	27.5	24.2	28.1	30.1	28.3
La	9.88	10.2	11.0	8.3	11.6	10.3	11.5	10.6	7.0	11.7	12.4	12.9
Ce	24.1	24.8	26.6	21.1	27.6	25.6	27.0	24.9	18.3	26.6	28.3	30.4
Nd	16.9	17.7	22	13	24	16	19	18	11	21	18	23
Sm	4.50	4.72	5.13	4.11	5.44	4.81	5.31	5.00	3.47	5.56	5.59	5.93
Eu	1.50	1.53	1.65	1.37	1.81	1.55	1.70	1.56	1.16	1.62	1.76	1.83
Gd	3.8	3.6	6.2	4.8	6.7	5.5	6.5	5.3	4.1	6.0	6.4	6.0
Tb	.71	.72	.88	.62	.97	.77	.85	.84	.58	.80	.96	.96
Tm	.20	.241	.27	.22	.38	.27	.31	.29	.19	.40	.29	.32
Yb	1.76	1.83	1.93	1.56	2.24	1.76	2.13	1.85	1.45	2.02	2.23	2.24
Lu	.259	.265	.287	.238	.34	.25	.299	.27	.21	.310	.30	.319

Sample symbol	UWE-46 O	UWE-47 O	UWE-48 O	UWE-49 O	UWE-50 O	UWE-51 O	UWE-47A A	UWE-50A A	UWE-52A A
SiO_2	49.0	47.4	47.5	48.4	50.0	50.1	49.8	50.0	49.6
Al_2O_3	11.5	11.5	12.4	12.4	12.8	13.1	13.6	13.2	13.5
Fe_2O_3	3.9	3.7	2.4	5.0	2.7	2.4	3.0	3.0	3.4
FeO	8.5	8.8	9.8	7.0	9.0	9.2	8.5	9.0	8.3
MgO	13.3	13.0	9.8	10.4	10.1	7.5	7.1	7.4	7.8
CaO	9.0	10.4	12.2	11.2	11.2	11.4	12.1	11.1	11.3
Na_2O	1.9	2.0	2.3	2.2	2.1	2.2	2.2	2.3	2.3
K_2O	.35	.37	.41	.42	.39	.44	.49	.50	.44
H_2O	.82	.24	.30	.08	.19	.36	.54	.36	.52
TiO_2	2.3	2.2	2.6	2.5	2.3	2.6	2.7	2.6	2.6
P_2O_5	.25	.29	.22	.33	.26	.31	.31	.29	.29
MnO	.18	.18	.20	.18	.18	.18	.18	.20	.18
Ba	<200	<200	120	133	103	123	148	128	127
Co (INAA)	68	61	51	52	54	45	44	44	45
Co (AA)	75	67	56	58	60	52	48	50	50
Cr	946	753	555	597	739	395	285	334	347

TABLE 13.2.—*Chemical analyses of Uwekahuna Bluff samples*—Continued

Sample symbol	UWE-46 O	UWE-47 O	UWE-48 O	UWE-49 O	UWE-50 O	UWE-51 O	UWE-47A A	UWE-50A A	UWE-52A A
Ni	670	460	220	240	290	120	100	110	120
Cu	71	100	130	120	98	100	91	67	110
Hf	2.99	3.5	3.8	3.68	3.4	3.9	4.01	3.98	3.8
Rb	<30	<30	<30	14	<30	15	<30	14	<20
Ta	.70	.93	1.02	.94	.85	1.03	1.10	1.13	1.08
Th	.70	.73	.80	.78	.68	.86	.97	.98	.92
U	.28	<0.5	<0.5	.29	.32	<0.6	<0.5	.30	<0.6
Zn	108	106	113	113	101	121	106	115	112
Zr	102	<200	140	130	152	154	125	202	179
Sc	25.4	27.2	29.9	30.0	30.0	31.8	31.1	31.4	31.3
La	9.6	11.1	12.7	11.7	10.7	12.4	13.4	13.8	13.3
Ce	23.9	26.9	29.8	28.3	26.3	29.3	32.4	32.7	31.3
Nd	21	18	19	20	15	20	24	21	23
Sm	4.61	5.28	5.83	5.48	5.11	5.75	5.82	5.88	5.61
Eu	1.46	1.68	1.88	1.81	1.69	1.89	1.93	1.92	1.84
Gd	4.6	6.1	6.4	6.2	5.6	7.0	7.2	6.9	5.8
Tb	.72	.80	1.00	.90	.75	.91	.95	.91	.88
Tm	.29	.28	.33	.35	.28	.34	.32	.31	.27
Yb	1.80	2.06	2.24	2.19	1.89	2.25	2.19	2.17	2.05
Lu	.244	.27	.30	.297	.27	.34	.36	.304	.297

TABLE 13.3.—*Olivine control lines*

[Coefficients for equations of the form $y = ax + b$, where y is the major oxide or element, x is the MgO content, a is the slope, and b is the y intercept value at MgO = 0 weight percent. Values for oxides in weight percent; values for trace elements in parts per million; uncertainty is one standard deviation either side of the mean slope. Data for PHKILCAL (prehistoric Kilauea caldera and Hilina flows), KIL1959 (Kilauea Iki, 1959), HISTML (historic Mauna Loa), and PPPC (prehistoric pahoehoe picrite complex flows from Wright, 1971). FeO_t, total iron oxide = FeO + 0.9 Fe_2O_3; n.d., not determined]

Element	Suites A–D		Suite C		PPPC		PHKILCAL		KIL1959		HISTML	
	(*a*)	(*b*)	(*a*)	(*b*)	(*a*)	(*b*)	(*a*)	(*b*)	(*a*)	(*b*)	(*a*)	(*b*)
SiO_2	−0.315±.028	52.842	−0.248±.064	51.828	−0.289±0.023	52.894	−0.317±0.021	53.327	−0.266±0.005	51.922	−0.312±0.010	54.260
Al_2O_3	−.348±.012	16.036	−.336±.025	15.852	−.357±.010	16.643	−.354±.028	16.585	−.325±.008	15.943	−.338±.007	16.527
FeO_t	.027±.020	11.456	.071±.037	10.811	.068±.017	10.480	.081±.030	10.260	.035±.003	11.046	.025±.006	10.747
CaO	−.204±.027	12.298	−.306±.056	12.797	−.288±.017	12.184	−.266±.016	13.044	−.284±.010	12.674	−.263±.005	12.400
Na_2O	−.073±.005	2.852	−.070±.008	2.822	−.053±.007	2.691	−.065±.005	2.753	−.059±.002	2.705	−.059±.003	2.702
K_2O	−.013±.002	.524	−.015±.003	.556	−.014±.003	.561	−.012±.003	.497	−.015±.001	.658	−.006±.002	.409
TiO_2	−.060±.008	2.946	−.086±.015	3.348	−.065±.006	2.906	−.057±.012	2.843	−.072±.003	3.263	−.045±.004	2.380
P_2O_5	−.009±.001	.359	−.008±.003	.348	−.006±.001	.266	−.005±.001	.259	−.007±.001	.324	−.004±.001	.246
MnO	−.002±.001	.182	−.002±.002	.183	.000±.001	.164	n.d.		n.d.		n.d.	
Ba	−1.277±1.505	126.440	.565±2.649	100.346	n.d.		n.d.		n.d.		n.d.	
Co (INAA)	3.047±.096	22.648	3.297±.253	19.006	n.d.		n.d.		n.d.		n.d.	
Co (AA)	3.184±.144	23.350	2.772±.353	29.385	n.d.		n.d.		n.d.		n.d.	
Cr	76.943±3.049	−191.459	63.771±6.067	2.147	n.d.		n.d.		n.d.		n.d.	
Ni	63.766±1.882	−349.095	65.268±5.240	−368.050	n.d.		n.d.		n.d.		n.d.	
Cu	−3.240±.858	139.767	−3.969±1.398	151.439	n.d.		n.d.		n.d.		n.d.	
Hf	−.094±.011	4.525	−.113±.025	4.831	n.d.		n.d.		n.d.		n.d.	
Rb	.040±.202	12.028	−.289±.345	16.829	n.d.		n.d.		n.d.		n.d.	
Ta	−.015±.006	1.013	−.032±.009	1.272	n.d.		n.d.		n.d.		n.d.	
Th	−.027±.004	1.023	−.025±.005	1.001	n.d.		n.d.		n.d.		n.d.	
U	.000±.010	.282	−.005±.012	.369	n.d.		n.d.		n.d.		n.d.	
Zn	−.378±.239	113.205	−.700±.600	118.175	n.d.		n.d.		n.d.		n.d.	
Zr	−3.090±1.128	171.309	−3.137±2.066	171.211	n.d.		n.d.		n.d.		n.d.	
Sc	−.654±.052	36.464	−.635±.074	36.140	n.d.		n.d.		n.d.		n.d.	
La	−.259±.057	13.718	−.409±.079	15.931	n.d.		n.d.		n.d.		n.d.	
Ce	−.600±.110	33.117	−.800±.162	36.090	n.d.		n.d.		n.d.		n.d.	
Nd	−.421±.150	23.420	−.578±.267	25.673	n.d.		n.d.		n.d.		n.d.	
Sm	−.135±.015	6.669	−.170±.033	7.194	n.d.		n.d.		n.d.		n.d.	
Eu	−.047±.004	2.189	−.056±.008	2.333	n.d.		n.d.		n.d.		n.d.	
Gd	−.185±.054	7.549	−.291±.070	9.128	n.d.		n.d.		n.d.		n.d.	
Tb	−.025±.003	1.129	−.029±.008	1.186	n.d.		n.d.		n.d.		n.d.	
Tm	−.009±.003	.402	−.011±.004	.432	n.d.		n.d.		n.d.		n.d.	
Yb	−.054±.007	2.595	−.068±.012	2.822	n.d.		n.d.		n.d.		n.d.	
Lu	−.006±.001	.354	−.009±.002	.392	n.d.		n.d.		n.d.		n.d.	

TRACE-ELEMENT CHEMISTRY AND RARE-EARTH-ELEMENT CHEMISTRY

Nearly all flows in the section were analyzed for a suite of 22 trace elements (table 13.2). Most of the trace elements show negative linear trends when plotted against MgO (fig. 13.5*B*; table 13.3), indicating that olivine abundance exerts the principal control on trace-element content. However, several trace elements correlate positively with MgO (table 13.3). Ni and Co, which resembles Ni in its behavior, are strongly partitioned from the melt into the olivine crystal structure (Gunn, 1971; Hart and Davis, 1978). The positive correlation between Cr and MgO probably reflects the presence of inclusions of chrome spinel in olivine (Gunn, 1971). Our results for Cu differ from those of Gunn (1971), who found a significant positive correlation between MgO and Cu, probably indicating sulfide saturation in his samples. We found no correlation between Cu and MgO, and this may indicate varying levels of sulfur in the magmas supplying suite C flows (T.L. Wright, oral commun., 1985).

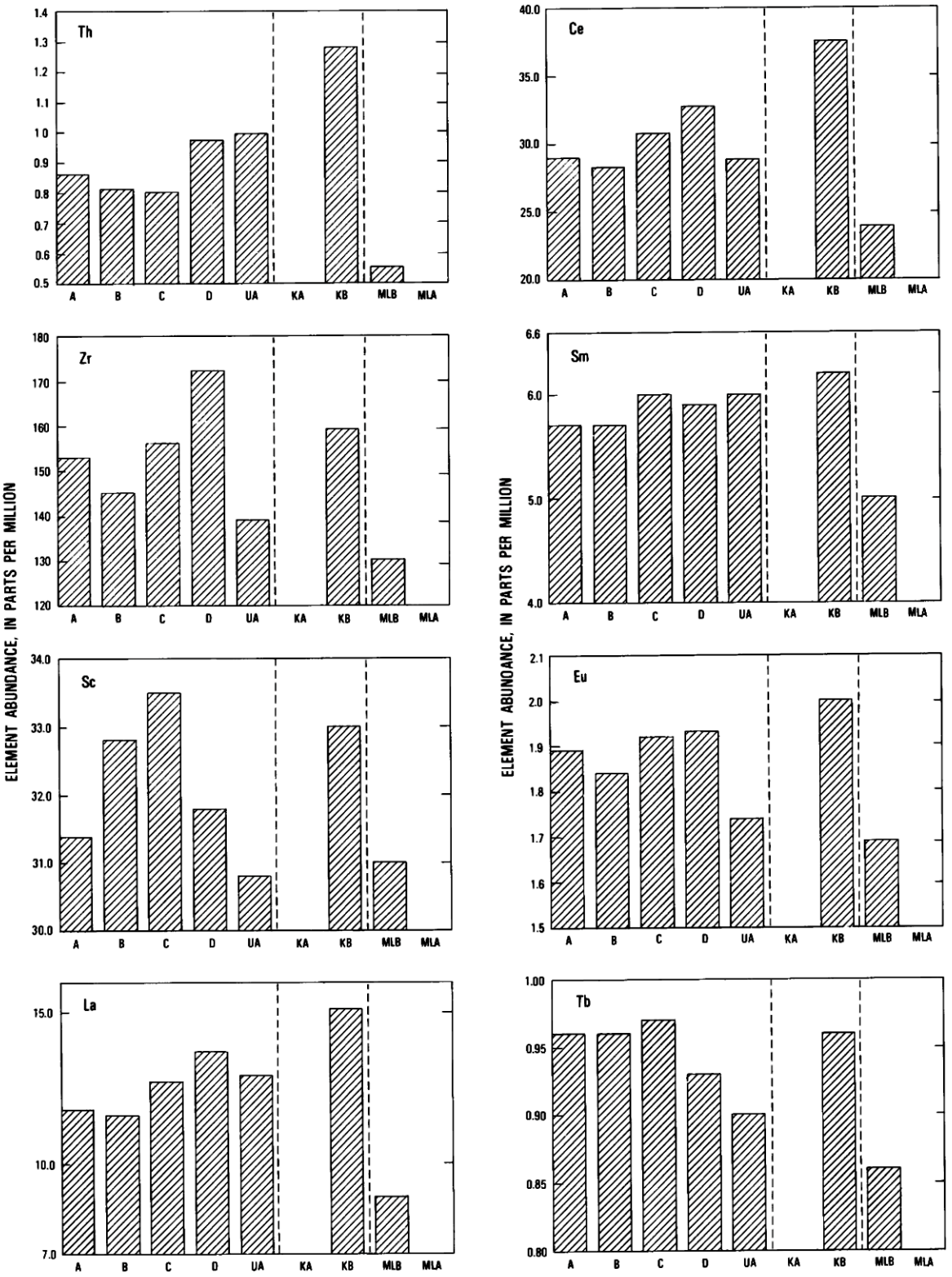

average from Wright (1971); KB, Kilauea average from Basaltic Volcanism Study Project (1981); MLB, Mauna Loa average from Basaltic Volcanism Study Project (1981); MLA, Mauna Loa average from Wright (1971). Vertical lines separate Uwekahuna Bluff data (left) from Kilauea averages (middle), and from Mauna Loa averages (right).

The rare-earth-element (REE) concentrations correlate negatively with MgO (fig. 13.5C), owing to the diluting effect of olivine crystals on the absolute concentrations of REE (Hanson, 1980). Chondrite-normalized REE data for selected flows from each suite show smooth curves with similar slopes (fig. 13.7*A*). In flows of suite C, differences in the positions of the curves reflect the large range in olivine content, whereas flows of suites A, B, and D have a smaller range in REE abundances. The shapes and slopes of the curves for all flows within the Uwekahuna Bluff section are similar, suggesting that the parent magmas had a similar origin.

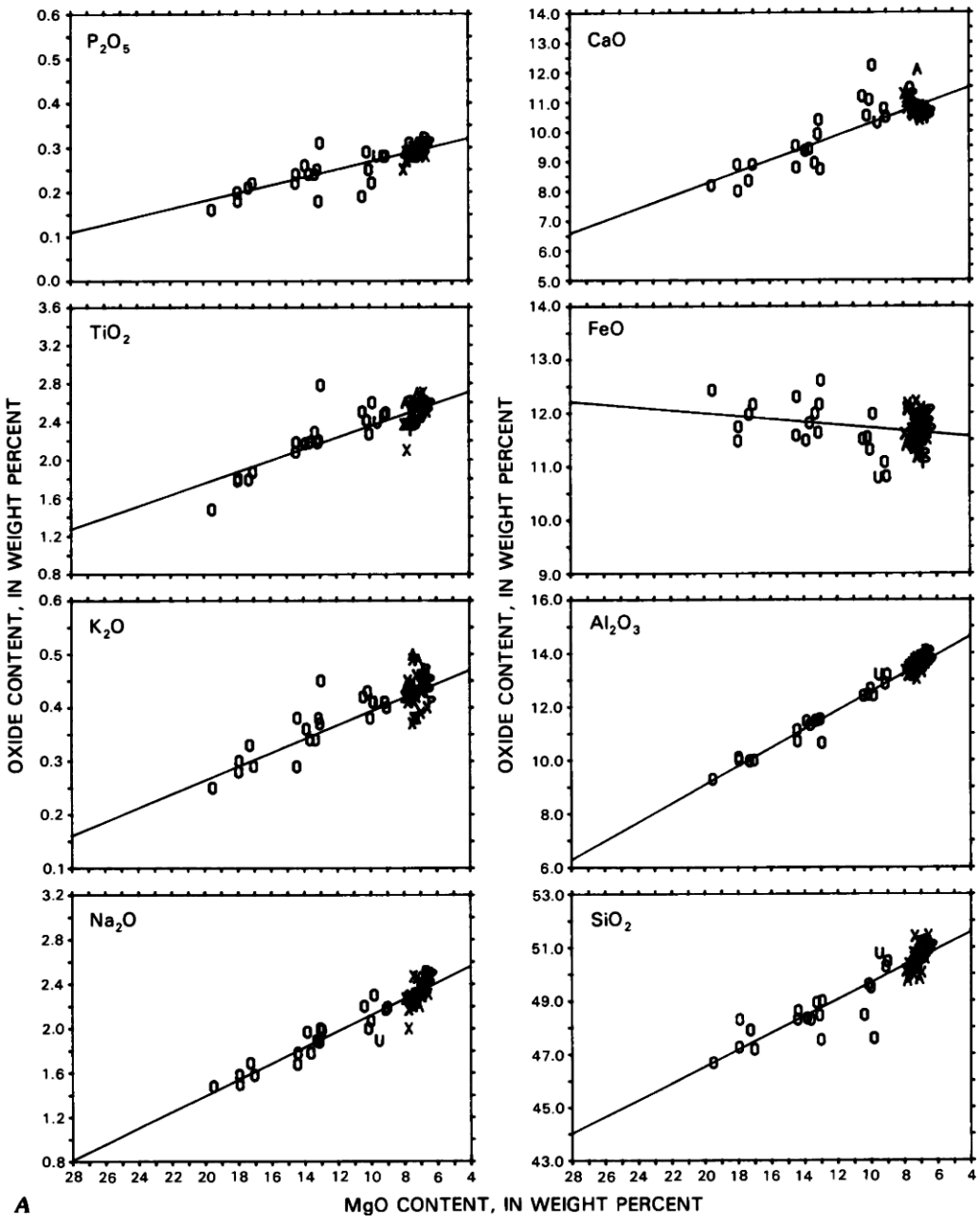

FIGURE 13.5.—MgO variation diagrams for flows of Uwekahuna Bluff section. Data symbols: P, flows of suite A, plagioclase porphyritic; X, flows of suite B, mostly aphyric; O, flows of suite C, olivine porphyritic; U, Uwekahuna Ash Member (unit 43); A, flows of suite D, aphyric. Lines are olivine-control lines for these data determined by linear least-squares regression. See table 13.3 for coefficients and figure 13.8 for comparison with olivine-control lines for other Kilauea lavas. ***A***, Plots of major-element oxides versus MgO. ***B***, Plots of trace elements versus MgO. ***C***, Plots of rare-earth elements versus MgO.

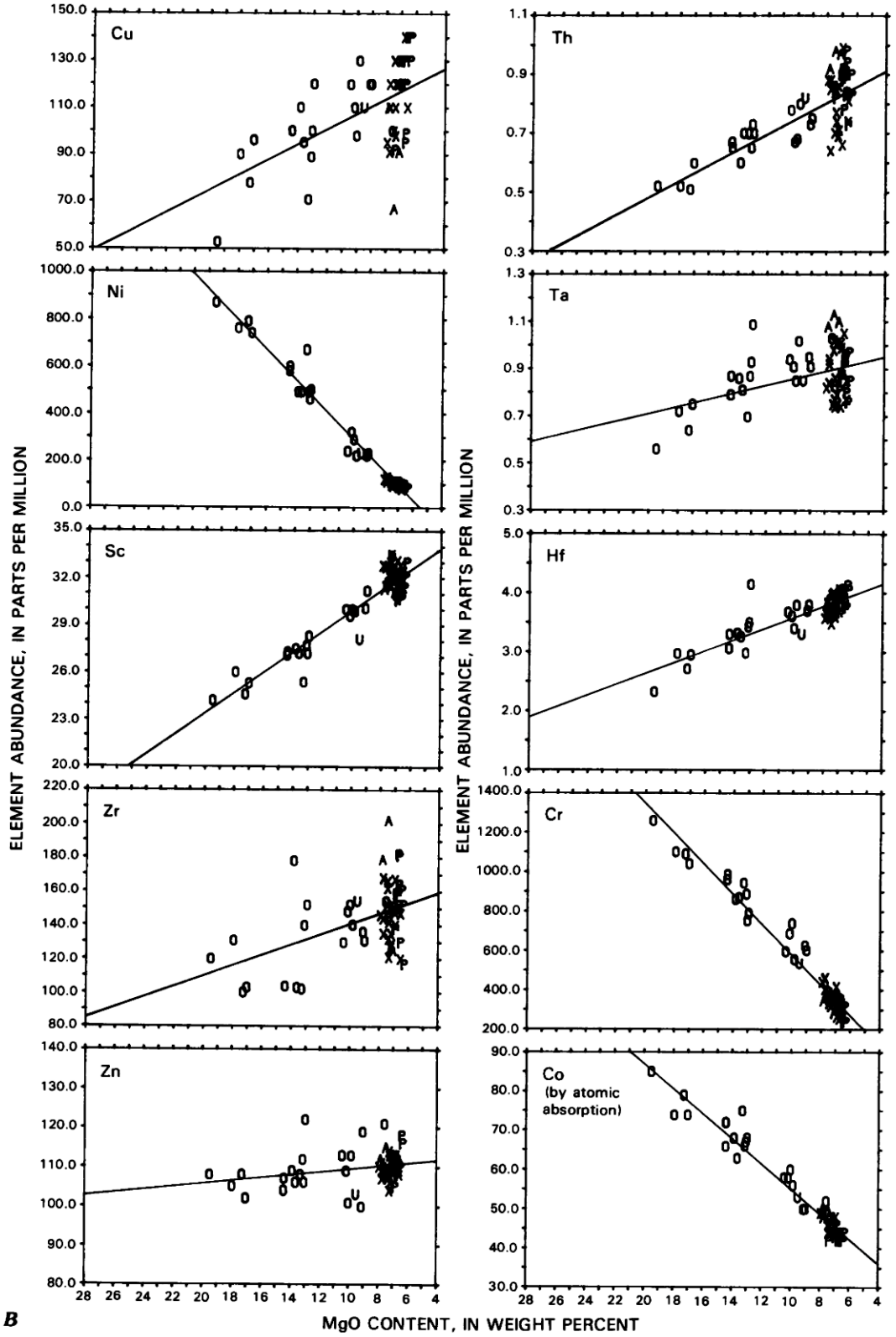

FIGURE 13.5.—Continued.

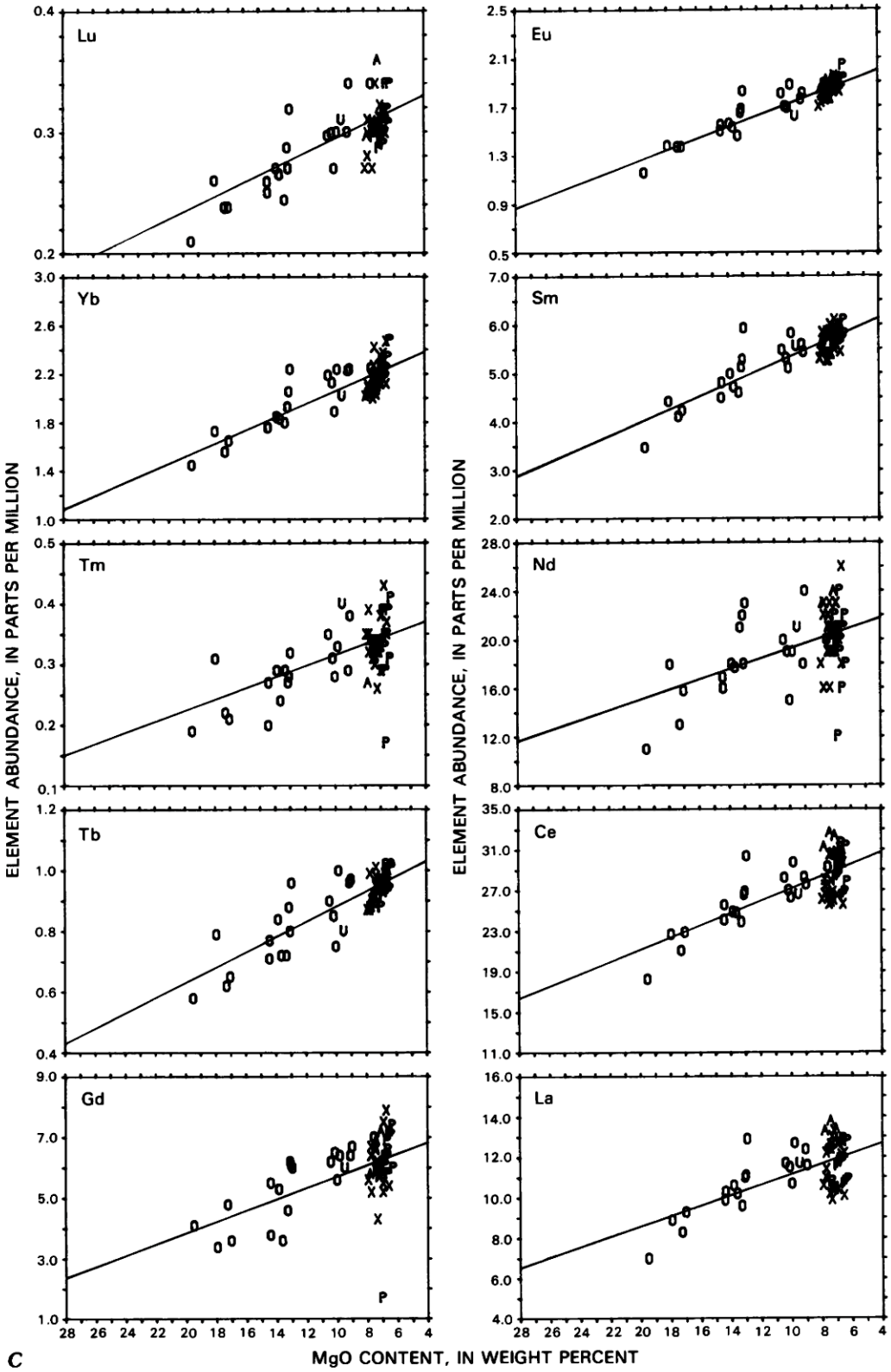

FIGURE 13.5.—Continued.

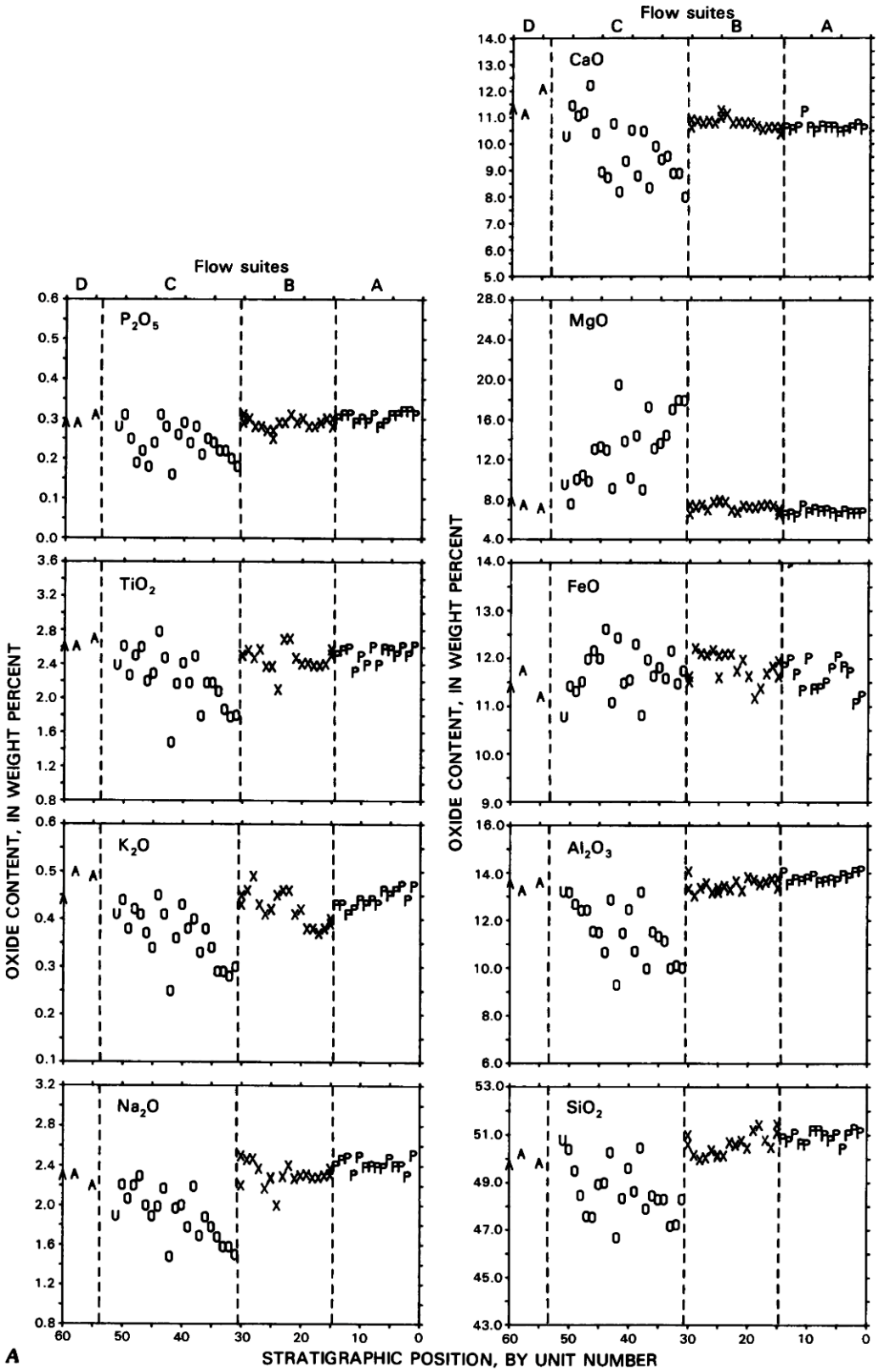

FIGURE 13.6.—Plots of chemical composition versus stratigraphic position within the Uwekahuna Bluff section. Data symbols: P, flows of suite A, plagioclase porphyritic; X, flows of suite B, mostly aphyric; O, flows of suite C, olivine porphyritic; U, Uwekahuna Ash Member (unit 43); A, flows of suite D, aphyric. Dashed lines separate suites. *A*, Plots of major-element oxides versus MgO. *B*, Plots of trace elements versus MgO. *C*, Plots of rare-earth elements versus MgO.

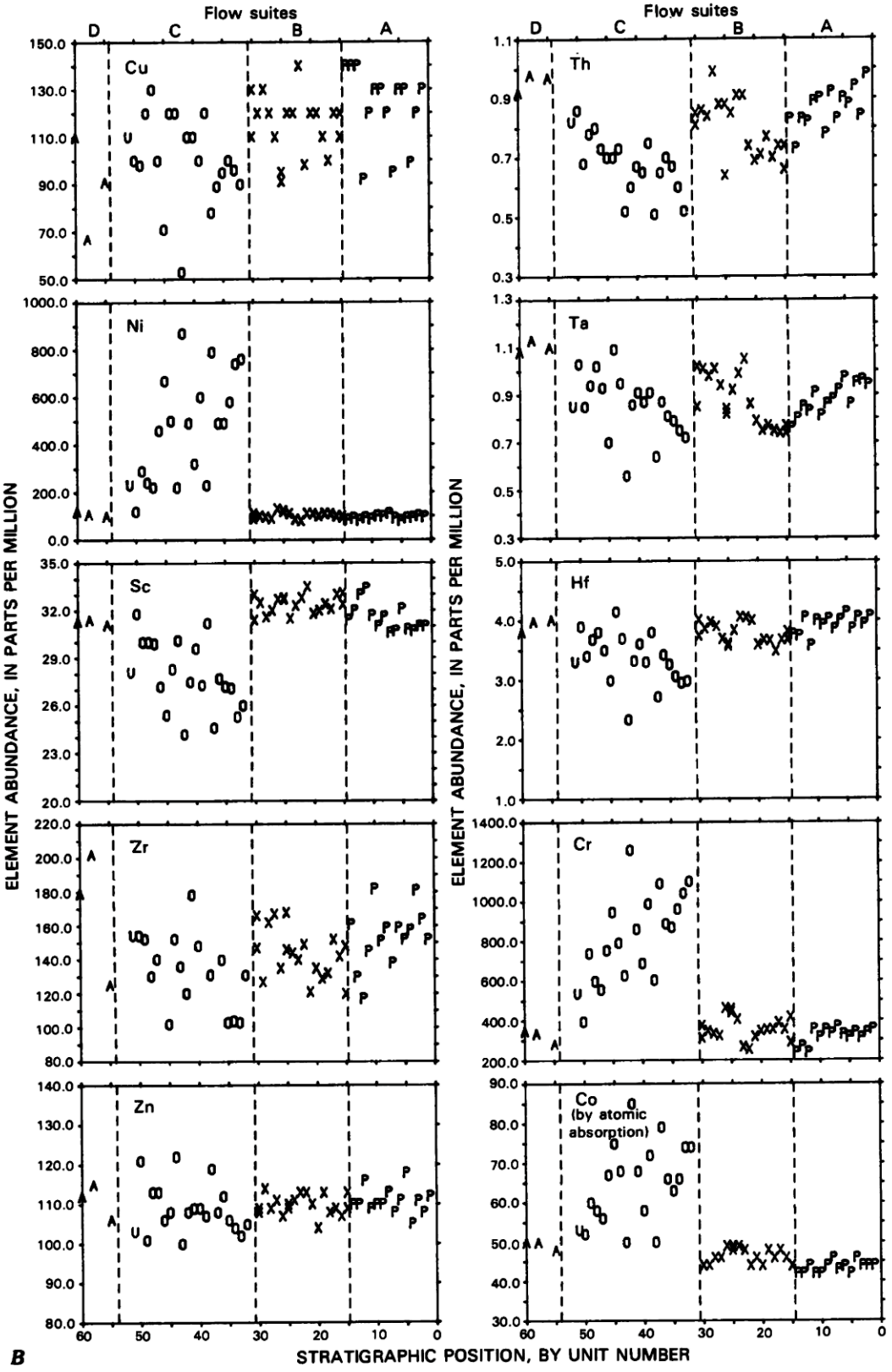

FIGURE 13.6.—Continued.

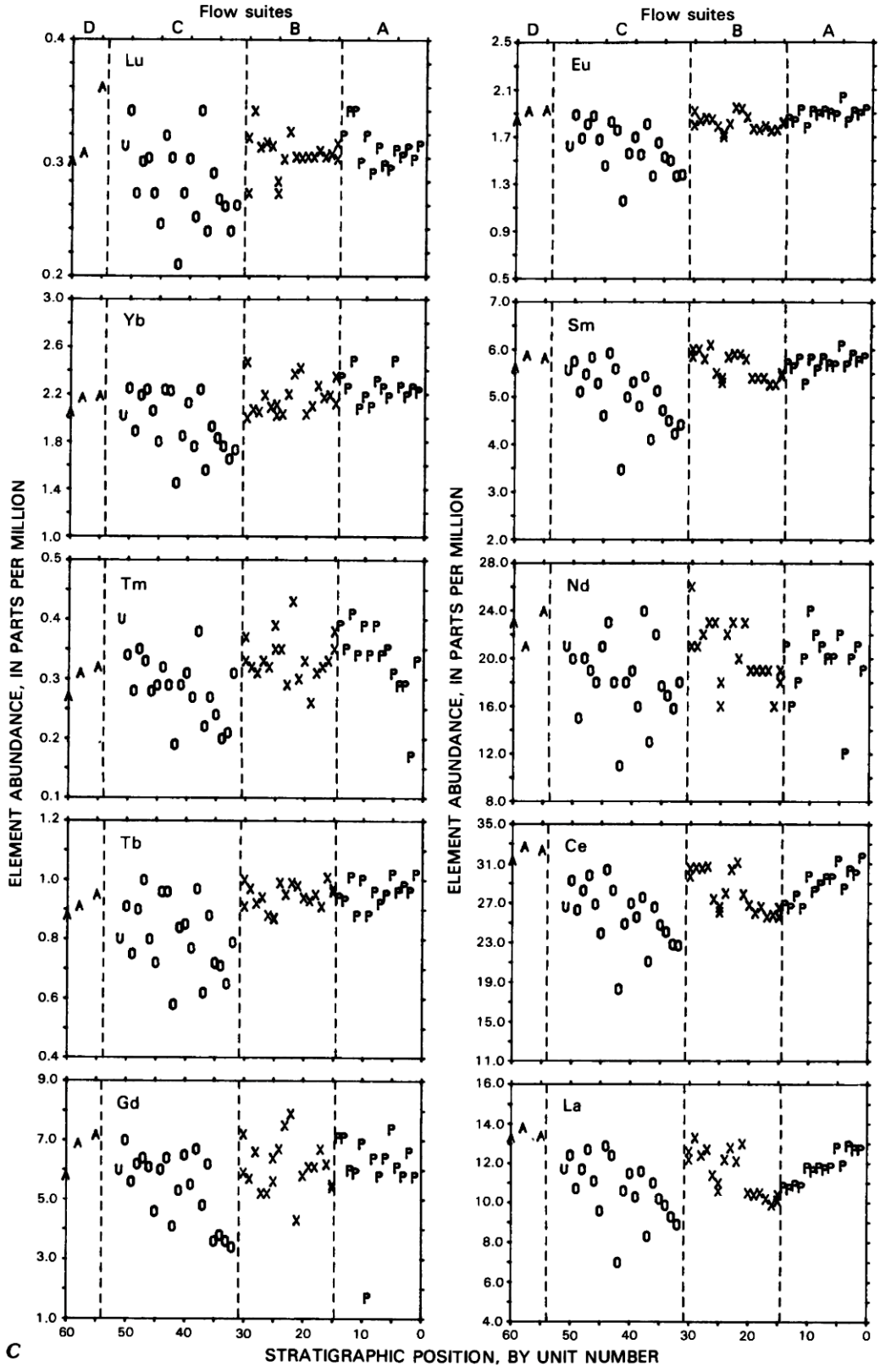

FIGURE 13.6.—Continued.

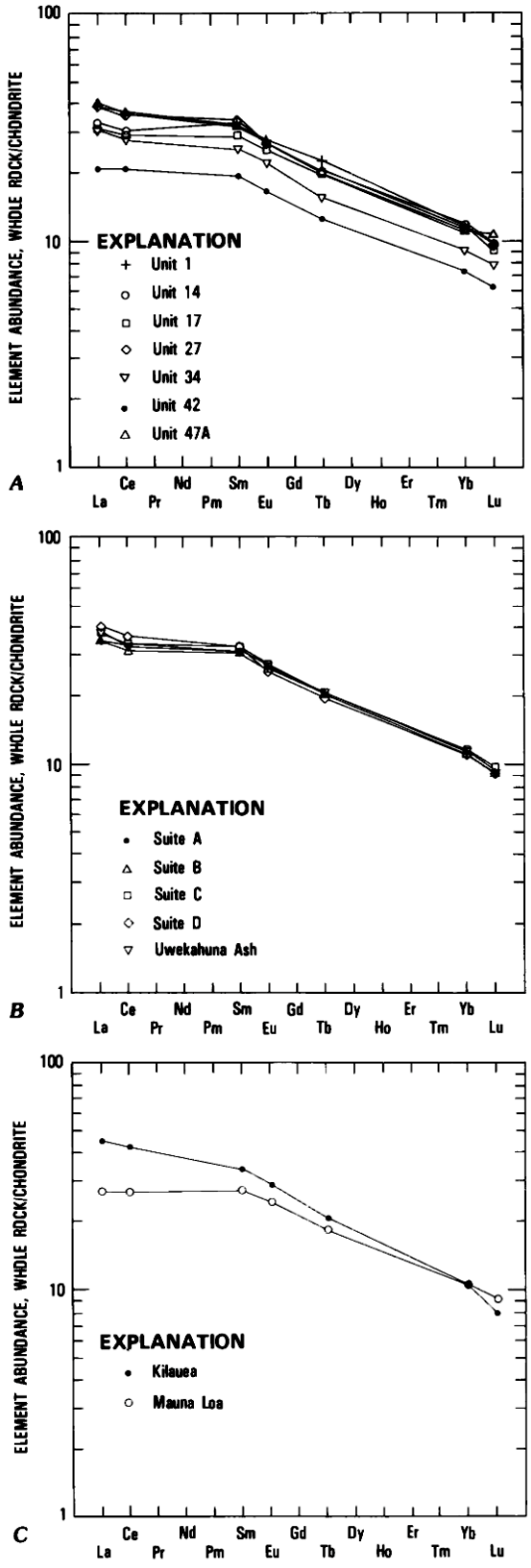

FIGURE 13.7.—Chondrite-normalized abundances of rare-earth elements in Uwekahuna Bluff samples. Abundances are normalized to chondrite values of Haskin and others (1968). Precision for most rare-earth-element (REE) abundances determined by neutron activation (Baedecker, 1979) is better than ±3 percent of reported value (see text). Precision for Nd, Gd, and Tm is poorer, and these elements are not used in plots of chondrite-normalized rare-earth abundances. ***A***, REE abundances in selected flows from Uwekahuna Bluff. ***B***, Averaged and normalized REE data for each suite of flows in Uwekahuna Bluff section and for the Uwekahuna Ash Member. ***C***, Averaged and normalized REE data for historical Mauna Loa and Kilauea flows (data from Basaltic Volcanism Study Project, 1981).

DISCUSSION

SOURCES OF MAGMAS

Flows of suites A and B have broadly similar major-element and trace-element chemistry (fig. 13.6*A*, *B*), and we detect no abrupt changes in composition such as might indicate exotic sources. The similarities in the REE patterns for these units likewise suggest a fairly homogeneous source. We interpret these data to indicate that the flows from suites A and B are comagmatic in the broad sense: they were derived from the same magma batch or from different batches with nearly identical source chemistry and crystallization histories.

Because flows of suite C contain various amounts of olivine, MgO content has a range sufficiently wide to define olivine-control lines. Wright (1971) showed that different comagmatic suites may be characterized by different olivine-control lines. The slopes and intercepts for suite C olivine-control lines are comparable to those calculated for various other suites of Kilauea lavas (Murata and Richter, 1966b; Wright, 1971). The similarity of these control lines (fig. 13.8) indicates that olivine is the only significant mineral phase affecting chemical variation in suite C flows and that the composition of that olivine is homogeneous. We interpret the flows of suite C to be derived from a Kilauea source, because their olivine-control lines resemble those of other Kilauea suites.

TRACE-ELEMENT DATA

Abundances of trace elements are similar within a restricted range among the flows from Uwekahuna Bluff and other Kilauea localities. Ba, Rb, Th, Zr, La, Ce, Sm, and Tb values fall within the ranges exhibited by historic Kilauea lavas (fig. 13.9; Basaltic Volcanism Study Project, 1981). No trace-element abundances in Uwekahuna Bluff flows are within the ranges that are unique to Mauna Loa.

The striking similarity among chondrite-normalized curves for each suite (fig. 13.7*B*) suggests that the magmas for the various suites of flows, as well as for the Uwekahuna Ash Member, are comagmatic. They may have a common parent in the upper mantle, have been affecetd by similar processes after leaving the mantle, or both.

Abundances of light REE are typically lower for Mauna Loa than for Kilauea (fig. 13.7C; Leeman and others, 1977, 1980; Basaltic Volcanism Study Project, 1981), whereas abundances of heavy REE are similar for Kilauea and Mauna Loa lavas. Curves for the flows in Uwekahuna Bluff more closely resemble those for Kilauea than those for Mauna Loa (fig. 13.7*B*, *C*). Thus, on the basis of major-, trace-, and rare-earth-element chemistry, it appears that no Mauna Loa flows occur in the Uwekahuna Bluff section.

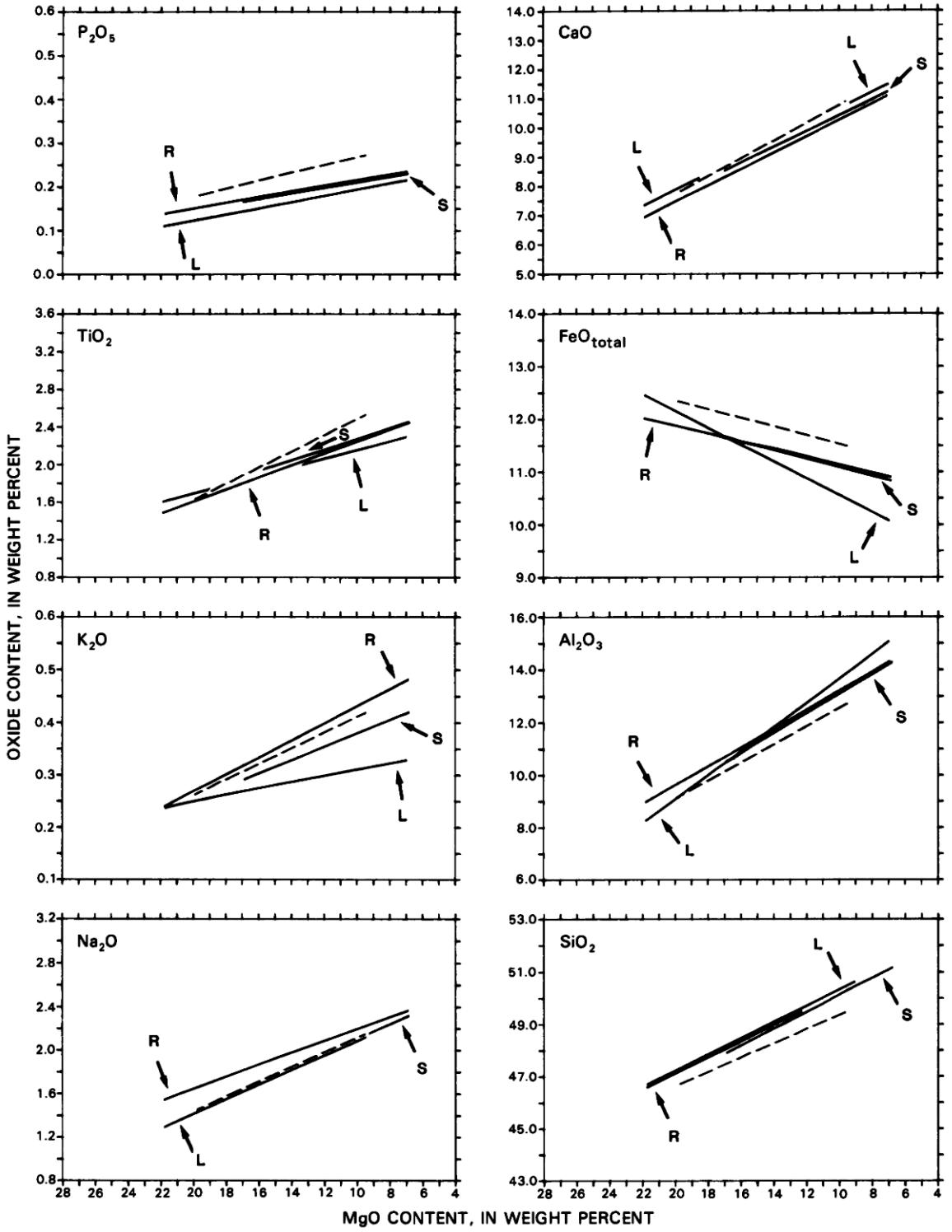

FIGURE 13.8.—Lines of olivine control for Kilauea lavas. Dashed line is for flows of picritic suite C at Uwekahuna Bluff. Other lines labeled by letters: S, Kilauea prehistoric summit lavas (Murata and Richter, 1966a; Wright, 1971); R, Kilauea southwest-rift-zone prehistoric picrites (Wright, 1971); and L, Uwekahuna laccolith (recalculated from data in Murata and Richter, 1961).

SECULAR TRENDS

Olivine control is the dominant mineral control affecting suite C flows. The flows from suites A, B, and D have MgO contents in excess of 6.4 weight percent and show no evidence of fractionation in the sense of Wright and others (1975). We assume that the minor chemical variation displayed by these flows is also olivine controlled. To look for evidence of chemical variability beyond that imposed by olivine control, we recalculated the compositions in table 13.2 to a constant 7.0 weight percent MgO by adding or subtracting olivine from the bulk compositions (Macdonald, 1944; Wright, 1971), using the composition of olivine from the Uwekahuna laccolith (Murata and Richter, 1961). That composition does not account for chrome spinel, which commonly occurs within olivine in Hawaiian lavas, and so we did not recalculate the Cr contents for the Uwekahuna Bluff samples. Listed in table 13.4 are average compositions for each of the lava suites at Uwekahuna Bluff and for juvenile material from the Uwekahuna Ash Member, all normalized to 7.0 weight percent MgO.

The following secular trends are recognized for the Uwekahuna Bluff section (fig. 13.9): (1) SiO_2 increases from 50.2 weight percent for the flows of suite D to 51.1 percent for the flows of suite A; (2) Al_2O_3, FeO_t, Na_2O, P_2O_5, and MnO remain nearly constant (table 13.4); and (3) CaO and TiO_2 decrease slightly from suite D to suite A. These secular changes differ in sense from those recognized by Wright (1971) for historical Kilauea lavas, in which SiO_2 decreases to the present and CaO and TiO_2 increase.

Historical olivine-controlled flows from Mauna Loa have more SiO_2 and less K_2O, TiO_2, and P_2O_5 than any of the flows from Uwekahuna Bluff (table 13.4; fig. 13.9). The ranges in the contents of these oxides for flows from Uwekahuna Bluff strongly resemble those for historical Kilauea flows.

CYCLIC VARIATIONS IN THE CHEMISTRY OF SUMMIT LAVAS

Plots of chemical composition versus position in the section for lavas of suites A and B (units 1–30) show essentially straight-line relationships (fig. 13.6), but small cyclic(?) departures are discernible. The olivine-rich flows of suite C display considerable scatter in MgO-variation diagrams (fig. 13.5A), but some evidence for cyclicity can be seen when all compositions are normalized to 7.0 weight percent MgO and plotted against stratigraphic position (fig. 13.10). Although the frequency of the apparent cycles varies from element to element, the data do suggest that cyclic variations occur in the compositions of Kilauea summit lavas.

Wright and others (1975) and Wright and Tilling (1980), on the basis of major-element chemistry, identified 10 distinct chemical variants or magma batches among the materials erupted by Kilauea in the period 1968–1974. They interpreted these variants as the unmodified products of separate partial melting events. Hofmann and others (1984) examined trace- and rare-earth-element data from Kilauea for 1968–1971; they concluded that incompatible trace-element concentrations in the lavas fit a pattern of continuous,

TABLE 13.4.—*Average chemical compositions of prehistoric lavas and ash from Uwekahuna Bluff, compared with historical Mauna Loa and prehistoric and historical Kilauea*

[Recalculated from original analyses by normalizing to 100 percent dry weight after converting all iron to FeO_{total}. Normalized to 7.0 weight percent MgO by subtracting or adding olivine of Uwekahuna laccolith composition (Murata and Richter, 1961, analysis 10). A, suite A flows; B, suite B flows; C, suite C flows; D, suite D flows; UA, Uwekahuna Ash Member, (UA = average of 5 rinds from cored bombs within Uwekahuna Ash Member (Dzurisin and Casadevall, 1986)); Kilauea A (Kil A = Kilauea summit 1911–1924) and Mauna Loa A (MLoa A) (Wright, 1971); Kilauea B (Kil B) and Mauna Loa B (MLoa B) (Basaltic Volcanism Study Project, 1981); n.d., not determined; uncertainty expressed as one standard deviation (1 sigma)]

	A	B	C	D	UA	Kil A	Kil B	MLoa B	MLoa A
SiO_2	51.10±0.23	50.90±0.39	50.60±0.78	50.23±0.25	51.08±0.35	50.33, n.d.	50.70±0.31	52.45±0.31	52.18, n.d.
Al_2O_3	13.7±0.2	13.6±0.2	13.6±0.3	13.7±0.2	13.73±0.9	14.00, n.d.	13.57±0.12	13.94±0.10	14.17, n.d.
FeO	11.7±0.3	11.8±0.3	11.3±0.5	11.4±0.3	11.63±1.00	11.09, n.d.	11.03±0.20	10.62±0.49	10.94, n.d.
MgO	7.0	7.0	7.0	7.0	7.0	7.0	7.0	7.0	7.0
CaO	10.6±0.2	10.9±0.3	11.7±0.7	11.7±0.4	11.05±0.28	11.58, n.d.	11.65±0.33	10.73±0.15	10.58, n.d.
Na_2O	2.4±0.1	2.3±0.1	2.3±0.1	2.3±0.1	2.14±0.25	2.28, n.d.	2.32±0.04	2.36±0.06	2.29, n.d.
K_2O	.44±0.02	.43±0.03	.44±0.04	.48±0.03	.45±0.02	.55, n.d.	.53±0.04	.39±0.03	.37, n.d.
TiO_2	2.51±0.08	2.49±0.12	2.62±0.21	2.68±0.04	2.51±0.09	2.72, n.d.	2.73±0.11	2.10±0.04	2.07, n.d.
P_2O_5	.30±0.01	.29±0.01	.28±0.04	.30±0.01	.26±0.06	.27, n.d.	.29±0.01	.24±0.02	.21, n.d.
MnO	.17±0.02	.17±0.01	.16±0.02	.19±0.01	.16±0.02	.17, n.d.	.17±0.01	.17±0.01	.17, n.d.
Ba	118±19	118±23	127±29	136±11	120±29	n.d.	138±18	84±14	n.d.
Cu	122±16	116±12	119±17	91±22	132±7	n.d.	n.d.	n.d.	n.d.
Hf	3.91±0.14	3.83±0.16	4.02±0.30	3.99±0.08	3.58±0.02	n.d.	4.58±0.17	3.59±0.11	n.d.
Rb	12±3	13±1	16±3	14, n.d.	13, n.d.	n.d.	11±3	6±1	n.d.
Ta	.88±0.06	.88±0.11	1.02±0.10	1.12±0.02	.93±0.05	n.d.	n.d.	n.d.	n.d.
Th	.86±0.07	.81±0.10	.80±0.06	.97±0.02	.89±0.09	n.d.	1.28±0.22	.55±0.03	n.d.
Zn	111±3	111±3	132±14	113±5	112±3	n.d.	n.d.	n.d.	n.d.
Zr	153±17	145±15	156±25	172±41	139±18	n.d.	159±20	130±5	n.d.
Sc	31.4±0.9	32.8±0.7	33.5±1.4	31.8±0.4	30.8±0.2	n.d.	33.0±2.0	31.0±1.2	n.d.
La	11.8±0.8	11.6±1.2	12.7±1.0	13.7±0.3	12.9±0.4	n.d.	15.1±1.7	8.9±0.6	n.d.
Ce	28.9±1.6	28.3±2.0	30.7±1.9	32.7±0.5	28.8±0.5	n.d.	37.5±3.2	23.9±1.4	n.d.
Nd	20±3	21±3	22±3	23±2	23±3	n.d.	n.d.	n.d.	n.d.
Sm	5.7±0.1	5.7±0.3	6.0±0.4	5.9±0.1	6.0±0.1	n.d.	6.2±0.2	5.0±0.2	n.d.
Eu	1.89±0.05	1.84±0.06	1.92±0.10	1.93±0.03	1.74±0.04	n.d.	2.00±0.07	1.69±0.04	n.d.
Gd	6.1±1.4	6.2±0.9	6.4±1.0	6.7±0.7	7.1±0.7	n.d.	n.d.	n.d.	n.d.
Tb	.96±0.04	.96±0.04	.97±0.10	.93±0.03	.90±0.02	n.d.	.96±0.03	.86±0.04	n.d.
Tm	.33±0.06	.34±0.04	.34±0.05	.31±0.02	.34±0.08	n.d.	n.d.	n.d.	n.d.
Yb	2.25±0.11	2.20±0.13	2.31±0.14	2.17±0.06	2.18±0.05	n.d.	2.05±0.03	2.10±0.04	n.d.
Lu	.31±0.02	.31±0.02	.33±0.02	.32±0.03	.31±0.01	n.d.	.26±0.10	.31±0.01	n.d.

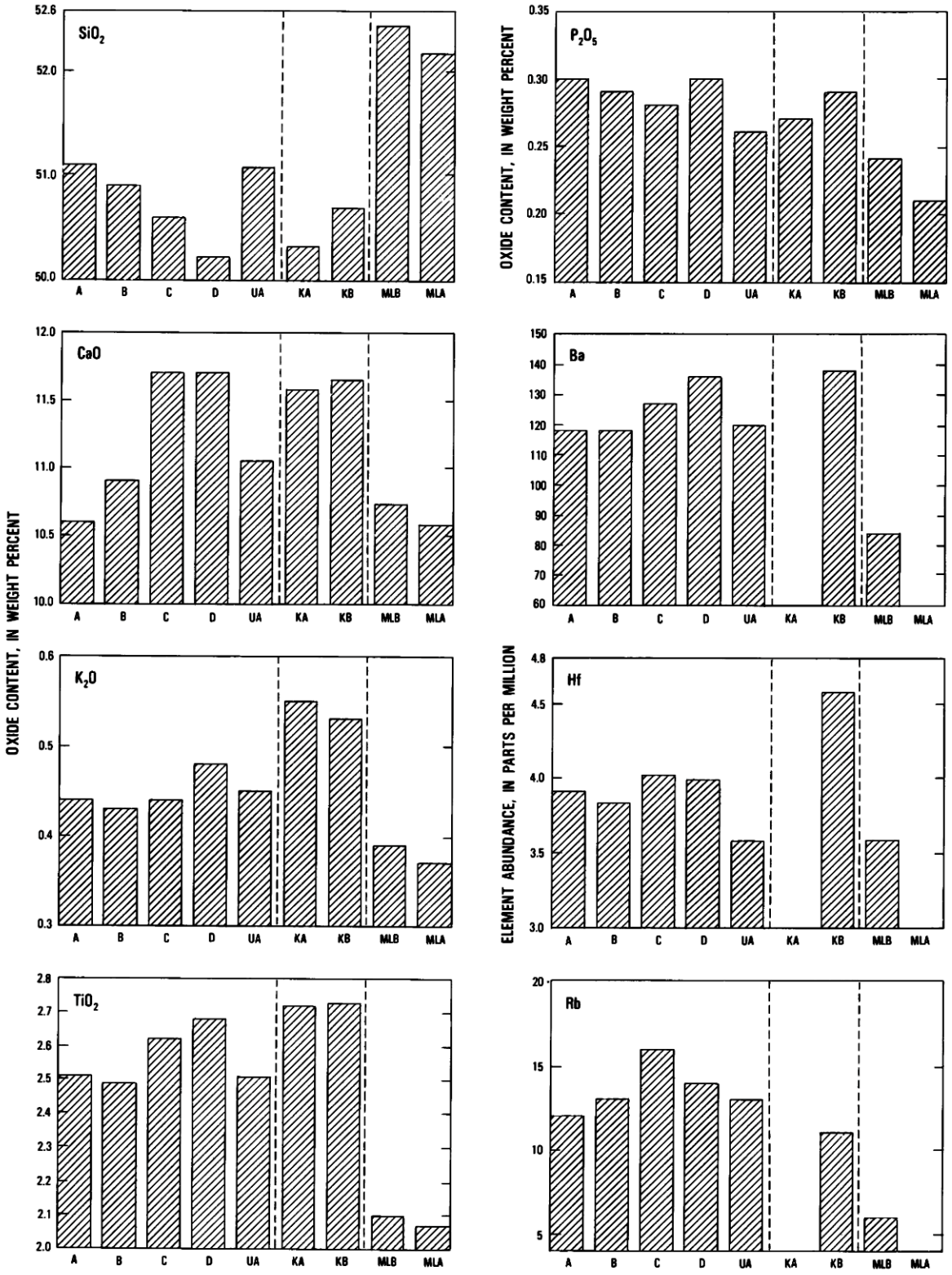

FIGURE 13.9.—Bar graphs showing averaged normalized abundances of selected major oxides and trace elements in Uwekahuna Bluff rocks and in Mauna Loa and Kilauea flows. Averages are recalculated from original analyses by normalizing to 100 percent dry weight after converting all iron to FeO. Averages have been normalized to 7.0 weight percent MgO by subtracting or adding olivine of Uwekahuna laccolith composition (Murata and Richter, 1961, analysis 10). A–D, Suites of flows from Uwekahuna Bluff; UA, Uwekahuna Ash Member; KA, Kilauea

monotonic decrease and that "there was no longer a need to invoke the existence of distinct magma batches to explain either the trace elements or the major elements" (Hofmann and others, 1984, p. 32). Shaw (chapter 51) argues that cyclic behavior on many time scales may be the norm for Hawaiian volcanism and suggests mechanisms to account for such cycles. The apparent cycles at Uwekahuna Bluff are too pronounced to be explained by analytical uncertainty; they may reflect subtle variations in the chemistry of the parental magma stored in the shallow reservoir.

CHRONOLOGY OF UWEKAHUNA BLUFF

To appreciate more fully the significance of the various rock suites exposed at Uwekahuna Bluff, an understanding of the time

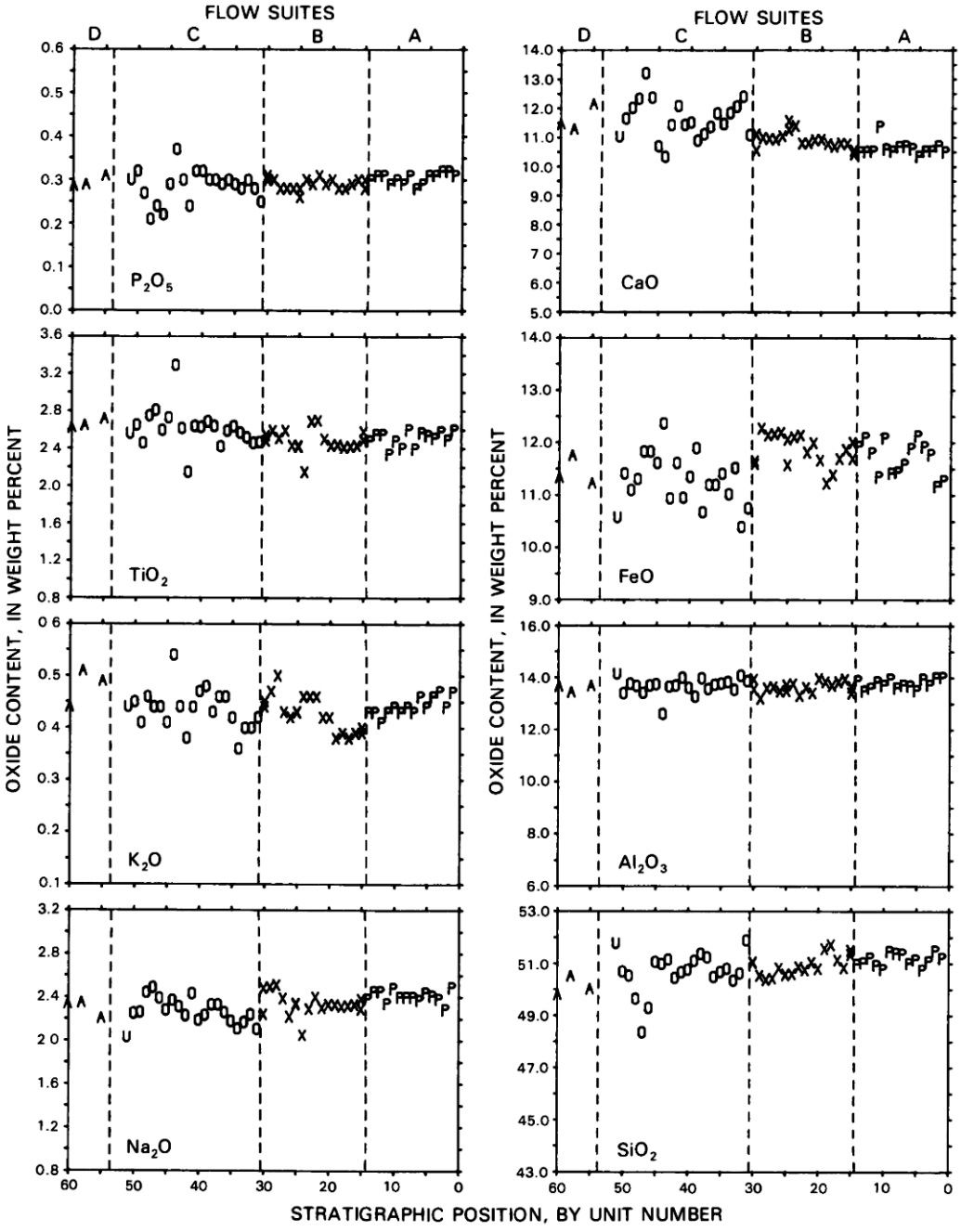

FIGURE 13.10.—Plot of recalculated major-element analyses versus stratigraphic position in the Uwekahuna Bluff section. Analyses have been recalculated to 7.0 weight percent MgO through addition or subtraction of olivine of the composition given in Murata and Richter (1961). Dashed lines separate suites of flows. U indicates sample of the Uwekahuna Ash Member. See figure 13.6 for explanation of other letter symbols.

intervals involved is essential. We offer here a tentative chronology of the sequence at Uwekahuna Bluff and a conceptual model to explain the chemical and petrologic variations observed there.

The Uwekahuna Ash Member, which underlies nearly the entire western wall of Kilauea caldera, is interpreted as the product of large explosive eruptions in the Kilauea summit region about 2.1 ka (Dzurisin and Casadevall, 1986; Lockwood and Rubin, 1986). We found no carbonaceous material within the Uwekahuna Bluff section, so no radiocarbon ages are available for the section above the Uwekahuna Ash Member. However, control on the age of flows within the various suites is available from study of paleomagnetism of the rocks from Uwekahuna Bluff.

Paleomagnetism in the flows of Uwekahuna Bluff has been studied since 1961, when 10 lava flows from the lower half of the section were sampled (Doell and Cox, 1965, 1972). We relocated those holes, which were drilled in units 29, 32, 34, 36, 37, 39, 42, 47A, 48A, and 49A (table 13.1). In 1981, nine additional flows (units 1, 2, 3, 4, 5, 15, 20, 27, and 51) were drilled (R.T. Holcomb and D.E. Champion, unpub. data).

The 1981 samples and the Doell and Cox samples record at least three distinct pole positions (D.E. Champion, oral commun., 1985). Three of the older samples of suite D (units 47A–49A) have paleomagnetic directions consistent with the directions of a lava flow that has been dated at 2.77 ± 0.15 ka (Lockwood and Rubin, 1986; sample W-5345). This age relationship is consistent with the geology of Uwekahuna Bluff, where units 47A–49A underlie the Uwekahuna Ash Member, but it implies a 600–700 yr hiatus in the Uwekahuna Bluff section between the emplacement of suite D flows and deposition of the ash.

A second time unit includes flows 15 through 51 from suites B and C. Flow 51 directly overlies the 2.1-ka Uwekahuna Ash Member. Samples from these flows show a continuous variation in paleomagnetic direction consistent with rapid and steady change of the local magnetic field vector from about 2.1 to 1.5 ka (D.E. Champion, oral commun., 1985). Field evidence indicates no major weathering surface in this sequence of flows. This consistency indicates that the flows of suites C (picrite) and B (aphyric) accumulated in roughly 600 years; no major time breaks are recognized.

The weathered top of unit 15, the uppermost flow of suite B, indicates a hiatus of unknown duration. Paleomagnetic directions within the top five flows of the section (flows of suite A) are consistent with dated field directions of about 0.35 ka (Holcomb, 1981). However, lack of paleomagnetic data for flows 6 through 14 precludes estimating the length of time represented by suite A.

Thus, five major events between 2.8 ka and 0.2 ka are recognized in the Uwekahuna Bluff section on the basis of field occurrence, radiocarbon dating of flows and tephra (Kelley and others, 1979; Lockwood and Rubin, 1986), and paleomagnetic studies (Holcomb, 1981; D.E. Champion, oral commun., 1985). We infer the following eruptive sequence for the rocks exposed at Uwekahuna Bluff:

1. Eruption of aphyric lavas of pre-Uwekahuna Ash Member age (suite D) about 2.8 ka.

2. Eruption of the Uwekahuna Ash Member about 2.1 ka.

3. Eruption of picritic lavas, replenishment of shallow reservoir, and eruption of aphyric lavas (suites C and B) about 2.1 to 1.5 ka (?).

4. Eruption of plagioclase-porphyritic lavas (suite A) about 0.8 to 0.2 ka (?).

5. Formation of present caldera and eruption of Keanakakoi Ash about 0.2 ka.

KILAUEA SUMMIT HISTORY FOR THE PAST 2,800 YEARS

Holcomb (chapter 12) has outlined one sequence of events for the recent evolution of the Kilauea summit area, but alternatives are possible. Our interpretation is generally similar, but we prefer a sequence in which some of the stratigraphic units in Uwekahuna Bluff are older than the ages assigned by Holcomb.

Holcomb (chapter 12) has used paleomagnetic data to assign an age of 2.0–1.5 ka to lava of suite D in Uwekahuna Bluff, as well as several flows outside of the caldera. A similarly magnetized lava flow on Mauna Loa has recently been dated by ^{14}C methods at 2.8 ka (D.E. Champion, oral commun., 1985). As discussed below, we believe that the Uwekahuna Ash Member is older than the 1.5 ka favored by Holcomb and others (in press), so we prefer the age of about 2.8 ka for the lava flows of suite D. These flows should be compared with pre-Uwekahuna Ash Member flows outside of the caldera to see if they may be coeval.

Holcomb (chapter 12) concludes that the present caldera of Kilauea was preceded by an older Powers caldera whose formation may have been associated with explosions that produced the Uwekahuna Ash Member in a manner similar to that proposed for the present caldera and the Keanakakoi Ash Member. The mechanism proposed for this association (Jaggar, 1947; Macdonald, 1965; Christiansen, 1979) involves large-scale summit collapse in response to rapid magma withdrawal into the volcano's rift zones, triggering phreatomagmatic explosions by providing ground water access to the volcano's plumbing system. Though the collapse of the current caldera preceded the explosive Keanakakoi eruption, the interval between collapse and explosion could have been short (Decker and Christiansen, 1983).

Several radiocarbon ages have been determined for the Uwekahuna Ash Member. When the original paleomagnetic chronology of Holcomb and others (in press) was worked out, the available measurements indicated an age of about 1.5 ka. Additional ages have been obtained since then, ranging from 1.0 ka to 2.2 ka. Lockwood and Rubin (1986) argue that the younger ages are affected by sample contamination and adopt 2.1 ka as the most representaive age for the ash. Holcomb (chapter 12) prefers to retain the earlier, younger age but we prefer the 2.1-ka ages of Lockwood and Rubin (1986).

Holcomb (chapter 12) suggests that collapse of the Powers caldera was followed by a period of caldera filling which did not affect the Uwekahuna Bluff section for about 0.75 ka, implying that the flows of suite C and suite B are younger than 0.75 ka. D.E. Champion (oral commun., 1985) believes that those flows record continuous variation in paleomagnetic field direction from about 2.1 to 1.5 ka. Dzurisin and Casadevall (1986) argue that the uppermost

pumice of the Uwekahuna Ash Member was buried quickly by picritic lava flows of suite C, because the pumice was uneroded when it was buried. We therefore assign an age of 2.1 to 1.5 ka to suite C and suite B flows and suggest that at least 30 m of suite C flows accumulated rapidly soon after the Uwekahuna Ash Member eruptions.

Our interpretation and that of Holcomb (chapter 12) converge on the age and origin of the suite A flows at Uwekahuna Bluff. These plagioclase-phyric flows are Holcomb's Observatory flows, so named because they form the substrate for the Hawaiian Volcano Observatory. He assigned them an age of 0.25–0.35 ka in figure 12.5, but also noted that they could be as old as 0.75 ka. We suggest that the weathered surface of the uppermost suite B flow records a hiatus of at least a few centuries, and adopt an age of 0.8–0.2 ka for the overlying suite A flows. Following extrusion of the suite A flows, the Uwekahuna Bluff section was capped by the Keanakakoi Ash Member.

The two main differences between our interpretation and that of Holcomb (chapter 12) are: (1) the age of the Uwekahuna Ash Member, and (2) the age and significance of the suite C and suite B lava flows. The differences are caused primarily from differing interpretations of available radiocarbon ages for summit flows and should be resolved by future work.

Our preferred interpretation is that the suite C picrites ponded in the Powers caldera soon after its formation and quickly buried the Uwekahuna Ash Member. Holcomb (chapter 12) agrees that collapse was soon followed by caldera filling, but infers that the Uwekahuna Bluff area was not covered for about 750 years. We interpret the suite C picrites as crystal cumulates or residua from a shallow magma reservoir that was rapidly drained during the Uwekahuna Ash Member eruptions, probably by a large effusive eruption low on the volcano's flank (Dzurisin and Casadevall, 1986). We infer that the lower parts of this magma reservoir were rich in olivine, because of the accumulation of settled olivine crystals (Macdonald, 1944; Murata and Richter, 1966a, b).

Murata and Richter (1966b) proposed that in the 1959 eruption of Kilauea Iki, the eruptive force mobilized olivine sludge from the depths of the shallow reservoir feeding that eruption. Helz (chapter 25) argues that the ascent rate of a juvenile component of the 1959 eruption was sufficient to entrain large olivine grains from a source in the upper mantle. We speculate that the suite C flows at Uwekahuna Bluff represent olivine sludge from the lower part of a compositionally zoned shallow magma reservoir and that unloading during the Uwekahuna Ash Member eruption was responsible for extrusion of the picrites. Preservation at the top of the Uwekahuna Ash Member of a thin pumice layer, which we tentatively assume to be related to emplacement of the ash at about 2.1 ka, indicates that at least 30 m of suite C lava flows accumulated on the floor of the Powers caldera and buried the pumice soon after it was erupted. The absence of weathered flow surfaces at the contacts of suite C flows also implies that most of their 60-m thickness accumulated rapidly after eruption of the ash. This model is attractive because it explains the presence of picrites, which are otherwise unusual in the Kilauea summit area, as a direct consequence of the equally unusual Uwekahuna Ash Member eruptions.

We speculate that the flows of suites B and A ponded within the Powers caldera and that they are genetically related. The plagioclase-porphyritic flows of suite A may represent a later eruptive product of a shallow reservoir that earlier was the source for the aphyric lavas of suite B. We tentatively interpret this sequence of aphyric lavas followed by plagioclase-porphyritic lavas as the product of a two-stage drawdown of a post-Uwekahuna Ash Member shallow magma reservoir. A possible problem with this interpretation is that paleomagnetic evidence suggests a hiatus of at least a few centuries between emplacement of the suite B and the suite A flows, and a hiatus is also indicated by the weathered contact between the suites. According to Holcomb (chapter 12), the hiatus lasted from 0.5 ka to 0.25 ka; according to D.E. Champion (oral commun., 1985) and the model proposed here, the hiatus lasted from 1.5 ka to 0.8 ka.

CONCLUSIONS

We conducted this study in an attempt to answer questions about how the summit region of Kilauea developed: (1) How important were intrusive bodies (sills, laccoliths, and dikes) to the growth of the summit region? (2) Are any lava flows from Mauna Loa exposed in the western wall of Kilauea caldera? (3) Can distinct suites of rocks be recognized in the caldera wall and give a record of the recent chemical evolution of Kilauea summit lavas? (4) Is there any evidence that distinct eruptive centers or source regions have supplied lavas to the summit region during Kilauea's recent past? In terms of these questions, we summarize our results as follows:

(1) Intrusive bodies such as sills and laccoliths are absent at Uwekahuna Bluff. The dikes and laccoliths found elsewhere in the western wall of the caldera account for less than 1 percent of the surface area of the wall (Casadevall and Dzurisin, chapter 14).

(2) The flows of Uwekahuna Bluff are similar in textural variety, phenocryst mineralogy, and major- and trace-element chemistry to prehistoric and historical Kilauea lavas. On the basis of these similarities and the lack of hypersthene, which is found in Mauna Loa flows (Macdonald, 1949), we suggest that all flows within the Uwekahuna Bluff section are from a Kilauea source.

(3) Four distinct suites of flows are recognized at Uwekahuna Bluff on the basis of field occurrence, petrography, and chemistry. Many flows represent near-vent accumulations of fluid lavas. The uniform thickness, lateral continuity, and extensive horizontality of many of the lava flows exposed in the western wall, especially above the Uwekahuna Ash Member, suggest a caldera-fill sequence.

(4) Our data do not require distinct source regions or eruptive centers for the Uwekahuna Bluff lavas, although those possibilities cannot be discounted. We attribute the petrographic differences between lava suites to processes within a single shallow magma reservoir beneath the summit area. The Uwekahuna Bluff lavas could have erupted from a single center or from several in the summit area. Our results are generally compatible with those of Holcomb (chapter 12), but remaining differences of opinion about absolute ages point out the need for additional stratigraphic study.

REFERENCES CITED

Baedecker, P.A., 1979, Instrumental neutron activation analysis program of the U.S. Geological Survey (Reston, Va.) *in* Carpenter, B.F., D'Agostino, F., and Yule, H.P., eds., Computers and activation analysis and gamma-ray spectroscopy: Contract 78042, U.S. Dept. Energy, p. 373–385.

Basaltic Volcanism Study Project, 1981, Basaltic volcanism on the terrestrial planets; New York, Pergamon Press, 1286 p.

Christiansen, R.L., 1979, Explosive eruption of Kilauea Volcano in 1790 [abs.]: International Association of Volcanology and Chemistry of the Earth's Interior, Symposium on Intraplate Volcanism and Submarine Volcanism, Hilo, Hawaii, July 1979, p. 174.

Daly, R.A., 1911, Magmatic differentiation in Hawaii: Journal of Geology, v. 19, p. 289–316.

de Saint Ours, P., 1982, Map of tectonic features of Kilauea Volcano summit region, Hawaii: U.S. Geological Survey Miscellaneous Field Studies Map, MF–1368, scale 1:24,000.

Decker, R.W., and Christiansen, R.L., 1983, Explosive eruptions of Kilauea Volcano, Hawaii, *in* Explosive Volcanism: inception, evolution, and hazards: Washington, National Academy Press, p. 122–132.

Doell, R.R.,and Cox, A.V., 1965, Paleomagnetism of Hawaiian lava flows: Journal of Geophysical Research, v. 70, p. 3377–3405.

——— 1972, The Pacific geomagnetic secular variation anomaly and the question of lateral uniformity in the lower mantle, in Robertson, E.C., ed., The nature of the solid Earth: New York, McGraw-Hill, p. 245–284.

Dutton, C.E., 1884, Hawaiian volcanoes: U.S. Geological Survey 4th Annual Report, p. 75–219.

Dzurisin, D., and Casadevall, T.J., 1986, Stratigraphy and chemistry of the Uwekahuna Ash: Product of prehistoric phreatomagmatic eruptions at Kilauea Volcano, Hawaii [abs.]: International Volcanological Congress, Auckland-Hamilton-Rotorua, New Zealand, Abstracts, February 1986, p. 100.

Dzurisin, D., Koyanagi, R.Y., and English, T.T., 1984, Magma supply and storage at Kilauea Volcano, Hawaii: Journal of Volcanology and Geothermal Research, v. 21, p. 177–206.

Fuller, R.E., 1939, Gravitational accumulation of olivine during the advance of basaltic flows: Journal of Geology, v. 47, p. 303–313.

Gunn, B.M., 1971, Trace element partition during olivine fractionation of Hawaiian basalts: Chemical Geology, v. 8, p. 1–13.

Hanson, G.N., 1980, Rare earth elements in petrogenetic studies of igneous systems: Annual Reviews of Earth and Planetary Science Letters, v. 8, p. 371–406.

Hart, S.R., and Davis, K.E., 1978, Nickel partitioning between olivine and silicate melt: Earth and Planetary Science Letters, v. 40, p. 203–219.

Haskin, L.A., Haskin, M.A., Frey, F.A., and Wildman, T.R., 1968, Relative and absolute terrestrial abundances of the rare earths, *in* Ahrens, L.H., ed., Origins and distribution of the elements: New York, Pergamon Press, p. 889–912.

Hofmann, A.W., Feigenson, M.D., and Raczek, I., 1984, Case studies on the origin of basalt: III. Petrogenesis of the Mauna Ulu eruption, Kilauea, 1969–1971: Contributions to Mineralogy and Petrology, v. 88, p. 24–35.

Holcomb, R.T., 1981, Kilauea Volcano, Hawaii: chronology and morphology of the surficial lava flows: U.S. Geological Survey Open-File Report 81–354, 321 p.

Holcomb, R.T., Champion, D.E., and McWilliams, M.O., in press, Dating recent Hawaiian lava flows using paleomagnetic secular variation: Geological Society of America Bulletin.

Jaggar, T.A., 1947, Origin and development of craters: Geological Society of America Memoir 21, 508p.

Kelley, M.L., Spiker, E.C., Lipman, P.W., Lockwood, J.P., Holcomb, R.T., and Rubin, M., 1979, U.S. Geological Survey radiocarbon dates XV: Mauna Loa and Kilauea Volcanoes, Hawaii: Radiocarbon, v. 21, p. 306–320.

Leeman, W.P., Budahn, J.R., Gerlach, D.C., Smith, D.R., and Powell, B.N., 1980, Origin of Hawaiian tholeiites: trace element constraints: American Journal of Science, v. 280–A, p. 796–821.

Leeman, W.P., Murali, A.V., Ma, M.S., and Schmitt, R.A., 1977, Mineral constitution of mantle source regions for Hawaiian basalts—rare earth element evidence for mantle heterogeneity, *in* Magma Genesis: Oregon Department of Mineral Industries Bulletin 96, p. 169–183.

Lockwood, J.P., and Rubin, M., 1986, Distribution and age of the Uwekahuna Ash, Kilauea Volcano, Hawaii [abs.]: International Volcanological Congress, Auckland-Hamilton-Rotorua, New Zealand, Abstracts, February 1986, p. 112.

Macdonald, G.A., 1944, The 1840 eruption and crystal differentiation in the Kilauean magma column: American Journal of Science, v. 242, p. 177–189.

——— 1949, Petrography of the Island of Hawaii; U. S. Geological Survey Professional Paper 214–D, 96 p.

——— 1965, Hawaiian calderas: Pacific Science, v. 19, p. 320–334.

Murata, K.J., and Richter, D.H., 1961, Magmatic differentiation in the Uwekahuna laccolith, Kilauea caldera, Hawaii: Journal of Petrology, v. 2, p. 424–437.

——— 1966a, Chemistry of the lavas of the 1959–60 eruption of Kilauea Volcano, Hawaii: U.S. Geological Survey Professional Paper 537–A, 26 p.

——— 1966b, The settling of olivine in Kilauean magma as shown by the 1959 eruption: American Journal of Science, v. 264, p. 194–203.

Peterson, D.W. 1967, Geologic map of the Kilauea Crater quadrangle, Hawaii: U.S. Geological Survey Geologic Quadrangle Map GQ–667, scale 1:24,000.

Powers, H.A., 1948, A chronology of the explosive eruptions of Kilaeua: Pacific Science, v. 2, p. 278–292.

——— 1955, Composition and origin of basaltic magma of the Hawaiian Islands: Geochimica et Cosmochimica Acta, v. 7, p. 77–107.

Powers, S., 1916, Intrusive bodies at Kilauea: Zeitschrift fur Vulkanologie, v. 3, p. 28–33.

Shapiro, Leonard, 1975, Rapid analysis of silicate, carbonate, and phosphate rocks: U.S. Geological Survey Bulletin 1401, 56 p.

Stearns, H.T., and Clark, W.O., 1930, Geology and water resources of the Kau district, Hawaii: U.S. Geological Survey Water Supply Paper 616, 194 p.

Stearns, H.T., and Macdonald, G.A., 1946, Geology and ground-water resources of the Island of Hawaii: Hawaii Division of Hydrography Bulletin 9, 363 p.

Swanson, D.A., 1973, Pahoehoe flows from the 1969–1973 Mauna Ulu eruption: Kilauea Volcano, Hawaii: Geological Society of America Bulletin, v. 84, p. 615–626.

Swanson, D.A., Christiansen, R.L. 1973, Tragic base surge in 1790 at Kilauea Volcano: Geology, v. 1, p. 83–86.

Walker, G.W., 1969, Geologic map of the Kau Desert Quadrangle, Hawaii: U.S. Geological Survey Geologic Quadrangle Map GQ–827, scale 1:24,000.

Washington, H.S., 1923, Petrology of the Hawaiian Islands, III: Kilauea and general petrology of Hawaii: American Journal of Science, v. 6, p. 338–367.

Wright, T.L., 1971, Chemistry of Kilauea and Mauna Loa in space and time: U.S. Geological Survey Professional Paper 735, 40 p.

——— 1974, Presentation and interpretation of chemical data for igneous rocks: Contribution to Mineralogy and Petrology, v. 48, p. 233–248.

——— 1984, Origin of Hawaiian tholeiite: a metasomatic model: Journal of Geophysical Research, v. 89, p. 3233–3252.

Wright, T.L., Swanson, D.A., and Duffield, W.A., 1975, Chemical composition of Kilauea east-rift lava, 1968–1971: Journal of Petrology, v. 16, p. 110–133.

INTRUSIVE ROCKS OF KILAUEA CALDERA

By Thomas J. Casadevall *and* Daniel Dzurisin

ABSTRACT

Eighteen prehistoric dikes exposed in the west wall of Kilauea caldera have been mapped and analyzed for major, trace, and volatile elements. Twelve dikes occur along Uwekahuna Bluff and to the north and east; six dikes occur south of the bluff. Alignment of many dikes approximates the northeasterly trend common for several tectonic elements at Kilauea: the 6 southern dikes generally follow the N. 48° E. strike of the southwest rift zone, and 9 of 12 dikes in the north set strike roughly parallel to the linear western wall of the caldera (N. 40° E.). Chemical analyses of the dikes show that all are tholeiitic basalts, typical of Kilauea summit flows and similar to the lava flows making up the western caldera wall.

Five dikes of the north set occupy fractures cutting the entire section of flows in the caldera wall and therefore must be fairly young. Their age relative to the A.D. 1790 Keanakakoi Ash Member of the Puna Basalt is unknown, but we suggest that they formed just before or shortly after the explosive eruption and presumed caldera collapse responsible for the ash. Dikes of the south set show a close parallelism with recent prehistoric and historical fissures in the southwest rift zone. They are also young and may be closely related to recent activity in the upper southwest rift zone. The more northerly strike of the north set of dikes may reflect the combined influences of stresses caused by flexing of Kilauea's shallow summit magma reservoir and gravitational slumping of the volcano's south flank.

PURPOSE AND BACKGROUND

At Kilauea Volcano on the Island of Hawaii, much effort has been directed to identify and understand subsurface processes responsible for eruption-related seismicity and surface deformation (Eaton and Murata, 1960). Models invariably refer to the causative bodies as dikes (Ryan and others, 1981; Duffield and others, 1982; Epp and others, 1983; Pollard and others, 1983; Dvorak and others, 1986), and the shallow magma reservoir is usually envisioned as a plexus of dikes and sills (Fiske and Kinoshita, 1969; Fiske and Jackson, 1972; Ryan and others, 1983). Despite the many references to intrusive bodies, little effort has been spent in examining those exposed in Kilauea caldera.

Kilauea is one of the youngest of the Hawaiian volcanoes, and erosional dissection of the edifice has been insufficient to expose intrusive bodies. However, the walls of the 3×5 km summit caldera are as much as 140 m high and provide a window into the upper level of the Kilauea edifice. The western caldera wall comprises numerous lava flows, at least 18 dikes, the Uwekahuna laccolith (Murata and Richter, 1961), and 3 thin pyroclastic units (the lithic ash of 1924, the Keanakakoi Ash Member of the Puna Basalt, of about A.D. 1790; and the Uwekahuna Ash Member of the Puna Basalt, of about 2.1 ka).

In this paper, we describe the distribution, form, dimensions, and chemistry of intrusive bodies exposed in the western wall of the Kilauea summit caldera. From Uwekakuna Bluff to Steaming Bluff, this wall is an unbroken, nearly vertical cliff averaging 130 m high. The wall south of Uwekahuna Bluff is lower (15–40 m) and it has a stepped profile that has been attributed to normal faulting along the caldera rim (Dutton, 1884; Peterson, 1967; Holcomb, 1981; Saint Ours, 1982). We studied the intrusive bodies exposed in the caldera walls in order to compare them petrologically with the flows that they cut, to assess their volumetric importance, and to evaluate their relationship to the structural setting and state of stress in the summit region.

PREVIOUS STUDIES

KILAUEA INTRUSIVE BODIES

The largest intrusive body exposed at Kilauea is the Uwekahuna laccolith, which Daly (1911) first described and inferred to have an intrusive origin. Powers (1916) mapped this laccolith and noted that "about 20 dikes also occur in the [caldera] walls at various points, but especially at the northeast end of the sink." Washington (1923) published two chemical analyses of a dike (11N of this report) from the wall below Steaming Bluff. Murata and Richter (1961) and Aramaki (1968) studied the petrology of the Uwekahuna laccolith, accepted its intrusive origin, and concluded that its compositional variation could be explained by gravity settling of olivine followed by filter-pressing of the residual liquid.

Walker (1969) mapped several dikes in the Hilina system of normal faults on the south flank of Kilauea, about 12 km from the summit caldera and far from any known eruptive vent. He interpreted those dikes as fillings of deep ground cracks by surface lava flows. Easton and Lockwood (1983) presented data on the volatile contents of those dikes to support that interpretation.

MECHANISMS OF INTRUSION

Several mechanisms have been proposed to explain the origin of intrusive bodies at Kilauea. One is the intrusion of magma from a deep source; in this mechanism, magmatic pressure and increasing buoyancy owing to exsolution of volatiles combine to overcome effects of gravity and lithostatic load, forcing magma upward or laterally into country rock (Ryan and others, 1981).

A second mechanism is the lateral injection of degassed lava from a ponded lava lake. Daly (1911) and Murata and Richter (1961) proposed such an origin for the Uwekahuna laccolith, and Swanson and Peterson (1973) hypothesized a similar mechanism during the filling of Alae lava lake. The driving force for such lateral injection is limited to the weight of the lava column in the lake.

A third mechanism is the filling of fractures by lava flows. Deep vertical ground cracks are common both at the summit and along the rift zones of Kilauea (de Saint Ours, 1982), and lava flows have frequently been observed cascading into these cracks (Duffield and others, 1982). Solidification of the crack filling would form a tabular body of rock indistinguishable in most respects from upwardly or laterally fed dikes. Walker (1969) and Easton and Lockwood (1983) support such an origin for the dikes in the Hilina fault system. The low volatile contents that characterize lava flows some distance from their vents (Swanson and Fabbi, 1973) aid in distinguishing such surface-fed bodies from dikes intruded from depth (Easton and Lockwood, 1983).

ACKNOWLEDGMENTS

Our appreciation of the intrusive bodies at Kilauea caldera has grown during conversations with many colleagues, particularly P.T. Delaney, R.T. Holcomb, D.W. Peterson, and D.A. Swanson. Analytical results are from the Branch of Analytical Services, U.S. Geological Survey, Reston, Va. Major-element chemistry by J. Reid and D. Kay, INAA analyses by L. Schwarz, and AA analyses by D. Golightly and P. Aruscavage were indespensible to this work. F. Brown provided rapid analyses of sulfur and chloride from the dike samples. W. Melson and T. O'Hearn (Smithsonian Institution) kindly provided the microprobe analyses of glasses from the chilled margins of several of the intrusives. The hydration-rind ages of two dike samples were measured by J. Halbig (University of Hawaii-Hilo). We greatly appreciate these considerable analytical efforts. D. Johnson assisted in computer analysis of the data. Reviews of this manuscript by D.A. Swanson and P.T. Delaney have substantially helped our presentation.

METHODS

Our work included field mapping and description, petrographic study, and chemical analysis. Most field work was done in 1979–1980 and focused on the west wall of the caldera for reasons of easy access and good exposure. We briefly examined sections of the wall near Keanakakoi, in the Byron Ledge-Waldron Ledge area, and north of Steaming Bluff (fig. 14.1), but found no dikes. Sections of these walls are covered by vegetation, talus, or young lava flows, however, so that small intrusive bodies might be obscured.

FIELD CRITERIA FOR RECOGNIZING INTRUSIONS

The Uwekahuna laccolith (fig. 14.2*A*) has a dense, blocky texture that gives it a light color and smooth, massive surface appearance. Similar light-colored, smooth-surfaced rock lenses occur throughout the western caldera wall; many have prismatic jointing similar to that in the laccolith. Based on these similarities we originally suspected that many of these bodies might be sills or laccoliths. To distinguish between surface flows and sills we focused attention on contact relations, particularly evidence for cross-cutting relations, deformation of wall rocks, and textures of the top and bottom surfaces of a unit. Textures such as pahoehoe ropes, evidence for collapsed pahoehoe shells, and the rubbly surfaces of aa flows indicate a surface flow. Internal features such as visible mineralogy and vesicle abundance and distribution were of secondary importance in mapping flow units. When these criteria were applied to the suspected sills, contact relations invariably revealed an extrusive origin. In particular, the contacts between the dikes and their wall rocks often showed signs of rapid cooling, including fine grain size and glassy margins.

Vesicles of various sizes and shapes are abundant in most flows at Uwekahuna Bluff; flows below the Uwekahuna Ash Member are generally less vesicular than those above (Casadevall and Dzurisin, chapter 13). In contrast, vesicles are rare in dikes and in the Uwekahuna laccolith. Vesicles in dike interiors are typically small (1–10 mm) and spherical. The paucity of vesicles in the dikes and laccolith suggests either that confining pressure was too large to permit formation of an extensive separate gas phase or that the intruding magma was largely degassed. Additional details of the petrography and volatile content of the intrusions are discussed later.

RESULTS

DISTRIBUTION AND DESCRIPTION OF INTRUSIVE BODIES

About 20 intrusive bodies are exposed in the western wall of the caldera. The largest and most conspicuous is the Uwekahuna laccolith (fig. 14.2*A*), which consists of two bodies having a total outcrop length of about 300 m and a maximum thickness of about 30 m. The dense, light-colored laccolith contains 15–40 percent olivine phenocrysts concentrated in its central and lower parts by gravitational settling (Murata and Richter, 1961). Similar patterns of olivine concentration occur in the thicker picritic flows of the Uwekahuna Bluff section (Casadevall and Dzurisin, chapter 13). The laccolith is the only body in the western caldera wall that visibly deformed its host rocks, except for the obvious extensions caused by dikes: 10–15 m of the overlying picritic lavas are deformed (fig. 14.2*A*).

A possible sill or low-angle dike is exposed in the western wall about 1 km north of the laccolith, but is not easily accessible from the caldera floor (fig. 14.2*B*). This massive body, which we refer to as the manta ray because of its shape, has two limbs extending outward and upward and appearing to cut across adjacent flows. We tentatively conclude that the body is an intrusion, but it could also be a flow that filled a small surface depression. The major lenticular bodies of rock in the Uwekahuna Bluff section are thick subaerial lava flows, as judged from contact relations (Casadevall and Dzurisin, chapter 13).

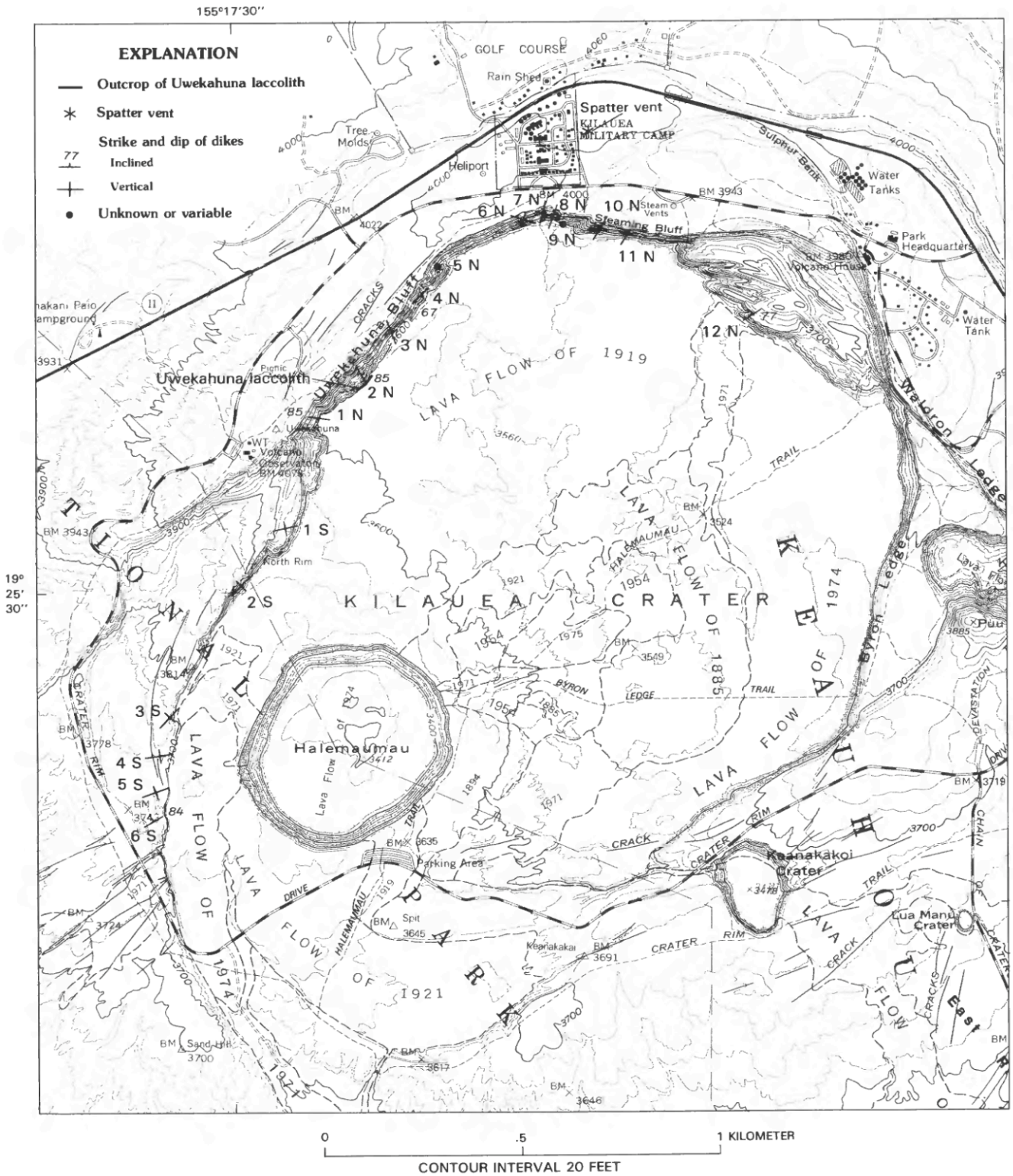

FIGURE 14.1.—Kilauea caldera showing location and attitude of dikes and locations of Uwekahuna laccolith and young spatter vent in Steaming Bluff area. Topographic map modified from U.S. Geological Survey Kilauea Crater 7.5-minute quadrangle, scale 1:24,000, 1981. Geology and structure modified from Peterson (1967) and de Saint Ours (1982). Dikes of north (N) and south (S) sets separately numbered.

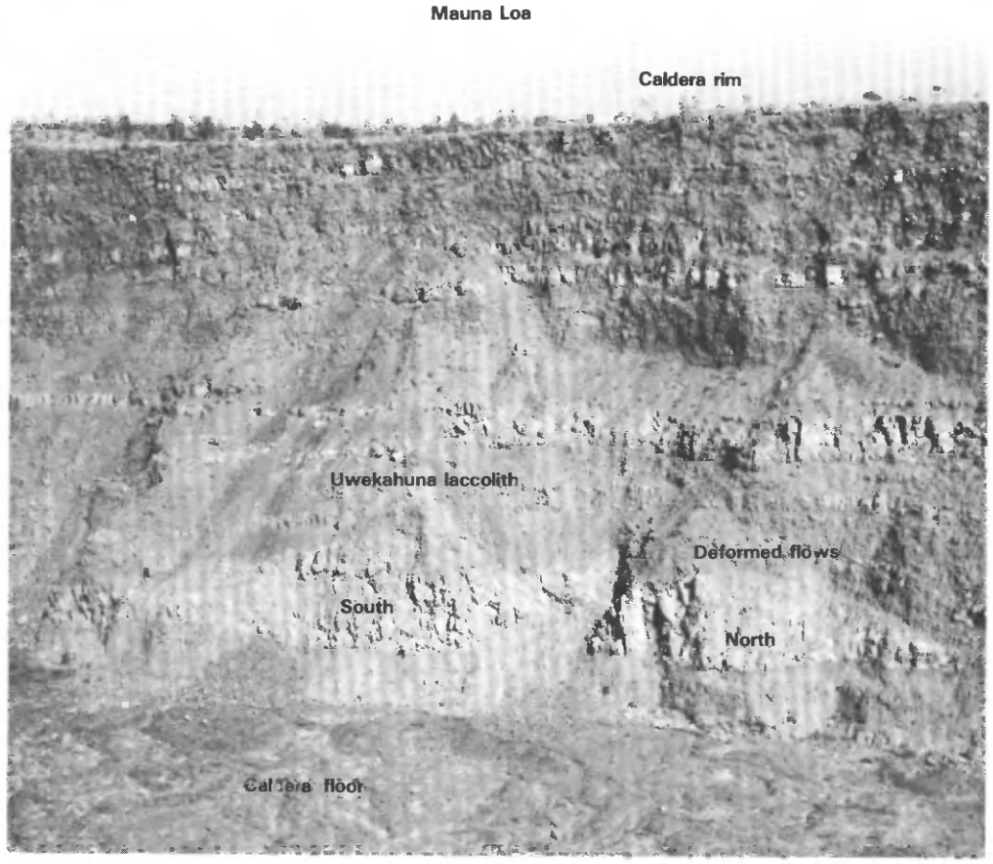
Mauna Loa
Caldera rim
Uwekahuna laccolith
Deformed flows
South
North
Caldera floor

A

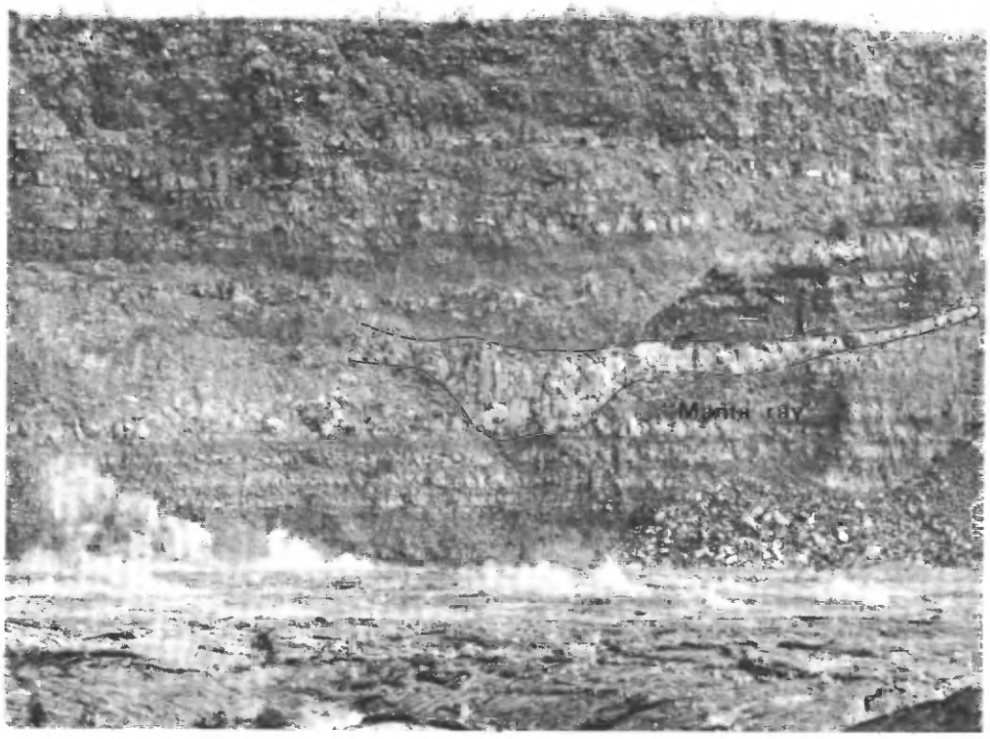
Mauna Loa

B

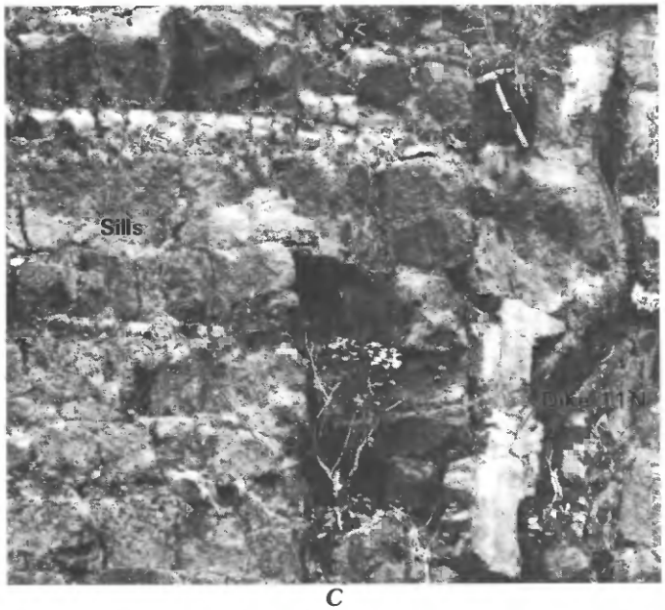

C

D

E

We identified 18 dikes in the western caldera wall that we subdivided into a north set (dikes 1N–12N) and a south set (dikes 1S–6S) based on their position relative to Uwekahuna Bluff (fig. 14.1). Most of the dikes trend northeasterly, roughly parallel to the strike of the southwest rift zone (N. 48° E.) and the linear segment of the western caldera wall (N. 40° E.; see fig. 14.6). Dike widths range from 5 cm to 2 m (table 14.1). The combined width of all dikes is only about 15 m, less than 1 percent of the length of the west wall.

DIKES OF THE NORTH SET

Dikes of the north set are oriented more northerly than those of the south set (fig. 14.1; table 14.1). Olivine-rich dikes 1N and 2N differ from other dikes of the north set in both composition and orientation (fig. 14.1); neither penetrates above the picritic lavas overlying the Uwekahuna Ash Member (Casadevall and Dzurisin, chapter 13). Dike 1N cuts the 2.1-ka Uwekahuna Ash Member and the lowermost flows of the picritic sequence at Uwekahuna

FIGURE 14.2.—Intrusive bodies in the west wall of Kilauea caldera. ***A***, Aerial view showing the two main parts (north and south) of the Uwekahuna laccolith; note tilted attitude of thin flows along northern edge of body. ***B***, Small manta ray-shaped body that is either an intrusion or formed by lava filling a surface depression. ***C***, Small sills coming off from main mass of dike 11N. ***D***, Detail of southwest caldera wall showing September 1971 eruptive fissure. ***E***, Dike 10N showing sets of prismatic joints perpendicular to dike walls.

TABLE 14.1.—*Thickness, orientation, MgO content, and brief description of dikes in the west wall of Kilauea caldera*

[n.d., not determined]

Dike	Thickness (cm)	Orientation		MgO content (weight percent)	Comments
		Strike	Dip		
North set					
1N	40–60	N. 83° W.	85° N.	6.9 (margin) 14.3 (core)	Glass margin, picritic core.
2N	85–110	N. 33° W.	85° NE.	26.6	Margin of Uwekahuna laccolith.
3N	5–10	N. 10° W.–N. 30° W.	vertical	n.d.	Thin dikelets in section of thin picritic pahoehoe flows.
4N	80 (minimum)	N. 45° E.	67° SE.	n.d.	Tabular dike; east wall is missing.
5N	8–10	n.d.	n.d.	n.d.	Thin dikelet, top of talus cone against caldera wall.
6N	20–30	N. 73° W.	vertical	6.7	Complex of dikes and dikelets with glassy margins.
7N	50	N. 17° E.	vertical	7.3	
8N	65	N. 29° E.	vertical	7.8	Glassy margins.
9N	20–30	NE. (varies)	n.d.	7.2	Complex of dikes and sills; glassy margins.
10N	60	N. 34° E.	vertical	7.0	Portion of dike by caldera floor has open, vuggy interior; glassy margins. Fills fracture that cuts entire section; dike stops 15 m below rim.
11N	100–180	N. 38° E.	vertical	7.5	Widest dike within caldera wall.
12N	100–150	N. 64° E.	77° NW.	6.9	Cuts flows in bench above 1974 flow on crater floor; glassy margins.
South set					
1S	8–12	N. 45° E.	vertical	6.7–7.7	Complex of dikelets and sills; glassy margins.
2S	75 (maximum)	N. 53° E.	vertical	6.6–7.5	Glassy margins.
3S	85–120	N. 42° E.–N. 53° E.	vertical	6.7–7.0	Above 1974 flows; glassy margins.
4S	35	N. 67° E.	vertical	7.0–7.2	Glassy margins.
5S	20–35	N. 85° E.	vertical	6.7–7.2 (margin) 20.1 (core)	Glassy margins.
6S	90 (maximum)	N. 60° E.	84° N.	n.d.	Glassy margins.

Bluff. Dike 2N occurs along the southern margin of the north part of the Uwekahuna laccolith, and it is olivine-rich throughout. It cuts several flows below the laccolith, but we did not find it above the laccolith.

The wider dikes display crude columnar jointing perpendicular to their margins. Dikes 10N and 11N have multiple cooling surfaces parallel to their walls that suggest more than one period of filling (fig. 14.2*E*). Small sills along flow contacts sprout from many dikes (fig. 14.2*C*); examples as much as 7 m long were observed.

Most samples for petrographic and chemical study were collected from the base of the exposure on the caldera floor. Along dike 10N, we rapelled from the caldera rim to collect samples and inspect the higher part of the dike about 15 m below the rim (fig. 14.3), where it terminates abruptly. This dike has fine-grained margins, 10–15 cm wide, which adhere to the walls of the fracture. The interior of the dike in its upper part is an open space about 80 cm wide, partly filled with soil and rock talus. We noted no spatter, drapery, or increased vesicularity of the dike rock to indicate eruption of the dike. The dike neither appeared to feed nor be fed from a surface flow. The host fracture, however, continued to the surface. Several factors, which we discuss later, may have prevented the magma from filling the fracture and reaching the surface, at least in the cross-section view we examined.

All but one of the 12 dikes in the north set occur in the unbroken part of the west caldera wall; dikes 6N–11N occupy fractures that cut through the entire sequence of flows in the wall (fig. 14.3). In the Steaming Flats area above these dikes, we found no evidence within several hundred meters of the rim that any dikes had vented. Where these fractures intersect the caldera rim, they are typically filled with vegetation, talus, and the Keanakakoi Ash Member. This cover obscures contact relations between the dikes and the ash.

Anecdotal evidence suggests that recent eruptive activity has occurred in the Steaming Flat area. Perret (1913, p. 615–616, fig. 6) noted that "miniature bombs or lava drops *** were discovered by the writer on the top, and surrounding the base, of several small, dome-topped cones of very scoriaceous lava situated on the northern rim of Kilauea near 'Kaniakolea', and therefore *outside* of the great pit crater, although within one of the surrounding areas of subsidence and not very far from Sulphur Banks*** ." H.A. Powers (oral commun., 1979) reported that following a large earthquake in the 1930's he found fresh spatter on the road at the western edge of Steaming Bluff, where Crater Rim Road ascends toward Kilauea Military Camp (fig. 14.1).

We did locate a spatter vent mapped by Macdonald and others (1983, fig. 19.19) (fig. 14.1). This feature is actually a series of echelon spatter ramparts that range in height from 2–8 m. They extend from the access road along the eastern boundary of Kilauea Military Camp to the northeast for approximately 150 m. The ramparts are mantled by the Keanakakoi Ash Member as much as 80 cm thick, indicating that they predate the 1790 eruption.

The area of Steaming Flats is currently aseismic (R.Y. Koyanagi, oral commun., 1979), and there is no local center of deformation in the area (A.T. Okamura, oral commun., 1984). However, nearby Sulfur Bank (fig. 14.1) is an area of active fumaroles (Casadevall and Hazlett, 1983), suggesting that a magmatic source of heat and gas is located at a shallow depth beneath the Steaming Flats area.

DIKES OF THE SOUTH SET

The six dikes south of Uwekahuna Bluff cut a thinner section of flows (15–40 m) than do the dikes north of Uwekahuna Bluff (120–140 m). Five of these southern dikes are fine grained and only

FIGURE 14.3.—Dike 10N in caldera wall below Steaming Bluff. Caldera floor at base of cliff just below bottom of view. Top of dike is about 15 m below caldera rim.

sparsely porphyritic, but dike 5S contains abundant olivine phenocrysts (tables 14.1, 14.2). Most of the dikes have open or rubble-filled interiors that resemble the 1971 eruptive fissure (Duffield and others, 1982) (fig. 14.2*D*). These dikes may have formed in a manner similar to that observed during the September 1971 eruption, in which the same fissure served first as a source of lava and later as a drain for surface flows.

The glassy margins of dikes 4S and 6S were dated by J. Halbig (written commun., 1985) using hydration-rind techniques. The hydration-rind ages have been calibrated elsewhere at Kilauea for lava flows dated by the radiocarbon method. The dikes have ages ranging from 0.55 to 0.45 ka. No ages are available for lava flows in this part of the caldera, so it is difficult to evaluate the accuracy of these ages. If, as we suspect, the flows cut by these dikes are equivalent to the upper flows exposed at Uwekahuna Bluff (suite A, 1.5–0.35 ka; see Casadevall and Dzurisin, chapter 13), the hydration-rind ages are reasonable.

PETROGRAPHY

We examined 28 thin sections from the dikes and identified three rock types on the basis of crystallinity and phenocryst content. The margins of most of the dikes and related thin sills consist of dark brown to olive glass with sparse microlites and scattered euhedral phenocrysts of olivine. The margins range from a few millimeters to several centimeters thick and pass gradually into the finely crystalline interiors of the dikes.

The cores of the thicker dikes are of two textural varieties, a porphyritic picrite (5S and 1N) with a fine- to medium-grained groundmass and an aphanitic basalt with sparse olivine phenocrysts in a groundmass of brown glass and plagioclase microlites. Olivine phenocrysts in the cores are generally corroded and resorbed, in contrast to their distinctly euhedral habit in the glassy margins. Dike 2N is medium to coarsely crystalline rock with only minor glass. It is distinct from all other dikes at Kilauea and closely resembles the Uwekahuna laccolith, which it appears to intrude and may have fed.

CHEMISTRY

MAJOR AND TRACE ELEMENTS

Fourteen dikes were analyzed for major and trace elements, including rare-earth elements, sulfur, and chlorine (table 14.2). The major-element data were determined using rapid-rock methods (Shapiro, 1975) and were supplemented by electron-microprobe analyses of glass from the margins of dikes. All analyses were recalculated on a dry-weight basis after converting iron to FeO_t ($FeO_t = FeO + 0.9Fe_2O_3$) to facilitate comparison of the data. Our objective in obtaining these data was to use chemistry, in conjunction with field occurrence and petrography, to characterize dikes or sets of dikes and to relate the dikes to the flows in the Uwekahuna Bluff section (Casadevall and Dzurisin, chapter 13). Water (H_2O^+), sulfur, and chlorine were measured to estimate the extent to which the dikes had degassed.

TABLE 14.2.—*Chemical analyses of samples from dikes in the west wall of Kilauea caldera*

[Values for oxides in weight percent; values for trace elements in parts per million. Symbols (numbers and letters) used to distinguish samples in fig. 14.4; INAA, neutron-activation analysis; AA, atomic absorption analysis; n.d., not determined; <, less than. Sources of data: for WASH-11, Washington (1923); for Uwekahuna laccolith, Murata and Richter (1961)]

Dike	1S	1S	2S	2S	3S	3S	3S	4S	4S	4S	5S
Sample	5614	W-211577	5615	W-211567	5616	5617	W-211575	5620	5621	W-211574	5618
Symbol	1	1	2	2	3	3	3	4	4	4	5
SiO_2	51.84	50.2	51.75	49.7	50.64	50.78	50.2	50.96	51.65	50.0	51.62
Al_2O_3	13.96	13.7	14.06	13.5	13.99	13.91	13.4	13.58	13.70	13.7	13.95
Fe_2O_3	n.d.	1.9	n.d.	2.2	n.d.	n.d.	2.9	n.d.	n.d.	2.0	n.d.
FeO	10.75	9.1	10.94	9.3	11.09	11.10	8.9	11.18	11.16	9.5	11.05
MgO	6.71	7.7	6.63	7.4	6.84	6.77	7.0	7.24	7.10	7.0	6.76
CaO	10.88	10.9	10.96	10.9	11.03	11.09	11.4	11.33	11.22	11.2	10.95
Na_2O	2.43	2.3	2.39	2.2	2.22	2.30	2.1	2.31	2.25	2.2	2.12
K_2O	.47	.45	.41	.40	.39	.41	.41	.45	.44	.43	.34
H_2O	n.d.	.16	n.d.	.01	n.d.	n.d.	.13	n.d.	n.d.	.04	n.d.
TiO_2	2.71	2.5	2.48	2.3	2.50	2.58	2.4	2.38	2.48	2.4	2.35
P_2O_5	.27	.26	.23	.27	.23	.24	.27	.26	.25	.27	.20
MnO	n.d.	.16	n.d.	.15	n.d.	n.d.	.18	n.d.	n.d.	.17	n.d.
CO_2	n.d.	n.d.	n.d.	n.d.	n.d.	n.d.	n.d.	n.d.	n.d.	n.d.	n.d.
Cl	n.d.	.004	n.d.	.004	n.d.	n.d.	.005	n.d.	n.d.	.006	n.d.
F	n.d.	n.d.	n.d.	n.d.	n.d.	n.d.	n.d.	n.d.	n.d.	n.d.	n.d.
S	n.d.	.042	n.d.	.049	n.d.	n.d.	.066	n.d.	n.d.	.049	n.d.
Ba	n.d.	121	n.d.	117	n.d.	n.d.	109	n.d.	n.d.	139	n.d.
Co (INAA)	n.d.	44.3	n.d.	44.5	n.d.	n.d.	43.3	n.d.	n.d.	43.6	n.d.
Co (AA)	n.d.	45	n.d.	45	n.d.	n.d.	45	n.d.	n.d.	47	n.d.
Cr	n.d.	454	n.d.	408	n.d.	n.d.	315	n.d.	n.d.	309	n.d.
Ni	n.d.	190	n.d.	140	n.d.	n.d.	100	n.d.	n.d.	100	n.d.
Cu	n.d.	120	n.d.	120	n.d.	n.d.	110	n.d.	n.d.	120	n.d.
Hf	n.d.	3.87	n.d.	3.55	n.d.	n.d.	3.99	n.d.	n.d.	3.83	n.d.
Rb	n.d.	11	n.d.	14	n.d.	n.d.	13	n.d.	n.d.	13	n.d.
Ta	n.d.	.87	n.d.	.76	n.d.	n.d.	.99	n.d.	n.d.	1.08	n.d.
Th	n.d.	.86	n.d.	.7	n.d.	n.d.	.95	n.d.	n.d.	.96	n.d.
U	n.d.	<0.6	n.d.	<0.5	n.d.	n.d.	.34	n.d.	n.d.	.37	n.d.
Zn	n.d.	111	n.d.	108	n.d.	n.d.	108	n.d.	n.d.	114	n.d.
Zr	n.d.	119	n.d.	81	n.d.	n.d.	167	n.d.	n.d.	76	n.d.
Sc	n.d.	29.9	n.d.	30.6	n.d.	n.d.	31.7	n.d.	n.d.	31.6	n.d.
La	n.d.	12.8	n.d.	10.6	n.d.	n.d.	12.3	n.d.	n.d.	12.3	n.d.
Ce	n.d.	29.0	n.d.	25.3	n.d.	n.d.	27.8	n.d.	n.d.	28.9	n.d.
Nd	n.d.	21	n.d.	21	n.d.	n.d.	9	n.d.	n.d.	23	n.d.
Sm	n.d.	5.50	n.d.	5.2	n.d.	n.d.	5.35	n.d.	n.d.	5.39	n.d.
Eu	n.d.	1.92	n.d.	1.80	n.d.	n.d.	1.74	n.d.	n.d.	1.78	n.d.
Gd	n.d.	5.1	n.d.	4.7	n.d.	n.d.	3.3	n.d.	n.d.	4.2	n.d.
Tb	n.d.	.87	n.d.	.79	n.d.	n.d.	.80	n.d.	n.d.	.83	n.d.
Tm	n.d.	.27	n.d.	.23	n.d.	n.d.	.27	n.d.	n.d.	.22	n.d.
Yb	n.d.	2.05	n.d.	2.05	n.d.	n.d.	2.10	n.d.	n.d.	2.20	n.d.
Lu	n.d.	.286	n.d.	.310	n.d.	n.d.	.302	n.d.	n.d.	.301	n.d.

Dike	5S	5S	5S	1N	1N	2N	6N	7N	8N	9N	10N
Sample	5619	W-211407	W-211573	5622	W-211408	W-211409	5623	W-211410	W-211411	W-211415	W-211412
Symbol	5	5	5	A	A	B	F	G	H	I	J
SiO_2	51.06	46.6	50.3	51.38	48.7	44.8	51.63	50.5	50.6	51.3	51.0
Al_2O_3	13.61	9.5	13.9	14.18	11.3	6.9	13.9	12.7	13.1	13.7	13.9
Fe_2O_3	n.d.	1.5	2.1	n.d.	2.0	2.8	n.d.	2.3	2.1	2.2	2.5
FeO	11.00	10.7	9.4	9.96	9.6	10.8	10.87	9.9	9.4	9.1	8.8
MgO	7.17	20.2	7.2	6.94	14.3	26.8	6.78	7.3	7.8	7.2	7.0
CaO	11.23	7.7	10.9	11.47	9.3	5.9	11.10	10.4	11.0	10.6	10.9
Na_2O	2.23	1.6	2.4	2.36	1.9	.99	2.37	2.4	2.2	2.5	2.5
K_2O	.40	.33	.44	.47	.37	.19	.41	.50	.45	.41	.44
H_2O	n.d.	.35	.33	n.d.	.13	.31	n.d.	.25	.13	.22	.16
TiO_2	2.45	1.7	2.3	2.65	2.1	1.0	2.39	2.9	2.5	2.4	2.4
P_2O_5	.19	.21	.27	.23	.25	.13	.23	.35	.28	.30	.28
MnO	n.d.	.19	.17	n.d.	.18	.20	n.d.	.20	.18	.19	.18
CO_2	n.d.	n.d.	n.d.	n.d.	n.d.	n.d.	n.d.	n.d.	n.d.	n.d.	n.d.
Cl	n.d.	.004	.005	n.d.	.004	.004	n.d.	.005	.006	.004	.004
F	n.d.	n.d.	n.d.	n.d.	n.d.	n.d.	n.d.	n.d.	n.d.	n.d.	n.d.
S	n.d.	.024	.045	n.d.	.027	.015	n.d.	.063	.068	.048	.025
Ba	n.d.	101	121	n.d.	<200	66	n.d.	148	130	103	<200
Co (INAA)	n.d.	87.9	40.5	n.d.	65.1	110	n.d.	44.6	46	42.4	41.7
Co (AA)	n.d.	89	45	n.d.	66	110	n.d.	50	52	48	48
Cr	n.d.	1220	328	n.d.	934	1620	n.d.	289	355	331	347
Ni	n.d.	980	90	n.d.	600	1400	n.d.	97	110	85	82
Cu	n.d.	68	120	n.d.	99	49	n.d.	140	120	120	100
Hf	n.d.	2.48	3.54	n.d.	3.21	1.50	n.d.	4.52	3.7	3.6	3.57
Rb	n.d.	<30	19	n.d.	<30	<30	n.d.	<30	16	<30	<30
Ta	n.d.	.66	.82	n.d.	.81	.39	n.d.	1.13	.91	.77	.77
Th	n.d.	.47	.84	n.d.	.65	<.4	n.d.	.87	.90	.68	.69
U	n.d.	.33	<.4	n.d.	.29	<.5	n.d.	.43	<.6	.31	<.6
Zn	n.d.	104	103	n.d.	106	105	n.d.	119	111	110	110
Zr	n.d.	89	168	n.d.	<100	<200	n.d.	185	157	118	<200
Sc	n.d.	20.9	29.5	n.d.	26.5	19.2	n.d.	31.9	31.2	30.1	30.5
La	n.d.	8.9	10.8	n.d.	10.2	4.6	n.d.	14.9	11.5	10.9	11.1
Ce	n.d.	21.3	25.0	n.d.	24.8	12.6	n.d.	35.5	29.0	25.8	26.0
Nd	n.d.	15	16	n.d.	18	9	n.d.	25	19	17	19
Sm	n.d.	3.92	5.22	n.d.	4.65	2.30	n.d.	6.64	5.49	5.39	5.4
Eu	n.d.	1.26	1.68	n.d.	1.54	.748	n.d.	2.17	1.78	1.81	1.72
Gd	n.d.	4.8	3.8	n.d.	5.4	3.0	n.d.	8.1	6.4	6.4	6.4
Tb	n.d.	.56	.74	n.d.	.70	.46	n.d.	1.01	.84	.86	1.05
Tm	n.d.	.17	.26	n.d.	.26	.10	n.d.	.40	.24	.34	.27
Yb	n.d.	1.40	2.15	n.d.	1.70	.91	n.d.	2.45	2.03	2.18	2.03
Lu	n.d.	.196	.298	n.d.	.253	.132	n.d.	.35	.30	.30	.29

TABLE 14.2.—*Chemical analyses of samples from dikes in the west wall of Kilauea caldera*—Continued

Dike	10N	11N	12N	11N	11N	LAC	LAC	LAC	LAC	LAC	LAC	LAC
Sample	W-211416	W-211414	W-211413	WASH-11	WASH-11	UWEMR-1	UWEMR-2	UWEMR-3	UWEMR-4	UWEMR-5	UWEMR-6	UWEMR-7
Symbol	J	K	L	K	K	U	U	U	U	U	U	U
SiO_2	51.2	50.9	51.7	51.77	50.53	48.37	48.25	46.59	46.32	48.56	49.50	52.04
Al_2O_3	14.3	13.4	13.7	13.54	13.61	11.19	10.72	7.69	8.58	11.62	12.67	13.20
Fe_2O_3	1.8	2.1	2.0	.75	1.69	3.08	2.14	2.20	1.58	2.9	4.89	2.86
FeO	9.2	9.3	9.2	9.63	9.30	8.65	9.50	10.46	10.98	8.56	6.36	8.55
MgO	7.0	7.5	6.9	7.33	7.01	15.26	16.45	21.79	21.98	14.65	11.55	5.84
CaO	10.6	10.6	10.6	10.57	10.75	8.94	8.79	7.41	7.11	9.36	10.05	8.83
Na_2O	2.3	2.4	2.4	2.18	2.16	1.76	1.61	1.33	1.28	1.74	1.99	2.79
K_2O	.43	.41	.42	.45	.35	.28	.25	.28	.21	.26	.32	.83
H_2O	.29	.10	.30	n.d.	n.d.	.13	.11	.41	.15	.17	.14	.41
TiO_2	2.4	2.4	2.3	4.01	3.68	1.88	1.75	1.83	1.44	1.92	2.14	4.16
P_2O_5	.30	.29	.30	.26	.20	.16	.16	.11	.11	.14	.18	.49
MnO	.18	.19	.17	.15	.13	.17	.17	.18	.17	.16	.16	.16
CO_2	n.d.	n.d.	n.d.	n.d.	n.d.	n.d.	n.d.	n.d.	n.d.	n.d.	n.d.	n.d.
Cl	.005	.004	.005	n.d.	n.d.	n.d.	n.d.	n.d.	n.d.	n.d.	n.d.	n.d.
F	n.d.	n.d.	n.d.	n.d.	n.d.	n.d.	n.d.	n.d.	n.d.	n.d.	n.d.	n.d.
S	.034	.027	.065	n.d.	n.d.	n.d.	n.d.	n.d.	n.d.	n.d.	n.d.	n.d.
Ba	112	99	105	n.d.	n.d.	n.d.	n.d.	n.d.	n.d.	n.d.	n.d.	n.d.
Co (INAA)	37.9	45	41.5	n.d.	n.d.	n.d.	n.d.	n.d.	n.d.	n.d.	n.d.	n.d.
Co (AA)	45	48	48	n.d.	n.d.	n.d.	n.d.	n.d.	n.d.	n.d.	n.d.	n.d.
Cr	309	370	318	n.d.	n.d.	n.d.	n.d.	n.d.	n.d.	n.d.	n.d.	n.d.
Ni	97	120	94	n.d.	n.d.	n.d.	n.d.	n.d.	n.d.	n.d.	n.d.	n.d.
Cu	120	100	120	n.d.	n.d.	n.d.	n.d.	n.d.	n.d.	n.d.	n.d.	n.d.
Hf	3.30	3.6	3.6	n.d.	n.d.	n.d.	n.d.	n.d.	n.d.	n.d.	n.d.	n.d.
Rb	<20	<30	<30	n.d.	n.d.	n.d.	n.d.	n.d.	n.d.	n.d.	n.d.	n.d.
Ta	.68	.79	.75	n.d.	n.d.	n.d.	n.d.	n.d.	n.d.	n.d.	n.d.	n.d.
Th	.68	.83	.76	n.d.	n.d.	n.d.	n.d.	n.d.	n.d.	n.d.	n.d.	n.d.
U	<.3	<.6	<.6	n.d.	n.d.	n.d.	n.d.	n.d.	n.d.	n.d.	n.d.	n.d.
Zn	98	120	115	n.d.	n.d.	n.d.	n.d.	n.d.	n.d.	n.d.	n.d.	n.d.
Zr	88	113	141	n.d.	n.d.	n.d.	n.d.	n.d.	n.d.	n.d.	n.d.	n.d.
Sc	27.5	31.0	30.1	n.d.	n.d.	n.d.	n.d.	n.d.	n.d.	n.d.	n.d.	n.d.
La	10.8	10.7	10.7	n.d.	n.d.	n.d.	n.d.	n.d.	n.d.	n.d.	n.d.	n.d.
Ce	24.1	24.9	25.5	n.d.	n.d.	n.d.	n.d.	n.d.	n.d.	n.d.	n.d.	n.d.
Nd	18	19	17	n.d.	n.d.	n.d.	n.d.	n.d.	n.d.	n.d.	n.d.	n.d.
Sm	5.34	5.24	5.24	n.d.	n.d.	n.d.	n.d.	n.d.	n.d.	n.d.	n.d.	n.d.
Eu	1.61	1.71	1.77	n.d.	n.d.	n.d.	n.d.	n.d.	n.d.	n.d.	n.d.	n.d.
Gd	6.6	6..1	5.7	n.d.	n.d.	n.d.	n.d.	n.d.	n.d.	n.d.	n.d.	n.d.
Tb	.85	.86	.83	n.d.	n.d.	n.d.	n.d.	n.d.	n.d.	n.d.	n.d.	n.d.
Tm	.23	.25	.33	n.d.	n.d.	n.d.	n.d.	n.d.	n.d.	n.d.	n.d.	n.d.
Yb	2.07	2.15	2.32	n.d.	n.d.	n.d.	n.d.	n.d.	n.d.	n.d.	n.d.	n.d.
Lu	.28	.318	.321	n.d.	n.d.	n.d.	n.d.	n.d.	n.d.	n.d.	n.d.	n.d.

The dikes are tholeiitic basalt and have compositions similar to those of typical Kilauea summit flows (Macdonald, 1949; Wright, 1971; Casadevall and Dzurisin, chapter 13), for which the main control on composition is the gain or loss of olivine (Powers, 1955; Murata and Richter, 1966a, b; Wright, 1971). Dikes of the north set and those of the south set are chemically similar. MgO variation diagrams show no obvious linear trends because most analyses cluster between 6.6 and 7.8 weight percent MgO (fig. 14.4A). The cores of the three picrite dikes (5S, 1N, and 2N) have MgO in excess of 14 weight percent; dikes 5N and 1S have glassy margins with MgO contents near 7.0 weight percent. The olivine-control lines for these two dikes are similar to those for lava flows of Uwekahuna Bluff (fig. 14.4; table 14.3; Casadevall and Dzurisin, chapter 13).

Thirteen dikes were analyzed for a suite of 24 trace elements using a combination of instrumental neutron activation (Baedecker, 1979), atomic absorption, and X-ray fluorescence methods (table 14.2). Most of the trace elements correlate negatively with MgO content (fig. 14.4*B*) but dilution by settled olivine causes Ni, Co, and Cr to show positive correlations (fig. 14.4*B*) for reasons discussed in Casadevall and Dzurisin (chapter 13). The rare-earth-element (REE) abundances and the shapes and slopes of chondrite-normalized REE plots for the dike samples (fig. 14.5) closely resemble those for Kilauea lava flows (Leeman and others, 1977, 1980; Basaltic Volcanism Study Project, 1981), including those from Uwekahuna Bluff (Casadevall and Dzurisin, chapter 13).

VOLATILE CONSTITUENTS

The dikes contain concentrations of water, sulfur, and chlorine that are higher than in typical surface-degassed lava, but lower than in primitive basaltic magma (table 14.4). Water content for glassy margins of most of the dikes is in the range of 0.13–0.35 weight percent; in dikes 2S and 4S it is considerably lower (0.01 and 0.04 weight percent, respectively). Sulfur content of glassy margins of the dikes ranges from 0.042 to 0.068 weight percent, and that of chlorine from 0.004 to 0.006 weight percent. Interiors of the dikes generally have less H_2O, S, and Cl than do their glassy margins. This difference probably reflects the fact that glassy margins quench in higher volatile contents compared to the more crystalline interior portions of the dikes. The concentrations in the glassy margins are low compared to the postulated abundances for parental Hawaiian basaltic magma (table 14.4): 0.30–0.45 weight percent H_2O; 0.10–0.15 weight percent S, and 0.008–0.011 weight percent Cl (Harris and Anderson, 1983; Gerlach and Graeber, 1985; Greenland and others, 1985; L.P. Greenland, written commun., 1985).

Gerlach and Graeber (1985) and Greenland and others (1985) have demonstrated that Hawaiian magma loses volatiles on the way to the surface as well as during eruption. Loss of carbon dioxide probably begins soon after the magma leaves the upper mantle. Significant loss of water and sulfur, on the other hand, occurs when the magma is at a confining pressure equivalent to several tens of meters of lithostatic load (Moore, 1970; Moore and Fabbi, 1971), although some is lost while the magma temporarily resides in the shallow summit reservoir (Gerlach and Graeber, 1985; Greenland and others, 1985).

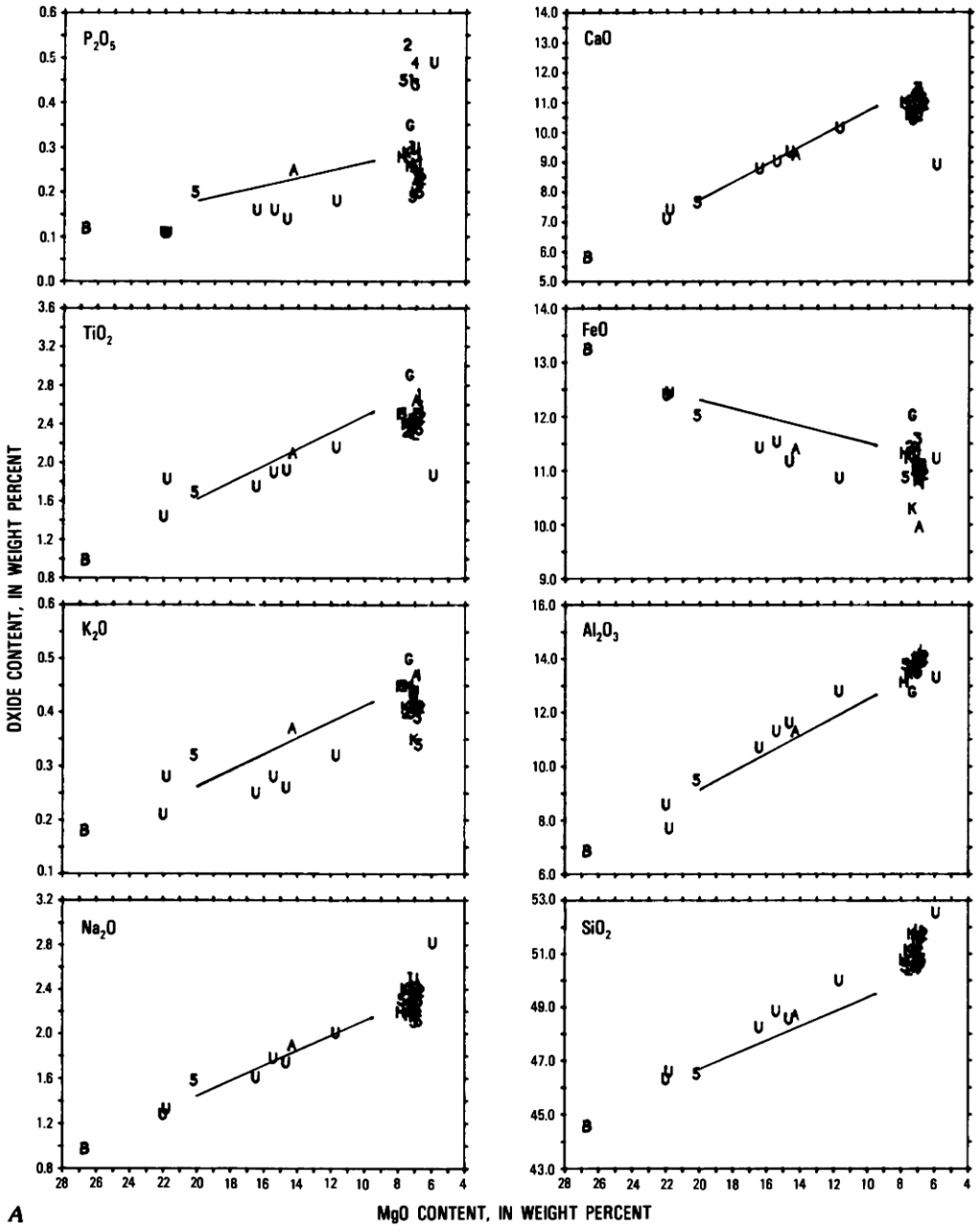

FIGURE 14.4.—MgO variation diagrams for intrusive rocks of Kilauea caldera. A, dike 1N; J, dike 10N; K, dike 11N; L, dike 12N; O, dike 10N; U, Uwekahuna laccolith. Also plotted are olivine-control lines for the picritic suite C lava flows at Uwekahuna Bluff (Casadevall and Dzurisin, chapter 13); these lines are not derived from the plotted data but instead provide a comparison between the caldera intrusions and the lava flows they intruded. Data for Uwekahuna laccolith from Murata and Richter (1961). Other number and letter symbols refer to samples listed in table 14.2. ***A***, Major-element abundances. ***B***, Trace-element abundances. ***C***, Rare-earth-element abundances.

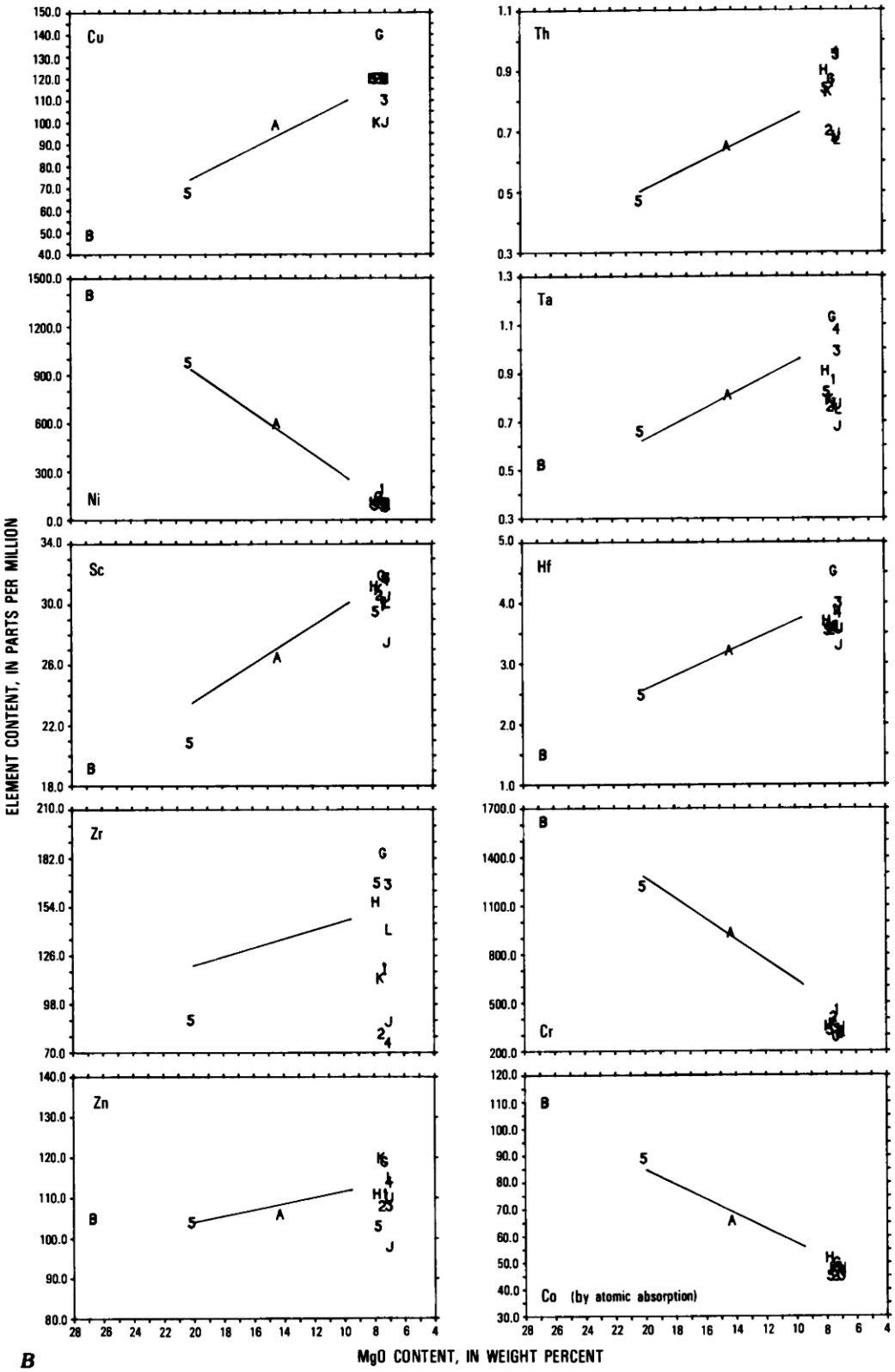

FIGURE 14.4.—Continued.

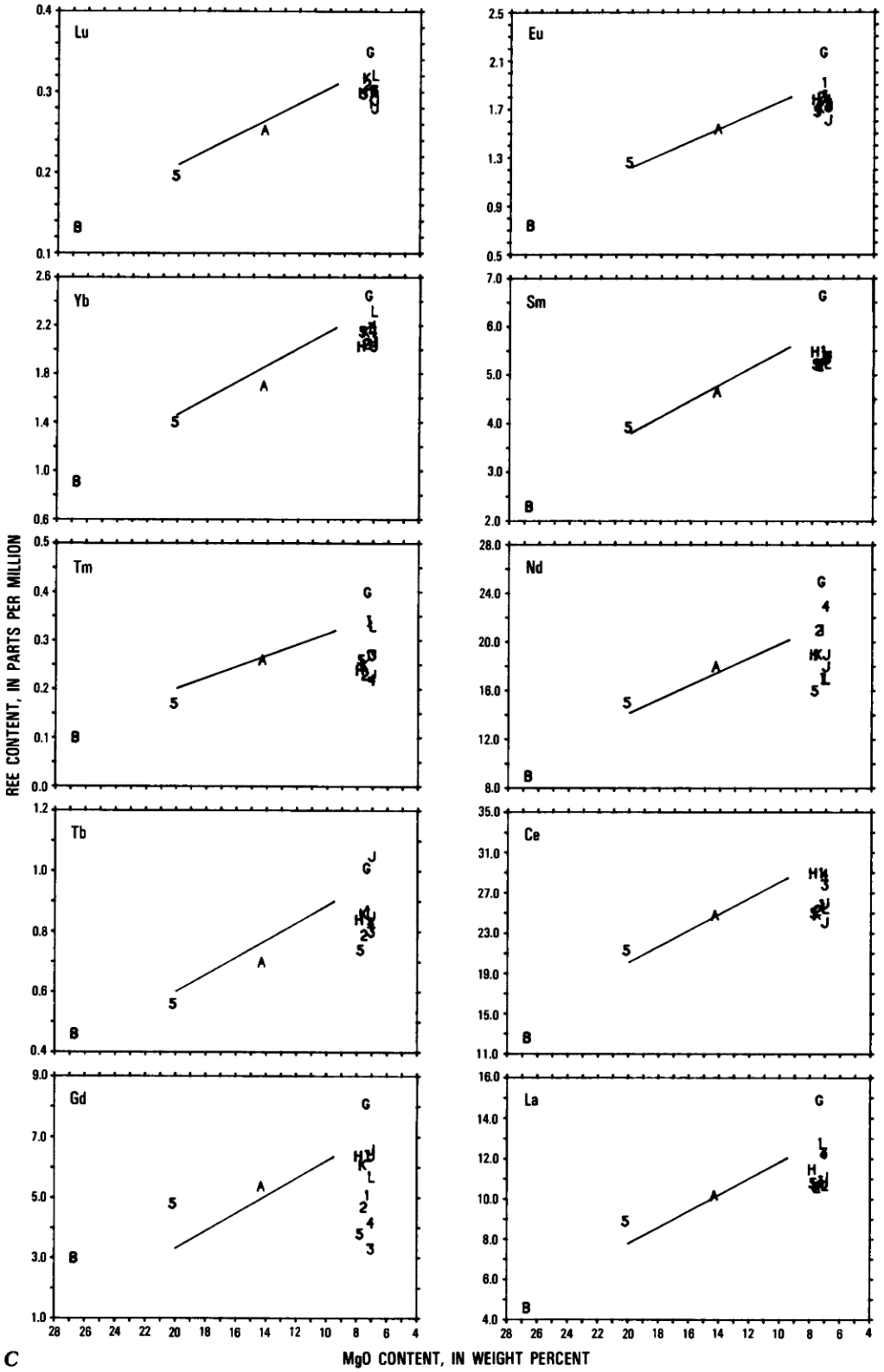

FIGURE 14.4.—Continued.

TABLE 14.3.—*Coefficients of olivine control lines (equations of the form $y = ax + b$) for Kilauea intrusive rocks and lava flows*

[y is the major oxide or element, x is the MgO content, a is the slope, and b is the y intercept value at MgO = 0 weight percent. Values for oxides in weight percent; values for trace elements in parts per million. Data sources: Dikes, this paper; Uwekahuna laccolith, Murata and Richter (1961); Uwekahuna Bluff suite C flows, Casadevall and Dzurisin (chapter 13); prehistoric pahoehoe picrite complex (PPPC) flows and prehistoric Kilauea caldera and Hilina (PHKILCAL) flows, Wright (1971). FeO_t, total iron oxide = FeO + 0.9 Fe_2O_3; n.d., not determined]

Element/oxide	Slope (a)	Uncertainty	Intercept (b)
Dike 5S			
SiO_2	−0.356	±0.047	53.651
Al_2O_3	−.332	±.024	16.181
FeO	.808	±.016	10.404
CaO	−.262	±.025	12.931
Na_2O	−.048	±.015	2.563
K_2O	−.005	±.007	.435
TiO_2	−.057	±.014	2.845
P_2O_5	−.005	±.019	.314
MnO	.002	n.d.	.148
Dike 1N			
SiO_2	−0.363	n.d.	53.898
Al_2O_2	−.391	n.d.	16.896
FeO	.196	n.d.	8.602
CaO	−.300	n.d.	13.554
Na_2O	−.063	n.d.	2.794
K_2O	−.014	n.d.	.564
TiO_2	−.075	n.d.	3.169
P_2O_5	.003	n.d.	.211
MnO	n.d.	n.d.	n.d.
Uwekahuna laccolith			
SiO_2	−0.307	±0.017	53.394
Al_2O_3	−.455	±.056	18.202
FeO	.160	±.013	8.935
CaO	−.275	±.019	13.342
Na_2O	−.066	±.005	2.744
K_2O	−.006	±.005	.367
TiO_2	−.045	±.023	2.603
P_2O_5	−.006	±.002	.253
MnO	.001	±.001	.144
Uwekahuna Bluff suite C flows			
SiO_2	−0.248	±0.064	51.828
Al_2O_3	−.336	±.025	15.852
FeO	.071	±.037	10.811
CaO	−.306	±.056	13.797
Na_2O	−.070	±.008	2.822
K_2O	−.015	±.003	.556
TiO_2	−.086	±.015	3.348
P_2O_5	−.008	±.003	.348
MnO	−.002	±.002	.183
Ba	.565	±2.649	100.346
Co (INAA)	3.297	±.253	19.006
Co (AA)	2.772	±.353	29.385
Cr	63.771	±6.067	2.147
Ni	65.268	±5.240	−368.050
Cu	−3.969	±1.398	151.439
Hf	−.113	±.025	4.831
Rb	−.289	±.345	16.829
Ta	−.032	±.009	1.272
Th	−.025	±.005	1.001
U	−.005	±.012	.369
Zn	−.700	±.600	118.175
Zr	−3.137	±2.066	171.211
Sc	−.635	±.074	36.140
La	−.409	±.079	15.931
Ce	−.800	±.162	36.090
Nd	−.578	±.267	25.673
Sm	−.170	±.033	7.194
Gd	−.291	±.070	9.128
Tb	−.029	±.008	1.186
Tm	−.011	±.004	.432
Yb	−.068	±.012	2.822
Lu	−.009	±.002	0.392
Prehistoric pahoehoe picrite complex (PPPC) flows			
SiO_2	−0.289	±0.023	52.894
Al_2O_3	−.357	±.010	16.643
FeO	.068	±.017	10.480
CaO	−.288	±.017	13.184
Na_2O	−.053	±.007	2.691
K_2O	−.014	±.003	.561
TiO_2	−.065	±.006	2.906
P_2O_5	−.006	±.001	.266
MnO	.000	n.d.	.164
Cr_2O_3	.008	.001	−.009
Prehistoric Kilauea caldera and Hilina flows (PHKILCAL)			
SiO_2	−0.317	±0.021	53.327
Al_2O_3	−.354	±.029	10.585
FeO	.081	±.030	10.260
CaO	−.266	±.016	13.044
Na_2O	−.065	±.005	2.753
K_2O	−.012	±.003	.497
TiO_2	−.057	±.012	2.843
P_2O_5	−.005	±.001	.259
MnO	n.d.	n.d.	n.d.

Lava flows from Kilauea and Mauna Loa that have traveled several kilometers from their feeding vents have low water contents of 0.01–0.10 weight percent, low total sulfur (0.004–0.007 weight percent), and chloride contents of 0.005–0.006 weight percent (Swanson and Fabbi, 1973; L.P. Greenland, written commun., 1985). These volatile contents are similar to those of surface-fed fracture fillings at Hilina Pali (Easton and Lockwood, 1983; table 14.4), but lower than most dikes in the west caldera wall. Surface flows within a few hundred meters of a vent may have higher volatile contents (0.01 weight percent S; 0.009 weight percent Cl) (Swanson and Fabbi, 1973).

DISCUSSION OF CHEMISTRY

The major- and trace-element chemistry of the dikes and Uwekahuna laccolith is similar to that of lava flows at Uwekahuna Bluff. In a companion paper (Casadevall and Dzurisin, chapter 13), we compare the composition of lava flows at Uwekahuna Bluff at a constant MgO content of 7.0 weight percent, by addition or subtraction of olivine from the bulk composition. We apply the same approach here to the intrusions. We used the olivine composition for the Uwekahuna laccolith determined by Murata and Richter (1961) and recalculated the composition for each analysis to 7.0 weight percent MgO. We then averaged the normalized magma compositions for dikes of the south set and the north set (table 14.5). The major-element and trace-element compositions of the intrusive bodies strongly resemble those of the succession of flows at Uwekahuna Bluff.

Olivine-control lines for dikes 5S and 1N, as well as for the Uwekahuna laccolith, have slopes similar to those for prehistoric Kilauea summit flows and the regional prehistoric pahoehoe picrite complex (PPPC) of the summit region (Wright, 1971), and the picritic flows (suite C) of the Uwekahuna Bluff section (table 14.3; fig. 14.4*A*; Casadevall and Dzurisin, chapter 13). These similarities indicate that the magma of the picritic dikes and the laccolith is chemically similar to other magmas of the Kilauea summit region.

TABLE 14.4.—*Volatile contents of samples from Kilauea caldera dikes and other Hawaiian intrusive and extrusive rocks*

[All values in weight percent. For Kilauea dikes, H_2O^+ content by modified Penfield method, analyses by CHN water analyzer (uncertainty ±3–5 percent of reported value); total sulfur analyses by Leco sulfur analyzer with infrared detector (uncertainty ±0.005 weight percent); total chlorine analyses using separation by Conway cell method, measured by selective ion electrode (uncertainty ±0.002 weight percent). Other samples: 1–9, Easton and Lockwood (1983), Swanson and Fabbi (1973); 10–12, L.P. Greenland, written commun. (1984); data for primitive Hawaiian magma from Greenland (in press), Greenland and others (1985), and Gerlach and Graeber (1985), also includes 0.65 weight percent CO_2]

Sample	Laboratory number	H_2O^+	Sulfur	Chloride	Total volatiles	Comments
Kilauea caldera dikes, south set						
1S	W-211577	0.16	0.042	0.004	0.206	Glass margin.
2S	W-211576	.01	.049	.004	.064	Glass margin.
3S	W-211575	.13	.066	.005	.201	Glass margin.
4S	W-211574	.04	.049	.006	.095	Glass margin.
5S	W-211573	.33	.045	.005	.380	Glass margin.
5S	W-211407	.35	.024	.004	.378	Picrite interior.
Kilauea caldera dikes, north set						
1N	W-211408	.13	.027	.004	.161	Picrite interior.
2N	W-211409	.31	.015	.004	.329	Cuts laccolith.
7N	W-211410	.25	.063	.005	.318	Glass margin.
8N	W-211411	.13	.068	.006	.204	Glass margin.
9N	W-211415	.22	.048	.004	.272	Glass margin.
10N	W-211412	.16	.025	.004	.189	Interior.
10N	W-211416	.29	.034	.005	.329	15 m below rim.
11N	W-211414	.10	.027	.004	.131	Margin.
12N	W-211413	.30	.065	.005	.370	Glass margin.
Other samples						
Field number		H_2O^+	Sulfur	Chloride	Total volatiles	Comments
(1) L-78-6B		---	0.09	0.04	0.2	0.33 Mauna Loa dike.
(2) L-78-7		.13	.05	.004	.184	Mauna Loa dike.
(3) L-78-8		.15	.03	<.05	<.23	Mauna Loa dike.
(4) L-78-9		.13	.05	.1	.28	Mauna Loa dike.
(5) L-77-35B		.05	.011	.006	.067	Hilina dike.
(6) L-77-35C		.06	.011	.007	.078	Hilina dike.
(7) --------		.09	.005	.007	.102	Uwekahuna laccolith.
(8) DAS71-1213-136		.04	.02	.009	.069	Kilauea surface flow.
(9) DAS71-1213-137		.04	.02	.009	.069	Kilauea surface flow.
(10) K 71		.13	.016	.008	.154	Puu Oo, April 1984.
(11) K 72		.16	.008	.008	.176	Puu Oo, April 1984.
(12) ML 117		.10	.016	.006	.122	Mauna Loa, April 1984.
Primitive Hawaiian magma (undegassed)						
		.30–.45	.10–.15	.008–.011	.41–.65	

The lava flows deformed by the laccolith are picritic, and we have interpreted them as ponded in an ancient caldera (Casadevall and Dzurisin, chapter 13).

The chilled margin of the Uwekahuna laccolith has a low total volatile content (table 14.4) that Easton and Lockwood (1983) attributed to degassing in a surface lake before intrusion. The picritic nature and low sulfur contents of dikes 1N (0.027 weight percent S) and 2N (0.015 weight percent S) indicate an origin similar to that of the laccolith. We concur with the interpretation of Murata and Richter (1961, p.433) that the laccolith was derived from "lateral injection during a prehistoric period of refilling of the caldera." We further suggest that dikes 1N and 2N formed by lateral injection from a picritic lava lake, since destroyed by collapse of the caldera. This lake may have been produced by eruption of the picritic lava of suite C. The intrusives may have derived from the lake and invaded its earlier overflows.

Dike 5S, on the other hand, cuts flows that are younger than the picritic flows of suite C, and therefore cannot be considered contemporaneous with either dikes 1N and 2N or with the laccolith. This dike cuts several tens of meters of lava flows in the southwest caldera wall; it may have fed a nearby olivine-rich lava flow exposed along Crater Rim Drive. That flow forms part of the regional prehistoric pahoehoe picritic complex (PPPC) of Wright (1971), as mapped by Walker (1969). R.T. Holcomb (oral commun., 1985), suggests that the PPPC probably represents a series of overflows from the summit region, a suggestion consistent with the possibility that dike 5S fed at least part of the PPPC.

The water, sulfur, and chlorine contents of the Kilauea intrusive rocks (table 14.4) indicate that about half of the parental abundance of these constituents was lost before the dikes solidified. Easton and Lockwood (1983) suggested that low total volatile content for the chilled margin of an intrusive body indicates that the body was fed by a surface flow draining into an existing fissure or by lateral injection from a surface lake, and not by intrusion from depth. The combined water, sulfur, and chlorine contents for Kilauea summit dikes (table 14.4) are high compared to those of degassed surface flows that have traveled some distance from their vent (Swanson and Fabbi, 1973) and to those of Hilina Pali crack fillings (Easton and Lockwood, 1983). However, we have no data on the volatile abundances in summit lava, which contains a higher initial volatile

TABLE 14.5.—*Chemical composition of intrusive and extrusive rocks from Uwekahuna Bluff, Kilauea compared with averages for Kilauea and Mauna Loa Volcanoes*

[Analyses recalculated to 100 percent dry weight after converting all iron to FeO_{total} and normalized to 7.0 weight percent MgO by subtracting or adding olivine of Uwekahuna laccolith composition (Murata and Richter, 1961, analysis 10). Sources of data: Kilauea caldera dike sets, this paper; Uwekahuna laccolith, Murata and Richter (1961); Uwekahuna Bluff flow suites, Casadevall and Dzurisin (chapter 13); Kilauea (1911–24 summit lavas) and Mauna Loa (historical eruptions) averages, Basaltic Volcanism Study Project (1981). n.d., not determined]

	Kilauea caldera dikes		Uwekahuna laccolith	Uwekahuna Bluff flow suites				Kilauea	Mauna Loa
	North set	South set		A	B	C	D		
SiO_2	51.31±0.44	51.14±0.50	51.20±0.17	51.10±0.23	50.90±0.39	50.60±0.78	50.23±0.25	50.70±0.31	52.45±0.31
Al_2O_3	13.8 ±0.4	13.9 ±0.2	14.0 ±0.8	13.7 ±0.2	13.6 ±0.2	13.6 ±0.3	13.7 ±0.2	13.57±0.12	13.94±0.10
FeO	11.1 ±0.6	11.2 ±0.2	10.8 ±0.4	11.7 ±0.3	11.8 ±0.3	11.3 ±0.5	11.4 ±0.3	11.03±0.20	10.62±0.49
MgO	7.0	7.0	7.0	7.0	7.0	7.0	7.0	7.0	7.0
CaO	11.0 ±0.4	11.2 ±0.2	11.6 ±0.2	10.6 ±0.2	10.9 ±0.3	11.7 ±0.7	11.7 ±0.4	11.65±0.33	10.73±0.15
Na_2O	2.3 ±0.1	2.3 ±0.1	2.2 ±0.1	2.4 ±0.1	2.3 ±0.1	2.3 ±0.1	2.3 ±0.1	2.32±0.04	2.36±0.06
K_2O	.43±0.04	.43±0.04	.37±0.05	.44±0.02	.43±0.03	.44±0.04	.48±0.03	.53±0.04	.39±0.03
TiO_2	2.68±0.58	2.45±0.12	2.46±0.24	2.51±0.08	2.49±0.12	2.62±0.21	2.68±0.04	2.73±0.11	2.10±0.04
P_2O_5	.28±0.04	.33±0.12	.19±0.02	.30±0.01	.29±0.01	.28±0.04	.30±0.01	.29±0.01	.24±0.02
MnO	.18±0.02	.17±0.01	.17±0.01	.17±0.02	.17±0.01	.16±0.02	.19±0.01	.17±0.01	.17±0.01
Ba	121 ±20	128 ±17	n.d.	118 ±19	118 ±23	127 ±29	136 ±11	138 ±18	84 ±14
Cu	117 ±13	117 ±7	n.d.	122 ±16	116 ±12	119 ±17	91 ±22	n.d.	n.d.
Hf	3.70±0.41	3.80±0.16	n.d.	3.91±0.14	3.83±0.16	4.02±0.30	3.99±0.08	4.58±0.17	3.59±0.11
Rb	16, n.d.	14 ±3	n.d.	12 ±3	13 ±1	16 ±3	14, n.d.	11 ±3	6 ±1
Ta	.86±0.15	.93±0.12	n.d.	.88±0.06	.88±0.11	1.02±0.10	1.12±0.02	n.d.	n.d.
Th	.77±0.10	.85±0.11	n.d.	.86±0.07	.81±0.10	.80±0.06	.97±0.02	1.28±0.22	.55±0.03
Zn	127 ±36	118 ±21	n.d.	111 ±3	111 ±3	132 ±14	113 ±5	n.d.	n.d.
Zr	135 ±35	126 ±41	n.d.	153 ±17	145 ±15	156 ±25	172 ±41	159 ±20	130 ±5
Sc	32.0 ±3.5	31.2 ±0.9	n.d.	31.4 ±0.9	32.8 ±0.7	33.5 ±1.4	31.8 ±0.4	33.0 ±2.0	31.0 ±1.2
La	11.5 ±1.6	12.2 ±1.1	n.d.	11.8 ±0.8	11.6 ±1.2	12.7 ±1.0	13.7 ±0.3	15.1 ±1.7	8.9 ±0.6
Ce	27.8 ±3.7	28.4 ±2.7	n.d.	28.9 ±1.6	28.3 ±2.0	30.7 ±1.9	32.7 ±0.5	37.5 ±3.2	23.9 ±1.4
Nd	20 ±3	19 ±5	n.d.	20 ±3	21 ±3	22 ±3	23 ±2	n.d.	n.d.
Sm	5.5 ±0.5	5.5 ±0.3	n.d.	5.7 ±0.1	5.7 ±0.3	6.0 ±0.4	5.9 ±0.1	6.2 ±0.2	5.0 ±0.2
Eu	1.78±0.19	1.83±0.09	n.d.	1.89±0.05	1.84±0.06	1.92±0.10	1.93±0.03	2.00±0.07	1.69±0.04
Gd	6.6 ±0.7	4.8 ±1.4	n.d.	6.1 ±1.4	6.2 ±0.9	6.4 ±1.0	6.7 ±0.7	n.d.	n.d.
Th	.91±0.08	.82±0.04	n.d.	.96±0.04	.96±0.04	.97±0.10	.93±0.03	.96±0.03	.86±0.04
Tm	.29±0.06	.25±0.02	n.d.	.33±0.06	.34±0.04	.34±0.05	.31±0.02	n.d.	n.d.
Yb	2.16±0.17	2.14±0.06	n.d.	2.25±0.11	2.20±0.13	2.31±0.14	2.17±0.06	2.05±0.03	2.10±0.04
Lu	.31	.30	n.d.	.31	.31	.33	.32	.26	.31

content than rift-zone lava (Gerlach and Graeber, 1985) or on those of any flow close to its vent. This makes it difficult to use volatile content as an indicator of origin for the dikes.

We interpret the major-, trace-, and volatile-element data for the dikes to indicate that they are composed of Kilauea magma that had an origin and evolution similar to that of the prehistoric flows of Uwekahuna Bluff. On the basis of contact relations and the higher volatile-element abundances in the dike rocks than in surface flows, we tentatively conclude that most or all of the dikes were injected from depth or laterally, not fed by surface flows.

ORIGIN OF THE DIKES

Igneous dikes are classically interpreted (Anderson, 1938) to form by forceful injection, in which magma pressure exceeds the least compressive stress acting across a potential dike plane. The extent to which existing fractures and regional structural fabric influence the propagation of dikes varies from one tectonic setting to another (Delaney and others, 1986). Most dikes in Kilauea caldera trend northeasterly, roughly parallel to major structural elements such as the southwest and east rift zones, the Hilina and Koae fault systems, and the linear west wall of the caldera. These elements were created by seaward migration of the south flank of the volcano (Fiske and Jackson, 1972; Swanson and others, 1976).

STRUCTURAL SETTING

The dikes in the summit region are confined to the west wall (fig. 14.1). Most have a northeast orientation, similar to that of surface fractures around the west rim of the caldera and to the strike of the southwest rift zone (N. 48° E.; fig. 14.6). Ground cracks extend southwestward into the southwest rift zone and northeastward only to the Steaming Flats area (de Saint Ours, 1982).

The pattern of dikes and other structural elements suggests that the dikes formed in a stress field reflecting the combined influences of the summit magma reservoir (radial) and a linear zone of weakness related to the contact between the edifices of Kilauea and Mauna Loa (N. 40° E.). That contact might be a zone of reduced compression if gravity pulls the unbuttressed Kilauea edifice seaward away from Mauna Loa (Fiske and Jackson, 1972; Swanson and others, 1976). We postulate that this zone offers a preferred path to the surface for magma in fractures in the volcano's summit region. According to this model, the southwest rift zone, the caldera rim at Uwekahuna Bluff, and the northeasterly dikes all reflect control by a structural element related to the contact between Mauna Loa and Kilauea.

SHALLOW DIKE EMPLACEMENT AT KILAUEA

The northeasterly orientation of many of the modern eruptive fissures within the Kilauea summit region (those of 1954, 1971, 1974, 1975, 1982) indicates that the northeasterly trend is still the favored orientation for fissure-fed eruptions. These fissures are typically discontinuous and in places show echelon offsets along their strike (Pollard and others, 1983). They often propagate in the form of slowly migrating surface cracks as an eruption develops (Duffield and others, 1982); seldom do these ground cracks and fissures erupt along their entire length (Pollard and others, 1983). Intrusions of

magma into the summit region and rift zones, some of which cause surface deformation and ground breakage, account for about 65 percent of the magma supplied from Kilauea's shallow magma reservoir; only about 35 percent is erupted (Dzurisin and others, 1984). Most of these intrusions probably form dikes (Swanson and others, 1976; Pollard and others, 1982; Dvorak and others, 1986) that reach shallow depths without erupting.

A number of the dikes in Kilauea caldera occupy fractures that continue to the caldera rim (fig. 14.3) but provide no evidence of having vented. We tentatively conclude that many of the dikes reached or started from very shallow depths but simply did not vent, at least not on the surface directly overlying their present host fractures in the caldera wall. We reason that the driving force of vesiculation, which increases as the dike nears the surface, is opposed by the weight of the magma, which also increases as the dike nears the surface. Partly for this reason, many shallow dikes move laterally more than vertically and vent only when their paths intersect the volcano's sloping flanks along a rift zone. Intrusions into Kilauea's rift zones commonly cause surface deformation and fractures, indicating that magma reached within a few tens to hundreds of meters of the surface without venting (Pollard and others, 1983; Dvorak and others, 1986). Once the top of a dike is shallow enough to cause ground fractures, loss of magmatic volatiles through those fractures may cause the dike's movement to stall without venting. Even if a dike succeeds in reaching the surface somewhere along its length, field observations during eruptions at Kilauea show that vents are typically separated by cracked or deformed areas that do not vent; in other words, the dike does not vent along much of its length.

We therefore conclude that (1) many shallow dikes at Kilauea do not vent; (2) dikes can stall at almost any depth because of loss of volatiles or increasing potential energy; and (3) dikes that do vent usually do so along only a part of their total length. If these inferences are correct, the lack of identifiable vent deposits above

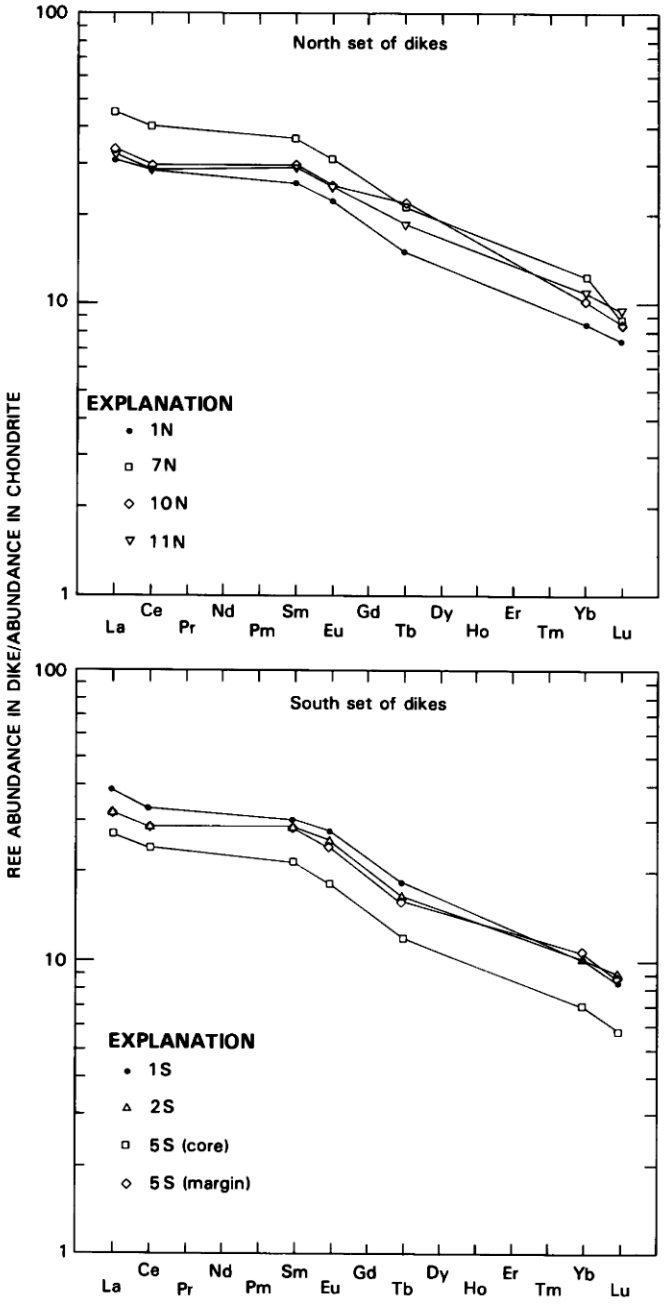

FIGURE 14.5.—Rare-earth-element (REE) plots showing chondrite-normalized abundances for north and south dike sets. Abundances are normalized to chondrite values (Haskin and others, 1968). Analytical precision for Nd, Gd, and Tm is poor (greater than ±6 percent of reported value in table 14.2), and these elements are not plotted.

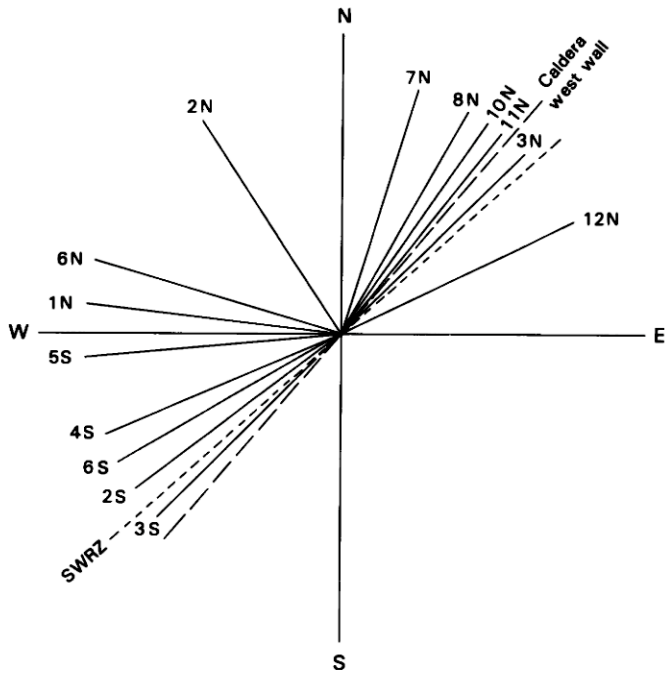

FIGURE 14.6.—Rose diagram showing orientation of dikes, west wall of Kilauea caldera. Also plotted are the orientations of the southwest rift zone (SWRZ) and the western wall of the caldera at N. 48° E. and N. 40° E., respectively.

many dikes at Kilauea caldera does not preclude an origin by forceful injection, either laterally or from below.

CONCLUSIONS

The main results of our study are the following:

(1) The Uwekahuna laccolith is the largest intrusive mass exposed in the west wall of the caldera. Contact relations indicate that most or all of the other dense lenses of rock in the wall are thick subaerial lava flows.

(2) Eighteen dikes occur in the western wall of Kilauea caldera, 12 north of and in Uwekahuna Bluff and 6 south of the bluff. The combined width of these dikes is only about 15 m and accounts for less than 1 percent of the length of the west wall.

(3) Of the 12 dikes in the north set, 5 occupy fractures cutting through the entire section of flows making up the west wall. Thus, these dikes were emplaced after all the flows had been extruded, but before the current caldera had formed.

(4) The composition of all dikes is remarkably uniform after the effects of olivine control are removed. The dikes are chemically similar to the undifferentiated summit lavas exposed at Uwekahuna Bluff and elsewhere in the Kilauea summit region.

(5) Contact relations and the volatile abundances of the dikes imply that most formed through injection, either laterally or from depth. Dikes 1N and 2N have low volatile contents and are chemically similar to the Uwekahuna laccolith and to the picritic lava flows of Uwekahuna Bluff; they may have formed by lateral injection of magma from a lava lake into a ponded sequence of picritic flows.

(6) The orientations of 15 dikes are similar to the structural grain formed by the western half of Kilauea caldera, the southwest rift zone, and the east rift zone. We conclude that the dikes formed under the combined influences of stresses caused by flexing of the summit magma reservoir and gravitational separation of Kilauea and Mauna Loa.

(7) The dikes of Kilauea caldera's west wall cut a succession of lavas that accumulated after the eruption of the Uwekahuna Ash Member, possibly as early as 2.1 ka (Dzurisin and Casadevall, 1986; Lockwood and Rubin, 1986), but before the formation of the present caldera.

FUTURE STUDIES

Several ideas about the origin of intrusive bodies at Kilauea caldera could be tested through further study. The relative ages of the dikes and the Uwekahuna laccolith could be determined by systematic paleomagnetic study supplemented by hydration-rind dating of glass from the margins of the dikes. The possible influence of regional structural fabric on dike propagation could be investigated through careful measurements of structural features such as fractures and joint sets in the vicinity of each dike (Delaney and others, 1986). More careful examination of the tops of the dikes and a thorough search for possible vent deposits could provide additional clues to their origins. Finally, additional measurements of volatile content of summit flows are necessary if the abundance of volatiles, especially sulfur and chlorine, is to be rigorously used as an indicator of dike provenance.

REFERENCES CITED

Anderson, E.M., 1938, The dynamics of sheet intrusion: Proceedings of the Royal Society of Edinburgh, v. 58, p. 242–251.

Aramaki, Shigeo, 1968, Segregation vein in the Uwekahuna laccolith, Kilauea Caldera, Hawaii: Bulletin of the Earthquake Research Institute, v. 46, p. 155–160.

Baedecker, P.A., 1979, Instrumental neutron activation analysis program of the U.S. Geological Survey (Reston, Va.) in Computers and activation analysis and gamma-ray spectroscopy, *in* Carpenter, B.F., D'Agostino, F., and Yule, H.P., eds., Contract 78042, U.S. Department of Energy, p. 373–385.

Basaltic Volcanism Study Project, 1981, Basaltic volcanism on the terrestrial planets: New York, Pergamon Press, 1286 p.

Casadevall, T.J., and Hazlett, R.W., 1983, Thermal areas of Kilauea and Mauna Loa: Journal of Volcanology and Geothermal Resources, v. 16, p. 173–188.

Daly, R.A., 1911, Magmatic differentiation in Hawaii: Journal of Geology, v. 19, p. 289–316.

de Saint Ours, P., 1982, Map of tectonic features of Kilauea Volcano summit region, Hawaii: U.S. Geological Survey Miscellansous Field Studies Map MF–1368, scale 1:24,000.

Delaney, P.T., Pollard, D.D., Ziony, J.I., and McKee, E.H., 1986, Field relations between dikes and joints: emplacement processes and paleostress analysis: Journal of Geophysical Research, v. 91, no. B5, p. 4920–4938.

Duffield, W.A., Christiansen, R.L., Koyanagi, R.Y., and Peterson, D.W., 1982, Storage, migration, and eruption of magma at Kilauea Volcano, Hawaii, 1971–1972: Journal of Volcanology and Geothermal Research, v. 13, p. 273–307.

Dutton, C.E., 1884, Hawaiian volcanoes: U.S. Geological Survey 4th Annual Report, p. 75–219.

Dvorak, J.J., Okamura, A.T., English, T.T., Koyanagi, R.Y. Nakata, J.S., Sako, M.K., Tanigawa, W.R., and Yamashita, K.M., 1986, Mechanical response of the south flank of Kilauea Volcano, Hawaii, to intrusive events along the rift zones: Tectonophysics, v. 124, p. 193–209.

Dzurisin, Daniel, and Casadevall, T.J., 1986, Stratigraphy and chemistry of the Uwekahuna Ash: Product of prehistoric phreatomagmatic eruptions at Kilauea Volcano, Hawaii [abs.]: International Volcanological Congress, Auckland-Hamilton-Rotorua, New Zealand, Abstracts, February 1986, p. 100.

Dzurisin, Daniel, Koyanagi, R.Y., and English, T.T., 1984, Magma supply and storage at Kilauea Volcano, Hawaii: Journal of Volcanology and Geothermal Resources, v. 21, p. 177–206.

Easton, R.M., and Lockwood, J.P., 1983, "Surface-fed dikes", The origin of some unusual dikes along the Hilina fault zone, Kilauea Volcano, Hawaii: Bulletin Volcanologique, v. 46, p. 45–53.

Eaton, J.P., and Murata, K.J., 1960, How volcanoes grow: Science, v. 132, p. 925–938.

Epp, D., Decker, R.W., and Okamura, A.T., 1983, Relation of summit deformation to east rift zone eruptions on Kilauea Volcano, Hawaii: Geophysical Research Letters, v. 10, p. 493–496.

Fiske, R.S., and Jackson, D.E., 1972, Orientation and growth of Hawaiian volcanic rifts: the effects of regional structure and gravitational stresses: Proceeding of the Royal Society of London, Series A, v. 329, p. 299–326.

Fiske, R.S., and Kinoshita, W.T., 1969, Inflation of Kilauea Volcano prior to its 1967–1968 eruption: Science, v. 165, p. 341–349.

Gerlach, T.M., and Graeber, E.J., 1985, Volatile budget of Kilauea Volcano: Nature, v. 313, p. 273–277.

Greenland, L.P., in press, Original volatile content of basaltic magmas: Bulletin of Volcanology.

Greenland, L.P., Rose, W.I., and Stokes, J.B., 1985, An estimate of gas emissions and magmatic gas content from Kilauea Volcano: Geochimica et Cosmochimica Acta, v. 49, p. 125–129.

Harris, D.M., and Anderson, A.T., 1983, Concentrations, sources, and losses of H_2O, CO_2, and S in Kilauean basalt: Geochimica et Cosmochimica Acta, v. 47, p. 1139–1150.

Haskin, L.A., Haskin, M.A., Frey, F.A., and Wildman, T.R., 1968, Relative and absolute terrestrial abundances of the rare earths, *in* Ahrens, L.H., ed., Origins and distribution of the elements: New York, Pergamon Press, p. 889–912.

Holcomb, R.T., 1981, Kilauea Volcano, Hawaii: chronology and morphology of the surficial lava flows: U.S. Geological Survey Open-File Report 81–354, 321 p.

Leeman, W.P., Murali, A.V., Ma, M.S., and Schmitt, R.A., 1977, Mineral constitution of mantle source regions for Hawaiian basalts—rare earth element evidence for mantle heterogeneity, *in* Magma Genesis: Oregon Department of Mineral Industries, Bulletin 96, p. 169–183.

Leeman, W.P., Budahn, J.R., Gerlach, D.C., Smith, D.R., and Powell, B.N., 1980, Origin of Hawaiian tholeiites: trace element constraints: American Journal of Science, v. 280-A, p. 796–821.

Lockwood, J.P., and Rubin, M., 1986, Distribution and age of the Uwekahuna Ash, Kilauea Volcano, Hawaii [abs.]: International Volcanological Congress, Auckland-Hamilton-Rotorua, New Zealand, Abstracts, February 1986, p. 112.

Macdonald, G.A., 1949, Petrography of the Island of Hawaii; U.S. Geological Survey Professional Paper 214–D, 96 p.

Macdonald, G.A., Abbott, A.T., and Peterson, F.L., 1983, Volcanoes in the sea: the geology of Hawaii (2d ed): Honolulu, University of Hawaii Press, 517 p.

Moore, J.G., 1970, Water content of basalt erupted on the ocean floor: Contributions to Mineralogy and Petrology, v. 28, p. 272–279.

Moore, J.G., and Fabbi, B.P., 1971, An estimate of the juvenile sulfur content of basalt: Contributions to Mineralogy and Petrology, v. 33, p. 118–127.

Murata, K.J., and Richter, D.H., 1961, Magmatic differentiation in the Uwekahuna laccolith, Kilauea caldera, Hawaii; Journal of Petrology, v. 2, p. 424–437.

——— 1966a, Chemistry of the lavas of the 1959–60 eruption of Kilauea Volcano, Hawaii; U.S. Geological Survey Professional Paper 537–A, 26 p.

——— 1966b, The settling of olivine in Kilauean magma as shown by the 1959 eruption: American Journal of Science, v. 264, p. 194–203.

Perret, F.A., 1913, Some ejectamenta from Kilauea: American Journal of Science, v. 35 p. 611–618.

Peterson, D.W., 1967, Geologic map of the Kilauea Crater quadrangle, Hawaii: U.S. Geological Survey Geologic Quadrangle Map GQ–667, scale 1:24,000.

Pollard, D.D., Delaney, P.T., Duffield, D.A., Endo, E.T., and Okamura, A.T. 1983, Surface deformation in volcanic rift zones: Tectonophysics, v. 94, p. 541–584.

Powers, H.A., 1955, Composition and origin of basaltic magma of the Hawaiian Islands: Geochimica et Cosmochimica Acta, v. 7, p. 77–107.

Powers, S., 1916, Intrusive bodies at Kilauea: Zeitschrift fur Vulkanologie, v. 3, p. 28–33.

Ryan, M.P., Koyanagi, R.Y., and Fiske, R.S., 1981, Modeling the three-dimensional structure of magma transport systems: application to Kilauea Volcano, Hawaii: Journal of Geophysical Research, v. 86, p. 7111–7129.

Ryan, M.P., Blevins, J.Y.K., Okamura, A.T., and Koyanagi, R.Y., 1983, Magma reservoir subsidence mechanics: theoretical summary and applications to Kilauea Volcano, Hawaii: Journal of Geophysical Research, v. 88, p. 4147–4188.

Shapiro, Leonard, 1975, Rapid analysis of silicate, carbonate, and phosphate rocks: U.S. Geological Survey Bulletin 1401, 56 p.

Swanson, D.A., and Fabbi, B.P., 1971, Loss of volatiles during fountaining and flowage of basaltic lava at Kilauea Volcano, Hawaii: Journal of Research of the U.S. Geological Survey, v. 1, p. 649–658.

Swanson, D.A., and Peterson, D.W., 1973, Partial draining and crustal subsidence of Alae lava lake, Kilauea Volcano, Hawaii: U.S. Geological Survey Professional Paper 800–C, p. C1–C14.

Swanson, D.A., Duffield, W.A., and Fiske, R.S., 1976, Displacement of the south flank of Kilauea Volcano: the result of forceful injection of magma into the rift zones: U.S. Geological Survey Professional Paper 963, 39 p.

Walker, G.W., 1969, Geologic map of the Kau Desert quandrangle, Hawaii: U.S. Geological Survey Geologic Quadrangle Map GQ–827, scale 1:24,000.

Washington, H.S., 1923, Petrology of the Hawaiian Islands, III: Kilauea and general petrology of Hawaii: American Journal of Science, v. 6, p. 338–367.

Wright, T.L., 1971, Chemistry of Kilauea and Mauna Loa in space and time: U.S. Geological Survey Professional Paper 735, 40 p.

——— 1984, Origin of Hawaiian tholeiite: a metasomatic model: Journal of Geophysical Research, v. 89, p. 3233–3252.

AN EARLY 19TH CENTURY RETICULITE PUMICE FROM KILAUEA VOLCANO

By Robert P. Sharp[1], Daniel Dzurisin, *and* Michael C. Malin[2]

ABSTRACT

Remnants of a fragmented reticulite pumice deposit, referred to as the golden pumice, along the southwest rim of Kilauea caldera are the product of episodes of lava fountaining of undocumented date within the caldera. At its best locality, the 2.8-m deposit consists of a basal fine-grained, well-bedded unit, 20 cm thick; an intermediate massive homogeneous unit, 1 m thick, consisting of coarse, jagged, firmly packed fragments; and an upper fine-grained unit, 1.6 m thick, of well-sorted and well-bedded pumice. The intermediate unit may be a product of massive direct fallout from lava fountains, and the finer grained upper and lower units may be pumice wind-drifted from a plume plus pumiceous debris reworked by wind. The pumice locally rests with angular unconformity on beds of 1790 pyroclastic debris and is overlain by a thin layer of 1924 lithic tephra. Layers of reworked pumiceous debris and 1790 lithic debris within the golden pumice suggest that its emplacement was episodic and may have occurred over a year or two. The stratigraphic succession and recorded observations of volcanic activity since 1823 indicate that the pumice formed between 1790 and 1823. The amount of erosion and deposition occurring between emplacement of the 1790 deposits and the pumice favors a date in the later part of this interval, possibly around 1820. We speculate that the golden pumice represents early phases in development of the lava conduit for the current fire-pit crater, Halemaumau, the most active center within Kilauea caldera during the 19th and 20th centuries.

INTRODUCTION

Surficial deposits of fragmented reticulite pumice at the southwest edge of Kilauea Crater were thought by Jaggar (1925, p. 3, 8) to be part of an underlying deposit of pyroclastic debris erupted in 1790, and they were included, by inference at least, within the Keanakakoi Formation by Wentworth (1938, p. 93). Christiansen interprets this pumice as a product of high lava fountains following an earlier episode of phreatomagmatic activity about 1790 (Christiansen, 1979; Decker and Christiansen, 1984, p. 125); Macdonald and Abbott (1970, p. 315) seemingly agree. The deposit is clearly not related to pumice at the base of the Keanakakoi Formation of Wentworth (1938, p. 95–96, 101) or to pumiceous products of post-1924 events (Wentworth, 1938, p. 149; Macdonald, 1955, p. 57; Macdonald and Abbott, 1970, p. 92–93; Richter and others, 1970, p. E5–E36). In order to distinguish this particular reticulite pumice from such older and younger deposits of similar nature, it is here informally called the golden pumice. Its stratigraphic position, between materials erupted in 1790 and 1924, was recognized by Macdonald (1949, p. 70, 72) and Macdonald and Abbott (1970, p. 315), who did not, however, discuss its origin or precise age. In this paper we present evidence that it represents a distinct event, separate from 1790 activity but early within the 1790–1924 interval, an interpretation seemingly favored, but without supporting arguments, by Finch (1947), Powers (1948, plate 3D), and Stearns (1966b, p. 40).

ACKNOWLEDGMENTS

Kilauea lies within Hawaii Volcanoes National Park, and we are indebted to park authorities for the privilege of access. The study was warmly and cooperatively supported by the U.S. Geological Survey's Hawaiian Volcano Observatory and financially aided by Grant W–13, 709 from the National Aeronautics and Space Administration. R.L. Christiansen has generously made available unpublished information from his extensive studies of the 1790 Keanakakoi Formation. Appreciation is expressed for constructive critical reviews and suggestions by Christiansen, D.A. Swanson, T.L. Wright, and R.T. Holcomb. W.G. Melson of the Smithsonian Institution kindly supplied records of a chemical analysis of 1820(?) Kilauea glass.

LOCATION AND DISTRIBUTION

Accumulations of the golden pumice are best preserved along the southwest margin of Kilauea caldera (fig. 15.1). The nearly circular, 1-km-wide pit crater of Halemaumau, last active in 1982, indents the caldera floor within 1 km of the best pumice exposures. The thickest accumulations of the golden pumice are trapped within open cracks and stream-cut gullies dissecting the southwest caldera wall and the immediately adjacent outer slope of the volcano, northwest and southeast of Crater Rim Road where it descends to the caldera floor (fig. 15.1). For convenience, the channels are termed caldera-wall gullies, although the larger ones extend headward tens of meters outside the caldera rim. The first 13 larger gullies south-southeast (fig. 15.2) of the descending reach of Crater

[1]California Institute of Technology, Pasadena, California 91125
[2]Arizona State University, Tempe, Arizona 85281

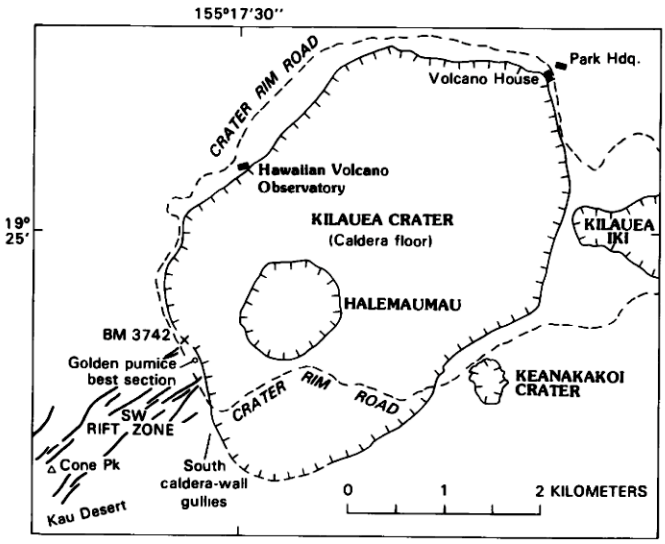

FIGURE 15.1.—Major features of Kilauea Crater and location of best section of the golden pumice.

Rim Road expose particularly informative sections. For identification, these gullies are sequentially numbered south from Crater Rim Road as 1–S, 2–S, and so on.

Remnants of the golden pumice also lie in protected places within the Kau Desert from the caldera rim southwestward more than 3 km, to and beyond Cone Peak (fig. 15.1). Their greater abundance in the northwestern part of the Kau Desert presumably reflects the direction of the dominant trade-wind flow (S. 60°–70° W.) somewhat oblique to the S. 45° W. axial trend of the desert tract.

MICROSTRATIGRAPHIC UNITS AND RELATIONS (SEE FIG. 15.3)

THE 1790 PART OF THE KEANAKAKOI FORMATION OF WENTWORTH (1938)

Stratigraphy of the Keanakakoi Formation of Wentworth (1938, p. 92–104; see also, Powers, 1948) has been most thoroughly and recently investigated by Christiansen (1979; Decker and Christiansen, 1984, p. 124–127) in a study not yet fully published. During investigation of stripping of Keanakakoi debris in Kau Desert, Malin and others (1983, p. 1149–1150) divided the 1790 part of the formation into three units: upper lithic, intermediate predominantly vitric, and lower mixed lithic and vitric; this subdivision is employed here.

Sherzer (1923, p. 460–461), Finch (1947, p. 2), and Powers (1948, p. 288) felt that only the upper lithic unit, or part of it, was emplaced by the 1790 phreatomagmatic eruptions of Kilauea, but Christiansen (1979) attributes the bulk of the Keanakakoi Formation of Wentworth (1938) to an evolutionary cycle of such activity that began around 1790. Malin and others (1983, p. 1151, 1155) favor Christiansen's interpretation, but they suggest, largely because of evidence of penecontemporaneous redistribution of tephra, that the successive eruptions occurred over a period of several years, including 1790. Easton (chapter 11) has reduced the rank of the Keanakakoi and included it in his Puna Basalt. Easton's Keanakakoi Ash Member consists mostly of deposits of the 1790 eruption, but slightly older reticulite pumice occurs at the base and the golden pumice at the top. In this paper we will use the modifier 1790 to designate that part of the Keanakakoi thought to have been formed by these explosive eruptions, without meaning to imply that all the material was necessarily emplaced within the single year 1790.

THE RETICULITE (GOLDEN) PUMICE

The thickest, most complete section of golden pumice observed (fig. 15.4) lies within the head of a gully extending outward from the caldera rim along a crack bearing S. 55° W. in the southwest rift zone (fig. 15.1). This exposure is about 30 m from the caldera brink, roughly 50 m northeast of Crater Rim Road, 78 m N. 15° E. from the SW Rift sign at the parking turnout, and 205 m S. 37° E. of BM 3742 (Kilauea Crater quadrangle). Within the 2.8-m section exposed here, upper, intermediate, and basal units are distinguished (fig. 15.3).

The basal 20 cm are well layered and consist of abraded-looking pumice fragments, mostly about 1 cm in size, in a sparse sand-size matrix of angular vitric fragments. This basal unit includes much Pele's hair and a few scattered lithic clasts as large as 6 mm, and near the top it contains a coarse sandy layer rich in lithic grains.

The massive, homogeneous intermediate unit, 1 m thick, consists of closely packed jagged pumice fragments, mostly 2–5 cm in diameter but ranging from 1 cm to 10 cm. It is nearly devoid of matrix, except for irregular vitric fragments broken from compacted pumice clasts. Tight packing has made the jagged pumice fragments interlock, giving the unit a cohesion that is expressed in a near-vertical outcrop face and in the toughness of detached pieces. No lithic fragments have been found within primary deposits of this coarse pumice, either here or in many other exposures.

The upper unit consists of 1.6 m of thinly and evenly bedded pumice, the fragments being mostly of 1-cm size. These clasts, although still angular, are consistently smaller, more regularly shaped, less jagged, and far more uniform in size than clasts of the intermediate unit. However, 53 cm above the base of the upper unit is a 5-cm layer of coarser fragments with intermediate-unit characteristics. Beds in the upper unit are mostly 3–4 cm thick, though ranging from 1 cm to 7 cm, and generally have a sparse matrix of sand-size vitric fragments. They do not display the inverse grading that typically results from flow emplacement (Sparks, 1976). Distributed throughout the upper unit are 1-cm-thick continuous beds principally composed of dense glass fragments; these layers emphasize the well-bedded aspect of this unit. Much Pele's hair is also present, especially in the lower part of the unit, and a few sparsely scattered lithic fragments, several millimeters in diameter, have been found. In the best section, a 4-cm sandy layer 10 cm from the top contains numerous lithic and crystal grains, some well worn. More

FIGURE 15.2.—View south-southeast from Crater Rim Road showing 20-m-high tephra-mantled southwest wall of Kilauea Crater, caldera-wall gullies, and 1974 lava flow along left margin. Light reflects from patches of crusted veneer on the detrital apron. U.S. Geological Survey photograph by J.D. Griggs.

and larger lithic fragments are seen within the upper unit at some other localities, where secondary reworking has clearly occurred (figs. 15.5*A*, 15.6).

In the best section, contacts between these units are sharp but conformable. Elsewhere, the contact between upper and intermediate units is unconformable (fig. 15.7) or marked by layers containing reworked lithic materials (fig. 15.5*A*). Disconformities and layers of reworked pumiceous and lithic debris also are found within the upper unit.

At the best section, the golden pumice rests with sharp contact upon coarse lithic-vitric sand, possibly dating from 1790; elsewhere it rests upon fluvial gravels, 1790 pyroclastic beds, or lava bedrock. Not all exposures of pumice display all units, the basal and intermediate units being more nearly ubiquitous and of less varying thickness than the upper unit. Remnant patches of pumice in the Kau Desert immediately southwest of the caldera rim are slablike and probably primary, but within a few hundred meters farther southwest the stratigraphy of the best section disappears and the packing and shape of pumice fragments change; preservation of these accumulations in settings protected from the northeast trade winds suggests secondary eolian reworking and redistribution. A secondary surficial crust of grayish chocolate-brown hue and irregular lumpy texture has formed on most such deposits, masking the nature of the underlying material. This crust, 2–4 mm thick, fractures easily owing to fragility of the understratum, but the crust itself is firm. Even though surficial crusts are known to form rapidly on surfaces in the Kau Desert (Malin and others, 1983, p. 1150). the thickness and firmness of this crust indicate at least slight antiquity for the deposits.

The golden pumice is primarily a reticulite (Wentworth and Williams, 1932, p. 41, 47–50) consisting of delicate, interconnected filaments of sideromelane glass (Heiken, 1974, p. 5) outlining oval and crudely polygonal patterns 0.5–2 mm in diameter. It is not as close to a perfect reticulite (Stone, 1926, p. 29; Macdonald, 1972, p. 127) as the basal Keanakakoi pumice (Wentworth, 1938, p. 95–96; Heiken, 1974, p. 5; Christiansen, 1979) or as that produced by the 1969–1974 Mauna Ulu fountains, because it has a wider range in the size and shape of openings and a more copious coating of dense black, gray, or brown glass on fragments. The golden pumice is light, having a specific gravity near 0.06 and a

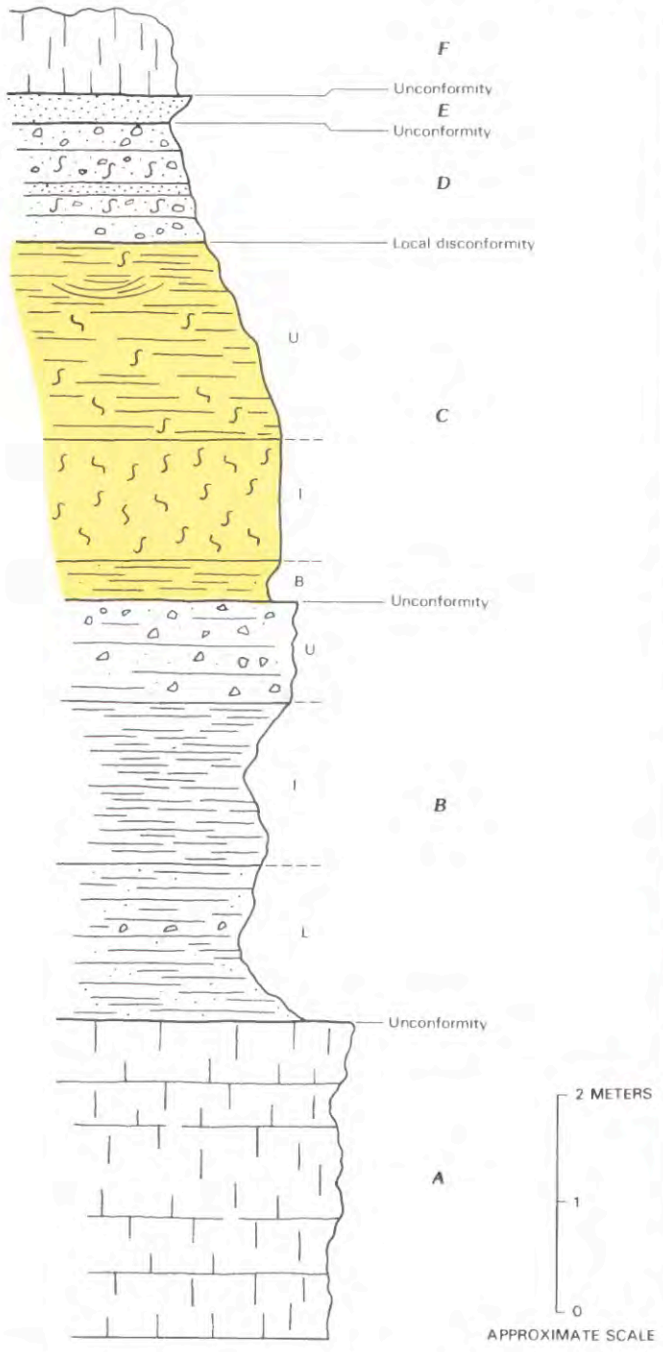

FIGURE 15.3.—Schematic columnar section, within area of southwest caldera rim. Units shown: ***A***, Crater-wall lava flows, >100 m thick, age at top 0.2–0.35 ka (Holcomb, 1980, p. 253). ***B***, ***C***, Keanakakoi Ash Member. ***B***, 1790 deposits; lower (L), intermediate (I), and upper (U) units (Malin and others, 1983), 4 m thick. ***C***, Golden pumice; basal (B), intermediate (I), and upper (U) units, 2.8 m thick, date about 1820. ***D***, Reworked mixed pumiceous and 1790 lithic debris, 1 m thick, date about 1820. ***E***, Lithic tephra, 1–7 cm thick, date 1924. ***F***, Pahoehoe lava flows, 2–3 m thick, dates 1971 and 1974.

porosity probably approaching 97 percent, and is so fragile that it crushes easily in the hand. In more perfect Hawaiian reticulite, Wentworth (1938, p. 149) measured a specific gravity of 0.043 and estimated a porosity of about 98 percent, consistent with Dana's (1891, p. 163) earlier figures. Although reticulite can form as a froth on the surface of some ponded gas-rich lava flows near vents, most Hawaiian reticulite is regarded as the product of vigorous lava fountaining.

REWORKED 1790 LITHIC DEBRIS AND PUMICE

Within the deposits constituting the detrital apron (fig. 15.8) dissected by the caldera-wall gullies are layers of reworked material derived from the adjacent tephra-mantled caldera wall. These layers, mostly 10–40 cm thick, may consist solely of 1790 lithic fragments, solely of pumice, or of mixtures of lithic and pumiceous fragments. Such layers lying below, between, and above beds composed solely of primary pumice (figs. 15.5–15.7) indicate that reworked debris was being intermittently delivered to the detrital apron before, during, and after emplacement of the golden pumice.

1924 LITHIC TEPHRA

The historically observed (Jaggar and Finch, 1924; Stearns, 1925; Jaggar, 1947, p. 205–259) explosive phreatic eruption of

FIGURE 15.4.— Best section of golden pumice exposed in gully near southwest rim of Kilauea caldera. B, bedded basal unit; I, massive intermediate unit; U, upper well-layered unit. The golden pumice is here overlain by 1924 crusted lithic tephra. U.S. Geological Survey photograph by J.D. Griggs.

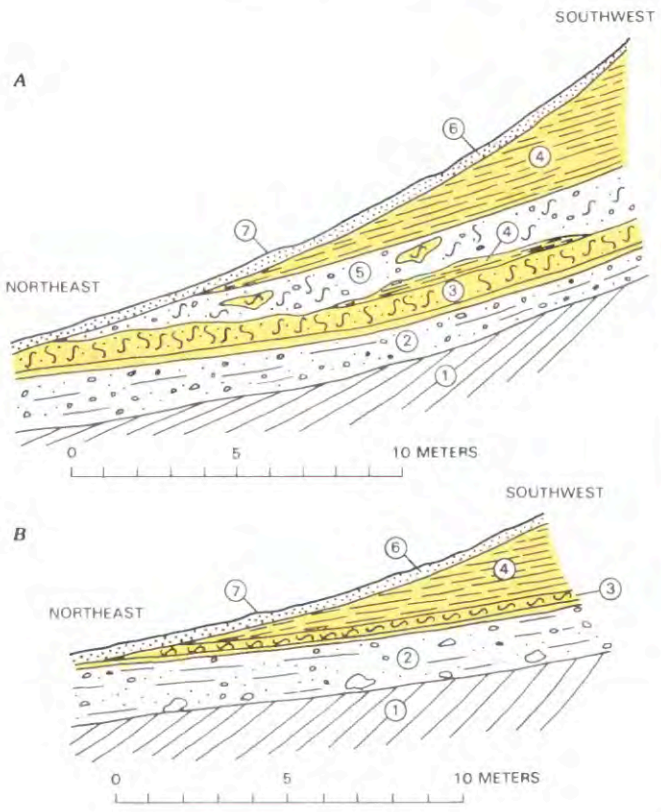

FIGURE 15.5.—Examples of angular unconformities of golden pumice and associated beds with 1790 deposits below and crusted apron veneer above. 1, 1790 beds; 2, reworked 1790 lithic debris, 20–40 cm thick; 3, basal and intermediate units of golden pumice, 45 cm; 4, upper unit of pumice, >1 m; 5, reworked mixed pumiceous and lithic debris, 60 cm; 6, apron veneer of reworked loose lithic-vitric sand, 20 cm; 7, crust on apron veneer. Angular unconformities below 2 and 6, and disconformity below 5. ***A***, South wall of caldera-wall gully 6–S. ***B***, South wall of caldera-wall gully 9–S.

Kilauea in 1924 produced a thin mantle, now crusted, of fine ash and sand- to granule-size fragments, mostly of dense lava, which covered much of the study area (Finch, 1925; Powers, 1948, plate 3D; Macdonald, 1949, p. 72; Macdonald and Abbott, 1970, p. 315). Scattered remnants of this mantle remain, filling shallow swales or forming residual scabs rising a few centimeters in relief on the present surface near and for a few hundred meters southwest of the southwest caldera rim.

Most such patches cover areas of only a few square meters or less. They are as much as 7 cm thick, but more commonly 2–4 cm. Although variable, the deposits display a reasonably consistent microstratigraphy: a basal 1–4 cm of distinctive pink, irregularly laminated fine ash, in many places containing accretionary lapilli, is succeeded by 0.3–0.5 cm of loose, matrix-free angular lithic granules, overlain by 1–2 cm of gray ash containing coarse sand and angular lithic granules, topped by a firm 1–3 mm crust in which abundant angular lithic granules are embedded. The crust has a distinctive rough texture, imparted by the projecting granules, and a medium brown color. Occasional larger lithic fragments (2–4 cm) in this crust may have been secondarily introduced from nearby exposures of 1790 lithic debris, because fragments that large do not here characterize the 1924 material beneath the crust. Lithologies of the lithic clasts in this deposit appear to duplicate those in the block field created around Halemaumau by the 1924 explosions. In the study area, the 1924 tephra rests upon golden pumice (Stone, 1926, p. 29) or, where that is lacking, directly upon the 1790 upper lithic unit.

APRON VENEER AND CRUST

A layer of loose sand and granule particles, 5–20 cm thick, capped by a firm crust, 1–3 cm thick, veneers large parts of the interfluve surface of the detrital apron in the area of caldera-wall gullies, south-southeast of Crater Rim Road (fig. 15.2). In its texture, firmness, setting, and general appearance, this crust so closely resembles the 1924 crust that it was initially and mistakenly so identified. However, it is pinkish rather than brown and lacks the characteristic underlying microstratigraphy, especially the fine ash. Furthermore, the sand and granule grains of this crust and the underlying conformable layers are a mixture of vitric and lithic particles, not solely lithic as in the 1924 deposit.

The apron veneer is a reworked deposit, which may contain 1924 debris but also includes older material, much of it vitric and probably derived from the golden pumice. It presumably dates from later than 1924, but because of its thickness and coherence perhaps only one or two decades later. It has been undermined by lateral recession of the walls of arroyo-like gullies, 1–2 m deep, cut into the alluvial apron, and so the crust may antedate that episode of dissection. In many exposures, the apron crust makes a spectacular

FIGURE 15.6.—North wall, lower reach of gully 5–S. A, reworked lithic debris. B, basal and intermediate (coarse) pumice units. C, primarily reworked lithic debris. D, reworked mixed pumiceous and lithic material. E, detrital apron crust. U.S. Geological Survey photograph by J.D. Griggs.

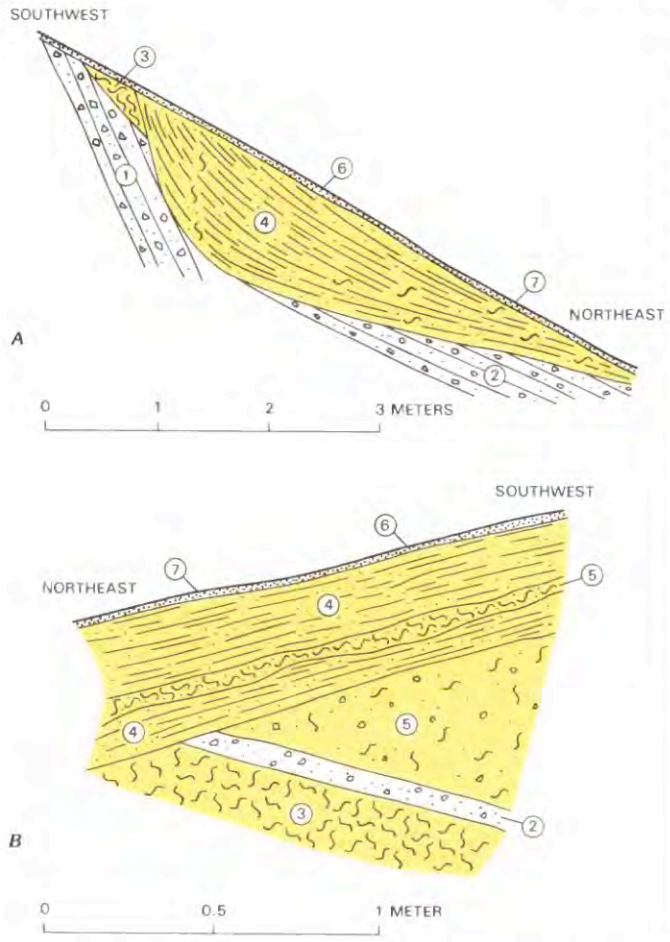

FIGURE 15.7.—Examples of unconformity between upper and intermediate units of golden pumice. 1, 1790 beds; 2, reworked 1790 lithic debris; 3, basal and intermediate units of pumice; 4, upper unit of pumice; 5, reworked coarse pumice; 6, reworked mixed pumiceous and lithic debris; 7, crusted apron veneer. ***A***, North wall of gully 8–S; ***B***, South wall of gully 1–S.

angular unconformity with the golden pumice and associated deposits (figs. 15.5, 15.7*A*).

SETTING AND RELATIONS

Microstratigraphic relations are best exposed in the first 13 major caldera-wall gullies south of Crater Rim Road. Each gully consists of a steep V-shaped upper reach indenting the caldera wall and a gentler, flat-floored arroyo-like reach cut into the detrital apron below (fig. 15.8), and each gully has experienced at least three episodes of dissection. Initially, narrow steep-walled slots, 2–3 m deep, were formed in the nearly horizontal lava flows composing the steep caldera walls, presumably by rock falls, avalanching, and fluvial erosion. These bedrock slots were subsequently partly or wholly filled by 1790 debris, forming some spectacular examples of tephra-bed draping or base-surge plastering on steep bedrock faces (fig. 15.9). Much of the 1790 debris was subsequently removed by further erosion, which locally cut through to bedrock. Deposits of pumice then partly refilled the gullies, mantled the upper gully walls, and added to the detrital apron. Such gully-wall pumice mantles form a striking large-angle unconformity with the more steeply inclined 1790 beds (fig. 15.9). Continued erosion has subsequently removed much of this caldera-wall pumice, but remnants are still seen on walls in the upper reaches of many gullies, particularly 8–S (fig. 15.10). A smaller angle unconformity between 1790 beds and the golden pumice, or associated conformable layers of reworked materials, is displayed in the walls of the lower reaches of many gullies (figs. 15.5, 15.11). A sharp angular unconformity also separates 1790 ash beds from reworked deposits of golden pumice in the Kau Desert (fig. 15.12).

Storm-water erosion within the gullies and colluvial reworking of debris mantling the caldera wall, both of which occurred contemporaneously with deposition of the upper golden pumice unit, added material to the detrital apron. Eventually most of the easily transportable debris was removed from the caldera wall, and regrading and dissection of the depositional apron occurred as the detrital load decreased. Lavas emplaced in 1971 and 1974 now bury the outer margin of the detrital apron (fig. 15.8).

ORIGIN AND EMPLACEMENT OF THE GOLDEN PUMICE

Historically, deposits of fragmented reticulite in Hawaii have been formed by high lava fountains associated with fissure eruptions on the flanks (Swanson and others, 1971) and in the summit calderas of Kilauea (Macdonald and Abbott, 1970, p. 82, 93; Richter and others, 1970) and Mauna Loa (Macdonald and Abbott, 1970, p. 62). The golden pumice has generally been regarded as the product of lava fountaining at an unidentified site or sites within Kilauea caldera. One can speculate concerning the changes that occurred at that source to produce the differences between the coarse, homoge-

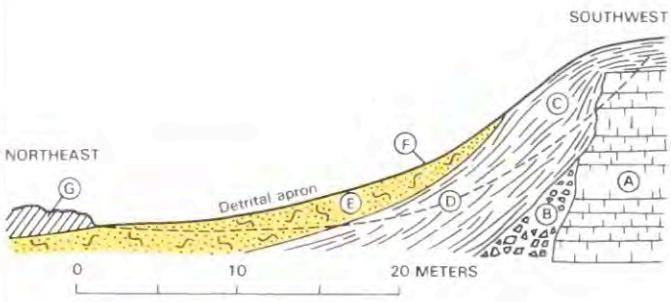

FIGURE 15.8.—Schematic cross section of detrital apron at caldera-wall gullies. A, lava flows of caldera wall; B, talus from caldera wall; C, 1790 beds; D, longitudinal profile of floor of caldera-wall gully; E, golden pumice and associated reworked pumiceous and lithic debris; F, crusted apron veneer; G, 1971 and 1974 pahoehoe lava flows.

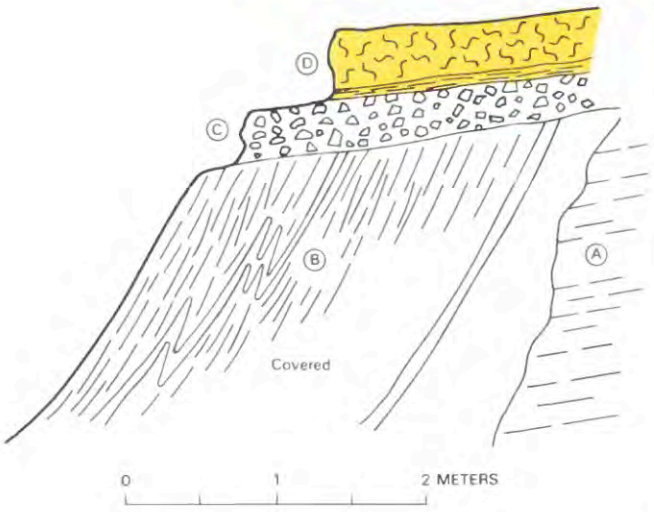

FIGURE 15.9.—Slump-deformed 1790 ash layers plastered on caldera wall and unconformably overlain by reworked lithic rubble and golden pumice, south side of caldera-wall gully 3–S. A, inferred caldera wall; B, 1790 ash beds; C, lithic-cobble rubble; D, lower and intermediate units of golden pumice.

neous, massive, tightly packed intermediate unit and the finer, well-layered, better sorted, more loosely packed basal and upper units.

Reticulite is so light that the behavior of individual fragments is strongly influenced by air currents; smaller particles, those with minimal glass coating, and those thrown highest are presumably the most strongly affected. Motion pictures of lava fountains show a central cone of debris falling back to the ground close to the fountain. This we shall term direct fallout to distinguish it from the more diaphanous plumes of material that drift for greater distances downwind (fig. 15.13). Most direct fallout follows a reasonably normal trajectory and consists largely of dense lapilli, glass, spatter and other forms of consolidated lava. A transition presumably exists between such direct fallout and drifted plume material. The coarse, closely packed pumice fragments of the intermediate unit appear to have come down directly out of the air, without significant secondary tumbling, wear or reworking. We speculate that it accumulated in the outermost part of the fallout zone and that large pumice fragments were so abundant they formed a clotted mass. We therefore refer to it as direct-fallout pumice, even though it probably drifted to some degree with the wind before coming to the ground.

Deposits of plume pumice should consist of smaller and better sorted fragments, possibly showing some evidence of attrition owing to buffeting contacts within the plume. If strong winds accompany the eruption, as commonly happens in Hawaii, such fragments may experience some eolian transport over the ground surface before coming to rest. Despite this complexity in their history, accumulations of both fallout and plume pumice are herein treated as primary. Both are highly susceptible to reworking by wind or water subsequent to their initial deposition, and such reworking imposes differences in texture, packing, coherence, fragment shape, contamination, and degree of layering that identify the resulting accumulations as of secondary origin.

Indications that much of the material composing the upper and basal units of the golden pumice has been secondarily transported by wind include the following: Good sorting; thin, even, regular layering; local cross-lamination; wear on pumice particles that has made them less jagged and removed some of the surficial glass coating; open packing; thin discrete layers of fine glass fragments; and inclusion of scattered lithic fragments, 2–3 mm in size, and thin layers rich in lithic sand. The well-bedded appearance of the upper and basal units results largely from the presence of numerous thin, continuous, even layers of fine vitric fragments that have specific gravities at least 25 times that of reticulite. These layers most likely formed as lag concentrates at times when strong trade winds removed accumulated pumice particles from the study area, leaving the smaller, denser glass fragments. Less probably, they may represent either changes in material being ejected or in the sorting of materials within plumes. Although the upper and lower units of the golden pumice contain a number of thin layers that may be primary plume pumice, and the upper unit clearly contains one 5-cm layer of primary fallout pumice, both units are inferred to be largely secondary in origin, on the basis especially of their excellent thin, regular bedding.

Deposition of fallout pumice and of plume or secondary pumice at the same site at different times could be caused by changes in the magnitude of fountaining at a fixed source or by migration of fountaining along a rift. Both are known to occur in Hawaii. Whatever the change was during the formation of the golden pumice, it was abrupt, not transitional, because the contacts between units

FIGURE 15.10.—Remnants of draped basal and intermediate units of golden pumice resting with angular unconformity on 1790 beds on northwest wall of gully 8–S. A, caldera-wall lavas; B, 1790 beds; C, golden pumice. U.S. Geological Survey photograph by J.D. Griggs.

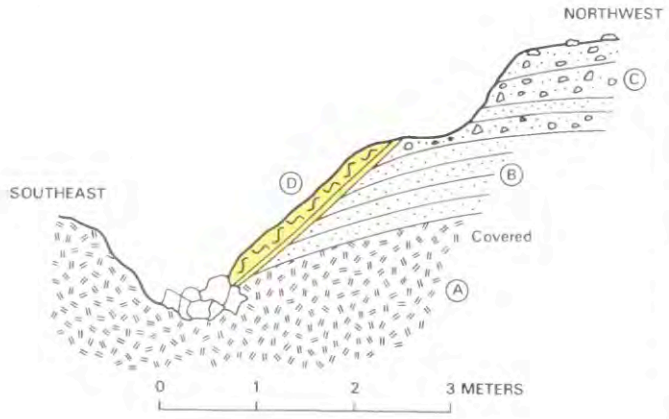

FIGURE 15.11.—Angular unconformity of draped basal and intermediate units of golden pumice on 1790 beds, north wall of gully 7–S. A, lavas; B, lower and intermediate units of 1790 deposits; C, upper lithic unit of 1790 deposits; D, basal and intermediate units of golden pumice.

are sharp. We find no compelling evidence to choose between these two alternatives, but it is perhaps simpler to imagine variations in fountaining at a fixed site, especially in accounting for the isolated 5-cm coarse fallout layer in the upper unit. The microstratigraphy of the golden pumice and associated deposits in the caldera-wall gullies (figs. 15.5–15.7) suggests that fountaining ceased completely on occasion, allowing both deposition by other processes and erosion to occur.

TEMPORAL CONSIDERATIONS

When, within the 1790–1924 period, was the golden pumice emplaced, and how much time was involved? Dana (1891, p. 43) visited Kilauea in 1877 and described deposits of reticulite along the caldera rim resting on coarse lithic conglomerate. This was almost certainly the golden pumice on the 1790 upper lithic unit. Wilkes's 1841 description (1845, p. 169–170) of coarse pumice filling open cracks of the southwest rift is almost identical to our description of the golden pumice intermediate unit. Observations of spumose lava, light as a sponge, wind-drifted, and visible all around on the surface of the Kau Desert a short walk southwest of Kilauea on August 1, 1823 (Goodrich, 1826, p. 22; Ellis, 1827, p. 162), strongly suggest that the golden pumice had been formed by that time. Probably it had formed not long before, because the pumice fragments were abundant and widely scattered and the deposits apparently not crusted, as they are now. These observations, and the improbability that lava fountaining adequate to create the golden pumice would go unrecorded after 1823 (Dana, 1891), point to the 1790–1823 interval as the likely time for the unit's origin.

A time late in that period would be particularly favored if the considerable erosion and reworking of 1790 lithic debris that occurred before pumice emplacement had been accomplished by normal fluvial and colluvial processes. However, the possibility that a more powerful process, such as base surge, might have produced the effects rather quickly deserves consideration in view of the fact that base surges are thought to have played a major role in emplacement of the 1790 deposits (Swanson and Christiansen, 1973, p. 85; Christiansen, 1979; Decker and Christiansen, 1984, p. 125). Spectacular U-shaped scour channels, local unconformities, and large bedforms within 1790 deposits for at least 0.5 km outward from the caldera rim are strong evidence for the action of base surges.

Kilauea caldera is large enough to have contained an intracaldera base surge that could have traversed the caldera floor and ascended the caldera wall. Accumulations of 1790 ash, showing base-surge characteristics, on large slump blocks on the caldera wall below Volcano House indicate to R.L. Christiansen (written commun., 1984) that this indeed happened. Likewise, the steep (60°–80°) inclination of fine 1790 ash beds (fig. 15.9) on the low southwest caldera wall is more likely to be the product of plastering of fine moist debris against the steep bedrock face by a steaming base surge than of draping by airfall deposition. These steep beds have been sharply truncated by erosion at the heads of nearly all the major caldera-wall gullies studied south of Crater Rim Road. A base surge acting in an erosive mode could have affected nearly universal truncation almost instantly. Such a surge would have had to occur late in the 1790 activity because at least part of the upper lithic unit is truncated (fig. 15.7*A*). The erosion required to form the uncomformity between golden pumice and 1790 beds might have been caused either by a base surge or by other more common surface processes.

It seems unlikely that the sandy gravel layers (figs. 15.5, 15.6) and the cobbly rubble (fig. 15.9) lying between golden pumice and the truncated 1790 beds in both the upper and lower reaches of the caldera-wall gullies are the result of base surges, because this reworked debris has been transported back toward the caldera floor rather than outward. Such debris layers were probably deposited by

FIGURE 15.12.—Angular unconformity of coarse pumice on fine-grained, well-layered 1790 ash on southwest flank of Cone Peak, about 80 m N. 16° E. from benchmark. U.S. Geological Survey photograph by J.D. Griggs.

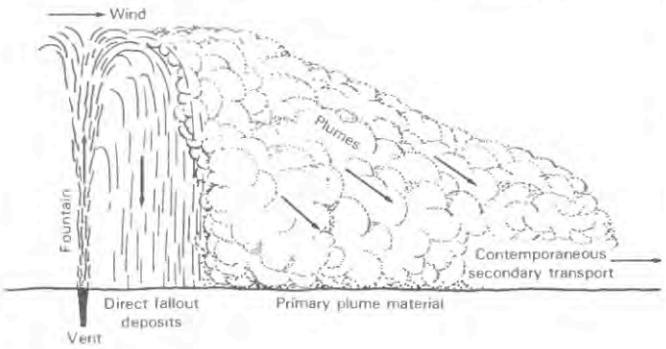

FIGURE 15.13.—Diagrammatic sketch of lava fountain, wind-drifted plumes, and related deposits. Variations in fountain height and character can produce superimposition or interlayering of different types of primary pumice deposits.

more slowly acting colluvial and fluvial processes. Relations in the caldera-wall gullies thus suggest that erosional truncation of 1790 beds could have occurred as a final gasp of the 1790 activity, but the deposition of reworked lithic layers may have occurred later and more slowly.

Pumice accumulations in the Kau Desert provide some insight on these relations. Along the western edge of the desert, a little northwest of the Kau Desert trail and about 1 km outward from the caldera rim (Kilauea Crater quadrangle), a wide fluvial arroyo 1 m deep has been eroded in 1790 deposits and older lava. Within this channel is a dissected alluvial fill of gravel, sand, and silt composed largely of reworked 1790 lithic material, capped by the golden pumice (fig. 15.14). The amount of fluvial work accomplished here before pumice deposition must have required a significant part of the 1790–1823 interval. In this same area, the golden pumice in many places rests directly upon lava bedrock from which the 1790 deposits must have been stripped before the pumice was laid down.

A favored setting for remnants of golden pumice in the Kau Desert is small niches on the flanks of little residual scabs, 30–50 cm high, on the eroded crusted surface of the 1790 upper lithic unit. Resistant overhanging ledges on such scabs make the pumice superficially appear to be interbedded with the lithic layers, and excavation is required to reveal that it is only inset (fig. 15.15). A secondary crust on the pumice, incorporating lithic fragments shed from the overhanging ledge, further obscures relations. Considerable modification of the surface of the crusted and irregularly cemented 1790 lithic layer by differential weathering, rainbeat, aqueous sapping, and probably eolian erosion had occurred to produce the scabs and their niches before the pumice was emplaced. Such modification could easily have required two or three decades. The overhanging ledges strongly suggest that erosion occurred after rather than before cementation. Even though most accumulations of golden pumice in the Kau Desert more than a few hundred meters from the caldera have probably formed by eolian reworking, such reworking likely occurred soon after pumice eruption, because newly formed pumice is very susceptible to eolian transport by the strong and prevailing northeast trade winds. Relations in the Kau Desert thus suggest pumice emplacement late in the 1790–1823 interval.

Another temporal question is the time involved in depositing the golden pumice and associated materials. The microstratigraphy of these units, as exposed in the walls of the caldera-wall gullies, strongly suggests that this was not a single brief episode. Successive eruptions of pumice were separated by intervals during which erosion created disconformities within the deposits, and stripping of detritus from the adjacent caldera wall introduced layers of pumiceous, lithic, or mixed pumiceous-lithic debris. During the period of golden pumice eruption, construction of the detrital apron at the base of that wall by colluvial, fluvial, eolian, and airfall processes was continuing.

Under current climatic conditions, the Kilauea summit is occasionally subjected to downpours of rain that create freshets and sheet floods across the surface of the detrital apron. In some years, several such events occur, in others none. Similar events probably occurred within the 1790–1823 interval and would have been capable of creating the erosional disconformities within the pumice sequence and introducing the interlayers of reworked debris. The time required to produce the golden pumice sequence may therefore have been anywhere from part of a year to several years.

Eruptive activity within Kilauea was greater than normal from about 1820 to 1832 (Hitchcock, 1911, p. 160–182; Macdonald and Abbott, 1970, p. 69–72), and it involved refilling of eruptive centers and associated lava fountaining. Native reports (Dana, 1891, p. 45) suggest that eruptive activity in Kilauea between March and June of 1823, before Ellis' visit of August 1 that year, was greater than anything occurring between 1790 and 1820

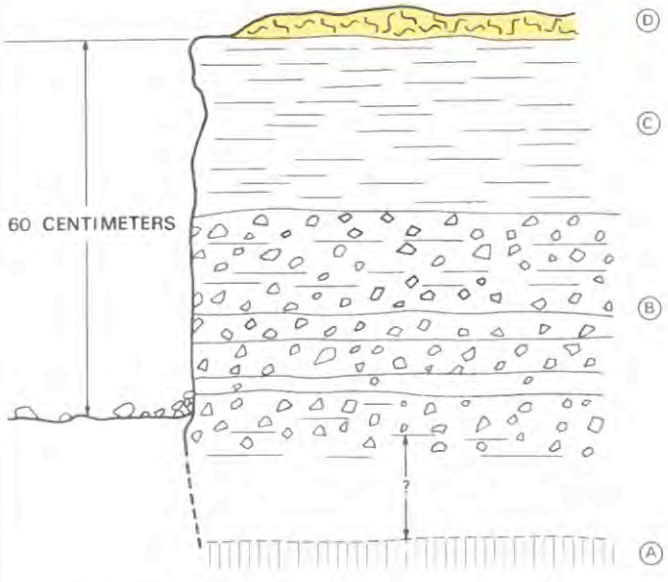

FIGURE 15.14.—Streambank exposure showing floodplain sand and silt (C) and fluvially reworked 1790 gravelly lithic debris (B) lying between coarse golden pumice (D) and the 1790 upper lithic unit or lava bedrock (A), northwest margin Kau Desert, 1 km southwest of Kilauea caldera.

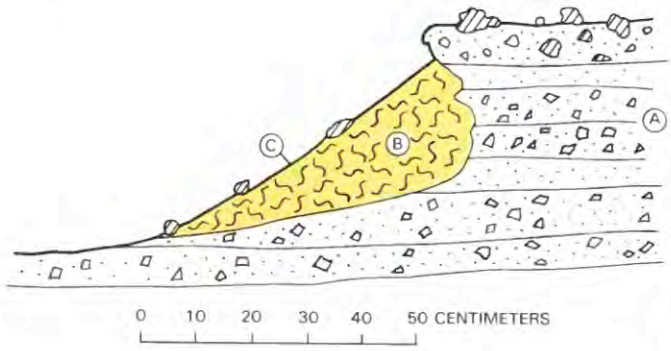

FIGURE 15.15.—Inset of crusted golden pumice within niche on flank of erosional scab on surface of upper lithic unit of 1790 deposits, Kau Desert. A, crusted upper lithic layer (1790); B, golden pumice; C, surface crust incorporating secondary lithic fragments.

(Goodrich, 1826, p. 27). The interval 1820–1823 appears adequate to accommodate the golden pumice, and the reported high degree of activity in Kilauea starting about 1820 favors that period.

Exactly when Halemaumau came into existence is not known. The crater probably did not exist as a specific topographic feature until some time after the 1790 outburst, for whose deposits it apparently was not the source (Stearns, 1966a, p. 134). A map drawn by Byron's lieutenant, Malden, in 1825 (Brigham, 1909, p. 45) shows a fairly large pit at the Halemaumau site, and various other early observers (Goodrich, 1826, p. 24; Ellis, 1827, p. 164, 170; Dana, 1891, p. 46–54; Brigham, 1909, p. 43–44) identified the southwestern part of Kilauea caldera, near the present Halemaumau, as the site of most intense activity. Although Halemaumau did not become a single crater until about 1905 (Richter and others, 1962, p. B53), we are intrigued with the speculative thought that the golden pumice may be a product of early activity of the volcanic conduit destined to determine the location of this present-day fire pit of Kilauea.

REFERENCES CITED

Brigham, W.T., 1909, The volcanoes of Kilauea and Mauna Loa: Bernice Pauahi Bishop Museum of Polynesian Ethnology and Natural History, Memoirs, v. 2, 222 p.

Christiansen, R.L., 1979, Explosive eruption of Kilauea Volcano in 1790 [abs.]: Proceedings of the Hawaii symposium on intraplate volcanism and submarine volcanism, Hilo, Hawaii, International association of volcanology and chemistry of the earth's interior, p. 158.

Dana, J.D., 1891, Characteristics of volcanoes: New York, Dodd, Mead, and Company, 399 p.

Decker, R.W., and Christiansen, R.L., 1984, Explosive eruptions of Kilauea Volcano, Hawaii: *in* Explosive volcanism: Inception, evolution and hazards: Washington, National Academy of Sciences, p. 122–132.

Ellis, William, 1827, Journal of William Ellis, Narrative of a tour of Hawaii, with remarks on the history, traditions, manners, customs, and language of the inhabitants of the Sandwich Islands: Honolulu, Hawaii, Advertiser Publishing Company, reprint of the London 1827 edition, 342 p.

Finch, R.H., 1925, The ash deposits at Kilauea Volcano: The Volcano Letter, No. 17, Hawaiian Volcano Research Association, 1 p.

———1947, Kilauea in 1790 and 1823: The Volcano letter, No. 496, Hawaiian Volcano Research Association, 2 p.

Goodrich, Joseph, 1826, Notice of the volcanic character of the Island of Hawaii: American Journal of Science, v. 11, p. 2–36.

Heiken, Grant, 1974, An atlas of volcanic ash: Smithsonian contributions to earth science, no. 12, p. 1–12.

Hitchcock, C.H., 1911, Hawaii and its volcanoes: Honolulu, Hawaiian Gazette, 314 p.

Holcomb, R.T., 1980, Kilauea Volcano, Hawaii: Chronology and morphology of the surficial lava flows: U.S. Geological Survey Open File Report 80-796, 321 p.

Jaggar, T.A., 1925, Discussion of special features: Hawaiian Volcano Observatory Monthly Bulletin, v. 13, p. 1–8.

———1947, Origin and development of craters: Geological Society of America Memoir 21, 508 p.

Jaggar, T.A., and Finch, R.H., 1924, The explosive eruption of Kilauea in Hawaii: American Journal of Science, v. 208, p. 353–374.

Macdonald, G.A., 1949, Petrography of the Island of Hawaii: U.S. Geological Survey Professional Paper 214-D, p. 51–96.

———1955, Hawaiian volcanoes during 1952: U.S. Geological Survey Bulletin 1021-B, p. 15–108.

———1972, Volcanoes: Englewood Cliffs, New Jersey, Prentice-Hall, 510 p.

Macdonald, G.A., and Abbott, A.T., 1970, Volcanoes in the sea: Honolulu, Hawaii, University of Hawaii Press, 441 p.

Malin, M.C., Dzurisin, Daniel, and Sharp, R.P., 1983, Stripping of Keanakakoi tephra on Kilauea Volcano, Hawaii: Geological Society of America Bulletin, v. 94, p. 1148–1158.

Powers, H.A., 1948, A chronology of the explosive eruptions of Kilauea: Pacific Science, v. 2, p. 278–292.

Richter, D.H., Eaton, J.P., Murata, K.J., Ault, W.U., and Krivoy, H.L., 1970, Chronological narrative: The 1959–60 eruptions of Kilauea Volcano, Hawaii: U.S. Geological Survey Professional Paper 537E, p. E1–E73.

Richter, D.H., Moore, J.G., and Haugen, R.T., 1962, Recent growth of Halemaumau, Kilauea Volcano, Hawaii: U.S. Geological Survey Professional Paper 450B, p. B53–B56.

Sherzer, W.H., 1923, Explosive eruptions of Kilauea: Science, v. 57, p. 459–461.

Sparks, R.S.J., 1976, Grain size variations in ignimbrites and implications for the transport of pyroclastic flows: Sedimentology, v. 23, no. 2, p. 147–188.

Stearns, H.T., 1925, The explosive phase of Kilauea Volcano, Hawaii, in 1924: Bulletin Volcanologique, v. 2, p. 193–209.

———1966a, Geology of the state of Hawaii: Palo Alto, California, Pacific Books, 266 p.

———1966b, Road guide to points of geologic interest in the Hawaiian Islands: Palo Alto, California, Pacific Books, 66 p.

Stone, J.B., 1926, The products and structure of Kilauea: Bishop Museum Bulletin 33, 59 p.

Swanson, D.A., and Christiansen, R.L., 1973, Tragic base surge in 1790 at Kilauea Volcano: Geology, v. 1, no. 2, p. 83–86.

Swanson, D.A., Jackson, D.B., Duffield, W.A., and Peterson, D.W., 1971, Mauna Ulu eruption, Kilauea Volcano: Geotimes, v. 16, p. 12–16.

Wentworth, C.K., 1938, Ash formations of the Isle of Hawaii: Hawaiian Volcano Observatory Third Special Report, 183 p.

Wentworth, C.K., and Williams, Howel, 1932, The classification and terminology of the pyroclastic rocks: National Research Council Bulletin 89, p. 19–53.

Wilkes, Charles, 1845, Narrative of the United States Exploring Expedition: Philadelphia, Lea and Blanchard, v. 4, 539 p.

THE 1972–1974 MAUNA ULU ERUPTION, KILAUEA VOLCANO: AN EXAMPLE OF QUASI-STEADY-STATE MAGMA TRANSFER

By Robert I. Tilling, Robert L. Christiansen, Wendell A. Duffield, Elliot T. Endo, Robin T. Holcomb, Robert Y. Koyanagi, Donald W. Peterson, *and* John D. Unger

ABSTRACT

The eruption at Mauna Ulu from February 3, 1972, to July 22, 1974, renewed the sustained activity on Kilauea's east rift zone that had previously ceased in October 1971. During 901 days of virtually continuous activity, about 162×10^6 m^3 of basaltic lava was erupted. Vent activity was confined to the Mauna Ulu-Alae area except for two short-lived outbreaks near Pauahi and Hiiaka Craters in May and November 1973. The minimum average magma production rate through April 1973 was 8×10^6 m^3/mo, comparable to rates for other periods of sustained eruptive activity at Kilauea.

The 1972–74 lava (1) covered an area of about 46 km^2; (2) raised the summit of the shield built at Mauna Ulu during the 1969–71 eruptions to a maximum height of 121 m above the pre-1969 ground surface; (3) greatly increased the size and height of the complex shield at Alae, which attained a maximum height of nearly 90 m above the pre-1969 ground surface; (4) filled the west pit of Makaopuhi Crater; and (5) entered the sea in August–October 1972 and February–May 1973 after traveling more than 12 km through well-developed lava-tube systems.

The 1972–74 eruption was dominated by active lava lakes at Mauna Ulu and Alae, their vents linked by an efficient tube system. The lava lakes exhibited a wide range of behavior, including (1) complex circulation patterns of the lake surface and low-level fountaining at drainback areas; (2) cyclic fluctuations of as much as a few tens of meters in the level of the lava column, accompanied by violent degassing during column collapse (the so-called gas-piston activity); (3) complete or partial draining of the lava lakes caused by major changes in eruptive mode or lava-supply system; (4) repeated short-duration overflows and levee construction leading to shield growth; and (5) sustained overflows and the development of lava tubes to feed long flows.

Records of Kilauea summit tilt during 1972–74, as measured at Uwekahuna vault, show two periods (February 1972 to April 1973 and December 1973 to July 1974) of oscillations within a narrow range and little or no net change in tilt. Each of these periods is interpreted to reflect a quasi-steady-state regime of magma transfer from a mantle source to Kilauea's summit reservoir and to the upper east rift zone. The first period apparently was terminated by subsurface blockage in the magma-transfer system, possibly caused by a 6.2-magnitude earthquake on April 26, 1973, which also disrupted a well-established tube system and halted lava entry into the sea. The second period marked the reestablishment of a highly efficient magma-transfer system following the November–December 1973 eruption at Pauahi. Our postulated periods of quasi-steady-state regime of magma transfer are compatible with the speculation of Daniel Dzurisin and others that the sustained eruptive activity at Mauna Ulu may be linked to increased deep magma production, as evidenced by above-average occurrence of deep harmonic tremor beneath Kilauea.

Ground deformation measured by periodic resurveying of level, ground tilt, and trilateration networks in the Kilauea summit region generally is compatible with patterns seen in continuous records of Uwekahuna tilt, seismicity, and observed eruptive activity. However, some deformation patterns during the periods of quasi-steady-state magma-transfer regime are diffuse and not amenable to simple analysis. The most coherent patterns obtained are related to the Pauahi-Hiiaka (May) and Pauahi (November) eruptions during the net inflation period of 1973; each of these was associated with a deflation at Uwekahuna of about 20 microradians. Perhaps a threshold volume or rate of change in summit magma storage must be exceeded before coherent ground-deformation patterns can be derived from geodetic surveys; the volcano may possess a characteristic yield strength, such that a finite amount of inelastic deformation must be accommodated before geodetic response can reflect elastic behavior.

INTRODUCTION

The 1969–71 Mauna Ulu eruption (figs. 16.1 and 16.2), which lasted about 2½ years and produced 185×10^6 m^3 of lava, was one of the most voluminous and long-lived historical rift eruptions of Kilauea Volcano, Hawaii (Swanson and others, 1971, 1979). The waning stage of that eruption was characterized by monotonic subsidence of the surface of a lava lake in Mauna Ulu crater, accompanied by sharp summit inflation, and was punctuated by a brief eruption within the summit caldera during August 1971 and another, in the caldera and southwest rift zone, during September 1971 (Duffield and others, 1982). The end of the 1969–71 Mauna Ulu eruption was October 15, 1971, the date when lava was last seen in the vent (Swanson and others, 1979). No eruptions occurred at Kilauea for the next 3½ months, a period of steady summit inflation.

In early February 1972, lava quietly reentered the crater of Mauna Ulu, initiating a period of sustained eruption that ultimately lasted until mid-July 1974. The 1972–74 activity was confined to the Mauna Ulu-Alae area except for an outburst from vents within and near Pauahi and Hiiaka Craters on May 5, 1973, and a month-long eruption at Pauahi in November–December 1973 (fig. 16.2). For convenience of discussion, the eruptions of Mauna Ulu (which

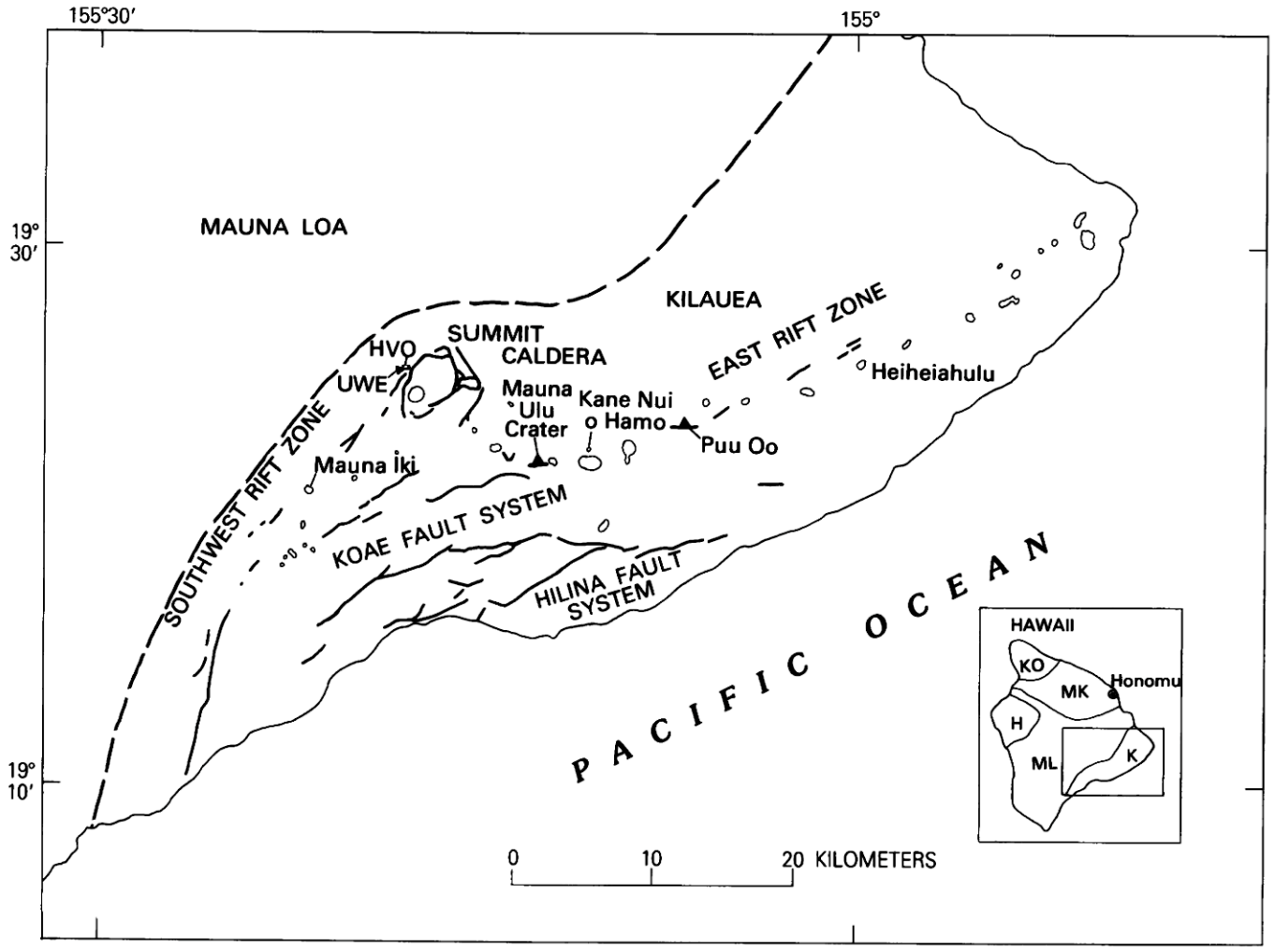

FIGURE 16.1.—Map of Kilauea Volcano showing summit caldera, rift zones, and principal fault systems; locations of the Hawaiian Volcano Observatory (HVO) and Uwekahuna vault (UWE) are also shown. Inset shows volcanoes making up Island of Hawaii: KO, Kohala; MK, Mauna Kea; H, Hualalai, ML, Mauna Loa; and K, Kilauea. Mauna Ulu eruption site (1969–1974) is on upper east rift zone, and Puu Oo eruption site (1983–present) is on middle east rift zone; these sites are indicated by solid triangles. Mauna Iki (1919–20), Heiheiahulu (1750?), and Kane Nui o Hamo (prehistoric) are volcanic shields developed on rift zones before 1969. Modified from Dzurisin and others (1984, fig. 2).

means "growing mountain" in Hawaiian), Pauahi, and Hiiaka during 1972–74 are considered collectively as the 1972–74 Mauna Ulu eruption because of their close association in space and time and the persistence of harmonic tremor thoroughout almost the entire period. The end of eruptive activity at Mauna Ulu is taken to be July 22, 1974, following a three-day summit eruption (Peterson and others, 1976), after which no molten lava could be observed at Mauna Ulu and harmonic tremor ceased.

Following the 1972–74 Mauna Ulu eruption, activity at Kilauea shifted to the summit region, where short-lived outbursts during July and September were followed by a brief eruption and intrusion in the southwest rift zone in December 1974 (Peterson and others, 1976; Dzurisin and others, 1984, table 1). Following various other short-lived eruptions and intrusions at several sites on the volcano during 1975–82 (Tilling and others, 1976b; Moore and others, 1980; Dzurisin and others, 1984), the beginning of the Puu Oo eruption in the middle east rift zone in 1983 (Wolfe and others, chapter 17) marked the return to Kilauea of a long-lived, voluminous flank eruption, like the Mauna Ulu eruptions during 1969–74.

The 1972–74 activity was particularly notable for active lava lakes that occupied the summit craters of Mauna Ulu and Alae shields for long periods of time. We consider a lava lake active if it is linked, directly or indirectly, to a feeding magma column, in contrast

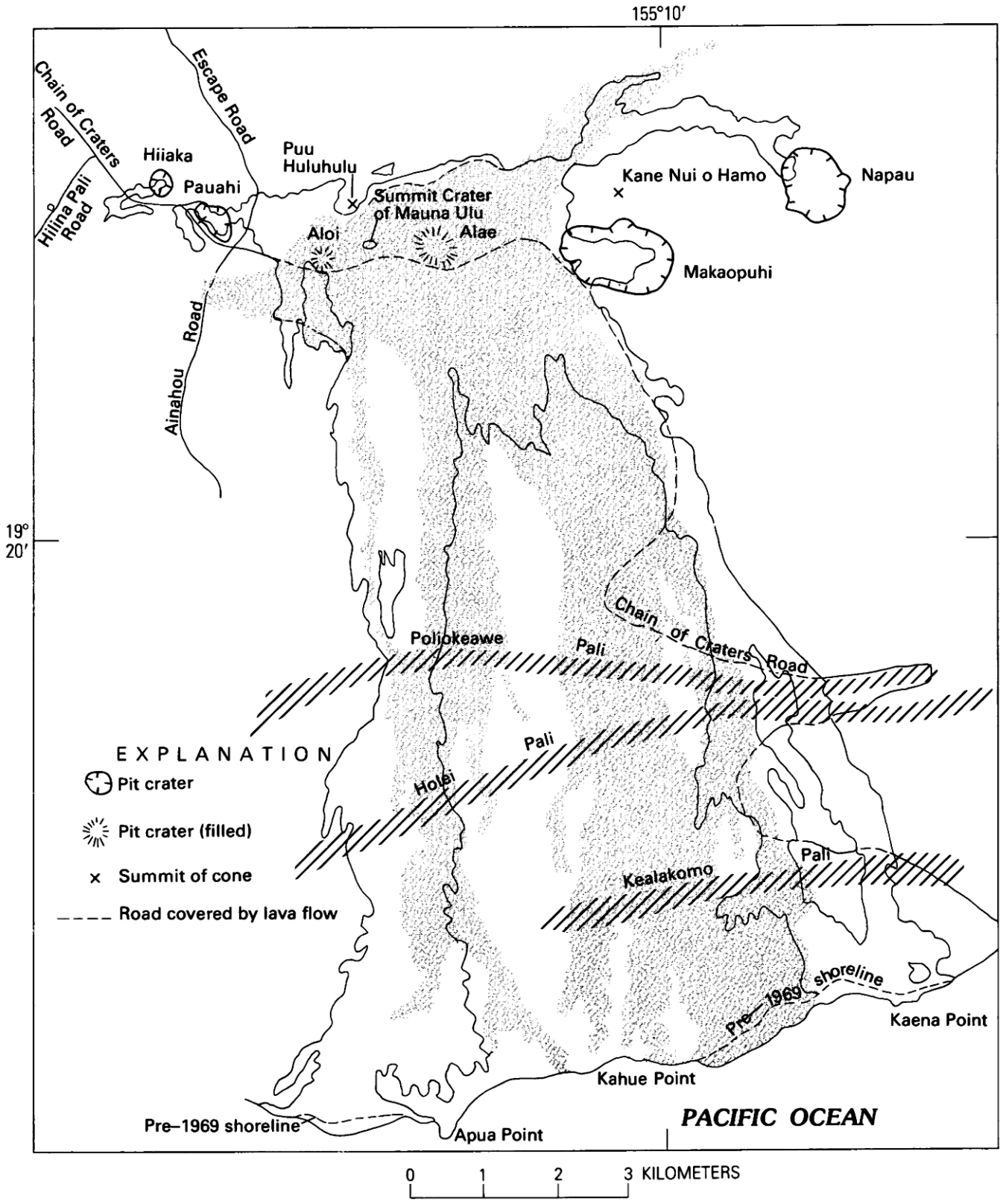

FIGURE 16.2.—Sketch map showing lava fields produced by the 1969–1971 Mauna Ulu eruption (shaded) and the 1972–74 Mauna Ulu eruption (outlined by solid line); pali means cliff in Hawaiian. Modified from Swanson and others (1979, fig. 4) and Holcomb (1976).

TABLE 16.1.—*Some published topical studies on aspects of the 1972–1974 Mauna Ulu eruption and general works on Kilauea that include data relevant to processes, products, or effects of the eruptions*

Topic	Reference
General summaries and field guidebooks.	Greeley (1974) Hazlett (1981) Macdonald and Hubbard (1982) Peterson and others (1976)
Geologic maps	Holcomb (1976) Holcomb (1980)
Lava chemistry	Wright and Tilling (1980)
Lava tubes	Peterson (1983)
Lava lakes, variations in depth to surface.	Tilling and others (1986)
Pahoehoe-aa transition	Peterson and Tilling (1980) Kilburn (1981)
Volcanic landforms	Tilling and others (1973) Holcomb (1973) Holcomb and others (1974) Tilling and others (1976b, c) Dzurisin (1978)
Lava deltas	Peterson (1976)
Lava movement under water and pillow formation.	Grigg (1973) Tepley (1975) Moore (1975)
Rockfall activity and seismicity	Tilling (1976a) Tilling and others (1975)
Pattern of historical eruptions	Klein (1982)
Ground deformation, including modeling.	Ryan and others (1983) Epp and others (1983) Dvorak and others (1983)
Magma intrusion into rift zones	Koyanagi and others (1973) Klein (1982) Dzurisin and others (1984)
Magma budget	Dzurisin and Koyanagi (1981) Dzurisin and others (1984)
Magma reservoir shape and mechanics	Ryan and others (1981) Ryan and others (1983)
Seismicity	Koyanagi and others (1976a, b) Ellesworth and Koyanagi (1977) Unger and others (1973) Unger and Ward (1979) Aki and Koyanagi (1981)
Geoelectrical studies of volcanic processes.	Zablocki (1976) Zablocki (1978)
Thermal studies	Casadevall and Hazlett (1983)
Gas and sublimate studies	Cadle and others (1973) Naughton and others (1973)
Miscellaneous	Sicks (1975) Dzurisin (1980)

to an inactive lava lake formed by passive ponding of magma within preexisting pit craters (see Swanson and others, 1979, p. 10). The long duration and easy accessibility of the 1972–74 Mauna Ulu eruption permitted frequent and numerous direct observations of the activities of these lava lakes, as well as of the development and evolution of volcanic shields, lava levees, flow channels, and lava tubes.

Many features of the 1972–74 Mauna Ulu eruption were virtually identical to those well described and illustrated by Swanson and others (1979) for the lava-lake-dominated activity of episodes 3 and 4 (called stages by them) of the 1969–71 Mauna Ulu eruption, and we refer where appropriate to those excellent descriptions rather than unnecessarily describing processes anew.

Many topical studies were undertaken during the course of the 1972–74 Mauna Ulu eruption, and several recent syntheses of Kilauea's magmatic behavior included data obtained in the 1972–74 period. A listing of some of these studies is given in table 16.1 to complement similar summaries for the 1969–71 Mauna Ulu eruption (Swanson and others, 1979, tables 1 and 2). The main purposes of this paper are to describe the eruptive phenomena in 1972–74, provide a general framework for topical studies already completed, and identify directions for possible further topical research.

ACKNOWLEDGMENTS

This paper could not have been written without the enthusiastic efforts of the many present and former members of the Hawaiian Volcano Observatory (HVO) staff who contributed to the systematic observation and monitoring of the 1972–74 Mauna Ulu eruption. Particular thanks go to John C. Forbes, William H. Francis, Kenneth T. Honma, George Kojima, John P. Lockwood, Jennifer S. Nakata, Arnold T. Okamura, Reginald T. Okamura, Marie S. Onouye, Gary S. Puniwai, James C. Ratte, Maurice K. Sako, Akira Yamamoto, and Charles J. Zablocki. Our National Park Service colleagues at Hawaii Volcanoes National Park also assisted our studies by their administrative support and additional observations of the eruptive phenomena.

During the course of the eruption, we benefited from stimulating discussions with members of the HVO staff, other U.S. Geological Survey colleagues, guest investigators, and visiting scientists, especially Michael H. Carr, Robert W. Decker, Richard S. Fiske, Ronald Greeley, John E. Guest, (the late) Everett D. Jackson, Jeffrey Judd, Peter W. Lipman, (the late) Gordon A. Macdonald, Harold Masursky, James G. Moore, Willard H. Parsons, Dallas L. Peck, Howard A. Powers, Daniel Rubel, Donald A. Swanson, Peter L. Ward, and Thomas L. Wright. Special thanks go to John Dvorak, Arnold Okamura, and Wil Tanigawa for assistance in the computer retrieval and reduction of ground-deformation data pertinent to the eruption. Support from the U.S. National Aeronautics and Space Administration (NASA) Planetology Program provided opportunities for instructive comparisons between Hawaiian and extraterrestrial volcanism and resultant landforms. Constructive reviews of an earlier draft of this paper by Donald A. Swanson and Edward W. Wolfe are greatly appreciated.

TABLE 16.2.—*Summary of east-rift eruptive activity of Kilauea Volcano, Hawaii, from February 1972 to July 1974 (modified from Peterson and others, 1976)*

Time period	Duration (days)	Location of vents (see fig. 16.3)	Esimated lava volume[1] (10^6 m^3)	Area covered by lava (km^2)
February 3, 1972 to May 4, 1973	457	Mauna Ulu and Alae	125	[2] 35
May 5, 1973	1	Pauahi and Hiiaka and nearby fissures	1	.6
May 6, 1973 to November 9, 1973	188	Mauna Ulu and Alae	2.5	.9
November 10, 1973 to December 9, 1973	30	Pauahi and nearby fissures	3	1.1
December 10, 1973 to July 22, 1974	225	Mauna Ulu	30	8
Total	901		161.5	45.6

[1]Includes only volume remaining on surface and excludes volume that drained back into fissures before eruption ended.
[2]Includes 0.47 km of new land added to south coast of Hawaii from lava entry into sea (Peterson, 1976).

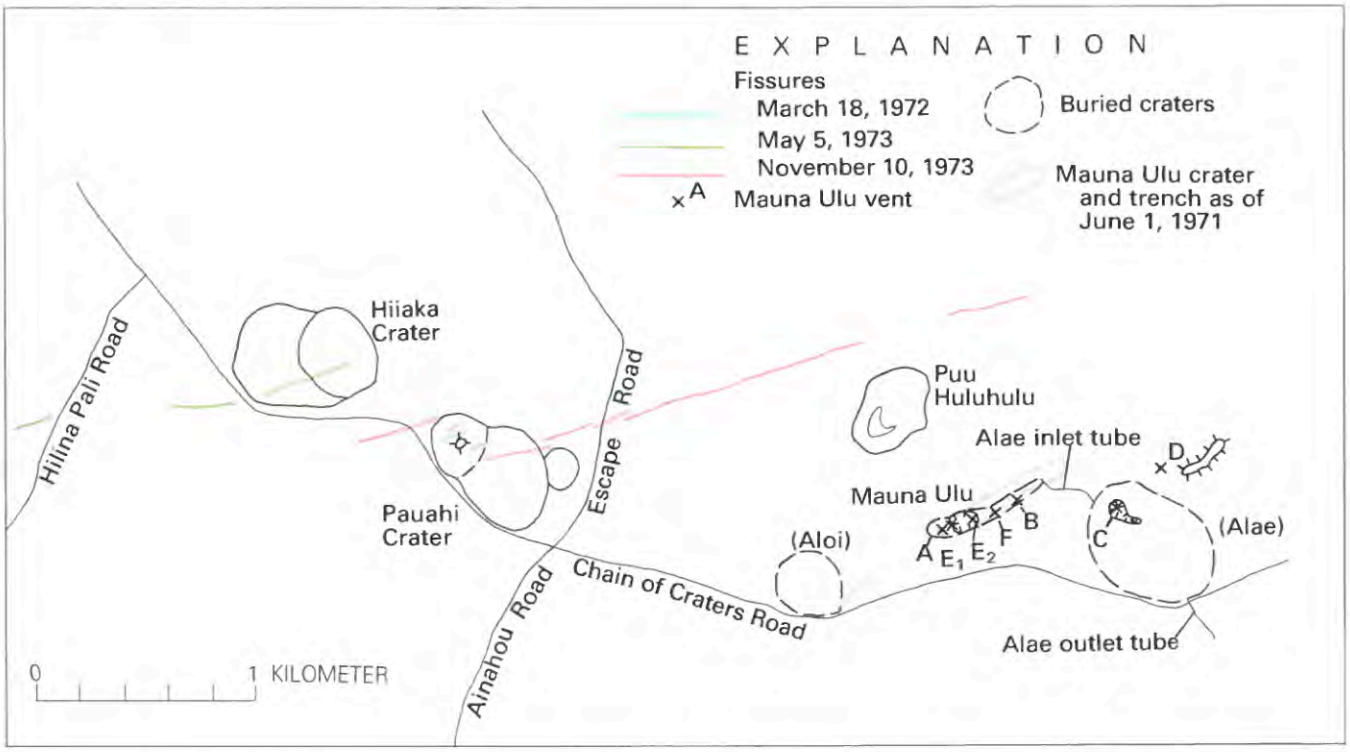

FIGURE 16.3.—Sketch map showing location of vents active during 1972–1974 eruption. The locus of 1972–74 Mauna Ulu vents (A,B,C,D,E_1,E_2, and F) essentially coincides with that of the vents active during July 1970–June 1971 (see Swanson and others, 1979, pl. 4).

OVERVIEW OF THE 1972–74 ERUPTION

Peterson and others (1976) summarized the general features of the 1972–74 eruptive activity of Kilauea Volcano; the overview given here draws on and adds to that earlier summary. The major events, locations of vents, and variation in summit tilt, as measured at Uwekahuna, throughout the 1972–74 Mauna Ulu eruption are summarized in table 16.2 and figures 16.3 and 16.4.

The eruption began in early February 1972 and was dominated through early June 1973 by active lava lakes and associated phenomena, such as overflows, lava-tube formation, and volcanic shield growth, at both Mauna Ulu and Alae (fig. 16.2). The lava lakes were clearly connected beneath the surface, but lava passageways between Mauna Ulu, Alae, and the summit reservoir are not well known. Through May 4, 1973, periodic voluminous overflows of lava from Mauna Ulu and Alae totaled 125×10^6 m^3. An unknown additional volume drained back into vents and intruded into the east rift zone. This volume of surface eruptive products, not adjusted for lava vesicularity or ground deformation, yields a minimum average magma supply rate of approximately 8×10^6 m^3/mo, comparable to the rates for the 1969–71 Mauna Ulu eruption (Swanson and others, 1979) and the 1971 summit eruptions (Duffield and others, 1982).

Many short-lived overflows from Alae, traveling only short distances, built a new shield, approximately 100 m high, abutting the eastern flank of the Mauna Ulu shield (Tilling and others, 1973, fig. 2). In contrast, long-lived overflows, instead of adding to the shield, evolved into lava tubes that were able to transport the lava for great distances from the vent. Some tube-fed lava from the Alae vent cascaded into Makaopuhi Crater and entered the sea during August–October 1972 and February–April 1973 (fig. 16.2; Tilling and others, 1973; Peterson, 1976).

The 6.2-magnitude Honomu earthquake on April 26, 1973 (Unger and others, 1973; Unger and Ward, 1979), although centered more than 60 km away (fig. 16.1, inset), apparently disrupted the well-integrated lava-tube system from Alae to the coast, and all flow into the sea stopped by about May 1. This earthquake probably also altered the magma conduit system from the summit to Mauna Ulu, as well as the lava-tube link between Mauna Ulu and Alae. Early on the morning of May 5, strong harmonic tremor and summit deflation accompanied the complete drainage of the lava lakes at Mauna Ulu and Alae. About 3½ hours later, lava fountained from a fissure in Pauahi Crater, 2 km uprift from Mauna Ulu (fig. 16.2), in the first historical eruption there. The Pauahi eruption began to wane after about 2 hours, and early in the afternoon new vent fissures opened within and near Hiiaka Crater. Near the closing stages of this activity, lava erupted briefly from a fissure in the eastern part of the Koae fault zone about 1 km west of Hiiaka, in the first historical outbreak in that area (Koyanagi and others, 1973; Duffield, 1975, p. 11–12).

By May 7, 1973, lava had quietly returned to the Mauna Ulu

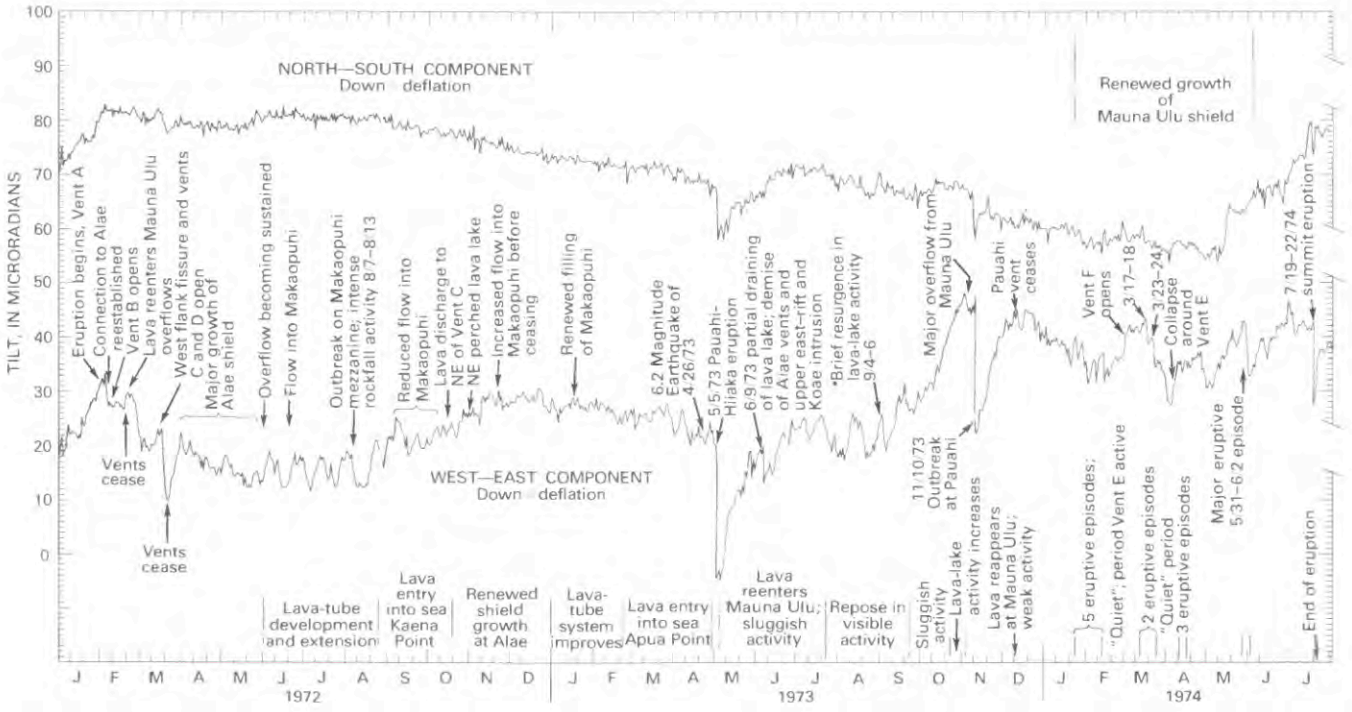

FIGURE 16.4.—Variation in Uwekahuna tilt for the period January 1972–July 1974, and its correlation with significant eruptive events (see text). Tilt data adjusted for the 18-microradian offset (east-west component) caused by the April 1973 Honomu earthquake (fig. 16.1 inset); zero point on tilt scale is arbitrary and referenced to January 1, 1972. The same data are also shown in figure 16.37 at reduced scale and not adjusted for earthquake offset.

crater. Moderate lava-lake activity had resumed at Mauna Ulu by early June, and a small lava lake reappeared at Alae. In the early hours of June 9, preceded and accompanied by harmonic tremor and abrupt summit deflation, drainage of lava partly emptied Mauna Ulu; Alae drained completely and stayed inactive for the remainder of the eruption. Almost immediately following its partial draining, Mauna Ulu lava lake began to rise again and to circulate sluggishly. Subsequent activity was summarized by Peterson and others (1976, p. 652): "Although the lava lake rose gradually with time, the surface area of the actively circulating lake steadily diminished. By mid-July the lava lake became practically stagnant, and the occasional small overflows of lava traveled only short distances on the crater floor. In late September, after nearly two months of virtual quiet, activity increased and voluminous flows flooded the crater floor."

Activity increased throughout October and early November, and Mauna Ulu lava lake rose to the crater rim, feeding voluminous overflows during November 4–8. On November 10, harmonic tremor and summit deflation again accompanied the abrupt drainage of the lake, which subsequently remained inactive for more than a month. A few hours after this sudden draining of lava from Mauna Ulu, an eruption began at Pauahi Crater (fig. 16.2) and continued vigorously for several hours, forming lava ponds in both the east and west pits fed by vents within the crater as well as by lava cascades from fissures outside Pauahi. Weak activity persisted in the west pit of Pauahi for about a month. Then, from December 9 to 12, 1973, no visible activity occurred anywhere on Kilauea.

On December 12, the seismic station located closest to the Pauahi-Mauna Ulu area began to record bursts of barely detectable harmonic tremor. By the next day, tremor had increased and become sustained, and lava quietly reentered Mauna Ulu. For the next one and one-half months, weak to moderate activity produced several short-lived flows that flooded the crusted surface of the rising lava lake.

Mauna Ulu eruptive activity in 1974 was unlike that during 1972–73. Beginning in late January, short vigorous eruptive episodes, lasting typically less than two days, produced moderately high lava fountains (40–80 m) that fed short-lived overflows. These brief eruptive periods were separated by 3-day to 5-week intervals of only feeble activity. The pattern of alternating vigorous and weak activity mimicked, albeit on a smaller scale, the episodes of high fountaining interspersed with longer periods of low activity that characterized the first stage of the 1969–71 Mauna Ulu eruption (Swanson and others, 1979).

Some overflows during the period January–June 1974 advanced as far as 9 km from the vent, but most traveled shorter distances. Consequently, the Mauna Ulu volcanic shield grew substantially in 1974, particularly during March–June, reaching a maximum height of 121 m above its pre-1969 base (Peterson and others, 1976). After June 2, the circulation of the lava lake became

increasingly sluggish, and the crusted and rubbly lake surface gradually subsided and became largely obscured by fumes. The summit region of Kilauea remained highly inflated during this period. The waning activity at Mauna Ulu apparently was unaffected by the July 19–22 summit eruption (Peterson and others, 1976), but the small, subsiding lava pool in Mauna Ulu disappeared below the rubble-covered crater bottom soon after. Harmonic tremor in the Mauna Ulu area also ceased after July 22, the arbitrary date taken for the end of the 1972–74 Mauna Ulu eruption.

The 1972–74 Mauna Ulu eruption produced a total volume of 162×10^6 m^3 of lava, 97 percent of which came from vents at Mauna Ulu and Alae, and 3 percent from vents in the Pauahi-Hiiaka area (table 16.2). During the period January–June 1974, the average magma eruption rate was about 4×10^6 m^3/mo, one-half that for the 1972–73 Mauna Ulu activity. This reduction in average magma eruption rate perhaps augured the eventual cessation of the eruption.

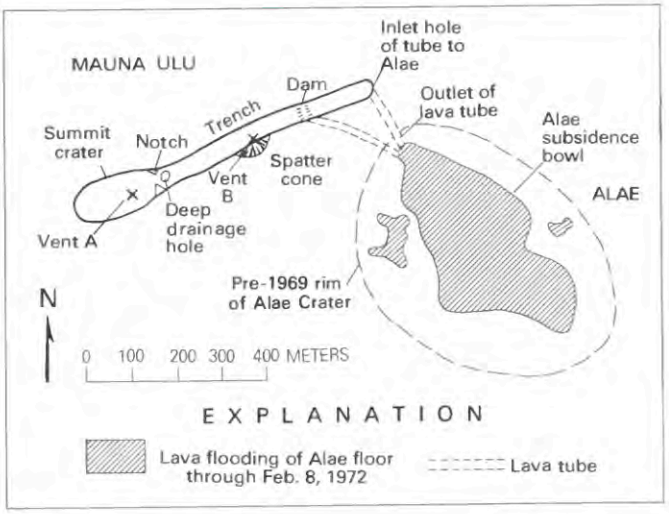

FIGURE 16.5.—Sketch map showing configuration of the summit area of Mauna Ulu shield and of Alae when the 1972–1974 eruption began in early February 1972. Summit crater, notch, trench, and lava-tube system linking Mauna Ulu and Alae had been developed by early 1971 during the 1969–71 Mauna Ulu eruption. Easternmost lava tube reopened on February 7, 1972, and fed lava onto the floor of Alae subsidence bowl, which filled to the brim by February 12.

CHRONOLOGICAL NARRATIVE

FEBRUARY 3–DECEMBER 31, 1972

REBIRTH OF MAUNA ULU LAVA LAKE

The start of the 1972–74 eruption was preceded by several months of net summit inflation and of increased seismicity from shallow sources at the summit and upper east rift. About one dozen earthquakes of magnitude 2.5 were felt by local residents between 0037 and 0200 (all times given are Hawaii standard time, H.s.t.) on January 21; these earthquakes, accompanied by shallow harmonic tremor, were centered in the caldera and Keanakakoi areas.

On the morning of February 5, 1972, a ground party discovered that lava had filled about half of the summit crater of Mauna Ulu. The reactivation of the lava lake may have occurred as early as February 2. This possible starting date is based on a telephone call from a passing motorist, who reported seeing "lava fountains on Hilina Pali" around 2130 while driving northeast from Pahala. Hilina Pali lies almost directly in line between Pahala and Mauna Ulu; thus, lava fountains or glow from Mauna Ulu might appear to issue from the pali (fig. 16.2). Though fog prevented its independent confirmation, there is little reason to doubt the February 2 eruption sighting of the motorist, a longtime resident who had witnessed many eruptions. The "bright and solid" glow witnessed by him could well have represented an early stage in refilling Mauna Ulu crater. However, seismograms for February 2 and 3 showed no unusual seismic activity or detectable harmonic tremor, which typically accompanies Kilauea eruptions.

The number of small east-rift earthquakes increased gradually about 0320 on February 4, and tremor began between 0500 and 0600. A strong storm struck the Island of Hawaii during this time, however, and the tremor recorded by several seismographs was thought at the time to be caused by high winds. The instrument at Puu Huluhulu (fig. 16.2) appeared to have been affected the most by the storm, even though some other instruments were equally exposed to the wind. In retrospect, the recorded tremor on February 4 was probably only partly due to the storm; when the storm slackened on February 5, tremor continued.

Available evidence thus indicates that lava was almost certainly flowing into Mauna Ulu crater on the morning of February 4 and possibly as early as the night of February 2. We arbitrarily use February 3 as the starting date of the 1972–74 Mauna Ulu eruption. This date is consistent with a starting time of the eruption of about 1900 on February 3, calculated by simple backward projection of the lava's rate of rise during February 5–6 (about 1.6 m/h).

REOPENING OF THE MAUNA ULU-ALAE CONNECTION

When discovered on the morning of February 5, the new lava lake had already filled about half of Mauna Ulu Crater and was slowly rising. No fountaining or surface circulation was observed. In the afternoon, the surface of the lava lake was 78 m below the crater rim, about the same elevation as the lava pool in a 30-m-diameter hole immediately east of the notch at the east end of the crater (fig. 16.5). All activity was confined to the western part of Mauna Ulu summit.

During the next two days, harmonic tremor increased, lava gradually rose, and fountaining as high as 10 m became localized at a point in the east-central part of the crater (fig. 16.5, vent A). Vent A is located in the same part of the lava lake as one of the vents active during stages 3 and 4 of the 1969–71 Mauna Ulu eruption (Swanson and others, 1979, plate 4). By 1030 on February 7, lava had risen to about 25 m below the rim of the crater and began to cascade over the notch into the pool. It flowed eastward down the

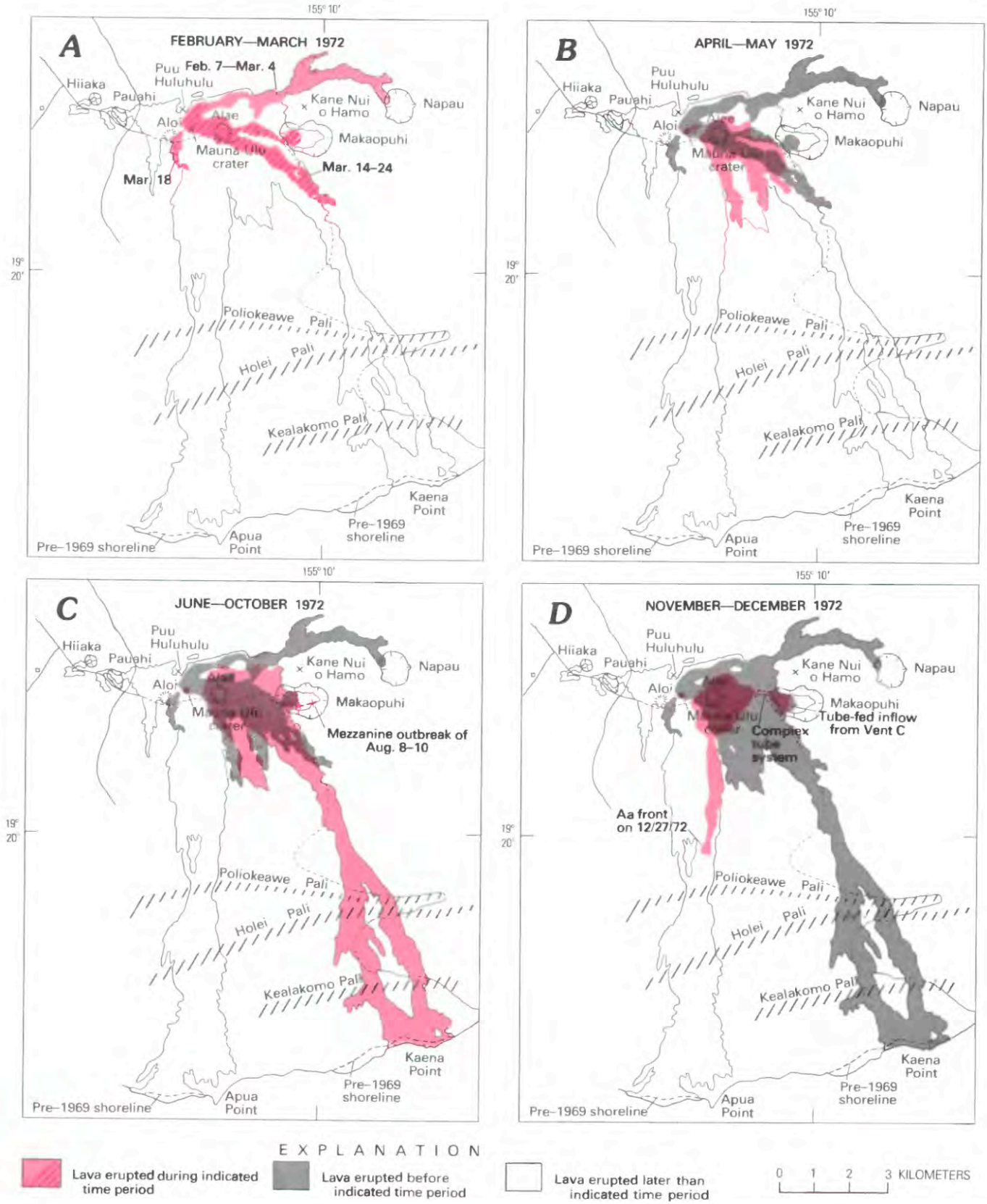
A
FEBRUARY—MARCH 1972
Feb. 7—Mar. 4
Mar. 14–24
Mar. 18
B
APRIL—MAY 1972
C
JUNE—OCTOBER 1972
Mezzanine outbreak of Aug. 8–10
D
NOVEMBER—DECEMBER 1972
Tube-fed inflow from Vent C
Complex tube system
Aa front on 12/27/72
Puu Huluhulu
Hiiaka
Pauahi
Kane Nui o Hamo
Napau
Aloi
Alae
Makaopuhi
Mauna Ulu crater
Poliokeawe Pali
Holei Pali
Kealakomo Pali
Kaena Point
Apua Point
Pre–1969 shoreline
155° 10'
19° 20'
EXPLANATION
Lava erupted during indicated time period
Lava erupted before indicated time period
Lava erupted later than indicated time period
0 1 2 3 KILOMETERS

trench, reaching the eastern end at 1200. The lave-tube system that linked Mauna Ulu and Alae during the 1969–71 eruption was still in existence, as later confirmed by thermal infra-red scanning imagery obtained during a pre-dawn flight in February 1973; lava apparently reentered this tube system and emerged at 1225 at the northwestern edge of the Alae subsidence bowl (fig. 16.5; see also Swanson and Peterson, 1972, fig. 1*B*). Activity in the lava lake continued steadily, and lava flowing in the trench developed a well-defined channel that fed directly into the Alae inlet tube(s).

LAVA-LAKE ACTIVITY AT MAUNA ULU AND ALAE AND PERIODIC OVERFLOWS

Activity on February 8 was similar to that the day before, except that rising lava now covered the notch between the summit crater and trench. Lava was overflowing a channel obstruction (the dam in fig. 16.5) that had developed about 165 m west of the end of the trench. Low fountaining continued at vent A, but a new fountain appeared near the south wall of the trench 130 m west of the dam (fig. 16.5, vent B). Vent B was to become the dominant vent for the remainder of the 1972–74 eruption.

For the next several days, activity remained much the same, with both vents A and B spurting lava fountains 10–20 m high, and a prominent spatter cone formed at vent B. Except for local variations around these two active vents, lava movement was generally eastward through the trench to the inlet for the tubes to Alae. By February 12, the Alae subsidence bowl had filled with a lava lake that remained intermittently active until early June 1973. Lava spilled over some low areas along the rim of the Alae lake but advanced only a few meters before levees developed.

During February 13–14, the vigor of vent A began to decline, while vent B produced a sustained overflow that advanced east-southeast about 1.1 km from Alae's rim toward Makaopuhi Crater (fig. 16.6*A*). Activity at vent A ceased on February 16, and the lava level at Mauna Ulu began to drop; although the fountaining at vent B temporarily increased, lava entry into Alae also ceased shortly thereafter. The surface of Alae lava lake crusted over and subsided 1–2 m, and all lava overflows stopped. For the next several days, the lava level in the summit crater continued to decline while weak fountaining persisted at vent B. By the morning of February 22, all surface activity terminated, but lava was still visible through three glowing holes at the site of vent B.

Lava reentered Mauna Ulu on February 24, and, fed by fountains 5–20 m high at vents A and B, the lake rose rapidly several tens of meters to spill over both the south and north rims of the trench. Fountains 40–75 m high at vent B were the highest observed since the eruption began. A major east-northeast-trending overflow advanced north of Kane Nui o Hamo as aa and spilled into Napau Crater on February 29 (figs. 16.6*A* and 16.7). For the next several days, numerous overflows raised the rim of the eastern part of the trench. Meanwhile, the spatter cone at vent B became the highest point on Mauna Ulu, more than 10 m higher than the rim of the summit crater (hereinafter the summit crater will be referred to simply as the crater). The episode of vigorous activity and overflows ended on March 5, when the lake surface subsided to more than 30 m below the rim of the crater (fig. 16.8). During the next several days, the lake surface continued to drop, and activity at vent B was reduced to sporadic low spurts.

Activity at vents A and B increased beginning on March 11, and on March 14 another overflow episode began. Periodic overflows, some lasting for several hours, alternated with drainbacks of 5–10 m accompanied by vigorous degassing. This cyclic activity resembled the so-called gas-piston described by Swanson and others (1979) but was larger in scale, involving the entire lake instead of a chimney-like vent. Virtually all parts of Mauna Ulu, except its extreme western end, were flooded by the overflows (fig. 16.9).

At 1800 on March 18, a new fissure vent, 200 m long, opened on the west flank of Mauna Ulu over the southeastern edge of the buried Aloi Crater (fig. 16.3). This fissure nearly coincided with that formed in April 1970 (Swanson and others, 1979, pls. 1, 3). The lava level in both the crater and trench rapidly dropped several tens of meters. Activity at the new fissure was short lived; after feeding a small flow (fig. 16.6*A*), the fountains stopped during the morning of March 19. However, accompanied by high-amplitude harmonic tremor and summit deflation, eruptive activity then shifted to the Alae area, where two new vents opened (fig. 16.11, vents C and D), each feeding fountains about 20 m high. The subsidence bowl at Alae again quickly filled; a perched lava lake soon developed by repeated overflows and levee construction, initiating the growth of a volcanic shield at Alae. During March 19–20, vents C and D fed two lava streams that advanced 2 km or more east and southeast; one of these streams poured into the deep western pit of Makaopuhi Crater (fig. 16.6*A*). Activity at the two vents then began to wane and ceased by March 24.

DOMINANT ACTIVITY SHIFTS TO ALAE: VOLCANIC SHIELD GROWTH

The opening of the vents during March 18–20 (the west-flank fissure at Mauna Ulu and vents C and D at Alae) ended the period of overflows from Mauna Ulu in 1972 (fig. 16.10): the next overflow was not to occur until early November 1973. For the remainder of 1972 and until mid-1973, generally weak activity continued intermittently at vent A within the crater, but vents C and D and various openings at or near vent B dominated the eruptive activity at Mauna

FIGURE 16.6.—Lava flows developed during 1972 in the Mauna Ulu region. Outlines of flows are approximate in this and subsequent similar figures tracing the development of lava flows during 1972–1974 Mauna Ulu eruption. Outline of the entire field, as well as the outlines of portions of lava flows not covered by younger flows, taken from geologic map of Holcomb (1976). See figure 16.3 for locations of vents. ***A***, February–March. Lava erupted during March 14–24 indicated by hachuring. ***B***, April–May. ***C***, June–October. For details about lava delta at Kaena Point, see Peterson (1976). ***D***, November–December. Except for late December flow and tube-fed inflow into western pit of Makaopuhi Crater, most flows were short-lived and accreted near vent, resulting in shield growth.

FIGURE 16.7.—View of 10-m-wide pahoehoe flow advancing through forest east of Puu Huluhulu on February 28, 1972, during overflow from Mauna Ulu (fig. 16.6*A*). Note burned vegetation adjacent to flow. Photograph taken by R.I. Tilling.

Ulu and Alae. In effect, the lava lake in Mauna Ulu's crater became mainly a passive holding tank, fluctuating in level but distinctly subordinate in activity to vents C and D, which are rootless and probably supplied from vent B through the Alae inlet tube. Whether vent B itself was a primary vent or tapped another, primary vent beneath Mauna Ulu is not known. However, we regard vent B as primary, at least for the period February 1972–April 1973 (see Tilling and others, 1973, fig. 2). All visible activity at Mauna Ulu from May 1973 on involved vents located west of vent B, and the primary vent may therefore have shifted westward at about that time.

The last week in March 1972 was marked by a lull in harmonic tremor and summit inflation; visible vent activity was restricted to weak spattering at vent A. On April 3, tremor increased and the lake in the crater rose. A new (unnamed) vent between vent B and the west end of the trench (fig. 16.3, near vent F) opened and fed a cascade of lava westward over the septum separating the trench and crater (fig. 16.11) and into the lava lake. Vent C was reactivated and began again to fill Alae lava lake. Overflows from vent D built a 20-m-high satellitic shield on the northern flank of the growing Alae shield.

For the next several months, the eruptive activity changed little. At Mauna Ulu, low fountains spouted locally from the circulating lava lake, whose level fluctuated from 20 to 30 m (generally 22–26 m) below the rim. The circulation pattern generally involved a net east-to-west movement; however, during brief episodes lasting a few minutes to half an hour, circulation reversals occurred, accompanied by turbulent disruption of the lake surface and fountaining as high as 25 m, presumably from vent A. A number of small vents and open, glowing holes in the trench, between the septum and the vent B spatter cone, intermittently ejected spatter or spawned short lava flows that covered the trench bottom. Gas-piston activity and attendant degassing were commonly observed at these vents. The lava level was generally about the same in both the crater and the trench, suggesting the existence of hydraulic connection through the septum.

The dominant vent during this period, however, was C, which quietly pumped out a virtually uninterrupted stream of lava into the

FIGURE 16.8.—Lava from the trench fed by vent B falling approximately 20 m over the septum (fig. 16.11) into the lava lake in Mauna Ulu Crater. Photograph taken by D.W. Peterson, March 5, 1972.

perched Alae lava lake, which measured about 200 m across and perhaps 5–10 m deep. Overflows from this lake fed many short lava flows, mainly to the south and southeast (fig. 16.6*B*), raised the confining levees, and accreted lava to the surrounding areas. By May, the irregular summit area of the rapidly growing volcanic shield was more than 40 m above the mid-1971 surface of the subsidence bowl at Alae.

The generally steady and quiet output of vent C was dis-

FIGURE 16.9.—Aerial view showing Mauna Ulu Crater filled with lava during March 14–24 period of overflow and shield growth. Circular structure, about 700 m across, in background is Alae subsidence bowl (fig. 16.5). Photograph taken by W.A. Duffield, March 17, 1972.

rupted, at intervals ranging from about 30 minutes to more than 2 hours, by abrupt and brief (5–30 seconds) drainbacks, causing considerable turbulence of the nearby lava-lake surface. Little or no gas was emitted during such behavior and the entire process occurred silently. Furthermore, simultaneous observations indicated that the drainback events at Alae did not correlate with gas-piston activity at Mauna Ulu.

Within Alae lava lake itself, quasi-solid but still highly mobile island-like and peninsula-like masses began to develop in late April (fig. 16.12). These islands and peninsulas eventually became fixed in position, grew, and coalesced to form a discontinuous, roughly northwest-southeast divider across the center of the lake, nearly separating it into two compartments, each of which contained lava pools (fig. 16.11). Beginning in late May, the principal inflow of lava from vent C was into the northeastern compartment; subsequent periodic overflows raised its surface about 5 m higher than that of the southwestern compartment. Spillage across the divider kept the southwestern pool active. Voluminous overflows from both compartments of the lake built the complex Alae shield to an estimated height of 80 m above the pre-1969 southeastern rim of former Alae Crater (fig. 16.13).

SUSTAINED OVERFLOWS, LAVA TUBES, AND LAVA ENTRY INTO THE SEA

Starting in June 1972, the eruption began to depart from the mode of activity characteristic of the preceding months. The level of Mauna Ulu lava lake dropped and then fluctuated between 30 and 45 m below the crater rim. Construction of the volcanic shield continued by periodic overflows around the margin of Alae lava lake, but some of the overflows were more sustained and gradually became channelized. Consequently, an integrated system of lava channels and tubes developed and carried lava great distances from

the immediate flanks of the growing shield. At times the surface of the Alae lake fell 1–10 m below the confining levees as lava drained from the lake through the tube system and emerged at the surface as far as 2 km from Alae. By June 20, surface and tube-fed lava flows from Alae again began to spill into the deep west pit of Makaopuhi Crater (fig. 16.6C).

The activity at Mauna Ulu remained essentially unchanged for the next several months. Lava entered the lake from the vent complex between vent B and the west end of the trench; surface circulation of the lava lake was predominantly from east to west; and lava fountains 5–10 m high played sporadically from various parts of the lake margin where surface lava and crust circulated downward. Meanwhile, vent C at Alae continued to feed lava through tubes into Makaopuhi's west pit. Near-vertical tubes developed around the two dominant lava cascades down the west wall of Makaopuhi and fed lava directly into the molten pool beneath the crusted floor, gradually raising it in piston-like fashion, as also happened during the filling of Alae Crater in 1969 (Swanson and others, 1972, 1979). In addition, prominent talus-and-lava cones formed against the west wall (fig. 16.14).

By early August, inflow into Makaopuhi declined, but tube-fed Pahoehoe flows accumulated in the area southeast of the Alae shield and began to advance southeastward. During August 7–13, intense rockfall activity in Makaopuhi 's west pit generated about 0.27×10^6 m^3 of rockfall debris. Many of these rockfalls were observed and photographed as they happened; correlations of field observations and seismic data suggested that this unusually energetic flurry of rockfalls was caused by eruption-induced changes in stress patterns of the crater walls (Tilling and others, 1975). The peak rockfall activity coincided with a small-volume eruption from echelon fissures on the mezzanine of Makaopuhi observed on August 9 and 10 (Tilling and others, 1975, figs. 2, 4); this eruption began between late afternoon of August 7 and early morning of August 9. Because the mezzanine vent fissures were rootless, the cause of this outbreak is problematic. It may in part be attributed to hydrofracturing induced by the weight of the lava lake and rockfall debris in the west pit exceeding the tensile strength of the mezzanine.

By mid-August, the tube-fed southeastward-flowing lava from Alae had advanced over Poliokeawe Pali and Holei Pali, buried a segment of Chain of Craters Road not covered during the 1969–71 activity, and covered flows of 1970–71 and older ages along the coastal flat. On August 23, lava reached the ocean at Kaena Point, about 1.5 km east of the lava delta of March–May 1971 (fig. 16.6C), marking the fourth time that lava had entered the sea along the south coast of Hawaii since June of 1969. The processes of lava entry into the sea and formation of lava deltas were essentially identical to those described earlier for the 1969–71 eruption of Mauna Ulu (Moore and others, 1973) and have been summarized by Peterson (1976). Substantial stretches of new black-sand beaches formed along the new shoreline when molten lava shattered upon quenching by seawater and was comminuted in the surf zone. SCUBA-diving scientists observed pillow formation and the submarine movement of lava (Grigg, 1973; Moore, 1975; Tepley, 1975).

Similar activity continued at Mauna Ulu and Alae throughout September and until mid-October. The lake level at Mauna Ulu varied between 33 and 50 m below the crater rim; the lake at Alae occasionally dropped to about 20 m below the crater rim and, at other times, briefly overflowed its levees to add to the bulk and height of the Alae shield. The volume rate of inflow of tube-fed lava into Makaopuhi Crater slackened. Temperature, flow velocity, and dimensions of lava channels were measured or estimated through openings or skylights formed by local collapse of the roof in the upstream parts of the principal tube systems (figs. 16.15, 16.16). Optical pyrometer and thermocouple measurements indicated minimum temperatures ranging between 1,130 and 1,165 °C. Average flow rates were 1.5–3.0 m/s; at times of low stands of Alae lake (for example. on October 17), flow rates in the tube systems decreased to about 0.2–0.5 m/s.

Lava flowage to the sea from Alae lake through the well developed southeast-trending tube system continued until mid-October, when lava from vent C was diverted to the east and northeast, away from the tube system. By November 8, the diverted lava had accumulated to form a well-defined lava pond, in effect a much smaller version of the Alae lake. This northeast pond periodically overflowed to construct a satellitic shield on the northeastern flank of the larger and complex Alae shield.

The diversion of vent C lava to the northeast diminished the rate of lava supply to Alae lake and to the tube system between Alae and the sea. Consequently, lava entry into the sea ceased completely by about October 20, after having formed a lava delta about 8.6×10^6 m^3 in volume and 0.18 km^2 in area (Peterson, 1976, table 1).

By early November the main lava tube draining Alae had become choked off at a point near the southeastern rim. Lava from Alae spilled into Makaopuhi again briefly in late October and more voluminously in mid-November (fig. 16.6*D*). The west pit of Makaopuhi was then virtually full of lava, the irregular surface of which sloped gently eastward from the west wall and averaged 2–3 m below the floor of the eastern mezzanine (fig. 16.17*A*).

ADDITIONAL GROWTH OF ALAE SHIELD

Activity at Mauna Ulu and Alae varied little for the remainder of 1972; the Mauna Ulu lake level fluctuated between 28 and 36 m below the crater rim, but was most commonly at about 31 m. Steady outpouring of lava from vent C through surface channels or short tubes fed numerous flows, which built the complex Alae shield higher and wider. The areas of major growth included Alae summit (around vent C) and three secondary vent areas on the southern flank of the complex shield. Accretions around these secondary vents, presumably the outlets of tubes within the shield, rose as much as 10 m above the sloping flanks of the main shield. Overflows also flooded the crusted surfaces of both compartments of the Alae lava lake, obliterating their former distinct edges.

The growth of the Alae shield was the dominant and most conspicuous activity in November–December 1972, but significant overflows to the south built a new system of lava channels and tubes,

FIGURE 16.10.—Profile of Mauna Ulu volcanic shield as seen from Alae, following February–March 1972 overflows; prominent knob is the 10-m-high

which gradually became well integrated. Toward the end of December, lava was being transported progressively greater distances from vent C through an increasingly efficient channel-tube system; as a result, shield-building processes became sporadic and subordinate. By December 27, a partly roofed, south-trending channel fed a flow that advanced to within 1 km of the edge of Poliokeawe Pali (fig. 16.6*D*). The continuing lava-lake activity at Mauna Ulu was not affected by the change of Alae's main activity from shield building to lava-tube development. In the months to come, shield building would be only an intermittent and minor eruptive process at Alae.

JANUARY 1–MAY 4, 1973

RENEWED OVERFLOWS, LAVA-TUBE FORMATION, AND LAVA ENTRY INTO SEA

Eruptive activity during January–April 1973 was dominated by continued voluminous lava output from vents at Alae, development of well-integrated lava-tube systems, and renewed entry of lava into the sea. Mauna Ulu's behavior during this interval remained basically the same as that during much of 1972; the lava-lake level was fairly steady, mostly fluctuating between 30 and 35 m below the crater rim (total range 24–41 m). Whereas during 1972 the surface movement of the lake was most commonly from east to west, in 1973 no net circulation direction prevailed.

Vent C remained the principal source of lava output at Alae during January–April 1973, and secondary nearby sources were intermittently active. Gas-piston activity became notable at vent C: a cycle consisted of the slow, quiet rise of the lava column for 15 minutes to one hour, followed by vigorous degassing and an abrupt drop of 5–20 m in the level of the column. As degassing ended, the quiet rise of lava resumed and the cycle repeated.

Associated with the steady activity at Alae during January–February, two major tube systems developed, one a south-trending system that began in December 1972 and the other a rejuvenated east-northeast-trending system toward Makaopuhi (fig. 16.18*A*). Tube-fed lava from the south-trending system spilled over Poliokeawe Pali and Holei Pali by January 12 and began to pond at the base of Holei Pali. Extension of the east-northeast-trending system resulted in renewed filling of Makaopuhi beginning on January 24. By mid-February the west pit of Makaopuhi was filled to the mezzanine level, and soon thereafter pahoehoe lava covered more than half of the mezzanine floor (fig. 16.17*B*).

Pahoehoe flows fed by the south-trending tube system continued to spread slowly over the coastal flat and on February 24 reached the ocean about 1 km west of Apua Point (fig. 16.18*A*), marking the fifth consecutive year that lava from Mauna Ulu eruptions had entered the sea. By March 20, the subaerial part of the lava delta at Apua Point had grown to about 0.18 km^2. Lava entered the sea at Apua Point throughout March and April, and the lava delta attained an area of about 0.29 km^2 and a volume of 13.0×10^6 m^3 (Peterson, 1976, table 1). As in 1972, SCUBA-diving scientists were again able to observe lava movement and pillow formation beneath the sea surface.

While inflow into Makaopuhi dwindled and finally stopped in early March, numerous overflows issued from two lava-tube skylights about 100–120 m east-northeast of vent C. These overflows and several from vent C itself resulted in a brief period of shield building at Alae summit, but the rate of flow in the south-trending system showed no decrease.

spatter cone of vent B. This profile changed little through late 1973. Composite of photographs taken by R.T. Holcomb, February 6, 1973.

Activity at Mauna Ulu and Alae through April varied little from that of earlier 1973. At times during this period, Mauna Ulu and Alae lava lakes varied roughly in concert (fig. 16.19). In mid-March, part of the east wall of Mauna Ulu crater collapsed and the lava lake lengthened eastward by about 20 m into the area of the trough. However, within about a week, the collapsed part of the wall was rebuilt and the lake perimeter retreated to near its former position. Beginning in early April, the western part of the Mauna Ulu trench subsided, and lava from vent B reached the lake in the western crater by periodic surface flows across part or all of the trench floor, rather than by flow beneath it.

EFFECT OF THE APRIL 26, 1973, HONOMU EARTHQUAKE

At 1026 on April 26, an earthquake of magnitude 6.2 shook the Island of Hawaii. The hypocenter was 48 km beneath Honomu (fig. 16.1, inset) on the northeast coast of Hawaii (Unger and others, 1973; Unger and Ward, 1979). Observations from the air and on the ground showed no appreciable immediate effect of this earthquake on the eruptive activity at Mauna Ulu and Alae, but the south-trending lava-tube system feeding the flows entering the ocean near Apua Point apparently was severely disrupted by subsurface collapse-induced obstructions that impeded and ultimately halted lava transport.

The rate of lava entering the sea showed a temporary increase immediately after the earthquake but then declined rapidly. By May 1, lava entry into the sea had ceased. Blockage of the tubes above Poliokeawe Pali caused several copious overflows from upstream skylights, which in turn fed spectacular cascades down the face of

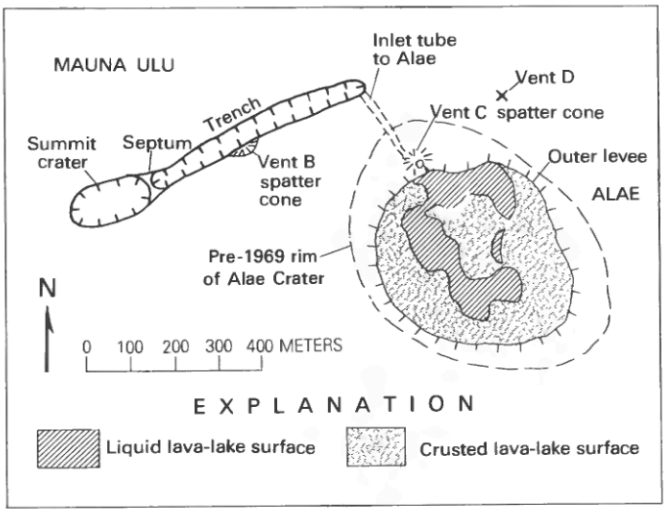

FIGURE 16.11.—Sketch map showing two compartments in lava lake at Alae and location of vents C and D. Vent C was fed through lava tubes from Mauna Ulu trench and in turn supplied vent D through surface channels and tubes. Configuration of Alae lava-lake surface varied daily, but the distinction of southwest and northeast compartments persisted for many weeks. See also Holcomb and others (1974, figs. 5-12, 5-13).

FIGURE 16.12.—View to west showing island-like masses of semisolid lava developed in Alae lava lake, which was fed by lava issuing from opening at base of fuming vent C spatter cone (center). Mauna Ulu shield, with its prominent vent B spatter cone, and Puu Huluhulu are seen in upper left. Photograph taken by D.W. Peterson, April 23, 1972.

Poliokeawe Pali and Holei Pali a few hundred meters east of the blocked tube system. These cascades continued until May 5. Tube blockage may also have caused the overflows and 5-m-high fountains on May 1 from vent C and several secondary vents on the southwest and south rim of the crusted Alae lake. By May 3, the activity at the secondary vents had nearly ended, and the lava column in vent C dropped to about 7 m below the ground surface.

We assume but cannot prove that this rather abrupt cessation in

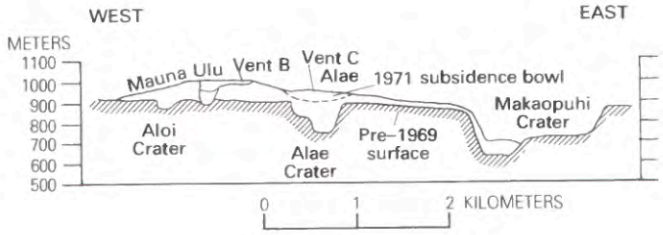

FIGURE 16.13.—Schematic cross section showing Mauna Ulu and Alae volcanic shields in late May 1972; line of section is approximately east-west but is bent at several points so as to traverse summits of Mauna Ulu and Alae, as well as Makaopuhi Crater and buried Aloi Crater. Vertical exaggeration is 2.5. Modified from Tilling and others (1973, fig. 2).

early May of the virtually continuous activity that had prevailed through April 1973 resulted from blockages in the magma conduits caused by the Honomu earthquake. A 7.2-magnitude earthquake in November 1975 (Tilling, 1976b; Tilling and others, 1976a) caused major changes in Kilauea's magma regime (Dzurisin and others, 1984). Yet, the 6.7-magnitude Kaoiki earthquake in November 1983 apparently produced no observable effects on the Puo Oo eruption (Wolfe and others, chapter 17; E.W. Wolfe, written commun., 1985). Though the coincidence in timing between cessation of activity and the Honomu earthquake may be fortuitous, we favor the working hypothesis that the disruption in magma-transfer regime perhaps was induced by the earthquake.

FIGURE 16.14.—Streams of tube-fed lava cascading down the western wall (200 m high) of Makaopuhi Crater, forming lava-and-talus cones. Photograph taken by W.A. Duffield on June 30, 1972; see Holcomb and others (1974, p. 51 and figs. 5-25, 5-26) for additional information.

FIGURE 16.15.—Geologist probing the depth of a lava stream with stainless steel pipe inserted through lava-tube skylight. Photograph taken by R.I. Tilling in January 1973.

PAUAHI-HIIAKA ERUPTION OF MAY 5, 1973

ACTIVITY WITHIN PAUAHI CRATER

At 0703 on May 5, an intense flurry of small shallow earthquakes began in the vicinity of Mauna Ulu and Alae. Subsequent smaller earthquakes were soon masked on seismograms by increasing harmonic tremor, accompanied by rapid deflation of the summit of Kilauea. Observations at 0915 showed that Mauna Ulu lava lake, whose level was 39 m below the crater rim only two days before, had completely drained to leave a very deep, rubble-choked crater, whose walls were crumbling amid thick dust clouds. The crater formerly containing the lava lake was now composed of two parts, a western pit about 180 m deep and an eastern pit about 200 m deep, both of which were entirely devoid of molten lava (figs. 16.20, 16.22*A*). The western pit approximately coincided with the general area of vent A. The empty crater extended eastward into the trench of Mauna Ulu as far as the area of the vent B spatter-and-pumice cone (fig. 16.20). Observations at 0945 showed that molten lava within the Alae volcanic edifice also had drained completely, as expressed by the collapse of the area of vent C to form a rubble-filled crater about 60 m by 100 m across and 30 m deep.

A magnitude-3 earthquake occurred at 0932 near Puu Huluhulu and was followed during the next hour by several comparable and larger shocks, some of which were felt as far away as Hilo. These earthquakes prompted inspection of the Chain of Craters Road area and a recommendation to officials of Hawaii Volcanoes National Park that the road be closed to traffic. An observer arrived at Pauahi Crater (fig. 16.18*B*) at 1020, just in time to watch the last of a series of large rockfalls from the north crater wall. At 1023 he heard a sharp loud sound and saw a dense fume cloud beginning to issue from a new opening near the deepest part of the western pit of the composite crater. At 1025 lava spurted from that opening, marking the first historical eruption in Pauahi. Within a few minutes, lava emerged from several additional openings aligned across the northern side of Pauahi, and by 1050 lava was fountaining along a 120-m-long fissure trending about N. 85° E. (figs. 16.3, 16.18*B*). At 1120 the lava fountains at the first and third vents to open on the crater floor reached their maximum height of about 20 m. Fountaining then declined rapidly along the length of the fissure, except at the two sites of maximum fountaining; drainback into the stagnant segments of the vent fissure immediately followed.

The decline of the lava fountains and increase in rate of drainback were rapid. By 1125, the remaining fountains were feeble, the level of the lava pond had dropped 17 m, and a new vent had broken out at a site a few tens of meters east-southeast of the original fissure and about 40 m above the level of the lava pond (fig. 16.18*B*). This new vent increased in vigor as the original fountains died about 1140. By then lava was draining at the two former vents on the original fissure much more rapidly than the new vent was supplying lava to the pond. Activity at the new vent soon began to weaken, and it ceased at about 1200. The lava surface in the crater had dropped to 20 m below its highest level by the time active drainback ended about 30 minutes later, leaving a pond of lava 20 m deep in the lowest part of the crater.

The total volume of lava erupted into Pauahi Crater during this first stage of the eruption was about 0.14×10^6 m^3, of which 0.12×10^6 m^3 drained back down the fissure. A few small bubbling vents were later observed to have remained intermittently active until early morning of May 6, but these contributed negligible additional volume to the lava fill within the crater.

ERUPTION SHIFTS TO HIIAKA CRATER AND NEARBY FISSURES

Earthquake activity and harmonic tremor remained high after the eruption within Pauahi. At 1255 on May 5, fountaining broke out along a set of fissures extending N. 70° E. from just east of the Chain of Craters Road to within the southeastern part of Hiiaka Crater (figs. 16.3, 16.18*B*). The highest fountains played along the fissure within the crater, reaching heights of nearly 50 m at times. Smaller fountains erupted from the fissures outside the crater and fed a spectacular cascade of lava down Hiiaka's southwestern wall. At

FIGURE 16.16.—Branch floating on lava stream bursts into flame as it encounters oxygen in the atmosphere at skylight (opening about 3 m wide) of principal lava tube leading from Alae. Passage of such branches is timed at successive downstream skylights by observers with stop watches who communicate by radio. Average rates of lava movement so determined are minimum rates, because the length of the meandering lava stream is greater than the length obtained by summing the linear distances measured between skylights and because cascades, pools, and eddies along the lava stream slow a branch's progress. Except at skylights, little oxygen is available in the lava tubes, so a branch can be carried hundreds of meters before being totally consumed. This method was used to estimate average flow velocities throughout the tube-fed stages of the 1969–71 and 1972–74 Mauna Ulu eruptions (Peterson and Swanson, 1974; this paper). Photograph taken by R.I. Tilling, September 19, 1972.

1307 lava broke out from a new fissure southwest of the Chain of Craters Road and initially ponded around the erupting vents and against one of the Koae fault scarps about 200 m farther south. The lava crossed the Chain of Craters Road at 1325 and added to the cascade down the crater wall, while fountaining continued at full force within Hiiaka.

The fissure southwest of the Chain of Craters Road, the latest near Hiiaka to open, was the first to die. Its decline was apparent by about 1500, and activity ended at about 1535. By that time, the fissures northeast of the road were erupting very gassy spatter in fountains no more than 3 or 4 m high, and the height of the lava fountains in Hiiaka had decreased as well. By 1700 the last (easternmost) vent in Hiiaka was virtually dead, spattering only feebly at long intervals, and slow drainback was underway (fig. 16.21).

At 1645, a dense fume cloud rose from a fissure 120 m west of the Hilina Pali Road (fig. 16.18*B*), 1 km southwest of its intersection with the Chain of Craters Road. Aerial observations around 1700 showed a continuous line of spattering only a few meters high along a fissure about 180 m long. A small flow was puddled around the eruptive fissure. By 1740, when this fissure was observed from the ground, it no longer was erupting lava but instead was degassing with a deafening roar and visible pale flames. The degassing gradually declined over a few hours, but the fissure fumed profusely through the next two days. This outbreak was only the second to occur within the Koae fault system in historical time, the first having been on May 24, 1969, and was much farther within the Koae system than the 1969 fissures (Koyanagi and others, 1973; Duffield, 1975; Swanson and others, 1979).

The maximum volume of the new fill in Hiiaka Crater from this

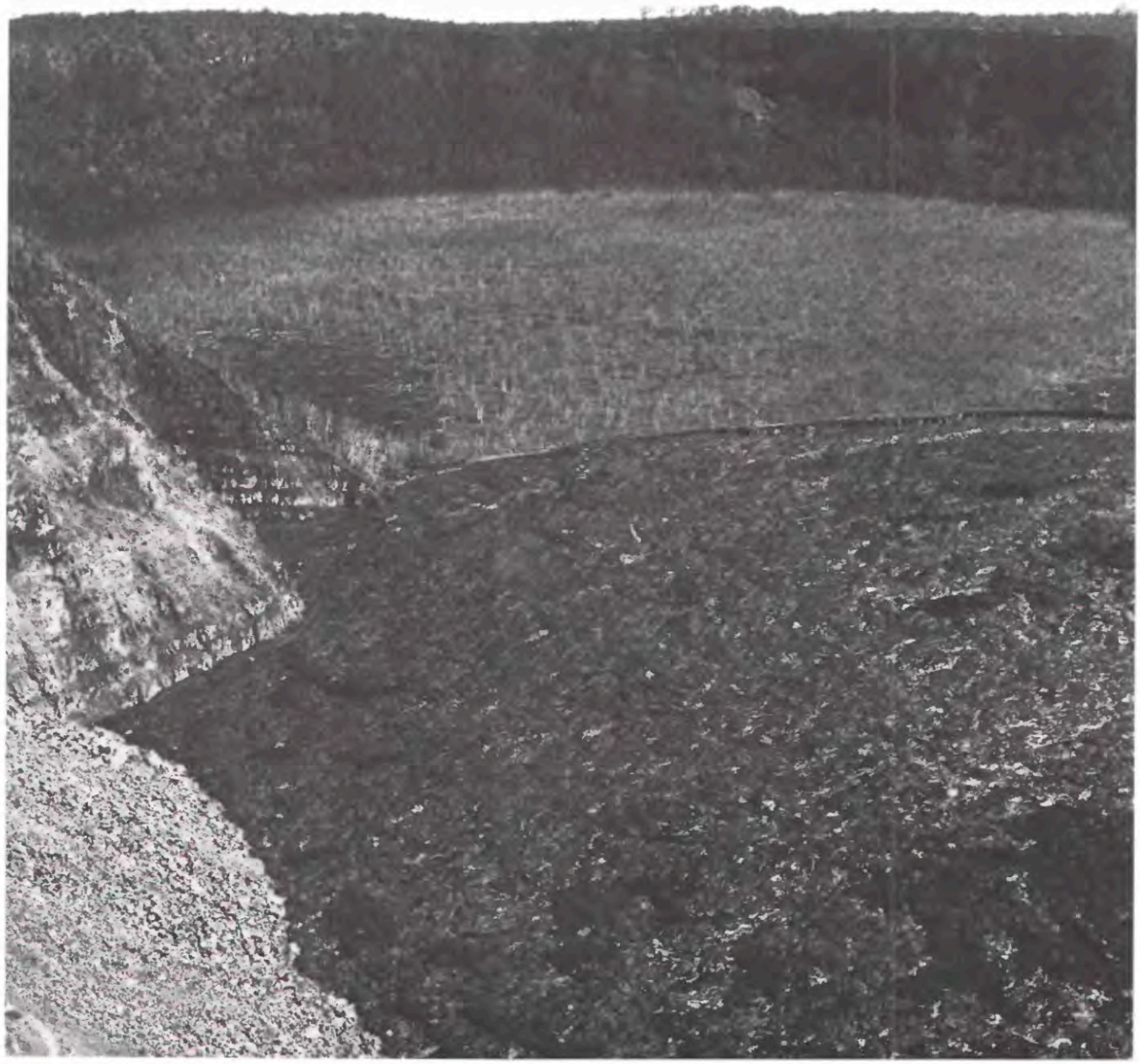

A

FIGURE 16.17.—Views of Makaopuhi Crater in early 1973. ***A,*** View on January 26, 1973, from the southwestern rim showing the west pit filled by tube-fed lava from vent C to within a few meters of the mezzanine surface. Part of 1965 lava on mezzanine (Wright and others, 1968) can still be seen (center left). Photograph taken by D.W. Peterson. ***B,*** View from nearly the same point on February 5, 1973, showing the mezzanine surface (center) more than half covered by new flow. Vegetation on mezzanine was killed earlier by fire set by the outbreak in August 1972. Photograph taken by R.T. Holcomb.

second stage of the eruption was 0.56×10^6 m^3, of which 0.12×10^6 m^3 drained back. In addition, flows covered about 0.37 km^2 of ground outside the crater, probably accounting for an additional volume of at least 0.5×10^6 m^3. Together with the 0.14×10^6 m^3 at Pauahi, these amounts make the total volume of lava erupted during the 7-hour eruption 1.2×10^6 m^3, of which 0.2×10^6 m^3 drained back into the vent fissures, resulting in a net volume remaining on the surface of about 1×10^6 m^3 (table 16.2).

MAY 6–NOVEMBER 9, 1973

The combination of the April 26 magnitude-6.2 Honomu earthquake and the May 5 Pauahi-Hiiaka eruption caused only a temporary disruption of the eruptive activity at Mauna Ulu.

B

FIGURE 16.17.—Continued.

However, these events may have been sufficient to weaken, and soon sever, the magma connection between Mauna Ulu and Alae that had operated so efficiently since February 1972.

RETURN OF LAVA TO MAUNA ULU AND ALAE

Mauna Ulu's 200-m-deep crater, emptied several hours before the Pauahi-Hiiaka eruption of May 5, was highly unstable now that its walls were no longer buttressed by the lava lake. Rockfall dust cleared sufficiently to allow the crater floor to be seen and its level measured on the morning of May 6 (fig. 16.20), but large rockfalls continued to spall from its walls for many days, generating dust clouds that rose as high as 500 m above the crater rim (see, for example, Tilling and others, 1975, fig. 9).

Harmonic tremor as recorded on the Puu Huluhulu seismograph was at a very low level from the morning of May 6 until about 1900 on the evening of May 7, when it increased noticeably. On the morning of May 8, two small pools of lava were observed in

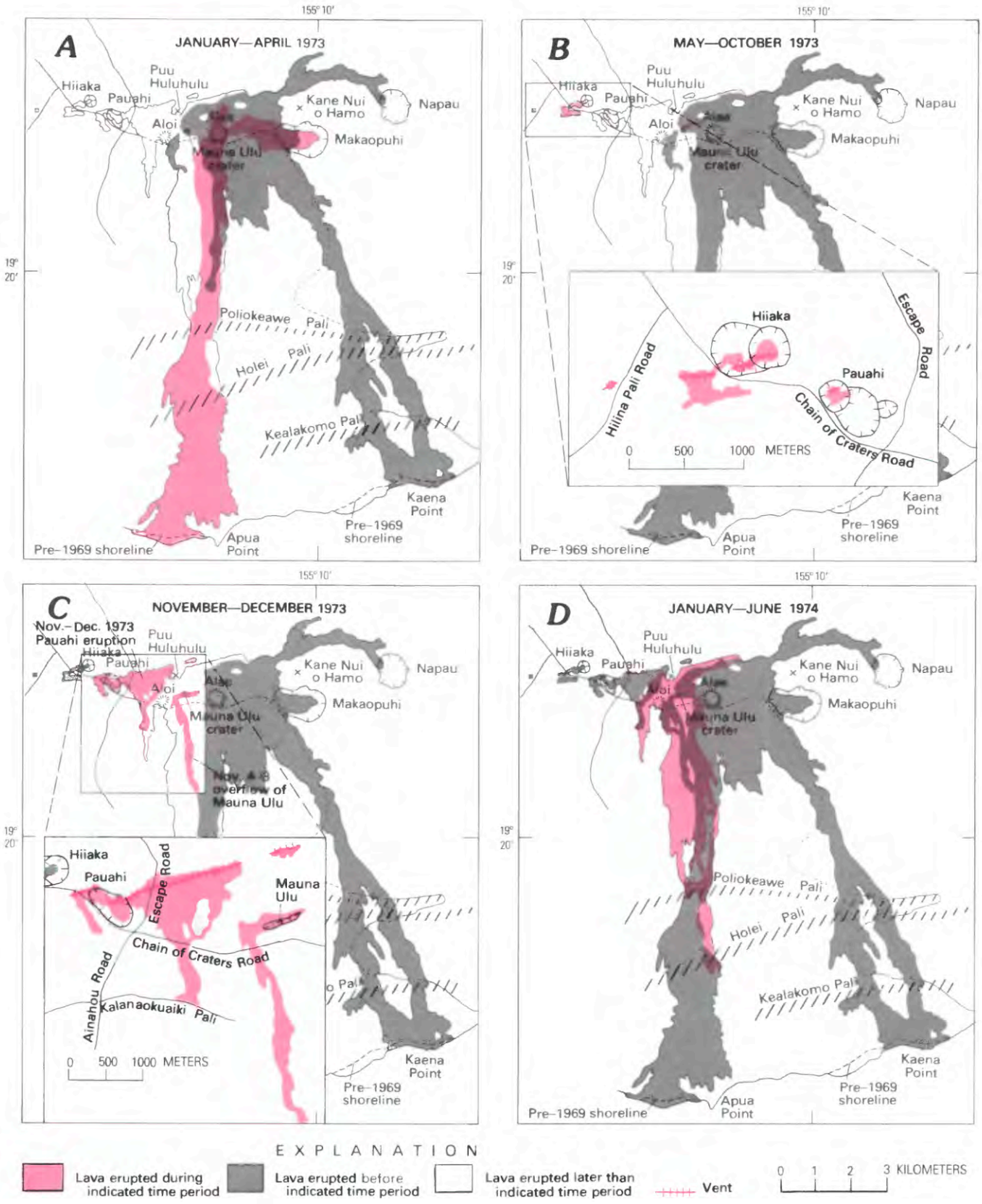
A
JANUARY—APRIL 1973
B
MAY—OCTOBER 1973
C
NOVEMBER—DECEMBER 1973
Nov.–Dec. 1973 Pauahi eruption
Nov. 4–8 overflow of Mauna Ulu
D
JANUARY—JUNE 1974
155°10'
19°20'
Hiiaka
Pauahi
Puu Huluhulu
Aloi
Kane Nui o Hamo
Napau
Makaopuhi
Mauna Ulu crater
Poliokeawe Pali
Holei Pali
Kealakomo Pali
Kaena Point
Apua Point
Pre–1969 shoreline
Escape Road
Hilina Pali Road
Chain of Craters Road
Ainahou Road
Kalanaokuaiki Pali
0 500 1000 METERS
EXPLANATION
Lava erupted during indicated time period
Lava erupted before indicated time period
Lava erupted later than indicated time period
Vent
0 1 2 3 KILOMETERS

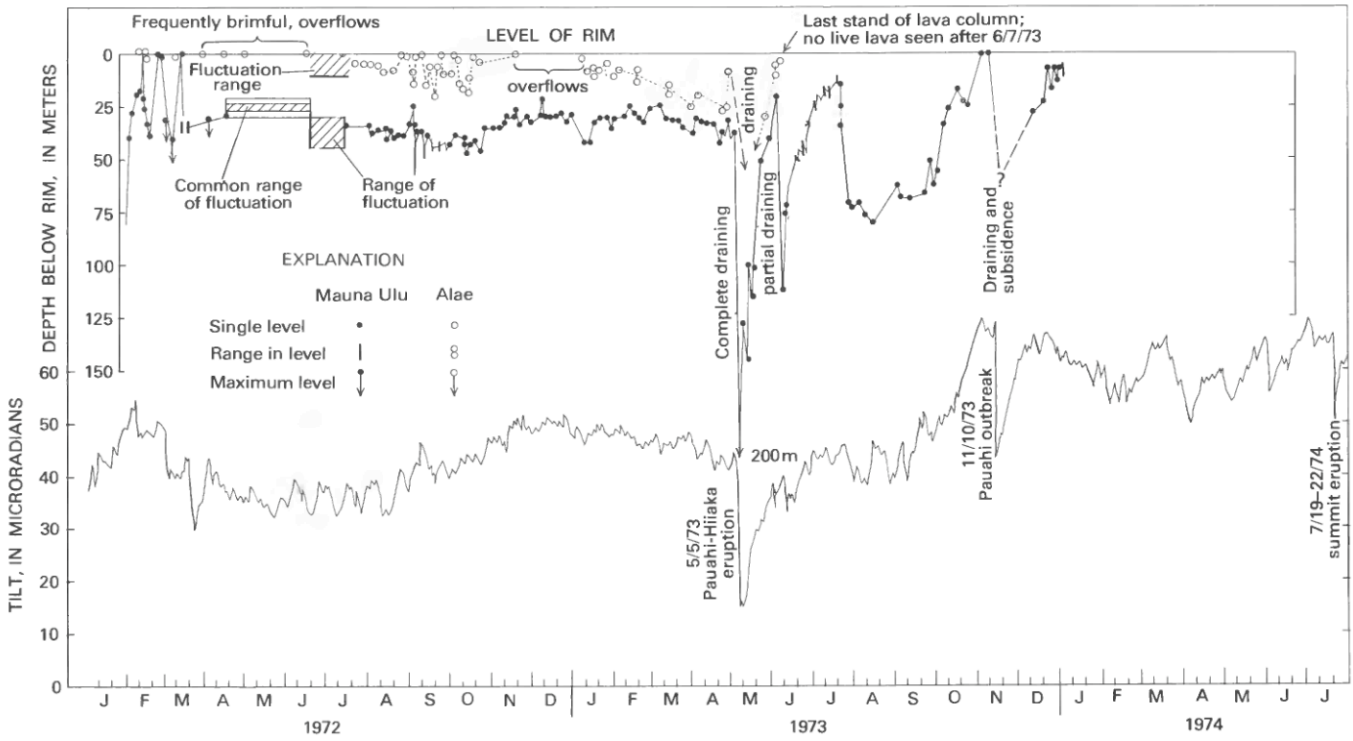

FIGURE 16.19.—Fluctuations in the depth from crater rim to the surface of lava lakes at Mauna Ulu and Alae compared with variations in the east-west component of summit tilt measured at Uwekahuna. Data plotted are from Tilling and others (1986) and figure 16.4; tilt record has been adjusted to remove the 18-microradian offset caused by the April 26, 1973 Honomu earthquake (see also figs. 16.4, 16.37).

the two deep pits of the crater; presumably lava had returned quietly during the night. Each pool rose rapidly, particularly that in the eastern deep pit. By May 15, the lava level in the eastern pit had reached as high as 97 m below the crater rim, but the level for both pits then fluctuated between 100–120 m below the rim during the next several days (fig. 16.22*B*). Then the level again rose rapidly and by May 25 the two pools had coalesced and the surface was 50 m below the crater rim. The level had risen another 10 m by May 30, and a small island of semisolid lava protruded above the surface of the lake (fig. 16.22C). This island, though changing somewhat in size and position and occasionally disappearing, persisted during much of the subsequent lava-lake activity (figs. 16.22 *D–F*). Prior to the 1972–74 Mauna Ulu eruption, the development and movement of such semisolid masses in liquid lava had only been observed at Halemaumau Crater within Kilauea's summit caldera (see, for example, Jaggar, 1920, 1947).

The lake continued to rise and on June 5 reached a level only 18 m below the rim, the highest stand since the overflows of February–March 1972, before subsiding to a depth of 23 m by June 7. Although the recovery of the lava lake was rapid, the sluggish lava circulation that prevailed throughout this time suggests that the effective viscosity of the lake lava was greater than before the May 5 draining.

On May 30, when the lava reached the 40-m level in Mauna Ulu, fresh lava was observed about 34 m below the crater rim in vent C of Alae. As the lava rose at Mauna Ulu, the level correspondingly rose at Alae, confirming the general sympathetic variation in the levels of the two lakes noted earlier (fig. 16.19). On June 5, when Mauna Ulu was at its highest level, the 100-m-diameter crater of Alae was filled to within 5 m of the rim by an active, bubbling lava lake. On June 7 the level at Alae subsided to 12 m, simultaneously with the drop at Mauna Ulu, and the lake surface became entirely crusted over.

FIGURE 16.18.—Lava flows developed during 1973 and 1974 in the Mauna Ulu region. ***A***, January–April, 1973. ***B***, May–October, 1973. Flows and vents of the May 5 Pauahi-Hiiaka eruption are shown in greater detail in the inset. No molten lava was seen at Alae after the June 9 draining of Mauna Ulu lava lake. ***C***, November–December, 1973. Major overflow from Mauna Ulu during November 4–8 and flows and vents of the November 10–11 outbreak at and near Pauahi are shown in greater detail in the inset. The flow field of Pauahi eruption was formed in less than 9 hours of activity, but weak activity associated with the vent and perched lava pond within the west pit of Pauahi persisted through December 9 (see fig. 16.29). ***D***, January–June 1974. All flows were produced in eleven relatively short-lived (no longer than 2 days) eruptive episodes: five in January–February, two in March, three in April, and one in May–June (see text). The only flow that advanced beyond Holei Pali in 1974 formed during the most voluminous eruptive episode (May 31–June 2).

FIGURE 16.20.—Aerial view looking east on May 6, 1973, showing dust-choked Mauna Ulu Crater and western half of trench (to vent B spatter cone, indicated by arrow), which collapsed during draining of lava lake on May 5 (see text). Contrast between February–March 1972 overflows (dark) and 1969–71 lava (light) is obvious in this photograph. Trail to left of crater leads to viewing platform established by the National Park Service for visitors to Hawaii Volcanoes National Park. Photograph taken by R.T. Holcomb.

JUNE 9 DRAINING OF LAVA LAKES: DEMISE OF ALAE VENT

At 2346 on June 8, strong harmonic tremor began abruptly, accompanied by rapid summit deflation and earthquakes in the eastern part of the Koae fault system. This activity ended equally abruptly at 0350 on June 9, by which time the summit had deflated by 8 microradians (fig. 16.4). When observers reached Mauna Ulu summit after daybreak, they discovered that the lava lake had fallen to about 112 m below the crater rim—a drop of 94 m from its stand

FIGURE 16.21.—Hiiaka Crater after the eruption of May 5, 1973, showing flat, crusted lava pond ringed by a lava-subsidence terrace (Holcomb, 1973), the top of which (about 6 m above pond surface) marks highest stand of lava lake during the eruption. Photograph taken by R.T. Holcomb, May 6, 1973.

just four days earlier (fig. 16.19). The large drop again triggered a rash of rockfalls from the unstable crater walls. The crusted lake at Alae also had dropped, and no molten lava could be seen anywhere on the rubble-covered floor of vent C, which was about 20 m below the crater rim. In effect, the events of June 8–9 were a smaller scale repetition of the May 5 draining of the lava lakes, but accompanied this time by intrusion into the upper east rift zone and the eastern part of the Koae fault system (Dzurisin and others, 1984, table 1) without a surface outbreak.

The lava lake at Alae never recovered from the June 9 draining, and all vent activity ceased there for the remainder of the eruption. However, the lava lake at Mauna Ulu immediately began

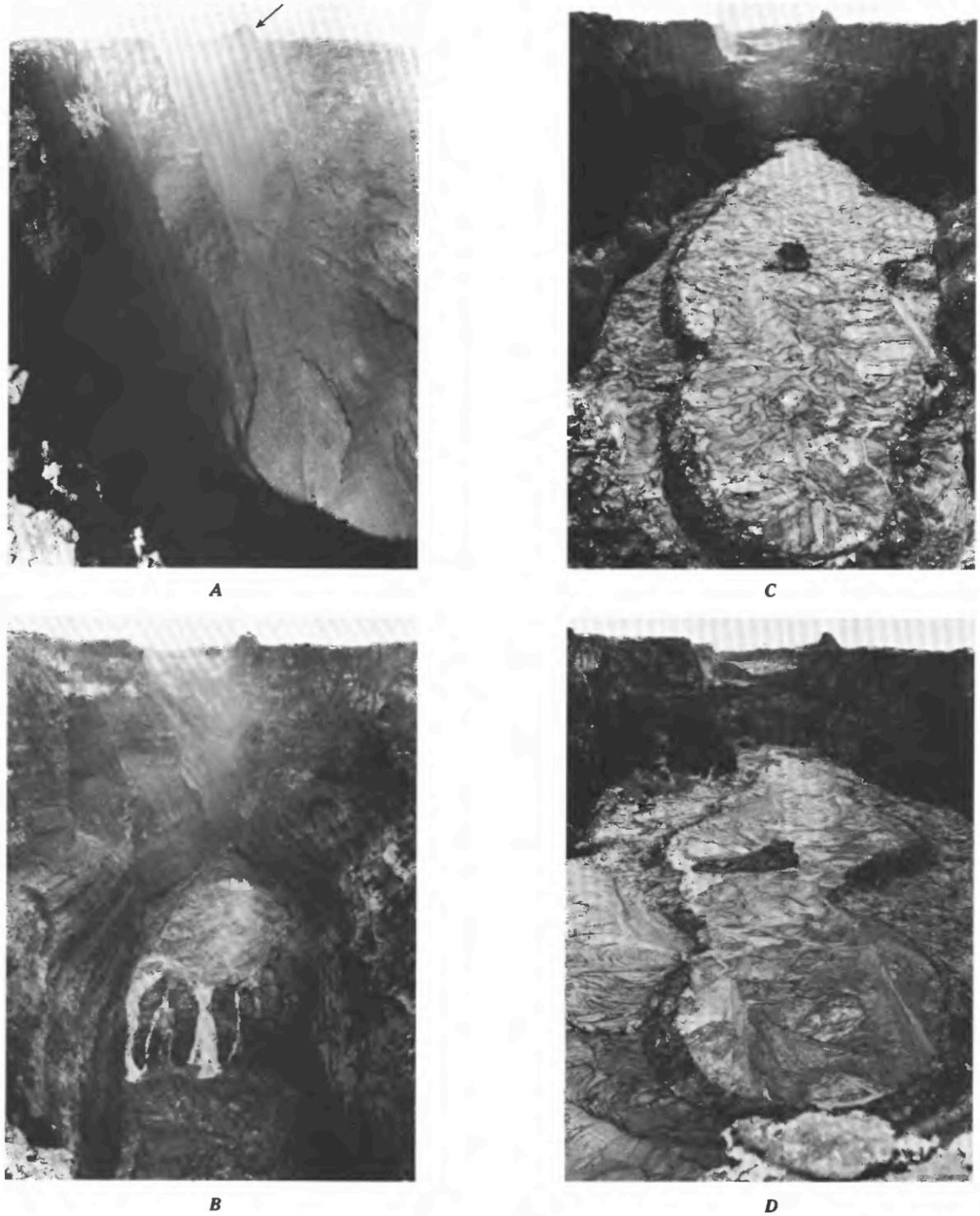

FIGURE 16.22.—Filling and draining of Mauna Ulu Crater during the period May–November 1973; all views are eastward from the western end of the crater. ***A***, Summit crater one day after the lava lake drained; crater is approximately 100 m wide and 200 m deep. Vent B spatter cone (arrow) serves as reference landmark in later views. Photograph taken by R.I. Tilling, May 6, 1973. ***B***, Renewed eruption has begun to fill the crater. Lava is shown here flowing over the levee of the lava lake in the eastern part of the crater and into deeper western part. Photograph taken by R.I. Tilling,. May 18, 1973. ***C***, Filling of the crater resumed following draining of the lava lake on June 9. Here levees confine an active lava lake that frequently overflowed into the surrounding moat. A semisolid island in center of lake, which first formed in late May and then briefly foundered following the June 9 draining, reappeared as the lake rose. Photograph taken by R.I. Tilling, June 15, 1973. ***D***, The island has grown larger, and the surface of active lake has decreased also as levees grew inward from the crater walls. Dominant flow direction of lake

E

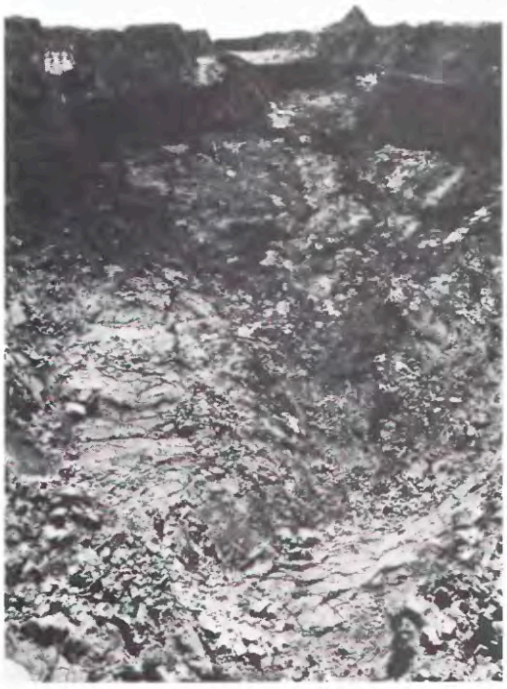

G

F

H

surface toward camera. Photograph taken by D.W. Peterson, June 21, 1973. ***E***, As lake level rose, the surface area of active lake continued to decrease. The former island has grown to become a peninsula that nearly divides the lake into two ponds. Photograph taken by R.I. Tilling, June 24, 1973. ***F***, Rise in lake surface has flooded the levees with new lava. Photograph taken by R.I. Tilling, June 28, 1973. ***G***, Gradual draining of lava during July resulted in collapse of perched lake and surrounding crust, beginning a two-month repose at Mauna Ulu (see text). Photograph taken by R.I. Tilling, July 25, 1973. ***H***, Rapid filling of the crater during October and early November produced a lava lake without levees, and the lake surface reached the lowest point on Mauna Ulu's western rim. Fountain in background fed lake and built spatter cone (fig. 16.23). Photograph taken by R.I. Tilling, November 4, 1973.

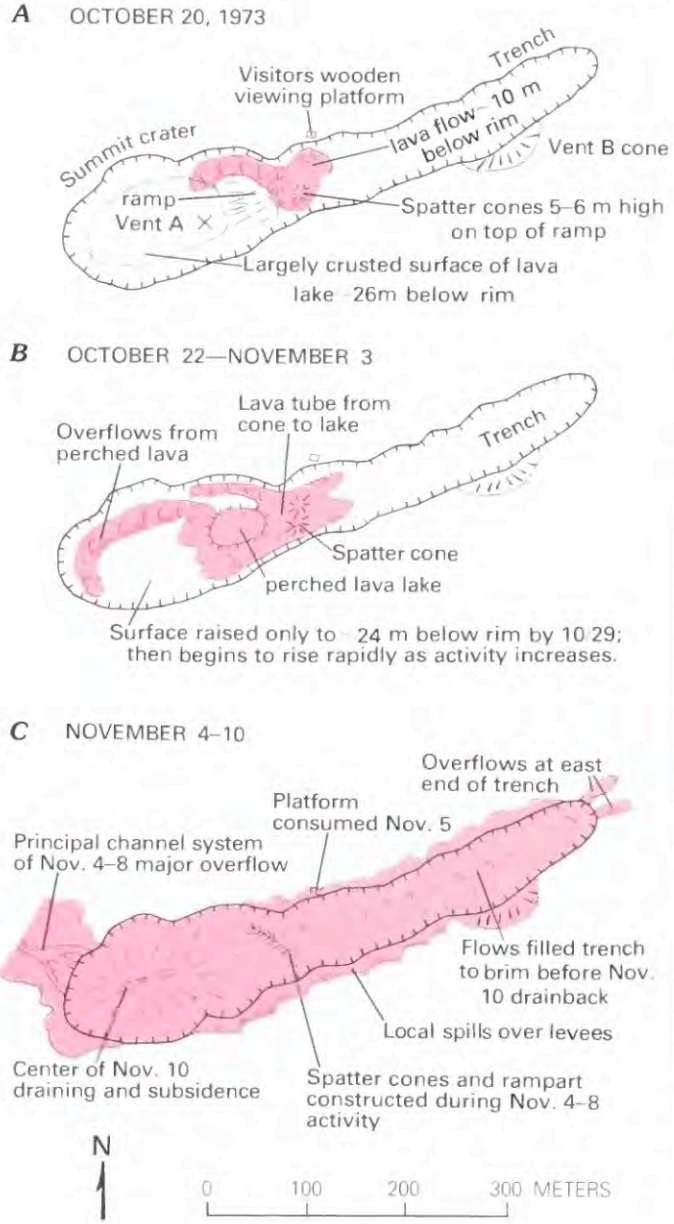

FIGURE 16.23.—Sketches showing eruptive activity at Mauna Ulu from October 20 through November 10, 1973. ***A***, October 20. ***B***, October 22–November 3. ***C***, November 4–10. Major overflow of November 4–8 was first from Mauna Ulu since March 1972.

to rise, reaching 51 m below the rim by June 19. The island of semisolid lava that first formed in late May briefly disappeared following the June 9 draining but soon reappeared and rose together with the lake surface (fig. 16.22*C–F*). The lava appeared even more viscous than following the May 5 draining. As the lava lake rose gradually, the area of sluggishly circulating lava steadily decreased. Activity was confined to a central part, perched behind natural levees and separated from the crater walls by a moat 3–20 m wide and 3–4 m deep. Periodic overflows into the moat raised the

FIGURE 16.24.—Overflow of Mauna Ulu Crater in November 1973. Lake level stabilized when overflows began on November 4, and levees again developed (compare fig. 16.22*H*), confining a perched lake at an elevation higher than the initial crater rim. Site from which photographs of figure 16.22 were taken is in foreground where stream on right overflows levee. Photograph taken by R.I. Tilling, November 7, 1973.

confining natural levees and the perched lake, as well as the level of the moat.

Sluggish lava-lake activity continued at Mauna Ulu for the next several months; lava level rose while the area of active surface lava shrank (fig. 16.22*D*, *E*). By mid-July, active lava was restricted to two circular areas 10–15 m in diameter, one of which included the active vent. Gas-piston cycles and associated small overflows occurred at intervals of 5–20 minutes. The declining activity, coupled with concurrent inflation at Kilauea summit, indicated that the connection between the summit reservoir and Mauna Ulu was not fully reestablished. By July 24 the lava lake had become stagnant, with the crusted surface at the vent about 15 m below the rim. No molten lava was visible, and the crusted surface began to subside (fig. 16.22*G*), beginning the longest repose in visible activity since the eruption began in February 1972. This repose period, except for the brief reappearance of lava in early September, lasted nearly two months. Subsidence was rapid for one week, averaging 5–6 m/d, and then slackened; it continued throughout August, and the lake crust fell to about 81 m below the rim. Harmonic tremor, varying from very low to moderate in intensity, persisted throughout the repose.

RESUMPTION OF LAVA-LAKE ACTIVITY AT MAUNA ULU: A MAJOR OVERFLOW

No molten lava was visible at Mauna Ulu from July 24 to September 3. Harmonic tremor markedly increased at 0435 on September 4, and observations later that morning revealed a lava lake in Mauna Ulu Crater with a few fountains up to 5 m high. The lake surface was 62 m below the crater rim, up from its 81-m level in mid-August. About 1400, tremor abruptly decreased and the low fountaining ceased. The lake persisted through September 6, by

FIGURE 16.25.—Telephoto view (300-mm lens) from Puu Huluhulu showing slabs of crust and molten material of Mauna Ulu lava lake being lifted in vortex of thermally generated whirlwind. Photograph was taken by R.I. Tilling on January 30, 1974, but similar and more vigorous activity occurred on November 8, 1973.

which time a solid, slowly subsiding crust had again developed across its entire surface.

Lava-lake activity resumed sometime between noon of September 25 and the afternoon of September 26 with the reopening of a vent in the eastern part of Mauna Ulu Crater. Lava flooded the crater floor, and within a few days the lake level rose from 68 m to 61 m below the rim; the familiar circulation pattern with periodic crustal overturns was reestablished. During the next three weeks, lava-lake activity alternated between active circulation and stagnation with the formation of crust, and the irregular surface of the lake gradually rose to 15 m below the rim in the eastern part of the crater and to 32 m in the western part.

Sharply increased summit inflation continued during October (fig. 16.4) and by October 20 the activity at Mauna Ulu was the most vigorous for many months; lava fountains from parts of the lake surface commonly attained heights of 15 m. The principal vents, whose lava columns periodically exhibited gas-piston behavior, were localized between former vents A and B, near the position of the septum that formerly separated the crater and the trench (figs. 16.11, 16.23*A*). Lava mostly flowed westward from these vents down a sloping ramp, at the base of which a perched lake developed (fig. 23*B*). Overflows from this perched lake, together with flows fed directly by the vents, flooded much of Mauna Ulu's crater floor during the next few weeks. The area of active surface greatly increased, and the lava lake continued to rise.

Mauna Ulu's activity substantially increased during the morning of November 3, when the lava surface was about 25 m below the lowest point of the western crater rim. Voluminous flows from three closely clustered vents (fig. 16.23B) raised the lava surface to 12 m below the rim by midday. The next morning fountaining was 40 m high, and modest deflation began at Kilauea summit. At 0900 on November 4, the lava level was only 3 m below the low point of the western rim, and it continued to rise at a rate of about 0.5 m/h. Soon the perched lava lake was inundated by the rising lava, and the two-level aspect (western crater and eastern trench) that had characterized the configuration of Mauna Ulu throughout much of the 1972–73 activity was lost. Mauna Ulu now resembled the brimfull lake that existed at times during February–March 1972.

By 1445 on November 4, lava had risen to the lowest point of the western rim (fig. 16.22*H*), and slow outflow commenced at 1600, marking the first overflow from the crater since March 18, 1972. This overflow, however, advanced only about 35 m, because construction of confining levees nearly kept pace with the now more slowly rising Mauna Ulu lake, whose surface area was now almost 55,000 m^2 (fig. 16.23C). Throughout the night of November 4–5, the lava lake continued to rise, and levees, typically 1–2 m high, were built along low areas of the old crater rim.

A major overflow from the western end of the crater began early on November 5, as a lava stream several meters wide flowed across a levee 8–10 m higher than the original low point on the rim (fig. 16.24). Subsequently, two or three lava streams spilled over the levees on the northwestern rim, converged into a single stream within about 30 m of the rim, and turned southward to pass east of the buried Aloi Crater (fig. 16.18C). An irregular overflow apron formed along most of the northwest crater rim, and other smaller short-lived spills occurred elsewhere, including two at the eastern end. However, voluminous outflow was confined to the south-trending stream spilling out of the western end of the crater; this flow advanced about 2.6 km before stopping in the early morning of November 8 (fig. 16.18C).

A wooden viewing platform at Mauna Ulu (fig. 16.23) was kept open to the public by the National Park Service through the night of November 4, allowing hundreds of park visitors to view the filling lava lake and 30 to 40-m-high fountains. Heat from the rising lava and continued high fountaining forced the viewing platform to be abandoned late on the night of November 4. The platform was consumed early the next morning as lava overflowed the rim.

On November 8, observers witnessed a thermally generated whirlwind that played erratically across the Mauna Ulu lava-lake surface for about 10 minutes. The whirlwind lifted crustal slabs 2–3 meters in diameter to heights of 20–30 m, and smaller pieces went much higher (fig. 16.25). Molten lava exposed beneath the vortex also was lifted high into the air and deposited, in part, as blobs of spatter and Pele's hair beyond the crater rim.

PAUAHI ERUPTION OF NOVEMBER 10–DECEMBER 9, 1973

VIGOROUS INITIAL ACTIVITY ASSOCIATED WITH FISSURE VENTS, NOVEMBER 10–11

About 1730 on November 10, seismic stations in the vicinity of Mauna Ulu and Pauahi Crater began to record a moderate to high level of harmonic tremor accompanied by a flurry of earthquakes. At the same time, a National Park Service ranger at Puu Huluhulu radioed a report to HVO that he felt ground shaking and could see greatly increased turbulence and degassing of the still brimful lava lake at Mauna Ulu. A drainback of Mauna Ulu lava lake was underway, similar to those that had occurred on May 5 and June 9. Summit deflation commenced about 15 minutes later and, combined with intensified seismic activity localized in the Pauahi-Mauna Ulu area, suggested the possibility of another eruptive outbreak.

HVO observers arrived at Mauna Ulu about 1830, in time to watch drainback; the surface of the lake in the western part of the crater had already subsided to a level of about 40 m below the rim

FIGURE 16.26.—Draining of lava from Mauna Ulu on November 10, 1973, left a rubble-covered crater floor about 40 m deep. During draining, the levees on the rim, left unsupported, collapsed. Photograph taken by D.W. Peterson, November 12, 1973.

(fig. 16.26). By 2100 subsidence (fig. 16.23C) had largely ceased, and partially cooled lava continued to spall from the crater walls amid showers of glowing debris. Meanwhile, rockfalls were reported in Pauahi Crater. At 2135 an earthquake was felt in the Puu Huluhulu area and triggered rockfalls at Pauahi.

At 2147, gassy lava broke out in Pauahi Crater about midway up the north wall of the east pit and began to pool at the bottom of the crater. Echelon fissures opened eastward up the wall to the crater rim. A few minutes later, a fissure trending N. 70° E., aligned with the northwest corner of the western pit, cut the Chain of Craters Road west of Pauahi (fig. 16.18C); fountaining of lava from this fissure was observed at 2200, and within minutes the road was blocked by lava. At 2215, a vent opened in the north wall of the west pit, approximately midway between the two fissures of the May 5 eruption, and lava began to pool in the west pit as well as in the east pit.

At 2245, several additional fissures opened and extended about 1.5 km east-northeast toward Puu Huluhulu; pahoehoe flows fed by fountains from these fissures ultimately covered about 1.1 km^2 of land (fig. 16.18C). Fountaining as high as 70 m continued within and outside Pauahi Crater throughout the night of November 10–11 and fed lava pools in both the east and west pits (fig. 16.27).

Shortly after midnight, lava filled the east pit to the level of the septum that separated it from the west pit and began to cascade westward and circulate clockwise (fig. 16.28). At 0135 on November 11, new lava outbreaks occurred high on the northwest wall of the west pit. Lava from these sources poured into the pit, but the rate of drainback, presumably into the May 5 fissures, was greater; the lava level in the west pit consequently began to lower. At 0150, the fissure in the east pit stopped erupting, and by 0200 flow

FIGURE 16.27.—View from the south rim of Pauahi Crater at 0015 on November 11, 1973, showing fountains 20–30 m high along fissure that cuts the north wall of the east pit of Pauahi and supplies lava to the rising lake, which at this point is still below the septum separating east and west pits. Lava fountains from other vents in the west pit (left center, near edge) feed another lava lake in the west pit. Five minutes after this photograph was taken, lava in the eastern lake had risen to the lowest point along the septum and began to spill into the west pit (see fig. 16.28). Photograph taken by R.I. Tilling.

across the septum between the pits had stopped. Soon lava was draining back into fissures in both pits, though it continued to cascade at a decreasing rate from the northwest wall of the west pit until 0545. At 0440, fountains as high as 20 m were active near the east end of the fissure system near Puu Huluhulu, but all activity along these fissures stopped by 0600.

PERSISTENT, FEEBLE ACTIVITY AT A LOCALIZED VENT WITHIN THE WEST PIT, NOVEMBER 11–DECEMBER 9

On November 12, the level of the largely crusted lava pool in the east pit of Pauahi was about 100 m below the crater rim and about 21 m below the high lava mark established before drainback. The northwest vent on the floor of the west pit of Pauahi continued to emit lava after all other activity had ceased. Lava fountains 15–35 m high still played at the vent through November 12, but four days later only a slow upwelling of lava could be seen. By November 19, a perched lava lake about 30 m in diameter had developed at the base of a spatter cone 5–10 m high situated near the west end of the northwest fissure vent (fig. 16.3). Lava level in the west pit slowly rose as the result of periodic overflows from the perched lava lake, and by November 21 it reached within 5 m of the lowest point on the septum between the two pits. On November 28, lava from the west pit trickled over the septum and descended into the east pit (fig. 16.29).

On about December 3, the activity in the west pit declined appreciably, and overflows from the perched lava lake ended. Vent activity virtually stopped, and during the next several days circulation became progressively more sluggish. By December 8, no circulation could be seen in the lake, and the crusted surface had subsided 7 m below the levees. Further subsidence of the lava crust occurred the next day, and fuming from the vent largely ceased. Cessation of tremor about noon on December 9 marked the end of the November–December Pauahi eruption.

FIGURE 16.28.—View from south rim of Pauahi Crater at 0050 on November 11, 1973, showing lava from lake in east pit cascading over septum into lava lake in west pit. Two smaller vents on western wall of west pit also feed lava into the lake, which here is about 150 m across and shows clockwise circulation. Photograph taken by R.I. Tilling.

DECEMBER 10, 1973–JULY 22, 1974

REAPPEARANCE OF THE LAVA LAKE AT MAUNA ULU

No eruption occurred at Kilauea between December 9 and 12. On December 10 and 11, a portable seismometer in the Pauahi-Mauna Ulu area detected no harmonic tremor above normal background noise. Then, on December 12, the permanent seismometer closest to the Pauahi-Mauna Ulu area began sensing intermittent harmonic tremor. This tremor increased in intensity and became sustained by the next day, when lava quietly reappeared at Mauna Ulu and quickly rose to 30 m below the crater rim. Thus visible activity at Mauna Ulu resumed on December 13 (not December 12 as stated by Peterson and others, 1976). Vent activity was localized a short distance west of the vigorous vents that fed the November 4–8 overflows (fig. 16.23).

Over the next few days the lake level rose to 18–20 m below the crater rim. Initially the entire surface of the lake was active, but by December 20 activity was reduced to sporadic oozing of lava, punctuated by brief degassing bursts, from a spatter cone feeding a small perched lava lake. This low-level activity continued into mid-January 1974, and the floor of Mauna Ulu crater became irregular because of differential subsidence.

DEPARTURE FROM 1972–73 BEHAVIOR: RENEWED GROWTH OF MAUNA ULU SHIELD

Rather than the sustained lava-lake and associated eruptive behavior that generally prevailed during 1972–73, Mauna Ulu activity in 1974 was characterized by short eruptions (no more than two days) in which lava fountains 40–80 m high fed short-lived but voluminous overflows. Episodes of fountaining and overflow were separated by 3-day to 5-week periods of only feeble activity.

The voluminous overflows, augmented by spatter-cone growth during the quiet periods, resulted in renewed growth of the Mauna Ulu shield. Most overflows traveled only short distances, but several extended 5 km or more from the vent and one advanced about 9 km.

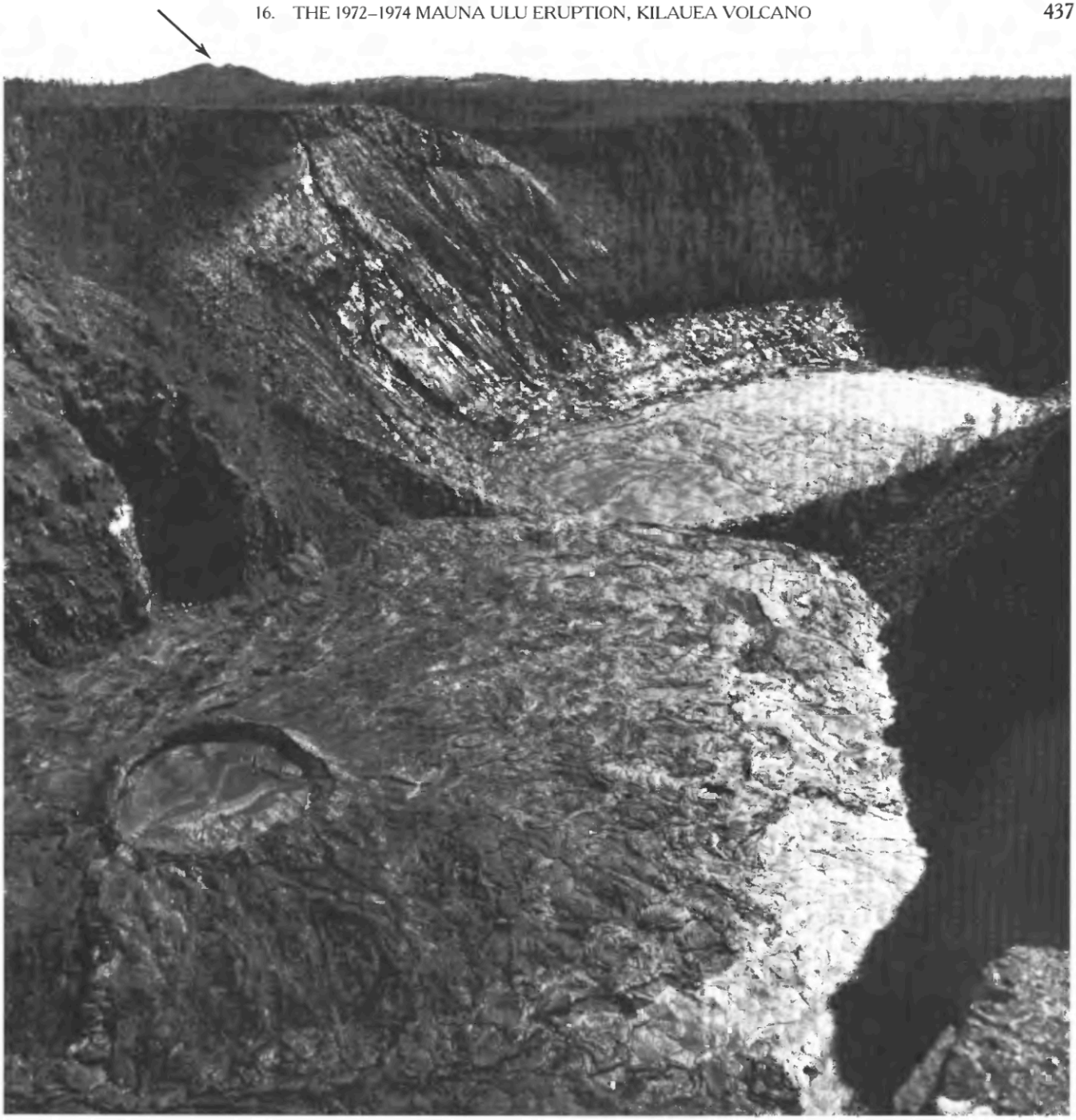

FIGURE 16.29.—View from Pauahi's west pit on December 5, 1973, toward Puu Huluhulu (arrow) and Mauna Ulu shield to right of it. Continued eruption in Pauahi's west pit through December 9 built a low lava shield, the small summit crater of which contains a perched pond of molten lava (lower left). Small amounts of lava from this perched pond have flowed across septum into the east pit. Also seen are the high mark of lava lake in east pit before drainback, and the fissure that fed the east-pit lake. Photograph taken by R.T. Holcomb.

The first of the 1974 eruptive episodes began on January 24 and was preceded by several days of heightened harmonic tremor, increased shallow summit earthquakes, and summit inflation (fig. 16.30). During the ensuing 36-hour burst of activity, a 60-m-high lava fountain (figs. 16.31, 16.32) fed by vent E_1 (fig. 16.3) filled Mauna Ulu to the brim, built a 15-m-high spatter cone atop the shield, and fed numerous overflows, one of which advanced more than 1 km from the vent. This episode was accompanied at Kilauea

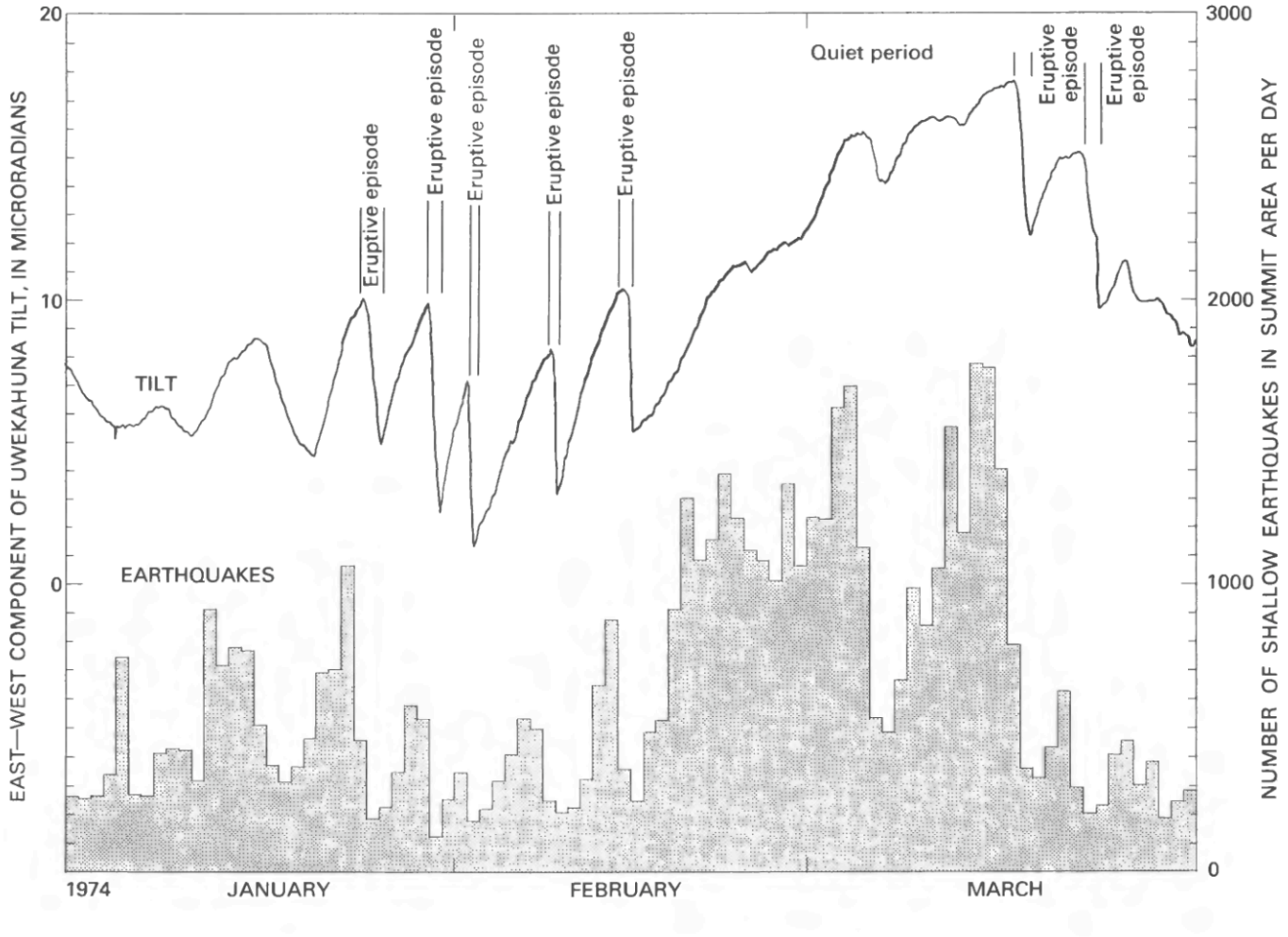

FIGURE 16.30.—Correlation of the eruptive episodes during January–March 1974, characterized by vigorous fountaining and voluminous overflows, with variations in Uwekahuna tilt and daily number of shallow (depth less than 5 km) summit earthquakes (see table 16.3 and text).

summit by abrupt but modest deflation and a decrease in seismicity. Once the episode ended, inflation began again and seismicity increased immediately, culminating in another eruptive episode on January 29. During the quiet period between the two eruptive episodes, low-level activity persisted at Mauna Ulu. The crusted lava-lake surface sagged to about 3 m below the rim, and bursts of spatter from vigorous gas-piston degassing reached heights of 20 m above the vent.

The time, duration, amount of inflation or deflation, tilt variations, and summit seismicity for five exceptionally well documented eruptive episodes during January–February 1974 are summarized in table 16.3 and figure 16.30. Lava spilled over all flanks of the Mauna Ulu shield during each episode, but the most voluminous overflows were directed northward. Much lava ponded in the saddle between Mauna Ulu and Puu Huluhulu, and a well-defined levee grew around the pond during the January 24–26 episode (fig. 16.32).

A month-long quiet period followed these January–February eruptive episodes; during the first part of this (February 15–March 5), vent activity was restricted entirely to the vent E_1 spatter cone at Mauna Ulu summit. On March 5 a new vent (designated F) opened about 140 m east-northeast of vent E_1 (fig. 16.3), accompanied by summit deflation of about 2 microradians. Both vents E_1 and F operated until March 17, and lava output from each varied within the range 2–5 m^3/s. Both vents exhibited gas-piston activity that generated spatter, enlarged their cones, and fed numerous short-lived flows. Their activities, however, could not be closely correlated in time; any connection between them was apparently complex despite their close proximity.

Two eruptive episodes occurred in March (table 16.3 and fig. 16.30). The first began in the early evening of March 17, lasted about 30 hours, and resulted in a summit deflation of about 5.5 microradians. In contrast to the January–February episodes, this one produced a maximum fountain height of only 15 m, even though lava output was equally great. South-directed overflows advanced 3 km (fig. 16.18*D*). The eruptive episode of March 23–24 (fig.

FIGURE 16.31.—Lava fountain and thermal plume produced during January 24–26 eruptive episode of Mauna Ulu viewed from Hawaiian Volcano Observatory more than 12 km away. Photograph taken by R.T. Holcomb, January 24, 1974.

16.30) produced copious overflows mainly directed southward and built the vent E_1 spatter cone even higher (fig. 16.33). This episode also included strong rockfall activity at Pauahi Crater. These frequent and large rockfalls, combined with high-amplitude tremor and rapid deflation, were reminiscent of the precursors to the May 1973 and November 1973 eruptions in the Pauahi area. This time, however, the movement of magma into the Pauahi area remained entirely underground and fed a brief intrusion into Kilauea's east rift

FIGURE 16.32.—View from the summit of Puu Huluhulu on January 25, 1974, during first of a series of brief eruptive episodes that were interspersed with longer quiet periods of only feeble visible activity. The lava fountain was about 60 m high. The lava lake surrounding the vent overflowed the confining levee and fed a copious flow that ponded in the saddle between Mauna Ulu and Puu Huluhulu (middle foreground). Ponded flow developed levees and evolved into a perched lava pond. Topographic feature to the left of lava fountain is the spatter cone of vent B. Photograph taken by R.T. Holcomb.

zone (Dzurisin and others, 1984, table 1), which had no observable effect on activity at Mauna Ulu. The sharp deflation ceased at 0700 on March 24, signaling the end of the episode. However, even though vigorous vent activity and voluminous surface overflows had largely ended by the morning of March 24, lava primarily from vent F continued to feed a south-moving flow through a channel-tube system. This flow cascaded over Poliokeawe Pali on April 3 and stopped several hundred meters farther two days later. During March, the southeastern flank of Mauna Ulu became underlain by a complex maze of anastomosing lava tubes, and there were abundant opportunities to observe lava-tube processes.

During the first half of April, relatively quiet activity prevailed at Mauna Ulu. The spatter cone at vent E_1 (fig. 16.33) collapsed on April 2, and continuing collapse resulted in a small (20 m by 15 m) active lava lake, which commonly exhibited gas-piston behavior. This activity apparently was confined to the area of the Mauna Ulu vents, as it was not reflected by Kilauea summit deflation or inflation. However, three larger eruptive episodes in mid-April (Apirl 13–14, 16–17, and 18–19) were accompanied by summit deflations of 5, 1.5, and 2 microradians, respectively. These episodes produced overflows, which moved down all sides of Mauna Ulu but did not enter the eastern part of the trench. The April 13–14 overflows continued virtually nonstop for 16 hours, and a dome fountain 5–10 m high played for many hours from an opening between vents E_1 and F (an excellent example of a dome fountain is shown by Swanson and others, 1979, fig. 28).

No well-defined eruptive episodes occurred during late April, but activity during this time was nonetheless fairly strong. All vent activity was confined to E_1 and a 2-m-wide new opening (designated E_2) 30 m farther east (fig. 16.3); vent F became inactive.

TABLE 16.3.—*Date and time of beginning and end of eruptive and associated premonitory quiet periods, and duration and amplitude of Kilauea summit deflation and inflation as measured by Uwekahuna mercury-pool tiltmeter January 20 to February 15, 1974*

[All times given are in Hawaii standard time]

Quiet periods				Eruptive episodes							
Inflation					Activity			Deflation			
Beginning	End	Duration (hours)	Amount (microradians)	No.	Beginning intermittent	Beginning continuous	End	Beginning	End	Duration (hours)	Amount (microradians)
1/20, 2200	1/24, 1900	93	5.6	I	1/24, 0800	1/24, 1400	1/26, 0500	1/24, 1900	1/26, 0530	35	5.1
1/26, 0530	1/29, 1400	90	5.0	II	1/29, 1800	1/29, 2400	1/30, 2400	1/29, 2400	1/30, 2400	24	7.3
1/30, 2400	2/2, 0400	52	4.5	III	2/1, 1100	Not observed, but continuous by 2/2, 0545	2/2, 1607	2/2, 0400	2/2, 1600	12	5.8
2/2, 1600	2/8, 2000	148	6.9	IV	2/8, 1900	2/9, 0100	2/9, 0600	2/8, 2000	2/9, 0700	11	5.0
2/9, 0700	2/14, 2000	133	6.8	V	2/14, 0300	Never continuous, but intermittent fountaining became strongest on 2/14, 2200	2/15, 0830	2/14, 2000	2/15, 0900	13	4.9

FIGURE 16.33.—View of Mauna Ulu shield from the west on March 27, 1974, showing steep-sided spatter cone of vent E_1, which collapsed on April 2. Flank of Puu Huluhulu is seen center left; Alae shield is behind and to right of Mauna Ulu. Photograph taken by R.I. Tilling.

Many brief but copious overflows from E_1 and E_2 added to the shield, burying vent F in the process. By the end of April, the height of the Mauna Ulu shield had increased about 15 m, to 117 m above the pre-1969 base, and its width increased proportionately. During the period of rapid shield growth, a sustained flow fed by vent E_2 formed a tube system that extended southward. Lava spilled over Poliokeawe Pali on April 30, and on May 7 the flow front reached the lip of Holei Pali before stopping the next day.

Gas-piston processes dominated the behavior of the overflows: a strong overflow would issue from vent E_1 or E_2 for a period of 5 minutes to more than one hour; then a brief but spectacular burst of degassing would abruptly terminate the overflow, and the lava column would drop 10–20 m. The lava column would then rise slowly over a period of 15 minutes to several hours. When the lava reached the rim of the vent, a new overflow would begin. The gas-piston cycles of vents E_1 and E_2 apparently operated independently.

During May, the eruptive activity at Mauna Ulu progressively declined: overflows stopped, lava in channels and tubes solidified, and the lava column dropped several meters. Piecemeal wall collapse enlarged vents E_1 and E_2; by May 12 the two openings coalesced to form an elongate crater, which measured approximately 40 m by 90 m on May 20. The lava lake within the western part of this crater was about 15–20 m below the rim. Lava circulated from west to east and then plunged over a septum into a pit at least 50 m deep in the eastern part of the crater.

During late May, lava-lake circulation became increasingly sluggish until the late evening of May 29, when summit deflation began and harmonic tremor increased. By the next morning the summit crater at Mauna Ulu had refilled, and low fountains were active along much of the lake margin. Lava was spilling over at two points on the southeast rim, and a flow already had advanced nearly 2 km southward. As the day progressed, the activity increased, as did the rate of summit deflation. During the night of May 30, gassy fountains at the lava lake threw spatter about 20 m high, and voluminous overflows began to cascade down all sides of the Mauna Ulu shield.

Fountains and overflows continued until June 1, when weather conditions permitted excellent aerial photography during peak activity (fig. 16.34). Most of the lava traveled southward, and the main flow poured over Poliokeawe Pali and Holei Pali (fig. 16.35). At about midnight the summit deflation stopped and inflation resumed; overflows ended about 0200 on June 2.

The May 29–June 2 eruptive episode was the largest of 1974 and was accompanied by about 10 microradians of summit deflation. It added another 4 m of lava to the Mauna Ulu shield to raise its summit to the maximum height reached during the 1972–74 eruption, 121 m above the pre-1969 ground surface (Peterson and others, 1976), and sent lava over Holei Pali for the first time in 1974

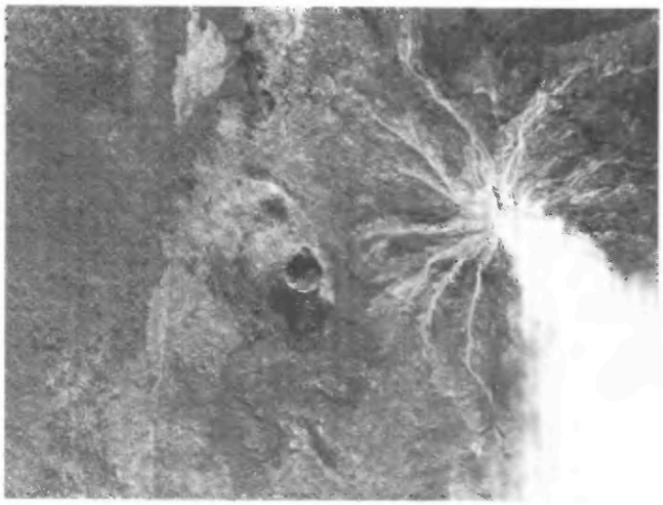

FIGURE 16.34.—Vertical aerial photograph (north is to left) taken June 1, 1974, showing active radial overflows from Mauna Ulu lava lake during the May–June eruptive episode. Also shown (center) are summit crater of Puu Huluhulu and lava pond in saddle between Mauna Ulu and Puu Huluhulu, which first formed in January 1974 (fig. 16.32) and was reactivated during several later eruptive episodes. Photograph taken by R.M. Towill Corporation.

(fig. 16.18*D*). This episode, as it turned out, also knelled the end of the 1972–74 Mauna Ulu eruption.

CESSATION OF THE 1972–74 MAUNA ULU ERUPTION

Soon after the May–June eruptive episode, Mauna Ulu's summit lake subsided, and lava circulated sluggishly 20–32 m below the crater rim. In response to the lower lake level, numerous rockfalls from steep and overhanging walls enlarged the crater at its rim from 40 m by 90 m on May 20 to 107 m by 147 m by June 20. Lava activity declined through June and much of July; the lava lake changed little in configuration and was largely obscured by fumes. Circulation became increasingly sluggish, and the crusted and rubbly lake surface continued to subside gradually, approaching about 40 m below the rim by mid-July.

FIGURE 16.35.—Lava stream of May–June 1974 eruptive episode becomes braided during cascade over Poliokeawe Pali (about 165 m high). Northwest is to left; lava flows from upper left to lower right. Vertical aerial photograph taken by R.M. Towill Corporation on June 1, 1974.

As Mauna Ulu activy waned, the summit region of Kilauea remained highly inflated, the tilt at Uwekahuna fluctuating within a range of 4 microradians. A summit eruption on July 19–22 (Peterson and others, 1976) caused no observable changes in the already feeble activity at Mauna Ulu. Following the summit eruption, however, the small, subsiding lava pool disappeared beneath the rubble-covered crater bottom. After July 22, no molten lava was visible anywhere on Kilauea, and harmonic tremor in the Mauna Ulu area ceased.

Months after July 22, Mauna Ulu Crater was obscured by extremely heavy emission of fumes. Visible observations of the crater were impossible, but sounds of rockfalls were commonly heard, indicating continued piecemeal collapse of the walls and possible subsidence of its rubbly floor. During November 1974, attempts were made to determine the depth of the crater by hurling percussion-impact, noise-emitting probes into the crater and measuring the time elapsed between release and impact. These measurements yielded six depth estimates ranging from 56 m below the rim in the shallow northwestern part of the crater to 133 m in the considerably deeper eastern part. Large uncertainties are attached to these measurements, but they nevertheless suggest that the deepest parts of Mauna Ulu Crater in November 1974 (averaging perhaps 130 m) were considerably shallower than the maximum depth of 200 m measured following the complete drainage of the lake in May 1973. The decrease in depth presumably reflected solidification of residual lava and partial filling of the crater by rockfall debris. The depth of the Mauna Ulu crater at the end of the 1969–71 eruption was 145 m (Swanson and others, 1979, fig. 7).

GROUND DEFORMATION AND SEISMICITY

The general relations between eruption, intrusion, ground deformation, and seismicity at Kilauea Volcano have been well documented from systematic studies by scientists of the Hawaiian Volcano Observatory since its founding in 1912. A comprehensive model that integrates the data on subsurface structure, magma storage and transport, and eruptive processes was first described in the early 1960's (see Eaton and Murata, 1960; Eaton, 1962); many subsequent studies have refined and increasingly quantified this model (for example, Fiske and Kinoshita, 1969; Swanson, 1972; Kinoshita and others, 1974; Koyanagi and others, 1976a, b; Swanson and others, 1976b; Ryan and others, 1981, 1983; Aki and Koyanagi, 1981: Dvorak and others, 1983; Dzurisin and others, 1984). In the discussion to follow, we assume that the reader is familiar with the well-documented behavior typically observed for Kilauea rift activity: between eruptions, summit inflation occurs as

TABLE 16.4.—*Dates of reoccupations of the ground-deformation networks of Kilauea summit pertinent to 1972–74 Mauna Ulu eruption*

[Measurements obtained during these reoccupations provide the data for figures 16.38–16.43. Some reoccupation periods were prolonged because of inclement weather. Reoccupations of two or more types of networks during a closely bracketed time period are indicated by an asterisk (*). Data are stored on magnetic tapes at the Hawaiian Volcano Observatory]

	Level	Tilt	Trilateration
		Inflation period before eruption	
*	9/29-30/71	10/1-7/71	10/4-7/71
		10/20-22/71	
		11/1-2/71	
		11/11-12/71	
		11/19-24/71	
*	11/30-12/1/71	11/29-12/1/71	
		12/13-14/71	
*		12/27-30/71	12/20-23/71
		1/10-11/72	
*	1/17-20/72	1/26-28/72	1/26-28/72
		During the 1972-74 Mauna Ulu eruption	
		2/7-9/72	
		2/22-25/72	
		3/7-9/72	
		4/3-7/72	
		4/17-18/72	
*	6/12-13/72	6/5-8/72	6/5-14/72
		7/17-20/72	
		8/21-29/72	
		9/27-29/72	
*	12/4-13/72	12/4-11/72	12/5-29/72
		3/13-26/73	
*	5/10-11-73	5/7-14/73	5/7-10/73
		5/21-6/1/73	5/29-6/1/73
		6/26-28/73	(partial)
*	9/19-20/73	9/20-10/3/73	9/24-27/73
*	11/13-14/73	11/11-14/73	11/15-21/73
		12/10-20/73	
		1/14-29/74	
		3/12-25/74	
*	4/4-5/74		4/1-3/74
		5/22-30/74	
*	7/26-31/74	7/22-26/74	7/22-25/74

magma is supplied from the upper mantle to a reservoir 2–4 km deep; during flank eruptions, summit deflation occurs as magma moves into a rift zone.

Ground-deformation and seismic data for the 1972–74 Mauna Ulu eruption are summarized in table 16.4 and figures 16.4 and 16.36–16.46. In general, crustal deformation and seismicity during the 1972–74 Mauna Ulu eruption were typical for Kilauea east-rift eruptions. Periods of weak or no vent activity generally correlated with net inflation and increased number of shallow earthquakes in the summit region, whereas vigorous eruptive activity correlated with deflation and reduced summit seismicity.

VARIATION IN SUMMIT TILT MEASURED AT UWEKAHUNA

Tilt at Kilauea summit, especially as measured daily by the 3-m-base, water-tube tiltmeters at Uwekahuna vault (fig. 16.1) to a precision of about 1 μrad (1 microradian), provides a sensitive and continuous record of the inflation-deflation state of the shallow magma reservoir. These daily measurements are augmented by continuously recording mercury-pool capacitance tiltmeters at the same site; data from these instruments correlate well with the daily water-tube measurements. In addition to these tilt-measurement instruments, Kilauea caldera is laced by the summit electronic-distance-measurement (EDM) monitor (fig. 16.36). The five EDM lines of the summit monitor are measured on a fairly frequent basis between periodic occupations of the entire summit trilateration network of 47 lines (Kinoshita and others, 1974, fig. 9). In general, summit inflation is indicated by extensions on these EDM lines and deflation by contractions.

Summit tilt measured at Uwekahuna (figs. 16.4, 16.37) generally correlates systematically with evidence of inflation and deflation from leveling, trilateration, and gravimetric data (Dzurisin and others, 1980, 1984; Dvorak and others, 1983). Because the locus of maximum uplift most commonly lies southeast of the Uwekahuna site, northward down tilt on the north-south axis or westward-down tilt on the east-west axis almost always indicates inflation; similarly, opposite senses of relative tilt of the two components generally indicate deflation. As will be seen, however, exceptions to this general relationship sometimes occur.

For the 1972–74 Mauna Ulu eruption, the east-west component of the Uwekahuna tilt shows the variations more clearly than does the north-south component; for convenience we discuss the summit tilt in terms of change in microradians (+, apparent inflation; −, apparent deflation) only in this east-west component (fig. 16.4). Whether the apparent inflation or deflation registered by the Uwekahuna tilt corresponds to actual inflation or deflation of the entire summit region can be evaluated by comparison of level, ground tilt, and trilateration surveys. With the exception of those related to non-elastic rotation of tectonic blocks, large changes in Uwekahuna tilt indicate true summit inflation or deflation, but small changes may not be amenable to simple interpretation. Like Dzurisin and others (1984, p. 191), we assume that net summit inflation reflects increased summit storage and cumulative summit deflation reflects increased rift-zone storage, which can be manifested as eruptive activity, intrusive activity, or both.

The variation curve for Uwekahuna tilt during 1972–74 shows two plateau-like segments (fig. 16.37), each of which is characterized by variations in tilt of less than 25 μrad during periods of at least 8 months. The first of these segments encompasses the period from the start of the eruption through April 1973, and the second period from December 1973 to the end of the eruption.

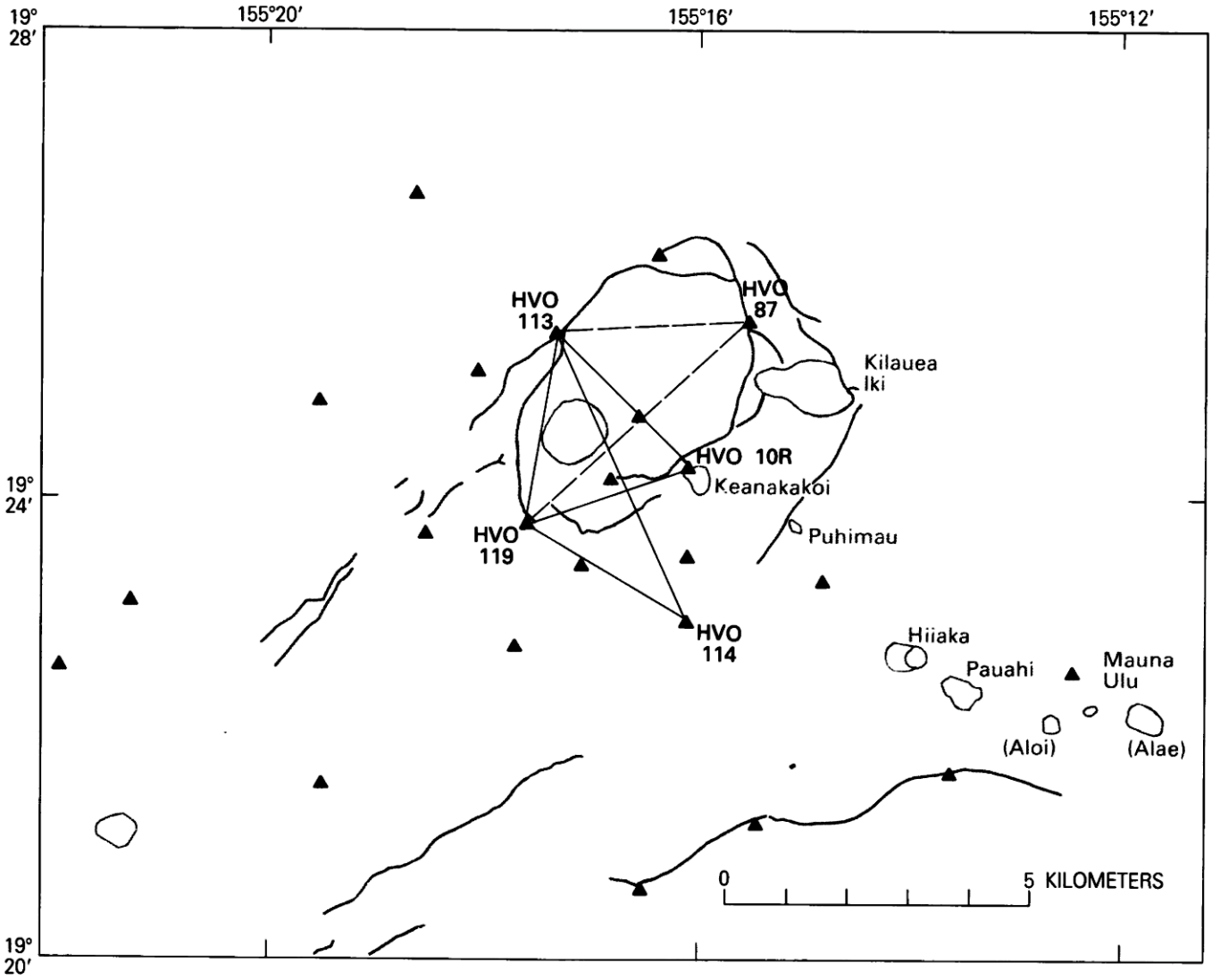

FIGURE 16.36.—Map showing location of the electronic-distance-measurement (EDM) bench marks (triangles) of the Kilauea summit trilateration network. The straight lines shown make up the so-called summit EDM monitor: solid lines are remeasured more frequently than dashed lines (see fig. 16.39). Distances between all other bench marks in the summit network (Kinoshita and others, 1974, fig. 9) are remeasured periodically depending on eruptive activity. Craters, the summit caldera, and faults in the rift zones shown for reference. HVO, Hawaiian Volcano Observatory.

These two prolonged periods of little net change in summit tilt suggest that a quasi-steady-state regime prevailed in the summit magma reservoir: supply of magma to the reservoir was counterbalanced by migration of magma into the east rift zone. This delicate balance was upset in early May 1973, possibly as a consequence of the Honomu earthquake (April 26, 1973), after which magma entered the reservoir faster than it was transferred to the rift zone, and net summit inflation occurred for the next seven months. December 1973 marked the reestablishment of open communication between the summit reservoir and the Pauahi-Mauna Ulu area, and the second period of quasi-steady state magma transfer began.

The amount of summit deflation during the May 1973 and November 1973 eruptions, about 20 μrad for each (fig. 16.37), is similar to the range of tilt oscillations during the various stages of the 1972–74 Mauna Ulu eruption (variation within the shaded bands in fig. 16.37). We suggest that the gross equivalence of the ranges of tilt changes reflects transfer of magma from the summit reservoir to the rift zone in increments just sufficient to maintain a quasi-steady-state condition that prevailed during most of the eruptive period.

A more detailed plot of the Uwekahuna tilt record for the 1972–74 Mauna Ulu eruption (fig. 16.4), adjusted for the 18-μrad tectonic offset caused by the April 1973 Honomu earthquake, reveals interesting second-order variations. The reappearance of lava at Mauna Ulu on February 3, 1972, did not appreciably disrupt the marked trend of net inflation that began in mid-1971. On February 5, the summit tilt reached a maximum since

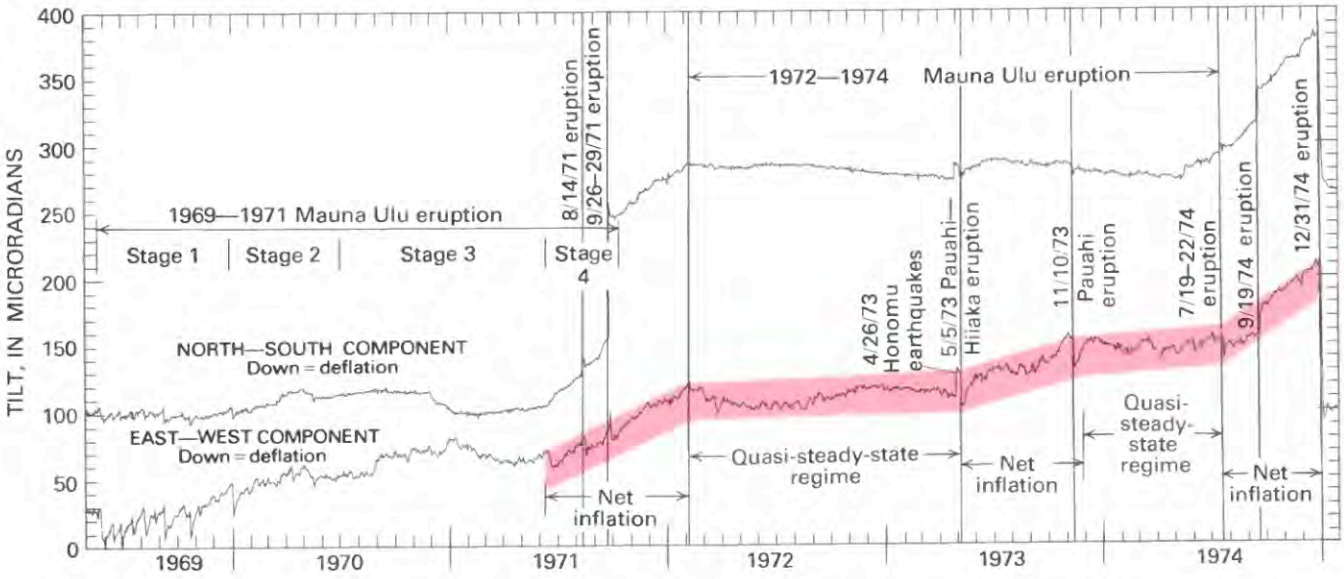

FIGURE 16.37.—Variation in Kilauea summit tilt for the period May 1969–January 1975, as measured by short-base water-tube tiltmeter at Uwekahuna vault; microradian scale arbitrary, with value at May 1, 1969, taken as zero. The magnitude-6.2 Honomu earthquake (April 26, 1973) caused an 18-microradian offset of the east-west component of tilt. Tilt record for 1972–1974 Mauna Ulu eruption is characterized by two distinctive plateau-like segments separated by period of net inflation (see text).

daily measurements were initiated at Uwekahuna in July 1956. This inflationary trend then was terminated by a 6-μrad deflation during the next two days as the lava lake rose rapidly in Mauna Ulu Crater. Thereafter, most of the larger variations in summit tilt can be related to significant changes in observed surface activity, the most prominent of which are annotated in figure 16.4.

Even many of the smaller tilt oscillations (5 μrad or less) can be correlated with changes in lava-lake level or episodes of vigorous vent activity, such as above-average lava fountaining or overflows from the vent. One of the best documented examples of such correlation is associated with the five eruptive episodes during January–February 1974 (table 16.3, fig. 16.30). Other good, but less well documented, examples are evident in figure 16.4.

Parts of the summit (Uwekahuna) tilt record cannot, however, be readily correlated with eruptive behavior. Possible reasons for such lack of correlation include: (1) Diagnostic field observations are lacking. (2) The tilt reflects subsurface magma migration processes that caused no visible change in eruptive activity, such as intrusion or leakage into secondary storage reservoirs in the rift zone(s). (3) Unrecognized time lags exist between changes in summit tilt and changes at the site of eruption. Some particularly intriguing tilt oscillations, larger than usual and more periodic and cyclical in amplitude, cannot be fully accounted for by changes in visible activity. The June–August 1972 oscillations (figs. 16.4, 16.37) occurred during a quasi-steady-state period when a well-integrated tube system supplied sustained overflows. Similar oscillations in late July–September 1973 occurred during a two-month repose in visible activity (fig. 16.4) when the summit was inflating.

These cyclical oscillations have a period of 20 to 21 days and are therefore unlikely to be related to fortnightly earth tides. They may reflect pulses of magma entry into shallow secondary reservoirs within the east rift zone, which caused localized intrusion and associated ground deformation rather than observable changes in surface activity at Mauna Ulu or Alae. Dzurisin and others (1984, fig. 4) demonstrated that similar oscillations (though more variable in amplitude), in April–August 1980 reflected periodic leakage of magma from the summit reservoir into the east rift zone. Unfortunately, the Mauna Ulu flows during 1969–74 repeatedly destroyed instrument sites and buried much of the established geodetic network in Kilauea's upper east rift zone. Periodic reoccupations that had been planned for these sites might have provided critical data on the possible existence of subsidiary magma storage reservoirs between the summit and the Mauna Ulu-Alae area or even farther downrift. Evidence for a secondary reservoir near Makaopuhi Crater before May 1969 was presented by Jackson and others (1975) and by Swanson and others (1976a).

If adjusted for the offset caused by the April 1973 Honomu earthquake, the net change in summit tilt during the entire eruption, February 3, 1972 to July 22, 1974, was no more than +8 μrad. Thus the 1972–74 Mauna Ulu eruption, despite the tilt excursions related to the two 1973 outbreaks near Pauahi (figs. 16.4, 16.37), resulted in negligible net inflation in terms of Uwekahuna tilt.

Throughout the eruption, the east-west component of summit tilt and the north-south component varied sympathetically, except during two intervals: August–December 1972 and June–October 1973. Individual tilt peaks during these intervals can be correlated, but the east-west component indicates apparent net inflation and the north-south component shows apparent net deflation (figs. 16.4, 16.37). Such a pattern can be produced either by an inflation center northeast of the Uwekahuna vault or by a subsidence center

southwest of it. Abundant studies of other historical Kilauea eruptions (for example, Fiske and Kinoshita, 1969; Duffield and others, 1982) provide no support for the possibility of an inflation center northeast of Uwekahuna. Although the alternative interpretation seems to be more plausible, given the well-documented and wide-ranging lateral shifts in inflation centers in the southern part of the summit, it too is unsatisfactory (see section below titled "Results of level, tilt, and trilateration surveys"). A departure from the general correspondence between the east-west and north-south components also characterized the period September 1970–April 1971 (Swanson and others, 1979, fig. 2) during stage 3 of the 1969–71 Mauna Ulu eruption, when lava-lake and associated processes were well developed and dominated the eruptive activity.

RESULTS OF LEVEL, TILT, AND TRILATERATION SURVEYS

Variations in Uwekhuna tilt provide a useful guide to the behavior of the summit magma reservoir, but they only represent measurements at a single locality and should be interpreted within the context of other geodetic data from ground-deformation networks spanning the entire summit of Kilauea.

SEPTEMBER 1971–JANUARY 1972: PRE-ERUPTION INFLATION

Ground-deformation networks in the summit region of Kilauea were reoccupied periodically before and during the 1972–74 Mauna Ulu eruption (table 16.4). Particularly useful are the results of closely bracketed surveys that included the reoccupation of the level or trilateration network in addition to the more frequently measured tilt network (tilt surveys were made by the spirit-level tilting or dry-tilt technique described by Kinoshita and others, 1974, p. 91). These data allow comparison of the geodetic response of the entire summit region with the tilt changes observed at Uwekahuna. For example, the 4-month net inflation (+43 μrad) preceding the 1972–74 Mauna Ulu eruption was clearly recorded by all three types of surveys, which delineated a well-defined center of inflation located about 1 km south-southeast of Halemaumau Crater (fig. 16.38*A*; Duffield and others, 1982, fig. 10*B*).

FEBRUARY 1972–APRIL 1973: QUASI-STEADY-STATE ACTIVITY

Only data from tilt surveys are available for the first several months of the eruption, a period of relatively small tilt changes at Uwekahuna but substantial visible activity at Mauna Ulu and Alae. The pre-eruption inflation, which during January 1972 resulted in a net Uwekahuna tilt change of about +15 μrad, is well expressed by plots of tilt vectors determined from measurements during January 26–28, about a week before resumption of activity at Mauna Ulu, and during the next survey on February 7–9 (fig. 16.38*B*). The period bracketed by these two surveys, though it included the start of eruption on February 3 and the tilt peak on February 5, showed virtually no net change in the east-west component of Uwekahuna tilt (figs. 16.4, 16.37). Given the measurement uncertainty of 2–3 μrad, the solid line vectors in figure 16.38*B* should have been essentially random in direction, if the Uwekahuna tilt was representative of the entire summit region. However, the vectors for the field surveys yield a fairly well-defined pattern consistent with slight summit inflation. Moreover, vectors calculated from the east-west and north-south components of Uwekahuna tilt are compatible with this inflation pattern (fig. 16.38*B*).

During the next survey period, the net Uwekahuna tilt change was negligibly small (+3 μrad), and the almost random array of vectors was not amenable to simple interpretation (fig. 16.38*C*). The next period, February 22–25 to March 7–9, encompassed major overflow activity at Mauna Ulu and net Uwekahuna deflation of about 9 μrad. The resulting tilt vectors for this period show a weak but nevertheless coherent deflation pattern (fig. 16.38*D*), in agreement with tilt data from Uwekahuna.

These results indiate that the measurable geodetic response of the entire summit region may not correspond to that at Uwekahuna vault during periods of minor inflation or deflation. Indeed, these observations in turn raise intriguing questions about the magma-conduit system: Is there some threshold value in the rate or volume of magma transport that must be exceeded before surface response becomes coherent over the entire summit region? Because Kilauea does not deform purely elastically (see Davis and others, 1974) but possesses a finite yield strength, must time elapse to accommodate inelastic deformation before elastic behavior dominates and integrated geodetic response is established?

It is difficult, perhaps impossible, to answer such questions with existing data, because the tilt surveys are significantly less precise than the water-tube tilt measurements at Uwekahuna. In addition, some ground displacements considerably larger than those discussed show widely diverse geodetic responses of the summit region: the center of inflation or deflation can migrate as much as 3 km in any direction within weeks; deflation generally is not a simple reversal of the preceding inflation; and the complexity of Kilauea's overall magma reservoir system allows local behavior to be almost independent for short periods of time (Fiske and Kinoshita, 1969; Swanson and others, 1976a; Duffield and others, 1982; Ryan and others, 1983; Dzurisin and others, 1984).

No appropriately paired deformation surveys are available to evaluate the effects of the mid-March deflation (13 μrad at Uwekahuna), the largest during 1972 (figs. 16.4, 16.37), which accompanied the opening of the west-flank fissure at Mauna Ulu and of Alae vents C and D that fed voluminous overflows. However, this deflation is reflected in the frequently measured lines of the summit EDM monitor (fig. 16.39).

Through May 1972 the eruption was characterized by a net Uwekahuna tilt change of −20 μrad, associated with a broad, kidney-shaped area of subsidence across the eastern part of the summit region (fig. 16.40*A*). The tilt vectors are consistent with the vertical displacements. However, similarly paired trilateration surveys (table 16.4) yield a pattern of vectors of horizontal ground displacements that is incompatible with the deflation pattern derived from tilt and level data. The reasons for this incompatibility are unknown but are under study. In addition, net summit deflations of

small magnitude, especially those involving several wider oscillations in summit tilt may in general yield less simple patterns than summit inflations.

The period June–December 1972, an interval of nearly continuous eruptive activity at Mauna Ulu and Alae, was characterized by a few months of periodic tilt oscillations (fig. 16.19) with virtually no net change in Uwekahuna tilt, followed by modest apparent net inflation of +15 μrad. However, during part of this period, the north-south component of Uwekahuna tilt indicated apparent net deflation. Perhaps these tilt data are best interpreted as indicating deflation localized south and west of Uwekahuna, as suggested by the vector calculated from the east-west and north-south tilt components (fig. 16.40*B*, vector UWE). Such deflation accords with the results of level and tilt surveys, which also suggest minor subsidence east of Pauahi (fig. 16.40*B*), but the azimuth of vector UWE appears to be incompatible with the deflation center defined by level data and vectors for other tilt sites. This incompatibility demonstrates that during the second half of 1972 Uwekahuna tilt changes were not representative of Kilauea summit as a whole. The trilateration data for the same period also yield a pattern of horizontal ground displacements that, despite being locally aberrant, can be reconciled with a model of complex net deflation (fig. 16.40*C*).

Comparing the surveys bracketing the entire period from mid-January to mid-December 1972 accumulates the effects of small changes and results in a coherent pattern of net deflation; the secondary low in the Pauahi-Mauna Ulu area is also reasonably defined (fig. 16.40*D*). The azimuth of the tilt vector for UWE, however, still appears anomalous with respect to the well-defined deflation center south of Halemaumau.

A weak trend of net deflation through April 1973 was expressed by both east-west and north-south components of Uwekahuna tilt and the summit EDM lines (figs. 16.37, 16.39). Remeasurement of the summit tilt network during mid-March 1973 yielded tilt vectors of about 15 μrad or less relative to the previous survey in mid-December 1972; these small changes yield a diffuse pattern (not shown) similar to those obtained during 1972.

Collectively, these data demonstrate the difficulty in making an internally consistent interpretation of ground displacements during a period dominated by quasi-steady-state eruptive activity and attendant subsurface magma transfer. In the absence of major shifts of magma from summit to rift, the geodetic response of the ground surface to small changes affecting the volcanic conduit system is apparently influenced by independent adjustments to local stresses. In addition, the Uwekahuna tilt changes, especially during June–December 1972, seem aberrant and permit interpretations incompatible with deformation patterns derived from tilt, level, and trilateration surveys.

The April 1973 Honomu earthquake, which perhaps caused or accelerated the termination of the quasi-steady-state activity, seemingly produced only minor dislocations of the volcano's surface. Other than the 18-μrad earthquake-induced offset of the Uwekahuna tiltmeter (fig. 16.37) and a 2-cm dilation of a crack at the rim of Mauna Ulu crater (Tilling, 1976a, fig. 3), no data exist to suggest other measurable geodetic response to the April 26 main shock and the 57 located aftershocks.

MAY–NOVEMBER 1973: NET SUMMIT INFLATION AND CHANGE IN ERUPTIVE MODE

The May–November 1973 period was characterized by substantial net inflation at Uwekahuna (+30 μrad) and encompassed the short-lived outbreaks at Pauahi-Hiiaka in May and at Pauahi in November, as well the partial draining of Mauna Ulu lava lake on June 9.

The May 5 Pauahi-Hiiaka eruption was accompanied by deflation of about 20 μrad at Uwekahuna. Posteruption ground-deformation surveys (table 16.4) yield a pattern typical for Kilauean east-rift eruptions or intrusions (for example, Jackson and others, 1975, figs. 13, 32; Swanson and others, 1976a, fig. 20): a distinct deflation at the summit coupled with uplift and associated local collapse at the eruption site (fig. 16.41*A*). The level data indicate maximum subsidence of 209 mm centered southeast of Halemaumau, slightly north of the center of inflation during the quasi-steady-state activity of 1972. The May 5 eruption was accompanied by intrusion in the Pauahi-Hiiaka area and into the Koae fault system, resulting in maximum measured uplift as great as 117 mm. Geodetic control is not good, but contours of equal vertical displacement can be drawn that reflect dike intrusion into the Koae fault system indicated by seismicity (Koyanagi and others, 1973). Within the uplifted area, graben-like collapse occurred along existing and new cracks in the vicinity of the eruptive fissures and resulted in vertical displacements as great as 250 mm (fig. 16.41*A*). Some ground cracks widened by as much as 0.5 m.

The results of tilt and trilateration surveys are consistent with the deformation pattern derived from the level data (figs. 16.41*A*, *B*). The tilts associated with the May 5 eruption are an order of magnitude greater than those recorded during 1972. The large horizontal displacements near Pauahi and Hiiaka reflect distension related to eruptive fissures and inferred intrusion into the Koae fault system (fig. 16.41*B*). However, the displacement vectors for benchmarks in the western part of the network, which are far removed from the sites of eruption and intrusion, appear anomalous and are not understood at present.

The summit reinflated rapidly following the May 5 eruption, and by early June the Uwekahuna tilt had essentialy recovered from its 20-μrad deflation. This rapid inflation is well shown by tilt surveys, which indicate a broad area of uplift east and south of Halemaumau (fig. 16.41*C*). Tilt site Escape Road No. 2 (fig. 16.41*C*), however, shows downtilting toward the eruption area; apparently this site had not fully recovered from the localized collapse and ground cracking of the May 5 eruption (figs. 16.41*A*, *B*). A few horizontal displacements (not shown) obtained from partial reoccupation of the trilateration network are compatible with the summit-inflation pattern defined by the tilt.

Partial draining of Mauna Ulu lava lake and related minor intrusion on June 9 were marked by a deflation of 7 μrad at Uwekahuna. The two tilt surveys that bracket this event (table

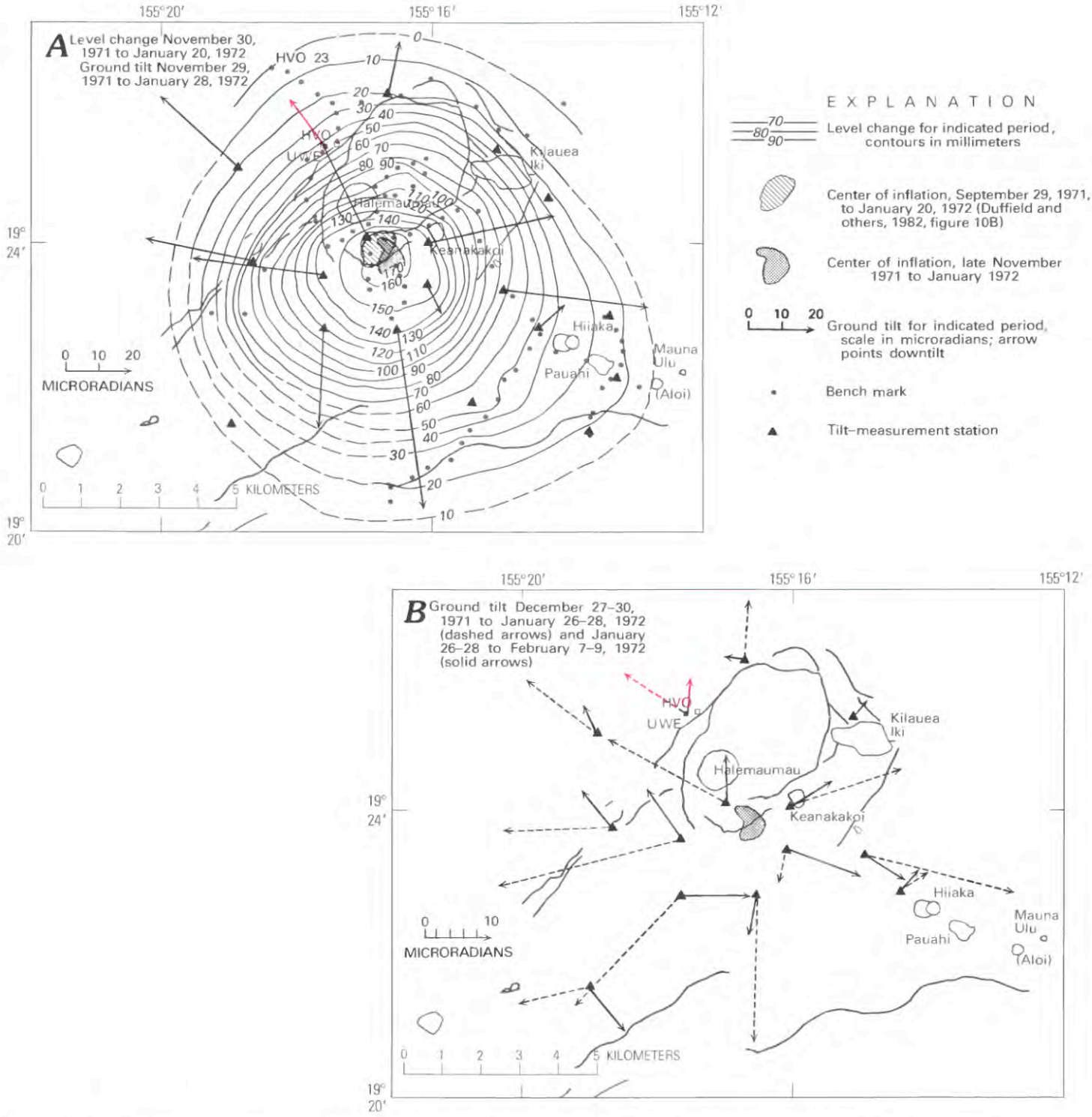

FIGURE 16.38.—Results of level and tilt surveys on Kilauea before and during first two months of the 1972–74 Mauna Ulu eruption. Vector UWE (red) calculated from east-west and north-south components of Uwekahuna tilt. Contours of level data referenced to bench mark HVO 23, assumed to be stable. ***A***, Well-defined pre-eruption inflation between November 1971 and January 1972. Inflation center defined for this 2-month period is virtually coincident with that obtained by Duffield and others (1982, fig. 10) for the 4-month period building toward the 1972–1974 Mauna Ulu eruption. ***B***, Tilt for periods spanning the final month of pre-eruption inflation (dashed vectors) and first days of the eruption beginning on February 3, 1972 (solid vectors). Survey period bracketing the start of eruption involved no net change in Uwekahuna tilt (see text). ***C***, Tilt vectors between February 7–9 and February 22–25, 1972, an interval with only about +3 microradians net change in Uwekahuna tilt (apparent inflation). ***D***, Tilt vectors between February 22–25 and March 7–9, 1972; net change in Uwekahuna tilt was about −9 microradians (apparent deflation), consistent with deflation indicated by vectors.

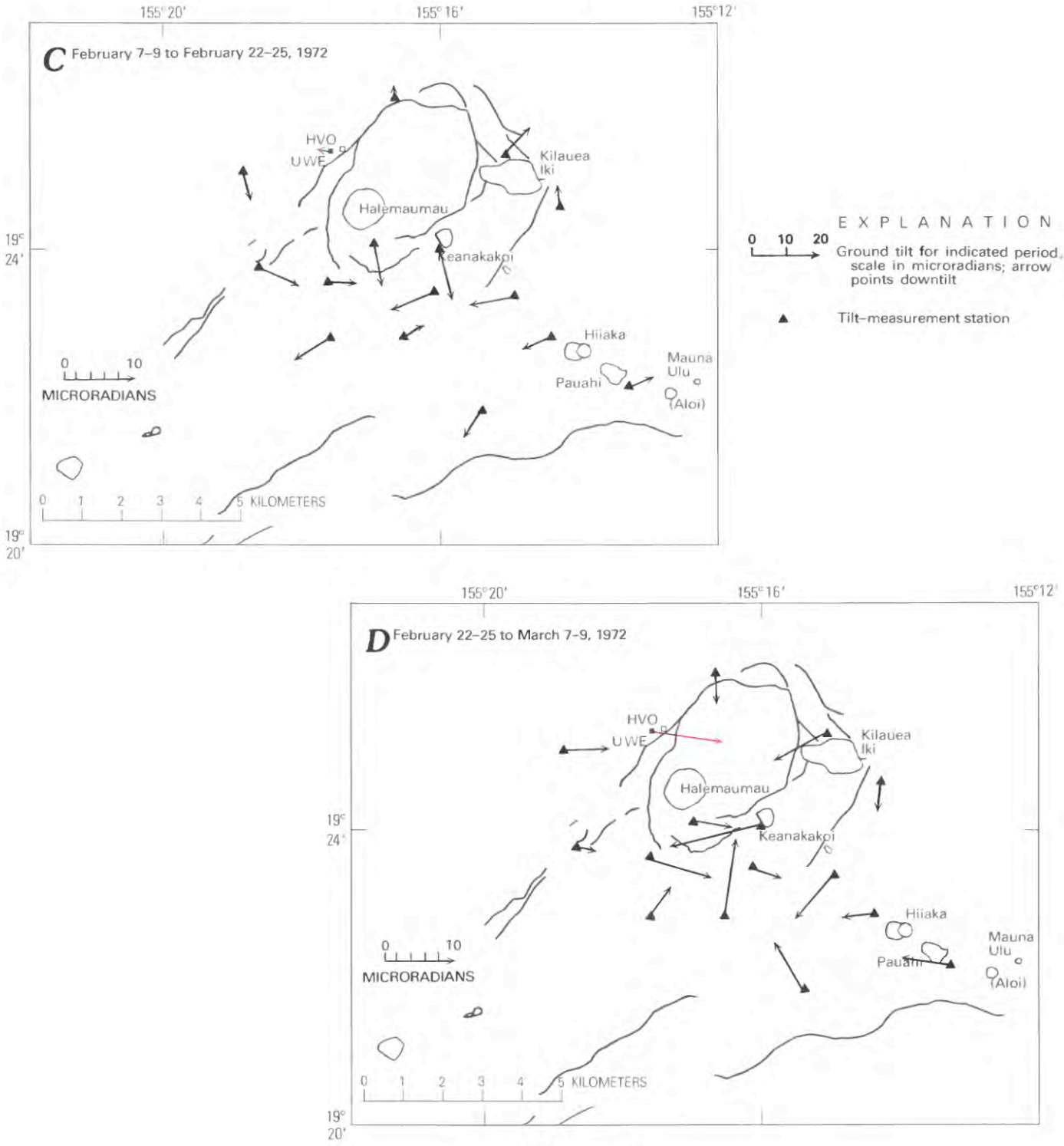

FIGURE 16.38.—Continued.

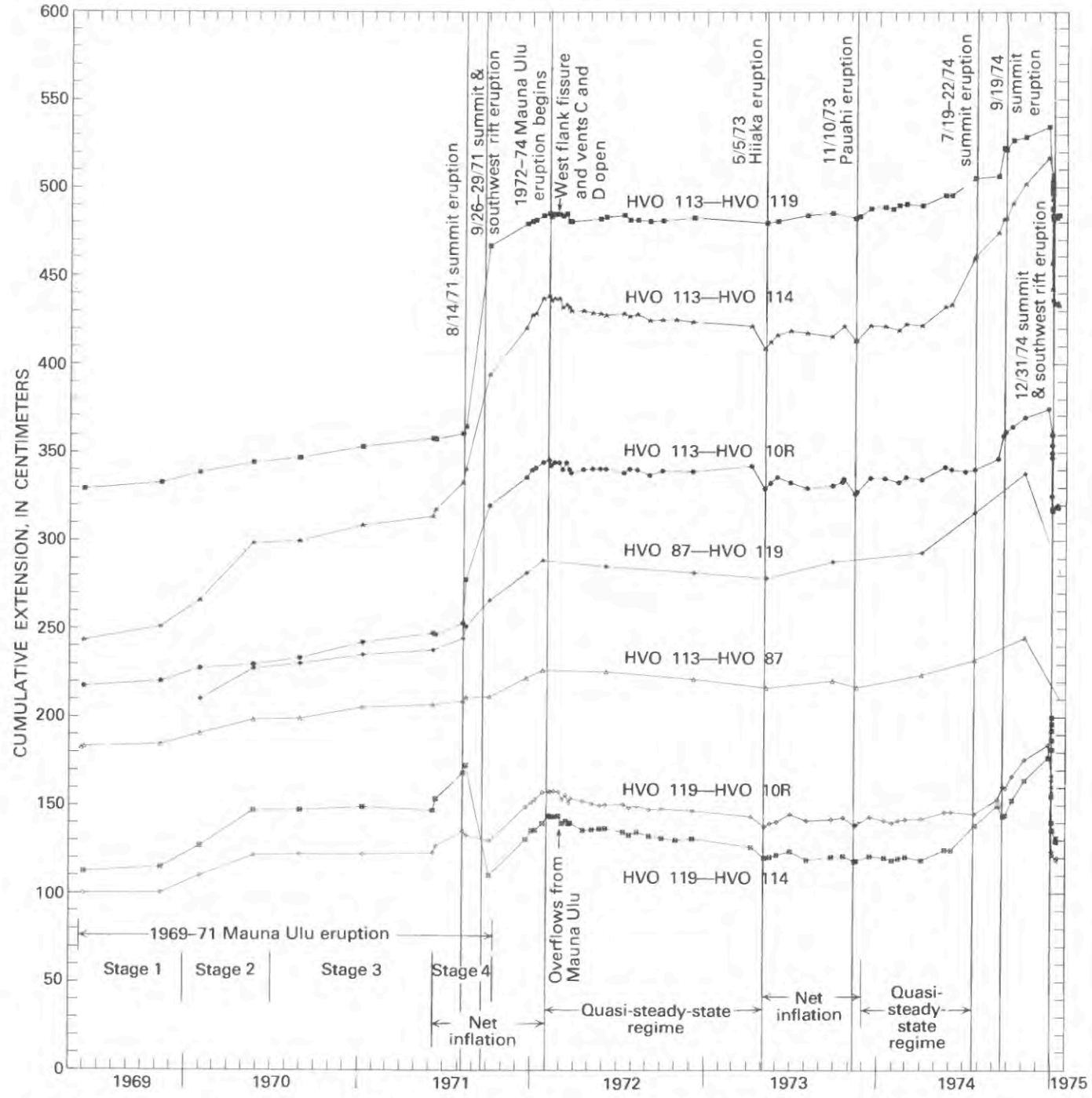

FIGURE 16.39.—Variations of distances within the summit EDM monitor between May 1969 and January 1975; locations of lines are shown in figure 16.36. Cumulative extension scale (in centimeters) is arbitrary. Frequent measurements detected small deflations in February and March 1972 related to overflows from Mauna Ulu and opening of new vents, respectively. Dotted parts of the curves for the 1973–74 period show probable variations if more frequent measurements had been made. Frequency of measurement during 1969–71 was about same as during 1972–75 (see Swanson and others, 1979, fig. 2; Duffield and others, 1982, fig. 2) but not all data plotted here.

16.4) yielded a diffuse net inflation pattern similar in shape but of slightly smaller magnitude to that obtained for the preceding survey period (see figs. 16.41*C*, *D*). Measurable geodetic response to the events of June 9, if any, apparently was largely masked by the net inflation and continued localized adjustments to the May 5 eruption that prevailed during May and June.

The reoccupation of all summit deformation networks beginning in mid-September provided data documenting the complex reinflation process following the May 5 eruption. Level and tilt data suggest a very broad zone of posteruption uplift, including the southeastern sector of the caldera and the upper part of the east rift zone (fig. 16.42*A*). The maximum vertical displacements occurred adjacent to the periphery of the eruption site on the north and southeast. The area of least vertical displacement coincides with the eruption site, indicating incomplete recovery from the localized collapse associated with the eruption (compare figs. 16.41 and 16.42). The pattern of horizontal ground displacements for the same survey period (fig. 16.42*B*) is expectedly complex but reasonably compatible with that derived from ground tilt and level data.

Net inflation during the May–October 1973 period was ended by the eruption at Pauahi on November 10 and the associated Uwekahuna deflation of about 21 μrad. All summit deformation networks were reoccupied in mid-November (table 16.4), when weak vent activity was continuing within Pauahi Crater. The previous reoccupation was completed on October 3, which was during the inflation (fig. 16.37). The differences between the surveys therefore record only about 25 percent of the total Uwekahuna deflation: the maximum measured subsidence in the summit deflation area barely exceeded 40 mm at two distinct centers (fig. 16.42*C*). Otherwise, the deformation pattern accompanying the November eruption—weak summit deflation coupled with stronger uplift and associated local collapse at the eruption site—closely resembles that for the May 1973 Pauahi-Hiiaka outbreak (see figs. 16.41, 16.42). As in May, the results of the level, tilt, and trilateration surveys bracketing the November eruption are mutually consistent.

Rapid reinflation of the summit began as soon as the peak eruptive activity of November 10–11 had dwindled to weak vent activity that persisted for nearly a month. This inflation was expressed by a tilt survey in mid-December, which shows a relatively well-defined inflation center east of Halemaumau, as well as local tilt changes presumably reflecting weak vent activity in December (fig. 16.42*D*).

DECEMBER 1973–JULY 1974: RETURN TO QUASI-STEADY-STATE REGIME AND DEPARTURE FROM 1972–73 ERUPTIVE BEHAVIOR

Kilauea apparently returned to quasi-steady-state activity in December, following rapid recovery from the November 10 outbreak at Pauahi. This is inferred from variations in Uwekahuna tilt, which showed little net change for the December 1973–July 1974 period, even though the tilt oscillations were larger than those in the quasi-steady-state period in 1972–73. The existence at this time of a highly efficient hydraulic connection between the summit reservoir and Mauna Ulu is illustrated by the close correlation between minor variations in summit tilt and visible activity during the eruptive episodes, especially the well-documented episodes during January–February 1974 (fig. 16.30). However, because of inclement weather and instrument breakdown, few deformation surveys were conducted during 1974, and we do not know whether slight shifts from equilibrium might have been detected by more frequent remeasurements.

The tilt network was remeasured in January 1974 and again in March (table 16.4). Deviations in Uwekahuna tilt were small (no more than 5 μrad), and the survey periods were prolonged by bad weather and instrument problems; the results obtained do not permit good definition of patterns. Nonetheless, tilt vectors for the December 1973–January 1974 period can be interpreted as indicating weak deflation, and those for the January–March 1974 survey, as slight inflation (patterns not shown). For both survey periods the measured tilts were 15 μrad or less, and most of the larger values were at sites near Hiiaka and Pauahi, probably because of continuing adjustments to the November–December Pauahi eruption, or possibly reflecting the influence of the eruptive activity at Mauna Ulu itself.

The level and trilateration networks in the summit area were reoccupied in early April (table 16.4). The level data indicate summit inflation (fig. 16.43*A*), consistent with the net tilt change at Uwekahuna of about +5 μrad for the period November 1973–April 1974. Residual effects of local uplift and associated collapse during November–December 1973 were still evident in April near Pauahi. The location of the inflation center, about 1 km northeast of Halemaumau indicates a substantial northward shift from the pre-eruption inflation center and the net 1972 deflation center (fig. 16.43*A*). The deformation pattern (not shown) obtained from the trilateration data is not diagnostic, but it is compatible with that shown in figure 16.43*A*. No tilt-survey data exist for April 1974 for comparison with level and trilateration measurements. However, tilt vectors for the period between November 1973–May 1974 also indicate net inflation with a center northeast of Halemaumau (fig. 16.43*B*).

Dvorak and others (1983, table 2, fig. 3) used a least-squares inversion technique and a point-source elastic model to analyze the surface displacements for the November 1973–April 1974 period. They found that: (1) the inflation centers determined separately for level and trilateration data coincide reasonably well; and (2) the model depth to the point source (summit magma reservoir) ranges from 2.2 to 2.6 km, depending on whether level data, trilateration data, or both are used.

Following the July 19–22 summit eruption, which terminated the 1972–74 Mauna Ulu eruption on the east rift, geodetic surveys were run in late July (figs. 16.43*C*, *D*). Their results reflect the prolonged inflation that preceded the July summit eruption but are complicated by the 15-μrad deflation at Uwekahuna that accompanied the eruption (Peterson and others, 1976). Level and tilt surveys were not completed until July 31 and thus bracketed part of the summit reinflation. As is typical of Kilauea summit eruptions, the area of maximum displacement coincided with the loci of eruptive fissures in the southeastern part of the caldera and in and near Keanakakoi and Lua Manu Craters (figs. 16.43*C*, *D*). The complex area of weak subsidence along the east rift zone between Hiiaka and Mauna Ulu reflects lingering effects of the November 1973 Pauahi eruption.

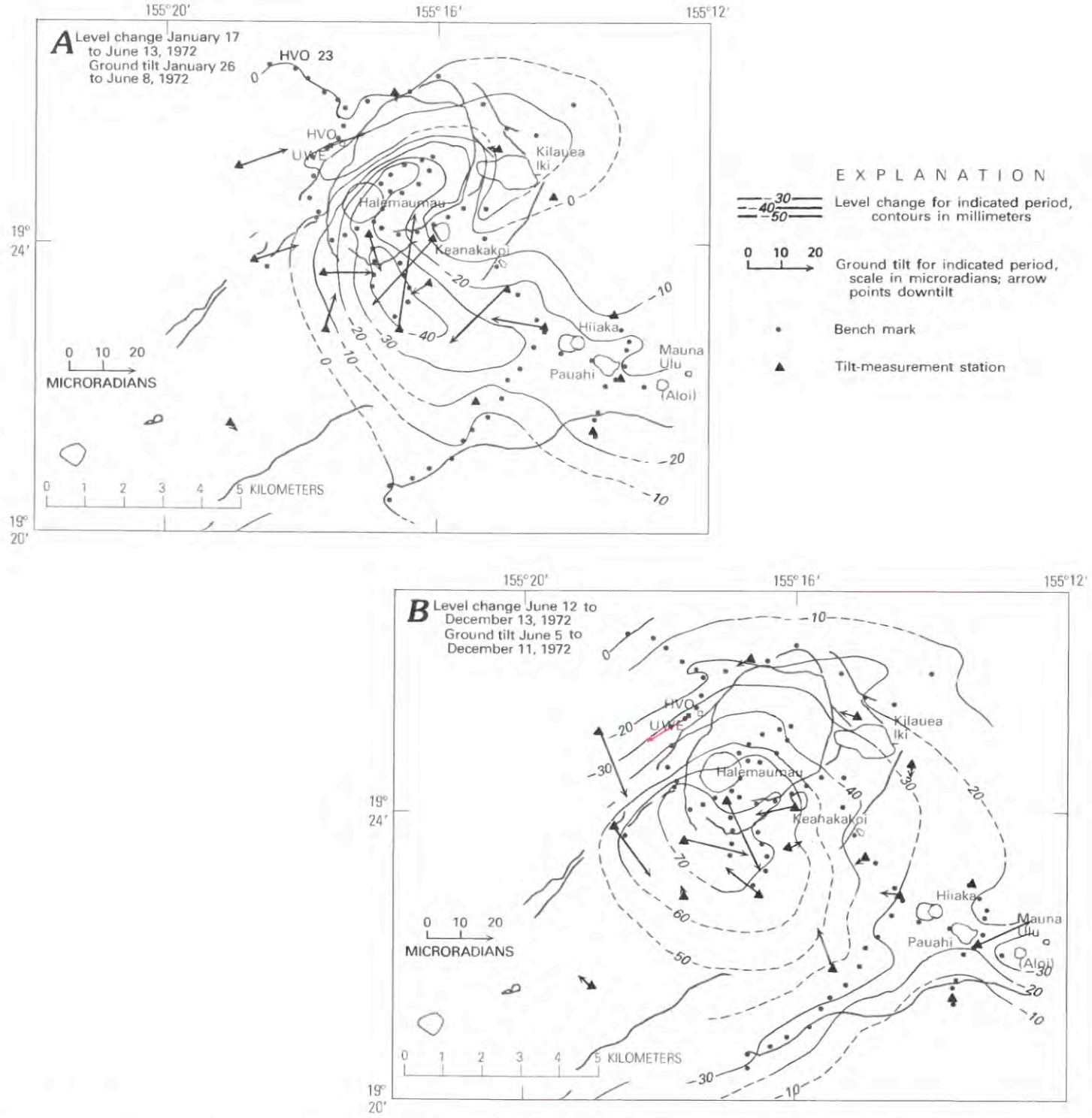

FIGURE 16.40.—Results of level, tilt, and trilateration surveys during 1972. Vector UWE (red) calculated from east-west and north-south components of Uwekahuna tilt. Contours of level data referenced to bench mark HVO 23, assumed to be stable. ***A***, Changes in elevation and tilt between January and June 1972; note change in vector scale from figures 16.38*B–D*. ***B***, Changes in elevation and tilt between June and December 1972, showing a weak but relatively well-defined pattern of net deflation; azimuth of vector UWE appears anomalous. ***C***, Horizontal displacements from trilateration surveys of Kilauea summit between June and December 1972. Displacement vectors determined by reference to assumed stable bench marks on southeastern flank of Mauna Loa Volcano (see Kinoshita and others, 1974). ***D***, Changes in elevation and tilt between January and December 1972. Combining the two survey periods shown in *A* and *B* yields a coherent deflation pattern; the azimuth of vector UWE is still anomalous. Note secondary area of subsidence in Pauahi-Mauna Ulu area.

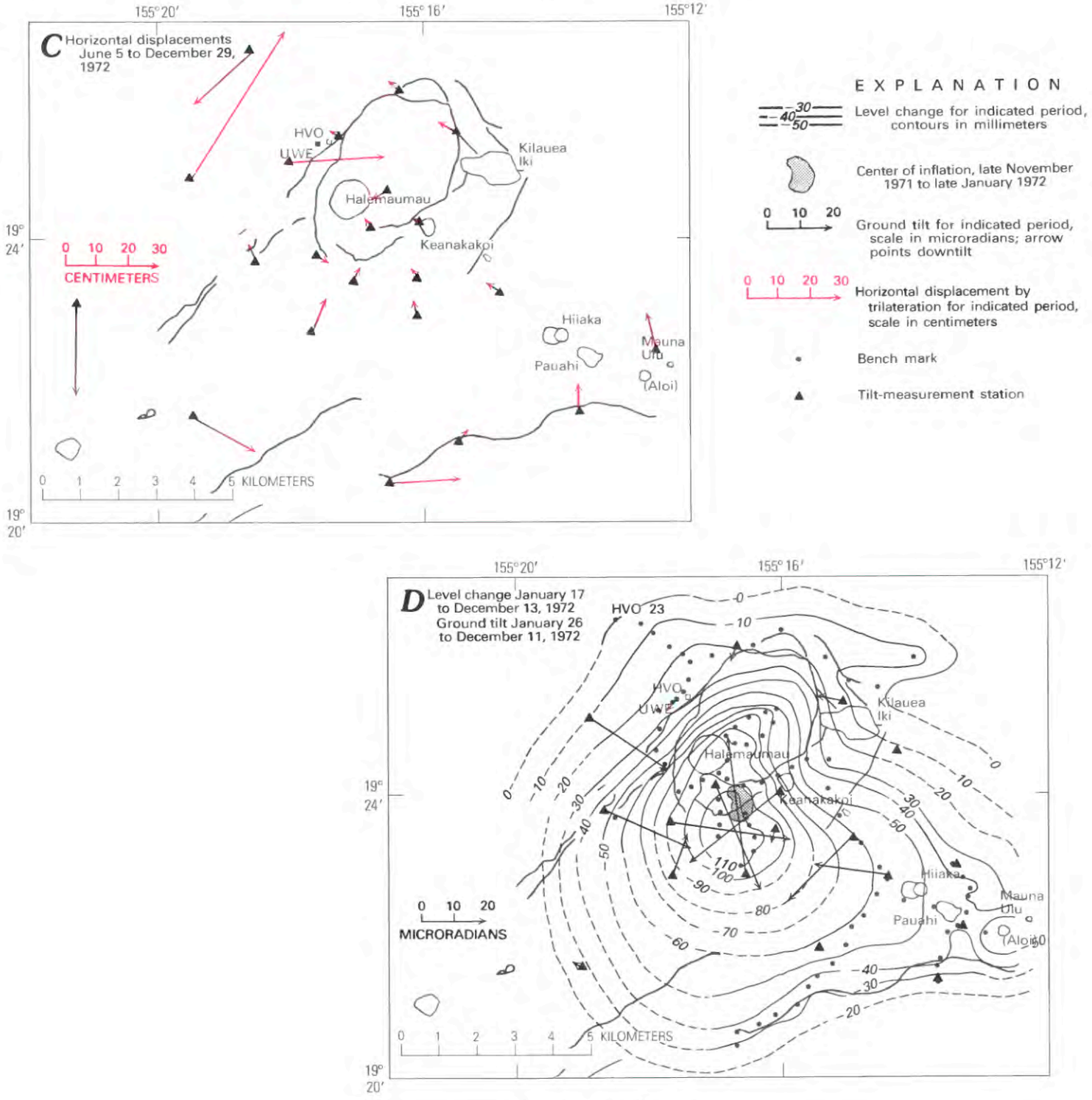

FIGURE 16.40.—Continued.

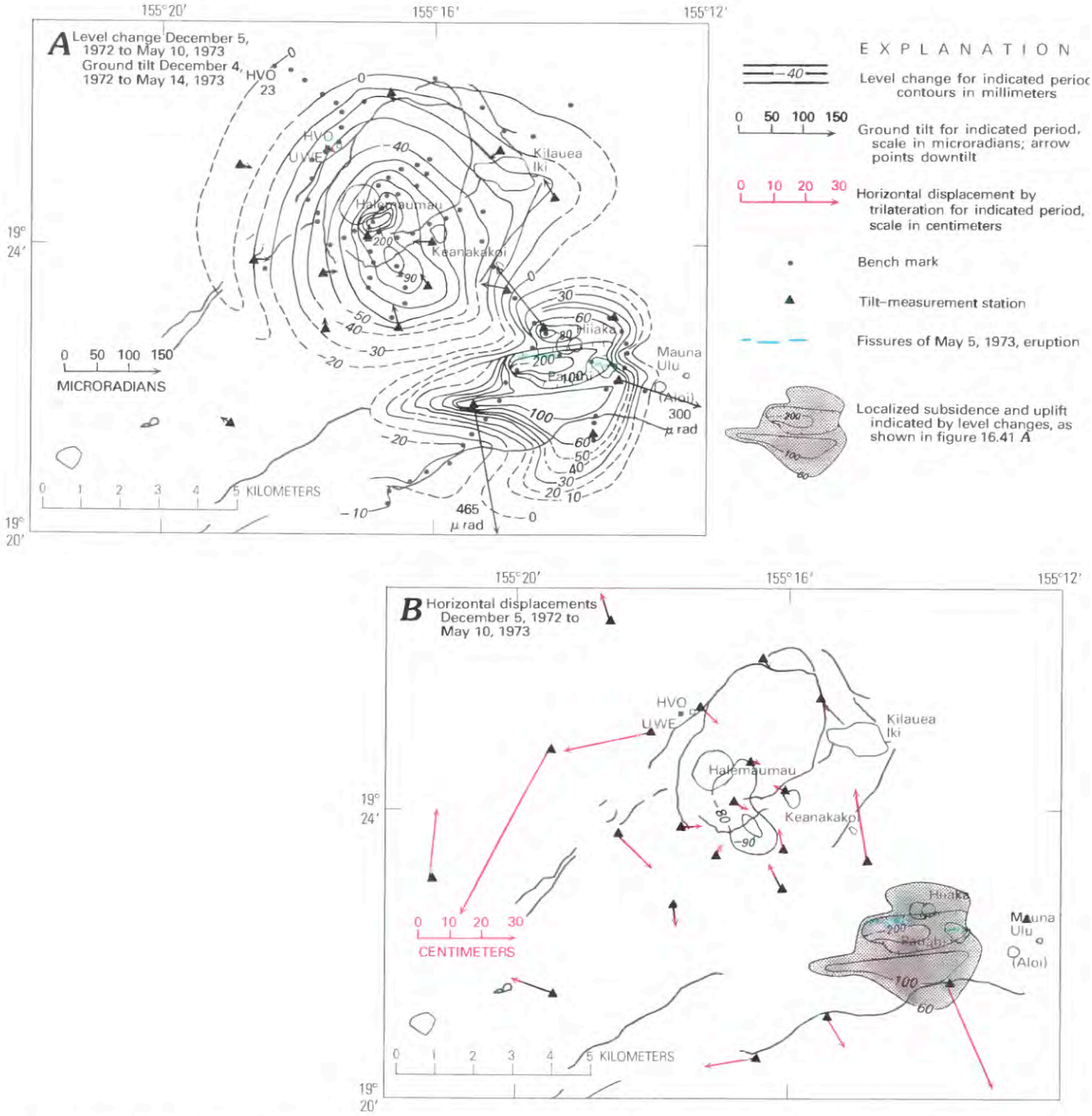

FIGURE 16.41.—Results of level, tilt, and trilateration surveys from December 1972 to June 1973. Vector UWE (red) calculated from east-west and north-south components of Uwekahuna tilt. Contours of level data referenced to bench mark HVO 23, assumed to be stable. ***A***, Changes in elevation and tilt between December 1972 and May 1973, showing the effect of the May 5 Pauahi-Hiiaka eruption and intrusion into eastern end of the Koae fault system (see text for discussion). Magnitude of tilt vectors and vertical displacements considerably larger than those in 1972 (compare with figs. 16.38 and 16.40). ***B***, Horizontal displacements from trilateration surveys between December 1972 and May 1973. Also shown are areas of localized subsidence and uplift determined from level data (see *A*). ***C***, Changes in tilt between May 7 and June 1, 1973, showing relatively small changes (note change in vector scale from *A*) that generally reflect summit inflation following May 5 eruption. Tilt in Pauahi-Hiiaka area reflects local adjustments (see text). ***D***, Changes in tilt between May 21 and June 28, 1973; this period includes the June 9 partial draining of the lava lake at Mauna Ulu. Effect of partial draining and associated intrusion is apparently masked by net inflation. Note change in vector scale from *A* and *C*.

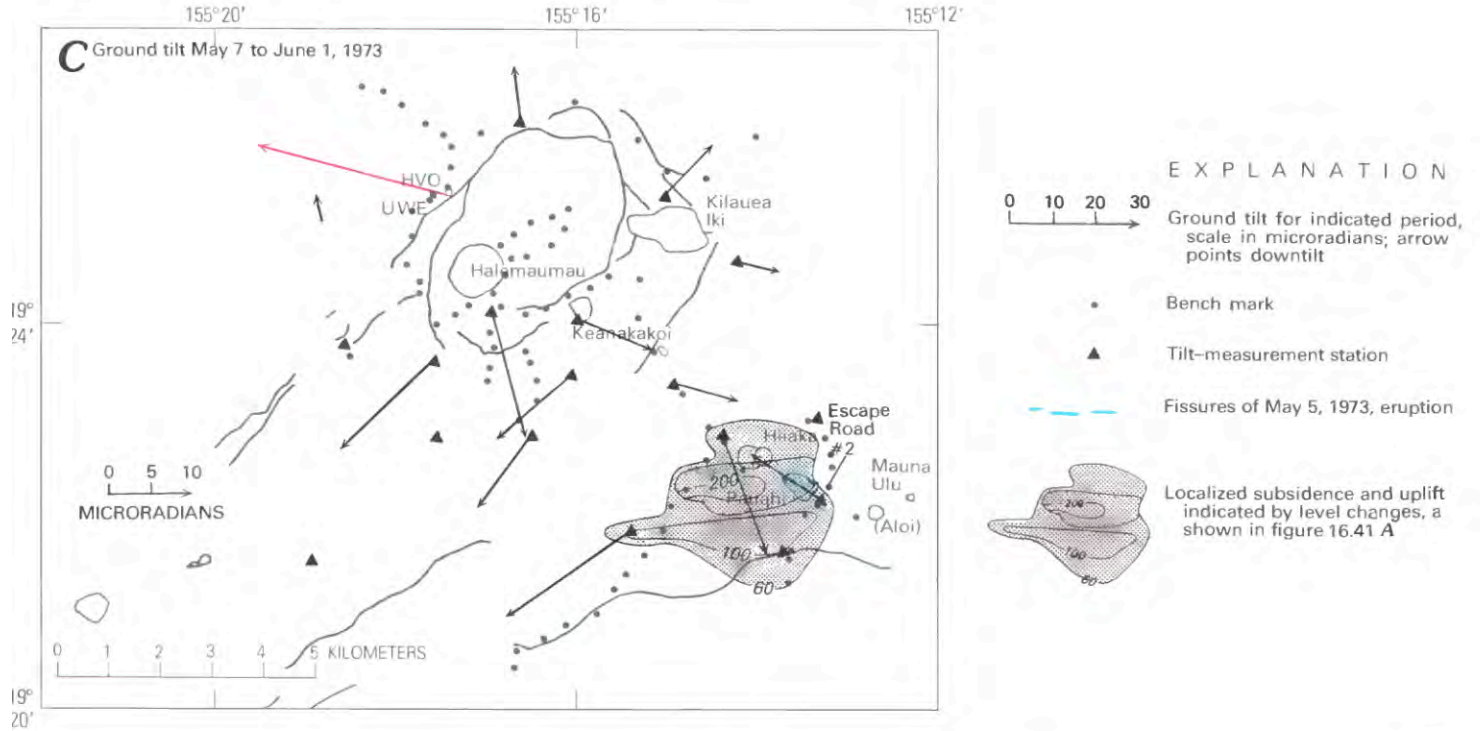

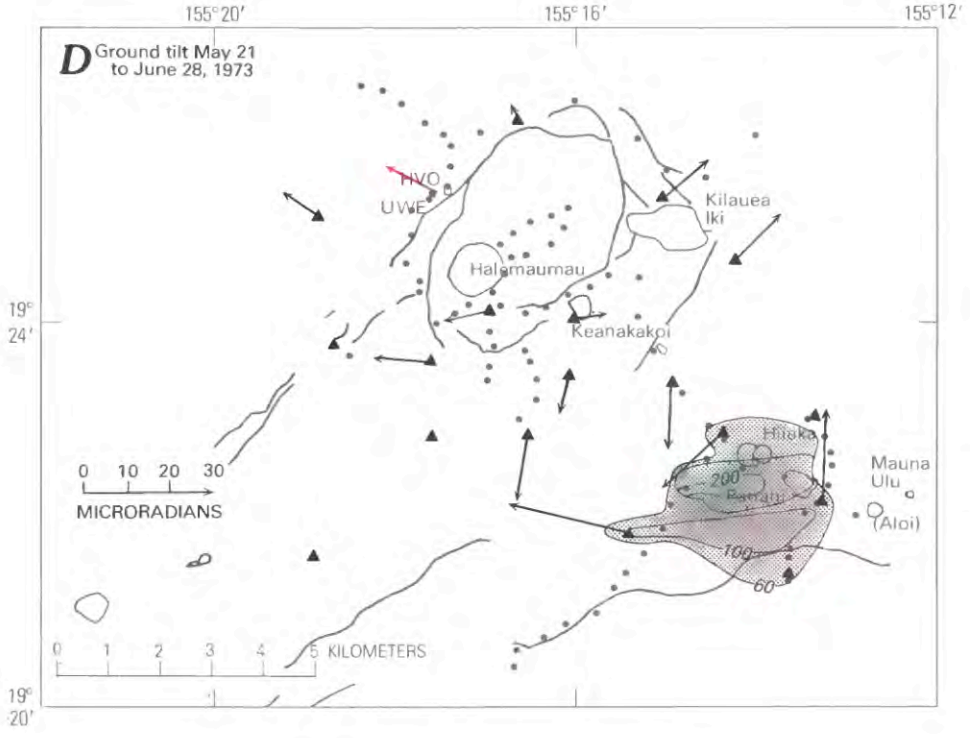

FIGURE 16.41.—Continued.

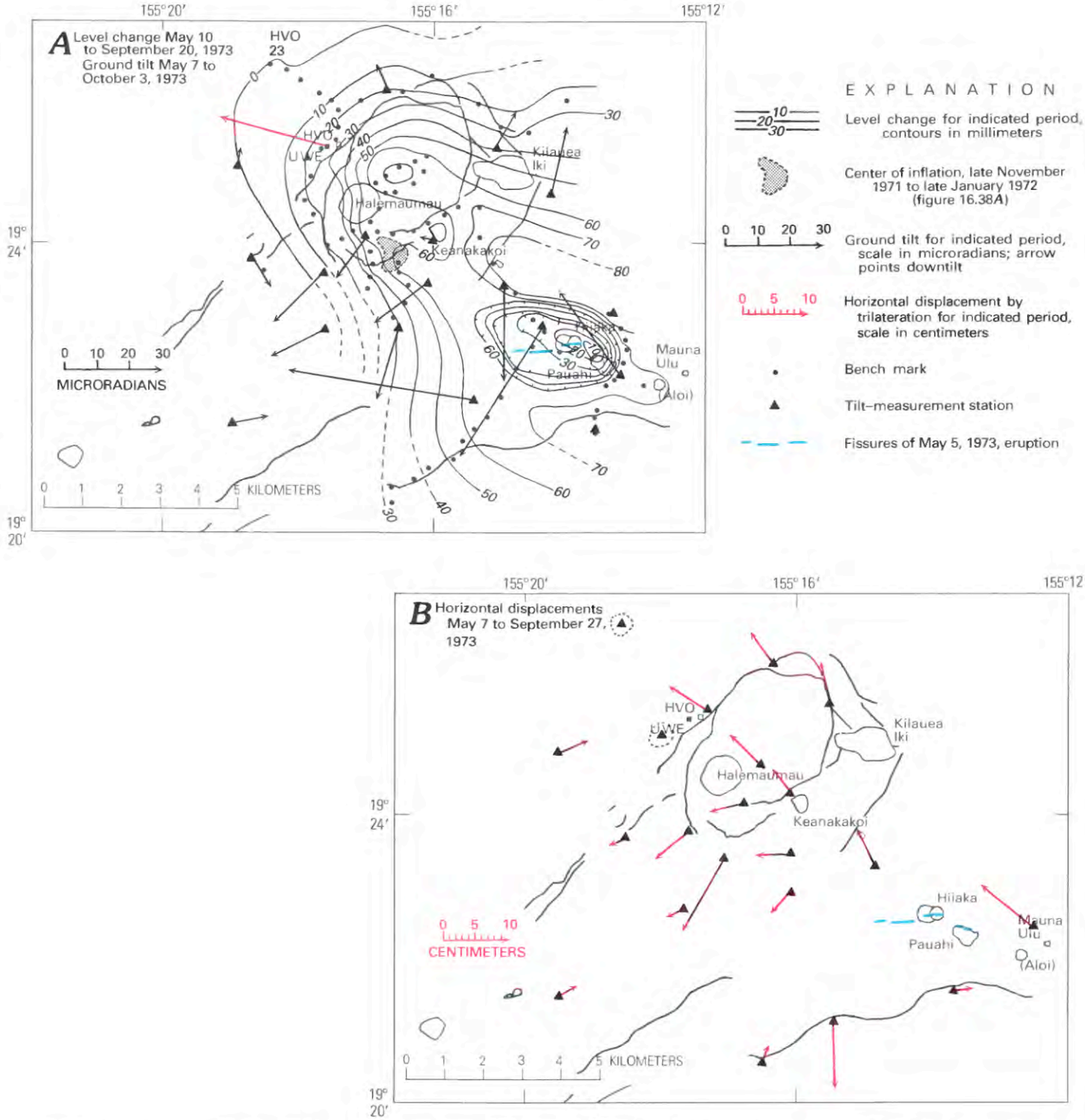

FIGURE 16.42.—Results of level, tilt, and trilateraton surveys from May to December 1973. Vector UWE (red) calculated from east-west and north-south components of Uwekahuna tilt. Contours of level data referenced to bench mark HVO 23, assumed to be stable. ***A***, Changes in elevation and tilt between May and September 1973. Effects of May 5 eruption and intrusion still evident. Elongate uplifted area shifted northward from previous inflation and deflation centers. ***B***, Horizontal displacements from trilateration surveys between May and December 1973. Changes are relatively small and resulting pattern diffuse; bench marks in dotted circles show northerly vectors that are masked by plot symbols (triangles). ***C***, Changes in elevation and tilt between September and November 1973, showing deformation associated with November 10–11 eruption at Pauahi. Deformation pattern generally similar to that for the May 5 eruption and other eruptions in Kilauea's upper east-rift zone (see text). ***D***, Changes in tilt between November and December 1973, reflecting summit inflation following the November 10–11 Pauahi eruption, which persisted feebly until December 9.

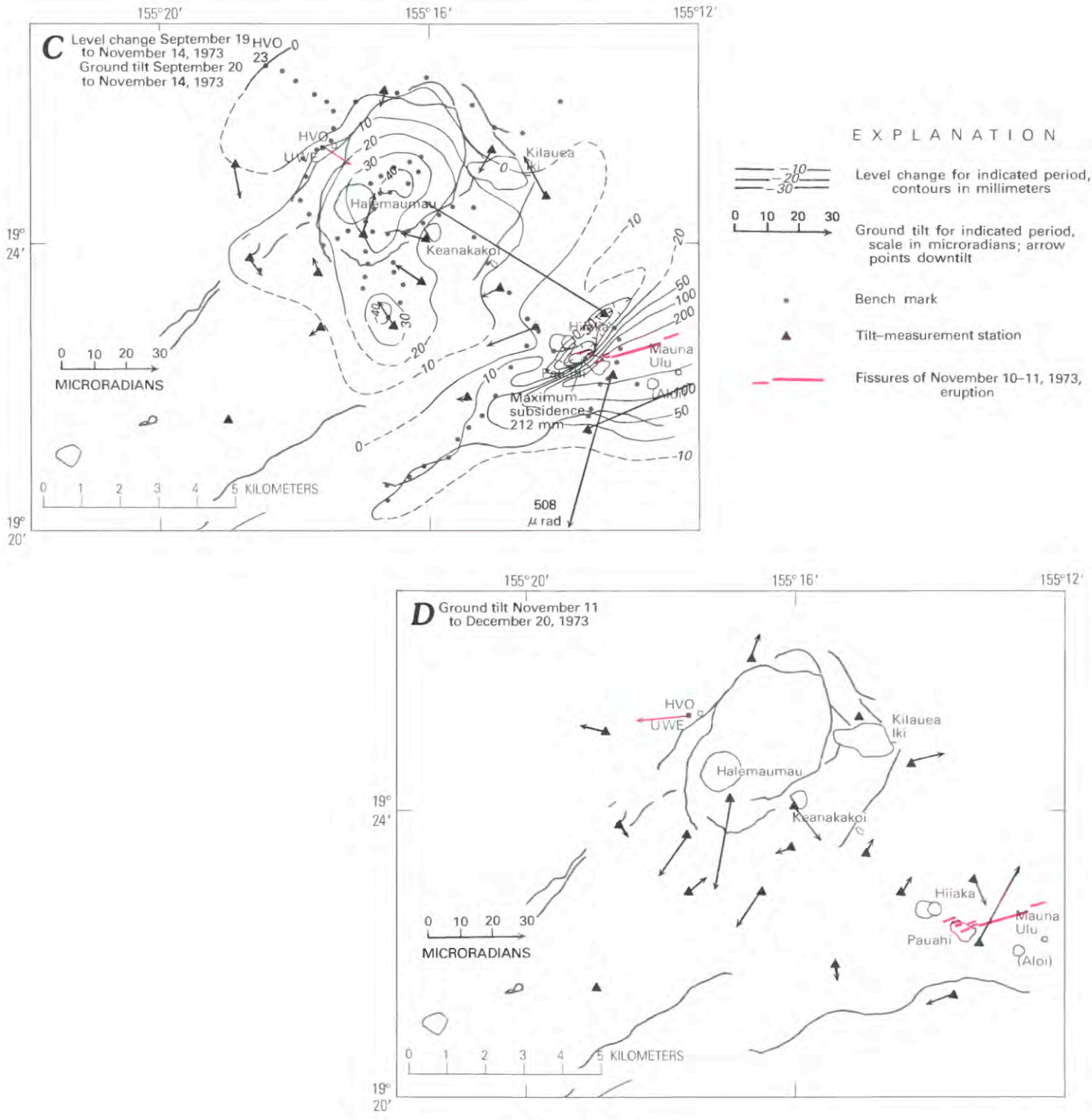

FIGURE 16.42.—Continued.

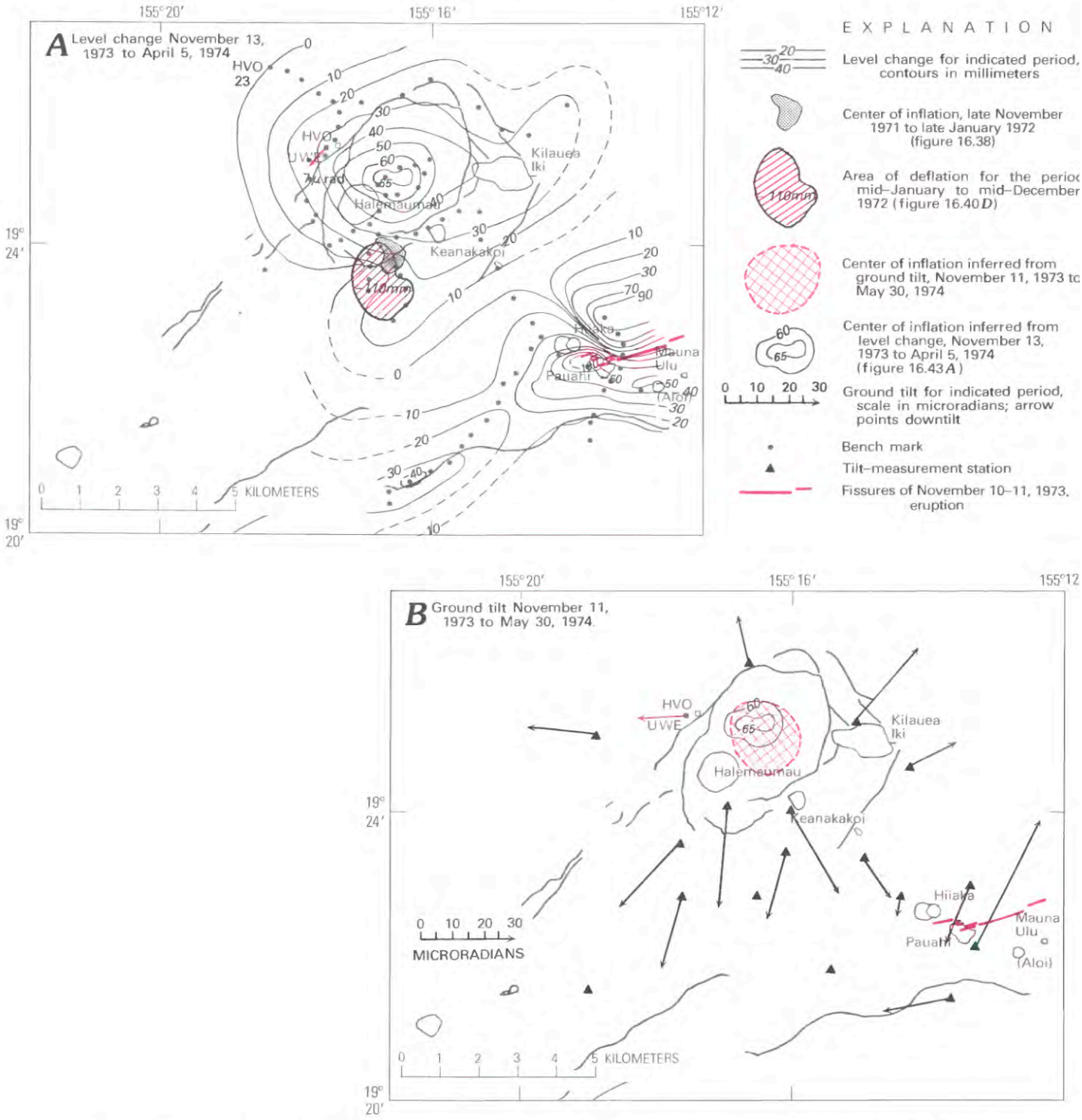

FIGURE 16.43.—Results of level, tilt, and trilateration surveys from November 1973 to July 1974. Vector UWE (red) calculated from east-west and north-south components of Uwekahuna tilt. Contours of level data referenced to bench mark HVO 23, assumed to be stable. ***A***, Changes in elevation between November 1973 and April 1974. Pattern of vertical displacements is complex and shows: (a) well-defined inflation center near northern end of uplifted area shown in figure 16.42*A*; (b) area of greater uplift north of Pauahi that perhaps reflects continued adjustments to November–December eruption; and (c) subsidence at and east of Pauahi, as well as in the eastern part of the Koae fault system. No corresponding data from tilt surveys available, but see *B*; azimuth of vector UWE appears anomalous. ***B***, Tilt vectors between November 1973 and May 1974. Broad inflation center corresponds well with previous centers determined from level data (see figs. 16.41, 16.42). Vector UWE is incompatible with radial pattern of vectors from tilt surveys. ***C***, Changes in elevation and tilt between March and July 1974, the period that includes the July 19–22 summit eruption and the end of the 1972–74 Mauna Ulu eruption on July 22. Well-defined uplift area coincides with active fissures of eruption in southern part of caldera near Keanakakoi and Lua Manu Craters. Bench mark at rim of Lua Manu (shown in red) collapsed about 2 m and not considered in contouring of the level data. ***D***, Horizontal displacements from trilateration surveys between March and July 1974. Displacement vectors point away from the eruptive fissures.

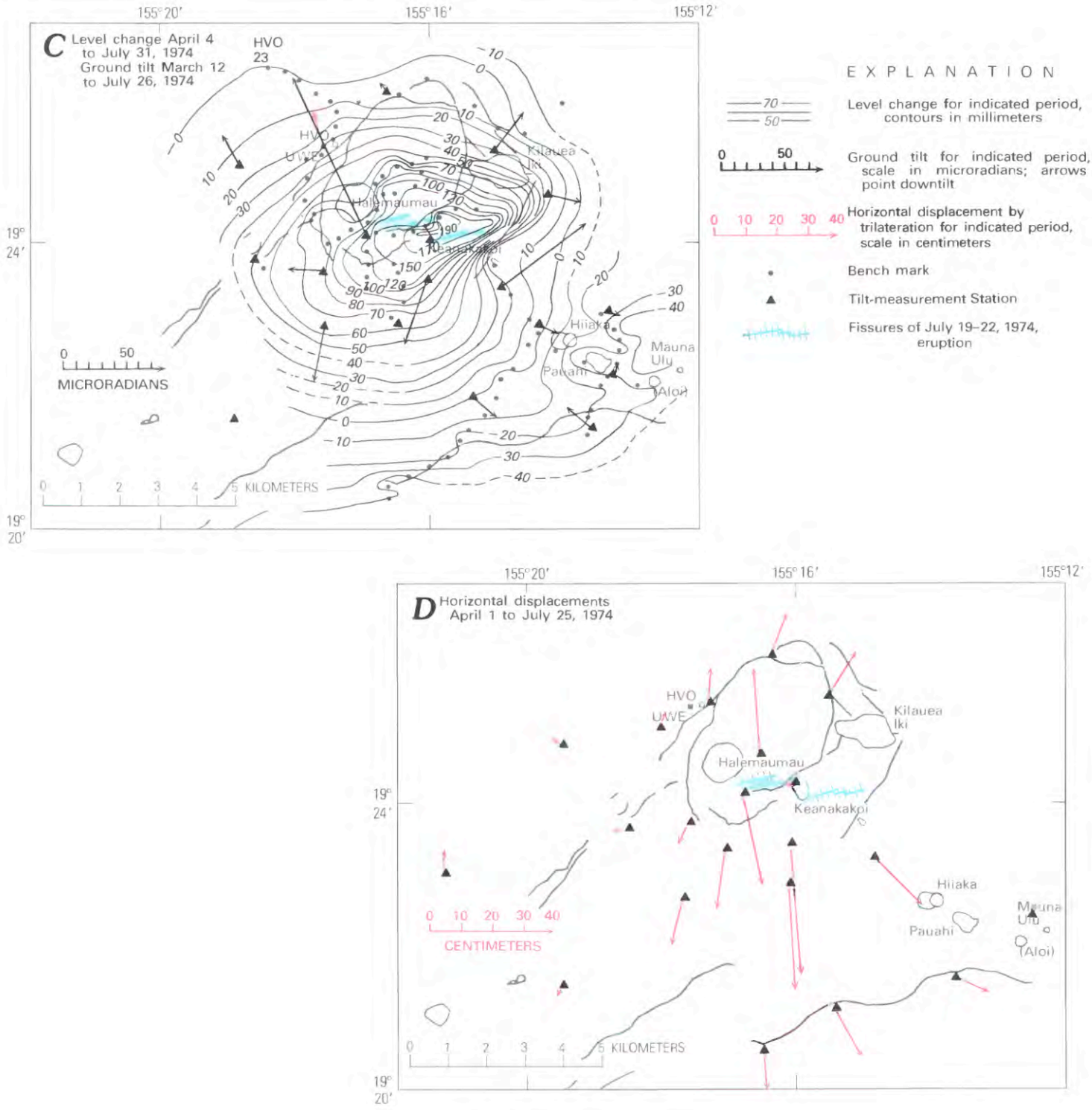

FIGURE 16.43.—Continued.

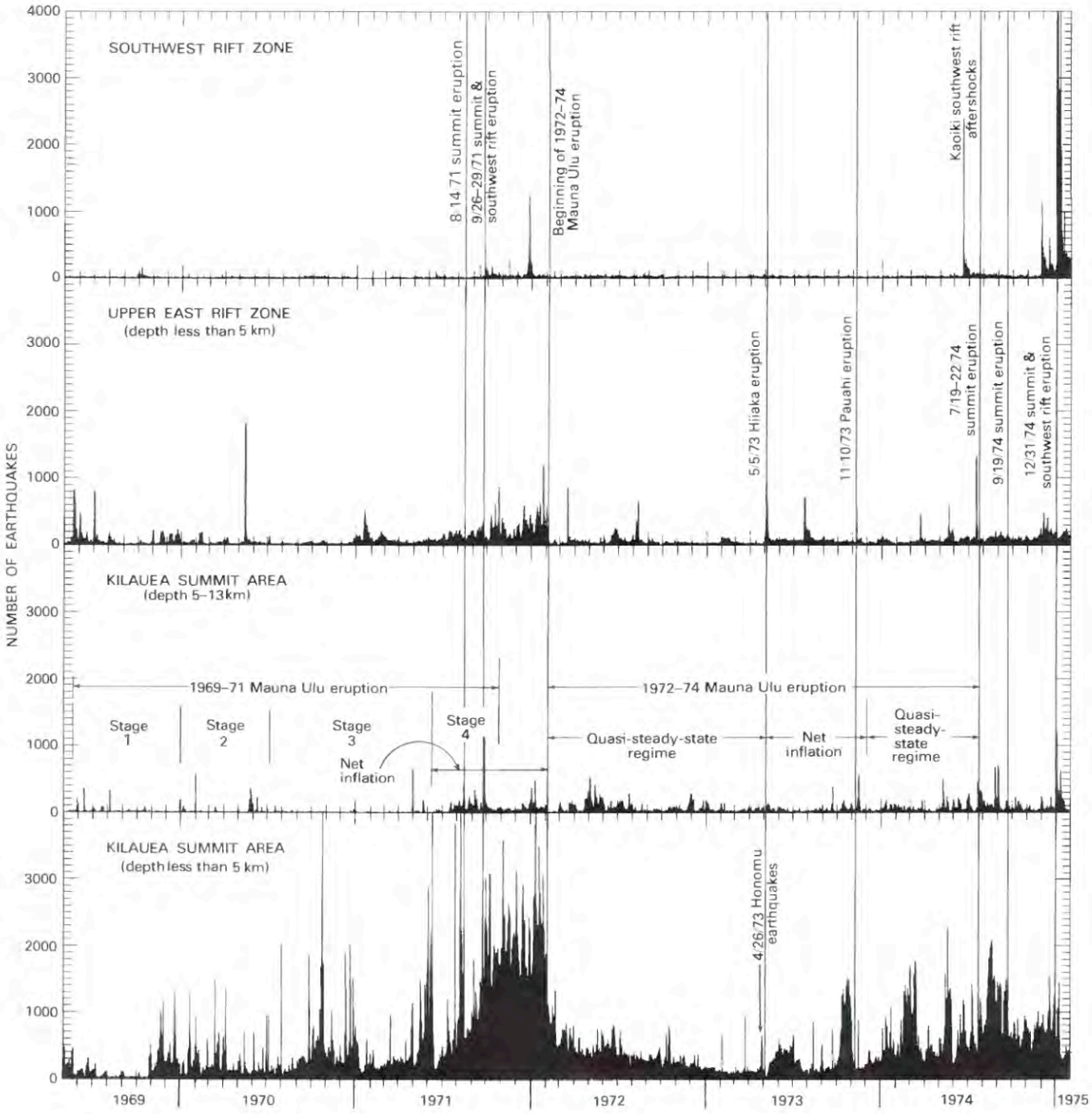

FIGURE 16.44.—Numbers of earthquakes in summit area (shallow and crustal depth), upper east rift zone, and southwest rift zone of Kilauea from May 1969 to January 1975. All events are counted, whether or not their hypocenters are well determined; counts for the southwest rift earthquakes include those in the Kaoiki fault system.

VARIATION IN SEISMICITY

Tabulations of earthquake counts and located events for 1972–74, as well as descriptions of the seismic network and instruments, have been published in summary form (Hawaiian Volcano Observatory, 1977a, 1977b, 1977c, 1977d, 1977e, 1977f, 1977g, 1977h, 1978). Some aspects of seismic activity during the 1972–74 period were discussed elsewhere (Koyanagi and others, 1973; Tilling and others, 1975; Koyanagi and others, 1976a, 1976b; Ellsworth and Koyanagi, 1977; Unger and Ward, 1979; and Aki and Koyanagi, 1981). We present in this paper a

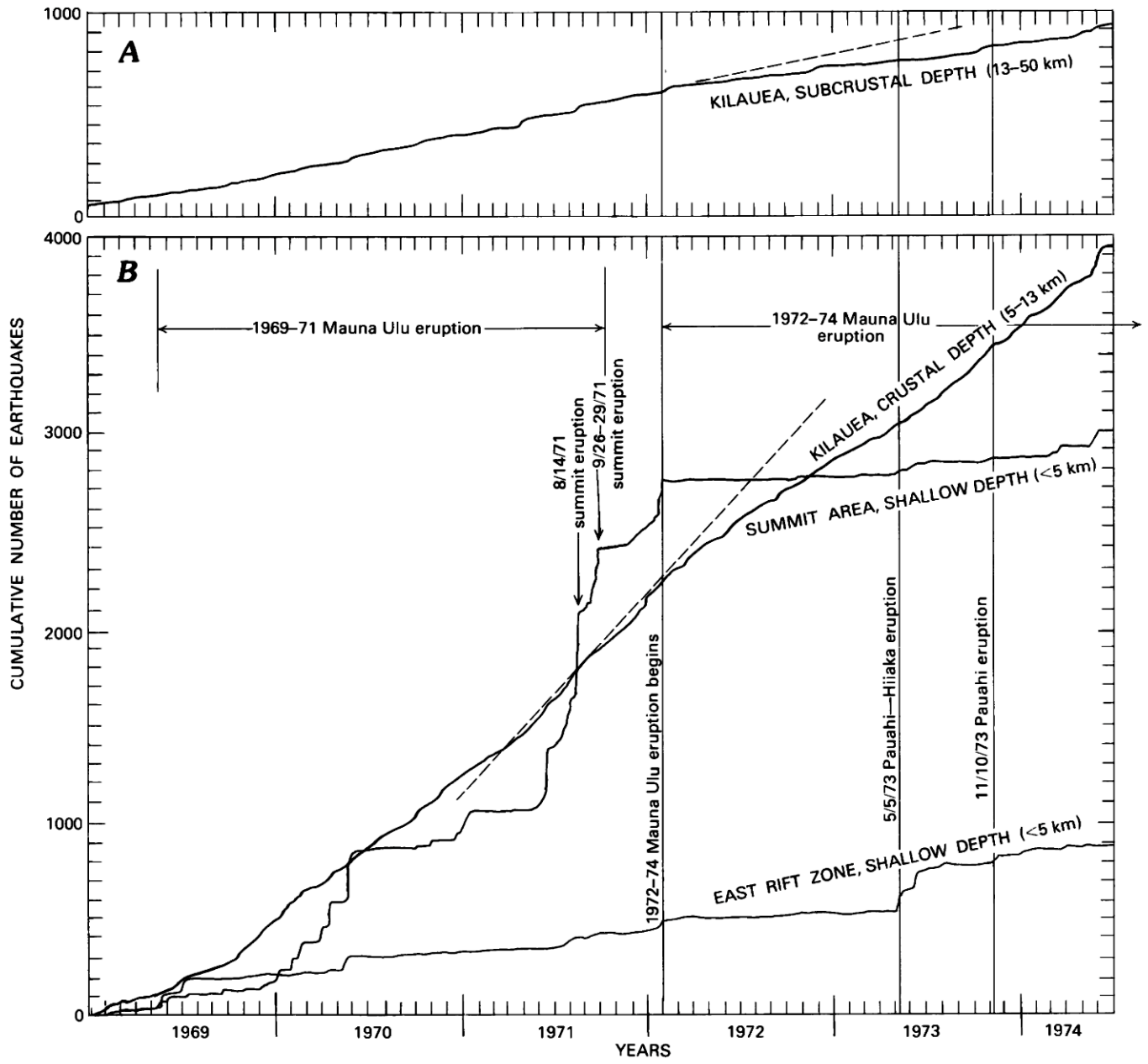

FIGURE 16.45.—Cumulative numbers of earthquakes with well-determined hypocenters, magnitude 1 or greater, at Kilauea from January 1969 to June 1974. ***A***, Subcrustal earthquakes (reference area: lat 19°11′ to 19°33′ N., long 154°48′ to 155°20′ W.). Dashed line is extrapolation of slope for period before onset of 1972–74 Mauna Ulu eruption. ***B***, Earthquakes of crustal depth (reference area: same as for subcrustal earthquakes) and shallow earthquakes in the summit area and east rift zone (reference areas: lat 19°23′ to 19°27′ N., long 155°13′ to 155°19′ W. and lat 19°20′ to 19°23′ N., long 155°06′ to 155°15′ W., respectively). Dashed line is extrapolation of slope of crustal-earthquake plot for pre-eruption net summit inflation beginning in mid-June 1971 (fig. 16.37); slope decreases after onset of 1972–74 eruption and then is similar to that during the 1969–71 Mauna Ulu eruption.

brief overview of the variation in seismicity (figs. 16.44–16.46) within the framework of the chronological narrative of volcanic activity. Systematic, more quantitative studies of the seismicity associated with the 1972–74 Mauna Ulu eruption are pending.

SEISMICITY BEFORE AND AFTER THE 1972–74 MAUNA ULU ERUPTION

Seismicity during the 1972–74 Mauna Ulu eruption was moderate relative to that of the preceding and subsequent periods.

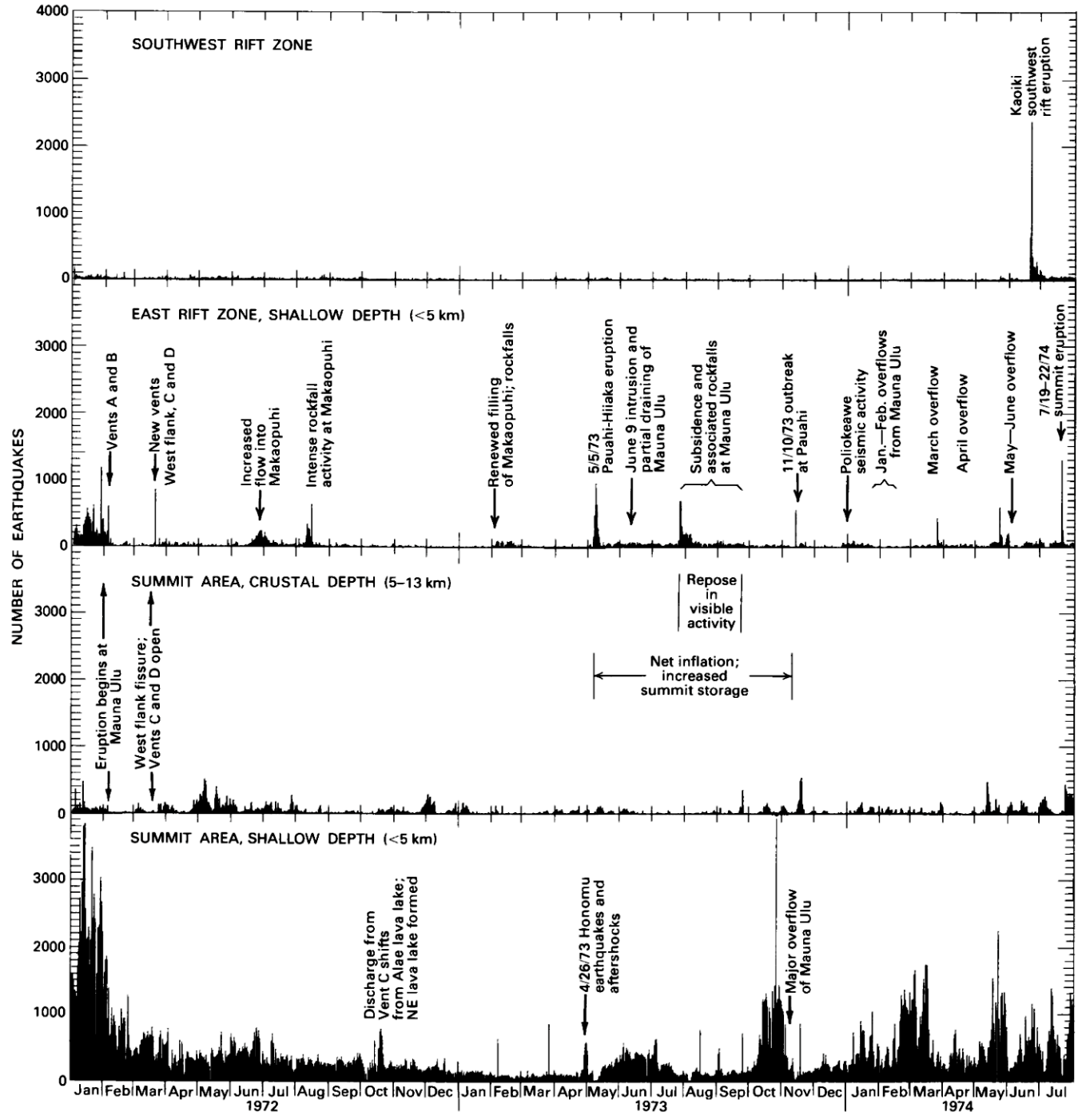

FIGURE 16.46.—Variation in seismicity during 1972–1974 Mauna Ulu eruption. Data also shown at smaller scale in figure 16.44. Significant changes in eruptive activity correlate with increased seismicity. Shallow summit-area earthquakes for the period January to March 1974 are shown in greater detail in figure 16.30.

Occurrence of long-period earthquakes at crustal depths (5–13 km) beneath Kilauea's summit became more frequent beginning in June 1971 (figs. 16.44, 16.45*B*), at about the same time as summit inflation. The generally reduced level of seismicity during the 1972–74 Mauna Ulu eruption, particularly of shallow (short-period) summit and east-rift earthquakes (depth less than 5 km), is especially evident during the first period of quasi-steady-state activity during February 1972–April 1973. Moreover, the occurrence of deeper Kilauea earthquakes (13–50 km) during the 1972–74 Mauna Ulu eruption decreased, as compared with that

during the 1969–71 Mauna Ulu eruption (fig. 16.44*A*).

As commonly observed at Kilauea, variations in the number of shallow summit earthquakes correlate closely with variations in tilt measured at Uwekahuna (see figs. 16.4, 16.37, 16.44–16.46). This correlation is well exhibited during the June 1971–January 1972 period, when the 1969–71 Mauna Ulu eruption gradually ended and the summit inflated in response to increased storage of magma in the summit reservoir (Duffield and others, 1982). A similar correlation exists between net inflation and incidence of upper-east-rift earthquakes during this period, implying periodic leakage of magma into the rift zone as the stressed summit reservoir failed repeatedly during reestablishment of the magma conduit system leading to Mauna Ulu. Within this context, the August 1971 summit eruption and the September 1971 southwest-rift eruption may be considered as massive and rather abrupt leakages by surface venting, inasmuch as the strong net summit inflation was only briefly interrupted by these events (Duffield and others, 1982).

SEISMICITY DURING THE ERUPTION

Sporadic bursts of low-level harmonic tremor in the summit region and upper east rift were recorded throughout the September 1971–January 1972 period of summit inflation. However, tremor increased in amplitude and became sustained in the early morning of February 4, 1972, only a day after the start of renewed eruption at Mauna Ulu. Within the next two days, as the new lava lake rose rapidly and vent activity increased, the numbers of shallow summit and upper-east-rift earthquakes decreased dramatically and thereafter remained low through April 1973 (fig. 16.46). This prolonged period of low seismicity implies the existence of a highly efficient and open system of magma transfer between the summit reservoir and the eruption site. We interpret the gradual net decline of shallow summit earthquakes during this period as reflecting a progressive improvement in the ability of the conduit system to transfer magma freely. Most of the conspicuous departures from the prevailing background of low seismicity can be correlated with changes in eruptive and associated activity and are so annotated in figure 16.46. Perhaps the most notable seismic events in 1972, however, were those associated with the continuous lava inflow into Makaopuhi in June–July and with the intense rockfall activity at Makaopuhi in August (Tilling and others, 1975), rather than with vent activity at Mauna Ulu or Alae.

An abrupt change in the magma-transfer regime, beginning in early May 1973, is clearly reflected in a seismic signature that that is distinct from that for the previous 15 months (figs. 16.44, 16.46). We correlate this change with obstruction of the magma transfer conduit caused by the April 26, 1973, Honomu earthquake, although we concede that their coincidence in timing could be fortuitous. Whatever the cause, the changed magma regime was expressed initially by an immediate increase in the number of shallow summit earthquakes, followed by increased east-rift seismicity in early May that preceded and accompanied the May 5 draining of Mauna Ulu and Alae lava lakes, the Pauahi-Hiiaka eruption, and the associated intrusion into the Koae fault system. After the eruption, the level of earthquake activity and harmonic tremor remained high until the early morning hours of May 6. Most of the earthquakes during this time occurred in the upper east rift zone and in the middle and eastern portions of the Koae fault system, with a secondary zone of seismicity around the summit caldera. Weak tremor, fluctuating in intensity, continued for about a week afterward.

Lava returned to Mauna Ulu's crater on May 7 and to Alae on May 30. Alae was probably entirely tube fed from Mauna Ulu, although local, limited feeding by dikes could also have occurred. The posteruption reinflation and related increase in the number of shallow summit earthquakes suggest that the reestablished link between the summit reservoir and Mauna Ulu and Alae was not a good conductor of magma. Alternatively, the increase in seismicity may reflect adjustment in brittle rock of the summit region and east rift zone during reinflation of the magma reservoir. After May 5, both the east-rift and summit seismicity were characterized by higher background levels than previously (fig. 16.46). The partial draining of Mauna Ulu lava lake and the demise of the Alae vent in early June are not clearly recognizable in the record of east-rift seismicity, though they are reflected by brief deflation at Uwekahuna and associated slight decrease in summit seismicity. The next significant increase in east-rift seismicity after the May 5 eruption occurred in late July 1973 (fig. 16.46), when collapse of the Mauna Ulu Crater floor triggered a flurry of rockfalls.

The month-long dramatic increase in the number of shallow summit earthquakes during October 1973 was the most noteworthy seismic activity since late 1971 and coincided with a period of strong inflation. The heightened seismicity began to wane in late October, when renewed vigorous activity in the rapidly rising Mauna Ulu lava lake indicated increased east-rift magma storage, and returned to background levels with the onset of the overflow from Mauna Ulu during November 4–8. Curiously, the east-rift seismicity preceding and accompanying the draining of Mauna Ulu lava lake and the November 10 outbreak at Pauahi was relatively weak and short-lived compared to that for similar events in May 1973 (fig. 16.46). The reappearance of Mauna Ulu lava lake on December 13 was heralded by increased local harmonic tremor, but otherwise it was not expressed seismically, either at the summit or the east rift zone.

We have postulated a period of quasi-steady-state activity from December 1973 to July 1974, largely on the basis of the small net change in Uwekahuna tilt. However, we have shown that this period differs from the quasi-steady-state period of February 1972–April 1973 in eruptive style. It also has a different seismic signature, characterized by significantly greater variation in the number of shallow summit earthquakes, which generally can be correlated with more variable oscillations in Uwekahuna tilt. The variations in both seismicity and Uwekahuna tilt during the final 8 months of the eruption bear a crude resemblance to those during stages 2 and 3 (January 1970–June 1971) of the 1969–71 Mauna Ulu eruption (fig. 16.44; Swanson and others, 1979, pl. 2).

The irregular increase in the number of shallow summit earthquakes following the November 10, 1973, Pauahi outbreak is inferred to reflect increased summit storage, even while the conduit

system between the summit and Mauna Ulu was gradually becoming more open and efficient in magma transfer. By mid-January 1974, the magma pathway between the summit reservoir and Mauna Ulu was fully reestablished, as evidenced by the precise correlation among the bursts of high fountaining and overflows, summit seismicity, and minor changes in Uwekahuna tilt during the five closely spaced eruptive episodes during January–February 1974 (figs. 16.30, 16.46; table 16.3). We believe that such an exact correlation can be achieved only if the magma transfer system between the summit reservoir and Mauna Ulu is fully engorged in order to maintain hydraulic equilibrium.

Shallow summit earthquakes typically increased in number before observed eruptive episodes during January–June 1974, but summit seismicity dropped abruptly and summit deflation began immediately before the high lava fountaining and voluminous overflows of the eruptions. As the summit deflated and magma moved to the eruption site during most such episodes, east-rift seismicity increased and summit seismicity decreased, in a manner like that during some of the high-fountaining events in stage 1 of the 1969–71 Mauna Ulu eruption (Swanson and others, 1979, pl. 2) and the well-documented example of summit to east rift magma transfers during April–August 1980 (Dzurisin and others, 1984, fig. 4).

VARIATION IN HARMONIC TREMOR

At Kilauea and well-monitored volcanoes elsewhere in the world, harmonic tremor has been shown to be linked to magma movement, surficial as well as subterranean, and to commonly precede and accompany intrusions and eruptions (Aki and Koyanagi, 1981). As during the 1969–71 Mauna Ulu eruption, shallow harmonic tremor in the upper east rift zone and summit area occurred at varying intensities throughout the 1972–74 Mauna Ulu eruption. Harmonic tremor typically increased in intensity and (or) became sustained shortly before and during changes in loci of energetic vent activity, including the opening of new vents. When visible activity was feeble or absent, harmonic tremor typically was more sporadic and barely detectable; on rare occasions, for as long as a few days, tremor decreased to levels too low to be discerned from background with normal gain settings of the seismic instruments.

Of perhaps greater significance is the increased occurrence of the so-called deep harmonic tremor during the period 1969–75 (Dzurisin and others, 1984). Such tremor is believed to originate in Kilauea's deep magma source region at a depth of approximately 40–50 km and to reflect the production and ascent of magma supplying Kilauea's shallow summit reservoir. A marked increase in the amplitude and duration of recorded deep tremor was observed coincident with the onset of the 1969–71 Mauna Ulu eruption.

The trend of increasing deep tremor peaked at the end of 1972, but occurrence remained much above average through 1975 (Dzurisin and others, 1984, fig. 10). We suggest that the period of maximum deep tremor correlates with the February 1972–April 1973 period of quasi-steady-state activity at Mauna Ulu. However, the increased occurrence in deep tremor apparently was not accompanied by concomitant increase in deep or crustal earthquakes at Kilauea (fig. 16.45). The foci of Kilauea crustal earthquakes (depth 5–13 km) are interpreted to define the feeding conduits from the deep magma source region to the shallow summit reservoir (Koyanagi and others, 1976a, fig. 5). Thus, our data may corroborate the speculation of Dzurisin and others (1984, p. 203) that "the rates of deep magma production and shallow supply to Kilauea may be closely linked" and that "a pulse of relatively rapid magma supply during 1968–1975 may have been responsible for the sustained eruptions at Mauna Ulu during 1969–1971 and 1972–1974." We recognize, however, that the correlation between deep tremor, magma supply, and eruptive activity is imperfect. For example, the 1967–68 Halemaumau eruption (Kinoshita and others, 1969) had the same magma supply rate as the 1969–1971 Mauna Ulu eruption (Swanson, 1972) but there was little associated deep tremor (Dzurisin and others, 1984, fig. 10).

SIGNIFICANCE OF THE 1972–74 MAUNA ULU ERUPTION

During the 1969–71 eruption, volcanic shield development was greatest during periods characterized by numerous short-distance and short-duration overflows from the main vents at Mauna Ulu. Swanson and others (1979, fig. 6) traced in detail the growth of Mauna Ulu shield, whose height grew at an average rate of about 6 m/mo and reached 80 m above the pre-eruption ground surface by the end of the major overflow activity in July 1970. At Alae, the complex filling, overflows, and draining of the lava lake between February 1969 and April 1971 resulted in net accretion of 29–40 m of lava above the rim of buried Alae Crater (Swanson and Peterson, 1972, fig. 2; Swanson and others, 1972, fig. 10). However, when activity ended in 1971, the altitude of the lowest point on the Alae lake surface, which rose or dropped by much as 19 m in response to the individual episodes of filling and subsidence, was determined in June 1971, after final settling, to be about 6 m higher than the pre-1969 datum (Swanson and Peterson, 1972, table 1).

During the 1972–74 eruption, countless overflows from vent C and subsidiary vents at Alae again filled the shallow subsidence bowl formed in 1971, and they accreted approximately another 60 m onto the complex Alae shield, increasing its height to about 100 m above the pre-1969 datum (the pre-eruption southeast rim of Alae Crater at 915 m above sea level, the same datum used by Swanson and Peterson, 1972).

At Mauna Ulu, the shield grew only slightly and irregularly from many small overflows during February–March 1972 and again during early November 1973. Vigorous growth comparable to that during 1969–70 occurred only during voluminous but short-lived eruptive episodes in 1974. By the end of April 1974, the height of the Mauna Ulu shield was 117 m above the pre-May 1969 ground surface (datum is 951 m above sea level, the same as used by Swanson and others, 1979, fig. 6) and its width increased proportionately. The final and most voluminous overflow of May 29–June 2, 1974, added another 4 m to the summit of the shield, resulting in its maximum height of 121 m above the pre-May 1969 base at the

end of the eruption. The May 1972 configuration of Mauna Ulu and Alae shields in May 1972 and of a mound filling the deep west pit of Makaopuhi Crater is schematically shown in figure 16.13. This configuration essentially persisted throughout the 1972–74 Mauna Ulu eruption, but the elevations of the landforms were modified by posteruption settling.

A comparison of the 1963 1:24,000 topographic map (based on 1954 aerial photographs) and the 1981 topographic map (based on 1977 aerial photographs) shows the following changes associated with the 1969–74 Mauna Ulu eruptions:

(1) The summit area of Mauna Ulu shield in 1977 is about 111 m above the pre-eruption ground surface, and the summit crater is deeper than 30 m.

(2) The site of buried Aloi Crater is well expressed topographically by a crudely circular area of minor subsidence (not more than 5 m) on the west flank of Mauna Ulu shield.

(3) The highest areas on the complex Alae shield, which rim the small collapse pit in the area of the (former) vent C, are nearly 90 m above the pre-1969 datum. The subsidence bowl that existed in 1971 is still reflected by a broad area of subsidence roughly coincident with the deeper compartment of the buried Alae Crater.

(4) Benchmarks not buried by 1969–74 flows have been raised or lowered a few meters, presumably in response to complex ground deformation related to eruptions during the period 1954–1977, principally the Mauna Ulu eruptions.

(5) Comparison of the maximum heights attained by Mauna Ulu and Alae during the eruption (121 m and 100 m, respectively) with their heights in 1977, as indicated by the 1981 topographic map (111 m and 90 m, respectively), demonstrates posteruption settling of about 10 m.

SUSTAINED OVERFLOWS: DEVELOPMENT OF LAVA-TUBE SYSTEMS

The 1969–74 Mauna Ulu eruptions afforded the opportunity, for the first time at Kilauea, to study the formation and evolution of lava tubes (see Greeley, 1971, 1972; Cruikshank and Wood, 1972; Peterson and Swanson, 1974; Peterson, 1983). Lava-tube and related flow processes have been described in detail by these geologists; we wish here only to outline some general observations especially pertinent to the 1972–74 eruption:

This paper is in general a sequel to the study by Swanson and others (1979) of the 1969–71 Mauna Ulu eruption. Indeed, we have presented our observations and inferences on the 1972–74 Mauna Ulu eruption in a format parallel to theirs in order to emphasize the continuity of similar eruptive processes and to facilitate the comparison of these two eruptions, separated by about 3½ months of inactivity, in the same area of Kilauea's east rift zone. Not surprisingly, much of Swanson and others' (1979) perception of the significance of the 1969–71 Mauna Ulu eruption applies also to the 1972–74 eruption.

LONG-LIVED FLANK ACTIVITY

It has previously been noted (Peterson and others, 1976; Swanson and others, 1979) that the Mauna Ulu eruptions were the longest nearly continuous rift activity at Kilauea in historical times (that is, since about A.D. 1750): the 1969–71 eruption lasted 875 days and the 1972–74 eruption lasted 901 days. Most historical flank eruptions of Kilauea have lasted a few weeks at most and more typically a few days or less. The Mauna Ulu eruptions of 1969–74 included several prolonged periods of remarkably continuous lava-lake activity, previously observed only at Halemaumau within the summit caldera during the 19th and early 20th centuries.

CONTINUOUS LAVA-LAKE ACTIVITY

Throughout much of the 1972–74 Mauna Ulu eruption, active lava lakes operated within the summit crater of Mauna Ulu and at Alae. Mauna Ulu lava lake was apparently fed directly by the magma conduit leading from the summit reservoir, whereas Alae lava lake was supplied through a very efficient tube system connected to Mauna Ulu. Lake circulation patterns and persistent vent activity suggest that magma from Kilauea summit most likely entered the Mauna Ulu system at an intricately branched inlet located beneath the area between vents A and B (fig. 16.3). The magma was directed from there through complex branches westward to feed Mauna Ulu lava lake and eastward to supply Alae lake, generally through vent C. We speculate that from mid-March 1972 through April 1973, eastward shunting of lava from the inlet dominated and resulted in vigorous activity at or near Alae and relatively sluggish activity at Mauna Ulu lava lake. The tube system connecting Mauna Ulu and Alae never fully recovered from its disruption in early May 1973, and vent C at Alae was severed from the inlet by early June. Magma thereafter was shunted westward from the inlet area to feed activity at Mauna Ulu for the remainder of the eruption.

Gas-piston activity associated with rises and falls of lava columns at Mauna Ulu and Alae was commonly observed during the 1969–74 eruptive activity. Short-term minor fluctuations in level of Mauna Ulu and Alae lava lakes may simply be due to larger scale gas-piston activity of a magma column of greater volume and lateral extent. However, large variations in lake levels over a period of time probably reflect major changes affecting either the magma-transfer system linking the Kilauea summit reservoir and the eruption site, or possibly even changes in the reservoir itself. The levels of Mauna Ulu and Alae lava lakes often varied sympathetically (fig. 16.19); at no time during 1972 did a drop in level at Mauna Ulu correlate with a rise in level at Alae or vice versa, but this correlation was weaker in early 1973. Moreover, the variations in lake level at times exhibited an unmistakable positive correlation with summit tilt (fig. 16.19). These observations suggest that a hydrostatic balance existed between the Kilauea summit reservoir, the Mauna Ulu holding tank, and the vent at Alae, compatible with the postulated quasi-steady-state magma regime operating during two long periods of the 1972–74 eruption. Detailed study of the hydrodynamics and evolution of active lava lakes at Mauna Ulu and Alae should bear importantly on the overall magma-transfer regime of Kilauea during sustained rift activity.

SHORT-DURATION OVERFLOWS: VOLCANIC SHIELD DEVELOPMENT

Volcanic shields are built by repeated eruptions of fluid lava from centralized vents. A number of small shields dot the flanks of Kilauea Volcano; examples include Kane Nui o Hamo (prehistoric) and Heiheiahulu (circa A.D. 1750?) on the east rift zone, and Mauna Iki (1919–20) on the southwest rift zone (fig. 16.1). However, it was not until the 1969–74 Mauna Ulu eruptions that shield development at Kilauea could be systematically observed and documented.

(1) Steady lava output from the vent over a long period of time (weeks to months) is the most important prerequisite in the development of channelized flows and, ultimately, lava tubes. Short-lived or erratic vent activity, even if of high volume, does not allow the formation of lava tubes.

(2) As shown in the chronological narrative, periods of sustained overflows leading to lava-tube development and periods of frequent short-duration overflows leading to shield growth generally are not coincident. On occasion, however, these two types of eruptive activity may grade from one into the other over a transition interval of several weeks; thus, both activities may go on concurrently for short periods of time.

(3) Systematic field observations of the transition of pahoehoe to aa during the sustained overflows permitted the documentation of several modes of transition and demonstrated that moving lava flows function as natural viscometers. Peterson and Tilling (1980) proposed the concept of a transition threshold zone to portray the observed inverse critical relation between viscosity and shear rate in the transition from pahoehoe to aa; this model was refined by Kilburn (1981).

(4) Sustained overflows and development of well-integrated tube systems enabled lava to be transported as far as 12 km from vents at Mauna Ulu and Alae. Flows that filled the deep west pit of Makaopuhi Crater were tube fed, as were those that entered the sea in August–October 1972 and in February–May 1973.

(5) Lava-tube systems are efficient but fragile conductors of lava and can be easily blocked or disrupted, as evidenced by the apparent drastic effect of the April 26, 1973, Honomu earthquake on the tube system feeding lava into the sea. By May 1, earthquake-induced impediments and blockage caused all flow to cease.

CHEMICAL VARIATIONS (MAGMA BATCHES)

The long-lived Mauna Ulu eruptions provided a unique opportunity to study and model subtle variations in major-element chemistry during the course of a lengthy eruption. Using the chemical composition of the lava from the 1967–68 summit eruption at Halemaumau (Kinoshita and others, 1969) as the reference analysis, Wright and others (1975) identified, after adjusting for olivine control, five chemical variants (magma batches) for the 1969–71 Mauna Ulu lava. Identification of these subtly different chemical variants in turn enabled Wright and others (1975) to demonstrate that the lava from a new fissure cutting Aloi Crater and the adjacent west flank of Mauna Ulu shield in early April 1970 was identical to that erupted by Mauna Ulu on the same date but distinct from that in preceding Mauna Ulu eruptions. Swanson and others (1979, p. 38–39) concluded that "a batch of new magma entered both the Mauna Ulu and Aloi plumbing systems just before the outbreak, implying that the systems were interconnected at some unknown depth." Hoffman and others (1984) contend, however, that the variations in the composition of the 1969–71 Mauna Ulu lava can be interpreted in terms of a partial melting model without resort to different magma batches from the mantle.

Wright and Tilling (1980) extended such chemical studies to include lava erupted during the two 1971 summit eruptions, the 1972–74 Mauna Ulu eruption, and the eruptions of July, September, and December 1974. They recognized five new magma batches (chemical variants) and concluded that the following processes were common to all eruptions in the period 1969–1974 (Wright and Tilling, 1980, p. 786):

"1. appearance of new chemically distinct batches of magma,
2. mixing of two or more of these batches prior to eruption,
3. subordinate isolation and cooling of magma followed by flow differentiation leading to eruption of differentiated compositions."

Analysis of the distribution in time and space of the chemically distinct magma batches makes it possible to estimate the residence times and volumes of these batches. For example, on the basis of such information, Wright and Tilling (1980, p. 777) suggest that the appearance of fractionated magma in July 1974 can be related to the isolation and cooling of magma introduced into shallow storage 2½ to 4 years before.

QUASI-STEADY-STATE ACTIVITY

The small amount of net summit inflation observed, together with other evidence presented earlier in this paper, suggests that a quasi-steady-state magma-transfer regime prevailed throughout much of the 1972–74 eruption. If our concept of quasi-steady-state activity is valid, then the magma influx from the deep source region must be approximately constant, at least on a time-averaged basis, and nearly equal to the increments transferred into the rift zone.

The ground-deformation patterns derived from level, ground tilt, and trilateration surveys during the periods of quasi-steady-state magma transfer, which show little net summit inflation or deflation between surveys, are not always in good agreement with the variations in Uwekahuna tilt (see section titled "Results of level, tilt, and trilateration surveys"). In contrast, deformation patterns during the period of net summit inflation related to the 1973 eruptions in the Pauahi-Hiiaka area, are more coherent. These observations suggest that a threshold amount or rate of summit tilt change must be exceeded in order for the results of ground-deformation surveys encompassing the entire summit region to yield definitive interpretations. This in turn implies that the volcanic edifice has a yield strength and that a finite amount of inelastic deformation must be accommodated before elastic behavior sets in.

COMPARISON WITH 1969–71 MAUNA ULU ERUPTION

The 1972–74 Mauna Ulu eruption shares many characteristics with the 1969–71 eruption. It differs, however, in the following aspects:

(1) The later eruption lacked the high-fountaining episodes (maximum 540 m) and associated larger summit deflation (maximum about 30 μrad) of the 1969 activity (stage 1 of Swanson and others, 1979). Although the behavior in 1974—brief eruptive episodes separated by longer intervals of weak vent activity—was qualitatively reminiscent of the stage 1 activity, fountain heights were smaller by an order of magnitude (40–80 m).

(2) The 1972–74 eruption occurred with practically no net summit inflation, whereas the 1969–71 activity resulted in a net summit inflation of approximately 60 μrad, suggesting that a more efficient magma-transfer regime existed during 1972–74.

(3) The February 1972–April 1973 period of low seismicity on the summit and east rift has no counterpart in the 1969–71 Mauna Ulu eruption.

SUMMARY REMARKS

The 1969–71 and 1972–74 Mauna Ulu eruptions provided an unparalleled opportunity to conduct systematic studies of ongoing eruptive processes associated with long-lived active lava lakes. Many of these studies have already been published (table 16.1; Swanson and others, 1979, table 1), others are in progress. Long-lived lava lakes were commonly active within or near Halemaumau Crater during the 19th and early 20th centuries, but it was not until the Mauna Ulu eruptions that such lava lakes were observed in a flank eruption. As of this writing (June 1985), the current long-lived eruption at Puu Oo in Kilauea's middle east (Wolfe and others, chapter 17) resembles activity during stage 1 of the 1969–71 Mauna Ulu eruption. Will it later evolve into a subsequent stage dominated by one or more active lava lakes? Our experience at Mauna Ulu suggests that it is possible.

REFERENCES

Aki, Keiiti, and Koyanagi, R.Y., 1981, Deep volcanic tremor and magma ascent mechanism under Kilauea, Hawaii: Journal of Geophysical Research, v. 86, no. B8, p. 7095–7109.

Cadle, R.D., Wartburg, A.F., Pollock, W.H., Gandrum, B.W., and Shedlovksy, J.P., 1973, Trace constituents emitted to the atmosphere by Hawaiian volcanoes: Chemosphere, v. 6, p. 231–234.

Casadevall, T.J., and Hazlett, R.W., 1983, Thermal areas on Kilauea and Mauna Loa Volcanoes, Hawaii: Journal of Volcanology and Geothermal Research, v. 16, p. 173–188.

Cruikshank, D.P., and Wood, C.A., 1972, Lunar rilles and Hawaiian volcanic features: possible analogues: The Moon, v. 3. no. 4, p. 412–447.

Davis, P.M., Hastie, L.M., and Stacey, F.D., 1974, Stresses within an active volcano—with particular reference to Kilauea: Tectonophysics, v. 22. no. 3-4, p. 355–362.

Duffield, W.A., 1975, Structure and origin of the Koae fault system, Kilauea Volcano, Hawaii: U.S. Geological Survey Professional Paper 856, 12 p.

Duffield, W.A., Christiansen, R.L., Koyanagi, R.Y., and Peterson, D.W., 1982, Storage, migration, and eruption of magma at Kilauea Volcano, Hawaii, 1971–72: Journal of Volcanology and Geothermal Research, v. 13, p. 273–307.

Dvorak, John, Okamura, Arnold, and Dietrich, J.H., 1983, Analysis of surface deformation data, Kilauea Volcano, Hawaii, October 1966 to September 1970: Journal of Geophysical Research, v. 88, no. B11, p. 9295–9304.

Dzurisin, Daniel, 1978, Planetary studies of Kilauea Volcano, Hawaii: the role of satellitic shields in Kilauea's recent evolution, *in* Strom, Robert and Boyce, Joseph, compilers, Reports of Planetary Geology Program 1977–1978 : NASA Technical Memorandum 79729, p. 192–193.

———1980, Influence of fortnightly earth tides at Kilauea Volcano, Hawaii: Geophysical Research Letters, v. 7, no. 11, p. 925–928.

Dzurisin, Daniel, Anderson, L.A., Eaton, G.P., Koyanagi, R.Y., Lipman, P.W., Lockwood, J.P., Okamura, R.T., Puniwai, G.S., Sako, M.K., and Yamashita, K.M., 1980, Geophysical observations of Kilauea Volcano, Hawaii, 2. Constraints on the magma supply during November 1975–September 1977: Journal of Volcanology and Geothermal Research, v. 7, p. 241–269.

Dzurisin, Daniel, and Koyanagi, R.Y., 1981, Changed magma budget since 1975 at Kilauea Volcano, Hawaii: U.S. Geological Survey Open-File Report 81–571, 46 p.

Dzurisin, Daniel, Koyanagi, R.Y., and English, T.T., 1984, Magma supply and storage at Kilauea Volcano, Hawaii, 1956–1983: Journal of Volcanology and Geothermal Research, v. 21, p. 177–206.

Eaton, J.P., 1962, Crustal structure and volcanism in Hawaii: American Geophysical Union, Geophysical Monograph 6, p. 13–29.

Eaton, J.P., and Murata, K.J., 1960, How volcanoes grow: Science, v. 132, no. 3432, p. 925–938.

Ellsworth, W.L., and Koyanagi, R.Y., 1977, Three-dimensional crust and mantle structure of Kilauea Volcano, Hawaii: Journal of Geophysical Research, v. 82, no. 33, p. 5379–5394.

Epp, David, Decker, R.W., and Okamura, A.T., 1983, Relation of summit deformation to east rift zone eruptions on Kilauea Volcano, Hawaii: Geophysical Research Letters, v. 10, no. 7, p. 493–496.

Fiske, R.S., and Kinoshita, W.T., 1969, Inflation of Kilauea Volcano prior to the 1967–68 eruption: Science, v. 165, no. 3891, p. 341–349.

Greeley, Ronald, 1971, Observations of actively forming lava tubes and associated structures, Hawaii: Modern Geology, v. 2, no. 3, p. 207–223.

———1972, Additional observations of actively forming lava tubes and associated structures, Hawaii: Modern Geology, v. 3, no. 3, p. 157–160.

———1974, editor, Guidebook to the Hawaiian Planetology Conference: NASA TMX 62362, Washington, D.C., 257 p.

Grigg, Rick, 1973, Fire under the sea: Oceans, v. 6, no. 2, p. 6–11.

Hawaiian Volcano Observatory, 1977a, Summary 65: January, February, and March 1972: Menlo Park, California, U.S. Geological Survey, 54 p.

———1977b, Summary 66: April, May, and June 1972: Menlo Park, California, U.S. Geological Survey, 44 p.

———1977c, Summary 67: July, August, and September 1972: Menlo Park, California, U.S. Geological Survey, 27 p.

———1977d, Summary 68: October, November, and December 1972: Menlo Park, California, U.S. Geological Survey, 29 p.

———1977e, Summary 69: January, February, and March 1973: Menlo Park, California, U.S. Geological Survey, 24 p.

———1977f, Summary 70: April, May, and June 1973: Menlo Park, California, U.S. Geological Survey, 61 p.

———1977g, Summary 71: July, August, and September 1973: Menlo Park, California, U.S. Geological Survey, 38 p.

———1977h, Summary 72: October, November, and December 1973: Menlo Park, California, U.S. Geological Survey, 42 p.

———1978, Summary 74: January to December, 1974: Menlo Park, California, U.S. Geological Survey, 164 p.

Hazlett, R.W., 1981, Guide to points of geologic interest in Hawaii Volcanoes National Park, Hawaii: Circum-Pacific Energy and Mineral Resources Conference, 55 p.

Hoffman, A.W., Feigenson, M.D., and Raczek, Ingrid, 1984, Case studies on the

origin of basalt: III. Petrogenesis of the Mauna Ulu eruption, Kilauea, 1969–71: Contributions to Mineralogy and Petrology, v. 88, p. 24–35.

Holcomb, R.T., 1973, Lava-subsidence terraces of Kilauea Volcano, Hawaii: International Union for Quaternary Research, Christchurch, New Zealand, Dec. 2–10, 1973, Ninth Congress Program, p. 152–153 (extended abstract).

———1976, Preliminary map showing products of eruptions, 1962–1974 from the upper east rift zone of Kilauea Volcano, Hawaii: U.S. Geological Survey Miscellaneous Field Studies Map MF–811, scale 1:24,000.

———1980, Preliminary geologic map of Kilauea Volcano, Hawaii: U.S. Geological Survey Open-File Report 80–796, scale 1:50,000, 2 sheets.

Holcomb, R.T., Peterson, D.W., and Tilling, R.I., 1974, Recent landforms at Kilauea Volcano, a selected photographic compilation, *in* Greeley, R.W., ed., Guidebook to the Hawaiian Planetology Conference, Washington, D.C., NASA TMX 62362, p. 49–86.

Jackson, D.B., Swanson, D.A., Koyanagi, R.Y., and Wright, T.L., 1975, The August and October 1968 east rift eruptions of Kilauea Volcano, Hawaii: U.S. Geological Survey Professional Paper 890, 33 p.

Jaggar, T.A., 1920, Seismometric investigation of the Hawaiian lava column: Seismological Society of America Bulletin, v. 10, no. 4, p. 155–275.

———1947, Origin and development of craters: Geological Society of America Memoir 21, 508 p.

Kilburn, C.R.J., 1981, Pahoehoe and aa lavas: a discussion and continuation of the model of Peterson and Tilling: Journal of Volcanology and Geothermal Research, v. 11, no. 2-4, p. 373–382.

Kinoshita, W.T, Koyanagi, R.Y., Wright, T.L., and Fiske, R.S., 1969, Kilauea Volcano—The 1967–68 summit eruption: Science (AAAS), v. 166, no. 3904, p. 459–468.

Kinoshita, W.T., Swanson, D.A., and Jackson, D.B., 1974, The measurement of crustal deformation related to volcanic activity at Kilauea Volcano, Hawaii, *in* Civetta, L., Luongo, G., and Rapolla, A., eds., Physical Volcanology, Developments in solid earth Geophysics: Amsterdam, Elsevier Publishers, v. 6, p. 87–116.

Klein, F.W., 1982, Patterns of historical eruptions at Hawaiian volcanoes: Journal of Volcanology and Geothermal Research, v. 12, p. 1–35.

Koyanagi, R.Y., Endo, E.T., and Ward, P.L., 1976a, Seismic activity on the island of Hawaii, 1970 to 1973, *in* Sutton, G.H., Manghnani, M.H., and Moberly, Ralph, eds., The Geophysics of the Pacific Ocean Basin and its margin: Geophysical Monograph 19, American Geophysical Union, Washington, D.C., p. 169–172.

Koyanagi, R.Y., Unger, J.D., and Endo, E.T., 1973, Seismic evidence for magma intrusion in the eastern Koae fault system, Kilauea Volcano, Hawaii [abs.]: Eos. American Geophysical Union Transaction, v. 54, no. 11, p. 1216.

Koyanagi, R.Y., Unger, J.D., Endo, E.T., and Okamura, A.T., 1976b, Shallow earthquakes associated with inflation episodes at the summit of Kilauea Volcano, Hawaii: International Association of Volcanology and Chemistry of the Earth's Interior, Symposium on Andean and Antarctic Volcanology Problems, p. 621–631.

Lipman, P.W., 1980, Rates of volcanic activity along the southwest rift zone of Mauna Loa Volcano, Hawaii: Bulletin Volcanologique, v. 43-4, p. 703–725.

Macdonald, G.A., and Hubbard, D.H., 1982, Volcanoes of the National Parks in Hawaii (8th ed.): Hawaii, Hawaii Natural History Association, Hawaii Volcanoes National Park, 64 p.

Moore, J.G., 1975, Mechanism of formation of pillow lava: American Scientist, v. 63, p. 269–277.

Moore, J.G., Phillips, R.L., Grigg, R.W., Peterson, D.W., and Swanson, D.A., 1973, Flow of lava into the sea, 1969–1971, Kilauea Volcano, Hawaii: Geological Society of America Bulletin, v. 84, no. 2, p. 537–546.

Moore, R.B., Helz, R.T., Dzurisin, Daniel, Eaton, G.P., Koyanagi, R.Y., Lipman, P.W., Lockwood, J.P., and Puniwai, G.S., 1980, The 1977 eruption of Kilauea Volcano, Hawaii: Journal of Volcanology and Geothermal Research, v. 7, p. 189–210.

Naughton, J.J., Lee, J.H., Keeling, D., Finlayson, J.B., and Dority, G., 1973, Helium flux from the Earth's mantle as estimated from Hawaiian fumarolic degassing: Science (AAAS), v. 180, no. 4081, p. 55–57.

Peterson, D.W., 1976, Processes of volcanic island growth, Kilauea Volcano, Hawaii, 1969–1973: International Association of Volcanology and Chemistry of the Earth's Interior, Symposium on Andean and Antarctic Volcanology Problems, Proceedings, p. 172–189.

———1983, Processes of development of lava tubes at Mauna Ulu, Kilauea Volcano, Hawaii [abs.]: The NSS Bulletin (Quarterly Journal of the National Spelelogical Society), v. 45, no. 1, unpaginated insert following p. 8.

Peterson, D.W., Christiansen, R.L., Duffield, W.A., Holcomb, R.T., and Tilling, R.I., 1976, Recent activity of Kilauea Volcano, Hawaii: International Association of Volcanology and Chemistry of the Earth's Interior, Symposium on Andean and Antarctic Volcanology Problems, Proceedings, p. 646–656.

Peterson, D.W., and Swanson, D.A., 1974, Observed formation of lava tubes during 1970–71 at Kilauea Volcano, Hawaii: Studies in Speleology, v. 2, part 6, p. 209–222.

Peterson, D.W., and Tilling, R.I., 1980, Transition of basaltic lava from pahoehoe to aa, Kilauea Volcano, Hawaii: field observataions and key factors: Journal of Volcanology and Geothermal Research, v. 7, p. 271–293.

Ryan, M.P., Blevins, J.Y.K., Okamura, A.T., and Koyanagi, R.Y., 1983, Magma reservoir subsidence mechanics: theoretical summary and application to Kilauea Volcano, Hawaii: Journal of Geophysical Research, v. 88, no. B5. p. 4147–4181.

Ryan, M.P., Koyanagi, R.Y., and Fiske, R.S., 1981, Modeling the three-dimensional structure of macroscopic magma transport systems: application to Kilauea Volcano, Hawaii: Journal of Geophysical Research, v. 86, no. B8, p. 7111–7129.

Sicks, G.C., 1975, The kinetics of silica dissolution from volcanic glass in the marine environment: HIG–75–23, Hawaii Institute of Geophysics, University of Hawaii, 82 p.

Swanson, D.A., 1972, Magma supply rate of Kilauea Volcano, 1952–1971: Science (AAAS), v. 175, no. 4018, p. 169–170.

Swanson, D.A., Duffield, W.A., and Fiske, R.S., 1976b, Displacement of the south flank of Kilauea Volcano: the result of forceful intrusion of magma into the rift zones: U.S. Geological Survey Professional Paper 963, 39 p.

Swanson, D.A., Duffield, W.A., Jackson, D.B., and Peterson, D.W., 1972, The complex filling of Alae Crater, Kilauea Volcano, Hawaii: Bulletin Volcanologique, v. 36, no. 1, p. 105–126.

———1979, Chronological narrative of the 1969–71 Mauna Ulu eruption of Kilauea Volcano, Hawaii: U.S. Geological Survey Professional Paper 1056, 55 p.

Swanson, D.A., Jackson, D.B., Duffield, W.A., and Peterson, D.W., 1971, Mauna Ulu eruption, Kilauea Volcano: Geotimes, v. 16, no. 5, p. 12–16.

Swanson, D.A., Jackson, D.B., Koyanagi, R.Y., and Wright, T.L., 1976a, The February 1969 east rift eruption of Kilauea Volcano, Hawaii: U.S. Geological Survey Professional Paper 891, 30 p.

Swanson, D.A., and Peterson, D.W., 1972, Partial draining and crustal subsidence of Alae lava lake, Kilauea Volcano, Hawaii: U.S. Geological Survey Professional Paper 800–C, p. C1–C14.

Tepley, Lee, 1975, Fireworks erupt when hot lava pours into the sea, 1975, Smithsonian, v. 6, no. 8. p. 70–75.

Tilling, R.I., 1976a, Rockfall activity in pit craters, Kilauea Volcano, Hawaii: International Association of Volcanology and Chemistry of the Earth's Interior, Symposium on Andean and Antarctic Volcanology Problems, Proceedings, p. 518–528.

———1976b, The 7.2 magnitude earthquake, November 1975, Island of Hawaii: Earthquake Information Bulletin, v. 8, no. 6, p. 5–13.

Tilling, R.I., Christiansen, R.L., Duffield, W.A., Holcomb, R.T., and Peterson, D.W., 1986, Determinations of the depth to the surfaces of active lava lakes at Mauna Ulu and Alae, Kilauea Volcano, Hawaii: U.S. Geological Survey Open-File Report 86–367, 16 p.

Tilling, R.I., Holcomb, R.T., Lipman, P.W., and Lockwood, J.P., 1976b, Rates of structural and landform evolution of Hawaiian volcanoes: role of short-lived and catastrophic processes: NASA Technical Memorandum X–3364, p. 157–158.

Tilling, R.I., Holcomb, R.T., Lockwood, J.P., and Peterson, D.W., 1976c,

Recent eruptions of Hawaiian volcanoes and the evolution of basaltic landforms: Geologica Romana, v. 15, p. 519–521.

Tilling, R.I., Koyanagi, R.Y., and Holcomb, R.T., 1975, Rockfall seismicity: correlation with field observations, Makaopuhi Crater, Kilauea Volcano, Hawaii: Journal of Research, U.S. Geological Survey, v. 3, no. 3, p. 345–361.

Tilling, R.I., Koyanagi, R.Y., Lipman, P.W., Lockwood, J.P., Moore, J.G., and Swanson, D.A., 1976a, Earthquake and related catastrophic events, Island of Hawaii, November 29. 1975: a preliminary report: U.S. Geological Survey Circular 740, 33 p.

Tilling, R.I., Peterson, D.W., Christiansen, R.L., and Holcomb, R.T., 1973, Development of new volcanic shields at Kilauea Volcano, Hawaii, 1969–1973: International Union for Quaternary Research, Christchurch, New Zealand, December 2–10, 1973, Ninth Congress Program, p. 366–367 (extended abstract).

Unger, J.D., Koyanagi, R.Y., and Ward, P.L., 1973, An important Hawaiian earthquake [abs.]: Eos, Transaction American Geophysical Union, v. 54, no. 11. p. 1136.

Unger, J.D., and Ward, P.L., 1979, A large, deep Hawaiian earthquake—the Honomu, Hawaii event of April 26, 1973: Bulletin of the Seismological Society of America, v. 69, no. 6, p. 1771–1781.

Wright, T.L., Kinoshita, W.T., and Peck, D.L., 1968, March 1965 eruption of Kilauea Volcano and the formation of Makaopuhi lava lake: Journal of Geophysical Research, v. 73, p. 3181–3205.

Wright, T.L., Swanson, D.A., and Duffield, W.A., 1975, Chemical compositions of Kilauea east-rift lava, 1968–1971: Journal of Petrology, v. 16, no. 1, p. 110–133.

Wright, T.L., and Tilling, R.I., 1980, Chemical variation in Kilauea eruptions 1971–74: American Journal of Science, v. 280–A, part 2, p. 777–793.

Zablocki, C.J., 1976, Mapping thermal anomalies on an active volcano by the self-potential method, Kilauea, Hawaii, *in* United Nations Symposium on the Development and Use of Geothermal Resources, 2nd, San Francisco, California, May 1975, Proceedings, v. 2, p. 1299–1309.

———1978, Applications of the VLF induction method for studying some volcanic processes of Kilauea Volcano, Hawaii: Journal of Volcanology and Geothermal Research. v. 3, p. 155–195.

THE PUU OO ERUPTION OF KILAUEA VOLCANO, EPISODES 1–20, JANUARY 3, 1983, TO JUNE 8, 1984

By Edward W. Wolfe, Michael O. Garcia[1], Dallas B. Jackson, Robert Y. Koyanagi, Christina A. Neal, *and* Arnold T. Okamura

ABSTRACT

The Puu Oo eruption began at Napau Crater in the east rift zone of Kilauea Volcano on January 3, 1983. After an initial series of intermittent fissure eruptions, the style changed to one of episodic central-vent eruptions. By early June 1984, 20 eruptive episodes had occurred, including the initial fissure-eruption episode, and approximately 240×10^6 m^3 of new basalt covered an area of more than 30 km^2. Fountains ranging up to nearly 400 m high built large cones at the central vents.

The eruption occurred in a part of the rift zone that had a long history as a locus for intrusions. Tilt changes and flurries of shallow earthquakes recorded accumulation of magma from 1978 through 1980 and again in late 1982. We interpret geodetic and seismic evidence to indicate a shallow magma reservoir in the area before emplacement of the feeder dike in early January 1983. Lava erupted during the first several months was differentiated beyond olivine control and was apparently derived from magma that had undergone prolonged storage and crystal fractionation in the rift zone.

The central-vent eruptive episodes, which began in February 1983 with episode 2, lasted from 9 hours to 12 days. They were characterized by high-volume discharge of lava, vigorous fountaining, rapid summit subsidence, and strong harmonic tremor in the vent area. The repose periods lasted from 8 to 65 days and were characterized by gradual reinflation of Kilauea's summit and persistence of weak harmonic tremor in the vent area. Alternating inflation and deflation in the summit and vent areas occurred sympathetically, suggesting that reservoirs in the rift zone and summit area were hydraulically linked.

After the initial episode, lava was erupted at an average rate of 13.4×10^6 m^3/mo. Long-term tilt change in the summit region was minimal, and, following the approach of Swanson (1972), we have calculated an average magma-supply rate of approximately 10×10^6 m^3/mo after correction for 25 percent porosity. This rate is higher than some estimates for long-term supply to the volcano, but evidence from SO_2-emission rates in the summit region also indicates that the Puu Oo eruption may have coincided with a period of increased magma supply.

After Puu Oo became established as the sole vent, olivine-controlled lava was erupted. Beneath Puu Oo, a column of magma, which may have been nearly vertical and several kilometers long, underwent short-term compositional changes during repose periods that apparently reflected fractionation of olivine. This process repeatedly produced a finite volume of MgO-depleted magma, which would be exhausted whenever the volume of the next eruptive episode exceeded that of MgO-depleted melt. A long-term compositional change manifested by gradually increasing CaO and MgO may have been a consequence either of gradually decreasing contamination of fresh summit melt by differentiated magma present in the rift zone or of gradually changing composition of the melt generated in the mantle.

INTRODUCTION

The Puu Oo eruption began at Napau Crater in the east rift zone of Kilauea Volcano (fig. 17.1) on January 3, 1983. An initial series of intermittent fissure eruptions was followed by a long and continuing series of central-vent eruptions. In the 17-month period reviewed in this paper, twenty major eruptive episodes occurred. Because it is difficult to maintain terminology that is both concise and consistent, for eruptive activity, we apply the term eruption both collectively to the entire series of related eruptive events in the east rift zone during 1983–84 and singly to individual periods of significant lava discharge within that series. Following the usage of Swanson and others (1979), we use the term episode to identify occurrences of fountaining and lava-flow production separated by relatively long quiescent periods during which Kilauea's summit reservoir inflated. Many of the eruptive episodes consisted of single fountaining and flow-production events. Others, however, such as episodes 1, 13, and 19, consisted of two or more such events separated by relatively brief quiescent periods. Thus, some of the episodes were, themselves, series of episodic events.

During those 17 months of activity, nearly 240×10^6 m^3 of basalt was erupted, covering more than 30 km^2 of largely forested country in the middle part of the rift zone and the adjacent part of the south flank of the volcano. Several flows entered sparsely populated areas and destroyed a total of 18 dwellings. Spatter falling from fountains that ranged up to nearly 400 m in height built large cones at the central vents. A 60-m-high cone, Puu Halulu, was formed within the first three months of the eruption; by the end of the twentieth episode, Puu Oo, the cone at the principal vent, stood about 130 m above the preeruption ground surface. At the time of writing (June 1985), the Puu Oo eruption continues unabated and has become the most voluminous historical eruption of Kilauea.

[1]Hawaii Institute of Geophysics, University of Hawaii, Honolulu.

Observational, instrumental, and laboratory results from the first one and one-half years of the Puu Oo eruption are presented in detail in separate papers covering geologic observations (Wolfe and others, in press), data on temperature and composition of sampled lavas (Neal and others, in press), gas studies (Greenland, in press; Greenland and others, in press), seismology (Koyanagi and others, in press), deformation studies (Okamura and others, in press), geoelectric studies (Jackson, in press), and petrology (Garcia and Wolfe, in press). Those papers provide a detailed foundation for this synthesis, and we refer the reader to them for details of topics treated here in summary fashion. Hereinafter, we draw on those papers extensively without further citation except as needed for clarity.

ACKNOWLEDGMENTS

In monitoring this long-lived eruption and organizing and analyzing the data, we received intensive and dedicated help from many associates. We especially thank geologic colleagues N.G. Banks, J. Buchanan-Banks, J.P. Lockwood, R.B. Moore, and G.E. Ulrich, who often joined or relieved us in observing eruptive activity and sampling the lavas. We also thank the staff of the Hawaiian Volcano Observatory for excellent and sustained support in all aspects of the work. John P. Hoffmann called our attention to the relation, illustrated in figure 17.27, between changes in effusion and changes in tilt rate during episode 19. Constructive reviews by T.L. Wright and D.A. Swanson are gratefully acknowledged.

GEOLOGIC SETTING FOR THE PUU OO ERUPTION

STRUCTURE AND MAGMATIC PLUMBING OF KILAUEA

A consistent generalized model of the geologic structure and magmatic plumbing of Kilauea Volcano has been developed from geologic and geophysical studies, particularly over the last three decades. This model has been recently reviewed and expanded by Ryan and others (1981, 1983), and additional recent reviews are given by Duffield and others (1982) and Dzurisin and others (1984). A brief summary of the model follows.

Basaltic magma generated at a probable depth of 60–90 km (Wright, 1984) rises through a system of fractures from deep in the mantle below Kilauea and accumulates within a relatively aseismic reservoir zone (Koyanagi and others, 1974) that lies approximately 2–6 km below the southern part of Kilauea caldera. Most likely the reservoir is a complex of interconnected sills and dikes. Continuing accumulation of magma causes inflation of the reservoir, which is manifested by uplift and distention of the crust that overlies it. Episodic relief from the magmatic stress that develops during filling of the reservoir is provided by summit eruptions and by intrusions that transfer magma from the summit to the rift zones of the volcano. During rift-zone intrusions and eruptions, subsidence and contraction occur in the crust overlying the reservoir; subsidence does not necessarily accompany summit eruptions. Inflations and deflations of the summit reservoir cause measurable tilts on the flanks of the zone of uplift or subsidence. The east-west component of such ground tilt, measured with a sensitivity better than 1 microradian by a continuously recording Hg-capacitance tiltmeter at the Uwekahuna vault (fig. 17.1), approximately 3 km northwest of the center of uplift and subsidence, is used to track the episodes of inflation and deflation. The frequency of shallow earthquakes in the vicinity of the summit reservoir also provides a continuous record of strain manifested as adjustments in the brittle country rock during eposides of inflation and deflation.

Intrusions into a rift zone are commonly accompanied by harmonic tremor and by swarms of shallow (depth <5 km) earthquakes that reflect fracturing of brittle rocks in response to dike emplacement or to volume changes in the magmatic conduit. Dike emplacement is commonly accompanied by ground cracking, extension perpendicular to the rift-zone axis, and vertically directed displacement above and flanking the dike (Pollard and others, 1983). Propagation of a dike to the surface results in an eruption. The close association of subsidence at the summit with intrusion in the rift zone implies a hydraulic link between the summit and the rift zone.

In some cases, either an aseismic zone separates the area of rift intrusion from the summit-reservoir region, or an intrusion occurs without generating an earthquake swarm in the rift zone. In the latter case, the intrusion is manifested by subsidence and related shallow earthquakes at the summit, geodetic and possibly electrical potential-field disturbances in the rift zone, and harmonic tremor. Aseismic transfers of magma, which are common, imply the presence of a preexisting magmatic conduit (Swanson and others, 1976b).

Kilauea abuts the seaward-sloping southeast flank of Mauna Loa, a much larger shield volcano that forms a massive buttress on Kilauea's northwest flank. Kilauea's summit is approximately 5 km above the adjacent sea floor, and its unbuttressed southeast flank is gravitationally unstable. Fiske and Jackson (1972) showed that this geometric arrangement results in orientation of the axis of least compressive stress perpendicular to the boundary between Mauna Loa and Kilauea. Consequently, extension and dike emplacement occur along two steeply dipping zones (the east and southwest rift zones) that approximately parallel the Kilauea-Mauna Loa boundary.

Repeated intrusion, extension, surface cracking, and extrusion have created, in each of the rift zones, a broad, gentle topographic ridge with numerous open cracks, normal faults of small throw, and linear vents, all aligned perpendicular to the direction of least compressive stress. The upper few kilometers of a rift zone must be laced by a complex of dikes that strike parallel to the rift-zone axis. The currently active part of the rift zone, as indicated by the distribution of historical (the last 200 yr) eruptive vents (Holcomb, 1980) is as much as about 2 km wide.

Geophysical evidence, including recognition of local inflation centers (see, for example, Jackson and others, 1975) and the occurrence of aseismic intrusions, indicates that magma persists along at least parts of the rift-zone interior for extended periods of time. This inference is supported by petrologic evidence, which

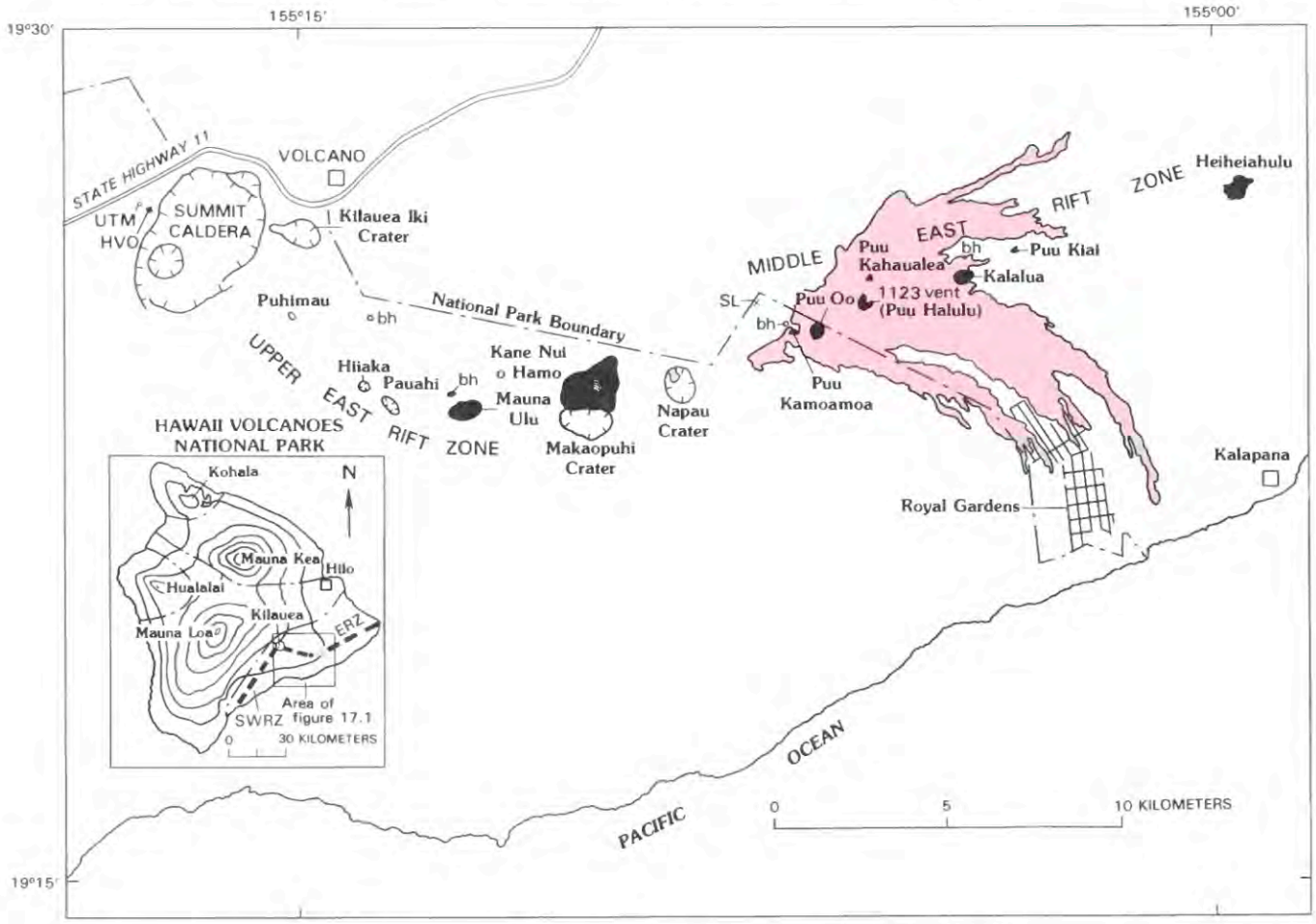

FIGURE 17.1.—Kilauea summit, upper and middle parts of east rift zone, and features discussed in text. HVO, Hawaiian Volcano Observatory; UTM, Uwekahuna tiltmeter; bh, borehole tiltmeter; SL, spirit-level tilt station. Red, flows of episodes 1–20, Puu Oo eruption. Black, shields and large cinder and spatter cones; all except Puu Oo and Puu Halulu predate the Puu Oo eruption. Inset shows location of area and outlines of volcanoes on Island of Hawaii. ERZ, east rift zone of Kilauea; SWRZ, southwest rift zone of Kilauea.

shows that melt of differentiated composition has been a significant component of rift-zone eruptions. Wright and Fiske (1971) have interpreted the differentiated melt as the product of cooling and partial crystallization of magma intruded into the rift zones from the summit region. Furthermore, geologic mapping in the lower east rift zone (Moore, 1983) has revealed areas where repeated eruption of differentiated melt has occurred, implying that local zones favorable to storage of intruded magma have persisted for hundreds of years.

Kilauea's seaward flank, generally called the south flank, is detached from the rest of the volcano along the rift zones, and it undergoes compression and seaward dislocation in response to intrusive activity in the rift zones (Swanson and others, 1976a). The approximate base of the mobile block is recorded by a zone of earthquake hypocenters, 8–9 km deep, that forms a belt parallel to the rift-zone axis but displaced southeastward from it (see fig. 17.8). Focal mechanisms indicate that fault movements occur parallel to a plane dipping 2–3° northwestward (Crosson and Endo, 1982); this subhorizontal zone of decoupling may correspond to a sediment-bearing layer at the interface between the young volcanic rocks that comprise the Island of Hawaii and the isostatically downbowed older sea floor beneath the island (Swanson and others, 1976a; Crosson and Endo, 1982).

The magma supplied to Kilauea from the mantle, then, is accommodated in summit storage, summit and rift-zone eruptions, and rift-zone intrusions. Growth of the volcano results primarily from addition of erupted basalt to its surface and from intrusion accompanied by seaward dislocation of the south flank. Dzurisin and others (1984) concluded that between 1956 and 1983 more than 2×10^9 m^3 of magma had entered Kilauea, at an average rate of about 7×10^6 m^3/mo. Approximately 35 percent of this magma was extruded during that period; the rest was stored in the rift zones, 55 percent in the east rift zone and 10 percent in the southwest rift zone. Apparently the summit reservoir has functioned in recent years, at least, mainly as a temporary holding tank.

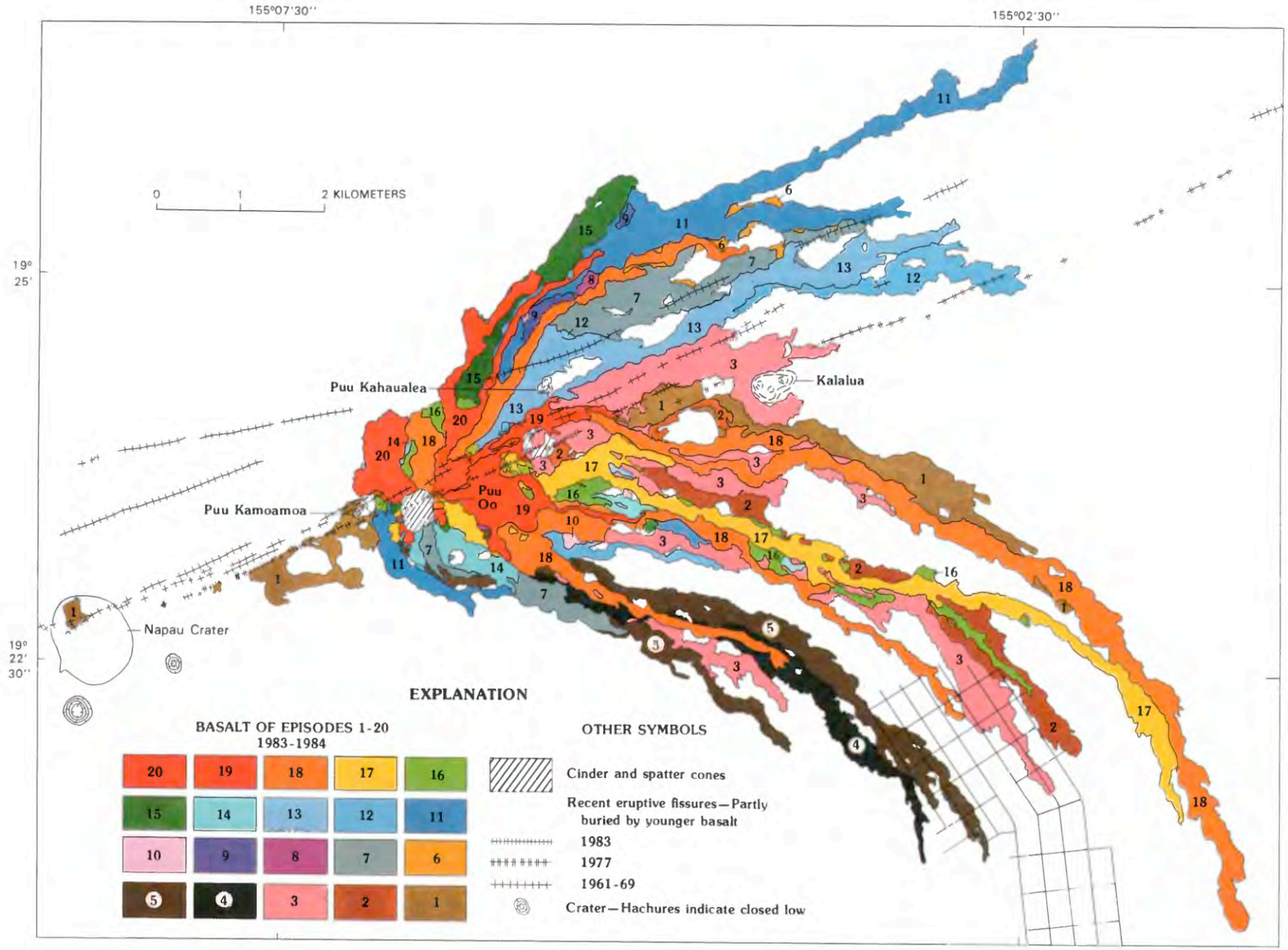

FIGURE 17.2.—Simplified geologic map of vents and flows for episodes 1–20 of the Puu Oo eruption. Also shows traces of recent pre-1983 fissure vents, which include 1977 vents (Moore and others, 1980; R.B. Moore, written commun., 1985) and 1961-69 vents (Moore and Koyanagi, 1969; Swanson and others, 1976b; Swanson and others, 1979). Flows were mapped and field checked using aerial photographs taken, when possible, after each eruptive episode.

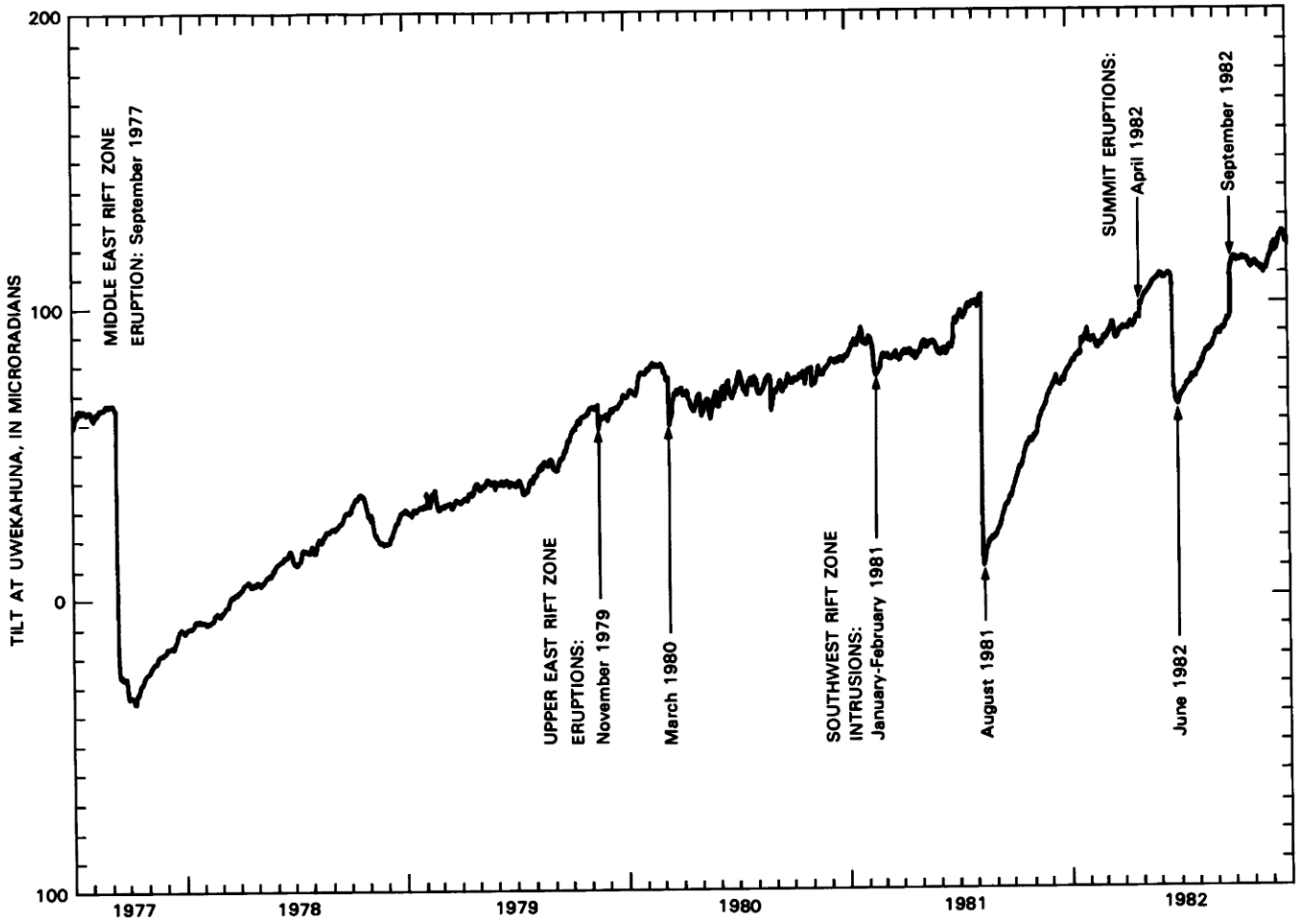

FIGURE 17.3.—East-west summit tilt at Uwekahuna, late 1977 to end of 1982. Increasing values indicate westward-directed (inflationary) tilt change; decreasing values indicate eastward-directed (deflationary) tilt change.

RECENT ACTIVITY IN THE EAST RIFT ZONE, 1955–1982

Eruptions occurred along the lower east rift zone of Kilauea in 1955 and 1960, following a virtual hiatus of 115 years (Macdonald and others, 1983). Thereafter, eruptive activity was confined to the upper and middle parts of the east rift zone. Since 1960, the frequency of earthquake occurrence has been low in the lower east rift and in the adjacent part of the volcano's south flank. Much higher seismicity, in both the rift zone and the south flank, west of the longitude of Heiheiahulu (fig. 17.1) indicates that post-1960 intrusive activity in the east rift zone has been confined to the upper and middle parts.

Fissure eruptions occurred repeatedly in the middle east rift zone from 1961 through 1969 (fig. 17.2). From 1969 through 1974, the two upper-east-rift eruptions at Mauna Ulu (Tilling and others, chapter 16; Swanson and others, 1979) dominated activity at Kilauea. Seaward displacement of Kilauea's south flank and consequent dilation of the rift zone during and after the large ($M = 7.2$) Kalapana earthquake on November 29, 1975, apparently changed the conduit system so that thereafter intrusions dominated rather than eruptions (Dzurisin and others, 1980). Dzurisin and others (1984) identified nine small but distinct intrusions that occurred in the east rift zone from 1976 through 1980. During that period, two minor eruptions (fig. 17.3) occurred in the upper part of the east rift zone, and a relatively voluminous ($35 \times 10^6 m^3$) eruption (Moore and others, 1980) occurred in the middle part (figs. 17.2 and 17.3) in September 1977.

The intrusions in the middle east rift zone were documented in part by tilt measurements. Except where covered by new flows, the middle east rift zone is heavily forested, access is difficult, and deformation data are limited. During the years between the later (1972–74) Mauna Ulu eruption and the 1977 eruption, spirit-level tilt stations in the east rift zone were largely limited to the upper part of the zone and to the part from Heiheiahulu eastward. In that eastern area, tilt measurements in early and mid-1977 showed a middle-east-rift inflation center near Heiheiahulu (Dzurisin and others, 1980). We do not know how far uprift the inflation extended. Following the 1977 eruption and through 1980, an expanded

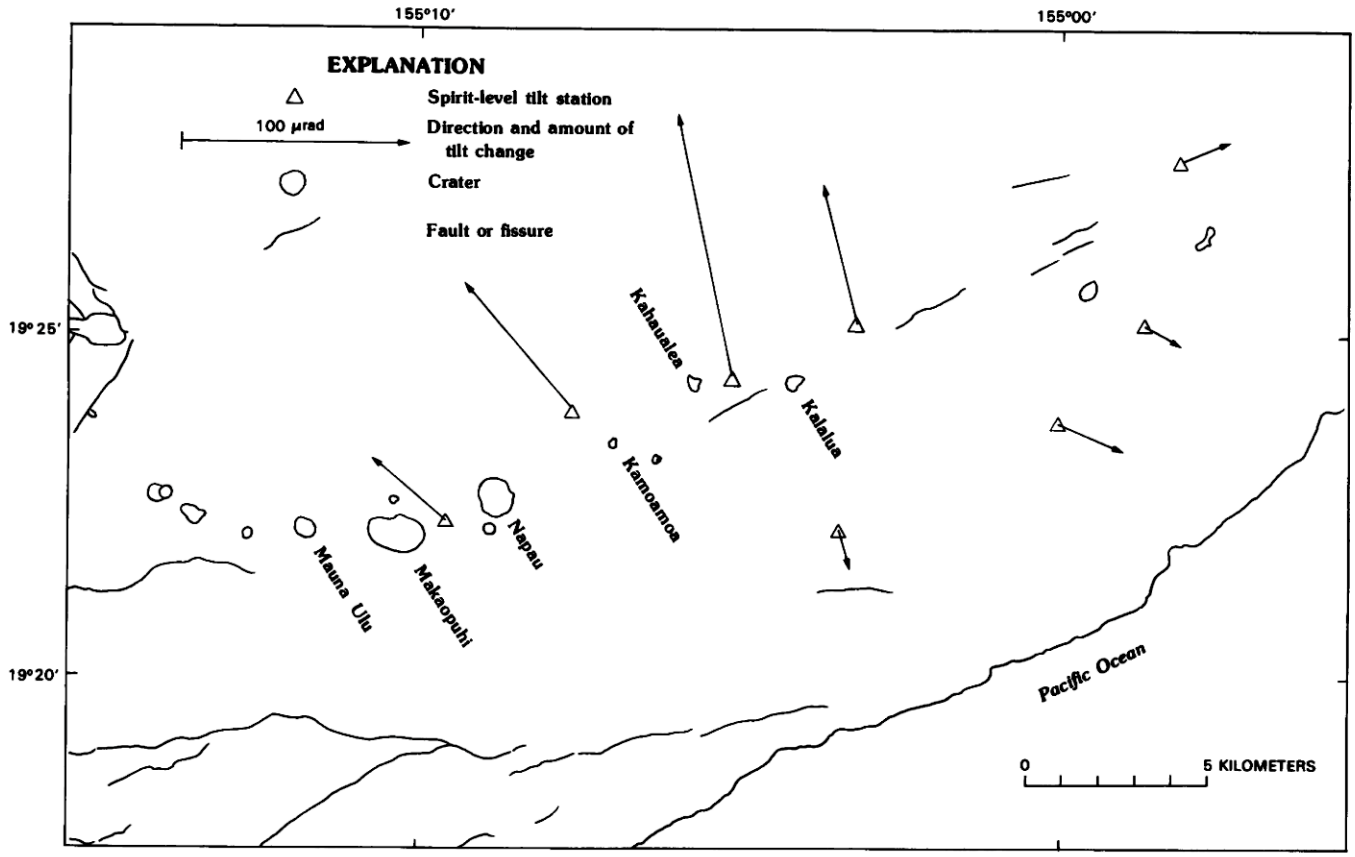

FIGURE 17.4.—Spirit-level tilt results, middle east rift zone, Kilauea Volcano, January 1978 through March 1981.

network of spirit-level tilt stations showed a broad inflationary zone approximately centered on the Puu Kamoamoa-Kalalua area (fig. 17.4).

Intermittent flurries of shallow earthquakes were recorded in the Puu Kamoamoa-Puu Kahaualea region between late 1978 and late 1980 (figs. 17.5*A*, 17.6). The flurries often occurred during or near the ends of episodes of gradual summit deflation. They may identify intrusive pulses that added magma to storage in the middle east rift zone as reflected by the increasing tumescence (fig. 17.4).

Intrusions into the east rift zone virtually ceased early in 1981 at the beginning of a series of southwest-rift-zone intrusions that continued intermittently through June 1982 (figs. 17.3, 17.5*B*). In addition to the seismic quiescence in the east rift zone during that time, there was an almost total absence of deformation, as shown by the borehole tiltmeter near Puu Kamoamoa (fig. 17.1), between early 1981 and late 1982.

Between 1956 and 1983, therefore, at least $1 \times 10^9 m^3$ of magma was added to east-rift-zone storage, according to the calculations of Dzurisin and others (1984). Earthquake distribution patterns indicate that magma accumulated only in the upper and middle parts of the rift zone after the eruption of 1960. Tilt measurements begun in the middle east rift zone after the 1975 Kalapana earthquake show that it was inflating through 1980 and was thus a major locus of magma storage. Magma reservoirs apparently became engorged, and the middle east rift zone became primed for the eruptive activity that began in 1983. The distribution of earthquake epicenters between late 1978 and late 1980 (fig. 17.5*A*) further indicates that intermittent intrusions were adding magma to a reservoir near the future main vents for the Puu Oo eruption.

IMMEDIATE PRECURSORS TO THE PUU OO ERUPTION

After a major intrusion in the southwest rift zone in August 1981, fairly sustained inflation of Kilauea's summit prevailed until late September 1982. A small summit eruption on April 30–May 1, 1982, and a second large southwest-rift intrusion in June 1982 punctuated the inflationary episode. An abrupt intrusion in the already inflated summit region on September 25 caused pronounced uplift (fig. 17.3) and led to a minor eruption in the southernmost part of Kilauea caldera. During the eruption and immediately following it, a swarm of shallow earthquakes migrated into the uppermost part of the east rift zone in the vicinity of Puhimau Crater (fig. 17.5*C*), and concomitant geoelectrical disturbances were meas-

ured in that area and also 4 km farther southeast near Pauahi Crater. However, no measurable surface deformation was detected at that time in the upper east rift, which suggests that no shallow dike was emplaced. Therefore, we infer that a surge of supply within the upper east-rift-zone conduit system led to fracturing of the shallow crustal rocks and development of an electrical anomaly.

Shallow earthquakes continued in the area between Puhimau and Pauahi Craters through early November, but with diminishing frequency after mid-October. A slow tilt change recorded by automatic tiltmeters along the upper east rift zone began on October 6, together with changes in self-potential near Pauahi. These events, which continued until about the end of the month, indicated that a gradual intrusion was under way in the upper east rift zone. Beginning about October 8, additional shallow earthquakes migrated from the upper east rift zone downrift as far as the Napau Crater area, where intermittent shallow earthquakes occurred in late October and early November (fig. 17.7). A gradual tilt change at the automatic tiltmeter near Puu Kamoamoa, beyond the downrift end of the flurry of earthquakes, began on November 8 and continued until about the middle of the month, indicating renewed accumulation of magma in the middle east rift zone.

A second intense earthquake swarm occurred in the upper east rift zone on December 9 and 10, 1982. Geoelectric response to this event was indistinct. However, a 70-mm subsidence northwest of Puhimau Crater, detected by leveling, may have been a response to emplacement of a dike within 2 km of the surface sometime between October 29 and December 9. As in the previous earthquake swarm, the shallow hypocenters once again migrated downrift to the vicinity of Napau Crater (fig. 17.7), where seismic activity continued through the end of the month. No tiltmeter disturbances occurred during early December in the upper east rift zone or near Puu Kamoamoa, but gradual tilt changes in the upper east rift and at Puu Kamoamoa began in both areas on December 20 and continued to the end of the year. The inferred intrusions during the last quarter of 1982 apparently reactivated the upper- and middle-east-rift-zone conduit system and set the stage for the Puu Oo eruption.

EMPLACEMENT OF THE FEEDER DIKE AND FISSURE ERUPTIONS OF THE FIRST EPISODE

The premonitory seismic swarm, accompanied by weak harmonic tremor, began about 1 km west of Makaopuhi Crater (fig. 17.8) at approximately 0030 (H.s.t.) January 2, 1983. When compared to the late-December seismicity, the swarm appears as an intensification of the already established earthquake pattern (fig. 17.9). However, tiltmeters located 2–4 km uprift near Mauna Ulu and Puhimau showed tilt changes virtually coincident with the onset of the swarm. Neither shallow earthquakes nor electrical changes occurred uprift in conjunction with the tiltmeter disturbances. Thus, the swarm was apparently initiated in response to a new surge of magma through melt-filled passages in which a pressure change could be transmitted rapidly and easily. An hour after the beginning of the swarm, the Uwekahuna tiltmeter began to register subsidence of the summit of Kilauea (fig. 17.10).

The located earthquakes of the swarm, mostly 2–4 km deep, formed a narrow band, 1–2 km wide, that apparently recorded magma intrusion in the form of a dike. The swarm elongated northeastward as its tip migrated downrift at a rate of approximately 0.7 km/h (fig. 17.11). The northeast end of the swarm had extended downrift nearly to Napau Crater by about 0400 January 2. Characterized by a sharply defined leading edge, the swarm continued downrift toward Puu Kamoamoa until about 0600. From then until the onset of eruptive activity early the next morning, the swarm lost its distinct leading edge (fig. 17.11) and was largely localized between Napau Crater and Puu Kamoamoa.

Surface deformation caused by the northeastward-migrating dike was detected by tiltmeters in the rift zone near both Puu Kamomoa and Kalalua while the earthquake swarm was still between Napau and Puu Kamoamoa. At 0430 January 2, the Puu Kamoamoa instrument, located north of the rift axis, started to detect a southeastward tilt of the ground, and two hours later, at 0630, the instrument north of Kalalua responded to a southward tilt. At 1030 at Puu Kamoamoa, the east-west tilt component, which was nearly parallel to the strike of the dike and thus more sensitive to passage of the dike tip (Maruyama, 1964), reversed direction from east down to west down; this reversal probably indicated the passing of the dike tip. In 10 hours, the dike tip had migrated slightly more than 7 km from the assumed starting point near Makaopuhi Crater. The migration rate based on the tilt reversal at the Puu Kamoamoa station, 0.7 km/h, agrees with the rate of downrift migration of the earthquake swarm.

The vertical surface-displacement field caused by the dike tip is expected to migrate downrift ahead of the tip, but the two should travel at the same rate (Maruyama, 1964), 0.7 km/h in this case. The initial tiltmeter disturbance at Kalalua, however, occurred at 0630, only 2 hours after that at Puu Kamoamoa, 5.4 km uprift, and nearly 6 hours earlier than predicted by downrift migration at 0.7 km/h.

This anomalous early arrival could have resulted from passage of a hydraulically induced surge of magma when the dike tip encountered another magma body. If that was the case, the migration of the pressure-induced surge from the dike tip to Kalalua may have been nearly instantaneous. At 0630, when the Kalalua tiltmeter first recorded movement, the dike tip should have been 4.2 km (0.7 km/h times 6 h) from the point of origin of the earthquake swarm. Thus it would have been between Napau Crater and Puu Kamoamoa, in the area where the leading edge of the swarm lost its definition (fig. 17.11).

About 20 hours after passage of the leading edge of the earthquake swarm, lava fountaining began at Napau Crater at 0031 January 3. The initial outbreak continued for 9.5 hours; it produced a 6-km-long, discontinuous line of erupting fissures that extended progressively downrift from Napau Crater and reached its temporary eastern limit, south of Puu Kahaualea, at 0740 (fig. 17.12). The overall migration of the vent system was downrift (fig. 17.13), but the sequence of vent opening was complicated in detail; at times, new vents opened uprift of already active ones. The sequence of

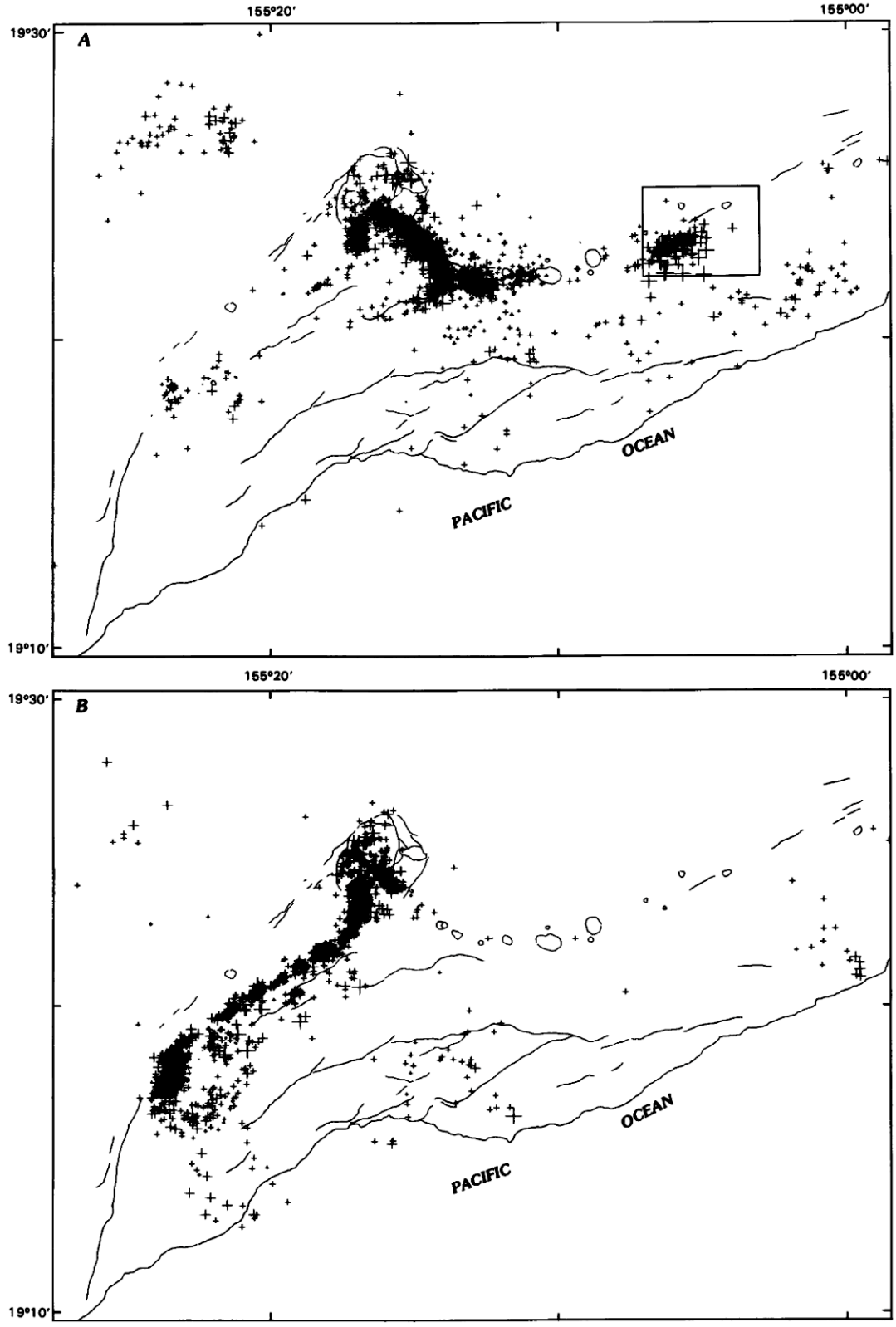

FIGURE 17.5.—Located shallow (<5-km depth) earthquakes at Kilauea from November 1978 through December 1982. ***A***, November 1978 through December 1980. Box shows location of earthquakes plotted in figure 17.6. ***B***, January 1981 through September 24, 1982. ***C***, September 25, 1982, through December 1982.

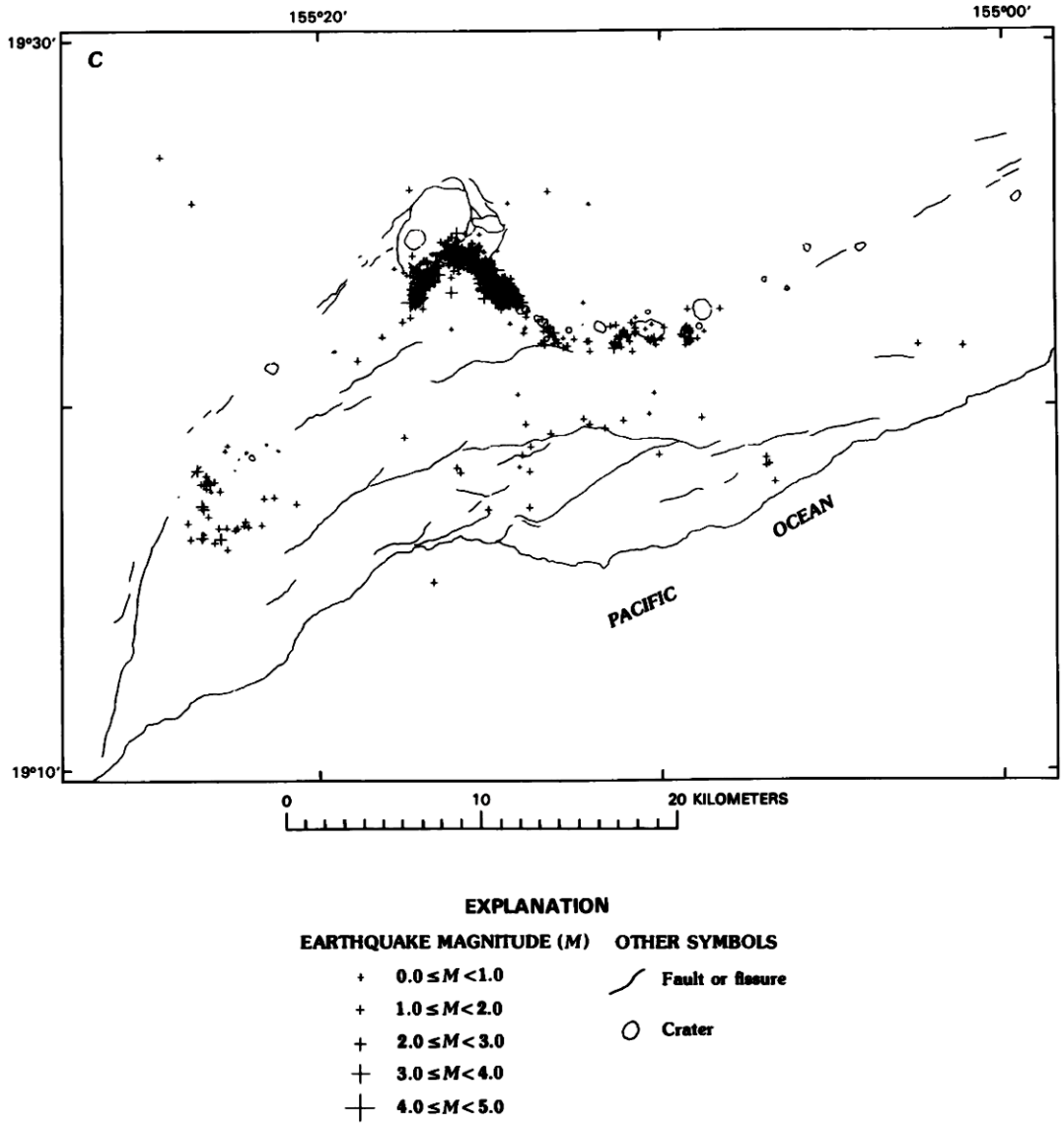

FIGURE 17.5.—Continued.

termination of eruption was also complex. The last vents to shut down, at 1000 that morning, were those at the middle of the fissure system, near Puu Kamoamoa.

Except for brief fountaining later that afternoon of the easternmost vent, which had opened at 0740, the initial outbreak was over; no further eruption occurred for approximately 2 days. Rapid subsidence of the summit stopped abruptly when extrusion stopped at 1000 January 3, and the summit reinflated until late on January 4, at which time subsidence resumed (fig. 17.10). During the respite in eruption from January 3 to January 5, shallow seismicity was distributed in a zone that extended nearly from Napau Crater to Kalalua (fig. 17.11).

Fountaining resumed at 1123 January 5, and nearly continuous fissure eruptions occurred alternately or sometimes simultaneously through January 5 and 6 at this 1123 vent, the previously active 0740 vent, and a third nearby vent that opened at 1708 January 5. Intermittent minor fissure eruptions also occurred during this period in the vicinity of Puu Kamoamoa.

Extension manifested by ground-cracking occurred on January 5 and 6 along zones that flanked the 0740-1123-1708 vent alignment (fig. 17.12). An estimated 0.5×10^6 m^3 of lava poured into an open crack south of the 0740 vent. On strike with the open crack, widening of 2–3 m occurred on cracks cutting a flow that was emplaced sometime on January 5–6; flows erupted on January 8–9

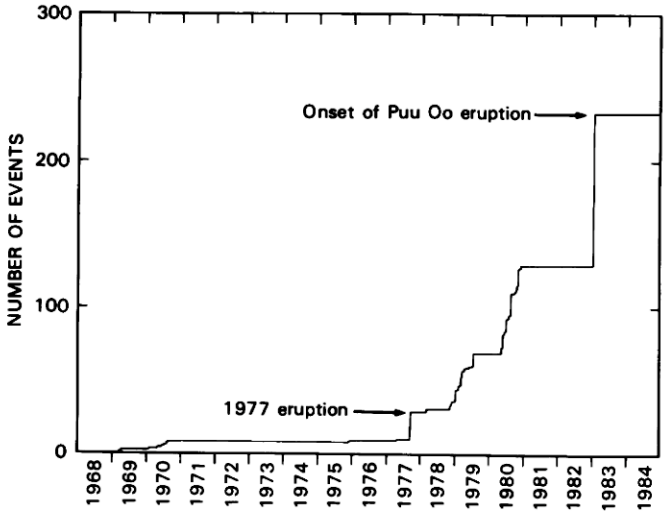

FIGURE 17.6.—Cumulative frequency of located shallow (<5-km depth) earthquakes in the Puu Kamoamoa-Puu Kahaualea area, 1978 through 1982. See figure 17.5*A* for location.

buried the cracks and showed no subsequent displacement.

Shallow earthquakes, sufficiently large to be well located, persisted in the eruption area between January 2 and 7. Early on January 7, seismicity increased markedly to form a renewed earthquake swarm near Kalalua, farther downrift than it had previously extended (fig. 17.11). Accelerated surface deformation in the same general area began during the evening of January 6 and, by midnight, had caused a large disturbance of the borehole tiltmeter about 300 m north of Kalalua. This event also perturbed the self potential in the same area. Daylight on January 7 showed the tiltmeter to be within a northeast-trending zone of new cracks that bounded a shallow graben. Immediate remeasurement of a horizontal distance across the zone of cracks north of Kalalua indicated that about 1.8 m of extension normal to the trend of the rift zone had occurred since the previous measurement on January 5 (Dvorak and others, in press; an additional 0.4 m of extension of the line was measured on January 11, after which there were no further changes). These events apparently recorded emplacement of the easternmost segment of the new dike system that had been delivering magma to the surface since January 3. Fountaining and flow production began on this segment of the dike at 1030 January 7 and continued for about 18 hours (fig. 17.13).

Forcible emplacement of a shallow dike apparently occurred near Kalalua on late January 6 and early January 7, but the effects of magmatic activity were evident earlier. An aseismic dislocation of the tiltmeter, discussed above, occurred at 0630 January 2, approximately 6 hours after the onset of the seismic swarm. Reoccupation, on the afternoon of January 3, of a self-potential measurement line crossing the rift zone near the tiltmeter showed a voltage increase, which contrasted with a previous long-term trend of generally decreasing self-potential. At the same time, production of profuse, hot, SO_2-rich fume was observed along newly lengthening cracks about 1 km east of the 0740 vent, where new vents would erupt four days later on January 7.

The earthquake swarm ended late on January 7. Thereafter, through at least the 20 eruptive episodes summarized here, no further concentrations of locatable shallow earthquakes occurred in the eruptive zone. The major subsidence of Kilauea's summit ended at about 0700 January 8. Thereafter, intermittent fissure eruptions, accompanied by sporadic minor tilt changes at the summit, occurred through January 15 at the 1123 and 1708 vents. An additional small eruption occurred near Puu Kamoamoa on January 23.

Fissure vents were dominant during the first episode of the Puu Oo eruption. They produced linear fountains as long as several hundred meters. Spatter from the fountains built low ramparts adjacent to the fissures, and thin fluid flows of pahoehoe, which changed locally to aa, normally spread near the erupting vents. A major exception occurred on January 7, when particularly intense effusion generated a fluid lava flow that rapidly moved 5.5 km down Kilauea's south flank at a rate that reached about 2 km/h. At the peak of that event, the discharge rate was greater than $1 \times 10^6 m^3/h$. Normal discharge in episode 1 was much lower, usually by an order of magnitude. In approximately 99 hours of actual eruption, episode 1 produced about $14 \times 10^6 m^3$ of new flows and vent deposits.

Subsidence related to the dike emplacement and the January eruptions occurred in Kilauea's summit area (fig. 17.14). The maximum vertical displacement, at least 55 cm, was in the southern part of the caldera, southeast of Halemaumau. The topographic volume loss, calculated from levelling data, was approximately $60 \times 10^6 m^3$ (Dvorak and others, in press). A concentration of shallow earthquakes in the southern caldera region (fig. 17.8) recorded brittle-fracture events coincident with the subsidence.

The earthquake swarm was approximately 16 km long (fig. 17.8), and its base was about 3–4 km deep. The feeder dike intersected the ground surface along an 8-km-long part of the earthquake zone. Using an 8-km length, 2.2-m width (from the measured extension near Kalalua), and average 3.5-km distance from top to bottom, we calculate an approximate volume of $60 \times 10^6 m^3$ for the dike, a value that is almost certainly an underestimate. Using the full 16-km length gives $120 \times 10^6 m^3$, twice as much as the topographic volume change in the summit area and probably an overestimate because the dike did not reach the surface over the full length of the earthquake swarm.

Horizontal distance measurements over the period from January–May 1982 to September–October 1983 indicated a seaward displacement of Kalalua, with respect to reference points on Mauna Loa, of more than 3 m (Hawaiian Volcano Observatory data). During the same period, stations in the upper east rift zone and downrift at Heiheiahulu showed no movement. Stations on the south flank, near the coast, were displaced seaward approximately 0.5–1 m; maximum movement was in the same sector as the earthquake swarm and diminished to the northeast and southwest. The large disparity between the apparent displacements of Kalalua and the stations closer to the coast indicates that substantial compression of the south flank resulted from intrusion of the dike. Modeling a theoretical dike that would best account for the measured horizontal displacements, Dvorak and others (in press) found that the best fit

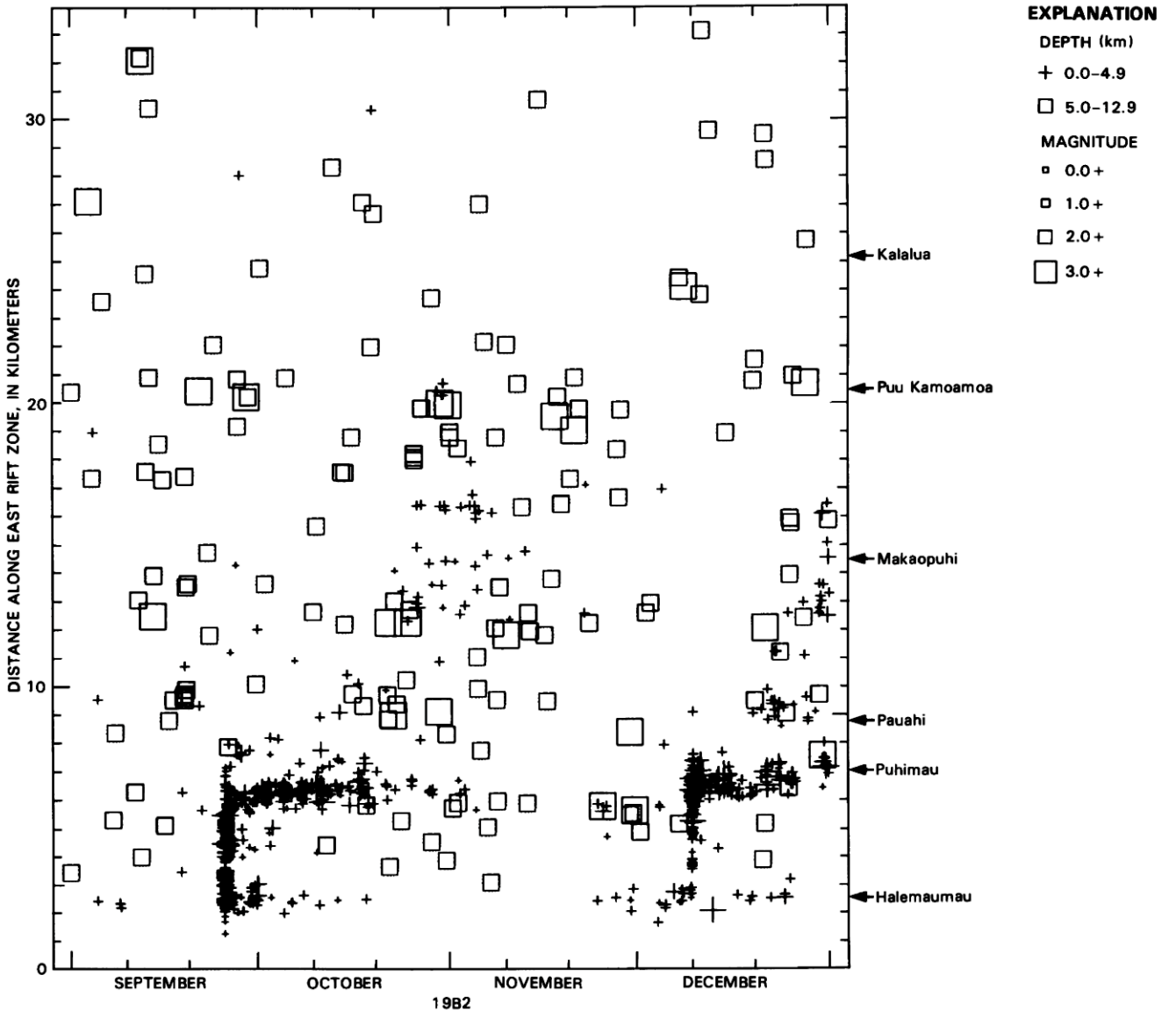

FIGURE 17.7.—Space-time diagram of earthquake epicenters in the summit, upper and middle east rift zone, and adjacent part of the south flank, Kilauea Volcano, from September through December 1982. Epicenters projected onto an east-west line.

was for a dike 11.4 km long, 2.4 km from top to bottom, and 3.6 m wide. These dimensions yield a volume of about $100 \times 10^6 m^3$, which is probably a reasonable approximation.

During the earthquake swarm, the area from Puu Kamoamoa to between Puu Kahaualea and Kalalua (fig. 17.8) showed a lower concentration of seismic activity. This area contains the major vents of the Puu Oo eruption: the 0740-1123-1708-vent complex south of Puu Kahaualea and the Puu Oo vent northeast of Puu Kamoamoa. It also coincides closely with the zone of shallow earthquake flurries that recurred repeatedly from late 1978 to late 1980 (figs. 17.5*A*, 17.6). Furthermore, the initial displacement field migrating downrift ahead of the dike tip passed through this area at a higher speed than in its passage farther uprift and produced the anomalous early tilt near Kalalua. Taken together, these data suggest that the major vents overlie a local magma reservoir established before the eruption started. The lower seismicity may record upward propagation of the dike through crust that, because of the magma reservoir, was more distended, fractured, and hotter than normal when dike emplacement occurred.

A zone of low seismicity was also found farther south in the same sector of the south flank (fig. 17.8), where it had been a persistent feature since at least the early 1960's (Hawaiian Volcano Observatory data). The quiet zone in the south flank may be related to the one in the 1983 earthquake swarm. If so, the persistence of

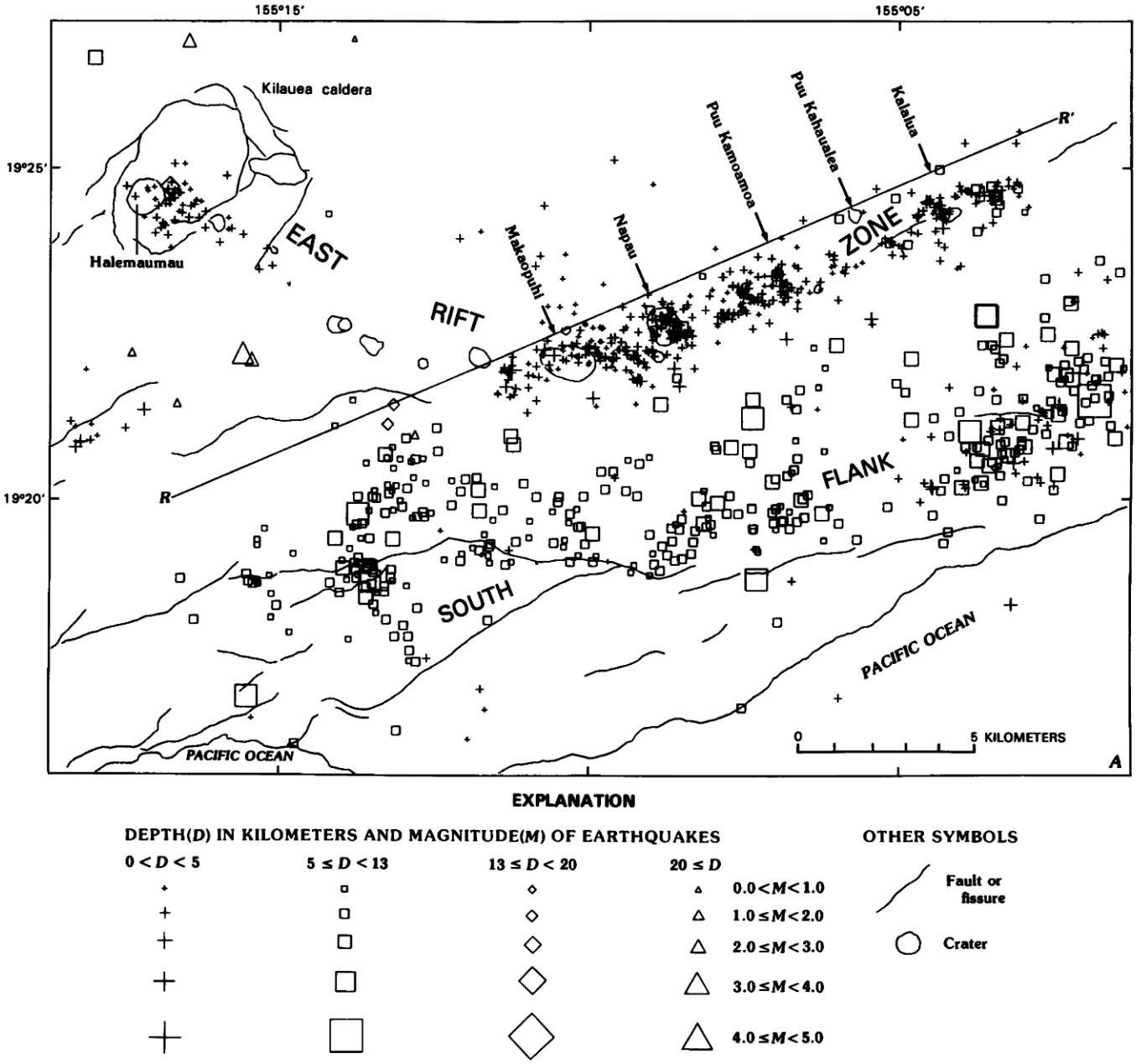

FIGURE 17.8.—Located earthquakes, January 1983, Kilauea caldera, east rift zone, and south flank. *A*, Distribution of epicenters. Cross section *R-R′* shown in figure 17.8*B*. *B*, Depth-distance distribution of hypocenters, projected onto line *R-R′*.

the south-flank feature may indicate that the Puu Kamoamoa-Puu Kahaualea area has had a magma reservoir for two decades or more. Two alternative explanations are that the south-flank seismic gap represents either a zone of aseismic slip or a locked zone that could yield abruptly to cause a large earthquake. Neither of these alternatives has a genetic or predictive relationship to the region of postulated magma storage in the rift zone.

EPISODIC CENTRAL-VENT ERUPTIONS: EPISODES 2–20

LOCATION, EPISODICITY, AND LAVA-DISCHARGE RATE

During episodes 2 and 3, the 1123 vent was the main eruptive vent, producing major flows that extended northeast within the rift

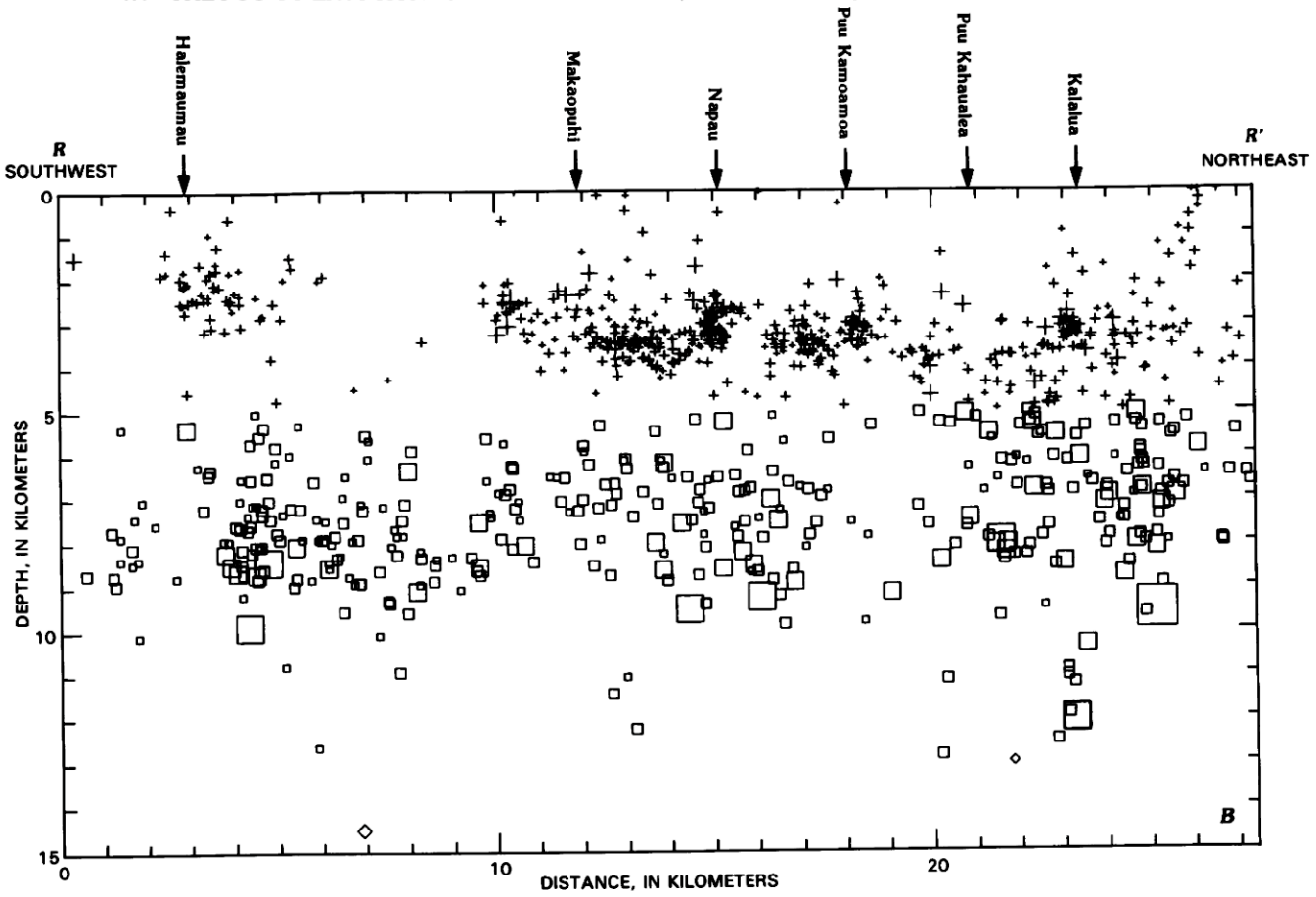

FIGURE 17.8.—Continued.

zone and southeast to the Royal Gardens subdivision (fig. 17.2). Less voluminous eruption also occurred in the area where Puu Oo would subsequently grow. Beginning with episode 4, the Puu Oo vent, supplemented on a few occasions by nearby local fissure vents, was the sole eruptive locus. During episodes 4 and 5, the major flows emerged from the south flank of Puu Oo and traveled southeast toward Royal Gardens. Thereafter, the major flows emerged from the northeast flank of Puu Oo. Many extended into dense forest north of Puu Kahaualea; others turned southeastward and advanced down the south flank toward the ocean.

An episodic pattern quickly developed (table 17.1, fig. 17.15). Eruptive episodes, which ranged in length from 9 hours to 12 days, were characterized by high-volume discharge of lava flows, vigorous fountaining, rapid summit subsidence, and strong harmonic tremor in the vent area. Repose periods, which ranged in length from 8 to 65 days, were characterized by reinflation of Kilauea's summit and weak harmonic tremor in the vent area; at times the upper surface of a magma column was evident in the conduit beneath the vent. The pattern was strikingly similar to that of the first 7 months (May–December 1969) of the 1969–71 Mauna Ulu eruption (Swanson and others, 1979). However, after 12 episodes with rapid discharge and high or sustained fountaining, the style of eruption at Mauna Ulu changed to one dominated by steady slow discharge that built the Mauna Ulu shield and transported large volumes of pahoehoe great distances from the vent through lava tubes (Tilling and others, chapter 16; Peterson and Swanson, 1974; Peterson, 1976; Swanson and others, 1979). In contrast, the episodic Puu Oo eruption has continued through episode 20 and beyond (33 episodes as of June 1985), producing one of the largest vent structures at Kilauea Volcano and creating an extraordinary complex of interleaved aa flows (fig. 17.2).

Both the duration of repose between eruptive episodes and the volume discharged during eruptive episodes varied significantly. Nevertheless, a striking regularity developed (fig. 17.16) that was particularly pronounced during episodes 4–12 and 13–17. During those two intervals, the time from the end of one eruptive episode to the end of the next varied from 9 to 31 days (from data of table 17.1) and averaged 19 ± 7 (1 standard deviation) days; erupted volumes of lava ranged from 6 to $14 \times 10^6 m^3$ and averaged $10 \pm 3 \times 10^6$ (1 standard deviation) m^3. These intervals were times of slightly higher than normal supply of lava, averaging about $15.7 \times 10^6 m^3$/mo. This difference is due largely to abnormally

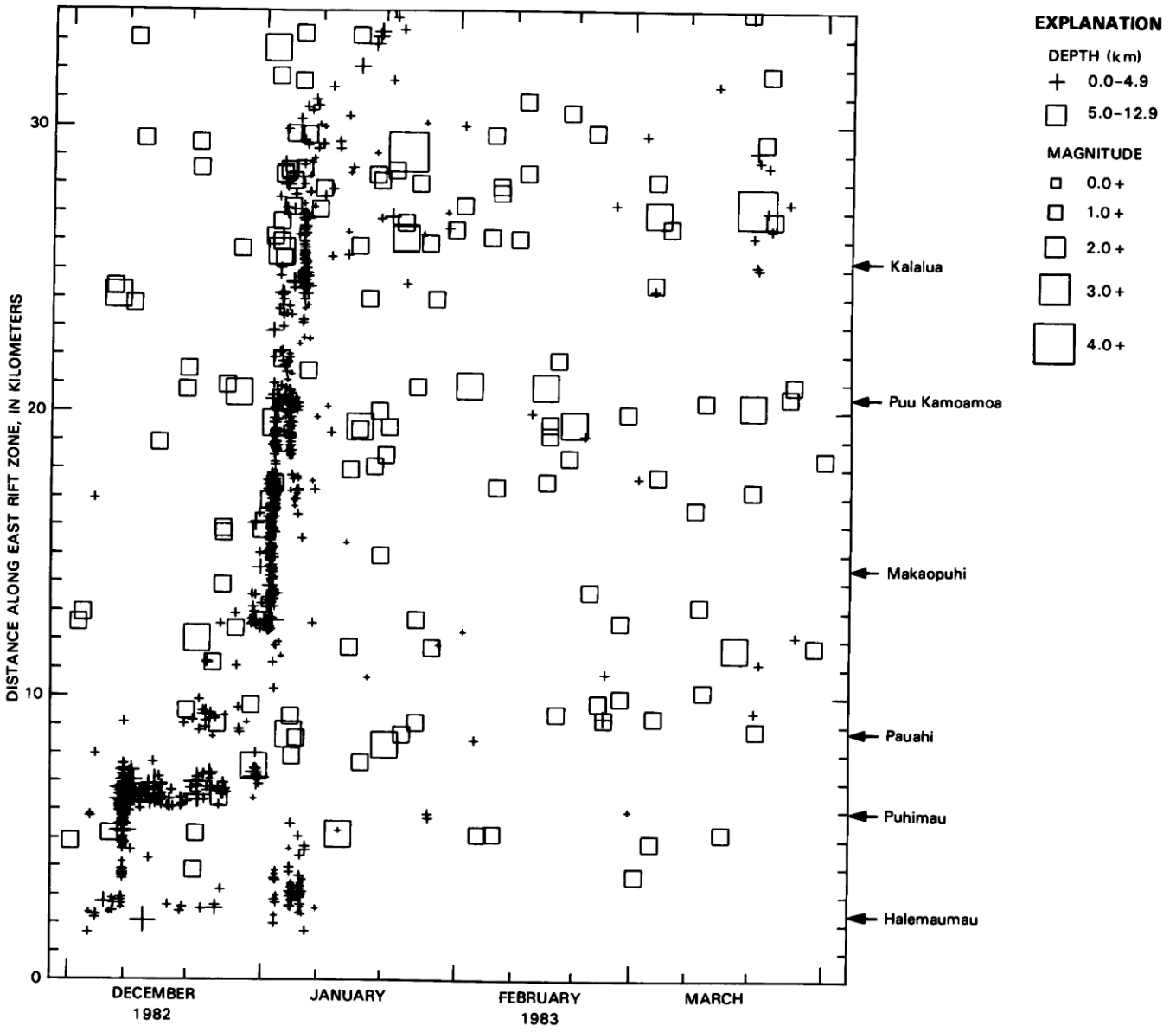

FIGURE 17.9.—Space-time diagram of earthquake epicenters in the summit, upper and middle east rift zone, and adjacent part of the south flank, Kilauea Volcano, for December 1982 through March 1983. Epicenters projected onto an east-west line.

prolonged repose before episodes 4 and 13. For comparison, during the 12 episodes of sustained fountaining that occurred in the early months of the 1969–71 Mauna Ulu eruption, lava was delivered to the surface at an approximate rate of $10 \times 10^6 m^3$/mo. During that period, average erupted volumes and average recurrence intervals at Mauna Ulu were also smaller than for the Puu Oo eruption (fig. 17.16).

As the Puu Oo eruption went on, the durations of individual episodes tended to decrease and the discharge rates to increase (table 17.1, fig. 17.17); thus comparable volumes of lava were delivered more rapidly in successive episodes. Presumably this reflected progressive enlargement and streamlining of the conduit system between the summit reservoir and the vent area.

MAGMA SUPPLY TO THE VOLCANO

Swanson (1972) examined the rate of lava production during three long eruptions of Kilauea—the 1952 Halemaumau eruption, the 1967–68 Halemaumau eruption, and the 1969–71 Mauna Ulu eruption—that were characterized by minimal net change in the degree of summit inflation as indicated by the summit tilt record. Assuming that minimal net tilt change at the summit implied minimal

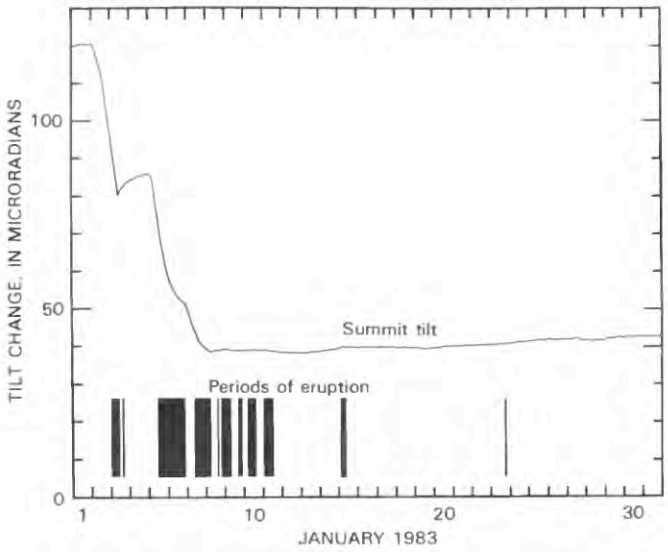

FIGURE 17.10.—East-west summit tilt record (Hg-capacitance tiltmeter at Uwekahuna) and episode 1 eruptive periods, Puu Oo eruption, January 1983. Increasing values indicate westward-directed (inflationary) tilt change; decreasing values indicate eastward-directed (deflationary) tilt change. Full magnitude of tilt change from January 5 through January 7 is greater than shown because of nonlinear response of tiltmeter to tilt change during that period.

change in the stored volume, he concluded that the erupted volumes approximated the supply of magma from the mantle. Correcting for an estimated 15 percent vesicularity, he calculated a magma-supply rate of approximately $9 \times 10^6 m^3$/mo for the three sustained eruptions. Before applying Swanson's technique to infer magma supply from the rate of lava delivery during the Puu Oo eruption, we evaluate several factors, including the large subsidence related to dike emplacement in episode 1, a long-term decrease in average tilt value, and the correction for vesicularity.

A large subsidence of Kilauea's summit occurred at the beginning of the Puu Oo eruption, and we infer that a large volume of magma, on the order of $100 \times 10^6 m^3$, remained in the intruded dike and this was not accounted for in the measured volume of episode 1 lava. After episode 1, the much smaller, alternately inflationary and deflationary tilt changes were roughly similar in magnitude and nearly cancelled each other. However, they were superimposed on a gradual, long-term decrease in average tilt that amounted to about 30 microradians by the end of episode 20 (fig. 17.15) after correction for the offset caused by the November 1983 Mauna Loa earthquake. This tilt change is equivalent to an apparent volume decrease of about $10 \times 10^6 m^3$ of magma over 17 months (see discussion in subsequent section titled "Relation of Summit Tilt Changes to Rift-Zone Activity"), which is within the uncertainty of our volume measurements. Furthermore, in an analysis of deformation and gravity data for the caldera region, Johnson (chapter 47) found that cross-caldera distances measured perpendicular to the coast have been steadily increasing at a rate of about 2 microstrain (parts per million) per month. Thus the subsidence indicated by gradually decreasing average tilt values may not reflect

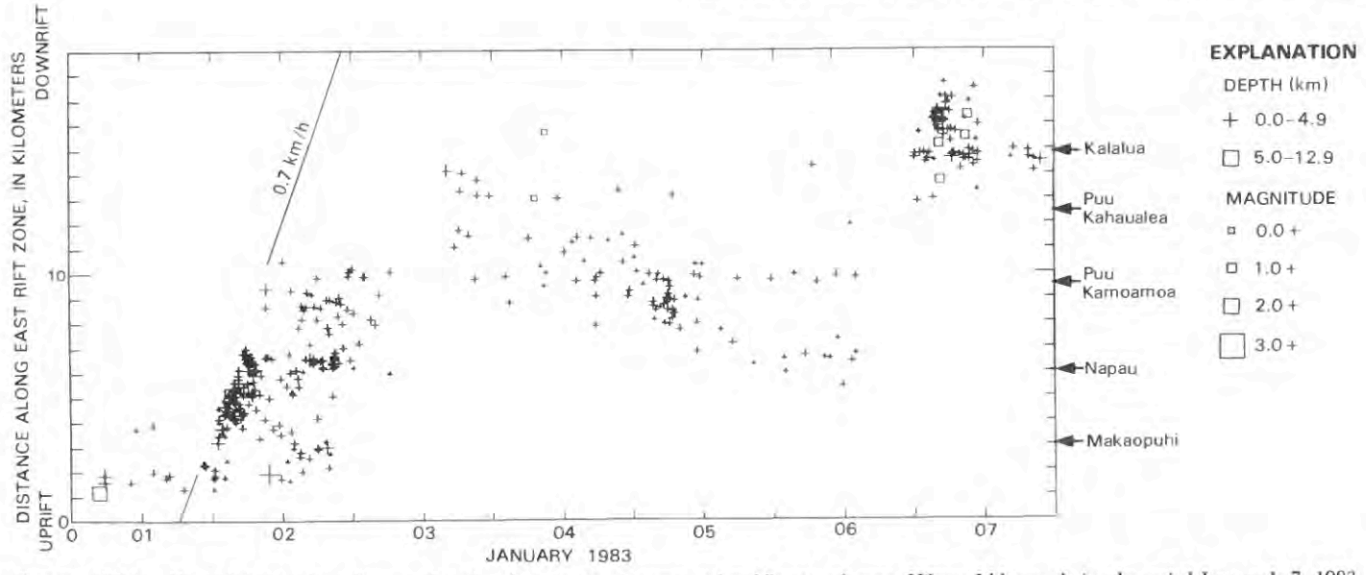

FIGURE 17.11.—Expanded space-time diagram of earthquake epicenters in upper and middle east rift zone, Kilauea Volcano, during the period January 1–7, 1983. Epicenters projected onto a line parallel to the axis of the middle east rift zone. A downrift migration rate of 0.7 km/h is inferred for the leading edge of the concentrated zone of shallow earthquakes during the morning of January 2. Location accuracy, based on horizontal and vertical standard error (Klein, 1978) for these earthquakes, is ±1 km.

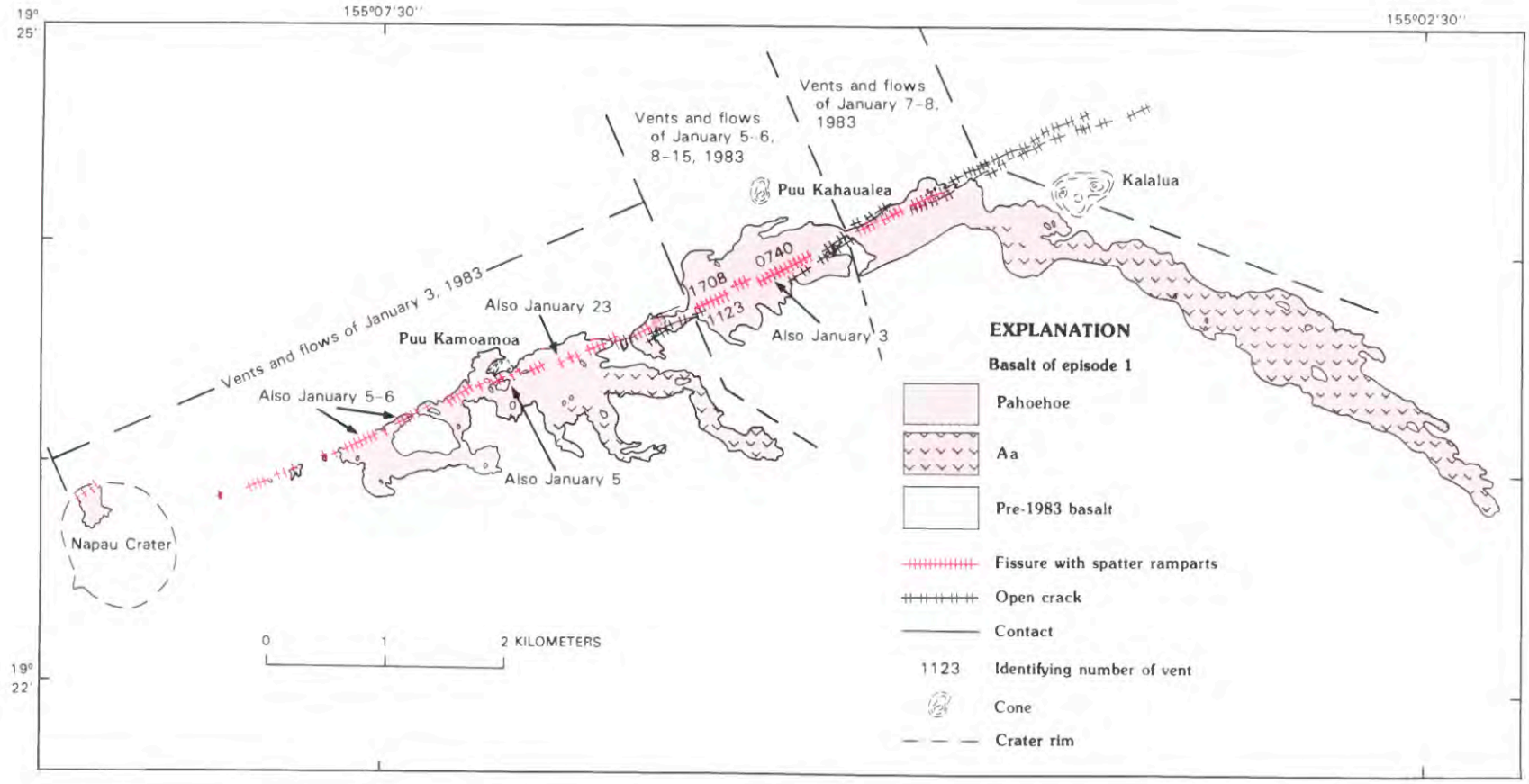

FIGURE 17.12.—Vents and flows of episode 1, Puu Oo eruption, Kilauea Volcano, January 1983.

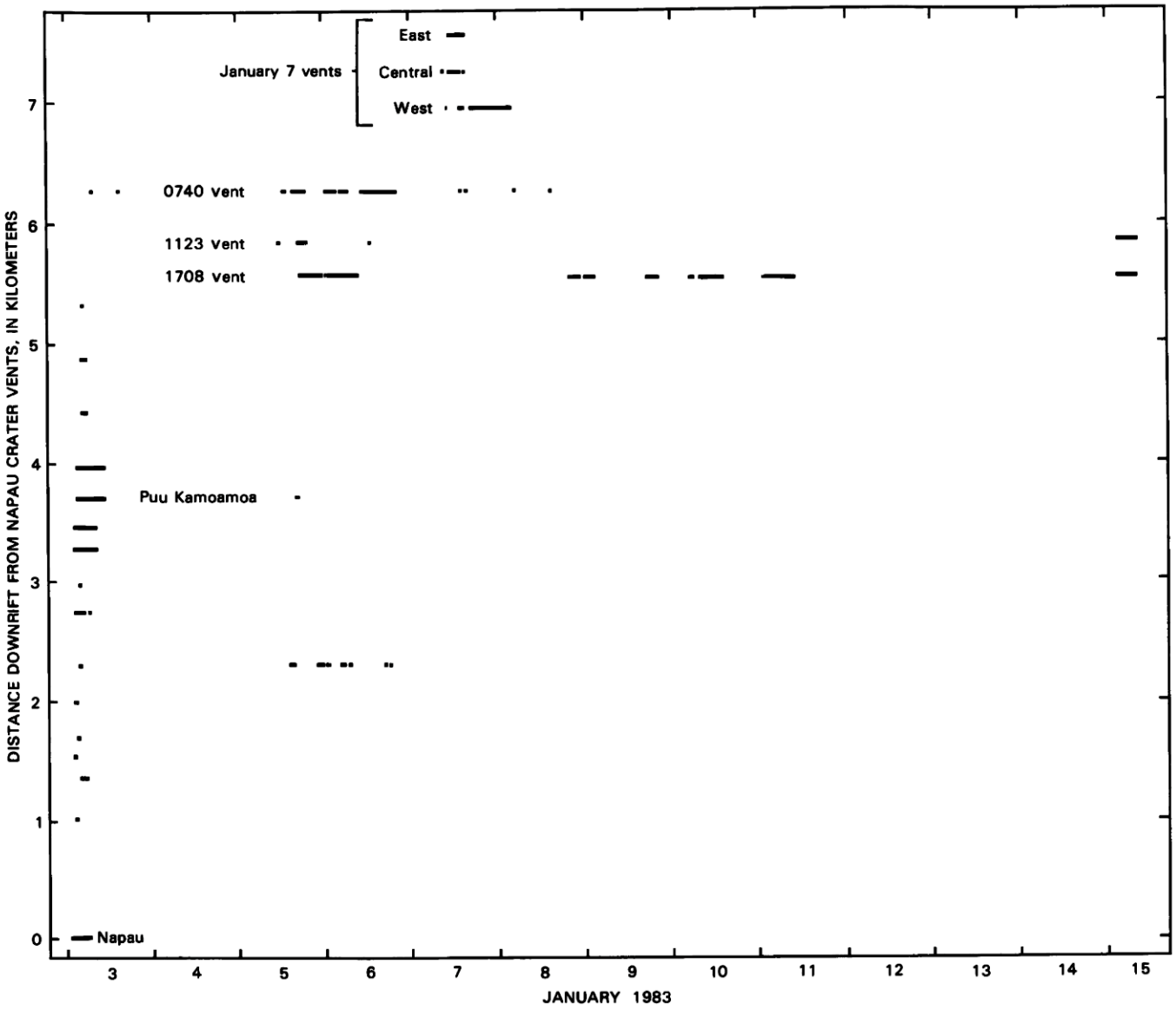

FIGURE 17.13.—Space-time diagram showing vent activity for January 3–15, episode 1 of the Puu Oo eruption. Approximate locations of centers of individual eruptive-fissure segments shown by distance downrift from the Napau Crater vents.

a reduction in reservoir magma volume but rather a gradual change in shape resulting from southeastward extension of the summit region. In addition, repeated gravity surveys from the beginning of 1984 through the time of writing (May 1985) have shown no long-term change in mass in the summit region, indicating that the average reservoir magma volume remained constant. We ignore both this gradual long-term subsidence and episode 1 with its dike emplacement in applying Swanson's technique for determining magma supply to the Puu Oo eruption.

The Puu Oo flows are dominantly vesicular rubbly aa. Average bulk densities of 1.94 and 2.17 g/cm^3 were determined from the results of two gravimeter and spirit-level profiles across the surface of an episode 3 aa flow where it overlies paved streets in a subdivision (D.J. Johnson, written commun., December 1984). These values suggest that the porosity is approximately 25 percent. Multiplying the average monthly lava supply of 13.4×10^6 m^3 by 0.75 to correct it to its dense-rock equivalent gives a rate of 10×10^6 m^3/mo of void-free lava. Thus, we infer an average magma-supply rate for episodes

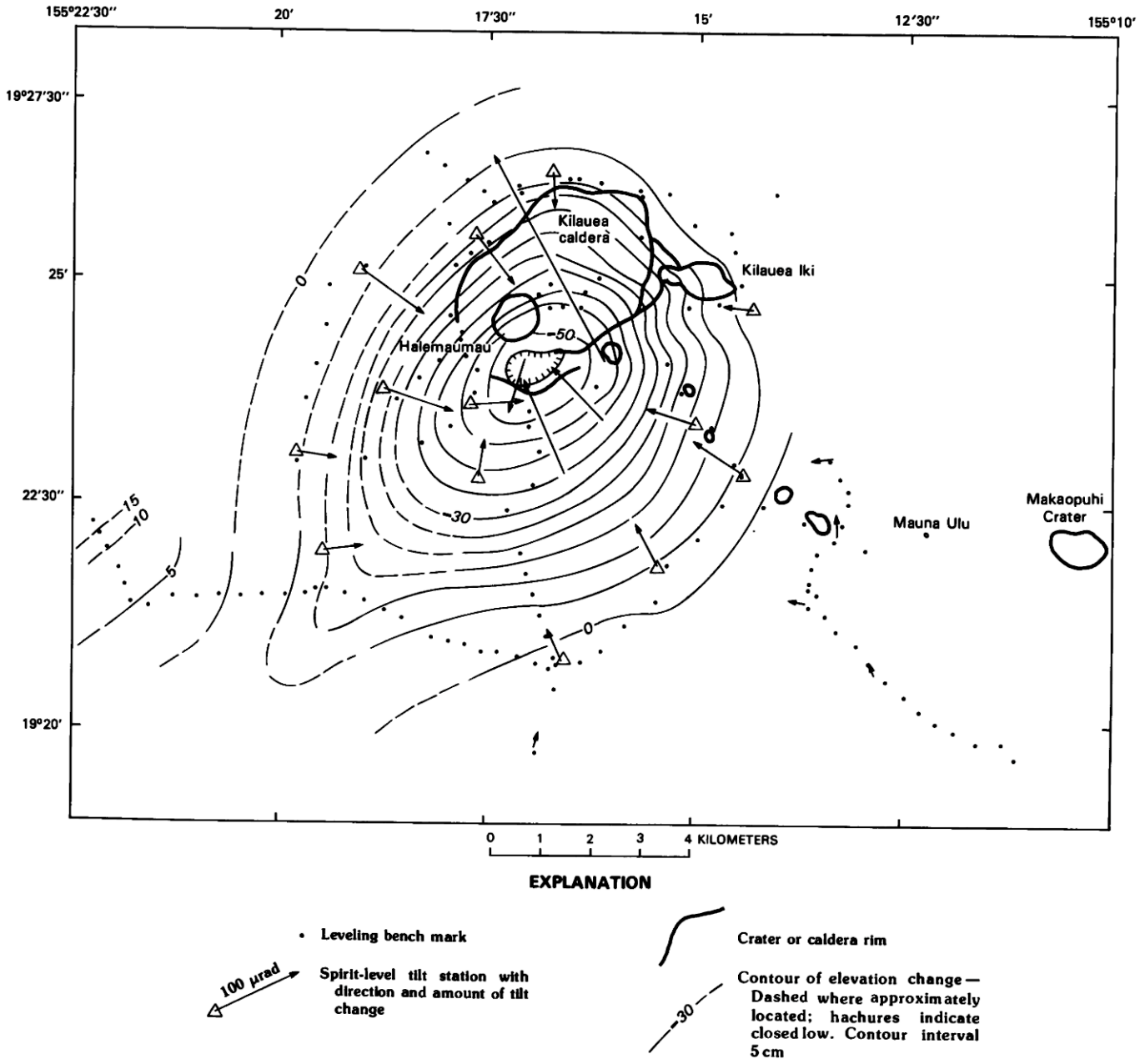

FIGURE 17.14.—Subsidence and tilt in the Kilauea summit region during the period from September 27–October 5, 1982, to February 7–11, 1983. Contours show relative elevation change.

2–20 of approximately $10 \times 10^6 m^3$/mo. Because volume-measurement errors may amount to 10 percent, this supply rate for the Puu Oo eruption is compatible with the rate determined by Swanson (1972) for other periods of sustained eruption. A slightly higher rate, approximately $11.8 \times 10^6 m^3$/mo, may be represented by the intervals encompassing episodes 4–12 and 13–17. The limited variation in recurrence interval and erupted volume (fig. 17.16) during those intervals indicates that an approximately steady-state condition had developed in the magma supply and transport system.

The question remains whether the Puu Oo magma-supply rate of at least $10 \times 10^6 m^3$/mo represents a period of elevated supply. Dzurisin and others (1984) reviewed magma-supply estimates more recent than Swanson's (Dzurisin and others, 1980; Duffield and others, 1982; Dvorak and others, 1983). They found a range of from 6×10^6 to $9 \times 10^6 m^3$/mo and concluded, from their analysis of the summit tilt record, that $7.2 \times 10^6 m^3$/mo is a reasonable minimum value for the average supply of magma from 1956 through 1983. Uncertainty arises from the possible addition of undetected

TABLE 17.1.—*Eruption data for episodes 1–20, Puu Oo eruption, Kilauea*

[All times are in Hawaii standard time (H.s.t.). ___, did not occur or was not observed]

Episode	First report of low-level eruption[1]		Beginning of vigorous eruption[2]		End of vigorous eruption[3]		Duration of vigorous eruption (hours)	Area covered (10^6 m^2)	Erupted volume (10^6 m^3)	Discharge rate[4] (10^3 m^3/h)
	Day	Hour	Day	Hour	Day	Hour				
1983										
1	___		Jan 3	0031	[5]		[5]	4.8	14	[5]
[6]2	Feb 10	1030	Feb 25	0900	Mar 4	1451	174	2.7	14	80
3	Mar 21	0600	Mar 28	0100	Apr 9	0257	290	7.9	38	130
4	___		Jun 13	1025	Jun 17	1413	100	2.2	11	110
5	Jun 29	1000	Jun 29	1251	Jul 3	0715	90	3.4	13	140
6	Jul 21	0600	Jul 22	1530	Jul 25	1630	73	2.0	9	120
7	Aug 8	0610	Aug 15	0741	Aug 17	1600	56	3.7	14	250
8	Sep 2	0900	Sep 6	0511	Sep 7	0526	24	[7]2.0	[7]8	[7]330
9	Sep 14	0009	Sep 15	1541	Sep 17	1920	52	[7]2.1	[7]8	[7]150
10	Oct 2	0800	Oct 5	0106	Oct 7	1650	64	2.7	14	220
11	___		Nov 5	2350	Nov 7	1845	43	4.3	12	280
12	Nov 29	1600	Nov 30	0447	Dec 1	1545	35	3.0	8	230
1984										
[8]13	Jan 20	1100	Jan 20	1724	Jan 22	1123	42	[7]2.6	[7]10	[7]230
[7]14	Jan 22	1123	Jan 30	1745	Jan 31	1318	19	[7]2.1	[7]6	[7]320
15	Feb 3	1000	Feb 14	1940	Feb 15	1501	19	2.2	8	420
16	Feb 27	1900	Mar 3	1450	Mar 4	2231	32	3.2	12	380
17	Mar 20	0910	Mar 30	0448	Mar 31	0324	23	3.0	10	430
18	Apr 5	1340	Apr 18	1800	Apr 21	0533	60	6.6	24	410
[9]19	Apr 23	0830	May 16	0500	May 18	0050	44	1.4	2	50
20	May 18	0800	Jun 7	2104	Jun 8	0625	9	1.6	4	480

[1]For episode 2, low-level eruption refers to a period of prolonged slow extrusion (averaging approximately 1,400 m^3/h) from February 10 to 25, 1983. For episodes 3–20, it refers to a period, preceding major eruption, during which any or all of the following phenomena were observed at the active vent: intermittent gas-piston activity, intermittent spattering, occasional extrusion of small pahoehoe flows, occurrence of a visible lava surface (sometimes partly crusted) in the conduit extending downward from the crater floor. Normally, low-level eruptive activity was confined to the interior of the crater, but on rare occasions short-lived pahoehoe flows spilled from Puu Oo.

[2]Normally, the onset of vigorous eruption was recognized in the following ways (order indicates priority): (1) direct observation of continuous emission of lava from the crater; (2) time-lapse camera record of beginning of continnous emission of lava from crater; (3) where spillway activity was not recorded, time-lapse camera record of first appearance of fountaining above the crater rim; (4) beginning of rapid increase in harmonic-tremor amplitude.

[3]The end of vigorous eruption was recognized in the following ways (order indicates priority): (1) direct observation of the cessation of lava discharge; (2) time-lapse camera record of cessation of fountaining; (3) rapid decay of harmonic-tremor amplitude.

[4]Discharge rate is calculated only for period of vigorous eruption. Except for episode 2, the volume of lava erupted during periods of low-level activity was negligible.

[5]Episode 1 was characterized by intermittent eruptive activity for nearly three weeks. Periods of active eruption totalled approximately 99 hours. The last sizeable event occurred on January 15; a minor one occnrred on January 23.

[6]During episode 2, approximately 0.5×10^6 m^3 of basalt was discharged during low-level eruption from February 10 to 25. The remaining 13.6×10^6 m^3 was discharged during the period of vigorous eruption at a rate of approximately 70,000 m^3/h.

[7]Flow was partly buried by younger basalt before it could be mapped. Thus uncertainty is increased in estimates of area, volume, and discharge rate.

[8]Fountaining and flow production during episode 13 occurred in two main periods. The first, approximately 31 hours long, was separated by about 5 hours from the 6-hour-long second period.

[9]Episode 19 was characterized by low fountain activity and intermittent low-volume overflows from the lava pond within the crater of Puu Oo. This activity was interrupted by four periods 1–3 h long, totalling about 7 hours altogether, of higher fountaining and increased lava discharge estimated as about $100–200\times10^3$ m^3/hr.

magma to rift-zone storage. Furthermore, Tilling and others (chapter 16) recognized two distinct episodes during the latter part of the Mauna Ulu eruption, February 1972 through April 1973 and December 1973 through July 1974, in which sustained lava extrusion coincided with negligible summit-tilt change. During the earlier episode, the lava-extrusion rate was about 8×10^6 m^3/mo; during the later one, it was 4×10^6 m^3/mo. Neither value is corrected for vesicularity. R.I. Tilling (oral commun., May 1985) regards the values as minimum estimates of magma-supply rate because of the unevaluated possibility that magma was being stored in the upper east rift zone during the 1972–74 Mauna Ulu eruption.

The data summarized above are only permissive evidence that the Puu Oo eruption coincided with a period of greater than normal magma supply. More substantial support may come from measurement of SO_2 flux to the atmosphere in the Kilauea summit area. The average flux increased abruptly after the beginning of the eruption in January 1983 from 130 t/d to 250 t/d; the elevated flux was maintained through at least episode 20 (fig. 17.18; Greenland and others, 1985). The near coincidence of the SO_2-flux change with the beginning of the Puu Oo eruption strongly suggests that the two events were related. The increased SO_2 flux may have been a direct and rapid response to an increased rate of supply of new magma to the summit reservoir; if so, the Puu Oo eruption coincided with a period of increased magma supply.

CHARACTER OF THE CENTRAL-VENT ERUPTIONS

Central-vent eruptions occurred during episodes 2 through 20. A nearly vertical pipe-like conduit delivered a spray of gas and fragmented vesiculating magma through a vent in the floor of a broad crater within a growing pyroclastic cone. Directed upward as a jet, the spray formed the fountain that was invariably present in the central-vent eruptions. Initial fallout from the fountain built a spatter ring, which, in repeated eruptive episodes, grew upward and outward by the addition of spatter, rootless flows, and unconsolidated lapilli and bombs.

The crater of Puu Oo evolved to a broad bowl mostly enclosed by steep walls. The diameter of its gently sloping floor gradually increased from about 20 m to 100 m. A deep breach that developed in the crater wall provided a passage through which lava left the

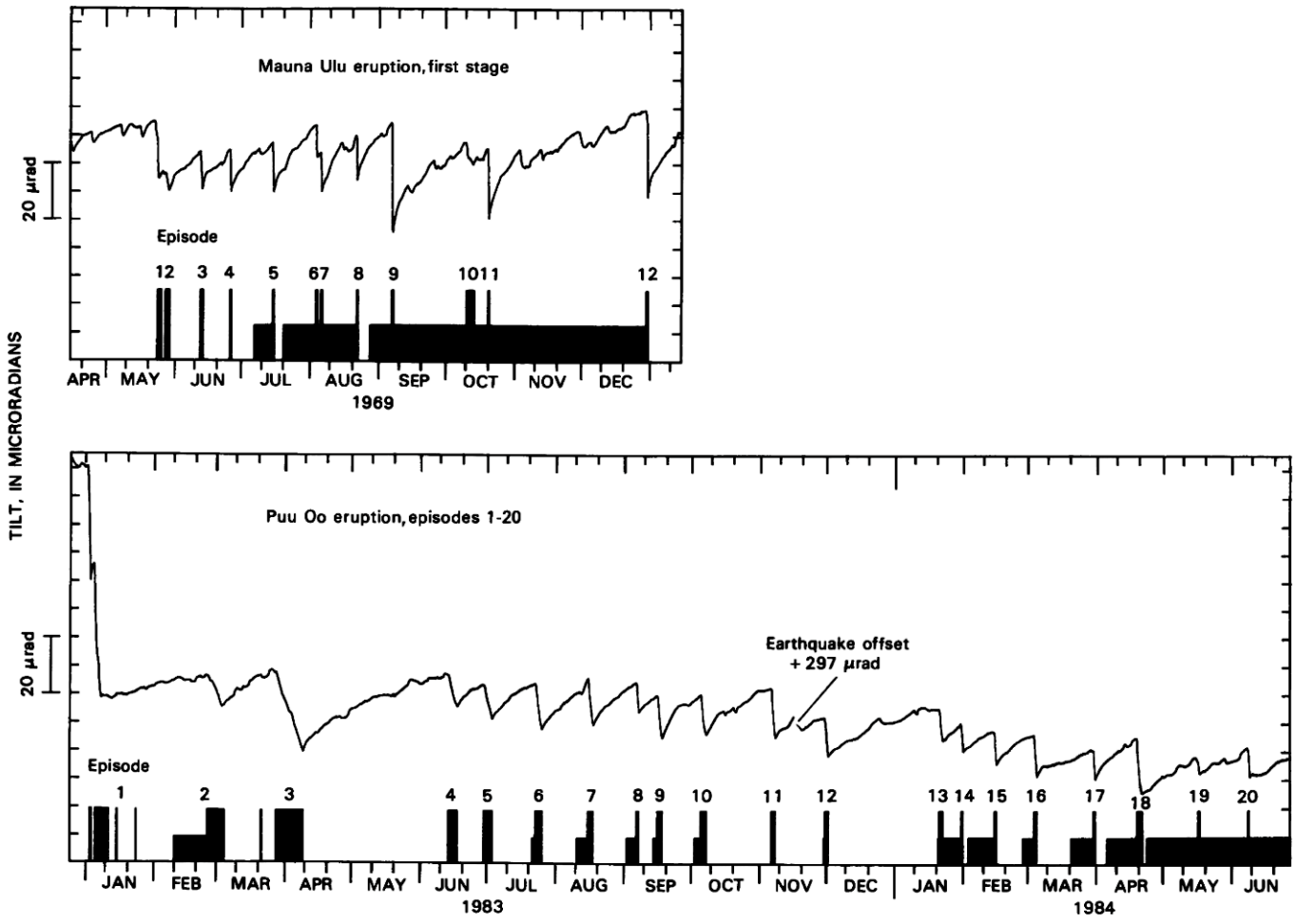

FIGURE 17.15.—East-west tilt at Kilauea summit (measured by the Uwekahuna Hg-capacitance tiltmeter), eruptive episodes (full- height bars), and observed repose-period eruptive activity (half- height bars) during episodes 1–20 of the Puu Oo eruption and the first stage of the 1969–71 Mauna Ulu eruption (Swanson and others, 1979).

crater. The floor of the breach was generally 5–15 m higher than the crater floor.

Before episode 13, rubble on the crater floor concealed the feeder conduit during most periods of repose. From episode 13 on, a persisting vertical and nearly cylindrical conduit about 20 m in diameter was revealed. Its walls exposed crudely layered platy to rubbly basalt; at its top, the pipe flared upward to meet the crater floor and was commonly draped with pahoehoe.

During eruptive episodes, the crater contained a lava pond and one or more fountains. The pond overflowed at the breach in the crater rim. Normally the spillway at the breach was fairly constricted, so that the surface of the hydraulically-dammed pond was several meters higher than the floor of the spillway. We estimate that the pond was normally at least 10–20 m deep. When high, broad fountains seemed to fill the crater, we could not see the pond, but continuing flow of lava over the spillway indicated its presence. However, flows produced during such periods were sometimes more sluggish than when a well-developed pond was seen to be present.

Though the pond shared the crater with a vigorous fountain, it maintained a fairly smooth surface that was commonly marked by a thin, flexible skin of slightly cooled lava undisrupted by effervescence. We infer that the pond consisted of mostly degassed lava that had coalesced from fragmented melt in the crater and the upper part of the conduit.

Fountains at the central vents during episodes 2–20 ranged in height from a few meters during periods of slow discharge to a maximum of nearly 400 m. In some of the eruptive episodes at Puu Oo, as, for example, episode 16, the fountain was highest in the early hours (fig. 17.19); this suggests that volatiles may have become more highly concentrated in the upper part of the conduit beneath the vent during periods of repose.

Fountain height was related at least in part to the rate of discharge. During both episodes 2 and 3, fountain height at the 1123 vent approximately doubled in concert with 2- to 3-fold increases in lava output. From episode 4 on, at Puu Oo, we normally saw no abrupt changes in discharge during an eruptive

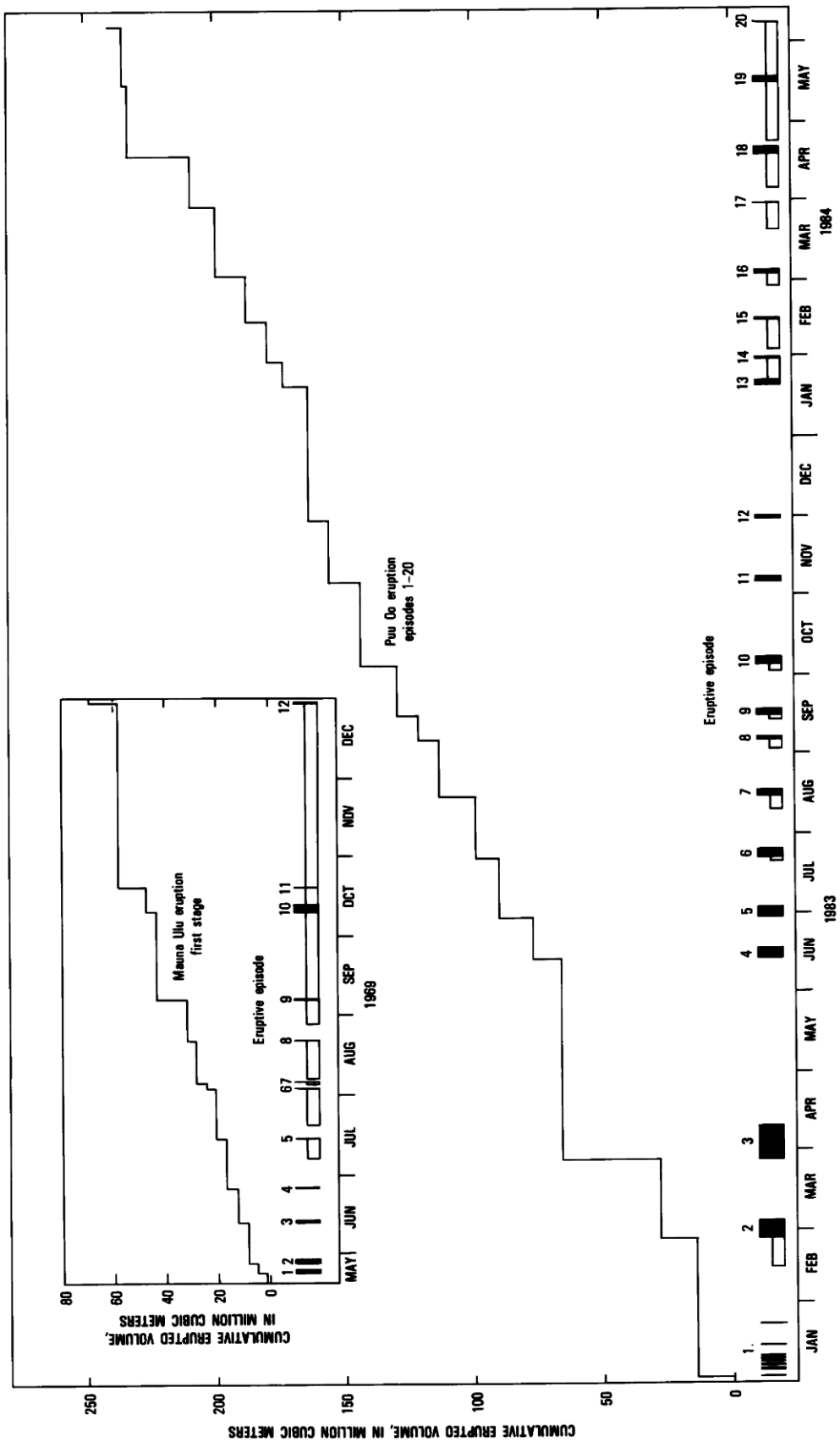

FIGURE 17.16.—Cumulative erupted volumes during episodes 1–20 of the Puu Oo eruption and the first stage of the Mauna Ulu eruption (Swanson and others, 1979). Solid full-height bar, eruptive episodes; open half-height bar, observed repose-period activity. Basalt volumes for Puu Oo eruption were determined by mapping flows and vent deposits of the individual episodes, measuring thicknesses by hand level at the flow edges, and measuring mapped area on a computerized digitizing tablet.

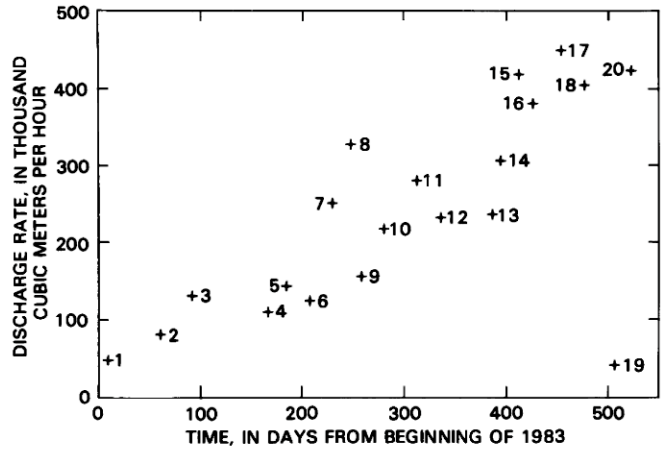

FIGURE 17.17.—Average lava-discharge rate for each of episodes 1-20, Puu Oo eruption, plotted against time.

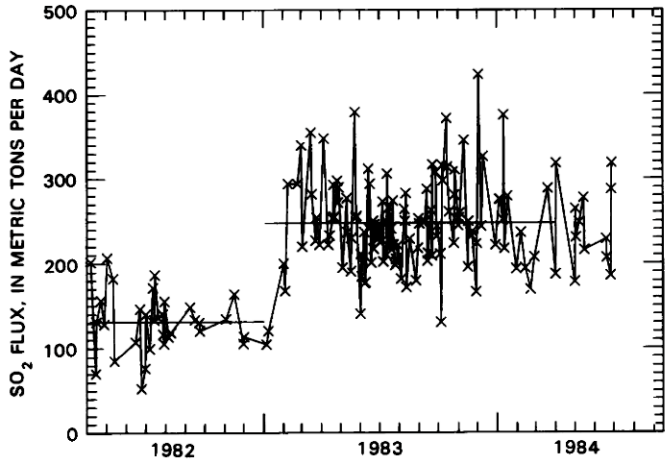

FIGURE 17.18.—Total sulfur dioxide (SO_2) flux from summit fumaroles of Kilauea Volcano, April 1982 through June 1984, based on ground measurements. Horizontal lines show change in average flux after the beginning of the Puu Oo eruption in January 1983. Modified from Greenland and others (1985); data extended through June 1984 by L.P. Greenland.

episode, but the rate was greater in successive episodes (fig. 17.17). Average fountain height at Puu Oo correlated roughly with average discharge (fig. 17.20), but appreciable scatter resulted from effects that may have included changing conduit conditions, enrichment of gas during repose periods, and damping of fountains by coalesced melt within the crater and upper part of the conduit.

Normally, each central-vent fountain episode produced one or more major elongate aa flows supplied by a river of fluid pahoehoe that originated from the steady overflow of the pond. Subordinate flows originated mainly from persistent near-vent overflows of the river and from mobilization of molten spatter that accumulated either rapidly or persistently on the flanks of the cone.

The river-fed flows evolved downstream through a similar progression of zones as that recognized in the aa lobes of the 1984 Mauna Loa eruption (Lipman and Banks, chapter 57). As at Mauna Loa, fluid channelized lava near the vent was inflated by gas but rapidly deflated downstream. The sustained cascade of spatter and the turbulence where the fountain burst from the pond apparently churned vent gases, including air, into the lava supplying the pond. Thus the pond was a continuing source of gas-rich fluid melt and was apparently fundamental in developing the long river-fed aa flows at Kilauea. Minimal development of the pond, such as during periods of high fountaining, was associated at times with production of less fluid flows. Furthermore, supply from a fountain with no basin or pond often produced thick, slow-moving aa directly.

Generally, the major flows were 4–8 km long and from 100–500 m wide. A few flows were significantly longer; the longest, produced during episode 18, extended more than 13 km from the vent (fig. 17.2). The average thickness of most of the river-fed aa flows was between approximately 3 and 5 m. However, the range of measured thicknesses was greater; locally, the distal parts of some flows were as thick as 10 m. The major river-fed flows advanced at average rates of 50–500 m/h. Surges of fluid lava at the flow fronts (Neal and Decker, 1983) resulted in more rapid advances that were sustained for tens of minutes at rates of as much as 2 km/h. Significant flow movement stopped when the lava supply was cut, generally at the vent but sometimes by diversion to a new flow. After the supply was terminated, however, slow creeping of the front sometimes continued for hours.

Low-level eruptive activity was evident during many repose periods. At Puu Oo, it was dominated by two phenomena: the gradual ascent of the magma column toward the surface and gas-piston activity much like that seen at Mauna Ulu (Swanson and others, 1979). After the open conduit descending from the crater floor became a permanent feature following episode 13, we could see that the magma-column surface rose gradually and sometimes spasmodically toward the crater floor during each repose period. If visibility was good, we would first see the top of the column when it was about 50 m down the conduit; the first sighting usually occurred at least 5 days and sometimes more than 3 weeks before the next major episode (fig. 17.15).

We were able to watch the beginnings of several of the fountaining episodes at Puu Oo. First the crater filled with lava, which steadily overflowed the spillway. Gas-piston activity, if it had been occurring, gave way to an open, roiled pond with a low dome fountain. Over a period ranging from tens of minutes to about two hours, the rate of overflow progressively increased from $1–10\times10^3$ m^3/h to normal discharge rates of 100×10^3 m^3/h or more. At the same time, the height of the fountain increased from less than 10 m to tens or hundreds of meters.

Central-vent activity at the 1123 vent during episodes 2 and 3 died gradually, as indicated by progressive decrease of fountain vigor during the last day of each episode. In contrast, eruptive episodes at the Puu Oo vent ended more abruptly. Sometimes the eruption suddenly stopped with no warning. More often, the fountain diminished and became less steady in the last 3–10 minutes

of the episode; during that brief period, we sometimes saw pauses of a few seconds or tens of seconds in fountain and flow production. Normally the output of lava from Puu Oo was steady until the terminating moments of fountain activity, after which no further discharge occurred.

SEISMIC EFFECTS IN THE ERUPTION ZONE

Intense harmonic tremor occurred in the vent area coincident with vigorous eruption. However, the amplitude of the harmonic tremor did not vary systematically with major changes in fountain height during individual eruptive episodes (fig. 17.19). Throughout the central-vent activity, the amplitude showed a positive correlation with discharge (fig. 17.21) but not with the average fountain height (fig. 17.22). Thus, the recorded tremor reflected primarily processes at levels deeper than those from which fountaining originated. The symmetry, with respect to Puu Oo, of tremor-attenuation patterns implies that the tremor source and the vent were vertically aligned, but the depth of the tremor source is uncertain.

Harmonic tremor continued at low amplitude throughout repose periods and increased rapidly at the beginning of each episode of fountaining. Relatively deep south-flank earthquakes continued throughout the period of central-vent activity, but there was no shallow seismic swarm like that during emplacement of the dike in episode 1. We infer from the absence of seismic swarms after episode 1 and also from the continuous harmonic tremor and visible evidence of magmatic activity during repose periods that a continuous magma-filled conduit between the summit reservoir and the vents persisted after episode 1.

GEODETIC EFFECTS IN THE ERUPTION ZONE

Geodetic measurements in the eruption zone were limited by the difficulty and expense of obtaining access and by burial of measurement stations by new lava flows. However, two major inferences for the period of central-vent activity can be made from the available data: (1) over the long term, slight net deflation occurred; (2) over the short term, gradual inflation accompanied repose periods, and abrupt deflation accompanied eruptive episodes.

Measurements at a spirit-level tilt station about 1.5 km northwest of Puu Kamoamoa showed that the ground tilted northwestward, away from the rift-zone axis, during the early part of the eruption (table 17.2). The major change between December 15, 1982, and January 18, 1983, undoubtedly reflects deformation resulting from emplacement of the dike in early January. A smaller change between January 18 and March 8, 1983, may record inflation of the rift zone; a measured distance across the eruptive fissure farther downrift near Puu Kahaualea gradually lengthened during the same period. During episode 3, however, the ground tilted 12 μrad southeastward toward the rift axis, consistent with subsidence there. Measurements made after episode 3 and again 16 months later after episode 24 show an additional 19 μrad of tilt toward the rift-zone axis.

The automatic borehole tiltmeter 250 m northwest of Puu Kamoamoa operated during episodes 1–10 and from shortly after episode 15 through episode 20. No recognizable tilt change was associated with episode 2. However, beginning with southeast-directed tilt during episode 3, the ground normally tilted gradually northwest during repose periods and rapidly southeast during periods of fountaining (fig. 17.23). These opposed tilt changes were commonly of similar magnitude, in the range of 3–9 μrad, and were directed approximately normal to the rift-zone axis. They presumably recorded alternating inflation and deflation in the rift zone near Puu Kamoamoa. The largest deflations occurred during episodes 3 and 18, which were the most voluminous eruptions (table 17.1). No detectable tilt change occurred during episode 19.

SUMMIT BEHAVIOR

Repeated uplift and subsidence of Kilauea's summit region, recorded by the rising and falling trace of the Uwekahuna tiltmeter (fig. 17.15), dominated summit response to the episodic eruptions. Summit inflation occurred during repose periods and was accompanied by increasing numbers of shallow, short-period earthquakes beneath Kilauea caldera (fig. 17.24). Daily frequency of earthquakes generally increased to a maximum of 100–200 in the latter part of each repose period, then decreased sharply during and following the deflation. The earthquakes apparently recorded fracturing of country rock as it adjusted to distention of the summit reservoir.

Shallow long-period earthquakes, intergradational with related harmonic tremor, were abundant beneath the caldera during the later parts of summit subsidence and the early parts of the repose periods. Before episode 8, the daily number of long-period earthquakes seldom exceeded 100, but thereafter peak counts of many hundreds of events per day were normal (fig. 17.24). Greater intensity of long-period-earthquake activity was associated with higher rates of sustained deflation. Thus the long-period events and associated tremor in the caldera area were apparently responses to rapid evacuation of magma from the summit reservoir.

RELATION OF SUMMIT TILT CHANGES TO RIFT-ZONE ACTIVITY

COMPARISON OF SUBSIDENCE AND LAVA-DISCHARGE RATES

The average rate of summit subsidence as reflected in tilt changes at Uwekahuna (fig. 17.25) increased steadily from episode 2 through episode 8. Unlike the lava-discharge rate, which continued to increase thereafter (fig. 17.17), the subsidence rate later was variable and appeared to peak at an upper limit of about 0.5 μrad/h. In the following section we discuss some possible reasons for such a variable relationship between summit tilt change and erupted volume. Dvorak and Okamura (in press) attribute the early increase in deflation rate to progressive decrease of flow resistance in the conduit system. We agree and interpret the continued increase in effusion rate to indicate that the efficiency of magma delivery to the

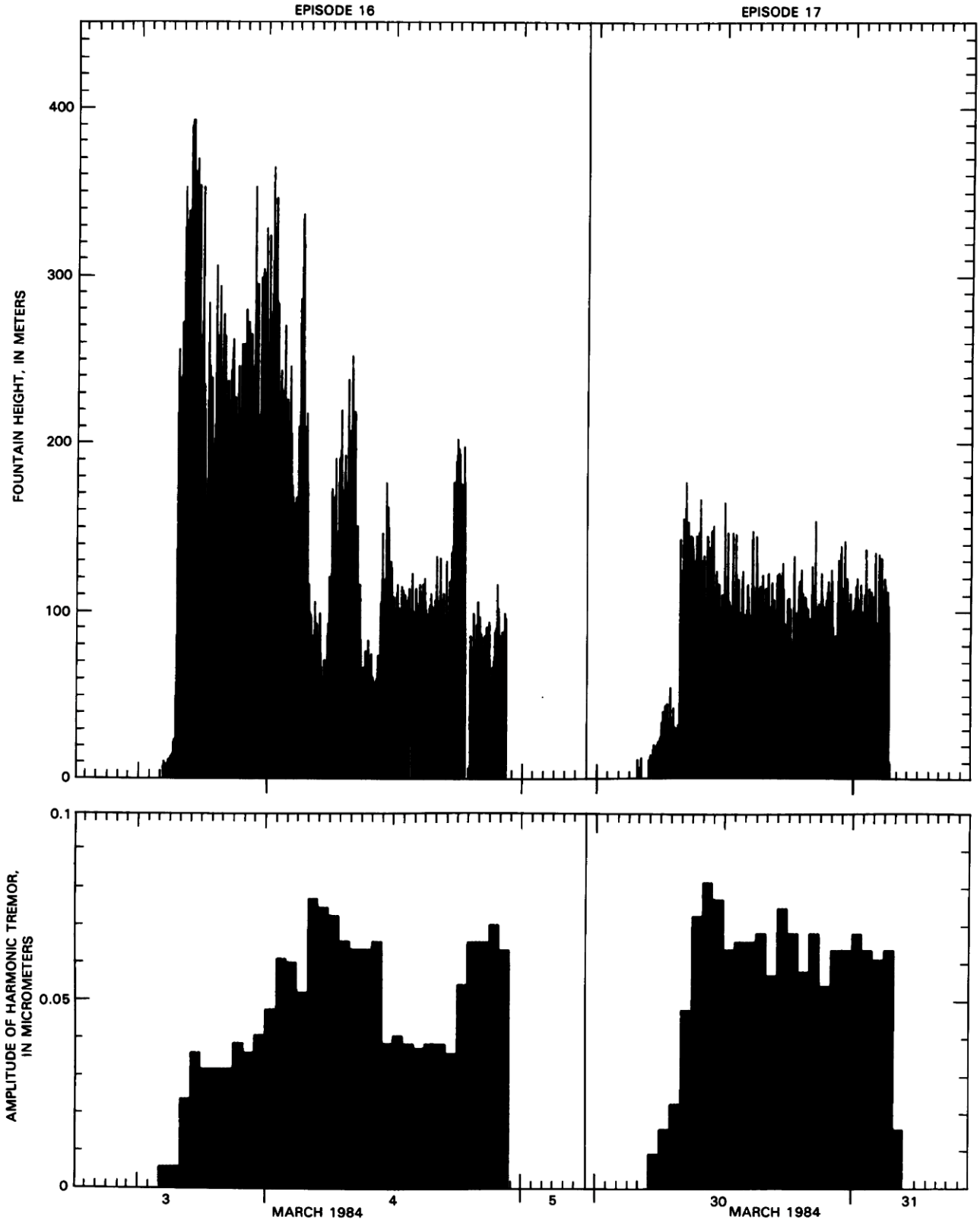

FIGURE 17.19.—Fountain height and amplitude of vent-area harmonic tremor recorded by seismometer at Makaopuhi Crater, episodes 16 and 17, Puu Oo eruption. Fountain height was measured from time-lapse film records. Gaps in fountain-height data record periods of poor visibility or inoperative camera.

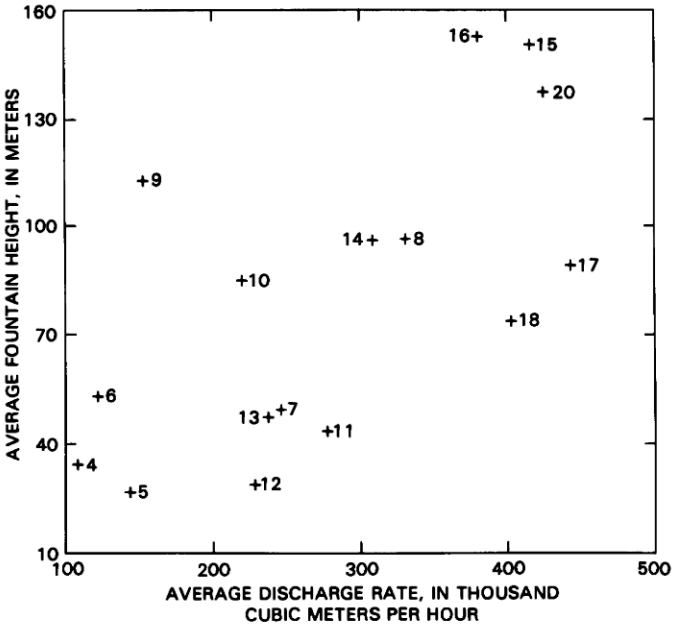

FIGURE 17.20.—Average fountain height versus average discharge rate at Puu Oo, episodes 4–18 and 20, Puu Oo eruption. Episode 19 is excluded because its intermittent fountaining yields a meaningless average.

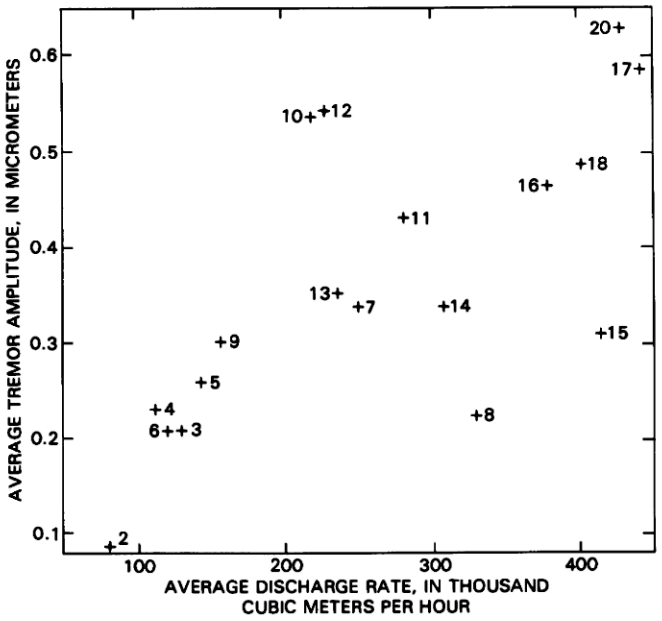

FIGURE 17.21.—Average harmonic-tremor amplitude, measured as ground displacement at the Makaopuhi Crater seismometer, versus average discharge rate at Puu Oo, episodes 2–18 and 20, Puu Oo eruption.

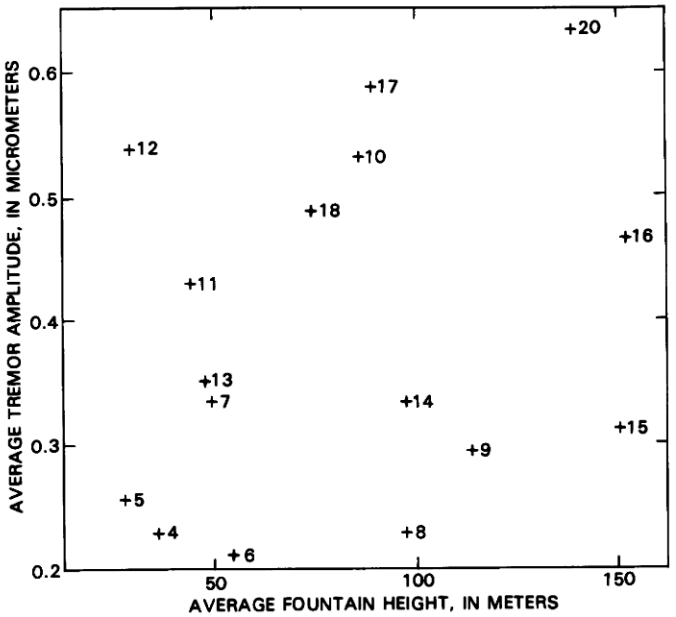

FIGURE 17.22.—Average harmonic-tremor amplitude, measured as ground displacement at the Makaopuhi Crater seismometer, versus average fountain height at Puu Oo, episodes 4–18 and 20, Puu Oo eruption. Fountain height value is a time-averaged arithmetic mean of fountain heights measured from time-lapse film records.

vent continued to increase after episode 8, even though the rate of tilt change at Uwekahuna did not.

VOLUMETRIC CONSIDERATIONS

The volume of lava erupted in each episode, adjusted for 25 percent porosity, ranged from approximately 0.3 to $1.0 \times 10^6 m^3$ per microradian of summit subsidence (table 17.3) measured on the east-west component of Uwekahuna tilt during episodes 2–20. The average value is 0.63 ± 0.21 (1 standard deviation) $\times 10^6 m^3/\mu rad$. The large variation may reflect several factors, including variable inequality between duration of eruption (table 17.1) and duration of subsidence (table 17.3), nonuniform summit response to reservoir-volume changes, variable rate of magma transfer from the summit reservoir to the rift zone during repose periods, and shifting position of the center of inflation and deflation with respect to the tiltmeter. The center of deflation did in fact shift within the region from east to

TABLE 17.2.—*Spirit-level tilt measurements at station 1.5 km northwest of Puu Kamoamoa*

[Vector azimuth gives direction of downward tilt]

Survey period	Vector magnitude (μrad)	Vector azimuth (degrees)
12/15/82–1/18/83	48	292
1/18/83–3/8/83	14	310
3/8/83–4/21/83	12	148
4/21/83–8/23/84	19	155

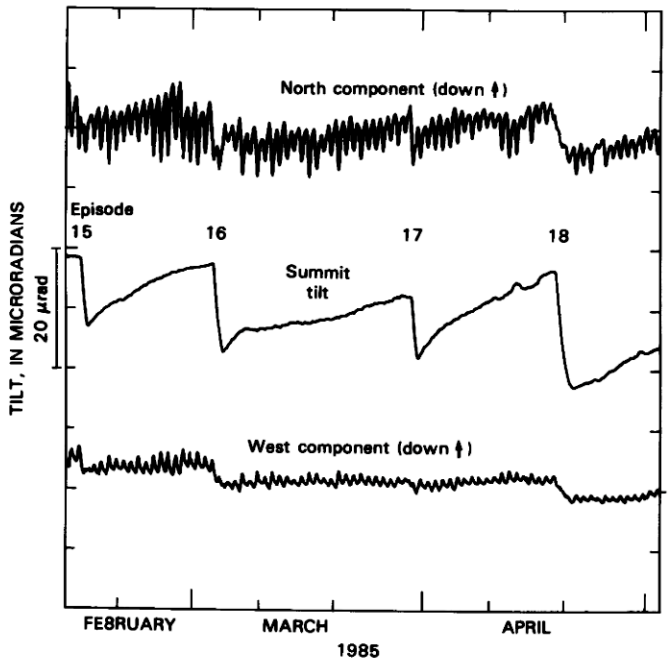

FIGURE 17.23.—East-west summit tilt and Kamoamoa borehole tilt (north and west components), episodes 15–18, Puu Oo eruption.

south of Halemaumau, as shown by levelling and spirit-level tilt surveys for the periods from February 7 to December 28, 1983, and December 28, 1983, to July 23, 1984 (fig. 17.26).

The first 12 fountaining episodes of the 1969–71 Mauna Ulu eruption produced lava at the rate of $0.34 \pm 0.09 \times 10^6 m^3/\mu rad$ of tilt change for a N. 60° W. vector calculated from Uwekahuna water-tube tilt data (Dzurisin and others, 1984). The first episode had a much lower than normal ratio of erupted volume to tilt change and was accompanied by an east-rift earthquake swarm (Swanson and others, 1979, plate 2). Thus, some of the volume of magma involved in the initial episode apparently formed a dike and is not represented at the surface. Eliminating the first episode from consideration, correcting for porosity (15 percent; Swanson, 1972), and adjusting the vector from N. 60° W. to east-west, we calculate a ratio for episodes 2–12 of the 1969–71 Mauna Ulu eruption of $0.35 \pm 0.08 \times 10^6 m^3$ of magma per microradian of east-west tilt change. This is slightly more than 50 percent of the value for episodes 2–20 of the Puu Oo eruption.

The ratio of volume change to tilt change has also been estimated by considering surficial volume change at the summit, determined from leveling surveys, as a measure of reservoir-volume change. Recent calculations of the ratio of surficial volume change to east-west Uwekahuna tilt change are $0.38 \pm 0.07 \times 10^6 m^3/\mu rad$ by Dzurisin and others (1984; value adjusted from N. 60° W. vector) and $0.45 \pm 0.13 \times 10^6 m^3/\mu rad$ by Dvorak and others (in press).

Johnson (chapter 47) attempts to relate elevation changes, Uwekahuna tilt changes, and summit-reservoir volume changes estimated from gravity measurements made from episodes 13–32 of the Puu Oo eruption, and he concludes that changes in reservoir volume may have been appreciably larger (perhaps 2.5 times) than measured surface-volume changes. If this is true, it could account for the high ratio of erupted-magma volume to tilt change for the Puu Oo eruption (0.63) compared to the lower ratio for the early Mauna Ulu episodes (0.35) and to the lower ratio calculated for surface--volume changes (0.38–0.45). We note that the ratio of erupted volume to tilt change for Mauna Ulu is slightly lower than the ratio of surface volume to tilt change; this relation implies that average reservoir-volume changes did not exceed surface-volume changes during the early Mauna Ulu episodes.

As an alternative, we suggest that the higher ratio for the Puu Oo eruption may have resulted from alternating additions to and subtractions from rift-zone storage. The rift zone, at least in the Puu Kamoamoa region, apparently inflated and deflated in tandem with Kilauea's summit (fig. 17.23). Thus we infer that successively accumulated and extruded volumes were accommodated in hydraulically connected summit and rift-zone reservoirs. If this is true, the volume of magma supplied to Kilauea during repose periods was accommodated by volume increases in both the summit and rift-zone reservoirs, and the volume of magma erupted during fountaining episodes was accommodated by volume decreases in both the summit and rift-zone reservoirs. Because part of the volume accommodation occurred in the rift-zone reservoir during Puu Oo eruptive episodes, surficial volume changes at the summit and related Uwekahuna tilt changes are insufficient measures of erupted volume.

The generally similar average ratios of volume to tilt change determined for the early Mauna Ulu episodes (0.35) and for surficial volume changes (0.38–0.45) represent about 55–70 percent of the average ratio of erupted volume to tilt change (0.63) for episodes 2–20 of the Puu Oo eruption. If the Mauna Ulu and surficial volume ratios are applied to Puu Oo episodes as a measure of summit-reservoir volume change, 55–70 percent, on the average, of the erupted volume (considered vesicle-free) was accommodated by summit-reservoir volume changes. The remaining 30–45 percent could have been accommodated by changes in the volume of rift-zone storage.

We emphasize that, because of large scatter in the ratios of erupted volume to tilt change for specific episodes (table 17.3), estimates of reservoir-volume change are at best generalized approximations. Furthermore, variations in summit-inflation rate (compare summit tilt-change patterns preceding episodes 16 and 17, fig. 17.24), including occasional deflationary episodes during repose periods, suggest that transfer of magma from the summit to the rift zone may have occurred during repose periods in an irregular and unpredictable pattern. Thus, we cannot predict the volume of rift-zone accommodation or the erupted volume for a single episode with reasonable precision from the Uwekahuna tilt record.

TIMING OF TILT CHANGES AND ERUPTIVE ACTIVITY

During eruptive episodes, changes in tilt rate or direction at the summit were often closely related to changes in eruptive activity.

Once the vent became established at Puu Oo, the tilt changes tended to lag behind the changes at the vent (table 17.3).

Typically, such changes occurred only at the beginnings and endings of eruptive episodes. However, discharge stopped and then resumed once during episode 13 and three times during episode 19. The rate of tilt change at the summit responded to each of these changes at the vent (fig. 17.27), emphasizing the effectiveness of the connection between vent and summit areas. In each case, however, the rate of summit tilt change reached a minimum several hours after the end of the related fountaining event. Similarly, the rate of tilt change reached a maximum in each case several hours after fountaining resumed.

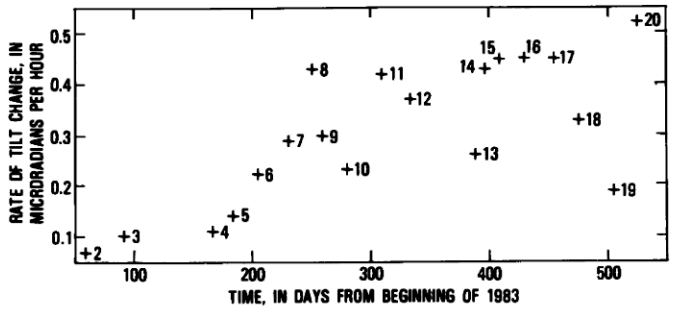

FIGURE 17.25.—Average rate of deflationary, east-west tilt change at Uwekahuna tiltmeter, episodes 2–20, Puu Oo eruption.

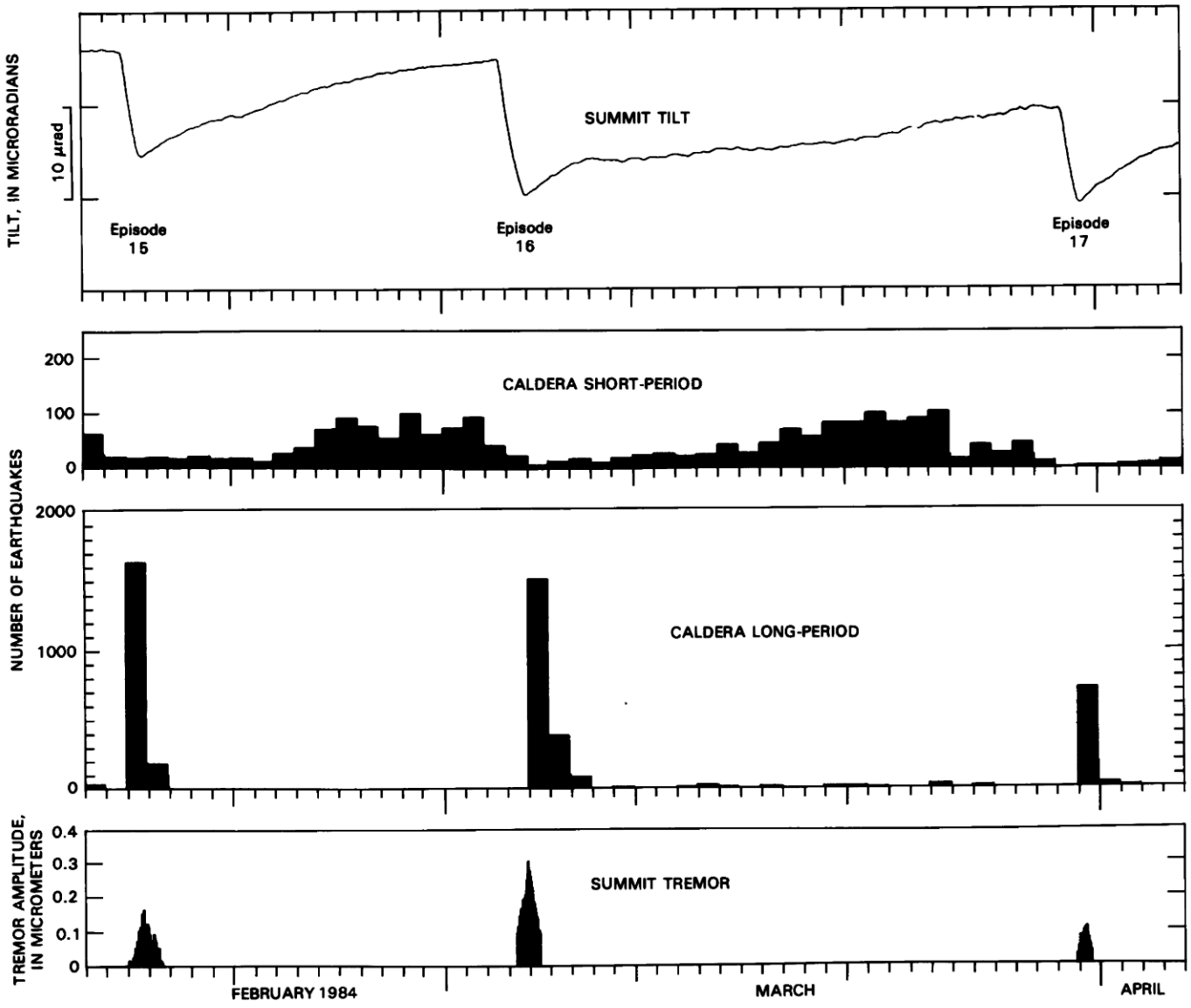

FIGURE 17.24.—East-west summit tilt, daily frequency of short-period and long-period caldera earthquakes, and amplitude of shallow harmonic tremor beneath Kilauea caldera, episodes 15–17, Puu Oo eruption.

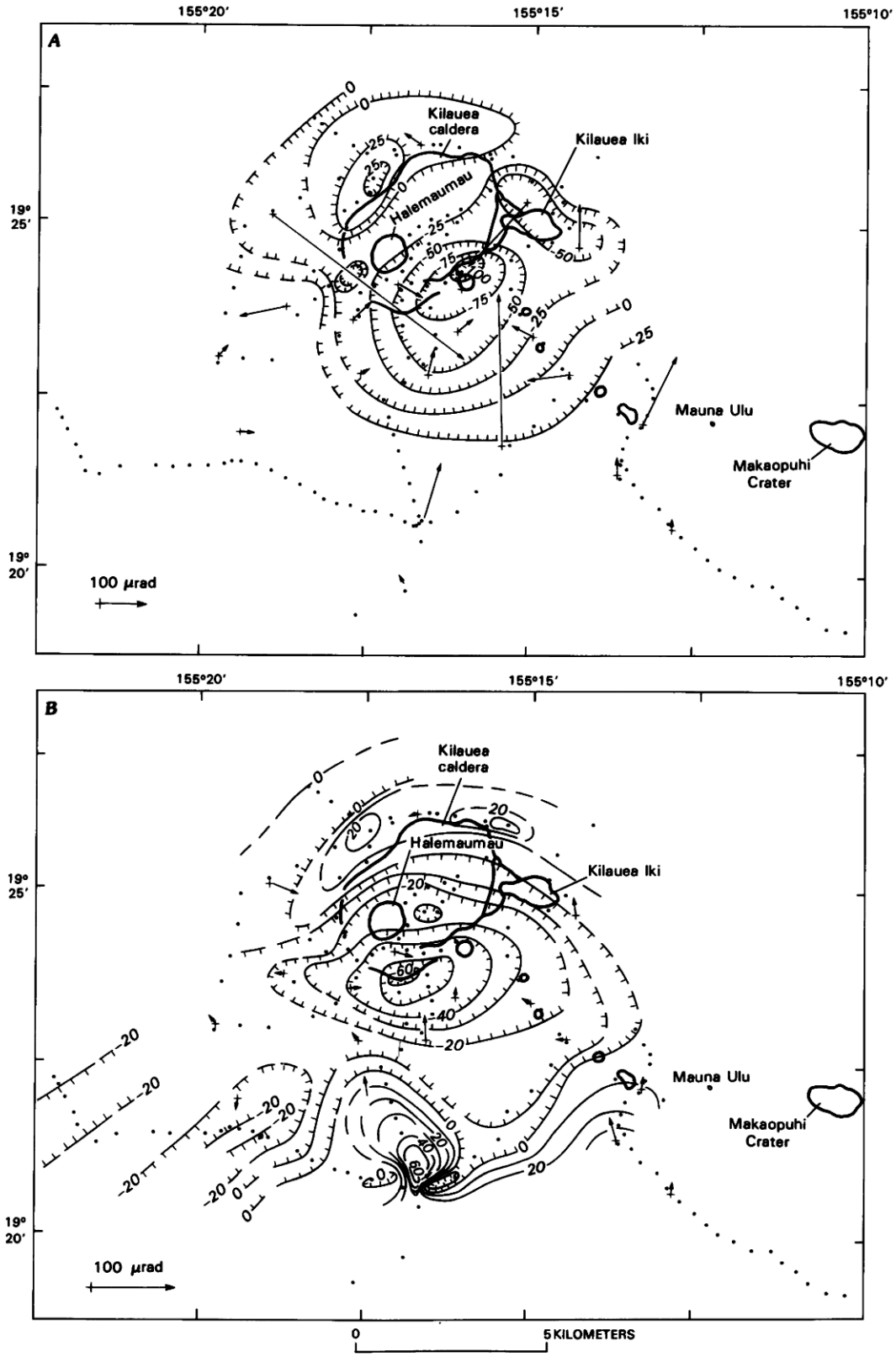

FIGURE 17.26.—Kilauea summit level change and tilt change during two periods of the Puu Oo eruption. *A*, February 7 to December 28, 1983. *B*, December 28, 1983, to July 23, 1984.

TABLE 17.3.—*Subsidence and relation to erupted volume, episodes 2–20, Puu Oo eruption, Kilauea*

[Tilt change is eastward on the east-west component of Uwekahuna tilt. Beginning lag is the time from start of eruption to start of accelerated, sustained deflation. For some episodes, uncertainty arises from the gradual nature of the onset of eruption or deflationary tilt change and from the absence of direct observation of the onset of eruption. Ending lag is the time from end of eruption to end of deflationary tilt change. Erupted volume corrected to remove 25 percent porosity.]

Episode	Tilt change (μrad)	Subsidence			Erupted volume/ tilt change ($10^6 m^3/\mu rad$)
		Duration (h)	Beginning lag (h)	Ending lag (h)	
2	10.9	151	−2.0	−24.8	.964
3	28.1	292	−1.0	1.0	1.014
4	11.2	98	4.6	3.3	.735
5	11.9	86	6.7	2.2	.819
6	16.2	72	3.5	2.5	.416
7	16.7	57	2.3	3.0	.630
8	10.0	23	5.8	4.5	.601
9	14.9	50	3.3	1.7	.402
10	14.1	60	3.9	.2	.745
11	17.4	41	2.2	.2	.517
12	13.8	37	.2	2.3	.434
13	11.1	43	3.6	4.6	.676
14	9.8	23	2.3	5.7	.458
15	11.3	25	.3	6.0	.531
16	14.8	33	1.2	2.5	.609
17	10.2	23	3.2	3.6	.732
18	19.4	58	2.0	.5	.928
19	4.1	21	6.0	[1]−16.8	.366
20	9.4	18	.9	9.6	.318

[1]Episode 19 included lava-pond activity and low-volume overflows that continued for a day after the end of intermittent fountaining and high-volume flow production. Ending lag = 6.6 h when considered with respect to end of high fountains and high-volume flow production.

From episode 3 on, summit deflation continued for as long as several hours beyond the end of lava production (table 17.3). From episode 4 on, the beginning of sustained rapid deflation lagged behind the beginning of steady lava production. In contrast, we note that, during episode 2, lava production continued for a full day after summit deflation had stopped. The starts of episodes 2 and 3 were gradual and the time relations therefore somewhat subjective (table 17.3), but our interpretation is that vigorous discharge lagged slightly behind the onset of rapid deflation.

The approximate balance between Uwekahuna tilt changes during repose periods and during fountaining periods for episodes 2–20 (fig. 17.15) implies that eruptive episodes began and ended in response to increased and decreased pressure in the reservoir system. However, the abrupt terminations of fountaining from episode 4 on and the delayed response of summit tilt to eruptive changes suggest that a valve nearer to the vent than to the summit reservoir was the immediate control over the timing of fountaining.

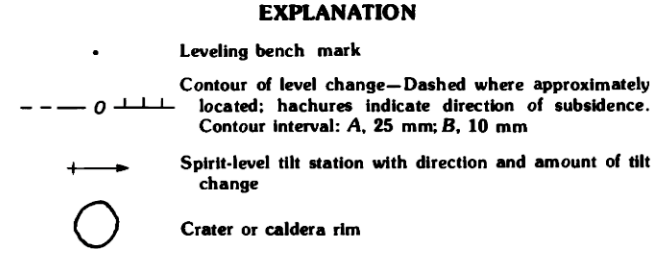

FIGURE 17.26.— Continued.

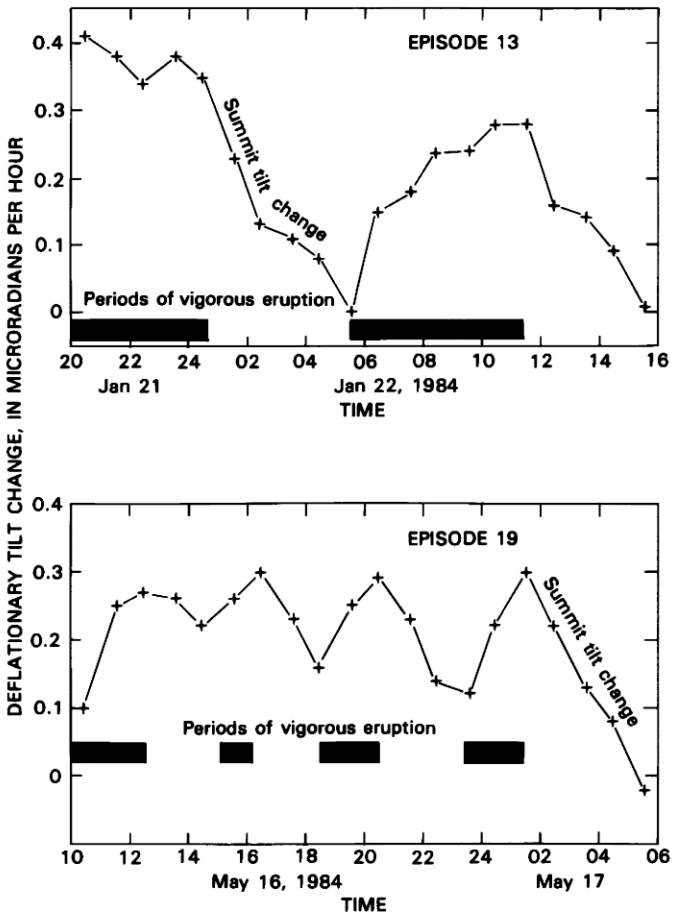

FIGURE 17.27.—Periods of vigorous discharge and variations in rate of summit tilt change for parts of episodes 13 and 19, Puu Oo eruption.

PETROLOGY

EPISODES 1–3

Samples of lava erupted during episodes 1–3 contain less than 6.8 percent MgO (figs. 17.28, 17.29) and thus represent differentiated basalt in the terminology of Wright and Fiske (1971) and Wright (1971). They are also depleted in CaO and enriched in FeO_t ($FeO_t = FeO + 0.9Fe_2O_3$) and in the incompatible elements. Following Wright and Fiske (1971), we interpret this lava as having resulted from fractionation of clinopyroxene and plagioclase as well as olivine from magma that had partly cooled and crystallized during prolonged storage within the rift zone.

The lava of episodes 1–3 is compositionally heterogeneous, even among samples collected during a limited time from a small geographic area. For example, nearly the full compositional range of lava sampled during episodes 1–3 was produced during episode 1 within the relatively restricted area of the 0740 and 1123 vents. Thus the lava apparently originated from several magma bodies that had differentiated to varying degrees within the rift zone. Partly resorbed xenocrysts and reversely zoned phenocrysts are present in

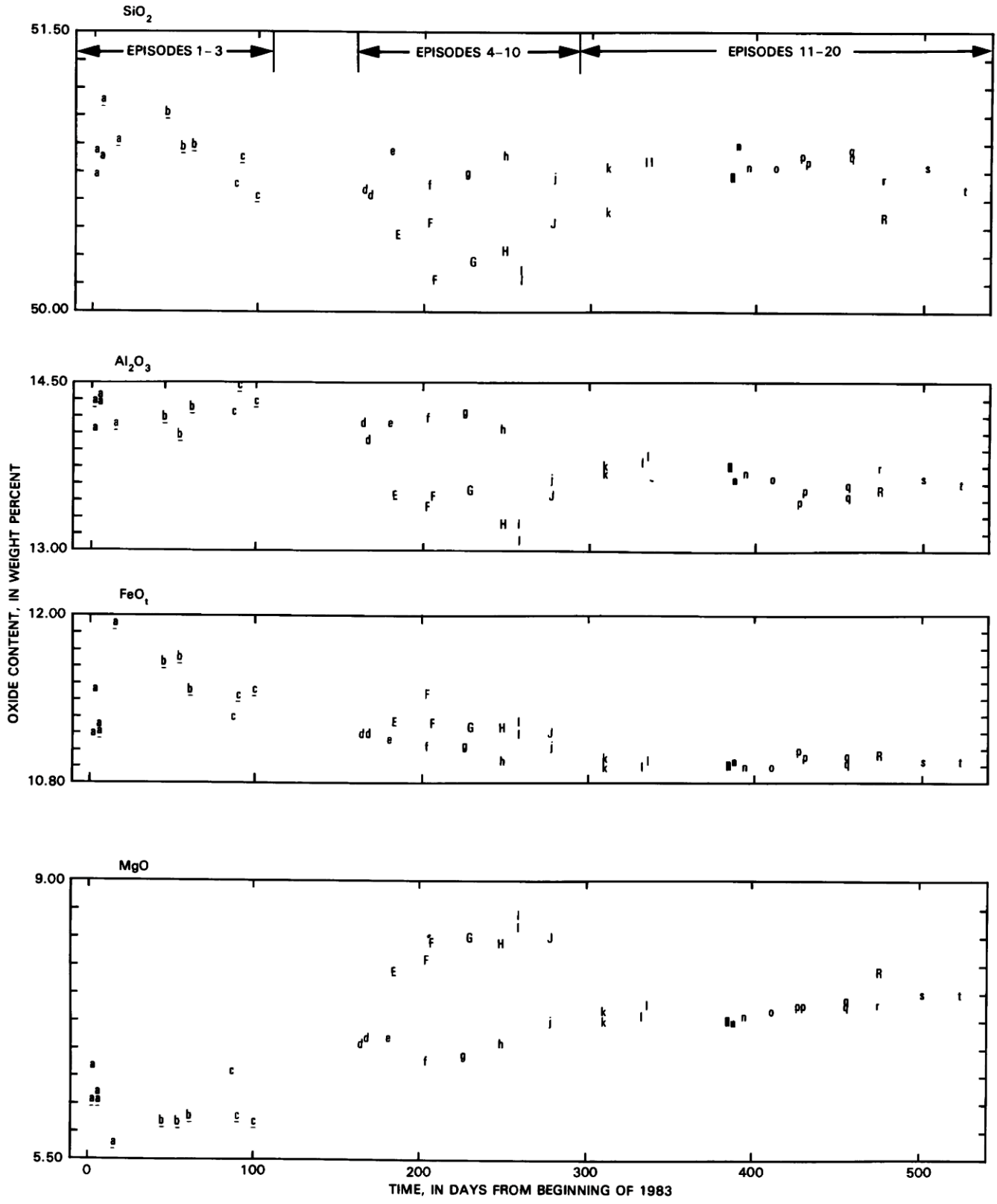

FIGURE 17.28.—Major-oxide concentrations in samples from Puu Oo eruption versus time of eruption. Letters identify episodes: a, episode 1; b, 2; c, 3; d, 4; e, 5; f, 6; g, 7; h, 8; i, 9; j, 10; k, 11; l, 12; m, 13; n, 14; o, 15; p, 16; q, 17; r, 18; s, 19; t, 20.

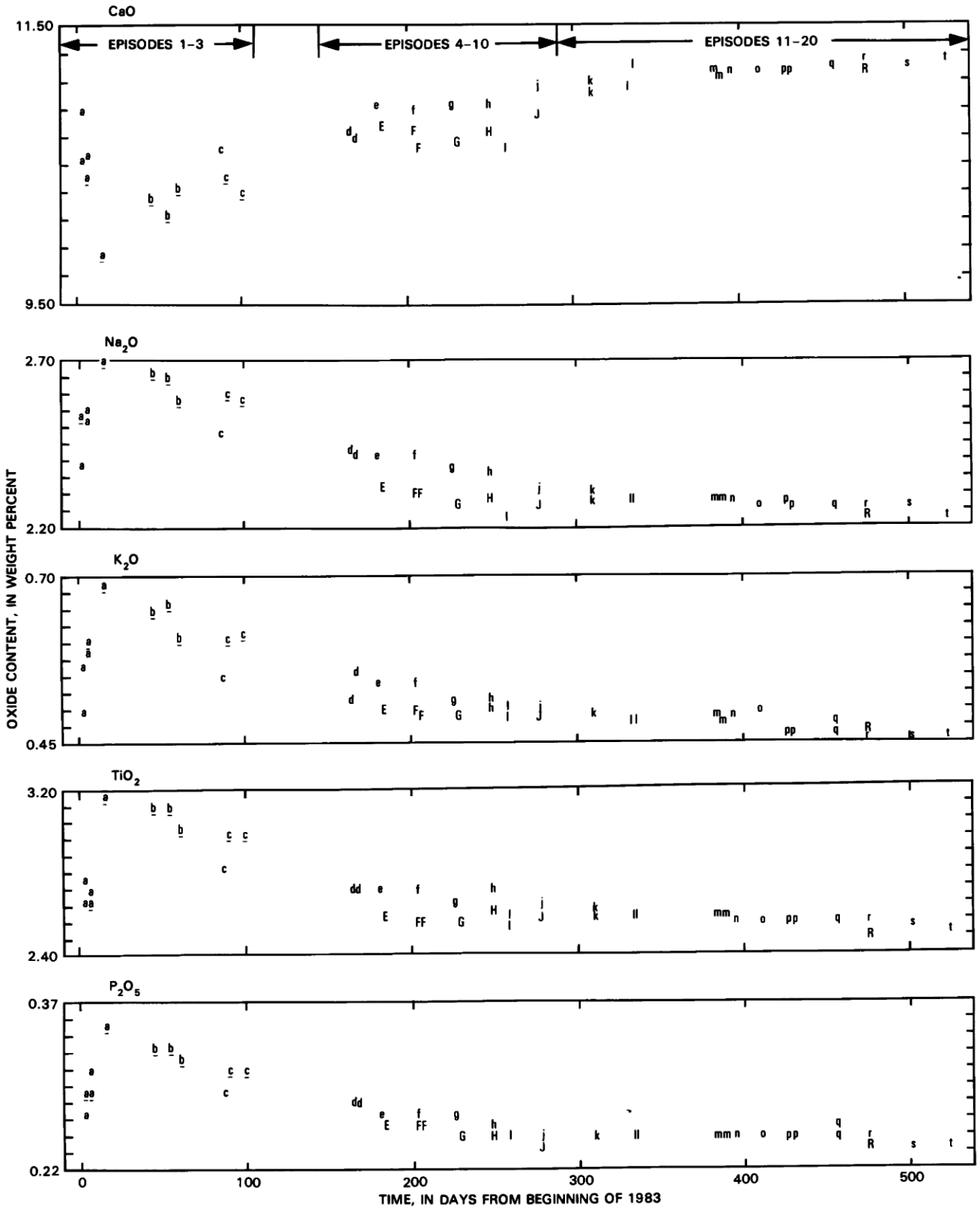

Capital letters designate MgO-rich lava erupted late in episodes 5–10 and 18. Underlined letters indicate samples from 0740 and 1123 vents (see fig. 17.12 for location). Compositions are from classical wet chemical analyses (see Neal and others, in press).

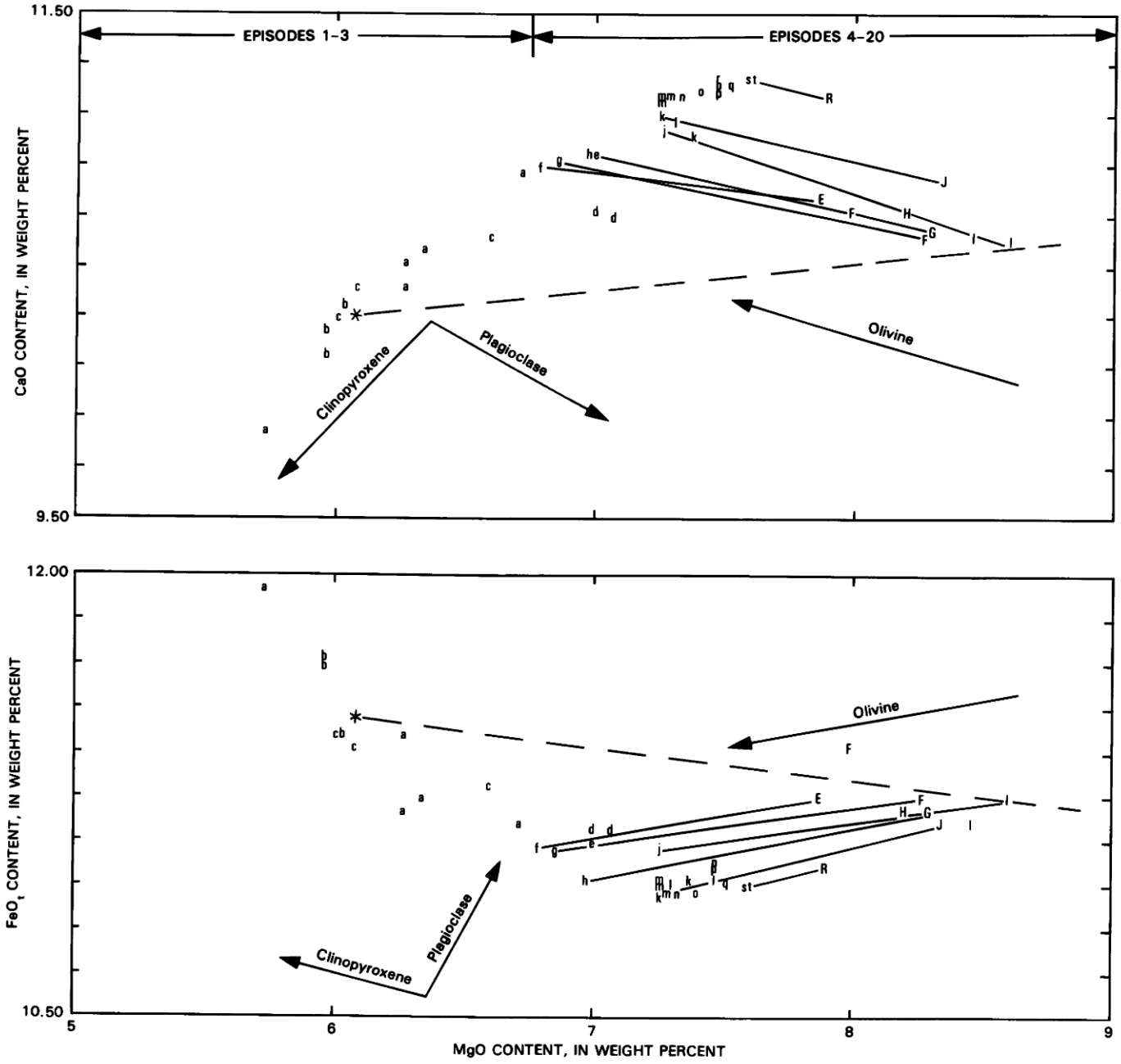

FIGURE 17.29.—CaO versus MgO and total iron (FeO_t) as FeO versus MgO for samples from Puu Oo eruption. Arrows show mineral-control lines calculated for samples with the same MgO content as the origins for the control lines (control lines have been shifted vertically to separate them from the other plotted data). Solid lines connect composition of MgO-rich lava erupted late in an episode with composition of MgO-poor lava erupted early in the succeeding episode. Long-dashed line connects average composition (*) for episode 1–3 lava (excluding the two most MgO-rich samples) and the most MgO-rich Puu Oo lava composition and is an approximate mixing line. Letters indicate episodes and capital letters MgO-rich lavas as in figure 17.28.

some of the samples, evidence that magma mixing had occurred to produce hybrid magmas.

EPISODES 4–20

Lava from episodes 4–20, all of which erupted from Puu Oo, contains 6.8 percent or more MgO. The most conspicuous compositional variation, which occurred within individual episodes 5 through 10 and to a lesser degree during episode 18, can be largely explained as a consequence of olivine fractionation; thus the lava is olivine-controlled in the terminology of Wright and Fiske (1971) and Wright (1971). An additional subtle long-term compositional change is not related to olivine control.

TABLE 17.4.—*Comparison of early episode 10 basalt and composition calculated by subtracting 3.74 percent late episode 9 olivine from late episode 9 basalt*

[Values given are in weight percent]

Oxide	(a) Early episode 10 basalt	(b) Calculated composition	Residual (a minus b)
SiO_2	50.91	50.88	0.03
Al_2O_3	13.71	13.70	.01
FeO_t	11.11	11.10	.01
MgO	7.30	7.30	.00
CaO	11.09	11.07	.02
Na_2O	2.32	2.33	−.01
K_2O	.50	.51	−.01
TiO_2	2.64	2.68	−.04
P_2O_5	.25	.26	−.01
MnO	.17	.18	−.01

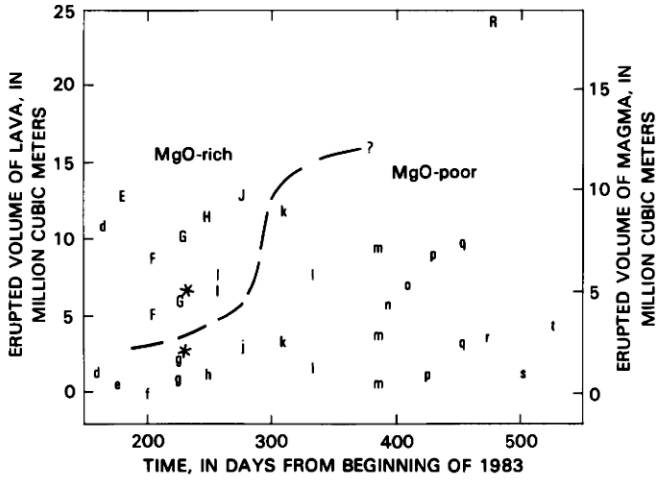

FIGURE 17.30.—Volume of lava (left axis) or magma (right axis) erupted in each episode (4–20) of the Puu Oo eruption at the time of collection of each analyzed sample. Letters indicate episodes and capital letters MgO-rich lavas as in figure 17.28. *, composition from microprobe analysis. Volume erupted by time of collection was estimated by multiplying the subsequently determined discharge rate by the time elapsed from the beginning of the eruptive episode.

During episodes 5–10 and 18, a transition to more MgO-rich lava occurred as the eruptive episode progressed, and all of the other oxides decreased in abundance as MgO increased (figs. 17.28, 17.29). Thus, eruption from a zoned body produced relatively MgO-poor lava early in an episode, and MgO-rich lava was erupted late. Samples for classical analyses represented in figures 17.28 and 17.29 were usually taken in the early and late parts of each eruptive episode. Additional analyses by electron microprobe, from episode 7 (not shown in figures 17.28, 17.29), indicate that the compositional change during the fountaining episode was gradational. Lava sampled during the period of small intracrater pahoehoe flows and pond activity that commonly preceded the major eruptive episodes was similar in composition to the early, MgO-poor lava of the following fountaining episode. Apparently magma in the column beneath the Puu Oo crater floor underwent a compositional change from MgO-rich to MgO-poor during some of the repose periods. Extension of the trends for the MgO-poor lava of episodes 5–10 indicates that only the MgO-poor variety was erupted during episodes 11–17 and 19–20.

Even though the repose periods were brief, crystal fractionation within the magma column seems the most plausible explanation for the compositional change that occurred between eruptive episodes. The most compelling example is the change from MgO-rich lava at the end of episode 9 to MgO-poor lava early in episode 10; it can be precisely accounted for by removal of 3.74 percent of late episode 9 olivine from late episode 9 basalt (table 17.4). Other repose-period compositional changes are fit less precisely by olivine fractionation alone. Nevertheless, the joins connecting the compositions of MgO-rich lava from late in one episode and MgO-poor lava from early in the next (fig. 17.29) are nearly parallel to the olivine-control line (calculated for late episode 9 basalt and its contained olivine). This near coincidence suggests that subtraction of olivine was the dominant cause of the compositional variation during single eruptive episodes. Petrographic data show that the higher MgO content of lava erupted late in a fountain episode does not reflect increased abundance of olivine crystals.

Episode 4 lava did not show the compositional change typical of episodes 5–10. Perhaps the specific magma-column geometry that led to fractionation of a limited melt volume during repose periods originated during episode 4. Thus, the fractionation occurred only during later repose periods.

The MgO-depleted magma in the zoned body was completely erupted in each of episodes 5 through 10. Thereafter, the MgO-depleted volume was too large to be exhausted in an eruptive episode, except for episode 18, which produced an appreciably greater volume than its predecessors at Puu Oo (table 17.1).

We have estimated the volume of lava that had been erupted in each episode at the time that each analyzed sample was collected (fig. 17.30). The first occurrence of both MgO-poor and MgO-rich lava in a single episode was during episode 5, but the volume of early MgO-poor lava is not well constrained. During episodes 6 through 9, MgO-poor lava gave way to MgO-rich lava after about 2.3×10^6 to $5.2\times10^6\,m^3$ of lava had been produced. The volume of MgO-poor lava in episode 10 is poorly constrained but it was less than $12.7\times10^6\,m^3$. Episode 11 produced $12\times10^6\,m^3$ of lava that was all MgO-poor, as was the lava of subsequent episodes except for 18. Lava collected at the end of episode 18, after eruption of $24\times10^6\,m^3$, was richer in MgO than early episode 18 lava but less so than most of the other MgO-rich lavas.

The volumes of MgO-poor lava, considered void-free so as to approximate magma volumes, indicate that about $3\times10^6\,m^3$ of MgO-poor magma was available in the reservoir during the early parts of episodes 5 through 9. Between episodes 9 and 11, this increased to more than $9\times10^6\,m^3$, but episode 18 indicates it did not exceed $18\times10^6\,m^3$.

Subsidence of the Puu Oo crater floor and collapse of the crater walls occurred late in episode 10. In the next two episodes, fountain heights were dramatically lower, and lava issued from several vents

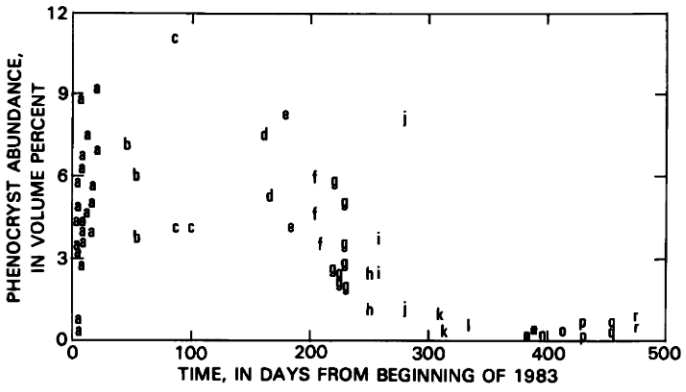

FIGURE 17.31.—Total percentage of olivine, augite, and plagioclase phenocrysts versus time of collection of lava samples from Puu Oo eruption. Letters indicate episodes as in figure 17.28.

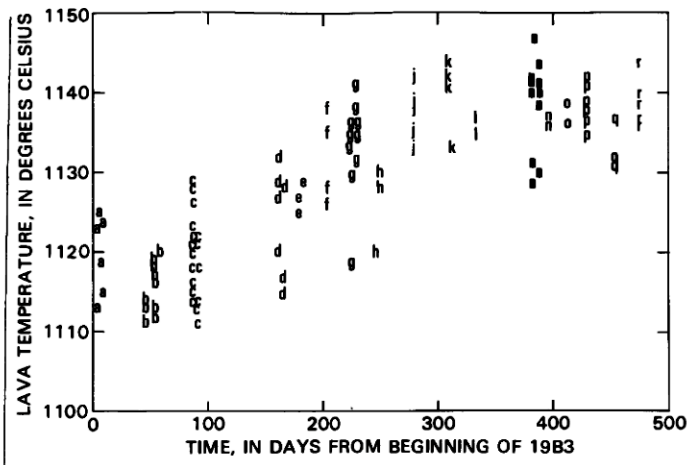

FIGURE 17.32.—Lava temperatures measured by chromel-alumel thermocouple, episodes 1–20 of Puu Oo eruption. Letters indicate episodes as in figure 17.28.

both within and outside the crater. These observations suggest that collapse in the conduit had partly blocked access to the normal vent. The marked increase in the erupted volume of MgO-depleted magma between episodes 9 and 11 may have recorded enlargement of the subcrater reservoir by the same event that caused crater collapse and disrupted the fountains.

If our hypothesis that MgO-depleted magma originated by crystal fractionation of MgO-rich magma in the magma-filled conduit beneath Puu Oo is correct, then the volume of MgO-depleted magma represents a minimum value for the volume of the magma column. We have no direct measure of the column length. However, we inferred previously from the distribution of earthquakes in the shallow swarm associated with episode 1 that the feeder dike was intruded upward to the surface from an aseismic zone at a depth of 3–4 km. If the aseismic zone persisted through the subsequent fountaining episodes as the subhorizontal zone of magma supply from the summit reservoir to the vent region, we can surmise that the magma column beneath Puu Oo was 3–4 km long. Using a 3.5-km length and the volume estimate of 3×10^6 m^3 for episodes 5–9, we calculate a minimum average diameter for the magma column of about 30 m. For the volume estimates for the later episodes (9×10^6 to 18×10^6 m^3), the calculated minimum average diameter is 60–80 m. These values are in close agreement with estimates of average conduit diameters of 40–70 m inferred from volumes of gas-enriched melt that caused high fountains early in some episodes (Wolfe and others, in press) and 50 ± 30 m inferred from interpretation of gas-flux and geodetic measurements (Greenland and others, in press).

The lava of episodes 4–20 shows a long-term compositional change marked by gradual increase in CaO and MgO and decrease in FeO_t and incompatible elements (figs. 17.28, 17.29). The changes are small, and the progression is imperfect. Nevertheless, figure 17.29 shows unmistakably that, in both the MgO-poor and MgO-rich lavas, CaO and MgO gradually increased together through time and FeO_t concomitantly decreased through time. Imposition of this progressive compositional change on both lava types supports our interpretation that each volume of MgO-depleted magma was derived from an associated volume of MgO-rich magma. In a sense, the two share a common fingerprint imposed by the gradual long-term compositional change.

Two possible reasons for the long-term compositional trend involve rift-zone mixing (see, for example, Wright and Fiske, 1971; Wright and others, 1975) and gradual compositional change of the melt produced in the mantle (see, for example, Hofmann and others, 1984). If mixing is the reason, fresh magma from the summit would become contaminated to progressively decreasing degrees from contact during its passage through the rift zone with older CaO- and MgO-depleted magma still in storage. We do not know the possible end-member compositions, but for illustration we have drawn an approximate mixing line (fig. 17.29) connecting the most MgO-rich sample (late episode 9) and an average composition that includes all analyzed lava from episodes 1–3 except for two samples that have significantly higher MgO contents (6.59 and 6.72 wt percent) and may reflect more recent involvement of summit magma than do other lavas of episodes 1–3.

If changing parent composition is the reason, then the progressive increase in CaO and depletion of incompatible elements, emphasized when the compositions from episodes 5–20 are normalized to a common MgO value by adjusting for olivine control, may have resulted from increasing melting of clinopyroxene in the mantle.

Reversely zoned phenocrysts in some samples from episodes 4–10 suggest magma mixing. Lava of episodes 11–20 was nearly aphyric (fig. 17.31), and no phenocrysts suggestive of disequilibrium were found. Lava-temperature measurements show much scatter (fig. 17.32) but suggest that the temperature increased through the early episodes, perhaps through episode 11, and then leveled off. This increase could have been a consequence of decreasing contamination of hotter summit melt by cooler rift-zone melt. We note that the change in phenocryst content and the change in measured temperatures through time roughly mimic the compositional changes

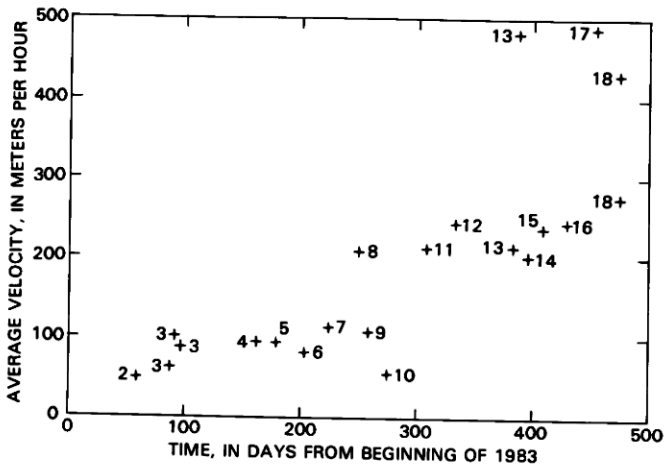

FIGURE 17.33.—Average flow-advance rate versus time of eruption for the major river-fed flow(s) of eruptive episodes 2–18, Puu Oo eruption. Flow-advance velocity was determined by periodic mapping of flow-front position.

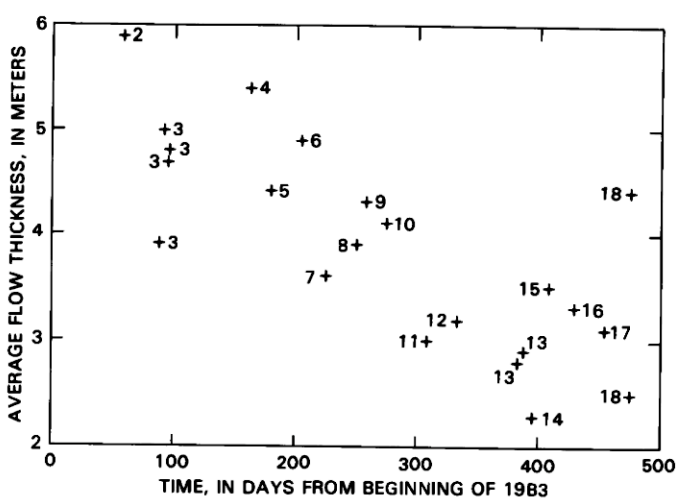

FIGURE 17.34.—Average flow thickness versus time of eruption, episodes 2–18 of Puu Oo eruption. Thickness was measured at numerous localities along flow margin. Average thickness was obtained from calculated volume/measured area.

recorded from episode 4 through 20. Average velocity and average thickness of the major river-fed lava flows (figs. 17.33 and 17.34) also roughly mimic these patterns. Velocity was greater and thickness less during episodes 11–20, suggesting that lava viscosity decreased, in accord with changing lava composition, petrography, and temperature.

NEGLIGIBLE EFFECTS OF MAUNA LOA EARTHQUAKE AND ERUPTION

A large ($M = 6.7$) earthquake (Buchanan-Banks, chapter 44; Koyanagi and others, 1984) occurred beneath Mauna Loa's southeast flank on November 16, 1983, between episodes 11 and 12 of the Puu Oo eruption. The earthquake caused an abrupt tilt change of nearly 300 μrad at the Uwekahuna tiltmeter (fig. 17.15), but it produced no recognizable change in the continuing events at Puu Oo.

A Mauna Loa eruption occurred from March 25 to April 15, 1984 (Lockwood and others, 1985); for the first time since 1919, Kilauea and Mauna Loa were in eruption simultaneously. Episode 17 of the Puu Oo eruption occurred on March 30–31, during the Mauna Loa eruption, and episode 18 on April 18–21 following the Mauna Loa eruption. The volume of episode 18 was larger than usual (table 17.1), but otherwise Puu Oo activity during and immediately after the Mauna Loa eruption was normal.

INTERPRETIVE SUMMARY

The east rift zone of Kilauea has been a major locus of magma storage as well as eruption; Dzurisin and others (1984) estimated that at least $1 \times 10^9 m^3$ of magma was added to east-rift-zone storage between 1956 and 1983. From late 1978 through 1980, the Puu Kamoamoa-Puu Kahaualea area, where the major vents of the Puu Oo eruption are located, was the site of repeated intrusions that caused flurries of shallow earthquakes and increasing tumescence of that part of the rift zone.

After a period of quiescence during 1981 and part of 1982, small intrusions into the Puu Kamoamoa area resumed following a summit intrusion and eruption on September 25–26, 1982. In early January 1983 a voluminous east-rift intrusion resulted in large subsidence of the previously distended summit reservoir, emplacement of a new feeder dike, and onset of the Puu Oo eruption.

The intrusion was initiated by an aseismic magmatic surge through magma-filled passages in the uppermost part of the east rift zone and by the onset of dike emplacement near Makaopuhi Crater. The distribution of shallow earthquakes indicates that the dike propagated upward from an aseismic region at a depth of 3–4 km within the rift zone, and its tip migrated downrift as intrusion continued. The upper edge of the dike eventually intersected the ground surface from Napau Crater to Kalalua, initiating nearly two weeks of intermittent fissure eruptions.

Over most of its length, the fissure system soon stopped erupting. Intermittent fissure eruptions during episode 1 of the series, in January 1983, became localized primarily south of Puu Kahaualea. During episodes 2 and 3, a central vent south of Puu Kahaualea, the 1123 vent, was the dominant eruptive locus, and a lesser one was located 1.5 km uprift in the area where Puu Oo was to develop. From episode 4 on, the Puu Oo vent was the main locus, and, except for fissures in the immediate vicinity of Puu Oo that were briefly active a few times, eruption has never recurred elsewhere along the fissure system (as of June 1985).

After episode 1, low harmonic tremor continued during repose periods, and subsequent fountaining episodes began without shallow earthquake swarms. Both these observations indicate that an active magma conduit was maintained between the summit and vent areas.

As the eruptive series progressed, the rift-zone conduit became more efficient in transporting magma, as indicated by the general increase in average lava-discharge rate. Factors that may have contributed to more rapid magma transport include enlargement and streamlining of passageways and reduction of melt viscosity as a consequence of increased temperature or decreased crystallinity. We have no direct means of evaluating the character of the magma-filled passageways, but enlargement or streamlining seem likely consequences of repeated passage of melt through them. We note that the lava generally became hotter and less porphyritic as the Puu Oo eruption progressed.

Several different phenomena, considered together, suggest that the main vents, located in the general Puu Kamoamoa-Puu Kahaualea area, overlay a zone of magma storage that antedated the beginning of the eruption. Effects specifically related to such a zone include: (1) anomalously rapid downrift passage of surface deformation preceding the tip of the dike; (2) dissipation of the tightly clustered concentration of shallow earthquakes that farther uprift recorded a systematic, steady downrift advance of the dike tip; (3) decreased concentration of shallow earthquakes associated with dike emplacement and establishment of the new vents; and (4) localization of repeated small intrusions from late 1978 through 1980.

The petrologic evidence suggests that a magma-storage zone had existed for a long time beneath the Puu Kamoamoa-Puu Kahaualea area. Lava erupted from the inferred storage zone during episodes 1–3 was differentiated beyond olivine control and was significantly cooler than olivine-controlled lava erupted later from Puu Oo. Following Wright and Fiske (1971), we infer that the lava of episodes 1–3 evolved as a consequence of crystal fractionation resulting from cooling and partial crystallization during prolonged storage in the rift zone. Additional compositional modification apparently resulted from magma mixing, as indicated by partly resorbed xenocrysts and reversely zoned phenocrysts. Approximately $50 \times 10^6 m^3$ of such differentiated and hybrid magma was erupted in episodes 1–3, and perhaps an additional $100 \times 10^6 m^3$ of this magma remained in the new dike.

Once the Puu Oo vent became established, the composition of lava was within the range of olivine control. Magma in the conduit beneath Puu Oo underwent a compositional change during repose periods that can be largely or entirely explained by fractionation of a few percent olivine. This produced MgO-depleted magma that was exhausted whenever the volume of the next eruptive episode exceeded the volume of MgO-depleted magma. During episodes 5–9, such MgO-poor magma gave way to MgO-rich magma after about $3 \times 10^6 m^3$ of magma had been erupted; in episodes 11–20, the volume of MgO-depleted magma available in each eruptive episode was between $9 \times 10^6 m^3$ and $18 \times 10^6 m^3$. The reservoir in which fractionation occurred during repose periods apparently was significantly enlarged between episodes 9 and 11.

Gradual enrichment of both CaO and MgO in the olivine-controlled magma erupted during episodes 4–20 may imply either decreasing levels of contamination of olivine-controlled summit magma by differentiated magma stored in the rift zone or gradually changing composition of magma generated in the mantle. The occurrence of reversely zoned phenocrysts in some of the lava of episodes 4–10 and the progressive increase in lava temperature through those episodes support the hypothesis that the lava composition was affected by magma mixing at least through episode 10.

Intrusion of summit magma into the rift zone apparently displaced differentiated magma already in storage, causing it to erupt during episodes 1–3. If olivine-controlled magma from the summit was contaminated thereafter by differentiated magma from the rift zone, the rift-zone conduit must have intersected one or more bodies of differentiated magma. Such magma bodies were possibly stored below the zone of brittle fracture indicated by shallow earthquakes generated during upward propagation of the dike. Thus, the bodies of stored magma and the rift-zone conduit were most likely at a depth of at least 3–4 km, within the normally aseismic deeper part of the rift zone.

Symmetry of patterns of attenuation of harmonic tremor with respect to Puu Oo indicates that, although the depth is uncertain, the tremor source and the vent were in vertical alignment. Furthermore, rift-zone dikes are generally near vertical (Pollard and others, 1983), and local, approximately cylindrical conduits that transport magma upward at higher flow rates and with lower heat loss than do dikes, can evolve from dikes by local erosion of wallrock as adjacent dike segments solidify and become inactive (Delaney and Pollard, 1981, 1982). These considerations suggest that a nearly vertical conduit descended from the Puu Oo vent in the plane of the initial dike. We suppose that the junction between the approximately vertical feeder conduit and the subhorizontal rift-zone conduit was located near the base of the episode 1 dike at a depth of 3–4 km. The mouth of the conduit, about 20 m in diameter, was nearly continuously visible in the crater floor after episode 13. The diameter may have increased downward. Erupted volumes of MgO-depleted melt were too large to have been accommodated in a conduit only 20 m in diameter and 3–4 km long; average diameters of 30 m for episodes 5–9 and 60–80 m for episodes 11–20 are implied if all of the inferred fractionation took place within this vertical magma column.

As eruptive activity became localized at Puu Oo, the presence of a nearby magma reservoir became evident from rift-zone tilt changes. Beginning with a subsidence during episode 3, rift-zone tumescence developed gradually during repose periods and rift-zone subsidence occurred rapidly during eruptive episodes, as indicated by a borehole tiltmeter northwest of Puu Kamoamoa. This deformation was congruent with tilt changes at the summit. Thus an approximate hydraulic equilibrium with the summit reservoir was continually maintained along the rift-zone conduit.

The limited range and approximate equivalence of opposed inflationary and deflationary tilt changes at the summit and also in the rift zone indicate that eruptive episodes began and ended in response to magmatic pressure in the reservoir system. The secondary reservoir in the rift zone apparently acted as a valve, controlling eruptive activity from the rift zone rather than from the summit. Thus, from the end of episode 3, starts and stops of vigorous eruption normally preceded, respectively, the onset of rapid summit deflation or the resumption of summit inflation as recorded by the

Uwekahuna tiltmeter. Summit response also lagged behind pauses and resumptions of lava discharge during individual eruptive episodes.

Eruptive episodes started gradually, possibly reflecting non-Newtonian behavior of the magma in the conduit system (Hardee, chapter 54). Reservoir pressure had to build sufficiently to overcome the yield strength of the melt, after which flow of magma accelerated.

The central-vent episodes at the 1123 vent died gradually, fountain height decreasing apparently in response to gradually diminishing magmatic pressure. However, lava discharge at Puu Oo normally stopped abruptly, without the gradual decay that characterized the earlier episodes. Perhaps this change was related to development of the rift-zone reservoir. Progressive depletion of the rift-zone reservoir, reflected by subsidence in the rift zone during eruptive episodes at Puu Oo, apparently led to abrupt termination of the eruption when pressure in the near-vent part of the reservoir system fell below a critical level sufficient to maintain the supply of fresh, nonvesiculated magma to the column below the vent. Summit deflation continued briefly as pressure was equalized in the linked summit and rift-zone reservoir systems.

We calculate an overall magma-supply rate of $10 \times 10^6 m^3$/mo for episodes 2–20. Allowing for errors in volume measurement, this value is not different from the rate of $9 \times 10^6 m^3$/mo determined by Swanson (1972) for earlier periods of prolonged eruption for which the relationships between volume change in the summit reservoir and the volume erupted could be evaluated. Higher rates, nearly $12 \times 10^6 m^3$/mo, prevailed at Puu Oo during episodes 4–12 and 13–17. In these two sequences, recurrence intervals and erupted volumes had a miniminal range, indicating that an approximately steady relationship was maintained between magma supply to the reservoir system and frequency and volume of eruption. Each of these periods of elevated supply of magma to the vent was preceded by an unusually long repose period. Thus, the long-term supply rate was less.

Inferred magma-supply rates during the Puu Oo eruption equal or exceed estimates of long-term supply given by Dzurisin and others (1984), causing us to speculate that the Puu Oo eruption may coincide with a period of increased magma supply to Kilauea. A marked increase in SO_2 flux to the atmosphere in the Kilauea caldera region occurred about one month after the beginning of the eruption and may reflect increased rate of supply of magma to the summit reservoir. We are unable to evaluate the rate of percolation of exsolved gas from the reservior region to the surface, and we have no other independent, short-term measure of supply to the reservoir. Thus, like Dzurisin and others (1984), we cannot distinguish whether the Puu Oo eruption was a response to possible increase in magma supply rate or whether it may have triggered increased supply. Nevertheless, a substantial rate of supply was apparently maintained through and beyond episode 20. It led to establishment of a comparatively unimpeded transport system from the summit reservoir to the vent at Puu Oo that is likely to remain open until disrupted by a tectonic event or until diminution of supply to the rift-zone conduit allows cooling, crystallization, and eventual termination of magma transport to the vent.

REFERENCES

Crosson, R.S., and Endo, E.T., 1982, Focal mechanisms and locations of earthquakes in the vicinity of the 1975 Kalapana earthquake aftershock zone of 1970–1979: implications for tectonics of the south flank of Kilauea Volcano, Island of Hawaii: Tectonics, v. 1, p. 495–542.

Delaney, P.T., and Pollard, D.D., 1981, Deformation of host rocks and flow of magma during growth of minette dikes and breccia-bearing intrusions near Ship Rock, New Mexico: U.S. Geological Survey Professional Paper 1202, 61 p.

———1982, Solidification of basaltic magma during flow in a dike: American Journal of Science, v. 282, p. 856–885.

Duffield, W.A., Christiansen, R.L., Koyanagi, R.Y., and Peterson, D.W., 1982, Storage, migration, and eruption of magma at Kilauea Volcano, Hawaii: Journal of Volcanology and Geothermal Research, v. 13, p. 273–307.

Dvorak, J.J., and Okamura, A.T., 1985, Variations in tilt rate and harmonic tremor during the January-August 1983 east rift eruptions of Kilauea Volcano, Hawaii: Journal of Volcanology and Geothermal Research, v. 25, p. 249–258.

Dvorak, J.J., Okamura, A.T., and Dietrich, J.H., 1983, Analysis of surface deformation data, Kilauea Volcano, Hawaii: October 1966 to September 1970: Journal of Geophysical Research, v. 88, p. 9295–9304.

Dvorak, J.J., Okamura, A.T., English, T.T., Koyanagi, R.Y., Nakata, J.S., Sako, M.K., Tanigawa, W.R., and Yamashita, K.M., in press, Mechanical response of the south flank of Kilauea Volcano, Hawaii, to intrusive events along the rift zones: Tectonophysics.

Dzurisin, D., Anderson, L.A., Eaton, G.P., Koyanagi, R.Y., Lipman, P.W., Lockwood, J.P., Okamura, R.T., Puniwai, G.S., Sako, M.K., and Yamashita, K.M., 1980, Geophysical observations of Kilauea Volcano, Hawaii, 2. Constraints on the magma supply during November 1975–September 1977: Journal of Volcanology and Geothermal Research, v. 7, p. 241–269.

Dzurisin, D., Koyanagi, R.Y., and English, T.T., 1984, Magma supply and storage at Kilauea Volcano, Hawaii, 1956–1983: Journal of Volcanology and Geothermal Research, v. 21, p. 177–206.

Fiske, R.S., and Jackson, E.D., 1972, Orientation and growth of Hawaiian volcanic rifts: the effect of regional structure and gravitational stresses: Royal Society [London] Proceedings, v. 329, p. 299–326.

Garcia, M.O., and Wolfe, E.W., *in* press, Petrology of the lavas from the Puu Oo eruption of Kilauea Volcano, Hawaii: episodes 1–20, in Wolfe, E.W., ed., The Puu Oo eruption of Kilauea Volcano, Hawaii: the first 1½ years: U.S. Geological Survey Professional Paper.

Greenland, L.P., in press, Gases from the 1983–84 east rift eruption of Kilauea Volcano, *in* Wolfe, E.W., ed., The Puu Oo eruption of Kilauea Volcano, Hawaii: the first 1½ years: U.S. Geological Survey Professional Paper.

Greenland, L. P., Okamura, A. T., and Stokes, J. B., in press, Constraints on the mechanics of eruption of Puu Oo, *in* Wolfe, E.W., ed., The Puu Oo eruption of Kilauea Volcano, Hawaii: the first 1½ years: U.S. Geological Survey Professional Paper.

Greenland, L.P., Rose, W.I., and Stokes, J.B., 1985, An estimate of gas emissions and magmatic gas content from Kilauea Volcano: Geochimica et Cosmochimica Acta, v. 49, p. 125–129.

Hofmann, A.W., Feigenson, M.D., and Raczek, I., 1984, Case studies on the origin of basalt: III, Petrogenesis of the Mauna Ulu eruption, Kilauea, 1969–71: Contributions to Mineralogy and Petrology, v. 88, p. 24–35.

Holcomb, R.T., 1980, Preliminary geologic map of Kilauea Volcano, Hawaii: U.S. Geological Survey open-file report 80–796, scale 1:50,000.

Jackson, D.B., in press, Geoelectric observations: September 1982 summit eruption and the first year of the 3 January 1983 east rift zone eruption, Kilauea volcano, Hawaii, *in* Wolfe, E.W., ed., The Puu Oo eruption of Kilauea Volcano, Hawaii: the first 1½ years: U.S. Geological Survey Professional Paper.

Jackson, D.B., Swanson, D.A., Koyanagi, R.Y., and Wright, T.L., 1975, The August and October 1968 east rift eruptions of Kilauea Volcano, Hawaii: U.S. Geological Survey Professional Paper 890, 33 p.

Klein, F.W., 1978, Hypocenter location program HYPOINVERSE, part 1: user's guide to versions 1, 2, 3, and 4: U.S. Geological Survey Open-File Report 78–694, 113 p.

Koyanagi, R.Y., Endo, E.T., Tanigawa, W.R., Nakata, J.S., Tomori, A.H., and Tamura, P.N., 1984, Kaoiki, Hawaii earthquake of November 16, 1983: a preliminary compilation of seismographic data at the Hawaiian Volcano Observatory, U.S. Geological Survey Open-File Report 84–798, 35p.

Koyanagi, R.Y., Tanigawa, W.R., and Nakata, J.S., in press, Seismicity associated with the eruption of Kilauea Volcano from January 1983 to July 1984, *in* Wolfe, E.W., ed., The Puu Oo eruption of Kilauea Volcano, Hawaii: the first 1½ years: U.S. Geological Survey Professional Paper.

Koyanagi, R.Y., Unger, J.D., Endo, E.T., and Okamura, A.T., 1974, Shallow earthquakes associated with inflation episodes at the summit of Kilauea Volcano, Hawaii, *in* Gonzales-Ferran, O., ed., Proceedings of the symposium on Andean and Antarctic volanology problems, Santiago, Chile, September 1974, International Association of Volcanology and Chemistry of the Earth's Interior, Special Series.

Lockwood, J.P., Banks, N.G., English, T.T., Greenland, L.P., Jackson, D.B., Johnson, D.J., Koyanagi, R.Y., McGee, K.A., Okamura, A.T., and Rhodes, J.M., 1985, The 1984 eruption of Mauna Loa Volcano, Hawaii: Eos, Transactions of the American Geophysical Union, v. 66, p. 169–171.

Macdonald, G.A., Abbott, A.T., and Peterson, F.L., 1983, Volcanoes in the sea: the geology of Hawaii, second edition: Honolulu, University of Hawaii Press, 517 p.

Maruyama, T., 1964, Statical elastic dislocations in an infinite and semi-infinite medium: Bulletin of the Earthquake Research Institute, v. 42, p. 289–368.

Moore, J.G., and Koyanagi, R.Y., 1969, The October 1963 eruption of Kilauea Volcano, Hawaii: U.S. Geological Survey Professional Paper 614–C, 13 p.

Moore, R.B., 1983, Distribution of differentiated tholeiitic basalts on the lower east rift zone of Kilauea Volcano, Hawaii: a possible guide to geothermal exploration: Geology, v. 11, p. 136–140.

Moore, R.B., Helz, R.T., Dzurisin, D., Eaton, G.P., Koyanagi, R.Y., Lipman, P.W., Lockwood, J.P., and Puniwai, G.S., 1980, The 1977 eruption of Kilauea Volcano, Hawaii: Journal of Volcanology and Geothermal Research, vol 7, p. 189–210.

Neal C.A., and Decker, R.W., 1983, Surging of lava flows at Kilauea Volcano, Hawaii [abstract]: Eos, Transactions of the American Geophysical Union, v. 64, no. 5, p. 904.

Neal, C.A., Duggan, T.J., Wolfe, E.W., and Brandt, E.L., in press, Lava samples, temperatures, and compositions, Puu Oo eruption of Kilauea Volcano, Hawaii, episodes 1–20, January 3, 1983–June 8, 1984, *in* Wolfe, E.W., ed., The Puu Oo eruption of Kilauea Volcano, Hawaii: the first 1½ years: U.S. Geological Survey Professional Paper.

Okamura, A.T., Dvorak, J.J., Koyanagi, R.Y., and Tanigawa, W.R., in press, Surface deformation associated with the 1983 Kilauea eruption, *in* Wolfe, E.W., ed., The Puu Oo eruption of Kilauea Volcano, Hawaii: the first 1½ years: U.S. Geological Survey Professional Paper.

Peterson, D.W., 1976, Processes of volcanic island growth, Kilauea Volcano, Hawaii, 1969–1973: International Association of Volcanology and Chemistry of the Earth's Interior, Symposium on Andean and Antarctic Volcanology Problems, Proceedings, p. 172–189.

Peterson, D.W., and Swanson, D.A., 1974, Observed formation of lava tubes during 1970-71 at Kilauea Volcano, Hawaii: Studies in Speleology, v. 2, p. 209–222.

Pollard, D.D., Delaney, P.T., Duffield, W.A., Endo, E.T., and Okamura, A.T., 1983, Surface deformation in volcanic rift zones: Tectonyphysics, v. 94, p. 541–584.

Ryan, M.P., Blevins, J.Y., Okamura, A.T., and Koyanagi, R.Y., 1983, Magma reservoir subsidence mechanics: theoretical summary and application to Kilauea Volcano, Hawaii: Journal of Geophysical Research, v. 88, p. 4147–4181.

Ryan, M.P., Koyanagi, R.Y., and Fiske, R.S., 1981, Modeling the three-dimensional structure of macroscopic magma transport systems: application to Kilauea Volcano, Hawaii: Journal of Geophysical Research, v. 86, p. 7111–7129.

Swanson, D.A., 1972, Magma supply rate at Kilauea Volcano, 1952–1971: Science, v. 175, p. 169–170.

Swanson, D.A., Duffield, W.A., and Fiske, R.S., 1976a, Displacement of the south flank of Kilauea Volcano: the result of forceful intrusion of magma into the rift zones: U.S. Geological Survey Professional Paper 963, 39 p.

Swanson, D.A., Duffield, W.A., Jackson, D.B., and Peterson, D.W., 1979, Chronological narrative of the 1969-71 Mauna Ulu eruption of Kilauea Volcano, Hawaii: U.S. Geological Survey Professional Paper 1056, 55 p.

Swanson, D.A., Jackson, D.B., Koyanagi, R.Y., and Wright, T.L., 1976b, The February 1969 east rift eruption of Kilauea Volcano, Hawaii: U.S. Geological Survey Professional Paper 891, 30 p.

Wolfe, E.W., Neal, C.A., Banks, N.G., and Duggan, T.J., in press, Geologic observations and chronology of eruptive events during the first 20 episodes of the Puu Oo eruption, January 3, 1983 through June 8, 1984, *in* Wolfe, E.W., ed., The Puu Oo eruption of Kilauea Volcano, Hawaii: the first 1½ years: U.S. Geological Survey Professional Paper.

Wright, T.L., 1971, Chemistry of Kilauea and Mauna Loa lava in space and time: U.S. Geological Survey Professional Paper 735, 40 p.

———1984, Origin of Hawaiian tholeiite: a metasomatic model: Journal of Geophysical Research, v. 89, p. 3233–3252.

Wright, T.L., and Fiske, R.S., 1971, Origin of the differentiated and hybrid lavas of Kilauea Volcano, Hawaii: Journal of Petrology, v. 12, p. 1–65.

Wright, T.L., Swanson, D.A., and Duffield, W.A., 1975, Chemical composition of Kilauea east rift lava, 1968–1971: Journal of Petrology, v. 16, p. 110–133.

HOLOCENE ERUPTIVE HISTORY OF MAUNA LOA VOLCANO

By John P. Lockwood *and* Peter W. Lipman

ABSTRACT

In order to evaluate the Holocene eruptive history of Mauna Loa, surface lava flows have been classified by age and a semiquantitative analysis made of their mapped areas. A new map depicting the age distribution of these surface lavas shows that flows are generally older at lower elevations and at greater distances from eruptive sources as a consequence of the fact that there are fewer long flows than short ones. Earlier estimates of the areas and volumes of historical eruptive products have been revised on the basis of new mapping and study of written records.

Lavas of known historical age (1843 and later) cover 13 percent of Mauna Loa's surface; their total volume is about 4 km^3. This figure includes extensive buried lavas, especially within Mokuaweoweo, Mauna Loa's summit caldera. The historical lavas were erupted at an average rate of 45×10^6 m^3/yr from 1843–76, but at less than half that rate since 1877. This change in eruptive rate coincides with an abrupt change in lava chemistry and may be related to effects of the magnitude-7.5 1868 earthquake.

The average historical (1843 and later) production rate of 29×10^6 m^3/yr is higher than average rates for the preceding six and one-half centuries, as reflected by lava-flow areal coverage rates. That period, from about A.D. 1200 to 1843, began shortly before the formation of the present Mokuaweoweo and was characterized by low levels of rift-zone activity and an increased incidence of eruption from northwest flank vents radial to the summit. The preceding period of about 750 years was characterized by voluminous pahoehoe overflows from a summit lava lake—over one-fourth of the volcano is covered with these lavas. The record becomes increasingly fragmentary with age, as over one-half of Mauna Loa has been buried during the past 1,500 years (since the arrival of man on Hawaii); almost 90 percent of the surface is covered with rocks of age less than 4 ka.

Pahoehoe and aa are present in nearly equal amounts at Mauna Loa's surface, but aa is more typical of rift than of summit eruptions. The ratio of aa to pahoehoe commonly increases with transport distance, and it appears to increase with time in the Holocene, aa being more common among lavas younger than about 750 years than among older flows.

INTRODUCTION

> I have not yet discovered any native traditions respecting eruptions from the larger volcano [Mauna Loa]. It is uninhabitable, and therefore its eruptions would not usually be frought with disaster to the inhabitants, and thus would be scarcely mentioned in the traditions. When Hawaii shall have been studied carefully it will be possible to give the sequence of several pre-historic eruptions.
>
> —*C.H. Hitchcock, 1909, p. 56–57.*

Mauna Loa, which rises nearly 9 km above the isostatically depressed floor of the central Pacific (to 4,167 m above sea level), is the largest volcano on Earth; its volume has been estimated at about 40,000 km^3 (Macdonald, 1972, p. 258). That volume is probably too high, however, because older, separate volcanoes are likely buried at depth. Mauna Loa's lavas cover about 5,125 km^2 of the Island of Hawaii (fig. 18.1). These subaerial lava flows preserve the most readily accessible record of the volcano's prehistoric eruptive activity, and evidence yielded by them forms the principal basis of this report. Limited exploration of the approximately 4,000 km^2 of Mauna Loa beneath sea level has also begun (Fornari and Campbell, chapter 4; Fornari and others, 1979; Moore and others, 1985).

PREVIOUS WORK

The first systematic geologic study of any part of Mauna Loa was that of Stearns and Clark (1930), who mapped the southwestern part of the volcano. They recognized the widespread pyroclastic deposit called the Pahala Ash and proposed the name "Kamehame basalt" for lavas of both Mauna Loa and Kilauea that overlie the ash and the name "Pahala formation" for underlying flows. Stearns and Macdonald (1946) refined the stratigraphic nomenclature and proposed the terms "Kau volcanic series" (now Kau Basalt) for Mauna Loa flows overlying the Pahala Ash and "Kahuku volcanic series" (now Kahuku Volcanics) for underlying flows. Individual prehistoric lava flows were not differentiated in these previous studies, nor was the chronology of prehistoric eruptive activity examined. Modern detailed mapping of Mauna Loa is limited to the northeast and southwest rift zones of the volcano (Lipman and Swenson, 1984; Lockwood, 1984); Lipman (1980b) has made an analysis of eruptive activity for the southwest rift zone.

METHODS

To reconstruct the eruptive history of Mauna Loa, a reconnaissance geologic map of the entire volcano was compiled at 1:24,000 scale (47 7½-minute quadrangles) utilizing unpublished mapping, aerial photographic interpretation, aerial inspection, and spot field checking. For quantitative analysis of flow distribution, the map was later divided into 164 subregions on the basis of elevation, quadrangle, and eruptive subdivision (see following section entitled "Geography"). The surface areas (in square kilometers) of all geologic map units in each subregion were then determined by

tracing geologic contacts on a digitizing tablet, and the resulting areal information was entered into a computer database for sorting and analysis. A highly generalized version of the map at about 1:500,000 scale (fig. 18.2) shows the gross distribution of lava flows of different ages.

Computation of historical eruptive volumes (table 18.1) is based on estimates of original flow areas (before burial by later flows) and average flow thicknesses. Detailed planetable topographic maps made for Mauna Loa between 1912 and 1927 (U.S. Geological Survey Advance Sheets, 1:31,680 scale) proved invaluable in interpreting the distribution of pre-1930 lava flows, and aerial photographs taken in 1942, 1965, and 1977 were studied to determine original extent of flows later buried. Thicknesses of flows outside Mokuaweoweo were determined by estimates from aircraft and by scattered ground measurements. Volumes of lava erupted within Mokuaweoweo were evaluated from the decreasing caldera depths and changing caldera configurations determined since the earliest accurate measurements by Wilkes (1845, p. 157). This progressive infilling was then compared with eyewitness accounts of the duration and vigor of summit activity to apportion cumulative volumes among the various eruptions. Most accounts are vague, and for eruptions before 1933 the volumes of erupted lavas within the caldera were generally prorated to fit the observed decreases of caldera volume between surveys. Although estimates from individual flows within Mokuaweoweo may involve possible errors of more than 40 percent, cumulative totals are much more accurate owing to occasional constraints provided by various topographic surveys.

Systematic recovery of organic material from beneath prehistoric lava flows and subsequent radiocarbon dating has been one of our key methods. An improved understanding of the conditions under which charcoal is formed and preserved under lava flows (Lockwood and Lipman, 1980) has enabled us to collect charcoal for radiocarbon dating from beneath most flows that extend to vegetated areas. A total of 174 radiocarbon ages has been obtained for Mauna Loa lava flows (Rubin and others, chapter 10; Kelley and others, 1979), and these data have revolutionized our understanding of prehistoric Mauna Loa eruptive chronology.

LIMITATIONS

The data summarized in the following text and figures are only as good as the generalized, preliminary geologic mapping on which they are based. Furthermore, 10 percent of Mauna Loa remains unmapped, even in reconnaissance; most of this unmapped area is covered by dense rain forest, which is concentrated at middle elevations of the east, south, and west flanks of Mauna Loa (see figs. 18.2, 18.21). As future detailed mapping becomes available, revision of the data and interpretations presented in this report can be expected.

ACKNOWLEDGMENTS

History described without chronology would be an empty shell of conjecture, and this paper could not have been written were it not for the careful radiocarbon age determinations by Meyer Rubin and his colleagues at the USGS Radiocarbon Laboratory in Reston, Va. Our gratitude to Meyer is deep, for both lab work and field discussions.

Our quantitative summary of areal and volume relations is based on a reconnaissance geologic map of Mauna Loa that was compiled by Lisa Petersen. The Mauna Loa mapping program has been aided greatly by Duane Champion and J.M. Rhodes, whose numerous paleomagnetic determinations and chemical analyses have assisted in the correlation of prehistoric lava flows. Dan Fornari provided unpublished observations on historical submarine lava flows, and Doak Cox provided information on the previously unreported brief summit eruption of September 1, 1903. Joan Blandett provided copies of important planetable maps from the USGS Western Mapping Center historical Archives, and Bill Sanders and others at the USGS Menlo Park library went to extraordinary efforts to ferret out obscure Mauna Loa literature. Jim Hutton, Marti Lockwood, Marjorie Summers, and Rick Warschauer contributed to many aspects of this paper. The careful reviews of D.R. Mullineaux and F.W. Klein are much appreciated. All photographs in this paper were taken by the senior author.

GEOGRAPHY

Mauna Loa's summit is occupied by Mokuaweoweo, a 3-km by 5-km collapse caldera elongate northeast-southwest (see figs. 18.1, 18.27). Rift zones, which are the loci of numerous linear eruptive vents, trend from Mokuaweoweo to the east-northeast (northeast rift zone—NERZ) and to the southwest (southwest rift zone—SWRZ). The subaerial part of the SWRZ is 65 km long, but it extends about 35 km farther to the south below sea level. The SWRZ is marked by a conspicuous bend in its middle, probably a result of westward migration of the middle part of the rift zone (Lipman, 1980a). Only 50 km of the NERZ is exposed, and historical eruptive activity has been limited to the upper 19 km of the rift. This rift zone becomes progressively wider and more diffuse eastward to the point where it is buried by younger Kilauea lavas; it may be traced geophysically at least 50 km farther east beneath the Kilauea flows (Flannigan and Long, chapter 39). A north rift zone, proposed by Stearns and Macdonald (1946, p. 96, fig. 6) does not exist; instead, isolated eruptive vents, oriented radially to Mokuaweoweo, are spread rather homogeneously over the entire northwest flank (see fig. 18.17).

Mauna Loa's historical activity has long been divided into (1) *summit eruptions*, which are restricted to the immediate area of Mokuaweoweo, and (2) *flank eruptions*, which begin with summit activity but erupt most of their volume at lower altitude vents (Dutton, 1884, p. 140; Stearns and Macdonald, 1946, p. 82; Klein, 1982, p. 21–24). For this report we consider flows derived from vents below 3,660 m (12,000 ft) elevation to be products of flank eruptions, and those from vents above 3,660 m to be from summit activity. This classification of Mauna Loa flows (fig. 18.3) also allows consistent separation of summit and flank phases of typical historical eruptions (for example, 1942, 1950, 1984), which

begin with summit activity and terminate with flank extrusion. Flows referred to as northeast- or southwest-rift-zone flows are those on Mauna Loa's flanks erupted from vents below 3,660 m elevation.

HISTORICAL ERUPTIVE ACTIVITY

Polynesian settlers, who first reached Hawaii about 1,500 years ago, preserved no record of Mauna Loa's eruptive activity, and the earliest references are fragmentary accounts of activity in the late 18th and earliest 19th centuries (Hitchcock, 1909, p. 80; Colnett, 1940). The first extended account of a Mauna Loa eruption was by the Rev. Joseph Goodrich, who witnessed the June 1832 eruption from Lahaina, Maui, 190 km away. The 1832 flows have not been identified, although a possible candidate is the young flow underlying the U.S. National Oceanic and Atmospheric Administration (NOAA) Mauna Loa Observatory, on the north side of the upper NERZ (Lockwood, 1978). The paucity of eruption reports between the time of Hawaii's discovery by Europeans in 1778 and the year 1832 suggests the correctness of Hitchcock's statement: "It is very probable that Mokuaweoweo showed less activity after 1780 and before 1832 than in the decades since" (Hitchcock, 1909, p. 80).

The oldest Mauna Loa lava flows to be positively associated with a specific dated eruption are those of 1843 (fig. 18.4), which were derived from both the upper NERZ and a north-flank radial vent. The 1843 eruption was well documented by the Rev. Titus Coan, who during this eruption climbed to the upper active vent in a perilous winter journey and provided the first published description of active lava tubes (Coan, 1844). Coan sent many eruption descriptions to his friend James Dana, editor of the Silliman Journal (later the American Journal of Science) over the next 40 years, and these letters, published by Dana, form much of the basis for the excellent accounts of 19th century eruptive activity later summarized by Dana (1890), Hitchcock (1909), and Brigham (1909). Largely owing to Coan's observations, more is perhaps known about Mauna Loa's eruptions between 1843 and 1881 than is known about the following 40 years of activity! Jaggar (1947) described Mauna Loa's activity in the first four decades of this century, and Macdonald published descriptions of the eruptions of 1940, 1942, and 1950 (for references, see Macdonald and Abbott, 1970). The eruptions of 1975 and 1984 are described by Lockwood and others (chapter 19).

AREAL AND VOLUMETRIC RELATIONS AND SURFACE COVERAGE RATES

Fourteen percent of Mauna Loa's mapped surface (12.5 percent of the total area) is covered by lava flows of the 1843 and later eruptions (see figs. 18.5, 18.10). Since 1859, the rate of coverage has been about seven percent per century, although it was much higher (about 17 percent per century) in the period between 1843 and 1859 (fig. 18.5). A contemporary observation of the decrease in "copiousness of the subaerial discharges [of Mauna Loa] since 1859" was made by J.D. Dana (1888, p. 85). This historical eruptive activity has been concentrated along the two rift zones; coverage rates on the flanks of these two rift zones are similar and since 1843 have averaged about 13 percent per century for their combined totals (fig. 18.6). Our calculated areas and volumes of some individual flows (table 18.1) differ substantially from values reported by Macdonald and Abbot (1970, table 2), but our value for the cumulative volume of all historical lavas exposed outside Mokuaweoweo is similiar to theirs.

Large volumes of lava that have accumulated within Mokuaweoweo (including South Pit and North Bay) since 1843 were previously ignored or greatly underestimated (Stearns and Macdonald, 1946, p. 88). On the basis of an evaluation of changing caldera dimensions, we estimate that about 1 km^3 of lava has accumulated within the caldera since 1843.

Mauna Loa erupted approximately 4.2 km^3 of lava in the period 1843–1984 at an average extrusion rate of 30×10^6 m^3/yr, a rate substantially lower than recently inferred magmatic production rates at Kilauea (120×10^6 m^3/yr: Swanson, 1972a; Dzurisin and others, 1984). The Mauna Loa values, which have not been adjusted for density, are considered accurate to about ± 20 percent.

Lava production rates are clearly different before and after 1877 (fig. 18.7). The rate was approximately 47×10^6 m^3/yr in the 34 years prior to 1877, but it dramatically lowered after that time to about 21×10^6 m^3/yr (averaged over 107 years). This abrupt rate change approximately coincided in time with a major shift in minor-element composition of Mauna Loa lava which occurred sometime between 1868 and 1877 (Rhodes and others, 1982). We propose that these changes in eruption rate and composition may be related to the great ($M = 7.5$) 1868 earthquake (Wood, 1914).

FREQUENCY AND DURATION OF ERUPTIONS

Virtually all historical eruptions have begun with activity within or near Mokuaweoweo, and so the greatest frequency of activity is at the summit (fig. 18.4; Klein, 1982). Half the historical summit eruptions have been followed within a few days by more voluminous flank eruptions, of which there have been 17: 8 on the NERZ, 7 on the SWRZ, and 2 on the north flank.

The duration of individual eruptions has varied from less than one day for several summit eruptions (table 18.1) to the 4½ years of almost continual activity during the summit eruption of 1872–77. Flank eruptions have varied in duration from 5 days (1868) to about 450 days (1855–56). Historical NERZ eruptions have mostly been of longer duration (mean 117 days) than those of the SWRZ (mean 16 days). The cumulative volume of historically erupted lava on the NERZ (1.3×10^6 m^3 is also greater than is that of the SWRZ (0.86×10^6 m^3, but the rift zone eruption with the greatest volume (1950) occurred on the SWRZ.

PREHISTORIC ERUPTIVE ACTIVITY

PROBLEMS

Our understanding of Mauna Loa's prehistoric activity is

based almost entirely on the rocks exposed on land, thus ignoring the near-equal area of the volcanic edifice beneath the sea. The eruptive record becomes less complete as one goes back in time, owing both to burial of older flows by younger lavas and to deeper weathering. Better exposures on the northwest flank bias the data toward that area relative to the largely unmapped southeast flank.

RADIOCARBON DATING

Of 174 radiocarbon ages obtained from carbonaceous matter beneath Mauna Loa flows, 143 are considered geologically reasonable for the overlying flows. The 31 rejected ages were regarded as invalid because of conflicting stratigraphic relationships. These incompatible ages are mostly caused by contamination of the sampled material by young charcoal derived from later forest fires or by old carbonaceous material in sooty soils, or by contamination of the original plant material by juvenile CO_2 devoid of ^{14}C (Rubin and others, chapter 9). The data from 143 samples give ages for 94 separate lava flows (fig. 18.8). Radiocarbon ages are most numerous for the NERZ; 44 of the 108 surface flows mapped in that area have been dated.

AGE UNITS

During our early mapping we assigned relative ages to surface lava flows on the basis of their degree of weathering (Lipman, 1980b, table 2). Flows were divided into five groups (from oldest to youngest: I to V). As radiocarbon ages became available, approximate limits were defined for each of these weathering categories.

Radiocarbon ages are presently available for almost 20 percent of the 463 surface lava flows recognized to date on Mauna Loa. The remaining undated flows were subdivided on the basis of the previously defined weathering categories and on their stratigraphic relationships with adjoining dated flows. In this paper, group V (undated flows of historical and latest prehistoric age) was combined with group IV. The age boundaries of the four groups were slightly changed from those given by Lipman (1980b) and are as follows:

Group	^{14}C age (ka)
IV	0.75–0.107 (the interval just before A.D. 1843)
III	1.5–0.75
II	4.0–1.5
I	>4.0

ERUPTIVE FREQUENCY

A total of 463 individual surface lava flows have been mapped to date on Mauna Loa. The age distribution of these flows (fig. 18.9) shows the low level of eruptive activity during group IV time relative to earlier and later periods.

The actual number of group IV flows is probably even lower than shown because (1) several small, unweathered flows of probable 19th century age high on Mauna Loa were counted with group IV flows because they could not be assigned to specific historical eruptions, (2) geographically extensive historical flows (such as those of 1950 and 1984) were only counted once but would likely have been counted as separate flows if they were of prehistoric age, and were preserved as widely separated remnants beneath younger flows, and (3) group IV flows erupted from more than one vent may have been counted more than once, in contrast to multiple-vent historic flows. As an example, 1926 lavas were only counted once, although they are exposed at isolated sites along more than 20 km of the SWRZ (Lipman and Swenson, 1984); they would likely have been counted as three separate flows if of prehistoric age.

Complete burial by younger lavas has not substantially lowered the total number of group IV flows, but does significantly lower the recognized number of older flows. Because of this, the increased number of group III flows (1.5–0.75 ka) documents a genuine increase in eruptive frequency during this period.

AREAL DISTRIBUTION

The distribution of surface flows of the various age categories in the principal geographic subdivisions (fig. 18.10) shows that flows of historical age are equal in areal extent to flows of group IV for Mauna Loa as a whole and nearly equal in each geographic subdivision. The historical flows were, however, formed in a 141-year period (1843–1984), whereas age IV flows accumulated in about 650 years before 1843. The increased extrusion rate for the historical period is also evident in figure 18.11, where the rates of surface coverage are shown as a function of time. An increased rate of historical flow coverage relative to the preceding 650 years is clear, demonstrating that such an increase, inferred by Lipman (1980b) for the SWRZ applies to the entire volcano. Additionally, small areas of probable 19th century flows of uncertain age (originally mapped as group V) were counted as group IV flows; their classification as historical flows would further accentuate the areal differences between these two groups.

More than one-fourth of Mauna Loa's surface is covered by group III lava flows, which accumulated in only about 750 years. These flows are concentrated on the northwest and southeast flanks of Mauna Loa (figs. 18.2, 18.10); most are tube-fed pahoehoe flows derived from steady overflows of a persistent lava lake at the summit.

Group I and II lava flows are substantially buried by younger lavas, so that their original coverage rates cannot be determined. Age I flows are exposed over only 10 percent of the mapped area; approximately 90 percent of Mauna Loa's surface has thus been buried in the past 4,000 years. An extrapolation of average coverage rates to earlier times, assuming steady eruption rates (fig. 18.11), suggests that flows older than 10 ka should be exposed on less than 2 percent of the volcano's surface.

As expected, average flow ages are younger at higher elevations and at lesser distances from source vents (figs. 18.12, 18.13). Most flows are relatively short and do not travel far from eruptive vents, and most eruptive vents are located high on the volcano. Because the short flows accumulate in a small area near the summit,

they eventually bury almost all of the older flows in that area. Longer flows that reach the larger flank areas are less frequent, the rate of burial at lower elevations is consequently less, and the older flows cover a larger surface area there. The classic shield shape of Mauna Loa is maintained by the overall balance between short and long flows. The more numerous short flows accumulate near the summit and tend to make the volcano's overall slope steeper, whereas the long flows are thicker at their distal ends and thus tend to flatten Mauna Loa's profile.

COMPARISON OF ACTIVITY ON THE NORTHEAST AND SOUTHWEST RIFT ZONES

The age distribution of flows derived from the NERZ and SWRZ is generally similiar (fig. 18.14), although the proportion of group II flows is higher on the SWRZ (Lipman, 1980b, p. 722). Group I flows are more extensive on the flanks of the NERZ, but this is probably due to geometric differences between the two rift zones: because of the proximity of the ocean to the SWRZ, older, long-traveled flows there are not exposed subaerially, whereas older, long flows tend to be preserved along the flanks of the NERZ (fig. 18.13). The proportion of older lavas on the NERZ would be even greater if the northeast continuation of the rift (Flannigan and Long, chapter 39, fig. 39.6) were not buried by young Kilauea lavas. The percentage of the surface downslope from each rift zone covered by historical and group IV flows is about the same.

Lipman (1980b, fig. 10) noted that there were substantial differences between the lava-flow age distribution on either flank of the SWRZ; lava coverage rates on the east flank of that rift zone are uniformly less than those on the west flank. There are no such systematic differences on opposite sides of the NERZ (fig. 18.15), although historical flows have preferentially been directed north of that rift zone, whereas group IV flows have preferentially flowed to the south. This pattern may be about to change again, however, as shown by the southward migration of historical vents (Lockwood and others, chapter 19).

DISTRIBUTION OF ERUPTIVE VENTS

Eruptive vents are found in four areas of Mauna Loa: Mokuaweoweo, the northeast and southwest rift zones, and the northwest flank. Vents are most numerous between 2,500 and 3,500 m (fig. 18.16), and the concentration of eruptive activity at these elevations has created topographic highs along both rift zones, near Puu Ulaula on the NERZ, and near Puu O Keokeo on the southwest rift zone (Lockwood and others, chapter 19, fig. 19.23; Lipman, 1980b, fig. 11, p. 714–715).

The northwest flank, buttressed by Mauna Kea and Hualalai, is cut by numerous linear eruptive fissures oriented radially to the Mauna Loa summit (fig. 18.17). Sixty-six of these radial vents have been recognized to date. Most of them are marked by linear curtain-of-fire spatter ramparts and one or more horseshoe-shaped spatter cones (fig. 18.18), although thirteen of them lack near-vent structures and are represented only by inconspicuous cracks from which voluminous, highly fluid flows quietly issued (fig. 18.19). Lava that fed these spatterless vents was apparently derived from degassed magma in shallow storage areas or from high-standing lava lakes at Mauna Loa's summit. Most of these spatterless radial vents are of group III age, a period characterized by summit lava-lake activity.

Two major radial vents have formed in historical time (1859, 1877), and two NERZ eruptions have developed radial vents after initial eruption within the rift zone (1843, 1935). Few prehistoric radial vents have yet been dated radiometrically, but the relations of their flows to adjoining lavas allows age classification (fig. 18.20). Radial vents of group IV age are most abundant; that was a time of diminished eruptive activity elsewhere on Mauna Loa and of an increased rate of formation of radial vents on the northwest flank. The rate has remained high into historical time.

DISTRIBUTION OF AA AND PAHOEHOE

The distribution of aa and pahoehoe on Mauna Loa reflects the volatile content of source eruptions, the length of individual flows, and the steepness of the terrain over which the lava flows traveled. Flow over steep slopes can cause pahoehoe to convert to aa, as well as travel for long distances. Aa and pahoehoe are merely different textures of otherwise identical lava and will form from the same material depending principally on temperature and flowage strain rates (Peterson and Tilling, 1980). Aa is produced from eruptions characterized by high fountaining of relatively volatile-rich lava, whereas extensive pahoehoe flows are derived from the stable upwelling of volatile-poor lava. Many Mauna Loa vents that are initially characterized by aa-producing high fountains later evolve to sustained pahoehoe production, resulting in the common occurrence of pahoehoe overlying aa of the same eruptive sequence. Because of differential weathering rates, the overlying pahoehoe commonly looks younger than the related aa and may easily be mistaken for an unrelated flow, especially in older terranes.

The proportions of aa and pahoehoe on Mauna Loa are about equal for the entire volcano, but they vary greatly for flows derived from the rift zones and the summit area (fig. 18.21). The greater abundance of aa flows on both rift zones reflects the dominance of fountain-fed lavas in those areas. Aa is nearly twice as abundant as pahoehoe on the SWRZ, whose slopes are steeper than those of the NERZ. Pahoehoe is much more characteristic of flows derived from Mauna Loa's summit area, where sustained lava lake activity occurred before the formation of the present Mokuaweoweo caldera.

Length of flow transport also affects the ratio of aa to pahoehoe: aa is more abundant at greater distances from eruptive sources (fig. 18.22). The proportions of aa and pahoehoe also vary with age (fig. 18.23): pahoehoe is more typical of older flows and aa more typical of group IV and historical lavas.

RELATIONS WITH ADJOINING VOLCANOES

The oldest lavas in contact with surface Mauna Loa flows are

the deeply eroded Ninole lavas on its south flank. Only 19 km^2 of the Ninole flows remain exposed; they are preserved as steep-walled, isolated ridges that rise above encroaching Mauna Loa lavas (fig. 18.24).

Radiometric dating of the Ninole flows (G.B. Dalrymple, written commun., 1978) suggests an age of about 200 ka. Stearns and Macdonald (1946, p. 66–68) considered them remnants of an older, pre-Mauna Loa volcano, but Lipman (1980a, p. 767) suggested they could be block-faulted remnants of earlier Mauna Loa lavas. Despite their age, the Ninole lavas have primary dips parallel to the younger Mauna Loa flows that surround them, indicating a source near the present upper SWRZ. We mapped them as a separate unit, since they are separated from adjacent Mauna Loa lavas by a major erosional unconformity, but we consider them most likely to be derived from the same magmatic system that fed younger Mauna Loa flows. The proposed Mohokea caldera in the area of the Ninole Hills (Hitchcock, 1906) appears to be only an erosional feature.

Late Mauna Kea cinder cones and flows overlie group I Mauna Loa lavas on the Humuula Saddle between the two volcanoes (fig. 18.25), although the contacts are mostly covered by younger Mauna Loa flows. Numerous kipukas (inliers) of Mauna Kea flows, not shown on earlier maps, are surrounded by Mauna Loa flows near the Mauna Kea–Mauna Loa contact (fig. 18.2). The total area of these kipukas is about 10 km^2.

Hualalai and Kilauea Volcanos differ greatly from Mauna Loa in their Holocene coverage rates, as is reflected by the distribution of kipukas of each volcano within the other. Four km^2 of Hualalai lava flows and cinder cones are preserved as kipukas surrounded by Mauna Loa lavas, but only 0.4 km^2 of Kilauea lavas are so surrounded. The eastern flank of Mauna Loa is covered by thin Kilauea flows, and 1.2 km^2 of Mauna Loa lavas are exposed as kipukas surrounded by Kilauea flows (fig. 18.26). The rate of coverage of Kilauea's surface (90 percent per 1,000 years; Holcomb, chapter 12, fig. 12.12) is much greater than Mauna Loa's rate, whereas Hualalai's average Holocene rate is less than Mauna Loa's (Moore and others, chapter 20, fig. 20.18). Because of Mauna Loa's larger size, however, the total area covered by Mauna Loa lava per unit time is greater than the area covered by Kilauea and Hualalai lavas combined.

GENERALIZED HISTORICAL NARRATIVE

OBSCURED EARLY HISTORY

We do not know when Mauna Loa began to form, or if the first lava was erupted on land or beneath the sea, but we can conjecture by extrapolation of Holocene activity rates that this happened more than 500,000 years ago. We do know that Kohala Volcano was then a large active structure, probably a separate island, to the north. Mauna Kea was also actively growing immediately to the north. Hualalai Volcano, to the west, has surface lavas as old as 200 ka (R.B. Moore, oral commun., 1985) and was probably also growing at the time of Mauna Loa's birth. Because Mauna Loa grew contemporaneously with Mauna Kea and Hualalai, flows of these three volcanoes interfingered. Kilauea began to grow on Mauna Loa's south flank, possibly beneath the sea, after Mauna Loa had already reached large size, perhaps before 100 ka. Lava flows and pyroclastic deposits from Kilauea also began to interlayer with flows from Mauna Loa along their contact.

RECORDED EARLY HISTORY

Flows older than 30 ka are exposed along fault scarps or river banks, or rarely as ash-mantled surface flows; these flows were derived from the same source directions as the flows that overlie them. Thus, the lower subaerial slopes of Mauna Loa existed in essentially the present shape by that time. It is probable that the present Mauna Loa geometry of a central feeder area and northeast and southwest rift zones also existed far back into Mauna Loa's unrecorded past.

The central feeder area, presently marked by Mokuaweoweo caldera (fig. 18.27), has long been the locus of multiple collapse structures. The buried rim of an earlier caldera lies to Mokuaweoweo's south and is marked by a low fault scarp (fig. 18.28), and other collapse structures at various scales have typified the Mauna Loa summit for a long period (see figs. 18.29, 18.34). Pit craters have formed and filled repeatedly at Mauna Loa's summit; cross sections of filled, dissected pit craters are well exposed in Mokuaweoweo's west wall (fig. 18.30). During the period of about 1.5–0.75 ka Mauna Loa's summit was marked by a sustained lava lake, which quietly supplied the tube-fed pahoehoe flows that now mantle the northwest and southeast flanks (figs. 18.10, 18.21).

Mauna Loa's two rift zones continued to erupt lava in nearly equal amounts as summit growth proceeded, although rates of eruptive activity have varied slightly between them, as indicated by a comparison of the areas covered downslope from each rift zone as a function of time (fig. 18.14). Because more than half the eruptive vents along the SWRZ are within 20 km of the coast, many flows from eruptions on this rift zone reached the sea, including flows from five of its seven historical eruptions. In contrast, the distance between most NERZ eruptive vents and the sea is more than 40 km, and flows from them rarely reached the ocean; none has in historical time. Flows from the NERZ did frequently enter streams on the wet windward side of the Island of Hawaii, however, and pillow lavas are well developed at the bases of several of these flows (Takahashi and Griggs, chapter 36, fig. 36.50). Prehistoric flows from the NERZ repeatedly dammed and diverted the Wailuku River (fig. 18.1).

The long flows that reached the sea enlarged Mauna Loa's surface area, in competition with subsidence and the forces of wave erosion. Where aa lava flows reached the sea, explosive contact between lava and sea water threw large amounts of lava and ash skyward, commonly forming littoral cones (fig. 18.31). Scores of these rootless cones are found along the shoreline west of the SWRZ, where the steep upland slopes have caused aa flows to predominate (fig. 18.21). Where fluid pahoehoe flows entered the

sea they commonly formed large deltalike additions to the land (fig. 18.32). Diving along the Mauna Loa coast has shown that many of these pahoehoe flows continued underwater through the formation of self-insulating conduits, as described by Moore and others (1973).

EVOLUTION OF MOKUAWEOWEO

Lava flows as young as 0.59 ± 0.07 ka are truncated by the edge of Mokuaweoweo (fig. 18.33). These fountain-fed pahoehoe flows were in part derived from arcuate fractures parallel to Mokuaweoweo's present rim and predate formation of the present caldera. Remnants of the dikes which fed these fountains are preserved along the caldera's northwest wall. Collapse of the caldera involved complex block subsidence (fig. 18.34) and was apparently accompanied by small phreatic explosions which showered blocks of hornfelsed basalt as far as 150 m beyond the present caldera rim (fig. 18.35).

Mokuaweoweo formed shortly after the beginning of group IV time, ending a period marked by the copious production of summit-fed pahoehoe flows. Group IV time was characterized by reduced output of surface lava flows from Mauna Loa's rift zones and increased activity on northwest flank radial vents. A great amount of group IV lava may have been erupted into a deep Mokuaweoweo (one-fourth of the historical lava has been erupted there), and would thus not be preserved as surface flows; this may account for some of the variations in recorded output over the past 600–700 years. Holcomb (chapter 12) suggests that a similar period of low surface coverage on Kilauea (1.5–1.0 ka) also coincided with a period of Kilauea caldera filling.

The original maximum depth of Mokuaweoweo cannot be known, although it was described as "about 400 yards" deep when first viewed by Archibald Menzies in 1794 (Wilson, 1920, p. 128). The first accurate survey of Mokuaweoweo was made in 1841 (Wilkes, 1845), when the maximum depth of the inner pit was 240 m below the summit. Major collapse of the inner pit occurred later; when next surveyed by Lydgate in 1874 (Brigham, 1909; Jaggar, 1931), it had a maximum depth of 320 m and was being rapidly filled by near-continuous lava-lake activity. By 1885, however, the inner pit had filled to 244 m below the summit (Alexander, 1888). The inner pit first overflowed in 1914, and the maximum depth of the caldera floor was 210 m below the summit by 1922 (Stearns and Clark, 1930, plate 2). In 1985 the caldera floor lay 183 m below the summit.

SUMMARY AND CONCLUSIONS

We have evaluated semiquantitatively the rates of Mauna Loa's volcanic activity over the past 10,000 years and have documented the range of behavior responsible for the formation of its surficial lavas. One can assume that similar behavior will typify the future. Mauna Loa has generated 22 flows outside Mokuaweoweo over the past 150 years, but at substantially lower production rates after 1876. There was less activity on the flanks of the volcano in the several centuries before 1843, and much of that lava output was apparently confined to Mokuaweoweo. In the preceding period, 1.5–0.75 ka, summit overflows blanketed much of the upper flanks with pahoehoe. About 40 percent of the Mauna Loa surface has been covered in the past 1,000 years (fig. 18.11), though coverage rates have varied during this period. This contrasts with coverage rates of 90 percent per 1,000 years for Kilauea (Holcomb, chapter 12) and 20 percent per 1,000 years for Hualalai (Moore and others, chapter 20). The record before 1.5 ka is fragmentary and will require much more work to refine.

The Mauna Loa coverage rate for the historical period has averaged 9 percent per 100 years. We do not know how much longer this relatively high rate of activity will persist, but we note no indication of abatement. Mauna Loa eruptions will of course continue to be a source of concern on the Island of Hawaii, but residents can take comfort in the knowledge that lava flows infrequently reach heavily populated coastal areas. Continuing investigations will provide more detailed knowledge of the varying frequency with which lava flows have covered various parts of the Mauna Loa surface. Such studies of the past provide the best guide to future volcanic behavior, behavior that will continue to impact human activities on the slopes of this great volcano.

REFERENCES

Alexander, J.M., 1888, On the summit crater in October, 1885, and its survey: American Journal of Science (3d ser.), v. 36, p. 5–39.

Brigham, W.T., 1909, The volcanoes of Kilauea and Mauna Loa on the Island of Hawaii: Bishop Museum Memoirs, v. 2, no. 4, 222 p.

Coan, T.M., 1844, Journey to Mauna Loa: The Missionary Herald (Boston), v. 40, no. 2, p. 44–47.

Colnett, James, 1940, The Journal of Captain James Colnett aboard the Argonaut from April 26, 1789 to Nov. 3, 1791: The Champlain Society (Toronto) Pub. 26, 328 p. [Reprinted 1968 by the Greenwood Press, New York].

Dana, J.D., 1888, History of changes in the Mt. Loa craters, pt. 2, on Mokuaweoweo: American Journal of Science (3d ser.), v. 36, no. 212, p. 81–112.

——— 1890, Characteristics of volcanoes, with contributions of facts and principles from the Hawaiian Islands: New York, Dodd, Mead, & Co., 339 p.

Dutton, C.E., 1884, Hawaiian volcanoes: U.S. Geological Survey 4th Annual Report, p. 79–219.

Dzurisin, Daniel, Koyanagi, R.Y., and English, T.T., 1984, Magma supply and storage at Kilauea Volcano, Hawaii, 1956–1983: Journal of Volcanology and Geothermal Research, v. 21, p. 177–206.

Fornari, D.J., Peterson, D.W., Lockwood, J.P., Malahoff, Alexander, and Heezen, B.C., 1979, Submarine extension of the southwest rift zone of Mauna Loa Volcano, Hawaii—visual observations from the U.S. Navy Deep Submergence Vehicle DSV *Sea Cliff*: Geological Society of America Bulletin, v. 90, p. 435–443.

Hitchcock, C.H., 1906, Mohokea caldera: Geological Society of America Bulletin, v. 17, p. 485–496.

——— 1909, Hawaii and its volcanoes: Honolulu, The Hawaiian Gazette Co., 314 p.

Jaggar, T.A., 1931, The crater of Mauna Loa: Hawaiian Volcano Observatory Volcano Letter 360, p. 1–4.

——— 1947, Origin and development of craters: Geological Society of America Memoir 21, 508 p.

Kelley, M.L., Spiker, E.C., Lipman, P.W., Lockwood, J.P., Holcomb, R.T.,

and Rubin, Meyer, 1979, U.S. Geological Survey, Reston, Virginia, radiocarbon dates XV—Mauna Loa and Kilauea Volcanoes, Hawaii: Radiocarbon, v. 21, no. 2, p. 306–320.

Klein, F.W., 1982, Patterns of historical eruptions at Hawaiian volcanoes: Journal of Volcanology and Geothermal Research, v. 12, no. 1, p 1–35.

Lipman, P.W., 1980a, The southwest rift zone of Mauna Loa—implications for structural evolution of Hawaiian volcanoes: American Journal of Science, v. 280-A, p. 752–776.

——— 1980b, Rates of volcanic activity along the southwest rift zone of Mauna Loa Volcano, Hawaii: Bulletin Volcanologique, v. 43, n. 4, p. 703–725.

Lipman, P.W., and Swenson, Alan, 1984, Generalized geologic map of the southwest rift zone of Mauna Loa Volcano, Hawaii: U.S. Geological Survey Miscellaneous Investigations Map I–1323, scale 1:100,000.

Lockwood, J.P., 1978, The volcanic environment of Mauna Loa Observatory, Hawaii—history and prospects, *in* Miller, John, ed., Mauna Loa Observatory—a 20th Anniversary Report: National Oceanic and Atmospheric Administration (NOAA) Special Report, p. 28–34.

——— 1984, Geologic map of the Kulani quadrangle, Hawaii (preliminary): U.S. Geological Survey Open-File Report 84–12, scale 1:24,000.

Lockwood, J.P.,and Lipman, P.W., 1980, Recovery of datable charcoal beneath young lavas—lessons from Hawaii: Bulletin Volcanologique, v. 43, no. 3, p. 609–615.

Macdonald, G.A., 1972, Volcanoes: Englewood Cliffs, N.J., Prentice-Hall, 510 p.

Macdonald, G.A., and Abbott, A.T., 1970, Volcanoes in the sea—the geology of Hawaii: Honolulu, University of Hawaii Press, 441 p.

Moore, J.G., Fornari, D.J., and Clague, D.A., 1985, Basalts from the 1877 submarine eruption of Mauna Loa, Hawaii: new data on the variation of palagonitization rate with temperature: U.S. Geological Survey Bulletin 1663, 11 p.

Moore, J.G., Phillips, R.L., Griggs, R.W., Peterson, D.W., and Swanson, D.A., 1973, Flow of lava into the sea, 1969—1971, Kilauea Volcano, Hawaii: Geological Society of America Bulletin, v. 84, p. 537–546.

Peterson, D.W., and Tilling, R.I., 1980, Transition of basaltic lava from pahoehoe to a'a, Kilauea Volcano, Hawaii—field observations and key factors: Journal of Volcanology and Geothermal Research, v. 7, p. 271–293.

Rhodes, J.M., Lockwood, J.P., and Lipman, P.W., 1982, Episodic variations in magma chemistry, Mauna Loa Volcano, Hawaii [abs.]: IAVCEI-IAGC Science Assembly, Generation of major basaltic types Reykjavik, Aug. 15–22, 1982, Abstracts Volume, p. 43.

Stearns, H.T., and Clark, W.O., 1930, Geology and water resources of the Kau District, Hawaii: U.S. Geological Survey Water-Supply Paper 616, 194 p.

Stearns, H.T., and Macdonald, G.A., 1946, Geology and ground-water resources of the Island of Hawaii: Hawaii Division of Hydrography Bulletin 9, 363 p.

Swanson, D.A., 1972a, Magma supply rate of Kilauea Volcano, 1952–1971: Science, v. 175, p. 169–170.

——— 1972b, Pahoehoe flows from the 1969–1971 Mauna Ulu eruption, Kilauea Volcano, Hawaii: Geological Society of America Bulletin, v. 84, p. 615–626.

Wilkes, Charles, 1845, Narrative of the United States Exploring Expedition during the years 1838–1842: Philadelphia, Lea and Blanchard, v. 4, 539 p.

Wilson, W.F., 1920, Hawaii nei 128 years ago—the journal of Archibald Menzies: Honolulu, private publication, 199 p.

Wood, H.O., 1914, On the earthquakes of 1868 in Hawaii: Seismological Society of America Bulletin, v. 4, no. 4, p. 169–203.

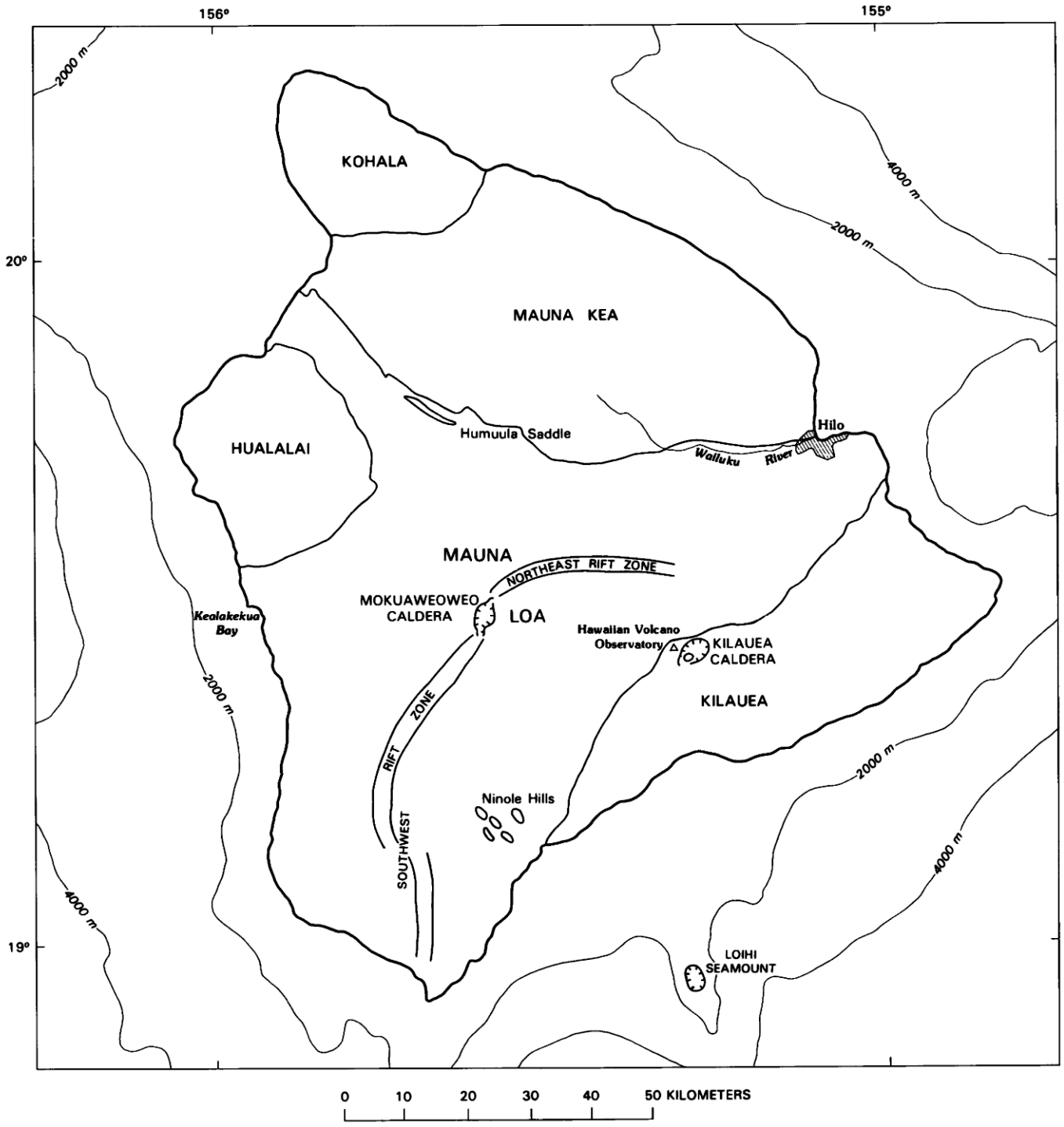

FIGURE 18.1.—Island of Hawaii, showing five volcanoes, some major structural and geographic features, and bathymetry of adjacent sea. Bathymetric contour interval 2,000 m.

TABLE 18.1.—*Ages, durations, areas, and volumes of historical Mauna Loa eruptions 1843–1984*

[Eruptive subdivisions: S, summit; NE, northeast rift zone; SW, southwest rift zone; NF, north flank. Estimated errors: 1, ±20 percent; 2, ±20–40 percent; 3, greater than ±40 percent; n.d., no data]

Date of start		Duration (days)		Eruptive subdivision(s)	Area (km^2)					Volume ($m^3 \times 10^6$)				Estimated error
(yr)	(mo-d)	Summit	Flank		Exposed outside Mokuaweoweo	Buried outside Mokuaweoweo	Original outside Mokuaweoweo	Original inside Mokuaweoweo	Total	Subaerial outside Mokuaweoweo	Estimated inside Mokuaweoweo	Estimated beneath sea level	Total	
1984	3-26	<1	22	S, NE	42	0	42	6	48	208	12	0	220	1
1975	7-05	1	0	S	3	4	7	6	13	18	12	0	30	1
1950	6-01	1	23	S, SW	112	0	112	0	112	306	0	70	376	2
1949	1-06	145	0	S	15	2	17	4	22	86	30	0	116	1
1942	4-26	2	13	S, NE	28	5	33	1	34	169	7	0	176	1
1940	4-17	134	0	S	1	5	6	7	13	14	96	0	110	1
1935	11-21	6	40	S, NE, NF	30	1	31	2	33	81	6	0	87	2
1933	12-02	17	0	S	0	1	1	5	6	2	98	0	100	2
1926	4-10	<1	14	S, SW	25	10	35	0	35	116	0	5	121	2
1919	9-26	<1	38	S, SW	21	7	28	0	28	83	0	100	183	2
1916	5-19	0	12	SW	14	3	17	0	17	31	0	0	31	2
1914	11-25	48	0	S	0	0	0	5	5	0	55	0	55	2
1907	1-09	<1	15	S, SW	25	0	25	3	28	116	5	0	121	2
1903	10-06	61	0	S	0	0	0	5	5	0	70	0	70	3
1903	9-01	<1	0	S	0	0	0	1	1	0	3	0	3	n.d.
1899	7-01	4	21	S, NE	21	0	21	2	23	73	8	0	81	2
1896	4-21	16	0	S	0	0	0	5	5	0	25	0	25	3
1892	11-30	3	0	S	0	0	0	3	3	0	12	0	12	3
1887	1-16	<1	7	S, SW	28	0	28	1	29	115	3	10	128	2
1880	11-05	0	280	NE	50	1	51	0	51	130	0	0	130	2
1880	5-01	6	0	S	0	0	0	5	5	0	10	0	10	n.d.
1879	3-09	<1	0	S	0	0	0	1	1	0	1	0	1	n.d.
1877	2-14	<1	<1	S,NF	1	0	1	0	1	1	0	7	8	3
1872	8-09	~1,200 (near ~continuous)	0	S	0	0	0	5	5	0	630	0	630	2
1871	8-10	~20	0	S	0	0	0	3	3	0	20	0	20	n.d.
1868	3-27	<1	5	S, SW	23	0	23	1	24	73	0	50	123	2
1865	12-30	~125	0	S	0	0	0	5	5	0	50	0	50	n.d.
1859	1-23	<1	~300	S, NF	90	0	90	1	91	287	1	95	383	3
1855	8-11	<1	~450	S, NE	62	4	66	0	66	280	0	0	280	3
1852	2-17	1	20	S, NE	18	15	33	0	33	182	0	0	182	2
1851	8-08	4	0	S	5	7	12	0	12	35	0	0	35	2
1849	5(?)	~15	0	S	0	0	0	5	5	0	25	0	25	n.d.
1843	1-10	5	~90	S, NE, NF	37	8	45	0	45	202	0	0	202	3
		Total			651	73	724	82	806	2,608	1,179	337	4,124	

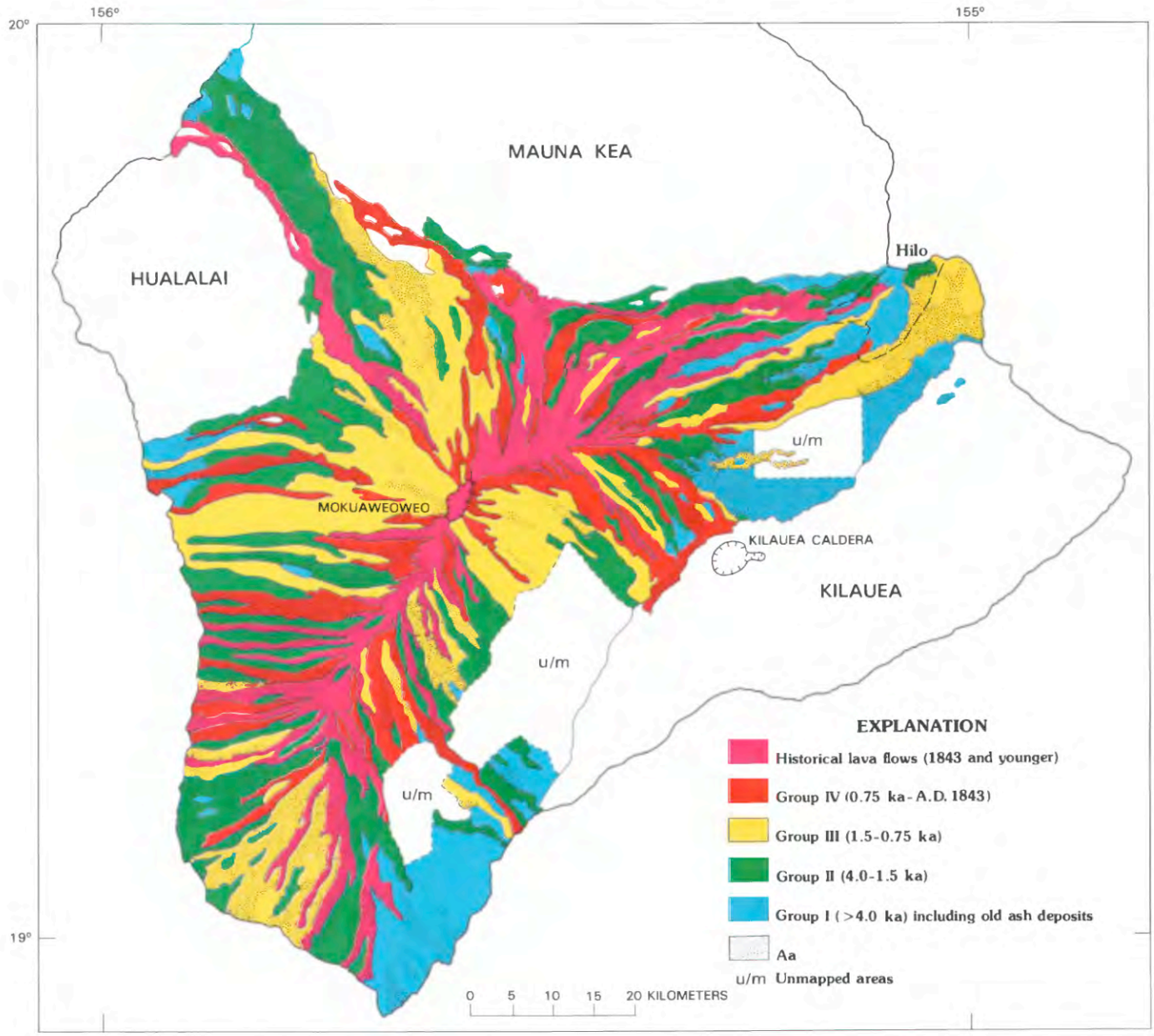

FIGURE 18.2.—Age-distribution map of Mauna Loa lava flows, greatly generalized from 1:24,000 mapping, including unpublished work in Hilo area by J.M. Buchanan-Banks.

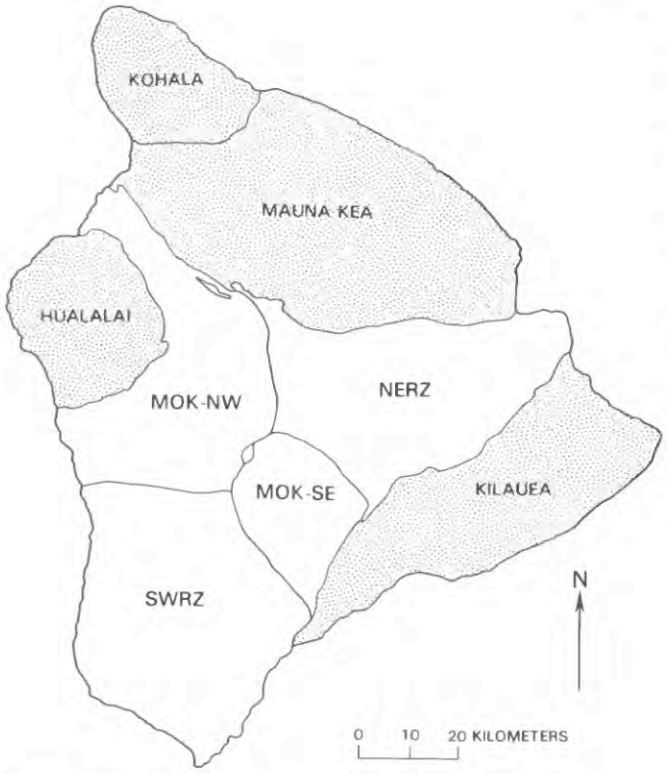

FIGURE 18.3.—Geographic subdivisions of Mauna Loa lava flows used in this paper. MOK-NW, northwest flank summit flows; MOK-SE, southeast flank summit flows; NERZ, northeast rift zone flows; SWRZ, southwest rift zone flows. Shaded areas show Island of Hawaii's other four volcanoes.

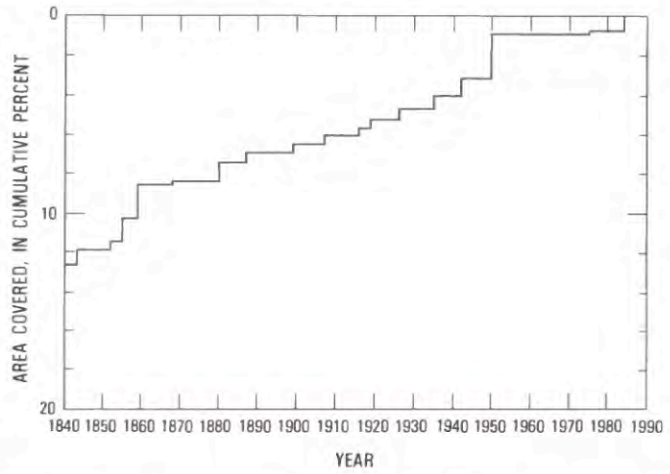

FIGURE 18.5.—Cumulative percentages of Mauna Loa's mapped surface covered by flows of historical age. Percentage given for a particular year is that covered by flows of that age or younger.

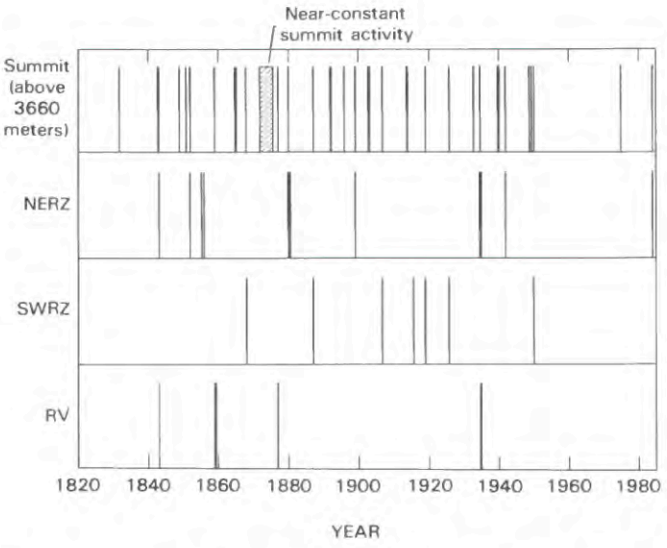

FIGURE 18.4.—Chronology of historical Mauna Loa eruptions. NERZ, northeast rift zone; SWRZ, southwest rift zone; RV, northwest flank radial vent eruptions.

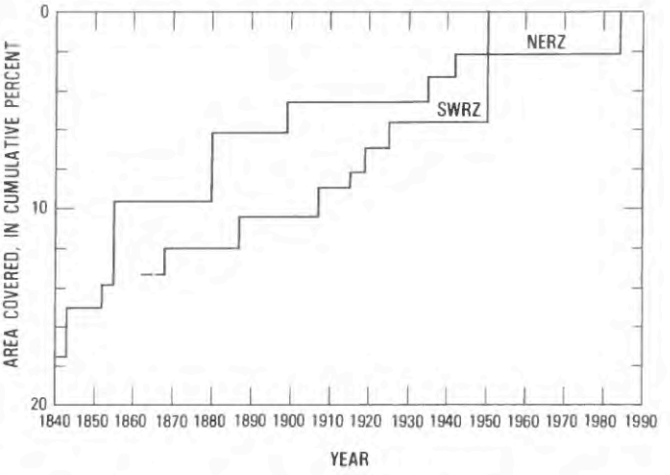

FIGURE 18.6.—Cumulative percentages of Mauna Loa's northeast and southwest rift zone flanks covered by flows of historical age. Percentage given for a particular year is that covered by flows of that age or younger.

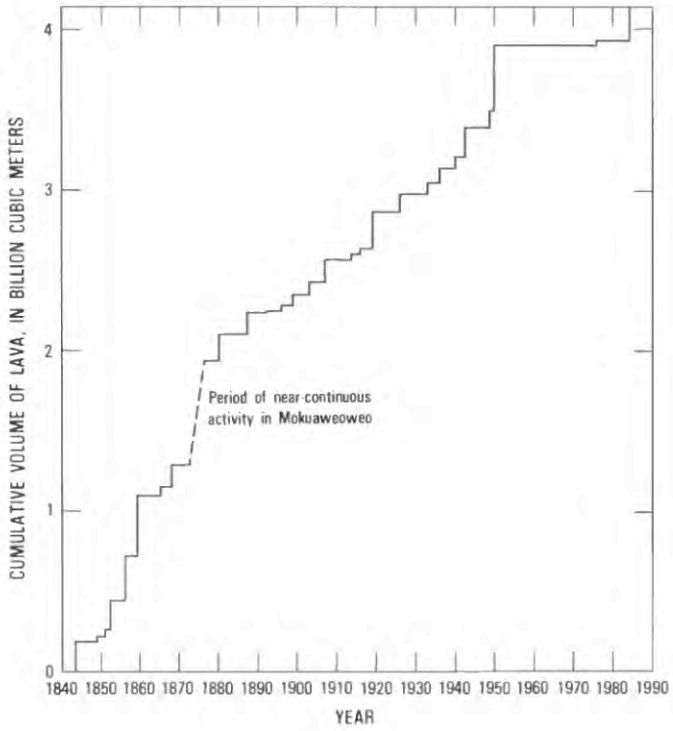

FIGURE 18.7.—Mauna Loa lava production, 1843 to 1984.

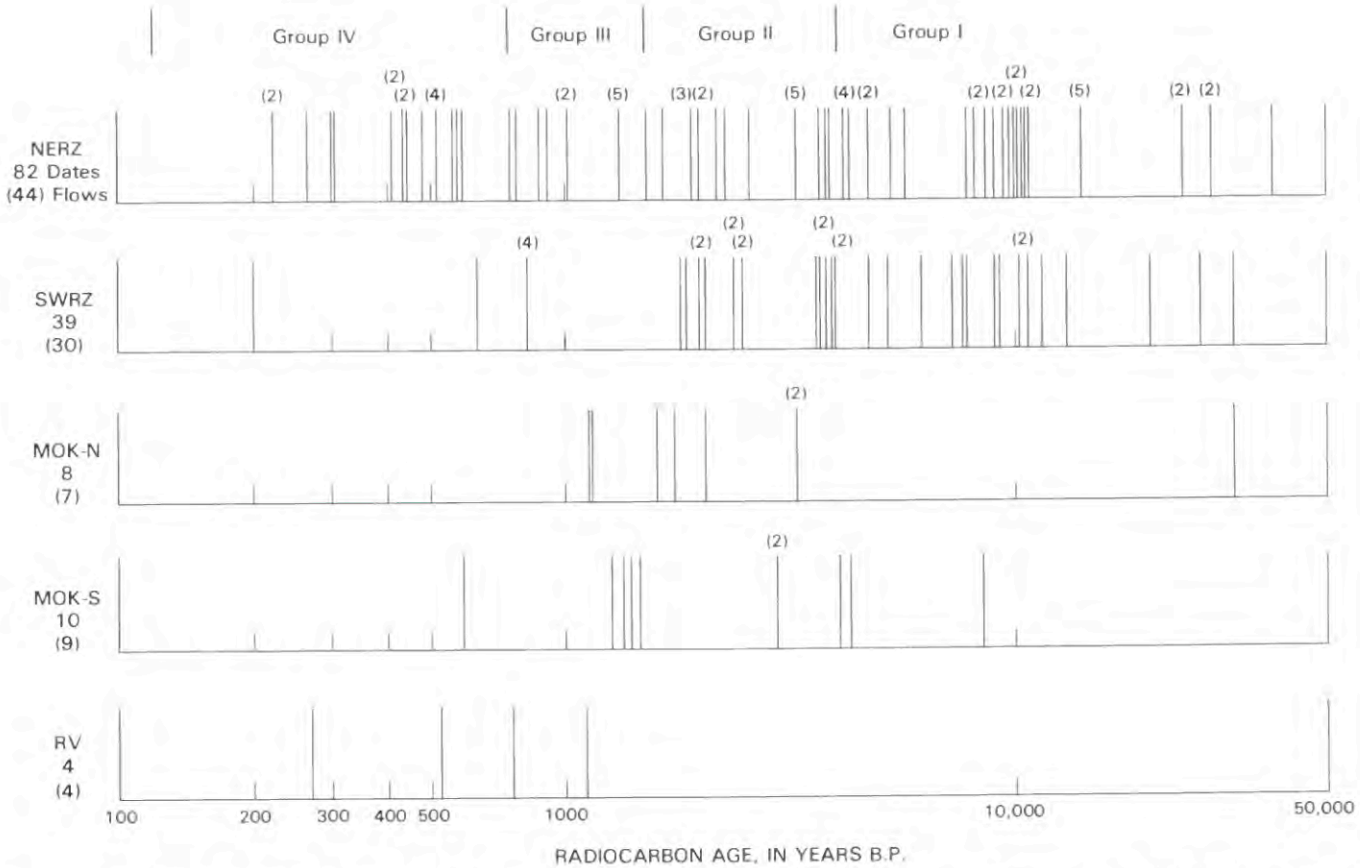

FIGURE 18.8.—Age distribution of radiocarbon-dated Mauna Loa lava flows, plotted on a logarithmic scale of time. Where multiple ages are available for individual flows, the number of these ages is plotted above bar at the mean value. All ages by Meyer Rubin. Flow sources: NERZ, northeast rift zone; SWRZ, southwest rift zone; MOK-NW, Mokuaweoweo overflows to the northwest; MOK-SE, Mokuaweoweo overflows to the southeast; RV, radial vents on northwest flank.

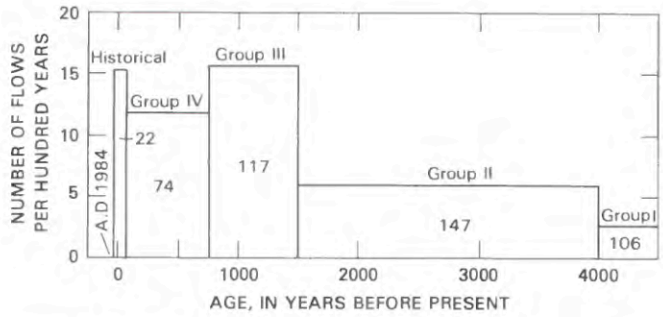

FIGURE 18.9.—Average number of flows per century for various age categories. Numbers within boxes give total numbers of flows in each age group.

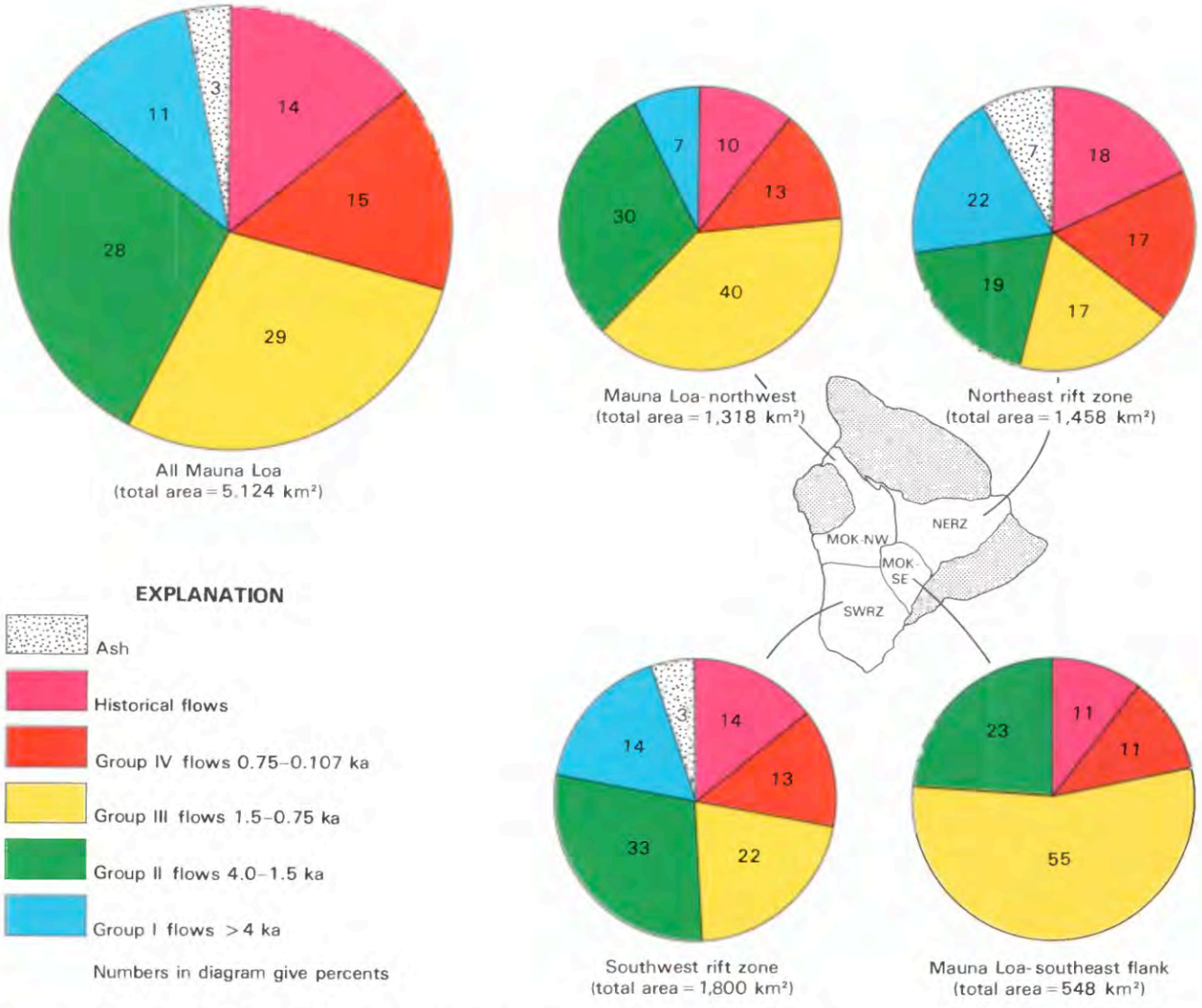

FIGURE 18.10.—Age and geographic distribution of Mauna Loa lava flows, recalculated to exclude unmapped areas. Percentages of excluded unmapped areas shown in figure 18.21.

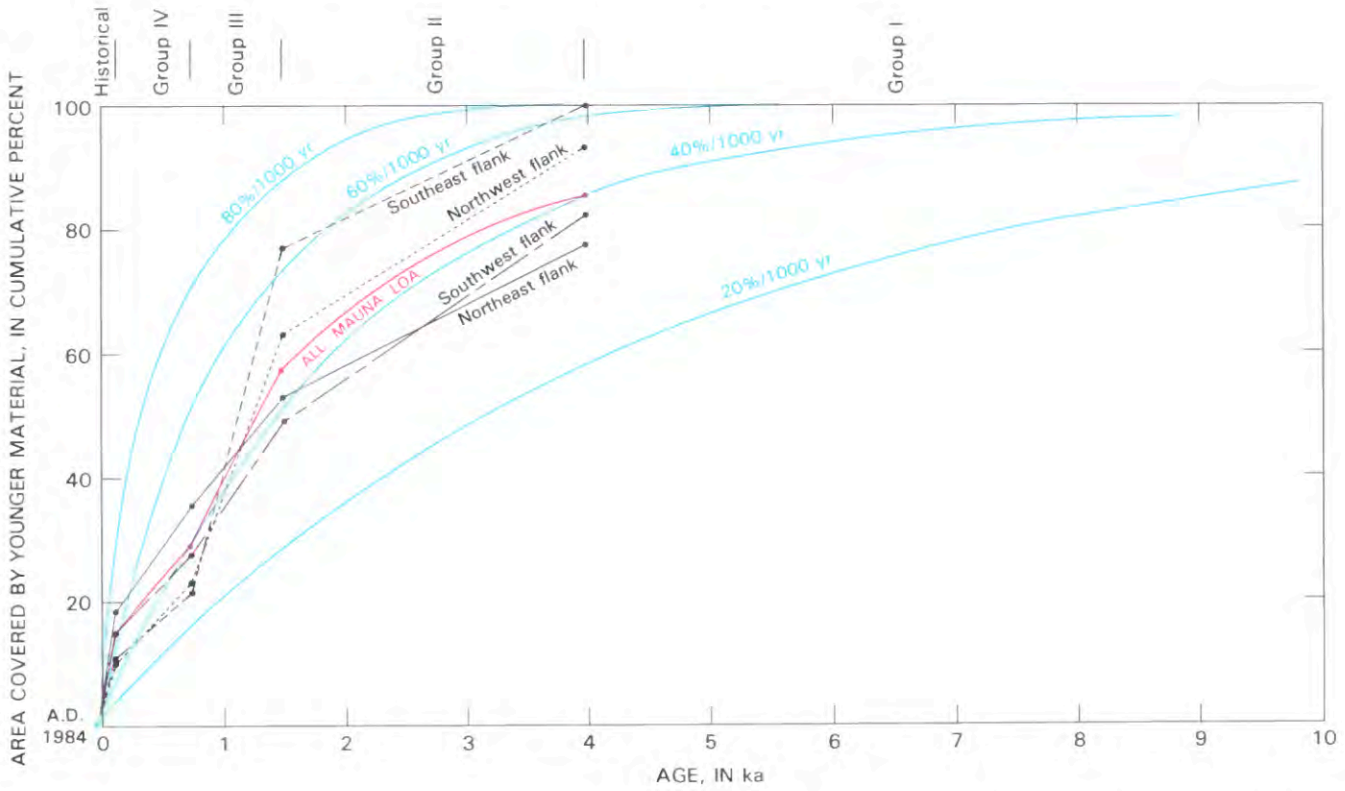

FIGURE 18.11.—Coverage of Mauna Loa's mapped surface as a function of time. Curves for areal subdivisions defined in figure 18.3 and for all areas combined (red curve) show actual age distribution of present surface. Ash deposits are included with group I lavas. Southeast flank plot is dashed because of the large areas unmapped in that region. Numbered curves (blue) are from Lipman (1980b, fig. 9A) and show expected cumulative areal coverage for indicated uniform coverage rate in percent per per 1,000 years.

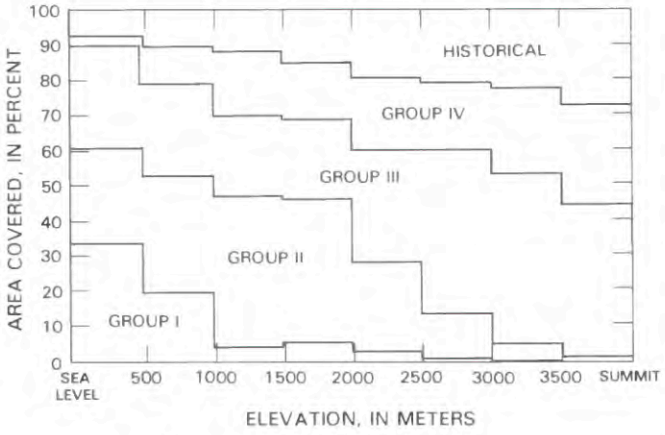

FIGURE 18.12.—Age distribution of Mauna Loa surface flows as a function of elevation.

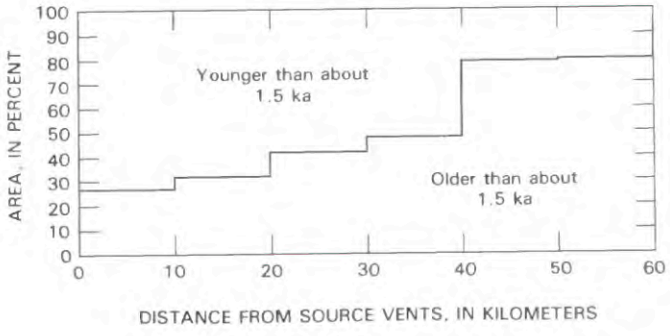

FIGURE 18.13.—Age distribution of Mauna Loa surface flows as a function of transport distance from eruptive sources.

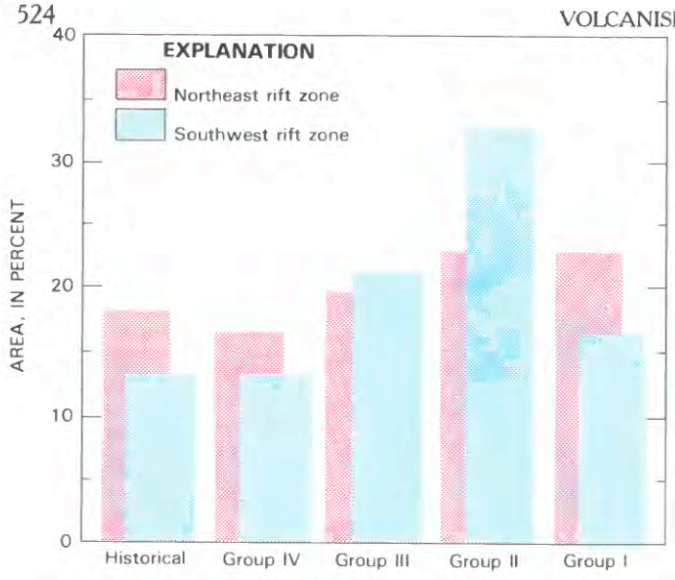

FIGURE 18.14.—Comparison of ages of flows from northeast and southwest rift zones, showing percentages of each flank covered by flows of different ages.

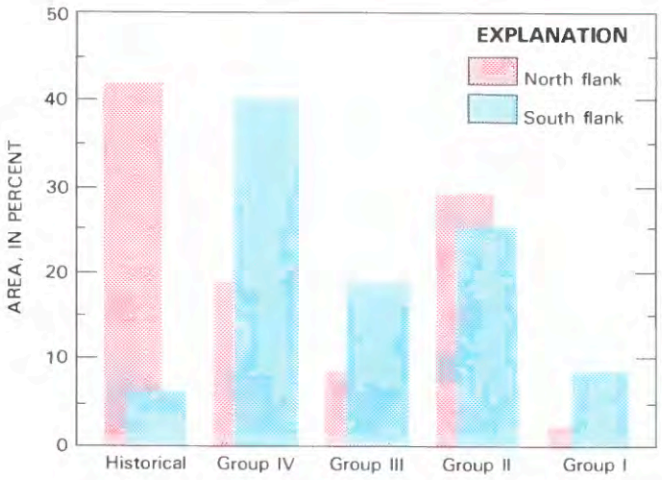

FIGURE 18.15.—Age distribution of lava flows on north and south flanks of northeast rift zone, above 1,500 m elevation, showing areal percentages of each flank covered by flows of different ages.

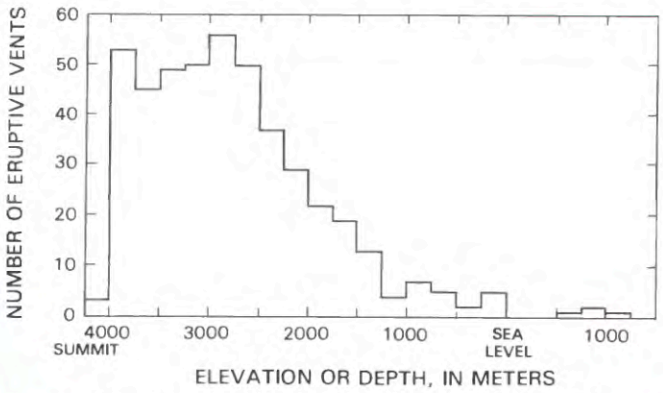

FIGURE 18.16.—Elevation distribution of Mauna Loa eruptive vents, showing total number of eruptive vents recognized within each 250-m-elevation interval of Mauna Loa. Vents on NERZ, SWRZ, and northwest flank are summed together for each elevation interval. Long vents that extend across elevation boundaries are counted in each interval.

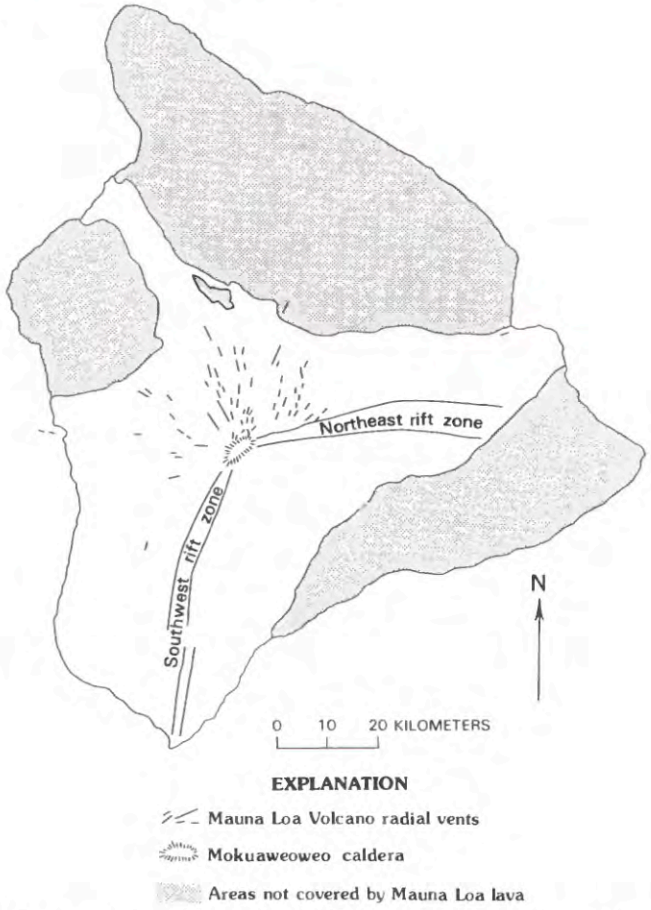

FIGURE 18.17.—Geographic distribution of northwest flank radial vents. Northeast and southwest rift zones are loci of hundreds of closely spaced vents, not shown here.

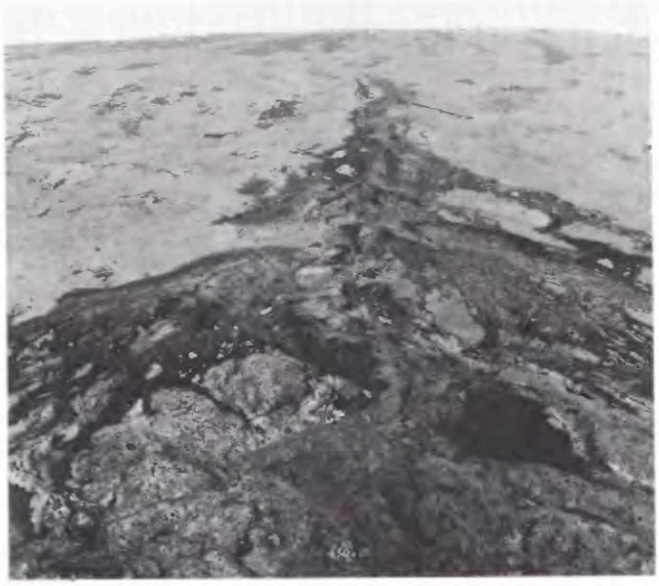

FIGURE 18.18.—Aerial view of spatter cones along a typical radial vent (1859). View to south. Strongly foreshortened view, about 500 m wide at bottom.

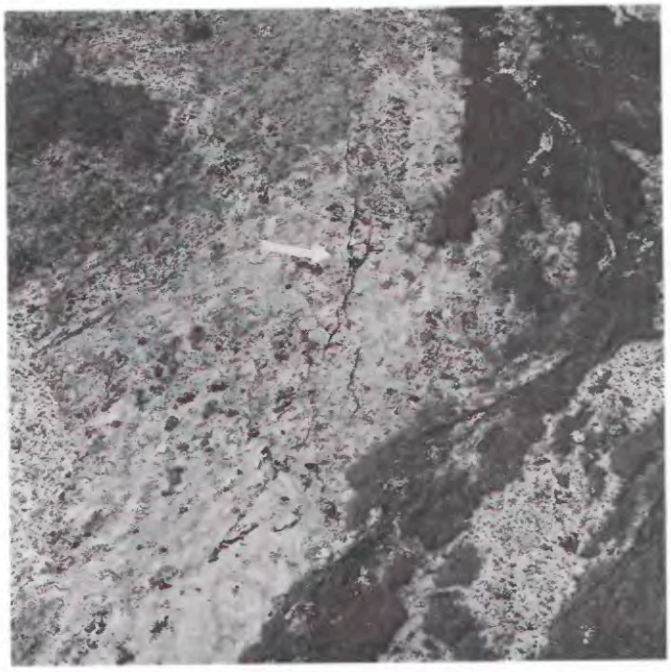

FIGURE 18.19.—Aerial view of radial vent (arrow) along which no spatter ramparts or cones developed. Top to bottom about 400 m.

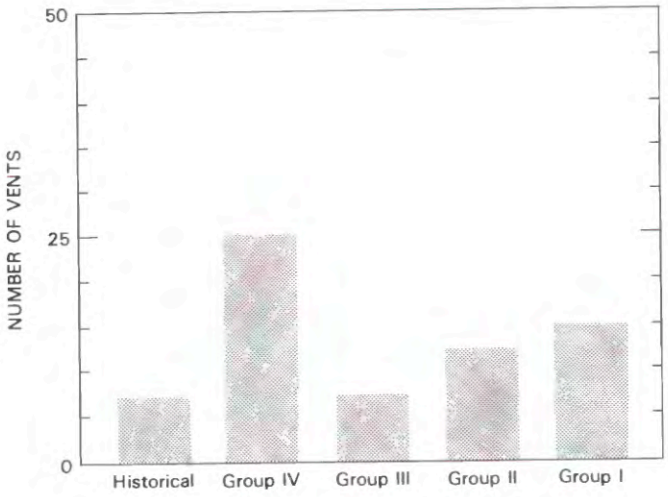

FIGURE 18.20.—Age distribution of northwest flank radial vents.

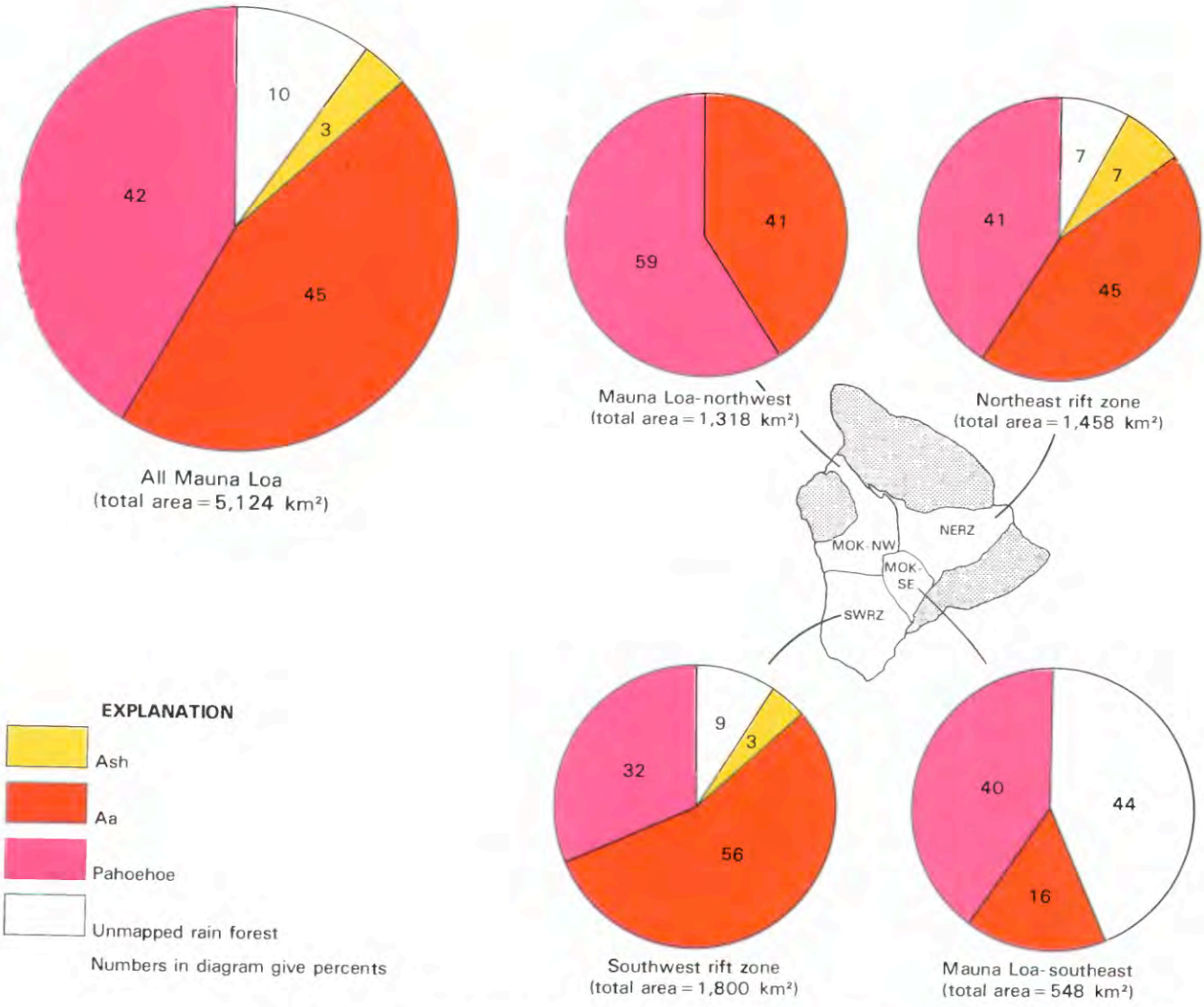

FIGURE 18.21.—Distribution of aa, pahoehoe, and unmapped areas on Mauna Loa.

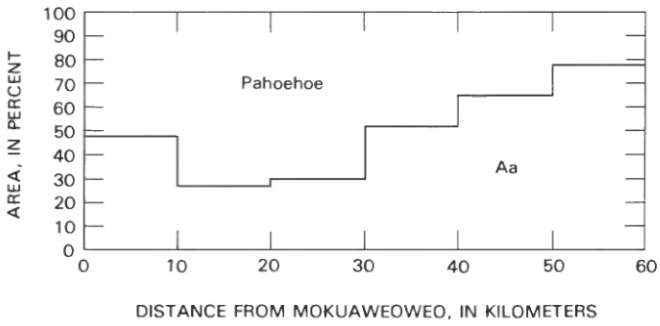

FIGURE 18.22.—Distribution of aa and pahoehoe on Mauna Loa's northwest flank as a function of transport distance from Mokuaweoweo; 1859 flows excluded.

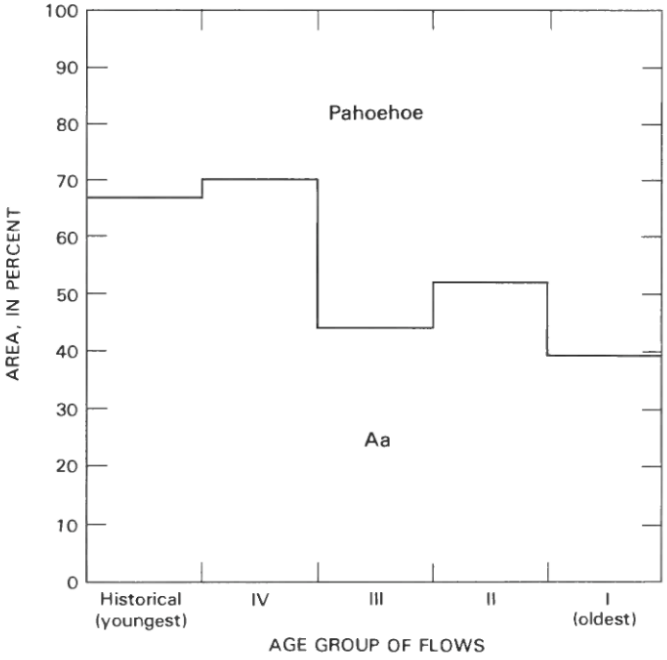

FIGURE 18.23.—Distribution of aa and pahoehoe on Mauna Loa's surface as a function of age.

FIGURE 18.24.—Aerial view of Ninole Hills from southwest, showing remnants of older Ninole flows rising above encroaching Mauna Loa lava flows north of town of Pahala.

FIGURE 18.25.—Aerial view of Mauna Loa's north flank, in Humuulu Saddle. View to south. Mauna Kea vents cut this flank of Mauna Loa and formed prominent cinder cones 20,000 to 8,000 years ago. These cones and their flows are preserved as kipukas (inliers) surrounded by younger Mauna Loa lavas.

FIGURE 18.26.—Aerial view of Mauna Loa's east flank near town of Keaau, showing kipukas (inliers) of Mauna Loa lava surrounded by young flows from Kilauea Volcano. View to southwest. Ash-covered, older kipukas support sugarcane fields.

FIGURE 18.27.—Aerial view of Mokuaweoweo caldera at summit of Mauna Loa, looking northeast. South Pit in foreground, Mauna Kea in background. Most of caldera floor is covered by pahoehoe erupted in March 1984.

FIGURE 18.28.—Aerial view of Mauna Loa's summit area from south, showing fault developed along inferred eastern boundary of old caldera. Fault cuts group III pahoehoe (light) and group IV aa (dark).

FIGURE 18.29.—Aerial view of Lua Poholo from north. This pit crater, in northeast corner of Mokuaweoweo, has a volume of about 7×10^6 m^3 and formed about 1880, probably during flank eruption of that year. Precollapse ground surface is preserved on rotated block at bottom of crater.

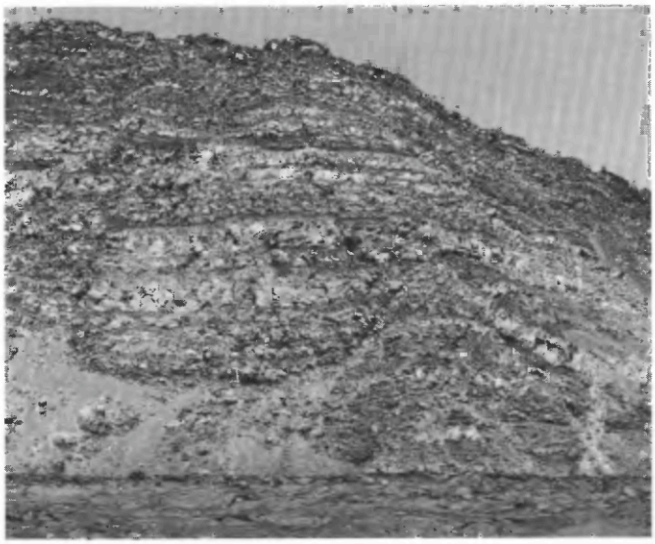

FIGURE 18.30.—Cross section of filled pit crater exposed on west wall of Mokuaweoweo caldera. Lowest of thick flows that fill crater overlies basal talus breccia (marked by a 4-meter rod). Filled crater is informally called "Lua Piha" (filled pit). Note crosscutting lopolith on right.

FIGURE 18.31.—Aerial view of Puu Hou, an 85-m-high littoral cone formed where 1868 SWRZ flow entered the sea near south tip of Hawaii Island.

FIGURE 18.32.—Aerial view of Kaawaloa Point, where a group III pahoehoe flow from Mauna Loa's summit mantles Kealakekua fault scarp and forms a typical lava delta.

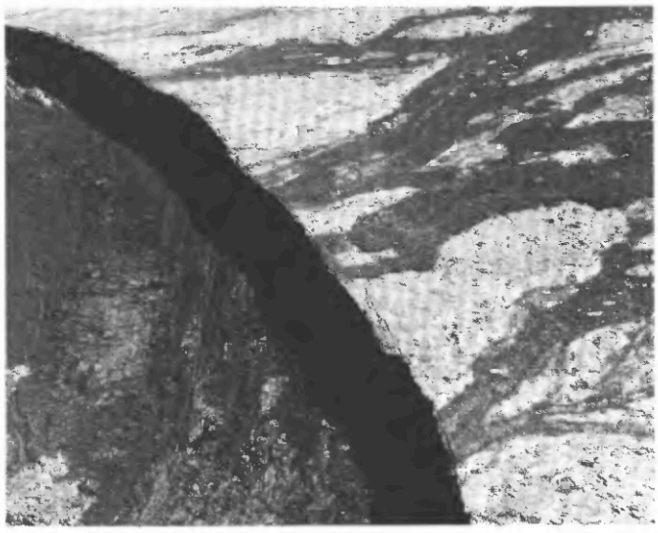

FIGURE 18.33.—Aerial view of southeast rim of Mokuaweoweo, showing truncation of group IV aa flows (dark) and underlying group III pahoehoe. Caldera rim here is 50 m high.

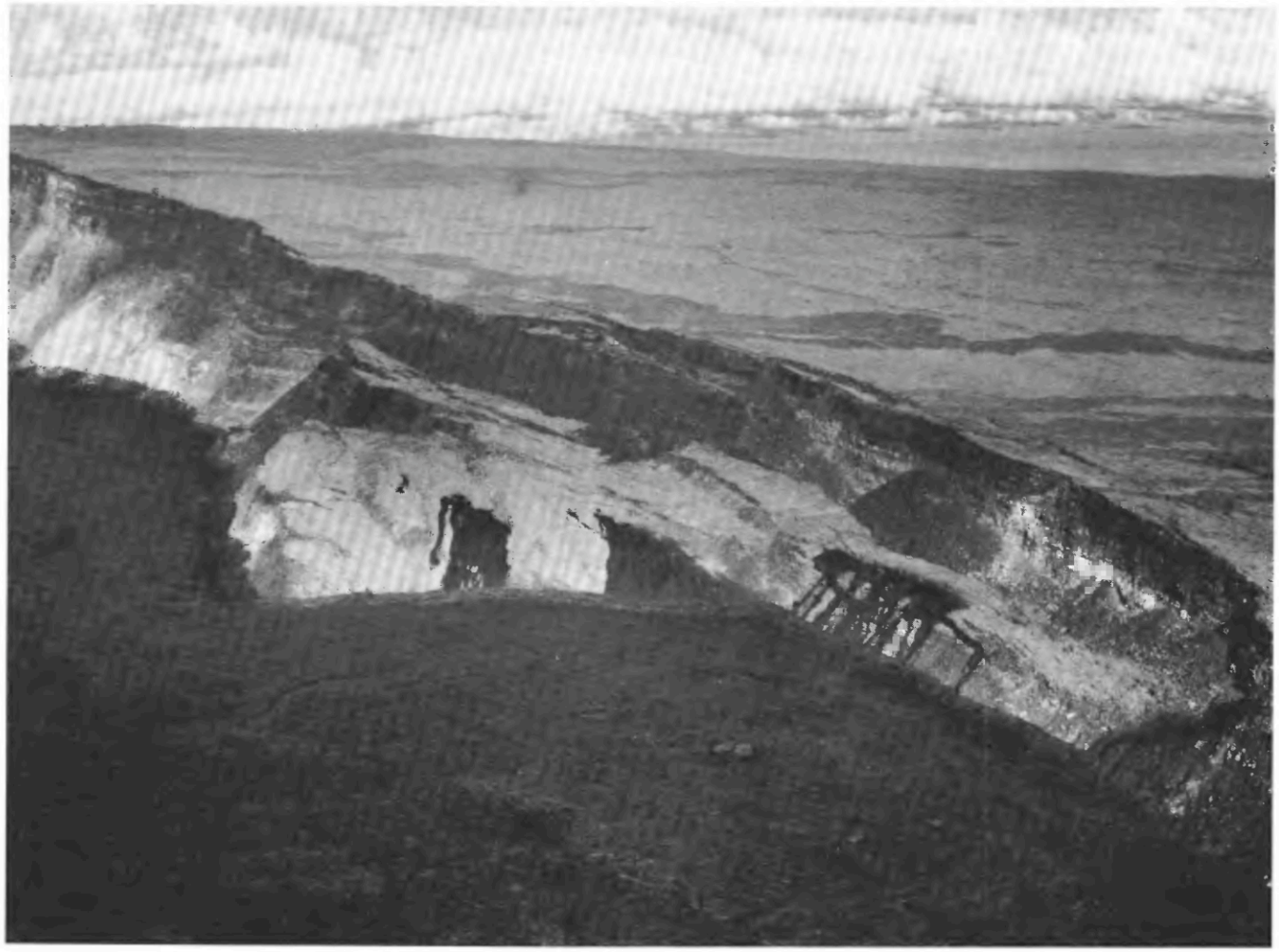

FIGURE 18.34.—Aerial view of north wall of Mokuaweoweo caldera, showing details of caldera subsidence fractures. Slump blocks are cut by summit lavas of 1942 eruption. Caldera floor is covered by lavas erupted in July 1975.

FIGURE 18.35.—Phreatic-explosion breccia fragments 100 m north of Mokuaweoweo caldera's north rim. These angular blocks of hornfelsic textured basalt here overlie a group IV aa flow.

MAUNA LOA 1974–1984: A DECADE OF INTRUSIVE AND EXTRUSIVE ACTIVITY

By John P. Lockwood, John J. Dvorak, Thomas T. English, Robert Y. Koyanagi, Arnold T. Okamura, Marjorie L. Summers, *and* Wilfred R. Tanigawa

ABSTRACT

The 1975 and 1984 eruptions of Mauna Loa Volcano were both related to a decade-long period of seismic and geodetic unrest (inflation) that was first detected in April 1974. The 1975 eruption, the first of Mauna Loa in 25 years, began just before midnight on July 5, but lasted less than 19 hours. Eruptive vents were confined to the summit region and produced about 30 million cubic meters of uniform tholeiite, which covered nearly 14 square kilometers of the summit area and north flank. Intense seismic activity continued in a localized area along the middle northeast rift zone (NERZ) for a week following the eruption and was accompanied by extensions across the rift, which suggested the intrusion of magma into this area. This led to a forecast of renewed activity on the NERZ sometime before the summer of 1978. The forecast timing proved erroneous, but the scenario was correct as to the place and character of the subsequent eruption.

The Mauna Loa summit inflated rapidly during the first two years after the 1975 eruption, but at lesser rates after 1977. Modeling of geodetic data showed that this inflation was caused by magma accumulation in a shallow storage reservoir beneath the southern edge of the summit caldera. Seismic activity was steady, although rates of intermediate-depth earthquakes began to increase in 1980, as did rates of summit deformation, resulting in a renewed forecast (1983) for an eruption of Mauna Loa within the next two years.

The 1984 summit-flank eruption began at 0125 H.s.t., March 25 (during a fortnightly earth tidal minimum). Eruptive fissures, which initially opened in the southwest corner of Mokuaweoweo, quickly propagated down the upper southwest rift and northeast rift zones, but eruptive activity was soon limited to the NERZ. A dike propagated down the NERZ at an average rate of 1.2 km/h during the day and was marked at the surface by discontinuous echelon eruptive fissures and earth cracks. The lowest eruptive vents were 15 km from the edge of Mokuaweoweo, between 2,770 and 2,930 m elevation; activity was restricted to these vents for the last three weeks of the eruption. Eruptive temperatures throughout this period remained constant at about 1,140 °C. Lava production began to diminish by early April, and lava steadily became more viscous, blocking supply channels at higher and higher elevations. When the eruption ended on April 15, approximately 220 million cubic meters of uniform tholeiite had been erupted, covering about 48 square kilometers of the Mauna Loa surface. Aa lava flowed as far as 27 km from eruptive vents to the 900-m elevation, to within 6 km of the nearest buildings in the city of Hilo.

Repeated geodetic and gravity measurements made throughout the eruption documented a substantial deflation of the Mauna Loa summit. The maximum measured subsidence, in the southern part of the summit, was 630 mm, and typical trilateration survey lines across Mokuaweoweo contracted an average of 300 mm, after initial dike-related extensions of about 600 mm. The summit area of Mauna Loa began to re-inflate immediately after the 1984 eruption, indicating the recharge processes for the volcano's next eruption have already begun.

INTRODUCTION

Mauna Loa, the largest active volcano on Earth, is a classic basaltic shield on the Island of Hawaii and rises to 4,170 m above the north-central Pacific Ocean. Mauna Loa erupted in July 1975 for the first time in 25 years. Another much larger summit and flank eruption followed in March and April 1984. Both eruptions were clearly related to a continuum of seismicity and deformation that began in 1974. This paper documents some of the events of this decade, but is only preliminary to more detailed analyses.

At the beginning of 1974 Mauna Loa had not erupted since the large eruption of June 1950 (Macdonald, 1954). Geophysical monitoring of Mauna Loa was provided principally by Hawaiian Volcano Observatory (HVO) instruments located on Kilauea prior to 1964, when the first modern seismometer was installed at the summit. Thomas A. Jaggar had previously placed seismographs at the summit at various times, but telemetry logistics limited their utility. R.W. Decker established a single EDM (Electronic Distance Measurement) survey line across Mokuaweoweo caldera in 1964, and annual reoccupation of this line (expanded to three lines by 1973) provided the only geodetic control. These transcaldera lines showed no significant changes prior to 1974. Earthquake activity was at low levels, as it had been for the previous 24 years.

The historical record of Mauna Loa's past eruptive behavior is lamentably brief—the first specific account describes the eruption of 1832, viewed from 150 km away. From 1832 to 1950 Mauna Loa had erupted an average of once every four years; the 24 years of quiescence from 1950 to 1974 was the longest noneruptive period in the volcano's brief recorded history. At the beginning of 1974 there were no premonitory indications of the decade of volcanic unrest and eruption which was soon to begin.

ACKNOWLEDGMENTS

Data and observations presented in this report came from the

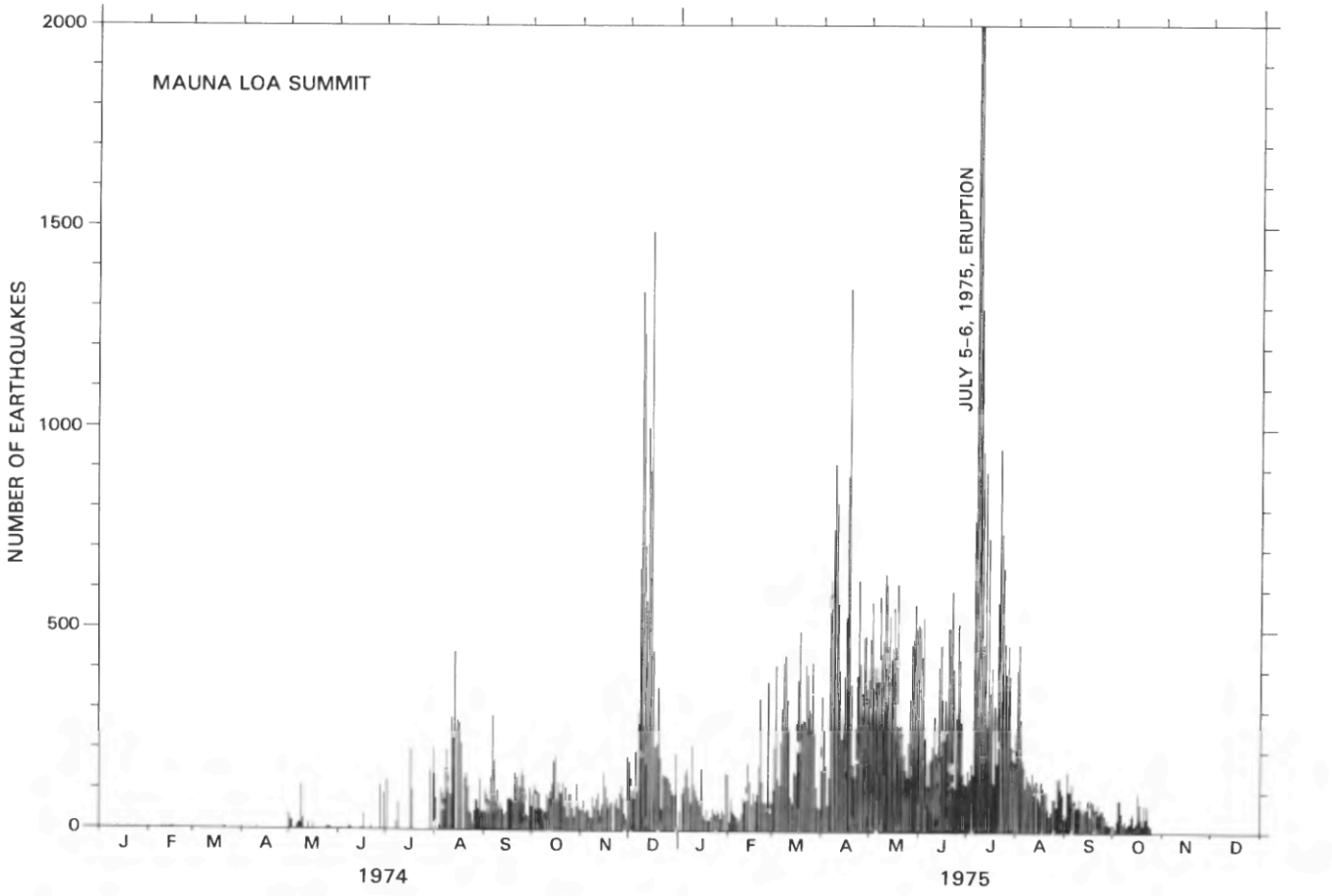

FIGURE 19.1.—Daily frequency of Mauna Loa short-period summit earthquakes ($M>0.1$), January 1974 to October 1975 (modified from Lockwood and others, 1976, fig. 5).

field and laboratory efforts of the entire staff of the Hawaiian Volcano Observatory from 1974 to 1984. This article incorporates previously published data of N.G. Banks, L.P. Greenland, D.B. Jackson, D.J. Johnson, K.A. McGee, Motoaki Sato, and J.M. Rhodes (see Lockwood and others, 1985). The careful review and thoughtful comments of P.W. Lipman greatly improved the manuscript as did review comments by T.L. Wright.

BEGINNING OF UNREST

An increase in the number of summit microearthquakes was detected in April 1974. The seismic activity continued to increase into the summer, and the possibility of future eruptive activity was noted (Koyanagi and others, 1975). Efforts to monitor the Mauna Loa activity more closely were frustrated by the fact that Kilauea was in near-continuous eruption at the Mauna Ulu eruptive vent during the first half of the year (Tilling and others, chapter 16), and brief Kilauea summit eruptions occurred in July, September, and December.

Trilateration measurements across Mokuaweoweo caldera in August 1974 revealed that significant dilation of the summit caldera had occurred since the previous measurements in 1973. This finding, together with continued increase in seismicity in the summit area, prompted expansion of the trilateration network to eight lines and the addition of two seismometers, placed around the rim of the caldera. Civil authorities were briefed on the situation, and through extensive news media interest, the island populace was alerted to the possibility of Mauna Loa eruptive activity. In mid-December 1974 the microearthquake rate ($M>0.1$) increased to 1,500 per day (fig. 19.1), and the conclusion that Mauna Loa was awakening was unescapable.

Trilateration measurements at the summit on December 14 showed significant dilation (to 4 cm) had occurred since August. On the morning of December 15, an earthquake of magnitude 4.6 below the southeastern part of the summit area was felt widely on the Island of Hawaii, and public concern was intensified.

From late December 1974 to February 1975 heavy snowfall blanketed Mauna Loa down to the 2,800-m elevation and covered all survey stations, preventing their reoccupation until early June. Aerial inspection of the summit area in April showed possibly

FIGURE 19.2.—Pit craters along upper southwest rift zone of Mauna Loa showing possibly anomalous melting of snow in April 1975. Lua Hou is in lower right corner. Photograph by J.P. Lockwood.

anomalous melting of snow in two pit craters on the upper southwest rift zone and along parts of the caldera floor (fig. 19.2).

In early spring of 1975 additional trilateration survey networks were established at lower elevations in order to measure strain across Mauna Loa's southwest rift zone (SWRZ) and northeast rift zone (NERZ). The Mokuaweoweo trilateration network was occupied on June 4 and showed as much as 10 cm of dilation of the summit since December.

Earthquakes between January 1974 and June 1975 occurred at intermediate depths (5–13 km) northwest of the summit and at shallow depths (<5 km) beneath and to the southwest of Mokuaweoweo (fig. 19.3). The number of intermediate-depth earthquakes increased first and was soon followed by an increase in the number of shallow earthquakes, commonly exceeding several hundred per day. Intense swarms occurred in August and December 1974, and again from February through June 1975.

During the week of June 30 to July 4 three borehole tiltmeters were installed on Mauna Loa's summit and north flank. One of these tiltmeters was to be destroyed by a lava flow in a few hours, before final adjustments could be made.

THE ERUPTION OF JULY 5–6, 1975

No unusual activity was noted on the Mauna Loa seismograms during the early evening of July 5; seismicity was at relatively low levels. At 2318 H.s.t. (all times given in Hawaii standard time), however, seismic alarms, signifying prolonged high-amplitude volcanic tremor, were activated in homes of HVO staff. The tremor had been first recorded by three seismometers (stations MOK,

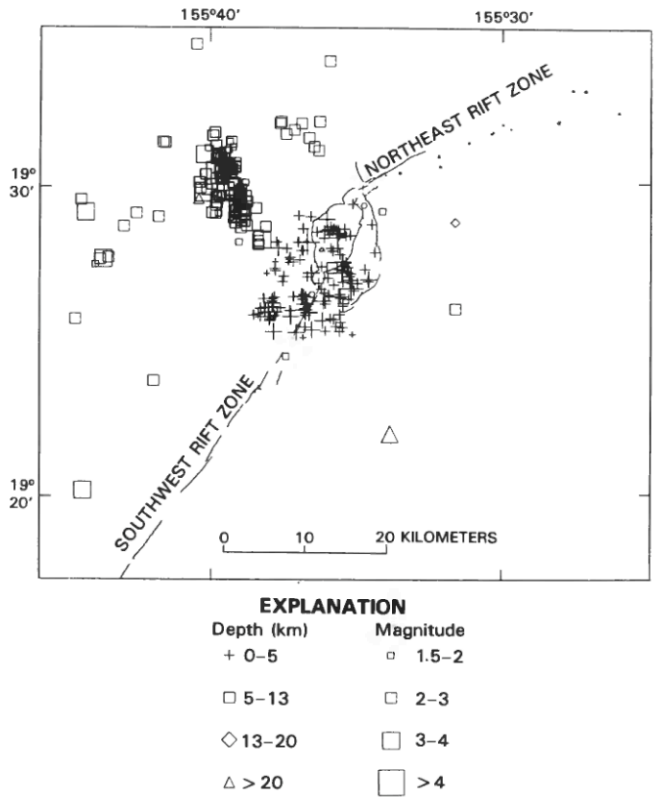

FIGURE 19.3.—Earthquake foci ($M \geq 1.5$) beneath Mauna Loa summit region in 18-month period prior to 1975 eruption (January 1, 1974, to June 30, 1975).

SWR, and WIL, see fig. 19.19) near Mokuaweoweo at 2251. Staff reached HVO at 2330 and saw that harmonic tremor was being recorded on all Mauna Loa and Kilauea seismographs. National Park and civil defense authorities were alerted to the imminent probability of a Mauna Loa eruption, and at 2342 a small glow was noted above the southwest end of Mokuaweoweo. Within one minute the glow extended across the entire summit area, and a fume cloud more than one thousand meters high was illuminated with a bright orange-red glow from the unseen lava fountains on the caldera floor.

A light airplane with two HVO staff members aboard reached the summit area at 0148; a line of fountains 20–50 m high crossed the entire floor of Mokuaweoweo at this time and extended about 1 km down the SWRZ. Lava cascades 90 m high were pouring into the three pit craters on the upper SWRZ (fig. 19.4). Flows were rapidly advancing to the west and southeast from the SWRZ vents. The eruptive fissures extended rapidly northeastward, across North Pit, and into the upper NERZ at 0225. At 0245 lava from the North Pit vents began cascading into another summit pit crater, Lua Poholo (see fig. 19.6). By 0315, the lava fountains on the SWRZ and within Mokuaweoweo were waning, and the lava flows moving to the west and southeast had stagnated. Fountains continued to migrate eastward along the NERZ, but by dawn eruptive activity was largely restricted to echelon vents near the NERZ 3,700-m level (fig. 19.5).

A voluminous aa flow moved about 2 km/h down Mauna Loa's north flank and threatened to cut the paved access road and powerlines to the Mauna Loa Observatory (an atmospheric research station operated by the National Oceanic and Atmospheric Administration, fig. 19.6). At about 0715 fountains feeding this aa flow subsided, and it soon stopped about 100 m from the Observatory road, having traveled 5.2 km. Fountaining continued at greatly diminished levels throughout the day, but ceased by nightfall. Approximately 30×10^6 m^3 of lava had been erupted, and 13.5 km^2 of the Mauna Loa summit area had been covered (fig. 19.6).

The erupted lava includes both aa and pahoehoe. This lava consists of dense pahoehoe within the caldera and mostly highly vesicular, shelly pahoehoe near eruptive vents on the rift zones. The flows are mostly blocky aa more than 500 m from eruptive vents and become more dense toward the distal ends of flows. The rock is nearly aphyric tholeiite (table 19.1), with sparse (<1 percent) olivine phenocrysts to 3 mm diameter. About 90 percent of these flows were subsequently buried by 1984 lava (see fig. 19.33).

A trilateration survey on July 7 showed that individual survey lines across Mokuaweoweo had extended by as much as 760 mm since the previous measurements in 1974, principally reflecting the July 5 intrusion of a dike across the caldera.

THE POSSIBILITY OF RENEWED ACTIVITY

July 7–12 was a period of great public concern, as an outbreak of lava lower along the NERZ seemed possible, in light of both the on-going seismicity and the numerous historical examples of brief summit eruptions followed within a few days by flank outbreaks (for example, April 1942, see Macdonald, 1954). Magma was clearly being intruded into the middle NERZ from July 6–12, as harmonic tremor continued, and several hundred small earthquakes occurred daily within the NERZ. Epicenters of these earthquakes, dozens of which were felt, were concentrated near the 2,900-m level on the NERZ, just southeast of Puu Ulaula (fig. 19.7). A trilateration network near Puu Ulaula was reoccupied on July 8 and showed significant dilation since installation of the network on May 28. On July 9, the network was again reoccupied and indicated continued dilation (as much as 4 cm extension on individual survey lines). Also on July 9, an earthquake of magnitude 4.5 near Puu Ulaula was felt throughout the island. Trilateration measurements at the summit on July 10 showed that the caldera had contracted since July 7 (as much as 5 cm of negative extension on some lines), presumably as magma drained into the NERZ. Harmonic tremor began to diminish in amplitude on July 10, and between July 9 and 12 the geodimeter lines near Puu Ulaula also contracted as much as 5 cm. With this information, the week-long 24-hour alert ended.

The historical record of Mauna Loa activity shows that isolated eruptions similar to that of July 1975 (those not followed within a few days by flank outbreaks) are nearly always followed by more voluminous flank eruptions after a period of 2–3 years (Dutton, 1882, p. 140; Stearns and Macdonald, 1946, p. 82). On

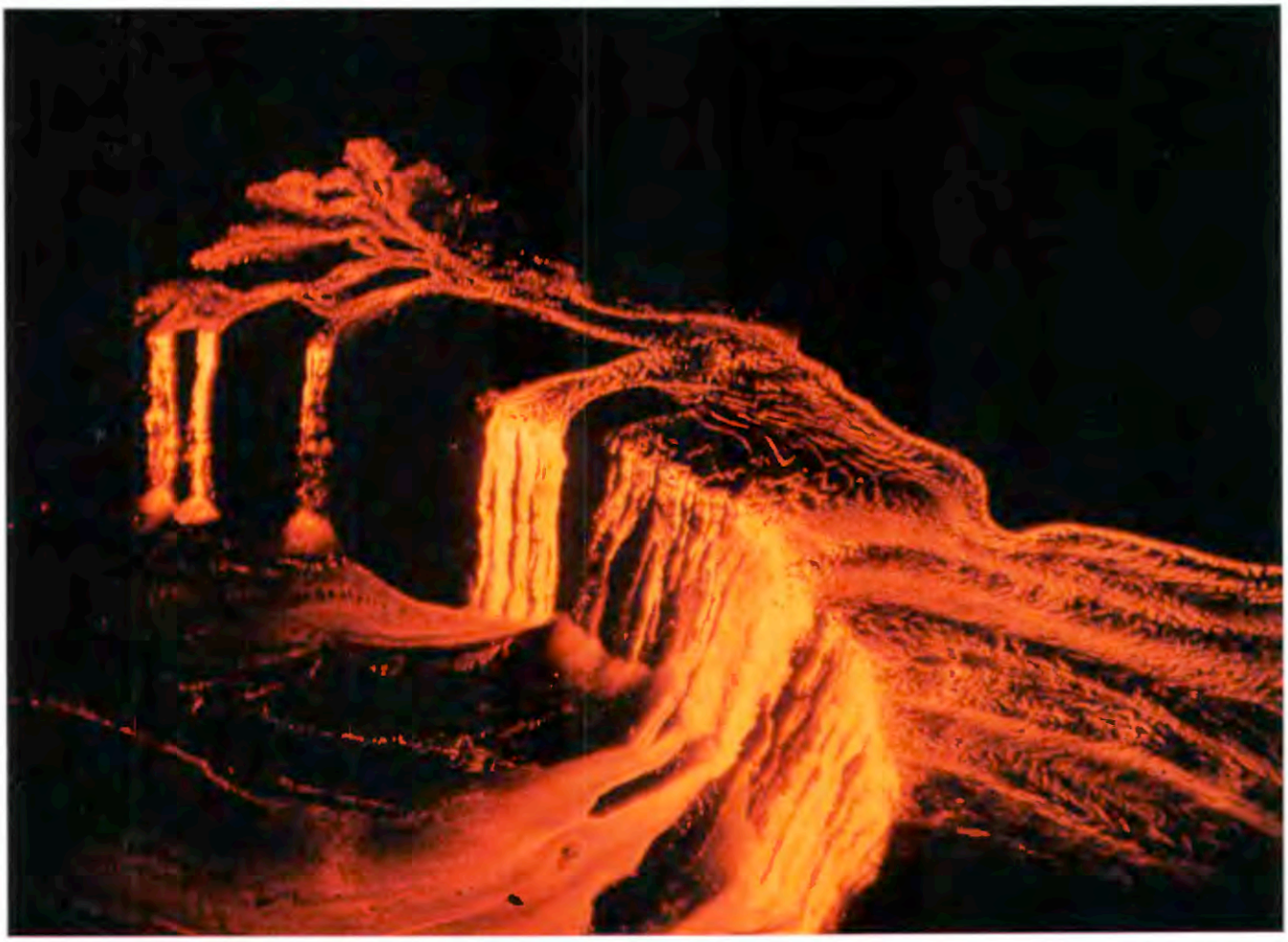

FIGURE 19.4.—Aerial view of lava cascades into Lua Hou, upper southwest rift zone, July 6, 1975, 0240 H.s.t. Cascade height about 90 m. Photograph by R.T. Holcomb.

FIGURE 19.5.—Oblique aerial view, looking west, of echelon eruptive fissures in Pohaku Hanalei area at dawn on July 6, 1975. Photograph by D.W. Peterson.

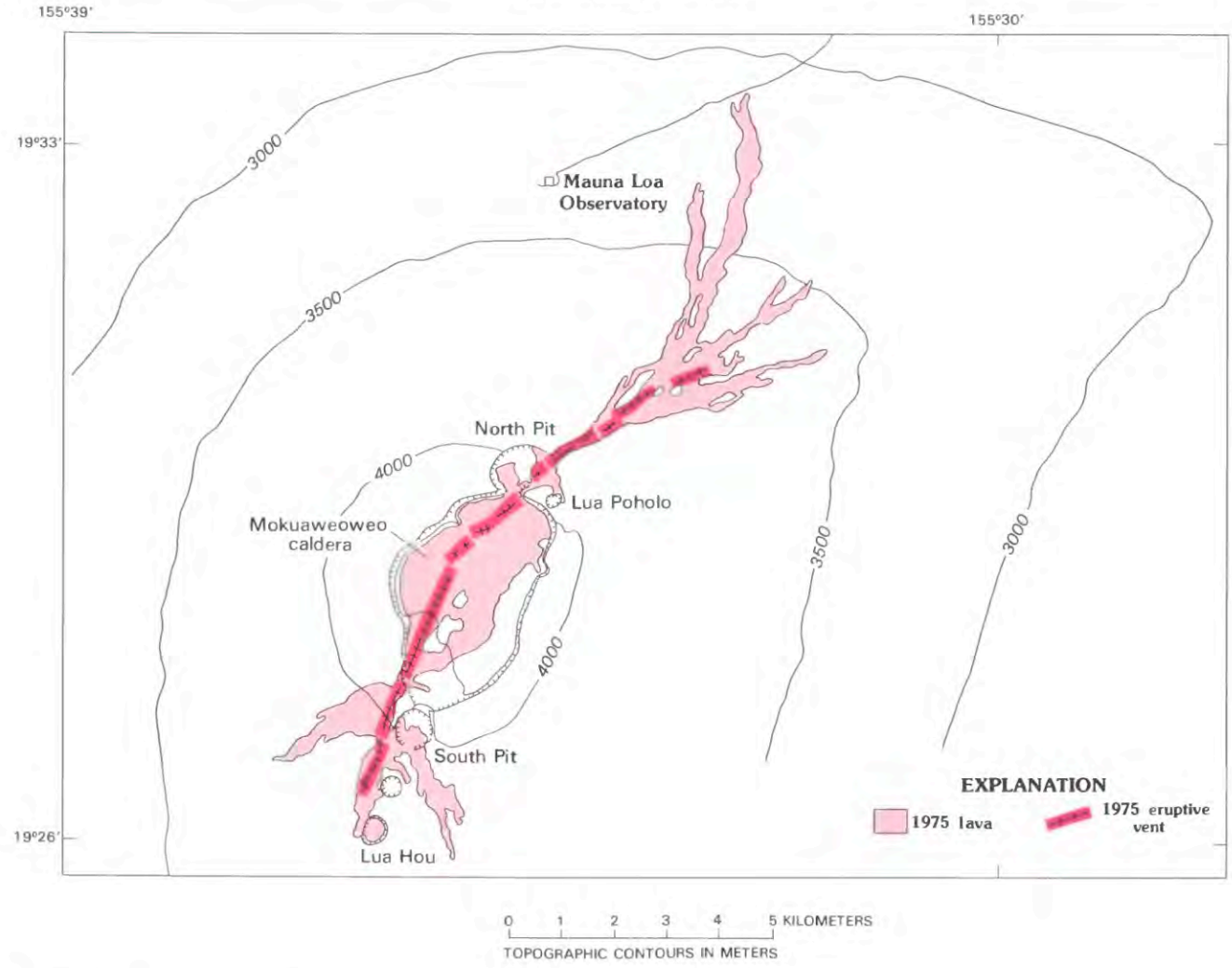

FIGURE 19.6.—Distribution of July 5–6, 1975 lava and geographic features of Mauna Loa summit area. Map by R.T. Holcomb, U.S. Geological Survey, 1975.

TABLE 19.1.—*Major-element compositions of 1975 Mauna Loa lava*

[NERZ, northeast rift zone; SWRZ, southwest rift zone; MOK, Mokuaweoweo. ML775-1 to -27, conventional rock analyses by V.C. Smith; ML-4 to -127, X-ray fluorescence analyses by J.M. Rhodes, reported on volatile-free basis, with total iron reported as Fe_2O_3. —, data not available]

Sample	ML775-1	ML775-17	ML775-21	ML775-22	ML775-23	ML775-24	ML775-26	ML775-27	ML-4	ML-5	ML-76	ML-78	ML-126	ML-127
Location	NERZ	MOK	NERZ	MOK	SWRZ	SWRZ	NERZ	SWRZ	MOK	NERZ	MOK	SWRZ	NERZ	SWRZ
Rock	aa	spatter	spatter	spatter	spatter	pahoehoe	spatter	aa	spatter	spatter	spatter	spatter	aa	spatter
SiO_2	52.04	52.01	52.13	52.31	52.13	52.15	52.11	51.93	51.76	51.64	51.81	51.54	51.87	51.58
TiO_2	2.09	2.07	2.14	2.23	2.19	2.19	2.19	2.19	2.11	2.11	2.10	2.09	2.11	2.10
Al_2O_3	14.26	14.32	14.04	13.96	14.26	14.21	14.22	14.16	13.72	13.76	13.72	13.73	13.72	13.77
Fe_2O_3	2.81	1.49	1.44	1.44	1.34	1.46	1.33	4.95	12.18	12.24	13.30	12.22	12.38	12.34
FeO	8.55	9.64	9.84	9.88	9.76	9.70	9.79	6.57	—	—	—	—	—	—
MnO	.18	.17	.17	.18	.17	.17	.17	.17	.16	.16	.17	.16	.18	.17
MgO	6.65	6.64	6.61	6.40	6.67	6.65	6.65	6.65	6.53	6.61	6.55	6.50	6.50	6.56
CaO	10.60	10.63	10.58	10.46	10.61	10.63	10.60	10.60	10.55	10.53	10.48	10.49	10.53	10.61
Na_2O	2.34	2.34	2.34	2.60	2.38	2.34	2.33	2.40	2.33	2.09	2.11	2.19	2.19	2.29
K_2O	.37	.36	.34	.40	.38	.38	.38	.38	.39	.39	.38	.39	.39	.39
P_2O_5	.23	.23	.23	.25	.23	.23	.22	.22	.26	.24	.23	.22	.24	.23
Cl	.01	0	.01	.01	0	0	.01	.01	—	—	—	—	—	—
F	.03	.03	.03	.03	.03	.03	.03	.03	—	—	—	—	—	—
S	.01	.02	.01	.02	.02	.04	.02	.01	—	—	—	—	—	—
CO_2	.01	0	.01	.01	.01	.01	.01	.01	—	—	—	—	—	—
H_2O^+	.01	0	.02	.01	.04	.04	.07	.05	—	—	—	—	—	—
H_2O^-	.07	.15	.04	.06	.01	0	0	0	—	—	—	—	—	—
Total	100.26	100.10	99.98	100.25	100.23	100.23	100.13	100.33	99.99	99.77	99.85	99.53	100.11	100.04

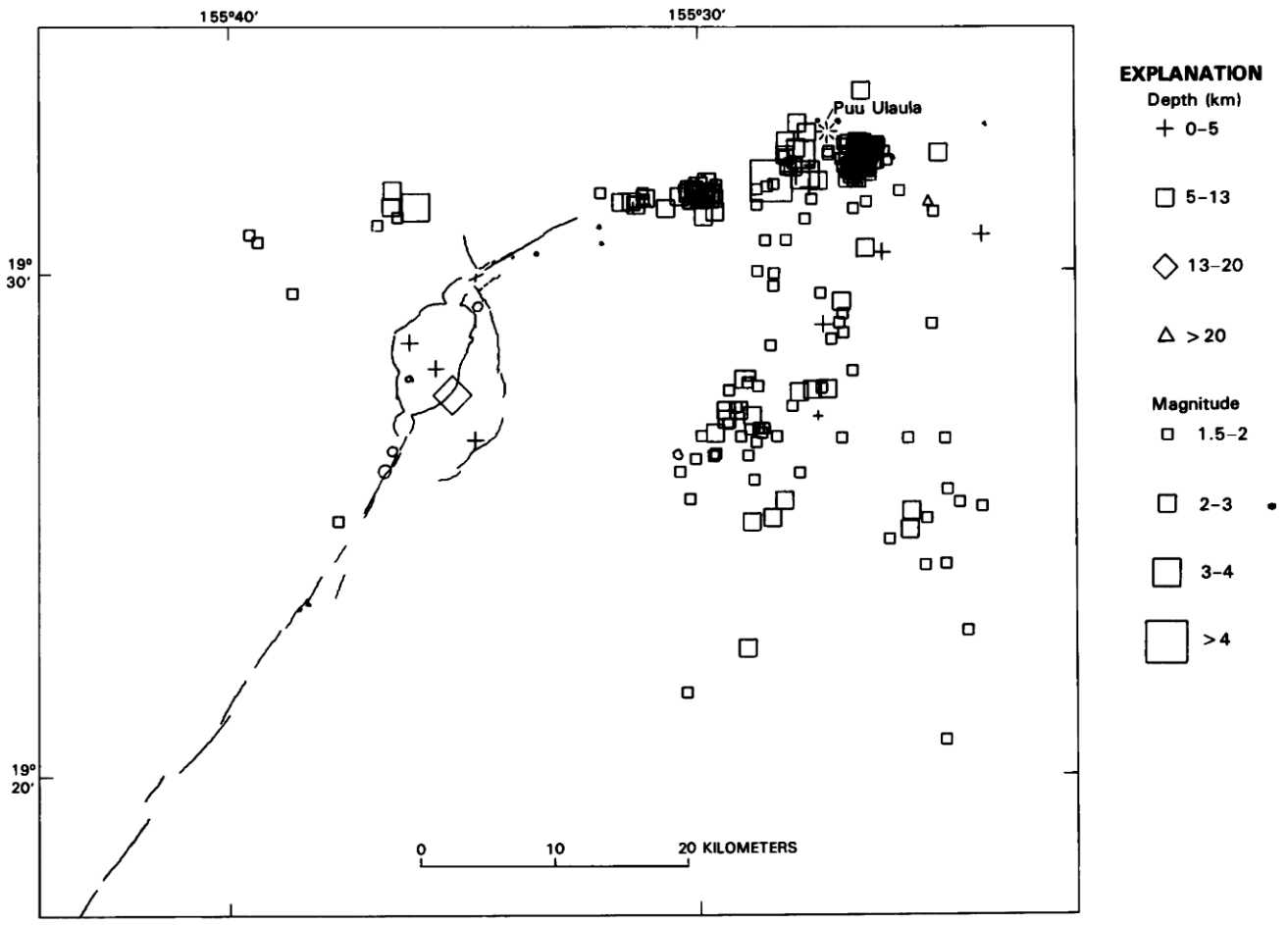

FIGURE 19.7.—Earthquake foci ($M \geq 1.5$) July 1–31, 1975. Earthquakes west of long 155° 34′ W. occurred before eruption, those to east occurred after July 5, mostly during critical period July 6–12.

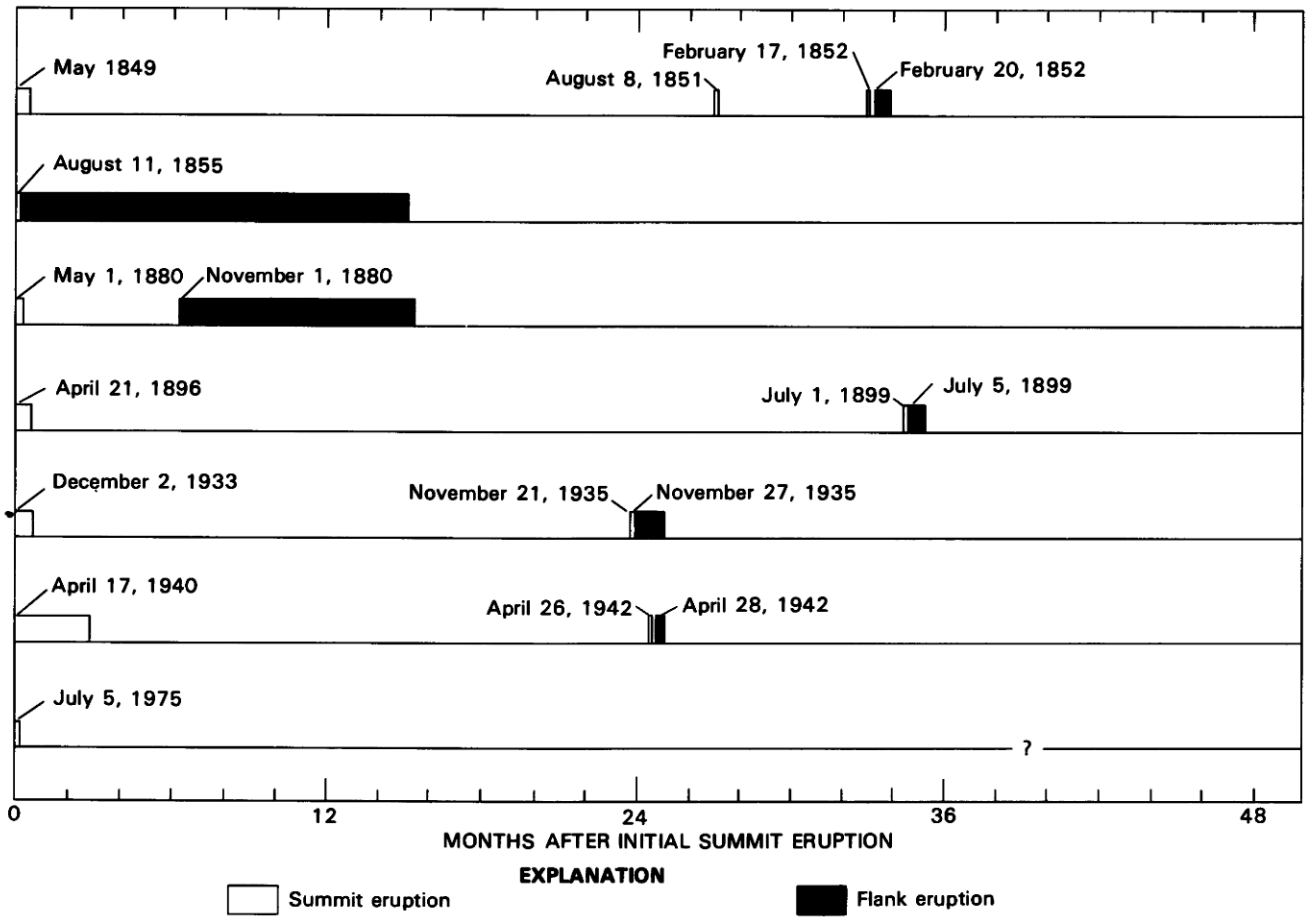

FIGURE 19.8.—Chronology of summit and northeast rift zone flank eruptions, 1849 to 1975 (modified from Lockwood and others, 1976, fig. 4).

the basis of this pattern (fig. 19.8), and the accumulating geophysical information on Mauna Loa's post-eruptive inflation, the 1975 eruption was recognized as the forerunner of future activity (Lockwood and others, 1976, p. 15):

> The historical record thus suggests that the summit eruption of July 1975 was the first phase of an eruptive sequence that will culminate with a major eruption on the flanks of Mauna Loa sometime before the summer of 1978. This flank eruption will likely be closely preceded by brief summit activity. If the Mauna Loa activity of July 6–10 is a reliable indicator, we can expect the flank vents to open between 2,800 and 3,000 m on the northeast rift zone in the vicinity of Puu Ulaula. On the basis of the historical record, we can expect relatively low fountains (50–75 m high) to form a 'curtain of fire' extending 1 to 3 km along the rift zone. The initial rate of lava production will be high, as are slope gradients high on Mauna Loa, so that lava may travel up to 10 km from eruptive vents during the first 24–48 hours. Because the rate of lava production should diminish, because the slopes of Mauna Loa become more gentle at lower elevations, and because lava will be farther from its supply vents, the flow rate will soon slow dramatically.

This scenario proved to be correct in all details, except for the timing, which was in error by almost six years (!).

THE INTERERUPTIVE PERIOD: 1975–1984

During this period the number of earthquakes beneath Mauna Loa's summit gradually increased in frequency. Geodetic monitoring showed that Mauna Loa continued to inflate at an essentially continuous, but irregular rate, reflecting the rise of magma into a shallow reservoir beneath Mokuaweoweo. The seismic and deformation data together allowed definition of the general location and depth of this reservoir (Decker and others, 1983). Civil authorities were kept apprised of Mauna Loa's inflation and the potential threat to the city of Hilo, and contingency plans were prepared for the diversion of lava flows above Hilo should that prove necessary (Lockwood and Torgerson, 1980; U.S. Army, 1980).

SEISMICITY

Over the 22-year period 1962–1984 shallow earthquakes (<5 km deep) were concentrated beneath Mokuaweoweo and the

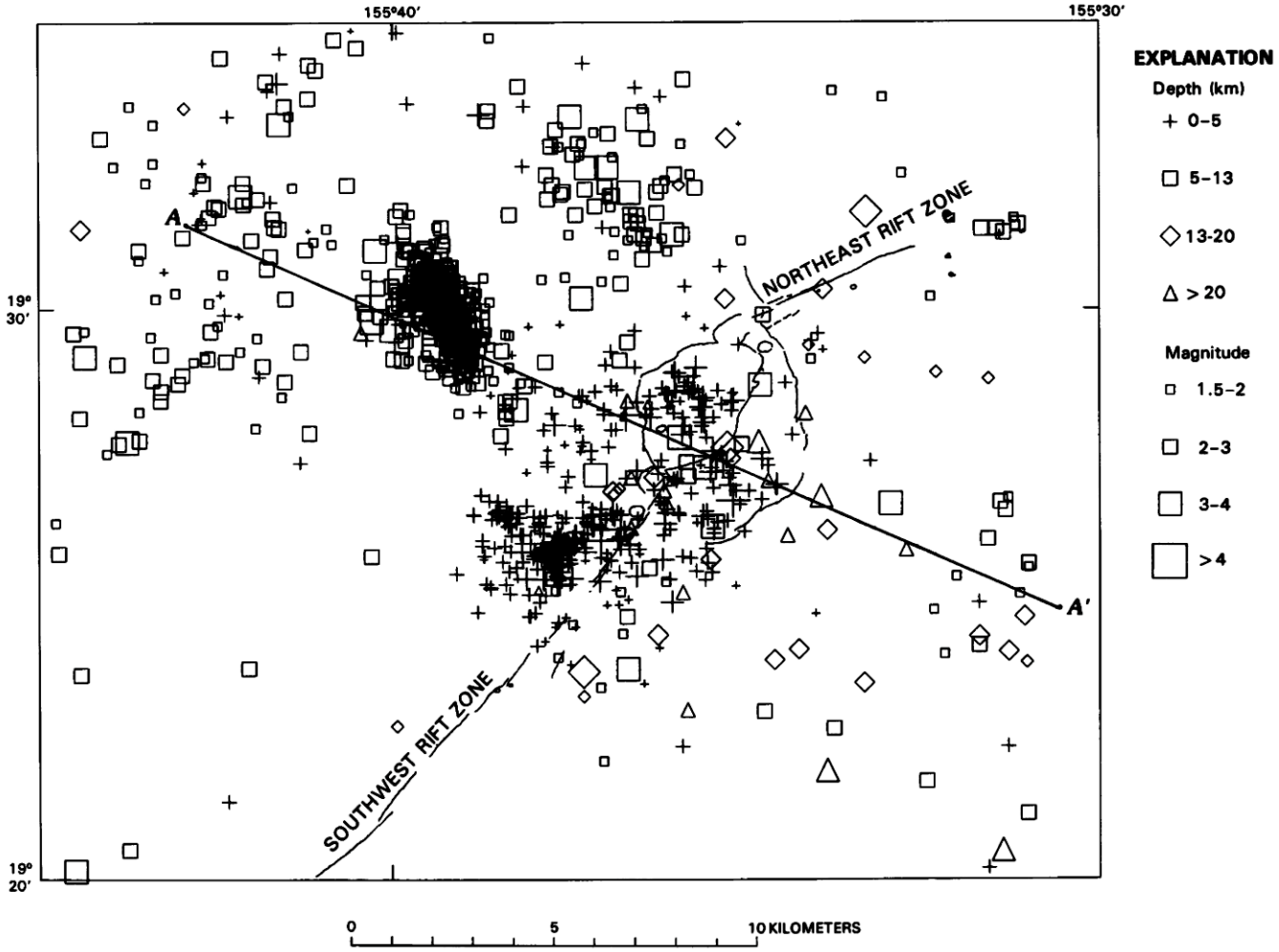

FIGURE 19.9.—Earthquake foci ($M \geq 1.5$) beneath Mauna Loa summit region from January 1, 1962, to December 31, 1984. A–A', line of cross section in figure 19.10. The earthquake foci have been obtained from a network of about 50 seismic stations covering the entire Island of Hawaii. To eliminate any bias from increasing number of earthquakes processed, owing to the increased density of seismometers over this period, only earthquakes of magnitude equal to or larger than 1.5 with horizontal and vertical location uncertainties of less than 2 km are plotted.

upper SWRZ, whereas intermediate depth earthquakes (5–13 km deep) were concentrated beneath the northwest flank (figs. 19.9, 19.10). After the 1975 eruption and the posteruption swarm of intrusion-related earthquakes in the NERZ (fig. 19.7), shallow earthquakes ceased beneath the summit, but 2–3 intermediate-depth earthquakes were noted each year until 1977, when they increased to about 20 per year (fig. 19.11). The number of deeper earthquakes (>13 km) per year was unchanged over the entire intereruptive period. Shallow earthquakes began again in 1977, and their rate generally continued to increase until the 1984 eruption (fig. 19.12).

SEISMIC INTERPRETATION

The shallow earthquakes are believed to occur in brittle rocks capping a magma storage reservoir. The intermediate-depth earthquakes northwest of the summit are of tectonic origin (E. Endo, written commun., 1983) and may be related to stresses built up in response to the wedging effects of shallow dikes emplaced along the summit caldera and rift zones. The deeper earthquakes may be caused by the opening of deep feeder conduits between the mantle magma source and the higher magma storage reservoirs.

DEFORMATION

Following the large dike-related dilation of Mokuaweoweo on July 5, 1975, and the subsequent slight contraction, trilateration lines across the caldera continued to extend (fig. 19.13). Repeated trilateration measurements between the summits of Mauna Loa, Mauna Kea, and Hualalai revealed that the extensions across Mokuaweoweo were mostly accommodated by southeastward translation of Mauna Loa's southeast flank. The northwest flank was only slightly compressed by the Mauna Loa inflation. The summit inflation is also indicated by spirit-level (dry-tilt) measurements (fig. 19.14). Spirit-level measurements were made by precise, repeated

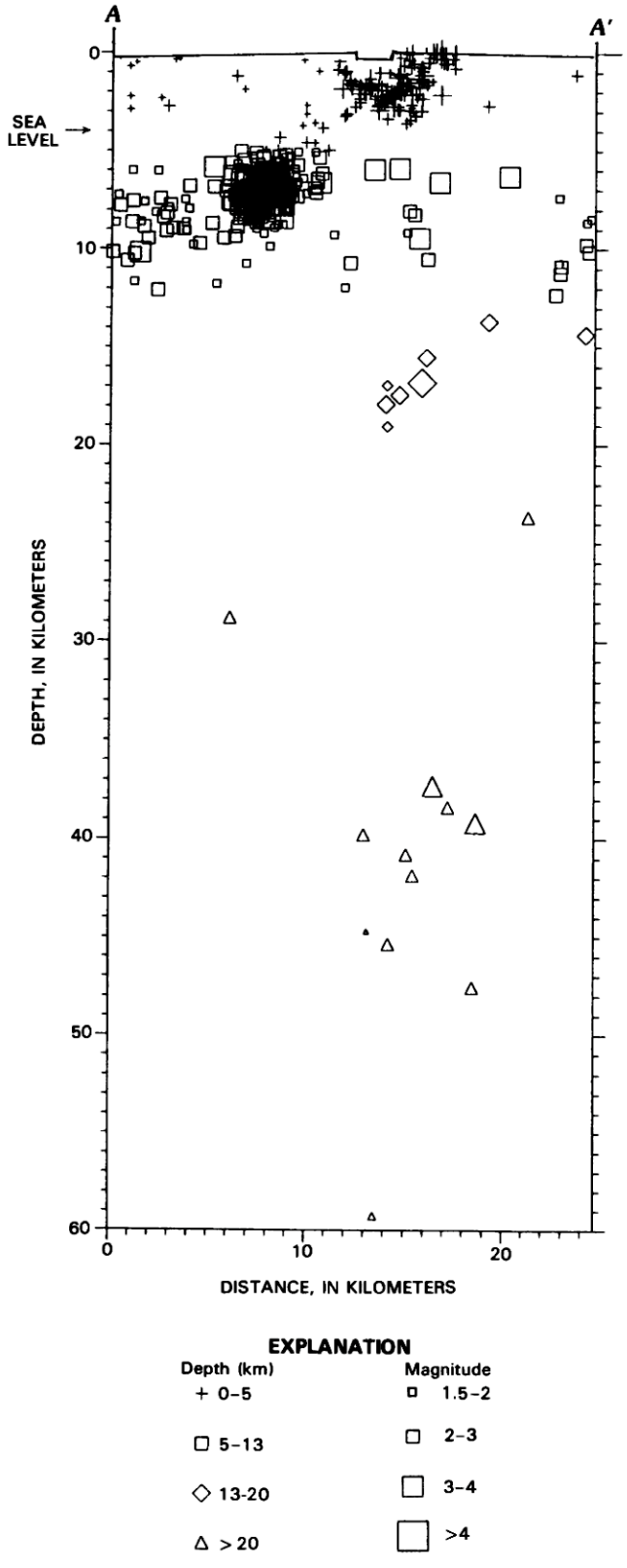

FIGURE 19.10.—Cross section of earthquake hypocenters within 2.5 km of line *A–A'* of fig. 19.9.

optical levels on stadia rods placed at bench marks arranged in a triangle with approximately 30- to 40-m base legs (Yamashita, 1981). Rapid outward tilt rates (inflation) persisted for one year after the 1975 eruption, followed by more moderate, though continuous, inflation after 1976. Level data for the summit region show greatest vertical uplift near the summit. The uplift profile (fig. 19.15) fits the theoretical uplift (Mogi, 1958) calculated for a pressure point source at 3.1 km depth.

DEFORMATION INTERPRETATION

Simultaneous inversion of horizontal, vertical, and tilt data for the period 1977–1981, using the methods of Dvorak and others (1983), further refined the location of the shallow inflation source (table 19.2; see fig. 19.19). In table 19.2 the longitude and latitude of the apex of inflation are x and y, respectively, and z is the depth to the point pressure source beneath the apex of inflation, referred to the elevation of the caldera floor. The volume values show, for each data source, the total volume of swelling, which represents the minimum volume of increased magma storage at depths of 3 to 4 km. The bulk rigidity and compressibility of the system are not known; thus magma-volume changes cannot be estimated. The base values show the amounts of theoretical uplift of the reference bench mark required to make the elastic model best fit the observations. The sigma values show the quality of fit between the least-squares model and the observations.

It is clear from all the deformation measurements that they fit a point-source elastic model reasonably well and that they define a common center of uplift and a surprisingly shallow pressure source. The similarity between the surface-deformation pattern of the summit areas of Mauna Loa and Kilauea Volcanoes is striking. On Kilauea, the pressure source is about 3 km deep (Fiske and Kinoshita, 1969; Swanson and others, 1976), and inflations and deflations of the summit area show similar patterns to those measured on Mauna Loa. Even though the lower zones of the magma chambers beneath Mauna Loa and Kilauea reach to several kilometers depth on the basis of seismic evidence (Koyanagi and others, 1975; Ryan and others, 1981), the changes in surface deformation on both volcanoes indicate that the zone of active magma input and removal is quite shallow, near the upper portion of the aseismic zones underlying both calderas.

The injection of magma into Mauna Loa's shallow storage reservoir over the 1977–1981 period caused an average surface-volume change of about 4×10^6 m^3/yr. This value is only 14 percent of the average historical Mauna Loa effusion rate of 29×10^6 m^3/yr (Lockwood and Lipman, chapter 18), and if characteristic of the entire 1975–1984 inter-eruptive period the cumulative amount intruded would account for only 16 percent of the volume erupted in 1984. For these reasons it is probable that magma was also accumulting at deeper levels within Mauna Loa during the 1975–1984 period. A schematic cross section of one possible model for the shallow magma-reservoir system beneath Mauna Loa shows the top of this shallow reservoir to be at about sea level (fig. 19.16).

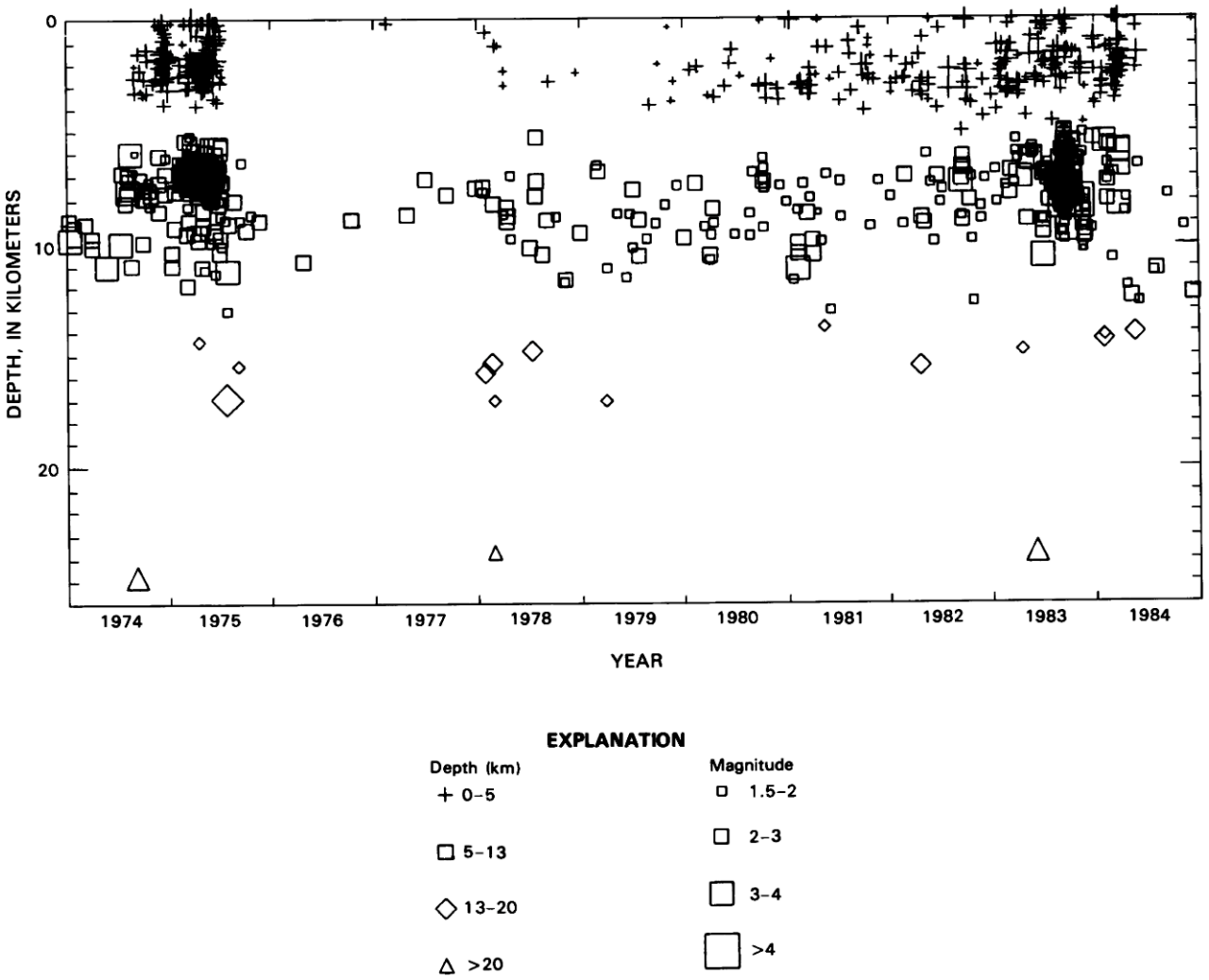

FIGURE 19.11.—Time, magnitude, and depth distribution of Mauna Loa earthquakes for period January 1, 1974, to December 31, 1984. Earthquakes plotted are those with $M>1.5$ located in area shown in fig. 19.9. Absence of earthquakes between 3 and 6 km depth suggests location of Mauna Loa's shallow magma storage reservoir.

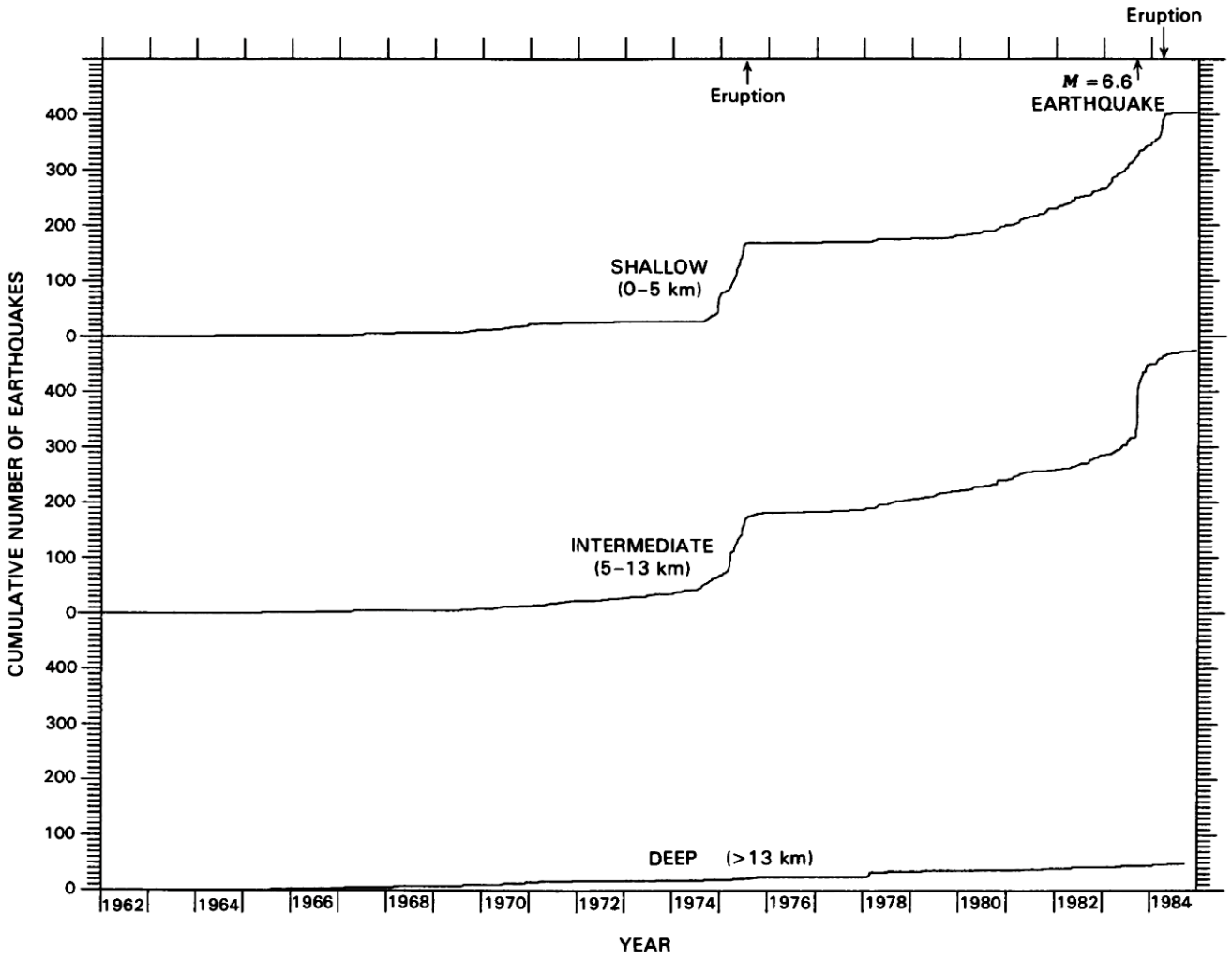

FIGURE 19.12.—Cumulative frequency plot of all earthquakes of magnitude equal to or greater than 1.5 beneath Mauna Loa summit region, from January 1, 1962, to December 31, 1984. Area included shown in figure 19.9. Note increase in intermediate depth earthquakes associated with $M = 6.6$ earthquake of November 16, 1983, and its aftershocks.

Zone A, the part of the magma-reservoir system that most influences summit geodetic changes, is probably a region that inflates slowly between eruptions and deflates rapidly during eruptive activity. Zone B may also be a region of magma storage, but is less active than zone A; it has less impact on surface deformation monitors. Both zones are inferred to be plexi of molten intrusions separated by screens of hot but more solid rock.

High-temperature (to 350 °C) fumaroles were continuously active along the central part of the 1975 eruptive fissures during the entire nine-year inter-eruptive period. These fumaroles produced visible fume (fig. 19.17) in dry as well as in humid weather and commonly produced a dense blue haze on Mauna Loa's upper north flank, especially during morning hours. This fume, mostly of atmospheric composition, contained relatively high concentrations of CO_2, which was frequently detected at the NOAA Mauna Loa Observatory during morning hours of downslope air movement (Miller and Chin, 1978). This fuming ceased immediately after cessation of the 1984 eruptive activity, and the Mauna Loa summit is now clear of visible fume (see Lockwood and Lipman, chapter 18, fig. 18.27).

Kilauea erupted more than six times during the 1975–1984 inter-eruptive period (1977, 1979, 1980, twice in 1982, and multiple episodes in 1983–1984). Mauna Loa exhibited no known sympathetic behavior with any of the Kilauea activity, suggesting the independence of their magma storage systems.

THE 1984 ERUPTION

Based on the post-1975 deformation and seismic data, Decker and others (1983) forecast an "increased probability for an eruption

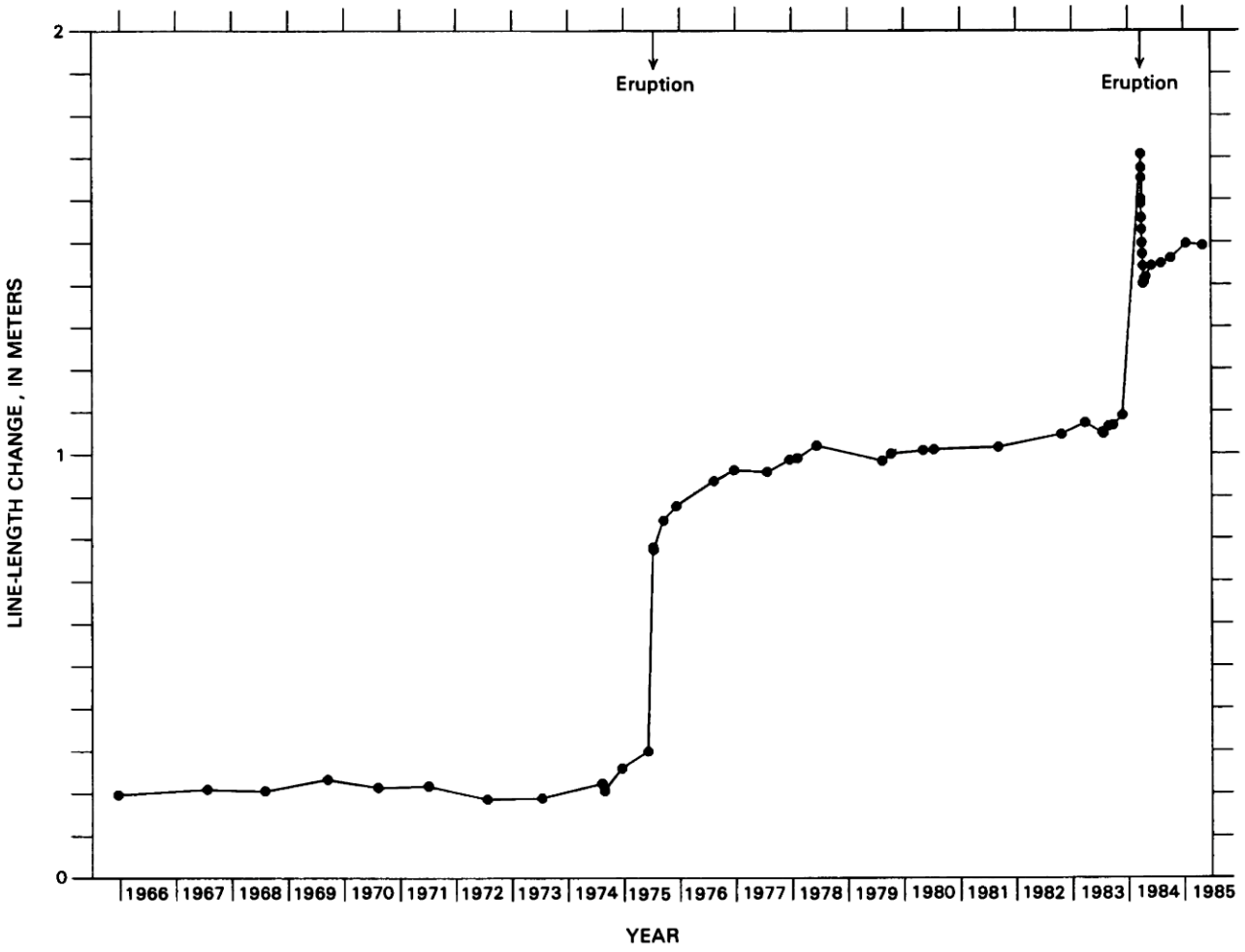

FIGURE 19.13.—Dilation of Mokuaweoweo, December 1965 to May 1985, as measured by trilateration surveys between stations HVO 92 and HVO 93 (station locations shown on fig. 19.19). Abrupt extensions on July 5, 1975, and on March 25, 1984, were associated with dike emplacement during 1975 and 1984 eruptions.

of Mauna Loa during the next two years." The inflation center was determined to underlie the south rim of Mokuaweoweo, and it was suggested that the eruption would follow historical patterns by beginning in the summit area.

PREMONITORY PHENOMENA

PREERUPTION SEISMICITY

Shallow- and intermediate-depth earthquakes increased in frequency beneath Mauna Loa from 1980 to 1983, culminating with a swarm of intermediate-depth earthquakes (5–13 km deep) beneath the northwest flank in mid-September 1983 (fig. 19.18). First-motion analyses suggest that these September earthquakes resulted from increasing lateral stresses generated in the summit and upper SWRZ, possibly as a consequence of intrusion of magma beneath the summit and upper rift zones (E. Endo, written commun., 1983).

At 0613 H.s.t. November 16, 1983, a damaging $M=6.6$ earthquake occurred beneath Mauna Loa's southeast flank (fig. 19.19). The earthquake generated an extensive aftershock sequence 20 km across, with the northern perimeter bordering Mauna Loa's NERZ. Seismicity remained high in the vicinity of Puu Ulaula until merging with eruptive seismicity on March 25, 1984.

The number of larger earthquakes ($M>1.5$) rose persistently as the time of eruption approached (figs. 19.11, 19.12). The daily frequency of smaller earthquakes ($M<1.5$) showed a more episodic increase, peaking one week before the eruption but decreasing to below average on the day before the outbreak (fig. 19.20). The overall distribution of earthquakes in the 16 months before the eruption (fig. 19.18) is remarkably similar to distribution of earthquakes in the 16 month period before the July 5, 1975, eruption (fig. 19.3).

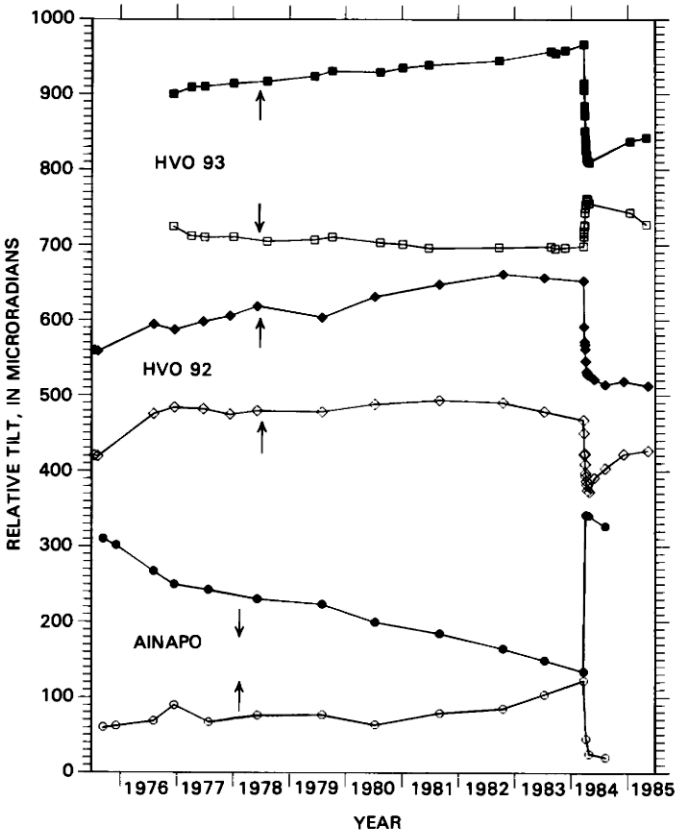

FIGURE 19.14.—Spirit-level tilt changes at three Mauna Loa summit stations, 1975 to 1985 (see fig. 19.19 for station locations). Darkened symbols are north-south component; open symbols are east-west component. Positive tilt changes indicate north or east down. Arrows show inflation direction for individual tilt components. Summit inflation is recorded at all stations prior to and after March 25 to April 15, 1984 eruption.

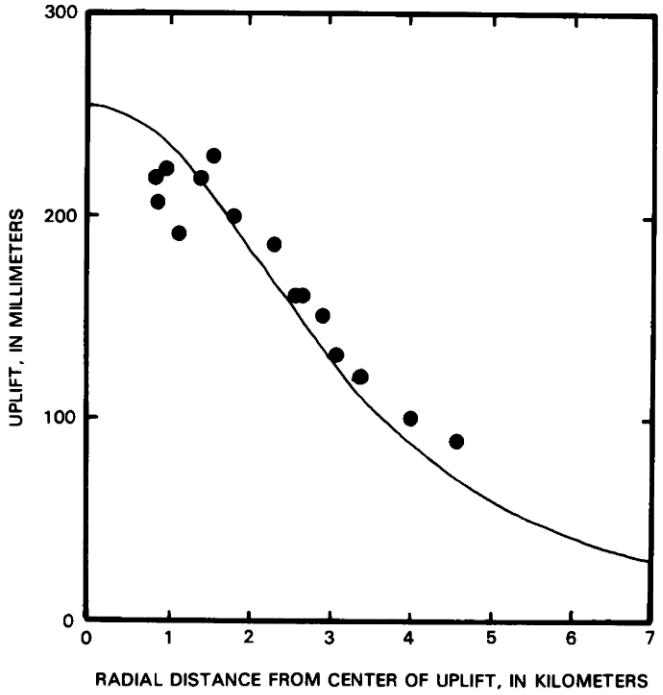

FIGURE 19.15.—Comparison of observed elevation changes in summit area (from 1977 to 1981 leveling surveys) with best-fit elastic deformation model (solid curve); see figure 19.19 for level station locations and calculated uplift center (from Decker and others, 1983, fig. 10).

TABLE 19.2.—*Mauna Loa geodetic data, 1977–1981*

[From Decker and others, 1983]

Data	x		y		z	Volume	Base	σ	σ EDM		σ Tilt
	Longitude (West)	(km)	Latitude (North)	(km)	(km)	(10^6 m^3)	(mm)	Level (mm)	mm	μ strain	(μrad)
Leveling	155°34.5′	±0.2	19°27.5′	±0.2	3.1±0.5	17±3	59±24	4	--	--	--
Tilt	155°35.2′	±0.6	19°27.5′	±0.6	2.6±1.2	8±5	--	--	--	--	27
EDM	155°35.1′	±0.7	19°27.2′	±0.4	3.2±1.2	19±8	--	--	37	25	--
All	155°35.0′	±0.4	19°27.3′	±0.3	3.9±0.8	22±6	88±50	16	40	26	30

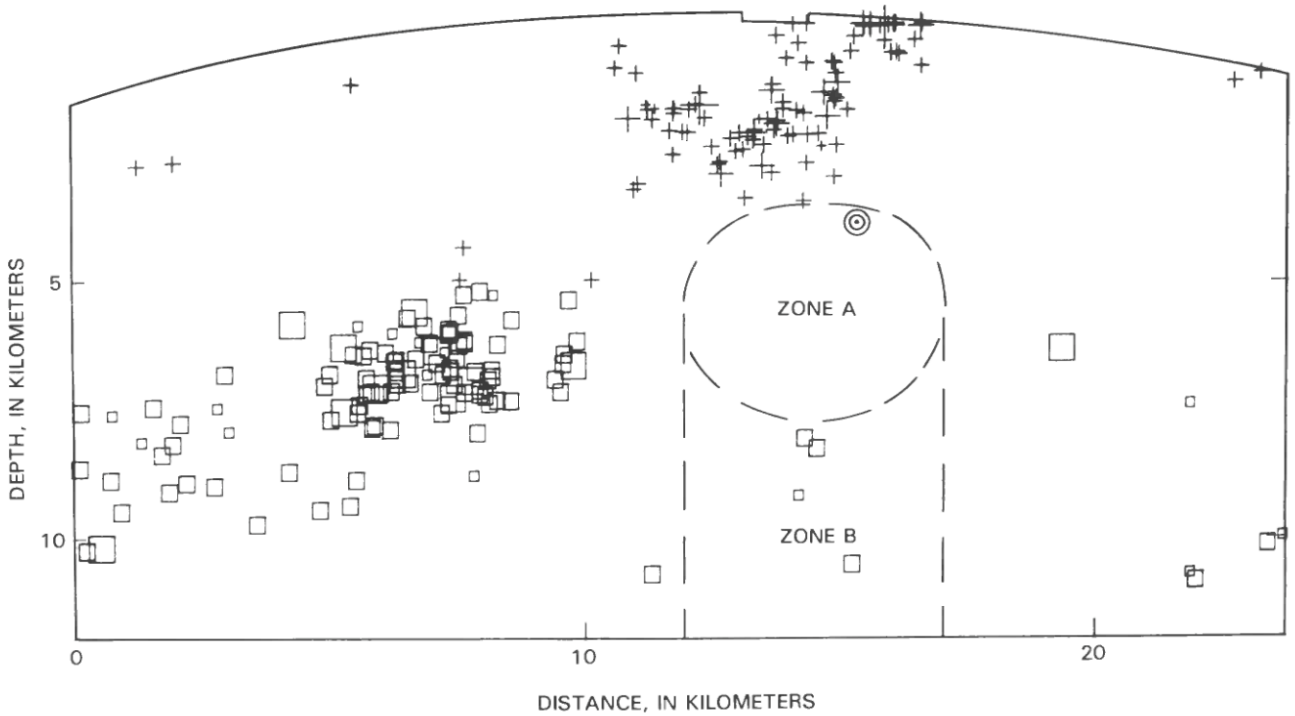

FIGURE 19.16.—Approximately true-scale schematic cross section of proposed magma reservoir system beneath Mokuaweoweo defined by an aseismic zone. Cross section and earthquake hypocenters same as in upper 12 km of figure 19.10, except earthquakes after May 1983 omitted. Double circle in zone A shows point-source inflation center calculated with 1977–81 deformation data (from Decker and others, 1983, fig. 14).

FIGURE 19.17.—Fumaroles along 1975 eruptive fissures in Mokuaweoweo caldera, view to north-northeast. 1940 cone in lower left, Mauna Kea in background. Photograph taken December 1977 by J.P. Lockwood.

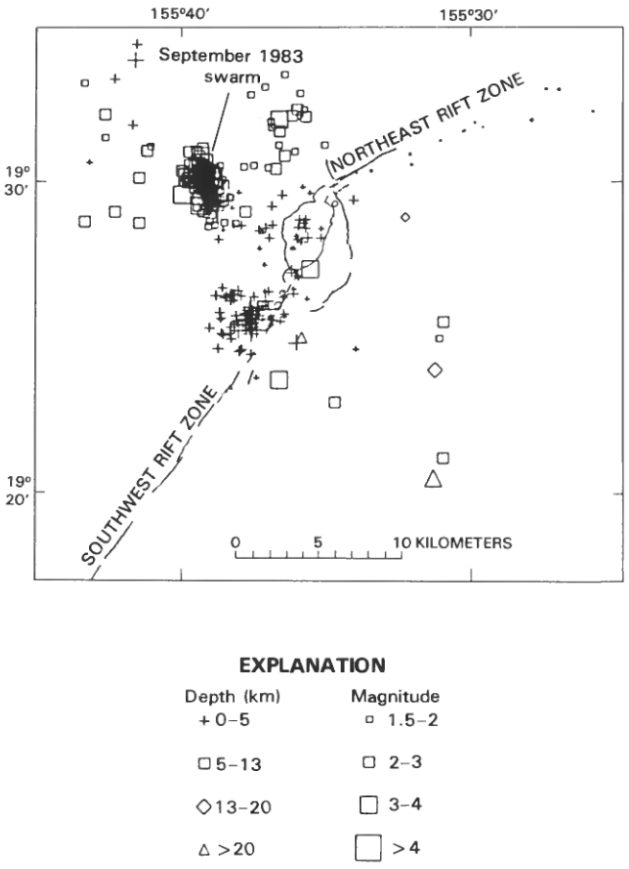

FIGURE 19.18.—Earthquake locations in summit region for 16-month period before 1984 eruption (September 24, 1982, to March 24, 1984). Compare with figure 19.3.

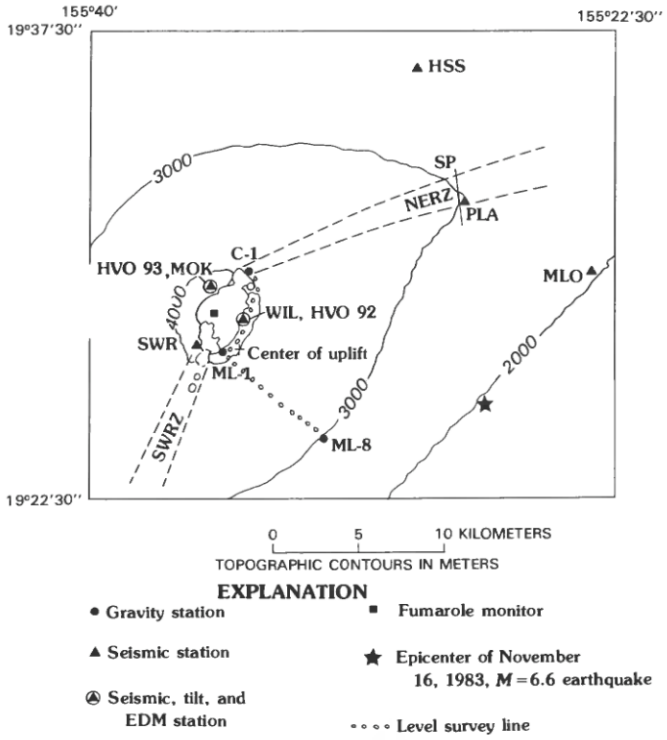

FIGURE 19.19.—Mauna Loa summit area, showing location of stations and features. NERZ, northeast rift zone; SWRZ, southwest rift zone; SP, electrical self-potential survey line.

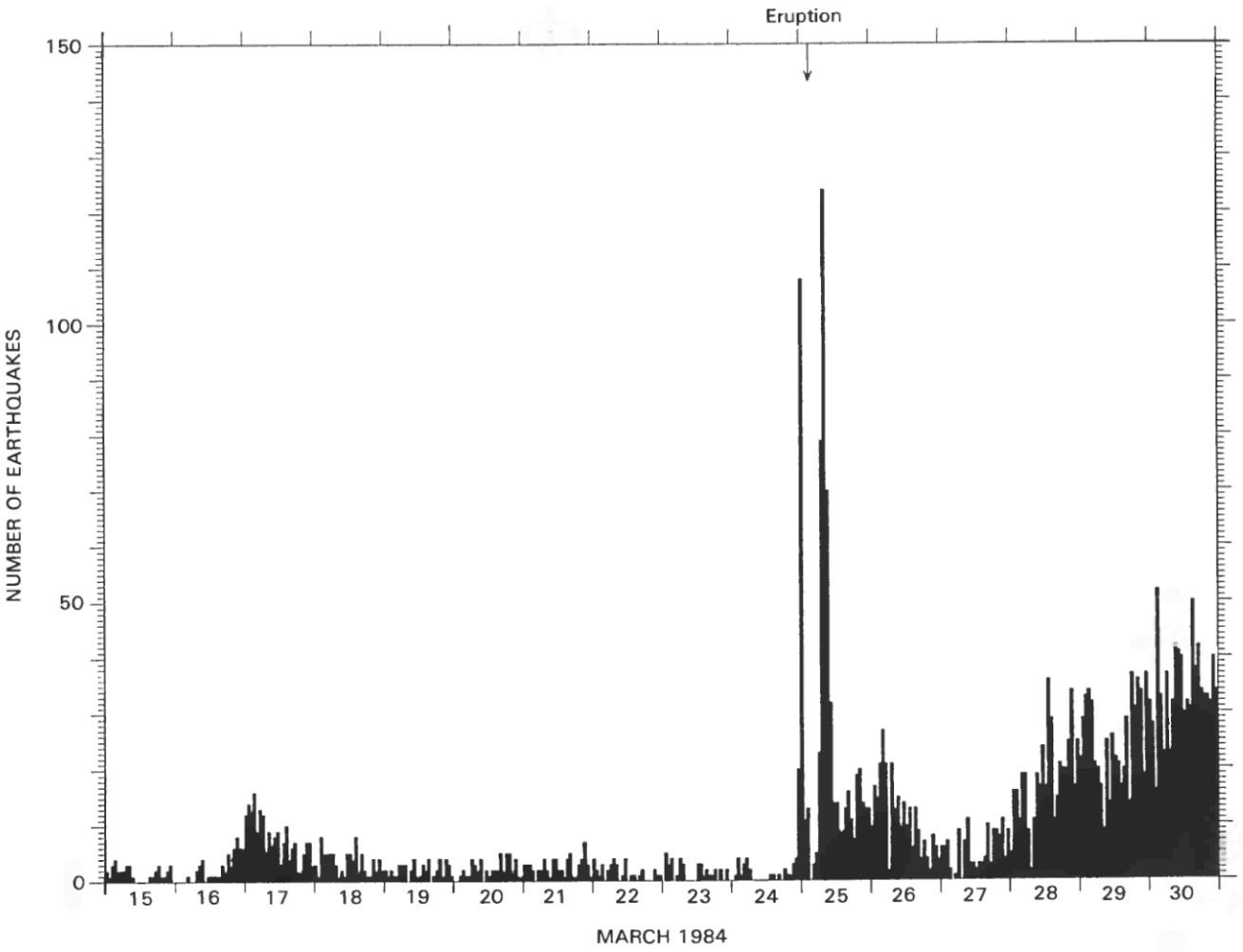

FIGURE 19.20.—Hourly counts of Mauna Loa short-period summit earthquakes for period March 15–30, 1984. Increase in earthquake frequency after March 27 accompanied deflation of Mauna Loa summit. Low counts on the morning of March 25 reflect period of masking by background of high-amplitude tremor.

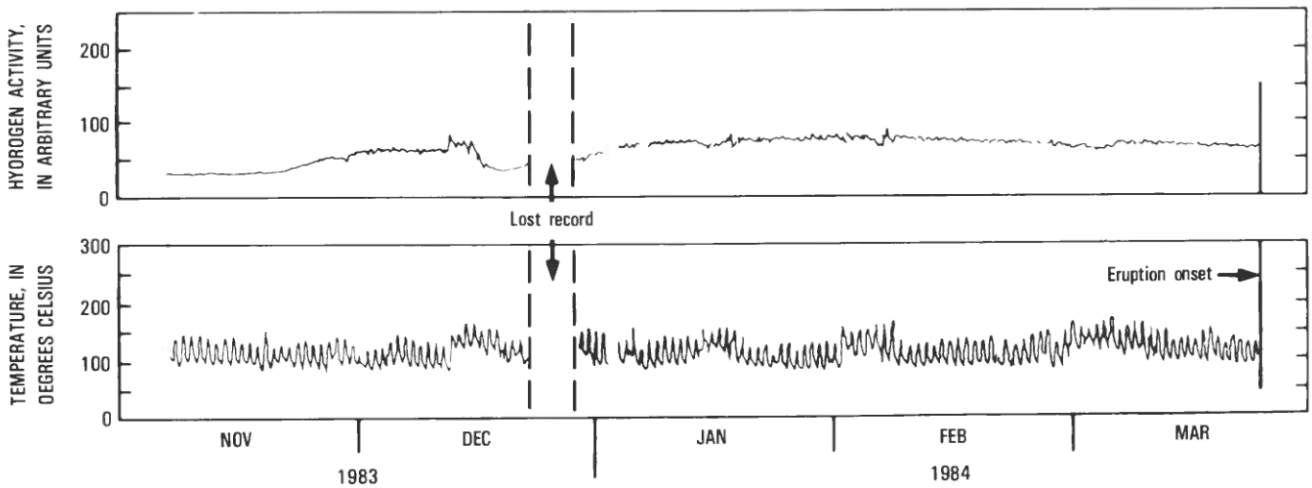

FIGURE 19.21.—Variation of temperature (t) and hydrogen (H_2) activity in a fumarole on 1975 eruptive fissure, Mokuaweoweo caldera, between November 5, 1983, and March 24, 1984. Temperature values are not field calibrated. Large diurnal temperature variations may be caused by artificial instrumental amplification. Hydrogen activity is referenced to a nonquantitative instrumental standard. Data from M. Sato and K. McGee, U.S. Geological Survey (from Lockwood and others, 1985, fig. 3).

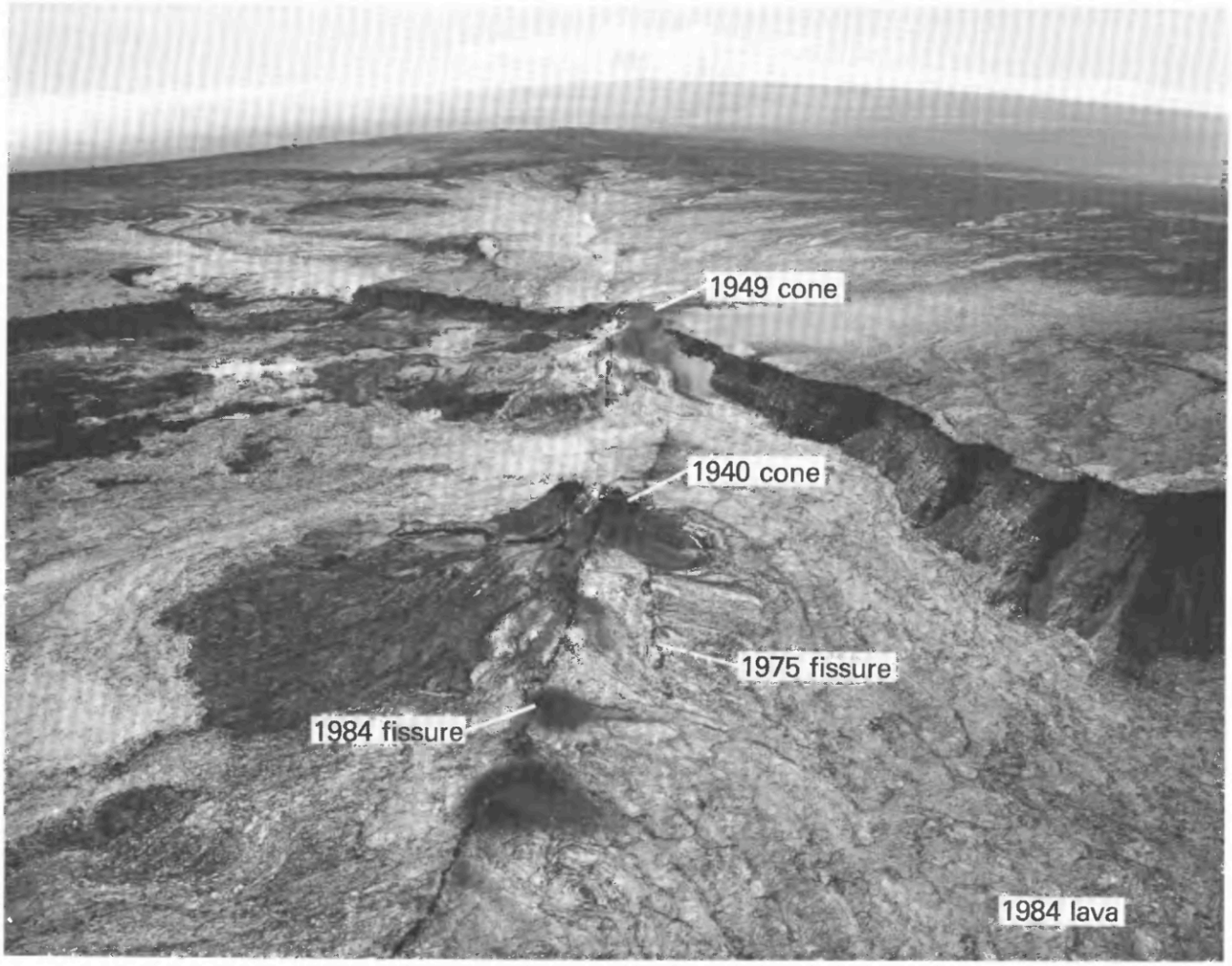

FIGURE 19.22.—Oblique aerial view, looking southwest, of 1984 eruptive fissure at southwest edge of Mokuaweoweo. Fissure extends across Mokuaweoweo, across 1940 and 1949 cones, and down the southwest rift zone. Reflective pahoehoe flows on caldera floor and down upper southwest rift were all erupted on March 25. Note 1975 eruptive fissure at northwest base of 1940 cone. Photograph by F.R. Warshauer.

PRE-ERUPTION DEFORMATION

Trilateration and tilt surveys showed that the inflation continued at a steady, but nonincreasing rate almost to the 1984 outbreak and gave no cause for alarm (figs. 19.13, 19.14).

FUMAROLE MONITORING

A remote station for monitoring H_2 activity and temperature was installed in a fumarole situated along a 1975 eruptive fissure in Mokuaweoweo on November 5, 1983 (Lockwood and others,' 1985). The first rise in temperature above the diurnal fluctuations was observed in the afternoon of November 18, 1983 (fig. 19.21).

A brief, small increase in H_2, as measured by activity of an H_2-O_2 fuel cell, was recorded concurrently with this temperature increase. The H_2 level had been stable before then, but gradually began to rise on November 21. Could these November changes have been related to the $M=6.6$ earthquake of November 16? Both temperature and H_2 increased on December 13, and on December 14 an anomalous steam cloud was seen rising to about 1 km above Mokuaweoweo. The fumaroles were visited on December 17, but temperatures and fuming were normal.

The H_2 level gradually increased again through late December and early January. Three thermal events lasted for 4 to 9 days in mid-January, early February, and early March. The H_2 levels showed concurrent changes, but the correlations were negative in 1984, contrary to the positive correlations observed in 1983. The reversal may indicate a change in the nature of emitted gases from reducing (H_2-rich) to more oxidized (H_2O, O_2-rich). The last data

FIGURE 19.23.—Echelon eruptive fissures in Pohaku Hanalei area, northeast rift zone at dawn on March 25, 1984. Compare with 1975 vent locations (fig. 19.5). View to west. Photograph by J.D. Griggs.

transmission (1 h before the sensors were destroyed at the eruption onset) showed normal background levels with no portent of the imminent events.

VISUAL OBSERVATIONS

On March 18, 1984, dull red glow was spotted along a crack (1975 fissures?) on the Mokuaweoweo floor by a hiker, but his report did not reach HVO until after the eruption began. On March 23, several observers spotted "steam clouds" rising above Mokuaweoweo. On March 24, the day before the eruption, M.M. Godchaux of Mount Holyoke College reportedly saw rocks and steam being ejected from the 1975 fissures, near the center of Mokuaweoweo, but there was no means to alert HVO.

ERUPTION NARRATIVE

Seismic stations MOK, WIL, and SWR along the rim of Mokuaweoweo (fig. 19.19) began to record an increase of shallow earthquakes at 2255 H.s.t., March 24 (fig. 19.20). Earthquakes less than $M = 0.1$ were recorded at a rate of 2–3 per minute after this time. At 2330 an increase in seismic background marked the onset of harmonic tremor. The onset of tremor, which presumably recorded the beginning of magma ascent to the surface, coincided with a fortnightly earth tidal minimum. A correlation between eruptive activity and fortnightly tidal minima was also noted at a 19th century eruption of a volcano in El Salvador (Golombek and Carr, 1978), but this is not a general characteristic of Mauna Loa eruptions (Dzurisin, 1980). The earthquake swarm and tremor strengthened rapidly just before 0100, March 25. At 0056 it became impossible to stabilize astronomical telescopes on the summit of Mauna Kea, 42 km to the northwest, owing to ground oscillations, and observations were impossible for the next 2 hours.

An infrared sensor in a military satellite recorded a "strong signal" from Mauna Loa at 0125:16 on March 25; this signal indicated the first surface outbreak of the eruption. At 0130 observers at the Mauna Kea summit and at Puu Ulaula spotted a red glow reflected off fume clouds above the southwest part of Mokuaweoweo (at about 4,015 m elevation). Eruptive fissures migrated rapidly down the upper SWRZ to 3,890 m, across the 1940 cone, and to the northeast across Mokuaweoweo, a few meters southeast of the 1975 fissures (fig. 19.22). At 0357 fountains extended into the upper NERZ and migrated in a series of south-stepping echelon fissures eastward (fig. 19.23), south of the 1975 fissures (compare with fig. 19.5). At about this time the fountains died out on the SWRZ and began to wane within Mokuaweoweo. By 0700 the fountaining was restricted to a zone on the NERZ between 3,700 and 3,780 m. At 0910, however, new fountains appeared 7 km farther east, at 3,410 m. The fissure feeding this new outbreak migrated rapidly uprift and downrift, and by 0930 a 2-km-long "curtain of fire" was active between 3,400 and 3,470 m elevation. Fountains were 10–50 m high along this fissure, and lava output was estimated at $1–2 \times 10^6$ m^3/h. A narrow flow moved about 5 km down the southeast flank from these vents, southwest of the 1880 flow. At 1030, profuse steaming was noted along a 1-km-long fracture system between 3,260 and 3,170 m, but there was no further downrift migration of fountains for several hours, and lava production again waned.

At 1641 a new eruptive fissure opened below Puu Ulaula at about 2,850 m elevation, 19 km east of the original outbreak point within Mokuaweoweo. These vents opened south and slightly uprift from the principal vent of the previous NERZ eruption, that of 1942 (fig. 19.24). The dike feeding these vents had migrated down the NERZ at an average rate of 1,200 m/h (fig. 19.25). The new eruptive fissure migrated rapidly both uprift and downrift, and by 1830 a 1,700-m-long "curtain of fire" was active between 2,770 and 2,930 m elevation. All fountains farther uprift quickly waned, and for the next three weeks eruptive activity was confined to these lower vents, hereafter called the 2,900 m vents. Six principal structures eventually formed around localized vents along this fissure, including a cinder cone at the uprift end and a lava shield at the downrift end (fig. 19.26). Lava fountains were low and never exceeded 50 m in height. By daybreak on March 26, a fast-moving flow from the 2,900 m vents had traveled 9 km to the northeast, and three shorter flows moved eastward. These latter flows directly threatened two penal facilities at 1,600 m elevation—the abandoned Mauna Loa Boy's School and the Kulani Honor Camp (figs. 19.27, 19.28). Inmates were prepared for evacuation on March 26 but the flows ceased forward movement within 48 hours and never crossed the Powerline Road above these facilities (fig. 19.28). On March 28 a 100-m-long east-west steaming fissure was noted on the north side of a prehistoric spatter cone at 2,435 m elevation, 4 km east of the lowest eruptive vents. A dike may have been intruded below this area, but if so it never broke the surface. The principal flow (flow 1 on fig. 19.28) advanced as a narrow, well-channelized

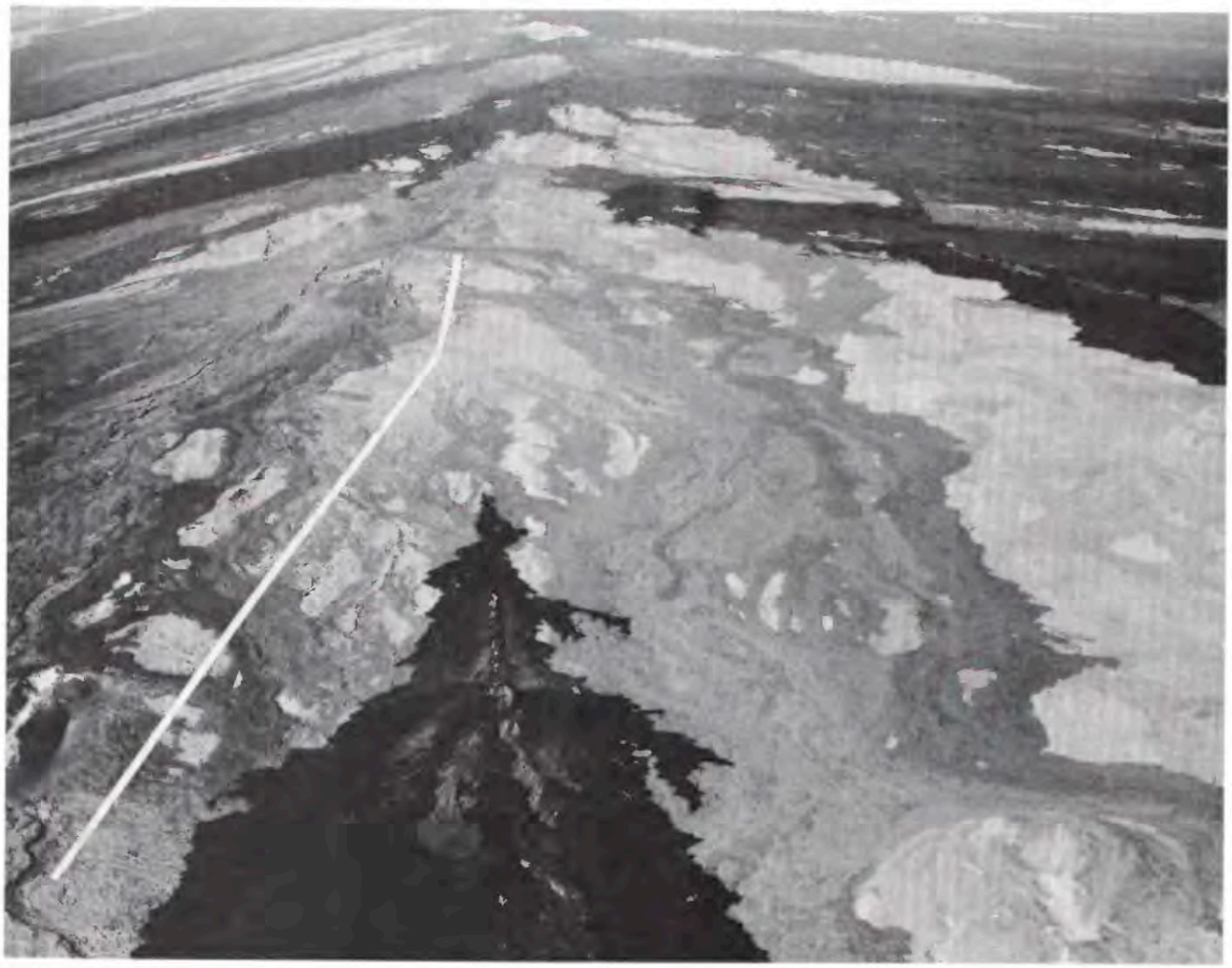

A

FIGURE 19.24.—Oblique views of middle northeast rift in area of 2,900-m vents. ***A***, Area before eruptive activity; photograph taken on September 6, 1978. ***B***, Area after March 25, 1984 eruption; photograph taken on May 5, 1984. Location where 1984 eruptive fissure later opened shown by white line in *A*. Note 1984 lava shield (arrow) at left margin of *B*. Photographs by J.P. Lockwood.

aa flow on top of and between the flows of 1852 and 1942. Although flow-advance rates slowed as the lava moved farther from the 2,900 m vents, the flow had traveled 25 km by March 29, reaching the 915 m elevation and causing concern in the city of Hilo, whose nearest buildings were then 6 km away. Several square kilometers of native rainforest were destroyed, and the copious smoke from burning vegetation (fig. 19.29), as well as large explosions from accumulations of methane gas near flow margins, accentuated the apprehension of Hilo residents.

On the morning of March 29, however, a channel levee on flow 1 collapsed at the 1,740 m elevation, 13 km upstream from the flow front. Here lava was diverted to form a second flow parallel to the first, and most of the supply to the initial lava flow was cut off. The new flow (flow 1A on fig. 19.28) also moved rapidly downslope, but did not overtake flow 1 until April 4. Another channel collapse and diversion occurred on April 5 at 2,070 m elevation, cut off the supply to flow 1A, and started a new branch (flow 1B). Lava production at the 2,900 m vents had begun to decrease in late March (Lipman and Banks, chapter 57, table 57.3) and rates of flow within the feeder channels clearly decreased (fig. 19.30). Lava in the channels became steadily more viscous (see section "Lava Petrography and Temperatures"), and channel blockages and levee

B

FIGURE 19.24.—Continued.

collapses occurred more and more frequently. These collapses restricted lava supply to the lower flow fronts, and the elevation of the lowest active flows moved steadily upslope (fig. 19.31), easing the threat to Hilo. By April 14 no active lava flows extended more than 2 km below the 2,900 m vents; the eruption ended on April 15.

On April 2 the north margin of flow 1A abutted against a 40-m-long segment of a lava diversion test barrier constructed at the 1,150 m elevation in 1977. The 4- to 5-m-high barrier impeded advance of this 10- to 12-m-thick portion of flow 1A for 6 days, but was finally overtopped by a short aa tongue on April 8, as the flow, now cut off from fresh lava supply, continued to creep forward because of gravitational downslope movement of its molten core (fig. 19.32).

The 1984 lava covered an area of about 48 km^2 (figs. 19.28, 19.33), and about 220×10^6 m^3 of lava was erupted. About 90 percent of the total volume was erupted from the 2,900 m vents. Flow thicknesses ranged from less than 1 m near short-lived vents to as much as 18 m at the distal ends of major aa flows.

As the flows cooled, a thin sublimate coating of *thenardite* (Na_2SO_4), as identified by T.E.C. Keith (written commun., 1984), formed on protected surfaces, and in late April many flows at higher, dry areas looked as if they had been dusted by a light snow.

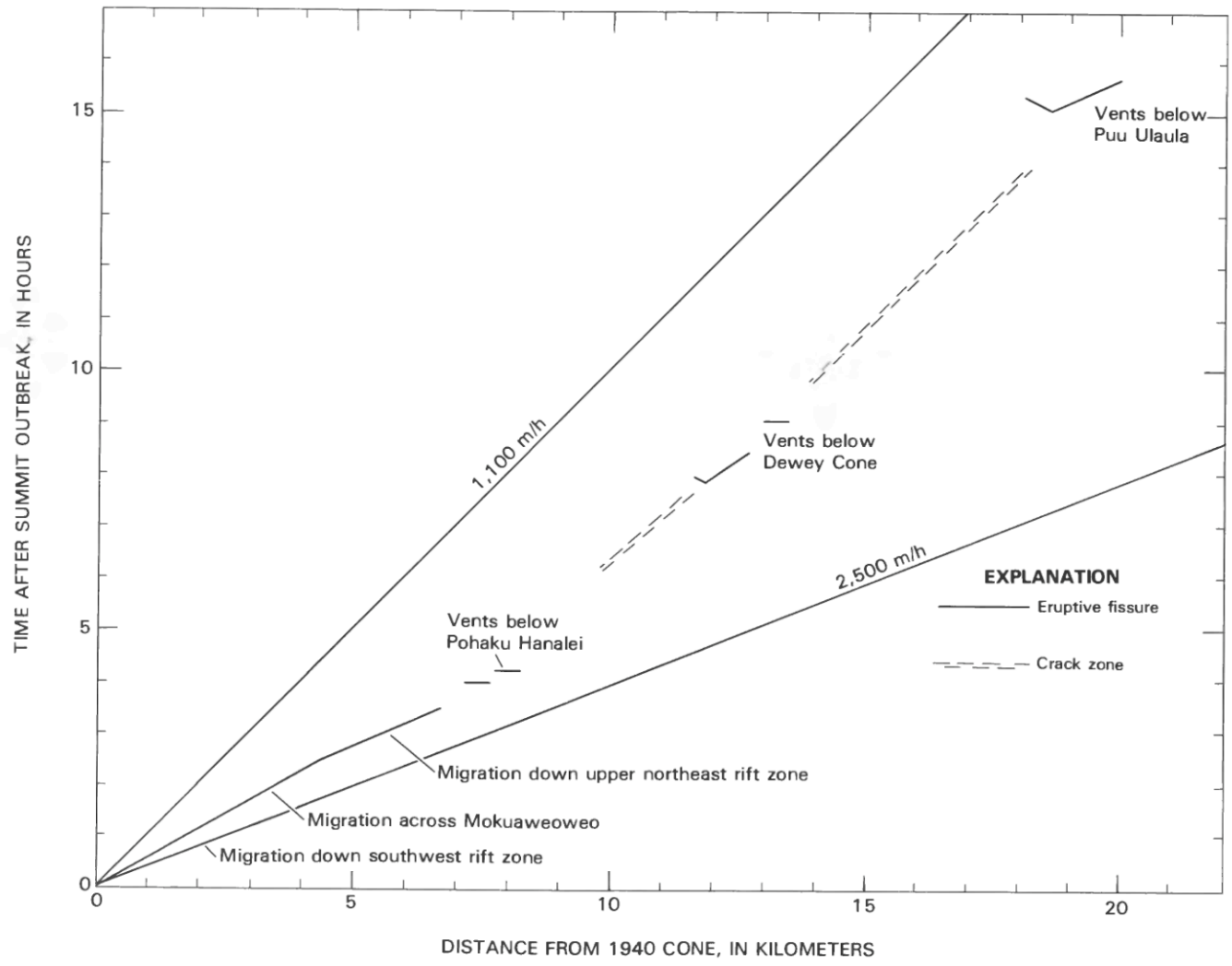

FIGURE 19.25.—Eruptive fissure (dike propagation) rates on March 25, 1984. Upside-down chevron fissure plots indicate propagation both uprift and downrift after initial surface rupture.

The thenardite was as thick as 5 mm as a mat of very fine, acicular crystals and formed after the rocks cooled below incandescence, but while still at over 100 °C. The mineral was especially common on low density (more permeable ?) aa blocks. This mineral is fragile, and water soluble, and was easily blown away by high winds; it was not seen after light rains in early May. This occurrence has apparently not been previously reported on Hawaiian lavas, although it is likely a common, but ephemeral mineral on cooling aa flows. It has also been reported as a high-temperature sublimate on the growing andesite dome of Mount St. Helens volcano (Keith and others, 1981).

A brief but spectacular eruption of Kilauea Volcano on March 30 (episode 17 of a protracted east rift zone eruption) had no effect on activity at Mauna Loa. These were the first simultaneous eruptions of Mauna Loa and Kilauea since 1919 and served to demonstrate the magmatic independence of these two volcanoes.

SEISMIC OBSERVATIONS

Although lava did not reach the surface until 0126, seismic activity had reached high levels earlier, and seven moderate earthquakes of 3.0–4.2 magnitude occurred between 0050 and 0210. This intrusion-related earthquake swarm and harmonic tremor at the summit decreased at 0215, marking the beginning of about 5 h of comparatively low seismicity (fig. 19.20), as magma migrated into the NERZ. Perhaps the elevated NERZ seismicity associated with aftershocks of the November 16, 1983, $M=6.6$ earthquake (Koyanagi and others, 1984) caused a substantial decrease in stress, which facilitated the subsequent rapid and relatively aseismic migration of magma from the summit into and along the NERZ on this morning. Or, perhaps the magma that intruded into the middle NERZ on July 6–10, 1975, was still liquid and capable of maintaining open conduits.

Between 0700 and 0915 the frequency of small earthquakes

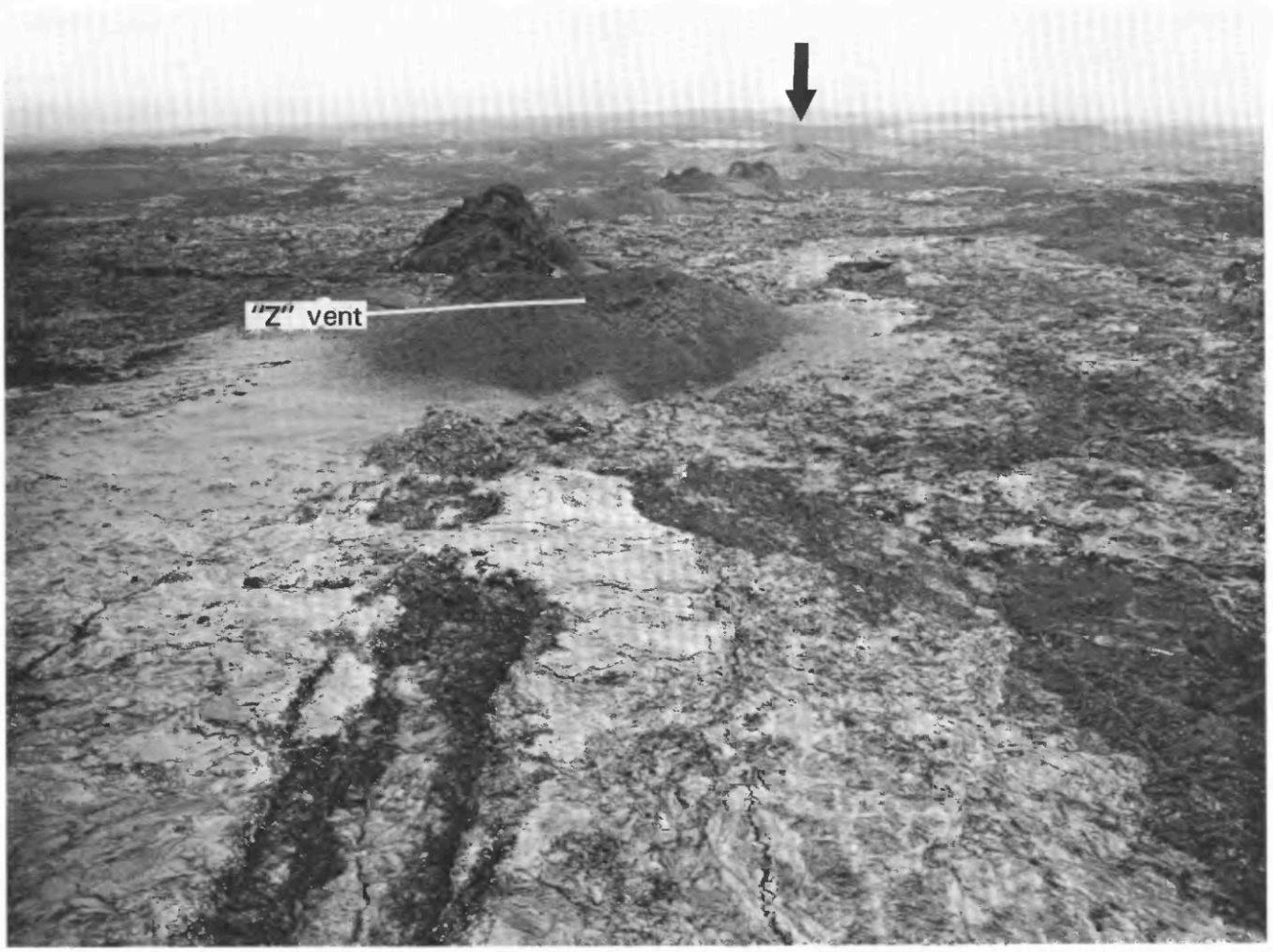

FIGURE 19.26.—Oblique view of 2,900-m vents looking downrift, with 25-m-high "Z" vent cinder cone and its tephra blanket at uprift end of vent system. This cone formed on April 8–12, and was the only vent to produce reticulite. Note lava shield at lower end of vent system (dark arrow). Cracks in foreground converge on "Z" vent and mark subsurface position of feeder dike. Note 20° bend in 1984 eruptive fissure. Photograph by J. P. Lockwood, April 30, 1985.

increased beneath the summit (fig. 19.20) and the NERZ midway between Mokuaweoweo and Puu Ulaula (fig. 19.28). At 0917 harmonic tremor increased in the NERZ, and high tremor was recorded on stations more than 30 km away. For the remainder of the vigorous eruption, tremor was centered along the NERZ and generally decreased in amplitude as a function of distance from Puu Ulaula. The dominant period of the tremor signals varied from about 0.2 to 0.7 s and also varied with recording distance from the eruption zone. Shorter period tremor dominated at stations within a few kilometers of the eruptive center. Short-period tremor was also dominant during the pre-eruptive and early eruptive stages. Tremor remained consistently strong on the seismometer nearest the eruptive site (PLA) until April 12, and after several days of low activity decayed to nearly background levels on April 15. The more distant stations MLO and HSS, located about 8 km from the center of eruption, showed highest tremor from March 25–28, followed by a lower level until April 2 and a gradual decay until the end of the eruption on April 15 (fig. 19.34).

The frequency of shallow, short-period earthquakes associated with summit subsidence started to increase on March 28. Counts peaked at 50–100 per hour on April 5–8, and they remained relatively high throughout April. These events decreased slowly thereafter and reached nearly average pre-eruption levels by mid-May. Earthquakes related to summit subsidence were mostly smaller than magnitude 1, shallower than 5 km, and centered in the caldera region. An exceptionally large earthquake on April 9, which measured $M=3.9$, was located 2 km beneath the caldera.

Numerous small, short- and long-period earthquakes near the active vents on the northeast rift followed the cessation of eruptive activity. These events (mostly $M<0.1$), which numbered many

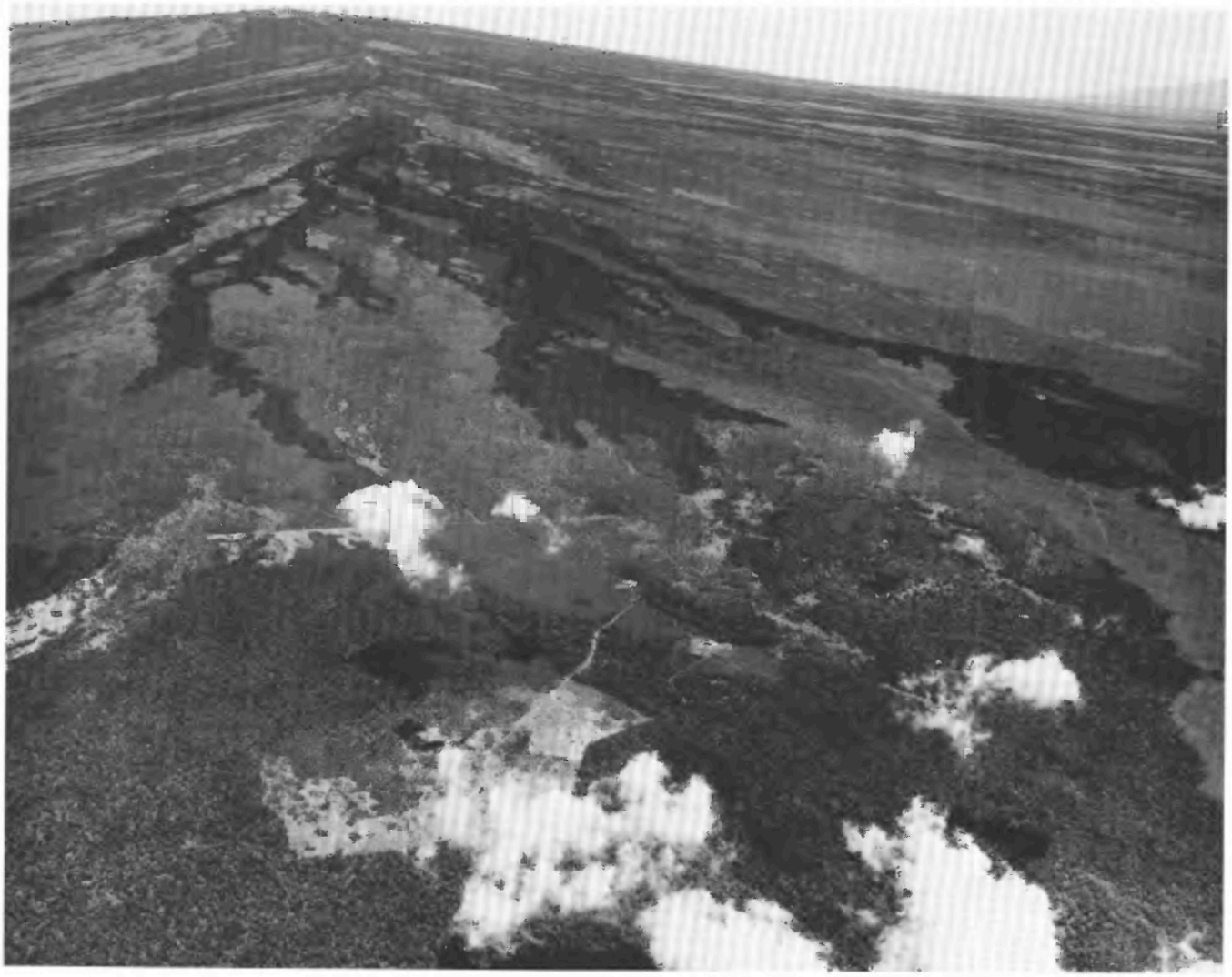

FIGURE 19.27.—Oblique aerial view of northeast rift zone showing 1984 lava (dark areas) between 2,000 and 3,000 m. Mauna Loa Boy's School is in right foreground. Kulani Honor Camp is located left of photograph margin. Lineament across center of photograph is Powerline Road. View is to west. Photograph by J.P. Lockwood.

hundreds per day in late April and throughout May 1984, were apparently caused by vent degassing activity as well as by local stresses induced by gravitational and thermal gradients; they gradually decreased to background levels (fig. 19.34).

GEODETIC OBSERVATIONS

An automatic tiltmeter located near the seismic station MOK at Mauna Loa's summit (fig. 19.19) recorded rapid surface displacements beginning at 0100 on March 25 (fig. 19.35). The initial tilt change, a sharp downward deflection to the north and west, indicated uplift of the summit region, probably caused by the sudden upward migration of magma.

A reversal in tilt direction at 0150 marked the beginning of summit subsidence and may also have corresponded to the eastward migration of eruptive vents. Subsequent spirit-level measurements at several dry tilt stations around the summit (network shown in Decker and others, 1983, fig. 13) indicated that subsidence of the summit region continued, though at a decreasing rate, for the duration of the eruption (fig. 19.36). A similar pattern of summit subsidence—contraction of several horizontal lines across the caldera—was indicated by trilateration surveys (fig. 19.37). The curves shown in figure 19.37 are similar to the decreasing lava production rate determined at the 2,900 m vents (Lipman and Banks, chapter 57, fig. 57.17). Net tilt changes between July 1983 and May 1984

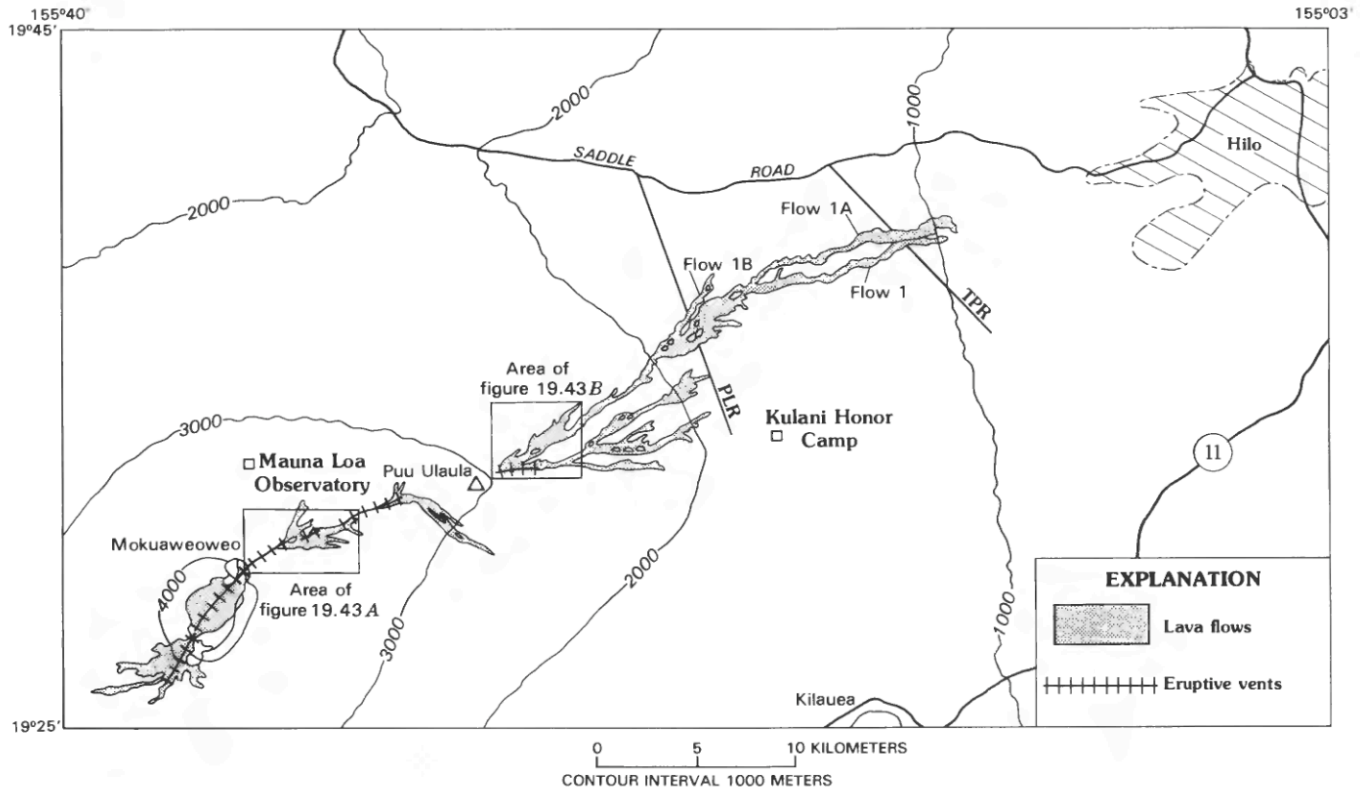

FIGURE 19.28.—Distribution of 1984 eruptive vents and lava flows and locations of figures 19.43*A*, *B*. PLR, Powerline Road; TPR, Tree-planting Road. (Modified from Lockwood and others, 1985, fig. 5.)

were 100–300 microradians at summit dry-tilt stations (fig. 19.38). The computed center of subsidence was in the southeastern area of the summit, a position identical to the center of uplift identified in 1977–1983 geodetic surveys (Decker and others, 1983). The volume of subsidence since July 1983, determined from the tilt vectors, was at least 100×10^6 m^3. Reoccupation of a 14-km-long level line that passes within 1.2 km of the subsidence center indicated that the Mauna Loa summit subsided at least 630 mm during the eruption. A resurvey of an extensive trilateration network (about 200 lines) that encompasses much of Mauna Loa indicated extension of more than 800 mm across the NERZ and compression of the adjacent flanks, which reflects dike emplacement. The dilation of the summit region was mostly accommodated by southeastward translation of the upper southeast flank, as revealed by distance measurements between the northwest summit of Mauna Loa and the summits of Mauna Kea and Hualalai Volcanoes.

GRAVITY OBSERVATIONS

A network of gravity stations on the upper slopes and summit of Mauna Loa was partly reoccupied on February 13–14, 1984. This survey, which preceded the 1984 eruption by 40 days, provided a precise datum for subsequent major changes and showed that a gravity change of only -20 ± 10 microgals (uplift) had occurred at station C-1 (fig. 19.19) in the preceding 8 years. Gravity values were determined to a precision of 10 microgals relative to a base station located 14 km distant, using two LaCoste and Romberg Model G gravimeters transported by helicopter between readings.

Reoccupation of station ML-1 (fig. 19.19) was begun within 10 h of the eruption onset and was continued on a near-daily basis. Gravity increased about 150 microgals at ML-1 during the eruption, at an exponentially decreasing rate (fig. 19.39). Because the gravity change is a function of both elevation and mass transfer changes, the exact amount of subsidence is not known.

The rate of gravity change is very similar to the exponentially diminishing rates of tilt change and horizontal strain (figs. 19.36, 19.37), which implies that the elevation change was closely tracking mass transfer changes with time. Processes such as incomplete summit collapse or extensive subaerial vesiculation are thus unlikely.

Gravity increases at C-1 (5 km from the deformation center) and ML-8 (7 km) were 61 and 19 microgals, respectively. Measurements at gravity stations on Mauna Loa's northeast flank (9, 13, and 27 km from the summit subsidence center) showed no significant changes. The rapid decay of the gravity changes with distance is consistent with a relatively shallow pressure source, as suggested by geodetic measurements.

FIGURE 19.29.—Lava flow advancing through rain forest at 950-m elevation on March 30. Flow is covering 1852 lava; more heavily forested area in lower left corner is underlain by prehistorical lava. View is to southeast. Photograph by J.P. Lockwood.

A ***B***

FIGURE 19.30.—Lava channel at 2,500 m, showing changing eruptive volumes from second to tenth day. View to east, 1852 spatter cone to left of channel. ***A***, March 26, 1984. ***B***, April 4, 1984. Photographs by J.D. Griggs.

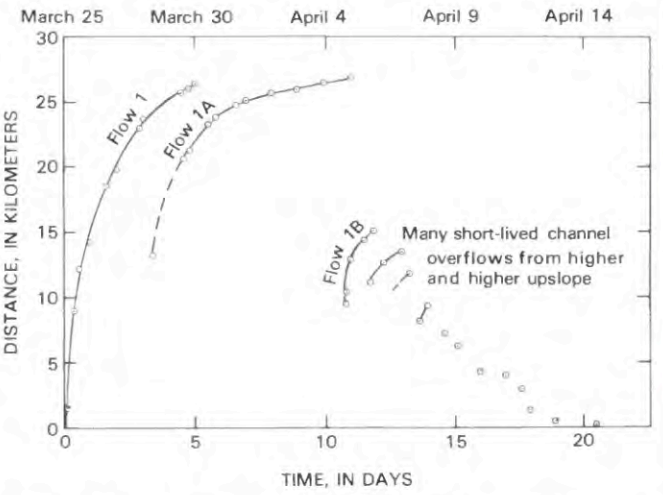

FIGURE 19.31.—Advance rates of lava flows from 2,900-m vents. Time plotted as days after initial outbreak on afternoon of March 25, 1984 (from Lockwood and others, 1985, fig. 4).

FIGURE 19.32.—Diversion of 1984 lava by U.S. Army Corps of Engineers test barriers constructed in 1977. The 4- to 5-m-high earthen barrier temporarily impeded the 1984 flows, here 14 m thick, but eventually was overtopped (arrow). View is to southeast.

GEOELECTRICAL OBSERVATIONS

A 3.8-km-long SP (electrical self-potential) line normal to the NERZ of Mauna Loa was established at about 3,000 m elevation (fig. 19.19) 9 months before the 1984 eruption. The pre-eruption SP data (fig. 19.40) show an anomaly centered over the area of the July 6–10, 1975, intrusion (Lockwood and others, 1976, p. 15). The relatively large data noise is attributed to the lack of soil or ash cover and low rainfall in this area, which produce very high electrode contact resistances.

This anomaly may indicate a zone of structural weakness that allowed upward transfer of heat. A profile along the same line on March 27, 2 days after the eruption began, shows a general increase of potentials, highest near the center of the traverse and coincident with a zone of ground cracks formed on the afternoon of March 25 (fig. 19.40).

Five days after the eruption began, VLF (very low frequency) measurements of tilt angle and ellipticity of the electromagnetic field, from a high-powered U.S. Navy radio transmitter at Lualualei, Oahu, were made along the SP profile (fig. 19.41). The steepest gradients on both the percent tilt angle and percent ellipticity curves occur approximately where they intersect at the zero crossover, a point that is nearly over the center of the anomaly-producing body.

The form of the curves suggests that the VLF anomaly is caused by a good conductor, probably with a high-angle tabular shape, directly beneath the SP high and near the center of the ground-crack zone. VLF resistivity measurements away from the conductive anomaly show high resistivity values (8,000–12,000 ohm/m); these values suggest, from an estimate of plane-wave penetration at the radio frequency used, that the depth to the top of the conductive zone is 100–150 m. The conductive body could be magma or a zone of hot, moist rocks leading to a heat source at greater depth. No emission of either steam or fume was noted from the ground cracks in this area, however, suggesting that a nonbrittle zone may have been present between the top of the shallow intrusion and the bottom of the ground cracks.

LAVA PETROGRAPHY AND TEMPERATURES

The 1984 lava consists of uniform, sparsely porphyritic tholeiitic basalt. Phenocrysts (generally less than 1 percent by volume) are euhedral to anhedral, 1- to 3-mm-diameter kinked olivine of forsteritic composition (Fo_{88-90}; M. Garcia, University of Hawaii, written commun., 1984) that is slightly to strongly resorbed, with granular pyroxene-plagioclase coronas. Similar kinked olivine in the 1959 Kilauea Iki lava has been interpreted to be of mantle origin (Helz, chapter 25). Rare clots of olivine and olivine-clinopyroxene-plagioclase intergrowths are also present. Microphenocrysts (3–30 percent) consist mostly of plagioclase laths, with slightly less abundant clinopyroxene and some olivine; all are generally less than 0.3 mm in maximum dimension. The groundmass consists of brown glass with plagioclase, granular clinopyroxene, and opaque minerals. The size and abundance of microphenocrysts increased steadily over the course of the eruption, apparently causing a concurrent increase in lava viscosity (Lipman and Banks, chapter 57; Lipman and others, 1986).

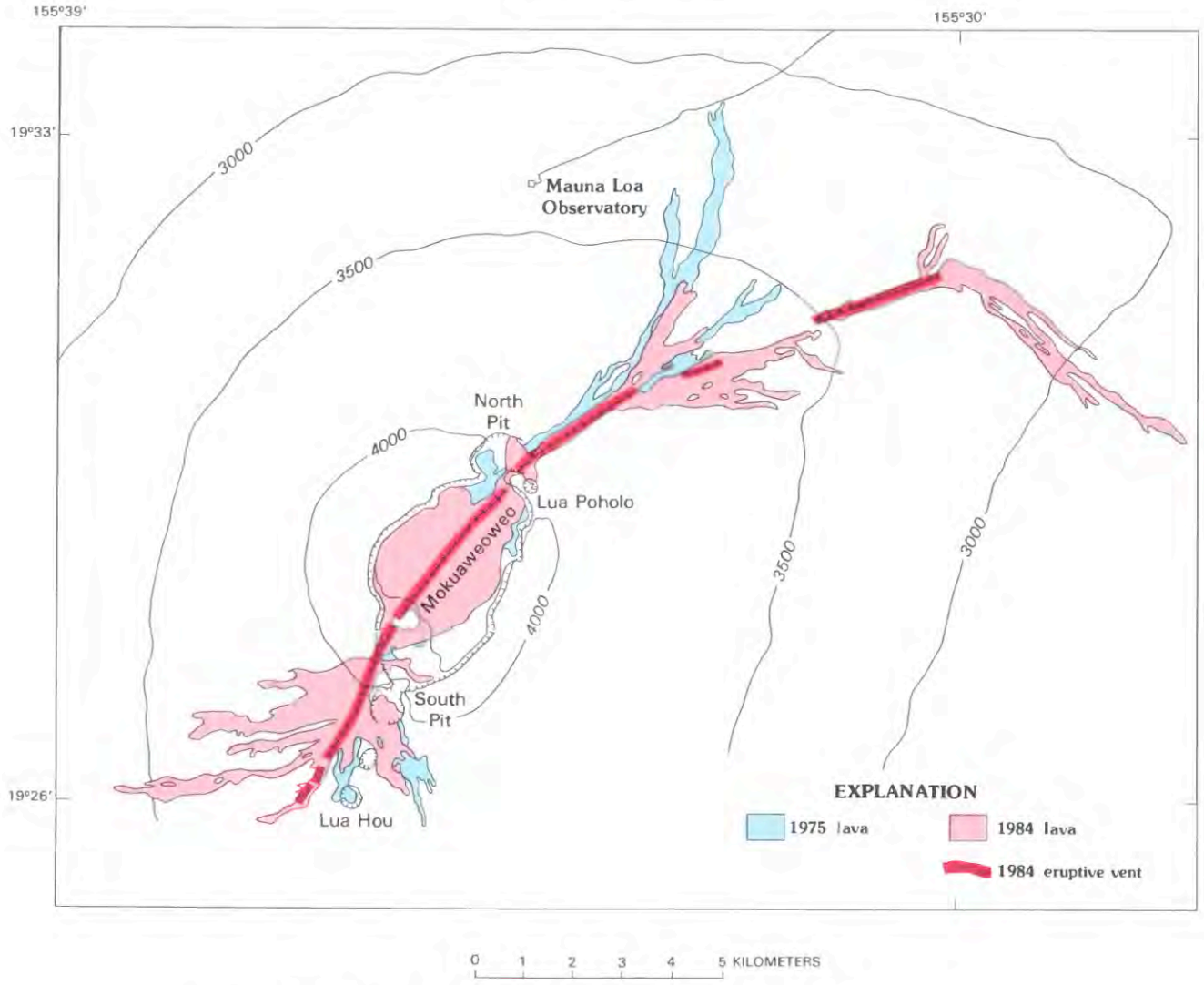

FIGURE 19.33.—Distribution of March 25, 1984, lava in summit region, showing relation to 1975 lava.

Lava temperatures were monitored throughout the eruption by Chromel/Alumel thermocouples and digital meters; the total range measured was between 1,120 °C and 1,144 °C. Fountain temperatures, measured by 2-color infrared radiometer, were generally in close agreement with the highest thermocouple temperatures obtained adjacent to the vents (Lipman and Banks, chapter 57). No changes were observed in either the fountain temperatures or in the temperatures of lava in the uppermost supply channels over the course of the eruption. The highest temperatures were obtained in lava tubes that issued from the base of spatter ramparts, although similar temperatures were obtained several kilometers downstream in the main lava channels or in overflows immediately adjacent to these channels. The lowest temperatures were obtained in thin sheet flows and in lava that appeared to have been stored for many hours or days in lava tubes. Temperatures measured in the main distributary channels decreased less than 20 °C over a total distance of 11 km downstream from the vents.

LAVA CHEMISTRY

Major-element analyses by X-ray fluorescence (table 19.3) show that the 1984 lava is remarkably uniform in composition except for one significantly more evolved sample from the SWRZ. This anomalous sample, which apparently represents contamination by older, stored magma, is not included in the analytical averages of table 19.3. With this exception, and the exception of small fluctuations in MgO content of lava erupted from the lower NERZ vents between March 25 and 30, there is little apparent difference between lava erupted along the upper SWRZ, the summit caldera, and the upper, middle, and lower segments of the NERZ. Such

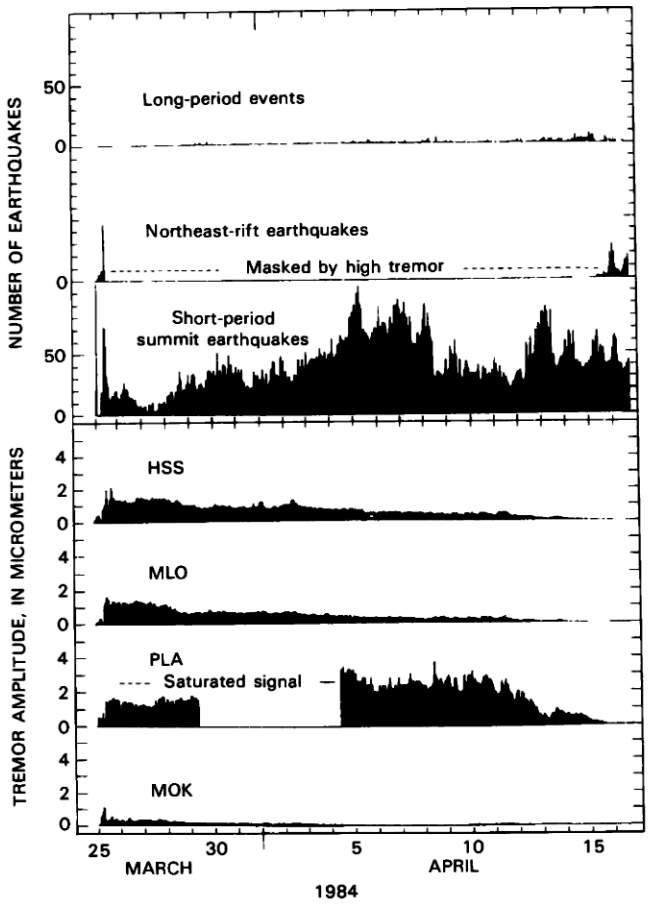

FIGURE 19.34.—Earthquake frequency (upper three plots) and tremor amplitude (lower four plots), March 25–April 16, 1984. Earthquakes as small as $M = -1$ were plotted when not masked by harmonic tremor. Harmonic tremor was read hourly at four seismic stations and plotted as micrometers of ground motion. Signals from PLA station (fig. 19.19) were saturated until April 4, when instrument sensitivity was lowered (from Lockwood and others, 1985, fig. 6).

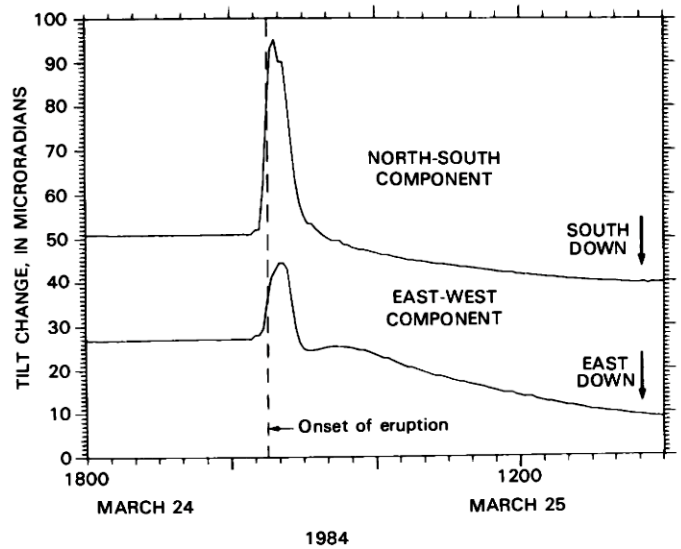

FIGURE 19.35.—Continuously recording tiltmeter record from MOK instrument for a 24-hour period beginning at 1800 H.s.t. on March 24. A positive tilt change (inflation) corresponds to a downward deflection in north and west directions (modified from Lockwood and others, 1985, fig. 7).

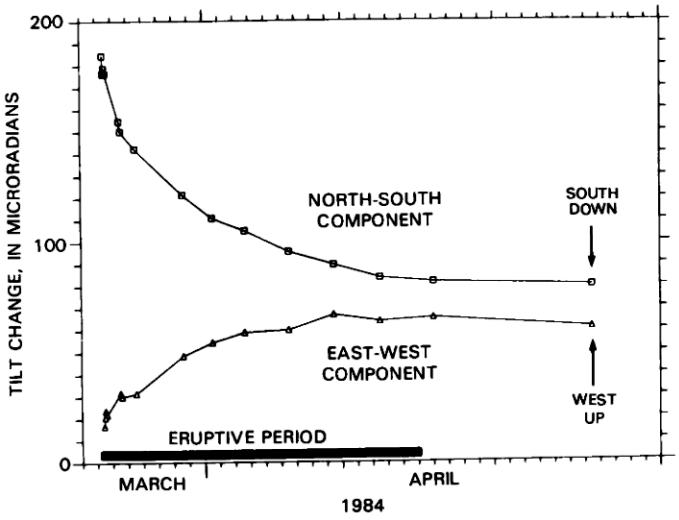

FIGURE 19.36.—Summit deflation curve determined from spirit-level (dry-tilt) measurements made near MOK station. A positive tilt change corresponds to a downward deflection in north and east directions (modified from Lockwood and others, 1985, fig. 8).

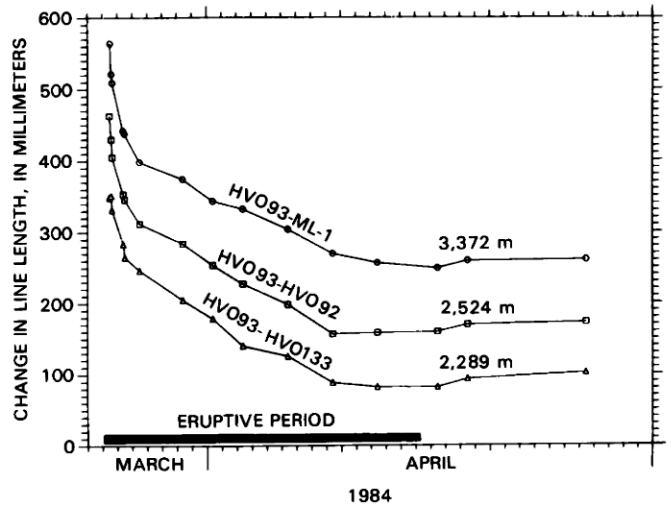

FIGURE 19.37.—Summit deflation curve determined from measurement of horizontal distances across Mokuaweoweo. Locations of survey lines are shown in Decker and others (1983, fig. 7). Line lengths from Lockwood and others (1985, fig. 9).

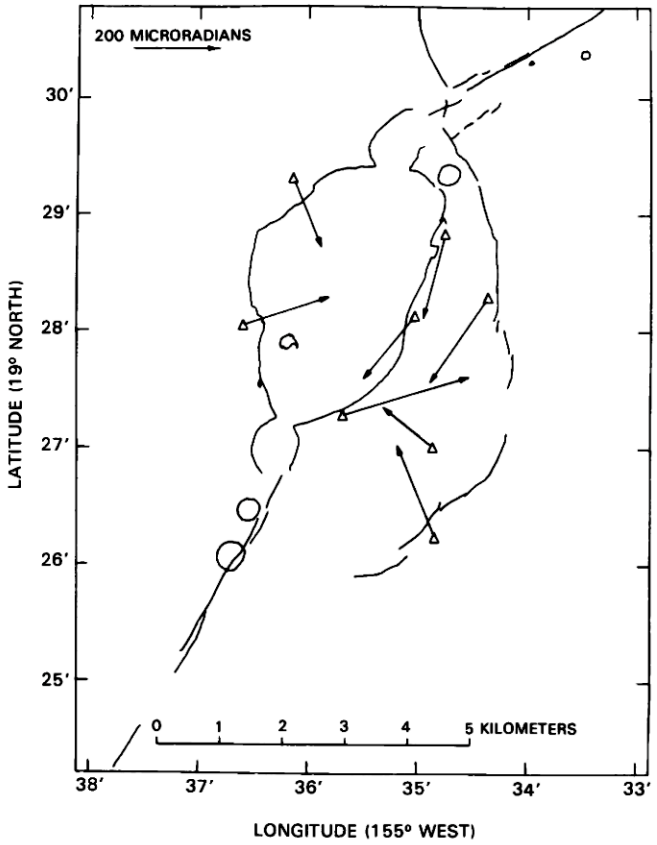

FIGURE 19.38.—Net tilt changes in summit region of Mauna Loa between June 1983 and May 1984. Triangles indicate location of spirit-level (dry tilt) stations. Vectors are drawn in direction of downward deflection of surface; length of vector shows amount of deflection (from Lockwood and others, 1985, fig. 10).

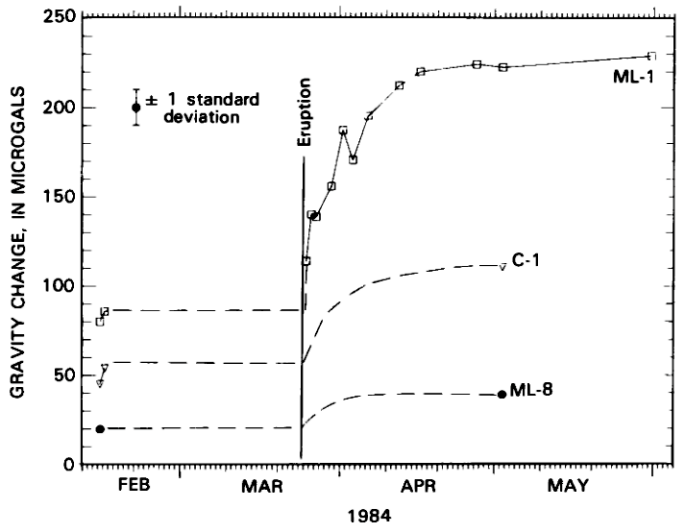

FIGURE 19.39.—Relative gravity changes at stations ML-1, C-1, and ML-8 from February 13 to May 28, 1984. Values plotted are not absolute, but only relative to February 13 datum. Dashed lines where data inferred. Data from D.J. Johnson, U.S. Geological Survey (modified from Lockwood and others, 1985, fig. 11).

homogeneity in lava composition is typical of historical Mauna Loa eruptions (Wright, 1971; Rhodes, 1983) and is consistent with the uniform lava temperature measurements.

The 1984 lava, which is slightly lower in MgO content compared with most historical Mauna Loa lava, has a composition indicative of multiple saturation with respect to olivine, clinopyroxene, and plagioclase. This lava is somewhat less evolved than the 1975 lava (table 19.1); it contains slightly less K_2O and TiO_2 and more MgO. Consequently, the 1984 lava cannot simply be residual magma remaining in shallow storage following the 1975 eruption, unless any magma stored in 1975 was less evolved than the lava erupted at that time. The combination of remarkably uniform lava composition and large eruptive volume over a 21-day period points to the ultimate derivation of this lava from a deeper reservoir of substantial size.

ERUPTIVE GASES

The 1984 eruption has yielded the first analyses ever reported for eruptive gases from Mauna Loa (Greenland, chapter 30). The gases are similar to those collected from the adjacent Kilauea Volcano, although they are lower in water and halogen content relative to sulfur (table 19.4). The low atomic C/S ratio (0.2, as at Kilauea) is attributed to pre-eruptive degassing of the magma during storage in a shallow (3–4 km deep) summit reservoir.

Thermodynamic calculations show that most samples contain excess water above that required for equilibrium with other species. Subtracting excess water from the analyses results in a calculated pO_2-temperature relation close to one directly measured in a Kilauea lava lake by Sato and Wright (1966). The excess water over that required for equilibrium in these analyses is not a meteoric contaminant but is believed to be magmatic water that has not equilibrated with the other gases because of the rapid magma rise rate.

Geographic factors had considerable influence on lava degassing. Much of the lava erupted at the 2,900 m vents was apparently partially degassed through high-temperature fumaroles along the March 25 vents between 3,400 and 3,470 m (Greenland, chapter 30). Aerial correlation spectrometer (COSPEC) monitoring showed this area of incandescent fumaroles to be a voluminous source of magmatic gas for the duration of the eruption; these fumaroles were the only source of detectable SO_2 after the end of lava production at the 2,900 m vents (J.B. Stokes, written commun., 1984). At the 2,900 m vents, high fountaining (high gas production) was most characteristic of the farthest uprift vents (including a reticulite-producing cinder cone, see fig. 19.26). At the lower end of this 1,700-m-long vent system, largely degassed pahoehoe issued continuously from a vent with almost no fountaining, constructing a 45-m-high lava shield (fig. 19.24*B*). Visible

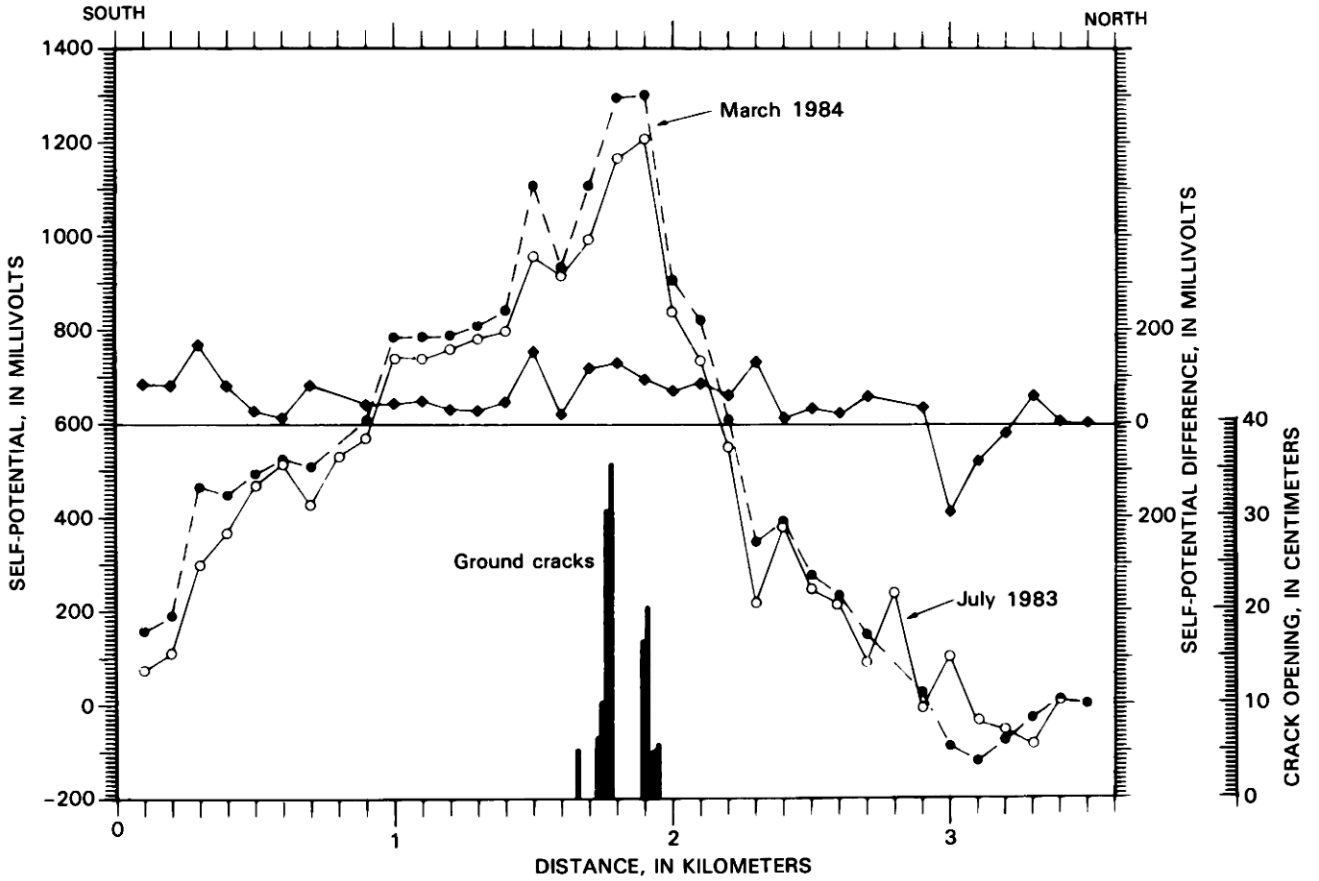

FIGURE 19.40.—Electrical self-potential (SP) profiles normal to northeast rift zone of Mauna Loa at about 3,000-m elevation, taken 9 months before 1984 eruption, and 2 days after eruption began. Locations of ground cracks that opened along profile line on March 25, 1984, are plotted on abscissa. SP data July 14, 1983 (solid lines and open circles), SP data March 27, 1984 (dashed lines and solid circles), differences between 1984 and 1983 SP data (solid lines and diamonds). Data from D.B. Jackson, U.S. Geological Survey (from Lockwood and others, 1985, fig. 12).

fume was also largely restricted to the farthest uprift of the 2,900 m vents. These circumstances may be due to vertical stratification of gas within laterally transported magma (fig. 19.42).

CONCLUSIONS: THE FUTURE

The 1975–1984 Mauna Loa eruptive sequence was the first for which extensive observations of geodetic, geoelectrical, geochemical, gravity, and temperature phenomena were possible; more has been learned about Mauna Loa inflation and eruption processes during this period than in all earlier historical eruptions.

This was Mauna Loa's first eruptive sequence since 1950 and involved the first flank eruption on the northeast rift zone since 1942. Intervals between NERZ flank eruptions have, however, been as short as 41 months (1852–1855), and posteruption geodetic measurements (figs. 19.13, 19.14) suggest inflation of Mauna Loa for her *next* eruption has already begun. As regards the volcano's long-term future behavior, we must look to the record of the past. Lava has covered the subaerial Mauna Loa surface during Holocene time at an average rate of about 40 percent per 1,000 years (Lockwood and Lipman, chapter 18, fig. 18.11). This coverage rate is likely to also characterize the long-term future, although substantial variations from this average are to be expected for shorter periods.

Most of the 32 eruptions since 1832 began with initial activity above 3,000 m elevation; 15 eruptions were limited to the summit area. The other 17 eruptions involved flank extrusion: 2 principally on the northwest flank, 7 on the southwest rift zone, and 8 primarily on the northeast rift zone. This general spatial distribution of flank eruptions will probably also characterize future activity.

Southwest rift zone eruptive loci generally migrated uprift from 1868 to 1950 (Lipman, 1980). Eruptive loci on the northeast rift zone have shown no such longitudinal distribution pattern, but have instead shown a strong tendency for southward migration with time, especially in the 20th century (fig. 19.43). The common pattern of south-stepping offset of echelon vents (fig. 19.23) is another apparent indication of this tendency for southward migration. Although

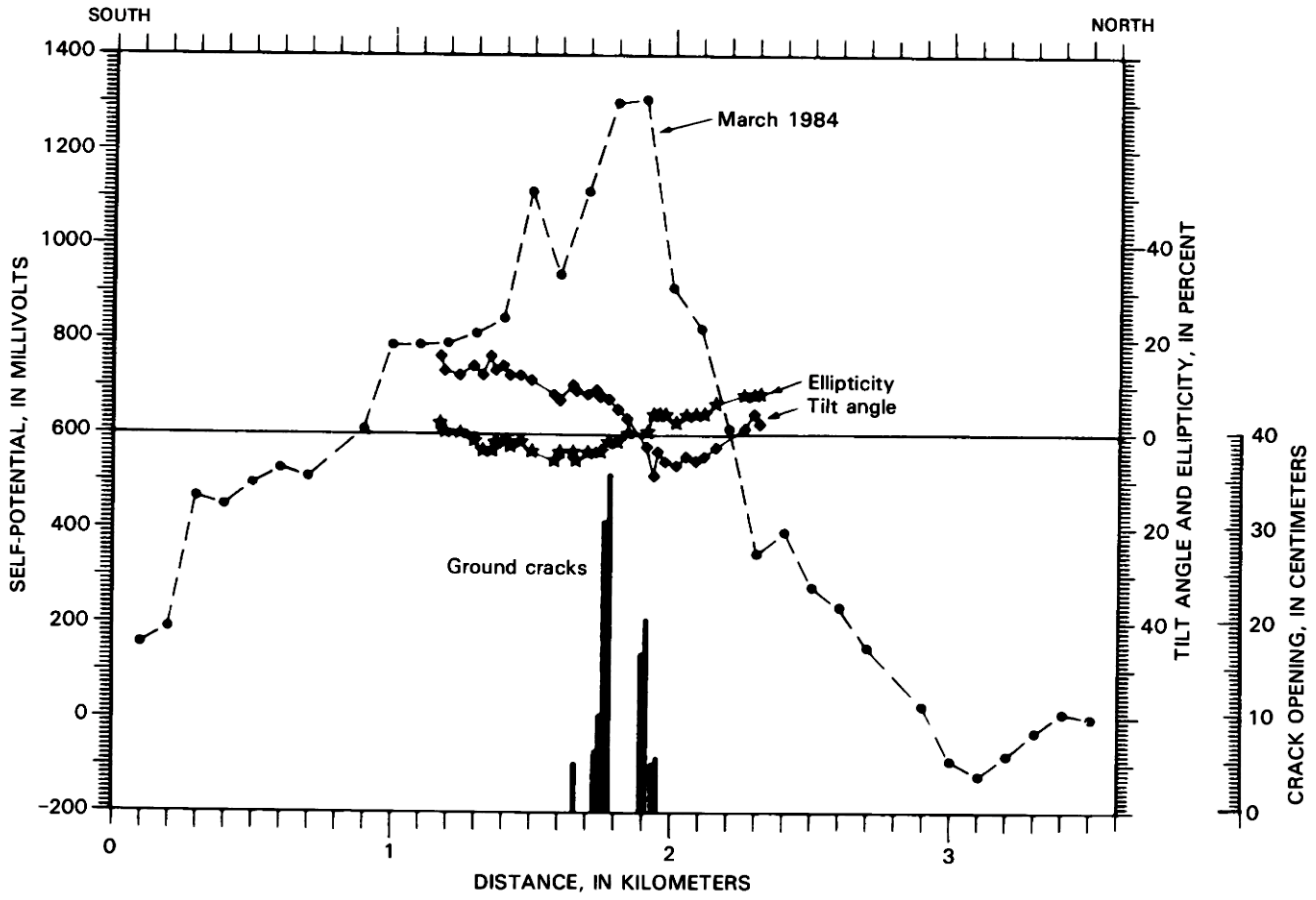

FIGURE 19.41.—Very low frequency profiles across northeast rift zone of Mauna Loa obtained on March 30, 1984. Ellipticity (stars) and tilt angle (diamonds) are shown with March 27, 1984, SP profile and ground cracks along same survey line. Data from D.B. Jackson, U.S. Geological Survey (from Lockwood and others, 1985, fig. 13).

TABLE 19.3.—*Average major-element compositions of 1984 Mauna Loa lava*

[X-ray fluorescence analyses by J.M. Rhodes. Analyses reported on volatile-free basis, with total iron reported as Fe_2O_3. *n*, sample size]

	Upper SWRZ *n*=5	Summit caldera *n*=9	Upper NERZ *n*=5	Middle NERZ *n*=5	Lower NERZ *n*=10	1975 Lava *n*=6
SiO_2	51.37	51.37	51.82	51.59	51.63	51.70
TiO_2	2.06	2.08	2.09	2.07	2.09	2.10
Al_2O_3	13.59	13.65	13.72	13.64	13.65	13.73
FeO^+	11.97	12.06	12.14	12.05	12.09	12.23
MnO	.19	.18	.18	.19	.19	.16
MgO	6.75	6.73	6.68	6.66	6.81	6.55
CaO	10.54	10.51	10.55	10.48	10.51	10.51
Na_2O	2.55	2.59	2.52	2.53	2.48	2.18
K_2O	.38	.38	.38	.38	.38	.39
P_2O_5	.24	.24	.24	.24	.24	.24
Total	99.55	99.79	100.32	99.84	100.05	99.79

TABLE 19.4.—*Relative atomic compositions of Mauna Loa and Kilauea eruptive gases*

[Values shown are the ratios of atoms of the indicated elements per atoms of sulfur. Analyses by L.P. Greenland]

	Mauna Loa	Kilauea
H	6.4	16
C	.21	.26
O	5.4	10
S	1.0	1.0
Cl	.0036	.021
F	.0035	.023

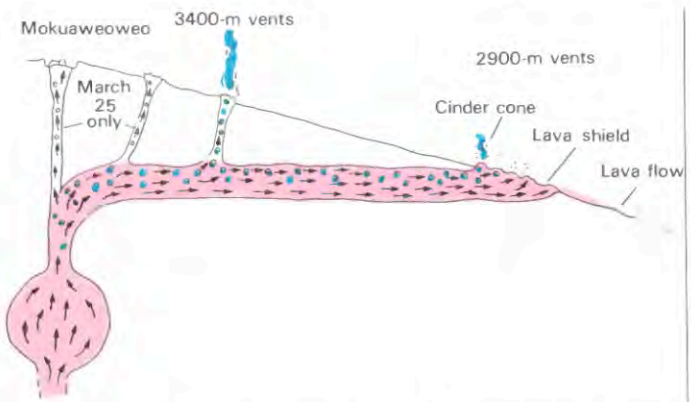

FIGURE 19.42.—Schematic longitudinal section of northeast rift zone, showing proposed degassing processes in laterally transported magma during period March 25 to April 15, 1984. Scale not internally consistent.

volumetrically more than 90 percent of historical lava flows have moved down the north side of the northeast rift zone (Lockwood and Lipman, chapter 18, fig. 18.15), future flows will preferentially flow down the south flank if the southward migration of eruptive vents continues.

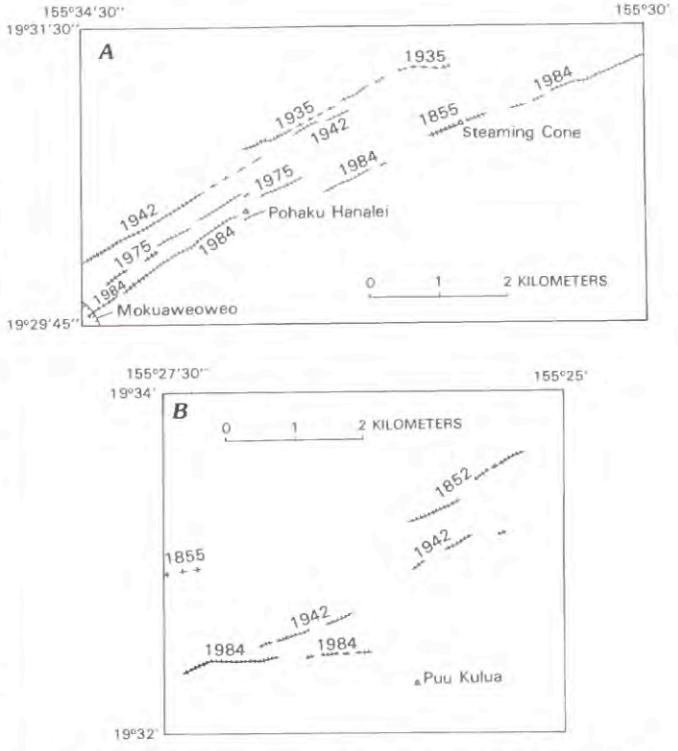

FIGURE 19.43.—Loci of historical eruptive vents at two localities on northeast rift zone. ***A***, Upper northeast rift zone, near Pohaku Hanalei. ***B***, Middle northeast rift zone, below Puu Ulaula. Figure locations shown on figure 19.28.

REFERENCES CITED

Decker, R.W., Koyanagi, R.Y., Dvorak, J.J., Lockwood, J.P., Okamura, A.T., Yamashita, K.M., and Tanigawa, W.R., 1983, Seismicity and surface deformation of Mauna Loa Volcano, Hawaii: American Geophysical Union Transactions, Eos, v. 64, no. 37, p. 545–547.

Dutton, C.E., 1882, Hawaiian volcanoes, *in* U.S. Geological Survey Annual Report, 4th, p. 79–219.

Dvorak, J.J., Okamura, A.T., and Dieterich, James, 1983, Analysis of surface deformation data, Kilauea Volcano, Hawaii: Journal of Geophysical Research, v. 88, no. B11, p. 9295–9304.

Dzurisin, Daniel, 1980, Influence of fortnightly Earth tides at Kilauea Volcano, Hawaii: Geophysical Research Letters, v. 7, no. 11, p. 925–928.

Fiske, R.S., and Kinoshita, W.T., 1969, Inflation of Kilauea Volcano prior to its 1967–1968 eruption: Science, v. 165, p. 341–349.

Golombek, M.P., and Carr, M.J., 1978, Tidal triggering of seismic and volcanic phenomena during the 1879–1880 eruption of Islas Quemadas Volcano in El Salvador, Central America: Journal of Volcanology and Geothermal Research, v. 3, no. 3–4, p. 299–307.

Keith, T.E.C., Casadevall, T., and Johnson, D. , 1981, Fumarole encrustations—occurrence, mineralogy, and chemistry, *in* Lipman, P.W., and Mullineaux, D.L., eds., The 1980 eruptions of Mount St. Helens, Washington: U.S. Geological Survey Professional Paper 1250, p. 239–250.

Koyanagi, R.Y., Endo, E.T., and Ebisu, J.S., 1975, Reawakening of Mauna Loa Volcano, Hawaii: A preliminary evaluation of seismic evidence: Geophysical Research Letters, v. 2, no. 9, p. 405–408.

Koyanagi, R.Y., Endo, E.T., Tanigawa, W.R., Nakata, J.S., Tomori, A.H., and Tamura, P.N., 1984, Kaoiki earthquake of November 16, 1983—a preliminary compilation of seismographic data at the Hawaiian Volcano Observatory: U.S. Geological Survey Open-File Report 84–798, 30 p.

Lipman, P.W., 1980, The southwest rift zone of Mauna Loa—implications for structural evolution of Hawaiian volcanoes: American Journal of Science, v. 280-A, p. 752–776.

Lipman, P.W., Banks, N.G., Rhodes, J.M., 1985, Degassing—induced crystallization of basaltic magma and effects on lava rheology: Nature, v. 317, p. 604–607.

Lockwood, J.P., Banks, N.G., English, T.T., Greenland, L.P., Jackson, D.B., Johnson, D.J., Koyanagi, R.Y., McGee, K.A., Okamura, A.T., and Rhodes, J.M., 1985, The 1984 eruption of Mauna Loa Volcano, Hawaii: American Geophysical Union Transactions, Eos, v. 66, no. 16, p. 169–171.

Lockwood, J.P., Koyanagi, R.Y., Tilling, R.I., Holcomb, R.T., and Peterson, D.W., 1976, Mauna Loa threatening: Geotimes, v. 21, no.6, p. 12–15.

Lockwood, J.P., and Torgerson, F.A., 1980, Diversion of lava flows by aerial bombing—lessons from Mauna Loa Volcano, Hawaii: Bulletin Volcanologique, v. 43, no. 4, p. 727–741.

Macdonald, G.A., 1954, Activity of Hawaiian volcanoes during the years 1940–1950: Bulletin Volcanologique, Series 2, v. 15, p. 119–179.

Miller, J.M., and Chin, J.F.S., 1978, Short-term disturbances in the carbon dioxide record at Mauna Loa Observatory: Geophsical Research Letters, v. 5, no. 8, p. 669–671.

Mogi, K., 1958, Relations between the eruptions of various volcanoes and the deformation of the ground surface around them: Tokyo University, Earthquake Research Institute Bulletin, v. 36, p. 99–134.

Rhodes, J.M., 1983, Homogeneity of lava flows: chemical data for historic Mauna Loan eruptions: Journal of Geophysical Research, v. 88, p. A869–A879.

Ryan, M.P., Koyanagi, R.Y., and Fiske, R.S., 1981, Modeling the three-dimensional structure of macroscopic magma transport systems—application to Kilauea Volcano, Hawaii: Journal of Geophysical Research, v. 86, p. 7111–7129.

Sato, Motoaki, and Wright, T.L., 1966, Oxygen fugacities of magmatic gases from crystallizing Hawaiian tholeiite [abs.]: American Geophysical Union Transactions, Eos, v. 17, no. 1, p. 209.

Stearns, H., and Macdonald, G.A., 1946, Geology and ground-water resources of the Island of Hawaii: Hawaii Division of Hydrography Bulletin 9, 363 p.

Swanson, D.A., Duffield, W.A., and Fiske, R.S., 1976, Displacement of the south flank of Kilauea Volcano—the result of forceful intrusion of magma into the rift zones: U.S. Geological Survey Professional Paper 963, 39 p.

U.S. Army Corps of Engineers, 1980, Lava flow control, Island of Hawaii: U.S. Army Engineer District, Pacific Division [Honolulu] Review Report and Environmental Impact Statement, May 1980, 116 p.

Wright, T.L., 1971, Chemistry of Kilauea and Mauna Loa lavas in space and time: U.S. Geological Survey Professional Paper 735, p. 1–45.

Yamashita, K.M., 1981, Dry tilt—a ground deformation monitor as applied to active volcanoes in Hawaii: U.S. Geological Survey Open-File Report 81–523, 14 p.

HUALALAI VOLCANO: A PRELIMINARY SUMMARY OF GEOLOGIC, PETROLOGIC, AND GEOPHYSICAL DATA

By Richard B. Moore, David A. Clague, Meyer Rubin, *and* Wendy A. Bohrson

ABSTRACT

Hualalai Volcano is the third youngest on the Island of Hawaii. Three rift zones striking northwest, north, and south-southeast have been the loci of all late Pleistocene and Holocene eruptions. Recent detailed and reconnaissance geologic mapping and ^{14}C age determinations indicate that about 95 percent of Hualalai's surface is Holocene, about 55 percent is less than 3,000 years old, and 25 percent is less than 1,000 years old.

Tholeiitic basalt does not occur on the subaerial surface of Hualalai, but has been encountered in a few drillholes and has been dredged from the submarine portion of the northwest rift zone. We infer that Hualalai, like other Hawaiian volcanoes, is dominantly tholeiitic lava and has a thin cap of alkalic lava. The available tholeiitic basalt is mostly olivine-controlled lava that has as much as 30.8 percent MgO. Major-element, trace-element, and isotopic data indicate that Hualalai tholeiitic basalt is most similar to that of Mauna Loa but that their garnet-bearing mantle sources are different.

The subaerial alkalic lava is chiefly alkali olivine basalt with minor hawaiite and trachyte. The alkalic basalt contains varied amounts of olivine, clinopyroxene, and plagioclase phenocrysts and has as much as 16 percent MgO (ankaramite); much is differentiated beyond olivine control. Xenoliths of mafic and ultramafic rocks are common in many alkalic vent deposits and flows. The alkalic basalt of Hualalai can be produced by 5–10 percent partial melting of a source enriched in the light rare-earth elements.

Trachyte occurs in one large cone and its associated flow, as xenoliths in several basaltic vents, and in one drillhole. Gravity and aeromagnetic data support the interpretation that these rocks, the most silicic lava on the Island of Hawaii, were erupted in significant amounts during the late Pleistocene and subsequently have been thinly mantled by alkalic basalt lava flows.

Seismic studies indicate that seismicity within Hualalai is low, and there is no evidence of current magmatic movement such as occurs on Kilauea and Mauna Loa. An intrusion probably occurred in 1929, when earthquakes shook the region for more than a month. Resistivity and electrical self-potential surveys indicate that residual heat from magmatic intrusions may lie at shallow levels. We believe that Hualalai may well erupt again within the next few decades and that precursory seismic activity may be short.

INTRODUCTION

LOCATION AND GEOLOGIC SETTING

Hualalai Volcano occupies the western part of the Island of Hawaii (fig. 20.1) and makes up about half of the area commonly referred to as the Kona district. Hualalai rises to a height of 2,523 m (8,271 ft) above sea level, covers an area of about 850 km^2 (about 325 mi^2), and has a subaerial volume of about 600 km^3 (about 144 mi^3). Alkalic lava on its southern, eastern, and northeastern flanks is interbedded with tholeiitic Mauna Loa lava.

Hualalai has three rift zones that strike northwest, north, and south-southeast from a point about 5 km east of its summit. The subaerial part of the prominent northwest rift zone, 2–4 km wide (fig. 20.2), is 24 km long to the ocean; bathymetry suggests that it may continue another 70 km offshore. The ill-defined north rift zone (fig. 20.3), about 10 km long and 5 km wide, contains less than 5 percent of the vents and has been inactive during the last 2,000 years. The south-southeast-trending rift zone (fig 20.4), 3–5 km wide, is about 13 km long and, like the others, is marked by prominent cinder and spatter cones.

This progress report summarizes recent work by the U.S. Geological Survey on Hualalai, including geologic mapping, ^{14}C age determinations, petrographic studies, major-element chemical analyses, trace-element analyses, and geophysical studies.

PREVIOUS WORK

Stearns and Macdonald (1946) mapped Hualalai in reconnaissance fashion, and named all of the alkalic rocks the Hualalai Volcanic Series, which included the Waawaa Volcanics (trachyte cone and flow) at its base. These units are currently called the Hualalai Volcanics and Waawaa Trachyte Member. Macdonald (1968) noted that most of the surface vents and flows are alkali olivine basalt. Richter and Murata (1961) and Jackson and others (1981) studied xenoliths in a lava flow erupted in 1800.

Clague and others (1980) discussed the petrology of 19 prehistoric and historical alkali basalt flows of Hualalai. Clague

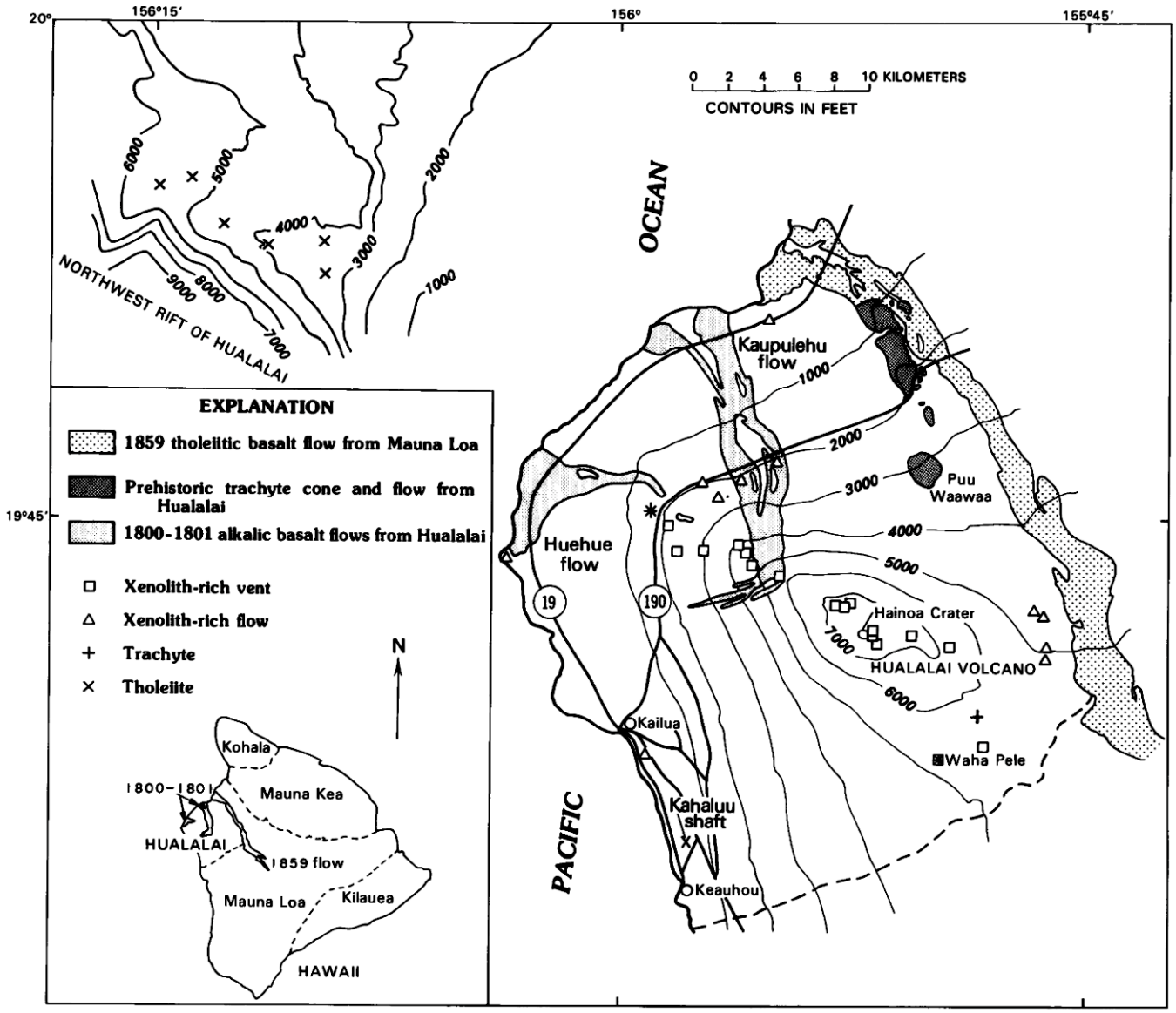

FIGURE 20.1.—Hualalai Volcano, including part of submarine northwest rift zone. Inset shows location of Hualalai on Island of Hawaii. Samples dredged from northwest rift are all tholeiitic basalt and picritic tholeiitic basalt. Symbol at Waha Pele indicates picritic tholeiitic basalt and trachyte blocks in maar deposit and xenoliths in flow from same vent. Other location with both trachyte and tholeiitic basalt, 1 km southwest of 1801 vent, is water well that encountered trachyte overlying tholeiitic basalt, both beneath more than 300 m (1,000 ft) of alkalic basalt flows. Third tholeiitic basalt location is from Kahaluu water shaft, where tholeiitic basalt occurs as shallow as 75 m (229 ft) below surface. Bathymetry from Campbell and Erlandson (1979). Dashed line marks approximate southern edge of Hualalai.

(1982) described tholeiitic basalt from the submarine northwest rift zone; much of our discussion of the tholeiitic shield lying hidden beneath the surficial alkali basalt flows is based on that study.

ACKNOWLEDGMENTS

We thank the B.P. Bishop Estate, Puu Waawaa Ranch, Huehue Ranch, Palani Ranch, and Hualalai Ranch for access to their land. Debby Kay of the USGS in Reston, Va., did the rapid-rock chemical analyses. Frank Trusdell, Jacqueline Eaby Dixon, and Richard Murnane assisted in the field. Dallas Jackson and Thomas Wright reviewed the manuscript.

STRATIGRAPHY

We have mapped all of Hualalai Volcano in reconnaissance fashion and have completed detailed mapping of lava flows and vent deposits in most of the area, including five of the eight 7½-minute

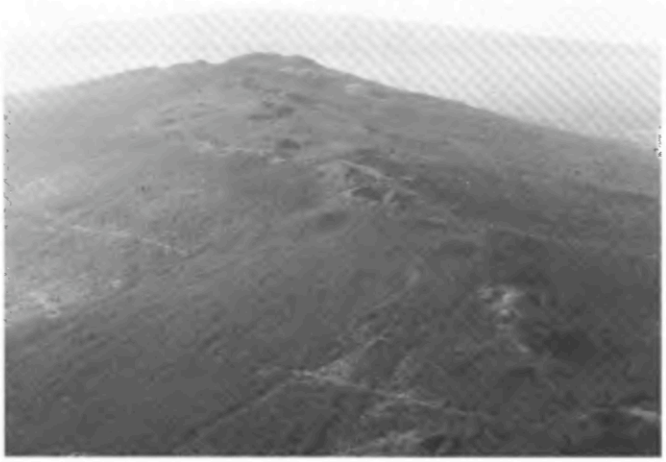

FIGURE 20.2.—Aerial view looking southeast over part of northwest rift zone of Hualalai Volcano. Mauna Loa is in background. Main 1800 vent is in center (no light-colored grass on flow), and another previously unmapped 1800 vent and flow are in lower right corner. Cone slightly to left of main 1800 vent and in front of it was nearly buried by 1800 flow.

FIGURE 20.3.—Aerial view of Hualalai Volcano from north. Dark flow in foreground is 1859 Mauna Loa flow. Large cone with pronounced radial drainage is Puu Waawaa, consisting of trachyte. A trachyte flow from that cone forms steep hummocky topography, partly casting a shadow, in center of photograph. Dark flow in front of Puu Waawaa is dated at 2,030 ± 80 yr B.P. A few small basaltic cones of the diffuse north rift zone are visible behind Puu Waawaa.

quadrangles that cover Hualalai. The mapping has been supplemented by ^{14}C ages presented in table 20.1. The generalized age-distribution map that summarizes this effort is shown in figure 20.5, and data on areas covered by lava of different age are given in table 20.2. Paleomagnetic studies (D.E. Champion, unpub. data, 1985) and future ^{14}C ages may modify these numbers slightly. The data in table 20.2 show that about 95 percent of Hualalai's surface is Holocene, as noted by Stearns and Macdonald (1946), and 25 percent is covered by lava that is <1,000 years old.

FIGURE 20.4.—Aerial view looking north-northwest across upper south-southeast rift zone of Hualalai Volcano. Most visible cones and flows are Holocene in age. Haleakala Volcano on Maui is in distance.

Hualalai has erupted about 0.2 km^3 of basalt per century during the last 3,000 years. This figure is an order of magnitude less than the 2.9 and 2.2 km^3 erupted per century by Mauna Loa and Kilauea, respectively, during historical (post-1820) time (Lockwood and Lipman, chapter 18; Macdonald, 1955).

PLEISTOCENE UNITS

Rocks of Pleistocene age that crop out on the subaerial surface of Hualalai include the Waawaa Trachyte Member (fig. 20.3), a few vent deposits and associated short flows of hawaiite, and a few alkalic basalt lava flows. Funkhouser and others (1968) reported a K-Ar age of 0.4 ± 0.3 Ma for the Waawaa Trachyte Member; more recent K-Ar determinations suggest that the trachyte is about 105 ka (G.B. Dalrymple, written commun., 1985). The volume of the Waawaa cone and flow is about 5.5 km^3, the largest volume single eruption known on the island.

The oldest dated basaltic flows on Hualalai are three flows of age 12–13 ka; each overlies another basalt flow of limited areal extent. We consider it unlikely that any older large flows will be discovered.

A cluster of cones that are mostly Pleistocene in age occurs in the summit area of the volcano (fig. 20.6). Lava dated at 12,950 ± 150 yr B.P. underlies the northeastern part of the village of Kailua and could have come only from the summit area. The summit crater (fig. 20.6) exposes dozens of flow units that suggest eruption on a satellitic shield, like Mauna Ulu on Kilauea Volcano. Near the end of the shield-building eruption, phreatic explosions ejected blocks of gabbro and diabase from a subsurface intrusion. Overlying the resulting tuff is a thin (≤1 m) lava flow of mixed hawaiite and alkali olivine basalt. A cone that overlies all of these deposits has been dated at 8,770 ± 200 yr B.P.

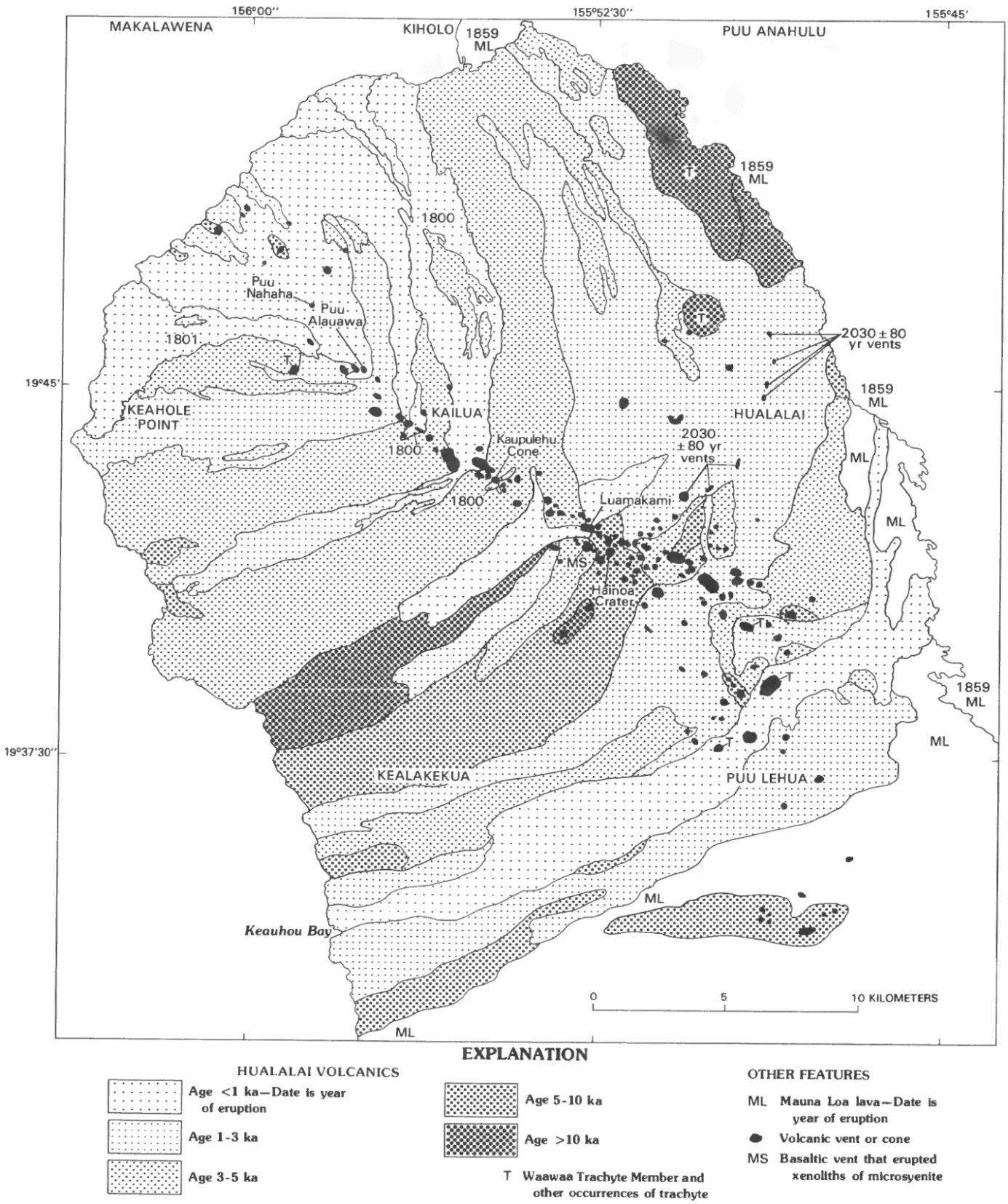

FIGURE 20.5.—Generalized geologic map of Hualalai Volcano showing age distribution of lava and locations of vents. Not all smaller vents are shown. Names of USGS 7½-minute topographic quadrangles used in mapping are shown in all capital letters.

TABLE 20.1.—*Carbon-14 ages of samples from Hualalai Volcano*

Sample	Laboratory Number	Age (yr B.P.)	Unit from which sample taken
79-15	W-4634	<200	An A.D. 1800 lava flow
82-75	W-5124	<200	An A.D. 1800 lava flow
79-8	W-4394	300±60	Young Luamakami flow
84-175	W-5531	710±150	Waha Pele flow
84-150	W-5491	900±110	Flow from large vent 3 km northeast of Waha Pele
82-129	W-5130	1030±60	Flow from cone 2 km northwest of Luamakami
84-170	W-5522	1180±200	Flow from vent 4.5 km north-northwest of Waha Pele
78-2	W-4171	2030±80	Flow from vent 3 km southeast of Puu Waawaa
79-3	W-4388	2290±70	Flow from vent 1 km west of Waha Pele
82-20	W-5068	2350±80	Old Luamakami flow
82-8	W-5073	2390±60	Cone 3 km northeast of Hainoa Crater
82-19	W-5076	2670±80	Cone 700 m east-northeast of Hainoa Crater
84-115	W-5559	3030±200	Flow 8 km northwest of Hainoa Crater
82-113	W-5127	3100±80	Cone 700 m northwest of Luamakami
78-12	W-4376	3600±70	Flow along Highway 190 4 km north-northwest of Kailua
84-119	W-5562	3610±200	Flow 900 m west of Puu Waawaa
82-131	W-5132	3990±70	Spatter 300 m northwest of Hainoa Crater
82-23	W-5070	4390±70	Flow from cone 1 km west of Hainoa Crater
79-10	W-4378	4720±80	Second highest flow in west Malekule pit crater
83-9	W-5297	6360±100	Flow from cone 1.6 km southeast of Hainoa Crater
83-14	W-5299	8770±200	Cone 60 m north of Hainoa Crater
78-5	W-4371	9490±100	Flow 10 km north-northwest of Puu Waawaa
78-11	W-4391	10,370±150	Flow 3 km north-northwest of Keauhou Bay
79-1	W-4365	12,230±150	Flow 4 km north of Puu Waawaa
82-1	W-5056	12,950±150	Flow 3 km east northeast of Kailua

TABLE 20.2.—*Areas of Hualalai Volcano's surface covered by lava of different ages*

[Quadrangle names refer to USGS 7½-minute topographic map sheets; percent figures give the percentage of the Hualalai part of each quadrangle covered by lava of that age group]

Quadrangle	Age group of lava: <1 ka		1-3 ka		3-5 ka		5-10 ka		>10 ka	
	(km^2)	(percent)	(km^2)	(percent)	(km^2)	(percent)	(km^2)	(percent)	(km^2)	(percent)
Makalawena -----	22	68.3	5	15.5	5	15.5	0.2	0.6	0	0
Kiholo ---------	95	59.2	25	15.6	40	24.9	0.5	0.3	0	0
Puu Anahulu ----	0	0	48	57.5	8	9.6	0.5	0.6	27	32.3
Hualalai -------	29	18.1	72	45.0	42	26.3	17	10.6	0	0
Kailua ---------	16	8.8	27	14.8	78	42.9	44	24.2	17	9.3
Keahole Point --	2	3.6	16	28.6	36	64.3	2	3.6	0	0
Kealakekua -----	21	27.3	24	31.2	10	13.0	22	28.6	0	0
Puu Lehua ------	16	27.1	25	42.4	2	3.4	16	27.1	0	0
Total ----------	201	24.8	242	30.0	221	27.3	102.2	12.6	44	5.4
Cumulative Percent -------		24.8		54.8		82.1		94.7		100.1

HOLOCENE UNITS

We have divided the Holocene lava flows of Hualalai into four age groups, based on our detailed and reconnaissance mapping and on ^{14}C ages: 10–5 ka, 5–3 ka, 3–1 ka, and <1 ka. About 55 percent of the surface has an age of less than 3 ka and 25 percent less than 1 ka. In contrast, Holcomb (1981) determined that 90 percent of the surface of Kilauea Volcano is younger than 1 ka, and Lockwood and Lipman (chapter 18) found that 40 percent of Mauna Loa is younger than 1 ka.

Inspection of figure 20.5 suggests that locations of vents of different ages are generally random; however, two important aspects of the volcano's overall morphology require discussion. First, the coastal part of the volcano north of the town of Kailua (figs. 20.5, 20.7) is a lava delta that has been built mostly in the last 3,000 years. The northwest rift zone, marked by spatter cones and ramparts, forms the axis of this feature; lava has built the volcanic pile nearly equally on both sides of the rift zone.

Second, the coast south of Kailua is relatively straight (fig. 20.7), and lava deltas are fewer. Some of the oldest subaerial flows on the volcano occur in this area; marine erosion typically has straightened the shoreline, whereas farther north erosion has not overcome the constructional landforms.

Several vent deposits and associated flows of Holocene age merit individual description. The eruptions of 1800–01 occurred from five separate vent areas (fig. 20.5) and extruded more than

FIGURE 20.6.—Aerial view looking north over summit area of Hualalai Volcano. Actual summit at elevation 2,521 m (8,271 ft) is between two large craters in center of photograph. Small crater barely visible just beyond Hainoa Crater (largest crater) is dated at 8,770 ± 200 yr B.P.; cone in right middle distance is dated at 2,670 ± 80 yr B.P.

300×10^6 m^3 of alkali olivine basalt. The main 1800 flow swept more than 30 m up a cone 450 m north of the vent (fig. 20.2), carried hundreds of thousands of large mafic and ultramafic xenoliths (fig. 20.8) farther downslope, and destroyed fishing villages when it reached the sea (Brigham, 1909).

The 1801 vents of the Huehue flow form a spatter rampart aligned down the slope of the volcano. This orientation caused the lava to flow longitudinally within the rampart. The flows are almost entirely tube-fed pahoehoe. A second vent slightly uphill and south of the main 1801 vents fed a small flow that overlies the main 1801 flows. This younger 1801 vent must have had extremely gentle eruptive activity because no rampart or cone was constructed along the eruptive fissure. A previously undiscovered 1800–01 vent at 1,296-m (4,250 ft) elevation on the northwest rift zone fed small aa flows down both the north and west flanks of the rift system. The fifth 1800–01 vent occurs within the much older Kaupulehu cone. The eruption veneered part of the cone and fed small flows in three directions. The eruptive sequence of the five vents is not known, but the main activity of the eruptive sequence appears generally to have migrated downslope.

The next youngest major eruption apparently occurred from Luamakami, 1 km northwest of the summit, at 300 ± 60 yr B.P., and produced flows that swept down both the north and southwest flanks of Hualalai. After extrusion of about 200×10^6 m^3 of alkali olivine basalt, collapse at one vent caused a minor phreatic explosion that deposited fragments of contact-metamorphosed basalts derived from the walls of the conduit (fig. 20.9).

FIGURE 20.7.—Aerial view looking north along western coast of Hualalai Volcano. Keauhou Bay is in foreground, dark flow from Waha Pele forming its north side. Town of Kailua is in middle distance. Lava flow of 1801 is large dark patch in distance.

The next youngest major eruption occurred at Waha Pele, on the south-southeast rift zone (figs. 20.10, 20.11), at 710 ± 150 yr B.P. As basaltic magma approached the surface, it apparently intersected a perched water table, resulting in massive phreatic explosions. Fragments of trachyte and basalt as large as 0.4 m in diameter were distributed over an area of at least 10 km^2. Later in the eruption, basaltic magma reached the surface, vigorous Strombolian activity built a wide low cone of spatter, and a large flow was extruded. This flow, which has a subaerial volume of at least 400×106 m^3, entered the sea, forming the north side of Keauhou Bay (fig. 20.7), and continued underwater for less than 1 km (J.G. Moore and D.A. Clague, unpublished data). Xenoliths of gabbro and dunite are locally common in the flow.

Another sequence of eruptions occurred on the northwest rift about 800 years ago. The vents formed then include Puu Nahaha, Puu Alauawa, and an unnamed vent about 200 m uprift from Puu Alauawa. Puu Nahaha is the oldest of these three vents and erupted mainly olivine-poor aa that flowed to the ocean on a broad front. Puu Alauawa is the next youngest and erupted plagioclase-rich pahoehoe that formed a large channel and tube system on the steep

FIGURE 20.8.—Xenoliths of 1800 Hualalai flow. Note that most of host basalt has drained away.

FIGURE 20.9.—East rim of Luamakami, Hualalai Volcano. Light-colored rocks, mainly on right, are thermally metamorphosed basalt ejected during phreatic explosion at end of eruption 300 ± 60 yr B.P.

slopes near the vent. Finally, the unnamed vent erupted and formed both pahoehoe and aa flows of olivine-rich lava. A perched lava pond formed above the eruptive fissure; no rampart or cone exists. These flows were dominantly constrained within the channel and tube system developed during the eruption of Puu Alauawa, and the result was a large flow that traveled about 10 km (northwestward) to the ocean, forming a lava delta about 3 km wide. Most of the short flows near the vent are dense aa flows, whereas the main flow is pahoehoe that partly transforms to a slabby aa near the ocean. These eruptive vents migrated uprift during the eruptive sequence. The ages of their flows are constrained by identical and unique paleomagnetic orientations for the earliest and latest flows (D.E. Champion, written commun., 1985).

FIGURE 20.10.—Waha Pele area of Hualalai Volcano from the east. Waha Pele, dated at 710 ± 150 yr B.P., is in center of photograph (arrow); dark flow from it extends to left out of photograph. Cone and flow just beyond it is dated at 2,290 ± 70 yr B.P. Light-colored areas in foreground and middle distance are underlain by trachytic debris ejected during phreatic first phase of Waha Pele eruption. Cone in right foreground consists of ankaramite with abundant mafic and ultramafic xenoliths. Part of Kailua is visible in distance.

FIGURE 20.11.—Aerial view north across part of the south-southeast rift zone of Hualalai Volcano. Waha Pele and its flow are in foreground; grassy light-colored areas just beyond Waha Pele are underlain by explosively ejected trachyte debris. Flow in right middle distance is dated at 900 ± 110 yr B.P. Large lava channel below horizon in center is part of extensive flow dated at 1,180 ± 200 yr B.P. Sharp cone on left horizon probably is about 3,000 years old; note prominent pahoehoe channel issuing from it. Part of Kohala Volcano is in distance.

An unnamed vent 3 km northeast of Waha Pele (fig. 20.12) erupted about 900 ± 110 years ago. Initial high fountaining distributed basaltic cinders and small xenoliths of trachyte over a wide area and built a large low spatter cone about 1 km in diameter and 40–60 m high. Continued voluminous production of lava constructed a satellitic shield within the older cone, and floods of lava

FIGURE 20.12.—Unnamed vent 3 km northeast of Waha Pele. This vent, dated at 900 ± 110 yr B.P., is source of flow on right side of figure 20.10. Note partly collapsed satellitic shield in lower left corner; shield fills crater of older spatter cone that formed during early stages of eruption.

rafted away parts of the cone. The flow, which has an estimated volume of 800×10^6 m^3 (one of the largest in Hawaii), moved 4 km south and 12 km north-northeast of the vent. The final events in the eruptive history of this remarkable vent were collapse of the summit of the shield to form small nested pit craters and a small eruption of alkali olivine basalt, richer in olivine and plagioclase phenocrysts than the previously erupted material, that built a small cone and flow within one of the pit craters.

Underlying part of the previously described flow are the products of another large eruption that occurred at 1,180 ± 200 yr B.P. The vent for this eruption, again unnamed, is 4.5 km north-northeast of Waha Pele. High fountaining distributed basaltic cinders and xenoliths of trachyte over a wide area. Voluminous pahoehoe flows spread northeast and southeast. These flows, which we have not yet finished mapping, are thinner than those of the 900-year-old eruption but still have a volume in excess of 400×10^6 m^3.

The youngest eruption on the diffuse north-trending rift zone occurred at about 2,030 ± 80 yr B.P. This eruption was unusual in that left-stepping echelon eruptive vents, which occur over a distance of 8 km, cut obliquely across the general strike of the rift zone, changing orientation from N. 10° W. at the northern end to N. 50° E. at the southwestern end (fig. 20.5). Similar changes in vent alignment occur over shorter distances on the northeast rift zone of Mauna Loa. It appears that the eruptive dike was fed from a reservoir beneath Hualalai's summit and followed a radial fracture extending northeastward. When it reached the northeast flank of Hualalai, a stress field probably induced by Mauna Kea caused a change in strike of the eruptive vents until they were parallel to the edge of the Mauna Kea edifice. Lava erupted at the lower elevation (1,130 m; about 3,700 ft) first and gradually broke out higher on the volcano's flank to the south and southwest as the eruption progressed, reaching elevations around 1,830 m (about 6,000 ft). We estimate the volume of this eruption to be at least 400×10^6 m^3.

PETROLOGY

THOLEIITIC SHIELD STAGE

Flows of tholeiitic basalt and picritic tholeiitic basalt of the shield stage are not exposed on the subaerial surface of Hualalai. However, the presence of a tholeiitic shield beneath the subaerial alkalic flows is confirmed by the recovery of tholeiitic basalt by dredging on the submarine northwest rift zone (Clague, 1982). In addition, tholeiitic basalt has been recovered in several water wells, and picritic tholeiitic basalt occurs as xenoliths at Waha Pele; these rocks probably are from subsurface parts of Hualalai.

The locations where tholeiitic lava has been found are shown in figure 20.1, and chemical analyses of several samples are presented in table 20.3. The discovery of tholeiitic basalt from Hualalai indicates, as with other Hawaiian volcanoes, that the vast bulk of the volcano is made of tholeiitic lava and that alkalic lava occurs in relatively small volume in the late stages of volcano growth (Clague, 1982).

The submarine tholeiitic basalt samples contain only olivine and spinel phenocrysts with the exception of two samples that also contain plagioclase and clinopyroxene. The picritic tholeiitic basalt samples contain euhedral olivine phenocrysts, subhedral to anhedral kink-banded olivine xenocrysts, extremely rare orthopyroxene

TABLE 20.3.—*Compositions of tholeiitic basalt samples from Hualalai Volcano*

[Major elements analyzed by X-ray fluorescence by J.S. Wahlberg, J. Taggart, and J. Baker; partial chemistry by B. Lai, H. Neiman, and E. Engleman, trace elements by X-ray fluorescence by H.J. Rose, J. Lindsay, B. McCall, G. Sellers, and R. Johnson; all of the USGS. KK7812–11 and KK9–2 are submarine samples from the northwest rift zone; K–11 and K–13 are from the Kahaluu water shaft (fig. 20.1)]

Sample	KK7812-11	K-13	K-11	KK9-2
	Major elements (weight percent)			
SiO_2	46.8	51.1	51.4	50.8
Al_2O_3	8.48	13.0	13.8	13.3
Fe_2O_3	1.29	3.03	5.67	2.33
FeO	10.4	8.16	5.79	8.43
MgO	23.0	9.79	7.86	7.57
CaO	6.49	10.3	10.6	10.6
Na_2O	1.36	2.01	2.05	2.15
K_2O	.20	.25	.22	.33
H_2O^+	.20	.04	.17	.36
H_2O^-	.08	.07	.27	.05
TiO_2	1.33	1.95	1.97	2.14
P_2O_5	.14	.18	.16	.24
MnO	.12	.17	.17	.16
CO_2	.04	.03	.28	<.01
Total	100.0	100.1	100.4	98.4
	Trace elements (ppm)			
Rb	4	3	<2	8
Sr	168	244	244	296
Y	14	22	25	24
Zr	77	100	97	131
Nb	<5	<5	7	12

xenocrysts, and rare small gabbroic xenoliths. The olivine-porphyritic and picritic samples plot on olivine-control lines and can be related by fractionation and accumulation of olivine of variable forsterite content. Hualalai tholeiitic basalt has trace-element and isotopic ratios distinct from Mauna Loa, Kilauea, and Loihi tholeiitic basalt and is also isotopically distinct from the overlying alkalic basalt (Clague, 1982). These differences are illustrated in table 20.4, which shows that Hualalai tholeiitic basalt is most similar to that of Mauna Loa, but that the trace-element and isotopic differences between tholeiitic basalt from the different volcanoes require that the source regions be different compositionally. The large variations in La/Yb and La/Y ratios indicate a major role for garnet in the generation of Hawaiian tholeiitic basalt. Further modeling of the major-element, trace-element, and isotopic data is in progress and will be presented elsewhere.

TABLE 20.4.—*Elemental and isotopic ratios in tholeiitic lava from Hualalai and other Hawaiian volcanoes*

[Helium data from Kurz and others (1983); other data from Clague (1982)]

	Hualalai	Mauna Loa	Kilauea	Loihi
La/Sm	2.2	1.8–2.0	2.2–2.8	2.4
La/Yb	3.6	4–5	6–8	6.0
La/Y	.36	.4	.5– .7	.55
K_2O/P_2O_5	1.7	1.8	2.0	1.5
$^{87}Sr/^{86}Sr$	.70373	.70374–.70386	.70348–.70379	.70347–.70357
$(^3He/^4He)_{Atm}$	14.4–17.6	8.0–8.6	13.4–14.7	24.4–31.9

TABLE 20.5.—*Compositions of trachyte samples from Hualalai Volcano*

[Data for HAW-15 from Basaltic Volcanism Study Project (1981). Samples 67–101A and 67–104 are accidental blocks collected by T. Wright. Analyses are classical wet chemistry by G. Riddle of the USGS; --, not determined]

Vent	Pau Waawaa	Waha Pele	Unnamed vent 3 km northeast of Waha Pele
Sample	HAW-15	67-101A	67-104
	Major elements (weight percent)		
SiO_2	62.99	63.10	62.84
Al_2O_3	18.04	17.79	17.86
Fe_2O_3	4.42	2.24	2.67
FeO	0	1.35	.90
MnO	.32	.52	.49
CaO	.71	0.79	.66
Na_2O	7.19	7.63	7.18
K_2O	4.87	4.97	4.90
H_2O^+	1.31	.26	.67
H_2O^-	1.31	.04	.16
TiO_2	.45	.50	.48
P_2O_5	.13	.12	.13
MnO	.29	.30	.27
CO_2	.11	.00	.00
Cl	--	.06	.01
F	--	.09	.08
Total	100.8	99.71	99.27
	Trace elements (ppm)		
Rb	108	--	--
Sr	48	--	--
Y	23	--	--
Zr	905	--	--
Nb	127	--	--

ALKALIC STAGE

The surficial flows of Hualalai Volcano are alkali olivine basalt or basalt transitional to hawaiite, with the exception of the Waawaa Trachyte Member cone and its flow. Trachyte also occurs as blocks in the maar deposit at Waha Pele, as a subsurface flow (drilled near the 1801 vents, figs. 20.1, 20.5), and as small chips in the cinder deposits of two other vents. These occurrences suggest that trachyte is relatively widespread on Hualalai, but that most exposures have been buried beneath subsequent alkalic basalt flows. Chemical analyses of trachyte from three of these locations are presented in table 20.5, and the locations are shown in figure 20.1. Some of the trachyte samples contain rare (<2 percent) modal nepheline.

Clague and others (1980) presented geochemical data for 17 samples of prehistoric alkali basalt flows and 15 samples from the 01 eruptions. They reached the following conclusions: (1) The historical flows are nearly homogeneous, although several samples reflect accumulation and resorption of olivine, plagioclase, and clinopyroxene xenocrysts. (2) The prehistoric flows are chemically similar to the historical flows, although they include lava that underwent fractionation leading to hawaiite. (3) The alkalic basalt magma can be derived by 5–10 percent partial melting of a garnet-bearing source that is enriched in the light rare-earth elements. (4) The source region for alkalic basalt beneath Hualalai is particularly rich in K_2O compared to that beneath other Hawaiian volcanoes.

Some of the alkali basalt vent deposits are aphyric, whereas others contain phenocrysts of olivine, olivine and plagioclase, or olivine, clinopyroxene, and plagioclase (table 20.6). The most abundant lava type is olivine-porphyritic basalt. There is no clear correlation of phenocryst mineralogy with either age or location of the vents on the volcano; however, as noted earlier, clusters of vents with similar mineralogy occur locally.

TABLE 20.6.—*Comparative abundance of phenocryst assemblages in samples of alkali basalt from Hualalai Volcano*

[Based on study of 256 samples of vent deposits, bombs, and cognate blocks]

Phenocryst assemblage	Percent of samples
Olivine	37
Olivine + plagioclase	24
Olivine + pyroxene	8
Olivine + plagioclase + pyroxene	24
Plagioclase	2
Aphyric	5

We now have analyses of about 300 samples of alkalic lava representing all the vents and many flows on the modern surface. Chemical analyses of 21 dated flows are presented in table 20.7. The analyses of alkalic basalt, trachyte, and tholeiitic basalt from tables 20.3, 20.5, and 20.6 and other unpublished analyses are plotted on the Macdonald-Katsura alkali-silica diagram in figure 20.13. We have also plotted magnesium-variation diagrams (fig. 20.14) using all available analyses of Hualalai lava. In addition, Peterson and Moore (chapter 7) compare Hualalai analyses with those from other Hawaiian volcanoes. Most of the plots display wide scatter that partly reflects varied phenocryst populations. The plot of Al_2O_3 against MgO has the tightest cluster of data and best shows the importance of olivine control; some scatter occurs at the low-magnesia end, as differentiation has proceeded beyond olivine control. Alkalic lava is olivine-controlled only at relatively high MgO contents.

Part of this study was designed to evaluate changes in lava chemistry through time. Because we have not yet completed mapping all of the volcano, we cannot at this time construct a detailed stratigraphic history of the surface flows. However, we have analyses of 18 alkalic basalt flows dated by ^{14}C that range in age from 12,950 yr B.P. to the historical 1800–01 flows. These samples can be used to evaluate time-dependent compositional changes. The major- and trace-element data from these samples are given in table 20.6, arranged from oldest to youngest. We have examined K_2O/P_2O_5, Zr/Nb, Zr/Y, Rb/Sr, and K/Rb ratios as a function of time and find no correlations that indicate systematic chemical changes through the last 13,000 years of volcanic history. In addition, we have analyzed samples from the 1800 flow, the 1801 flow, and one prehistoric vent deposit for $^{87}Sr/^{86}Sr$ ratio, and all are within analytical precision at 0.70362 ± 0.00001.

The data for the younger alkalic lava, combined with that for the much older tholeiitic lava recovered from the submarine northwest rift zone, display the same inverse correlation between $^{87}Sr/^{87}Sr$ and Rb/Sr (or La/Sm) ratios seen at other Hawaiian volcanoes (Chen and Frey, 1983; Clague and others, 1983; Feigenson, 1984; Roden and others, 1984). More detailed analysis of the alkalic basalt erupted during the last 13,000 yr may show subtle time-dependent chemical variations. However, at the present time we can only compare the groups of tholeiitic and alkalic lava flows to evaluate chemical changes over long time periods. As at Haleakala, East Molokai, Kauai, and Oahu, the samples with the most enriched trace-element ratios and the least radiogenic isotopic ratios are of younger alkalic basalt. These data can be explained by mixing of melts derived from several sources (see Chen and Frey, 1983), but they imply a complex petrogenesis of the lava.

XENOLITHS

The A.D. 1800 Kaupulehu flow on Hualalai Volcano is well known for its abundant coarse-grained xenoliths (Richter and Murata, 1961; Jackson, 1968; Jackson and others, 1981), and many prehistoric vent deposits and flows also contain abundant

TABLE 20.7—*Composition of alkali basalt samples from historical and prehistoric dated flows of Hualalai Volcano*

[All ages given in years B.P. and derived from ^{14}C determinations, except for historical 1800–01 flows. Major element data from rapid wet-chemical analyses by D. Kobilis, except those for sample 67–101, average 1800, 1801 toe, and vent, which are classical wet chemical analyses from Clague and others (1980). Trace elements analyzed by energy-dispersive X-ray flourescence by W. Bohrson; except those from the historical 1800– flows, which are from Clague and others (1980). --, not determined]

Sample	82-1A	79-1	78-11	78-5	79-10	82-23	82-131	78-12	81-22	82-7	81-92	81-47	81-86	82-129	81-152	81-153	67-101	81-91	Avg 1800	Toe 1801	Vent 1801
Age	12,950	12,230	10,370	9,490	4,720	4,390	3,990	3,600	2,670	2,390	2,350	2,290	1,180	1,030	900	900	710	300	150	149	149
Major elements (weight percent)																					
SiO_2	45.6	46.2	47.0	46.0	46.5	46.1	46.3	47.7	46.9	47.9	46.7	47.5	45.9	47.1	46.6	47.3	46.74	47.3	46.55	46.10	46.48
Al_2O_3	13.7	11.8	10.9	12.8	13.2	12.9	13.9	15.2	14.8	15.4	14.1	13.8	13.9	14.4	14.9	13.9	14.60	16.2	14.64	13.18	14.67
Fe_2O_3	3.8	1.5	1.8	2.9	3.2	2.6	5.7	2.6	7.9	2.8	2.5	5.5	4.6	2.1	3.0	3.4	2.12	1.8	2.97	3.30	2.36
FeO	8.4	10.4	10.4	9.1	9.1	9.6	6.8	10.1	5.2	10.3	9.5	7.0	8.1	10.7	9.6	9.7	10.35	10.3	9.80	8.86	10.24
MgO	10.8	13.5	14.7	10.5	10.7	11.2	11.3	5.4	6.7	6.0	9.6	10.0	9.7	9.7	8.7	10.3	9.20	6.1	9.04	11.86	9.17
CaO	10.4	10.1	9.3	11.5	10.2	10.1	10.0	10.1	10.3	8.7	10.3	10.4	9.8	10.4	10.2	8.0	10.67	8.3	10.15	11.41	10.35
Na_2O	2.2	2.2	2.1	2.3	2.5	2.3	2.4	3.2	3.3	3.6	2.5	2.5	2.4	2.6	2.8	3.0	2.71	3.6	2.90	2.26	2.77
K_2O	.65	.65	.56	.78	.83	.76	.69	1.27	1.17	1.2	.69	1.03	1.21	.9	.85	1.15	.811	1.37	.91	.66	.87
H_2O^+	.99	.21	.21	.25	.13	.67	.83	.22	.46	.57	.20	.22	.19	.65	.38	.48	.10	.16	.07	.02	.09
H_2O^-	--	.05	.03	.11	.05	--	--	.12	.10	--	.07	.19	.22	--	.09	--	.06	.19	.05	.02	.05
TiO_2	2.1	1.9	1.9	2.0	2.0	1.9	2.0	2.9	2.5	2.7	1.9	2.2	2.3	2.3	2.2	2.2	2.06	2.6	2.40	1.82	2.27
P_2O_5	.24	.22	.20	.27	.28	.25	.27	.38	.37	.43	.27	.32	.33	.31	.31	.36	.25	.47	.28	.22	.28
MnO	.19	.20	.18	.21	.21	.14	.16	.20	.18	.17	.17	.19	.18	.18	.23	.21	.18	.19	.19	.18	.19
CO_2	.01	.02	.02	.02	.02	.02	.02	.02	.02	.02	.02	.02	.02	.04	.02	.02	.01	.02	.01	.02	.01
Cl	--	--	--	--	--	--	--	--	--	--	--	--	--	--	--	--	.02	--	.03	.03	.03
F	--	--	--	--	--	--	--	--	--	--	--	--	--	--	--	--	.06	--	.05	.04	.06
Total	99.1	99.0	99.3	98.7	98.9	98.5	100.4	99.4	99.9	99.8	98.5	100.9	98.9	101.4	99.9	100.0	99.94	98.6	100.04	99.98	99.89
Trace elements (ppm)																					
Rb	15	11	14	--	16	30	28	28	32	37	19	25	32	35	24	21	18	40	34	31	34
Sr	380	340	267	--	411	408	412	510	487	599	347	425	468	430	441	438	424	582	456	360	417
Y	19	21	14	--	21	21	22	29	28	25	21	20	22	22	21	19	23	31	21	17	18
Zr	114	113	87	--	123	119	122	181	177	202	121	138	144	151	134	134	137	215	147	115	143
Nb	15	18	13	--	22	19	20	35	31	32	16	18	24	22	18	18	22	38	--	--	--
Ni	252	420	533	--	312	331	330	58	101	71	229	210	233	206	166	134	187	76	152	520	290

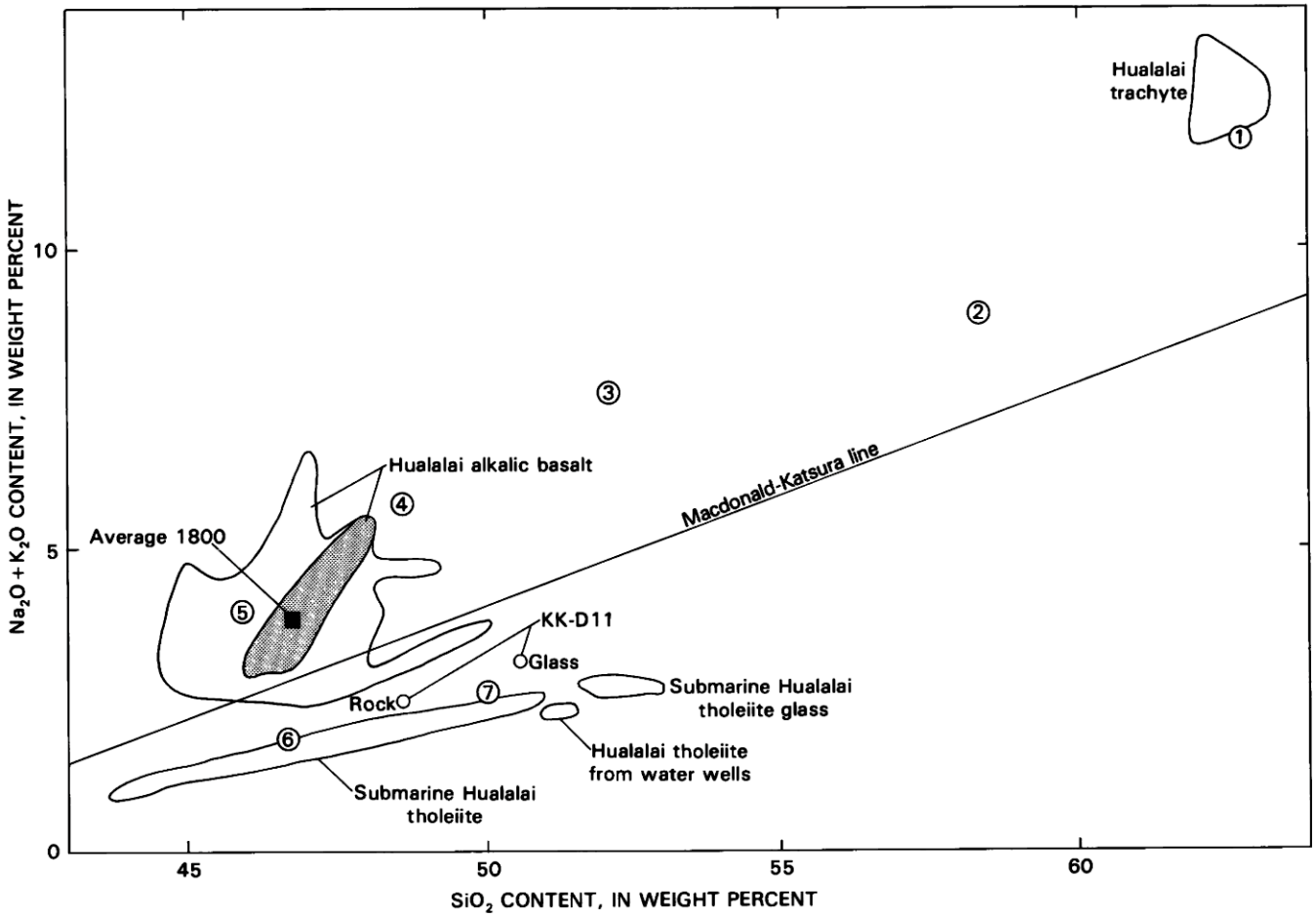

FIGURE 20.13.—Alkali-silica diagram showing the fields for Hualalai lava groups. Shaded Hualalai alkalic basalt field is from Clague and others (1980) and large unshaded field is based on about 300 new analyses. Sample KK–D11, dredged from northwest rift zone, is chemically distinct from other dredged or drilled tholeiitic samples in that it has higher alkali contents and has trace-element signature intermediate between tholeiitic basalt and alkalic basalt. Circled numbers are average Hawaiian compositions from Macdonald (1968): 1, trachyte; 2, benmoreite; 3, mugearite; 4, hawaiite; 5, alkalic basalt; 6, picritic tholeiitic basalt; 7, tholeiitic basalt.

xenoliths. Richter and Murata (1961) briefly described the remarkable occurrence of xenoliths in discrete cobble beds at about 950 m elevation in the Kaupulehu flow. More recently, Jackson and Clague (1982) presented a detailed plane-table map of this site, and Jackson and others (1981) presented data on the lithology, size, shape, density, mineralogy, and chemistry of xenoliths from the site. During our detailed mapping of Hualalai Volcano we have discovered numerous additional vents and flows and several pyroclastic deposits that contain xenoliths, commonly in great numbers. These sites are shown on figure 20.1. With a few exceptions, these new sites, like those described previously, contain dunite and gabbro xenoliths; no lherzolite or garnet-bearing xenoliths have been found. A few vents and flows have either nearly all dunite or nearly all gabbro.

Three sites are distinctive in that the coarse-grained xenoliths occur in pyroclastic deposits; these include the gabbro and diabase xenoliths in a tuff at Hainoa Crater (fig. 20.1), angular blocks of gabbro and syenite as loose blocks on the surface in the vicinity of Malekule (fig. 20.5), and a lag deposit of mainly dunite with less common wehrlite and gabbro from just east of Hainoa Crater. The lag deposit apparently formed as a wind-winnowed cinder deposit, but the other two deposits resulted from phreatic eruptions. The xenoliths in the tuff surrounding Hainoa Crater are mostly diabase with accumulated olivine and clinopyroxene; they probably formed as cumulates in a lava lake within the crater. The xenoliths in the area of Malekule include gabbro and varieties of syenite bearing biotite, apatite, or zircon. These samples apparently represent the cumulates formed in a shallow magma reservoir associated with trachyte erupted early in the alkalic stage at Puu Waawaa and other locations.

Xenoliths in the 1800 Kaupulehu flow are dominantly dunite and wehrlite with metamorphic textures (Kirby and Green, 1980). Only five percent of the xenoliths are dikes, sills, and veins, whereas about one-third are cumulates ranging from dunite, wehrlite, troctolite, clinopyroxene gabbro, and olivine-clinopyroxene gabbro to anorthosite. Orthopyroxene-bearing xenoliths are rare but include

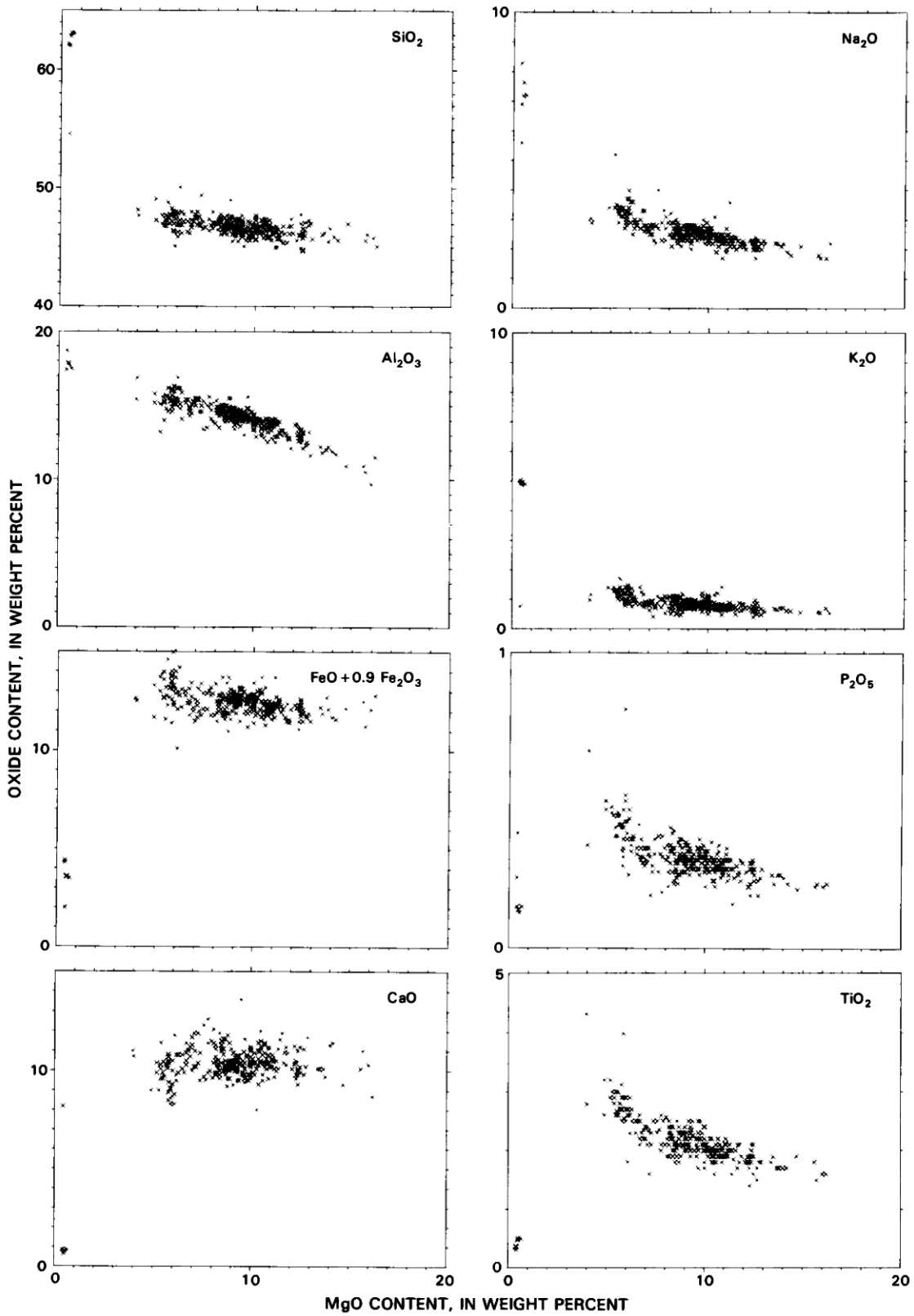

FIGURE 20.14.—Magnesia-variation diagrams for alkalic lava samples from Hualalai Volcano.

websterite and norite. Preliminary analysis of these samples indicates that some are probably cumulates related to the alkalic and tholeiitic lava of Hualalai Volcano, whereas others are related to tholeiitic basalt of the underlying oceanic crust (D.A. Clague, unpub. data, 1985).

The presence of rocks from the oceanic crust, and the pressure inferred from CO_2 inclusions in olivine (Roedder, 1965) in the dunite xenoliths, indicate that the host lava rose rapidly from a depth of about 15–20 km. Clague and others (1980) infer from the lava compositions that some fractionation occurred prior to incorporation of the xenoliths and suggest that the magma fractionated at depth. We propose that this fractionation occurred near the base of the oceanic crust at a depth of about 20 km.

The few rare xenoliths found in the tholeiitic lava dredged from the northwest rift zone are shallow level cumulates similar to those that occur in tholeiitic lava from other Hawaiian volcanoes (Jackson, 1968).

GEOPHYSICAL STUDIES AND GEOTHERMAL POTENTIAL

SEISMICITY

The Hawaiian Volcano Observatory (HVO) has maintained a seismic station 3 km east of Hualalai's summit since 1971. During the last 16 years, no swarms of microearthquakes nor any harmonic tremor from a source beneath Hualalai were recorded. Each year, however, several magnitude-4 earthquakes occur on Hualalai, most commonly from a fairly deep source just off the coast near the northwest rift zone (HVO, unpub. data). This seismicity apparently is not related to magmatic movement within the volcano.

In 1929, an intense swarm of earthquakes, lasting over a month, occurred beneath Hualalai (Macdonald and others, 1983). It seems likely that magma was intruded close to the surface at that time.

GRAVITY

Hualalai is unique among the five volcanoes on the Island of Hawaii in having a gravity high of rather low amplitude that is offset from its summit and rift zones (Kinoshita and others, 1963). The amplitude of this anomaly is 50–60 mGal less than the anomalies over the other four volcanoes. The closed high is nearly 20 km south of Hualalai's summit and appears to be more related to the Kealakekua fault system on the west flank of Mauna Loa than to Hualalai. We suggest that the relatively low gravity (250 mGal) over Hualalai's summit and rift zones reflects the presence of relatively low density trachyte that is thinly mantled with mafic lava.

AEROMAGNETICS

The aeromagnetic data for Hualalai (Godson and others, 1981) are even more striking than the gravity data. Hualalai is the only one of Hawaii's five volcanoes with a pronounced aeromagnetic low over its rift zones and summit area. We interpret these results in the same manner as the gravity data: Hualalai's rift zones and summit are underlain by relatively nonmagnetic material, that is, trachyte. The alternative view, that there is abundant magma above the Curie temperature at shallow levels, seems less likely, given the relative lack of seismicity or significant ground deformation.

ELECTRICAL GEOPHYSICAL STUDIES

Jackson and Sako (1982) have run numerous electrical self-potential traverses across the rift zones and summit area of Hualalai. They report that Hualalai has anomalies similar to those over known heat sources on Kilauea Volcano. They estimate that the depths to the tops of the sources of anomalies near the 1800 vents and near the summit are 200 m and 500 m, respectively. We suggest that the heat probably is residual and associated with a cooling magma body emplaced in 1800.

Kauahikaua and Mattice (1981) carried out resistivity surveys on Hualalai; they found low-resistivity layers beneath the summit and near the 1801 vents and suggested that they might be targets for future geothermal exploration. We suggest that further exploration of the entire northwest rift zone for potential geothermal resources is warranted. The infrequency of eruptions combined with the significant self-potential and resistivity anomalies make Hualalai an attractive target.

VOLCANIC HAZARDS

The stratigraphic and geochronologic data that we have obtained permit a preliminary assessment of the hazards that future eruptions of Hualalai pose to the burgeoning population in the Kona district. These hazards are of two general types, caused by pyroclastic materials and by lava flows.

Pyroclastic deposits on Hualalai generally are of two types: the dominant type is cinders and spatter associated with cone or rampart building at vents; less abundant is debris resulting from explosive phreatic eruptions. The latter are quite rare, although two of the last three major eruptions (those of Luamakami about 300 years ago and Waha Pele about 700 yr ago) included explosive events. At Luamakami (fig. 20.8), phreatic explosions near the end of the eruption ejected blocks of thermally metamorphosed basalt as much as 1 m in diameter at least 100 m from the vent. The affected area was quite small, however; probably less than 0.5 km^2 was devastated.

Explosive phreatic eruptions that preceded basaltic effusion at Waha Pele were more significant. As mentioned earlier, ascending basaltic magma caused violent steam eruptions that ejected blocks of trachyte, picritic tholeiite, and alkali basalt as large as 0.4 m in diameter; fine ash covered an area of at least 10 km^2. This eruption likely would have destroyed anything living nearby, but its effects did not extend to the coast 16 km away, where both ancient and modern people as well as commerce have been concentrated.

Eruptions near sea level on the lower northwest rift zone, by analogy with the 1960 eruption of Kilauea (Richter and others, 1970), could result in local phreatic explosions during dominant Strombolian and effusive activity. Most vent deposits on Hualalai have formed typical cinder-and-spatter cones and spatter ramparts. Although the wide dispersal of cinders from some vents indicates that the eruptions may have been sub-Plinian, it seems unlikely that such eruptions would threaten populated areas.

Lava flows pose by far the greater danger. Hualalai's summit is only 15 km from Kailua; the average topographic gradient across the distance is 168 m/km, corresponding to a 9.5° slope. A flow as voluminous and fluid as that of 1800 could cover that distance in a few hours. Recent (younger than 3,000 yr B.P.) flows have originated at vents that are fairly evenly spaced along the northwest and south-southeast rift zones (fig. 20.5). Thus we cannot predict on that basis where the next activity will occur. On the other hand, the youthfulness of the terrain north of Kailua and the presence of the large self-potential anomaly near the 1800 vents imply that the next eruption may occur on the northwest rift zone. The location of the vent relative to the topographic axis of the rift is critical; a few tens or hundreds of meters to the north or south may determine whether the flows go north over relatively unpopulated ranchland or southwest into populated, industrialized areas. A flow from the southeast rift zone, if it gets within one or two kilometers of the sea, could also be devastating; total property values on the 700-year-old Waha Pele flow are approaching $1 billion. It seems unlikely that mitigating measures, such as diversion barriers, would be effective—the Waha Pele flow locally is more than 15 m thick and is 1.3 km wide at the ocean. Depending on the speed and size of any future flow, evacuation may be the only feasible measure.

The eruptive recurrence interval of Hualalai for all of Holocene time is on the order of 50 years (about 200 eruptions in 10,000 yr), though much longer for any specific point on it. However, our mapping and ^{14}C dating indicate that eruptions have occurred in clusters (groups of several eruptions over a few hundred years, separated by several centuries of inactivity). The current lack of magma-related seismicity and deformation provides no information about when the next eruption might occur. In 1800 the magma ascended quite rapidly from a depth of 15–20 km (Clague and others, 1980), judging from the size and abundance of the mafic and ultramafic xenoliths that it carried up from that depth. This rapid ascent implies that seismic detection of shallow, magmatic movement may precede actual eruptive activity by only a short time. The intervals between the latest Holocene eruptions, including the 186 years since the last one, lead us to suggest that a Hualalai eruption is highly probable within the next 200 years and could well occur during the next few decades.

REFERENCES CITED

Basaltic Volcanism Study Project, 1981, Basaltic volcanism of the terrestrial planets: New York, Permagon Press, 1,286 p.

Brigham, W.T., 1909, The volcanoes of Kilauea and Mauna Loa: B.P. Bishop Museum Memoir, v. 2, no. 4, 222 p.

Campbell, J.F., and Erlandson, D., 1979, OTEC-1 anchor site survey: Hawaii Institute of Geophysics Report, 55 p.

Chen, C.-Y., and Frey, F.A., 1983, Origin of Hawaiian tholeiites and alkalic basalts: Nature, v. 302, p. 785–789.

Clague, D.A., 1982, Petrology of tholeiitic basalt dredged from Hualalai Volcano, Hawaii [abs.]: Eos, American Geophysical Union Transactions, v. 63, p. 1138.

Clague, D.A., Frey, F.A., and Beeson, M., 1983, Rare-earth element and Sr isotopic evidence for the origin of the East Molokai Volcanics, Hawaii: Eos, American Geophysical Union Transactions, v. 64, p. 902.

Clague, D.A., Jackson, E.D., and Wright, T.L., 1980, Petrology of Hualalai Volcano, Hawaii: Implications for mantle composition: Bulletin Volcanologique, v. 43–4, p. 641–656.

Feigenson, M.D., 1984, Geochemistry of Kauai Volcanics and a mixing model for the origin of Hawaiian alkalic basalts: Contributions to Mineralogy and Petrology, v. 87, p. 109–119.

Funkhouser, J.G., Barnes, I.L., and Naughton, J.J., 1968, The determination of a series of ages of Hawaiian volcanoes by the potassium-argon method: Pacific Science, v. 22, p. 369–372.

Godson, R.H., Zablocki, C.J., Pierce, H.A., Frayser, J.B., Mitchell, C.M., and Sneddon, R.A., 1981, Aeromagnetic map of the Island of Hawaii: U.S. Geological Survey Geophysical Investigations Map GP–946, scale 1:250,000.

Holcomb, R.T., 1981, Kilauea Volcano, Hawaii: chronology and morphology of the surficial lava flows: U.S. Geological Survey Open-File Report 81–0354, 321 p.

Jackson, D.B., and Sako, M.K., 1982, Self-potential surveys related to probable geothermal anomalies, Hualalai Volcano, Hawaii: U.S. Geological Survey Open-File Report 82–127, 10 p.

Jackson, E.D., 1968, The character of the lower crust and upper mantle beneath the Hawaiian Islands: International Geological Congress, Prague, 23d, Proceedings, p. 135–150.

Jackson, E.D., and Clague, D.A., 1982, Map showing distribution of the nodule beds of the 1800–1801 Kaupulehu flow of Hualalai Volcano, Island of Hawaii: U.S. Geological Survey Miscellaneous Field Studies Map MF–1355, scale 1:1200.

Jackson, E.D., Clague, D.A., Engleman, E., Friesen, W.F., and Norton, D., 1981, Xenoliths in the alkalic basalt flows of Hualalai Volcano, Hawaii: U.S. Geological Survey Open-File Report 81–1031, 33 p.

Kauahikaua, J.P., and Mattice, M., 1981, Geophysical reconnaissance of prospective geothermal areas on the Island of Hawaii using electrical methods: U.S. Geological Survey Open-File Report 81–1044, 50 p.

Kinoshita, W.T., Krivoy, H.L., Mabey, D.R., and Macdonald, R.R., 1963, Gravity survey of the Island of Hawaii: U.S. Geological Survey Professional Paper 475–C, p. C114–C116.

Kirby, S.H., and Green, H.W., 1980, Dunite xenoliths from Hualalai Volcano: Evidence for mantle diapiric flow beneath the Island of Hawaii: American Journal of Sciences, v. 280-A, p. 550–575.

Kurz, M.D., Jenkin W.J., Hart, S.R., and Clague, D.A., 1983, Helium isotopic

variations in volcanic rocks from Loihi Seamount and the Island of Hawaii: Earth and Planetary Science Letters, v. 66, p. 388–406.

Macdonald, G.A., 1955, Hawaiian Islands: Catalog of the active volcanoes of the world including solfatara fields, Part III: International Volcanological Association, Naples, Italy, 37 p.

———1968, Composition and origin of Hawaiian lavas: Geological Society of America Memoir 116, pp. 477–522.

Macdonald, G.A., Abbott, A.T., and Peterson, F.L., 1983, Volcanoes in the sea (2nd ed.): Honolulu, University of Hawaii Press, 517 p.

Richter, D.H., Eaton, J.P., Murata, K.J., Ault, W.U., and Krivoy, H.L., 1970, Chronological narrative of the 1959–60 eruption of Kilauea Volcano, Hawaii: U.S. Geological Survey Professional Paper 537–E, 73 p.

Richter, D.H., and Murata, K.J., 1961, Xenolithic nodules in the 1800–1801 Kaupulehu flow of Hualalai Volcano, Hawaii: U.S. Geological Survey Professional Paper 424–B, p. B215–B217.

Roden, M.F., Frey, F.A., and Clague, D.A., 1984, Geochemistry of tholeiitic and alkalic lavas from the Koolau Range, Oahu, Hawaii: Implications for Hawaiian volcanism: Earth and Planetary Science Letters, v. 69, p. 144 158.

Roedder, E., 1965, Liquid CO_2 inclusions in olivine-bearing nodules and phenocrysts from basalts: American Mineralogist, v. 50, p. 1746–1782.

Stearns, H.T., and Macdonald, G.A., 1946, Geology and ground-water resources of the Island of Hawaii: Hawaii Division of Hydrography Bulletin 9, 363 p.

PLEISTOCENE SUBGLACIAL ERUPTIONS ON MAUNA KEA

By Stephen C. Porter[1]

ABSTRACT

A distinctive assemblage of pyroclastic cones and lava flows inside the limit of Pleistocene glaciation on the upper slopes of Mauna Kea Volcano is attributed to subglacial eruptions during two intervals when an ice cap mantled the summit of the mountain. During the Waihu glaciation, when an ice cap of about 140 km² formed, eruptions built two pyroclastic cones composed of hyaloclastite tuff capped by subaerially erupted bomb-bearing cinder deposits. Associated lava flows have steep embayed margins and glassy surfaces, and are locally palagonitized. A bouldery conglomerate on the southwestern flank of the volcano is inferred to have resulted from floods caused by failure of glacier-impounded lakes that formed over the erupting vents.

A younger group of cones and lava flows was erupted during the Makanaka glaciation, when a smaller ice cap (70 km²) mantled the summit. A seismic discontinuity in one of these cones may mark a boundary between a hyaloclastite core and overlying hydrothermally altered cinders that are exposed locally. Associated lavas are characterized by steep margins, pillows, glassy surfaces, spiracles, and palagonitized zones. The morphology of flow margins suggests that ice was thin along rift zones but thickened away from them.

Stratigraphic relations and radiometric ages show that the Waihu-age eruptions occurred during marine isotope stage 6 and the Makanaka-age eruptions took place either during stage 3 or near the end of stage 4. Although firm evidence of subglacial eruptions earlier than the Waihu glaciation is lacking, such events are likely to have occurred during the Pohakuloa glaciation (isotope stage 8) at the close of the tholeiitic shield-building phase of Mauna Kea's growth.

INTRODUCTION

The phenomenon of subglacial volcanic eruptions has been well documented through studies of distinctive ice-contact volcanic rocks and landforms in Iceland, western Canada, and Antarctica. In each of these regions volcanoes have erupted in environments subjected to repeated and widespread glaciation. In tropical latitudes, where modern and former snowlines lie at high elevations and evidence of past glaciation is far more restricted, the opportunities for glacier-volcano interaction are less common. One of the best-documented records of such activity is from the upper slopes of Mauna Kea, the only Hawaiian volcano on which evidence of past glaciation has been found (fig. 21.1).

Glacial features on Mauna Kea were first reported by Daly (1910) and investigated more fully by Wentworth and Powers (1941) and by Stearns (1945) and Stearns and Macdonald (1946). Although Stearns speculated that a distinctive conglomerate on the south slope of the mountain may have resulted from floods caused by eruptions that melted an ice cap, supportive evidence for such events has been forthcoming only during recent stratigraphic and sedimentologic studies of the glacial and volcanic succession on the upper slopes of the mountain (Porter, 1979a, b). This evidence points to subglacial volcanic activity during at least two intervals when the summit region was mantled with an extensive ice cap. The resulting landforms and deposits, which are analogous to subglacial phenomena described from higher latitudes, are unique in Hawaii and are confined to the area within the defined limits of successive Pleistocene glaciers.

Stratigraphic nomenclature used in this chapter is that of Langenheim and Clague (chapter 1, part II).

ACKNOWLEDGMENTS

Critical reviews and constructive suggestions by William E. Scott and William S. Wise are gratefully acknowledged. This research was supported by the Earth Sciences Section, National Science Foundation through Grants GA–20320 and DES74–16379.

GLACIAL RECORD

STRATIGRAPHIC SEQUENCE ON MAUNA KEA

Exposed volcanic rocks and sediments on Mauna Kea are divided into two major lithologic successions (fig. 21.2). The Hamakua Volcanics includes a thick tholeiitic assemblage, which forms the main volcanic shield, and the overlying Hopukani Volcanic Member and the Pohakuloa Glacial Member. The Hopukani Volcanic Member comprises lavas and related pyroclastic cones exposed mainly below an elevation of 1,000 m, where they are discontinuously mantled by younger lavas.

The sediments of the Pohakuloa Glacial Member lie at or near the top of the Hopukani lavas, which were their source rocks. Although the Pohakuloa sediments were inferred by Stearns (1945) to be an explosion breccia, a variety of characteristics, including

[1]Quaternary Research Center, University of Washington, Seattle, Washington 98195.

sedimentary facies (till and outwash), grain-size distribution, clast fabric and angularity, faceted clasts, presence of striated lava surfaces underlying the unit, and absence of bomb sags, point to a glacial origin (Porter, 1979a). Exposed only in several gulches that indent the upper south slope of the volcano, the Pohakuloa Glacial Member constitutes the oldest exposed evidence of glaciation on Mauna Kea.

The overlying Laupahoehoe Volcanics consists of a widely exposed sequence of alkalic lavas and pyroclastic layers (Waikahalulu Volcanic Member), and sedimentary strata; it is much thinner than the Hamakua Volcanics. Lavas are predominantly blocky hawaiite aa flows that issued from vents near the summit and along the rift zones. On the upper slopes, a succession of superimposed flows reaches a thickness of 100 m or more, but on the lower slopes, where commonly only a single flow overlies lavas of the Hamakua Volcanics, thicknesses of 30 m or less are typical. Associated pyroclastic cones are composed of dark-gray or reddish cinders, scoria, and bombs.

Three layers of glacial drift are interstratified with lavas of the Laupahoehoe Volcanics. The Waihu Glacial Member is exposed mainly in kipukas (inliers) on the southwest slope of the volcano below an elevation of about 3,350 m. Elsewhere it is largely covered by younger lava flows and glacial deposits. A belt of Waihu moraines west of Waikahalulu Gulch is overlapped by younger lavas that pass upslope beneath post-Waihu end moraines. Where the Waihu drift is exposed at the surface, it has been substantially modified by weathering and erosion. Commonly the drift is highly indurated and forms steep cliffs along gulches. End moraines,

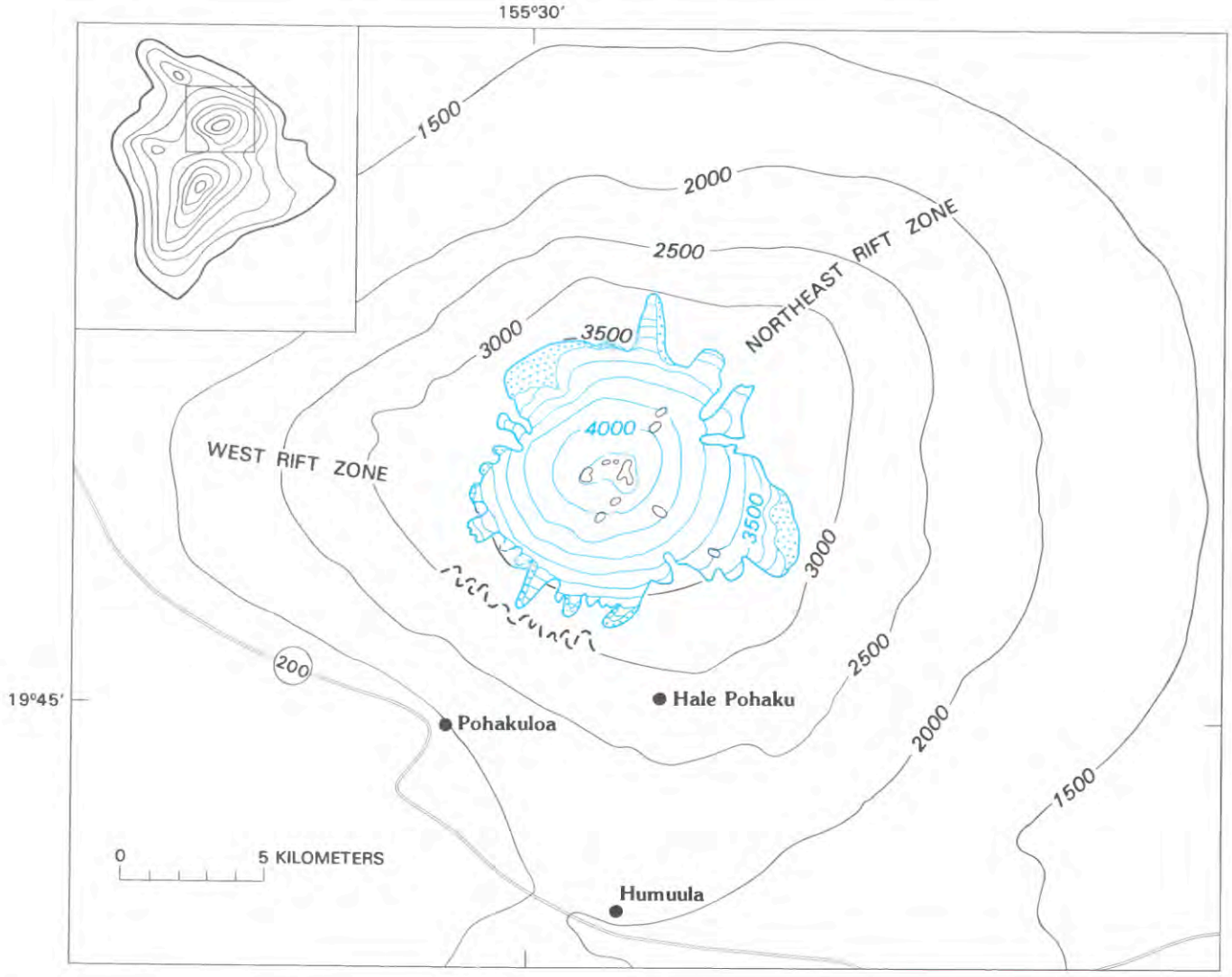

FIGURE 21.1.—Map of upper slopes of Mauna Kea showing reconstructed ice cap (blue) of the late Makanaka glaciation and the nunataks (white) that rose above it. Contour interval 500 m, with 100-m interval for ice cap. Shaded pattern shows extent of early Makanaka drift beyond late Makanaka ice limit. Known extent of more-extensive Waihu glacier is shown by heavy dashed line on the southwest flank.

however, are subdued. In places, tor-like pinnacles of drift standing up to 3 m high indicate the minimum erosion that has occurred since the moraines were deposited. Associated outwash gravels mantle the lower southwest slope of the mountain below the belt of moraines, and a dissected outwash fan lies at the base of Waikahalulu Gulch. Surface stones tend to be deeply pitted or spalled, and most have brownish oxidation rinds 1–2 mm thick.

The Makanaka Glacial Member includes two bodies of drift, the older of which is bordered by end moraines that are exposed discontinuously around the summit area. The older Makanaka drift is less indurated than Waihu drift, and surface stones are stained light yellowish brown. In many places it is buried by younger lavas or by younger drift of late Makanaka age. The younger drift forms conspicuous arcuate moraines around much of the summit area at about the 3,500-m level, as well as prominent lateral moraines along several major gulches. Above the drift limit, low recessional moraines are found, especially on the southeast and southwest slopes of the mountain. Striated lava surfaces are widespread on the summit plateau above about 3,600 m. The younger drift is little weathered, and soil profiles are thin and weakly developed. Associated meltwater sediments are confined largely to the floors of gulches and to the plain at the south base of the mountain.

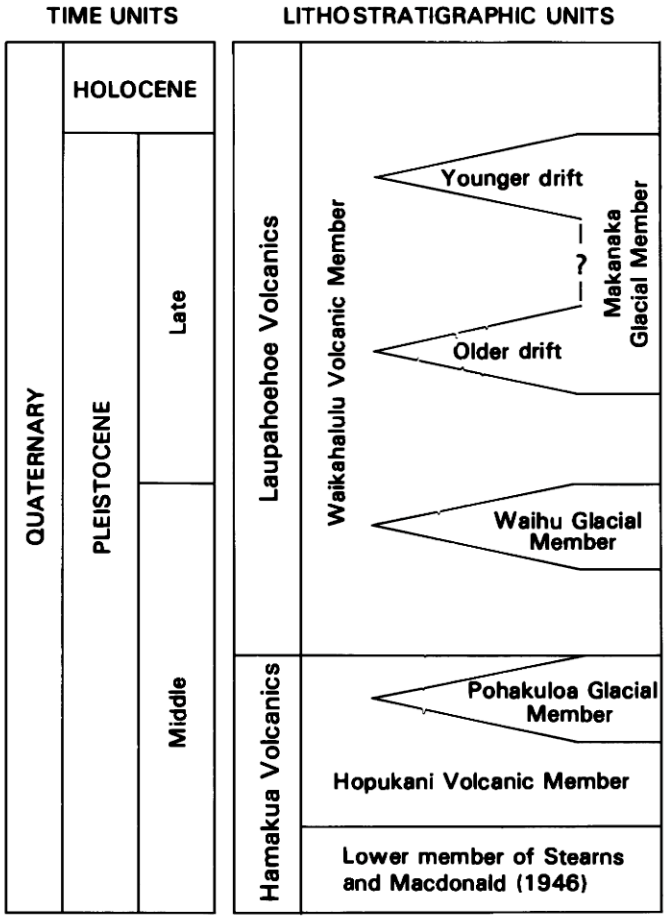

FIGURE 21.2.—Lithostratigraphic units on upper slopes of Mauna Kea, showing relation to geologic time scale (modified from Porter, 1979a).

PLEISTOCENE ICE CAPS

The ice cap of late Makanaka time can be reconstructed in considerable detail using abundant ice-limit data in the summit region (Porter, 1979b). Radial profiles, based on end moraines and on upper limits of erratic stones on cinder cones within the drift limit, were constructed along various flow lines, as inferred from striations and other ice-flow directional indicators. The profiles were then extrapolated to the summit less than 2 km away. Using these as a basis for contouring, the topographic configuration of the former ice cap was obtained (fig. 21.1). At its maximum advance, the glacier measured about 10.5 km in diameter, had an area of 70.5 km^2, and averaged about 75 m thick. Its volume is estimated to have been close to 5 km^3. The glacier margin was irregular, especially along the rift zones, where high-standing cinder cones caused divergence of ice flow. Tongues of ice flowing down the deepest gulches extended as low as 3,160 m, while broad lobes occupied the slopes between rift zones. Although the ice cap was broadly symmetrical about the summit region, its margin averaged somewhat higher in the northwest and northeast quadrants (3,570 m and 3,510 m, respectively) than in the southwest and southeast quadrants (3,465 m and 3,420 m, respectively), implying a southerly or southeasterly source of moisture (Porter, 1979b).

The early Makanaka ice cap apparently was only slightly larger than the younger ice cap, for in those places where the older drift limit can be mapped or inferred from stratigraphic data it lies no more than 100–200 m downslope from the late Makanaka limit. However, because early Makanaka moraines were not positively identified through some sectors on the eastern slope of the mountain (fig. 21.1), the exact shape of the glacier is not known. Although it probably was broadly similar to the late Makanaka ice cap, in detail it must have differed; during the period between the two advances, lava flows and cinder cones were erupted in the summit area, thereby causing local reorientation of glacier flow lines. During the earlier ice advance, the bedrock surface beneath the glacier must have been, on average, at least several tens of meters lower than during the later glaciation.

Less is known about the still-older Waihu ice cap, for few deposits or erosional features are exposed. In the southwestern quadrant of the mountain, the Waihu glacier deposited a belt of moraines that lie about 1.5 km beyond the Makanaka moraines and close to 3,000-m elevation (fig. 21.3). Assuming a symmetrical distribution of ice about the summit, the glacier covered an estimated area of 140 km^2. The estimated minimum ice thickness in the summit region was at least 150 m, based on analogy with the better-constrained late Makanaka glacier. The average diameter of the ice cap was between 12 and 13 km. Assuming an average thickness of 100 m, the total ice volume would have been close to 14 km^3. Because no large pyroclastic cones had yet been built near the summit, few, if any, nunataks rose above the glacier surface during the initial part of this glaciation. The glacier terminus apparently was less irregular than that of subsequent ice caps, probably because deep gulches had not yet been eroded into the flanks of the mountain and there were no prominent cinder cones that would have produced a lobate margin. Ice flow, inferred from preserved striations and

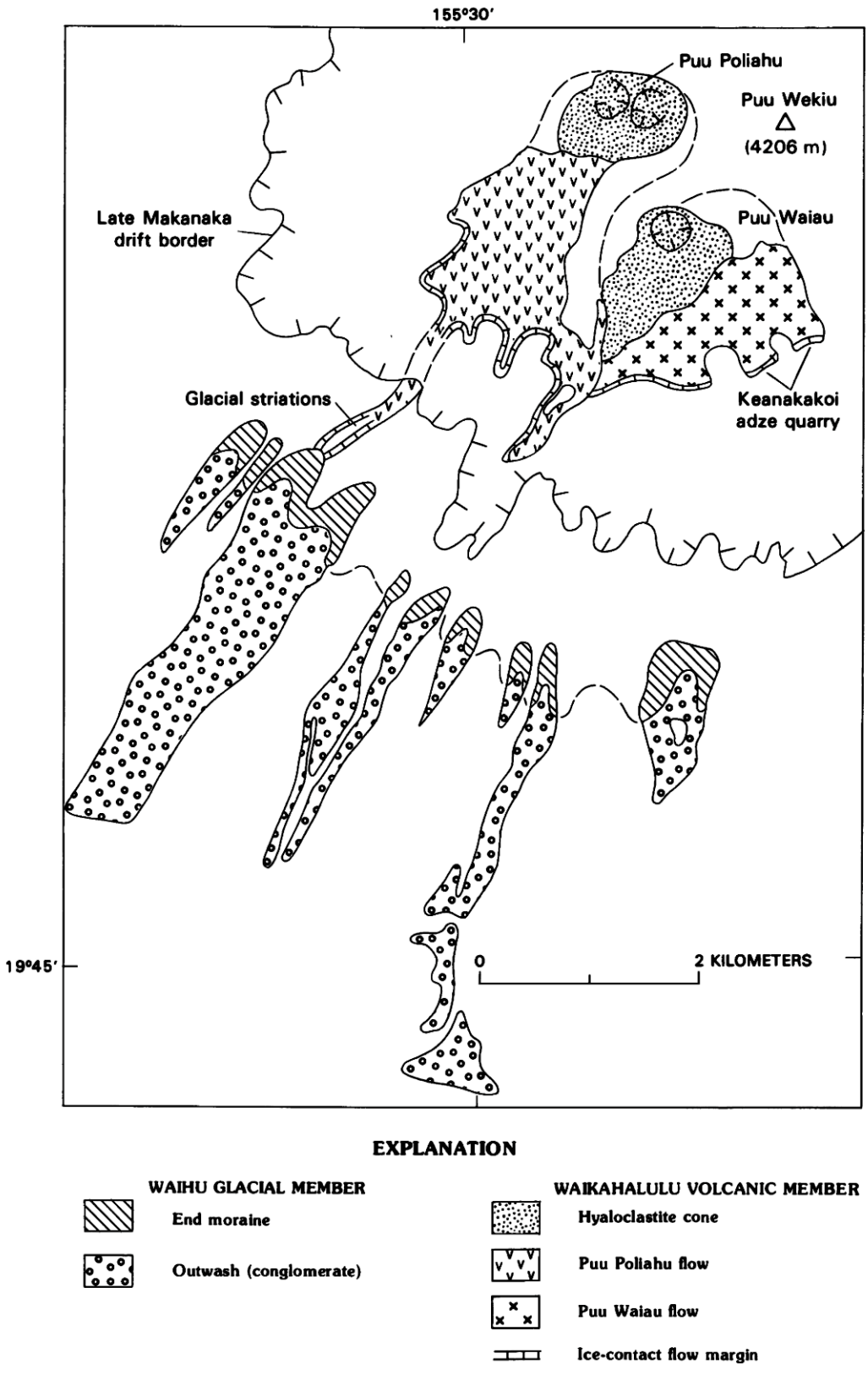

FIGURE 21.3.—Map of upper southwest slope of Mauna Kea showing distribution of intra-Waihu cones and flows with respect to Waihu end moraines and outwash deposits and to late Makanaka drift border. Dashed lines show possible extent of Waihu lava flows and moraine belt beneath younger lavas and glacial deposits.

from till fabrics, was approximately radial from the summit region.

Pohakuloa drift is seen only in several gulches on the southwest slope of the volcano, where the thickest exposures lie beneath early Waikahalulu lavas under the Waihu moraine belt. Accordingly, the Pohakuloa glacier is inferred to have been comparable in size to the Waihu ice cap, again assuming that it was symmetrically distributed about the summit region. On this basis, its areal extent was probably 130–150 km^2.

SUBGLACIAL ERUPTIONS

A distinctive assemblage of volcanic units found within the mapped limits of glaciation on Mauna Kea is unique in the Hawaiian Islands. It includes both lava flows and pyroclastic cones, built during the interval of alkalic eruptive activity, as well as associated fluvial sediments that have no known counterpart on other Hawaiian volcanoes. Detailed mapping has shown that these rocks are coeval with the Waihu and Makanaka Glacial Members, rather than with Waikahalulu volcanic rocks erupted during nonglacial intervals. Their stratigraphic association, distinctive morphology, and similarity to subglacially erupted volcanic assemblages in other parts of the world imply that they were emplaced during Pleistocene glacial episodes on Mauna Kea.

WAIHU GLACIATION

PYROCLASTIC CONES

Nearly two dozen pyroclastic cones and cone complexes lie inside the limit of the last ice cap in the summit region. Most are older than late Makanaka drift, as shown by their glacially eroded and oversteepened flanks, by erratic blocks strewn about their flanks, or by drift filling their craters. Most also are composed of dark-grayish or dark-reddish cinders, vitric ash, and bombs, as are the numerous cinder cones that lie below the limit of glaciation on the mountain.

Two cones near the summit, however, have surface morphologies and internal characteristics that are distinctly different from those of nearby cones. Puu Waiau has been largely buried by lavas on all but its southern flank, while Puu Poliahu is partly covered by younger lavas on its north, east, and southeast sides (fig. 21.3). Puu Waiau has a single crater, which contains Lake Waiau (3,968 m; fig. 21.4), whereas Puu Poliahu has two juxtaposed craters lying along an east-west axis. The slopes of nonglaciated cinder cones on Mauna Kea have angles of as great as 26°, the typical repose angle of the cinders (Porter, 1972), but the glacially eroded flanks of Puu Waiau and Puu Poliahu reach angles as great as 36° (fig. 21.5).

The uppermost 25–35 m of each of these two cones consists of typical subaerially erupted dark-gray cinders and ash containing numerous spindle bombs. Below this, however, the tephra changes character rather abruptly into a light-yellowish-brown or varicolored hyaloclastite tuff consisting of waxy, vitric particles as much as 2 cm in diameter and having concoidally fractured surfaces. The <2-mm size fraction averages 55 percent sand, 35 percent silt, and 10 percent clay. This well-bedded tuff dips 18°–20° in Puu Waiau and 20°–26° in Puu Poliahu (fig. 21.6). Bombs scattered throughout the tuff in Puu Waiau average about 50 cm in diameter, but some have diameters as great as 3 m; such bombs are less plentiful in exposed parts of Puu Poliahu. Some bombs have glassy surfaces, and some are palagonitized. Being less erodible than the enclosing tuff, bombs often remain as caps on pillars of tuff up to 2 m high.

FIGURE 21.4.—Summit region of Mauna Kea showing Puu Waiau (foreground) overlapped by steep ice-contact margin of Puu Hau Kea flow rising above Lake Waiau. Behind Puu Hau Kea (right, middle distance) rises Puu Wekiu, showing the roadcut along which hydrothermal alteration is exposed. Upper part of flow north of Puu Poliahu is visible to left of Puu Wekiu. Photograph by Agatin T. Abbott. Reprinted, by permission of University of Hawaii Press, from *Volcanoes in the Sea: The Geology of Hawaii*, second edition, by Gordon A. Macdonald, Agatin T. Abbott, and Frank L. Peterson.

FIGURE 21.5.—Puu Poliahu rising above surface of Puu Hau Kea flow; view looking north. Glacially oversteepened slope of cone facing camera has angle of 36°.

LAVA FLOWS

Distinctive hawaiite lava flows adjacent to Puu Waiau and Puu Poliahu are believed to represent later phases of the eruptions that built the cones (fig. 21.3). However, the stratigraphic relationships at the head of each flow are obscured by overlapping younger lavas and by colluvium. Their alkalic composition and their position beneath younger lavas that are coeval with Makanaka glaciation indicate that these flows are broadly post-Pohakuloa and pre-Makanaka in age (Porter, 1979a).

The front margin of the flow southwest of Puu Poliahu is marked by a steep cliff, locally up to 80 m high. In places it is deeply embayed, in contrast to the lobate fronts of most hawaiite flows. Where erosion has been slight, the flow margin has a glassy zone near its surface and is locally palagonitized. A similar flow lying south and east of Puu Waiau has similar characteristics. Associated with this latter flow, especially along its abrupt front that rises in a cliff 15–25 m high (fig. 21.7), are many prehistoric lithic workshops where early Hawaiians mined the stone for making adzes. The flow, which is very fine grained and hard, fractures into slabs appropriate for such artifacts and apparently was ideal for stone working. Its glassy groundmass contains randomly oriented microlites of plagioclase, rather than fully developed crystals, making the rock tougher than other flows and therefore easier to shape. Although the flow is remote and lies at a high elevation, the large number of adze quarries on this unit implies that the Hawaiians found its attributes to be uniquely valuable.

The high, steep margins of the Puu Waiau and Puu Poliahu flows are unlike those of most other hawaiite lavas on the mountain, which tend to be both lower and lobate. Elsewhere on the island (for example, Kohala volcano, Puu Waawaa), steep flow fronts occur in viscous lavas and on associated domes that consist of more alkalic rocks (mugearite, benmoreite, trachyte), but such flows lack embayed margins, glassy surfaces, and palagonite.

FIGURE 21.6.—Hyaloclastite tuff on northwest flank of Puu Waiau, with interbedded bombs standing in relief above eroded surface of cone.

CONGLOMERATE

A bouldery conglomerate on the south flank of Mauna Kea is traceable from the belt of Waihu end moraines to the base of the mountain in the Mauna Kea-Mauna Loa saddle. Stearns (1945), who described its occurrence and character, referred to it as the "Waihu fanglomerate" and attributed it to possible floods caused by eruptions that melted an ice cap. The deposit consists of bouldery gravel, so indurated that clasts are difficult to dislodge with a hammer (fig. 21.8). Where buried by lavas, the deposit is less indurated and resembles outwash gravels of Makanaka age. Its stratigraphic position is demonstrable in deep gulches on the south flank of the mountain, where it lies above Pohakuloa drift and early Waikahalulu lavas but below late Waikahalulu lavas and the lower drift of the Makanaka Glacial Member. Where exposed at the

FIGURE 21.7.—Ice-contact margin of Puu Waiau flow at Keanakakoi adze quarry (elevation 3,770 m) on south slope of Mauna Kea. Debris from prehistoric quarrying operations litters surface below and above steep, embayed margin of flow.

FIGURE 21.8.—Poorly sorted conglomerate facies of Waihu Glacial Member exposed in a shallow gulch on the upper southwest slope of Mauna Kea.

surface, boulders of the conglomerate are oxidized to yellowish brown and have weathering rinds 1–2 mm thick; many are spalled, pitted, or fractured. Where it meets the Waihu moraine belt the deposit has a thickness of 10–20 m, but it thins progressively downslope and is seldom more than 1 m thick near the base of the mountain.

INTERPRETATION

The assemblage of volcanic features that formed at the time of Waihu glaciation are adequately explained by attributing them to subglacial eruptions. The thick pile of hyaloclastite forming the bulk of Puu Waiau and Puu Poliahu imply eruption under water. The cones stand 100–170 m above the surrounding terrain at the crest of the mountain, and therefore the topography offers no means of ponding a body of water. In addition, the volcanic rocks that comprise the summit region are porous. If magma reached the surface beneath a summit ice cap, however, melting of ice above the vent would likely have generated a meltwater lake in which the bedded hyaloclastite could have accumulated. The observed thickness of eruptive products (about 170 m) is consistent with the reconstructed thickness of an ice cap over the summit having the areal extent indicated by the Waihu drift limit. When the accumulating hyaloclastite deposit reached the level of the lake surface and kept water from reaching the vent, subaerial eruptive activity would have commenced and produced cinders and bombs like those seen capping the hyaloclastite in both cones. The explosive character of the early phases of activity that produced Puu Waiau is suggested by the large number of spindle-shaped bombs that are interbedded with the hyaloclastite; evidently pieces of fluid lava were ejected above the surface of the postulated lake, acquired their distinctive aerodynamic shapes as they fell back to the surface, and settled through the water onto the accumulating pyroclastic pile.

Similar subglacially erupted volcanic units in Iceland have been described by Jones (1970), who inferred deposition of a basal pillow sequence in meltwater lakes as deep as 500 m. A change to explosive volcanism occurred as the water depth over the accumulating volcanic pile decreased to less than 200 m. Hyaloclastite tuff, characteristic of basaltic eruptions from vents in shallow water, then piled up above the pillow lavas as water interacted with lava rising rapidly through the conduit. In neither of the Mauna Kea cones are the lowermost eruptive products exposed, so the presence or absence of basal pillow lavas cannot be confirmed. However, the inferred water depth of less than 200 m suggests that the lower parts of the cones consist mostly or entirely of hyaloclastite.

As explosive activity waned, lava that was erupted from the Puu Poliahu and Puu Waiau vents is inferred to have flowed downslope, melting the glacier in the process. The unusual thickness and steep embayed fronts of the flows, their abundant pillow structures, the fine grain size and glassy margins of the dense flow rock, and the presence of zones of palagonite are all consistent with such an interpretation.

The exact number and sequence of eruptive events remains uncertain, largely because the flows and cones have been partly buried by younger volcanic units and partly eroded during subsequent glaciations. Puu Waiau appears to be a simple cone with a crater at its apex; however, its north side is not exposed. Related to it is a single lava flow that lies along its east and southeast sides. The source area for the flow is not evident, but it may lie near the highest exposed part of the flow. The source could also be buried beneath younger lava on the north or northeast side of the cone, in which case the lava would have issued from the upslope side of the cone and flowed downslope around its eastern side.

Puu Poliahu, by contrast, is a complex cone consisting of two adjacent craters. The two vents may have given rise to separate lava flows that coalesced downslope, as suggested by the dashed lines in figure 21.3, or possibly only one of the vents produced a flow. Alternatively, lava may have emerged from a vent unrelated to the hyaloclastite eruption, but in the same general area. Possible source areas are now covered by younger lavas that surround Puu Poliahu on all but the southwestern side.

The map pattern south of Puu Waiau suggests that the Poliahu flow may overlap the margin of the Waiau flow (fig. 21.3), but the field relations are not diagnostic. In any event, the period of time separating the eruptions is not known.

The subglacial eruptions would have melted a substantial body of ice from the glacier. The minimum areas covered by Puu Poliahu and Puu Waiau and their associated flows are 4 km^2 and 2.8 km^2, respectively. Assuming a mean ice thickness of 150 m for areas of the glacier directly affected by the eruptions, the volume of ice melted amounted to at least 1 km^3, or about 7 percent of the estimated volume of the entire ice cap. Some of the water would have interacted explosively with the erupting magma and escaped as steam, but the bulk is likely to have been ponded in one or more lakes within the ice cap, from which it would eventually have drained downslope either slowly or catastrophically. The fluvial conglomerate facies of the Waihu Glacial Member (the "Waihu fanglomerate" of Stearns, 1945) is exposed downslope from Puu Poliahu and Puu Waiau (fig. 21.3), principally along primary drainage routes that would have channeled meltwater from the summit region. The bulk of the coarse conglomeratic outwash facies is likely to have been deposited by floods resulting from sudden dumping of glacially impounded lakes that contained nearly 1 km^3 of meltwater, a mechanism consistent with Stearns' hypothesis for the origin of the conglomerate.

EVIDENCE OF RENEWED GLACIATION

Two lines of evidence suggest that the Waihu glacier reformed following the Puu Poliahu eruption and advanced across the Poliahu flow. Fragments of glassy flow margin and palagonitized hawaiite lava have been found in the Waihu end moraine system. A tongue of the Poliahu flow that emerges from beneath the Makanaka moraine belt and retains remnants of glacially chilled margins is a possible source of these fragments. The flow tongue apparently reached or nearly reached the glacier margin at the 3,200-m level. Glacial striations on the top surface of the flow (fig. 21.3) indicate that the glacier must have readvanced across the cooled lava tongue, abrading its surface and eroding fragments of the chilled margin. Because the striated flow surface lies well beyond the limit reached by Makanaka ice advances, the readvance must have occurred either

shortly after the eruptions, as the melted part of the ice cap reformed, or during a subsequent stadial advance. In either case the glacier must have achieved nearly the same size it had at the time of the Poliahu eruption.

MAKANAKA GLACIATION

LAVA FLOWS

Four additional lava flows that originated at vents near the summit possess features indicating that they also were erupted while glacier ice mantled the upper slopes of Mauna Kea. These flows lie stratigraphically above the Waihu-age eruptive units and the lavas that were extruded before the Makanaka glaciation, but they are stratigraphically lower than post-Makanaka flows and pyroclastic cones on the upper south flank of the mountain. Accordingly, these lavas must have been erupted sometime during the Makanaka glaciation.

The flows are associated with an arcuate cluster of pyroclastic cones from which they radiate in a nearly symmetrical pattern (fig. 21.9). Like the two older intraglacial lava flows, they possess locally steep and abrupt margins that rise as much as 30 m above surrounding rock surfaces (fig. 21.4) and that in places are strongly embayed. The marginal scarps are lowest on flows erupted along the topographically prominent rift zones, and highest on thicker flows that moved down slopes between rift zones. If the eruptions were contemporaneous, these relations imply that ice was relatively thin along the rift zones and thicker in the broad regions between, an interpretation consistent with reconstructed isopachs for the late Makanaka glacier (Porter, 1979b).

Each flow has been glacially abraded and quarried since it formed, but substantial sectors of the flow margins are relatively intact. The flow north of Puu Poliahu, which originates near a cone ("McCrae Cone" in earlier reports) just west of Puu Hauoki, displays a typical array of distinctive features along its southern margin that point to an ice-contact origin. Here the flow margin forms a steep scarp 3–10 m high marked by numerous pillows as much as 3 m in diameter (figs. 21.10 and 21.11). The pillows display radial jointing, have knobby surfaces that are often glassy to depths as great as 5 mm, and are locally palagonitized. Where pillows are lacking, flow margins frequently are marked by palagonitized vitric breccias.

Spiracles are also visible along the margins of some flows. Those developed in the flow north of Puu Poliahu rise as high as 2 m above the flow base, where they are as much as 60 cm wide (fig. 21.12). The longer ones tend to narrow upward and to bend in the downflow direction, implying that the flow was mobile during their formation.

PYROCLASTIC CONES

Pyroclastic cones associated with the four intra-Makanaka lava flows displaying ice-contact features resemble typical cinder cones on the upper slopes of Mauna Kea (fig. 21.4). Their flanks have been steepened by glacial erosion, but their surfaces are mantled with colluvium consisting of loose cinders and bombs. Hyaloclastite tuff like that composing the Waihu-age cones is not visible. However, seismic surveys of Puu Wekiu ("Summit Cone" in earlier reports) conducted before construction of the large astronomical observatory there provide important evidence of the internal structure of the cone.

Furomoto and Adams (1968) identified three zones within Puu Wekiu characterized by different seismic velocities (fig. 21.13). The uppermost, having a velocity of 0.49 km/s, was interpreted as a layer of loose colluvial cinders on the flank of the cone. A second zone, having a velocity of 0.76 km/s, underlies most of the surface of the cone to a depth of as much as 150 m. The deepest zone, with a velocity of 1.83 km/s, forms the core of the cone. Its measured velocity is well below that of weathered basalt (2.74 km/s) and it must therefore be formed of a less rigid material. Furomoto and Adams inferred that this zone probably consisted of "scoriae compressed by the overburden," but the proposed subglacial origin of the eruption makes it more likely that the seismic properties of the deepest zone indicate a hyaloclastite core, which is likely to have a rigidity intermediate between those of weathered basalt and consolidated cinders. If this interpretation is correct, then the hyaloclastite extends to an elevation of about 4,040 m within the cone, a level that is consistent with the thickness of the glacier at the time of the eruption, based on the height of the ice-contact flow margins downslope.

Exposures along the summit access road, which has been excavated several meters into the southwest flank of Puu Wekiu (fig. 21.4), display evidence of extensive hydrothermal alteration beneath the surface (fig. 21.14). The altered clay-rich zone also is enriched in phyllosilicates and has a redder color than pedogenic profiles of typical cinder cones outside the glacial limit (Ugolini, 1974). Those profiles generally extend no deeper than about 15 cm. The deep and extensive subsurface reddish zone of alteration therefore cannot be attributed to normal soil-forming processes. It is instead interpreted as having resulted from the upward movement of hot solutions into the cinder- and bomb-rich superstructure of the cone during the waning phase of the subglacial eruption. The presence of alteration products in the upper part of the cone may explain the greater seismic velocity there than in thin surficial layer of unconsolidated cinders mantling the outer slope.

OUTWASH DEPOSITS

Unlike the Waihu conglomerate, which forms a broad sheet across the southwestern side of the mountain below the moraine belt, outwash related to the Makanaka ice advances is confined mainly to gulches that indent the mountain side and to fans at the south base of the volcano. If floods were generated by the Makanaka subglacial eruptions, they apparently were confined to the preexisting drainage channels and were of smaller magnitude than those of Waihu time. In contrast to the postulated Waihu floods, which appear to have been concentrated on the southwest side of the volcano, meltwater flows during Makanaka eruptions were more dispersed, having been directed primarily down gulches that descend the mountain flanks beyond the lava tongues (fig. 21.9).

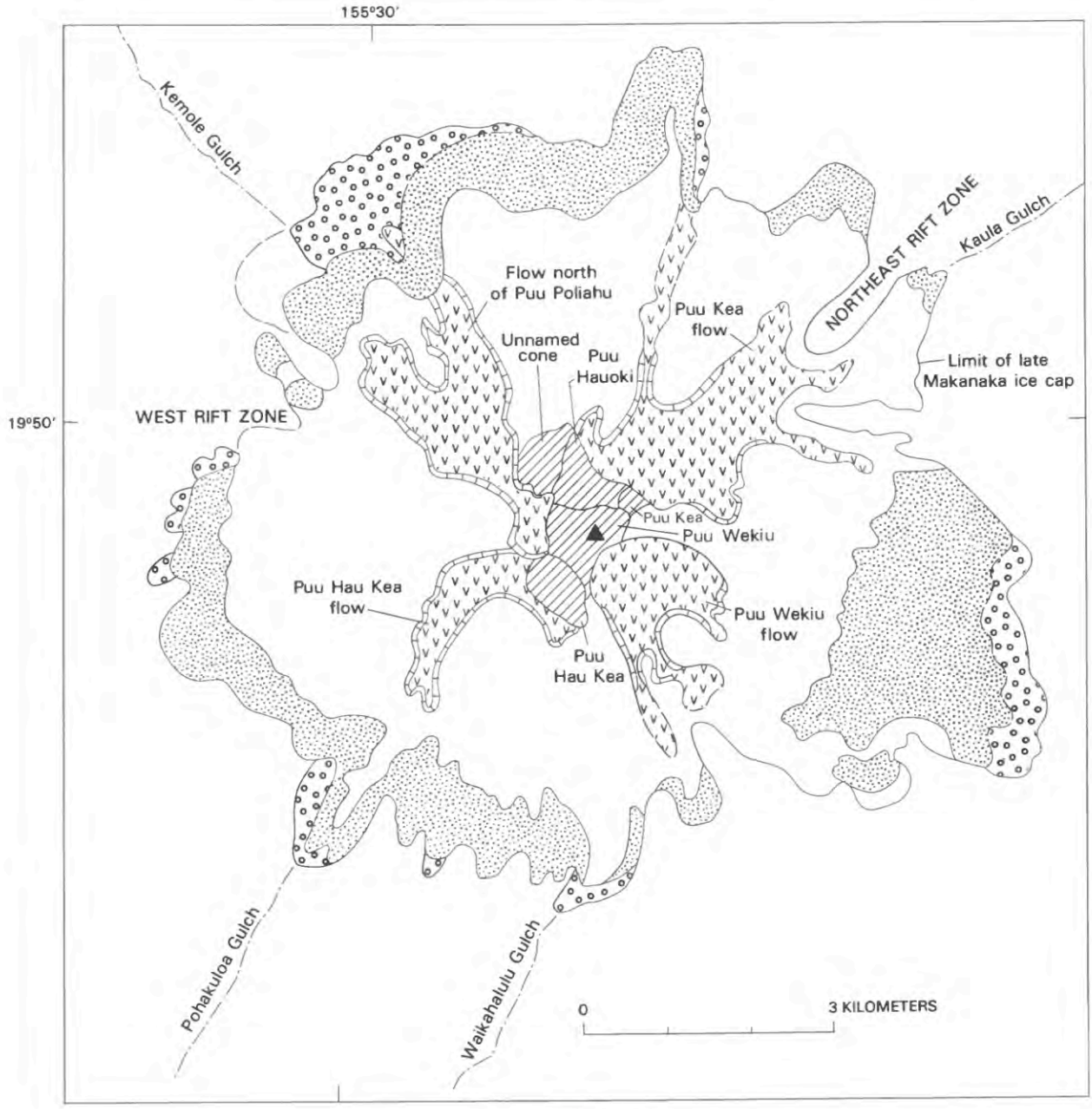

EXPLANATION

WAIKAHALULU VOLCANIC MEMBER

- Intraglacial lava flow
- Intraglacial pyroclastic cone
- Ice-contact flow margin

MAKANAKA GLACIAL MEMBER

- Late Makanaka end moraine
- Early Makanaka end moraine
- Contact—Dashed where approximately located; dotted where concealed or inferred
- ▲ Summit of Mauna Kea (4206 m)

FIGURE 21.9.—Map of summit region of Mauna Kea showing relationship of intra-Makanaka ice-contact lava flows and pyroclastic cones to early and late Makanaka end moraines.

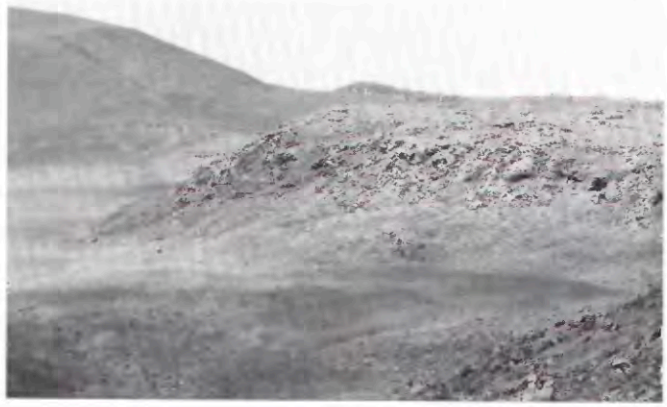

FIGURE 21.10.—Ice-contact margin of flow exposed along north side of Puu Poliahu (off picture to right). The steep margin (10–15 m high) is marked by pillow structures with radial jointing, palagonitized zones, and well-developed spiracles that rise into the flow from its base.

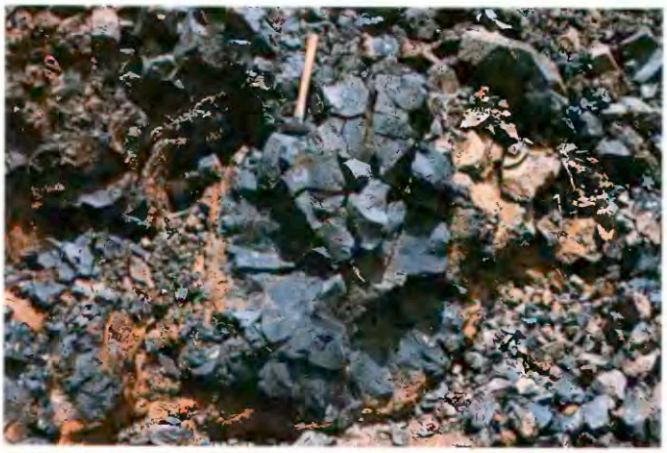

FIGURE 21.11.—Pillow structure at margin of flow north of Puu Poliahu. The pillow is about 1 m in diameter and marked by glassy margin, palagonite, and radial jointing.

FIGURE 21.12.—Spiracles exposed at lateral margin of flow along north side of Puu Poliahu. Interior surfaces are glassy. Spiracles are bent toward left, in direction lava flowed.

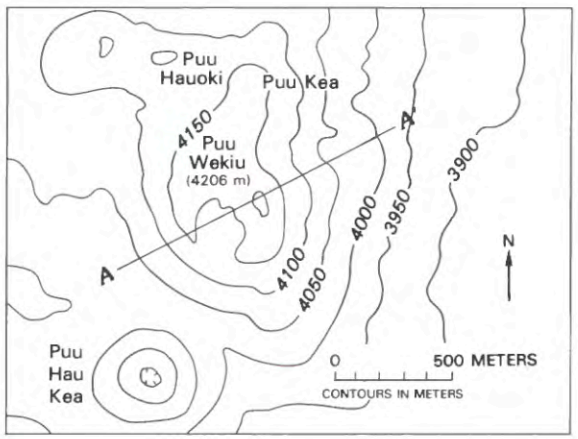

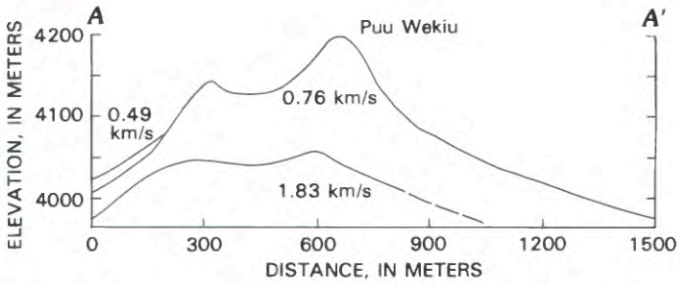

FIGURE 21.13.—Map and structure section of Puu Wekiu showing seismic-velocity zones defined by Furomoto and Adams (1968). Zone of highest velocity (1.83 km/s) is inferred to represent a core of hyaloclastite that is mantled by hydrothermally altered cinders forming a zone of lower velocity (0.76 km/s). A surficial layer of unconsolidated colluvium on the southwest slope forms a zone of still lower velocity (0.49 km/s).

FIGURE 21.14.—Hydrothermally altered pyroclastic deposits exposed along access road on south slope of Puu Wekiu (see fig. 21.4). Reddish rock is enriched in clay and phyllosilicates.

STRATIGRAPHIC RELATIONS

Stratigraphic relations and glacial features in the summit region provide constraints on the age of the subglacial eruptions. An unglaciated tongue of the flow north of Puu Poliahu emerges from beneath the late Makanaka end moraine near the head of Kemole Gulch (fig. 21.9) and overlies drift of the early Makanaka advance. These relationships imply that the flow postdates the early Makanaka maximum and antedates the late Makanaka maximum. Fragments of the chilled flow margins can be found in the late Makanaka end moraines, and the slopes of cones associated with the intra-Makanaka lavas have been glacially eroded and oversteepened. The slight erosional modification of the flows, in comparison to the erosion of the Waihu-age lavas, suggests only a single overriding advance, rather than two. These relationships imply that the eruptions date to an interval between the glacial maxima, when the ice cap was present but in a somewhat contracted state. The ice-contact flow margins can be followed downslope nearly to the late Makanaka moraine belt (fig. 21.15), but they generally are lower than the Waihu flow margins and so imply thinner ice; the size of the postulated hyaloclastite core of Puu Wekiu also points to thinner ice than during the late Makanaka glacial maximum. Because the extent and height of the several flow margins are similar, the geometry of the ice cap apparently was nearly the same during each eruptive event. The eruptions, therefore, may have been synchronous or nearly so.

CHRONOLOGY OF GLACIATIONS AND SUBGLACIAL ERUPTIONS

The timing of the Hawaiian glaciations is constrained by K-Ar ages of lava flows and radiocarbon ages of organic matter related stratigraphically to the glacial and interglacial units (Porter, 1979a). These ages show that the Pohakuloa glaciation occurred after, but probably not long after, a flow dated at 278.5 ± 68.5 ka. Thus this earliest glaciation is very likely correlative with marine oxygen-isotope stage 8, which culminated between about 276 ka and 247 ka (Hays and others, 1976). K-Ar ages of samples of the Puu Waiau and Puu Poliahu flows, and of a bomb collected from the top of Puu Waiau, cluster between 170 ka and 175 ka (171.9 ± 2.8, 174 ± 37.4, and 174.4 ± 26.5 ka), implying correlation of the Waihu glaciation with marine isotope stage 6 (190–127 ka; fig.

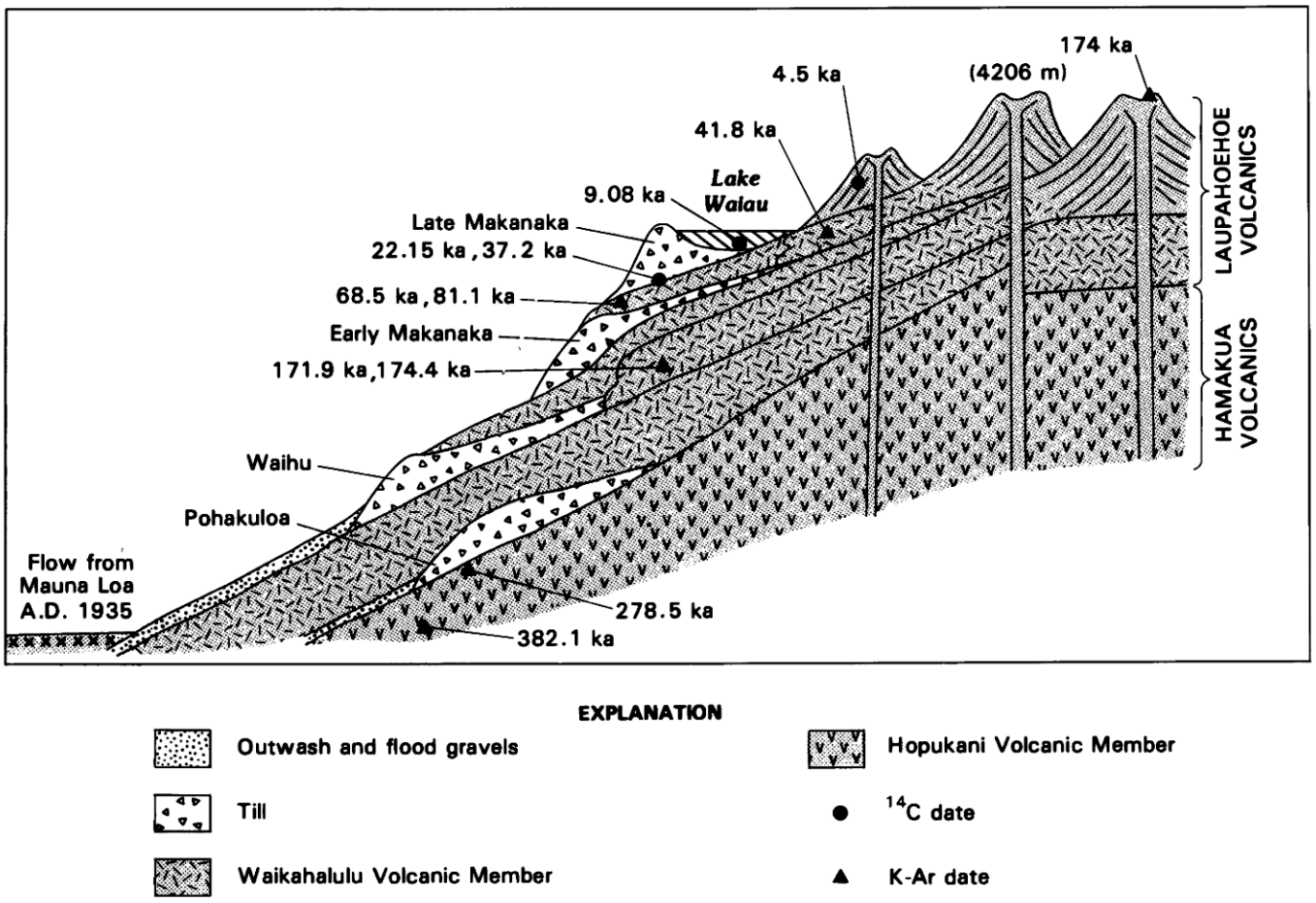

FIGURE 21.15.—Diagrammatic section showing stratigraphic relations and radiometric ages for glacial and volcanic units on upper slopes of Mauna Kea.

21.16). The early Makanaka glaciation occurred after 69.6±2.6 ka (K-Ar age) and before 37.2±1.4 ka (^{14}C age), making it a probable correlative of isotope stage 4 (73–61 ka). The late Makanaka advance culminated sometime between 29.75±0.5 (or possibly 22.15±0.25) ka and 9.08±0.2 ka (^{14}C ages), indicating equivalence to isotope stage 2 (29–10 ka).

A lava sample collected from the ice-contact margin of the flow north of Puu Poliahu has a K-Ar age of 41.3±8.3 ka. This would place it within isotope stage 3 (61–29 ka; fig. 21.16). However, the downslope extent of the ice-contact flow margins implies a large ice cap at the time of the eruptions; the subglacial eruptions may therefore have occurred either late in isotope stage 4 or early in stage 2, when the ice cover probably was more extensive. Calculations suggest that the snowline must be lowered at least 400 m before a glacier can begin to form at the summit of Mauna Kea (Porter, 1979b), and the extent of the intra-Makanaka ice-contact flows indicates snowline depression nearly as great then as during the late Makanaka maximum. It is therefore less likely that the eruptions occurred during isotope stage 3, which was an interstade marked by reduced global ice volume and general glacier recession (see, for example, Nilsson, 1983), than during either stage 4 or stage 2. These correlations are based on a single K-Ar age; dating other intra-Makanaka subglacially erupted flow units on Mauna Kea could help to resolve the present uncertainty.

Inasmuch as there is evidence for summit eruptions during the Waihu and Makanaka glaciations, might there also have been such activity during the Pohakuloa glaciation? Because the recurrence interval of eruptions is shorter during the tholeiitic shield-building phase, it seems unlikely that an ice cap as large as that of Pohakuloa time (130–150 km^2) could have existed for thousands of years without at least some eruptions occurring subglacially. The exposed Pohakuloa deposits provide no firm evidence of such activity, but the abundance of Pohakuloa meltwater sediments exposed in Waikahalulu and Pohakuloa gulches and their coarseness and poor sorting suggest that they may be related to subglacial eruptions that generated floods like those of Waihu time. Although the very limited outcrops of Pohakuloa drift make it unlikely that definitive evidence will be found, such eruptions remain a possibility.

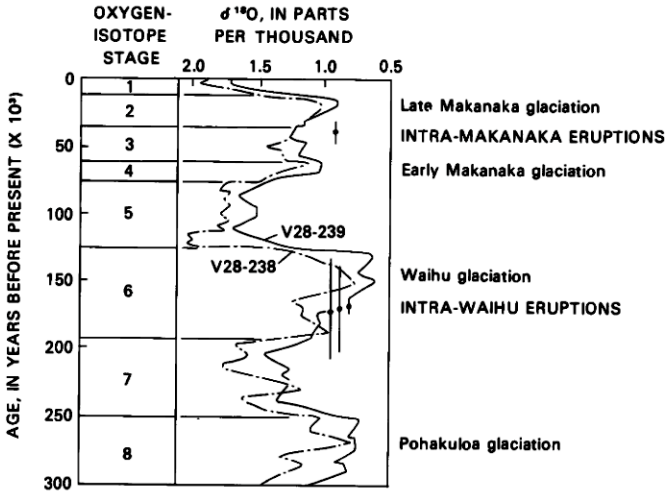

FIGURE 21.16.—Oxygen-isotopic variations in Pacific deep-sea cores V28–238 and V28–239 (Shackleton and Opdyke, 1976), showing isotope stages 1–8; inferred correlation with Mauna Kea glaciations; and K-Ar ages (dots), with error range of one standard deviation (bars), of products of subglacial eruptive activity.

REFERENCES CITED

Daly, R.A., 1910, Pleistocene glaciation and the coral reef problem: American Journal of Science, v. 298, p. 297–308.

Furomoto, A.A., and Adams, W.M., 1968, Seismic refraction study of the internal structure of a volcanic cinder cone, *in* Knopoff, Leon, Drake, C.L., and Hart, P.J., eds., The crust and upper mantle of the Pacific area: American Geophysical Union Geophysical Monograph 12, p. 112–121.

Hays, J.D., Imbrie, J., and Shackleton, N.J., 1976, Variations in the Earth's orbit: pacemaker of the Ice Ages: Science, v. 194, p. 1121–1132.

Jones, J.G., 1970, Intraglacial volcanoes of the Laugarvatn region, southwest Iceland, II: Journal of Geology, v. 78, p. 127–140.

Porter, S.C., 1972a Distribution, morphology, and size frequency of cinder cones on Mauna Kea Volcano, Hawaii: Geological Society of America Bulletin, v. 83, p. 3607–3612.

———1972b, Buried caldera of Mauna Kea Volcano, Hawaii: Science, v. 175, p. 1458–1460.

———1979a, Quaternary stratigraphy and chronology of Mauna Kea, Hawaii: a 380,000-year record of mid-Pacific volcanism and ice-cap glaciation: Geological Society of America Bulletin, Part II, v. 90, p. 980–1093.

———1979b, Hawaiian glacial ages: Quaternary Research, v. 12, p. 161–187.

Shackleton, N.J., and Opdyke, N.D, 1976, Oxygen-isotope and paleomagnetic stratigraphy of Pacific core V28–239, late Pliocene to latest Pleistocene, *in* Cline, R.M., and Hays, J.D., eds., Investigation of Late Quaternary paleoceanography and paleoclimatology: Geological Society of America Memoir 145, p. 449–464.

Stearns, H.T., 1945, Glaciation of Mauna Kea, Hawaii: Geological Society of America Bulletin, v. 56, p. 267–1526.

Stearns, H.T., and Macdonald, G.A., 1946, Geology and ground-water resources of the Island of Hawaii: Hawaii Division of Hydrography Bulletin 9, 363 p.

Ugolini, F.C., 1974, Hydrothermal origin of the clays from the upper slopes of Mauna Kea, Hawaii: Clays and Clay Minerals, v. 22, p. 189–194.

Wentworth, C.K., and Powers, W.E., 1941, Multiple glaciation of Mauna Kea, Hawaii: Geological Society of America Bulletin, v. 52, p. 1193–1218.

VOLCANIC HAZARDS IN THE HAWAIIAN ISLANDS

By Donal R. Mullineaux, Donald W. Peterson, *and* Dwight R. Crandell

ABSTRACT

Volcanic eruptions have built the Hawaiian Islands, and similar eruptions in the future will affect many areas in them, especially on Kilauea and Mauna Loa Volcanoes on the Island of Hawaii. Some of those eruptions will endanger people and property. Hazards that result directly from eruptions include lava flows, tephra falls, volcanic gases, and pyroclastic surges. Less direct hazards associated with eruptions include ground fractures and subsidence, earthquakes, and tsunamis.

The Islands of Hawaii and Maui have been subdivided on maps, for some kinds of hazards, into various zones of differing magnitude of hazard. These hazard-zone maps can be used for making land-use decisions before eruptions occur and for responding to actual or threatened eruptions. Hazard-zone maps for earthquakes and tsunamis are not included in this report; however, earthquakes of both volcanic and nonvolcanic origin can affect extensive areas in the islands, and tsunamis can be highly damaging in narrow coastal zones.

Because most volcanic events cannot be effectively controlled, volcanic hazards are best avoided by land-use planning before eruptions occur and by evacuation when they do occur. Mitigation measures to reduce effects from lava flows can be effective, at least temporarily, but such measures are generally more effective for some other hazards such as tephra falls and volcanic gases.

INTRODUCTION

All the Hawaiian Islands have been built by volcanic eruptions over a period of millions of years. Similar eruptions have continued into historical time on the islands of Hawaii and Maui and undoubtedly will occur in the future, especially on Kilauea and Mauna Loa Volcanoes. Most Hawaiian eruptions form lava flows that endanger chiefly property; explosive eruptions are relatively rare but are more likely to threaten people. As intensive land development expands toward areas of relatively high hazard, the threat to life and property will increase accordingly.

This report discusses the characteristics, frequency, location, and extent of various hazardous phenomena typical of Hawaiian volcanoes, assesses the likely future extent, frequency, and relative severity of these phenomena, and shows distribution of some hazards on hazard-zone maps. Although they have distinct limitations, these maps can be useful for planning long-range mitigation of volcanic hazards and for organizing short-term response to eruptions.

The character of volcanic eruptions in Hawaii has been described at length in many previous reports (for example, Macdonald and Abbott, 1970; Macdonald, 1972) and is treated at length elsewhere in this volume. Brief descriptions of volcanic activity in this assessment are intended to emphasize certain characteristics that can help the public and public officials to understand volcanic hazards and ways of mitigating them. Hazards resulting from eruptions that bring rock materials to or above the ground surface are here termed direct hazards. Hazards termed indirect are events that accompany such eruptions, or are secondary effects of eruptions, or result from movement of magma that does not reach the ground surface.

The term hazard in this report refers either to a hazardous event or to its products; examples are an explosive eruption or a lava flow. The term risk refers to the likelihood of losses to people, such as the loss of life, homes, or productive land. Volcanic hazards in the nearly uninhabited upper part of the east rift zone of Kilauea, for example, are of about the same frequency and severity as those in the lower, more highly populated part of the rift zone. Risk, however, is much higher in the lower part because of its greater population and more intensive land use. The potential hazards from volcanic eruptions in the islands will remain about the same in the foreseeable future, but increased risk from those eruptions will accompany growth in population and economic development.

ACKNOWLEDGMENTS

This report has been based in large part on information published by past and present scientists at the Hawaiian Volcano Observatory, on pre-1970 mapping by H.T. Stearns and G.A. Macdonald, and on more recent published and unpublished mapping and interpretations of R.T. Holcomb, P.W. Lipman, J.P. Lockwood, and R.B. Moore. In addition, much information has been provided by many other scientists who have carried on investigations at the volcano observatory. This report includes additions to and modifications of reports on volcanic hazards on the Island of Hawaii by Mullineaux and Peterson (1974), and on Oahu and Maui by Crandell (1975 and 1983).

HAWAIIAN VOLCANIC ACTIVITY

The Hawaiian Islands (fig. 22.1) lie at the southeastern end of a largely submerged volcanic chain about 6,000 km long, which extends from the Emperor Seamounts to the Island of Hawaii (Dalrymple and others, 1973). This chain consists of volcanoes that are progressively younger toward the southeast; Kilauea and Mauna Loa Volcanoes on the southeastern part of the Island of Hawaii (fig.

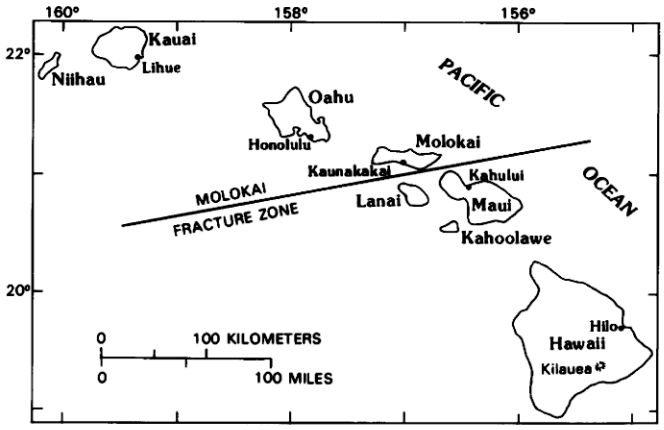

FIGURE 22.1.—Index map of the Hawaiian Islands, showing location of the Molokai fracture zone.

22.2) are now the most active in the chain. Another volcano, Loihi, is growing on the ocean floor off the southeast coast of Hawaii (Moore and others, 1982; fig. 22.2), though it probably will not rise above the ocean surface for many thousands of years.

Hawaiian volcanoes consist largely of basaltic lava flows that were highly fluid and traveled as much as tens of kilometers from their source vents. Their cones typically are broad in comparison to their height and are called shield volcanoes. During their growth, many of these volcanoes developed elongate systems of near-vertical fractures along zones of weakness called rifts or rift zones, which lead from the volcano centers outward through their flanks. Magma moving up into a volcano rises along the central conduit, and much is erupted from vents at the summit, but some magma may spread outward into the rift zones and be erupted there. In addition, a few eruptions occur at vents on the volcanoes' flanks outside the rift zones.

Hawaiian volcanoes typically follow an evolutionary pattern. In an early stage, during which the main shield is built, eruptions of highly fluid lava are frequent and voluminous; Kilauea and Mauna Loa on the Island of Hawaii are in such a stage now. Later, eruptions become less frequent but commonly are more explosive. Hualalai and Mauna Kea on the Island of Hawaii are now in this stage and probably also Haleakala on the Island of Maui; none of these volcanoes can be regarded as extinct. Sporadic eruptions can occur on Hawaiian volcanoes for many tens of thousands of years after their shield building stage has ended.

Most eruptions that build the volcanoes are not explosive, but activity at the onset of an eruption often is vigorous enough to produce fountains of molten lava that reach tens to hundreds of meters above the vent. Large lava clots fall back and may be included in spatter ramparts or lava flows, but small particles of molten and solidified lava from the fountains are carried by wind away from the vent area and fall to produce deposits of tephra. Continued and less vigorous emission of lava produces lava streams that flow away from the vent. Lava that flows into the sea can be explosively disrupted by steam, producing mounds of lava fragments called littoral cones along the shore.

Explosive eruptions are not as frequent as lava flows, but they have occurred repeatedly in Hawaii and produce a variety of products. Large clots of lava and solid rock fragments thrown high into the air by explosions fall back close to the vent to form cinder cones. Finer particles are carried away by wind, forming ash deposits that can be as much as a few meters thick near the cone. Explosions can also create cloudlike mixtures of rock fragments and gases, called pyroclastic surges, which typically spread from vents outward along the ground surface at high speed. Ash-laden clouds that rise above pyroclastic surges can also be carried away by winds and form beds of ash.

Volcanic gases are emitted during every kind of eruption and at many vents during intervening dormant periods. Gases generally are quickly diluted by air as they are dispersed downwind, although their odor may be detectable for many tens of kilometers.

Eruptions have been frequent in historical time, about the last 200 years. Kilauea and Mauna Loa have each erupted dozens of times during this period, and Hualalai erupted as recently as A.D. 1801 (Moore and others, chapter 20; Macdonald and Abbott, 1970). Haleakala Volcano on Maui last erupted about 1790 and

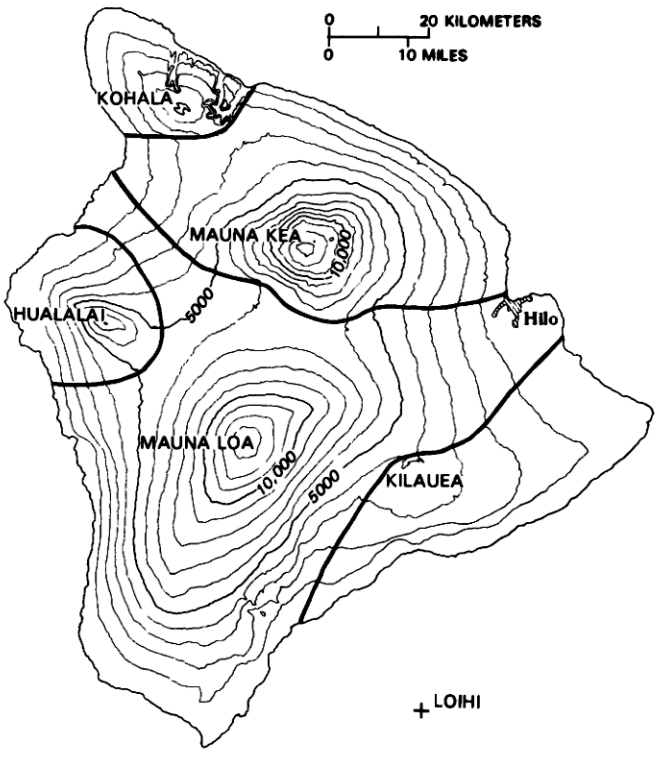

FIGURE 22.2.—Location and topography of the five volcanoes that form the Island of Hawaii, and location of the still-submerged offshore volcano Loihi. Contour interval 1,000 feet (approx. 300 m). Heavy solid lines mark boundaries of the five volcanoes.

has been active at least 10 times within the last 1,000 years (Crandell, 1983).

Several other volcanoes, though dormant during the last 200 years, are not extinct. Mauna Kea has erupted several times within the last 10,000 years (Porter, 1973) and, among those other volcanoes, has the highest eruptive probability. Other potentially active volcanic areas, such as the southeastern part of Oahu, apparently have not erupted for more than 10,000 years. The possibility of future eruptions in those areas should be recognized, even though specific preparation for such eruptions may not be economically or socially practical.

DIRECT VOLCANIC HAZARDS

Among direct volcanic hazards, lava flows occur most frequently and are the greatest hazard to property. Eruptions of tephra are also frequent but do not represent a severe hazard to people or property. Although pyroclastic surges are relatively infrequent, they can be a great danger to human life. Volcanic-gas emissions, in contrast, are common and continuous but represent relatively little danger to people or property.

LAVA FLOWS

Lava is erupted from single vents and from long fissures, and typically forms tongue-shaped to broadly lobate flows that extend downslope from the vent (fig. 22.3). The size, extent, and kind of movement of lava flows vary greatly, depending on such factors as the rate and volume of eruption and the topography over which the lava moves.

Hawaiian lava flows generally advance more slowly than the speeds at which people normally walk (3–5 km/h) but some may move much faster. Fronts of voluminous flows on steep ground have advanced as rapidly as 9 km/h, and lava streams in well-established channels on steep slopes may reach speeds of 55 km/h (Macdonald and Abbott, 1970, p. 23). Contrasting flow behavior and surface features divide most lava flows in Hawaii into two types, termed pahoehoe and aa. Pahoehoe lava is relatively fluid and forms flows that are thinner than the more viscous aa flows, and pahoehoe flows are more strongly controlled by minor topographic features. Individual pahoehoe flows range in thickness from a few tens of centimeters to as much as 3 m. During the course of a single eruption, however, successive pahoehoe flows moving along the same path may build up thicknesses of many tens of meters. Individual aa flows are generally 2–8 m thick, but locally they can be as thick as 20 m.

Hawaiian lava flows range from a few meters to more than 50 km in length, and from a meter or two to about 3 km in width. A critical factor in assessing hazards from future lava flows is the maximum distance they can be expected to extend. Although the majority of past flows from Mauna Loa have not extended more than 10–15 km from their vents, some have reached much farther in only one or a few days. The longest lava flows apparently reached their maximum extents quickly, before the loss of heat or gases caused their fluidity to decrease, or they formed lava tubes that minimized loss of heat and gases. Of many factors that influence the length of lava flows, Walker (1973) proposed that rate of eruption of the lava is most important, and that it could be used to predict the distance a lava flow will travel. Malin (1980), however, pointed out that rate of lava eruption does not correlate well with length of lava flows from Kilauea or Mauna Loa; those flows correlate more closely to volume. In 1984, a lava flow from Mauna Loa extended more than 25 km toward Hilo in less than 5 days (Lipman and Banks, chapter 57). Decreases in eruption rate then triggered channel blockages and branching of the flow (Lipman and Banks, chapter 57), and the flow did not reach closer to the city. A high sustained rate of lava eruption clearly indicates that a lava flow could reach far from the vent. The most useful clues to the probable final length of such a flow may be determination of whether the rate of eruption is constant or changing, and whether or not the flow forms a lava tube.

The paths followed by lava flows are generally downslope, but they may vary in detail. Because parts of a flow are continually cooling and becoming more viscous, the flow may not move directly into the lowest available ground as would a stream of water. Lava flows may move diagonally down slopes or even cross low ridges.

The chief threat presented by lava flows is to property that cannot be removed. They burn, crush, bury, or surround structures that lie in their paths, and reduce the value of land that is covered. Although most lava flows move so slowly that they do not threaten

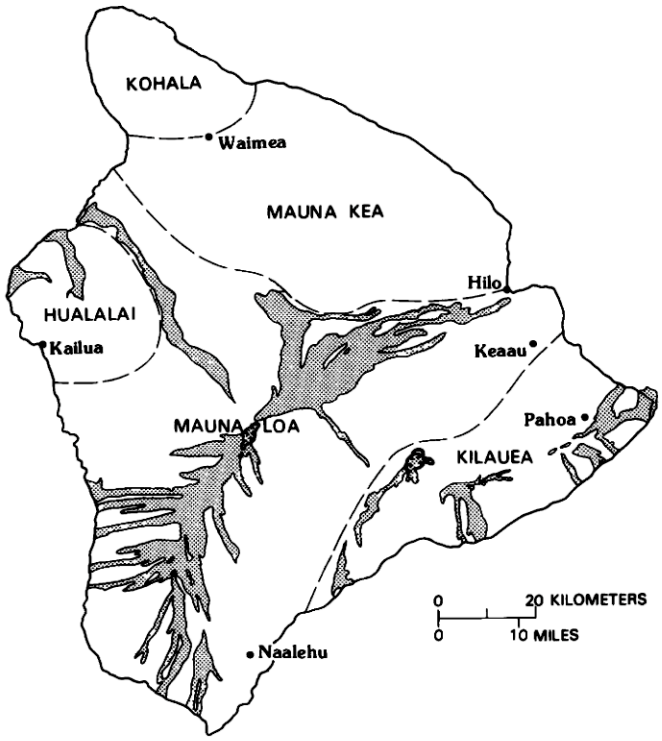

FIGURE 22.3.—The Island of Hawaii, showing approximate areas covered by pre-1975 historical and some prehistorical lava flows (stippled). Dashed lines mark the boundaries of the five volcanoes that form the island.

lives, voluminous flows, especially those on steep slopes, can move rapidly enough to endanger people.

TEPHRA FALLS

Tephra, which consists of volcanic ash and coarser fragments, is produced most frequently in Hawaii by lava fountains, but it can also be formed by explosive magmatic eruptions and by steam-blast (phreatic) explosions, both of which throw large and small fragments of molten and solid rock into the air. Large clots of lava erupted in fountains may still be molten when they fall to the ground, where they may become part of a flow or form spatter cones and ridges near the vents. Fragments ejected during eruptions that are more vigorous, and often more continuous, partly or wholly solidify before they fall back to the ground surface, and these form cinder cones around the vent. Tephra produced by steam explosions generally consists of pieces of previously solidified rock. Steam-blast eruptions such as those at Kilauea in 1924 probably resulted when ground water entered hot zones inside the volcano (Macdonald, 1972, p. 245; Decker and Christiansen, 1984). Locally, mounds of tephra (littoral cones) can be built by steam explosions where lava flows enter the ocean.

Large tephra fragments fall close to their source vents, but smaller particles commonly are carried away by winds to form widespread ash deposits. Tephra deposits are also thick near source vents, and thin rapidly with increasing distance. Tephra from lava fountains at Kilauea Iki in 1959, for example, is more than 3 m thick at 0.5 km from the vent, but thins to about 15 cm and 3 cm at distances of 2 km and 4 km, respectively (Richter and others, 1970; figs. 22.4, 22.5). Tephra from eruptions that built cinder cones on Mauna Kea is as much as a meter thick at distances of 1–2 km and 10 cm thick at about 5 km (Porter, 1973). An ash layer about 2,500 years old on the west flank of Haleakala on Maui is as much as 10 cm thick at about 9 km from the crater. Repeated eruptions of tephra from the same or nearby vents can result in even thicker deposits; widespread, prehistoric ash deposits on the Island of Hawaii are locally nearly 20 m thick (Stearns and Macdonald, 1946), and similar deposits as thick as 6 m blanket a large area on the upper northwest flank of Haleakala. Traces of ash from lava fountains commonly have been seen at distances of 40–50 km during historical eruptions of Kilauea and Mauna Loa. Tephra from steam-blast eruptions generally is coarse-grained and no more than a few tens of centimeters thick. Large fragments from the 1924 eruption at Kilauea, some weighing several tons, were thrown hundreds of meters, and smaller rocks were thrown as far as about 2 km (Jaggar, 1947; Macdonald and Abbott, 1970).

Lava fountains and eruptions that form cinder cones are spectacular but seldom endanger people or animals, who can move upwind or out of the range of the falling material. No human deaths or serious injuries from such eruptions have been reported in Hawaii during the 19th or 20th centuries. Steam-blast eruptions, however, can occur abruptly and eject large fragments that represent a distinct threat to people and animals. At least one person, in 1924, has been struck and killed by large fragments ejected in an explosive eruption (Macdonald and Abbott, 1970).

Tephra can seriously affect vegetation and manmade structures and machinery. Property may be burned and abraded by airborne particles, damaged by impact of large fragments, or buried by a blanket of ash. Ash can also cause discomfort and even injury to eyes and respiratory systems, and can smother vegetation, clog water and sewage systems, and damage machinery.

Tephra from eruptions during historical time that is thick enough to have caused severe damage has been limited to areas less than about 2 km from active vents. Tephra deposits from eruptions of Kilauea and Mauna Loa have covered the ground to thicknesses of more than 15 cm only within about 2 km from the vents. The thickness of tephra and the damage it causes gradually decrease at progressively greater distances.

PYROCLASTIC SURGES

Some explosive eruptions produce pyroclastic surges, which are clouds of ash, rock fragments, and gases that move at high speed outward from a source vent. Although pyroclastic surges move along the ground surface, they may or may not follow topographic depressions. The temperature of rock material in some surges is higher than the boiling point of water, but in others can be lower. Pyroclastic surges are commonly caused by steam explosions or by explosions of magma and steam. These explosions can originate in at least four ways: (1) interaction between ground water and molten rock in a fluctuating magma column; (2) sudden depressurization of a shallow hydrothermal system; (3) intrusion by magma into water-saturated rocks; and (4) movement of sea water directly into a conduit during submarine eruptions. Prehistoric explosive eruptions of Kilauea have been attributed to the first two causes (Decker and Christiansen, 1984).

Explosive eruptions can produce, in their early stages, a primary surge that moves laterally away from the explosion site in all directions, as well as a vertical eruption column. Secondary pyroclastic surges can develop when material falls back to the ground from the vertical column. Although velocities of 50 km/h to as much as 300 km/h can be inferred for some surges, they decelerate rapidly and typically stop less than 10 km from their source (Crandell and others, 1984).

Pyroclastic surges formed by eruptions at basaltic volcanoes have affected areas as far as 10 km from their source vents (Crandell, 1983; Dzurisin and others, in press). The probability that an area will be affected by a surge, as well as the severity of the effects, decrease progressively away from a vent. Because surges do not necessarily follow topographic lows, high areas may not be safe. Pyroclastic surges formed by eruptions at Rotomahana-Waimangu, New Zealand, in 1886 extended at least 6 km from their source area and surmounted steep hills as high as 360 m above the vents and 200 m above the adjacent land surface (Nairn, 1979).

A series of explosive eruptions at the summit of Kilauea about 2,000 years ago produced at least three pyroclastic surges (Dzurisin and others, in press). The first two were separated by lava-fountain

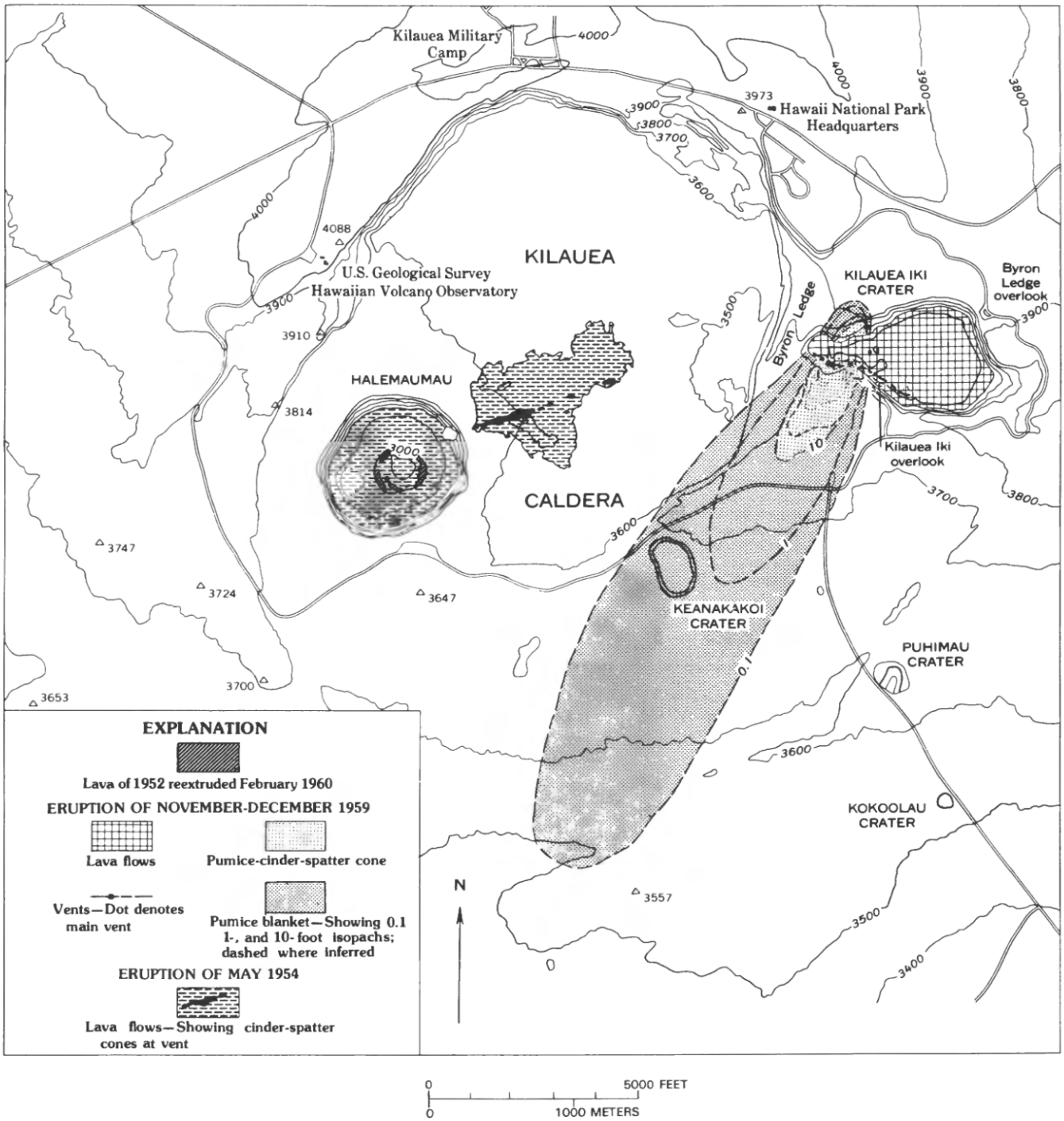

FIGURE 22.4.—The summit area of Kilauea, showing extent of tephra (pumice) blanket from Kilauea Iki vent in 1959. From Richter and others (1970). Topographic contours in feet.

eruptions, and the second and third by lava fountaining and an explosion that produced a shower of rock fragments. The last surge was followed by more fountains and by lava flows. These surges affected areas at least 10 kilometers from the vent area. Pyroclastic surges originating in the same area about 1790 left deposits of rock debris locally more than 10 m thick near Kilauea's summit caldera (Decker and Christiansen, 1984; fig. 22.6) and may have affected areas as far as 9 km from the vent. Prehistoric pyroclastic-surge

FIGURE 22.5.—Tephra (pumice) blanket in former picnic area 1 km southwest of Kilauea Iki vent, on November 30, 1959. Small shelter after 3rd phase of activity; about 1 m of tephra covers ground. From Richter and others (1970).

FIGURE 22.7.—Volcanic gases issuing from the Mauna Ulu vent on the upper east rift zone of Kilauea in about 1972. Distance across the photograph from left to right, through the vent, is about 2 km.

deposits also have been recognized at many localities on the southeastern part of Oahu, and on the islet of Molokini off the southwest coast of Maui.

Although less frequent than lava flows, explosive eruptions that produce pyroclastic surges represent a severe hazard to lives. The chief hazards to people are from asphyxiation by hot ash, impact by rock fragments traveling at high speed, and burns from hot and perhaps wet, clinging ash. The positions and condition of bodies of persons killed by pyroclastic surges during the 1790 eruptions of Kilauea indicated that asphyxiation and heat caused the deaths, rather than injuries resulting from impact by rock fragments (Swanson and Christiansen, 1973). The chief hazards of pyroclastic surges to property are impact and blast effects; vegetation as well as structures can also be burned, buried, and abraded.

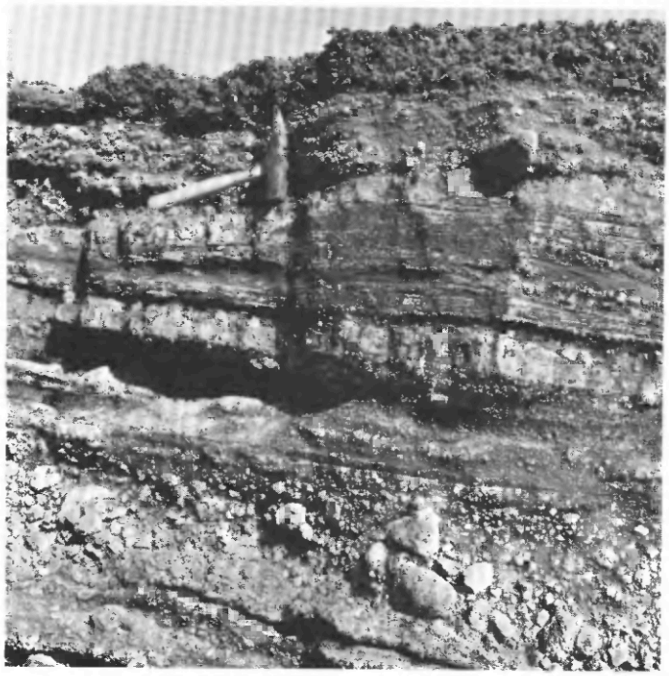

FIGURE 22.6.—Interbedded tephra-fall deposits and pyroclastic-surge deposits (with inclined bedding) that were explosively erupted from Kilauea caldera in 1790. Photograph by R.L. Christiansen, U.S. Geological Survey.

VOLCANIC GASES

Volcanic gases are emitted during all types of eruptions (fig. 22.7) and can continue to be released for many years after other eruptive activity ceases. Gas can also be expelled at vents that have never erupted lava; some fumaroles have produced gases for more than a century. The most abundant constituents of volcanic gas in Hawaii are water vapor, sulfur dioxide, and carbon dioxide, but many other gases have been detected (Macdonald, 1972, p. 50). The gases of most concern to human health are various combinations of sulfur, oxygen, and hydrogen, such as hydrogen sulfide and sulfur dioxide; other dangerous gases include chlorine, fluorine, and carbon monoxide. Carbon dioxide can collect in closed depressions and cause asphyxiation. Small amounts of mercury have also been detected in gases emitted from vents along the east rift zone of Kilauea (Siegel and Siegel, chapter 35; Siegel and Siegel, 1978).

No deaths from volcanic gases have been reported on Hawaii, although gases have killed people elsewhere, notably in Indonesia (LeGuern and others, 1982). Brief exposure to gases generally does not harm otherwise healthy persons, but it can endanger people with heart and lung ailments. The hazard is greatest downwind from and near active vents, and it may persist at vents that continue to fume during inactive periods. Gases mix with air as they drift downwind, and their concentrations and effects diminish with increasing distance from the source. Even small concentrations of sulfur-bearing gases

can affect the lungs, eyes, and skin, and may cause gastric upsets. Furthermore, these gases can combine with water to form sulfuric acid, which can damage live tissue, cloth, metal, and other materials. Many types of vegetation cannot survive near gas-emitting vents, and many varieties may be killed as far as 30 km from the source vents. Some volcanic gases, such as carbon monoxide and carbon dioxide, are odorless and heavier than air, and during windless periods they may become concentrated in topographic depressions and present an invisible danger of asphyxiation. The presence of sulfur-bearing volcanic gases generally can be detected by their odor.

INDIRECT VOLCANIC HAZARDS

Ground fractures, subsidence, and earthquakes commonly occur together as a result of magma movement. They are especially common in the summit areas and rift zones of Kilauea and Mauna Loa but are generally not severe. These hazards also occur on a larger scale along the flanks of Kilauea and Mauna Loa as a result of massive landslides (Lipman and others, 1985), and tsunamis accompanying earthquakes may affect coastlines of the islands. Such earthquakes endanger property, and the tsunamis are a great threat to lives. Earthquakes that affect Hawaii are also caused by crustal movements underneath the volcanoes, and many tsunamis that affect the islands are generated elsewhere in the Pacific Ocean.

GROUND FRACTURES

Ground fractures in rock and soil are caused when the mass on one side shifts away from or slides past an adjacent mass along a crack. Fractures may form scarps where one mass moves up or down relative to another. Cracks as much as several meters across can remain open for long periods, and some are many kilometers in length.

Cracks can form rapidly or slowly, and by repeated discrete movements or by slow, more continuous movements. Repeated vertical displacements along the same fracture can produce a scarp as high as several hundred meters.

Most fractures in the Hawaiian Islands result from magma movement, subsidence of landslide blocks, or earthquake shaking. Fractures of historical age caused by magma movement are very abundant in summit areas and rift zones on Kilauea and Mauna Loa (fig. 22.8), and prehistoric fractures, probably of similar origin, are common along the southwest rift zone of Haleakala. The gravitational subsidence of large landslide blocks on the flanks of Kilauea and Mauna Loa also creates fractures.

Earthquakes cause fractures by ground vibration and also by triggering landslides, especially in loose soils. The earthquakes of April 26, 1973, November 29, 1975, and November 16, 1983, for example, caused cracks at many places on the Island of Hawaii.

Ground fractures are a minor but persistent hazard to people and animals. Cracks that open suddenly could trap them, and a danger would remain for as long as the cracks stayed open, especially where they are hidden by thick vegetation. Ground fractures also threaten property: they can disrupt roads and buildings as well as water, sewer, power, and telephone lines.

FIGURE 22.8.—Subsidence of a graben in the Kapoho area on the lower east rift zone of Kilauea, on January 13, 1960, prior to outbreak of eruption in the area. View eastward along the Kapoho fault scarp in the village of Kapoho. Maximum vertical displacement is about 1 m (3.5 feet). Photography by R.T. Haugen, National Park Service.

GROUND SUBSIDENCE

Ground subsidence consists mainly of four kinds that differ greatly in scale: (1) subsidence of entire islands, (2) subsidence of parts of a volcano's flanks, (3) settling of small areas as a result of underground movement of magma, and (4) local collapse of the roofs of lava tubes.

Subsidence of some islands is slow but continuous, and the resulting submergence along shorelines is augmented by slow, worldwide rise of sea level. The rate of subsidence for the Island of Hawaii, which differs from place to place on the island, has been calculated as 1.4–4.1 mm/yr (Moore, chapter 2; Apple and Macdonald, 1966; Moore and Fornari, 1984). The worldwide rise of sea level is 1–2 mm/yr, thus the island is being submerged at approximately 3–6 mm/yr, equivalent to 1–2 feet per century. At Kahului, Maui, the rate of island subsidence may be as much as 1.7 mm/yr (Moore, chapter 2; Moore, 1970) and the overall submergence about 3 mm/yr, equivalent to 1 foot per century. Subsidence of such large areas is believed to result from depression of the sea floor under the weight of the islands. Coral reefs, beach rock, and soils encountered in drill holes on Oahu at depths as much as 336 m below sea level (Stearns, 1966, p. 21) indicate that the Island of Oahu also has subsided in the past. Tide-gauge records indicate that the island is now being submerged at the same rate as the worldwide rise in sea level, thus it apparently is stable now (Moore, chapter 2; Moore and Fornari, 1984).

FIGURE 22.9.—Stepped topography produced by subsidence of large landslide blocks on the south flank of Kilauea. The scarps are formed by repeated downward movement of blocks south of faults. Each episode of movement develops new ground cracks; such cracks are visible on face of scarp in foreground. Scarps are partly mantled with lava erupted from Mauna Ulu in 1969–74. Photograph by R.I. Tilling, U.S. Geological Survey.

Submergence from slow, continuous subsidence and sea-level rise will eventually endanger shoreline facilities. Low-lying coastal sites will become increasingly threatened by damage from storm waves and tsunamis, and eventually by inundation. Submergence is thus a factor to be considered in long-range plans for buildings and other facilities in all coastal areas of the Hawaiian Islands, and especially on the Islands of Hawaii and Maui.

Most other types of subsidence are more rapid. Large parts of the flanks of Kilauea and Mauna Loa, for example, sometimes subside abruptly. The areas affected may be several tens of kilometers long and involve hundreds of square kilometers of land (Lipman and others, 1985). Steep scarps and stair-step topography along fault zones on the flanks of both volcanoes were formed by repeated movements during the recent geologic past (fig. 22.9). These movements result from instability of the volcanoes' flanks caused in part by intrusion of magma into rift zones and in part by the load of the unbuttressed seaward flanks of the growing volcanoes (Moore and Fiske, 1969; Swanson and others, 1976).

Rapid subsidence can damage or destroy manmade structures by tilting, shaking, and fracturing the ground. It endangers areas along shorelines because they may suddenly become inundated or lowered enough to be vulnerable to damage from storm waves and tsunamis.

Shallow underground movements of magma can also cause subsidence. Withdrawal of magma from beneath summit areas and rift zones may remove support from tracts of land and cause them to subside. Such movements may be no more than a few meters, but the summation of repeated settling can amount to tens or hundreds of meters. This process produced the summit calderas and pit craters of Mauna Loa and Kilauea, which are as much as several hundred meters deep.

Subsidence caused by withdrawal of magma is restricted to summit areas and rift zones; manmade structures in those areas can be damaged or destroyed by tilting or by differential settling of underlying rock. Some depressed areas may become more vulnerable to inundation by water or lava flows. This type of subsidence is so commonly associated with eruptions and so restricted to summit and rift-zone areas that its effects are overshadowed by those caused directly by eruptions.

Collapse of roofs of lava tubes is a minor subsidence hazard. Roof collapse can occur while lava is still moving through a tube, or later, especially if new loads are added by construction or heavy equipment. This hazard can be minimized by investigating for the presence of lava tubes at construction sites and along paths to be followed by heavy construction equipment. The hazard is highest on young pahoehoe lava flows of Mauna Loa and Kilauea, but it may also exist along the southwest rift zone of Maui and on the Kalaupapa Peninsula of Molokai.

EARTHQUAKES

Thousands of earthquakes occur each year in the Hawaiian Islands; most of them originate on the Island of Hawaii and result from the movement of magma at shallow depths (see Klein and others, chapter 43). These earthquakes commonly are associated with volcanic eruptions, but they also accompany movements of magma that does not reach the surface. The greatest number of earthquakes on the Island of Hawaii originate beneath the summit areas and along or near the rift zones of Kilauea and Mauna Loa. Most are so small that they can only be detected by instruments and cause no damage, but some are strong enough to be felt, and a few cause minor to moderate damage.

Some earthquakes are less directly associated with volcanic activity, and a few of these cause major damage (Klein and others, chapter 43). Such earthquakes originate every few years under the Island of Hawaii and are less frequent beneath and between other islands of the Hawaii group. Some of these earthquakes probably originate within or at the base of the volcanoes (Lipman and others, 1985) and others in the Earth's crust beneath the volcanoes. A major zone of structural weakness, the Molokai fracture zone, extends westward from North America and intersects the Hawaiian Islands (fig. 22.1). It has been the site of occasional strong earthquakes, some of which were centered close enough to the islands to be damaging. This structural zone holds the potential for generating major, though infrequent, earthquakes in the future.

The two largest earthquakes in Hawaii, in 1868 and 1975, had magnitudes greater than 7 and probably were caused indirectly by movement of magma into rift zones of Mauna Loa and Kilauea, respectively. Magma forced the flanks of the volcanoes outward, and the earthquakes resulted from the abrupt subsidence of part of the south flank (Swanson and others, 1976; Tilling and others, 1976; Lipman and others, 1985).

Earthquakes endanger people and property directly by shaking structures and by causing ground fractures, ground settling, and landslides. Earthquakes can also be associated with tsunamis when

both result from the sudden subsidence of a volcano's flank. Strong earthquakes in the past have damaged buildings, water tanks, and bridges, and have disrupted water, sewer, and telephone lines. Locally, such damage can be intensified where soft, saturated sediments amplify earthquake ground motions. Earthquakes also trigger rockfalls and other kinds of landslides, fracture the ground, and cause confined bodies of water to slosh back and forth. Indirect effects from shaking, such as fire, can be even more severe than direct effects.

Only a few earthquakes in Hawaii have been strong enough to cause severe and widespread damage. The frequent earthquakes caused directly by magma movement do not seriously endanger life or property; most damage resulting from the strongest earthquakes of this type has been related to the falling of loose objects. The strongest historical earthquake, in 1868, was centered beneath the south coast of the Island of Hawaii (Wood, 1914). It caused widespread and locally major damage across the entire island, triggered a destructive mudflow near the community of Pahala, and was accompanied by a devastating tsunami. The combined effects of this earthquake claimed 40–50 lives. A similar earthquake in 1975 caused widespread damage, and an accompanying tsunami claimed two lives (Tilling and others, 1976).

TSUNAMIS

Tsunamis, also called seismic sea waves or tidal waves, are large, rapidly moving ocean waves. Most tsunamis are associated with earthquakes and are generated when an abrupt movement of the ocean floor displaces a large mass of water. Tsunamis also have resulted directly from volcanism and from landsliding. Tsunamis that have originated around the rim of the Pacific Ocean at great distances from Hawaii have destructive effects similar to those that originate locally, and they are discussed along with locally generated tsunamis.

Tsunamis reportedly have swept onshore to heights as great as 40 m above sea level at some localities in the world, but the maximum recorded height reached by such a wave anywhere in Hawaii has been 16–17 m (Tilling and others, 1976). The heights and distances inland reached by different tsunamis, and on different coasts by the same tsunami, however, have varied greatly. The tsunami of November 29, 1975, reached as high as 14.6 m on the south coast of the Island of Hawaii (Tilling and others, 1976), but waves were only 1–2.4 m high on other parts of that island and less than 1 m high on the other islands. Recently, Moore and Moore (1984) have suggested that coral-bearing gravel deposits on some of the islands, formerly interpreted as beaches formed during high stands of sea level, are actually the result of a truly giant wave possibly generated by a submarine landslide.

Although the effects of tsunamis that originate at great distances are similar to those generated locally, the latter are potentially more dangerous because the time between their origin and arrival at the shoreline may be too brief to warn and evacuate people or property.

Tsunamis sometimes move onshore as turbulent waves that can damage or destroy virtually everything in their paths. People may be battered or drowned, buildings moved off their foundations or knocked over, trees uprooted, and boats carried inland. As the waves recede, they may carry people and property out to sea. Tsunamis can also rise quietly as they move onshore and inundate nearshore areas. The salt water can kill crops, poison soil, corrode metal, and damage objects and structures in other ways. The actual effects of a tsunami at any specific site will be determined by the details of local topography, both offshore and onshore, and the direction of approach of the wave, and they are difficult to predict.

The locally generated tsunami of April 2, 1868, destroyed most villages along the south coast of the Island of Hawaii and killed an estimated 46 people (Brigham, 1909, p. 495–496; Hitchcock, 1909; Wood, 1914). Five successive tsunamis that accompanied the earthquake of November 29, 1975, caused the loss of two lives and about $1.4 million in property damage.

Tsunamis have been reported in Hawaii about 50 times since the early 19th century (Macdonald and others, 1947). Those of 1837, 1868, 1877, 1946, 1960, and 1975 caused major damage. The tsunaumi of 1946 originated in Alaska and reached the islands without warning; it caused 150 deaths and $25 million damage (Macdonald and others, 1947; Shepard and others, 1950). Although adequate warnings accompanied the 1960 tsunami, which originated in Chile, they were not fully heeded, and the toll included 61 deaths as well as millions of dollars of property damage (Eaton and others, 1961).

HAZARD ZONES

Volcanic-hazard zonation maps have been prepared only for the Islands of Hawaii and Maui. Volcanic eruptions on the other islands are so unlikely in the near future that similar hazard zonation is not warranted. Likewise, no hazard-zone maps have been drawn for earthquakes or tsunamis. The threat from earthquakes is widespread across the islands, and earthquake effects are strongly influenced by local conditions. The danger from tsunamis exists only along the coasts of the islands in a narrow zone whose width depends on local topographic conditions. The danger from large tsunamis is somewhat greater along the southeast and southwest coastlines of the Island of Hawaii, because highly destructive tsunamis are occasionally generated there by large landslides.

The hazard-zone maps distinguish areas in which the general level of hazard is different from that of adjacent areas. However, the level of hazard can vary considerably within any hazard zone, either gradually or abruptly. Direct volcanic hazards, for example, decrease in magnitude gradually across zones away from active vents. For such hazards as lava flows, the frequency with which a specific site is affected decreases with increasing distance; for other hazards such as tephra and gases, the severity of effects diminishes gradually with increasing distance. Such gradational changes in the hazard may extend across an entire zone. Abrupt changes in magnitude of hazard within a zone commonly occur along sharp topographic features, and local topographic features in a zone may have a magnitude of hazard very different from that of the zone as

whole. The hills behind Ninole, for example, stand well above the adjacent slopes of modern Mauna Loa and so have a much lower lava-flow hazard than do those slopes. Consequently, the magnitude of hazard assigned to a zone applies only to that zone as a whole, and differences within it are not shown. Such differences can best be determined by specific site studies.

The change in degree of hazard across most zone boundaries is gradual rather than abrupt, and it may be apparent only over a distance of a few kilometers or more. Boundaries between many zones are approximations that serve chiefly as guidelines to show that a difference in hazard does exist and to facilitate description of the zones. Although adjacent hazard zones are separated on the maps by single lines, changes in the degree of hazard across most zone boundaries are so gradational that they might better be shown by numerous lines or a continuous change in shading.

Some zones that theoretically exist are not shown on the hazard maps. For example, in an area south of Kilauea caldera, the distribution of lava flows indicates that the hazard from future flows is much less than on the nearby southeast flank of the volcano. Zones intermediate between the two hazard zones that are shown must exist, but these intermediate zones are not drawn on the map because multiple narrow zones would suggest greater accuracy than is warranted.

Hazard zones are based chiefly on the assumption that future eruptions will be like those in the past that are known from oral and written histories and from geologic investigations. Some kinds and scales of eruptive events could occur that are not foreseen by these hazards assessments.

ISLAND OF HAWAII

HAZARD ZONES FOR LAVA FLOWS

Hazard zones for lava flows are based chiefly on lava-flow coverage of different areas during specific time periods. The zones are also based partly on the current structural conditions within the volcanoes, on fault scarps and other topographic features that would limit the distribution of lava flows, and on the frequency of past eruptive events. Recent studies of Kilauea by Holcomb (chapter 12), Mauna Loa by Lockwood and Lipman (chapter 18), and Hualalai by Moore and others (chapter 20) provide most of the data on lava-flow coverage for the time periods on which hazard zones are based. Similar data for Mauna Kea are from Porter (1973). Hazard zones and definitions used for the Island of Hawaii in this report are modified from those used for a previous volcanic-hazards assessment of the island (Mullineaux and Peterson, 1974; U.S. Geological Survey, 1976).

To facilitate comparison of the hazard from place to place across the Island of Hawaii, lava-flow hazard zones for its five volcanoes have been fit into a single scale of decreasing hazard. The overlap of hazard zones shown for Kilauea and Mauna Loa is approximate, in part because both volcanoes have changed their eruptive patterns within the past several hundred years, and their future patterns are only partly predictable. Between A.D. 1200 and A.D. 1800, for example, Kilauea erupted voluminous lava flows from precaldera summit vents; the flows covered more than 80 percent of the volcano, including its northeast and northwest flanks (Holcomb, chapter 12, fig. 12.42). Since 1800, lava has covered significant areas of its flanks only south of its east rift zone. In contrast, lava flows on Mauna Loa since about A.D. 1840 have covered more area than those of the previous several hundred years (Lipman, 1980). Neither volcano shows signs of changing its current pattern. The hazard zones shown on fig. 22.10 are based on the assumption that present kinds and rates of activity at both volcanoes will continue unchanged for at least the next few years and probably for the next few decades.

Zone 1 (fig. 22.10) consists of the summit areas and active parts of the rift zones of Kilauea and Mauna Loa; in those areas, 25 percent or more of the land surface has been covered by lava within historical time, during the 19th and 20th centuries. These areas contain the sites of most historical eruptions, and a large majority of the lava flows that will affect other zones on Kilauea and Mauna Loa in the near future probably will originate in zone 1.

Zone 2 consists of several areas that are adjacent to and downslope from the active rift zones of Kilauea and Mauna Loa and therefore are subject to burial by lava flows of even small volume erupted in those rift zones. On Kilauea south of its east rift zone, as much as 25 percent of the land surface has been covered by lava during historical time, and 10–15 percent has been covered since 1950. Lava flows have covered parts of this area as recently as January 1986, and the history of Kilauea suggests that they will continue until some significant change occurs within the volcano. Although very little of the area in zone 2 north of the lower east rift zone of Kilauea has been affected by lava since 1950, about 15 percent of that surface has been covered during historical time. On Mauna Loa, long and voluminous lava flows have repeatedly entered the areas included in zone 2, covering about 5 percent of those areas since 1950 and about 20 percent within historical time.

Zone 3 includes other areas on Kilauea and Mauna Loa in which the hazard is gradationally lower than that in zone 2. On Kilauea, less than 5 percent of the areas in zone 3 has been covered with lava during historical time. However, more than 75 percent of those areas has been covered by lava flows within the last 750 years. The hazard is less in zone 3 on the flanks of Kilauea than in zone 2 because ground subsidence within much of Kilauea's rift zones prevents lava flows of small volume from extending beyond those rift zones. On Mauna Loa, only about 1-3 percent of the land surface in most of zone 3 has been covered by lava during historical time; however, a single lava flow during the 19th century covered about 10 percent of the area in zone 3 on the northwest flank of the volcano. During the last 750 years, lava flows have covered about 15-20 percent of the flanks of Mauna Loa within zone 3. The hazard on Mauna Loa decreases progressively downslope from its summit and

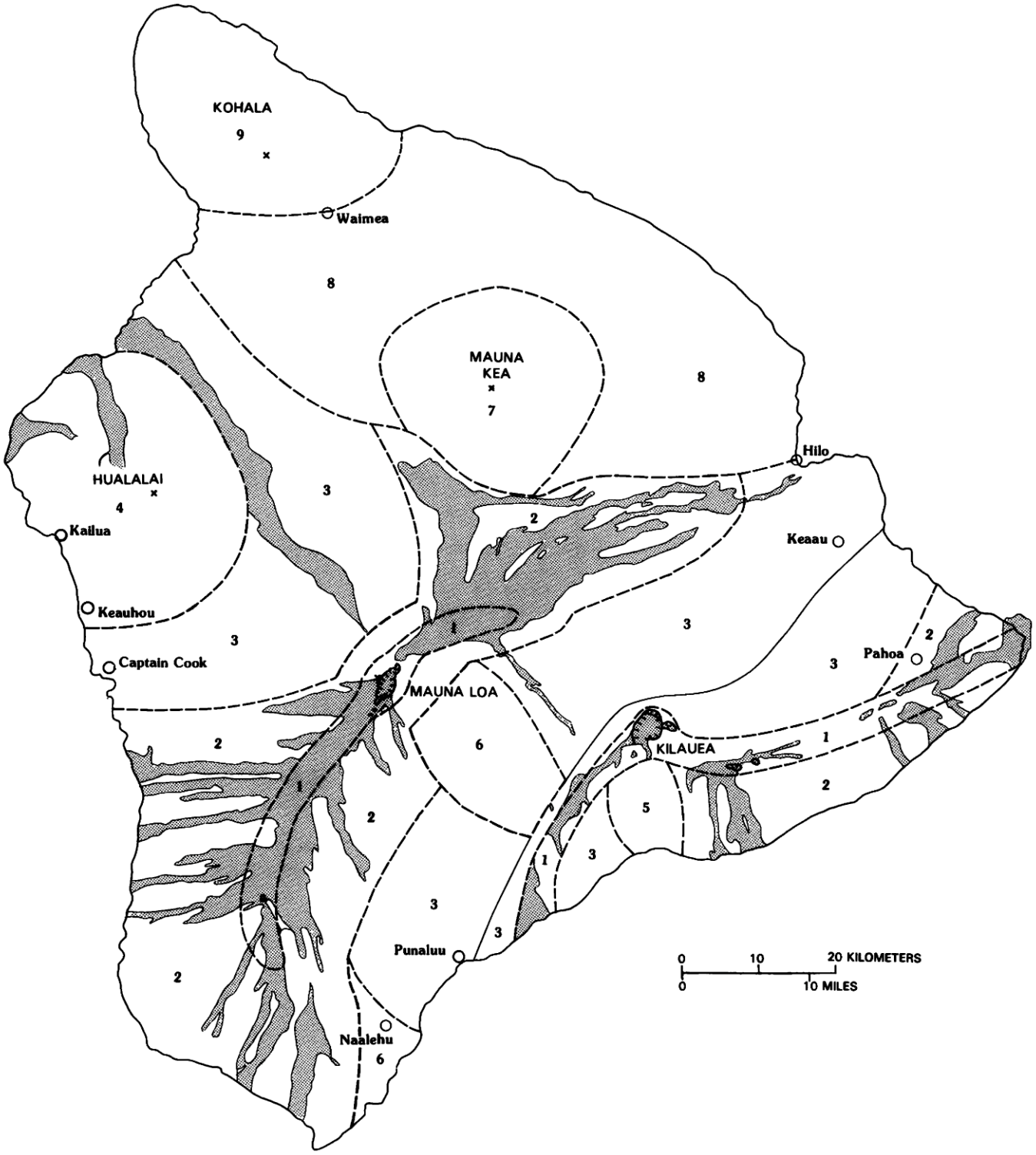

FIGURE 22.10.—Hazard zones for lava flows on the Island of Hawaii. See text for explanation of numbered zones. Thin, solid line marks boundary between Mauna Loa and Kilauea Volcanoes. Stipple pattern indicates areas covered by pre-1975 historical lava flows.

rift zones across zones 2 and 3. The hazard is lower in zone 3 because lava flows on Mauna Loa typically do not extend all the way from the source vents to the coastline; only about half of the flows on this volcano during the last 1,500 years have reached its lower flanks (Lockwood and Lipman, chapter 18). Within zone 3 on Mauna Loa, the hazard is currently less in the part that lies southeast of the rift zones than on the northwest flank of the volcano and should remain so in the near future. The hills behind Ninole, east of the southwest rift zone, are not identified on the hazard-zone map. They may be an upthrown block of Mauna Loa or part of an older volcano (Lipman, 1980), and they stand as much as a hundred meters above the younger surface of Mauna Loa. The lava-flow hazard on these hills decreases with height and is about as low as that in zone 8 at their highest points.

Zone 4 embraces only Haulalai Volcano, where a few percent of the land surface was covered by lava flows in A.D. 1800-1801, but less than 15 percent has been covered during the last 750 years. Recent prehistoric as well as historical eruptions on Haulalai have been less frequent than on Kilauea and Mauna Loa. Lava flows on Hualalai have typically covered large areas, and the rift zones of the volcano do not seem to have a distinctly higher degree of hazard than do its flanks.

Zone 5, on the lower flank of Kilauea south of its caldera, has been almost unaffected by lava flows during historical time, although nearly half of this area has been covered within the last 750 years. This flank of Kilauea is currently protected by the presence of the Kilauea summit caldera and by fault scarps in the Koae fault zone that face upslope. Zone 5 seems to be relatively safe from lava-flow burial under present conditions, but it could be threatened by a new episode of voluminous eruption of lava that spilled southward from the summit caldera.

Zone 6 includes one area on the flank of Mauna Loa south-southeast of its caldera and another that is east of the lower part of its southwest rift zone. The age and extent of flows in these areas are not well known, but the oldest flows at the surface of Mauna Loa are on this flank (Lipman, 1980). These areas seem relatively unlikely to be affected by lava flows in the near future. The magnitude of the hazard south-southeast of the summit could change significantly, however, if the caldera of Mauna Loa were to fill with lava.

Zone 7 includes the summit and upper flanks of Mauna Kea; this is an area in which no eruptions have occurred since about 3,500 years ago, but lava covered about 20 percent of the land surface between 5,000 and 3,500 years ago.

Zone 8 is a large area on the lower flanks of Mauna Kea that has not been affected by lava flows for at least 10,000 years. However, zone 8 could be affected by an unusually long lava flow issuing from a vent higher on Mauna Kea.

Zone 9 consists of Kohala Volcano. No eruption has occurred there for about 60,000 years, but even though the hazard there is extremely low the volcano cannot be regarded as extinct.

HAZARD ZONES FOR TEPHRA FALLS

Hazard zones for tephra (fig. 22.11) are based on eruption frequency, proximity to potential vents, and wind directions. Frequency and proximity largely control the location of tephra hazard zones on the Island of Hawaii, because the potential hazard diminishes rapidly in severity with increasing distance from vents as both fragment size and thickness of deposits decrease. Winds have less influence on the distribution of these hazard zones because the prevailing northeasterly trade winds are not dominant over the entire Island of Hawaii; antitrade and storm winds, especially at the altitudes of vents high on Mauna Loa, and upslope and downslope winds as well as sea and land breezes result in great variations from trade-wind directions. However, antitrade winds seldom blow from Kilauea, Mauna Loa, or Hualalai across Mauna Kea or Kohala, and storm winds blowing in those directions are infrequent.

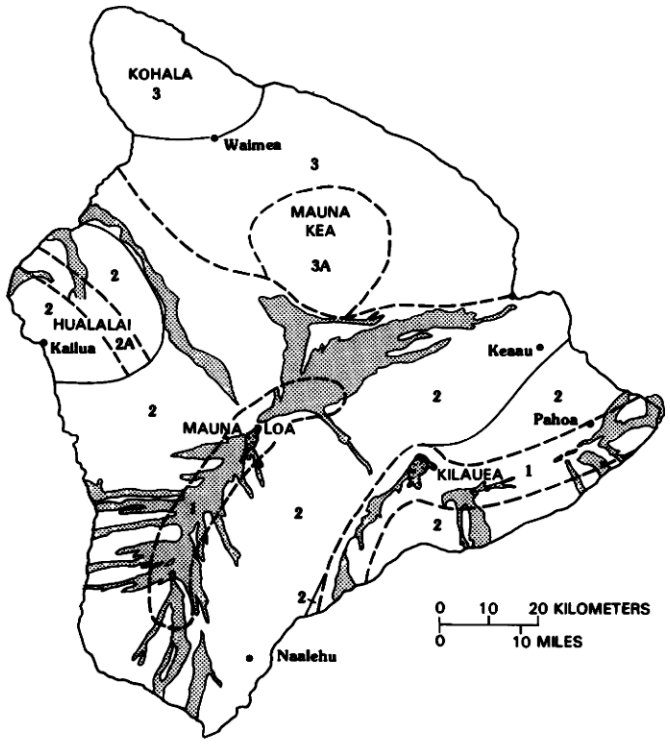

FIGURE 22.11.—Hazard zones for tephra on the Island of Hawaii. See text for explanation of numbered zones. Thin, solid lines mark boundaries between volcanoes. Stipple pattern indicates areas covered by pre-1975 historical lava flows.

Tephra is produced most frequently by lava fountains in the summit areas and rift zones of Kilauea and Mauna Loa. Such eruptions have occurred at least once every few years in historical time, and they have produced tephra as much as 1 m thick at a distance of 1 km from the vents and 10 cm thick at about 2 km (Richter and others, 1970). Steam-blast explosions have occurred at the summits of Kilauea and Mauna Loa and where the east rift zone of Kilauea intersects the shoreline. Tephra-fall deposits from steam-blast eruptions have included large rock fragments, but such eruptions rarely produce layers more than about 1 cm thick at localities

more than about 2 km from the source vents. Outside those zones, a few historical eruptions on the upper north slope of Mauna Loa suggest that tephra could be produced there by future lava fountains. Tephra mounds (littoral cones) can also be formed wherever lava flows enter the ocean; thus, they are limited to the seacoast, mostly on Kilauea and Mauna Loa. The hazard from tephra of this origin is not identified on a hazard map, inasmuch as it accompanies and is inseparable from the lava-flow hazard along the shoreline.

Tephra eruptions have been much less frequent on Hualalai; none are known in historical time. Such eruptions have been even less frequent on Mauna Kea and Kohala. The youngest eruptions on Mauna Kea occurred more than 3,500 years ago, but they produced tephra layers as thick as 5 m about 1 km from the source vents, 1 m at 2 km, and 10 cm at 4 km (Porter, 1973). No eruptions have occurred on Kohala for several tens of thousands of years.

Tephra-hazard zone 1 includes the summit areas and rift zones of Kilauea and Mauna Loa, the areas of highest eruption frequency, and extends about 2 km beyond the rift-zone boundaries. Tephra more than 10 cm thick, as well as large fragments, will likely be restricted to this zone during virtually all future eruptions from the summits and rift zones of Kilauea and Mauna Kea.

Tephra-hazard zone 2, in which tephra falls from lava fountains should be frequent but thin, includes the flanks of Kilauea and Mauna Loa and all of Hualalai. The potential hazard within this zone is locally somewhat greater on the upper north flank of Mauna Loa, where there are several vents along minor fractures. A subzone, 2A, of somewhat different character exists on Hualalai. In addition to the hazard there represented by thin tephra erupted from within zone 1, a potential exists for burial by cinder cones and thinner, more widespread tephra 10 cm or more thick from infrequent eruptions of Hualalai. This subzone includes the rift zone on Hualalai and the areas within about 4 km on both sides of the rift zone.

Tephra hazard zone 3 includes areas in which only thin deposits of tephra erupted from Kilauea, Mauna Loa, or Hualalai are likely to fall. The low frequency of winds that blow northward across Mauna Kea and Kohala from the three more active volcanoes indicates that even thin ash is likely from only a minority of eruptions. The subzone 3A marks an area of Mauna Kea above about a 2,000-m elevation in which cinder-cone eruptions could produce locally thick tephra deposits; although such eruptions have a very low probability, their effects could be locally severe.

HAZARD ZONES FOR PYROCLASTIC SURGES

On the Island of Hawaii, the deposits of pyroclastic surges have been recognized only adjacent to the caldera of Kilauea. The single hazard zone for pyroclastic surges surrounds the caldera and extends to a distance of 10 km from its center.

Pyroclastic surges conceivably could be initiated at other places where ground water or sea water can interact with magma. Magma could encounter ground water under the rift zones of Kilauea and the summit and rift zones of Mauna Loa and possibly at scattered sites elsewhere on Mauna Loa and on Hualalai. Magma and sea water could interact where both rift zones of Kilauea and the southwest rift zone of Mauna Loa meet the coastline.

HAZARD ZONES FOR VOLCANIC GASES

Hazard zones for volcanic gases are the same as hazard zones for tephra (fig. 22.11); like tephra, gases are emitted chiefly from the summit areas and rift zones of Kilauea and Mauna Loa; they are distributed by winds and their effects decrease with distance. Hazard zone 1 consists of the summit areas and rift zones of Kilauea and Mauna Loa, and extends about 2 km beyond the rift-zone boundaries.

Hazard zone 2 for gases includes Hualalai as well as the other parts of Kilauea and Mauna Loa. Although the hazard is less in zone 2, historical events show that gas effects can be significant far beyond the source vents. In 1977, gases from eruptions on Kilauea killed vegetation as far as 30 km from their source (J.P. Lockwood, written commun., 1978). From 1967 to 1974, trade winds carried gases from Kilauea's summit and east rift zone southwestward into the Kau District, reportedly causing a decline in sugar yields. Fumes then drifted around to the Kona District on the west coast and were blamed for the decline of other crops.

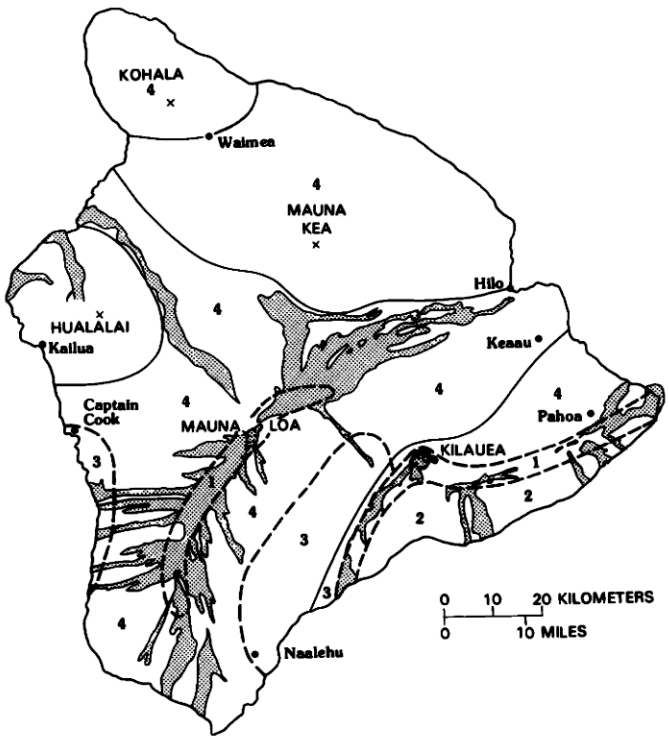

FIGURE 22.12.—Hazard zones for ground fractures and subsidence on the Island of Hawaii. See text for explanation of numbered zones. Location of areas subject to fracture and subsidence on flanks of Mauna Loa from Lipman (1980). Thin, solid lines mark boundaries between volcanoes. Stipple pattern indicates areas covered by pre-1975 historical lava flows.

Hazard zone 3 covers Mauna Kea and Kohala, which are subject to a lower degree of hazard because of their distance from vent areas and the infrequency of winds that blow across them from the south.

HAZARD ZONES FOR GROUND FRACTURES AND SUBSIDENCE

The Island of Hawaii is divided into four hazard zones for ground fracture and small-scale subsidence (fig. 22.12). The zone of highest hazard, zone 1, includes the summit areas and rift zones of Mauna Loa and Kilauea, where fractures and subsidence occur most frequently. Zone 2 consists of the south flank of Kilauea, where fracturing and subsidence occur somewhat less frequently than in the summit and rift zone areas. Fracturing and subsidence of the south flank occur chiefly along the Koae and Hilina fault zones but are not limited to them (Holcomb, chapter 12; Duffield, 1975; Lipman and others, 1985.

Hazard zone 3 embraces the areas of the Kaoiki and Kealakekua fault systems on Mauna Loa, where fractures and subsidence caused by magma movement are less frequent than on Kilauea. Zone 4, in which these hazards are least, includes the remainder of the island.

Abrupt large-scale subsidence of fault blocks causes an additional hazard from inundation along the coast seaward of the Kaoiki and Kealakekua fault systems on the flanks of Kilauea and Mauna Loa. Subsidence-induced tsunamis, however, can be a more serious hazard than the abrupt inundation. In addition, inundation hazard from slow regional subsidence exists along the entire shoreline of the island.

MAUI

The Island of Maui comprises two volcanoes, West Maui and Haleakala (Stearns and Macdonald, 1942; fig. 22.13). Potassium-argon ages of lavas of the West Maui volcano range from about 1.97 to 1.3 million years before present (McDougall, 1964; Naughton and others, 1980), and Crandell (1983) concluded that even the youngest lava flows on the volcano are more than 25,000 years old. The likelihood of a future eruption on West Maui seems remote.

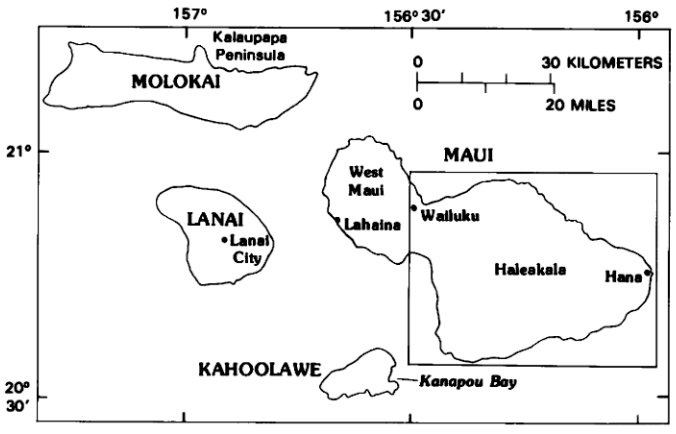

FIGURE 22.13.—The Islands of Maui, Molokai, Lanai, and Kahoolawe. Rectangle indicates area on Maui shown in figures 22.14 and 22.16.

Potassium-argon ages on lava flows of Haleakala volcano range from about 0.91 to 0.36 million years before present (McDougall, 1964; Naughton and others, 1980). Radiocarbon ages ranging from about 26,800 to 200 years before present have been reported on more recent ash deposits and lava flows (Crandell, 1983). Crandell inferred that the average frequency of eruptions on the volcano as a whole has been nearly one per 100 years during the last 1,000 years. The latest eruption occurred about 1790 at a vent in the lower part of the southwest rift zone, and it produced a 3-km-long lava flow.

HAZARD ZONES FOR LAVA FLOWS

Five zones of differing lava-flow hazard proposed by Crandell (1983) on Haleakala were based on the inferred frequency of eruptions and the ages of recent lava flows. The geologically recent eruptive history of Haleakala differs in many respects from that of the volcanoes on the Island of Hawaii. Because of these differences, lava-flow hazard zones recognized on Haleakala do not correspond exactly to hazard zones on Hawaii, and they are defined here from highest (1) to lowest (5) degree of hazard. The zones described here are the same as those outlined on a previous lava-flow hazard map of Haleakala (Crandell, 1983), but the definitions of some zones have been modified.

On Maui, lava-flow hazard zone 1 includes areas in which about 50 percent of the land surface has been covered by lava flows during the last 1,000 years, and it covers the crater of Haleakala and the southwest rift zone (fig. 22.14). The inferred frequency of lava flows has been at least one per 120 years in the crater during the last 2,500 years, and at least one per 150–200 years in the southwest rift zone during the last 1,000 years.

Zone 2 includes two areas in which 10–30 percent of the land surface has been covered by lava flows during the last 1,000 years. These areas are situated south of the southwest rift zone, where about 10 percent of the surface has been covered during the last 1,000 years, and north of the east rift zone, where lava flows have covered about 30 percent of the land surface during the same period. Lava flows are inferred to have occurred within these areas at an average rate of at least one per 500 years, and the last flow occurred less than 1,000 years ago.

Zone 3 includes areas in which eruptions have not occurred for more than 1,000 years, but where much of the land surface has been covered by lava flows within the last 20,000 years. The best evidence of rate of coverage in this zone on Haleakala is north of the southwest rift zone, where lava flows inferred to be less than 20,000 years old have covered about 75 percent of the land surface. Flows have occurred at an average rate of at least one per 2,000 years in this area, although the last flow was erupted about 4,000 years ago. The valleys that extend from the crater northward and southward to

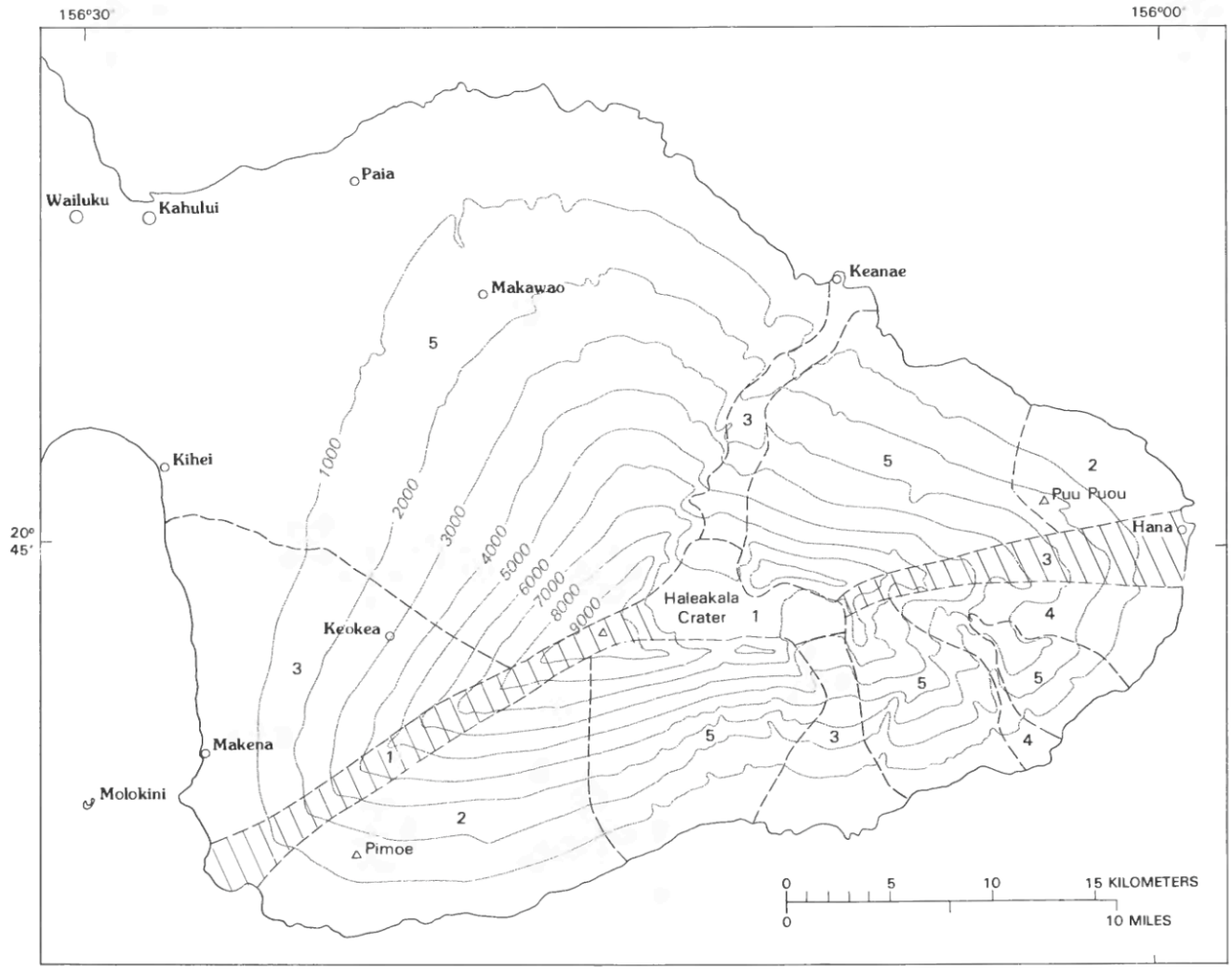

FIGURE 22.14.—Lava-flow hazard zones on Haleakala Volcano, eastern Maui. See text for description of the numbered zones. Lined areas indicate the southwest and east rift zones of the volcano. Topographic contours at 1,000-ft intervals.

the coasts, as well as the east rift zone, are included in zone 3. The two youngest flows recognized in the lower part of the southern valley were tentatively assigned an age of more than 1,000 but less than 10,000 years by Crandell (1983). A flow in the upper part of the east rift zone is radiocarbon dated at about 9,400 years before present, and one in the lower part of the rift zone is dated at 12,760 years before present. The rate of lava flow eruptions along the east rift zone probably is less than one per 2,000 years.

Zone 4 is defined solely from the average frequency of lava flows, which is inferred to be less than one per 10,000 years, but is at least one per 20,000 years. The last lava flows in these areas probably were formed more than 10,000 years ago. The rate of lava coverage is not known, but probably less than 10 percent of the area has been covered in the last 20,000 years.

Zone 5 includes areas that have not been affected by lava flows for at least 20,000 years.

Lava-flow hazard zones on Maui are compared with those on the Island of Hawaii in table 1, but the frequency of eruptions or the percentage of lava-flow cover during a specified period on one island may correspond only approximately with similar data on the other island.

TABLE 22.1.—*Comparison of lava-flow hazard zones on the Islands of Maui and Hawaii*

[N.R., not represented]

Lava-flow hazard zone on Hawaii	Lava-flow hazard zone on Maui
1	N.R.
2	N.R.
3	1 (?)
4	2
5	N.R.
6	N.R.
7	3
8	4
9	5

FIGURE 22.15.—View southeastward across lava flows (foreground) and cinder cones in the crater of Haleakala Volcano, eastern Maui. Cone at right side of photograph is about 150 m (500 feet) high. Average rate of eruptions in the crater during the last 2,500 years may be at least one per 100 years, but the age of the last eruption is not known.

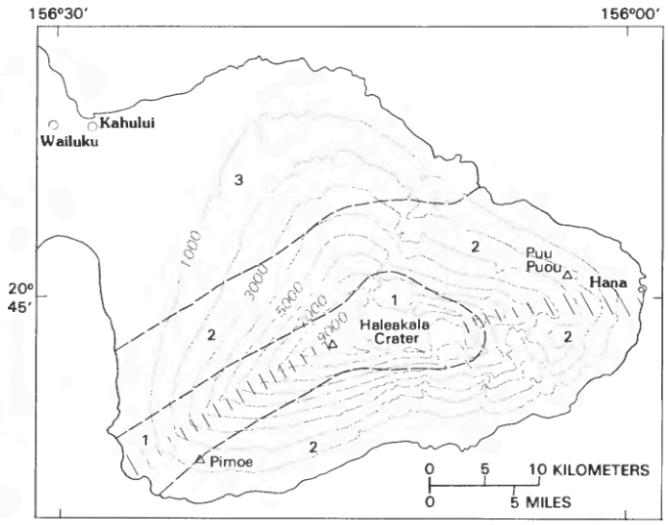

FIGURE 22.16.—Ashfall-hazard zones on Haleakala Volcano, eastern Maui. See text for description of the three zones. Lined areas indicate the southwest and east rift zones of the volcano. Topographic contours at 1,000-ft intervals.

HAZARD ZONES FOR TEPHRA FALLS

Because of the low frequency of eruptions on Maui in comparison with the Island of Hawaii, the likelihood of areas being affected by ashfall is much lower. If an ash-producing eruption does occur, the active vent probably will be within the crater (fig. 22.15) or somewhere along the southwest rift zone. Such an eruption might also occur at a flank vent, such as that represented by the Pimoe cone on the southwest side of Haleakala. Cindery ash on the northeast flank of Haleakala, northwest of Hana, probably came from a vent at or near Puu Puou (fig. 22.16). This ash is older than a 500-year-old lava flow and may be several thousand years old.

Three zones of different ashfall hazard on Maui (fig. 22.16) are based on the estimated frequency and range of thickness of future ashfalls. Within each ashfall-hazard zone, maximum thicknesses should be expected near the source vent, with rapidly decreasing thicknesses at increasing distance downwind. Zone 1 includes areas that could be affected at a rate of one ashfall per 200–500 years with thicknesss of 1–100 cm. Zone 2 includes areas in which 1–100 cm of ash could fall less often than once per 500 years but more often than once per 1,000 years and in which less than 1 cm of ash is expected once per 200–500 years. Zone 3 includes areas in which less than 1 cm of ash is expected to fall at an average rate of once per 1,000 years. This zone also includes areas in which 10 cm or more of ash may fall at least once per 3,000 years.

OTHER VOLCANIC HAZARDS

Hazard zones are not designated on Maui for pyroclastic surges, volcanic gases, ground fracture and subsidence, or earthquakes, but a few general statements can be made.

For the purpose of pyroclastic-surge hazard assessment, vents near or beneath sea level, and those in areas of high ground-water table, are regarded as areas of potential hazard from pyroclastic surges during eruptions. The most likely locations of such vents are near the coastline along the two rift zones of Haleakala. In addition, eruptions elsewhere on the windward, relatively wet, northeast side of Haleakala are more likely to be accompanied by explosions and pyroclastic surges than are eruptions at vents on drier parts of the island. The deposits of pyroclastic surges are present on the islet of Molokini, but have not been recognized on Maui.

The area of greatest potential danger to human health from volcanic gases probably is within the crater of Haleakala, because the crater is a natural basin in which heavier-than-air gases may be trapped. The crater floor would be a zone of relatively high gas hazard during an eruption. Gases erupted within the crater could also be carried by tradewinds toward the southwest and west slopes of the volcano.

Most future destructive earthquakes on Maui probably will be generated along the Molokai fracture zone (fig. 22.1) and thus could affect all or most parts of the island. For example, the earthquake of 1938, which had an epicenter about 40 km north of the island, damaged roads and structures on both Maui and Molokai (Macdonald and Abbott, 1970, p. 252; Furumoto and others, 1973).

The most likely area of ground fracture and subsidence in the future coincides with the crater and southwest rift zone of Haleakala, and these events would most likely be associated with an eruption. In addition, regional subsidence of possibly 1.7 mm/yr is occurring on Maui (Moore, chapter 2; Moore and Fornari, 1984), but this directly creates a hazard only along a narrow shoreline zone.

VOLCANIC HAZARDS ON THE OTHER ISLANDS

On islands other than Hawaii and Maui, the likelihood of an

eruption in the foreseeable future is so low that no preparation seems warranted unless premonitory signs indicate an approaching eruption. Each of these other islands is briefly discussed in the following sections.

KAHOOLAWE

The uninhabited Island of Kahoolawe is a single shield volcano with an erosionally breached caldera at its east end (Stearns, 1940; fig. 22.13). Deep weathering of rocks at the ground surface across the island (Macdonald and Abbott, 1970) and a potassium-argon age (Naughton and others, 1980) both indicate that Kahoolawe lava flows are one million or more years old. The most recent activity on the island, which is undated but much younger, produced small amounts of cinders and lava in the area of the breached caldera at Kanapou Bay (Macdonald and Abbott, 1970). The likelihood of a future eruption on Kahoolawe seems very low, but if an eruption should occur, it probably would produce a small amount of ash and lava in the Kanapou Bay area.

LANAI

Lanai also is a single shield volcano (fig. 22.13). Potassium-argon ages of lava flows reported from the island range from about 1.46 million years before present (Bonhommet and others, 1977) to 700,000 years before present (Naughton and others, 1980). More recent volcanism has not been recognized, and the likelihood of future eruptions on Lanai seems to be extremely low.

MOLOKAI

The Island of Molokai is formed chiefly by two large volcanoes, both of which are more than 1 million years old on the basis of potassium-argon ages (McDougall, 1964; fig. 22.13). The Kalaupapa Peninsula, which projects 4 km from the north side of the island, is a younger lava cone. Stearns and Macdonald (1947) noted that the lava flows on the peninsula are locally overlain by gravel which they thought was deposited by a stream graded to a stand of sea level 7.6 m higher than the present. This higher sea level has been dated at 120,000 years before present on Oahu (Ku and others, 1974); thus, the lava flows that form the peninsula seem to be older than 120,000 years before present. Three recent potassium-argon ages on the Kalaupapa lava flows, between 570,000 and 344,000 years before present, support that age assessment (Clague and others, 1982). Another vent appeared, perhaps at about the same time, off the east coast of the island. Explosions initially built a small tuff cone, but they were followed by the extrusion of lava flows (Macdonald and Abbott, 1970, p. 348).

Despite evidence cited above that the lava flows of the Kalaupapa peninsula are more than 100,000 years old, depth of weathering on the flows is less than that on some flows on the southwest flank of Haleakala that are younger than 25,000 years before present. This apparent discrepancy has not yet been resolved.

The probability of future volcanism on Molokai seems extremely low. If eruptions do occur, they probably would originate at vents at or near the Kalaupapa Peninsula or off the east end of the island.

OAHU

The eruptive activity that built Oahu occurred during three major periods. Potassium-argon age determinations on lavas from the shield volcano that forms western Oahu (fig. 22.17) range from about 3.5 to 2.74 million years before present, and lavas from the Koolau Volcano of eastern Oahu range in age from about 2.5 to 2 million years before present (McDougall, 1964). A third eruptive period began not long after 1 million years ago, and intermittent volcanism continued at least until about 30,000 years ago (Gramlich and others, 1971). All the vents active during the youngest period lie southeast of a line between Pearl Harbor and the Mokapu Peninsula (figs. 22.17, 22.18). Some of these eruptions formed such well-known features as Punchbowl and Diamond Head and produced airfall ash, lava flows, and pyroclastic-surge deposits that now underlie parts of the Honolulu metropolitan area. One flow of this period originated at the Sugar Loaf Crater on a ridge about 3 km east-northeast of Punchbowl and extended eastward into Manoa Valley, where it now underlies the University of Hawaii campus and the Honolulu suburb of Moiliili (Stearns and Vaksvik, 1935, p. 158). The ages of these events are not well known. Despite previously reported potassium-argon ages of about 900,000 and 100,000 years before present on the flow, Macdonald and Abbott (1970, p. 269) pointed out that the small amount of weathering and erosion on it suggest an age of only a few thousand years before present. Subsequent age determinations, however, gave ages of 68,000 and 66,000 years before present (Gramlich and others, 1971).

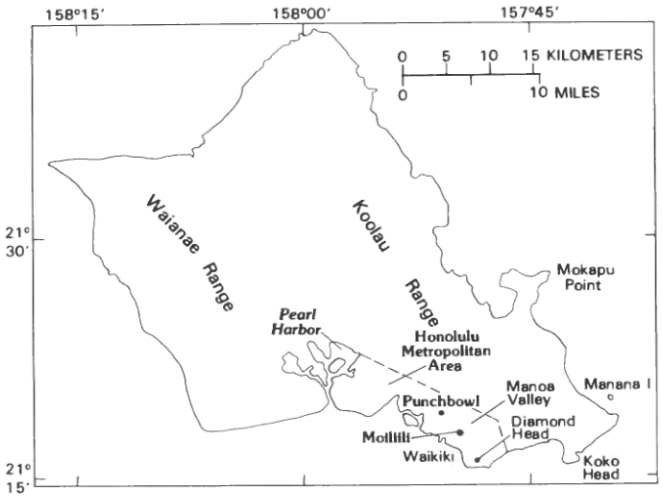

FIGURE 22.17.—The Island of Oahu. The Wainae and Koolau Ranges are each deeply eroded shield volcanoes more than 2 million years old. The most recent eruptions on Oahu originated at vents located between Koko Head and Manana Island.

FIGURE 22.18.—Aerial view southeastward across Koko Crater (center) and Koko Head (right center) on the southeast coast of Oahu. The most recent eruptions on Oahu, between about 43,000 and 31,000 years ago, occurred in the area between Koko Head and Manana Island, which is out of view 4 km to the left of the photograph.

The most recent dated eruptive activity on Oahu, between about 43,000 and 31,000 years ago, was concentrated along the shoreline in the southeasternmost part of the island between Koko Head (figs. 22.17, 22.18) and Manana (Rabbit) Island.

The restriction of the most recent eruptions to that part of the island suggests that if volcanic activity recurs, it will be located in the same general area, although not necessarily at the same vents as before. Eruptions there, if not affected by sea water, probably would produce cindery ash, whose distribution would be predominantly to the west and southwest, and perhaps lava flows. Eruptions in areas at or near sea level, or offshore, probably would be explosive and throw large rock fragments to distances of as much as several kilometers, produce airfall ash that would be carried downwind, and create pyroclastic surges (referred to as lateral blasts by Crandell, 1975). The specific areas that could be affected by these events cannot be predicted now and would not be known until an eruption began.

KAUAI AND NIIHAU

The bulk of the Island of Kauai (fig. 22.1) is formed of lava flows whose potassium-argon ages range from 5.7 to 3.8 million years before present (McDougall, 1964). The most recent eruptive activity occurred at about 40 vents scattered over the eastern two thirds of the island. These eruptions probably were spread over a long period of time, and all probably are older than 100,000 years before present (McDougall, 1964).

Ages of the lava flows that form Niihau (fig. 22.1) are not known, but even the youngest volcanic rocks on the island are older than the stand of sea level that was 7.6 m above that of the present (Macdonald and Abbott, 1970), and that evidently dates from about 120,000 years ago (Ku and others, 1974).

The absence of any eruptive activity on Kauai and Niihau for more than 100,000 years indicates that the likelihood of future eruptions on these islands is virtually nil.

MITIGATION OF VOLCANIC HAZARDS

Volcanic hazards can be mitigated chiefly by avoiding or controlling the hazards and by minimizing their effects. Hazards can be avoided on a long-term basis by land-use zoning that prevents building of structures in areas of high danger. On a short-term basis, people can be evacuated and some property removed from threatened areas when an eruption is imminent or even underway. Control

of hazardous volcanic events generally is not feasible, although diversion of some lava flows has been at least partly successful. Minimizing effects by protective measures generally is less useful for lava flows than for other volcanic hazards such as tephra and volcanic gases.

Predictions of future eruptions can also help people prepare for and respond effectively to those events. Long-range forecasts can include hazard assessments stating the probable frequency of hazardous events and areas they could affect, based on eruptions of the past. These forecasts can be accompanied by hazard-zonation maps such as those in this report, which show the relative magnitudes of certain hazards in different areas. This information can be used for making decisions regarding both long-term land use and short-term response to eruptions threatened or in progress.

Short-range forecasts are based chiefly on geophysical monitoring that measures the effects, especially earthquakes and deformation, of magma rising into the volcano. Such forecasts probably will provide warning of impending eruptions for most if not all lava-flow eruptions in Hawaii. Premonitory signs of explosive eruptions are less well known, but sudden or major lowering of magma levels, especially at the Kilauea caldera, should be regarded as a strong danger signal.

LAVA FLOWS

Avoidance through land-use zoning and evacuation is virtually the only way to reduce losses from lava flows. Areas in which lava-flow hazard is high can be zoned to restrict use. Even after eruptions have begun, flows can generally be avoided by people, and enough time often is available to remove some property from threatened localities.

Lava flows generally cannot be controlled. Although some diversions of lava flows have been successful, they can raise legal and social problems, and they require favorable conditions.

Diversion or control of flowing lava can be attempted by (1) construction of barriers and diversion channels; (2) use of explosives to block or divert lava streams, including those in lava tubes; and (3) use of water to cool and solidify lava flows. Each of these methods can be temporarily effective, and its success will ultimately depend on an early end to the eruption. The first two methods have been tried in Hawaii with limited success, and diversion barriers have recently been used successfully on Mount Etna in Italy (Lockwood and Romano, 1985). The third method was employed in 1973 at Heimaey, Iceland, and helped prevent destruction of parts of a town and harbor.

Generally, the larger and more rapidly moving the lava flows are, the more difficult it is to control or divert them. Moreover, decisions to attempt to control lava flows should be based on many factors, such as the path and other characteristics of the flow, the type of topography toward which it is moving, the economic and engineering feasibility of control measures, and the social and economic value of areas from which and toward which the lava would be diverted.

BARRIERS AND DIVERSION CHANNELS

Even small obstructions such as rock walls have changed the course of lava flows; thus barriers are an obvious diversion technique. During the 1955 and 1960 Kilauea eruptions, hastily erected barriers temporarily impeded lava flows, although the barriers were ultimately overwhelmed. Theoretically, structures of sufficient size and strength could be constructed to divert lava flows as large as any historic Hawaiian flows. For such barriers to be effective, however, wide and smooth channels would have to be provided as alternate paths. Without such channels, a voluminous flow could thicken behind the barrier and ultimately either overflow or break through it.

Plans have been proposed to protect the city of Hilo by systems of barriers and diversion channels (Jaggar, 1945; Macdonald, 1958, 1962). Their probable effectiveness has been debated (Wentworth and others, 1961), and costs and commitments to existing land use apparently have prevented any such projects from being carried out. The 1975 eruption of Mauna Loa renewed awareness of the lava-flow threat and led to consideration of lava diversion plans (Lockwood and Torgerson, 1980). Technical feasibility is, however, only one of the several difficult aspects of lava diversion. For example, artificial diversion of lava onto property that would otherwise have been spared could lead to complex legal and other problems.

DISRUPTION OF LAVA CHANNELS AND TUBES BY EXPLOSIVES

Attempts were made in 1935 and 1942 to divert Mauna Loa flows by bombing, because of potential threats to Hilo (Jaggar, 1936; Finch and Macdonald, 1949; Macdonald, 1958). It was reasoned that if a lava tube or channel were breached or blocked near its source, the advancing lava front would lose its source of supply, and the flow would halt. Lava issuing from any breach would then have to build a new channel and tube system before a flow would again reach the former front, and during this time the eruption might come to a stop. The bombings of 1935 and 1942 demonstrated the potential of this method, but the eruptions stopped before the method had been fully tested. New plans for use of explosives to divert lava flows were developed after the 1975 Mauna Loa eruption (Lockwood and Torgerson, 1980).

Attempts to divert high-volume, rapid flows might be ineffective, especially those which are not confined to channels or tubes, such as the voluminous flows from the southwest rift zone of Mauna Loa during the early part of the 1950 eruption.

COOLING LAVA FLOWS WITH WATER

During early 1973, lava flows on the island of Heimaey, Iceland, were advancing into the town of Vestmannaeyjar and threatening its harbor. Because a small-scale test indicated that water sprayed on the flow front cooled the lava sufficiently to impede its advance, huge pumps and large quantities of plastic pipe were used to implement the method on a large scale (Williams and Moore, 1973; Einarsson, 1974). As seawater was pumped from the harbor

and sprayed onto the flow, the chilled lava formed a barrier behind which new lava accumulated. The barrier eventually became high enough and strong enough to divert the oncoming lava into a new path, away from the town and harbor.

Such a technique might be feasible in Hawaii on relatively low-volume flows close to sea level. Plastic pipes enabled the water-delivery system on Heimaey to be moved readily in response to changing needs; such pipes, however, could not withstand the high pressures if water were to be delivered more than a few tens of meters above sea level. Even with such limitations, this technique might prove to be valuable under favorable conditions.

Protection from the effects of lava flows, other than by such methods of diversion or control, is generally not feasible. An individual lava flow will have roughly the same effects all the way from its source to its terminus, and attempts to protect buildings and other structures from the hot, crushing lava generally are not effective.

Long-term forecasts of the location of high-hazard areas can facilitate selection, before as well as during eruptions, of areas suitable for various uses, such as relatively safe evacuation routes. In addition, short-term forecasts of eruptions can almost always provide warnings. Even after lava-flow eruptions have begun, time generally is available to carry out evacuation plans.

TEPHRA FALLS

It is not possible to prevent widespread distribution of tephra, but hazard-zone maps can be used for choosing sites for specific uses that avoid areas of high hazard from tephra falls. Even after a tephra-producing eruption has begun, areas sometimes can be evacuated, and its effects can be effectively reduced for people who remain. People close to a vent during a tephra eruption should move upwind of the vent if possible; if they cannot, they should find suitable cover to prevent death or injury from falling fragments. Most other adverse effects can be decreased by placing damp or even dry cloths over noses and mouths to screen out ash particles. Structures in high-hazard zones can be designed to withstand impacts and loads imposed by falling material. In addition, airtight construction and filtering systems can reduce the likelihood that dust-sized particles will infiltrate structures and mechanized equipment.

PYROCLASTIC SURGES

The principal mitigative action for pyroclastic surges is to avoid them. Evacuation must be accomplished, however, before surge-forming eruptions occur, because pyroclastic surges move so rapidly that escape is not possible after they have begun.

Control of surges is not possible, although they can be deflected by natural barriers. Partial protection from the effects of surges is also possible but limited. Structures in areas of high hazard, for example, could be designed to withstand pyroclastic surges typical of Hawaiian volcanoes. Because many surges extend only short distances and become less severe near their margins, the chances of surviving them increase rapidly with increasing distance from the source vent. The people killed by a probable pyroclastic surge from Kilauea in 1790 were not seriously burned or battered, and they probably died from breathing hot air laden with volcanic gas and ash. People overrun by a pyroclastic surge could improve their chances of survival by finding any shelter, such as a vehicle, to reduce the effects of blast and impact. In addition, use of a filter could be critical because breathing of hot gas and ash is especially dangerous. A wet mask, clothing, or any other material that could filter ash and cool the air inhaled could be especially valuable.

VOLCANIC GASES

Effects of gas can be minimized by selecting building sites in zones of low hazard, and serious short-term effects can be avoided by evacuating some areas during periods of strong gas emission. However, gas probably cannot be completely avoided anywhere on the southern two-thirds of the Island of Hawaii. The emission or distribution of gas cannot be controlled.

For personal safety, topographic depressions near erupting vents should be avoided to eliminate the possibility of being overcome by odorless gases that are heavier than air. Persons with heart or respiratory ailments should avoid areas where concentrations of volcanic gas are possible. A filtering mask or damp cloth held over the face can reduce the effects of sulfur-bearing gas and temporarily lessen discomfort (see Wilcox, 1952, p. 443). No method is known, however, to eliminate gas damage to vegetation and mechanical equipment.

GROUND FRACTURES AND SUBSIDENCE

Ground-fracture and subsidence hazards to people or structures can be avoided only by staying away from areas in which they might occur, for the hazards cannot be controlled and generally cannot be economically minimized. The minor danger to people represented by these hazards can generally be avoided by using care in the areas affected. People living or working in fracture- and subsidence-prone areas should be wary of large open cracks, especially when leaving established trails or in heavily vegetated areas. Damage to structures rarely is catastrophic, but fractures with differential movements of more than a few tens of centimeters, or significant tilting from subsidence, could destroy some buildings. Thus, facilities that have unusual value or that are essential to public health and safety should not be built in areas where these hazards are high. Structures could be designed to resist fractures, but design to resist effects of tilting or submergence from subsidence probably is not economically practical.

The frequency of ground fracturing and subsidence and the localities that are susceptible can generally be predicted, and specific sites could be studied to determine the local magnitude of hazard.

EARTHQUAKES

Potential damage from strong earthquakes is widespread in

Hawaii and cannot be avoided, especially on the Island of Hawaii, but future damage could be reduced by land-use zoning and by earthquake-resistant design and construction. Areas can be avoided that are on or near steep slopes that could fail during earthquakes. Some areas that are underlain by materials susceptible to ground failure during earthquakes are shown on maps (Buchanan-Banks, 1983). Similarly, some areas could be identified in which structures could be damaged by the amplification of ground motion during earthquakes. Construction in such areas can be regulated by zoning or other measures where appropriate, and structures can be designed to resist damage from future earthquakes. Assessments of the magnitudes and frequency of future earthquakes, and of effects of past earthquakes (see Buchanan-Banks, chapter 44, and references therein), can contribute to decisions regarding appropriate future land-use and building requirements.

TSUNAMIS

Zoning to avoid tsunamis would require restricting land use along all the coastlines of the Hawaiian Islands, areas that are now intensively utilized for commercial, residential, and recreational purposes. Nevertheless, avoiding tsunamis through site selection for critical facilities, tsunami-resistant construction, and evacuation plans all could be effective for minimizing future losses. Zoning, for example, could restrict land uses along the coasts to those judged to be compatible with the tsunami hazard, and structures can be designed to resist the forces from tsunamis of predicted size. In addition, tsunami warnings often can be made in time to evacuate threatened coastal zones.

At present, the International Tsunami Information Center in Honolulu is alerted whenever potentially dangerous waves are generated by an earthquake anywhere in the Pacific region, and warnings are issued when appropriate. Low-lying areas generally can be evacuated before tsunamis from distant sources arrive. Tsunami-hazard zones on most islands are shown in telephone books in Hawaii, and people could choose in advance what routes to use in leaving threatened areas. People should be aware, however, that tsumanis could conceivably extend beyond some of the zones shown in telephone books, and they should be prepared to move farther inland or to higher ground if a large tsunami is predicted.

If a tsunami were generated locally, time might be too short for an official warning to be effective. Thus, any earthquake strong enough to make standing difficult can be taken as a warning that a tsunami may soon follow, and people along shorelines should immediately move inland or to higher ground.

FUTURE VOLCANIC ACTIVITY

Future eruptions can be expected at several volcanoes in Hawaii, and they will occur most frequently at Kilauea and Mauna Loa. The historical record suggests that no more than about 5 years will elapse without an eruption at one or the other of those two (Klein, 1982). Lava will be emitted chiefly from vents in the summit areas and along rift zones, but almost all parts of both volcanoes can be affected by lava flows. Based on historical records, about 5–10 percent of Kilauea and Mauna Loa could be covered during any 50-year period. Although wide fluctuations can be expected in eruptive rates from one decade to another, the overall rates likely will remain about the same. It is not possible, however, to predict where the next eruptive centers will be, how frequent or copious eruptions will be in a specific area, or which specific areas will be covered by lava.

The volcanic activity along Kilauea's east rift zone in historical time illustrates a difficulty in using the short historical record to predict future activity in a specific area. Between 1800 and 1950, approximately 2 percent of the eastern flanks of the volcano had been covered by lava from the east rift zone. In 1950, the probability based on these figures that a site in that region would be covered would have been 0.013 percent per year. However, between 1950 and 1975 about 8 percent of Kilauea's east flank was covered by lava, and so the coverage in that interval was actually about 0.32 percent per year. Estimates of future coverage may be no more accurate.

Mapping and dating of prehistoric lava flows also show that rates of burial have also varied widely in recent prehistoric time on both Kilauea and Mauna Loa. Overall rates of burial have changed markedly on Mauna Loa since 1868 (Lockwood and Lipman, chapter 18; Lipman, 1980); areas of high burial rates have switched from one flank of Kilauea to another at various times within the last 500 years (Holcomb, chapter 12; Holcomb, 1979). Accurate predictions of short-term probabilities of lava-flow coverage for any specific area clearly are not yet feasible.

Although lava flows are the most common volcanic hazard on Mauna Loa and Kilauea, explosive eruptions almost certainly will occur in the future. Two large explosive eruptions that produced pyroclastic surges have occurred within the last 2,000 years (Decker and Christiansen, 1984), and another in the future is a distinct possibility. While the hazard from such eruptions may seem small because of their infrequency, the potential threat to life should not be ignored.

Accurate statements of probabilities for frequency of eruptions or rate of burial by lava at Hualalai are not yet possible. However, at least four major eruptions have occurred at this volcano in the last 1,000 years (Moore and others, chapter 20; Moore and others, 1979). The lava flows from Hualalai in 1800–1801 were voluminous and highly fluid, but late prehistoric explosive eruptions near the summit built many large cinder and spatter cones. Future eruptions likely will originate both in the summit area and along the northwest and southeast rift zones, and some areas downslope from active vents will be buried by lava flows.

Neither Mauna Kea nor Kohala has been active during man's occupation of Hawaii. Mauna Kea has erupted within the last 5,000 years, however, most recently about 3,600 years ago (Porter, 1973), and it probably will erupt again. Future eruptions of Mauna Kea will probably be accompanied by mild to moderate explosive activity, producing ash and cinders that will build cones similar to those on its summit area and upper flanks, and produce ash deposits adjacent to the cones. Ash from such eruptions might drift for tens of kilometers downwind. If lava flows were erupted, they probably

would be relatively viscous and thick and would not travel more than a few kilometers from their sources. All the most recent eruptions have occurred at elevations above about 2,000 m, and future activity on Mauna Kea would most likely also originate on the upper part of the mountain.

Kohala is less likely to erupt in the near future than is Mauna Kea. The youngest flow of Kohala, a single flow that occurred long after the major growth of the volcano, has been dated at about 60,000 years before present (McDougall and Swanson, 1972). The probability of future activity of this volcano is very low compared to that for other volcanoes on the Island of Hawaii.

On Maui, Haleakala Volcano has been quiet for nearly two centuries, yet the inferred average rate of eruptions on the volcano as a whole has been nearly 1 per 100 years during the last 1,000 years (Crandell, 1983). This eruptive history suggests that an eruption could occur somewhere on Haleakala within the next 100 years. Recent eruptions have been most frequent within the crater and along the southwest rift zone, so one or the other of these areas seems to be the most likely location of the next eruption, but there is as yet no way to predict its specific time or place.

Future eruptions on Oahu and other islands are possible, but are likely to be so infrequent and scattered that preparation for such eruptions does not seem warranted now.

REFERENCES CITED

Apple, R.A., and Macdonald, G.A., 1966, The rise of sea level in contemporary times at Honaunau, Kona, Hawaii: Pacific Science, v. 20, no. 1, p. 125–136.

Bonhommet, Norbert, Beeson, M.H., and Dalrymple, G.B., 1977, A contribution to the geochronology of the Island of Lanai, Hawaii: Geological Society of America Bulletin, v. 88, p. 1282–1286.

Brigham, W.T., 1909, The volcanoes of Kilauea and Mauna Loa on the Island of Hawaii: Bernice Pauahi Bishop Museum Memoirs v. 2, no. 4, p. 379–608.

Clague, D.A., Dao-Gong, Chen, Murnane, Richard, Beeson, M.H., Lanphere, M.A., Dalrymple, G.B., Friesen, Walter and Holcomb, R.T., 1982, Age and petrology of the Kalaupapa Basalt, Molokai, Hawaii: Pacific Science v. 36, p. 411–420.

Crandell, D.R., 1975, Assessment of volcanic risk on the Island of Oahu, Hawaii: U.S. Geological Survey Open-File Report 75–287, 18 p.

———1983, Potential hazards from future volcanic eruptions on the Island of Maui, Hawaii: U.S. Geological Survey Miscellaneous Investigations Series Map I–1442.

Crandell, D.R., Booth, Basil, Kusumadinata, K., Shimozuru, Daisuke, Walker, G.P.L., and Westercamp, Denis, 1984, Source-book for volcanic-hazards zonation: UNESCO, 97 p.

Dalrymple, G.B., Silver, E.A., and Jackson, E.D., 1973, Origin of the Hawaiian Islands: American Scientist, v. 61, p. 294–308.

Decker, R.W., and Christiansen, R.L., 1984, Explosive eruptions of Kilauea Volcano, Hawaii, *in* Explosive volcanism: inception, evolution, and hazards: National Academy Press, p. 122–132.

Duffield, W.A., 1975, Structure and origin of the Koae fault system, Kilauea Volcano, Hawaii: U.S. Geological Survey Professional Paper 856, 12 p.

Dzurisin, Daniel, Lockwood, J.P., Casadevall, Thomas, and Rubin, Meyer, (in press), The Uwekahuna Ash: product of a large phreato-magmatic eruption of Kilauea Volcano, Hawaii: Bulletin of Volcanology.

Eaton, J.P., Richter, D.H., and Ault, W.V., 1961, The tsunami of May 23, 1960, on the Island of Hawaii: Seismological Society of America Bulletin, v. 51, p. 135–157.

Einarsson, T.M., 1974, The Heimaey eruption in words and pictures: Reykjavik, Heimskringla, 56 p.

Finch, R.H., and Macdonald, G.R., 1949, Bombing to divert lava flows: Volcano Letter 506, p. 1–30.

Furumoto, A.S., Nielsen, N.N., and Phillips, W.R., 1973, A study of past earthquakes, isoseismic zones of intensity, and recommended zones for structural design for Hawaii: Hawaii University Institute of Geophysics Report HIG–73–4, 50 p.

Gramlich, J.W., Lewis, V.A., and Naughton, J.J., 1971, Potassium-argon dating of Holocene basalts of the Honolulu volcanic series: Geological Society of America Bulletin, v. 82, p. 1399–1404.

Hitchcock, C.H., 1909, Hawaii and its volcanoes [2d ed., with supplement, 1911]: Honolulu, Hawaiian Gazette, 314 p.

Holcomb, R.T., 1979, Century-scale changes in eruptive behavior of Hawaiian volcanoes [abs.]: Hawaii Symposium on Intraplate Volcanism and Submarine Volcanism, Hilo, July 16–22, 1979, Abstract Volume, p. 164.

Jaggar, T.A., 1936, The bombing operation at Mauna Loa: Volcano Letter 431, p. 4–6.

———1945, Protection of harbors from lava flows: American Journal of Science, v. 243–A, p. 333–351.

———1947, Origin and development of craters: Geological Society of America Memoir 21, 508 p.

Klein, F.W., 1982, Patterns of historical eruptions at Hawaiian volcanoes: Journal of Volcanology and Geothermal Research, vol. 12, p. 1–35.

Ku, Teh-Lung, Kimmel, M.A., Easton, W.H., and O'Neil, T.J., 1974, Eustatic sea level 120,000 years ago on Oahu, Hawaii: Science, v. 183, p. 959–962.

LeGuern, F., Tazieff, H., and Faivre Pierret, R., 1982, An example of health hazard, people killed by gas during a phreatic eruption: Dieng Plateau (Java, Indonesia), February 20, 1979: Bulletin Volcanologique, v. 45 (2), p. 152–156.

Lipman, P.W., 1980, Rates of volcanic activity along the southwest rift zone of Mauna Loa Volcano, Hawaii: Bulletin Volcanologique, v. 43–4, p. 703–725.

Lipman, P.W., Lockwood, J.P., Okamura, R.T., Swanson, D.W., and Yamashita, K.M., 1985, Ground deformation associated with the 1975 magnitude-7.2 earthquake and resulting changes in activity of Kilauea Volcano, Hawaii: U.S. Geological Survey Professional Paper 1336, 45 p.

Lockwood, J.P., and Romano, Romolo, 1985, Lava diversion proved in 1983 test at Etna: Geotimes, v. 30, no. 5, p. 10–12.

Lockwood, J.P., and Torgerson, S.A., 1980, Diversion of lava flows by aerial bombing—lessons from Mauna Loa Volcano, Hawaii: Bulletin Volcanologique, v. 43–4, p. 727–741.

Macdonald, G.A., 1958, Barriers to protect Hilo from lava flows: Pacific Science, v. 12, p. 258–277.

———1962, The 1959 and 1960 eruptions of Kilauea Volcano, Hawaii, and the construction of walls to restrict the spread of the lava flows: Bulletin Volcanologique, v. 24, p. 249–294.

———1972, Volcanoes: Englewood Cliffs, New Jersey, Prentice-Hall, 510 p.

Macdonald, G.A., and Abbott, A. T., 1970, Volcanoes in the sea: Honolulu, University of Hawaii Press, 441 p.

Macdonald, G.A., Shepard, F.P., and Cox, D.C., 1947, The tsunami of April 1, 1946, in the Hawaiian Islands: Pacific Science, v. 1, p. 21–37.

McDougall, Ian, 1964, Potassium-argon ages from lavas in the Hawaiian Islands: Geological Society of America Bulletin, v. 75, p. 107–128.

McDougall, Ian, and Swanson, D.A., 1972, Potassium-argon ages of lavas from the Hawi and Pololu volcanic series, Kohala Volcano, Hawaii: Geological Society of America Bulletin, v. 83, p. 3731–3738.

Moore, J.G., 1970, Relationship between subsidence and volcanic load, Hawaii: Bulletin Volcanologique, v. 34, no. 2, p. 562–576.

Moore, J.G., and Fiske, R.S., 1969, Volcanic substructure inferred from dredge samples and ocean-bottom photographs, Hawaii: Geological Society of America Bulletin, v. 80, no. 7, p. 1191–1202.

Moore, J.G. and Fornari, D.J., 1984, Drowned reefs as indicators of the rate of subsidence of the Island of Hawaii: Journal of Geology, v. 92, p. 752–759.

Moore, J.G., Clague, D.A., and Normark, W.R., 1982, Diverse basalt types from Loihi Seamount, Hawaii: Geology, v. 10, no. 2, p. 88–92.

Moore, J.G., and Moore, G.W., 1984, Deposit from a giant wave on the Island of Lanai, Hawaii: Science, v. 226, p. 1312–1315.

Moore, R.B., Rubin, Meyer, and Spiker, E.C., 1979, Recent geologic investigations on Hualalai Volcano Hawaii [abs.]: Eos, v. 61, no. 6, p. 70.

Mullineaux, D.R., and Peterson, D.W., 1974, Volcanic hazards on the Island of Hawaii: U.S. Geological Survey Open-File Report 74–239, 61 p.

Nairn, I.A., 1979, Rotomahana-Waimangu eruption, 1886: base surge and basalt magma: New Zealand Journal of Geology and Geophysics, v. 22, no. 3, p. 363–378.

Naughton, J.J., Macdonald, G.A., and Greenberg, V.A., 1980, Some additional potassium-argon ages of Hawaiian rocks: the Maui volcanic complex of Molokai, Maui, Lanai and Kahoolawe: Journal of Volcanology and Geothermal Research, v. 7, p. 339–355.

Porter, S.C., 1973, Stratigraphy and chronology of late Quaternary tephra along the south rift zone of Mauna Kea Volcano, Hawaii: Geological Society of America Bulletin, v. 84, p. 1923–1940.

Richter, D.H., Eaton, J.P., Murata, K.J., Ault, W.U., and Krivoy, H.L., 1970, Chronological narrative of the 1959–60 eruption of Kilauea Volcano, Hawaii: U.S. Geological Survey Professional Paper 539–E, 73 p.

Shepard, F.P., Macdonald, G.A., and Cox, D.C., 1950, The tsunami of April 1, 1946: Scripps Institute of Oceanography Bulletin, v. 5, p. 391–528.

Siegel, B.Z., and Siegel, S.M., 1978, Mercury emission in Hawaii—aerometric study of the Kalalua eruption of 1977: Environmental Science and Technology, v. 12, no. 9, p. 1036–1039.

Stearns, H.T., 1940, Geology and ground-water resources of the Islands of Lanai and Kahoolawe, Hawaii: Hawaii Division of Hydrography, Bulletin 6, 177 p.

———1966, Geology of the State of Hawaii: Palo Alto, California, Pacific Books, 266 p.

Stearns, H.T., and Macdonald, G.A., 1942, Geology and ground-water resources of the Island of Maui, Hawaii Division of Hydrography, Bulletin 7, 344 p.

———1946, Geology and ground-water resources of the Island of Hawaii: Hawaii Division of Hydrography, Bulletin 9, 363 p.

———1947, Geology and ground-water resources of the Island of Molokai, Hawaii: Hawaii Division of Hydrography, Bulletin 11, 113 p.

Stearns, H.T., and Vaksvik, K.N., 1935, Geology and ground-water resources of the Island of Oahu, Hawaii: Hawaii Division of Hydrography, Bulletin 1, 479 p.

Swanson, D.A., and Christiansen, R.L., 1973, A tragic base surge in 1790 at Kilauea Volcano: Geology, v. 1, no. 2, p. 83–86.

Swanson, D.A., Duffield, W.A., and Fiske, R.S., 1976, Displacement of the south flank of Kilauea Volcano—the result of forceful intrusion of magma into the rift zones: U.S. Geological Survey Professional Paper 963, 39 p.

Tilling, R.I., Koyanagi, R.Y., Lipman, P.W., Lockwood, J.P., Moore, J.G., and Swanson, D.A., 1976, Earthquake and related catastrophic events, Island of Hawaii, November 29, 1975—A preliminary report: U.S. Geological Survey Circular 740, 33 p.

U.S. Geological Survey, 1976, Natural hazards on the Island of Hawaii: Washington, U.S. Government Printing Office, 15 p.

Walker, G.P.L., 1973, Lengths of lava flows: Philosophical Transactions, Royal Society of London, Series A, v. 274, p. 107–118.

Wentworth, C.K., Powers, H.A., and Eaton, J.P., 1961, Feasibility of a lava-diverting barrier at Hilo, Hawaii: Pacific Science, v. 15, no. 3, p. 352–357.

Wilcox, R.E., 1959, Some effects of recent volcanic ash falls, with especial reference to Alaska: U.S. Geological Survey Bulletin 1028–N, p. 409–476.

Williams, R.S., Jr., and Moore, J.G., 1973, Iceland chills a lava flow: Geotimes, v. 18, no. 8, p. 14–17.

Wood, H.O., 1914, On the earthquakes of 1868 in Hawaii: Seismological Society of America Bulletin, v. 4, no. 4, p. 169–203.

Fume cloud produced by eruption of Puu Oo, Kilauea east rift zone, as seen from Hawaiian Volcano Observatory. View is toward east, across Kilauea caldera, on October 21, 1985. Photograph by J.D. Griggs.

PETROGENESIS AND VOLCANIC GASES

Petrologic and geochemical studies come alive in Hawaii because such processes as igneous differentiation and exsolution of volatile species in magma can be studied as they happen. Many igneous processes can in fact be quantitatively understood only through direct observation of igneous events. Such events, accurately delineated in time and space in turn, constrain deeper processes related to the construction of Hawaiian volcanoes. The first chapter in this section gives an overview of what we have learned about the petrogenesis of Hawaiian volcanoes, with an emphasis on the contributions made by studies of active volcanism.

The second and third chapters provide petrologic observations on recent volcanic activity; chapter 25, combined with chapter 48 in the section on dynamics, provides fascinating insights into one of Kilauea's most famous eruptions, the 1959 eruption in Kilauea Iki Crater. Chapters 26 and 27 address one of the most fundamental problems of Hawaiian petrology—the characterization of mantle sources for Hawaiian magma.

Chapters 28 through 34 treat comprehensively the study of volatile species associated with active Hawaiian volcanism, including a report on the first systematic collection of gases during an eruption of Mauna Loa. Chapter 34 outlines a new technique for rapid transmission of data from gas monitoring. The section closes with an interdisciplinary study of elemental mercury, tracing its path from volcanic emanations, through concentration in plants, to possible effects on human health.

Rainbow Men
Hawaiian Petroglyph
Nuuanu, Oahu

RECENT ADVANCES IN HAWAIIAN PETROLOGY AND GEOCHEMISTRY

By Thomas L. Wright *and* Rosalind T. Helz

ABSTRACT

Hawaiian petrology continues to be a subject of great scientific interest. Several developments over the last three decades have substantially increased our knowledge of the processes by which basaltic magma is generated in the mantle, transported to storage in the crust, and erupted onto the surface. Significant areas of study include the following:

(1) Active volcanism at Kilauea Volcano, including the study of lava lakes ponded in pit craters. Lava lakes have provided natural laboratories in which numerous petrologic processes associated with cooling, crystallization, and differentiation of basaltic magma have been quantified. The detailed study of Kilauea lava chemistry in time and space has resulted in recognition of other petrologic processes, including storage of chemically distinct mantle-derived magma batches and mixing of these parental magma batches with magma stored and fractionated in the rift zones. Geodetic and seismologic studies at Kilauea have been critical in establishing a context in which the petrologic data can be evaluated. One unsolved question is the source of magma for each active volcano. Seismic evidence suggests a common staging area at 40 km depth, whereas petrologic studies show that each active volcano has unique chemical characteristics, indicating isolated storage regions.

(2) Detailed study of the recently discovered Loihi Seamount, the newest volcano in the Hawaiian Chain, has revealed a preshield alkalic stage similar, but not identical, to the postshield alkalic stages on the subaerial volcanoes.

(3) Detailed stratigraphic studies of individual volcanoes, using major element chemistry, trace-element chemistry, and radioactive-isotope systems, show diversity of chemical evolution in each volcano in the chain, particularly within the alkalic stage that follows construction of a tholeiitic shield. There is also diversity in the chemical and isotopic relations linking shield lava to postshield lava. The combined isotopic and chemical data has revealed significant complexity in the source mantle for Hawaiian lava, both within the stratigraphic record of a single volcano and among different volcanoes.

(4) The origin of Hawaiian magma, as defined by depth and degree of partial melting, enriched versus depleted sources, and mineralogy of the source mantle, is unresolved at present. The increasing amount of data indicates a need for more definition of the structure and composition of the Earth's mantle from such diverse disciplines as seismic tomography and the experimental physics of melting and melt transport.

Finally, all models that address the origin of the Hawaiian Islands, whether geochemical or geophysical, need to take into account the constraints imposed by seismic, geodetic, and petrologic studies of the active volcanoes in the chain.

INTRODUCTION

The Hawaiian Islands occupy a unique place in igneous petrology. Early in the development of the science Hawaii was recognized as a locale of petrologic significance, partly because of its active and approachable volcanoes, partly because of its location in the middle of the Pacific Ocean—uncomplicated by the presence of other kinds of terrain—and finally because of the wide variety of volcanic rock types available for study. Long before the recognition of plate tectonics, the Hawaiian Islands were recognized from the degree of erosion and the location of volcanic activity as having formed in an orderly progression from northwest to southeast. J.D. Dana saw that the islands were distributed in a way that defined parallel, but offset, segments that he related to tectonic controls (see Clague and Dalrymple, chapter 1, part I). Early visitors to Kilauea outlined in vivid descriptions the general nature of Hawaiian eruptions, and early visits to the bubbling lava at Halemaumau resulted in gas collections that still rank among the best ever obtained from an active volcano (Greenland, chapter 28).

With the advent of plate tectonics, the Hawaiian Chain became a classic example of midplate volcanism. The orderly progression of volcanism was quantified by radiometric dating, and the historical development was extended by recognition that the chain continued to the northwest past Midway Island, defined by long submerged seamounts of the Emperor Chain (see Clague and Dalrymple, chapter 1, part I). These seamounts were also sampled as part of the Deep Sea Drilling Project, and subsequent study revealed a remarkable uniformity, starting about 70 Ma, of both the rate of progression of volcanism and of the products of volcanism. For example, tholeiitic basalt from the 69-Ma Suiko Seamount (Clague and Dalrymple, chapter 1, part I) is geochemically similar to basalt presently being erupted at Kilauea and Mauna Loa (Clague and Frey, 1980; Kirkpatrick and others, 1980).

Earlier land-based studies by numerous workers, notably H.S. Stearns and G.A. Macdonald, had identified a sequence of compositional changes in the building of Hawaiian volcanoes that appeared to be the same, although not always complete, in each studied volcano (Clague and Dalrymple, chapter 1, part I; Macdonald and others, 1983). From these studies each Hawaiian volcano was inferred to pass through the following stages: (1) An early and voluminous tholeiitic stage that constructed huge shields rising from the ocean floor, exemplified by the active volcano Mauna Loa; (2) a period of much less voluminous alkalic volcanism, forming a small cap of mildly undersaturated alkalic lava on the tholeiitic shield, for example, the younger lava of Mauna Kea; (3) a period of erosion, which has been determined to be 0.5–2 m.y. long, in which the volcanic mass above sea level was thoroughly dissected; and (4) a period of basanitic or nephelinitic volcanism following the erosion of the old shield. The famous Oahu landmark Diamond Head is the product of eruption in this last period. This framework has been

modified as more volcanoes have been sampled and studied in detail. For example, work on Loihi Seamount has identified a preshield alkalic stage (Clague, in press). In no single volcano are all stages fully represented. Nephelinitic volcanism is rare, but well-developed series are presented on Kauai (Koloa Volcanics) and in the Koolau Range on Oahu (Honolulu Volcanics). The Kiekie Basalt on Niihau (which includes Lehua Island, Macdonald and others, 1983) and some of the Leeward Islands (Kaula, Macdonald and others, 1983) may include nephelinitic rocks. The latest, most undersaturated rocks to the southeast are not separated from the earlier alkalic series by nearly as long an interval of erosion (<500,000 years versus 2 m.y. for Kauai and Oahu) and are basanites, not nephelinites. The volcanoes that have a nephelinitic series show very little development of an earlier mildly alkalic series, whereas the basanites (the Lahaina Volcanics on West Maui Volcano, the Hana Volcanics on Haleakala Volcano) tend to overlie a lower, more mildly alkalic series. In this paper we will use the terms "nephelinitic series" to describe the truly posterosional rocks, bearing in mind that these rocks range in composition from alkali basalt through true nephelinites, and "upper alkalic series" for the rocks of other volcanoes that show a lesser erosional break.

The older Hawaiian volcanoes can be subdivided into groups on the basis of variations in the character of the mildly alkalic rock series present. This subdividing was first done by Macdonald and Katsura (1964), who recognized a Haleakala type and Kohala type. Further study suggests four significant variants:

(1) Haleakala type: characterized by a thick, transitional zone of interbedded tholeiite, transitional basalt, and ankaramite overlain by hawaiite and mugearite. Most analyzed alkali basalt in this type is slightly hypersthene-normative. Other volcanoes of this type are Mauna Kea (Macdonald and Katsura, 1964) and East Molokai (Beeson, 1976).

(2) Kohala type: mafic alkalic rocks are subordinate. The dominant rock types are hawaiite and mugearite, which form a thin cap of lava that was erupted from vents scattered around the tholeiitic shield. Trachyte may be present. As in the first type, alkali basalt in these alkalic series is slightly hypersthene-normative. Other examples are Waianae, West Molokai, and West Maui (Macdonald and Katsura, 1964).

(3) Hualalai type: characterized by an almost bimodal suite of nepheline-normative alkali basalt and trachyte (Macdonald, 1968; Clague and others, 1980). No other representatives of this type are known.

(4) Koolau type: mildly alkalic series is either absent, or present only as a few flows at the top of the tholeiitic sequence. Other examples are Lanai (Bonhommet and others, 1977), Kauai, Niihau, and Kahoolawe (Macdonald and others, 1983).

The distribution of these various types of Hawaiian volcanoes is not random. All the volcanoes are distributed on several locus lines (fig. 23.1). Two locus lines are defined for the southeastern islands of the Hawaiian Chain: the Loa line, passing through Mauna Loa, and the Kea line, passing through Mauna Kea (fig. 23.1). When looking at figure 23.1 with the above classification in mind, two features stand out. First, adjacent volcanoes are almost always of different types. Second, some types occur *only* on the Loa or Kea locus. For example, the Haleakala type is found only on the Kea locus, and the Koolau type only on the Loa locus. The existence of the four subtypes suggests that the groups result from significant differences in either source or plumbing, or both. The observations on the spatial array further suggest that adjacent volcano sources interact in some fashion at this stage in the volcano's development and that consistent differences in source may exist between the Loa and Kea locus lines. The latter possibility is supported by the trace-element data of Budahn and Schmitt (1985) on tholeiitic basalt from the Hawaiian volcanoes. Also, some correlation may exist between these four types and the nature of the various later alkalic rock series. In particular, the nephelinitic series has so far been observed only on Koolau-type volcanoes, found on the Loa locus. A more thorough examination of the upper alkalic series, seen mostly on Haleakala- and Kohala-type volcanoes on the Kea locus, may reveal other differences between the various late alkalic series that correlate either with volcano type or location.

In the last two decades, our understanding of Hawaiian volcanism has been greatly expanded as a result of the following important studies: (1) Detailed seismic, geodetic, and petrologic studies of Kilauea, conducted at the Hawaiian Volcano Observatory, have provided quantitative data on the processes of cooling, crystallization, and differentiation of tholeiitic basalt, and an understanding of how tholeiitic magma is transported and stored during construction of an Hawaiian shield; (2) the discovery, first by bathymetry, and secondly by seismic swarms and dredging, of an active undersea Hawaiian volcano—the Loihi Seamount—confirmed the continued southeastward progression of Hawaiian volcanism and, more importantly, overturned ideas about the uniformity of the tholeiitic stage of volcanism; (3) modern petrologic and geochemical studies of volcanoes in the Hawaiian Chain in all stages of development have been definitive in establishing the nature of oceanic midplate volcanism and the complexities that can occur in even this most simple of geologic settings; and (4) the study of xenoliths, high pressure phase relations, and seismic structure of the Earth have yielded insights into the structure of the Earth's mantle beneath the oceans. These four topics are emphasized in this overview. The first topic will be covered in detail; the others will be largely referenced to recent literature and to other comprehensive papers in these volumes.

ACKNOWLEDGMENTS

This overview has benefited from my discussions over the years with many persons. In particular, Al Hofmann and Fred Frey have kept me aware of the contribution of isotopic and trace-element data to the study of Hawaiian geologic problems, whereas my own research has been principally concerned with major-oxide mass balances as they relate to constraints provided by geologic, geodetic, and geophysical information. I appreciate correspondence and preprints from D.L. Anderson. The manuscript has benefited from reviews by Christina Heliker, Dave Clague, and Rosalind (Roz) Helz. Roz' review resulted in a substantially expanded content, much of it her own ideas; therefore, she was included here as a coauthor.

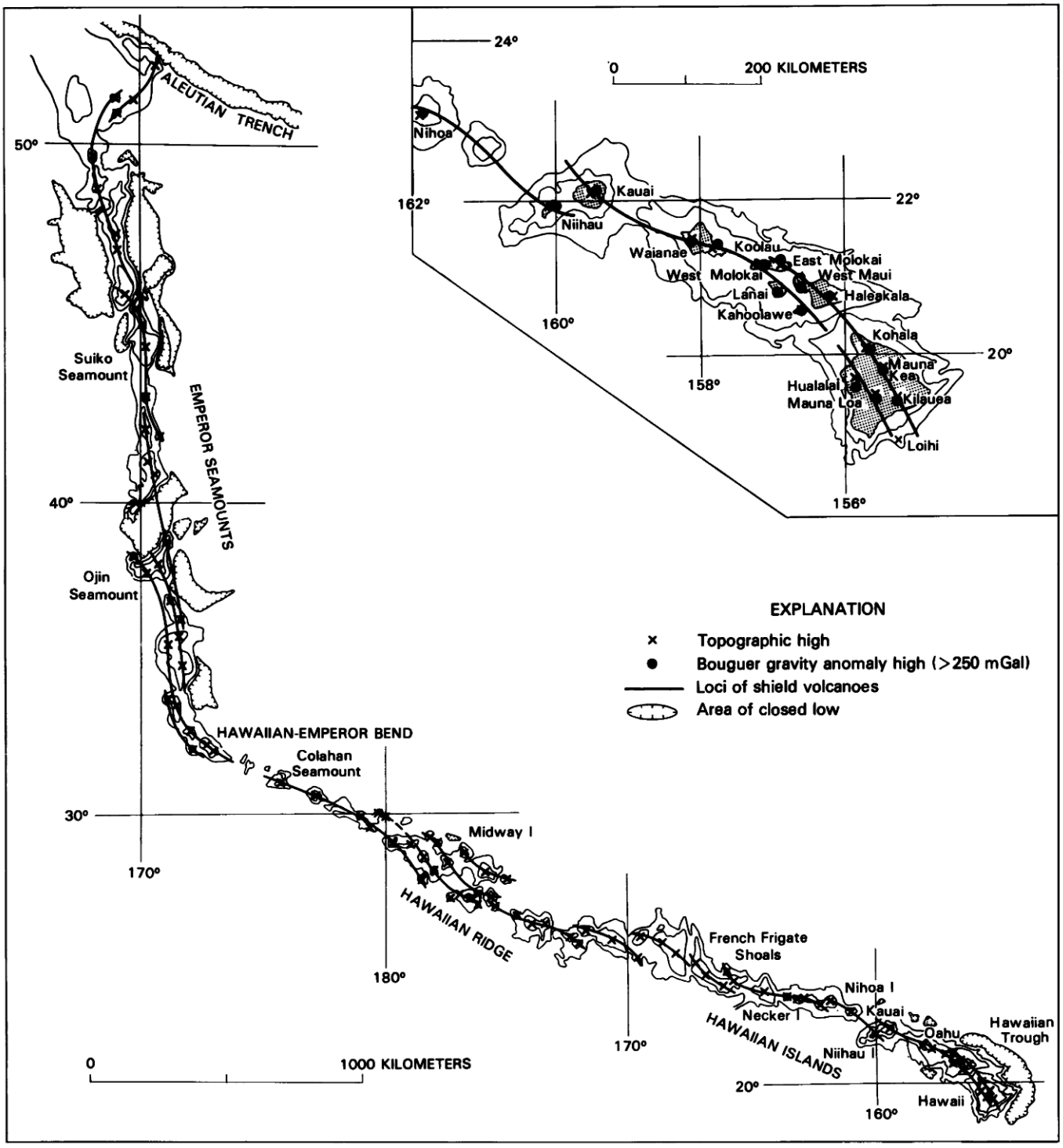

FIGURE 23.1.—Loci of shield volcanoes in the Hawaiian-Emperor Chain. Inset shows the detailed relation between topographic highs (crosses), Bouguer gravity anomaly highs (circles), and loci (heavy lines) for the principal Hawaiian Islands. From Jackson and others (1972).

THOLEIITIC VOLCANISM: WHAT HAVE WE LEARNED?

Modern petrologic study of Hawaiian volcanoes began in the 1940's and 1950's with G.A. Macdonald's work on the development of Hawaiian volcanoes and his analyses of the different lava types (Macdonald and Katsuura, 1964), with H.A. Powers' (1955) recognition that olivine played a dominant role in tholeiitic differentation, and with the work of Tilley and Scoon (1961), emphasizing chemical and mineralogic distinctions between lava from Kilauea and lava from Mauna Loa. These workers established that Hawaiian tholeiite ranges in composition from about 5.5 to 20 percent MgO, that lava with over 7 percent MgO had magnesian olivine as the dominant phenocryst, that lava with less than 7 percent MgO had augite and plagioclase in addition, and that Mauna Loa was distinguished from Kilauea by the presence of hypersthene, in combination with all three of the other silicate phases. Powers and Tilley had both demonstrated that once the chemical signature of olivine addition or subtraction has been removed, different tholeiitic volcanoes have subtly different compositions (the range of compositions related by a single set of olivine control lines are termed "magma batches") that characterized each volcano uniquely. Powers, in addition, had recognized that even more subtle variations occurred to produce separate magma batches within the products of a single tholeiitic shield.

Another level of inquiry began with modern studies at the Hawaiian Volcano Observatory, beginning about 1952, when Kilauea became active after 18 years of dormancy. From 1952 to the present (1986), every eruption has been sampled and analyzed, and eruptions that extended over periods of days, weeks, or even years, have been sampled at regular intervals to cover both the spatial and temporal distribution of eruptive products. This sampling is of critical importance because significant changes in lava composition during an eruption have occurred, and earlier (particularly the earliest) eruptive products are likely to be covered by later phases of the eruption and thus never encountered in conventional studies of older lava. This burial process is amply demonstrated, for example, by the 1983–1984 eruption of Kilauea (see Wolfe and others, chapter 17).

In another development, the occurrence of a series of eruptions in pit craters (1959, 1963, 1965) provided molten lakes of tholeiitic basalt for large, outdoor laboratory experiments in the cooling and crystallization of basalt. These studies were complementary to a study made of a prehistoric lava lake exposed in the walls of Makaopuhi Crater (Moore and Evans, 1967; Evans and Moore, 1968). In the next two subsections we address first what we have learned from the lava lakes, and secondly, we apply this information to interpret petrologic processes important to understanding the entire sequence of eruptive activity from 1952 to the present.

KILAUEA LAVA LAKES

Core drilling in the lava lakes, after they crusted over, provided a means of studying the processes of crystal-liquid movement during slow cooling. An overview of the importance of the lava-lake studies with a description of what was done on each lake, including an annotated bibliography, was written by Wright and others (1976). Subsequently, papers on the March 1965 Makaopuhi lava lake (Wright and Okamura, 1977), the August 1963 Alae lava lake (Peck and Kinoshita, 1976; Peck, 1978; Wright and Peck, 1978), and thermal-modeling studies (Peck and others, 1977; Shaw and others, 1977) have contributed further details; Peck and others (1979) demonstrated the breadth of interest in the lava lakes. Makaopuhi and Alae have both been covered by subsequent eruptions, further attesting to the value of real-time volcanic studies. The November–December 1959 Kilauea Iki lava lake, documented by Murata (1966), Murata and Richter (1966), Richter and Moore (1966), Richter and Murata (1966), and Richter and others (1970), is still being studied. Drilling programs in 1976, 1979, and 1981 were performed as a joint project of the U.S. Geological Survey and Sandia National Laboratories. Geophysical results of the 1976 drilling are given by Hermance and Colp (1982), and a description of the 1981 drilling is given by Hardee and others (1981). Thermal modeling of the lake (Hardee, 1980) and a study of the seismic structure of the lake (Chouet and Aki, 1981) have also been accomplished. Further petrologic results are reported by Helz (chapter 25; 1980) and by Helz and Wright (1983). Description of drill core is provided by Helz and Wright (1983) and by Helz and others (1984). New interpretations of the mechanics of the 1959 eruption are given by Eaton and others (chapter 48) and by Helz (chapter 25).

The studies of Alae and Makaopuhi lava lakes have quantitatively documented several processes of importance to Hawaiian petrology. These processes include the following:

(1) Settling of olivine occurs under the influence of gravity at temperatures greater than 1,150 °C. This settling is by no means as straightforward a process as that predicated by theory, as it can be shown that the observed rates of settling are far less than those predicted by Stokes' law. This difference is partly due to the presence of gas bubbles moving upward as olivine is sinking, thus impeding the progress of both, and partly to the fact that the liquid behaves as a Bingham fluid, as was discovered by direct experimentation in Makaopuhi lava lake (Shaw and others, 1968). Further study of Kilauea Iki led to the suggestion that with a large population of olivine the crystals might settle with a boundary layer of melt, decreasing the rapidity with which olivine can be segregated (Helz, 1980, p. 693–696). Helz (chapter 25) has shown, in line with earlier studies of a frozen prehistoric lava lake (Moore and Evans, 1967; Evans and Moore, 1968), that olivine, after settling, rapidly re-equilibrates to more iron-rich compositions and that the final olivine composition may be very different from that present at the time of eruption. All of these data place constraints on the interpretation of olivine abundance in natural lava.

(2) Differential separation of augite and plagioclase occurs under the influence of convective flow at temperatures between 1,150 °C and 1,080 °C This separation is a more subtle process than olivine segregation and is shown to occur at crystal sizes far smaller than those that could be gravitationally segregated in a reasonable time. Differential separation of augite and plagioclase is inferred to take place only in the absence of a separate volatile phase, because upward movement of vesicles will reverse the density gradients

needed to initiate convection in a body of molten basalt. The time at which convection in Makaopuhi lava lake was initiated has been inferred from thermal anomalies in temperature profiles taken in the melt, correlated with decreased vesicularity in core collected below a certain depth in the lake. Within months of the time at which convection was initiated, the bulk composition of the lava lake began to change in a manner reflecting loss of chemical components present in augite and plagioclase, in addition to those present in olivine (Wright and Okamura, 1977). A complementary effect of convective transfer is to enrich the margins and probably the basal parts of the lava lake in the components of augite and plagioclase, in addition to those of olivine, causing a chemical profile through a lava lake to depart from strict olivine control. The chemical effect is nicely shown in analyses from the lower part of the prehistoric Makaopuhi lava lake (Moore and Evans, 1967).

(3) Melt is physically segregated from a rigid crystal framework at temperatures below 1,080 °C. The lava lakes provide a quantitative demonstration of the process known as filter pressing, and they contribute toward an understanding of the origin of segregations of basaltic liquids with variably fractionated chemistry. Natural segregations are common in thick basaltic flows and sills throughout the world. The term "segregation vein" was applied to these bodies in the 19th century and has remained in use since. Basaltic segregations generally stand out from the host rock by their lighter color and coarser texture, and they commonly fill subhorizontal fractures. Segregation of this kind only occurs at temperatures below the critical temperature at which the lake behaves as a rigid body (see discussion in Wright and others, 1976). First demonstrated as an artifact of the drilling process (that is, melt flowing into open drill holes during thermal recovery toward predrilling temperatures), this process also results in natural segregations (segregation veins) where melt has flowed into zones of lower pressure. Most segregations have sharp contacts with the host rock, suggesting filling of an open fracture. Others have more subtle boundaries, suggesting that the wall rocks were ductile at the time of segregation. The presence of segregations is a function of the rate of cooling, and their orientation (that is, whether fillings are horizontal, vertical, or some other angle) gives important information on the stress distribution in the cooling lava. Whether segregation takes place is a function of temperature, which controls both the chemical composition and viscosity of the melt fraction, the rigidity of the crystal network, and the time during which a pressure gradient favorable to segregation is present. In the lava lakes, a combination of cooling curves and viscosity temperature relations limit the normal process of segregation to temperatures above about 1,050 °C, at which temperature melt compositions are still in the basaltic range. However, Kilauea Iki lava lake contains rare examples of small segregations of much more siliceous melt, with silica content as much as 70 percent. This mechanism may operate in basaltic intrusions to produce small bodies of rhyolite or dacite for later eruption as lava.

Several lines of evidence indicate that Hawaiian eruptions are supersaturated in volatile constituents at the time of eruption. Thus, the vesicle distribution in thick lava lakes is, in large part, a frozen record of incomplete volatile removal at high temperature. We must emphasize that lava erupted at, or under, saturation would behave very differently in terms of processes defined for the Kilauea lava lakes.

Results of the study of Makaopuhi and Alae lava lakes define classic, closed-system fractional crystallization in which mass-balance calculations document various kinds of crystal movement in liquids that vary along a regular liquid line of descent (see Wright and Peck, 1978, fig. 4). The study of processes documented by study of major oxides have been extended to show that trace elements vary consistently with major oxide relations (Lindstrom and Haskin, 1984).

Kilauea Iki, the remaining lava lake, is distinguished from Alae and Makaopuhi by its more magnesian bulk composition (average MgO content is 15–16 weight percent), larger volume, and more complex filling history. As a result, the core obtained from Kilauea Iki shows many features unlike those seen in the other lava lakes. For example, core recovered below 12 m depth has a chemistry that does not fit the olivine-controlled chemistry defined by samples collected during the eruption (Wright, 1973). Although, by definition, this lava lake also represents a closed system, the mass balances relating the chemistry of crystallizing minerals, liquid segregation, and bulk rock at different levels in the lake depart significantly from the rather straightforward relations summarized in papers on the other lava lakes. Fractionation processes identified in Kilauea Iki are listed below. Some of these processes occur at higher temperatures than in the other lakes (Nos. 1, 2, and 5), whereas others have been observed only in Kilauea Iki (Nos. 3, 4, and 6).

(1) Gravitative settling of coarse (>2 mm) olivine, resulting in a zone in which large olivine crystals are absent, occurring between 20–40 m below the surface of the lake. The composition of the moving olivine averaged Fo_{86}, that is, the chemistry of the drill core defines a set of olivine control lines on variation diagrams of Al_2O_3 versus MgO or SiO_2 versus MgO that extrapolate to an olivine composition of Fo_{86}. This composition implies that temperatures were ≥1,180 °C in the part of the lake through which the olivine settled (Helz, 1980; Helz and Thornber, in press).

(2) Horizontal redistribution of augite microphenocrysts, by convection. Within the olivine-depleted zone, small (1–2 mm) clots of augite microphenocrysts are present in core from near the edge of the lake and absent in the middle. This differential concentration of augite raises the CaO content of the core from 10.5 weight percent in the middle to 11.6 weight percent at the edge. In contrast to Makaopuhi, this flow differentiation has not involved plagioclase, hence it occurred only at temperatures above 1,160 °C.

(3) Diapiric upwelling of lower density melt from within the olivine-rich mush at the base of the lens of melt. The moving liquid is that present at temperatures of 1,145–1,160 °C, just below the incoming of plagioclase. This liquid is inferred to rise to the uppermost part of the lens of melt where it mixes with the melt just below the base of the upper crust. This process causes the lava below 12 m to deviate from olivine controlled chemistry. The upper mixed zone is enriched in low melting constituents such as TiO_2 and alkalis and is depleted in FeO and CaO relative to what would be expected for olivine-controlled chemistry (Helz, 1980). The source region undergoes complementary depletion in TiO_2 and alkalis relative to olivine-controlled chemistry. Helz (1980), citing data for

the upper, enriched zone only, tentatively described the enrichment to filter pressing of liquid formed during partial remelting of foundered crust deep in the lake. Recovery and analysis of deeper core has led to our present recognition that, first, this process does not require foundered crust, and second, it has affected the chemistry of the lava at virtually all levels in the lake. This process occurs only in olivine-rich rock. The requisite density inversion is much smaller in melts in bulk compositions with MgO $\leq$7.5 percent. Hence, this process would not have been expected to occur in the other lava lakes.

(4) Diapiric rise of streams of vesicles with or without entrained melt, from within the lower crust. The vesicles first entrain melt, then coarse olivine from the lower part of the lake. As the plume rises into cooler material it begins to segregate, with the vesicles and melt detaching themselves from the trail of coarse olivine. These trails remain as vertical olivine-rich bodies, which can be seen in every drill core recovered from Kilauea Iki between 40 and 58 m (Helz, 1980). These olivine-rich bodies contain excess iron-rich olivine (Fo_{77-79}) and differentiated liquid (temperature range of 1,140–1,120 °C), relative to the adjacent host rock, so they are active at lower temperatures than the diapirs in process 3. Analogous vuggy, vertical bodies also are present between 26 and 40 m, but they are much harder to spot as they lack coarse olivine (Helz, 1980). The melt- and vesicle-rich top of the vertical olivine-rich bodies looks like a segregation vein, which led Helz (1980) to suggest that segregations might be related to these bodies in some way. Similar bodies, described as "indistinct, pipe-like masses rich in olivine" occur in the lower part of the prehistoric Makaopuhi lava lake (Moore and Evans, 1967), though in that lake there was no evident connection with segregation veins.

(5) Formation of segregation veins, which are coarse-grained diabasic sills, generated by processes internal to the lava lake. Segregation veins in Kilauea Iki are more abundant than in the other lakes and form an apparently continuous set of sills, concentrated between 18 and 56 m, where they comprise 5–10 volume percent of the lake (Helz, 1980). Their bulk compositions correspond to liquids produced at 1,135–1,100 °C, using the calibration of Helz and Thornber (in press). In Kilauea Iki, segregation veins are more magnesian and presumably form at higher temperatures than those in Alae and Makaopuhi.

(6) Filling of late fractures or large vesicles by highly differentiated liquids, produced at 1,060–1,000 °C. The fractures are produced by brittle failure of the lake lava as it shrinks during crystallization and cooling. The bulk compositions of these tiny bodies are andesitic to rhyolitic (SiO_2, 56–70 weight percent, MgO, 0.5–3.0 weight percent); their existence demonstrates the mobility of interstitial liquid even when very little (<10 percent melt is present (Helz, 1984). The driving mechanism is inferred to be gas filter-pressing (Anderson and others, 1984).

In addition to these processes involving differential movement of crystals, vesicles, and liquid, Kilauea Iki illustrates very well the extent to which interstitial liquid compositions are controlled by *local* bulk composition. As discussed in Helz (1984), interstitial liquid becomes progressively depleted in FeO as olivine content increases. Other oxides (SiO_2, Al_2O_3, alkalis) increase as FeO decreases, whereas a few oxides (MgO, CaO, TiO_2) are buffered by the phase assemblage. Thus, at a given MgO content of interstitial liquid, the liquids in olivine-rich rocks are richer in SiO_2 and alkalis than liquids in olivine-poor rocks or segregation veins. Where a segregation vein occurs in an olivine-rich host, the difference in glass composition across the contact can be as great as 4 weight percent FeO within a single thin section.

The later stage mineral assemblages closely reflect these variations in interstitial melt composition. In olivine-rich rock, the low-calcium pyroxene is orthopyroxene (opx), the dominant Fe-Ti oxide is ferropseudobrookite (fpsb). With decreasing olivine content opx is replaced by pigeonite, and the oxide assemblage changes to fpsb + ilmenite, fpsb + ilmenite + magnetite, and finally ilmenite + magnetite, as observed in the low-MgO lakes Alae and Makaopuhi.

Thus, gravitative settling of olivine, followed by closed-system crystallization, has created a magma chamber in which different liquid lines of descent are being generated in rocks meters apart. Important implications of these observations, applied to larger differentiating chambers, are that one chamber may be capable of erupting two or more dissimilar lava series produced solely by processes operating within the chamber and not necessarily from different sources.

TIME-SPACE RELATIONS OF KILAUEA LAVA

Studies based on the chemistry of erupted lava from 1952 to 1985 have extended our knowledge of differentation processes in Hawaiian tholeiite. Interpretation of Kilauea's chemistry is also dependent on seismic and geodetic studies (Eaton and Murata, 1960; Eaton, 1962), which clearly identify a complex holding reservoir beneath the Kilauea summit through which magma for eruptions anywhere on the volcano must pass (fig. 23.2; also see Wright and Fiske, 1971, fig. 9; Ryan and others, 1981). Helz (chapter 25) presents data that supports the earlier suggestion of Wright (1973) that magma erupted in 1959 is an exception and might have bypassed storage in the normal summit-reservoir complex. Two early summaries (Wright, 1971; Wright and Fiske, 1971) document the general changes of bulk chemistry with time, quantify the concept of olivine control, describe the differentiation processes operating within Kilauea's rift zones, and treat the problem of magma batches and the mixing of liquids of different composition prior to eruption. A model was developed in Wright and Fiske (1971) in which magma batches of subtly differing bulk chemistry arrive in the storage complex beneath Kilauea summit and are displaced to higher levels in the storage complex, where they become chemically zoned due to gravitational settling of olivine as newer batches of olivine-rich magma arrive from the mantle. During eruption or intrusion within the rift zones, some portion of magma moving into the rift is separated from the main source of heat, resulting in cooling and differentiation. Rift eruptions are inferred to be fed from the lower parts of the summit reservoir complex and, more often than not, mix with fractionated magma present from previous episodes of rift intrusion to form hybrid magma. Because of

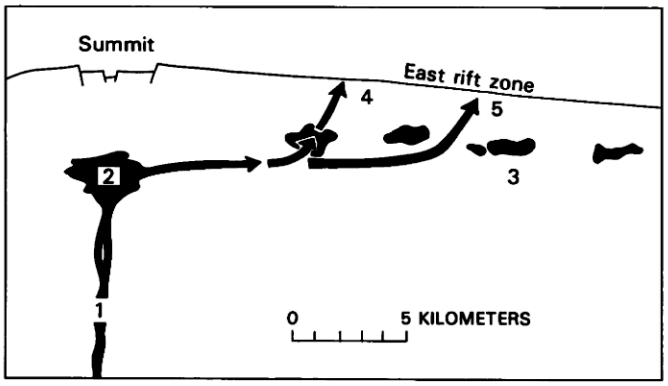

FIGURE 23.2.—Simplified model of magma storage and eruption at Kilauea (modified from Wright and Fiske, 1971, fig. 9): (1) Conduit through the oceanic crust defined seismically; (2) shallow storage reservoir, defined from both geodetic measurements and as an aseismic zone; (3) isolated pockets of magma produced by intrusions into the rift zones. Eruptions at the summit are fed directly from the top of the central reservoir. Most eruptions on the rift are also fed from lower in the central reservoir and may either become mixed with stored rift magma (4) or have direct access to the surface (5). Infrequently, stored rift magma may be erupted independently.

the compositional layering in the summit reservoir resulting from the sequence of magma batches supplied from the mantle, rift eruptions tend to be richer in olivine than summit eruptions and have a summit component in their composition that predates eruption of that component at the summit. These inferences were presented for Kilauea eruptions through 1974 in Wright and Fiske (1971), Wright and others (1975), and Wright and Tilling (1980).

In 1971 and 1974 intrusions beneath the south part of Kilauea caldera were evident (Duffield and others, 1982; HVO, unpublished data). These intrusions resulted in development of mildly differentiated lava as a component of subsequent hybrid eruptions at Kilauea summit in 1974 and 1982 (Wright and Tilling, 1980; HVO, unpublished data).

Direct eruption of fractionated lava on the east rift zone occurred in 1955, 1962, and 1968 (see Wright and Fiske, 1971; Wright and others, 1975) and again in 1977 (Moore and others, 1980) and 1983 (Wolfe and others, chapter 17; Garcia and others, in press). The parent composition, time of rift storage, and rate of crystallization in storage have been quantitatively determined for recent mildly fractionated lava (see Wright and Tilling, 1980). The processes of differentiation within the rift zone appear to be very similar to both the high-temperature and low-temperature differentiation observed in Makaopuhi and Alae lava lakes, suggesting that magma in storage is under sufficient pressure to maintain volatile components in solution, thus enabling convection to take place, and that lower temperature segregation can sometimes occur on a large scale, creating separate reservoirs of fractionated magma. The 1955 eruption requires the latter, as the early erupted lava shows an intratelluric phenocryst assemblage (hypersthene, augite, plagioclase, Fe-Ti oxides) very different from the normal assemblage of olivine and minor augite and plagioclase characterizing lava whose bulk composition is unfractionated.

In addition to study of petrologic processes demonstrated in single eruptions, it should be eventually possible to quantitatively evaluate the times of arrival of magma batches from the mantle, specify where these batches will be stored and for how long, and relate these to when and where they will be erupted to the surface. The seismic data on earthquake swarms related to magmatic intrusions (Klein and others, chapter 43), combined with detailed petrochemical study (for example, Wright and Tilling, 1980), should provide the basic data to do this within the broad framework of geodetic and geophysical observations related to magma storage (Dzurisin and others, 1984).

The processes defined at Kilauea are by no means restricted to Hawaiian tholeiite. The same processes of storage, fractionation, and mixing of magma have been amply documented for midocean ridge basalts (see, for example, Basaltic Volcanism Study Project, 1981, p. 132–160). Thus, both voluminous oceanic basalt types, whose chemistry remains fairly constant with time, behave similarly in spite of the differences in bulk chemistry. However, studies of recent Hawaiian eruptions illustrate a problem that must be considered in looking at older basaltic lava sequences in Hawaii and elsewhere; that is, samples from a single stratigraphic section may represent only a fraction of the lava from any single eruption, and significant compositional changes that occurred during the eruption may be missed. Interpreting contacts between flows to define related eruptive sequences is virtually impossible in older flows, especially in flows of small volume. In the prehistoric record, contacts preserved in a sequence of flows from Mauna Ulu (1969–1974) may look no different than a contact between lava erupted in 1961 and any one episode of Mauna Ulu that happened to cover it. This possibility underscores the fact that petrologic studies of older lava fields may lack much of the critical information that is made available when an eruption or sequence of eruptions is actually observed.

COLLECTION AND ANALYSIS OF HAWAIIAN GASES

One of the most important opportunities afforded by active volcanoes is the sampling of volatile constituents either from active fumaroles or during eruptions. Collection of usable gas samples at an active vent is far from an easy task, as it entails being able to approach an erupting fissure or lava pond, collect a sample with minimal atmospheric contamination, and analyze the sample within hours of collection in order to prevent reaction of the gas species with one another. Some of the best samples ever obtained were collected in the early 20th century from the continuously active lava lake in Kilauea caldera (Shepherd, 1921; Gerlach, 1980). Later in the century, collections were made through drill holes in Makaopuhi lava lake (Finlaysen and others, 1968) and the 1977 eruption of Kilauea (Graeber and others, 1979). In 1980, permanent gas analysis facilities were established at the Hawaiian Volcano Observatory. Greenland (chapters 28 and 30) summarizes information on extensive collections of gases from Kilauea and the first modern samples of eruptive gases from Mauna Loa. Franczyk and others (chapter 31) give complementary data on the amount of carbon and sulfur that remains in the lava after eruption.

The importance of volcanic gas analyses lies both in the estimates of primary volatile compositions of magma and in the budget of volatile species put into the Earth's atmosphere as a result of volcanic eruption. The latter subject is addressed by Casadevall and others (chapter 29) and by Gerlach and Graeber (1985). Volcanic pollutants, mainly CO_2 and SO_2, are found to be significantly less than the contribution from modern industry. The composition of gases arriving from the mantle, after storage beneath Kilauea summit, and residual gas left in erupted lava is estimated for Kilauea (table 23.1) using data of Greenland and others (1985). These estimates are close to those made by Gerlach and Graeber (1985). Estimates of volatile budgets for the 1983–1985 Kilauea eruption also provide an estimate of volatile emission rates consistent with magma supply rates obtained by seismic and geodetic methods (Gerlach and Graeber, 1985; Greenland and others, 1985). Finally, study of gases from the ongoing Kilauea east rift eruption has led to estimates of the rates of magma ascent in the conduit, the diameter of the conduit, and the vertical gradients of pressure and density within the magma column (Greenland and others, in press).

TABLE 23.1.—*H_2O-CO_2-S budget in Kilauea magma*

[Values reported are in weight percent]

	H_2O	CO_2	S
Magma arriving from mantle	0.32	0.32	0.09
Magma after storage and before eruption	.28	.03	.08
Residual volatiles in erupted lava	.05	<.01	.02

PETROLOGY IN CONTEXT: A MODEL FOR STORAGE AND TRANSPORT OF KILAUEA MAGMA

Petrologic and geochemical studies at Kilauea are not in themselves sufficient to translate chemical variations into physical processes. The framework for interpretation of time- and space-related petrologic processes at Kilauea is provided by seismic and geodetic studies. These studies provide direct evidence both for regions of magma storage and for the distribution of and relief of stress associated with magma movement at crustal and upper mantle depths (see Decker, chapter 42). A primary storage region beneath Kilauea summit is defined both seismically (Koyanagi and others, chapter 45, part I; Thurber, chapter 38; Koyanagi and others, 1976) and from ground deformation measurements (for example, Fiske and Kinoshita, 1969; Dvorak and others, 1983). Secondary, and apparently transient, areas of active storage in the rift zones are also defined by a combination of seismic and geodetic measurements (see Klein and others, chapter 43, Jackson and others, 1975; Swanson and others, 1976b). Ryan and others (1981) have incorporated both kinds of data into a generalized three-dimensional model for Kilauea.

A simplified, two-dimensional representation of magma transport and storage is shown in figure 23.2. The depth to both primary and secondary storage is from about 2 km to 6 km beneath the ground surface. The summit storage reservoir is approximately the volume of Kilauea caldera minus the lava flows of historical age that have partially filled it; massive draining of the reservoir has probably occurred during caldera formation in the past.

The rate of magma supply to the Hawaiian system, as estimated from calculated volumes of dated volcanic edifices, is greater for the Island of Hawaii than at any time past (Clague and Dalrymple, chapter 1, part I; also see Moore, chapter 2, for an alternative interpretation). The magma supply to Kilauea, estimated from geodetic and gravity data, is intruded as dikes and sills and extruded as flows in nearly equal amounts; this relation appears to be constant over periods of years (Swanson, 1972; Dzurisin and others, 1984). Recent evidence suggests that the magma supply to Kilauea has increased over the past decade (see Wolfe and others, chapter 17; Greenland and others, 1985). The passage of magma into the rift zones causes a buildup of strain in the south flank that is marked by changes in length of geodetic lines and by high seismicity. The strain is relieved when the unbuttressed south flank of Kilauea moves oceanward (Swanson and others, 1976a). Seismicity, associated both with the rift zones and the south flank, is also high during intrusion or during emplacement of a dike preceding eruption at a new location. Commonly earthquake epicenters migrate ahead of the dike tip to define the magma transport path (see Wolfe and others, chapter 17; Koyanagi and others, chapter 45, part I; Klein and others, chapter 43). Long continued eruptions such as Mauna Ulu (1969–1974) or the current Kilauea eruption at Puu Oo (Wolfe and others, chapter 17) create an open transport system in which seismicity along transport paths is greatly reduced (Koyanagi and others, chapter 45, part I).

Magma supply from the mantle during 1952–1975 was describable in terms of batches of distinct composition (Wright and others, 1975; Wright and Tilling, 1980). Following a large south flank earthquake ($M = 7.2$) in 1975 (Lipman and others, 1985), magma compositions during 1979–1984 were no longer easily divided into discrete batches. Possibly the earthquake effectively broke down internal boundaries in the storage system, so that stored magma and new magma mixed on a large scale. An earthquake of similar magnitude occurred in 1868 and had an apparent effect on both the subsequent rate of eruption and chemical composition of lava from Mauna Loa (Lockwood and Lipman, chapter 18; Tilling and others, chapter 24). This effect further emphasizes the need to know volcanotectonic constraints in order to properly interpret petrochemical data.

The high rates of magma supply from depth in the past decade are also reflected in patterns of deeper seismicity. A zone between 15 and 30 km depth (that is, in the very uppermost mantle) is less seismic than the regions above and below, perhaps defining, as with the lowered seismicity around shallow rift transport systems, a greater openness of the magma transport path (Koyanagi and others, chapter 45, part I).

The distribution in time and space of deep tremor and long-period earthquakes is of great significance, providing evidence for magma movement at depths of 40–60 km (Koyanagi and others,

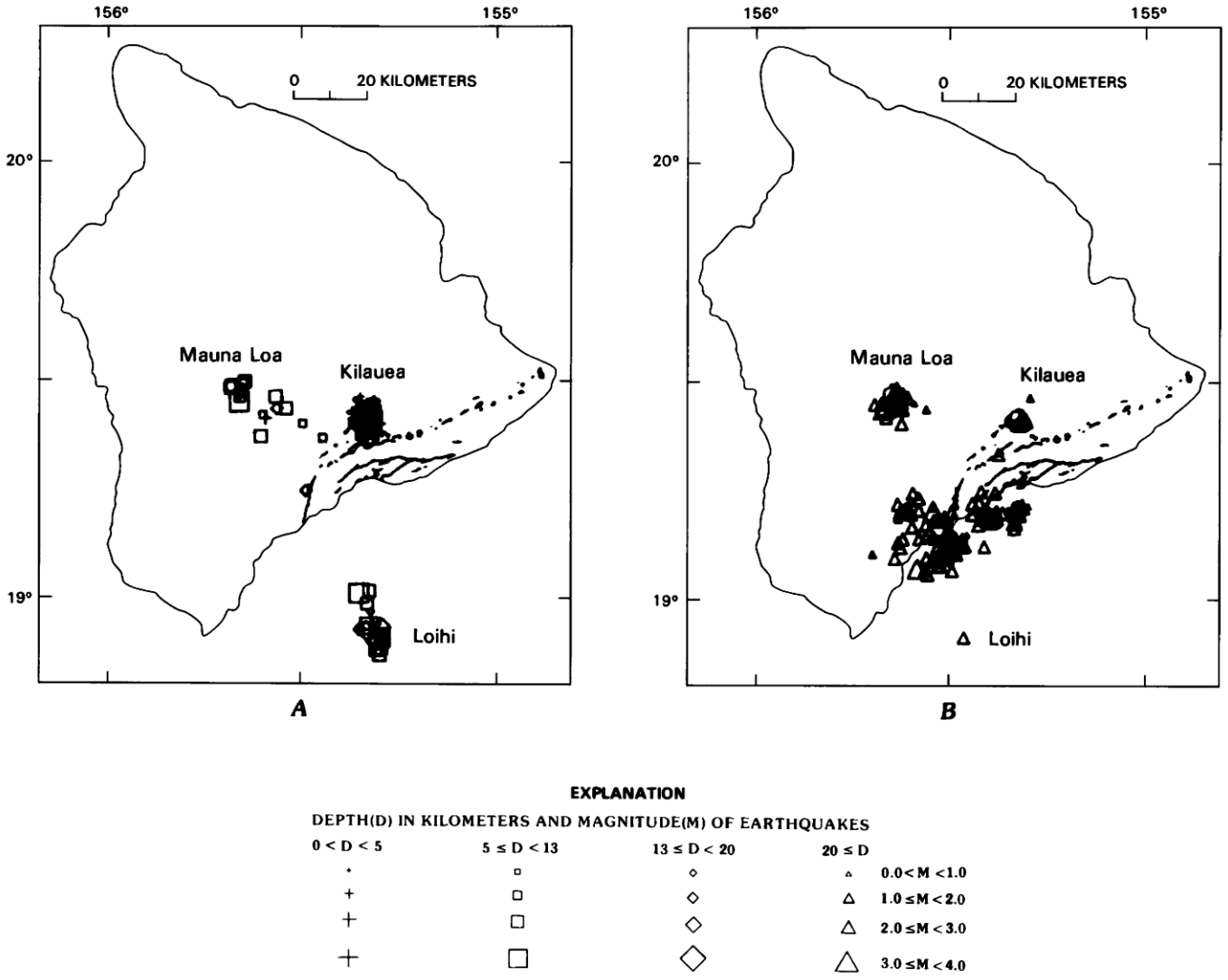

FIGURE 23.3.—Long-period seismicity of the Island of Hawaii, 1972–85. ***A***, Epicenters of long-period earthquakes with hypocenters <15 km deep. Note clustering at the three active volcanic centers. ***B***, Long-period earthquakes and locatable bursts of harmonic tremor with hypocenters >30 km deep (maximum is about 55 km). Note the dominant clustering in a broad zone between the three active volcanic centers.

chapter 45, part I; Klein, 1982). The zone of deep, long-period seismicity is centrally located with respect to all three active volcanoes—Loihi, Kilauea, and Mauna Loa—contrasting with the concentration of shallow long-period earthquakes in each volcanic edifice above and below the storage reservoir; these relations are shown in figure 23.3. The connections between deep and shallow transport systems are not clear. If, indeed, the zone shown in figure 23.3*B* defines the deeper end of magma transport systems for all three volcanoes, then it severely constrains the explanations for the distinctive chemistry and lava associations in each volcano. Either the zone of magma collection is compartmented at a scale not seen by the seismic data, or the chemical differences are produced in transit toward the surface, at much higher levels than the zone of melting. Isotopic data, as currently understood, probably rule out the latter conclusion, leaving one with a challenge to relate the observed seismicity to magma transport in a way that preserves chemical differences that originate in the melting zones (see Chen and Frey, 1985, however, for discussion of the possible influence of the transport path to the surface on chemical and isotopic variation).

Deeper yet, the zone of melting beneath Hawaii has been postulated to be within the uppermost asthenosphere, at depths greater than 60 km (see Wright, 1984). The unique chemistries of magma at the three volcanoes suggest that discrete regions of melting within the asthenosphere each have their own isotopic and trace-element signature. This problem will be discussed further in the final section.

LOIHI SEAMOUNT: A LOOK AT THE BEGINNING OF A HAWAIIAN VOLCANO

Loihi Seamount was discovered in 1955 from looking at a compilation of bathymetric data around the Hawaiian Islands (Emery, 1955). Later, with an expanded Hawaiian seismic net and a new computer system for locating earthquake foci, F.W. Klein and R.Y. Koyanagi noted swarms of shallow crustal earthquakes off the southeast coast of the Island of Hawaii (Klein and Koyanagi, 1979; Klein, 1982). Together, these observations suggested the existence of an active Hawaiian volcano in the making. Plans to dredge the seamount were carried out, samples were taken, more precise bathymetry was obtained, and preliminary results were published (Malahoff and others, 1982; Moore and others, 1982). A summary of more recent bathymetry and geophysical study is given in Malahoff (chapter 6). The dredge hauls contained both tholeiitic and alkalic basalt. Some of the latter contained xenoliths. Dating of samples showed an age range of from 0.5 to 1.6 ka, with alkalic basalt older, for the most part, than tholeiite. Thus, the newest volcano in the Hawaiian Chain showed apparent reversal in the accepted age relations of alkalic and tholeiitic basalt.

Research on Loihi was subsequently treated in a manner similar to the lunar program; we now know more about Loihi (isotopes, trace elements, major oxides) than any other single Hawaiian volcano (see Craig, 1983). Study of Loihi has generated many new questions about the growth of Hawaiian shields and the nature of the melting process(es). Workers on Loihi have concluded that the earliest stage of Hawaiian volcanism is alkalic. The Loihi data also raise the possibility that alkalic volcanism may occur at any stage in shieldbuilding, perhaps when the rate of melting in the mantle slows down for some reason. The bathymetry of the undersea portions of most Hawaiian volcanoes defines a shield shape, and this requires that the dominant shield-building lava be fluid tholeiite and that the alkalic component be at most a minor intercalation. All conclusions need to be tempered by the fact that above water we have sampled less than 10 percent of any Hawaiian shield, and the sampling at Loihi comprises only the surface lava on its shield.

Detailed petrologic and geochemical studies of Loihi (Frey and Clague, 1983; Hawkins and Melchior, 1983), combined with isotopic studies of Sr (Lanphere, 1983; Staudigel and others, 1984) and Pb and Nd (Staudigel and others, 1984), bring about the unanimous conclusions that significant heterogeneity exists within the Hawaiian hotspot and that it is difficult to relate Loihi samples with subaerial lava sequences. The tholeiite samples have a demonstrably Hawaiian chemistry that differs in small ways from both Kilauea and Mauna Loa. The alkalic samples differ from the subaerial alkalic caps on other Hawaiian volcanoes and from the nephelinitic series. Furthermore, these samples lack the garnet-bearing xenoliths of the latter series, but contain lherzolite xenoliths not found in the former series. Isotopic study of rare gases (Kaneoka and others, 1983; Kurz and others, 1983; Rison and Craig, 1983) unequivocally define the source material as primitive and undegassed mantle material, unmodified by crustal processes, relative to data from other volcanoes. Thus, the discovery and subsequent study of Loihi has provided additional constraints and new questions to be asked in relation to our understanding of Hawaiian volcanic cycles.

PUTTING IT ALL TOGETHER: INTEGRATED MODELS OF THE PETROGENESIS OF VOLCANIC SEQUENCES IN THE HAWAIIAN ISLANDS

Earlier studies of Hawaiian volcanism were based on geologic mapping and sampling stratigraphic sections for petrographic study and major-oxide chemistry. Work on trace elements and isotopes was of a reconnaissance nature confined to widely scattered samples, only some of which were tied to major-oxide study. Compilation of these data resulted in generalities about the geochemical signature of Hawaiian volcanism and recognition of the systematic differences between midplate and midocean ridge volcanism (see, for example, summaries by O'Nions and others, 1977; Lanphere and Dalrymple, 1980; Basaltic Volcanism Study Project, 1981), but contributed little to understanding the details of the evolution of individual Hawaiian shields. Recently, more concentrated studies on specific volcanoes and stratigraphically defined sequences within those volcanoes have been undertaken to establish the details of isotopic, trace-element, and major-oxide behavior. These studies have focused on Molokai (Beeson, 1976; Clague and others, 1983), Kohala (Feigenson and others, 1983; Lanphere and Frey, in press), Kilauea (Casadevall and Dzurisin, chapter 13; Hofmann and others, 1985), Haleakala (Chen and Frey, 1983, 1985), Koolau (Stille and others, 1983; Roden and others, 1984), Kauai (Feigenson, 1984), and Loihi (see above). The Honolulu Volcanics have also been studied comprehensively (Clague and Frey, 1982). The principal conclusions reached from stratigraphic studies are the following:

(1) The transition from tholeiitic basalt to alkalic basalt at the end stages of Hawaiian volcanism is commonly, but not always, gradual, with interfingering of the two rock types with rocks of transitional chemistry.

(2) Sr isotopic signatures are inversely correlated to Rb/Sr ratios and may be systematically different for the tholeiitic shield, lower alkalic lava, and uppermost alkalic lava. The progression is subtle and is best illustrated by data from Haleakala using $^{87}Sr/^{86}Sr$ ratios (Chen and Frey, 1983, 1985) for tholeiite (0.7037–0.704) through lower alkalic (0.7032–0.7035) and upper alkalic lava (0.7030–0.7033). In addition, $^{143}Nd/^{144}Nd$ ratios show a smaller variation and are inversely correlated to $^{87}Sr/^{86}Sr$ ratios. These data are interpreted to show participation of different source regions in the formation of the three series. In other volcanoes, including Waianae, West Maui, and Mauna Kea, no systematic differences exist between radiogenic-isotope signatures in the tholeiitic and alkalic stages (Hegner and others, 1986; Stille and others, in press).

(3) Pb isotopes differ for each volcano, vary independently of Sr and Nd, and appear to be related to the age and location of individual volcanoes in the Hawaiian Chain (that is, to the Loa and Kea locus lines (fig. 23.1; see also Tatsumoto, 1978; Stille and others, in press). The absolute variation of all isotopic ratios and the uncorrelated variations of Pb with Nd and Sr have led workers in Hawaii to postulate mixing of at least three kinds of variably enriched or depleted sources. Beyond defining the need for three sources, no consensus has been made as to their position in the mantle or the details of their origin (see Tatsumoto and others,

chapter 26; Tatsumoto, 1978; Staudigel and others, 1984; Kaneoka, in press; Stille and others, in press).

Other geochemical studies, using trace and major elements, address further the relations between tholeiitic and alkalic volcanism. On the basis of field mapping, petrologic study of volcanic sequences, and experimental study of basaltic phase equilibria, two hypotheses have been proposed (see Macdonald, 1968, p. 512–516, for a good summary of these hypotheses). The first hypothesis, based principally on field studies and later on high-pressure phase equilibria, is that alkalic series on Hawaiian volcanoes are derived directly by fractionation of tholeiitic magma in storage. For this process to work, pressures must be great enough to stabilize hypersthene as a liquidus phase, the crystallization of which reduces the SiO_2 of the derivative magma (see Green and Ringwood, 1964). This hypothesis is attractive from consideration of the very small volumes of the alkalic caps and was defended by Wright and others (1979) as a logical consequence of an active tholeiitic shield-building system breaking the connection with the hotspot as the plate drifts to the northwest. The second hypothesis, first presented by Kuno and others (1957), Yoder and Tilley (1962) and later, in modified form, by O'Hara (1965), all working with experimental data, postulates that alkalic magma is independently derived from a different source region at a greater depth than that which produced the tholeiite.

Evidence based on geochemistry shows that the first hypothesis is clearly untenable as a simple single-stage fractionation process, even for those volcanoes for which isotopic ratios are similar in the two rock types. Mass-balance calculations made using hypersthene as a dominant crystallizing phase satisfy major oxides, but leave minor and incompatible trace elements out of balance; that is, the alkalic basalt always has greater amounts of incompatible elements (K, P, light rare-earth elements, and so on) than can be explained by balancing SiO_2, Al_2O_3, FeO, MgO, and CaO. Chondrite-normalized rare-earth-element patterns are always steeper for alkalic basalt than for tholeiite, a relation not explainable by removal of hypersthene in which solid-liquid partition coefficients for rare-earth elements are too low to significantly steepen the patterns for derivative liquids. The mismatch between trace elements and major oxides might be rectified in a model involving a continuously replenished magma system (see O'Hara, 1977). However, replenishment does not have much appeal in explaining the waning stage of Hawaiian volcanism. Hypothesis 1 is also difficult to apply to an earlier stage of alkalic volcanism, such as Loihi, where alkalic magma is preceding, rather than following, tholeiitic magma.

Modern evidence favors the first part of hypothesis 2, that the alkalic basalt is generated independently of the tholeiite in an isotopically different source mantle. The depths at which either type of magma is generated or last equilibrated is an unresolved issue. The identification of mantle metasomatism, isotopic heterogeneity, and possible mixing of source mantle materials with each other and with basaltic melt provide little certainty as to the absolute depths of generation of any basaltic melt, with the exception that the depths are in the mantle and below the deepest earthquake foci (60 km for Hawaii). At Loihi further complications arise. The data require simultaneous eruption of magma that has equilibrated at different depths and that does not show the same isotopic relations as shown for the tholeiitic-alkalic transition at the end of Hawaiian volcanism.

The origin of the nephelinitic series, those containing modal nepheline and (or) melilite, is yet another story. Clague and Frey (1982) have exhaustively analyzed data for the Honolulu Volcanics on Oahu. They conclude that this series was produced at degrees of melting ranging from 5–11 percent and requires some premelting metasomatism of a garnet peridotite source. They specify melting at a pressure of 2.5–3.0 GPa, corresponding to a maximum depth of about 100 km. Other workers, for example Jackson and Wright (1970) and Wright (1984), favor an origin in the low velocity zone, deeper than 100 km. Because as much as 2 m.y. separates the truly nephelinitic series from underlying lava at the same locality, the nephelinite series should be only indirectly related to the thermal plume assumed to exist for the building of the large-volume Hawaiian shields. Jackson and Wright (1970, p. 427) hypothesised that post-erosional lava erupts due to release of pressure following the re-establishment of isostatic equilibrium, which was upset during the vast extrusions of shield-building lava. A more recent evaluation (Clague and Dalrymple, chapter 1, part I) finds that the time separating the shield-building lava and the uppermost alkalic lava is decreasing downchain and that the occurrence of post-erosional volcanism maintains a constant distance from contemporaneous shield-building activity. This evaluation is consistent with the Jackson-Wright model.

MELTING MODELS AND THE NATURE OF THE HAWAIIAN MANTLE

Numerous recent models for Hawaiian volcanism have been based on very different premises and data sets. Not surprisingly, the various authors come to different conclusions regarding some of the fundamental facts needed to specify the history of Hawaiian magma from its source in the mantle to its eruption at the Earth's surface. These facts are, in part, the following, each of which has been or needs to be ascertained for each major rock type or stage of volcanism, that is, shield-building tholeiite, preshield and caldera-filling alkalic basalt, and uppermost alkalic to nephelinitic rocks.

1. Mantle sources: depth, mineralogy, and bulk composition.
2. Depth of partial melting.
3 Melt fraction produced at time of melting.
4. Degree to which primary magma is changed on the way to storage in the shallow crust or to eruption, for example, loss of olivine, interaction with wall rocks, and mixing during ascent.

An excellent summary of current models to explain the Hawaiian magma system is presented by Frey and Roden (in press). The geochemical models are grouped into those based primarily on isotopic data (Kaneoka, chapter 27; Kaneoka, in press; Tatsumoto and others, chapter 26; Staudigel and others, 1984; Stille and others, in press), those based on trace-element data (Leeman and others, 1980; Clague and Frey, 1982; Hofmann and White, 1982; Budahn and Schmitt, 1985), or those based on a combination of isotopic and chemical data (Chen and Frey, 1983, 1985; Feigenson, and others, 1983; Feigensen, 1984; Roden and others, 1984;

Hofmann and others, 1984; Clague, in press; Feigensen, in press; Lanphere and Frey, in press). The geochemical models are in general formulated to fit established geochemical assumptions (such as nonfractionation of isotopes and chondritic source compositions) and pay little attention to either geophysical considerations or the constraints afforded by study of active volcanism. Some additional models (Presnall and Helsley, 1982; Sen, 1983) are based on the interpretations of geophysical data and on experimentally determined phase equilibria for basalt and for mantle rocks, but fail to apply their interpretations to actual geochemical balances. Anderson (1981) has proposed models based on seismologic data using the velocity structure of the mantle and has attempted to reconcile these models with the existing geochemical data, again without quantitative verification. Wright (1984) has considered geochemical balances consistent with the physical processes involved in constructing an Hawaiian volcano. However, the various authors find little agreement on items 1–4 above.

On item 1, disagreement arises as to the existence of a deep mantle plume, whether such a plume would supply the material to be melted (as opposed to the heat for melting at upper mantle depths), and as to the nature of the residual assemblage after melting. The $^3He/^4He$ ratios for some volcanoes support, in a striking way, the primitive nature of Hawaiian magma sources (see Kaneoka, chapter 27). Additional constraints on mantle sources, as determined by study of rare gas data, are given by Clague (in press). As noted earlier, there is agreement that several isotopically distinct sources participate at some point prior to melting and (or) storage at crustal levels. On the composition of the residual assemblage present after melting, two extreme views are presented: (1) Budahn and Schmitt (1985) use convergence of chondrite-normalized rare-earth-element patterns at the heavy end to infer the necessity of garnet in the residual assemblage for melting all Hawaiian basalt, and (2) Wright (1984) argues for a metasomatic process by which the garnet-like rare-earth-element signature is imparted to a depleted mantle source formed by melting of midocean ridge basalt before melting to produce Hawaiian tholeiite.

Most workers agree on item 2 that the actual partial melting occurs at uppermost mantle depths (that is, 100 ± 50 km) but disagree as to whether lithosphere or asthenosphere is directly melted. Presnall and Helsley (1982) and Sen (1983) favor lithospheric melting, which has been strongly criticized on both geochemical and physical grounds (see Feigenson, in press). Most authors favor primary melting of the asthenosphere. Wright (1984) differs from both in postulating that melting takes place in asthenosphere that begins as oceanic lithosphere, but through a combination of metasomatic enrichment and lithospheric thinning was converted to asthenosphere before melting. Chen and Frey (1983, 1985) propose that melts are generated in the asthenosphere and subsequently modified during passage through the lithosphere.

Arguments about item 3 follow from the consideration of residual assemblages. The geochemical models, whether using incompatible element enrichment, or garnet as a residual phase, infer small (less than 10 percent) degrees of melting, even for tholeiite. This model results in a conundrum regarding the supply of material to be melted. As aptly stated by Chen and Frey (1983, p. 789) "the entire lower lithosphere and much of the asthenosphere beneath a Hawaiian volcano must be involved in its creation." Hofmann and others (1984) in a study of short-term chemical variation at Kilauea, remain noncommittal on absolute degree of melting, although their requirement that garnet be a residual phase restricts the degree of melting to less than 20 percent, in consideration of high-pressure phase relations in ultramafic systems. O'Hara (1985) points out some important constraints on assumptions of the degree of partial melting, based on evaluation of the real shape of the melting anomaly.

Conclusions regarding item 4 are largely a consequence of inferences made for items 1–3. As stated above, isotopic data appear to require a more complicated history than one might infer from other data. The existence of magma batches at Kilauea (see Wright and others, 1975) requires heterogeneity, either inherited from the melt source or produced between initial melting and shallow storage. Even this concept (that is, magma batches at Kilauea), carefully outlined in a series of papers (Wright and Fiske, 1971; Wright and others, 1975; Wright and Tilling, 1980), has been questioned by Hofmann and others (1984), who claim that the data define a continuum in all elements. We disagree and leave this subject as a point to emphasize how difficult it is to reach a consensus of interpretation on any observations of Hawaiian volcanism.

Finally, Anderson (1984, 1985) has questioned all of the conventional ideas regarding items 1–4. He favors a source for magma in the transition region at 200–250 km depth where large scale melting is followed by processes such as eclogite fractionation during ascent and mixing with melts from enriched mantle at shallow depth, to produce the rocks forming both the oceanic crust and the oceanic islands such as Hawaii. Time will tell whether these provocative ideas can be quantified and tested against all of the geochemical and geophysical constraints provided by study of active volcanism.

One additional way of determining the composition of the mantle and the melting process is through study of xenoliths brought up with basalt. The processes by which xenoliths arrive at the surface of the earth is somewhat enigmatic. Both tholeiitic magma and alkalic magma show abundant evidence of shallow storage, although the general absence of mantle inclusions from tholeiite and their frequent association with alkalic magma remains unexplained. Clague (in press) suggests that xenoliths are filtered out of tholeiitic magma during storage in large magma chambers. Wright (1984) makes a further suggestion that the rates of tholeiitic-magma transport are too slow and the coalescing transport paths too thin to permit xenoliths to arrive at the surface. Nephelinitic magma is inferred to erupt directly from the mantle and carry the only lherzolite and garnet-bearing xenoliths. Frey and Roden (in press) provide an excellent summary of the relations of xenoliths to both basalt and mantle sources. They point out that virtually all xenoliths have undergone modification prior to their inclusion in the ascending magma in the form of interaction with fluids that may change trace-element content, isotopic ratios, or deposit hydrous minerals. Therefore, because of these factors, combined with their small size, no xenolith can be interpreted as representing the bulk mantle, or any part of the mantle large enough to be considered as a source

composition in melting models. Nonetheless, their presence is useful in assessing the depth of origin of some Hawaiian basalt.

Perhaps no single model works for all volcanoes in the chain. As Frey and Roden (in press) point out, a problem in developing a general model is that it must explain both the unique geochemical features that characterize individual Hawaiian volcanoes and simultaneously explain the geochemical variations among all Hawaiian volcanoes. As a final point, we want to reemphasize the necessity for comprehensive study of everything relevant to construction of an individual Hawaiian volcano as well as the entire volcanic chain (see Wright and others, 1979; Wright, 1984). Recent advances in our understanding of seismology (Anderson and others, 1984), phase relations of ultramafic rocks (Takahashi and Scarfe, 1985; Walker and Herzberg, 1985), and the physical processes of melt separation (MacKenzie, 1984; Richter and MacKenzie, 1984) may eventually resolve both the depth and degree of partial melting in a way that can accommodate the constraints provided by active volcanic processes.

SUGGESTIONS FOR FURTHER STUDY

The acquisition of more chemical data on Hawaiian lava has increased our qualitative and quantitative understanding of Hawaiian petrology and has also raised new questions for further study. Obviously, the location of Hawaii, in the interior of an oceanic plate far removed from influences of spreading centers or continental margins, continues to provide a setting in which possible determinations can be made as to the nature of the oceanic crust and mantle and the dynamics of plume or hotspot volcanism. Presently the heterogeneities in the hotspot magma sources are being emphasized. Yet over the long term it is important to keep in mind that the Hawaiian chain has shown an identifiable eruptive style and geochemical signature for over 70 million years. Thus, a gross uniformity must exist in the source and some unifying principles in the production of Hawaiian magma, the mechanics of its segregation from the mantle, and its transport to areas of storage within the crust. Further study of the following topics ought to bring us to a better understanding of the processes important in the formation of Hawaiian volcanoes: (1) Continued detailed geochemical study of stratigraphically constrained samples; (2) geophysical study of the mantle; (3) more detailed petrographic study (both field and thin section) of lava samples, including detailed electron probe analysis of phase chemistry; and (4) more study of the submarine portions of active or young rift zones. For example, cursory petrographic study of submarine rift samples identified mineral forms and textures such as anhedral olivine and sieved plagioclase that suggest that processes involved in submarine lava are different from those in subaerial equivalents on the same rift zones.

REFERENCES

Anderson, A.T., Swihart, G.H., Artioli, G., and Geiger, C.A., 1984, Segregation vesicles, gas filter-pressing, and igneous differentiation: Journal of Geology, v. 92, p. 55–72.

Anderson, D.L., 1981, Hotspots, basalts, and the evolution of the mantle: Science, v. 213, p. 82–89.

———1984, The Earth as a planet: paradigms and paradoxes: Science, v. 223, p. 347–355.

———1985, Hotspot magmas can form by fractionation and contamination of mid-ocean ridge basalt: Nature, v. 318, p. 145–149.

Basaltic Volcanism Study Project, 1981, Basaltic volcanism on the terrestrial planets: Elmsford, Pergamon Press, 1,286 p.

Beeson, M.H., 1976, Petrology, mineralogy and geochemistry of the East Molokai Volcanic Series, Hawaii: U.S. Geological Survey Professional Paper 961, 53 p.

Bonhommet. N., Beeson, M.H., and Dalrymple, G.B., 1977, A contribution to the geochronology and petrology of the Island of Lanai, Hawaii: Geological Society of America Bulletin, v. 88, p. 1281–1286.

Budahn, J.R., and Schmitt, R.A., 1985, Petrogenetic modeling of Hawaiian basalts: a geochemical approach: Geochimica et Cosmochimica Acta, v. 49, p. 67–87.

Chen, C.-Y., and Frey, F.A., 1983, Origin of Hawaiian tholeiite and alkalic basalt: Nature, v. 302, p. 785–789.

———1985, Trace element and isotopic geochemistry of lavas from Haleakala Volcano, East Maui, Hawaii: implications for the origin of Hawaiian basalts: Journal of Geophysical Research, v. 90, p. 8743–8768.

Chouet, B., and Aki, K., 1981, Seismic structure and seismicity of the cooling lava lake of Kilauea Iki, Hawaii: Journal of Volcanology and Geothermal Research, v. 9, p. 41–56.

Clague, D.A., in press, Hawaiian alkaline volcanism: Proceedings of the Royal Society of Edinburgh.

Clague, D.A., and Frey, F.A., 1980, Trace element geochemistry of tholeiitic basalts from site 433C, Suiko Seamount, *in* Shambach, J., ed., Initial reports of the Deep Sea Drilling Project [leg 55], v. 55: Washington, U.S. Government Printing Office, p. 559–569.

———1982, Petrology and trace element geochemistry of the Honolulu Volcanics, Oahu: Implications for the oceanic mantle below Hawaii: Journal of Petrology, v. 23, p. 447–504.

Clague, D.A., Frey, F.A., and Beeson, M.H., 1983, Rare-earth element and Sr isotopic evidence for the origin of the East Molokai Volcanics, Hawaii [abs.]: Eos, v. 64, p. 902.

Clague, D.A., Jackson, E.D., and Wright, T.L., 1980, Petrology of Hualalai Volcano, Hawaii: implication for mantle composition: Bulletin Volcanologique, v. 43, p. 641–656.

Craig, H., 1983, Introduction to Loihi Seamount: collected papers: Earth and Planetary Science Letters, v. 66, p. 334–336.

Duffield, W.A., Christiansen, R.L., Koyanagi, R.Y., and Peterson, D.W., 1982, Storage, migration, and eruption of magma at Kilauea Volcano, Hawaii, 1971–1972: Journal of Volcanology and Geothermal Research, v. 13, p. 273–307.

Dvorak, J.D., Okamura, A., and Dieterich, J.H., 1983, Analysis of surface deformation data, Kilauea Volcano, Hawaii: October 1966 to September 1970: Journal of Geophysical Research, v. 88, p. 9295–9304.

Dzurisin, D., Koyanagi, R.Y., and English, T.T., 1984, Magma supply and storage at Kilauea Volcano, Hawaii, 1956–1983: Journal of Volcanology and Geothermal Research, v. 21, p. 177–206.

Eaton, J.P., 1962, Crustal structure and volcanism in Hawaii, *in* Macdonald, G.A., and Kuno, H., eds., The crust of the Pacific Basin: Washington, American Geophysical Union, Monograph 6, p. 13–29.

Eaton, J.P., and Murata, K.J., 1960, How volcanoes grow: Science, v. 132, p. 925–938.

Emery, K.O., 1955, Submarine topography south of Hawaii: Pacific Science, v. 9, p. 286–291.

Evans, B.W., and Moore, J.G., 1968, Mineralogy as a function of depth in the prehistoric Makaopuhi tholeiitic lava lake, Hawaii: Contributions to Mineralogy and Petrology, v. 17, p. 85–115.

Feigenson, M.D., 1984, Geochemistry of Kauai volcanics and a mixing model for the origin of Hawaiian alkali basalts: Contributions to Mineralogy and Petrology, v. 87, p. 109–119.

———in press, Geochemical and geophysical constraints on the origin of Hawaiian lavas: Journal of Geophysical Research.

Feigenson, M.D., Hofmann, A.W., and Spera, F.J., 1983, Case studies on the origin of basalt: II. The transition from tholeiitic to alkalic volcanism on Kohala Volcano, Hawaii: Contributions to Mineralogy and Petrology, v. 84, p. 390–405.

Finlayson, J.B., Barnes, I.L.. and Naughton, J.J., 1968, Developments in volcanic gas research in Hawaii, *in* The upper crust and upper mantle of the Pacific area: American Geophysical Union Geophysics Monograph 12, p. 428–438.

Fiske, R.S., and Kinoshita, W., 1969, Inflation of Kilauea Volcano prior to its 1967–1968 eruption: Science, v. 165, p. 341–349.

Frey, F.A., 1980, The origin of pyroxenites and garnet pyroxenites from Salt Lake Crater, Oahu, Hawaii: trace element evidence, *in* Irving, J., ed., The Jackson Volume; American Journal of Science, v. 280-A, pt. 2, p. 427–449.

Frey, F.A., and Clague, D.A., 1983, Geochemistry of diverse basalt types from Loihi Seamount, Hawaii: petrogenetic implications, *in* Loihi Seamount: collected papers: Earth and Planetary Science Letters, v. 66, p. 337–355.

Frey, F.A., and Roden, M., in press, The mantle source for the Hawaiian Islands: constraints from the lavas and ultramafic inclusions, *in* Menzies, M., and Hawkesworth, C., eds., Mantle metasomatism: New York, Academic Press.

Garcia, M.O., Wolfe, E.W., and Byers, C.D., in press, Petrology of the lavas from the Puu Oo eruption of Kilauea Volcano, Hawaii: Phases 1–20, *in* Wolfe, E.W., ed., The Puu Oo eruption of Kilauea Volcano, Hawaii: the first 1½ years: U.S. Geological Survey Professional Paper.

Gerlach, T.M., 1980, Evaluation of volcanic gas analyses from Kilauea Volcano: Journal of Volcanology and Geothermal Research, v. 7, p. 295–317.

Gerlach, T.M., and Graeber, E.J., 1985, Volatile budget of Kilauea Volcano: Nature, v. 313, p. 273–277.

Graeber, E.J., Modreski, P.J., and Gerlach, T.M., 1979, Compositions of gases collected during the 1977 east rift eruption, Kilauea Volcano, Hawaii: Journal of Volcanology and Geothermal Research, v. 5, p. 337–344.

Green, D.H., and Ringwood, A.E., 1964, Fractionation of basalt magmas at high pressures: Nature, v. 201, p. 1276–1279.

Greenland, L.P., in press, Estimated mantle content of volatiles from basaltic gas compositions: Bulletin of Volcanology.

Greenland, L.P., Okamura, A.O., and Stokes, J.B., in press, Constraints on the mechanics of eruption of Puu Oo, *in* Wolfe, E.W., ed., The Puu Oo eruption of Kilauea Volcano, Hawaii: the first 1 ½ years: U.S. Geological Survey Professional Paper.

Greenland, L.P., Rose, W. I., and Stokes, J.B., 1985, An estimate of gas emissions and magmatic gas content from Kilauea Volcano: Geochimica et Cosmochimica Acta, v. 49, p. 125–129.

Hardee, H.C., 1980, Solidification in Kilauea Iki lava lake: Journal of Volcanology and Geothermal Research, v. 7, p. 211–223.

Hardee, H.C., Dunn, J.C., Hills, R.G., and Ward, R.W., 1981, Probing the melt zone of Kilauea Iki lava lake, Kilauea Volcano, Hawaii: Geophysical Research Letters, v. 8, p. 1211–1214.

Hawkins, J., and Melchior, J., 1983, Petrology of basalts from Loihi Seamount, Hawaii, *in* Loihi Seamount: collected papers: Earth and Planetary Science Letters, v. 66, p. 356–368.

Hegner, E., Unruh, D., and Tatsumoto, M., 1986, Pb, Sr, and Nd isotope evidence for the origin of the West Maui Volcanic Suite, Hawaii: Nature, v. 319, no. 6053, 478–480.

Helz, R.T., 1980, Crystallization history of Kilauea Iki lava lake as seen in drill core recovered in 1967–1979: Bulletin Volcanologique, v. 43-4, p. 675–701.

———1984, In situ fractionation of olivine tholeiite, Kilauea Iki lava lake, Hawaii [abs.]: Geological Society of America Abstracts with Programs, v. 16, p. 536–537.

Helz, R.T., Banks, N.G., Casadevall, T.J., Fiske, R.S., and Moore, R.B., 1984, A catalogue of drill core recovered from Kilauea Iki lava lake from 1967 to 1979: U.S. Geological Survey Open-File Report 84–484, 72 p.

Helz, R.T., and Thornber, C.R., in press, Geothermometry of Kilauea Iki lava lake, Hawaii: Journal of Geophysical Research.

Helz, R.T., and Wright, T.L., 1983, Drilling report and core logs for the 1981 drilling of Kilauea Iki lava lake (Kilauea Volcano, Hawaii), with comparative notes on earlier (1967–1979) drilling experiences: U.S. Geological Survey Open-File Report 83–326, 66 p.

Hermance, J.F., and Colp, J.L., 1982, Kilauea Iki lava lake: geophysical constraints on its present (1980) physical state: Journal of Volcanology and Geothermal Research, v. 13, p. 31–61.

Hofmann, A.W., Feigenson, M.D., and Raczek, I., 1984, Case studies on the origin of basalt: III. Petrogenesis of the Mauna Ulu eruption, Kilauea, 1969–1971: Contributions to Mineralogy and Petrology, v. 88, p. 24–35.

Hofmann, A.W., and White, W.M., 1982, Mantle plumes from ancient oceanic crust: Earth and Planetary Science Letters, v. 57, p. 421–436.

Jackson, D.B., Swanson, D.A., Koyanagi, R.Y., and Wright, T.L., 1975, The August and October 1968 east rift eruptions, Kilauea Volcano, Hawaii: U.S. Geological Survey Professional Paper 890, 33 p.

Jackson, E.D., Silver, E.A., and Dalrymple, G.B., 1972, Hawaiian-Emperor Chain and its relation to Cenozoic tectonics: Geological Society of America Bulletin, v. 83, p. 601–618.

Jackson, E.D., and Wright, T.L., 1970, Xenoliths in the Honolulu volcanic series, Hawaii: Journal of Petrology, v. 11, p. 405–430.

Kaneoka, I., in press, Constraints on the origin of Hawaiian basalts and evidence for a multi-component mantle: Geochimica et Cosmochimica Acta.

Kaneoka, I., Takaoka, N., and Clague, D.A., 1983, Noble gas systematics for coexisting glass and olivine crystals in basalts and dunite xenoliths from Loihi Seamount, *in* Loihi Seamount: collected papers: Earth and Planetary Science Letters, v. 66, p. 427–437.

Kirkpatrick, R.J., Clague, D.A., and Friesen, W.B., 1980, Petrology and geochemistry of volcanic rocks, *in* Initial reports of the Deep Sea Drilling Project [leg 55], v. 55: Washington, U.S. Government Printing Office, p. 509–557.

Klein, F.W., 1982, Earthquakes at Loihi Submarine Volcano and the Hawaiian hotspot: Journal of Geophysical Research, v. 87, p. 7719–7726.

Klein, F.W., and Koyanagi, R.Y., 1979, Seismicity of Kilauea and Loihi Volcanoes, Hawaii [abs.]: Hawaii Symposium on Intraplate Volcanism and Submarine Volcanism, International Association of Volcanology and Chemistry of the Earth's Interior, Hilo, Hawaii, July 16–22, 1979, Abstract Volume, p. 24.

Koyanagi, R.Y., Unger, J.D., Endo, E.T., and Okamura, A.T., 1976, Shallow earthquakes associated with inflation episodes at the summit of Kilauea Volcano, Hawaii, *in* Gonzales-Ferran, O., ed., Symposium on Andean and Antarctic Volcanology Problems, Santiago, Chile, September 1974, Proceedings, p. 621–631.

Kuno, H., Yamasaki, K., Iida, C., and Nagashima, K., 1957, Differentiation of Hawaiian magmas: Japanese Journal of Geology and Geophysics, v. 28, p. 179–218.

Kurz, M.D., Jenkins, W.J., Hart, S.R., and Clague, D., 1983, Helium isotopic variations in volcanic rocks from Loihi Seamount and the Island of Hawaii, *in* Loihi Seamount: collected papers: Earth and Planetary Science Letters, v. 66, p. 388–406.

Lanphere, N., 1983, $^{87}Sr/^{86}Sr$ ratios for basalt from Loihi Seamount, Hawaii, *in* Loihi Seamount: collected papers: Earth and Planetary Science Letters, v. 66, p. 380–387.

Lanphere, M.A., Dalrymple, G.B., and Clague, D., 1980, Rb-Sr systematics of basalts from the Hawaiian-Emperor volcanic chain, *in* Shambach, J., ed., Initial reports of the Deep Sea Drilling Project [Leg 55], v. 55: Washington, Government Printing Office, p. 695–706.

Lanphere, M.A., and Frey, F.A., in press, Geochemical evolution of Kohala Volcano, Hawaii: Contributions to Mineralogy and Petrology.

Leeman, W.P., Budahn, J.R., Gerlach, D.C., Smith, D.R., and Powell, B.N., 1980, Origin of Hawaiian tholeiites: trace element constraints, *in* Irving, A.J., ed., The Jackson Volume: American Journal of Science, v. 280-A, pt. 2, p. 794–819.

Lindstrom, M.M., and Haskin, L.H., 1984, Studies of trace element behavior during crystallization of Makaopuhi lava lake, Hawaii: National Science Foundation Final Report EAR–7904888, 5 p.

Lipman, P.W., Lockwood, J.P., Okamura, R.T., Swanson, D.A., and Yamashita, K.M., 1985, Ground deformation associated with the 1975 magnitude 7.2 earthquake and resulting changes in activity of Kilauea Volcano, Hawaii: U.S. Geological Survey Professional Paper 1276, 45 p.

Macdonald, G.A., 1968, Composition and origin of Hawaiian lavas: Geological

Society of America Memoir 116, p. 477–522.

Macdonald, G.A., Abbott, A.A., and Peterson, F.L., 1983, Volcanoes in the sea: the geology of Hawaii: Honolulu, Hawaii, University of Hawaii Press, 517 p.

Macdonald, G.A., and Katsura, T., 1964, Chemical composition of Hawaiian lavas: Journal of Petrology, v. 5, p. 82–133.

Mackenzie, D.S., 1984, The generation and compaction of partial melts: Journal of Petrology, v. 5, pt. 1, p. 82–133.

Malahoff, A., McMurtry, G.M., Wiltshire, J.C., and Yeh, H.W., 1982, Geology and chemistry of hydrothermal deposits from active submarine volcano Loihi, Hawaii: Nature, v. 298, p. 234–239.

Moore, J.G., Clague, D.A., and Normark, W.R., 1982, Diverse basalt types from Loihi Seamount, Hawaii: Geology, v. 10, p. 88–92.

Moore, J.G., and Evans, B.W., 1967, The role of olivine in the crystallization of the prehistoric Makaopuhi tholeiitic lava lake, Hawaii: Contributions to Mineralogy and Petrology, v. 15, p. 202–223.

Moore, R.B., Helz, R.T., Dzurisin, D., Eaton, G.P., Koyanagi, R.Y., Lipman, P.W., Lockwood, J.P., and Puniwai, G.P., 1980, The 1977 eruption of Kilauea Volcano, Hawaii: Journal of Volcanology and Geothermal Research, v. 7, p. 189–210.

Murata, K.J., 1966, An acid fumarolic gas from Kilauea Iki: U.S. Geological Survey Professional Paper 537–C, 6 p.

Murata, K.J., and Richter, D.H., 1966, Chemistry of the lavas of the 1959–60 eruption of Kilauea Volcano, Hawaii: U.S. Geological Survey Professional Paper 537–A, p. A1–A26.

O'Hara, M.J., 1965, Primary magmas and the origin of basalts: Scottish Journal of Geology, v. 1, p. 19–40.

———1977, Geochemical evolution during fractional crystallization of a periodically refilled magma chamber: Nature, v. 266, p. 503–507.

———1985, Importance of the "Shape" of the melting regime during partial melting of the mantle: Nature, v. 314, p. 58–60.

O'Nions, R.K., Hamilton, P.J., and Evensen N.M., 1977, Variations in $^{143}Nd/^{144}Nd$ and $^{87}Sr/^{86}Sr$ ratios in oceanic basalts: Earth and Planetary Science Letters, v. 34, p. 13–22.

Peck, D.L., 1978, Cooling and vesiculation of Alae lava lake, Hawaii: U.S. Geological Survey Professional Paper 935–B, 59 p.

Peck, D.L., Hamilton, M.S., and Shaw, H.R., 1977, Numerical analysis of lava lake cooling models: Part II, application to Alae lava lake, Hawaii: American Journal of Science, v. 277, p. 415–437.

Peck, D.L., and Kinoshita, W.T., 1976, The eruption of August 1963 and the formation of Alae lava lake, Hawaii: U.S. Geological Survey Professional Paper 935–A, 33 p.

Peck, D.L., Wright, T.L., and Decker, R.W., 1979, The lava lakes of Kilauea: Scientific American, v. 241, p. 114–129.

Powers, H.A., 1955, Composition and origin of basaltic magma of the Hawaiian Islands: Geochimica et Cosmochimica Acta, v. 7, p. 77–107.

Presnall, D.C., and Helsley, C.E.. 1982, Diapirism of depleted peridotite—a model for the origin of hot spots: Physics of the Earth and Planetary Interiors, v. 29, p. 148–160.

Richter, D.H., Eaton, J.P., Murata, K.J., Ault, W.U., and Krivoy, H.L., 1970, Chronologic narrative of the 1959–60 eruption of Kilauea Volcano, Hawaii: U.S. Geological Survey Professional Paper 537–E, 73 p.

Richter, D.H., and Moore, J.G., 1966, Petrology of the Kilauea Iki lava lake, Hawaii: U.S. Geological Survey Professional Paper 537–B, 26 p.

Richter, D.H., and Murata, K.J., 1966, Petrography of the lavas of the 1959–60 eruption of Kilauea Volcano, Hawaii: U.S. Geological Survey Professional Paper 537–D, 12 p.

Richter, F.M., and Mackenzie, D., 1984, Dynamical models for melt segregation from a deformed matrix: Journal of Geology, v. 92, p. 729–740.

Rison, W., and Craig, H., 1983, Helium isotopes and mantle volatiles in Loihi Seamount and Hawaiian Island basalts and xenoliths: Earth and Planetary Science Letters, v. 66, p. 407.

Roden, M.G., Frey, F.A., and Clague, D.A., 1984, Geochemistry of tholeiitic and alkalic lavas from the Koolau Range, Oahu, Hawaii: implications for Hawaiian volcanism: Earth and Planetary Science Letters, v. 69, p. 141–158.

Ryan, M.P., Koyanagi, R.Y., and Fiske, R.S., 1981, Modeling the three-dimensional structure of macroscopic magma transport systems: application to Kilauea Volcano, Hawaii: Journal of Geophysical Research, v. 86, p. 7111–7129.

Sen, G.A., 1983, A petrologic model for the constitution of the upper mantle and crust of the Koolau Shield, Oahu, Hawaii, and Hawaiian magmatism: Earth and Planetary Science Letters, v. 62, p. 215–228.

Sen, G., and Presnall, D.C., 1980, Dunite nodules from the Koolau shield, Hawaii: crystal cumulates from a tholeiitic magma chamber [abs.]: Geological Society of America Abstracts with Programs, v. 12, p. 519.

Shaw, H.R., Hamilton, M.S., and Peck, D.L., 1977, Numerical analysis of lava lake cooling models: Part I. Description of the method: American Journal of Science, v. 277, p. 384–414.

Shaw, H.R., Wright, T.L., Peck, D.L., and Okamura, R., 1968, The viscosity of basaltic magma: an analysis of field measurements in Makaopuhi lava lake, Hawaii: American Journal of Science, v. 266, p. 225–264.

Shepherd, E.S., 1921, Kilauea gases, 1919: Hawaiian Volcano Observatory Bulletin, v. 9, p. 83–88.

Staudigel, H., Zindler, A., Hart, S.R., Leslie, T., Chen, C.-Y., and Clague, D., 1984, The isotope systematics of a juvenile intraplate volcano. Pb, Nd, and Sr isotope ratios of basalts from Loihi Seamount, Hawaii: Earth and Planetary Science Letters, v. 69, p. 13–29.

Stille, P., Unruh, D.M., and Tatsumoto, M., 1983, Pb, Sr, Nd and Hf isotopic evidence of multiple sources for Oahu, Hawaii basalts: Nature, v. 304, p. 25–29.

———in press, Pb, Sr, Nd, and Hf isotopic constraints on the origin of Hawaiian basalts and evidence for a multi-component mantle: Geochimica et Cosmochimica Acta.

Swanson, D.A., 1972, Magma supply rate at Kilauea Volcano, 1952–1971: Science, v. 175, p. 169–170.

Swanson, D.A., Duffield, W.A., and Fiske, R.S., 1976a, Displacement of the south flank of Kilauea Volcano: the result of forceful intrusions of magma into the rift zones: U.S. Geological Survey Professional Paper 963, 39 p.

Swanson, D.A., Jackson, D.B., Koyanagi, R.Y., and Wright, T.L., 1976b, The February 1969 east rift eruption of Kilauea Volcano, Hawaii: U.S. Geological Survey Professional Paper 891, 30 p.

Takahashi, E., and Scarfe, C.M., 1985, Melting of peridotite to 14 GPa and the genesis of Komatiite magmas [abs.] : Eos, v. 66, p. 403.

Tatsumoto, M., 1978, Isotopic composition of lead in oceanic basalt and its implication to mantle evolution: Earth and Planetary Science Letters, v. 38, p. 63–87.

Tilley, C.E., and Scoon, J.H., 1961, Differentiation of Hawaiian basalts: trends of Mauna Loa and Kilauea historic magma: American Journal of Science, v. 259, p. 60–68.

Walker, D., and Herzberg, C.T., 1985, Implications of possible liquidus-solidus convergence in mantle peridotite at high pressure [abs.]: Eos, v. 66, p. 403.

Wright. T.L., 1971, Chemistry of Kilauea and Mauna Loa lava in space and time: U.S. Geological Survey Professional Paper 735, 40 p.

———1973, Magma mixing as illustrated by the 1959 eruption, Kilauea Volcano, Hawaii: Geological Society of America Bulletin, v. 84, p. 849–858.

———1984, Origin of Hawaiian tholeiite: a metasomatic model: Journal of Geophysical Research, v. 89, p. 3233–3252.

Wright, T.L., and Fiske, R.S., 1971, Origin of the differentiated and hybrid lavas of Kilauea Volcano, Hawaii: Journal of Petrology, v. 12, p. 1–65.

Wright, T.L., and Okamura, R.T., 1977, Cooling and crystallization of tholeiitic basalt, 1965 Makaopuhi lava lake, Hawaii: U.S. Geological Survey Professional Paper 1004, 78 p.

Wright, T.L., and Peck, D.L., 1978, Crystallization and differentiation of the Alae magma, Alae lava lake, Hawaii: U.S. Geological Survey Professional Paper 935–C, 20 p.

Wright, T.L., Peck, D.L., and Shaw, H.R., 1976, Kilauea lava lakes: natural laboratories for study of cooling, crystallization and differentiation of basaltic magma, *in* The geophysics of the Pacific Ocean Basin and its margin: American Geophysical Union, Geophysical Monograph 19, p. 375–392.

Wright, T.L., Shaw, H.R., Tilling, R.I., and Fiske, R.S., 1979, Origin of Hawaiian tholeiitic basalt: a quantitative model [abs.]: Hawaii Symposium on Intrapiate Volcanism and Submarine Volcanism, International Association of

Volcanology and Chemistry of the Earth's Interior, Hilo, Hawaii, July 16–22, 1979, Abstract Volume, p. 104.

Wright, T.L., Swanson, D.A., and Duffield, W.A., 1975, Chemical composition of Kilauea east-rift lava, 1968–1971: Journal of Petrology, v. 16, p. 110–133.

Wright, T.L., and Tilling, R.I., 1980, Chemical variation in Kilauea eruptions 1971–1974, *in* Irving, A., ed., The Jackson Volume: American Journal of Science, v. 280–A, pt. 2, p. 777–793.

Yoder, H.S., Jr., and Tilley, C.E., 1962, Origin of basalt magmas—an experimental study of natural and synthetic rock systems: Journal of Petrology, v. 3, pt. 3, p. 342–532.

TRACE-ELEMENT CHEMISTRY OF KILAUEA AND MAUNA LOA LAVA IN SPACE AND TIME: A RECONNAISSANCE

By Robert I. Tilling, Thomas L. Wright, *and* Hugh T. Millard, Jr.

ABSTRACT

Rare-earth and other trace elements have been determined in 75 Kilauea and Mauna Loa tholeiite samples selected from the same rock powders previously analyzed by Wright (USGS Prof. Paper 735, 1971), to provide a representative sampling in space and time. Preliminary interpretations of the results include the following:

(1) Abundance-variation patterns for well-determined trace elements confirm the long-term temporal variation previously demonstrated by major-element data for olivine-controlled Kilauea lava. Younger lava is richer in olivine-incompatible constituents (such as K, Ti, P, LREE, Sc, and Hf): the behavior of uranium is more varied but fits the overall pattern. Results for less well determined incompatible elements provide supporting permissive evidence.

(2) Subtle systematic differences are observed between the mean compositions of olivine-controlled lava from the summit and rift-zone areas of Kilauea and, perhaps, Mauna Loa, indicating a possible, heretofore unrecognized, compositional variation with eruption locus.

(3) Our results confirm the observation of Budahn and Schmitt (Geochim et Cosmo., v. 49, 1985) that prehistoric Mauna Loa olivine-controlled lava differs systematically from its historical counterpart. Furthermore, our data demonstrate significant differences between 19th-century and 20th-century Mauna Loa lava, suggesting systematic long-term secular variation not previously detected from major-element studies alone.

(4) Mauna Loa's long-term variation trend, in contrast to Kilauea's, is characterized by decreasing abundances of olivine-incompatible constituents with time. Thus, the composition of lava from the two volcanoes diverges with time, resulting in maximum differences between them in the 20th century. The chemical distinction between Kilauea and Mauna Loa has existed for over 30,000 years.

(5) Superimposed on the long-term (centuries to millenia) variations for both volcanoes are short-term (years to decades) variations that cannot be explained by olivine control.

(6) Rhodes' (Jour. of Geophys. Res., v. 88, 1983) data for 114 analyses of Mauna Loa historical lava are interpreted to illustrate not only long-term variation, marked by an irregular decrease in the incompatible elements K, Ti, P, Nb, Zr, and Sr, but also short-term variation (<1 year). A sharp compositional break exists between the lava of the 1868 and 1880 eruptions, and we speculate that this break may reflect disruption of magmatic processes in Mauna Loa's reservoir and conduits caused by the catastrophic 1868 earthquake, the largest to strike the Island of Hawaii in historical time.

Our tentative findings have general implications for processes of intraplate (hot spot) volcanism. Specifically, any complete petrogenetic model for Hawaiian tholeiite must take into account both long-term and short-term variations in olivine-controlled lava of Kilauea and Mauna Loa.

INTRODUCTION

Kilauea and Mauna Loa Volcanoes, on the Island of Hawaii (fig. 24.1), are composed entirely of tholeiitic basalt erupted in an intraplate tectonic setting. Because of their generally nonexplosive character, the eruptions of these two volcanoes—among the most active in the world—have been systematically monitored, documented, and sampled. The papers in this volume attest to the wealth of observational data and the comparatively good general understanding of Hawaiian magmatic and eruptive mechanisms that have

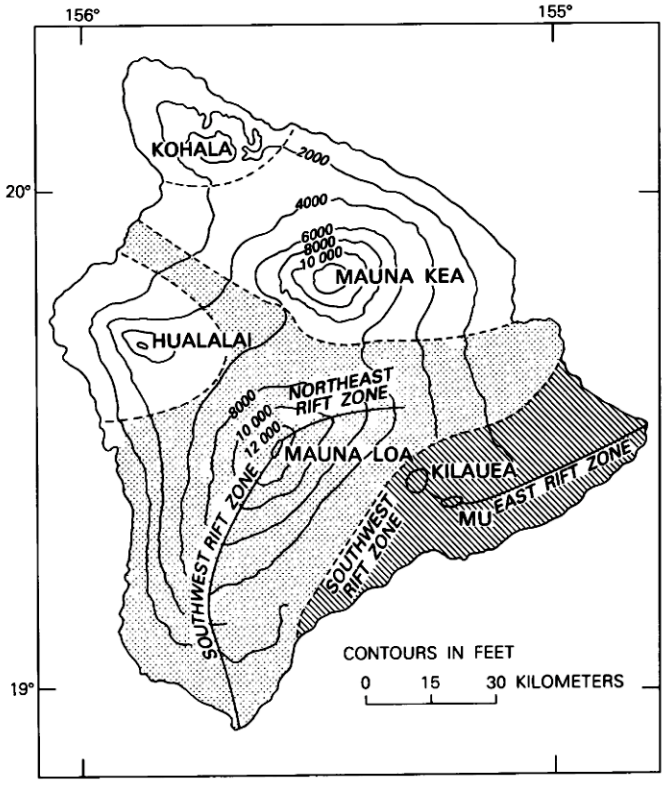

FIGURE 24.1.—Index map showing five volcanoes that make up Island of Hawaii and rift zones of Kilauea and Mauna Loa Volcanoes. MU, site of 1969–74 Mauna Ulu eruption on Kilauea's upper east rift zone. (From Wright, 1971, fig. 1).

been achieved by many decades of modern, multifaceted studies since the founding of the Hawaiian Volcano Observatory in 1912.

This paper reports results from the initial phase of a comprehensive investigation into the trace-element geochemistry of Kilauea and Mauna Loa lava undertaken as a complement to the systematic major-element geochemical study of Wright (1971). There were three primary objectives of this initial phase: (1) to conduct a reconnaissance trace-element survey of representative samples of Kilauea and Mauna Loa lava to determine possible compositional variations with location of eruptive vents or with time; (2) to improve our understanding of the distribution of trace elements in olivine-controlled lava, whose major-element variations can be explained largely by the addition or subtraction of olivine only (see, for example, Powers, 1955; Murata and Richter, 1966a,b; Wright, 1971, 1973); and (3) to identify selected trace elements whose abundances could be determined precisely and accurately to serve as the focus for subsequent, more quantitative studies of specific suites of olivine-controlled, differentiated, and hybrid lava to bear on the petrogenesis, transport and storage, and eruption of Hawaiian tholeiite.

Our study, involving 75 representative samples, considerably increases the body of trace-element data for Kilauea and Mauna Loa lava, especially lava erupted in prehistoric times (before about A.D. 1750). The analytical data we report here, though not published previously, were acquired more than a decade ago; possibly some analyses may be of lower quality than might be obtained today. Therefore, we have paid particular attention to their precision and accuracy, evaluated by comparison with more recent published analyses of Kilauea and Mauna Loa tholeiite (for example, Casadevall and Dzurisin, chapter 13; Leeman and others, 1977, 1980; Basaltic Volcanism Study Project, 1981; Rhodes, 1983; Hoffman and others, 1984; Budahn and Schmitt, 1985). As will be seen, our reconnaissance data agree well for many elements with analytical results obtained by other laboratories on similar, or, in some cases, the same samples. These data should provide a broader context for the evaluation of recent petrogenetic models of the origin of Hawaiian tholeiite (for example, Hoffman and others, 1984; Wright, 1984; Budahn and Schmitt, 1985), as well as for the design of specific, topical studies to refine our understanding of olivine-controlled basaltic lava.

ACKNOWLEDGMENTS

This study was facilitated by the cooperation, assistance, and encouragement of our colleagues at the Hawaiian Volcano Observatory as well as at the USGS centers in Denver and Reston. Philip J. Aruscavage made the fission-track spark-counting (FTSC) determinations of uranium and performed the instrumental neutron activation analyses of the samples through the gamma-counting step. The staff of the USGS Triga Reactor (Denver) were most helpful in performing neutron irradiations of the samples. Anthony F. Dorrzapf made a special effort to obtain the best possible emission-spectrographic analyses from the semi-quantitative technique used. The cheerful help of Margaret Mangan in the computer reduction and plotting of the analytical results is greatly appreciated. Joseph Arth made available his computer program for plotting chondrite-normalized rare-earth elements, and Thomas Casadevall and Daniel Dzurisin kindly provided us their analytical data on the Uwekahuna Bluff section (Kilauea caldera) prior to their publication in this volume. Rosalind T. Helz and David Gottfried, USGS, reviewed the manuscript and offered constructive criticism and useful suggestions that materially improved the paper; however, any remaining flaws rest solely with us.

PREVIOUS WORK

Pioneering petrologic and chemical studies of Kilauea and Mauna Loa lava include those of Macdonald (1949a, b; 1968), Powers (1955), Tilley and Scoon (1961), Murata and Richter (1966a, b), and Aramaki and Moore (1969). From these and other previous studies, several important conclusions developed: (1) For most of the lava from a given volcano, chemical variations can be largely explained by addition or subtraction of olivine (this is known as olivine control), although some marked exceptions have been noted; (2) systematic petrographic and chemical differences exist between the lavas of these two volcanoes; for example, orthopyroxene commonly occurs in small amounts in Mauna Loa lava but is almost totally absent in Kilauea lava; (3) composition of Kilauea lava during some eruptions varied with time; and (4) variations in composition in space and (or) time may be related to separate and chemically distinct batches of magma.

These observations, based almost exclusively on petrographic and major-element analyses, were comprehensively documented and extended not only for olivine-controlled lava, but also for differentiated and hybrid lavas, by Wright and coworkers (Wright, 1971, 1973; Wright and Fiske, 1971; Wright and others, 1975; Wright and Tilling, 1980). As defined and demonstrated empirically (Wright, 1971; Wright and Fiske, 1971), Hawaiian olivine-controlled lava characteristically has MgO contents greater than 6.80 weight percent, differentiated lava invariably contains less than 6.80, and hybrid lava varies in MgO content depending on the mixture of olivine-controlled and differentiated magmas.

Beginning in the mid-1960's, numerous trace-element and isotopic studies obtained data on Hawaiian tholeiite and other basalt types (for example, Powell and Delong, 1966; Tatsumoto, 1966,1978; Frey and others, 1968; Gast, 1968; Hubbard, 1969; Schilling and Winchester, 1969; Peterman and Hedge, 1971; DePaolo and Wasserburg, 1976; O'Nions and others, 1977). Most pertinent for our present purposes are the studies that contain analytical data on lava from Kilauea and Mauna Loa (for example, Gunn, 1971; Wright, 1971; Leeman and others, 1977, 1980; Rhodes and Lipman, 1979; Easton and Garcia, 1980; Basaltic Volcanism Study Project, 1981; Rhodes and others, 1982; Rhodes, 1983; Budahn and Schmitt, 1985). The significance of trace-element and isotopic constraints on petrogenetic models for the derivation of Hawaiian tholeiite is readily apparent from several recent papers (for example, Clague and Frey, 1982; Frey and Clague, 1983; Staudigel and others, 1984; Wright, 1984). In this paper we will touch briefly on how our reconnaissance data might bear on these models.

SAMPLE SELECTION AND ANALYTICAL TECHNIQUES

SAMPLE SELECTION

Because of the reconaissance nature of this study, the materials analyzed were selected with the following requirements in mind:

(1) Representative sampling of the eruptions of each volcano in space (summit, rift zones, flanks) and in time (prehistoric, 18th–19th centuries, 20th century).

(2) Representative sampling of the range in MgO content, if applicable, for each time-space lava group. This was done in order to compare the variations in trace-element distribution with variations expected from olivine control. Accordingly, the samples chosen for study are predominantly those demonstrated by Wright (1971) from major-element chemistry to be olivine controlled. For comparative purposes, we also selected several samples of differentiated and hybrid lava.

(3) Use of the same rock powders analyzed chemically for previous studies (Wright, 1971; Wright and Fiske, 1971). This permitted direct comparison with published major-element compositions and minimized variation stemming from sample inhomogeneity. Some samples initially chosen could not be studied because none of the original rock powder was available for analysis; where possible, suitable alternative samples meeting the other requirements were substituted. In all, 75 samples (44 from Kilauea, 31 from Mauna Loa) were analyzed by the techniques described below.

ANALYTICAL TECHNIQUES

The concentrations of 28 major, minor, and trace elements (Cs, Rb, Ba, Sr, K, Na, Th, U, La, Ce, Nd, Sm, Eu, Gd, Tb, Dy, Tm, Yb, Lu, Ta, Zr, Hf, Sb, Sc, Mn, Fe, Cr, and Co) were determined using the instrumental neutron activation analysis (INAA) procedure outlined in Zielinski and others (1977) and in Dodge and others (1982). The analytical procedure uses 1.1- to 2.3-g splits of the powdered basalt samples; USGS standard rocks G–2 and CQS–2 (a synthetic standard prepared by adding solutions of the elements of interest to a high-purity quartz powder, drying, and mixing) are used as standards. Sets of the samples and standards are irradiated for 20 min in a neutron flux of 30×10^9 n/cm^2/s, allowed to decay for 1 h: the short-lived nuclides are then gamma-counted twice on a coaxial Ge(Li) detector. The samples and standards are then reirradiated for 8 h in a flux of 3×10^{12} n/cm^2/s and counted on the coaxial Ge(Li) detector and also on a low-energy planar Ge(Li) detector. The counting conditions of our procedure are given in table 24.1. Five separate irradiations were required to analyze the 75 samples, grouped as shown in table 24.2.

A computer is used to calculate the areas under the photopeaks and apply corrections for pulse pileup, decay time, and interfering activities at the same gamma energies caused by other nuclides or by the fission of uranium and thorium. The pulse-pileup correction is computed by comparing the concentrations of iron determined by INAA to those determined by classical rock analysis or X-ray fluorescence techniques. The concentration of an element in the sample is computed by multiplying the concentration in the standard by the ratio of the corrected photopeak area in the sample to that in the standard and by the weight ratio of standard to sample. Values for the various isotopes of each element and for different decay times are weighted according to the reciprocal of the variance based on counting statistics and combined to yield a single concentration for each element.

A direct assessment of the precision and accuracy of our INAA analytical procedure is provided by results for five splits of basalt standard BCR–1 (Columbia River basalt) shown in table 24.3. The accuracy for the determinations of Rb, Sr, Th, Sm, Tb, Tm, and Sb is poor, as is the precision for Gd, Tb, Tm, Ta, and Sb (coefficient of variation >20 percent). Another diagnostic evaluation of our INAA procedure is afforded by interlaboratory comparison of results obtained for Hawaiian tholeiite (tables 24.4, 24.5, 24.6; fig. 24.2). Such comparisons indicate that our rare-earth element (REE) data agree well with published values on the same or similar samples, but the accuracy of our INAA determinations of Th and Zr is unsatisfactory, even though their precision may be acceptable. Our determination of Sm abundance is high relative to other values for the BCR–1 basalt standard (table 24.3) but systematically low compared with reported values for Kilauea and Mauna Loa lava (table 24.2; fig. 24.2). For reasons of poor accuracy and (or) precision, our INAA determinations of Rb, Sr, Zr, Th, U, Sb, Gd, Tb, and Tm are not given in the tabulations of individual analyses (tables 24.9–24.12, 24.15–24.19) despite good agreement for occasional samples (see tables 24.4, 24.5). However, possibly significant qualitative differences in the concentration ranges and averages of some of the determinations with poor precision, but with acceptable accuracy, are noted where appropriate. The INAA results for the major elements Na, K, Fe, and Mn, which accord well with values determined previously by classical rock analysis (Wright, 1971), are not reported.

The abundances of V, Ni, Cu, Mo, Zn, Ga, Nb, Y, and Pb reported were determined by a computerized emission-spectrographic (ES) technique described by Dorrzapf (1973). Even though this method is only semiquantitative in approach, results for some of the reported elements compare favorably with values determined by quantitative techniques (tables 24.4, 24.5). According to Dorrzapf (1973, p. 561), the precision of the technique "is within the range of +50 to −30 percent of the amount present*** and approaches +10–15 percent for many elements***." However, strong biases were observed for some elements (for example, Nb) that exceeded this stated uncertainty.

Comparison of available data (tables 24.4, 24.5) indicates that the emission-spectrographic determinations of Zn and Pb appear to be accurate, but the values for Cu and Nb are low compared to determinations by more quantitative techniques (table 24.4; Gunn, 1971, table 1). Fair agreement exists between the available reported analyses of V, Ni, Ga, and Y, despite wide scatter in data stemming from differences in techniques, samples analyzed, possible laboratory biases, and other factors. Other than the analyses of standard BHVO–1, we know of no published data for Mo concentration in Hawaiian tholeiite to compare with our results. Thus, we have excluded the determinations of Cu and Nb in the individual analyses, but have retained the other emission-

TABLE 24.1.—*Instrumental gamma-counting conditions for neutron-activation analysis*

[Efficiency of coaxial GE(Li), 10 percent; area of planar Ge(Li), 0.785 cm²]

	Coaxial Ge(Li)			Planar Ge(Li)		
Decay time	Source-detector distance	Counting time (min)	Resolution (eV FWHM at 1,333 keV)	Source-detector distance	Counting time (min)	Resolution (eV FWHM at 122 keV)
1-5 h	6.0	16.7	2,000	--	--	500
7 d	6.0	16.7	2,000	3.0	16.7	500
14 d	3.0	33.3	2,000	3.0	33.3	500
60 d	.5	167	2,000	1.0	167	500

TABLE 24.2.—*Number of samples of spatial and temporal basalt groups irradiated and analyzed by neutron activation*

[Basalt groups: SUM, summit; ERZ, east rift zone; SWRZ, southwest rift zone; NERZ, northeast rift zone; FLKS, northwest and southwest flanks; DIFF, differentiated; P, prehistoric; T, 18th and 19th centuries; H, 20th century]

	Irradiations				
Basalt group	TIL973	TIL008	TIL694	TIL746	TIL997
			Kilauea		
SUM	1	10	1	1	7
ERZ	3	0	0	3	7
SWRZ	0	1	3	7	0
P	1	4	0	9	3
T	0	0	2	2	4
H	3	7	2	0	7
			Mauna Loa		
SUM	1	0	0	1	3
SWRZ	1	3	1	4	1
NERZ	0	0	4	0	0
FLKS	0	4	1	2	0
DIFF	1	0	4	0	0
P	2	4	3	3	1
T	1	1	5	2	2
H	0	2	2	2	1

TABLE 24.3.—*Comparison of elemental composition by neutron-activation analyses (INAA) of five splits of USGS standard rock BCR-1 and previously published values*

[--, value not given in publication]

Element	Mean (ppm)	INAA results: Coefficient of variation (percent of mean)	Published values (ppm): Gladney and others (1983)	Published values (ppm): Abbey (1983)
Cs	0.98	7	0.97	0.96
RB	62	11	47.1	47
Ba	700	7	678	680
Sr	450	4	330	330
K	14,440	9	14,000	14,000
Na	23,600	1	24,300	24,500
Th	5.6	3	6.04	6.1
U	1.95	12	1.71	1.7
La	25.6	4	25.0	27
Ce	51.9	6	53.7	53
Nd	30.8	5	28.7	--
Sm	7.6	9	6.58	6.5
Eu	2.05	4	1.96	2.0
Gd	7.3	21	6.68	--
Tb	1.3	28	1.05	1.0
Dy	5.9	11	6.35	--
Tm	.4	39	.59	--
Yb	2.9	9	3.39	3.4
Lu	.57	10	.512	--
Ta	.79	25	.79	--
Zr	220	12	191	185
Hf	4.9	7	4.9	5
Sb	.4	61	.62	.6
Sc	33	5	32.8	33
Mn	1,405	1	1,410	1,400
Fe	93,200	4	93,800	94,000
Cr	18	12	16	15
Co	36	1	36.3	36

TABLE 24.4.—*Average compositions of samples from 20th-century Kilauea summit eruptions compared with standard basalt BHVO-1 from 1919 eruption*

[MgO and K_2O reported in weight percent; other values all ppm. --, value not given in publication. Samples from 20th-century eruptions adjusted to 7.00 weight percent MgO]

	Standard basalt BHVO-1 1919 eruption, Kilauea summit				20th-century Kilauea summit eruptions			
	1	2	3	4	5 n=4	6 n=5	7 n=7	8 n=2
MgO	6.95	7.3	7.31	7.00	7.00	7.00	7.00	7.00
K_2O	.52	.46	.54	.54	.55	.55	.52	.55
Rb	15	--	10	10.1	14.4	--	11.0	9.1
Cs	--	--	* .15	.15	.19	--	--	.10
Sr	--	445	420	423	360	--	386	370
Ba	185	150	135	136	146	114	136	128
Sc	33	30	31	31.2	32.1	30	32.3	--
V	--	328	*320	322	315	--	--	--
Cr	290	266	300	279	200	--	182	--
Co	46	44	45	43.8	43.4	--	--	--
Ni	--	110	120	101	56	--	--	--
Cu	--	--	140	141	65	--	--	--
Mo	--	--	* 1	1.0	4.3	--	--	--
Zn	--	--	105	105	130	--	--	--
Ga	--	--	* 21	21.2	18.6	--	22.5	--
Zr	--	200	180	181	202	--	158	--
Hf	--	4.5	4.3	4.3	4.2	--	4.5	--
Nb	--	--	19	19.2	7.9	--	--	--
Ta	1.1	1.3	* 1.1	1.1	1.1	--	--	--
Y	--	--	* 27	27.2	18.5	--	25	--
Th	--	1.0	1.0	1.0	1.5	--	1.3	--
U	--	.3	* .4	.40	.44	--	--	--
Pb	--	--	--	--	2.1	--	[a]6	--
Sb	--	--	* .17	.17	.18	--	--	--
La	15.0	15.0	* 17	17.1	15.4	16.6	14.9	--
Ce	37	39.0	39	39.3	39.9	39.2	37.2	--
Nd	24	25.5	24	24.2	24.2	23.3	--	--
Sm	6.2	6.37	6.1	6.15	5.51	6.2	6.12	--
Eu	2.10	2.05	2.0	2.02	1.99	2.13	1.99	--
Gd	--	--	6.0	6.05	8.08	--	--	--
Tb	.9	.91	* 1.0	1.01	.74	.93	.95	--
Dy	--	5.2	* 5	5.0	5.1	5.2	5.6	--
Tm	--	--	* .3	.30	.55	--	--	--
Yb	2.08	1.97	1.9	1.92	1.93	2.03	2.04	--
Lu	.30	.28	--	--	.24	.29	.30	--

1 Frey (1980, table 1).
2 Budahn and Schmitt (1985, table 1).
3 Govindaraju (1984, appendix 1; * denotes proposed value only).
4 Values in (3) adjusted to 7.00 weight percent MgO.
5 This paper (1959 and 1967-68 eruptions).
6 Budahn and Schmitt (1985, table 2; 1924, 1952, 1954, 1961, 1967 eruptions).
7 Basaltic Volcanism Study Project (1981, tables 1.2.6.2. and 1.2.6.3; 1921, 1924, 1954, 1959, 1971, and 1974 eruptions).
8 Hoffman and others (1984, table 2; 1968 eruption).
[a]Value seems high; Tatsumoto (1978) reports isotope-dilution values of 1.32-2.03 ppm for Kilauea historical eruptions.

TABLE 24.5.—*Interlaboratory comparison of analyses of samples of Mauna Loa lava*

[MgO and K_2O reported in weight percent; other values all ppm. R, Rhodes (1983), average of n samples; BSVP, Basaltic Volcanism Study Project (1981); BS, Budahn and Schmitt (1985); T, this paper; --, not given in publication or not analyzed. For some comparisons, the same sample was analyzed, for others, different samples of the same eruption]

	Prehistoric						1859			1868		
	BS (TLW 67-29)	T	BS (TLW 67-70B)	T	BS (TLW 67-119)	T	R (n=6)	BSVP (HAW-4)	T (DPH-77)	R (n=8)	BSVP (HAW-5)	T (1868ML)
MgO	6.3	6.99	7.4	6.93	6.6	6.74	8.68	7.25	7.75	17.69	21.02	23.64
K_2O	.40	.42	.43	.46	.43	.46	.39	.42	.43	.31	.27	.26
Rb	-	16.9	21.7	-	-	-	-	6.9	-	-	4.4	9.2
Sr	349	273	361	445	383	419	324	344	461	249	213	207
Ba	85	140	91	92	120	94	-	-	147	-	70	108
Sc	28	29.4	29	30.3	29	29.3	-	29.5	28.7	-	21	20.9
V	279	311	290	297	291	293	252	-	305	200	-	202
Cr	222	224	237	248	185	183	458	350	278	1,040	1,405	1,250
Co	40	41.9	40	43.0	40	38.6	-	-	-	-	-	-
Ni	105	88	85	84	100	75	166	-	98	771	-	846
Zn	-	133	-	111	-	128	112	-	113	110	-	106
Ga	-	19.3	-	17.4	-	21.3	-	20	15.6	-	14	8.4
Zr	95	179	95	148	115	141	129	129	181	101	88	142
Hf	3.6	3.3	3.6	3.6	3.4	3.0	-	3.48	3.3	-	2.38	2.0
Nb	-	3.0	-	6.1	-	-	9.9	9	2.2	7.8	6	2.2
Ta	.6	.38	.7	.35	.7	.53	-	-	-	-	-	-
Y	-	19.2	-	19.6	-	17.1	-	23	19.6	-	15	8.5
Th	.4	.57	.4	.9	.45	.78	-	.56	.7	-	.34	.9
U	.1	.22	.1	.23	.1	.23	-		.192	-	-	-
Pb	-	1.0	-	2.4	-	2.0	-	<1	2.0	-	4	3.0
La	9.8	9.4	10.9	10.4	10.6	10.3	-	9.38	8.8	-	6.16	5.68
Ce	26.1	25.9	28.7	28.7	26.8	24.8	-	25.0	25.9	-	16.4	12.5
Nd	20	19.5	21	18.0	20	17.0	-	-	-	-	-	-
Sm	4.88	4.57	5.41	5.10	5.20	4.42	-	4.80	4.77	-	3.30	2.67
Eu	1.78	1.63	1.85	1.83	1.79	1.52	-	1.70	1.72	-	1.10	.99
Tb	.77	1.42	.80	.72	.79	1.91	-	.81	.24	-	.54	.38
Dy	4.8	5.0	5.0	5.2	4.7	4.6	-	-	-	-	-	-
Yb	1.99	1.92	1.99	1.88	2.00	2.03	-	2.00	1.75	-	-	-
Lu	.23	.23	.25	.26	.27	.29	-	.29	.25	-	.20	.15

	1887				1899		1907		1919	
	R (n=12)	BVSP HAW-6	BS (TLW 67-59)	T	R (n=5)	BS (TLW 67-65)	R (n=10)	BS (TLW 67-56)	BS (TLW 67-77)	T H-34
MgO	8.16	8.53	7.1	7.50	7.28	7.5	7.38	7.3	7.3	7.09
K_2O	.33	.33	.30	.33	.35	.35	.36	.37	0.36	0.35
Rb	-	4.9	-	-	-	-	-	-	-	6.0
Sr	281	273	294	350	299	280	305	250	305	235
Ba	-	75	65	134	-	60	-	50	80	116
Sc	-	29.5	28	30.3	-	29	-	30	29	29.6
V	248	-	261	335	263	282	258	282	280	362
Cr	378	480	285	260	310	235	300	260	240	237
Co	-	-	44	46.2	-	43	-	43	42	42.8
Ni	144	-	75	83	100	75	119	125	100	90
Zn	112	-	-	119	117	-	111	-	-	-
Ga	-	20	-	16.6	-	-	-	-	-	20.7
Zr	121	119	120	74	131	160	131	150	120	146
Hf	-	3.34	2.9	3.0	-	3.6	-	3.3	3.6	3.2
Nb	8.7	8	-	3.9	9.3	-	9.1	-	-	-
Ta	-	-	.55	.30	-	.6	-	.5	.5	.5
Y	-	23	-	21.2	-	-	-	-	-	23.9
Th	-	.50	.35	.84	-	.3	-	.4	.6	1.0
U	-	-	< .1	.148	-	.1	-	.2	.2	.286
Pb	-	6	-	2.3	-	-	-	-	-	-
La	-	7.58	8.0	7.8	-	8.5	-	8.6	8.8	8.6
Ce	-	21.0	22.1	21.4	-	23.6	-	23.5	23.4	18.8
Nd	-	-	17	16.2	-	19	-	19	20	16.0
Sm	-	4.40	4.60	-		4.87	-	4.85	4.79	4.20
Eu	-	1.60	1.64	1.51	-	1.75	-	1.75	1.70	1.45
Tb	-	.84	.74	.67	-	.74	-	.79	.76	.55
Dy	-	-	4.6	5.0	-	4.0	-	4.4	4.6	4.34
Yb	-	1.98	1.92	2.02	-	1.99	-	2.03	2.00	2.00
Lu	-	.29	.25	.28	-	.25	-	.28	.25	.26

TABLE 24.5.—*Interlaboratory comparison of analyses of samples of Mauna Loa lava*—Continued

	1926			1935		1942				1950				
	R	BSVP	T	R	BS	R	BS	T	BS	R	BSVP	BS	T	T
	(n=6)	HAW-8	TLW67-67	(n=6)	TLW67-67	(n=8)	TLW67-62	TLW67-62 (NE rift)	TLW67-68 (Summit)	(n=12)	(HAW-10)	(TLW67-73)		(TLW67-79)
MgO	7.39	7.90	7.82	6.99	7.1	7.10	8.8	7.21	7.1	8.17	8.99	7.0	6.87	9.22
K_2O	.37	.37	.35	.37	.37	.37	.38	.36	.32	.38	.35	.41	.37	.36
Rb	-	5.4	-	-	-	-	-	22.9	-	-	5.2	-	-	5.7
Sr	312	302	374	316	260	313	330	483	350	306	294	285	240	177
Ba	-	82	110	-	70	-	60	241	70	-	72	100	143	58
Sc	-	30.4	30.3	-	29	-	30	30.9	29	-	29.0	29.0	31.0	28.6
V	264	-	317	268	283	265	278	309	282	287	-	282	337	311
Cr	301	390	277	275	250	291	300	270	260	369	490	220	202	395
Co	-	-	47.1	-	42	-	43	45.0	43	-	-	43	44.9	49.7
Ni	112	-	145	86	90	91	75	76	85	170	-	105	82	131
Zn	117	-	104	117	-	116	-	135	-	114	-	-	114	126
Ga	-	20	19.0	-	-	-	-	20.4	-	-	19	-	20.4	18.2
Zr	134	123	185	133	120	132	200	169	-	132	121	150	174	174
Hf	-	3.45	3.0	-	3.3	-	3.6	3.3	3.3	-	3.43	3.3	2.8	2.8
Nb	9.5	8	4.5	9.4	-	9.6	-	-	-	9.6	8	-	5.4	5.4
Ta	-	-	-	-	.6	-	.6	.27	.6	-	-	.5	.40	-
Y	-	23	21	-	-		-	16.0	-	-	23	-	20.40	18.8
Th	-	.58	.59	-	.4	-	.3	1.0	.4	-	.55	.4	.60	.70
U	-	-	-	-	.1	-	.2	.160	.2	-	-	.2	.177	.194
Pb	-	3	3.1	-	-	-	-	-	-	-	5	-	3.1	2.8
La	-	8.81	8.8	-	8.8	-	8.8	8.86	8.8	-	8.52	8.9	9.00	7.5
Ce	-	23.3	23.4	-	24.5	-	24.6	22.9	23.2	-	22.5	23.8	23.3	18.8
Nd	-	-	-	-	17	-	19	16.3	19	-	-	19	16.8	16.2
Sm	-	4.97	4.44	-	4.85	-	4.86	4.53	4.88	-	4.85	5.00	4.36	3.97
Eu	-	1.61	1.61	-	1.71	-	1.73	1.57	1.68	-	1.55	1.75	1.67	1.26
Tb	-	.80	-	-	.71	-	.74	.90	.75	-	.86	.75	.56	.58
Dy	-	-	-	-	4.3	-	5.4	5.15	4.4	-		4.6	5.9	4.7
Yb	-	2.07	1.88	-	1.83	-	1.96	1.89	1.97	-	2.00	2.08	2.01	1.94
Lu	-	.30	.28	-	.27	-	.27	.25	.28	-	.29	.31	.29	.24

TABLE 24.6.—*Interlaboratory comparison of selected elements in analyses of lava samples from Kilauea Iki and Kapoho*

[MgO and K_2O reported in weight percent; other values all ppm. Gunn (1971, table I), average of n samples; BVSP, Basaltic Volcanism Study Project (1981); T, this paper. --, not given or not analyzed]

	Kilauea Iki									Kapoho	
	Iki-22, 11/18/59			Iki-42, 11/16/59		Iki-5, 11/21/59		Iki-12, 12/4/59		KP-25, 2/13/60	
	G (KI0022) (n=2)	BSVP (HAW-23)	T (S-5)	G (KI0053) (n=2)	T (S-3)	G (KI0051) (n=3)	T (S-8)	G (KI0016)	T (S-14)	BSVP (HAW-26)	T (F-17)
MgO	19.30	18.90	19.55	8.21	8.85	9.54	10.45	8.68	8.55	13.62	13.16
K_2O	.38	.38	.35	.54	.50	.51	.54	.55	.53	.49	.49
Sr	246	270	290	340	394	330	262	357	253	310	404
Ba	130	115	75	175	126	169	198	178	174	135	230
Sc	--	25.0	24.4	--	31.2	--	28.1	--	29.5	27.1	27.3
Cr	1,150	1,550	1,170	373	407	497	369	386	256	710	440
Co	95.4	--	85.1	56.7	50.8	61.4	56.6	59.6	49.8	--	65.5
Ni	812	--	542	126	168	211	170	190	149	--	269
Zn	99	--	116	102	123	100	127	105	120	--	--
Ga	11.8	--	9.3	17.4	16.9	16.2	14.6	18.9	19.6	--	15.6
Zr	--	118	145	--	--	--	--	--	--	159	158
Hf	--	3.15	3.0	--	--	--	--	--	--	4.62	3.8
Y	17.4	17	10.1	24.5	15.6	23.2	13.9	24.3	18.0	23	13.5
La	--	11.5	11.1	--	15.0	--	15.1	--	14.7	14.9	15.2
Ce	--	27.6	24.1	--	31.8	--	41.5	--	42.0	36	35.8
Sm	--	4.50	3.78	--	5.10	--	5.11	--	5.23	5.80	--
Eu	--	1.39	1.34	--	2.01	--	1.88	--	1.83	1.92	--
Yb	--	1.40	1.36	--	1.84	--	1.83	--	2.07	1.95	2.05
Lu	--	.21	.17	--	.22	--	.35	--	.21	.28	.31

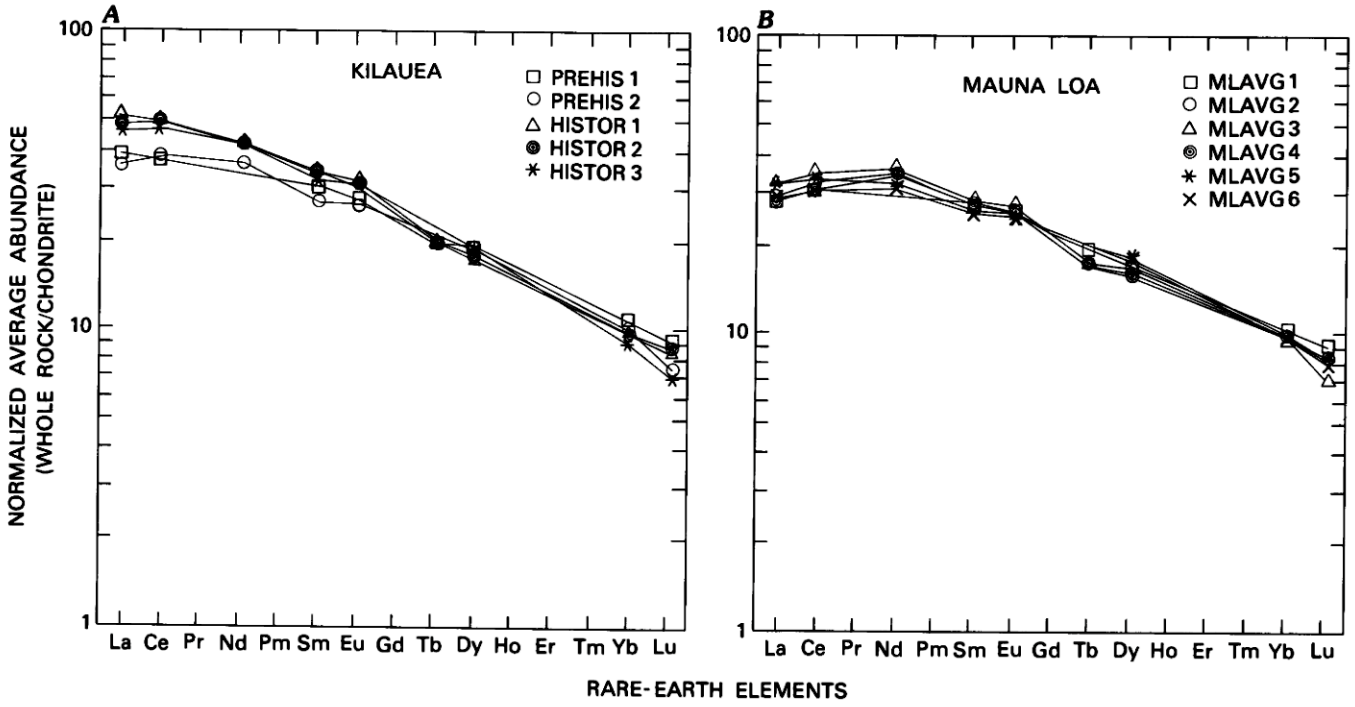

FIGURE 24.2.—Interlaboratory comparisons of MgO-adjusted average chondrite-normalized REE abundances. Patterns for data from this paper in this and subsequent figures reflect the systematic, slightly lower determination of Sm abundance in our INAA procedure relative to reported values for Hawaiian tholeiite (see table 24.4). ***A***, Kilauea samples. Prehistoric lava: PREHIS1, Budahn and Schmitt (1985); PREHIS2, this paper. Historical lava: HISTOR1, Budahn and Schmitt (1985); HISTOR2, Leeman and others (1980); HISTOR3, this paper. ***B***, Mauna Loa samples. Prehistoric lava: MLAVG3, Budahn and Schmitt, 1985; MLAVG5, this paper. Prehistoric and historical combined: MLAVG2, Leeman and others, 1980. Historical lava: MLAVG1, Basaltic Volcanism Study Project, 1981; MLAVG4, Budahn and Schmitt, 1985; MLAVG6, this paper.

spectrographic determinations (V, Ni, Mo, Zn, Ga, Y, and Pb.) In any case, systematic relative differences in the variations of some of these elements clearly reflect olivine control and suggest that their more precise determination by quantitative methods might prove to be important in subsequent studies.

Uranium concentrations we report were determined by a modification of a fission-track spark-counting technique (FTSC) first published by Cross and Tommasino (1970). Because this particular FTSC procedure has not been described previously, it is outlined in detail here. The method involves the etching of fission tracks recorded in a thin plastic detector until they become holes, which are then counted rapidly by sparking across them. A thin aluminum film is used as one of the electrodes and is destroyed behind each hole as the spark passes through, thus preventing multiple sparking through the same hole.

The specific FTSC procedure used in this study was adapted from that of Bertine and others (1970). Pellets of 0.25-inch diameter are prepared from cellulose powder (ion-exchange grade) in a pellet press. About 50 mg of sample powder is then pressed onto the top of the pellet at 34.5 MPa (5,000 psi); duplicate pellets are prepared for each sample. Standards are prepared from Dowex 1×8 anion-exchange resin that has been loaded with uranium from a $7N$ HNO_3 solution and calibrated against USGS standard basalt BCR–1 using the delayed neutron counting technique (Millard and Keaten, 1982). Double-sided adhesive tape is affixed to the top of a cellulose pellet and the resin sprinkled on top, creating a monolayer of resin beads. Pieces of 2.5×7.6 cm (1×3 in) of Lexan foil (Kimfoil, 10 μm thick) are pressed against the top of each standard and sample pellet, and this assembly is irradiated with a neutron dose of 1×10^{14} n/cm^2. This dose yields about 500 holes/ppm U and keeps the density of the holes below the upper limit for counting of 3,000 holes/cm^2. Following irradiation, the foils are etched for 30 minutes at 70 °C with $7N$ NaOH to produce holes of 2μm to 3μm diameter and then placed in the spark-counting apparatus.

The counting apparatus consists of a brass upper electrode 1 cm in diameter, an aluminum-coated Mylar lower electrode, a high voltage supply, an amplifier, and a scaler. The electrical circuit contains appropriate capacitors and resistors to shape the pulses from the sparks and to provide time for recovery after each spark. A presparking is performed at 800 V to enlarge the holes to 8 μm diameter, and then the foil is moved and the actual counting performed at 500 V. The counting is completed in less than a minute and can be repeated by simply moving to a new place on the Mylar. The accuracy and precision of the technique are shown in table 24.7 and discussed below.

The results obtained by the FTSC method proved to be considerably better than our INAA determinations for uranium. The accuracy and precision of the technique are good (table 24.7);

TABLE 24.7.—*Accuracy and precision of fission-track spark counting determination of uranium in replicates of USGS standard rocks and the Hinsdale Formation basalt*

Sample	Uranium content by fission-track spark counting			Published values (ppm)		
	Replicate analyses (ppm)	Mean (ppm)	Coefficient of variation (percent of mean)	Gladney and others (1983)	Abbey (1983)	Others
PCC-1	0.0038 .0054 .0030 .0019 .0035	0.0035	37	0.0045±0.0007	--	--
DTS-1	.0053 .0043 .0043 .0023 .0042	.0041	27	.0036±0.0005	--	--
BHVO-1	.45 .46 .50 .53	.49	8	--	--	[1].42±0.06
Basalt of Hinsdale Formation	.93 .95 .76 .69	.83	16	--	--	[2].88
BCR-1	1.66 1.76 1.76 1.68	1.72	3	1.72±0.6	1.71	1.7
GSP-1	2.42 2.45 2.20 2.34	2.35	5	2.2±0.3	2.1	--

[1]Gladney and Goode (1981).
[2]Isotope-dilution mass spectrometry (Doe and others, 1969).

the relative precision at the average level of concentration in the samples analyzed (about 0.2 ppm) should be about 10 percent or better. The mean relative difference between duplicate determinations of uranium in basalt samples of this study is 6.4 percent.

Conservative estimates of the analytical uncertainties for the concentrations of the elements analyzed in this study are given in table 24.8. The analytical data for the lava suites studied are given in tables 24.9–24.12 and 24.15–24.19 and plotted in magnesia-variation diagrams (figs. 24.4, 24.5, 24.10). Unless noted otherwise, all major-element data (water-free basis) for Kilauea and Mauna Loa lava appearing in tables and plots in this paper are from Wright (1971) or Wright and Fiske (1971), who also summarize other pertinent information on the samples studied. Our data set covers Kilauea eruptions through the 1967–68 activity at Halemaumau, and Mauna Loa eruptions through the 1950 eruption on its southwest rift zone.

TABLE 24.8.—*Estimated uncertainties of the trace-element determinations for Hawaiian basalt samples*

[Analytical methods: INAA, instrumental neutron-activation analysis; ES, emission spectrography; FTSC, fission-track spard counting. Uncertainties for INAA values based on counting statistics only. n.d., not determined]

Element	Uncertainty (percent of determined value)		
	Range	Mean	Analytical method
Rb	10-30	22	
Cs	10-30	20	INAA
Sr	10-30	15	
Ba	10-30	16	
Sc	1-5	3	INAA
V		10-15?	ES
Cr	10-25	15	INAA
Co	1-3	2	INAA
Ni			
Cu			
Mo		10-15	ES
Zn			
Ga			
Zr	1-10	3	INAA
Hf	1-10	3	INAA
Nb		10-15?	ES
Ta	1-15	6	INAA
Y		10-15?	ES
Th	5-30	9	INAA
U		≤10	FTSC
Pb		10-15?	ES
Sb	10-50	28	INAA
La	1-5	3	
Ce	1-10	4	
Nd	1-15	7	
Sm	1-5	2	
Eu	1-15	4	
Gd	5-20	11	INAA
Tb	n.d.	n.d.	
Dy	1-10	3	
Tm	n.d.	n.d.	
Yb	1-10	4	
Lu	1-10	5	

KILAUEA LAVA

Trace-element determinations for Kilauea lava samples are given in tables 24.9–24.12. Most elements listed are conservatively judged to be of good accuracy and precision, but a few determinations of adequate accuracy but poorer precision (for example, Cs and Ba) are also included.

To facilitate the comparison of differences between various olivine-controlled lava suites, we utilize average compositions computed after the individual analyses are adjusted to 7.00 weight percent MgO (see appendix 24.1) to eliminate the elemental differences stemming from variation in olivine content only (fig. 24.3). In the computation of these average MgO-adjusted compositions, we omit all differentiated samples (<6.8 weight percent MgO), even though Wright (1971) and Wright and Fiske (1971) included a few whose compositions fall within the range of summit (that is, olivine-controlled) lava.

The relatively large scatter in data points in some of the MgO-variation diagrams reflects both analytical uncertainty and compositional differences not accounted for by olivine control alone. As will be seen, these compositional differences appear to vary with space and, especially, time. One of the best examples of olivine-controlled lava is afforded by the tholeiite erupted during the November–December 1959 eruption of Kilauea Iki, which, however, is not typical of Kilauea summit eruptions (see Wright, 1973). Data for the Kilauea Iki lava will be treated separately and contrasted with those of the differentiated and hybrid lavas of the January–February 1960 eruption (fig. 24.5; table 24.12).

VARIATION IN SPACE

Within analytical uncertainty, the MgO-adjusted mean trace-element compositions of the olivine-controlled lava of Kilauea's summit (SUM) and its southwest rift zone (SWRZ) are similar (table 24.13), consistent with earlier observations based on major-element data (Wright, 1971). The apparent low adjusted means for Ni and Cr for lava of Kilauea's east rift zone (ERZ), relative to those of the SUM and SWRZ (table 24.13), are inconsistent with the raw data (fig. 24.4) and reflect the unsatisfactory MgO adjustment for these two elements discussed in appendix 24.1. However, if Ni and Cr are not considered, the mean composition of the ERZ lava is characterized by generally higher abundances of olivine-incompatible elements relative to those of summit lava. Differences between many of the means are small and, strictly speaking, not statistically significant, but we are impressed by their nonrandom nature (fig. 24.6).

Because these nonrandom, subtle differences are within analytical uncertainty, it is appropriate to ask whether they might have been introduced by nonrandom grouping of samples preparatory to the five separate irradiations required to analyze the 75 samples. However, in almost all cases, samples belonging to each lava grouping—whether according to space (vent location) or to time (prehistoric, 18th–19th centuries, 20th century)—were spread over two or more irradiations, and only rarely did one irradiation contain appreciably more than half of the samples from one category

TABLE 24.9.—*Composition of olivine-controlled tholeiite of Kilauea's summit.*

[Oxide values (in weight percent) from Wright (1971, table 4), recast to 100 percent dry weight; values for elements in parts per million]

	Prehistoric						Historical					
	Hilina Basalt			Puna Basalt			18th–19th centuries		20th century			
									1959		1967–68 eruption	
Sample	57F-15	57F-17	57F-97	8X078-0	8X067-0	8X002-0	1790	1866(?)	S-1	S-2	1967HM	HM68-15
SiO_2	48.53	49.43	50.79	48.07	49.19	51.17	50.64	50.05	50.04	50.05	50.40	50.30
MgO	15.17	10.97	8.14	17.06	13.26	6.95	8.31	6.61	8.10	7.23	7.61	7.64
K_2O	.33	.38	.38	.31	.30	.46	.45	.50	.55	.60	.54	.55
TiO_2	1.91	2.21	2.51	1.98	2.00	2.44	2.64	2.70	2.63	2.75	2.66	2.62
P_2O_5	.18	.22	.24	.18	.17	.24	.25	.26	.25	.28	.26	.26
Cs	.15	.00	.16	.19	.30	.03	.12	.76	.21	.22	.00	.14
Ba	161.00	77.00	72.00	79.00	129.00	43.00	65.00	150.00	158.00	164.00	159.00	94.00
Sc	26.80	29.90	29.40	25.40	28.50	29.10	28.90	31.20	31.60	30.40	32.60	31.60
V	.00	254.00	.00	205.00	278.00	287.00	282.00	308.00	296.00	300.00	318.00	327.00
Cr	707.00	485.00	299.00	889.00	819.00	357.00	291.00	195.00	251.00	148.00	295.00	283.00
Co	75.20	61.40	45.60	79.70	65.70	41.80	47.90	43.40	45.00	44.70	46.70	46.70
Ni	.00	131.00	.00	490.00	278.00	90.00	121.00	72.00	104.00	80.00	89.00	106.00
Mo	.00	4.00	.00	4.20	6.00	4.50	3.30	3.90	4.90	4.10	3.60	4.10
Zn	.00	124.00	.00	131.00	122.00	125.00	129.00	133.00	143.00	137.00	107.00	128.00
Ga	.00	13.10	.00	10.80	13.80	17.40	18.80	17.60	16.00	18.20	19.10	19.90
Hf	2.90	3.40	3.40	3.10	3.10	3.20	3.50	4.20	3.70	4.20	4.30	4.20
Y	.00	15.40	.00	11.50	14.10	17.00	17.70	19.70	16.40	19.10	17.80	19.50
U	.41	.71	.52	.21	.33	.17	.34	.47	.48	.51	.37	.35
Pb	.00	1.20	.00	1.70	1.60	2.00	2.10	1.60	1.10	1.40	2.50	3.50
La	9.60	9.90	10.60	9.00	8.90	8.40	11.40	13.20	14.70	16.10	15.20	14.60
Ce	26.70	26.90	30.30	21.60	21.40	18.50	29.20	38.20	44.00	42.10	34.90	35.70
Nd	18.00	17.60	17.50	14.50	15.20	16.00	21.50	22.70	24.50	25.60	21.60	23.30
Sm	3.86	4.35	4.28	4.04	3.98	4.10	5.25	5.50	4.71	5.65	5.73	5.60
Eu	1.41	1.66	1.79	1.63	1.54	1.68	1.71	2.00	1.88	1.94	2.05	1.99
Dy	.00	3.60	6.00	4.60	3.90	4.30	.00	5.40	4.50	5.30	4.00	6.20
Yb	1.55	1.92	1.98	1.77	1.82	1.93	2.02	1.86	1.89	1.97	1.66	2.08
Lu	.34	.21	.29	.23	.20	.27	.27	.26	.19	.26	.28	.25

(table 24.2). Therefore, we believe that the observed minor but systematic differences (table 24.13; fig 24.6) cannot be ascribed to nonrandom sample groupings during irradiations. Such small intravolcano systematic differences between eruption loci on the volcano have not been observed or considered in previous studies (for example, Leeman and others, 1980; Budahn and Schmitt, 1985), which were based on more limited sampling and emphasized the larger intervolcano variations between Kilauea and Mauna Loa.

The relatively higher content of olivine-incompatible elements in the ERZ lava is even better illustrated by reference to the SWRZ samples (fig. 24.6) and by REE patterns (fig. 24.7*A*). The sole exception is the ratio for uranium, which is less than unity, offset from the range of other ratios, and yet varies sympathetically with them. The apparent departure in the behavior of uranium relative to other olivine-incompatible elements is not understood. Analytical bias probably is not the explanation, because the uranium appears to be as accurately determined as the other elements (see tables 24.3, 24.4, 24.7). The explanation may be related in part to unrepresentative sampling of ERZ lava, thus resulting in a biased mean. The mean computed for the ERZ is based only on data for older (prehistoric and 18th–19th centuries) lavas, which are low in uranium compared to 20th century lava (tables 24.10; fig. 24.4).

Major-element studies have shown that differentiated lava is more prevalent in the ERZ than elsewhere at Kilauea (Wright, 1971; Wright and Fiske, 1971; Moore, 1983). Our trace-element data also indicate that the olivine-controlled lava of the ERZ is more fractionated, as compared to the olivine-controlled lava of the SUM and, especially, the SWRZ. Even though eruptions in the ERZ and the SWRZ are fed from a common shallow (2–6 km deep) reservoir beneath Kilauea summit, these two rift zones intrinsically differ in topographic expression, structural setting, and eruption frequency during the past 2,000 years (see, for example, Swanson and others, 1976b; Holcomb, 1980, 1981; Duffield and others, 1982; Moore, 1983). The volume of magma intruded into and erupted in the ERZ is estimated to be more than two orders of magnitude greater than that of the SWRZ. Moreover, geophysical studies have demonstrated the existence of several secondary magma reservoirs in the ERZ (see, for example, Jackson and others, 1975; Swanson and others, 1976a; Zablocki and Koyanagi, 1979; Moore, 1983). Thus, the more differentiated and hybridized compositions of the ERZ lava may simply reflect greater opportunity for magma fractionation and mixing because of the following: (1) More voluminous and frequent transfers of magma from the summit reservoir into the ERZ relative to the SWRZ; (2) longer uninter-

TABLE 24.10.—*Composition of olivine-controlled tholeiite of Kilauea's east rift zone*

[Oxide values (in weight percent) from Wright (1971, table 6) for prehistoric samples, and from Wright and Fiske (1971, table 4) for historical samples, recast to 100 percent dry weight; values for elements in parts per million. Samples TLW67-130 and TLW68-6 fit definition of differentiated (less than 6.80 weight percent MgO) and are omitted in calculation of averages and not plotted in figure 24.4]

	Prehistoric				Historical			
					18th-19th centuries			
					1790?	1840		
Sample	TLW67130	TLW67131	TLW67132	MP-57	H-23	TLW68-5	TLW68-6	TLW68-12
SiO_2	50.72	49.45	50.37	50.12	50.96	50.62	51.21	48.08
MgO	6.13	10.05	8.08	8.73	7.16	9.35	6.03	17.54
K_2O	.51	.52	.45	.41	.44	.40	.55	.33
TiO_2	2.92	2.67	2.53	2.53	2.71	2.32	3.06	1.92
P_2O_5	.28	.25	.23	.24	.25	.25	.30	.18
Cs	.26	.28	.14	.11	.19	.17	.12	.16
Ba	137.00	140.00	157.00	163.00	189.00	130.00	165.00	110.00
Sc	30.20	29.60	31.80	27.90	32.50	31.50	32.30	25.40
V	344.00	337.00	308.00	377.00	373.00	304.00	400.00	244.00
Cr	83.00	419.00	335.00	281.00	179.00	405.00	47.00	812.00
Co	43.30	55.00	50.40	47.40	48.80	55.60	49.00	82.70
Ni	57.00	196.00	112.00	146.00	99.00	167.00	62.00	512.00
Mo	4.80	4.20	4.20	4.40	5.60	4.60	5.50	3.80
Zn	158.00	145.00	128.00	141.00	135.00	145.00	161.00	124.00
Ga	22.30	21.40	20.30	25.40	22.50	21.20	24.10	15.00
Hf	3.80	3.90	3.60	3.60	4.40	3.90	5.30	3.20
Y	23.40	22.50	21.80	21.10	24.60	18.00	25.20	13.90
U	.30	.37	.34	.36	.39	.21	.35	.19
Pb	4.80	2.50	2.70	4.10	2.90	2.10	4.40	2.60
La	13.80	13.60	11.90	11.20	12.10	11.20	15.70	9.20
Ce	35.60	33.20	30.40	31.50	36.30	30.60	42.30	24.30
Nd	24.60	24.00	22.80	21.20	24.80	22.20	32.70	17.20
Sm	6.02	5.52	4.91	4.56	5.58	5.02	6.73	3.85
Eu	1.96	1.88	1.88	1.45	2.04	1.92	2.43	1.47
Dy	6.40	6.60	5.80	5.70	7.60	5.70	7.20	.00
Yb	2.19	2.03	1.94	2.21	2.15	2.14	2.79	1.57
Lu	.31	.24	.29	.21	.28	.30	.32	.19

rupted storage of summit magma in isolated secondary reservoirs or pockets, thereby allowing greater cooling and fractionation before eruption to yield more differentiated lava; and (3) increased incidence of magma mixing to produce hybrid lava by repeated filling of the secondary reservoirs by new magma, either from storage pockets uprift or from the summit reservoir.

VARIATION IN TIME

Wright (1971) showed that for olivine-controlled Kilauea lava, at any given MgO content, three time groupings (prehistoric, 18th–19th centuries, and 20th century) could be distinguished on the basis of major-element composition. Younger lava is characterized by higher K_2O, TiO_2, and P_2O_5 and by several other chemical distinctions. One of the principal objectives of our study was to try to further document such secular variation using trace elements. Leeman and others (1980, p. 802), citing unpublished, limited data for prehistoric Kilauea lava, tentatively concluded that there is "little or no difference in trace element contents with time at Kilauea, but additional analyses are required to confirm this conclusion." More recently however, Budahn and Schmitt (1985, table 2), referring to the same unpublished data as did Leeman and others (1980), presented the ranges and means of selected trace elements (REE, Sr, Ba, and Sc) for 7 Kilauea lava samples (20th century, 5; prehistoric, 2).

Budahn and Schmitt (1985, p. 71) noted that with respect to light-rare-earth-element (LREE) abundance patterns the 20th-century and prehistoric lavas were "compositionally distinct." Our more extensive data (tables 24.9–24.11 and fig. 24.4) confirm their finding and suggest that the mean contents of Sc, Co, Hf, and the LREE of lava from the 18th–19th centuries are intermediate between those for prehistoric and 20th century lavas (table 24.13; figs. 24.7*B*, 24.8). This relation is similar to progressive changes of some major elements (for example, K_2O and TiO_2) for these three time groupings (Wright, 1971).

Some historical summit eruptions of Kilauea have chemically distinct major-element compositions (Wright, 1971, fig. 12), supporting the concept of so-called magma batches, originally suggested by Powers (1955). We are aware that, in treating our trace element data in terms of means, we overlook the differences between such chemically distinct eruptions (magma batches) within the broader space or time grouping; this problem is particularly serious in dealing with the samples of prehistoric lava, for which time relations are poorly known. For example, recent work by Easton and Garcia (1980) on the Hilina Basalt, the oldest exposed rocks of Kilauea Volcano (25 ka and older), indicates considerable chemical variation. Similarly, the study of Casadevall and Dzurisin (chapter 13),

TABLE 24.11.—*Composition of olivine-controlled tholeiite of Kilauea's southwest rift zone*

[Oxide values (in weight percent) from Wright (1971, table 5), recast to 100 percent dry weight; values for elements in parts per million. Sample TLW67-12 fits definition of differentiated and is omitted in calculation of averages and not plotted in figure 24.4]

	Prehistoric						Historical				
							19th century			20th century	
							1823	1868		1920	
Sample	TLW67140	TLW67-134	KD-32	KD-32	KD-56	TLW67-28	TLW67-24	1868-SW	TLW67-12	TLW67-4	TLW67-6
SiO_2	50.23	51.17	46.59	49.07	51.13	50.16	51.01	50.62	51.40	49.75	50.26
MgO	10.03	6.81	21.98	13.30	7.32	9.12	7.29	8.61	6.79	9.21	7.49
K_2O	.40	.47	.28	.36	.40	.36	.43	.45	.50	.49	.51
TiO_2	2.34	2.48	1.52	1.98	2.42	2.22	2.43	2.39	2.80	2.55	2.66
P_2O_5	.21	.25	.15	.19	.23	.20	.22	.27	.24	.23	.25
Cs	.03	.24	.00	.20	.00	.27	.14	.00	.18	.25	.01
Ba	152.00	126.00	429.00	76.00	152.00	61.00	53.00	103.00	168.00	71.00	202.00
Sc	26.90	31.30	21.00	22.00	30.40	29.50	31.50	31.20	29.40	30.30	33.60
V	277.00	261.00	166.00	185.00	284.00	245.00	326.00	329.00	316.00	279.00	337.00
Cr	541.00	309.00	847.00	667.00	244.00	341.00	307.00	438.00	186.00	571.00	575.00
Co	50.10	40.50	88.40	69.80	42.90	51.70	45.30	47.90	39.50	51.10	50.60
Ni	191.00	97.00	787.00	510.00	91.00	186.00	111.00	182.00	106.00	178.00	150.00
Mo	3.40	3.50	4.10	3.30	3.80	3.80	4.20	4.20	4.50	4.50	4.80
Zn	123.00	157.00	110.00	110.00	128.00	134.00	119.00	108.00	131.00	146.00	140.00
Ga	20.80	17.40	9.80	14.10	22.00	17.20	20.50	20.90	24.40	19.10	24.90
Hf	2.70	3.70	2.20	2.70	3.40	3.20	3.80	3.90	4.00	4.20	4.50
Y	16.80	17.60	8.40	10.60	18.80	15.80	19.50	22.50	20.60	14.50	18.90
U	.19	.27	.19	.21	.26	.27	.33	.22	.52	.30	.51
Pb	1.00	1.00	3.00	2.90	2.40	1.20	2.70	3.00	3.80	2.00	2.50
La	10.30	12.30	6.90	8.20	10.90	10.60	11.50	10.90	12.90	13.50	14.10
Ce	24.10	29.80	20.30	21.70	33.30	27.60	31.30	31.00	34.30	35.80	36.40
Nd	19.60	21.90	12.00	13.10	19.80	16.60	20.90	18.10	22.10	21.80	23.40
Sm	4.62	5.11	2.98	3.60	4.70	4.50	5.01	5.01	5.70	5.39	5.81
Eu	1.41	1.78	1.13	1.28	1.67	1.74	1.91	1.86	1.85	1.91	2.19
Dy	5.10	6.10	3.20	3.90	5.40	5.70	6.10	4.90	6.50	5.60	5.80
Yb	2.15	2.12	1.02	1.40	1.90	1.79	2.08	2.00	2.06	1.68	1.79
Lu	.25	.28	.14	.18	.25	.26	.30	.28	.29	.24	.20

which involves the most thorough sampling of prehistoric Kilauea lava at a single locality to date, demonstrates wide variation in the composition of prehistoric lava of the Puna Basalt (2.8 ka and younger) well exposed in the northwestern wall (Uwekahuna Bluff) of Kilauea caldera.

For prehistoric Kilauea lava in our study, we note that the uranium abundance in the three samples of the Hilina Basalt analyzed (0.41–0.71 ppm) was considerably higher than that in the Puna Basalt (0.17–0.33 ppm) with no overlap (table 24.9). However, it should be noted that Easton and Garcia (1980) suggested, on the basis of sample location, that only one of the five samples (57F–15) designated by Wright (1971, table 4) as from the Hilina Series (now Hilina Basalt) truly belonged to that stratigraphic unit. In any case, sample 8X002–0 of the Puna Basalt (table 24.9) is characterized by the lowest LREE content of any of the 15 prehistoric Kilauea lava samples we analyzed. Thus, we are keenly aware of the wide internal variations within the prehistoric Kilauea and several other lava groupings, as well as the related problems in attempting to evaluate differences between mean compositions. Indeed, our reconnaissance study is intended to identify specific petrologic and geochemical topics for subsequent systematic sampling and detailed investigations.

LAVA OF THE KILAUEA IKI AND KAPOHO ERUPTIONS

The November–December 1959 summit eruption at Kilauea Iki, the related January–February 1960 lower ERZ eruption at Kapoho, and their eruptive products have been subject of many studies (for example, Helz, chapter 25, 1980; Murata and Richter, 1966a, b; Richter and Murata, 1966; Gunn, 1971; Wright, 1973; Wright and others, 1976). The Kilauea Iki lava provides one of the best documented examples of olivine control (Murata and Richter, 1966a; Gunn, 1971; Wright, 1973), whereas the Kapoho lava has been shown to include differentiated and hybrid types (Wright and Fiske, 1971). Yet, despite the abundance of petrologic and major-element data, there are few systematic trace-element data, other than the work of Gunn (1971), for the Kilauea Iki lava. For our study, we selected a suite of samples (Kilauea Iki, 10; Kapoho, 5) that spanned the duration of the eruptions and showed a wide range in MgO content (tables 24.12, 24.14; figs. 24.5, 24.9*A*). Several of the samples we studied have also been analyzed previously, but, unfortunately, the interlaboratory agreement between the results is unsatisfactory for some of the elements determined (table 24.6).

The mean composition for the Kilauea Iki lava is distinct from those for other olivine-controlled Kilauea lavas, as evidenced by its

TABLE 24.12.—*Composition of olivine-controlled tholeiite of the Kilauea Iki eruption and of differentiated and hybrid lavas of the Kapoho eruption*

[Oxide values (in weight percent) from Murata and Richter (1966a, tables 1 and 2) recast to 100 percent dry weight; values for elements in parts per million. Samples S-1 through S-9 were erupted in November, 1959; S-14 through S-25 in December, 1959; and F-1 through F-17 during January–February, 1960]

	Kilauea Iki eruption, 1959										Kapoho eruption, 1960				
Sample	S-1	S-2	S-3	S-5	S-7	S-8	S-9	S-14	S-15	S-25	F-1	F-5	F-8	F-12	F-17
SiO_2	50.04	50.05	49.67	46.74	48.28	49.31	48.46	49.51	46.88	49.53	50.57	50.79	49.96	49.39	48.88
MgO	8.10	7.23	8.86	19.55	13.69	10.49	13.35	8.56	18.89	8.87	6.56	6.09	8.28	10.59	13.16
K_2O	.55	.60	.50	.35	.45	.54	.47	.53	.36	.53	.65	.69	.60	.54	.49
TiO_2	2.63	2.75	2.55	1.80	2.27	2.54	2.30	2.62	1.86	2.67	3.11	3.37	2.92	2.69	2.43
P_2O_5	.25	.28	.26	.18	.23	.25	.23	.26	.19	.26	.35	.36	.33	.28	.26
Cs	.21	.22	.11	.11	.00	.25	.32	.00	.23	.19	.25	.19	.19	.06	.23
Ba	158.00	164.00	126.00	75.00	172.00	198.00	151.00	174.00	95.00	132.00	144.00	347.00	149.00	353.00	230.00
Sc	31.60	30.40	31.20	24.40	27.30	28.10	26.20	29.50	24.50	29.30	29.90	31.60	31.10	29.60	27.30
V	296.00	300.00	277.00	208.00	223.00	264.00	251.00	287.00	249.00	291.00	0.00	362.00	.00	301.00	254.00
Cr	251.00	148.00	407.00	1170.00	721.00	369.00	543.00	256.00	1020.00	338.00	134.00	97.00	231.00	339.00	440.00
Co	45.00	44.70	50.80	85.10	67.60	56.60	65.50	49.80	79.80	50.60	46.10	48.60	53.30	60.10	65.50
Ni	104.00	80.00	168.00	542.00	296.00	170.00	293.00	149.00	525.00	130.00	.00	82.00	.00	191.00	269.00
Mo	4.90	4.10	4.20	4.30	3.20	4.20	3.80	5.50	4.60	4.10	.00	3.90	.00	3.60	3.60
Zn	143.00	137.00	123.00	116.00	109.00	127.00	108.00	120.00	133.00	131.00	.00	122.00	.00	114.00	111.00
Ga	16.00	18.20	16.90	9.30	12.30	14.60	14.60	19.60	14.20	20.40	.00	27.60	.00	16.70	15.60
Hf	3.70	4.20	4.20	3.00	3.20	4.10	3.60	4.20	3.00	3.90	5.50	6.00	5.20	4.70	3.80
Y	16.40	19.10	15.60	10.10	9.80	13.90	12.20	18.00	15.00	15.40	.00	25.90	.00	15.40	13.50
U	.48	.51	.60	.32	.49	.34	.43	.72	.75	.45	.55	.54	.47	.40	.64
Pb	1.10	1.40	1.90	1.00	1.10	1.60	2.20	2.40	4.60	2.30	.00	3.70	.00	1.70	1.30
La	14.70	16.10	15.00	11.10	13.70	15.10	13.30	14.70	11.90	15.90	18.60	23.00	18.10	18.30	.00
Ce	44.00	42.10	31.80	24.10	30.10	41.50	36.20	42.00	24.30	31.90	45.50	51.80	49.30	45.20	.00
Nd	24.50	25.60	21.20	16.00	.00	21.80	.00	.00	15.70	22.60	.00	34.20	32.60	32.80	.00
Sm	4.71	5.65	5.10	3.78	4.65	5.11	4.79	5.23	4.02	5.22	7.05	7.27	6.87	6.10	.00
Eu	1.83	1.94	2.01	1.34	1.63	1.88	1.74	1.83	1.40	1.94	2.48	2.78	2.36	2.19	.00
Dy	4.50	5.30	5.10	4.10	5.30	7.10	4.80	4.80	4.40	5.50	7.30	7.40	5.50	7.20	5.70
Yb	1.89	1.97	1.84	1.36	1.83	1.83	1.44	2.07	1.59	1.77	2.79	2.93	2.36	1.98	2.05
Lu	.19	.26	.22	.17	.22	.35	.21	.21	.13	.26	.35	.43	.29	.38	.31

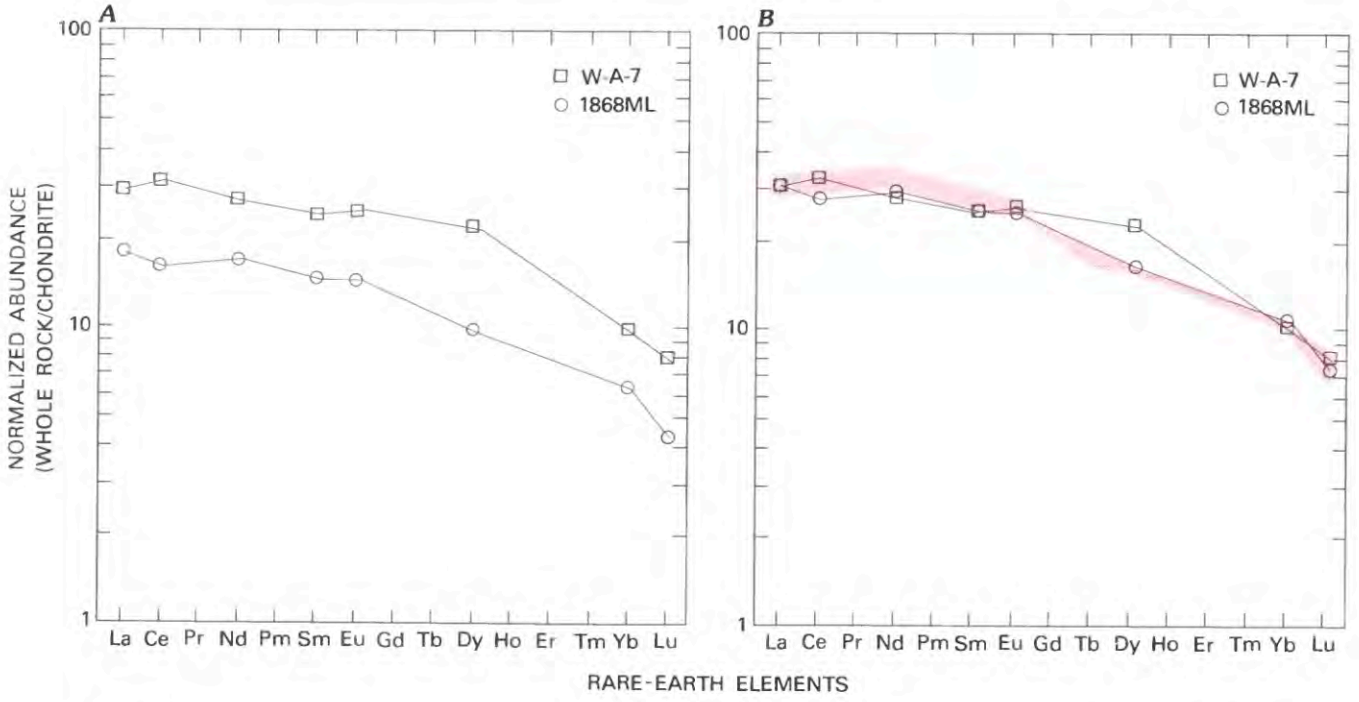

FIGURE 24.3.—Chondrite-normalized REE abundances of two samples of olivine-controlled lava of the 1868 Mauna Loa eruption plotted (***A***) from raw data (table 24.17) and (***B***) after adjustment to 7.00 weight percent MgO (see appendix 24.1), showing good convergence. Band (red) brackets the range of mean values for Mauna Loa lava plotted in figure 24.2; Dy value for sample W-A-7 and Ce value for sample 1868ML plot outside this band and may be spurious.

TABLE 24.13.—*Average compositions of spatial and temporal groups of olivine-controlled lava of Kilauea, adjusted to 7.00 weight percent MgO*

[Calculated from data in table 24.9–24.11; average for Kilauea Iki (1959) and Kapoho (1960) given in table 24.14. S.d., standard deviation. Oxide values in weight percent; values for elements in parts per million. Numbers of samples where different from numbers (n) given: summit, 7 for Cs, V, Ni, Mo, Zn, Ga, Y, Pb, and Dy (excludes Kilauea Iki eruption of 1959); east rift zone, 5 for Dy (excludes Kapoho eruption of 1960); southwest rift zone, 7 for Cs; Prehistoric, 14 for Dy, 13 for V, Ni, Mo, Zn, Ga, Y, and Pb, 12 for Cs; 18th and 19th centuries, 5 for Cs, and Dy; 20th century, 3 for Cs; historical, 8 for Cs, 9 for Dy.]

	Spatial groups						Temporal groups							
	Summit n=9		East rift zone n=6		Southwest rift zone n=10		Prehistoric n=15		18th-19th centuries n=6		20th century n=4		Historical (all) n=10	
	Mean	S.d.	Mean	S.d.	Mean	S.d.	Mean	S.d.	Mean	S.d.	Mean	S.d.	Mean	S.d.
MgO	7.00	-	7.00	-	7.00	-	7.00	-	7.00	-	7.00	-	7.00	-
K_2O	.45	.07	.46	.05	.45	.05	.43	.05	.45	.02	.54	.02	.48	.05
TiO_2	2.56	.14	2.66	.14	2.50	.12	2.51	.15	2.58	.13	2.69	.02	2.68	.08
P_2O_5	.24	.02	.26	.01	.24	.02	.24	<.02	.26	.02	.25	.01	.25	<.02
Cs	.19	.10	.19	.06	.18	.10	.20	.09	.17	.04	.14	.12	.16	.08
Ba	114	62	161	18	[1]115	51	[1]128	53	118	52	134	60	124	53
Sc	32.1	1.8	32.5	1.9	31.3	2.3	31.5	2.4	32.5	1.7	32.8	.9	32.6	1.4
V	300	26	348	33	287	42	291	48	330	28	322	20	327	24
Cr	250	90	183	78	[2]325	110	[2]251	83	214	100	368	147	276	138
Co	43.1	1.9	44.1	2.9	[8]43.1	3.1	[8]42.7	2.5	44.4	2.6	45.0	2.6	44.6	2.5
Ni	[3]63	23	[4]39	32	[5]88	32	[7]68	42	[4]65	33	45	19	73	34
Mo	4.7	1.3	4.9	.5	3.8	1.3	4.5	1.0	4.6	.8	4.4	.6	4.5	.7
Zn	127	10	140	8	119	38	132	13	129	14	131	18	130	15
Ga	17.4	2.3	22.8	2.2	20.1	3.0	19.0	3.7	21.3	1.2	21.3	2.6	21.3	1.8
Hf	3.8	.4	4.1	.3	3.7	.5	3.6	.4	4.1	.3	4.4	.1	4.2	.3
Y	17.5	1.3	22.0	2.4	16.5	5.5	17.9	3.4	20.7	2.7	18.1	1.9	19.7	2.6
U	.42	.18	.33	.98	.30	.9	.36	.16	.30	.07	.4	.09	.34	.09
Pb	2.2	.7	3.1	.7	2.5	1.2	2.4	1.2	2.8	.5	2.7	.6	2.7	.6
La	11.9	2.1	12.6	1.1	10.8	3.6	11.4	1.4	11.9	.5	14.7	.5	13.0	1.5
Ce	30.0	5.5	33.8	2.0	31.6	4.0	29.8	4.4	32.7	2.1	36.7	1.0	34.3	2.6
Nd	20.2	2.6	24.0	1.3	19.3	4.4	20.1	2.8	22.4	2.2	23.1	.8	22.7	1.7
Sm	5.05	.59	5.34	.42	5.06	.46	4.87	.45	5.32	.19	5.78	.09	5.50	.28
Eu	1.90	.17	1.93	.21	1.83	.21	1.79	.19	1.96	.11	2.08	.09	2.01	.11
Dy	5.1	1.1	6.6	.8	5.6	.5	5.5	.9	6.2	1.0	5.6	1.0	5.9	1.0
Yb	2.06	.19	2.18	.11	1.94	.22	2.05	.22	2.15	.07	1.85	.18	2.03	.19
Lu	[6].27	.03	.27	.04	.26	.03	[6].26	.03	.29	.02	.24	.03	.27	.03

[1]Anomalously high adjusted value (702 ppm) for sample KD-32 omitted.
[2]Adjusted value for sample HD-32 is negative and omitted from average (see appendix 24.1).
[3]Three negative adjusted values (samples 57F-17, 8X078-0, and 8X067-0) omitted (see appendix 24.1).
[4]Negative adjusted value for sample TLW68-12 omitted.
[5]Two negative adjusted values (samples TLW67-140 and KD-32) omitted.
[6]Anomalously high adjusted value (0.43 ppm) for sample 57F-15 omitted.
[7]Five negative adjusted values (samples 57F-17, 8X08-0, 8X067-0, TLW67-140, and KD-32) omitted.
[8]Anomalously low value (23.7 ppm) for sample KD-32 omitted.

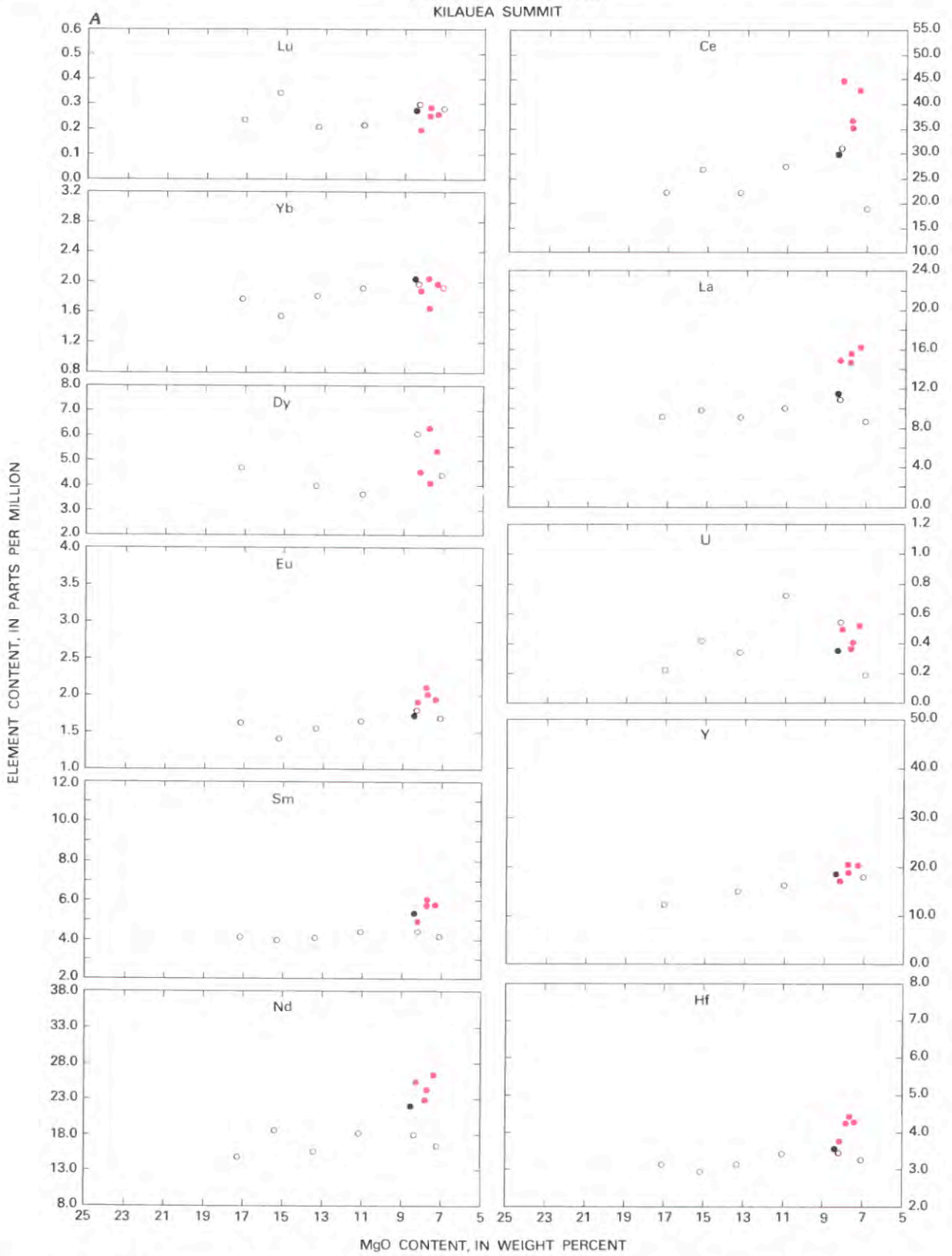

FIGURE 24.4.—MgO-variation diagrams for olivine-controlled Kilauea lava. ***A,*** Summit. ***B,*** Southwest rift zone (SWRZ). ***C,*** East rift zone (ERZ). Open symbols, prehistoric; solid black symbols, 18th–19th centuries; solid red symbols, 20th century. Data from tables 24.9–24.11; elements showing wider scatter not plotted.

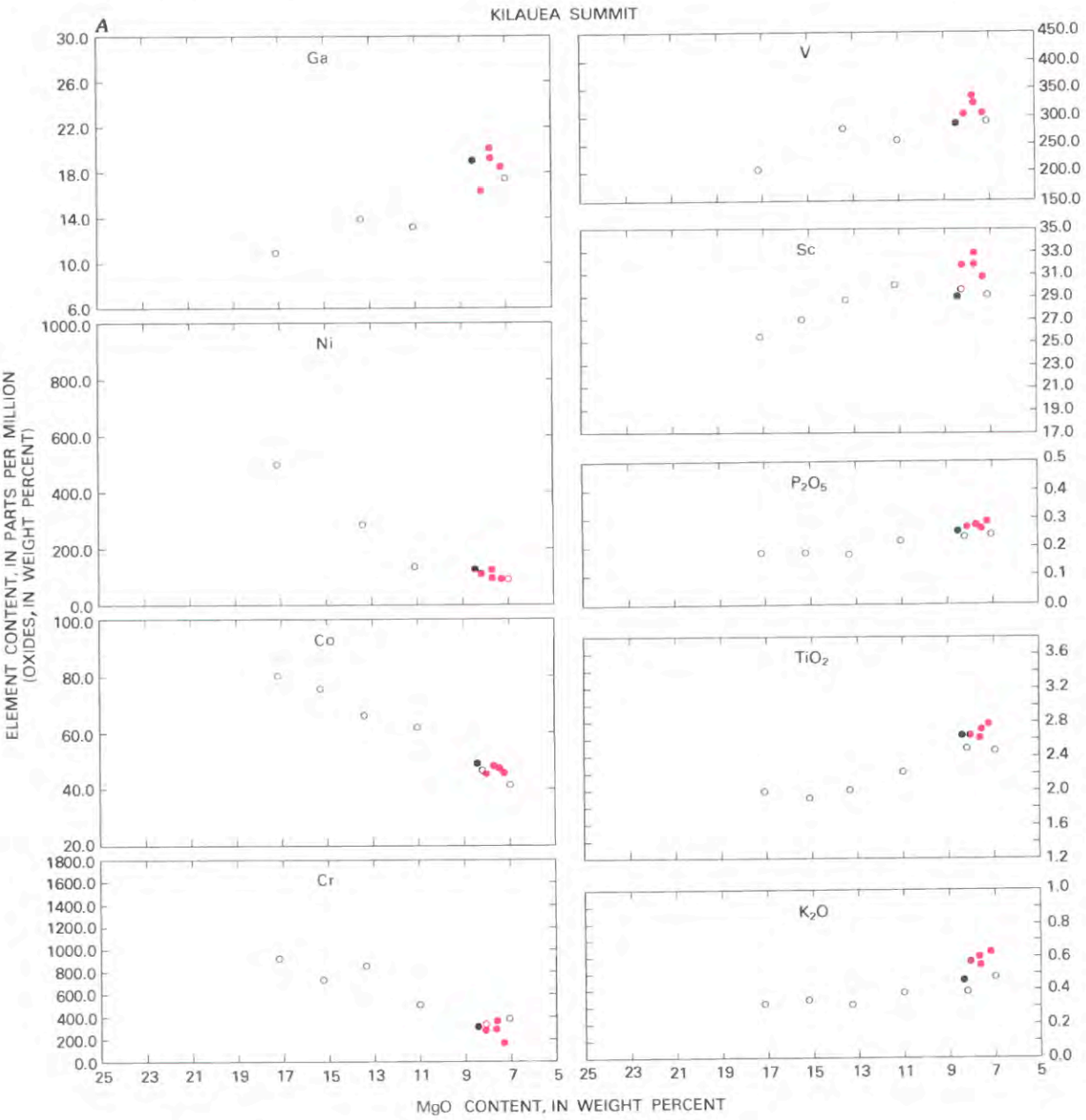

FIGURE 24.4.—Continued.

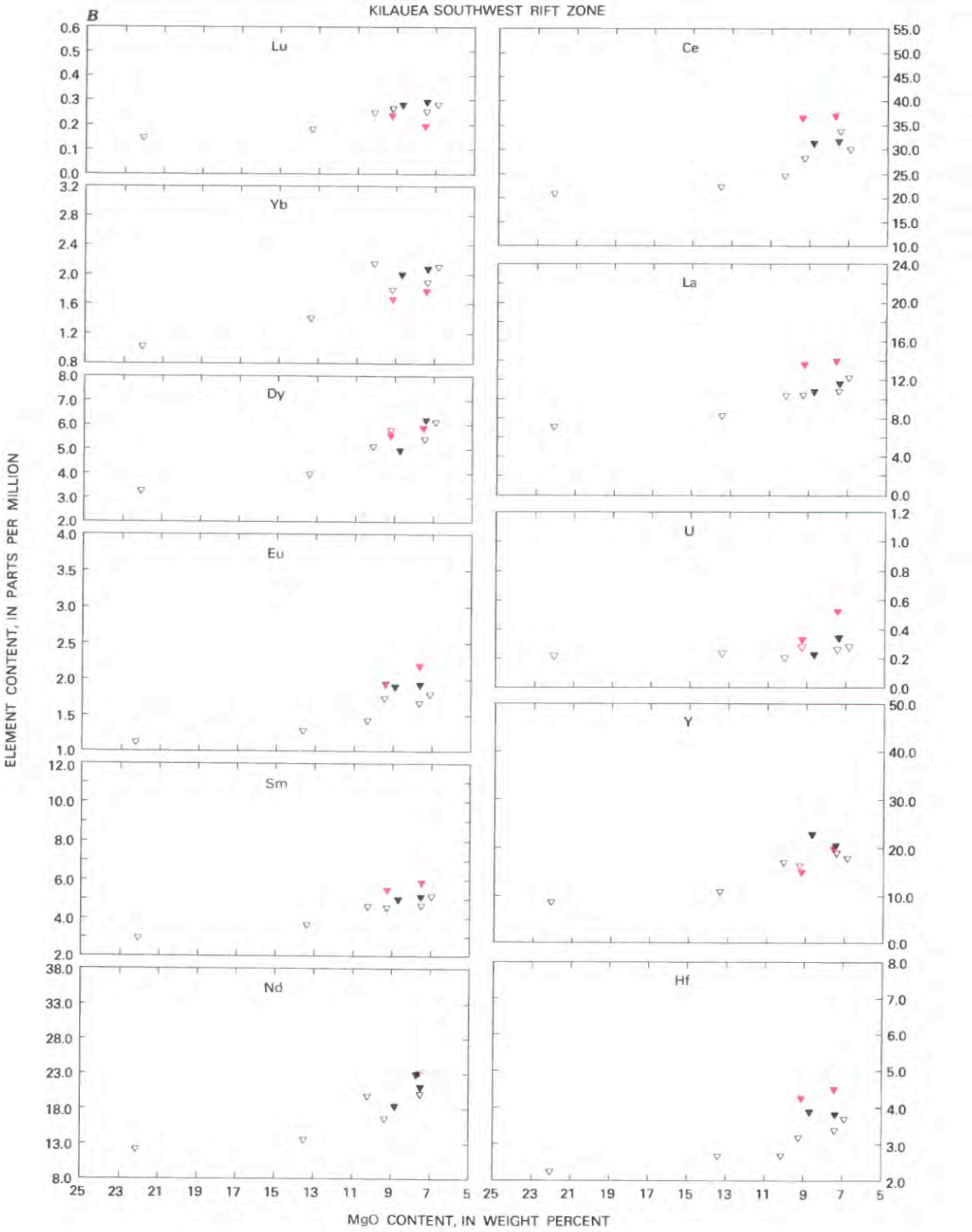

FIGURE 24.4.—Continued.

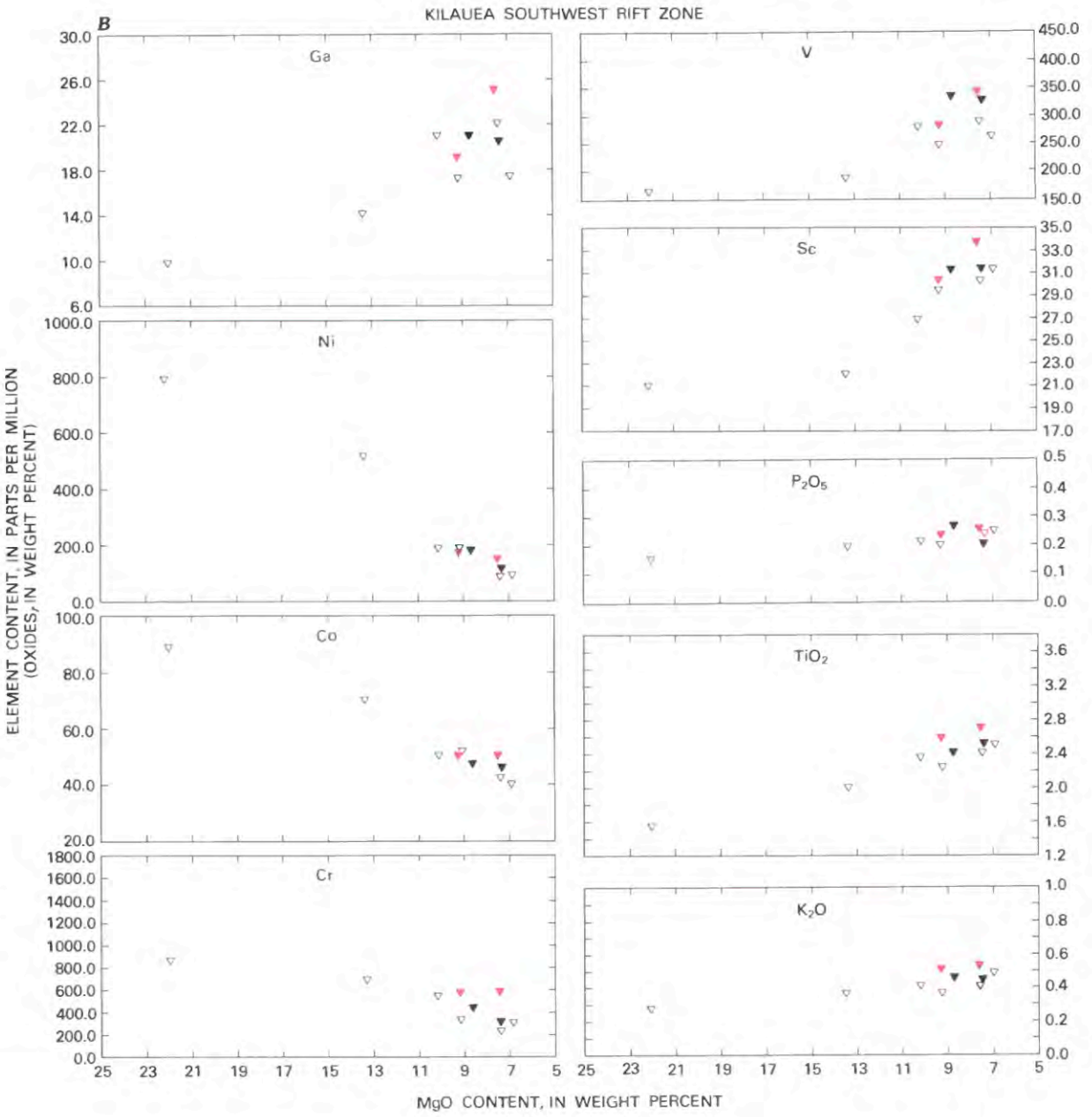

FIGURE 24.4.—Continued.

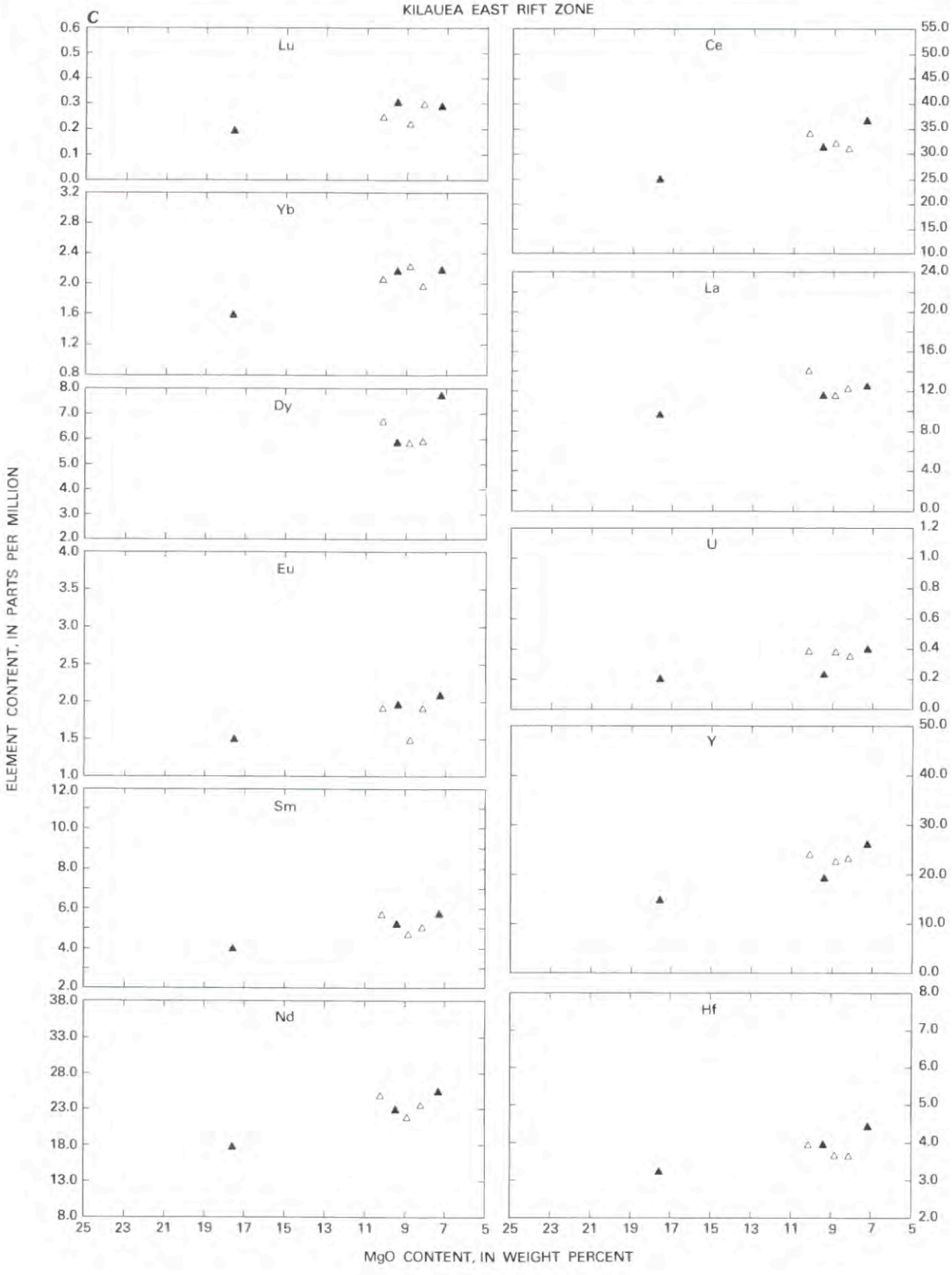

FIGURE 24.4.—Continued.

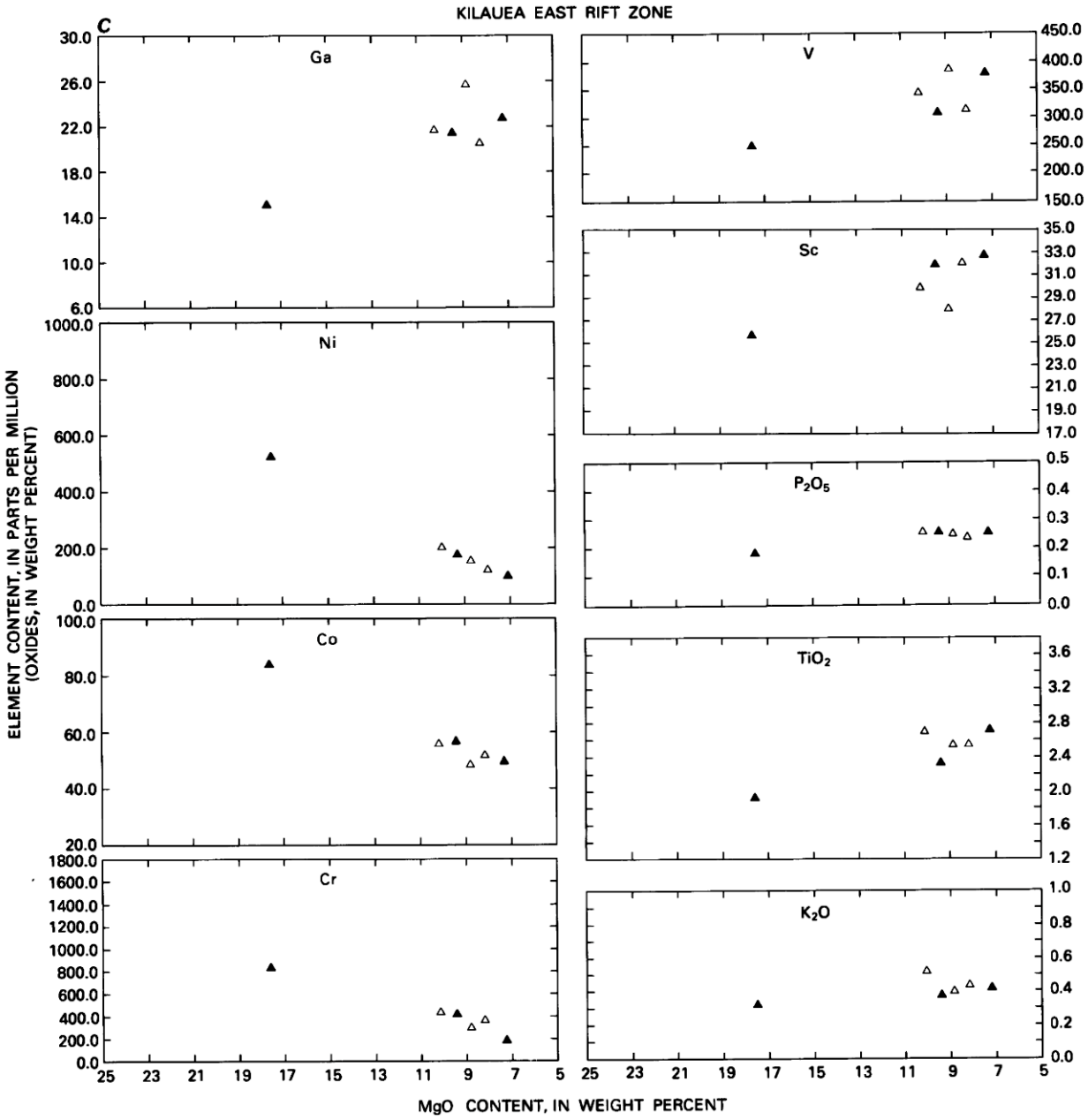

FIGURE 24.4.—Continued.

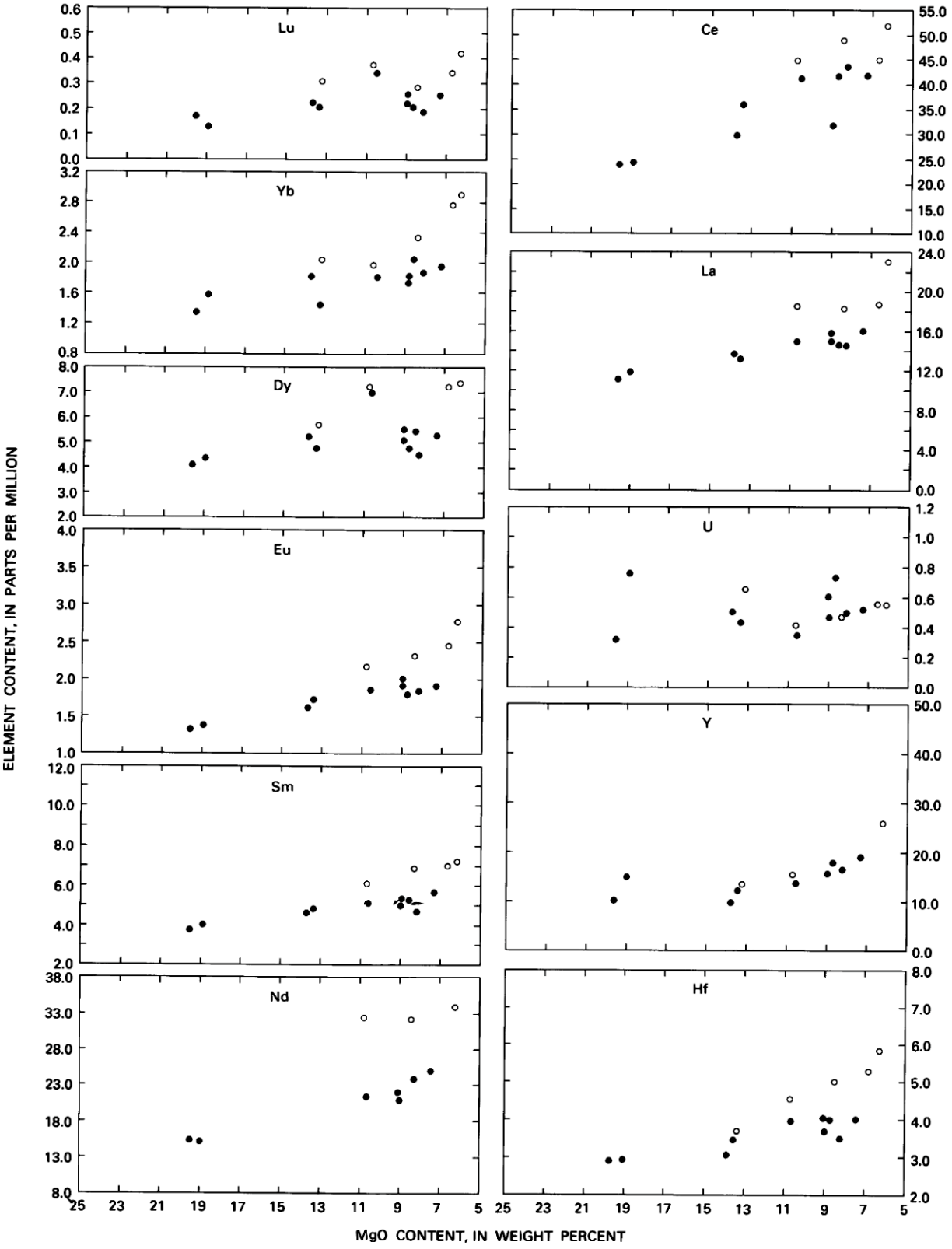

FIGURE 24.5.—MgO-variation diagrams for olivine-controlled lava of 1959 Kilauea Iki eruption (dots) and for hybrid lava of 1960 Kapoho eruption (circles). Data from table 24.12.

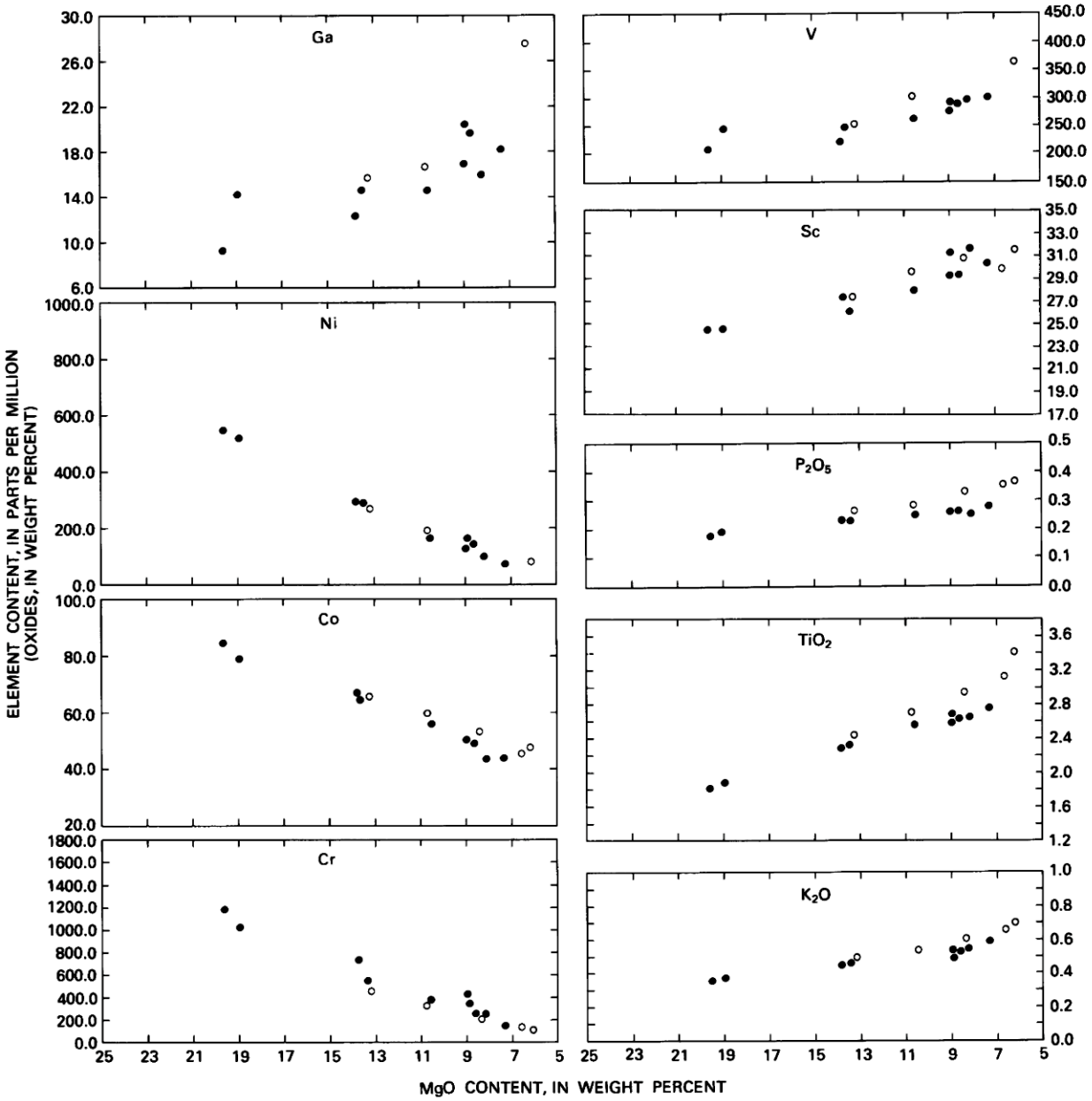

FIGURE 24.5.—Continued.

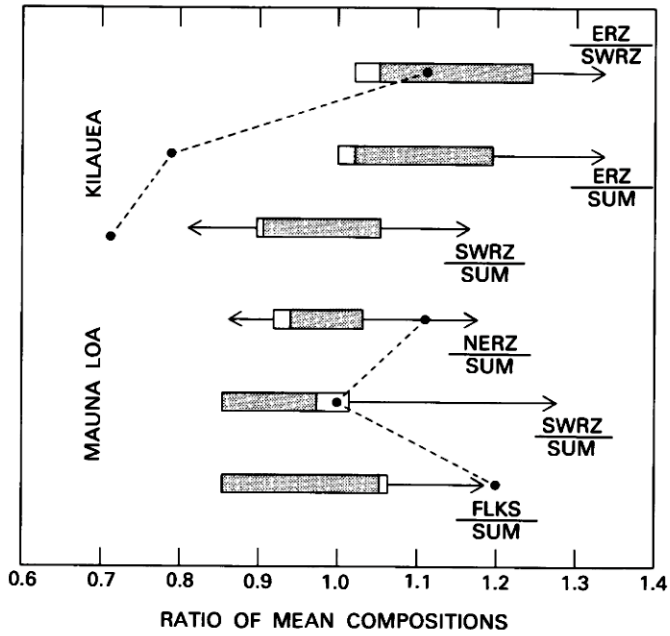

FIGURE 24.6.—Ratios of MgO-adjusted mean compositions (computed from data in tables 24.13, 24.20) of lava samples grouped according to space. SUM, summit; ERZ, east rift zone; SWRZ, southwest rift zone; NERZ, northeast rift zone; FLKS, northwest and southeast flanks. Bars show ranges of ratios for well-determined olivine-incompatible elements (K_2O, TiO_2, P_2O_5, Sc, Hf, and REE); shaded parts of bars bracket values for LREE only). Arrows indicate extension of a given range of values if less precisely determined values for V, Mo, Zn, Ga, Y, and Pb are considered; Cs and Ba are omitted because of wide scatter. Dots linked by dashed lines are ratios for uranium.

higher concentration of K_2O, TiO_2, P_2O_5, Ba, Hf, U, and the REE except for Yb and Lu (see tables 24.13, 24.14). The relatively elevated concentrations of U are especially conspicuous, and many samples contain more U than do samples of differentiated or hybrid lava. The reason for the (to date) unique composition of the Kilauea Iki lava is unknown, but major-oxide variations and other evidence prompted Wright (1973, p. 849) to suggest these lavas "were fed from a source different from that which fed other summit eruptions" in the 1952–68 period. Our trace-element data are compatible with Wright's postulation. Wright's (1973) mixing calculations show that the variations in composition of the Kilauea Iki lava can be explained by mixing olivine (plus chromite) with various proportions of two end-member magmas, represented by samples S–1 and S–2 (table 24.12) erupted the first day of the eruption.

Because of their compositional complexity and uniqueness, Kilauea Iki samples are not included in any of the space or time groupings of Kilauea lava (tables 24.9–24.11). Nor have we incorporated them in the estimate of the average composition of Kilauea Volcano as a whole (table 24.14), as was done by Leeman and others (1980, table 1 and appendix); of the ten analyses they averaged, five are of Kilauea Iki lava.

Compositional differences in the 1960 Kapoho lava are not related to olivine control alone; they were interpreted by Wright and Fiske (1971) as the result of complex mixing of undifferentiated and differentiated magmas. Their calculations showed that the lava erupted through January 26, 1960 (samples F–1 and F–5, table 24.14) can be produced by mixing undifferentiated 1961 magma and early 1955 differentiated magma, whereas lava erupted later (samples F–8, F–12, and F–17) resulted from mixing of olivine, one or more undifferentiated magmas (1959, 1961, 1967), and the early 1960 hybrid magma (Wright and Fiske, 1971, tables 10 and 11). Mixing calculations incorporating our trace-element constraints have not yet been done for the Kapoho hybrid lava, nor for any of the differentiated lava samples we analyzed, but the results of such studies should confirm or refine magma-mixing models based solely on major-element variations. For example, the decreased mean Sc contents of the differentiated and hybrid lavas (table 24.14), relative to those for olivine-controlled lava, clearly reflect the effect of pyroxenes joining olivine as phenocryst phases. In any case, the Kapoho lava (not MgO adjusted) is characterized by the highest concentrations of K, Ti, P, Ba, Hf, and REE of any of the Kilauea lava samples analyzed in this study (table 24.14; figs. 24.4, 24.5, and 24.9*A*).

MAUNA LOA LAVA

Analytical data for 31 Mauna Loa lava samples are given in tables 24.15–24.19) and plotted in magnesia-variation diagrams (fig. 24.10). The individual analyses were MgO-adjusted to a uniform MgO content of 7.00 weight percent to remove effects of olivine control (see appendix 24.1) before computation of mean compositions of samples grouped according to space or time (table 24.20). Several of the lava samples we studied also have been analyzed in previous studies, and the interlaboratory comparison of analytical results (table 24.5) indicates fair to good agreement for most elements.

POSSIBLE SPATIAL VARIATION

In comparison to Kilauea, Mauna Loa exhibits less chemical variation. Wright (1971) could not detect any significant systematic variation in major-element composition of Mauna Loa lava over space or time. More recently, Rhodes (1983), whose study represents the most thorough sampling of historical Mauna Loa lava to date, demonstrated each flow is remarkably homogeneous, despite the large areal extent and volume and the wide differences in the duration of eruptions (1–450 days). Many historical lava fields studied by Rhodes (1983, p. A869) "have compositional variability that is within, to close to, the analytical error for most elements." This observation has important implications for assessing possible systematic variation of Mauna Loa lava with time, discussed later.

Our trace-element data, within analytical uncertainty, do not indicate any obvious differences between the mean compositions of the various groupings of olivine-controlled lava (tables 24.15–24.18, 24.20). However, possible minor compositional differences as a function of space, though subtle and not significant statistically, are suggested by the comparison of ratios of mean compositions (fig. 24.6). The mean abundances of the well-deter-

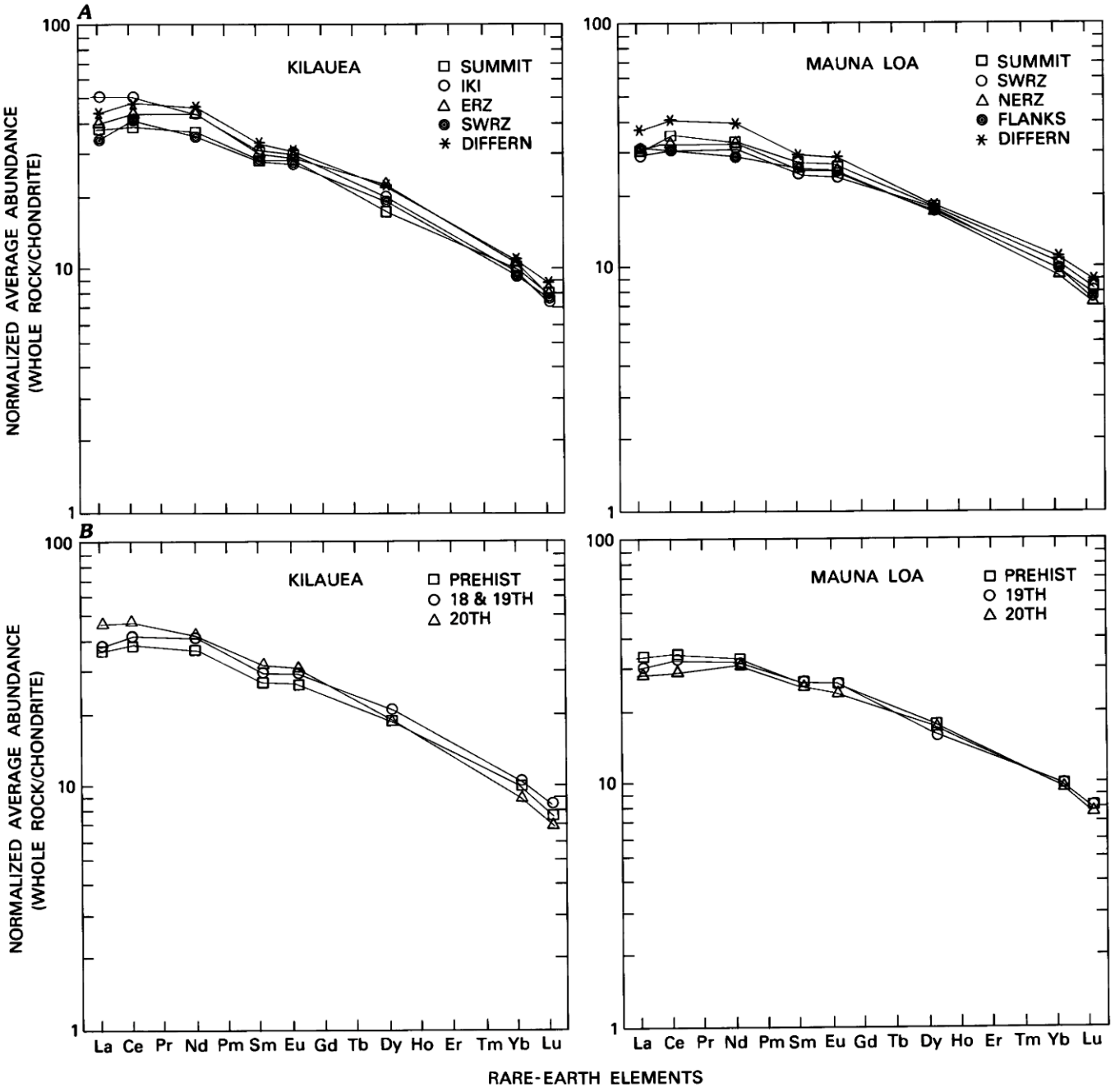

FIGURE 24.7.—Comparison of MgO-adjusted, chondrite-normalized average REE abundances of Kilauea and Mauna Loa lava samples, grouped as in tables 24.13 and 24.20 according to space (*A*) and according to time (*B*). For spatial groups, abbreviations are same as in figure 24.6; IKI, lava of 1959 Kilauea Iki eruption. Abundances of differentiated lava (DIFFERN) shown for comparison are not MgO adjusted. If DIFFERN curves are not considered, variability in space and time for Mauna Loa lava is less than Kilauea lava, which exhibits a discernible compositional gap between east rift zone (ERZ) lava and that of summit and southwest rift zone (SWRZ). Temporal variations discussed in text.

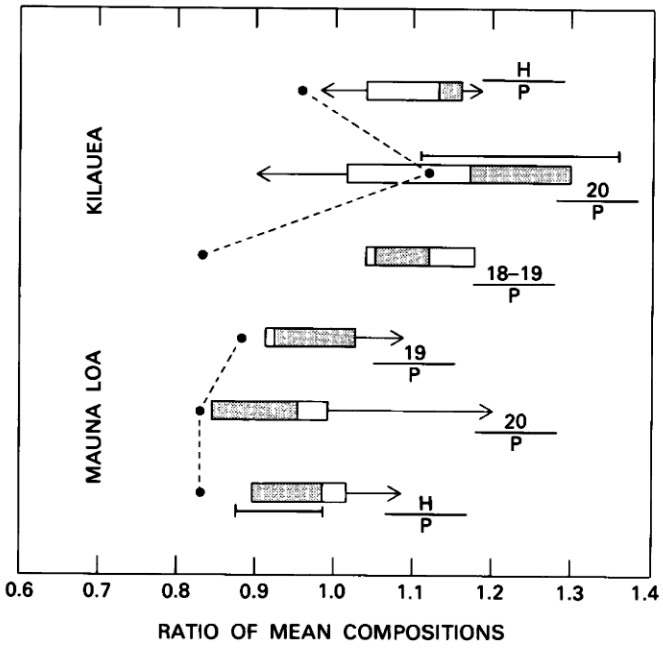

FIGURE 24.8.—Ratios of MgO-adjusted mean compositions of lava samples (listed in tables 24.13, 24.20) grouped according to time. P, prehistoric (erupted before A.D. 1750); 18 and 19, 18th and 19th centuries, respectively; 20, 20th century; H, historical undivided. Double-ended heavy line, range of ratios for LREE data of Budahn and Schmitt (1985, table 2); other symbols and explanation same as in fig. 24.6.

mined elements (K, Ti, P, Sc, Hf, and LREE) for lava of the SWRZ appear to be lower than their counterparts for SUM lava (figs. 24.6, 24.7*A*). Similar, but even more subtle, differences are hinted by the ratio shifts between the summit lava and the lava of Mauna Loa's northwest and southeast flanks (FLKS) and northeast rift zone (NERZ). Specifically, for the ratios FLKS/SUM and NERZ/SUM, the values for all REE other than La are less than unity.

We emphasize that our sampling of FLKS and NERZ lava is small and may not be representative. Furthermore, the samples of southeast-flank lava are from the Ninole Hills, whose major-element composition is unusual and highly varied (Wright, 1971, table 12). Because the Ninole lava (currently called the Ninole Basalt) comprises the oldest known rocks of Mauna Loa, as indicated by provisional K-Ar ages of 0.7 to 0.5 Ma for two dated flows (Evernden and others, 1964, table 4), it is not nearly as fresh as other Mauna Loa lava analyzed. Its chemical variability probably in part reflects posteruption weathering or possible alteration.

In any case, Rhodes and Lipman (1979) also found the Ninole Hills lava to differ compositionally from both prehistoric and historical lavas of Mauna Loa's southwest rift zone and suggested that it may be derived from a source different from that for most Mauna Loa lava. Indeed, Wright (1971, p. 18) even suggested that "The Ninole lavas may represent remnants of a separate volcano older than Mauna Loa." If so, then the apparent shift in FLKS/SUM ratios is intervolcano rather than intravolcano. Alternatively, given the wide analytical uncertainty, the apparent shifts in ratios plotted in figure 24.6 could be completely fortuitous, could represent sampling bias, or both. Nevertheless, as in the case of Kilauea lava, we are impressed by the seemingly nonrandom nature of the ratio shifts (fig. 24.6). As mentioned earlier in the discussion of Kilauea lava, such minor but nonrandom differences cannot be ascribed to grouping of samples for irradiations (table 24.2). Clearly, our speculation that the lava samples from the western sector of Mauna Loa may vary in composition as a function of space must be tested with many more precise analyses of fresher samples.

VARIATION IN TIME

Until recently, few published data on prehistoric Mauna Loa lava were available to test the possibility that it might differ compositionally from historical lava, as had been well demonstrated for Kilauea (Wright, 1971). Rhodes and his colleagues, in presenting the preliminary results of an integrated mapping and geochemical study of both prehistoric and historical lavas of Mauna Loa, concluded that "there is no evidence of major changes in compositional characteristics throughout the 31,000 years of eruptive history covered by our samples" (Rhodes and Lipman, 1979, p. 97). They recognized small "episodic" compositional variations for the historical Mauna Loa lava and suggested that processes that produced such variations "occurred episodically throughout the past 30,000 years" (Rhodes and others, 1982). However, as discussed below, we suggest that the prehistoric lava differs chemically from historical lava and that systematic minor secular variations may exist.

To our knowledge, Budahn and Schmitt (1985) were the first to report a compositional difference between the prehistoric and historical lavas of Mauna Loa. The results of our study, based on more comprehensive sampling, confirm their observation. Assuming that our mean trace-element compositions for the groupings of Mauna Loa lava are representative, our data suggest a compositional distinction between the 19th-century and 20th-century lavas as well (there are no known 18th-century eruptions). Our data suggest small but systematic relative decreases with time in the abundances of K, Ti, P, Sc, Hf, and LREE (table 24.20; figs. 24.7*B*, 24.8, 24.11). For certain of the other olivine-incompatible elements, the trend of inferred secular variation is convincingly demonstrated, we believe, by the more comprehensive and precise data of Rhodes (1983) for the historical Mauna Loa lava (table 24.21; fig. 24.12). As mentioned in the abstract by Rhodes and others (1982), the general features of the variation shown in figure 24.12 are also reflected in the variation of a few other incompatible elements and the ratios LREE/HREE, Zr/Y, and K/Ti. The striking parallelism between the variation patterns evident in figure 24.12, even at the scale of the small change between the 1949 and 1950 eruptions, attests to the high precision of Rhodes' data.

As earlier noted by Rhodes and others (1982), a significant compositional break occurs between lava erupted before and after 1870 (fig. 24.12). For this reason, we chose to lump the 1880, 1887, and 1899 eruptions with the 20th-century eruptions in computing the averages in table 24.21. However, even if the

TABLE 24.14.—*Average compositions of tholeiite samples analyzed in this study*

[Calculated from data in table 24.9–24.12 and 24.15–24.19. S.d., standard deviation. Oxide values in weight percent; values for elements in parts per million]

	Olivine-controlled lava (adjusted to 7.00 weight percent MgO)						Differentiated and hybrid lavas, (not adjusted for MgO)			
	Kilauea Iki n = 10		Kilauea[1] n = 25		Mauna Loa[2] n = 24		Differentiated[3] n = 11		Kapoho n = 5	
	Mean	S.d.	Mean	S.d.	Mean	S.d.	Mean	S.d.	Mean	S.d.
MgO	7.00	-	7.00	-	7.00	-	6.45	.42	8.94	2.95
K_2O	.55	.03	.45	.05	[4] .41	.04	.49	.09	.59	.08
TiO_2	2.73	.05	2.56	.14	2.14	.15	2.58	.41	2.90	.36
P_2O_5	.27	<.01	.24	.02	[4] .23	.02	.27	.05	.32	.04
Cs	.24	.09	.19	.08	.25	.23	.19	.20	.18	.07
Ba	164	34	[5]126	52	127	48	154	51	245	102
Sc	32.4	2.0	31.9	2.1	31.4	1.6	29.9	1.7	29.9	1.7
V	297	20	307	43	314	22	332	35	306	54
Cr	200	85	[6]261	108	[7]224	55	151	59	248	143
Co	40.7	4.6	43.5	2.6	[8]41.1	9.4	42.6	2.9	54.7	8.0
Ni	44	20	[9]68	36	[10]77	21	79	17	181	94
Mo	5.0	1.0	4.6	1.0	4.5	1.3	4.3	.7	3.7	.2
Zn	128	13	131	13	125	16	138	15	116	6
Ga	17.7	2.5	20.0	3.2	17.5	2.1	20.5	2.6	20.0	6.6
Hf	4.2	0.2	3.8	.4	3.4	.3	4.1	1.1	5.0	.8
Y	16.6	2.8	18.7	3.1	18.7	2.4	23.2	6.4	18.3	6.7
U	.59	.20	.35	.13	.22	.05	.38	.24	.52	.09
Pb	[11]1.8	.6	2.5	1.1	2.5	1.0	3.3	1.1	2.2	1.3
La	16.2	.7	12.0	1.6	9.5	1.3	12.4	1.8	19.5	2.3
Ce	39.5	5.0	31.6	4.4	24.5	3.8	33.4	8.1	48.0	3.2
Nd	23.9	1.2	21.1	2.7	17.2	1.6	23.1	6.0	33.2	.9
Sm	5.52	.27	5.12	.5	4.61	.35	5.55	1.2	6.82	.51
Eu	2.01	.07	1.88	.19	1.64	.27	1.97	.38	2.45	.25
Dy	5.8	.9	5.6	.9	5.2	.6	5.8	1.4	6.6	.9
Yb	2.01	.17	2.04	.20	2.02	.15	2.24	.42	2.42	.4
Lu	.25	.05	.26	.03	.27	.02	.31	.05	.35	.06

[1]Some trace elements not determined for all samples: n = 23 for V, Ni, Mo, Zn, Ga, Y, Pb; 22 for Dy; and 20 for Cs.

[2]Some trace elements not determined for all samples: n = 23 for Ga, Yb, and Lu; n = 23 for V, Ni, Zn, Mo, Ga, Y, U, Pb, and Sm; and 21 for Nd, 20 for Cs.

[3]So-called differentiated samples of Mauna Loa and Kilauea (MgO <6.80 weight percent include those in table 24.19 and those indicated in tables 24.9-24.11. These data are not adjusted to 7.00 weight percent MgO.

[4]Samples ID-275-2 and ID-214-2 omitted because of anomalously low values.

[5]Adjusted value for sample KD-32 (702 ppm) omitted.

[6]The adjusted value for HD-32 was negative and omitted (see appendix).

[7]Four negative adjusted values (samples TLW67-84, TLW67-89, C819, and 1868 ML) omitted.

[8]Anomalously low values (<30.0 ppm) for samples TLW67-84, C819, and 1868 ML omitted.

[9]Six negative adjusted values omitted (samples 57F-17, 8X078-0, 8X067-0, TLW68-12, TLW67-140 and KD-32).

[10]Ten negative adjusted values omitted (samples TLW67-84, TLW67-89, 65MAN-1, 1868 ML, TLW67-79, TLW67-61, TLW67-63, TLW 67-117A, ID-275-2, and ID-214-2).

[11]Anomalous value (6.6 ppm) for sample S-15 omitted.

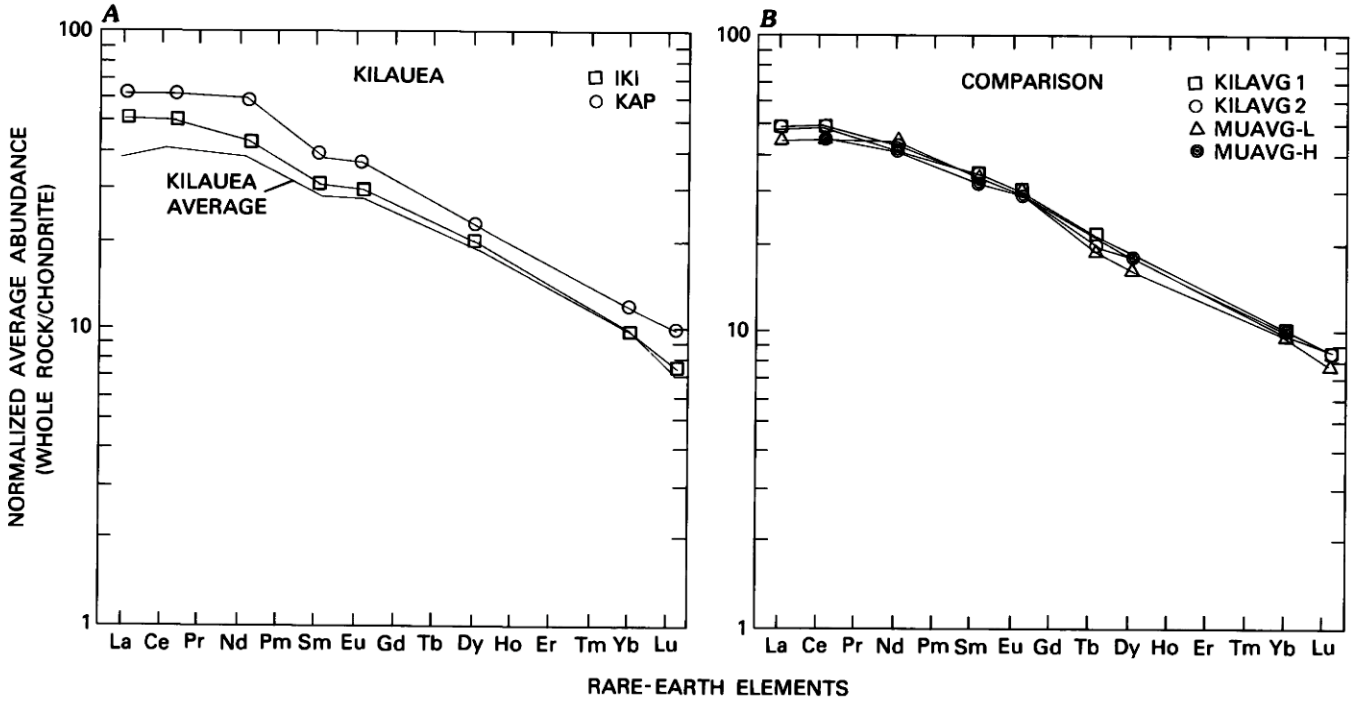

FIGURE 24.9.—Comparison of chondrite-normalized average REE abundances for groups of Kilauea lava. ***A***, Curves for MgO-adjusted Kilauea Iki lava (IKI), Kapoho lava, not MgO adjusted (KAP), and overall Kilauea average (data from table 24.14). ***B***, Curves for MgO-adjusted averages of historical Kilauea lava and averages for 1969–71 Mauna Ulu lava groups: KILAVG1 (Basaltic Volcanism Study Project, 1981), KILAVG2 and MUAVG-L (Leeman and others, 1980), and MUAVG-H (Hoffman and others, 1984). Curves for Mauna Ulu lava lie slightly below averages previously determined for historical Kilauea lava in (***B***), but slightly above our Kilauea average (***A***), which excludes data for Kilauea Iki lava (see text).

TABLE 24.15.—*Composition of olivine-controlled tholeiite of Mauna Loa's summit*

[Oxide values (in weight percent) from Wright (1971, table 8), recast to 100 percent dry weight; values for elements in parts per million]

	Prehistoric		Historical		
			19th century		20th century
			1877?	1880?	1949
Sample	TLW67-84	TLW67-70B	TLW67-88	TLW67-89	M-56-2
SiO_2	49.20	52.12	52.20	51.29	52.16
MgO	16.29	6.93	6.85	10.74	7.07
K_2O	.32	.46	.41	.30	.40
TiO_2	1.76	2.12	2.01	1.74	2.04
P_2O_5	.17	.25	.23	.23	.21
Cs	.00	.24	.05	.00	.30
Ba	67.00	92.00	86.00	157.00	94.00
Sc	25.50	30.30	32.20	30.20	32.60
V	211.00	297.00	319.00	273.00	.00
Cr	582.00	248.00	185.00	501.00	211.00
Co	59.80	43.00	46.80	64.40	50.80
Ni	565.00	84.00	80.00	149.00	.00
Mo	3.60	3.70	3.80	4.00	.00
Zn	108.00	111.00	142.00	153.00	.00
Ga	10.80	17.40	16.80	16.10	.00
Hf	2.80	3.60	3.60	3.10	3.80
Y	12.10	19.60	18.60	16.70	.00
U	.18	.23	.16	.14	.00
Pb	2.10	2.40	2.20	1.40	.00
La	7.90	10.40	10.20	7.20	8.60
Ce	23.10	28.70	27.20	21.40	.00
Nd	14.50	18.00	19.90	14.80	17.10
Sm	3.85	5.10	4.82	4.05	4.89
Eu	1.28	1.83	1.79	1.60	1.87
Dy	4.10	5.30	5.60	5.30	4.80
Yb	.00	1.88	2.34	2.02	2.16
Lu	.26	.26	.28	.26	.26

TABLE 24.16.—*Composition of olivine-controlled tholeiite of Mauna Loa's northeast rift zone*

[Oxide values (in weight percent) from Wright (1971, table 10), recast to 100 percent dry weight; values for elements in parts per million]

	Prehistoric	Historical		
		19th century		20th century
		1852	1855	1942
Sample	TLW67-29	TLW67-61	TLW67-63	TLW67-62
SiO_2	52.02	48.92	50.74	51.92
MgO	6.99	16.88	9.79	7.21
K_2O	.41	.33	.38	.36
TiO_2	2.10	1.62	2.02	2.06
P_2O_5	.24	.19	.21	.21
Cs	.11	.00	.11	.06
Ba	140.00	174.00	97.00	241.00
Sc	29.40	24.90	29.40	30.90
V	311.00	240.00	298.00	309.00
Cr	224.00	938.00	488.00	270.00
Co	41.90	76.90	53.70	45.00
Ni	88.00	472.00	179.00	76.00
Mo	3.80	4.30	5.40	4.30
Zn	133.00	108.00	145.00	135.00
Ga	19.30	11.80	19.10	20.40
Hf	3.30	2.60	3.00	3.10
Y	19.20	11.80	16.60	16.00
U	.22	.20	.22	.16
Pb	1.00	2.20	1.40	2.20
La	9.40	7.70	9.80	8.90
Ce	25.90	20.40	22.20	22.90
Nd	19.50	13.50	15.90	16.30
Sm	4.57	3.64	4.08	4.53
Eu	1.63	1.40	1.57	1.57
Dy	5.00	4.20	4.40	5.20
Yb	1.92	1.45	1.76	1.89
Lu	.23	.19	.24	.25

averages were computed using the arbitrary time groupings used elsewhere in this study for historical lava (18th and 19th centuries versus 20th century), the two resulting averages would still yield the same results, although the differences between them would be smaller.

In summary, as with the inferred secular variation in Kilauea lava, we admit that the differences observed for Mauna Loa lava also are largely within analytical uncertainty, but we attach significance to the nonrandom pattern of variations defined by the mean compositions of the prehistoric and historical lavas. If the variations were truly statistically random, then there would be no reason for the observed systematic shifts in the ratios of the mean compositions. It is also apparent from our data that the patterns of compositional variation of Mauna Loa lava in time and, possibly, space differ in trend from those for Kilauea lava, as discussed below.

DISCUSSION

DIVERGENCE IN SECULAR VARIATION PATTERNS FOR KILAUEA AND MAUNA LOA LAVAS

Systematic differences in petrographic and major-element characteristics of Kilauea and Mauna Loa lavas have been recognized in numerous previous studies, beginning with Macdonald (1949a, b), and comprehensively documented by Wright (1971). More recently, a few studies, based on limited sampling, have shown that the tholeiite lava of these two volcanoes, not surprisingly, also differ in the abundance patterns of various trace elements (Murata, 1970; Leeman and others, 1977, 1980; Basaltic Volcanism Study Project, 1981; Budahn and Schmitt, 1985). Our study reinforces the findings of these previous workers (fig. 24.13). At a given MgO content, Kilauea olivine-controlled lava has distinctly greater abundances of olivine-incompatible elements than Mauna Loa olivine-controlled lava; these distinctions are enhanced if the Kilauea Iki samples are included in the computation of average composition of Kilauea lava (table 24.14). All recent studies conclude that the chemical differences between Kilauea and Mauna Loa cannot be explained solely by shallow fractionation processes and reflect heterogeneities in the mantle source regions and (or) different melting mechanisms to produce the chemically distinct magmas (see, for example, Leeman and others, 1980; Wright, 1984; Budahn and Schmitt, 1985).

If our inferred time-space-composition relations (tables 24.13, 24.20; figs. 24.6–24.9) are valid, then an intriguing pattern emerges. For Kilauea, the MgO-adjusted mean abundances of K, Ti, P, Sc, Hf, U, and the LREE tend to increase progressively with time, whereas, for Mauna Loa, these elements tend to decrease with time (figs. 24.14, 24.15). These relations are also indicated by the data of Budahn and Schmitt (1985, table 2). The lava of the 1969–71 Mauna Ulu eruption of Kilauea shows considerable major-element variation with time and exhibits at least a temporary reversal in TiO_2 and K_2O content relative to the overall secular change for Kilauea olivine-controlled lava (Wright and others, 1975). However, the limited trace-element data for the Mauna Ulu lava (Leeman and others, 1980; Hoffman and others, 1984) and the November 1975 summit lava (one analysis, Basaltic Volcanism Study Project, 1981), if MgO-adjusted, fall close to our computed mean for 20th-century olivine-controlled Kilauea lava.

The combined effects of these two apparently diverging trends cause the difference in composition between Kilauea and Mauna Loa lava to increase with time (figs. 24.14, 24.15). Our data for other olivine-incompatible elements lack sufficient precision to define other such trends, but the limited data of Budahn and Schmitt (1985, table 2) may indicate a similar divergence of variation trends for Ba and Ta. In addition, the data of Rhodes (1983) for Nb, Zr, and Sr abundances in historical Mauna Loa lava, as discussed earlier, yields a decreasing trend with time; unfortunately, however, comparably precise data for these elements in Kilauea lava needed to fully define the diverging trends for the two volcanoes are lacking.

Samples analyzed in this study include historical eruptions through July 1968 at Kilauea and through 1950 at Mauna Loa. Only limited published trace-element data exist for Hawaiian lava erupted since then to test our observations. The few data on lava of the July 1975 summit eruption at Mauna Loa (Rhodes, 1983; Budahn and Schmitt, 1985) show that its composition falls within the range for other 20th-century eruptions.

Thus, at the present time, available trace-element data are insufficient to ascertain whether the apparent diverging secular variation trends for the two volcanoes continue in lava erupted since

TABLE 24.17.—*Composition of olivine-controlled tholeiite of Mauna Loa's southwest rift zone*

[Oxide values (in weight percent) from Wright (1971, table 9), recast to 100 percent dry weight; values for elements in parts per million. Sample C820 fits definition of differentiated and is omitted in calculation of averages and not plotted in figure 24.10]

	Prehistoric			Historical						
				19th century			20th century			
				1868		1887	1919	1926	1950	
Sample	C819	C820	65MAN-1	W-A-7	1868ML	TLW67-59	H-34	TLW-67-76	TLW67-73	TLW67-79
SiO_2	46.29	49.35	50.44	51.39	46.88	52.27	52.10	51.69	52.03	51.48
MgO	24.25	6.12	13.13	8.84	23.64	7.50	7.09	7.82	6.87	9.22
K_2O	.28	.36	.34	.41	.26	.33	.35	.35	.37	.36
TiO_2	1.24	2.82	1.66	2.07	1.34	1.95	2.12	2.05	2.10	1.93
P_2O_5	.15	.28	.19	.23	.14	.19	.21	.20	.22	.21
Cs	.54	.19	.38	.19	.45	.14	.29	.14	.10	.17
Ba	50.00	230.00	48.00	174.00	108.00	134.00	116.00	110.00	143.00	58.00
Sc	17.70	31.30	25.50	29.30	20.90	30.30	29.60	30.30	31.00	28.60
V	.00	353.00	236.00	295.00	202.00	335.00	362.00	317.00	337.00	311.00
Cr	924.00	78.00	652.00	369.00	1250.00	260.00	237.00	277.00	202.00	395.00
Co	95.70	44.90	61.70	47.00	95.40	46.20	42.80	47.10	44.90	49.70
Ni	.00	62.00	293.00	152.00	846.00	83.00	90.00	145.00	82.00	131.00
Mo	.00	4.30	4.50	4.40	4.00	3.80	5.00	4.60	4.60	5.00
Zn	.00	137.00	123.00	148.00	106.00	119.00	119.00	104.00	114.00	126.00
Ga	.00	21.40	14.80	16.10	8.40	16.60	20.70	19.00	20.40	18.20
Hf	2.00	4.40	2.40	3.20	2.00	3.00	3.20	3.00	3.60	2.80
Y	.00	25.40	15.10	16.20	8.50	21.20	23.90	21.00	20.40	18.80
U	.00	1.00	.16	.21	.16	.15	.25	.17	.18	.19
Pb	.00	3.80	1.50	2.60	3.00	2.30	2.00	3.10	2.30	2.80
La	6.70	11.50	7.20	9.30	5.70	7.80	8.60	8.80	9.00	7.50
Ce	18.20	27.10	20.80	24.40	12.50	21.40	18.80	23.40	23.30	18.80
Nd	11.40	21.80	15.10	14.80	9.50	16.20	16.00	.00	16.80	16.20
Sm	.00	4.66	3.59	4.40	2.67	.00	4.20	4.44	4.36	3.97
Eu	1.02	2.32	1.32	1.69	.99	1.51	1.45	1.61	1.67	1.26
Dy	3.00	6.00	3.80	6.50	2.90	5.00	4.30	5.40	5.90	4.70
Yb	1.21	2.63	1.47	2.00	1.30	2.02	2.00	1.88	2.01	1.94
Lu	.00	.32	.22	.27	.15	.28	.26	.28	.29	.24

TABLE 24.18.—*Composition of olivine-controlled tholeiite of Mauna Loa's northwest and southwest flanks*

[Oxide values (in weight percent) from Wright (1971, tables 11 and 12), recast to 100 percent dry weight; values for elements in parts per million. Sample TLW67-119 fits definition of differentiated and is omitted in calculation of averages and not plotted in figure 24.10]

	Northwest flank				Southwest flank		
	Prehistoric			Historical	Prehistoric (Ninole Hills)		
				1859			
Sample	TW67117A	TLW67119	TLW67125	DPH-77	ID-098-2	ID-275-2	ID-214-2
SiO_2	49.59	52.30	50.84	51.46	50.53	50.08	47.50
MgO	14.37	6.74	7.85	7.75	7.17	9.99	17.45
K_2O	.34	.46	.43	.43	.46	.09	.08
TiO_2	1.70	2.16	2.24	2.17	2.68	2.05	1.61
P_2O_5	.19	.25	.23	.25	.26	.17	.14
Cs	.00	.05	.16	.27	.10	.12	.13
Ba	101.00	94.00	117.00	147.00	138.00	93.00	73.00
Sc	24.80	29.30	29.20	28.70	31.20	30.10	24.90
V	252.00	293.00	290.00	305.00	334.00	312.00	240.00
Cr	628.00	183.00	377.00	278.00	235.00	463.00	854.00
Co	61.50	38.60	46.90	44.50	47.80	53.80	79.60
Ni	371.00	75.00	118.00	98.00	111.00	135.00	477.00
Mo	4.00	2.90	4.40	2.80	5.40	4.60	3.50
Zn	106.00	113.00	107.00	113.00	124.00	123.00	126.00
Ga	12.10	17.60	15.40	15.60	17.00	17.00	11.20
Hf	2.50	3.00	3.30	3.40	4.20	3.00	2.30
Y	12.60	17.10	20.10	19.60	21.90	17.80	12.50
U	.17	.23	.36	.19	.31	.16	.15
Pb	2.60	2.00	1.30	2.00	1.20	3.20	3.40
La	7.90	10.30	10.20	8.80	13.40	7.80	6.70
Ce	19.70	24.80	25.30	25.90	29.30	16.00	14.20
Nd	14.20	17.00	0.00	16.70	0.00	12.60	11.10
Sm	3.64	4.42	4.76	4.77	5.49	3.78	3.10
Eu	1.21	1.52	1.58	1.72	2.08	1.50	1.21
Dy	3.90	4.60	5.30	4.70	6.40	4.20	3.70
Yb	1.65	2.03	1.94	1.75	2.18	1.82	1.49
Lu	.21	.29	.27	.25	.25	.24	.19

TABLE 24.19.—*Composition of differentiated lava of Mauna Loa. These samples are not olivine-controlled in terms of major-element composition*

[Oxide values (in weight percent) from Wright (1971, table 13), recast to 100 percent dry weight; values for elements in parts per million]

	Prehistoric	Historical			
		19th century			20th century
		1843			1926
Sample	9	W-A-22	W-A-23	TLW67-66	TLW67-72
SiO_2	52.49	51.74	51.99	52.05	52.16
MgO	5.54	6.76	6.81	6.68	6.70
K_2O	.73	.46	.45	.47	.42
TiO_2	3.19	2.16	2.16	2.16	2.23
P_2O_5	.42	.25	.25	.26	.23
Cs	.19	.12	.11	.08	.02
Ba	100.00	96.00	137.00	253.00	159.00
Sc	25.90	29.30	29.30	29.30	31.60
V	375.00	299.00	309.00	.00	325.00
Cr	139.00	195.00	226.00	138.00	190.00
Co	41.20	40.50	40.90	43.20	44.50
Ni	86.00	83.00	106.00	.00	78.00
Mo	4.20	4.20	4.20	.00	4.30
Zn	128.00	152.00	131.00	.00	131.00
Ga	21.30	20.20	17.70	.00	18.90
Hf	6.70	3.10	3.30	3.30	3.50
Y	39.30	17.80	19.90	.00	23.30
U	.45	.20	.18	.25	.19
Pb	3.60	2.80	4.00	.00	2.40
La	14.90	11.00	10.30	11.60	11.00
Ce	51.10	30.40	28.50	30.70	24.10
Nd	36.00	18.70	20.20	20.00	18.40
Sm	8.50	4.77	5.22	4.59	4.95
Eu	2.76	1.65	1.70	1.76	1.77
Dy	8.95	4.80	4.60	4.50	5.20
Yb	3.01	1.81	1.73	2.19	2.33
Lu	.42	.26	.24	.37	.30

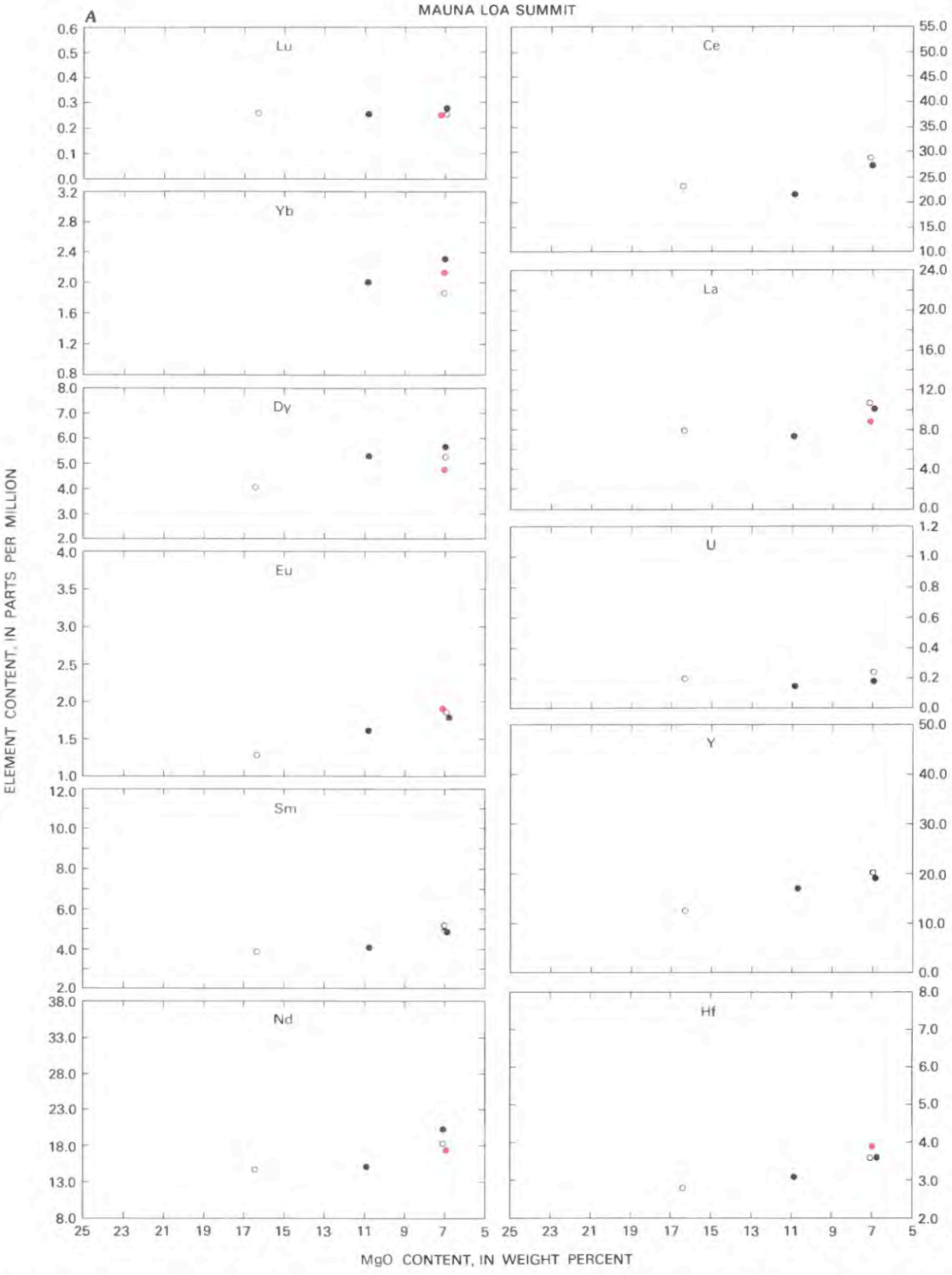

FIGURE 24.10.—MgO-variation diagrams for olivine-controlled lava of Mauna Loa. ***A,*** Summit (SUM). ***B,*** Southwest rift zone (SWRZ). ***C,*** Northeast rift zone (NERZ). ***D,*** Northwest and southeast flanks (FLKS). Open symbols, prehistoric; solid black symbols, 19th century; solid red symbols, 20th century. Differentiated lava (MgO <6.8 weight percent) of Mauna Loa (table 24.19) and of Kilauea (samples specified in headings of tables 24.9–24.11) would plot in dashed fields.

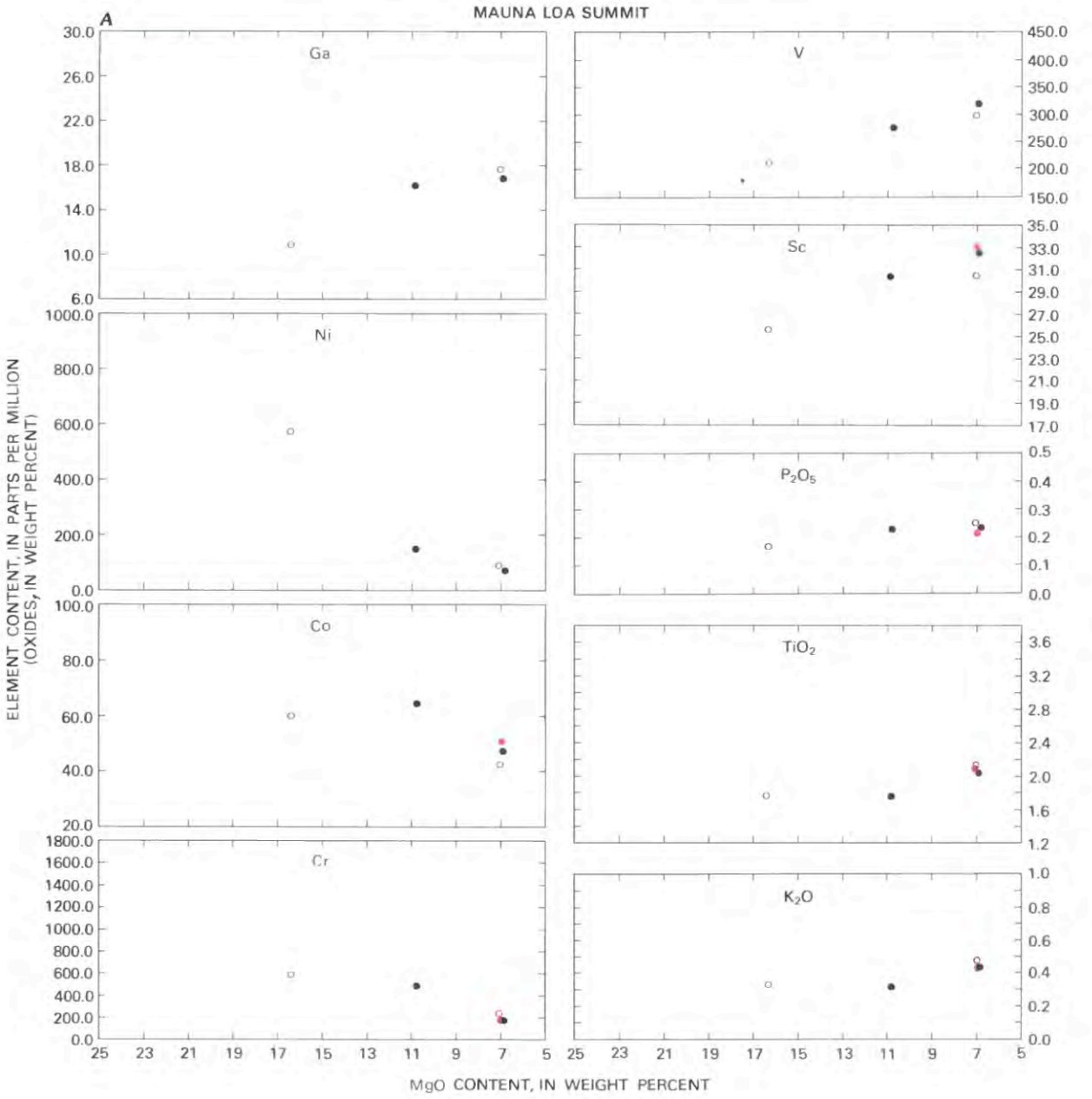

FIGURE 24.10.—Continued.

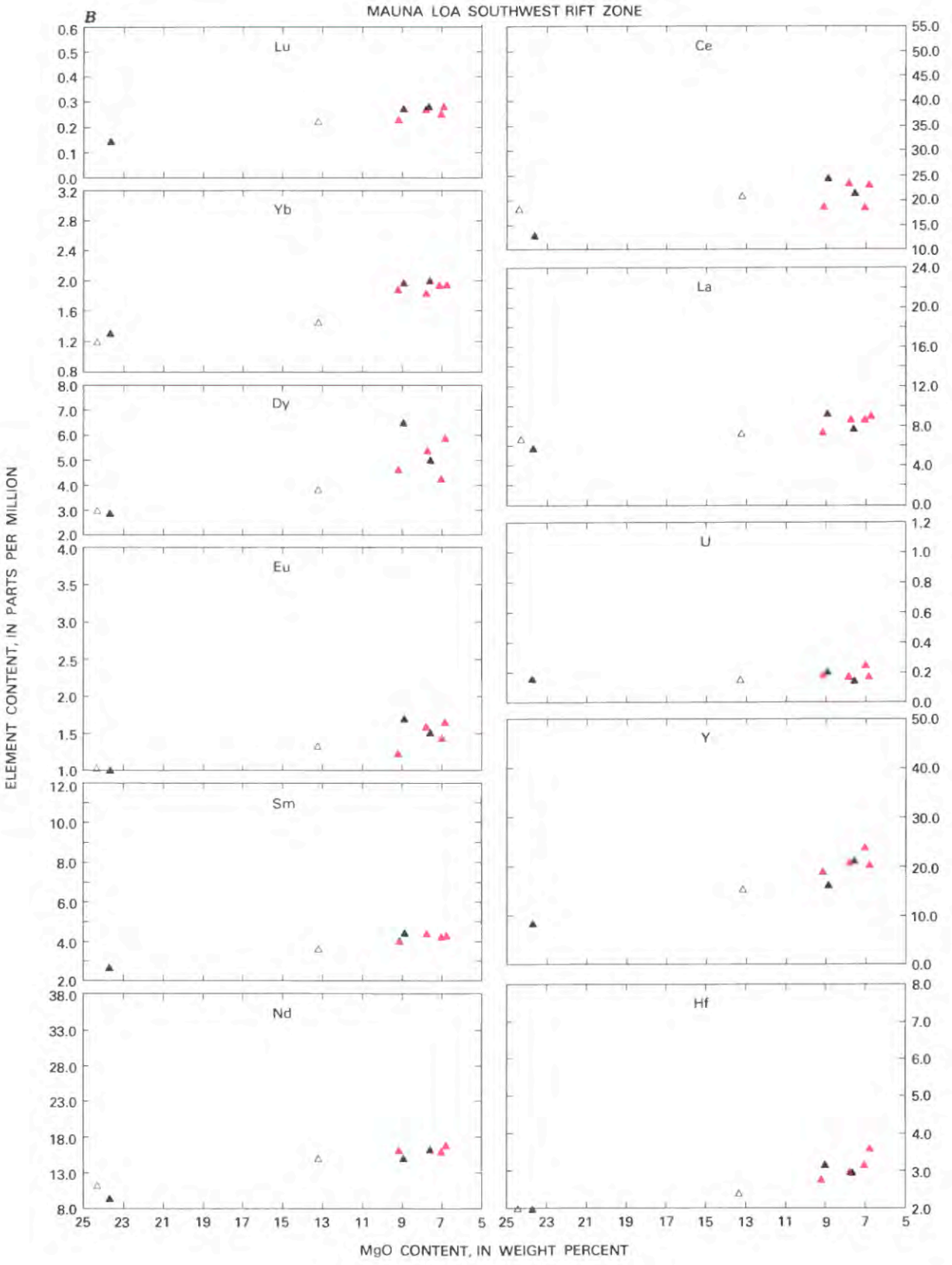

FIGURE 24.10.—Continued.

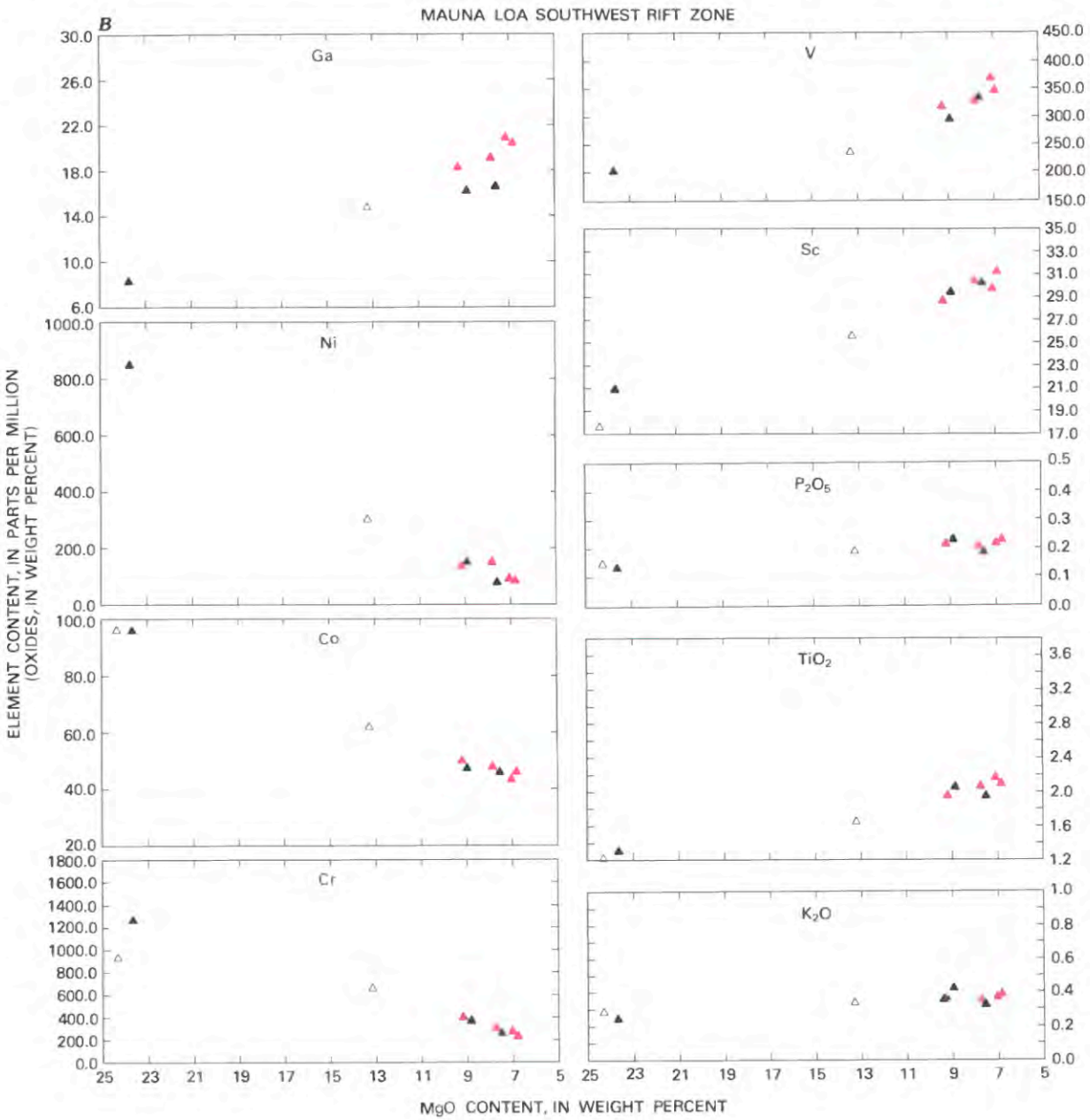

FIGURE 24.10.—Continued.

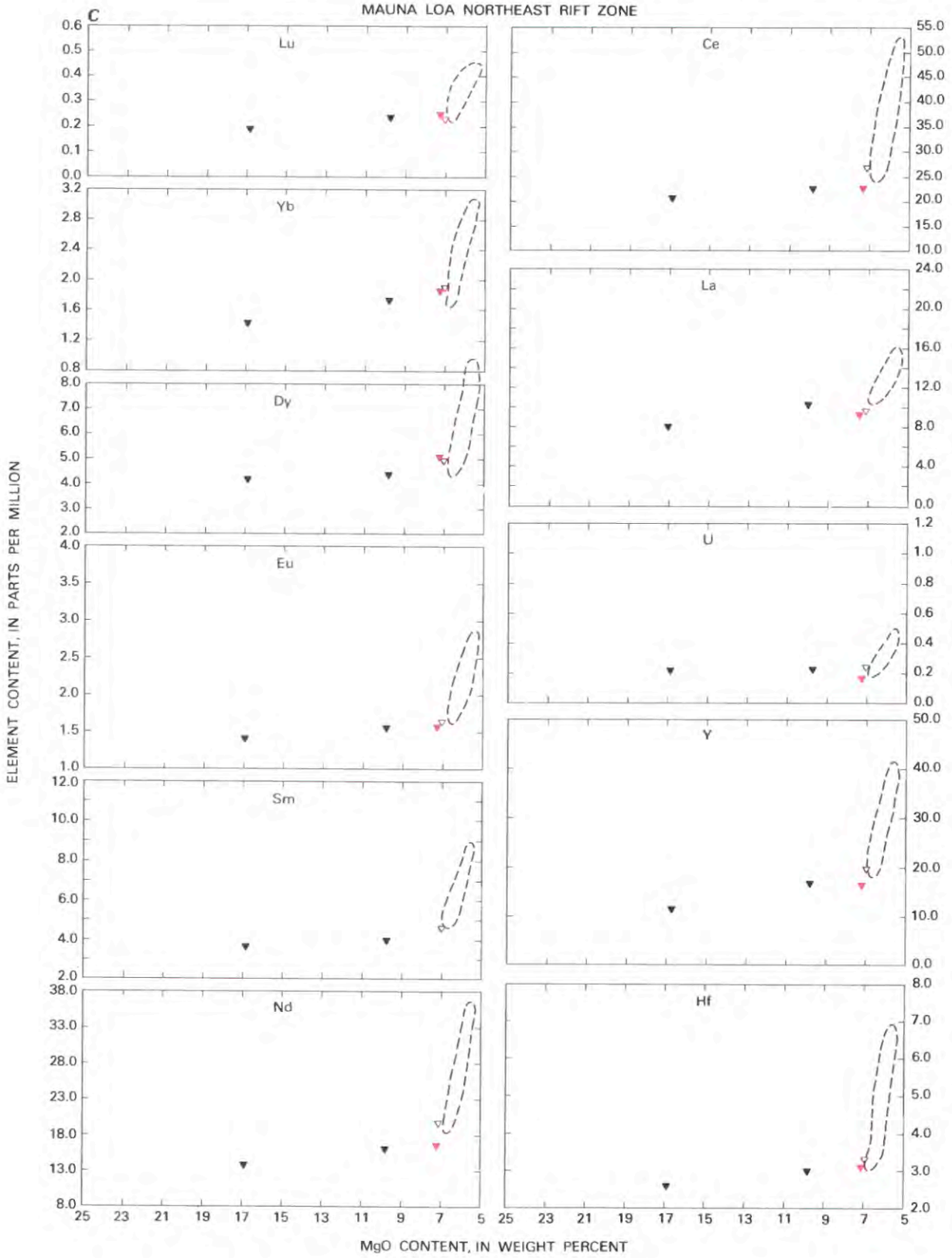

FIGURE 24.10.—Continued.

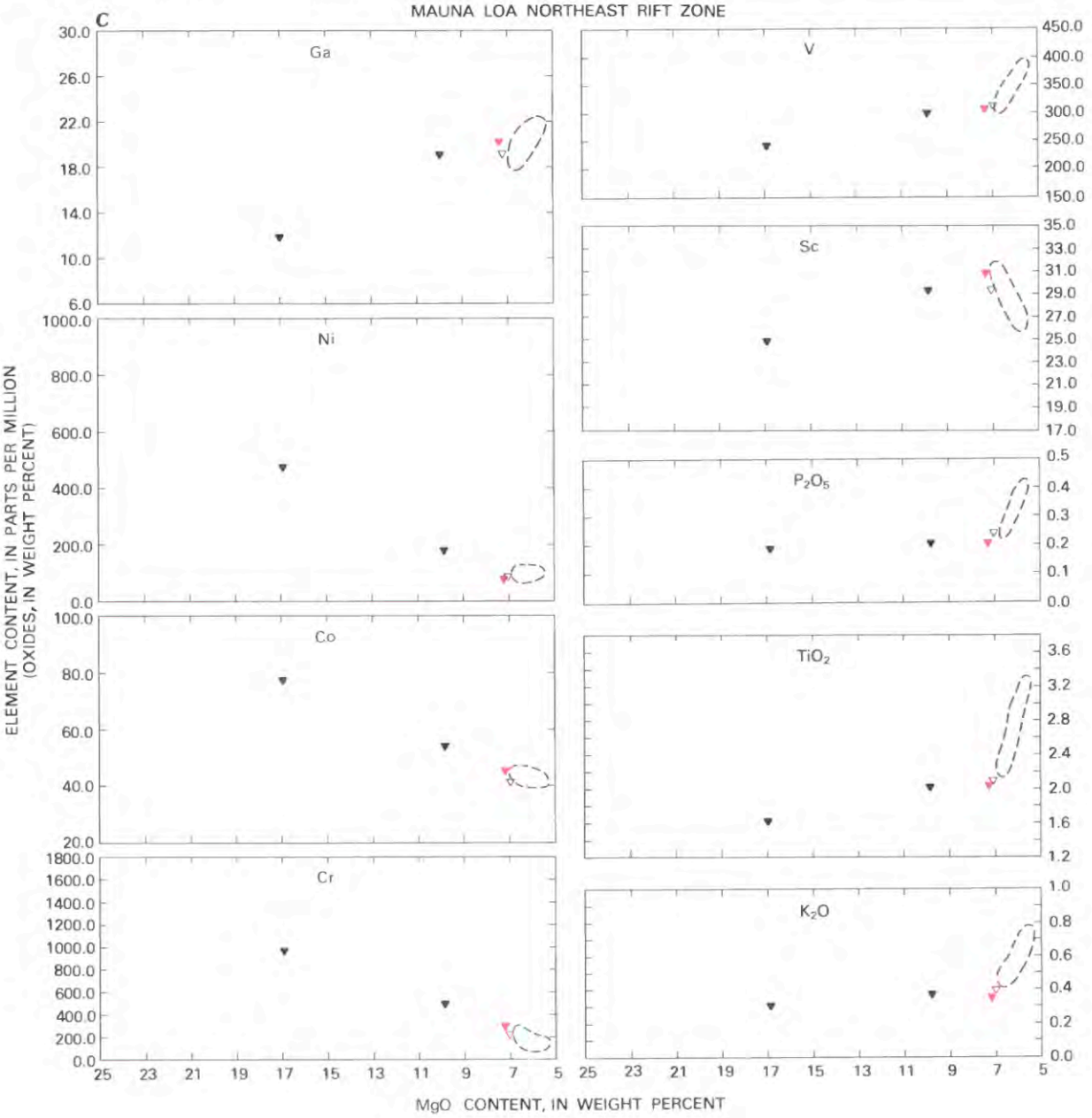

FIGURE 24.10.—Continued.

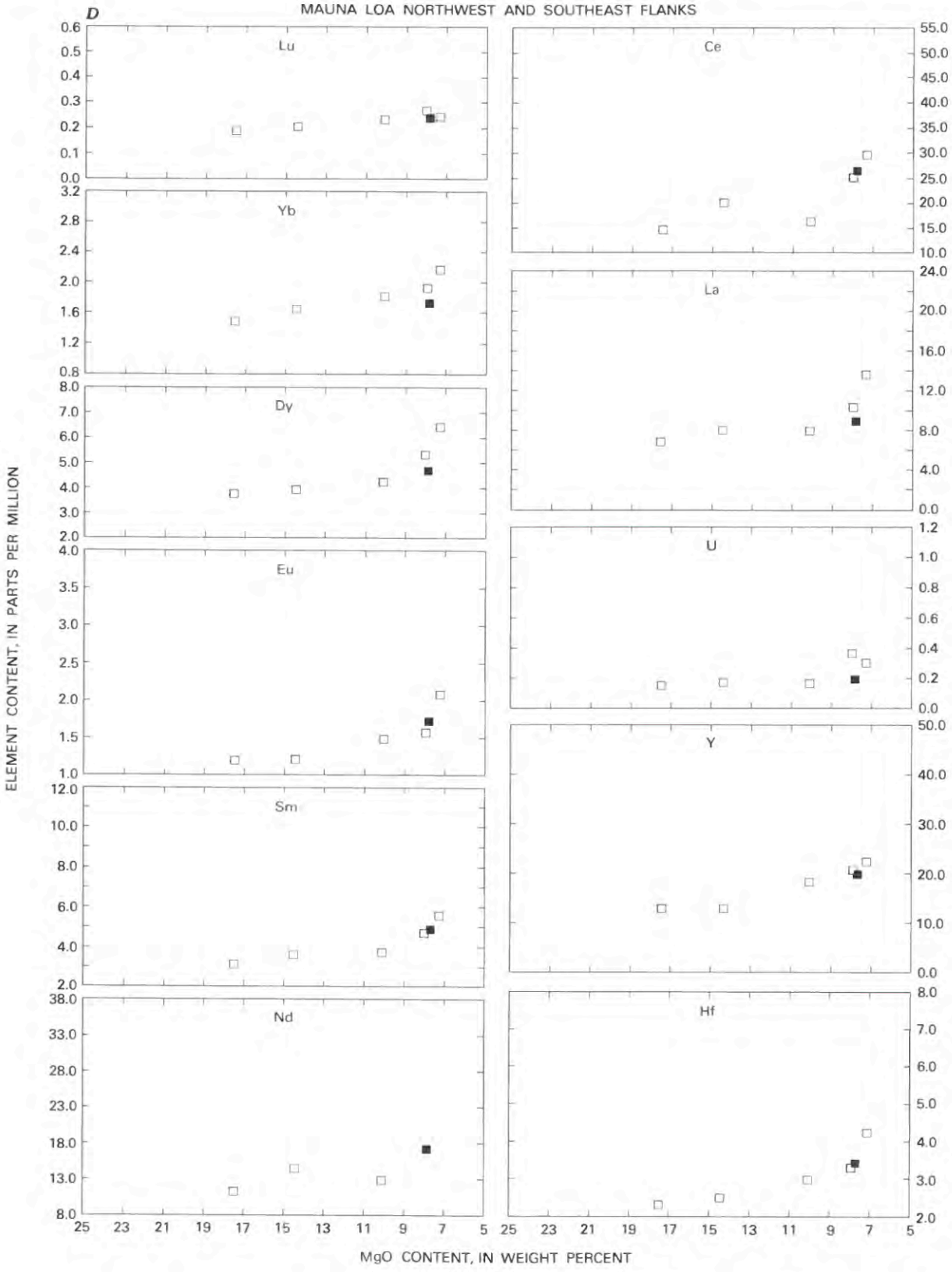

FIGURE 24.10.—Continued.

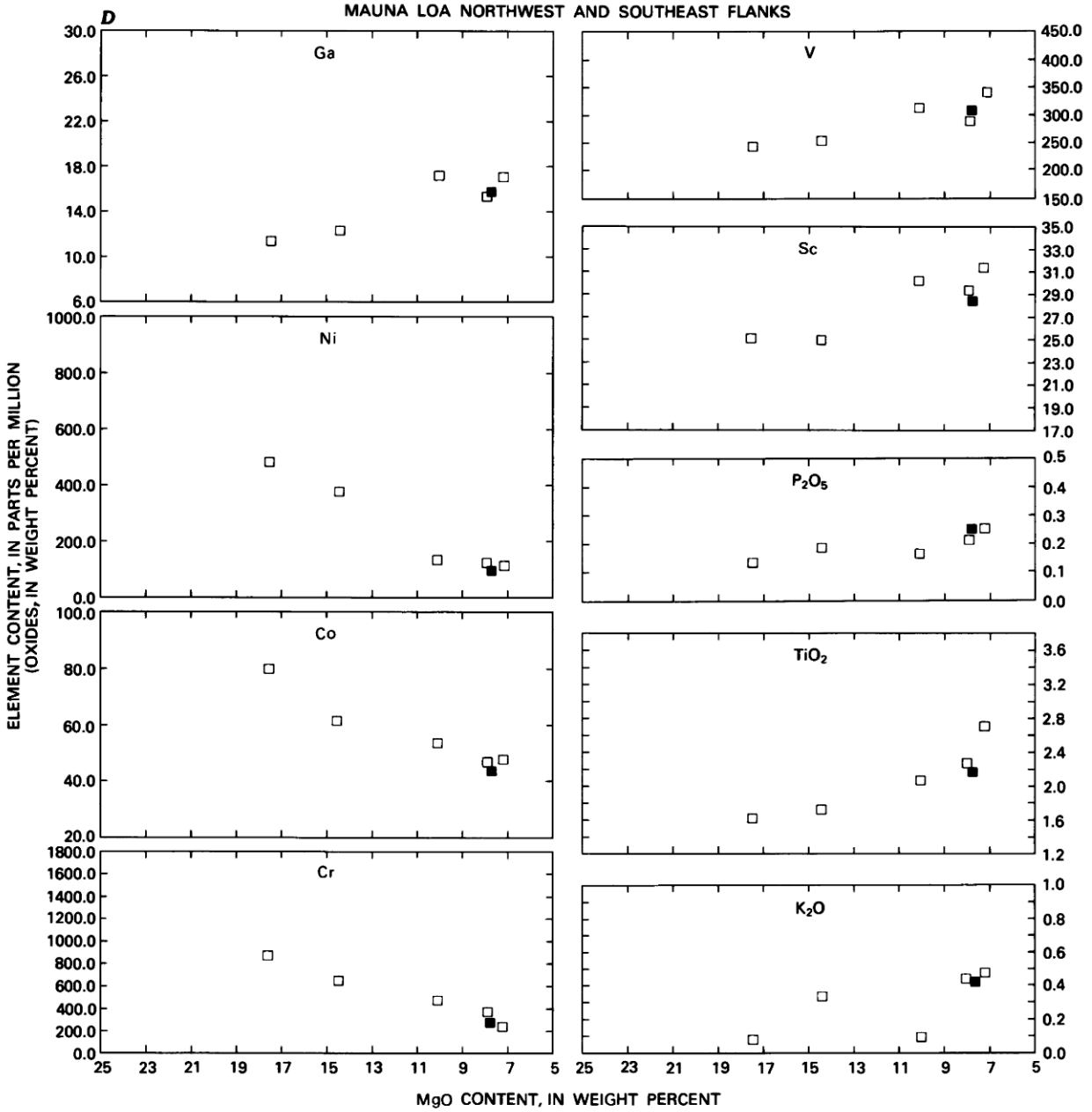

FIGURE 24.10.—Continued.

TABLE 24.20.—*Average compositions of spatial and temporal groups of olivine-controlled lava of Mauna Loa, adjusted to 7.00 weight percent MgO*

[Calculated from data in table 24.15–24.18: S.d., standard deviation. Oxide values in weight percent; values for elements in parts per million. Numbers of samples where different from numbers (n) given: summit, 3 for Cs and 4 for V, Ni, Mo, Zn, Ga, Y, U, Pb, Ce, and Yb; northeast rift zone, 3 for Cs; southwest rift zone, 8 for V, Ni, Mo, Zn, Ga, Y, U, Pb, Nd, and Lu, 7 for Sm; northwest and southeast flanks, 5 for Cs, 4 for Nd; prehistoric, 9 for V, Ni, Mo, Zn, Ga, Y, U, Pb, Sm, and Yb, 8 for Cs and Nd; 18th and 19th centuries, 7 for Sm and 6 for Cs; 20th century, 5 for V, Ni, Mo, Zn, Ga, Y, U, Pb, Ce, and Nd]

	Spatial groups								Temporal groups							
	Summit		Northeast rift zone		Southwest rift zone		Northwest and Southeast flanks		Prehistoric		18th-9th centuries		20th century		Historical (all)	
	n=5		n=4		n=9		n=6		n=10		n=8		n=6		n=14	
	Mean	S.d.	Mean	S.d.	Mean	S.d.	Mean	S.d.	Mean	S.d.	Mean	S.d.	Mean	S.d.	Mean	S.d.
MgO	7.00	-	7.00	-	7.00	-	7.00	-	7.00	-	7.00	-	7.00	-	7.00	-
P_2O	.40	.05	.40	.03	.40	.05	[1] .44	<.02	[1] .44	.03	.40	.05	.37	<.02	.39	.04
TiO_2	2.07	.14	2.12	.04	2.10	.10	[2]2.20	.08	[2]2.16	.11	2.11	.13	2.08	.03	2.10	.10
P_2O_5	.23	<.02	.23	<.02	.22	.02	.24	.01	[1] .24	<.02	.23	.02	.21	<.01	.22	.02
Cs	.20	.13	.10	.03	.36	.32	[1] .17	.07	.29	.29	.26	.26	.18	.10	.22	.20
Ba	107	37	180	68	120	47	118	22	102	25	156	47	128	62	144	54
Sc	32.3	1.3	31.3	1.6	[3]30.6	.5	31.2	1.7	31.2	1.5	[3] 31.6	1.5	30.9	1.0	31.6	1.8
V	294	22	312	5	324	26	315	16	302	24	315	12	332	20	321	17
Cr	[4]218	30	258	30	228	11	200	94	[4]210	82	[4]240	34	227	19	234	27
Co	[5]48.1	3.7	42.2	2.2	[5]42.6	3.0	41.2	5.1	[5]41.2	4.2	[5]44.1	4.4	44.7	3.2	44.5	3.
Ni	[4]88	1	[6]76	18	[7]72	25	[8]73	25	[9]86	15	[10]58	22	[11]83	14	7	
Mo	4.2	.5	4.9	1.0	5.0	.09	4.6	.9	4.7	.6	4.7	1.3	4.8	.4	4.7	1.0
Zn	131	24	132	15	123	14	119	12	121	11	133	19	121	13	128	18
Ga	16.5	1.7	19.0	2.3	18.2	2.1	16.2	1.3	16.6	1.7	16.9	1.8	20.0	.6	18.1	2.1
Hf	3.6	.1	3.3	.2	3.2	.3	3.4	.4	3.4	.4	3.4	.2	3.3	.3	3.3	.2
Y	18.1	1.6	17.2	1.6	19.6	3.0	19.0	2.4	18.5	2.2	18.0	2.2	20.3	2.8	18.9	2.6
U	.20	.05	.22	.05	.20	.04	.24	.08	.24	.06	.21	.05	.20	.04	.20	.04
Pb	2.2	.5	1.9	.8	2.8	1.1	2.6	1.4	2.4	1.2	2.5	1.2	2.5	.5	2.5	1.0
La	9.5	1.1	9.8	.7	9.2	1.2	10.0	1.8	10.2	1.5	9.4	1.0	8.7	.4	9.1	.9
Ce	27.4	2.8	25.0	1.9	23.5	3.9	23.7	4.6	25.8	4.7	24.6	2.3	21.8	2.2	23.5	2.6
Nd	18.0	1.4	17.8	1.3	17.0	1.5	15.8	1.8	17.6	2.2	17.1	1.4	16.7	.5	16.9	1.1
Sm	4.86	.24	4.59	.19	4.39	.19	4.67	.52	4.68	.48	4.66	.19	4.45	.26	4.56	.24
Eu	1.79	.08	1.69	.12	1.61	.15	1.70	.21	1.70	.17	1.73	.10	1.58	.19	1.67	.15
Dy	5.4	.4	5.1	.4	5.3	.8	5.2	.7	5.2	.6	4.8	1.7	5.1	.6	5.3	.6
Yb	2.15	.20	1.91	.02	2.03	.14	2.02	.13	1.98	.13	2.07	.19	2.00	.10	2.04	.16
Lu	.29	.03	.25	.01	.27	.01	.26	.01	.28	.03	.27	<.02	.26	<.02	<.27	<.02

[1]Anomalously low values of K_2O and TiO_2 (samples ID-275-2 and ID-214-2) omitted.
[2]High adjusted value of 2.69 ppm (sample ID-098-2) omitted.
[3]High adjusted value of 36.0 ppm (sample 1868 ML) omitted.
[4]Two negative adjusted values (samples TLW67-84 and TLW67-89) omitted. (See text, appendix 24.1).
[5]Anomalously low adjusted values (<30 ppm) (samples TLW67-84, C819, 1868 ML) omitted.
[6]Two negative adjusted values (samples TLW67-61 and TLW67-63) omitted.
[7]Two negative adjusted values (samples C819 and 1868 ML) omitted.
[8]Three negative adjusted values (samples TLW67-117A, ID-275-2, and ID-214-2) omitted.
[9]Five negative adjusted values (samples TLW67-84, 65 MAN-1, TLW67-117A, ID-275-2, and ID-214-2) omitted.
[10]Four negative adjusted values (samples TLW67-89, TLW67-61, TLW67-63, and 1868 ML) omitted.
[11]The negative adjusted value for sample TLW67-79 omitted.

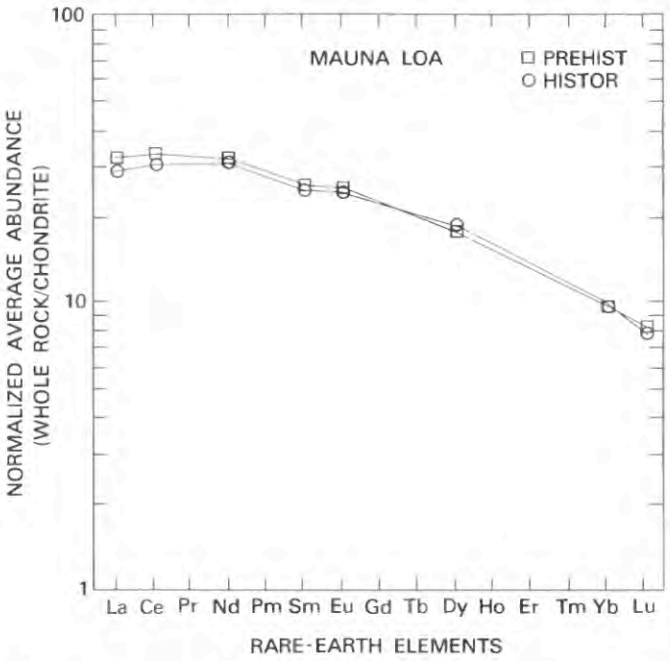

FIGURE 24.11.—Chondrite-normalized average REE abundances showing difference in LREE between prehistoric (PREHIST) and historical (HISTOR) lava of Mauna Loa (see table 24.20). Data of Budahn and Schmitt (1985, table 2) demonstrate a similar systematic difference.

TABLE 24.21.—*Averages of MgO-adjusted mean abundances of selected incompatible elements in historical lava of Mauna Loa*

[Calculated from data of Rhodes (1983, table 1). S.d., standard deviation. Oxide values in weight percent, values for trace elements in parts per million; see text and figure 24.12 for rationale in grouping eruptions]

	Average of 5 pre-1870 eruptions[1]		Average of 11 post-1870 eruptions[2]	
	Mean	S.d.	Mean	S.d.
K_2O	0.43	0.02	0.36	0.02
TiO_2	2.13	.02	2.06	.03
P_2O_5	.26	.01	.23	.01
Nb	10.5	.2	9.4	.2
Zr	140	5	131	4
Sr	350	16	309	10

[1]Total of 31 analyses for the following eruptions: 1843, 1852, 1855, 1859, and 1868 (see Rhodes, 1983, for the individual means and standard deviations of these and the eruptions listed below).

[2]Total of 83 analyses for the following eruptions: 1880, 1887, 1899, 1907, 1916, 1926, 1935, 1942, 1949, 1950, and 1975.

July 1968. It is beyond the scope of this paper to review the various petrogenetic models proposed for Hawaiian tholeiite in the light of the possible space-time-composition relations suggested by our reconnaissance study. It is clear, however, that any complete model involving partial melting and fractionation must reconcile not only the compositional differences between Mauna Loa and Kilauea lava, but also the time-space chemical variations within the lava of each volcano.

LONG-TERM AND SHORT-TERM VARIATIONS

Differences in MgO-adjusted composition within the summit (olivine-controlled) lava are interpreted to represent chemically distinct batches of magma derived from a source, or sources, whose composition evolves with time. A long-term secular major-element variation for Kilauea lava, on the scale of centuries to millenia, has been well documented by Wright (1971, p. 29), who showed that younger lava becomes progressively "richer in the olivine-incompatible constituents (K_2O, P_2O_5, TiO_2)" with time. The results of this study, as well as those of other recent studies (for example, Casadevall and Dzurisin, chapter 13; Easton and Garcia, 1980; Budahn and Schmitt, 1985) show that long-term temporal variations are also evident in trace-element abundance patterns.

Superimposed on this long-term temporal variation for Kilauea lava are shorter term (years to decades) variations, as shown by the chemically distinct MgO-adjusted lava compositions for five summit eruptions, including Kilauea Iki, during the 16-year period from 1952 to 1968 (Wright, 1971, fig. 12). An excellent recent example of short-term compositional variation at Kilauea is afforded by the olivine-controlled lava of the 1969–74 Mauna Ulu eruption (Tilling and others, chapter 16; Swanson and others, 1979). During its 5-year period, this eruption produced 10 chemically distinct variants, interpreted by Wright and others (1975) and Wright and Tilling (1980) to represent new magma batches entering Kilauea's storage reservoir. Hoffman and others (1984) confirmed the short-term secular compositional variation in the Mauna Ulu lava, defined by "monotonic decrease" in the abundances of certain elements, but interpreted it in terms of an equilibrium partial melting model not requiring magma batches. The major-element composition of the Mauna Ulu lava appears to show at least a short-term reversal of the long-term secular variation at Kilauea (Wright and others, 1975). Whether this change represents a permanent departure from the overall trend remains to be tested by systematic evaluation of the chemistry of lava erupted at Kilauea since June 1974.

Possible short-term secular variations, as expressed by compositional changes with small differences in stratigraphic position, also are apparent in recent studies on prehistoric Kilauea lava (Casadevall and Dzurisin, chapter 13; Easton and Garcia, 1980), but it is not possible to place precise time constraints on these samples. However, from detailed data on 20th-century olivine-controlled Kilauea lava, particularly from the Mauna Ulu eruption, we know that significant changes, not explainable by olivine control, can occur on a time scale of a year or less.

Perhaps the most significant conclusions from this reconnaissance study are that: (1) Mauna Loa lava, like Kilauea lava, shows long-term secular variation in composition; and (2) the trends of such variation for the two volcanoes diverge, providing additional evidence that their magmatic systems operate independently. The focus and sampling of our study were not intended to identify possible short-term variations in the MgO-adjusted olivine-controlled Mauna Loa lava. However, we believe that the comprehensive data of Rhodes (1983), in addition to confirming our suggestion of secular variation between the 19th century and 20th-century lava, also provides good evidence of short-term variation on a time scale as

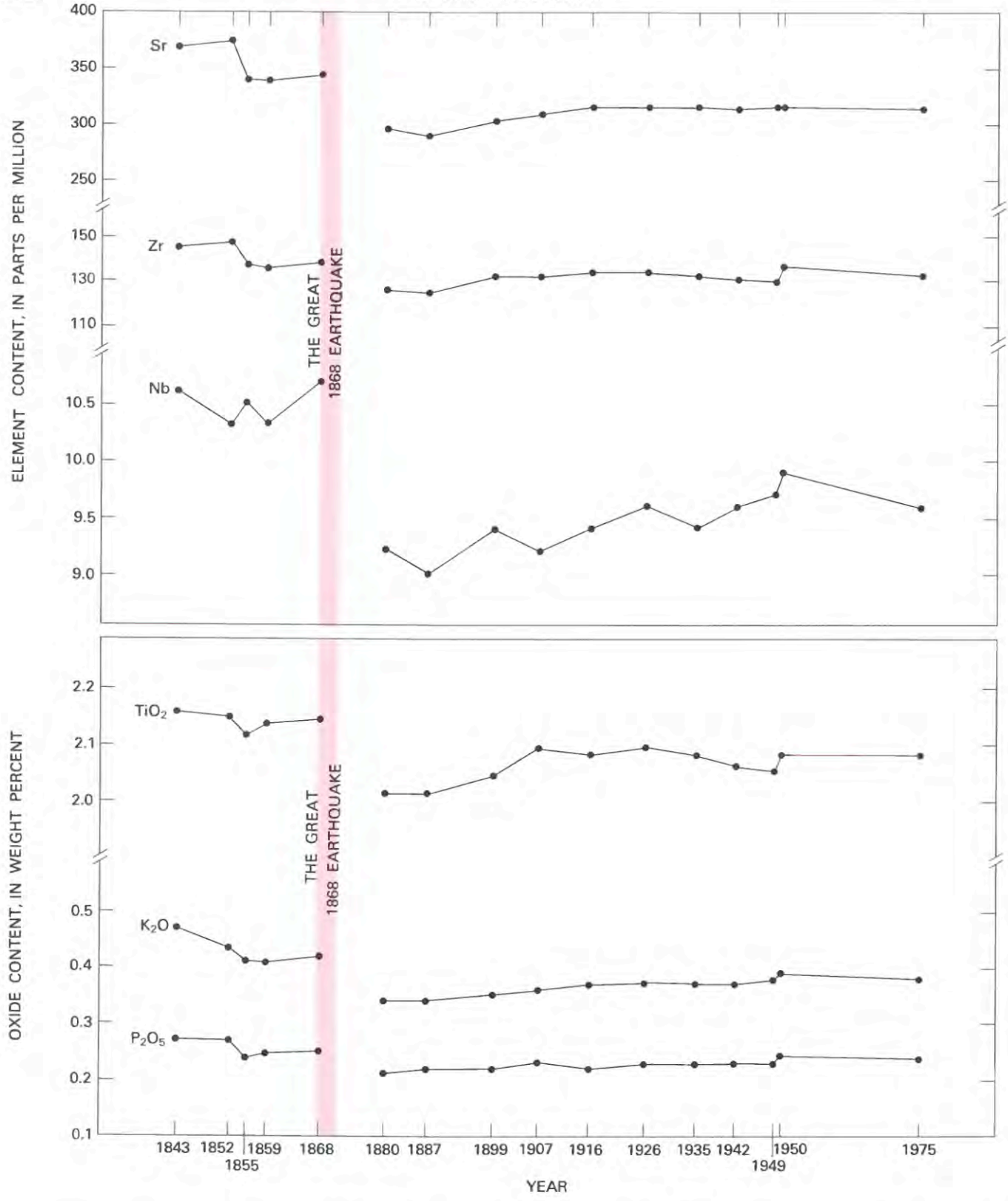

FIGURE 24.12.—MgO-adjusted average contents of olivine-incompatible elements and oxides in lava of historical Mauna Loa eruptions (data of Rhodes, 1983) plotted against year of eruption. Data published as averages; thus, individual analyses could not be adjusted for MgO content before computation of mean, as generally done in this paper (see appendix 24.1). Compositional break between 1868 and 1880 eruptions may reflect disruptive effects of catastrophic 1868 earthquake (see text).

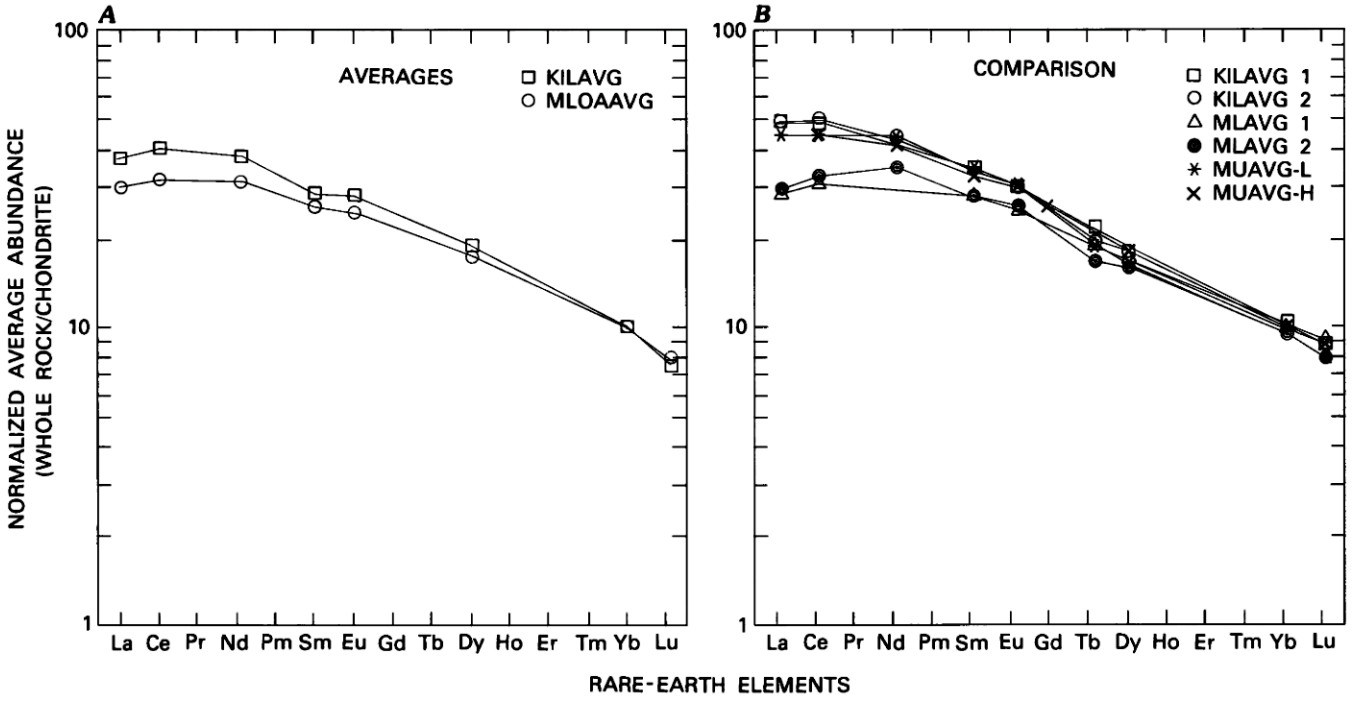

FIGURE 24.13.—Difference in MgO-adjusted average REE abundances between Kilauea (KIL), including Mauna Ulu (MU), and Mauna Loa (ML) lava samples. *A*, Data of this paper. *B*, Previously published data: KILAVGl and MLAVG 1 (Basaltic Volcanism Study Project, 1981); KILAVG2 MLAVG2, and MUAVG-L (Leeman and others, 1980); MUAVG-H (Hoffman and others, 1984). See also figure 24.4 for data of Budahn and Schmitt (1985) showing compositional distinction between Mauna Loa and Kilauea.

small as one year (fig. 24.12; Rhodes and others, 1982; Rhodes, 1983). Although the variations shown in figure 24.12 may in some instances be within analytical uncertainty, the nonrandom nature of the variations and the remarkable conformity of the trends convince us that the differences shown are real. Rhodes and others (1982, abstract 43) labeled the compositional changes observed for historical Mauna Loa lava, including the "sudden drop between 1868 and 1880," as "episodic" variations. However, we interpret these compositional variations (fig. 24.12) as a segment of a long-term secular trend of decreasing abundances of the incompatible elements considered. This trend was abruptly disrupted by the processes accompanying or immediately following the 1868 eruption, but a gradual recovery afterward reestablished conformance with the general trend.

Some observations concerning the 1868 eruption are pertinent and might bear on the sharp compositional break. Some of the lava from the 1868 eruption is picritic—containing as much as 50 percent olivine phenocrysts—and has the highest mean MgO content (17.69 weight percent) of any historical Mauna Loa lava (Rhodes, 1983, table 1). This eruption began at Mauna Loa summit on March 27, 1868, and initially produced lava of moderate MgO content (~9 percent, according to Rhodes, 1983). On April 2, a catastrophic earthquake struck the Island of Hawaii; this earthquake was the largest historical earthquake in Hawaii and estimated to be greater than the magnitude-7.2 event at Kalapana on November 29, 1975 (Tilling and others, 1976). The 1868 eruptive activity shifted to the southwest rift zone on April 7, and picritic lava began to be erupted from a 5-km-long fissure, marking the first major historical activity in Mauna Loa's southwest rift zone. As noted by Lipman (1980, p. 709), the eruptive fissure was localized at the lowest elevation of any historical vent (600–900 m) in a segment of the southwest rift where "no large eruption appears to have occurred for several thousand years previously." Lipman (p. 709) suggests that the earthquake, apparently centered along the southeast flank of Mauna Loa, "may have been significant in opening up a lower part of the rift zone from which access of magma had previously been blocked for a long time."

The eruption, which ended on April 11, 1868, is interpreted to have successively tapped first the upper (olivine-poor) and then the lower (olivine-rich) part of a zoned magma reservoir developed by olivine settling (Lipman, 1980). We further suggest that the 1868 earthquake may have caused a sudden, drastic change in Mauna Loa's magma regime, as expressed by the abrupt compositional discontinuity and decades-long subsequent recovery in the long-term secular variation trend for Mauna Loa lava (fig. 24.12). Lockwood and Lipman (chapter 18, fig. 18.7) show that the average lava-production rate for Mauna Loa after 1877 was less than half that before 1877 and note that this marked change coincides with the compositional shift in historical lava (Rhodes and others, 1982). Lockwood and Lipman (chapter 18) also, independently from our study, suggest that this change in rate and composition might be related to the 1868 earthquake.

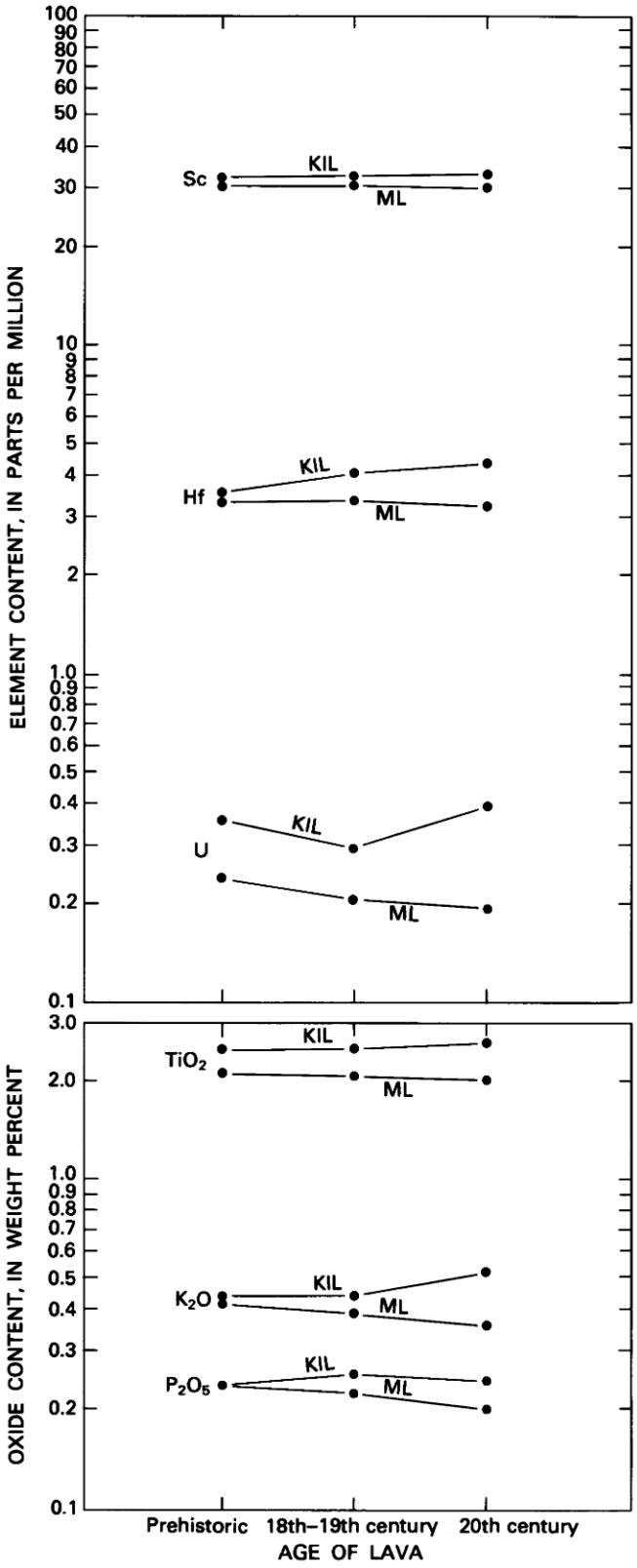

FIGURE 24.14.—Apparent diverging long-term secular compositional trends for Kilauea (KIL) and Mauna Loa (ML) olivine-controlled lava, as suggested by variations in MgO-adjusted mean contents of K, Ti, P, Sc, Hf, and U. (Data from tables 24.13 and 24.20).

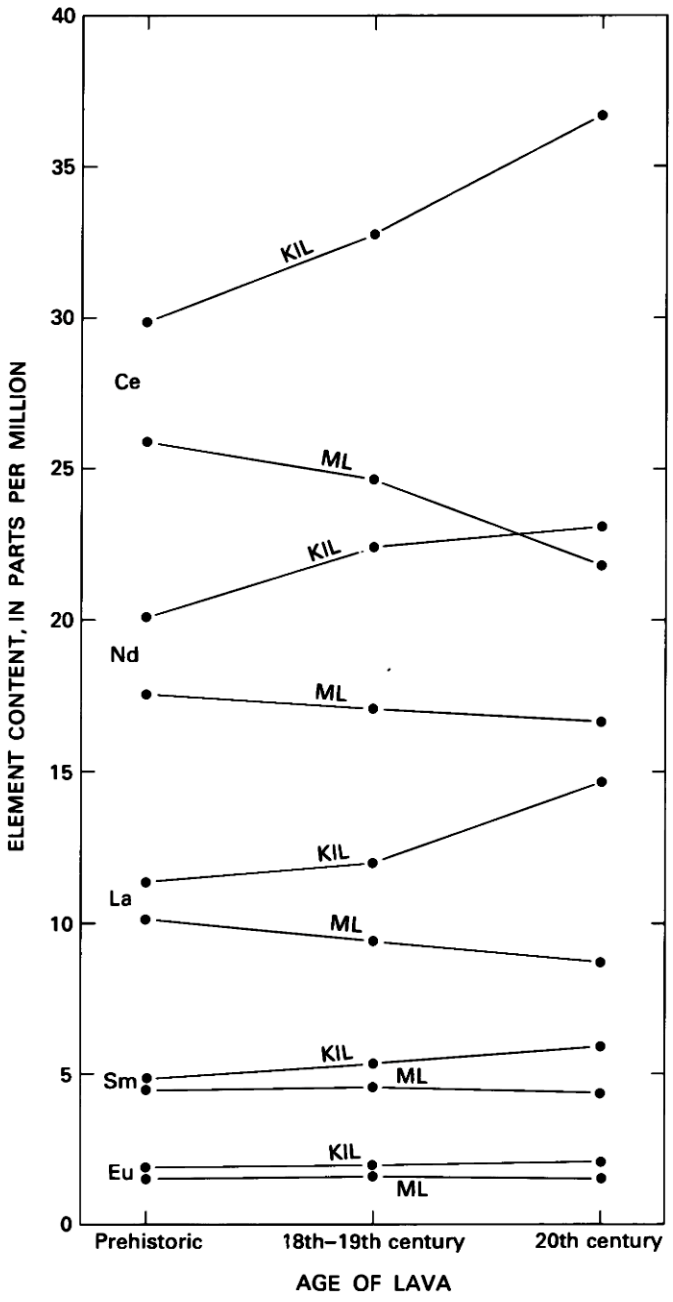

FIGURE 24.15.—Diverging long-term secular compositional trends of Kilauea (KIL) and Mauna Loa (ML) lava, as shown by variations in MgO-adjusted mean LREE abundances (data of tables 24.13 and 24.20). HREE abundance patterns of two volcanoes tend to converge, and no systematic differences are evident within analytical uncertainty.

The apparent coincidence between the compositional break, the change in lava-production rate, and the catastrophic 1868 earthquake may be purely fortuitous, but we speculate that these phenomena are at least indirectly related. If so, it would be of interest to determine whether a similar compositional break might exist for Kilauea lava, in view of the fact that the 1868 earthquake also apparently triggered, on the same day, (1) a brief eruptive outbreak at Kilauea Iki; (2) extrusion of a small amount of lava in the southwest rift zone about 15 km from the summit; and (3) approximately 100 m of subsidence of the floor of Kilauea caldera, without affecting the ongoing lava-lake activity at Halemaumau (Tilling and others, 1976; Lipman, 1980). A major change in Kilauea magma regime related to the 1975 Kalapana earthquake (magnitude 7.2) has been well documented (Dzurisin and others, 1981, 1984). Moreover, a much lower energy (magnitude 6.2) earthquake in April 1973 is interpreted to have caused substantial disruption in the magma conduit system during the 1972–74 Mauna Ulu eruption (Tilling and others, chapter 16), but the possibility that the 1973 and 1975 earthquakes might also coincide with detectable compositional changes in Kilauea lavas erupted since 1971 has not been evaluated.

DIRECTIONS FOR FUTURE STUDIES

This reconnaissance study clearly needs to be followed by more quantitative studies to confirm, refine, or reject our preliminary findings. Subsequent investigations ought to include, though not be limited to, the following.

PRECISE AND ACCURATE DETERMINATIONS OF ADDITIONAL TRACE ELEMENTS

The tentative conclusions we reached in this study are based primarily on analytical data for the well determined olivine-incompatible elements (K, Ti, P, Sc, Hf, U, and the REE), although some of the less well determined elements provide permissive evidence. It would be important to test our findings with comparably well determined abundances of other selected key incompatible elements, ideally in the same rock powders (to minimize effects of possible sample inhomogeneity) that we have analyzed. Some of the other key incompatible elements that should be investigated include Rb, Cs, Sr, Ba, Zr, Nb, Ta, and Th. In addition, the abundances of Ir, Au, and Ag in volcanic rocks, which can be precisely and accurately determined at concentrations of less than one part per billion, have been shown to be highly sensitive to differentiation processes as well as source-area effects (see, for example, Gottfried and Greenland, 1972; Bornhorst and others, 1984). Thus, systematic studies of Au, Ag, and the platinum metals, as well as studies of Cu and S to assess the effect of possible immiscible sulfide melt in tholeiite magma (for example, Skinner and Peck, 1969; Moore and Fabbi, 1971; Gottfried, 1983) should provide important trace-element data to complement the already abundant data for incompatible elements.

QUANTITATIVE OLIVINE-CONTROL LINES FOR SELECTED ELEMENTS

Excellent olivine-control lines are available for the major elements of interest, but the limited data of Rhodes (1983) and Gunn (1971) are the only systematic analytical data for both olivine-compatible and olivine-incompatible trace elements available in the published literature. Such studies should include as a critical component the analysis of olivine (and included chromite) mineral separates, preferably from the lava analyzed; however, even analysis of unrelated, but more easily concentrated, olivine separates of comparable bulk compositions could at least provide some general compositional constraints. Lava suites from the 1959 Kilauea Iki eruption, or from the 1868 Mauna Loa eruption, would serve as ideal samples for initial detailed analytical studies to establish quantitative olivine-control lines for key trace elements. It is anticipated that, with sufficiently precise determinations of olivine-compatible trace elements, several olivine-control lines could be defined for the various groupings of Mauna Loa lava, rather than only the one determined for the historical lava; in contrast, four separate control lines have already been determined for Kilauea lava in terms of major elements alone (Wright, 1971, table 3).

SYSTEMATIC STUDY OF PREHISTORIC LAVA SUITES

Studies in recent years have greatly improved our understanding of the chronology and distribution of the prehistoric lava of Kilauea and Mauna Loa (for example, Lockwood and Lipman, chapter 18; Holcomb, 1980, 1981; Lipman, 1980a, b; Moore, 1983; Lipman and Swenson, 1984). Systematic geochemical studies of these rocks now can be interpreted in a fairly well understood space and time framework. An obvious objective of further studies would be to detect temporal and spatial patterns that would better define longer term variation trends. Another important objective would be to determine how long the chemical distinction between Mauna Loa and Kilauea has been in existence. Available data suggest that the distinction has existed for more than 30,000 years (Rhodes and Lipman, 1979; Easton and Garcia, 1980).

SYSTEMATIC STUDY OF DIFFERENTIATED AND HYBRID LAVAS

The acquisition of precise data to establish quantitative control lines for olivine-controlled lava would make it possible to apply trace-element constraints to lava whose composition is determined by other major liquidus phases (clinopyroxene, orthopyroxene, and plagioclase) in addition to, or instead of, olivine. Once variation patterns are well defined for both olivine-controlled and differentiated lava, then trace-element abundances can be incorporated to provide additional variables in mixing calculations to determine the lineage of hybrid lavas. Such studies would extend the work of Wright and Fiske (1971) and serve to test their models based on major-element variations alone.

DEVELOPMENT OF COMPLETE PETROGENETIC MODELS FOR HAWAIIAN THOLEIITE

Most proposed models for the generation, transport, storage, and eruption of Hawaiian basalt are incomplete because they do not fully take into account both the long-term and the short-term secular variations in composition of the erupted lava. The preliminary results of this study, we believe, are compatible with the earlier conclusion of Wright (1971) that both the long-term and short-term variations in the MgO-adjusted composition of olivine-controlled lava reflect high-pressure fractionation processes that occur before storage in shallow magma reservoirs. However, if our speculations concerning the 1868 eruption and earthquake are valid, then the possibility that some short-term variations are produced by other processes cannot be entirely discounted.

We suggest that such complex secular chemical variation requires the magma source region(s) to be heterogeneous and possibly compositionally zoned laterally and vertically. Assuming that our inferred short-term and long-term variations, including the divergence of long-term variation trends for Kilauea and Mauna Loa, withstand the test of more data, we recommend that future petrogenetic models for Hawaiian basaltic volcanism incorporate such secular variations to furnish additional model constraints.

REFERENCES

Abbey, S., 1983, Studies in "standard samples" of silicate rocks and minerals: Geological Survey of Canada Paper 83–15, 114 p.

Aramaki, Shigeo, and Moore, J.G., 1969, Chemical composition of prehistoric lavas at Makaopuhi Crater, Kilauea Volcano, and periodic change in alkali content of Hawaiian tholeiitic lavas: Tokyo University Earthquake Research Institute Bulletin, v. 47, pt. 2, p. 257–270.

Basaltic Volcanism Study Project, 1981, Basaltic Volcanism on the Terrestrial Planets: Elmsford, N.Y., Pergamon Press, 1,286 p.

Bertine, K.K., Chan, L.H., and Turekian, K.K., 1970, Uranium determinations in deep-sea sediments and natural water using fission tracks: Geochimica et Cosmochimica Acta, v. 34, p. 641–648.

Bornhorst, T.J., Rose, WI., Jr., and Wolfe, S.P., 1984, Abundance of gold and silver in fresh calc-alkalic Quaternary volcanic rocks [abs.]: Geological Society of America Abstracts with Program, v. 16, no. 6, p. 450.

Budahn, J.R., and Schmitt. R.A., 1985, Petrogenetic modeling of Hawaiian tholeiitic basalts: A geochemical approach: Geochimica et Cosmochimica Acta, v. 49, p. 67–87.

Clague, D.A., and Frey, F.A., 1982, Petrology and trace element geochemistry of the Honolulu Volcanics, Oahu: Implications for the oceanic mantle below Hawaii: Journal of Petrology, v. 23, p. 447–504.

Cross, W.G., and Tommasino, L., 1970, A rapid reading technique for nuclear particle damage tracks in thin foils: Radiation Effects, v. 5, p. 85–89.

DePaolo, D.J., and Wasserburg, G.J., 1976, Nd isotopic variations and petrogenetic models: Geophysical Research Letters, v. 3, p. 249–252.

Dodge, F.C.W., Millard, H.T., Jr., and Elsheimer, H.N., 1982, Compositional variations and abundances of selected elements in granitoid rocks and constituent minerals, central Sierra Nevada batholith, California: U.S. Geological Survey Professional Paper 1248, 24 p.

Doe, B.R., Lipman, P.W., Hedge, C.E., and Kurasawa, H., 1969, Primitive and contaminated basalts from the southern Rocky Mountains, U.S.A.: Contributions to Mineralogy and Petrology, v. 21, p. 142–156.

Dorrzapf, A.F., Jr., 1973, Spectrochemical computer analysis—Argon-oxygen D-C arc method for silicate rocks: U.S. Geological Survey Journal of Research, v. 1, no. 5, p. 559–562.

Duffield, W.A., Christiansen, R.L., Koyanagi, R.Y., and Peterson, D.W., 1982, Storage, migration, and eruption of magma at Kilauea Volcano, Hawaii, 1971–1972: Journal of Volcanology and Geothermal Research, v. 13, p. 273–307.

Dzurisin, Daniel, and Koyanagi, R.Y., 1981, Changed magma budget since 1975 at Kilauea Volcano, Hawaii: U.S. Geological Survey Open-File Report 81–571, 46 p.

Dzurisin, Daniel, Koyangi, R.Y., and English, T.T., 1984, Magma supply and storage at Kilauea Volcano, Hawaii, 1956–1983: Journal of Volcanology and Geothermal Research, v. 21, no. 3/4, p. 177–206.

Easton, R.M., and Garcia, M.O., 1980, Petrology of the Hilina Formation, Kilauea Volcano, Hawaii: Bulletin Volcanologique, v. 43, p. 657–674.

Evernden, J.F., Savage, D.E., Curtis, G.H., and James, G.T., 1964, Potassium-argon dates and the Cenozoic mammalian chronology of North America: American Journal of Science, v. 262, p. 145–198.

Frey, F.A., 1980, The origin of pyroxenites and garnet pyroxenites from Salt Lake Crater, Oahu, Hawaii: Trace element evidence: American Journal of Science, v. 280–A, pt. 2, p. 427–449.

Frey, F.A., and Clague, D.A., 1983, Geochemistry of diverse basalt types from Loihi Seamount, Hawaii: petrogenetic implications: Earth and Planetary Science Letters, v. 66, p. 337–355.

Frey, F.A., Haskin, L.A., Poetz, J., and Haskin, M.A., 1968, Rare earth abundances in some basic rocks: Journal of Geophysical Research, v. 73, p. 6085–6098.

Gast, P.W., 1968, Trace-element fractionation and the origin of tholeiitic and alkaline magma types: Geochimica et Cosmochimica Acta, v. 32, p. 1057–1086.

Gladney, E.S., Burns, C.E., and Roelandts, I., 1983, 1982 compilation of elemental concentrations in eleven United States Geological Survey rock standards: Geostandards Newsletter, v. 7, p. 3–226.

Gladney, E.S., and Goode, W.E., 1981, Elemental concentrations in eight new United States Geological Survey rock standards: Geostandards Newsletter, v. 5, p. 31–64.

Gottfried, David, 1983, Cu, Ni, and Co fractionation patterns in Mesozoic tholeiitic magmas of eastern North America: Evidence for sulfide fractionation [abs.]: Geological Society of America Abstracts with Program, v. 15, no. 2, p. 92.

Gottfried, David, and Greenland, L.P., 1972, Variation of iridium and gold in oceanic and continental basalts: International Geological Congress, 24th, Montreal, Canada, Proceedings, Section 10, p. 135–144.

Govindaraju, K., 1984, 1984 compilation of working values and sample description for 170 international reference samples of mainly silicate rocks and minerals: Special Issue, July 1984, Geostandards Newsletter, p. 3–16 (exclusive of appendices).

Gunn, B.M., 1971, Trace element partition during olivine fractionation of Hawaiian basalts: Chemical Geology, v. 8, p. 1–13.

Helz, R. T., 1980, Crystallization history of Kilauea Iki lava lake as seen in drill core recovered in 1967–1979: Bulletin Volcanologique, v. 43, no. 4, p. 675–702.

Hoffman, A.W., Feigenson, M.D., and Raczek, Ingrid, 1984, Case studies on the origin of basalt: III. Petrogenesis of the Mauna Ulu eruption, Kilauea, 1969–1971: Contributions to Mineralogy and Petrology, v. 88, p. 24–35.

Holcomb, R.T., 1980, Preliminary geologic map of Kilauea Volcano, Hawaii: U.S. Geological Survey Open-File Report 80–796, 2 map sheets, scale 1:50,000.

———1981, Kilauea Volcano, Hawaii: Chronology and morphology of the surficial lava flows: U.S. Geological Survey Open-File Report 81–354, 321 p.

Hubbard, N. J., 1969, A chemical comparison of oceanic ridge, Hawaiian tholeiitic and Hawaiian alkalic basalts: Earth and Planetary Science Letters, v. 5, p. 346–352.

Jackson, D.B., Swanson, D.A., Koyanagi, R.Y., and Wright, T.L., 1975, The August and October 1968 east rift eruptions of Kilauea Volcano, Hawaii: U.S. Geological Survey Professional Paper 890, 33 p.

Leeman, W.P., Budahn, J.R., Gerlach, D.C., Smith, D.R., and Powell, B.N., 1980, Origin of Hawaiian tholeiites: trace element constraints: American Journal of Science, v. 280–A, part 2, p. 794–819.

Leeman, W.P., Murali, A.V., Ma, M.S., and Schmitt, R.A., 1977, Mineral

constitution of mantle source regions for Hawaiian basalts—rare earth element evidence for mantle heterogeneity, *in* Magma genesis: Oregon Department of Mineral Industries Bulletin 96, p. 169–183.

Lipman, P.W., 1980a, Rates of volcanic activity along the southwest rift zone of Mauna Loa Volcano. Hawaii: Bulletin Volcanologique, v. 43. no. 4, p. 703–726.

———1980b, The southwest rift zone of Mauna Loa: Implications for structural evolution of Hawaiian volcanoes: American Journal of Science, v. 280-A, part 2, p. 752–776.

Lipman, P.W., and Swenson, Alan, 1984, Generalized geologic map of the southwest rift zone of Mauna Loa Volcano, Hawaii: U.S. Geological Survey Miscellaneous Investigations Series Map I–1312, scale 1:100,000.

Macdonald, G.A., 1949a, Petrography of the Island of Hawaii: U.S. Geological Survey Professional Paper 214–D, p. 51–96.

———1949b, Hawaiian petrographic province: Geological Society of America Bulletin, v. 60, p. 1541–1596.

———1968, Composition and origin of Hawaiian lavas: Geological Society of America Memoir 116, p. 477–522.

Millard, H.T., Jr., and Keaten, B.A., 1982, Precision of uranium and thorium determinations by delayed neutron counting: Journal of Radioanalytical Chemistry, v. 72, p. 489–500.

Moore, J.G., and Calk, Lewis, 1971, Sulfide spherules in vesicles of dredged pillow basalt: American Mineralogist, v. 56, p. 476–488.

Moore, J.G., and Fabbi, B.P., 1971, An estimate of the juvenile sulfur content of basalt: Contributions to Mineralogy and Petrology, v. 41, p. 105–118.

Moore, R.B., 1983, Distribution of differentiated tholeiitic basalts on the lower east rift zone of Kilauea Volcano, Hawaii: A possible guide to geothermal exploration: Geology, v. 11, p. 136–140.

Murata, K.J., 1970, Tholeiitic basalt magmatism of Kilauea and Mauna Loa Volcanoes of Hawaii: Naturwissenschaften, v. 57, p. 108–113.

Murata, K. J., and Richter, D.H., 1966a, Chemistry of the lavas of the 1959–60 eruption of Kilauea Volcano, Hawaii: U.S. Geological Survey Professional Paper 537–A, 26 p.

———1966b, The settling of olivine in Kilauean magma as shown by lavas of the 1959 eruption: American Journal of Science, v. 264, p. 194–203.

O'Nions, R.K., Hamilton, P.J., and Evensen, N.M., 1977, Variations in $^{143}Nd/^{144}Nd$ and $^{87}Sr/^{86}Sr$ ratios in oceanic basalts: Earth and Planetary Science Letters, v. 34, p. 13–22.

Peterman, Z.E., and Hedge, C.E., 1971, Related strontium isotopic and chemical variations in oceanic basalts: Geological Society of America Bulletin, v. 82, p. 493–499.

Powell, J.L., and Delong, S.E., 1966, Isotopic composition of strontium in volcanic rocks from Oahu: Science. v. 153. p. 1239–1242.

Powers, H.A., 1955, Composition and origin of basaltic magma of the Hawaiian Islands: Geochimica et Cosmochimica Acta, v. 7, p. 77–107.

Rhodes, J.M., 1983, Homogeneity of lava flows: Chemical data for historic Mauna Loan eruptions: Journal of Geophysical Reserach. v. 88 (supplement), p. A869–A879.

Rhodes, J.M., and Lipman, P.W., 1979, Chemistry of prehistoric lavas erupted along the southwest rift zone of Mauna Loa [abs.]: Hawaii Symposium on Intraplate Volcanism and Submarine Volcanism, July 1979, Hilo, Hawaii, Abstract Volume, p. 97.

Rhodes, J.M., Lockwood, J.P., and Lipman, P.W., 1982, Episodic variation in magma chemistry, Mauna Loa Volcano, Hawaii [abs.]: International Association of Volcanology and Chemistry of the Earth's Interior–International Association of Geochemistry and Cosmochemistry Scientific Assembly, Generation of major basalt types, August 1982, Reykjavik, Iceland, Abstract Volume, Abstract No. 43.

Richter, D.H., Eaton, J.P., Murata, K.J., Ault, W.U., and Krivoy, H.L., 1970, Chronological narrative of the 1959–60 eruption of Kilauea Volcano, Hawaii: U.S. Geological Survey Professional Paper 537–E, 73 p.

Richter, D.H., and Murata, K.J., 1966, Petrography of the lavas of the 1959–60 eruption of Kilauea Volcano, Hawaii: U.S. Geological Survey Professional Paper 537–D, 12 p.

Schilling, J.G., and Winchester, J.W., 1969, Rare earth contribution to the origin of Hawaiian lavas: Contributions to Mineralogy and Petrology, v. 23, p. 27–37.

Skinner, B.J., and Peck, D.L., 1969, An immiscible sulfide melt from Hawaii, *in* Wilson, H.D.B., and Bateman, A.M., eds., Magmatic ore deposits—a symposium: Economic Geology Monograph, p. 310–322.

Staudigel, H., Zindler, A., Hart, S.R., Leslie, T., Chen, C.-Y., and Clague, D., 1984, The isotope systematics of a juvenile intraplate volcano: Pb, Nd, and Sr isotope ratios of basalts from Loihi Seamount, Hawaii: Earth and Planetary Science Letters, v. 69, p. 13–29.

Swanson, D.A., Duffield, W.A., and Fiske, R.S., 1976b, Displacement of the south flank of Kilauea Volcano: The result of forceful intrusion of magma into the rift zones: U.S. Geological Survey Professional Paper 963, 39 p.

Swanson, D.A., Duffield, W.A., Jackson, D.B., and Peterson, D.W., 1979, Chronological narrative of the 1969–71 Mauna Ulu eruption of Kilauea Volcano, Hawaii: U.S. Geological Survey Professional Paper 1056, 55 p.

Swanson, D.A., Jackson, D.B., Koyanagi, R.Y., and Wright, T.L., 1976a, The February 1969 east rift eruption of Kilauea Volcaho, Hawaii: U.S. Geological Survey Professional Paper 891, 30 p.

Tatsumoto, M., 1966, Isotopic composition of lead in volcanic rocks from Hawaii, Iwo Jima, and Japan: Journal of Geophysical Research, v. 71, p. 1721–1733.

———1978, Isotopic composition of lead in oceanic basalt and its implication to mantle evolution: Earth and Planetary Science Letters, v. 38, p. 63–87.

Tilley, C.E., and Scoon, J.H., 1961, Differentiation of Hawaiian basalts—trends of Mauna Loa and Kilauea historic magma: American Journal of Science, v. 259, p. 60–68.

Tilling, R.I., Koyanagi, R.Y., Lipman, P.W., Lockwood, J.P., Moore, J.G., and Swanson, D.A., 1976, Earthquake and related catastrophic events, Island of Hawaii, November 29, 1975: A preliminary report: U.S. Geological Survey Circular 740, 33 p.

Wright, T.L., 1971, Chemistry of Kilauea and Mauna Loa lava in space and time: U.S. Geological Survey Professional Paper 735, 40 p.

———1973, Magma mixing as illustrated by the 1959 eruption, Kilauea Volcano, Hawaii: Geological Society of America Bulletin, v. 84, p. 849–858.

———1984, Origin of Hawaiian tholeiite: A metasomatic model: Journal of Geophysical Research, v. 89, no. B5, p. 3233–3252.

Wright, T.L., and Fiske, R.S., 1971, Origin of the differentiated and hybrid lavas of Kilauea Volcano, Hawaii: Journal of Petrology, v. 12, p. 1–65.

Wright, T.L., Peck, D.L., and Shaw, H.R., 1976, Kilauea lava lakes: Natural laboratories for the study of cooling, crystallization, and differentiation of basaltic magma, *in* Sutton, G.H., Manghnani, and Moberly, R., eds., The Geophysics of the Pacific Ocean Basin and its margin: American Geophysical Union, Washington, D.C., Geophysical Monograph Series, v. 19, p. 375–390.

Wright, T.L., Swanson, D.A., and Duffield, W.A., 1975, Chemical compositions of Kilauea east-rift lava, 1968–1971: Journal of Petrology, v. 16, p. 110–133.

Wright, T.L., and Tilling, R.I., 1980, Chemical variation in Kilauea eruptions 1971–74: American Journal of Science, v. 280–A, pt. 2, p. 777–793.

Zablocki, C.J., and Koyanagi, R.Y., 1979, An anomalous structure in the lower east rift zone of Kilauea Volcano, Hawaii, inferred from geophysical data [abs.]: Hawaii Symposium on Intraplate Volcanism and Submarine Volcanism, July 1979, Hilo, Hawaii, Abstract Volume, p. 177.

Zielinski, R.A., Lipman, P.W., and Millard, H.T., Jr., 1977, Minor-element abundances in obsidian, perlite, and felsite of calc-alkalic rhyolites: American Mineralogist, p. 426–437.

APPENDIX 24.1

PROCEDURE TO ADJUST ANALYSES TO MgO = 7.00 WEIGHT PERCENT FOR OLIVINE-CONTROLLED LAVA

The procedure for this adjustment will be outlined briefly here. In it, we accept the average compositions of olivine (plus chromite) to be added or removed previously used by Wright (1971). For Kilauea lava, we use an olivine composition of $Fo_{86.2}$, for Mauna Loa lava, $Fo_{87.5}$ (table 24.22). The major elements in these average olivines are fairly well constrained, but their trace elements

TABLE 24.22.—*Assumed average compositions of olivine (plus chromite) used to adjust MgO to 7.00 weight percent for olivine-controlled lava of Kilauea (KAVOL) and Mauna Loa (MLAVOL)*

[KAVOL, average composition of olivine (+1.8 percent chromite) that controls composition of 1959 Kilauea Iki lava; MLAVOL, average composition of olivine (+1.5 percent chromite) that controls composition of historical flows of Mauna Loa. Oxide values (in weight percent) are from Wright (1971, table 15); Al_2O_3 primarily reflects melt inclusions of chromite. Trace-element values (in parts per million) from regression-equation estimates of: G, Gunn 1971, table 2; R, Rhodes, 1983, fig. 1]

	KAVOL ($Fo_{86.2}$)	MLAVOL ($Fo_{87.5}$)
SiO_2	39.48	39.70
Al_2O_3	1.17	.98
"FeO"	13.23	12.08
MgO	45.51	46.60
CaO	.39	.39
Na_2O	.00	.00
K_2O	.00	.00
TiO_2	.04	.03
P_2O_5	.00	.00
MnO	.22	.22
V	38 R	3 R
Cr	2,840 G	2,990 R
Co	190 G	190 G
Ni	2,430 G	2,465 R
Cu	5 G	5 G
Zn	97 G	94 G

are not. For the elements V, Cr, Co, Ni, Cu, and Zn, we use the regression-equation estimates from the olivine-control lines (Gunn, 1971; Rhodes, 1983); we assume the other trace elements to be present in negligibly small amounts or absent in olivine. However, even using significantly different assumed olivine compositions causes minimal effect on the derived adjusted values for incompatible elements and the relative differences between them.

The most convenient way to calculate the MgO-adjusted average composition of a group of related lava samples is to simply compute the mean and then adjust it to the desired MgO content. We chose, however, to adjust each individual analysis and then compute the mean and standard deviation. A comparison of these two adjustment procedures (table 24.23), using the data set showing the greatest range in MgO content (6.87 to 24.25 percent) of the lavas we studied, illustrates the following:

(1) The two mean compositions obtained are similar except for some of the transition elements, particularly Ni, which is compatible with olivine, and Cr, which is included in chromite. The significant differences in the computed mean values for Cr and Ni, however, suggest that the assumed concentrations of these elements in the olivine (table 24.22) used in the MgO adjustment are too high and (or) that the INAA and ES determinations of these elements are biased to low values in high-MgO (picritic) lava. In other words, the slope of the olivine-control line used in the adjustment procedure appears to be too steep for Cr and Ni.

In the comparison of procedures (table 24.23), MgO adjustment after the calculation of the mean occasionally results in negative adjusted values of Ni. Such negative averages are avoided by adjusting the individual analyses prior to computation of the mean; specific samples that yield negative adjusted values can then be identified and omitted from the mean. In general, lava that contains about 10 weight percent or more MgO yields negative adjusted values for Ni and, more rarely, Cr. Quantitative trace-element data are needed before the problem with the MgO adjustment of compatible elements in olivine-controlled lava can be resolved. Thus, in this study, we emphasize the variations in the olivine-incompatible elements (assumed to be negligible or absent in olivine) after MgO adjustment, because their relative differences between samples or lava suites remain valid despite the adjustment procedure.

(2) As expected, computing the average after adjustment of individual analyses substantially reduced the standard deviations of the means of the trace elements determined with relatively good precision (for example, Sc, V, Cr, Co, Ni, Ga, Hf, Eu, Sm) that show good linear correlation with MgO (see figs. 24.4, 24.5, 24.10). For the elements that show wide scatter in the MgO-variation diagrams, their standard deviations remain large regardless of the adjustment procedure used.

TABLE 24.23.—*Comparison of compositions of olivine-controlled lava of Mauna Loa's southwest rift zone (see table 24.17) after adjustment to 7.00 weight percent MgO by two different methods*

[MLAVOL olivine composition ($Fo_{87.5}$) used for adjustment; oxide values in weight percent; values for elements in parts per million]

	Adjustment after calculation of average				Adjustment of individual analyses before calculation of average		
	Range	Average (n = 9)	Standard deviation	Adjusted average	Range	Average (n = 9)	Standard deviation
MgO	6.87-24.25	12.04	7.01	7.00		7.00	0.0
K_2O	.26-.41	.34	.05	.39	.33-.50	.40	.05
[1]Rb	5.7-19.4	11.5	6.4	13.2	6.0-30.5	15.7	10.4
Cs	.10-.54	.27	.16	.31	.10-.96	.36	.32
[1]Sr	177-426	292	84	334	188-507	346	112
Ba	48-174	105	44	120	57-186	120	47
Sc	17.7-31.0	27.0	4.7	30.9	29.7-36.0	31.2	1.9
V	202-362	299	54	337	272-363	324	26
Cr	202-1250	507	364	145	211-241	228	11
Co	42.8-95.7	58.9	21.4	39.8	22.9-46.8	38.7	8.3
Ni	82-846	228	259	[3](98)	39-96	[2]72	25.3
[1]Cu	40.0-54.6	49.3	5.5	55.8	43.0-86.0	55.3	13.5
Mo	3.8-5.0	4.5	0.4	5.2	3.8-6.9	5.0	.9
Zn	104-148	120	14	138	104-151	123	14
Ga	8.4-20.7	16.8	4.0	19.2	14.5-20.7	18.2	2.1
[1]Zr	74-185	144	32	165	75-245	172	49
Hf	2.0-3.6	2.8	.6	3.2	2.8-3.6	3.2	.3
[1]Nb	2.2-7.3	4.8	1.5	5.5	3.8-7.3	5.2	1.4
[1]Ta	.30-.57	.41	.09	.47	.30-.80	.49	.16
Y	8.5-23.9	18.1	4.8	20.7	14.7-24.0	19.6	3.0
[1]Th	.6-2.7	1.0	.7	1.1	.6-4.8	1.3	1.3
U	.15-0.25	.18	.04	.21	.15-.27	.20	.04
Pb	1.5-3.1	2.4	.5	2.8	1.8-5.2	2.8	1.1
[1]Sb	.10-.18	.14	.04	.16	.10-.31	.19	.11
La	5.7-9.3	7.8	1.2	8.9	7.9-11.9	9.2	1.2
Ce	12.5-24.4	20.2	3.6	23.1	18.8-32.2	23.5	3.9
Nd	9.5-16.8	14.5	2.6	16.6	15.5-20.2	17.0	1.5
Sm	2.67-4.44	3.95	.64	4.53	4.20-4.61	4.39	.19
Eu	.99-1.69	1.39	.26	1.59	1.33-1.81	1.61	.15
[1]Gd	3.21-6.00	4.79	1.19	5.49	4.05-6.34	5.58	.73
[1]Tb	.38-.67	.55	.11	.63	.55-.68	.61	.06
Dy	2.9-6.5	4.6	1.2	5.3	4.3-6.8	5.27	.75
[1]Tm	.12-.59	.38	.17	.44	.12-.69	.47	.21
Yb	1.21-2.02	1.76	.33	2.02	1.74-2.24	2.03	.14
[1]Lu	.15-.29	.25	.05	.29	.25-.29	.27	.01

[1]Not listed in individual analyses.
[2]Negative adjusted value (see text for discussion).
[3]Three negative adjusted values for individual analyses omitted.

DIVERSE OLIVINE TYPES IN LAVA OF THE 1959 ERUPTION OF KILAUEA VOLCANO AND THEIR BEARING ON ERUPTION DYNAMICS

By Rosalind Tuthill Helz

ABSTRACT

The lava of the 1959 eruption of Kilauea Volcano, containing about 20 weight percent olivine, is the only picritic lava erupted in the summit area in historical time. The olivine population can be divided into several distinct classes: (1) irregular, blocky crystals (1–12 mm long), many of which contain multiple planar extinction discontinuities, which appear to be deformation features; (2) euhedral or skeletal crystals (0.5–5 mm long); (3) round or otherwise strongly resorbed grains; (4) angular or conchoidal fragments; and (5) subhedral crystals containing sulfide-bearing inclusions. Also present are dunitic aggregates, some with deformed or annealed textures, and rare olivine megacrysts.

Olivine in drill core from Kilauea Iki lava lake, quenched as much as 22 years after the eruption, has the same petrographic features seen in eruption samples or early lake samples. In particular, the deformation features in olivine have survived 22 years at 1,140–1,190 °C.

Olivine phenocrysts in samples of eruption pumice have core compositions of $Fo_{83.5-88.7}$ and contain 0.10–0.25 weight percent NiO. Zoning is moderate (≤3 percent Fo within most crystals); normally and reversely zoned crystals are about equally abundant. There is no correlation between petrographic class and core composition or style of zoning. This variable but moderate zoning seen in olivines in the eruption pumices is not preserved in olivines in drill core from the lake. Lake olivine is all normally zoned, varying by 5 percent Fo or more, and appears to have re-equilibrated with the melt during slow cooling.

The eruption samples are, for the most part, poorly equilibrated. Disequilibrium features observed include: (1) compositional heterogeneity in glasses (away from olivines); (2) presence of a boundary layer of MgO-poor glass near 30 percent of the olivine grains analyzed; (3) widespread occurrence of partially resorbed olivines, in all classes; (4) presence of reversely zoned, unzoned and (or) normally zoned olivines in the same thin section; (5) presence of olivines of very different core compositions in the same section; and (6) presence of olivines of different rim compositions in the same section. These features appear to record mixing immediately before or during the eruption. In particular, the resorption of olivine, seen in grains of all classes, at all but the earliest stages of the eruption, is interpreted as resulting from mixing of thermally disparate magmas, in which the hotter component was dominant.

Many aspects of this eruption are unusual for a Kilauean summit eruption, including: (1) High olivine content; (2) very magnesian glasses, recording high eruption temperatures; (3) the presence of deformed olivine, as single grains or in aggregates, like that commonly found in Hawaiian alkalic rocks; (4) occurrence of rare olivine megacrysts; (5) presence of olivine with sulfide-bearing inclusions; and, perhaps, (6) presence of reversely zoned olivines. These features can be explained by a model in which one of the two mixing components of the eruption, previously defined by Wright (1973), came directly from the mantle, without being stored for a significant time in the shallow summit reservoir. The lava component erupted from the east end of the initial fissure appears to represent this juvenile component. The ascent rate of this component from its source at a depth of 45–60 km is estimated to be 0.6–0.8 cm/s. This rate is sufficient to entrain the largest olivine grains and dunitic aggregates found in the 1959 lavas.

INTRODUCTION AND HISTORICAL BACKGROUND

The 1959 summit eruption of Kilauea Volcano was unique in the history of the Hawaiian Volcano Observatory (HVO) and of Kilauea in that it was the first major eruption for which most of the array of modern volcano-monitoring techniques now available was used. This eruption lasted from November 14 to December 20, 1959, and formed a conspicuous cinder cone (Puu Puai) and a large lava lake in Kilauea Iki pit crater (see fig. 25.1). The eruption consisted of seventeen phases of high fountaining and lava output, separated by periods of quiescence, during which some of the erupted material drained from the lake back down the throat of the main vent. HVO personnel made detailed records of this eruptive activity, its timing and patterns, including fountain heights and temperatures, and the depth of filling of the pit crater. The pumice and lava were then studied petrographically and chemically. These results were published in a series of professional papers (Murata and Richter, 1966a; Richter and Murata, 1966; Richter and others, 1970) that, taken together, give a very detailed picture of the eruption. In addition, Kilauea Volcano had been monitored seismically for several years before 1959; also, summit deformation before and during the eruption was monitored using the tiltmeter network established in 1957. Descriptions of the relationship between earthquake activity, summit deformation and the 1959–60 eruptions of Kilauea, by Eaton (1962) and Eaton and Murata (1960), constituted a quantum jump in our understanding of the physical behavior of active volcanoes.

The lava lake formed during the 1959 summit eruption has also been much studied. The upper crust of the lake has been drilled repeatedly (in 1960, 1961, 1962, 1967, 1975, 1976, 1979, and

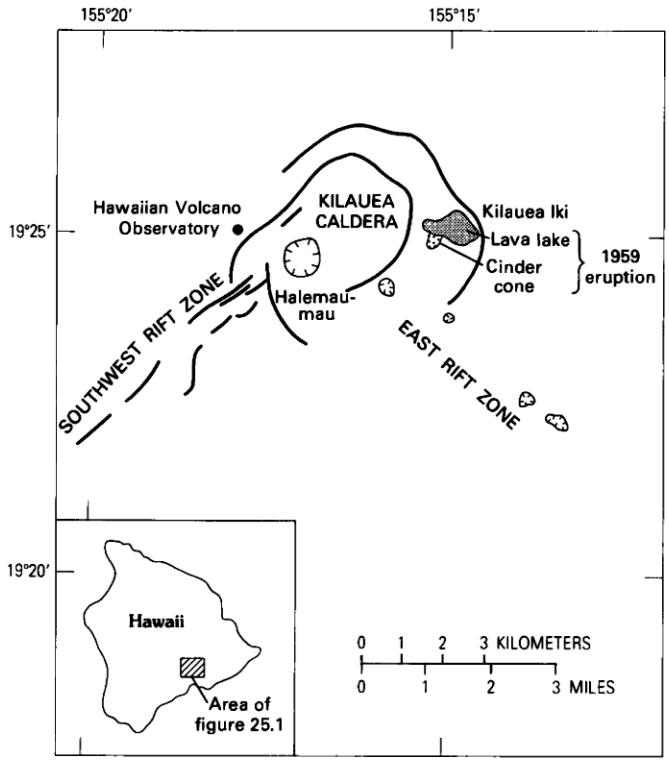

FIGURE 25.1.— Index map of the summit area of Kilauea Volcano, showing the location of Kilauea Iki lava lake and the 1959 cinder cone relative to the main caldera and the upper east rift zone of Kilauea.

1981), resulting in almost 1,200 m of drill core. Richter and Moore (1966) present a detailed petrographic and chemical description of the 1960–62 core. Partial data on petrography and (or) chemistry for the drill core recovered in 1967–1981 may be found in Helz (1980), Luth and Gerlach (1980), Luth and others (1981), Helz and Wright (1983), Helz and others (1984), and Helz (1984). The thermal history of the lake has also been monitored from the earliest days; Helz and Thornber (in press) give a partial summary of that literature. Lastly, the lake has been the object of several geophysical investigations, such as those of Zablocki and Tilling (1976), Chouet and Aki (1981), Hardee and others (1981), and Hermance and Colp (1982).

The 1959 summit lava is unique in several respects, the most conspicuous of which is its olivine content: it is the only picritic basalt erupted at or near Kilauea's summit in historical time. The average MgO content of the eruption pumice was estimated by Wright (1973) to be 15.43 percent by weight, which corresponds to about 20 percent by weight olivine crystals. Other historical eruptions with comparable olivine content have occurred on the rift zones, for example, the 1840 east-rift eruption (see analyses in Macdonald, 1944; Wright and Fiske, 1971). Other young summit eruptions have 7.0–8.5 percent MgO and correspondingly smaller amounts of phenocrystic olivine (Wright, 1971).

Consequently, the eruption pumice and the 1959 lava lake contain an enormous population of olivine crystals, occurring singly and in aggregates. This paper presents the results of a petrographic and chemical study of selected olivine crystals and aggregates, both in eruption pumice and in drill core from the lava lake. The study supplements earlier work on the eruption (cited above) by providing detailed electron microprobe data on a large suite of eruption samples. A limited amount of microprobe data on the 1959 eruption pumices has already been published (Leeman and Scheidegger, 1977; Harris and Anderson, 1983), but coverage of the eruptive suite was very incomplete.

ACKNOWLEDGMENTS

This paper builds on the past and present work of many people who have studied the 1959 eruption. In particular, I would like to thank J.G. Moore of the United States Geological Survey (USGS), Menlo Park, for access to his thin sections of submarine east-rift lava and T.L. Wright (USGS, Hawaiian Volcano Observatory) for access to his collection of thin sections of subaerial Kilauea lava. B.C. Hearn (USGS, Reston) and S.H. Kirby (USGS, Menlo Park) helped with the interpretation of the textures of the annealed olivine aggregates. In addition, I have benefited from conversations with D.A. Clague, J.P. Eaton, P. Delaney and S.W. Kieffer, all of the USGS, A.T. Anderson, Jr. of the University of Chicago, and C.-Y. Chen of the University of Illinois at Urbana. Lastly, I wish to thank B.C. Hearn and M.P. Ryan for constructive reviews of the manuscript.

SAMPLING AND ANALYTICAL PROCEDURES

SAMPLE SELECTION

The 1959 summit eruption consisted of 17 distinct phases. These phases, and the variations of lake level with time, are described in detail in Murata and Richter (1966a) and Richter and others (1970) and are summarized in figure 25.2. During each phase, eruptive materials were sampled, often both pumice from the fountain and flow material from the edge and upper crust of the lava lake. In selecting a subset of samples for this study, preference was given to pumice samples, because they were quenched much faster than flow samples, and to samples previously studied, especially those for which a bulk analysis was presented in Murata and Richter (1966). The collection dates of samples examined petrographically is indicated by the dots along the curve in figure 25.2. Although samples from only twelve of the seventeen phases were checked, they are fairly evenly distributed in time throughout the eruption.

In addition to these eruption samples, I have examined 600 thin sections of drill core from the lava lake. The drill-core sections contain all the types of olivine seen in the eruption samples. In addition, I found in the drill core two olivine megacrysts and a dozen dense polycrystalline olivine aggregates of distinctive texture. These unusual aggregates and megacrysts, of types not seen in the eruption pumice, are the only lake samples that will be discussed in detail in this paper.

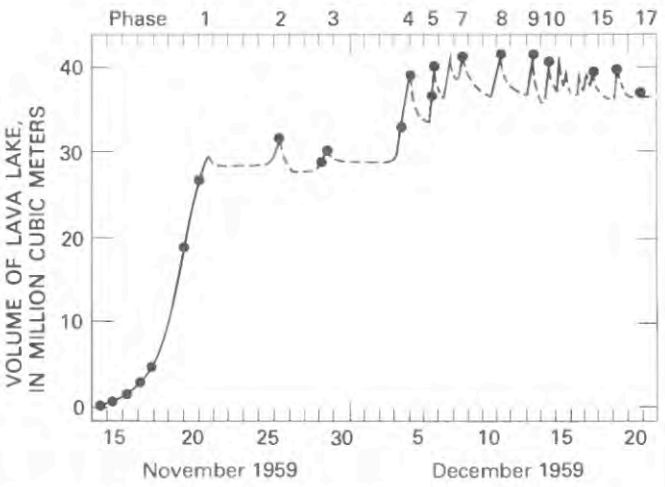

FIGURE 25.2.—Volume of Kilauea Iki lava lake versus time (after Richter and Moore, 1966, fig. 3). Decrease in lake volume at the end of each phase represents drainback down the eruptive vent. Each dot corresponds to a sample examined in this study. Phases represented in this study are numbered along the top of the diagram.

PETROGRAPHIC METHODS

All thin sections have been examined in transmitted light. All polished sections have also been checked in reflected light to verify the identification of opaque and near-opaque phases. No universal-stage work has been done.

In addition to the thin-section work, the drill core from the lake has been examined macroscopically in detail, with emphasis on the size and distribution of olivine phenocrysts. The results of this work are presented in Helz (1980), Helz and Wright (1983), and Helz and others (1984) and form part of the background to the present paper.

ANALYTICAL METHODS

Olivine and glass analyses were obtained using an ARL-SEMQ nine-channel electron microprobe. Operating conditions were an accelerating voltage of 15 kV and a beam current of 0.1 μA. Natural mafic silicates and basaltic glasses were used as standards. Counting times were 40 s for most major elements, 20 s for some of the minor elements (Ti, Cr, P, and K in glass; Ni and Cr in olivine). All data were reduced using a modified Bence-Albee routine (Bence and Albee, 1968; Albee and Ray, 1970). In addition, the glass analyses were renormalized, using a glass of known composition, following the method of Melson and others (1976). The glass selected for this was sample 69–1–22 from the 1965 Makaopuhi lava lake (Wright and Okamura, 1977). The revised analysis of Jarosewich and others (1979) was used for the renormalization procedure. This process eliminates minor day-to-day variations in analyses caused by slight shifts in the instrument and produces a data set of great internal precision. The accuracy of the analyses, which depends on the uniformity of the standards, the accuracy of the standard analyses, and of the Bence-Albee corrections, is not affected by the renormalization procedure. All analyses reported correspond to the composition of a single point unless the number of points included is specified.

CLASSIFICATION OF OLIVINES

The olivine in the lava of the 1959 Kilauea eruption is not only abundant but quite varied petrographically. The earliest description is that of Richter and Murata (1966), who described three classes of olivine: euhedral, rounded, and skeletal. The euhedral and skeletal olivine they reported to be fairly iron-rich (Fo_{82}), whereas the larger, blocky grains with rounded corners were more magnesian (Fo_{87-88}). The compositions were determined by X-ray techniques. Richter and Murata further remarked that the larger, rounded grains were obviously out of equilibrium with their present host liquid just before quenching, whereas the more iron-rich euhedral grains appeared to have the equilibrium olivine composition.

Based on examination of drill core from the lake, Helz (1980) divided the olivine phenocryst population in the lake into two groups. Type 1 were large, blocky crystals, the overall form of which was irregular. These commonly, but not always, contain multiple planar extinction discontinuities, bounding kink-bands, or subgrains with rectangular boundaries; similar features have been described by Kirby and Green (1980) in olivine in dunite xenoliths from Hualalai Volcano. Type 2 grains, in this classification, were smaller, euhedral olivines, which were free of deformation features. Type 2 olivine is more abundant than type 1 by a ratio of roughly 5:1.

Further study of samples from both the lava lake and the eruption pumice has led to the following five-fold classification:

(1) Class 1 (formerly type 1) consists of large grains (1–12 mm long), generally blocky in form, but irregular in overall outline, as described in Helz (1980). They commonly contain planar extinction discontinuities, bounding kink-bands, which extend all the way across the crystal (see figs. 25.4*A–B*, 25.5*A*). More rarely, the subgrains may be rectangular (see fig. 25.5*B*). Grains of this class rarely contain melt inclusions. Although planar extinction discontinuities may be quite abundant in a given grain, the total amount of strain involved is usually not large. The extinction position of different parts of the grains never varies by more than 15° of rotation and the usual range is 5°–10°. These grains may exhibit local rounding or resorption at their edges. If resorption is present, the subgrain boundaries are preferentially resorbed by the melt (as in figs. 25.4*A*, 25.5*A*). Olivine grains in this class are the most conspicuous in any given thin section (see fig. 25.3).

(2) Class 2, containing all euhedral and skeletal grains (see figs. 25.3, 25.4*C* and 25.5*C*), is the most abundant class of olivine. The distinguishing feature of this class is that the form of the grains suggests that they have grown from a melt in the recent past. Minor rounding of tips and corners of grains may occur, but in general class 2 olivine exhibits much less resorption than class 1 grains do. They are completely free of multiple planar extinction discontinuities. They commonly contain melt inclusions, most often a single large inclusion, of negative crystal form, in the center of the grain. Grains

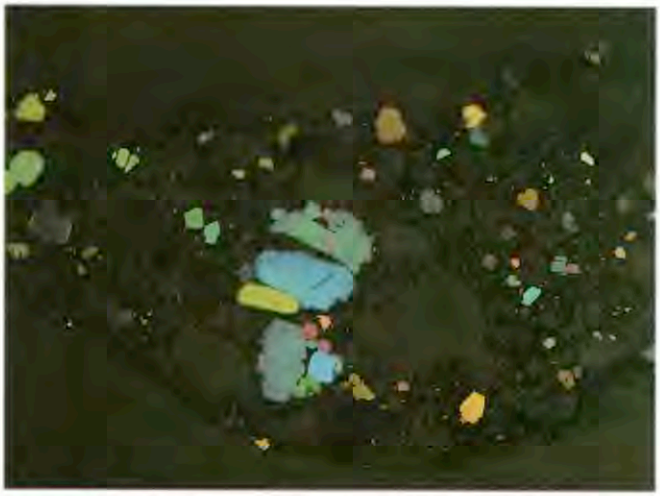

FIGURE 25.3.—Eruption sample Iki–24, from phase 9 of the 1959 eruption. All birefringent grains are olivine; matrix is moderately vesicular brown glass. Note large range in size that exists for both olivine and vesicles. Nicols partly crossed. Field of view is 2.2 cm across.

of this type are commonly 0.5–2 mm long, but they may reach 5 mm in length. A large skeletal grain is shown in figure 25.4*D*; skeletal grains of this size are rare in the 1959 lavas.

(3) Class 3 includes a small population of grains whose shapes have been so extensively modified by resorption that they cannot be assigned to group 1 or 2 on the basis of shape. Most class 3 grains are almost perfectly rounded. More rarely they may be amoeboid, but are never skeletal. These grains do not contain kink-bands; any grain with such features, even though strongly rounded, has been put in class 1.

(4) Class 4 includes rare angular or conchoidal fragments of olivine. Some care is needed to distinguish between broken pieces of olivine and crystals that have odd shapes because they have been sectioned obliquely. Nevertheless, there are a few grains of olivine that are clearly bounded by fracture surfaces. This class provides evidence for local brittle failure of olivine under conditions quite different from those under which the deformation features seen in class 1 olivine formed. Some of these angular fragments may be slightly modified by resorption (see fig. 25.4*C*). Others have survived for decades in the lake without significant resorption or overgrowth of olivine (see fig. 25.5*D*).

(5) Class 5 olivine grains are those containing swarms of inclusions of opaque minerals and pale glass, in which the opaques consist partly or entirely of sulfide. Chromite (or chromian spinel) is the other opaque phase that may be present. Class 5 grains are very rare, melt-bearing inclusions in most grains being sulfide-free. Sometimes the entire core of the olivine grain is so charged with inclusions that it looks dirty in thin section. More often, the inclusions occur only in patches within an otherwise clear grain. Inclusions also occur as a continuous necklace, separating a clear core and a clear rim. Examples of these various types are shown in figures 25.4*E* and 25.5*E*. Grains in this class are usually small (1–4 mm long) and are equant but not conspicuously euhedral in outline. A few class 5 grains contain planar extinction discontinuities, but most are undeformed. The presence of included sulfide is the crucial feature in assigning a grain to this class. Some olivine grains have inclusion swarms similar to the class 5 swarms in all respects, except that they lack sulfide. These grains have been excluded from class 5 as presently defined, though more detailed work on their inclusions might justify extending this class to include them.

This five-fold classification was first published in Helz (1983). Almost simultaneously, and quite independently, Schwindinger and others (1983) published a different classification scheme for olivine in the 1959 lava. Schwindinger and coworkers leached the olivine grains out of the glass of several samples of eruption pumice to view them in three dimensions. Their classification thus emphasizes three-dimensional form and surface morphology. Also, they worked exclusively with eruption pumice. These differences in scope and technique have led inevitably to different classification schemes. The two schemes are not in conflict, however; rather, the two studies complement each other.

The present classification scheme was developed by looking at olivine as it appears in thin section, that is, in two dimensions. I have considered chiefly the overall form of the grain (complexly blocky, euhedral, round, fragmental) and the presence of certain internal features (multiple planar extinction discontinuities, swarms of sulfide-bearing inclusions) in assigning a grain to a given class. Features not used here to classify grains include: Size of grain; presence or absence of inclusions of chromite or brown glass; and presence or absence of minor or local resorption. Certain classes do exhibit group characteristics with respect to this set of features. For example, class 1 grains tend to be larger than any other type. Inclusions of brown basaltic glass are very common in class 2 grains, and rare in all other classes. However, this clustering of additional traits is a matter of observation, and not part of the classification process.

With so many types of olivine present, the possibility obviously arises that only some classes of crystals (for example, class 2) are cognate with the host, whereas others (perhaps class 1) may be largely xenocrystic. As will become evident below, there are many gradations between cognate and xenocrystic, and so these terms will be little used in this paper. Instead, the term phenocryst is used to mean any olivine grain big enough to see with the unaided eye, without genetic implications, while the terms grain or crystal may include smaller olivine grains as well.

PETROGRAPHY OF THE ERUPTION PUMICE

The eruption samples examined in this study are listed in table 25.1, together with their dates of collection and petrographic notes on the olivine present. Two sample designations are given. The first is the collection number assigned in the field, which will be used in this paper. The second number (S-number in parentheses) is the number used in Murata and Richter (1966a) and Richter and Murata (1966); it is reproduced here to facilitate comparison with those papers. Some samples investigated here were not analyzed in

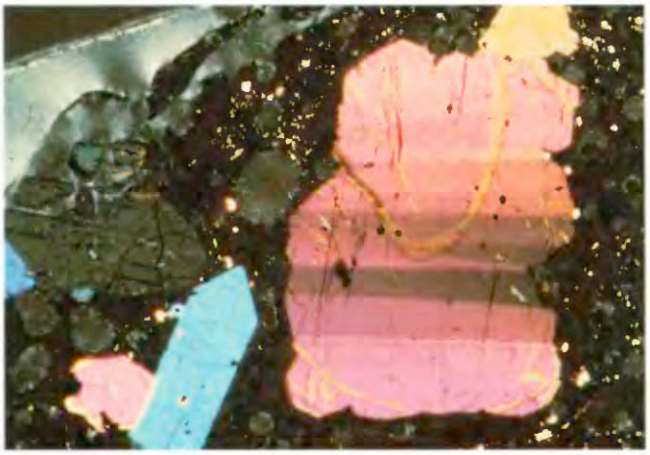

A

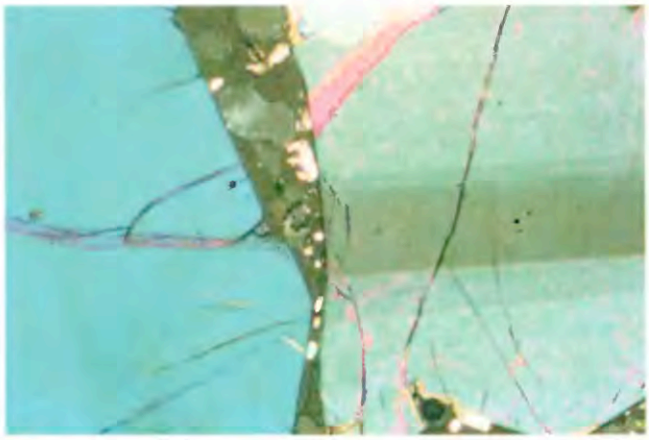

B

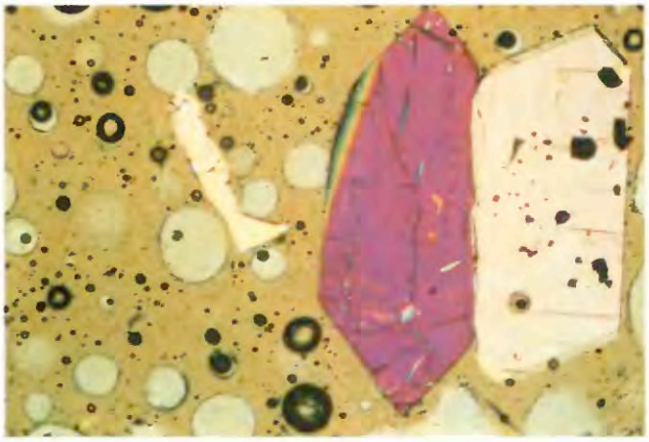

C

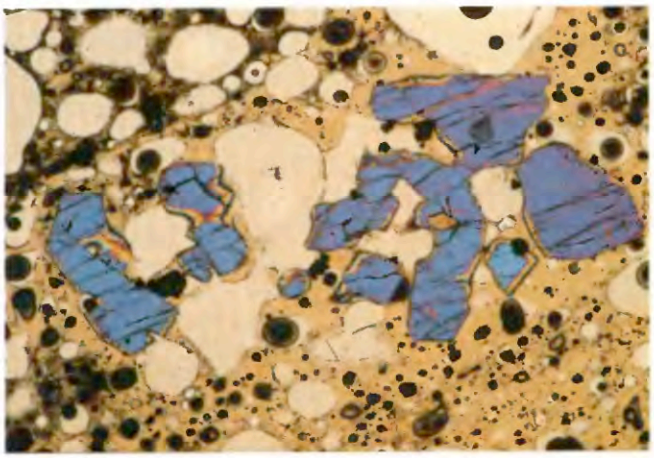

D

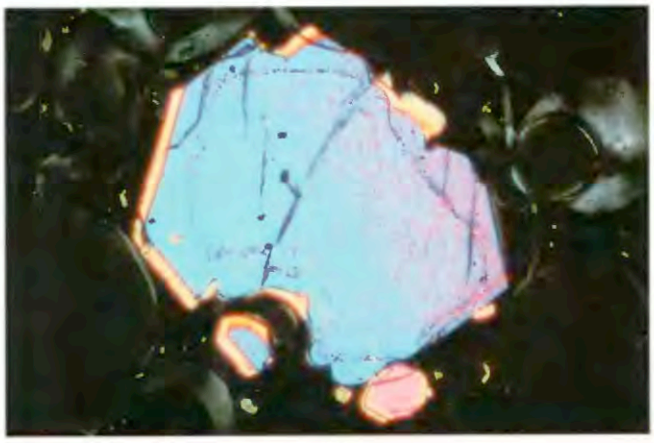

E

FIGURE 25.4.—Representative olivine grains from the eruption pumice of the 1959 Kilauea eruption. ***A***, Deformed (class 1) olivine grain, 2 mm long from Iki–21 (phase 8). The edges are resorbed and show preferential resorption along the planar extinction discontinuities bounding the kink-bands. Two euhedral (class 2) grains are visible to the left. Crossed nicols. ***B***, Deformed (class 1) olivine grain (right), showing relationship between the curved (possibly bent?) edge of the grain and the position of the extinction discontinuities, along an edge where resorption has not occurred. This grain, from Iki–24, is visible in the center of figure 25.3. Field of view 2 mm across. Crossed nicols. ***C***, Euhedral (class 2) and fragmental (class 4) olivine grains in Iki–7 (phase 1). The euhedral grains are 1 mm long. Nicols partly crossed. ***D***, Coarse skeletal (class 2) olivine grain, 3 mm in length, in Iki–21 (phase 8). Such grains are very rare in the 1959 lava. Nicols slightly crossed. ***E***, Class 5 olivine (1 mm long) with necklace of tiny inclusions, from sample Iki–32 (phase 15). The edge of this crystal shows local resorption (cuspate edges) but is euhedral elsewhere around its rim. Nicols partly crossed.

the earlier studies, and therefore have no S-numbers.

All samples in table 25.1 contain abundant brown glass, mostly very fresh and clear, but locally charged with fine-grained opaques. All glasses are quite vesicular, some of them so vesicular that less than a third of the area of the thin section is glass and crystals. A typical olivine-rich, moderately vesicular eruption sample is shown in figure 25.3. All of the birefringent material in this section is olivine; clearly the size range of olivine present is very large.

The crystalline material present in the eruption pumice consists almost entirely of olivine plus chromite. Both phases are always present; there are few chromite-free olivine grains and no chromite-free samples. Chromite occurs principally as inclusions in olivine; most crystals not included in olivine are immediately adjacent to

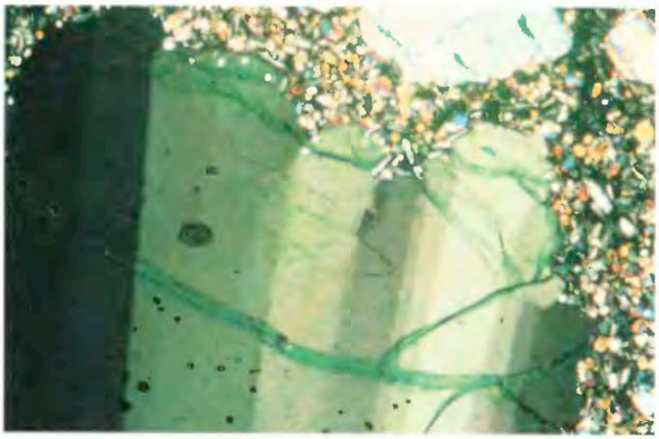

A

B

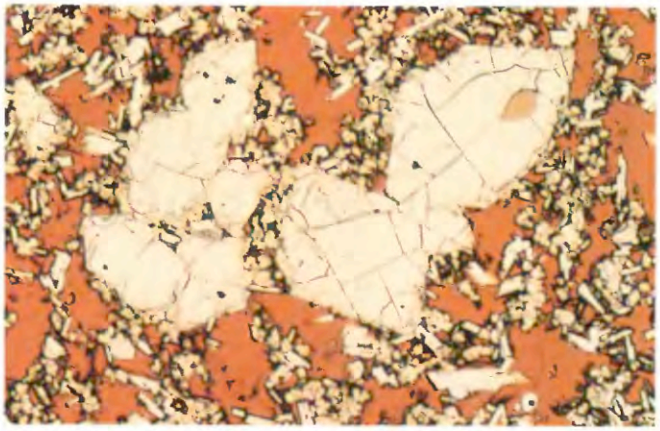

C

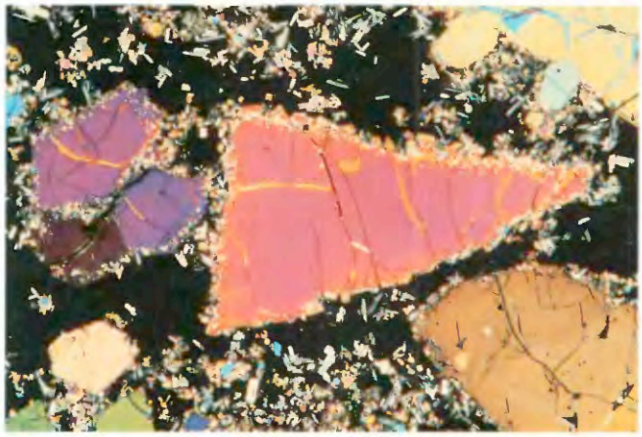

D

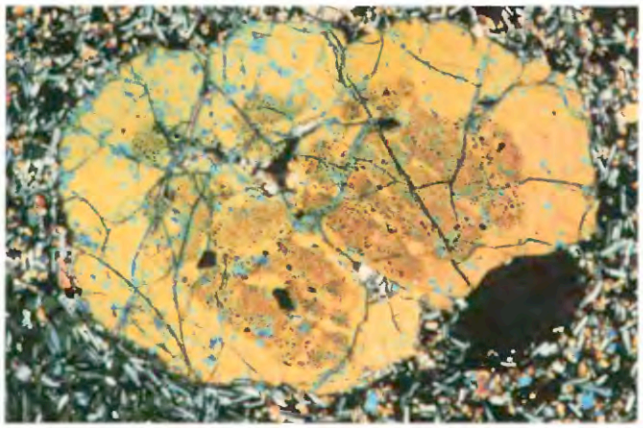

E

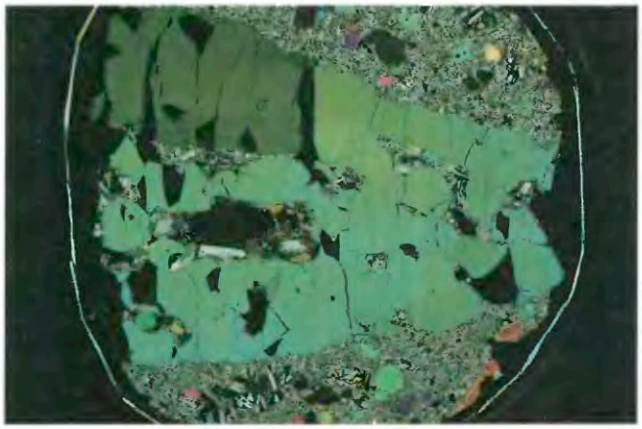

F

FIGURE 25.5.—Representative olivine from Kilauea Iki lava lake. ***A***, Deformed (class 1) olivine grain from KI81–2–226, quenched from 1,140 °C in 1981. It has multiple planar extinction discontinuities and cuspate margins like the grain in figure 25.4*A*. Part of grain visible is 2 mm long. Crossed nicols. ***B***, Deformed (class 1) grain in aggregate KI79–1–189.0(b), quenched from 1,130–1,135 °C in 1979. The olive-green grain shows rectangular subgrain boundaries instead of planar extinction discontinuities extending across the whole grain. This grain is 5 mm long. Black area at lower right is the edge of the rock section. Crossed nicols. ***C***, Euhedral (class 2) olivine grains from KI76–1–149.1, quenched from 1,105 °C in 1976. These are grouped into clusters of 2–3 grains each. Smaller crystals are groundmass phases, including olivine, augite, and plagioclase, in brown glass. Field of view 3 mm across. Plane-polarized light. ***D***, Fragmental (class 4) olivine grain from sample KI75–1–145.1, quenched from 1,120 °C in 1975. All surfaces of the pink triangular grain are slightly conchoidal. This grain is 5 mm long. Class 1 (yellow grain, lower right) and class 2 (purple grains to left) olivine phenocrysts are also visible. The glass is at extinction. Crossed nicols. ***E***, Class 5 olivine phenocryst (3 mm across) with inclusion-rich core, from sample KI81–1–306.7, quenched from 1,085 °C in 1981; smaller, attached grain is at extinction. Crossed nicols. ***F***, Olivine megacryst from sample KI76–2–20.5. It is mounted on a glass slide, just visible in the picture, which is 2.54 cm across. The grain is somewhat skeletal, with former melt inclusions now visible as areas of mesostasis. Irregular black areas within the crystal are the result of fragmentation and plucking during sectioning. Faint extinction discontinuities (visible in upper part of crystal) are present throughout the grain. Crossed nicols.

TABLE 25.1.—*Samples of 1959 eruption pumice investigated*

Sample	Phase of eruption	Date	Type of sample	Olivine classes present	Resorption observed?	Kink bands present in olivines?	Types (numbers) of sections examined
Iki-1(S-2)	1	11/14/59	Flow	2	No	No	TS, PTS
Iki-58(S-1)	1	1/14	Flow	2	No	No	TS, PTS
Iki-42	1	1/16	Flow	2	No	No	TS(2)
Iki-2(S-4)	1	11/17	Pumice	2	No	No	TS
Iki-22 (S-5)	1	11/18	Pumice	1,2,3	Yes	Yes	TS, PTS
Iki-44 (S-7)	1	11/20	Pumice	1,2,3	Yes	Yes	TS, PTS
Iki-5 (S-8)	1	11/21	Pumice	1,2	No	Yes	TS
Iki-7 (S-9)	1	11/21	Pumice	1,2,3,4	Yes	Yes	TS, PTS
Iki-8(S-10)	2	11/26	Flow	1,2	Yes	Yes	TS
Iki-11(S-11)	2	11/26	Pumice	1,2,3,5	Yes	Yes	TS, PTS
Iki-9(S-12)	3	11/28	Pumice	2	Yes	No	TS, PTS(2)
Iki-10(S-13)	3	11/29	Pumice	2	Yes	No	TS
Iki-12(S-14)	4	12/4	Flow	2	No	No	TS
Iki-13(S-15)	4	12/5	Pumice	1,2,3,4	Yes	No	TS, PTS
Iki-14(S-16)	5	12/6	Pumice	1,2,4,5	Yes	Yes	TS, PTS
Iki-15(S-17)	5	12/7	Pumice	1,2	Yes	Yes	TS
Iki-19(5-18)	7	12/8	Pumice	1,2,3,5?	Yes	Yes	TS
Iki-20	7	12/8	Pumice	2,5	Yes	No	PTS
Iki-21(S-19)	8	12/11	Pumice	1,2,4,5	Yes	Yes	TS, PTS
Iki-24	9	12/13	Pumice	1,2,4	Yes	Yes	PTS
Iki-36	9	12/13	Pond Surface	1,2,4	Yes	Yes	TS(2)
Iki-26(S-21)	10	12/14	Pumice	1,2,3	Yes	Yes	TS, PTS
Iki-32(S-22)	15	12/17	Pumice	1,2,3,5	Yes	Yes	TS, PTS
Iki-33(S-24)	16	12/19	Pumice	1,2	Yes	Yes	TS, PTS
Iki-38(S-25)	17?	12/19?	Ooze	1,2	No	No	TS

olivine. Crystals of chromite occurring in the glass, at some distance from olivine, are rare. This pattern of association of olivine and chromite suggests that spinel nucleates on olivine, whenever possible.

A few eruption samples also contain minor amounts of fine-grained augite, with or without tiny laths or plates of plagioclase. These phases occur in all of the earliest phase 1 pumice samples (Iki–58, Iki–1, Iki–42) plus some phase 2 and 3 samples (Iki–11, Iki–9). These minerals are never sufficiently coarse grained to be considered phenocrystic. They do not survive in recognizable form in the lake (Helz, 1980), but must make up part of the groundmass.

As can be seen in table 25.1, the petrographic character of the olivine in the eruption pumice varies with time. The early phase 1 samples (Iki–58, Iki–1, Iki–42, Iki–2) contain only minor amounts of euhedral class 2 olivine showing little or no resorption. Lava temperature evidently increased during this period, however, as the latest of this series of samples does not contain the tiny augite ± plagioclase crystals seen in pumice erupted on November 14–16. On November 18, 1959, the olivine content of the lava increased and the olivine assemblage became more complex, now including representatives of classes 1, 2, and 3. This situation persisted to the end of the first phase, with some fragmental olivine (class 4) occurring in the latest sample (see fig. 25.4C).

Phase 2 samples also have a complex olivine assemblage, including the earliest known class 5 olivine. Phase 3, by contrast, marks a reversion to a depleted olivine population like the early phase 1 pumice, but with more rounding of the olivine. An early phase 4 sample is similarly olivine-poor, but later phase 4 and the phase 5 samples again contain a complex olivine assemblage, which contains the first fragmental olivine seen since the end of phase 1.

Phase 6 is not represented, but phase 7 pumice continues to have a very complex olivine assemblage, containing all classes of olivine except the fragmental class 4. Phases 8 and 9 contain abundant and very variable olivine (see figs. 25.3, 25.4*A–B*), including class 4 fragments, but without any class 3 (round or strongly resorbed) grains. These are the last eruption samples known to contain fragmental olivine. In phases 10 and 15, rounded

class 3 olivine reappears, but class 4 olivine is absent. Later samples from phase 16 and 17(?) contain abundant olivine, but it is, like that in the earliest pumice, less variable in form. In the latest sample, an ooze, the olivine shows neither resorption nor kink-bands; the only other samples like it are the earliest (November 14–17) phase 1 samples.

Thus, the sequence of appearance of the different classes is: first, class 2, followed by 1 and 3, then 4, then 5. Class 3 and class 4 olivine tend not to occur in the same sample: of the eight samples with class 3 grains and 6 samples with class 4 fragmental olivine, only two (Iki–7, Iki–13) contain both classes. Class 5 olivine, the last class to appear, is found in phases 2, 5, 7, 8, and 15 and may occur in association with any of the other classes. The sequence of disappearance, as the eruption went on, was: first, 4, then 3 and 5, leaving only 1 and 2 present in the last phase.

Certain of these classes are uncommon, and it might be thought that the apparent gaps in the occurrence of classes 3, 4, and 5 would disappear, if more thin sections were examined. For many samples, however, more than one section is available already, and the olivine population is almost always the same in both sections. Thus, it appears that the occurrence of class 3, 4, and 5 olivine as reported in table 25.1 is not an accident of sectioning but a characteristic of particular samples.

PETROGRAPHY OF OLIVINE PHENOCRYSTS AND MEGACRYSTS IN THE LAVA LAKE

The same five classes of olivine that occur in the eruption pumice can be found in samples from the lake. Such samples cannot he related to individual phases, however, because of mixing in the lake, drainback between phases, and re-eruption of some of the same material in later phases. In addition to these complications, there has been significant redistribution of olivine within the lake after it crusted over, as discussed in Helz (1980). The dominant process was probably gravitative settling, as the coarser class 1 olivine grains have been affected more than the smaller class 2 phenocrysts. For these reasons, it is not possible to develop an olivine stratigraphy for the lake that would correlate with the time sequence observed in table 25.1. Posteruptive redistribution of olivine has produced essentially three zones in the lake: an upper, olivine-rich zone down to a depth of 18 m, an olivine-depleted zone from 18–40 m, and a second olivine-rich zone from 40 m down to within 2 m of the bottom of the lake (Helz, 1980; Helz and Wright, 1983; Helz and others, 1984). Both olivine-rich zones contain all five classes of olivine. The olivine-depleted zone generally contains only class 2 grains, which are commonly rounded and may be locally rimmed with pyroxene.

It might be thought that some of the features used to classify olivine in the eruption pumice would disappear during prolonged annealing in the lake. In fact, the only type of grain significantly affected is the skeletal olivine. Skeletal grains do occur in the pumice, though usually only in the microphenocryst size range (<0.5 mm). Lake samples, having cooled more slowly, contain virtually no skeletal olivine. Sample KI79–1–189.0 contains the only known example of a coarse skeletal olivine in the lake. Typical grains of class 2 lake olivine are shown in figure 25.5C. These look very much like their equivalents in the eruption pumice, as overgrowths of olivine are minor and glass inclusions tend to crystallize later than the melt outside the olivine.

Other types of olivine have also survived as much as 22 years of slow cooling unscathed. For example, figure 25.5*A* shows a class 1 olivine, with multiple planar extinction discontinuities, and strongly resorbed outline, which is virtually identical to the grain shown in figure 25.4*A*. The first grain was quenched from 1,198 °C on December 11, 1959 (see table 25.1). The second was quenched from 1,140 °C on April 22, 1981 (Helz and Wright, 1983; Helz and Thornber, in press). The extinction discontinuities have not been removed by annealing, nor have the crystallographically irrational curved surfaces of the resorbed grains healed. Apparently they are very unfavorable sites for further growth of olivine. Fragmental olivine also survives in the lake (see fig. 25.5*D*), perhaps for the same reason: the broken surfaces are not favorable growth sites, compared with the abundant rational faces and edges available on the class 2 phenocrysts and groundmass olivine.

The distribution of class 5 grains in the lake, which appears to be random, is of particular interest. These grains occur in olivine-rich samples at the edge of the lake, and in the center, at all depths, wherever class 1 grains occur. One of the best examples of this class (fig. 25.5*E*) is from the bottom of the deepest drill hole in the center of the lake. As indicated in table 25.1, class 5 grains have not yet been observed in any phase 1 samples. The bulk of the lake, however, was erupted during phase 1 and did not drain back down the vent (see fig. 25.2). Therefore, if the apparent absence of class 5 grains from phase 1 is real, the presence of grains of this class throughout the lake, including its most northerly and (or) deepest parts, implies that the bulk of the lake was very well mixed during phases 2–17, and perhaps for some time thereafter, even though there was little net increase in lava in the lake after phase 1.

OLIVINE MEGACRYSTS

The principal reason for considering lake samples in a paper on the dynamics of the 1959 eruption is that the lake contains a sparse population of very large olivine grains and aggregates of olivine, distinct from any observed in the available thin sections of eruption pumice. Perhaps the most curious are the two olivine megacrysts that have been found in the lake. One of these is shown in fig. 25.5*F*; data on both are presented in table 25.2.

The actual size of these large single crystals, or megacrysts, of olivine is unknown, but the parts of the grains visible in drill core and thin section are 20 mm by 10 mm. Though found at very different levels in the lake, the two grains are so much alike that they look like pieces of the same crystal. Both are wedge-shaped in section and contain as inclusions large areas of glass plus augite, plagioclase, and other groundmass phases. Presumably the original grains were skeletal, with irregular cavities in their cores. Their external form is not euhedral; their present grain boundaries appear to be fracture surfaces, at least in part. Both megacrysts contain abundant planar

extinction discontinuities (as in fig. 25.5*F*), but the total angle of rotation is very slight in both megacrysts. The planes are decorated with minute inclusions or voids, a style of decoration that is not commonly observed in ordinary class 1 olivine phenocrysts. Megacrysts of this sort have not previously been reported in Kilauean lava.

PETROGRAPHY OF OLIVINE AGGREGATES

Schwindinger and others (1983) reported that 95 percent of the olivine in the eruption samples studied by them occur in aggregates. This figure is not unreasonable for other eruption samples as well, but may be a little high for lake samples. Whatever the exact figure, isolated single crystals of olivine are uncommon. Large clots of crystals are also exceptional, however; most clumps of crystals appear, at least in thin section, to consist of 2–6 individual grains (see fig. 25.3).

If one considers only the largest aggregates, there are two distinct types present. The more common type of large olivine aggregates consists of relatively open or skeletal clusters of grains, like that shown in figure 25.6*A–B*. These open clusters consist of class 2 grains, rounded or otherwise, which have a common crystallographic orientation. A subordinate set, rotated 90° from the first set, is not uncommon, but other crystal orientations are rare. The crystals in these open aggregates are not sorted by size (see fig. 25.6*B* especially). These networks of crystals are open, with glass and vesicles along boundaries and at interstices. Schwindinger and others (1983) studied this type of open aggregate in some detail and recognized several subcategories. They have suggested that these aggregates form by synneusis, the swimming together of crystals suspended in a melt. Similar aggregates are common in the lake; these differ from the one shown in figure 25.6*A* chiefly in that they contain fewer crystals and less interstitial glass. The significance of these aggregates is that, whatever their exact origin, everything about them suggests that they formed in the presence of abundant melt, most probably in Kilauea's summit reservoir.

The second group of olivine aggregates differs markedly in character from the open, glomerocrystic clots described above. This group, which will be referred to as dense olivine aggregates or dunite aggregates, consists of clusters of non-euhedral olivine, for the most part very tightly interlocked or intergrown. The grains are not oriented crystallographically relative to each other. Such olivine aggregates, or dunite fragments, are uncommon; the one dozen examples known to date are described in table 25.2.

The dunitic aggregates in table 25.2 are from drill core, and so have undergone variable periods of slow cooling in the lake between eruption and quenching. Therefore, table 25.2 includes the dates on which the various samples were drilled and the temperatures from which they were quenched. The temperature estimates are based on the composition of the glass found in the groundmass of the host rock of each sample, using the empirical calibration presented in Helz and Thornber (in press) for Kilauean samples, except for sample KI76–2–20.5, which was collected long after the rock crystallized. For this sample, the temperature (about 100 °C) was determined by downhole thermocouple measurement. From these data it can be seen that individual aggregates were stored anywhere from 9 months to 22 years in the lake and quenched from temperatures ranging from 950 °C to 1,140 °C.

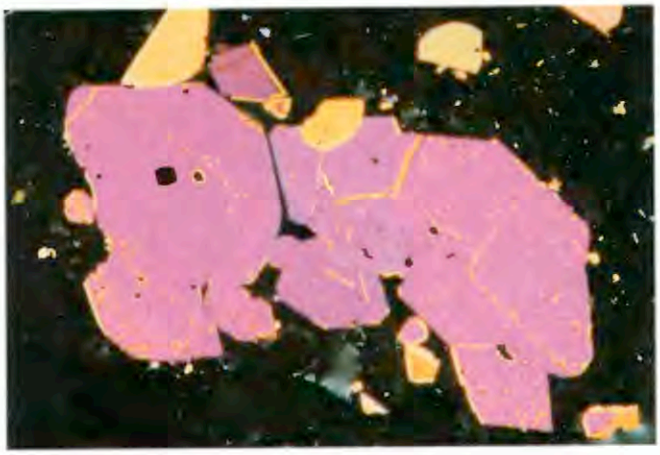

A

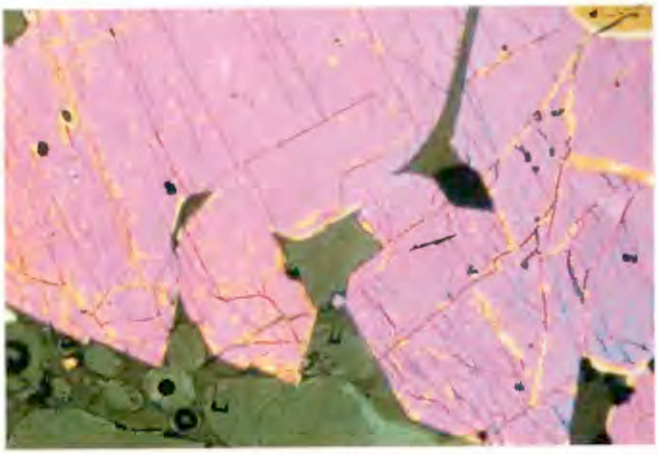

B

FIGURE 25.6.—Skeletal olivine aggregate from the 1959 Kilauea eruption. ***A***, Aggregate of euhedral grains in sample Iki–33 (phase 16). Note the strong preferred orientation of the crystals. The aggregate is 6 mm long. Crossed nicols. ***B***, Close-up of the same aggregate, showing its open nature. Interior grain margins are slightly rounded, exterior margins strictly euhedral.

It is evident from table 25.2 that these twelve dunitic aggregates are not distinctive in size; most are similar in size to the largest individual class 1 olivine grains. Even the largest are no bigger than the megacrysts described above. It is not surprising, therefore, that they occur randomly within the upper and lower olivine-rich zones, associated with the coarser olivine phenocrysts. Because the lake appears to have become very well mixed during the eruption, it is not possible to associate the aggregates and megacrysts with a particular phase or phases, even though they may have been far from random in their occurrence in the eruption samples.

This group of dense olivine aggregates can be divided into three subcategories: (1) seven aggregates consisting dominantly of

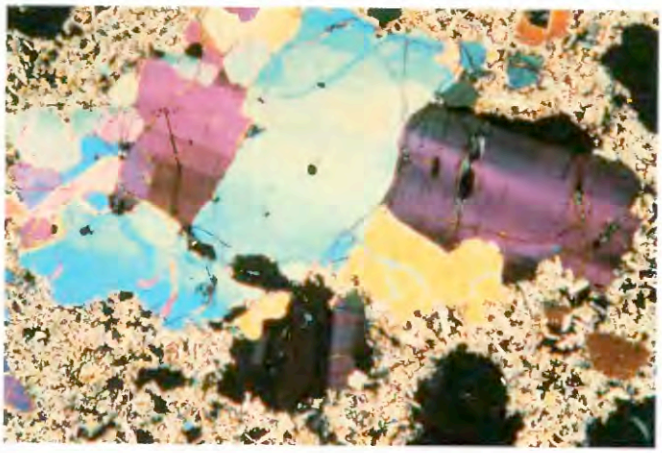

A

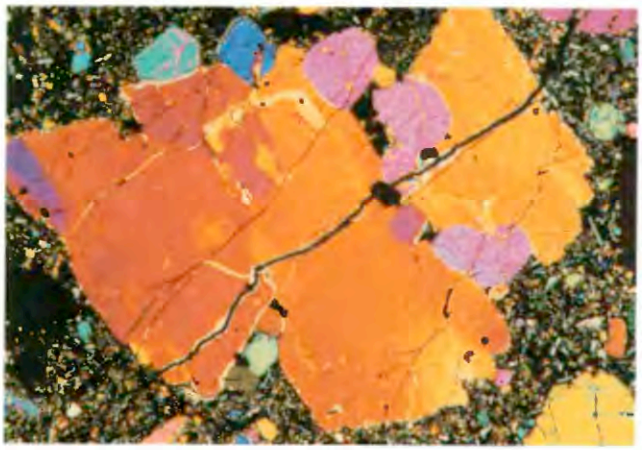

C

B

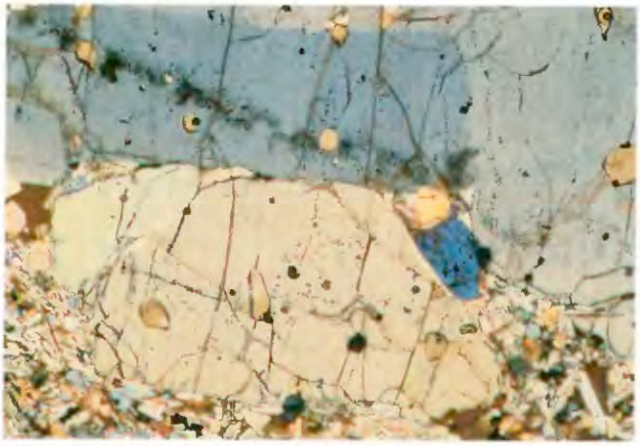

D

FIGURE 25.7.—Dunitic aggregates from Kilauea Iki lava lake. ***A***, Aggregate of deformed olivines from KI–113, quenched from 1,090 °C–1,095 °C in 1960. All but a few of the small grains are deformed. The aggregate is 8 mm across. Crossed nicols. ***B***, Close-up of a triple junction in aggregate, showing irregular grain boundaries, plus lack of 120° angles, and minimal penetration of melt from host along boundaries and at triple junction. (The black strip that intersects the triple junction is an epoxy-filled crack formed during sectioning.) Note cracks radiating from chromite inclusion in blue grain at left. Field of view 2.5 mm across. Crossed nicols. ***C***, Aggregate of class 1 olivine (6 by 5 mm), from KI81–1–230.4, quenched from 1,140 °C in 1981. The large grains contain irregular blocky subgrains, the boundaries of which are oblique to the section. Chromite (black) and smaller, strain-free olivine grains occur along the margins of the coarse olivine. Grain boundaries at triple junctions intersect at angles near 120°, and most grain boundaries are planar. Melt penetration of this aggregate is minimal, even after 22 years in the lava lake. Crossed nicols. ***D***, Aggregate of class 5 olivine in KI67–2–87.5, quenched from 1,073 °C in 1967, showing swarms of inclusions. Most inclusions are very tiny. Note densest inclusion swarm trends obliquely to grain boundaries. Field of view is 1 mm across. Partly crossed nicols.

interlocking class 1 grains: (2) two clusters of class 5 grains: and (3) three aggregates containing areas of a mosaic of unstrained olivine grains.

DENSE AGGREGATES OF CLASS 1 GRAINS

This is the commonest type of dense aggregate, with seven known examples. One of these, recovered in 1960 from a depth of 6.86 m in the lake, is shown in figure 25.7*A–B*. It consists of anhedral grains, for the most part tightly interlocked, most containing multiple planar extinction discontinuities. Some grains contain chromite inclusions, surrounded by fractures radiating from the inclusion wall into the olivine (see fig. 25.7*B*). Triple junctions, generally not intersecting at 120°, contain very small pools of glass. Two-grain boundaries can be highly irregular (fig. 25.7*A–B*) and are mostly unmarked by inclusions of vapor, glass, or other material. The aggregate contains a population of smaller, equant, usually unstrained grains that occur at the margins of the large grains but do not completely surround them. In the textural classifications developed for olivine-rich xenoliths from basalts and kimberlites, this and other aggregates in this group are transitional between the coarse and porphyroclastic categories of Harte (1977), or the protogranular and porphyroclastic categories of Mercier and Nicolas (1975).

The aggregate in KI–113 was quenched only nine months after the eruption ceased, so its texture may be presumed to be

relatively little affected by long-term storage in the lake. The other aggregates of class 1 grains, from 26–70 m below the surface of the lake, were cooled slowly from about 1,190 °C to the quenching temperature indicated in table 25.2 over periods of 8 to 22 years. However, the only textural change consistently observed in the latter aggregates is that the grain boundaries become more planar, and the angle of their intersections at triple junctions approach 120° (see figs. 25.5*D*, 25.7*C*). There is some tendency for greater penetration of the aggregate by melt, but, as figure 25.7*C* shows, this is not necessarily extensive, even after 22 years. In some of the more recently quenched samples there is a tendency for chromite to occur interstitially in the aggregate, rather than as inclusions in olivine (fig. 25.7*C*); but other aggregates (fig. 25.5*D*) have included chromite preserved.

Some aspects of the fabric of these seven aggregates are unaffected by annealing in the lake. For example, the aggregates are notably inequigranular, with the ratio of largest to smallest olivine grains present varying from 10 to 30 (see table 25.2). There is no tendency for the proportion of small grains to increase or decrease with time, nor does average grain size change in any other way as length of storage in the lake increases. Also, as in the isolated crystals, there is no discernable tendency for the kink bands or rectangular subgrains to disappear with time. The lack of internal reorganization of the large deformed grains suggests that the apparent expulsion of chromite to grain boundaries seen in some aggregates (fig. 25.7*C*) was accomplished during an earlier cycle of deformation and recrystallization. The present generation of subgrains, then, must have been produced in a second deformation event, the effects of which have not been eliminated by recrystallization during storage in the lake.

By decrease in number of adhering grains, these aggregates appear to grade into the dispersed class 1 olivine phenocrysts. It seems possible that all the class 1 grains and clusters found in the eruption samples and in the lake may have been disaggregated from rocks like this first group of dense, dunitic aggregates.

AGGREGATES OF CLASS 5 GRAINS

Three of the dense aggregates listed in table 25.2 contain olivine with sulfide-bearing inclusions. The two smaller ones (KI67–2–87.5 and KI79–1–203.6), consisting exclusively of class 5 grains, will be discussed here. The description below applies equally to rare smaller clusters of class 5 grains, containing 2 to 6 grains each.

A close-up view of the KI67–2–87.5 aggregate (fig. 25.7D) shows most of the features of this type. The grains are full of inclusions; some inclusions are large, of brown glass with or without opaques and vapor, but most are tiny and any glass present is pale. Included crystalline phases are chromite and sulfide. In some cases, the sulfide bleb appears to be too large to be a daughter phase, in the terminology of Roedder (1984), suggesting that such inclusions were polyphase initially, the melt already being saturated with an immiscible sulfide liquid (±chromite) at the time the inclusions formed. No daughter silicates have been observed. Grain shapes are irregular, but grain boundaries are tight only locally. These aggregates all show extensive penetration of melt along grain boundaries, independent of storage time in the lake. This and the abundant inclusions give these aggregates a dirty, moth-eaten appearance in thin section.

The localization of some inclusions in the KI67–2–87.5 aggregate (fig. 25.7*D*) in planar arrays suggests that they formed when melt ± sulfide, chromite, and vapor were injected into fractures in a previously existing grain or aggregate of grains. This distribution of inclusions is different from that in most class 5 grains, in which the inclusions commonly occupy either the core (as in fig. 25.5*E*) or a well-defined necklace (as in fig. 25.4*E*). The latter arrangements are more characteristic of primary inclusions, that is, inclusions incorporated during the growth of the individual olivine grain. The inclusion arrays in figure 25.7*D*, by contrast, appear to be secondary crack fillings (see Roedder, 1984, for a discussion of primary versus secondary inclusions). Sulfide-bearing inclusions also occur in irregular trails, swirls, and patches that cannot, from their geometry, be unequivocally designated as primary or secondary.

Class 5 grains are very rare, occurring in only 3 percent of the thin sections of drill core examined. The fact that aggregates of class 5 grains occur at all suggests that the single grains may formerly have been in aggregates, as it is highly improbable that these rare grains would coalesce into pure class-5 clusters after having been dispersed in the 1959 lava. Because of their rarity and in spite of the variation in distribution of inclusions, it seems likely that all these sulfide-bearing grains and aggregates came from a fairly limited source region.

DENSE AGGREGATES CONTAINING POLYGONAL MOSAICS OF OLIVINE

Three of the dunitic aggregates described in table 25.2 consist partly or entirely of a mosaic of equigranular polygonal olivine. Two of these (in KI79–5–171.4 and KI81–1–181.5) are the largest known aggregates in the lake. Each of the three is slightly different in character, having a different range of grain sizes in the mosaic areas, as follows:

KI67–2–87.9	0.6–2.5 mm
KI79–5–171.4	0.4–1.0 mm
KI81–1–181.5	0.05–0.2 mm

The grain size of the mosaics is independent of storage time in the lake, as the coarsest was quenched in 1967 and the finest grained in 1981. Mosaic textures similar to those shown in figure 25.8*A–C* have been produced experimentally by thermal annealing (Mercier, 1979, p. 200, fig. 2d). None of the grains in the mosaics show any sign of strain, suggesting that they were not produced by recrystallization during steady-state deformation of the sort studied by Ross and others (1980). The lack of correlation between mosaic grain size and time of storage in the lake suggests that none of these mosaics was produced during post-eruptive annealing in the lake.

The smallest and simplest of these three aggregates (fig. 25.8C) consists of strain-free grains with curvilinear boundaries and limited size range. This texture corresponds to the equant gran-

TABLE 25.2.—*Data on olivine aggregates and megacrysts found in Kilauea Iki lava lake*

Sample	Depth of sample (m)	Date drilled (mo/d/yr)	Quenching temperature (°C)	Location in lake	Size of aggregate in section (mm)	Crystal size range: Largest (mm)	Crystal size range: Smallest (mm)	Size ratio (largest/smallest)	Dominant crystal class
Olivine Aggregates									
KI-113	6.86	8/24/60	1090-1095	center	8 x 5	4	0.2	20	1
KI67-2-87.5	26.67	6/14/67	1073	north edge	7 x 5	6	0.5	12	5
KI67-2-87.9	26.79	7/6/67	1090	north edge	(a)[1] 12 x 7	8	0.8	10	1
					(b) 9 x 3	2.5	0.6	4	Polygonal mosaic
KI79-5-171.4	52.24	2/1/79	950-980	north edge	[1] 14 x 10	7	0.4	28	Polygonal mosaic
KI81-1-181.5	55.32	4/10/81	1010-1030	center	[1,2] 16 x 4	2	< 0.1	> 20	Polygonal mosaic
KI79-1-189.0	57.61	12/21/78	1130-1135	center	(a)[1] 8 x 6	6	0.4	15	1
					(b)[1] 6 x 6	6	0.6	10	1
KI79-6-190.3	58.00	2/14/79	1130-1135	between center and north edge	5 x 4	5	0.5	10	1
KI79-1-203.6	62.06	12/21/78	1140	center	3 x 2	2	0.3	7	5
KI81-1-224.4	68.40	4/13/81	1140	center	10 x 5	8	0.5	16	1
KI81-1-230.4	70.23	4/13/81	1140	center	6 x 5	6	0.2	30	1
Megacrysts									
KI76-2-20.5	6.25	8/30/76	~100	center	[1] 20 x 10	single crystal		-	-
KI81-1-238	72.54	4/14/81	1135-1140	center	[1] 20 x 10	single crystal		-	-

[1]Cut by edge of section. Area given is that within the section.

[2]Area of aggregate on drill core surface 16 mm x 10 mm. The section was cut perpendicular to the core surface.

uloblastic category of Harte (1977) or the mosaic equigranular category of Mercier and Nicolas (1975, fig. 6b, p. 464), a texture attributed to lengthy annealing at high temperatures. The olivines in this inclusion contain abundant healed discoid fractures similar to textures in olivines from San Carlos and elsewhere, which have been interpreted (Wanamaker and Evans, 1985) as produced by decrepitation of fluid inclusions during rapid decompression. Similar healed fractures occur in inclusions KI67–2–87.5 and KI79–1–189.0(a), but are not as common in these aggregates as in figure 25.8*C*.

The KI81–1–181.5 aggregate is more complex, in that it contains, in addition to the fine-grained mosaic shown in figure 25.8*B*, a population of coarser, more euhedral crystals, commonly containing a necklace of inclusions, some with sparse, tiny sulfide blebs. The coarser grains probably represent a second stage of grain coarsening, with the larger crystals having grown at the expense of smaller ones. The necklace of inclusions would correspond to impurities along former boundaries of the grains, swept up as the olivine grains grew outward. For the following reasons, this interpretation is preferred to a model in which the coarser grains would be considered to be later cumulates that attached themselves to a preexisting fine-grained substrate: First, some of the coarse grains occur within the mosaic, not at its edge. Second, the grains are very tightly intergrown and randomly oriented (unlike the open cumulate aggregates shown in fig. 25.6*A–B*). Third, the small mosaic grains contain very tiny inclusions similar in character to those in the coarser grains, suggesting that the coarse grains grew by incorporating this mosaic and its grain-boundary phases. Clearly the second-stage coarsening did not take place in the lava lake; the mosaic at the left end of the aggregate (fig. 25.8*D*) is in direct contact with the host and shows no coarsening whatever. Therefore, both stages predate incorporation in the present host.

The third of these aggregates, from sample KI79–5–171.4 (fig. 25.8*D*), is the most heterogeneous and also the most enigmatic. It contains areas where deformed class 1 grains are partly enclosed by strain-free polygonal grains, but elsewhere it contains euhedral, class-2-like grains. This aggregate also shows more extensive penetration by melt (now groundmass crystals) than any other aggregate. Of all the aggregates in table 25.2, this one appears to have the most complex history.

In contrast to the other two groups of aggregates, which correspond to one or another of the olivine classes described above, the mosaic grains do not occur as a recognizable separate class of dispersed grains. It is possible that some of the smallest class 1 and some class 3 grains might be former polygonal mosaic, but this seems unlikely: there are very few such grains in the eruption pumice. A more likely explanation is that strongly annealed dunites are simply rarer than the mildly deformed ones.

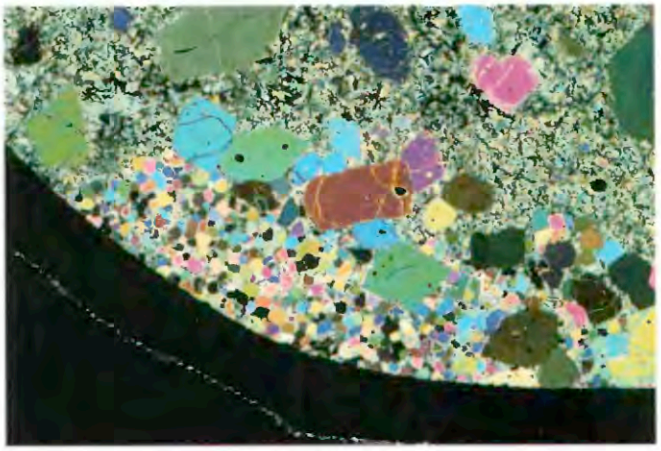

A

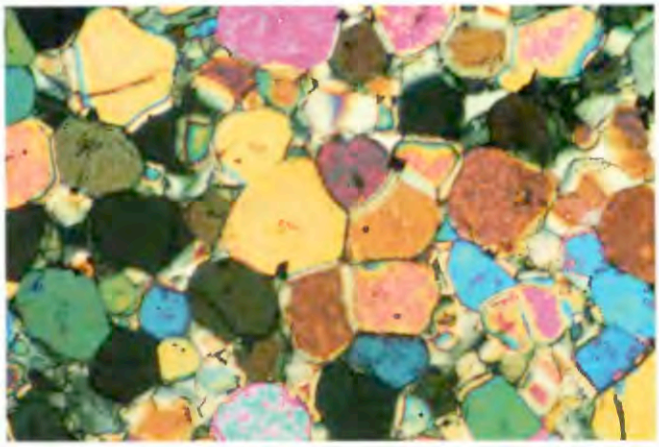

B

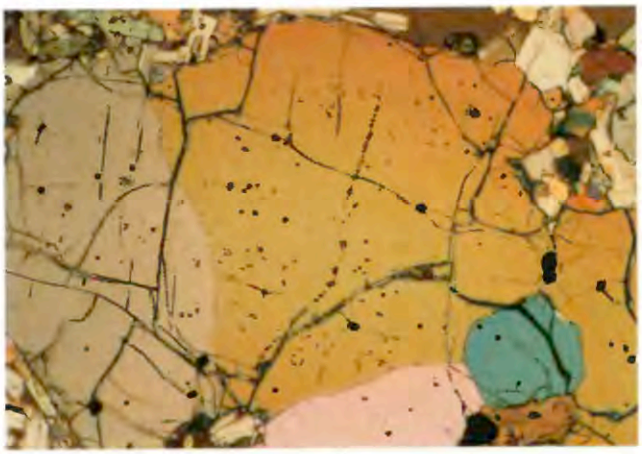

C

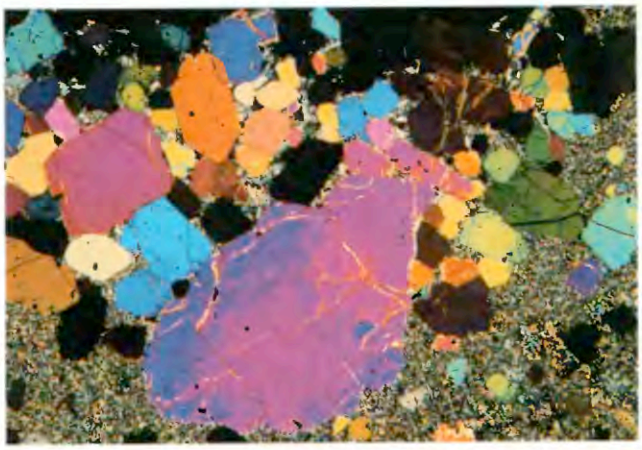

D

FIGURE 25.8.—Dunitic aggregates found in Kilauea Iki lava lake. ***A***, Olivine aggregate and host in KI81–1–181.5, quenched from 1,010–1,030 °C in 1981. Field of view is 1 cm across. The aggregate consists of areas of fine-grained polygonal mosaic of olivine, with coarser, more euhedral olivine present along the edge or (lower right) within the mosaic. At the left end of the aggregate, the mosaic is in direct contact with the groundmass of the host. Crossed nicols. ***B***, Close-up of polygonal mosaic in aggregate in KI81–1–181.5. Field of view 1 mm across. Most grains are olivine. Most of the olivine grains contain a central swarm of tiny inclusions (see yellow grains in center). Chromite grains (opaque) occur at margins of olivine. Minor interstitial plagioclase and augite are present locally. Crossed nicols. ***C***, Close up of the smaller olivine aggregate from KI67–2–87.9, quenched from 1,090 °C in 1967. Grain boundaries intersect at angles near 120° at triple junctions, but are otherwise curvilinear, so that grain shapes are irregular. The color variation seen in the tan olivine grains reflects zoning toward the host; it follows the outline of the aggregate, not of individual grains. Black grains within the aggregate are chromite. Fuzzy inclusions are healed discoid fractures containing asterisk-like inclusions of brown glass and chromite. Field of view is 4 mm across. Nicols partly crossed. ***D***, Olivine aggregate (10 by 14 mm) in sample KI79–5–171.4, quenched from 950–980 °C in 1979. This aggregate has been extensively penetrated by melt, now visible as interstitial groundmass-size crystals. It contains local areas of polygonal olivine, surrounding coarser deformed olivine (the green grains on right side), and areas of randomly oriented euhedral olivine (center and left). Crossed nicols.

In summary, then, rare dunitic aggregates have been found in Kilauea Iki lava lake. The textures of the various aggregates, which record multiple deformation events, multiple annealing events, and (or) rapid decompression, match those observed in ultramafic xenoliths of mantle origin. The fact that the history recorded in these aggregates appears to predate entirely their incorporation in the 1959 lava implies that all aggregates are xenolithic. To the extent that class 1 and class 5 olivine grains in the 1959 lava are derived by disaggregation from similar preexisting dunite, crystals in those classes may likewise be considered xenocrystic.

OLIVINE PHENOCRYSTS AND DUNITIC AGGREGATES IN OTHER HAWAIIAN ROCKS

Olivine is virtually ubiquitous as a phenocryst phase in Hawaiian tholeiites and mafic alkalic rocks. With the petrographic description of the phenocrysts, megacrysts, and dense aggregates found in the Kilauea Iki lava in hand, it is now appropriate to review the information available on the petrography of olivine from other Kilauea lava and from those of other Hawaiian volcanoes.

No comparably detailed petrographic work on Kilauea

olivines has been done previously. Even studies focused on the picritic lava of Kilauea (Macdonald, 1944; Muir and Tilley, 1957; Murata and Richter, 1966a, 1966b) have not mentioned the occurrence of kink-banded olivine, for example. Therefore I have re-examined all of the thin sections of subaerial Kilauea basalt available to me, with the present classification scheme in mind. The available sections included samples of the historical eruptions described in Wright (1971), including the 1920 eruption, the relatively magnesian 1921 summit eruption, and the 1840 east-rift picrite. In addition, samples of the 1977, April 1982, and September 1982 eruptions, and samples of phases 1–8 of the ongoing (as of January 1986) Puu Oo eruption have been examined. The earlier samples were available only as covered thin sections; for the 1977–1983 samples, polished sections were available for examination.

One good example of a kink-banded olivine phenocryst was found in this search, in TLW 67–1g, the most magnesian lava of the 1920 southwest-rift eruption (Wright, 1971). No other class 1 or probable class 5 olivine has been observed in any of them. The olivine phenocyrsts present all fall in class 2 of the present classification system, being either euhedral or skeletal. Skeletal grains are much more common, proportionately, than they are in Kilauea Iki samples. Resorbed grains, though present (in some Puu Oo samples, for instance), are rare.

The olivine-rich precaldera intrusive rocks exposed in Kilauea's caldera wall, including the Uwekahuna laccolith, were also examined, with the thought that they might represent samples of olivine-rich sludge from the bottom of Kilauea's summit reservoir. The olivine phenocrysts in these intrusives are uniform in grain size (1–5 mm long) in contrast to the more variable olivine in Kilauea Iki (see fig. 25.3). Planar extinction discontinuities were observed in very few grains. These grains are small, and the bands very faint. In about one-half the cases, the discontinuities exist only at the margin of the grain and are absent from the interior. No such grains have been observed in the 1959 lava, and it is not clear whether these marginal extinction discontinuities are deformation or growth features.

Examination of the submarine east-rift lava described by Moore (1965) turned up deformed olivine in two samples, No. 1742, from 1,400 m below sea level, and No. 1706, from 5,000 m below sea level. Another dredged sample of Kilauea east-rift lava, shown to me by M.O. Garcia (University of Hawaii) also contains good examples of blocky, deformed olivine crystals, strikingly similar to those in the 1959 lava.

In addition to these instances of kink-banded olivine in Kilauea tholeiite, such olivine has been reported from tholeiite of Hualalai, dredged from 2 km below sea level (Clague, 1982) and in one Haleakala tholeiite in the suite studied by Chen and Frey (1983) (C.-Y. Chen, written commun., 1984). Thus, the kink-banded olivine in the 1959 Kilauea tholeiite are not unique. However, they appear to be virtually absent from other subaerial Kilauea eruptions.

Dunitic aggregates containing deformed olivine and (or) mosaics of unstrained grains occur very widely in alkalic rocks in Hawaii. They have been described from Hualalai (Kirby and Green, 1980; Jackson and others, 1981), from the Honolulu Volcanics (formerly the Honolulu Volcanic Series; Jackson and Wright, 1970; Sen, 1983), and from Loihi Seamount (Moore and others, 1982; Roedder, 1983). Other reports of similar materials in Hawaiian tholeiite are lacking, however. Jackson (1968), in his very extensive survey of coarse-grained xenoliths in Hawaiian rocks, stated that all coarse-grained xenoliths he had found in tholeiitic lavas were cumulates, and that "none of the minerals is strained or deformed" (Jackson, 1968, p. 142). He further presented data showing that pure olivine rocks, containing no other cumulus or interstitial phases, were very rare in Hawaiian tholeiite. The deformed dunitic aggregates found in Kilauea Iki appear to be the first such material recognized in any Hawaiian tholeiite.

OLIVINE AND GLASS COMPOSITIONS: ERUPTION PUMICE

This section presents compositional data on olivine and glass in the eruption samples. Of particular interest are (1) variations in composition and zoning of the olivine phenocrysts as a function of petrographic class and of time, (2) variations in average glass composition with time, and (3) more detailed data on the glasses immediately adjacent to olivine phenocrysts in the eruption pumice. As will become evident, these rapidly quenched samples preserve a significant amount of internal disequilibrium, as might be expected in an eruption long-recognized as involving magma mixing (Wright, 1973).

Analyses of representative olivine grains are presented in table 25.3. These analyses cover the range of phenocryst composition observed. The forsterite contents shown are reproducible to ± 0.1 percent, MnO ± 0.02 percent, CaO to ± 0.03 percent absolute. NiO is more variable, reproducible to perhaps ± 0.05 percent absolute. The intragrain chemical variation (see table 25.3, columns 1 and 2, for example) is modest, but it exceeds the analytical uncertainty and is generally systematic, with the cores being uniform and all variation (zoning) confined to the rims. There are a few grains, especially in the later samples, where forsterite content varies more irregularly, but the total range of intragrain variation in these grains is ≤ 0.8 mol percent Fo. Therefore, it seems justifiable to document, and to interpret, the zoning patterns of most of these olivines.

Table 25.4 includes average glass compositions for the fifteen eruption samples studied. These include only glass analyses taken some distance (>1 mm) away from the olivine phenocrysts. All of the glass compositions are olivine-controlled (Powers, 1955; Wright, 1971); that is, they are related to each other chiefly by addition or removal of olivine ($\pm$chromite), the only phenocryst phase present. Hence, the most variable component is MgO, which ranges from 6.35 to 10.03 weight percent and is reproducible to ± 0.10 percent. Other oxides are less variable: total iron as FeO only varies from 11.00 to 11.65 percent, for example. As documented in Helz and Thornber (in press), the MgO content of Kilauea glass in equilibrium with olivine varies linearly with temperature and appears to be a usable geothermometer. The quenching

temperature assigned each glass in table 25.4 is based on this calibration.

OLIVINE PHENOCRYST COMPOSITION VERSUS PETROGRAPHIC CLASS

Olivine compositional data as a function of the petrographic classes established above are presented in figures 25.9*A–B* and 25.10. Figure 25.9*A* shows histograms of the forsterite content of the cores of all the olivine phenocrysts analyzed to date. Each symbol corresponds to one analyzed point. For grains showing <0.5 percent variation in forsterite, all points are plotted. Most such grains are strongly resorbed (class 3 or 1) or fragmental (class 4) and may not have any real rims preserved on them.

The most important feature of figure 25.9*A* is that there is extensive overlap in core compositions between the euhedral class 2 olivine and the less regularly shaped, kink-banded and (or) sulfide-bearing olivine in classes 1 and 5. Class 1 and 5 cores extend to higher forsterite contents (88.7 percent), and class 2 cores to lower forsterite contents (85.0 percent), but the bulk of both subsets fall between 85 and 88 percent Fo. The class 3 and 4 grains are not distinctive, with most having 86.5–87.7 percent Fo. It should be noted that the composition of olivine from phase 1 (which made up most of the lake; see fig. 25.2) is no different from that of olivine in the later phases, except that the most iron-rich class 2 grains are absent.

TABLE 25.3.—*Composition of selected olivine grains from the 1959 eruption pumice, showing extremes of composition and zoning*

[Oxide contents in weight percent]

	1	2	3	4	5
Sample	Iki-22		Iki-9		Iki-24
	core	rim	core	rim	core
Olivine class	1	1	2	2	1
Points in analysis	5	4	2	4	3
SiO_2	39.44	39.90	40.09	38.95	40.22
TiO_2	.01	.01	.05	.04	.00
Al_2O_3	.03	.02	.00	.02	.00
Cr_2O_3	.02	.00	.04	.02	.01
FeO	14.22	12.09	12.26	18.16	11.03
NiO	.10	.19	.15	.01	.17
MnO	.20	.17	.12	.20	.17
MgO	45.86	47.76	47.38	42.37	47.87
CaO	.24	.20	.24	.32	.25
Na_2O	.00	.00	.00	.02	.02
Total percent	100.12	100.34	100.33	100.11	99.74
Mol% Fo	85.2	87.6	87.3	80.6	88.6
Comments	Reverse zoning		Extreme normal zoning		Most magnesian

Most of the olivine phenocrysts in the eruption samples are zoned, and figure 25.9*B* summarizes the available data on zoning patterns for the same population of grains whose core compositions were given in figure 25.9*A*. Most grains vary over a range of 3 percent Fo or less, the zoning generally being confined to the outermost 10–30 μm of the crystal. Only two small class 2 grains are more strongly zoned, showing as much as an 8 percent decrease in Fo from core to rim. The class 3 and 4 grains are essentially unzoned.

Three features of figure 25.9*B* are particularly noteworthy. First, normally zoned and reversely zoned grains are almost equally abundant. Second, there is little difference between the euhedral class 2 grains and the class 1 and 5 grains in this respect. If anything, reverse zoning is more frequent in the class 2 population. Lastly, the olivine phenocrysts analyzed so far from phase 1 samples are mostly either reversely zoned or unzoned. Normally zoned phenocrysts do not become common until phase 2.

The variation in NiO content of olivine cores for this same population of grains is shown in figure 25.10. NiO content was of particular interest because potentially it might allow one to distinguish between cognate and xenocrystic (peridotite-derived) olivine, or perhaps between olivine that coexisted with sulfide and olivine that did not. As can be seen in figure 25.10, however, the various populations appear not to have distinctive NiO contents. The few class 5 sulfide-bearing grains in the eruption pumice tend to fall below the median NiO content for the class 1 + 5 grains overall, but even here the difference is not very marked. (It should be noted that all the sulfides in the class 5 grains in the eruption samples are tiny, hence do not unequivocally predate entrapment and therefore do not prove that the basaltic melt from which the olivine in fig. 25.10 grew was sulfide-saturated.) From the analyses in table 25.3 one might suppose that there was a positive correlation between NiO and forsterite contents, but when the entire data set is considered there is no such correlation. The NiO contents observed here (0.10–0.30 percent) are the same as reported by other workers for Kilauea basalt (Häkli and Wright, 1969; Bence and others, 1981) and other mafic rocks (Fleet and others 1977; Fleet and MacRae, 1983).

It is evident from figures 25.9*A–B* and 25.10 that the various petrographic classes of olivine described earlier are not distinct with respect to Fo content or NiO content or style of zoning. They are not distinguishable on the basis of MnO or CaO contents either. This suggests that the olivine grains formed under some continuous range of conditions and that none of the classes can be singled out on the basis of composition as being xenocrystic to their host.

The results presented above are slightly at variance with those of some earlier workers. Richter and Murata (1966) reported that large blocky olivine phenocrysts were magnesian (Fo_{87-88}) and small euhedral olivine crystals more iron-rich (Fo_{82}). Certainly individual crystals can be found with these characteristics, but the composition ranges of the two populations overlap almost completely. Even the microphenocrysts (not shown in figs. 25.9*A–B*, 25.10) range from Fo_{87} to Fo_{74}. Thus, the various olivine groups cannot be considered to be successive generations of crystals grown

TABLE 25.4.—*Composition of glass away from olivine phenocrysts in selected samples of the 1959 Kilauea eruption pumice*

[Oxide contents in weight percent; total iron reported as FeO]

	1	2	3	4	5	6	7	8	9	10	11	12	13	14	15
Sample No.	Iki-1	Iki-58	Iki-22	Iki-44	Iki-7	Iki-11	Iki-9	Iki-13	Iki-14	Iki-20	Iki-21	Iki-24	Iki-26	Iki-32	Iki-33
Date (mo/d) sample collected	11/14	11/15	11/18	11/20	11/21	11/26	11/28	12/5	12/6	12/8	12/11	12/13	12/14	12/17	12/19
Phase of eruption	1	1	1	1	1	2	3	4	5	7	8	9	10	15	16
SiO_2	49.91	50.23	49.18	49.46	49.62	49.32	50.46	49.84	49.43	49.81	49.76	49.88	49.26	49.65	49.63
TiO_2	2.96	2.91	2.49	2.66	2.64	2.64	2.82	2.62	2.60	2.60	2.63	2.68	2.67	2.63	2.63
Al_2O_3	13.99	13.98	12.10	12.82	12.88	12.69	13.51	12.74	12.73	13.02	12.85	13.19	12.98	12.93	13.03
Cr_2O_3	.01	.00	.08	.07	.05	.06	.01	.07	.06	.04	.07	.07	.06	.04	.06
FeO	11.40	11.65	11.33	11.27	11.25	11.15	11.00	11.14	11.27	11.28	11.21	11.04	10.92	11.08	11.22
MnO	.13	.14	.13	.14	.13	.12	.14	.13	.13	.13	.13	.13	.13	.13	.12
MgO	6.35	6.46	10.03	8.55	8.60	8.48	6.93	9.04	9.49	8.21	9.09	8.61	8.67	8.73	8.70
CaO	11.25	11.50	11.17	11.25	11.33	11.39	11.56	11.39	11.38	11.33	11.41	11.51	11.51	11.55	11.67
Na_2O	2.67	2.62	2.33	2.53	2.46	2.51	2.48	2.36	2.29	2.32	2.39	2.17	2.46	2.45	2.28
K_2O	.62	.60	.52	.54	.56	.56	.58	.55	.58	.54	.55	.58	.52	.54	.60
P_2O_5	.28	.26	.22	.26	.25	.27	.31	.23	.21	.27	.26	.24	.24	.23	.24
Total	99.57	100.35	99.58	99.55	99.77	99.19	99.80	100.11	100.17	99.51	100.35	100.10	99.42	99.96	100.18
Points in average	8	14	6	6	7	4	6	9	5	5	7	4	6	5	4
Quenching temperature (°C)	1142	1144	1216	1187	1188	1185	1154	1196	1205	1181	1197	1188	1189	1191	1190

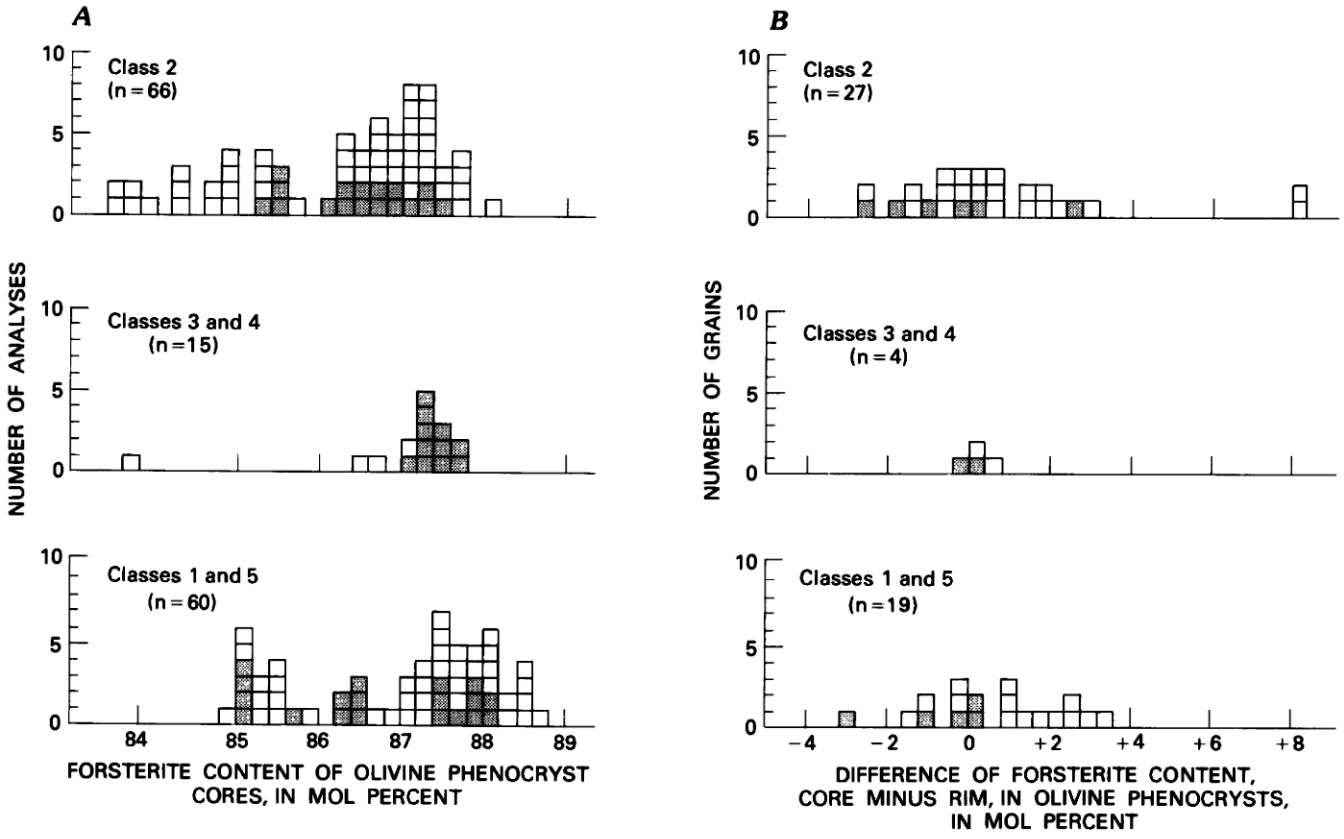

FIGURE 25.9.—Compositional data for olivine phenocrysts from the 1959 Kilauea eruption. Shaded squares, olivine from phase 1; open squares, olivine from later phases. ***A***, Frequency distribution of forsterite content of the cores of olivine phenocrysts in eruption samples. Each square represents one analyzed point. ***B***, Frequency distribution of different types of Mg-Fe zoning observed in olivine phenocrysts in eruption samples, for the same olivine population as in fig. 25.9*A*. Each square represents one grain. Negative abscissa values indicate reverse zoning.

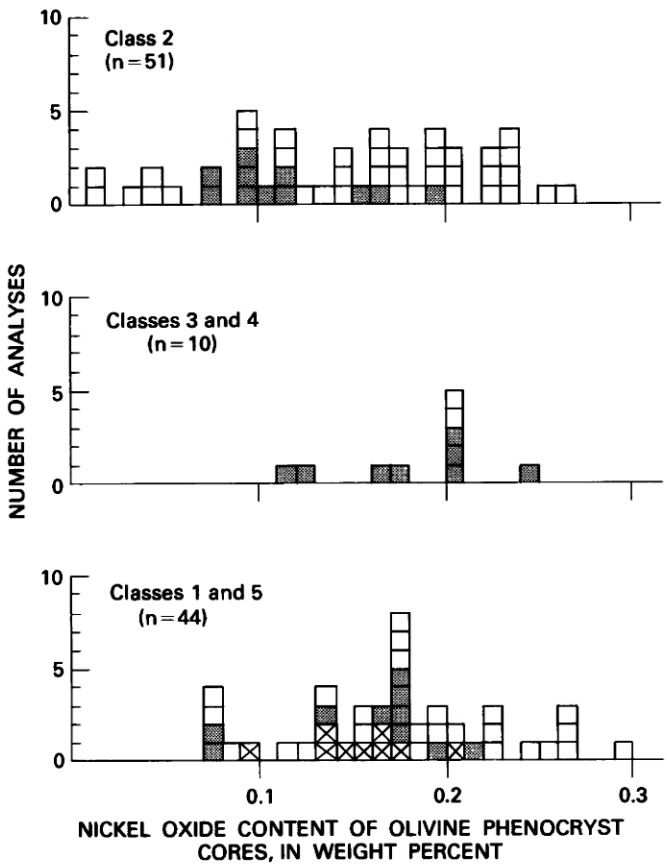

FIGURE 25.10.—NiO content of the cores of olivine phenocrysts in the 1959 Kilauea eruption samples, for the same population of olivine grains as in fig. 25.9. Each square represents one analyzed point. There are fewer points in this figure than in figure 25.9 because Ni was not always analyzed for. Shaded squares, phase 1 olivine; squares with x, class 5 olivine, from phases 2–16; open squares, other olivine from phases 2–16. The calculated limit of detection of NiO is 0.08 weight percent.

from a single batch of magma.

The data in figure 25.9*B*, showing that most olivine phenocrysts are zoned, are superficially in conflict with Leeman and Scheidegger's (1977) statement that the olivine in the 1959 eruption is not zoned. This is a question of semantics, however: Leeman and Scheidegger chose to regard any grain that varied by less than 5 percent Fo as unzoned, and it is true that strongly zoned grains are rare in the 1959 lava.

OLIVINE PHENOCRYST COMPOSITIONS VERSUS TIME

It is evident from figure 25.9*A*–*B* that olivine compositions and zoning patterns vary slightly from phase to phase of the eruption. These variations from sample to sample are shown in figure 25.11. Note that in this figure, in contrast to figures 25.9*A* and 25.10, symbols correspond to more than one analyzed point. For example, in sample Iki–11, three grains have been analyzed, one each from classes 1, 2, and 5. There are six analyzed core points and three rim points on the class 5 grain, but some of the core points fall on top of each other, so are not visible as separate points in figure 25.11. Average MgO content of the glass in each sample (see table 25.4) is plotted below the olivine data. The range of MgO content shown is that observed in glass more than 1 mm away from any olivine phenocryst. The fields in figure 25.11 outline the range of core compositions for the two groups of olivine.

As noted above, olivine is sparse in the cool (1,140–1,145 °C), early phase 1 samples. The olivine grains are small and euhedral, but with variable zoning. Iki–22, the first of the olivine-rich samples, has a much more magnesian glass with a quenching temperature of 1,217 °C (see table 25.4) and a phenocryst population of large, reversely zoned olivine crystals. Previous workers (Leeman and Scheidegger[1] 1977; Ford and others, 1983; Harris and Anderson, 1983) have noted that the cores of these olivine phenocrysts would be in equilibrium with the glass in the sample at about 1,250 °C. None has reported the existence of the more magnesian rims, however.

In contrast to Iki–22, Iki–44 has only fairly magnesian olivine grains in it, all virtually unzoned. The glass in this sample was quenched from a lower temperature (1,189 °C) than that in Iki–22. The glass in Iki–7 is similar to that in Iki–44 but it includes, besides magnesian, unzoned olivines like those in Iki–44, reversely zoned euhedral olivines, some of which are shown in figure 25.4C. Thus, in phase 1 we see a large range in glass composition and a significant range in olivine composition (Fo_{88} to $Fo_{84.5}$). However, there is no correlation between glass composition and olivine core composition, olivine rim composition, or the style of zoning, if any. As noted above, all large zoned olivine grains in phase 1 are reversely zoned.

Phase 2 (Iki–11) contains the first coarse, normally zoned olivine, in addition to reversely zoned crystals. The crystals do not converge on a common rim composition, however: the class 1 crystals range from $Fo_{87.8}$ (core) to Fo_{85} (rim), whereas the class 2 crystals go from Fo_{85} (core) to $Fo_{87.4}$ (rim). Further evidence of internal disequilibrium is the observation that the glass in this sample is appreciably more heterogeneous than that in any individual phase 1 sample, with MgO ranging from 8.07 to 8.60 percent, for glasses well away from olivine.

Phase 3 (Iki–9), like Iki–58 from phase 1, though olivine-poor, does not contain a uniform olivine population. Only two small class 2 olivines occur in the thin section, but they show very different zoning patterns: one ranges from $Fo_{87.4}$ to $Fo_{79.3}$ and is euhedral at the edges; the other varies from $Fo_{84.9}$ to $Fo_{83.1}$ and is resorbed at the edges. The glass in this sample was quenched from a lower temperature (1,154 °C) and is more differentiated than that in any but the earliest phase 1 samples.

Phase 4 glass (Iki–13) is again more magnesian, with a quenching temperature of 1,196 °C, and the glass is more hetero-

[1]Leeman and Scheidegger (1977) refer to Iki–22 as KI–7 and to what is probably Iki–7 as KI–22. This is a numbering mixup: Iki–22 has a unique high-MgO glass not found in any other phase 1 pumice. Ford and others (1983), using Leeman and Scheidegger's data, reproduce the same numbering error.

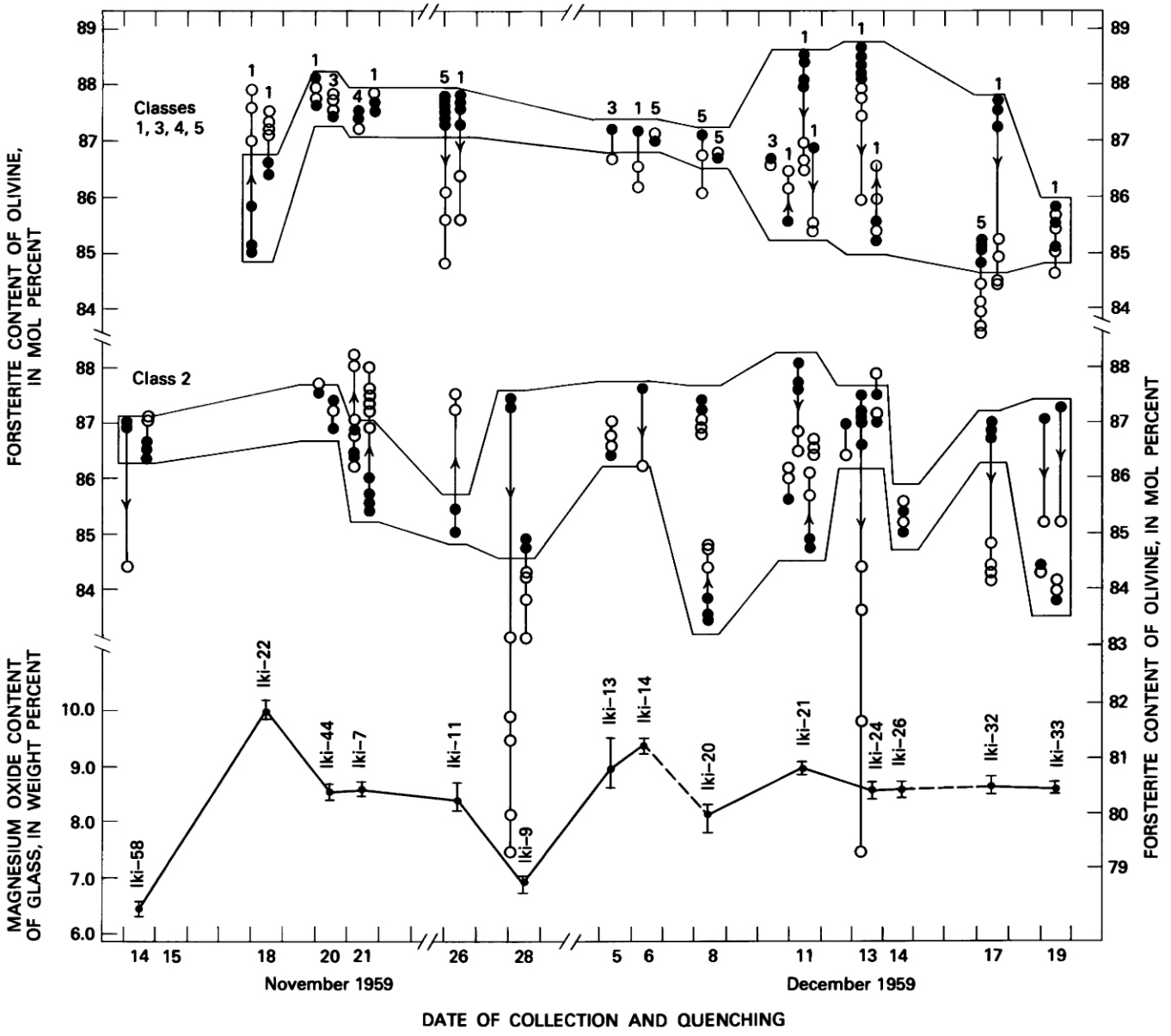

FIGURE 25.11.—Composition of olivine phenocrysts (mol percent Fo) and of glass (weight percent MgO) in samples from the 1959 eruption of Kilauea, plotted against the dates of eruption and quenching. For olivine, each symbol includes all analyzed points on a given grain having the same composition, rounded to 0.1 percent Fo. All data from a given grain are connected by a line. Solid circles, analyzed points from the cores of grains; open circles, points around the rims of the same grains. Grains in classes 1, 3, 4 and 5 are individually labeled. Arrows pointing toward rim compositions emphasize the direction of zoning. For glass, the small dots give the average MgO content of glass, from table 25.4, whereas the bar indicates the total range of MgO content observed, for glass more than 1 mm away from olivine.

geneous than any other sample, with MgO varying from 8.70 to 9.48 percent. Phase 5 (Iki–14) contains a still hotter (1,205 °C) but more uniform glass, with 9.32 to 9.55 percent MgO. In both samples, olivine phenocrysts are weakly zoned, in both normal and reverse senses, and are consistently magnesian ($Fo_{87.5}$ to $Fo_{86.0}$).

Phase 6 is not represented here. Phase 7 (Iki–20) is, again, a cooler phase (1,181 °C), though not as differentiated or olivine-poor as phase 3. The olivine population within the section is more diverse than ever: Both normally and reversely zoned grains are present, and the class 2 olivine exhibits a wide range of core compositions ($Fo_{87.5}$ to $Fo_{83.4}$). For the first time, however, the rim compositions of the different grains converge toward a common composition, as though they had been trying to equilibrate, either with each other or with a common melt.

Phase 8 (Iki–21) is hotter again (1,197 °C) and very olivine-rich, with a very heterogeneous olivine population. As in phase 7, the rims of the various class 2 grains appear to be converging on a common composition. This sample contains the most magnesian ($Fo_{88.1}$) class 2 olivine found.

Phase 9 (Iki–24, see fig. 25.3) contains a slightly cooler (1,188 °C) glass. Like Iki–21, it contains a very varied group of olivine crystals, with the class 1 grains converging on a common rim composition. It also contains the only strongly zoned grain ($Fo_{87.5}$ to $Fo_{79.3}$) found since phase 3, and the most magnesian olivine ($Fo_{88.7}$) in the whole analyzed population shown in figure 25.11.

From phase 10 through phase 16 (samples Iki–26, Iki–32, and Iki–33), glass composition is constant, implying uniform quenching temperatures of 1,188–1,190 °C. The glass is quite homogeneous, away from olivine, within each section. The olivine grains are either normally zoned or unzoned; none shows pronounced reverse zoning. Also, although core composition remains quite varied, olivine rim compositions are consistently more iron-rich ($Fo_{85.5}$ to $Fo_{83.5}$) than in all previous phases but phase 3. This trend toward simpler, better equilibrated olivine compositional variations begins earlier than the simplification in the petrographic variants, which is confined to phases 16 and 17 (see table 25.1).

COMPOSITION OF GLASS ADJACENT TO OLIVINE

The glass compositions presented in table 25.4 and discussed above are those found more than 1 mm away from any olivine phenocryst. Glass closer to olivine grains is more variable in composition, in ways that cannot be explained as the result of quench overgrowths on olivine. This section presents data on selected pairs of olivine rim and adjacent glass that illustrate both this greater variation in the glass and its apparent correlation with the condition (euhedral or resorbed) of the adjacent olivine rim.

The olivine rim compositions (shown in fig. 25.11) were taken on points within 10 μm (and usually within 3–5 μm) of the contact of the olivine with the glass. The adjacent glass analyses are taken at distances of 20–30 μm away from the contact. Most of the rim points shown in figure 25.11 have a corresponding analysis of adjacent glass. From this data set, figure 25.12 includes data on only three samples: two phase 1 samples (Iki–22, Iki–44) and the latest analyzed sample (Iki–33, from phase 16).

In Iki–22, glass adjacent to the large reversely zoned phenocrysts is less magnesian than glass elsewhere in the section. Around the edge of each crystal, glass adjacent to euhedral corners and faces is more magnesian than glass adjacent to resorbed edges. Some of this resorption is very local (fig. 25.13). It is possible that all the adjacent glass has been depleted in MgO by growth of olivine during quenching, but the variation within the adjacent glass cannot be so explained; the analyzed points are all equally far from olivine.

The glass in Iki–44 is less magnesian and the olivine more magnesian than Iki–22, as noted above. Here we see data from four different grains, two in a cluster and two isolated phenocrysts. Three of these grains have adjacent glass analyses with MgO

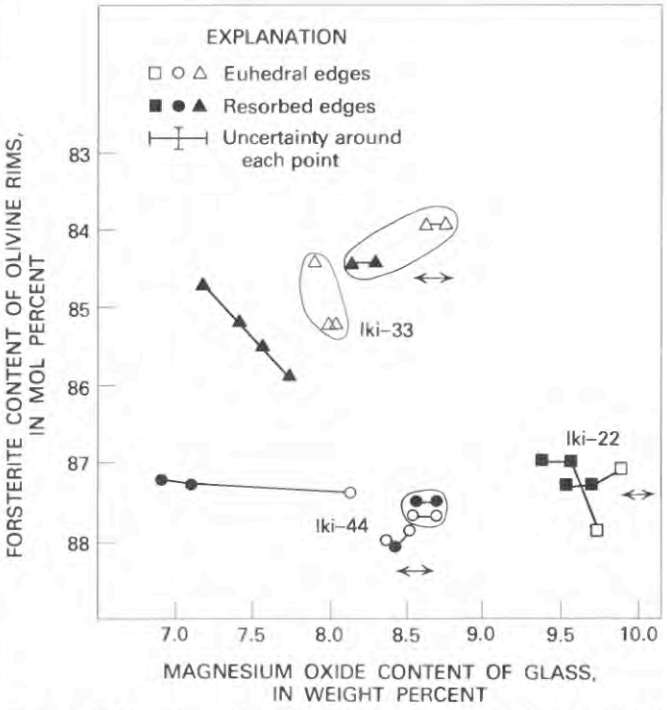

FIGURE 25.12.—Composition of rims of olivine phenocrysts (mol percent Fo) plotted against the MgO content (weight percent) of glass adjacent to the olivine rim, for three samples from the 1959 Kilauea eruption. Squares, data from Iki–22; circles, data from Iki–44; triangles, data from Iki–32. In this figure, points connected by a line are from around the periphery of a single grain. Data within a circle represents points on two or more different grains from a cluster of olivine grains. The double-ended arrow shows the range of MgO in glass more than 1 mm from olivine for each of the samples. The uncertainty in Fo and in MgO is ±0.1 percent.

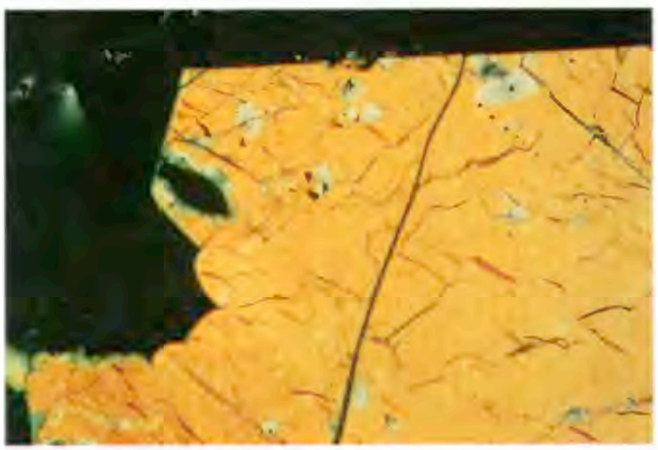

FIGURE 25.13.—Large olivine grain from Iki–22, showing euhedral form locally modified by resorption. Cuspate edges like this are also visible in figure 25.4*E*. Field of view 2 mm across. Crossed nicols.

contents close to the average MgO content of the distant glass; these glasses appear to be unaffected by any quench overgrowths on olivine. The fourth grain is surrounded by a sheath of variable, but less magnesian glass, some of which is grossly different in composition from glass elsewhere in the thin section. As in Iki–22, the euhedral parts of this crystal have relatively magnesian glass adjacent to them, while the resorbed parts are next to glass with 7 percent MgO.

Iki–33 provides evidence that this same kind of heterogeneity was present almost to the end of the eruption. One grain, completely euhedral, is surrounded by glass identical to the distant glass. An adjacent resorbed grain is surrounded by glass with significantly less MgO. The cluster of euhedral grains shown in figure 25.6*A–B* lies in a pool of glass with 8 percent MgO; these grains show only minor resorption. A last grain, of class 1, is surrounded by a sheath of glass with 7.2 to 7.7 percent MgO and is strongly resorbed on all sides.

Similar patterns occur in the other eruption samples analyzed so far. The main variants may be summarized as follows:

(1) In the first type of rim-glass relationship, the adjacent glass contains 0.2 to 1.5 weight percent less MgO than the glass more than 1 mm away from olivine. The enclosed olivine shows signs of resorption, such as rounding of corners and wavy or cuspate margins, as seen in figures 25.4*E*, 25.5*A*, and 25.13. Resorption may be partial, or the entire rim of the crystal may be affected. Glass next to resorbed surfaces is consistently less magnesian than glass adjacent to euhedral corners and edges, even on the same grain. A dozen such grains, partly or completely rimmed by low-MgO glass, have been found. They occur in samples Iki–7, 11, 9, 14, 20, 24, and 32, in addition to the samples in figure 25.12.

(2) In the second type of rim-glass relationship, the adjacent glass has a composition essentially equal (within ± 0.2 weight percent MgO) to that of the more distant glass. There is no correlation between crystal form and glass composition; the grain may be locally resorbed or completely euhedral. Thirty-one such grains have been analyzed, of which 12 are essentially euhedral.

In addition, there are two small euhedral grains, one in Iki–9 and the other in Iki–32, which have skins of low-MgO glass but show little resorption, like the cluster of grains in Iki–33 (fig. 25.6*A–B*). No cases are known in which an olivine grain has a sheath of glass appreciably more magnesian (>0.2 percent MgO) than the distant glass.

The existence of these boundary layers (or sheaths) of contrasting glass composition was not evident from petrographic examination, as no color difference exists between the various compositions; their presence was only detected with the microprobe. These MgO-poor boundary layers cannot simply result from quench overgrowth on olivine, because 31 out of 46 grains do not have them. Sheathed grains are not rare, though; they make up 30 percent of the grains analyzed. The possibility that olivine (or other) crystals might carry a boundary layer of melt with them as they move has been suggested before (Helz, 1980), but the layers themselves have not previously been observed.

COMPOSITION OF OLIVINE IN THE LAKE

The rapidly quenched eruption pumice samples preserve many sorts of disequilibrium and evidence of magma mixing. Olivine phenocrysts in the lake, by contrast, have had months or years to exchange Mg for Fe with the surrounding host liquids before being quenched during drilling. Table 25.5 presents data for olivine in the aggregates and megacrysts described in table 25.2. These grains differ from isolated phenocrysts in the same samples in that core compositions may be slightly more forsteritic, but they are otherwise quite representative of phenocrystic olivine in the lake.

The shallow samples (KI–113 and KI76–2–20.5 in table 25.5) show strong normal zoning, from $Fo_{88–86}$ (cores) to $Fo_{78–72}$ (rims). Such extensive zoning, with a range of 10–14 percent Fo, is unknown so far in the eruption samples. This zoning probably developed in the lake, during crystallization of the groundmass. Note that the holocrystalline sample (KI76–2–20.5), quenched from about 100 °C, shows more extensive zoning than the KI–113 clot, which was quenched from 1,090 °C. Extensive normal zoning of this sort is common in olivine phenocrysts in older Hawaiian lava flows (Maaloe and Hansen, 1982). In the flows, some uncertainty exists over whether the narrow, iron-rich rims are overgrowths or result from exchange of Fe and Mg between preexisting olivine and the differentiating melt. In these lake samples, there is no ambiguity; the zoning is produced by re-equilibration, not by overgrowth.

Samples from deeper in the lake show progressively less zoning, always in the normal sense. In KI67–2–87.9 (table 25.5) the range in forsterite content is 10 mol percent. The intragrain color variations seen in the olivine cluster in figure 25.8*D* are produced by this zoning. It is evident that the zoning follows the outline of the whole aggregate, not of individual grains within the cluster. In the 1981 samples (table 25.5, columns 5–6 and 9–10) the range of forsterite variation is only 4–5 mol percent. In these later samples, there is a positive correlation between maximum forsterite content and core quenching temperature, as follows:

Sample	Percent Fo	Temperature (°C)
KI81–1–238	85.1	1,135–1,140
KI67–2–87.9	82.7	1,090
KI81–1–181.5	79.2	1,010–1,030

Even more extensive re-equilibration of olivine phenocrysts has been described by Moore and Evans (1967) in samples from deep within the prehistoric Makaopuhi lava lake. There, the phenocrysts were almost unzoned and had the same composition as groundmass olivine. Maaloe and Hansen (1982) present calculations showing how zoning in initially forsteritic olivine phenocrysts would be expected to change with time, as exchange of Fe for Mg proceeds. The olivine in both lava lakes follows the model very well.

The feature of these data most relevant to the present paper, however, is that they suggest that even the largest olivine aggregates and megacrysts have been affected by exchange of Fe and Mg with the melt during slow cooling. The zoning complexities present in the eruption olivine phenocrysts are gone, even in the earliest drill core.

TABLE 25.5.—*Composition of olivine megacrysts and grains in dunitic aggregates from Kilauea Iki lava lake, 1959 Kilauea eruption*

	1	2	3	4	5	6	7	8	9	10
Sample type	KI-113 class 1 aggregate		KI67-2-87.9 class 1 aggregate		KI81-1-181.5 mosaic		KI76-2-20.5 megacryst		KI81-1-238 megacryst	
Points in analysis	3	1	2	1	5	1	7	1	4	3
SiO_2	39.61	37.53	39.82	38.14	38.52	37.87	39.70	37.18	39.68	38.8
TiO_2	.00	.00	.04	.07	.00	.00	.00	.01	.00	.02
Al_2O_3	.00	.00	.04	.06	.00	.00	.00	.00	.00	.01
Cr_2O_3	.00	.00	.02	.03	.00	.00	.02	.00	.00	.00
FeO	11.93	21.95	16.20	24.83	19.54	23.26	12.88	25.08	14.12	18.19
NiO	.17	.04	-	-	.09	.11	.20	.11	.14	.02
MnO	.17	.32	.15	.21	.28	.33	.19	.34	.18	.25
MgO	47.03	39.47	43.62	36.74	41.79	38.55	46.49	37.17	45.29	42.30
CaO	.24	.24	.30	.28	.15	.17	.22	.20	.23	.29
Na_2O	.01	.00	.05	.07	.01	.01	.02	.01	.02	.02
Total percent	99.16	99.55	100.24	100.43	100.38	100.30	99.72	100.10	99.66	99.96
Mol percent Fo	87.5	77.8	82.7	72.51	79.2	74.7	86.6	72.5	85.1	80.6
Location	core	rim	core	rim	small grain, center of mosaic	rim of larger crystal at edge of aggregate	core	rim	core	rim
	largest grain in aggregate		large single crystal							
Quenching temperature (°C)	1090-1095°C		1090°C		1010-1030°C		~ 100°C		1135-1140°C	

Only the sizes and textures of the aggregates and megacrysts may preserve information relevant to the dynamics of the 1959 eruption.

DISCUSSION

The olivine phenocryst population in the 1959 eruption samples is very heterogeneous petrographically. It is somewhat more uniform chemically, but zoning patterns are varied, with normally and reversely zoned grains almost equally abundant in the population analyzed. There is no correlation between petrographic class and chemical composition. The petrographic and chemical characteristics of this olivine phenocryst population vary from phase to phase of the eruption, supporting a model of magma mixing and progressive internal equilibration that will be advanced below.

Olivine in Kilauea Iki lava lake retains all of the textures seen in the eruption samples. In addition to abundant olivine phenocrysts, the lake contains rare olivine megacrysts and dunitic aggregates. Though textures are stable for decades in the lake, chemical composition is not. The lake olivines are all normally zoned, and their cores may be relatively Fe-rich, because of continued exchange of Fe and Mg with the melt during slow cooling of the lava lake.

Many features of this population of phenocrysts and aggregates are unusual and bear on the dynamics of the 1959 eruption. These features are (1) the presence of deformed olivine grains, (2) the presence of dense olivine aggregates of complex history, (3) the occurrence of rare olivines containing sulfide-bearing inclusions, (4) the presence of reversely zoned and of oppositely zoned crystals in a single thin section, and (5) the occurrence of resorbed olivine. The significance of these will be considered in turn.

DEFORMATION FEATURES IN OLIVINE

Olivine with multiple planar extinction discontinuities extending across the whole grain or with complex rectangular subgrains is present in the 1959 eruption pumice and in Kilauea Iki lava lake. The grains occur singly, in small clusters, or in larger aggregates.

Irregularly shaped, deformed crystals like this are common in Hawaiian alkalic rocks (see, among others, White, 1966). Similar kink-banded olivine, as isolated grains or in small clusters, has been reported from many other localities as well (Blanchard and others, 1976; Imsland, 1984; Francis, 1985). The kink-banded olivines are always among the coarsest grains present, as at Kilauea Iki. In most of these occurrences, the deformed grains are all very forsteritic (Fo_{90}), which is not the case in the 1959 pumice. Most authors consider the deformed olivine to be xenocrystic. Imsland (1984) considers it (and the chromian diopside associated with it in the ankaramites of Jan Mayen) to be mantle-level phenocrysts precipitated from the ankaramitic parental liquid.

Extinction discontinuities, or rectangular subgrain boundaries like those shown in figure 25.5*B*, have been produced experimentally in olivine at high temperatures and pressures (Raleigh, 1968; Carter and Ave Lallemant, 1970; Raleigh and Kirby, 1970). They form in olivine in a crystalline matrix, in response to non-hydrostatic stress. As yet there are no studies that investigate the minimum amount of interstitial melt necessary to prevent olivine from deforming in this manner. Kink-bands do not form under hydrostatic conditions, however; kink-banded crystals surrounded by melt (figs. 25.3, 25.4*A–B*) must have been deformed in a very different environment.

Aggregates of deformed olivine are the most numerous class of dense olivine aggregates in Kilauea Iki (table 25.2). The deformed olivine in these aggregates is similar in size and petrographic character to the isolated, deformed phenocrysts. It was suggested above that the isolated class I crystals were produced by disaggregation of coarse, mildly deformed dunite like the seven dense, melt-poor aggregates found in the lake. In fact, the literature on olivine deformation virtually requires such an origin for any grain with deformation features. Their depth of origin cannot be tightly constrained merely from the presence of deformation features, however, as olivine deforms readily over a wide range of pressures and temperatures. Nevertheless, minimum confining pressures of several hundred megapascals, much higher than the 100 MPa (1 kbar) in Kilauea's summit reservoir, seem indicated (Carter and Ave Lallemant, 1970).

DENSE OLIVINE AGGREGATES

Kilauea Iki lava lake contains several dense aggregates of olivine, as discussed above. Most consist of coarse, mildly deformed class I grains; others contain polygonal mosaics of unstrained olivine (table 25.2). Neither of these types contains significant amounts of basaltic melt, and where melt does occur, it appears to be the host melt penetrating the aggregate, rather than being indigenous to the aggregate. The mineralogy and textures of these aggregates are matched by those of the dunite tectonite xenoliths that are so common in Hawaiian mafic alkalic rocks, whether from the Honolulu Volcanics (Jackson and Wright, 1970), Hualalai (Kirby and Green, 1970), Loihi Seamount (Moore and others, 1982; Roedder, 1983), or elsewhere (White, 1966; Jackson, 1968). Similar textures occur in other types of olivine-rich xenoliths and in alpine peridotite (see, for example, Mercier and Nicolas, 1975; Mercier, 1979). Textures like those seen in the coarse, mildly deformed aggregates of table 25.2 are considered by these authors to be produced by plastic deformation in the upper mantle, the polygonal mosaics by recrystallization of deformed grains and subsequent annealing. It seems possible that the textures of the Kilauea Iki aggregates were produced the same ways.

The olivine in the dunite tectonite xenoliths from Hawaiian alkalic rocks are more iron-rich than the olivine in most peridotite. Jackson and Wright (1970) give $Fo_{87.5–84}$ and Sen (1983) gives $Fo_{90–81}$ for the olivine in the dunite xenoliths in the Honolulu Volcanics, while White (1966) reports $Fo_{89–84}$ for all dunite xenoliths from the Hawaiian Islands. This range is similar to the range of compositions seen in class I olivines in the pumice samples ($Fo_{88.7–85}$) and to the core compositions seen in the dunitic aggregates in the lake ($Fo_{87.5–83}$). However, the same compositional range is observed for other classes of olivine phenocrysts in this eruption (fig. 25.9*A*) and for olivine from other Hawaiian tholeiite (Maaloe and Hansen, 1982; Basaltic Volcanism Study Project, 1981).

The origin of these relatively iron-rich dunite tectonites has been controversial. Their compositions and the fact that they tend to occur in lavas that have come up near the central conduit of tholeiitic shields (Jackson and Wright, 1970) suggest a relationship with the tholeiitic series, even though the dunite is normally found in alkalic rocks. They have been considered to be residual (Jackson and Wright, 1970) cumulates from shallow crustal magma chambers (Sen, 1983) or perhaps from the mantle (Wright, 1984), or metamorphic mantle rocks of indeterminate origin (Kirby and Green, 1980). None of these ideas explains simultaneously (1) the iron-rich olivine compositions identical to those of tholeiitic phenocrysts, (2) the general scarcity of minerals other than olivine + chromite, and (3) the absence of cumulate textures and the ubiquity of deformed or annealed textures in this rock type.

The model favored here is that the dunitic inclusions in the 1959 lava are cumulates from tholeiite, as suggested by Sen (1983) and Wright (1984), but that they precipitated on conduit walls at mantle and deep crustal levels, rather than in shallow crustal reservoirs. Their composition suggests they are cumulates from tholeiite, and their limited mineralogy suggests they formed in a thermally buffered environment. Heating of the conduit wall, by frequent passage of tholeiitic liquid, seems more likely to forestall precipitation of interstitial pyroxene and other minerals than periodic replenishment of more isolated, shallow crustal reservoirs. Also, the occurrence of similar dunite inclusions in summit lava of the very young volcano Loihi suggests that they start forming early in the development of the tholeiitic shield, and that at that stage they are already located very near the main conduit. Lastly the rarity of undeformed representatives of this type implies they come from an environment where low melt fractions and a plastic response to non-hydrostatic stress are the norm. These conditions are not likely to be met in shallow magma chambers. In this model, megacrysts like those found in Kilauea Iki would be presumed to form in melt-rich pockets along the conduit wall. Disruption of these pockets by a

later batch of magma would then incorporate the megacrysts into a magma capable of erupting.

By contrast with these dunite tectonites, the cumulate-textured xenoliths described by Jackson (1968) are much more likely candidates to be cumulates from crustal magma chambers of the sort visualized by Sen (1983). This suite contains minor dunite. Most of its representatives contain appreciable pyroxene and plagioclase, as well as olivine, in contrast to the dunite tectonites, which rarely contain other minerals. Also, the members of this suite, including its rare dunite, were described by Jackson (1968) as exhibiting no deformation features.

An alternate way of producing Fe-rich dunite tectonite might be to have the spinel-lherzolite, typical of the Hawaiian upper mantle away from tholeiitic conduits (Jackson, 1968; Jackson and Wright, 1970) react completely with passing tholeiitic liquid, removing pyroxene and changing the composition of the remaining olivine + chromite. Whatever path was followed, it seems likely that the iron-rich, deformed dunite is produced at upper mantle or deep crustal levels, in the immediate vicinity of the tholeiitic conduit. The geochemistry of the included rare gases in some dunite tectonites is MORB-like (Kaneoka and others, 1983; Rison and Craig, 1983), which suggests they are associated somehow with the oceanic lithosphere that underlies all Hawaiian volcanoes, or at least, that they may have exchanged the isotopes with such material. The isotopic composition of the 1959 dunite samples is unknown, but after months or years of storage in the lake, they will not be pristine in any case.

The questions then arise of how the dunite is deformed, and what the timing of the deformation is, relative to the time of eruption. Mercier (1979) compared textures of xenoliths in kimberlite with experimentally observed rates of recrystallization for deformed olivine and concluded that at 1,400–1,600 °C the deformation textures, especially in kink-banded paleoblasts, would be entirely recrystallized within hours or days. For those xenoliths, he suggested that the textures must have been produced by the host kimberlite itself, as it moved through the mantle to the surface.

In the present case, it has been observed that deformed olivine grains have persisted for 22 years in the lava lake at 1,140–1,190 °C. The expected temperatures in the upper part of Kilauea's conduit and in the deeper parts of the shallow reservoir are probably 1,250–1,350 °C, based on estimates of parental MgO contents by Wright (1984) and the resulting liquidus temperatures suggested from the calibration of Helz and Thornber (in press). At these temperatures, the deformation features observed in single grains and in aggregates would be expected to survive for days to years, but beyond that their age cannot be constrained, as there are no data on static olivine-annealing rates in the temperature range of interest. Consequently, it is not possible to say that all of the deformation features seen in the 1959 olivine were produced by the host magma; at these lower temperatures, some may have been produced in earlier deformation events. Indeed the localization of chromite at grain boundaries in some aggregates where the coarsest olivine still contains deformation features (fig. 25.7C) may indicate that these aggregates have been subject to repeated deformation.

Nevertheless, the absence of primary igneous (cumulate) textures supports the idea that the dense aggregates come from an environment where deformation is almost unavoidable during sampling by the host, if not before. Furthermore, the scarcity of strongly deformed olivine or olivine aggregates in most Kilauea lava, including very olivine-rich shallow intrusives like the Uwekahuna laccolith, suggests that these dense aggregates have not formed in the shallow reservoir and do not survive there indefinitely. The more abundant glomerocrystic clusters of oriented, undeformed olivine, like that shown in figure 25.5*A–B*, are more likely representatives of olivine cumulates from Kilauea's shallow reservoir. The dense, deformed aggregates must have come from much deeper parts of Kilauea's plumbing.

The presence of two annealed aggregates (KI67.2–87.9b and KI81–1–181.5) containing no deformed grains complicates the picture somewhat. Their textures reflect prolonged thermal annealing in a hydrostatic environment. If the deepest parts of the conduit sampled are characterized by extremely low melt fractions and nonhydrostatic stress, these two aggregates must have been annealed at higher levels, suggesting that they were relatively high in the plumbing for some time prior to eruption.

SULFIDE-BEARING OLIVINE

Sulfides are rare in Kilauea basalt. They have been found included in, or associated with, ilmenite and titanomagnetite separates from differentiated rift lava (Desborough and others, 1968). They also occur as immiscible blebs in glass or as inclusions in augite in early scoria of the 1977. eruption (Moore and others, 1980), and as a late phase in interstitial liquid in Alae lava lake (Skinner and Peck, 1969) and in Kilauea Iki lava lake (R.T. Helz, unpub. data, 1985).

This paper reports the first known occurrence of sulfide in Kilauea summit lava. In the 1959 samples, it occurs in olivine as one phase in swarms of inclusions, which consist otherwise of chromite, glass, and vapor. This occurrence is very similar to the occurrence of sulfide as inclusions in olivine in the dunite xenoliths from Loihi (Roedder, 1983). Such grains and aggregates are very rare in the 1959 lava, and it was suggested above that they all came from the same limited source region.

The question is, where is that source? Sulfide is stable as a separate phase only at appropriate combinations of temperature, silicate melt composition, and sulfur and oxygen fugacities. The occurrence of sulfide as inclusions in some olivine phenocrysts demonstrates that the necessary combinations exist, at least locally, but the scarcity of sulfide-bearing melt inclusions in the 1959 and other summit lava suggests that the conditions are rarely met. It is known that melt composition and oxygen fugacity of Kilauea lava vary within rather narrow limits (Wright, 1971; Anderson and Wright, 1972). To the extent that magma temperatures of the 1959 lava were higher than most summit eruptions, the lava would be less likely than most to contain sulfide. One can conclude, therefore, that the sulfur fugacity was, at least locally, higher than usual. Recent studies of gases emitted from the summit area of Kilauea Volcano

show a tremendous flux of magmatic gas (CO_2, SO_2), which is lost from stored magma even between eruptions (Greenland and others, 1985; Gerlach and Graeber, 1985). Most melt inclusions in olivine are sulfide-free, suggesting that the melt in the summit reservoir generally contains much less sulfur than would be required to stabilize a separate sulfide liquid. It seems likely, therefore, that the sulfide-bearing inclusions formed at greater depth than the other melt inclusions, either in the lowest parts of the summit reservoir or deeper. Geobarometry on the sulfide-bearing olivine, using the methods of Roedder (1983) or Harris and Anderson (1983), might help constrain the depth of origin of these and other olivine xenocrysts. The observations that the sulfide-bearing, inclusion-rich olivine almost never contains deformation features and that aggregates of such olivine tend to be less densely compacted (fig. 25.7*D*) than the deformed olivine aggregates are compatible with the idea that class 5 olivine is derived from higher levels than the deformed class 1 olivine and the dense aggregates. The presence of sulfide-bearing inclusions in one of the annealed aggregates (shown in fig. 25.8*A–B*) suggests that this particular aggregate was stored and annealed at a level close to the source of the other sulfide-bearing olivine, though this very dense aggregate may have originated at still greater depths.

SIGNIFICANCE OF OLIVINE ZONING IN THE ERUPTION PUMICE

A complete evaluation of olivine zoning in the 1959 lava must wait on the availability of detailed compositional profiles of the olivine. However, the isolated point analyses presented here are sufficient to characterize the nature and extent of zoning and its gross variation with time during the eruption.

The most curious feature of the olivine zoning is the presence of a substantial number of reversely zoned crystals. Mechanisms for producing reverse zoning in olivine include magma mixing and decompression at constant temperature. Crystals entrained in a hotter magma might develop more magnesian rims eventually, but the usual effect in the 1959 lava is partial resorption. Some of the reversely zoned crystals in the 1959 lava are perfectly euhedral (fig. 25.4*C*) and show no sign of resorption or any other kind of hiatus in crystal growth, suggesting that some other mechanism is involved. The analysis of van Kooten and Buseck (1978) suggests that reverse zoning in olivine forms when a water-bearing melt, saturated with olivine, undergoes isothermal decompression. This results in an increase in oxygen fugacity, an increase in the Fe^{+3}/Fe^{+2} ratio, and hence an increase in the $Mg/Mg+Fe^{+2}$ ratio in olivine crystallizing from the melt. Their calculations showed that forsterite content would increase 3–5 percent for a 200-Mpa (2 kbar) drop in pressure, at 1,000 °C, for a melt containing 2.5 weight percent H_2O. The pressure effect in a dry magma has been determined by Takahashi and Kushiro (1983) and is much smaller: if Kilauea magma were completely dry, a 3 percent reversal in Fo content would record 2,500 MPa (25 kbar) of isothermal decompression. The amount of water in Hawaiian tholeiite is of the order of 0.3–0.6 weight percent H_2O (Moore, 1965), so a pressure drop of between 200–2,500 MPa (2–25 kbar) would be required to produce the maximum reverse zoning seen in the 1959 eruption.

The question arises as to what stage of decompression might be recorded in the reversely zoned phenocrysts. Every crystal in the eruption pumice was moved from the level of Kilauea's shallow reservoir, which is 2–6 km below the summit of the volcano (Eaton, 1962; Ryan and others, 1981), to the surface, and so has undergone a pressure drop of roughly 100 ± 50 MPa (1 ± 0.5 kbar). If this were sufficient to produce detectable reverse zoning, then all phenocrysts would be reversely zoned; in fact, only some of them are (see figs. 25.9*B*, 25.11). Furthermore, the number of reversely zoned olivine grains and the extent of reverse zoning tended to decline as the eruption progressed (fig. 25.14*A–B*). The trends are irregular but suggest that the reverse zoning is neither stable in shallow storage nor being produced there. Those olivine grains showing pronounced reverse zoning were probably brought up by the 1959 magma from below the level of the shallow reservoir.

Another question of interest is, how long could the variable zoning seen in the eruption samples last before internal equilibrium would be restored? Detailed calculations for each sample are beyond the scope of this paper, but the calculations of Maaloe and Hansen (1982) suggest that the time interval is between a month and a year, for zoned margins typically 10–30 μm thick. This is compatible with the observations that (1) the kind of zoning changed, and internal equilibrium in the eruption samples increased perceptibly over the 5-week period of the eruption and (2) shallow lake samples quenched as little as 9 months later show only strong normal zoning, of a sort rarely seen in the eruption samples. Thus many of the olivine grains from eruption pumice analyzed here were quenched within weeks, or at most a few months, of the time their zoning was produced.

SIGNIFICANCE OF RESORBED OLIVINES

Partial resorption of olivine is widespread in the 1959 eruption pumice and has been noted by previous workers (Richter and Murata, 1966). Resorption textures, including cuspate margins like those shown in figures 25.4*A*, *D* have been produced experimentally by Thornber and Huebner (1985); these are not simply unusual growth forms. This resorption occurs in samples quenched from 1,160–1,217 °C (see table 25.4), far above the incoming of pigeonite, which lies at 1,090–1,100 °C in the 1959 lava (Helz and Thornber, in press; unpub. data, 1985). Consequently, the resorption cannot be the result of a reaction relationship between olivine and liquid.

As discussed above, about 30 percent of the olivine grains analyzed from eruption samples are partly or completely enclosed in a sheath of glass significantly less magnesian than glass elsewhere in the same section. Glass next to resorbed edges is significantly less magnesian than glass next to euhedral parts of the same grain. That these MgO-depleted glass sheaths are not produced by quench overgrowths in olivine seems clear from the fact that 70 percent of the olivine grains are bordered by glass identical in composition to glass farther away from olivine.

These observations suggest that the resorption was produced as follows: Olivine crystals from a cooler part of the magma

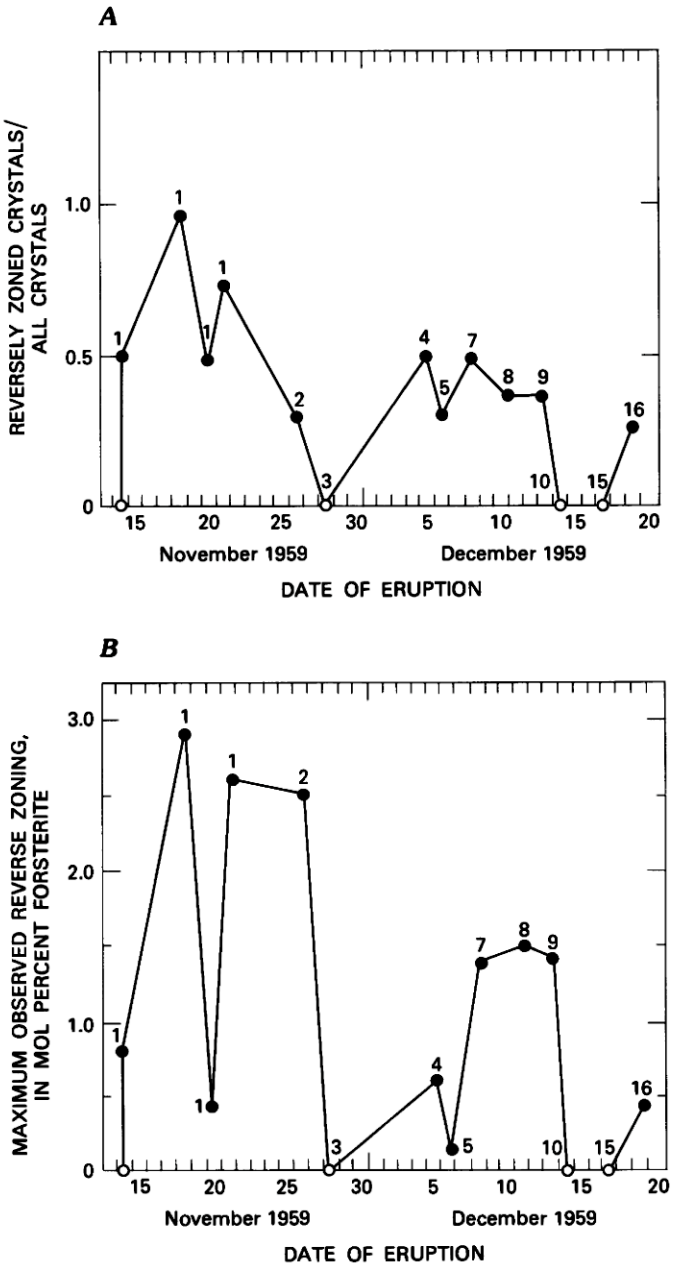

FIGURE 25.14.—Occurrence of reversely zoned olivine in 1959 eruption samples. *A*, Frequency of occurrence of reversely zoned crystals in 1959 eruption pumice, as a fraction of the total number of analyzed crystals, plotted against time of eruption. Points are labeled with the number of phase in which the sample was erupted. *B*, Maximum observed reverse zoning (as difference in mol percent Fo between core and rim) observed in 1959 eruption pumice, plotted against time of eruption. Samples containing no reversely zoned crystals plot on abscissa. Phase numbers as in figure 25.14*A*.

chamber were swept up in hotter, more mobile liquid. A thin layer of less magnesian, cooler, and hence slightly more viscous liquid moved with the crystals. (This layer might tend to gradually slough off the leading edge of the grain as it moves farther into the hotter liquid.) Thermal equilibrium between the new host and the crystal with its liquid boundary layer was established very rapidly (within minutes), at which point the melt in the boundary layer was superheated and no longer in equilibrium with olivine of any composition. The melt began to resorb the adjacent olivine, stopping when equilibrium was reached, that is, when the composition of the adjacent melt was equal to that of the rest of the melt. Once equilibrium was attained, the resulting odd-shaped grain persisted for decades without healing of the resorbed surfaces.

This model explains not only the occurrence of local resorption in olivine, but the fact that resorption is independent of rim composition or style of zoning. Of the 15 grains or clusters in low-MgO glass, 6 are normally zoned, 5 are unzoned, and 4 are reversely zoned. Rim compositions ranging from $Fo_{88.0}$ to $Fo_{80.7}$ have all been resorbed. This model also explains the occurrence of resorbed edges on 19 grains for which no compositionally distinct glass rims were found but which nevertheless show at least local resorption. Under this model, these would have had MgO-poor boundary layers at one time, but chemical equilibrium within the melt was re-established prior to quenching of the sample. The widespread occurrence of partial resorption of olivine in the 1959 samples implies that mixing of thermally disparate magmas was very common during the 1959 eruption.

These results have implications that may be important in other areas. First, resorption does not necessarily indicate that a given crystal is xenocrystic to the magma system. Second, one must be wary about calculating crystal-liquid distribution ratios in systems where magma mixing may have occurred, even where the glass is uniform in color, unless the glass has been thoroughly checked for chemical uniformity.

MODEL FOR THE 1959 ERUPTION

The physical processes preceding this eruption have been described by Eaton and Murata (1960), Eaton (1962), and Eaton and others (Chapter 48). In the late 1950's, seismic activity at Kilauea included intermittent swarms of deep (45–60 km) earthquakes. A minor swarm occurred in January 1959. The summit was inflating during the January swarm, and continued to do so thereafter, but subsided again between May and August 1959. This long period of subsidence was followed by an intense deep earthquake swarm on August 14–19. Reinflation of the summit began in late September and continued until the outbreak of the eruption on November 14, 1959 (Eaton and Murata, 1960, fig. 7). Other precursory seismic activity included weak harmonic tremor at depths of 5–15 km, presumably resulting from upward migration of magma in the conduit. Beginning in September, shallow earthquakes occurred in the northern part of the caldera. These were numerous, but very small until November 14, just before the eruption. The seismic and tilt data combined to give a picture of magma, originating at 45–60 km, migrating upward and becoming lodged slightly to the north of Halemaumau, prior to triggering an eruption. The overall magma path was not unlike that outlined in Ryan and others (1981) for the period 1961–1974 at Kilauea. The 1958–1960

period was exceptional, however, in having earthquakes at 45–60 km; such deep earthquakes have not been seen since. Also, the intense swarm of tiny earthquakes seen only on the north pit seismograph (Eaton, 1962; Eaton and others, chapter 48) are unique to the 1959 eruption.

Neither Eaton and Murata (1960) nor Eaton (1962) states specifically that the lava erupted in November and December 1959 included any of the magma liberated during the August earthquake swarm. It was not at first evident that this might be so, as can be seen by considering the usual pattern of magma storage in the summit reservoir (see Wright, 1971; and Wright and Fiske, 1971).

In these papers, it was shown that summit lava, though olivine controlled (Powers, 1955), typically lies at the olivine-depleted end of the olivine control line; that is, it contains minor phenocrystic olivine but has no fractionated augite or plagioclase. Variation in the amount of olivine, as observed in the 1959 eruption, was considered to be achieved by tapping different levels of a magma reservoir that was olivine-rich at the bottom and melt-rich at the top (Murata and Richter, 1966b; Wright, 1971).

In addition to varying in olivine content, the summit lava exhibits batch-to-batch compositional differences unrelated to olivine control. Different batches are chemically distinctive, some being unique, and can be followed through the volcanic plumbing. Wright and Fiske (1971) presented evidence that magma batches erupted at the summit in the 1950's and 1960's had appeared in flank eruptions 1–6 years earlier. They inferred that (1) magma batches arriving at the summit reservoir do not mix with each other in storage; (2) flank eruptions tap lower levels of the reservoir than summit eruptions do; and (3) summit eruptions usually tap magma that has been in storage in the shallow (2–4 km) reservoir for years, or even decades, prior to eruption.

Wright and Fiske (1971) recognized the 1959 eruption as exceptional in that neither of its two component magma batches (3a and 3b in the terminology of Wright and Fiske, 1971) had ever appeared in flank lava or as major eruptions in Halemaumau. In particular, the 1960 Kapoho eruption, which immediately followed the 1959 summit eruption, was not related chemically to the summit eruption. The picture of the summit reservoir that emerged from this work was of a highly compartmentalized magma storage zone, like that shown by Fiske and Kinoshita (1969), such that even closely spaced eruptions might drain completely unconnected parts of the reservoir. This draining of discrete reservoirs has been demonstrated to occur at Kilauea during other time periods as well, including 1967–1969 (Dvorak and others, 1983) and 1972–1973 (Ryan and others, 1983). The isolation of the 1959 magma from all other parts of Kilauea's reservoir that were active from 1955 to 1965 led Wright and Fiske to hypothesize that the 1959 magma occupied chambers "separated from the main conduits of the central reservoir" (Wright and Fiske, 1971, p. 54).

Other exceptional features of this eruption, besides its unusual seismicity, chemistry, and inferred deviant path to the surface, include its having (1) the highest lava fountains observed at the summit (580 m, or 1,900 feet, observed December 17, 1959); (2) the hottest eruption temperatures ever measured (1,192 °C on December 5, 1959); and (3) the most magnesian glass recovered for a historical Kilauea eruption. In addition, the pumice blanket produced during phase 3 is unusual in a historical Kilauea summit eruption. (All data is from Richter and others, 1970.) Thus, at least some of the 1959 lava was hotter and more gas-rich than typical Kilauea summit lava.

This paper has presented evidence that the 1959 lava contains material that appears to have originated below the level of the shallow reservoir. This includes (1) deformed olivine grains, singly and in aggregates, (2) aggregates of thermally annealed olivine, and (3) olivine megacrysts. Such materials are common in Hawaiian alkalic lava, but rare to absent in subaerial tholeiite, from Kilauea and elsewhere in Hawaii. In addition, the 1959 eruption contains rare olivine with sulfide-bearing inclusions and olivine with significant reverse zoning, neither of which appear to be produced in Kilauea's summit reservoir.

The unusual features of this eruption would be most easily explained if one of the two magmatic components erupted was the same magma that was liberated during the August earthquake swarm and reached the base of the shallow reservoir in late September. The hypothesis is that at that point the magma followed a seldom-used path to the north of the main reservoir (that is, the reservoir as located in Fiske and Kinoshita, 1969, and Ryan and others, 1981), encountering an older batch of stored magma. It broke through this older chamber to the surface on November 14, bringing some of the stored magma with it. The unusual features of the eruption are considered to be a direct consequence of the presence of the juvenile component.

THE MODEL AT MANTLE LEVELS

Kilauea tholeiite may originate as highly magnesian (>20 percent MgO) melt and fractionate appreciably, to MgO contents of 13–14 weight percent, enroute to the surface (Wright, 1984). The average MgO content of the 1959 eruption has been estimated as 15.43 percent (Wright, 1973) and hence is closer to the primitive melt than to the hypothesized parental one. Can this inferred differentiation from 20 to 15 percent MgO be made compatible with the apparent presence in the 1959 Kilauean lava of possible mantle-level material?

The answer to this potential contradiction is implicit in the theoretical model for the migration of fluid-filled cracks, as developed by Stevenson (1983), modifying earlier work by Weertman (1971a,b). In Stevenson's model, material from the lower end of the rising packet of fluid precipitates to close the crack below. In fact, healing the crack in this fashion is essential to migration of a discrete packet of melt. All that is necessary for a Kilauean tholeiite to contain mantle or deep crustal material and to differentiate is that the amount of material precipitated to seal the crack at the lower end exceed the amount picked off the walls at the upper end of the body of melt.

This model of crack migration dovetails with the hypothesized origin for the iron-rich dunite xenoliths proposed above. The dunite would correspond to this crack-healing material, because, for

TABLE 25.6.—*Calculated settling velocities of olivine phenocrysts and aggregates in Kilauea Iki lava lake, assuming Newtonian behavior*

Particle radius (cm)	Settling velocity (cm/s)
For viscosity 150 P, pressure 0.1 MPa (1 bar)	
0.25	0.05
0.5	0.21
1.0	0.85
For viscosity 50 P, pressure 1.5 GPa (15 kbar)	
0.25	0.16
0.5	0.65
1.0	2.6

tholeiite, the precipitate would be olivine + chromite. The exact composition of the olivine would vary slightly with depth, as the migrating melt fractionated enroute to the shallow reservoir. The deformation observed in the dunite xenoliths would be produced as the leading edge of a melt packet opened the crack, by analogy with the process Mercier (1979) inferred for deformed olivines in xenoliths in kimberlite. Because the Kilauea conduit is re-opened at frequent intervals, however, it is possible that some of the deformation observed in the dunitic aggregates was produced by an earlier packet of melt, not the host magma.

MAGMA ASCENT RATE

If the hypothesized model for the 1959 eruption is correct, we can calculate the average ascent velocity of the new magma package. To travel from depths of 45–60 km to the surface in the period from August 14–19 to November 14, the magma would have to move at 0.58–0.77 cm/s. This is compatible with ascent velocities for fluid-filled cracks, estimated by Stevenson (1983) to be 0.1–10 cm/s. It falls at the extreme low end of the range of ascent velocities Spera (1984) cites for xenolith-bearing lava (10^{-2} m/s to 30 m/s).

Is this velocity fast enough to entrain the largest objects found in the lake? Table 25.6 presents the results of calculating the Stokes' law settling velocities of olivine in basalt, for objects of different sizes. The first set of results is for a viscosity typical of very magnesian basalt at 0.1 MPa (1 atmosphere), the second set for the lower viscosity that the same melt would have at 1,500 MPa (15 kbar). Both viscosity estimates are taken from Kushiro and others (1976). The calculated settling rates for the largest particles found, which have average radii between 0.5 and 1.0 cm, would be 0.21–0.85 cm/s at low pressures and 0.65–2.6 cm/s at the high pressure limit. Non-Newtonian effects were neglected, on the assumptions that (1) much of the olivine phenocryst load (the very numerous class 2 olivine crystals and open aggregates) in the 1959 lava was in fact picked up from the lowest part of the older, stored magma, in Kilauea's summit reservoir and (2) the lava did not vesiculate until it was well up into the crust. The calculated Newtonian settling velocities are maximum values; to the extent that the magma was non-Newtonian, settling velocities would be lower, and the magma could more easily retain the larger olivine and olivine aggregates.

The calculated settling velocities are close to the average ascent velocity inferred above. If the eruption model is correct, this agreement means that the juvenile component was moving just fast enough to entrain the largest olivine and olivine aggregates found. It implies, further, that no significantly larger dunite inclusions will be found in the lake and that the magma never stopped moving from the time it picked up the aggregates until it began vesiculating, when non-Newtonian behavior took over. These deep-seated ascent rates are irrelevant to near-surface processes such as venting, fountaining, and so on, which involve the presence of a gas phase (see Eaton and others, chapter 48), resulting in strongly non-Newtonian behavior. The ability of the lava to entrain olivine in the shallow chamber was a function of magma discharge rate (Murata and Richter, 1966b); this rate increased during eruption, as the magma became more non-Newtonian (Wadge, 1981).

OLD VERSUS NEW MAGMA

It remains to be established which of the two recognized mixing components of the 1959 eruption was stored, old magma and which was the more juvenile. Early on it was noticed that the lava erupted from the east end of the initial fissure (Iki–58, or S–1 of Wright, 1973; or 3b of Wright and Fiske, 1971) was enriched in an augite-like component relative to west-end lavas (Iki–1 or S–2, or magma 3a). Murata and Richter (1966a) hypothesized that the former lava was derived by settling of augite phenocrysts into hotter parts of the magma chamber, where they were redissolved to give the east-end melt compositions. Calculations by Wright and Fiske (1971) supported this observation, though Wright (1973) noted that the implied physical model was very complex.

There are three problems with this augite-resorption hypothesis. First, it would require both components to be stored magma, rather than one stored and one juvenile, for if the Iki–1 (S–2) parent were not a stored component, the apparent relationship tested by the calculation would not exist, and the calculation would be meaningless. Second, the amount of augite (6 percent, Wright, 1973) required by the calculation is so small that the calculation cannot distinguish with certainty between low-pressure and high-pressure augite. Lastly, there is no petrographic evidence, in the form of phenocrystic augite, for the process. The tiny augite crystals

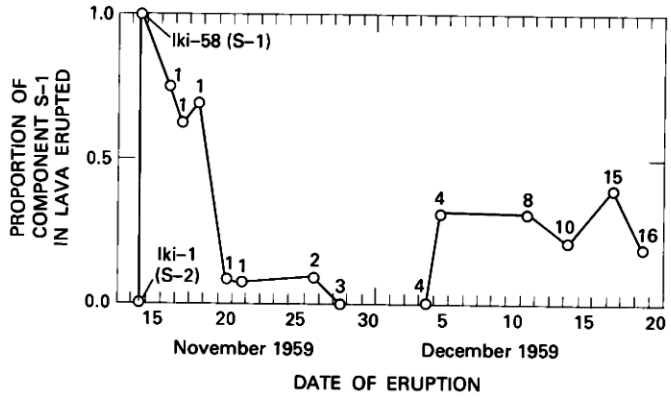

FIGURE 25.15.— Proportion of S–1 magmatic component present in various 1959 eruption samples (taken from Wright, 1973) plotted against date of eruption. The mixing components used by Wright (1973), namely samples Iki–58 (S–1) and Iki–1 (S–2), plot at 1.0 and zero respectively. Numbers by points identify the phase of the eruption.

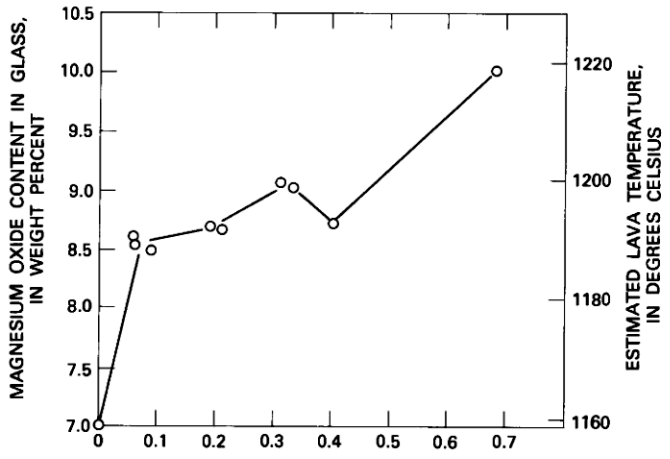

FIGURE 25.16.—MgO content of the glass (weight percent, left side) and estimated glass quenching temperature (right side) plotted against the fraction of S–1 component present for all samples erupted after November 17, for which both a bulk analysis and a glass analysis are available.

in the initial eruption samples are not phenocryst-sized and are almost always associated with plagioclase. This is a problem because plagioclase is not required by the calculation, and augite could not be readily separated from plagioclase by flow differentiation of the sort described by Wright (1973). Careful search for augite phenocrysts in the lake, including samples of foundered crust and of the basal chill zone, has failed to uncover any phenocrystic augite, resorbed or otherwise; nor does augite occur as an inclusion in olivine in any eruption sample.

Another line of evidence that must be considered is shown in figure 25.15, which plots the change in mixing ratio found by Wright (1973) against time (see also Wright, 1973, fig. 3). Early phase 1 lava is disproportionately rich in S–1 (Iki–58, the east-end component), later phases richer in S–2 (west-end). This might be interpreted as showing that stagnant S–1 magma was pushed out first, as the chamber was flooded by new, hot S–2 magma.

However, three other lines of evidence favor the east-end lava (Iki–58 or S–1 or 3b) as the new component, with the west-end lava the stored component. The first is the recognition of Wright and Fiske (1971, p. 54) that the brief 1954 Halemaumau eruption was of west-end (their 3a) type. Thus, west-end lava had been in storage near the surface for five years prior to 1959. Second is the occasional recurrence of the west-end component in almost pure (>90 percent) form after the initial curtain of fire shrank to a single vent on November 15. Figure 25.15 shows that the late phase 1 and phase 3, and early phase 4 samples are pure, or nearly pure west-end (S–2) material. The east-end component is never seen in pure form, except of course in the type sample Iki–58, where its purity is a matter of definition only. This pattern is more compatible with east-end material being the newer material, seen only as it filters through older, stored magma.

The last piece of evidence that the east-end component may be the more juvenile is shown in figure 25.16, which shows the correlation between the amount of S–1 (east-end) material and MgO content in glass (which covaries with temperature), for eruption samples from November 18 on. The more S–1, the hotter the sample, with the exception of Iki–32 from phase 15. This suggests that the S–1 component was consistently hotter than S–2 melts, hence probably more juvenile.

If one accepts that S–1 is the new and S–2 is the stored component, the above interpretation of the data in figure 25.15 must be revised. Instead of old magma being pushed out first, the new, more fluid magma must have streamed through the more stagnant material, to be erupted first. The stored magma was more prominent in later phases because it was remobilized by picking up heat and perhaps gas bubbles, from the newer, gassier material.

ERUPTION CHRONOLOGY

Using the above model and the data presented in this paper, the 1959 eruption can now be described in terms of progressively more intimate intermingling and internal equilibration of two separate types of olivine tholeiitic magma, a previously stored component and a new component that originated at 45–60 km depth and began its ascent in the August earthquake swarm.

The initial eruption fissure broke open along the south side of Kilauea Iki pit crater on November 14, 1959. Iki–1 (or S–2) was erupted at the west end, while Iki–58 (or S–1) was erupted at the east end. Initial samples of both components were relatively cool and differentiated, with a sparse population of class 2 olivine. Iki–58 is slightly hotter than Iki–1, however, and contains more phenocrystic olivine, including at least one reversely zoned grain (fig. 25.11), all features consistent with its being the new component. From November 14 to 17, lava continued to be dominantly east-end material (fig. 25.15), but gradually got hotter. On November 18, the hottest known sample, Iki–22, was erupted. This sample

contains a complex olivine assemblage that includes the most extensive reverse zoning found (tables 25.1, 25.3; figs. 25.11 and 25.14*B*).

No samples from November 19 have been analyzed, but by November 20, the lava being erupted was very nearly pure west-end material, though quite olivine-rich (fig. 25.15). The first such sample, Iki–44, contains a cooler glass than Iki–22, but the olivine is more magnesian and weakly zoned. Kink-banded olivine is present, but the banding is very faint, as the amount of deformation is slight. Compositionally, all the olivines appear to be in equilibrium with each other and (or) in equilibrium with a common melt. Such olivines might have come from the lowest (hottest) part of the west-end magma chamber.

A later sample from phase 1, Iki–7, is similar to Iki–44 in temperature in melt composition, and in the character of its class 1 olivines, but contains reversely zoned euhedral (class 2) olivines that are probably juvenile. Iki–7 also contains fragmental (class 4) olivine. Phase 2 (Iki–11) is slightly hotter and richer in the east-end component than Iki–44 and Iki–7. It contains the first normally zoned class 1 olivine found, the first sulfide-bearing class 5 olivine known, and more reversely zoned class 2 olivine. Clearly more new material was being tapped; the greater heterogeneity of the glass in Iki–11 (fig. 25.11) suggests that this mixing was very recent.

Phase 3 (Iki–9) was so extremely gas-rich that very little of it got into the lake; instead, it formed a pumice blanket downwind of the vent (Richter and others, 1970). It is pure west-end material, though slightly hotter than Iki–1 (S–2). Presumably this phase was derived from the gas-charged, differentiated upper part of the west-end magma chamber. The only puzzling feature of this phase is why this material did not erupt in phase 1. Two possible explanations are: (1) It came from an isolated cupola that was not breached by the initial fracture, or (2) the extra gas was derived from the new magma, which, after it had accumulated in a layer of differentiated west-end material near the roof, blew that material out as phase 3.

Early phase 4 lava was similar to that of phase 3. Later samples, like Iki–13, were much hotter (1,196 °C, table 25.4) and richer in east-end component (fig. 25.15) and olivine. The glass in Iki–13 is uniquely heterogeneous (fig. 25.11), suggesting that it was produced by very recent mixing of two components. Phase 5 (Iki–14) was hotter still (1,205 °C), but its glass is homogeneous, as though the disequilibrium of the Iki–13 mixing event had begun to dissipate. Both of these samples contain a complex assemblage (table 25.1) of very magnesian olivine (fig. 25.11) that shows little zoning. The combination of a change in mixing ratio of S–1 and S–2 (fig. 25.15), and the increase in temperature suggest that new material was fed into the base of the S–2 chamber about December 5. The presence of fragmental (class 4) olivine in these samples, presumably produced by brittle failure (shallow diking?), is compatible with this suggestion. The fact that both S–1/S–2 mixing ratios and glass quenching temperatures vary rather little after phase 5 suggests that this was the last significant influx of new material into the part of the chamber that was feeding the eruption.

Phase 7 (Iki–20) marks the reappearance of cooler lava (1,181 °C, see table 25.4). It also marks the first appearance of (1) very diverse, non-overlapping core compositions within a single sample, and (2) convergence of olivine rim compositions from those very different cores toward a common rim composition. Earlier eruption samples, though exhibiting great diversity of zoning pattern, generally included only a narrow range of core compositions in classes 1, 3, 4, and 5 (taken together) and class 2 (see fig. 25.11). From phase 7 through phase 16, by contrast, one or both of these olivine groups include very varied phenocryst cores within a single thin section. These varied cores must have formed initially in different parts of the magmatic plumbing. Hence, their close juxtaposition in the later samples is evidence for increasingly intimate commingling of all parts of the active magmatic system. The convergent zoning suggests that this mingling resulted in accelerated internal equilibration of the samples. Rapid fine-scale mixing was possible because both components were basaltic and quite fluid, with only minimal viscosity contrasts.

Phases 8 and 9, represented by Iki–21 and Iki–24, include the last evidence for new material entering the actively erupting part of the chamber. They contain (1) the most magnesian olivine observed; (2) the only class 1 olivine with significant reverse zoning other than those in Iki–22 (figs. 25.11, 25.14*B*); and (3) the latest known fragmental olivine (table 25.1). The thermal perturbation at the onset of phase 8 (1,197 °C, compared with 1,181 °C in phase 7) is smaller than that at phase 4 (1,196 °C vs. 1,154 °C in phase 3), and Iki–24 (phase 9) is cooler still, rather than hotter, as Iki–14 (phase 5) was. This suggests that the amount of new material introduced was rather slight and may simply represent more thorough in-mixing of the deepest part of the chamber. On the other hand, these observations do agree with evidence presented by Eaton and others (chapter 48) that the magma reservoir was being intruded by new magma from the end of phase 1 through phases 8 and 9.

Subsequent samples from phases 10, 15, and 16, show some variation in the S–1/S–2 ratio but no thermal perturbations, suggesting that thermal equilibrium within the mixed volume was complete. Reverse zoning is scarce (figs. 25.11, 25.14*A*), and olivine rims are consistently iron-rich (fig. 25.11). Chemical equilibration was still incomplete, however, as evidenced by the occurrence even in phase 16 (Iki–33) of olivine with rims of low-MgO glass.

SUMMARY

This paper documents the petrographic and chemical diversity of the olivine phenocrysts and aggregates in the 1959 lava of Kilauea Volcano. The lava contains five petrographically distinct classes of olivine, dunitic aggregates with deformed or annealed textures, and two olivine megacrysts (10×20 mm in section). Olivine cores vary from $Fo_{83.5}$ to $Fo_{88.7}$. Zoning is moderate (≤3 percent Fo within most crystals); normal and reverse zoning are about equally abundant. There is no correlation between petrographic class and core composition or style of zoning. Olivine in drill core from Kilauea Iki lava lake has the same petrographic features as olivine in the rapidly quenched eruption samples. Pre-eruption zoning and overall chemical composition is not preserved in the lake olivine, as it has

exchanged Mg for Fe with the melt.

Many features of the 1959 eruption are unusual for a historical Kilauea summit eruption and can be explained by a model in which one of the two observed magmatic components of this mixed-magma eruption came directly from the mantle, bypassing the main shallow reservoir. The component erupted from the east end of the initial fissure appears to be the juvenile component, responsible for the very hot, gas-rich, olivine-rich nature of the 1959 lava. The various components of the olivine population were picked up by the rising magma in roughly the following sequence:

(1) Deepest are the deformed olivine grains, aggregates of deformed olivine, and megacrysts, though the actual depths are poorly constrained. The thermally annealed aggregates may be strictly deep seated, or may have been annealed in shallower storage. All these materials are hypothesized to be derived originally from material lining the conduit wall at mantle or deep crustal levels. They are xenocrystic to the S–1 magma, but accumulated from earlier Kilauea tholeiite, so are not compositionally distinct.

(2) Euhedral olivine crystals with significant reverse zoning are deep-seated phenocrysts of the S–1 magma, recording large (several hundred MPa, or several kbar), but poorly constrained amounts of near-isothermal decompression. Reversely zoned class 1 olivine grains were picked off the walls deeper than unzoned class 1 olivine and erupted sooner after sampling, as this style of zoning is not stable in the shallow reservoir.

(3) Sulfide-bearing olivine grains and aggregates, rarely deformed and never showing reverse zoning, come from somewhere above the source of the deformed and (or) reversely zoned olivine, but below the shallow reservoir, where SO_2 is liberated from the magma. They may be cognate but are more probably xenocrystic to the S–1 magma.

(4) The occurrence of fragmental class 4 olivine, presumably formed by brittle failure, correlates fairly well with other indicators for episodes of influx of new S–1 liquid into the shallow chamber at the end of phase 1, and at phases 4–5 and 8–9. These fragments are hypothesized to result from fracture of old shallow olivine cumulates within the volcanic edifice.

(5) The bulk of the phenocrysts present, including most euhedral and rounded class 3 grains, unzoned or with some normal zoning, were picked up from the lower parts of the stored (S–2) magma. The widespread resorption observed in all classes of olivine is a consequence of mixing of thermally disparate melts at this stage.

(6) The small, euhedral olivine crystals with strong (8 percent Fo) normal zoning formed in the most rapidly cooled margin of the stored magma; they were only rarely sampled during the eruption.

Disequilibrium features present in the eruption samples include: (1) the presence of heterogeneous glass (away from olivine); (2) the presence of boundary layers of MgO-poor glass near olivine; (3) the presence of reversely zoned, unzoned and (or) normally zoned olivine in the same thin section; (4) the presence of olivine with very different core compositions in the same section; and (5) the presence of olivine with different rim compositions in the same section. Comparison with other data (Maaloe and Hansen, 1982) suggests that the mixing event(s) recorded by these features took place weeks before the eruption, or perhaps only within the 36 days of the eruption itself. Further analysis of these various indicators of change, or "geospeedometers," is deferred to a later paper.

The presence of kink-banded olivine is, by comparison, a relatively slow geospeedometer, as these deformation textures may last months to a few years at shallow-reservoir conditions. Their rarity in subaerial tholeiite, even picritic lava, suggests that they do not survive for decades in subsurface reservoirs, in contrast to their survival for 22 years in Kilauea Iki lava lake. However, deformed olivine occurs frequently in submarine east-rift lava of Kilauea. This suggests that some lower rift lava may move out laterally into the rift before reaching the shallow reservoir and so, like the 1959 lava, avoid prolonged shallow storage before their eruption. It would be of interest to search this submarine lava for the other types of deeper seated material found in the 1959 lava.

REFERENCES CITED

Albee, A.L., and Ray, L., 1970, Correction factors for electron probe microanalysis of silicates, oxides, carbonates, phosphates, and sulfates: Analytical Chemistry, v. 42, p. 1408–1414.

Anderson, A.T., Jr., and Wright, T.L., 1972, Phenocrysts and glass inclusions, and their bearing on oxidation and mixing of basaltic magmas, Kilauea Volcano, Hawaii: American Mineralogist, v. 57, p. 188–216.

Basaltic Volcanism Study Project, 1981, Basaltic volcanism on the terrestrial planets: New York, Pergamon Press, Inc., 1,286 p.

Bence, A.E., and Albee, A.L., 1968, Empirical correction factors for the electron microanalysis of silicates and oxides: Journal of Geology, v. 76, p. 382–403.

Bence, A.E., Brande, S., Indelicato, G., and Allen, F., 1981, Analysis of trace and minor elements in rock-forming minerals using an automated electron microprobe: Proceedings of the 8th International Conference on X-ray Optics and Microanalysis, p. 538–548.

Blanchard, D.P., Rhodes, J.M., Dungan, M.A., Rodgers, K.V., Donaldson, C.H., Brannon, J.C., Jacobs, J.W., and Gibson, E.K., 1976, The chemistry and petrology of basalts from leg 37 of the deep-sea drilling project: Journal of Geophysical Research, v. 81, p. 4231–4246.

Carter, N.L., and Avé Lallemant, H.G., 1970, High temperature flow of dunite and peridotite: Geological Society of America Bulletin, v. 81, p. 2181–2202.

Chen, C.-Y. and Frey, F.A., 1983, Origin of Hawaiian tholeiite and alkali basalt: Nature, v. 302, p. 785–789.

Chouet, B., and Aki, K., 1981, Seismic structure and seismicity of the cooling lava lake of Kilauea Iki, Hawaii: Journal of Volcanology and Geothermal Research, v. 9, p. 41–56.

Clague, D.A., 1982, Petrology of tholeiitic basalt dredged from Hualalai Volcano, Hawaii [Abs.]: Eos, v. 63, p. 1138.

Desborough, G.A., Anderson, A.T., Jr., and Wright, T.L., 1968, Mineralogy of sulfides from certain Hawaiian basalts: American Mineralogist, v. 63, p. 636–644.

Dvorak, J., Okamura, A., and Dieterich, J.H., 1983, Analysis of surface deformation data, Kilauea Volcano, Hawaii from October 1966 to September 1970: Journal of Geophysical Research, v. 88, p. 9295–9304.

Eaton, J.P., 1962, Crustal structure and volcanism in Hawaii: American Geophysical Union Geophysical Monograph, v. 6, p. 13–29.

Eaton, J.P., and Murata, K.J., 1960, How volcanoes grow: Science, v. 132, p. 925–938.

Fiske, R.S., and Kinoshita, W.T., 1969, Inflation of Kilauea Volcano prior to its 1967–1968 eruption: Science, v. 165, p. 341–349.

Fleet, M.E., and MacRae, N.D., 1983, Partition of Ni between olivine and sulfide and its application to Ni-Cu sulfide deposits: Contributions to Mineralogy and Petrology, v. 83, p. 75–81.

Fleet, M.E., MacRae, N.D., and Herzberg, C.T., 1977, Partition of nickel between olivine and sulfides: a test for immiscible sulfide liquids: Contributions to Mineralogy and Petrology, v. 65, p. 191–197.

Ford, C.E., Russell, D.G., Craven, J.A., and Fisk, M.R., 1983, Olivine-liquid equilibria: temperature, pressure, and composition dependence of the crystal/liquid cation partition coefficients for Mg, Fe^{2+}, Ca and Mn: Journal of Petrology, v. 24, p. 256–266.

Francis, D., 1985, The Baffin Bay lavas and the value of picrites as analogues of primary magmas: Contributions to Mineralogy and Petrology, v. 89, p. 144–154.

Gerlach, T.M., and Graeber, E.S., 1985, The volatile budget of Kilauea Volcano. Nature, v. 313, p. 273–277.

Greenland, L.P., Rose, W.I., and Stokes, J.B., 1985, An estimate of gas emissions and magmatic gas content from Kilauea Volcano: Geochimica et Cosmochimica Acta, v. 49, p. 125–130.

Häkli, T., and Wright, T.L., 1967, The fractionation of nickel between olivine and augite as a geothermometer: Geochimica et Cosmochimica Acta, v. 31, p. 877–884.

Hardee, H.C., Dunn, J.C., Hills, R.G., and Ward, R.W., 1981, Probing the melt zone of Kilauea Iki lava lake, Kilauea Volcano, Hawaii: Geophysical Research Letters, v. 8, p. 1211–1214.

Harris, D.M., and Anderson, A.T., Jr., 1983, Concentrations, sources and losses of H_2O, CO_2, and S in Kilauean basalt: Geochimica et Cosmochimica Acta, v. 47, p. 1139–1150.

Harte, Ben, 1977, Rock nomenclature with particular relation to deformation and recrystallization textures in olivine-bearing xenoliths: Journal of Geology, v. 85, p. 279–288.

Helz, R.T., 1980, Crystallization history of Kilauea Iki lava lake as seen in drill core recovered in 1967–1979: Bulletin Volcanologique, v. 43–4, p. 675–701.

———1983, Diverse olivine population in lavas of the 1959 eruption of Kilauea Volcano, Hawaii [abs.]: Eos, v. 64, p. 900.

———1984, In situ fractionation of olivine tholeiite: Kilauea Iki lava lake, Hawaii [abs.]: Geological Society of America Abstracts with Programs, v. 16, p. 536–537.

Helz, R.T., Banks, N.G., Casadevall, T.J., Fiske, R.S., and Moore, R.B., 1984, A catalogue of drill core recovered from Kilauea Iki lava lake from 1967–1979: U.S. Geological Survey Open File Report 84–484, 72 p.

Helz, R.T., and Thornber, C.R., in press, Geothermometry of Kilauea Iki Lava Lake, Hawaii.

Helz, R.T., and Wright, T.L., 1983, Drilling report and core logs for the 1981 drilling of Kilauea Iki lava lake (Kilauea Volcano, Hawaii) with comparative notes on earlier (1967-1979) drilling experiences: U.S. Geological Survey, Open File Report 83–326, 66 p.

Hermance, J.F., and Colp, J.L., 1982, Kilauea Iki lava lake: geophysical constraints on its present (1980) physical state: Journal of Volcanology and Geothermal Research, v. 13, p. 31–61.

Imsland, P., 1984, Petrology, mineralogy and evolution of the Jan Mayen magma system: Reykjavik, Visindafelag Islendinga, Rit 43, Prentsmidjan Oddi, 332 p.

Jackson, E.D., 1968, The character of the lower crust and upper mantle beneath the Hawaiian Islands: International Geological Congress, 23d, Prague, Proceedings, v. 1, p. 135–150.

Jackson, E.D., Clague, D.A., Engleman, E., Friesen, W.B., and Norton, D., 1981, Xenoliths in the alkalic basalt flows from Hualalai Volcano, Hawaii: U.S. Geological Survey Open-File Report 81–1031.

Jackson, E.D., and Wright, T.L., 1970, Xenoliths in the Honolulu Volcanic Series, Hawaii: Journal of Petrology, v. 11, p. 405–430.

Jarosewich, E., Nelen, J.A., and Norberg, J.A., 1979, Electron microprobe reference samples for mineral analyses: Smithsonian Contributions to the Earth Sciences, v. 22, p. 68–72.

Kaneoka, I., Takaoka, N., and Clague, D.A., 1983, Noble gas systematics for coexisting glass and olivine crystals in basalts and dunite xenoliths from Loihi Seamount: Earth and Planetary Science Letters, v. 66, p. 427–437.

Kirby, S.H., and Green, H.W., II, 1980, Dunite xenoliths from Hualalai Volcano: evidence for mantle diapiric flow beneath the Island of Hawaii: American Journal of Science, v. 280-A, p. 550–575.

Kushiro, I., Yoder, H.S., Jr., and Mysen, B.O., 1976, Viscosities of basalt and andesite melts at high presure: Journal of Geophysical Research, v. 81, p. 6351–6356.

Leeman, W.P., and Scheidegger, K.F., 1977, Olivine/liquid distribution coefficients and a test for crystal-liquid equilibrium: Earth and Planetary Science Letters, v. 35. p. 247–257.

Luth, W.C., and Gerlach, T.M., 1980, Composition and proportions of major phases in the 1959 Kilauea Iki lava lake in December 1978 [abs.]: Eos, v. 61, p. 1142.

Luth, W.C., Gerlach T.M., and Eichelberger, J.C., 1981, Kilauea Iki lava lake: April 1981 [abs.]: Eos, v. 62, p. 1073.

Maaloe, S., and Hansen, B., 1982, Olivine phenocrysts of Hawaiian olivine tholeiite and oceanite: Contributions to Mineralogy and Petrology, v. 81, p. 203–211.

Macdonald, G.A., 1944, The 1840 eruption and crystal differentiation in the Kilauean magma column: American Journal of Science, v. 242, p. 177–189.

Melson, W.G., Vallier, T.L., Wright, T.L., Byerly, G., and Nelen, J., 1976, Chemical diversity of abyssal volcanic glass erupted along Pacific, Atlantic, and Indian Ocean seafloor spreading centers: American Geophysical Union Geophysical Monograph, v. 19, p. 351–368.

Mercier, J-C.C., 1979, Peridotite xenoliths and the dynamics of kimberlite intrusion, *in* The mantle sample: inclusions in kimberlites and other volcanics: Proceedings of the Second International Kimberlite Conference, v. 2, p. 197–212.

Mercier, J-C.C., and Nicolas, A., 1975, Textures and fabrics of upper mantle peridotites as illustrated by xenoliths from basalts: Journal of Petrology, v. 16, p. 454–487.

Moore, J.G., 1965, Petrology of deep-sea basalt near Hawaii: American Journal of Science, v. 263, p. 40–52.

Moore, J.G., Clague, D.A., and Normark, W.R., 1982, Diverse basalt types from Loihi Seamount, Hawaii: Geology, v. 10, p. 88–92.

Moore, J.G., and Evans, B.W., 1967, The role of olivine in the crystallization of the prehistoric Makaopuhi lava lake, Hawaii: Contributions to Mineralogy and Petrology, v. 15, p. 202–223.

Moore, R.B., Helz, R.T., Dzurisin, D., Eaton, G.P., Koyanagi, R.Y., Lipman, P.W., Lockwood, J.P., and Puniwai, G.S., 1980, The 1977 eruption of Kilauea Volcano, Hawaii: Journal of Volcanology and Geothermal Research, v. 7, p. 189–210.

Muir, I.D., and Tilley, C.E., 1957, Contributions to the petrology of Hawaiian basalts 1. The picrite-basalts of Kilauea: American Journal of Science, v. 255, p. 241–253.

Murata, K.J., and Richter, D.H., 1966a, Chemistry of the lavas of the 1959–60 eruption of Kilauea Volcano, Hawaii: U.S. Geological Survey Professional Paper 537–A, 26 p.

———1966b, The settling of olivine in Kilauean magma as shown by lavas of the 1959 eruption: American Journal of Science, v. 264, p. 194–203.

Powers, H.A., 1955 Composition and origin of basaltic magma of the Hawaiian Islands: Geochimica et Cosmochimica Acta, v. 7, p. 77–107.

Raleigh, C.B., 1968, Mechanisms of plastic deformation in olivine: Journal of Geophysical Research, v. 73, p. 5391–5406.

Raleigh, C.B., and Kirby, S.H., 1970, Creep in the upper mantle: Mineralogical Society of America Special Paper 3, p. 113–121.

Richter, D.H., Eaton, J.P., Murata, K.J., Ault, W.U., and Krivoy, H.L., 1970, Chronological narrative of the 1959–60 eruption of Kilauea Volcano, Hawaii: U.S. Geological Survey Professional Paper 537–E, 73 p.

Richter, D.H., and Moore, J.G., 1966, Petrology of the Kilauea Iki lava lake, Hawaii: U.S. Geological Survey Professional Paper 537–B, 26 p.

Richter, D.H., and Murata, K.J., 1966, Petrography of the lavas of the 1959–60 eruption of Kilauea Volcano, Hawaii: U.S. Geological Survey Professional Paper 537–D, 12 p.

Rison, W., and Craig, H., 1983, Helium isotopes and mantle volatiles in Loihi Seamount and Hawaiian Island basalts and xenoliths: Earth and Planetary Science Letters, v. 66, p. 407–426.

Roedder, E., 1983, Geobarometry of ultramafic xenoliths from Loihi Seamount, Hawaii, on the basis of CO_2 inclusions in olivine: Earth and Planetary Science

Letters, v. 66, p. 369–379.
———1984, Fluid inclusions: Reviews in Mineralogy, v. 12, 644 p.
Ross, J.V., Avé Lallement, H.G., and Carter, N.L., 1980, Stress dependence of recrystallized-grain and subgrain size in olivine: Tectonophysics, v. 70, p. 39–61.
Ryan, M.P., Blevins, J.Y.K., Okamura, A.T., and Koyanagi, R.Y., 1983, Magma reservoir subsidence mechanics: theoretical summary and application to Kilauea Volcano, Hawaii: Journal of Geophysical Research, v. 88, p. 4147–4181.
Ryan, M.P., Koyanagi, R.Y., and Fiske, R.S., 1981, Modelling the three-dimensional structure of macroscopic magma transport systems: application to Kilauea Volcano: Journal of Geophysical Research, v. 86, p. 7111–7129.
Schwindinger, K.R., Roppo, P.S., and Anderson, A.T., Jr., 1983, Synneusis of olivine phenocrysts into glomeroporphyritic clusters [abs.]: Geological Society of America Abstracts with Programs, v. 15, p. 682.
Sen, G., 1983, A petrologic model for the constitution of the upper mantle and crust of the Koolau shield, Oahu, Hawaii, and Hawaiian magmatism: Earth and Planetary Science Letters, v. 62, p. 215–228.
Skinner, B.J., and Peck, D.L., 1969, An immiscible sulfide melt from Hawaii: Economic Geology Monograph, v. 4, p. 310–322.
Spera, F.J., 1984, Carbon dioxide in petrogenesis III: role of volatiles in the ascent of alkaline magma with special reference to xenolith bearing mafic lavas: Contributions to Mineralogy and Petrology, v. 88, p. 217–232.
Stevenson, D.J., 1983, Magmatic transport by the migration of fluid-filled cracks [abs.]: Eos, v. 64, p. 848.
Takahashi, E., and Kushiro, I., 1983, Melting of a dry peridotite at high pressures and basalt magma genesis: American Mineralogist, v. 68, p. 859–879.
Thornber, C., and Huebner, J.S., 1985, Dissolution of olivine in basaltic liquids I: Experimental observations and applications: American Mineralogist, v. 70, p. 934–945.
Van Kooten, G.K., and Buseck, P.R., 1978, Interpretation of olivine zoning: study of a maar from the San Francisco volcanic field, Arizona: Geological Society of American Bulletin, v. 89, p. 744–754.
Wadge, G., 1981, The variation of magma discharge during basaltic eruptions: Journal of Volcanology and Geothermal Research, v. 11, p. 139–168.
Wanamaker, B.J., and Evans, B., 1985, Experimental diffusional crack healing in olivine, *in* Schock, R.N., ed., American Geophysical Union Monograph 31: p. 194–210.
Weertman, J., 1971a, Theory of water-filled crevasses in glaciers applied to vertical magma transport beneath oceanic ridges: Journal of Geophysical Research, v. 76, p. 1171–1183.
———1971b, Velocity at which liquid-filled cracks move in the Earth's crust or in glaciers: Journal of Geophysical Research, v. 76, p. 8544–8553.
White, R.W., 1966, Ultramafic inclusions in basaltic rocks from Hawaii: Contributions to Mineralogy and Petrology, v. 12, p. 245–314.
Wright, T.L., 1971, Chemistry of Kilauea and Mauna Loa lava in space and time: U.S. Geological Survey Professional Paper 735, 40 p.
———1973, Magma mixing as illustrated by the 1959 eruption, Kilauea Volcano, Hawaii: Geological Society American Bulletin, v. 84, p. 849–585.
———1984, Origin of Hawaiian tholeiite: a metasomatic model: Journal of Geophysical Research, v. 89, p. 3233–3252.
Wright, T.L., and Fiske, R.S., 1971, Origin of the differentiated and hybrid lavas of Kilauea Volcano, Hawaii: Journal of Petrology, v. 12, p. 1–65.
Wright, T.L., and Okamura, R.T., 1977, Cooling and crystallization of tholeiitic basalt, 1965 Makaopuhi lava lake, Hawaii: U.S. Geological Survey Professional Paper 1004, 78 p.
Zablocki, C.J., and Tilling, R.I., 1976, Field measurements of apparent Curie temperatures in a cooling basaltic lava lake, Kilauea Iki, Hawaii: Geophysical Research Letters, v. 3, p 487–490.

ORIGIN OF THE WEST MAUI VOLCANIC ROCKS INFERRED FROM Pb, Sr, AND Nd ISOTOPES AND A MULTICOMPONENT MODEL FOR OCEANIC BASALT

By Mitsunobu Tatsumoto, Ernst Hegner,[1] *and* Daniel M. Unruh

ABSTRACT

Isotope ratios of Pb, Sr, and Nd for West Maui volcanic rocks fall within the range of those from other volcanoes of the Kea trend. Shield-building and caldera-filling rocks have indistinguishable Sr and Nd isotope ratios, but the latter rocks have slightly more radiogenic Pb. Posterosional volcanic rocks have lower $^{87}Sr/^{86}Sr$ ratios and less radiogenic Pb than underlying rocks. Isotope data for West Maui, as well as those for other Hawaiian volcanoes, are not adequately explained by binary mixing, but must be accounted for by mixing of at least three end members: the oceanic crust (Kilauea end member), the depleted upper mantle (posterosional end member). and a deep-mantle plume (Koolau end member). Isotope data thus far reported for oceanic basalt can also be described by a three-component mixing model: the depleted upper mantle (MORB source), Austral-St. Helena source, and recycled oceanic and continental crust (plumes?). However, data trends for oceanic basalt from individual areas suggest that mantle plumes may have only moderately radiogenic Pb, Sr, and Nd, requiring that such basalt was derived by mixing of these plumes with the chemically heterogeneous upper mantle (at least seven isotopically different components). Lithospheric contamination may also be involved.

INTRODUCTION

The geology and geophysics of the Hawaiian Islands have been extensively studied in order to understand intraplate volcanism and the formation of linear island chains. It has been thought for some time that the Emperor-Hawaiian Chain was formed by the northwestward motion of the Pacific plate over a fixed mantle hot spot (Wilson, 1963). It follows from the hot-spot hypothesis that the volcanoes of the chain are progressively older northwestward from the currently active volcanoes of Kilauea, Mauna Loa, and Loihi. The progression of ages has been well documented by K-Ar age measurements of Hawaiian rocks (McDougall, 1964; Dalrymple and others, 1973; Dalrymple and Clague, 1976).

The loci of the Hawaiian volcanoes follow two parallel curves (fig. 26.1): the Loa (southwestern) and Kea (northeastern) trends (Jackson and others, 1972, and references therein). From youngest to oldest, volcanoes on the Loa trend are Loihi, Mauna Loa (Hawaii), Hualalai (Hawaii), Kahoolawe, Lanai, West Molokai, Koolau (Oahu), Waiane (Oahu), and Kauai; those on the Kea trend are Kilauea (Hawaii), Mauna Kea (Hawaii), Kohala (Hawaii), Haleakala (East Maui), West Maui, and East Molokai.

Hawaiian volcanoes usually evolve in three stages: a shield-building stage, producing mostly tholeiite, a caldera-filling stage (alkalic rocks), and a posterosional stage (nephelinitic rocks) (Macdonald, 1968). However, recent studies of Loihi reveal a seamount stage in which basanite and alkali basalt with subordinate tholeiite are erupted before the shield-building tholeiitic stage (Moore and others, 1982). Although the earlier three-stage division may be too simple, subaerial Hawaiian rocks can be conveniently subdivided according to the three major stages. The two volcanoes on Maui, Haleakala in the east and the smaller West Maui Volcano, have developed to the posterosional stage. Those on the Island of Hawaii, however, 100 km to the southeast, have not yet erupted lava of posterosional type.

Strontium isotopes have been used for two decades to trace the origin of Hawaiian volcanic rocks (see, for example, Lessing and Catanzaro, 1964; Hamilton, 1965; Powell and Delong, 1966). From the Sr isotope difference between the Koolau Basalt (shield-building stage) and Honolulu Volcanics (posterosional alkalic-nephelinitic stage) on Oahu, Powell and Delong (1966) suggested that the two volcanic sequences were not derived from a common parent magma and that the upper mantle source regions are chemically and isotopically heterogeneous. Later isotope studies of Pb, Nd, Sr, and Hf (for example, Lanphere and Dalrymple, 1980; Stille and others, 1983; Roden and others, 1984) support this contention.

Chen and Frey (1983), in an extensive geochemical and isotopic study of Haleakala, found inverse correlations between $^{143}Nd/^{144}Nd$ and Sm/Nd abundance ratios and between $^{87}Sr/^{86}Sr$ and Rb/Sr abundance ratios. These findings are consistent with mixing of two kinds of melt, one derived from an enriched mantle and another formed by melting of a fraction (less than two percent of the total volume) of midocean-ridge basalt source.

[1]Department of Geological Sciences, University of Saskatchewan, Saskatoon, Saskatchewan, S7N OWO, Canada.

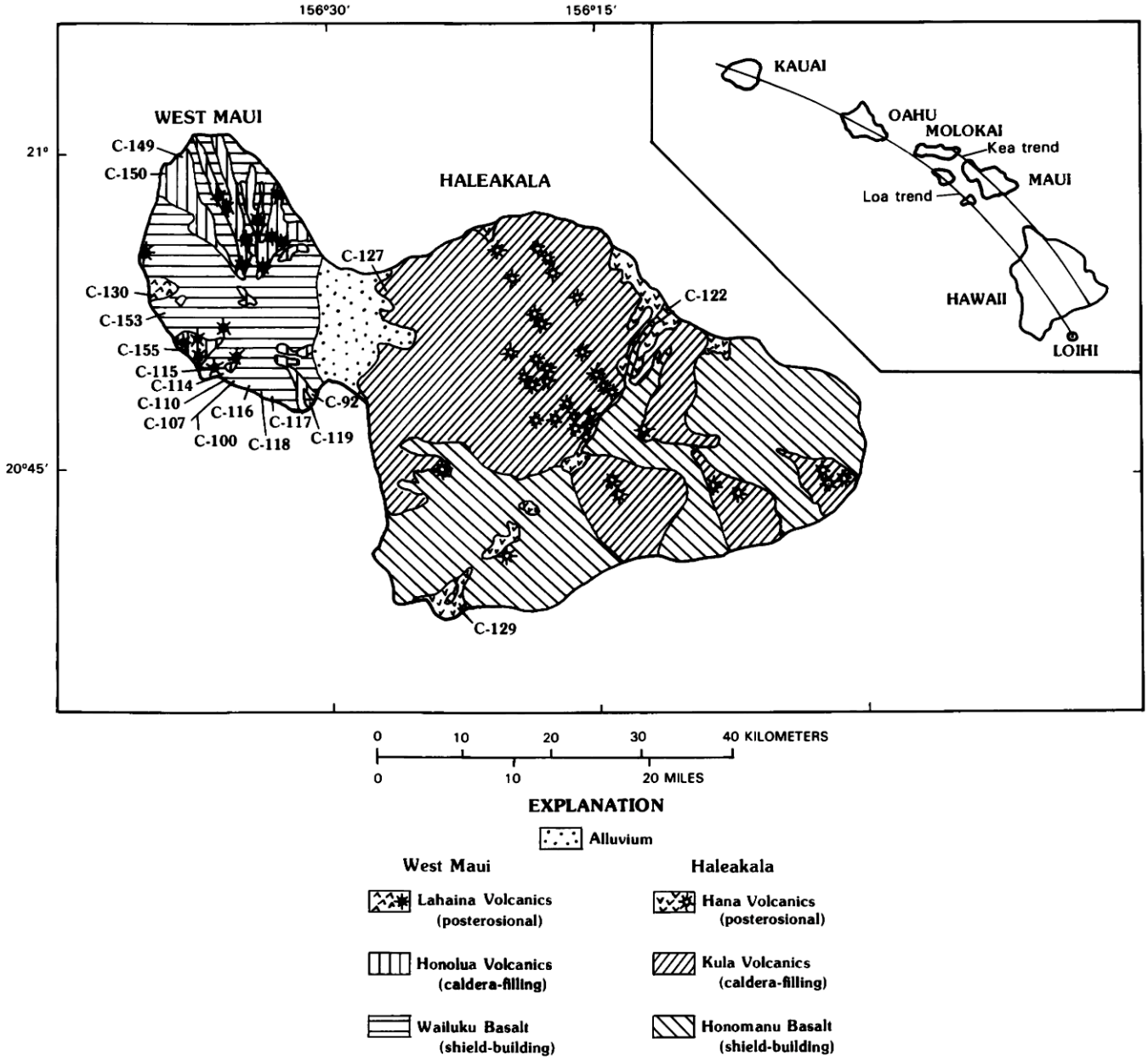

FIGURE 26.1.—Geologic map of the Island of Maui, simplified from Macdonald (1949). Sample locations are shown by numbers (for exact location, see Macdonald and Katsura, 1964, table 6 and 7; and this study). Inset shows location of Kea and Loa lineaments of volcanic centers in Hawaiian Islands.

Stille and others (1983) analyzed Pb, Sr, Nd, and Hf isotopes in volcanic rocks from Oahu and found that the isotope systematics can be best explained by a model involving mixing of three or more independent magma sources. Staudigel and others (1984) concurred with this view in an isotopic study of Loihi Seamount volcanic rocks. In order to place additional isotopic constraints on Hawaiian basalt petrogenesis, we measured Pb, Sr, and Nd isotopes in volcanic rocks from West Maui Volcano. The results were reported in brief previously (Hegner and others, 1986). In this paper we report concentrations of U, Th, Pb, Rb, Sr, Sm, and Nd, as well as Pb, Sr, and Nd isotopic ratios, in Maui volcanic rocks, and we discuss the origins of both Hawaiian volcanic rocks and oceanic basalt in general.

Stratigraphic nomenclature used in this report is that from Langenheim and Clague (chapter 1, part II).

ACKNOWLEDGMENTS

We are indebted to the late Dr. G.A. Macdonald for the C-series basalt samples. The supplemental samples were kindly

provided by Dr. J.A. Philpotts from the Macdonald collection. One of the authors (M.T.) thanks Drs. J.M. Sinton and Alan Zindler for their help with the field work.

GEOLOGY AND SAMPLES

The geology of Maui has been described in Stearns and Macdonald (1942) and Macdonald (1949). The Island of Maui comprises two volcanoes, both of which lie on the Kea trend. These volcanoes are the youngest in which post-erosional volcanics have erupted (fig. 26.1). The West Maui Volcano is wholly prehistoric and about one-fourth the size of the Haleakala (East Maui) Volcano, which last erupted in A.D. 1790. The Wailuku Basalt (formerly Wailuku Volcanic Series) represents the shield-building stage of West Maui and is composed mostly of tholeiite and intercalated alkali basalts with minor ankaramite near the top. Caldera-filling lava of the Honolua Volcanics (formerly Honolua Volcanic Series) is dominantly differentiated alkalic rock ranging from mugearite to soda trachyte in composition. After cessation of the Honolua volcanism and prolonged erosion, basanitic lava of the Lahaina Volcanics (formerly Lahaina Volcanics Series) was erupted.

The shield-building lava of Haleakala has been designated the Honomanu Basalt, and the composition of exposed rocks ranges only from tholeiitic olivine basalt to oceanite. The Honomanu Basalt is overlain by the Kula Volcanics, which are dominantly composed of hawaiite. The Hana Volcanics represents Haleakala's posterosional volcanism; this unit is less silica-saturated and consists of alkalic olivine basalt and basanitoid in contrast to the basanite-dominated Lahaina Volcanics of West Maui.

We analyzed 6 samples of tholeiitic basalt and 2 of alkali olivine basalt collected from the Wailuku Basalt (shield building), 8 samples of alkalic differentiates from the Honolua Volcanics (caldera filling), and 3 samples of basanite from the Lahaina Volcanics (posterosional). Sample numbers prefixed by a "C" were collected by the late Dr. Gordon A. Macdonald. Rock names and locations of samples C–92 to C–130 are listed by Macdonald and Katsura (1964) and are shown in figure 26.1. Samples collected by Macdonald from other sites have the following identities and places of collection (G.A. Macdonald, written commun., 1966): C–149, mugearite, transitional toward trachyte, roadcut at top of grade on west side of Pohakupule Gulch, West Maui, Honolua Volcanics; C–150, mugearite, transitional toward trachyte; dikelike body cutting mugearite flow in roadcut at berm where road starts to descend the west side of Honolua Gulch, West Maui, Honolua Volcanics; C–153, hawaiite, boulder in Kanaha Stream below Paupau Hill, just above Kelawea Village on outskirts of Lahaina, West Maui, Honolua Volcanics; C–155, mugearite, south branch of Makamakaole Gulch, 25 feet southeast of culvert under road, West Maui, Honolua Volcanics.

Samples designated "HMT" series were collected by one of us (M.T.) under the guidance of Dr. J.M. Sinton, University of Hawaii. Sample localities are the same as those of the C-series of Macdonald and Katsura (1964, tables 6 and 7), except HMT–2b, which is an alkalic olivine basalt from above an ash bed separating it from tholeiite (HMT–2a). Three samples from Haleakala Volcano were analyzed for comparison with Chen and Frey's (1983) data; they include a tholeiite from the Honomanu Basalt (shield building), a hawaiite of the Kula Volcanics (caldera filling), and a basanitoid of the Hana Volcanics (posterosional). Haleakala samples are also from the late Dr. Macdonald's collection. K-Ar ages by McDougall (1964) are 1.20 ± 0.02 Ma for olivine basalt from the upper part of the Wailuku Basalt, 1.16 ± 0.01 Ma for mugearite and trachyte of the Honolua Volcanics, and 0.44–0.86 Ma for alkalic rocks of the Kula Volcanics of Haleakala. Therefore, the isotopic data obtained from these samples require no age correction.

EXPERIMENTAL PROCEDURES

About 100 mg of each sample were dissolved in HF and HNO_3 with spike mixtures of ^{233}U-^{236}U-^{230}Th-^{205}Pb, ^{87}Rb-^{84}Sr, and ^{150}Nd-^{149}Sm in a PFA Teflon vial. First, Pb was separated in a $1N$ HBr medium using a single anion-exchange resin column of 100 μL volume (Tatsumoto and Unruh, 1976). The effluent was converted into $7N$ HNO_3 solution. The U and Th were then separated using an anion-exchange resin column of 600 μL volume. The effluent was converted into HCl solution, and Rb, Sr, and rare-earth elements (REE) were separated using a cation-exchange resin column of 4 mL volume. The Sr was purified using a 400 μL cation-exchange resin column, and the Nd and Sm were separated using 2-methyllactic acid in a 600 μL cation-exchange

TABLE 26.1.—*Standard analyses for selected elements and isotope ratios*

[Uncertainties refer to last significant figure(s) and represent 95 percent confidence level]

Sample	$^{143}Nd/^{144}Nd$	$^{87}Sr/^{86}Sr$	Rb (ppm)	Sr (ppm)	Sm (ppm)	Nd (ppm)
La Jolla standard	0.511865±10	--	--	--	--	--
NBS SRm-987 standard	--	.710255±30	--	--	--	--
BCR-1	.512654±15	.705009±20	46.47	329.6	6.64	29.06

resin column (Nakamura and others, 1976).

Pb isotopes were measured using single Re filaments with a phosphoric acid-silica gel in a NBS tandem-type mass spectrometer equipped with a 10^{11}-Ω resistor. The beam intensities of ^{206}Pb ranged from 3×10^{-12} to 1×10^{-10} A. A mass-fractionation correction of 0.12 ± 0.03 percent per atomic mass unit was applied to the raw Pb data. The U, Th, and Rb were measured using Re triple filaments in the same tandem mass spectrometer. The Sr, Nd, and Sm isotopic analyses were done in a VG 54R mass spectrometer using oxidized Ta filaments for Sr and Re-Ta triple filaments for Nd and Sm (Nakamura and others, 1976). Sr and Nd isotopic compositions of samples were deduced from the spiked runs by normalizing $^{86}Sr/^{88}Sr=0.1194$ and $^{146}Nd/^{144}Nd=0.7219$, respectively, using a linear fractionation law (Dodson, 1970). The NBS Sr standard SRM–982 and La Jolla Nd standard were measured in runs of varying (normal ^{86}Sr)/(spike ^{84}Sr) and (normal ^{144}Nd)/(spike ^{150}Nd) ratios (up to unity), and we found that spiked runs agree with unspiked runs to within 0.005 percent. Four samples (powdered) that showed somewhat high $^{87}Sr/^{86}Sr$ ratios compared to other samples were leached with 6*N* HCl at ≈80 °C for 10 h in order to eliminate alteration effects (O'Nions and others, 1977; Zindler and others, 1984). The leached samples were

TABLE 26.2.—*Selected elemental concentration and elemental and isotope ratios in samples of Maui volcanic rocks*

Sample		Rb (ppm)	Sr	Rb/Sr	Sm (ppm)	Nd	Sm/Nd	Pb (ppm)	U	Th	$\frac{^{238}U}{^{204}Pb}$	$\frac{^{232}Th}{^{238}U}$
WEST MAUI												
Lahaina Volcanics												
C-130	basanite	8.4	245	0.034	4.59	19.91	0.23	1.38	0.39	1.16	17.7	3.1
C-115	basanite	43.8	705	.062	4.82	25.94	.19	3.03	1.40	4.05	28.9	3.0
HMT 79-5	(C-115)	40.5	667	.061	7.97	39.42	.20	4.51	1.54	5.60	21.4	3.7
Honolua Volcanics												
C-155	mugearite	49.8	1,331	.037	17.62	87.05	.20	4.27	1.22	5.56	18.1	4.7
	--	--	--	--	--	--	--	1.18	5.33	--	4.7	--
C-153	hawaiite	8.7	499	.017	9.06	40.33	.22	1.59	.46	1.51	18.6	3.4
C-150	mugearite	44.1	1,149	.038	15.15	71.00	.21	4.23	1.66	78.05	24.7	4.4
C-149	mugearite	48.2	1,041	.046	14.95	64.91	.23	5.04	2.07	6.14	25.9	3.1
C-128	trachyte	59.1	400	.148	14.63	78.24	.19	7.27	1.84	7.24	16.0	4.1
C-116	trachyte	64.5	432	.149	20.33	98.84	.21	6.15	2.35	7.45	24.3	3.0
	--	--	--	--	--	--	--	2.55	8.42	--	3.4	--
C-92	trachyte	50.0	1,040	.048	15.67	81.33	.19	4.56	1.86	4.84	25.7	2.7
[1]HMT79-2b	alkali basalt	3.4	525	.006	8.58	31.05	.28	2.04	.29	1.46	8.9	5.3
Wailuku Basalt												
HMT 79-3	tholeiitic olivine basalt (C-120)	.6	360	.002	5.51	20.51	.27	.95	.11	.70	7.3	6.1
C-119	tholeiitic olivine basalt	7.7	489	.016	8.10	25.94	.31	1.16	.35	1.15	19.1	3.4
C-118	alkalic olivine basalt	1.4	254	.006	4.20	16.49	.25	1.20	.23	.61	11.8	2.8
C-117	tholeiitic olivine basalt	3.6	382	.009	4.14	16.96	.24	1.14	.22	.76	12.1	3.6
[1]C-114	alkalic olivine basalt	3.1	739	.004	6.88	27.41	.25	1.37	.27	1.23	12.5	4.7
C-110	tholeiite	4.2	319	.013	4.93	17.92	.27	2.85	.23	.62	5.0	2.8
[1]C-107	tholeiite	5.1	356	.014	6.97	25.99	.27	.96	.27	.77	17.8	2.9
C-100	tholeiite	3.1	346	.009	3.45	13.07	.26	.87	.20	.68	14.5	3.5
EAST MAUI (HALEAKALA)												
Hana Volcanics												
C-129	basanitoid	23.9	523	.046	6.16	27.58	.22	1.63	.61	2.09	23.6	3.5
[2]H65-11	alkalic basalt	18.8	582	.032	6.01	26.1	.23	--	--	2.6	--	--
Kula Volcanics												
C-127	hawaiite	29.8	831	.036	7.53	37.40	.20	2.27	.97	3.05	26.8	3.3
[2]H65-4	alkalic basalt	19.9	616	.032	6.83	30.7	.22	--	--	2.1	--	--
Honomanu Basalt												
C-122	tholeiitic olivine basalt	4.72	225	.021	4.23	14.71	.29	1.08	.20	.51	11.6	2.6
[2]C-122		4.11	207	.020	3.73	12.3	.30	--	--	.8	--	--

[1]Analyses from Unruh and others (oral commun., 1985).
[2]Chen and Frey (1983).

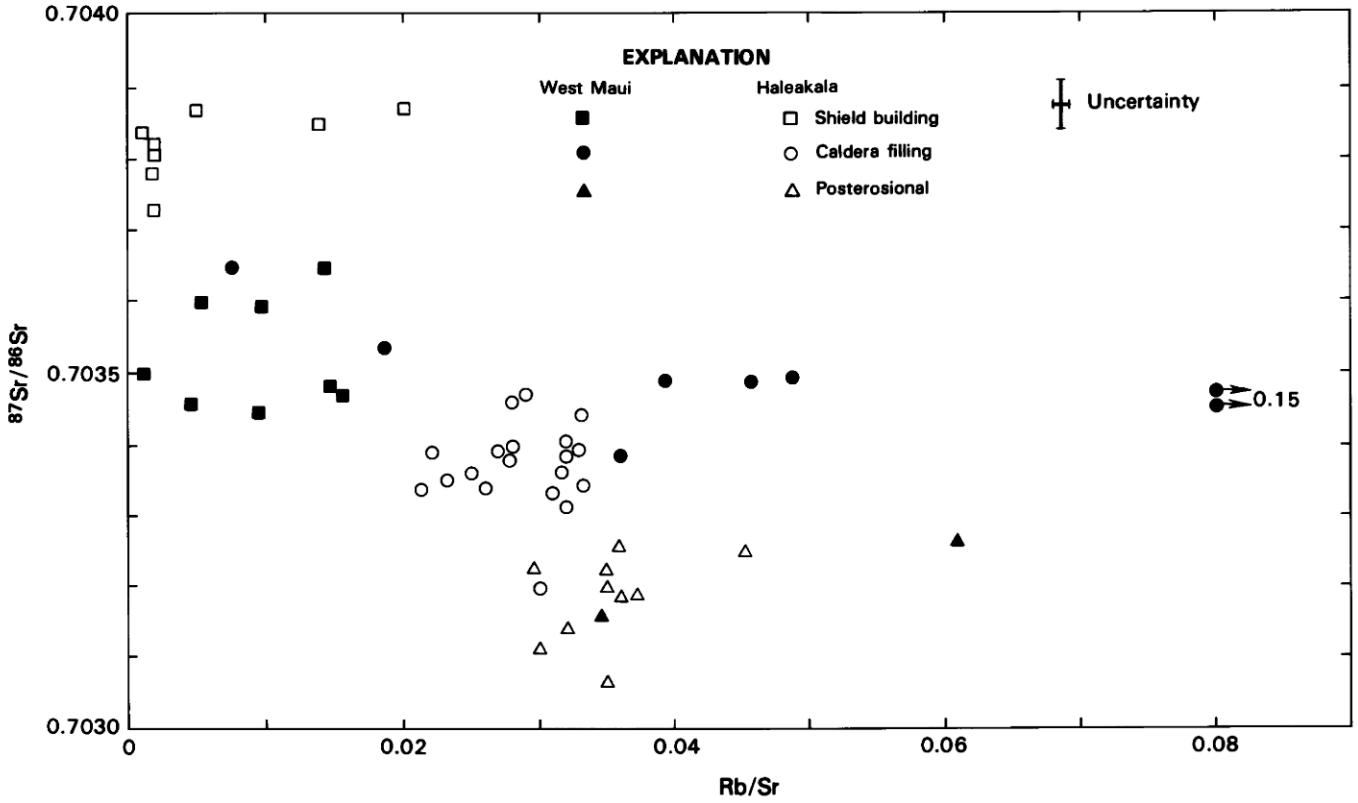

FIGURE 26.2.—Plot of $^{87}Sr/^{86}Sr$ ratio against Rb/Sr ratio for samples of volcanic rocks from Maui. Data for Haleakala from Chen and Frey (1983) included. Uncertainty bars apply to all data.

analyzed only for Sr isotopic composition. The standard runs during this study averaged $^{143}Nd/^{144}Nd = 0.511865 \pm 0.000010$ for the La Jolla Nd, and $^{87}Sr/^{86}Sr = 0.710265 \pm 0.000030$ for NBS SRM–987 (table 26.1). No instrumental bias corrections were applied to the isotope data in table 26.3. The USGS rock standard BCR–1 was analyzed once during the course of this study, and the results are listed in table 26.1. Blanks for the analyses are in ng: Pb, 0.1–0.15; U, <0.01; Th, <0.01; Rb, 0.1–0.2; Sr, 0.5–1; Sm, <0.03; Nd, <0.1.

RESULTS

TRACE-ELEMENT CONCENTRATIONS

The elemental concentration data for volcanic rocks from West Maui and Haleakala are listed in table 26.2. Data for Haleakala samples from Chen and Frey (1983) are also included. The trace-element abundances of Rb, Sr, Sm, Nd, Pb, U, and Th of West Maui and Haleakala are similar to those in other subaerial Hawaiian basalts (Tatsumoto, 1978; Clague and Frey, 1982; Roden and others, 1984).

Plots of the ratios $^{87}Sr/^{86}Sr$ versus Rb/Sr and $^{143}Nd/^{144}Nd$ versus Sm/Nd for West Maui and Haleakala samples are shown in figures 26.2 and 26.3, which include data from Haleakala obtained by Chen and Frey (1983). The variation in Rb/Sr ratios of West

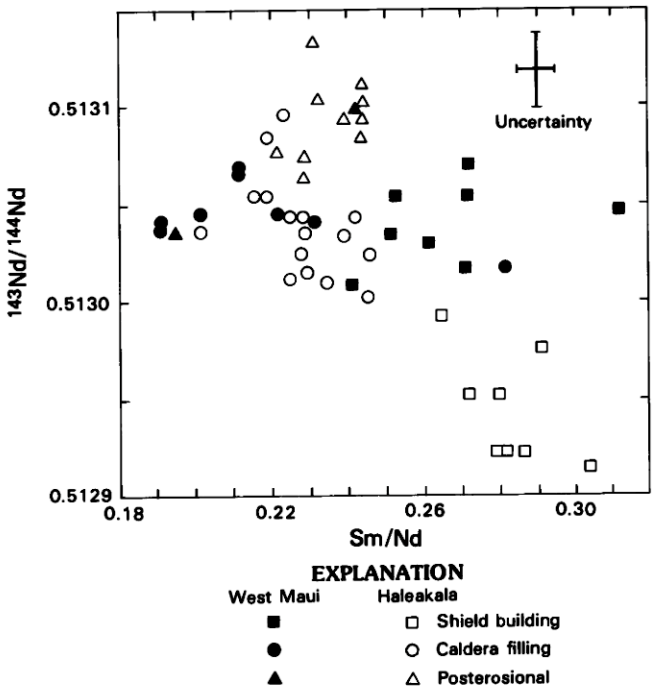

FIGURE 26.3.—Plot of $^{143}Nd/^{144}Nd$ ratio against Sm/Nd ratio for samples of volcanic rock from Maui. Uncertainty bars apply to all data.

Maui volcanic rocks (fig. 26.2) is large compared to that of the Haleakala volcanic rocks, because West Maui samples contain highly fractionated alkalic rocks such as trachyte that do not occur at Haleakala. Sm/Nd ratios (fig. 26.3) of West Maui vary from 0.31 to 0.19 and are similar to those of the Haleakala volcanic rocks. The lowest values are for trachyte and basanite, and Rb/Sr ratios of these rocks are correspondingly high. In contrast, $^{143}Nd/^{144}Nd$ values of West Maui volcanics are almost constant. Chen and Frey (1983) discovered profound negative correlations between parent/daughter abundance ratios and radiogenic isotope abundances in the

TABLE 26.3.—*Isotope data for Sr, Nd, and Pb in samples of Maui volcanic rocks*

[Uncertainties correspond to last significant figure(s) and are 95 percent confidence level. Uncertainties for lead are limited to a few values because of correction uncertainties for mass fractionation]

Sample	Rock type	$^{87}Sr/^{86}Sr$	ϵ_{Sr}	$^{143}Nd/^{144}Nd$	ϵ_{Nd}	$^{206}Pb/^{204}Pb$	$^{207}Pb/^{204}Pb$	$^{208}Pb/^{204}Pb$
WEST MAUI								
Lahaina Volcanics								
C-130	basanite	0.70315±3	-22.0	0.513086±28	8.7	18.169±11	15.452±14	37.750±49
				.513107±10				
C-115	basanite	.70326±2	-20.4	.513034±20	7.7	18.191±11	15.460±14	37.833±49
HMT79-5	(C-115)	.70325±4	--	.513031±18	--			
		.70327±3						
Honolua Volcanics								
C-155	mugearite	.70343±4	-18.0	.513043±8	7.9	18.513±11	15.494±14	38.050±49
C-153	hawaiite	.70353±3	-16.6	.513041±7	7.8	18.447±11	15.456±14	37.917±49
C-150	mugearite	.70349±3	-17.2	.513065±9	8.3	18.502±11	15.483±14	38.033±49
C-149	mugearite	.70349±3	-17.2	.513037±64	7.7	18.509±11	15.489±14	38.030±49
C-128	trachyte	.70347±3	-17.5	.513034±20	7.7	18.492±11	15.476±14	38.008±49
C-116	trachyte	.70348±5	-17.3	.513064±7	8.3	18.523±11	15.471±14	37.961±49
C-92	trachyte	.70350±3	-17.0	.513035±16	7.7	18.482±11	15.466±14	37.957±49
HMT79-1a	(C-92)	.70355±4	--	.513033±20	--	18.487±11	15.462±14	37.947±49
HMT79-2b	alkali basalt	.70354±3	--	.513033±20	7.3	18.506±11	15.560±14	38.040±49
[1]HMT79-2b		.70352±4	--	.513005±16	--	18.474±16	15.535±16	37.974±49
Wailuku Basalt								
HMT79-3	tholeiitic olivine basalt (C-120)	.70349±4	-17.2	.513014±19	7.3	18.462±11	15.456±14	37.925±50
C-119	tholeiitic olivine basalt	.70347±4	-17.5	.513044±28	7.9	18.426±11	15.472±14	37.904±49
HMT79-2A	(C-119)	.70356±3	--	.513025±20		18.462±11	15.454±14	37.899±49
C-118	alkalic olivine basalt	.70364±4	--	.513049±12	8.0	18.258±11	15.471±14	37.762±49
		[3].70359±2	-15.8					
C-117	tholeiitic olivine basalt	.70359±3	-15.8	.513007±15	7.2	18.404±15	15.429±14	37.940±49
		.70361±2						
[1]C-114	alkalic olivine basalt	.70346±4	-17.6	.513032±22	8.9	18.412±11	15.472±14	37.906±49
C-110	tholeiite	.70363±3	--	.513053±13	8.1	18.309±11	15.476±14	37.874±49
		[3].70365±3	-14.9					
[1]C-107	tholeiite	.70348±3	-17.3	.513070±12	8.1	18.438±11	15.499±14	37.948±49
C-100	tholeiite	.70361±4		.513027±13	7.5	18.365±11	15.470±14	37.877±49
		[3].70344±3	-17.9					
EAST MAUI (HALEAKALA)								
Hana Volcanics								
C-129	basanitoid	.70325±3	-20.6	.513070±13	8.4	18.259±11	15.453±14	37.828±49
[2]H65-1	alkalic basalt	.70314±4	-22.1	.51310±2	9.0	--	--	--
Kula Volcanics								
C-127	hawaiite	.70339±4	-18.6	.513030±15	7.6	18.351±11	15.468±14	37.938±49
[2]H65-4	alkalic basalt	.70334±3	-19.3	.51302±1	7.4	--	--	--
Honomanu Basalt								
C-122	tholeiite olivine basalt	.70378±3	-13.1	.512976±16	6.6	18.303±11	15.452±14	37.924±49
		.70374±4						
		.70374±3						
[2]C-122		.70387±4	-11.8	.51291±2	5.3	--	--	--

[1]Analyses from Stille and others (1985).
[2]Chen and Frey (1983).
[3]On acid leached samples (6N HCl, 10 hours).

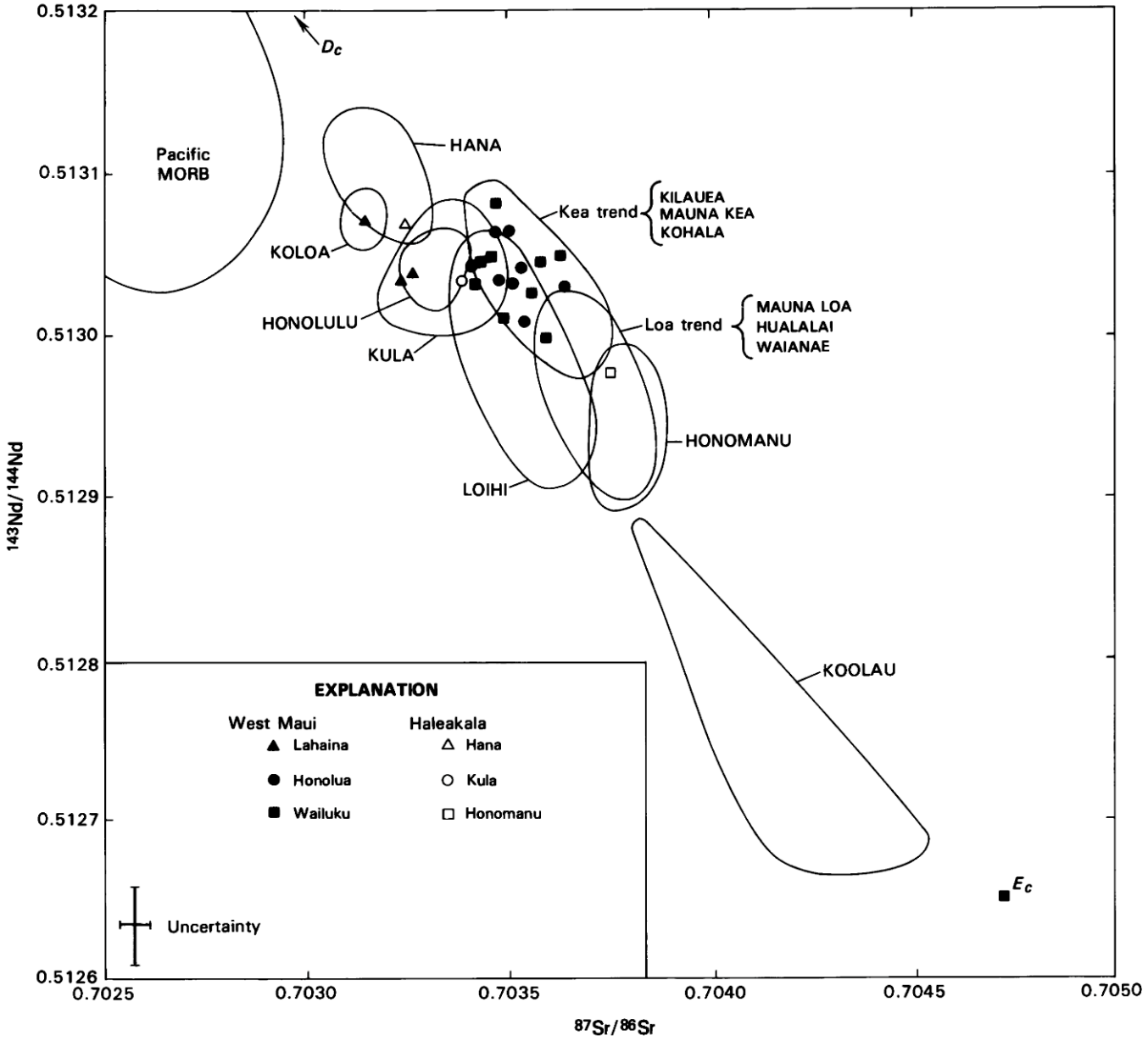

FIGURE 26.4.—Plot of $^{87}Sr/^{86}Sr$ ratio against $^{143}Nd/^{144}Nd$ ratio for Hawaiian basalt. Data for samples from Maui are shown by symbols. Data for Honomanu Basalt, Kula Volcanics, and Hana Volcanics of Haleakala from Chen and Frey (1983) are also shown. Also shown are fields for Koolau Basalt and Waianae Volcanics, Oahu; (Stille and others, 1983; Roden and others, 1984); Loihi (Staudigel and others, 1984); Koloa Volcanics, Kauai, (O'Nions and others, 1977); and volcanics from Island of Hawaii (Stille and others, in press). Data for posterosional basalt appears to be shifted slightly to left from main Hawaiian trend and close to East Pacific Ridge basalt (Pacific MORB) field. D_c and E_c, possible depleted and enriched members, respectively, in hypothetical two-component mixing model. Uncertainty bars apply to all individual symbols.

Rb-Sr and Sm-Nd systems. Although such negative correlations for West Maui samples are somewhat indistinct, our results clearly do not support the mantle-isochron concept of Brooks and others (1976), who proposed that a positive correlation of Rb/Sr with $^{87}Sr/^{86}Sr$ corresponds to an age of mantle differentiation of 1.8 Ga. The trace-element concentrations of Maui tholeiite (this study; Chen and Frey, 1983) are distinctly higher than those of normal mid-ocean-ridge basalt (N-MORB) but are comparable to those in enriched MORB (P-MORB) (see, for example, Tatsumoto and others, 1965; Cohen and O'Nions, 1982).

For seven samples from the Wailuku Basalt, West Maui, Rb and Sr concentrations and Rb/Sr ratios are similar to those of the Koolau Basalt, Oahu (Roden and others, 1984) (sample HMT 79–3 is omitted because of its weathered nature). However, the Rb concentrations and Rb/Sr ratios of Wailuku rocks appear to be distinctly lower than those of Loihi tholeiite (Frey and Clague,

1983; Staudigel and others, 1984), although their $^{87}Sr/^{86}Sr$ ratios are similar.

ISOTOPIC COMPOSITIONS

The Sr, Nd, and Pb isotopic data for West Maui and Haleakala are listed in table 26.3. The Sr and Nd data of Haleakala by Chen and Frey (1983) are also included in the table. The Nd-Sr data of West Maui basalt are plotted on a Nd-Sr correlation diagram in figure 26.4.

The C-series samples generally appear to be fresh; however, a $^{87}Sr/^{86}Sr$ value higher than 0.7036 in one of the three Wailuku samples proved to be related to alteration. Sample HMT 79–2b also shows slight alteration and a higher $^{87}Sr/^{86}Sr$ value.

The $^{87}Sr/^{86}Sr$ ratio of all samples from West Maui varies from 0.70315 to 0.70364, which correspond to an ε_{Sr} range of 7.0 (0.07 percent) and is well within the range (0.7031–0.7046; ε_{Sr} range, 21.3) of Hawaiian volcanic rocks so far reported (Lanphere and others, 1980; Chen and Frey, 1983; Stille and others, 1983, in press; Roden and others, 1984). The ε_{Sr} is the deviation in parts per ten thousand from the present day bulk earth value of $^{87}Sr/^{86}Sr = 0.7047$ (O'Nions and others, 1977). Although the bulk-earth value has been debated (for example, Zindler and others, 1982), we use the ε_{Sr} just for convenience to compare $^{87}Sr/^{86}Sr$ variations in the present paper. The variation is smaller than that for the three Haleakala volcanic sequences (0.70307–0.70387; ε_{Sr} range, 11.4) and the tholeiitic series of Koolau (0.70367–0.70458; ε_{Sr} range, 12.9), but it is similar to that for the Loihi Seamount volcanics (0.7033–0.7037; ε_{Sr} range, 5.7, Staudigel and others, 1984). Similar $^{87}Sr/^{86}Sr$ ratios (0.70346–0.70370) for West Maui volcanic rocks are also reported by Feigenson and others (1984). The shield-building Wailuku Basalt and the late-stage Honolua alkalic rocks from West Maui have an almost constant $^{87}Sr/^{86}Sr$ ratio of 0.70353 ± 0.00010, corresponding to an ε_{Sr} range of only 1.4. The $^{87}Sr/^{86}Sr$ ratios are distinctly smaller than those of Honomanu Basalt but slightly higher than those of Kula alkalic rocks from Haleakala. The $^{87}Sr/^{86}Sr$ ratio of Lahaina basanite from West Maui is distinctly smaller than that of volcanic rocks of the earlier stages, but similar to those in the Hana Volcanics at Haleakala (fig. 26.2) and in the Honolulu Volcanics on Oahu (Stille and others, 1983).

Chen and Frey (1983, fig. 1) reported that the $^{143}Nd/^{144}Nd$ ratio in Haleakala rocks varies from 0.51313 to 0.51291. This variation corresponds to an ε_{Nd} variation of 4.2, and Nd isotopic ratios are negatively correlated with Sm/Nd ratios. Like ε_{Sr}, ε_{Nd} is the deviation in parts per ten thousand from the present day bulk-earth value of $^{143}Nd/^{144}Nd = 0.51264$ (DePaolo and Wasserburg, 1976). In contrast to Haleakala, the $^{143}Nd/^{144}Nd$ ratio of all samples analyzed from West Maui exhibits almost constant values (0.51301 to 0.51309), which correspond to an ε_{Nd} range of only 1.6. Furthermore, $^{143}Nd/^{144}Nd$ ratios for shield-building Wailuku Basalt and alkalic Honolua Volcanics vary from only 0.51301 to 0.51307, these valves correspond to a narrow range of ε_{Nd} of 1.2.

The Sr and Nd ratios of West Maui volcanic rocks are inversely correlated and plot at the upper end of the Hawaiian data array shown in figure 26.4 (Stille and others, 1983, 1985; Roden and others, 1984; Staudigel and others, 1984). The Lahaina Volcanics (posterosional) has similar $^{143}Nd/^{144}Nd$ ratios to the underlying rocks but smaller $^{87}Sr/^{86}Sr$ ratios. Consequently, the Lahaina data are shifted slightly to the left, close to the MORB field, and plot in the fields of Hana (Haleakala) and Honolulu (Oahu) data.

The Pb isotopic compositions of West Maui samples are shown in a diagram plotting $^{206}Pb/^{204}Pb$ against $^{207}Pb/^{204}Pb$ and $^{208}Pb/^{204}Pb$ in figure 26.5. Note that the scale for $^{207}Pb/^{204}Pb$ is expanded five times relative to those for $^{206}Pb/^{204}Pb$ and $^{208}Pb/^{204}Pb$. The variation in Pb isotopic compositions (table 26.3) is partly caused by measurement errors associated with mass fractionation. However, the ratios of West Maui samples vary beyond measurement errors.

The Pb isotopic compositions of West Maui volcanic rocks fall within the field for Hawaiian volcanic rocks between Waianae (Oahu) and Kilauea (Hawaii); in contrast to the Sr and Nd isotopes; however, the West Maui rocks display the largest range in Pb isotopic composition of any single Hawaiian volcano so far determined except Loihi. On the other hand, Pb isotopic compositions of Honomanu, Kula, and Hana rocks from Haleakala show smaller variations compared to West Maui, although Nd and Sr show larger variations (Chen and Frey, 1983). However, only three samples from Haleakala were analyzed in the present study. The Pb data for Haleakala measured by Chen and Frey are not published and were compiled from Staudigel and others (1984, fig. 5), and the actual sample population is not known to us. The least radiogenic Pb in Wailuku samples is similar to those in the Haleakala samples, but Pb in upper Wailuku samples is more radiogenic. The Pb in the alkalic late-stage Honolua Volcanics is more radiogenic than that of the Wailuku samples showing oceanic-crust assimilation as discussed later. Alkali basalt sample HMT 79–2b has a significantly high $^{207}Pb/^{204}Pb$ ratio compared to other samples (fig. 26.5). The data fall on the "1.8-Ga MORB trend" instead of the "0.9-Ga Hawaiian trend" in the plot of $^{206}Pb/^{204}Pb$ versus $^{207}Pb/^{204}Pb$ (Tatsumoto, 1978) and indicate a Pb-isotopic diversity in Hawaiian

FIGURE 26.5.—Plots of $^{206}Pb/^{204}Pb$ ratio against $^{207}Pb/^{204}Pb$ and $^{208}Pb/^{204}Pb$ ratios for Hawaiian volcanic rocks. Data from Maui (this study), Island of Hawaii (Tatsumoto, 1978), Oahu (Stille and others, 1983), Koloa Volcanics, Kauai (Sun, 1980), and Loihi (Staudigel and others, 1984). Data of shield building and caldera-filling rocks from West Maui plot in large area similar to Loihi data but with lower $^{208}Pb/^{204}Pb$, whereas posterosional rocks are less radiogenic and plot close to Hana Volcanics (Haleakala) and Honolulu Volcanics (Oahu). Hawaiian basalt data fall on apparent isochron of ~0.9 Ga, whereas some data plot near 1.8-Ga MORB trend. In upper diagram, reference lines with K ($^{232}Th/^{238}U$) = 3.0 are shown for ages of 0.9 and 1.8 Ga. Uncertainty ellipses apply to data of this study.

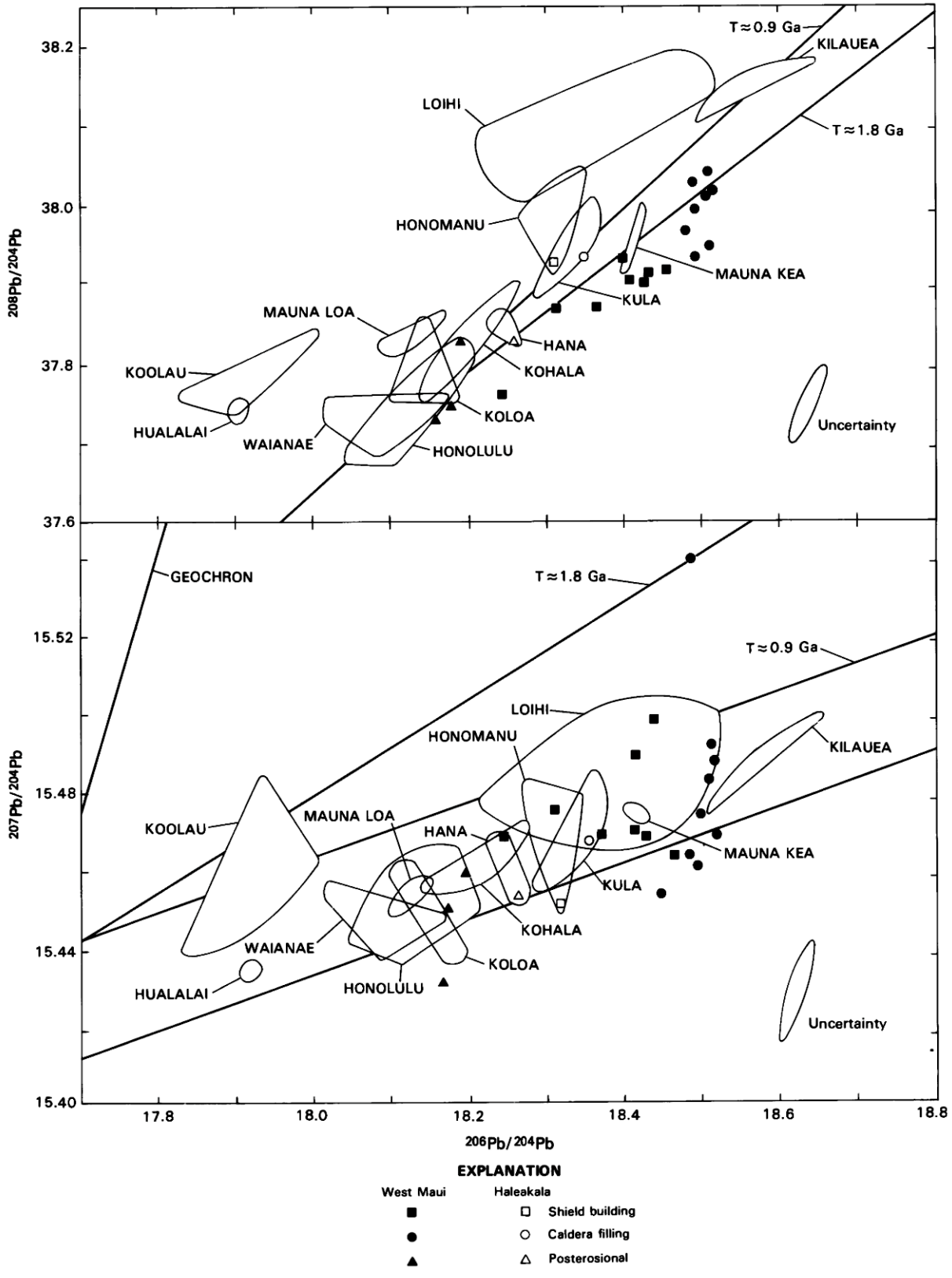
T≈0.9 Ga
KILAUEA
LOIHI
T≈1.8 Ga
HONOMANU
MAUNA KEA
KULA
MAUNA LOA
HANA
KOHALA
KOOLAU
KOLOA
HUALALAI
WAIANAE
HONOLULU
Uncertainty
38.2
38.0
37.8
37.6
208Pb/204Pb
GEOCHRON
T≈1.8 Ga
T≈0.9 Ga
15.52
15.48
15.44
15.40
207Pb/204Pb
17.8
18.0
18.2
18.4
18.6
18.8
206Pb/204Pb
EXPLANATION
West Maui
Haleakala
Shield building
Caldera filling
Posterosional

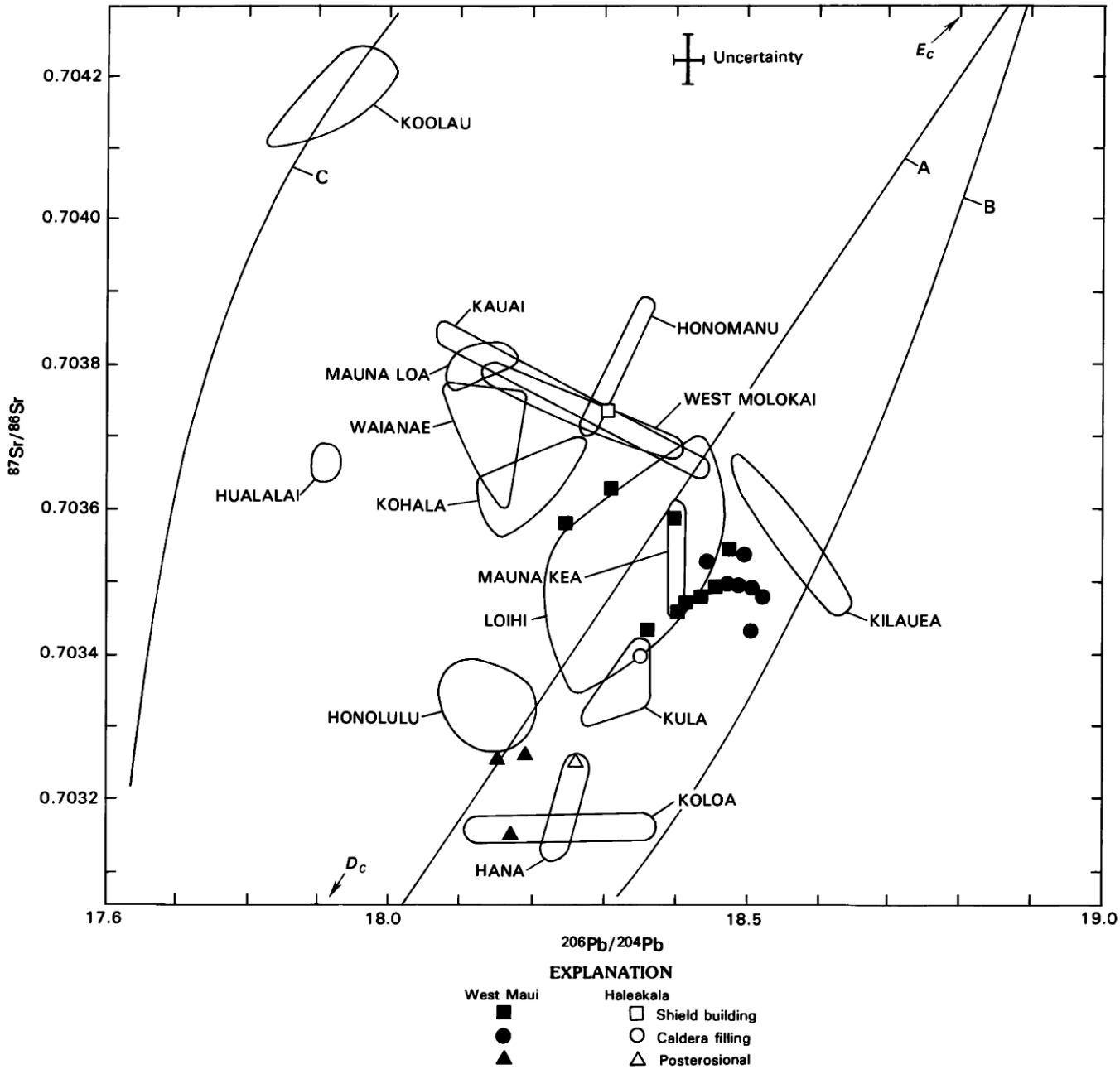

FIGURE 26.6.—Plot of $^{206}Pb/^{204}Pb$ ratio against $^{87}Sr/^{86}Sr$ ratio for Hawaiian rocks. Sources of data as in figures 26.4 and 26.5. Shield-building and caldera-filling rocks from West Maui plot in and near field for Loihi, whereas posterosional rocks plot to less radiogenic side of trend. Also shown are hypothetical mixing curves between depleted and enriched sources: A, $Q_l = 1$; B, $Q_l = 0.5$; C, $Q_l = 10$. See discussion in text. D_c and E_c, inferred depleted and enriched components, respectively.

basalt. Although these peculiar data need confirmation, it is conceivable that the high $^{207}Pb/^{204}Pb$ ratio is the reflection of oceanic lower crust involvement; the basalt locally contains 1-cm gabbroic clots. Basanite of the Lahaina sequence has less radiogenic Pb than Wailuku tholeiite, indicating a different origin from the underlying volcanic rocks.

The Pb, Sr, and Nd data for Hawaiian volcanic rocks are shown in plots of $^{206}Pb/^{204}Pb$ versus $^{87}Sr/^{86}Sr$ and $^{143}Nd/^{144}Nd$ diagrams in figures 26.6 and 26.7. Differences between the posterosional Lahaina Volcanics and the underlying rocks are more evident on the Sr-Pb diagram. The Pb becomes slightly more radiogenic, and the Sr becomes slightly less radiogenic moving from

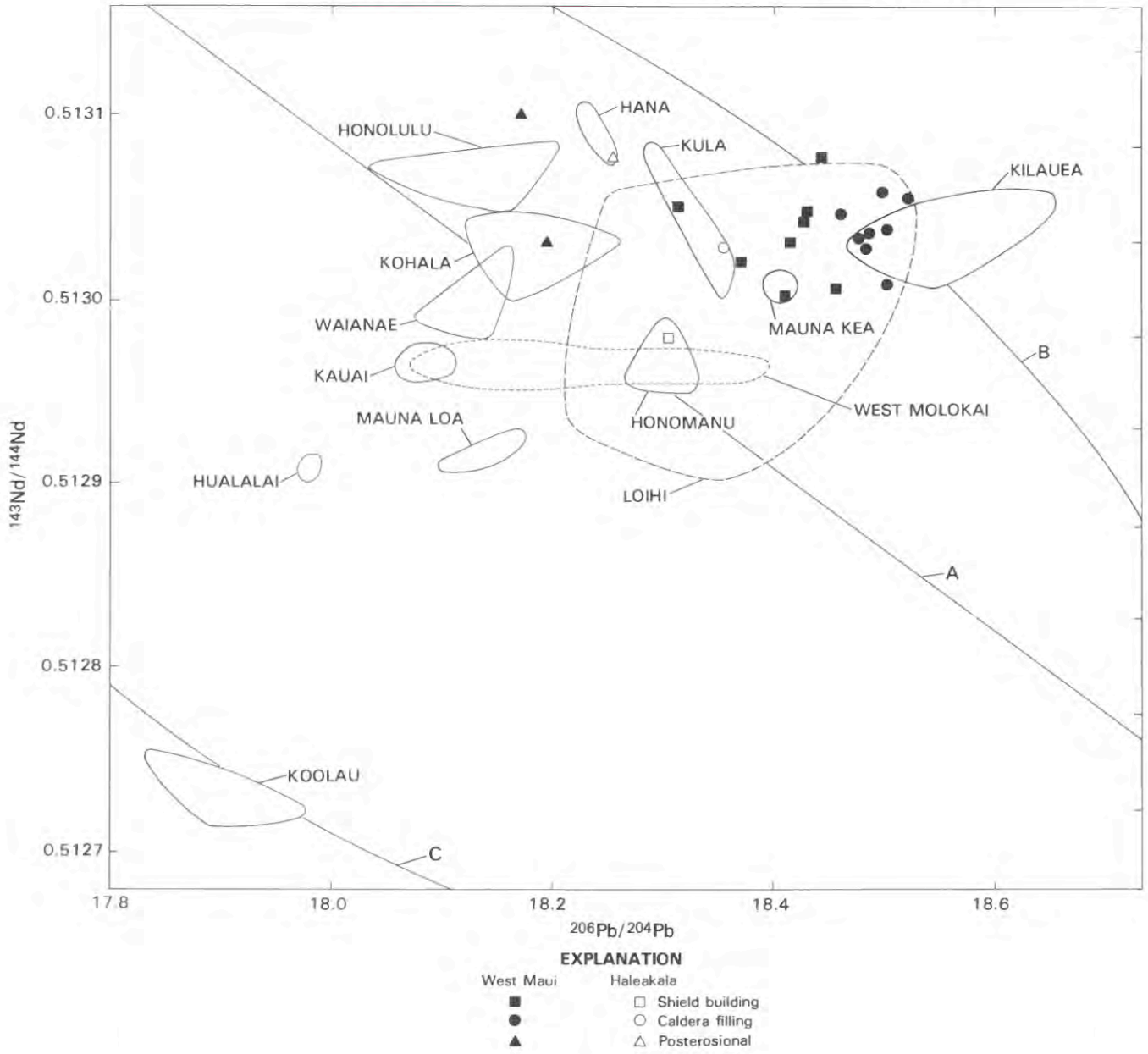

FIGURE 26.7.—Plot of $^{206}Pb/^{204}Pb$ ratio against $^{143}Nd/^{144}Nd$ ratio for Hawaiian rocks. Sources of data as in figures 26.4 and 26.5. Plot can be regarded as upside-down image of figure 26.6. Hypothetical mixing curves calculated as in figure 26.6: A, $Q_2=1$; B, $Q_2=0.5$; C, $Q_2=10$.

tholeiite to caldera-filling basalt, and the data define a crude negative correlation. The negative correlation is similar to the main Hawaiian trend that supports a model in which two-component mixing occurs between a mantle plume and depleted mantle or lithosphere. The mixing with depleted mantle progressively increases as the volcano evolves (Chen and Frey, 1983). However, the data for posterosional basalt do not appear to be related to the main trend and indicate the possible presence of a second depleted source with relatively non-radiogenic Pb and Sr.

DISCUSSION

Results of high-pressure experiments show that alkali olivine basalt can be produced from olivine tholeiite magma by orthopyroxene and olivine fractionation at pressures greater than 1.2 GPa (12 kbar)(see, for example, Kushiro, 1969; Presnall and others, 1979). No significant differences in Pb isotopes between tholeiite and alkali basalt were found for Kohala and Mauna Kea (Tatsumoto, 1978) nor for Pb, Sr, Nd, and Hf isotopic composition between the two

rock types from the Waianae Volcano (Stille and others, 1983). These isotopic similarities between tholeiite and alkali basalt appear to be consistent with results of high-pressure experiments. Distinct differences in $^{87}Sr/^{86}Sr$ ratio between shield-building Koolau tholeiite and nephelinitic Honolulu Volcanics from Oahu have been observed for about two decades (Powell and Delong, 1966). Recent Sr-isotope measurements (Lanphere and Dalrymple, 1980) as well as studies of Pb, Nd, and Hf isotopes in Oahu volcanic rocks (Stille and others, 1983; Roden and others, 1984) have confirmed the isotopic differences between the two rock series. Thus Tatsumoto (1978) and Stille and others (1983) suggested a close genetic relationship exists between tholeiite and late-stage alkali basalt, but that nephelinitic rocks are of independent origin. This suggestion derived from isotopic studies is consistent with Jackson and Wright's (1970) view; from a study of xenoliths they concluded that the Honolulu Volcanics originated from garnet lherzolite at greater depths than the Koolau tholeiite magma.

In contrast, Chen and Frey (1983) found that Sr and Nd isotopic compositions of Honomanu Basalt (shield-building stage), Kula Volcanics (alkalic basalt), and Hana Volcanics from Haleakala are distinctly different among the three sequences and are inversely correlated with Rb/Sr and Sm/Nd ratios. Chen and Frey invoked a two-component melt-mixing model to account for the isotopic and incompatible-element relationships. Present Nd and Sr isotopic data for West Maui volcanics do not show such clear distinctions as Chen and Frey observed for the east. These results may indicate that Haleakala late-stage magma had crustal contamination along differentiation and changed its isotopic signature, while West Maui magma had little assimilation along differentiation.

Staudigel and others (1984) stated that the heterogeneous isotopic character of Loihi Seamount volcanic rocks may attest to Loihi's inability to homogenize lava before eruption, whereas parental magma of more mature and active volcanoes may be well mixed in established magma chambers. Waianae (Stille and others, 1983) and West Maui data seem to support such a hypothesis.

Staudigel and others (1984) argued that Honolulu and Koolau data define two extreme positions in the $^{143}Nd/^{144}Nd$-$^{87}Sr/^{86}Sr$ correlation diagram, with Kilauea data falling in the center, but that the Honolulu and Koolau data fall close to one end of the $^{206}Pb/^{204}Pb$-$^{207}Pb/^{204}Pb$ trend (fig. 26.5). They used this inconsistency to preclude simple mixing of two end members. We observe, as shown in the previous section, that on the plot of $^{87}Sr/^{86}Sr$ versus $^{143}Nd/^{144}Nd$ (fig. 26.4) Kilauea and Koolau are two extremes (Kilauea does not fall in the center) that define the general trend (tholeiite and late-stage samples) of the Hawaiian volcanic rocks. Posterosional volcanic rocks of Honolulu, Hana, and Lahaina deviate to the left of the general trend, implying a three-component system.

On the $^{206}Pb/^{204}Pb$-$^{207}Pb/^{204}Pb$ plot of figure 26.5, Koolau deviates slightly from the general trend of Waianae, Honolulu, and Kilauea. This deviation is even more pronounced in the plot of $^{206}Pb/^{204}Pb$ versus $^{208}Pb/^{204}Pb$. In these Pb-Pb diagrams, the denominator of the ratios on each axis is the same (^{204}Pb); therefore, data representing two-component mixing should

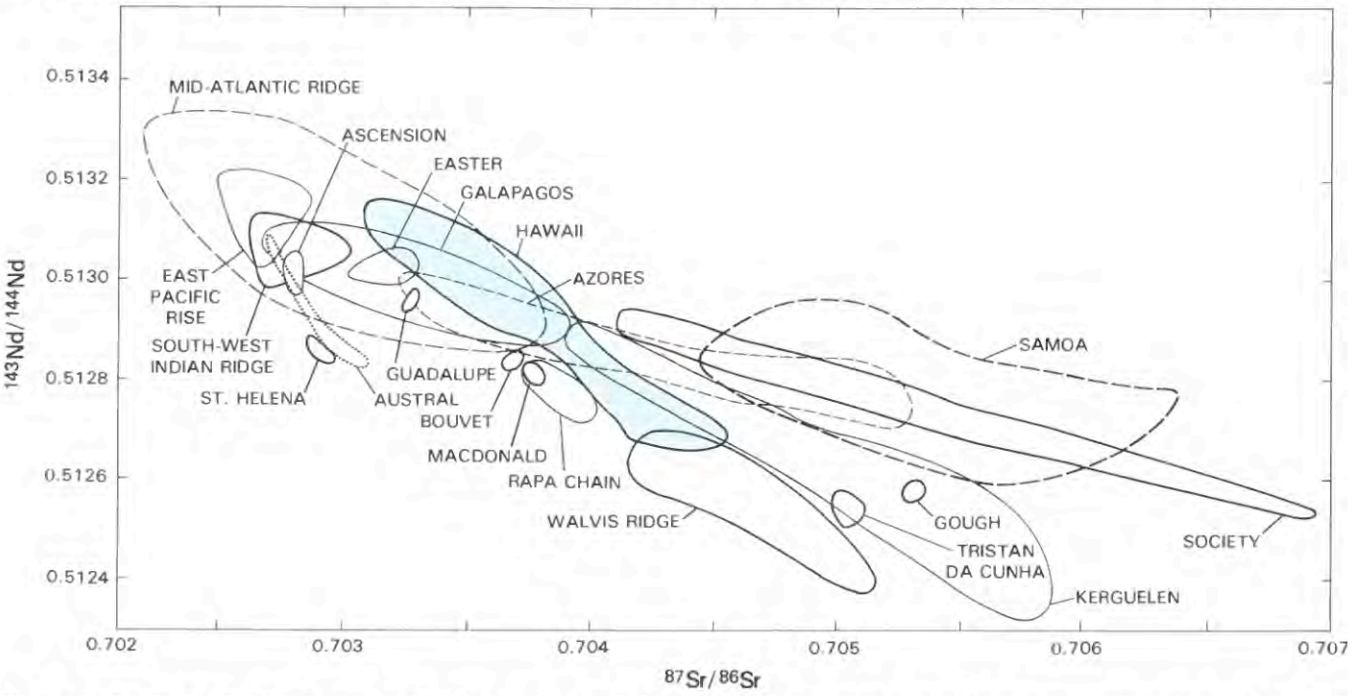

FIGURE 26.8.—Plot of $^{87}Sr/^{86}Sr$ ratio against $^{143}Nd/^{144}Nd$ ratio for oceanic basalt. All data can possibly be explained by three-component mixing model with end-member isotopic compositions close to N-MORB, Austral-St. Helena, and Kerguelen-Society Islands. Data from literature as summarized by Zindler and others (1982), Hart (1984), and White (1985). Data sources for Indian MORB and Rapa-Macdonald chain are from Hamelin and Allègre (1985) and Tatsumoto and others (1984), respectively.

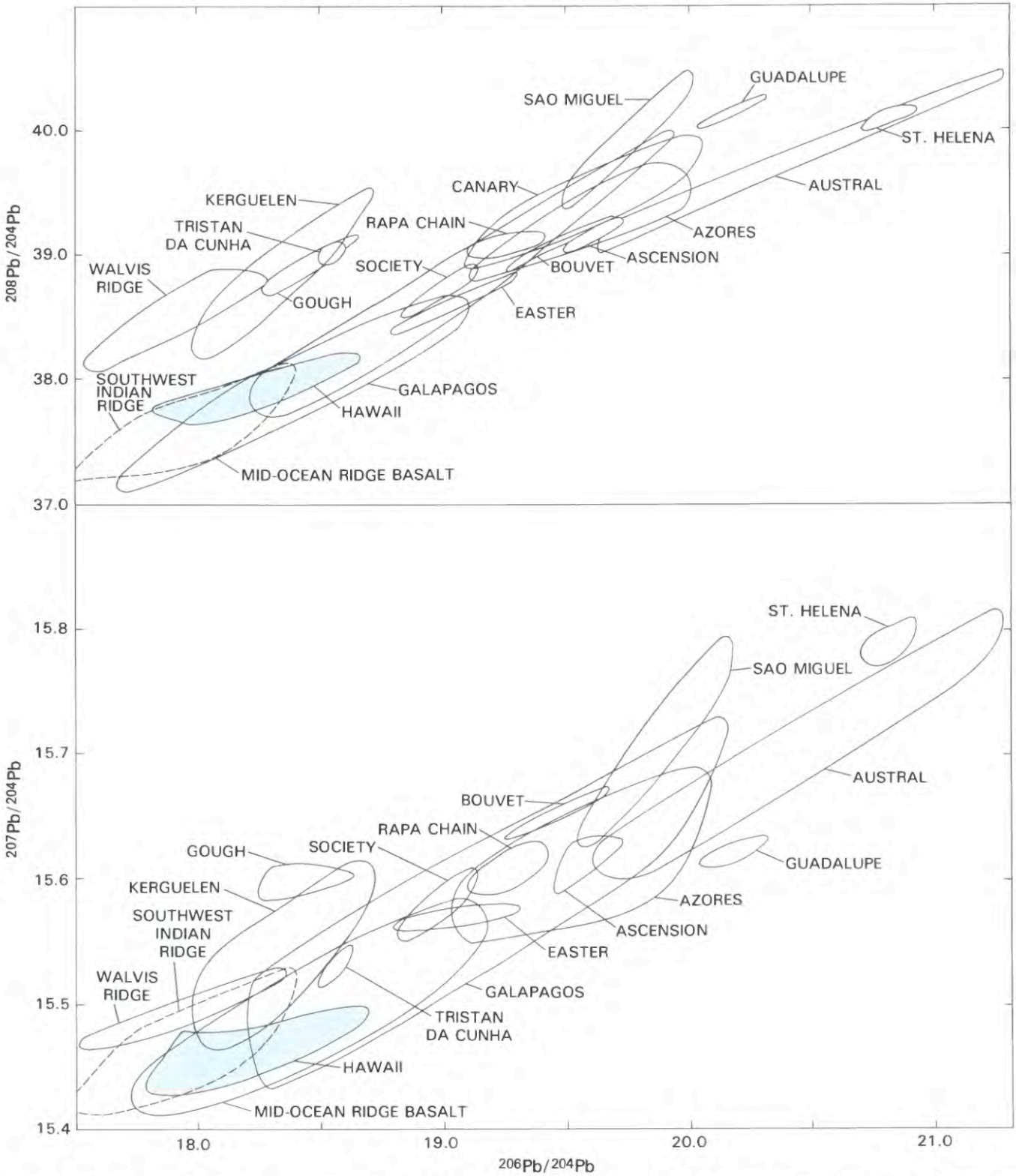

FIGURE 26.9.—Plot of $^{206}Pb/^{204}Pb$ ratio against $^{207}Pb/^{204}Pb$ and $^{208}Pb/^{204}Pb$ ratios for oceanic basalt. Data from Tatsumoto (1978), Sun (1980), Zindler and others (1982), Dupré and Allègre (1983), Stille and others (1983, in press), and Staudigel and others (1984).

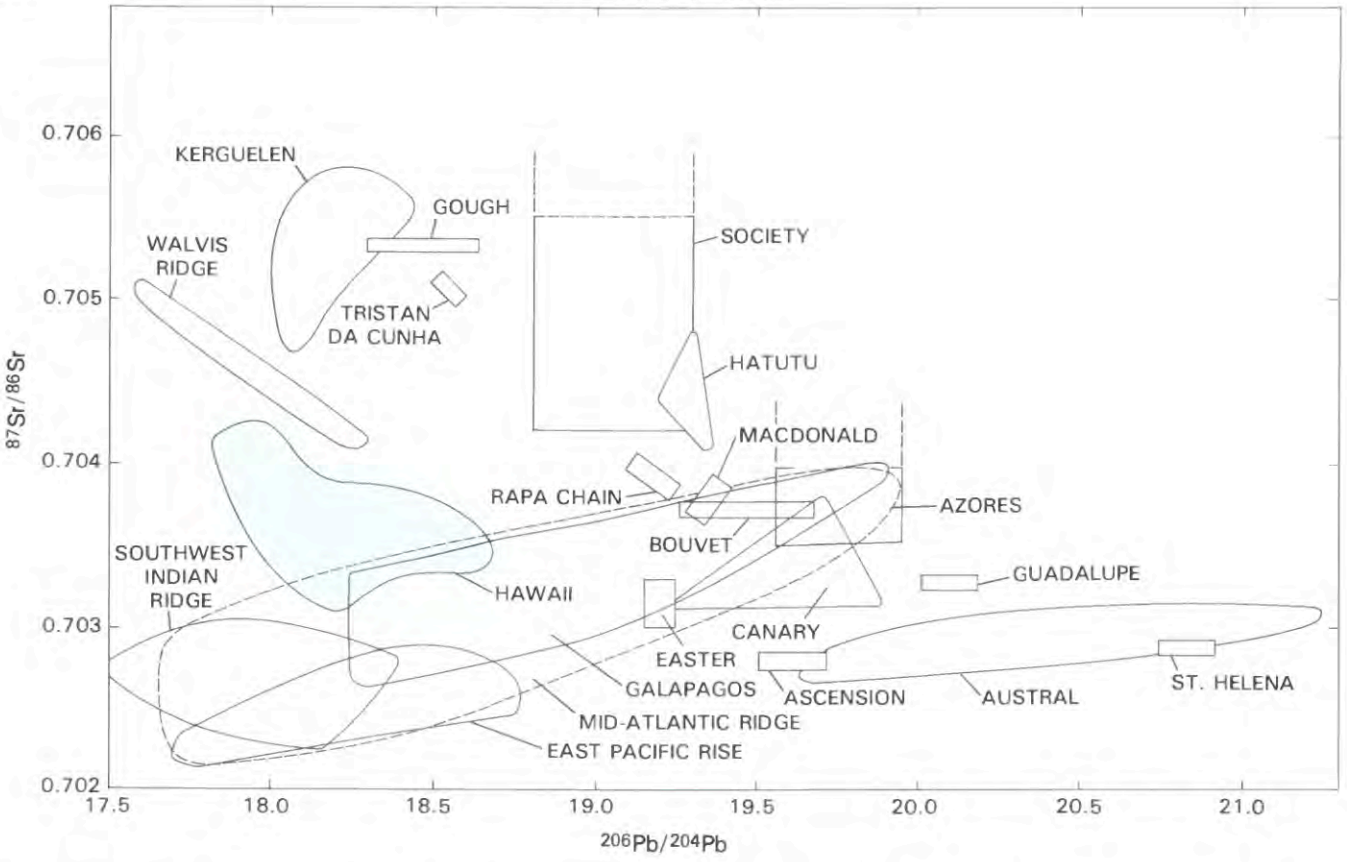

FIGURE 26.10.—Plot of $^{206}Pb/^{204}Pb$ ratio against $^{87}Sr/^{86}Sr$ ratio for oceanic basalt. Data from Tatsumoto (1978), Sun (1980), Zindler and others (1982), Dupré and Allègre (1983), Stille and others (1983, in press), and Staudigel and others (1984).

define a linear correlation. It is evident from the Pb data that Hawaiian volcanics must be described by a model using at least three components.

Evidence for at least three components can also be obtained from the Pb-Sr and Pb-Nd relations among Hawaiian basalt, as shown in figures 26.6 and 26.7. Relative positions of data points for Hawaiian basalt on the $^{206}Pb/^{204}Pb$-$^{87}Sr/^{86}Sr$ diagram (fig. 26.6) are very similar to those on the $^{206}Pb/^{204}Pb$-$^{207}Pb/^{206}Pb$ diagram (fig. 26.5), and the former resembles an expanded (y-axis) plot of the latter. This resemblance is observable not only for Hawaiian rocks but also on a global scale for all oceanic-island basalt (OIB) (see figs. 26.8 and 26.9). The plot $^{206}Pb/^{204}Pb$ versus $^{143}Nd/^{144}Nd$ is an upside-down image of the plot of $^{206}Pb/^{204}Pb$ versus $^{87}Sr/^{86}Sr$ (see figs. 26.10 and 26.11). The shield-building Wailuku Basalt and the late-stage Honolua Volcanics lie close to the Koolau-Kilauea trend, but the posterosional Lahaina Volcanics plots near Hana Volcanics data on both diagrams (figs. 26.6 and 26.7).

In our previous paper (Hegner and others, 1986), in order to test Chen and Frey's two-component mixing model, we followed their premise that the enriched component has isotopic compositions close to those of bulk-earth Sr and Nd (similar to Koolau) and the depleted source has isotopic compositions similar to MORB or to Kilauea. However, the Pb isotopic compositions of the depleted MORB and Kilauea are not similar, and we use the depleted-MORB-like Pb for the present discussion instead of Kilauea-like Pb used in our previous paper. Posterosional alkali basalt of the Lahaina (West Maui), Hana (Haleakala), Honolulu (Oahu), and Koloa (Kauai) sequences all have similar Pb values near $^{206}Pb/^{204}Pb = 18.2$, which is higher than that ($\sim$17.9) of Koolau, and these rocks cannot be one of the end members in the two-component mixing model, even though their Sr-Nd characteristics are closest to MORB among Hawaiian basalt. In figures 26.6 and 26.7, we set the following values of ratios for the two hypothetical end members in order to demonstrate the shortcomings of a two-component mixing model: $^{206}Pb/^{204}Pb = 17.3$, 19; $^{87}Sr/^{86}Sr = 0.702$, 0.7045; $^{143}Nd/^{144}Nd = 0.5134$, 0.51264—for the depleted and enriched components, respectively.

Chen and Frey's (1983) model proposed that a melt produced from the enriched end member (mantle plume) mixes with melt formed by low degrees of melting (<2 percent) of a depleted MORB source. The melting degree of MORB progressively decreases (thereby abundances of incompatible elements increase) but mixing amounts progressively increase from tholeiite through late-stage alkalic rocks to posterosional volcanic rocks. According to this model, elements with stronger incompatibility in mantle minerals

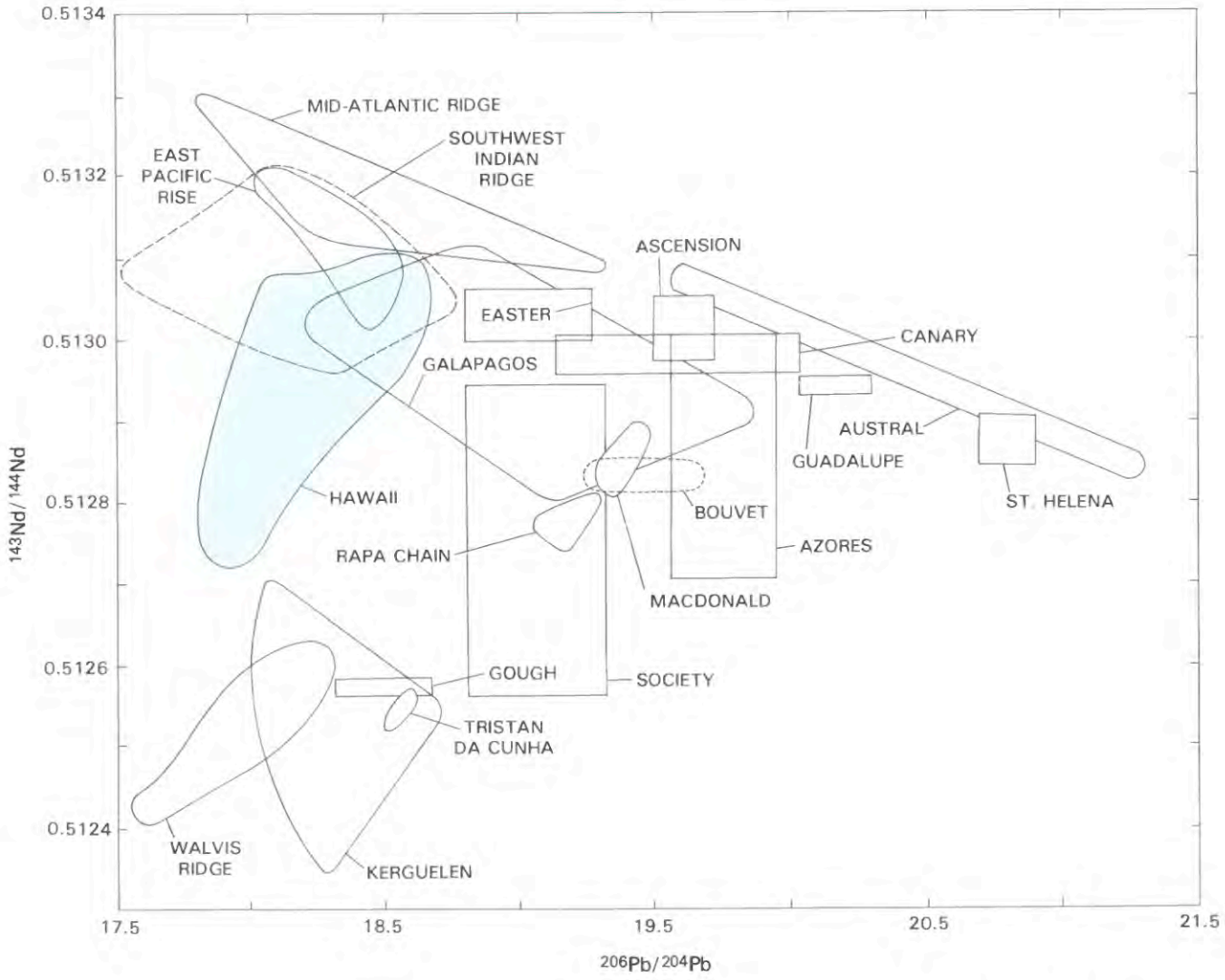

FIGURE 26.11.—Plot of $^{206}Pb/^{204}Pb$ ratio against $^{143}Nd/^{144}Nd$ ratio for oceanic basalt. Data are from Tatsumoto (1978), Sun (1980), Zindler and others (1982), Dupré and Allègre (1983), Stille and others (1983, in press), and Staudigel and others (1984).

are more enriched in later stage volcanic products. Because isotopic compositions of Pb, Sr, and Nd do not change by melting, these elements must have more MORB characteristics in posterosional volcanic rocks than in underlying volcanic rocks. Consequently, parent-daughter elemental abundances and isotopic compositions of Sr and Nd are negatively correlated in Haleakala volcanic rocks.

General equations for two-component mixing have been discussed by Vollmer (1976) and Langmuir and others (1978). Mixing curves of ratio-to-ratio plots of $^{206}Pb/^{207}Pb$ versus $^{87}Sr/^{86}Sr$ (fig. 26.6) and $^{206}Pb/^{204}Pb$ versus $^{143}Nd/^{144}Nd$ (fig. 26.7) are hyperbolae, whose curvature is controlled by the ratio of elemental abundance ratios of the two elements in a MORB melt relative to that in a melt of enriched component (that is, $Q_1 = (Pb/Sr)_{MORB}/(Pb/Sr)_{enriched}$ or $Q_2 = (Pb/Nd)_{MORB}/(Pb/Nd)_{enriched}$. When Q_1 or Q_2 is in unity, the mixing curve will be a straight line. Partition coefficients of common mantle minerals are listed in table 26.4. The values for Rb, Sr, La, Ce, Nd, and Sm are from Chen and Frey (1984) and Clague and Frey (1982). For setting the Th values, those reported by Clague and Frey (1982), Tatsumoto (1978), and Sun (1980) are used. The values for U and Pb are selected rather arbitrarily from the consideration of U/Pb and U/Th ratio changes in basaltic rocks. Incompatibility of Pb is assumed to be less than U, but higher than Sr, considering that the U/Pb ratio in a melt increases from that in the source during partial melting. The actual Pb partition coefficient for mantle silicate minerals may be smaller than the value estimated. However, Pb is one of the chalcophile elements, and the bulk partition coefficient for the mantle may not be much different from the value estimated from

TABLE 26.4.—*Partition coefficients of orthopyroxene (opx), olivine, clinopyroxene (cpx), and garnet for selected elements*

[Coefficients other than for Pb, U, and Th are from Chen and Frey (1983)]

Element	Opx	Olivine	Cpx	Garnet
Rb	0.00010	0.0001	0.0080	0.0010
Sr	.00020	.0005	.0720	.0070
Nd	.00190	.0013	.0900	.0184
Sm	.00280	.0019	.1400	.0823
Pb	.00015	.0002	.0500	.0050
U	.00010	.0001	.0180	.0015
Th	.00010	.0001	.0150	.0010
La	.00050	.0005	.0200	.0010
Ce	.00090	.0008	.0400	.0033

U/Pb ratios in basalt.

The initial concentrations of the relevant elements for MORB and enriched sources are listed in table 26.5. The values, except U, Th, and Pb, are from Chen and Frey (1983). The values for U, Th, and Pb were chosen on the basis of the concentration data reported in this study and previously reported (for example, Tatsumoto, 1978; Sun, 1980) and on the basis of partition coefficients listed in table 26.4.

Modal compositions of the MORB and enriched sources, melt compositions, and partition-coefficient values for Sr and Nd are from Chen and Frey (1983). The bulk solid/liquid partition coefficients of Th, U, Pb, and Sr calculated for a basaltic liquid in equilibrium with a solid composed of 60 percent olivine, 25 percent orthopyroxene, 10 percent clinopyroxene, and 5 percent garnet (Chen and Frey, 1983) are 0.00164, 0.00196, 0.00541, and 0.00790, respectively. We assumed that the melts composed of olivine (10 percent), orthopyroxene (10 percent), clinopyroxene (40 percent), and garnet (40 percent). If these partition coefficients and concentrations in the two end members of table 26.5 are used, Q_1 and Q_2 must both be about 10 in order to cover Koolau data on the hyperbolae. However, if the values in tables 26.4 and 26.5 are used, the maximum calculated Q_1 and Q_2 are only 1.23 and 1.34, respectively, even for an extreme mixing case of 0.001 percent melt of the MORB source with 20 percent melt of the enriched source.

Tests were made using varying D_{Pb} in the range of 0.0025–0.010 and Pb concentrations of the enriched mantle source in the range of 0.08–1.7 ppm. However, we could not obtain Q_1 and Q_2 larger than 4 in any conceivable combination. Therefore, we conclude that the two-component mixing model is not adequate to explain Hawaiian isotope data and that at least three isotopically distinct sources are required to account for the observed data. Stille and others (in press) reached the same conclusion by using depleted and enriched end members similar to those listed above but with the Pb isotopic compositions of the two end members reversed.

Recent isotope studies of Hawaiian volcanic rocks also imply multicomponent hypotheses (for example, Stille and others, 1983, in press; Roden and others, 1984; Staudigel and others, 1984; Hegner and others, 1986), but some differences exist between studies in the assignment of the isotopic components to specific mantle sources. From the preceding discussion on the Pb-Sr-Nd isotopic characteristics, it is essential that Koolau, Kilauea, and the

TABLE 26.5.—*Elemental compositions of the inferred MORB and enriched mantle sources of West Maui volcanic rocks*

Component	MORB	Enriched mantle
Initial concentration (ppm)		
Rb	0.1	0.73
Sr	13.2	23.7
Nd	.86	1.2
Sm	.32	.39
Pb	.08	.17
U	.009	.02
Th	.028	.077
La	.31	.71
Ce	.95	1.9
Isotope ratios		
$^{238}U/^{204}Pb$	7.08	8.12
$^{232}Th/^{238}U$	3.21	3.98

posterosional volcanic rocks (Lahaina, Hana, and Honolulu) are the most extreme in terms of isotopic composition, and all other Hawaiian data fall in a field bounded by these end members. In the following discussion on the origin of Hawaiian basalt, we will refer to these as the Koolau, Kilauea, and PE (posterosional) components (Stille and others, in press), although we recognize that the pure end members are probably more extreme in composition than the Koolau, Kilauea, and PE. A rigorous test using three-dimensional regressions of the Hawaiian data was made in our previous paper (Stille and others, in press) and will not be repeated here.

Staudigel and others (1984) proposed that the Koolau component represents an enriched portion of the oceanic lithosphere, Kilauea the mantle plume, and PE the uppermost lithosphere or crust. We have previously proposed (Tatsumoto, 1978; Stille and others, 1983, in press; Hegner and others, 1986) that the main tholeiite and late-stage alkalic trend is predominantly a plume-lithosphere mixing trend with Koolau having the largest proportion of plume and Kilauea having the largest proportion of oceanic crust or lithosphere. In our previous model, the PE component was derived from the depleted upper mantle (MORB source or material residual from MORB production). The reasoning behind this interpretation is presented below.

The Koolau component has low $^{206}Pb/^{204}Pb$ and $^{143}Nd/^{144}Nd$ ratios, but high $^{207}Pb/^{204}Pb$, $^{208}Pb/^{204}Pb$, and $^{87}Sr/^{86}Sr$ ratios; Koolau data therefore plot distinctly below the mantle plane of Zindler and others (1982). Such isotopic characteristics might be assigned to recycled oceanic lithosphere (Hofmann and White, 1982). However, as will be discussed later (fig. 26.9), Koolau and Walvis Ridge data fall on the left side of the mantle array in a Nd-Sr correlation diagram with Kerguelen as the enriched member, whereas Samoa and Society Island data, which are considered to present the most convincing evidence for having a recycled-crust component (White and Hofmann, 1982), plot on the opposite side of the mantle array.

Staudigel and others (1984) alternatively proposed that the Koolau component may represent an enriched part of the (lower)

oceanic lithosphere, which originated from ancient metasomatized mantle and accreted to the lithosphere at or near the ridge. Such an interpretation may be possible, but the proposed physical process should be tested as more OIB data become available. The process of metasomatism is not well understood, and the chemical composition of the hydrothermal fluids proposed to be involved in metasomatism appear to vary widely depending on the type of process postulated. This obscurity is, we believe, largely caused by a tendency to arbitrarily attribute unexplainable enrichments in incompatible elements to metasomatism.

Wright (1984) postulates, from rigorous comparison of chemical composition between MORB and Hawaiian tholeiite, that the latter originated from depleted mantle that has been metasomatized by a liquid with a composition of nephelinite plus amphibole (plus some minor phases); hence such metasomatism is characterized by H_2O and alkali-rich fluids (Hawkesworth and others, 1979). The metasomatized rocks would have high Rb/Sr ratios and eventually high $^{87}Sr/^{86}Sr$ ratios. Consequently, Nd-Sr data for these rocks would plot on the right-hand side of the mantle array on a Nd-Sr diagram. Most Nd-Sr data of the Hawaiian tholeiite plot is indeed on the right-hand side and support Wright's postulation. However, Koolau data plot on the lower left side of the array. Furthermore, because Koolau Pb-Sr data appear to be unique among all OIB (see next section), we interpret Koolau as a unique end member. If Koolau originated from metasomatized mantle, the proposed metasomatizing fluids would also have to have been unique in their enrichment in alkali and light REE without enrichment in U relative to Pb.

In contrast, we have postulated that ancient metasomatism would slightly decrease the Rb/Sr ratio and increase U/Pb if the metasomatizing fluid is carbonatite-like (Tatsumoto and others, 1984) so that fairly low $^{87}Sr/^{86}Sr$ but high ^{206}Pb and ^{207}Pb values would result from the process. Koolau data plot on the lower left of the mantle array on the Nd-Sr correlation diagram but show very low ^{206}Pb values. Thus, Koolau isotope data are not consistent with a hypothesis of such a metasomatized source. Kilauea tholeiite, however, could be related to metasomatism because those data plot on the right-hand side of the Nd-Sr mantle array and show a high $^{206}Pb/^{204}Pb$ ratio (although in this paper we interpret the Kilauea end member to represent lithosphere contamination instead of metasomatism).

Stille and others (1983, in press) have shown that the isotopic characteristics of Koolau samples are consistent with an origin from primitive lower mantle and that the Koolau component may be unique among oceanic basalt. Alternatively, the Koolau component may represent a less depleted or possibly even enriched upper mantle material that exists as a distinct body (see, for example, Davies, 1984) or is preserved in the center of a concentrically zoned convection cell (see, for example, Tatsumoto, 1978).

The Honolulu, Hana, and Lahaina Volcanics all have $^{206}Pb/^{204}Pb \simeq 18.2$, $^{87}Sr/^{86}Sr \simeq 0.71031$, and $^{143}Nd/^{144}Nd \simeq 0.51315$. In the Nd-Sr correlation diagram (fig. 26.4) it is evident that these PE volcanic rocks are most depleted and are isotopically closest to MORB among Hawaiian rocks. Because basanite may originate, in the presence of garnet, at greater depth than tholeiite (Presnall and others, 1979; Jackson and Wright, 1970), the PE component may represent the depleted upper mantle.

The Kilauea component has moderately radiogenic Pb, but MORB-like isotopic compositions of Sr, Nd, and Hf (Stille and others, in press). The Pb isotopic compositions in volcanics from the Kea trend are generally more radiogenic than those from the Loa trend (Tatsumoto, 1978). The isotopic difference was thought to reflect contamination of the ~80-Ma lithosphere (MORB) under Hawaii, and Kilauea was thought to represent a lithosphere component. The half-life of ^{238}U (4.47×10^9 yr) is short compared to those of ^{87}Rb (4.9×10^{10} yr) and ^{147}Sm (1.06×10^{11} yr), and so an increase in the $^{206}Pb/^{204}Pb$ ratio may be detected in ~100-Ma lithosphere (a $^{207}Pb/^{204}Pb$ increase is not detectable because of the small amount of ^{235}U). Recent detailed studies of Nd, Sr, and Hf isotopes support this view (Stille and others, in press). However, Staudigel and others (1984) assigned the Kilauea component to the plume, and the differences between Loa and Kea isotope trends were considered to have been generated by mixing of plume material with the sublithospheric Koolau component. While such a model may be formally allowed, we maintain that the isotopic differences observed between the presently active Kilauea and Mauna Loa would be extremely difficult to produce if mixing occurs below the lithosphere. Furthermore, the isotopic characteristics of the Kilauea component are not those considered typical for mantle plumes but are actually quite MORB-like. Thus we maintain our earlier conclusions that the Kilauea component represents MORB-related old oceanic lithosphere and that the isotopic differences among volcanoes of the Loa and Kea trends are best explained if mixing occurs within the lithosphere.

COMPARISON OF HAWAIAN DATA WITH THOSE OF OTHER OCEANIC BASALT

In this section we compare isotopic data of Hawaiian basalt with those of other oceanic basalt and discuss the genesis of oceanic basalt.

The Nd-Sr, Pb-Pb, Pb-Sr, and Pb-Nd isotopic correlation diagrams for selected OIB and MORB from the literature are shown in figures 26.8–26.11 and an explanatory combined diagram in figure 26.12. The diagrams contain data for Walvis Ridge basalt that are not corrected for in-place growth of radiogenic isotope during the 70–80 m.y. of their existence (Richardson and others, 1982). However, the isotopic compositions are very similar to those of Koolau Basalt, and in-place growth of radiogenic isotope should not change the overall picture.

Recently, several researchers (for example, Allègre, 1982; Hart, 1984) have argued that the isotopic characteristics of oceanic basalt could be correlated geographically. Allègre (1982) contends that systematic variations occur within each ocean basin and are probably related to convection units in the mantle. Hart (1984) emphasizes that isotopic differences can be observed between the northern and southern hemispheres. However, for the sake of

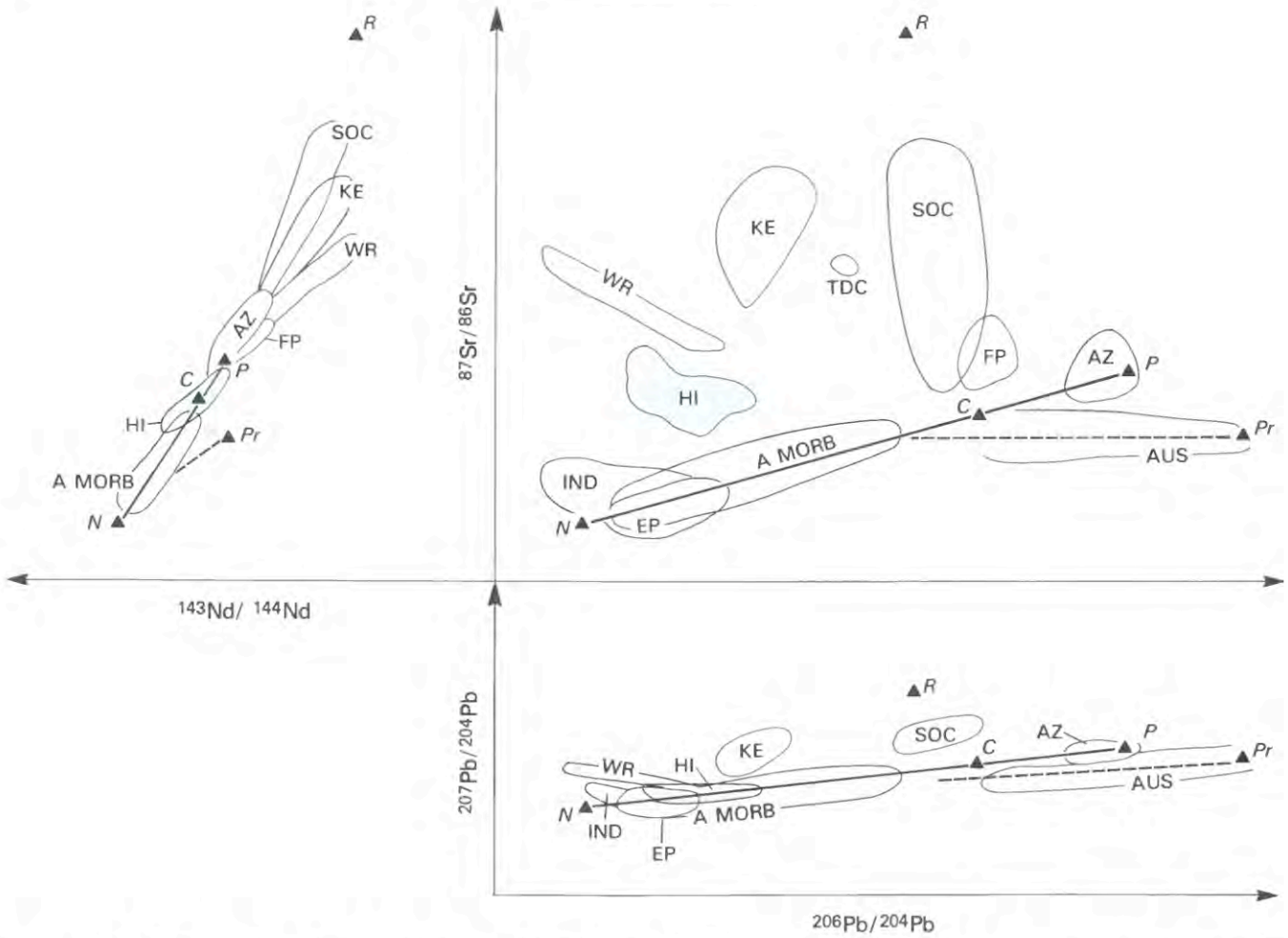

FIGURE 26.12.—Explanatory diagram for oceanic-basalt isotope data. Combined diagram consists of plots of $^{206}Pb/^{204}Pb$ versus $^{207}Pb/^{204}Pb$, $^{206}Pb/^{204}Pb$ versus $^{87}Sr/^{86}Sr$, and $^{87}Sr/^{86}Sr$ versus $^{143}Nd/^{144}Nd$. Triangles, hypothetical parent materials in possible three-component mixing of *N* (depleted MORB), *Pr* (enriched source represented by Austral-St. Helena), and *R* (recycled crust). Data for islands on or near ridges fall on *N*–*P* line (depleted–enriched MORB) or its extension. In alternative multicomponent mixing model, plume (stars labeled *C*) ascending from lower mantle mixes with heterogeneous upper mantle and oceanic crust. Fields represent Mid-Atlantic Ridge (A MORB), East Pacific Rise (EP), Indian Ocean Ridge (IND), Hawaiian Islands (HI), Walvis Ridge (WR), Kerguelen (KE), Tristan da Cunha (TDC), Society Islands (SOC), French Polynesia islands other than Society and Austral (FP), Azores (AZ), and Austral (AUS). For scales on plots and sources of data, see figures 26.8–26.10.

simplicity, we will proceed with our discussion on the basis of oceanic basalt in general, and later we will demonstrate that the systematic geographic variations that occur are probably caused by upper mantle heterogeneity.

It is widely accepted from isotope data of oceanic basalt that their sources are chemically heterogeneous and that such heterogeniety has existed for a long time (>1 b.y.). The variety of trace-element and isotope signatures in oceanic basalt has often been explained by a layered-mantle model involving mixing of partial melts from a depleted upper mantle and an undepleted lower mantle (see for example, Schilling, 1973; Sun and Hansen, 1975; Allègre and others, 1983). When Nd isotopic data became available (for example, DePaolo and Wasserburg, 1976), the layered-mantle hypothesis appeared to be substantiated. Mass balance, computed with Sm-Nd and Rb-Sr data, indicated that only 30–50 percent of the whole mantle could be involved in continental crust formation (Jacobsen and Wasserburg, 1979: O'Nions and others, 1979; Allègre and others, 1980; DePaolo, 1980). In these computations, the boundary between depleted and enriched mantle was set at a depth of 700 km, which coincides with the seismic discontinuity.

The mantle array observed for MORB and OIB in the Nd-Sr correlation diagram was often interpreted as a mixing line between the depleted mantle and the mantle plumes. However, as more data for oceanic basalt were accumulated, more exceptions that did not plot on a linear mantle array were found (fig. 26.8). In the Nd-Sr diagram, one can easily see that data trends for oceanic basalt do not form a linear mantle array. McCulloch and others (1983) and Anderson (1986) argued that, if some extreme isotopic

values are assigned to depleted and enriched reservoirs, a two-component mixing model may be sufficient to explain all basalt data. However, as discussed above for Hawaiian data, the Pb data plotted in figure 26.9 cannot be explained by a two-component mixing model because the denominator is the same and two-component mixing must therefore define a straight line. The negative correlations of Hawaiian and Walvis Ridge data in the Pb-Sr plot (fig. 26.10) are also difficult to explain by a two-component mixing model.

The diversity of isotope data for oceanic basalt may be adequately explained by a three-component model. The depleted MORB component (N-type) has the least radiogenic Pb and Sr and the most radiogenic Nd and occupies one corner in the Pb-Sr-Nd correlation diagrams (figs. 26.8–26.11). N-MORB and trace-element-rich P-MORB form a single trend that corresponds to a 1.8-Ga isochron on the Pb-Pb diagram. Data for oceanic islands on or near ridges, such as the Iceland-Reykjanes Ridge, Galapagos Islands, Easter Island , and the Azores, also lie on this line (defined as N–P in figure 26.12). This line has been interpreted as a mixing line between a depleted component and mantle plumes instead of a differentiation trend, and the Pb isotopic composition of the plume as defined from Pb-Sr-Nd relations is $^{206}Pb/^{204}Pb = 20.6$, $^{207}Pb/^{204}Pb = 15.75$, $^{208}Pb/^{204}Pb = 40.8$ (Tatsumoto and others, 1984). A similar composition was defined by Dupré and Allègre (1980) as the "Planetary Lead Atlantic" value, although they did not specify that this could represent the plume component. Very radiogenic Pb from St. Helena and Ascension (Sun, 1980) appears to lie on an extension of the N–P trends in the Pb-Pb diagram (fig. 26.9), whereas radiogenic Pb from the Australs plots on a slightly shallower trend (Tatsumoto and others, 1984; Vidal and others, 1984). In the Pb-Sr diagram, however, data from St. Helena, the Australs, and Ascension form a trend that is distinctly shallower than the N–P trend. We define the component that shows extremely radiogenic Pb (but less radiogenic Sr and Nd) as Pr in figure 26.12.

Enrichment of incompatible elements or metasomatism in some part of the depleted mantle may have occurred by mixing or contamination with carbonatite-like fluid (high in CO_2, and U/Pb and Sr/Rb ratios and slightly enriched in light REE), which originated somewhere else in the depleted mantle within the last ~1.8 b.y. Thus, when time passed, this contaminated mantle (*Pr*) source has extremely radiogenic Pb, moderately radiogenic Nd, but less radiogenic Sr. Consequently, the *Pr* component plots on a distinctly lower position from the mantle array (Tatsumoto and others, 1984; White, 1985). The Austral Pb may represent a more recently contaminated mantle source because it plots below the N–P line in the diagram $^{206}Pb/^{204}Pb$ versus $^{207}Pb/^{204}Pb$.

As can be seen in figure 26.12, all oceanic data can be explained by a three-component mixing model with *N*, *Pr*, and another component (R) that has high $^{87}Sr/^{86}Sr$ (>0.706), moderate $^{206}Pb/^{204}Pb$ (~18.2), and very low $^{143}Nd/^{144}Nd$ (<0.5123) ratios. Such a component is most likely recycled crust. If so, then the Koolau and Walvis Ridge data that plot above the N–P line on the Pb-Sr diagram might indicate involvement of a small amount of recycled oceanic crust, and data for Kerguelen and Society Islands indicate involvement of large amounts of this crust component.

According to this interpretation, Koolau may contain the largest proportion of the recycled crust among Hawaiian volcanoes because its Sr is the most radiogenic. Therefore, if the subducted oceanic crust penetrates down to the mantle-core boundary, as proposed by Hofmann and White (1982), then Koolau could represent a recycled crustal plume at Hawaii. If this hypothesis is correct, all OIB that plot above the N–P line in the Pb-Sr diagram contain a component of recycled oceanic crust (R) whose isotope ratios vary regionally. Those OIB that plot on the N–P or N–Pr trends contain little or no R component.

On the Nd-Sr correlation diagram (fig. 26.8), the so-called mantle array (N–P line) extends to Kerguelen. Society Islands data plot above the extension of the N–P line, but Koolau and Walvis Ridge plot below the line. This positioning is not consistent with that observed above on the Pb-Sr diagram.

Dupré and Allègre 983) and Hamelin and Allègre (1985) found that the depleted end member of Indian MORB, which they considered to represent the asthenosphere, is characterized by particularly nonradiogenic $^{206}Pb/^{204}Pb$, but higher $^{207}Pb/^{204}Pb$, $^{208}Pb/^{204}Pb$, and $^{87}Sr/^{86}Sr$ and lower $^{143}Nd/^{144}Nd$ ratios compared to Atlantic and Pacific MORB. This means that the asthenosphere is heterogeneous but there is still a regional similarity that may be related to each convection unit. Thus, in the same manner, the higher $^{207}Pb/^{204}Pb$, $^{208}Pb/^{204}Pb$, and $^{87}Sr/^{86}Sr$ and low $^{143}Nd/^{144}Nd$ ratios of Koolau and Walvis Ridge basalt may be interpreted as due to regional upper mantle heterogeneities instead of a contribution from the recycled oceanic crust.

In any case, Koolau basalt is unique with respect to its relatively primitive isotopic composition (Stille and others, in press). Hawaiian basalt contains the highest $^{3}He/^{4}He$ ratios thus far reported for oceanic basalt (Lupton and Craig, 1975; Kaneoka and Takaoka, 1978; Kurz and others, 1982; Allègre and others, 1983; Rison and Craig, 1983). If our argument is correct, Koolau would have had the highest $^{3}He/^{4}He$ value among Hawaiian basalt (Stille and others, in press). Conversely, the Hawaiian basalt with a high $^{3}He/^{4}He$ and relatively primitive Pb, Nd, and Sr isotopic composition would not support the assumption of radiogenic plume lead proposed by Tatsumoto and others (1984).

White (1985) argued that at least five trends can be observed in Pb-Sr-Nd isotopic systematics: MORB, St. Helena, Kerguelen, Society Islands, Hawaii (see figs. 26.10 and 26.12). Extrapolations of the latter four trends all intersect the central part (C) of the N–P trend, but they do not trend toward *P* or *Pr*. The intersection corresponds to $^{206}Pb/^{204}Pb \simeq 18.5–19.5$, $^{87}Sr/^{86}Sr \simeq 0.7030–0.7035$, and $^{143}Nd/^{144}Nd \simeq 0.5129–0.5130$. It is conceivable that this point represents the plume component instead of *P* in figure 26.12. According to this interpretation, more than five trends are easily observable, because each hot spot creates its own trend by mixing C with upper mantle of variable isotopic composition.

In this context, the Galapagos and Azores trends should be separated from the N–C trend if the radiogenic components do not lie on the N–C trend but on the extension. Walvis Ridge and Rapa-Macdonald may be separated from Hawaii and Society

Islands trends, respectively, because the Walvis Ridge and Hawaii may not plot on the same trends in the Pb-Sr and Pb-Nd diagrams and Rapa Macdonald data plot apart from Society Islands data on the Nd-Sr diagram. This means that as more data become available, more trends will show up as regional variations. The fact that C cannot be defined as a unique point but has a small range in isotopic compositions may indicate that small regional variations also exist for the lower mantle values.

It should be noted that Austral-St. Helena data do not appear to converge to C on the Nd-Sr plot. Their Pb is extremely radiogenic and indicates extremely enriched sources, while their slightly radiogenic Sr indicates a moderately depleted source. We retain our earlier interpretation that these data reflect an old metasomatized component enriched in U and Sr from carbonatite-like fluids derived from a previously depleted (MORB) source (Tatsumoto and others, 1984). Thus the Austral-St. Helena-Ascension trend is predominantly an upper mantle trend.

We previously suggested that Kilauea contains the most MORB component derived from the oceanic crust because of the depleted nature of its Sr and Nd isotopes. Alternatively, Kilauea might be considered to contain the most plume component since Kilauea occupies the position closest to C (Staudigel and others, 1984). However, as previously mentioned, this interpretation does not adequately account for the observed isotopic differences among simultaneously active volcanoes: Kilauea and Mauna Loa.

The important role of subduction of oceanic crust and sediments for isotope evolution of the crust-mantle system was first suggested by Armstrong (1968), and influences of subducted material on Pb isotopes were detected for volcanics from the Japanese Islands (Tatsumoto, 1969) and the Aleutian Island arc (Kay and others, 1978) but not detected for those from the Mariana arc (Maijer, 1976). Extremely low $^{238}U/^{204}Pb$ ratios (as low as 2.1) in Japanese arc volcanics (Tatsumoto, 1960; Tatsumoto and Knight, 1969) indicate that volatile Pb is preferentially extracted from the subducted material by arc volcanism, whereas $^{238}U/^{204}Pb$ ratios of the Mariana arc volcanics are about 7. Thus, plumes generated from the recycled crust are likely to have variations in isotope ratios depending on their storage times and environments; this implies the existence of a heterogeneous lower mantle (see for example, Davies, 1984) providing that the subducted crust penetrates into the lower mantle.

Several seismic studies have presented evidence that subducting slabs penetrate into the lower mantle (Jordan, 1977; Creager and Jordan, 1984). Although some workers suggest that the penetration is only a few hundred kilometers below the seismic boundary at a depth of 670 km (see for example, Christensen and Yuen, 1984), others consider that the subducted slabs reach the core-mantle boundary (Hofmann and White, 1982; Davies, 1984; Loper, 1985). Loper (1985) suggested that numerous narrow axisymmetric plumes rise up into the upper mantle. Thus, it may be possible that numerous plumes with various isotope signatures rise from the lower mantle. However, with the presently available isotopic evidence, we prefer a convective layered mantle model with a chemically heterogeneous upper mantle and a nearly homogeneous (less differentiated) lower mantle because (1) the upper mantle is strongly differentiated by magma extraction and (2) no high $^{87}Sr/^{86}Sr$ signature of subducted material is found for volcanics from Hawaii where the volcanism is most likely related to a mantle plume as evidenced by high $^{3}He/^{4}He$ ratios. Contamination of magmas as they rise through the oceanic lithosphere makes the isotopic signatures more complicated.

CONCLUSIONS

Pb, Sr, and Nd isotope data of Hawaiian basalt provide strong evidence for the involvement of three distinct sources in the production of these rocks. The volcanoes or groups of rocks that most closely approach the three end members are Koolau (representing the mantle plume), Kilauea (the oceanic crust), and the Honolulu-Hana-Lahaina posterosional volcanic rocks (the depleted mantle). Pb, Sr, and Nd relationships are not compatible with a two-component mixing model for Hawaiian basalt genesis.

Pb, Sr, and Nd isotope characteristics of oceanic basalt from other areas are also compatible with a three-component mixing model. The three main sources are the depleted upper mantle, enriched lower or upper mantle, and recycled oceanic crust. However, the oceanic basalt data form several trends that intersect in the middle of the three-component field. These trends may indicate multicomponent mixing between a heterogeneous upper mantle and a nearly homogeneous lower mantle, plus contamination by the lithosphere.

REFERENCES CITED

Allègre, C.J., 1982, Chemical geodynamics: Tectonophysics, v. 81, p. 109–132.

Allègre, C.J., Brevart, O., Dupré, BH., and Minster, J.-F., 1980, Isotopic and chemical effects produced in a continuously differentiating convecting Earth mantle: Philosophical Transactions of the Royal Society of London, Ser. A, v. 297, p. 447–477.

Allègre, C.J., Staudacher, T., Sarda, P., and Kurz, M., 1983, Constraints on the evolution of Earth's mantle from rare gas systematics: Nature, v. 303, p. 762–766.

Anderson, D.L., 1985, Hotspot magmas can form by fractionation and contamination of MORB: Nature, v. 318, p. 145–149.

Armstrong, R.L., 1968, A model for Sr and Pb isotope evolution in a dynamic Earth: Review of Geophysics, v, 6, p. 175–199,

Brooks, C., Hart, S.R., Hofmann, A., and James, D.E., 1976, Rb-Sr mantle isochrons from oceanic regions: Earth and Planetary Science Letters v. 32, p. 51–61.

Chen, C.-Y., and Frey, F.A., 1983, Origin of Hawaii tholeiite and alkalic basalt: Nature, v. 302, p. 785–789.

Christensen, U.R., and Yuen, D.A., 1984, The interaction of a subducting lithospheric slab with a chemical or phase boundary: Geophysical Research, v. 89, p. 4389–4402.

Clague, D.A., Frey, F.A., 1982, Petrology and trace element geochemistry of the Honolulu volcanics, Oahu: Implications for the oceanic mantle below Hawaii: Journal of Petrology, v. 23, p. 447–504.

Cohen, R.S., and O'Nions, R.K., 1982, The lead, neodymium and strontium isotopic structure of ocean ridge basalts: Journal of Petrology, v. 23, p. 299–324.

Creager, K.C., and Jordan, T.H., 1984, Slab penetration into the lower mantle: Journal of Geophysical Research, v. 89, p. 3031–3050.

Dalrymple, G.B., and Clague, D.A., 1976, Age of the Hawaii-Emperor bend: Earth and Planetary Science Letters, v. 31, p. 313–329.

Dalrymple, G.B., Silver, E.A., and Jackson, E.D., 1973, Origin of the Hawaiian Islands: American Scientist, v. 61, p. 294–308.

Davies, G.F., 1984, Geophysical and isotopic constraints on mantle convection: An interim synthesis: Journal of Geophysical Research, v. 89, p. 6017–6040.

DePaolo, D.J., 1980, Crustal growth and mantle evolution: Inferences from models of element transport and Nd and Sr isotopes: Geochimica et Cosmochimica Acta, v. 44, p. 1185–1196.

DePaolo, D.J., and Wasserburg, G.J., 1976, Inferences about magma sources and mantle structure from variations of $^{143}Nd/^{144}Nd$: Geophysical Research Letters, v. 3. p. 743–746.

Dodson, M.H., 1970, Simplified equations for double-spiked isotopic analyses: Geochimica et Cosmochimica Acta, v. 34, p. 1241–1244.

Dupré, B., and Allègre, C.J., 1980, Pb-Sr-Nd isotopic correlation and the chemistry of the North Atlantic mantle: Nature, v. 286, p. 17–22.

———1983, Pb-Sr isotope variation in Indian Ocean basalts and mixing phenomena: Nature, v. 303, p. 142–146.

Feigenson, M.D., Korr, K., and Raczek, I., 1984, Trace element and isotopic evidence for the formation of transitional basalts of West Maui Volcano [abs.]: Eos, v. 65. p. 300.

Frey, F.A., and Clague, D.A., 1983, Geochemistry of diverse basalt types from Loihi Seamount, Hawaii: petrogenetic implications: Earth and Planetary Science Letters, v. 66, p. 337–355.

Hamelin, B., and Allègre, C.J., 1985, Large scale regional units in the depleted upper mantle revealed by an isotope study of the South-West Indian Ridge: Nature, v. 315, p. 196–199.

Hamilton, E.I., 1965. Distribution of some trace elements and the isotopic composition of strontium in Hawaiian lavas: Nature, v. 206, p. 251–253.

Hart, S.R., 1984, A large scale isotope anomaly in the Southern Hemisphere mantle: Nature, v. 309. p. 753–757.

Hawkesworth, C.J., Norry, M.J., Roddick, J.C., and Vollmer, R., 1979, $^{143}Nd/^{144}Nd$ and $^{87}Sr/^{86}Sr$ ratio from Azores and their significance in LIL-element enriched mantle: Nature, v. 280, p. 28–31.

Hegner, E., Unruh, D.M., and Tatsumoto, M., 1986, Sr, Nd, and Pb isotopic evidence for the origin of the West Maui volcanic suite, Hawaii: Nature, v. 319. p.478–480.

Hofmann, A., and White, W., 1982, Mantle plumes from ancient oceanic crust: Earth and Planetary Science Letters, v. 57, p. 421–436.

Jackson, E.D., Silver, E.A., and Dalrymple, G.B., 1972, Hawaiian-Emperor chain and its relation to Cenozoic circum-Pacific tectonics: Geological Society of America Bulletin, v. 83, p. 601–618.

Jackson, E.D., and Wright, T.L., 1970, Xenoliths in the Honolulu volcanic series, Hawaii: Journal of Petrology, v. 11, p. 405–430.

Jacobsen, S.B., and Wasserburg, G.J., 1979, The mean age of mantle and crustal reservoirs: Journal of Geophysical Research, v. 84, p. 7411–7427.

Jordan, T.H., 1977, Lithospheric slab penetration into the lower mantle beneath the Sea of Okhotsk: Journal of Geophysical Research, v. 79, p. 2679–2685.

Kaneoka, I., and Takaoka, N., 1978, Excess ^{129}Xe and high $^{3}He/^{4}He$ ratio in olivine phenocrysts of Kapuho lava and xenolithic dunites from Hawaii: Earth and Planetary Science Letters, v. 39, p. 382–386.

Kay, R.W., Sun, S.-S., and Lee-Hu, C.-N., 1978, Pb and Sr isotopes in volcanics from Aleutian Islands and Pribilof Island, Alaska: Geochimica et Cosmochimica Acta, v. 42, p. 263–274.

Kurz, M.P., Jenkins, W.J., and Hart, S.R., 1982, Helium isotopic systematics of oceanic islands and mantle heterogeneity: Nature, v. 297, p. 43–47.

Kushiro, I., 1969, The system forsterite-diopside-silica with and without water at high pressures: American Journal of Science, v. 267A, p. 269–294.

Langmuir, C.H., Vocke, R.D., Jr., and Hanson, G.N., 1978, A general mixing equation with applications to Iceland basalts: Earth and Planetary Science Letters, v. 37, p. 380–392.

Lanphere, M.A., and Dalrymple, G.B , 1980, Age and strontium isotopic composition of the Honolulu volcanic series, Oahu, Hawaii: American Journal of Science, v. 280A, p. 736–751.

Lanphere, M.A., Dalrymple, G.B., and Clague, D.A., 1980, Rb-Sr systematics of basalts from the Hawaiian-Emperor volcanic chain: Initial Report of the Deep Sea Drilling Project, Volume 55: Washington, U.S. Government Printing Office, p. 695–706.

Lessing, P., and Catanzaro, E.J., 1964, $^{87}Sr/^{86}Sr$ in Hawaiian lavas: Journal of Geophysical Research, v. 69, p. 1599–1601.

Loper, D.E., 1985, A simple model of whole-mantle convection: Journal of Geophysical Research, v. 90, p. 1809–1836.

Lupton, J.E., and Craig, H., 1975, Excess ^{3}He in oceanic basalts: evidence for terrestrial primordial helium: Earth and Planetary Science Letters, v. 26, p. 133–139.

Macdonald, G.A., 1949, Hawaiian petrographic province: Geological Society of America Bulletin, v. 60, p. 1541–1596.

———1968, Composition and origin of Hawaiian lavas: Geological Society of America Memoirs, v. 116, p. 477–522.

Macdonald, G.A., and Katsura, T., 1964, Chemical composition of Hawaiian lavas: Journal of Petrology, v. 5, p. 82–133.

McCulloch, M.T., Jaques, A.L., Nelson, D.R., and Lewis, J.D., 1983, Nd and Sr isotopes in kimberlites and lamproites from western Australia: an enriched mantle origin: Nature, v. 302, p. 400–403.

McDougall, I., 1964, Potassium-argon ages from lavas of the Hawaiian Islands: Geological Society of America Bulletin, v. 75, p. 107–128.

Meijer, A., 1976, Pb and Sr isotopic data bearing on the origin of volcanic rocks from the Mariana island-arc system: Geological Society of America Bulletin, v. 87, p. 1358–1369.

Moore, J.G., Clague, D.A., and Normark, W.R., 1982, Diverse basalt types from Loihi seamount, Hawaii: Geology, v. 10, p. 88–92.

Nakamura, N., Tatsumoto, M., Nunes, P.D., Unruh, D.M., Schwab, A.P., Wildeman, T.R., 1976, 4.4 b.y.-old clast in Boulder 7, Apollo 17: A comprehensive chronological study of U-Pb, Rb-Sr and Sm/Nd methods: Proceedings of the Lunar Scientific Conference, 7th, p. 2309–2333.

O'Nions, R.K., Evensen, N.M., and Hamilton, P.J., 1979, Geochemical modelling of mantle differentiation and crustal growth: Journal of Geophysical Research, v. 84, p. 6091–6101.

O'Nions, R.K., Hamilton, P.J., and Evensen, N.M., 1977, Variations in $^{143}Nd/^{144}Nd$ and $^{87}Sr/^{86}Sr$ ratios in oceanic basalts: Earth and Planetary Science Letters, v. 34, p. 13–22.

Powell, J.L., and DeLong, S.E., 1966, Isotopic composition of strontium in volcanic rocks from Oahu: Science, v. 153, p. 1239–1242.

Presnall, D.C., Dixon, S.A., Dixon, J.R., O'Donnell, T.H., Brenner, N.L., Schrock,, R.L., Dycus, D.W., 1979, Liquidus phase relations on the join diopside-forsterite-anorthite from 1 atm to 20 kbar: Their bearing on the generation and crystallization of basaltic magma: Contributions to Mineralogy and Petrology, v. 66, p. 203–220.

Richardson, S.H., Erlank, A.J., Duncan, A.A., and Reid, D.L., 1982, Correlated Nd, Sr and Pb isotope variation in Walvis Ridge basalts and implications for the evolution of their mantle source: Earth and Planetary Science Letters, v. 59, p. 327–342.

Rison, W., and Craig, H., 1983, Helium isotopes and mantle volatiles in Loihi Seamount and Hawaiian Island basalts and xenolights: Earth and Plantetary Science Letters, v. 66, p. 407–426.

Roden, M.F., Frey, F.A., and Clague, D.A., 1984, Geochemistry of tholeiitic and alkalic lavas from the Koolau Range, Oahu, Hawaii: implications for Hawaiian volcanism: Earth and Planetary Science Letters, v. 69, p. 141–158.

Schilling, J.G., 1973. Iceland mantle plume: Geochemical study of the Reykjanes Ridge: Nature, v. 242, p. 565–571.

Staudigel, H., Zindler, A., Hart, S.R., Leslie, T., Chen, C.-Y., and Clague, D., 1984, The isotope systematics of a juvenile intraplate volcano: Pb, Nd, and Sr isotope ratios of basalts from Loihi Seamount, Hawaii: Earth and Planetary Science Letters, v. 69. p. 13–29.

Stearns, H.T., and Macdonald, G.A., 1942, Geology and ground-water resources of the island of Maui, Hawaii: Hawaii Division of Hydrography Bulletin, v. 7, p. 344.

Stille, P., Unruh, D.M., and Tatsumoto, M., 1983, Pb, Sr, Nd and Hf isotopic evidence of multiple sources for Oahu, Hawaii basalts: Nature, v. 304, p. 25–29.

———in press, Pb, Sr, Nd and Hf isotopic constraints on the origin of Hawaiian basalts and evidence for a unique mantle source: Geochimica et Cosmochimica Acta.

Sun, S.-S., 1980, Lead isotope study of young volcanic rocks from mid-ocean ridges, ocean islands and island arcs: Philosophical Transactions of the Royal Society of London, v. A. 297, p. 409–445.

Sun, S.-S, and Hanson, G., 1975, Evolution of the mantle: Geology, v. 3, p. 297–301.

Tatsumoto, M., 1969, Lead isotopes in volcanic rocks and possible ocean floor thrusting beneath island arcs: Earth and Planetary Science Letters, v. 6, p. 369–376.

———1978, Isotopic composition of lead in oceanic basalt and its implication to mantle evolution: Earth and Planetary Science Letters, v. 38, p. 63–87.

Tatsumoto, M., Hedge, C.E., and Engle, A.E.J., 1965, Potassium, rubidium, strontium, thorium, uranium, and the ratio of strontium-87 to strontium-86 in oceanic tholeiitic basalts: Science, v. 150, p. 886–889.

Tatsumoto, M., and Knight, R.J., 1969, Isotopic composition of lead in volcanic rocks from Central Honshu—with regard to basalt genesis: Geochemical Journal, v. 3, p. 53–86.

Tatsumoto, M., and Unruh, M., 1976, KREEP basalt age: Grain by grain U-Th-Pb systematics study of the quartz monzodiorite clast 15405,88: Proceedings of the 7th Lunar Scientific Conference, Geochimica et Cosmochimica Acta, Supplement 7, v. 2, p. 2107–2129.

Tatsumoto, M., Unruh, D.M., Stille, P., and Fujimaki, H., 1984, Pb, Sr, and Nd isotopes in oceanic island basalts: International Geological Congress, 27th, Proceedings, v. 11, p. 485–501.

Vidal, P., Chauvel, C., and Brousse, R., 1984, Large mantle heterogeneity beneath French Polynesia: Nature, v. 307, p. 536–538.

Vollmer, R., 1976, Rb-Sr and U-Th-Pb systematics of alkaline rocks: the alkaline rocks from Italy: Geochimica et Cosmochimica Acta, v. 40, p. 283–295.

White, W.M., 1985, Sources of oceanic basalts: Radiogenic isotopic evidence: Geology, v. 13. p. 115–118.

White, W.M., and Hofmann, A.W., 1982, Sr and Nd isotope geochemistry of oceanic basalts and mantle evolution: Nature, v. 296, p. 821–825.

Wilson, J.T., 1963, A possible origin of the Hawaiian Islands: Canadian Journal of Physics, v. 41, p. 863–870.

Wright, T.L., 1984, Origin of Hawaiian tholeiite: a metasomatic model: Journal of Geophysical Research, v. 89. p. 3233–3252.

Zindler, A., Jagoutz, E., and Goldstein, S.T., 1982, Nd, Sr and Pb isotopic systematics in a three component mantle: a new perspective: Nature, v. 298, p. 519–523.

Zindler, A., Staudigel, H., and Batiza, R., 1984, Isotope and trace element goechemistry of young Pacific seamounts: implications for the scale of upper mantle heterogeneity: Earth and Planetary Science Letters, v. 70, p. 175–195.

CONSTRAINTS ON THE CHARACTERISTICS OF MAGMA SOURCES FOR HAWAIIAN VOLCANOES BASED ON NOBLE-GAS SYSTEMATICS

By Ichiro Kaneoka[1]

ABSTRACT

The implications of noble-gas-isotope signatures of Hawaiian volcanic rocks and ultramafic nodules for the characteristics of Hawaiian volcanism are discussed. Hawaiian volcanic rocks have higher $^{3}He/^{4}He$ ratios and lower $^{40}Ar/^{36}Ar$ ratios than MORB, strongly indicating that they derived from a source enriched in volatile and primordial components. That source is probably located in the deeper part of the Earth's interior (lower mantle?). These observations are compatible with the hot-spot hypothesis.

The variations in the observed $^{3}He/^{4}He$ and $^{40}Ar/^{36}Ar$ ratios for Hawaiian volcanic rocks and nodules can be explained in terms of varying degrees of mixing among noble-gas components of three types: *P*(plume), *M*(MORB), and *A*(atmosphere). Mixing of *P* and *M* components occurs during ascent of a diapir through the asthenosphere and lithosphere, followed by introduction of the *A* component during eruption.

Systematic variations in the $^{3}He/^{4}He$ ratios with the volume of individual volcanoes, together with other radiogenic-isotope signatures, indicate a possible model for the evolution of Hawaiian volcanism based on the rise of volatile-enriched diapirs from the Earth's deep interior. However, the amount of noble-gas (volatile) components would vary at each stage of a volcano's evolution. The model suggests that the partially melted zone plays an important role during the evolution of Hawaiian volcanism. It is further pointed out that the voluminous outpourings of Hawaiian volcanoes do not always reflect the direct material supply from the hot-spot source but may reflect the combined effects of material transfer and heat supply.

INTRODUCTION

Because the Hawaiian Islands have formed far from any lithospheric plate boundary, they provide a good opportunity to study the characteristics of intraplate volcanism, especially of hot-spot areas as identified by Wilson (1963) and Morgan (1971).

Noble gases are chemically inert and include both radiogenic and stable isotopes. Furthermore, their isotopic ratios are rather insensitive to the physical and chemical processes occurring during magmatic fractionation. Hence, the isotopic ratios of noble gases can give us unique information concerning the characteristics of source materials. In this paper, I summarize the noble-gas data so far obtained for Hawaiian samples and discuss the characteristics of source materials for Hawaiian rocks based on those noble-gas data.

Dalrymple and Moore (1968) identified that recent submarine pillow basalts erupted on the east rift zone of Kilauea showed excess ^{40}Ar. Similar results were obtained for the same kind of samples by Noble and Naughton (1968). It has been realized that magmatic Ar is trapped in glassy rims because of rapid cooling under a high hydrostatic pressure of sea water, which hinders the degassing. Compared to the atmospheric values of 295.5, the $^{40}Ar/^{36}Ar$ ratio in these samples is as high as about 1,200. However, these ratios are not so high as those observed in some glassy pillow samples of midocean ridge basalt (MORB), which reach as high as about 10,000 (Funkhouser and others, 1968).

Funkhouser and Naughton (1968) examined radiogenic He and Ar in ultramafic inclusions from Hualalai Volcano, Hawaii, and Salt Lake Crater, Oahu, and concluded that they include magmatic radiogenic components in fluid and gaseous inclusions in the minerals of the nodules. This confirmed the previous results by Lovering and Richards (1964), who suggested the presence of excess ^{40}Ar in clinopyroxene from a pyroxenite nodule erupted at Salt Lake Crater that showed an apparently very old K-Ar age of 1.4 Ga. The radiogenic components in these ultramafic nodules were further investigated by Gramlich and Naughton (1972), who inferred, on the basis of diffusion experiments of He and Ar, that the $^{4}He/^{40}Ar$ ratio in the environment where the minerals of lherzolite nodules were concentrated at Salt Lake Crater had a value of 1.2 ± 0.2. These investigations demonstrate the occurrence of radiogenic noble gases such as ^{4}He and ^{40}Ar of magmatic origin in pillow glass and ultramafic nodules. At that time, these data were interpreted to show the characteristics of noble-gas isotopes in the Earth's interior in a general sense, and it was premature to discuss the characteristics of noble-gas isotopes that might be unique for Hawaiian samples.

The value of noble-gas isotope studies on Hawaiian samples was illustrated by Hennecke and Manuel (1975) when they found excess ^{129}Xe in ultramafic nodules. Furthermore, Craig and Lupton (1976) found a higher $^{3}He/^{4}He$ ratio in Kilauea fumaroles than in those of MORB, which is known to be relatively uniform on a global scale. Such data are significant because they might characterize the uniqueness of Hawaiian magma sources. The occurrence of high $^{3}He/^{4}He$ ratios and excess ^{129}Xe in Hawaiian samples was confirmed in both lava flows and ultramafic nodules (Kaneoka and

[1]Geophysical Institute, University of Tokyo, Bunkyo-ku, Tokyo 113, Japan.

Takaoka, 1978; Kaneoka and others, 1978). On the basis of systematic differences in $^{3}He/^{4}He$ and $^{40}Ar/^{36}Ar$ ratios, Kaneoka and Takaoka (1980) discussed the difference of magmatic sources between lava flows and ultramafic nodules. Further data on these samples were accumulated, discussed, and compared with similar data from other areas (Kyser and Rison, 1982). Detailed studies on samples from Loihi Volcano have revealed that high $^{3}He/^{4}He$ ratios for Hawaiian magma sources are real but rather variable even between different eruptions of the same volcano (Kaneoka and others, 1983; Kurz and others, 1983; Rison and Craig, 1983). However, no excess ^{129}Xe has been found in samples of Loihi pillow glass (Allègre and others, 1983; Kaneoka and others, 1983). Furthermore, large variation in the $^{3}He/^{4}He$ ratio is found even for different volcanoes on the same island (Kurz and others, 1983). These data could indicate more complexity in magmatic sources for Hawaiian magmatism, which however still remain distinct from those of MORB.

ACKNOWLEDGMENTS

For my experimental work on noble-gas systematics of Hawaiian samples, I have benefited much from using a mass spectrometer developed by N. Takaoka of Yamagata University. R.W. Decker of the U.S. Geological Survey and K. Nakamura of the Earthquake Research Institute, University of Tokyo, have given me the chance to write this review paper and gave encouragement through the work. The constructive reviews by G.B. Dalrymple and T.L. Wright of U.S. Geological Survey were very helpful for improving the manuscript.

This study was financially supported in part by a Grant-in-Aid for Scientific Research from the Ministry of Education, Science and Culture, Japan, under contracts No. 58540220 and No. 59065001.

ABUNDANCES AND TRAPPING SITES OF NOBLE GASES IN HAWAIIAN ROCK SAMPLES

Noble-gas abundances in a sample reflect both the characteristics of the source and the sample's subsequent history (see, for example, Dymond and Hogan, 1978; Kaneoka and Takaoka, 1985). If we can evaluate the latter contribution properly, it is possible to get some information on the characteristics of the sample source, though it is generally not easy to do so. Noble gases in selected samples of different kinds from the Kilauea region are compared in table 27.1. Since these samples can be regarded as almost recent, it is not necessary to consider the effect of radiogenic components formed after extrusion on the surface. Hence, these samples should show similar isotopic ratios and characteristic abundances of noble gases reflecting the processes involved in their magmatic history. Judging from the $^{40}Ar/^{36}Ar$ ratio and relative noble-gas abundance patterns, Kapoho lava seems to have lost most magmatic gas and to have been equilibrated with atmospheric noble gases. The observed amount of ^{40}Ar in this sample (2.0×10^{-7} cm^3/g at standard temperature and pressure) is just the value expected in a molten magma in equilibrium with the Earth's atmosphere as inferred from the solubility data of Ar in melt of tholeiitic basalt (Hayatsu and Waboso, 1982). However, there still remain small amounts of magmatic noble gases in this sample, which is shown by the relative enrichment of ^{4}He and ^{132}Xe compared with Ar (see the data for lava in figure 27.1).

On the other hand, olivine phenocrysts (diameter >1 mm) in this sample contain lesser amounts of noble gases (except for ^{4}He) than lava, but they show definitely higher $^{3}He/^{4}He$ and $^{40}Ar/^{36}Ar$ ratios than the atmosphere. These phenocrysts are considered to have been formed in the magma reservoir at depth without atmospheric contaminations. Hence, these values can be considered to approximate the values for the magmatic noble gases, or at least for their isotopic ratios.

It has been known that the chilled margins of submarine basalt pillows contain magmatic noble gases (see, for example, Dalrymple and Moore, 1968; Funkhouser and others, 1968; Noble and Naughton, 1968). However, the efficiency of trapping of noble gases is dependent on both the cooling rate and the ambient hydrostatic pressure. As shown in table 27.1, tholeiite from the east rift zone reflects such tendencies (Kyser and Rison, 1982). The sample from the derived depth of 2,960 m clearly shows the evidence of magmatic noble gases, but that from the depth of 30 m does not, though the latter seems to retain a small amount of ^{4}He.

In a subaerial sample (glassy spatter), the observed amounts of noble gases are quite large, but the $^{40}Ar/^{36}Ar$ ratio is atmospheric and the noble-gas abundance pattern is similar to that of the atmosphere (fig. 27.1). Hence, it is not likely that these gases truly represent those in the original magma. Many microscopic gas pores are observed in this sample; atmospheric noble gases were probably trapped in such pores when it erupted.

The high $^{3}He/^{4}He$ ratio reported in Kilauea gas samples (Craig and Lupton, 1976) is similar, within their analytical uncertainties, to those observed in phenocrysts and pillow glass from this region. However, we have no guarantee that the observed values for fumarolic gases approximate those of the magmatic gases for heavier noble gases, since they are much more easily contaminated from the atmosphere (see, for example, Ozima and Podosek, 1983; Kaneoka and Takaoka, 1985).

Thus it is essential in noble-gas analyses to select appropriate samples to infer the conditions of magmatic noble gases. For this purpose, pillow glass and large olivine and pyroxene phenocrysts have been regarded as suitable. Ultramafic nodules also contain magmatic noble gases, since they are formed at depth without atmospheric contaminations. For $^{3}He/^{4}He$ analyses, fumarolic gas and even water samples can be used, because the effect of atmospheric contamination is generally quite small for He compared with the abundance of magmatic He in these samples.

Noble-gas abundances in different kinds of samples from the Hawaiian region are compared in figure 27.1. To exclude the ambiguity from the addition of secondary atmospheric components, low-temperature (500–700 °C) and high-temperature (1,700–1,800 °C) fractions were taken for most samples, and the values for the higher temperature fraction are shown in figure 27.1. These samples include some from Loihi Seamount and from Hawaii, Maui, and Oahu Islands. Except for some quite different

TABLE 27.1—*Comparison of noble gases in different kinds of samples from Kilauea Volcano*

[Values for gas contents are at standard temperature and pressure; atmospheric values calculated from total amount in atmosphere divided by mass of the Earth; R/R_A given by $(^3He/^4He)_{sample}/(^3He/^4He)_{air}$; —, not determined]

Sample	Noble-gas content ($cm^3/g \times 10^{-8}$)			Noble-gas content ($cm^3/g \times 10^{-10}$)		Ratios			Reference
	^4He	^{20}Ne	^{36}Ar	^{84}Kr	^{132}Xe	$^3He/^4He$ ($\times 10^{-6}$)	R/R_A	$^{40}Ar/^{36}Ar$	
Kapoho lava	.063	.0111	.0674	.256	.0796	<226	<161	297.0±1.6	1
Olivine phenocrysts in Kapoho lava	4.43	.0100	.0245	.0476	.0058	25.1±3.4	17.9±2.4	732.0±2.2	2
Glassy splatter on Kilauea caldera floor, erupted November29, 1975	2.46	4.25	9.76	26.9	.682	———	———	294.0±1.4	3
Pillow glass Tholeiite of east rift zone, depth=30 m	1.9	.0103	.039	.084	.0058	0±14	0±10	296±22	4
Tholeiite of east rift zone, depth=2,960 m	32.6	.129	.213	.473	.0245	17±2	12±1	1175±22	4
Kilauea gas	——	——	——	——	——	20.9±1.1	14.9±0.8	———	5
Atmosphere	.347	1.09	2.08	4.31	.152	1.399	1	295.5	

1. Kaneoka and Takaoka (unpublished data).
2. Kaneoka and Takaoka (1978).
3. Kaneoka and others (1978).
4. Kyser and Rison (1982).
5. Craig and Lupton (1976).

samples (lava and glassy spatter in table 27.1), the samples show generally similar noble-gas abundance patterns, in which high enrichment of He is significant. Among different kinds of samples, lighter noble gases (He, Ne) are generally more enriched in ultramafic nodules and glassy samples than in phenocrysts. Nodule samples include dunite, lherzolite, and pyroxenite; however, their noble-gas abundance patterns are similar.

Noble gases are generally more abundant in dunite nodules than in olivine phenocrysts. Numerous microscopic gas or liquid inclusions (probably CO_2) are observed in such ultramafic nodules, and most noble gases are expected to have been entrapped in such inclusions. This inference has been supported by crushing or decrepitation of samples (see, for example, Funkhouser and Naughton, 1968), which showed that rather large amounts of He and radiogenic ^{40}Ar were released. Furthermore, it has been demonstrated that most He is included in vesicles and not dissolved in the glass itself in pillow-glass samples from Loihi Seamount (Kurz and others, 1983; Rison and Craig, 1983). Hence, the noble-gas abundances in these samples would correspond to those in inclusions or vesicles.

Phenocrysts seem to contain fewer inclusions than nodules and glassy samples, and this probably affects the noble-gas abundances. Olivine phenocrysts from Hawaii contain amounts of noble gases comparable to those in samples from Reunion Island, whereas samples from Iceland contain lesser amounts of the lighter noble gases than those from Hawaii and Reunion (Kaneoka and Takaoka, 1985). This difference may reflect different tectonic environments for extrusion of magma; the samples from Hawaii may be closer to the original abundances of noble gases in the magma reservoir than those from Iceland.

Noble-gas abundances in MORB are also shown in figure 27.1 for comparison (plotted to the right of the Hawaii data). MORB samples are typically enriched in lighter noble gases, especially He. There is no reason to believe that U(+Th) is more abundant in the MORB source than in that of Hawaii, and such enrichment probably reflects secondary processes that occurred during the formation and transportation of MORB magma to the surface.

NOBLE-GAS ISOTOPIC CHARACTERISTICS OF HAWAIIAN SAMPLES

HELIUM ISOTOPES

As noted in the previous section, the concentrations of noble gases in a sample are susceptible to secondary processes and it is therefore useful to evaluate such processes. To infer the characteristics of magma sources, however, isotopic ratios are more useful than elemental concentrations, since they are much less affected by the processes of formation, transportation, and extrusion of a magma, except for the effects of mass fractionation and mixing among different sources. Among the many aspects of noble-gas isotope systematics, the $^3He/^4He$ ratio ($=R$) has been most

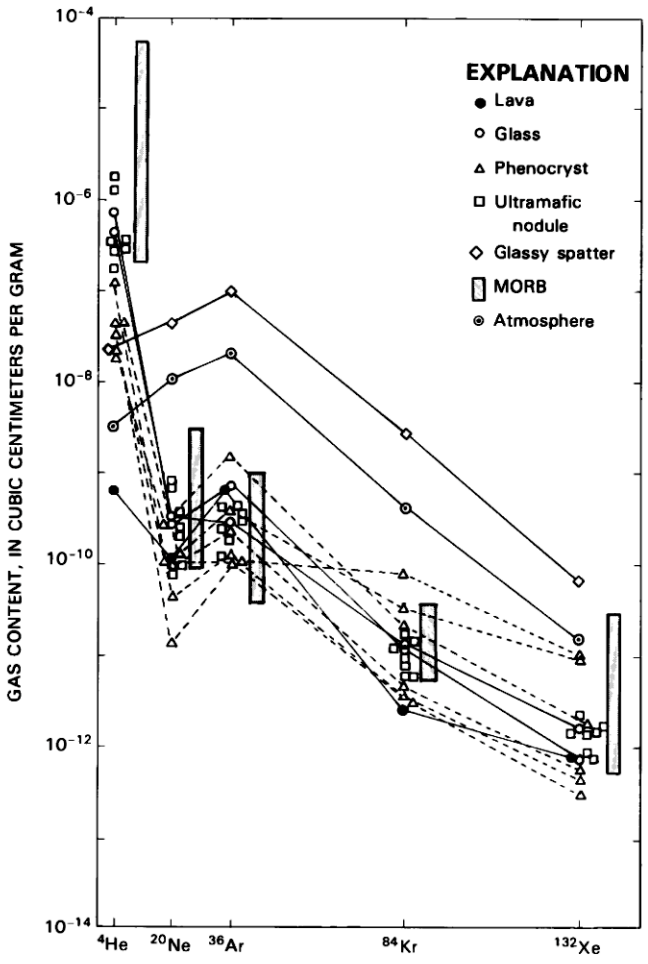

FIGURE 27.1.— Noble-gas abundances in Hawaiian rock samples. Values plotted are total amounts of noble gases in the samples adjusted to standard temperature and pressure. Values for atmosphere derived from total amounts of noble gases in the atmosphere divided by mass of the Earth. Data sources for Hawaiian samples: Hennecke and Manuel (1975); Kaneoka and Takaoka (1978, 1980); Kaneoka and others (1983). Data sources for MORB: Kyser and Rison (1982); Allègre and others (1983); Ozima and Zashu (1983).

successfully used so far because He is least contaminated by the atmosphere.

It has been revealed that MORB shows a rather uniform $^{3}He/^{4}He$ ratio that varies from 1.1×10^{-5} to 1.4×10^{-5} ($R=8$–$10R_A$, where R_A is the ratio of $^{3}He/^{4}He$ for air) irrespective of regional differences and elemental fractionation, whereas other samples show more variability and some systematic differences. For example, crustal gases generally show a lower $^{3}He/^{4}He$ ratio than that of atmospheric He ($R_A=1.4\times10^{-6}$). Examples are shown in figure 27.2, where the $^{3}He/^{4}He$ ratio is plotted against the $^{4}He/^{20}Ne$ ratio for each sample. The $^{3}He/^{4}He$ ratio for MORB is rather uniform, though the $^{4}He/^{20}Ne$ ratio varies by a factor of more than 10^{4}. Such uniformity in the $^{3}He/^{4}He$ ratio for MORB surely reflects a characteristic of the magma source.

Hawaiian samples show rather different characteristics from those of MORB in figure 27.2. Although most ultramafic nodules show similar $^{3}He/^{4}He$ ratios to that of MORB, which has an $^{4}He/^{20}Ne$ ratio of 0.5×10^{3}–5×10^{3}, phenocryst samples have higher $^{3}He/^{4}He$ ratios. This indicates that Hawaiian magma sources are isotopically different from that of MORB.

Detailed studies of the $^{3}He/^{4}He$ ratio have revealed that it varies among different volcanoes on each Hawaiian island and even within the individual volcanoes (Kaneoka and Takaoka, 1980; Kurz and others, 1983; Rison and Craig, 1983). The geographical variation of the $^{3}He/^{4}He$ ratio for Hawaiian samples is summarized in figure 27.3.

Such variations in the $^{3}He/^{4}He$ ratio surely reflects the conditions in the magma sources for these volcanoes. Furthermore, the variation in the $^{3}He/^{4}He$ ratio seems to be related to the rock type and the sequence of volcano formation. For example, tholeiite from Loihi Seamount shows higher $^{3}He/^{4}He$ ratios than alkali basalt (Kurz and others, 1983; Rison and Craig, 1983). Kurz and others (1983) further reported that the $^{3}He/^{4}He$ ratio for basalt on the Island of Hawaii seems to decrease with either increase in the volume of a volcano or decrease in the eruption age. Such observations are significant for interpreting Hawaiian volcanism and will be discussed later in more detail.

ARGON ISOTOPES

It has been known that ultramafic nodules from Hawaii, such as those from Hualalai and the Salt Lake Crater region, contain large amounts of excess ^{40}Ar, resulting in high $^{40}Ar/^{36}Ar$ ratios of more than a few thousand (see, for example, Funkhouser and Naughton, 1968). Since these ultramafic nodules are mantle derived (they are mostly cumulates with minor amounts of mantle materials), such values have sometimes been considered to represent the $^{40}Ar/^{36}Ar$ value in the mantle. Although submarine glassy pillows from the east rift zone of Kilauea show $^{40}Ar/^{36}Ar$ ratios as high as about 1,200 (see, for example, Dalrymple and Moore, 1968; Kyser and Rison, 1982), these $^{40}Ar/^{36}Ar$ ratios are still much lower than those observed in MORB. Furthermore, Kaneoka and Takaoka (1980) have demonstrated that higher $^{3}He/^{4}He$ ratios that exceed the MORB value seem to be associated with lower $^{40}Ar/^{36}Ar$ ratios. Hence, there is a possibility that such relatively low $^{40}Ar/^{36}Ar$ ratios represent the characteristics of the source materials for hot-spot areas.

The most serious problem in the measurement of the $^{40}Ar/^{36}Ar$ ratio is that the value is easily modified by the addition of atmospheric components, since the atmosphere (and sea water) contains fairly large amount of Ar. For this reason, it is often argued that the observed low $^{40}Ar/^{36}Ar$ ratios that are closer to the atmospheric value were caused by atmospheric contamination (see for example, Fisher, 1983). Such effects should be properly evaluated to infer the significance of the Ar isotopic ratios. One solution is to make comparison with other isotopic ratios that are not seriously affected by the atmospheric contamination. Another solution is to check the observed data in a plot of $^{40}Ar/^{36}Ar$ against $1/^{36}Ar$, in which samples contaminated with atmospheric component should be

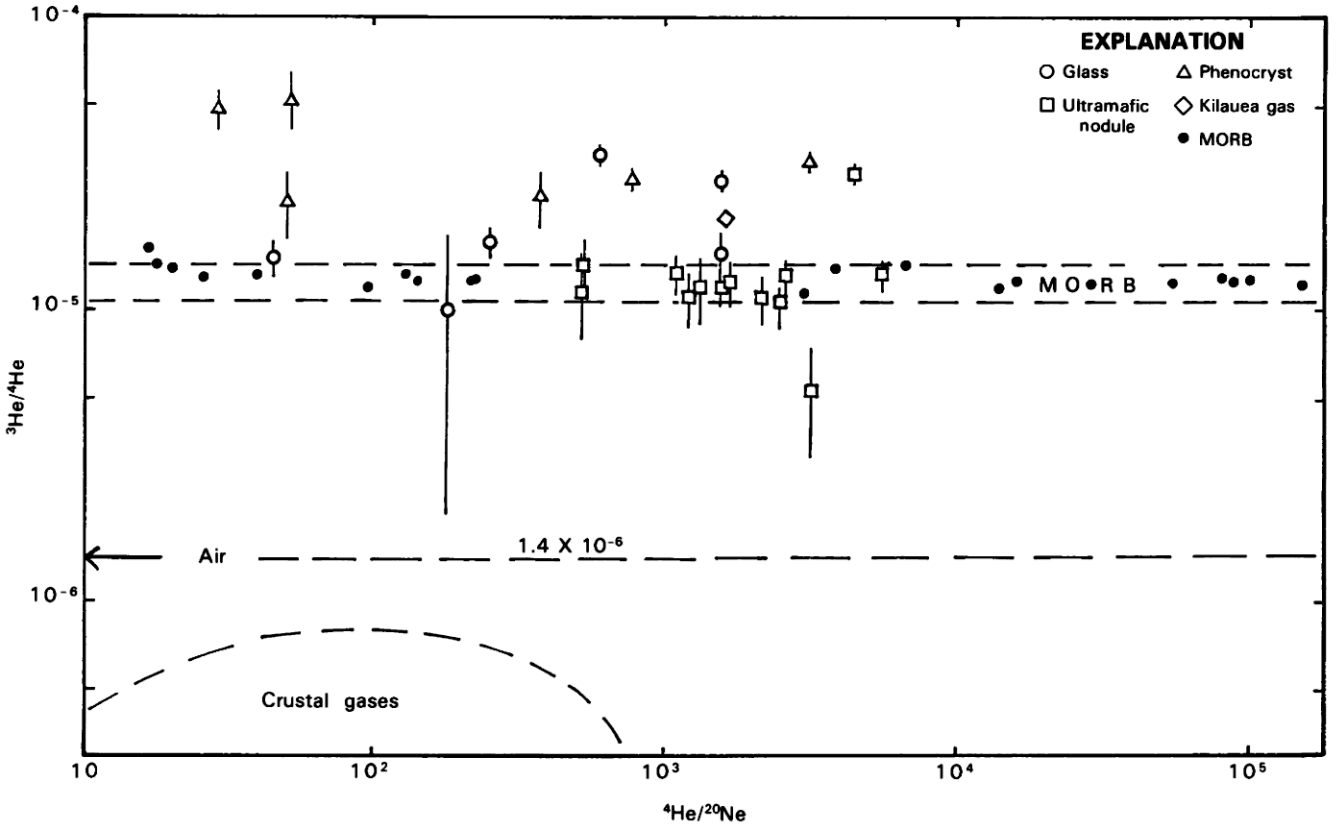

FIGURE 27.2.—Plot of $^3He/^4He$ ratio against $^4He/^{20}Ne$ ratio for Hawaiian samples and MORB. Vertical lines show uncertainty in the $^3He/^4He$ ratio measured. In spite of large variation in $^4He/^{20}Ne$ ratio for MORB, its $^3He/^4He$ ratio is rather uniform (as shown by brochetting dashed lines), but $^3He/^4He$ ratios for Hawaiian samples are generally higher than those of MORB. Data sources: Lupton and Craig (1975); Craig and Lupton (1976); Kaneoka and Takaoka (1978, 1980); Kyser and Rison (1982); Kaneoka and others (1983); Ozima and Zashu (1983).

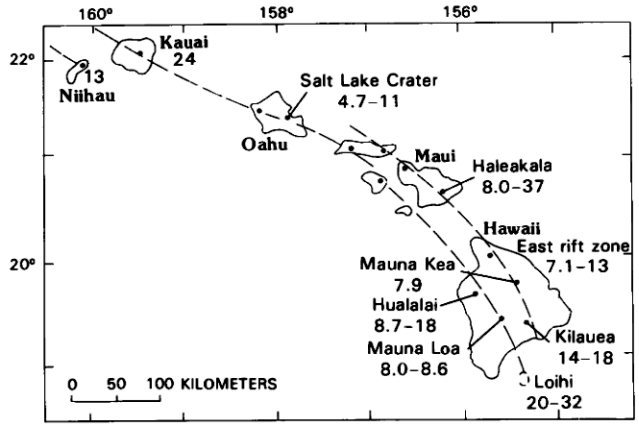

FIGURE 27.3.—Distribution of $^3He/^4He$ ratio for rock and gas samples from the Hawaiian Islands. Each number corresponds to the value or range of values of R/R_A, where R is the $^3He/^4He$ ratio in the sample(s) and R_A indicates the atmospheric value (1.4×10^{-6}). Dashed lines mark the two lines of volcanic centers (dots). Data sources: Craig and Lupton (1976); Kaneoka and Takaoka (1978, 1980); Kyser and Rison (1982); Kaneoka and others (1983); Kurz and others (1983); Lupton (1983); Rison and Craig (1983).

on a line that connects the atmospheric $^{40}Ar/^{36}Ar$ ratios (295.5) on the ordinate and the point for uncontaminated sample, as long as the samples contain the same amount of ^{36}Ar (see, for example, Dymond and Hogan, 1978). The data for Hawaiian samples are plotted on such a diagram in figure 27.4; in this diagram, the data scatter and do not define any single line. However, it is worthwhile to point out that most ultramafic nodules show systematically higher $^{40}Ar/^{36}Ar$ ratios of more than 1,000, whereas glass samples and phenocrysts show mostly values of less than 1,000, irrespective of the amount of ^{36}Ar. These submarine glass samples are not different in their eruptive conditions from MORB. Hence there is no reason why they should be much more contaminated with atmospheric components through sea water than MORB. In effect, these glass samples retain magmatic He. Hence, even if the relatively low $^{40}Ar/^{36}Ar$ ratios observed are affected by the atmospheric contamination for some samples, it does not preclude the possibility of a low $^{40}Ar/^{36}Ar$ ratio for magmatic Ar in Hawaii. This point will be discussed again later in discussing the $^3He/^4He$ - $^{40}Ar/^{36}Ar$ diagram.

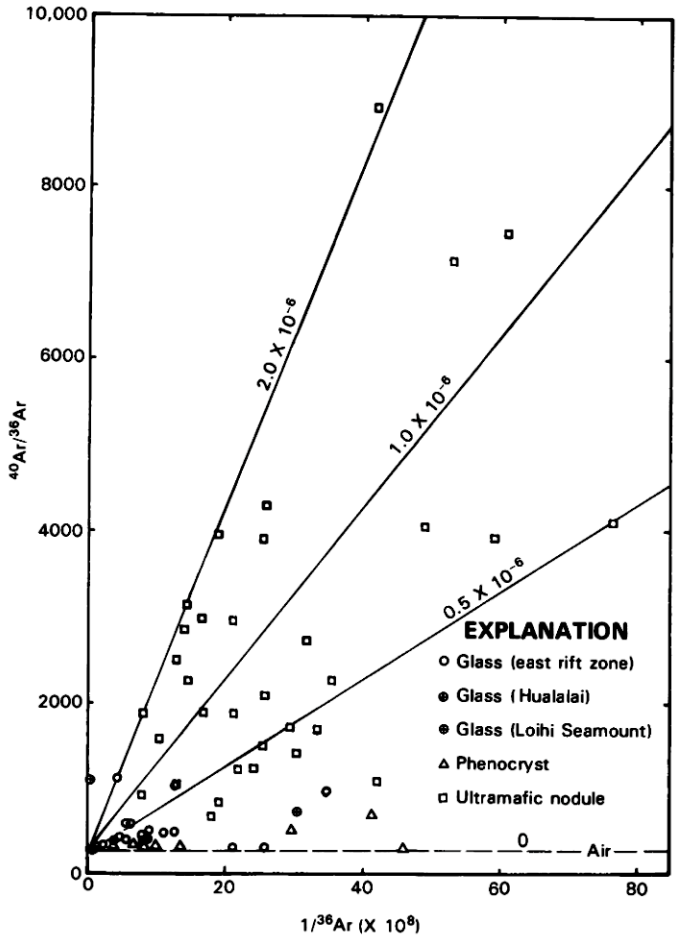

FIGURE 27.4.—Plot of $^{40}Ar/^{36}Ar$ ratio against $1/^{36}Ar$ for Hawaiian rock samples. Value of $^{40}Ar/^{36}Ar$ in air indicated by dashed line. The lines in the figure indicate reference lines which correspond to the mixing line between the original magmatic Ar and the atmospheric Ar, where the concentration of magmatic ^{40}Ar in each sample is assumed as the numerical figures on each line in the unit of cubic centimeters at standard temperature and pressure for one gram sample. Data sources: Dalrymple and Moore (1968); Funkhouser and Naughton (1968); Noble and Naughton (1968); Hennecke and Manuel (1975); Kaneoka and Takaoka (1978, 1980); Kyser and Rison (1982); Allègre and others (1983); Fisher (1983); Kaneoka and others (1983).

OTHER NOBLE GAS ISOTOPES

In Kilauea gas and in MORB, a higher $^{20}Ne/^{22}Ne$ ratio (10.3) than the atmospheric value (9.80) was reported by Craig and Lupton (1976), who considered it as evidence that the primordial Ne component of solar type may be still retained in the Earth's deep interior. However, this value and the corresponding $^{21}Ne/^{22}Me$ ratio can also be explained by mass fractionation from the atmospheric value (Kaneoka, 1980), and the occurrence of primordial Ne component has not yet been confirmed.

On the other hand, the occurrence of higher $^{129}Xe/^{130}Xe$ ratios than the atmospheric value has been confirmed in ultramafic nodules from Hualalai (Hennecke and Manuel, 1975; Kaneoka and others, 1978; Kyser and Rison, 1982). Even olivine phenocrysts of Kapoho lava, Kilauea, seem to contain excess ^{129}Xe (Kaneoka and Takaoka, 1978). However no excess ^{129}Xe has been confirmed in Loihi samples (Allègre and others, 1983; Kaneoka and others, 1983). Since excess ^{129}Xe has been regarded as the decay product of extinct ^{129}I (half-life, 17 m.y.), its occurrence indicates that the magma source was not totally equilibrated with the surrounding part for more than 4 b.y. Allègre and others (1983) reported the occurrence of excess ^{129}Xe in MORB.

The $^{129}Xe/^{130}Xe$ ratio is plotted in figure 27.5 against the $^{40}Ar/^{36}Ar$ ratio for Hawaiian samples and some MORB samples. Although the uncertainty in the $^{129}Xe/^{130}Xe$ ratio is fairly large, the array of samples seems to indicate on a mixing line of $r \geqq 0.5$, where r is defined as the ratio of $^{130}Xe/^{36}Ar$ for air divided by $^{130}Xe/^{36}Ar$ for the MORB source and the value of $^{130}Xe/^{36}Ar$ for air is 1.13×10^{-4}. For $^{130}Xe/^{36}Ar$ of the MORB source, if we adopt the value observed for a pillow glass that showed the highest excess ^{129}Xe in MORB (Allègre and others, 1983), it becomes 11.6×10^{-4}. Hence, mixing between this component and the atmosphere indicates a value of r close to about 0.1. The data array observed in figure 27.5 do not seem to be explained by the addition of an atmospheric component alone. This may imply that the Hawaiian magma source, which may be a typical hot-spot area, shows an atmospheric $^{129}Xe/^{130}Xe$ ratio and a rather low $^{40}Ar/^{36}Ar$ ratio close to the atmospheric value. Large analytical

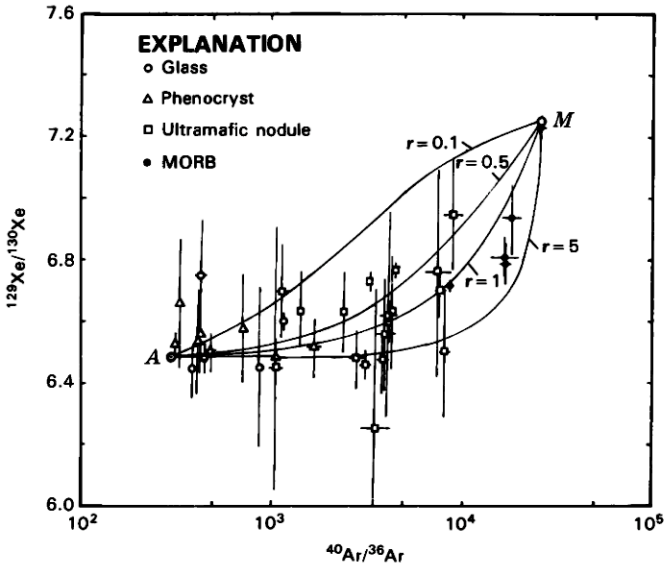

FIGURE 27.5.—Plot of $^{129}Xe/^{130}Xe$ ratio against $^{40}Ar/^{36}Ar$ ratio for Hawaiian rock samples and a few MORB samples. Mixing lines between the atmospheric component (*A*: $^{40}Ar/^{36}Ar = 295.5$; $^{129}Xe/^{130}Xe = 6.48$) and an assumed MORB source component (*M*: $^{40}Ar/^{36}Ar = 25{,}000$; $^{129}Xe/^{130}Xe = 7.25$) are drawn with a function of r, where r is $(^{130}Xe/^{36}Ar)air/(^{130}Xe/^{36}Ar)_{MORB}$ source. Vertical and horizontal lines indicate uncertainty. Data sources: Hennecke and Manuel (1975); Kaneoka and Takaoka (1978, 1980); Kyser and Rison (1982); Allègre and others (1983); Kaneoka and others (1983).

uncertainties remain, however, concerning the $^{129}Xe/^{130}Xe$ ratio for most samples from Hawaii. Hence more precise data are necessary to draw a definite conclusion.

THE $^{3}He/^{4}He$-$^{40}Ar/^{36}Ar$ SYSTEM

A magma source would be more clearly characterized by an appropriate combination of isotopic ratios than by a single one. For this purpose, the $^{3}He/^{4}He$-$^{40}Ar/^{36}Ar$ system is one of the most effective ones among possible combinations of noble-gas isotopic ratios. The merits of using this system have been discussed in detail elsewhere (Kaneoka and Takaoka, 1985).

All the available data for samples from Hawaiian volcanoes are plotted on the $^{3}He/^{4}He$-$^{40}Ar/^{36}Ar$ diagram in figure 27.6. Except for a dunite nodule from Loihi Seamount, higher $^{3}He/^{4}He$ ratios seem to be accompanied by lower $^{40}Ar/^{36}Ar$ ratios. Furthermore, ultramafic nodules are located in the region defined by MORB. Such relations for Hawaiian samples were first identified by Kaneoka and Takaoka (1980), who argued for different magma sources for Hawaiian magma and ultramafic nodules. As pointed out previously, the accumulation of data on the $^{3}He/^{4}He$ ratio in lava phases has suggested that Hawaiian volcanism is characterized by some complexity of processes in each locality, but this would not change the main scheme fundamentally from that stated above. This point will be discussed later in more detail.

However, the plot in figure 27.6 strongly suggests at least that a magma source enriched in primordial noble-gas components exists under the Island of Hawaii. If we extend such data to other areas, the same tendencies as observed for Hawaiian samples are also identified (fig. 27.7). The most remarkable feature of figure 27.7 is that higher $^{3}He/^{4}He$ ratios than the MORB value are always associated with relatively lower $^{40}Ar/^{36}Ar$ ratios, except for a few cases, and such high $^{3}He/^{4}He$ ratios are observed in typical hot-spot areas. This does not mean that samples from all hot-spot areas show such a trend. For example, volcanic rocks from the Tristan da Cunha and Gough Islands show lower $^{3}He/^{4}He$ ratios than that of MORB, but the ratios are still higher than that of the atmospheric component (Kurz and others, 1982). Such a trend may be explained by the addition of a crustal component to the pure plume-type component that has a high $^{3}He/^{4}He$ ratio (see, for example, Kurz and others, 1982; Kaneoka and Takaoka, 1985).

On the basis of the $^{3}He/^{4}He$-$^{40}Ar/^{36}Ar$ systematics, we can identify at least four end members as shown in figure 27.7: *P*(plume-type), *M*(MORB-type), *A*(atmosphere-type), and *C*(crust-type) (Kaneoka, 1983; Kaneoka and Takaoka, 1985). *C* components are multi-divided further depending on the local and regional inhomogeneities including time-integrated effects. Although *P* and probably *M* components can be subdivided on a local scale, we need not do so to discuss general trends on rather global scales. The observed noble-gas data can be explained by mixing among these components, including the data observed at subduction zones, which may be mixtures of *M*, *A*, and *C* components.

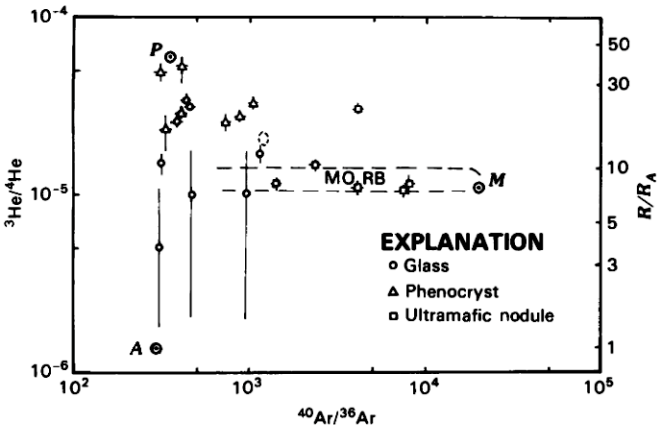

FIGURE 27.6.—Plot of $^{3}He/^{4}He$ ratio against $^{40}Ar/^{36}Ar$ ratio for Hawaiian rock samples. For most samples, only the results from high-temperature fractions are shown here. *A*, atmosphere; *P*, plume-type source; *M*, MORB source; dashed lines, approximate range of MORB samples. Vertical and horizontal lines indicate analytical uncertainties for each sample. Dashed circle indicates a combined value for samples for Kilauea, where $^{3}He/^{4}He$ ratios were obtained for fumarolic gases and $^{40}Ar/^{36}Ar$ ratios for pillow glasses from east rift zone. Data sources: Kaneoka and Takaoka (1978, 1980); Kyser and Rison (1982); Allègre and others (1983); Kaneoka and others (1983).

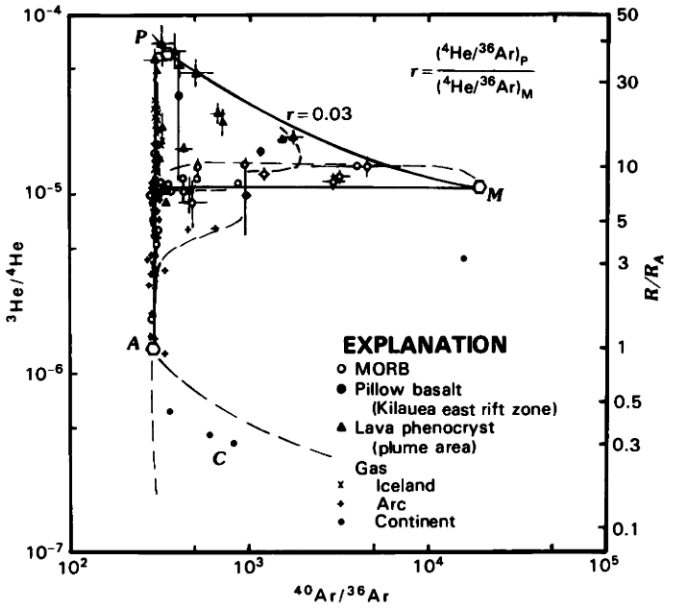

FIGURE 27.7.—Plot of $^{3}He/^{4}He$ ratio against $^{40}Ar/^{36}Ar$ ratio for samples that represent the recent state of the Earth's interior. *P*, *M*, *A*, and *C* represent assumed typical values for source materials of plume, MORB, atmosphere and crust types, respectively. Uncertainties are indicated by short vertical and horizontal lines. Solid lines show calculated mixing lines between sources. Dashed lines indicate regions where each component is dominant (though arc-type source material is not discussed in the present study) (after Kaneoka and Takaoka, 1985).

In this context, it is interesting to examine the data for Hawaiian samples in figure 27.7. Most data for Hawaiian samples are located in a region bordered by the three mixing lines, *P–M*, *M–A*, and *P–A*. Since *A* component is composed of atmospheric noble gases from the atmosphere, sea water, and ground water, those data located away from the mixing line *P–M* would have been secondarily contaminated on the surface or at a relatively shallow depth. On the other hand, some Hawaiian samples seem to lie on the *P–M* mixing line. Since the fit for mixing line is fairly good, the variation in the observed data bas been interpreted as showing the mixing between these probably mantle-derived components (Kaneoka and Takaoka, 1980, 1985; Kyser and Rison, 1982; Kaneoka, 1983).

Because this diagram is composed of two kinds of noble-gas isotopic ratios, the variation in it can be explained rather simply as long as He and Ar behave similarly in the main process concerned. On the other hand, if we take a set of elements of different kind, such as He and Sr (see, for example, Kurz and others, 1982), the system is more easily disturbed because of the different transfer of elements caused by the difference in the chemical behavior. Hence, the occurrence of completely different components (*P* and *M*) in the $^{3}He/^{4}He$-$^{40}Ar/^{36}Ar$ systematics is of great significance in inferring chemical characteristics of the Earth's interior. The component *P* would surely represent the source material of less depleted or fertile mantle that lies under the *M*-type (MORB) source, which is considered to have been much depleted in incompatible elements (Kyser and Rison, 1982; Kaneoka, 1983; Kaneoka and Takaoka, 1985). Although some investigators argue for the occurrence of fertile mantle as a result of enrichment process in the asthenosphere (for example, Anderson, 1982), this seems unlikely on the basis of noble-gas systematics (Kaneoka, 1983).

Thus, noble-gas isotopes for Hawaiian samples clearly suggest that the Hawaiian rocks are derived from fertile mantle, which is richer in primitive noble gases and incompatible elements such as K and U than the MORB source. Although similar inferences have been made on the basis of Nd-Sr systematics (see, for example, Jacobsen and Wasserburg, 1979; DePaolo, 1981), the identification of the typical component for the fertile mantle has remained hypothetical and could be interpreted in a different way in the $^{143}Nd/^{144}Nd$-$^{87}Sr/^{86}Sr$ diagram. In the $^{3}He/^{4}He$-$^{40}Ar/^{36}Ar$ diagram, however, we can identify it clearly as the *P* component. This component seems to be found in samples from typical hot-spot areas such as Hawaii, Iceland, and Reunion. Thus, noble-gas data give clear evidence for the inference that Hawaiian volcanism has been caused by a mantle plume or plumes from a hot spot that lies at a relatively deeper level (lower mantle?) in the Earth's interior (see Kaneoka, 1983, for further discussion).

NOBLE GAS ISOTOPES AS CONSTRAINTS TO INFER THE GENETIC RELATIONS FOR HAWAIIAN ROCKS

In attempts to reveal the orgin of Hawaiian volcanic rocks by petrological, mineralogical, and geochemical studies, it has often been assumed that the ultramafic nodules included in Hawaiian volcanic rocks represent either the source materials of these volcanic rocks or cumulates from them (for example, Jackson and Wright, 1970). On the basis of $^{3}He/^{4}He$ and $^{40}Ar/^{36}Ar$ ratios, however, it has been shown that phenocrysts in Hawaiian volcanic rocks (tholeiite and alkalic basalt) and ultramafic nodules would have been derived from different sources (Kaneoka and Takaoka, 1978, 1980). The source for ultramafic nodules seems to be similar to that for MORB. Such results have been supported by subsequent work (Kyser and Rison, 1982). It has been known that $^{87}Sr/^{86}Sr$ ratios for ultramafic nodules (0.7031–0.7032) (Shimizu, 1975) are slightly lower than those of Hawaiian tholeiite (0.7034–0.7038) (see, for example, O'Nions and others, 1977). However, the difference in the $^{3}He/^{4}He$ and $^{40}Ar/^{36}Ar$ ratios is so large between phenocrysts and ultramafic nodules (see fig. 27.6) that we cannot regard them as derived from similar sources. Recent summarized studies on the origin of Hawaiian tholeiite have also suggested that most ultramafic nodules are not directly related to the origin of Hawaiian volcanic rocks (Wright, 1984).

As discussed in the previous section, Hawaiian ultramafic nodules show similar $^{3}He/^{4}He$ and $^{40}Ar/^{36}Ar$ ratios to those of MORB. These analyzed nodules were mostly samples from Hualalai Volcano and Salt Lake Crater, and their rock types include dunite, spinel lherzolite, and garnet pyroxenite. As far as noble-gas data are concerned, these ultramafic nodules include gas components that were derived from the same source or a quite similar source to that of MORB. Hence, these nodules might have been the source rock or cumulates of MORB, or they might represent rocks formed in the asthenosphere to constitute the lower part of the lithosphere. More strictly, if the accompanying volcanic rocks also show *M*-type noble-gas isotopes, we cannot preclude the possibility of a genetic relation between such ultramafic nodules and the volcanic-rock source. However, dredged tholeiite samples from Hualalai show definitely higher $^{3}He/^{4}He$ ratios (14-18 R_A) than those of ultramafic nodules (8.6-9.2 R_A) (Kurz and others, 1983). Hence they have no direct genetic relation between them.

For the samples from Salt Lake Crater, we unfortunately have no noble-gas data on volcanic rocks. Since volcanic rocks of the Honolulu Volcanics are reported to have rather lower $^{87}Sr/^{86}Sr$ ratios (about 0.7033) than those of the Koolau Basalt[2] (about 0.7039) (Lanphere and Dalrymple, 1980), there is a possibility that volcanic rocks of the Honolulu Volcanics may have *M*-type noble-gas isotopes. If this is so, then we can regard those ultramafic nodules as related to some source rocks or cumulates that also were a source for volcanic rocks of the Honolulu Volcanics.

In a detailed study of $^{3}He/^{4}He$ ratios for volcanic rocks from the Island of Hawaii, Kurz and others (1983) have revealed that each volcano shows different $^{3}He/^{4}He$ ratios and that the ratio seems to decrease with increasing volume of a volcano and with decreasing age of the volcano. In their results, it is noteworthy that tholeiite samples from Mauna Loa and an alkali basalt from Mauna Kea show very similar $^{3}He/^{4}He$ ratios (7.9-8.6 R_A) to that of

[2]Stratigraphic nomenclature used in chapter is from Langenheim and Clague (chapter 1, part II).

MORB. Rison and Craig (1983) also report a similar value (8.5 R_A) for one Mauna Loa sample from analyzing olivine phenocrysts. Unfortunately, we have no heavier noble-gas data for these samples. However, even these data give us important information to infer the processes that are occurring underneath the Island of Hawaii.

With reference to He isotopes, the He sources should be similar to that of MORB. Hence in the present frame of ideas the He source should be either in the asthenosphere or in the lithosphere itself, since *P*-type noble gases are assumed to be derived from the deeper part of the Earth's interior.

Samples from Loihi give us a unique chance to study the relations of rock types and nodule gas isotopes. Because Loihi Seamount is regarded as the most recent volcano in the evolution of the Hawaiian-Emperor Chain, from it we can get information on an earlier state of a volcano's evolution along the chain. Furthermore, the dredged rocks from the seamount show diverse basalt types, including tholeiitic, transitional, and alkali basalt and basanite, including dunite nodules (Moore and others, 1982).

The He isotopic measurements have shown very high $^3He/^4He$ ratios (up to 32 R_A) and tholeiite samples show generally higher $^3He/^4He$ ratios than those of alkali rocks (Kurz and others, 1983; Rison and Craig, 1983). Since dunite nodules show $^3He/^4He$ ratios similar to that of alkalic lava that included nodules, Kurz and others (1983) have conjectured that the apparent lower $^3He/^4He$ ratios for alkalic rocks might be due to contamination by He included in xenocrysts of nodules. On the other hand, Kaneoka and others (1983), who examined all noble gases in both tholeiitic and alkalic rocks, found that the $^{40}Ar/^{36}Ar$ ratios for lava are not so high as observed in MORB and are still located in the region defined by the three kinds of mixing lines among *P*, *M*, and A components in the $^3He/^4He$-$^{40}Ar/^{36}Ar$ diagram. Only a dunite nodule from Loihi Seamount seems to be an exception. Although this nodule shows a high $^3He/^4He$ ratio (22 R_A), its $^{40}Ar/^{36}Ar$ ratio is also high (4,200). To explain this, Kaneoka and others (1983) have conjectured that only He was equilibrated with the surrounding magma and the nodule had originally *M*-type noble gases.

In Loihi samples, fairly large variation in the $^3He/^4He$ ratio has been observed. This may be a characteristic of the initial state of a volcano's evolution caused by different degrees of contamination with lithospheric and (or) asthenospheric components that are similar to that of MORB.

On the other hand, apparent uniformity in the observed value of noble gases may simply reflect the sampling problem, because we have data only on lava flows of relatively limited time periods of young active volcanoes such as Mauna Loa and Kilauea. In fact, for Haleakala Volcano, we have observed very high $^3He/^4He$ ratios for olivine and augite phenocrysts of ankaramite (32–36 R_A) from the vent known as White Hill Cone (Kaneoka and Takaoka, 1980; Rison and Craig, 1983), which probably belongs to the Pleistocene Kula Volcanics (hawaiite). However, both pyroxene phenocrysts from the A.D. 1790 ankaramite flow in the post erosional Hana Volcanics and olivine phenocrysts from the tholeiitic shield lava of the Honomanu Basalt show *M*-type $^3He/^4He$ ratios of 8.1 R_A and 8.0 R_A, respectively (Rison and Craig, 1983). Except for the Hana Volcanics, such tendency is at variance with that predicted from some trace-element data and from Sr and Nd isotopic ratios for Haleakala Volcano (Chen and Frey, 1983). This means that noble gases (and probably some volatile elements, too) may not always behave similarly with other nonvolatile elements, even in a mantle plume.

HAWAIIAN VOLCANISM AS INFERRED FROM NOBLE-GAS DATA

As discussed previously, Hawaiian volcanism seems to be strongly related to a mantle plume or plumes of deep origin. Noble-gas data require a source material that still retains more of primitive components than does that of MORB (see, for example, Kyser and Rison, 1982; Kaneoka, 1983). If Hawaiian volcanism was initiated by propagation of a tensional fracture through the lithosphere, the magma source should be located in the uppermost part of the asthenosphere. However, it seems difficult to keep such a source in a relatively shallow part of the Earth's interior for a long time, because the source material is inferred to retain primitive components, including He, which would show one of the largest mobilities in the Earth's interior (Kaneoka, 1983).

The $^3He/^4He$ ratios for each volcano in the Hawaiian Islands are plotted against the volume of each volcano in figure 27.8. If we consider only the Island of Hawaii, volcanoes with small volume show high $^3He/^4He$ ratios, and volcanoes with large volume show $^3He/^4He$ ratios similar to that of MORB (for example, Mauna Kea and Manua Loa). This suggests that the contribution of *P*-type source material is larger in the early stage of a volcano's evolution relative to that of *M*-type source material. Such a relation has been shown by Kurz and others (1983). If we include other volcanoes from different islands, however, such systematics seem to be disturbed, as shown in figure 27.8. Volcanic rocks from Haleakala on Maui Island and those from Kauai Island indicate relatively high $^3He/^4He$ ratios in spite of the large volumes of their volcanoes. From Haleakala Volcano, volcanic rocks with $^3He/^4He$ ratios similar to that of MORB have also been reported (Rison and Craig, 1983). Ultramafic nodules from Salt Lake Crater, Oahu Island, show $^3He/^4He$ ratios fairly similar to that of MORB. Hence, the situation may be not so simple as reported initially for samples from the Island of Hawaii. Relatively high $^3He/^4He$ ratios observed for samples from Haleakala Volcano indicate that the *P*-type component of noble gases could have been added even at a later stage in a volcano's evolution.

On the basis of the systematic changes in elemental ratios and $^{87}Sr/^{86}Sr$ and $^{143}Nd/^{144}Nd$ ratios with eruption age for volcanic rocks of Haleakala Volcano, Chen and Frey (1983) have predicted a systematic decrease over time in the rate of contribution of plume-derived material to the formation of a magma. Basically their model seems to explain well the variations of elemental and isotopic data for Hawaiian volcanism. However, the data in figure 27.8 do not always follow the model. As suggested by Rison and Craig (1983), the Honomanu Basalt (shield-building tholeiite) of Haleakala Volcano shows *M*-type He component, whereas *P*-type He component would be expected in the model. Although higher $^3He/^4He$ ratios seem to be accompanied by higher $^{87}Sr/^{86}Sr$ ratios or lower

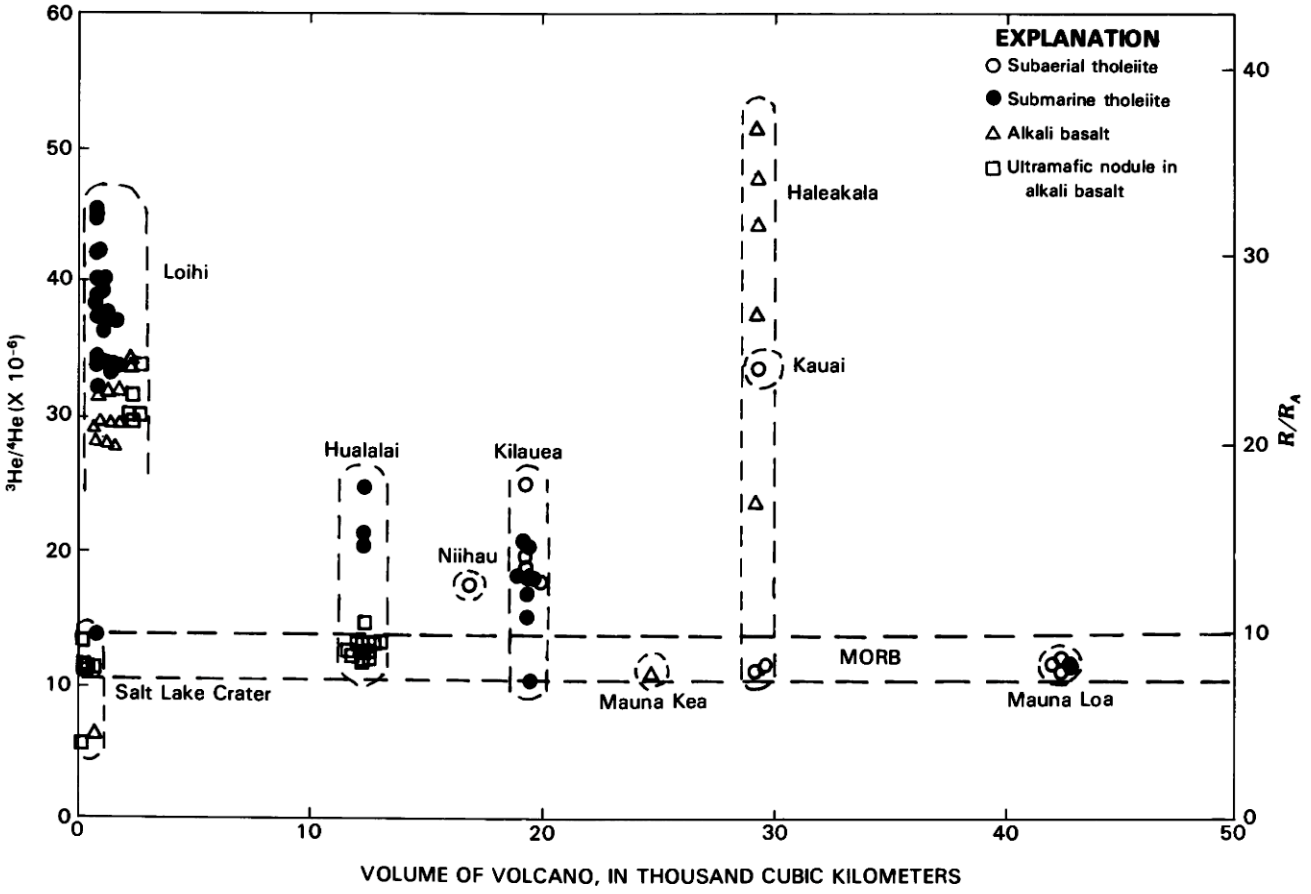

FIGURE 27.8.—Plot of $^3He/^4He$ ratio against volcano volume for Hawaiian volcanoes. Volcano volumes taken from Bargar and Jackson (1974). Typical range of $^3He/^4He$ values for MORB indicated by horizontal dashed lines. Data sources: Craig and Lupton (1976); Kaneoka and Takaoka (1978, 1980); Kyser and Rison (1982); Kurz and others (1982, 1983); Kaneoka and others (1983); Lupton (1983); Rison and Craig (1983).

$^{143}Nd/^{144}Nd$ ratios for Loihi samples (Kurz and others, 1983; Staudigel and others, 1984), such trends are not always retained when the data from other volcanoes are included. Furthermore, although tholeiitic shield lava from the Hawaiian Islands shows generally slightly higher $^{87}Sr/^{86}Sr$ and lower $^{143}Nd/^{144}Nd$ ratios that those of MORB (see, for example, Staudigel and others, 1984), the $^3He/^4He$ ratio is quite similar to the MORB value, at least for Mauna Kea and Mauna Loa. Thus, noble-gas isotopes seem to be not always correlated with the other radiogenic isotopes such as Sr, Nd, and Pb. Such differences probably reflect the different geochemical behavior of noble gases from the other nonvolatile elements. This implies that noble gases would be transported in varying degrees together with other volatile components during the different stages of evolution of Hawaiian volcanoes. Furthermore, the $^3He/^4He$ ratios for Hawaiian rocks have not always varied smoothly. Such noble gases may have been transported in a mantle diapir rather than in a mantle plume.

So far, a number of models for Hawaiian volcanism have been proposed (see, for example, Macdonald, 1968; Chen and Frey, 1983; Sen, 1983; Staudigel and others, 1984). However, those do not take properly into account the noble-gas-isotope signature. As discussed in previous sections, the most significant feature of this signature is the occurrence in Hawaiian lava of much higher $^3He/^4He$ ratios than that of MORB, which strongly suggests the involvement of a source material that contains fairly primordial components and is located in the deeper part of the Earth's interior (lower mantle?). We cannot deny the involvement of oceanic lithosphere during the formation of a magma. As far as the noble gases (and probably volatile components) are concerned, however, the contribution from the oceanic lithosphere would be not so significant as has been suggested for nonvolatile elements (Staudigel and others, 1984). If the age of the oceanic lithosphere is great enough to have increased the $^{87}Sr/^{86}Sr$ ratio, the $^3He/^4He$ ratio would have been lowered by the addition of radiogenic ^4He, resulting in a lower $^3He/^4He$ ratio than that of MORB. When the $^3He/U$ ratio can be postulated to be similar to that of the MORB source, the $^3He/^4He$ ratio would have to be similar also. However, it is very difficult to conjecture that the $^3He/U$ ratio is maintained

higher than that of the MORB source, because He would be easily lost during formation of the lithosphere around the ridge, resulting in lowering the $^3He/U$ ratio. If the lower part of the oceanic lithosphere is formed by the addition of the components of the asthenosphere, its isotopic composition would be similar to that of MORB. At least some Hawaiian ultramafic nodules might have been derived from such lower lithosphere.

Volcanic rocks from Loihi Seamount show definitely higher $^3He/^4He$ ratios than those of Kilauea (fig. 27.8). This implies that the contribution of *P*-type component is larger for Loihi samples than for Kilauea samples as indicated by the He data. Large variations in the observed values can be explained by varying degrees of addition of *M*-type component during the ascent of volatile-enriched mantle diapirs. It is true that magma chemistry as determined by the last depth of equilibration would have little bearing on the initial depth of origin for source diapirs (Staudigel and others, 1984). Even the voluminous outpourings are not always good indicators for characterizing the source material of a plume, because we cannot exclude the possibility of interaction during the ascent of a mantle diapir with *M*-type source materials. The $^3He/^4He$ ratio may be used more efficiently to indicate the plume component for noble-gas (volatiles) components.

From the noble-gas data together with those of other radiogenic isotopes, we can summarize a model for Hawaiian volcanism as shown schematically in figure 27.9.

The initial (infant) stage of Hawaiian volcanism would be exemplified by Loihi Seamount (fig. 27.9*A*). When the relatively cold lithosphere approaches the hot spot, volcanism would be initiated by the rise of volatile-enriched mantle diapirs with *P*-type noble gases derived from the deeper part of the Earth's interior

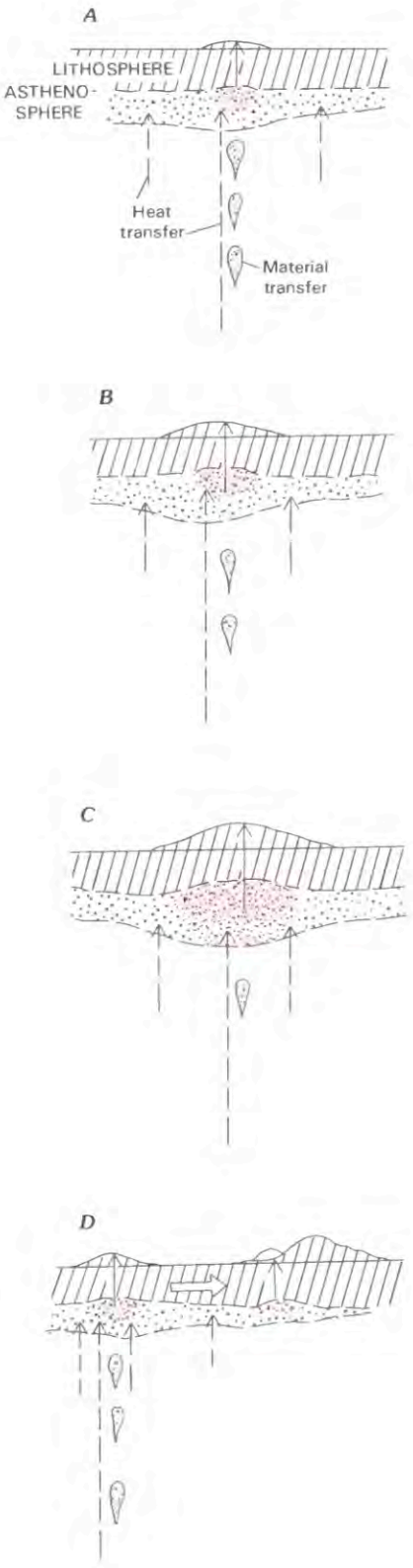

FIGURE 27.9.—Schematic model to show the evolution of Hawaiian volcanism. Red color shows regions of intensive partial melting. ***A,*** Infant stage: volcanism is initiated by rise of diapir(s) from hot-spot source in Earth's deep interior (lower mantle?). Diapir will be enriched in volatile components. Possible example of this stage is Loihi Seamount. ***B,*** Early part of tholeiitic shield-building stage: diapirs still rise through asthenosphere and lithosphere. Partially melted zone will be increased because of accumulation of heat energy through diapirs and conduction, causing downward swelling and thinning of lithosphere over hot spot. Plume-type source material will mix with surrounding MORB-type source material during rise of diapirs(s) through asthenosphere and lithosphere (example, Kilauea Volcano). ***C,*** Later part of tholeiitic shield-building stage: contribution from diapir(s) probably much reduced. Instead, most melt may be derived from partially melted zone in uppermost part of asthenosphere. Most MORB-type He might be supplied from this portion (example, Mauna Loa). Although no example is shown here, in a volcano at the postcaldera stage, no significant contribution from diapirs can be expected. Diminishing heat and material supplies from hot-spot source cause eruption frequency of a volcano to decrease. Degrees of partial melting also decrease, resulting in production of alkalic basalt (example, Kula Volcanics, Haleakala Volcano). ***D,*** Posterosional stage: when a volcano migrates far away from hot-spot area, some melt would still remain at bottom of lithosphere. Addition of conductive heat from initial thermal anomaly and release of latent heat from solidification of melt may form some melt pockets under the volcano and produce alkalic and (or) nephelinitic rocks. Source material for such rocks is quite similar to that of MORB (example, Honolulu Volcanics, Oahu Island).

(lower mantle?). During ascent to the surface, such diapirs will interact with surrounding materials at various depths both in the asthenosphere and the lithosphere. Such interaction would have caused large variation in both isotopic and chemical signatures of magmas. We assume the existence under the lithosphere of a partially melted zone enriched with *M*-type noble gases that is indicated seismically as the low-velocity zone. The occurrence of such a zone may help the interaction between the diapirs and the surrounding materials.

The second stage is that of tholeiitic shield-building (fig. 27.9*B*, *C*). During this stage, melting in the partially melted zone of the asthenosphere would be increased because of the addition of heat from the ascending diapirs and by conduction. This may cause swelling of the partially melted zone and thinning of the lithosphere over the hot-spot area. During such processes, *M*-type noble gases might be enriched in the partially melted zone under the lithosphere. At Kilauea Volcano (fig. 27.9*B*), the contribution from mantle diapirs will still be significant, but the mixing rate of *M*-type noble gas will increase, resulting in lower $^{3}He/^{4}He$ and $^{87}Sr/^{86}Sr$ ratios and higher $^{143}Nd/^{144}Nd$ ratios compared with those of the infant stage.

On the other hand, for Mauna Kea and Mauna Loa Volcanoes (fig. 27.9*C*), the role of diapirs may be much less than for Kilauea Volcano. As shown in figure 27.8, we observe no difference in the $^{3}He/^{4}He$ ratio between these volcanoes and MORB. This implies that even when voluminous out-pourings occur from these volcanoes, it does not always mean a contribution from mantle diapirs as far as He isotopes are concerned. On the other hand, $^{87}Sr/^{86}Sr$ and $^{143}Nd/^{144}Nd$ ratios are still different for these volcanoes from those of MORB (see, for example, Staudigel and others, 1984). This suggests that most He was derived from the partially melted zone in the uppermost asthenosphere and that the voluminous outpourings of lava were also caused by the expansion of the partially melted zone compared with the infant stage. At this stage, the hot spot may act mainly as a heat source, but not the main source for adding materials, though some small diapirs will still rise. The isotopic ratios for Sr and Nd may be explained by the interaction of melts formed in the asthenosphere with the oceanic lithosphere. The occurrence of mantle metasomatism is possible (Wright, 1984).

Another possibility is that the contribution from diapirs still continues but the diapirs are less enriched in volatile components than those of the infant stage. Hence, even if isotopic ratios for nonvolatile elements are still different from those of MORB, the $^{3}He/^{4}He$ ratio might become similar to that of MORB because of mixing with the volatile-enriched *M*-type source in the partially melted zone. At present, we have no good evidence to select one or the other possibility. In both cases, however, most He would have been derived from the partially melted zone in the uppermost asthenosphere, and the occurrence of such a zone is significant for Hawaiian volcanism at this stage.

When the volcano migrates away from the hot spot, the supply of heat and materials will be diminished. The rate of melting in the partially melted zone also decreases, resulting in the decrease of eruption frequency of a volcano. Total amounts of melt produced would also decrease. Since the degree of partial melting would also decrease, alkalic basalt would be dominant. Isotopic ratios for both nonvolatile elements and noble gases may approach those of MORB. However, relatively primitive ratios may still be observed in some cases, since the addition of diapir components would dominate the isotopic ratios in the melt because of the mass balance between melts from diapirs and the surrounding materials. The very high $^{3}He/^{4}He$ ratios for the Kula Volcanics of Haleakala Volcano (Kaneoka and Takaoka, 1980; Rison and Craig, 1983) might have originated in such a way.

The final stage of Hawaiian volcanism is identified as the posterosional stage, which occurs after a period of volcanic quiescence. In this stage, no contribution from diapirs is expected because the volcano has migrated far away from the hot spot. At the bottom of the oceanic lithosphere, some melt remains after producing alkalic basalt. The addition of conductive heat from the initial thermal anomaly together with the release of some latent heat during solidification of melt may form some melt pockets under a volcano that produce alkalic and or nephelinitic rocks. In this case, the source materials would be mostly the *M*-type material in the uppermost asthenosphere. Thus, it is reasonable to conjecture that such volcanic rocks would show values for isotopic ratios, including $^{3}He/^{4}He$ ratios, very similar to those of MORB. The Honolulu Volcanics on Oahu Island and the Hana Volcanics at Haleakala Volcano, Maui Island, are good examples of such late volcanism (fig. 27.9*D*).

This model is rather qualitative, and the major scheme is not seriously different from those which have been proposed before. Furthermore, the present scheme shows only a general trend; small variations would occur on a local scale. However, it is worth noting that voluminous outpourings of Hawaiian volcanoes do not always reflect direct matieral supply from the hot-spot source but may rather reflect the combined effects of material transfer plus heat supply. The occurrence of a partially melted zone under the lithosphere would play an important role in controlling the activity and characteristics of Hawaiian volcanoes. The occurrence of such a partially melted zone might be related to the conductive transfer of heat from the deeper part of the Earth together with the existence of the overlying, less conductive lithosphere acting as an insulator.

To clarify further and in greater detail the evolutionary scheme for Hawaiian volcanism, more systematic isotopic surveys, both of the noble gases and of other elements are required.

REFERENCES CITED

Allègre, C.J., Staudacher, T., Sarda, P. and Kruz, M., 1983, Constraints on evolution of Earth's mantle from rare gas systematics: Nature, v. 303, no. 5920, p. 762-766.

Anderson, D.L., 1982, Isotopic evolution of the mantle: a model: Earth and Planetary Science Letters, v. 57, no. 1, p. 13-24.

Barger, K.E., and Jackson, E.D., 1974, Calculated volumes of individual shield volcanoes along the Hawaiian-Emperor Chain: Journal of Research of the U.S. Geological Survey, v. 2, p. 545-550.

Chen, C.-Y., and Frey, F.A., 1983, Origin of Hawaiian tholeiite and alkalic basalt: Nature, v. 302, no. 5911, p. 785-789.

Craig, H., and Lupton, J.E., 1976, Primordial neon, helium and hydrogen in oceanic basalts: Earth and Planetary Science Letters, v. 31, no. 3, p. 369-385.

Dalrymple, G.B., and Moore, J.G., 1968, Argon-40: excess in submarine pillow basalts from Kilauea Volcano, Hawaii: Science, v. 161, no. 3846, p. 1132-1135.

DePaolo, D.J., 1981, Nd isotopic studies: some new perspectives on earth structure and evolution: Eos, Transactions, American Geophysical Union, v. 62, no. 14, p. 137-140.

Dymond, J., and Hogan, L., 1978, Factors controlling the noble gas abundance patterns of deep sea basalts: Earth and Planetary Science Letters, v. 38, no. 1, p. 117-128.

Fisher, D.E., 1983, Rare gases from the undepleted mantle?: Nature, v. 305, no. 5932, p. 298-300.

Funkhouser, J.G., Fisher, D.E., and Bonatti, E., 1968, Excess argon in deep-sea rocks: Earth and Planetary Science Letters, v. 5, no. 2, p. 95-100.

Funkhouser, J.G., and Naughton, J.J., 1968, Radiogenic helium and argon in ultramafic inclusions from Hawaii: Journal of Geophysical Research, v. 73, no. 14, p. 4601-4607.

Gramlich, J.W., and Naughton, J.J., 1972, Nature of source material for ultramafic minerals from Salt Lake Crater, Hawaii, from measurement of helium and argon diffusion: Journal of Geophysical Research, v. 77, no. 17, p. 3032-3042.

Hayatsu, A., and Waboso, C.E., 1982, The solubility of rare gases in rock melts: implications for K-Ar dating and Earth degassing: *in* Abstracts for the Fifth International Conference on Geochronology, Cosmochronology and Isotope Geology, p.139.

Hennecke, E.W., and Manuel, O.K., 1975, Noble gases in Hawaiian xenoliths: Nature, v. 257, no. 5529, p. 778-780.

Jackson, E.D., and Wright, T.L., 1970, Xenoliths in the Honolulu Volcanic Series, Hawaii: Journal of Petrology, v. 11, part 2, p. 405-430.

Jacobsen, S.B., and Wasserburg, G.J., 1979, The mean age of mantle and crustal reservoirs: Journal of Geophysical Research, v. 84, no. B13, p. 7411-7427.

Kaneoka, I., 1980, Rare gas isotopes and mass fractionation: an indicator of gas transport into or from a magma: Earth and Planetary Science Letters, v. 48, no. 2, p. 284-292.

———1983, Noble gas constraints on the layered structure of the mantle: Nature, v. 302, no. 5910, p. 689-700.

Kaneoka, I., and Takaoka, N., 1978, Excess ^{129}Xe and high $^{3}He/^{4}He$ ratios in olivine phenocrysts of Kapuho lava and xenolithic dunites from Hawaii: Earth and Planetary Science Letters, v. 39, no. 3, p. 382- 386.

———1980, Rare gas isotopes in the Hawaiian ultramafic nodules and volcanic rocks: constraints on genetic relationships: Science, v. 208, no. 4450, p. 1366-1368.

———1985, Noble-gas state in the Earth's interior—some constraints on the present state: Chemical Geology, v. 52, no. 1, p. 75-95.

Kaneoka, I., and Takaoka, N., and Aoki, K., 1978, Rare gases in mantle-derived rocks and minerals, *in* Alexander, E.C., Jr., and Ozima, M., eds., Terrestrial Rare Gases: Tokyo, Center for Academic Publications, p. 71-84.

Kaneoka, I., and Takaoka, N., and Clague, D.A., 1983, Noble gas systematics for coexisting glass and olivine crystals in basalts and dunite xenoliths from Loihi Seamount: Earth and Planetary Science Letters, v. 66, p. 427-437.

Kurz, M.D., Jenkins, W.J., and Hart, S.R., 1982, Helium isotopic systematics of oceanic islands and mantle heterogeneity: Nature, v. 297, no. 5861, p. 43-47.

Kurz, M.D., Jenkins, W.J., Hart, S.R., and Clague, D., 1983, Helium isotopic variations in volcanic rocks from Loihi Seamount and the Island of Hawaii: Earth and Planetary Science Letters, v. 66, p. 388-406.

Kyser, T.K., and Rison, W., 1982, Systematics of rare gas isotopes in basic lavas and ultramafic xenoliths: Journal of Geophysical Research, v. 87, no. B7, p. 5611-5630.

Lanphere, M.A., and Dalrymple, G.B., 1980, Age and strontium isotopic composition of the Honolulu Volcanic Series, Oahu, Hawaii: American Journal of Science, v. 280-A, part 2, p. 736-751.

Lovering, J.F., and Richards, J.R., 1964, Potassium-argon age study of possible lower-crust and upper-mantle inclusions in deep-seated intrusions: Journal of Geophysical Research, v. 69, no. 22, p. 4895-4901.

Lupton, J.E., 1983, Terrestrial inert gases: isotope tracer studies and clues to primordial components in the mantle: Annual Review of the Earth and Planetary Sciences, v. 11, p. 371-414.

Lupton, J.E., and Craig, H., 1975, Excess ^{3}He in oceanic basalts: evidence for terrestrial primodial helium: Earth and Planetary Science Letters, v. 26, no. 2, p. 133-139.

Macdonald, G.A., 1968, Composition and origin of the Hawaiian lavas: Memoir of the Geological Society of America, no. 116, p. 477-522.

Moore, J.G., Clague, D.A., and Normark, W.R., 1982, Diverse basalt types from Loihi Seamount, Hawaii: Geology, v. 10, no. 2, p. 88-92.

Morgan, W.J., 1971, Convection plumes in the lower mantle: Nature, v. 230, no. 5288, p. 42-43.

Noble, C.S., and Naughton, J.J., 1968, Deep-ocean basalts. Inert gas content and uncertainties in age dating: Science, v. 162, no. 3850, p. 265-269.

O'Nions, R.K., Hamilton, P.J., and Evensen, N.M., 1977, Variations in $^{143}Nd/^{144}Nd$ and $^{87}Sr/^{86}Sr$ ratios in oceanic basalts: Earth and Planetary Science Letters, v. 34, no. 1, p. 13-22.

Ozima, M., and Podosek, F.A., 1983, Noble gas geochemistry: Cambridge University Press, 367 p.

Ozima, M., and Zashu, S., 1983, Noble gases in submarine pillow volcanic glasses: Earth and Planetary Science Letters, v. 62, no. 1, p. 24- 40.

Rison, W., and Craig, H., 1983, Helium isotopes and mantle volatiles in Loihi Seamount and Hawaiian Island basalts and xenoliths: Earth and Planetary Science Letters, v. 66, p. 407-426.

Sen, G., 1983, A petrologic model for the constitution of the upper mantle and crust of the Koolau shield, Oahu, Hawaii, and Hawaiian magmatism: Earth and Planetary Science Letters, v. 62, no. 2, p. 215-228.

Shimizu, N., 1975, Geochemistry of ultramafic inclusions from Salt Lake Crater, Hawaii and from Southern African kimberlites: Physical Chemistry of the Earth, v. 9, p. 655-669.

Staudigel, H., Zindler, A., Hart, S.R., Leslie, T., Chen, C.-Y., and Clague, D.A., 1984, The isotopic systematics of a juvenile intraplate volcano: Pb, Nd, and Sr isotope ratios of basalts from Loihi Seamount, Hawaii: Earth and Planetary Science Letters, v. 69, no. 1, p. 13-19.

Wilson, J.T., 1963, A possible origin of the Hawaiian Islands: Canadian Journal of Physics, v. 41, p. 863-870.

Wright, T.L., 1984, Origin of Hawaiian tholeiite: a metasomatic model: Journal of Geophysical Research, v. 89, no. B5, p. 3233-3252.

HAWAIIAN ERUPTIVE GASES

By L. Paul Greenland

ABSTRACT

Analysis of eruptive gases began at Kilauea Volcano in 1912. After the classic gas collections of 1917–19, there was a lapse of 40 years until sampling of eruptive gases recommenced in 1960. This paper summarizes results of gas analyses from Kilauea for the 1912–19 and 1968 Halemaumau eruptions, two summit eruptions in 1982, the 1960, 1965, 1977, and 1983–84 east-rift eruptions, and a shallow southwest-rift intrusion in 1981. Also included are results from the 1919 and 1984 eruptions of Mauna Loa. These data show the following: (1) Hawaiian eruptive gases predominantly have one of two compositions, defined by an atomic carbon/sulfur ratio (C/S) of ~0.2 for gases exsolving from magma that has had even brief storage in shallow summit reservoirs, and (much less commonly) a C/S ratio of ~2 for gases associated with eruptions of magma directly from the mantle. (2) The major causes of compositional variation in these gases is the introduction of varied amounts of assimilated crustal water and near-surface mixing of meteoric water. (3) The total volatile content of Hawaiian magma stored in summit reservoirs is approximately uniform and amounts to less than 0.5 weight percent.

INTRODUCTION

Studies of eruptive gas at Kilauea Volcano began in 1912 with collections from an active lava lake by Day and Shepherd (1913). Because of the sampling technique, only partial analyses of these gases could be obtained. Improvements in sampling and analytical procedures resulted in the first complete volcanic gas analyses in 1917 (Shepherd, 1919) and the culminating studies of T.A. Jaggar's classic collections of 1918–19 (Shepherd, 1921). Between 1919 and 1980, sporadic collections of volcanic gas associated with eruptive activity at Kilauea were obtained from vents during the 1960 east-rift eruption (Heald and others, 1963), from an actively filling lava lake (Finlayson and others, 1968), and from the 1977 east-rift eruption (Graeber and others, 1979).

Systematic gas studies were reinstituted at the Hawaiian Volcano Observatory with the installation of modern gas-analysis facilities in 1980. Partial analyses were obtained of gases from a near-surface intrusion in 1981 and from two summit eruptions in 1982; both partial and complete analyses have been obtained from the episodic east-rift eruption of 1983-4 and from the 1984 eruption of Mauna Loa. The present paper summarizes previous work on eruptive gases and describes heretofore unpublished results of the 1981–84 partial analyses. Complete gas analyses of the 1983–84 east-rift eruption of Kilauea and of the Mauna Loa eruption are being described concurrently (Greenland, chapter 30) and will not be considered here.

To improve comparability, all analyses cited from the literature have been recalculated to an air-free basis. Furthermore, I have followed Matsuo (1962) in apportioning the S_2 reported in the 1917–19 analyses to H_2S and SO_2, and, where reported, SO_3 to SO_2; for the 1981–84 partial analyses, I have assumed thermodynamic equilibrium in the gases in order to estimate apparent-equilibrium H_2O and H_2S contents. The effects of oxidation and of temperature on the composition of volcanic gas samples have been avoided by considering the analyses on an atomic basis (that is, all hydrogen-bearing species are combined to yield a value for total atomic hydrogen, and so on), and these values form the basis for most of the discussion.

ACKNOWLEDGMENTS

I am grateful to E. Wolfe and T. Wright for thorough and helpful reviews of the manuscript.

RESULTS AND DISCUSSION

GAS COLLECTIONS FROM 1912 TO 1919

Analyses of gases collected from a continuously active lava lake in Kilauea's caldera over this period are fiven in table 28.1, which also includes two samples from the 1919 eruption of Mauna Loa. The equilibrium compositions of the 1918–19 gas collections as estimated by Gerlach (1980) also are included in table 28.1 for reference.

The 1912 gases were collected by a pumping technique, and thus only the concentrations of gases insoluble in the acid aqueous condensate (CO_2, H_2, and CO) could be determined; these provide too little information for interpretation, though it is notable that temperatures (1,150–1,250 °C) inferred from the CO_2/CO ratio (from equations 1 and 5, see below) are reasonable for a protracted summit eruption.

The 1917–19 analyses have been discussed extensively (Shepherd, 1938; Jaggar, 1940; Matsuo, 1962; Nordlie, 1971; Gerlach, 1980); conclusions have ranged from Shepherd's (1921, p. 87) "We are not here dealing with a mixture of gas which is definite in composition and given off steadily by the magma. Each bubble has its own composition, ***" to Gerlach's (1980, p. 303) "***(after making allowance for meteoric water contamination)***(1) the erupted gases initially had compositions closely approaching equilibrium, and (2) the reacting gases were quenched at some temperature near the collection temperature." These views are less far

TABLE 28.1.—*Composition of Hawaiian eruptive gases, 1912–1919*

[n.d., not determined; --, not detected]

Sample	Constituents (mole percent)						Atomic ratios	
	H_2O	H_2	CO_2	CO	SO_2	H_2S	H/S	C/S
1912 Kilauea Summit (Day and Shepherd, 1913)								
D–1	n.d.	7.2	23.8	5.6	n.d.	n.d.	n.d.	n.d.
D–2	n.d.	6.7	58.0	3.9	n.d.	n.d.	n.d.	n.d.
D–8	n.d.	7.5	62.3	3.5	n.d.	n.d.	n.d.	n.d.
D–11	n.d.	7.0	59.2	4.6	n.d.	n.d.	n.d.	n.d.
D–17	n.d.	10.2	73.9	4.0	n.d.	n.d.	n.d.	n.d.
1917 Kilauea Summit (Shepherd, 1919)								
S–1	87.8	5.45	3.42	1.34	.809	1.20	96.7	2.36
S–2	61.4	2.16	28.7	.575	6.13	1.04	18.0	4.08
S–3	20.5	1.78	38.1	1.62	35.3	2.72	1.31	1.04
S–4	69.7	1.28	10.0	3.53	5.16	10.3	10.5	.875
S–5	70.2	1.66	10.3	1.21	12.7	3.93	9.11	.692
S–6	90.6	.212	1.99	.827	2.77	3.63	29.5	.440
S–7	67.8	.803	18.2	.655	11.0	1.50	11.2	1.51
S–8	75.5	.704	15.4	.452	7.35	.657	19.2	1.98
S–9	64.7	1.96	8.98	.885	19.9	3.57	5.98	.420
S–10	90.5	.372	1.55	.433	2.39	4.78	26.7	.277
1918–19 Kilauea Summit (Shepherd, 1921)								
J–2	85.3	--	6.58	--	8.14	--	21.0	0.808
J–3	83.6	.156	6.90	.229	9.10	--	18.4	.783
J–4	87.4	.175	6.99	.144	5.05	.206	33.4	1.36
J–6	98.4	.088	1.09	.200	.175	--	1130.	7.37
J–8	37.1	.493	48.9	1.50	11.9	.055	6.30	4.22
J–10	60.0	.118	19.4	.130	20.2	.079	5.94	.963
J–11	64.2	.334	21.8	.615	12.7	.348	9.95	1.72
J–12	97.8	.081	1.43	.050	.561	.094	299.0	2.26
J–13	69.9	.994	17.6	.601	10.8	.124	13.0	1.67
J–14	79.1	.175	15.2	.484	4.88	.137	31.7	3.13
J–15	79.0	.107	12.3	.139	8.40	.043	18.7	1.47
J–16	68.4	.692	18.6	.578	11.5	.206	11.8	1.64
J–17	80.2	.587	11.7	.374	6.72	.324	23.0	1.71
J–18	64.8	.869	18.4	.775	14.8	.307	8.73	1.27
1918–19 Kilauea Summit: estimated equilibrium composition (Gerlach, 1980)								
J–8	37.1	.490	48.9	1.51	11.8	0.040	6.36	4.26
J–11	40.1	.550	36.7	1.03	21.1	.200	3.84	1.77
J–13	69.3	1.01	17.8	.620	10.9	.080	12.8	1.68
J–14	35.1	.540	47.4	1.52	15.1	.150	4.69	3.21
J–16	60.4	.870	23.2	.740	14.3	.140	8.50	1.66
J–17	66.0	1.02	20.3	.620	11.4	.320	11.5	1.78
J–18	58.1	1.03	21.8	.930	17.5	.170	6.71	1.29
1919 Mauna Loa (Shepherd, 1920)								
ML–1	75.4	--	3.84	0.03	3.30	--	45.7	1.16
ML–2	67.4	.01	6.42	.19	10.07	--	13.5	.66

apart than one might think: Gerlach (1980) recognizes the effects of oxidation and of shallow degassing of CO_2 on these compositions; furthermore, thermodynamic analyses such as Gerlach's are concerned with the relative proportions of oxidized and reduced species rather than the relative proportions of all hydrogen-bearing, carbon-bearing, and sulfur-bearing species. In addition, it may indeed be possible that each bubble has its own composition and yet approaches equilibrium when one considers the possible effects of differential degassing with pressure and of the incorporation of air and water into the vent system by a chimney effect. The highly porous edifice of Kilauea combines with the high-temperature vertical pipes of the fissure system to produce a chimney effect whereby air, water vapor, and other gases are pulled through the edifice into the depths of the fissure, heated, expanded, and expelled to the surface. A similar effect has been observed at Pagan Volcano (see Banks and others, 1984.)

The effects of oxidation and temperature, but not of water contamination, can be avoided by considering the analyses on an atomic basis. Table 28.1 includes the analytical values normalized to atoms of S for ease of comparison, and figure 28.1 is a ternary atomic H-C-S plot of these data. If all of these analyses were related simply by water contamination (with or without oxidation effects), the analyses would plot along a water-control line such as the two shown in figure 28.1; in fact, however, there is a large amount of scatter in figure 28.1, implying considerable variation in carbon/sulfur ratio independent of the obvious water variation. Gerlach (1980) attributed this variation to the preferential degassing of the very insoluble CO_2, and he suggested that the most CO_2-rich samples are most characteristic of undegassed magma. On the other hand, preferential degassing of CO_2 at least raises the possibility of the contamination of eruptive magma with deeper released CO_2. Several observations may be made from the plot in figure 28.1: (1) although the 1917 samples show considerably more scatter than the 1918–19 collections, perhaps because of the poorer sampling conditions of 1917 noted by Shepherd (1921), the compositions of the two groups overall are indistinguishable. (2) As noted by Shepherd (1920), the two Mauna Loa samples are similar in composition to the Kilauea samples. (3) The 1918–19 analyses selected as superior by Gerlach (1980) show much less scatter and much closer adherence to a water-control line than does the original complete set. (4) Nearly all samples have an atomic C/S ratio much higher than do collections made since 1979, which follow the water-control line with C/S = 0.18 in figure 28.1. The third observation

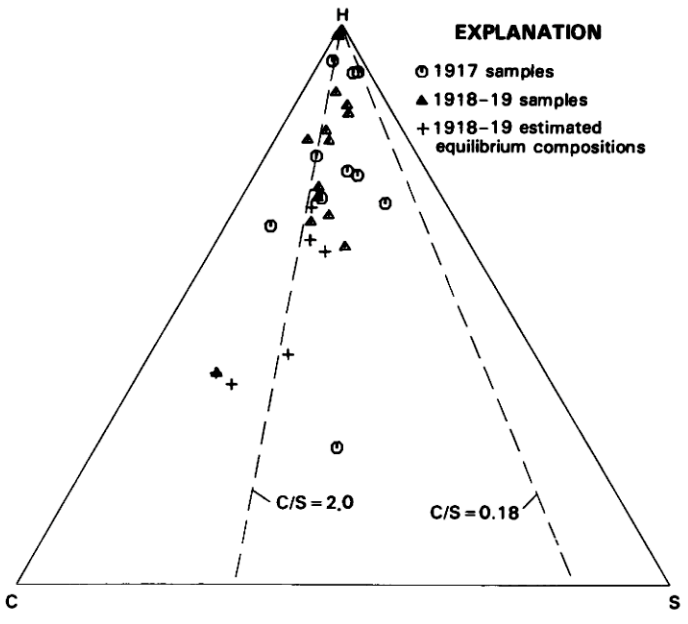

FIGURE 28.1.—Ternary H-C-S plot for 1917–19 Hawaiian eruptive gases. Data from table 28.1. Dashes indicate water-control lines for specific values of the C/S ratio. Atomic hydrogen has been reduced by a factor of 0.5 to increase clarity.

above raises the unanswerable question of how much of the observed scatter in the 1917–19 analyses might be due to analytical error; a modern analyst reading Shepherd's (1925) account of his analytical procedure can only be awed by his skill and meticulous attention to detail, while remaining aware of the inherent limitations imposed by the equipment available to him. The fourth observation above has been attributed to degassing of CO_2 during storage of magma in the summit reservoir of Kilauea, and it forms the basis of recent models (Gerlach and Graeber, 1985; Greenland and others, 1985) of magma-degassing processes at Kilauea.

The two samples from Mauna Loa have been largely neglected in the literature, perhaps because both are highly oxidized and both were collected from a low-temperature (~300 °C) ground crack near advancing lava and about 100 m from the eruptive fissure. However, oxidation does not affect the atomic composition, and it has been my experience that such sampling sites at Kilauea frequently provide excellent gas samples. The significance of these samples is that their C/S ratio is closer to that of the 1917–19 Kilauea collections than to the much lower ratio found for the 1984 Mauna Loa eruption. The distinction between high 1917–19 and low 1983–84 C/S ratios at Kilauea has been attributed to degassing during storage in the summit reservoir (Gerlach and Graeber, 1985; Greenland, and others, 1985; Greenland, in press), and the same mechanism has been invoked to account for the low C/S ratios of the 1984 Mauna Loa gases (Greenland, chapter 30). However, the 1919 Mauna Loa eruption was also a rift eruption and thus the magma would be expected to have passed through, and been degassed in, the summit reservoir; therefore, it is not obvious how the different C/S ratios of the 1919 and 1984 eruptions are to be accounted for. Perhaps the very high content of SO_3 shown in the analysis of 1919 gas (Shepherd, 1920) led to condensation of H_2SO_4 and reaction with wallrock; also, the chemistry of lava erupted on the southwest rift zone differs from that of the northeast rift zone (T.L. Wright, written commun., 1985), indicating a possibility of different storage reservoirs for the two rifts.

KILAUEA GAS COLLECTIONS FROM 1920 TO 1979

Gas collections representing the 1959 Kilauea Iki eruption were made from the degassing cinder cone of Puu Puai and from drill holes in the cooling lava lake (Heald and others, 1963). Both of these sites give information on the degassing of lava after eruption but are only indirectly related to eruptive magmatic gas compositions and will not be considered here.

Three samples were collected from the 1960 east-rift eruption at Kapoho (table 28.2). These samples, collected from a high-temperature fumarole near a lava fountain, are remarkable in showing a significant amount of CH_4 and extremely high water content and C/S ratio. Heald and others (1963) suggest, very reasonably, that these samples have been contaminated by meteoric water and by buried organic matter. In view of the probable high degree of contamination, these analyses shed little light on the nature of magmatic gases.

TABLE 28.2.—*Composition of eruptive gases from Kilauea, 1920–1979*

[n.d., not determined; --, not detected]

Sample	Constituents (mole percent)							Atomic ratios	
	H_2O	H_2	CO_2	CO	SO_2	H_2S	CH_4	H/S	C/S
Kapoho, 1960 East Rift (Heald and others, 1963)									
Ka–1	97.2	0.373	2.34	0.059	0.009	--	0.047	22,000.0	267.0
Ka–2	97.5	.394	1.97	.019	.152	--	.034	1,290.0	13.1
Ka–4	97.2	.432	2.21	.086	.001	.031	.023	6,100.0	71.8
Makaopuhi, 1965 East Rift Lava Lake (Finlayson and others, 1968)									
26–M	67.1	--	8.54	--	24.4	--	--	5.50	0.35
27–M	98.0	.057	1.90	--	--	--	--	n.d.	n.d.
28–M	87.5	.137	1.96	--	6.61	3.79	--	17.6	.19
29–M	97.0	1.125	1.92	--	--	--	--	n.d.	n.d.
38–M	95.8	.011	.597	--	3.60	--	--	26.6	.17
Halemaumau Fountain, 1968 (Naughton and others, 1969)									
HMM–1	95.0	n.d.	4.0	n.d.	1.0	n.d.	n.d.	190.0	4.0
1977 East Rift (Graeber and others, 1979)									
G–5	89.1	--	5.06	--	5.45	--	--	32.7	0.93
G–6	96.9	--	1.99	--	.84	--	--	235.	2.38
G–7	93.6	--	1.87	--	4.42	--	--	42.3	.42

Table 28.2 gives the analyses of five gas samples collected from the filling lava lake at Makaopuhi during the 1965 east-rift eruption. (For further analyses of gas samples from the cooling lava lake, see Finlayson and others, 1968). As shown by the low content of H_2 and the absence of CO, these samples are highly oxidized; the very high water content in four of the samples and the absence of sulfur species in two also raises doubts about the quality of the samples. Nevertheless, on an atomic basis, the three samples that contain detectable sulfur have C/S ratios very similar to the ratios observed in the 1983–84 east-rift eruption (see below) and two of these have H/S ratios in the range of the later analyses. Therefore, although these samples have been subjected to oxidation and, probably, contamination with meteoric water, they are consistent with suggestions (Gerlach and Graeber, 1985; Greenland and others, 1985) that all summit-stored magma at Kilauea has about the same composition of volatiles.

In 1968, Naughton and others (1969) made an interesting direct measurement of the major gases in a lava fountain (Halemaumau eruption of 1967–68, table 28.2) using an infrared technique. Naughton and others (1969) stress the exploratory nature of their study and the tentativeness of the results; nonetheless, fountain-gas measurements obviously are impossible to obtain by conventional sampling procedures, and it is encouraging to note the similarity of this analysis, particularly in C/S ratio, to those of the 1917–19 Halemaumau samples (table 28.1). The high water content in this analysis may be due to uncertainties inherent in the technique (a very large, and not entirely certain, correction was required for atmospheric water in the light path). However, in view of the observation that degassing of melt continues within the fountain (Swanson and Fabbi, 1973), it may be that fountain gas is enriched in water, which, because of its high solubility in the melt, is the last gas to be exsolved. It is unfortunate that this potentially rewarding technique has not been pursued.

Table 28.2 gives analyses of three gas samples from the 1977 east-rift eruption (Graeber and others, 1979). These samples were collected from one of the main vents of the fissure eruption three days after eruption of the sampled vent had ceased; the observation that the samples were almost entirely air and completely oxidized parallels my experience in sampling similar sites during the 1982 summit eruptions, the 1983–84 east-rift eruption, and the 1984 Mauna Loa eruption: sampling gases from major vents after fountaining ceases during fissure eruptions seems unrewarding. A remarkable feature of these analyses is the great variation in C/S ratio, which ranges from 0.4 to 2.4 in the three samples collected within 15 minutes of each other at the same vent. This is a greater range than shown in 14 months of the 1983–84 eruption (see below). Graeber and others (1979) observed reddish flame at this vent during the night, and it may be that the varying C/S ratio reflects pyrolyzing organic matter swept into the vent by the chimney effect, a phenomenon recognized frequently during early stages of the 1983–84 eruption.

KILAUEA GAS COLLECTIONS FROM 1980 TO 1982

During this period, gas samples were collected from a shallow intrusion into the southwest rift zone and from two summit eruptions. Gas samples during these events were collected in flowthrough bottles. The sampling technique and subsequent gas chromatographic analysis have been described previously and the results compared with conventional techniques (Greenland, 1984).

Only partial analyses (H_2, CO_2, CO, and SO_2) could be made of these samples, and, for comparison with other eruptions, it is necessary to make an estimate of the H_2O and H_2S content of the gases. Following the procedure described elsewhere (Greenland, chapter 30), equilibrium constants for the elementary oxidation reactions of the major gases can be expressed as

$$\log K1 = 2\log[CO_2/CO] - \log[O_2] \quad (1)$$

$$\log K2 = 2\log[H_2O/H_2] - \log[O_2] \quad (2)$$

$$\log K3 = 2\log[SO_2/H_2S] + \log[H_2] - \log[O_2] \quad (3)$$

and, over a limited temperature range, the temperature dependence of the equilibrium constant can be approximated by

$$\log K = [A/T] + B, \quad (4)$$

where A and B are thermodynamic constants. Complete gas analyses of both the 1983–84 east-rift eruption (Greenland, in press) and of the 1984 Mauna Loa eruption (Greenland, chapter 30) have shown that the partial pressure of oxygen in these gases was buffered by the magma; therefore, $\log[O_2]$ is a linear function of the reciprocal of temperature. Averaging the results from the cited complete analyses yields

$$\log[O_2] = -[18{,}600/T] + 4.06. \quad (5)$$

Combining equations 1, 4, and 5 makes it possible to estimate an equilibrium temperature for a gas sample from the observed CO_2/CO ratio, and equations 2 and 3 provide estimates of the equilibrium amounts of H_2O and H_2S in the sample.

Table 28.3 provides the estimated equilibrium composition of gas samples collected in the 1980–82 period. These estimates depend on the assumptions that (1) the gases were in thermodynamic equilibrium and (2) there has been no oxidation of CO or H_2. That many eruptive gas samples approximate equilibrium assemblages has been demonstrated widely (Greenland, chapter 30; Gerlach, 1980, 1982; Greenland, in press). Examination of equations 1 and 2 show that oxidation of CO would yield a low estimate of temperature and a high estimate of water, whereas oxidation of H_2 would result in a low estimate of water. There can be no independent check on the oxidation state of these samples, and therefore the water and temperature estimates should not be taken too literally; on the other hand, as shown below, results from this calculation procedure appear to be generally reasonable and are preferable to no estimate at all. Note that this procedure does not alter the observed gas ratios, and thus the original analyses may be recovered directly from table 28.3.

A major intrusion into the southwest rift zone of Kilauea occurred on August 10, 1981, and resulted in ground cracking over a large area. A small segment of the dike reached within 250 m of the surface (estimated from deformation measurements, A. Okamura, oral commun., 1981) and magmatic gases issued from low-temperature ground cracks in this local area. The estimated equilibrium compositions of samples of these gases (table 28.3) show a rapid change with time. The initial sample has a composition similar to some of the east-rift Makaopuhi and 1983–84 east-rift gases (this paper), but subsequent samples are water-rich and show increasing C/S ratios with continued outgassing. A sample collected the following morning (August 11), after the intrusion had ended, had a C/S ratio of >100 and too little CO to attempt an equilibrium estimate. Because CO_2 is much less soluble than S, the increase of C/S ratio with time cannot reflect degassing of the near-surface melt. Perhaps CO_2 that exsolved from the deeper part of the dike percolated through the local, shallow segment as an easy route to the surface; this would account for the observation that CO_2 emissions from these cracks ceased after a few weeks when, presumably, freezing of the shallow segment of the dike blocked egress for the CO_2.

A brief fissure eruption adjoining Halemaumau occurred in April 1982. It was impossible to obtain gas samples from the erupting vents, and samples obtained from these vents after fountaining ceased consisted only of air. Two strongly fuming ground cracks, on strike with the fissure and less than 100 m from fountains, provided the analyses given in table 28.3. The initial sample from crack no. 1 has a composition similar to east-rift samples, but the C/S ratio increases rapidly in the subsequent samples, which also become very water rich. The first sample from crack no. 2 already has a high C/S ratio and high water content, and subsequent samples show increases in both parameters. The probable explanation for the increase in C/S ratio with time at these cracks lies in their location at the edge of Halemaumau: it is likely that these cracks tap into the extensive Halemaumau fumarole system; they have continued to emit CO_2-rich gases typical of these fumaroles through May 1985. The composition of the magmatic gas probably is best

TABLE 28.3.—*Composition of eruptive gases from Kilauea, 1980–1982*
[--, no data]

Collection		Temperature (°C)		Constituents (mole percent)						Atomic ratios	
Date	Hour	Collection	Equilibrium	H_2O	H_2	CO_2	CO	SO_2	H_2S	H/S	C/S
AUGUST 1981 SOUTHWEST-RIFT-ZONE INTRUSION											
8/10/81	0800	84	878	83.222	0.524	3.772	0.029	11.379	1.073	13.623	0.305
	1200	84	810	93.688	.388	1.497	.006	3.906	.515	42.792	.340
	1530	82	919	90.178	.714	3.165	.034	5.421	.487	30.930	.541
	1730	82	823	91.709	.413	3.713	.017	3.692	.456	44.630	.899
APRIL 1982 SUMMIT ERUPTION											
Ground crack No. 1											
4/30/82	1540	94	1,002	79.712	0.962	3.064	0.063	15.228	0.972	10.080	0.193
	1745	85	755	94.943	.268	3.766	.008	.872	.143	187.923	3.719
	1940	80	712	94.487	.192	4.713	.006	.503	.097	315.613	7.859
	2210	79	689	94.143	.159	5.427	.006	.218	.046	713.306	20.537
	2400	--	652	93.509	.115	6.241	.004	.105	.026	1,432.087	47.747
Ground crack No. 2											
	1530	82	909	89.578	0.672	3.333	0.033	5.846	0.538	28.442	0.527
	1735	86	816	92.110	.397	4.211	.018	2.897	.367	56.906	1.296
	1940	85	743	93.566	.242	4.844	.009	1.145	.194	140.410	3.625
	2220	82	698	94.369	.172	5.343	.006	.091	.019	1,732.875	49.017
SEPTEMBER 1982 SUMMIT ERUPTION											
Ground cracks											
9/25/82	1910	22	1,128	87.644	1.813	1.732	0.080	8.297	0.434	20.591	0.208
	1920	40	1,113	88.580	1.726	1.236	.052	7.971	.435	21.589	.153
	2000	85	1,132	87.261	1.833	1.299	.062	9.076	.469	18.766	.143
Active vent											
9/25/82	2300	1,120	1,004	47.068	0.573	6.239	0.129	44.316	1.675	2.145	0.138
	2325	1,070	1,042	72.311	1.048	3.261	.088	22.129	1.164	6.399	.144
9/26/82	0125	--	995	78.632	.914	3.488	.067	15.878	1.020	9.536	.210
	0405	--	958	91.220	.887	.974	.014	6.384	.521	26.830	.143

approximated by the first sample from crack no. 1.

Another brief summit eruption of Kilauea took place in the south caldera in September 1982. Actively fountaining vents were unapproachable, but fuming ground cracks (the leading edge of the progressively opening fissure) yielded three gas samples (table 28.3). One isolated vent erupted very briefly and then continued to emit a continuous blue-green flame with spatter and occasional small lava overflows for the rest of the eruption; this provided the gas samples identified as from an active vent in table 28.3. Unlike those from the preceding eruption and intrusion, these samples maintain an approximately constant C/S ratio throughout; this ratio is the same as that of the samples considered best from the April 1982 eruption and the 1983–84 east-rift eruption. The active-vent samples show an increase in apparent water content with time. Whether this is a real effect or an anomaly caused by the procedure for estimating water is uncertain. An important observation is the similarity of the gas compositions in very low temperature samples from ground cracks and in high-temperature samples at the active vent: apparently, gases are quenched very rapidly by contact with the cold country rock, a significant result to consider when attempting to sample fissure eruptions.

KILAUEA GAS COLLECTIONS FROM 1983

A middle-east-rift eruption of Kilauea began in January 1983 and has continued episodically (through February 1986). Results of complete analyses of gas samples from this eruption are described elsewhere (Greenland, in press) and will not be considered here. More than 400 gas samples were collected for partial analysis (CO_2, CO, H_2, and SO_2); more than half of these contained too much air or organic gases or were too greatly oxidized to be of much significance. Tables 28.4–28.8 present the results for the remainder of the samples, selected with the constraints that (1) CO_2 and SO_2 constitute more than 0.1 percent and CO and H_2 more than 0.001 percent of the original sample to ensure adequate determination and (2) the CO/H_2 ratio be less than 0.3 to exclude samples with organic contamination and some of the oxidized samples. Estimated equilibrium temperatures and H_2O and H_2S contents (see above) are included in tables 28.4–28.8; as noted above, these estimates have large uncertainties and only the general tendency of the results can be regarded as significant.

This eruption began as a fissure eruption that provided an abundance of gas sampling sites along a line of vents several kilometers long through January and part of February 1983; by June 1983, the eruption had become localized at a single vent that has provided far fewer gas-sampling opportunities. With the restriction of sampling sites, samples were increasingly collected for complete analysis rather than the rapid partial analyses described here; therefore most of the results in tables 28.4–28.8 refer to the January–March 1983 interval.

These results are summarized in the ternary atomic H-C-S diagram of figure 28.2. This diagram shows that most of the samples adhere closely to a water-control line with a C/S ratio of 0.18. A few of the samples, particularly at higher water contents,

TABLE 28.4.—*Composition of gases from east rift eruption of Kilauea, 1983: actively erupting vents*

[--, no data]

Sample	Date (mo/d)	Temperature (°C)		Constituents (mole percent)						Atomic ratios	
		Collection	Equilibrium	H_2O	H_2	CO_2	CO	SO_2	H_2S	H/S	C/S
70	1/10	--	823	68.427	0.308	6.503	0.030	22.611	2.121	5.730	0.264
71	1/10	--	811	67.474	.282	6.508	.026	23.450	2.260	5.447	.254
259	3/31	--	827	57.568	.266	9.151	.043	30.584	2.387	3.653	.279
386	8/12	--	830	65.766	.309	6.453	.031	25.217	2.223	4.978	.236
387	8/13	--	920	74.629	.595	3.485	.038	19.772	1.482	7.218	.166
389	8/13	1,048	1,089	87.004	1.538	1.488	.054	9.386	.530	17.965	.156
390	8/13	820	954	56.578	.539	6.660	.095	34.348	1.780	3.260	.187
391	8/13	820	966	78.035	.790	3.413	.053	16.570	1.139	9.031	.196
393	8/14	820	919	64.112	.508	5.227	.056	28.265	1.831	4.416	.176
394	8/14	820	977	83.633	.895	2.629	.045	11.946	.852	13.343	.209
395	8/14	1,120	1,083	84.515	1.457	2.153	.076	11.177	.623	14.677	.189
396	8/14	1,120	1,035	92.098	1.289	2.158	.055	4.121	.279	42.575	.503
404	9/02	1,115	1,039	85.476	1.222	1.692	.045	10.887	.678	15.110	.150
405	9/02	1,115	1,051	80.879	1.216	2.359	.067	14.636	.841	10.717	.157
406	9/02	1,115	1,024	83.432	1.115	1.972	.047	12.635	.798	12.707	.150
407	9/02	1,110	982	79.500	.870	1.976	.035	16.511	1.108	9.249	.114
408	9/02	1,110	863	58.040	.335	4.311	.029	34.849	2.437	3.262	.116
409	9/03	1,113	1,074	90.476	1.502	1.319	.044	6.279	.381	27.735	.205
410	9/04	1,110	1,078	85.853	1.451	1.435	.049	10.605	.606	15.683	.132
411	9/04	1,110	1,076	85.390	1.429	1.514	.051	10.987	.628	15.058	.135
414	10/28	--	658	68.036	.088	4.118	.003	23.398	4.330	5.228	.149

TABLE 28.5.—*Composition of gases from east rift eruption of Kilauea, 1983: presently inactive*

[--, no data]

Sample	Date (mo/d)	Temperature (°C)		Constituents (mole percent)						Atomic ratios	
		Collection	Equilibrium	H_2O	H_2	CO_2	CO	SO_2	H_2S	H/S	C/S
10	1/05	721	1,025	74.674	1.000	4.647	0.111	18.519	1.408	7.842	0.243
11	1/05	721	1,023	71.293	.948	5.543	.131	20.948	1.137	6.645	.257
20	1/05	92	1,025	88.274	1.185	5.412	.130	4.688	.311	35.915	1.109
49	1/07	--	1,116	65.527	1.295	5.373	.233	26.503	1.070	4.925	.203
50	1/07	--	1,108	67.292	1.286	4.934	.203	25.221	1.064	5.299	.195
54	1/09	285	820	48.154	.212	10.515	.046	38.491	2.581	2.481	.257
61	1/09	95	837	56.567	.278	10.208	.053	30.624	2.270	3.594	.312
69	1/09	941	1,071	71.143	1.170	3.295	.108	23.164	1.120	6.048	.140
88	1/13	498	978	50.672	.543	9.150	.156	37.831	1.648	2.678	.236
90	1/14	720	1,083	67.925	1.173	6.170	.217	23.460	1.055	5.723	.261
93	1/14	935	1,082	57.134	.984	6.672	.234	33.697	1.279	3.396	.197
98	1/15	500	963	59.777	.594	4.708	.072	33.079	1.771	3.566	.137
113	1/15	888	1,084	64.240	1.115	6.300	.224	26.976	1.145	4.730	.232
115	1/15	890	1,118	68.469	1.363	5.283	.231	23.660	.993	5.746	.224
116	1/16	888	1,076	71.707	1.202	4.874	.164	21.039	1.014	6.704	.228
118	1/16	888	1,092	71.225	1.277	4.249	.159	22.071	1.019	6.368	.191
119	1/17	887	1,064	75.852	1.209	3.346	.104	18.520	.969	8.008	.177
120	1/17	887	1,048	67.626	1.006	4.054	.114	25.940	1.260	5.139	.153
122	1/18	863	1,052	57.602	.871	5.590	.161	34.364	1.412	3.348	.161
123	1/18	863	1,054	73.850	1.124	3.952	.115	19.918	1.041	7.254	.194
143	2/12	900	990	47.358	.539	5.482	.102	44.752	1.766	2.135	.120
144	2/12	350	1,101	65.042	1.208	4.234	.167	28.181	1.168	4.594	.150
154	2/14	1,008	950	59.720	.557	2.779	.038	34.967	1.938	3.372	.076
155	2/14	1,006	677	58.464	.089	2.734	.002	33.758	4.952	3.281	.071
156	2/14	--	796	33.420	.126	9.531	.033	54.144	2.746	1.276	.168
165	2/15	985	987	67.390	.754	2.113	.039	28.116	1.589	4.695	.072
178	2/17	867	1,023	73.915	.981	3.115	.074	20.746	1.169	6.942	.146
179	2/17	867	1,003	50.070	.607	5.613	.115	41.905	1.690	2.402	.131
187	2/23	975	963	63.474	.631	3.242	.049	30.851	1.752	4.040	.101
188	2/23	975	866	77.200	.452	2.309	.016	18.345	1.678	7.924	.116
194	2/24	930	898	69.084	.487	3.968	.036	24.597	1.828	5.404	.152
195	2/24	930	896	69.048	.480	3.972	.035	24.622	1.843	5.394	.151
250	3/29	230	765	30.731	.093	8.753	.022	57.391	3.010	1.120	.145
275	4/05	900	716	41.175	.086	7.202	.010	47.427	4.099	1.761	.140
279	4/07	--	873	80.300	.492	2.025	.015	15.711	1.457	9.582	.119
281	4/08	832	842	82.835	.421	1.840	.010	13.470	1.424	11.371	.124
285	4/08	862	817	73.319	.317	3.067	.013	21.114	2.170	6.511	.132
311	5/06	810	685	48.394	.079	5.679	.006	41.046	4.797	2.324	.124
315	5/16	795	805	83.659	.334	2.477	.009	12.058	1.462	12.641	.184
317	5/20	765	839	71.198	.354	4.160	.022	22.212	2.053	6.067	.172
322	5/24	750	778	85.187	.284	2.143	.006	10.897	1.483	14.047	.174
323	5/24	750	783	85.164	.294	2.225	.007	10.860	1.450	14.120	.181

TABLE 28.6.—*Composition of gases from east rift eruption of Kilauea, 1983: ground cracks near eruptive center*

[--, no data]

Sample	Date (mo/d)	Temperature (°C)		Constituents (mole percent)						Atomic ratios	
		Collection	Equilibrium	H_2O	H_2	CO_2	CO	SO_2	H_2S	H/S	C/S
2	1/03	140	1,143	63.183	1.388	7.571	0.385	26.498	0.974	4.772	0.290
3	1/03	141	1,296	74.433	2.771	4.913	.557	16.782	.545	8.974	.316
22	1/05	205	1,034	68.096	.952	4.723	.121	24.852	1.256	5.386	.186
23	1/05	88	1,012	71.712	.907	3.752	.082	22.295	1.252	6.274	.163
24	1/06	80	1,023	86.327	1.144	2.894	.068	8.979	.588	18.409	.310
25	1/06	77	970	91.516	.944	2.283	.037	4.838	.383	35.565	.444
26	1/06	78	1,070	80.157	1.312	3.563	.116	14.085	.766	11.075	.248
27	1/06	67	1,045	85.588	1.253	4.105	.113	8.423	.518	19.541	.472
28	1/06	82	1,075	88.020	1.472	3.915	.131	6.103	.359	27.809	.626
29	1/06	78	1,052	86.814	1.315	4.781	.138	6.551	.401	25.469	.708
30	1/06	78	1,047	87.346	1.293	4.826	.135	6.025	.375	27.817	.775
31	1/06	77	1,056	89.185	1.370	4.605	.136	4.429	.276	38.610	1.008
32	1/06	--	1,054	90.351	1.376	4.401	.128	3.521	.223	49.119	1.210
34	1/06	335	1,084	77.589	1.343	3.263	.115	16.829	.861	9.021	.191
46	1/06	48	1,107	83.573	1.589	6.113	.250	8.055	.420	20.196	.751
47	1/07	69	1,091	76.085	1.359	5.081	.188	16.475	.812	9.054	.305
72	1/11	90	919	64.839	.514	5.442	.059	27.354	1.792	4.607	.189
73	1/11	91	830	62.308	.293	6.589	.032	28.402	2.376	4.222	.215
74	1/11	--	860	72.512	.411	5.159	.033	20.122	1.762	6.826	.237
75	1/11	88	888	76.237	.508	4.909	.041	16.884	1.421	8.540	.270
162	2/14	330	941	45.600	.406	8.355	.107	43.638	1.894	2.104	.186
167	2/15	835	1,007	62.530	.771	2.588	.055	32.439	1.617	3.812	.078
168	2/15	835	1,010	60.083	.751	2.693	.058	34.762	1.654	3.432	.076
169	2/15	440	791	69.461	.252	1.661	.005	25.844	2.776	5.066	.058
198	2/27	385	1,031	62.644	.863	4.091	.102	30.850	1.449	4.022	.130
199	2/27	275	1,045	50.472	.740	4.979	.137	42.127	1.544	2.416	.117
205	3/01	270	892	44.853	.305	9.908	.085	42.741	2.108	2.108	.223
211	3/04	83	712	68.129	.139	11.184	.015	17.969	2.563	6.900	.545
212	3/04	244	766	40.682	.125	10.502	.027	45.520	3.143	1.806	.216
244	3/28	210	661	43.642	.058	7.842	.006	43.346	5.106	2.015	.162
249	3/29	125	660	61.175	.081	6.607	.005	27.576	4.556	4.096	.206
251	3/29	--	749	40.860	.111	7.646	.016	47.811	3.556	1.734	.149
329	6/13	67	965	55.816	.561	2.267	.035	39.361	1.961	2.824	.056
330	6/13	85	1,010	87.580	1.094	.517	.011	10.105	.693	16.553	.049
331	6/13	117	999	57.747	.687	2.199	.044	37.559	1.765	3.062	.057

TABLE 28.7.—*Composition of gases from east rift eruption of Kilauea, 1983: ground cracks distant from eruption center*

[--, no data]

Sample	Date (mo/d)	Temperature (°C)		Constituents (mole percent)						Atomic ratios	
		Collection	Equilibrium	H_2O	H_2	CO_2	CO	SO_2	H_2S	H/S	C/S
13	1/05	571	1,079	61.882	1.051	5.253	0.180	30.375	1.258	4.058	0.172
14	1/05	561	1,106	69.929	1.326	4.113	.167	23.434	1.031	5.909	.175
15	1/05	441	1,108	68.678	1.313	5.441	.224	23.339	1.004	5.833	.233
16	1/05	441	1,111	70.619	1.370	4.614	.194	22.228	.975	6.289	.207
17	1/05	420	1,079	65.772	1.117	5.367	.185	26.398	1.160	4.939	.201
18	1/05	--	1,066	64.907	1.041	4.991	.157	27.665	1.239	4.649	.178
51	1/09	72	858	85.494	.478	5.663	.036	7.551	.778	20.831	.684
52	1/09	86	816	66.681	.287	6.933	.030	23.838	2.231	5.309	.267
53	1/09	6	894	77.888	.535	9.650	.084	10.924	.919	13.399	.822
55	1/09	160	803	55.117	.218	10.728	.040	31.350	2.546	3.415	.318
62	1/09	150	923	58.210	.470	5.872	.065	33.432	1.951	3.427	.168
63	1/09	150	921	54.940	.439	6.501	.071	36.051	1.998	3.016	.173
65	1/09	70	802	69.317	.272	7.870	.029	20.426	2.085	6.368	.351
66	1/09	90	807	79.636	.322	4.267	.017	14.134	1.624	10.354	.272
67	1/09	90	768	53.077	.165	5.892	.015	37.484	3.368	2.771	.145
68	1/09	91	847	74.979	.391	9.323	.053	13.940	1.313	10.055	.615
82	1/13	90	838	58.741	.291	11.954	.063	26.896	2.056	4.220	.415
83	1/13	90	812	74.217	.310	8.945	.036	14.922	1.569	9.229	.545
85	1/13	82	835	56.364	.273	12.964	.066	28.235	2.098	3.873	.430
87	1/13	88	923	57.383	.465	10.472	.117	29.854	1.709	3.774	.335
89	1/14	145	859	54.313	.305	10.186	.065	32.950	2.182	3.234	.292
91	1/14	85	815	60.104	.257	8.989	.038	28.217	2.396	4.100	.295
114	1/15	87	843	76.489	.389	15.664	.086	6.721	.650	21.036	2.137
117	1/16	87	830	78.725	.371	12.576	.061	7.489	.778	19.324	1.529
133	1/24	732	745	75.602	.198	3.363	.007	18.292	2.539	7.521	.162
180	2/17	869	633	42.954	.044	5.198	.003	45.656	6.145	1.897	.100
226	3/08	--	830	40.895	.192	9.740	.048	46.564	2.561	1.777	.199

TABLE 28.8.—*Composition of gases from east rift eruption of Kilauea, 1983: January 23 crack*

[--, no data]

Sample	Date (mo/d)	Temperature (°C)		Constituents (mole percent)						Atomic ratios	
		Collection	Equilibrium	H_2O	H_2	CO_2	CO	SO_2	H_2S	H/S	C/S
130	1/24	540	779	65.687	0.220	4.913	0.014	26.369	2.796	4.711	0.169
132	1/24	732	757	70.251	.201	3.780	.009	22.933	2.826	5.690	.147
135	2/04	508	688	63.512	.106	4.915	.005	27.348	4.113	4.306	.156
139	2/10	406	657	63.532	.082	4.512	.003	27.140	4.731	4.289	.142
140	2/12	385	696	44.111	.079	8.844	.010	42.657	4.298	2.065	.189
141	2/12	385	666	55.642	.077	6.624	.005	32.844	4.808	3.215	.176
176	2/17	410	744	45.538	.119	8.866	.018	41.914	3.545	2.165	.195
177	2/17	410	747	49.863	.133	7.814	.016	38.629	3.545	2.539	.186
185	2/23	407	688	33.766	.057	9.415	.010	52.559	4.194	1.340	.166
186	2/23	407	711	48.525	.098	7.338	.010	39.883	4.145	2.397	.167
192	2/24	403	738	41.876	.104	8.466	.016	45.871	3.667	1.843	.171
193	2/24	403	715	39.490	.083	8.788	.012	47.675	3.952	1.686	.170
196	2/27	403	851	37.138	.199	8.283	.049	51.917	2.413	1.463	.153
197	2/28	403	853	42.441	.230	7.798	.047	46.995	2.489	1.825	.159
202	3/01	452	764	37.414	.113	7.651	.019	51.495	3.308	1.490	.140
203	3/01	452	758	38.045	.110	7.649	.018	50.787	3.391	1.534	.142
210	3/04	435	765	45.426	.138	6.660	.017	44.318	3.441	2.052	.140
227	3/08	--	720	52.150	.113	6.601	.010	37.141	3.985	2.735	.161
228	3/08	--	733	51.516	.123	6.543	.011	37.986	3.820	2.653	.157
236	3/22	423	754	49.671	.140	5.898	.013	40.666	3.612	2.413	.133
237	3/22	423	756	47.385	.135	6.237	.014	42.638	3.592	2.211	.135
242	3/22	419	620	39.594	.036	7.780	.003	46.437	6.150	1.741	.148
243	3/28	419	663	45.064	.061	6.403	.005	43.255	5.211	2.077	.132
247	3/29	409	743	53.558	.139	5.317	.011	37.251	3.724	2.803	.130
252	3/30	394	665	54.701	.076	5.088	.004	35.051	5.081	2.983	.127
257	3/31	401	671	54.481	.079	5.058	.004	35.405	4.972	2.949	.125
262	4/01	405	676	65.667	.100	3.824	.003	26.125	4.281	4.608	.126
270	4/04	385	654	55.888	.070	5.035	.003	33.734	5.270	3.140	.129
276	4/05	392	655	54.748	.069	5.014	.003	34.843	5.323	2.995	.125
280	4/08	410	660	56.312	.074	4.820	.003	33.644	5.147	3.173	.124
286	4/08	402	666	57.777	.081	4.800	.004	32.410	4.928	3.363	.129
288	4/11	411	664	57.985	.079	4.731	.004	32.232	4.969	3.389	.127
291	4/13	398	654	59.521	.074	4.457	.003	30.820	5.124	3.601	.124

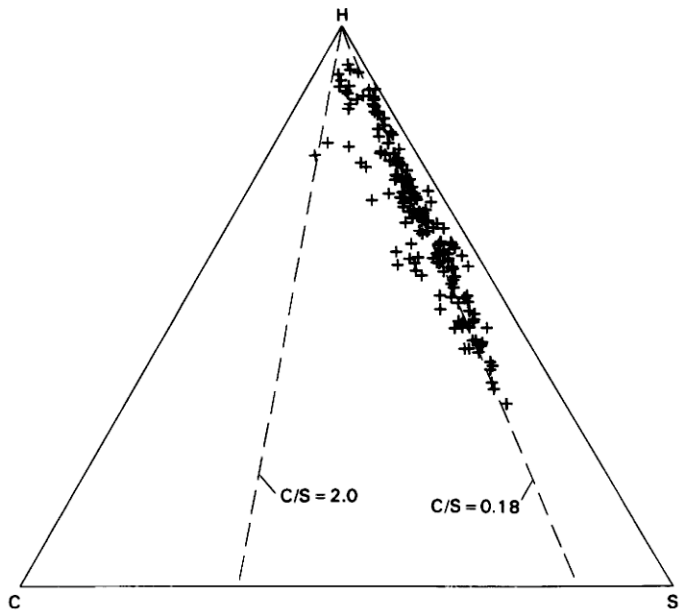

FIGURE 28.2.—Ternary H-C-S plot for gas samples from 1983 Kilauea east-rift-zone eruption. Data from tables 28.4–28.8. Dashes indicate water-control lines for specific values of the C/S ratio. Atomic hydrogen has been reduced by a factor of 0.5 to increase clarity.

deviate considerably from this line, becoming carbon-rich. Examination of the tables shows that almost all of the samples with a C/S ratio >0.3 were collected from ground cracks during January 1983; the eruption began in a heavily vegetated area, and thus contamination of the magmatic gas with organic pyrolysis products is likely. Furthermore, the eruptive area contained numerous preexisting low-temperature fumaroles emitting CO_2-rich steam, and mixing of these vapors with the magmatic gas may account for some of the samples rich in H_2O and CO_2. Samples with a C/S ratio <0.1 are associated with vents at which fountaining had ceased and with ground cracks near eruptive centers, and all were collected after the January activity; remobilization of S from the January lava is a possible explanation for the low C/S ratios of these samples.

The samples from actively erupting vents (table 28.4) were all collected within a few meters, usually a few centimeters, of actively churning, spattering or fountaining melt. All but three of these were collected in the period after July 1983, when eruptive episodes were preceded by the formation of a lava lake in the central vent that persisted for several hours to several days before full-scale eruption. This lava lake frequently became crusted over, with small vents emitting spatter, gas, and occasional overflows of lava through the crust; the August–October samples in table 28.4 were obtained from such vents. The three January–March samples in table 28.4 were collected from small holes in vigorously fountaining spatter cones. Examination of table 28.4 reveals a clear trend for apparent water (that is, the thermodynamic estimate of water content) to

increase and for the C/S ratio to decrease from the pre-April samples through the August samples to the September samples; however, this trend is not apparent in samples collected from other sites (tables 28.5–28.7) and it seems more likely to reflect vagaries in the degassing process rather than a change in the volatile composition of the magma.

The samples of gas from vents no longer active (table 28.5) collected before March 1983 were invariably from very small vents that had erupted only weakly, forming spatter ramparts less than a meter high. Samples collected from vents that had erupted vigorously either consisted solely of air or were thoroughly oxidized, often to the point where not even SO_2 was detectable. The March–April eruptive episodes ended with partial collapse of the crater wall in the central vent cone (the later Puu Oo), which completely blocked the main vent; the samples in table 28.5 from this period were obtained from degassing cracks in the debris pile. The observed variation in the C/S ratio of these samples might well be accounted for by remobilization of sulfur from the edifice and adjoining lava and by incorporation of pyrolyzed organic matter through the chimney effect.

Gas samples collected from fuming ground cracks have been distinguished as "near" (table 28.6), meaning within 200 m of an actively erupting vent, and "distant" (table 28.7), usually meaning more than 1 km from any eruptive site or collected during a noneruptive period of this episodic eruption. Comparison of tables 28.6 and 28.7, however, shows this to be a distinction without a difference; the composition of gas issuing from ground cracks appears to be unrelated to the relative proximity of eruptive centers or to whether an eruption is actually occurring. A notable feature of gas samples from these ground cracks is the high temperature of apparent gas equilibrium in spite of the very low collection temperatures, many less than 100 °C. This result, as with the 1981–82 gas collections (see above), indicates that an abundance of gas samples should be easily obtainable from Hawaiian fissure eruptions. (On the other hand, an abundance of samples is required from such sites: about half of the analyses excluded from tables 28.4–28.8 as being too oxidized or too contaminated were obtained from low-temperature ground cracks.) Comparison of these samples with samples collected in immediate contact with melt (table 28.4) shows a general tendency for the apparent water content of the crack samples to be lower; this distinction may be related to the depth at which gas became separated from the melt (see Greenland, chapter 30) but the possibility of greater oxidation of H_2, leading to low estimates of H_2O, in the low-temperature samples cannot be excluded.

On January 23, 1983, an isolated very small eruption took place at a single vent. Associated with this eruption, a ground crack formed starting at a point about 30 m from the vent and extending for about 100 m. This crack fumed strongly into April, making possible a study of the change of gas composition at a single site with time (table 28.8). These data show a general decrease in observed collection temperature with time and a corresponding, though smaller, decrease of apparent equilibrium temperature. Within this general trend, there was a notable increase in collection temperature on March 1, preceded by an equally notable increase in apparent equilibrium temperature two days earlier; it may be significant that these temperature increases accompany the main episode 2 eruptive activity (February 25 to March 4). Paralleling the overall trend of temperature decrease is a decrease of the C/S ratio in the gas. However, the eruptive activity of episode 2 and episode 3 (March 28 to April 9) produced lava that encroached upon and even overran parts of the crack, and it is possible that significant contributions of remobilized sulfur came from these flows.

MAUNA LOA GAS COLLECTIONS FROM 1984

Complete gas analyses of collections from the recent Mauna Loa eruption are discussed in detail elsewhere in this volume (Greenland, chapter 30) and will not be considered here. Two types of gas-sampling sites were available for this eruption: "active" vents that were emitting spatter interspersed with occasional low fountains or small lava flows or both, and "feeder" vents uprift of the active vents. The feeder vents at 3,350 m elevation produced major fountains and lava flows early in the eruption but ceased activity when the lower vents at 2,930 m elevation became active. Abundant fume produced from the feeder vents after lava emission ceased there originated from magma degassing as it flowed through the conduit to the actively erupting vents. Flowthrough-bottle collections of gases for partial analysis largely overlap the collections for complete analysis, which were mostly being made at the same vent at the same time.

Results of these analyses are given in table 28.9, which includes estimates of the equilibrium temperature and content of H_2O and H_2S made as described above. These data are summarized in a ternary H-C-S plot in figure 28.3, which shows the analyses to lie along a water-control line with a C/S ratio very close to that of the 1983 Kilauea east-rift gases and very much lower than the C/S ratio of the 1919 Mauna Loa eruptive gases (see above). The low C/S ratio in these gases has been attributed, as at Kilauea, to degassing of the magma during storage in the shallow summit storage reservoir (Greenland, chapter 30).

There is no obvious difference in composition or apparent equilibrium temperature between samples collected from actively erupting vents and those from feeder vents (table 28.9). As with Kilauea (see table 28.4), apparent equilibrium temperatures of samples collected at magmatic temperatures (~1,100 °C) are uniformly lower than collection temperatures, whereas samples collected at temperatures below 900 °C almost always have apparent equilibrium temperatures that are higher than the collection temperature. This result indicates that quenching of the high-temperature flowthrough collections is not sufficiently fast to prevent gas reactions down to ~1,000 °C. The similarity of apparent equilibrium water contents of samples from the two kinds of sites contrasts with the observation from the complete analyses (Greenland, chapter 30) that the active vents have a higher total water content than do the feeder vents. However, estimating equilibrated water in the complete analyses yields the same results given here for the partial analyses (Greenland, chapter 30); the distinction between total and equilibrated water was attributed to nonequilibrium degassing of the erupting magma.

TABLE 28.9.—*Composition of gases from Mauna Loa, 1984*

[--, no data]

Date (mo/d)	Temperature (°C)		Constituents (mole percent)						Atomic ratios	
	Collection	Equilibrium	H_2O	H_2	CO_2	CO	SO_2	H_2S	H/S	C/S
Actively erupting vents										
3/25	1,075	969	54.713	0.562	6.754	0.108	36.124	1.739	3.012	0.181
3/26	1,100	1,016	62.186	.800	5.635	.127	29.811	1.442	4.123	.184
3/26	1,100	975	47.237	.499	8.324	.139	42.079	1.723	2.258	.193
3/26	1,120	955	53.429	.510	6.534	.094	37.594	1.839	2.829	.168
3/27	1,100	978	63.592	.683	5.680	.097	28.400	1.548	4.396	.193
3/27	1,130	981	55.892	.608	7.480	.130	34.257	1.632	3.240	.212
3/30	1,100	903	52.966	.385	8.922	.084	35.641	2.003	2.941	.239
3/31	1,100	941	51.902	.461	7.672	.098	37.989	1.877	2.721	.195
4/02	1,100	1,098	57.307	1.055	8.137	.316	32.010	1.175	3.588	.255
4/02	1,100	1,073	58.389	.965	7.668	.253	31.478	1.249	3.704	.242
4/02	--	837	41.372	.204	9.987	.052	45.894	2.491	1.821	.207
4/05	835	944	44.512	.402	8.520	.112	44.582	1.873	2.014	.186
Feeder vents										
4/03	1,100	1,007	51.039	0.631	8.819	0.187	37.790	1.535	2.706	0.229
4/03	--	911	48.799	.369	10.795	.108	38.005	1.924	2.559	.273
4/05	1,010	1,078	71.865	1.214	4.309	.147	21.434	1.031	6.598	.198
4/05	1,100	1,097	58.075	1.063	6.842	.264	32.541	1.215	3.576	.211
4/05	895	983	50.474	.555	7.658	.136	39.487	1.690	2.561	.189
4/07	880	976	51.350	.544	7.412	.124	38.843	1.726	2.643	.186
4/09	875	957	49.212	.474	8.574	.124	39.830	1.785	2.474	.209
4/09	875	972	51.808	.540	8.514	.139	37.312	1.687	2.771	.222
4/11	840	946	49.270	.450	8.109	.108	40.204	1.858	2.452	.195
4/11	840	906	56.669	.417	6.900	.067	33.922	2.025	3.289	.194
4/13	820	939	48.468	.427	8.742	.111	40.381	1.871	2.403	.210

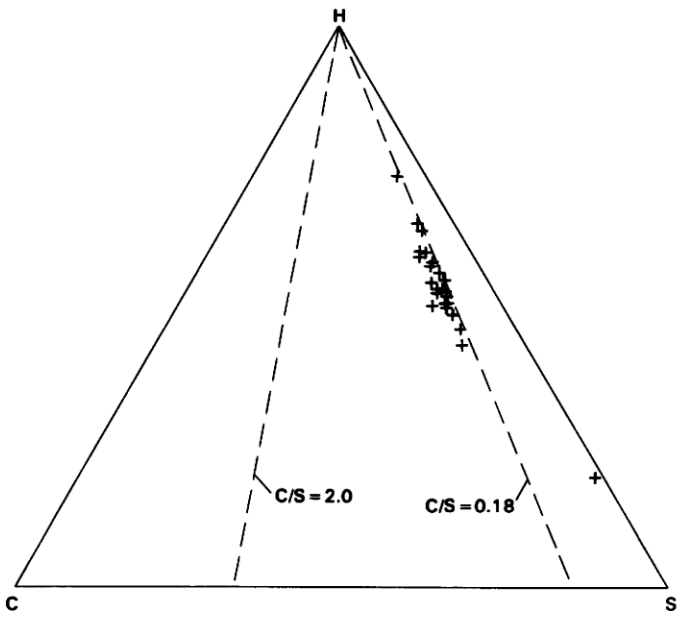

FIGURE 28.3.—Ternary H-C-S plot for gas samples from 1984 Mauna Loa eruption. Data from table 28.9. Dashes indicate water-control lines for specific values of the C/S ratio. Atomic hydrogen has been reduced by a factor of 0.5 to increase clarity.

CONCLUSIONS

Compositions of Hawaian eruptive gas are summarized in figure 28.4. Plotted in a ternary H-C-S diagram are averages for the 1917, 1919, 1965, September 1982, and 1983 eruptions of Kilauea, and the initial (best) compositions of the April 1982 eruption and 1981 intrusion at Kilauea, and averages for the 1919 and 1984 eruptions of Mauna Loa.

It is apparent from figure 28.4 that eruptive gases in Hawaii predominantly have C/S ratios of ~2.0 or ~0.2; exceptions are the 1968 Halemaumau Fountain gas (C/S = 4.0) and the 1919 Mauna Loa eruption (C/S = 0.9), both of which are particularly uncertain determinations. The high (2.0) C/S ratio is associated with protracted summit eruptions of Kilauea and the low (0.2) ratio is associated with rift and brief summit eruptions. Current degassing models of Kilauea (Gerlach and Graeber, 1985; Greenland and others, 1985) and of Mauna Loa (Greenland, chapter 30) indicate that mantle-derived magma arrives in shallow (2–6 km) summit storage reservoirs bearing an immiscible CO_2-rich fluid phase and having an overall C/S ratio of about 2. Degassing of the CO_2-rich fluid phase through summit fumaroles is rapid, at least at Kilauea (days to weeks; see Greenland and others, 1985), leaving the magma with a C/S ratio of about 0.2. A consequence of this view is that eruptive gas in Hawaii will have the low C/S ratio if the magma has resided even briefly in the summit reservoir. The high ratio will be found only when magma passes directly through the reservoir to

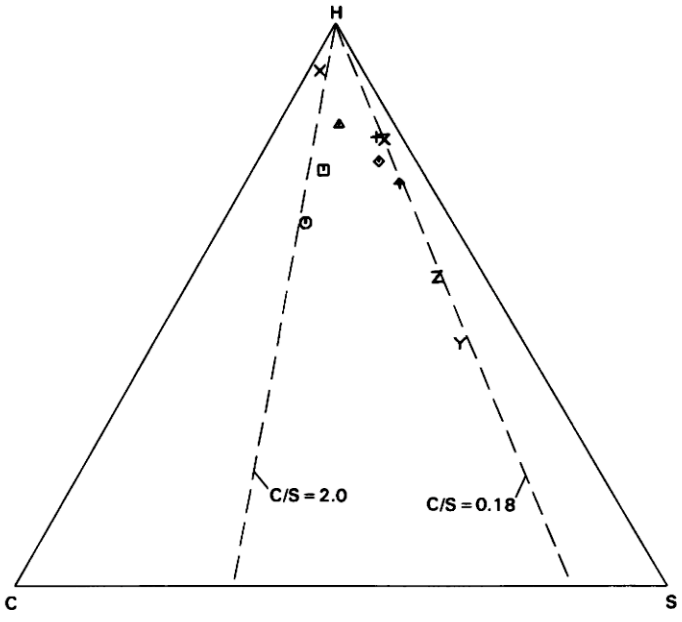

FIGURE 28.4.—Summary ternary H-C-S plot of Hawaiian eruptive gas compositions from 1917 through 1984. Dashes indicate water-control lines for specific values of the C/S ratio. Atomic hydrogen has been reduced by a factor of 0.5 to increase clarity.

the eruption center, which in practical terms means only for continuous summit eruptions that are lengthy enough to flush a passageway through the reservoir. An actual suite of gas samples collected from an eruption, however, can be expected to exhibit a considerable range of C/S ratios because of contamination by organic matter and by remobilized sulfur.

The major source of variation in these eruptive gases within a particular eruption is the water content, as is shown by figures 28.1–28.3, and water is also the primary distinguishing variable between eruptions, as indicated by figure 28.4. Hydrogen isotope studies yield convincing evidence that magma absorbs crustal water somewhere between its formation in the mantle and eruption (Kyser and O'Neil, 1984), and studies of submarine basalt (Moore, 1965) show that water is undersaturated in Hawaiian magma at the pressure and temperature conditions of the summit reservoir. It seems probable, then, that much of the water variation in these eruptive gases is due to varying amounts of assimilation of water by magma in transit between mantle and eruption site. A further source of water variation in gas samples is contamination of the magmatic gas with meteoric water both in the vent system and from the atmosphere at the sampling site; this problem is exacerbated because meteoric water in the vent system may be equilibrated with the magmatic gas, and it is possible that the last exsolved magmatic water may be collected before equilibration with previously exsolved gas is complete (Greenland, chapter 30). It may be that variation of water among eruptions is due primarily to variable assimilation and that variation within an eruption largely reflects meteoric contamination, but only hydrogen isotope studies can resolve this problem.

Studies of gas composition as summarized here offer no direct information about the actual content of gas in the magma, which is an important question to those concerned with petrology and eruptive mechanics. If the degassing model described above is correct, however, it can be inferred that the carbon and sulfur content of Hawaiian summit-stored magma is constant and is fixed by the pressure and temperature conditions of the summit reservoir; the equilibrium amounts of carbon and sulfur dissolved in reservoir magma have been estimated (Gerlach and Graeber, 1985; Greenland and others, 1985) as about 0.03 percent CO_2 and 0.1 percent S by weight. The water content of summit-stored magma, which is not fixed by solubility limits, probably varies with the extent of assimilation of crustal water. The water content is difficult to estimate because of uncertainties about meteoric water contamination of gas samples; Greenland and others (1985) and Gerlach and Graeber (1985) independently estimate about 0.3 weight percent H_2O, which, even with the uncertainties, probably is close to correct. Therefore, excluding protracted summit eruptions, the total content of volatiles in Hawaiian eruptive magma probably is less than 0.5 percent by weight and probably varies little from eruption to eruption.

REFERENCES

Banks, N.G., Koyanagi, R.Y., Sinton, J.M., and Honma, K.T., 1984, The eruption of Mount Pagan Volcano, Mariana Islands, 15 May 1981: Journal of Volcanology and Geothermal Research, v. 22, p. 225–269.

Day, A.L., and Shepherd, E.S., 1913, L'eau et les gaz magmatiques: Comptes Rendu Seances de l'Academie des Sciences, v. 157, p. 1–7.

Finlayson, J.B., Barnes, I.L., and Naughton, J.J., 1968, Developments in volcanic gas research in Hawaii, *in* The Upper Crust and Upper Mantle of the Pacific Area: American Geophysical Union, Geophysical Monograph, v. 12, p. 428–438.

Gerlach, T.M., 1980, Evaluation of volcanic gas analyses from Kilauea Volcano: Journal of Volcanology and Geothermal Research, v. 7, p. 295–317.

———1982, The interpretation of volcanic gas data from tholeiitic and alkaline mafic magmas: Bulletin Volcanologique, v. 45-3, p. 235–244.

Gerlach, T.M., and Graeber, E.J., 1985, Volatile budget of Kilauea Volcano: Nature, v. 313, p. 273–277.

Graeber, E.J., Modreski, P.J., and Gerlach, T.M., 1979, Compositions of gases collected during the 1977 east rift eruption, Kilauea, Hawaii: Journal of Volcanology and Geothermal Research, v. 5, p. 337–344.

Greenland, L.P., 1984, Gas composition of the January 1983 eruption of Kilauea Volcano, Hawaii: Geochimica et Cosmochimica Acta, v. 48, p. 193–195.

———in press, Gases from the 1983–84 east-rift eruption of Kilauea Volcano, *in* Wolfe, E.W., ed., The Puu Oo eruption of Kilauea Volcano, Hawaii: the first 1½ years: U.S. Geological Survey Professional Paper.

Greenland, L.P., Rose, W.I., and Stokes, J.B., 1985, An estimate of gas emissions and magmatic gas content from Kilauea Volcano: Geochimica et Cosmochimica Acta, v. 49, p. 125–129.

Heald, E.F., Naughton, J.J., and Barnes, I.L. Jr., 1963, Use of equilibrium calculations in the interpretation of volcanic gas samples: Journal of Geophysical Research, v. 68, p. 545–557.

Jaggar, T.A., 1940, Magmatic gases: American Journal of Science, v. 238, p. 313–353.

Kyser, T.K., and O'Neil, J.R., 1984, Hydrogen isotope systematics of submarine basalts: Geochimica et Cosmochimica Acta, v. 48, p. 2123–2133.

Matsuo, S., 1962, Establishment of chemical equilibrium in the volcanic gas obtained from the lava lake of Kilauea, Hawaii: Bulletin Volcanologique, v. 24, p. 59–71.

Moore, J.G., 1965, Petrology of deep-sea basalt near Hawaii: American Journal of Science, v. 263, p. 40–52.

Naughton, J.J., Derby, J.V., and Glover, R.B., 1969, Infrared measurements on volcanic gas and fume: Kilauea eruption, 1968: Journal of Geophysical Research, v. 74, p. 3273–3277.

Nordlie, B.E., 1971, The composition of the magmatic gas at Kilauea and its behavior in the near surface environment: American Journal of Science, v. 271, p. 417–463.

Shepherd, E.S., 1919, The composition of the gases of Kilauea: Hawaiian Volcano Observatory Bulletin, v. 7, no. 7, p.94–97.

———1920, Two gas collections from Mauna Loa: Hawaiian Volcano Observatory Bulletin, v. 8, no. 5, p. 65–67.

———1921, Kilauea gases, 1919: Hawaiian Volcano Observatory Bulletin, v. 9, no. 5, p. 83–88.

———1925, The analysis of gases obtained from volcanoes and from rocks: Journal of Geology, v. 33, p. 289–370.

———1938, The gases in rocks and some related problems: American Journal of Science, v. 236, p. 311–351.

Swanson, D.A., and Fabbi, B.F., 1973, Loss of volatiles during fountaining and flowage of basaltic lava at Kilauea Volcano, Hawaii: Journal of Research of the U.S. Geolgical Survey, v. 1, p. 649–658.

SO_2 AND CO_2 EMISSION RATES AT KILAUEA VOLCANO, 1979–1984

By Thomas J. Casadevall, J. Barry Stokes, L. Paul Greenland, Lawrence L. Malinconico, John R. Casadevall, *and* Bruce T. Furukawa

ABSTRACT

Quiescent outgassing of the summit region of Kilauea Volcano produces a plume of gas and particles that contains sulfur dioxide and carbon dioxide as principal constituents. The SO_2 and CO_2 are derived from outgassing of magma temporarily stored in the shallow reservoir at a depth of 2–6 km beneath the summit.

Since June 1979 we have made regular measurements of SO_2 emission rates from Kilauea. In 1983 and 1984, measurements of CO_2 emission rates were also made for Kilauea. The average daily SO_2 emission rate from 1979 through 1982 was 170 ± 50 t/d; from 1983–1984, the average daily emission rate had increased to 260 ± 90 t/d. The 1979–1982 rate occurred during a time when no major eruptive activity occurred at Kilauea summit. The increase in 1983 is coincidental with the start of major eruptive activity at the Puu Oo vent on the east rift zone and probably reflects an increase in the rate of magma supply.

The total SO_2 production in 1979–1982 is calculated at approximately 63,000 tonnes annually. In 1983–1984, this annual production is calculated at 95,000 tonnes annually. The SO_2 from quiescent outgassing of Kilauea Volcano contributes less than 1 percent of the total annual global contribution from volcanoes. The 1983–1984 episodes of the Puu Oo eruption produced about 370,000 tonnes of SO_2, or as much as 3 percent of the annual volcanic contribution.

INTRODUCTION

A plume of gas and microscopic particles continuously enters the atmosphere from fumaroles in the southern half of Kilauea caldera. The plume is generally transparent with a light-bluish-gray color due to scattering of light by tiny particles. It contains H_2O, CO_2, and SO_2 as the major gaseous constituents (Cadle and others, 1969, 1971; Darzi, 1981; Darzi and Winchester, 1982c).

In this paper we describe the techniques used to measure SO_2 and CO_2 emission rates at Kilauea, the results from June 1979 through December 1984, and the interpretation of the data. These measurements form a part of the program to monitor Kilauea Volcano from the Hawaiian Volcano Observatory. Their purpose is to determine the long-term emission rates for SO_2 from Kilauea; to evaluate the usefulness of the measurements for forecasting eruptions; and to integrate geochemical observations with geophysical and geologic observations of activity to refine our understanding of how Kilauea Volcano works.

We will show that (1) during periods of relative quiescence, Kilauea emitted a nearly constant flux of SO_2; (2) during the 1983–1984 eruptions at Puu Oo on Kilauea's east rift zone, the rate of SO_2 release at the summit doubled and has remained at an elevated level; and (3) eruption plumes from Kilauea are characterized by increases in SO_2 of about two orders of magnitude over rates of non-eruptive or quiescent degassing.

BACKGROUND AND PREVIOUS STUDIES

The principal gases released from fumaroles at Kilauea are H_2O, CO_2, and SO_2 (Heald and others, 1963; Cadle and others, 1969, 1971; Gerlach, 1980; Greenland, 1984; Gerlach and Graeber, 1985; Greenland and others, 1985). The SO_2 is interpreted to be of magmatic origin (Sakai and others, 1982). The summit fumaroles at Halemaumau Crater and along the 1971 and 1974 eruptive fissures are the most notable sources of SO_2 in the summit region (Casadevall and Hazlett, 1983) and overly a shallow magma reservoir, envisioned as a plexus of sills and dikes, at a depth of 2 to 6 km (Fiske and Kinoshita, 1969; Ryan and others, 1981). Magma is fed into this shallow reservoir from a zone of generation at a minimum depth of 60 km (Eaton and Murata, 1960; Wright, 1984). Pre-eruptive degassing of magma while enroute to and temporarily stored in the shallow reservoir produces a CO_2-rich gas phase (atomic C/S ratio greater than 10); eruptive degassing produces a CO_2-rich gas phase during summit eruptions (atomic C/S is 5 or less) (Gerlach and Graeber, 1985; Greenland and others, 1985). An SO_2-rich gas phase (atomic C/S less than 1) is produced during rift eruptions from a magma which had already lost much of its CO_2 during equilibration at the pressure conditions of the shallow reservoir (Greenland, 1984; Gerlach and Graeber, 1985).

The preeruption content of sulfur in Hawaiian magma has been determined by Harris and Anderson (1983) to be about 1,300 ppm based on examination of melt inclusions in olivine phenocrysts. Basalt erupted on the sea floor under high confining pressure has lost some sulfur, but still contains between 700 and 1,000 ppm (Moore and Fabbi, 1971; Fornari and others, 1979) and surface flows contain from 50 to 200 ppm (Moore and Fabbi, 1971; Swanson and Fabbi, 1973; Sakai and others, 1982).

The continuous loss of sulfur during noneruptive periods to produce the volcanic plume is due largely to distillation of gas from magma as it reequilibrates to the pressure conditions of the shallow summit reservoir (Harris and Anderson, 1983; Greenland and others, 1985). Greenland and others (1985) suggest this mechanism results in about 150 ppm sulfur loss, while Gerlach and Graeber (1985) suggest a loss of between 300 and 600 ppm from the magma prior to eruption. Magma intruded to shallower depths in the

summit or rift zones may lose additional volatiles including SO_2. Further SO_2 loss occurs through effervescence of the basaltic magma (Swanson and Fabbi, 1973; Naughton and others, 1974; Harris and Anderson, 1983) during eruptions, a process which decreases the concentration of sulfur by approximately 600 ppm (Moore and Fabbi, 1971).

ACKNOWLEDGMENTS

Early support and encouragement for this program came from G. Eaton, Scientist-in-Charge at the Hawaiian Volcano Observatory from 1977–1979, and from R. Christiansen, Coordinator for the U.S. Geological Survey Geothermal Program which funded the purchase of the COSPEC. Continued support from the staff of the Hawaiian Volcano Observatory, in particular R. Decker, R. Okamura, and J. Forbes, is appreciated and gratefully acknowledged. Measurements during July and August 1982 were made by J.T. Prosser of Dartmouth College. The airborne measurements of SO_2 emission rates at Kilauea in July 1983 were made with the assistance of R. Symonds. W.I. Rose, Jr. (Michigan Technological University) and T.M. Gerlach (Sandia Laboratory) provided helpful reviews of earlier drafts of this paper. We dedicate this paper to our friend and teacher Richard E. Stoiber.

ACTIVITY OF KILAUEA, 1979–1984

Since June 1979, Kilauea has experienced two short-lived eruptions in the summit caldera (April and September 1982), a brief eruption at Pauahi Crater on the upper east rift zone (November 1979), a long-lived eruption in the middle east rift zone (January 1983–March 1985), and 13 intrusions (table 29.1). Each intrusion was accompanied by ground deformation and intense seismic activity that included discrete earthquakes and harmonic tremor (Dvorak and others, 1986). Five intrusions were also accompanied by the release of heat and (or) gases at the ground surface in the area of the intrusion.

METHODS, UNCERTAINTIES, AND ASSUMPTIONS

SO_2 emission rates have been measured at volcanoes since 1972 (Casadevall and others, 1981, 1984; Stoiber and others, 1983) including Kilauea in February 1975 (Stoiber and Malone, 1975) and in October 1978 (Stoiber and others, 1979). Regular ground-based measurements of SO_2 emission rates at Kilauea began in June 1979. Airborne measurements of SO_2 and CO_2 emission rates of the non-eruptive plume at Kilauea caldera and the eruption plume at the Puu Oo began in December 1983.

The emission rates of SO_2 and CO_2 are calculated by multiplying the plume velocity and the gas concentration in a cross-sectional profile of the plume. In this section we describe the methods and uncertainties for the measurements of wind speed, SO_2, and CO_2.

TABLE 29.1.—*Summary of activity, Kilauea Volcano: 1979–1984*

[S, summit: ERZ, east rift zone; SWRZ, southwest rift zone; I, intrusion; E, eruption; *, gas and (or) heat detected at ground surface above intrusion; n.d., not determined. Intruded volume calculated from Uwekahuna summit tilt (0.33×10^6 m^3 = 1 microradian). Modified from Dzurisin and others (1984)]

Date	Duration (days)	Location			Erupted volume	Intruded volume
		S	ERZ	SWRZ	(in million cubic meters)	
1979						
May 29	1	I				1.0
Aug 12	1		I			.6
Nov 16	1		E		0.4	
1980						
Mar 2	1		I			0.6–1.0
Mar 10	2–3		I*			5.3
Aug 27	1		I*			2.3
Oct 22	1		I*			.6
Nov 2	1		I			2.0
1981						
Jan 19	2	I				n.d.
Jan 24	16			I		>8.0
Jun 25	1	I				1.6
Aug 10	2			I*		35.0
1982						
Apr 30	1	E			0.5	
Jun 22	3			I*		14.1
Sept 25	2	E			3.0	
Dec 9	1		I			1.0
1983						
Jan 3	800+		E		360+	

WIND SPEED MEASUREMENTS

On the east side of the Island of Hawaii northeasterly trade-winds travel from 3 to 20 m/s. These winds carry the plume of gas from the fumaroles on the caldera floor out into the southwest rift zone of Kilauea (fig. 29.1). During winter months this wind pattern is frequently reversed as Kona winds blow from the southwest. We usually assume that the wind speed stays constant during the period of measurement.

For ground measurements of SO_2, the plume velocity is measured at Uwekahuna Bluff on the west side of Kilauea caldera (fig. 29.1) using a hand-held anemometer. Five 1-minute measurements of wind velocity are taken before and after the SO_2 measurements. The average of the before and after wind measurements is used to calculate the SO_2 emission rate.

For airborne measurements of SO_2 and CO_2, we rely primarily on wind direction and speed determinations made twice daily at Hilo Airport by the NOAA radiosonde. These are checked during flight. When possible, we compare true air speed of the aircraft determined while flying in the plume with true ground speed measured by flying a fixed distance (usually 10 miles) both with (tailwind) and against (headwind) the wind. The difference between the true ground speed and true air speed gives the wind speed.

The uncertainty in the measurement of wind speed is typically between 10 and 30 percent. This measurement is the largest single source of uncertainty in measuring the rates of SO_2 and CO_2 emission.

SO_2 MEASUREMENTS

The emission rates of SO_2 are measured using the Correlation Spectrometer (COSPEC; Barringer Research Ltd. of Canada) originally designed for use in pollution studies (Millan and others, 1976; Millan and Hoff, 1978) and adapted to the study of volcanoes (Stoiber and others, 1983). Correlation spectrometry is a remote-sensing technique that uses solar ultraviolet light scattered by the Earth's atmosphere as a source. The spectrally tuned instrument measures the amount of uv absorption by SO_2 present along the optical path through the plume in units of concentration-pathlength (ppm·m) at one atmosphere. Calibration is performed using an internal standard with a known concentration-pathlength of SO_2. A cross-section profile of the plume is determined by multiplying the plume width (m) with the concentration-pathlength. The product of this profile (ppm·m^2) and the wind speed (m/s) is the mass flux (ppm·m^3/s) and is usually expressed as tonnes per day (t/d).

Most measurements reported here were made with the COSPEC mounted in an automobile that is driven at a constant velocity of 40 km/h beneath the plume as it passes over a road that encircles Kilauea caldera (fig. 29.1*B*). An SO_2 cross section of the plume is continuously recorded on a chart recorder, and the changes in SO_2 pathlength concentration and geographic position are recorded. Four to six traverses can be made beneath the plume in about one hour. The techniques for airborne measurements are the same as those used at Mount St. Helens (Casadevall and others, 1981).

The large amounts of SO_2 and the enormous size of the eruption plumes at Kilauea presented added problems for airborne measurements. During eruptions in 1979, 1982, 1983, and 1984, the concentrations of SO_2 in the eruption plumes exceeded the measurable capacity using the COSPEC technique and caused saturation of the signal. In April 1984, we installed a high concentration SO_2 disc and calibration cells into the COSPEC to permit measurement of higher concentrations of SO_2. An additional problem is that the large plumes produced during eruptions of Kilauea often remain close to the ground, thereby preventing the aircraft from flying completely beneath the plume. Thus, many of the airborne measurements of SO_2 emission rates of eruption plumes are minimum values.

UNCERTAINTIES

The reported emission rate of SO_2 incorporates uncertainties due to both instrumental factors and variations from natural causes (Casadevall and others, 1981; Stoiber and others, 1983). The latter include real-time variation in gas emission, short-term (minutes to hours) variation in wind speed, and changes in cloud cover. Estimated uncertainties arising from operator and instrumental factors include uncertainty in the instrument calibration (±5 percent); variation in speed of vehicle used to measure the plume (±10 percent); uncertainty in data processing (±5 percent); and uncertainty in the measurement of wind speed (±10–30 percent). The effect of these uncertainties and variations on the reported SO_2 emission rate can be minimized by averaging the results of from 4 to 20 traverses each day. In practice, the average of these traverses, that is the average daily emission rate, usually has an uncertainty of ±10 to ±30 percent of the reported value.

CO_2 MEASUREMENTS

The emission rates of CO_2 have been measured within the noneruptive summit plume and at the Puu Oo eruption site (Greenland and others, 1985) beginning in 1983. The technique uses an infrared spectrometer that is flown through the plume at successively higher altitudes while the concentration of CO_2 is continuously measured (Harris and others, 1981). The concentration of CO_2 in excess of the background atmospheric CO_2 content is inferred to be from the volcano. This excess CO_2 generally ranges from 1 to 15 ppm (by volume), compared to an average atmospheric concentration of approximately 320±20 ppm. The altitude-concentration data are used to make a map of excess CO_2 concentration in a cross section of the plume. The product of the cross section-concentration (ppm·m^2) and the plume velocity (m/s) gives the emission rate of CO_2 (ppm·m^3/s) and is reported as tonnes per day. Each daily value represents a single cross section of the plume requiring between 90 and 120 minutes of continuous in-flight measurement.

The utility of the CO_2 method is limited by the practicality of flying repeatedly through a plume that is usually not visible, as well as by the threshold emission rate. We are aided in tracking the plume by simultaneously using the COSPEC to measure SO_2. Experience at Mount St. Helens (Casadevall and others, 1981; Harris and others, 1981) has shown that SO_2 and CO_2 are usually well mixed in the plume and that maximum CO_2 concentration is typically coincident with maximum SO_2 concentration.

The threshold value for detecting excess CO_2 in the plume depends on the wind speed and dispersion of the plume and the distance from the source at which measurements are made (that is, degree of air dilution). Excess CO_2 of less than 2 ppm is difficult to determine accurately. This concentration effectively becomes our threshold value for detecting excess CO_2 in the plume; in practical terms, emission rates of less than 1,000 t/d are difficult to measure. We estimate a maximum uncertainty in these measurements of ±40 percent of the reported value.

DATA QUALITY

In addition to real changes in the emission rates of gases, other factors, both natural and operator related, affect the quality of the data. These factors include changes in cloud cover, variation in wind speed and direction, experience of the operators, and instrumentation. Operator experience is important both in making the measurements of SO_2 and wind speed, as well as in reduction of data. Judgment must be used to evaluate the quality of a given day's measurement conditions and in interpreting the chart records. Judgment improves with practice and becomes more uniform with experience. Measurements made daily or at least several times each

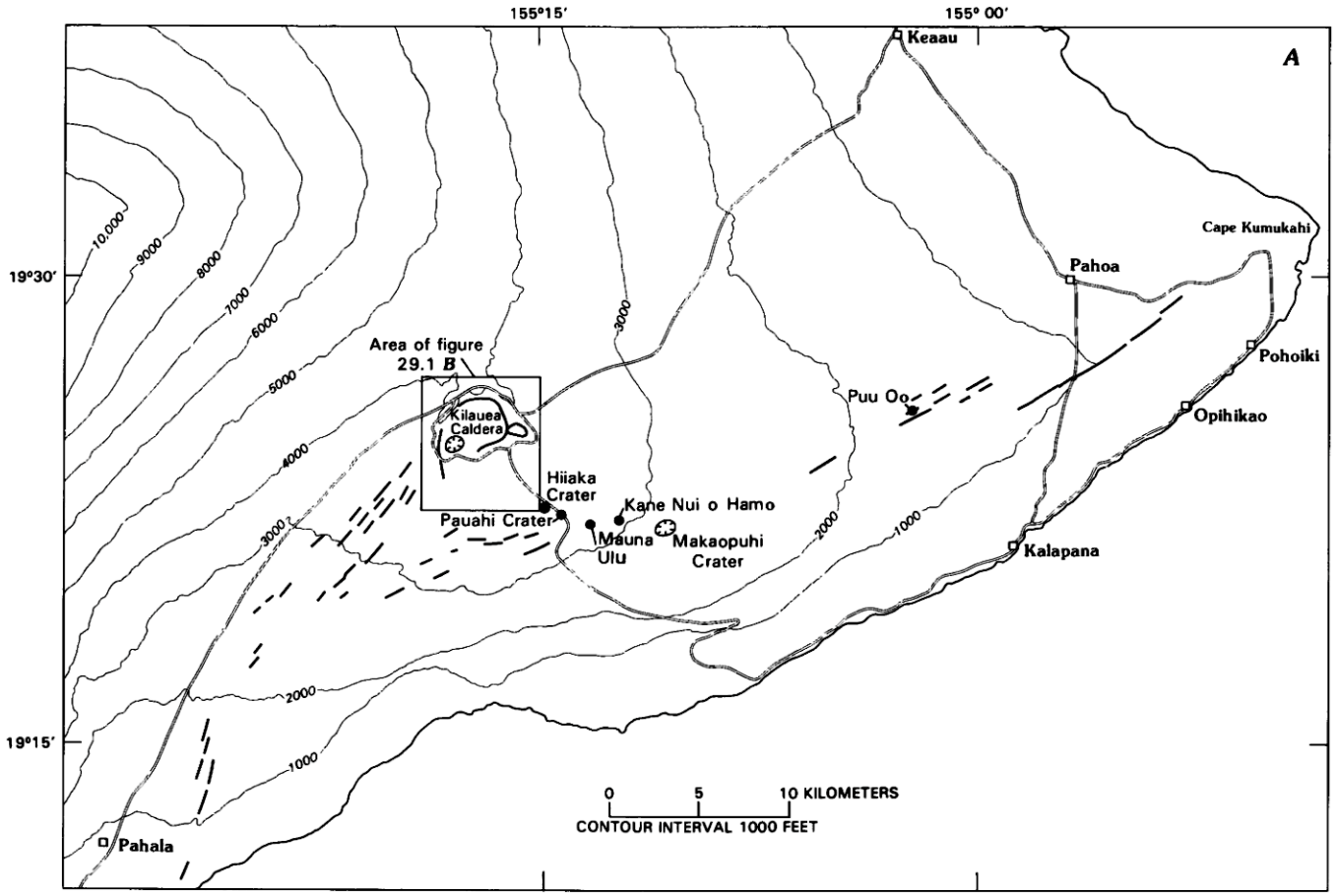

FIGURE 29.1.—Index map of Kilauea Volcano. ***A***, Summit area and rift zones. ***B***, Kilauea caldera area.

week provide a more reliable indication of background values than measurements made only weekly or less frequently. We have designated data quality as good if the frequency of measurement was weekly or better and if the measurements were made by the same experienced operator. Data of good quality include the summit measurements from June 1979 to June 1980, and from November 1981 through December 1984. Data of poor quality are those which have been collected infrequently by one or more inexperienced operators. The data collected from September 1980 through October 1981 are generally considered to be of poor quality. In addition, during many of the airborne measurements, the concentration of SO_2 exceeded that measurable by the COSPEC. These data should be treated with caution since they likely represent minimum rates for SO_2 emission.

REMOVAL OF SO_2 FROM THE PLUME

We have assumed that the SO_2 measured in the plume accurately represents the mass of sulfur released from the summit fumaroles. We recognize that while enroute to the surface, the SO_2-bearing gas mixture may be affected by a variety of conditions and processes that reduce the amount of sulfur reaching the fumaroles (Gerlach and Graeber, 1985). Measurements made during the season of heavy rainfall (December through March) show no significant change in SO_2 emission rate, suggesting that removal of SO_2, at least by the shallow ground-water table, is probably minimal. Eruption plumes do not appear to be affected by subsurface removal of SO_2 as there is little evidence for magma-ground water interaction during eruption (Greenland, 1984).

SO_2 in the plume may be removed through rainout and through dry deposition. Dry deposition occurs onto soil and vegetation as well as onto atmospheric particles such as sea spray and tropospheric dust (Darzi and Winchester, 1982a, 1982b). Direct deposition of SO_2 may damage vegetation (Winner and Mooney, 1980) and acidify rainfall (pH = 3.0–4.0), owing to scavenging of SO_2 by rain droplets (Harding and Miller, 1982; Russell, 1982). Salt and dust particles have been detected at the summit of Kilauea (Woodcock, 1960; Darzi and Winchester, 1982b), but their efficiency as scavengers of SO_2 and other gases is unknown. In eruption plumes, where the concentration of particles is higher than in noneruptive plumes, scavenging of SO_2 by tephra particles may be significant (Naughton and others, 1974; Rose, 1977).

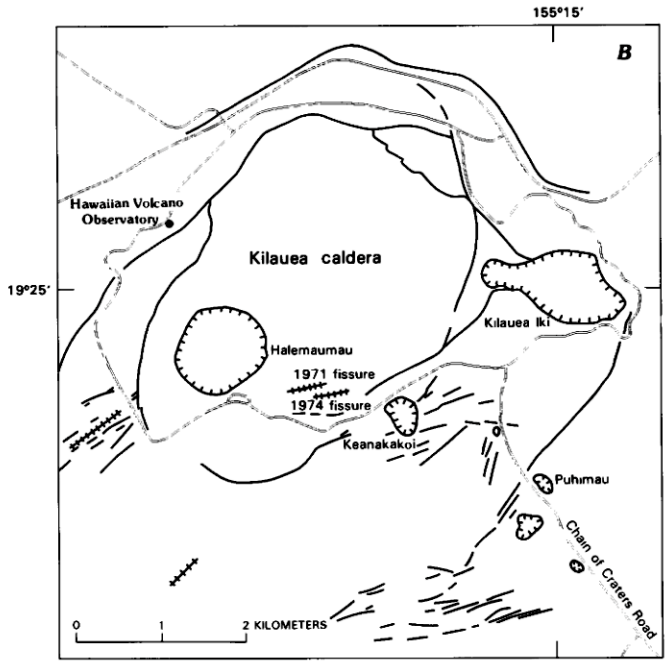

FIGURE 29.1.—Continued.

Some SO_2 in the plume is eventually converted to sulfate; however, studies of Kilauea fume by Cadle and others (1971) indicate that SO_2 dominates over other oxidized forms of sulfur. When the plumes at Kilauea summit and at Puu Oo were measured, they had usually been in the atmosphere for less than a few minutes; some measurements of the larger Puu Oo eruptive plumes require flying farther downwind where plumes may be as much as 1 hour old. This time is short as compared to the removal rates calculated from study of industrial plumes (Roberts and Williams, 1979; Williams and others, 1981) and estimated (Graedel, 1977; Maahs, 1983a; Martin, 1983; Barrie, 1985) as being on the order of less than about 1 percent SO_2 per hour. Removal rates increase only slightly with humidity and with acidity of the water droplets (Maahs, 1983b). The short-lived (usually tens of seconds) condensation cloud at Halemaumau may temporarily absorb some SO_2, but as the condensate evaporates the sulfur is probably released to the atmosphere as SO_2 (Hegg and Hobbs, 1978).

RESULTS

QUIESCENT SUMMIT EMISSIONS OF SO_2

The average daily emission rates of SO_2 from June 1979 through December 1984 are tabulated in table 29.2 and all data are plotted in figure 29.2. To examine these data for trends and changes, we have applied several statistical methods, including analysis of variance, multiple range test (Duncan), and regression analysis with step-wise selection of data to determine the timing and magnitude of changes in SO_2 emission rates. We have applied these

TABLE 29.2.—*Summary of SO_2 emission rates for the quiescent plume, Kilauea: 1979–1984*

[Values given in tonnes per day; *b*, the slope coefficent of the model; B estimate of *b*; R^2, percent of the SO_2 emission rate explained by the model; N, number of measurements]

Period	Dates	Daily rate (mean)	95 percent confidence interval for mean	B	$b=0$	R^2
1A	June 1979 to Mar 15, 1980	160 (N=120)	151–169	0	yes	--
1B	Mar 15 to Jun 1980(?)	100 (N=23)	75–120	0	yes	--
2	Sept 1980 to Aug 11, 1981	190 (N=43)	162–210	0	yes	--
3	Aug 11 to Dec 1981	300 (N=13)	265–326	0	yes	--
4	Feb 1982 to Jan 1983	160 (N=34)	100–220	0	yes	--
5	Jan 1983 to Dec 30, 1984	260 (N=172)	250–265	+0.04	no	2.8

tests to address the following questions: (1) Is it possible to identify periods during which SO_2 emission rates remained relatively constant? (2) If yes, what are the mean SO_2 emission rates during those periods and are there statistically significant differences between means for the different periods? (3) Which means are different and by how much? (4) Are there significant variations within periods which might not be apparent from visual inspection of the data? We have not weighted the data for instrument-related uncertainty, owing mainly to the difficulty in distinguishing between variation due to instrumental or operator errors and variation due to natural causes.

To begin, we visually inspected the data of figure 29.2 and selected 5 periods during which emission data appeared to have remained constant and calculated the mean SO_2 emission rate for each period. These periods include: (1) June 1979–June 1980, (2) September 1980–mid-August 1981, (3) mid-August 1981–December 1981, (4) February 1982–January 1983, and (5) late-January 1983–December 1984. Using the analysis of variance, we tested the null hypothesis (H_o) that the means for periods 1, 2, 3, 4, and 5 are the same ($H_o = u_1 = u_2 = u_3 = u_4 = u_5$ versus H_1 such that at least one pair u_i is not equal to u_j) where u_j is the mean SO_2 flux for period j. The test statistic (F-ratio) is highly significant (50.48), and we may conclude that the means are not all identical. Table 29.2 contains a summary of the analysis of variance for the five phases including the means of the data and the 95 percent confidence intervals.

To examine if the data within each period are constant within the 95 percent confidence limits, we performed a regression analysis using the least-squares method to test the regression model:

$$Y_i = a + bx_i$$

where Y_i is the SO_2 flux and x_i is the number of days since December 31, 1978. The coefficient a is of no particular use in this application since the origin is arbitrary. The important test statistics are B (the estimate of b, the slope coefficient of the model) and R^2 (the proportion of the SO_2 flux explained by the model). The analysis of variance (table 29.2) for each period tests the hypothesis that $b=0$, which indicates that the slope of a least-squares line is flat. In the initial test for periods 1 and 5, b was not equal to 0, indicating that there are trends to the data for these periods.

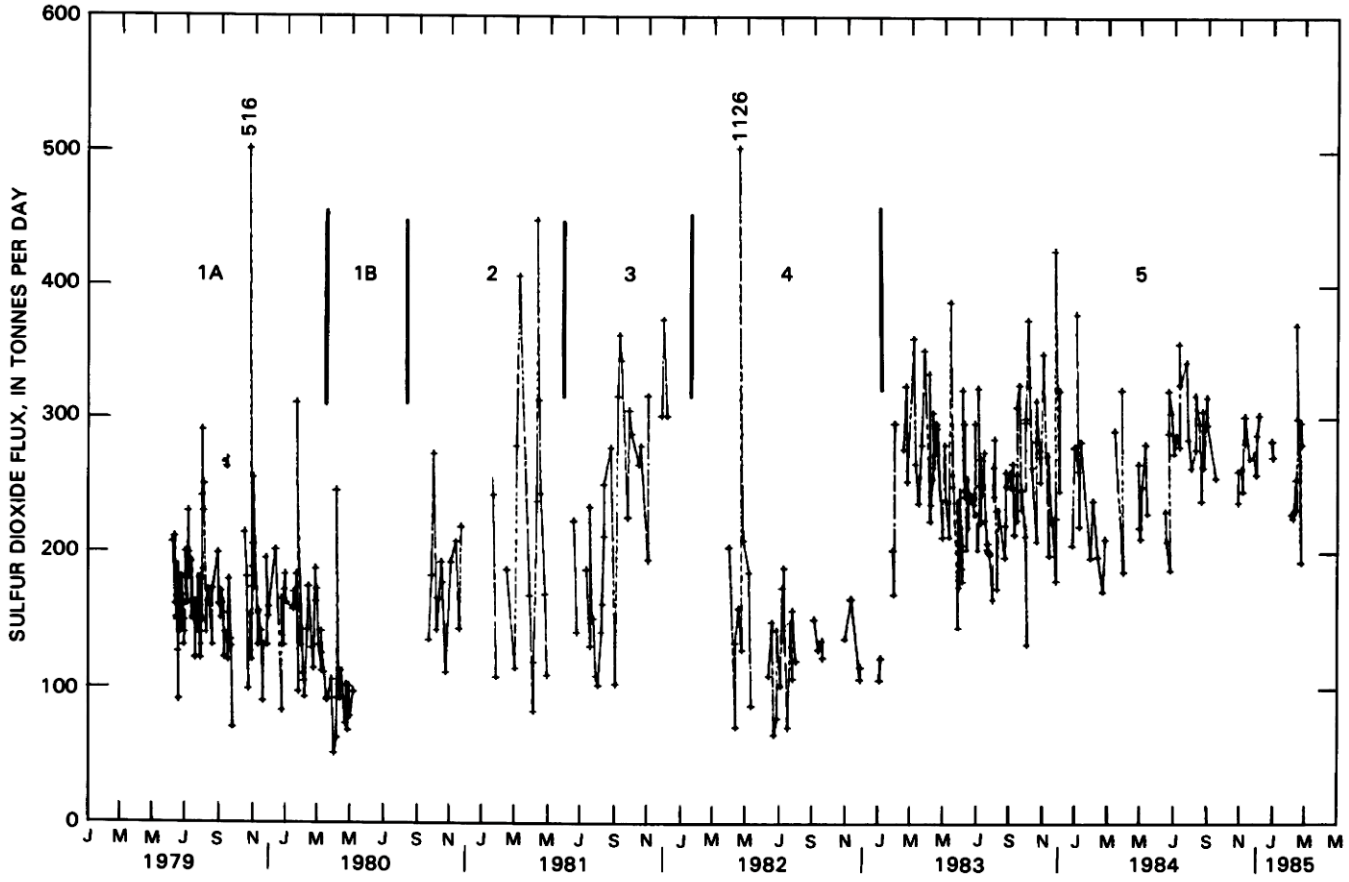

FIGURE 29.2.—SO_2 emission rate data obtained from COSPEC for Kilauea summit area, 1979–1984. Periods 1A–5 separated by heavy black lines.

However, the high R^2 value and negative sign for B (−0.17) for period 1 indicates that the trends in the data for this period are not smooth, but may be due instead to an abrupt decrease in the SO_2 emission rate.

By applying an iterative procedure using step-wise selection of data, we find that a significant decrease in SO_2 emission rates in period 1 occurred in mid-March 1980. On the basis of this test we have subdivided period 1 into 1A and 1B with the break occurring in mid-March 1980. The mean for period 1A (to mid-March 1980) is 160 t/d; the mean for period 1B (after mid-March 1980) is only 100 t/d. Regression analyses show that *b* for periods 1A and 1B equals 0, indicating that the trends for these two subsets of the data are flat.

We used the multiple range test (Duncan) to identify if the mean emission rates are significantly different from one another. Period 1B has the lowest mean and is significantly different from means for all the other periods at the 0.05 level. Periods 1A, 2, and 4 are not significantly different from each other at the 0.05 level. Periods 3 and 5 have the highest means, but are not significantly different from one another at the 0.05 level.

Lack of measurements for part of the second half of 1980 prevent us from determining whether the transition from period 1B to period 2 is abrupt or gradual. For period 5, the slope of the regression equation is slightly positive with a low value of B indicating that the data fit a trend of slight increase in SO_2, equivalent to about 0.05 t/d.

SO_2 EMISSION RATES DURING SUMMIT AND UPPER EAST RIFT ZONE ERUPTIONS

On April 30, 1982, a summit eruption lasted for 19 hours and produced about 0.5×10^6 m^3 of lava from an eruption fissure located northeast of Halemaumau Crater on the floor of Kilauea caldera. A peak emission rate of 1,150 t/d was measured during the middle of the eruption, and rates dropped to pre-eruption values quickly after activity ceased. On September 25, 1982, another summit eruption began at about 1900 (H.s.t.) and was over by the next morning after the eruption of about 3.0×10^6 m^3 of lava. The September eruption took place at night from vents located south of the Crater Rim Road, so COSPEC measurements were not possible. In contrast to the August 1971 and the July 1974 eruption fissures, which host prominent solfataras within the caldera, both 1982 eruptive fissures quickly cooled to ambient temperature and ceased emitting sulfur gases at the end of eruptive activity.

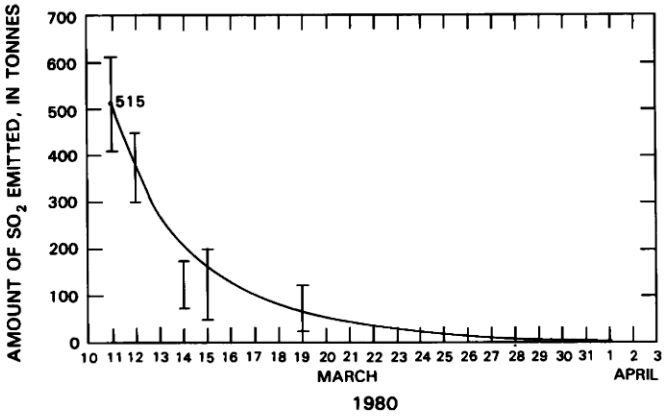

FIGURE 29.3.—SO_2 emission rates following Mauna Ulu intrusion, March–April 1980.

In November 1979, a 22-hour-long eruption occurred from vents east and west of, as well as within Pauahi Crater (fig. 29.1*A*) and approximately 3.5×10^6 m^3 of lava was erupted. COSPEC measurements were possible only during the first several hours of the eruption, before the Chain of Craters Road was closed by a lava flow, and an emission rate of 700 t/d of SO_2 was measured for the vent within Pauahi Crater. The 1979 fissures ceased emitting sulfur gases at the end of eruptive activity.

THE MARCH 10–12, 1980, INTRUSION

On March 2 and 10–12, 1980, two intrusions into the upper east rift zone of Kilauea (fig. 29.1*A*) between Pauahi Crater and Mauna Ulu were followed within minutes by deflation of the summit region. No lava was observed during these events; however, field studies in 1982 discovered a small volume (about 1 m^3) of fresh lava at 770 m elevation along the southeast end of the March 12 fracture (R. Moore, oral commun., 1982).

The March 10–12 intrusion released large amounts of CO_2 and SO_2 from the summit crater of the Mauna Ulu shield and from a 300-m-long N. 60° E. fracture set located between Mauna Ulu and Kane Nui o Hamo (fig. 29.1*A*). The fractures were quickly coated by elemental sulfur and fumed heavily for several days. The maximum temperature of the gas coming from the cracks was 98 °C. SO_2 emission rates from March 11 to 19 decreased from approximately 520 to 100 t/d, and within 30 days emission rates were less than 3 t/d (fig. 29.3). Approximately 3,000 tonnes of SO_2 was produced from March 11 through April.

SO_2 AND CO_2 EMISSIONS: AIRBORNE MEASUREMENTS: 1983–1984

Airborne measurements of SO_2 and CO_2 emission rates were made for eruption and intra-eruptive plumes at Puu Oo and for non-eruptive plumes at Kilauea caldera beginning in 1983 (table 29.3). The plumes from the eruptive episodes of Puu Oo are enormous in terms of SO_2 burden and physical size. The high concentration of SO_2 saturated the COSPEC signal, and plume widths often exceeded 50 km.

TABLE 29.3.—*Emission rates of SO_2 and CO_2 during Puu Oo eruption episodes: 1983–1984*

[—, no data; n.d., not determined]

Phase	Duration (hr)	Date	SO_2 (tonnes/day)	[1]CO_2 (tonnes/day)	Lava volume ($m^3 \times 10^6$)	Rate (m^3/hr)
			1983			
6	73	Jul 24	24,000 ± 4,700	--	9.4	0.13
7	56	Aug 15	15,700 ± 4,200	--	10.2	.18
7	56	Aug 17	17,500 ± 5,500	--	n.d.	n.d.
8	24	Sept 6	6,700 ± 1,800	--	7.0	.29
9	52	Sept 16	17,600 ± 10,300	--	8.7	.17
			1984			
14	19	Jan 31	11,800 ± 4,300	--	5.9	[3]0.31
15	19	Feb 15	[2]27,000	[1]4,700	8.6	.42
16	31	Mar 4	[2]18,000	[1]3,200	11.8	.37
17	22	Mar 30	5,100 ± 3,100	--	9.6	[3] .46
21	8	Jun 30	28,000 ± 6,200	--	5.7	[3] .71
28	15	Dec 4	32,000 ± 10,400	--	n.d.	[3] .85

[1]From Greenland and others (1985).
[2]Calculated values (see Greenland and others, 1985).
[3]Calculated from HVO monthly reports.

The episodes of the Puu Oo eruption have been well documented (Wolfe and others, chapter 17), including accurate measurements of erupted volumes and rates of lava production (table 29.3). Emission rates of SO_2 were measured during 8 eruptive episodes (6, 7, 8, 9, 14, 17, 21, and 28) of Puu Oo in 1983–1984; these rates range from 5,100 to 32,000 t/d (table 29.3). Rates for episodes 15 and 16 have been calculated from CO_2 flux measurements and fumarole gas composition (Greenland and others, 1985). The uncertainty in these measurements ranges from 15 to 40 percent of the reported values.

Between eruptive episodes at Puu Oo, gas is emitted continuously. On December 2, 1983, 24 hours after the end of phase 12, the SO_2 emission rates averaged 260 t/d; a week later the emission rates were 20 t/d. The CO_2 emission rates at Puu Oo were below the level of detection (less than 800–1,000 t/d) on both December 2 and 9. These data are consistent with gas sampling from the Puu Oo vent and with airborne measurements of eruptive plumes that indicate the CO_2/SO_2 ratio has been less than 1 (Greenland, 1984; Greenland and others, 1985).

On December 9, 1983, the emission rate of SO_2 in the summit region was 300 ± 30 t/d; the emission rate for CO_2 was 3,600 t/d. On February 13, 1984 the emission rates for SO_2 and CO_2 were 220 and 1,600 t/d, respectively (Greenland and others, 1985). These airborne measurements indicate a CO_2/SO_2 ratio greater than 5, in general agreement with measurements of fumaroles in the summit region.

DISCUSSION AND INTERPRETATION

RATES OF SO_2 EMISSION: NON-ERUPTIVE PLUME

The statistical analysis of the COSPEC data for 1979–1984 reveals that levels of SO_2 release remain relatively constant for

periods of months to years. Changes in the SO_2 flux generally correlate with other events at Kilauea such as eruptions or intrusions. We suggest that rates of SO_2 emissions, and changes in those rates, closely reflect magmatic processes at Kilauea. The relatively constant rates of SO_2 emission during periods 1A (before mid–March 1980), 3 (from August through December 1981), and 4 (February 1982 through January 1983) reflect the steady supply of magma to the shallow reservoir. The intrusions of magma into the upper east rift zone in March 1980 apparently diverted some magma out of the shallow reservoir and caused a 35 percent decrease in the rate of SO_2 emission from the summit region. In contrast, the southwest rift zone intrusion of August 1981 was followed by an increase in SO_2 emission rates (period 3), reflecting a temporary increase in the rate of magma supply as indicated by rapid reinflation of the summit chamber (Dvorak and others, 1986). Another rapid increase in the emission rate starting in January 1983 (period 5) occurred coincidently with an increase in magma supply rate that began with the Puu Oo eruption (Wolfe and others, chapter 17; Greenland and others, 1985).

For the period 1976–1982, magma was supplied to the shallow reservoir at about 5.6×10^6 m^3/mo (Dzurisin and others, 1984), and at 12×10^6 m^3/mo for the period 1983–1984 (chapter 17). From the mean rate of SO_2 emission from 1979–1982, we calculate that between 150 and 400 ppm sulfur were released by the magma stored in the shallow reservoir. A similar amount of sulfur was released during 1983-1984 using the higher rates of magma supply (Wolfe and others, chapter 17) and higher rates of SO_2 emission. This calculation suggests that about 10 to 30 percent of the 1,300 ppm sulfur (Harris and Anderson, 1983) initially dissolved in the parental melt is released to provide the daily rates of SO_2 measured in the non-eruptive plumes.

We noted earlier that distillation of magma as it re-equilibrates in the shallow reservoir may account for a sulfur loss of between 150 ppm (Greenland and others, 1985) and from 300 to 600 ppm (Gerlach and Graeber, 1985) prior to eruption. Thus, though some overlap exists in the amount of sulfur lost as determined from magma supply rates and SO_2 emission rates (150–400 ppm) as compared to the range of sulfur expected, the quantity of sulfur detected at the surface is apparently less than the amount of sulfur actually released from the magma. Gerlach and Graeber (1985) suggest that some SO_2 may be prevented from reaching the surface due to removal in the hydrothermal alteration of the volcanic pile or reaction with the deep hydrothermal brine, or it may be lost by separation of an immiscible sulfide melt during summit storage.

To discuss this problem more thoroughly, we need (1) to know more about the nature of the hydrothermal system postulated to overly the shallow magma reservoir, (2) more careful study of the volatile contents of intrusive bodies, and (3) additional study of melt inclusions to determine more precisely the primary sulfur content in Hawaiian basaltic magmas.

MAUNA ULU INTRUSION, MARCH 10–12, 1980

The fate of the sulfur remaining in the magma after its partial distillation in the shallow reservoir depends on its subsequent history. For the period 1956–1983, Dzurisin and others (1984) have shown that approximately 65 percent of the magma supplied to the shallow reservoir was stored through intrusion into the summit and rift zones of the volcano; approximately 35 percent was erupted. Only the extruded volume is largely outgassed of sulfur, whereas the intruded magma is less completely outgassed.

If intrusion is sufficiently shallow, further gas loss may be quite efficient. The initially large flux and subsequent rapid decrease in SO_2 emission rates which followed the intrusion near Mauna Ulu in mid-March 1980 is interpreted to reflect the pattern of outgassing of a portion of magma following its intrusion to a shallow depth. The SO_2 emission rates at the summit decreased significantly after this intrusion and remained low for at least three months. The volume of intruded magma estimated from the net summit deflation (16 microradians) during the event is approximately 5.2×10^6 m^3 (that is 0.33 million m^3 per microradian; Dzurisin and others, 1984). Assuming efficient degassing of 2.2 kg/m^3 of sulfur (loss of 800 ppm S; $p = 2.8$ g/cm^3), the 3,000 tonnes of SO_2 released during this event require a magma volume of 1.4×10^6 m^3. However, overburden pressures require greater solubility of sulfur in the melt, thus only about 30 percent of the dissolved sulfur in the reservoir-equilibrated magma would have had to escape to produce the SO_2 emissions of this event.

SO_2 FROM KILAUEA—ANNUAL BUDGET AND GLOBAL IMPACT

From the averaged monthly emission rates for SO_2 (table 29.2) we have calculated the average annual emission rates of SO_2 from quiescent outgassing of Kilauea from 1979–1984. These are: 1979, $58,500\pm15,000$ t/yr; 1980, $52,000\pm15,000$ t/yr; 1981, $83,000\pm30,000$ t/yr; 1982, $58,500\pm18,000$ t/yr; 1983, $95,000\pm33,000$ t/yr; and 1984, $95,000\pm33,000$ t/yr. The global anthropogenic contribution of SO_2 to the atmosphere is estimated at between 100×10^6 t/yr (Likens, 1979; Cadle, 1980) and 150×10^6 t/yr (Berresheim and Jaeschke, 1983). The global volcanic contribution is estimated to be 15×10^6 t/yr (Berresheim and Jaeschke, 1983) with the majority coming from a few large eruptive events. The contribution of SO_2 from quiescent outgassing of Kilauea contributes less than 1 percent of the annual global contribution from volcanoes.

The 1983–1984 eruptions of Puu Oo produced about 0.37×10^6 t/yr of SO_2 (calculated from the 1983–1984 total erupted magma of 307×10^6 m^3, corrected to dense rock equivalent, or DRE, using a 20 percent vesicularity correction, and estimated to release 3 kg of SO_2 per cubic meter of DRE lava) and may have contributed as much as 3 percent of the annual volcanic contribution. Though the individual eruptive episodes of Puu Oo contributed large amounts of SO_2 to the atmosphere, these emissions were confined to the lower troposphere, and eruptions seldom continued for longer than 72 hours. The local impact of such emissions on vegetation and rainfall chemistry may be dramatic (Winner and Mooney, 1980); however, their global impact remains small.

ERUPTION PREDICTION USING EMISSION RATE DATA

At Asama Volcano, Japan, Noguchi and Kamiya (1963) demonstrated that the amounts of sulfur gas emitted by the volcano increased prior to explosive eruptions. At Mount Etna, large increases in the rate of SO_2 emission were observed before each of two Strombolian eruptions in 1977 (Malinconico, 1979). At Mount St. Helens, increases in SO_2 emission rates were noted two to four weeks prior to 2 of 12 eruptions between 1981 and 1983 (Casadevall and others, 1983). These studies indicate that increases in SO_2 emission rates precede some, but not necessarily all, types of eruptive activity.

From experience with emission-rate data at Mount St. Helens, Casadevall and others (1983) note that confidence in using the data for prediction of activity increases with the frequency and regularity of measurements. We have scrutinized the present data for Kilauea and find no hindsight indication of pending activity. If such increases happen only days or hours before activity, it is unlikely that we would recognize them using the frequency of measurements made during 1979–1984.

Measurements of SO_2 and CO_2 emission rates require considerable investments of time and effort, and the present techniques simply are not practical for making continuous measurements. Different methods of measurement, as well as more careful integration of geochemical data with other geophysical measurements, are necessary if we hope to use emission rates to improve our abilities to predict impending activity.

REFERENCES

Barrie, L.A., 1985, Scavenging ratios, wet deposition and in-cloud oxidation: an application to the oxides of sulphur and nitrogen: Journal of Geophysical Research, v. 90, p. 5789–5799.

Berresheim, H., and Jaeschke, W., 1983, The contribution of volcanoes to the global atmospheric sulfur budget: Journal of Geophysical Research, v. 88, p. 3732–3740.

Cadle, R.D., 1980, A comparison of volcanic with other fluxes of atmospheric trace gas constituents: Reviews of Geophysics and Space Physics, v. 18, p. 746–752.

Cadle, R.D., Lazrus, A.L., and Shedlovsky, J.P., 1969, Comparison of particles in the fume from eruptions of Kilauea, Mayon, and Arenal volcanoes: Journal of Geophysical Research, v. 74, p. 3372–3378.

Cadle, R.D., Wartburg, A.F., and Grahek, F.E., 1971, The proportion of sulfate to sulfur dioxide in Kilauea Volcano fume: Geochimica et Cosmochimica Acta, v. 35, p. 503–507.

Casadevall, T.J., and Hazlett, R.W., 1983, Thermal area of Kilauea and Mauna Loa: Journal of Volcanology and Geothermal Research, v. 16, p. 173–188.

Casadevall, T.J., Johnston, D.A., Harris, D.M., Rose, W.I., Jr., Malinconico, L.L., Stoiber, R.E., Bornhorst, T.J., Williams, S.N., Woodruff, Laurel, and Thompson, J.M., 1981, SO_2 emission rates at Mount St. Helens from March 29 through December, 1980, *in* Lipman, P.W., and Mullineaux, D.L., eds., The 1980 eruptions of Mount St. Helens, Washington: U.S. Geological Survey Professional Paper 1250, p. 193–200.

Casadevall, T.J., Rose, W.I., Jr., Fuller, W.H., Hunt, W., Hart. M., and Moyers, J.L., 1984, SO_2 and particles in quiescent volcanic plumes from Poas, Arenal, and Colima Volcanos, Costa Rica and Mexico: Journal of Geophysical Research, v. 89. p. 9633–9641.

Casadevall, T.J., Rose, W.I., Jr., Gerlach, T.M., Greenland, L.P., Ewert, J., Wunderman, R., and Symonds, R., 1983. Gas emissions and the eruptions of Mount St. Helens through 1982: Science, v. 221, p. 1383–1385.

Darzi, Michael, 1981, Fumarolic aerosols from Kilauea volcano, Hawaii: Nuclear Instrumentation Methods, v. 181, p. 359–365.

Darzi, Michael, and Winchester, J.W., 1982a, Aerosol characteristics at Mauna Loa observatory, Hawaii, after East Asia dust storm: episodes: Journal of Geophysical Research, v. 87, p. 1251–1258.

——— 1982b, Resolution of basaltic and continental aerosol components during spring and summer within the boundary layer of Hawaii: Journal of Geophysical Research, v. 87, p. 7262–7272.

——— 1982c, Volcanic aerosol phosphorus, chlorine, and sulfur at Kilauea, Hawaii: Journal of Geophysical Research, v. 87, p. 11,095–11,101.

Dvorak, J.J., Okamura, A.T., English, T.T., Koyanagi, R.Y. Nakata, J.S., Sako, M.K., Tanigawa, W.T., and Yamashita, K.M., 1986, Mechanical response of the south flank of Kilauea Volcano, Hawaii, to intrusive events along the rift systems: Tectonophysics, v. 124, p. 193–209.

Dzurisin, Daniel, Koyanagi, R.Y., and English, T.T., 1984, Magma supply and storage at Kilauea Volcano, Hawaii: Journal of Geophysical Research, v. 21, p. 177–206.

Eaton, J.P., and Murata, K.J., 1960, How volcanoes grow: Science, v. 132, p. 925–938.

Fiske, R.S., and Kinoshita, W.T., 1969, Inflation of Kilauea Volcano prior to its 1967–1968 eruption: Science, v. 165, p. 341–349.

Fornari, D.J., Moore, J.G., and Calk, L., 1979. A large submarine sand-rubble flow on Kilauea Volcano, Hawaii: Journal of Volcanology and Geothermal Research, v. 5, p. 239–256.

Gerlach, T.M., 1980, Evaluation of volcanic gas analyses from Kilauea Volcano: Journal of Volcanology and Geothermal Research, v. 7. p. 295–317.

Gerlach, T.M., and Graeber, E.J., 1985, The volatile budget of Kilauea: Nature, v. 313, p. 273–277.

Graedel, T.E., 1977, The homogeneous chemistry of atmospheric sulfur: Reviews of Geophysics and Space Physics, v. 15, p. 421–426.

Greenland, L.P., 1984, Gas composition of the January 1983 eruption of Kilauea Volcano, Hawaii: Geochimica et Cosmochimica Acta, v. 48, p. 193–195.

Greenland, L.P., Rose, W.I., Jr., and Stokes, J.B., 1985, An estimate of gas emissions and magmatic gas content from Kilauea Volcano: Geochimica et Cosmochimica Acta, v. 49. p. 125–129.

Harding, Duane, and Miller, J.M., 1982, The influence of volcanic outgassing on rain chemistry of the Hawaiian volcano Kilauea: Journal of Geophysical Research, v. 87, p. 1225–1230.

Harris, D.M., and Anderson, A.T., Jr., 1983, Concentrations, sources, and losses of H_2O, CO_2, and S in Kilauean basalt: Geochimica et Cosmochimica Acta, v. 47, p. 1139–1150.

Harris, D.M., Sato, Motoaki, Casadevall, T.J., Rose, W.I., Jr., and Bornhorst, T.J., 1981, Emission rates of CO_2 from plume measurements, *in* Lipman, P.W., and Mullineaux, D.L., eds., The 1980 eruptions of Mount St. Helens, Washington: U.S. Geological Survey Professional Paper 1250, p. 201–207.

Heald, E.F., Naughton, J.J., and Barnes, I.L., 1963, The chemistry of volcanic gases. 2. Use of equilibrium calculations in the interpretation of volcanic gas samples: Journal of Geophysical Research, v. 68, p. 545–557.

Hegg, D.A., and Hobbs, P.V., 1978, Oxidation of sulfur dioxide in aqueous systems with particular reference to the atmosphere: Atmospheric Environment, v. 12, p. 241–253.

Likens, G.E., 1979, Acid rain: Scientific American, v. 241, p. 43–51.

Maahs, H.G., 1983a, Measurements of the oxidation rate of sulfur (IV) by ozone in aqueous solution and their relevance to SO_2 conversion in nonurban tropospheric clouds: Atmospheric Environment, v. 17. p. 341–345

——— 1983b, Kinetics and mechanism of the oxidation of S(IV) by ozone in aqueous solution with particular reference to SO_2 conversion in nonurban tropospheric clouds: Journal of Geophysical Research, v. 88, p. 10,721–10,732.

Malinconico, L.L., 1979, Fluctuations in SO_2 emission during recent eruptions of Etna: Nature, v. 278, p. 43–45.

Martin, L.R., 1983, Kinetic studies of sulfite oxidation in aqueous solution, *in*

Calvert, J.G., ed., SO_2, NO, NO_2 oxidation mechanism: atmospheric considerations, v. 3, of Acid precipitation series: Boston, Butterworth, p. 63–100.

Millan, M.M., Gallant, A.J., and Turner, H.E., 1976, The application of correlation spectroscopy to the study of dispersion from tall stacks: Atmospheric Environment, v. 10, p. 499–511.

Millan, M.M., and Hoff, R.M., 1978, Remote sensing of air pollutants by correlation spectroscopy—instrumental response characteristics: Atmospheric Environment, v. 12, p. 853–864.

Moore, J.G., and Fabbi, B.P., 1971. An estimate of the juvenile sulfur content of basalt: Contributions to Mineralogy and Petrology, v. 33, p. 118–127.

Naughton, J.J., Lewis, V.A., Hammond, D., and Nishimoto, D., 1974, The chemistry of sublimates collected directly from lava fountains at Kilauea Volcano, Hawaii: Geochimica et Cosmochimica Acta, v. 38, p. 1679–1690.

Noguchi, K., and Kamiya, H., 1963, Prediction of volcanic eruption by measuring the chemical composition and amounts of gases: Bulletin Volcanologique, v. 26, p. 367–378.

Roberts, D.B., and Williams, D.J., 1979. The kinetics of oxidation of sulphur dioxide within the plume from a sulphide smelter in a remote region: Atmospheric Environment, v. 13, p. 1485–1499.

Rose, W.I., Jr., 1977, Scavenging of volcanic aerosol by ash: atmospheric and volcanic implications: Geology, v. 5, p. 621–624.

Russell, C., 1982, The effects of acid environments on metabolic gas exchange in *Usena australis* Fr.: Honolulu, University of Hawaii, MS thesis, 131 p.

Ryan, M.P., Koyanagi, R.Y., and Fiske, R.S., 1981, Modeling the three-dimensional structure of magma transport systems: Application to Kilauea Volcano, Hawaii: Journal of Geophysical Research, v. 86, p. 7111–7129.

Sakai, H., Casadevall, T.J. and Moore, J.G., 1982, Chemistry and isotope ratios of sulfur in basalts and volcanic gases at Kilauea Volcano, Hawaii: Geochimica et Cosmochimica Acta, v. 46, p. 729–738.

Stoiber R.E., Malinconico, L.L., and Casadevall, T.J., 1979. SO_2 monitoring by remote sensing at Kilauea Volcano, Hawaii [abs.]: Hawaii Symposium on Intraplate Volcanism and Submarine Volcanism, Hilo, HI, Abstract volume, p. 174.

Stoiber R.E., Malinconico, L.L., and Williams, S.N., 1983, Use of the correlation spectrometer at volcanoes, *in* Tazieff, H., and Sabroux, J.C., eds., Forecasting Volcanic Events: Amsterdam, Elsevier, p. 425–444.

Stoiber R.E., and Malone, G.B., 1975, SO_2 emission at the crater of Kilauea, at Mauna Ulu and at Sulfur Banks, HI [abs.]: Eos, v. 56, p. 461.

Swanson, D.A., and Fabbi, B.P., 1973, Loss of volatiles during fountaining and flowage of basaltic lava at Kilauea Volcano, Hawaii; U.S. Geological Survey Journal of Research, v. 1, p. 649–658.

Williams, D.J., Carras, J.N., Milne, J.W., 1981, The oxidation and long-range transport of sulphur dioxide in a remote region: Atmospheric Environment, v. 15, p. 2255–2262.

Winner, W.E., and Mooney, H.A., 1980, Response of Hawaiian plants to volcanic sulfur dioxide: stomatal behavior and foliar injury: Science, v. 210, p. 789–791.

Woodcock, A.H., 1960, The origin of trade-wind orographic shower rains: Tellus, v. 12, p. 315–326.

Wright, T.L., 1984, Origin of Hawaiian tholeiite: a metasomatic model: Journal of Geophysical Research, v. 89. p. 3233–3252.

COMPOSITION OF GASES FROM THE 1984 ERUPTION OF MAUNA LOA VOLCANO

By L. Paul Greenland

ABSTRACT

The March–April 1984 eruption of Mauna Loa Volcano provided an excellent opportunity for sampling eruptive gases. These Mauna Loa gases are similar to those from adjacent Kilauea Volcano, but they have less Sater and halogens relative to sulfur than Kilauea gases. The very low atomic C/S ratio (0.2, as at Kilauea) is attributed to pre-eruption degassing of the magma during storage in Mauna Loa's shallow (3–4 km) summit reservoir. Thermodynamic calculations show that most of these samples contain excess water above that required for equilibrium with other species. It is suggested that the excess water in these analyses is not a meteoric contaminant but is magmatic water which has not equilibrated with the other gases because of the rapid rate of rise of the magma in the vent system.

INTRODUCTION

A flank eruption of Mauna Loa Volcano, Hawaii, began on March 25, 1984, and ended by April 14. The eruption began in the summit caldera and extended about 3 km down the southwest rift zone and about 19 km down the northeast rift zone. By 0930 Hawaiian standard time (H.s.t.) of March 25, fountaining was restricted to a 21-km-long curtain of fire between about 3,400-m and 3,470-m elevation on the northeast rift zone; by 0640 H.s.t. the next day, activity had ceased at these vents except for profuse fume emission, which continued through May 5. As eruptive activity at these vents waned, new vents opened downrift at about 2,800-m elevation; these vents were active along a 500-m segment of the fissure until April 14. A preliminary summary of geologic, deformational, and seismic studies of this eruption may be found in Lockwood (1984).

Many of the vents in the active area of the fissure at 2,800-m elevation were fully productive only intermittently, having long intervals of only low-level spatter activity and occasional small lava flows overflowing the vent. These provided nearly ideal sites for sampling gases. Continued eruptive activity made these sites inaccessible after April 5, and gas sampling was then restricted to the fuming, noneruptive vents above 3,400 m. Gases emitted by the noneruptive vents originated from magma in the feeder dike as it passed through the conduit system to be erupted downrift. This paper reports the results of gas collections made in these two areas.

ACKNOWLEDGMENTS

I am greatly indebted to T.M. Gerlach for a thorough and trenchant review of an earlier draft of this paper. I have also benefited from thoughtful comments by I. Barnes, M. Sato, and A. Truesdell.

EXPERIMENTAL METHODS

SAMPLING SITES

Two classes of sampling sites will be distinguished in this paper: "active" sites are those where gas samples were taken from, or immediately adjacent to, vents actively emitting spatter, fountains, and (or) lava flows; "feeder" sites were at posteruptive vents through which the magma was degassing as it flowed through the conduit to the actively erupting vents. After March 25, the active sites were located at 2,800-m to 3,000-m elevation, while the feeder sites were in the area of 3,400-m elevation. Only active sites were sampled until April 3; these then became generally inaccessible, and subsequently attention was concentrated on the feeder sites.

SAMPLING TECHNIQUE

Gas samples were collected through lead-in tubes using evacuated bottles as described elsewhere (Greenland, 1984). Lead-in tubes used at various times were lengths of titanium, stainless steel, quartz, or mullite tubing 1–2 m long and 1–4 cm in diameter; they were inserted up to two-thirds of their length into the vent and left for several minutes in order for the natural gas flow to flush out air. At the active vents, the entrance of the tube was always within a meter or so of molten magma and often within centimeters. When first used, metal tubes were inserted in a vent for as long as 30 min to develop corrosion; no samples were taken during this conditioning process. Experience in Hawaii has shown that 1–2 min of flushing is adequate, while more than 10–15 min of flushing of stainless steel or titanium at temperatures above 1,000 °C results in samples having increased H_2 content; all samples reported here were collected within 5 minutes of tube insertion when stainless steel or titanium was used. Quartz or mullite tubes are much less reactive than the metal ones, but they are discouragingly fragile under rough field conditions. With the sampling technique used here, there appears to be no difference in sample composition related to composition of lead-in tube.

The evacuated bottles used for gas collection were similar to those described by Giggenbach (1975) but contained a different aqueous solution. Piccardi and Cellini-Legittimo (1983) discussed the advantages of a Cd solution for separating H_2S, and T.M. Gerlach (oral commun., 1983) suggested replacing caustic solutions with NH_4OH. (Subsequently, Gerlach has returned to caustic solutions). The present collections were made with bottles containing 25–45 mL of 3*M* NH_4OH–0.1*M* $NH_4CH_3CO_2$–0.04*M* CdO. Gas collections were made by covering the exit of the lead-in tube with a metal washer to reduce air contamination, inserting the stem (2–4 cm) of the inverted bottle, and opening the stopcock allowing the gases to bubble through the ammonia solution; H_2S was immediately precipitated as CdS, the acid gases were absorbed in the aqueous solution, and H_2 and CO passed into the headspace.

Temperatures were measured with a chromel-alumel thermocouple. Because of the difficult conditions, measured temperatures at the active vents may be as much as 25–50 °C lower than actual temperatures.

Extreme precautions to exclude air from the samples were not taken. An abundance of experiments made in Hawaii have shown that gas collections made in this way are stable for 4–6 h even with 95 percent air in the sample; left overnight for analysis, however, such gas samples usually become oxidized. Because of the proximity of laboratory facilities and the availability of helicopter transport, it usually was possible to complete the gas chromatography analyses within 5 h of collection; on the few occasions when this was not possible, the samples were discarded. The aqueous solutions of the acid gases are unaffected by air contamination except for the possible oxidation of SO_3^{2-} to SO_4^{2-}; all S in these solutions was calculated as SO_2, and these analyses could be performed at leisure.

GAS CHROMATOGRAPHY

The H_2 and CO collected in the headspace of the evacuated bottles were determined by gas chromatography. Because of the high temperature of the sampling and because sampling was occasionally interrupted before the bottles were completely full, air was admitted to the bottles just before analysis to adjust the pressure to atmospheric pressure. The H_2 was separated on 4.9 m (16 ft) of 5A molecular sieve with N_2 carrier gas at room temperature and determined by thermal conductivity (helium was sought simultaneously but was not present at >0.001 percent). The gas chromatograph for this determination was assembled locally from a commercially available sampling valve, detector, and integrator. For the determination of CO and CH_4, samples were injected onto 3.6 m (12 ft) chromosorb 102 with He carrier gas in a Hewlett-Packard 5840 gas chromatograph; a valve permitted backflushing of CO_2, H_2O, and SO_2 while the more rapidly eluted gases passed to 2.4 m (8 ft) of 5A molecular sieve. After elution of oxygen from this column, a valve switched the gas stream to enable reaction of CO with H_2 in the presence of a nickel catalyst to form CH_4 (CH_4 originally present in the sample eluted subsequently and passed through this converter unchanged). The CO (converted to CH_4) and CH_4 were then determined with a flame ionization detector. Analytical precision of the gas chromatography analyses was ±3–5 percent.

WET CHEMISTRY

The CO_2, SO_2, H_2S, HCl, and HF were determined in aliquants of the aqueous solution in the evacuated-bottle collections. For CO_2, 0.5 mL was added to 1 mL of 6*M* H_2SO_4 saturated with $K_2Cr_2O_7$ in a closed vial; the CO_2 liberated into the headspace was then determined by gas chromatography. The HF was determined by specific-ion electrode after adjusting the pH of an aliquant to 6 with dilute H_2SO_4. The HCl also was determined by specific-ion electrode after acidification with 6*M* H_2SO_4 and oxidation of SO_3^{2-} with $NaNO_2$. The Cd remaining in the supernatant solution was determined by atomic-absorption spectrometry; the difference from that originally present was attributed to CdS, thus H_2S. The SO_3^{2-} and SO_4^{2-} were determined by conventional ion chromatography with 3m*M* $NaHCO_3$–Na_2CO_3 as eluent; SO_3^{2-} and SO_4^{2-} were combined and calculated as SO_2. The analytical precision of these determinations was ±10–15 percent.

The evacuated bottles were weighed before and after sample collection. The weight gained, after subtraction of CO_2 and SO_2, was taken as water.

RESULTS

Analyses of the evacuated-bottle collections on an air-free basis are given in table 30.1. The water content of these samples ranges from 55 to 91 percent, and, because of the constant sum condition, this variation induces an apparent variability in the less abundant components. Furthermore, the abundances of H_2, CO, and H_2S are thermodynamic functions of the temperature and partial pressure of oxygen at which they were last in equilibrium, and thus variations in these gases may simply reflect the temperature and oxidation state of the gases. These effects are reduced in table 30.2, which gives the analyses on the basis of atomic ratios (atoms per sulfur atom) and compares their average with the composition of gas from the recent east-rift-zone eruption of adjacent Kilauea Volcano. Even on this basis, the compositional variability remains fairly large, with the range of each component extending over more than a factor of three.

Two samples were collected after the eruption ended on April 15. Table 30.1 shows these samples to be greatly depleted in SO_2 and enriched in H_2O; by April 18, halogen acids also became more abundant.

The abundance of halogen acids is generally very low in these gases, less than 1 percent of the sulfur content, and quite variable, ranging over more than an order of magnitude. It is obvious from table 30.1 that the halogens are highly correlated with each other, but statistical tests show that they vary independently of H, C, or S species. The average atomic Cl/F ratio, 1.1 ± 0.46, is not significantly different from the ratio (0.92) found for the 1983 eruption of Kilauea (table 30.2), although the halogen/S ratios from Kilauea are almost an order of magnitude higher than these Mauna Loa

TABLE 30.1.—*Composition of gas samples from 1984 Mauna Loa eruption*

[Lead-in tube materials: 1, Ti: 2, stainless steel; 3, quartz; 4, mullite]

Sample	Collection date (mo/d)	Constituents (mole percent)								Temperature (°C)	Tube Materials
		H_2O	H_2	CO_2	CO	SO_2	H_2S	HCl	HF		
Active vents											
1	3/25	75.6	0.36	3.22	0.108	19.9	0.58	0.074	0.064	1,080	1
2	3/25	59.2	.66	6.34	.156	32.9	.62	.018	.100	1,075	1
3	3/25	64.9	.55	4.57	.157	28.7	.92	.130	.101	1,080	1
4	3/26	73.0	.64	3.23	.146	22.1	.69	.108	.051	1,100	1
5	3/26	73.4	.48	4.15	.158	21.0	.56	.161	.096	1,100	1
6	3/26	77.6	.49	2.38	.090	18.0	1.05	.194	.118	1,120	4
7	3/26	75.7	.30	4.25	.073	19.0	.51	.066	.072	1,050	4
8	3/27	77.2	.73	2.23	.150	19.0	.56	.077	.036	1,130	1
9	3/27	79.8	.86	3.05	.168	15.3	.74	.094	.098	1,130	1
10	3/27	70.2	.80	3.45	.115	24.5	.79	.059	.103	1,100	1
11	3/27	78.5	.75	2.45	.137	16.9	1.01	.174	.086	1,100	1
12	3/27	69.4	.66	4.57	.164	24.7	.38	.015	.025	1,130	1
13	3/30	73.1	.32	5.34	.117	20.1	.81	.049	.055	825	3
14	3/30	70.7	.27	6.64	.094	21.0	1.11	.089	.110	825	3
15	3/31	64.9	.94	7.79	.346	25.0	.85	.093	.116	1,080	3
16	4/ 1	71.7	1.31	6.61	.322	17.9	2.02	.065	.054	1,100	1
17	4/ 1	78.7	.93	4.69	.238	14.0	1.35	.048	.039	1,100	1
18	4/ 2	82.3	.33	4.36	.143	11.7	1.11	.028	.030	1,050	1
19	4/ 2	79.8	.60	4.54	.102	13.9	.97	.049	.060	1,050	1
24	4/ 5	71.8	.31	2.11	.063	25.1	.47	.063	.073	1,010	1
25	4/ 5	65.6	.90	6.13	.109	24.8	2.45	.040	.029	1,010	1
26	4/ 5	65.8	1.30	6.53	.306	23.3	2.49	.139	.174	1,100	1
Feeder vents											
20	4/ 3	71.1	.17	5.21	.096	22.2	1.02	.082	.102	735	1
21	4/ 3	64.2	.28	4.91	.083	29.2	1.15	.059	.078	870	1
22	4/ 3	71.3	.15	5.11	.072	22.2	1.02	.092	.099	775	1
23	4/ 3	62.0	.30	6.58	.078	29.1	1.41	.208	.265	835	1
27	4/ 5	61.1	.41	6.54	.125	30.4	1.23	.119	.124	875	3
28	4/ 5	55.3	.58	8.72	.157	33.2	1.61	.165	.199	895	1
29	4/ 7	59.8	.57	6.16	.129	31.6	1.63	.035	.019	880	1
30	4/ 9	65.0	.46	5.88	.122	27.5	1.01	.024	.018	875	2
31	4/11	70.2	.29	5.07	.060	23.6	.80	.020	.022	840	1
32	4/11	66.1	.28	5.06	.089	27.2	1.12	.061	.056	840	2
33	4/13	64.9	.25	5.34	.107	27.5	1.64	.097	.136	820	1
34	4/13	64.7	.16	6.01	.046	28.0	1.03	.042	.045	820	2
Posteruption samples											
35	4/16	91.2	.51	1.66	.009	5.1	1.44	.042	.077	760	2
36	4/18	86.8	.07	4.05	.004	6.7	1.72	.193	.469	745	2

ratios. The great difference in halogen/S ratios may reflect a difference in the magma chemistry of Mauna Loa versus that of Kilauea; alternatively, eruptive degassing may have been more efficient for the Kilauea samples than for those from Mauna Loa.

Examination of tables 30.1 and 30.2 suggests a difference in water content between samples taken in the area of actively eruptive vents and samples taken where the feeder dike was degassing through posteruptive vents. Student's t-test (Fisher, 1936) confirms the difference in means (72.6 and 64.6 percent H_2O, respectively) to be significant at the 99-percent confidence level. A ternary plot of atomic H-C-S (fig. 30.1) shows the clear distinction between active vents and feeder vents in their content of water, the major contributor to atomic H. Samples from both types of vent plot closely along the same atomic-H control line, defined by a C/S ratio of ~0.2, indicating that the major source of variability among these samples is a process that has added or subtracted water to or from the gas. Most of the samples from the feeder sites were taken after the lower vents became inaccessible; it is possible,therefore, that the lower water content of these samples reflects a change in the gas composition with time. But, as discussed below, it seems more probable that this difference reflects the greater depth (thus greater solubility of water) of the degassing in the feeder dike compared with the near-surface degassing in the eruption area.

DISCUSSION

EQUILIBRIUM CONSIDERATIONS

A fundamental question concerning the complete analyses given in table 30.1 is the extent to which they represent an equilibrium assemblage. There are several techniques for studying volcanic gas equilibria (Heald and others, 1963; Nordlie, 1971; Gerlach, 1980). A simple, rapid technique that does not require a computer will be described here. The following three oxidation reactions include all of the gas species commonly reported in a volcanic gas analysis:

$$2CO + O_2 = 2CO_2 \quad (1)$$

$$2H_2 + O_2 = 2H_2O \quad (2)$$

$$H_2S + O_2 = SO_2 + H_2 \quad (3)$$

All other reactions of the common volcanic gases can be derived

TABLE 30.2.—*Atomic composition of gas samples from 1984 Mauna Loa eruption*

[Figures are atoms per atom of S; Mauna Loa average excludes posteruption samples; Kilauea average is of east-rift-zone eruption of 1983 (Greenland, 1984)]

Sample	Collection date (mo/d)	Element					
		H	C	O	S	Cl ($\times 10^3$)	F ($\times 10^3$)
Active vents							
1	3/25	7.48	0.163	5.96	1.00	3.61	3.15
2	3/25	3.62	.194	4.12	1.00	.53	2.98
3	3/25	4.49	.160	4.44	1.00	4.39	3.41
4	3/26	6.52	.148	5.43	1.00	4.74	2.22
5	3/26	6.92	.200	5.75	1.00	7.47	4.45
6	3/26	8.31	.129	6.21	1.00	10.17	6.18
7	3/26	7.84	.221	6.26	1.00	3.35	3.68
8	3/27	8.03	.122	6.13	1.00	3.92	1.83
9	3/27	10.16	.201	7.27	1.00	5.85	6.13
10	3/27	5.68	.141	4.99	1.00	2.35	4.05
11	3/27	8.99	.145	6.56	1.00	9.71	4.83
12	3/27	5.61	.188	5.10	1.00	.60	.98
13	3/30	7.11	.261	5.94	1.00	2.33	2.65
14	3/30	6.53	.305	5.70	1.00	4.03	4.98
15	3/31	5.17	.315	5.06	1.00	3.61	4.49
16	4/ 1	7.54	.348	6.08	1.00	3.25	2.70
17	4/ 1	10.56	.321	7.58	1.00	3.14	2.53
18	4/ 2	13.08	.352	8.94	1.00	2.17	2.31
19	4/ 2	10.95	.312	7.86	1.00	3.28	4.01
24	4/ 5	5.68	.085	4.94	1.00	2.45	2.85
25	4/ 5	5.06	.229	4.68	1.00	1.48	1.05
26	4/ 5	5.41	.265	4.88	1.00	5.39	6.75
Feeder vents							
20	4/ 3	6.23	.229	5.43	1.00	3.55	4.39
21	4/ 3	4.33	.165	4.37	1.00	1.93	2.57
22	4/ 3	6.25	.223	5.43	1.00	3.98	4.24
23	4/ 3	4.19	.218	4.37	1.00	6.82	8.69
27	4/ 5	3.98	.211	4.27	1.00	3.76	3.92
28	4/ 5	3.31	.255	4.00	1.00	4.74	5.72
29	4/ 7	3.73	.189	4.08	1.00	1.06	.58
30	4/ 9	4.66	.211	4.63	1.00	.85	.64
31	4/11	5.85	.210	5.23	1.00	.84	.89
32	4/11	4.77	.182	4.62	1.00	2.16	1.98
33	4/13	4.59	.187	4.49	1.00	3.33	4.67
34	4/13	4.54	.209	4.57	1.00	1.44	1.54
Posteruption vents							
35	4/16	28.59	.256	16.06	1.00	6.37	11.84
36	4/18	21.22	.484	12.92	1.00	23.03	55.97
Mauna Loa average							
		6.39	.214	5.45	1.00	3.59	3.47
Kilauea average							
		15.5	.260	10.0	1.00	21.6	23.4

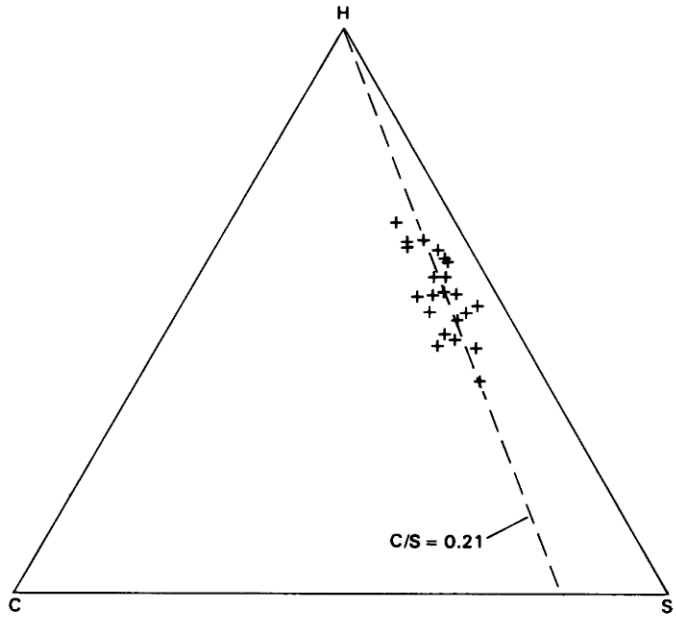

FIGURE 30.1.—Ternary plot of atomic H, C, and S from data in table 30.2. Atomic H has been divided by a factor of 5 for clarity of plotting. Dashes indicate water-control line for a C/S value of 0.21.

from these elementary reactions. Equilibrium constants, K, for these reactions can be expressed in the form

$$\log(O_2) = 2\log(CO_2/CO) - \log\ K_1 \quad (4)$$

$$\log(O_2) = 2\log(H_2O/H_2) - \log\ K_2 \quad (5)$$

$$\log(O_2) = \log(SO_2/H_2S) + \log(H_2) - \log\ K_3 \quad (6)$$

where the individual species have been written to indicate their respective partial pressures.

Because the heat of reaction for gaseous reactions is nearly constant over a limited temperature range, the temperature dependence of the equilibrium constant can be approximated by

$$\log\ K = (A/T) + B \quad (7)$$

where T is the temperature in Kelvin and A and B are thermodynamic constants. From the functional temperature dependence of the equilibrium constant, it is obvious that a plot of $\log(pO_2)$ versus $1/T$ for equations 4–6 will yield three straight lines intersecting at a single point if the analysis represents an equilibrium assemblage; equally, divergence to three distinct intersections implies disequilibrium. The major virtue of such plots is that they can easily be constructed during an analysis from a table giving equilibrium constants at two temperatures, thus serving as an immediate control on analyses.

Alternatively, an analytic solution may be obtained by combining equations 1–3 to eliminate oxygen:

$$CO + H_2O = CO_2 + H_2 \quad (8)$$

$$2CO + SO_2 + H_2 = 2CO_2 + H_2S \quad (9)$$

$$3H_2 + SO_2 = 2H_2O + H_2S \quad (10)$$

Temperatures calculated from equation 7 for these reactions necessarily will be the same if all species are in equilibrium.

Applying this procedure to the samples of table 30.1 shows that some are close to equilibrium, while many others are far from equilibrium. Equilibrium temperatures (table 30.3) were calculated for all the analyses of table 30.1 from equations 8–10 with the partial pressure of oxygen calculated from equation 4 at the temperature given by equation 9. The results demonstrate a consistent pattern of equation 8 yielding temperatures above the measured magma temperature (1,150 °C), temperatures from equation 9 being close to gas-collection temperatures, and temperatures from equation 10 being less than those of collection. Because changes in the H_2O/H_2 ratio change the calculated temperatures of equations 8 and 10 in opposite directions, this ratio is the obvious candidate for

TABLE 30.3.—*Observed temperature, calculated equilibrium temperatures, and calculated oxygen partial pressure for gas samples from 1984 Mauna Loa eruption*

[Oxygen partial pressure (pO_2) calculated from equation 4 at the temperature given by equation 9]

Sample	Observed temperature (°C)	Equilibrium temperature (°C) From equation 8	From equation 9	From equation 10	log pO_2
Active vents					
1	1,080	2,063	1,039	889	−10.461
2	1,075	1,120	1,060	1,044	−9.838
3	1,080	1,494	1,058	968	−10.166
4	1,100	1,703	1,096	982	−9.796
5	1,100	1,829	1,071	942	−10.043
6	1,120	1,861	1,032	898	−10.687
7	1,050	1,547	972	866	−11.084
8	1,130	2,076	1,150	1,002	−9.316
9	1,130	1,695	1,109	998	−9.755
10	1,100	1,271	1,074	1,025	−9.881
11	1,100	1,835	1,092	964	−10.035
12	1,130	1,440	1,111	1,036	−9.363
13	825	1,675	979	859	−11.174
14	825	1,427	923	827	−11.896
15	1,080	1,300	1,110	1,062	−9.559
16	1,100	1,218	1,074	1,036	−10.212
17	1,100	1,540	1,068	973	−10.334
18	1,050	2,286	978	814	−11.540
19	1,050	1,284	985	917	−11.087
24	1,010	2,038	1,042	894	−10.309
25	1,010	903	966	987	−11.228
26	1,100	1,156	1,072	1,049	−10.204
Feeder vents					
20	735	2,192	931	773	−11.954
21	870	1,459	951	854	−11.476
22	775	1,996	904	758	−12.275
23	835	1,173	916	857	−11.878
27	875	1,256	978	914	−11.080
28	895	1,008	980	971	−10.989
29	880	1,118	990	956	−10.934
30	875	1,273	994	930	−10.386
31	840	1,259	929	857	−11.609
32	840	1,513	953	849	−11.481
33	820	1,712	943	819	−11.781
34	820	1,306	869	782	−12.527
Post-eruptive samples					
35	760	810	813	814	−13.541
36	745	883	661	610	−16.499

the source of disequilibrium in these samples. Oxidation of CO, on the other hand, would increase the temperature from equation 8 (which is already too high), whereas oxidation of H_2S would leave this temperature unaffected. Gerlach (1980, 1982) has noted the importance of the addition of meteoric water and of the oxidation of H_2 in volcanic-gas collections. Either excess, unequilibrated, H_2O or a lack of H_2 in the analyses because of oxidation could account for the discrepant temperatures of table 30.3: Subtracting H_2O or adding H_2 to the analytical values decreases the temperature from equation 8 and increases that from equations 9 and 10 (water affects equation 9 because the constant sum of partial pressures requires a change in H_2 opposite to that of H_2O).

Forcing the analyses in table 30.1 to apparent equilibrium by adjusting either H_2O or H_2 yields the results shown in table 30.4. Assuming only oxidation of H_2 as the cause of disequilibrium, apparent equilibrium H_2 was obtained by combining equations 8 and 9 to eliminate H_2:

$$3CO + H_2O + SO_2 = 3CO_2 + H_2S \qquad (11)$$

With an equilibrium temperature from this reaction, oxygen was calculated from equation 1 and apparent equilibrium H_2 from equation 2. Alternatively, assuming disequilibrium to be due solely to H_2O, apparent equilibrium H_2O was obtained by subtracting H_2O incrementally from a starting partial pressure of 1.0 (simultaneously correcting H_2 for the constant sum requirement) until the temperatures calculated from equations 8–10 agreed within 10 °C. The apparent equilibrium temperatures from these two processes (see table 30.4) agree within 20 °C and are close to collection temperatures. Both processes also require very large changes from the observed values (table 30.4): about half of the samples require more than half of the H_2 to have been oxidized, and a fifth of the samples have apparent equilibrium water contents of less than 45 percent. Thus neither process alone seems an entirely plausible explanation for the observed disequilibrium in the samples.

That neither oxidation of H_2 nor excess H_2O is the sole cause of disequilibrium may be seen from the size of deviations from the analytical values required for apparent equilibrium. One can define the magnitude of the correction required to force apparent equilibrium as the positive difference between observed and calculated (table 30.4) values divided by the observed value. If disequilibrium is attributed solely to oxidation of H_2, then the observed H_2O content is the equilibrium amount, and the extent of oxidation of H_2 should be independent of H_2O content. In fact, there is a positive correlation, significant at the 99-percent confidence level, between the required deviation of H_2 and the observed H_2O content in both active-vent and feeder-vent samples. This correlation, indicating a tendency for samples with higher H_2O contents to require greater apparent oxidation corrections of H_2, implies that forcing apparent equilibrium by adding H_2 to the analysis is correcting, at least partially, for excess, unequilibrated, water in the samples rather than solely for oxidation.

Because of the constant sum of partial pressures and because the greatest deviations of H_2O are associated with higher water contents, there is necessarily an inverse correlation between the required correction in H_2O and other components of the sample: the negative correlation of H_2O deviation with CO_2, for example, is significant at the 99-percent confidence level for both active and feeder vents. This problem is eliminated by considering the H_2/CO_2 ratio: the negative correlation of H_2O deviation with this ratio is significant at the 99-percent confidence level for the feeder vents, but not significant (<90 percent) at the active vents. Negative correlations of H_2/CO and H_2/H_2S with water deviation also are significant at the feeder vents but not at the active vents. This result implies that, at least at the feeder vents, forcing equilibrium in the samples by subtracting water is compensating, at least partially, for the oxidation of H_2 in the samples. It seems probable, then, that both addition of unequilibrated water and oxidation processes have contributed significantly to the observed disequilibrium.

Gerlach (1982) noted that magma tends to have an oxygen fugacity in the area bounded by the quartz-magnetite-fayalite (QMF) and nickel-nickel oxide (NNO) buffers and showed that most equilibrated volcanic gases also plot in this area. A similar plot of these Mauna Loa samples (fig. 30.2) shows that they follow an oxygen-temperature curve very close to QMF, regardless of whether the analyses are forced to apparent equilibrium by subtracting H_2O or by adding H_2, and that both processes yield the same relation

TABLE 30.4.—*Apparent equilibrium values of temperature and oxygen partial pressure assuming excess H_2O or oxidation of H_2 for gas samples from 1984 Mauna Loa eruption*

Sample	Observed temperature (°C)	Assuming excess H_2O: Temperature (°C)	Assuming excess H_2O: $\log(pO_2)$	Assuming excess H_2O: Estimated H_2O (mole percent)	Observed H_2O (mole percent)	Assuming oxidation of H_2: Temperature (°C)	Assuming oxidation of H_2: $\log(pO_2)$	Assuming oxidation of H_2: Estimated H_2 (mole percent)	Observed H_2 (mole percent)
Active vents									
1	1,080	1,078	−9.813	47.0	75.6	1,101	−9.455	1.196	0.360
2	1,075	1,064	−9.781	56.2	59.2	1,066	−9.740	.741	.660
3	1,080	1,078	−9.832	48.0	64.9	1,092	−9.608	1.070	.550
4	1,100	1,125	−9.351	53.8	73.0	1,140	−9.119	1.435	.640
5	1,100	1,104	−9.522	50.2	73.4	1,122	−9.234	1.260	.480
6	1,120	1,069	−10.069	53.4	77.6	1,086	−9.790	1.428	.490
7	1,050	1,001	−10.561	54.8	75.7	1,014	−10.320	.747	.300
9	1,130	1,141	−9.274	64.0	79.8	----	------	-----	----
10	1,100	1,086	−9.680	62.4	70.2	1,092	−9.595	1.125	.800
11	1,100	1,129	−9.477	58.4	78.5	1,143	−9.257	1.897	.750
12	1,130	1,129	−9.089	57.4	69.4	1,138	−8.945	1.087	.660
13	825	1,008	−10.630	48.2	73.1	1,026	−10.314	.893	.320
14	825	946	−11.427	48.8	70.7	960	−11.149	.658	.270
15	1,080	1,121	−9.388	57.2	64.9	1,127	−9.296	1.287	.940
16	1,100	1,083	−10.056	66.0	71.7	1,087	−9.995	1.696	1.310
17	1,100	1,096	−9.897	64.4	78.7	1,105	−9.750	1.867	.930
18	1,050	1,025	−10.679	50.4	82.3	1,047	−10.309	1.434	.330
19	1,050	1,004	−10.733	69.2	79.8	1,010	−10.626	1.040	.600
24	1,010	1,078	−9.715	42.6	71.8	1,103	−9.322	1.006	.310
25	1,010	962	−11.318	69.2	65.6	960	−11.360	.768	.900
26	1,100	1,077	−10.118	62.0	65.8	1,080	−10.072	1.520	1.300
Feeder vents									
20	735	967	−11.253	33.0	71.1	998	−10.674	.783	.170
21	870	972	−11.075	42.0	64.2	989	−10.754	.662	.280
22	775	938	−11.591	34.6	71.3	965	−11.044	.652	.150
23	835	929	−11.617	48.2	62.0	938	−11.429	.513	.300
27	875	991	−10.828	47.6	61.1	1,001	−10.642	.692	.410
28	895	981	−10.960	53.6	55.3	982	−10.936	.618	.580
29	880	997	−10.806	53.0	59.8	1,002	−10.714	.741	.570
30	875	1,009	−10.571	52.2	65.0	1,018	−10.408	.766	.460
31	840	947	−11.260	54.6	70.2	956	−11.069	.552	.290
32	840	976	−11.042	42.6	66.1	993	−10.711	.702	.280
33	820	969	−11.275	35.6	64.9	994	−10.822	.785	.250
34	820	887	−12.111	42.4	64.7	902	−11.797	.383	.160
Posteruptive samples									
35	760	813	−13.559	91.2	91.2	813	−13.549	.505	.510
36	745	676	−15.977	75.6	86.8	679	−15.877	.147	.070

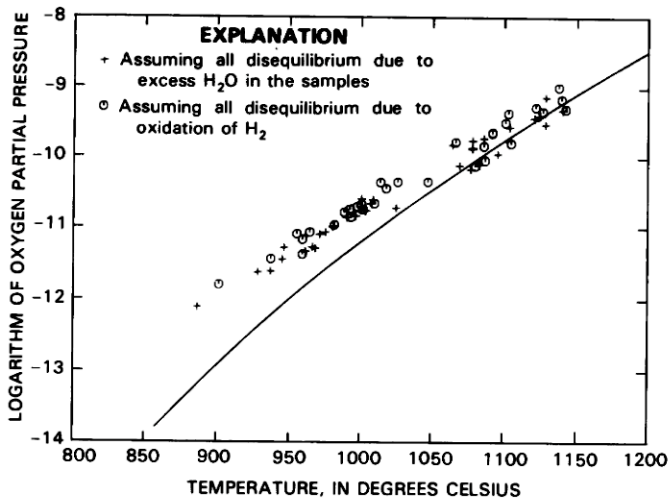

FIGURE 30.2.—Apparent equilibrium partial pressure of oxygen plotted against apparent equilibrium temperature for gas samples from the 1984 Mauna Loa eruption. Line indicates the quartz-magnetite-fayalite buffer.

between temperature and partial pressure of oxygen. This relationship,

$$\log(pO_2) = -19300/T + 4.46 \qquad (12)$$

provides a means of estimating the equilibrium partial pressures of H_2O and H_2 independently of each other. Because the lower temperature of the posteruption samples involves considerable extrapolation of this relation, those samples are excluded from the following.

With equation 12, an equilibrium temperature for an analysis can be estimated from equation 4, the H_2 content from equation 6, and the H_2O content from equation 5, assuming that the CO_2/CO and SO_2/H_2S ratios are equilibrium values. When this procedure is followed, nine of the analyses from table 30.1 yield temperatures above 1,150 °C or partial pressures of H_2O above 1.0 or both, implying that the assumption is not justified for these samples, which are therefore rejected. About half the remaining samples have estimated H_2 contents less than the observed values (after correction for constant sum), indicating either that oxidation is not a major effect or that the either CO_2/CO or SO_2/H_2S or both ratios are not equilibrium values. Examination of equation 6 shows that oxidation

TABLE 30.5.—*Comparison of observed and estimated equilibrium temperature and composition of gas samples from 1984 Mauna Loa eruption*

[Compositional figures in mole percent; observed values of H_2 from table 30.1 corrected for the new sum of partial pressures, (see text)]

Sample	Temperature (°C)		H_2O		H_2		H_2S	
	estimated	observed	estimated	observed	estimated	observed	estimated	observed
Active vents								
1	1,075	1,080	47.127	75.6	0.789	0.780	0.628	0.580
2	1,028	1,075	54.684	59.2	.747	.733	1.342	.620
3	1,079	1,080	48.289	64.9	.821	.810	.920	.920
4	1,123	1,100	53.860	73.0	1.097	1.094	.718	.690
5	1,095	1,100	50.759	73.4	.924	.889	.683	.560
7	978	1,050	54.161	75.7	.584	.566	.871	.510
9	1,157	1,130	85.935	79.8	1.993	.599	.740	.740
10	1,074	1,100	62.176	70.2	1.037	1.015	1.022	.790
12	1,085	1,130	56.242	69.4	.984	.944	.908	.380
13	1,012	825	51.871	73.1	.656	.573	.810	.810
14	953	825	58.400	70.7	.555	.383	1.110	1.110
15	1,120	1,080	57.151	64.9	1.151	1.148	.867	.850
24	1,057	1,010	41.521	71.8	.644	.643	.727	.470
Feeder vents								
20	988	735	55.665	71.1	.629	.261	1.020	1.020
21	976	870	46.298	64.2	.494	.420	1.150	1.150
22	952	775	50.680	71.3	.480	.258	1.020	1.020
23	930	835	50.312	62.0	.425	.392	1.410	1.410
27	993	875	49.651	61.1	.574	.531	1.230	1.230
28	985	895	58.279	55.3	.648	.541	1.610	1.610
29	1,005	880	65.353	59.8	.803	.491	1.630	1.630
30	1,004	875	52.233	65.0	.638	.628	1.137	1.010
31	930	840	54.385	70.2	.459	.444	1.237	.800
32	981	840	49.082	66.1	.538	.421	1.120	1.120
33	999	820	74.401	64.9	.888	.182	1.640	1.640
34	879	820	42.403	64.7	.269	.261	1.332	1.030

of H_2S would lead to underestimating H_2; table 30.5 shows the result of reversing this oxidation by adding H_2S incrementally to the analyses and recalculating H_2 and H_2O until the estimated H_2 content is at least as great as that observed. (Note that the H_2S/SO_2 ratio is used in equation 6, and thus the comparison of observed versus estimated H_2S in table 30.5 is not affected by the new sum of partial pressures; H_2, on the other hand, is estimated in absolute terms from equation 6 and thus comparison requires correction of the observed value for the new sum produced by the change in H_2O.)

An interesting feature of table 30.5 is the distinction between active and feeder vents: oxidation appears to have affected primarily H_2S rather than H_2 at the active vents, whereas at the feeder vents H_2 appears to have been oxidized to a greater extent than H_2S. This is consistent with the observation noted above that simple subtraction of H_2O from the analysis to force apparent equilibrium results in a negative correlation between excess H_2O and H_2/CO_2 at the feeder vents (implying that oxidation of H_2 is actually being "corrected") but not at the active vents. The distinction between oxidation of H_2 and H_2S may be related to the lower temperature, or to the longer time between separation of the gases from magma and their collection at the feeder vents relative to active vents. Regardless of the vent type and of the extent of apparent oxidation, most samples in table 30.5 yield considerably less H_2O in the apparent equilibrium composition than in the observed analysis.

The calculations for table 30.5 depend on the assumptions that the samples follow rigidly an oxygen-temperature buffer relationship and that the CO_2/CO and SO_2/H_2S ratios are equilibrium values, assumptions which table 30.5 makes manifest are not valid for at least half the table 30.1 samples. An alternative set of assumptions, relying on the buffer relationship and the CO_2/CO ratio and water content, fares even less well. Estimating temperature from equation 1, H_2 from equation 2, and H_2S from equation 3 yields less than the observed H_2S content in one-third of the samples and, as previously, a strong correlation between the extent of apparent oxidation and the observed water content, implying that the oxidation "correction" is actually correcting for excess, unequilibrated water in the samples. It is apparent that a multiplicity of effects has been the cause of disequilibrium in these samples, and it is most improbable that all effects have been equally operative in all samples.

WATER CONTENT

The data in table 30.5 demonstrate that these gas samples have been affected by incorporation of unequilibrated water and by oxidation of both H_2 and H_2S. Because H_2S is separated immediately on collection as CdS, and because H_2 is stable in these collections (after quenching) over the 4–6 h period before analysis (see above), oxidation of these gases must occur in the vent or immediately during collection; opportunity exists in both cases. Because this oxidation is a nonequilibrium process (equilibrium oxidation obviously would not produce a disequilibrium assemblage), high-temperature reaction rates must be slow relative to the few seconds between separation of the gas from the melt and quenching in a sample bottle. This is also shown by the observation that even the best gas collections, where near-perfect equilibrium can be demonstrated, actually contain a partial pressure of oxygen orders of magnitude higher than the equilibrium value (0.01 percent air in the sample yields 4–5 orders of magnitude more oxygen than

equilibrium). The slow (seconds) rate of reaction suggests the possibility that un-equilibrated water in the samples is magmatic water that, because its solubility in the melt is much greater than those of CO_2 and S, is exsolved in abundance in the last few seconds of the magma's rise and may be collected before reaction with C and S species is complete.

The observed water contents from table 30.1 are compared in figure 30.3 with the apparent equilibrium water content of those samples from table 30.5 that show no evidence of oxidation of H_2S. Whether one restricts consideration to only the samples in which neither H_2S nor H_2 appears to be oxidized or includes all of the table 30.5 values does not affect the conclusions. A notable feature of figure 30.3 is that the bimodal distribution of water in the original analyses disappears in the apparent equilibrium water values, which show no distinction between active and feeder vents. The mean apparent equilibrium water content of the samples giving no evidence of H_2S oxidation in table 30.5 is 56 percent; in comparison, the observed water content is 65 percent at the feeder vents and 73 percent at the active vents (table 30.1). There is no reason to expect the active vents to be more contaminated with meteoric water than the feeder vents (one would expect the contrary, given the longer passage through country rock before collection at the feeder vents), and thus the lower total water at the feeder vents probably is related to the greater depth of degassing (greater solubility of water) at the feeder vents. A consequence of this is that neither the feeder-vent nor the active-vent samples reflect the gas composition of the magma: degassing a water-poor gas from the magma through the feeder vents prior to eruption results in the gas at the active vents being depleted in CO_2 and SO_2, thus enriched in water.

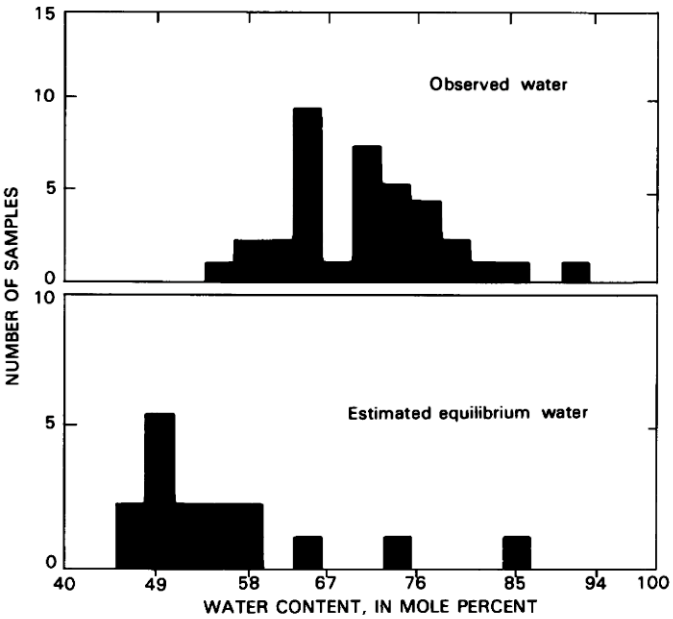

FIGURE 30.3.—Comparison of observed water content (from table 30.1) with apparent equilibrium water content (from table 30.5 data for samples showing no H_2S oxidation) for gas samples from 1984 Mauna Loa eruption.

Both the apparent equilibrium atomic H/S ratio and the observed ratio at the feeder vents is very low (table 30.6) compared with adjacent Kilauea Volcano or other basaltic volcanoes; even basing the ratio on total water at the active vents still leaves Mauna Loa with among the lowest H/S ratios in table 30.6. Comparison of the atomic H/S ratio of undegassed intrusive dike rocks collected from the summit caldera of Mauna Loa with the gas ratios (table 30.6) shows no reason to expect Mauna Loa magma to be unusually deficient in water. The very low atomic H/S ratio of the gas samples can be explained by assuming that (1) this particular batch of Mauna Loa magma had a remarkably low initial water content, (2) eruptive degassing was so inefficient that equilibrium at atmospheric pressure between melt and gas was not even approached, leaving the melt supersaturated in water, or (3) gases were sampled and quenched before they could react completely with the newly exsolved water, implying that total water in these samples represents equilibrated plus unequilibrated magmatic water. I suggest that some combination of the last two alternatives provides a more plausible explanation for the low H/S ratio of these gases than does invoking a special origin for the magma.

Anderson (1975) pointed out that a spectrum of gas compositions may be derived from the same melt with varying pressure and suggested this as a plausible mechanism to account for varying proportions of volcanic gases. About 77 percent of the mean total water at active vents and 86 percent of the mean total at feeder vents is in apparent equilibrium with other gases. Studies of submarine basalt (Moore, 1965) indicate that the saturation pressure for water in the melt is about 8 MPa (80 bars). Given a rock density of 2.3 g/cm^3, this corresponds to a depth of 350 m. If the solubility curve above this point is linear, 25 percent of the total water is exsolved in the final 90 m of magma rise. Thus the final eruptive surge and degassing of the melt might well be too rapid to maintain equilibrium in samples collected in virtual contact with erupting melt.

PRE-ERUPTION DEGASSING

The average atomic C/S ratio in these Mauna Loa gas samples is 0.21 (table 30.2). This value is similar to the ratio (0.25) found for the current east-rift-zone eruption of Kilauea (Greenland, 1984)

TABLE 30.6.—*Atomic H/S ratios of gases from basaltic volcanoes*

Gas source	Atomic H/S ratio	Source of data
Mauna Loa	3.4	Equilibrated H_2O, this paper
Mauna Loa, feeder vents	4.7	Total H_2O, this paper
Mauna Loa, active vents	7.3	Total H_2O, this paper
Mauna Loa, intrusive dikes	11	Easton and Lockwood (1983)
Kilauea, Halemaumau	7.2	Equilibrated H_2O, Gerlach (1980)
Kilauea, Halemaumau	15	Total H_2O, Gerlach (1980)
Kilauea, original magma	13	Greenland and others (1985)
Kilauea, original magma	8.6	Gerlach and Graeber (1985)
Kilauea, east rift	15	Greenland (1984)
Erta Ale, 1971	13	Equilibrated H_2O, Gerlach (1982)
Erta Ale, 1973	21	Equilibrated H_2O, Gerlach (1982)
Erta Ale, 1974	18	Equilibrated H_2O, Gerlach (1982)
Ardoukoba	8.8	Equilibrated H_2O, Gerlach (1982)
Surtsey, 1971	36	Equilibrated H_2O, Gerlach (1982)
Surtsey, 1965	58	Equilibrated H_2O, Gerlach (1982)
Surtsey, 1967	55	Equilibrated H_2O, Gerlach (1982)

but is much lower than most basaltic gases, in which carbon is usually more abundant than sulfur (Gerlach, 1982). Gerlach (1980, 1982) has emphasized the importance of shallow degassing of CO_2-rich gas for controlling the composition of volcanic gases, and Greenland and others (1985) and Gerlach and Graeber (1985) have suggested that the composition of Kilauea gas is controlled by degassing of magma to equilibrium in the shallow summit reservoir of Kilauea. Mauna Loa also has a summit storage chamber (Decker and others, 1983) at about the same depth as at Kilauea (3–4 km); thus the coincidence of Kilauea and Mauna Loa magmas being depleted in CO_2 to the same extent probably reflects their common degassing to equilibrium at the temperature and pressure of the summit storage reservoir. If this is so, then the eruptive gases sampled here reflect the composition of the reservoir rather than the composition of the initial magma formed in the mantle.

Gerlach (1980, 1982) has shown the usefulness of H/C versus S/C diagrams for indicating the effect of early CO_2 degassing on the composition of volcanic gas. Such a diagram yields a vertical trend if H_2O is the only significant source of variation and a diagonal trend if CO_2 variation is important; figure 30.1 has shown that H_2O is the major cause of variation in these gases, but figure 30.4 shows that an independent variation of CO_2 also is an important contributor to the total variance of composition. (In the following, I exclude the anomalous active vent sample with a C/S ratio of 0.085). The trend, shown in figure 30.4, for H/C to increase with increasing S/C is statistically significant at the 95-percent confidence level and implies that pre-eruption degassing of CO_2 has had a significant effect on eruptive gas composition. Examination of figure 30.4 shows, however, that the CO_2-degassing trend in these samples is produced almost entirely by the early samples from the active vents. Student's t-test confirms the higher mean S/C ratio of samples collected in the March 25–27 period relative to both the later active vents and the feeder vents at the 99-percent confidence level; the latter two sample groups also are significantly (99 percent) different from each other in S/C ratio. The daily average S/C ratio, plotted in figure 30.5, shows a high initial value for the gases, a decline after March 28 at the active vents, and a subsequent small increase at the later feeder vents. Removing the pre-March 30 samples from the population removes the CO_2 degassing trend from figure 30.4 (no statistical correlation between H/C and S/C) suggesting that the early eruptive magma was degassed of CO_2 relative to the later, more uniform, eruptive magma.

Equilibrium degassing of magma at pressures less than the solubility limit of CO_2 and S cannot change the S/C ratio of the emitted gas. Assuming a linear pressure dependence of the solubility, the mass M of gas exsolved per cubic meter of magma at any pressure P is:

$$M = aP + M_o \qquad (13)$$

where M_o is the initial mass of gas per cubic meter dissolved in the saturated melt. It is obvious that for two gases, the slopes, a, of equation 13 will be in the same proportion as the initial contents, and thus the exsolved gas will have the same composition regardless of decreasing pressure after both gases have become saturated. Degassing of Kilauea magma during storage in the shallow summit reservoir (Gerlach and Graeber, 1985; Greenland and others, 1985) and, presumably, of this Mauna Loa magma in Mauna Loa's reservoir (see above) leaves the melt saturated in CO_2 and S; therefore changes in S/C ratio must reflect variations in retention of the CO_2-rich fluid phase with which the magma entered the

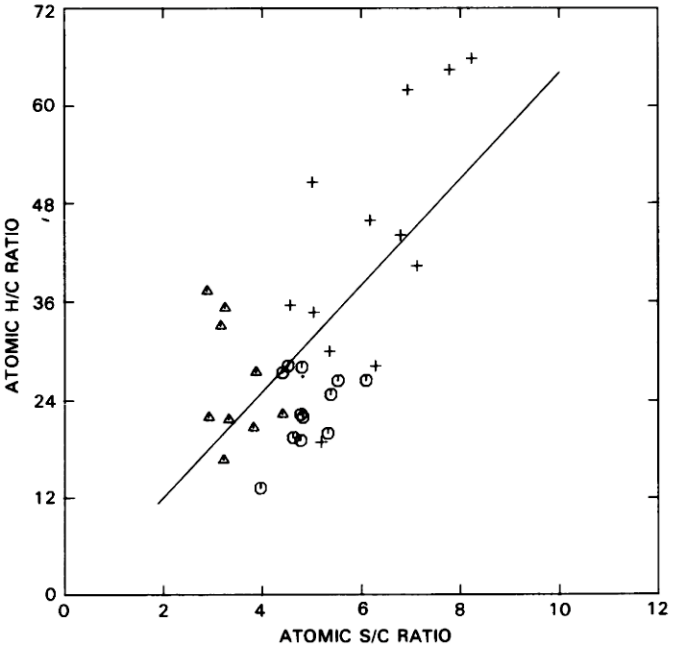

FIGURE 30.4.—Plot of atomic H/C ratio against atomic S/C ratio for gas samples from 1984 Mauna Loa eruption, showing effect of carbon degassing. Crosses, active-vent samples, March 25–27; triangles, active-vent samples, March 30 through April 5; circles, feeder-vent samples, April 3–13. Least-squares line fitted to the data.

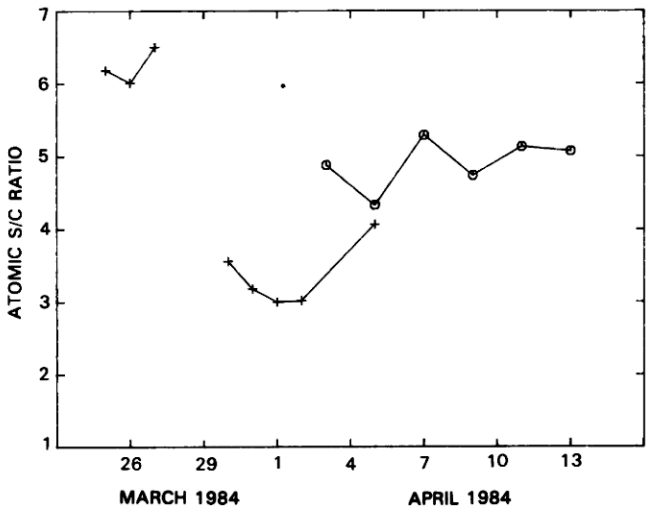

FIGURE 30.5.—Daily average atomic S/C ratio of gas samples from 1984 Mauna Loa eruption plotted against collection date. Crosses, active-vent samples; circles, feeder-vent samples.

reservoir. Seismic evidence suggests (R.Y. Koyanagi, oral commun., 1984) that some of this magma had been injected into the rift at a depth of ~3 km over a period of years prior to eruption. This rift-stored magma would be the first to be erupted, and it may be that storage of a small body of magma in the rift would provide a better opportunity for separation and loss of the original CO_2-rich fluid phase than would storage in the larger summit reservoir system. If this is so, then the change in S/C ratio of the gas suggests that at least three but less than six days of eruption were required to flush the rift conduit. Lipman and Banks (chapter 57) report a ~10-fold decrease in lava-effusion rate beginning about April 6; perhaps the lower flow rate through the conduit permitted a greater loss of the residual fluid phase from the reservoir by degassing during transit to the feeder vents, accounting for the higher S/C ratio at the feeder vents relative to the later active vents. In any case, the change in S/C ratio with time observed in these gases seems to require at least two magma batches having retained different fractions of a CO_2-rich fluid phase exsolved during ascent to the reservoir.

POSTERUPTION DEGASSING

It was noted above that the two posteruption gas samples in table 30.1 are greatly enriched in water. By April 18, halogens also became greatly enriched relative to S (table 30.2). This pattern is consistent with the final degassing of a cooling dike, in which the most soluble components (water and halogens) become enriched relative to less soluble ones (CO_2, SO_2). This pattern has been observed repeatedly at posteruptive vents and cones during the 1983–1984 east-rift-zone eruption of Kilauea (upublished data).

However, CO_2 actually became enriched relative to S by April 18; further samples collected on May 5 had CO_2 as much as five times more abundant than SO_2. The posteruption enrichment of CO_2 relative to SO_2 in the gas cannot be due to degassing of a static dike and implies the existence of another source of CO_2. Tentatively, I suggest a refilling of the shallow summit reservoir from the mantle (see above) and degassing of CO_2 from this new magma through vents created by the eruption.

CONCLUSIONS

Most of the gas samples collected from this eruption of Mauna Loa contain more water than is compatible with an equilibrium assemblage of gases. The apparent equilibrium compositions contain much lower atomic H/S ratios than have been observed for other basaltic gases or in un-degassed dikes from Mauna Loa; basing the H/S ratio on total, rather than equilibrated, water content of the active vents alleviates but does not completely solve the problem posed by these very low H/S ratios. This observation suggests that the latest exsolved water may not have reacted completely with the other gases before being quenched during sampling.

Halogen/sulfur ratios also are very much lower than those in eruptive gases from the adjacent Kilauea Volcano, whereas atomic C/S ratios are almost identical at the two volcanoes. On the basis of evidence for a shallow (3–4 km) magma storage reservoir under Mauna Loa, and by analogy with Kilauea, it can be suggested that this Mauna Loa magma was largely degassed of CO_2 during storage before eruption. Degassing at this depth, however, does not account for the low water and halogen contents of these gases. I suggest that the rate of flow of magma through the eruptive vent was too great for maintenance of equilibrium between magma and exsolved gases; thus variations in the water content of these samples reflect variations in the amount of water exsolved, a rate phenomenon rather than an equilibrium phenomenon. The low abundance of halogens also may be a result of incomplete exsolution, but the possibility of a low initial abundance in the magma cannot be excluded.

This study suggests that Hawaiian magmas degas in stages: CO_2 is primarily degassed from 3–4 km depth long before the start of eruption, SO_2 as the eruptive magma begins its ascent from the reservoir, and H_2O and halogens only as the magma nears the surface. An implication of this hypothesis is that gas samples collected from eruptive vents do not reflect the gas composition of the original magma and may not even reflect the gas composition of the erupting magma. Additionally, if physical rate processes create significant variations in observed gas compositions, then recalculating a gas analysis to an equilibrium assemblage may prove more misleading than enlightening.

REFERENCES CITED

Anderson, A.T., 1975, Some basaltic and andesitic gases: Review of Geophysics and Space Physics: v. 13, p. 37–55.

Decker, R.W., Koyanagi, R.Y., Dvorak, J.J., Lockwood, J.P., Okamura, A.T., Yamashita, K.M., and Tanigawa, W.R., 1983., Seismicity and surface deformation of Mauna Loa Volcano, Hawaii: Eos, v. 64, p. 545–547.

Easton, R.M. and Lockwood, J.P., 1983, Surface-fed dikes—The origin of some unusual dikes along the Hilina fault zone, Kilauea Volcano, Hawaii: Bulletin Volcanologique, v. 46-1, p. 45–53.

Fisher, R.A., 1936, Statistical methods for research workers (6th ed.): Edinburgh, Oliver and Boyd, 360 p.

Gerlach, T.M., 1980, Evaluation of volcanic gas analyses from Kilauea Volcano: Journal of Volcanology and Geothermal Research, v. 7, p. 295–317.

——— 1982, The interpretation of volcanic gas data from tholeiitic and alkaline mafic lavas: Bulletin Volcanologique, v. 45-3, p. 235–244.

Gerlach, T.M., and Graeber, E.J., 1985, Volatile budget of Kilauea Volcano: Nature, v. 313, p. 273–277.

Greenland, L.P., 1984, Gas composition of the January 1983 eruption of Kilauea Volcano, Hawaii: Geochimica et Cosmochimica Acta, v. 48, p. 193–195.

Greenland, L.P., Rose, W.I., and Stokes, J.B., 1985, An estimate of gas emissions and magmatic gas content from Kilauea Volcano: Geochimica et Cosmochimica Acta, v. 49, p. 125–129.

Giggenbach, W.F., 1975, A simple method for the collection and analysis of volcanic gas samples: Bulletin Volcanologique, v. 39, p. 132–145.

Heald, E.F., Naughton, J.J., and Barnes, I.L., Jr., 1963, The chemistry of volcanic gases: Journal of Geophysical Research, v. 68, p. 545–557.

Lockwood, J.P., 1984, Mauna Loa Volcano, Hawaii: SEAN Bulletin 9 (3), p. 1–9.

Moore, J.G., 1965, Petrology of deep-sea basalt near Hawaii: American Journal of Science, v. 263, p. 40–52.

Nordlie, B.F., 1971, The composition of the basaltic gas phase: NASA Technical Report R–348, 81 p.

Piccardi, G., and Cellini-Legittimo, P., 1983, A sampling and chemical analysis procedure for fumarolic gases: Mikrochimica Acta, v. 11, p. 159–167.

SULFUR AND CARBON ABUNDANCES IN HAWAIIAN THOLEIITE LAVAS: 1972–1975 ERUPTIONS OF KILAUEA AND 1975 ERUPTION OF MAUNA LOA

By Karen J. Franczyk, Everett K. Gibson, Jr.[1], *and* Robert I. Tilling

ABSTRACT

Analysis of sulfur and carbon abundances in 135 samples of fresh Hawaiian basalts erupted subaerially during 1972–1975 indicates that the different degassing behavior of sulfur and carbon volatiles and the ease of contamination by atmospheric carbon explain the different relationships observed between the sulfur and carbon contents in the samples and their density, flowage distance, and type of eruptive material. Sulfur abundances range from 37 to over 15,000 μg/g (median value 153 μg/g); these values are lower by a factor of 4 to 6 than those for submarine tholeiitic basalts. Decreases in sulfur abundance away from the vent further document previous findings that sulfur is progressively lost by degassing during lava fountaining and flowage; the greatest loss occurs within about 2 km of the active vent. Sulfur abundance is best preserved in spatter (mean value 177 μg/g) and more depleted in pahoehoe (mean value 152 μg/g) and aa (mean value 96 μg/g) flows, a distribution controlled largely by increasing distance from the vent. A weaker inverse relation was found between sulfur content and relative sample density.

The carbon content measured in this study reflects the combined contribution from the magmatic carbon (CO_2 dissolved in the basaltic glass) and a nonmagmatic surficial component adsorbed after eruption and even after sample collection. Total carbon abundances range from 11 to 1,099 μg/g; the median value (69 μg/g) falls within the range of total carbon abundances reported for submarine basalts, but the value range is considerably greater. This distribution is opposite from that expected from a comparison between submarine (nondegassed) and subaerial (degassed) samples; posteruption contamination by atmospheric carbon is inferred to account for the wide dispersion in our data. In contrast to the sulfur data, the carbon data show no systematic relation of measured abundance to sample type, relative density, or distance from the vent. Such an observation is compatible with recent experimental and volcanic-gas studies that demonstrate extensive and rapid loss of CO_2 from the magma during storage in Kilauea's shallow summit reservoir and at the onset of an eruption. Alternatively, this absence of any recognizable degassing pattern for carbon volatiles during lava fountaining and flowage could mean simply that any variations in magmatic carbon content are obscured by contamination-caused variations in nonmagmatic carbon. Subsequent studies involving stepwise combustion in the analytical procedure are required to determine the carbon budget for subaerial basalts.

INTRODUCTION

The sudden escape of volatiles from magma provides the driving force for volcanic eruptions. Many investigations have been conducted, therefore, of the distribution of volatiles, principally water, sulfur, and carbon, in the gaseous and solid eruptive products of volcanoes. Because of their high eruption frequency and good accessibility, Kilauea and Mauna Loa Volcanoes on the Island of Hawaii (fig. 31.1) have provided abundant materials for such studies.

The staff of the Hawaiian Volcano Observatory (HVO) systematically sampled, in time and space, the eruptive products of the long-lived 1972–74 Mauna Ulu activity (Tilling and others, chapter 16), as well as eruptive products of the following short-lived activity: the July, September, and December 1974 Kilauea eruptions (Lockwood and others, chapter 19); the July 1975 eruption at Mauna Loa summit (Lockwood and others, 1976); and the small eruption at Kilauea summit triggered by the magnitude −7.2 Kalapana earthquake on November 29, 1975 (Tilling and others, 1976).

We have determined the total sulfur and carbon abundances in 135 selected samples from these events (tables 31.1–31.2) in an attempt to describe their variation and to document any patterns of volatile behavior during subaerial eruption. To the best of our knowledge, the data set presented herein is the most comprehensive obtained to date for subaerially erupted tholeiitic basalts. Problems involving initial degassing, collection state of the samples, and ease of sample contamination by atmospheric carbon (Des Marais and Moore, 1984) combine to introduce a large degree of uncertainty in interpretation of the data. Nonetheless, in this paper we note several general systematic relations. The validity of these relations remains to be tested by additional studies specifically designed to eliminate or minimize posteruption carbon contamination by utilizing better controlled field sampling, sample storage and preparation, and modified analytical procedures.

ACKNOWLEDGMENTS

Our thanks go to the staff members of the Hawaiian Volcano Observatory for their diligent and timely efforts in making the systematic collection of eruptive products of Kilauea and Mauna Loa during 1972–1975. Some of the materials, had they not been sampled at, or shortly after, the time of their eruption, would have been unavailable for study because of burial by later flows. Robert L. Engram assisted with sample preparation and some of the analyses. Careful and incisive reviews of earlier versions of this paper by our USGS colleagues L. Paul Greenland (Hawaiian Volcano Observatory) and James G. Moore (Menlo Park) were most helpful and greatly appreciated.

[1]Johnson Space Center, NASA, Houston, Texas.

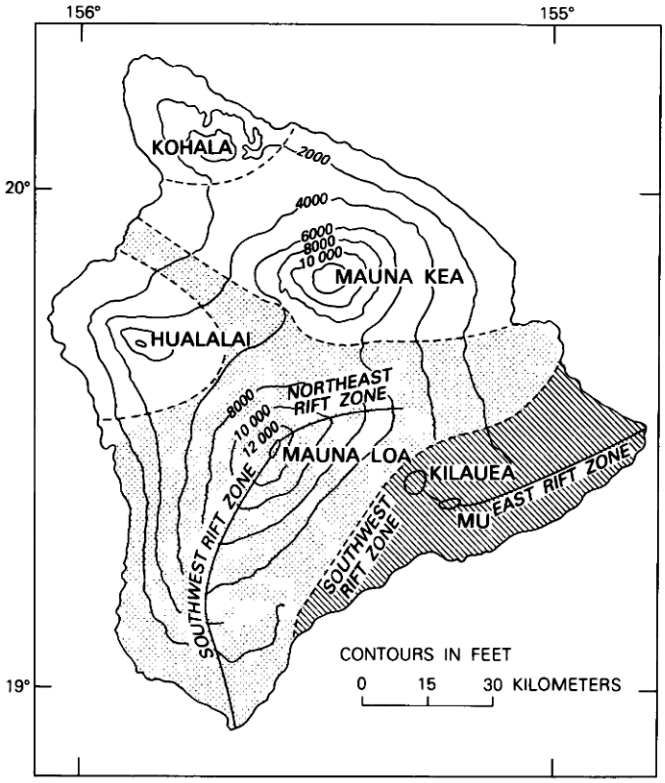

FIGURE 31.1.—Index map of Hawaii from Tilling and others (chapter 24) showing the five volcanoes that make up the island. Elevation contours are in feet. The site of the 1969–74 Mauna Ulu eruptions on Kilauea's upper east rift zone is also shown. (For more details on the Mauna Ulu eruptions, see Tilling and others, chapter 16).

ANALYTICAL METHODS

Sulfur and carbon abundances were determined in 127 samples from the 1972–75 eruptions of Kilauea Volcano and 8 samples from the 1975 Mauna Loa eruption. The analytical data, together with pertinent information on the samples (location, type, relative density, distance from the vent, and collection state), are given in tables 31.1–31.2.

Measurements of total sulfur and carbon were made using a LECO IR–32 sulfur analyzer and a LECO IR–12 carbon analyzer following the procedures of Gibson and Moore (1973). Powdered samples of approximately 300 mg were combusted in oxygen at 1,800 °C, and the resulting SO_2 and CO_2 measured with an infrared Luft-cell detector. Detection limits were 1 μg sulfur or carbon. Each sample was ground and divided into three parts that were individually analyzed and the results averaged to provide the reported sulfur and carbon abundances given in tables 31.1–31.2. The accuracy of the sulfur and carbon analyzers were checked against the National Bureau of Standards reference steel 55e (S: 110 ± 10 μg/g; C: 112 ± 10 μg/g). The analytical uncertainty of the determinations is estimated to be less than 10 percent of the amount of S or C in the samples.

The relative density of each sample was qualitatively assigned after visual examination. Samples with very few or no vesicles were designated as having a high relative density, and those with extremely abundant or large vesicles were designated as having very low relative density. Samples falling between these two extremes were ranked as moderately high, moderate, moderately low, and low.

PREVIOUS WORK

During the past two decades, significant advances have been made in the understanding of the distribution and the isotopic compositions of volatiles in ocean-floor and Hawaiian basalts (Moore and Fabbi, 1971; Moore and Schilling, 1973; Swanson and Fabbi, 1973; Mathez, 1976; Javoy and others, 1978, 1982; Muenow and others, 1979; Harris, 1981; Harris and Anderson, 1983; Des Marais and Moore, 1984; Kyser and O'Neil, 1984; Mattey and others, 1984; Sakai and others, 1984). More recently, complementary studies of the volcanic gases emitted at Hawaiian volcanoes have made possible improved models of the magmatic budgets of carbon and sulfur for the Kilauea and Mauna Loa volcanic systems (Greenland, chapter 28, 1984, in press; Gerlach, 1980, 1982; Gerlach and Graeber 1985; Greenland and others, 1985, in press). Many of these studies have focused on estimations of the juvenile contents of sulfur and carbon and their implications for the abundance and occurrence of these elements in the magma source regions. It is now well known that submarine basalts erupted under conditions of great hydrostatic pressure are the least degassed, and hence the measurements of their sulfur and carbon abundances most closely approximate juvenile concentrations. Subaerially erupted basalts are typically lower in total sulfur abundance than submarine basalts because of the substantial degassing loss to the atmosphere during fountaining at the vent and lava flowage (Moore and Fabbi, 1971; Gibson and Moore, 1974, fig. 5).

Des Marais and Moore (1984) have demonstrated that carbon abundance in submarine basalt decreases with decreasing ocean depth of eruption site. This relation reflects the increased solubility of CO_2 in the melt at high pressure and the attendant greater tendency for volatiles to escape from magma at shallow water depths (that is, at lower confining pressure). Several recent studies (Des Marais and Moore, 1984; Mattey and others, 1984; Sakai and others, 1984) have shown that carbon typically occurs in three forms: (1) posteruption carbon on sample surfaces (adsorbed gases, organic matter, weathering coatings, and other nonmagmatic carbon species acquired by the basaltic glasses); (2) magmatic carbon dioxide trapped in vesicles; and (3) magmatic carbon dissolved in basaltic glasses. For the 12 midocean basalts they analyzed, Des Marais and Moore (1984) found that forms (1) and (3) provide the bulk of the measured total carbon content. Furthermore, they demonstrated that posteruption carbon can be easily acquired by the sample, as evidenced by the 19 μg/g of surficial carbon yielded by reanalysis of a sample exposed to the atmosphere for four days following a previous analysis (maximum combustion temperatures 504 °C).

We designed our study as a broad survey of the carbon and sulfur abundances in Hawaiian tholeiitic basalts in order to build on the earlier studies of Moore and Fabbi (1971), Swanson and Fabbi (1973), and Swanson (1973) with the following general objectives: (1) To obtain a larger data base for fresh subaerially erupted Hawaiian basalts that have not been subjected to weathering; (2) to examine the relation between volatile content and the different materials produced during the course of an eruption; (3) to document better the degassing behavior of sulfur and carbon during lava fountaining and flowage; and (4) to detect changes, if any, in volatile content of magma through time. We did not anticipate the magnitude of the problem of sample contamination by atmospheric carbon recently brought to light and the additional uncertainty in data interpretation created by posteruption contamination effects. Despite the difficulty in data interpretation presented by these factors, we believe that it is useful to report our carbon data because they constitute the best available data set for subaerial basalts obtained to date.

DISTRIBUTION OF SULFUR AND CARBON CONTENT IN DIFFERENT ERUPTIVE PRODUCTS

The gas content and degassing patterns of magma are some of the primary controls on the morphology of lava flows (Swanson, 1973). In our study, spatter (near-vent) and pahoehoe and aa flows were extensively sampled, but we did not differentiate between the varieties of pahoehoe (see, for example, Swanson, 1973) nor the varieties transitional between pahoehoe and aa (see, for example, Peterson and Tilling, 1980). Because these products have undergone different degassing histories and the lavas may have varied in original volatile content, the eruptive products might be expected to differ in measured sulfur and carbon contents.

To facilitate comparison of the data, which show great scatter, we computed mean sulfur and carbon values according to sample type for each of the eruptive episodes of Kilauea, for Kilauea samples as a whole, and for the 1975 Mauna Loa eruption (tables 31.3–31.5). The small sample populations for many of the eruptive episodes allow only a general comparison between the products of the same episode. However, the mean values for aggregated Kilauea data provide a better statistical basis for comparison.

On the basis of the aggregated Kilauea data, the mean sulfur content of 177 μg/g for spatter is the highest, followed by 152 μg/g for pahoehoe, and 96 μg/g for aa. There are deviations from this general pattern when the products of a single eruptive event are compared, but these probably result from the small sample populations for most of the single events, as well as from the lumping of pahoehoe varieties and the disregard of the transitional flow types between pahoehoe and aa. Comparison of the products of the 1975 Mauna Loa eruption is hampered by a small sample population; the one pahoehoe sample exceeds in sulfur content the mean for spatter, but some individual spatter samples contain more sulfur than the pahoehoe sample.

The time of formation and location of deposition of these three eruptive products explain the general decrease in sulfur content from spatter to pahoehoe to aa. Spatter, deposited by lava fountaining in the vicinity of the active vent, commonly represents material ejected early in the eruption or during more vigorous vent activity. Because spatter is an air-quenched product, it undergoes minimal degassing and thus retains a relatively high sulfur content. In contrast, the pahoehoe and aa form lava streams that are continually degassing as they advance from the vent.

Swanson (1973) documented numerous types of pahoehoe and concluded that gas content and mode of flowage of the lava determine the resultant morphology and gross texture. Different types of pahoehoe were not differentiated in our study, but some of the variations we found in sulfur content in the pahoehoe samples no doubt reflect different morphologic types, distances from the vent, and multiple phases of pahoehoe formation. The role of gas loss in the transition from pahoehoe to aa has been debated. Pahoehoe is generally regarded to be richer in gas than aa (see, for example, Williams and McBirney, 1979). Swanson (1973), however, believed that a higher rate of cooling, and not the loss of gases, causes the transition from pahoehoe to aa. Others (Sparks and Pinkerton, 1978) have attributed aa formation to the high yield strength of lava that has lost a significant amount of gas. Peterson and Tilling (1980), though not directly addressing the issue of gas loss, proposed that lava changes from pahoehoe to aa once a certain critical relation (the so-called transition threshold) between viscosity and rate of shear is attained. In general, magma viscosity increases with decreasing gas content, and we interpret the lower mean sulfur values for aa to indicate that it had degassed to a greater extent than the pahoehoe or spatter. This interpretation is consistent with the observation that aa lava is predominantly found at the toe of an advancing flow, hence farther from the vent, and so has had more opportunity to degas than its associated pahoehoe lava.

The carbon values for spatter, pahoehoe, and aa show more variation and, unlike the sulfur values do not exhibit any systematic trend. Swanson and Fabbi (1973) similarly did not observe any demonstrable trends in the behavior of carbon volatiles and suggested that their analytical techniques were not precise enough to detect small but possibly significant changes. However, the low solubility of CO_2 in the melt and its tendency to degas rapidly before or during eruption (see Greenland, chapter 28; Basaltic Volcanism Study Project, 1981; Gerlach and Graeber, 1985; Greenland, in press) may better explain the incoherent variation pattern for carbon abundances. If indeed most of the CO_2 is lost by degassing during storage in the shallow summit reservoir or immediately with the onset of eruption, then products that formed later in the eruption and flowage sequence would not on average contain noticeably less carbon than those formed early in the eruption. Moreover, the great range in carbon content within each category of material analyzed and the slightly higher mean carbon value for pahoehoe than for spatter, contrary to expected degassing behavior, probably also reflect scatter in the data resulting from posteruption contamination by atmospheric carbon. Given these great uncertainties, the difference between the mean carbon values for Kilauea aa (85 μg/g)

TABLE 31.1.—*Sulfur and carbon contents and other characteristics of selected lava samples from Kilauea Volcano*

[For most samples, the date given is both the date of eruption and the date of sample collection; where they differ, the collection date is given in parentheses. Relative density estimated by visual inspection of sample vesicularity before crushing: H, high; MH, moderately high; M, moderate; ML, moderately low; L, low; VL, very low; *, density not estimated. Physical state of sample at time of collection: S, solid; H, hot; W, warm; C, cool; L, liquid. Most spatter samples collected in the immediate vicinity of the vent; approximate distances from vent are given for other samples]

Sample	Date erupted (Date collected)	Material	Relative density	Collection state	S (μg/g)	C (μg/g)	Distance from vent	Remarks
			Mauna Ulu eruption (upper east rift zone), February 1972 - May 1973					
MU272-2	2/8/72	Spatter	M	S,H	164	46	0	Still glowing when collected
MU272-3	2/9/72	Pahoehoe	MH	L	153	223	1 km	Toe of active flow
MU272-16	2/27/72	Spatter	M	S,H	182	270	0	
MU372-23	3/18/72 (3/19/72)	Spatter	L	S,W	232	181	0	
MU372-27	3/21/72	Pahoehoe	ML	L	170	245	20 m	
MU472-30	4/11/72	Pahoehoe	L	L	258	350	40 m	Dipped from Alae lava lake
MU472-32	4/14/72	Aa	MH	L	120	68	200 m	Pasty, glowing core of moving flow
MU472-33	3/18/72 (4/14/72)	Spatter	ML	S,C	216	226	0	
MU572-34	5/8/72	Pahoehoe	VL	L	299	561	0	Dipped from Alae lava lake (air-quenched)
MU572-35	5/8/72	Pahoehoe	VL	L	163	114	0	Dipped from Alae lava lake (water-quenched)
MU572-39	5/23/72	Spatter	MH	S,H	189	94	0	Alae lava lake
MU672-41	6/1/72	Pahoehoe	M	S,H	301	112	0	N. rim overflow, Alae lake
MU672-43	6/9/72	Spatter	M	S,W	162	119	0	
MU772-47	7/11/72	Spatter	MH	S,C	201	60	0	
MU772-48	7/11/72	Pahoehoe	M	L	197	123	2 km	Flowing from Alae
MU872-51	8/4/72	Pahoehoe	H	L	105	54	2 km	Makaopuhi Crater floor
MU872-55	8/12/72	Pahoehoe, spinose	M	L	132	68	2 km	Liquid cooled on thermocouple tip
MU972-57	9/3-5/72 (9/5/72)	Spatter	M	S,C	201	56	0	
MU972-61	9/28/72	Pahoehoe	H	L	123	77	10 km	Very viscous flow, lava lake
MU1072-64	9/28/72 10/13/72	Stalactite and wall glaze	M	S,H	15,025	68	1.5 km	Edge of skylight, active tube
MU1072-65	10/16/72 (10/17/72)	Spatter	MH	S,W	227	115	0	
MU1072-66a	10/25/72	Lava	MH	L	133	66	2 km	Quenched; outside of steel bucket; glassy
MU1072-66b	10/25/72	Lava	M	L	157	221	2 km	Inside of bucket; more slowly cooled
MU1172-68	11/7/72	Pahoehoe	H	L	153	36	3 km	
MU1172-69	11/28/72	Pahoehoe	M	L	182	92	250 m	
MU1272-70	11/29-12/1/72 (12/1/72)	Spatter	M	S,C	197	74	0	
MU1272-74	12/14/72	Pahoehoe	ML	L	190	47	1 km	
MU173-76	1/9/73	Pahoehoe	M	L	102	107	2.5 km	Temperature measured
MU173-77	1/9/73	Pahoehoe	M	L	100	84	3 km	
MU173-78a	1/9/73	Aa	H	L	64	36	7.2 km	Pasty, glowing core; air-quenched
MU173-78b	1/9/73	Aa	H	L	57	68	7.2 km	Water-quenched
MU173-79a	1/9/73	Pahoehoe	M	L	105	94	7 km	Air-quenched
MU173-79b	1/9/73	Pahoehoe	M	L	92	83	7 km	Water-quenched
MU173-80	1/9-1/10/73 (1/10/73)	Spatter	L	S,W	166	157	0	
MU173-89	1/31/73	Pahoehoe	MH	L	85	21	8 km	
MU273-95	2/28/73	Pahoehoe	H	L	111	31	1 km	Leaking from tumulus
MU273-97	2/28/73	Pahoehoe	H	S,H	94	23	10 km	5-m depth sea
MU373-98	3/3/73	Pahoehoe	H	S,H	223	66	10 km	Average S and C values for entire sample
MU373-98a					389	67		Glassy rim, 1 cm thick
MU373-98b					157	92		21-cm thick fine-grained interior
MU373-98c					123	39		Glassy lower rim
MU373-99	3/4/73	Pahoehoe	MH	S,H	120	24	10 km	Collected in tide pool
MU373-101	3/6/73	Black sand	*	S,C	121	53	10 km	Newly formed
MU373-103	3/14/73	Spatter	MH	S,C	190	51	0	
MU373-107	3/23/73	Pahoehoe	H	L	107	20	10 km	Temperature measured
MU473-108	4/10/73	Spatter	MH	S,H	133	26	0	
MU473-109	4/10/73	Pahoehoe	M	L	112	11	10 km	Temperature measured
MU573-111	5/1/73	Spatter	M	S,W	217	25	0	
MU573-112	5/1/73	Pahoehoe	M	L	150	48	1.5 km	

TABLE 31.1.—*Sulfur and carbon contents and other characteristics of selected lava samples from Kilauea Volcano—Continued*

[For most samples, the date given is both the date of eruption and the date of sample collection; where they differ, the collection date is given in parentheses. Relative density estimated by visual inspection of sample vesicularity before crushing: H, high; MH, moderately high; M, moderate; ML, moderately low; L, low; VL, very low; *, density not estimated. Physical state of sample at time of collection: S, solid; H, hot; W, warm; C, cool; L, liquid. Most spatter samples collected in the immediate vicinity of the vent; approximate distances from vent are given for other samples]

Sample	Date erupted (Date collected)	Material	Relative density	Collection state	S (μg/g)	C (μg/g)	Distance from vent	Remarks
			Pauahi-Hiiaka eruption (upper east rift zone), May 5, 1973					
PH573-1	5/5/73	Pumice	VL	S,C	213	437	0	Highest fountaining
PH573-2	5/5/73	Pahoehoe	M	L	135	99	1 km	
PH573-3	5/5/73	Spatter	M	S,H	161	110	0	
PH573-4	5/5/73	Spatter	M	S,W	165	85	0	
PH573-5	5/5/73 (5/23/73)	Pahoehoe	MH	S,C	324	123	0	High lava lake, Hiiaka stand
PH573-6	5/5/73 (5/23/73)	Pumice	VL	S,C	210	181	0	Hiiaka Crater
PH973-8	5/5/73 (9/10/73)	Spatter	M	S,C	177	109	0	Pauahi Crater
PH973-10	5/5/73 (9/10/73)	Pahoehoe	ML	S,C	121	119	0	Pauahi, high lava lake stand
PH973-11	prehistoric 9/10/73	Lava	H	S,C	37	106		Prehistoric lava; wall of Pauahi
			Mauna Ulu eruption (upper east rift zone), June 1973 - November 1973					
MU673-115	6/5/73? (6/7/73)	Pahoehoe	L	S,W	413	77	100 m	Glassy rind of shelly pahoehoe, Alae
MU673-116	6/7/73	Pahoehoe	M	L	175	13	0	Dipped from Mauna Ulu lava lake
			(Mauna Ulu not sampled again until October)					
MU1073-117	10/30/73	Spatter	L	S,H	234	114	0	
MU1173-120	11/4/73	Spatter	ML	S,W	229	15	0	
MU1173-122	11/4/73	Pahoehoe	ML	L	253	32	200 m	Lava lake overflow
MU1173-125	11/8/73	Pahoehoe	M	L	140	29	150 m	Dipped lava lake
			Pauhi eruption (upper east rift zone), November - December, 1973					
PH1173-12	11/10/73	Spatter	L	S,C	187	146	50 m	Watch it fall
PH1173-15	11/11/73	Pahoehoe, glassy rind	ML	S,H	197	118	0	Glowing toe
PH1173-16	11/11/73	Spatter	*	S,W	318	135	300 m	Fissure 300 m from Puu Huluhulu
PH1173-21	11/29/73	Spatter	M	S,C	102	135	0	
PH574-25	12/9/73 (5/1/74)	Pahoehoe, glassy skin	M	S,C	86	119	0	Last erupted material in west pit
			Mauna Ulu eruption (upper east rift zone), December 1973 - June 1974					
MU1273-127	12/14/73 (12/27/73)	Pahoehoe	M	S,C	286	62	<100 m	Lava-lake high stand
MU174-131	1/25/74	Pahoehoe	M	L	78	66	<25 m	
MU174-132	1/25/74	Spatter	L	S,W	243	69	0	Collected as it fell
MU174-133	1/25/74	Pahoehoe	M	L	81	46	140 m	
MU174-134	1/25/74	Pahoehoe	M	L	80	69	400 m	Slabby pahoehoe
MU274-142	1/25-26/74 (2/2/74)	Aa	*	S,C	208	91	2 km	Terminus of 1/25/74 flow
MU274-143	1/25-26/74 (2/2/74)	Pahoehoe, spinose	M	S,C	70	81	0.6 km	Edge of 1/25-26/74 flow
MU274-147	2/14/74	Pahoehoe	ML	L	144	58	10 m	
MU274-148	2/14/74	Pahoehoe	ML	L	168	31	50 m	
MU374-154	3/5/74	Spatter	ML	S,C	149	67	0	Vent F
MU374-155	3/17/74 (3/18/74)	Spatter	L	S,W	202	36	0	Vent E
MU374-156	3/23/74	Spatter	L	S,H	229	41	0	Collected as it fell
MU374-157	3/23/74	Pahoehoe	M	L	168	45	24 m	
MU374-158	3/23/74	Pahoehoe	M	L	118	48	0.6 km	
MU474-161	4/3/74	Pahoehoe, interior	MH	S,H	93	67	5 km	Collected 3 minutes after solidification
MU474-161a	4/3/74	Pahoehoe, crust	MH	S,H	119	77	5 km	Collected 3 minutes after solidification
MU474-162	4/5/74	Spatter	ML	S,C-W	141	57	0	
MU474-163	4/8/74	Spatter	MH	S,H	146	53	0	
MU474-168	4/22/74	Pahoehoe	*		162	115	5 m	Vent F
MU574-169a	5/3/74	Pahoehoe	H	S,H	159	62	5 km	Collected a few hours after solidification
MU574-169b	5/3/74	Pahoehoe	MH	S,H	151	143	5 km	Collected a few hours after solidification
MU574-170	5/6/74	Spatter	H	S,W	162	83	0	
MU574-171	5/30/74	Spatter	L	S,H	155	98	0	Watched it fall
MU574-172	5/31/74	Pahoehoe	ML	L	149	127	25 m	
MU674-173	6/3-5/74 (6/8/74)	Spatter	M	S,W	147	82	0	

TABLE 31.1.—*Sulfur and carbon contents and other characteristics of selected lava samples from Kilauea Volcano—Continued*

[For most samples, the date given is both the date of eruption and the date of sample collection; where they differ, the collection date is given in parentheses. Relative density estimated by visual inspection of sample vesicularity before crushing: H, high; MH, moderately high; M, moderate; ML, moderately low; L, low; VL, very low; *, density not estimated. Physical state of sample at time of collection: S, solid; H, hot; W, warm; C, cool; L, liquid. Most spatter samples collected in the immediate vicinity of the vent; approximate distances from vent are given for other samples]

Sample	Date erupted (Date collected)	Material	Relative density	Collection state	S (μg/g)	C (μg/g)	Distance from vent	Remarks
			Summit eruption, July 19-22, 1974					
KIL774-1	7/19/74	Pahoehoe	L	L	149	84	0	
KIL774-2	7/19/74	Spatter	L	S,H	177	81	0	Watched it fall
KIL774-6a	7/20/74	Pahoehoe	M	L	107	67	0	Fissure F
KIL275-10	7/19/74 (2/16/75)	Spatter	ML	S,C	166	70	0	Fissure A
KIL275-11	7/19/74 (2/16/75)	Spatter	M	S,C	154	159	0	
KIL275-12	7/19/74 (2/16/75)	Pahoehoe	M	S,C	110	135	0.5 km	Terminus of flow fed by fissure F
KIL275-13	7/19/74 (2/16/75)	Aa	H	S,C	111	97	2 km	Terminus of flow fed by fissure A
			Summit eruption, September 19, 1974					
KIL974-8	9/19/74	Spatter	MH	S,H	141	64	0	
KIL375-14a	9/19/74 (3/24/75)	Pahoehoe	M	S,C	123	139	0	
KIL375-14b	9/19/74 (3/24/75)	Spatter	ML	S,C	152	114	0	Same location as KIL375-14a
KIL375-15	9/19/74 (3/24/75)	Pahoehoe	M		123	149	1 km	Glassy skin of toe
			Southwest flank eruption, December 31, 1974					
SWR1274-1	12/31/74	Spatter	L	S,H	135	127	0	First material, fissure E
SWR1274-2	12/31/74	Spatter	ML	S,H	122	89	0	Last material, fissure E
SWR1274-3	12/31/74	Spatter	L	S,W-C	192	191	0	Fissure B
SWR1274-4	12/31/74	Spatter	M	S,C	122	35	0	Fissure B
SWR1274-5	12/31/74	Spatter	MH	S,C	125	137	0	Fissure I
SWR1274-6	12/31/74	Spatter	L	S,C	156	147	0	Last material, last fountain, fissure D
SWR175-7	12/31/74 (1/18/75)	Pahoehoe	MH	S,C	65	118	1.5 km	Average S and C content for entire sample
SWR175-7a					79	117		Glassy top rim
SWR175-7b					61	92		Fine-grained interior
SWR175-7c					56	144		Fine-grained bottom rim
SWR175-8	12/31/74 (1/18/75)	Pahoehoe	M	S,C	80	110	2.5 km	
SWR175-9	12/31/74 (1/18/75)	Pahoehoe	M	S,C	78	142	5.5 km	
SWR175-10	12/31/74 (1/18/75)	Aa	H	S,C	48	38	5.5 km	
SWR175-11	12/31/74 (1/18/75)	Pahoehoe	MH	S,C	58	159	9 km	Transitional pahoehoe
SWR175-12	12/31/74 (1/18/75)	Aa	H	S,C	66	200	10.5 km	Weathered - terminus of 12/31/74 flow
			Summit eruption, November 29, 1975					
KIL75-1	11/29/75	Pahoehoe	L	S,H	334	99	400 m	From vent A
KIL75-2	11/29/75 (12/3/75)	Spatter	M	S,C	132	38	10 m	From vent B-1
KIL75-3	11/29/75 (12/3/75)	Spatter	MH	S,C	160	48	0	Irregular, clinkery
KIL75-4	11/29/75 (12/3/75)	Cinder	*	S,C	695	49	0	Irregular
KIL75-5	11/29/75 (12/4/75)	Spatter	L		200	69	0	
KIL75-6	11/29/75 (12/4/75)	Pahoehoe	M		174	443	1 km	Average S and C content for entire sample
KIL75-6a					172	163		Glassy rim
KIL75-6b					179	68		Fine-grain interior; vesicles 1-2 mm
KIL75-6c					173	1099		Fine-grained basal, rim; vesicles <1 mm

TABLE 31.2.—*Sulfur and carbon contents and other characteristics of selected lava samples from the July 5–6, 1975, summit eruption of Mauna Loa Volcano*

[For most samples, the date given is both the date of eruption and the date of sample collection; where they differ, the collection date is given in parentheses. Relative density estimated by visual inspection of sample vesicularity before crushing: H, high; MH, moderately high; M, moderate; ML, moderately low; L, low; VL, very low; *, density not estimated. Physical state of sample at time of collection: S, solid; H, hot; W, warm; C, cool; L, liquid. Most spatter samples collected in the immediate vicinity of the vent; approximate distances from vent are given for other samples.]

Sample	Date erupted (Date collected)	Material	Relative density	Collection state	S (μg/g)	C (μg/g)	Distance from vent	Remarks
ML775-1	7/6/75	Aa	MH	S,H	48	28	5 km	Red hot when collected at active flow front
ML775-17	7/6/75) (7/15/75)	Spatter	ML	S,C	227	199	0	
ML775-21	7/6/75 (7/15/75)	Spatter	H	S,C	108	58	40 m	
ML775-22	7/6/75 (7/15/75)	Spatter	ML	S,C	134	52	0	
ML775-23	7/5/75 (7/21/75)	Spatter	L	S,C	238	205	8 m	
ML775-24	7/5/75 (7/21/75)	Pahoehoe	L	S,C	196	115	0.5 km	
ML775-26	7/6/75) (7/29/75)	Spatter	ML	S,C	184	73	0	
ML775-27	7/5/75 (7/31/75)	Aa	H	S,C	28	41	2.5 km	

TABLE 31.3.—*Distribution of mean sulfur and carbon contents in spatter from Kilauea and Mauna Loa Volcanoes*

Location and month of eruption	Number of samples	Mean S (μg/g)	Mean C (μg/g)
Kilauea Volcano, all samples	45	117	96
Mauna Ulu 2/72-5/73	14	191	99
Pauahi-Hiiaka 5/73	3	168	101
Mauna Ulu 6/73-11/73	2	231	64
Pauahi-Hiiaka 11/73-12/73	3	202	139
Mauna Ulu 12/73-6/74	9	175	65
Summit 7/74	3	166	103
Summit 9/74	2	147	89
Southwest flank 12/74	6	142	121
Summit 11/75	3	164	52
Mauna Loa Volcano 7/75	5	178	117

TABLE 31.4.—*Distribution of mean sulfur and carbon contents in pahoehoe from Kilauea and Mauna Loa Volcanoes*

Location and month of eruption	Number of samples	Mean S (μg/g)	Mean C (μg/g)
Kilauea Volcano, all samples	60	152	103
Mauna Ulu 2/72-5/73	25	153	108
Pauahi-Hiiaka 5/73	3	193	114
Mauna Ulu 6/73-11/73	4	245	38
Pauahi-Hiiaka 11/73-12/73	2	141	119
Mauna Ulu 12/73-6/74	15	130	68
Summit 7/74	3	122	95
Summit 9/74	2	123	144
Southwest flank 12/74	4	70	132
Summit 11/75	2	254	271
Mauna Loa Volcano 7/75	1	196	115

and for spatter (96 μg/g) is probably not significant, even though the difference is compatible with the presumed greater degassing of the aa samples.

Several eruptive products other than the three general types discussed above were sampled and analyzed. The only cinder sample collected (KIL75–4) has the highest sulfur content (695 μg/g) of any of the material (excluding the stalactite) we analyzed but a low carbon content (49 μg/g). The relatively low carbon content is suggestive of little posteruption contamination; therefore, if sulfur has not been adsorbed, then the sulfur content, which is similar to the mean (680 μg/g) for submarine basalts (Moore and Fabbi, 1971), perhaps approaches the original sulfur content of the basaltic magma erupted in November 1975 at Kilauea. Two pumice samples (PH573–1 and PH573–6), collected during the May 1973 Kilauea eruption at Pauahi and Hiiaka craters, also contain high sulfur contents (213 and 210 μg/g, respectively) and high carbon contents (437 and 181 μg/g, respectively). Sample PH573–1 formed during the highest fountaining observed for the Pauahi-Hiiaka eruption. If this sample was not contaminated, then the comparison of this carbon value to a spatter sample (MU1173–120) that contains only 14 μg/g carbon indicates that almost complete degassing of CO_2 is possible during eruption. Alternatively, the wide ranges in sulfur and carbon contents observed for the cinder and pumice samples could simply reflect adsorption trapping of plume gases during high fountaining, as suggested by unpublished data of L. Paul Greenland of the

TABLE 31.5.—*Distribution of mean sulfur and carbon contents in aa from Kilauea and Mauna Loa Volcanoes*

Location and month of eruption	Number of samples	Mean S (μg/g)	Mean C (μg/g)
Kilauea Volcano, all samples	7	96	85
Mauna Ulu 2/72-5/73	3	80	57
Mauna Ulu 12/73-6/74	1	208	91
Summit 7/74	1	111	97
Southwest flank 12/74	2	57	119
Kilauea Volcano totals	7	96	85
Mauna Loa Volcano 7/75	2	38	35

Hawaiian Volcano Observatory (written commun., 1985) from the Puu Oo eruption on Kilauea's east rift zone that began in 1983 (Wolfe and others, chapter 17).

A sample of red, oxidized, hollow-cored stalactite (MU1072–64) taken from the roof of an active lava tube through a skylight has an extremely high sulfur content of 15,025 μg/g but a low carbon content of 68 μg/g. The high sulfur content possibly results from degassed sulfur volatiles that condensed and formed a sulfide-mineral phase near the skylight because of changes in temperature and Eh conditions. The very low carbon content suggests that most of the CO_2 degassed before the lava entered the lava tube or that carbon escaped through the skylight without reacting with the wall material.

A sample of prehistoric lava (PH973–11) from the wall of Pauahi crater has a very low sulfur content of 37 μg/g, which would place it in the range of modern aa samples analyzed in this study. The moderate carbon content of 106 μg/g provides no clues to its origin or its distance from the vent, because carbon abundances vary greatly in all categories of eruptive products. In addition, such a prehistoric (older than A.D. 1750) lava must have a higher probability of being affected by atmospheric carbon contamination than the fresh materials erupted during 1972–75 at Kilauea.

Three samples of pahoehoe were selected for analysis of sulfur and carbon contents in each of several distinct textural zones (glassy upper rind; fine grained, moderately vesicular interior; and glassy or fine-grained, slightly vesicular basal rim) for comparison with results of zoned pillow basalts analyzed by Moore and Fabbi (1971). Two samples (MU373–98 and SWR175–7) have sulfur content highest in the upper glassy rim and lowest in the lower rim. Sample KIL75–6 showed no significant variation in sulfur content among the zones. Thus, the sulfur distribution in our zoned subaerial pahoehoe samples generally follows the trend observed by Moore and Fabbi (1971) for zoned submarine pillow basalts, but the sulfur contents in the pahoehoe are much lower. The carbon distribution for the three zoned pahoehoe samples is irregular, most probably because of posteruption contamination; carbon was not analyzed in the Moore and Fabbi pillow-basalt study.

VARIATIONS IN SULFUR AND CARBON CONTENT WITH DISTANCE FROM VENT

Degassing of lava during fountaining and flow from the vent has been previously observed and documented (Swanson, 1973; Swanson and Fabbi, 1973; Gibson and others, 1975). If the degassing process is efficient and systematic, eruptive products that have travelled greater distances from the vent should show progressively lower sulfur and carbon contents.

In general, sulfur abundance does tend to decrease with increasing distance from the vent, the greatest loss occurring within 2 km of the vent (fig. 31.2). Sulfur abundances in samples collected 2–10 km from the vent do not show a well-defined decreasing trend, indicating that variations caused by differences in sample type,

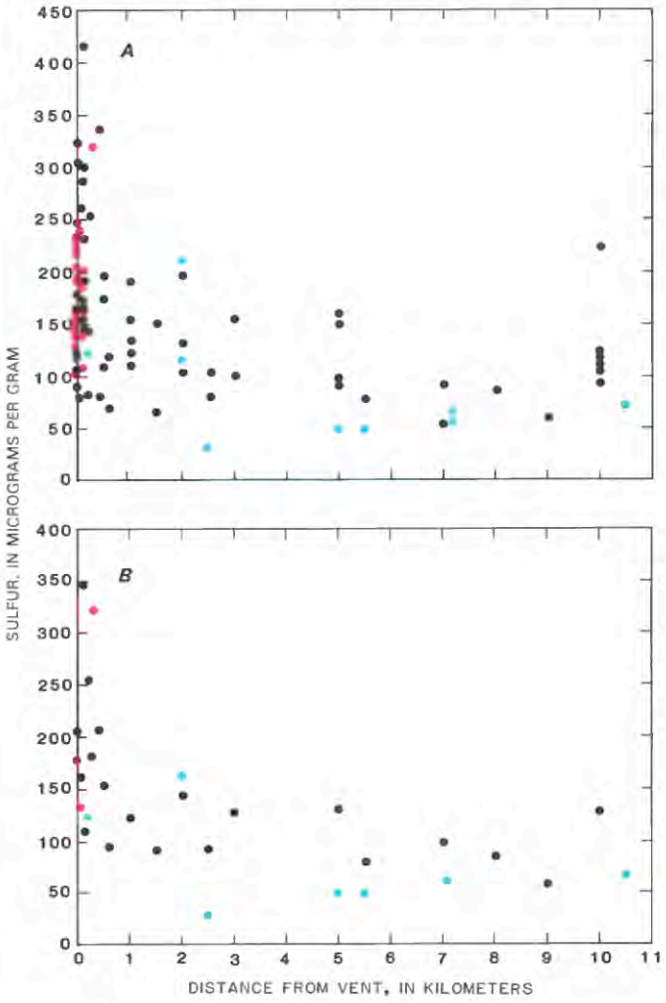

FIGURE 31.2.—Sulfur contents of Kilauea and Mauna Loa lavas plotted against distance from eruptive vent. Red, spatter; black, pahoehoe; blue, aa. ***A***, Sulfur content of individual samples. ***B***, Mean sulfur content of samples grouped by distance from eruptive vent. Samples collected 5–50 m from vent are grouped together and the mean value is plotted at 0.05 km.

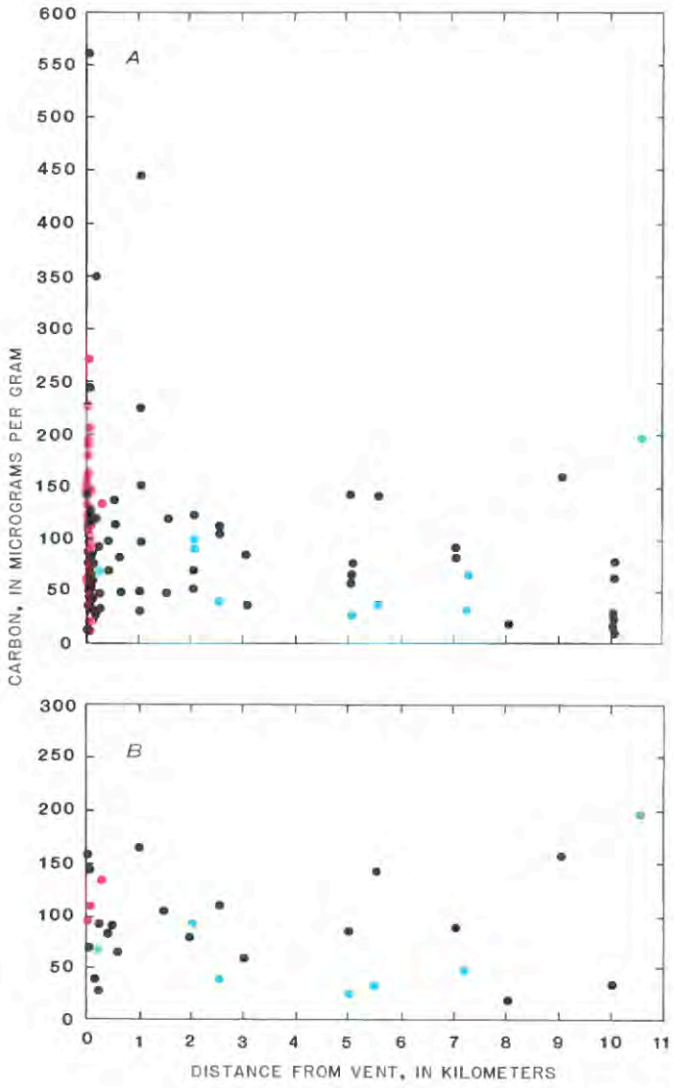

FIGURE 31.3.—Carbon contents of Kilauea and Mauna Loa lavas plotted against distance from eruptive vent. Red, spatter; black, pahoehoe; blue, aa. ***A***, Carbon content of individual samples. ***B***, Mean carbon content of samples grouped by distance from eruptive vent. Samples collected 5–50 m from vent are grouped together and the mean value is plotted at 0.05 km.

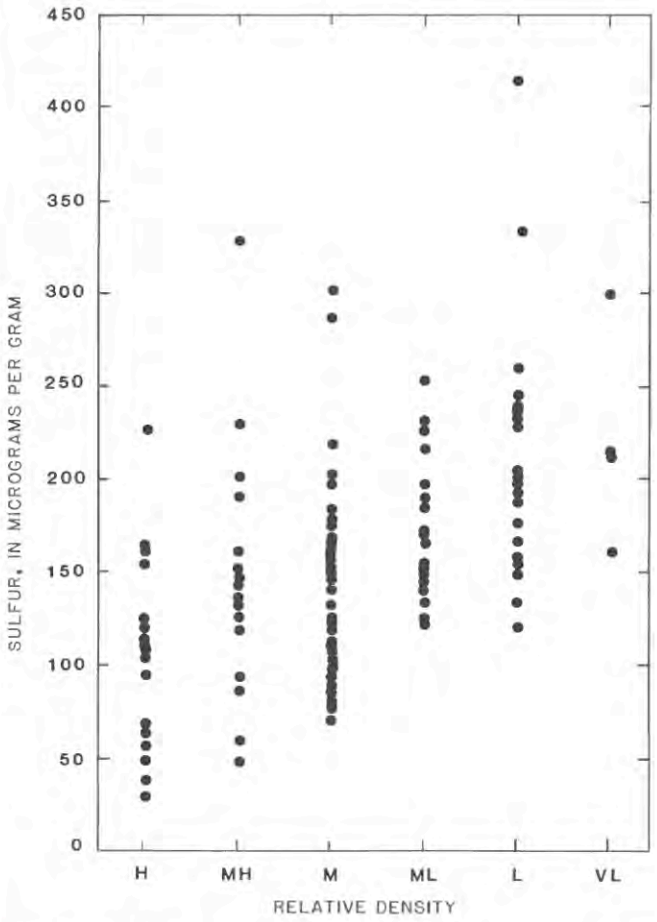

FIGURE 31.4.—Sulfur contents of Kilauea and Mauna Loa lava samples plotted by relative density estimated qualitatively from visible vesicularity. H, high; MH, moderately high; M, moderate; ML, moderately low; L, low; VL, very low.

especially for pahoehoe, are greater in that interval than those related to degassing alone. Although the distance the lava flows from the vent is an important determinant of the type of pahoehoe formed, it is not the sole control. Swanson (1973) has shown that the original volatile content, the rate of flow of the lava, the gradient of the surface over which the lava flows, and the mode of lava extrusion all help control the type of pahoehoe formed. Presumably pahoehoe with different morphologies and volatile contents can occur at the same distance from the vent; the sampling in our study was inadequate to permit such distinctions.

Carbon abundance shows little apparent correlation with distance from the vent (fig. 31.3). Although the highest carbon values do occur closest to the vent, whatever progressive degassing trend may exist is obscured by contamination-caused variations in total carbon content. If immediate, sudden release of most carbon volatiles occurs during the initial phases of the eruption, then the high carbon contents in some samples collected far from the vent are difficult to explain and are almost certainly related to posteruption contamination.

VARIATION IN SULFUR AND CARBON WITH SAMPLE DENSITY

Sulfur and carbon abundances show different general patterns when plotted against relative density (figs. 31.4 and 31.5). Although high sulfur contents may be encountered in most of the arbitrarily defined density classes, sulfur values generally become lower as the density increases. This general trend corresponds to a decrease in lava vesicularity as degassing of volatiles progresses. For

example, Swanson (1973) noted a 10-percent decrease in lava vesicularity that he attributed to gas loss during 4 km of flowage. Without actual measurements of the density, we cannot estimate the average decrease in vesicularity with lava flowage, but our qualitative data affirm the occurrence of generally lower concentrations of sulfur volatiles in denser, more degassed lavas.

A similar plot of carbon content against relative density (fig. 31.5) yields an almost random pattern. The highest carbon contents are not restricted to the samples with lowest density, and the lowest carbon values are distributed almost equally among all density classes. This lack of correlation is compatible with the notion that carbon volatiles may degas rapidly before or during the earliest vent activity rather than systematically during flowage. The wide range and scatter in carbon contents may again reflect the ease of posteruption contamination of the samples.

POSSIBLE VARIATION IN SULFUR AND CARBON CONTENT WITH TIME

Temporal and spatial variations in the chemical composition of Hawaiian basalts, even those formed during a single eruption, have been well documented in many previous studies (see, for example, Tilling and others, chapter 24; Wright, 1971; Wright and others, 1975; Wright and Tilling, 1980; Hoffman and others, 1984). Theoretically, variations in the volatile content of the eruptive products might be expected to correlate with differences in the composition of the magma in equilibrium with the volatiles. Swanson and Fabbi (1973) suggested that the differences in the energy level of vent fountaining might be linked to changes in volatile content of the magma; the most vigorous fountaining indicated the highest volatile content. They did not believe that the original volatile content of a magma could be estimated by analyzing subaerial eruptive products, because more than 80 percent of that content would have been lost. Swanson and Fabbi (1973) concluded, however, that spatter samples would retain the original volatiles better than any other eruptive product.

Although we cannot estimate the original volatile content of the magma associated with each eruptive event, we have plotted the sulfur and carbon content of spatter as a function of time (figs. 31.6, 31.7) in an attempt to ascertain any systematic secular changes in volatile content. Sulfur values (fig. 31.6) for most spatter samples fall in the range 125–250 μg/g, but the distribution appears random and no systematic temporal trend is apparent. Spatter samples collected during the same eruptive suquence may vary by as much as 130 μg/g. The plot of carbon content versus time (fig. 31.7) shows even more variation than that for sulfur. Spatter samples formed during the same eruption may differ in carbon content by as much as 156 μg/g. Such variations indicate that many more analyses of spatter samples, together with modifications in analytical procedure (such as stepwise combustion for carbon analysis), are needed before the possible existence of systematic temporal variations in volatile content of magma can be tested with any confidence. Furthermore, recent studies of volcanic gases from Kilauea rift eruptions indicate remarkable uniformity in the contents and proportions of the carbon and sulfur gases (Greenland, 1984; Gerlach and Graeber, 1985; Greenland and others, 1985). Such uniformity implies that the magma source region in the mantle beneath Hawaii is very homogeneous in volatile contents and, correspondingly, that variation in the volatile content of Hawaiian eruptive magmas may be so slight as to be extremely difficult to demonstrate with presently available sampling and analytical techniques.

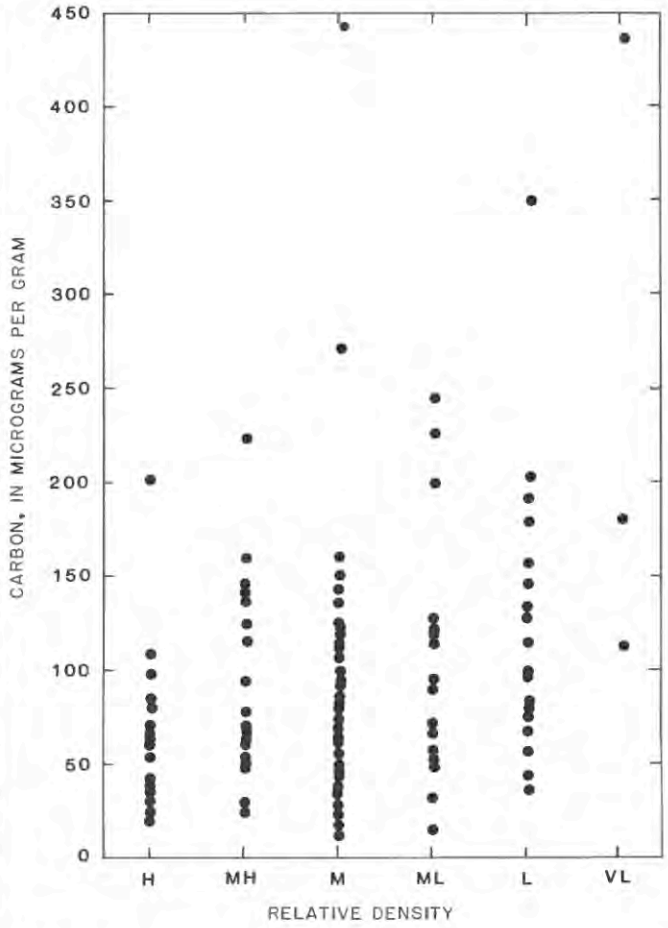

FIGURE 31.5.—Carbon contents of Kilauea and Mauna Loa lava samples plotted by relative density estimated qualitatively from visible vesicularity. H, high; MH, moderately high; M, moderate; ML, moderately low; L, low; VL, very low.

DISCUSSION

In our broad survey of recently erupted subaerial Hawaiian basalts, the total sulfur abundances ranged from 37 to 15,025 μg/g (median value 153 μg/g). The greatest sulfur abundances were found in a stalactite sample and wall glaze from an active lava tube. Presumably the stalactite sample served as a cold surface on which sulfur had condensed and accumulated; evidence of elemental sulfur deposits could be observed on the sample. The sulfur abundances for the subaerial basalts we analyzed are lower by a factor of 4 to 6

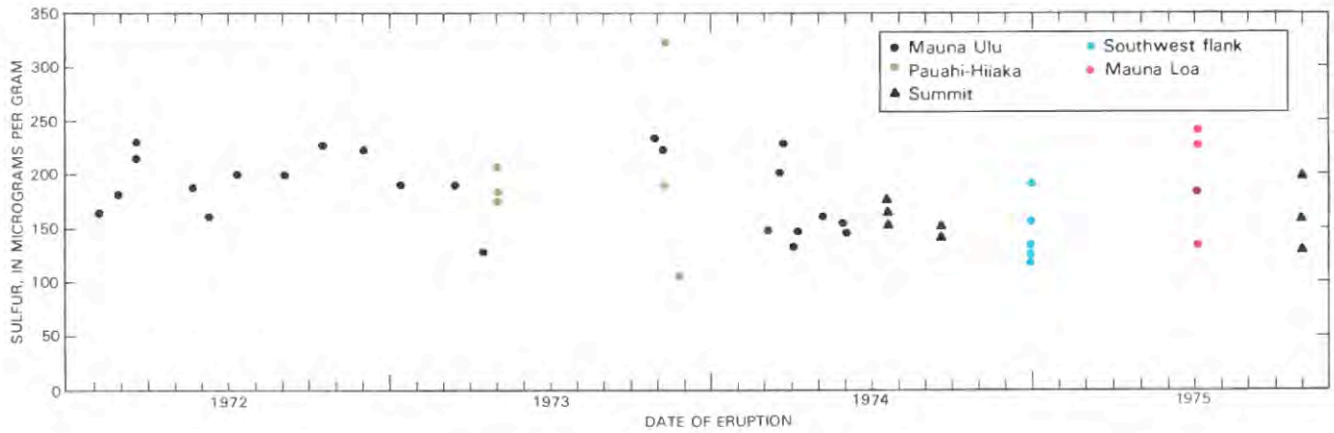

FIGURE 31.6.—Sulfur content of Kilauea and Mauna Loa lava spatter samples plotted by date of eruption.

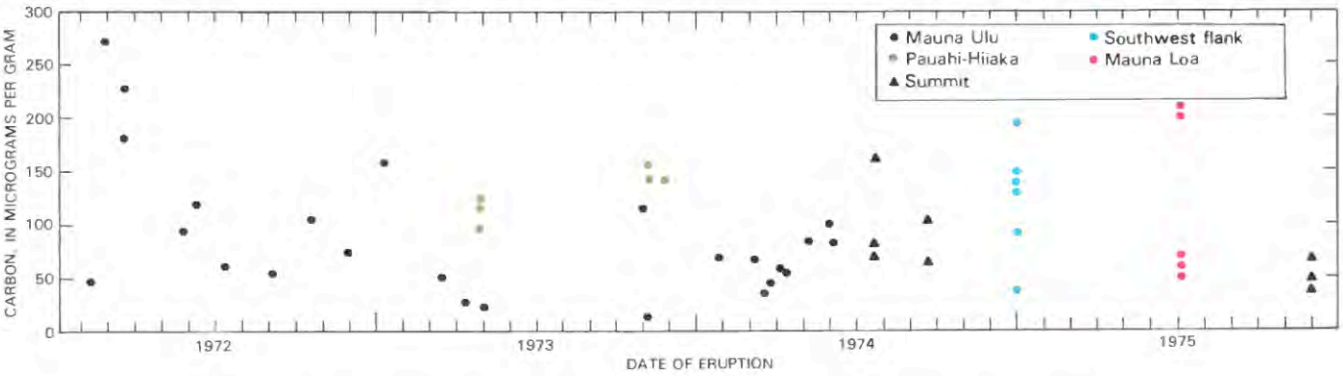

FIGURE 31.7.—Carbon content of Kilauea and Mauna Loa lava spatter samples plotted by date of eruption.

than those reported for submarine basaltic glasses (Des Marais and Moore, 1984; Sakai and others, 1984).

Sulfur abundances for ocean-floor basalts range from 60 to 990 μg/g (Moore and Fabbi, 1971; Moore and Schilling, 1973; Killingley and Muenow, 1975; Delaney and others, 1978; Naldrett and others 1978; Garcia and others, 1979; Des Marais and Moore, 1984; Sakai and others, 1984). The upper value approaches the inferred limit of saturation for lavas dredged at water depths exceeding 200 meters (Moore and Calk, 1971; Mathez, 1976). Swanson and Fabbi (1973) noted that recent subaerially erupted basalts contain 50 to 2,000 μg/g S, with the lower value typical of degassed samples and the upper value characteristic only of glass inclusions in phenocrysts (Anderson, 1974). Naldrett and Goodwin (1977) and Naldrett and others (1978) found that the sulfur contents of Archean basalts range between zero and 8,000 μg/g, with a maximum frequency near 1,000 μg/g. Their interpretation of these S concentrations, which are extraordinarily high compared to those of recent basalts, is that the retention of sulfur, despite extensive redistribution by metamorphism, resulted from the rapid accumulation of the Archean volcanic pile, allowing little interaction with seawater.

Carbon abundances of the basalts we analyzed range from 11 to 1,099 μg/g (median value 69 μg/g). The median value falls within the range of total carbon values reported for submarine basalts (see Des Marais and Moore, 1984; Sakai and others, 1984). However, our range of carbon contents in the subaerial basalts of Kilauea and Mauna Loa is considerably greater (by a factor of 4–5) than that for submarine basalts, contrary to what would be expected from subaerial (degassed) samples. Although additional factors may help account for this anomaly, we suspect that posteruption contamination by atmospheric carbon is most likely the principal cause of the wide dispersion observed in our data.

In terrestrial basalts, carbon is present usually as CO_2, the second most abundant volatile associated with volcanic systems. Most other volcanic gases are far more soluble in basaltic melts than CO_2 (Anderson, 1975), and this carbon gas species should dominate the vapor phase at fairly high pressures (about 400 MPa), in accordance with the experimental data of Kadik and others (1972).

Because the samples analyzed in this study were powders, most or all of the carbon dioxide that might have been present within vesicles in the rock has been lost during sample preparation. The total carbon abundances we measured represent the combined contributions of magmatic carbon (dissolved CO_2 in the glass) and nonmagmatic carbon acquired by the sample after eruption. Some of the samples contained olivine phenocrysts, generally making up less than 2 percent of the sample, and these phenocrysts were not removed from the sample. Any CO_2 inclusions in the phenocrysts therefore also contributed, though probably only a minor amount, to the total carbon abundance. For several submarine basalts from Kilauea's east rift zone, the carbon dissolved in the glass (released at combustion temperatures 1,200 to 1,270 °C) constituted 49 to 85 percent of the total carbon abundance (Des Marais and Moore, 1984, table 1). However, for a subaerial Kilauea basalt they analyzed, the carbon released in the high-temperature combustion represented only 5 percent of the total carbon.

For subaerial basaltic volcanism, Swanson and Fabbi (1973), on the basis of limited data, suggested that carbon dioxide volatilization does not vary appreciably with fountaining activity or with distance of lava flowage. If this is so, it implies that because of its low solubility in basaltic melt, CO_2 escapes very rapidly during the onset of eruptive activity and during the effervescent stage immediately preceding. In addition, recent studies of volcanic gases at Kilauea (Gerlach and Graeber, 1985; Greenland and others, 1985; Greenland, in press) indicate that substantial loss of CO_2 from the magma may occur during storage in the volcano's summit reservoir (at a depth of 2–6 km). In order to obtain a direct estimate of the magmatic carbon in subaerially erupted basalts and of the variations in its abundance induced by degassing, it would require determination of individual abundances for the various forms of carbon that contribute to the total carbon abundance. Such studies would need to use analytical procedures involving stepwise combustion and sample preparation methods similar to those used in the recent detailed studies of submarine basalts (for example, Des Marais and Moore, 1984). We hope that our broad data base of total carbon and sulfur abundances in fresh subaerial basalts from Kilauea and Mauna Loa will provide a starting point for the subsequent, more systematic studies required to evaluate the carbon budget in the subaerial eruption and attendant degassing of basaltic lavas.

REFERENCES CITED

Anderson, A.T., 1974, Chlorine, sulfur, and water in magmas and oceans: Geological Society of America Bulletin, v. 85, no. 9, p. 1485–1492.

——— 1975, Some basaltic and andesitic gases: Review of Geophysics and Space Physics, v. 13, no. 1, p. 37–55.

Basaltic Volcanism Study Project, 1981, Volatiles in planetary basalts: hydrogen, carbon, and sulfur gas species, *in* Basaltic Volcanism on the Terrestrial Planets: New York, Pergamon Press, Inc., p. 385–398.

Delaney, J.R., Muenow, D.W., and Graham, D.G., 1978, Abundance and distribution of water, carbon and sulfur in the glassy rims of submarine pillow basalts: Geochimica et Cosmochimica Acta, v. 42, no. 6B, p. 581–594.

Des Marais, D.J., and Moore, J.G., 1984, Carbon and its isotopes in mid-oceanic basaltic glasses: Earth and Planetary Science Letters, v. 69, p. 43–57.

Garcia, M.O., Liu, N.W., and Muenow, D.W., 1979, Volatiles in submarine volcanic rocks from the Mariana Island arc and trough: Geochimica et Cosmochimica Acta, v. 43, no. 3, p. 305–312.

Gerlach, T.M., 1980, Evaluation of volcanic gas analyses from Kilauea Volcano: Journal of Volcanology and Geothermal Research, v. 7, no. 3–4, p. 295–317.

——— 1982, Interpretation of volcanic gas data from tholeiitic and alkaline mafic lavas: Bulletin Volcanologique, v. 45–3, p. 235–244.

Gerlach, T.M., and Graeber, E.J., in press, The volatile budget of Kilauea Volcano: Nature.

Gibson, E.K., Jr., Chang, S., Lennon, K., Moore, G.W., and Pearce, G.W., 1975, Sulfur abundances and distributions in mare basalts and their source magmas: Proceedings 6th Lunar Science Conference, p. 1287–1301.

Gibson, E.K., Jr., and Moore, G.W., 1973, Carbon and sulfur abundances in lunar fines: Proceedings 4th Lunar Science Conference, p. 1577–1586.

——— 1974, Sulfur abundances and distributions in the valley of Taurus-Littrow, *in* Lunar Science Conference, 5th, Houston, Tex., 1974, Proceedings: Geochimica et Cosmochimica Acta, supp. 5, v. 2, p. 1823–1837.

Greenland, L.P., 1984, Gas composition of the January 1983 eruption of Kilauea Volcano, Hawaii: Geochimica et Cosmochimica Acta, v. 48, p. 193–195.

——— in press, Estimated mantle content of volatiles from basaltic gas composition: Journal Geology.

Greenland, L.P., Casadevall, T.J., and Stokes, J.B., in press, Emission rate of CO_2 and SO_2 from Kilauea Volcano, Hawaii: Nature.

Greenland, L.P., Rose, W.I., and Stokes, J.B., 1985, An estimate of gas emissions and magmatic gas content from Kilauea Volcano: Geochimica et Cosmochimica Acta, v. 49, no. 1, p. 125–130.

Harris, D.M., 1981, The concentration of CO_2 in submarine basalts: Journal of Geology, v. 89, . 689–701.

Harris, D.M., and Anderson, A.T., 1983, Concentrations, sources and losses of H_2O, CO_2, and S in Kilauean basalt: Geochimica et Cosmochimica Acta, v. 47, p. 1139–1150.

Hoffman, A.W., Feigenson, M.D., and Raczek, Ingrid, 1984, Case studies on the origin of basalt: III. Petrogenesis of the Mauna Ulu eruption, Kilauea, 1969–71: Contributions to Mineralogy and Petrology, v. 88, p. 24–35.

Javoy, M., Pineau, F., and Allegre, C., 1982, Carbon geodynamic cycle: Nature, v. 300, p. 171–173.

Javoy, M., Pineau, F., and Iiyama, I., 1978, Experimental determination of the isotopic fractionation between gaseous CO_2 and carbon dissolved in tholeiitic magma: Contributions to Mineralogy and Petrology, v. 67, p. 35–39.

Kadik, A.A., Lukanin, O.A., Lebedev, Y.B., and Korovushkina, E.Y., 1972, Solubility of H_2O and CO_2 in granite and basalt melts at high pressures: Geochemistry International, v. 6, p. 1041–1050.

Killingley, L.S., and Muenow, D.W., 1975, Volatiles from Hawaiian submarine basalts determined by dynamic high temperature mass spectrometry: Geochimica et Cosmochimica Acta, v. 39, p. 1467–1473.

Kyser, T.K., and O'Neil, J.R., 1984, Hydrogen isotope systematics of submarine basalts: Geochimica et Cosmochimica Acta, v. 48, p. 2123–2133.

Lockwood, J.P., Koyanagi, R.Y., Tilling, R.I., Holcomb, R.T., and Peterson, D.W., 1976, Mauna Loa threatening: Geotimes, v. 21, no. 6, p. 12–15.

Mathez, E.A., 1976, Sulfur solubility and magmatic sulfides in submarine basalt glass: Journal of Geophysical Research, v. 81, p. 4269–4276.

Mattey, D.P., Carr, R.H., Wright, I.P., and Pillinger, C.T., 1984, Carbon isotopes in submarine basalts: Earth and Planetary Science Letters, v. 70, p. 196–206.

Moore, J.G., and Calk, L., 1971, Sulfide spherules in vesicles of dredged pillow basalt: American Mineralogist, v. 56, p. 476–488.

Moore, J.G., and Fabbi, B.P., 1971, An estimate of the juvenile sulfur content of basalt: Contributions to Mineralogy and Petrology, v. 33, p. 118–127.

Moore, J.G., and Schilling, J.G., 1973, Vesicles, water, and sulfur in Reykjanes Ridge basalts: Contributions to Mineralogy and Petrology, v. 41, p. 105–118.

Muenow, D.W., Graham, D.G., and Liu, N.W.K., 1979, The abundance of volatiles in Hawaiian tholeiitic submarine basalts: Earth and Planetary Science Letters, v. 42, p. 71–76.

Naldrett, A.J., and Goodwin, A.M., 1977, Volcanic rocks of the Blake River Group, Abitibi Greenstone Belt, Ontario, and their sulfur content: Canadian Journal of Earth Sciences, v. 14, p. 539–550.

Naldrett, A.J., Goodwin, A.M., Fisher, T.L., and Ridler, R.H., 1978, The

sulfur content of Archean volcanic rocks and a comparison with ocean-floor basalts: Canadian Journal of Earth Sciences, v. 15, p. 715–728.

Peterson, D.W., and Tilling, R.I., 1980, Transition of basaltic lava from pahoehoe to aa, Kilauea Volcano, Hawaii: Field observations and key factors: Journal of Volcanology and Geothermal Research, v. 7, p. 271–293.

Sakai, H., Des Marais, D.J., Ueda, A., and Moore, J.G., 1984, Concentrations and isotope ratios of carbon, nitrogen, and sulfur in ocean-floor basalts: Geochimica et Cosmochimica Acta, v. 48, no. 12, p. 2433–2442.

Sparks, R.S.J., and Pinkerton, H., 1978, The effect of degassing on the rheology of basaltic lava: Nature, v. 276, p. 385–386.

Swanson, D.A., 1973, Pahoehoe flows from the 1969–71 Mauna Ulu eruption, Kilauea Volcano: Geological Society of America Bulletin, v. 84, p. 615–626.

Swanson, D.A., and Fabbi, B.P., 1973, Loss of volatiles during fountaining and flowage of basaltic lava at Kilauea Volcano, Hawaii: U.S. Geological Survey Journal of Research, v. 1, p. 649–658.

Tilling, R.I., Koyanagi, R.Y, Lipman, P.W., Lockwood, J.P., Moore, J.G., and Swanson, D. A., 1976, Earthquake and related catastrophic events, Island of Hawaii, November 29, 1975: A preliminary report: U.S. Geological Survey Circular 740, 33 p.

Williams, Howel, and McBirney, A.R., 1979, Volcanology: San Francisco, Freeman, Cooper & Co, 397 p.

Wright, T.L., 1971, Chemistry of Kilauea and Mauna Loa lava in space and time: U.S. Geological Survey Professional Paper 735, 40 p.

Wright, T.L., Swanson, D.A., and Duffield, W.A., 1975, Chemical compositions of Kilauea east-rift lava, 1968–1971: Journal of Petrology, v. 16, p. 110–133.

Wright, T.L., and Tilling, R.I., 1980, Chemical variations in Kilauea eruption 1971–74: American Journal of Science, v. 280-A, p. 777–793.

VARIATION OF $\delta^{13}C$ IN FUMAROLIC GASES FROM KILAUEA VOLCANO

By Irving Friedman, Jim Gleason, *and* Trevor Jackson

ABSTRACT

Values of $\delta^{13}C$ in fumarolic gases from Sulphur Bank, the Puhimau thermal area, and a fumarole at Halemaumau have been determined for samples collected from June 1984 through December 1985. Samples from Sulphur Bank and Halemaumau have a $\delta^{13}C$ of -3.5 ± 0.2 parts per thousand (permil) and show little change during this period. In contrast, the $\delta^{13}C$ of samples from the Puhimau thermal area increased from -3.5 to values of -2.7 permil at the end of the collection period. Applying an equilibrium fractionation factor of 1.004 for the ^{13}C distribution between carbon dissolved in the magma and the CO_2 gas in equilibrium with the magma resulted in a calculated primary $\delta^{13}C$ value of -7.5 permil for carbon dissolved in the Kilauea magma. The change of $\delta^{13}C$ at Puhimau can be the result of cooling of a pod of magma beneath Puhimau caused by the closure of its feeder passage from the main magma body.

INTRODUCTION

The $\delta^{13}C$ values of fumarolic gases are of interest for several reasons. The isotopic composition of mantle carbon is still a matter of conjecture, and the isotopic composition of mantle-derived gases is of importance in understanding the carbon cycle. Fumarolic gases are an important source of CO_2 to the atmosphere, and a knowledge of the $\delta^{13}C$ of such gases will help in understanding the atmospheric CO_2 cycle.

The first analyses of fumarolic gases from Hawaii were made by Naughton and Terada (1954). Conversion of their published atomic ratios to modern δ notation gives the following values in parts per thousand, permil to a precision of about ± 2 permil.

Sulphur Bank fumarolic gas	
1949, Mauna Loa in eruption	0 permil
1952, Kilauea in eruption	0 permil
1953, both volcanoes quiet	0 permil
Gas collected from Mauna Loa lava flow	−24 permil
CO_2 extracted from 1950 Mauna Loa olivine basalt	−19 permil

Those authors commented on the constancy of the Sulphur Bank ratios and on the relative enrichment of Sulphur Bank samples in ^{13}C as compared to the gas extracted from the chilled lava or from above the active lava flow. Thomas (1977) reported data on samples collected at Sulphur Bank as well as at 1971 and 1974 fissures at Halemaumau. His data are given in table 32.1.

EXPERIMENTAL PROCEDURE

In order to determine whether the variations found by Thomas were related to eruptive events, we initiated frequent sample collections at Sulphur Bank, Halemaumau, and at the Puhimau thermal area. Samples were collected by drawing the gases with a hand vacuum pump through a metal sample tube fitted with valves at both ends. The samples have been shipped to our laboratory in Denver where they were drawn through a metal trap cooled with liquid nitrogen. After the water was separated from the CO_2 at dry ice temperature, SO_2 was separated from the CO_2 by distillation at the temperature of melting ethanol. Analysis for $\delta^{13}C$ was carried out in the conventional manner on a 12-inch, triple-collector 90°-sector mass spectrometer.

RESULTS

Our results are given in table 32.2 and plotted in figure 32.1. Analysis of probable errors indicates two standard deviations (2σ) equal 0.1 permil.

There does not appear to be any correlation between $\delta^{13}C$ values of gases collected at any of the three collection sites and the short-term phases of the eruption at Puu Oo.

TABLE 32.1.—*Values of $\delta^{13}C$ obtained by Thomas (1977) for samples of fumarole from Sulphur Bank, Kilauea Volcano, Hawaii*

[Values given in permil (parts per thousand)]

Location	Date	$\delta^{13}C$
Sulphur Bank	5 Aug 75	−3.2
		−2.6
	18 Aug 75	−3.4
		−2.3
	8 Nov 75	−3.2
		3.0
	Dec 75	2.5
	13 Aug 76	−3.4
	17 Aug 76	−3.4
	13 Aug 76	−3.0
	1 Dec 76	−2.7
	28 Dec 76	−3.5
	28 Jan 77	−3.3
1971 fissure	13 Aug 75	−3.4
	19 Aug 75	−3.2
	8 Nov 75	−3.3
		−3.2
	1 Dec 75	−3.3
	9 Aug 76	−3.2
		−3.3
	26 Aug 76	−3.4
		−2.8
	13 Oct 76	−2.8
		−3.5
	1 Dec 76	−3.2
	28 Dec 76	−4.2
	29 Dec 76	−3.6
1974 fissure	29 Jan 77	−3.1
	10 Feb 77	−3.0

TABLE 32.2.—*Values of $\delta^{13}C$ for samples of fumarolic gas from localities on Kilauea Volcano, Hawaii*

[Values given in permil; date is date of collection of sample]

Date	Puhimau	Halemaumau	Sulphur Bank
	1984		
26 June	−3.6	−3.5	------
25 July	−3.2	−3.8	−3.9
6 Aug	−3.1	−3.6	−3.2
24 Aug	−3.0	−3.2	−3.4
11 Sept	−3.3	−3.6	------
19 Sept	−3.2	−3.5	−3.3
26 Sept	−4.0	−3.9	−3.3
2 Oct	−3.0	−3.6	−3.5
12 Oct	−3.2	−3.8	−3.4
29 Oct	−2.7	−3.5	−3.5
31 Oct	−2.8	−3.6	−3.4
13 Nov	−2.5	−3.5	−3.5
27 Nov	−2.7	−3.5	−3.4
4 Dec	−2.7	−3.4	−3.3
	1985		
10 Mar	−2.9	−3.5	−3.3
21 Mar	−2.9	−3.5	−3.4
1 Apr	−2.9	------	−3.1
3 Apr	-------	------	−3.3
12 Apr	−2.6	−3.4	------
19 Apr	−2.6	[1]−1.9	−3.1
1 May	−2.6	−3.0	−3.1
14 May	−2.6	------	−3.0
20 May	−2.7	−3.1	−3.3
31 May	−2.6	−3.5	------
4 June	−2.7	------	−3.4
17 June	−2.7	−3.5	−3.5
24 June	−2.7	−3.5	−3.2
28 June	−2.7	−3.4	−3.6
3 July	−2.8	−3.4	−3.5
19 July	−2.6	−3.3	−3.7
24 July	−2.7	−3.3	−3.4
9 Aug	−2.6	−3.4	−3.4
20 Aug	−2.8	−3.3	−3.5
13 Sept	−2.8	−3.4	−3.5
23 Sept	−2.5	−3.2	−3.3
30 Sept	−2.6	−3.5	−3.2
4 Oct	−2.7	−3.3	−3.3
11 Oct	−2.7	------	------
16 Oct	−2.8	−3.7	−3.6
25 Oct	−2.7	−3.4	------
31 Oct	−2.8	−3.3	−3.5
8 Nov	−2.7	−3.4	−3.4
14 Nov	−2.1	−2.8	−3.5
19 Nov	−1.9	−3.3	−3.4
22 Dec	−3.2	−3.5	−3.5
30 Dec	−3.2	−3.5	−3.4

[1]We have no explanation for this apparent anomalous value.

The $\delta^{13}C$ values of gases from both Halemaumau and Sulphur Bank appear to be fairly constant at -3.5 ± 0.3 permil, in reasonable agreement with the results of Thomas. We plan to continue to research long enough to determine if this constancy of $\delta^{13}C$ will persist during periods of quiescence at Kilauea.

Gases emitted at the Puhimau thermal area show greater variation and indicate an increase in $\delta^{13}C$ from -3.6 permil in late June, 1984, to -2.7 permil in November, followed by a slow decrease to -2.9 permil in March 1985. The $\delta^{13}C$ at Puhimau remained constant until early November, when it increased to -1.9, and then decreased to -3.2 in late December. These changes may have been caused by a temperature decline in the gas source, related to either cooling of an isolated body of magma beneath the thermal area or to withdrawal of magma from under the site, followed in December by reintroduction.

DISCUSSION

Pineau and others (1976) found the $\delta^{13}C$ of CO_2 released from vesicles in tholeiitic basalt from the mid-Atlantic ridge to be -7.6 ± 0.5 permil and postulated that this value represents the $\delta^{13}C$ of primary deep-seated carbon in the ridge area. Mattey and others (1983) postulated that the $\delta^{13}C$ of volcanic carbon is -4.2 to -7.5 for basalt midocean ridges, -2.8 to -6.7 permil in glass from Hawaiian and Explorer Seamounts, and -7.7 to -16.3 permil for glass from basalts in backarc basins.

The $\delta^{13}C$ of dissolved carbon in 11 samples of glass from midocean basalt was determined by Des Marais and Moore (1984) to range from -5.6 to -7.5.

Javoy and others (1978) determined experimentally that CO_2 in equilibrium with carbon dissolved in tholeiitic magma at 1,120–1,280 °C and 7.0–8.4 Kb, is enriched in ^{13}C by 4.0 to 4.6 permil relative to the magma. Therefore, if basaltic magma containing dissolved carbon with a $\delta^{13}C$ of -7.5 permil loses carbon dioxide to the atmosphere, we can expect that the initial fumarolic CO_2 will have a $\delta^{13}C$ of about -3 to -3.5 permil. Our results obtained at Halemaumau and Sulphur Bank agree with these expected values.

If the magma continues to lose CO_2 in an equilibrium distillation (a Rayleigh process), then the $\delta^{13}C$ of the CO_2 will continuously decrease as the amount of carbon in the magma decreases with time because of CO_2 loss.

The fairly constant $\delta^{13}C$ of the gases sampled at Halemaumau and Sulphur Bank indicate that only a small amount of CO_2 is lost from a large amount of magma, or that new magma enters the system in a continuous manner.

The increase of $\delta^{13}C$ with time observed at Puhimau thermal area can be explained by a decrease in the temperature of isotopic equilibration from about 1,250 to 1,100 °C. This could occur by the cooling of a small pod of magma isolated by interruption of its feeder dike from a larger magma body, which has been the source of heat for the thermal area since its formation in 1936 or 1937. If this explanation is correct, the isolation must have occurred just before our initial sampling in late June 1984. The decrease in $\delta^{13}C$ observed in December 1985 may be due to reintroduction of fresh magma beneath the site.

Monitoring the $\delta^{13}C$ of fumarolic CO_2 at Kilauea can yield important insights into magma movement and the opening and closing of feeder dikes.

REFERENCES

Des Marais, D.J., and Moore, J.G., 1984, Carbon and its isotopes in mid-oceanic basaltic glasses: Earth and Planetary Science Letters, v. 69, p. 43–57.

Javoy, M., Pineau,F., and Iiyama, I., 1978, Experimental determination of the isotopic fractionation between gaseous CO_2 and carbon dissolved in tholeiitic magma: Contributions to Mineralogy and Petrology, v. 67, p. 35–39.

Mattey, D.P., Carr, R.H., Wright, I.P., and Pillinger, C.T., 1983, Carbon isotopes in submarine basalts: Earth and Planetary Science Letters, v. 70, p. 196–206.

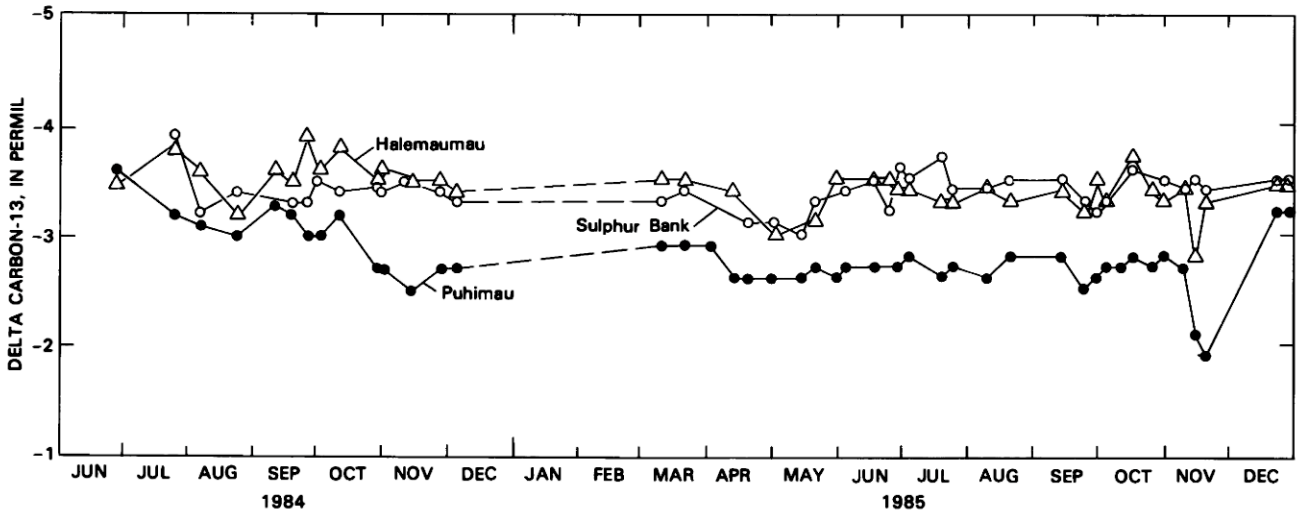

FIGURE 32.1.—Variation of $\delta^{13}C$ in samples of fumarolic gas from three localities on Kilauea Volcano, Hawaii.

Naughton, J.J., and Terada, K., 1954, Effect of eruption of Hawaiian volcanoes on the composition and carbon isotopic composition of associated volcanic and fumarolic gases: Science, v. 120, p. 580–581.

Pineau, F., Javoy, M., and Bottinga, Y., 1976, $^{13}C/^{12}C$ ratios of rocks and inclusions in popping rocks of the Mid-Atlantic Ridge and their bearing on the problem of isotopic composition of deep-seated carbon: Earth and Planetary Science Letters, v. 29, p. 413–421.

Thomas, D.M., 1977, The isotopic profile of gases from the summit and flank of Kilauea Volcano: Honolulu, University of Hawaii, Department of Chemistry, Ph. D. thesis.

HELIUM AT KILAUEA VOLCANO

Part I
Spatial and Temporal Variations at Sulphur Bank

By Irving Friedman *and* G. Michael Reimer

ABSTRACT

A survey of helium in soil gas was conducted at Sulphur Bank, Kilauea Volcano. The resulting helium-isograd map shows the highest helium abundance in an area about 75 m southwest of the experimental well drilled about 50 years ago.

Variation of helium abundance over time was investigated using an automated helium analyzer installed adjacent to Sulphur Bank. The gas effluent from a new well drilled at Sulphur Bank was piped to the instrument. The gas was analyzed every 3 hours and the equipment was operated periodically for 2 years. Helium data from July 1982 to August 1984 show periods of higher helium from August 1982 to January 1983 and again from February to August 1984.

INTRODUCTION

In 1978, a helium sniffer shipped from Denver to the Hawaiian Volcano Observatory was used by Irving Friedman and Ted Denton to conduct a survey of helium in soil gas at Sulphur Bank, on Kilauea Volcano. In order to conduct this survey, sampling was carried out by first pounding a thick-wall steel tube of 6-mm (0.25-in) diameter into the ground to a depth of about 0.5 m. A rubber septum was attached to the top of the tube and a plastic hypodermic syringe was used to withdraw a gas sample. Immediately upon withdrawal of the sidehole hypodermic needle from the septum, the hole in the needle was sealed by placing a piece of close-fitting, soft silicone-rubber tubing over the needle. At the laboratory, the gas sample was injected from the syringe through another rubber septum into the inlet system of the helium mass spectrometer. The spectrometer response was calibrated by frequent injections of gas standards of known helium content. Errors in the sampling and analysis process are estimated to be less than ± 5 percent of the amount of helium present. The data from this survey at Sulphur Bank are given in figure 33.1.

The uranium and thorium contents of soil derived from Hawaiian basalt are very low, and the parent rocks at Kilauea are very young. Thus, these soils contain very little helium derived in place from radioactive decay of uranium and thorium. The content of helium in the soil gas at Sulphur Bank, however, is very high, even compared to that in soils developed on old granitic rocks, in which the concentrations of uranium and thorium are orders of magnitude greater than at Sulphur Bank.

The high helium content of the soil gas at Sulphur Bank reinforced the authors' earlier inference that Sulphur Bank taps a deep magma source, even though it does not appear to be along a major rift zone.

ACKNOWLEDGMENTS

We wish to thank the following: Reggie Okamura and the Hawaiian Volcano Observatory crew for drilling the new well; Don McNair for constructing the original electronics and assembling the unit in Hawaii; Joe Jurceka for constructing the automated inlet system; and Barry Stokes for maintaining the instrument, as well as making many modifications to the wellhead and sampling equipment.

PRESENT SURVEY

Shortly after the completion of the (earlier) survey of Friedman and Denton, Thomas and Naughton (1979) observed changes in the ratio of helium to carbon dioxide at both Sulphur Bank and Halemaumau before inflation and eruptive events at Kilauea.

In 1979 we decided to install at Sulphur Bank an automated helium analyzer similar to that at a site 5 miles north of Gardiner, Montana, near Yellowstone National Park (Friedman and others, in press).

A new well at Sulphur Bank was successfully drilled about 100 m east of the old well (see fig. 33.1). The well was drilled to a depth of about 25 m, and the upper 13 m was cased with heavy-wall stainless steel pipe. The new well is shown in figure 33.2. Although the well casing was not cemented in place, alteration of the surrounding rock by the acid gases emitted along the casing has resulted in self-sealing of the casing. A slight positive gas pressure is observed in the casing.

The helium sniffer was placed in a trailer parked in the Park Service service area above Sulphur Bank Pali (see fig. 33.3). A 12-mm-diameter polyethylene tube inside a protective polyethylene pipe was used to convey the gas sample from well to trailer, a distance of 100 m, including 30 m of vertical rise.

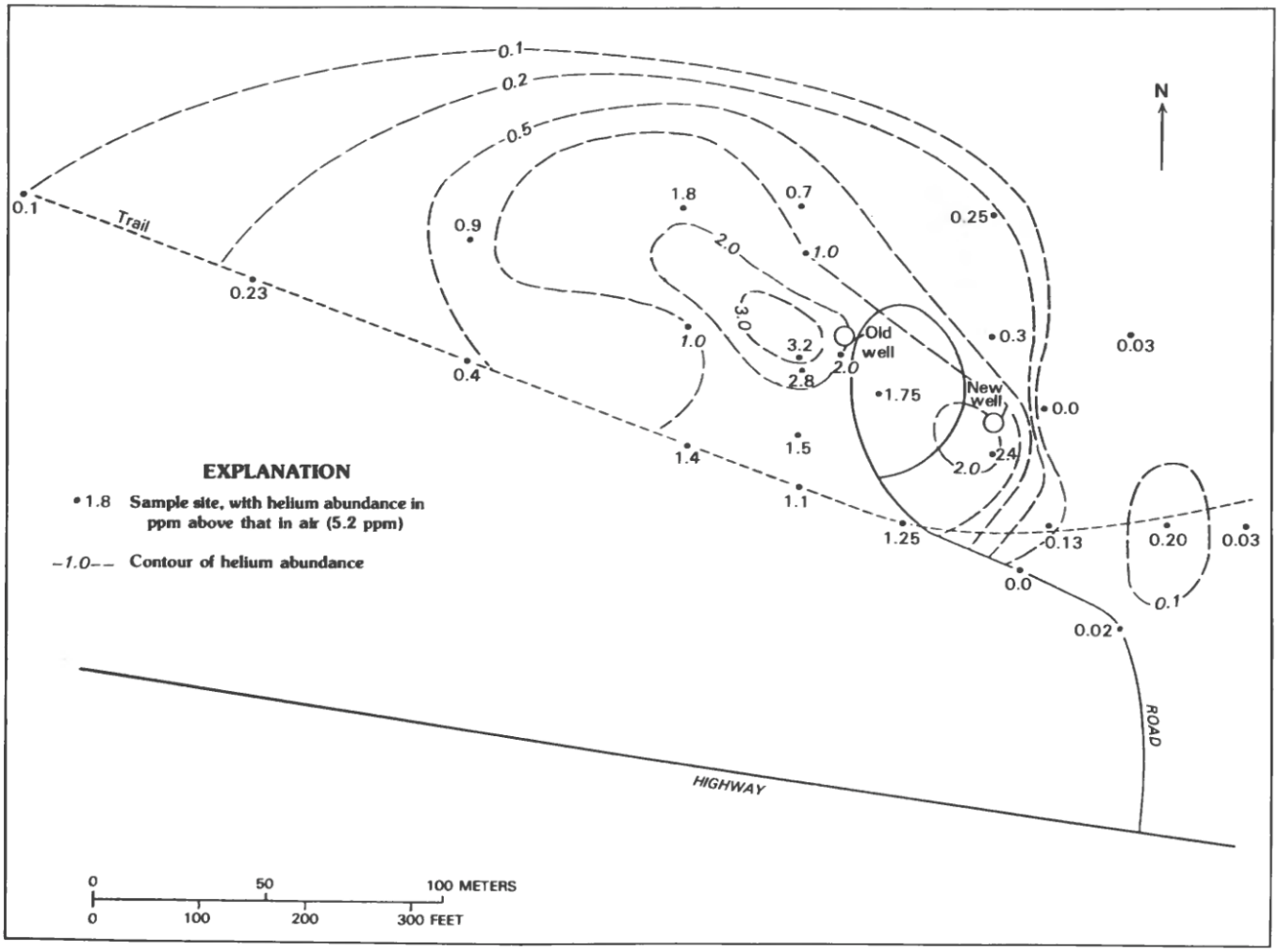

FIGURE 33.1.—Distribution of helium abundance in soil gas in the Sulphur Bank area, Kilauea Volcano, Hawaii. For location of Sulphur Bank, see figure 33.6.

Several attempts were made to condense the steam emitted by the well before it entered the polyethylene tube. Some schemes would work during dry periods when the steam flow was minimal, only to fail during increased steam flow associated with rainy intervals. In addition, metal condenser parts corroded at a very rapid rate, particularly at junctions of dissimilar metals. This problem was eventually solved by making all the wellhead fittings of Kynar plastic. A teflon tube connects these wellhead fittings to the steam condenser, which consists of 13 m of 37-mm-diameter thick wall copper pipe drained through a U-shaped tube. We found that the first few meters of copper pipe would corrode completely through in about 6 months, and it was replaced as needed. All parts, except for the two copper pipes joined with a plastic coupling, are now plastic.

FIGURE 33.2.—Wellhead of new well, completed 1979, for sampling soil gas at Sulphur Bank, Kilauea Volcano. White teflon tube carries gas from actual wellhead (left) to end of dark copper condensing tube. Note U-shaped glass tube (about 15 cm high) that allows condensed water to escape but prevents air from entering.

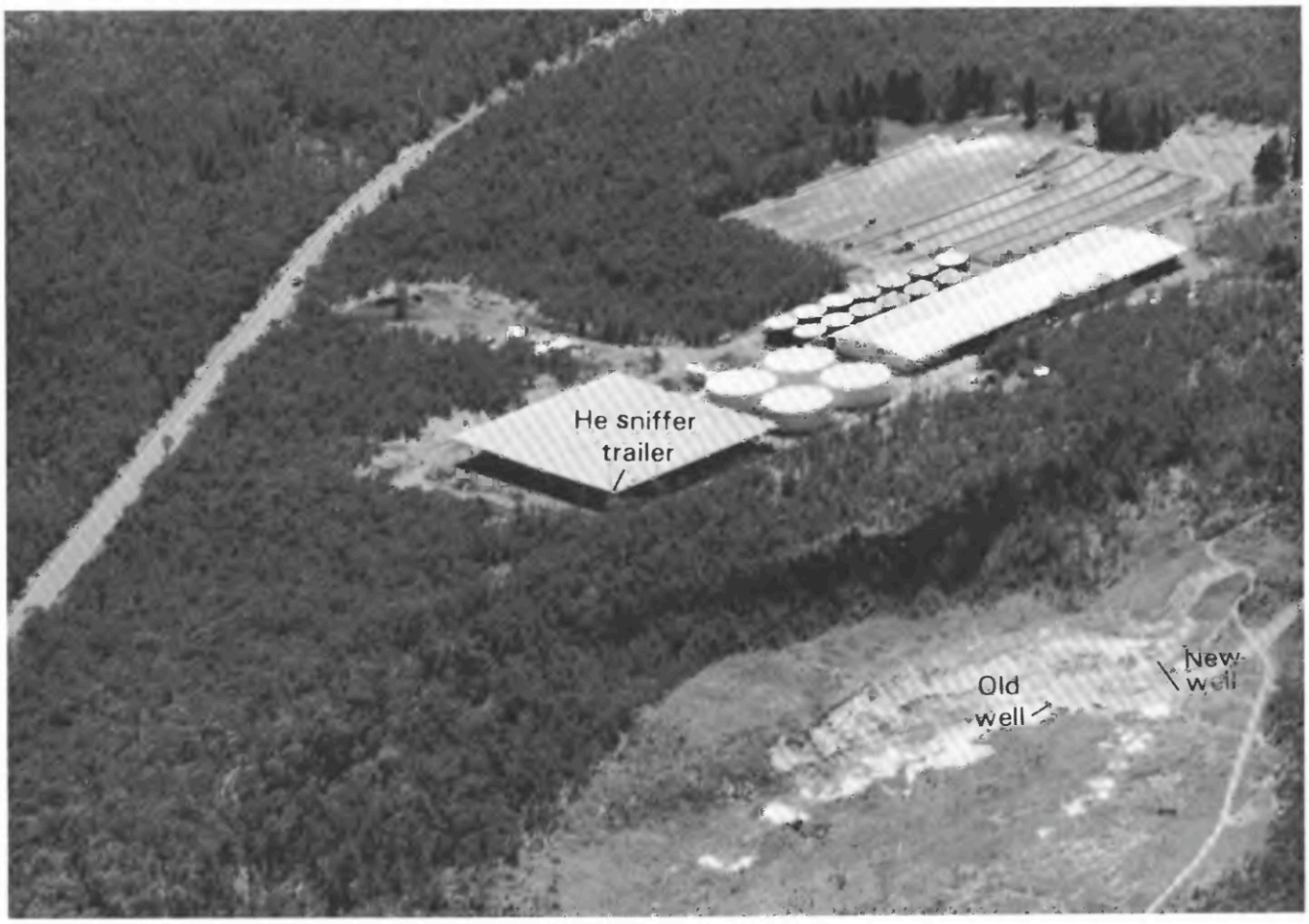

FIGURE 33.3.—Aerial view of Sulphur Bank area, Kilauea Volcano, showing location of old and new gas wells and of trailer containing helium sniffer (under corner of rain shed).

A small vacuum pump continuously pumped the well at about 100 mL/min. In order to remove water vapor that was not removed by the copper condenser pipe at the well site, the gas was passed through a silica-gel trap before entering the mass spectrometer sampling system.

At regular intervals (hourly at first, later changed to every 3 hours) the valve was opened automatically to admit a sample into the helium spectrometer for analysis. Immediately before and after each sample analysis, an aliquot of standard gas was analyzed, and after the second standard, a sample of ambient air was also analyzed. The results of these analyses were recorded on analog charts, an example of which is shown in figure 33.4.

Besides this automated mode of operation, it was possible to manually inject samples and compare the results to those for the standard gas. Approximately once a day, a sample of gas was collected manually at the wellhead by a sidehole hypodermic needle through a rubber septum; it was then analyzed manually on the automated instrument. These manually collected samples were used as a check on the operation of the automated system. In general, results from the two types of samples agreed within experimental error (± 50 ppb).

For a time, until the failure of the western GOES satellite, we were able to telemeter the results of the analysis via satellite to Wallops Island, Virginia and by land-line to Denver.

RESULTS

The helium concentrations in the samples show both short-term and long-term changes, as well as one abrupt change that preceded the January 1983 east-rift-zone eruption (fig. 33.5). From August 1982 through December 1983. the helium content decreased from about 11 ppm to 8 ppm. The helium content then rose again from about 8 ppm in mid-January 1984, to 16 ppm in mid-July 1984 at which time the instrument was decommissioned. An abrupt decrease occurred during December 21–28, 1982, coinciding with a hydrogen-gas increase noted on Kilauea (McGee and others, 1984) and preceding the January 1983 eruption.

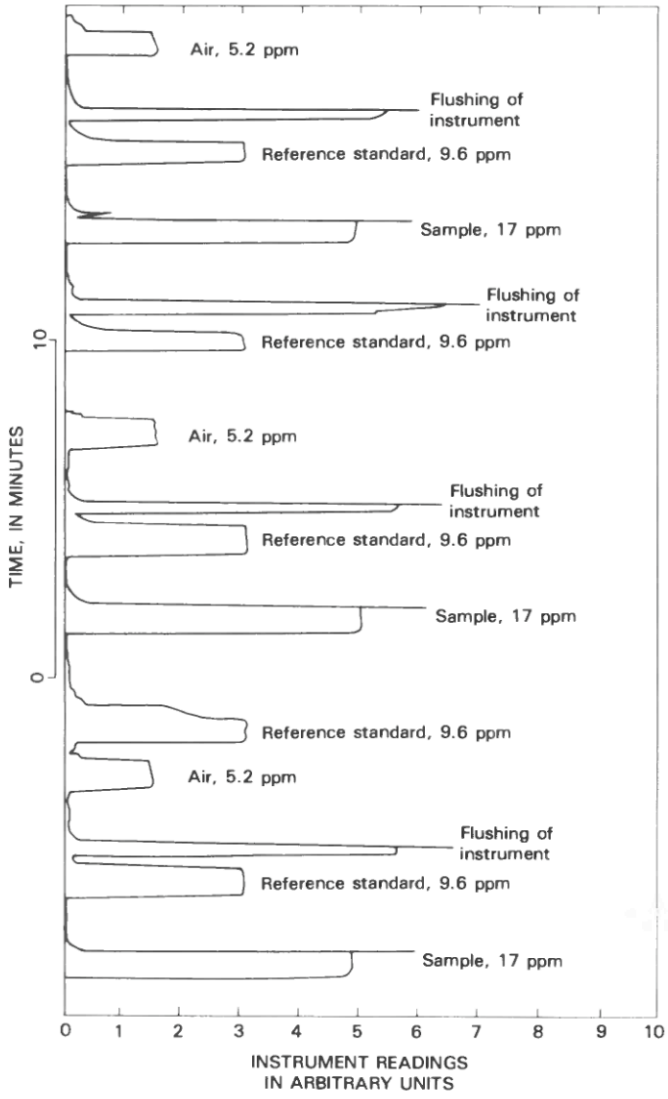

FIGURE 33.4.—Example of segment of instrument chart from the helium sniffer at Sulphur Bank, showing a typical helium analysis.

Other large and abrupt changes in helium abundance have been observed for which there is no obvious correlation with eruptive or meteorological events. If there is a link between the gas events and the east-rift-zone eruptions, we suspect that a change in the pressure regime of the magma source feeding the eruption should have been sufficient to be seen throughout the caldera.

Although the installation was automatic, it required weekly maintenance of the filters and occasional servicing of the mass spectrometer. Because the project investigators resided in Denver and could only visit the field site periodically, suitable personnel were not continuously available near the site, and even the usual teething problems required a long time to solve. These difficulties finally led us to abandon the effort and to substitute daily manual sample collection, the samples being mailed to Denver for analysis.

CONCLUSIONS

The map of helium abundance in soil gas at Sulphur Bank (fig. 33.1) shows a high concentration of helium in the vicinity of the old experimental well drilled in the 1920's.

Although helium abundance in the gases emitted from the newly drilled well vary with time (fig. 33.5), we were not able to correlate these variations conclusively with eruptive events during the two years in which we have collected data. A longer term record would be desirable, and this is now being collected.

REFERENCES

Friedman, I., Jurceka, J., Doering, W., Long, W., and McNair, D., in press, An automated helium analysis station. U.S. Geological Survey Professional Paper.

McGee, K.A., Sutton, A.J., and Sato, M., 1984, Observations of hydrogen gas events prior to volcanic seismicity [abs.]: International Chemical Congress of Pacific Basin Societies, American Chemical Society, Honolulu, December 16–21, 1984.

Thomas, D.M., and Naughton, J.J., 1979, Helium/carbon dioxide ratios as premonitors of volcanic activity: Science, v. 204, p. 1195–1196.

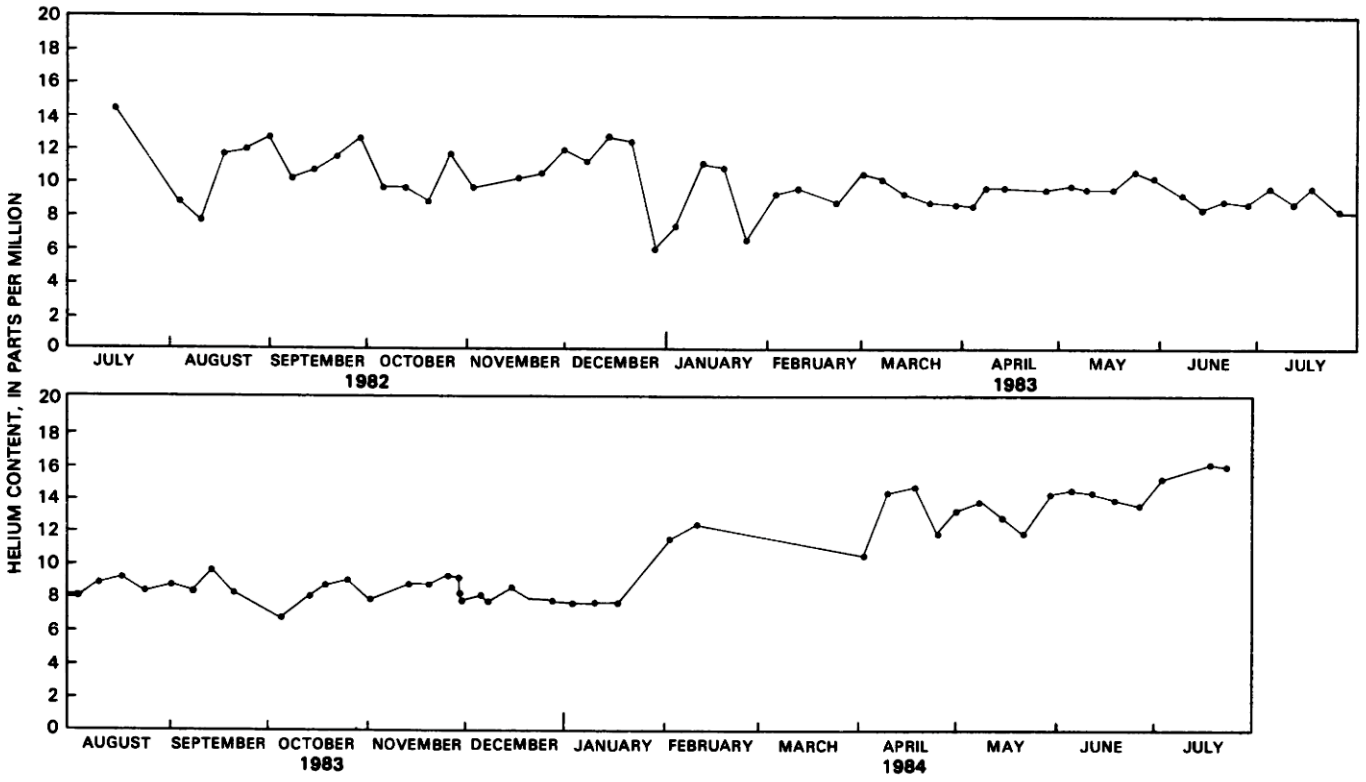

FIGURE 33.5.—Variation of helium abundance in soil gas at Sulphur Bank, Kilauea Volcano, from July 1982 to July 1984. All readings on samples from new gas well.

HELIUM AT KILAUEA VOLCANO

Part II
Distribution in the Summit Region

By G. Michael Reimer

ABSTRACT

A helium soil-gas survey was performed in the summit region of Kilauea Volcano, Hawaii. The average concentration found was about 5,250 parts per billion, only a little in excess of the atmospheric concentration of 5,240 parts per billion. High helium concentrations are not always associated with steaming areas which are most likely responding to meteoric water reacting with hot subsurface rocks. One anomalous area at Sulphur Bank and Steaming Bluff contained over 8,000 parts per billion helium and is interpreted as originating from at least as deep as the Kilauea magma reservoir and possibly from a mantle source. The anomalous Sulphur Bank area and a few higher than average helium concentrations at the village of Volcano occur along strike of the southwest rift zone and may be indicative of a northeast extension of that rift zone across Kilauea caldera. If the areal extent of the helium anomaly and the flux rate could be determined, it would be possible to estimate the mantle helium concentration at Kilauea.

INTRODUCTION

The helium-4 isotope is produced by the natural alpha-particle radioactive decay of uranium and thorium. On a gross scale, its distribution in the earth is controlled by the presence and concentration of the parent generating material, various trapping mechanisms, pathways for migration, and the primordial distribution. Primordial helium is characterized by high concentrations of the helium-3 isotope such that it may be on the order of 10^5 times more abundant (as in chondrites) than in minerals containing mostly radiogenically produced helium. The data in this paper refer only to helium-4 unless otherwise noted.

Helium has unique chemical and physical properties that make it an excellent gas for use in geochemical surveys. It is chemically inert, biogenically neither produced nor consumed, radioactively stable, highly diffusive, and has a low solubility in water. These characteristics provide helium with some advantages over other gases commonly used in surveys such as radon, which has a 3.8 day half-life, or methane and carbon dioxide, which can be involved in biological reactions.

Most helium soil-gas analyses have been performed as a geochemical guide in the search for oil and gas or uranium energy resources (Dyck, 1976; Reimer and others, 1979; Roberts, 1981). Several studies have shown the usefulness of helium in locating, tracing the extent of, or generally characterizing hot-water geothermal occurrences (Roberts and others, 1975; McCarthy and others, 1982; Baldi and others, 1984). An interesting observation from many of the energy-related studies has been that there is frequently unequivocal control of helium concentrations by geologic structure, such as faulting or jointing (Reimer and Adkisson, 1977; Jones and Drozd, 1983). This observation is presently being explored for potential applications in tracing faults or monitoring faults for helium variations that may be precursory to seismic activity (Reimer, 1980).

Very few helium soil-gas studies have been performed in volcanic areas. Hinkle (1978) performed a limited survey at the Puhimau Steaming Area on Kilauea. Friedman (chapter 33, part I) performed a survey at Sulphur Bank on Kilauea in 1978 preparatory to establishing an automated helium analyzer near the site. Hinkle and Kilburn (1980) and Green (1984) performed field surveys at the Long Valley caldera, California. A change in the helium distribution occurred there in the 4 years separating those two surveys, and the change is speculatively thought to be related to subsurface movement of magma and concomitant degassing within the system. Lombardi and others (1984) performed surveys at the Phlegraean Fields near Pozzuoli, Italy, in July and September 1983 and recorded a pronounced change in the helium distribution. The change is thought to be the effect of an increase of earthquakes which released 10 times the strain as in previous months and possibly reopened older fissures and fractures.

This study presents the results of a systematic survey of the helium soil-gas distribution at the Kilauea summit. It will provide a data base for future studies that will be especially important if the dramatic changes observed by Lombardi at Pozzuoli are characteristic precursors of seismic or eruptive events. In addition, this study will augment the data obtained by Cox (1983) on the soil content of radon and mercury at Kilauea. Various volatile species have their own unique chemical and physical properties; when considered collectively, they provide a better insight into the mechanisms controlling surface distribution and concentration of the gases.

ACKNOWLEDGMENTS

I thank Trevor Jackson and Barry Stokes for assistance with the sample collection and Josh Been and Don Murrey for help with the analyses.

STUDY AREA AND SAMPLING METHODS

This helium soil-gas survey was conducted in the vicinity of the summit of Kilauea Volcano on the Island of Hawaii. At the time of the survey in December 1984, eruptive activity on the east rift zone, which commenced in January 1983, was in the post-phase 28 interim. Kilauea has formed primarily from the extrusion of tholeiitic basalts and ash. Subsurface magma intrusion and movement contribute to the formation of the numerous and complex fault zones in the area, and the prominent Kilauea caldera and Halemaumau crater were formed by subsidence. Several of the fracture systems give rise to large steaming areas such as those at the northeast edge of the Kilauea caldera and at Sulphur Banks 0.6 km farther northeast. Numerous other vents from smaller areas of fractures and cracks produce gas, the bulk of which is water but containing varying amounts of other trace gases such as CO_2, SO_2, and He (Gerlach, 1980; Greenland, 1984).

There is a diversity in soil type and ground cover around Kilauea. The areas north and east of the caldera have well-developed soils capable of supporting tropical vegetation; the areas south and west have poorly developed or non-existing soils and are covered by historical lava flows, ash, and cinders.

Soil gas is that gas accumulated within the soil pores and is in quasi-equilibrium with the soil moisture. The gas is mobile to an extent controlled principally by the soil permeability, and represents a time-integrated sample, the period of which is also controlled by mobility. Mobility, in turn, especially in near-surface samples, is strongly influenced by external meteorological factors. Precipitation can provide water that decreases permeability; temperature differences can create convective pumping effects; wind-speed variations can create venturi pumping effects. Soil gases reside in a dynamic environment but the gas concentration variations induced in the environment are not so great that they limit the usefulness of the method (Reimer, 1980).

In this study, soil gases were collected by pounding an 8-mm-diameter hollow steel probe into the soil to a depth of 0.5 m. A septum-containing cap was placed on the probe to create an air-tight seal, and the gas was slowly withdrawn through the system by a hypodermic syringe. The probe nominally contains a dead volume of 2 cm^3 and was first purged by withdrawing and discarding 5 cm^3, of gas. A sample of 15–20 cm^3 was then withdrawn into the syringe and transferred to a pre-evacuated stainless steel container of 6-cm^3 internal volume for shipment to the laboratory for analysis. The container is overpressurized with sample and sealed with a single valve on one end with a septum in series through which the sample was injected. Soil-gas samples collected by the probe method commonly are taken from a depth of 0.75 or 1.0 m. This depth represents a compromise between ease of sampling and reduction of variation from meteorological conditions (Reimer, 1980). However, meteorology is usually a factor when a survey takes several days to perform. Because of the variation in soil depth at the Kilauea summit a sample depth of 0.5 m was chosen to permit uniformity. All samples were collected in a 9-hour daylight period on December 11, and the weather conditions at the summit were extremely consistent throughout the sampling: clear to partly cloudy, trade winds 15–30 km/h, temperature 17–22 °C, and no precipitation. The good fortune of uniform weather minimized site-to-site variation in the samples taken at the 0.5-m depth.

Samples were analyzed using a small leak-detector mass spectrometer tuned specifically for the helium mass-to-charge ratio of 4+. The minor modifications to this type of instrument, commercially used for testing leaks in vacuum systems, to allow it to be used for high precision analytical work are described by Reimer and others (1979). Analytical precision for helium is ±10 parts per billion (10 in 10^9). The atmosphere nominally contains 5,240 parts per billion helium and is a remarkably constant reservoir (Glueckauf, 1949; Oliver and others, 1984). Samples are withdrawn from the stainless steel cylinders by inserting a hypodermic needle through the septum and opening the valve. The syringe rebounds in response to the overpressure in the cylinder. Knowing the amount of sample injected into the cylinder and the amount of rebound during extraction, a gross check on the integrity of the cylinder is obtained. Samples with rebounds not within 1 cm^3 of that anticipated are rejected. The sample is injected into the spectrometer inlet system, where gases other than helium and neon are removed on activated charcoal at liquid-nitrogen temperatures. The sensitivity of the spectrometer is determined every 10 samples by analyzing two reference gases containing different helium concentrations, and each unknown sample is bracketed by two reference analyses. From the calibrated instrument sensitivity and the difference in peak height for the sample-standard combination, the concentration of helium in the sample is determined.

DATA AND DISCUSSION

The area of the survey and location of sample collection points are shown in figure 33.6. This area is roughly equivalent to that sampled by Cox (1983) for radon and mercury, but the exact stations were not reoccupied. A total of 93 soil-gas samples were collected and analyzed. The distribution of the helium concentration was fairly uniform, with only three samples from Sulphur Bank and Steaming Bluff being anomalously high. The average helium concentration, excluding the 3 high values, is 5,248 ± 23 ppb, which is about that of the nominal atmospheric concentration. Table 33.1 presents the helium concentrations of the samples keyed to figure 33.6. The ΔHe is the difference in helium from the atmospheric concentration. Concentrations of soil-gas helium less than the atmospheric content are the result of dilution by other gases such as carbon dioxide or water vapor. Concentrations of helium greater than atmospheric content result when a subsurface source is present. Overall, the helium concentration throughout the Kilauea summit

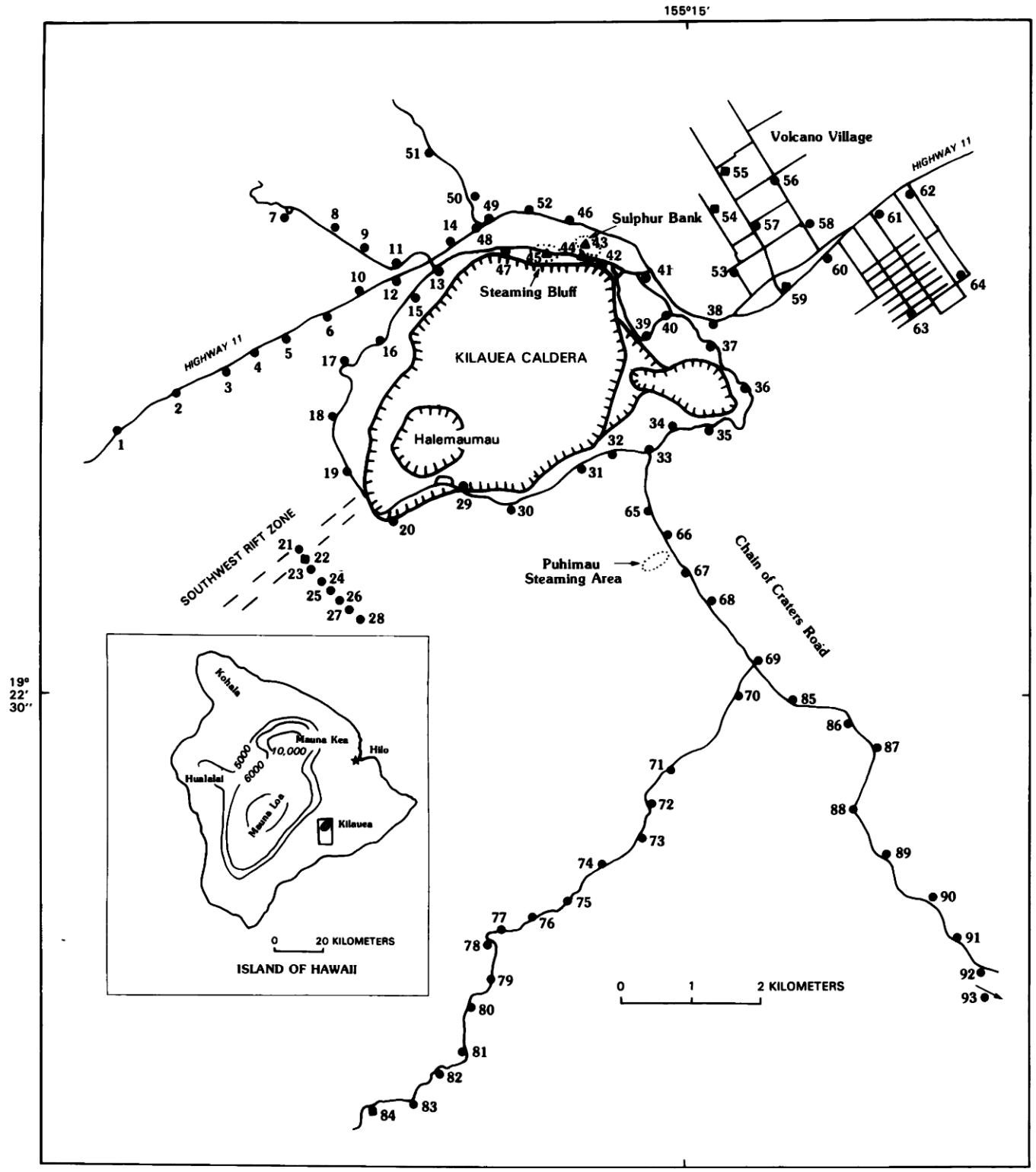

FIGURE 33.6.—Summit region of Kilauea Volcano, Hawaii, showing sampling sites for survey of helium in soil gas. Dots, samples yielding average helium concentrations; squares, slightly higher helium concentrations (greater than two standard deviations from that of air); triangles, the anomalously high concentrations at Sulphur Bank and Steaming Bluff. Sample numbers keyed to table 33.1. Hachures indicate infacing scarps of caldera and craters.

TABLE 33.1.—*Helium concentrations in soil-gas samples from Kilauea Volcano, Hawaii*

[All samples collected December 11, 1984; sample locations shown in figure 33.6. Δ helium is the difference in the helium concentration between the sample and the air reference at 5240 ppb. N.A. for sample 8 means it was not analyzed because of obvious leakage of the sample cylinder. The precision of the analyses was ±10 ppb helium; the reported concentrations are those determined by the signal processing computer and do not imply greater precision]

Sample number	Helium (ppb)	Δ helium (ppb)	Sample number	Helium (ppb)	Δ helium (ppb)	Sample number	Helium (ppb)	Δ helium (ppb)
1	5244	4	32	5261	9	63	5229	−11
2	5239	−1	33	5226	−14	64	5257	17
3	5222	−18	34	5250	10	65	5265	25
4	5240	0	35	5260	20	66	5224	25
5	5254	14	36	5248	8	67	5226	−14
6	5268	28	37	5227	−13	68	5251	11
7	5252	12	38	5200	−40	69	5233	−7
8	N.A.	N.A.	39	5245	5	70	5233	−7
9	5265	25	40	5217	−23	71	5253	13
10	5255	15	41	5261	21	72	5260	20
11	5238	−2	42	5229	−11	73	5259	19
12	5265	25	43	8084	2844	74	5211	−29
13	5250	10	44	8774	3534	75	5215	−25
14	5265	25	45	5712	472	76	5249	9
15	5249	9	46	5252	12	77	5249	9
16	5270	30	47	5227	−13	78	5295	−45
17	5246	6	48	5241	1	79	5277	37
18	5248	8	49	5277	37	80	5265	25
19	5230	−10	50	5262	22	81	5294	54
20	5224	−16	51	5232	−8	82	5263	23
21	5252	12	52	5253	13	83	5284	44
22	5257	67	53	5243	3	84	5295	55
23	5245	5	54	5294	54	85	5248	8
24	5262	22	55	5309	69	86	5228	−12
25	5247	7	56	5270	30	87	5241	1
26	5248	8	57	5263	23	88	5235	−5
27	5227	−13	58	5236	−4	89	5270	30
28	5252	12	59	5296	56	90	5219	−21
29	5223	−17	60	5236	−4	91	5218	−22
30	5241	1	61	5267	27	92	5215	−25
31	5249	9	62	5265	25	93	5277	37

area is similar to that found in other regional surveys such as those in the Powder River Basin of Wyoming (Reimer and others, 1980) and the Basin and Range Province of Utah and Nevada (Reimer and Bowles, 1983). This observation is consistent with the fact that there are no high concentrations of uranium or thorium contributing to a high helium background at Kilauea.

The helium concentration of Sulphur Bank and Steaming Bluff is quite anomalous, in excess of 8,000 ppb for some samples. This is the area in which Cox (1983) reported the highest radon concentrations from his survey. The high helium and radon concentrations are typical of areas where there is a surface manifestation of hot spring activity (Roberts and others, 1975; McCarthy and others, 1982; Baldi and others, 1984). The high concentrations of radiogenic byproducts from hot springs, however, may be the result of local concentrations of uranium daughter isotopes, notably radium in precipitates. Samples collected in the vicinity of the Puhimau Steaming Area did not show similarly anomalous helium or radon concentrations. The steaming activity at Puhimau is attributable to meteoric water contacting the residual heat of the 1938(?) intrusion in that area. In neither area, Puhimau nor Steaming Bluff and Sulphur Bank, is there a known, near-surface concentration of helium-producing daughter isotopes. It is inferred, therefore, that there is a large helium component to the gases venting on the northeast side of the Kilauea caldera. Helium-3/helium-4 ratios have indicated that the helium component is derived in large part from the mantle (Craig and others, 1978). Steaming areas alone do not necessarily imply gas supply from a deep source. If the areal extent of the helium anomaly and the flux rate through the soil could be determined by future studies, the volume of mantle-derived helium could be determined from Kilauea alone and compared to the total Earth values derived by Naughton and others (1973), who used helium/carbon ratios. In contrast to the earlier view of Macdonald and Abbott (1977), these recent helium data support the idea of connection of Sulphur Bank gases to a magma source, most likely that feeding Kilauea.

Another area at the Kilauea summit with slightly higher helium concentrations is within the village of Volcano. The values are not exceptionally high, only 50 to 70 ppb above the atmospheric concentration, but they are interesting because they occur in an area of low radon concentrations (Cox, 1983).

Cox interprets the low radon concentrations to represent either low permeability of strata or downflow of gas in that vicinity. For the helium, the similarity of soils in the area (U.S. Dept. of Agriculture, 1973) tends to rule out permeability differences very near the surface or at the sampling depth, and the positive values are not representative of inhalation. I suggest that this region may be an extension of the area receiving mantle-derived helium because of the proximity to Sulphur Bank, only 2.5 km southwest. Alternatively, these higher concentrations, with those at Steaming Bluff and Sulphur Bank, could be indicative of a northeast extension of the

southwest rift zone. They all occur along the strike of the rift across the caldera. A more detailed survey could indicate if the areas might be linked.

CONCLUSIONS

The reconnaissance helium soil-gas survey at the summit of Kilauea Volcano has indicated only one broad area of high helium concentration. That area, comprising Sulphur Bank and Steaming Bluff on the northeast side of the caldera, had soil-gas helium concentrations greater than 8,000 ppb. Thermally induced concentration and release of helium is typical in areas where the host rock can provide the uranium or thorium alpha-particle-producing daughters that ultimately produce the helium. At Kilauea, the character of the host rock and its young age generally preclude the concentrating of uranium and thorium (Newman and others, 1984). The high bulk helium concentration is thought, therefore, to be the result of a mantle-derived source. It may be possible with future studies to estimate the amount of helium contributed from the mantle at Kilauea, or at least set limits on the amount. In addition, the helium soil-gas technique may be useful in finding areas in which the mantle helium is being degassed at the surface and distinguishing those areas from the ordinary thermal steaming areas. It would be a particularly helpful method to locate areas not marked by surface fracture systems where gases in magma reservoirs have the most permeable pathway to the surface.

REFERENCES CITED

Baldi, P., Ceccarelli, A., Bertrami, R., Friedman, I., and Lombardi, S., 1984, Helium in soil gases in geothermal areas: Seminar on the utilization of geothermal energy for electric power production and space heating, Florence, Italy, May 14–17, 1984, United Nations Economic Commission, EP/SEM.9/R.10, 12 p.

Cox, M.E., 1983, Summit outgassing as indicated by radon, mercury, and pH mapping, Kilauea Volcano, Hawaii: Journal of Volcanology and Geothermal Research, v. 16, p. 131–151.

Craig, H., Lupton, J.E., and Horibe, Y., 1978, A mantle helium component in circum-Pacific volcanic gases: Hakone, the Marianas, and Mt. Lassen, *in* Alexander, E.C., and Ozima, M., eds., Terrestrial Rare Gases: Tokyo, Japan Scientific Societies Press, Advances in Earth and Planetary Sciences, v. 3, p. 3–16.

Dyck, Willy, 1976, The use of helium in mineral exploration: Journal of Geochemical Exploration, v. 5, p. 3–20.

Gerlach, T.M., 1980, Evaluation of volcanic gas analyses from Kilauea Volcano: Journal of Volcanology and Geothermal Research, v. 7. 295–317.

Glueckauf, E., 194 A micro-analysis of the helium and neon contents of air: Proceedings of the Royal Society of London, v. 185, p. 98–119.

Green, K.R., 1984, An algorithm for determining soil and water helium concentrations from headspace analyses: Examples of geochemical applications in Long Valley, California, and the Fiji Islands: Golden, Colorado, Colorado School of Mines, Master's thesis, 197 p.

Greenland, L.P., 1984, Gas composition of the January, 1983, eruption of Kilauea Volcano, Hawaii: Geochimica et Cosmochimica Acta, v. 48, p. 193–196.

Hinkle, M.E., 1978, Helium, mercury, sulphur compounds, and carbon dioxide in soil gases of the Puhimau Thermal Area, Hawaii Volcanoes National Park, Hawaii: U.S. Geological Survey Open-File Report 78–246, 14 p.

Hinkle, M.E., and Kilburn, J.E., 1980, Survey of helium in soil gases of Long Valley, California: U.S. Geological Survey Open-File Report 80–612, 19 p.

Jones, V.T., and Drozd, R.J., 1983, Predictions of oil or gas potential by near-surface geochemistry: American Association of Petroleum Geologists Bulletin, v. 67. p. 932–952.

Lombardi, S., DiFilippo, M., and Zantedeschi, L., 1984, Helium in Phlegraean Fields soil gases: July 20–26, September 19–25. 1983: Bulletin Volcanologique, v. 47-2, p. 259–265.

Macdonald, G.A., and Abbott, A.T., 1977, Volcanoes in the sea: Honolulu, Hawaii, University of Hawaii Press, 441 p.

McCarthy, K.P., Been, J.M., Reimer, G.M., Bowles, C.G., and Murrey, D.G., 1982, Helium and ground temperature surveys at Steamboat Springs, Colorado: Denver, Colorado, Colorado Geological Survey, Special Publication 21, 11 p.

Naughton, J.J., Lee, J.H., Keeling, D., Finlayson, J.B., and Dority, G., 1973, Helium flux from the Earth's mantle as estimated from Hawaiian fumarolic degassing: Science, v. 180, p. 55–57.

Newman, S., Finkel, R.C., Macdougall, J.D., 1984, Comparison of ^{230}Th–^{238}U disequilibrium systematics in lavas from three hot spot regions: Hawaii, Prince Edward and Samoa: Geochimica et Cosmochimica Acta, v. 48, p. 315–324.

Oliver, B.M., Bradley, J.G., and Farrar, Harry, 1984, Helium concentration in the Earth's lower atmosphere: Geochimica et Cosmochimica Acta, v. 48, p. 1759–1768.

Reimer, G.M., 1980, Use of soil-gas helium concentrations for earthquake prediction: limitations imposed by diurnal variations: Journal of Geophysical Research, v. 85, p. 3107–3114.

Reimer, G.M., and Adkisson, C.W., 1977, Reconnaissance survey of the helium content of soil gas in Black Hawk, Eldorado Springs, Evergreen, Golden, Morrison, Ralston Buttes and Squaw Pass quadrangles, Colorado: U.S. Geological Survey Open-File Report 77–464, 10 p.

Reimer, G.M., and Bowles, C.G., 1983. Helium concentration in soil-gas of the Ely and Delta 1° by 2° quadrangles, Basin and Range Province: U.S. Geological Survey Open-File Report 83–589, 26 p.

Reimer, G.M., Denton, E.H., Friedman, Irving, and Otton, J.K., 1979, Recent developments in uranium exploration using the U.S. Geological Survey's mobile helium detector: Journal of Geochemical Exploration, v. 11, p. 1–12.

Reimer, G.M., Murrey, D.G., and Been, J.M., 1980, Helium soil-gas concentrations in the Torrington, Newcastle, Gillette, and Ekalaka 1° x 2° quadrangles: Data from a reconnaissance survey: U.S. Geological Survey Open-File Report 80–452, 14 p.

Roberts, A.A., 1981, Helium emanometry in exploration for hydrocarbons II, *in* Gottlieb, B.M., ed., Unconventional methods for exploration for petroleum and natural gas: Dallas, Texas, Southern Methodist University Press, p. 136–149.

Roberts, A.A., Friedman, I., Donovan, T.J., and Denton, E.H., 1975, Helium survey, a possible technique for locating geothermal reservoirs: Geophysical Research Letters, v. 2, p. 209–210.

U.S. Department of Agriculture, 1973, Soil survey of the Island of Hawaii, State of Hawaii: Washington, D.C., Soil Conservation Service, U.S. Department of Agriculture, 115 p., 195 plates.

USE OF SATELLITE TELEMETRY FOR MONITORING ACTIVE VOLCANOES, WITH A CASE STUDY OF A GAS-EMISSION EVENT AT KILAUEA VOLCANO, DECEMBER 1982

By Kenneth A. McGee, A. Jefferson Sutton, *and* Motoaki Sato

ABSTRACT

A telemetry system using geostationary satellites for data relay has several advantages over ground-based systems that are widely used as a means for relaying geophysical and geochemical data from volcanoes. The National Oceanic and Atmospheric Administration's NESDIS (National Environmental Satellite, Data, and Information Service) maintains two operating Geostationary Operational Environmental Satellites (GOES) to monitor the Earth's weather systems. These satellites are part of a worldwide network of meteorological satellites, and each is equipped to relay data transmissions from networks of data-collection platforms. A degassing event at Kilauea Volcano in December 1982, observed and recorded some 9,000 km away, is cited as an example of how satellite telemetry can be a viable alternative for monitoring potentially active volcanoes.

INTRODUCTION

Radio telemetry is widely used as a means for relaying geophysical and geochemical data from active volcanoes to observatories or other data-collection centers. Most existing telemetry networks are ground based and are constrained by topographic conditions. In order to extend the range of the telemetry, repeater stations may be installed or telephone lines leased. However, the cost of maintaining these systems adds substantially to the total cost of the operation. Moreover, the complexity of the system increases and the flow of data becomes more vulnerable to equipment failure as more links are added to the data-relay chain.

A telemetry system using geostationary satellites for data relay has advantages over ground-based systems (McGee and Sato, 1982). The need for repeaters, multiple telemetry links, and dedicated telephone lines is eliminated. Although the initial cost of the transmitters may be higher, the elimination of repeater stations and leased telephone lines reduces the operational costs and, more importantly, extends the potential useful range to thousands of kilometers. Since the telemetry antennas must be pointed skyward at a high angle (30° to 60° depending on latitude), the elevation and local topography of the monitoring site become less important. Also, because satellite-relayed telemetry systems operate at higher radio frequencies than typical ground-based systems they have shorter antenna element lengths and fewer interference problems. Smaller antenna systems in turn reduce the vulnerability of monitoring sites to damage from wind or ice. Finally, a telemetry system using geostationary satellites for data relay allows more than one observatory or laboratory to collect data from volcanoes scattered across continents or oceans.

DESCRIPTION OF A SATELLITE DATA-COLLECTION SYSTEM

The National Oceanic and Atmospheric Administration's NESDIS (National Environmental Satellite, Data, and Information Service) operates a series of Geostationary Operational Environmental Satellites (GOES) to image and monitor the Earth's cloud cover and weather systems (National Oceanic and Atmospheric Administration, 1983). These satellites, placed in orbits coincident with the Earth's equatorial plane at an altitude of about 35,500 km, rotate at the same speed as the Earth and appear from the Earth to be in a fixed position. Unlike earlier polar-orbiting satellites, these geostationary or geosynchronous satellites, which are part of a worldwide network of meteorological satellites, have nearly a full hemisphere of continuous view (fig. 34.1). NESDIS maintains operational satellites at 75° and 135° west longitudes. One or more older satellites, located about midway between these two operational sites, are used if one of the primary satellites fails. These in-orbit spares can be turned on and moved to the operational location to provide continuity of coverage.

Each of the satellites is equipped to relay data transmissions from networks of data-collection platforms to one or more receiving sites. The onboard instrumentation that performs the relay function is a satellite transponder, which is a combination radio receiver and transmitter that receives data and instantaneously retransmits it back to Earth with no change except for frequency. Each of the two NESDIS satellites can relay environmental data from as many as several thousand individual data-gathering devices located at virtually any point in the Western Hemisphere. Likewise, the large beam width of the satellite transmitter antenna permits reception of the signal from the satellites over the same wide area.

In addition to the spacecraft itself, a satellite data-collection system is made up of four major parts: (1) sensors; (2) data-collection platforms; (3) Earth receiving stations; and (4) a data processing and storage system (fig. 34.2). Because NESDIS operates a central Earth Receiving Station, the user need only

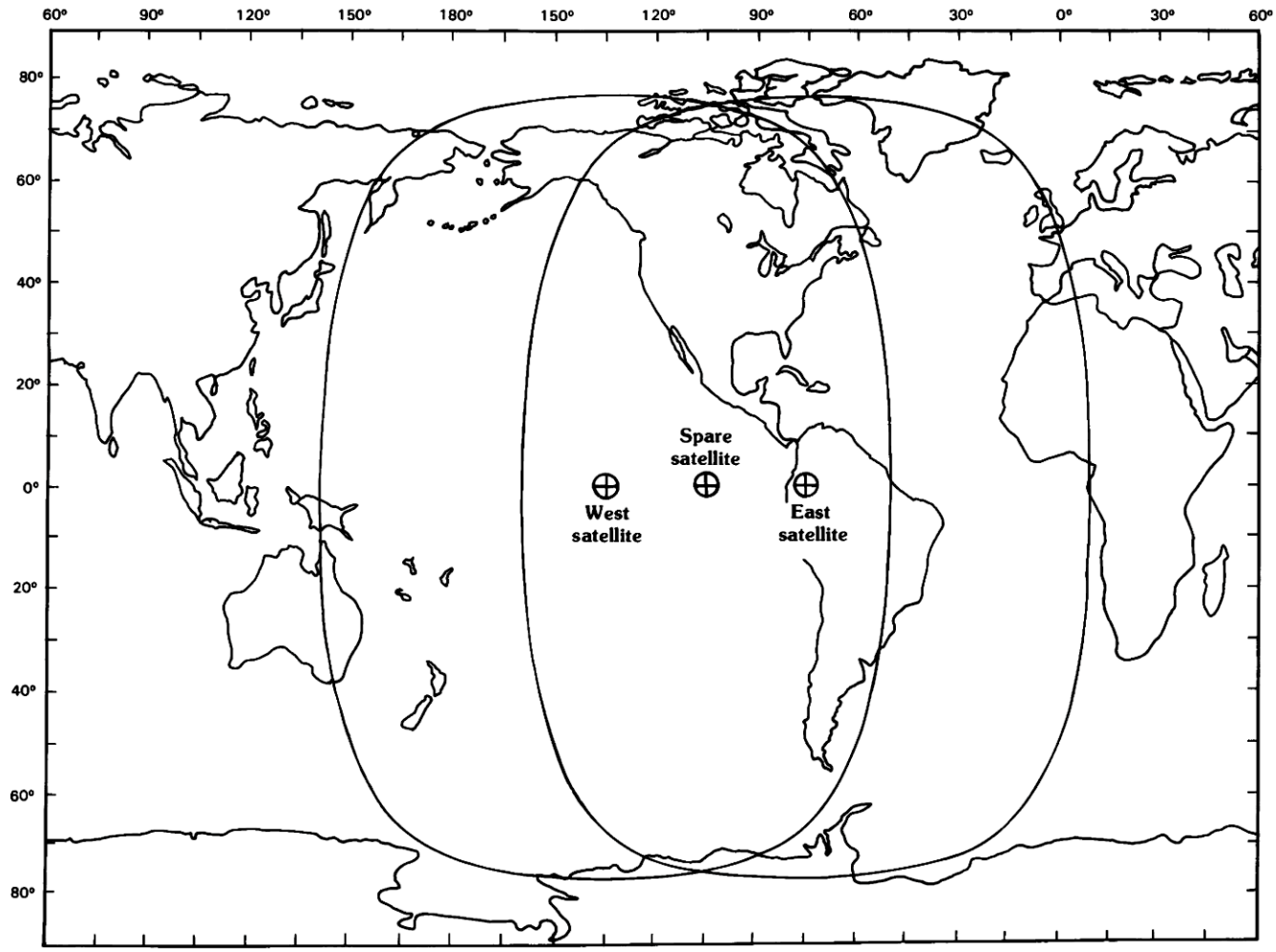

FIGURE 34.1.—Areal coverage of the Earth's surface by geostationary satellites located at long 75° and 135° W. (from National Oceanic and Atmospheric Administration, 1983, fig. 1–2, p. 4).

supply the remaining three parts. In a minimum network configuration (1–20 monitoring sites), the user provides only the sensors, data-collection platforms, and some sort of data processing and storage system. As the number of monitoring sites increases, it may be beneficial to acquire a direct-readout ground receiving station.

The GOES system is particularly suited to monitoring slowly varying parameters. In a volcanic region, parameters of interest may include tilt, magnetic field strength, self-potential, gas emissions, fumarole temperatures, and meteorological data. In some instances, it is possible to transmit higher frequency data through the system if some onsite preprocessing is done. For example, seismicity, in the form of earthquake counts, can easily be accommodated. This might have particular application to remote volcanoes where recording the number of earthquakes may be more pertinent to assessing the level of activity than recording the actual waveforms. GOES data-collection platforms (DCP's) typically require sensors with analog voltage outputs in the range 0–5 V, although other output ranges and certain sensing devices with digital outputs can often be accommodated.

GOES DCP's are small, battery-powered, 402-megahertz radio transmitters that transmit data to the satellite at a rate of 100 bits per second (National Oceanic and Atmospheric Administration, 1984). Higher data rates are possible though not currently used. The major components of a DCP are the sensor interface, programmable microprocessor, memory, radio, clock, and antenna. Many GOES DCP's operate in the self-timed mode, which requires the platform periodically to transmit its data under the command of a precise timer. In this self-timed mode, the platform, under control of the timer and microprocessor, scans its sensor interface. A typical DCP sensor interface can accommodate as many as 16 sensors. Data from each scan may be stored in the memory of the DCP until the prescribed transmission interval. Some DCP's are capable of performing preliminary data manipulation including data conversion, averaging, slope computation, and warning-level assessment, for emergency transmissions. Reliable, environmentally hardened DCP's are commercially available from a number of sources. A complete site installation, exclusive of sensors, can be performed in less than four hours.

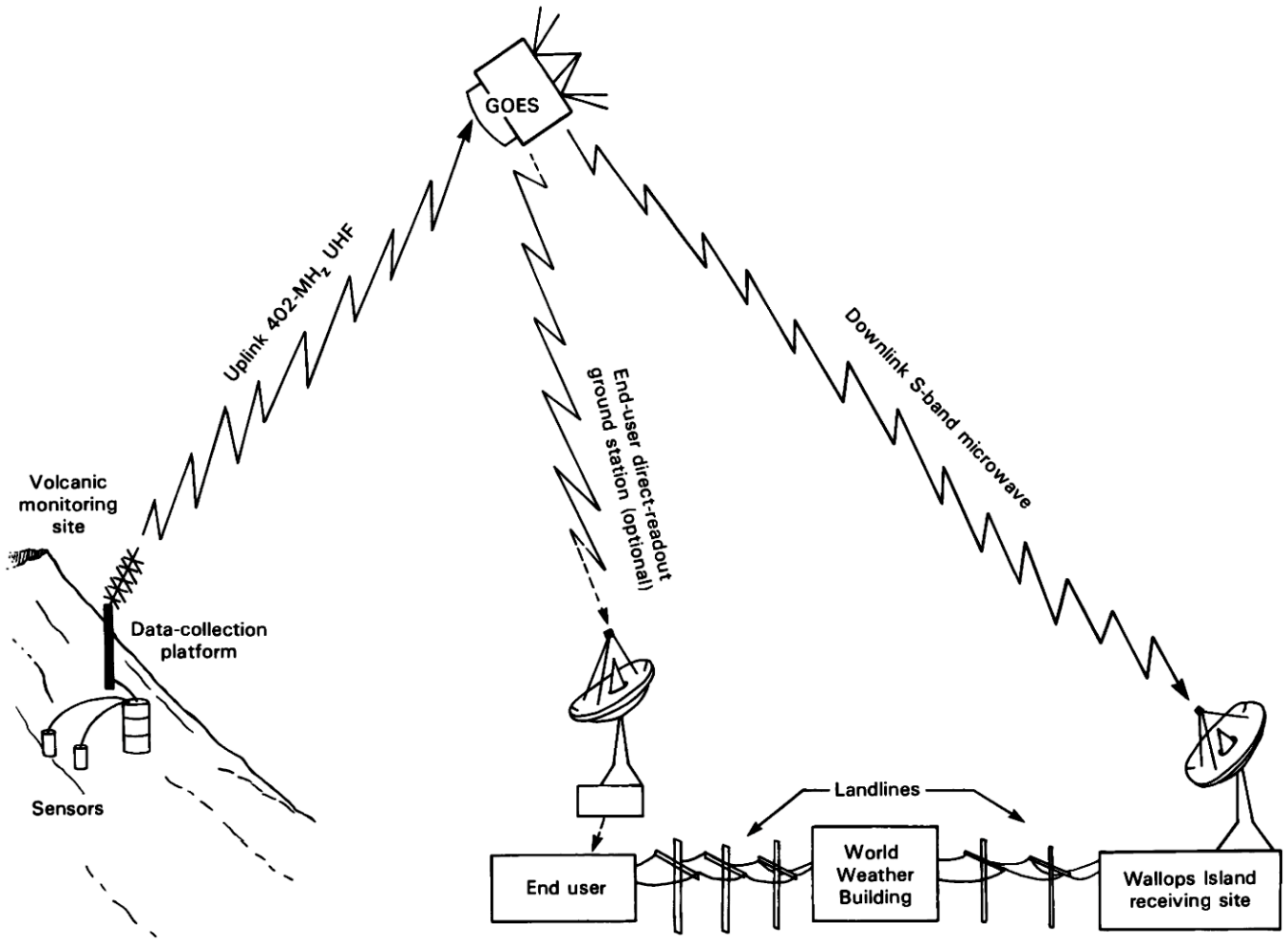

FIGURE 34.2.—Diagram of Geostationary Operational Environmental Satellite (GOES) data-flow path from remote site through satellite to end user.

Each satellite can support more than 250 radio channels, many of which are dedicated to self-timed platforms. The technique for defining the schedule of DCP reporting is called frequency-division multiple access with time-shared channel occupancy. A GOES platform typically uses a 1-min time interval every 3 h on its assigned radio channel for transmission of its data to the satellite. Sensor data can be collected as often as every 10 min and stored in memory until the prescribed transmission interval. Depending on the number of sensors and data points, transmission message lengths average about 30 s. In addition to self-timed transmission, two other modes of DCP transmission initiation are possible in the GOES system: (1) interrogation by the satellite, and (2) emergency transmission because of a predetermined sensor-threshold value being exceeded. The latter capability can be useful in providing warnings of imminent floods or mudflows.

NESDIS operates only one Earth receiving site, located at Wallops Island, Va., for the GOES satellite data-collection system. This receiving site performs a number of functions including command and control of the spacecraft, reception of data, and monitoring of signal quality. From the Wallops Island location, NESDIS forwards data from the satellites to a computer in the World Weather Building at Camp Springs, Md. From there, the data are distributed to users via the telephone system using either dedicated circuits or dial-in lines. Many users of the GOES system, in an effort to reduce system complexity and dependence on land lines, are establishing their own local direct-readout ground station terminals. These terminals are becoming less expensive and can provide a user with immediate access to the data transmitted from the satellite.

Because NESDIS does not store data in its computer for longer than a few days, it is necessary for the user to transfer the data regularly to his own computer system for processing and storage. Collecting data from one sensor at 10-min intervals produces more than 52,000 data points in a year. A network of several DCP's, each with several sensors, can thus produce a large data base. In addition, since the data are in numerical form, a mechanism for converting the data to graphical form for viewing is a must. Frequent visual inspection of the recorded data for significant sensor variations is necessary to take full advantage of the nearly real-time

nature of satellite-relayed telemetry. An optimum computer system for end users of the GOES system would include screen and hard-copy graphics capability and several megabytes of online data-storage capacity.

EXAMPLE OF A WIDE-AREA NETWORK FOR MONITORING VOLCANOES

The current U.S. Geological Survey network of volcanic-gas monitoring stations at several widely scattered volcanoes is an excellent example of a wide-area network using satellite telemetry. In the summer of 1981, satellite-relayed hydrogen-gas monitoring stations were installed at Mount Baker and Mount St. Helens, Wash., and Lassen Peak, Calif. Similar monitoring stations were installed in 1982, at Long Valley Caldera, Calif., and Kilauea, Hawaii, and in 1983 at Mauna Loa, Hawaii, and Coso Hot Springs, Calif. Until mid-1984, data from all of these stations were scrutinized and recorded at the U.S. Geological Survey National Center in Reston, Va. (more than 4,000 km from the nearest monitoring site). In June 1984, the responsibility for collecting data from these stations was transferred to the Cascades Volcano Observatory in Vancouver, Wash. This change of recording facility was completed without the necessity for a single visit to any field site and clearly demonstrates the extreme flexibility of a satellite-relayed telemetry system.

Although some of the field sites in the gas network are located near existing ground-based telemetry systems, many of the monitoring locations are in remote areas where there is no possibility of linking into a ground-based telemetry system or telephone line. That any data can be collected at all from these sites in nearly real-time fashion is a tremendous accomplishment. Clearly, the wide-area gas monitoring network owes its existence to the availability of satellite telemetry.

CASE STUDY—EVIDENCE FOR A WIDESPREAD GAS EVENT AT KILAUEA VOLCANO, DECEMBER 1982

Hydrogen gas sensors were strategically deployed in or near fumaroles at the Kilauea summit caldera ('71 Fissure and Halemaumau West), along the east rift zone (Mauna Ulu and Puu Kiai), and on the southwest rift zone (Kau Desert) in the late 1970's with conventional ground-based telemetry used at each site to transmit the data to the Hawaiian Volcano Observatory for recording (McGee, 1979). In mid-December 1982, a GOES satellite data-collection platform was interfaced with the receivers of the land-based telemetry system to produce an integrated telemetry system. Previous data acquisition involved the mailing of strip-chart recordings to a distant laboratory for analysis (months later). This marriage of ground-based and satellite telemetry allowed a wide area of Kilauea to be monitored using a single central DCP for data relay to the satellite.

On December 23, 1982, a degassing event was recorded at both Kilauea summit stations and at Mauna Ulu in the upper east rift zone (fig. 34.3). Although the distance between the summit monitoring sites and the Mauna Ulu site is about 8 km, the onset time and duration (2 days) of the gas event are essentially concurrent at the three locations. In addition, hydrogen sensors with on-site recording at two nearby locations, Puhimau and a different fumarole at Mauna Ulu, recorded similar peaks. On December 26, a distinct gas event that had rapid onset and lasted only a few hours was recorded at Puu Kiai. This event is noteworthy because it is the only hydrogen gas event ever recorded at that location. Puu Kiai is located about 13 km down the east rift zone from Mauna Ulu.

Other independent evidence also points to a widespread gas release during this time period. Friedman and Reimer (chapter 33, part I) report a distinct helium anomaly at Sulfur Bank in late December 1982. In addition, a substantial radon peak was observed near the western rim of Kilauea's caldera at about the same time (Donald Thomas, oral commun., 1984). It is likely that this widespread gas release was a precursory manifestation of the intrusion of a large body of magma into the Kilauea summit area. Subsequent injection of this magma into the east rift zone resulted, on January 3, 1983, in the first of a long series of east-rift eruptions.

The crucial point to note here is that the degassing event, as detected in satellite-relayed data from the hydrogen-monitoring stations, was identified and recorded 9,000 km away almost instantly, leaving ample opportunity for telephone notification of personnel near the site of the event before the onset of eruptive activity. This episode illustrates the utility of using satellite telemetry for monitoring pertinent parameters of potentially active volcanoes from long distances.

CONCLUSIONS

The potential for utilizing geostationary satellites for monitoring remote and widely scattered volcanoes has not yet been fully realized. The techniques recently developed are directly applicable to many areas of the world where real-time data on natural hazards are required. The availability of low-cost and reliable data-collection platforms and direct-readout ground stations can provide a data-telemetry system free from the usual communications infrastructure (Shope and Paulson, 1981). The United States, the European Space Agency, and the Japanese Meteorological Agency all currently operate geostationary satellites capable of data relay. There are few areas in the world where potential users could not gain access to a geostationary satellite. The example cited earlier clearly demonstrates that satellite telemetry is now a viable alternative to other types of data-collection systems for monitoring potentially active volcanoes.

REFERENCES CITED

McGee, K.A., 1979, An analog data telemetry system for remote monitoring applications, version II: U.S. Geological Survey Open-File Report No. 79–946, 11 p.

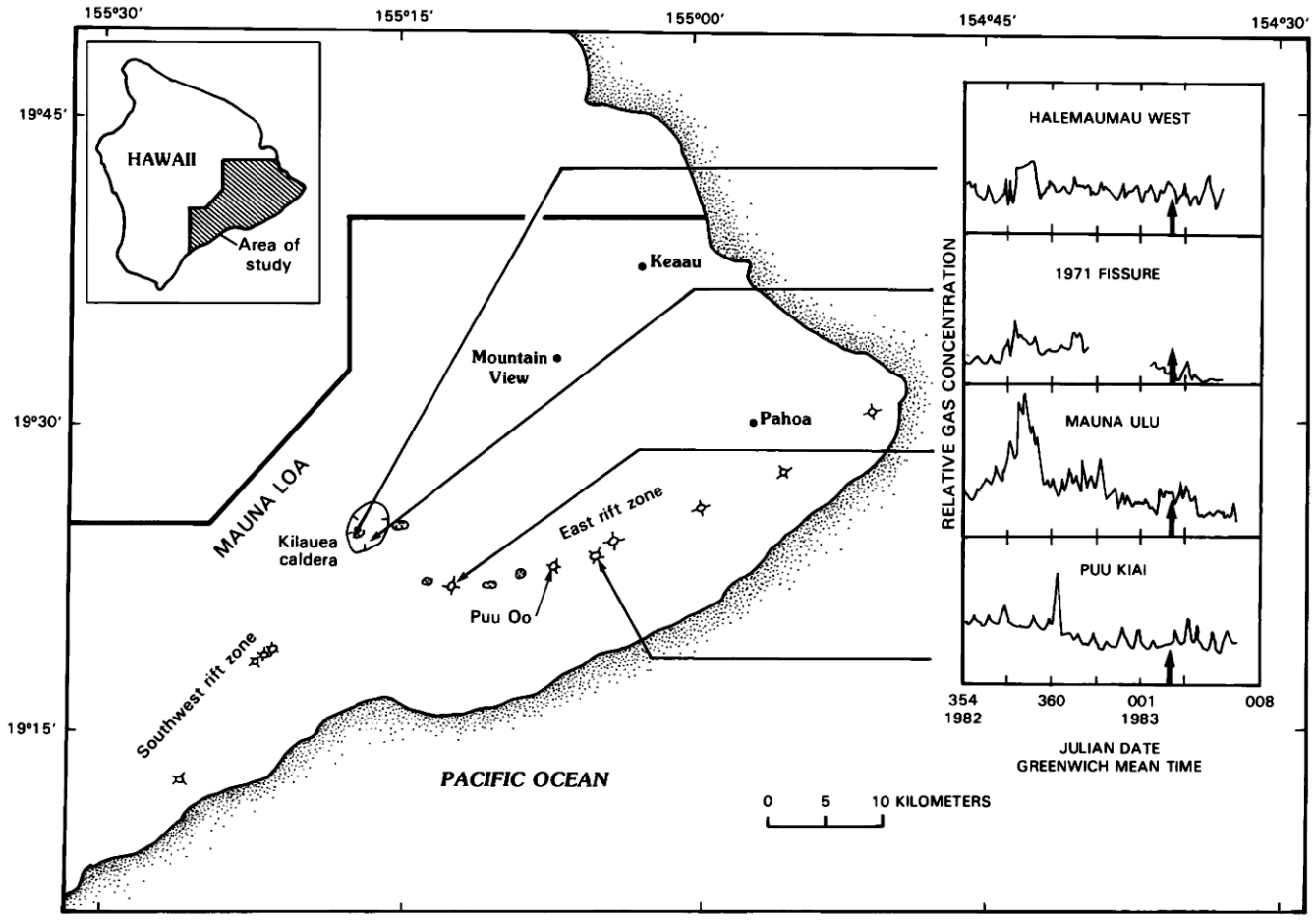

FIGURE 34.3.—Results from satellite-telemetered gas monitoring stations at Kilauea for late December 1982 to early January 1983. Occurrence of gas-emission event is essentially simultaneous at the two caldera stations and Mauna Ulu. Vertical arrow marks onset of eruptive activity at Puu Oo.

McGee, K.A. and Sato, Motoaki, 1982, The use of satellite telemetry for monitoring active volcanoes [abs.]: International Association of Volcanology and Chemistry of the Earth's Interior, Symposium on the Generation of Major Basalt Types, Reykjavik, Iceland, 1982, Proceedings, p. 109.

National Oceanic and Atmospheric Administration, 1983, The geostationary operational environmental satellite data collection system: Washington, D.C., National Oceanic and Atmospheric Administration Technical Memorandum National Environmental Satellite Data and Information System 2.

———1984, GOES data collection system and data processing system: Washington, D.C., National Environmental Satellite Data and Information System User Interface Manual, 132 p.

Shope, W.G., and Paulson, R.W., 1981, Data collection via satellite for water management: Transportation Engineering Journal, American Society of Civil Engineers, 107, no. TE4, p. 445–455.

HAWAIIAN VOLCANOES AND THE BIOGEOLOGY OF MERCURY

By Barbara Z. Siegel[1] *and* Sanford M. Siegel[1]

ABSTRACT

The global importance of volcanoes as a source of mercury appears to have been underestimated. The highly active Kilauea Volcano in Hawaii lies in the middle of one of the world's most productive forest ecosystems; hence it provides an ideal situation for the study of biological-geological-chemical interactions and interrelationships.

Mercury-rich emissions from Hawaiian volcanoes were discovered in 1971. Since then, the local sources of mercury in Hawaii, its chemical species, accompanying gases, release during lava weathering, dispersal, and vertical distribution have been studied. Parallel investigations have been made of bioaccumulation, biotransformation, and biovolatilization of mercury.

The most significant results during the period covered in this report, 1970–84, are:

1. Mercury emission data have been obtained from the Mauna Loa and Kilauea summit calderas, the Kilauea east rift and nearby fumaroles.

2. A provocative drop in mercury output was observed during the recent (1983–84) Puu Oo eruption compared to the 1977 Kalalua event.

3. The first measurements of mercury over a vertical range (rift level to 2,500-m elevation) were made during the 1977 Kalalua eruption.

4. The relation between Hg^0 and HgX_2 have been studied with respect to site, time, and distance, and a specific Hg-CO_2 correlation has been derived.

5. The regulatory role of vegetation in mercury distribution as a sink and secondary source through facile conversion of the ion to Hg^0 and its continuous release has been established.

6. It has been found that seedlings have a 300-fold greater sensitivity to Hg^0 than mature plants, which respond by premature senescence.

INTRODUCTION

Mercury is produced by Hawaii's active volcanoes, Kilauea and Mauna Loa, and by many other volcanoes the world over, including Hekla, Erebus, and St. Helens, irrespective of their chemical description (basaltic or andesitic) or location (midplate or plate margin). In spite of the element's global scarcity, mercury appears to be a ubiquitous constituent of volcanic gases, lavas, and pyroclastic deposits.

Recent flux measurements indicate that the amount of mercury attributable to volcanic activity has been underestimated in the past. Output figures from Mount St. Helens and several Central American volcanoes are remarkably similar to those reported from Halemaumau, the main vent of Kilauea, which produces approximately 270 tons annually (Varekamp and Buseck, 1981; Siegel and Siegel, 1984a). If, in fact, 200–300 tons of mercury were released annually by each of the 50–60 terrestrial volcanoes considered active (1975–80 annual average from Simkin and others, 1981), then the volcanic contribution to the global total would equal or exceed the commonly cited value of 10×10^9–20×10^9 g/yr for all mercury transfer to the atmosphere (U.S. National Academy of Sciences, 1977; Andren and Nriagu, 1979).

In 1970 we identified Kilauea as the major source of mercury in air over Oahu, 320 km away. Our work since that time has attempted to develop a comprehensive picture of the primary and secondary sources of the mercury, its sites of temporary storage, transfer modes, and sinks.

The cool upland forest in and around Hawaii Volcanoes National Park on the Island of Hawaii is one of the most productive ecosystems on this planet. Few volcanoes are situated in environments so heavily covered with vegetation as is Kilauea. Since the biosphere exerts a remarkable degree of control over the chemistry of the air, water, and soil, the location of Kilauea on Hawaii offers an exceptional opportunity to examine the transformation and distribution of volcanic mercury in a geobotanical and biogeochemical framework. On the other hand, few volcanoes are situated in locations so barren that their activity can be studied and their behavior interpreted without reference to geobiology; Mount Erebus in Antarctica may be one of those few (Siegel and others, 1980b) and therefore allow for interesting comparisons.

We have worked more than 15 years on this problem in Hawaii and elsewhere; much information has also been contributed by many others. Nevertheless, a great deal still remains unknown about the cycling of mercury on Earth, and this paper is only a progress report.

ACKNOWLEDGMENTS

Our research was made possible by the generous research funds, travel support, and facilities provided by many organizations and institutions. We thank the National Aeronautics and Space Administration; National Geographic Society; National Science Foundation, Division of Polar Programs; National Institutes of Health, Division of Research Resources; Department of Energy,

[1]University of Hawaii, Honolulu, Hawaii.

Lawrence-Livermore Laboratory (Institutional Grants Program); North Atlantic Treaty Organization; the Cottrell Foundation; the Environmental Center, the Hawaii Natural Energy Institute, and the Office of Research Administration of the University of Hawaii at Manoa; the University of British Columbia; and the British Columbia Science Council.

Thanks are also due Professor Gudmunder Sigvaldasson, Nordic Institute of Volcanology, University of Iceland; Professors Neil Towers and Harry Warren, Department of Botany and Geology, respectively, University of British Columbia; Gordon Eaton and Robert Decker, past Scientists-in-Charge, Hawaii Volcano Observatory (HVO), U.S. Geological Survey; and to Hawaii Volcanoes National Park Superintendents Bryan Harry, Robert Barbee, and David Ames.

Individuals who have generously shared data or field time include Paul Greenland, Thomas Casadevall, John P. Lockwood, Reginald Okamura, and many other members of the HVO staff, and also Thomas Speitel and Gary McMurtry, University of Hawaii at Manoa; Alan Eshleman, Berkeley, CA; Conrad Bachmann, University of Heidelberg; David Penny, Massey University, and Pauline Penny, Ministry of Works, New Zealand.

Finally, we dedicate this paper to the late Gordon A. Macdonald, Professor of Geology and Geophysics, University of Hawaii at Manoa, and the late Irving Breger, United States Geological Survey, who actively encouraged us in the exciting interdisciplinary maze that is biogeochemistry.

MINERALOGY, GEOCHEMISTRY, AND CHEMISTRY

For a more comprehensive review of mercury's physical parameters, the reader is referred to several excellent texts (King, 1951; Goldschmidt, 1954; Rankama and Sahama, 1950; Hem, 1970; Aylett, 1973).

The mineralogy of mercury is comparatively simple. Cinnabar is the only common mineral; it can be primary or found as an alteration product of more complicated base-metal sulfides containing mercury. Native mercury is frequently an oxidation product of cinnabar. The other known mercury minerals are curiosities; among them the oxysalts are indicators of arid climatic conditions. Traces of mercury may occur in some minerals, including tetrahedrite and tennantite (they are then called schwazite and hermesite), penroseite, argyrodite, clausthalite, altaite, and sphalerite.

Mercury has a high ionization potential (I.P.) and tends strongly to remain in the elemental state. Its first I.P. is 10.39 eV (gold's is 9.20 eV and silver 7.53 eV), and its second I.P. is 18.65 eV.

Mercury has a uniquely low melting point (-39 °C) and high vapor pressure (1.9×10^{-3} mmHg at 25 °C), indicative of its very low interatomic forces. Its viscosity, similar to that of water, is also low.

Mercury vapor is almost all monatomic, even at room temperature; apart from the noble gases, mercury is the only element to show this behavior at such low temperatures. Viscosity measurements suggest that the closest interatomic approach in the vapor phase is about 3.25 A at 850 K, little greater than in the liquid state. Both absorption and emission spectra of mercury vapor yield data that indicate the presence of a very small proportion of weakly bonded Hg_2 molecules.

The solubility (6×10^{-6} g/100 g water at 25 °C) of Hg^0 in air-free water is exceptional, being much higher than that of most other metals. Addition of air increases the solubility 700 times, up to a value almost identical with the solubility of HgO in water. Mercury is also appreciably soluble in n-hexane (2.7×10^{-7} g/100 g at 40 °C), benzene (2.0×10^{-7} g/100 g at 20 °C), methanol (3.6×10^{-7} g/100 g at 63 °C) and dioxane (7.0×10^{-7} g/100 g at 25 °C).

Oxygen and dry air do not react with mercury appreciably at room temperature, but the reaction may be greatly promoted by ultraviolet radiation. Ozone rapidly attacks mercury at room temperature to give Hg^{2+}.

All the halogens react directly with mercury at room temperature: mercurous halides seem to be formed first, followed by mercuric halides if halogen is in excess.

Air-free water below about 200 °C does not react chemically with mercury. Other elements that react directly with mercury, especially on heating, include sulphur, selenium, and tellurium; on the other hand, nitrogen, phosphorus, arsenic, carbon, silicon, and germanium do not seem to combine with it. Dry halides such as HX(X=F,Cl), H_2S, NH_3, PH_3, and AsH_3 do not react with mercury below about 200 °C. Some reaction with HBr, HI, and H_2Se occurs even at room temperature. Various nonmetallic halides react readily with mercury. Among oxides, SO_2, SO_3, N_2O, CO, and CO_2 are without effect at room temperature, but NO_2 reacts very rapidly to give mixtures of mercury (I) nitrite and nitrate as initial products.

Dilute hydrochloric and sulphuric acids do not react with mercury, but moderately concentrated solutions (>6*N*) attack it superficially to give a little mercurous salt. Concentrated hot H_2SO_4 dissolves mercury to yield Hg_2SO_4, $HgSO_4$, and SO_2, and nitric acid gives a range of products depending on conditions that include $Hg_2(NO_2)_2$, $Hg(NO_2)$, $Hg(NO_3)_2$, NO, and NO_3. Phosphoric acid does not react appreciably.

Mercury is not attacked by alkali, but ammonia solutions in air rapidly lead to the production of Millon's base, Hg_2NOH.

Under natural conditions of temperature and pressure that occur in river and lake water and water-saturated sediment, mercury can be present in one or more of its three different oxidation states. The most reduced, in a chemical sense, of these forms is the metal, which has a distinct tendency to vaporize because it is a liquid at ordinary temperatures. The other two forms are ionic: where the average valence of mercury is +1, the more reduced of the two ions is the mercurous ion Hg_2^{2+}; in oxidizing conditions, especially at low pH, the stable form is the mercuric ion, Hg^{2+} (Hem, 1970).

Although chemical oxidation reactions do not require the presence of oxygen, it is the most common oxidizing agent. Systems in contact with air tend to be oxidized, and in its absence reducing conditions readily become established. In moderately oxidizing conditions of pH above 5 the predominant mercury species in

solution is undissociated mercury. Its solubility, constant over the whole range of temperature where the liquid metal is stable, is fairly low (25 ppb), and the mercury exists as Hg^0. This solubility value represents the likely upper equilibrium limit of mercury in low-chloride surface streams and lakes.

Mildly reducing conditions, which are likely to occur in many lake and streambed sediments, can cause the mercury to be precipitated as cinnabar, which has an extremely low solubility. In the field at neutral pH, $Hg(HS)_2^0$ aq and HgS_2^{2-} have an equilibrium solubility lower than 0.002 ppb. Very strongly reducing conditions, however, may increase the solubility somewhat by converting the mercuric ion to free metal.

In solutions high in chloride the solubility of mercury in oxygenated water may be greatly increased by the formation of the uncharged $HgCl_2$ complex, or anionic complexes such as $HgCl_4^{2-}$ (Wagman, 1969).

The frequent departure of natural systems from equilibrium is well known and must be kept in mind when using equilibrium calculations. There are two aspects of mercury chemistry that are particularly important sources of departure from what is predicted theoretically. One of these is the formation of organic complexes and participation of mercury in biochemical processes, especially in the production of methyl mercury by sedimentary bacteria (Jensen and Jernelov, 1969). A secondary property of importance is the tendency for mercury to participate in dismutation reactions—that is, in reactions of the type $Hg_2^{2+} \rightleftharpoons Hg^0 + Hg^{+2}$ that provide a means whereby mercury can be first converted to the liquid form and then escape as vapor.

Although there is some understanding of the aqueous chemistry of mercury, a considerable amount of basic research is still needed, especially on rates and mechanisms of reaction and on the behavior of organic mercury complexes.

TOXICOLOGY

The onset of symptoms from mercury poisoning in humans is insidious, and the symptoms, with the exception of tremor, may often be ignored or attributed to other causes (Bidstrup, 1964). This is especially true of a peculiar emotional instability called erethism, which is defined by irritability, irrational outbursts of temper, excitability, shyness, and sometimes depression; such symptoms are often just attributed to an anxiety state.

The classic signs of poisoning by mercury in the inorganic form are gingivitis and stomatitis accompanied by excessive salivation or a metallic taste, burning, swelling and ashy discoloration of the mouth followed by intense thirst and abdominal pain; erethism; and tremor (Goldwater, 1951). Vomiting may occur, and in some cases circulatory collapse with a fatal outcome appears suddenly and at an early stage. Delayed effects on the kidneys or large intestine are generally the cause of death (Sollman, 1957). There is no clear difference between the acute, subacute, and chronic forms except that the symptoms develop more quickly and are of greater intensity, and generally the oral and gastrointestinal symptoms are more obvious in acute and subacute poisoning (Bidstrup, 1964). Mercuric chloride especially is irritating to the skin and mucous membranes, causing irritation, vesication, and corrosion. Absorption through the skin and mucous membranes may cause systemic poisoning.

Acrodynia (so-called pink disease) occurs in infants and young children; it is characterized by mental disturbances, insomnia, sweating, disordered sensation of the extremities, and peripheral vascular phenomena and is often fatal. Strong evidence exists that the absorption of mercury is the most important cause of this disease, although there is confusing etiology (Warkany and Hubbard, 1953).

When cinnabar, HgS, has been used for the red color in tattooing, mercury dermatitis has been reported, and occasionally an eczematous rash has spread to involve the entire body.

Acute poisoning from metallic mercury or its vapor rarely occurs now and is usually the result of an accidental exposure (Matthes and others, 1958), but historically it was a common occurrence among men exposed to mercury in certain occupations. Hunter (1955, p. 256) quotes from Ramazzini concerning miners and goldsmiths:

> It is from mercury mines that there issues the most cruel bane of all that deals death and destruction to miners.
>
> * * * * *
>
> We all know what terrible maladies are contracted from mercury by goldsmiths, especially those employed in gilding silver and copper objects. Hence craftsmen of this sort very soon become subject to vertigo, asthma and paralysis. Very few of them reach old age, and even when they die young their health is so terribly undermined that they pray for death.

and also mirror makers:

> you may see these workmen gazing with reluctance and scowling at the reflection of their own sufferings in their mirrors and cursing the trade they have adopted.

Acute and subacute poisoning among persons engaged in the mining and refining of mercury have been reported, but improvements in ventilation of mines, refinery processes, and the use of personal protective measures have reduced the numbers and severity of poisoning. Vouk and others (1950), reporting on environmental conditions in the Idria (Yugoslavia) mercury mines, stated that there were 93 cases in 1949 and 53 reported in the first half of 1950. In Idria mercury occurs both as cinnabar and in the free form, and the mining of Hg^0 is particularly hazardous.

Concentrations of mercury in the air in pits where cinnabar, alone or with free mercury, is mined are 50–59 $\mu g/m^3$. Dizon and others (1960) investigated a mercury mine in the Philippines, where it is a relatively new industry and the processes are highly mechanized. The highest atmospheric concentrations reported were 100–400 $\mu g/m^3$ in the vicinity of the ore crushers, and 6 of the 11 men employed at the crushers had symptoms of mercury poisoning. In Peru, Carlin and others (1960) reported that 16 out of 18 refinery workers were found to have high mercury excretion in the urine (average 224 $\mu g/L$), and 13 had definite evidence of mercury poisoning.

More general problems of animal toxicity have been discussed in detail in the compilations of Buhler (1973) and Nriagu (1979). Included are behavioral effects, cell and organ degeneration, and developmental abnormalities in birds, terrestrial vertebrates, and aquatic marine forms from mammals to fish.

In spite of the obvious role of plants in primary life support, the effect of mercury on vegetation has received little more than token attention until recently. From the first account of mercury intoxication of plants (Deiman and others, 1797), the only reports up to 1930 were those of Boussingault (1867a,b), Harrington (1917), and Le Van (1930). Zimmermann and Crocker (1933, 1934) and Ratsek (1933) revived the experimental study of mercury toxicity in conjunction with seed and greenhouse problems, but they did not recognize major developmental features of mercury toxicity and its dependency on the chemical species used.

Typically, plant-cell damage takes place with aqueous solutions containing as little as 10 μg/L of Hg ion (Siegel, 1977).

In contrast, when 18 species and varieties of seeds were germinated in air containing 14 μg/L of Hg^0 vapor (Siegel and Siegel, 1979a; Siegel and others, 1984a), root growth was stimulated in 4 species, inhibited by 25 percent or less in 6, and did not exceed 50 percent inhibition in the 8 remaining species. Shoot growth was even less adversely affected; only 4 species were inhibited by more than 25 percent.

Of castor bean seedlings 20 days old in air containing 0.05 μg/L of Hg^0, only 14 percent lost their leaves, and none showed zones of discoloration or morbidity after seven days. Coleus seedlings of the same age were even less affected. However, mature plants of both species after seven days in air containing 0.05 μg/L of Hg^0, lose 50–90 percent of their leaves. In terms of toxic thresholds, mature plants are approximately 300 times more sensitive to mercury than seedlings.

At the concentration of 0.05 μg/L $HgCl_2$ vapor has essentially no toxic effect on seedlings or mature plants.

The principal toxic effect of Hg^0 seems to be an acceleration of the aging process mediated by induction of the plant stress hormone ethylene (Siegel and others, 1973b; Goren and Siegel, 1976).

MERCURY IN HAWAII

DISCOVERY

Mercury in Hawaii was first found in stream sediments on the Island of Oahu and later in the air (Siegel and others, 1973b). To determine the source of this mercury, widespread monitoring, sampling, and analyses were carried out. Air mercury levels on Oahu were found to be highest in the southeastern part of the island and lowest at sites facing the northeast tradewinds; this indicated that the primary source was the thermally active Island of Hawaii (Eshleman and others, 1971). The verification of volcanic-fumarolic mercury sources in 1970–71 led in turn to a program of study that has continued to the present. The main focus has been the active volcanic areas of Hawaii, but the studies have also included Iceland, Alaska, New Zealand, and Antarctica.

The sources of mercury on Oahu, with its long-dormant (or extinct) volcanoes Kaala and Waianae (Macdonald and Abbott, 1970), have provided us with opportunities for research involving residual mercury, mercury transport, and biological compartments. These subjects will be discussed later.

PRIMARY SOURCES AND SPECIATION

There are two active centers of gas emission on the Island of Hawaii—the volcanoes Kilauea and Mauna Loa. Kilauea and the thermal features of the east rift zone have been studied extensively; the Mauna Loa summit caldera, Mokuaweoweo, has also been sampled, but emissions during flank eruption have only been measured for mercury during March 1984. The most commonly studied sites on Kilauea have been Halemaumau (the main vent) and the Sulphur Bank fumaroles, first sampled in 1970 (Siegel and Siegel, 1980, 1984a).

In our ongoing studies, air samples have been regularly collected in nitric acid/pyrex-fiberglass impingers at flow rates of 1–2 L/min for periods of 4–7 h, thus assuring a gas volume of at least 240 L (0.24 m^3). Samples have been analyzed by flameless atomic absorption (Eshleman and others, 1971; Siegel and Siegel, 1978, 1979; Siegel and others, 1985). Parallel sampling was also carried out by drawing air through gold-foil traps, which were subsequently stripped of mercury in nitric acid. Millipore filters were used to trap particles with diameters larger than 0.22 μm. The nitric acid traps collect total mercury; the gold foil collects Hg^0 only and millipore filters insoluble HgS (cinnabar). Cinnabar was verified by solubility in aqua regia and insolubility in cold nitric acid. Any difference observed between total mercury and particulate mercury plus Hg^0 is considered to be HgX_2, presumably a mixed halide (Cadle, 1975), but mainly the chloride.

Another approach to air sampling is fallout measurement or deposition (Siegel and Siegel, 1977). Here copper foil, which reduces Hg^{2+}, and gold foil, which amalgamates Hg^0, are used to distinguish the mercury species.

We assume that copper foil collects both Hg^0 and Hg^{2+}, hence the amount of mercury trapped on gold foil subtracted from the amount of mercury on copper foil yields a value for Hg^{2+}. This calculation is valid only if the HgS particulate fraction is negligible.

The average total mercury concentration in the open air 2 m above the ground (at right angles to the slope) at Sulphur Bank ranged from 2,700 to 40,600 ng/m^3 through 1977, but in subsequent years exceeded 1,000 ng/m^3 only during January–February 1982, at the start of the current Puu Oo eruption series (fig. 35.1; table 35.1). The Halemaumau vent of Kilauea (fig. 35.1, table 35.2) has also been highly productive, behaving similarly to Sulphur Bank in eruptive and quiescent periods. Overall, it would appear that the normal value for mercury in air in the Kilauea summit area ranges from 400 to 1,000 ng/m^3. Similar values are seen along the approach to Kilauea caldera from the northeast (as seen in the 500- to 1,000-m transects along the volcano highway; fig. 35.2). For the period 1971–78, the average mercury value in the immediate vicinity of the caldera lies between 400 and 1,400 ng/m^3, but it falls off dramatically to the northeast into the tradewinds.

Air samples taken at Royal Gardens during the Kalalua rift eruption of 1977 show the mercury level rising suddenly from a putative baseline (June–July) of about 300 ng/m^3 to 200,000 ng/m^3 (200 μg/m^3) or more by September 15, then dropping precipitously after the fountaining and tremor ended in October (Siegel and Siegel, 1978).

TABLE 35.1.—*Mercury concentration in air at the Sulphur Bank fumaroles Kilauea Volcano, 1971–1980*

[s.d., standard deviation; part., particulates]

Year	Number of samples	Total mercury (ng/m^3) (± s.d.)	Mercury species (percent)		
			Hg^0	Hg (part.)	HgX_2
1971	26	28,400±11,000	69	1	30
1972	27	3,700± 520	24	13	63
1973	10	4,900± 640	62	2	36
1974	9	4,500± 660	71	<1	29
1975	17	2,700± 390	44	<1	56
1976	24	8,600± 1,200	32	<1	68
1977	38	40,600± 4,680	28	<1	72
1978	26	500± 70	10	5	85
1979	29	880± 95	60	1	39
1980	29	500± 85	59	<1	41
	241 (total)	9,528± 1,464 (avg)	45.9 (avg)	2.2 (avg)	51.9 (avg)

In all the measurements of mercury concentration in air, there appears a consistent downward trend by as much as 95 percent after about 1978. This trend downward may even apply to Mauna Loa mercury output, although the sample data are limited.

It is clear from the record, however, that Kilauea's mercury output since 1977 has not approached that of the Kalalua rift emissions, in spite of the far greater output of fluids and gases since January 1983. This leads to the provocative question of whether the mercury output of Hawaiian volcanoes is really declining. If so, is this phenomenon a long-term downtrend or merely the downward limb of a cyclical process? Either alternative poses interesting challenges for interpretation.

With few exceptions, particulate mercury has not been found in samples of the air around Kilauea, even during periods of eruptive activity (table 35.1). The 10-year average of particulate mercury is 2.2 percent of the total, but commonly less than 1 percent of the total mercury was found on the filters.

The wide variation in Hg^0 and HgX_2 content of air samples was unexpected—Hg^0 ranged from 10–71 percent of the total at Sulphur Bank (Siegel and Siegel, 1979b). This was also seen in fallout data from the same location (Siegel and Siegel, 1977):

Date	Hg^0 (ng/m^3)	HgX_2 (ng/m^3)	Hg^0/HgX_2
1972 January	80±9	377±44	0.21
April	300±31	1,220±369	.25
1975 May	250±31	540±60	.46
December	438±48	42±7	10.43
1976 May	575±66	250±27	2.30
June	119±22	612±12	.20

On the other hand, concurrent fallout samples taken on Oahu, about 400 km northwest of Kilauea, always yielded far less total mercury (about 10 percent of that detected near Kilauea) and mostly as Hg^0. At Halemaumau, Hg^0 accounted for 15–21 percent of the total mercury released, but on the floor of Kilauea, at the very active

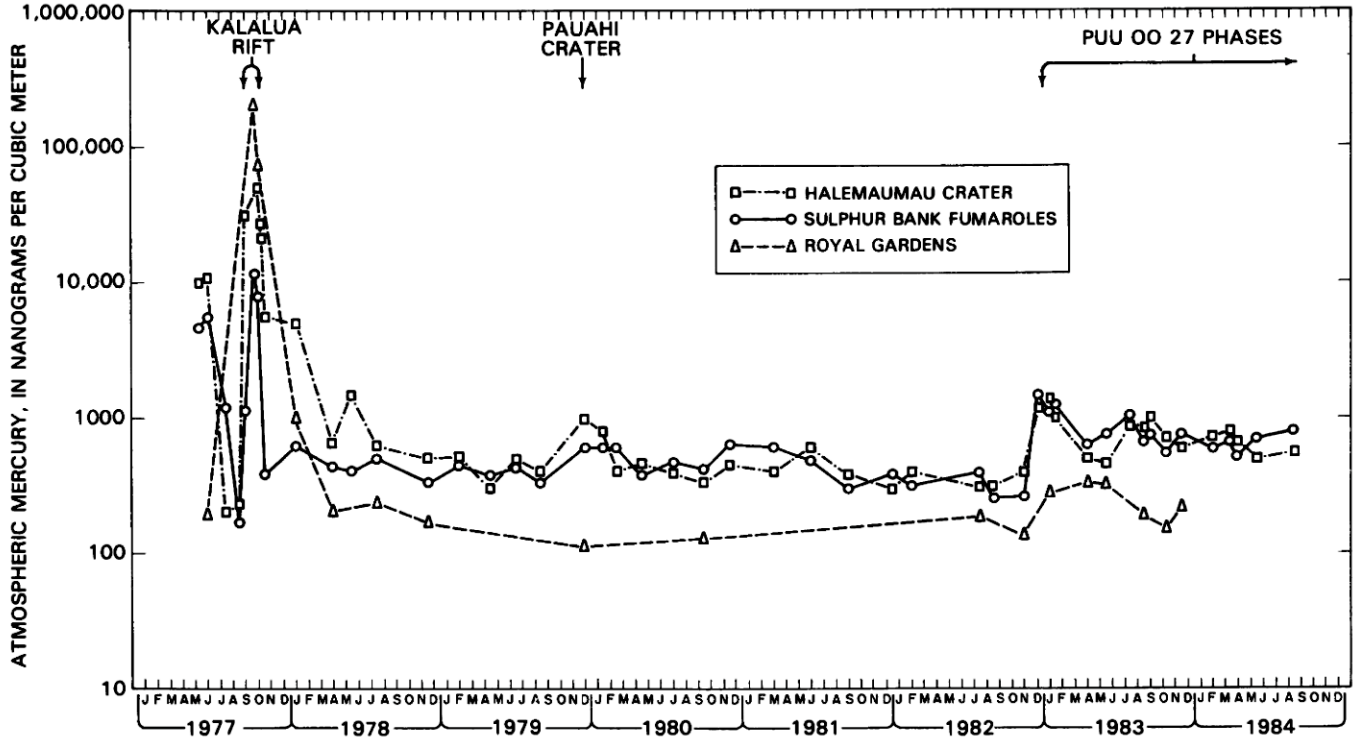

FIGURE 35.1.—Mercury emission record for Kilauea at Halemaumau main vent, the nearby Sulphur Bank fumaroles, and south of east rift at Royal Gardens, 1977–1984. Three events noted: major Kalalua rift eruption lasting nearly one month; one-day Pauahi Crater eruption of 1979; and exceptionally prolonged rift eruption at Puu Oo, beginning January 1983, through its 27th episode. Note that the ordinate scale is logarithmic.

TABLE 35.2.—*Measurements of mercury in air at various locations on Kilauea and Mauna Loa Volcanoes*

[See also Conners, 1979]

Site	Sampling period	Total mercury (ng/m^3)	Hg^0 (percent)
Kilauea Volcano			
Halemaumau	1971 August	40,500	16
	1977 August	48,100	21
	1978 August	1,400	15
Caldera floor			
1971 fissure	1978 August	79,900	1
	1981 August	3,600	2
1974 fissure	1978 August	29,800	2
	1981 August	1,900	5
Kalalua rift	1977 August	1,200	22
	1977 September	>200,000	50
	1977 October	18,500	58
	1977 November	500	80
Puhimau thermal area	1978 January	5,800	72
	1978 August	12,200	49
	1981 January	930	56
Mauna Loa Volcano			
Mokuaweoweo caldera	1978 July	24,600	35
Upper rift	1984 March	4,850	—

1971 and 1974 fissure the Hg^0 fraction fell to only 1–5 percent of the total emitted. During the 1977 eruption, the Hg^0 fraction rose from its minimum of 22 percent to a peak at 80 percent after the active phase ended.

Mercury is, of course, a minor constituent of volcanic and fumarolic gas emissions, wet or dry. It is accompanied by H_2S, SO_2, and CO_2 (Siegel and Siegel, 1979b, 1980). An exception is the Puhimau thermal dieback area, where sulfur in any form has only been detected in the parts per billion range (Phelps and others, 1979). This area formed in 1938–9 after an earthquake and magma shifting brought heat near the surface, causing several acres of forest to die; the ground temperature 5 cm below the surface here averages 97 °C.

At Halemaumau, measurements during 1971–78 gave mole ratios of 590 for H_2S, 6,300 for SO_2, and 2.10×10^6 for CO_2 (table 35.3). Obviously, sulfur-mercury relations are highly varied, even within a single volcanic system, and are highly site dependent. It is, therefore, of special interest to note that the ratio CO_2/Hg is nearly constant at Kilauea; individual measurements do differ somewhat, however, and data from other locations such as Mount St. Helens are distinctly different.

Lava flows constitute another source of mercury. Weathering brings about the slow release of soluble or solubilized constituents as the igneous materials degrade into soil minerals. Lava samples were analyzed by digestion of 100-mesh powder with 0.1*N* HCl to remove soluble and loosely bound mercury. This was followed by hot 2*N* HNO_3 digestion to remove any mercury complex with organic ligands, and then concentrated HF to destroy the silicate matrix

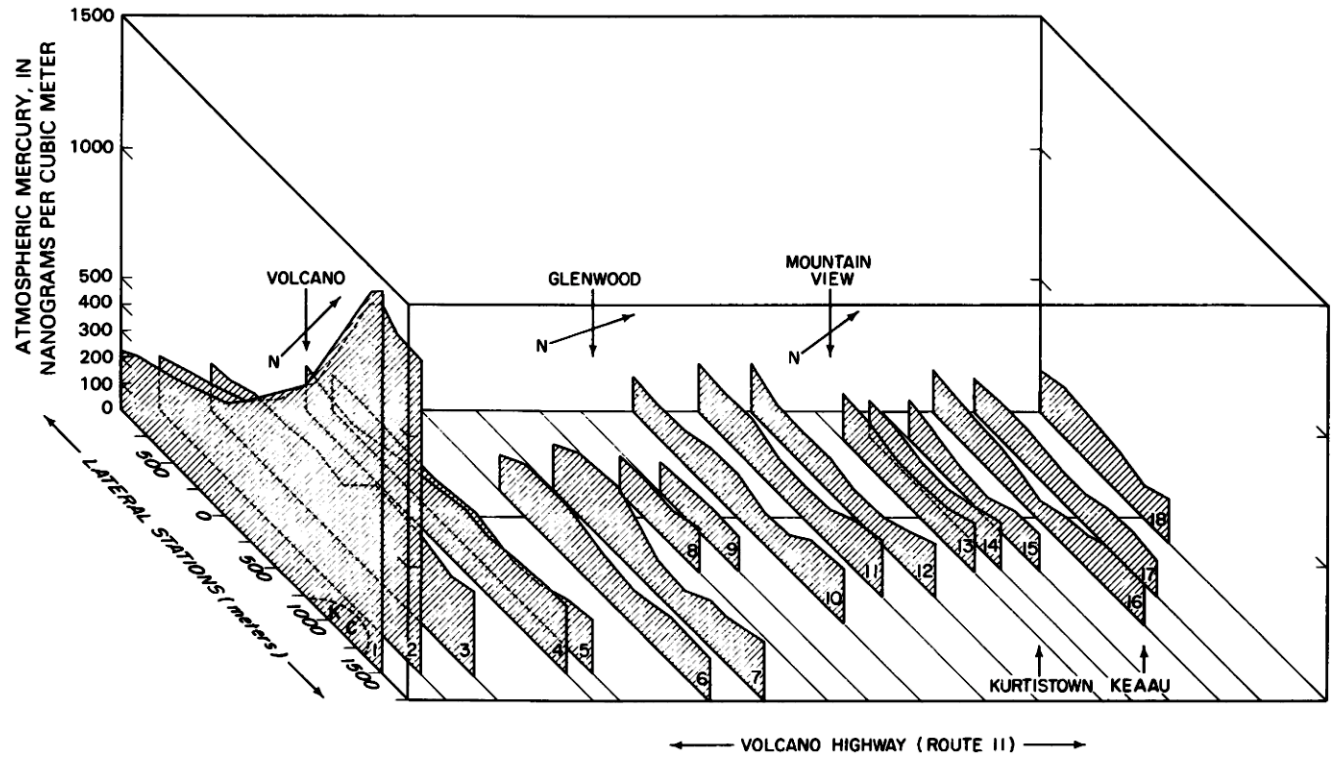

FIGURE 35.2.—Average atmospheric mercury concentration along volcano highway from Kilauea caldera (KC) northeast to the Village of Keaau. North is indicated at three villages. Highway is plotted as straight line perpendicular to transects 1–18.

TABLE 35.3.—*Relations between mercury and other gaseous omissions at thermal sites*

[s.d., standard deviation; n.d., not determined]

Thermal site	Number of samples	Sampling date	Flux (tons/yr)	Plume (μmol/m^3)	Mole ratios		
					H_2S/Hg	SO_2/Hg	$(CO_2/Hg)10^{-6}$
Kilauea Volcano							
Halemaumau	86	1971–80	260	0.054±0.014	590	6,300	2.10
Sulphur Bank	18	1976–78	—	.012±0.083	3,700	3,050	2.75
1971 Fissure	8	1977–78	—	.396±0.055	0	239	2.75
1974 Fissure	8	1977–78	—	.146±0.016	0	96	2.19
Puhimau Thermal	10	1976–78	—	.026±0.005	0	0	3.66
Mount St. Helens	5	1980	365	.005±0.002	—	2,750	.013
Costa Rica							
Fumarole Poas		1980–82	52	—	—	1,030,000	—
Volcan Arenas		1980–82	32	—	—	5,000	—

(Siegel and others, 1975). Samples from flows of 1840, 1923, and 1955 were obtained with the assistance of the late Gordon Macdonald; fresh Pauahi samples were collected in 1979. The results (below) suggest a 50 percent release in about 50 years and a gradual infiltration of oxidizable, presumably humic, complexing substrates.

Year of flow	HG concentration μ/kg in lava		
	HCl soluble	HNO_3 soluble	HF digest
1840	5	81	45
1923	16	66	310
1955	10	59	970
1979	0	15	1,290

If Kilauea lava typically cools with about 1,000 μg/kg of mercury and proceeds to release 90 percent, then this still constitutes only a minor source of the element. The 1840 eruption produced about 400×10^6 m^3 of lava weighing perhaps 16×10^9 kg. Thus, this lava contained a total of 16×10^6 g (16 tons) of mercury, of which about 14 tons was released in about a century. In contrast, Halemaumau yields 260 tons annually when it is not erupting (Siegel and Siegel, 1984a).

Of course, the impact of a small though continuous and localized release of mercury cannot be discounted as a possible selection factor for mercury tolerance in the endemic vegetation of Hawaii. It is clear, as we show below, that plants in volcanic areas can become well adapted to life in mercuric environments. Also, Hg^0 slowly released by lava at ground level will, like any heavy gas, tend to accumulate in enclosed pockets and depressions and form areas of local concentration.

At the end of the weathering process, some mercury remains in the clays and derivative soils. In areas of heavy precipitation, such as the Sulphur Bank, acid red clays are common and contain no readily soluble mercury, but when they are heated in closed vessels, their mercury output can be collected on gold foil and measured.

The following data on mercury release from Sulphur Bank soil were obtained in this way:

T(°C)	Rate (ng/kg·h)
25	0.254
70	5.67
120	68.1

Using this kind of data and the Arrhenius equation, we have calculated an apparent heat of activation of 13.81 kcal/mole (Siegel and Siegel, 1983). This value compares well with the molar heat of vaporization calculated similarly from CRC Handbook vapor-pressure data. Thus atmospheric mercury released from soils directly may have been held entirely as Hg^0.

DISPERSAL

The northeast tradewinds with velocity of 20–40 km/h constitute a major and well-known determinant of climate in Hawaii. However, the assumption that these winds continually cleanse the atmosphere of pollutants, conveniently displacing them to the southwest, is not borne out by experience. During the 1977 eruption, with tradewinds normal, measurements were made on samples of air from 30 m above ground level at a station on Oahu about 400 km northwest of Kilauea. The mercury content rose from 40 ng/m^3 to 160 ng/m^3 in only 30 hours after the first fountaining at Kalalua (Siegel and Siegel, 1978). The mercury released along the rift and at Halemaumau traveled no less than 13 km/h in a direction about 90° to the tradewind vector. Increases in atmospheric turbidity 1–3 days after the onset of fountaining in a volcanic eruption have often been observed, not only in Honolulu, but also on the west side of the Island of Kauai.

The tradewind air masses move southwestward across the North Pacific and then encounter the high relief and rough terrain of the Island of Hawaii, where they become turbulent. Furthermore, the major sources of emission extend from the tradewind zone upward into air masses moving in other directions. During the final stages of the 1977 eruption, mercury in the air showed a rapid dropoff above the Kalalua rift to an asymptotic value of about 1,000 ng/m^3 at elevations of 1,200–2,500 m (fig. 35.3). Mercury at these higher elevations was over 90 percent Hg^0. This observation agrees with the fallout data discussed above that showed the proportion of Hg^0 in total mercury was higher on Oahu (sea level) than at the Sulphur Bank when samples collected at the same time were compared (Siegel and Siegel, 1977). The comparison of the Hg^0/HgX_2 ratio at the two locations is as follows:

	January 1972	May 1975	June 1976
Hawaii	0.212	0.463	0.195
Oahu	2.86	3.16	3.31

It must also be recalled that the Mauna Loa caldera continually fumes at an elevation of about 4,500 m, and numerous fissures are always injecting hot mercuriferous gas into an often turbulent atmosphere. The gas column is subject in its dispersal to a variety of wind vectors, including some that carry the mercury northward and downward as it cools. These may account largely for the distribution of mercury on Oahu (fig. 35.4; see also, Siegel and Siegel, 1980), where higher values occur to the south and west. The same is true of the Island of Kauai. Residual thermal activity on Maui, however, tends to obscure the direct impact that the Island of Hawaii's volcanic activity may have on its mercury distribution, and anomalies are often related to anthropogenic pollution.

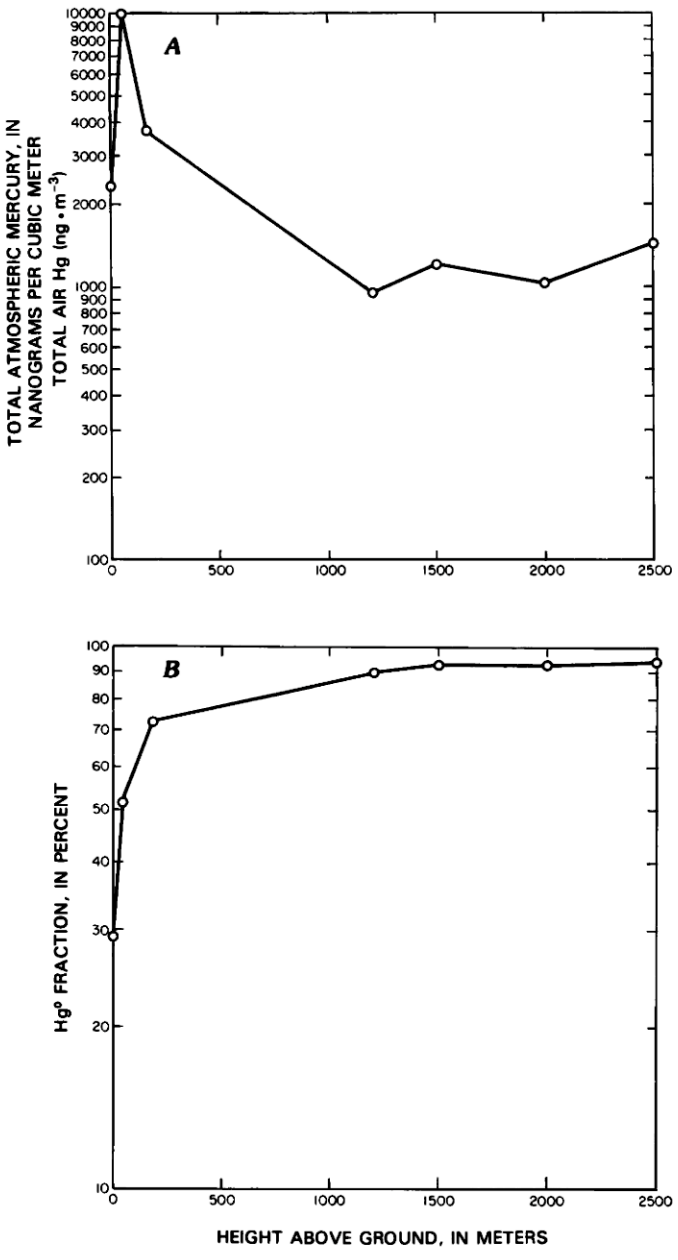

FIGURE 35.3.—Vertical distribution of atmospheric mercury over the Kalalau fissures during the 1977 eruption. Data obtained using dual-trap method: nitric-acid impinger and gold foil. *A*, Concentration from ground level to height of 2,500 m. *B*, Percentage of Hg^0 in total mercury.

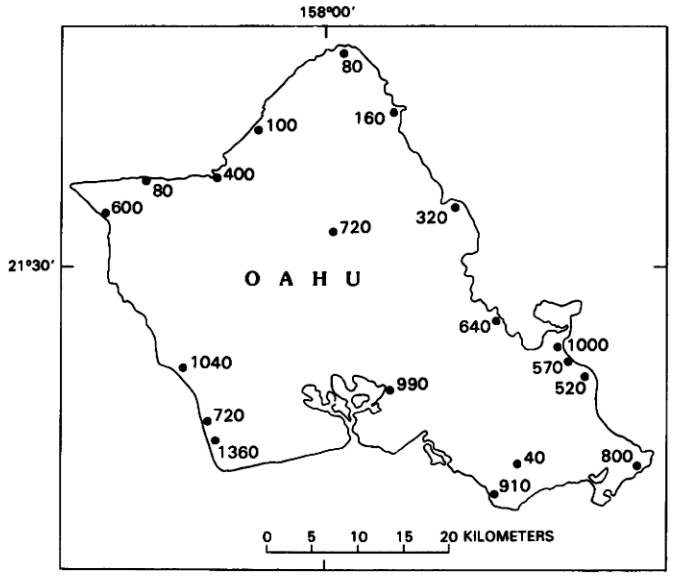

FIGURE 35.4.—Distribution of atmospheric mercury (in ng/m³) around Oahu at 2 m above ground. Figures are means of samples taken 1971–78.

GEOBOTANY AND BIOGEOCHEMISTRY

One factor relating to dispersal of mercury in Hawaii remains to be considered, however, and that is the role of vegetation in its cycling and dispersal. For example, toward the back of the Palolo Valley (Honolulu) the old, weathered soils contain little mercury, only 15×3 μg/kg (Siegel and others, 1975), yet the two grass species growing in that soil (*Digitaria and Andropogon*) contain much more (68 ± 8 and 79 ± 11 μg/kg, respectively). When these grasses die, their decaying residues retain most of the mercury (56 ± 6 μg/kg), which is then taken in by soil invertebrates, the earthworm *Lumbricus* (388 ± 21 μg/kg) and the millipedes *Trigonialis* (467 ± 21) and *Oxydus* (382 ± 12). In this simple example, the earthworm to soil mercury ratio is about 31.

All of the aquatic plants that we have encountered accumulate mercury (Siegel and others, 1973b, 1975, 1984b, 1985; Siegel and Siegel, 1982, 1984b), usually with sizeable enrichment (table 35.4). The same is true for marine animals including fish, but not limited to vertebrates. High ratios are in part a consequence of the low mercury concentrations found in natural (nonindustrial) waters. Near black sand (basaltic) beaches in Hawaii, the highest mercury levels yet found reach 2–3 μg/L.

Many terrestrial plants also accumulate mercury, but nearly 300 samples from four widely separated areas (table 35.5) show a clear bimodality in the concentration ratio. Overall, 55–77 percent

TABLE 35.4.—*Mercury accumulation in marine organisms*

Sample	Content in organism (μg/kg)	Concentration ratio (organism/water)
Algae		
Hawaii		
Ulva	40–200	25–145
Padina	140–185	65–88
Sargassum	26–46	12–23
Iceland		
Ulva	106	1,060
Mastigocladus	380	3,800
Antarctica		
Ulva	1.5–3.1	8–16
Fish		
Hawaii		
Marlin	>500	>250
Tuna	220–1,370	110–685
Iceland		
Tuna	287	2,870
Antarctica		
Cod	36	200

TABLE 35.5.—*Distribution of mercury concentration ratios in vascular plants at various localities*

[Figures in percent of species; number of species sampled given beneath each locality name; after Siegel and others, 1975]

Mercury concentration ratio (plant/soil)	Iceland (79)	Hawaii (105)	New England (38)	Alaska (66)
<0.1	13	14	32	30
.1 –0.67	10	22	10	0
.67–1.33	0	8	0	5
1.33–2.0	14	4	18	10
>2	63	54	40	55

of all the plants studied contained at least 1.33 times as much mercury as the soil around their roots, but 23–42 percent of the plants from the four locations contained less mercury than the soil in which they were growing.

Although it may seem reasonable to hypothesize a mechanism whereby plants exclude mercury, there are too many essential nutrient cations similar in charge and size to Hg^{2+}, among them, Ca^{2+} and Fe^{2+}, that could not be biologically distinguished. It is difficult to construct an energetically and structurally sound model that can include Hg^{2+} with virtually absolute selectivity. An alternate mechanism, however, was suggested when we found that mercury concentrations in air at Sulphur Bank were not determined by inorganic processes alone. Thus, an Arrhenius plot based on air samples taken at one meter over the vegetation on the flats, about 100 m from the fumaroles, shows that there are two slopes (fig. 35.5), implying two limiting processes or mechanisms. The higher temperature process (>20 °C) has a slope parallel to the vapor-pressure line, but at lower temperatures mercury in air is limited by a process other than evaporation, possibly biological in nature.

This surmise has been verified experimentally in more than 50 species of plants (Kama and Siegel, 1980; Siegel and others, 1980a; Siegel and Siegel, 1983). Examples of terrestrial Hg^0 producers include leaves of pineapple, sugar cane, ferns, mosses, lichens, and mushrooms (table 35.6).

This process that may be called biovolatilization is not unique to land species; the unicellular green alga *Chlorella* has been shown to possess a photosynthetic reduction system that generates Hg^0 vapor (Ben-Bassat and Meyer, 1975, 1977).

TABLE 35.6.—*Rates of elemental mercury release from various vascular plants*

[Uncertainty figures are one standard deviation; after Kama and Siegel, 1980; Siegel and others, 1980; Siegel and Siegel, 1983]

Vascular plant	Rate (ng/kg-m)	Plant	Rate (ng/kg-m)
Aloe	850±50	Lichens	
Pineapple	820±30	*Usnea*	660±190
Coconut	240±90	*Cladonia*	120±30
Nutgrass	340±45	*Stereocaulon*	840±91
Staghorn fern	730±45	Mosses	
Hibiscus	490±45	*Leucobryum*	50±215
Leucanea	3,050±300	*Bryum*	400±50
Pandanus	1,590±390	*Polytrichum*	400±160
Avocado	4,130±220	Fungi	
Mangrove	100±40	*Polyporus*	1,200±105
Sugarcane	650±40	*Fomes*	2,430±1200
Papyrus	700±49	*Trametes*	950±480

Most of these studies on release of Hg^0 from plants have emphasized Hawaiian species and the Hawaiian environment. However, the New Zealand manuka, *Leptospermum scoparium*, also appears to release mercury adaptively, keeping levels in tissue down and delaying or preventing toxic buildup (fig. 35.6). As soil

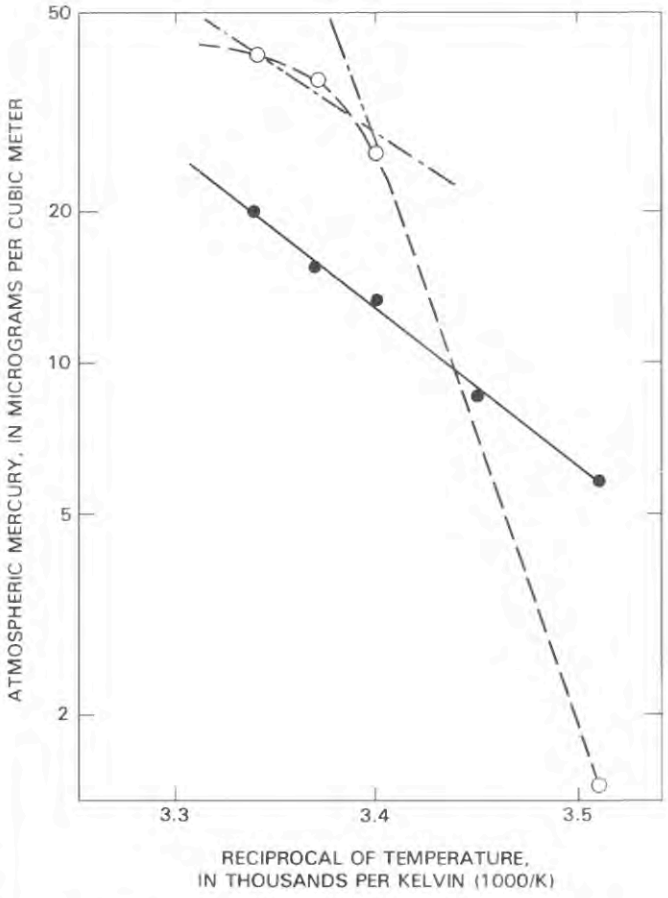

FIGURE 35.5.—Variation of atmospheric mercury concentration with air temperature over the vegetation near Sulphur Bank fumaroles. Data are presented as Arrhenius plot. Dashed curve, field data; dots and solid line, vapor pressure data. See text for discussion.

mercury rises approximately 30-fold from nonthermal Wellington to the Hell Gate thermal area, manuka shoots increase in mercury less than 5-fold. The detoxification mechanism, however, has increased the Hg^0 release rate by a factor of 9.

Presumably, Hg^{2+} is taken up from soil and ground water and translocated rapidly into the leaves, where reduction is followed by evaporative release. In a number of leguminous species growing in Hawaiian soils, it has been shown that mercury in seeds is selectively eliminated during the ripening process, thereby reducing the concentration below that at which cytological damage to the embryo may take place (Ramel, 1969; Siegel and Siegel, 1985).

Re-emission of Hg^0 may be followed by its direct uptake by nearby plants with or without toxic consequences according to species and concentration (Siegel and others, 1973a; Siegel and Siegel, 1979a). Accordingly, mercury as Hg^{2+} or its complexes may be taken up from soil or ground water and converted to Hg^0 for subsequent release and, perhaps, re-uptake.

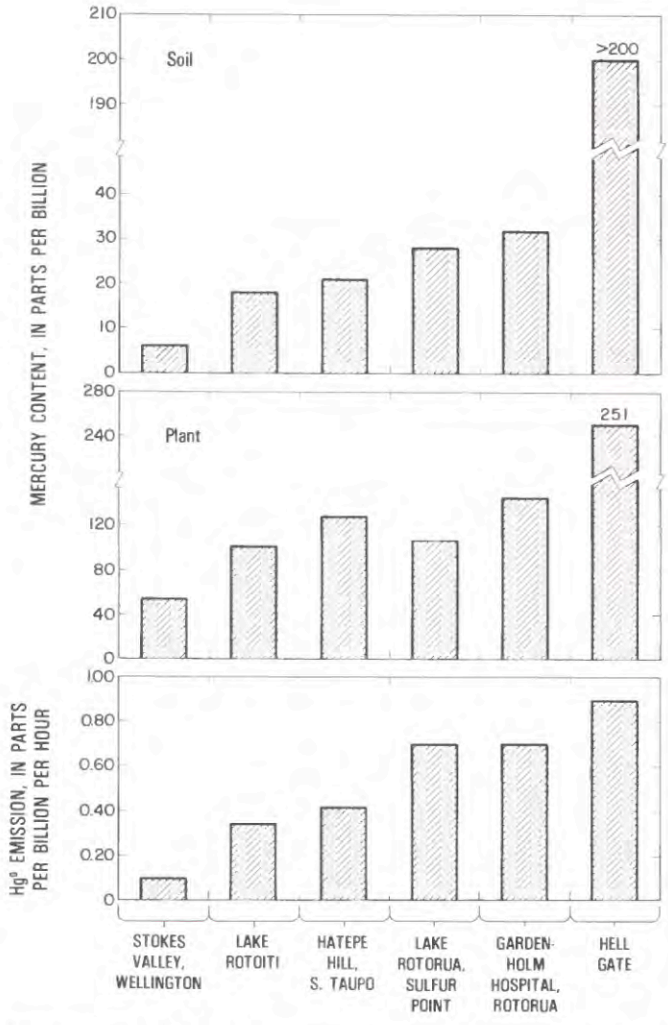

FIGURE 35.6.—Relation between mercury content of New Zealand soils and plants and rates of Hg^0 emission by *Leptospermum scoparium*.

Such recycling processes in local areas may well lead to diffuse patterns of mercury distribution. This has been noted in the lower Puna district, the eastern portion of the Island of Hawaii, site of the Kilauea east rift zone. Mercury levels in the leaves of the native forest tree ohia, *Metrosideros collina* var. *polymorpha*, follow approximately the mercury levels along the east rift zone, as does the mercury content of the soil in which the trees grow (figs. 35.7, 35.8). In contrast, the distribution of mercury in air (fig. 35.9) shows far more sharply defined areas of concentration than the mercury content of either plant or soil. This seems to imply the direct degassing process along the rift zone proceeds substantially faster than the release from soils and plants.

Biological release of Hg^0 is obviously a regulated process and it differs mechanistically from simple vaporization. Our data show that simple vaporization does occur in the soil; however, soil does not begin to release mercury until a concentration of about 25 μg/kg (ppb) is attained (fig. 35.10). It is, in any case, clear that the impact of the ecosystem on mercury cycling is as great as the impact of natural mercury emission on vegetation and the ecosystem, though they are of a different character.

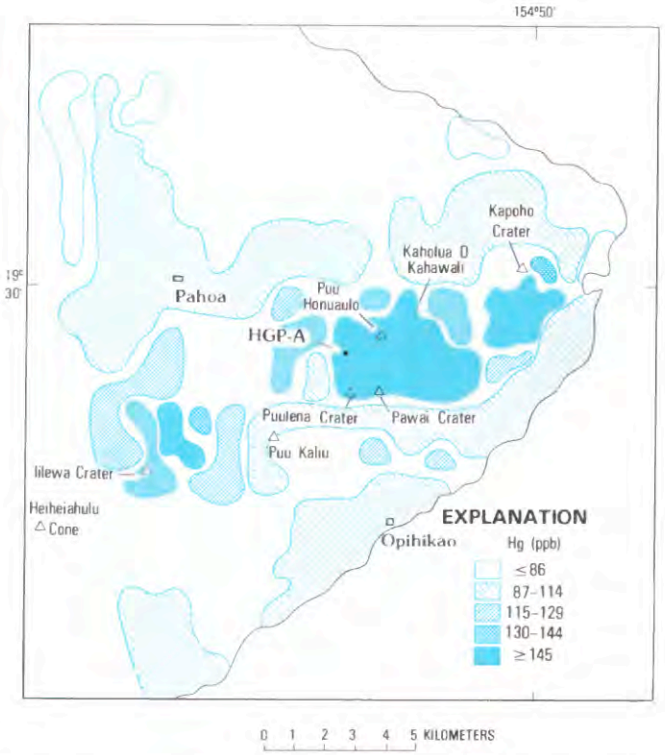

FIGURE 35.7.—Mercury content of ohia leaves (*Metrosideros*) East Puna District, Hawaii. Sampled areas delimited by closed lines; other areas not sampled because of poor access or other limitations. Samples collected between 1975 and 1982, excluding periods of heavy rains, strong winds, and volcanic eruptions. Midrange values of 87–114 ppb represent one standard error on either side of the mean for entire Puna collection.

REFERENCES CITED

Andren, W., and Nriagu, J., 1979, Global mercury, *in* Biochemistry of mercury in the environment: Amsterdam, Elsevier, p. 173–130.

Aylett, B.J., 1973, The chemistry of zinc, cadmium and mercury: New York, Pergamon Press, volume 18.

Ben-Bassat, D., and Mayer, A., 1975, Volatilization of mercury by algae: Physiologia Plantarum, v. 38, p. 128–132.

———1977, Reduction of mercury chloride by Chlorella: Physiologia Plantarum, v. 40, p. 157–162.

Bidstrup, P.L., 1964, Toxicity of mercury and its compounds: Amsterdam, Elsevier.

Boussingault, M., 1867a, Sur l'action deletere que la vapeur emanant du mercure exerce sur les plantes (premiere partie): Paris, Academie des Sciences Compte Rendu, v. 64, p. 924–928

———1867b, Sur l'action deletere que la vapeur emanant du mercure exerce sur les plantes (deuxieme partie): Paris, Academie des Sciences Compte Rendu, v. 64, p. 983–989.

Buhler, D.R. ed., 1973, Mercury in the western environment: Continuing Education Publication, Corvallis Oregon, Proceedings of a Workshop, Portland Oregon, February 25–26, 1971.

Cadle, R.D., 1975, Volcanic emissions of halides and sulfur compounds to the troposphere and stratosphere: Journal of Geophysical Research, v. 80, p. 1650–1652.

Carlin, C.E., Corigliana, P.J., Gastanaga, C.A., and Ochoa, L.R., 1960, Occupational risk in a mercury plant: Salud Ocupationale, v. 5, p. 3 (Abstract Bulletin of Hygeine, 1961, v. 36, p. 440).

Connor, J.J., 1979, Geochemistry of Vegetation, Puhimau Thermal Area, Hawaii: Science of Total Environment, v. 12, p. 241–250

Deiman, Paats, Van-Troostwyck, and Lauwerenburgh, 1979, Experiences sur l'action du mercure sur la vie vegetale: Annales de Chimie, Paris, v. 21, p. 122–127.

Dizon, G.D., Anselmo, J.E., and Villanueva, J., 1960, Examination of the risk in mercury mine in the Philippines: Medicale Seguridad Trabido, v. 8, p. 29. (Abstract Bulletin of Hygeine, 1961, v. 36, p. 745).

Eshleman, A., Siegel, S.M., and Siegel, B.Z., 1971, Is mercury from Hawaiian volcanoes a natural source of pollution?: Nature, v. 233, p. 471–472.

Goldschmidt, V., 1954, Geochemistry: Oxford, Clarendon Press, p. 287.

Goldwater, L.J., 1951, The toxicology of inorganic mercury: New York Academy of Sciences Annals, v. 65, p. 498–503.

Goren, R., and Siegel, S.M., 1976, Mercury-induced ethylene formation and abscission in citrus and coleus explants: Plant Physiology, v. 57, p. 628–631.

Harrington, 1917, Further studies of the germination of Johnson grass seeds: Proceedings of the Association of the Official Seed Analysts of North America 1916–1917, p. 71–70

Hem, J.D., 1970, Chemical behavior of mercury in aqueous media, *in* Mercury in the Environment: U.S. Geological Survey Professional Paper 713, p. 19–24.

Hunter, D., 1955, The Disease of Occupations: London, English Universities Press, p. 256.

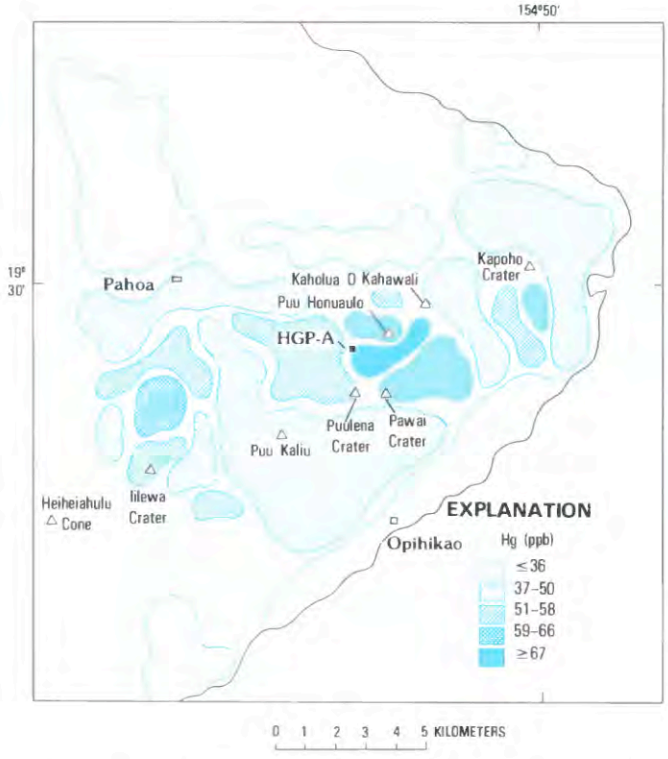

FIGURE 35.8.—Soil mercury content in East Puna District, Hawaii. Samples areas delimited by closed lines; other areas not sampled because of poor access or other limitations. Samples collected between 1975 and 1982, excluding periods of heavy rains, strong winds, and volcanic eruptions. Midrange values of 37–50 ppb represent one standard error on either side of the mean for entire Puna collection. Symbols same as in figure 35.7.

FIGURE 35.9.—Atmospheric mercury content in East Puna District, Hawaii. Sample areas delimited by closed lines; other areas not sampled because of poor access or other limitations. Midrange values of 96–191 ng/m^3 represent one standard error on either side of the mean for entire East Puna collection. Samples collected between 1975 and 1982, excluding periods of heavy rains, strong winds, and volcanic eruptions. Triangles, volcanic cones and vents; squares and rectangles, villages; dashed lines, roads; numbers in circles identify highways; HGP–A, Hawaii Geothermal Project—Abbott.

Jensen, S., and Jernelov, A., 1969, Biological methylation of mercury in aquatic organisms: Nature, v. 223, p. 753–754.

Kama, W., and Siegel, S.M., 1980, Volatile mercury release from vascular plants: Organic Geochemistry, v. 2, p. 99–101.

King, C.V., 1951, Mercury: Its scientific history and its role in physical chemistry and electrochemistry: New York Academy of Sciences Annals, v. 65, p. 360–368.

Le Van, W.C., 1930, The effects of metals on the respiration of *Lupine albus*: American Journal of Botany, v. 17, p. 381–395.

Macdonald, G.A., and Abbott, A. T., 1970, Volcanoes in the Sea, The Geology of Hawaii: Honolulu, Hawaii, The University Press of Hawaii, 441 p.

Matthes, R.T., Kirschner, R., Yow, M.D., and Brenna, J.C., 1958, Acute poisoning associated with inhalation of mercury vapor: Pediatrics, v. 22, p. 675.

Nriagu, J., ed., 1979, Biogeochemistry of Mercury in the Environment: Amsterdam, Elsevier North-Holland Biomedical Press, 696 p.

Phelps, D., Siegel, B., Siegel, S., Buseck, P.R., Copp, J., Hinkle, M., and Casadevall, T., 1979, The distribution of Hg in the Puhimau Area, Hawaii Volcanoes National Park: [abs.] American Geophysical Society Meeting, San Francisco, Dec. 3–7, 1979.

Piotrowski, J.K., and Coleman, D.O., 1980, Environmental hazards of heavy metals: Summary evaluation of lead, cadmium and mercury: Global Environmental Monitoring System Programme Activity, London.

Ramel, C., 1969, Genetic effects of organic mercury compounds. I. Cytological investigations on *Allium* roots: Hereditas, v. 61, p. 208–230.

Rankama, K., and Sahama, T.G., 1950, Geochemistry: Chicago, University of Chicago Press, p. 334.

Ratsek, J.C., 1933, Injury to roses from mercuric chloride used in soil for pests: Floral Review, v. 72, p. 11–12.

Siegel, B.Z., Lasconia, M., Yaeger, E. and Siegel, S.M., 1984a, The phytotoxicity of mercury vapor: Water, Air and Soil Pollution, v. 23, p. 15–24.

Siegel, B.Z., and Siegel, S.M., 1978, The Hawaii geothermal project: An aerometric study of the Kalalua eruption of 1977: Environmental Science and Technology, v. 12, p. 1036–1039.

———1979a, Biological indicators of atmospheric mercury, *in* Nriagu, J., ed., The biochemistry of mercury in the environment: Amsterdam, Elesevier/North-Holland Biomedical Press, p. 131–159

———1979b, Mercury and other toxic emissions from Kilauea: Site and time patterns: Division of Environmental Chemistry, ACS/CSJ Chemical Congress, Honolulu, Hawaii, April 1979, Abstracts, part 1, No. 30.

———1982, Mercury content of *Equisetum* plants around Mount St. Helens one year after the major eruption: Science, v. 216, p. 292–293.

Siegel, B.Z., Siegel, S.M., and Horsky, S., 1984, *Equisetum* plants and the cycling of mercury at Mount St. Helens: Environmental Science and Technology, v. 18, p. 174–181.

Siegel, S.M., 1977, The cytotoxic response of *Nicotiana* protoplasts to metal ions: A survey of the chemical elements: Water, Air, and Soil Pollution, v. 8, p. 293–304.

Siegel, S.M., Eshleman, A., Umeno, I., Puerner, N., and Smith, C.W., 1973a, The general and comparative biology of toxic metals and their derivatives: Mercury and Lead: Mercury in the western environment: Oregon, Continuing Education Publishing Company.

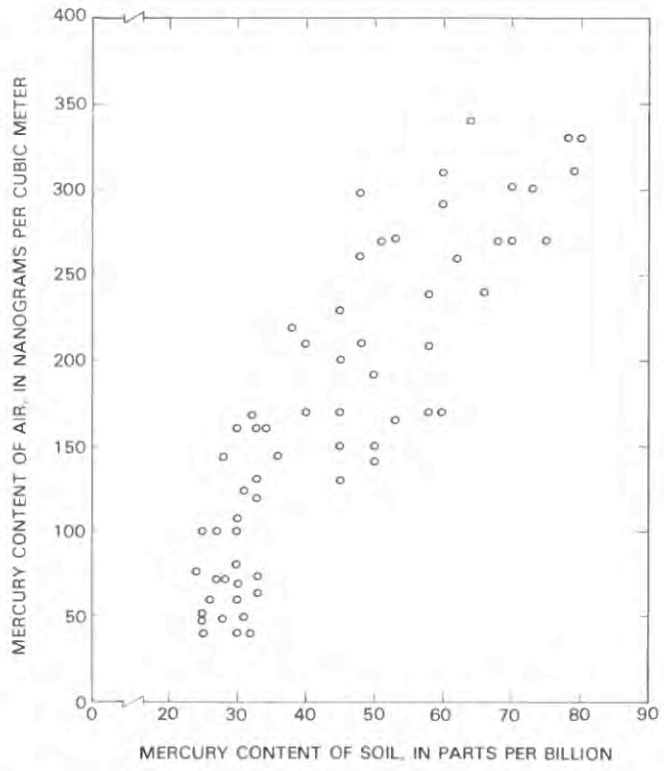

FIGURE 35.10.—Relation between atmospheric and soil mercury in East Puna District, Hawaii. Data represent replicated analyses of air and soil at same locations for 63 sample sites.

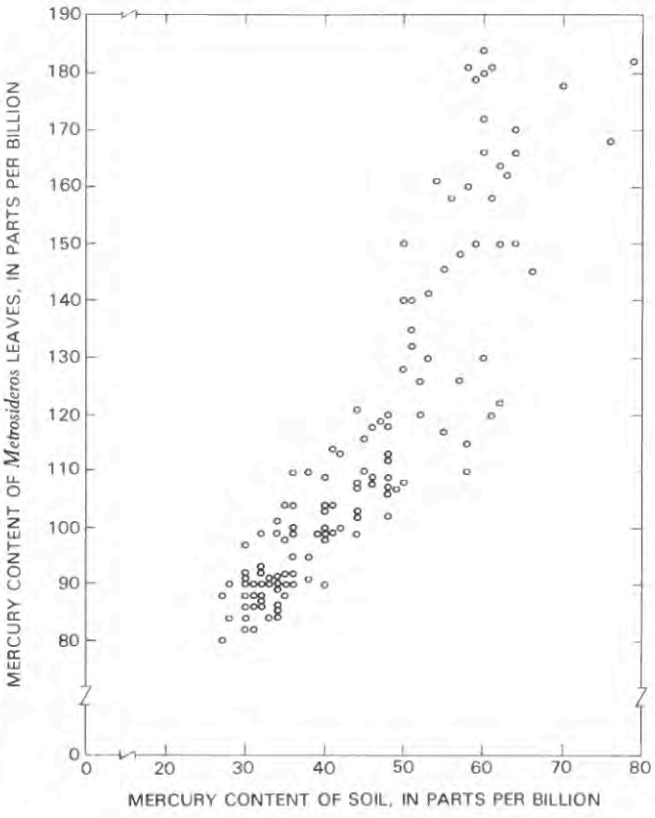

FIGURE 35.11.—Relation between mercury content of ohia leaves and soil in East Puna District, Hawaii. Data represent replicated analyses of leaves and soil at the same location for 121 sample sites.

Siegel, S.M., Okasako, J., Kaalakea, P., and Siegel, B.Z., 1980a, Release of volatile mercury from soils and non-vascular plants: Organic Geochemistry, v. 2, p. 139–140.

Siegel, S.M., and Siegel, B.Z., 1977, Mercury fallout in Hawaii: Water, Air, and Soil Pollution, v. 9, p. 113–118.

———1980, Hawaii Energy Resource Overview: Geothermal, Siegel, B., ed., The Environmental Impact, UCRL–1552. Vol. 4. National Technical Information Service (NTIS), DE830–12947. p. 7–14, 99–127, 138–146.

———1983, Vegetation and the atmospheric cycling of mercury: Advanced Space Research, v. 3, p. 135–139.

———1984a, First estimate of annual mercury flux at the Kilauea main vent: Nature, v. 309, no. 5964, p. 146–147.

———1984b, Regional differences in plant-soil mercury relations in *Equisetum*, *Plantago* and *Taraxacum*: Organic Geochemistry, v. 5, no. 4, p. 255–257.

———1985, Differential elimination of mercury during maturation of leguminous seeds: Phytochemistry, v. 24, p. 235–236.

Siegel, S.M., Siegel, B.Z., Eshleman, A.M., and Bachman, K., 1973b, Geothermal sources and distribution of mercury in Hawaii: Environmental Biology and Medicine, v. 2, p. 81–89.

Siegel, S.M., Siegel, B.Z., Lipp, C., Kruckeberg, A., Towers, G.H.N., and Warren, H., 1985, Indicator plant-soil mercury patterns in a mercury-rich mining area of British Columbia: Water, Air, and Soil Pollution, v. 27, p. 73–85.

Siegel, S.M., Siegel, B.Z., and McMurtry, G., 1980b, Atmosphere-soil mercury distribution: The biotic factor: Water, Air, and Soil Pollution, v. 13, p. 109–112.

Siegel, S.M., Siegel, B.Z., Puerner, N., and Speitel, T., 1975. Water and soil biotic relations in mercury distribution: Water, Air, and Soil Pollution, v. 4, p. 9–18.

Simkin, T., Siebert, L., McClelland, L., Bridge, D., Newhall, C., and Latter, J., Jr., 1981, Volcanoes of the World: Stroudsburg, Penn., Smithsonian Institute, Hutchinson Ross Publishing Co.

Solhnan, T., 1957, Manual of Pharmacology 8th ed.: Philadelphia, Sauders, p. 1310.

United States National Academy of Sciences, 1977, An assessment of mercury in the environment: Washington, D.C.

Varekamp, J.C., and Buseck, P.R., 1981, Mercury emissions from Mount St. Helens during September 1980: Nature, v. 293, p. 555–556.

Vouk, V.B., Fugas, M., and Topolnik, Z., 1950, Environmental conditions in the mercury mine of Idria: British Journal of Industrial Medicine, v. 7, p. 168.

Wagman, D.C., Evans, W.H., Parker, V.B., Harlow, I., Bailey, S.M., and Schum, R.H., 1968, Selected values of chemical thermodynamic properties: National Bureau of Standards (US) Technical Note 270-3, p. 1–264.

Warkany, J., and Hubbard, D.M., 1953, Acrodynia and mercury: Journal of Pediatrics, v. 42, p. 365.

Zimmerman, P.W., and Crocker, W., 1933, The injurious effect of mercury vapor from biochloride of mercury in soil of rose houses: Florists Exchange, v. 81, p. 13

———1934, Plant injury caused by vapors of mercury and compounds of mercury: Contributions of the Boyce Thompson Institute, v. 6, p. 167–187.

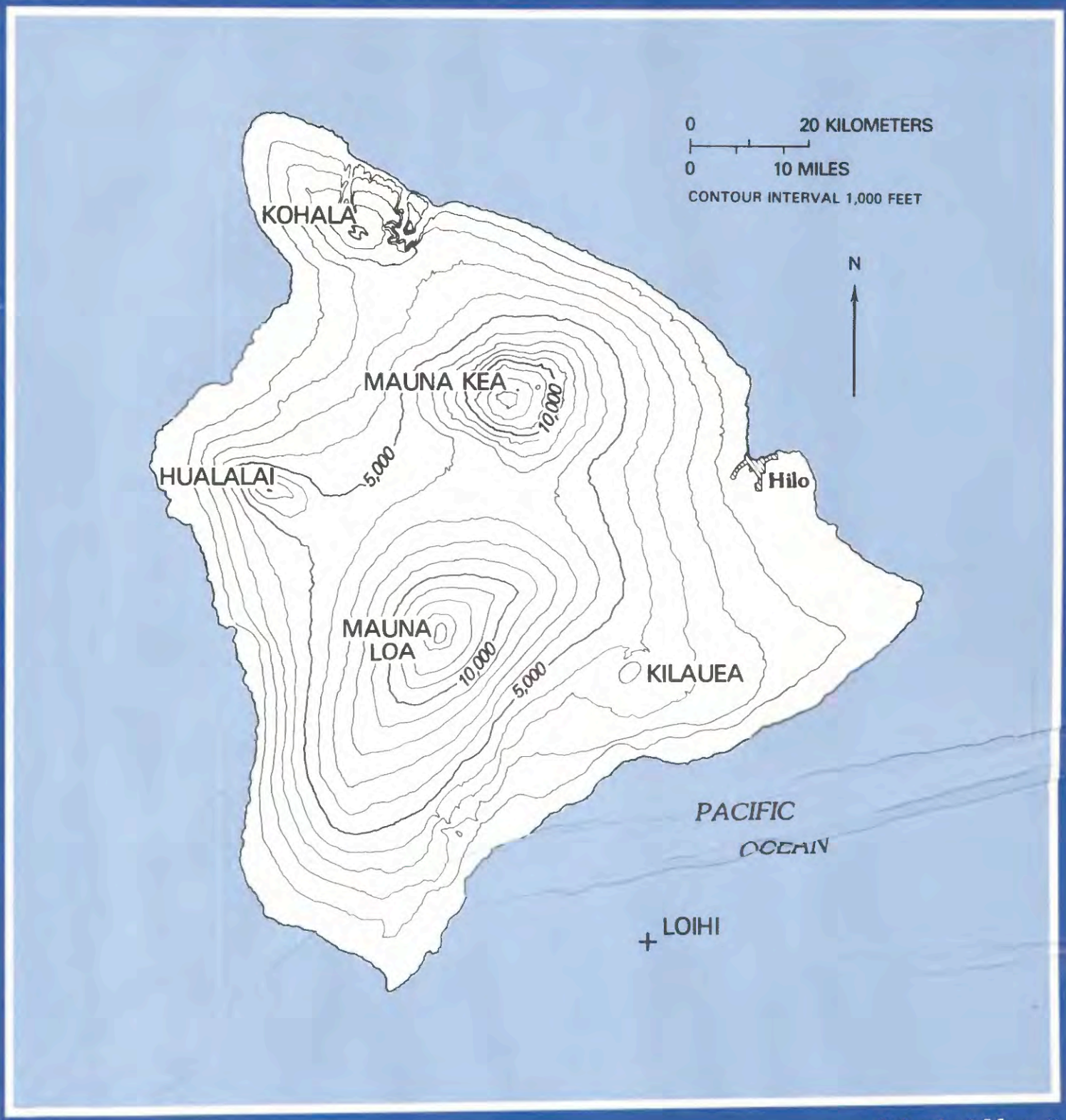

Island of Hawaii

U.S. DEPARTMENT OF THE INTERIOR
March 3 1849